がん幹細胞ニッチを標的とした新規治療法の開発

平成24年度～平成28年度　私立大学戦略的研究基盤形成支援事業

研究成果報告書

平成29年4月

学校法人名　　東海大学
大学名　　東海大学
研究組織名　　大学院医学研究科がん幹細胞研究センター
研究代表者　　安藤　潔（大学院医学研究科がん幹細胞研究センター長
教授）

目次

1、研究概要　及び　研究成果

研究代表者;安藤　潔

（1）研究プロジェクトの目的・意義及び計画の概要

がんは日本人の死亡原因の第一位を占めており、その撲滅は国民の悲願である。肺癌、大腸癌、乳癌、白血病、リンパ腫などの一部の腫瘍では近年の分子標的薬の開発で予後の改善が認められているが、多くの進行癌ではいまだに有効な治療法がなく、新しい発想による新規治療法の開発が望まれている。がんの維持と進展にはがん幹細胞およびそのニッチが重要な役割を果たしていることが明らかとなってきた。しかしながらがん幹細胞を標的とした治療研究が進展している一方で、ニッチを標的とした研究は未開拓の領域である。本学にはこの分野で先進的かつ独創性の高い研究を推進している複数のグループが存在しており、本プロジェクトにおいてこれらのグループを統合してがん幹細胞ニッチを標的とした新規治療法の開発を集約的に行う。具体的には、1）がん幹細胞のニッチからの離脱を促す PAI-1 阻害薬、2）ニッチ構成分子である Notch ligand を標的とした創薬、3）新規がん幹細胞分子を標的としたペプチドワクチン療法の開発、4）新規治療標的の探索を目指す。また本プロジェクトを遂行する過程でヒトの種々の疾患に対するモデル動物を開発するのみでなく、疾患の克服のために独自の方法で候補化合物（リード化合物）を見出し、NOG マウスを利用した異種移植系（ヒト化マウス）により前臨床試験をできるだけ迅速に進めるシステムを開発することができ、これらは他の標的に対しても利用可能となる。本研究により創出された新規治療はがんの治癒、進展の制御による QOL の向上をもたらし、国民の健康福祉に貢献することが期待される。

学術的特色・意義として以下の4点をあげておきたい。

1）がん治療研究においてがん幹細胞を標的とした治療研究が進展している一方で、ニッチを標的とした研究は未開拓の領域であり、それを推進する点が本研究計画の特色である。

2）ヒト癌幹細胞とニッチの相互作用を研究するためには in vivo モデルが必要であるが、そのためには申請者の安藤、中村が実験動物中央研究所と共同開発した NOG マウスを利用することが最も有効な方法であり、本研究計画の特色である。

3）本研究により創出された新規治療はがんの治癒、進展の制御による QOL の向上をもたらし、国民の健康福祉に貢献することに意義がある。

4）わが国発の新規薬剤を創出することにより、経済の活性化に貢献することに意義がある。

（2）研究組織

学内のがん研究、幹細胞ニッチ、血管新生の専門家を集約したグループにより、研究および若手研究者の育成の拠点としている。研究代表者は、5つの研究プロジェクトが相互に連携をとりながら、全体の研究計画の責任者として統括する。研究プロジェクトは1）血液腫瘍（安藤・中村・平山・八幡・松下・他研究員等・学外者（伊藤・宮田・Anderson）計 14 名）、2）乳癌骨転移(徳田・持田・佐藤・酒井・新倉・他研究員等計 12 名)、3）婦人科癌(三上・亀谷・椎名・他研究員等計 6 名)、4）消化器癌と血管ニッチ（猪口・浅原・小澤・増田・他研究員等計 5 名）、5）Notch ligand(穂積・稲垣・他研究員計 3 名)を研究テーマとするグループで構成されている。グループには医学部内の血液・腫瘍内科学、乳腺外科学、消化器外科学、婦人科学、分子生命科学、免疫学などの研究者、大学院生（2名）、奨励研究員（6名）等が参画し，各分担者がグループを統括する。また、国内外のグループと共同研究も推進する。研究進捗状況は、毎月の進捗状況報告会で議論され、各プロジェクトで研究内容の連携できる項目等を確認し、

評価指標の達成度も確認する。研究計画の倫理的側面および各種指針の遵守に関しては、学内の各種委員会で承認を得て遂行される。研究成果の評価は外部委員により評価を受け、必要に応じ研究方針を修正する。共同研究機関である実験動物研究所、東北大学の宮田研究室とは頻繁に研究打ち合わせ、報告会を設けて常に連携が取れる状況を作っている。研究支援体制は、研究補助の一部を生命科学統合支援センター、本事業の予算管理を伊勢原教学課、科研費・研究委託等の外部資金管理を伊勢原研究支援課と連携して行っている。

(3)研究施設・設備等

[研究施設]

本プロジェクトに係わる研究施設としては、伊勢原校舎1号館6階の各研究室(計 863.25 ㎡)を利用している。利用者は延べ50人を越えており、当初の申請に対し平成26年度より6G12a・b 研究室を追加した。

[装置・設備]

装置・設備では、下記のものを主に利用しており、細胞や組織解析のためにフル稼働している。

共焦点レーザスキャン顕微鏡システム[LSM510META](平成19年度整備):稼働時間12時間/日

凍結ミクロトーム[CM3050SIV](平成19年度整備)::稼働時間12時間/日

細胞分析器(平成24年度整備):稼働時間6時間/日

蛍光顕微鏡(平成24年度整備):稼働時間稼働時間6時間/日

実験動物用 X 線 CT 装置(平成25年度整備):稼働時間2時間/日

(4)研究成果の概要

本プロジェクトでは、がん幹細胞ニッチを標的とした新規治療法の開発を目的として学内外のグループと戦略的に研究を遂行するための基盤形成を行う。具体的には、1)造血腫瘍、2)乳癌骨転移、3)婦人科癌、4)消化器癌、5)Notch ligand を中心としたがんニッチ基礎研究、を研究テーマとするグループを構成し、相互に連携をとりながら全体の研究計画を遂行する。以下、テーマごとに研究の成果、課題、対応状況を報告する。

1 造血腫瘍グループ

造血器腫瘍の発症機序の解明や治療法の開発に取り組んでおり、以下にあげる(1)～(5)の成果を得ている。

＜優れた成果が上がった点＞

(1)造血幹細胞制御における PAI-1 の役割:ニッチ因子としての分泌性 PAI-1 の意義の解明

野生型 C57BL6 マウス、PAI-1 欠損マウスに致死量放射線を照射後、野生型マウスより採取した骨髄細胞を静脈内に移植した。生理食塩水あるいは PAI-1 阻害薬を移植当日から1日1回、5日間にわたって連続投与した。血漿と骨髄細胞を採取し、ELISA 法およびフローサイトメトリーを利用して、各種造血再生因子の発現や造血幹細胞の増幅等を解析した。また、組織科学的な手法により骨髄ニッチの状態を観察した。これらの解析により、以下の成果を得た。

放射線照射などの造血ストレスが負荷されると、造血ニッチ細胞は PAI-1 を高産生し、tPA 主導のサイトカイン産生を阻害することによって造血幹細胞の増殖を抑制することを明らかにした。

骨髄移植において、本学で開発した PAI-1 阻害薬を用いて PAI-1 活性を抑制することによって、造血再生の迅速化のみならず、長期間にわたる造血系の恒常性の維持が達成された。

(2)造血幹細胞制御における PAI-1 の役割:TGF-ぁによって誘導される細胞内 PAI-1 の意義の解明

野生型 C57BL6 マウスに PAI-1 阻害剤あるいは TGF-ぁ阻害剤を5日間連続投与後、末梢血を回収し、骨髄ニッチを離脱した造血幹細胞の割合を解析した。フローサイトメトリーを利用して PAI-1 や Furin の細胞内発現を検討した。また、PAI-1 阻害剤によるニッチからの離脱は MT1-MMP 依存的であることを確認するために、抗 MT1-MMP 抗体を投与した阻害実験を行った。これらの解析により、以下の成果を得た。

ニッチが産生する TGF-ぁによって造血幹細胞に PAI-1 発現が誘導されることを発見した。

造血幹細胞に発現する PAI-1 は細胞内で機能し、セリンプロテアーゼである Furin の活性を阻害することによって細胞表面の遊走因子である MT1-MMP が成熟型に変換することを抑制することを明らかにした。

細胞内 PAI-1 は、造血幹細胞の運動性を抑制し、ニッチに留めることを明確にした。

TGF-ぁ-PAI-1 シグナルを阻害すると、造血幹細胞はニッチから離脱し、末梢循環血中に動員されることを見出した。

(3)白血病幹細胞の TKI 耐性における PAI-1 の役割の解明

マウス造血前駆細胞株である 32D 細胞に BCR-ABL 遺伝子を導入し、CML 様細胞として TKI 感受性などを検討した。この細胞株に PAI-1 cDNA のトランスフェクションにより過剰発現させたもの、あるいは CRSPR/Cas9 法により PAI-1 発現を欠損させたものを作製した。CML 幹細胞の解析は、マウス造血幹細胞に BCR-ABL 遺伝子を導入し、移植することによって CML を発症させたマウス骨髄を利用した。治療実験は、生理食塩水群、TKI 単剤群、TKI と PAI-1 阻害剤の併用群を用意し、CML 細胞の生着や生存率を解析した。これらの解析により、以下の成果を得た。

造血幹細胞と同様に、ニッチが産生する TGF-ぁによって CML 幹細胞に PAI-1 発現が誘導されることを見出した。

CML 細胞に PAI-1 を過剰発現させると TKI 抵抗性になり、逆に PAI-1 を欠損させると TKI 感受性になることから、CML 細胞内に発現する PAI-1 の多寡が TKI 感受性を決定することを明らかにした。

CML モデルマウスを利用した治療実験系において、TKI と PAI-1 阻害剤を併用すると、CML 幹細胞の減少や生存率の向上など TKI 単剤群に比べて顕著な治療効果が認められた。

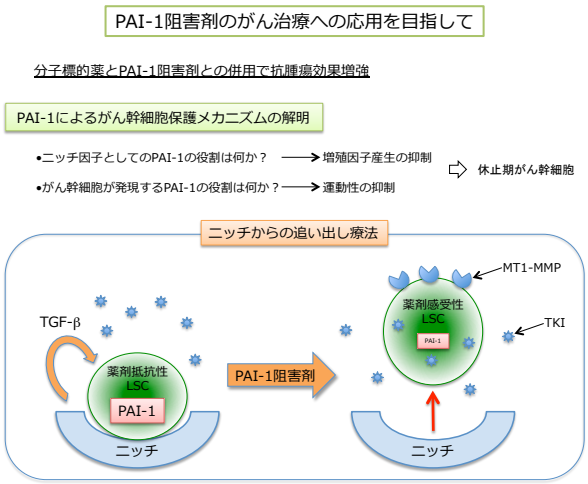

(4)低酸素ニッチにおけるがん幹細胞に対する VitC 治療の開発

白血病細胞は骨髄低酸素ニッチに存在し、HIF-1α 活性化による glucose transporter の発現上昇を介して glucose と同時に VitC の取り込みも上昇している。このことを利用して白血病に対する VitC(以下 L-AA)治療の有用性を示した。

L-AA がヒト正常造血幹細胞/前駆細胞の生存・増殖には影響を与えない濃度レベルで、様々なヒト白血病細胞株とリンパ腫細胞株の生存・増殖に対して著明な抑制効果を発揮することを確認した。

L-AA の抗腫瘍効果は、過酸化水素の産生だけではなく、腫瘍細胞のニッチとの interaction に深く関わっている低酸素誘導因子(HIF-1α)の発現を抑制することが大きく関与していることを、HIF-1α を過剰発現させたヒト白血病細胞株を移植した免疫不全マウスを用いた実験系で確認した

再発リンパ腫症例を対象に高濃度 L-AA の第 I 相臨床試験を実施して、その安全性とともに、非投与時に比して 250 倍以上の L-AA 血中濃度が得られることも確認した。

(5)がんニッチ間相互作用(インタラクトーム)解析により新規治療標的分子の特定

がんが生育する生体内では、「がん細胞」とニッチ(下図 b)、「がん細胞」同士(下図 a)、ニッチ細胞同士(下図 c)といった複雑な相互作用が、様々な強さで生じており、同一個体内でがんの多様性を生ずる要因となっている。中でも「がん細胞」とニッチの間で特異的に起こっている相互作用(下図b矢印等)は、がんの進行や治療抵抗性の獲得に重要な役割を果たしてい

る。本研究ではこのようなインタラクトーム解析を利用して多発性骨髄腫とニッチの相互作用を担う分子を同定した。

骨髄環境側に発現するSDF－1と骨髄腫細胞に発現するCCXCR4が高い依存性をもって相互作用していることが定量的に明らかとなった。つまり、多発性骨髄腫では正常造血細胞と同様の幹細胞維持機構が働いている。

本解析により、CD38はニッチ側のCD31と、CD138はHGFと高い依存性をもって結合することが明らかとなった。CD31は血管内皮やマクロファージに発現することが知られており、骨髄腫細胞の血流を介した転移やニッチへの局在に関与し、細胞増殖や生存に機能している。また、CD138はHGFとcMetのシグナルを安定化することで、骨髄腫細胞の増殖に寄与していると考えられる。

インタラクトームによる相互作用の強さと依存度の相対的定量評価により、骨髄腫細胞とニッチの間で特に相互依存度が高い組み合わせを10程度抽出した。

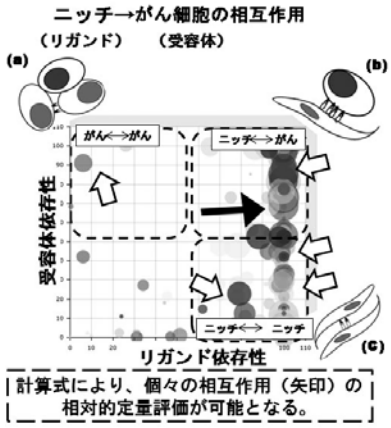

＜課題となった点＞

マウスで得られた知見がヒトにも応用できるものであるか否かは、臨床試験を実施することによって確かめる以外に方法がない。われわれが開発したPAI-1阻害薬のヒトにおける安全性、有効性を今後臨床試験により検証していく必要がある。インタラクトーム解析で同定された新規ニッチ因子は今後の機能解析が必要である。

＜自己評価の実施結果と対応状況＞

研究ミーティングの中で、各研究者は自己評価して適切に対応した結果、当初の期待以上の研究成果を得ることができた。

2　乳癌グループ

乳癌グループは胎盤と癌との類似性に着目し、がん幹細胞ニッシェが胎盤形成・維持機構を模倣すると仮定してヒト胎盤と癌の比較解析を行うとともに、妊娠免疫と腫瘍免疫がニッチ形成にどのように関わるのかを明らかにする為に免疫系の比較解析も行ってきた。また、霊長類モデルとしてのコモンマーモセットの評価も行ってきた。特に以下にあげる(1)～(3)の成果を得ている。

＜優れた成果が上がった点＞

(1)乳癌患者のHLAタイピングを行うと同時にin vitroでペプチド刺激を行い、IL-2産生能、細胞増殖能、活性化抗原の発現を指標にHLAとペプチドの有効性を解析し、効果の得られ

るHLAを同定した。
(2)実験動物中央研究所より提供されたヒトIL-4産生重度免疫不全マウスであるhIL4TgNOGマウスに様々な乳癌患者の末梢血単核球を移植し、申請者等が以前マウスで抗腫瘍効果を認めたHER2の部分ペプチドであるCH401MAPペプチドをアジュバントと共に投与した。このマウス末梢血の上清について抗腫瘍効果の評価を行ったところ、健常者と比較して特異抗体産生能が低いことが示された。ペプチドに対するHLA親和性をアルゴリズムで算出し、抗体産生能と比較したが、強い相関は観察されなかった。また、HER2/neu 抗原が発現していなくてもHER2抗体の産生が観察された。
(3)乳癌における新規Her2ペプチドワクチンCH401MAPの患者末梢血における反応性を明らかにした(Tsuda et al. 2012)。CH401MAPが、大部分の日本人HLAに提示されるモチーフを持つ事、末梢血を刺激する事によりリンパ球の反応性が得られる事が明らかになった。
＜課題となった点＞
以上の結果より、改良NOGマウスであるNOG-IL-4-Tgマウスを用いて、ヒト免疫系をある程度再構築できること、また、これらのマウスを用いて、新規 HER2 ペプチドワクチン候補であるCH401MAP に対する乳がん患者の抗体産生能を評価することができることが明らかになった。この系を用いて、検体のHLAと抗体産生能について比較解析を行ったが、今まで汎用されてきたアルゴリズムと抗体産生能は必ずしも一致せず、アルゴリズムによるペプチド提示能予測は必ずしも抗体産生能の予測とはならないことが明らかとなった。今後の検討が必要である。またヒトにおける臨床試験を予定している。
＜自己評価の実施結果と対応状況＞
研究ミーティングの中で、各研究者は自己評価して適切に対応した結果、十分な前臨床の成果を得ることができた。

3 婦人科癌グループ
婦人科癌グループは胎盤と癌との類似性に着目し、がん幹細胞ニッシェが胎盤形成・維持機構を模倣すると仮定してヒト胎盤と癌の比較解析を行うとともに、妊娠免疫と腫瘍免疫がニッシェ形成にどのように関わるのかを明らかにする為に免疫系の比較解析も行った。また、この研究に必須の in vivo 霊長類モデルとしてコモンマーモセットが使用できるのかについての評価も行った。その結果、特に以下にあげる(1)～(4)の成果を得ている。
＜優れた成果が上がった点＞
種々のサイトカインおよび TCR の発現を定量的に測定できる事を可能とし、マーモセットCD117+細胞が機能的なマスト細胞に分化する事を報告した。さらに、これらの細胞が T 細胞にも分化すること、ヒトと異なり、B 細胞分化は先行しないことを明らかにした。また、IL-2Rg 遺

伝子をゲノム編集によりノックアウトしたマーモセットのリンパ球を解析し、ヒトと異なり、IL-2Rgを KO しても T 細胞が分化することを明らかにした。
担癌状態で亢進する調節性 T 細胞に発現する HLA-G のマーモセットオーソログ遺伝子構造を明らかにした。また、ブタ MHC(SLA)については、遺伝子上の3種類の class-I 遺伝子が活性化とともに連動して発現亢進する事が明らかになった。さらに SLA のアロタイプ特異的なモノクローナル抗体を作製し、遺伝子座特異的な mRNA 発現とタンパク質発現の間に相違があることを明らかにした。
神経栄養因子受容体であり、卵胞の生育にも重要な役割を果たす癌遺伝子 TrkB アイソフォームの発現が、明細胞腺癌で異なる事を明らかにした。また、この遺伝子の発現をヒトおよびマーモセット胎盤で確認し、そのアイソフォームの発現が、胎盤局所において変化することについても明らかにした。これらの結果は、ヒト・マーモセットのいずれの動物種でも観察され、マーモセットがこの現象に関しては動物モデルとなりうることが示唆された。さらに、胎盤および癌の免疫学的ニッシェの同定に必要なマーモセット NK 細胞の性状を明らかにした。
(4)マーモセットおよびヒトの妊娠初期・中期・後期の末梢血より血漿を採取し、これらの血漿成分の LC/MS 解析を行った。その結果、ヒトでは妊娠中期に血漿中で亢進する PZP が、マーモセットでは亢進しないこと、代わりに、同じ arpha-2-macrogulobulin (A2M)ファミリーである arpha-2-macroblobulin-like 1 (A2ML1)が亢進することを明らかにした。
＜課題となった点＞
マウス、マーモセットで得られた知見がヒトでもあてはまるかいなかを今後臨床サンプルで確認する必要がある。
＜自己評価の実施結果と対応状況＞
研究ミーティングの中で、各研究者は自己評価して適切に対応した結果、十分な前臨床の成果を得ることができた。

4 消化器癌グループ
癌による腫瘍増大及び癌転移において重要な役割を担う癌ニッチの血液細胞群の修飾による癌ニッチ崩壊戦略を提案し、その基礎研究を実施した。癌ニッチは、炎症性血管を構築し、制御性 T 細胞や M2 マクロファージなどの抗炎症性および免疫制御性細胞を動員し、炎症性および免疫賦活化 CD8+T 細胞、NK 細胞、M1 マクロファージなどの癌細胞傷害性細胞浸潤が抑制された環境として、いわば「癌バリアー」を獲得し、癌細胞増殖、腫瘍増大を容易にしている。この癌ニッチにおけるを炎症性および免疫賦活性環境の表現型に変換することによる癌ニッチの「癌バリアー」崩壊を抗癌戦略として提案した。
＜優れた成果が上がった点＞

(1)抗 VEGF 抗体(Avastin)による炎症環境の修飾による癌ニッチに及ぼす影響を明らかにした。すなわち、Avastin は、癌幹細胞において炎症性、抗炎症性細胞群のいずれにおいてもEPC の血管形成能力を低下させると考えられ、腫瘍血管新生に抑制的に働く一方で、腫瘍の壊死を促進し、癌ニッチの炎症を促進する可能性が示唆された。(下図1, 2)

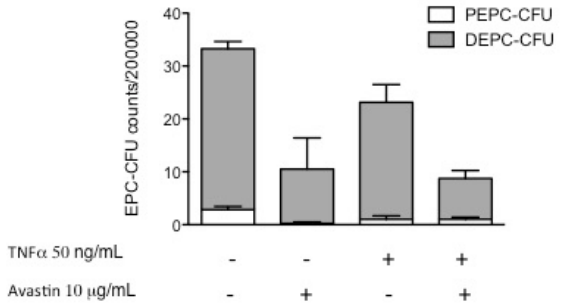

図1. AvastinによるEPCコロニー形成能抑制作用。
AvastinまたはTNF-alpha添加を添加したヒト末梢血単核球の抗炎症性・血管形成性培養細胞(AInVC)のEPCコロニー産生能。

(2)癌ニッチ制御による新たな制癌戦略の開発

傷害組織の再生と同様に、癌組織においても抗炎症及び血管の成熟化による機能性血管の構築が抗癌において重要であることが示された。この知見より新たな制癌戦略として、抗炎症性環境及び機能性血管の構築による癌ニッチの崩壊促進療法の開発が期待される。

＜課題となった点＞

マウスで得られた知見がヒトでもあてはまるかいなかを今後臨床サンプルで確認する必要がある。

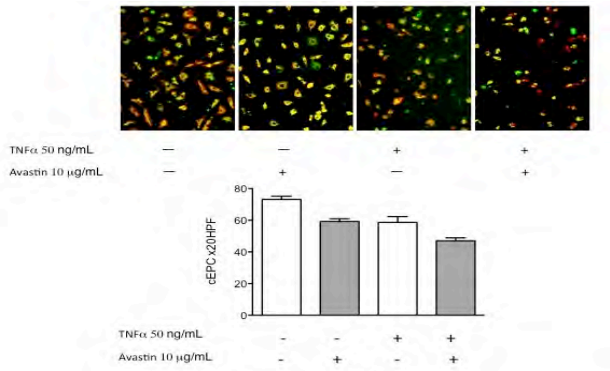

図2. Avastinによるコロニー非形成性EPC産生抑制作用。
AvastinまたはTNF-alpha添加を添加した末梢血単核球のEPC培養アッセイ。

＜自己評価の実施結果と対応状況＞

研究ミーティングの中で、各研究者は自己評価して適切に対応した結果、十分な前臨床の成果を得ることができた。

5　Notch ligand を中心としたがんニッチ基礎研究グループ

Notch 系は種を越えて広く保存され、細胞膜上に発現した Notch 分子（哺乳類では Notch1-4）がそのリガンド（NotchL；哺乳類では Dll1、Dll4、Jag1、Jag2）と結合することで誘導されるシグナルが種々の細胞の系列決定に寄与する、広く共有されたシステムである。Notch シグナルが基本的作用機構として分化抑制と増殖誘導を有することから、未分化細胞の「多能性」を保持するニッチ分子として NotchL の関与が想定されている。本研究では各組織に固有のニッチ分子として NotchL を想定し、特に骨髄、胸腺、膵臓での幹・前駆細胞ニッチとしての機能を追求した。また、増殖や生存維持、腫瘍化との関連における NotchL の機能について、血液腫瘍と NotchL 改変マウスを用い、NotchL の機能について検証した。さらに、NotchL 機能発現に重要な細胞外ドメインの NotchL 特異性について精査し、pan-Notch シグナル阻害薬（gamma-secretase inhibitor）に認められる腸管上皮細胞不全の誘導を回避し、Notch/NotchL の各分子相互作用に特異的な抑制薬の開発に向けた情報の整理を目指した。特に以下にあげる（1）～（4）の成果を得ている。

＜優れた成果が上がった点＞

（1）多発性骨髄腫（Multiple Myeloma、MM）のボルテゾミブ耐性を促す腫瘍ニッチ分子としての Notch リガンド：Jagged1 の役割を明らかにした。ヒト MM 細胞における Notch 分子の発現を詳細に調べ、Notch リガンド存在下での MM 細胞への挙動の変化について確認した。また、我々が独自に作製したヒト NotchL 発現 NOG マウスを用いて、Notch シグナル誘導環境における MM の振る舞いを、in vivo モデルにて検討した。さらに、BTZ 存在下での MM 細胞の治療抵抗性について精査した。この結果、MM 治療に際し大きな問題となる BTZ 耐性が、腫瘍環境要因としての Jag1 を介して誘導される Notch シグナルによってもたらされることを、初めて明確にした。

（2）Notch リガンド機能発現に寄与する細胞外ドメインの重要性を明らかにした。これまで機能的意義が不明瞭であった Dll 分子 N 末（MNNL）領域に着目し、キメラ分子を作製しその機能を調べた。その結果、Dll4 分子の MNNL 領域がきわめて機能的に重要であることが判明し、逆に、Dll1 分子の MNNL 領域はほとんどその機能に寄与していないことが示唆された。以上の結果は、2つの Dll 分子は、少なくとも Notch1 を介したシグナル発動に際し、それぞれ異なる領域を中心として機能していることを示している。この結論は、これまでの Notch リガンド研究からはまったく想定されてこなかったものであり、より詳細な分子機構の解明が待たれる。

（3）Notch リガンドによる幹細胞・未分化細胞の分化制御における役割を明らかにした。我々が独自に作製した a1Col-hDll1（D1 Tg）マウスは、マウス a1-collagen プロモーター制御下にヒト Dll1 を配した遺伝子改変マウスであり、未分化骨芽細胞を含む骨芽細胞系列にてヒト Dll1

の発現が確認できる。D1 Tg マウスでは、出生直後より、過剰な骨化が進行する一方、骨代謝回転は著しく低下していた。同マウス骨髄内では、胎齢後期よりOsterix 陽性未分化骨芽細胞の異常増殖を認め、その結果、幼若な骨組織の拡大と骨髄腔の縮小が観察された。この形質は、Dll1 に特徴的であり、同様に作製した hJag1 発現マウスでは、そうした形質は見出されなかった。D1 Tg マウスでは、Osterix 陽性細胞の異常増殖に伴い、Osteocalcin 陽性の骨細胞への分化が抑制されており、未分化骨芽細胞期にて分化が停滞しているものと推測された。また、骨芽細胞分化不全に付随して破骨細胞分化が抑制されており、結果として、骨代謝回転が大きく低下していた。同マウス骨間葉系細胞の培養から、そうした形質が再現される一方、本培養系での Dll1 遺伝子欠損の誘導により、未分化骨芽細胞が減少するとともに骨細胞への分化が促進される、Dll1 過剰発現系とは逆の形質を認め、Dll1 が Notch リガンドとして生理的重要性を有することが示唆された。以上の結果から、Dll1 が、未分化骨芽細胞期の増殖・分化を精密に制御し、骨組織形成のバランスを維持していることが推察された。

（4）ヒト Notch1 細胞内断片と変異型 IL7Ra 鎖の発現による T 細胞白血病（T acute lymphoblastic leukemia、T-ALL）発症の分子機構を明らかにした。我々は、独自にヒト T-ALL 細胞株より変異型 IL7Ra 鎖（細胞膜領域挿入型）を単離し、同変異が造血細胞に IL7 非依存的な増殖能を付与することを見出した。本研究では、変異 IL7Ra 鎖を様々なマウス造血未分化細胞に導入することにより、その造腫瘍性について調べた。その結果、同遺伝子を造血幹細胞画分に導入すると、骨髄増殖症（myeloproliferative disorder）を促し、さらに Notch 細胞内断片との協働により、悪性度の高い T-ALL を発症することを示した。また、リンパ性前駆細胞（common lymphoid progenitors、CLP）への導入では、B-ALL 様の症状を呈した。以上の結果は、ヒト T-ALL にて比較的高頻度に認められる細胞膜領域挿入型 IL7Ra 鎖変異は、明らかな造腫瘍性を有し、発現時期に依存した細胞系列の血液腫瘍を誘導した。すなわち、血液腫瘍に共通するシグナル伝達機構として、JAK3-STAT5 系が機能する可能性が示唆された。また、その中で、Notch シグナルにより、明確な T-ALL 誘導を認め、ヒト T-ALL 発生要因における Notch シグナルの役割が注目された。今後、Notch シグナル発生要因として、骨髄・骨芽細胞上に発現する Notch リガンド：Dll4 の関与を明確にする必要がある。

＜課題となった点＞

すべての Notch/NotchL を介したシグナルを抑制する pan-Notch inhibitor は、Notch シグナル依存的な腸管上皮細胞の分化を抑制（杯細胞などの粘液分泌細胞が過剰に誘導される）するなどの副作用が強く、臨床上、問題となる場合が多い。よって、Notch/NotchL の組み合わせを特異的に制御する方策を実現する必要がある。我々は、Dll4 と Dll1 の機能的差異を特定する過程で、両 NotchL が、異なる領域を用いて Notch 受容体と結合・シグナル誘導を行うことを初めて明らかにした（投稿中）。こうした取り組みから得られる情報を整理し、Dll4 特異的

な抑制を実現できれば、ETP-ALL の効果的治療薬の開発に有用と考えられる。

＜外部（第三者）評価の実施結果と対応状況＞

下記のようにシンポジウムを開催し、外部評価を頂いた。

評価員は

吉田輝彦　先生（国立がん研究センター研究所　遺伝医学研究分野分野長）

佐谷秀行　先生（慶應義塾大学医学部先端医学研究所　遺伝子制御研究部門教授）

公開シンポジウム

「がん幹細胞ニッチを標的とした新規治療法の開発」

文部科学省私立大学戦略的研究基盤形成支援事業

2015年9月19日（土）15:00－17:00

（東海大学校友会館（霞が関ビル35階　望星の間）

THE INSTITUTE OF ME
TOKAI UNIVERSITY

共同開催公開シンポジウ
「がん幹細胞ニッチを標的とした新規治療法の開発」

文部科学省私立大学戦略的研究基盤形成支援事業
がん幹細胞を標的とした新規治療法の開発プロジェクト／東海大学総合医学研究所

2015年9月19日(土)15：00～17：00
東海大学交友会館(霞ヶ関ビル35階　望星の間)(参加費無料)

司会　安藤　潔

●15:00 開会の挨拶
安藤　潔
(東海大学医学部　内科学系　血液・腫瘍内科　教授)

●15:15 中村　雅登
(東海大学医学部　基盤診療学系
再生医療科学　教授)
「がんゼノ患者システムのインタラクトーム解析による、がん幹細胞－微小環境相互作用の多面的、多次元解析」

●15:35 幸谷　愛
(東海大学総合医学研究所造血腫瘍分野　准教授
東海大学医学部 血液・腫瘍内科　准教授
JST さきがけ研究者)
「癌幹細胞階層性とニッチの相互作用
～マイクロRNAの役割」

●15:55 亀谷　美恵
(東海大学医学部　基礎医学系
分子生命科学　准教授)
「乳癌幹細胞を標的とした新規
Her2ペプチドワクチンの開発」

●16:15 八幡　崇
東海大学医学部　基盤診療学系
再生医療科学　准教授)
「ニッチ因子を標的とした
白血病幹細胞治療法の開発」

●16:35
講評　吉田　輝彦
(国立がんセンター研究所
遺伝医学研究分野分野長)
佐谷　秀行
(慶応義塾大学医学部
先端医科学研究所
遺伝子制御研究部門教授)

●16:55 閉会の挨拶
瀧澤　俊也 (東海大学総合医学研究所所長)

【お問合せ先】東海大学医学部再生医学センター　〒259-1193 神奈川県伊勢原市下糟屋143　TEL. 0463-93-1121(内線：2700)

(1) 中村雅登:がんゼノ患者システムのインタラクトーム解析による、がん幹細胞－微小環境、相互作用の多面的、多次元解析

評価者1

【総合評価】A

【意見・感想】

・独創性の高い、貴重なバイオリソースを構築している。様々な機能解析や創薬研究に必須の資源となる。

・このリソースを活用する研究として、独創性の高い仮説「がん－間質の発現プロファイルのバランスの中で、継代を繰り返しても維持されるものが、がん幹細胞の中核となる分子経路である可能性」を追求しており、極めて魅力的である。

・データ駆動型研究として、対象とする分子経路自体は仮説に依存しないアプローチである。そのため、今後、whole transcriptome sequencing への展開、proteome の追加、sample size の増強と tumor subtype の網羅、継代毎の腫瘍の phenotyping、正常組織のプロファイルデータの追加等々、期待が広がる研究である。

・バイオリソース構築・維持・品質管理の恒常的資金の確保も課題であろう。

評価者2

【総合評価】B

【意見・感想】

- 100 種 PDX を樹立されていることは高く評価できる。腫瘍の不均一性を評価する。
- システムとして優れているが、そのためには癌幹細胞数や分布を定量的に検出できる。
- 方法論が必要と考える。本システムの優位性を利用して何らかのプロジェクトが進展することを期待する。

(2) 幸谷愛:癌幹細胞階層性とニッチの相互作用～マイクロ RNA の役割

評価者1

【総合評価】A

【意見・感想】

・EBV+ HL の pathogenesis、特に炎症性 niche に関する新しい、極めて魅力的な仮説を提示し、様々な角度から検証を試みている。炎症とがんという、より一般的で、大きな世界につなが

る可能性がある。
・EBV は多くの組織に感染する。EBV(+)胃がんの話が少し出たが、本研究から他のがんや疾患においても exosome の関与が推測され、その波及効果も大きい。
・今後、miRNA(−) EBV との対比、EBV(−) HL との対比がさらに深化され、40 種の miRNA の機能がさらに解明されれば、たいへん楽しみである。

評価者2
【総合評価】A
【意見・感想】
研究の object,specific aim ともに極めて優れている。 EBV の miRNA が生物学的にマクロファージのニッチとしての役割を高めていることは驚きである。今後、EBVmiRNA によって刺激されたマクロファージが他の腫瘍浸潤マクロファージと性質の違いがあることを解析されることによって 新たな腫瘍ニッチに関する分子メカニズムが解明されると考える。

(3) 亀谷美恵:乳癌幹細胞を標的とした新規 Her2 ペプチドワクチンの開発

評価者1
【総合評価】A
【意見・感想】
・HER2 を標的にしたペプチドワクチンの中でも、日本人患者を想定した、独創的な抗原ペプチドを作成し、solid な基礎検討を積み重ねている。
・乳管上皮以外も含め、正常組織幹細胞における HER2 発現とその機能、ヒトにおける HER2 ペプチドの免疫原性等の課題の解明が期待される。
・ペプチドワクチンの臨床開発においては、その endpoint の設定の仕方など、多くの経験が積み重ねられてきた。乳がん再発予防を目的とした臨床試験は大規模にならざるを得ないが、有効な術後化学療法が確立していない triple negative を対象にするなどのアンメットな臨床ニーズがあると考えられる。

評価者2
【総合評価】A
【意見・感想】
基礎研究としても応用研究としてもレベルが極めて高い。ペプチドの活性に関して in vitro か

らin vivoまでよく検討されている。 IL-4　NOGマウスを用いた検討も素晴らしい。
応用面での問題として真に乳がん幹細胞にHer2が発現していないか否か　今後チェックする必要がある。

(4)八幡崇;ニッチ因子を標的とした白血病幹細胞治療法の開発

評価者1
【総合評価】A
【意見・感想】
・TM5275 を自ら開発し、造血機能改善薬としての臨床試験に進んでいることは極めて高く評価される。
・このようにPAI-1阻害剤が正常造血幹細胞の増殖・分化を促進しながらも、白血病細胞の増殖を抑制することは興味深い。そのメカニズムを多角的な解析技術で探索し、factor Y を初め、新しい分子機構の解明が進んでいる点が見事であり、たいへん期待が高まる。
・さらに白血病細胞自体が PAI-1 を高発現し、それが imatinib 耐性と相関していることもたいへん注目される知見である。もしこの耐性が imatinib 特異的であれば、その抗腫瘍効果に必要なタンパク質のprocessingを制御しているのかも知れない。

評価者2
【総合評価】A
【意見・感想】
発想も実験もオリジナリティが高く申し分ない。CMLを選択して実験に入っている点も深く考慮されていて優れている。臨床サンプル(薬剤投与後の)のPD解析が極めて興味深い。

＜研究期間終了後の展望＞
本研究期間内に PAI-1 阻害薬、乳がんに対するペプチドわくちん療法などは、今後直ちに臨床研究へ進むだけの前臨床知見を得られた。その他の知見も、今後ヒトサンプルを用いた解析ににより、動物データがヒトにも外挿できるのか否かを検討し、がん治療に貢献することが期待される。
＜研究成果の副次的効果＞
若手研究者の育成も行われ、本研究期間内に12名の学位論文を生み出すことができた。また、新規薬剤の導出に興味を示す企業との共同研究を予定している。

(5)研究業績

〈英文〉

本論文は全て「査読有」

1. ＊Suzuki R, Kikuchi S, Harada T, Mimura N, Minami J, Ohguchi H, Yoshida Y, Gorgun G, CirsteaD.Cottini F, Jakubikova J, Tai YT, Chauhan D, Richardson PG, Munshi N, Ando K, Utsugi T, Hideshima T and Anderson KC. Combination of a selective HSP90α/β inhibitor and a RAS-RAF-MEK-ERK signaling pathway inhibitor triggers synergistic cytotoxicity in multiple myeloma cells. PLoS One, 10e0143847, 2016
2. ＊Kawai H, Matsushita H, Ohmachi K, Kojima M, Machida S, Ogawa Y, Kawada H, Nakamura N, Ando K. Four hepatosplenic T-cell lymphoma cases of Japan. Leukemia Research Report, 5,11-13, 2016
3. ＊Yamamoto H, Lu J, Oba S, Kawamata T, Yoshimi A, Kurosaki N, Yokoyama K, Kurokawa M, Tojo A, Ando K, Morishita K, and Ai Kotani. miR-133 regulates dysregulated Evi1 expression in AML cells as potential therapeutic target without severe adverse effect. Scientific Reports, 12:6:19204, 2016
4. Watanabe T, Tobinai K, Matsumoto M, Suzuki K, Sunami K, Ishida T, Ando K, Chou T, Ozaki S, Taniwaki M, Uike N, Shibayama H, Hatake K, Izutsu K, Ishikawa T, Shumiya Y, Kashihara T and Iida S. A phase 1/2 study of carfilzomib in Japanese patients with relapsed and/or refractory multiple myeloma. Brit J Haematol, 172(5)745-756, 2016
5. ＊Nagao R, Kikuti YY, Carreras J, Kikuchi T, Miyaoka M, Matsushita H, Kojima M, Ando K, Sakata-Yanagimoto M, Chiba S, Nakamura N. Clinicopathological analysis of angioimmunoblastic T-cell lymphoma with or without RHOA G17V mutation using formalin-fixed paraffin-embedded sections. American Journal of Surgical Pathology, 40(8)1041-1050, 2016
6. Ichinohe T, Kuroda Y, Okamoto S, Matsue K, Iida S, Sunami K, Komeno T, Suzuki K, Ando K, Taniwaki M, Tobinai K, Chou T, Kaneko H, Iwasaki H, Uemura C, Tamakoshi H, Zak MHi, Doerr T, Hagiwara S. A multicenter phase 2 study of pomalidomide plus dexamethasone in patients with

relapsed and refractory multiple myeloma: the Japanese MM-011 trial. Experimental Hematology and Oncology, dol:10,1186/s40164-016-0040-7, 2016

7. ＊Amaki J, Matsushita H, Kitamura Y, Murayama H, Kojima M, and Ando K. The formation of an aberrant PAX5 transcript in a patient with mixed phenotype acute leukemia harboring der(9)t(7;9)(q11.2;p13). Leukemia Research Report, 5, 14-17, 2016
8. Kojima M, Ohgiya D, Ichiki A, Hara R, Amaki J, Kawai H, Numata H, Sato A, Miyamoto M, Suzuki R, Machida S, Matsushita H, Ogawa Y, Kawada H, and Ando K. Refractly acute promyelocytic leukemia successfully treated with combination therapy of arsenic trioxide and tamibarotene: A case report. Leukemia Res Report, 5, 11-13, 2016
9. ＊Nakai T, Sakai D, Nakamura Y, Nukaga T, Grad S, Li Z Alini M, Chan D, Masuda K, Ando K, and Mochida J. CD146 defines differentiation of cultured annulus fibrosus cells to express a contractile phenotype. Journal of Orthopaedic Research 34(8)1361-1372, 2016
10. Ohgiya D, Matsushita H, Murayama H, and Ando K. Chédiak-Higashi-like granules and waxy Auer bodies in a case of acute promyelocytic leukemia. Int J Hematol., 104,637-638, 2016
11. Machida S, Onizuka M, Toyosaki M, Aoyama Y, Kawai H, Amaki J, Hara R, Ichiki A, Ogawa Y, Kawada H, and Ando K. Danaparoid Reduces the Incidence of Hematopoietic Stem Cell Transplantation-Associated Thrombotic Microangiopathy. Bone Marrow Transplant, 52(2)307-309, 2017
12. Ichiki A, Hashimoto N, Ueda T, Hiraiwa S, Tajiri T, Nakamura N, Ando K, Yokoyama K. IgG4-related disease with bone marrow involvement. Int Med, 55, 2295-2299, 2016
13. ＊Muguruma Y, Hozumi K, Warita H, Yahata T, Uno T, Ito M and Ando K. Maintenance of bone homeostasis by Dll1-mediated Notch signaling. J Cell Physiol., dol:10.1002/jcp.25647 2016
14. Miyaoka M, Kikuchi T, Carreras J, Kikuchi YY, Ohmachi K, Kojima M, Ando K and Nakamura N. Composite follicular lymphoma and CD5-positive

nodal marginal zone lymphoma. J Clin Exp Hematopathology, 56, 55-58, 2016

15. Esteban JC, Kikuti YY, Tomiata S, Kikuchi T, Hiraiwa S, Sato A, Kojima M, Itoh J, Colomo L, Ando K, Nakamura N. Clinicopathological characteristics and genomic profile of primary de novo sinonasal tract diffuse large B-cell lymphoma reveals gain at 1q31 and RGS1 encoding protein. Histopathology, 2016
16. Ninomiya H, Obara N, Chiba S, Usuki K, Nishiwaki K, Matsumura I, Shichishima T, Okamoto S, Nishimura J, Ohyashiki K, Nakao S, Ando K, Kanda Y, Kawaguchi T, Nakakuma H, Harada D, Akiyama H, Kinoshita T, Ozawa K, Omine M, Kanakura K. Interim analysis of post-marketing surveillance of eculizumab for paroxysmalnocturnal hemoglobinuria in Japan. Int J Hematol. 25,2443-2452, 2016
17. Tefferi A, Al-Ali H K, G Barosi G, T Devos, Gisslinger H, Jiang Q, Kiladjian J-J, Mesa R, Passamonti F, Ribrag V, Schiller G, Vannucchi A M, Zhou D, Reiser D, Zhong J and R P Gale for the RESUME trialists (incl. Ando K). A randomized study of pomalidomide vs. placebo in persons with myeloproliferative neoplasm-associated myelofibrosis and RBC-transfusion-dependence. Leukemia, doi: 10.1038/leu.2016.3000, 2016
18. Ogura M, Ishizawa K, Maruyama D, Abe Y, Ando K, Izutsu K, Terui Y, Imaizumi Y, Tsukasaki K, Suzuki K, Izumi T, Usuki K, Kinoshita T, Taniwaki M, Uoshima N, Suzumiya J, Kurosawa M, Nagai H, Uchida T, Fukuhara N, Choi I, Ohmachi K, Yamamoto G, and Tobinai K. Bendamustine plus rituximab for previously untreated patients with indolent B-cell non-Hodgkin lymphoma or mantle cell lymphoma: A multicenter Phase II clinical trial in Japan. Int J Hematol., dol:10.1007/s12185-016-2146-4, 2016
19. Igarashi T, Ogura M, Itoh K, Taniwaki M, Ando K, Kuroda Y, Yamamoto K, Uike N, Tomita A, Nagai H, Kurosawa M, Mori S, Nawano S, Terauchi T, Ohashi Y, Tobinai K. Japanese phase II study of rituximab maintenance for untreated indolent B-cell non-Hodgkin lymphoma with high tumor burden. Int J Hematol.104, 700-708, 2016

20. Ogawa Y, Izutsu K, Kiguchi T, Choi I, Takatsuka Y, Ando K, and Suzumiya J. A multicenter, single-arm, Phase II clinical trial of bendamustine monotherapy in patients with chronic lymphocytic leukemia in Japan. Int J Hematol., dol:10.1007/s12185-016-2178-9, 2017
21. ＊Carreras J, Kikuti YY, Bea S, Miyaoka M, Hiraiwa S, Ikoma H, Nagao R, Tomita S, Martin-Garcia D, Salaverria I, Sato A, Ichiki A, Roncador G, Garcia JF, Ando K, Campo E, and Nakamura N. Clinicopathological characteristics and genomic profile of primary sinonasal tract diffuse large B cell lymphoma reveals gain at 1q31 and RGS1 encoding protein: poor overall survival in DLBCL not otherwise specific. Histopathology, in press, 2017
22. Kawai H, Matsushita H, Kawada H, Ogawa Y, Ando K. The successful use of rivaroxaban in the prevention of thromboembolism in a patient with antithrombin deficiency in the perioperative period. Int Med., in press, 2017
23. Maruyama D, Hatake K, Kinoshita T, Fukuhara N, Choi I, Taniwaki M, Ando K, Terui Y, Higuchi Y, Onishi Y, Abe Y, Kobayashi T, Shirasugi Y, Tobinai K. A multicenter phase II study of nivolumab in Japanese patients with relapsed or refractory classical Hodgkin lymphoma. Cancer Sci., in press, 2017
24. Robert Marcus, Andrew Davies, Kiyoshi Ando, Wolfram Klapper, Stephen Opat,Carolyn Owen, Elizabeth Phillips, Randeep Sangha, Rudolf Schlag, John F Seymour, William Townsend, Marek Trněný, Michael Wenger, Günter Fingerle-Rowson, Kaspar Rufibach, Tom Moore, Michael Herold, Wolfgang Hiddemann. Obinutuzumab or rituximab immunochemotherapy in previously untreated iNHL. New Eng J Med, in press, 2017
25. ＊Nakata T, Shimizu H, Nagata S, Ito G, Fujii S, Suzuki K, Kawamoto A, Ishibashi F, Kuno R, Anzai S, Murano T, Mizutani T, Oshima S, Tsuchiya K, Nakamura T, Hozumi K, Watanabe M and Okamoto R. Indispensable role of Notch ligand-dependent signaling in the proliferation and stem cell niche maintenance of APC-deficient intestinal tumors. *Biochem Biophys Res Commun.* in press, 2016.

26. ＊Ishige-Wada M, Kwon SM, Eguchi M, Hozumi K, Iwaguro H, Matsumoto T, Fukuda N, Mugishima H, Masuda H and Asahara T. Jagged-1 signaling in the bone marrow microenvironment promotes endothelial progenitor cell expansion and commitment of CD133+ human cord blood cells for postnatal vasculogenesis. *Plos One*. 11(11): e0166660, 2016.
27. ＊Furukawa T, Ishifune C, Tsukumo SI, Hozumi K, Maekawa Y, Matsui N, Kaji R and Yasutomo K. Transmission of survival signals through Delta-like 1 on activated CD4+ T cells. *Sci Rep*, doi: 10.1028/srep33692., 2016.
28. ＊Liu L, Wada H, Matsubara N, Hozumi K and Itoh M. Identification of domains for efficient Notch signaling activity in immobilized Notch ligand proteins. *J Cell Biochem*, in press, 2016.
29. ＊Hayashi Y, Nishimune H, Hozumi K, Saga Y, Harada A, Yuzaki M, Iwatsubo T, Kopan R and Tomita T. A novel non-canonical Notch signaling regulates expression of synaptic vesicle proteins in excitatory neurons. *Sci. Rep.* 6: 23969, April 4, 2016.
30. ＊Okano M, Matsuo H, Nishimura Y, Hozumi K, Yoshioka S, Tonoki A and Itoh M. Mib1 modulates dynamin 2 recruitment via Snx18 to promote Dll1 endocytosis for efficient Notch signaling. *Gene Cells.* 21: 425-441, 2016.
31. ＊Z. Zhang, J. Yang, W. Yan, Y. Li, Z. Shen, T. Asahara. Pretreatment of Cardiac Stem Cells With Exosomes Derived From Mesenchymal Stem Cells Enhances Myocardial Repair. *J Am Heart Assoc*. 2016;5:
32. ＊S. Tsukada, H. Masuda, S. Y. Jung, J. Yun, S. Kang, D. Y. Kim, J. H. Park, S. T. Ji, S. M. Kwon, T. Asahara. Impaired development and dysfunction of endothelial progenitor cells in type 2 diabetic mice. *Diabetes Metab*. 2016;
33. ＊S. Takizawa, E. Nagata, T. Nakayama, H. Masuda, T. Asahara. Recent Progress in Endothelial Progenitor Cell Culture Systems: Potential for Stroke Therapy. *Neurol Med Chir (Tokyo)*. 2016;56:302-9.
34. ＊T. Nakamura, H. Koga, H. Iwamoto, V. Tsutsumi, Y. Imamura, M. Naitou, A. Masuda, Y. Ikezono, M. Abe, F. Wada, T. Sakaue, T. Ueno, M. Ii, C. Alev, A. Kawamoto, T. Asahara, T. Torimura. Ex vivo expansion of circulating CD34(+) cells enhances the regenerative effect on rat liver

cirrhosis. *Mol Ther Methods Clin Dev*. 2016;3:16025.

35. J. H. Lee, S. T. Ji, J. Kim, S. Takaki, T. Asahara, Y. J. Hong, S. M. Kwon. Specific disruption of Lnk in murine endothelial progenitor cells promotes dermal wound healing via enhanced vasculogenesis, activation of myofibroblasts, and suppression of inflammatory cell recruitment. *Stem Cell Res Ther*. 2016;7:158.
36. ＊M. Ishige-Wada, S. M. Kwon, M. Eguchi, K. Hozumi, H. Iwaguro, T. Matsumoto, N. Fukuda, H. Mugishima, H. Masuda, T. Asahara. Jagged-1 Signaling in the Bone Marrow Microenvironment Promotes Endothelial Progenitor Cell Expansion and Commitment of CD133+ Human Cord Blood Cells for Postnatal Vasculogenesis. *PLoS One*. 2016;11:e0166660.
37. ＊ Mikio Mikami,Kazuhiro Tanabe,Koji Matsuo,Yuko Miyazaki,Masaki Miyazawa,
    Masaru Hayashi,Satoshi Asai,Masae Ikeda,Masako Sida,Takeshi Hirasawa,Nozomi Kojima,Ryuichiro Sho,Sadayo Iijima Fully-sialyated alpha-chain of complement 4-binding protein: Diagnostic utility for ovarian clear cell carcinoma. Gynecologic Oncology.2016
38. ＊Masako Shida,Masanori Yasuda,Mariko Fujita,Masaki Miyazawa,Hiroshi Kajiwara,Takeshi Hirasawa,Masae Ikeda,Naruaki Masui,Toshinari Muramatsu,Mikiko Mikami Possible role of thymidine phosphoryl in gynecological tumors as an individualized treatment strategy Oncology Letters Oncology Letters 12(5) 3215-3223,.2016
39. ＊Tanaka K,Mikami M,Aoki D,Kiguchi K,Ishiwata I,Iwamori M Expression of sulfatide and sulfated lactosylcermide among histological types of human ovarian carcinomas. Hum Cell 28 37-43.2016
40. ＊Naruaki Matsui,Hiroshi Kajiwara,Akihiro Morishita,Tetsuji Iida,Kazumi Nakazawa,MasakiMiyazawa,Mikio Mikami,Takafumi Ogawa,Naoya Nakamura,Shinkichi Sato Use of epithelial-specific antigen for cytological diagnosis of glandular lesions in the uterine cervix Pathology International 66(5) 305-308.2016
41. Chisa Narayama,Masae Ikeda,Miwa Yasaka,Yu-suke Sagara,Yasuhiro Kan-no,Io Hayashi,Atuya Narita,Satoshi Asai,Toshiki Tajima,Masako

Shida,Takeshi Hirasawa,Mikio Mikami Aggressive Angiomyxoma of the Vulva with No Recurrence on a 5-year Follow up:A Case Report Tokai J Exp Clin Med 41(1) 42-45. 2016

42. Yuji Ikeda, Akiko Furusawa,Ryo Kitagawa,Aya Tokinaga,Fuminori Ito,Masayo Ukita,Hidetaka Nomura,Wataru Yamagami,Hiroshi Tanabe,Mikio Mikami,Nobuhiro Takeshima,Nobuo Yaegashi, Practice patterns of adjuvant therapy for intermediate/high recurrence risk cervical cancer patients in japan Journal of Gynecologic Oncology 27(3) e29.2016
43. Satoshi Asai, Hitoshi Ishimoto,Akira Yabuno,Hironori Asada,Mikio Mikami,Yasunori Yoshimura A novel modification of two-port laparoscopic ovarian cystectomy using a needlescopic instrumant:One surgeon's initial experience Gynecology and Minimally Invasive Therapy in press 2016
44. Koji Matsuo, Sigita S.Cahoon,Kosuke Yoshihara,Masako Shida,Mamoru Kakuda,Sosuke Adachi,Aida Moeini,Hiroko Machida,Jocelyn Garcia-Sayre,Yutaka Ueda,Takayuki Enomoto,Mikio Mikami,Lynda D.Roman,Anil K.Sood Association of Loew-Dose Aspirin and Survival of Women With Endometrial Cancer Obstetrics&Gynecology 128(1) 127-37.2016.2016
45. Yasuhiko Ebina, Hidetaka Katabuchi,Mikio Mikami,Satoru Nagase,Nobuo Yaegashi,Yasuhiro Udagawa,Hienori Kato,Kaneyuki Kubushiro,Kiyoshi Takamatsu,Kasuhiro Ino,Hiroyuki Yoshikawa. Japan Society of Gynecologic Oncology guidelines 2013 for the treatment of uterine body neoplasms International Journal of Clinical Oncology 21 435-446.2016
46. Shinichi Komiyama, Hidetaka Katabuchi,Mikio Mikami,Satoru Nagase,Nobuo Yaegashi,Aikou Okamoto,Kiyoshi Ito,Kenicihro Morishige,Nao Suzuki,Masanori Kaneuchi,Nobuo Yaegashi,Yasuhiro Udagawa,Hiroyuki Yoshikawa Japan Society of Gynecologic Oncology guidelines 2015 for the treatment of ovarian cancer including primary pertioneal cancer and fallopian tube cancer International Journal of Clinical Oncology 21 419-434.2016
47. ＊Kyoko Tanaka,Masaki Miyazawa,Mikio Mikami,Daisuke Aoki,Kazushige Kiguchi,Masao Iwamori Enhanced expression of unique gangliosides with GM2-determinant in human uterine cervical carcinoma-derived cell lines Glycoconjugate Journal.2016

48. Toru Sugiyama,Aikou Okamoto,Takayuki Enomoto,Tetsutato Hamano,Eriko Aotani,Yasuhisa Terao,NaoSuzuki,Mikio Mikami,Nobuo Yaegashi,Kiyoko Kato,Hiroyuki Yoshikawa,Yoshihito Yokoyama,Hiroshi Tanabe,Koji Nishino,Hiroyuki Nomura,Jae-Weon Kim,Byoung-Gie Kim,Sandro Pignata,Jerome Alexandre,John Green,Seiji Isonishi,Fumitoshi Terauchi,Keiichi Fujiwara,Daisuke Aoki Randomized Phase Ⅲ Trial of Irinotecan Plus Cisplatin Compared With Paclitaxel PlusCarboplatin As First-Line Chemotherapy for Ovarian Clear Cell Carcinoma:JGOG3017/GCIG Trial Journal of Clinical Oncology.2016
49. ＊Toshiki Tajima, Masaki Miyazawa, Masaru Hayashi, Satoshi Asai, Masako Ikeda, Masae Shida, Takeshi Hirasawa, Masao Iwamori, Mikio Mikami Enhanced expression of hydroxylated ceramide in well-differentiated endometrial adenocarcinoma. Oncology Letters 13 45-50.2016
50. ＊Ogiya R, Niikura N, Kumaki N, Bianchini G, Kitano S, Iwamoto T, Hayashi N, Yokoyama K, Oshitanai R, Terao M, Morioka T, Tsuda B, Okamura T, Saito Y, Suzuki Y, Tokuda Y. Comparison of Tumour-infiltrating Lymphocytes between Primary and Metastatic Tumours in Breast Cancer Patients. Cancer Sci. 107: 1730-35, 2016.
51. Saito Y, Suzuki Y, Inomoto C, Kumaki N, Yokoyama K, Ogiya R, Oshitanai R, Terao M, Tsuda B, Morioka T, Niikura N, Okamura T, Masuda S, Tokuda Y. A Case of Giant Borderline Phyllodes Tumor of the Breast Associated with Hypoglycemia. Tokai J Exp Clin Med. 41:118-22, 2016.
52. Kataoka A, Iwamoto T, Tokunaga E, Tomotaki A, Kumamaru H, Miyata H, Niikura N, Kawai M, Anan K, Hayashi N, Masuda S, Tsugawa K, Aogi K, Ishida T, Masuoka H, Iijima K, Kinoshita T, Nakamura S, Tokuda Y. Young adult breast cancer patients have a poor prognosis independent of prognostic clinicopathological factors: a study from the Japanese Breast Cancer Registry. Breast Cancer Res Treat. 160:163-172, 2016.
53. Iwamoto T, Kumamaru H, Miyata H, Tomotaki A, Niikura N, Kawai M, Anan K, Hayashi N, Masuda S, Tsugawa K, Aogi K, Ishida T, Masuoka H, Iijima K, Matsuoka J, Doihara H, Kinoshita T, Nakamura S, Tokuda Y. Distinct

breast cancer characteristics between screen- and self-detected breast cancers recorded in the Japanese Breast Cancer Registry. Breast Cancer Res Treat. 156:485-94, 2016

54. Tang X, Yamashita T, Hara M, Kumaki N, Tokuda Y, Masuda S. Histopathological characteristics of breast ductal carcinoma in situ and association with imaging findings. Breast Cancer. 23: 491-8, 2016
55. ＊Niikura N, Hashimoto J, Kazama T, Koizumi J, Ogiya R, Terao M, Oshitanai R, Morioka T, Tsuda B, Okamura T, Saito Y, Iwaisako K, Iwamoto T, Hayashi N, Imai Y, Tokuda Y. Diagnostic performance of (18)F-fluorodeoxyglucose PET/CT and bone scintigraphy in breast cancer patients with suspected bone metastasis. Breast Cancer. 23: 662-7, 2016.
56. Kinoshita T, Fukui N, Anan K, Iwamoto T, Niikura N, Kawai M, Hayashi N, Tsugawa K, Aogi K, Ishida T, Masuoka H, Masuda S, Iijima K, Nakamura S, Tokuda Y. Comprehensive prognostic report of the Japanese Breast Cancer Society Registry in 2004. Breast Cancer 23: 39-49, 2016
57. Anan K, Fukui N, Kinoshita T, Iwamoto T, Niikura N, Kawai M, Hayashi N, Tsugawa K, Aogi K, Ishida T, Masuoka H, Masuda S, Iijima K, Nakamura S, Tokuda Y. Comprehensive prognostic report of the Japanese Breast Cancer Society Registry in 2005. Breast Cancer. 23: 50-61, 2016.
58. Iwamoto T, Fukui N, Kinoshita T, Anan K, Niikura N, Kawai M, Hayashi N, Tsugawa K, Aogi K, Ishida T, Masuoka H, Masuda S, Iijima K, Nakamura S, Tokuda Y. Comprehensive prognostic report of the Japanese Breast Cancer Society registry in 2006. Breast Cancer. 23: 62-72, 2016.
59. Niikura N, Tomotaki A, Miyata H, Iwamoto T, Kawai M, Anan K, Hayashi N, Aogi K, Ishida T, Masuoka H, Iijima K, Masuda S, Tsugawa K, Kinoshita T, Nakamura S, Tokuda Y. Changes in tumor expression of HER2 and hormone receptors status after neoadjuvant chemotherapy in 21 755 patients from the Japanese breast cancer registry. Ann Oncol. 27: 480-7, 2016.
60. Watanabe K, Shimo A, Tsugawa K, Tokuda Y, Yamauchi H, Miyai E, Takemura K, Ikoma A, Nakamura S. Safe and effective deodorization of malodorous fungating tumors using topical metronidazole 0.75 % gel

(GK567): a multicenter, open-label, phase III study (RDT.07.SRE. 27013). Support Care Cancer. 24: 2583-2590, 2016

61. Kawai M, Tomotaki A, Miyata H, Iwamoto T, Niikura N, Anan K, Hayashi N, Aogi K, Ishida T, Masuoka H, Iijima K, Masuda S, Tsugawa K, Kinoshita T, Nakamura S, Tokuda Y. Body mass index and survival after diagnosis of invasive breast cancer: a study based on the Japanese National Clinical Database-Breast Cancer Registry. Cancer Med. 5: 1328-40, 2016

62. ＊Yoshie Kametani*, Shino Ohshima, Asuka Miyamoto, Atsuko Shigenari, Masaki Takasu, Noriaki Imaeda, Tatsuya Matsubara, Masafumi Tanaka, Takashi Shiina, Hiroshi Kamiguchi, Ryuji Suzuki, Hitoshi Kitagawa, Jerzy K. Kulski, Noriaki Hirayama, Hidetoshi Inoko, Asako Ando Production of a Locus and Allele-Specific Monoclonal Antibody for the Characterisation of SLA-1*0401 mRNA and Protein Expression Levels in MHC-Defined Microminipigs. PLOS ONE11(10):e0164995. doi: 10.1371/journal.pone.0164995 2016

63. ＊Tatsuya Matsubara, Naohito Nishii, Satoshi Takashima, Masaki Takasu, Noriaki Imaeda, Kayo Aiki-Oshimo, Kazuaki Yamazoe, Michinori Kakisaka, Shin-nosuke Takeshima, Yoko Aida, Yoshie Kametani, Jerzy K Kulski, Asako Ando, Hitoshi Kitagaw Identification and characterization of two CD4 alleles in Microminipigs. BMC Veterinary Research Oct 7;12(1):222. 2016

64. ＊Sato K, Oiwa R, Kumita W, Henry R, Sakuma T, Ito R, Nozu R, Inoue T, Katano I, Sato K, Okahara N, Okahara J, Shimizu Y, Yamamoto M, Hanazawa K, Kawakami T, Kametani Y, Suzuki R, Takahashi T, Weinstein EJ, Yamamoto T, Sakakibara Y, Habu S, Hata JI, Okano H, Sasaki Generation of a Nonhuman Primate Model of Severe Combined Immunodeficiency Using Highly Efficient Genome Editing. E.Cell Stem Cell. 19(1):127-138 doi: 10.1016/j.stem.2016.06.003. PMID: 27374787 2016

65. Nakajima Y, Hattori Y, Ito S, Kawasaki R, Kuwabara H, Machida S, Shirasugi Y, Miyazaki K, Sakai R, Tomita N, Ando K, Higashihara M, Ishiguro Y, Fujisawa S. Acute leukemia during pregnancy:

an investigative survey of the past eleven years. Int J Hematol. 101(3), 286-294, 2015

66. Suzuki K, Ogura M, Abe Y, Suzuki T, Tobinai K, Ando K, Taniwaki M, Maruyama D, Kojima M, Kuroda J, Otani H, Iizuka K. Phase I study of siltuximab, an anti-IL-6 monoclonal antibody, in relapsed/refractory multiple myeloma. Int J Hematol. 101(3), 286-294, 2015
67. Kojima M, Nakamura N, Yabe M, Tokunaka M, Kikuti YY, Kikuchi T, Murayama H, Moriuchi M, Tsuboi K, Ogawa Y, and Ando K. A case of clonally distinct relapse of Burkitt lymphoma nine years after complete remission. Int J Hematol, 101(5), 520-524, 2015
68. Tateishi U, Tatsumi M, Terauchi T, Ando K, Niitsu, N, Kim, WS, Suh C, Ogura M, Tobinai K. Prognostic Significance of Metabolic Tumor Burden by FDG PET/CT in Patients with Relapsed/Refractory Diffuse Large B-cell Lymphoma. Cancer Science. 106(2); 186-193, 2015
69. ＊Amaki J, Onizuka M, Ohmachi K, Aoyama Y, Hara R, Ichiki A, Kawai K, Sato A, Miyamoto M, Toyosaki M, Machida S, Kojima M, Kawada H, Ogawa Y, and Ando K. Single nucleotide polymorphism of cytarabine metabolic genes influence clinical outcome in acute myeloid leukemia patients received high dose cytarabine therapy. Int J Hematol, 101(6), 543-553, 2015
70. ＊Shimada S, Nunomura S, Mori S, Suemizu H, Itoh T, Takabayashi S, Okada Y, Yahata T, Shiina T, Katoh H, Suzuki R, Tani K, Ando K, Yagita H, Habu S, Sasaki E, Kametani Y. Common marmoset CD117-positive hematopoietic cells, possess multipotency. Int Immunol. 27, 567-577, 2015
71. Onizuka M, Ohmachi K, Aoyama Y, Hara R, Ichiki A, Kawai K, Sato A, Miyamoto M, Toyosaki M, Machida S, Kojima M, Kawada H, Ogawa Y, and Ando K. Noninfectious pulmonary complications after stem cell transplantation and induction of an innate immune response. Journal of Blood Disorders & Transfusion 6(3): 1-6, 2015
72. Tomita S, Kikuti Y, Carreras J, Kojima M, Ando K, Takasaki H, Sakai R, Takata K, Yoshino T, Bea S, Campo E, Nakamura N. Genomic and

immunohistochemical profiles of enteropathy-associated T-cell lymphoma in Japan. Modern Pathology, 28, 1286-1296, 2015

73. Kojima M, Ohgiya D, Kawai H, Miyamoto M, Ohmachi K, Ogawa Y, Nakamura N, and Ando K. Two cases of successful autologous hematopoietic stem cell harvest after treatment with BrentuximabVedotin. Acta Hematol, 27, 134, 181-182, 2015
74. Kobayashi Y, Yamauchi T, Kiyoi H, Sakura T, Hata T, Ando K, Watabe A, Harada A, Taube T, Miyazaki Y, Naoe T. Phase I Trial of Volasertib, a Polo-like Kinase Inhibitor, in Japanese Patients with Acute Myeloid Leukemia. Cancer Sci. 106, 1590-1595, 2015 DOI: 10.1111/cas.12814
75. ＊Damdinsuren A, Matsushita H, Ito M, Tanaka M, Guilan J, Tsukamoto H, Asai S, Ando K, Miyachi H. FLT3-ITD drives Ara-C resistance in leukemic cells via the induction of RUNX3. Leukemia Res. 39, 1405-1403, 2015
76. Ogawa Y, Ogura M, Tobinai K, Ando K, Suzuki T, Watanabe T, Ohmachi K, Uchida T, Hanson M, Tanaka Y, Shimamoto T, Hotta T. MSD. A Phase I Study of Vorinostat combined with bortezomib in Patients With Relapsed or Refractory Multiple Myeloma. Int J Hematol. 103, 25-33, 2015
77. Kojima M, Ichinose A, Souri M, Osaki T, Kawai H, Amaki J, Numata H, Miyamoto M, Ogiya D, Tsuboi K, Ogawa Y, Ozawa S, Ando K. Successful bypass surgery for esophageal carcinoma under adequate factor XIII/13 replacement therapy in a case with intractable autoimmune hemorrhaphilia due to anti-Factor XIII/13 antibodie. Int J Hematol. 103, , 2015
78. ＊Imai J, Hozumi K, Sumiyoshi H, Yazawa M, Hirano K, Abe J, Higashi K, Inagaki Y and Mine T. Anti-fibrotic effects of a novel small compound on the regulation of cytokine production in a mouse model of colorectal fibrosis. *Biochem Biophys Res Commun.* 468: 554-560, 2015.
79. ＊Hirano K, Negishi N, Yazawa M, Yagita H, Habu S and Hozumi K. Delta-like 4-mediated Notch signaling is required for early T cell development in a three-dimensional thymic structure. *Eur J Immunol.* 45: 2252-2262, 2015.
80. ＊Nakano Y, Negishi N, Gocho S, Mine T, Sakurai Y, Yazawa M, Abe K, Yagita H, Habu S, Kageyama R, Kawaguchi Y and Hozumi K. Disappearance

of centroacinar cells in the Notch ligand-deficient pancreas. *Genes Cells.* 20: 500-511, 2015.

81. ＊Maekawa Y, Ishifune C, Tsukumo S, Hozumi K, Yagita H and Yasutomo K. Notch controls the survival of memory CD4+ T cells by regulating glucose uptake. *Nat. Med.* 21: 55-61, 2015.
82. Mokuyasu S, Suzuki Y, Kawahara E, Seto T, Tokuda Y. High-sensitivity cardiac troponin I detection for 2 types of drug-induced cardiotoxicity in patients with breast cancer. Breast Cancer. 2015 Nov;22(6):563-9
83. Masuda N, Tokuda Y, Nakamura S, Shimazaki R, Ito Y, Tamura K. Dose response of pegfilgrastim in Japanese breast cancer patients receiving six cycles of docetaxel, doxorubicin, and cyclophosphamide therapy: a randomized controlled trial. Support Care Cancer. 2015 Mar 3.
84. Kosaka Y, Rai Y, Masuda N, Takano T, Saeki T, Nakamura S, Shimazaki R, Ito Y, Tokuda Y, Tamura K. Phase III placebo-controlled, double-blind, randomized trial of pegfilgrastim to reduce the risk of febrile neutropenia in breast cancer patients receiving docetaxel/cyclophosphamide chemotherapy. Support Care Cancer. 23: 1137-43, 2015.
85. Ito Y, Masuda N, Iwata H, Mukai H, Horiguchi J, Tokuda Y, Kuroi K, Mori A, Ohno N, Noguchi S. [Everolimus plus exemestane in postmenopausal patients with estrogen-receptor-positive advanced breast cancer - Japanese subgroup analysis of BOLERO -2]. Gan To Kagaku Ryoho. 42: 67-75, 2015.
86. Kurebayashi J, Miyoshi Y, Ishikawa T, Saji S, Sugie T, Suzuki T, Takahashi S, Nozaki M, Yamashita H, Tokuda Y, Nakamura S. Clinicopathological characteristics of breast cancer and trends in the management of breast cancer patients in Japan: Based on the Breast Cancer Registry of the Japanese Breast Cancer Society between 2004 and 2011. Breast Cancer. 22: 235-44, 2015
87. Mukai H, Noguchi S, Akiyama F, Inaji H, Iwase H, Horiguchi J, Kurebayashi J, Hirata K, Toi M, Kurosumi M, Kohno N, Nishimura R, Nakamura S, Imoto S, Iwase T, Endo T, Saeki T, Ogawa Y, Ito Y, Tokuda Y, Ikeda T. 2013 clinical practice guidelines (The Japanese Breast Cancer Society): history,

policy and mission. Breast Cancer. 22:1-4, 2015.

88. ＊Tsuda B, Kametani Y, Miyamoto A, Miyako H, Kumaki N, Ogiya1 R, Oshitanai R, Terao M, Morioka T, Niikura N, Okamura1 T, Saito Y, Suzuki Y, Tokuda Y. The Effect of Peptide Treatment on the HLA-Binding and Antibody Production in Peripheral Blood Mononuclear Cells Obtained from Japanese Breast Cancer Patients. J Vaccines Vaccin 6:1, 2015

89. ＊Tatsuya Matsubara, Naohito Nishii, Satoshi Takashima, Masaki Takasu, Noriaki Imaeda, Kayo Aiki-Oshimo, Kazuaki Yamazoe, Yoshie Kametani, Asako Ando, Hitoshi Kitagawa Identification of a CD4 variant in Microminipigs not detectable with available anti-CD4 monoclonal antibodies. 2015 Veterinary immunology and Immunopathology 168(3-4):176-183 (IF 1.535) doi:10.1016/j.vetimm.2015.09.008

90. ＊Takenobu Nii, Tomotoshi Marumoto, Hiroshi Kohara, Saori Yamaguchi, Hirotaka Kawano, Erika Sasaki, Yoshie Kametani, Kenzaburo Tan Improved hematopoietic differentiation of primate embryonic stem cells by inhibition of the PI3K-AKT pathway under defined conditions. i. 2015 Exp Hematol 43:901-911 doi:10.1016/j.exphem.2015.06.001.

91. ＊Shin Shimada, Satoshi Nunomura, Shuya Mori, Hiroshi Suemizu, Toshio Itoh, Shuji Takabayashi, Yoshinori Okada, Takashi Yahata, Takashi Shiina, Hideki Katoh, Ryuji Suzuki, Kenzaburo Tani, Kiyoshi Ando, Hideo Yagita, Sonoko Habu, Erika Sasaki, Yoshie Kametani＊ Common marmoset CD117-positive hematopoietic cells possess multipotency. 2015 Int Immunol 27:567-577 (IF 2.536) doi: 10.1093/intimm/dxv031

92. ＊Imai J, Hozumi K, Sumiyoshi H, Yazawa M, Hirano K, Abe J, Higashi K, Inagaki Y and Mine T. Anti-fibrotic effects of a novel small compound on the regulation of cytokine production in a mouse model of colorectal fibrosis. *Biochem Biophys Res Commun.* 468: 554-560, 2015.

93. ＊Hirano K, Negishi N, Yazawa M, Yagita H, Habu S and Hozumi K. Delta-like 4-mediated Notch signaling is required for early T cell

development in a three-dimensional thymic structure. *Eur J Immunol.* 45: 2252-2262, 2015.

94. ＊Nakano Y, Negishi N, Gocho S, Mine T, Sakurai Y, Yazawa M, Abe K, Yagita H, Habu S, Kageyama R, Kawaguchi Y and Hozumi K. Disappearance of centroacinar cells in the Notch ligand-deficient pancreas. *Genes Cells.* 20: 500-511, 2015.
95. ＊Maekawa Y, Ishifune C, Tsukumo S, Hozumi K, Yagita H and Yasutomo K. Notch controls the survival of memory CD4+ T cells by regulating glucose uptake. *Nat. Med.* 21: 55-61, 2015.
96. Yasuhiko Ebina, Nobuo Yaegashi, Hidetaka Katabuchi, Satoru Nagase,Yasuhiro Udagawa, Toru Hachisuga, Tsuyoshi Saito, Mikio Mikami, Yoichi Aoki,Hiroyuki Yoshikawa Japan Society of Gynecologic Oncology guidelines 2011 for the treatment of uterine cervical cancer International Journal of Clinical Oncology 20, 240-248,2015
97. Yasuhiko Ebina, Nobuo Yaegashi, Hidetaka Katabuchi, Satoru Nagase,Yasuhiro Udagawa, Toru Hachisuga, Tsuyoshi Saito, Mikio Mikami, Yoichi Aoki,Hiroyuki Yoshikawa. Japan Society of Gynecologic Oncology guidelines 2011 for the treatment of uterine cervical cancer. International Journal of Clinical Oncology.20.240-248.2015
98. Mikio Mikami,Kazuhiro Tanabe,Koji Matsuo,Yuko Miyazaki,Masaki Miyazawa,
    Masaru Hayashi,Satoshi Asai,Masae Ikeda,Masako Sida,Takeshi Hirasawa,Nozomi Kojima,Ryuichiro Sho,Sadayo Iijima Fully-sialyated alpha-chain of complement 4-binding protein:Diagnostic utility for ovarian clear cell carcinoma Gynecologic Oncology.2015
99. Nishimura J, Yamamoto M, Hayashi S, Ohyashiki K, Ando K, Noji H, Kitamura K, Eto T, Ando T, Masuko M, Matsumoto T, Wano Y, Shichishima T, Shibayama T, Hase M, Li L, Johnson K, Tamburini P, Inazawa J, Kinoshita T, Kanakura Y. A rare genetic polymorphism in C5 confers poor response to the anti-C5 monoclonal antibody Eculizumab by eleven Japanese patients with PNH. New Eng J Med. 370, 632-639. 2014
100. Katakami N, Kunikane H, Takeda K, Takayama K, Sawa T, Saito H, Harada

M, Yokota S, Ando K, Saito Y, Yokota I, Ohashi Y, Eguchi K. Prospective study on the incidence of bone metastasis and skeletal-related events in patients with stage IIIB and IV lung cancer—CSP-HOR13. J Thorac Oncol. 9(2);231-238 2014

101. ＊Yamakawa N, Okuyama K, Kanai A, Helwak A, Takamatsu M, Ogata J, Takakura K, Chanda B, Kurosaki N, Yamamoto H, Ando K, Matsui H, Inaba T, Kotani A. Novel functional small RNAs are selectively loaded onto mammalian Ago 1. Nucleic Acid Research, 42(8);5289-5301, 2014 ＊
102. ＊Negishi N, Ito R, Irie N, Matsuo K, Suzuki D, Yahata T, Nagano K, Aoki K, Ohya K, Hozumi K, Ando K, Tamaoki N, Ito M, Habu S. Effective expansion of engrafted human hematopoietic stem cells in bone marrow of mice expressing human Jagged-1. Exp Hematol, 42(6);487-494, 2014 ＊
103. Suzuki R, Matsushita H, Kawai H, Matsuzawa H, Tsuboi K, Watanabe S, Kawada H, Ogawa Y, Ando K. Identification of a novel *SEPT9-ABL1* fusion gene in a patient with T-cell prolymphocytic leukemia. Leukemia Research Report, 3,54-57, 2014.＊
104. ＊Sato A, Nakamura N, Kojima M, Ohmachi K, Esteban JC, Kikuti YY, Numata H, Ohgiya D, Tazume K, Amaki J, Moriuchi M, Miyamoto M, Aoyama Y, Kawai H, Ichiki A, Hara R, Kawada H, Ogawa Y, Ando K. The clinical outcome of Epstein-Barr virus positive diffuse large B-cell lymphoma of the elderly in rituximab era. Cancer Science, in press,
105. , Murayama H, Matsushita H, Ohbayashi Y, Ando K. Erythrophagocytosis by blasts in acute myeloid leukaemia harboring the *BCR-ABL1* fusion gene. Brit. J Haematol. in press, 2014＊
106. Kawai H, Matsushita H, Suzuki R, Sheng Y, Lu J, Matsuzawa H, Yahata T, Kaneko M, Tsukamoto H, Kawada H, Ogawa Y, Ando K. Functional analysis of the *SEPT9-ABL1* chimeric fusion gene derived from T-prolymphocytic leukemia. Leukemia Research in press, ＊
107. Matsushita H, Yahata T, Sheng Y, Nakamura Y, Muguruma Y, Matsuzawa H, Tanaka M, Hayashi H, Damdinsuren A, Onizuka M, Ito M, Miyachi H, Pandolfi PP, Ando K. The common myeloid progenitor is a target for *PML-RARA* in human APL leukemogenesis. PLPS ONE in press, ＊

108. ＊Watanabe M, Kudo Y, Kawano M, Nakayama M, Nakamura K, Kameda M, Ebara M, Sato T, Nakamura M, Omine K, Kametani Y, Suzuki R, Ogasawara K. NKG2D functions as an activating receptor on natural killer cells in common marmoset (callithrix jacchus). Int Immunol. in press＊

109. ＊Goto Y, Kametani Y＊, Kikugawa A, Tsuda B, Miyazawa M, Kajiwara H, Terao Y, Takekoshi S, Nakamura N, Takeda S, Mikami M. Defect of tropomyosin-related kinase B isotype expression in ovarian clear cell adenocarcinoma. BioScience Trends 8:93-100 2014 ＊

110. ＊Kono A, Brameier M, Roos C, Suzuki S, Shigenari A, Kametani Y, Kitaura K, Suzuki R, Inoko H, Walter L, Shiina T. Genomic sequence analysis of the major histocompatibility complex (MHC) class I G/F segment in common marmoset (Callithrix jacchus). J. Immunol. (April) 192(7):3239-3246 2014 ＊

111. ＊Ashley I. Beyer, Marina E. Fomin, Rahul Thakker, Usha S. Mulvaney, Masato Nakamura, Hiroshi Suemizu, Alicia Ba´rcena, Marcus O. Muench, “The Adult Livers of Immunodeficient Mice Support Human Hematopoiesis, Evidence for a Hepatic Mast Cell Population that Develops Early in Human Ontogeny” PLoS ONE 9(5): e97312, 2014 ＊

112. ＊Daisuke Furukawa, Tsuyoshi Chijiwa, Masahiro Matsuyama, Masaya Mukai, Ei-ichi Matsuo, Osamu Nishimura, Kenji Kawai, Hiroshi Suemizu, Nobuyoshi Hiraoka, Toshio Nakagohri, Seiei Yasuda and Masato Nakamura, “Zinc finger protein 185 is a liver metastasis-associated factor in colon cancer patients” Molecular and Clinical Oncology, 2: 709-713, 2014 ＊

113. ＊Hiroshi Suemizu, Kazuaki Nakamura, Kenji Kawai, Yuichiro Higuchi, Mureo Kasahara, Junichiro Fujimoto, Akito Tanoue and Masato Nakamura “Hepatocytes buried in the cirrhotic livers of patients with biliary atresia proliferate and function in the livers of urokinase-type plasminogen activator-NOG mice” Liver Transplantation (Article first published online: 4 AUG 2014, DOI: 10.1002/lt.23916) ＊

114. ＊Goto Y, Kametani Y,Kikugawa A,Tsuda B,Miyazawa M,Kajiwara H,Terao Y,Takekoshi S,Nakamura N,Takeda S,Mikami M. Defect of tropomyosin-related kinase B isotype expression in ovarian clear cell adenocarcinoma Bio

Science Trends, 8(2) 93-100 2014.*

115. Ikeda M, Kanno H,Hayashi M, Tsukada H,Shida M, Hirasawa T, Muramatsu T,Ogushi Y,Mikami M. Predicting perioperative venous thromboembolism in Japanese gynecological patients. PLoS One.2014. 26;9(2):e89206.
116. ＊Sogabe M,Nakazawa H,Tanaka N,Kubota T,Kaji H, Kuno A,Togayachi A,Goto M,Nakanishi H,Mikami M,Suzuki N,Kiguchi K,Ikehara Y,Narimatsu H. Novel glycobiomarker for ovarian cancer that detects clear cell carcinoma, Journal of Proteome Research, 1624-1635 2014 *
117. ＊Shimizu, H., Okamoto, R., Ito, G., Fujii, S., Nakata, T., Murano, T., Mizutani, T., Tsuchiya, K., Nakamura, T., Hozumi, K. and Watanabe, M. Distinct expression patterns of Notch ligands, Dll1 and Dll4, in normal and inflamed mice intestine. Peer J. 2: e370, 2014.*
118. ＊Ishifune, C., Maruyama, S., Sasaki, Y., Yagita, H., Hozumi, K., Tomita, T., Kishihara, K and Yasutomo, K. Differentiation of CD11c+CXCR1+ cells in the small intestine requires Notch signaling. Proc. Natl. Acad. Sci. USA. 111: 5986-91, 2014.*
119. ＊Haji, Y., Suzuki, M., Moriya, K., So, T., Hozumi, K., Mizuma, M., Unno, M and Ishii, N. Activation of Notch1 promotes development of human CD8+ single positive T cells in humanized mice. Biochem. Biophys. Res. Commun. 2014.*
120. ＊Negishi, N., Suzuki, D., Ito, R., Irie, N., Matsuo, K., Yahata, T., Nagano, K., Aoki, K., Ohya, K., Hozumi, K., Ando, K., Tamaoki, N., Ito, M. and Habu, S. Effective expansion of engrafted human hematopoietic stem cells in bone marrow of mice expressing human Jagged-1. Exp. Hematol. 2014.*
121. Tanaka M, Ikeda K, Suganami T, Komiya C, Ochi K, Shirakawa I, Hamaguchi M, Nishimura S, Manabe I, Matsuda T, Kimura K, Inoue H, Inagaki Y, Aoe S, Yamasaki S, and Ogawa Y: Macrophage-inducible C-type lectin underlies obesity-induced adipose tissue fibrosis. Nat Commun in press *
122. Abe J, Shichino S, Ueha S, Hashimoto S, Tomura M, Inagaki Y, Stein JV, and Matsushima K: Lymph node stromal cells negatively regulate antigen-specific CD4+ T cell responses. J Immunol in press *
123. Reyes-Gordillo K, Shah R, Arellanes-Robledo J, Hernández-Nazara Z,

Rincón- Sánchez AR, Inagaki Y, Rojkind M, and Lakshman MR: Mechanisms of action of acetaldehyde in the up regulation of the human a2(I) collagen gene in hepatic stellate cells-key roles of Ski, SMAD3, SMAD4 and SMAD7. Am J Pathol 184: 1458-1467, 2014 *

124. Yamaoka H, Sumiyoshi H, Higashi K, Nakao S, Minakawa K, Sumida K, Saito K, Ikoma N, Mabuchi T, Ozawa A, and Inagaki Y: A novel small compound accelerates dermal wound healing by modifying infiltration, proliferation and migration of distinct cellular components in mice. J Dermatol Sci 74: 204-213, 2014
125. Kuroda R, Matsumoto T, Niikura T, Kawakami Y, Fukui T, Lee SY, Mifune Y, Kawamata S, Fukushima M, Asahara T, Kawamoto A, Kurosaka M., Local Transplantation of Granulocyte Colony Stimulating Factor-Mobilized CD34+ Cells for Patients With Femoral and Tibial Nonunion: Pilot Clinical Trial. Stem Cells Transl Med. 2014 Jan;3(1):128-34.
126. Fujita Y, Kinoshita M, Furukawa Y, Nagano T, Hashimoto H, Hirami Y, Kurimoto Y, Arakawa K, Yamazaki K, Okada Y, Katakami N, Uno E, Matsubara Y, Fukushima M, Nada A, Losordo DW, Asahara T, Okita Y, Kawamoto A., Phase II Clinical Trial of CD34+ Cell Therapy to Explore Endpoint Selection and Timing in Patients With Critical Limb Ischemia. Circ J. Jan 24;78(2):490-501.2014
127. Masuda H, Asahara T. Clonogenic Isolation of Colony-forming Endothelial Progenitor Cells. Manual of Research Techniques in Cardiovascular Medicine, published from Willey Blackwell, 71-93 2014
128. Tanaka R, Masuda H, Kato S, Imagawa K, Kanabuchi K, Nakashioya C, Yoshiba F, Fukui T, Ito R, Kobori M, Wada M, Asahara T, Miyasaka M. Autologous g-csf-mobilized peripheral blood cd34+ cell therapy for diabetic patients with chronic nonhealing ulcer. Cell Transplant. 23:167-179 2014;
129. Obi S, Masuda H, Akimaru H, Shizuno T, Yamamoto K, Ando J, Asahara T. Dextran induces differentiation of circulating endothelial progenitor cells. Physiological reports.;2:e00261 2014
130. Lee SH, Lee JH, Asahara T, Kim YS, Jeong HC, Ahn Y, Jung JS, Kwon SM. Genistein promotes endothelial colony-forming cell (ecfc) bioactivities and

cardiac regeneration in myocardial infarction. *PLoS One*.;9:e96155 2014

131. Masuda H, Tanaka R, Fujimura S, Ishikawa M, Akimaru H, Shizuno T, Sato A, Okada Y, Iida Y, Itoh J, Itoh Y, Kamiguchi H, Kawamoto A, Asahara T. Vasculogenic conditioning of peripheral blood mononuclear cells promotes endothelial progenitor cell expansion and phenotype transition of anti-inflammatory macrophage and t lymphocyte to cells with regenerative potential. Journal of the American Heart Association.;3:e000743 2014
132. Kuroda R, Matsumoto T, Niikura T, Kawakami Y, Fukui T, Lee SY, Mifune Y, Kawamata S, Fukushima M, Asahara T, Kawamoto A, Kurosaka M. Local transplantation of granulocyte colony stimulating factor–mobilized cd34+ cells for patients with femoral and tibial nonunion: Pilot clinical trial. *Stem Cells* Transl Med.;3:128-134 2014
133. Fukui T, Mifune Y, Matsumoto T, Shoji T, Kawakami Y, Kawamoto A, Ii M, Akimaru H, Kuroda T, Horii M, Yokoyama A, Alev C, Kuroda R, Kurosaka M, Asahara T. Superior potential of cd34–positive cells compared to total mononuclear cells for healing of nonunion following bone fracture. Cell Transplant. 2014
134. Fujita Y, Kinoshita M, Furukawa Y, Nagano T, Hashimoto H, Hirami Y, Kurimoto Y, Arakawa K, Yamazaki K, Okada Y, Katakami N, Uno E, Matsubara Y, Fukushima M, Nada A, Losordo DW, Asahara T, Okita Y, Kawamoto A. Phase ii clinical trial of cd34+ cell therapy to explore endpoint selection and timing in patients with critical limb ischemia. Circ J.;78:490-501 2014
135. ＊Fadini GP, Ferraro F, Quaini F, Asahara T, Madeddu P. Concise review: Diabetes, the bone marrow niche, and impaired vascular regeneration. *Stem Cells Transl Med*. 2014
136. Kwon SM, Lee JH, Lee SH, Jung SY, Kim DY, Kang SH, Yoo SY, Hong JK, Park JH, Kim JH, Kim SW, Kim YJ, Lee SJ, Kim HG, Asahara T. Cross talk with hematopoietic cells regulates the endothelial progenitor cell differentiation of cd34 positive cells. *PLoS One*.;9:e106310 2014 ＊

137. ＊Niikura N, Sakatani T, Arima N, Ohi Y, Honma N, Kanomata N, Yoshida K, Kadoya T, Tamaki K, Kumaki N *et al*: Assessment of the Ki67 labeling index: a Japanese validation ring study. Breast Cancer 2014 ＊
138. ＊Itoh M, Iwamoto T, Matsuoka J, Nogami T, Motoki T, Shien T, Taira N, Niikura N, Hayashi N, Ohtani S *et al*: Estrogen receptor (ER) mRNA expression and molecular subtype distribution in ER-negative/progesterone receptor-positive breast cancers. Breast Cancer Res Treat, **143**(2):403-409.2014 ＊
139. Sakai D, Grad S, Advancing the cellular and molecular therapy for intervertebral disc disease, Adv. Drug Deliv. Rev. 2014;http://dx.doi.org/10.1016/j.addr.2014.06.009. 2014
140. Likhitpanichkul M, Dreischarf M, Illien-Junger S, Walter BA, Nukaga T, Long RG, Sakai D, Hecht AC, Iatridis JC. Fibrin-genipin adhesive hydrogel for annulus fibrosus repair: performance evaluation with large animal organ culture, in situ biomechanics, and in vivo degradation tests. Eur Cell Mater.;28:25-38. 2014
141. Benneker LM, Andersson G, Iatridis JC, Sakai D, Härtl R, Ito K, Grad S. Cell therapy for intervertebral disc repair: advancing cell therapy from bench to clinics. Eur Cell Mater.;27:5-11. 2014
142. ＊Pattappa G, Peroglio M, Sakai D, Mochida J, Benneker LM, Alini M, Grad S. CCL5/RANTES is a key chemoattractant released by degenerative intervertebral discs in organ culture. Eur Cell Mater.;27:124-36; discussion 136. 2014
143. Watanabe M, Sakai D, Yamamoto Y, Nagai T, Sato M, Mochida J. Analysis of predisposing factors in elderly people with type II odontoid fracture. Spine J 2014
144. ＊Ibrahim AA, Yahata T, Takanashi T, Hiyama K, Onizuka M, Dan T, van Ypersele de Strihou C, Miyata T, and Ando K. Inhibition of plasminogen activator inhibitor type-1 activity enhances rapid and sustainable hematopoietic regeneration. Stem Cells 32, 946-958, 2013 ＊
145. Ohmachi K, Niitsu N, Uchida T, Kim SJ, Ando K, Takahashi N, Takahashi N, Uike N, Eom HS, Chae YS, Terauchi T, Tateishi U, Tatsumi M, Kim WS,

Tobinai K, Suh C, Ogura M. Multicenter Phase II Study of Bendamustine Plus Rituximab in Patients With Relapsed or Refractory Diffuse Large B-Cell Lymphoma. J Clin Oncol, 31, 2103-2109, 2013

146. Kojima M, Nishikii H, Takizawa J, Aoki S, Noguchi M, Chiba S, Ando K, and Nakamura N. MYC rearrangements are useful for predicting outcomes following rituximab and chemotherapy: multi-center analysis of Japanese patients with diffuse large B-cell lymphoma. Leuk. Lymphoma, 54:2149-54., 2013

147. ＊Kawada H, Kaneko M, Sawanobori M, Uno T, Matsuzawa H, Nakamura Y, Matsushita H, Ando K. High concentrations of L-ascorbic acid specifically inhibit the growth of human leukemic cells via downregulation of HIF-1α transcription. PLOS ONE, 8(4), e2717, , doi:10.1371/journal.pone.0062717 2013 ＊

148. ＊Harada Y, Inoue D, Ding Y, Imagawa J, Doki N, Matsui H, Yahata T, Matsushita H, Ando K, Sashida G, Iwama A, Kitamura T, and Harada H. RUNX1/AML1 mutant collaborates with BMI1 overexpression in the development of human and murine myelodysplastic syndromes. Blood, 121, 3434-3446, 2013 ＊

149. ＊Harkensee C, Oka A, Onizuka M, Middleton PG, Inoko H, Nakaoka H, Gennery AR, Ando K and Morishima Y. Scanning of the immunogenome with microsatellite markers for non-HLA associations with graft-versus-host disease in haematopoietic stem cell transplantation. Immunogenetics, 65; 417-427, 2013

150. Kojima M, Machida S, Miyamoto M, Moriuchi M, Ohbayash Y, Ando K. Deferasirox treatment improved hematopoiesis and led to complete remission in a patient with pure red cell aplasia. Int J Hematol, 98:719-22., 2013

151. Kantarjian H, Martinelli G, Jabbour E, Quintás-Cardama A, Ando K, Bay J-O, Wei A, Gröpper S, Papayannidis C, Owen K, Pike L, Schmitt N, Stockman P, Giagounidis A, on behalf of the SPARK-AML1 investigators. Stage I findings of a two-stage Phase II study to assess the efficacy, safety and tolerability of barasertib (AZD1152) compared with low dose cytosine arabinoside in elderly patients with acute myeloid leukemia. Cancer, 119

(14);2611-2619, 2013

152. Ogawa Y, Suzuki K, Sakai A, Iida S, Ogura M, Tobinai K, Matsumoto M, Matsue K, Terui Y, Ohashi K, Ishii M, Mukai H, Ando K, Hotta T. A phase I/II study of VMP (bortezomib-melphalan-prednisolone) for previously untreated patients with multiple myeloma in Japan. Cancer Sci, 104(7);912-919, 2013
153. ＊Okuyama K, Ikawa T, Harnprasopwat R, Lu J, Yamashita R, Ha D, Toyoshima T, Chanda B, Kawamata T, Yokoyama K, Gertner B, Wang S, Ando K, Lodish HF, Tojo A, Kawamoto H, Kotani A. miR-126-mediated control of cell fate in B cell-myeloid progenitors as a potential alternative to transcriptional factors. Proc Nat Acad Sci. 110(33);13410-13415, 2013 ＊
154. Murayama H, Matsushita H, Ando K. Atypical chronic myeloid leukemia harboring *NUP98-HOXA9.* Int J Hematol, 98,143-144, 2013 ＊
155. Ogawa Y, Ogura M, Suzuki T, Ando K, Uchida T, Shirasugi Y, Tobinai K, Lee JW, Kase M, Katsura K, Hotta T. A phase I/II study of ofatumumab (GSK1841157) in Japanese and Korean patients with relapsed or refractory B-cell chronic lymphocytic leukemia. Int J Hematol, 98;164-170, 2013
156. ＊Kikuchi T, Tokunaka M, Kikuti Y, Carreras J, Ogura G, Takekoshi S, Kojima M, Ando K, Hashimoto Y, Abe M, Takata K, Yoshino T, Muto A, Igarashi K, Nakamura N. Over-expression of Bach2 is related to ongoing somatic hypermutation of the immunoglobulin heavy chain gene variable region of de novo diffuse large B-cell lymphoma. Pathology International, 63,339-344, 2013 ＊
157. Muroi K, Miyamura K, Ohashi K, Murata M, Eto T, Kobayashi N, Taniguchi S, Imamura M, Ando K, Kato S, Mori T, Teshima T, Mori M, Ozawa K. Unrelated allogeneic bone marrow-derived mesenchymal stem cell for steroid-refractory acute graft-versus-host disease: a phase I/II study. Int J Hematol. 98,206-213, 2013
158. Ohnishi H, Sasaki H, Nakamura Y, Kato S, Ando K, Narimatsu H, Tachibana K. Regulation of cell shape and adhesion by CD34. Cell Adhesion & Migration, 7;426-433, 2013
159. Ohgiya D, Machida S, Tsuchiya T, Ichiki A, Amaki J, Aoyama Y, Kawai H,

Miyamoto M, Murayama H, Onizuka M, Ando K. Strong effect of mogamulizumab on splenic residual disease of adult T-cell leukemia/lymphoma. Ann Hematol. 93(4);719-720, 2013

160. Kanakura Y, Ohyashiki K, Shichishima T, Okamoto S, Ando K, Ninomiya H, Kawaguchi T, Nakao S, Nakakuma H, Nishimura J, Kinoshita T, Bedrosian CL, Ozawa K, Omine M. Long-term efficacy and safety of eculizumab in Japanese patients with PNH: AEGIS trial. Int J Hematol. 98(4);406-416, 2013
161. Ogura M, Ishida T, Hatake K, Taniwaki M, Ando K, Tobinai K, Fujimoto K, Yamamoto K, Miyamoto T, Uike N, Tanimoto M, Tsukasaki K, Ishizawa K, Suzumiya J, Inagaki H, Tamura K, Akinaga S, Tomonaga M, Ueda R. Multicenter phase II study of mogamulizumab (KW-0761), a defucosylated anti-CCR4 antibody, in patients with relapsed peripheral T-cell lymphoma and cutaneous T-cell lymphoma. J Clin Oncol 32(11);1157-63, 2013
162. Suzuki T, Yamauchi T, Ando K, Nagai T, Kakihana K, Miyata Y, Uchida T, Tabata Y, Ogura M. Phase I study of Clofarabine (JC0707) in adult Japanese patients with acute myeloid leukemia (AML) in Japan. JJCO, 43(12);1177-1183, 2013
163. Ogura M, Ando K, Suzuki T, Ishizawa K, Oh SY, Ito K, Yamamoto K, Au WA, Tien HF, Matsuno Y, Terauchi T, Yamamoto K, Mori M, Tanaka Y, Shimamoto T, Tobinai K, Kim WS. A Multicenter Phase II Study of Vorinostat in Patients With Relapsed or Refractory Indolent B-cell Non-Hodgkin Lymphoma or Mantle Cell Lymphoma. Brit J Haematol, 165(6)768-76, 2013
164. Miyamoto M, Onizuka M, Machida S, Toyosaki M, Amaki J, Aoyama Y, Kawai H, Sato A, Hayama N, Ogawa Y, Kawada H, Ando K. ACE deletion polymorphism is associated with a high risk of non-infectious pulmonary complication after stem cell transplantation. Int J Hematol, 99(2):175-83, 2013
165. ＊ Immune-Related Gene Expression Profile in Laboratory Common Marmosets Assessed by an Accurate Quantitative Real-Time PCR Using Selected Reference Genes. Fujii Y., Kitaura K., Matsutani T., Shirai K.,

Suzuki S., Takasaki T., Kumagai K., Kametani Y., Shiina T., Takabayashi S., Katoh H., Hamada Y., Kurane I., Suzuki R. Pros ONE 8(2) e56296 2013 *

166. * Kenji Kawai, Katsumi Tamura, Ikuko Sakata, Jiro Ishida, Masayoshi Nagata, Hideo Tsukada, Hiroshi Suemizu, Tsuyoshi Chijiwa, Masato Nakamura, Yoshiyuki Abe "New in vivo models to analyze hepatic metastasis of human colon cancer cell line (HCT116) in NOD/Shi-scid/IL-2R γ^{null} (NOG) mice by ^{18}F-FDG PET/CT" Oncology Reports, 29: 464-468, 2013 *

167. * Tomoko Shofuda, Daisuke Kanematsu, Hayato Fukusumi, Atsuyo Yamamoto, Yohei Bamba, Sumiko Yoshitatsu, Hiroshi Suemizu, Masato Nakamura, Yoshikazu Sugimoto, Miho Kusuda Furue, Arihiro Kohara, Wado Akamatsu, Yohei Okada, Hideyuki Okano, Mami Yamasaki, and Yonehiro Kanemura "Human Decidua-Derived Mesenchymal Cells are a Promising Source for the Generation and Cell Banking of Human Induced Pluripotent Stem Cells" Cell Medicine, 4:125-147, 2013 *

168. * Hayato Fukusumi, Tomoko Shofuda, Daisuke Kanematsu, Atsuyo Yamamoto, Hiroshi Suemizu, Masato Nakamura, Mami Yamasaki, Masatoshi Ohgushi, Yoshiki Sasai and YonehiroKanemura "Feeder-free generation and long-term culture of human induced pluripotent stem cells using Pericellular Matrix of Decidua derived Mesenchymal cells" PLoS ONE, 2013 PLoS ONE 8(1): e55226, 2013; (doi:10.1371/journal.pone.0055226, Received May 29, 2012; Accepted December 20, 2012; Published January 31, 2013)

169. * Hiroshi Yamazaki, Hiroshi Suemizu, Norie Murayama, Masahiro Utoh, Norio Shibata, Masato Nakamura, and F. Peter Guengerich "In vivo Drug Interactions of the Teratogen Thalidomide with Midazolam: Heterotropic Cooperativity of Human Cytochrome P450 in Humanized Liver TK-NOG Mice" Chemical Research in Toxicology, 26: 486—489, 2013 *

170. * Ai Tsukada, Hiroshi Suemizu, Norie Murayama, Ryohji Takano, Makiko Shimizu, Masato Nakamura, and Hiroshi Yamazaki, "Plasma concentrations of melengestrol acetate in humans extrapolated from the pharmacokinetics established in in vivo experiments with rats and chimeric mice with humanized liver and physiologically based pharmacokinetic modeling"

Regulatory Toxicology and Pharmacology, 65: 316-324, 2013 *

171. *Hiroshi Suemizu1, Kenji Kawai, Yuichiro Higuchi, Haruo Hashimoto, Tomoyuki Ogura, Toshio Itoh, Erika Sasaki, Masato Nakamura, "A Versatile Technique for the In Vivo Imaging of HumanTumor Xenografts Using Near-Infrared Fluorochrome-Conjugated Macromolecule Probes" PLoS ONE 8 (12): e82708, 2013; (doi:10.1371/journal.pone.0082708, Received April 1, 2013; Accepted October 26,; Published December 17, 2013) 2013 *
172. Mikami M, Aoki Y, Sakamoto M,Shimada M,Takeshima N,Fujiwara H,Matsumoto T,Kita T,Takizawa K. Current surgical principle for uterine cervical cancer of stages Ia2, Ib1, and IIa1 in Japan: A survey of the Japanese Gynecologic Oncology Group. International Journal of Gynecological Cancer.2013. 23(9):1655-60
173. Togo A, Izumi S, Sato S,Nakamura E,Goto K,Suzuki T,Ishimoto H,Mikami M. Isolated Tubal Torsion *in Adolescence: Case Report and Review. Journal of Gynecologic Surgery.29:39-44. 2013
174. Hirasawa T, Miyazawa M,Yasuda M,Shida M,Ikeda M ,Kajiwara H,Nakamura M,Fujita M,Muramatsu T, Mikami M. Alterations of Hypoxia-Induced Factor Signaling Pathway Due 5. Yokoyama, K., Yokoyama, N., Izawa, K., Kotani, A., Harashima, A., Hozumi, K. and Tojo, A. In vivo leukemogenic potential of an interleukin 7 receptor alpha chain mutant in hematopoietic stem and progenitor cells. Blood. 122: 4259-4263, 2013.
175. *Kawaguchi, D., Furutachi, S., Kawai, H., Hozumi, K. and Gotoh Y. Dll1 maintains quiescence of adult neural stem cells and segregates asymmetrically during mitosis. Nat Commun. 4: 1880 doi: 10.1038/ncomms2895, 2013.*
176. *Hiraoka, Y., Komine, O., Nagaoka, M., Bai, N., Hozumi, K. and Tanaka, K. Delta-like 1 regulates Bergmann glial monolayer formation during cerebellar development. Mol. Brain. 6: 25 doi:10.1186/1756-6606-6-25, 2013.*
177. Inoue, S., Sato, T., Suzuki-Utsunomiya K., Komori, Y., Hozumi, K., Chiba, T., Yahata, T., Nakai, K. and Inokuchi, S. Sepsis-induced hypercytokinemia and lymphocyte apoptosis in aging-accelerated Klotho knockout mice.

Shock. 39: 311-6, 2013.

178. Hirasawa T, Miyazawa M,Yasuda M,Shida M,Ikeda M ,Kajiwara H,Nakamura M,Fujita M,Muramatsu T, Mikami M. Alterations of Hypoxia-Induced Factor Signaling Pathway Due to Mammalian Target of Rapamycin (mTOR) Suppression in Ovarian Clear Cell Adenocarcinoma. International Journal of Gynecological Cancer..23:1210-1218. 2013 *

179. *Li X, Bian Y, Takizawa Y, Hashimoto T, Ikoma T, Tanaka J, Kitamura N, Inagaki Y, Komada M, and Tanaka T: ERK-dependent downregulation of Skp2 reduces Myc activity with HGF, leading to inhibition of cell proliferation through a decrease in Id1 expression. Mol Cancer Res 11: 1437-1447,2013*

180. Tsukui T, Ueha S, Abe J, Hashimoto S, Shichino S, Shimaoka T, Shand FHW, Arakawa Y, Oshima K, Hattori M, Inagaki Y, Tomura M, and Matsushima K: Qualitative rather than quantitative changes are hallmarks of fibroblasts in bleomycin-induced pulmonary fibrosis. Am J Pathol 183: 758-773, 2013

181. *Masuda H, Asahara T. Clonogenic Assay of Endothelial Progenitor Cells. Trends Cardiovasc Med. Jan 31. [Epub ahead of print] 2013.

182. Tsukada S, Kwon SM, Matsuda T, Jung SY, Lee JH, Lee SH, Masuda H, Asahara T. Identification of mouse colony forming endothelial progenitor cells for postnatal neovascularization: a novel insight highlighted by new mouse colony forming assay. Stem Cell Res Ther.;4(1):20. 2013 *

183. Tanaka R, Vaynrub M, Masuda H, Ito R, Kobori M, Miyasaka M, Mizuno H, Warren SM, Asahara T. Quality-control culture system restores diabetic endothelial progenitor cell vasculogenesis and accelerates wound closure. Diabetes.;62:3207-3217 2013

184. Lee JH, Lee SH, Yoo SY, Asahara T, Kwon SM. Cd34 hybrid cells promote endothelial colony-forming cell bioactivity and therapeutic potential for ischemic diseases. Arterioscler Thromb Vasc Biol.;33:1622-16341. 2013

185. Niikura N, Masuda S, Kumaki N, Xiaoyan T, Terada M, Terao M, Iwamoto T, Oshitanai R, Morioka T, Tuda B et al: Prognostic Significance of the Ki67 Scoring Categories in Breast Cancer Subgroups. Clinical breast cancer 2013.*

186. Niikura N, Odisio BC, Tokuda Y, Symmans FW, Hortobagyi GN, Ueno NT: Latest biopsy approach for suspected metastases in patients with breast cancer. Nat Rev Clin Oncol, **10**(12):711-719. 2013 *

187. Suzuki Y, Ogiya R, Oshitanai R, Terao M, Terada M, Morioka T, Tsuda B, Niikura N, Okamura T, Saito Y et al: Feasibility and pharmacokinetics of combined therapy with S-1 and trastuzumab in patients with human epidermal growth factor receptor 2-positive metastatic or recurrent breast cancer. Int J Clin Oncol 2013.

188. Niikura N, Kimura M, Iwamoto T, Hayashi N, Shintoku J, Saito Y, Suzuki Y, Tokuda Y: Women prefer adjuvant endocrine therapy to chemotherapy for breast cancer treatment. Breast Cancer, **20**(1):67-74. 2013

189. Hayashi N, Niikura N, Yamauchi H, Nakamura S, Ueno NT: Adding hormonal therapy to chemotherapy and trastuzumab improves prognosis in patients with hormone receptor-positive and human epidermal growth factor receptor 2-positive primary breast cancer. Breast Cancer Res Treat, **137**(2):523-531. 2013

190. Hayashi N, Costelloe CM, Hamaoka T, Wei C, Niikura N, Theriault RL, Hortobagyi GN, Madewell JE, Ueno NT: A prospective study of bone tumor response assessment in metastatic breast cancer. Clin Breast Cancer, **13**(1):24-30. 2013

191. Hiyama A, Yokoyama K, Nukaga T, Sakai D, Mochida J. A complex interaction between Wnt signaling and TNF-α in nucleus pulposus cells. Arthritis Res Ther.;15(6):R189. 2013

192. Guterl CC, See EY, Blanquer SB, Pandit A, Ferguson SJ, Benneker LM, Grijpma DW, **Sakai D,** Eglin D, Alini M, Iatridis JC, Grad S. Challenges and strategies in the repair of ruptured annulus fibrosus. Eur Cell Mater.;25:1-21. 2013

193. Tanaka M, Sakai D, Hiyama A, Arai F, Nakajima D, Nukaga T, Nakai T, Mochida J. Effect of cryopreservation on canine and human activated nucleus pulposus cells: a feasibility study for cell therapy of the intervertebral disc. Biores Open Access.;2(4):273-82. 2013

194. Yamamoto J, Maeno K, Takada T, Kakutani K, Yurube T, Zhang Z,

Hirata H, Kurakawa T, Sakai D, Mochida J, Doita M, Kurosaka M, Nishida K. Fas ligand plays an important role for the production of pro-inflammatory cytokines in intervertebral disc nucleus pulposus cells. J Orthop Res.;31:608-15. doi: 10.1002/jor.22274. 2013

195. Kawamata T, Jun L, Sato T, Tanaka M, Nagaoka H, Agata Y, Toyoshima T, Yokoyama K, Oyaizu N, Nakamura N, Ando K, Tojo A, Kotani A. Imatinib mesylate directly impairs class switch recombination through downregulation of AID: its potential efficacy as an AID suppressor. Blood, 119, 3123-3127,2012*
196. Ogura M, Hatake K, Ando K, Tobinai K, Tokushige K, Ono C, Ishibashi T, Vandendries E. Phase I Study of Anti-CD22 Immunoconjugate Inotuzumab Ozogamicin Plus Rituximab in Relapsed/Refractory B-cell Non-Hodgkin Lymphoma. Cancer Science, 103, 933-938, 2012
197. Matsushita H, Nakamura N, Tanaka Y, Ohgiya D, Tanaka Y, Damdinsuren A, Ogawa Y, Ando K, Miyachi H. Clinical and pathological features of B-cell non-Hodgkin lymphomas lacking surface expression of immunoglobulin light chains. Clinical Chemistry and Laboratory Medicine, 50,1665-1670, 2012
198. Shirasugi Y, Ando K, Miyazaki K, Tomiyama Y, Iwato K, Okamoto S, Kurokawa M, Kirito K, Hashino S, Ninomiya H, Mori S, Yonemura Y, Usuki K, Wei H, Lizambri R. An Open-Label Extension Study Evaluating the Safety and Efficacy of up to 3.5 years of Romiplostim in Thrombocytopenic Japanese Patients with Immune Thrombocytopenic Purpura (ITP) Int J Hematol, 95,652-659, 2012
199. Harkensee C, Oka A, Onizuka M, Middleton PG, Inoko H, Hirayasu K, Yabe T, Nakaoka H, Ando K, Gennery AR, Morishima Y. Single Nucleotide Polymorphisms and outcome risk in unrelated Haematopoietic Stem Cell Transplantation: An exploration study. Blood, 119, 6365-6372, 2012
200. Ohgiya D, Matsushita H, Onizuka M, Nakamura N, Amaki J, Aoyama Y, Kawai H, Ogawa Y, Kawada H and Ando K. PML affects IL-6 production and resistance to treatment in multiple myeloma. Acta Haematologica. 128, 213-222, 2012 *
201. Nunomura S, Shimada S, Kametani Y, Yamada Y, Yoshioka M, Suemizu H,

Ozawa M, Itoh T, Kono A, Suzuki R, Tani K, Ando K, Yagita H, Ra C, Habu S, Satake M, Sasaki E. Double expression of CD34 and CD117 on bone marrow progenitors is a hallmark of the development of functional mast cell of Calithrix Jucchus (common marmoset). Int Immunol. 24, 593-603, 2012 *

202. Ito R, Negishi N, Irie N, Matsuo K, Suzuki D, Katano I, Hayakawa E, Kawai K, Kamisako T, Eto T, Ogura T, Hozumi K, Ando K, Aiso S, Tamaoki N, Habu S and Ito M. Osteosclerosis and inhibition of human hematopoiesis in NOG mice expressing human Delta-like 1 in osteoblasts. Exp Hematol, 40,953-963, 2012 *
203. Moriya Y, Mizuma A, Uesugi T, Ohnuki Y, Nagata E, Takahashi W, Kobayashi H, Kawada H, Ando K, Takagi S, Takizawa S. Phase I study of intravenous low-dose granulocyte-colony stimulating factor in acute and sub-acute ischemic stroke. Journal of Stroke and Cerebrovascular Diseases, 22,1088-1097, 2012
204. Ohgiya D, Matsushita H, Kojima M, Ando K. Huge multinucleated megaloblasts found in a patient with refractory anemia with excess blasts-1. Int J Hematol., 96, 631-632, 2012
205. Ikoma N, Manabe Y, Yamaoka H, Akasaka E, Mabuchi T, Ozawa A, Nakamura N, Kojima M, Ando K. Random skin biopsy of intravascular large B-cell lymphoma: a case report. Tokai J Exp Clin Med. Sep 20;37(3):75-6 2012
206. Sakai D, Nakamura Y, Nakai T, Mishima T, Kato S, Grad S, Alini M, Risbud MV, Chan D, Cheah KSE, Masuda K, Ando K, Mochida J. Exhaustion of nucleus pulposus progenitor cells with ageing and degeneration of the intervertebral disc. Nature Comm, 3, 1264, DOI:10.1038/ncomms2226 2012
207. Tsuda B, Kametani Y*, Goto Y, Saito Y, Suzuki Y, Habu S, Inoko H, Tokuda Y A human B cell receptor epitope-based erbB-2 peptide (N:163-182) with pan-reactivity to the T cells of Japanese breast cancer patients. Vaccines and Vaccination, 3:7. Doi.org/10.4172/2157-7560.1000159 2012 *
208. Kitaura K, Fujii Y, Matsutani T, Shirai K, Suzuki S, Takasaki T, Shimada S, Kametani Y, Shiina T, Takabayashi S, Katoh H, Ogasawara K, Kurane I,

Suzuki R. A new method for quantitative analysis of the T cell receptor V region repertoires in healthy common marmosets by microplate hybridization assay.. J Immunol Methods 384:81-91 2012*

209. Nunomura S, Shimada S, Kametani Y*, Yamada Y, Yoshioka M, Suemizu H, Ozawa M, Itoh T, Kono A, Suzuki R, Tani K, Ando K, Yagita H, Ra C, Habu S, Satake M, Sasaki E. Double expression of CD34 and CD117 on bone marrow progenitors is a hallmark of the development of functional mast cell of *Calithrix Jucchus* (common marmoset). Int. Immunol24:593-603 2012 *
210. Kametani Y, Ohshima S, Kita YF, Shimada S, Kamiguchi H, Shiina T, Inoko H, Kulski JK and Ando A Porcine MHC classical class I genes are coordinately expressed in superantigen-activated mononuclear cells.Veterinary Immunology and Immunopathology 148:252-259 2012*
211. Hitoshi Yamazaki, Tsuyoshi Chijiwa, Yoshimasa Inoue, Yoshiyuki Abe, Hiroshi Suemizu, Kenji Kawai, Masatoshi Wakui, Daisuke Furukawa, Masaya Mukai, Sadahiro Kuwao, Makoto Saegusa, Masato Nakamura "Overexpression of the miRNA-34 family suppresses invasive growth of malignant melanoma with the wild - type p53 gene" Experimental and Therapeutic Medicine 3: 793-796, 2012 *
212. Yamazaki, H., Suemizu, H., Shimizu, M., Igaya, S., Shibata, N., Nakamura, M., Chowdhury, G. & Guengerich, F.P. " In Vivo Formation of Dihydroxylated and Glutathione Conjugate Metabolites Derived from Thalidomide and 5-Hydroxythalidomide in Humanized TK-NOG Mice" Chemical research in toxicology 25: 274-276, 2012.
213. Yoshihara K,Tsunoda T,Shigemizu D,Fujiwara H,Hatae M,Fujiwara H,Masuzaki H,Katabuchi H,Kawakami Y,Okamoto A,Nogawa T,Matsumura N,Udagawa Y,Saito T,Itamochi H,Takano M,Miyagi E,Sudo T,Ushijima K,Iwase H,Seki H,Terao Y,Enomoto T, Mikami M,Akazawa K,Tsuda H,Moriya T,Tajima A,Inoue I,Tanaka K Iwamori M. High-Risk Ovarian Cancer Based on 126-Gene Expression Signature Is Uniquely Characterized by Downregulation of Antigen Presentation Pathway.. Clinical Cancer Research. 18:1374-1385. 2012.*

214. Sugiyama T, Miyazawa M,Mikami M,Goto Y,Nishijima Y,Ikeda M,Hirasawa T,Muramatsu O,Takekoshi S,Iwamori M. Enhanced Expression of Sulfatide, a Sulfated Glycolipid, in Well-Differentiated Endometrial Adenocarcinoma..International Journal of Gynecological Cancer. 22:1192-1197 2012
215. Tanaka K, Takada H,Isonishi S,Aoki D,Mikami M, Kiguchi K,Iwamori M. Possible involvement of glycolipids in anticancer drug resistance of human ovarian serous carcinoma-derived cells. Journal of Biochemistry. 152:587-594. 2012.*
216. Nishijima Y, Toyoda M, Yamazaki M,Sugiyama T,Miyazawa M,Muramatsu T,Nakamura K,Narimatsu H,Umezawa A,Mikami M. Glycan profiling of endometrial cancers using lectin microarray. Genes to Cells. 17:826-836. 2012.*
217. Toita T, Kitagawa R, Hamano T,Umayahara K,Hirashima Y,Aoki Y,Oguchi M,Mikami M,Takizawa K. Phase II study of concurrent chemoradiotherapy with high-dose-rate intracavitary brachytherapy in patients with locally advanced uterine cervical cancer: Efficacy and toxicity of a low cumulative radiation dose schedule. Gynecologic Oncology. 126:211-216. 2012.
218. Tsukada H, Muramatsu T,Miyazawa M, Iida T,Ikeda M, Shida M,Hirasawa T,Kajiwara H,Murakami M,Yasuda M,Mikami M. Long Term Prognostic Implications of Expression of Glucose Transporter-1 and Hexokinase in Patients with Stage Uterine Leiomyosarcoma..45:147-154. 2012 *
219. Sato, T., Chiba, T., Ohno, S., Sato, C., Sugoh, T., Miyashita, K., Akatsuka, H., Hozumi, K., Okada, Y., Iida, Y., Akatsuka, A., Agata, Y., Chiba, M., Kohu, K., Satake, M., Tanabe, H., Saya, H. and Habu, S. Reciprocal control of G1-phase progression is required for Th-POK/Runx3-mediated CD4/8 thymocyte cell fate decision. *J. Immunol.* 189: 4426-36, 2012.*
220. Kamei, N., Kwon, S.M., Ishikawa, M., Ii, M., Nakanishi, K., Yamada, K., Hozumi, K., Kawamoto, A., Ochi, M. and Asahara, T. Endothelial progenitor cells promotes astrogliosis following spinal cord injury through Jagged1-dependent Notch signaling. J. Neurotraum. 29: 1758-69, 2012.*
221. Sekine, C., Koyanagi, A., Koyama, N., Hozumi, K., Chiba, S. and Yagita, H.

Differential regulation of osteoclastogenesis by Notch2/Delta-like 1 and Notch1/Jagged1 axes. Arthritis Res. Ther. 14: R45, 2012.*

222. Luo, H., Jin, K., Xie, Z., Qiu, F., Li, S., Zou, M., Cai, L., Hozumi, K., Shima, D.T. and Xiang, M. Forkhead box N4 (Foxn4) activates Dll4-Notch signaling to suppress photoreceptor cell fates of early retinal progenitors. Proc. Natl. Acad. Sci. USA. 109: E553-62, 2012.*
223. Jung SY, Choi JH, Kwon SM, Masuda H, Asahara T, Lee YM. Decursin inhibits vasculogenesis in early tumor progression by suppression of endothelial progenitor cell differentiation and function. **J Cell Biochem**. Feb 1. [Epub ahead of print], May;113(5):1478-87. 2012
224. Fadini GP, Rattazzi M, Matsumoto T, Asahara T, Khosla S. Emerging role of circulating calcifying cells in the bone-vascular axis. Circulation. 125(22):2772-2781. 2012;
225. Fukui T, Matsumoto T, Mifune Y, Shoji T, Kuroda T, Kawakami Y, Kawamoto A, Ii M, Kawamata S, Kurosaka M, Asahara T, Kuroda R. Local transplantation of granulocyte colony-stimulating factor-mobilized human peripheral blood mononuclear cells for unhealing bone fractures. *Cell Transplant*. 2012;21(4):707-721.
226. Kamei N, Kwon SM, Ishikawa M, Ii M, Nakanishi K, Yamada K, Hozumi K, Kawamoto A, Ochi M, Asahara T. Endothelial progenitor cells promote astrogliosis following spinal cord injury through Jagged1-dependent Notch signaling. J Neurotrauma.;29(9):1758-1769. 2012 *
227. Kamei N, Kwon SM, Kawamoto A, Ii M, Ishikawa M, Ochi M, Asahara T. Contribution of bone marrow-derived endothelial progenitor cells to neovascularization and astrogliosis following spinal cord injury. J Neurosci Res.;90(12):2281-2292. 2012 *
228. Kawakami Y, Ii M, Alev C, Kawamoto A, Matsumoto T, Kuroda R, Shoji T, Fukui T, Masuda H, Akimaru H, Mifune Y, Kuroda T, Horii M, Yokoyama A, Kurosaka M, Asahara T. Local transplantation of ex vivo expanded bone marrow-derived CD34-positive cells accelerates fracture healing. Cell Transplant.;21(12):2689-2709. 2012
229. Kinoshita M, Fujita Y, Katayama M, Baba R, Shibakawa M, Yoshikawa K,

Katakami N, Furukawa Y, Tsukie T, Nagano T, Kurimoto Y, Yamasaki K, Handa N, Okada Y, Kuronaka K, Nagata Y, Matsubara Y, Fukushima M, Asahara T, Kawamoto A. Long-term clinical outcome after intramuscular transplantation of granulocyte colony stimulating factor-mobilized CD34 positive cells in patients with critical limb ischemia. Atherosclerosis. 224(2):440-445. 2012;

230. Kwon SM, Alev C, Lee SH, Asahara T. The molecular basis of Notch signaling: a brief overview. Adv Exp Med Biol.;727:1-14. 2012
231. Masuda H, Iwasaki H, Kawamoto A, Akimaru H, Ishikawa M, Ii M, Shizuno T, Sato A, Ito R, Horii M, Ishida H, Kato S, Asahara T. Development of serum-free quality and quantity control culture of colony-forming endothelial progenitor cell for vasculogenesis. Stem Cells Transl Med.;1(2):160-171. 2012
232. Obi S, Masuda H, Shizuno T, Sato A, Yamamoto K, Ando J, Abe Y, Asahara T. Fluid shear stress induces differentiation of circulating phenotype endothelial progenitor cells. Am J Physiol Cell Physiol.;303(6):C595-606. 2012
233. Tanaka R, Masuda H, Kato S, Imagawa K, Kanabuichi K, Nakashioya C, Yoshiba F, Fukui T, Ito R, Kobori M, Wada M, Asahara T, Miyasaka M. Autologous G-CSF mobilized peripheral blood CD34(+) cell therapy for diabetic patients with chronic non-healing ulcer. *Cell Transplant.* [Epub ahead of print] 2012.
234. Niikura N, Liu J, Hayashi N, Mittendorf EA, Gong Y, Palla SL, Tokuda Y, Gonzalez-Angulo AM, Hortobagyi GN, Ueno NT: Loss of human epidermal growth factor receptor 2 (HER2) expression in metastatic sites of HER2-overexpressing primary breast tumors. *J Clin Oncol*, **30**(6):593-599. 2012 *
235. Niikura N, Liu J, Hayashi N, Palla SL, Tokuda Y, Hortobagyi GN, Ueno NT, Theriault RL: Retrospective analysis of antitumor effects of zoledronic acid in breast cancer patients with bone-only metastases. *Cancer*, **118**(8):2039-2047. 2012
236. Niikura N, Iwamoto T, Masuda S, Kumaki N, Xiaoyan T, Shirane M, Mori K, Tsuda B, Okamura T, Saito Y *et al*: Immunohistochemical Ki67 labeling index

has similar proliferation predictive power to various gene signatures in breast cancer. *Cancer Sci*, **103**(8):1508-1512.2012*

237. Niikura N, Ueno NT: Biomarker discordance during tumor progression. *Cancer Biomark* **12**(6):205-206.*
238. Niikura N, Ueno NT: Cange in HER2 status during breast tumor progression. *Cancer Biomark* 2012, **12**(6):251-255. 2012
239. Hiyama A, Arai F, Sakai D, Yokoyama K, Mochida J. The effects of oxygen tension and antiaging factor Klotho on Wnt signaling in nucleus pulposus cells. Arthritis Res Ther. 14:R105. 2012;
240. Abe K, Araki K, Tanigawa M, Semba K, Ando T, Sato M, Sakai D, Hiyama A, Mochida J, Yamamura K. A Cre knock-in mouse line on the Sickle tail locus induces recombination in the notochord and intervertebral disks. Genesis;50:758-65. 2012
241. Illien-Jünger S, Pattappa G, Peroglio M, Benneker LM, Stoddart MJ, **Sakai D,** Mochida J, Grad S, Alini M. Homing of mesenchymal stem cells in induced degenerative intervertebral discs in a whole organ culture system. ***Spine***;37:1865-73. 2012
242. Arai F, Hiyama A, Sakai D, Yokoyama K, Mochida J. The expression and role of non-canonical (PKC) signaling in nucleus pulposus cell metabolism. J Orthop Res.;30:1478-85. 2012

＜図書＞

1. (ガイドライン委員会)片渕秀隆、三上幹男、宇田川康博、八重樫伸生、永瀬智、金内優典　外陰がん・膣がん治療ガイドライン作成委員会、評価委員会　外陰がん・膣がん治療ガイドライン 2015 年版　　日本婦人科腫瘍学会　(金原出版)
2. 第 1 版委員会　日本産科婦人科学会婦人科腫瘍委員会　邦における卵巣腫瘍の登録のあり方検討小委員会　卵巣腫瘍取り扱い規約改訂小委員会(婦人科系委員会)青木大輔、牛島公生、岡本愛光、加来恒壽、片渕秀隆、紀川純三、小林裕明、小林浩、齋藤豪、齋藤俊章、田代浩徳、蜂須賀徹、馬場長、深澤一雄、万代

昌紀、三上幹男、八重樫伸生、山上亘　卵巣腫瘍・卵管癌・腹膜癌取扱い規約臨床編第 1 版　日本産科婦人科学会・日本病理学会 （金原出版）　2015
3. 寒河江悟、戸板孝文、三上幹男、岡本愛光、万代昌紀、落合和徳　子宮頸がん臨床試験の最前線　GCIG 2014Cervical Cancer Brainstorming Meeting in Melbourne の報告(1)　産婦人科の実際　第 64 巻第 4 号 549-544 2015
4. 寒河江悟、戸板孝文、三上幹男、岡本愛光、万代昌紀、落合和徳　子宮頸がん臨床試験の最前線　GCIG 2014Cervical Cancer Brainstorming Meeting in Melbourne の報告(2)　産婦人科の実際 産婦人科の実際 第 64 巻第 5 号 705-711 2015
5. 三上幹男、林優、浅井哲、池田仁惠、信田政子、平澤猛　広汎子宮全摘術に傍大動脈リンパ節郭清を追加すべき症例は？また郭清追加だけで十分か？　産婦人科の実際 64(13) 2021-206 2015
6. 金内優典、三上幹男、片渕秀隆　WV 婦人科疾患　2:子宮頸管・子宮体癌　日常診療に活かす診療ガイドライン UP-TO-DATE 2016→2017　メディカルレビュー社 857-64　2015
7. ガイドライン委員会委員長　片渕秀隆　副委員長　三上幹男　主幹事　永瀬智　編集幹事　金内優典　　婦人科がん治療ガイドラインエッセンシャル 2016 年版　日本婦人科腫瘍学会(金原出版株式会社)
8. ガイドライン委員会委員長　片渕秀隆　副委員長　三上幹男　主幹事　永瀬智　編集幹事　金内優典　患者さんとご家族のための子宮頸がん・子宮体がん・卵巣がん治療ガイドライン(第 2 版)　日本婦人科腫瘍学会(金原出版株式会社) 2016
9. 三上　幹男　産婦人科研修の必修知識 2016-2018　産科婦人科学会　初版　2016
10. K Matsuo,Y Takazawa,M.S.Ross,E Elishaev,I Podzielinski,M Yunokawa,T.B Sheridan,S.H.Bush,M.M.Klobocista,E.A.Blake,T Takano,S Matsuzaki,T Baba,S Satoh,M Shida,T Nishikawa,Y Ikeda,S Adachi,T Yokoyama,M Takekuma,K Fujiwara,Y Hazama,D Kadogami,M.N.Moffitt,S Takeuchi,M Nishimura,K Iwasaki,N Ushioba,M.S.Johnson,M Yoshida,A Hakam,S.W.Li,A.M.Richmond,H Machida,P.Mhawech-Fauceglia,Y Ueda,K Yoshino,K Yamaguchi,T Oishi,H Kajiwara,K Hasegawa,M Yasuda,K Kawana,K Suda,T.M.Miyake,T Moriya,Y Yuba,T Morgan,T Fukagawa,A Wakatsuki,T Sugiyama,T Pejovic,T Nagano,K

Shimoya,M Andoh,Y Shiki,T Enomoto,T Sasaki,K Fujiwara,M Mikami,M Shimada,I Konishi, TKimura, M.D.Post,M.M.Shahzad,D.D.Im,H Yoshida,K Omatsu,F.R,Ueland,J.L.Kelley,R.G.Karabakhtsian&L.D.Roman significance of histologic pattern of carcinoma and sarcoma components on survival outcomes of uterine carcinosarcoma Annals of Oncology 1 月 10 日 2016

11. 片渕秀隆、榎本隆之、井崑一彦、牛島公生、齋藤俊章、杉山徹、鈴木直、田代浩徳、永瀬智、万代昌紀、三上幹男、宮本新吾 報告 婦人科腫瘍委員会 産科婦人科学会雑誌 68(6) 1377-1380 2016
12. 三上幹男、万代昌紀 第 68 回日本産科婦人科学会・学術講演会 シンポジウム 2 子宮悪性腫瘍に対する低侵襲手術の確立に向けて 座長レビュー 日本産科婦人科学会雑誌 68(11) 2637-26402016
13. 矢坂美和、鈴木隆弘、菅野秀俊、西島義博、池田仁惠、三上幹男 発生機序が不明確な卵管子宮内膜症の 1 例 日本エンドメトリオーシス学会誌 37 165-168 2016
14. 三上幹男,他、メジカルビュー社出版、OGS NOW No.6、2011、70-81
15. 三上幹男、株式会社ヴァン メディカル、オンコロジストはこう治療している 婦人科がん診療と化学療法 全面改訂第 2 版 2012
16. 三上幹男,他、メジカルビュー社出版、OGS NOW No.14、2013、134-145
17. 三上幹男,他、メジカルビュー社出版、OGS NOW No.16 2013、18-25

＜学会発表＞

1. Hozumi K, Ochiai S and Hirano K. Essential role of Lmo2 for the maintenance of T-cell differentiation potential in Ebf1-deficient pro-B cells. 日本免疫学会・学術集会. 2016(沖縄)
2. Muguruma Y, Warita T, Yahata T, Itoh M, Hozumi K and Ando K. Jagged1-Notch interaction in the niche is responsible for acquisition of drug-resistance. 日本血液学会. 2016, パシフィコ横浜
3. Hozumi K and Hirano K. Idetification of the essential factors for receiving the Notch signaling in early T cell progenitors. 日本免疫学会・学術集会. 2015(札幌)
4. Hozumi K, Ochiai S and Hirano K. The structural-function relationship in Dll1/Dll4 chimeric molecules for supporting the T cell development. 日本分子生物学会・年

会. 2015(神戸)

5. Muguruma Y, Warita T, Nakamura Y, Yahata T, Suzuki R, Ishikawa S, Isagawa T and Ando K. Identification of molecular interactions in MM cell niche in vivo.日本血液学会. 2015(金沢)
6. Hozumi K, Hirano K and Habu S. Distinct function of Notch ligand Dll1 and Dll4 on lymphocyte development in vivo. 日本免疫学会・学術集会. 2014(京都)
7. Muguruma Y, Yahata T, Itoh M, Hozumi K and Ando K. Jagged1-Notch signal supports human myeloma cell survival. 日本血液学会. 2014(大阪)
8. Hozumi K, Hirano K and Habu S. Comparison between Dll1 and Dll4 for T cell induction in the thymus using cre-dependent conditional Tg mice. 日本免疫学会・学術集会. 2013(幕張)
9. Hozumi K, Hirano K and Habu S. Dll4-mediated Notch signaling is partially transduced by c-Myc at the transition of DN3/DP stages in the thymus. 日本免疫学会・学術集会. 2012(神戸)
10. 穂積勝人. Notch リガンド欠損マウスにおける膵腺房中心細胞の消失. 日本分子生物学会・年会. 2012(福岡)
11. 増田治史、Batroxobin Facilitates Vascular Regeneration via Abrogating Inflammatory 第16回日本再生医療学会、2017.3.7-9 (3.8)、仙台国際センター
12. 増田治史、Mouse Blood-Regeneration Associating Cells Potentiates Vascular Regeneration in Ischemic Hindlimb 16回日本再生医療学会、2017.3.7-9 (3.8)、仙台国際センター
13. Kazuya Kabayama, Yoshiyuki Manabe, Yoshie Kametani , Koichi Fukase Comparative study of fully synthetic self-adjuvanting cancer vaccine candidates containing tandem repeats of B Cell epitope from HER2 Qi Feng, 日本生化学会第97春季大会 2017年3月16-19日(横浜・慶応義塾大学日吉キャンパス)
14. Tsung-Che Chang, Yoshiyuki Manabe, Yukari Fujimoto, Yoshie Kametani, Kazuya Kabayama, Koichi. FukaseSynthesis and Immunological Evaluation of Self-Adjuvanting N-modified Clustered Sialyl-Tn Conjugate Vaccine Candidate 日本生化学会第97春季大会 2017年3月16-19日(横浜・慶応義塾大学日吉キャンパス)
15. Asuka Miyamoto, Ikumi Katano, Ryoji Ito, Banri Tsuda, Yutaka Tokuda, Sonoko Habu,Production of specific IgG against HER2 peptide CH401MAP in NOG-IL-

4-Tg mice. Mamoru Ito, Yoshie Kametani 第45回日本免疫学会総会・学術集会 2016年12月　5-7日　沖縄　沖縄コンベンションセンター

16. Aska Miyamoto, Ikumi Katano, Ryoji Ito, Banri Tsuda, Yutaka Tokuda, Sonoko Habu, Mamoru Ito, Yoshie Kametani .Production of specific IgG against HER2 peptide CH401MAP in NOG-IL-4-Tg International Congress of Immunology 2016 2016 August 21th-26th (Melbourne)
17. Yoshie Kametani, Asuka Miyamoto, Ikumi Katano, Banri Tsuda, Kiyoshi Ando, Yutaka Tokuda, Mamoru Ito, Sonoko Habu PBL-NOG-hIL-4 mouse promotes GVHD-free human humoral immunity. 5th International Workshop of Humanized Mice 2016 Jan 28-30, University of Zurich, Switzerland
18. Negishi Naoko, Uchida Koichiro, Sato Takehito, Kametani Yoshie, Okumura Ko, Habu Sonoko .Possible potential of TIGIT for serial transfer of anergy status into activated naïve T cells. The 44rd Annual meeting of the Japanese Society for Immunology. 2015. Nov. 18-20, Sapporo Sapporo Convention Center
19. Asuka Miyamoto, Banri Tsuda, Yoshie Kametani, Yutaka Tokuda .Antibody-based Her2 peptide CH401MAP as a candidate of breast cancer vaccine. The 74th Annual Meeting of the Japanese Cancer Association 2015 Oct 8-10, Nagoya, Nagoya Congress Center
20. Negishi Naoko, Sato Takehito, Kametani Yoshie, Hori Shohei, Yagita Hideo, Okumura Ko, Habu Sonoko The suppression of naïve T cells are required cell to cell contact by TSST-1 induced anergy T cells. The 43rd Annual meeting of the Japanese Society for Immunology. 2014. Dec. 10-12, Kyoto, Kyoto International Conference Center
21. iyamoto Asuka, Tsuda Banri, Tokuda Yutaka, Kametani Yoshie. Analysis of the humoral immunity of breast cancer patients as the candidates of a new Her2 peptide vaccine CH401MAP. M The 43rd Annual meeting of the Japanese Society for Immunology. 2014. Dec. 10-12, Kyoto, Kyoto International Conference Center
22. Kikuchi Yusuke, Miyamoto Asuka, Tsuda Banri, Katano Ikumi, Tokuda Yutaka, Ito Mamoru, Kametani Yoshie, Analysis of the human immunological system reconstructed in the hIL4-Tg NOG mouse. The 43rd Annual meeting of the Japanese Society for Immunology. 2014. Dec. 10-12, Kyoto, Kyoto International Conference Center

23. 小島美香、森　修弥、嶋田　新、大島　志乃、伊藤　守、鈴木　隆二、安藤　潔、亀谷　美恵 NOG マウス環境下で分化する transitional B 細胞の抗体産生細胞の解析　第 37 回日本分子生物学会年会　2014. 11 月 25-27 日　パシフィコ横浜
24. 森修弥、沼尾絵里奈、大島志乃、嶋田新、岡原純子、佐々木えりか、鈴木隆二、石本人士、椎名隆、亀谷美恵　コモンマーモセット胎盤における妊娠免疫系の解析　2014 年 5 月 17 日　第 61 回日本実験動物学会総会　札幌・札幌コンベンションセンター
25. 小島美香、森修弥、大島志乃、伊藤守、安藤潔、亀谷美恵　ヒト免疫系再構築マウス Transitional B 細胞の抗体産生能解析　2014 年 5 月 17 日　第 61 回日本実験動物学会総会　札幌・札幌コンベンションセンター
26. 大島志乃、嶋田新、森修弥、小島美香、宮本あすか、椎名隆、安藤麻子、亀谷美恵　c-kit 発現細胞の増結能に関する比較生物学的解析　2014 年 5 月 17 日　第 61 回日本実験動物学会総会　札幌・札幌コンベンションセンター
27. 椎名隆、重成敦子、森修弥、北浦一孝、亀谷美恵、鈴木隆二, コモンマーモセット MHC 遺伝子に置ける DNA タイピング法の開発と多型解析 2014 年 5 月 17 日　第 61 回日本実験動物学会総会　札幌・札幌コンベンションセンター
28. Yoshie Kametani, Shuya Mori, Shin Shimada, Ryoji Ito, Mamoru Ito, Sonoko Habu Antibody secreting B cell subsets developed in humanized NOG mouse, 2013 年 12 月 12 日　第 42 回日本免疫学会・学術集会　（千葉・幕張メッセ）
29. 大島志乃、森修弥、重成敦子、高須正規、今枝紀明、布村聡、田中正史、北川均、安藤麻子、亀谷美恵　ブタ c-kit に対するモノクローナル抗体作製と性状解析　2013 年 5 月 15 日　第 60 回日本実験動物学会総会　茨城・筑波国際会議場
30. 森修弥、嶋田新、大島志乃、岡田義則、安藤潔、亀谷美恵　ヒト免疫系再構築 NOG マウス B 細胞の性状解析　2013 年 5 月 15 日第 60 回日本実験動物学会総会　茨城・筑波国際会議場
31. 北浦一孝、藤井克樹、松谷隆治、白井顕治、鈴木さつき、高崎智彦、亀谷美恵、倉根一郎、鈴木隆二　コモンマーモセットにおけるリアルタイム PCR を用いた免疫関連遺伝子発現解析　2013 年 5 月 16 日第 60 回日本実験動物学会総会　茨城・筑波国際会議場
32. 亀谷美恵、嶋田新、森修弥、佐々木えりか、安藤潔　免疫不全マウスを用いた非ヒト霊長類コモンマーモセットの造血幹細胞同定　第 46 回日本無菌生物ノートバイオロジー学会 2013 年　1 月 26 日　フォーラム 246

33. 後藤優美子、高橋千果、布田孝代、石本人士、和泉俊一郎、亀谷美恵、三上幹男　卵巣、癌化における脳由来神経栄養因子(BDNF)受容体 TrkB のシグナル変容 2012 年 12 月 8 日　東京ステーションコンファレンス
34. 亀谷美恵他　Human transitional B cells secrete antigen specific IgM in humanized NOG mouse. 第 41 回日本免疫学会　12 月 6 日　神戸国際会議場
35. 根岸尚子他　Induction of antigen specific unresponsive T cells de novo from naïve T cells for generations in an IL-10 dependent manner.　第 41 回日本免疫学会 12 月 5 日神戸国際会議場
36. 津田万里、亀谷美恵他**日本人 HLA 汎親和性の Her-2 ペプチドによる乳癌患者末梢血単核球反応性の解析**　2012 年 9 月 15-17 日　日本組織適合性学会　東京

    津田万里、亀谷美恵他　Human IL-4 transgenic NOG mouse における乳癌患者 HLA 型に依存する抗 Her-2/neu 抗体エピトープペプチド CH401 の抗腫瘍効果の解析　2012 年 7 月 26-28 日　第 10 回日本臨床腫瘍学会　大阪
37. 津田万里、亀谷美恵他　**Her2 部分配列を持つ CH401MAP ペプチドの乳癌患者血液細胞に対する反応性の解析** 2012 年 6 月 28-30 日　第 20 回日本乳癌学会　熊本
38. 阿部　良行, 川井　健司, 塚田　秀夫, 末水　洋志, 千々和　剛, 中村　雅登　“PET analysis of in vivo hepatic metastases human colon cancer xenografts in NOD/Shi-scid/IL-2 Hayato Fukusumi, Tomoko Shofuda, Daisuke Kanematsu, Atsuyo Yamamoto, Hiroshi Suemizu, Masato Nakamura, Mami Yamasaki, Yoshiki Sasai, Yonehiro Kanemura “Pericellular Matrix of Decidua-derived Mesenchymal Cells is a Versatile Human Substrate to Use both Feeder Cells Free Generation and Long-term Maintenance of Human Induced Pluripotent Stem Cells”（2012 年 6 月）国際幹細胞学会 International Society for Stem Cell Research (ISSCR) **第 10 回年次大会**
39. Tomoko Shofuda, Daisuke Kanematsu, Atsuyo Yamaoto, Hayato Fukusumi, Mika Mizutani, Yohei Bamba, Hiroshi Suemizu, Masato Nakamura, Hideyuki Okano, Mami Yamasaki, Yonehiro Kanemura “Comprehensive Analysis on Stability of Human Induced Pluripotent Stem Cells from Decidua-Derived Mesenchymal Cells”（2012 年 6 月）国際幹細胞学会 International Society for Stem Cell Research (ISSCR) **第 10 回年次大会**
40. Yonehiro Kanemura, Tom 田中京子、久布白兼行、石渡勇、青木大輔、三上幹男、木口一成、岩森正男、Change in the phenotype of human endometrial carcinoma cells by transfection with glycolipid sulfotransferase gene、第 72 回日本癌学会学術総会、2013 年 10 月 3 日-5 日　パシィフィコ横浜
41. 後藤優美子、亀谷美恵、宮澤昌樹、三上幹男、Unique expression profile of tropomyosin-related kinase B variants in ovarian clear cell adenocarcinoma、第 72 回日本癌学会学術総会、2013 年 10 月 3 日-5 日　パシィフィコ横浜

42. 宮澤昌樹、杉山太朗、宮澤麻里子、藤井幸子、池田仁惠、信田政子、平澤猛、村松俊成、松井成明、梶原博、岩森正男、三上幹男、Enhanced Expression of Sulfatide, a Sulfated Glycolipid, In Uterine Cervical Adenocarcinomas、第 72 回日本癌学会学術総会、2013 年 10 月 3 日-5 日　パシィフィコ横浜
43. 曽我部万紀、野崎浩文、久保田智巳、久野敦、梶裕之、栂谷内晶、中西速夫、中西透、鈴木直、木口一成、三上幹男、池原譲、成松久、Novel glyco-biomarker for epithelial ovarian cancer sensitive to clear cell adenocarcinoma、第 71 回日本癌学会学術総会、2012 年 9 月 19 日-21 日、ロイトン札幌
44. 宮澤昌樹、杉山太朗、西島義博、平澤猛、内藤佳津子、上条あけみ、松井成明、宮澤麻里子、村松俊成、岩森正男、三上幹男 An orthotopic uterine cervical cancer model in rats to determine the role of glycolipids fore lymph node metastasis 第 71 回日本癌学会学術総会、2012 年 9 月 19 日-21 日、ロイトン札幌
45. 田中京子、礒西成治、青木大輔、三上幹男、木口一成、岩森正男、Possible involvement of glycolipids in anticancer drug resistance of human ovarian serous carcinoma-derived cells、第 71 回日本癌学会学術総会、2012 年 9 月 19 日-21 日、ロイトン札幌
46. 宮澤昌樹、杉山太朗、西島義博、池田仁惠、信田政子、平澤猛、村松俊成、竹腰進、宮澤麻里子、松井成明、岩森正男、三上幹男、Overexpression of Sulfatide in Uterine cervical adenocarcinomas、第 70 回日本癌学会学術総会、2011 年 10 月 3 日-5 日、名古屋国際会議場
47. 田中京子、塚崎克己、三上幹男、青木大輔、吉村泰典、ヒト漿液性卵巣癌由来細胞における抗がん剤耐性糖脂質の変化、第 63 回日本産科婦人科学会学術講演会、2011 年 8 月 29 日-31 日、大阪国際会議場
48. 西島義博、後藤優美子、杉山太朗、平澤猛、村松俊成、石本人士、和泉俊一郎木直、木口一成、三上幹男、レクチンアレイを用いた子宮内膜・子宮体癌（高分化型・低分化型）に発現する糖蛋白糖鎖の検索、第 63 回日本産科婦人科学会学術講演会、2011 年 8 月 29 日-31 日、大阪国際会議場
49. 日本免疫学会、穂積勝人・平野健一・垣生園子、Comparison between Dll1 and Dll4 for T cell induction in the thymus using cre-dependent conditional Tg mice.、千葉、2013.12.11
50. 日本免疫学会、穂積勝人・平野健一・垣生園子、Dll4-mediated Notch signaling is partially tr ansduced by c-Myc at the transition of DN3/DP stages in the thymus.、神戸、2012.12.6
51. 住吉秀明、三上健一郎、茂呂　忠、紙谷聡英、稲垣　豊：細胞系譜特異的 Notch/Jagged-1 シグナルによる肝線維化と前駆細胞動員の制御機構. 第 49 回日本肝臓学会総会、2013 年 6 月 6 日、東京
52. 稲垣　豊：肝臓の線維化とその治療. 第 111 回内科学会総会・講演会、シンポジウム3「臓器の線維化とその治療」、2014 年 4 月 13 日、東京
53. 増田治史、浅原孝之、第78回日本循環器学会（2014 年 3 月 21-23 日、東京）; Vasculogenic Culture of Blood Mononuclear Cell Enhances Regenerative and Anti-inflammatory Potential
54. 増田治史、浅原孝之、第13回日本再生医療学会（2014 年 3 月 4-6 日,京都）; Vasculogenic Culture of Blood Mononuclear Cell Enhances Regenerative and

Anti-inflammatory Potential

55. 増田治史、浅原孝之、第 11 回回国際幹細胞学会(ISSCR) (2013 年 6 月 12-15 日,ボストン) ; Establishment of Serum-Free Culture System of Peripheral Blood Mononuclear Cells to Potentiate Vascular Regeneration.
56. 津田万里、亀谷美恵、齋藤雄紀、鈴木育宏、猪子英俊、徳田裕 Her2 部分配列を持つ CH401MAP ペプチドの乳癌患者血液細胞に対する反応性の解析 2012年7月 日本乳癌学会
57. 津田万里(筆頭者)、亀谷美恵、扇屋りん、大下内理紗、寺尾まやこ、寺田瑞穂、森岡徹、新倉直樹、齋藤雄紀、鈴木育宏、猪子英俊、徳田裕 Human IL-4 transgenic NOG mouse における乳癌患者 HLA 型に依存する抗 Her-2/neu 抗体エピトープペプチド CH401 の抗腫瘍効果の解析 2012年7月日本臨床腫瘍学会
58. 津田万里(筆頭者)、亀谷美恵、吉川枝里、安藤麻子、猪子英俊、徳田裕 日本人 HLA 汎親和性の Her-2 ペプチドによる乳癌患者末梢血単核球反応性の 2013年9月 日本組織適合性学会
59. 津田万里、扇屋りん、大下内理紗、寺尾まやこ、寺田瑞穂、森岡徹、新倉直樹、岡村卓穂、齋藤雄紀、鈴木育宏、亀谷美恵、徳田裕 HER2 部分配列を持つ CH401MAP peptide の乳がん患者 T 細胞/B 細胞 相互作用の解析 2013年7月 日本乳癌学会
60. 津田万里、亀谷美恵、宮本あすか、齋藤雄紀、鈴木育宏、徳田裕 ペプチドワクチンの効果予測因子としての CH401MAP による in vitro 刺激の検討 2014年7月日本乳癌学会

2、造血腫瘍ニッチを標的とした新規治療法の開発

造血幹細胞制御における PAI-1 の役割

分担研究者　再生医療科学科　八幡　崇
研究協力者　血液・腫瘍内科　アブドゥル　アジズ、金子聡子、渡邊伸央

【研究の背景と目的】

不治の病とされた慢性骨髄性白血病（CML）は、100 万人に 10～20 名程度の発症率の希少疾患で、かつては造血幹細胞移植を施行しなければ急性転化期に進行して、ほぼ全ての患者が 7～8 年以内に死亡する予後不良の疾患であった。しかしその治療は、2001 年の BCR-ABL 遺伝子蛋白を分子標的とする第一世代チロシンキナーゼ阻害剤（TKI）のイマチニブ（IM）の登場により一変し、IM による 8 年間の治療成績（IRIS 試験）では、CML 関連死は 7%にまで激減した。しかし、IM によって分子遺伝学的完全寛解（CMR。以下、「完全寛解」という。）が 2 年以上得られていても、投与を中止すると完全寛解維持率は 1 年後で 41%と半数以上の患者で再発（完全寛解の喪失）することが示され、CML 幹細胞の関与が示唆されている。すなわち、CML 幹細胞は骨髄ニッチで休止期（G0）にあるために、TKI に抵抗性を示すと考えられる。

CML 幹細胞は CML の発症起点であり、供給源でもある。したがって、CML の完全寛解を実現するためには、CML 幹細胞の性状を理解し、その根絶を達成する必要がある。CML 幹細胞は骨髄のニッチと呼ばれる場所で休眠した状態で『静止』している。TKI は活動的な CML 細胞に作用するので、休眠 CML 幹細胞には効きにくい。このことが、がんの完治を困難にしている最大の要因である。しかし逆に言えば、CML 幹細胞をニッチから離脱させれば、TKI に対する抵抗力を弱めることが期待できる。幹細胞はニッチから産生される因子（TGF-β）によって休眠状態に誘導される。TGF-βはニッチや幹細胞の plasminogen activator inhibitor-1 (PAI-1)の発現を強力に誘導し、増殖や細胞遊走を抑制する。従って、幹細胞をニッチに休止期で静止させているのは PAI-1 である蓋然性が高い。つまり、PAI-1 活性を制御できれば、CML 幹細胞をニッチから人為的に引き離し、TKI 感受性を向上させることが期待される。

CML 幹細胞は、休止期で骨髄ニッチに存在し、成熟細胞を産生し続けるなど、正常造血幹細胞と多くの共通した性質を持つ。したがって、造血幹細胞研究と CML 幹細胞研究は車の両輪の関係にある。そこで本プロジェクトでは、研究の過程を3段階に分けて、（1）まず CML 幹細胞のモデルケースとして造血幹細胞に焦点を絞り、PAI-1 による造血幹細胞制御機構の解明、特にニッチ細胞が産生する PAI-の役割の解明に取り組んだ。（2）次に、同じくニッチが産

生する造血幹細胞制御因子である TGF-βによって造血幹細胞内に発現誘導される PAI-1 の意義を明確にすることに取り組んだ。(3)最後に、CML 幹細胞の TKI 耐性における PAI-1 の役割を明確にし、分担研究者らが開発した PAI-1 阻害剤を利用した CML 幹細胞を標的とした新しい治療法の確立に取り組んだ。

【究方法と成果】

(1)造血幹細胞制御における PAI-1 の役割の解明:ニッチ因子としての分泌性 PAI-1 の意義

野生型 C57BL6 マウス、PAI-1 欠損マウスに致死量放射線を照射後、野生型マウスより採取した骨髄細胞を静脈内に移植した。生理食塩水あるいは PAI-1 阻害薬を移植当日から1日1回、5日間にわたって連続投与した。血漿と骨髄細胞を採取し、ELISA 法およびフローサイトメトリーを利用して、各種造血再生因子の発現や造血幹細胞の増幅等を解析した。また、組織科学的な手法により骨髄ニッチの状態を観察した。これらの解析により、以下の成果を得た。

- 放射線照射などの造血ストレスが負荷されると、造血ニッチ細胞は PAI-1 を高産生し、tPA 主導のサイトカイン産生を阻害することによって造血幹細胞の増殖を抑制することを明らかにした。
- 骨髄移植において、本学で開発した PAI-1 阻害薬を用いて PAI-1 活性を抑制することによって、造血再生の迅速化のみならず、長期間にわたる造血系の恒常性の維持が達成された。

(2)造血幹細胞制御における PAI-1 の役割の解明:TGF-βによって誘導される細胞内 PAI-1 の意義

野生型 C57BL6 マウスに PAI-1 阻害剤あるいは TGF-β阻害剤を5日間連続投与後、末梢血を回収し、骨髄ニッチを離脱した造血幹細胞の割合を解析した。フローサイトメトリーを利用して PAI-1 や Furin の細胞内発現を検討した。また、PAI-1 阻害剤によるニッチからの離脱は MT1-MMP 依存的であることを確認するために、抗 MT1-MMP 抗体を投与した阻害実験を行った。これらの解析により、以下の成果を得た。

- ニッチが産生する TGF-あによって造血幹細胞に PAI-1 発現が誘導されることを発見した。
- 造血幹細胞に発現する PAI-1 は細胞内で機能し、セリンプロテアーゼである Furin の活

性を阻害することによって細胞表面の遊走因子である MT1-MMP が成熟型に変換することを抑制することを明らかにした。

- 細胞内 PAI-1 は、造血幹細胞の運動性を抑制し、ニッチに留めることを明確にした。
- TGF-β-PAI-1 シグナルを阻害すると、造血幹細胞はニッチから離脱し、末梢循環血中に動員されることを見出した。

(3)CML 幹細胞の TKI 耐性における PAI-1 の役割の解明

マウス造血前駆細胞株である 32D 細胞に BCR-ABL 遺伝子を導入し、CML 様細胞として TKI 感受性などを検討した。この細胞株に PAI-1 cDNA のトランスフェクションにより過剰発現させたもの、あるいは CRSPR/Cas9 法により PAI-1 発現を欠損させたものを作製した。CML 幹細胞の解析は、マウス造血幹細胞に BCR-ABL 遺伝子を導入し、移植することによって CML を発症させたマウス骨髄を利用した。治療実験は、生理食塩水群、TKI 単剤群、TKI と PAI-1 阻害剤の併用群を用意し、CML 細胞の生着や生存率を解析した。これらの解析により、以下の成果を得た。

- 造血幹細胞と同様に、ニッチが産生する TGF-βによって CML 幹細胞に PAI-1 発現が誘導されることを見出した。
- CML 細胞に PAI-1 を過剰発現させると TKI 抵抗性になり、逆に PAI-1 を欠損させると TKI 感受性になることから、CML 細胞内に発現する PAI-1 の多寡が TKI 感受性を決定することを明らかにした。
- CML モデルマウスを利用した治療実験系において、TKI と PAI-1 阻害剤を併用すると、CML 幹細胞の減少や生存率の向上など TKI 単剤群に比べて顕著な治療効果が認められた。

【考察】

造血幹細胞や CML 幹細胞の制御に PAI-1 が深く関与していることが明らかになった。PAI-1 はセリンプロテアーゼ阻害因子(serpin)であり、分泌性蛋白として tPA/uPA/plasmin を主体とした線維素溶解系の抑制因子として機能することが知られていたが、分担研究者らの解析により細胞の内部においても serpin として機能し、細胞遊走や細胞死などを制御することが分かった。このことは、従来考えられていた以上に細胞内 serpin が多岐にわたる生命現象において重要な役割を担っていることを示唆しており、新しい学術領域を開拓する成果である。

幹細胞にとっての PAI-1 の重要な機能は、分泌性 serpin としてサイトカイン産生を抑制する

こと、そして細胞内 serpin として運動性を抑制することによって幹細胞がニッチに留まり休止期を維持することである。放射線照射後の造血再生においては、PAI-1 活性は造血幹細胞の増殖反応を阻害するため、PAI-1 阻害剤の投与は造血再生の効率化に有効である。この知見をもとに、本プロジェクト遂行期間中に造血再生の効率化を期待した臨床試験を実施した。第1相臨床試験の結果、PAI-1 阻害剤の投与は重篤な副作用を引き起こさなかったことから、新規 PAI-1 阻害剤の安全性は確認された。PAI-1 阻害剤は造血幹細胞のニッチからの離脱を促進することから、ニッチで保護されている治療抵抗性 CML 幹細胞においても同様の効果を発揮することが期待された。実際、CML モデル実験系において PAI-1 阻害剤の有効性は証明されたことから、CML の完全寛解を目指した新しい治療法となることが期待され、次年度より CML 患者を対象とした臨床試験を実施する予定である。

がんニッチ間相互作用（インタラクトーム）解析による治療標的分子の特定

研究分担者：六車　ゆかり
研究協力者：割田　貴之

【研究の目的】

多発性骨髄腫は、その発症や進行に骨髄腫細胞と周りの微小環境（ニッチ）との相互作用が特に深く関与していると考えられる難治性の血液がんであり、近年の新薬開発などによる治療方法の進歩にもかかわらず、再発例や治療抵抗例が多い不治の病である。したがって、その課題を克服する根治療法の開発は、患者の QOL の向上のみならず、医療経済の観点からも必要とされている。本研究は、ヒト多発性骨髄腫モデルマウスを利用したがんニッチ間相互作用（インタラクトーム）解析という画期的な手法によって、骨髄腫細胞と宿主であるマウス環境とのがんとニッチ相互作用全体を定量的に同定し、がん病態に深く関与している「がん幹細胞」とニッチの分子間相互作用と、その相互作用によって惹起される「がん幹細胞」特異的な分子シグナルを解明することによって、治療標的を特定することを目的とする。

【研究の概要】

本研究は、以下の具体的開発項目を達成することによって、難治性血液がんである多発性骨髄腫における、ニッチを介したがん細胞の治療抵抗性獲得機構を解明し、多発性骨髄腫の根治療法の確立を目指すものである。

＜がん幹細胞の実態・治療抵抗性の解明と創薬標的の同定＞

ヒト多発性骨髄腫モデルマウスの移植片について全トランスクリプトーム解析を行い、がん細胞とニッチに由来する遺伝子を、ヒトとマウスの塩基配列の違いから判別して振り分けるという全く新しい手法（インタラクトーム解析）を用いて、これまで不可能であった生体内における「がん幹細胞」とニッチの相互作用の全体像を定量的に同定する。そして、正常造血幹細胞モデルの解析結果を対照とすることで、がんの発症・進行と治療抵抗性獲得の要因となっているがんとニッチの分子間相互作用と、その相互作用の結果として、「がん幹細胞」特異的に変化している分子シグナルを同定して、「がん幹細胞」の治療抵抗性獲得機構を解明し、「がん幹細胞」を直接ターゲットとする創薬標的を特定する。

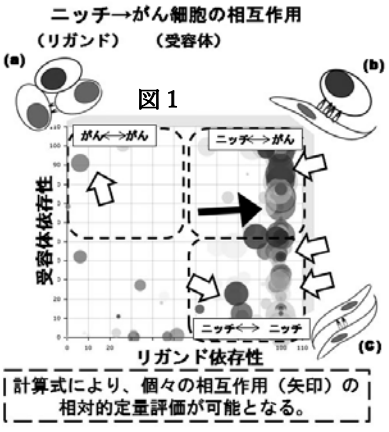

図 1

相互作用の定量評価に用いる計算式

	ニッチ→がん細胞への相互作用
リガンド依存性	$\frac{Ln}{Lc + Ln}$
受容体依存性	$\frac{Rc}{Rc + Rn}$
相互作用の強さ	$\sqrt{Ln \cdot Rc}$

定量化した遺伝子発現
Ln: ニッチリガンド
Lc: がん細胞リガンド
Rn: ニッチ受容体
Rc: がん細胞受容体

【研究結果】

＜インタラクトーム解析＞

がんが生育する生体内では、「がん細胞」とニッチ（右図 b）、「がん細胞」同士（右図 a）、ニッチ細胞同士（右図 c）といった複雑な相互作用が、様々な強さで生じており、同一個体内でがんの多様性を生ずる要因となっている。中でも「がん細胞」とニッチの間で特異的に起こっている相互作用（右図b矢印等）は、がんの進行や治療抵抗性の獲得に重要な役割を果たしている。

本研究では、左に示す計算式を用いて、個別の相互作用の強さと特異性を相対的に評価して、病態の特定に最も寄与している骨髄腫細胞とニッチの相互作用を解析した。

＜多発性骨髄腫に特徴的な相互作用の特定＞

1. 骨髄ニッチに発現するSDF1と骨髄腫細胞側のCXCR4

SDF1－CXCR4シグナルは正常細胞の増殖や局在といった生理的機能を担っているが、多発性骨髄腫においても骨髄腫細胞間におけるシグナル伝達がその生存に寄与しているという報告がある。本研究における骨髄ニッチでの相互作用解析の結果、骨髄環境側に発現するSDF－1と骨髄腫細胞に発現するCCXCR4が高い依存性をもって相互作用していることが定量的に明らかとなった。つまり、多発性骨髄腫では正常造血細胞と同様の幹細胞維持機構が働いていると考えられる。また、脾臓などの髄外で腫瘤を形成した場合にはその依存度が低いことから、相互作用は骨髄腫細胞の局在によって差異があることも示唆された。

2. 既知の骨髄腫細胞のマーカーの相手方の特定

骨髄腫細胞においては、細胞表面分子であるCD38、CD138等が高頻度で発現することが知られており、臨床診断の指標として用いられているほか、それらを標的とする抗体医薬も開発されている。しかし、それらの分子が生体内でどのような生理分子と結合し、多発性骨髄腫の病態にどのように関与しているかは知られていない。本解析により、CD38はニッチ側のCD31と、CD138はHGFと高い依存性をもって結合することが明らかとなった。CD31は血管内皮やマクロファージに発現することが知られており、骨髄腫細胞の血流を介した転移やニッチへの局在に関与し、細胞増殖や生存に機能していると考えられる。また、CD138はHGFとcMetのシグナルを安定化することで、骨髄腫細胞の増殖に寄与していると考えられる。

3. 未知の相互作用の抽出

インタラクトームによる相互作用の強さと依存度の相対的定量評価により、骨髄腫細胞とニッチの間で特に相互依存度が高い組み合わせを10程度抽出しており、それらの生理的機能を解析していく予定である。

造血腫瘍ニッチを標的とした新規治療法の開発

分担研究者：東海大学医学部血液腫瘍内科　川田浩志
研究協力者：東海大学医学部癌幹細胞研究センター　金子光代

【研究の背景と目的】

我々は、造血腫瘍に対する非侵襲的治療法の開発に取り組んでいる。その中の 1 つが、比較的大量ビタミン C（L-ascorbic acid）療法(以下 L-AA）である。2000 年代になり、NIH の研究グループが、L-AA の抗腫瘍効果は、そのプロオキシダント作用によって過酸化水素を発生させることによっており、過酸化水素の分解能力が正常細胞よりも劣っている腫瘍細胞に対して L-AA が特異的に増殖抑制効果を発揮することを見いだした。そこで我々は、L-AA が造血腫瘍に対する新しい治療戦略になり得るか検討を行った。

【研究の方法】

様々な造血腫瘍細胞株を用いて in vitro における L-AA の抗腫瘍効果とメカニズムを検討するとともに、免疫不全マウスに対する移植モデルを用いて in vivo の検討を行った。

【研究成果】

L-AA がヒト正常造血幹細胞/前駆細胞の生存・増殖には影響を与えない濃度レベルで、様々なヒト白血病細胞株とリンパ腫細胞株の生存・増殖に対して著明な抑制効果を発揮することを確認した。また、この L-AA の抗腫瘍効果は、過酸化水素の産生だけではなく、腫瘍細胞のニッチとの interaction に深く関わっている低酸素誘導因子（HIF-1α）の発現を抑制することが大きく関与していることを、HIF-1α を過剰発現させたヒト白血病細胞株を移植した免疫不全マウスを用いた実験系で確認した（Kawada H et al. PLoS One 2013）。さらに、これらの知見を踏まえつつ、再発リンパ腫症例を対象に高濃度 L-AA の第 I 相臨床試験を実施して、その安全性とともに、非投与時に比して 250 倍以上の L-AA 血中濃度が得られることも確認できた(Kawada H et al. Tokai J Exp Clin Med 2014)。

【研究考察】

L-AA が、多くのがん細胞が治療抵抗性を発揮する大きな原因の1つである HIF-1α の発現を強力に抑えて抗白血病作用を示すことを見出した。しかも、その効果は正常の造血幹細胞／前駆細胞にはほとんど発揮されず、ほぼ白血病細胞特異的であった。現在、我々は L-AA の造血腫瘍細胞に対する効果を最大限に誘導する条件を同定しつつあり、今後も造血腫瘍

ニッチを標的とする、患者に負担が少なく、腫瘍細胞には強力に作用する腫瘍細胞特異的治療の臨床応用を目指して、さらなる検討を続けたいと考えている。

J Clin Exp Hematop
Vol. 56, No. 1, June 2016

Case Study

Composite Follicular Lymphoma and CD5-Positive Nodal Marginal Zone Lymphoma

Masashi Miyaoka,[1)] Tomoki Kikuchi,[1)] Joaquim Carreras,[1)] Yukie Yara Kikuti,[1)] Ken Omachi,[2)] Minoru Kojima,[2)] Kiyoshi Ando,[2)] and Naoya Nakamura[1)]

Composite CD10-positive low-grade B-cell and CD5-positive low-grade B-cell lymphoma is extremely rare. We report a case of a composite follicular lymphoma (FL) and CD5-positive nodal marginal zone lymphoma (NMZL) in a resected inguinal lymph node of a 72-year-old Japanese male. Histologically, multiple follicles had reactive-germinal centers with tingible body macrophages, a thin mantle zone and a wide marginal zone. The wide marginal zone consisted of medium-sized cells having slightly indented nuclei and clear cytoplasm, indicating monocytoid cells with CD5-positive B-cells. Several follicles had germinal centers filled with many centrocytes, with CD10-positive B-cells. Polymerase chain reaction/sequence analysis of the immunoglobulin heavy chain gene obtained from microdissected regions of CD5-positive NMZL and FL showed different sequences within the CDR3 region. To our knowledge, this is the first report of FL and CD5-positive NMZL. 〔*J Clin Exp Hematop 56(1):55-58, 2016*〕

Keywords: composite lymphoma, follicular lymphoma, CD5-positive nodal marginal zone lymphoma

INTRODUCTION

Composite lymphoma (CL) is defined as two histologically distinct variants of malignant lymphoma occurring in the same organ or mass.[1,2] CL is quite rare, with frequency ranging from 1 to 4.7% of lymphoma cases.[3] Many combinations of lymphoma types have been reported in CLs, including composite B-cell lymphoma, composite B- and T-cell lymphoma, and composite Hodgkin lymphoma (HL) and non-Hodgkin lymphoma (NHL).[2] Previously reported cases of composite HL and NHL were combinations of HL and B-cell non-Hodgkin lymphoma, such as HL and follicular lymphoma (FL), as well as HL and diffuse large B-cell lymphoma.[4-6] In some cases, polymerase chain reaction (PCR) amplification and sequence analysis of the immunoglobulin heavy chain gene (IGH) demonstrated common clonal origins in the two abovementioned cases,[5,6] suggesting the clonal relationship in combination HL and NHL.

Received: November 16, 2015
Revised : December 5, 2015
Accepted: January 7, 2016
[1)]Department of Pathology and [2)]Division of Hematology/Oncology, Department of Internal Medicine, Tokai University School of Medicine, Isehara, Japan
Corresponding author: Masashi Miyaoka, M.D., Department of Pathology, Tokai University School of Medicine, 143 Shimokasuya, Isehara, Kanagawa, 259-1193, Japan
E-mail: miyaokamasasi828@yahoo.co.jp

Several combinations of low grade B-cell lymphoma, including FL and mantle cell lymphoma (MCL), FL and B-chronic lymphocytic leukemia/small lymphocytic lymphoma, and MCL and nodal marginal zone lymphoma (NMZL), have also been reported.[7-9] Some of these cases showed clonal relation whereas other cases were clonally unrelated.[7-9]

We report a case of CL of FL and CD5-positive NMZL in a lymph node, and demonstrated different B-cell clones in the FL and CD5-positive NMZL.

CASE REPORT

A 72-year-old, Japanese male had been treated for hypertension and suspicion of Parkinson's disease by his family doctor. The patient noticed a mass in the left groin one year prior. The mass was small, and the patient did not have fever or any other symptoms. After 6 months, the size of the mass began to increase. His family doctor then referred him to a hematologist at our hospital, and masses were identified in the left groin, right neck, and left flank. Excisional biopsy of an inguinal lymph node was performed for pathological diagnosis with flow cytometry and karyotype analyses. Peripheral blood evaluation revealed a hemoglobin level of 13.0 g/dL, a platelet count of 13.7 x 10^4/μL, a white blood cell count of 5.0 x 10^3/μL, LD 155 U/L, and soluble interleukin-2 receptor of 2,380 U/L. Positron emission tomography

showed abnormal accumulation in the right neck, right clavicles, para-aorta, left ilium, and left groin. Flow cytometry demonstrated predominant B-cells, and $CD19^+CD5^+$ and $CD20^+CD10^+$ fractions were observed. No restriction of the light chain (κ/λ) was observed, which may have been due to the $CD20^+CD10^+$ fraction involving neoplastic and reactive cells.

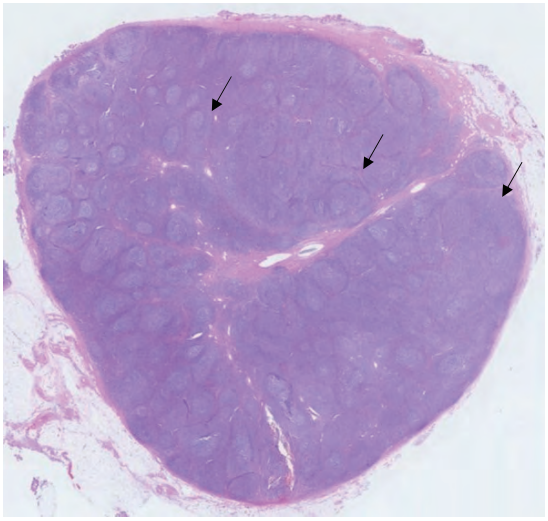

Fig. 1. Low power view of resected lymph node. Many follicles are distributed throughout the lymph node. Most follicles show marginal zone lymphoma, but several follicles show follicular lymphoma (*arrows*). H&E stain.

The patient's karyotype was normal, 46/XY[20/20]. Bone marrow involvement was not observed by histology and immunohistochemistry evaluation of the clot section. Low grade B-cell lymphoma was diagnosed. The patient underwent R-CHOP (rituximab, cyclophosphamide, doxorubicin, vincristine, and prednisolone) therapy and achieved remission.

PATHOLOGICAL FINDINGS

Histological evaluation of the resected lymph node demonstrated multiple follicles evenly distributed throughout (Fig. 1). Most follicles had a reactive-germinal center (GC) with tingible body macrophages, thin mantle zone, and wide marginal zone (Fig. 2). The wide marginal zone consisted of medium-sized cells having a slightly indented nucleus and clear cytoplasm, indicating monocytoid cells (Fig. 2). There were several follicles that had GCs filled with numerous centrocytes (Figs.1 & 2). Plasma cell differentiation was unclear in both the wide marginal zone and centrocyte-rich GC.

Immunohistochemically, monocytoid cells in the wide marginal zone were $CD3^-$, $CD5^+$, $CD10^-$, $CD20^+$, $BCL\text{-}2^+$, $BCL\text{-}6^-$, $MUM\text{-}1^-$ and cyclin $D1^-$, and lymphocytes in the GC

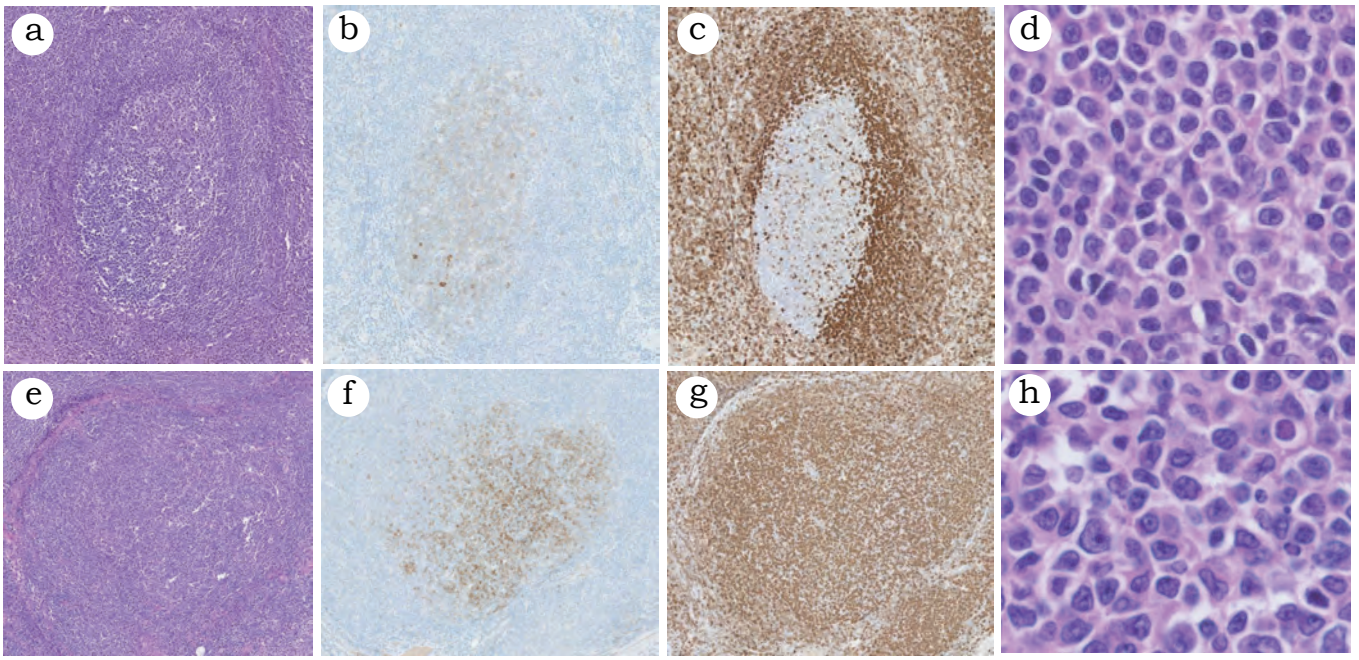

Fig. 2. Histopathology and immunohistochemistry of marginal zone lymphoma and follicular lymphoma. Nodal marginal zone lymphoma show a wide marginal zone (MgZ), mantle zone (MZ) and germinal center (GC)(***2a***). CD10 positivity is observed in the GC, but not the MgZ (***2b***), and BCL-2 positivity is observed in the MgZ and MZ, but not the GC (***2c***). Under high power view, the MgZ consists medium-sized cells having slightly indented nuclei and clear cytoplasm, indicating monocytoid cells (***2d***). Follicular lymphoma shows GC swelling (***2e***). Both CD10 and BCL-2 positivity is observed in the GC (***2f***, ***2g***). Under high power view, the GC consisted of small cleaved cells (***2h***). (*2a*), (*2d*), (*2e*) & (*2h*), H&E stain.

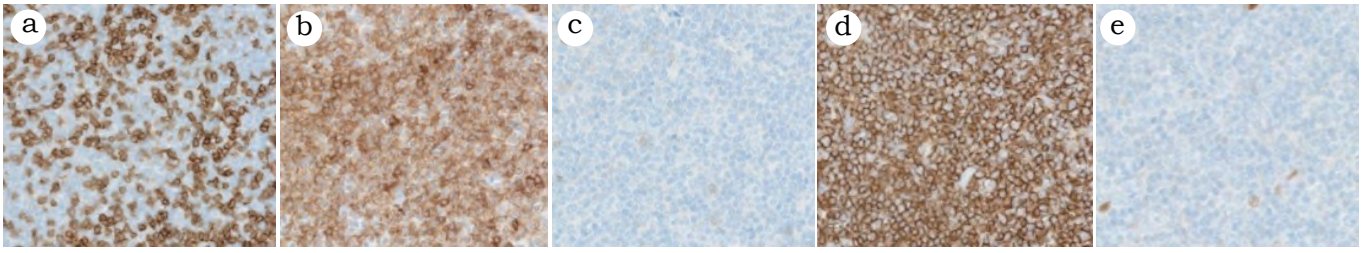

Fig. 3. Immunohistochemistry of nodal marginal zone lymphoma. Marginal zone cells were CD3-negative (***3a***), CD5-positive (***3b***), CD10-negative (***3c***), CD20-positive (***3d***), and Cyclin D1-negative (***3e***).

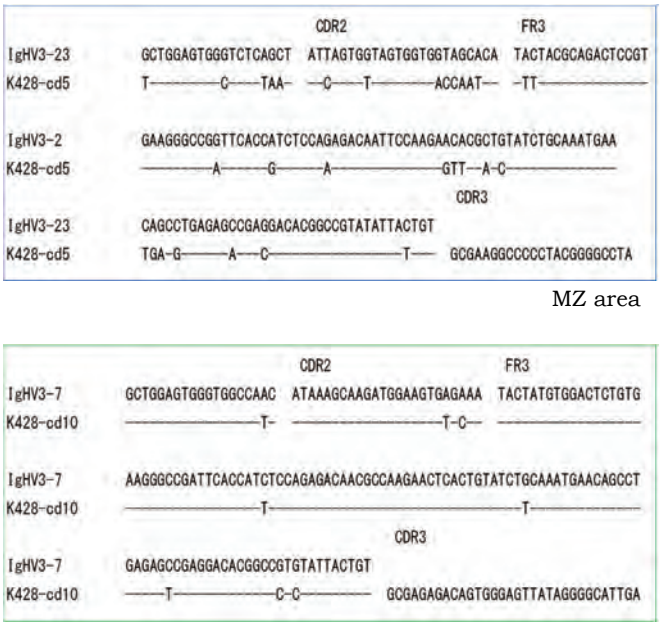

Fig. 4. Nucleotide sequence of the immunoglobulin heavy chain gene (IGH). Polymerase chain reaction and sequencing of IGH demonstrated that the marginal zone and centrocyte-rich germinal center had different sequences in the complementary determining region (CDR) 2, flame work region (FR) 3, and CDR3. Differences in the CDR3 indicate that these were two different clones.

were CD10$^+$ (weak), CD20$^+$, and BCL-2$^-$ (Figs. 2 & 3). These findings indicated CD5-positive NMZL. On the other hand, centrocytes in the GC were CD3$^-$, CD5$^+$, CD10$^+$, CD20$^+$, BCL-2$^+$, BCL-6$^+$, MUM-1$^-$, and cyclin D1$^-$, indicate FL (Fig. 2). Both κ^+ plasma cells and λ^+ plasma cells were observed in *in situ* hybridization, showing no restriction of the light chain.

PCR sequencing of the IGH from microdissected samples of the CD5-positive NMZL and FL showed different sequences in the CDR3 region, with IGHV3-23 in the CD5-positive NMZL and IgHV3-7 in the FL (Fig. 4).

DISCUSSION

We presented an unusual variation of CL composed of CD10-positive FL and CD5-positive NMZL, which to the best of our knowledge is the first case of such combination. Considering the results from the histological and immunohistochemical analysis, three possibilities were raised; (1) FL with marginal zone differentiation and CD5 expression, (2) CD5-positive NMZL with follicular colonization, or (3) composite lymphoma of FL and CD5-positive NMZL. Clarification of the clonal relationship is important in CL, and it is recommended to use not only morphological and immunohistochemical techniques, but also Southern blotting or PCR sequencing of the IGH and T cell receptor gene rearrangements, cytogenetics, and fluorescence *in situ* hybridization (FISH). In our case, PCR and sequence analysis of IGH demonstrated the different clones of the FL and CD5-positive NMZL.

Cases of CL containing a CD5-positive low grade B-lymphoma component have been previously reported.[7,8,10] In four of these cases, PCR sequencing of IGH was performed;[7,8] three of the cases showed common clonal origin and the other case had different clonal origins. Although the progenitor cells of CL containing CD5-positive low grade B-lymphoma with common clonal origin may be lymphoid stem cells or immature B-cells, the latter case and our case may have developed by chance.

MCL and chronic lymphocytic leukemia/small lymphocytic lymphoma are the main components observed in CL, and there has been a previously reported case of CL composed of CD5-positive splenic marginal zone lymphoma and FL with uncertain clonal relationship.[10] Due to the small number of cases, we were unable to determine the factor leading to the pathogenesis of CL composed of CD10-positive FL and CD5-positive low grade B-cell lymphoma, including MZL. Although such cases occur by chance, further accumulation of cases is important for identification of the factors involved in the pathogenesis of CL composed of FL and CD5-positive NMZL, as well as other CL.

In our case, the FL area was small, suggesting possible *in situ* FL. *In situ* FL has been recognized by the recent World Health Organization (WHO) classification system, but the incidence rate remains unknown due to the limited number of published cases and series.[11,12] *In situ* FL shows preservation of the nodal architecture, and most follicles appear to be

cytologically reactive, whereas rare germinal centers appear to be monotonous and lack tingible body macrophages.[11] The later follicles show strongly positive staining for BCL-2 and CD10, whereas the majority of follicles in the same lymph node are negative for BCL-2. In most cases of FL, tumor cells involve the majority of the follicles and infiltrate into the inter-follicular region; however, in *in situ* FL, tumor cells involve only a few follicles, and do not infiltrate into the many remaining reactive follicles or the inter-follicular region. There is also a possibility of overt FL of the systemic lymph nodes.

NMZL is currently defined in the WHO classification as a primary nodal B-cell lymphoma that morphologically resembles extranodal or splenic MZL, but without evidence of extranodal or splenic disease.[13] NMZL is uncommon, accounting for less than 2% of all lymphomas.[13] Generally, NMZL do not express CD5, but a few have been shown to do so. CD5-positive NMZL have histologic and immunophenotypic features typical of NMZL in addition to the expression of CD5. Jaso *et al*. reported the proportion of CD5-positive NMZL to typical NMZL to be 8.6% (7/91 cases).[14] Of the CD5-positive NMZL patients, 86% (6/7 cases) showed lymphadenopathy above and below the diaphragm, 6 cases underwent bone marrow check, and all cases had bone marrow invasion.[14] In our case, lymphadenopathy above and below the diaphragm was observed, but not bone marrow invasion.

In NMZL, CD5 has been reported to be expressed in only 8.6% cases, and CD5 expression correlates with a higher frequency of dissemination and bone marrow invasion.[14] However, patients with CD5-positive NMZL generally have an indolent clinical course and excellent overall survival.[14] In our case, although bone marrow invasion was not observed, dissemination above and below the diaphragm was present. In CD5-positive NMZL, the mechanism of CD5 expression and progenitor identification remain unclear; however, CD5 expression in NMZL may be associated with wide dissemination.

CONFLICT OF INTEREST

The authors declare no conflict of interest.

REFERENCES

1 Kim H, Hendrickson R, Dorfman RF: Composite lymphoma. Cancer 40:959-976, 1977

2 Kim H: Composite lymphoma and related disorders. Am J Clin Pathol 99:445-451, 1993

3 Thirumala S, Esposito M, Fuchs A: An unusual variant of composite lymphoma: a short case report and review of the literature. Arch Pathol Lab Med 124:1376-1378, 2000

4 Jaffe ES, Zarate-Osorno A, Kingma DW, Raffeld M, Medeiros LJ: The interrelationship between Hodgkin's disease and non-Hodgkin's lymphomas. Ann Oncol 5 (Suppl 1):7-11, 1994

5 Bellan C, Lazzi S, Zazzi M, Lalinga AV, Palummo N, *et al*.: Immunoglobulin gene rearrangement analysis in composite Hodgkin disease and large B-cell lymphoma: evidence for receptor revision of immunoglobulin heavy chain variable region genes in Hodgkin-Reed-Sternberg cells? Diagn Mol Pathol 11:2-8, 2002

6 Bräuninger A, Hansmann ML, Strickler JG, Dummer R, Burg G, *et al*.: Identification of common germinal-center B-cell precursors in two patients with both Hodgkin's disease and non-Hodgkin's lymphoma. N Engl J Med 340:1239-1247, 1999

7 Wang S, Tzankov A, Xu-Monette ZY, Hoeller S, Wang SA, *et al*.: Clonally related composite follicular lymphoma and mantle cell lymphoma with clinicopathologic features and biological implications. Hum Pathol 44:2658-2667, 2013

8 Boiocchi L, Witter RE, He B, Subramaniyam S, Mathew S, *et al*.: Composite chronic lymphocytic leukemia/small lymphocytic lymphoma and follicular lymphoma are biclonal lymphomas: a report of two cases. Am J Clin Pathol 137:647-659, 2012

9 Rodig SJ, Healey BM, Pinkus GS, Kuo FC, Dal Cin P, *et al*.: Mantle cell lymphoma arising within primary nodal marginal zone lymphoma: a unique presentation of two uncommon B-cell lymphoproliferative disorders. Cancer Genet Cytogenet 171:44-51, 2006

10 Demurtas A, Aliberti S, Bonello L, Di Celle PF, Cavaliere C, *et al*.: Usefulness of multiparametric flow cytometry in detecting composite lymphoma: study of 17 cases in a 12-year period. Am J Clin Pathol 135:541-555, 2011

11 Carbone A, Gloghini A, Santoro A: *In situ* follicular lymphoma: pathologic characteristics and diagnostic features. Hematol Oncol 30:1-7, 2012

12 Harris NL, Nathwani BN, Swerdlow SH, de Jong D, Jaffe ES, *et al*.: Follicular lymphoma. In: Swerdlow SH, Campo E, Harris NL, Jaffe ES, Pileri SA, *et al*. (eds): World Health Organization Classification of Tumours, WHO Classification of Tumours of Haematopoietic and Lymphoid Tissues. 4th ed, Lyon, International Agency for Research on Cancer (IARC), pp.220-226, 2008

13 Campo E, Pileri SA, Jaffe ES, Müller-Hermelink HK, Nathwani BN. Nodal marginal zone lymphoma. In: Swerdlow SH, Campo E, Harris NL, Jaffe ES, Pileri SA, *et al*. (eds): World Health Organization Classification of Tumours, WHO Classification of Tumours of Haematopoietic and Lymphoid Tissues. 4th ed, Lyon, International Agency for Research on Cancer (IARC), pp.218-219, 2008

14 Jaso JM, Yin CC, Wang SA, Miranda RN, Jabcuga CE, *et al*.: Clinicopathologic features of CD5-positive nodal marginal zone lymphoma. Am J Clin Pathol 140:693-700, 2013

bjh research paper

A phase 1/2 study of carfilzomib in Japanese patients with relapsed and/or refractory multiple myeloma

Takashi Watanabe,[1,2] Kensei Tobinai,[1] Morio Matsumoto,[3] Kenshi Suzuki,[4] Kazutaka Sunami,[5] Tadao Ishida,[6] Kiyoshi Ando,[7] Takaaki Chou,[8] Shuji Ozaki,[9] Masafumi Taniwaki,[10] Naokuni Uike,[11] Hirohiko Shibayama,[12] Kiyohiko Hatake,[13] Koji Izutsu,[14] Takayuki Ishikawa,[15] Yoshihisa Shumiya,[16] Tomohisa Kashihara[16] and Shinsuke Iida[17]

[1]Department of Haematology, National Cancer Centre Hospital, Tokyo, [2]Department of Haematology, Komaki City Hospital, Komaki, [3]Department of Haematology, National Hospital Organization Nishigunma National Hospital, Shibukawa, [4]Department of Haematology, Japanese Red Cross Medical Centre, Tokyo, [5]Department of Haematology, National Hospital Organization Okayama Medical Centre, Okayama, [6]Department of Gastroenterology, Rheumatology and Clinical Immunology, Sapporo Medical University School of Medicine, Sapporo, [7]Department of Haematology and Oncology, Tokai University School of Medicine, Isehara, [8]Department of Internal Medicine, Niigata Cancer Centre Hospital, Niigata, [9]Department of Haematology, Tokushima Prefectural Central Hospital, Tokushima, [10]Division of Haematology and Oncology, Graduate School of Medical Science, Kyoto Prefectural University of Medicine, Kyoto, [11]Department of Haematology, National Hospital Organization Kyushu Cancer Centre, Fukuoka, [12]Department of Haematology and Oncology, Osaka University Graduate School of Medicine, Suita, [13]Department of Haematology and Oncology, The Cancer Institute Hospital of Japanese Foundation for Cancer Research, Tokyo, [14]Department of Haematology, Toranomon Hospital, Tokyo, [15]Department of Haematology, Kobe City Medical Centre General Hospital, Kobe, [16]Department of Oncology Clinical Development Planning, Ono Pharmaceutical Co., Ltd., Osaka, and [17]Department of Haematology and Oncology, Nagoya City University

Summary

We conducted a phase 1/2 study of single-agent carfilzomib in Japanese patients with relapsed/refractory multiple myeloma. Safety, pharmacokinetics and pharmacodynamics of carfilzomib were examined in phase 1. The primary endpoint in phase 2 was the overall response rate (ORR). Carfilzomib was administered in a twice-weekly, consecutive-day dosing schedule. In Phase 1, doses of 15 or 20 mg/m^2 were administered on this schedule or 20 mg/m^2 on Days 1 and 2 of Cycle 1 and then 27 mg/m^2 in the 20/27 mg/m^2 cohort. Patients had a median of five prior therapies, including bortezomib and an immunomodulatory agent. The dose level did not reach the maximum tolerated dose. The most common adverse events were haematological. Notably, carfilzomib either induced new hypertension (n = 4) or aggravated previously existing hypertension (n = 6) in 10 of 50 patients. Four of the eight patients who previously experienced peripheral neuropathy (PN) experienced a recurrence with carfilzomib use, but no new cases of PN occurred. The ORR of the 20/27 mg/m^2 40 patient cohort was similar to that in the pivotal US study. The dose was efficacious and tolerable in heavily pre-treated Japanese patients; however, meticulous control of hypertension may be necessary for further carfilzomib use.

Keywords: multiple myeloma, carfilzomib, hypertension peripheral neuropathy, cardiovascular AEs.

doi: 10.1111/bjh.13900

Graduate School of Medical Sciences, Nagoya, Japan

Received 14 September 2015; accepted for publication 6 November 2015
Correspondence: Dr Takashi Watanabe, Haematology Division, Komaki City Hospital, 1-20 Jobushi, Komaki, Japan.
E-mail: takawata@komakihp.gr.jp

Multiple myeloma (MM) is characterized by the abnormal accumulation of clonal plasma cells in the bone marrow. In the United States (US), an estimated 21 700 new cases of MM and 10710 deaths were predicted in 2012 (American Cancer Society 2012); in Japan, an estimated 6860 new cases of MM and 4066 deaths (http://ganjoho.jp/reg_stat/statistics/dl/) were predicted. Over the past decade, the introduction of immunomodulators, such as thalidomide and lenalidomide, and a proteasome inhibitor (PI) bortezomib (Velcade®, Millennium Pharmaceuticals, Cambridge, MA, USA) has significantly improved the overall survival (OS) of MM patients (Jemal *et al*, 2010).

Carfilzomib (Kyprolis®, Onyx Pharmaceuticals, an Amgen subsidiary, South San Francisco, CA, USA) is one of the second-generation epoxyketone PIs that can irreversibly inhibit chymotrypsin-like activity (Demo *et al*, 2007; Parlati *et al*, 2009). Carfilzomib induced apoptosis in myeloma cell lines and primary myeloma cells from patients whose disease was resistant to available therapies, including bortezomib (Kuhn *et al*, 2007). In addition, carfilzomib has fewer off-target effects, which may explain a lack of neurodegeneration *in vitro*, and less neurotoxicity in animal studies (Arastu-Kapur *et al*, 2011). Therefore, carfilzomib was expected to circumvent some of the clinical adverse events (AEs) of bortezomib, particularly peripheral neuropathy (PN) (Bruna *et al*, 2010; Arastu-Kapur *et al*, 2011).

In fact, PN did not appear to be clinically limiting for extended carfilzomib treatment (Vij *et al*, 2012a,b). An alternative subcutaneous route of administration for bortezomib reduced the incidence of PN without reducing efficacy (Moreau *et al*, 2011). Despite these facts, the subcutaneous administration of bortezomib has still caused gastrointestinal (GI) AEs in patients with MM (Moreau *et al*, 2011). Carfilzomib has also caused GI AEs; however, those occurring with carfilzomib use were mild and manageable with routine supportive care (Siegel *et al*, 2012; Vij *et al*, 2012b).

Almost all patients with MM will eventually relapse, and new treatment options are needed. Accordingly, to change the intrinsic natural behaviour of MM, it was suggested that the use of higher doses, combination regimens and early treatment of the disease course without AEs are required for the new treatment using carfilzomib (Reece, 2012). However, discontinuation or dose reduction was inevitable because of increased toxicities in some of the carfilzomib trials using combination therapies (Bringhen *et al*, 2014; Sonneveld *et al*, 2015).

In an open-label, phase 2 pilot study (PX-171-003-A0) of carfilzomib in 46 patients with relapsed/refreactory MM (RRMM), patients treated with carfilzomib 20 mg/m^2 achieved an overall response rate (ORR) of 16·7%, with manageable toxicities (Jaganath *et al*, 2012). The study was subsequently amended to include an expanded dosing cohort with a scheduled dose escalation from 20 to 27 mg/m^2 beginning in the second cycle (PX-171-003-A1 [003-A1]). In 003-A1, which included 266 patients with RRMM, the ORR was 23·7%; these results were the basis for the accelerated approval of carfilzomib by the US Food and Drug Administration (Siegel *et al*, 2012). In the present study, we used the same dose escalation schedule as 003-A1, with one exception: 27 mg/m^2 was started on Day 8 of Cycle 1. With this method, we carefully characterized the AEs of carfilzomib in a phase 1/2 single-agent carfilzomib study in Japanese patients with RRMM.

Methods

Study design

This was a multicentre, open-label phase 1/2 study (ONO-7057-01) in Japanese patients with RRMM. The safety, tolerability, efficacy, pharmacokinetics (PK) and pharmacodynamics of carfilzomib were examined in phase 1 for intravenously administered carfilzomib at doses of 15, 20 and 20/27 mg/m^2. Phase 2 examined the safety and efficacy of carfilzomib at the recommended dose determined in phase 1. The primary endpoint in phase 2 was the ORR. Secondary endpoints included the duration of response (DOR), Progression-free survival (PFS) and OS. It was planned that three or six patients for each cohort in phase 1 and 24 patients in phase 2 were enrolled. If dose-limiting toxicity (DLT) occurred in one of three patients, an additional three patients were enrolled; if the incidence of DLT was two of three patients or three of six patients, the previous dose level was used as the recommended dose in phase 2.

Eligibility

The main patient inclusion criteria were age ≥20 years and Eastern Cooperative Oncology Group (ECOG) performance status (PS) of 0–2. Patients were required to have relapsed myeloma and measurable disease (either serum M protein level of ≥5·0 g/l or urinary M protein of ≥0•2 g/24 h) responsive to at least one previous therapeutic regimen (≥25% of reduction in M or total protein) and refractory to their most recent therapy (disease progression either during treatment or within 60 days after therapy completion). Patients were to be exposed to at least three prior treatments, including bortezomib, an immunomodulatory agent (lenalidomide and/or thalidomide), an alkylating agent, a corticosteroid and anthracycline (except for patients ineligible or clinically unsuitable for transplantation). Patients were excluded if they had Grade ≥3 or Grade 2 PN with pain or a past history of interstitial lung disease (ILD), congestive heart failure (CHF) of New York Heart Association class ≥III, symptomatic myocardial ischaemia or uncontrolled conduction abnormalities.

This study was conducted in compliance with the Good Clinical Practice guidelines. The study protocol was approved by the Institutional Review Board of each institution, and written informed consent was obtained from each patient enrolled in this study.

Dose-limiting toxicity definition

DLT was defined as any of the following AEs in Cycle 1 that were at least possibly related to carfilzomib and met one of the following criteria: Grade 3 or 4 PN or Grade 2 PN with pain; Grade ≥3 non-haematological toxicities; Grade ≥3 nausea, vomiting or diarrhoea that was uncontrolled after an adequate administration of anti-emetic or anti-diarrhoeal medications; febrile neutropenia; Grade 4 neutropenia persisting for >8 days without using granulocyte-colony stimulating factor (G-CSF) for supportive therapy and Grade 4 thrombocytopenia that required platelet transfusion or was accompanied by bleeding. Administration of G-CSF was not permitted during the DLT evaluation period.

Treatment

Carfilzomib was intravenously administered for 10 min at doses of 15, 20 and 20/27 mg/m^2 on Days 1, 2, 8, 9, 15 and 16 of each 28-day cycle until withdrawal of consent, disease progression or the occurrence of unacceptable toxic effects. For the 20/27 mg/m^2 dosage, 20 mg/m^2 was dosed on Days 1 and 2 of Cycle 1 and escalated to 27 mg/m^2 on Day 8 of Cycle 1 and thereafter.

Oral or intravenous dexamethasone (4 mg) was administered before each dose of carfilzomib in Cycle 1 and thereafter if necessary as pre-medication to prevent infusion reactions. Intravenous and oral hydrations were also required during Cycle 1 and in subsequent cycles as needed. In Cycle 1, all patients were required to receive prophylactic antibiotics, and patients with a medical history of herpes infection received acyclovir.

Assessment of response and safety

The efficacy analysis set comprised all patients who received at least one dose of carfilzomib and had at least one assessment of efficacy or pharmacodynamics. The primary endpoint of phase 2 was the ORR based on central laboratory data according to the International Myeloma Working Group (IMWG) Uniform Response Criteria (Durie *et al*, 2006), including the minimal response (MR), as defined by the European Group for Blood and Marrow Transplantation criteria (Bladé *et al*, 1998). The ORR with 95% confidence interval (CI) was determined for each dose level. The investigational period ended when Cycle 6 was completed for all patients enrolled in the study, and subsequent cycles were included in the analysis for patients whose therapy lasted more than six cycles.

The safety analysis set comprised all patients who received at least one dose of carfilzomib, and all AEs were graded according to the National Cancer Institute Common Terminology Criteria for Adverse Events version 4•0 (http://evs.nci.nih.gov/ftp1/CTCAE/CTCAE_4·03_2010-06-14_QuickReference_8·5x11.pdf).

Pharmacokinetics and pharmacodynamics

Samples for determining the plasma concentrations of carfilzomib were collected on Days 1 and 16 of Cycle 1 before administration, 5 min after the start of administration, immediately before the completion of administration and 5, 15 and 30 min and 1, 2 and 4 h after administration was completed. Moreover, whole blood and peripheral blood mononuclear cells (PBMCs) were collected on Days 1, 2 and 8 of Cycle 1 and Day 1 of Cycle 2 before administration as well as at 1 h after administration was completed to analyse proteasome activity.

Statistical analyses

All statistical analyses were performed using SAS® version 9•3 (SAS Institute Inc., Cary, NC, USA). Two-sided 95% CI of the best ORR was determined according to Willson (1927) for evaluable patients whose best response was classified as stringent complete response (sCR), complete response (CR), very good partial response (VGPR) and partial response (PR).

The analysis of the ORR was performed in subgroups, defined by the patient baseline characteristics of age, sex, cytogenetics/fluorescence *in situ* hybridization (FISH) and International Staging System (ISS) for MM stage (Greipp *et al*, 2005) as exploratory analyses. Patients were classified as

having standard-risk or high-risk cytogenetic abnormalities, as defined by IMWG criteria (Munshi *et al*, 2011). High-risk cytogenetic markers included either del 13 or hypodiploidy by metaphase cytogenetic analysis and/or del 17p13, t(4;14), t(14;16) by interphase FISH. Hence, patients without these abnormalities were considered to be standard risk.

The ORR was estimated within each subgroup along with its 95% Wilson CI. The clinical benefit rate (CBR) is the percentage of patients whose best response was classified as CR, VGPR, PR and MR. The CBR was estimated along with its 95% Wilson CI. Analysis for time-to-event (PFS and OS) was performed by preparing Kaplan–Meier estimates of the median and plotting Kaplan–Meier curves. In addition, two-sided 95% CIs for the medians were estimated.

Results

Patients and characteristics

Fifty patients were enrolled from 15 centres in Japan between August 2011 and January 2014; patient characteristics are shown in Table I. The median age was 67 years (range, 48–81 years), and the median time from initial diagnosis to study entry was 4·7 years (range 1·6–12·6 years). Most patients had either immunoglobulin G- (70%) or immunoglobulin A-type (16%) myeloma, and 58% had ISS stage II or III at diagnosis. A significant proportion of patients (32%) had poor/unfavourable karyotypes, as determined by FISH analysis. The majority of patients (70%) had Grade 1 or 2 PN at baseline, and 40 of the 50 enrolled patients had past medical history of PN.

The patients had previously received a median of five (range 3–10) therapies, and 42% had previously received at least six therapies. All patients had received bortezomib and an immunomodulatory agent in previous regimens, and 48% had received at least two lines of bortezomib-containing regimens. Twenty (40%) patients had undergone autologous stem cell transplantation (ASCT) (Table I).

Dose escalation

Seventeen of the 50 patients enrolled in the study were enrolled in phase 1. Four patients, including one patient who was not evaluable for DLT, were enrolled in the 15 mg/m^2 cohort; no DLT was observed.

One of the first three patients experienced DLT (thrombotic microangiopathy, cardiomyopathy, hepatic disorder and sensorimotor disorder) in the 20 mg/m^2 cohort; therefore, an additional three patients were enrolled at this level. No further DLT was observed in the three patients; subsequently, no DLT was observed in a total of seven patients (including one who was not evaluable for DLT) enrolled in the 20/27 mg/m^2 cohort, thereby suggesting that a higher dose could reasonably be tested. However, 20/27 mg/m^2 was determined to be the recommended dose in phase 2 of this Japanese study at that time, considering the results in the previous carfilzomib studies conducted overseas (Siegel *et al*, 2012).

Efficacy

Fifty patients were included in the efficacy analysis set; the ORR was 20·0% and the CBR was 28·0% (Table II). In the 40 patients who received the 20/27 mg/m^2 dose, the ORR was 22·5% and the CBR was 27·5%. Subgroup analysis of the 20/27 mg/m^2 group demonstrated that the ORR was not affected by age and ISS stage (Table III). The comparison of the 20/27 mg/m^2 group in this study with that in the 003-A1 study (Siegel *et al*, 2012) showed that the results were similar (22·5% vs. 23·7%) (Table III). In the 20/27 mg/m^2 group, the median DOR was not reached (95% CI, 2·3 months–not reached), and the median PFS was 5·1 months (95% CI: 2·8–7·0 months), whereas the median OS was not reached (95% CI: 7·4 months–not reached) at the time of the data cut-off. The median follow-up times for PFS and OS were 6·0 months (95% CI: 5·8–6·7 months) and 6·5 months [95% CI: 6·0–7·2 months], respectively.

Safety

Fifty patients who received at least one dose of carfilzomib were included in the safety population. All patients experienced at least one AE, and 88% had at least one AE of Grade ≥3. All AEs encountered in ≥20% of the patients are shown in Table SI. The most commonly observed AEs were haematological toxicities, including lymphopenia (86%), thrombocytopenia (68%), anaemia (58%), neutropenia (56%) and leucopenia (50%). The most commonly observed AEs of Grade ≥3 were lymphopenia (68%), neutropenia (38%), anaemia (30%), thrombocytopenia (26%) and leucopenia (26%).

Although PN was observed in eight patients (16%), none were of Grade ≥3, and four of the eight patients had PN of Grade 1 or 2 at the baseline of the study. Moreover, all eight patients had a past history of PN before enrolment in the study (Table IV). According to the detailed analysis of the history of PN, 45 (90%) of 50 patients had experienced PN before they were enrolled in the study; however, PN in 10 of the 45 patients resolved before enrolment. Subsequently, four of the 10 patients encountered PN again after carfilzomib treatment (Patients 2, 3, 5 and 7 in Table IV). In total, eight (18%) of the 45 patients developed PN again after carfilzomib treatment and, of the 35 patients who had PN at baseline (Table I), carfilzomib exacerbated PN in three patients (6% of 50 enrolled patients, 8·6% of the 35 patients) (Patients 1, 4 and 6 in Table IV). In contrast, the remaining five patients who had never experienced PN before enrolment into the carfilzomib study did not develop PN after carfilzomib treatment. One patient who had Grade 2 PN of the lower extremities at baseline newly developed a trigeminal nerve

Table I. Patients' baseline characteristics.

Characteristic	15 mg/m^2 (n = 4)		20 mg/m^2 (n = 6)		20/27 mg/m^2 (n = 40)		Total (N = 50)	
Sex, *n* (%)								
Male	3	(75)	5	(83)	18	(45)	26	(52)
Median age, years (range)	67	(57–80)	71	(59–80)	66	(48–81)	67	(48–81)
ECOG PS, *n* (%)								
0	3	(75)	3	(50)	23	(58)	29	(58)
1	1	(25)	3	(50)	17	(43)	21	(42)
ISS stage*, *n* (%)								
I	2	(50)	2	(33)	12	(30)	16	(32)
II	1	(25)	3	(50)	14	(35)	18	(36)
III	1	(25)	1	(17)	9	(23)	11	(22)
Unknown	0	(0)	0	(0)	5	(13)	5	(10)
Ig subtype, *n* (%)								
IgG	3	(75)	1	(17)	31	(78)	35	(70)
IgA	1	(25)	5	(83)	2	(5)	8	(16)
IgD	0	(0)	0	(0)	2	(5)	2	(4)
Bence–Jones	0	(0)	0	(0)	5	(13)	5	(10)
Cytogenetic/FISH prognostic markers, *n* (%)								
Normal/Favourable	1	(25)	5	(83)	25	(63)	31	(62)
Unfavourable†	3	(75)	1	(17)	12	(30)	16	(32)
Unknown	0	(0)	0	(0)	3	(8)	3	(6)
Peripheral neuropathy, *n* (%)								
Grade 0	0	(0)	1	(17)	14	(35)	15	(30)
Grade 1	2	(50)	4	(67)	20	(50)	26	(52)
Grade 2	2	(50)	1	(17)	6	(15)	9	(18)
Previous lines of therapy, median (range)	5	(4–7)	6	(3–8)	5	(3–10)	5	(3–10)
≥6, *n* (%)	2	(50)	3	(50)	16	(40)	21	(42)
Baseline anti-hypertensive therapy, *n* (%)								
Yes	3	(75)	1	(17)	14	(35)	18	(36)
No	1	(25)	5	(83)	26	(65)	32	(64)
Previous therapy, *n* (%)								
Bortezomib	4	(100)	6	(100)	40	(100)	50	(100)
Immunomodulatory agent								
Lenalidomide	4	(100)	6	(100)	33	(83)	43	(86)
Thalidomide	2	(50)	4	(67)	23	(58)	29	(58)
Corticosteroid	4	(100)	6	(100)	40	(100)	50	(100)
Alkylating agent	4	(100)	6	(100)	40	(100)	50	(100)
Anthracycline	2	(50)	4	(67)	26	(65)	32	(64)
Stem cell transplantation	1	(25)	2	(33)	17	(43)	20	(40)

ECOG PS, Eastern Cooperative Oncology Group performance status; FISH, fluorescence *in situ* hybridization; Ig, immunoglobulin; ISS, International Staging System.

*At diagnosis.

†Includes either t(4;14), t(14;16) or del (17p).

disorder of Grade 1 during carfilzomib treatment, whereas the pre-existing PN was not aggravated by carfilzomib (Table IV). No ILD was observed.

We particularly highlighted cardiovascular and infectious AEs in this study, and the details are presented in Table V. In total, the occurrence rate of hypertension (HT) was low and similar to that reported in the previous study (17%) (Grade ≥3; 6%) (Vij *et al*, 2012a). In the present study, HT (10/50 patients; 20%) was relatively common among the cardiovascular AEs. Although HT (8%) of Grade ≥3 and cardiomyopathy (2%) of Grade ≥3 were observed, severe CHF was not reported. The AEs considered to be autonomic are also shown in Table SII, although they were mild, except HT. Among AEs of any grade, HT was the most commonly noted; moreover, as observed in four patients, HT was the only Grade ≥3 AE that was attributed to autonomic neuropathy.

With respect to infectious AEs, it is notable that nasopharyngitis and pharyngitis were relatively common, but the incidence of other infectious AEs was low, a finding

Table II. Best overall response.

	15 mg/m^2 (n = 4)		20 mg/m^2 (n = 6)		20/27 mg/m^2 (n = 40)		Total (N = 50)	
Best response, *n* (%)								
CR	0	(0)	0	(0)	0	(0)	0	(0)
VGPR	0	(0)	0	(0)	2	(5·0)	2	(4·0)
PR	1	(25·0)	0	(0)	7	(17·5)	8	(16·0)
MR	0	(0)	2	(33·3)	2	(5·0)	4	(8·0)
SD	1	(25·0)	1	(16·7)	16	(40·0)	18	(36·0)
PD	0	(0)	1	(16·7)	9	(22·5)	10	(20·0)
NE	2	(50·0)	2	(33·3)	4	(10·0)	8	(16·0)
ORR (≥PR), *n* (%)	1	(25·0)	0	(0)	9	(22·5)	10	(20·0)
CBR (≥MR), *n* (%)	1	(25·0)	2	(33·3)	11	(27·5)	14	(28·0)
DOR, median (95% CI), months	9·5	(NR–NR)	–	–	NR	(2·3–NR)	9·5	(2·3–9·5)
PFS, median (95% CI), months	2·8	(1·7–15·9)	11·1	(0·9–11·1)	5·1	(2·8–7·0)	5·1	(2·8–7·0)
OS, median (95% CI), months	17·9	(3·0–NR)	17·8	(3·4–23·4)	NR	(7·4–NR)	23·4	(10·3–NR)

CR, complete response; VGPR, very good partial response; PR, partial response; MR, minimal response; SD, stable disease; PD, progressive disease; NE, not evaluable; ORR, overall response rate; CBR, clinical benefit rate; DOR, duration of response; NR, not reached; PFS, progression-free survival; CI, confidence interval; OS, overall survival; NR, not reached.

Table III. Comparison of overall response rate in the 20/27 mg/m^2 cohort according to baseline characteristics.

	ONO-7057-01*			PX-171-003-A1†					
Characteristic	*n*	ORR	95% CI	*n*	ORR	95% CI	Odds ratio	95% CI	*P*-value‡
Overall	40	22·5	12·3–37·5	257	23·7	18·7–29·4	0·93	0·42–2·07	0·8640
Age									
<65 years	12	25·0	8·9–53·2	139	25·2	18·2–33·2	0·99	0·25–3·87	0·9890
≥65 years	28	21·4	10·2–39·5	118	22·0	14·9–30·6	0·97	0·35–2·63	0·9445
Sex									
Female	22	13·6	4·7–33·3	108	29·6	21·2–39·2	0·38	0·10–1·36	0·1232
Male	18	33·3	16·3–56·3	149	19·5	13·4–26·7	2·07	0·72–5·98	0·1720
Cytogenetics/FISH prognostic markers									
Normal/Favourable	25	28·0	14·3–47·6	158	22·8	16·5–30·1	1·32	0·51–3·40	0·5677
Unfavourable	12	16·7	4·7–44·8	71	29·6	19·3–41·6	0·48	0·10–2·36	0·3554
ISS stage									
I	12	25·0	8·9–53·2	76	31·6	21·4–43·3	0·72	0·18–2·91	0·6461
II	14	7·1	1·3–31·5	96	24·0	15·8–33·7	0·24	0·03–1·97	0·1547
III	9	33·3	12·1–64·6	78	17·9	10·2–28·3	2·29	0·51–10·26	0·2704

ORR, overall response rate; CI, confidence interval; FISH, fluorescence *in situ* hybridization; ISS, International Staging System.
*Present study. For the 20/27 mg/m^2 cohort, 20 mg/m^2 was dosed on Days 1 and 2 of Cycle 1 and escalated to 27 mg/m^2 on Day 8 of Cycle 1 and thereafter.
†Siegel *et al* (2012). The dose for Cycle 1 was 20 mg/m^2, which was escalated to 27 mg/m^2 on Day 1 of Cycle 2 and thereafter.
‡χ^2 test.

similar to those for the upper respiratory tract documented previously in patients treated with bortezomib (Shah *et al*, 2004; Teh *et al*, 2014a,b) and carfilzomib (31–34%) (Vij *et al*, 2012a,b). Regarding AEs of Grade ≥3, pneumonia, bronchopneumonia, viral pneumonia, staphylococcal infection and herpes virus infection were observed in one patient each in the study (Table V).

No AEs led to death during the administration period of carfilzomib or within 30 days after the final administration of carfilzomib. Eight patients (16%) discontinued treatment, and dosing was interrupted or reduced in 24 patients (48%) because of AEs. It is noteworthy that infection was the most frequent reason for the interruption of carfilzomib treatment. Of the 24 patients whose treatment was interrupted, 11 (46%) experienced viral or upper respiratory diseases, including one patient with flu, one with viral disease, eight with upper respiratory diseases and one with fever who was given an anti-inflammatory drug commonly used

Table IV. Patients with peripheral neuropathy under study treatment.

Patient No.	Dose level (mg/m^2)	Preferred terminology (Grade)	Baseline PN Grade	Worst PN Grade before the study
1	20	Peripheral neuropathy (2)	1	3
2	20/27	Peripheral neuropathy (1)	0	2
3	20/27	Peripheral sensory neuropathy (1)	0	2
4	20/27	Peripheral sensory neuropathy (2)	1	3
5	20/27	Peripheral sensory neuropathy (1)	0	2
6	20/27	Peripheral sensory neuropathy (2)	1	3
7	20/27	Peripheral sensory neuropathy (1)	0	1
8*	20/27	Trigeminal nerve disorder (1)	2	2

PN, peripheral neuropathy.
*Developed trigeminal nerve disorder during carfilzomib treatment. Patient had Grade 2 PN of the lower extremities at baseline, which was not aggravated by carfilzomib.

Table V. Adverse events related to cardiovascular disorders and infections of all grades or ≥Grade 3.

Dose (mg/m^2)	15 mg/m^2 (n = 4)		20 mg/m^2 (n = 6)		20/27 mg/m^2 (n = 40)		Total (N = 50)	
Patients Grade	All Grades	≥Grade 3	All Grades	≥Grade 3	All Grades	≥Grade 3	All Grades	≥Grade 3
Cardiovascular disorder								
Hypertension	2	0	2	0	6	4	10	4
Congestive Heart failure	0	0	0	0	2	0	2	0
Vascular pain	0	0	0	0	2	0	2	0
Hot flush	0	0	0	0	2	0	2	0
Atrioventricular block first degree	0	0	0	0	1	0	1	0
Palpitations	0	0	0	0	1	0	1	0
Dyspnoea*	0	0	0	0	1	0	1	0
Vasculitis	0	0	0	0	1	0	1	0
Troponin T increased	0	0	0	0	1	0	1	0
Orthostatic hypotension	1	0	0	0	0	0	1	0
Cardiomyopathy	0	0	1	1	0	0	1	1
Infections								
Nasopharyngitis	0	0	1	0	10	0	11	0
Pharyngitis	1	0	0	0	5	0	6	0
Gingivitis	1	0	0	0	1	0	2	0
Pneumonia	0	0	1	1	1	0	2	1
Bronchopneumonia	0	0	0	0	1	1	1	1
Influenza	0	0	0	0	1	0	1	0
Viral pneumonia	0	0	0	0	1	1	1	1
Upper respiratory tract infection	0	0	0	0	1	0	1	0
Enteritis infection	0	0	0	0	1	0	1	0
Lip infection	0	0	0	0	1	0	1	0
Oropharyngeal candidiasis	0	0	1	0	0	0	1	0
Staphylococcal infection	0	0	1	1	0	0	1	1
Herpes virus infection	0	0	1	1	0	0	1	1

*Dyspnoea is classified as a respiratory adverse event according to National Cancer Institute Common Terminology Criteria for Adverse Events (NCI-CTCAE) version 4•0 (http://evs.nci.nih.gov/ftp1/CTCAE/CTCAE_4·03_2010-06-14_QuickReference_8·5x11.pdf).

as a medicine for cold. In addition, three patients were believed to have infections leading to treatment interruption; these three patients included one patient with pneumonia and two with fever (of three events), for which levofloxacin or acetaminophen was prescribed. The treatment was interrupted in five other patients who developed neutropenia (of seven events).

Our findings indicate that carfilzomib 20/27 mg/m^2 is feasible for Japanese patients with RRMM.

Pharmacokinetics and pharmacodynamics

PK analyses were performed in a total of 17 patients in phase 1. The PK parameters for carfilzomib are shown in

Table SIII. The plasma carfilzomib concentration showed a rapid decrease after intravenous administration with terminal half-lives ($T_{1/2}$) of 0·424–0·706 h. In the dose range of 15–27 mg/m^2, the area under the plasma concentration–time curve from time 0 to the time of last quantifiable concentration (AUC_{last}) and maximum plasma concentration (C_{max}) increased in a dose-dependent manner. There was no trend toward increasing or decreasing the clearance and volume of distribution at steady state over the dose range. Following repeated doses of carfilzomib at 15 and 20 mg/m^2, the PK parameters were similar on Days 1 and 16. Although C_{max} was measured, the results were not compared with those of previous studies because the duration of intravenous administration of carfilzomib was 10 min in the present study and 2–10 min in the overseas studies (PX-171-007; Papadopoulos *et al*, 2013) Therefore, we concluded that there was no remarkable ethnic difference in the PK parameters of carfilzomib compared with the AUC_{last} and $T_{1/2}$ in PX-171-007.

For all dosing levels of carfilzomib, the proteasome activities in whole blood and PBMCs were reduced 1 h after administration on Days 1, 2 and 8 of Cycle 1 and on Day 1 of Cycle 2 with ≥80% inhibition. Furthermore, although proteasome activity in whole blood before the administration of carfilzomib on Day 1 of Cycle 2 slightly recovered (≥70% inhibition) because drug interruption was longer during this period than during other parts of the administration period, administration of carfilzomib resulted in a similar level of inhibition of proteasome activity. The level of inhibition was ≥80%, which was similar to that obtained in the overseas studies (Alsina *et al*, 2012).

Discussion

The present study aimed to evaluate the efficacy and safety of single-agent carfilzomib in Japanese patients with RRMM. The dose level did not reach the MTD, but the recommended dose in phase 2 was determined to be 20/27 mg/m^2 on the basis of the results of phase 1. The results of single-agent carfilzomib at a 20/27 mg/m^2 dose showed good responses in heavily pre-treated patients, with an ORR of 22·5% and a median PFS of 5·1 months.

A comparison of the 20/27 mg/m^2 group in this study with that in the pivotal US study (003-A1) (Siegel *et al*, 2012) showed that the results of the ORR were similar (22·5% and 23·7%, respectively), the median number of previous lines of therapy of the 20/27 mg/m^2 group of each study were the same and the proportion of patients with poor prognosis according to cytogenetic abnormalities was 30% in this study (Table I) and 28% in 003-A1. However, the median PFS was better in this study than in 003-A1 (5·1 months vs. 3·7 months, respectively). The following factors account for the difference: 1) no patients with ECOG PS 2 were enrolled in this study, whereas 13% of the enrolled patients in 003-A1 were PS 2, and 2) the median cumulative carfilzomib dose in this study was 796 mg/m^2 (range 80–1363 mg/m^2), which was much higher than the 470 mg/m^2 (range 20–2647 mg/m^2) in 003-A1. On the other hand, ethnic differences in the efficacy of carfilzomib did not seem to be significant, and both studies demonstrated good efficacy in patients with RRMM.

The incidences of PN were similar: PN of any grade occurred in 73/526 (13·9%) patients; Grade ≥3 PN occurred in seven (1·3%) patients in the integrated analysis of four phase 2 studies of single-agent carfilzomib (Siegel *et al*, 2013), whereas PN of any grade was encountered in eight (16·0%) patients and no patient developed PN of Grade ≥3 in the present study. In addition, of the 35 patients who had PN at baseline, carfilzomib aggravated PN in three patients (8·6%), which contrasts with the results of a previous study (Vij *et al*, 2012b). However, none of the patients who had not previously experienced PN developed new PN. There may be some patients who are prone to develop PN induced by PIs (Broyl *et al*, 2010; Corthals *et al*, 2011; Watanabe *et al*, 2013), and the choice of carfilzomib among PIs decreases the chance of encountering PN that hinders patients with MM from continuing to receive currently efficacious treatment or future treatment for RRMM.

Adverse effects of particular interest have been cardiac events, previously reported for single-agent carfilzomib treatment (Siegel *et al*, 2012; 2013). Aggregated cardiac AEs, including arrhythmia, CHF, ischaemic heart disease and cardiomyopathy, have been reported in 116 of 526 patients (22·1%), with 50 patients (9·5%) being Grade ≥3, in the integrated analysis (Siegel *et al*, 2013). However, in the present study, regarding Grade ≥3 cardiac AEs, only one (2·0%) patient in the 20 mg/m^2 cohort had cardiomyopathy, and no deaths occurred. Cardiotoxicities have been unexpectedly induced by PIs (Voortman & Giaccone, 2006; Orciuolo *et al*, 2007). In addition, unexplained deaths have been reported in the single-agent bortezomib study, which were attributed to CHF and sudden death, although they were regarded as probably not related to bortezomib (Richardson *et al*, 2009).

The previous integrated analysis reported that HT was documented in 14·3% and that more than half of those had a history of HT (Siegel *et al*, 2013). Although HT was more frequently recorded in our study (10 of 50 enrolled patients; 20%) than in the previous studies, four of the 10 patients were newly induced; however, in the remaining six patients who were prescribed hypertensive drugs before enrolment (Table SIV), HT was aggravated after carfilzomib treatment. As PIs have a potential to exacerbate impaired hypertensive states, blood pressure should be carefully monitored during the treatment, particularly in those who have a history of HT, and should be strictly controlled with additional anti-hypertensive drugs during carfilzomib treatment. It is noteworthy that there was a case reported in which the female patient developed severe CHF after bortezomib treatment, for which HT was the sole cardiovascular risk factor

(Bockorny *et al*, 2012); hence, we highlight this point. Moreover, intriguingly, in pressure-overload hearts of mice, it has been shown that proteasome activities in cardiomyocytes were depressed, resulting from cardiomyocyte apoptosis through the accumulation of pro-apoptotic proteins caused by impaired degradation, before the onset of cardiac dysfunction (Tsukamoto *et al*, 2006). Therefore, there is a great need for the pre-control of HT to mitigate the risk of cardiac toxicity, including heart failure, and control of HT is likely to be an important component of the successful management of MM patients treated with PIs.

GI disorders are caused by bortezomib; however, the rate of GI disorders was 21% lower for the subcutaneous administration of bortezomib than for intravenous administration, of which the incidence of diarrhoea was 12% lower (Moreau *et al*, 2011). The GI disorders may be ascribed to autonomic neuropathy (Mele *et al*, 2015) because it is a well-known fact that autonomic neuropathy is induced by bortezomib (Shah *et al*, 2004; Giannoccaro *et al*, 2011; Stratogianni *et al*, 2012; Mele *et al*, 2015); therefore, autonomic neuropathy may also account for PI-induced HT.

Although 222 (42·2%) and 67 (1·7%) patients experienced dyspnoea and pneumonia of any grade, respectively, in the integrated analysis (Siegel *et al*, 2013), only one (2·0%) and two (4·0%) of the patients in the present study experienced dyspnoea and pneumonia of any grade, respectively (Table V). The aetiology of dyspnoea remained unknown (Siegel *et al*, 2012) and has been debated (Siegel *et al*, 2013) because ILD was scarcely reported with regard to carfilzomib. Therefore, although dyspnoea was considered as pulmonary toxicity in the previous report (Siegel *et al*, 2013), it is more likely a symptom caused by pulmonary oedema owing to reversible acute left ventricular failure induced by PIs because it has been reported as a transient symptom that appeared on the day of or the day after carfilzomib dosing (Siegel *et al*, 2013). Consequently, in the present study, similar to a recent report (Sonneveld *et al*, 2015), we assumed dyspnoea to be a cardiovascular disorder (Table V) so that they would not be underestimated.

If carfilzomib can replace bortezomib as the mainstay of triple combination therapy (Jakubowiak *et al*, 2012; Niesvizky *et al*, 2013; Wang *et al*, 2013; Bringhen *et al*, 2014; Sonneveld *et al*, 2015; Stewart *et al*, 2015), it may be necessary to optimize the use of carfilzomib, although carfilzomib and lenalidomide combined with dexamethasone has an extremely compelling efficacy and is well tolerated (Stewart *et al*, 2015). To explain this, illustrative results of phase 1 or 2 carfilzomib trials using combination therapies were as follows: 1) a total of 33% of patients required carfilzomib dose reduction and 20% discontinued treatment because of AEs in combination with cyclophosphamide and dexamethasone for patients with newly diagnosed MM (Bringhen *et al*, 2014), 2) notably, a total of 31% of the patients enrolled in a dose-escalating study (up to 56 mg/m^2) of carfilzomib experienced at least one Grade ≥3 dyspnoea when combined with 300 mg/m^2 of cyclophosphamide and low-dose dexamethasone (Bensinger *et al*, 2014) and 3) furthermore, the rate of any cardiac-related AEs increased up to 19% with 5% Grade 3 after consolidation therapy following autologous stem cell transplantation in a phase 2 study, in which combination of carfilzomib, thalidomide and dexamethasone was used (Sonneveld *et al*, 2015). In this study, notably, only 59% of the patients were able to complete the original treatment schedule without either delays, reductions, interruptions or premature stoppage of carfilzomib during the induction therapy. Furthermore, a slower (30 min) infusion of carfilzomib was better tolerated and permitted the administration of higher doses (20/45 mg/m^2 or 20/56 mg/m^2) according to the dissociation constant (Kd); however, higher incidences of AEs were reported, including cough (40·9%), dyspnoea (31·8%) and HT (31·8%), with 13·6% of Grade ≥3as the most common non-haematological Grade ≥3 AE (Badros *et al*, 2013).

Moreover, because our study showed that lymphopenia was the most common (Grade ≥3, 68%), haematological AE (Table SI), in addition to upper respiratory disease being the most common reason for interruption of the treatment, additional care should be taken should carfilzomib be introduced into combination therapy in the future, particularly with pomalidomide and dexamethasone.

Lessons have been learned regarding the optimal administration of PIs from experiences with the use of the first-generation PI, bortezomib. Supportive care to avoid or prevent AEs induced by bortezomib and carfilzomib is important in continuous treatment with PIs (Delforge *et al*, 2010; Siegel, 2013). MM eventually develops resistance to all existing available therapies, and patients succumb to the disease (Kumar *et al*, 2012). Therefore, it is important to judiciously use PIs to reduce toxicities and to maintain the drug efficacy against currently existing MM in patients through a consecutive treatment of patients with MM through their life. To optimize the dose of carfilzomib, prescribing prophylactic drugs in advance for potential AEs in its earliest stages when toxicities are anticipated will be crucial for patients with MM to continue carfilzomib treatment and achieve more profound responses, which should prolong survival (Chanan-Khan & Giralt, 2010; Gay *et al*, 2011; Martínez-López *et al*, 2013).

In conclusion, in terms of safety, we did not find any clinically important ethnic differences in safety when carfilzomib was administered in a 20/27 mg/m^2 dosing regimen in Japanese MM patients. Although the PN rates with carfilzomib are low, it may worsen pre-existing PN. Cardiotoxicities were the major concern in previous carfilzomib studies, but they were less frequently observed in the present study; hypertensive status seemed to be exacerbated by the administration of carfilzomib and bortezomib, an affect that may be caused by PI-induced autonomic neuropathy. Therefore, we highlight the importance of managing AEs, including HT, by early treatment to alleviate PI-induced AEs so that

PI treatment can continue. With respect to efficacy, Japanese patients with RRMM achieved relatively longer PFS after higher total doses of carfilzomib than those administered in previous studies.

Acknowledgements

We thank all of the patients who participated in this study and their families as well as all investigators, physicians, nurses and clinical research coordinators who helped with this study. We would also like to thank Dr. Hirokazu Murakami (Gunma University Graduate School of Health Science, Maebashi) who was the medical consultant as well as Dr. Yutaka Ariyoshi (Aichi Cancer Centre Aichi Hospital, Okazaki), Dr. Chihiro Shimazaki (Japan Community Health care Organization Kyoto-Kuramaguchi Medical Centre, Kyoto), Dr. Masahiro Kizaki (Saitama Medical Centre, Saitama Medical University, Saitama), Dr. Takao Katoh (International University of Health and Welfare, Mita Hospital, Tokyo), Dr. Masashi Takahashi (Yujin-Yamazaki Hospital, Hikone) and Dr. Terufumi Kato (Kanagawa Cardiovascular and Respiratory Centre, Yokohama) for their strict review of the clinical data as members of the Efficacy and Safety Evaluation Committee. We also acknowledge the statistical support of Naokazu Gion (Ono Pharmaceutical Co., Ltd., Osaka) and critical review of the manuscript by Sanjay K. Aggarwal, G. Prabhakar Reddy, and Alan Hopkins (Onyx Pharmaceuticals, an Amgen subsidiary, South San Francisco). Editorial assistance was provided by SunFlare Co., Ltd. (Tokyo) and funded by Ono Pharmaceutical Co., Ltd. (Osaka). This study was supported by Ono Pharmaceutical Co., Ltd. (Osaka).

Author contributions

T. Watanabe performed the research and wrote this manuscript. Y. Shumiya and T. Kashihara designed the protocol and wrote the draft manuscript. K. Tobinai, M. Matsumoto, K. Suzuki, K. Sunami, T. Ishida, K. Ando, T. Chou, S. Ozaki, M. Taniwaki, N. Uike, H. Shibayama, K. Hatake, K. Izutsu, T. Ishikawa and S. Iida performed the research and contributed to the final version of the manuscript.

Conflict of interest

The authors declare the following: TW: personal fees from Celgene. K.K., Janssen Pharmaceutical K.K., Takeda Pharmaceutical Co., Ltd., Nippon Kayaku Co., Ltd., Eisai Co., Ltd., Nippon Shinyaku Co., Ltd., Daiichi Sankyo Co., Ltd., Zenyaku Kogyo Co., Ltd., outside the submitted work. KT: grants from Ono Pharmaceutical Co., Ltd., during the conduct of the study; grants and other funding from Eisai and Takeda; grants from Chugai Pharma, Kyowa Hakko Kirin, Celgene, Janssen Pharmaceuticals, GlaxoSmithKline, Mundipharma, SERVIER, Abbvie; other funding from Zenyaku Kogyo and Spectrum Pharmaceuticals, outside the submitted work. MM: personal fees from Celgene K.K., Janssen Pharmaceutical K.K. and Ono Pharmaceutical Co.,LTD, outside the submitted work. KS: No relevant financial relationship(s) to disclose. TI: grants and personal fees from TAKEDA, personal fees from CELGENE and JANSSEN, outside the submitted work. KA: No relevant financial relationship(s) to disclose. TC: Honoraria, lecture fee from Jansen Japan Pharmaceutical Co., Ltd., Celgene Japan Pharmaceutical Co., Ltd., BMS Japan Pharmaceutical Co., Ltd., Takeda Japan Pharmaceutical Co., Ltd., Chugai Japan Pharmaceutical Co., Ltd. SO: No relevant financial relationship(s) to disclose. MT: grants from Kyowa Hakko Kirin, Chugai Pharma, Janssen Pharma, Novartis, Bristol-Myers Squibb, Celgene, Pfizer Inc, Takeda Pharma, Asahikasei Pharma and Dainippon Sumitomo Pharma, outside the submitted work. NU: No relevant financial relationship(s) to disclose. HS: grants from Ono Pharmaceutical Company, during the conduct of the study; grants and personal fees from Celgene K.K. and Takeda Pharmaceutical Co. Ltd., personal fees from Janssen Pharmaceutical Co. Ltd. and grants from Bristol-Meyers Squibb Company, outside the submitted work. KH: No relevant financial relationship(s) to disclose. KI: grants from Ono Pharmaceutical Co. Ltd., during the conduct of the study; personal fees from Janssen Pharmaceutical K. K., Eisai Co., Ltd., Kyowa Hakko Kirin Co., Ltd., Takeda Pharmaceutical Co., Ltd., Genzyme Japan K. K., Celgene K. K., Shionogi & Co., Ltd., MSD K. K., Eli Lilly Japan K. K., Chugai Pharmaceutical Co., Ltd., Sumitomo Dainippon Pharma Co., Ltd., Nihon Servier Co. Ltd. and Zenyaku Kogyo Co., Ltd., grants and personal fees from Ono Pharmaceutical Co. Ltd., outside the submitted work. TI: No relevant financial relationship(s) to disclose. YS: Ono Pharmaceutical Co.,Ltd. employee (sponsor company). TK: Ono Pharmaceutical Co., Ltd. employee (sponsor company). SI: grants from Ono Pharmaceutical Co. Ltd., during the conduct of the study; grants and personal fees from Celgene K.K., Ono Pharmaceutical Co. Ltd. and Chugai Pharmaceutical Co. Ltd., personal fees from Janssen Pharmaceutical Company, Kyowa Hakko Kirin Inc., Eli Lilly Japan K.K., Bristol-Myers Squibb Company, Taiho Pharmaceutical Co., Ltd and Nippon Kayaku Co. Ltd., outside the submitted work.

Supporting Information

Additional Supporting Information may be found in the online version of this article:

Table SI. Adverse events (≥20%) of all grades or ≥Grade 3.

Table SII. Adverse events attributable to autonomic neuropathy.

Table SIII. Pharmacokinetic parameters.

Table SIV. Adverse event of hypertension.

References

Alsina, M., Trudel, S., Furman, R.R., Rosen, P.J., O'Connor, O.A., Comenzo, R.L., Wong, A., Kunkel, L.A., Molineaux, C.J. & Goy, A. (2012) A phase I single-agent study of twice-weekly consecutive-day dosing of the proteasome inhibitor carfilzomib in patients with relapsed or refractory multiple myeloma or lymphoma. *Clinical Cancer Research*, **18**, 4830–4840.

American Cancer Society (2012) Cancer Facts & Figures 2012. American Cancer Society Inc., Atlanta, GA, USA.

Arastu-Kapur, S., Anderi, J.L., Kraus, M., Parlati, F., Shenk, K.D., Lee, S.J., Muchamuel, T., Bennett, M.K., Driessen, C., Ball, A.J. & Kirk, C.J. (2011) Non-proteasomal targets of the proteasome inhibitors bortezomib and carfilzomib: a link to clinical adverse events. *Clinical Cancer Research*, **17**, 2734–2743.

Badros, A., Papadopoulos, K.P., Zojwalla, N., Lee, J.R.J. & Siegel, D.S.(2013) 30-minute infusion of carfilzomib plus dexamethasone in patients with relapsed and/or refractory multiple myeloma. (International Myeloma Workshop Meeting Abstracts), A278.

Bensinger, W.I., Vescio, R., Gasparetto, C., Camacho, E.S., Nath, R., Gomes, C.L., Smith, D.D., Shah, J.J. & Durie, B.G.M. (2014) A multi-center phase 1b, open-label, dose-finding pilot study to evaluate the combination of carfilzomib and cyclophosphamide with dexamethasone (CCyD) prior to autologous stem cell transplant (ASCT) in patients with transplant eligible newly diagnosed multiple myeloma. *Blood (ASH Annual Meeting Abstracts)*, **124**, A4739.

Bladé, J., Samson, D., Reece, D., Apperley, J., Björkstrand, B., Gahrton, G., Gertz, M., Giralt, S., Jagannath, S. & Vesole, D. (1998) Criteria for evaluating disease response and progression in patients with multiple myeloma treated by high-dose therapy and haemopoietic stem cell transplantation. *British Journal of Haematology*, **102**, 1115–1123.

Bockorny, M., Chakravarty, S., Schulman, P., Bockorny, B. & Bona, R. (2012) Severe heart failure after bortezomib treatment I a patient with multiple myeloma: a case report and review of the literature. *Acta Haematologica*, **128**, 244–247.

Bringhen, S., Petrucci, M.T., Larocca, A., Conticello, C., Rossi, D., Magarotto, V., Musto, P., Boccadifuoco, L., Offidani, M., Omedé, P., Gentilini, F., Ciccone, G., Benevolo, G., Genuardi, M., Montefusco, V., Oliva, S., Caravita, T., Tacchetti, P., Boccadoro, M., Sonneveld, P. & Palumbo, A. (2014) Carfilzomib, cyclophosphamide, and dexamethasone in patients with newly diagnosed multiple myeloma: a multicenter, phase 2 study. *Blood*, **124**, 63–69.

Broyl, A., Corthals, S.L., Jongen, J.L., van der Holt, B., Kuiper, R., de Knegt, Y., van Duin, M., el Jarari, L., Bertsch, U., Lokhorst, H.M., Durie, B.G., Goldschmidt, H. & Sooneveld, P. (2010) Mechanisms of peripheral neuropathy associated with bortezomib and vincristine in patients with newly diagnosed multiple myeloma: a prospective analysis of data from the HOVON-65/GMMG-HD4 trial. *Lancet Oncol*, **11**, 1057–1065.

Bruna, J., Udina, E., Alé, A., Vilches, J.J., Vynckier, A., Monbaliu, J., Silverman, L. & Navarro, X. (2010) Neurophysiological, histological and immunohistochemical characterization of bortezomib-induced neuropathy in mice. *Experimental Neurology*, **223**, 599–608.

Chanan-Khan, A.A. & Giralt, S. (2010) Importance of achieving a complete response in multiple myeloma, and the impact of novel agents. *Journal of Clinical Oncology*, **28**, 2612–2624.

Corthals, S.L., Kuiper, R., Johnson, D.C., Sonneveld, P., Hajek, R., van der Holt, B., Magrangeas, F., Goldschmidt, H., Morgan, G.J. & Avert-Loiseau, H. (2011) Genetic factors underlying the risk of bortezomib induced peripheral neuropathy in multiple myeloma patients. *Haematologica*, **96**, 1728–1732.

Delforge, M., Bladé, J., Dimopoulos, M.A., Facon, T., Kropff, M., Ludwig, H., Palumbo, A., Van Damme, P., San-Miguel, J.F. & Sonneveld, P. (2010) Treatment-related peripheral neuropathy in multiple myeloma: the challenge continues. *The Lancet Oncology*, **11**, 1086–1095.

Demo, S.D., Kirk, C.J., Aujay, M.A., Buchholz, T.J., Dajee, M., Ho, M.N., Jiang, J., Laidig, G.J., Lewis, E.R., Parlati, F., Shenk, K.D., Smyth, M.S., Sun, C.M., Vallone, M.K., Woo, T.M., Molineaux, C.J. & Bennett, M.K. (2007) Antitumor activity of PR-171, a novel irreversible inhibitor of the proteasome. *Cancer Research*, **67**, 6383–6391.

Durie, B.G., Harousseau, J.L., Miguel, J.S., Bladé, J., Barlogie, B., Anderson, K., Gertz, M., Dimopoulos, M., Westin, J., Sonneveld, P., Ludwig, H., Gahrton, G., Beksac, M., Crowley, J., Belch, A., Boccadoro, M., Cavo, M., Turesson, I., Joshua, D., Vesole, D., Kyle, R., Alexanian, R., Tricot, G., Attal, M., Merlini, G., Powles, R., Richardson, P., Shimizu, K., Tosi, P., Morgan, G. & Rajkumar, S.V. (2006) International uniform response criteria for multiple myeloma. *Leukemia*, **20**, 1467–1473.

Gay, F., Larocca, A., Wijermans, P., Cavallo, F., Rossi, D., Schaafsma, R., Genuardi, M., Romano, A., Liberati, A.M., Siniscalchi, A., Petrucci, M.T., Nozzoli, C., Patriarca, F., Offidani, M., Ria, R., Omede, P., Bruno, B., Passera, R., Musto, P., Boccadoro, M., Sonneveld, P. & Palumbo, A. (2011) Complete response correlates with long-term progression-free and overall survival in elderly myeloma treated with novel agents: analysis of 1175 patients. *Blood*, **117**, 3025–3031.

Giannoccaro, M.P., Donadio, V., Pèrez, C.G., Borsini, W., Stasi, V.D. & Liguori, R. (2011) Somatic and autonomic small fiber neuropathy induced by bortezomib therapy: an immunofluorescence study. *Neurological Sciences*, **32**, 361–363.

Greipp, P.R., San Miguel, J., Durie, B.G., Crowley, J.J., Barlogie, B., Bladé, J., Boccadoro, M., Child, J.A., Avet-Loiseau, H., Kyle, R.A., Lahuerta, J.J., Ludwig, H., Morgan, G., Powles, R., Shimizu, K., Shustik, C., Sonneveld, P., Tosi, P., Turesson, I. & Westin, J. (2005) International staging system for multiple myeloma. *Journal of Clinical Oncology*, **23**, 3412–3420.

Jaganath, S., Vij, R., Stewart, A.K., Trudel, S., Jakubowiak, A.J., Reiman, T., Somlo, G., Bahlis, N., Lonial, S., Kunkel, L.A., Wong, A.F. & Wang, M. (2012) An open-label single-arm pilot phase II study (PX-171-003-A0) of low-dose, single-agent carfilzomib in patients with relapsed and refractory multiple myeloma. *Clinical Lymphoma Myeloma Leukemia*, **12**, 310–318.

Jakubowiak, A.J., Dytfeld, D., Griffith, K.A., Lebovic, D., Vesole, D.H., Jagannath, S., Al-Zoubi, A., Anderson, T., Nordgren, B., Detweiler-Short, K., Stockerl-Goldstein, K., Ahmed, A., Jobkar, T., Durecki, D.E., McDonnell, K., Mietzel, M., Couriel, D., Kaminski, M. & Vij, R. (2012) A phase 1/2 study of carfilzomib in combination with lenalidomide and low-dose dexamethasone as a frontline treatment for multiple myeloma. *Blood*, **120**, 1801–1809.

Jemal, A., Siegel, R., Xu, J. & Ward, E. (2010) Cancer Statistics, 2010. *CA Cancer Journal for Clinicans*, **60**, 277–300.

Kuhn, D.J., Chen, Q., Voorhees, P.M., Strader, J.S., Shenk, K.D., Sun, C.M., Demo, S.D., Bennett, M.K., van Leeuwen, F.W.B., Chanan-Khan, A.A. & Orlowski, R.Z. (2007) Potent activity of carfilzomib, a novel, irreversible inhibitor of the ubiquitin-proteasome pathway, against preclinical models of multiple myeloma. *Blood*, **110**, 3281–3290.

Kumar, S.K., Lee, J.H., Lahuerta, J.J., Morgan, G., Richardson, P.G., Crowley, J., Haessler, J., Feather, J., Hoering, A., Moreau, P., LeLeu, X., Hulin, C., Klein, S.K., Sonneveld, P., Siegel, D., Bladé, J., Goldschmidt, H., Jagannath, S., San Miguel, J., Orlowski, R., Palumbo, A., Sezer, O., Rajkumar, S.V. & Durie, B.G.M. on behalf of the International Myeloma Working Group. (2012) Risk of progression and survival in multiple myeloma relapsed after therapy with IMiDs and bortezomib: A multicenter international myeloma working group study. *Leukemia*, **26**, 149–157.

Martínez-López, J., Fernández-Redonondo, E., García-Sánz, R., Montalban, M.A., Martínez-Sánchez, P., Pavia, B., Mateos, M.V., Rosiñol, L., Martin, M., Ayala, R., Martínez, R., Blanchard., M.J., Alegre, A., Besalduch, J., Bargay, J., Hernandez, M.T., Sarasquete, M.E., Sanchez-Godoy, P., Fernández, M., Blade, J., San Miguel, J.F. & Lahuerta, J.J. (2013) Clinical applicability and prognostic significance of molecular response assessed by fluorescent-PCR of immunoglobulin genes in multiple myeloma Results from a GEM/PETHEMA study. *British Journal of Haematology*, **163**, 581–589.

Mele, G., Coppi, M.R., Melpignano, A. & Quarta, G. (2015) Paralytic ileus following "*subcutaneous bortezomib*" therapy: focus on the clinical emergency-report of two cases. *Clinical and Experimental Medicine*. doi:10.1007/s10238-015-0337-6

Moreau, P., Pylypenko, H., Grosicki, S., Karamanesht, I., Leleu, X., Grishunina, M., Rekhtman, G., Masliak, Z., Robak, T., Shubina, A., Arnulf, B., Kropff, M., Cavet, J., Esseltine, D.L., Feng, H., Girgis, S., van de Velde, H., Deraedt, W. & Harousseau, J.L. (2011) Subcutaneous versus intravenous administration of bortezomib in patients with relapsed multiple myeloma: a randomised, phase 3, non-inferiority study. *The Lancet Oncology*, **12**, 431–440.

Munshi, N.C., Anderson, K.C., Bergsagel, P.L., Shaughnessy, J., Palumbo, A., Durie, B., Fonseca, R., Stewart, A.K., Harousseau, J.L., Dimopoulos, M., Jagannath, S., Hajek, R., Sezer, O., Kyle, R., Sonneveld, P., Cavo, M., Rajkumar, S.V., San Miguel, J., Crowley, J. & Avet-Loiseau, H. on behalf of the International Myeloma Workshop Consensus Panel 2 (2011) Consensus recommendations for risk stratification in multiple myeloma: report of the International Myeloma Workshop Consensus Panel 2. *Blood*, **117**, 4696–4700.

Niesvizky, R., Martin, T.G. III, Bensinger, W.I., Alsina, M., Siegel, D.S., Kunkel, L.A., Wong, A.F., Lee, S., Orlowski, R.Z. & Wang, M. (2013) Phase 1b dose-escalation study (PX-171-006) of carfilzomib, lenalidomide, and low-dose dexamethasone in relapsed or progressive multiple myeloma. *Clinical Cancer Research*, **19**, 2248–2256.

Orciuolo, E., Buda, G., Cecconi, N., Galimberti, S., Versari, D., Cervetti, G., Salvetti, A. & Petrini, M. (2007) Unexpected cardiotoxicity in haematological bortezomib treated patients. *British Journal of Haematology*, **138**, 396–397.

Papadopoulos, K.P., Burris, H.A. III, Gordon, M., Lee, P., Sausville, E.A., Rosen, P.J., Patnaik, A., Cutler, R.E. Jr, Wang, Z., Lee, S., Jones, S.F. & Infante, J.R. (2013) A phase I/II study of carfilzomib 2–10-min infusion in patients with advanced solid tumors. *Cancer Chemotherapy and Pharmacology*, **72**, 861–868.

Parlati, F., Lee, S.J., Aujay, M., Suzuki, E., Levitsky, K., Lorens, J.B., Micklem, D.R., Ruurs, P., Sylvain, C., Lu, Y., Shenk, K.D. & Bennett, M.K. (2009) Carfilzomib can induce tumor cell death through selective inhibition of the chymotrypsin-like activity of the proteasome. *Blood*, **114**, 3439–3447.

Reece, D.E. (2012) carfilzomib in multiple myeloma: gold, silver, or bronze? *Blood*, **120**, 2776–2777.

Richardson, P.G., Xie, W., Mitsiades, C., Chanan-Khan, A.A., Lonial, S., Hassoun, H., Avigan, D.E., Oaklander, A.L., Kuter, D.J., Wen, P.Y., Kesari, S., Briemberg, H.R., Schlossman, R.L., Munshi, N.C., Heffner, L.T., Doss, D., Esseltine, D.L., Weller, E., Anderson, K.C. & Amato, A.A. (2009) Single-agent bortezomib in previously untreated multiple myeloma: efficacy, characterization of peripheral neuropathy, and molecular correlations with response and neuropathy. *Journal of Clinical Oncology*, **27**, 3518–3525.

Shah, M.H., Young, D., Kindler, H.L., Webb, I., Kleiber, B., Wright, J. & Grever, M. (2004) Phase II study of the proteasome inhibitor bortezomib (PS-341) in patients with metastatic neuroendocrine tumors. *Clinical Cancer Research*, **10**, 6111–61118.

Siegel, D.S. (2013) From clinical trials to clinical practice: single-agent carfilzomib adverse events and their management in patients with relapsed and/or refractory multiple myeloma. *Therapeutic Advances in Hematology*, **4**, 354–365.

Siegel, D.S., Martin, T., Wang, M., Vij, R., Jakubowiak, A.J., Lonial, S., Trudel, S., Kureti, V., Bahlis, N., Alsina, M., Chanan-Khan, A., Buadi, F., Reu, F.J., Somlo, G., Zonder, J., Song, K., Stewart, A.K., Stadtmauer, E., Kunkel, L., Wear, S., Wong, A.F., Orlowski, R.Z. & Jagannath, S. (2012) A phase 2 study of single-agent carfilzomib (PX-171-003-A1) in patients with relapsed and refractory multiple myeloma. *Blood*, **120**, 2817–2825.

Siegel, D., Martin, T., Nooka, A., Harvey, R.D., Vij, R., Niesvizky, R., Badros, A.Z., Jagannath, S., McCulloch, L., Rajangam, K. & Lonial, S. (2013) Integrated safety profile of single-agent carfilzomib: experience from 526 patients enrolled in 4 phase II clinical studies. *Haematologica*, **98**, 1753–1761.

Sonneveld, P., Asselbergs, E., Zweegman, S., van der Holt, B., Kersten, M.J., Vellenga, E., van Marwijk-Kooy, M., Broyl, A., de Weerdt, O., Lonergan, S., Palumbo, A. & Lokhorst, H. (2015) Phase 2 study of carfilzomib, thalidomide, and dexamethasone as induction/consolidation therapy for newly diagnosed multiple myeloma. *Blood*, **125**, 449–456.

Stewart, A.K., Rajkumar, S.V., Dimopoulos, M.A., Masszi, T., Špička, I., Oriol, A., Hájek, R., Rosiñol, L., Siegel, D.S., Mihaylov, G.G., Goranova-Marinova, V., Rajnics, P., Suvorov, A., Niesvizky, R., Jakubowiak, A.J., San-Miguel, J.F., Ludwig, H., Wang, M., Maisnar, V., Minarik, J., Bensinger, W.I., Mateos, M.V., Ben-Yehuda, D., Kukreti, V., Zojwalla, N., Tonda, M.E., Yang, X., Xing, B., Moreau, P. & Palumbo, A. (2015) Carfilzomib, lenalidomide, and dexamethasone for relapsed multiple myeloma. *The New England Journal of Medicine*, **372**, 142–152.

Stratogianni, A., Tosch, M., Schlemmer, H., Weis, J., Katona, I., Isenmann, S. & Haensch, C.A. (2012) Bortezomib-induced severe autonomic neuropathy. *Clinical Autonomic Research*, **22**, 199–202.

Teh, B.W., Harrison, S.J., Pellegrini, M., Thursky, K.A., Worth, L.J. & Slavin, M.A. (2014a) Changing treatment paradigms for patients with plasma cell myeloma: Impact upon immune determinants of infection. *Blood Reviews*, **28**, 75–86.

Teh, B.W., Worth, L.J., Harrison, S.J., Thursky, K.A. & Slavin, M.A. (2014b) Risks and burden of viral respiratory tract infections in patients with multiple myeloma in the era of immunomodulatory drugs and bortezomib: experience at an Australian Cancer Hospital. *Supportive Care in Cancer*, doi:10.1007/s00520-014-2550-3

Tsukamoto, O., Minamino, T., Okada, K., Shintani, Y., Takashima, S., Kato, H., Liao, Y., Okazaki, H., Asai, M., Hirata, A., Fujita, M., Asano, Y., Yamazaki, S., Asanuma, H., Hori, M. & Kitakaze, M. (2006) Depression of proteasome activities during the progression of cardiac dysfunction in pressure-overloaded heart of mice. *Biochemical and Biophysical Research Communications*, **340**, 1125–1133.

Vij, R., Siegel, D.S., Jagannath, S., Jakubowiak, A.J., Stewart, A.K., McDonagh, K., Bahlis, N., Belch, A., Kunkel, L.A., Wear, S., Wong, A.F., Orlowski, R.Z. & Wang, M. (2012a) An open-label, single-arm, phase 2 study of single-agent carfilzomib in patients with relapsed and/or refractory multiple myeloma who have been previously treated with bortezomib. *British Journal of Haematology*, **158**, 739–748.

Vij, R., Wang, M., Kaufman, J.L., Lonial, S., Jakubowiak, A.J., Stewart, A.K., Kukreti, V., Jagannath, S., McDonagh, K.T., Alsina, M., Bahlis, N.J., Reu, F.J., Gabrail, N.Y., Belch, A., Matous, J.V., Lee, P., Rosen, P., Sebag, M., Vesole, D.H., Kunkel, L.A., Wear, S.M., Wong, A.F., Orlowski, R.Z. & Siegel, D.S. (2012b) An open-label, single-arm, phase 2 (PX-171-004) study of single-agent carfilzomib in bortezomib-naïve patients with relapsed and/or refractory multiple myeloma. *Blood*, **119**, 5661–5670.

Voortman, J. & Giaccone, G. (2006) Severe reversible cardiac failure after bortezomib treatment combined with chemotherapy in a non-small cell lung cancer patient: a case report. *BioMed Central Cancer*, **6**, 129.

Wang, M., Martin, T., Bensinger, W., Alsina, M., Siegel, D.S., Kavalerchik, E., Huang, M., Orlowski, R.Z. & Niesvizky, R. (2013) Phase 2 dose-expansion study (PX-171-006) of carfilzomib, lenalidomide, and low-dose dexamethasone in relapsed or progressive multiple myeloma. *Blood*, **122**, 3122–3128.

Watanabe, T., Mitsuhashi, M., Sagawa, M., Ri, M., Suzuki, K., Abe, M., Ohmachi, K., Nakagawa, Y., Nakamura, S., Chosa, M., Iida, S. & Kizaki, M. (2013) Phytohemagglutinin-induced IL2 mRNA in whole blood can predict bortezomib-induced peripheral neuropathy for multiple myeloma patients. *Blood Cancer Journal*, **3**, e150.

Willson, E.B. (1927) Probable inference, the law of succession, and statistical inference. *Journal of the American Statistical Association*, **22**, 209–212.

Ichinohe *et al. Exp Hematol Oncol (2016) 5:11*
DOI 10.1186/s40164-016-0040-7

Experimental Hematology & Oncology

RESEARCH Open Access

A multicenter phase 2 study of pomalidomide plus dexamethasone in patients with relapsed and refractory multiple myeloma: the Japanese MM-011 trial

Tatsuo Ichinohe[1*†], Yoshiaki Kuroda[1†], Shinichiro Okamoto[2], Kosei Matsue[3], Shinsuke Iida[4], Kazutaka Sunami[5], Takuya Komeno[6], Kenshi Suzuki[7], Kiyoshi Ando[8], Masafumi Taniwaki[9], Kensei Tobinai[10], Takaaki Chou[11], Hitomi Kaneko[12], Hiromi Iwasaki[13], Chie Uemura[14], Hiromi Tamakoshi[14], Mohamed H. Zaki[15], Thomas Doerr[15] and Shotaro Hagiwara[16]

Abstract

Background: The immunomodulatory agent pomalidomide in combination with low-dose dexamethasone has demonstrated efficacy and safety for the treatment of relapsed and refractory multiple myeloma (RRMM) in phase 2 and 3 trials. However, these trials enrolled very few Asian patients.

Methods: This phase 2 study investigated pomalidomide plus low-dose dexamethasone in 36 Japanese patients with RRMM after ≥2 prior therapies.

Results: Patients enrolled in the study had a relatively high disease burden (81 % Durie–Salmon stage II or III) and were heavily pretreated (median, 6.5 prior antimyeloma regimens). The overall response rate was 42 % (1 patient with complete response and 14 with partial response), with an additional 44 % (16 patients) achieving stable disease (SD). Response rates in patients aged ≤65 years and >65 years were 47 and 35 %, respectively. None of the five patients with extramedullary disease achieved a response, with three of them maintaining SD of short duration. Median progression-free survival was 10.1 months after a 7.7-month median follow-up, and the median overall survival was not reached. The most frequent grade ≥3 adverse events (AEs) were neutropenia (64 %), anemia (42 %), and thrombocytopenia (31 %). The most frequent nonhematologic grade ≥3 AEs were pneumonia and decreased appetite (8 % each). Adverse events in patients aged >65 years were similar to those in patients aged ≤65 years, except for a higher rate of grade ≥3 pneumonia.

Conclusions: Collectively, the results of this study demonstrate that pomalidomide plus low-dose dexamethasone is an effective and safe treatment for Japanese patients with RRMM, although careful attention needs to be paid to serious infections.

Trial registration: Clinicaltrials.gov NCT02011113

Keywords: Relapsed/refractory multiple myeloma, Pomalidomide, Phase 2, Japan, Asian, Plasmacytoma

*Correspondence: tatsuo.ichinohe@gmail.com
†Tatsuo Ichinohe and Yoshiaki Kuroda co-first authors contributed equally to this work
[1] Department of Hematology and Oncology, Research Institute for Radiation Biology and Medicine, Hiroshima University, 1-2-3 Kasumi, Minami-Ku, Hiroshima 734-8553, Japan
Full list of author information is available at the end of the article

Background

Although the introduction of thalidomide, lenalidomide, and bortezomib has improved the survival of patients with multiple myeloma (MM) [1], MM remains incurable, and median overall survival (OS) for patients who have become refractory to bortezomib and thalidomide or lenalidomide is only 9 months [2]. Pomalidomide is a distinct IMiD® immunomodulatory compound with a mechanism of action that includes tumoricidal, immunomodulatory, and antiangiogenic effects [3]. In combination with low-dose dexamethasone, pomalidomide was approved in the United States, Canada, and the European Union for the treatment of patients with relapsed and refractory MM (RRMM) who have received ≥2 prior therapies, including lenalidomide and bortezomib, and who have demonstrated disease progression on the last therapy (United States, Canada, European Union) or within 60 days of completion of the last therapy (United States) [4–6]. In addition, this regimen has recently been approved for the treatment of Japanese patients with RRMM.

In a North American phase 1/2 RRMM study (MM-002), pomalidomide plus low-dose dexamethasone significantly extended progression-free survival (PFS) compared with pomalidomide alone [7, 8]. Furthermore, the regimen significantly improved both PFS and OS compared with high-dose dexamethasone alone in an international phase 3 trial (MM-003) [9]. The safety profile of pomalidomide plus low-dose dexamethasone was acceptable in both studies [8, 9]. However, the number of Asian patients who were enrolled in these previous studies was very small. Additionally, there are no phase 2 studies demonstrating the efficacy and safety profile of pomalidomide in Asian patients with RRMM.

Because pharmacokinetic (PK) and safety profiles of a drug can be affected by ethnicity [10–12], the phase 1 MM-004 study evaluated the tolerated dose, PK, safety, and efficacy of pomalidomide, alone and in combination with low-dose dexamethasone, in Japanese patients with RRMM [13]. Pomalidomide 4 mg/day, the recommended dose in the United States, Canada, and European Union [4–6], was identified as the tolerated dose in this patient population [13], consistent with previous observations in Caucasian patients [7]. These results led us to the phase 2 study, which investigated the efficacy and safety of pomalidomide plus low-dose dexamethasone in Japanese patients with RRMM.

Results

Patient characteristics

A total of 36 patients were enrolled between December 2013 and July 2014 at 13 sites in Japan; all patients were of Asian origin (Fig. 1). The median age was 64.5 years, and 11 % of the patients were aged >75 years (Table 1). The median time from first diagnosis was 4.7 years. Five patients (14 %) presented with extramedullary plasmacytoma in bone (n = 4) and liver (n = 1). Patients had a relatively high disease burden, including Durie–Salmon stage II or III disease in 81 %, and were heavily pretreated, with a median of 6.5 prior antimyeloma regimens. All but 1 patient (97 %) were refractory to lenalidomide, and 58 % were refractory to both lenalidomide and bortezomib.

Study treatment

Median treatment duration was 5.5 months (range, 0.3–12.0 months), and the median number of treatment cycles was 6 (range, 1–13 cycles). At the data cutoff (February 3, 2015), 16 patients (44 %) remained on the protocol treatment. Disease progression was the most common reason for discontinuation (14 patients, 39 %). Three patients (8 %) discontinued because of an adverse event (AE), including 1 fatal AE of aggravated asthma and pneumonia, and three patients (8 %) discontinued for other reasons (Fig. 1).

Efficacy

All 36 patients received study treatment and were evaluable for efficacy. The overall response rate (ORR) was 42 % (15 patients; 95 % CI, 26–58 %), with 1 patient (3 %) achieving a complete response (CR) and 14 patients (39 %) achieving a partial response (PR; Table 2). Stable disease (SD) was recorded as the best response in 16 patients (44 %). Of these 36 evaluable patients, final pomalidomide doses at the last follow-up were 4 mg in 27 patiens, 3 mg in seven patients, and 2 mg in two patients with ORR of 44 % (12/27 patients, 1 CR and 11 PRs), 43 % (3/7 patients, all PRs) and 0 % in each dose

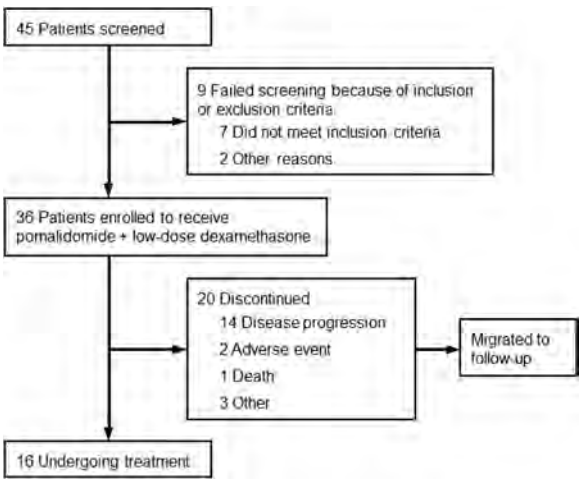

Fig. 1 Patient screening, enrollment, and follow-up in the trial

Table 1 Patient baseline characteristics

Characteristic	Pomalidomide plus dexamethasone (N = 36)
Age	
Median (range), years	64.5 (43–78)
>65 years, n (%)	17 (47.2)
>75 years, n (%)	4 (11.1)
Sex, n (%)	
Male	16 (44.4)
Female	20 (55.6)
Time from first diagnosis, median (range), years	4.7 (0.6–21.1)
ECOG performance status, n (%)	
0–1	33 (91.7)
2	3 (8.3)
Durie–Salmon stage, n (%)	
I	7 (19.4)
II	16 (44.4)
III	13 (36.1)
β_2-microglobulin level, n (%)	
<3.5 mg/L	24 (66.7)
3.5–<5.5 mg/L	10 (27.8)
≥5.5 mg/L	2 (5.6)
Bone lesions, n (%)	22 (61.1)
Extramedullary plasmacytoma, n (%)	5 (13.9)
Creatinine clearance, n (%)	
<30 mL/min	0
30–<45 mL/min	0
45–<60 mL/min	8 (22.2)
60–<80 mL/min	13 (36.1)
≥80 mL/min	15 (41.7)
Prior antimyeloma therapies, median (range)	6.5 (2–15)
Prior stem cell transplant, n (%)	19 (52.8)
Prior therapies, n (%)	
Lenalidomide	36 (100.0)
Bortezomib	36 (100.0)
Thalidomide	12 (33.3)
Dexamethasone	35 (97.2)
Melphalan	31 (86.1)
Last prior therapy, n (%)	
Lenalidomide	21 (58.3)
Bortezomib	15 (41.7)
Refractory to prior therapies, n (%)	
Lenalidomide	35 (97.2)
Bortezomib	21 (58.3)
Both lenalidomide and bortezomib	21 (58.3)

ECOG Eastern Cooperative Oncology Group

Table 2 Responses based on IMWG criteria

Variable	Pomalidomide plus dexamethasone (N = 36)
Response rate, n (%)	
Overall response	15 (41.7)
Complete response	1 (2.8)
Very good partial response	0
Partial response	14 (38.9)
Stable disease	16 (44.4)
Progressive disease	5 (13.9)
Not evaluable	0
Time to response, median (range), months	1.9 (0.9–5.5)
Duration of response, median (range), months	Not reached (1.9–11.1)

IMWG International Myeloma Working Group

Table 3 Best response by final daily dose of pomalidomide

Variable	Final daily dose of pomalidomide[a]		
	4 mg (n = 27)	3 mg (n = 7)	2 mg (n = 2)
Best response rate, n (%)			
Overall response	12 (44.4)	3 (42.9)	0
Complete response	1 (3.7)	0	0
Very good partial response	0	0	0
Partial response	11 (40.7)	3 (42.9)	0
Stable disease	11 (40.7)	3 (42.9)	2 (100)
Progressive disease	4 (14.8)	1 (14.3)	0

[a] Daily dose as of February 3, 2015

group, respectively (Table 3). The median time to first response was 1.9 months, including 2 patients whose response improved from SD after ≥4 cycles of treatment (Fig. 2). The median duration of response (DOR) was not reached (95 % CI, 4.6 months-not estimable). After a median follow-up of 7.7 months, the median PFS was 10.1 months (Fig. 3). A prespecified final OS analysis was conducted using a data cutoff of September 25, 2015; after median follow-up of 11.3 months, the 1-year OS was 58.5 %.

In patients aged ≤65 years, the ORR was 47 % (9/19 patients, all PRs), and in patients aged >65 years, an ORR of 35 % was observed (6/17 patients, 1 CR and 5 PRs). One of four patients aged >75 years achieved a PR. Analysis of impact of disease stage at the time of protocol enrollment showed that ORR in Durie–Salmon stage III disease (23 %) tended to be lower than that in stage I (57 %) or stage II (50 %) disease, although it is not statistically significant (P = 0.28). ORR was 43 % among patients who were refractory to lenalidomide (15/35 patients, 1 CR and 14 PRs) and 33 % among those refractory to both lenalidomide and bortezomib (7/21 patients, all PRs). Recent studies have shown that thalidomide is effective in patients refractory to

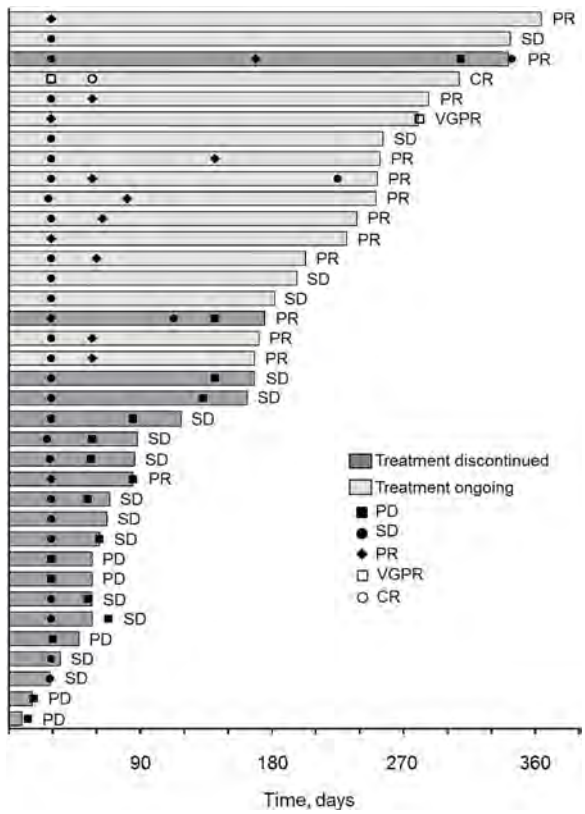

Fig. 2 Treatment exposure and response duration of the enrolled patients. *CR* complete response, *PD* progressive disease, *PR* partial response, *SD* stable disease, *VGPR* very good partial response

bortezomib and lenalidomide treatment [14, 15]. ORR among patients who had previously received thalidomide and those who did not receive thalidomide was 33 % (4/12 patients, all PRs) and 46 % (11/24 patients, with 1 CR and 10 PRs), respectively, with no significant difference between two groups (P = 0.72), although the latter showed a trend toward longer PFS (3.3 months versus not reached, P = 0.21). Median OS was not reached for patients who received or did not receive prior thalidomide. Of the five patients with plasmacytomas, none achieved a response, with SD recorded as the best response in three patients. The median PFS for these five patients was 1.8 months.

Safety

All 36 patients reported ≥1 AE, and 31 patients (86 %) experienced a grade ≥3 AE, regardless of causality (Table 4). The most frequently reported grade ≥3 hematologic AEs regardless of causality were neutropenia (23 patients, 64 %), anemia (15 patients, 42 %), and thrombocytopenia (11 patients, 31 %). The most frequently reported grade ≥3 nonhematologic AEs regardless of causality were pneumonia (three patients, 8 %) and decreased appetite (three patients, 8 %). Other frequently reported AEs (any grade) were pyrexia (nine patients, 25 %); nasopharyngitis (eight patients, 22 %); and gastrointestinal disorders, including constipation (eight patients, 22 %), diarrhea, and nausea (seven patients, 19 % each).

Peripheral neuropathy (PN) of any grade occurred in three patients (8 %) and was considered to be treatment-related in all cases. No occurrences of deep vein thrombosis or pulmonary embolism were reported; all patients received thromboprophylaxis, most commonly with aspirin (94 % of patients). Febrile neutropenia was observed in one patient (3 %), and severe infections and infestations occurred in three patients (8 %). Serious AEs were reported in 13 patients (36 %) and were considered treatment related in six patients (17 %). Constipation and

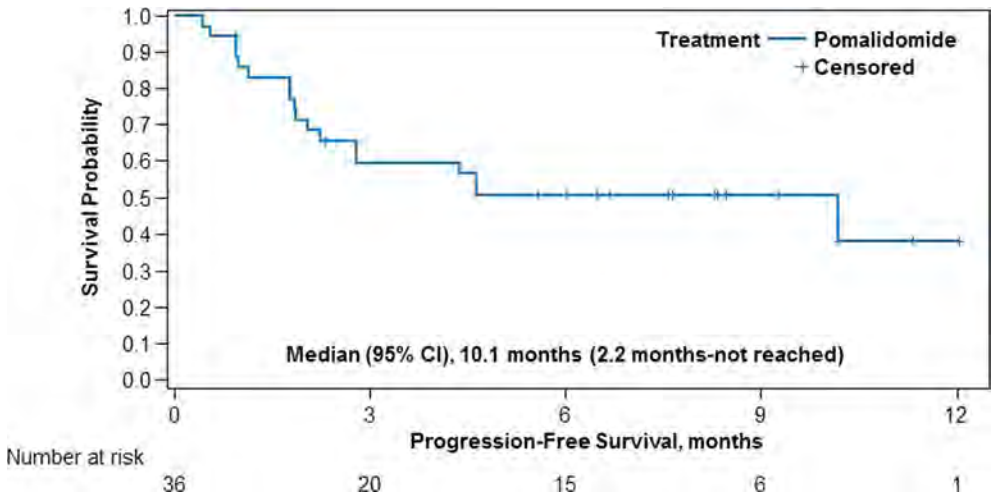

Fig. 3 Kaplan–Meier estimates of progression-free survival from the start of first treatment to first documented disease progression or death, whichever occurred earlier, among patients who received pomalidomide plus low-dose dexamethasone in MM-011

Table 4 Summary of the most commonly reported adverse events (regardless of causality and reported at any grade in ≥10 % of patients)

n (%)	All patients (N = 36)		Age ≤65 years (n = 19)		Age >65 years (n = 17)	
	All grades	Grade ≥ 3	All grades	Grade ≥ 3	All Grades	Grade ≥ 3
Patients with ≥ 1 AE	36 (100.0)	31 (86.1)	19 (100.0)	16 (84.2)	17 (100.0)	15 (88.2)
Neutropenia	26 (72.2)	23 (63.9)	16 (84.2)	14 (73.7)	10 (58.8)	9 (52.9)
Anemia	17 (47.2)	15 (41.7)	9 (47.4)	8 (42.1)	8 (47.1)	7 (41.2)
Thrombocytopenia	17 (47.2)	11 (30.6)	11 (57.9)	6 (31.6)	6 (35.3)	5 (29.4)
Pyrexia	9 (25.0)	0	5 (26.3)	0	4 (23.5)	0
Constipation	8 (22.2)	2 (5.6)	6 (31.6)	1 (5.3)	2 (11.8)	1 (5.9)
Nasopharyngitis	8 (22.2)	0	2 (10.5)	0	6 (35.3)	0
Lymphopenia	7 (19.4)	6 (16.7)	4 (21.1)	3 (15.8)	3 (17.6)	3 (17.6)
Diarrhea	7 (19.4)	0	5 (26.3)	0	2 (11.8)	0
Nausea	7 (19.4)	0	4 (21.1)	0	3 (17.6)	0
Leukopenia	6 (16.7)	4 (11.1)	3 (15.8)	2 (10.5)	3 (17.6)	2 (11.8)
Peripheral edema	6 (16.7)	0	2 (10.5)	0	4 (23.5)	0
Rash	6 (16.7)	0	4 (21.1)	0	2 (11.8)	0
Insomnia	6 (16.7)	0	2 (10.5)	0	4 (23.5)	0
Pneumonia	5 (13.9)	3 (8.3)	1 (5.3)	0	4 (23.5)	3 (17.6)
Decreased appetite	5 (13.9)	3 (8.3)	2 (10.5)	1 (5.3)	3 (17.6)	2 (11.8)
Malaise	5 (13.9)	0	4 (21.1)	0	1 (5.9)	0
Dysgeusia	5 (13.9)	0	2 (10.5)	0	3 (17.6)	0
Hypoxia	4 (11.1)	1 (2.8)	3 (15.8)	1 (5.3)	1 (5.9)	0
Epistaxis	4 (11.1)	0	2 (10.5)	0	2 (11.8)	0
Upper respiratory tract infection	4 (11.1)	0	2 (10.5)	0	2 (11.8)	0

AE adverse event

pneumonia were the only 2 treatment-related serious AEs that occurred in >1 patient (two patients, 6 % each).

Pomalidomide dosing was interrupted in 15 patients (42 %) and reduced in nine patients (25 %) due to AEs. AEs leading to dose reductions in >1 patient were thrombocytopenia (three patients, 8 %), anemia (two patients, 6 %), and leukopenia (two patients, 6 %). Three patients (8 %) had ≥1 AE that led to discontinuation of study treatment, all of which were considered treatment related. AEs leading to discontinuation were asthma, dyspnea, pleural effusion, anemia, pyrexia, and pneumonia. Nine patients (25 %) died during the study; eight deaths were due to progression of MM, and one was due to an AE of pneumonia and aggravated asthma that was suspected to be related to study treatment.

The AE profile in patients aged >65 years was broadly consistent with that in patients aged ≤65 years (Table 4), except for a higher rate of grade ≥3 pneumonia in the older patients.

Discussion

This study demonstrates that pomalidomide in combination with low-dose dexamethasone is an effective regimen that confers disease stabilization or regression in 86 % of heavily pretreated Japanese patients with RRMM, with an acceptable safety profile consistent with the prior studies in other regions. The phase 3 MM-003 trial, which was conducted in 93 centers in Europe, Russia, Australia, Canada, and the United States, previously investigated pomalidomide plus dexamethasone in 302 patients with RRMM who had received prior therapy with both lenalidomide and bortezomib [9]. MM-003 found that pomalidomide plus low-dose dexamethasone significantly improved PFS, OS, and ORR vs high-dose dexamethasone alone [9].

Due to the small sample size of MM-011, results may be less precise and the ability to compare with other trials such as MM-003 is limited, therefore findings in our study should be interpreted with caution. However, the results reported here, including an ORR of 42 % (compared with 31 % in MM-003), suggest that efficacy outcomes of pomalidomide-based salvage treatment in RRMM could be more favorable depending on the criteria used for patient selection [9]. It will be interesting to determine if, as in MM-003, patients with a greater response (either SD or ≥PR) experience a longer OS

compared with patients with progressive disease [16]. Additionally, median PFS in MM-011 was substantially longer than in the MM-003 trial (10.2 vs 4.0 months, respectively) [9], probably reflecting the differences in background characteristics of the patients participating in these studies.

One possible explanation for the observed differences in outcomes between MM-011 and MM-003 is the longer duration of treatment in MM-011 (median, 5.5 vs 4.2 months) [9]. Subgroup analysis of MM-003 showed that some patients who achieved only SD within four cycles of treatment went on to improve their response status with continued treatment beyond four cycles [16]. Thus, the improved outcomes in MM-011 may reflect prolonged time on therapy.

Additionally, the observed differences in outcomes may reflect variability in disease characteristics between the patient population of MM-011 and the pomalidomide plus low-dose dexamethasone arm of MM-003. Several factors associated with poor outcomes were less common in MM-011 than in MM-003. For example, impaired renal function (creatinine clearance <60 mL/min) was present in 22 % of patients in MM-011 compared with 31 % of patients in MM-003 [9]. Renal function may reflect the disease status of MM; however, preliminary data from the MM-008 study showed that pomalidomide dosing need not be reduced in patients with renal function impairment [17]. Additionally, slightly fewer patients in MM-011 had bone lesions compared with MM-003 (61 vs 68 %) [9]. Advanced lytic lesions were reported to be a risk factor associated with poor survival in patients who receive pomalidomide [18]. Finally, patients had lower levels of serum β_2-microglobulin in MM-011 vs MM-003 (Celgene Corporation, MM-003 clinical study report, unpublished observation). Higher serum β_2-microgloblin has been identified as a risk factor associated with shorter OS in patients refractory to bortezomib and IMiD immunomodulatory agents [2].

Of note, three out of five patients with plasmacytomas in MM-011 achieved SD following treatment with pomalidomide plus low-dose dexamethasone, albeit with a short median PFS of 1.8 months. Extramedullary disease associated with MM is known for poor prognosis, even after the introduction of novel agents, including lenalidomide and bortezomib, and thalidomide [19, 20]. Therefore, improved treatment options are urgently needed for this patient population. Because pomalidomide has been shown to have more potent in vitro antimyeloma activity compared with conventional IMiD agents [21–23], further studies are needed to determine whether pomalidomide plus low-dose dexamethasone provides a survival benefit in patients with extramedullary disease or nonsolitary plasmacytoma.

Use of prior treatment options also notably differed between MM-011 and MM-003. Fewer patients in MM-011 had received a prior stem cell transplant than patients in MM-003 (53 vs 71 %) [9]. Although patients had received a higher number of prior antimyeloma therapies in MM-011 vs MM-003 (median, 6.5 vs 5 therapies), median time from initial diagnosis was shorter in MM-011 (4.7 vs 5.3 years). A similar proportion of patients in MM-011 and MM-003 were refractory to lenalidomide (97.2 vs 95 %). Fewer patients in MM-011 were refractory to bortezomib alone (58 vs 79 %) or to both lenalidomide and bortezomib (58 vs 75 %). The lower levels of bortezomib refractory disease in MM-011 may result from differences in eligibility criteria: MM-003, but not MM-011, included patients with primary refractory disease and required that patients had experienced prior treatment failure with both lenalidomide and bortezomib. These differences suggest that patients in MM-011 had disease that was not advanced as in MM-003, potentially accounting for the higher response rates and longer PFS observed. However, subanalysis of MM-003 found no effect of prior treatment on response rate [16].

The chromosomal aberrations del(17p) and t(4;14) are associated with adverse prognosis, with median event-free survival from diagnosis of only 20.6 months and 15 months, respectively [24–27]. Therefore, the efficacy of pomalidomide plus low-dose dexamethasone in MM-011 may have been affected by the proportion of patients with these poor-risk chromosomal aberrations. However, collection of data on chromosomal aberrations was not included in the MM-011 protocol, and this analysis is not available.

The non-hematologic AE profile in MM-011 was generally consistent with that of pomalidomide plus low-dose dexamethasone treatment in MM-003, with a few exceptions. The incidence of severe infections was lower in MM-011 (8.3 % with grade $\geq$3 infection or infestation) than in MM-003 (30 % with grade 3/4 infection), as was the incidence of any grade febrile neutropenia (3 vs 10 %) [9]. Venous thromboembolism (VTE) is associated with decreased survival in MM [28] and is a rare but potentially serious AE that has been reported with IMiD therapy [29, 30]. In a preliminary study in 1035 Japanese patients with MM treated with thalidomide, the incidence of VTE was found to be lower than that in Western patients [31], potentially associated with genetic background and other factors related to ethnicity [32, 33]. In prior studies, appropriate thromboprophylaxis has been selected based on the risk of VTE for Japanese patients. With appropriate protocol-mandated thromboprophylaxis in MM-011, no cases of VTE were reported. Finally, PN is a common and potentially treatment-limiting AE

associated with thalidomide and bortezomib; however, pomalidomide as well as lenalidomide do not appear to cause substantial neurotoxicity [9, 34]. In MM-011, PN of any grade occurred in three patients (8 %) and did not lead to treatment discontinuation.

Grade ≥3 hematologic AEs occurred more frequently in MM-011 than in MM-003, including neutropenia (64 vs 48 %), anemia (42 vs 33 %), and thrombocytopenia (31 vs 22 %); however, the rate of all-grade hematologic AEs in MM-011 was similar to MM-003 [9]. In the Japanese MM-004 study, the incidence of grade ≥3 neutropenia was also higher than in MM-003 (67 vs 48 %) [9, 13]. This suggests that a greater number of Japanese patients may have a greater need for dose adjustments in response to hematologic AEs compared with those from other regions. The observed differences in AEs are not likely to be due to PK differences, as MM-004 found PK parameters of pomalidomide in Japanese patients with RRMM to be similar to those reported for pomalidomide in other RRMM populations, with limited accumulation after multiple doses [13]. Importantly, hematologic AEs were manageable with temporary discontinuation of treatment or with concomitant administration of granulocyte colony-stimulating factor. The successful management of AEs may have contributed to extended duration of treatment in MM-011.

Conclusions

In conclusion, pomalidomide 4 mg/day has been confirmed as the acceptable starting dose for Japanese patients, with dexamethasone administered at a dose of 40 mg/day (reduced to 20 mg/day for patients aged >75 years). Pomalidomide plus low-dose dexamethasone is a relatively safe and highly efficacious treatment for Japanese patients with RRMM who have previously received both lenalidomide and bortezomib. Patients who achieve stable disease or better response while on pomalidomide can continue to benefit from this therapy. Additional studies may be required to further define those patients that would derive the most benefit from pomalidomide-based therapies.

Methods

Patients

Eligible patients had documented MM and relapsed and refractory disease, defined as disease progression after ≥SD for ≥1 cycle of treatment or during or within 60 days of completing treatment. Other inclusion criteria were ≥2 prior therapies (including ≥2 cycles of lenalidomide and bortezomib, separately or in combination), age ≥20 years, and Eastern Cooperative Oncology Group performance status ≤2. Exclusion criteria included previous pomalidomide treatment; hypersensitivity to thalidomide, lenalidomide, or dexamethasone; absolute neutrophil count <1000/μL; platelet count <75,000/μL (or <30,000/μL if ≥50 % of bone marrow nucleated cells were plasma cells); creatinine clearance <45 mL/min using the Cockcroft-Gault formula; corrected serum calcium >14 mg/dL (>3.5 mmol/L); hemoglobin <8 g/dL (<4.9 mmol/L); liver enzyme concentrations >3.0× upper limit of normal (ULN); total bilirubin >2.0 mg/dL (34.2 μmol/L; or ≥3.0× ULN for hereditary benign hyperbilirubinemia); congestive heart failure (New York Heart Association Class III/IV); myocardial infarction within 12 months; unstable or poorly controlled angina pectoris; and PN grade ≥2.

All patients provided informed consent; the study was approved by each study site's institutional review board and was conducted in accordance with the Declaration of Helsinki and the International Conference on Harmonisation guidelines on good clinical practice. The trial is registered as clinicaltrials.gov identifier NCT02011113.

Study design

MM-011 was a phase 2 multicenter, single-arm, open-label study conducted in Japan (Fig. 1). Patients received pomalidomide (4 mg/day orally, days 1-21, 28-day cycles) and dexamethasone (40 mg/day [20 mg/day if aged >75 years] orally, days 1, 8, 15, and 22), consistent with United States and European Union approved dosing [4, 5]. Treatment was continued until disease progression, unacceptable toxicity, or withdrawal. All patients received thromboprophylaxis with low-dose aspirin, low-molecular-weight heparin, or equivalent.

Pomalidomide was interrupted for grade 4 neutropenia or thrombocytopenia, grade ≥3 constipation, VTE, rash, PN, or other pomalidomide-related AE, or grade ≥2 hypothyroidism or hyperthyroidism. Additionally, pomalidomide was interrupted for febrile neutropenia (any grade). Pomalidomide could be restarted at the same level or decreased by 1 mg. Discontinuation of pomalidomide was indicated for rash (grade 4 or blistering) or grade ≥4 PN. Dexamethasone dose was modified for grade ≥3 edema, hyperglycemia, or any other dexamethasone-related AE. Additionally, dexamethasone was modified for grade ≥2 confusion/mood alteration or muscle weakness, or any grade dyspepsia. Dexamethasone was discontinued for acute pancreatitis.

The primary endpoint was response rate according to the International Myeloma Working Group (IMWG) criteria [35]. Enrollment of 37 patients was planned using the expected response rate of 25 % based on the efficacy evaluable population, the threshold response rate of 10 %, on one-sided alpha of 0.05 and the statistical power of 80 % based on the test for one sample proportion. Secondary endpoints included response rate according to

European Group for Blood and Marrow Transplantation (EBMT) criteria [36], time to response (TTR), DOR, PFS, and safety.

Efficacy assessments

Response was assessed by investigators using IMWG criteria and was confirmed by the members of an independent response adjudication committee, who also confirmed responses using EBMT criteria. TTR was calculated as the time from first dose to first documented response. DOR was defined as the time from first documented response to first documented disease progression. PFS was the time from first dose to first documented disease progression or death, whichever occurred earlier, and was estimated using the Kaplan–Meier method.

Safety evaluation

AEs were graded according to the National Cancer Institute Common Terminology Criteria for Adverse Events version 4.0 [37] throughout treatment and for 28 days after last dose. Other safety assessments included VTE monitoring, physical examinations, vital signs, electrocardiograms, and standard clinical laboratory assessments (thyroid function, hematology, serum chemistry, urinalysis, creatinine clearance, and virology).

Abbreviations

AE: adverse event; CR: complete response; DOR: duration of response; EBMT: European Group for Blood and Marrow Transplantation; ECOG: Eastern Cooperative Oncology Group; IMWG: International Myeloma Working Group; ITT: intent to treat; MM: multiple myeloma; ORR: overall response rate; OS: overall survival; PFS: progression-free survival; PK: pharmacokinetics; PN: peripheral neuropathy; PR: partial response; RRMM: relapsed and refractory MM; SD: stable disease; TTR: time to response; ULN: upper limit of normal; VGPR: very good partial response; VTE: venous thromboembolism.

Authors' contributions

All authors were involved with data acquisition, interpretation of the data, review and revision of the manuscript for important intellectual content, and giving final approval of the version to be submitted. In addition, TI, YK, and SH were involved in the drafting of the manuscript, MZ, TD, CU, and HT contributed to the conception and design of the study, and analyzed the data. All authors read and approved the final manuscript.

Author details

[1] Department of Hematology and Oncology, Research Institute for Radiation Biology and Medicine, Hiroshima University, 1-2-3 Kasumi, Minami-Ku, Hiroshima 734-8553, Japan. [2] Key University Hospital, 35 Shinanomachi, Shinjuku-Ku, Tokyo 160-8582, Japan. [3] Kameda Medical Center, 929 Higashi-chou, Kamogawa, Chiba 296-8602, Japan. [4] Nagoya City University Hospital, 1 Kawasumi, Mizuho-chou, Mizuho-Ku, Nagoya 467-8601, Japan. [5] Okayama Medical Center, 1711-1, Tamasu, Kita-Ku, Okayama 701-1154, Japan. [6] Mito Medical Center, 280 Sakuranosato, Ibarakimachi, Higashi-Ibaraki-Gun, Ibaraki 311-3193, Japan. [7] Japanese Red Cross Medical Center, 4-1-22 Hiroo, Shibuya-Ku, Tokyo 150-8935, Japan. [8] Tokai University Hospital, 143 Shimokasuya, Isehara, Kanagawa 259-1193, Japan. [9] University Hospital Kyoto Prefectural University of Medicine, Kawaramachi-Hirokoji, Kamigyo-Ku, Kyoto 602-8566, Japan. [10] National Cancer Center Hospital, 5-1-1 Tsukiji, Chuo-Ku, Tokyo 104-0045, Japan. [11] Niigata Cancer Center Hospital, 2-15-3 Kawagishimachi, Chuo-Ku, Niigata 951-8133, Japan. [12] Osaka Red Cross Hospital, 5-30 Fudegasaki-cho, Tennouji-Ku, Osaka 543-8555, Japan. [13] Kyushu University Hospital, 3-1-1 Maidashi, Higashi-Ku, Fukuoka 812-8582, Japan. [14] Celgene, 1-21-1 Toyama, Shinjuku-Ku, Tokyo 162-8655, Japan. [15] Celgene Corporation, 86 Morris Avenue, Summit, NJ 07901, USA. [16] National Center for Global Health and Medicine Hospital, 15: 2-7-2 Marunouchi, Chiyoda-Ku, Tokyo 100-7010, Japan.

Acknowledgements

The authors would like to thank all the physicians and medical staff who dedicated their time for the care of patients who participated in this study. The authors also thank all the research coordinators and data managers who contributed to the study. The authors received editorial assistance from MediTech Media (Peter J. Simon, Ph.D and Roy Garcia, Ph.D), sponsored by Celgene Corporation. This study was supported by Celgene K.K.

Competing interests

TI received honoraria (Pfizer, Celgene) and research funding (Toyama Chemical, Kyowa Hakko Kirin, Pfizer, Chugai); SO and KM received honoraria (Celgene). SI received honoraria (Celgene, Janssen, Ono, Takeda, Bristol-Myers Squibb) and research funding (Celgene, Kyowa Hakko Kirin, Ono, Eli Lilly, Janssen, Bayer, Chugai, Takeda). KS received research funding (Takeda, Ono, Novartis, Celgene). KA received research funding (Kyowa Hakko Kirin). KT received honoraria (Zenyaku, Eisai, Spectrum, Takeda) and research funding (Chugai, Kyowa Hakko Kirin, Ono, Celgene, Janssen, GSK, Eisai, Mundipharma, Takeda, Servier, AbbVie). TC received honoraria and consultancy fee (Celgene, Janssen, Novartis, Ono). HK received research funding (Celgene). HI received honoraria (Celgene, Kyowa Hakko Kirin) and research funding (Kyowa Hakko Kirin, Bristol-Myers Squibb, Novartis). SH is a member of an advisory committee (Celgene). CU, HT, MZ and TD are employees of Celgene. The other authors declare that they have no competing interests.

Received: 23 February 2016 Accepted: 8 April 2016
Published online: 18 April 2016

References

1. Kumar SK, Rajkumar SV, Dispenzieri A, et al. Improved survival in multiple myeloma and the impact of novel therapies. Blood. 2008;111:2516–20.
2. Kumar SK, Lee JH, Lahuerta JJ, et al. Risk of progression and survival in multiple myeloma relapsing after therapy with IMiDs and bortezomib: a multicenter International Myeloma Working Group study. Leukemia. 2012;26:149–57 **(Erratum in: Leukemia. 2012;26(5):1153)**.
3. Quach H, Ritchie D, Stewart AK, et al. Mechanism of action of immunomodulatory drugs (IMiDs) in multiple myeloma. Leukemia. 2010;24:22–32.
4. AnonymousImnovid (pomalidomide) [Summary of Product Characteristics]. Uxbridge, UK:Celgene Europe; 2015.
5. AnonymousPomalyst (pomalidomide) [package insert]. Summit, NJ:Celgene Corporation; 2015.
6. AnonymousPomalyst (pomalidomide) [product monograph]. Mississauga, ON:Celgene Canada; 2015.
7. Richardson PG, Siegel D, Baz R, et al. Phase 1 study of pomalidomide MTD, safety, and efficacy in patients with refractory multiple myeloma who have received lenalidomide and bortezomib. Blood. 2013;121:1961–7.
8. Richardson PG, Siegel DS, Vij R, et al. Pomalidomide alone or in combination with low-dose dexamethasone in relapsed and refractory multiple myeloma: a randomized phase 2 study. Blood. 2014;123:1826–32.
9. San Miguel J, Weisel K, Moreau P, et al. Pomalidomide plus low-dose dexamethasone versus high-dose dexamethasone alone for patients with relapsed and refractory multiple myeloma (MM-003): a randomised, open-label, phase 3 trial. Lancet Oncol. 2013;14:1055–66.
10. Johnson JA. Predictability of the effects of race or ethnicity on pharmacokinetics of drugs. Int J Clin Pharmacol Ther. 2000;38:53–60.
11. Yasuda SU, Zhang L, Huang SM. The role of ethnicity in variability in response to drugs: focus on clinical pharmacology studies. Clin Pharmacol Ther. 2008;84:417–23.
12. Ramamoorthy A, Pacanowski MA, Bull J, Zhang L. Racial/ethnic differences in drug disposition and response: review of recently approved drugs. Clin Pharmacol Ther. 2015;97:263–73.
13. Matsue K, Iwasaki H, Chou T, et al. Pomalidomide alone or in combination with dexamethasone in Japanese patients with refractory or relapsed and refractory multiple myeloma. Cancer Sci. 2015;106:1561–7.

14. Guglielmelli T, Petrucci MT, Saglio G, Palumbo A. Thalidomide after lenalidomide: a possible treatment regimen in relapse refractory multiple myeloma patients. Br J Haematol. 2011;153:146.
15. Mateos MV, Richardson PG, Schlag R, et al. Bortezomib plus melphalan and prednisone compared with melphalan and prednisone in previously untreated multiple myeloma: updated follow-up and impact of subsequent therapy in the phase III VISTA trial. J Clin Oncol. 2010;28:2259–66.
16. San Miguel JF, Weisel KC, Song KW, et al. Impact of prior treatment and depth of response on survival in MM-003, a randomized phase 3 study comparing pomalidomide plus low-dose dexamethasone versus high-dose dexamethasone in relapsed/refractory multiple myeloma. Haematologica. 2015;100:1334–9.
17. Matous J, Siegel D, Lonial S, Harvey R, Kasserra C. MM-008: a phase 1 trial evaluating pharmacokinetics and tolerability of pomalidomide + low-dose dexamethasone in patients with relapsed or refractory and refractory multiple myeloma and renal impairment. Blood. 2014;124:4730.
18. Wang TF, Ahluwalia R, Fiala MA, et al. The characteristics and outcomes of patients with multiple myeloma dual refractory or intolerant to bortezomib and lenalidomide in the era of carfilzomib and pomalidomide. Leuk Lymphoma. 2014;55:337–41.
19. Varettoni M, Corso A, Pica G, Mangiacavalli S, Pascutto C, Lazzarino M. Incidence, presenting features and outcome of extramedullary disease in multiple myeloma: a longitudinal study on 1003 consecutive patients. Ann Oncol. 2010;21:325–30.
20. Pour L, Sevcikova S, Greslikova H, et al. Soft-tissue extramedullary multiple myeloma prognosis is significantly worse in comparison to bone-related extramedullary relpase. Haematologica. 2014;99:360–4.
21. Davies FE, Raje N, Hideshima T, et al. Thalidomide and immunomodulatory derivatives augment natural killer cell cytotoxicity in multiple myeloma. Blood. 2001;98:210–6.
22. Corral LG, Haslett PA, Muller GW, et al. Differential cytokine modulation and T cell activation by two distinct classes of thalidomide analogues that are potent inhibitors of TNF-alpha. J Immunol. 1999;163:380–6.
23. Zhu YX, Braggio E, Shi CX, et al. Cereblon expression is required for the anti-myeloma activity of lenalidomide and pomalidomide. Blood. 2011;118(18):4771–9.
24. Avet-Loiseau H, Attal M, Moreau P, et al. Genetic abnormalities and survival in multiple myeloma: the experience of the Intergroupe Francophone du Myelome. Blood. 2007;109:3489–95.
25. Avet-Loiseau H, Hulin C, Campion L, et al. Chromosomal abnormalities are major prognostic factors in elderly patients with multiple myeloma: the Intergroupe Francophone du Myelome experience. J Clin Oncol. 2013;31:2806–9.
26. Leleu X, Karlin L, Macro M, et al. Pomalidomide plus low-dose dexamethasone in multiple myeloma with deletion 17p and/or translocation (4;14): IFM 2010-02 trial results. Blood. 2015;125:1411–7.
27. Dimopoulos MA, Weisel KC, Song KW, et al. Cytogenetics and long-term survival of pomalidomide and low-dose dexamethasone in refractory or relapsed and refractory multiple myeloma. Haematologica. 2015;100:1327–33.
28. Kristinsson SY, Pfeiffer RM, Bjorkholm M, Schulman S, Landgren O. Thrombosis is associated with inferior survival in multiple myeloma. Haematologica. 2012;97:1603–7.
29. Leleu X, Rodon P, Hulin C, et al. MELISSE, a large multicentric observational study to determine risk factors of venous thromboembolism in patients with multiple myeloma treated with immunomodulatory drugs. Thromb Haemost. 2013;110:844–51.
30. Palumbo A, Rajkumar SV, Dimopoulos MA, et al. Prevention of thalidomide- and lenalidomide-associated thrombosis in myeloma. Leukemia. 2008;22:414–23.
31. Kato A, Takano H, Ichikawa A, et al. A retrospective cohort study of venous thromboembolism (VTE) in 1035 Japanese myeloma patients treated with thalidomide; lower incidence without statistically significant association between specific risk factors and development of VTE and effects of thromboprophylaxis with aspirin and warfarin. Thromb Res. 2013;131:140–4.
32. Roberts LN, Patel RK, Arya R. Venous thromboembolism and ethnicity. Br J Haematol. 2009;146:369–83.
33. Montagnana M, Favaloro EJ, Franchini M, Guidi GC, Lippi G. The role of ethnicity, age and gender in venous thromboembolism. J Thromb Thrombolysis. 2010;29:489–96.
34. Delforge M, Bladé J, Dimopoulos MA, et al. Treatment-related peripheral neuropathy in multiple myeloma: the challenge continues. Lancet Oncol. 2010;11:1086–95.
35. Durie BG, Harousseau JL, Miguel JS, et al. International uniform response criteria for multiple myeloma. Leukemia. 2006;20:1467–73.
36. Blade J, Samson D, Reece D, et al. Criteria for evaluating disease response and progression in patients with multiple myeloma treated by high-dose therapy and haemopoietic stem cell transplantation. Myeloma Subcommittee of the EBMT. European Group for Blood and Marrow Transplant. Br J Haematol. 1998;102:1115–23.
37. National Cancer Institute. Common Terminology Criteria for Adverse Events (CTCAE) Version 4.0; 2010.

bjh research paper

A phase 1/2 study of carfilzomib in Japanese patients with relapsed and/or refractory multiple myeloma

Takashi Watanabe,[1,2] Kensei Tobinai,[1] Morio Matsumoto,[3] Kenshi Suzuki,[4] Kazutaka Sunami,[5] Tadao Ishida,[6] Kiyoshi Ando,[7] Takaaki Chou,[8] Shuji Ozaki,[9] Masafumi Taniwaki,[10] Naokuni Uike,[11] Hirohiko Shibayama,[12] Kiyohiko Hatake,[13] Koji Izutsu,[14] Takayuki Ishikawa,[15] Yoshihisa Shumiya,[16] Tomohisa Kashihara[16] and Shinsuke Iida[17]

[1]Department of Haematology, National Cancer Centre Hospital, Tokyo, [2]Department of Haematology, Komaki City Hospital, Komaki, [3]Department of Haematology, National Hospital Organization Nishigunma National Hospital, Shibukawa, [4]Department of Haematology, Japanese Red Cross Medical Centre, Tokyo, [5]Department of Haematology, National Hospital Organization Okayama Medical Centre, Okayama, [6]Department of Gastroenterology, Rheumatology and Clinical Immunology, Sapporo Medical University School of Medicine, Sapporo, [7]Department of Haematology and Oncology, Tokai University School of Medicine, Isehara, [8]Department of Internal Medicine, Niigata Cancer Centre Hospital, Niigata, [9]Department of Haematology, Tokushima Prefectural Central Hospital, Tokushima, [10]Division of Haematology and Oncology, Graduate School of Medical Science, Kyoto Prefectural University of Medicine, Kyoto, [11]Department of Haematology, National Hospital Organization Kyushu Cancer Centre, Fukuoka, [12]Department of Haematology and Oncology, Osaka University Graduate School of Medicine, Suita, [13]Department of Haematology and Oncology, The Cancer Institute Hospital of Japanese Foundation for Cancer Research, Tokyo, [14]Department of Haematology, Toranomon Hospital, Tokyo, [15]Department of Haematology, Kobe City Medical Centre General Hospital, Kobe, [16]Department of Oncology Clinical Development Planning, Ono Pharmaceutical Co., Ltd., Osaka, and [17]Department of Haematology and Oncology, Nagoya City University

Summary

We conducted a phase 1/2 study of single-agent carfilzomib in Japanese patients with relapsed/refractory multiple myeloma. Safety, pharmacokinetics and pharmacodynamics of carfilzomib were examined in phase 1. The primary endpoint in phase 2 was the overall response rate (ORR). Carfilzomib was administered in a twice-weekly, consecutive-day dosing schedule. In Phase 1, doses of 15 or 20 mg/m^2 were administered on this schedule or 20 mg/m^2 on Days 1 and 2 of Cycle 1 and then 27 mg/m^2 in the 20/27 mg/m^2 cohort. Patients had a median of five prior therapies, including bortezomib and an immunomodulatory agent. The dose level did not reach the maximum tolerated dose. The most common adverse events were haematological. Notably, carfilzomib either induced new hypertension (n = 4) or aggravated previously existing hypertension (n = 6) in 10 of 50 patients. Four of the eight patients who previously experienced peripheral neuropathy (PN) experienced a recurrence with carfilzomib use, but no new cases of PN occurred. The ORR of the 20/27 mg/m^2 40 patient cohort was similar to that in the pivotal US study. The dose was efficacious and tolerable in heavily pre-treated Japanese patients; however, meticulous control of hypertension may be necessary for further carfilzomib use.

Keywords: multiple myeloma, carfilzomib, hypertension peripheral neuropathy, cardiovascular AEs.

First published online 5 January 2016
British Journal of Haematology, 2016, **172,** 745–756
doi: 10.1111/bjh.13900

Graduate School of Medical Sciences, Nagoya, Japan

Received 14 September 2015; accepted for publication 6 November 2015
Correspondence: Dr Takashi Watanabe, Haematology Division, Komaki City Hospital, 1-20 Jobushi, Komaki, Japan.
E-mail: takawata@komakihp.gr.jp

Multiple myeloma (MM) is characterized by the abnormal accumulation of clonal plasma cells in the bone marrow. In the United States (US), an estimated 21 700 new cases of MM and 10710 deaths were predicted in 2012 (American Cancer Society 2012); in Japan, an estimated 6860 new cases of MM and 4066 deaths (http://ganjoho.jp/reg_stat/statistics/dl/) were predicted. Over the past decade, the introduction of immunomodulators, such as thalidomide and lenalidomide, and a proteasome inhibitor (PI) bortezomib (Velcade®, Millennium Pharmaceuticals, Cambridge, MA, USA) has significantly improved the overall survival (OS) of MM patients (Jemal *et al*, 2010).

Carfilzomib (Kyprolis®, Onyx Pharmaceuticals, an Amgen subsidiary, South San Francisco, CA, USA) is one of the second-generation epoxyketone PIs that can irreversibly inhibit chymotrypsin-like activity (Demo *et al*, 2007; Parlati *et al*, 2009). Carfilzomib induced apoptosis in myeloma cell lines and primary myeloma cells from patients whose disease was resistant to available therapies, including bortezomib (Kuhn *et al*, 2007). In addition, carfilzomib has fewer off-target effects, which may explain a lack of neurodegeneration *in vitro*, and less neurotoxicity in animal studies (Arastu-Kapur *et al*, 2011). Therefore, carfilzomib was expected to circumvent some of the clinical adverse events (AEs) of bortezomib, particularly peripheral neuropathy (PN) (Bruna *et al*, 2010; Arastu-Kapur *et al*, 2011).

In fact, PN did not appear to be clinically limiting for extended carfilzomib treatment (Vij *et al*, 2012a,b). An alternative subcutaneous route of administration for bortezomib reduced the incidence of PN without reducing efficacy (Moreau *et al*, 2011). Despite these facts, the subcutaneous administration of bortezomib has still caused gastrointestinal (GI) AEs in patients with MM (Moreau *et al*, 2011). Carfilzomib has also caused GI AEs; however, those occurring with carfilzomib use were mild and manageable with routine supportive care (Siegel *et al*, 2012; Vij *et al*, 2012b).

Almost all patients with MM will eventually relapse, and new treatment options are needed. Accordingly, to change the intrinsic natural behaviour of MM, it was suggested that the use of higher doses, combination regimens and early treatment of the disease course without AEs are required for the new treatment using carfilzomib (Reece, 2012). However, discontinuation or dose reduction was inevitable because of increased toxicities in some of the carfilzomib trials using combination therapies (Bringhen *et al*, 2014; Sonneveld *et al*, 2015).

In an open-label, phase 2 pilot study (PX-171-003-A0) of carfilzomib in 46 patients with relapsed/refreactory MM (RRMM), patients treated with carfilzomib 20 mg/m^2 achieved an overall response rate (ORR) of 16·7%, with manageable toxicities (Jaganath *et al*, 2012). The study was subsequently amended to include an expanded dosing cohort with a scheduled dose escalation from 20 to 27 mg/m^2 beginning in the second cycle (PX-171-003-A1 [003-A1]). In 003-A1, which included 266 patients with RRMM, the ORR was 23·7%; these results were the basis for the accelerated approval of carfilzomib by the US Food and Drug Administration (Siegel *et al*, 2012). In the present study, we used the same dose escalation schedule as 003-A1, with one exception: 27 mg/m^2 was started on Day 8 of Cycle 1. With this method, we carefully characterized the AEs of carfilzomib in a phase 1/2 single-agent carfilzomib study in Japanese patients with RRMM.

Methods

Study design

This was a multicentre, open-label phase 1/2 study (ONO-7057-01) in Japanese patients with RRMM. The safety, tolerability, efficacy, pharmacokinetics (PK) and pharmacodynamics of carfilzomib were examined in phase 1 for intravenously administered carfilzomib at doses of 15, 20 and 20/27 mg/m^2. Phase 2 examined the safety and efficacy of carfilzomib at the recommended dose determined in phase 1. The primary endpoint in phase 2 was the ORR. Secondary endpoints included the duration of response (DOR), Progression-free survival (PFS) and OS. It was planned that three or six patients for each cohort in phase 1 and 24 patients in phase 2 were enrolled. If dose-limiting toxicity (DLT) occurred in one of three patients, an additional three patients were enrolled; if the incidence of DLT was two of three patients or three of six patients, the previous dose level was used as the recommended dose in phase 2.

Eligibility

The main patient inclusion criteria were age ≥20 years and Eastern Cooperative Oncology Group (ECOG) performance status (PS) of 0–2. Patients were required to have relapsed myeloma and measurable disease (either serum M protein level of ≥5·0 g/l or urinary M protein of ≥0•2 g/24 h) responsive to at least one previous therapeutic regimen (≥25% of reduction in M or total protein) and refractory to their most recent therapy (disease progression either during treatment or within 60 days after therapy completion). Patients were to be exposed to at least three prior treatments, including bortezomib, an immunomodulatory agent (lenalidomide and/or thalidomide), an alkylating agent, a corticosteroid and anthracycline (except for patients ineligible or clinically unsuitable for transplantation). Patients were excluded if they had Grade ≥3 or Grade 2 PN with pain or a past history of interstitial lung disease (ILD), congestive heart failure (CHF) of New York Heart Association class ≥III, symptomatic myocardial ischaemia or uncontrolled conduction abnormalities.

This study was conducted in compliance with the Good Clinical Practice guidelines. The study protocol was approved by the Institutional Review Board of each institution, and written informed consent was obtained from each patient enrolled in this study.

Dose-limiting toxicity definition

DLT was defined as any of the following AEs in Cycle 1 that were at least possibly related to carfilzomib and met one of the following criteria: Grade 3 or 4 PN or Grade 2 PN with pain; Grade ≥3 non-haematological toxicities; Grade ≥3 nausea, vomiting or diarrhoea that was uncontrolled after an adequate administration of anti-emetic or anti-diarrhoeal medications; febrile neutropenia; Grade 4 neutropenia persisting for >8 days without using granulocyte-colony stimulating factor (G-CSF) for supportive therapy and Grade 4 thrombocytopenia that required platelet transfusion or was accompanied by bleeding. Administration of G-CSF was not permitted during the DLT evaluation period.

Treatment

Carfilzomib was intravenously administered for 10 min at doses of 15, 20 and 20/27 mg/m^2 on Days 1, 2, 8, 9, 15 and 16 of each 28-day cycle until withdrawal of consent, disease progression or the occurrence of unacceptable toxic effects. For the 20/27 mg/m^2 dosage, 20 mg/m^2 was dosed on Days 1 and 2 of Cycle 1 and escalated to 27 mg/m^2 on Day 8 of Cycle 1 and thereafter.

Oral or intravenous dexamethasone (4 mg) was administered before each dose of carfilzomib in Cycle 1 and thereafter if necessary as pre-medication to prevent infusion reactions. Intravenous and oral hydrations were also required during Cycle 1 and in subsequent cycles as needed. In Cycle 1, all patients were required to receive prophylactic antibiotics, and patients with a medical history of herpes infection received acyclovir.

Assessment of response and safety

The efficacy analysis set comprised all patients who received at least one dose of carfilzomib and had at least one assessment of efficacy or pharmacodynamics. The primary endpoint of phase 2 was the ORR based on central laboratory data according to the International Myeloma Working Group (IMWG) Uniform Response Criteria (Durie *et al*, 2006), including the minimal response (MR), as defined by the European Group for Blood and Marrow Transplantation criteria (Bladé *et al*, 1998). The ORR with 95% confidence interval (CI) was determined for each dose level. The investigational period ended when Cycle 6 was completed for all patients enrolled in the study, and subsequent cycles were included in the analysis for patients whose therapy lasted more than six cycles.

The safety analysis set comprised all patients who received at least one dose of carfilzomib, and all AEs were graded according to the National Cancer Institute Common Terminology Criteria for Adverse Events version 4•0 (http://evs.nci.nih.gov/ftp1/CTCAE/CTCAE_4·03_2010-06-14_QuickReference_8·5x11.pdf).

Pharmacokinetics and pharmacodynamics

Samples for determining the plasma concentrations of carfilzomib were collected on Days 1 and 16 of Cycle 1 before administration, 5 min after the start of administration, immediately before the completion of administration and 5, 15 and 30 min and 1, 2 and 4 h after administration was completed. Moreover, whole blood and peripheral blood mononuclear cells (PBMCs) were collected on Days 1, 2 and 8 of Cycle 1 and Day 1 of Cycle 2 before administration as well as at 1 h after administration was completed to analyse proteasome activity.

Statistical analyses

All statistical analyses were performed using SAS® version 9•3 (SAS Institute Inc., Cary, NC, USA). Two-sided 95% CI of the best ORR was determined according to Willson (1927) for evaluable patients whose best response was classified as stringent complete response (sCR), complete response (CR), very good partial response (VGPR) and partial response (PR).

The analysis of the ORR was performed in subgroups, defined by the patient baseline characteristics of age, sex, cytogenetics/fluorescence *in situ* hybridization (FISH) and International Staging System (ISS) for MM stage (Greipp *et al*, 2005) as exploratory analyses. Patients were classified as

having standard-risk or high-risk cytogenetic abnormalities, as defined by IMWG criteria (Munshi *et al*, 2011). High-risk cytogenetic markers included either del 13 or hypodiploidy by metaphase cytogenetic analysis and/or del 17p13, t(4;14), t(14;16) by interphase FISH. Hence, patients without these abnormalities were considered to be standard risk.

The ORR was estimated within each subgroup along with its 95% Wilson CI. The clinical benefit rate (CBR) is the percentage of patients whose best response was classified as CR, VGPR, PR and MR. The CBR was estimated along with its 95% Wilson CI. Analysis for time-to-event (PFS and OS) was performed by preparing Kaplan–Meier estimates of the median and plotting Kaplan–Meier curves. In addition, two-sided 95% CIs for the medians were estimated.

Results

Patients and characteristics

Fifty patients were enrolled from 15 centres in Japan between August 2011 and January 2014; patient characteristics are shown in Table I. The median age was 67 years (range, 48–81 years), and the median time from initial diagnosis to study entry was 4·7 years (range 1·6–12·6 years). Most patients had either immunoglobulin G- (70%) or immunoglobulin A-type (16%) myeloma, and 58% had ISS stage II or III at diagnosis. A significant proportion of patients (32%) had poor/unfavourable karyotypes, as determined by FISH analysis. The majority of patients (70%) had Grade 1 or 2 PN at baseline, and 40 of the 50 enrolled patients had past medical history of PN.

The patients had previously received a median of five (range 3–10) therapies, and 42% had previously received at least six therapies. All patients had received bortezomib and an immunomodulatory agent in previous regimens, and 48% had received at least two lines of bortezomib-containing regimens. Twenty (40%) patients had undergone autologous stem cell transplantation (ASCT) (Table I).

Dose escalation

Seventeen of the 50 patients enrolled in the study were enrolled in phase 1. Four patients, including one patient who was not evaluable for DLT, were enrolled in the 15 mg/m^2 cohort; no DLT was observed.

One of the first three patients experienced DLT (thrombotic microangiopathy, cardiomyopathy, hepatic disorder and sensorimotor disorder) in the 20 mg/m^2 cohort; therefore, an additional three patients were enrolled at this level. No further DLT was observed in the three patients; subsequently, no DLT was observed in a total of seven patients (including one who was not evaluable for DLT) enrolled in the 20/27 mg/m^2 cohort, thereby suggesting that a higher dose could reasonably be tested. However, 20/27 mg/m^2 was determined to be the recommended dose in phase 2 of this Japanese study at that time, considering the results in the previous carfilzomib studies conducted overseas (Siegel *et al*, 2012).

Efficacy

Fifty patients were included in the efficacy analysis set; the ORR was 20·0% and the CBR was 28·0% (Table II). In the 40 patients who received the 20/27 mg/m^2 dose, the ORR was 22·5% and the CBR was 27·5%. Subgroup analysis of the 20/27 mg/m^2 group demonstrated that the ORR was not affected by age and ISS stage (Table III). The comparison of the 20/27 mg/m^2 group in this study with that in the 003-A1 study (Siegel *et al*, 2012) showed that the results were similar (22·5% vs. 23·7%) (Table III). In the 20/27 mg/m^2 group, the median DOR was not reached (95% CI, 2·3 months–not reached), and the median PFS was 5·1 months (95% CI: 2·8–7·0 months), whereas the median OS was not reached (95% CI: 7·4 months–not reached) at the time of the data cut-off. The median follow-up times for PFS and OS were 6·0 months (95% CI: 5·8–6·7 months) and 6·5 months [95% CI: 6·0–7·2 months], respectively.

Safety

Fifty patients who received at least one dose of carfilzomib were included in the safety population. All patients experienced at least one AE, and 88% had at least one AE of Grade ≥3. All AEs encountered in ≥20% of the patients are shown in Table SI. The most commonly observed AEs were haematological toxicities, including lymphopenia (86%), thrombocytopenia (68%), anaemia (58%), neutropenia (56%) and leucopenia (50%). The most commonly observed AEs of Grade ≥3 were lymphopenia (68%), neutropenia (38%), anaemia (30%), thrombocytopenia (26%) and leucopenia (26%).

Although PN was observed in eight patients (16%), none were of Grade ≥3, and four of the eight patients had PN of Grade 1 or 2 at the baseline of the study. Moreover, all eight patients had a past history of PN before enrolment in the study (Table IV). According to the detailed analysis of the history of PN, 45 (90%) of 50 patients had experienced PN before they were enrolled in the study; however, PN in 10 of the 45 patients resolved before enrolment. Subsequently, four of the 10 patients encountered PN again after carfilzomib treatment (Patients 2, 3, 5 and 7 in Table IV). In total, eight (18%) of the 45 patients developed PN again after carfilzomib treatment and, of the 35 patients who had PN at baseline (Table I), carfilzomib exacerbated PN in three patients (6% of 50 enrolled patients, 8·6% of the 35 patients) (Patients 1, 4 and 6 in Table IV). In contrast, the remaining five patients who had never experienced PN before enrolment into the carfilzomib study did not develop PN after carfilzomib treatment. One patient who had Grade 2 PN of the lower extremities at baseline newly developed a trigeminal nerve

Table I. Patients' baseline characteristics.

Characteristic	15 mg/m^2 (n = 4)		20 mg/m^2 (n = 6)		20/27 mg/m^2 (n = 40)		Total (N = 50)	
Sex, *n* (%)								
Male	3	(75)	5	(83)	18	(45)	26	(52)
Median age, years (range)	67	(57–80)	71	(59–80)	66	(48–81)	67	(48–81)
ECOG PS, *n* (%)								
0	3	(75)	3	(50)	23	(58)	29	(58)
1	1	(25)	3	(50)	17	(43)	21	(42)
ISS stage*, *n* (%)								
I	2	(50)	2	(33)	12	(30)	16	(32)
II	1	(25)	3	(50)	14	(35)	18	(36)
III	1	(25)	1	(17)	9	(23)	11	(22)
Unknown	0	(0)	0	(0)	5	(13)	5	(10)
Ig subtype, *n* (%)								
IgG	3	(75)	1	(17)	31	(78)	35	(70)
IgA	1	(25)	5	(83)	2	(5)	8	(16)
IgD	0	(0)	0	(0)	2	(5)	2	(4)
Bence–Jones	0	(0)	0	(0)	5	(13)	5	(10)
Cytogenetic/FISH prognostic markers, *n* (%)								
Normal/Favourable	1	(25)	5	(83)	25	(63)	31	(62)
Unfavourable†	3	(75)	1	(17)	12	(30)	16	(32)
Unknown	0	(0)	0	(0)	3	(8)	3	(6)
Peripheral neuropathy, *n* (%)								
Grade 0	0	(0)	1	(17)	14	(35)	15	(30)
Grade 1	2	(50)	4	(67)	20	(50)	26	(52)
Grade 2	2	(50)	1	(17)	6	(15)	9	(18)
Previous lines of therapy, median (range)	5	(4–7)	6	(3–8)	5	(3–10)	5	(3–10)
≥6, *n* (%)	2	(50)	3	(50)	16	(40)	21	(42)
Baseline anti-hypertensive therapy, *n* (%)								
Yes	3	(75)	1	(17)	14	(35)	18	(36)
No	1	(25)	5	(83)	26	(65)	32	(64)
Previous therapy, *n* (%)								
Bortezomib	4	(100)	6	(100)	40	(100)	50	(100)
Immunomodulatory agent								
Lenalidomide	4	(100)	6	(100)	33	(83)	43	(86)
Thalidomide	2	(50)	4	(67)	23	(58)	29	(58)
Corticosteroid	4	(100)	6	(100)	40	(100)	50	(100)
Alkylating agent	4	(100)	6	(100)	40	(100)	50	(100)
Anthracycline	2	(50)	4	(67)	26	(65)	32	(64)
Stem cell transplantation	1	(25)	2	(33)	17	(43)	20	(40)

ECOG PS, Eastern Cooperative Oncology Group performance status; FISH, fluorescence *in situ* hybridization; Ig, immunoglobulin; ISS, International Staging System.

*At diagnosis.

†Includes either t(4;14), t(14;16) or del (17p).

disorder of Grade 1 during carfilzomib treatment, whereas the pre-existing PN was not aggravated by carfilzomib (Table IV). No ILD was observed.

We particularly highlighted cardiovascular and infectious AEs in this study, and the details are presented in Table V. In total, the occurrence rate of hypertension (HT) was low and similar to that reported in the previous study (17%) (Grade ≥3; 6%) (Vij *et al*, 2012a). In the present study, HT (10/50 patients; 20%) was relatively common among the cardiovascular AEs. Although HT (8%) of Grade ≥3 and cardiomyopathy (2%) of Grade ≥3 were observed, severe CHF was not reported. The AEs considered to be autonomic are also shown in Table SII, although they were mild, except HT. Among AEs of any grade, HT was the most commonly noted; moreover, as observed in four patients, HT was the only Grade ≥3 AE that was attributed to autonomic neuropathy.

With respect to infectious AEs, it is notable that nasopharyngitis and pharyngitis were relatively common, but the incidence of other infectious AEs was low, a finding

Table II. Best overall response.

	15 mg/m^2 (n = 4)		20 mg/m^2 (n = 6)		20/27 mg/m^2 (n = 40)		Total (N = 50)	
Best response, *n* (%)								
CR	0	(0)	0	(0)	0	(0)	0	(0)
VGPR	0	(0)	0	(0)	2	(5·0)	2	(4·0)
PR	1	(25·0)	0	(0)	7	(17·5)	8	(16·0)
MR	0	(0)	2	(33·3)	2	(5·0)	4	(8·0)
SD	1	(25·0)	1	(16·7)	16	(40·0)	18	(36·0)
PD	0	(0)	1	(16·7)	9	(22·5)	10	(20·0)
NE	2	(50·0)	2	(33·3)	4	(10·0)	8	(16·0)
ORR (≥PR), *n* (%)	1	(25·0)	0	(0)	9	(22·5)	10	(20·0)
CBR (≥MR), *n* (%)	1	(25·0)	2	(33·3)	11	(27·5)	14	(28·0)
DOR, median (95% CI), months	9·5	(NR–NR)	–	–	NR	(2·3–NR)	9·5	(2·3–9·5)
PFS, median (95% CI), months	2·8	(1·7–15·9)	11·1	(0·9–11·1)	5·1	(2·8–7·0)	5·1	(2·8–7·0)
OS, median (95% CI), months	17·9	(3·0–NR)	17·8	(3·4–23·4)	NR	(7·4–NR)	23·4	(10·3–NR)

CR, complete response; VGPR, very good partial response; PR, partial response; MR, minimal response; SD, stable disease; PD, progressive disease; NE, not evaluable; ORR, overall response rate; CBR, clinical benefit rate; DOR, duration of response; NR, not reached; PFS, progression-free survival; CI, confidence interval; OS, overall survival; NR, not reached.

Table III. Comparison of overall response rate in the 20/27 mg/m^2 cohort according to baseline characteristics.

	ONO-7057-01*			PX-171-003-A1†					
Characteristic	*n*	ORR	95% CI	*n*	ORR	95% CI	Odds ratio	95% CI	*P*-value‡
Overall	40	22·5	12·3–37·5	257	23·7	18·7–29·4	0·93	0·42–2·07	0·8640
Age									
<65 years	12	25·0	8·9–53·2	139	25·2	18·2–33·2	0·99	0·25–3·87	0·9890
≥65 years	28	21·4	10·2–39·5	118	22·0	14·9–30·6	0·97	0·35–2·63	0·9445
Sex									
Female	22	13·6	4·7–33·3	108	29·6	21·2–39·2	0·38	0·10–1·36	0·1232
Male	18	33·3	16·3–56·3	149	19·5	13·4–26·7	2·07	0·72–5·98	0·1720
Cytogenetics/FISH prognostic markers									
Normal/Favourable	25	28·0	14·3–47·6	158	22·8	16·5–30·1	1·32	0·51–3·40	0·5677
Unfavourable	12	16·7	4·7–44·8	71	29·6	19·3–41·6	0·48	0·10–2·36	0·3554
ISS stage									
I	12	25·0	8·9–53·2	76	31·6	21·4–43·3	0·72	0·18–2·91	0·6461
II	14	7·1	1·3–31·5	96	24·0	15·8–33·7	0·24	0·03–1·97	0·1547
III	9	33·3	12·1–64·6	78	17·9	10·2–28·3	2·29	0·51–10·26	0·2704

ORR, overall response rate; CI, confidence interval; FISH, fluorescence *in situ* hybridization; ISS, International Staging System.
*Present study. For the 20/27 mg/m^2 cohort, 20 mg/m^2 was dosed on Days 1 and 2 of Cycle 1 and escalated to 27 mg/m^2 on Day 8 of Cycle 1 and thereafter.
†Siegel *et al* (2012). The dose for Cycle 1 was 20 mg/m^2, which was escalated to 27 mg/m^2 on Day 1 of Cycle 2 and thereafter.
‡χ^2 test.

similar to those for the upper respiratory tract documented previously in patients treated with bortezomib (Shah *et al*, 2004; Teh *et al*, 2014a,b) and carfilzomib (31–34%) (Vij *et al*, 2012a,b). Regarding AEs of Grade ≥3, pneumonia, bronchopneumonia, viral pneumonia, staphylococcal infection and herpes virus infection were observed in one patient each in the study (Table V).

No AEs led to death during the administration period of carfilzomib or within 30 days after the final administration of carfilzomib. Eight patients (16%) discontinued treatment, and dosing was interrupted or reduced in 24 patients (48%) because of AEs. It is noteworthy that infection was the most frequent reason for the interruption of carfilzomib treatment. Of the 24 patients whose treatment was interrupted, 11 (46%) experienced viral or upper respiratory diseases, including one patient with flu, one with viral disease, eight with upper respiratory diseases and one with fever who was given an anti-inflammatory drug commonly used

Table IV. Patients with peripheral neuropathy under study treatment.

Patient No.	Dose level (mg/m^2)	Preferred terminology (Grade)	Baseline PN Grade	Worst PN Grade before the study
1	20	Peripheral neuropathy (2)	1	3
2	20/27	Peripheral neuropathy (1)	0	2
3	20/27	Peripheral sensory neuropathy (1)	0	2
4	20/27	Peripheral sensory neuropathy (2)	1	3
5	20/27	Peripheral sensory neuropathy (1)	0	2
6	20/27	Peripheral sensory neuropathy (2)	1	3
7	20/27	Peripheral sensory neuropathy (1)	0	1
8*	20/27	Trigeminal nerve disorder (1)	2	2

PN, peripheral neuropathy.
*Developed trigeminal nerve disorder during carfilzomib treatment. Patient had Grade 2 PN of the lower extremities at baseline, which was not aggravated by carfilzomib.

Table V. Adverse events related to cardiovascular disorders and infections of all grades or ≥Grade 3.

Dose (mg/m^2)	15 mg/m^2 (n = 4)		20 mg/m^2 (n = 6)		20/27 mg/m^2 (n = 40)		Total (N = 50)	
Patients Grade	All Grades	≥Grade 3	All Grades	≥Grade 3	All Grades	≥Grade 3	All Grades	≥Grade 3
Cardiovascular disorder								
Hypertension	2	0	2	0	6	4	10	4
Congestive Heart failure	0	0	0	0	2	0	2	0
Vascular pain	0	0	0	0	2	0	2	0
Hot flush	0	0	0	0	2	0	2	0
Atrioventricular block first degree	0	0	0	0	1	0	1	0
Palpitations	0	0	0	0	1	0	1	0
Dyspnoea*	0	0	0	0	1	0	1	0
Vasculitis	0	0	0	0	1	0	1	0
Troponin T increased	0	0	0	0	1	0	1	0
Orthostatic hypotension	1	0	0	0	0	0	1	0
Cardiomyopathy	0	0	1	1	0	0	1	1
Infections								
Nasopharyngitis	0	0	1	0	10	0	11	0
Pharyngitis	1	0	0	0	5	0	6	0
Gingivitis	1	0	0	0	1	0	2	0
Pneumonia	0	0	1	1	1	0	2	1
Bronchopneumonia	0	0	0	0	1	1	1	1
Influenza	0	0	0	0	1	0	1	0
Viral pneumonia	0	0	0	0	1	1	1	1
Upper respiratory tract infection	0	0	0	0	1	0	1	0
Enteritis infection	0	0	0	0	1	0	1	0
Lip infection	0	0	0	0	1	0	1	0
Oropharyngeal candidiasis	0	0	1	0	0	0	1	0
Staphylococcal infection	0	0	1	1	0	0	1	1
Herpes virus infection	0	0	1	1	0	0	1	1

*Dyspnoea is classified as a respiratory adverse event according to National Cancer Institute Common Terminology Criteria for Adverse Events (NCI-CTCAE) version 4·0 (http://evs.nci.nih.gov/ftp1/CTCAE/CTCAE_4·03_2010-06-14_QuickReference_8·5x11.pdf).

as a medicine for cold. In addition, three patients were believed to have infections leading to treatment interruption; these three patients included one patient with pneumonia and two with fever (of three events), for which levofloxacin or acetaminophen was prescribed. The treatment was interrupted in five other patients who developed neutropenia (of seven events).

Our findings indicate that carfilzomib 20/27 mg/m^2 is feasible for Japanese patients with RRMM.

Pharmacokinetics and pharmacodynamics

PK analyses were performed in a total of 17 patients in phase 1. The PK parameters for carfilzomib are shown in

Table SIII. The plasma carfilzomib concentration showed a rapid decrease after intravenous administration with terminal half-lives ($T_{1/2}$) of 0·424–0·706 h. In the dose range of 15–27 mg/m^2, the area under the plasma concentration–time curve from time 0 to the time of last quantifiable concentration (AUC_{last}) and maximum plasma concentration (C_{max}) increased in a dose-dependent manner. There was no trend toward increasing or decreasing the clearance and volume of distribution at steady state over the dose range. Following repeated doses of carfilzomib at 15 and 20 mg/m^2, the PK parameters were similar on Days 1 and 16. Although C_{max} was measured, the results were not compared with those of previous studies because the duration of intravenous administration of carfilzomib was 10 min in the present study and 2–10 min in the overseas studies (PX-171-007; Papadopoulos *et al*, 2013) Therefore, we concluded that there was no remarkable ethnic difference in the PK parameters of carfilzomib compared with the AUC_{last} and $T_{1/2}$ in PX-171-007.

For all dosing levels of carfilzomib, the proteasome activities in whole blood and PBMCs were reduced 1 h after administration on Days 1, 2 and 8 of Cycle 1 and on Day 1 of Cycle 2 with ≥80% inhibition. Furthermore, although proteasome activity in whole blood before the administration of carfilzomib on Day 1 of Cycle 2 slightly recovered (≥70% inhibition) because drug interruption was longer during this period than during other parts of the administration period, administration of carfilzomib resulted in a similar level of inhibition of proteasome activity. The level of inhibition was ≥80%, which was similar to that obtained in the overseas studies (Alsina *et al*, 2012).

Discussion

The present study aimed to evaluate the efficacy and safety of single-agent carfilzomib in Japanese patients with RRMM. The dose level did not reach the MTD, but the recommended dose in phase 2 was determined to be 20/27 mg/m^2 on the basis of the results of phase 1. The results of single-agent carfilzomib at a 20/27 mg/m^2 dose showed good responses in heavily pre-treated patients, with an ORR of 22·5% and a median PFS of 5·1 months.

A comparison of the 20/27 mg/m^2 group in this study with that in the pivotal US study (003-A1) (Siegel *et al*, 2012) showed that the results of the ORR were similar (22·5% and 23·7%, respectively), the median number of previous lines of therapy of the 20/27 mg/m^2 group of each study were the same and the proportion of patients with poor prognosis according to cytogenetic abnormalities was 30% in this study (Table I) and 28% in 003-A1. However, the median PFS was better in this study than in 003-A1 (5·1 months vs. 3·7 months, respectively). The following factors account for the difference: 1) no patients with ECOG PS 2 were enrolled in this study, whereas 13% of the enrolled patients in 003-A1 were PS 2, and 2) the median cumulative carfilzomib dose in this study was 796 mg/m^2 (range 80–1363 mg/m^2), which was much higher than the 470 mg/m^2 (range 20–2647 mg/m^2) in 003-A1. On the other hand, ethnic differences in the efficacy of carfilzomib did not seem to be significant, and both studies demonstrated good efficacy in patients with RRMM.

The incidences of PN were similar: PN of any grade occurred in 73/526 (13·9%) patients; Grade ≥3 PN occurred in seven (1·3%) patients in the integrated analysis of four phase 2 studies of single-agent carfilzomib (Siegel *et al*, 2013), whereas PN of any grade was encountered in eight (16·0%) patients and no patient developed PN of Grade ≥3 in the present study. In addition, of the 35 patients who had PN at baseline, carfilzomib aggravated PN in three patients (8·6%), which contrasts with the results of a previous study (Vij *et al*, 2012b). However, none of the patients who had not previously experienced PN developed new PN. There may be some patients who are prone to develop PN induced by PIs (Broyl *et al*, 2010; Corthals *et al*, 2011; Watanabe *et al*, 2013), and the choice of carfilzomib among PIs decreases the chance of encountering PN that hinders patients with MM from continuing to receive currently efficacious treatment or future treatment for RRMM.

Adverse effects of particular interest have been cardiac events, previously reported for single-agent carfilzomib treatment (Siegel *et al*, 2012; 2013). Aggregated cardiac AEs, including arrhythmia, CHF, ischaemic heart disease and cardiomyopathy, have been reported in 116 of 526 patients (22·1%), with 50 patients (9·5%) being Grade ≥3, in the integrated analysis (Siegel *et al*, 2013). However, in the present study, regarding Grade ≥3 cardiac AEs, only one (2·0%) patient in the 20 mg/m^2 cohort had cardiomyopathy, and no deaths occurred. Cardiotoxicities have been unexpectedly induced by PIs (Voortman & Giaccone, 2006; Orciuolo *et al*, 2007). In addition, unexplained deaths have been reported in the single-agent bortezomib study, which were attributed to CHF and sudden death, although they were regarded as probably not related to bortezomib (Richardson *et al*, 2009).

The previous integrated analysis reported that HT was documented in 14·3% and that more than half of those had a history of HT (Siegel *et al*, 2013). Although HT was more frequently recorded in our study (10 of 50 enrolled patients; 20%) than in the previous studies, four of the 10 patients were newly induced; however, in the remaining six patients who were prescribed hypertensive drugs before enrolment (Table SIV), HT was aggravated after carfilzomib treatment. As PIs have a potential to exacerbate impaired hypertensive states, blood pressure should be carefully monitored during the treatment, particularly in those who have a history of HT, and should be strictly controlled with additional anti-hypertensive drugs during carfilzomib treatment. It is noteworthy that there was a case reported in which the female patient developed severe CHF after bortezomib treatment, for which HT was the sole cardiovascular risk factor

(Bockorny *et al*, 2012); hence, we highlight this point. Moreover, intriguingly, in pressure-overload hearts of mice, it has been shown that proteasome activities in cardiomyocytes were depressed, resulting from cardiomyocyte apoptosis through the accumulation of pro-apoptotic proteins caused by impaired degradation, before the onset of cardiac dysfunction (Tsukamoto *et al*, 2006). Therefore, there is a great need for the pre-control of HT to mitigate the risk of cardiac toxicity, including heart failure, and control of HT is likely to be an important component of the successful management of MM patients treated with PIs.

GI disorders are caused by bortezomib; however, the rate of GI disorders was 21% lower for the subcutaneous administration of bortezomib than for intravenous administration, of which the incidence of diarrhoea was 12% lower (Moreau *et al*, 2011). The GI disorders may be ascribed to autonomic neuropathy (Mele *et al*, 2015) because it is a well-known fact that autonomic neuropathy is induced by bortezomib (Shah *et al*, 2004; Giannoccaro *et al*, 2011; Stratogianni *et al*, 2012; Mele *et al*, 2015); therefore, autonomic neuropathy may also account for PI-induced HT.

Although 222 (42·2%) and 67 (1·7%) patients experienced dyspnoea and pneumonia of any grade, respectively, in the integrated analysis (Siegel *et al*, 2013), only one (2·0%) and two (4·0%) of the patients in the present study experienced dyspnoea and pneumonia of any grade, respectively (Table V). The aetiology of dyspnoea remained unknown (Siegel *et al*, 2012) and has been debated (Siegel *et al*, 2013) because ILD was scarcely reported with regard to carfilzomib. Therefore, although dyspnoea was considered as pulmonary toxicity in the previous report (Siegel *et al*, 2013), it is more likely a symptom caused by pulmonary oedema owing to reversible acute left ventricular failure induced by PIs because it has been reported as a transient symptom that appeared on the day of or the day after carfilzomib dosing (Siegel *et al*, 2013). Consequently, in the present study, similar to a recent report (Sonneveld *et al*, 2015), we assumed dyspnoea to be a cardiovascular disorder (Table V) so that they would not be underestimated.

If carfilzomib can replace bortezomib as the mainstay of triple combination therapy (Jakubowiak *et al*, 2012; Niesvizky *et al*, 2013; Wang *et al*, 2013; Bringhen *et al*, 2014; Sonneveld *et al*, 2015; Stewart *et al*, 2015), it may be necessary to optimize the use of carfilzomib, although carfilzomib and lenalidomide combined with dexamethasone has an extremely compelling efficacy and is well tolerated (Stewart *et al*, 2015). To explain this, illustrative results of phase 1 or 2 carfilzomib trials using combination therapies were as follows: 1) a total of 33% of patients required carfilzomib dose reduction and 20% discontinued treatment because of AEs in combination with cyclophosphamide and dexamethasone for patients with newly diagnosed MM (Bringhen *et al*, 2014), 2) notably, a total of 31% of the patients enrolled in a dose-escalating study (up to 56 mg/m^2) of carfilzomib experienced at least one Grade ≥3 dyspnoea when combined with 300 mg/m^2 of cyclophosphamide and low-dose dexamethasone (Bensinger *et al*, 2014) and 3) furthermore, the rate of any cardiac-related AEs increased up to 19% with 5% Grade 3 after consolidation therapy following autologous stem cell transplantation in a phase 2 study, in which combination of carfilzomib, thalidomide and dexamethasone was used (Sonneveld *et al*, 2015). In this study, notably, only 59% of the patients were able to complete the original treatment schedule without either delays, reductions, interruptions or premature stoppage of carfilzomib during the induction therapy. Furthermore, a slower (30 min) infusion of carfilzomib was better tolerated and permitted the administration of higher doses (20/45 mg/m^2 or 20/56 mg/m^2) according to the dissociation constant (Kd); however, higher incidences of AEs were reported, including cough (40·9%), dyspnoea (31·8%) and HT (31·8%), with 13·6% of Grade ≥3as the most common non-haematological Grade ≥3 AE (Badros *et al*, 2013).

Moreover, because our study showed that lymphopenia was the most common (Grade ≥3, 68%), haematological AE (Table SI), in addition to upper respiratory disease being the most common reason for interruption of the treatment, additional care should be taken should carfilzomib be introduced into combination therapy in the future, particularly with pomalidomide and dexamethasone.

Lessons have been learned regarding the optimal administration of PIs from experiences with the use of the first-generation PI, bortezomib. Supportive care to avoid or prevent AEs induced by bortezomib and carfilzomib is important in continuous treatment with PIs (Delforge *et al*, 2010; Siegel, 2013). MM eventually develops resistance to all existing available therapies, and patients succumb to the disease (Kumar *et al*, 2012). Therefore, it is important to judiciously use PIs to reduce toxicities and to maintain the drug efficacy against currently existing MM in patients through a consecutive treatment of patients with MM through their life. To optimize the dose of carfilzomib, prescribing prophylactic drugs in advance for potential AEs in its earliest stages when toxicities are anticipated will be crucial for patients with MM to continue carfilzomib treatment and achieve more profound responses, which should prolong survival (Chanan-Khan & Giralt, 2010; Gay *et al*, 2011; Martínez-López *et al*, 2013).

In conclusion, in terms of safety, we did not find any clinically important ethnic differences in safety when carfilzomib was administered in a 20/27 mg/m^2 dosing regimen in Japanese MM patients. Although the PN rates with carfilzomib are low, it may worsen pre-existing PN. Cardiotoxicities were the major concern in previous carfilzomib studies, but they were less frequently observed in the present study; hypertensive status seemed to be exacerbated by the administration of carfilzomib and bortezomib, an affect that may be caused by PI-induced autonomic neuropathy. Therefore, we highlight the importance of managing AEs, including HT, by early treatment to alleviate PI-induced AEs so that

PI treatment can continue. With respect to efficacy, Japanese patients with RRMM achieved relatively longer PFS after higher total doses of carfilzomib than those administered in previous studies.

Acknowledgements

We thank all of the patients who participated in this study and their families as well as all investigators, physicians, nurses and clinical research coordinators who helped with this study. We would also like to thank Dr. Hirokazu Murakami (Gunma University Graduate School of Health Science, Maebashi) who was the medical consultant as well as Dr. Yutaka Ariyoshi (Aichi Cancer Centre Aichi Hospital, Okazaki), Dr. Chihiro Shimazaki (Japan Community Health care Organization Kyoto-Kuramaguchi Medical Centre, Kyoto), Dr. Masahiro Kizaki (Saitama Medical Centre, Saitama Medical University, Saitama), Dr. Takao Katoh (International University of Health and Welfare, Mita Hospital, Tokyo), Dr. Masashi Takahashi (Yujin-Yamazaki Hospital, Hikone) and Dr. Terufumi Kato (Kanagawa Cardiovascular and Respiratory Centre, Yokohama) for their strict review of the clinical data as members of the Efficacy and Safety Evaluation Committee. We also acknowledge the statistical support of Naokazu Gion (Ono Pharmaceutical Co., Ltd., Osaka) and critical review of the manuscript by Sanjay K. Aggarwal, G. Prabhakar Reddy, and Alan Hopkins (Onyx Pharmaceuticals, an Amgen subsidiary, South San Francisco). Editorial assistance was provided by SunFlare Co., Ltd. (Tokyo) and funded by Ono Pharmaceutical Co., Ltd. (Osaka). This study was supported by Ono Pharmaceutical Co., Ltd. (Osaka).

Author contributions

T. Watanabe performed the research and wrote this manuscript. Y. Shumiya and T. Kashihara designed the protocol and wrote the draft manuscript. K. Tobinai, M. Matsumoto, K. Suzuki, K. Sunami, T. Ishida, K. Ando, T. Chou, S. Ozaki, M. Taniwaki, N. Uike, H. Shibayama, K. Hatake, K. Izutsu, T. Ishikawa and S. Iida performed the research and contributed to the final version of the manuscript.

Conflict of interest

The authors declare the following: TW: personal fees from Celgene. K.K., Janssen Pharmaceutical K.K., Takeda Pharmaceutical Co., Ltd., Nippon Kayaku Co., Ltd., Eisai Co., Ltd., Nippon Shinyaku Co., Ltd., Daiichi Sankyo Co., Ltd., Zenyaku Kogyo Co., Ltd., outside the submitted work. KT: grants from Ono Pharmaceutical Co., Ltd., during the conduct of the study; grants and other funding from Eisai and Takeda; grants from Chugai Pharma, Kyowa Hakko Kirin, Celgene, Janssen Pharmaceuticals, GlaxoSmithKline, Mundipharma, SERVIER, Abbvie; other funding from Zenyaku Kogyo and Spectrum Pharmaceuticals, outside the submitted work. MM: personal fees from Celgene K.K., Janssen Pharmaceutical K.K. and Ono Pharmaceutical Co.,LTD, outside the submitted work. KS: No relevant financial relationship(s) to disclose. TI: grants and personal fees from TAKEDA, personal fees from CELGENE and JANSSEN, outside the submitted work. KA: No relevant financial relationship(s) to disclose. TC: Honoraria, lecture fee from Jansen Japan Pharmaceutical Co., Ltd., Celgene Japan Pharmaceutical Co., Ltd., BMS Japan Pharmaceutical Co., Ltd., Takeda Japan Pharmaceutical Co., Ltd., Chugai Japan Pharmaceutical Co., Ltd. SO: No relevant financial relationship(s) to disclose. MT: grants from Kyowa Hakko Kirin, Chugai Pharma, Janssen Pharma, Novartis, Bristol-Myers Squibb, Celgene, Pfizer Inc, Takeda Pharma, Asahikasei Pharma and Dainippon Sumitomo Pharma, outside the submitted work. NU: No relevant financial relationship(s) to disclose. HS: grants from Ono Pharmaceutical Company, during the conduct of the study; grants and personal fees from Celgene K.K. and Takeda Pharmaceutical Co. Ltd., personal fees from Janssen Pharmaceutical Co. Ltd. and grants from Bristol-Meyers Squibb Company, outside the submitted work. KH: No relevant financial relationship(s) to disclose. KI: grants from Ono Pharmaceutical Co. Ltd., during the conduct of the study; personal fees from Janssen Pharmaceutical K. K., Eisai Co., Ltd., Kyowa Hakko Kirin Co., Ltd., Takeda Pharmaceutical Co., Ltd., Genzyme Japan K. K., Celgene K. K., Shionogi & Co., Ltd., MSD K. K., Eli Lilly Japan K. K., Chugai Pharmaceutical Co., Ltd., Sumitomo Dainippon Pharma Co., Ltd., Nihon Servier Co. Ltd. and Zenyaku Kogyo Co., Ltd., grants and personal fees from Ono Pharmaceutical Co. Ltd., outside the submitted work. TI: No relevant financial relationship(s) to disclose. YS: Ono Pharmaceutical Co.,Ltd. employee (sponsor company). TK: Ono Pharmaceutical Co., Ltd. employee (sponsor company). SI: grants from Ono Pharmaceutical Co. Ltd., during the conduct of the study; grants and personal fees from Celgene K.K., Ono Pharmaceutical Co. Ltd. and Chugai Pharmaceutical Co. Ltd., personal fees from Janssen Pharmaceutical Company, Kyowa Hakko Kirin Inc., Eli Lilly Japan K.K., Bristol-Myers Squibb Company, Taiho Pharmaceutical Co., Ltd and Nippon Kayaku Co. Ltd., outside the submitted work.

Supporting Information

Additional Supporting Information may be found in the online version of this article:

Table SI. Adverse events (≥20%) of all grades or ≥Grade 3.

Table SII. Adverse events attributable to autonomic neuropathy.

Table SIII. Pharmacokinetic parameters.

Table SIV. Adverse event of hypertension.

References

Alsina, M., Trudel, S., Furman, R.R., Rosen, P.J., O'Connor, O.A., Comenzo, R.L., Wong, A., Kunkel, L.A., Molineaux, C.J. & Goy, A. (2012) A phase I single-agent study of twice-weekly consecutive-day dosing of the proteasome inhibitor carfilzomib in patients with relapsed or refractory multiple myeloma or lymphoma. *Clinical Cancer Research*, **18**, 4830–4840.

American Cancer Society (2012) Cancer Facts & Figures 2012. American Cancer Society Inc., Atlanta, GA, USA.

Arastu-Kapur, S., Anderi, J.L., Kraus, M., Parlati, F., Shenk, K.D., Lee, S.J., Muchamuel, T., Bennett, M.K., Driessen, C., Ball, A.J. & Kirk, C.J. (2011) Non-proteasomal targets of the proteasome inhibitors bortezomib and carfilzomib: a link to clinical adverse events. *Clinical Cancer Research*, **17**, 2734–2743.

Badros, A., Papadopoulos, K.P., Zojwalla, N., Lee, J.R.J. & Siegel, D.S.(2013) 30-minute infusion of carfilzomib plus dexamethasone in patients with relapsed and/or refractory multiple myeloma. (International Myeloma Workshop Meeting Abstracts), A278.

Bensinger, W.I., Vescio, R., Gasparetto, C., Camacho, E.S., Nath, R., Gomes, C.L., Smith, D.D., Shah, J.J. & Durie, B.G.M. (2014) A multi-center phase 1b, open-label, dose-finding pilot study to evaluate the combination of carfilzomib and cyclophosphamide with dexamethasone (CCyD) prior to autologous stem cell transplant (ASCT) in patients with transplant eligible newly diagnosed multiple myeloma. *Blood (ASH Annual Meeting Abstracts)*, **124**, A4739.

Bladé, J., Samson, D., Reece, D., Apperley, J., Björkstrand, B., Gahrton, G., Gertz, M., Giralt, S., Jagannath, S. & Vesole, D. (1998) Criteria for evaluating disease response and progression in patients with multiple myeloma treated by high-dose therapy and haemopoietic stem cell transplantation. *British Journal of Haematology*, **102**, 1115–1123.

Bockorny, M., Chakravarty, S., Schulman, P., Bockorny, B. & Bona, R. (2012) Severe heart failure after bortezomib treatment I a patient with multiple myeloma: a case report and review of the literature. *Acta Haematologica*, **128**, 244–247.

Bringhen, S., Petrucci, M.T., Larocca, A., Conticello, C., Rossi, D., Magarotto, V., Musto, P., Boccadifuoco, L., Offidani, M., Omedé, P., Gentilini, F., Ciccone, G., Benevolo, G., Genuardi, M., Montefusco, V., Oliva, S., Caravita, T., Tacchetti, P., Boccadoro, M., Sonneveld, P. & Palumbo, A. (2014) Carfilzomib, cyclophosphamide, and dexamethasone in patients with newly diagnosed multiple myeloma: a multicenter, phase 2 study. *Blood*, **124**, 63–69.

Broyl, A., Corthals, S.L., Jongen, J.L., van der Holt, B., Kuiper, R., de Knegt, Y., van Duin, M., el Jarari, L., Bertsch, U., Lokhorst, H.M., Durie, B.G., Goldschmidt, H. & Sooneveld, P. (2010) Mechanisms of peripheral neuropathy associated with bortezomib and vincristine in patients with newly diagnosed multiple myeloma: a prospective analysis of data from the HOVON-65/GMMG-HD4 trial. *Lancet Oncol*, **11**, 1057–1065.

Bruna, J., Udina, E., Alé, A., Vilches, J.J., Vynckier, A., Monbaliu, J., Silverman, L. & Navarro, X. (2010) Neurophysiological, histological and immunohistochemical characterization of bortezomib-induced neuropathy in mice. *Experimental Neurology*, **223**, 599–608.

Chanan-Khan, A.A. & Giralt, S. (2010) Importance of achieving a complete response in multiple myeloma, and the impact of novel agents. *Journal of Clinical Oncology*, **28**, 2612–2624.

Corthals, S.L., Kuiper, R., Johnson, D.C., Sonneveld, P., Hajek, R., van der Holt, B., Magrangeas, F., Goldschmidt, H., Morgan, G.J. & Avert-Loiseau, H. (2011) Genetic factors underlying the risk of bortezomib induced peripheral neuropathy in multiple myeloma patients. *Haematologica*, **96**, 1728–1732.

Delforge, M., Bladé, J., Dimopoulos, M.A., Facon, T., Kropff, M., Ludwig, H., Palumbo, A., Van Damme, P., San-Miguel, J.F. & Sonneveld, P. (2010) Treatment-related peripheral neuropathy in multiple myeloma: the challenge continues. *The Lancet Oncology*, **11**, 1086–1095.

Demo, S.D., Kirk, C.J., Aujay, M.A., Buchholz, T.J., Dajee, M., Ho, M.N., Jiang, J., Laidig, G.J., Lewis, E.R., Parlati, F., Shenk, K.D., Smyth, M.S., Sun, C.M., Vallone, M.K., Woo, T.M., Molineaux, C.J. & Bennett, M.K. (2007) Antitumor activity of PR-171, a novel irreversible inhibitor of the proteasome. *Cancer Research*, **67**, 6383–6391.

Durie, B.G., Harousseau, J.L., Miguel, J.S., Bladé, J., Barlogie, B., Anderson, K., Gertz, M., Dimopoulos, M., Westin, J., Sonneveld, P., Ludwig, H., Gahrton, G., Beksac, M., Crowley, J., Belch, A., Boccadoro, M., Cavo, M., Turesson, I., Joshua, D., Vesole, D., Kyle, R., Alexanian, R., Tricot, G., Attal, M., Merlini, G., Powles, R., Richardson, P., Shimizu, K., Tosi, P., Morgan, G. & Rajkumar, S.V. (2006) International uniform response criteria for multiple myeloma. *Leukemia*, **20**, 1467–1473.

Gay, F., Larocca, A., Wijermans, P., Cavallo, F., Rossi, D., Schaafsma, R., Genuardi, M., Romano, A., Liberati, A.M., Siniscalchi, A., Petrucci, M.T., Nozzoli, C., Patriarca, F., Offidani, M., Ria, R., Omede, P., Bruno, B., Passera, R., Musto, P., Boccadoro, M., Sonneveld, P. & Palumbo, A. (2011) Complete response correlates with long-term progression-free and overall survival in elderly myeloma treated with novel agents: analysis of 1175 patients. *Blood*, **117**, 3025–3031.

Giannoccaro, M.P., Donadio, V., Pèrez, C.G., Borsini, W., Stasi, V.D. & Liguori, R. (2011) Somatic and autonomic small fiber neuropathy induced by bortezomib therapy: an immunofluorescence study. *Neurological Sciences*, **32**, 361–363.

Greipp, P.R., San Miguel, J., Durie, B.G., Crowley, J.J., Barlogie, B., Bladé, J., Boccadoro, M., Child, J.A., Avet-Loiseau, H., Kyle, R.A., Lahuerta, J.J., Ludwig, H., Morgan, G., Powles, R., Shimizu, K., Shustik, C., Sonneveld, P., Tosi, P., Turesson, I. & Westin, J. (2005) International staging system for multiple myeloma. *Journal of Clinical Oncology*, **23**, 3412–3420.

Jaganath, S., Vij, R., Stewart, A.K., Trudel, S., Jakubowiak, A.J., Reiman, T., Somlo, G., Bahlis, N., Lonial, S., Kunkel, L.A., Wong, A.F. & Wang, M. (2012) An open-label single-arm pilot phase II study (PX-171-003-A0) of low-dose, single-agent carfilzomib in patients with relapsed and refractory multiple myeloma. *Clinical Lymphoma Myeloma Leukemia*, **12**, 310–318.

Jakubowiak, A.J., Dytfeld, D., Griffith, K.A., Lebovic, D., Vesole, D.H., Jagannath, S., Al-Zoubi, A., Anderson, T., Nordgren, B., Detweiler-Short, K., Stockerl-Goldstein, K., Ahmed, A., Jobkar, T., Durecki, D.E., McDonnell, K., Mietzel, M., Couriel, D., Kaminski, M. & Vij, R. (2012) A phase 1/2 study of carfilzomib in combination with lenalidomide and low-dose dexamethasone as a frontline treatment for multiple myeloma. *Blood*, **120**, 1801–1809.

Jemal, A., Siegel, R., Xu, J. & Ward, E. (2010) Cancer Statistics, 2010. *CA Cancer Journal for Clinicans*, **60**, 277–300.

Kuhn, D.J., Chen, Q., Voorhees, P.M., Strader, J.S., Shenk, K.D., Sun, C.M., Demo, S.D., Bennett, M.K., van Leeuwen, F.W.B., Chanan-Khan, A.A. & Orlowski, R.Z. (2007) Potent activity of carfilzomib, a novel, irreversible inhibitor of the ubiquitin-proteasome pathway, against preclinical models of multiple myeloma. *Blood*, **110**, 3281–3290.

Kumar, S.K., Lee, J.H., Lahuerta, J.J., Morgan, G., Richardson, P.G., Crowley, J., Haessler, J., Feather, J., Hoering, A., Moreau, P., LeLeu, X., Hulin, C., Klein, S.K., Sonneveld, P., Siegel, D., Bladé, J., Goldschmidt, H., Jagannath, S., San Miguel, J., Orlowski, R., Palumbo, A., Sezer, O., Rajkumar, S.V. & Durie, B.G.M. on behalf of the International Myeloma Working Group. (2012) Risk of progression and survival in multiple myeloma relapsed after therapy with IMiDs and bortezomib: A multicenter international myeloma working group study. *Leukemia*, **26**, 149–157.

Martínez-López, J., Fernández-Redonondo, E., García-Sánz, R., Montalban, M.A., Martínez-Sánchez, P., Pavia, B., Mateos, M.V., Rosiñol, L., Martin, M., Ayala, R., Martínez, R., Blanchard., M.J., Alegre, A., Besalduch, J., Bargay, J., Hernandez, M.T., Sarasquete, M.E., Sanchez-Godoy, P., Fernández, M., Blade, J., San Miguel, J.F. & Lahuerta, J.J. (2013) Clinical applicability and prognostic significance of molecular response assessed by fluorescent-PCR of immunoglobulin genes in multiple myeloma Results from a GEM/PETHEMA study. *British Journal of Haematology*, **163**, 581–589.

Mele, G., Coppi, M.R., Melpignano, A. & Quarta, G. (2015) Paralytic ileus following "*subcutaneous bortezomib*" therapy: focus on the clinical emergency-report of two cases. *Clinical and Experimental Medicine*. doi:10.1007/s10238-015-0337-6

Moreau, P., Pylypenko, H., Grosicki, S., Karamanesht, I., Leleu, X., Grishunina, M., Rekhtman, G., Masliak, Z., Robak, T., Shubina, A., Arnulf, B., Kropff, M., Cavet, J., Esseltine, D.L., Feng, H., Girgis, S., van de Velde, H., Deraedt, W. & Harousseau, J.L. (2011) Subcutaneous versus intravenous administration of bortezomib in patients with relapsed multiple myeloma: a randomised, phase 3, non-inferiority study. *The Lancet Oncology*, **12**, 431–440.

Munshi, N.C., Anderson, K.C., Bergsagel, P.L., Shaughnessy, J., Palumbo, A., Durie, B., Fonseca, R., Stewart, A.K., Harousseau, J.L., Dimopoulos, M., Jagannath, S., Hajek, R., Sezer, O., Kyle, R., Sonneveld, P., Cavo, M., Rajkumar, S.V., San Miguel, J., Crowley, J. & Avet-Loiseau, H. on behalf of the International Myeloma Workshop Consensus Panel 2 (2011) Consensus recommendations for risk stratification in multiple myeloma: report of the International Myeloma Workshop Consensus Panel 2. *Blood*, **117**, 4696–4700.

Niesvizky, R., Martin, T.G. III, Bensinger, W.I., Alsina, M., Siegel, D.S., Kunkel, L.A., Wong, A.F., Lee, S., Orlowski, R.Z. & Wang, M. (2013) Phase 1b dose-escalation study (PX-171-006) of carfilzomib, lenalidomide, and low-dose dexamethasone in relapsed or progressive multiple myeloma. *Clinical Cancer Research*, **19**, 2248–2256.

Orciuolo, E., Buda, G., Cecconi, N., Galimberti, S., Versari, D., Cervetti, G., Salvetti, A. & Petrini, M. (2007) Unexpected cardiotoxicity in haematological bortezomib treated patients. *British Journal of Haematology*, **138**, 396–397.

Papadopoulos, K.P., Burris, H.A. III, Gordon, M., Lee, P., Sausville, E.A., Rosen, P.J., Patnaik, A., Cutler, R.E. Jr, Wang, Z., Lee, S., Jones, S.F. & Infante, J.R. (2013) A phase I/II study of carfilzomib 2–10-min infusion in patients with advanced solid tumors. *Cancer Chemotherapy and Pharmacology*, **72**, 861–868.

Parlati, F., Lee, S.J., Aujay, M., Suzuki, E., Levitsky, K., Lorens, J.B., Micklem, D.R., Ruurs, P., Sylvain, C., Lu, Y., Shenk, K.D. & Bennett, M.K. (2009) Carfilzomib can induce tumor cell death through selective inhibition of the chymotrypsin-like activity of the proteasome. *Blood*, **114**, 3439–3447.

Reece, D.E. (2012) carfilzomib in multiple myeloma: gold, silver, or bronze? *Blood*, **120**, 2776–2777.

Richardson, P.G., Xie, W., Mitsiades, C., Chanan-Khan, A.A., Lonial, S., Hassoun, H., Avigan, D.E., Oaklander, A.L., Kuter, D.J., Wen, P.Y., Kesari, S., Briemberg, H.R., Schlossman, R.L., Munshi, N.C., Heffner, L.T., Doss, D., Esseltine, D.L., Weller, E., Anderson, K.C. & Amato, A.A. (2009) Single-agent bortezomib in previously untreated multiple myeloma: efficacy, characterization of peripheral neuropathy, and molecular correlations with response and neuropathy. *Journal of Clinical Oncology*, **27**, 3518–3525.

Shah, M.H., Young, D., Kindler, H.L., Webb, I., Kleiber, B., Wright, J. & Grever, M. (2004) Phase II study of the proteasome inhibitor bortezomib (PS-341) in patients with metastatic neuroendocrine tumors. *Clinical Cancer Research*, **10**, 6111–61118.

Siegel, D.S. (2013) From clinical trials to clinical practice: single-agent carfilzomib adverse events and their management in patients with relapsed and/or refractory multiple myeloma. *Therapeutic Advances in Hematology*, **4**, 354–365.

Siegel, D.S., Martin, T., Wang, M., Vij, R., Jakubowiak, A.J., Lonial, S., Trudel, S., Kureti, V., Bahlis, N., Alsina, M., Chanan-Khan, A., Buadi, F., Reu, F.J., Somlo, G., Zonder, J., Song, K., Stewart, A.K., Stadtmauer, E., Kunkel, L., Wear, S., Wong, A.F., Orlowski, R.Z. & Jagannath, S. (2012) A phase 2 study of single-agent carfilzomib (PX-171-003-A1) in patients with relapsed and refractory multiple myeloma. *Blood*, **120**, 2817–2825.

Siegel, D., Martin, T., Nooka, A., Harvey, R.D., Vij, R., Niesvizky, R., Badros, A.Z., Jagannath, S., McCulloch, L., Rajangam, K. & Lonial, S. (2013) Integrated safety profile of single-agent carfilzomib: experience from 526 patients enrolled in 4 phase II clinical studies. *Haematologica*, **98**, 1753–1761.

Sonneveld, P., Asselbergs, E., Zweegman, S., van der Holt, B., Kersten, M.J., Vellenga, E., van Marwijk-Kooy, M., Broyl, A., de Weerdt, O., Lonergan, S., Palumbo, A. & Lokhorst, H. (2015) Phase 2 study of carfilzomib, thalidomide, and dexamethasone as induction/consolidation therapy for newly diagnosed multiple myeloma. *Blood*, **125**, 449–456.

Stewart, A.K., Rajkumar, S.V., Dimopoulos, M.A., Masszi, T., Špička, I., Oriol, A., Hájek, R., Rosiñol, L., Siegel, D.S., Mihaylov, G.G., Goranova-Marinova, V., Rajnics, P., Suvorov, A., Niesvizky, R., Jakubowiak, A.J., San-Miguel, J.F., Ludwig, H., Wang, M., Maisnar, V., Minarik, J., Bensinger, W.I., Mateos, M.V., Ben-Yehuda, D., Kukreti, V., Zojwalla, N., Tonda, M.E., Yang, X., Xing, B., Moreau, P. & Palumbo, A. (2015) Carfilzomib, lenalidomide, and dexamethasone for relapsed multiple myeloma. *The New England Journal of Medicine*, **372**, 142–152.

Stratogianni, A., Tosch, M., Schlemmer, H., Weis, J., Katona, I., Isenmann, S. & Haensch, C.A. (2012) Bortezomib-induced severe autonomic neuropathy. *Clinical Autonomic Research*, **22**, 199–202.

Teh, B.W., Harrison, S.J., Pellegrini, M., Thursky, K.A., Worth, L.J. & Slavin, M.A. (2014a) Changing treatment paradigms for patients with plasma cell myeloma: Impact upon immune determinants of infection. *Blood Reviews*, **28**, 75–86.

Teh, B.W., Worth, L.J., Harrison, S.J., Thursky, K.A. & Slavin, M.A. (2014b) Risks and burden of viral respiratory tract infections in patients with multiple myeloma in the era of immunomodulatory drugs and bortezomib: experience at an Australian Cancer Hospital. *Supportive Care in Cancer*, doi:10.1007/s00520-014-2550-3

Tsukamoto, O., Minamino, T., Okada, K., Shintani, Y., Takashima, S., Kato, H., Liao, Y., Okazaki, H., Asai, M., Hirata, A., Fujita, M., Asano, Y., Yamazaki, S., Asanuma, H., Hori, M. & Kitakaze, M. (2006) Depression of proteasome activities during the progression of cardiac dysfunction in pressure-overloaded heart of mice. *Biochemical and Biophysical Research Communications*, **340**, 1125–1133.

Vij, R., Siegel, D.S., Jagannath, S., Jakubowiak, A.J., Stewart, A.K., McDonagh, K., Bahlis, N., Belch, A., Kunkel, L.A., Wear, S., Wong, A.F., Orlowski, R.Z. & Wang, M. (2012a) An open-label, single-arm, phase 2 study of single-agent carfilzomib in patients with relapsed and/or refractory multiple myeloma who have been previously treated with bortezomib. *British Journal of Haematology*, **158**, 739–748.

Vij, R., Wang, M., Kaufman, J.L., Lonial, S., Jakubowiak, A.J., Stewart, A.K., Kukreti, V., Jagannath, S., McDonagh, K.T., Alsina, M., Bahlis, N.J., Reu, F.J., Gabrail, N.Y., Belch, A., Matous, J.V., Lee, P., Rosen, P., Sebag, M., Vesole, D.H., Kunkel, L.A., Wear, S.M., Wong, A.F., Orlowski, R.Z. & Siegel, D.S. (2012b) An open-label, single-arm, phase 2 (PX-171-004) study of single-agent carfilzomib in bortezomib-naïve patients with relapsed and/or refractory multiple myeloma. *Blood*, **119**, 5661–5670.

Voortman, J. & Giaccone, G. (2006) Severe reversible cardiac failure after bortezomib treatment combined with chemotherapy in a non-small cell lung cancer patient: a case report. *BioMed Central Cancer*, **6**, 129.

Wang, M., Martin, T., Bensinger, W., Alsina, M., Siegel, D.S., Kavalerchik, E., Huang, M., Orlowski, R.Z. & Niesvizky, R. (2013) Phase 2 dose-expansion study (PX-171-006) of carfilzomib, lenalidomide, and low-dose dexamethasone in relapsed or progressive multiple myeloma. *Blood*, **122**, 3122–3128.

Watanabe, T., Mitsuhashi, M., Sagawa, M., Ri, M., Suzuki, K., Abe, M., Ohmachi, K., Nakagawa, Y., Nakamura, S., Chosa, M., Iida, S. & Kizaki, M. (2013) Phytohemagglutinin-induced IL2 mRNA in whole blood can predict bortezomib-induced peripheral neuropathy for multiple myeloma patients. *Blood Cancer Journal*, **3**, e150.

Willson, E.B. (1927) Probable inference, the law of succession, and statistical inference. *Journal of the American Statistical Association*, **22**, 209–212.

INTERNAL MEDICINE

□ CASE REPORT □

IgG4-related Disease with Bone Marrow Involvement

Akifumi Ichiki[1,2], Norisato Hashimoto[1], Tomoki Ueda[1], Shinichiro Hiraiwa[3], Takuma Tajiri[3], Naoya Nakamura[4], Kiyoshi Ando[2] and Kenji Yokoyama[1]

Abstract

A 61-year-old Japanese woman with anemia, submandibular gland swelling, and enlarged lymph nodes was diagnosed with IgG4-related disease (IgG4-RD) by lymph node biopsy. Bone marrow involvement of IgG4-RD was detected by 18F-fluorodeoxyglucose positron emission tomography/computed tomography (FDG-PET/CT) and immunohistochemically proven by bone marrow biopsy in this patient. Anemia progressed gradually, and prednisolone treatment was initiated. Anemia and submandibular gland swelling improved soon after prednisolone treatment was initiated. We report a rare case of IgG4-RD involving the bone marrow. FDG-PET/CT and bone marrow biopsy were useful for diagnosis in this case.

Key words: IgG4-related disease, bone marrow involvement, FDG-PET/CT

(Intern Med 55: 2295-2299, 2016)
(DOI: 10.2169/internalmedicine.55.6749)

Introduction

IgG4-related disease (IgG4-RD) is a relatively new identified disease entity, characterized by histologically proven lymphoplasmacytic infiltration with the involvement of abundant IgG4-positive plasma cells in multiple organs. Kamisawa et al. reported 8 patients with sclerosing pancreatitis with abnormally increased serum IgG4 concentrations (1). They demonstrated IgG4-positive plasma cell infiltration of multiple organs and first proposed a new entity of systemic IgG4-related autoimmune disease. Mikulicz's disease subsequently showed infiltration of IgG4-positive plasma cells in swelling salivary glands (2). Thus far the term IgG4-RD is widely used in those conditions (3). Symmetrical swelling of the lachrymal, parotid, or submandibular glands, autoimmune pancreatitis, and retroperitoneal fibrosis are known to be common features of IgG4-RD. The involvement of various organs, including the central nervous system, thyroid gland, lungs, biliary duct, liver, gastrointestinal tract, kidneys, prostate gland, and lymph nodes has also been reported (3), however, only a few cases of IgG4-RD with bone or bone marrow involvement have been reported and little is known about this manifestation (1, 4, 5). We herein report an IgG4-RD patient with bone marrow involvement that was detected by fluorodeoxy glucose-positron emission tomography (FDG-PET)/CT and immunohistochemically confirmed by a bone marrow biopsy.

Case Report

A 61-year-old Japanese woman was referred to Tokai University Hachioji Hospital due to submandibular swelling. She was well until 2 months previously, when anemia was diagnosed at a routine medical checkup. She subsequently experienced malaise and submandibular swelling. She was slightly anemic and bilateral submandibular gland swelling was observed at the initial visit. The cervical and bilateral axillar lymph nodes were also palpable. Laboratory studies revealed hemoglobin (10.1 g/dL), increased level of total protein (10.9 g/dL) and decreased albumin (2.7 g/dL). Total cholesterol was low, 86 mg/dL. Serum iron was low, 16 μg/dL, while ferritin was 38 ng/mL. IgG and IgG4 were increased to 5,496 mg/dL and 2,180 mg/dL, respectively. β2 microglobulin was high, 6.3 mg/L, and C-reactive protein was 0.184 mg/dL. Serum free light chain κ and λ were 458 mg/L and 289 mg/L, respectively, and monoclonal protein was not detected by immunoelectrophoresis (Table). An

[1]Department of Hematology/Oncology, Tokai University Hachioji Hospital, Japan, [2]Department of Hematology/Oncology, Tokai University School of Medicine, Japan, [3]Department of Pathology, Tokai University Hachioji Hospital, Japan and [4]Department of Pathology, Tokai University School of Medicine, Japan

Received for publication October 27, 2015; Accepted for publication November 30, 2015

Correspondence to Dr. Kenji Yokoyama, yk092750@tsc.u-tokai.ac.jp

Table. **Laboratory Data at the Diagnosis.**

WBC	4,300/μL	β2 microglobulin	6.3 mg/L
Seg	56.0%	CRP	0.184 mg/dL
Lymph	39.0%	IgG	5,486 mg/dL
Mono	1.0%	IgG4	2,180 mg/dL
Eosino	4.0%	IgA	151 mg/dL
RBC	3.41×10^6/μL	IgM	272 mg/dL
Hemoglobin	10.1 g/dL	Free light chain	
Platelet	222×10^3/μL	κ	458 mg/L
		λ	289 mg/L
Total protein	10.9 g/dL	κ/λ	1.58
Albumin	2.7 g/dL		
Total cholesterol	86 mg/dL	Immunoelectrophoresis	
BUN	11 mg/dL		
Creatinine	0.99 mg/dL		
LDH	139 U/L		
AST	14 U/L		
ALT	8 U/L		
Fe	16 μg/dL		
TIBC	261 μg/dL		
Ferritin	38 ng/mL		

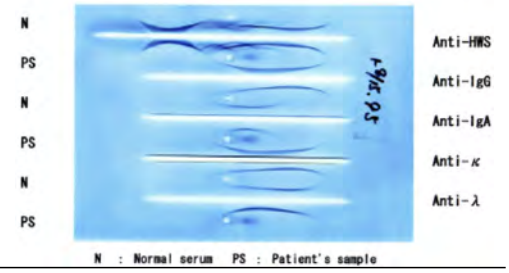

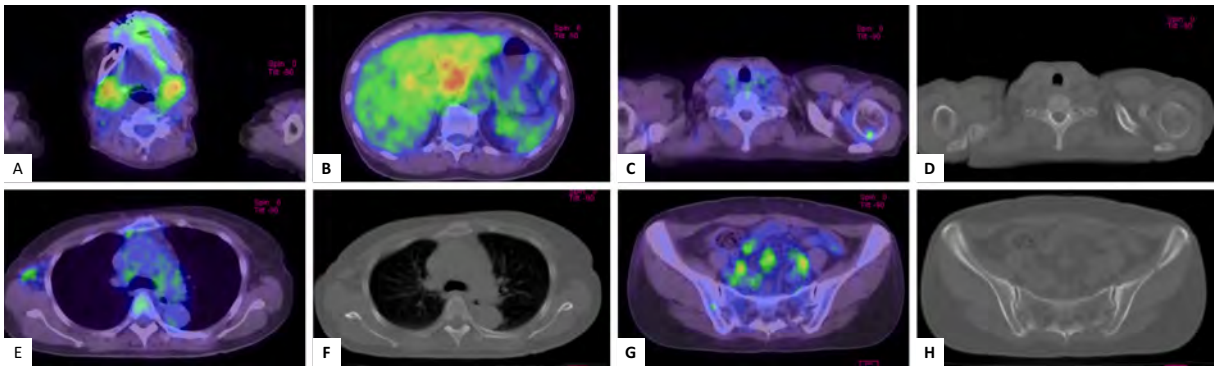

Figure 1. **FDG-PET/CT showed uptakes in multiple organs. (A) Bilateral submandibular glands, (B) Hepatic lymph nodes demonstrated the highest SUV max (6.3). Uptakes were also noted in the (C) left upper arm, (E) spine, and (G) iliac bone. (D, F, H) No lytic or sclerotic change was found on plain CT.**

FDG-PET/CT scan showed uptakes in the bilateral parotid gland, submandibular gland, and the cervical, axillar, paraaortic, mesentery, and inguinal lymph nodes (Fig. 1A, B). Although no lytic or sclerotic bone regions were observed on plain CT, uptakes were also detected in the upper arm, spine, and iliac bones (Fig. 1C-H). The highest uptake [standardized uptake value (SUV)max =6.3] was detected in the hepatic lymph nodes. Bone marrow aspiration and a biopsy and a biopsy of the right axillary lymph node were performed. No significant morphologic abnormalities were detected in myeloid, erythroid, or megakaryocyte lineage cells in the bone marrow aspiration materials. Plasma cells were increased to 5.3%, and 46.9% and 37.4% of CD38-positive cells expressed κ and λ chain, respectively, according to flow cytometry. The bone marrow karyotype was 46, XX and IgH-JH rearrangement was not detected by a Southern blot analysis. Biopsy specimens revealed normocellular marrow with mild infiltration of lymphocytes and plasma cells (Fig. 2A). CD138-positive plasma cells were scattered throughout the specimens, not clustered (Fig. 2B), and more than half of these cells were also positive for IgG4 (Fig. 2C). Short, thin reticulin fibers were observed in the bone marrow, but did not intersect to form a network. The lymph nodes showed reactive follicular hyperplasia and increasing plasma cells in the interfollicular area and outside of capsule (Fig. 3A-C). These plasma cells were positive for CD138 and IgG. More than half of these cells were positive for IgG4 (Fig. 3D-F). IgH-JH rearrangement was not detected by a Southern blot analysis using extracted DNA from lymph node mononuclear cells. According to these findings, a diagnosis of IgG4-RD was made. The patient was observed without medication, and her anemia progressed gradually. Her hemoglobin decreased to 7.1 g/dL 4 months later, and oral prednisolone 0.5 mg/kg/day was pre-

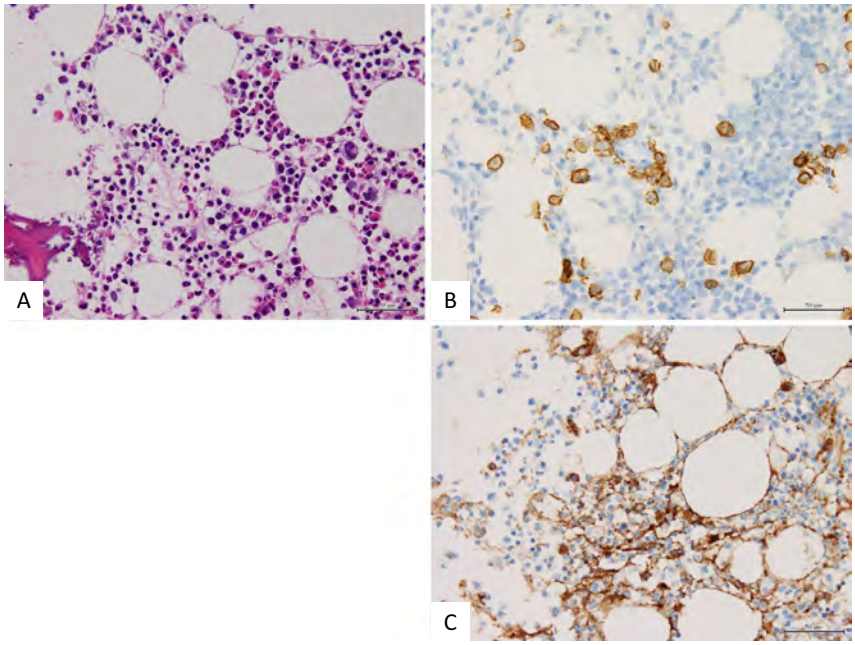

Figure 2. **Histopathological findings of the bone marrow. (A) Hematoxylin and Eosin staining. (B, C) Immunohistochemical findings of CD138 and IgG4, respectively. CD138- and IgG4-positive plasma cells were found in the bone marrow.**

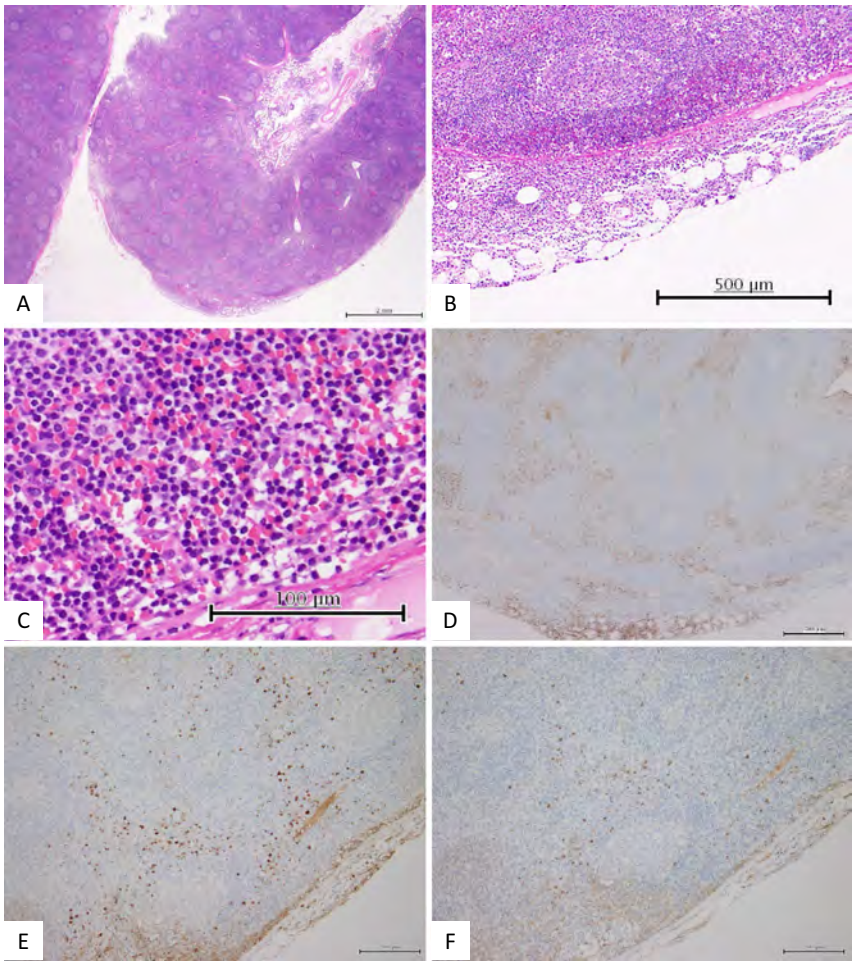

Figure 3. **Histopathological findings of the right axillar lymph node. (A, B, C) Hematoxylin and Eosin staining showed small lymphocytes and plasmacytes expanding into the interfollicular area. (D, E, F) Immunohistochemical findings of CD138, IgG, and IgG4, respectively, showed many of the interfollicular cells were CD138- and IgG-positive plasmacytes, and more than half of IgG-positive cells were also IgG4-positive.**

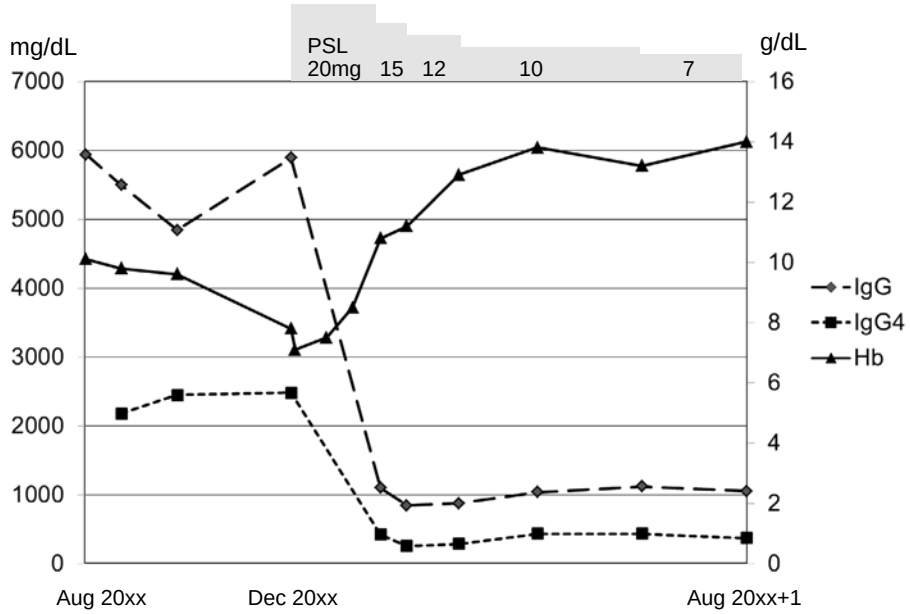

Figure 4. Clinical course. Four months after the diagnosis, treatment with 0.5 mg/kg of prednisolone was initiated due to the progression of anemia. Hemoglobin increased, and IgG and IgG4 decreased soon after initiating prednisolone treatment.

scribed. Her malaise improved soon after initiating prednisolone treatment, and 5 weeks later her IgG4 decreased to 421 mg/dL. Swelling of the parotid gland, submandibular gland, and lymph nodes disappeared, and her hemoglobin, albumin, and cholesterol increased to 10.8 g/dL, 3.4 g/dL, and 268 mg/dL, respectively (Fig. 4). Serum iron and ferritin increased to 88 μg/dL and 46.3 ng/mL, respectively, and β2 microglobulin decreased to 1.6 mg/L. The prednisolone dose was gradually decreased to 0.1 mg/kg/day, and the patient currently remains well.

Discussion

Our patient showed 18F-FDG uptakes in the spine, upper arm, and pelvic bones, suggesting bone marrow involvement of IgG4-RD. Bone marrow involvement was immunohistochemically confirmed according to the increased number of IgG4-positive cells in the bone marrow. FDG-PET/CT and a bone marrow biopsy are not always performed in IgG4-RD patients, and therefore the actual incidence of bone marrow involvement in IgG4-RD remains unknown. To the best of our knowledge, only a few cases of IgG4-RD with bone or bone marrow involvement have been reported. Kamisawa et al. demonstrated IgG4-positive plasma cell infiltration of the bone marrow in two patients with autoimmune pancreatitis (1). The distribution of IgG4-positive cells in the bone marrow of our patient was similar to that in the previously reported cases. Bittencourt et al. reported a patient with IgG4-RD of the temporal bone (4). Zen et al. reported a cross-sectional study of 114 IgG4-RD cases, the largest case series thus far, and none of the 35 patients with systemic IgG4-RD had radiographically or histologically confirmed bone or bone marrow involvement (6). IgG4-RD is characterized by multi-organ involvement, and biopsy specimens of suspected organs are often not easily obtained. Conventional imaging methods, such as ultrasonography, CT, and magnetic resonance imaging, also have limited value for detecting IgG4-RD organ involvement. FDG-PET/CT is commonly used in the field of clinical oncology, and several reports indicate that FDG-PET/CT is useful for diagnosing, assessing organ involvement, and monitoring the therapeutic response in Ig4-RD patients (5, 7-11). The FDG-PET/CT findings for 17 IgG4-RD patients were reported by Tokue et al. (7), 35 patients by Zhang et al. (8), and 8 patients by Takahashi et al. (9). None of these patients demonstrated a FDG uptake in the bone or bone marrow. Ebbo et al. retrospectively analyzed 21 IgG4-RD patients and reported only one patient with a diffuse FDG uptake in the bone marrow (5). FDG-PET/CT detected some localized bone marrow involvement in addition to submandibular gland and lymph node involvement in our patient.

Our patient had progressive anemia, severe hypocholesterolemia, and hypoalbuminemia at presentation, and these abnormalities improved soon after the initiation of prednisolone treatment. Anemia is rarely observed in IgG4-RD patients, and only one case report of a patient with IgG4-RD and autoimmune hemolytic anemia was found in the literature (12). We did not measure haptoglobin, however, both direct and indirect anti-globulin tests were negative in our patient, indicating that autoimmune hemolytic anemia was not the cause of anemia in our case. Although the number of IgG4-positive plasma cells increased in the bone marrow, erythroid progenitor cells were sparse, and the leukocytes and platelets were not found to have decreased in number, thus the patient's anemia was not likely due to bone marrow suppression caused by increased plasma cells. IgG4-RD is a

systemic inflammatory disease, therefore, it may cause anemia of chronic disorders, which is characterized by decreased serum iron, decreased total iron binding capacity, and increased ferritin (13). Although ferritin was not increased in the present patient, anemia was potentially due to anemia of a chronic disorder. The patient complained of mild bleeding from a hemorrhoid, which could result in underlying iron deficiency and decreased ferritin. Hypocholesterolemia and hypoalbuminemia might also reflect systemic inflammation in this patient. We did not measure erythropoietin, other inflammatory markers or cytokines, and therefore cannot confirm the mechanisms of anemia, hypocholesterolemia and hypoalbuminemia in this patient.

We herein reported a rare case of IgG4-RD with bone marrow involvement. FDG-PET/CT is useful for suspicious bone marrow involvement and it can be immunohistochemically confirmed by a bone marrow biopsy.

The authors state that they have no Conflict of Interest (COI).

References

1. Kamisawa T, Funata N, Hayashi Y, et al. A new clinicopathological entity of IgG4-related autoimmune disease. J Gastroenterol **38**: 982-984, 2003.
2. Yamamoto M, Takahashi H, Sugai S, Imai K. Clinical and pathological characteristics of Mikulicz's disease (IgG4-related plasmacytic exocrinopathy). Autoimmun Rev **4**: 195-200, 2005.
3. Umehara H, Okazaki K, Masaki Y, et al. A novel clinical entity, IgG4-related disease (IgG4RD): general concept and details. Mod Rheumatol **22**: 1-14, 2012.
4. Bittencourt A, Pereira LV, Cabral F Jr, et al. IgG4-related sclerosing disease of the temporal bone. Otol Neurotol **34**: e20-e21, 2013.
5. Ebbo M, Grados A, Guedj E, et al. Usefulness of 2-[18F]-fluoro-2-deoxy-D-glucose-positron emission tomography/computed tomography for staging and evaluation of treatment response in IgG 4-related disease: A retrospective multicenter study. Arthritis Care Res **66**: 86-96, 2014.
6. Zen Y, Nakamura Y. IgG4-related disease. A cross-sectional study of 114 cases. Am J Surg Pathol **34**: 1812-1819, 2010.
7. Tokue A, Higuchi T, Arisaka Y, et al. Role of F-18 FDG-PET/CT in assessing IgG4-related disease with inflammation of head and neck glands. Ann Nucl Med **29**: 499-505, 2015.
8. Zhang J, Hua C, Ma Y, et al. Characterizing IgG4-related disease with 18F-FDG-PET/CT: a prospective cohort study. Eur J Nucl Med Mol Imaging **41**: 1624-1634, 2014.
9. Takahashi H, Yamashita H, Morooka M, et al. The utility of FDG-PET/CT and other imaging techniques in the evaluation of IgG4-related disease. Joint Bone Spine **81**: 331-336, 2014.
10. Nakatani K, Nakamoto Y, Togashi K. Utility of FDG-PET/CT in IgG4-related systemic disease. Clin Radiol **67**: 297-305, 2012.
11. Lee LK, Sahani DV. Autoimmune pancreatitis in the context of IgG4-related disease: Review of imaging findings. World J Gastroenterol **20**: 15177-15189, 2014.
12. Hasegawa S, Mine S, Hagiwara S. IgG4-related disease combined with autoimmune hemolytic anemia and steroid-responsive transient hypercalcemia. Clin Med Insights Case Rep **8**: 51-55, 2015.
13. Bertero MT, Caligaris-Cappio F. Anemia of chronic disorders in systemic autoimmune diseases. Haematologica **82**: 375-381, 1997.

Int J Hematol (2016) 104:700–708
DOI 10.1007/s12185-016-2097-9

ORIGINAL ARTICLE

Japanese phase II study of rituximab maintenance for untreated indolent B-cell non-Hodgkin lymphoma with high tumor burden

Tadahiko Igarashi[1] · Michinori Ogura[2,17] · Kuniaki Itoh[3] · Masafumi Taniwaki[4] · Kiyoshi Ando[5] · Yoshiaki Kuroda[6,18] · Kazuhito Yamamoto[7] · Naokuni Uike[8,19] · Akihiro Tomita[9,20] · Hirokazu Nagai[10] · Mitsutoshi Kurosawa[11] · Shigeo Mori[12] · Shigeru Nawano[13] · Takashi Terauchi[14,21] · Yasuo Ohashi[15] · Kensei Tobinai[16]

Received: 3 July 2016 / Revised: 21 September 2016 / Accepted: 26 September 2016 / Published online: 6 October 2016

Abstract Recent large-scale randomized clinical trials in Europe and the US demonstrated that maintenance therapy with rituximab significantly improved the progression-free survival (PFS) in indolent B-cell non-Hodgkin lymphoma (B-NHL) patients, especially those with follicular lymphoma (FL). However, rituximab maintenance has not been approved in Japan, because there are no clinical data supporting the benefit of rituximab maintenance in Japanese patients. Therefore, we conducted a single-arm, multicenter bridging study in previously untreated indolent B-NHL patients with high tumor burden. The primary endpoint was 4-year PFS and was expected to be 70 % based on previous studies. Sixty-two patients, including 55 FL patients, were enrolled and received induction therapy with CHOP combined with rituximab (R-CHOP). Fifty-eight patients responding to R-CHOP induction received rituximab at 375 mg/m^2 every 8 weeks for 2 years as for the rituximab

✉ Tadahiko Igarashi
taigarash@gunma-cc.jp

[1] Division of Hematology/Oncology, Gunma Cancer Center, 617-1 Takabayashinishicho, Ohta 373-8550, Japan

[2] Department of Hematology and Oncology, Nagoya Daini Red Cross Hospital, Nagoya, Japan

[3] Department of Hematology, National Cancer Center Hospital East, Chiba, Japan

[4] Department of Hematology, Kyoto Prefectural University of Medicine, Kyoto, Japan

[5] Department of Hematology/Oncology, Tokai University School of Medicine, Kanagawa, Japan

[6] Department of Hematology, Hiroshima University School of Medicine, Hiroshima, Japan

[7] Department of Hematology and Cell Therapy, Aichi Cancer Center Hospital, Nagoya, Japan

[8] Department of Hematology, National Hospital Organization, Kyushu Cancer Center, Fukuoka, Japan

[9] Department of Hematology and Oncology, Nagoya University Graduate School of Medicine, Nagoya, Japan

[10] Department of Hematology, National Hospital Organization, Nagoya Medical Center, Nagoya, Japan

[11] Department of Hematology, National Hospital Organization, Hokkaido Cancer Center, Sapporo, Japan

[12] The University of Tokyo, Tokyo, Japan

[13] Department of Radiology, International University of Health and Welfare Mita Hospital, Tokyo, Japan

[14] Department of Diagnostic Radiology, National Cancer Center Hospital, Tokyo, Japan

[15] Faculty of Science and Engineering, Chuo University, Tokyo, Japan

[16] Department of Hematology, National Cancer Center Hospital, Tokyo, Japan

[17] Present Address: Department of Hematology, Tokai Central Hospital, Kakamigahara, Japan

[18] Present Address: Division of Stem Cell Regulation, Center for Molecular Medicine, Jichi Medical University, Tochigi, Japan

[19] Present Address: Department of Palliative Care, Saga Prefectural Hospital Koseikan, Saga, Japan

[20] Present Address: Department of Hematology, Fujita Health University School of Medicine, Toyoake, Japan

[21] Present Address: Department of Nuclear Medicine, Cancer Institute Hospital, Tokyo, Japan

maintenance arm in the PRIMA study. A 4-year PFS of 69.8 % was obtained (95 % confidence interval 55.9–80.0 %). Rituximab maintenance was well tolerated and common adverse events were infections, neutropenia, and/or leukopenia that were manageable with conventional supportive care. No patients died. These data were compatible with the PRIMA data. R-CHOP induction followed by rituximab is useful in Japanese patients with untreated indolent B-NHL having high tumor burden.

Clinical trial number UMIN000001191

Keywords Rituximab maintenance · Non-Hodgkin lymphoma · Phase II clinical trial · Progression-free survival

Introduction

Rituximab, an anti-CD20 chimeric monoclonal antibody, [1] has been used as monotherapy or in combination with chemotherapy for advanced indolent B-cell non-Hodgkin lymphoma (B-NHL). However, most indolent B-NHLs are incurable as the disease inevitably relapses. Several large-scale randomized clinical studies in Europe and the United States (US) have reported significant improvement in progression-free survival (PFS) with rituximab when used as maintenance therapy in patients with indolent B-NHL or follicular lymphoma (FL) who achieved responses by preceding induction therapy with chemotherapy alone or in combination with rituximab [2–7]. A prospective phase III study conducted by the European Organization for Research and Treatment of Cancer (EORTC) showed improved PFS in patients with recurrent/resistant FL who received rituximab maintenance treatment for 2 years following induction with rituximab in combination with CHOP (cyclophosphamide, doxorubicin, vincristine and prednisone) [2, 3]. The PRIMA (primary rituximab and maintenance) randomized phase III study also demonstrated an improvement in PFS with rituximab maintenance therapy in patients with previously untreated FL with high tumor burden, although no improvement in overall survival (OS) was seen in comparison with observation alone [8, 9].

While rituximab maintenance has already been approved in Europe and the US, it has been off-label in Japan because its efficacy and safety in Japanese patients have not yet been examined. Therefore, we conducted a non-randomized, single-arm, multicenter phase II study to evaluate whether rituximab maintenance is applicable to Japanese patients with previously untreated indolent B-NHLs bearing high tumor burden.

Materials and methods

Study design and patients

This open-label, single-arm multicenter phase II study between January 2009 and November 2013 was intended to evaluate the effectiveness of rituximab maintenance in Japanese indolent B-NHL with the Groupe d'Etude des Lymphomes Folliculaires (GELF) high tumor burden by comparing its efficacy and safety with those reported in the PRIMA study. All patients provided written informed consent prior to study entry. The study was approved by each institutional review board and was conducted according to the Declaration of Helsinki, Good Clinical Practice guidelines, and other related regulations. The trial was registered at the University Hospital Medical Information Network (No. UMIN000001191).

Patient eligibility

Study patients were aged 20–80 years, with previously untreated CD20-positive indolent B-NHL diagnosed by biopsy performed within 4 weeks of enrollment and classified into small lymphocytic lymphoma, lymphoplasmacytic lymphoma, splenic marginal zone B-cell lymphoma, extranodal marginal zone B-cell lymphoma of MALT type, nodal marginal zone B-cell lymphoma, or FL (grade 1, 2, or 3a), according to the WHO Classification of Tumours of Haematopoietic and Lymphoid Tissues [10]. Histology was later confirmed by a central pathology review committee consisting of three independent pathology experts. Eligible patients had to have a high tumor burden meeting at least one of the GELF criteria [11, 12]: bulky disease (one lesion >7 cm); presence of B symptoms; raised serum concentrations of lactate dehydrogenase or β2-microglobulin; involvement of three or more regional lymph nodes >3 cm; symptomatic splenic enlargement; and compressive syndrome, ascites or pleural effusion.

Patients were also required to have adequate organ function (bone marrow, liver, kidney, heart, and lung), a performance status (PS) of ≤2 on the Eastern Cooperative Oncology Group (ECOG) scale, and a life expectancy of at least 6 months at the time of study enrollment.

Patients with grade 3b FL or mantle cell lymphoma, histologically transformed from indolent B-NHL, central nervous system involvement, or any other active malignancy were excluded from the study. Patients were also excluded if they had human immunodeficiency virus infection, were sero-positive for hepatitis B virus or hepatitis C virus infection, had any underlying infectious disease or medical conditions known to affect life expectancy, had a previous history of monoclonal antibody therapy, or had

allergy or sensitivity to mouse-related proteins. Nursing or pregnant patients were also excluded.

Treatment schedule

Patients were assessed for their baseline characteristics prior to initial study treatment, including a physical examination, laboratory testing, and computed tomography (CT) assessment of tumor burden. In the induction phase of the study, patients were treated with rituximab and CHOP chemotherapy as follows: six cycles of standard CHOP therapy (cyclophosphamide 750 mg/m^2 i.v. on day 1; doxorubicin 50 mg/m^2 i.v. on day 1; vincristine 1.4 mg/m^2 [capped at 2 mg] i.v. on day 1; and prednisone 100 mg orally on days 1–5) and rituximab (375 mg/m^2) on day 1 of each CHOP cycle, with two additional infusions every 3 weeks after the last R-CHOP cycle. Patients who achieved a partial response (PR) or better after the induction phase stepped into the maintenance phase of the study, where patients received 12 infusions of rituximab monotherapy at 375 mg/m^2 i.v. once every 8 weeks, starting 8 weeks after the last induction treatment, for 2 years. After completion of rituximab maintenance, patients were followed for 18 months or until tumor progression, whichever was longer. Thus, the patients were studied up to 4 years (48 months, 192 weeks) from study entry until last observation. All patients received premedication with acetaminophen 400 mg and d-chlorpheniramine maleate 2 mg orally 30 min before each rituximab administration to minimize infusion-related reactions.

Patient evaluation and study endpoints

CT was used to assess tumor responses at study entry, after completion of induction therapy, and every 6 months during rituximab maintenance and during post-maintenance follow-up period. Tumor response was evaluated by a central CT review committee consisting of 3 radiologists according to the International Workshop NHL Response Criteria [13].

The primary endpoint of the study was the 4-year PFS rate from study entry. Secondary endpoints included the 4-year OS rate, overall response rate [ORR; complete response (CR) plus partial response (PR)] and CR rate at the end of maintenance therapy.

Adverse events (AEs) including abnormal laboratory values were assessed according to the Common Terminology Criteria for Adverse Events (CTCAE) version 3.0 from the Japan Clinical Oncology Group and the Japan Society of Clinical Oncology (JCOG/JSCO). All AEs observed were examined by extramural committee for severity and relationship to rituximab.

Statistical analysis

Based on previous studies, we expected to observe a 4-year PFS of 70 % with a two-sided 95 % confidence interval (CI) no lower than 50 % [2, 4, 8, 14–16]. A total of 50 patients were required to achieve at least 80 % power to show the expected 4-year PFS with two-sided 5 % significance in accordance with Fleming's one-stage procedure (e.g., $\alpha = 0.05$, $1 - \beta = 0.8$) [17]. We assumed that up to 8 patients (15 %) would be lost to follow-up and/or eligibility violation; thus, 58 patients were planned for enrollment.

All statistical analyses for efficacy were performed using the full analysis set (FAS, all enrolled patients). PFS and OS rates were estimated by the Kaplan–Meier method [18].

Baseline pretreatment factors affecting PFS were analyzed in FAS population by univariate and multivariate analysis using Cox proportional hazard regression model. The proportional hazard assumption was graphically checked using the log–log survival plot. The safety analysis population set was defined as patients who received at least one dose of rituximab.

SAS software version 9.2 (SAS Institute Inc., NC, USA) was used for all analyses. P values <0.05 were considered significant.

Results

Patient disposition and baseline characteristics

Figure 1 shows the patient disposition. Overall, 62 patients were enrolled and underwent induction therapy. Of these, 59 patients completed the 6 cycles of R-CHOP plus 2 additional cycles of rituximab monotherapy in the induction phase. Three patients were discharged during the course of induction therapy for the following reasons: one patient withdrew consent [this patient was later diagnosed as having diffuse large B-cell lymphoma (DLBCL) by central pathology review and was treated as a protocol violation]; treatment-related toxicity (prolonged leukopenia and neutropenia), $n = 1$; and serious deep venous thrombosis not related to rituximab, $n = 1$. All 59 patients who completed the induction therapy achieved PR or better tumor responses and stepped into the maintenance phase, except one patient who was positive for antibody against hepatitis B virus surface antigen (anti-HBs) and discharged from the study. Fifty-two of the 58 patients completed the maintenance phase and 6 patients discontinued the study because of lymphoma progression, $n = 4$; grade 3 AEs (back pain) not related to rituximab, $n = 1$; medical judgment because of ineligible pathology (diagnosed as having DLBCL by central pathology review), $n = 1$. Among 52 patients who

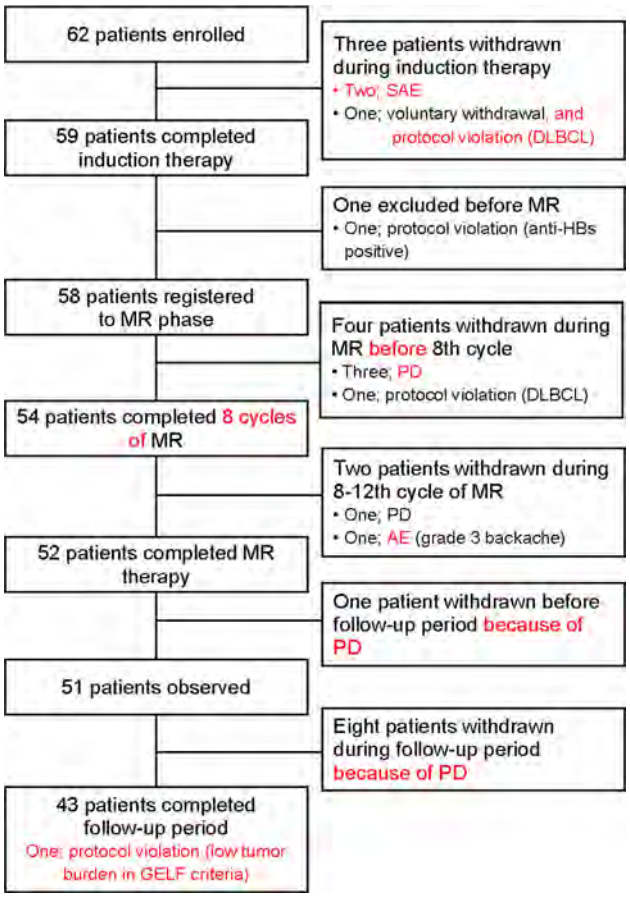

Fig. 1 Patient disposition. *MR* maintenance of rituximab therapy, *GELF* Groupe d'Etude des Lymphomes Folliculaires, *SAE* serious adverse event, *DLBCL* diffuse large B-cell lymphoma, *Anti-HBs* antibody against hepatitis B virus surface antigen, *PD* progressive disease, *AE* adverse event

completed rituximab maintenance, nine patients developed tumor progression and 43 patients completed 18 months of post-maintenance follow-up.

Table 1 shows baseline characteristics of the FAS. Sixty-one of 62 enrolled patients (98 %) fulfilled at least of one of the GELF high tumor burden criteria [11, 12]. Thirty-six patients (58 %) had bone marrow involvement. Fifty-two patients (84 %) had stage III or IV disease. The median age was 58.5 years (range 36–77 years). Baseline Follicular Lymphoma International Prognostic Index (FLIPI) scores categorized patients as low risk (zero-to-one risk factor) $n = 21$; intermediate risk (two risk factors) $n = 20$; and high risk (three-to-five risk factors) $n = 21$ [19]. Three patients were diagnosed as having composite lymphoma mixed with FL grade 3a and DLBCL by central pathology review, but were considered to be eligible by extramural review because they had an indolent clinical course correlated with FL, and thus, stayed in the study. Overall, 92 % (57/62) of patients enrolled had confirmed indolent B-NHL and 89 % (55/62) of patients had FL.

Table 1 Patient characteristics at baseline

	FAS, $n = 62$, (%)
Sex	
Female	33 (53)
Male	29 (47)
Age (years)	
Median	58.5
Range	36–77
Performance status (ECOG)	
0	48 (77)
1	13 (21)
2	1 (2)
Histopathology (WHO Classification)[a]	
Follicular, grade 1	23 (37)
Follicular, grade 2	25 (40)
Follicular, grade 3a	7 (11)
Nodal marginal zone	2 (3)
Diffuse large + Follicular	3 (5)
Diffuse large	2 (3)
Clinical stage (Ann Arbor)	
I	3 (5)
II	7 (11)
III	15 (24)
IV	37 (60)
B-symptom	
Absent	52 (84)
Present	10 (16)
LDH	
Normal	43 (69)
Elevated	19 (31)
Extra-nodal involvement	
Absent	51 (81)
Present	11 (19)
Bone marrow involvement	
Negative	26 (42)
Positive	36 (58)
Follicular Lymphoma International Prognostic Index	
Low	21 (34)
Intermediate	20 (32)
High	21 (34)

LDH lactate dehydrogenase, *ECOG* Eastern Cooperative Oncology Group, *FAS* full analysis set

[a] According to diagnosis by the central pathology review

Efficacy endpoints

Four-year PFS and 4-year OS from the date of enrollment were 69.8 % (95 % CI 55.9–80.0) and 100 %, respectively (Fig. 2a).

Table 2 shows the response rates after induction therapy and maintenance therapy. The ORR was 95.2 % (59/62;

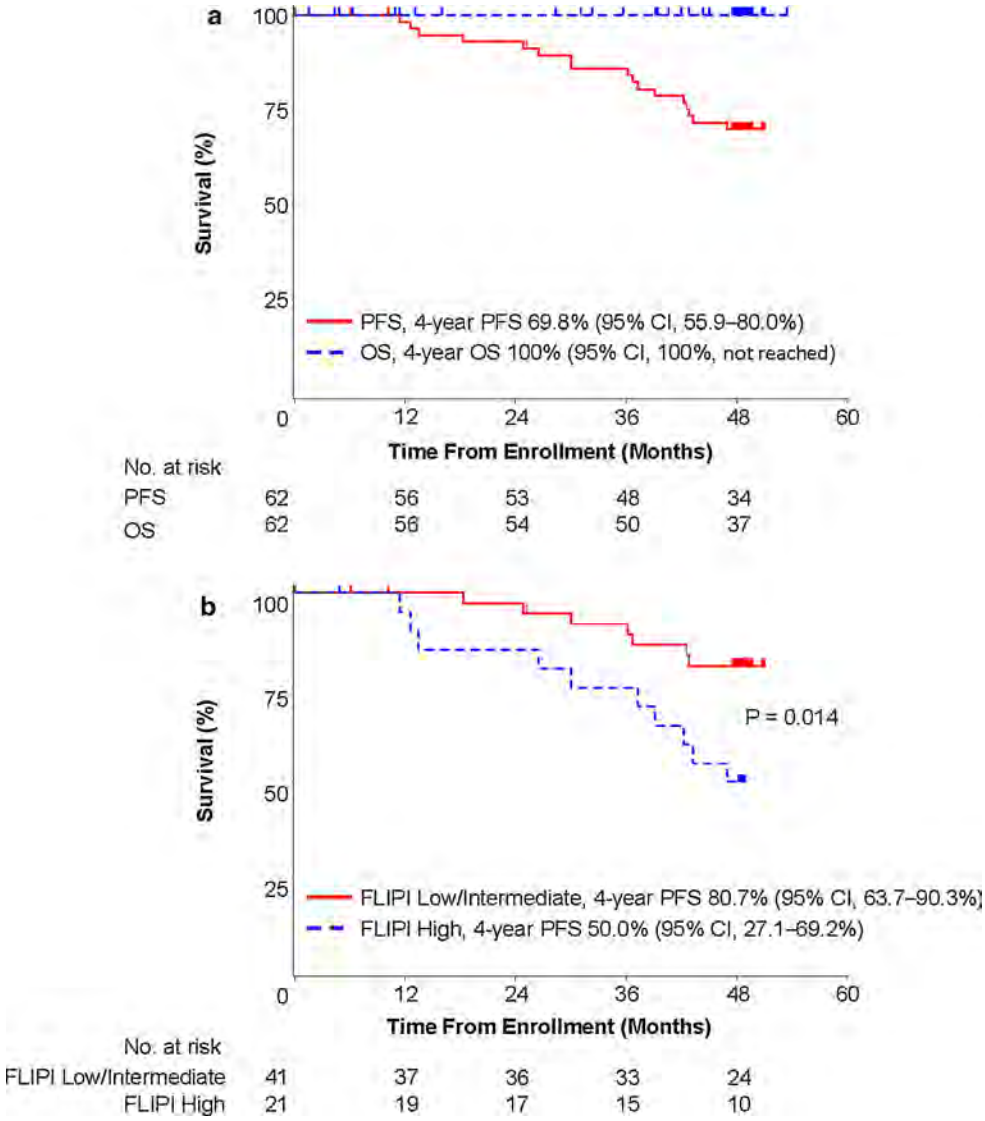

Fig. 2 Progression-free survival and overall survival. **a** PFS and OS. **b** PFS stratified by FLIPI score. *PFS* progression-free survival, *OS* overall survival, *FLIPI* Follicular Lymphoma International Prognostic Index, *CI confidence interval*. *P* = log-rank test

Table 2 Response to therapy

	n	No. of patients achieving response						Response rate (95 % CI)	
		CR	CRu	PR	SD	PD	NE	%ORR	%CR rate
After induction therapy									
Enrolled	62	38	0	21	1	0	2	95.2 % (86.5–99.0)	61.3 % (48.1–73.4)
After maintenance therapy									
Enrolled	58	45[a]	0	3	0	8	2	82.8 % (70.6–91.4)	77.6 % (64.7–87.5)

Response to induction therapy and maintenance therapy was evaluated after each therapy according to the International Workshop Criteria for Non-Hodgkin's Lymphoma

CI confidence interval, *CR* complete response, *CRu* complete response/unconfirmed, *NE* not evaluative because of insufficient follow-up, *ORR* overall response rate, *PD* progressive disease, *PR* partial response, *SD* stable disease

[a] Fourteen patients converted from PR to CR

95 % CI 86.5–99.0) after induction therapy and 82.8 % (48/58; 95 % CI 70.6–91.4) after maintenance therapy. Fourteen of 21 patients who achieved PR after induction therapy converted to CR during maintenance therapy. Sixteen patients experienced disease progression during the maintenance phase and follow-up period.

Factors affecting PFS

Baseline pretreatment factors affecting PFS were analyzed by univariate and multivariate analysis. In addition to conventional patient characteristics such as gender, ECOG PS, bone marrow involvement, extra-nodal involvement, and FLIPI score, we also selected the peripheral blood absolute lymphocyte count/absolute monocyte count ratio (ALC/AMC ratio) at study enrollment for analysis [20, 21]. As shown in Table 3 and Fig. 2b, PFS was significantly affected by FLIPI in both univariate and multivariate analyses, and patients in the low/intermediate-risk group had a significantly higher PFS rate over the 4-year period (80.7 %, 95 % CI 63.7–90.3) compared with the high-risk group (50.0 %, 95 % CI 27.1–69.2; $p = 0.014$; by log-rank test). By univariate analysis, PFS was significantly associated with ECOG PS, ALC/AMC ratio, and FLIPI score. As a result of the model selection by multivariate Cox proportional hazards regression analyses, FLIPI high risk was an independent unfavorable factor, whereas ECOG PS was not selected as a factor because of multicollinearity with FLIPI score.

Immunoglobulins

Serum concentrations of immunoglobulins (IgG, IgA, and IgM) that decreased from baseline during the induction and maintenance phase tended to recover during the follow-up period. Mean serum concentrations (mg/dL) of IgG/IgA/IgM at baseline, post-maintenance therapy, and after 2 years follow-up were 1,151/176/95, 798/104/44, and 828/133/53, respectively. No patients received supplemental immunoglobulins.

Other findings

One of 16 patients who experienced a recurrence/relapse had a histological transformation to high grade B-NHL from FL grade 3a. Peripheral blood $CD19^+$ and $CD20^+$ cells were immediately depleted after the first cycle of induction treatment, and depletion persisted through the maintenance phase. The depleted $CD19^+$ and $CD20^+$ cells remained nearly undetectable until approximately 12 months after the end of the maintenance phase, and then gradually recovered. Development of human anti-CD20 antibodies (HACA) was examined in 58 patients but was not detected throughout the study.

Safety analysis

Safety was assessed for all 62 patients who received at least one infusion of rituximab. A total of 7,018 AEs including laboratory value abnormalities were observed throughout the study (4230 events in induction phase, 2119 in maintenance phase, and 669 in follow-up period). Of these, 477 were grade 3 or 4 in severity, but no grade 5 (death) events were reported.

Table 4 shows the AEs of grade 3 that occurred in two or more patients and all AEs of grade 4. Most grade 3 or 4 AEs were hematological toxicities represented by leukopenia/neutropenia and were more frequently observed during the induction phase than during the maintenance phase

Table 3 Prognostic factors affecting PFS

Factor	Factor levels	*n*	Univariate analysis			Multivariate analysis		
			HR[a]	95 % CI	*P*[a]	HR[b]	95 % CI	*P*[b]
Sex	Male	29						
	Female	33	1.14	0.43–3.00	0.790	0.86	0.31–2.39	0.778
ECOG performance status	0	48						
	1,2	14	4.35	1.67–11.33	0.003	–	–	–
ALC/AMC ratio	<4.7	39						
	4.7 or more	23	0.27	0.08–0.95	0.042	0.37	0.10–1.36	0.133
Bone marrow involvement	Negative	26						
	Positive	36	0.93	0.36–2.45	0.886	0.66	0.23–1.91	0.446
Extra-nodal involvement	Absent	51						
	Present	11	1.62	0.53–4.97	0.400	1.81	0.55–5.93	0.329
FLIPI	Low or Intermediate risk	41						
	High risk	21	3.14	1.20–8.26	0.020	2.91	1.01–8.40	0.049

ECOG PS. FLIPI Follicular Lymphoma International Prognostic Index, *ALC/AMC ratio* the absolute lymphocyte count/absolute monocyte count ratio at enrollment, *ECOG* Eastern Cooperative Oncology Group, *CI* confidence interval

[a] Results of univariate hazard ratio (HR) analyzed by Cox regression model

[b] Results of multivariate hazard ratio analyzed by Cox regression model

Table 4 Grade 3 or greater hematological and non-hematological adverse events

Toxicity	During induction therapy ($n = 62$)		During maintenance therapy ($n = 58$)		During follow-up period ($n = 51$)	
	Grade 3[a]	Grade 4	Grade 3[a]	Grade 4	Grade 3[a]	Grade 4
Neutropenia	6 (10 %)	50 (81 %)	5 (9 %)	5 (9 %)	2 (4 %)	1 (2 %)
Leukopenia	29 (47 %)	22 (35 %)	3 (5 %)	0 (0 %)	0 (0 %)	0 (0 %)
Decreased CD4 + cells	2 (3 %)	0 (0 %)	7 (12 %)	0 (0 %)	0 (0 %)	0 (0 %)
Febrile neutropenia	11 (18 %)	1 (2 %)	0 (0 %)	0 (0 %)	0 (0 %)	0 (0 %)
Infections	3 (5 %)	0 (0 %)	3 (5 %)	0 (0 %)	0 (0 %)	0 (0 %)
Deep venous thrombosis	2 (3 %)	0 (0 %)	0 (0 %)	0 (0 %)	0 (0 %)	0 (0 %)
Back pain	2 (3 %)	0 (0 %)	0 (0 %)	0 (0 %)	0 (0 %)	0 (0 %)
Body weight decreased	2 (3 %)	0 (0 %)	0 (0 %)	0 (0 %)	0 (0 %)	0 (0 %)
Anaphylactoid reaction	0 (0 %)	1 (2 %)	0 (0 %)	0 (0 %)	0 (0 %)	0 (0 %)
Lung adenocarcinoma	0 (0 %)	0 (0 %)	0 (0 %)	0 (0 %)	0 (0 %)	1 (2 %)

Hematological toxicity was evaluated according to the Common Terminology Criteria for Adverse Events (CTCAE) version 3.0 by Japan Clinical Oncology Group and Japan Society of Clinical Oncology (JCOG/JSCO)

Only grade ≥3 hematological and non-hematological adverse events observed during the induction, maintenance therapy and follow-up period (for 18 months after the last rituximab infusion) are listed in this table

[a] Adverse events of grade 3 that occurred in two or more patients

and follow-up period. Nine of 12 patients who developed grade 3 or 4 febrile neutropenia during induction treatment received G-CSF. Four patients with grade 3 or 4 leukopenia/neutropenia during maintenance or follow-up received G-CSF (three patients during maintenance and one patient during maintenance and follow-up period).

Grade 3 or 4 non-hematologic toxicities were also frequently observed during the induction phase. Infections were the most common AEs and were observed in 52 patients throughout the study. Most infections were of grade 1 or 2 in severity, and grade 3 infections were neutropenic infection, cystitis, herpes simplex, pneumonia, pulmonary mycosis, pyelonephritis, and disseminated herpes zoster. Secondary malignancy, lung adenocarcinoma stage IA was found in one patient who received CT examination for assessment of lymphoma response during the follow-up period, for which endoscopic excision was applied and removed successfully.

Twenty-nine serious adverse events (SAEs) were reported in 19 patients; of these, 18 SAEs were suspected to be treatment-related. All treatment-related AEs and SAEs were recovered and remitted. One patient discontinued the study because of treatment-related toxicity (prolonged neutropenia during induction treatment). No deaths were reported in this study.

Discussion

We conducted a multicenter phase II study of rituximab maintenance in Japanese patients with newly diagnosed indolent B-NHL having GELF high tumor burden, with reference to the PRIMA study. Our study design was similar to the PRIMA study in terms of patient eligibility and treatment schedule, and we expected to obtain a 4-year PFS of 70 % starting from study enrollment in accord with previous rituximab maintenance studies in the Europe and US and R-CHOP combination study in Japan [2, 4, 8, 14–16].

Sixty-two patients were enrolled and 43 patients were free from progression at 4-years yielding 69.8 % (95 % CI 55.9–80.0 %) of 4-year PFS as originally expected. In the PRIMA study, a PFS of 74.9 % was obtained with a median follow-up of 36 months from initiation of rituximab maintenance in FL patients [8]. Considering that 88.7 % (55/62) of our patients had FL, the 4-year PFS we observed in our study is comparable to that in the PRIMA study [8]. The 4-year PFS of 70 % in the current study is longer than that reported in a previous R-CHOP study without rituximab maintenance in Japan [22]. An ORR of 95.2 % with CR rate of 61.3 % was obtained after R-CHOP induction therapy. These responses are consistent with the results of a US study of low-grade or follicular B-NHL patients receiving R-CHOP [23] and our previous study in which an ORR of 94 % with CR rate of 66 % was obtained [14]. Fourteen of 21 patients (67 %) who achieved PR after induction treatment converted to CR during maintenance in our study, similar to the PRIMA study in which 72/139 patients (52 %) converted from PR to CR [8]. Thus, our findings, taken together with previous studies, suggest that maintenance use of rituximab after first-line remission induction is useful to prolong PFS in Japanese patients.

Despite the superior PFS with the addition of rituximab maintenance therapy compared with the standard induction treatment for advanced indolent B-NHL, it remains unclear whether there is a benefit in terms of OS. The OS in the PRIMA study was approximately 90 % in both the observation and rituximab maintenance arms, and was not statistically different between the arms [8]. Because indolent B-NHL has a relatively slow-growing nature with a decade-long life expectancy, a longer follow-up period is necessary to observe the effects of rituximab maintenance on OS [9].

Safety of rituximab maintenance observed in our study was also consistent with that reported in the PRIMA study. In our current study, hematological toxicities and infections were commonly observed and 72 % of patients developed infections or infestations of any grade during the maintenance period. In the PRIMA study, infections were reported to be the most common AEs and grade 2–4 infections were significantly more common in the rituximab maintenance arm (39 %) than in the observation arm (24 %). Frequencies of grade 3/4 infections were similar between our study and PRIMA (5 and 4 %, respectively). Because we routinely employed sulfamethoxazole/trimethoprim as prophylaxis for *Pneumocystis jirovecii* infection in the induction phase (82 % in all patients) and afterwards by investigator direction, no *P. jirovecii* infections were observed in our study. All observed treatment-related AEs were manageable with standard supportive therapy and did not prevent the continuation of study treatment.

There was no difference in terms of secondary malignancies in the rituximab maintenance and observation arms in the PRIMA study [8]. Similarly, we observed only one case of lung adenocarcinoma during the follow-up period, and this patient underwent successful surgical resection for lung cancer.

Pretreatment factors affecting PFS in the present study included FLIPI, ECOG PS, and ALC/AMC ratio by univariate analysis. Only a high FLIPI score was independently associated with a shorter PFS by multivariate analysis. This result is consistent with analyses reported by the PRIMA study and other studies [8, 24]. The primary limitations of this study were its relatively small size and non-randomized design. However, the prospective nature of the trial, its long maintenance phase and follow-up period, as well as the consistency of the efficacy and safety results with those of several large-scale, randomized trials, including PRIMA and several other European and US studies, support the validity of our findings.

However, it remains unclear whether indolent B-NHL patients with low tumor burden and patients with non-FL could also benefit from rituximab maintenance, and this should be addressed by further investigations.

In conclusion, R-CHOP induction therapy followed by 2 years of rituximab maintenance every 8 weeks is a useful therapeutic option in Japanese patients with untreated indolent B-NHL with high tumor burden as defined by GELF criteria, with a 4-year PFS of nearly 70 %. The treatment regimen was feasible for routine practice, was well tolerated, and is also applicable to Japanese patients.

Acknowledgments This study was supported by Zenyaku Kogyo (Tokyo, Japan). The authors thank the patients and their families and all the investigators, including the physicians, nurses, clinical research coordinators (CRC), and laboratory technicians in the participating institutions of this multicenter trial. The authors are grateful to Drs K. Toyama (Tokyo Medical College, Tokyo, Japan), N. Horikoshi (Juntendo University School of Medicine, Tokyo, Japan), and M. Mori (Japanese Red Cross Medical Center, Tokyo, Japan) for their critical review of the clinical data as members of the Independent Data and Safety Monitoring Committee. The authors are also grateful to Drs S. Nakamura (Nagoya University Graduate School of Medicine, Nagoya, Japan), and Y. Matsuno (Hokkaido University Hospital, Sapporo, Japan) for their histopathological review as members of the Central Pathology Review Committee, and M. Matsusako (St. Luke's International Hospital, Tokyo, Japan) for their central radiological review as members of the CT Review Committee. The authors also acknowledge K. Endo, H. Harada, T. Ito, I. Okugaito, M. Watanabe, M. Abe, T Oba, S. Kamiyama, and T. Kayo (Zenyaku Kogyo) for their help with data collection and statistical analysis.

The authors would like to thank Ms Reiko Yamaura and Dr J. Ludovic Croxford of Edanz Group Ltd. for providing English writing support, which was funded by Zenyaku Kogyo.

Compliance with ethical standards

Conflict of interest Tadahiko Igarashi and Kiyoshi Ando received research funding from Zenyaku Kogyo. Masafumi Taniwaki and Kazuhito Yamamoto received research funding from Chugai Pharmaceutical. Hirokazu Nagai received honoraria from Chugai Pharmaceutical. Yasuo Ohashi is a board member and stockholder of Statcom and received honoraria from Chugai Pharmaceutical. Kensei Tobinai received research funding from Zenyaku Kogyo and Chugai Pharmaceutical, and honoraria from Zenyaku Kogyo. The remaining authors have no conflict of interests to disclose.

References

1. Reff ME, Carner K, Chambers KS, Chinn PC, Leonard JE, Raab R, et al. Depletion of B cells in vivo by a chimeric mouse human monoclonal antibody to CD20. Blood. 1994;83:435–45.
2. van Oers MH, Klasa R, Marcus RE, Wolf M, Kimby E, Gascoyne RD, et al. Rituximab maintenance improves clinical outcome of relapsed/resistant follicular non-Hodgkin lymphoma in patients both with and without rituximab during induction: results of a prospective randomized phase 3 intergroup trial. Blood. 2006;108:3295–301.
3. van Oers MH, Van Glabbeke M, Giurgea L, Klasa R, Marcus RE, Wolf M, et al. Rituximab maintenance treatment of relapsed/resistant follicular non-Hodgkin's lymphoma: long-term outcome of the EORTC 20981 phase III randomized intergroup study. J Clin Oncol. 2010;28:2853–8.
4. Hochster H, Weller E, Gascoyne RD, Habermann TM, Gordon LI, Ryan T, et al. Maintenance rituximab after cyclophosphamide, vincristine, and prednisone prolongs progression-free survival in advanced indolent lymphoma: results of the randomized phase III ECOG1496 study. J Clin Oncol. 2009;27:1607–14.

5. Hainsworth JD, Litchy S, Shaffer DW, Lackey VL, Grimaldi M, Greco FA. Maximizing therapeutic benefit of rituximab: maintenance therapy versus re-treatment at progression in patients with indolent non-Hodgkin's lymphoma—a randomized phase II trial of the Minnie Pearl Cancer Research Network. J Clin Oncol. 2005;23:1088–95.
6. Ghielmini M, Schmitz SF, Cogliatti SB, Pichert G, Hummerjohann J, Waltzer U, et al. Prolonged treatment with rituximab in patients with follicular lymphoma significantly increases event-free survival and response duration compared with the standard weekly × 4 schedule. Blood. 2004;103:4416–23.
7. Vidal L, Gafter-Gvili A, Salles G, Dreyling MH, Ghielmini M, Hsu Schmitz SF, et al. Rituximab maintenance for the treatment of patients with follicular lymphoma: an updated systematic review and meta-analysis of randomized trials. J Natl Cancer Inst. 2011;103:1799–806.
8. Salles G, Seymour JF, Offner F, López-Guillermo A, Belada D, Xerri L, et al. Rituximab maintenance for 2 years in patients with high tumour burden follicular lymphoma responding to rituximab plus chemotherapy (PRIMA): a phase 3, randomised controlled trial. Lancet. 2011;377:42–51.
9. Seymour JF, Feugier P, Offner F, Lopez-Guillermo A, Belada D, Xerri L, et al. Updated 6 year follow-up of the PRIMA Study confirms the benefit of 2-year rituximab maintenance in follicular lymphoma patients responding to frontline immunochemotherapy. Blood. 2013;122:509 **(abstract)**.
10. Jaffe ES, Harris NL, Stein H, Vardiman JW. World Health Organization classification of tumours: pathology and genetics of tumours of haematopoietic and lymphoid tissues. Lyon: IARC Press; 2001.
11. Decaudin D, Lepage E, Brousse N, Brice P, Harousseau JL, Belhadj K, et al. Low-grade stage III–IV follicular lymphoma: multivariate analysis of prognostic factors in 484 patients—a study of the Groupe d' Etude des Lymphomes de l'Adulte. J Clin Oncol. 1999;17:2499–505.
12. Solal-Céligny P, Lepage E, Brousse N, Tendler CL, Brice P, Haïoun C, et al. Doxorubicin-containing regimen with or without interferon alfa-2b for advanced follicular lymphomas: final analysis of survival and toxicity in the Groupe d'Etude des Lymphomes Folliculaires 86 Trial. J Clin Oncol. 1998;16:2332–8.
13. Cheson BD, Horning SJ, Coiffier B, Shipp MA, Fisher RI, Connors JM, et al. Report of an international workshop to standardize response criteria for non-Hodgkin's lymphomas. NCI Sponsored International Working Group. J Clin Oncol. 1999;17:1244.
14. Ogura M, Morishima Y, Kagami Y, Watanabe T, Itoh K, Igarashi T, et al. Randomized phase II study of concurrent and sequential rituximab and CHOP chemotherapy in untreated indolent B-cell lymphoma. Cancer Sci. 2006;97:305–12.
15. Tobinai K, Ogura M, Itoh K, Kinoshita T, Hotta T, Watanabe T, et al. Randomized phase II study of concurrent and sequential combinations of rituximab plus CHOP (cyclophosphamide, doxorubicin, vincristine and prednisolone) chemotherapy in untreated indolent B-cell non-Hodgkin lymphoma: 7-year follow-up results. Cancer Sci. 2010;101:2579–85.
16. Forstpointner R, Unterhalt M, Dreyling M, Böck HP, Repp R, Wandt H, et al. Maintenance therapy with rituximab leads to a significant prolongation of response duration after salvage therapy with a combination of rituximab, fludarabine, cyclophosphamide, and mitoxantrone (R-FCM) in patients with recurring and refractory follicular. Blood. 2006;108:4003–8.
17. Fleming TR. One-sample multiple testing procedure for phase II clinical trials. Biometrics. 1982;38:143–51.
18. El Kaplan, Meier P. Nonparametric estimation from incomplete observations. J Am Stat Assoc. 1958;53:457–81.
19. Solal-Coligny P, Roy P, Colombat P. Follicular lymphoma international prognostic index. Blood. 2004;104:1258–65.
20. Behl D, Ristow K, Markovic SN, Witzig TE, Habermann TM, Colgan JP, et al. Absolute lymphocyte count predicts therapeutic efficacy of rituximab therapy in follicular lymphomas. Br J Haematol. 2007;137:409–15.
21. Kumagai S, Tashima M, Fujikawa J, Iwasaki M, Iwamoto Y, Sueki Y, et al. Ratio of peripheral blood absolute lymphocyte count to absolute monocyte count at diagnosis is associated with progression-free survival in follicular lymphoma. Int J Hematol. 2014;99:737–42.
22. Watanabe T, Tobinai K, Shibata T, Tsukasaki K, Morishima Y, Maseki N, et al. Phase II/III study of R-CHOP-21 versus R-CHOP-14 for untreated indolent B-cell non-Hodgkin's lymphoma: JCOG 0203 trial. J Clin Oncol. 2011;29:3990–8.
23. Czuczman MS, Grillo-López AJ, White CA, Saleh M, Gordon L, LoBuglio AF, et al. Treatment of patients with low-grade B-cell lymphoma with the combination of chimeric anti-CD20 monoclonal antibody and CHOP chemotherapy. J Clin Oncol. 1999;17:268–76.
24. Czuczman MS, Weaver R, Alkuzweny B, Berlfein J, Grillo-López AJ. Prolonged clinical and molecular remission in patients with low-grade or follicular non-Hodgkin's lymphoma treated with rituximab plus CHOP chemotherapy: 9-year follow-up. J Clin Oncol. 2004;22:4711–6.

Int J Hematol
DOI 10.1007/s12185-016-2178-9

ORIGINAL ARTICLE

A multicenter, single-arm, Phase II clinical trial of bendamustine monotherapy in patients with chronic lymphocytic leukemia in Japan

Yoshiaki Ogawa[1] · Koji Izutsu[2] · Toru Kiguchi[3] · Ilseung Choi[4] · Yoshifusa Takatsuka[5] · Kiyoshi Ando[1] · Junji Suzumiya[6] · Japanese Bendamustine CLL Study Group

Received: 7 September 2016 / Revised: 27 December 2016 / Accepted: 27 December 2016

Abstract The present study was intended to examine the efficacy and safety of bendamustine monotherapy in patients with previously untreated chronic lymphocytic leukemia (CLL) for whom treatment with fludarabine (FLU) was not suitable, and in FLU-naïve patients with relapsed/refractory CLL. We intravenously administered bendamustine 100 mg/m^2/day on days 1 and 2 of each 28-day cycle to 10 patients (eight previously untreated; two relapsed/refractory) up to six cycles. The primary endpoint was overall response rate (ORR: partial remission or better) according to the 2008 International Workshop on the CLL guidelines. The ORR was 60.0% (6/10), with the 95% confidence interval of 26.2–87.8%. Neither disease progression nor mortality occurred during follow-up. Therefore, the medians for progression-free survival, duration of response, and overall survival were estimated to exceed 12.6, 8.7, and 12.6 months, respectively. Adverse events (AEs) occurred in all 10 patients. Grade 3/4 hematologic AEs included lymphopenia (90%), neutropenia (80%), CD4 lymphopenia (80%), and leukopenia (70%). Nonhematologic AEs included constipation (80%), nausea (80%), malaise (50%), and anorexia (50%). There was one case each of grade 3 infection and adenocarcinoma of the stomach. Bendamustine showed high efficacy for Japanese patients with previously untreated or relapsed/refractory CLL, and its safety profile was acceptable.

Keywords Bendamustine · Chronic lymphocytic leukemia · Japanese · Efficacy · Safety

✉ Yoshiaki Ogawa
yoshioga@is.icc.u-tokai.ac.jp

[1] Department of Hematology and Oncology, Tokai University Hospital, 143 Shimokasuya, Isehara, Kanagawa 259-1193, Japan

[2] Department of Hematology, Toranomon Hospital, Tokyo, Japan

[3] Department of Hematology, Chugoku Central Hospital of the Mutual Aid Association of Public School Teachers, Fukuyama, Japan

[4] Department of Hematology, National Hospital Organization Kyushu Cancer Center, Fukuoka, Japan

[5] Department of Hematology, Jiaikai Imamura Bun-in Hospital, Kagoshima, Japan

[6] Department of Oncology/Hematology, School of Medicine, Shimane University, Izumo, Japan

Introduction

Chronic lymphocytic leukemia (CLL) is the most prevalent form of adult leukemia in the Western world [1, 2], with a marked racial difference in age-adjusted incidence between the United States and Japan (3.5 and 0.2 cases per 100,000 person-years in 2008 [3], respectively). In contrast to the United States and Europe where a number of chemotherapeutic options are available and many new anticancer agents are under development [1, 2, 4, 5], the chemotherapeutic armamentarium for patients with CLL—especially, elderly patients with CLL for whom fludarabine (FLU) is not suitable—is very restricted in Japan [6]; therefore, the development of a therapeutic option for them remains as an unmet need.

Bendamustine is a unique cytotoxic agent with structural similarities to alkylating agents and antimetabolites; the former and latter properties are endowed by the mechlorethamine and benzimidazole rings, respectively [7, 8]. Hence, bendamustine has shown, when used alone or in combination with rituximab (BR), high efficacy and

Published online: 03 February 2017

an acceptable safety profile for patients with previously untreated or relapsed/refractory CLL [9–14]. Concretely, bendamustine monotherapy offers significantly greater efficacy than chlorambucil as first-line therapy for patients with advanced CLL [9, 10] and provides an alternative therapeutic option, compared to FLU, as second-line therapy for patients with relapsed CLL [11]. BR has also shown efficacy and safety for patients with previously untreated [12] or relapsed/refractory [13] CLL. Furthermore, the benefit of combining BR with B cell receptor signal inhibitors (e.g., Bruton's tyrosine kinase inhibitors) in patients with previously treated CLL has been suggested [14]. In contrast, the efficacy and safety of even bendamustine monotherapy has never been examined in Japan.

We conducted the present Phase II clinical study to investigate the above features of bendamustine monotherapy in Japanese patients with previously untreated or relapsed/refractory CLL.

Patients and methods

Study design and patients

A multicenter, single-arm, phase II clinical study was conducted at six medical institutions in Japan. Patients with previously untreated or relapsed/refractory CLL were considered eligible when meeting all of the following criteria: 20–80 years of age at entry; definite diagnosis of CLL in accordance with the 2008 International Workshop on the Chronic Lymphocytic Leukemia (IWCLL) guidelines [15]; Eastern Cooperative Oncology Group performance status of 0–2; no previous treatment with FLU and treatment with FLU is not suitable; Binet stage C or active stage B at entry [15]; two or less regimens of prior chemotherapy and antibody therapy; and the well-conserved function of main organs.

Patients were excluded from the study when falling under any of the following key exclusion criteria: the deletion of p53 (17p−) in the chromosomal test (fluorescent in situs hybridization); clinically recognized Richter syndrome; history of allogeneic hematopoietic stem cell transplantation; central nervous system involvement or clinical symptoms suggestive of it; double cancer or a history of another malignancy in the past 5 years; positivity for either the anti-human immunodeficiency virus antibody or the hepatitis C virus; positivity for the hepatitis B surface antigen; and pregnancy or lactation.

The mutational status analysis of the immunoglobulin heavy chain variable region gene was conducted by a central laboratory according the direct sequencing method [16] using two primer sets [framework 1c (FR1c)/LJH/VLJH and a mixture of six FR1 V_H family-specific primers/LJH/VLJH]. The base sequences obtained were examined with the database (the International Immunogenetics Information System®) to analyze homology thereof (homology cut-off value 98%) [17].

The study protocol was approved by the institutional review board at each institution, and all patients provided written informed consent before study enrollment. The present study complied with the Declaration of Helsinki, was conducted in compliance with the Good Clinical Practice guidelines, and was registered with ClinicalTrials.gov (NCT02042911).

Treatment

Bendamustine 100 mg/m^2/day was administered intravenously over 60 min on days 1 and 2 of each 28-day cycle. The administration of bendamustine was repeated up to six cycles. In cycle 2 or later, dose modification (dose delay, dose reduction, or dose discontinuation) was made based on adverse events (AEs) found in the previous cycle. In patients who had received bendamustine, outcomes were investigated every 3 months for a specified period of time.

In cycle 2 or later, administration was continued when the patient met the criteria for next cycle initiation that consisted of neutrophil count (≥1000/mm^3), platelet count (≥50,000/mm^3), aspartate aminotransferase (AST) [≤fivefold the upper limit of normal (ULN) at each institution], alanine aminotransferase (ALT) (≤fivefold the ULN at each institution), total bilirubin (≤threefold the ULN at each institution), serum creatinine (≤threefold the ULN at each institution), and the absence of persisting grade 3 or greater AEs at the time of assessment.

In cycle 3 or later, the dose of bendamustine in the next cycle was reduced according to its dose levels (level 1: 100 mg/m^2/day, level 2: 75 mg/m^2/day, and level 3: 50 mg/m^2/day) when the patient fell under any of the following criteria for dose reduction: criterion (1) any of AEs found in the previous cycle, as graded by the Common Terminology Criteria for Adverse Events (CTCAEs) Japanese version 4.03 published by Japan Clinical Oncology Group, which were grade 4 (<500/mm^3) neutropenia lasting for 1 or more weeks, platelet count (<25,000/mm^3), a need for platelet transplantation, and grade 3/4 nonhematologic toxicity (excepting electrolyte anomalies and hyperglycemia); and criterion (2) AEs other than those described above, for which the investigator considered dose reduction necessary. Dose increase after dose reduction was not permitted. The administration of bendamustine was discontinued when the patient fell under the criteria for dose reduction while receiving the drug at dose level 3.

To prevent or alleviate nausea and vomiting, the intravenous administration of dexamethasone (8–12 mg, once daily) and 5-hydroxytriptamine type 3 (5-HT_3) receptor antagonists

Table 1 Patient characteristics at baseline

Characteristics	*n*	Percentage
Gender	10	100
Male	6	60
Female	4	40
Age, years		
Median (range)	71.5 (50–78)	
<65	2	20
≥65	8	80
Binet clinical stage		
Stage B	3	30
Stage C	7	70
Prior treatment		
Absent	8	80
Present	2	20
Comorbidities		
Absent	1	10
Present	9	90
ECOG performance status		
0	8	80
1	2	20
Lymphoadenopathy		
Absent	2	20
Present	8	80
B symptoms		
Absent	2	20
Present	8	80

ECOG Eastern Cooperative Oncology Group

was recommended. In addition, the administration of neurokinin 1 receptor antagonists was also permitted. When the number of CD4+ lymphocytes decreased to 200 cells/mm^3 or below, sulfamethoxazole-trimethoprim and/or acyclovir was administered orally. When screening resulted positive for the HBs or HBc antibody, HBV-DNA was assayed once in each cycle. When the assay resulted positive for HBV-DNA, the administration of entecavir was initiated. When concern arose about tumor lysis syndrome, hydration and other appropriate measures were recommended. Furthermore, the administration of rasburicase was permitted. The administration of G-CSFs was considered when grade 4 (<500/mm^3) neutropenia, febrile neutropenia, or other AEs occurred.

Efficacy and safety assessments

The primary endpoint of the present study was the overall response rate [ORR: complete remission (CR), CR with incomplete marrow recovery (CRi), nodular partial remission (nPR), and PR] assessed by the independent review committee based on best overall response according to the 2008 IWCCL guidelines [15]. The secondary endpoints of the present study were the following: the ORR defined by the National Cancer Institute Working Group (NCI-WG)—CR, nPR, and PR; CR (CR and CRi) rate [18]; progression-free survival (PFS); duration of response (DOR); overall survival (OS); and safety.

Statistical analyses

Assuming that the expected response rate is 59.2%, the threshold response rate is 10.0%, the one-tailed significance level is 2.5%, and statistical power is 80%, the required number of patients was calculated to be eight. In consideration of 20% for withdrawals and others, we established 10 patients as the target number of patients.

The efficacy of bendamustine was analyzed primarily for the full analysis set (FAS) and secondarily for the per-protocol set (PPS). The safety of bendamustine was analyzed for the safety analysis set (SAS). SAS version 9.3 (SAS Institute, Cary, NC, USA) was used to conduct all statistical analyses.

Results

Patients

From May 2013 through June 2015, 10 eligible patients (six males and four females) were enrolled in the present study, and patient characteristics at baseline are shown in Table 1. The median age of patients was 71.5 years (range 50–78 years), and patients aged 65 years or older were predominant (eight). Three and seven patients were at Binet stages B and C, respectively. Eight patients presented with previously untreated CLL, and two patients were treated previously. Ten patients did not receive fludarabine due to the following reasons: eight, elderly over age 65; one, a history of pneumonia and peripheral neuropathy; and one, physician's discretion. Nine patients had comorbidities, and nine patients showed the diffuse infiltration of the marrow examination. Interphase fluorescence in situ hybridization (FISH) revealed trisomy of chromosome 12 in two patients, the deletion in the long arm of chromosome 13 [del(13q14.1)] in five patients, and the absence of deletions in chromosomes 11 [del(11q22–23)] and 17 [del(17p13)]. The immunoglobulin heavy chain gene was mutated in nine of 10 these patients.

The median number of the cycles delivered was six (range 2–6 cycles). Six patients completed six cycles. Four patients discontinued the treatment early for the following reasons: consent withdrawal ($n = 1$) in cycle 2, investigator's discretion ($n = 2$) in cycle 4, and prolonged neutropenia ($n = 1$) in cycle 5. Dose delays and dose

Table 2 Best overall responses in patients with chronic lymphocytic leukemia

	Best overall response, *n* (%)							ORR (95% CI) (%)	CR rate (95% CI) (%)
	CR	CRi	nPR	PR	SD	PD	NE		
IWCLL	2	0	0	4	3	0	1	60.0 (26.2–87.8)	20.0 (2.5–55.6)
NCI-WG	0	–	0	6	3	0	1	60.0 (26.2–87.8)	0

IWCLL International Workshop on Chronic Lymphocytic Leukemia, *NCI-WG* National Cancer Institute Working Group, *CR* complete remission, *CRi* complete remission with incomplete marrow recovery, *nPR* nodular partial remission, *PR* partial remission, *SD* stable disease, *PD* progressive disease, *NE* not evaluable, – not applicable

Table 3 Hematologic adverse events

Adverse events	Grades					
	All-grades (%)	3/4 (%)	1 (*n*)	2 (*n*)	3 (*n*)	4 (*n*)
Lymphopenia	90	90			5	4
Neutropenia	100	80		2	2	6
CD4 lymphopenia	100	80		2	6	2
Leukopenia	90	70		2	5	2
Thrombocytopenia	90	20	2	5	1	1
Anemia	10	0	1			

As graded according to Common Terminology Criteria for Adverse Events Japanese version 4.0

reductions were required in 21 and six of 51 cycles, respectively. The mean relative dose intensity was 76.2% (range 57.2–99.0%).

All of the patients in the present study received at least one dose of bendamustine, and none of them were excluded from SAS, FAS, or PPS. Therefore, all statistical analyses for efficacy and safety were made for 10 patients.

Efficacy

Best overall responses are shown in Table 2. The ORR (CR, CRi, nPR, and PR) as assessed according to the IWCLL criteria [15] was 60.0% (6/10; two patients in CR, four patients in PR, three patients in SD, and one patient in not evaluable), with the 95% confidence interval (CI) of 26.2–87.8%. Therefore, the ORR rate exceeded the previously established expected efficacy rate of 59.2%, and the lower limit for the 95% CI (26.2%) exceeded the threshold rate of 10.0% at the time of design. The ORR (CR, nPR, and PR) as assessed according to the NCI-WG criteria [18] was also 60.0% (6/10; six patients in PR, three patients in SD, and one patient in NE), with the 95% CI of 26.2–87.8%. In addition, the CR rate (CR and CRi) as assessed according to the IWCLL guidelines [15] was 20.0% (95% CI 2.5–55.6%). None of our patients reached CR according to the NCI-WG guidelines' criteria due to failure in meeting the criteria or in obtaining data for assessment at 8 weeks later as required by the criteria.

Neither disease progression nor deaths occurred during follow-up (median 12.6 months; range 2.6–21.7 months). Therefore, the medians for both progression-free survival and overall survival were estimated to exceed 12.6 months. Moreover, DOR was estimated to exceed the median (8.7 months) of follow-up.

Safety

A total of 340 episodes of AEs occurred in all 10 patients. Hematologic AEs are shown in Table 3, and grade 3/4 hematologic AEs were lymphopenia (90%), neutropenia (80%), CD4 lymphopenia (80%), leukopenia (70%), and thrombocytopenia (20%). Major nonhematologic AEs are shown in Table 4, with constipation (80%), nausea (80%), malaise (50%), anorexia (50%), increased AST (40%), decreased blood immunoglobulin (Ig) A (30%), decreased blood IgG (30%), decreased blood IgM (30%), pruritus (30%), and maculopapular rash (30%). Grade 3 infections—febrile neutropenia (10%), pneumonia (10%), and bacterial infection (10%)—occurred in one patient; all these infections resolved. Furthermore, conjunctivitis (20%), cytomegalovirus infection (10%), nasopharyngitis (10%), oral candidiasis (10%), and pneumonia (10%) developed as grade 1/2 infections. Grade 1/2 vascular disorders were phlebitis (20%), vascular pain (20%), and vasculitis (10%). Neither vascular event leading to the discontinuation of bendamustine nor serious injection site reaction occurred. Grade 3 rash occurred in one patient. Grade 1/2 skin disorders were pruritus (30%), maculopapular rash (30%), urticaria (20%), acne-like dermatitis (10%), rash (10%), erythema (10%), and multiform erythema (10%). Adenocarcinoma of the stomach with suspected hepatic metastasis developed in one patient.

Table 4 Nonhematologic adverse events

Adverse events	Grades					
	All-grades (%)	3/4 (%)	1 (*n*)	2 (*n*)	3 (*n*)	4 (*n*)
Constipation	80		7	1		
Nausea	80		6	2		
Malaise	50		4	1		
Anorexia	50		3	2		
Increased AST	40		4			
Decreased IgA in serum	30		3			
Decreased IgG in serum	30		3			
Decreased IgM in serum	30		3			
Pruritus	30		1	2		
Maculopapular rash	30		1	2		
Palpitation	20		2			
Gastritis	20			2		
Stomatitis	20		2			
Fatigue	20		2			
Fever	20		1	1		
Peripheral edema	20		2			
Conjunctivitis	20			2		
Pneumonia	20	10		1	1	
Increased ALT	20		2			
Prolonged QT interval	20		1	1		
Decreased uric acid in plasma	20		2			
Increased γ-GTP	20		1	1		
Myalgia	20		1	1		
Dysgeusia	20		2			
Insomnia	20		2			
Oropharyngeal pain	20		2			
Rash	20	10	1		1	
Urticaria	20			2		
Hypertension	20	10		1	1	
Phlebitis	20			2		
Vascular pain	20		1	1		

As graded according to Common Terminology Criteria for Adverse Events Japanese version 4.0

AST aspartate transaminase, *IgA* immunoglobulin A, *IgG* immunoglobulin G, *IgM* immunoglobulin M, *ALT* alanine transaminase, *γ-GTP* gamma-glutamyl transpeptidase

A total of 6 serious AEs occurred in three patients, with one episode each of hemorrhagic intestinal diverticulum, pneumonia, bacterial infection, iliac fracture, cytomegalovirus infection, and adenocarcinoma of the stomach.

Discussion

Standard first-line therapy for "fit" younger patients with CLL is the combination of FLU with cyclophosphamide and rituximab (FCR), and BR is an alternative therapeutic option for "fit" younger and elderly patients who are not eligible for FCR therapy in the United States and Europe [1, 2, 4, 5]. In Japan, however, bendamustine was recently approved for the treatment of CLL, but rituximab is not.

The present study demonstrated the efficacy of bendamustine 100 mg/m^2/day given by 2-day consecutive intravenous administration to patients with previously untreated CLL for whom FLU was not suitable and to FLU-naïve patients with relapsed/refractory CLL; however, definite consensus has not been obtained as to the unsuitableness of FLU administration for patients with CLL. In clinical practice, nevertheless, FLU is not recommend for elderly patients, patients with declined renal function, patients with infection, and others. In our study, 10 patients did not receive FLU due to the following reasons: advanced age

(≥65 years) in eight patients; a history of pneumonia and peripheral neuropathy in one patient; and physician's discretion in one patient. The safety profile of bendamustine observed in the present study was nearly similar to that found in prior clinical studies of bendamustine monotherapy in Japan [19, 20], although histologies examined and doses used were different; furthermore, any AEs specific to patients with CLL were not found.

In the present study, we used the same initial dose of 100 mg/m^2/day for both Japanese patients with previously untreated CLL and those who had FLU-naïve, treated CLL, based on the arguments to be described below. Regarding those who were previously untreated, we had verified the tolerability of bendamustine up to 120 mg/m^2/day in Japanese patients with relapsed or refractory indolent B-NHL [19, 20], and the efficacy and safety of bendamustine 100 mg/m^2/day had been demonstrated for patients with CLL in a Phase III clinical trial in Germany [9]. Therefore, we set 100 mg/m^2/day as the initial dose for Japanese patients with previously untreated CLL. Regarding those who presented treated CLL, previous German studies showed that the maximum tolerated dose (MTD) of bendamustine was 70 mg/m^2/day [21]. On the other hand, a Phase I/II study in Bulgaria described 110 mg/m^2/day as the MTD in patients who had FLU-naïve, pretreated CLL [22]. Therefore, we limited patients with treated CLL to those who had FLU-naïve, treated CLL in the present study. Patients with CLL usually necessitate time to recover from CLL- and/or chemotherapy-induced myelosuppression at the initial stage of chemotherapy. Indeed, dose delays were required in 21 of 51 cycles to meet the next cycle initiation criteria, which lowered RDI to 76.2%. Despite these facts, six of 10 patients completed six cycles as scheduled. Hence, we consider that the initial dose of 100 mg/m^2/day was set appropriately in our study. Nevertheless, an international consensus panel [23] has recommended an initial dose lower than 100 mg/m^2 for patients with refractory/relapsed CLL. Therefore, there is a need for dose adjustment in accordance with their fitness level and in light of real-world clinical practice.

The ORR (60.0%), calculated according to the IWCLL guidelines [15], achieved the expected ORR. In addition, the ORR calculated according to the NCI-WG criteria [18] was also 60.0%. Therefore, the ORR of bendamustine in our study was almost comparable to 68 and 76% in the phase III randomized studies of bendamustine in patients with previously untreated CLL [9] and FLU-naïve patients with relapsed/refractory CLL [11], respectively.

Hereafter, the comparability to the present study of the safety profile of bendamustine monotherapy in the Phase II study in Japanese patients with relapsed/refractory, indolent NHL and MCL [20] is discussed in more detail. Regarding hematologic AEs, namely, grade 3/4 lymphopenia, neutropenia, and leukopenia occurred in more than 70% of patients, while there were a few number of cases of thrombocytopenia and anemia. Among nonhematologic AEs, the incidences of vomiting (10 vs. 42%) and weight loss (10 vs. 35%) were lower. We consider that the recommended intravenous administration of a steroid and a 5-HT$_3$ receptor antagonist was effective in preventing chemotherapy-induced nausea and vomiting. The incidences of nonhematologic AEs other than vomiting and weigh loss were nearly comparable.

The present study has several limitations. First, sample size was small. Therefore, accumulating further clinical evidence in the real-world clinical settings will be required to more precisely delineate the safety profile of bendamustine treatment for Japanese patients with CLL. Second, the median of follow-up was as short as about 1 year; therefore, the investigation on delayed AEs, e.g., secondary cancer, was not sufficient. Since PFS in prior Phase III clinical studies reached approximately 20 months [9], further follow-up is required to calculate PFS in our patient population. Third, we used bendamustine monotherapy to conduct the present study. However, the recent guidelines recommend the combination of bendamustine and rituximab [1, 2, 4, 5]; indeed, the combined regimen is predominant in countries outside Japan [24–26]. In addition, dose levels and the number of cycles to be delivered differ between patients with previously untreated CLL and patients with relapsed CLL [23]. Hence, the dose levels of bendamustine and rituximab in combination regimens need to be verified.

In conclusion, bendamustine showed efficacy for patients with previously untreated or relapsed/refractory CLL for whom treatment with FLU was not suitable in Japan. Furthermore, bendamustine also exhibited an acceptable safety profile as was the case in Phase I and II clinical studies in patients with relapsed/refractory NHL and MCL in Japan. Therefore, bendamustine is a promising therapeutic option for these patient populations. Nevertheless, the accumulation of further clinical evidence on these features of bendamustine and a clinical study of bendamustine in combination with an anti-CD20 antibody and/or a B-cell receptor signal inhibitor will be required in the future.

Acknowledgements The authors thank patients, investigators, and staff who were involved in the present study. Research support was provided by SymBio Pharmaceuticals. This work was funded by SymBio Pharmaceuticals Ltd and Eisai Co., Ltd. No grant number applies. The authors also manifest our gratitude to the members of the Efficacy and Safety Monitoring Committee—Hirokazu Murakami, MD, PhD, Noriko Usui, MD, PhD, and Keisuke Toyama, MD, PhD, to the members of the Independent Review Committee—Sadao Aoki, MD, PhD, Naoya Nakamura, MD, PhD, and Ukihide Tateishi, MD, PhD, and to the medical advisor—Kazuo Tamura, MD, PhD. Furthermore, the authors thank Satoshi Sakima, MD, for his gracious review of the manuscript.

Compliance with ethical standards

Conflict of interest Dr. Izutsu has received honoraria from Chugai, Kyowa Hakko Kirin, and Takeda; and has received research funding from Kyowa Hakko Kirin, MSD, Celgene, and Pfizer. Dr. Ando has received research funding form Kyowa Hakko Kirin. Dr. Suzumiya has received honoraria from Chugai, Eisai, and Takeda; and has received research funding from Kyowa Hakko Kirin, Chugai, Astellas, and Toyama Chemical. All remaining authors have declared no conflicts of interest.

References

1. Hallek M. Chronic lymphocytic leukemia: 2015 update on diagnosis, risk stratification, and treatment. Am J Hematol. 2015;90:446–60.
2. Eichhorst B, Robak T, Montserrat E, Ghia P, Hillmen P, Hallek M, et al. Chronic lymphocytic leukaemia: ESMO Clinical Practice Guidelines for diagnosis, treatment and follow-up. Ann Oncol. 2015;26(Suppl 5):v78–84.
3. Chihara D, Ito H, Matsuda T, Shibata A, Katsumi A, Nakamura S, et al. Differences in incidence and trends of haematological malignancies in Japan and the United States. Br J Haematol. 2014;164:536–45.
4. Stilgenbauer S, Furman RR, Zent CS. Management of chronic lymphocytic leukemia. Am Soc Clin Oncol Educ Book 2015; 164–75.
5. NCCN Clinical Practice Guidelines in Oncology. Chronic lymphocytic leukemia/small lymphocytic lymphoma version 1. 2017. https://www.nccn.org/professionals/physician_gls/pdf/cll.pdf. Assessed 11 Nov 2016.
6. Aoki S. Chronic lymphocytic leukemia. Rinsho Ketsueki. 2014;55:213–22.
7. Cheson BD, Rummel MJ. Bendamustine: rebirth of an old drug. J Clin Oncol. 2009;27:1492–501.
8. Leoni LM, Hartley JA. Mechanism of action: the unique pattern of bendamustine-induced cytotoxicity. Semin Hematol. 2011;48(Suppl 1):S12–23.
9. Knauf WU, Lissichkov T, Aldaoud A, Liberati A, Loscertales J, Herbrecht R, et al. Phase III randomized study of bendamustine compared with chlorambucil in previously untreated patients with chronic lymphocytic leukemia. J Clin Oncol. 2009;27:4378–84.
10. Knauf WU, Lissitchkov T, Aldaoud A, Liberati AM, Loscertales J, Herbrecht R, et al. Bendamustine compared with chlorambucil in previously untreated patients with chronic lymphocytic leukaemia: updated results of a randomized phase III trial. Br J Haematol. 2012;159:67–77.
11. Niederle N, Megdenberg D, Balleisen L, Heit W, Knauf W, Weiß J, et al. Bendamustine compared to fludarabine as second-line treatment in chronic lymphocytic leukemia. Ann Hematol. 2013;92:653–60.
12. Fischer K, Cramer P, Busch R, Böttcher S, Bahlo J, Schubert J, et al. Bendamustine in combination with rituximab for previously untreated patients with chronic lymphocytic leukemia: a multicenter phase II trial of the German Chronic Lymphocytic Leukemia Study Group. J Clin Oncol. 2012;30:3209–16.
13. Fischer K, Cramer P, Busch R, Stilgenbauer S, Bahlo J, Schweighofer CD, et al. Bendamustine combined with rituximab in patients with relapsed and/or refractory chronic lymphocytic leukemia: a multicenter phase II trial of the German Chronic Lymphocytic Leukemia Study Group. J Clin Oncol. 2011;29:3559–66.
14. Chanan-Khan A, Cramer P, Demirkan F, Fraser G, Silva RS, Grosicki S, et al. Ibrutinib combined with bendamustine and rituximab compared with placebo, bendamustine, and rituximab for previously treated chronic lymphocytic leukaemia or small lymphocytic lymphoma (HELIOS): a randomised, double-blind, phase 3 study. Lancet Oncol. 2016;17:200–11.
15. Hallek M, Cheson BD, Catovsky D, Caligaris-Cappio F, Dighiero G, Döhner H, et al. Guidelines for the diagnosis and treatment of chronic lymphocytic leukemia: a report from the International Workshop on Chronic Lymphocytic Leukemia updating the National Cancer Institute-Working Group 1996 guidelines. Blood. 2008;111:5446–56.
16. Nakamura N, Kuze T, Hashimoto Y, Tasaki K, Hojo H, Sasaki Y, et al. Analysis of the immunoglobulin heavy chain gene variable region of 101 cases with peripheral B cell neoplasms and B cell chronic lymphocytic leukemia in the Japanese population. Pathol Int. 1999;49:595–600.
17. Ghia P, Stamatopoulos K, Belessi C, Moreno C, Stilgenbauer S, Stevenson F, et al. ERIC recommendations on IGHV gene mutational status analysis in chronic lymphocytic leukemia. Leukemia. 2007;21:1–3.
18. Cheson BD, Bennett JM, Grever M, Kay N, Keating MJ, O'Brien S, et al. National Cancer Institute-sponsored Working Group guidelines for chronic lymphocytic leukemia: revised guidelines for diagnosis and treatment. Blood. 1996;87:4990–7.
19. Ogura M, Uchida T, Taniwaki M, Ando K, Watanabe T, Kasai M, et al. Phase I and pharmacokinetic study of bendamustine hydrochloride in relapsed or refractory indolent B-cell non-Hodgkin lymphoma and mantle cell lymphoma. Cancer Sci. 2010;101:2054–8.
20. Ohmachi K, Ando K, Ogura M, Uchida T, Itoh K, Kubota N, et al. Multicenter phase II study of bendamustine for relapsed or refractory indolent B-cell non-Hodgkin lymphoma and mantle cell lymphoma. Cancer Sci. 2010;101:2059–64.
21. Bergmann MA, Goebeler ME, Herold M, Emmerich B, Wilhelm M, Ruelfs C, et al. Efficacy of bendamustine in patients with relapsed or refractory chronic lymphocytic leukemia: results of a phase I/II study of the German CLL Study Group. Haematologica. 2005;90:1357–64.
22. Lissitchkov T, Arnaudov G, Peytchev D, Merkle Kh. Phase-I/II study to evaluate dose limiting toxicity, maximum tolerated dose, and tolerability of bendamustine HCl in pre-treated patients with B-chronic lymphocytic leukaemia (Binet stages B and C) requiring therapy. J Cancer Res Clin Oncol. 2006;132:99–104.
23. Cheson BD, Brugger W, Damaj G, Dreyling M, Kahl B, Kimby E, et al. Optimal use of bendamustine in hematologic disorders: treatment recommendations from an international consensus panel—an update. Leuk Lymphoma. 2016;57:766–82.
24. Fornecker LM, Aurran-Schleinitz T, Michallet AS, Cazin B, Guieze R, Dilhuydy MS et al. Salvage outcomes in patients with first relapse after fludarabine, cyclophosphamide, and rituximab for chronic lymphocytic leukemia: the French intergroup experience. Am J Hematol. 2015; 90:511–4.
25. Laurenti L, Innocenti I, Autore F, Vannata B, Efremov DG, Ciolli S, et al. Bendamustine in combination with rituximab for elderly patients with previously untreated B-cell chronic lymphocytic leukemia: a retrospective analysis of real-life practice in Italian hematology departments. Leuk Res. 2015;39:1066–70.
26. Zoellner AK, Höhler T, Fries S, Böhme A, Kiewe P, Kellermann L, et al. Altered treatment of chronic lymphocytic leukemia in Germany during the last decade. Ann Hematol. 2016;95:853–61.

International Journal of Hematology

Bendamustine plus rituximab for previously untreated patients with indolent B-cell non-Hodgkin lymphoma or mantle cell lymphoma: A multicenter Phase II clinical trial in Japan

--Manuscript Draft--

Manuscript Number:	IJHM-D-16-00796R3
Full Title:	Bendamustine plus rituximab for previously untreated patients with indolent B-cell non-Hodgkin lymphoma or mantle cell lymphoma: A multicenter Phase II clinical trial in Japan
Article Type:	Original Article
Section/Category:	Japan
Corresponding Author:	Michinori Ogura, M.D., Ph.D. ***(06) Tokai Central Hospital Kakamigahara, Gifu JAPAN
Corresponding Author Secondary Information:	
Corresponding Author's Institution:	Tokai Central Hospital
Corresponding Author's Secondary Institution:	
First Author:	Michinori Ogura, M.D., Ph.D. ***(06)
First Author Secondary Information:	
Order of Authors:	Michinori Ogura, M.D., Ph.D. ***(06)
	Kenichi Ishizawa, MD
	Dai Maruyama, MD
	Naokuni Uike, MD
	Kiyoshi Ando, MD
	Koji Izutsu, MD
	Yasuhito Terui, MD
	Yoshitaka Imaizumi, MD
	Kunihiro Tsukasaki, MD
	Kenshi Suzuki, MD
	Tohru Izumi, MD
	Kensuke Usuki, MD
	Tomohiro Kinoshita, MD
	Masafumi Taniwaki, MD
	Nobuhiko Uoshima, MD
	Junji Suzumiya, MD
	Mitsutoshi Kurosawa, MD
	Hirokazu Nagai, MD
	Toshiki Uchida, MD
	Noriko Fukuhara, MD
	Ilseung Choi, MD

	Ken Ohmachi, MD
	Go Yamamoto, MD
	Kensei Tobinai, MD
Order of Authors Secondary Information:	
Funding Information:	
Abstract:	A Phase II, multicenter clinical trial of bendamustine plus rituximab (BR) regimen was conducted in previously untreated patients with high-tumor-burden indolent B-cell non-Hodgkin lymphoma (B-NHL) and previously untreated elderly patients with mantle cell lymphoma (MCL) in Japan. Bendamustine 90 mg/m2/day on days 1 and 2, as well as rituximab 375 mg/m2 on day 1 were administered intravenously up to six cycles. The primary endpoint was the complete response (CR) rate as assessed by the International Workshop Response Criteria (1999). Sixty-nine patients (59 with indolent B-NHL and 10 with MCL) were treated. The median number of delivered cycles was six (range: 1-6). The CR rates were 67.8% [95% confidence interval (CI): 54.4-79.4%] and 70.0% (95% CI: 34.8-93.3%) for indolent B-NHL and MCL, respectively. Estimated progression-free survival at 30 months was 72.1% (95% CI: 58.5-82.0%) in indolent B-NHL and was 67.5% (95% CI: 29.1-88.2%) in MCL. Major grade 3/4 toxicities were hematologic and included lymphopenia (97%), CD4 lymphopenia (91%), and neutropenia (86%), and leukopenia (83%). No treatment-related death was found. The BR regimen showed high efficacy, as evidenced by the expected CR rate, and durable response, as well as an acceptable safety profile for the study populations.
Response to Reviewers:	
Additional Information:	
Question	**Response**
Is your submission applicable to any of cases below? (Please refer to the latest *IJH* Information for Authors) 1) “Duplicate Publication” which has been published previously or currently under consideration for publication elsewhere. 2) “Secondary Publication” which is based on material published in other journals or online.	No

Bendamustine plus rituximab for previously untreated patients with indolent B-cell non-Hodgkin lymphoma or mantle cell lymphoma: A multicenter Phase II clinical trial in Japan

Michinori Ogura[1,2], Kenichi Ishizawa[3], Dai Maruyama[4], Naokuni Uike[5], Kiyoshi Ando[6], Koji Izutsu[7], Yasuhito Terui[8], Yoshitaka Imaizumi[9], Kunihiro Tsukasaki[10], Kenshi Suzuki[11], Tohru Izumi[12], Kensuke Usuki[13], Tomohiro Kinoshita[14], Masafumi Taniwaki[15], Nobuhiko Uoshima[16], Junji Suzumiya[17], Mitsutoshi Kurosawa[18], Hirokazu Nagai[19], Toshiki Uchida[1], Noriko Fukuhara[3], Ilseung Choi[5], Ken Ohmachi[6], Go Yamamoto[7], and Kensei Tobinai[4], for the Japanese Bendamustine Lymphoma Study Group

[1]Department of Hematology and Oncology, Nagoya Daini Red Cross Hospital, Nagoya;

[2]Department of Hematology, Tokai Central Hospital, Kakamigahara;

[3]Department of Hematology and Rheumatology, Tohoku University Graduate School of Medicine, Sendai;

[4]Department of Hematology, National Cancer Center Hospital, Tokyo;

[5]Department of Hematology, National Hospital Organization Kyushu Cancer Center, Fukuoka;

[6]Department of Hematology and Oncology, Tokai University Hospital, Isehara;

[7]Department of Hematology, Toranomon Hospital, Tokyo;

[8]Department of Hematology Oncology, the Cancer Institute Hospital of the Japanese Foundation for Cancer Research, Tokyo;

[9]Department of Hematology, Nagasaki University Hospital, Nagasaki;

[10]Department of Hematology, National Cancer Center Hospital East, Kashiwa;

[11]Department of Hematology, Japanese Red Cross Medical Center, Tokyo;

[12]Division of Hematology, Tochigi Cancer Center, Utsunomiya;

[13]Department of Hematology, NTT Medical Center Tokyo, Tokyo;

[14]Department of Hematology and Cell Therapy, Aichi Cancer Center, Nagoya;

[15]Division of Hematology and Oncology, Kyoto Prefectural University of Medicine, Kyoto;

[16]Department of Hematology, Matsushita Memorial Hospital, Moriguchi;

[17]Department of Oncology/Hematology, School of Medicine, Shimane University, Izumo;

[18]Department of Hematology, National Hospital Organization Hokkaido Cancer Center, Sapporo;

[19]Department of Hematology, National Hospital Organization Nagoya Medical Center, Nagoya;

Japan

Running head: Bendamustine-rituximab for untreated B-NHL

Type of manuscript: Original article

Correspondence should be addressed to:

Michinori Ogura, MD, PhD

Department of Hematology, Tokai Central Hospital, 4-6-2 Higashijimacho, Sohara,

Kakamigahara, Gifu 504-8601, Japan

Phone: +81-58-382-3101; FAX: +81-58-382-1762; e-mail address: mi-ogura@naa.att.ne.jp

Abstract

A Phase II, multicenter clinical trial of bendamustine plus rituximab (BR) regimen was conducted in previously untreated patients with high-tumor-burden indolent B-cell non-Hodgkin lymphoma (B-NHL) and previously untreated elderly patients with mantle cell lymphoma (MCL) in Japan. Bendamustine 90 mg/m^2/day on days 1 and 2, as well as rituximab 375 mg/m^2 on day 1 were administered intravenously up to six cycles. The primary endpoint was the complete response (CR) rate as assessed by the International Workshop Response Criteria (1999). Sixty-nine patients (59 with indolent B-NHL and 10 with MCL) were treated. The median number of delivered cycles was six (range: 1–6). The CR rates were 67.8% [95% confidence interval (CI): 54.4–79.4%] and 70.0% (95% CI: 34.8–93.3%) for indolent B-NHL and MCL, respectively. Estimated progression-free survival at 30 months was 72.1% (95% CI: 58.5–82.0%) in indolent B-NHL and was 67.5% (95% CI: 29.1–88.2%) in MCL. Major grade 3/4 toxicities were hematologic and included lymphopenia (97%), CD4 lymphopenia (91%), and neutropenia (86%), and leukopenia (83%). No treatment-related death was found. The BR regimen showed high efficacy, as evidenced by the expected CR rate, and durable response, as well as an acceptable safety profile for the study populations.

Key words: bendamustine, rituximab, indolent B-cell non-Hodgkin lymphoma, mantle cell lymphoma, first-line therapy

Introduction

Combination chemotherapy with rituximab is a standard of care for previously untreated patients with high-tumor-burden follicular lymphoma (FL)—a major indolent B-cell non-Hodgkin lymphoma (B-NHL). Despite arduous efforts to improve clinical outcomes of therapeutic modalities to date, the optimal initial immunochemotherapy with the demonstrated superiority of overall survival (OS) is still not established [1-3]. Although rituximab plus cyclophosphamide, doxorubicin, vincristine, and prednisone (R-CHOP) is a standard therapeutic option for previously untreated elderly patients with mantle cell lymphoma (MCL) [4, 5], R-CHOP has not demonstrated improvements in the OS or progression-free survival (PFS) in this population [6].

Bendamustine is a cytotoxic alkylating agent, a bifunctional mechlorethamine derivative with the purine-like benzimidazole ring [7]. Bendamustine, when used as monotherapy or in combination with rituximab, has shown high efficacy and an acceptable safety profile for patients with relapsed/refractory B-NHL and MCL [8-13]. Bendamustine is in extensive clinical use for these malignancies in many countries including Europe, Japan, and North America.

There are two major Phase III clinical trials of the bendamustine and rituximab (BR) regimen conducted by the German and international investigator groups in previously untreated patients with indolent B-NHL or MCL: the StiL NHL 1-2003 (StiL-1) [14] and the BRIGHT Study [15]. The former showed its superiority of the BR regimen to R-CHOP in PFS and less toxicity, while

the latter indicated its noninferiority to R-CHOP/R-cyclophosphamide, vincristine, and prednisone (R-CVP) in CR rate and differences in safety profile. In Europe, furthermore, recent clinical studies in patients with indolent non-follicular B-NHL or mucosa-associated lymphoid tissue lymphoma showed the efficacy and tolerability of the BR regimen [16, 17], and retrospective studies in patients with indolent B-NHL or MCL demonstrated the efficacy and safety of the BR regimen in real-world clinical practice [18, 19]. Therefore, the BR regimen has become recognized as a standard regimen for these patients in Western countries. In Asian countries, by contrast, no clinical evidence has been obtained to demonstrate the efficacy or safety of the BR regimen for the relevant patients. We hence conducted the present phase II study to obtain the evidence for previously untreated patients with indolent B-NHL and previously untreated elderly patients with MCL in Japan.

Patients and Methods

Study design and subjects

A prospective, multicenter, single-arm, open-label, phase II clinical study was conducted at 21 medical institutions in Japan from November 9, 2011, through November 15, 2013. Previously untreated patients were considered eligible when meeting all of the following criteria: 1) CD20-positive, advanced indolent B-NHL [small lymphocytic lymphoma, splenic marginal zone lymphoma, lymphoplasmacytic lymphoma, extranodal marginal zone lymphoma of mucosa-associated lymphoid tissue, nodal marginal zone lymphoma, and follicular lymphoma (grades 1, 2, and 3a)] or MCL that was histopathologically confirmed based on World Health Organization Classification 2008 [20]; 2) B-NHL patients aged 20-79 years and MCL in patients aged 66-79 years; 3) high-tumor-burden indolent B-NHL defined as follows—a) bulky disease more than 7 cm in major axis on CT scans (excluding the spleen), b) three or more lymph node regions more than 3 cm in major axis on CT scans, c) B symptoms, d) elevated serum lactate dehydrogenase or beta 2 microglobulin, e) symptomatic splenomegaly, f) compression symptoms, and g) pleural effusions/ascites; 4) a measurable lesion [major axis on computed tomography (CT) scans: > 1.5 cm]; 5) Eastern Cooperative Oncology Group performance status: 0-2; and 6) patients with the adequately maintained function of principal organs (bone marrow, liver, kidneys, lungs, and heart)—a) neutrophil count: $\geq 1{,}500/mm^3$, b) platelet count: $\geq 75{,}000/mm^3$, c) aspartate aminotransferase (AST): $\leq$ 3-fold the upper limit of normal (ULN) at the institution; d)

alanine aminotransferase (ALT): ≤ 3-fold the ULN at the institution; e) total bilirubin: ≤ 1.5-fold the ULN at the institution; f) serum creatinine: ≤ 1.5-fold the ULN at the institution; g) arterial partial pressure of oxygen (PaO_2): ≥ 65 mmHg; h) electrocardiogram showing no abnormalities that require treatment; and i) left ventricular ejection fraction: ≥ 55%. The key exclusion criteria were as follows: histopathologically confirmed transformation; administration or transfusion of cytokines; positivity for the HBs antigen, anti-HCV antibody, or anti-HIV antibody; involvement of the central nervous system or clinical symptoms suggesting the involvement; active double cancer; pregnant or probably pregnant women; and men and women who give no consent to contraception. At screening, histopathological diagnoses were made at each participating medical institution. An independent expert pathological review panel ensured the precision of histopathological diagnoses made among medical institutions after the termination of the treatment. All patients provided written informed consent, and the protocol was approved by the institutional review board at respective institutions. The present study complied with the Declaration of Helsinki, was conducted in compliance with the Good Clinical Practice guidelines in effect, and was registered with ClinicalTrials.gov (NCT01718691).

Treatment

Bendamustine 90 mg/m^2/day was administered intravenously on days 1 and 2, and rituximab 375 mg/m^2 on day 1 (day 0 in cycle 1). The 28-day cycle was conducted up to six cycles.

Furthermore, the dose of bendamustine was reduced from 90 mg/m^2/day to 60 mg/m^2/day when falling under any of the following dose reduction criteria in the previous cycle: grade 4 neutropenia (< 500/mm^3) lasting for 1 or more weeks; febrile neutropenia, ≥ grade 3 neutropenia (< 1,000/mm^3) involving fever ≥ 38°C that lasts for 3 days; platelet count: < 25,000/mm^3; a bleeding tendency requiring blood transfusion; and adverse events which the investigator has admitted the need for dose reduction. The administration of bendamustine was discontinued when again falling under any of the criteria at the dose of 60 mg/m^2/day. The second and subsequent cycles were initiated after having verified the following criteria: neutrophil count: ≥ 1,000/mm^3; platelet count, ≥ 75,000/mm^3; AST and ALT ≤ 5-fold the ULN at each institution; total bilirubin, ≤ 3-fold the ULN at each institution; serum creatinine, ≤ 3-fold the ULN at each institution; and no persistence of ≥ grade 3 adverse events at assessment.

Patients received acetaminophen and chlorpheniramine to prevent or alleviate the infusion-related reaction of rituximab, and the administration of the following drugs to patients was recommended: dexamethasone; 5-hydroxytryptamine 3 receptor antagonists and/or neurokinin 1 receptor antagonists to prevent or alleviate nausea/vomiting as needed; and sulfamethoxazole-trimethoprim and acyclovir to prevent opportunistic infections caused by *Pneumocystis jirovecii* (PJP) and herpes zoster virus, respectively, when CD4+ lymphocyte counts became 200/mm^3 or below. The administration of granulocyte colony-stimulating factors (G-CSFs) was allowed after the verification of grade 3 neutropenia in cycle 1 and on day 3 or later in cycles 2 to 6.

Efficacy and Safety Assessments

The primary endpoint was the complete response (CR) [CR plus unconfirmed CR] rate that was evaluated after cycle 3 and at the completion of the final cycle by the independent review committee (IRC) in accordance with International Workshop to Standardize Response Criteria for Non-Hodgkin's Lymphoma (IWRC) [21].

The secondary endpoints were the overall response rate [ORR: CR, unconfirmed CR, and partial response] that was assessed according to the IWRC, the CR rate and the ORR according to Revised Response Criteria for Malignant Lymphoma (revised RC) [22], PFS, duration of response (DOR), and OS. Furthermore, the follow-up investigation on PFS, OS, and safety was conducted for patients who gave consent after the completion of the present study.

CT was conducted at the time of recruitment, as well as in cycle 3 and the final cycle. Positron emission tomography was conducted in patients who had [^{18}F]fluorodeoxyglucose avidity at baseline [22]. The safety of the BR regimen was assessed using Common Terminology Criteria for Adverse Events (CTCAE) version 4.0.

Statistical analyses

Regarding indolent B-NHL, sample size was calculated to be 52 under the following conditions: the expected CR rate, 66% [95% confidence interval (CI): 47-81%]; the threshold CR rate, 47% [23]; α value: 0.025 (one-tailed); and β value: 0.20. The size was calculated to be 57 in

consideration of the exclusion rate of 10% from statistical analyses. Regarding MCL, sample size was calculated to be 10 under the following conditions: the expected CR rate: 38%; the threshold CR rate: 8%; α value, 0.05 (one-tailed); and β value, 0.20.

The safety analysis set (SAS) consisted of patients who received at least one medication, and the full analysis set (FAS) comprised patients who remained after the exclusion from the SAS. The CR rate and the ORR were calculated to precisely compute the 95% CI based on the binominal probability. PFS, DOR, and OS were computed according to the Kaplan-Meier method. The median value and its 95% CI were calculated according to Greenwoods formula. All statistical analyzes were made with SAS version 9.1.3 (SAS Institute Inc., Cary, NC, USA).

Results

Patient characteristics at baseline

Seventy patients were enrolled, and one was excluded due to positivity for the HBs antigen that was found after recruitment; therefore, 69 underwent the BR regimen and constituted each of the SAS and FAS. Patient characteristics at baseline are shown in Table 1. Fifty-nine of 69 patients had indolent B-NHL, with a median age of 62 years (range: 39-79 years). FL was most predominant (51 patients) by histology. Ten patients (median age: 70 years; range: 67-77 years) had MCL. The independent expert pathological review panel ensured the precision of histopathological diagnoses made among medical institutions after the termination of the treatment and then verified the absence of any discrepancies in the diagnoses.

Efficacy

Best overall responses assessed by the IRC according to the IWRC are shown in Table 2. The CR rate for all-type histology was 68.1% (47/69 patients; 95% CI: 55.8-78.8%). The CR rate for indolent B-NHL was 67.8% (40/59 patients; 95% CI: 54.4-79.4%), thus exceeding its expected CR rate of 66%; furthermore, the lowest limit for 95% CI (54.4%) exceeded the threshold CR rate of 47%. Similarly, the CR rate 70.0% (7/10 patients; 95% CI: 34.8-93.3%) for MCL exceeded the expected CR rate of 38%; furthermore, the lowest limit for 95% CI (34.8%) exceeded the threshold CR rate of 8%.

The ORR assessed by the IRC according to the IWRC was 95.7% (66/69 patients; 95% CI: 87.8-99.1%) for all-type histology, 96.6% (57/59 patients; 95% CI: 88.3-99.6%) for indolent B-NHL, and 90.0% (9/10 patients; 95% CI: 55.5-99.7%) for MCL. The same ORR for these histologies was obtained when calculated according to the revised RC as well. The CR rate was 66.7% (46/69 patients; 95% CI: 54.3-77.6%) for all-type histology, 64.4% (38/59 patients; 95% CI: 50.9-76.4%) for indolent B-NHL, and 80.0% (8/10 patients; 95% CI: 44.4-97.5%) for MCL. Subgroup analysis on patients with indolent B-NHL revealed that the CR rate and the ORR as assessed by the IRC according to the IWRC for follicular lymphoma (n = 51) were 66.7% and 98.0%, respectively.

At the median follow-up of 30.1 months (range: 1.9-39.3 months), 21 events (including 15 cases of progressive disease) occurred. Therefore, the median PFS was not reached (Figure 1). PFS at 30 months in patients with all-type histology was estimated to be 71.5% (95% CI, 58.9-80.8%). PFS at 30 months was estimated to be 72.1% (range: 58.5-82.0%) for patients with indolent B-NHL and to be 67.5% (range: 29.1-88.2%) for patients with MCL. No death occurred during the follow-up.

Safety

The median of delivered cycles was 6 (range: 1-6), and 52 patients (75%) received BR in six cycles. Thirteen patients discontinued treatment due to neutropenia, two due to disease progression, one due to the investigator’s discretion, and one due to grade 3 rash unrelated to the

BR regimen. Dose delay (54%, 37/69 patients) was required in one or more cycles delivered, and dose was reduced in 12% (8/69 patients). Relative dose intensity was 89.6 ± 9.4%.

A total of 2,278 episodes of adverse effects (AEs) developed in all 69 patients. Hematologic and nonhematologic AEs by grade are shown in Tables 3 and 4, respectively. Major AEs among grade 3/4 hematologic AEs were lymphopenia (97%), CD4 lymphopenia (91%), neutropenia (86%), and leukopenia (83%) (Table 3). Forty-eight patients (70%) received G-CSFs, 12 of whom discontinued treatment in less than six cycles due to neutropenia. Major nonhematologic AEs were nausea, constipation, malaise, decreased immunoglobulin M, anorexia, rash, and infusion-related reaction (Table 4). Major grade 3 nonhematologic AEs were two cases (3%) each of infusion-related reaction, increased alanine aminotransferase, increased aspartate aminotransferase, anorexia, erythroderma, maculopapular rash, and rash.

Ten episodes of serious AEs occurred in nine patients. There were three cases of febrile neutropenia, as well as one case each of tumor lysis syndrome, breast cancer, cytomegalovirus pneumonia, allergic dermatitis, chromosomal aberration, atrial tachycardia, and fever. All patients with these serious AEs recovered.

Infections occurred in 42 (61%) among 69 patients, the majority of which were grade 2 or lower AEs. The most predominant infections were fever (25%) and nasopharyngitis (20%) (Table 4). Grade 3 infections occurred in five patients: three patents with febrile neutropenia; and one patient each with cytomegalovirus pneumonia and bacterial infection. Grade 4 infection did not

occur. Sixty-seven patients (97%) underwent prophylaxis with sulfamethoxazole-trimethoprim, and PJP did not occur. Fifty-seven patients (83%) underwent prophylaxis with acyclovir, and the reactivation of varicella-zoster virus (VZV) occurred in one of 12 patients who had not undergone the prophylaxis. Treatment-related death was not found. Secondary cancer was diagnosed in one patient with breast cancer at 5 months after administration completion.

Discussion

To assess the clinical usefulness of the BR regimen as first-line therapy for indolent B-NHL and MCL in an attempt to make comparisons with previous clinical studies in countries outside Japan, we established the CR rate as the primary endpoint in the present explorative phase II study. The CR rate exceeded the expected and threshold CR rates, and we thus verified the efficacy of the BR regimen for the study population.

Two, randomized, open-label, noninferiority, phase III clinical trials of the BR regimen have been conducted in previously untreated patients with indolent B-NHL or MCL. One is the StiL-1 Study [14] that compared BR with R-CHOP, which described the comparable ORRs between the BR group and the R-CHOP group (93% vs. 91%); the BR group showed a significantly higher CR rate (40% vs. 30%; $P = 0.021$) and a significantly longer median PFS (69.5 months vs. 31.2 months; $P < 0.0001$). BR was better tolerated by patients than R-CHOP. Another is the BRIGHT Study [15] that compared BR with a standard rituximab-containing chemotherapy regimen—R-CHOP/R-CVP. The BR group showed a significantly better ORR (97% vs. 91%; $P = 0.0102$), and BR was not inferior to R-CHOP/R-CVP with respect to the CR rate assessed by the IRC (31% vs. 25%; CR rate ratio: 1.26; $P = 0.0225$). The data on time-to-event (i.e., PFS, event-free survival, and OS) remain to be collected.

The CR rate of patients with all-type histology in the present study was 68.1%, thus exceeding those of the StiL-1 Study (40%) and the BRIGHT Study (31%). On the other hand, the

ORRs were equivalent among the present study (95.7%), the StiL-1 Study (93%), and the BRIGHT Study (97%). Age range and the proportion of patients with MCL were nearly equivalent among these three studies. The proportions of patients with clinical stage III/IV and patients in the “follicular lymphoma international prognostic index high” subgroup (78% and 29%, respectively) were lower in the present study than in the StiL-1 Study (97% and 46%, respectively) and the BRIGHT Study (90% and 43%, respectively). Therefore, we speculate that the lower proportion of patients with high-risk indolent B-NHL at baseline possibly influenced the outcomes in favor of our study. PFS at 30 months in our study (72.1%) is nearly equivalent to the datum extractable from the figure of StiL-1 Study, thus inferring the long-term duration of response.

Comparisons among the StiL-1 Study [14], the BRIGHT Study [15], and the present study with respect to G3/4 hematologic AEs revealed no differences in the safety profile except for the incidence of neutropenia. Concretely, the incidences of neutropenia exceeded 80% in our study in contrast to those described in the prior two studies, thus indicating large differences. We cannot specify the causes for this fact, although a racial difference and/or differences in prophylaxis practice using G-CSFs in two studies [14, 15] as compared with our study are conceivable.

The incidences of nonhematologic AEs differ among these three studies, and the majority were categorized to grade 2 or lower and were manageable clinically. Concretely, the incidence of infections (61%) in our study was higher than 37% in StiL-1 Study and was nearly equivalent

to 54.3% in the BRIGHT Study. However, all the infections in our study were manageable clinically. We prospectively examined the immunological functions of patients in each cycle because of concern about CD4 lymphopenia potentially caused by the BR regimen [24, 25] and found the high incidence (91%, 63/69 patients) of grade 3/4 CD4 lymphopenia. In the present study, prophylaxis using sulfamethoxazole-trimethoprim and acyclovir was recommended for patients who had grade 3/4 CD4 lymphopenia. Indeed, 97% and 83% of patients underwent prophylaxis with the respective drugs. Consequently, PJP did not occur, and the reactivation of VZV occurred in one of 12 patients who had not undergone the prophylaxis. These findings suggest the need for the prophylaxis in patients undergoing the BR regimen. There were only one case of grade 1 alopecia and three cases of grade 1 peripheral neuropathy. Our study provides the safety profile similar to that described in previous clinical trials in Japanese patients with relapsed/refractory indolent B-NHL [12, 13].

In conclusion, the BR regimen showed high efficacy and an acceptable safety profile for previously untreated patients with high-tumor-burden indolent B-NHL and previously untreated elderly patients with MCL not eligible for ASCT in Japan. Therefore, the BR regimen is of clinical relevance and can be a therapeutic option also for these patient populations.

Acknowledgments

We thank patients, investigators, and staff who were involved in the present study. Research support was provided by SymBio Pharmaceuticals Ltd. We also thank Satoshi Sakima, MD, for his gracious review of the manuscript. This work was supported by SymBio Pharmaceuticals Ltd. and Eisai Co., Ltd.

Conflict of interest

Dr. Ogura has received research funding from SymBio; and has received honoraria from Takeda, Mundipharma, Meiji Seika Pharma, and Celgene. Dr. Ishizawa has received research funding from Kyowa Hakko Kirin, MSD, Celgene, and Pfizer; and has received honoraria form Kyowa Hakko Kirin, Chugai, and Takeda. Dr. Maruyama has received honoraria from Eisai, Takeda, Chugai, Janssen, Nippon Kayaku, Celgene, Mundipharma, Sanofi, Kyowa Hakko Kirin, Mochida, and Ono. Dr. Ando has received research funding form Kyowa Hakko Kirin. Dr. Izutsu has received honoraria and research funding from Eisai. Dr. Terui has received honoraria form Janssen. Dr. Tsukasaki has received research funding from Eisai, Celgene, Takeda, and Mundipharma; and has received honoraria from Zenyaku Kogyo, HUYA, and Chugai. Dr. Usuki has received honoraria from Nippon Shinyaku, MSD, Kyowa Hakko Kirin, Novartis, Bristol-Meyer-Squibb, and Dainippon Sumitomo. Dr. Kinoshita has received research funding form Eisai, Solasia, and has received honoraria from Eisai, Zenyaku Kogyo, Janssen, Chugai, and Kyowa Hakko Kirin. Dr. Suzumiya has received research funding from Eisai, Kyowa Hakko Kirin, Chugai, Astellas, and Toyama Chemical; and has received honoraria from Eisai, Chugai, and Takeda. Dr. Nagai has received research funding from CIMIC, Janssen, Mundipharma, Takeda, Bristol-Myers Squibb, and Otsuka; and has received honoraria from Chugai. GY has received honoraria form Takeda, Celgene, and Janssen. Dr. Tobinai has received research funding from Eisai, Chugai, Kyowa Hakko Kirin, Ono, Celgene, Janssen, GlaxoSmithKline,

Mundipharma, Takeda, Servier, and AbbVie; and has received honoraria from Eisai, Janssen, Mundipharma, Takeda, Zenyaku Kogyo, and HUYA.

All remaining authors have declared no conflicts of interest.

References

1. Dreyling M, Ghielmini M, Marcus R, Salles G, Vitolo U, Ladetto M. Newly diagnosed and relapsed follicular lymphoma: ESMO Clinical Practice Guidelines for diagnosis, treatment and follow-up. Ann Oncol. 2014; 25:iii76-82.
2. Hiddemann W, Cheson BD. How we manage follicular lymphoma. Leukemia. 2014;28: 1388-95.
3. Kahl BS, Yang DT. Follicular lymphoma: evolving therapeutic strategies. Blood. 2016; 127:2055-63.
4. Dreyling M, Geisler C, Hermine O, Kluin-Nelemans HC, Le Gouill S, Rule S, et al. Newly diagnosed and relapsed mantle cell lymphoma: ESMO Clinical Practice Guidelines for diagnosis, treatment and follow-up. Ann Oncol. 2014;25:iii83-92.
5. Dreyling M, Ferrero S, Hermine O. How to manage mantle cell lymphoma. Leukemia. 2014;28:2117-30.
6. Lenz G, Dreyling M, Hoster E, Wörmann B, Dührsen U, Metzner B, et al. Immunochemotherapy with rituximab and cyclophosphamide, doxorubicin, vincristine, and prednisone significantly improves response and time to treatment failure, but not long-term outcome in patients with previously untreated mantle cell lymphoma: results of a prospective randomized trial of the German Low Grade Lymphoma Study Group (GLSG). J Clin Oncol. 2005;23:1984-92.

7. Cheson BD, Rummel MJ. Bendamustine: rebirth of an old drug. J Clin Oncol. 2009;27: 1492-501.
8. Rummel MJ, Al-Batran SE, Kim SZ, Welslau M, Hecker R, Kofahl-Krause D, et al. Bendamustine plus rituximab is effective and has a favorable toxicity profile in the treatment of mantle cell and low-grade non-Hodgkin's lymphoma. J Clin Oncol. 2005;23:3383-9.
9. Robinson KS, Williams ME, van der Jagt RH, Cohen P, Herst JA, Tulpule A, et al. Phase II multicenter study of bendamustine plus rituximab in patients with relapsed indolent B-cell and mantle cell non-Hodgkin's lymphoma. J Clin Oncol. 2008;26:4473-9.
10. Friedberg JW, Cohen P, Chen L, Robinson KS, Forero-Torres A, La Casce AS, et al. Bendamustine in patients with rituximab-refractory indolent and transformed non-Hodgkin's lymphoma: results from a phase II multicenter, single-agent study. J Clin Oncol. 2008;26 204-10.
11. Kahl BS, Bartlett NL, Leonard JP, Chen L, Ganjoo K, Williams ME, et al. Bendamustine is effective therapy in patients with rituximab-refractory, indolent B-cell non-Hodgkin lymphoma: results from a Multicenter Study. Cancer. 2010;116:106-14.
12. Ogura M, Uchida T, Taniwaki M, Ando K, Watanabe T, Kasai M, et al. Phase I and pharmacokinetic study of bendamustine hydrochloride in relapsed or refractory indolent B-cell non-Hodgkin lymphoma and mantle cell lymphoma. Cancer Sci. 2010;101:2054-8.

13. Ohmachi K, Ando K, Ogura M, Uchida T, Itoh K, Kubota N, et al. Multicenter phase II study of bendamustine for relapsed or refractory indolent B-cell non-Hodgkin lymphoma and mantle cell lymphoma. Cancer Sci. 2010;101:2059-64.
14. Rummel MJ, Niederle N, Maschmeyer G, Banat GA, von Grünhagen U, Losem C, et al. Bendamustine plus rituximab versus CHOP plus rituximab as first-line treatment for patients with indolent and mantle-cell lymphomas: an open-label, multicentre, randomised, phase 3 non-inferiority trial. Lancet. 2013;381: 1203-10.
15. Flinn IW, van der Jagt R, Kahl BS, Wood P, Hawkins TE, Macdonald D, et al. Randomized trial of bendamustine-rituximab or R-CHOP/R-CVP in first-line treatment of indolent NHL or MCL: the BRIGHT study. Blood. 2014;123:2944-52.
16. Luminari S, Goldaniga M, Cesaretti M, Orsucci L, Tucci A, Pulsoni A, et al. A phase II study of bendamustine in combination with rituximab as initial treatment for patients with indolent non-follicular non-Hodgkin lymphoma. Leuk Lymphoma. 2016;57:880-7.
17. Salar A, Domingo-Domenech E, Panizo C, Nicolás C, Bargay J, Muntañola A et al. First-line response-adapted treatment with the combination of bendamustine and rituximab in patients with mucosa-associated lymphoid tissue lymphoma (MALT2008-01): a multicentre, single-arm, phase 2 trial. Lancet Haematol. 2014;1:e104-11.
18. Becker M, Tschechne B, Reeb M, Schwinger U, Bruch HR, Frank M, et al. Bendamustine as first-line treatment in patients with advanced indolent non-Hodgkin lymphoma and mantle cell lymphoma in German routine clinical practice. Ann Hematol. 2015;94:1553-8.

19. Mondello P, Steiner N, Willenbacher W, Wasle I, Zaja F, Zambello R, et al. Bendamustine plus rituximab versus R-CHOP as first-line treatment for patients with indolent non-Hodgkin's lymphoma: evidence from a multicenter, retrospective study. Ann Hematol. 2016;95:1107-14.
20. Swerdlow SH, Campo E, Harris NL, Jaffe ES, Pileri SA, Stein H, et al. WHO Classification of Tumours of Haematopoietic and Lymphoid Tissues, Fourth Edition. Lyon:IARC; 2008.
21. Cheson BD, Horning SJ, Coiffier B, Shipp MA, Fisher RI, Connors JM, et al. Report of an international workshop to standardize response criteria for non-Hodgkin's lymphomas. J Clin Oncol. 1999;17:1244-53.
22. Cheson BD, Pfistner B, Juweid ME, Gascoyne RD, Specht L, Horning SJ, et al. Revised response criteria for malignant lymphoma. J Clin Oncol. 2007;25:579-86.
23. Ogura M, Morishima Y, Kagami Y, Watanabe T, Itoh K, Igarashi T, et al. Randomized phase II study of concurrent and sequential rituximab and CHOP chemotherapy in untreated indolent B-cell lymphoma. Cancer Sci. 2006;97:305-12.
24. Ogura M, Ando K, Taniwaki M, Watanabe T, Uchida T, Ohmachi K, et al. Feasibility and pharmacokinetic study of bendamustine hydrochloride in combination with rituximab in relapsed or refractory aggressive B cell non-Hodgkin's lymphoma. Cancer Sci. 2011;102:1687-92.
25. Ohmachi K, Niitsu N, Uchida T, Kim SJ, Ando K, Takahashi N, et al. Multicenter phase II study of bendamustine plus rituximab in patients with relapsed or refractory diffuse large B-cell lymphoma. J Clin Oncol. 2013;31:2103-9.

Figure legends

Fig. 1 Progression-free survival (assessed by independent review committee)

iNHL: indolent B-cell non-Hodgkin lymphoma; MCL: mantle cell lymphoma

Int J Hematol (2016) 104:548–558
DOI 10.1007/s12185-016-2065-4

ORIGINAL ARTICLE

Interim analysis of post-marketing surveillance of eculizumab for paroxysmal nocturnal hemoglobinuria in Japan

Haruhiko Ninomiya[1,19] · Naoshi Obara[2,19] · Shigeru Chiba[2,19] · Kensuke Usuki[3,19] · Kaichi Nishiwaki[4,19] · Itaru Matsumura[5,19] · Tsutomu Shichishima[6,19] · Shinichiro Okamoto[7,19] · Jun-ichi Nishimura[8,19] · Kazuma Ohyashiki[9,19] · Shinji Nakao[10,19] · Kiyoshi Ando[11,19] · Yoshinobu Kanda[12,19] · Tatsuya Kawaguchi[13,19] · Hideki Nakakuma[14,19] · Daisuke Harada[15] · Hirozumi Akiyama[15] · Taroh Kinoshita[16,19] · Keiya Ozawa[17,19] · Mitsuhiro Omine[18,19] · Yuzuru Kanakura[8,19]

Received: 28 April 2016 / Revised: 13 July 2016 / Accepted: 13 July 2016 / Published online: 27 July 2016

Abstract Data characterizing the safety and effectiveness of eculizumab in patients with paroxysmal nocturnal hemoglobinuria (PNH) are limited. We describe the safety and effectiveness of eculizumab in PNH patients enrolled in a post-marketing surveillance study. Types and frequencies of observed adverse events were similar to those reported in previous clinical trials and no meningococcal infection was reported. Effectiveness outcomes included the reduction of intravascular hemolysis, the change in hemoglobin (Hb) level, the withdrawal of transfusion and corticosteroids, the change of renal function, and overall survival. The effect of eculizumab on intravascular hemolysis was demonstrated by a reduction in lactate dehydrogenase levels at all measurements after baseline. Significant increases in Hb levels from baseline were also observed after 1 month's treatment with eculizumab ($p < 0.01$). Of those who were transfusion-dependent at baseline, the median number of transfusions decreased significantly from 18 to 0 unit/year after 1 year of treatment with eculizumab ($p < 0.001$). An increase in Hb and a high rate of transfusion independence were observed, especially in patients with platelet count $\geq 150 \times 10^9$/L. Approximately 97 % of patients showed

✉ Haruhiko Ninomiya
ninomiya.haruhiko.ft@u.tsukuba.ac.jp

1 Department of Medical Sciences, Faculty of Medicine, University of Tsukuba, 1-1-1 Tennodai, Tsukuba, Ibaraki 305-8575, Japan

2 Department of Hematology, Faculty of Medicine, University of Tsukuba, Tsukuba, Japan

3 Department of Hematology, NTT Medical Center Tokyo, Tokyo, Japan

4 Division of Oncology and Hematology, Department of Internal Medicine, Jikei University Kashiwa Hospital, Kashiwa, Japan

5 Division of Hematology, Kinki University, Osakasayama, Japan

6 Department of Cardiology and Hematology, Fukushima Medical University, Fukushima, Japan

7 Division of Hematology, Department of Internal Medicine, Keio University, Tokyo, Japan

8 Department of Hematology and Oncology, Osaka University, Suita, Japan

9 Department of Hematology, Tokyo Medical University, Tokyo, Japan

10 Hematology/Respiratory Medicine, Kanazawa University, Kanazawa, Japan

11 Division of Hematology and Oncology, Tokai University, Isehara, Japan

12 Division of Hematology, Jichi Medical University, Shimotsuke, Japan

13 Departments of Hematology and Infectious Diseases, Kumamoto University, Kumamoto, Japan

14 Kagoshima Tokushukai Hospital, Kagoshima, Japan

15 Alexion Pharma G.K., Tokyo, Japan

16 Department of Immunoregulation, Research Institute for Microbial Diseases, Osaka University, Suita, Japan

17 IMSUT Hospital, Institute of Medical Science, University of Tokyo, Tokyo, Japan

18 Department of Hematology, Showa University Fujigaoka Hospital, Yokohama, Japan

19 Japan PNH Study Group, Tokyo, Japan

maintenance or improvement of renal function. Overall survival rate was about 90 % (median follow-up 1.9 years). These results suggest an acceptable safety profile and favorable prognosis after eculizumab intervention.

Keywords Paroxysmal nocturnal hemoglobinuria · Eculizumab · Effectiveness · Safety · Post-marketing surveillance

Introduction

Paroxysmal nocturnal hemoglobinuria (PNH) is primarily an acquired clonal disorder of hematopoietic stem cells caused by a somatic mutation of the phosphatidylinositol glycan complementation class A (*PIG-A*) gene [1, 2]. PNH is a progressive and debilitating disease, which is characterized by chronic complement-mediated intravascular hemolysis that can lead to thromboembolism, various organ function impairments, and death [3–7]. Patients with PNH suffer from a poor quality of life (QoL), including disabling symptoms of fatigue, recurrent abdominal pain, chest pain, and hemoglobinuria [3, 7–9].

Eculizumab, a recombinant humanized monoclonal antibody (h5G1.1-mAb), binds to the terminal complement protein C5 and inhibits cleavage of C5 into C5a and C5b, preventing both the release of the anaphylatoxin C5a and the formation of the membrane attack complex (MAC), which induces red blood cell lysis [10]. Several clinical trials of eculizumab in adults with PNH showed dramatic reductions in hemolysis, transfusion requirements, and episodes of hemoglobinuria, as well as improvement in QoL [11–17]. On the other hand, inhibition of the MAC formation might indicate a safety concern with eculizumab due to increased infection risk, particularly with meningococcus [18].

Following the approval of eculizumab in 2010 in Japan for the reduction of hemolysis in patients with PNH, a regulatory-mandated post-marketing surveillance (PMS) was initiated to characterize the long-term safety and effectiveness of eculizumab in PNH patients treated with eculizumab in a real-world setting. This interim analysis summarizes the safety and effectiveness of eculizumab in PNH patients treated with eculizumab between June 2010 and March 2014.

The objectives of the analyses were to: (1) evaluate the long-term safety of eculizumab, and (2) assess effectiveness of eculizumab on intravascular hemolysis reduction [as measured by lactate dehydrogenase (LDH)], change of hemoglobin (Hb) level, transfusion units, corticosteroid usage, estimated glomerular filtration rate (eGFR) as a marker for renal function, and overall survival. Some of the assessments were also stratified by the baseline presence of bone marrow failure (BMF).

Materials and methods

Study design and population

As PNH is an extremely rare disease and data regarding safety and efficacy of eculizumab are limited in patients with PNH, the Japan regulatory body requested Alexion Pharma GK (Alexion) to monitor all PNH patients who were treated with eculizumab (Soliris®).

As a mandatory condition of eculizumab approval, all PNH patients, who were diagnosed by flow cytometry (FCM) and/or 'Ham test and Sugar-water test' and treated with eculizumab in Japan, were enrolled in this prospective, observational, PMS study. Patients were diagnosed by physicians according to the Japanese Reference Guide on Clinical Practice for PNH [19] with the decision to treat with eculizumab made at the discretion of the treating physician. The PMS protocol was reviewed by the Institutional Review Board in each medical facility. However, since this was a mandatory surveillance study, informed consent from individual patients was not necessary, as per Japanese health authority regulations.

Data collection

Each physician entered patient-level data into a case report form (CRF) using patient medical records. CRFs are collected annually, however, patient-level data were collected at baseline and at the following intervals after the first eculizumab dose during the first year: 1 week, 2 weeks, 1 month, 3, 6, 9, and 12 months. Follow-up continues until death, or withdrawal of eculizumab for any reason. Follow-up for patients discontinuing treatment with eculizumab is continued until 8 weeks after withdrawal of eculizumab.

Data captured include demographics, method of PNH diagnosis, date and first dose of eculizumab, medical history, concomitant medications, comorbidities, adverse events (AEs), and clinical laboratory tests during eculizumab intervention, including LDH in serum, Hb, and creatinine measurements.

Treatment

Patients received 600 mg of intravenous eculizumab weekly for the first 4 weeks, followed by 900 mg for the fifth dose 1 week later, then 900 mg every 2 weeks thereafter. All patients must be vaccinated with a meningococcal vaccine at least 2 weeks prior to receiving the first dose of eculizumab.

Analytic cohort

This interim analysis includes all patients ($n = 319$) enrolled in the PMS database for eculizumab between June 2010 and March 2014 with physician agreement on data publication. Although 433 patients had been enrolled in the PMS database between June 2010 and March 2014, physician consent for publication had not been received for 114 patients at the time of this analysis. These 114 patients have been excluded from the current analysis.

Outcome definitions

Adverse events (AEs), serious adverse events (SAEs), adverse drug reactions (ADRs) and serious adverse drug reactions (SADRs) were defined based on ICH E2A guidelines. AEs were defined as any untoward medical events, not necessarily causally related to eculizumab treatment. SAEs were defined as any AE resulting in hospitalization, prolonged hospitalization, disability, permanent injury, death or that was life-threatening. ADRs were defined as any noxious or unintended responses deemed to be related to eculizumab treatment. SADRs were defined as any ADR resulting in hospitalization, prolonged hospitalization, disability, permanent injury, death or that was life-threatening. Data on all AEs, SAEs, ADRs, SADRs that occurred during the observation period were prospectively monitored and collected.

Transfusion independence, corticosteroid withdrawal, and renal function were outcome measures. Transfusion independence was defined as no transfusion required for 6 months, and was assessed in the subset of patients receiving transfusion at baseline. Corticosteroid withdrawal was defined as no corticosteroid medication use for 1 month. For the corticosteroid withdrawal analysis, patients using corticosteroids at baseline were included and stratified by BMF status at baseline. BMF status was determined by the presence of physician-diagnosed aplastic anemia or myelodysplastic syndrome. Renal function was assessed using the eGFR formula of the Japanese Society of Nephrology [20]. eGFR values at baseline and during eculizumab therapy were calculated using creatinine values before eculizumab and the maximum absolute values of change from baseline, respectively.

Statistical analysis

Patient demographics and disease characteristics at baseline were summarized using means. Frequency and percentages were reported for categorical variables.

The number and incidence of AEs and SAEs during follow-up between June 2010 and March 2014 are reported. Incidence was expressed as the percentage of patients experiencing the AE, SAE, ADR or SADR of interest and was calculated as the number of patients experiencing the AE, SAE, ADR or SADR of interest following first eculizumab dose divided by the total number of patients included in this analysis.

The effectiveness of eculizumab was examined using several outcome measures, including the reduction of LDH levels, the change of Hb levels and eGFR levels, the withdrawal of transfusion and corticosteroids, and overall survival.

Patients with missing baseline laboratory values, such as LDH, Hb, serum creatinine, platelet count, transfusion, and BMF were excluded from the respective analyses. The Steel test was used to examine the association between mean Hb level at baseline and duration of eculizumab treatment, stratified by baseline platelet level ($<50 \times 10^9$/L, ≥ 50 to $<100 \times 10^9$/L, ≥ 100 to $<150 \times 10^9$/L, and $\geq 150 \times 10^9$/L). The Chi-square and the Kruskal–Wallis tests were used to compare eGFR values between baseline and during eculizumab therapy.

Regarding transfusion withdrawal, patients with a history of transfusion within 1 year of baseline were examined in three ways.

1. Transfusion rate (units/year) between 1 year before and after 1 year of eculizumab treatment was compared using the paired *t* test.
2. Kaplan–Meier analyses and the log-rank test were used to assess the accumulated probability of transfusion withdrawal (transfusion independence) in patients with and without BMF.
3. Kaplan–Meier analyses and the log-rank test were used to assess the accumulated probability of transfusion withdrawal by baseline platelet count ($<50 \times 10^9$/L, ≥ 50 to $<100 \times 10^9$/L, ≥ 100 to $<150 \times 10^9$/L, and $\geq 150 \times 10^9$/L).

Patients with less than 1 year of eculizumab intervention, without a history of transfusion, and missing baseline BMF status and platelet count, were excluded from each analysis.

Kaplan–Meir analyses and the log-rank test were used to assess the accumulated probability of corticosteroid withdrawal and overall survival rate in patients with and without BMF.

Results

Patient characteristics

A total of 319 patients were included in the analysis. Patient demographics and disease characteristics are shown in

Table 1 Patient demographics and disease characteristics at baseline ($n = 319$)

Age: mean (SD)	55.1 (17.3)
Female: *n* (%)	165 (51.7)
Disease duration, months[a]: mean (SD)	113.2 (105.7)
Diagnosed by flow cytometry: *n* (%)	251 (78.7)
Comorbidity and history of thromboembolism: *n* (%)	
Aplastic anemia	146 (45.8)
Myelodysplastic syndrome	43 (13.5)
History of thromboembolism	35 (11.0)
Treatment history: *n* (%)	
Corticosteroids	121 (37.9)
Immunosuppressive therapy	62 (19.4)
Anticoagulant	62 (19.4)

SD standard deviation

[a] From PNH diagnosis to start of eculizumab treatment

Table 1. Mean age at baseline was 55.1 years and 51.7 % of the cohort was female. Mean disease duration at baseline was 113.2 months. The Japanese Reference Guide on Clinical Practice for PNH recommends the use of FCM to confirm the presence of glycosylphosphatidylinositol-anchored proteins deficient on peripheral blood cells. Nearly 80 % ($n = 251$) of patients had their disease diagnosed by FCM. It should be noted that the remaining ~20 % of patients enrolled in this PMS study were diagnosed with PNH by non-FCM methods. Most of those patients were diagnosed prior to the development of the Japanese Reference Guide on Clinical Practice for PNH. At the time of this analysis, patients were followed for a median of 1.9 years (range 0.02–6.1). Aplastic anemia and myelodysplastic syndrome were reported as comorbidity in 45.8 and 13.5 % of PNH patients, respectively. Thirty-five patients (11.0 %) had a history of thromboembolism at baseline. One hundred and twenty-one patients (37.9 %) had been treated with corticosteroids prior to baseline, while the number of patients treated with immunosuppressive therapy were 62 (19.4 %) and those with anticoagulants were 62 (19.4 %).

Safety

Between June 2010 and March 2014, 56.1 % (179/319), 26.3 % (84/319), 35.1 % (112/319), 8.5 % (27/319) patients experienced AEs, SAEs, ADRs, and SADRs, respectively. Table 2 shows the incidence of frequently reported AEs (reported in >1 % of patients), SAEs, ADRs and SADRs. Headache was the most commonly reported AE ($n = 69$, 21.6 %), followed by hemolysis ($n = 28$, 8.8 %), and renal impairment ($n = 14$, 4.4 %). The most commonly reported SAEs were pneumonia ($n = 9$, 2.8 %) and hemolysis ($n = 9$, 2.8 %), followed by sepsis ($n = 8$, 2.5 %). Twenty deaths were reported as the last outcome of 31 AEs or SAEs. Those events consisted of death (6), sepsis (3), cerebral hemorrhage, extradural hematoma, pneumonia, aggravated renal dysfunction (2), brain contusion, immunodeficiency, pancytopenia, sudden death, acute cardiac failure, cardiac failure, acute renal failure, acute respiratory failure, deteriorating general condition, disseminated intravascular coagulation (DIC), pulmonary empyema, hepatic cancer, bone cancer, and lung cancer (1). Of these, causal relationship with eculizumab could not be ruled out for sepsis (1 event/1 patient) and cancer (3 events/1 patient). No causal relationship with eculizumab was identified for the other events. As in previous studies [16, 21], no meningococcal infections were reported.

Hemolysis and hemoglobin

An analysis of the association between eculizumab treatment and LDH levels in 272 patients showed that LDH levels during eculizumab treatment were lower at all follow-up measurements compared to baseline (Fig. 1).

Figure 2a shows the effect of eculizumab treatment on mean Hb levels overall, and in Fig. 2b–e, stratified by baseline platelet levels, a possible marker of bone marrow function. Significant increases in Hb levels compared to baseline were observed from 1 month after the first eculizumab treatment, and persisted for 36 months. Mean Hb level at 36 months was 9.38 g/dL, a significant increase compared to the baseline value of 8.02 g/dL (Fig. 2a; $p < 0.001$). Similarly, in patients with platelet counts $\geq 150 \times 10^9$/L ($n = 103$), significant and clear increases in Hb levels compared to baseline were observed at 1 month following the start of eculizumab treatment, which were maintained for 36 months. In this subgroup of patients, mean Hb level at 36 months was 9.72 g/dL, a significantly increase compared to the baseline level of 8.06 g/dL (Fig. 2e; $p < 0.01$). In the subgroups with platelet counts $<150 \times 10^9$/L (Fig. 2b–d), Hb levels were slightly elevated, but were not consistently increased compared to baseline.

eGFR

A total of 196 patients had creatinine values to calculate eGFR at both baseline and during eculizumab treatment, and were analyzed to compare eGFR between baseline and during eculizumab treatment. A total of 49 patients (25 %) moved to the upper range of eGFR, 6 patients (3.1 %) moved to the lower range of eGFR, and 141 patients of 196 (71.9 %) maintained the same range of eGFR between baseline and during eculizumab treatment (Table 3).

Table 2 Incidence of frequently observed AEs (reported in >1 % of patients), SAEs, ADRs and SADRs reported during eculizumab treatment

	Eculizumab-treated patients ($n = 319$)			
	AEs *n* (%)	SAEs *n* (%)	ADRs *n* (%)	SADRs *n* (%)
Overall	179 (56.1)	84 (26.3)	112 (35.1)	27 (8.5)
Headache	69 (21.6)	1 (0.3)	67 (21.0)	1 (0.3)
Hemolysis	28 (8.8)	9 (2.8)	1 (0.3)	1 (0.3)
Renal impairment	14 (4.4)	4 (1.3)	2 (0.6)	1 (0.3)
Pneumonia	12 (3.8)	9 (2.8)	5 (1.6)	3 (0.9)
Nasopharyngitis	11 (3.5)	0	3 (0.9)	0
Upper respiratory tract infections	9 (2.8)	0	1 (0.3)	0
Gastroenteritis	8 (2.5)	1 (0.3)	2 (0.6)	0
Arthralgia	8 (2.5)	2 (0.6)	6 (1.9)	2 (0.6)
Sepsis	8 (2.5)	8 (2.5)	4 (1.3)	4 (1.3)
Urinary tract infections	7 (2.2)	0	1 (0.3)	0
Other infections[a]	6 (1.9)	2 (0.6)	3 (0.9)	2 (0.6)
Death[b]	6 (1.9)	6 (1.9)	0	0
Dizziness	5 (1.6)	0	2 (0.6)	0
Cholelithiasis	5 (1.6)	4 (1.3)	1 (0.3)	0
Back pain	5 (1.6)	2 (0.6)	4 (1.3)	2 (0.6)
Herpes zoster	4 (1.3)	1 (0.3)	2 (0.6)	1 (0.3)
Influenza	4 (1.3)	2 (0.6)	0	0
Upper respiratory tract inflammation	4 (1.3)	0	0	0
Diarrhea	4 (1.3)	0	2 (0.6)	0
Pyrexia	4 (1.3)	2 (0.6)	2 (0.6)	1 (0.3)

See text for definitions of AEs (adverse events), SAEs (serious adverse events), ADRs (adverse drug reactions), and SADRs (serious adverse drug reactions)

[a] Causative organisms unknown

[b] Cause of death not identified

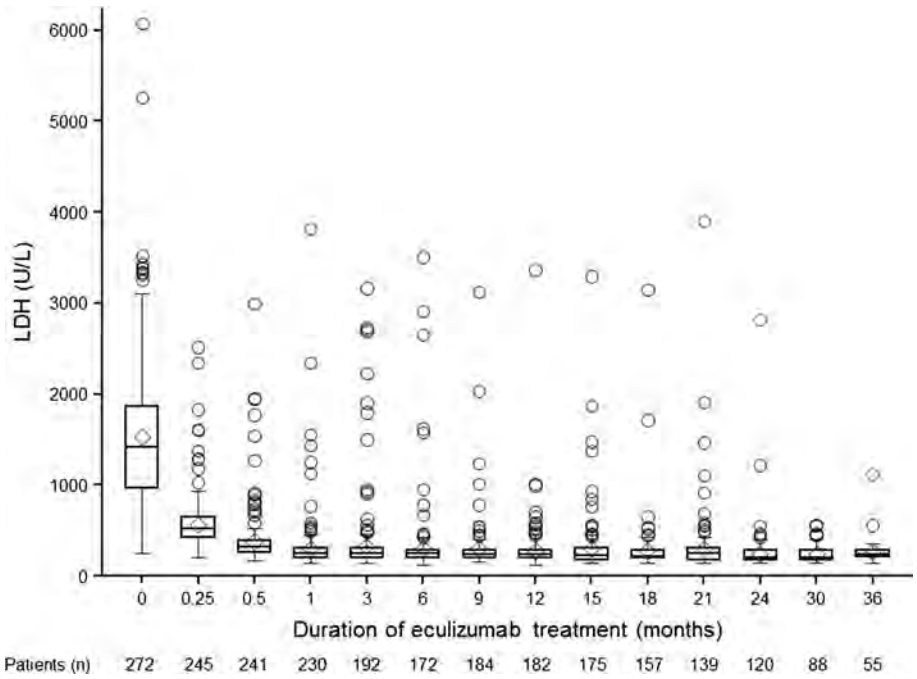

Fig. 1 LDH levels, a marker of intravascular hemolysis during eculizumab treatment. *Middle line in box* represents the median, *lower box* bounds the first quartile, *upper box* bounds the third quartile, and *whiskers* represent the 95 % confidence interval of the mean

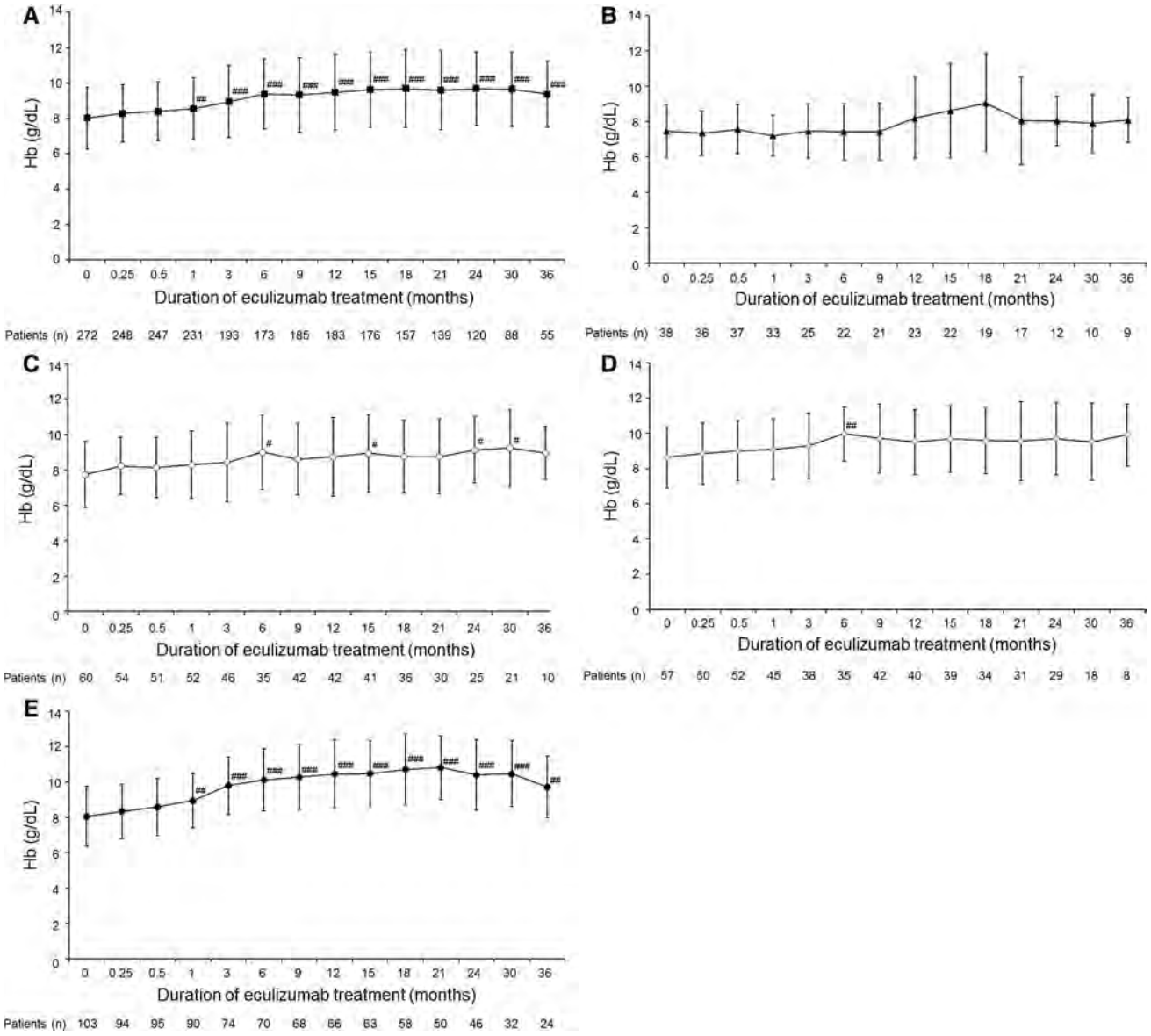

Fig. 2 Hb levels during eculizumab treatment according to baseline platelet level: **a** all patients; stratified by baseline platelet level <50 × 10^9/L (**b**), ≥50 to <100 × 10^9/L (**c**), ≥100 to <150 × 10^9/L (**d**), and ≥150 × 10^9/L (**e**), respectively. Each *symbol* and *vertical bar* represents mean ± SD. #, ##, ###: $p < 0.05$, $p < 0.01$, $p < 0.001$ vs baseline using Steel test

Transfusion

Among patients who were transfusion-dependent at baseline, the number of transfusion units/year was significantly decreased after 1 year of eculizumab treatment (median 18.0 units pre-eculizumab and 0 unit post-eculizumab) (Fig. 3a; $p < 0.001$). When examining the accumulated probability of transfusion independence in patients with and without BMF, the percentage of patients achieving transfusion independence rapidly increased immediately after eculizumab dosing and gradually increased as the number of months on eculizumab treatment increased (Fig. 3b). The proportion of patients achieving transfusion independence was not significantly different between patients with and without BMF. The accumulated probability of transfusion independence was highest in patients with platelet count ≥150 × 10^9/L, followed by patients with platelet count ≥100 to <150 × 10^9/L, ≥50 to <100 × 10^9/L, and <50 × 10^9/L (log-rank p value = 0.002) (Fig. 3c).

Corticosteroid withdrawal

The accumulated probability of corticosteroid withdrawal during eculizumab treatment in patients with and

Table 3 Shift in eGFR range ($n = 196$) from baseline during eculizumab therapy, n (%)

		During eculizumab treatment											
		90≤ eGFR (mL/min/1.73 m^2)		60≤ eGFR <90 (mL/min/1.73 m^2)		30≤ eGFR <60 (mL/min/1.73 m^2)		15≤ eGFR <30 (mL/min/1.73 m^2)		eGFR <15 (mL/min/1.73 m^2)		χ^2	Kruskal–Wallis
Baseline	90≤ eGFR (mL/min/1.73 m^2)	61	(31.1%)	4	(2.0%)	0	(0.0%)	0	(0.0%)	0	(0.0%)	p<0.001	p<0.001
	60≤ eGFR <90 (mL/min/1.73 m^2)	22	(11.2%)	35	(17.9%)	2	(1.0%)	0	(0.0%)	0	(0.0%)		
	30≤ eGFR <60 (mL/min/1.73 m^2)	1	(0.5%)	14	(7.1%)	35	(17.9%)	0	(0.0%)	0	(0.0%)		
	15≤ eGFR <30 (mL/min/1.73 m^2)	0	(0.0%)	0	(0.0%)	10	(5.1%)	8	(4.1%)	0	(0.0%)		
	eGFR <15 (mL/min/1.73 m^2)	0	(0.0%)	0	(0.0%)	0	(0.0%)	2	(1.0%)	2	(1.0%)		

Increase in eGFR range indicated by green shading; decrease in eGFR range indicated by red shading; no change in eGFR range indicated by yellow shading

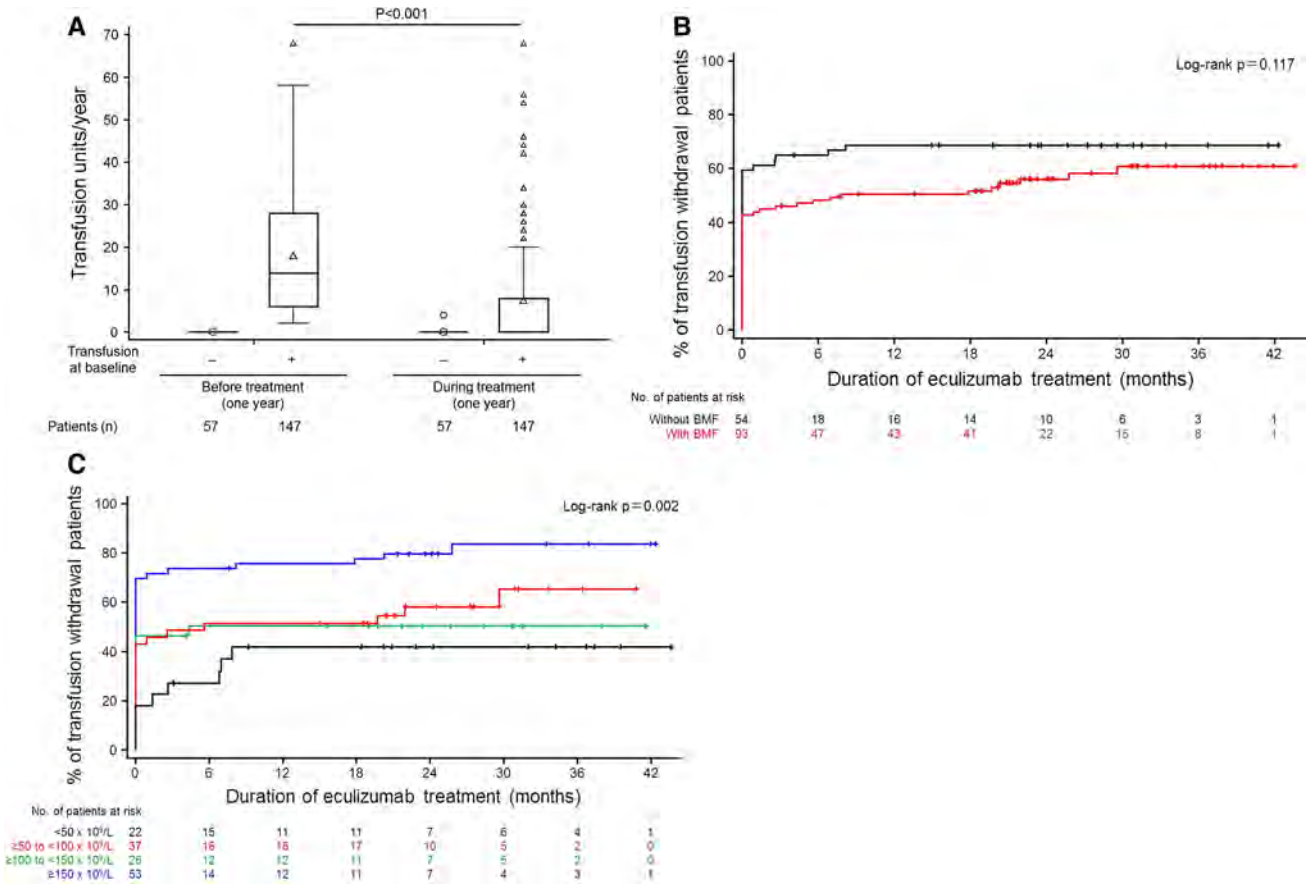

Fig. 3 Transfusion withdrawal during eculizumab treatment: **a** annual rate of transfusion according to the presence ($n = 147$) or absence ($n = 57$) of transfusion at baseline and after 1 year of eculizumab treatment; **b** accumulated probability of transfusion withdrawal in PNH patients with (*red line*) and without (*black line*) BMF; **c** accumulated probability of transfusion withdrawal according to baseline platelet count <50 × 10^9/L (*black line*), ≥50 to <100 × 10^9/L (*red line*), ≥100 to <150 × 10^9/L (*green line*), and ≥150 × 10^9/L (*blue line*), respectively. In **a**, *middle line in box* represents the median, *lower box* bounds the first quartile, *upper box* bounds the third quartile, and *whiskers* represent the 95 % confidence interval of the mean. p value was calculated using the paired t test (**a**) or the log-rank test (**b**, **c**)

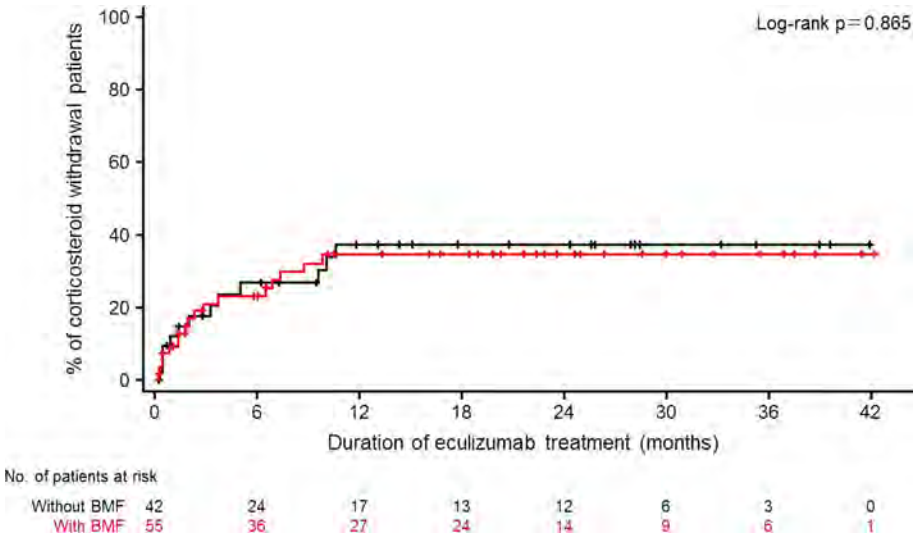

Fig. 4 Accumulated probability of corticosteroid withdrawal during eculizumab therapy in patients with (*red line*) and without BMF (*black line*). *P* value was calculated using the log-rank test

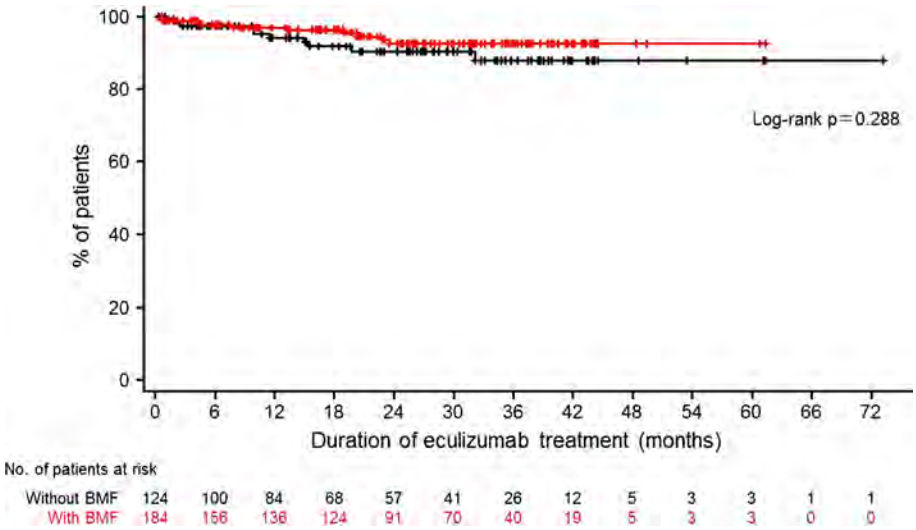

Fig. 5 Overall survival during eculizumab therapy in patients with (*red line*) and without BMF (*black line*). *p* value was calculated using the log-rank test

without BMF was similar (Fig. 4). About 40 % of patients in each group discontinued corticosteroids approximately 12 months after starting eculizumab treatment, and remained off corticosteroids throughout 42 months of eculizumab treatment (log-rank p value = 0.865).

Overall survival

A total of 20 deaths were reported during the observation period, of which ten occurred in patients with BMF. No significant differences in overall long-term survival were observed between patients with or without BMF over 72 months on eculizumab treatment (Fig. 5) (log-rank p value = 0.865).

Discussion

The Japanese PMS study in patients with PNH provides an opportunity to examine the long-term safety and effectiveness of eculizumab in a larger population than earlier clinical trials, using a variety of measures in a real-world setting.

The incidence of all safety events was low across all system organ classes, consistent with other studies [16, 21]. Twenty deaths were reported as the last outcome of 31 AEs or SAEs. The reported occurrence of meningococcal infection is between 0 and 1.5 % in patients with PNH treated with eculizumab [6, 11, 22]; however, there were no meningococcal infections during the follow-up period in our analysis.

LDH levels decreased rapidly after eculizumab dosing and were sustained during long-term (36 months) eculizumab treatment compared to baseline. Improvements in Hb levels from baseline were also observed, particularly in the group of patients with platelets $\geq 150 \times 10^9$/L. Statistically significant improvements of LDH level were consistently observed both in the short-term (starting at 1 month after eculizumab treatment) and long-term (throughout 36 months). These results are compatible with national and international research on eculizumab treatment [11, 13, 14, 16, 23]. It should be noted that missing laboratory values at baseline precluded the inclusion of some patients in specific analyses. The impact of these excluded patients on effectiveness measures is unclear.

Treatment with eculizumab led to an improvement in eGFR in 49 patients (25 %), including improvements in patients with <30 mL/min/1.73 m^2. The proportions of patients who showed no change or worsening of eGFR range were 71.9 and 3.1 %, respectively. This result is similar to that of previous studies [6, 15, 16, 23].

Among patients with a history of transfusions, patients receiving eculizumab had significantly lower rates of transfusion (units/year) after 1 year of treatment compared to baseline (before treatment), with nearly 50 % of patients becoming transfusion-independent following eculizumab treatment. While the fraction of patients achieving transfusion independence was slightly better for patients without BMF than with BMF, the association was not significant. However, patients without BMF appeared to show a tendency to improved and faster transfusion withdrawal. Transfusion dependence was considered to have a possible relation to bone marrow function, and we therefore examined transfusion withdrawal in terms of bone marrow function, based on platelet level. The accumulated probability of transfusion withdrawal was highest in patients with platelet count $\geq 150 \times 10^9$/L compared to patients with platelet count ≥ 100 to $< 150 \times 10^9$/L, ≥ 50 to $< 100 \times 10^9$/L, or $< 50 \times 10^9$/L. Röth et al. have reported that eculizumab-treated PNH patients with a high reticulocyte production index (>2), indicating adequate bone marrow function, could have a reduced need for blood transfusions [24]. This might suggest that higher bone marrow function supports transfusion withdrawal in response to eculizumab. Our results using platelet level as a marker for bone marrow function, are consistent with a previous report [24]. The effectiveness of eculizumab on transfusion withdrawal rapidly increased immediately after eculizumab dosing and gradually increased as the number of months on eculizumab treatment increased in patients with a platelet count $\geq 150 \times 10^9$/L, whereas it reached a plateau after several months in patients with $< 50 \times 10^9$/L. Previous reports have showed that eculizumab has no effect on bone marrow function, including the production of reticulocytes [11, 12, 25, 26]. The amount of reticulocyte production would not be recovered. This might be one of reasons that the efficacy of eculizumab reached the plateau in those patients. We think that eculizumab might have poor response to transfusion withdrawal on patients with lower bone marrow function, though additional study with longer follow-up is needed.

Treatment with corticosteroids in PNH is purely empirical, and long-term treatment with corticosteroids is contraindicated [27]. Physicians attempted to withdraw corticosteroids, and approximately 40 % of patients treated with corticosteroids at baseline finally completed corticosteroid withdrawal after 1 year of eculizumab treatment; however, we could not determine the reasons for continued corticosteroid administration in the remaining patients (~60 %) in this surveillance study. This result might suggest that eculizumab is effective in reducing corticosteroid dependence in all patients with PNH, independent of BMF status, another potential benefit of treatment with eculizumab. However, it is unclear why there was no significant difference in corticosteroid withdrawal between patients with and without BMF. Further analysis is required to elucidate the relationship between BMF status and corticosteroid withdrawal during eculizumab treatment.

Previous research in patients untreated with eculizumab has shown that PNH-cytopenia patients had a significantly greater risk of mortality compared with classic PNH patients [28]. We report here that patients treated with eculizumab demonstrate similar overall survival regardless of underlying BMF, suggesting that BMF might not be a significant risk factor of mortality in patients treated with eculizumab. These data, which are the first to describe overall survival during eculizumab therapy according to BMF status, are limited by the short follow-up period. Kelly et al. reported that 5-year survival in PNH patients treated with eculizumab ($n = 79$) was significantly higher compared to patients without eculizumab ($n = 30$) [17]. Loschi et al. also reported that 6-year survival in patients treated with eculizumab ($n = 123$) significantly improved overall survival compared to historical controls diagnosed after 1985 ($n = 100$) [29]. Thus, we expect that the long-term overall survival of PNH patients treated with eculizumab in this study would be the same in these two reports [17, 29].

The findings from this study are representative of PNH patients treated with eculizumab. The safety and effectiveness profiles observed in this PMS study were similar to results reported from previous eculizumab clinical trials in patients with PNH [15, 16]. In addition, although a larger proportion of patients in this study had a history of BMF compared to those of previous eculizumab clinical studies in the United States and Europe [11, 13, 14], we observed similar efficacy among patients with and without BMF.

In summary, results from this Japanese PMS study in patients with PNH showed an acceptable safety profile with

no cases of meningococcal infection and significant effectiveness of eculizumab, including sustained suppression of intravascular hemolysis, improvements in Hb values and increased transfusion independence regardless of BMF. The findings suggest that eculizumab improves the disease characteristics of patients with PNH. Further long-term results of PMS studies will help elucidate the longitudinal impact of eculizumab.

Acknowledgments We thank all participating physicians and registered patients who took part in this surveillance study. This study was sponsored by Alexion, and Alexion was involved in the process of the study design, data collection, analysis and manuscript preparation. Alexion approved the content of the manuscript and the submission of the manuscript for publication.

Compliance with ethical standards

Funding source Logistical and financial cost for the post-marketing surveillance of eculizumab is provided by Alexion Pharma GK.

Conflict of interest Dr. Ninomiya, Dr. Kawaguchi, and Dr. Kinoshita report personal fees from Alexion Pharma G.K., outside the submitted work; Dr. Ninomiya, Dr. Chiba, Dr. Nishiwaki, Dr. Shichishima, Dr. Ohyashiki, and Dr. Okamoto report grants from Alexion Pharma G.K., outside the submitted work; Dr. Nakao reports personal fees from Alexion Pharma G.K., outside the submitted work; Dr. Kanakura and Dr. Nishimura report grant and personal fees from Alexion Pharma G.K. during the conduct of the study; Dr. Omine reports nonfinancial support from Alexion Pharma G.K., during the conduct of the study; Dr. Obara, Dr. Usuki, Dr. Matsumura, Dr. Ando, Dr. Kanda, Dr. Nakakuma, and Dr. Ozawa have nothing to declare; Dr. Harada and Mr. Akiyama are employees of Alexion Pharma G.K. and may own stock or hold stock options in the company.

References

1. Takeda J, Miyata T, Kawagoe K, Iida Y, Endo Y, Fujita T, et al. Deficiency of the GPI anchor caused by a somatic mutation of the PIG-A gene in paroxysmal nocturnal hemoglobinuria. Cell. 1993;73:703–11.
2. Miyata T, Takeda J, Iida Y, Yamada N, Inoue N, Takahashi M, et al. The cloning of PIG-A, a component in the early step of GPI-anchor biosynthesis. Science. 1993;259:1318–20.
3. Brodsky R. Paroxysmal nocturnal hemoglobinuria. In: Hoffman R, et al., editors. Hematology basic principles and practices. 4th ed. Philadelphia: Elsevier Churchill Livingstone; 2005. p. 419–27.
4. Parker C, Omine M, Richards S, Nishimura J, Bessler M, Ware R, et al. Diagnosis and management of paroxysmal nocturnal hemoglobinuria. Blood. 2005;106:3699–709.
5. Lee JW, Jang JH, Kim JS, Yoon SS, Lee JH, Kim YK, et al. Clinical signs and symptoms associated with increased risk for thrombosis in patients with paroxysmal nocturnal hemoglobinuria from a Korean Registry. Int J Hematol. 2013;97:749–57.
6. Hillmen P, Elebute M, Kelly R, Urbano-Ispizua A, Hill A, Rother RP, et al. Long-term effect of the complement inhibitor eculizumab on kidney function in patients with paroxysmal nocturnal hemoglobinuria. Am J Hematol. 2010;85:553–9.
7. Hillmen P, Lewis SM, Bessler M, Luzzatto L, Dacie JV. Natural history of paroxysmal nocturnal hemoglobinuria. N Engl J Med. 1995;333:1253–8.
8. Weitz I, Meyers G, Lamy T, Cahn JY, Uranga MT, García Vela JA, et al. Cross-sectional validation study of patient-reported outcomes in patients with paroxysmal nocturnal haemoglobinuria. Int Med J. 2013;43:298–307.
9. Schrezenmeier H, Muus P, Socié G, Szer J, Urbano-Ispizua A, Maciejewski JP, et al. Baseline characteristics and disease burden in patients in the International Paroxysmal Nocturnal Hemoglobinuria Registry. Haematologica. 2014;99:922–9.
10. Thomas TC, Rollins SA, Rother RP, Giannoni MA, Hartman SL, Elliott EA, et al. Inhibition of complement activity by humanized anti-C5 antibody and single-chain Fv. Mol Immunol. 1996;33:1389–401.
11. Brodsky RA, Young NS, Antonoli E, Risitano AM, Schrezenmeier H, Schubert J, et al. Multicenter phase 3 study of the complement inhibitor eculizumab for the treatment of patients with paroxysmal nocturnal hemoglobinuria. Blood. 2008;111:1840–7.
12. Hill A, Hillmen P, Richards SJ, Elebute D, Marsh JC, Chan J, et al. Sustained response and long-term safety of eculizumab in paroxysmal nocturnal hemoglobinuria. Blood. 2005;106:2559–65.
13. Hillmen P, Hall C, Marsh JC, Elebute M, Bombara MP, Petro BE, et al. Effect of eculizumab on hemolysis and transfusion requirements in patients with paroxysmal nocturnal hemoglobinuria. N Engl J Med. 2004;350:552–9.
14. Hillmen P, Young NS, Schubert J, Brodsky RA, Socié G, Muus P, et al. The complement inhibitor eculizumab in paroxysmal nocturnal hemoglobinuria. N Engl J Med. 2006;355:1233–43.
15. Hillmen P, Muus P, Röth A, Elebute MO, Risitano AM, Schrezenmeier H, et al. Long-term safety and efficacy of sustained eculizumab treatment in patients with paroxysmal nocturnal haemoglobinuria. Br J Haematol. 2013;162:62–73.
16. Kanakura Y, Ohyashiki K, Shichishima T, Okamoto S, Ando K, Ninomiya H, et al. Long-term efficacy and safety of eculizumab in Japanese patients with PNH: AEGIS trial. Int J Hematol. 2013;98:406–16.
17. Kelly R, Hill A, Arnold LM, Brooksbank GL, Richards SJ, Cullen M, et al. Long-term treatment with eculizumab in paroxysmal nocturnal hemoglobinuria: sustained efficacy and improved survival. Blood. 2011;117:6786–92.
18. McKeage K. Eculizumab: a review of its use in paroxysmal nocturnal haemoglobinuria. Drugs. 2011;71:2327–45.
19. Nishimura J, Kanakura Y. Paroxysmal nocturnal hemoglobinuria. In: Ozawa K, et al., editors. Guidelines for the diagnosis and treatment of intractable anemia. Tokyo: Nankodo; 2011. p. 93–130.
20. Matsuo S, Imai E, Horio M, Yasuda Y, Tomita K, Nitta K, et al. Revised equations for estimating glomerular filtration rate (GFR) from serum creatinine in Japan. Am J Kidney Dis. 2009;53:982–92.
21. Kanakura Y, Ohyashiki K, Shichishima T, Okamoto S, Ando K, Ninomiya H, et al. Safety and efficacy of the terminal complement inhibitor eculizumab in Japanese patients with paroxysmal nocturnal hemoglobinuria: the AEGIS clinical trial. Int J Hematol. 2011;93:36–46.
22. Dmytrijuk A, Robie-Suh K, Cohen MH, Rieves D, Weiss K, Pazdur R. FDA report: eculizumab (Soliris®) for the treatment of patients with paroxysmal nocturnal hemoglobinuria. Oncologist. 2008;13:993–1000.
23. Marti-Caravajal AJ, Anand V, Cardona AF, Solà I. Eculizumab for treating patients with paroxysmal nocturnal hemoglobinuria. Cochrane Database Syst Rev. 2014;10:CD010340. doi:10.1002/14651858.CD010340.pub2.
24. Röth A, Hock C, Konik A, Christoph S, Dührsen U. Chronic treatment of paroxysmal nocturnal hemoglobinuria patients with eculizumab: safety, efficacy, and unexpected laboratory phenomena. Int J Hematol. 2011;93:704–14.
25. Röth A, Dührsen U. Treatment of paroxysmal nocturnal hemoglobinuria in the era of eculizumab. Eur J Hematol. 2011;87:473–9.

26. Hill A. Eculizumab in the treatment of paroxysmal nocturnal hemoglobinuria. Clin Med Insights Ther. 2009;1:1467–76.
27. Röth A, Dührsen U. Paroxysmal nocturnal hemoglobinuria. Dtsch Arztebl. 2007;104:A192–7.
28. Jang JH, Kim JS, Yoon SS, Lee JH, Kim YK, Jo DY, et al. Predictive factors of mortality in population of patients with paroxysmal nocturnal hemoglobinuria (PNH): results from a Korean PNH Registry. J Korean Med Sci. 2016;31:214–21.
29. Loschi M, Porcher R, Barraco F, Terriou L, Mohty M, de Guibert S, et al. Impact of eculizumab treatment on paroxysmal nocturnal hemoglobinuria: a treatment versus no-treatment study. Am J Hematol. 2015;. doi:10.1002/ajh.24278.

Int J Hematol (2016) 104:637–638
DOI 10.1007/s12185-016-2078-z

IMAGES IN HEMATOLOGY

Chédiak–Higashi-like granules and waxy Auer bodies in a case of acute promyelocytic leukemia

Daisuke Ogiya[1] · Hiromichi Matsushita[2,3] · Hiromichi Murayama[1] · Kiyoshi Ando[1]

Received: 30 March 2016 / Revised: 9 August 2016 / Accepted: 9 August 2016 / Published online: 18 August 2016

Keywords Chédiak–Higashi-like granule · Waxy Auer body · Acute promyelocytic leukemia

A 31-year-old man presented with pharyngeal pain and purpura on the right dorsal surface of the hand for 1 week. The complete blood count showed leukopenia and thrombocytopenia (white blood cell count, 1.8×10^9/L; platelet count, 51×10^9/L). Coagulation tests revealed the following: prothrombin time–international normalized ratio (PT–INR) of 1.46; fibrinogen level of 36 mg/dL; fibrin degradation products (FDP) level of 50.9 μg/mL; D-dimer level of 60.6 μg/mL; and thrombin–antithrombin III (TAT) complex level of 54.6 ng/mL. These results indicated disseminated intravascular coagulopathy (DIC). A bone marrow examination revealed hypocellularity with 77 % abnormal promyelocytes. Promyelocytes were variable in size, and contained round, ovoid, distorted, or folded nuclei, as well as rich cytoplasm with abundant azurophilic granules. Chédiak–Higashi-like granules were frequently observed in these promyelocytes (Fig. 1a). Auer bodies were often thick, and some were waxy (Fig. 1b). A diagnosis of acute promyelocytic leukemia (APL) was made on the detection of the t(15;17) (q22;q21) translocation and the resultant *PML/RARA* fusion transcript. *FLT3*–ITD mutation was negative.

The patient underwent single-agent induction therapy with all-*trans* retinoic acid (ATRA). Although supportive therapies were provided, including platelet concentrate, fresh frozen plasma, and recombinant thrombomodulin, the prolonged DIC resulted in pulmonary alveolar hemorrhage. Additional administration of idarubicin (12 mg/m^2 for 3 days) and cytarabine (100 mg/m^2 for 7 days) induced a complete remission of APL with an improvement in DIC. Complete molecular remission was attained after the first cycle of consolidation therapy with arsenic trioxide. The patient is currently undergoing maintenance therapy with no evidence of relapse.

Chédiak–Higashi-like granules have been described in rare cases of acute myeloid leukemia (AML). Electron microscopic studies have shown that the granules arise from fusion of azurophilic granules, in contrast to the lysosomal origin of the inclusions seen in Chédiak–Higashi syndrome. Chédiak–Higashi-like granules have been reported to co-occur with coagulation abnormalities in AML, although their significance is currently unknown. In addition, we occasionally observed thick and/or waxy Auer bodies in this case. Although the clinical significance of the

✉ Hiromichi Matsushita
hirommat@ncc.go.jp

[1] Department of Hematology and Oncology, Tokai University School of Medicine, Isehara, Kanagawa 259-1193, Japan

[2] Department of Laboratory Medicine, Tokai University School of Medicine, Isehara, Kanagawa 259-1193, Japan

[3] Division of Pathology and Clinical Laboratories, National Cancer Center Hospital, 5-1-1 Tsukiji, Chuo-ku, Tokyo 104-0045, Japan

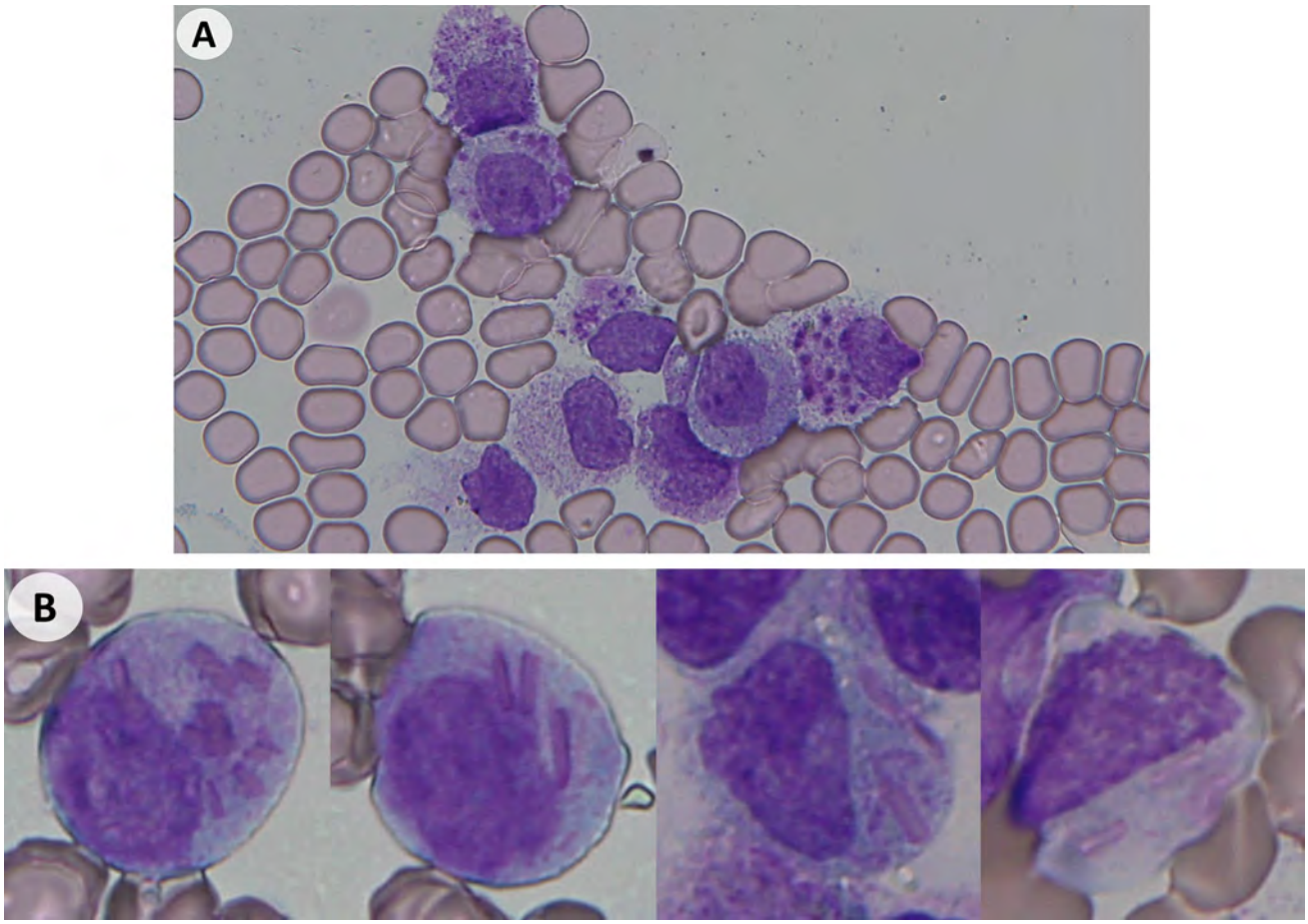

Fig. 1 Morphological features of the bone marrow aspirate. **a** Markedly increased promyelocytes with abundant azurophilic granules and Auer bodies. Chédiak–Higashi-like granules frequently observed in these promyelocytes (Wright–Giemsa stain, ×1000). **b** Thick and/or waxy Auer bodies occasionally observed in these promyelocytes (Wright–Giemsa stain, ×1000)

waxy Auer bodies was unclear, these Chédiak–Higashi-like granules and thick Auer bodies appeared to correspond to a DIC status, as DIC management was extremely difficult in the present case.

Compliance with ethical standards

Conflict of interest The authors have no conflict of interests.

Patient consent statement The patient's consent was obtained.

Int J Hematol (2017) 105:470–477
DOI 10.1007/s12185-016-2146-4

ORIGINAL ARTICLE

Bendamustine plus rituximab for previously untreated patients with indolent B-cell non-Hodgkin lymphoma or mantle cell lymphoma: a multicenter Phase II clinical trial in Japan

Michinori Ogura[1,2] · Kenichi Ishizawa[3] · Dai Maruyama[4] · Naokuni Uike[5] · Kiyoshi Ando[6] · Koji Izutsu[7] · Yasuhito Terui[8] · Yoshitaka Imaizumi[9] · Kunihiro Tsukasaki[10] · Kenshi Suzuki[11] · Tohru Izumi[12] · Kensuke Usuki[13] · Tomohiro Kinoshita[14] · Masafumi Taniwaki[15] · Nobuhiko Uoshima[16] · Junji Suzumiya[17] · Mitsutoshi Kurosawa[18] · Hirokazu Nagai[19] · Toshiki Uchida[1] · Noriko Fukuhara[3] · Ilseung Choi[5] · Ken Ohmachi[6] · Go Yamamoto[7] · Kensei Tobinai[4] · For the Japanese Bendamustine Lymphoma Study Group

Received: 29 September 2016 / Revised: 11 November 2016 / Accepted: 13 November 2016 / Published online: 29 November 2016

Abstract A Phase II, multicenter clinical trial of bendamustine plus rituximab (BR) regimen was conducted in previously untreated patients with high-tumor-burden indolent B-cell non-Hodgkin lymphoma (B-NHL) and previously untreated elderly patients with mantle cell lymphoma (MCL) in Japan. Bendamustine 90 mg/m^2/day on days 1 and 2, as well as rituximab 375 mg/m^2 on day 1 were administered intravenously up to six cycles. The primary endpoint was the complete response (CR) rate as assessed by the International Workshop Response Criteria (1999). Sixty-nine patients (59 with indolent B-NHL and 10 with MCL) were treated. The median number of delivered cycles was six (range 1–6). The CR rates were 67.8% [95% confidence interval (CI) 54.4–79.4%] and 70.0% (95% CI 34.8–93.3%) for indolent B-NHL and MCL, respectively. Estimated progression-free survival at 30 months was 72.1% (95% CI 58.5–82.0%) in indolent B-NHL and was 67.5% (95% CI 29.1–88.2%) in MCL. Major grade 3/4 toxicities were hematologic and included lymphopenia (97%), CD4 lymphopenia (91%), neutropenia (86%), and leukopenia (83%). No treatment-related death was found. The BR regimen showed high efficacy as evidenced by the expected CR

✉ Michinori Ogura
mi-ogura@naa.att.ne.jp

1 Department of Hematology and Oncology, Nagoya Daini Red Cross Hospital, Nagoya, Japan

2 Department of Hematology, Tokai Central Hospital, 4-6-2 Higashijimacho, Sohara, Kakamigahara, Gifu 504-8601, Japan

3 Department of Hematology and Rheumatology, Tohoku University Graduate School of Medicine, Sendai, Japan

4 Department of Hematology, National Cancer Center Hospital, Tokyo, Japan

5 Department of Hematology, National Hospital Organization Kyushu Cancer Center, Fukuoka, Japan

6 Department of Hematology and Oncology, Tokai University Hospital, Isehara, Japan

7 Department of Hematology, Toranomon Hospital, Tokyo, Japan

8 Department of Hematology Oncology, The Cancer Institute Hospital of the Japanese Foundation for Cancer Research, Tokyo, Japan

9 Department of Hematology, Nagasaki University Hospital, Nagasaki, Japan

10 Department of Hematology, National Cancer Center Hospital East, Kashiwa, Japan

11 Department of Hematology, Japanese Red Cross Medical Center, Tokyo, Japan

12 Division of Hematology, Tochigi Cancer Center, Utsunomiya, Japan

13 Department of Hematology, NTT Medical Center Tokyo, Tokyo, Japan

14 Department of Hematology and Cell Therapy, Aichi Cancer Center, Nagoya, Japan

15 Division of Hematology and Oncology, Kyoto Prefectural University of Medicine, Kyoto, Japan

16 Department of Hematology, Matsushita Memorial Hospital, Moriguchi, Japan

17 Department of Oncology/Hematology, School of Medicine, Shimane University, Izumo, Japan

18 Department of Hematology, National Hospital Organization Hokkaido Cancer Center, Sapporo, Japan

19 Department of Hematology, National Hospital Organization Nagoya Medical Center, Nagoya, Japan

rate and durable response, as well as an acceptable safety profile for the study populations.

Keywords Bendamustine · Rituximab · Indolent B-cell non-Hodgkin lymphoma · Mantle cell lymphoma · First-line therapy

Introduction

Combination chemotherapy with rituximab is a standard of care for previously untreated patients with high-tumor-burden follicular lymphoma (FL)—a major indolent B-cell non-Hodgkin lymphoma (B-NHL). Despite arduous efforts to improve clinical outcomes of therapeutic modalities to date, the optimal initial immunochemotherapy with the demonstrated superiority of overall survival (OS) is still not established [1–3]. Although rituximab plus cyclophosphamide, doxorubicin, vincristine, and prednisone (R-CHOP) is a standard therapeutic option for previously untreated elderly patients with mantle cell lymphoma (MCL) [4, 5], R-CHOP has not demonstrated improvements in the OS or progression-free survival (PFS) in this population [6].

Bendamustine is a cytotoxic alkylating agent, a bifunctional mechlorethamine derivative with the purine-like benzimidazole ring [7]. Bendamustine, when used as monotherapy or in combination with rituximab, has shown high efficacy and an acceptable safety profile for patients with relapsed/refractory B-NHL and MCL [8–13]. Bendamustine is in extensive clinical use for these malignancies in many countries including Europe, Japan, and North America.

There are two major Phase III clinical trials of the bendamustine and rituximab (BR) regimen conducted by the German and international investigator groups in previously untreated patients with indolent B-NHL or MCL: the StiL NHL 1-2003 (StiL-1) [14] and the BRIGHT Study [15]. The former showed its superiority of the BR regimen to R-CHOP in PFS and less toxicity, while the latter indicated its noninferiority to R-CHOP/R-cyclophosphamide, vincristine, and prednisone (R-CVP) in CR rate and differences in safety profile. In Europe, furthermore, recent clinical studies in patients with indolent non-follicular B-NHL or mucosa-associated lymphoid tissue lymphoma showed the efficacy and tolerability of the BR regimen [16, 17], and retrospective studies in patients with indolent B-NHL or MCL demonstrated the efficacy and safety of the BR regimen in real-world clinical practice [18, 19]. Therefore, the BR regimen has become recognized as a standard regimen for these patients in Western countries. In Asian countries, by contrast, no clinical evidence has been obtained to demonstrate the efficacy or safety of the BR regimen for the relevant patients. We hence conducted the present phase II study to obtain the evidence for previously untreated patients with indolent B-NHL and previously untreated elderly patients with MCL in Japan.

Patients and methods

Study design and subjects

A prospective, multicenter, single-arm, open-label, phase II clinical study was conducted at 21 medical institutions in Japan from November 9, 2011, through November 15, 2013. Previously untreated patients were considered eligible when meeting all of the following criteria: (1) CD20-positive, advanced indolent B-NHL [small lymphocytic lymphoma, splenic marginal zone lymphoma, lymphoplasmacytic lymphoma, extranodal marginal zone lymphoma of mucosa-associated lymphoid tissue, nodal marginal zone lymphoma, and follicular lymphoma (grades 1, 2, and 3a)] or MCL that was histopathologically confirmed based on World Health Organization Classification 2008 [20]; (2) B-NHL patients aged 20–79 years and MCL in patients aged 66–79 years; (3) high-tumor-burden indolent B-NHL defined as follows—(a) bulky disease more than 7 cm in major axis on CT scans (excluding the spleen); (b) three or more lymph node regions more than 3 cm in major axis on CT scans; (c) B symptoms; (d) elevated serum lactate dehydrogenase or beta 2 microglobulin; (e) symptomatic splenomegaly; (f) compression symptoms, and (g) pleural effusions/ascites; (4) a measurable lesion [major axis on computed tomography (CT) scans: >1.5 cm]; (5) Eastern Cooperative Oncology Group performance status: 0–2; and (6) patients with the adequately maintained function of principal organs (bone marrow, liver, kidneys, lungs, and heart)—(a) neutrophil count: $\geq$1500/mm^3; (b) platelet count: $\geq$75,000/mm^3; (c) aspartate aminotransferase (AST): $\leq$threefold the upper limit of normal (ULN) at the institution; (d) alanine aminotransferase (ALT): $\leq$threefold the ULN at the institution; (e) total bilirubin: $\leq$1.5-fold the ULN at the institution; (f) serum creatinine: $\leq$1.5-fold the ULN at the institution; (g) arterial partial pressure of oxygen (PaO_2): $\geq$65 mmHg; (h) electrocardiogram showing no abnormalities that require treatment; and (i) left ventricular ejection fraction: $\geq$55%. The key exclusion criteria were as follows: histopathologically confirmed transformation; administration or transfusion of cytokines; positivity for the HBs antigen, anti-HCV antibody, or anti-HIV antibody; involvement of the central nervous system or clinical symptoms suggesting the involvement; active double cancer; pregnant or probably pregnant women; and men and women who give no consent to contraception. At screening, histopathological diagnoses were made at each participating medical institution. An independent expert

pathological review panel ensured the precision of histopathological diagnoses made among medical institutions after the termination of the treatment. All patients provided written informed consent, and the protocol was approved by the institutional review board at respective institutions. The present study complied with the Declaration of Helsinki, was conducted in compliance with the Good Clinical Practice guidelines in effect, and was registered with ClinicalTrials.gov (NCT01718691).

Treatment

Bendamustine 90 mg/m^2/day was administered intravenously on days 1 and 2, and rituximab 375 mg/m^2 on day 1 (day 0 in cycle 1). The 28-day cycle was conducted up to six cycles. Furthermore, the dose of bendamustine was reduced from 90 to 60 mg/m^2/day when falling under any of the following dose reduction criteria in the previous cycle: grade 4 neutropenia (<500/mm^3) lasting for 1 or more weeks; febrile neutropenia, ≥grade 3 neutropenia (<1000/mm^3) involving fever ≥38 °C that lasts for 3 days; platelet count: <25,000/mm^3; a bleeding tendency requiring blood transfusion; and adverse events which the investigator has admitted the need for dose reduction. The administration of bendamustine was discontinued when again falling under any of the criteria at the dose of 60 mg/m^2/day. The second and subsequent cycles were initiated after having verified the following criteria: neutrophil count, ≥1000/mm^3; platelet count, ≥75,000/mm^3; AST and ALT ≤fivefold the ULN at each institution; total bilirubin, ≤threefold the ULN at each institution; serum creatinine, ≤threefold the ULN at each institution; and no persistence of ≥grade 3 adverse events at assessment.

Patients received acetaminophen and chlorpheniramine to prevent or alleviate the infusion-related reaction of rituximab, and the administration of the following drugs to patients was recommended: dexamethasone; 5-hydroxytryptamine 3 receptor antagonists and/or neurokinin 1 receptor antagonists to prevent or alleviate nausea/vomiting as needed; and sulfamethoxazole–trimethoprim and acyclovir to prevent opportunistic infections caused by *Pneumocystis jirovecii* (PJP) and herpes zoster virus, respectively, when CD4+ lymphocyte counts became 200/mm^3 or below. The administration of granulocyte colony-stimulating factors (G-CSFs) was allowed after the verification of grade 3 neutropenia in cycle 1 and on day 3 or later in cycles 2–6.

Efficacy and safety assessments

The primary endpoint was the complete response (CR) [CR plus unconfirmed CR] rate that was evaluated after cycle 3 and at the completion of the final cycle by the independent review committee (IRC) in accordance with International Workshop to Standardize Response Criteria for Non-Hodgkin's Lymphoma (IWRC) [21].

The secondary endpoints were the overall response rate (ORR: CR, unconfirmed CR, and partial response) that was assessed according to the IWRC, the CR rate and the ORR according to Revised Response Criteria for Malignant Lymphoma (revised RC) [22], PFS, duration of response (DOR), and OS. Furthermore, the follow-up investigation on PFS, OS, and safety was conducted for patients who gave consent after the completion of the present study.

CT was conducted at the time of recruitment, as well as in cycle 3 and the final cycle. Positron emission tomography was conducted in patients who had [^{18}F]fluorodeoxyglucose avidity at baseline [22]. The safety of the BR regimen was assessed using Common Terminology Criteria for Adverse Events (CTCAE) version 4.0.

Statistical analyses

Regarding indolent B-NHL, sample size was calculated to be 52 under the following conditions: the expected CR rate, 66% [95% confidence interval (CI) 47–81%]; the threshold CR rate, 47% [23]; α value, 0.025 (one-tailed); and β value, 0.20. The size was calculated to be 57 in consideration of the exclusion rate of 10% from statistical analyses. Regarding MCL, sample size was calculated to be 10 under the following conditions: the expected CR rate: 38%; the threshold CR rate: 8%; α value, 0.05 (one-tailed); and β value, 0.20.

The safety analysis set (SAS) consisted of patients who received at least one medication, and the full analysis set (FAS) comprised patients who remained after the exclusion from the SAS. The CR rate and the ORR were calculated to precisely compute the 95% CI based on the binominal probability. PFS, DOR, and OS were computed according to the Kaplan–Meier method. The median value and its 95% CI were calculated according to Greenwoods formula. All statistical analyses were made with SAS version 9.1.3 (SAS Institute Inc., Cary, NC, USA).

Results

Patient characteristics at baseline

Seventy patients were enrolled, and one was excluded due to positivity for the HBs antigen that was found after recruitment; therefore, 69 underwent the BR regimen and constituted each of the SAS and FAS. Patient characteristics at baseline are shown in Table 1. Fifty-nine of 69 patients had indolent B-NHL, with a median age

Table 1 Patient characteristics at baseline

Characteristics	iNHL ($n = 59$)	MCL ($n = 10$)
Age, years		
Median (range)	62 (39–79)	70 (67–77)
<65	36	0
≥65	23	10
Gender, male/female, *n*	22/37	9/1
ECOG PS, *n*		
0	42	7
1	16	3
2	1	0
Histology, *n*		
Small lymphocytic lymphoma	2	
Lymphoplasmocytic lymphoma	2	
MALT lymphoma	4	
Follicular lymphoma	51	
MCL		10
Ann Arbor stage, *n*		
I–II	15	0
III	9	0
IV	35	10
Number of involved lymph node regions, *n*		
0	0	0
1	12	1
2	6	1
3	4	2
≥4	37	6
Lactate dehydrogenase, *n*		
Upper limit of normal or lower	45	7
High	14	3
β2-Microglobulin, *n*		
Upper limit of normal or lower	15	3
High	44	7
Bulky disease, ≥7 cm in major axis, *n*	28	1
B symptoms, *n*		
Fever, present/absent	0/59	0/10
Nocturnal sweating, present/absent	3/56	0/10
Weight loss, present/absent	2/57	0/10
Bone marrow infiltration, *n*		
Positive	34	8
Negative	24	2
Undefined	1	0
FLIPI risk groups, *n* (=51)		
Low	17	
Intermediate	19	
High	15	

iNHL indolent B-cell non-Hodgkin lymphoma, *MCL* mantle cell lymphoma, *ECOG PS* Eastern Cooperative Oncology Group performance status, *MALT* extranodal marginal zone B-cell lymphoma of mucosa-associated lymphoid tissue, *FLIPI* Follicular Lymphoma International Prognostic Index

of 62 years (range 39–79 years). FL was most predominant (51 patients) by histology. Ten patients (median age 70 years; range 67–77 years) had MCL. The independent expert pathological review panel ensured the precision of histopathological diagnoses made among medical institutions after the termination of the treatment and then verified the absence of any discrepancies in the diagnoses.

Efficacy

Best overall responses assessed by the IRC according to the IWRC are shown in Table 2. The CR rate for all-type histology was 68.1% (47/69 patients; 95% CI 55.8–78.8%). The CR rate for indolent B-NHL was 67.8% (40/59 patients; 95% CI 54.4–79.4%), thus exceeding its expected CR rate of 66%; furthermore, the lowest limit for 95% CI (54.4%) exceeded the threshold CR rate of 47%. Similarly, the CR rate 70.0% (7/10 patients; 95% CI 34.8–93.3%) for MCL exceeded the expected CR rate of 38%; furthermore, the lowest limit for 95% CI (34.8%) exceeded the threshold CR rate of 8%.

The ORR assessed by the IRC according to the IWRC was 95.7% (66/69 patients; 95% CI 87.8–99.1%) for all-type histology, 96.6% (57/59 patients; 95% CI 88.3–99.6%) for indolent B-NHL, and 90.0% (9/10 patients; 95% CI 55.5–99.7%) for MCL. The same ORR for these histologies was obtained when calculated according to the revised RC as well. The CR rate was 66.7% (46/69 patients; 95% CI 54.3–77.6%) for all-type histology, 64.4% (38/59 patients; 95% CI 50.9–76.4%) for indolent B-NHL, and 80.0% (8/10 patients; 95% CI 44.4–97.5%) for MCL. Subgroup analysis on patients with indolent B-NHL revealed that the CR rate and the ORR as assessed by the IRC according to the IWRC for follicular lymphoma ($n = 51$) were 66.7 and 98.0%, respectively.

At the median follow-up of 30.1 months (range 1.9–39.3 months), 21 events (including 15 cases of progressive disease) occurred. Therefore, the median PFS was not reached (Fig. 1). PFS at 30 months in patients with all-type histology was estimated to be 71.5% (95% CI 58.9–80.8%). PFS at 30 months was estimated to be 72.1% (range 58.5–82.0%) for patients with indolent B-NHL and to be 67.5% (range 29.1–88.2%) for patients with MCL. No death occurred during the follow-up.

Safety

The median of delivered cycles was 6 (range 1–6), and 52 patients (75%) received BR in six cycles. Thirteen patients discontinued treatment due to neutropenia, two due to disease progression, one due to the investigator's discretion, and one due to grade 3 rash unrelated to the BR regimen. Dose delay (54%, 37/69 patients) was required in one or

Table 2 Best overall responses in patients with indolent B-cell non-Hodgkin lymphoma and patients with mantle cell lymphoma

Histology	*n*	Best overall response, *n* (%)						ORR, *n* (%) [95% CI]	CR rate, *n* (%) [95% CI]
		CR	CRu	PR	SD	PD	NE		
Overall	69	29 (42.0)	18 (26.1)	19 (27.5)	2 (2.9)	0 (0.0)	1 (1.4)	66 (95.7) [87.8–99.1]	47 (68.1) [55.8–78.8]
iNHL	59	24 (40.7)	16 (27.1)	17 (28.8)	1 (1.7)	0 (0.0)	1 (1.7)	57 (96.6) [88.3–99.6]	40 (67.8) [54.4–79.4]
MCL	10	5 (50.0)	2 (20.0)	2 (20.0)	1 (10.0)	0 (0.0)	0 (0.0)	9 (90.0) [55.5–99.7]	7 (70.0) [34.8–93.3]

CR complete response, *CRu* unconfirmed complete response, *PR* partial response, *SD* stable disease, *PD* progressive disease, *NE* not evaluated, *ORR* overall response rate, *CI* confidence interval, *iNHL* indolent B-cell non-Hodgkin lymphoma, *MCL* mantle cell lymphoma

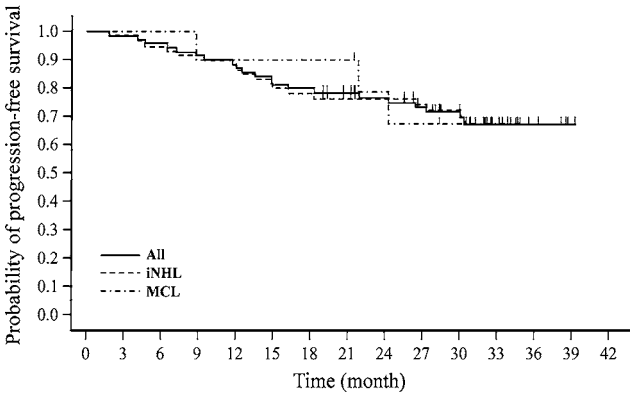

Fig. 1 Progression-free survival (assessed by independent review committee). *iNHL* indolent B-cell non-Hodgkin lymphoma, *MCL* mantle cell lymphoma

more cycles delivered, and dose was reduced in 12% (8/69 patients). Relative dose intensity was 89.6 ± 9.4%.

A total of 2278 episodes of adverse effects (AEs) developed in all 69 patients. Hematologic and nonhematologic AEs by grade are shown in Tables 3 and 4, respectively. Major AEs among grade 3/4 hematologic AEs were lymphopenia (97%), CD4 lymphopenia (91%), neutropenia (86%), and leukopenia (83%) (Table 3). Forty-eight patients (70%) received G-CSFs, 12 of whom discontinued treatment in less than six cycles due to neutropenia. Major nonhematologic AEs were nausea, constipation, malaise, decreased immunoglobulin M, anorexia, rash, and infusion-related reaction (Table 4). Major grade 3 nonhematologic AEs were two cases (3%) each of infusion-related reaction, increased alanine aminotransferase, increased aspartate aminotransferase, anorexia, erythroderma, maculopapular rash, and rash.

Ten episodes of serious AEs occurred in nine patients. There were three cases of febrile neutropenia, as well as one case each of tumor lysis syndrome, breast cancer, cytomegalovirus pneumonia, allergic dermatitis, chromosomal aberration, atrial tachycardia, and fever. All patients with these serious AEs recovered.

Infections occurred in 42 (61%) among 69 patients, the majority of which were grade 2 or lower AEs. The most predominant infections were fever (25%) and nasopharyngitis (20%) (Table 4). Grade 3 infections occurred in five patients: three patents with febrile neutropenia; and one patient each with cytomegalovirus pneumonia and bacterial infection. Grade 4 infection did not occur. Sixty-seven patients (97%) underwent prophylaxis with sulfamethoxazole–trimethoprim, and PJP did not occur. Fifty-seven patients (83%) underwent prophylaxis with acyclovir, and the reactivation of varicella-zoster virus (VZV) occurred in one of 12 patients who had not undergone the prophylaxis. Treatment-related death was not found. Secondary cancer was diagnosed in one patient with breast cancer at 5 months after administration completion.

Table 3 Hematologic adverse events

Adverse events	Patients affected ($N = 69$)					
	Grade, *n*				All grades *n* (%)	Grade 3/4 *n* (%)
	1	2	3	4		
Leukopenia	3	9	45	12	69 (100)	57 (83)
Lymphopenia	0	0	5	62	67 (97)	67 (97)
Neutropenia	1	5	25	34	65 (94)	59 (86)
CD4 lymphopenia	0	1	29	34	64 (93)	63 (91)
Thrombocytopenia	22	11	3	2	38 (55)	5 (7)
Anemia	12	9	3	0	24 (35)	3 (4)

CTCAE common terminology criteria for adverse events version 4.0

Table 4 Nonhematologic adverse events (≥10%)

Adverse events	Patients affected ($N = 69$)					
	Grade, *n*				All grades *n* (%)	Grade 3/4 *n* (%)
	1	2	3	4		
Nausea	32	13	1	0	46 (67)	1 (1)
Constipation	38	7	0	0	45 (65)	0
Malaise	31	6	0	0	37 (54)	0
Decreased immunoglobulin M	32	0	0	0	32 (46)	0
Anorexia	20	8	2	0	30 (43)	2 (3)
Rash	18	9	2	0	29 (42)	2 (3)
Infusion-related reaction	6	20	2	0	28 (41)	2 (3)
Increased aspartate aminotransferase	18	2	2	0	22 (32)	2 (3)
Increased lactate dehydrogenase	22	0	0	0	22 (32)	0
Decreased immunoglobulin A	21	0	0	0	21 (30)	0
Decreased immunoglobulin G	21	0	0	0	21 (30)	0
Vasculitis	9	11	0	0	20 (29)	0
Insomnia	18	0	1	0	19 (28)	1 (1)
Increased alanine aminotransferase	13	3	2	0	18 (26)	2 (3)
Increased C-reactive protein	17	1	0	0	18 (26)	0
Pyrexia	14	3	0	0	17 (25)	0
Increased GGT	7	7	1	0	15 (22)	1 (1)
Stomatitis	10	5	0	0	15 (22)	0
Nasopharyngitis	8	6	0	0	14 (20)	0
Vomiting	9	3	1	0	13 (19)	1 (1)
Increased alkaline phosphatase	13	0	0	0	13 (19)	0
Dysgeusia	13	0	0	0	13 (19)	0
Pruritus	10	2	1	0	13 (19)	1 (1)
Headache	12	0	0	0	12 (17)	0
Diarrhea	8	3	0	0	11 (16)	0
Vascular pain	11	0	0	0	11 (16)	0
Eosinophilia	11	0	0	0	11 (16)	0
Weight loss	6	3	0	0	9 (13)	0
Neutrophilia	9	0	0	0	9 (13)	0
Injection site reaction	7	1	0	0	8 (12)	0
Injection site pain	4	4	0	0	8 (12)	0
Decreased total protein	8	0	0	0	8 (12)	0
Noncardiac chest pain	6	1	0	0	7 (10)	0
Maculopapular rash	3	2	2	0	7 (10)	2 (3)

CTCAE common terminology criteria for adverse events version 4.0, *GGT* gamma-glutamyl transpeptidase

Discussion

To assess the clinical usefulness of the BR regimen as first-line therapy for indolent B-NHL and MCL in an attempt to make comparisons with previous clinical studies in countries outside Japan, we established the CR rate as the primary endpoint in the present explorative phase II study. The CR rate exceeded the expected and threshold CR rates, and we thus verified the efficacy of the BR regimen for the study population.

Two, randomized, open-label, noninferiority, phase III clinical trials of the BR regimen have been conducted in previously untreated patients with indolent B-NHL or MCL. One is the StiL-1 Study [14] that compared BR with R-CHOP, which described the comparable ORRs between the BR group and the R-CHOP group (93 vs. 91%); the BR group showed a significantly higher CR rate (40 vs. 30%; $P = 0.021$) and a significantly longer median PFS (69.5 vs. 31.2 months; $P < 0.0001$). BR was better tolerated by patients than R-CHOP. Another is the BRIGHT

Study [15] that compared BR with a standard rituximab-containing chemotherapy regimen—R-CHOP/R-CVP. The BR group showed a significantly better ORR (97 vs. 91%; $P = 0.0102$), and BR was not inferior to R-CHOP/R-CVP with respect to the CR rate assessed by the IRC (31 vs. 25%; CR rate ratio: 1.26; $P = 0.0225$). The data on time-to-event (i.e., PFS, event-free survival, and OS) remain to be collected.

The CR rate of patients with all-type histology in the present study was 68.1%, thus exceeding those of the StiL-1 Study (40%) and the BRIGHT Study (31%). On the other hand, the ORRs were equivalent among the present study (95.7%), the StiL-1 Study (93%), and the BRIGHT Study (97%). Age range and the proportion of patients with MCL were nearly equivalent among these three studies. The proportions of patients with clinical stage III/IV and patients in the "follicular lymphoma international prognostic index high" subgroup (78 and 29%, respectively) were lower in the present study than in the StiL-1 Study (97 and 46%, respectively) and the BRIGHT Study (90 and 43%, respectively). Therefore, we speculate that the lower proportion of patients with high-risk indolent B-NHL at baseline possibly influenced the outcomes in favor of our study. PFS at 30 months in our study (72.1%) is nearly equivalent to the datum extractable from the figure of StiL-1 Study, thus inferring the long-term duration of response.

Comparisons among the StiL-1 Study [14], the BRIGHT Study [15], and the present study with respect to G3/4 hematologic AEs revealed no differences in the safety profile except for the incidence of neutropenia. Concretely, the incidences of neutropenia exceeded 80% in our study in contrast to those described in the prior two studies, thus indicating large differences. We cannot specify the causes for this fact, although a racial difference and/or differences in prophylaxis practice using G-CSFs in two studies [14, 15] as compared with our study are conceivable.

The incidences of nonhematologic AEs differ among these three studies, and the majority were categorized to grade 2 or lower and were manageable clinically. Concretely, the incidence of infections (61%) in our study was higher than 37% in StiL-1 Study and was nearly equivalent to 54.3% in the BRIGHT Study. However, all the infections in our study were manageable clinically. We prospectively examined the immunological functions of patients in each cycle because of concern about CD4 lymphopenia potentially caused by the BR regimen [24, 25] and found the high incidence (91%, 63/69 patients) of grade 3/4 CD4 lymphopenia. In the present study, prophylaxis using sulfamethoxazole–trimethoprim and acyclovir was recommended for patients who had grade 3/4 CD4 lymphopenia. Indeed, 97 and 83% of patients underwent prophylaxis with the respective drugs. Consequently, PJP did not occur, and the reactivation of VZV occurred in one of 12 patients who had not undergone the prophylaxis. These findings suggest the need for the prophylaxis in patients undergoing the BR regimen. There were only one case of grade 1 alopecia and three cases of grade 1 peripheral neuropathy. Our study provides the safety profile similar to that described in previous clinical trials in Japanese patients with relapsed/refractory indolent B-NHL [12, 13].

In conclusion, the BR regimen showed high efficacy and an acceptable safety profile for previously untreated patients with high-tumor-burden indolent B-NHL and previously untreated elderly patients with MCL not eligible for ASCT in Japan. Therefore, the BR regimen is of clinical relevance and can be a therapeutic option also for these patient populations.

Acknowledgements We thank patients, investigators, and staff who were involved in the present study. Research support was provided by SymBio Pharmaceuticals Ltd. We also thank Satoshi Sakima, MD, for his gracious review of the manuscript. This work was supported by SymBio Pharmaceuticals Ltd. and Eisai Co., Ltd.

Compliance with ethical standards

Conflict of interest Dr. Ogura has received research funding from SymBio; and has received honoraria from Takeda, Mundipharma, Meiji Seika Pharma, and Celgene. Dr. Ishizawa has received research funding from Kyowa Hakko Kirin, MSD, Celgene, and Pfizer; and has received honoraria form Kyowa Hakko Kirin, Chugai, and Takeda. Dr. Maruyama has received honoraria from Eisai, Takeda, Chugai, Janssen, Nippon Kayaku, Celgene, Mundipharma, Sanofi, Kyowa Hakko Kirin, Mochida, and Ono. Dr. Ando has received research funding form Kyowa Hakko Kirin. Dr. Izutsu has received honoraria and research funding from Eisai. Dr. Terui has received honoraria form Janssen. Dr. Tsukasaki has received research funding from Eisai, Celgene, Takeda, and Mundipharma; and has received honoraria from Zenyaku Kogyo, HUYA, and Chugai. Dr. Usuki has received honoraria from Nippon Shinyaku, MSD, Kyowa Hakko Kirin, Novartis, Bristol-Meyer-Squibb, and Dainippon Sumitomo. Dr. Kinoshita has received research funding form Eisai, Solasia, and has received honoraria from Eisai, Zenyaku Kogyo, Janssen, Chugai, and Kyowa Hakko Kirin. Dr. Suzumiya has received research funding from Eisai, Kyowa Hakko Kirin, Chugai, Astellas, and Toyama Chemical; and has received honoraria from Eisai, Chugai, and Takeda. Dr. Nagai has received research funding from CIMIC, Janssen, Mundipharma, Takeda, Bristol-Myers Squibb, and Otsuka; and has received honoraria from Chugai. GY has received honoraria form Takeda, Celgene, and Janssen. Dr. Tobinai has received research funding from Eisai, Chugai, Kyowa Hakko Kirin, Ono, Celgene, Janssen, GlaxoSmith-Kline, Mundipharma, Takeda, Servier, and AbbVie; and has received honoraria from Eisai, Janssen, Mundipharma, Takeda, Zenyaku Kogyo, and HUYA.All remaining authors have declared no conflicts of interest.

References

1. Dreyling M, Ghielmini M, Marcus R, Salles G, Vitolo U, Ladetto M. Newly diagnosed and relapsed follicular lymphoma: ESMO Clinical Practice Guidelines for diagnosis, treatment and follow-up. Ann Oncol. 2014; 25:iii76–82.
2. Hiddemann W, Cheson BD. How we manage follicular lymphoma. Leukemia. 2014;28:1388–95.

3. Kahl BS, Yang DT. Follicular lymphoma: evolving therapeutic strategies. Blood. 2016;127:2055–63.
4. Dreyling M, Geisler C, Hermine O, Kluin-Nelemans HC, Le Gouill S, Rule S, et al. Newly diagnosed and relapsed mantle cell lymphoma: ESMO Clinical Practice Guidelines for diagnosis, treatment and follow-up. Ann Oncol. 2014; 25:iii83–92.
5. Dreyling M, Ferrero S, Hermine O. How to manage mantle cell lymphoma. Leukemia. 2014;28:2117–30.
6. Lenz G, Dreyling M, Hoster E, Wörmann B, Dührsen U, Metzner B, et al. Immunochemotherapy with rituximab and cyclophosphamide, doxorubicin, vincristine, and prednisone significantly improves response and time to treatment failure, but not long-term outcome in patients with previously untreated mantle cell lymphoma: results of a prospective randomized trial of the German Low Grade Lymphoma Study Group (GLSG). J Clin Oncol. 2005;23:1984–92.
7. Cheson BD, Rummel MJ. Bendamustine: rebirth of an old drug. J Clin Oncol. 2009;27:1492–501.
8. Rummel MJ, Al-Batran SE, Kim SZ, Welslau M, Hecker R, Kofahl-Krause D, et al. Bendamustine plus rituximab is effective and has a favorable toxicity profile in the treatment of mantle cell and low-grade non-Hodgkin's lymphoma. J Clin Oncol. 2005;23:3383–9.
9. Robinson KS, Williams ME, van der Jagt RH, Cohen P, Herst JA, Tulpule A, et al. Phase II multicenter study of bendamustine plus rituximab in patients with relapsed indolent B-cell and mantle cell non-Hodgkin's lymphoma. J Clin Oncol. 2008;26:4473–9.
10. Friedberg JW, Cohen P, Chen L, Robinson KS, Forero-Torres A, La Casce AS, et al. Bendamustine in patients with rituximab-refractory indolent and transformed non-Hodgkin's lymphoma: results from a phase II multicenter, single-agent study. J Clin Oncol. 2008; 26 204–10.
11. Kahl BS, Bartlett NL, Leonard JP, Chen L, Ganjoo K, Williams ME, et al. Bendamustine is effective therapy in patients with rituximab-refractory, indolent B-cell non-Hodgkin lymphoma: results from a Multicenter Study. Cancer. 2010;116:106–14.
12. Ogura M, Uchida T, Taniwaki M, Ando K, Watanabe T, Kasai M, et al. Phase I and pharmacokinetic study of bendamustine hydrochloride in relapsed or refractory indolent B-cell non-Hodgkin lymphoma and mantle cell lymphoma. Cancer Sci. 2010;101:2054–8.
13. Ohmachi K, Ando K, Ogura M, Uchida T, Itoh K, Kubota N, et al. Multicenter phase II study of bendamustine for relapsed or refractory indolent B-cell non-Hodgkin lymphoma and mantle cell lymphoma. Cancer Sci. 2010;101:2059–64.
14. Rummel MJ, Niederle N, Maschmeyer G, Banat GA, von Grünhagen U, Losem C, et al. Bendamustine plus rituximab versus CHOP plus rituximab as first-line treatment for patients with indolent and mantle-cell lymphomas: an open-label, multicentre, randomised, phase 3 non-inferiority trial. Lancet. 2013;381:1203–10.
15. Flinn IW, van der Jagt R, Kahl BS, Wood P, Hawkins TE, Macdonald D, et al. Randomized trial of bendamustine-rituximab or R-CHOP/R-CVP in first-line treatment of indolent NHL or MCL: the BRIGHT study. Blood. 2014;123:2944–52.
16. Luminari S, Goldaniga M, Cesaretti M, Orsucci L, Tucci A, Pulsoni A, et al. A phase II study of bendamustine in combination with rituximab as initial treatment for patients with indolent non-follicular non-Hodgkin lymphoma. Leuk Lymphoma. 2016;57:880–7.
17. Salar A, Domingo-Domenech E, Panizo C, Nicolás C, Bargay J, Muntañola A, et al. First-line response-adapted treatment with the combination of bendamustine and rituximab in patients with mucosa-associated lymphoid tissue lymphoma (MALT2008-01): a multicentre, single-arm, phase 2 trial. Lancet Haematol. 2014;1:e104–11.
18. Becker M, Tschechne B, Reeb M, Schwinger U, Bruch HR, Frank M, et al. Bendamustine as first-line treatment in patients with advanced indolent non-Hodgkin lymphoma and mantle cell lymphoma in German routine clinical practice. Ann Hematol. 2015;94:1553–8.
19. Mondello P, Steiner N, Willenbacher W, Wasle I, Zaja F, Zambello R, et al. Bendamustine plus rituximab versus R-CHOP as first-line treatment for patients with indolent non-Hodgkin's lymphoma: evidence from a multicenter, retrospective study. Ann Hematol. 2016;95:1107–14.
20. Swerdlow SH, Campo E, Harris NL, Jaffe ES, Pileri SA, Stein H, et al. WHO classification of tumours of haematopoietic and lymphoid tissues. 4th ed. Lyon: IARC; 2008.
21. Cheson BD, Horning SJ, Coiffier B, Shipp MA, Fisher RI, Connors JM, et al. Report of an international workshop to standardize response criteria for non-Hodgkin's lymphomas. J Clin Oncol. 1999;17:1244–53.
22. Cheson BD, Pfistner B, Juweid ME, Gascoyne RD, Specht L, Horning SJ, et al. Revised response criteria for malignant lymphoma. J Clin Oncol. 2007;25:579–86.
23. Ogura M, Morishima Y, Kagami Y, Watanabe T, Itoh K, Igarashi T, et al. Randomized phase II study of concurrent and sequential rituximab and CHOP chemotherapy in untreated indolent B-cell lymphoma. Cancer Sci. 2006;97:305–12.
24. Ogura M, Ando K, Taniwaki M, Watanabe T, Uchida T, Ohmachi K, et al. Feasibility and pharmacokinetic study of bendamustine hydrochloride in combination with rituximab in relapsed or refractory aggressive B cell non-Hodgkin's lymphoma. Cancer Sci. 2011;102:1687–92.
25. Ohmachi K, Niitsu N, Uchida T, Kim SJ, Ando K, Takahashi N, et al. Multicenter phase II study of bendamustine plus rituximab in patients with relapsed or refractory diffuse large B-cell lymphoma. J Clin Oncol. 2013;31:2103–9.

Leuk Res Rep. 2016; 5: 11–13. PMCID: PMC4840419
Published online 2016 Jan 22. doi: 10.1016/j.lrr.2016.01.001

Refractory acute promyelocytic leukemia successfully treated with combination therapy of arsenic trioxide and tamibarotene: A case report

Minoru Kojima,[a,b,*] Daisuke Ogiya,[a] Akifumi Ichiki,[a] Ryujiro Hara,[a] Jun Amaki,[a,b] Hidetsugu Kawai,[a] Hiroki Numata,[a] Ai Sato,[a] Mitsuki Miyamoto,[a] Rikio Suzuki,[a,c] Shinichiro Machida,[a] Hiromichi Matsushita,[d] Yoshiaki Ogawa,[a] Hiroshi Kawada,[a] and Kiyoshi Ando[a]

[a]Division of Hematology/Oncology, Department of Internal Medicine, Tokai University School of Medicine, 143 Shimokasuya, Isehara, Kanagawa, Japan
[b]Department of Hematology, Ebina General Hospital, Japan
[c]Division of Internal Medicine, Hadano Red Cross Hospital, Japan
[d]Department of laboratory Medicine, Tokai University School of Medicine, 143 Shimokasuya, Isehara, Kanagawa, Japan
Minoru Kojima: kojima@tokai-u.jp; Hiromichi Matsushita: hmatsu@is.icc.u-tokai.ac.jp
*Corresponding author at: Department of Hematology, Ebina General Hospital, 1320 Kawaraguchi, Ebina, Kanagawa 243-0433, Japan.Department of Hematology, Ebina General Hospital1320 KawaraguchiEbinaKanagawa243-0433Japan ; Email: kojima@tokai-u.jp

Received 2015 Sep 5; Revised 2015 Dec 2; Accepted 2016 Jan 7.

Abstract

A 40-year-old male developed refractory acute promyelocytic leukemia (APL) after various treatments including all-trans retinoic acid, tamibarotene, arsenic trioxide (As_2O_3), conventional chemotherapy, and autologous peripheral blood stem cell transplantation. We attempted to use both tamibarotene and As_2O_3 as a combination therapy, and he achieved molecular complete remission. Grade 2 prolongation of the QTc interval *on the electrocardiogram* was observed during the therapy. The combination therapy of As_2O_3 and tamibarotene may be effective and tolerable for treating refractory APL cases who have no treatment options, even when they have previously been treated with tamibarotene and As_2O_3*as a single agent*.

1. Introduction

Acute promyelocytic leukemia (APL) is driven by an oncogenic chromosomal translocation fusing the promyelocytic leukemia (*PML*) and retinoic acid receptor alpha (*RARA*) genes. The *PML*/*RARA* fusion protein causes a maturational block at the promyelocyte stage of myeloid differentiation. Differentiation therapy with all-trans retinoic acid (ATRA) alone or in combination with chemotherapy is a major advance in the treatment of APL and is regarded as the first paradigm of molecularly targeted therapy [1]. However, relapse/refractory APL patients demonstrating resistance to ATRA are recognized as a clinically critical problem.

Arsenic trioxide (As_2O_3) is also highly effective in the treatment of APL. Early studies conducted in China and the United States showed that this agent can induce sustained molecular remission when used as a single agent in patients who have a relapse after treatment with ATRA-containing regimens [2], [3]. As_2O_3 acts through specific binding of the *PML* moiety of the disease-specific *RARA* oncoprotein, leading to its degradation and resulting in partial differentiation and induction of apoptosis of leukemic promyelocytes. Synergy of As_2O_3 and ATRA, which binds the *RARA* moiety of *PML/RARA*, has been shown at both the biological and the clinical levels.

On the other hand, tamibarotene is in the same family of drugs as ATRA, induces the differentiation of APL cells,

and is applied to relapsed cases that have previously received ATRA treatment [4]. Tamibarotene has strong differentiation-inducing activity on human promyelocytic leukemia cells and is expected to be more effective and safe than ATRA [5].

While it has been reported that the combination therapy of As_2O_3 and ATRA is highly effective not only as the front-line treatment [6], but also in relapsed and treatment-refractory APL patients [7], showing fewer adverse events than the combination of ATRA and chemotherapeutic drugs, the efficacy and tolerability of the combination of As_2O_3 and tamibarotene are unknown. We herein report a patient with APL successfully treated with the combination therapy of As_2O_3 and tamibarotene, in whom both As_2O_3 and tamibarotene monotherapies had not been effective.

2. Case report

Go to: Go to:

A 40-year-old Japanese male was admitted to our hospital because he presented with purpura on both legs in May 2011. Laboratory examinations revealed significantly abnormal findings, including a white blood cell (WBC) count of 41,400/μL with 65.5% blasts and 22.5% promyelocytes, a hemoglobin level of 12.2 g/dL, and a platelet count of 20,000/μL. Blood coagulation parameters showed a fibrinogen level of 154 mg/dL, FDP level of 320.8 μg/mL, and D-dimer level of 70.9 μg/mL. A bone marrow aspiration study revealed the proliferation of blasts (65.5%) and promyelocytes (22.5%). A chromosome analysis based on a G-banding analysis showed the karyotype 46,XY,t(15;17)(q22;q21) [20/20]. On the basis of these findings, a diagnosis of acute promyelocytic leukemia was made. The patient received an induction therapy with JALSG APL 204 regimen-group C, which consisted of ATRA, cytarabine (Ara-C), and idarubicin, and achieved hematological complete remission (CR). Accordingly, he received three cycles of post-remission therapies and achieved molecular CR (Table 1).

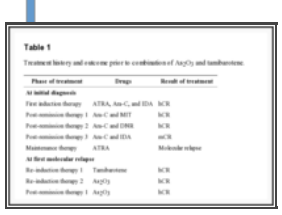

Table 1

Treatment history and outcome prior to combination of As_2O_3 and tamibarotene.

However, although hematological relapse was not detected, the *PML*/*RARA* mRNA transcripts came to be recognized by an RT-PCR test during the period of maintenance therapy using ATRA. Thus, the patient was diagnosed as having molecular relapse and received tamibarotene (6 mg/m^2/day) for eight weeks, but the *PML*/*RARA* mRNA transcripts did not disappear. He then received a therapy with JALSG APL 205R regimen composed of As_2O_3 single treatment as a re-induction therapy and two cycles of As_2O_3 single treatment as post-remission therapy. However, the *PML*/*RARA* mRNA transcripts did not disappear during the following consolidation therapy.

He received high-dose cytarabine (2000 mg/m^2 twice a day) for five days and achieved second molecular CR. Accordingly, autologous peripheral blood stem cell transplantation (aPBSCT) was performed after the high-dose chemotherapy consisting of busulfan (1 mg/kg four times a day) for three days and melphalan (70 mg/m^2/day) for two days in August 2014. Engraftment was subsequently observed and he was discharged while remaining in molecular CR.

However, a second molecular relapse occurred nine months after the aPBSCT. Tamibarotene was used again, but resulted in a hematological relapse.

Then, we attempted to use both tamibarotene and As_2O_3 as a combination therapy. He achieved hematological and molecular CR on day 28 and on day 61, respectively (Fig. 1). Hematologic toxicities and hypertriglyceridemia were not detected, and grade 2 prolongation of the QTc interval *on the electrocardiogram* was observed during the therapy.

Fig. 1

Clinical course after second molecular relapse. The patient received the con

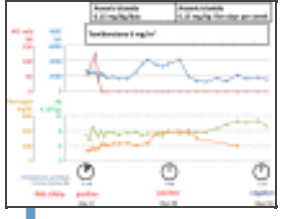

chemotherapy of tamibarotene and As_2O_3. He attained hematological CR a
on day 28 and on day 61, respectively. APL: acute promyelocytic leukemia,

Subsequently, the patient underwent allogeneic bone marrow transplantation in January 2015, and the molecular CR has persisted so far for eleven months since the transplantation.

3. Discussion

Go to: Go to:

Reports have included speculation on the molecular mechanisms of resistance to ATRA and As_2O_3. In terms of the mechanism of resistance to ATRA, genetic mutations (i.e. missense, nonsense, and deletions) have been identified on the *RARA* ligand binding domain (LBD) in *PML-RARA*. These mutations accumulate in the three subregions of the LBD domain [8]. In vitro analyses using ATRA-resistant NB4 cells and mutated-*PML-RARA* expressing Cos-1 cells [9] indicated that ATRA-binding affinity with mutated *PML-RARA* was lower than that with *PML-RARA* without mutations because of conformational changes in LBD. Furthermore, ligand-dependent N-CoR/SMRT co-repressor release and co-activator recruitment, which are critical for the transcriptional activation of genes with RARE sites and morphological cell differentiation, are impaired under the therapeutic dose of ATRA [9].

On the other hand, information on As_2O_3 resistance remains limited compared with that on ATRA resistance. Goto et al. reported the first molecular basis for clinical resistance to As_2O_3 in APL using two As_2O_3-resistant patients [10]. The authors concluded that *PML*-B2 domain mutations may play an important role in aberrant molecular responses to As_2O_3 and may be critical for As_2O_3 resistance in APL.

To overcome these resistance mechanisms in APL cells, a number of drugs have been tested. Tamibarotene is approximately 10 times more potent than ATRA as an in vitro inducer of differentiation, and is chemically more stable than ATRA [5]. Although the precise mechanism of the combination of tamibarotene and As_2O_3 in overcoming therapy resistance of APL cells is not known, we suppose a certain synergistic effect of the drugs, as is observed in the combination of ATRA and As_2O_3 [6], [7]. Most importantly, our refractory patient, who had previously been treated with both tamibarotene and As_2O_3 monotherapies and could not enter hematological CR, achieved molecular CR by the combination therapy without severe adverse events, and has been in the molecular CR although the subsequent allogenic stem cell transplantation might significantly affect the clinical course. The combination of As_2O_3 and tamibarotene may be effective and tolerable for treating patients with refractory APL who have previously received various treatments including tamibarotene and As_2O_3, and have no treatment options.

Author's contributions

Go to: Go to:

M.K. designed the experiments, performed the experiments and prepared the manuscript; D.A., F.I., R.H., J.A., Hid.K., H.N., A.S., M.M., R.S., S.M., and Y.O. designed the experiments and performed the experiments; H.M., Hir.K., and K.A. designed the experiments and prepared the manuscript.

Conflict of interest

Go to: Go to:

The authors have no conflicts of interests or funding to disclose.

References

Go to: Go to:

1. Ohno R., Asou N., Ohnishi K. Treatment of acute promyelocytic leukemia: strategy toward further increase of cure rate. Leukemia. 2003;17(8):1454–1463. [PubMed]

2. Shen Z.X., Chen G.Q., Ni J.H., Li X.S., Xiong S.M., Qiu Q.Y., Zhu J., Tang W., Sun G.L., Yang K.Q., Chen Y., Zhou L., Fang Z.W., Wang Y.T., Ma J., Zhang P., Zhang T.D., Chen S.J., Chen Z., Wang Z.Y. Use of arsenic

trioxide (As_2O_3) in the treatment of acute promyelocytic leukemia (APL): II. Clinical efficacy and pharmacokinetics in relapsed patients. Blood. 1997;89(9):3354–3360. [PubMed]

3. Soignet S.L., Frankel S.R., Douer D., Tallman M.S., Kantarjian H., Calleja E., Stone R.M., Kalaycio M., Scheinberg D.A., Steinherz P., Sievers E.L., Coutré S., Dahlberg S., Ellison R., Warrell R.P., Jr. United States multicenter study of arsenic trioxide in relapsed acute promyelocytic leukemia. J. Clin. Oncol. 2001;19(18):3852–3860. [PubMed]

4. Tobita T., Takeshita A., Kitamura K., Ohnishi K., Yanagi M., Hiraoka A., Karasuno T., Takeuchi M., Miyawaki S., Ueda R., Naoe T., Ohno R. Treatment with a new synthetic retinoid, Am80, of acute promyelocytic leukemia relapsed from complete remission induced by all-trans retinoic acid. Blood. 1997;90(3):967–973. [PubMed]

5. Hashimoto Y., Kagechika H., Kawachi E., Fukasawa H., Saito G., Shudo K. Correlation of differentiation-inducing activity of retinoids on human leukemia cell lines HL-60 and NB4. J. Cancer Res. Clin. Oncol. 1995;121(11):696–698. [PubMed]

6. Lo-Coco F., Avvisati G., Vignetti M., Thiede C., Orlando S.M., Iacobelli S., Ferrara F., Fazi P., Cicconi L., Di Bona E., Specchia G., Sica S., Divona M., Levis A., Fiedler W., Cerqui E., Breccia M., Fioritoni G., Salih H.R., Cazzola M., Melillo L., Carella A.M., Brandts C.H., Morra E., von Lilienfeld-Toal M., Hertenstein B., Wattad M., Lübbert M., Hänel M., Schmitz N., Link H., Kropp M.G., Rambaldi A., La Nasa G., Luppi M., Ciceri F., Finizio O., Venditti A., Fabbiano F., Döhner K., Sauer M., Ganser A., Amadori S., Mandelli F., Döhner H., Ehninger G., Schlenk R.F., Platzbecker U., Gruppo Italiano Malattie Ematologiche dell'Adulto; German-Austrian Acute Myeloid Leukemia Study Group; Study Alliance Leukemia Retinoic acid and arsenic trioxide for acute promyelocytic leukemia. N. Engl. J. Med. 2013;369(2):111–121. [PubMed]

7. Thirugnanam R., George B., Chendamarai E., Lakshmi K.M., Balasubramanian P., Viswabandya A., Srivastava A., Chandy M., Mathews V. Comparison of clinical outcomes of patients with relapsed acute promyelocytic leukemia induced with arsenic trioxide and consolidated with either an autologous stem cell transplant or an arsenic trioxide-based regimen. Biol. Blood Marrow Transplant. 2009;15(11):1479–1484. [PubMed]

8. Gallagher R.E., Moser B.K., Racevskis J., Poiré X., Bloomfield C.D., Carroll A.J., Ketterling R.P., Roulston D., Schachter-Tokarz E., Zhou D.C., Chen I.M., Harvey R., Koval G., Sher D.A., Feusner J.H., Tallman M.S., Larson R.A., Powell B.L., Appelbaum F.R., Paietta E., Willman C.L., Stock W. Treatment-influenced associations of PML-RARα mutations, FLT3 mutations, and additional chromosome abnormalities in relapsed acute promyelocytic leukemia. Blood. 2012;120(10):2098–2108. [PubMed]

9. Côté S., Zhou D., Bianchini A., Nervi C., Gallagher R.E., Miller W.H., Jr. Altered ligand binding and transcriptional regulation by mutations in the PML/RARalpha ligand-binding domain arising in retinoic acid-resistant patients with acute promyelocytic leukemia. Blood. 2000;96(9):3200–3208. [PubMed]

10. Goto E., Tomita A., Hayakawa F., Atsumi A., Kiyoi H., Naoe T. Missense mutations in PML-RARA are critical for the lack of responsiveness to arsenic trioxide treatment. Blood. 2011;118(6):1600–1609. [PubMed]

Leuk Res Rep. 2016; 5: 14–17. PMCID: PMC4840422
Published online 2016 Apr 12. doi: 10.1016/j.lrr.2016.04.001

The formation of an aberrant PAX5 transcript in a patient with mixed phenotype acute leukemia harboring der(9)t(7;9)(q11.2;p13)

Jun Amaki,[a,b] Hiromichi Matsushita,[c,d,*] Yuka Kitamura,[d] Ryoko Nagao,[e] Hiromichi Murayama,[b] Minoru Kojima,[a,b] and Kiyoshi Ando[b,d]

[a] Division of Hematology, Ebina General Hospital, Ebina, Kanagawa, Japan
[b] Division of Hematology and Oncology, Department of Internal Medicine, Tokai University School of Medicine, Isehara, Kanagawa, Japan
[c] Department of Laboratory Medicine, Tokai University School of Medicine, 143 Shimokasuya, Isehara, Kanagawa, Japan
[d] Research Center for Cancer Stem Cell, Tokai University School of Medicine, Isehara, Kanagawa, Japan
[e] Department of Pathology, Tokai University School of Medicine, Isehara, Kanagawa, Japan
Hiromichi Matsushita: hmatsu@is.icc.u-tokai.ac.jp
[*] Corresponding author at: Department of Laboratory Medicine, Tokai University School of Medicine, 143 Shimokasuya, Isehara, Kanagawa, Japan.Department of Laboratory Medicine, Tokai University School of MedicineIseharaKanagawaJapan ; Email: hmatsu@is.icc.u-tokai.ac.jp

Received 2015 Dec 9; Revised 2016 Mar 12; Accepted 2016 Apr 11.

Abstract

We experienced the case of a 56-year-old male with B-lymphoid/myeloid lineage mixed phenotype acute leukemia (MPAL). A cytogenetic analysis of the patient's bone marrow revealed a complex karyotype, including der(9)t(7;9)(q11.2;p13). We identified an aberrant *PAX5* transcript, including the exons 1A to 5 and the contiguous intron 5/6 sequence using the 3′ rapid amplification of cDNA ends-polymerase chain reaction method, and confirmed their expression in the leukemic cells. Our case suggests that der(9)t(7;9)(q11.2;p13) can cause the truncation of the *PAX5* transcript, which is supposed to contribute to the generation of MPAL, in addition to three previously reported types of *PAX5* fusion.

Keywords: MPAL, der(9)t(79)(q11.2p13), PAX5

1. Introduction

Mixed phenotype acute leukemia (MPAL) is a rare hematological malignancy which is characterized by the generation of leukemic blasts with multilineage potential. Genetic analyses revealed that the *BCR-ABL1* and *KMT2A* (*MLL1*) gene rearrangement in B-lymphoid/Myeloid MPAL are frequently detected, resulting in the formation of each subtype of MPAL. In addition, deletion 6 and 12p11.2 abnormalities have been observed in multiple cases [1], [2]. On the other hand, the frequency and significance of *PAX5* gene alteration located on 9p13.2, which have been reported in B-progenitor acute lymphoblastic leukemia (B-ALL), remains unknown in MPAL.

We herein report an MPAL patient with der(9)t(7;9)(q11.2;p13) which generated a truncated PAX5 transcript.

2. Case report

A 56-year-old male was referred to our hospital for evaluation of leukocytosis (29,800×10^9/L). A bone marrow examination showed a marked proliferation of blasts (88.3%) that were negative for myeloperoxidase (MPO) staining. These blasts were uniformly positive for CD19, CD10, TdT, CD34, MPO and HLA-DR based on the

findings of flow cytometry (Fig. 1**A**), thus suggesting the presence of biphenotypic acute leukemia. A chromosomal analysis of the bone marrow cells revealed a complex karyotype including the derivative chromosome der(9)t(7;9)(q11.23;p13) (Fig. 1**B**). Transcripts of *BCR-ABL1*, *ETV6-RUNX1*, *E2A-PBX1*, *MLL-AF4*, *MLL-AF6*, *MLL-AF9* and *MLL-ENL* were not detected. The patient was therefore diagnosed with MPAL of B-lymphoid/myeloid lineage (not otherwise specified).

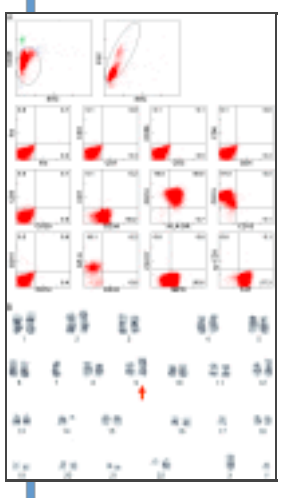

Fig. 1

The characterization of leukemic cells. A. A flow cytometry analysis of the cellular surface markers. The blasts were found to be positive for CD19, CD10, TdT, CD34, MPO and HLA-DR, while they were negative for CD13, CD33 and CD3. B. The cytogenetic analysis **...**

3. Result and discussion

Go to: Go to:

Three types of PAX5 fusion in B-ALL with t(7;9)(q11.2;p13) and der(9)t(7;9)(q11.2;p13), including *PAX5-ELN*, *PAX5-AUTS2* and *PAX5-POM12*, have been reported thus far [3]. In order to analyze the alteration of the *PAX5* gene in the present case, we utilized the 3′ RACE-PCR method. We detected an aberrant *PAX5* transcript, including exons 1A to 5 and the contiguous intron 5/6 sequence. The presumably truncated PAX5 protein was composed of 256 amino acids. It preserved the paired domain for DNA binding at the N-terminus and acquired an aberrant C-terminus, instead of the transactivation and inhibitory domains for transcription regulation. The expression of this transcript and wild-type transcript (derived from a wild-type allele) in the leukemic blasts was confirmed by reverse transcription (RT)-PCR (Fig. 2).

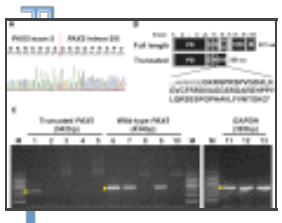

Fig. 2

The detection of the aberrant *PAX5* transcript. A. A sequence chromatogram of the aberrant *PAX5* transcript. B. The presumed structure of the truncated PAX5 protein. The amino acid sequence derived from the intron 5/6 sequence (5/6) is indicated at the **...**

The addition of the intron 5/6 sequence at the 3′ end was supposed to be generated by chromosomal translocation without the fusion partner gene at 9q13; The *PAX* gene was simply broken at intron 5/6 without the supply of a splice acceptor site at the 3′ end of the intron, resulting in the in-frame transcription of the unremoved intron sequence. An identical truncated transcript was also detected in 3 B-ALL cases including a case with dic(9;16)(p13;q11), but not der(9)t(7;9)(q11.2;p13) [4], suggesting that this genetic alteration can be generated by genomic instability that is not related to a specific rearrangement of *PAX5*.

The *PAX5* gene encodes a transcriptional factor, which is specifically expressed at the early stages of B-cell differentiation and it is required for B-cell development. Its dysregulation is involved in the leukemogenesis of B-ALL. The *PAX5* gene rearrangements account for approximately 2.5% of pediatric B-ALL cases [5]. A genome-wide analysis revealed that one-third of pediatric B-ALL cases had somatic mutations in PAX5, which resulted in the generation of a hypomorphic allele of the *PAX5* gene [6]. Chemical and retroviral mutagenesis significantly increases the penetrance of B-ALL in mice with a heterozygous loss-of-function mutation of *PAX5* [7], suggesting that the reduced expression and dysregulation of PAX5 function are closely related to the development of B-ALL.

However, the PAX5 function in bi-phenotypic B-lymphoid/myeloid cells remains obscure; one study showed that ectopic *PAX5* expression was required for their maintenance [8]. Another demonstrated that low-level *PAX5* expression was required for MPAL development [9]. To the best of the authors' knowledge, there are no other case reports of *PAX5* gene or 9p13.2 abnormalities in MPAL patients. The truncated PAX5 that was observed in

the present study behaves as a competitive inhibitor of wild-type PAX5 transcriptional activity [6], suggesting that the truncated PAX5 may also contribute to the development of MPAL by inhibiting the function of wild-type PAX5.

The leukemogenesis of MPAL could be heterogeneous and even complicated in some cases, because the development of MPAL requires the inhibition of multilineage differentiation in leukemic blasts. The complex karyotype in the present case indicates the possible combined involvement of PAX5 inhibition derived from truncated PAX5 and myeloid dysregulation provided by other genetic abnormalities such as deletion 6 and 12p11.2 cytogenetic aberrations resulting in the development of MPAL.

Regarding the technical effectiveness of RACE, RACE is not always successful at identifying chimeric transcripts even if PAX5 fusions are observed. As MPAL cases associated with 9p13 translocation are quite rare, a molecular analysis using these individual cases are thus considered to be important to understand the expression and function of PAX fusion in MPAL leukemogenesis. Therefore, comprehensive molecular techniques, such as RNA sequencing, may be helpful and informative for this purpose.

In conclusion, this is the first case of MPAL with der(9)t(7;9)(q11.2;p13), where an aberrant PAX5 transcript was detected.

Authors' contributions

Go to: Go to:

JA collected the clinical information and drafted the manuscript. HMa designed the study and drafted the manuscript. YK carried out the molecular analyses. RN carried out the histopathological analyses. HMu collected the clinical information and a bone marrow sample. MK supervised the study. KA supervised the study and drafted the manuscript. All authors read, discussed and approved the final version of the manuscript.

Competing interests

Go to: Go to:

The authors declare no competing interests in association with the present study.

Footnotes

Go to: Go to:

Appendix A Supplementary data associated with this article can be found in the online version at doi:10.1016/j.lrr.2016.04.001.

Appendix A. Supplementary material

Go to: Go to:

Supplementary material

Click here to view. (51K, docx)

.

References

Go to: Go to:

1. Owaidah T.M., Beihany Al A., Iqbal M.A., Elkum N., Roberts G.T. Cytogenetics, molecular and ultrastructural characteristics of biphenotypic acute leukemia identified by the EGIL scoring system. Leukemia. 2006;20(4):620–626. [PubMed]

2. Legrand O., Perrot J.Y., Simonin G., Baudard M., Cadiou M., Blanc C. Adult biphenotypic acute leukaemia: an entity with poor prognosis which is related to unfavourable cytogenetics and P-glycoprotein over-expression. Br. J. Haematol. 1998;100(1):147–155. [PubMed]

3. Denk D., Bradtke J., König M., Strehl S. PAX5 fusion genes in t(7;9)(q11.2;p13) leukemia: a case report and review of the literature. Mol. Cytogenet. 2014;7(1):13. [PubMed]

4. Coyaud E., Struski S., Prade N., Familiades J., Eichner R., Quelen C. Wide diversity of PAX5 alterations in B-

ALL: a groupe francophone de cytogenetique hematologique study. Blood. 2010;115(15):3089–3097. [PubMed]

5. Mullighan C.G. Molecular genetics of B-precursor acute lymphoblastic leukemia. J. Clin. Investig. 2012;122(10):3407–3415. [PubMed]

6. Mullighan C.G., Goorha S., Radtke I., Miller C.B., Coustan-Smith E., Dalton J.D. Genome-wide analysis of genetic alterations in acute lymphoblastic leukaemia. Nature. 2007;446(7137):758–764. [PubMed]

7. Dang J., Wei L., de Ridder J., Su X., Rust A.G., Roberts K.G. PAX5 is a tumor suppressor in mouse mutagenesis models of acute lymphoblastic leukemia. Blood. 2015;125(23):3609–3617. [PubMed]

8. Anderson K., Rusterholz C., Månsson R., Jensen C.T., Bacos K., Zandi S. Ectopic expression of PAX5 promotes maintenance of biphenotypic myeloid progenitors coexpressing myeloid and B-cell lineage-associated genes. Blood. 2007;109(9):3697–3705. [PubMed]

9. Simmons S., Knoll M., Drewell C., Wolf I., Mollenkopf H.J., Bouquet C. Biphenotypic B-lymphoid/myeloid cells expressing low levels of Pax5: potential targets of BAL development. Blood. 2012;120(18):3688–3698. [PubMed]

SCIENTIFIC REPORTS

OPEN

miR-133 regulates Evi1 expression in AML cells as a potential therapeutic target

Received: 21 October 2015
Accepted: 08 December 2015
Published: 12 January 2016

Haruna Yamamoto[1,*], Jun Lu[2,*], Shigeyoshi Oba[3], Toyotaka Kawamata[4], Akihide Yoshimi[5], Natsumi Kurosaki[1], Kazuaki Yokoyama[4], Hiromichi Matsushita[6], Mineo Kurokawa[5], Arinobu Tojo[4], Kiyoshi Ando[6], Kazuhiro Morishita[7], Koko Katagiri[8] & Ai Kotani[1,6,9]

The Ecotropic viral integration site 1 (Evi1) is a zinc finger transcription factor, which is located on chromosome 3q26, over-expression in some acute myeloid leukemia (AML) and myelodysplastic syndrome (MDS). Elevated Evi1 expression in AML is associated with unfavorable prognosis. Therefore, Evi1 is one of the strong candidate in molecular target therapy for the leukemia. MicroRNAs (miRNAs) are small non-coding RNAs, vital to many cell functions that negatively regulate gene expression by translation or inducing sequence-specific degradation of target mRNAs. As a novel biologics, miRNAs is a promising therapeutic target due to its low toxicity and low cost. We screened miRNAs which down-regulate Evi1. miR-133 was identified to directly bind to Evi1 to regulate it. miR-133 increases drug sensitivity specifically in Evi1 expressing leukemic cells, but not in Evi1-non-expressing cells The results suggest that miR-133 can be promising therapeutic target for the Evi1 dysregulated poor prognostic leukemia.

The human ecotropic viral integration site 1 (Evi1) gene is located on 3q26.2, a region frequently rearranged in acute myeloid leukemia (AML)[1,2]. Most patients with 3q26 rearrangements overexpress EVI1[2,3]. In all, 5–10% of AML patients show Evi1 upregulation[4]. While Evi1-low patients showed >80% overall survival (OS) at 5 years, Evi1-high patients showed <60%, indicating that high expression of Evi1 correlated with poor prognosis[5,6].

MicroRNAs (miRNAs) are 18–25 nt, single-stranded non-coding RNAs that are generated from primary miRNAs via pre-miRNAs. miRNAs can suppress post-transcriptional gene expression by base pairing with their target messenger RNAs (mRNAs) and inducing either translational repression or mRNA degradation[7,8]. miRNAs regulate a wide range of biological processes in animal development and human disease[9,10].

miRNAs are promising therapeutic targets for Evi1-overexpressing AML. The advantages of miRNAs for therapy are: 1) their multiple targets; 2) low toxicity due to biological therapy; 3) and low cost due to technological innovation[11]. Evi1 deficiency severely affects not only hematopoietic stem cells but also other systems[12]. Therefore, the suppression of Evi1 is presumed to cause systemic adverse effects. miRNAs could overcome this problem because they should be expressed at an optimal dose *in vivo* under the control of endogenous feedback regulation and should affect the dysregulated overexpression of Evi1 in leukemic cells but not in other systems. Accordingly, Evi1-overexpressing leukemia should be a good target for miRNA-based therapy. In this study, we aimed to identify miRNAs that suppress Evi1 for therapeutic purposes. We found that miR-133, which targets

[1]Department of Hematological Malignancy, Institute of Medical Science, Tokai University, 143 Shimokasuya, Isehara, Kanagawa 259-1193 Japan. [2]Department of Intractable Diseases, Institute of National Center for Global Health and Medicine, 1-21-1 Toyama, Shinjuku-ku, Tokyo 162-8655 Japan. [3]Department of Nephrology and Endocrinology, the University of Tokyo Hospital, 7-3-1 Hongo, Bunkyo-ku, Tokyo 113-8655 Japan. [4]Department of Hematology/Oncology, Institute of Medical Science, University of Tokyo, 4-6-1 Shirokanedai, Minato-ku, Tokyo 108-8639 Japan. [5]Department of Hematology and Oncology, Graduate School of Medicine, the University of Tokyo, 4-6-1 Shirokanedai, Minato-ku, Tokyo 108-8639 Japan. [6]Department of Hematology / Oncology, School of Medicine, Tokai University, 143 Shimokasuya, Isehara, Kanagawa 259-1193 Japan. [7]Department of Medical Science, Faculty of Medicine, University of Miyazaki, 5200 Kiyotakecho Kihara, Miyazaki-city, Miyazaki 889-1692 Japan. [8]Department of Biosciences, School of Science, Kitasato University 1-15-1, Kitasato, Minami-ku, Sagamihara, Knagawa 252-0373 Japan. [9]Japan Science and Technology Agency (JST) Science Plaza 5-3, Yonbancho, Chiyoda-ku, Tokyo 102-8666 Japan. *These authors contributed equally to this work. Correspondence and requests for materials should be addressed to A.K. (email: aikotani@k-lab.jp)

let-7b	miR-466a-3	miR-669f-3p
let-7c	miR-466b-3p	miR-669k
miR-30c	miR-466c-3p	miR-674
miR-32	miR-466d-3p	miR-702
miR-125b-1-3p	miR-466e-3p	miR-709
miR-133a	miR-466i-3p	miR-713
miR-133b	miR-468	miR-804
miR-210	miR-470	miR-833a-5p
miR-302a	miR-471-3p	miR-833b-5p
miR-302b	miR490-5p	miR-1199
miR-302c	miR-491	miR-1894-3p
miR-302d	miR-501-5p	miR-1897-3p
miR-423-5p	miR-532-5p	miR-1934
miR-431	miR-539-5p	miR-1982.1

Table 1. In silico predicted miRNAs which are potentially bound to the 3′UTR of human Evi1 mRNA. Candidate miRNAs.

Evi1, increased the drug sensitivity of Evi1-high-expressing leukemic cells, but not Evi1-non-expressing leukemic cells. This suggests that miR-133 is a promising therapeutic target for Evi1-overexpressing leukemia.

Results

We screened for miRNAs that potentially target Evi1 to suppress its expression using computational prediction and luciferase assays. *In silico* prediction of Evi1 targets using the miRanda software revealed that 42 miRNAs potentially bind to the Evi1 3′UTR. (Table 1) Next, we examined whether they suppress the translation of a luciferase reporter containing the 3′UTR of the human Evi1 mRNA. The precursors for 42 miRNAs were available in our miRNA precursor library. Pre-miR™ Precursor Molecules for these 42 miRNAs were co-transfected into NIH3T3 cells with a luciferase reporter vector containing the 3′UTR region of the *human Evi1* mRNA. (Figure 1a) Two miRNAs reproducibly downregulated luciferase activity: miR-133 and miR-466. (Figure 1b)

To examine whether the endogenous expression of Evi1 is affected by miR-133 and miR-466, we overexpressed miR-133 in HEL cell lines, which express high levels of Evi1. We found that miR-133 suppressed endogenous Evi1 expression in the HEL cell lines. (Figure 1c)

Overexpression of miR-466 did not affect endogenous Evi1 expression, but suppression of miR-466 activity by miR-466 TUD[13] resulted in upregulation of endogenous Evi1 expression. (Figure 1d)

Since miR-133 and miR-466 both regulated Evi1, we further analyzed their functions in leukemia cell lines. Evi1 overexpression is associated with poor prognosis and shorter survival in AML, because AML shows strong drug resistance. We examined whether miR-133 and miR-466 increase sensitivity to Adriamycin (ADR), one of the key drugs in chemotherapy for AML. HEL and K562 cells derive from AML patients with high Evi1expression, while HL60, U937 and THP1 cells are from ones without Evi1 expression. (Figure 1e,f) We compared drug sensitivity between the two groups of cell lines. Ectopic expression of miR-133 in HEL cells sensitized the cells to ADR. HEL cells were transduced with a retroviral expression vector, MDH, expressing miR-466, miR-133, or no miRNA (control). Transduced HEL and K562 cells were sorted for those expressing GFP (a marker gene in the MDH vector) and were treated with ADR for 44 h. Annexin V staining was used to measure apoptosis. Approximately 3–7% of cells expressing miR-133 were Annexin V-positive (apoptotic) in the absence of ADR treatment, similar to sorted control MDH HEL, K562, HL60, U937 and THP1 cells. (Figure 2a,b) Treatment with ADR for 48 h dose-dependently increased the number of Annexin V-positive miR-133-overexpressing HEL and K562 cells, but not HL60, U937 and THP1 cells, compared to control cells. (Figure 2a,b) These results clearly show that miR-133 induces apoptosis in Evi1-overexpressing cells, but not in cells without Evi1 expression. miR-466 did not show any effect on ADR sensitivity.

That miR-133 increases drug sensitivity in Evi1-high-expressing AML 1 cells was confirmed by caspase activation in these cells. ADR dose-dependently increased cleaved caspase-3 levels in miR-133-overexpressing cells compared with control cells. (Figure 2c) This indicates that miR-133 promoted apoptosis in the presence of ADR in Evi1-high-expressing HEL leukemic cells. (Figure 3)

Discussion

miR-1-2 and miR-133a-1 are clustered together at the same locus on chromosome 18[14] suggesting that their transcription might be regulated by similar mechanisms. It was previously reported that transcription of these two miRNAs was directly regulated by Evi1, which acts as a transcription factor for them[15].

Both miRNAs are upregulated by overexpression of Evi1, while only miR-1, and not miR-133, increased cell proliferation[16]. The function and significance of miR-133, which is transcriptionally upregulated by Evi1, needed to be explored. In this study, we demonstrated that miR-1 and miR-133 might act antagonistically, at least in Evi1-overexpressing leukemic cells. Similarly, a previous study showed that miR-1 and miR-133, which are preferentially expressed in cardiac and skeletal muscle and have been shown to regulate differentiation and proliferation of cells in these tissues, produce opposing effects: miR-1 is pro-apoptotic in cardiac cell apoptosis whereas miR-133 is anti-apoptotic. This suggests that the relative levels of miR-1 and miR-133 are more important than their

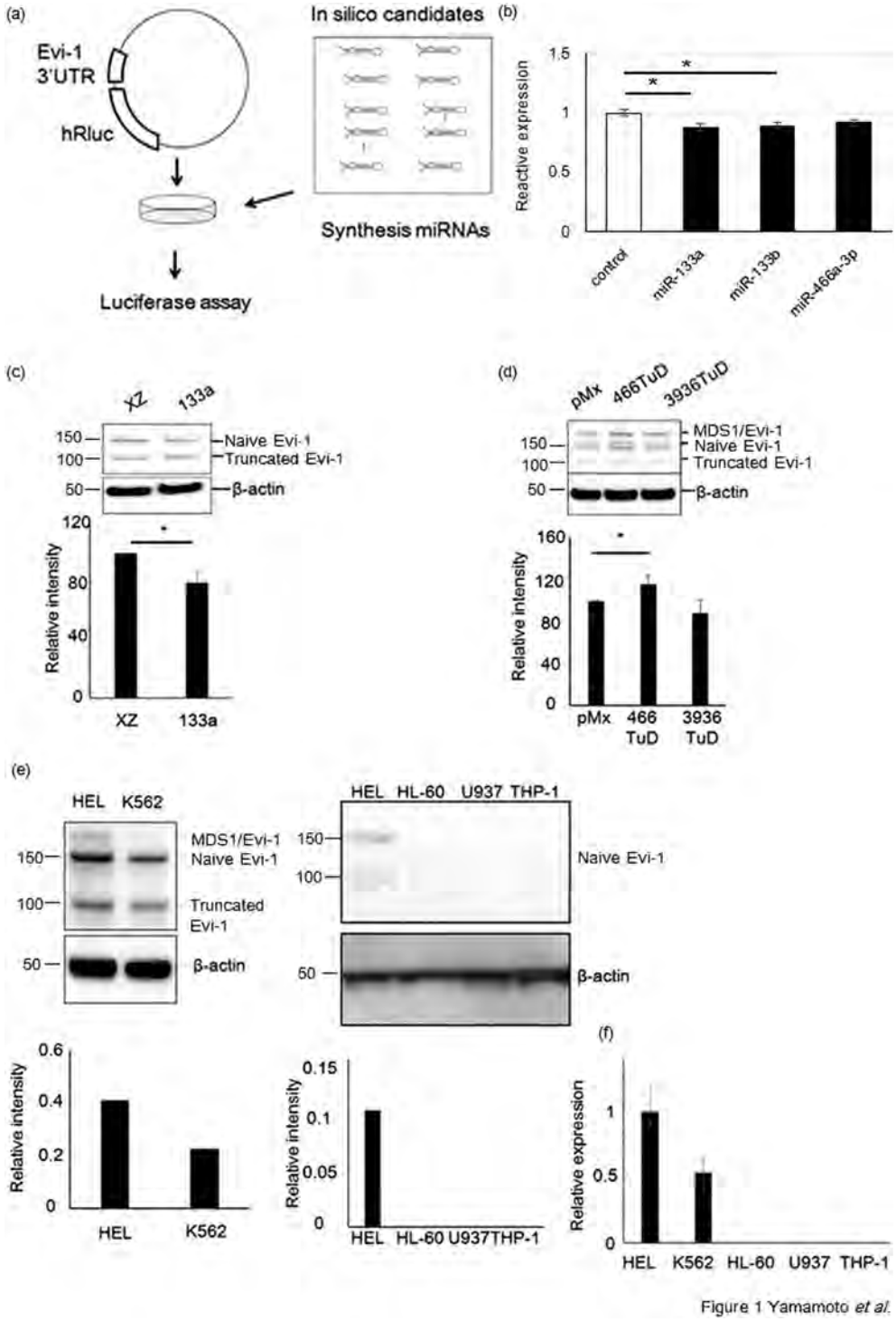

Figure 1 Yamamoto *et al.*

Figure 1. (**a**)The schema of the screening of miRNAs binding to the Evi1 3′UTR Synthetic miRNAs and the luciferase reporter containing the 3′-UTR of the human Evi1 mRNA were co-transfected into NIH3T3 cells to identify the miRNAs which downregulate luciferase by binding to Evi1 3′UTR. (**b**) The downregulated luciferase activity by binding of miR-133a,b, and miR-466a-3p to Evi1 3′UTR. The longtitude axis showed the relative luciferase to the control. (**c**) Exogenous miR-133 decreased Evi-1 expressions in HEL cells. The sum of naïve and truncated or MDS1 bands intensity was determined by densitometry and normalized to β-actin. Three experiments were done. (*$p < 0.05$). (**d**) In Hela cells which were transfected with miR-466 or miR-3936 tough decoy (TuD), all of Evi-1 variant proteins including MDS1/Evi-1, Evi-1 and truncated Evi-1 were specifically upregulated by miR-466 suppression. The band intensity was determined as above. Three experiments were done. (*$p < 0.05$). (**e**) Expression of Evi1 in HEL, K562, HL60, U937 and THP1 cells. The expression of Evi1 was high in HEL and K562 cells (Left), while that was not detected in HL60, U937 and THP-1 cells. The band intensity was determined by densitometry and normalized to β-actin. (**f**) Data of real-time PCR of expression of Evi1 in HEL, K562, HL60, U937 and THP-1 cells. Expression of Evi1 was detected only in HEL and K562 cells. (*$p < 0.05$)

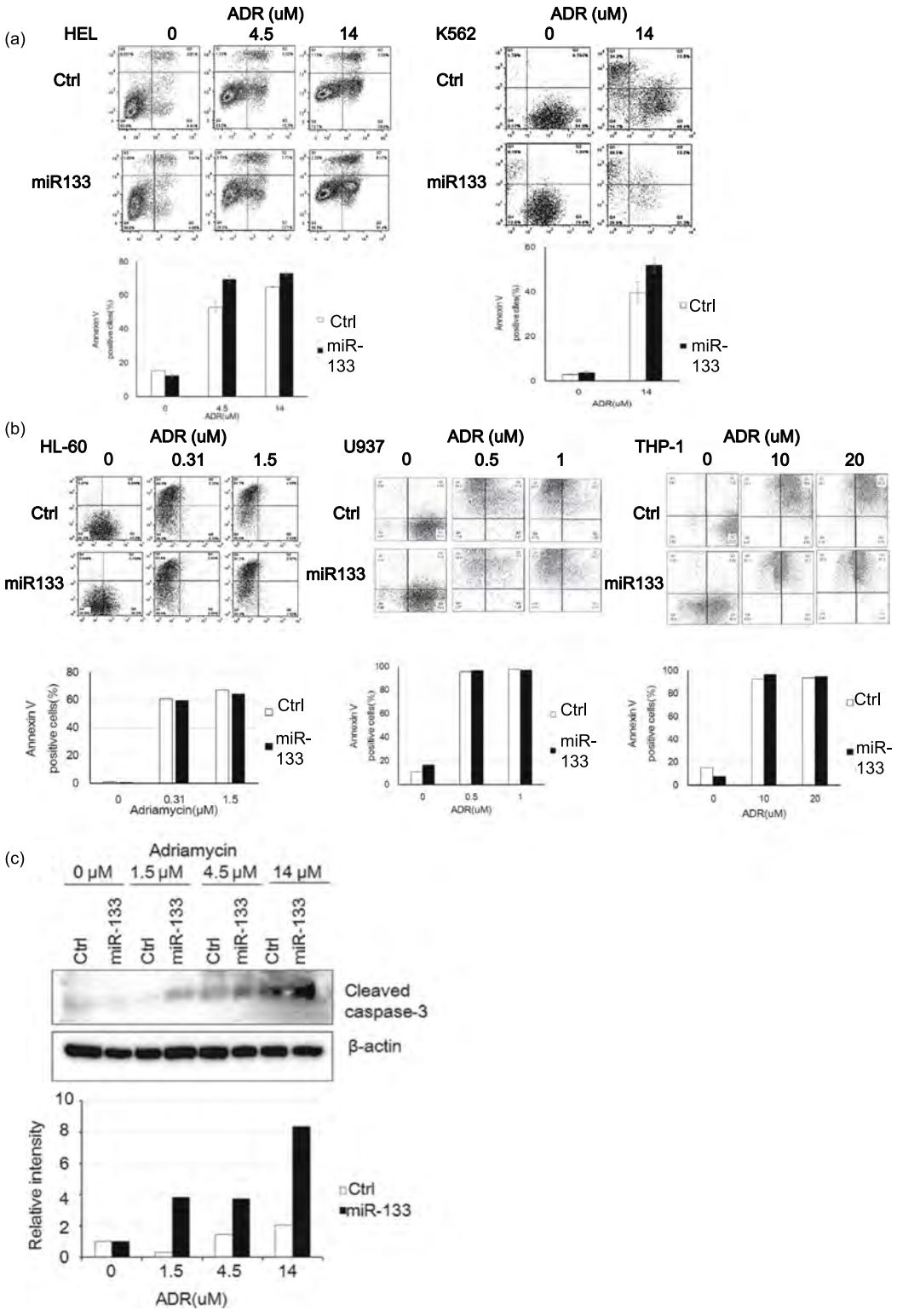

Figure 2. Functional Analysis for miR-133. (**a**) Exogenous expression of miR-133 in Evi-1^{high} HEL cells increases the sensitivity of ADR. Annexin V positive cells including PI positive and PI negative cells were measured by FACS analysis. miR-133 overexpressing Evi-1^{high} HEL cells and K562 cells showed more Annexin V positive cells in 4.5 and 14 μM ADR. ADR indicates Adriamycin.(*$p < 005$). (**b**) Exogenous expression of miR-133 in HL60 cells, U937 cells and THP1 cells had no effect on the sensitivity of ADR. Annexin V positive miR-133 overexpressing HL60 cells, U937cells, and THP-1 cells showed no difference with the control HL60 cells, U937 cells, and THP-1 cells at all the concentration of ADR. (c) Cleaved caspase 3 was increased by miR-133 in ADR dose dependent manner.

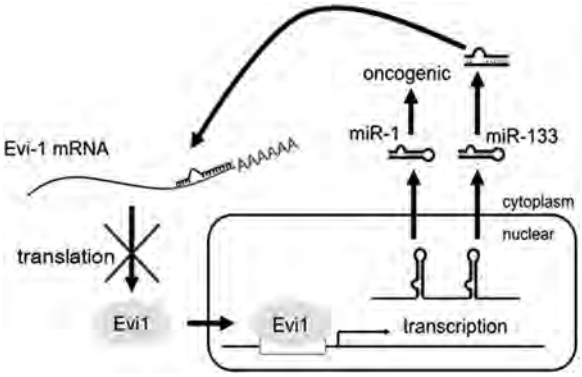

Figure 3. The schema of the function of miR-1 and miR-133 in Evi-1^{high} cells. Evi1 upregulates precursor of miR-1 and miR-133. While miR-1 shows oncogenic activity, miR-133 binds 3UTR of Evi1 to downregulate Evi1, which makes "negative feedback loop". The English in this document has been checked by at least two professional editors, both native speakers of English. For a certificate, please see: http://www.textcheck.com/certificate/cTxRPr

absolute levels in determining the fate (apoptosis or survival) of cardiac cells. The expression difference between miR-1 and miR-133 might be governed by their biogenesis because the primary miRNA for miR-1 and miR-133 is a single transcript.

Recently, an *in silico* study showed that a SNP in the predicted miR-133 binding site in the 3′UTR of Evi1 predicted worse prognosis in AML. This suggests that in patients miR-133 may play a critical tumor suppressive role whose abrogation results in a worse prognosis[17]. Our functional assay clearly showed that miR-133 is a tumor suppressor for Evi1-overexpressing leukemic cells. The restoration of miR-133 in gastric cancer suppresses cell proliferation and induces apoptosis, indicating that miR-133 is a promising therapeutic target, consistent with our study[18,19]. Accordingly, regulation of miR-133 processing, chemically modified mimics of miR-133, and drug delivery systems should be further studied to better understand the function of miR-133 in Evi1-overexpressing leukemia and its therapeutic potential. Target molecules of Evi1 that induce drug resistance include ITGA6, GPR5, and ANG1[20–22].

The target genes of miR-133 include MCL1, BCLxL, and IGF-1R, which have anti-apoptotic and oncogenic properties[23–27]. miR-133 may induce drug sensitivity through downregulation of Evi1 and these target genes.

In summary, we identified miR-133 as a miRNA that regulates Evi1, whose overexpression is associated with a poor prognosis in AML. Since miR-133 modulates dysregulated excess Evi1 expression but not normal expression, it could be a promising therapeutic target in Evi1-overexpressing AML patients.

Materials and Methods

Prediction of miRNAs using a computational target prediction system. To detect candidate miRNAs targeting Evi1, we first evaluated a series of miRNA precursors. To narrow the screened miRNAs to fewer than 100 miRNAs, we used a computational target prediction system (miRanda) containing updated sequences for all known miRNAs. Cutoff scores for selection of candidate miRNAs were <-20.0 for energy and >120 for binding[28].

Cell culture. Five cell lines (HEL, K562, U937, HL-60, and THP1) were maintained in RPMI 1640 medium (Wako, Japan) supplemented with 10% (v/v) fetal bovine serum (FBS), 50 U/mL penicillin, and 50 mg/mL streptomycin in a 10 cm dish (Corning, Inc., Corning, NY, USA). Cells were passaged twice per week.

Quantitative PCR for genes. For target gene detection, RT-PCR was performed using the High Capacity cDNA Reverse Transcription Kit (Applied Biosystems, Inc., CA, USA) and qPCR was carried out with the Fast SYBR Green Master mix. All real-time qPCR was conducted using the StepOnePlus real-time PCR system (Applied Biosystems). Threshold cycle (CT) values were calibrated to β-actin and analyzed by the $2^{-\Delta\Delta CT}$ method. Sequences of specific primers are listed in Supplementary Table 1.

Western blotting. For Western blot analyses, cells were harvested by centrifugation and washed twice with phosphate-buffered saline (PBS). Cells (1.0×10^5) were lysed in radioimmunoprecipitation assay (RIPA) buffer for 5 min on ice. Cell lysates were centrifuged to remove debris. Protein samples were separated electrophoretically on a 5–20% SDS-polyacrylamide gel and blotted onto PVDF membranes (Bio-Rad Laboratories, Tokyo, Japan). The blots were blocked with 2% low-fat dry milk in TBST (20 mM Tris-HCl, pH 7.5, 150 mM NaCl containing 0.1% Tween 20 [Sigma, MO, USA]) for 1 h at room temperature. The blocked membrane was incubated with anti-Evi1 (CST#2593) (1:2000) or anti-βactin (1:5000) for 2 h, followed by incubation with anti-rabbit IgG (CST#7074) (1:2000) secondary antibody for 1 h.

Drug sensitivity assay. Five cell lines (HEL, K562, U937, HL-60, and THP1) were seeded in 24-well plates with 2.0×10^5 cells per well in growth medium. Adriamycin was added at specific concentrations and incubated for 48 h, before being analyzed by FACS with immunostaining for APC-Annexin V (BioLegend, Japan).

References

1. Ihle, J. N., Morishita, K., Matsugi, T. & Bartholomew, C. Insertional mutagenesis and transformation of hematopoietic stem cells. *Prog Clin Biol Res* **352,** 329–337 (1990).
2. Morishita, K., Parganas, E., Parham, D. M., Matsugi, T. & Ihle, J. N. The Evi-1 zinc finger myeloid transforming gene is normally expressed in the kidney and in developing oocytes. *Oncogene* **5,** 1419–1423 (1990).
3. Morishita, K. *et al.* Activation of EVI1 gene expression in human acute myelogenous leukemias by translocations spanning 300–400 kilobases on chromosome band 3q26. *Proc Natl Acad Sci USA* **89,** 3937–3941 (1992).
4. Saito, Y. *et al.* CD52 as a molecular target for immunotherapy to treat acute myeloid leukemia with high EVI1 expression. *Leukemia* **25,** 921–931 (2011).
5. Lugthart, S. *et al.* High EVI1 levels predict adverse outcome in acute myeloid leukemia: prevalence of EVI1 overexpression and chromosome 3q26 abnormalities underestimated. *Blood* **111,** 4329–4337 (2008).
6. Nucifora, G., Laricchia-Robbio, L. & Senyuk, V. EVI1 and hematopoietic disorders: history and perspectives. *Gene* **368,** 1–11 (2006).
7. Bartel, D. P. MicroRNAs: genomics, biogenesis, mechanism, and function. *Cell* **116,** 281–297 (2004).
8. Bagga, S. *et al.* Regulation by let-7 and lin-4 miRNAs results in target mRNA degradation. *Cell* **122,** 553–563, doi: 10.1016/j.cell.2005.07.031 (2005).
9. Ambros, V. The functions of animal microRNAs. *Nature* **431,** 350–355 (2004).
10. Okuyama, K., Ogata, J., Yamakawa, N., Chanda, B. & Kotani, A. Small RNA as a regulator of hematopoietic development, immune response in infection and tumorigenesis. *Int J Hematol* **99,** 553–560, doi: 10.1007/s12185-014-1564-4 (2014).
11. Esau, C. C. & Monia, B. P. Therapeutic potential for microRNAs. *Adv Drug Deliv Rev* **59,** 101–114 (2007).
12. Hoyt, P. R. *et al.* The Evi1 proto-oncogene is required at midgestation for neural, heart, and paraxial mesenchyme development. *Mech Dev* **65,** 55–70 (1997).
13. Haraguchi, T., Ozaki, Y. & Iba, H. Vectors expressing efficient RNA decoys achieve the long-term suppression of specific microRNA activity in mammalian cells. *Nucleic Acids Res* **37,** e43 (2009).
14. Liu, N. *et al.* An intragenic MEF2-dependent enhancer directs muscle-specific expression of microRNAs 1 and 133. *Proc Natl Acad Sci USA* **104,** 20844–20849 (2007).
15. Chen, J. F. *et al.* The role of microRNA-1 and microRNA-133 in skeletal muscle proliferation and differentiation. *Nat Genet* **38,** 228–233 (2006).
16. Gómez-Benito, M. *et al.* EVI1 controls proliferation in acute myeloid leukaemia through modulation of miR-1-2. *Br J Cancer* **103,** 1292–1296, doi: 10.1038/sj.bjc.6605874 (2010).
17. Wang, T. Y., Huang, Y. P. & Ma, P. Correlations of common polymorphism of EVI-1 gene targeted by miRNA-206/133b with the pathogenesis of breast cancer. *Tumour Biol*, 2213–5 (2014).
18. Cheng, Z. *et al.* miR-133 is a key negative regulator of CDC42-PAK pathway in gastric cancer. *Cell Signal* **26,** 2667–2673 (2014).
19. Liu, Y. *et al.* Identification of miRNomes in human stomach and gastric carcinoma reveals miR-133b/a-3p as therapeutic target for gastric cancer. *Cancer Lett* **369,** 58–66 (2015).
20. Yamakawa, N., Kaneda, K., Saito, Y., Ichihara, E. & Morishita, K. The increased expression of integrin α6 (ITGA6) enhances drug resistance in EVI1 (high) leukemia. *PLoS One* **7,** e30706 (2012).
21. Saito, Y. *et al.* Maintenance of the hematopoietic stem cell pool in bone marrow niches by EVI1-regulated GPR56. *Leukemia* **27,** 1637–1649 (2013).
22. Ichihara, E., Kaneda, K., Saito, Y., Yamakawa, N. & Morishita, K. Angiopoietin1 contributes to the maintenance of cell quiescence in EVI1 (high) leukemia cells. *Biochem Biophys Res Commun* **416,** 239–245 (2011).
23. Bartram, I. *et al.* Inhibition of IGF1-R overcomes IGFBP7-induced chemotherapy resistance in T-ALL. *BMC Cancer* **15,** 663 (2015).
24. Koti, M. *et al.* Identification of the IGF1/PI3K/NF κB/ERK gene signalling networks associated with chemotherapy resistance and treatment response in high-grade serous epithelial ovarian cancer. *BMC Cancer* **13,** 549 (2013).
25. Ariës, I. M. *et al.* The synergism of MCL1 and glycolysis on pediatric acute lymphoblastic leukemia cell survival and prednisolone resistance. *Haematologica* **98,** 1905–1911 (2013).
26. Kiprianova, I. *et al.* Sorafenib Sensitizes Glioma Cells to the BH3 Mimetic ABT-737 by Targeting MCL1 in a STAT3-Dependent Manner. *Neoplasia* **17,** 564–573 (2015).
27. Zhou, W. *et al.* Inhibition of Bcl-xL overcomes polyploidy resistance and leads to apoptotic cell death in acute myeloid leukemia cells. *Oncotarget* **6,** 21557–21571 (2015).
28. Oba, S. *et al.* A useful method of identifying of miRNAs which can down-regulate Zeb-2. *BMC Res Notes* **6,** 470 (2013).

Acknowledgements

We thank Drs. Ryo Nasu, Kazuki Okuyama, Natsuko Yamakawa, and Bidisha Chanda, and the Education and Research Support Center, Tokai University, for technical assistance.

Author Contributions

H.Y., J.L., S.O. and A.K. performed research and analyzed data. A.K. designed research and wrote the paper. T.K., A.Y., N.K., K.Y., H.M., M.K., A.T., K.A., K.M. and K.K. contributed vital new reagents.

Additional Information

Supplementary information accompanies this paper at http://www.nature.com/srep

Competing financial interests: The authors declare no competing financial interests.

How to cite this article: Yamamoto, H. *et al.* miR-133 regulates Evi1 expression in AML cells as a potential therapeutic target. *Sci. Rep.* **6**, 19204; doi: 10.1038/srep19204 (2016).

J Clin Exp Hematop
Vol. 56, No. 1, June 2016

Case Study

Composite Follicular Lymphoma and CD5-Positive Nodal Marginal Zone Lymphoma

Masashi Miyaoka,[1)] Tomoki Kikuchi,[1)] Joaquim Carreras,[1)] Yukie Yara Kikuti,[1)] Ken Omachi,[2)] Minoru Kojima,[2)] Kiyoshi Ando,[2)] and Naoya Nakamura[1)]

Composite CD10-positive low-grade B-cell and CD5-positive low-grade B-cell lymphoma is extremely rare. We report a case of a composite follicular lymphoma (FL) and CD5-positive nodal marginal zone lymphoma (NMZL) in a resected inguinal lymph node of a 72-year-old Japanese male. Histologically, multiple follicles had reactive-germinal centers with tingible body macrophages, a thin mantle zone and a wide marginal zone. The wide marginal zone consisted of medium-sized cells having slightly indented nuclei and clear cytoplasm, indicating monocytoid cells with CD5-positive B-cells. Several follicles had germinal centers filled with many centrocytes, with CD10-positive B-cells. Polymerase chain reaction/sequence analysis of the immunoglobulin heavy chain gene obtained from microdissected regions of CD5-positive NMZL and FL showed different sequences within the CDR3 region. To our knowledge, this is the first report of FL and CD5-positive NMZL. 〔*J Clin Exp Hematop 56(1):55-58, 2016*〕

Keywords: composite lymphoma, follicular lymphoma, CD5-positive nodal marginal zone lymphoma

INTRODUCTION

Composite lymphoma (CL) is defined as two histologically distinct variants of malignant lymphoma occurring in the same organ or mass.[1,2] CL is quite rare, with frequency ranging from 1 to 4.7% of lymphoma cases.[3] Many combinations of lymphoma types have been reported in CLs, including composite B-cell lymphoma, composite B- and T-cell lymphoma, and composite Hodgkin lymphoma (HL) and non-Hodgkin lymphoma (NHL).[2] Previously reported cases of composite HL and NHL were combinations of HL and B-cell non-Hodgkin lymphoma, such as HL and follicular lymphoma (FL), as well as HL and diffuse large B-cell lymphoma.[4-6] In some cases, polymerase chain reaction (PCR) amplification and sequence analysis of the immunoglobulin heavy chain gene (IGH) demonstrated common clonal origins in the two abovementioned cases,[5,6] suggesting the clonal relationship in combination HL and NHL.

Received: November 16, 2015
Revised : December 5, 2015
Accepted: January 7, 2016
[1)]Department of Pathology and [2)]Division of Hematology/Oncology, Department of Internal Medicine, Tokai University School of Medicine, Isehara, Japan
Corresponding author: Masashi Miyaoka, M.D., Department of Pathology, Tokai University School of Medicine, 143 Shimokasuya, Isehara, Kanagawa, 259-1193, Japan
E-mail: miyaokamasasi828@yahoo.co.jp

Several combinations of low grade B-cell lymphoma, including FL and mantle cell lymphoma (MCL), FL and B-chronic lymphocytic leukemia/small lymphocytic lymphoma, and MCL and nodal marginal zone lymphoma (NMZL), have also been reported.[7-9] Some of these cases showed clonal relation whereas other cases were clonally unrelated.[7-9]

We report a case of CL of FL and CD5-positive NMZL in a lymph node, and demonstrated different B-cell clones in the FL and CD5-positive NMZL.

CASE REPORT

A 72-year-old, Japanese male had been treated for hypertension and suspicion of Parkinson's disease by his family doctor. The patient noticed a mass in the left groin one year prior. The mass was small, and the patient did not have fever or any other symptoms. After 6 months, the size of the mass began to increase. His family doctor then referred him to a hematologist at our hospital, and masses were identified in the left groin, right neck, and left flank. Excisional biopsy of an inguinal lymph node was performed for pathological diagnosis with flow cytometry and karyotype analyses. Peripheral blood evaluation revealed a hemoglobin level of 13.0 g/dL, a platelet count of 13.7 x 10^4/μL, a white blood cell count of 5.0 x 10^3/μL, LD 155 U/L, and soluble interleukin-2 receptor of 2,380 U/L. Positron emission tomography

showed abnormal accumulation in the right neck, right clavicles, para-aorta, left ilium, and left groin. Flow cytometry demonstrated predominant B-cells, and $CD19^+CD5^+$ and $CD20^+CD10^+$ fractions were observed. No restriction of the light chain (κ/λ) was observed, which may have been due to the $CD20^+CD10^+$ fraction involving neoplastic and reactive cells.

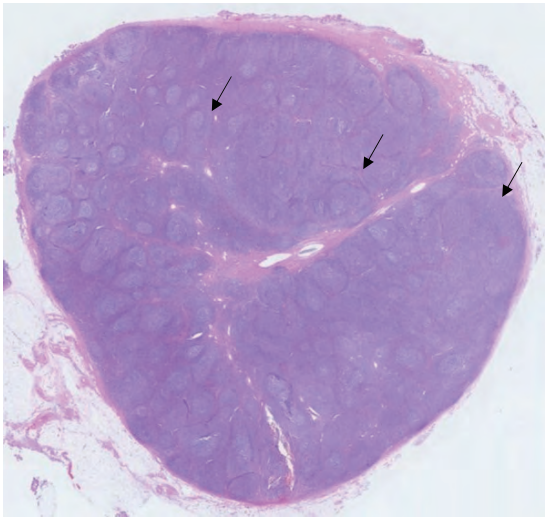

Fig. 1. Low power view of resected lymph node. Many follicles are distributed throughout the lymph node. Most follicles show marginal zone lymphoma, but several follicles show follicular lymphoma (*arrows*). H&E stain.

The patient's karyotype was normal, 46/XY[20/20]. Bone marrow involvement was not observed by histology and immunohistochemistry evaluation of the clot section. Low grade B-cell lymphoma was diagnosed. The patient underwent R-CHOP (rituximab, cyclophosphamide, doxorubicin, vincristine, and prednisolone) therapy and achieved remission.

PATHOLOGICAL FINDINGS

Histological evaluation of the resected lymph node demonstrated multiple follicles evenly distributed throughout (Fig. 1). Most follicles had a reactive-germinal center (GC) with tingible body macrophages, thin mantle zone, and wide marginal zone (Fig. 2). The wide marginal zone consisted of medium-sized cells having a slightly indented nucleus and clear cytoplasm, indicating monocytoid cells (Fig. 2). There were several follicles that had GCs filled with numerous centrocytes (Figs.1 & 2). Plasma cell differentiation was unclear in both the wide marginal zone and centrocyte-rich GC.

Immunohistochemically, monocytoid cells in the wide marginal zone were $CD3^-$, $CD5^+$, $CD10^-$, $CD20^+$, $BCL\text{-}2^+$, $BCL\text{-}6^-$, $MUM\text{-}1^-$ and cyclin $D1^-$, and lymphocytes in the GC

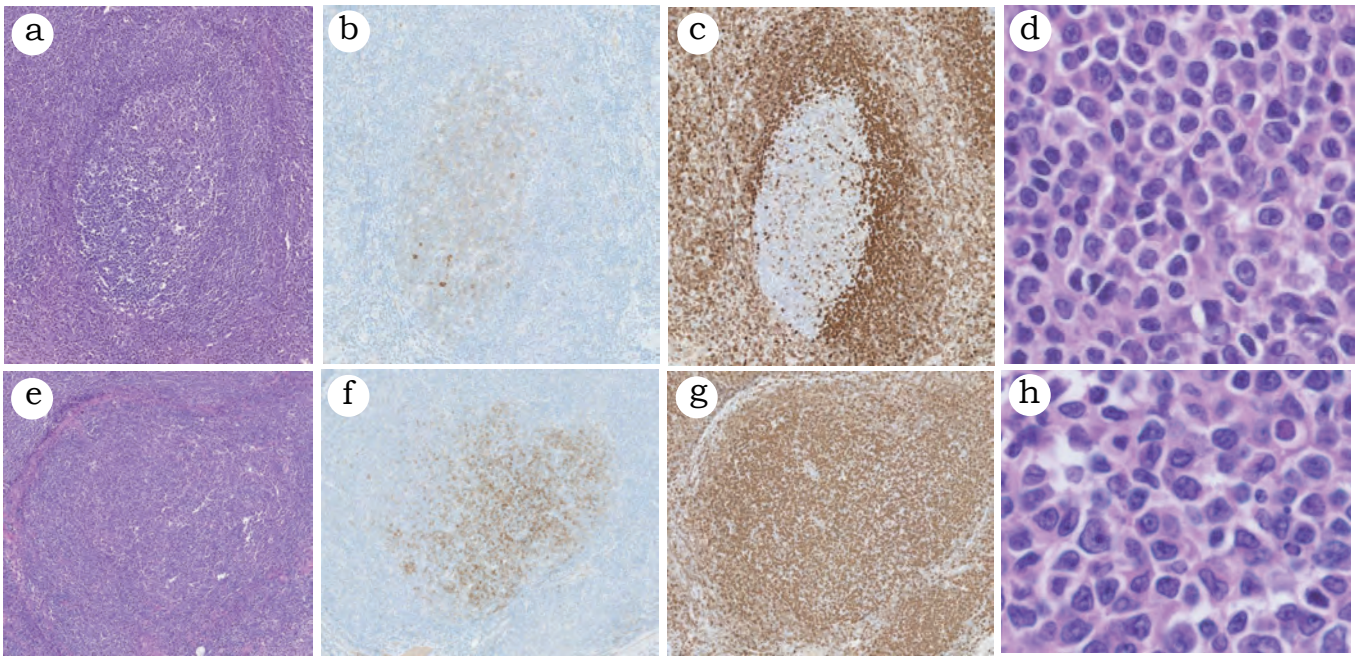

Fig. 2. Histopathology and immunohistochemistry of marginal zone lymphoma and follicular lymphoma. Nodal marginal zone lymphoma show a wide marginal zone (MgZ), mantle zone (MZ) and germinal center (GC)(***2a***). CD10 positivity is observed in the GC, but not the MgZ (***2b***), and BCL-2 positivity is observed in the MgZ and MZ, but not the GC (***2c***). Under high power view, the MgZ consists medium-sized cells having slightly indented nuclei and clear cytoplasm, indicating monocytoid cells (***2d***). Follicular lymphoma shows GC swelling (***2e***). Both CD10 and BCL-2 positivity is observed in the GC (***2f***, ***2g***). Under high power view, the GC consisted of small cleaved cells (***2h***). (*2a*), (*2d*), (*2e*) & (*2h*), H&E stain.

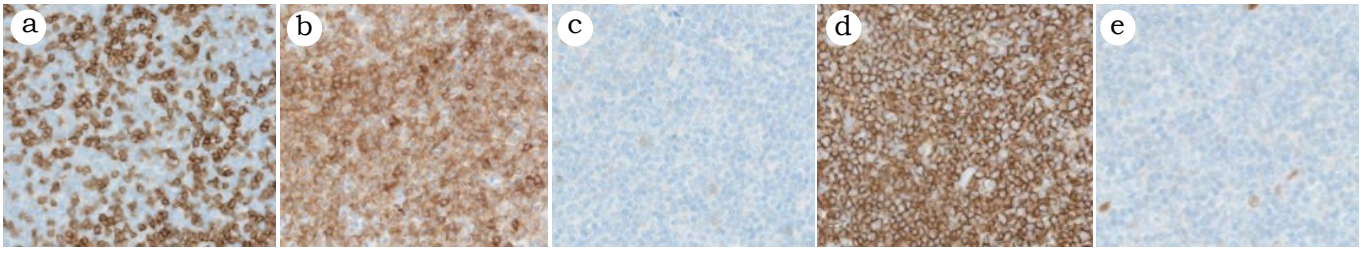

Fig. 3. Immunohistochemistry of nodal marginal zone lymphoma. Marginal zone cells were CD3-negative (***3a***), CD5-positive (***3b***), CD10-negative (***3c***), CD20-positive (***3d***), and Cyclin D1-negative (***3e***).

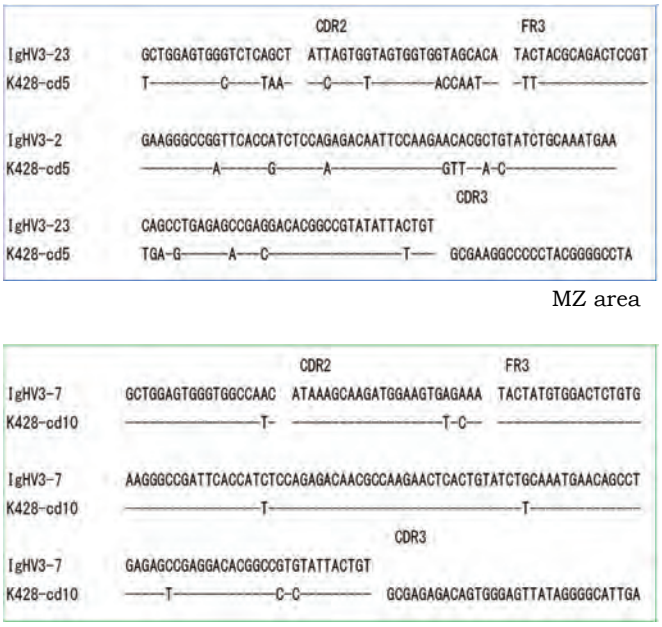

Fig. 4. Nucleotide sequence of the immunoglobulin heavy chain gene (IGH). Polymerase chain reaction and sequencing of IGH demonstrated that the marginal zone and centrocyte-rich germinal center had different sequences in the complementary determining region (CDR) 2, flame work region (FR) 3, and CDR3. Differences in the CDR3 indicate that these were two different clones.

were CD10$^+$ (weak), CD20$^+$, and BCL-2$^-$ (Figs. 2 & 3). These findings indicated CD5-positive NMZL. On the other hand, centrocytes in the GC were CD3$^-$, CD5$^+$, CD10$^+$, CD20$^+$, BCL-2$^+$, BCL-6$^+$, MUM-1$^-$, and cyclin D1$^-$, indicate FL (Fig. 2). Both κ^+ plasma cells and λ^+ plasma cells were observed in *in situ* hybridization, showing no restriction of the light chain.

PCR sequencing of the IGH from microdissected samples of the CD5-positive NMZL and FL showed different sequences in the CDR3 region, with IGHV3-23 in the CD5-positive NMZL and IgHV3-7 in the FL (Fig. 4).

DISCUSSION

We presented an unusual variation of CL composed of CD10-positive FL and CD5-positive NMZL, which to the best of our knowledge is the first case of such combination. Considering the results from the histological and immunohistochemical analysis, three possibilities were raised; (1) FL with marginal zone differentiation and CD5 expression, (2) CD5-positive NMZL with follicular colonization, or (3) composite lymphoma of FL and CD5-positive NMZL. Clarification of the clonal relationship is important in CL, and it is recommended to use not only morphological and immunohistochemical techniques, but also Southern blotting or PCR sequencing of the IGH and T cell receptor gene rearrangements, cytogenetics, and fluorescence *in situ* hybridization (FISH). In our case, PCR and sequence analysis of IGH demonstrated the different clones of the FL and CD5-positive NMZL.

Cases of CL containing a CD5-positive low grade B-lymphoma component have been previously reported.[7,8,10] In four of these cases, PCR sequencing of IGH was performed;[7,8] three of the cases showed common clonal origin and the other case had different clonal origins. Although the progenitor cells of CL containing CD5-positive low grade B-lymphoma with common clonal origin may be lymphoid stem cells or immature B-cells, the latter case and our case may have developed by chance.

MCL and chronic lymphocytic leukemia/small lymphocytic lymphoma are the main components observed in CL, and there has been a previously reported case of CL composed of CD5-positive splenic marginal zone lymphoma and FL with uncertain clonal relationship.[10] Due to the small number of cases, we were unable to determine the factor leading to the pathogenesis of CL composed of CD10-positive FL and CD5-positive low grade B-cell lymphoma, including MZL. Although such cases occur by chance, further accumulation of cases is important for identification of the factors involved in the pathogenesis of CL composed of FL and CD5-positive NMZL, as well as other CL.

In our case, the FL area was small, suggesting possible *in situ* FL. *In situ* FL has been recognized by the recent World Health Organization (WHO) classification system, but the incidence rate remains unknown due to the limited number of published cases and series.[11,12] *In situ* FL shows preservation of the nodal architecture, and most follicles appear to be

cytologically reactive, whereas rare germinal centers appear to be monotonous and lack tingible body macrophages.[11] The later follicles show strongly positive staining for BCL-2 and CD10, whereas the majority of follicles in the same lymph node are negative for BCL-2. In most cases of FL, tumor cells involve the majority of the follicles and infiltrate into the inter-follicular region; however, in *in situ* FL, tumor cells involve only a few follicles, and do not infiltrate into the many remaining reactive follicles or the inter-follicular region. There is also a possibility of overt FL of the systemic lymph nodes.

NMZL is currently defined in the WHO classification as a primary nodal B-cell lymphoma that morphologically resembles extranodal or splenic MZL, but without evidence of extranodal or splenic disease.[13] NMZL is uncommon, accounting for less than 2% of all lymphomas.[13] Generally, NMZL do not express CD5, but a few have been shown to do so. CD5-positive NMZL have histologic and immunophenotypic features typical of NMZL in addition to the expression of CD5. Jaso *et al*. reported the proportion of CD5-positive NMZL to typical NMZL to be 8.6% (7/91 cases).[14] Of the CD5-positive NMZL patients, 86% (6/7 cases) showed lymphadenopathy above and below the diaphragm, 6 cases underwent bone marrow check, and all cases had bone marrow invasion.[14] In our case, lymphadenopathy above and below the diaphragm was observed, but not bone marrow invasion.

In NMZL, CD5 has been reported to be expressed in only 8.6% cases, and CD5 expression correlates with a higher frequency of dissemination and bone marrow invasion.[14] However, patients with CD5-positive NMZL generally have an indolent clinical course and excellent overall survival.[14] In our case, although bone marrow invasion was not observed, dissemination above and below the diaphragm was present. In CD5-positive NMZL, the mechanism of CD5 expression and progenitor identification remain unclear; however, CD5 expression in NMZL may be associated with wide dissemination.

CONFLICT OF INTEREST

The authors declare no conflict of interest.

REFERENCES

1 Kim H, Hendrickson R, Dorfman RF: Composite lymphoma. Cancer 40:959-976, 1977

2 Kim H: Composite lymphoma and related disorders. Am J Clin Pathol 99:445-451, 1993

3 Thirumala S, Esposito M, Fuchs A: An unusual variant of composite lymphoma: a short case report and review of the literature. Arch Pathol Lab Med 124:1376-1378, 2000

4 Jaffe ES, Zarate-Osorno A, Kingma DW, Raffeld M, Medeiros LJ: The interrelationship between Hodgkin's disease and non-Hodgkin's lymphomas. Ann Oncol 5 (Suppl 1):7-11, 1994

5 Bellan C, Lazzi S, Zazzi M, Lalinga AV, Palummo N, *et al*.: Immunoglobulin gene rearrangement analysis in composite Hodgkin disease and large B-cell lymphoma: evidence for receptor revision of immunoglobulin heavy chain variable region genes in Hodgkin-Reed-Sternberg cells? Diagn Mol Pathol 11:2-8, 2002

6 Bräuninger A, Hansmann ML, Strickler JG, Dummer R, Burg G, *et al*.: Identification of common germinal-center B-cell precursors in two patients with both Hodgkin's disease and non-Hodgkin's lymphoma. N Engl J Med 340:1239-1247, 1999

7 Wang S, Tzankov A, Xu-Monette ZY, Hoeller S, Wang SA, *et al*.: Clonally related composite follicular lymphoma and mantle cell lymphoma with clinicopathologic features and biological implications. Hum Pathol 44:2658-2667, 2013

8 Boiocchi L, Witter RE, He B, Subramaniyam S, Mathew S, *et al*.: Composite chronic lymphocytic leukemia/small lymphocytic lymphoma and follicular lymphoma are biclonal lymphomas: a report of two cases. Am J Clin Pathol 137:647-659, 2012

9 Rodig SJ, Healey BM, Pinkus GS, Kuo FC, Dal Cin P, *et al*.: Mantle cell lymphoma arising within primary nodal marginal zone lymphoma: a unique presentation of two uncommon B-cell lymphoproliferative disorders. Cancer Genet Cytogenet 171:44-51, 2006

10 Demurtas A, Aliberti S, Bonello L, Di Celle PF, Cavaliere C, *et al*.: Usefulness of multiparametric flow cytometry in detecting composite lymphoma: study of 17 cases in a 12-year period. Am J Clin Pathol 135:541-555, 2011

11 Carbone A, Gloghini A, Santoro A: *In situ* follicular lymphoma: pathologic characteristics and diagnostic features. Hematol Oncol 30:1-7, 2012

12 Harris NL, Nathwani BN, Swerdlow SH, de Jong D, Jaffe ES, *et al*.: Follicular lymphoma. In: Swerdlow SH, Campo E, Harris NL, Jaffe ES, Pileri SA, *et al*. (eds): World Health Organization Classification of Tumours, WHO Classification of Tumours of Haematopoietic and Lymphoid Tissues. 4th ed, Lyon, International Agency for Research on Cancer (IARC), pp.220-226, 2008

13 Campo E, Pileri SA, Jaffe ES, Müller-Hermelink HK, Nathwani BN. Nodal marginal zone lymphoma. In: Swerdlow SH, Campo E, Harris NL, Jaffe ES, Pileri SA, *et al*. (eds): World Health Organization Classification of Tumours, WHO Classification of Tumours of Haematopoietic and Lymphoid Tissues. 4th ed, Lyon, International Agency for Research on Cancer (IARC), pp.218-219, 2008

14 Jaso JM, Yin CC, Wang SA, Miranda RN, Jabcuga CE, *et al*.: Clinicopathologic features of CD5-positive nodal marginal zone lymphoma. Am J Clin Pathol 140:693-700, 2013

Int J Hematol (2015) 101:543–553
DOI 10.1007/s12185-015-1766-4

ORIGINAL ARTICLE

Single nucleotide polymorphisms of cytarabine metabolic genes influence clinical outcome in acute myeloid leukemia patients receiving high-dose cytarabine therapy

Jun Amaki · Makoto Onizuka · Ken Ohmachi · Yasuyuki Aoyama · Ryujiro Hara · Akifumi Ichiki · Hidetsugu Kawai · Ai Sato · Mitsuki Miyamoto · Masako Toyosaki · Shinichiro Machida · Minoru Kojima · Yukari Shirasugi · Hiroshi Kawada · Yoshiaki Ogawa · Kiyoshi Ando

Received: 26 November 2014 / Revised: 23 February 2015 / Accepted: 23 February 2015 / Published online: 4 March 2015

Abstract Cytarabine arabinoside (Ara-C) is the most important agent for treating acute myeloid leukemia (AML). Here, we genotyped 11 single nucleotide polymorphisms (SNPs) of seven Ara-C metabolism-related genes in 39 AML patients who had received high-dose Ara-C as a single-agent treatment. Univariate analysis identified three SNPs that were significantly associated with shorter time-to-relapse (TTR): CTPS rs12144160 GG compared to AA/AG, DCTD rs9990999 AG/GG compared to AA, and SLC29A1 rs693955 CC compared to AA/AC. Multivariate analysis of TTR revealed the SLC29A1 rs693955 CC genotype and first induction failure to be significantly associated with a shorter TTR. The DCTD rs9990999 AG/GG and SLC29A1 rs693955 CC genotypes were also significantly associated with shorter duration of neutropenia. The results of our study suggest that SNP analysis can be an important tool in improving drug responsiveness and enabling a better understanding of this condition and the development of tailor-made treatments for AML patients who benefit from consolidated high-dose Ara-C therapy.

Keywords Cytarabine · Single nucleotide polymorphism · Acute myeloid leukemia

J. Amaki · M. Onizuka (✉) · K. Ohmachi · Y. Aoyama · R. Hara · A. Ichiki · H. Kawai · A. Sato · M. Miyamoto · M. Toyosaki · S. Machida · M. Kojima · Y. Shirasugi · H. Kawada · Y. Ogawa · K. Ando
Division of Hematology/Oncology, Department of Internal Medicine, Tokai University School of Medicine, 143 shimokasuya, Isehara, Kanagawa 259-1143, Japan
e-mail: moni5@mac.com

Introduction

Acute myeloid leukemia (AML) is hematological malignancy characterized by the rapid growth of abnormal white blood cells that accumulate in the bone marrow and interfere with the production of normal blood cells. Treatment strategies for AML that use one of the various cytarabine arabinoside (Ara-C) agents have remained the general choice of clinicians for more than 40 years. Multiple clinical trials have demonstrated complete remission (CR) rates of 50–60 % and overall survival rates of 30–40 % among AML patients receiving such Ara-C-based therapy [1–3]. However, many studies indicate that AML describes a heterogeneous collection of diseases characterized by distinct chromosomal abnormalities and cytogenetic mutations, and as such, the most suitable general treatment for AML is still unclear. Gene variations in leukemic cells significantly associated with prognosis have now been identified, with consequent prognostic improvement [4–7], and we propose that similar improvements in AML treatment could be achieved by better understanding the genetic polymorphisms related to the pharmacokinetics of Ara-C.

Ara-C is one of the nucleotide-analog therapeutic agents, which are transported into cells by nucleoside transporters including solute carrier family 29 member 1 (SLC29A1) [8]. Intracellular Ara-C is phosphorylated into Ara-C monophosphate (Ara-CMP) by deoxycytidine kinase (DCK) and eventually to Ara-C triphosphate (Ara-CTP), which competes with deoxycytidine triphosphate (dCTP) for incorporation into DNA and subsequent blocking of DNA synthesis causing cell death. In turn, cytidine deaminase (CDA) and deoxycytidylate deaminases (DCTD) catalyze the conversion of Ara-C and Ara-CMP into an inactive form [9], and 5′-nucleotidase cytosolic II (NT5C2) activity opposes that of DCK by dephosphorylating Ara-CMP.

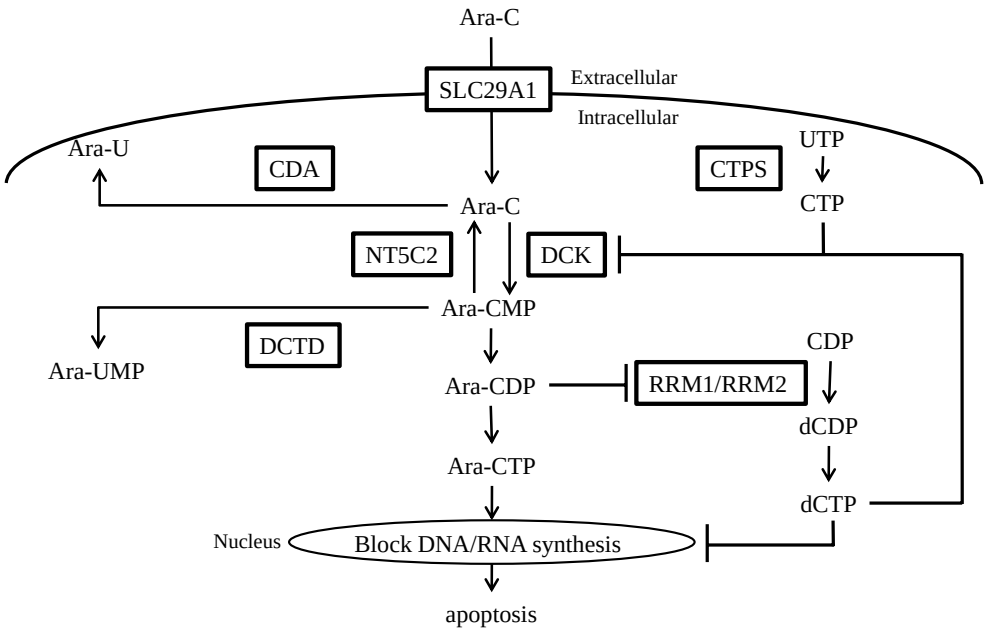

Fig. 1 Metabolic pathway of Ara-C. Ara-C is transported into cells by SLC29A1. Intracellular Ara-C is phosphorylated by DCK. Ara-CTP competes with dCTP for incorporation into DNA. CDA catalyzes the conversion of Ara-C into Ara-U, and DCTD catalyzes the conversion of Ara-CMP into Ara-UMP. CTPS catalyzes the conversion of UTP to CTP. Exhaustion of the CTP/dCTP pools due to facilitated Ara-C phosphorylation causes incorporation of Ara-CTP into DNA by reducing the feedback inhibition of DCK. RRM1/RRM2 is an enzyme involved in DNA synthesis. The enzyme regulates intracellular dCTP pools, which in turn, have been implicated in the development of Ara-C resistance

In addition, cytidine-5′-triphosphate synthetase (CTPS) and ribonucleotide reductase (RRM1/RRM2) are enzymes that regulate the intracellular CTP/dCTP pools, with exhaustion of the CTP/dCTP pools via facilitated Ara-C phosphorylation causing incorporation of Ara-CTP into DNA by reducing the feedback inhibition of DCK [10] (Fig. 1).

Understanding the pharmacogenetic response to Ara-C could lead to personalized treatment strategies and improved outcomes in AML patients. Indeed, each of the Ara-C metabolism-associated genes exhibits a significant degree of genetic variation, particularly via single nucleotide polymorphisms (SNPs), and several studies of individual SNPs in Ara-C metabolic genes have reported that genetic background plays an important role in the clinical outcomes of AML patients receiving Ara-C-based therapy [11–13]. In one such study, Gamazon et al. [11] conducted a meta-analysis of genome-wide association studies involving 523 lymphoblastoid cell lines from individuals of European, African, Asian, and African American ancestry, and identified 18 of 33 SNPs associated with either cytarabine 50 % inhibitory concentration in leukemia cells or clinical response parameters among patients randomized to receive low-dose or high-dose Ara-C plus daunorubicin and etoposide. In addition, Kim et al. [13] reported that the *SLC29A1* rs3734703 AA/AC genotype in combination with *TYMS* rs2612100 AA genotype was significantly associated with shorter relapse-free survival in Korean AML patients received an induction regimen of Ara-C and idarubicin followed by sequential consolidation therapy with Ara-C and anthracyclines or hematopoietic stem cell transplantation (HSCT). However, in these reports, the patient background included anthracycline agents or HSCT and thus might not accurately reflect the influence of genetic polymorphism on Ara-C metabolism.

Analyzing the combined effects of SNPs may provide evidence of drug response. Accordingly, we hypothesized that sensitivity to Ara-C could be influenced by SNP located in Ara-C metabolic genes and thus focused on high-dose Ara-C as single-agent therapy. In this study, we simply examined the association between SNPs in such genes and the clinical outcome of AML patients receiving high-dose Ara-C without HSCT.

Materials and methods

Study patients

We selected de novo AML patients who received high-dose Ara-C as consolidation therapy, and whose bone marrow or peripheral blood samples were stored in our laboratory. We excluded one patient diagnosed as M3 subtype and

one patient who received HSCT in the first CR. All subjects enrolled in this study provided informed consent for genetic analysis. This study was approved by the Institutional Review Board of Tokai University Hospital.

SNP selection

Seven Ara-C metabolic genes, *CDA*, *CTPS*, *DCK*, *DCTD*, *NT5C2*, *RRM1* and *SLC29A1*, were evaluated. SNPs were selected based on SNP frequency data from the International Hap-Map project (http://hapmap.ncbi.nlm.nih.gov/) and The National Center for Biotechnology Information (NCBI) (http://www.ncbi.nlm.nih.gov/). SNP frequency data were identified according to the HapMap Genome Browser release #27 (Phase 1, 2 and 3—merged genotypes and frequencies) of Japanese in Tokyo, Japan (JPT) database to estimate linkage disequilibrium (LD) blocks by Haploview software (version 4.2) [14]. The criteria for SNP selection were thus as follows: (1) minor allele frequency (MAF) >0.25 in JPT; (2) one or two SNPs were selected from each evaluated gene; (3) SNP reported by previous study [15], or located with each different LD blocks of the highest MAF. Allele frequency data of rs9937 was lacking in the JPT, so we instead search SNP frequency data of the CHB + JPT data in NCBI. Finally, eleven SNPs (*CDA*; rs10916827, rs477155, *CTPS*; rs4132440, rs12144160, *DCK*; rs12648166 *DCTD*; rs9542, rs9990999, *NT5C2*; rs3736922, *RRM1*; rs9937, *SLC29A1*; rs693955, 9394992) in each of the gene locus were selected.

SNP genotyping

Genomic DNA was isolated from bone marrow or peripheral blood individually using a QIAamp mini DNA kit (Qiagen, Valencia, CA, USA). SNP genotyping was performed using the TaqMan platform in 96-well plates and read with the Sequence Detection Software on a 7500 Real-Time PCR System according to the manufacturer's instructions (Applied Biosystems, Foster City, CA, USA). Primers and probes were supplied by Applied Biosystems.

Definition of clinical response and hematological toxicity

All clinical information about the patients was obtained from our institution database.

Overall survival (OS) was measured from the date of diagnosis to the date of death from any cause. Time to relapse (TTR) was measured from the date of diagnosis to the date of relapse. Relapse was defined as the presence of more than 5 % blast cells in the bone marrow or reappearance of blast cells in the peripheral blood. Hematological toxicity was measured by duration of neutropenia and thrombocytopenia during each high-dose Ara-C course. Neutropenia was defined as an absolute neutrophil count less than 500/μl. Thrombocytopenia was defined as an absolute platelet count less than 50,000/μl.

Statistical analysis

For SNP analysis, we tested two genetic models: the dominant model (major allele homozygous + heterozygous vs. minor allele homozygous) and the recessive model (major allele homozygous vs. heterozygous + minor allele homozygous). For univariate analysis, OS probabilities were estimated by the Kaplan–Meier method, and differences in the distributions between the dominant and recessive model of each SNP were evaluated using the log-rank test. TTR was estimated by the cumulative incidence method, and Gray's test was used to compare distribution differences between the genotypes [16]. Death without experiencing a relapse was considered a competing event with experiencing first relapse.

For multivariate analysis, the Fine–Gray regression model [5] was used for the sub-distribution hazard of a competing risk to analyze the effect of baseline risk factors on the cumulative incidence function of relapse. Factors associated with a two-side *P* value of less than 0.05 in the univariate SNP analysis and known prognostic risk factors for the Japanese population [17], such as age >50 years, performance status >2, myeloperoxidase (MPO) positivity of blasts >50 %, and first induction failure, were included in the multivariate analysis. We used a stepwise regression based on *P* values and retained only the statistically significant variables in the final model. This analysis did not include the factor of the DCTD rs9990999 AA genotype, because no patients with DCTD rs9990999 AA genotype experienced relapse. Thus, the DCTD rs9990999 AA genotype could not be treated as a single multivariate factor for the time-to-event analysis. For hematological toxicity analysis, comparisons between the dominant and recessive models of each SNP were performed using Student's *t* test.

All statistical analyses were performed with EZR (Saitama Medical Center, Jichi Medical University), which is a graphical user interface for R (The R Foundation for Statistical Computing, version 2.13.2) [18]. More precisely, it is a modified version of R commander (version 1.6–3) that includes statistical functions frequently used in biostatistics. For all analyses, *P* values were two-tailed, and a *P* value of less than 0.05 was considered significant.

Results

Patient characteristics and treatments

Thirty-nine AML patients were eligible for this study. Table 1 summarizes the patients' characteristics. The

Table 1 Patient characteristic

Factor	Group	Number (%) $n = 39$ (100 %)	Median (range)
Age			54.00 y/o (23.00, 71.00)
Gender	Male	26 (66.7)	
	Female	13 (33.3)	
FAB	M1	8 (20.5)	
	M2	22 (56.4)	
	M4	4 (10.3)	
	M5	5 (12.8)	
Karyotype	Normal	14 (35.9)	
	t(8;21)	12 (30.8)	
	inv(16)	2 (5.1)	
	del(7)	2 (5.1)	
	Complex	2 (5.1)	
	Others	7 (17.9)	
FLTIII-ITD mutation	Negative	16 (41.0)	
	Positive	3 (7.7)	
	Unknown	20 (51.3)	
WBC count at diagnosis			20,800/μl (900, 474,800)
MPO positivity of blasts	≤50 %	10 (25.6)	
	>50 %	29 (74.4)	
Performance status	0	24 (61.5)	
	1	12 (30.8)	
	2	2 (5.1)	
	4	1 (2.6)	
First induction regimen	DNR + Ara-C	8 (20.5)	
	IDA + Ara-C	31 (79.5)	
No. of induction	1	33 (84.6)	
	>1	6 (15.4)	
HSCT after relapse		7 (17.9)	
Relapse rate		19 (48.7)	
Time to relapse			306 days (152, 1271)
Non-relapse morality		4 (10.3)	
Overall survival			833 days (55, 3931)

FAB French–America–British classification, *WBC* white blood cell, *MPO* myeloperoxidase, *PS* performance status, *HSCT* hematopoietic stem cell transplantation

median age of patients was 54.0 years (range 23.0–71.0 years) and the male/female proportion was 26/13. The most frequent French–American–British (FAB) subtype was M2 (56.4 %) followed by M1 (20.5 %). M0, M6, and M7 subtypes were not represented in this population. In total, 14 patients had a good cytogenetic risk based on karyotype; 12 patients had t(8; 21) (q22;q22) and 2 patients had inv(16) (p13q22). Another 4 patients had a poor cytogenetic risk; 2 patients had del(7) and 2 patient had a complex karyotype. A total of 14 patients (35.9 %) were of normal karyotype, and 7 patients had an unspecified karyotype. Three of the 19 patients in whom the FLT3 internal tandem duplication (ITD) mutation information was identified had a FLT3/ITD mutation; however, the FLT3/ITD mutation was not examined for the other 20 patients and data on other molecular abnormalities were not available. Median white blood cell (WBC) count at diagnosis was 20,800/μl (range 900–47,4800/μl). Eight patients had received their first induction regimen consisting of Ara-C with daunorubicin, and another 31 patients received an induction regimen consisting of Ara-C with idarubicin. Thirty-three patients (84.6 %) achieved CR after the first induction regimen, and six patients (15.4 %) needed two or more induction regimens to achieve CR. Once patients achieved complete remission, the patients received consolidation therapy consisting of high-dose Ara-C. Seventeen patients received three courses of Ara-C dose of 2.0 g/m^2 for 5 days. Two patients received two courses of Ara-C dose of 2.0 g/m^2 for 5 days and one patient was died in the second course of consolidation therapy due to severe infection. Three patients died in the first course. Other patients received various doses and durations of Ara-C treatment according to the physician's clinical decision, as follows: one patient received three courses of Ara-C dose of 3.0 g/m^2 for 5 days; one patient received three courses of Ara-C dose of 3.0 g/m^2 for 4 days; two patients received four courses of Ara-C dose of 3.0 g/m^2 for 3 days; one patient received two courses and two patients received three of Ara-C dose of 2.0 g/m^2 for 3 days; and, one patient received two courses and four patients received three of Ara-C dose of 1.0 g/m^2 for 5 days. Nineteen patients (48.7 %) relapsed during the follow-up period and the median TTR was 306 days (range 152–1271 days). The median follow-up period overall survival was 833 days (range 55–3931 days).

Results of SNP genotyping

All SNP genotyping was successful among the AML patients, as summarized in Table 2.

The SNP genotypes could be divided into three groups, and comparison between groups only was analyzed statistically, due to insufficient minor allele frequency.

SNP effect on treatment outcomes

The effects of the two SNP genetic models on OS and TTR are summarized in Table 3. In the univariate analysis, no SNP was a significant prognostic factor for OS. However, three SNPs, individually, had associations with TTR (Fig. 2). The *CTPS* rs12144160 GG genotype was

Table 2 SNP genotype frequency and analysis model in our study

Gene; ref.SNP	Chromosome	Location	Genotype	*n*	Analysis model	
CDA; rs10916825	Chr1	Intron	AA	17	Dominant model	AA vs. AG + GG
			AG	20	Recessive model	AA + AG vs. GG
			GG	2		
CDA; rs477155	Chr1	Intron	AA	6	Dominant model	GG vs. GA + AA
			AG	20	Recessive model	GG + GA vs.AA
			GG	13		
CTPS; rs4132440	Chr1	Intron	AA	18	Dominant model	AA vs. AG + GG
			AG	18	Recessive model	AA + AG vs. GG
			GG	3		
CTPS; rs12144160	Chr1	Intron	AA	7	Dominant model	GG vs. GA + AA
			AG	20	Recessive model	GG + GA vs. AA
			GG	12		
DCK; rs12648166	Chr4	Intron	AA	10	Dominant model	AA vs. AG + GG
			AG	21	Recessive model	AA + AG vs. GG
			GG	8		
DCTD; rs9542	Chr4	Intron	CC	7	Dominant model	TT vs. TC + CC
			CT	18	Recessive model	TT + TC vs. CC
			TT	14		
DCTD; rs9990999	Chr4	Intron	AA	6	Dominant model	GG vs. GA + AA
			AG	14	Recessive model	GG + GA vs. AA
			GG	19		
NT5C2; rs3736922	Chr10	Intron	AA	9	Dominant model	GG vs. GA + AA
			AG	19	Recessive model	GG + GA vs. AA
			GG	11		
RRM1; rs9937	Chr11	Exon	AA	15	Dominant model	AA vs. AG + GG
			AG	16	Recessive model	AA + AG vs. GG
			GG	8		
SLC29A1; rs693955	Chr6	Intron	AA	1	Dominant model	CC vs. CA + AA
			AC	15	Recessive model	CC + CA vs. AA
			CC	23		
SLC29A1; s9394992	Chr6	Intron	CC	20	Dominant model	CC vs. CT + TT
			CT	16	Recessive model	CC + CT vs. TT
			TT	3		

significantly associated with shorter TTR compared to the AA/AG genotype (2-year relapse rate 0.694 [95 % CI 0.258–0.907] vs. 0.363 [95 %CI 0.177–0.552], $P = 0.0209$). The *DCTD* rs9990999 AG/GG genotype was significantly associated with shorter TTR compared to the AA genotype (2-year relapse rate 0.529 [95 % CI 0.331–0.692] vs. NA [NA–NA], $P = 0.0255$). The *SLC29A1* rs693955 CC genotype was significantly associated with shorter TTR compared to the AA/AC genotype (2-year relapse rate 0.683 [95 % CI 0.416–0.848] vs. 0.131 [0.019-0.353], $P = 0.00261$). There were 14 patients with CBF leukemia and 21 patients with intermediate risk group. The *SLC29A1* rs693955 CC genotype with intermediate risk ($n = 14$) was significantly associated with shorter TTR compared to the AA/AC genotype ($n = 7$) (2-year relapse rate 0.701 [95 % CI 0.295–0.902] vs. 0.214 [0.002–0.689], $P = 0.0498$). There was no statistical significance of the comparison for other SNPs and TTR regarding cytogenetic risk groups.

Multivariate analysis of TTR revealed that the *SLC29A1* rs693955 CC genotype (HR 7.659 [95 % CI 1.98–29.63], $P = 0.0096$) and first induction failure (HR 3.613 [95 % CI 1.37–9.55]) were significantly associated with shorter TTR (Table 4).

SNP effect on hematological toxicity

The total number of high-dose Ara-C was 109, and febrile neutropenia (FN) observed in 83 cases including 4 mortalities due to exacerbation of infections. The dead cases were

excluded from the duration analysis because they did not recover from the neutropenia or the thrombocytopenia. The duration of hematological toxicity analysis was therefore analyzed for 105 treatment courses. The mean durations of neutropenia and thrombocytopenia were 14.1 days (95 % confidential interval [CI]; 12.8–15.4 days) and 14.3 days (95 %CI; 12.6–16.0 days), respectively. Administration of granulocyte colony-stimulating factor (GCSF) was noted in 55/109 courses. Table 5 summarized the statistical analysis of SNPs compared to duration of neutropenia or thrombocytopenia. Figure 3 shows the three candidate SNPs and the association with duration of neutropenia. The *DCTD* rs9990999 AG/GG genotype was significantly associated with shorter duration of neutropenia compared to the AA genotype (13.2 ± 5.77 vs. 19.5 ± 9.11 days, $P = 0.000497$). The *SLC29A1* rs693955 CC genotype was significantly associated with shorter duration of neutropenia compared to the AA/AC genotype (13.1 ± 5.69 vs. 15.8 ± 7.87 days, $P = 0.0386$) and also thrombocytopenia (12.7 ± 7.89 vs. 16.9 ± 9.15 days, $P = 0.0116$). The frequency of GCSF administration was 1 in 16 of the *DCTD* rs9990999 AA genotypes and 54 in 93 of AG/GG genotypes, and was similar between the *SLC29A1* AA/AC genotype (20/42) and CC genotype (32/67). The *SLC29A1* AA/AC genotype required longer duration of GCSF administration than CC genotype (16.1 ± 5.54 vs. 13.1 ± 4.58 days, $P = 0.0377$). Concerning neutropenia without GCSF, the *DCTD* rs9990999 AG/GG genotype ($n = 39$) was significantly associated with shorter duration of neutropenia compared to the AA genotype ($n = 15$) (15.1 ± 5.44 vs. 19.5 ± 9.11 days, $P = 0.0314$), and the *SLC29A1* rs693955 CC genotype ($n = 32$) was significantly associated with shorter duration of neutropenia compared to the AA/AC genotype ($n = 22$) (14.8 ± 5.33 vs. 18.5 ± 5.27 days,

Table 3 Summary of *P* value of SNPs about OS and TTR

Gene	SNP	*P* Value (OS)		*P* value (TTR)	
		Dominant	Recessive	Dominant	Recessive
CDA	rs10916825	0.931	0.954	0.994	0.399
CDA	rs477155	0.252	0.0916	0.619	0.069
CTPS	rs4132440	0.615	0.228	0.891	0.967
CTPS	rs12144160	0.448	0.179	0.119	**0.0209**
DCK	rs1268166	0.991	0.805	0.232	0.896
DCTD	rs9542	0.345	0.334	0.828	0.22
DCTD	rs9990999	0.371	0.473	**0.0255**	0.579
NT5C2	rs3736922	0.984	0.544	0.916	0.843
RRM1	rs9937	0.601	0.633	0.483	0.845
SLC29A1	rs693955	0.74	0.814	**0.00261**	0.699
SLC29A1	rs9394992	0.921	0.2	0.626	0.248

Value of $P < 0.05$ were considered statistically significant

Bold value donate statistical significance

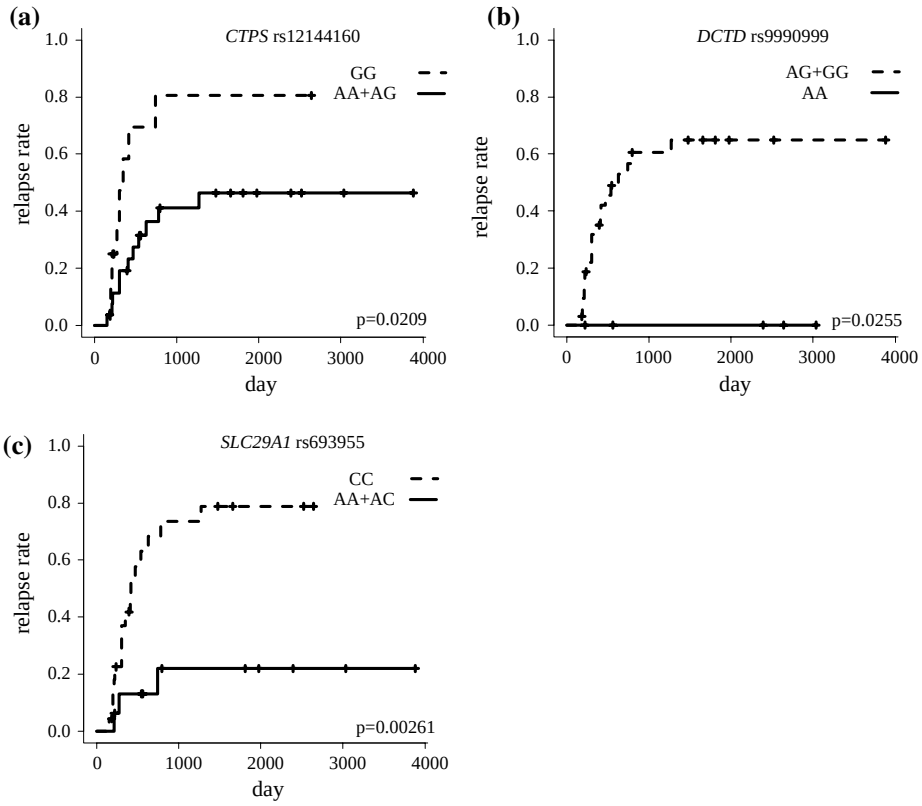

Fig. 2 Significant effect of SNP on time to relapse. Time to relapse was estimated by the cumulative incidence method, and Gray's test was used to compare differences between genotypes with respect to the SNP distributions. Death without experiencing a relapse was considered a competing event with experiencing first relapse. **a** SNP effect of *CTPS* rs12144160. **b** SNP effect of *DCTD* rs9990999. **c** SNP effect of *SLC29A1* rs693955

Table 4 Competing-risk model of variables associated with the cumulative incidence of relapse

Factor	Group	*n*	Univariant			Multivariant	
			2 year Relapse rate	Median TTR	*P* value	Hazard ratio	*P* value
Age	≤50	13	0.500 (0.231–0.614)	643	0.557		
	>50	26	0.433 (0.220–0.629)	NA			
No. of induction	1	33	0.414 (0.230–0.590)	1271	0.271		
	>1	6	0.667 (0.122–0.925)	291.5		3.613 (1.37–9.55)	**0.0032**
Karyotype	CBF-leukemia	14	0.429 (0.166–0.670)	NA	0.346		
	Others	25	0.539 (0.289–0.736)	745			
MPO positive blasts	≤50 (%)	10	0.594 (0.084–0.897)	647	0.518		
	>50 (%)	29	0.432 (0.242–0.609)	1271			
Performance status	1–2	38	0.437 (0.264–0.598)	782	0.357		
	3–4	1	NA (NA–NA)	415			
WBC count at diagnosis	≤20000/μl	19	0.369 (0.141–0.601)	782	0.274		
	>20000/μl	20	0.533 (0.280–0.733)	415			
CTPS rs12144160	AA/AG	27	0.363 (0.177–0.552)	NA	**0.0209**		
	GG	12	0.694 (0.258–0.907)	350			
DCTD rs9990999	AA	6	0.000 (0.000–0.000)	NA	**0.0255**		
	AG/GG	33	0.529 (0.331–0.692)	647			
SLC29A1 rs693955	AA/AC	16	0.131 (0.019–0.353)	NA	**0.00261**		
	CC	23	0.683 (0.416–0.848)	415		7.659 (1.98–29.63)	**0.0096**

Bold value donate statistical significance

Value of $P < 0.05$ were considered statistically significant

MPO myeloperoxidase, *WBC* white blood cell, *CBF* core binding factor

Table 5 Summary of *P* value of SNPs about duration of neutropenia and thrombocytopenia

Gene	SNP	Neutropenia (WBC <500/μl)		Thrombocytopenia (Platelet <50,000/μl)	
		Dominant	Recessive	Dominant	Recessive
CDA	rs10916825	0.175	0.734	0.832	0.636
CDA	rs477155	**0.00249**	0.619	0.0576	0.919
CTPS	rs4132440	0.648	0.327	0.680	0.460
CTPS	rs12144160	0.544	0.628	0.0681	0.909
DCK	rs1268166	0.419	0.689	0.0816	0.756
DCTD	rs9542	**0.00265**	**0.00989**	0.154	0.736
DCTD	rs9990999	0.0257	**0.000497**	0.0895	0.0558
NT5C2	rs3736922	0.861	0.962	0.859	0.721
RRM1	rs9937	0.926	0.884	0.705	0.911
SLC29A1	rs693955	**0.0386**	**0.000155**	**0.0166**	0.0995
SLC29A1	rs9394992	**0.0177**	0.994	**0.0116**	0.477

Value of $P < 0.05$ were considered statistically significant

Bold value donate statistical significance

$P = 0.0468$). The frequency of FN was 12 of 16 *DCTD* rs9990999 AA genotypes, 71 of 93 AG/GG genotypes, 30 of 42 *SLC29A1* AA/AC genotypes, and 53 of 67 CC genotypes. In addition, the four cases that died during high dose Ara-C treatment all had the same *SLC29A1* rs693955 AA/AC genotype. However, there was no severe acute neurotoxicity caused by high-dose Ara-C therapy observed in the patients, and other acute, severe non-hematologic side effects were not documented in the available clinical information.

Discussion

The present study suggested that the three SNPs, rs12144160 in the *CTPS* gene, rs9990999 in the *DCTD* gene, and rs693955 in the *SCL29A1* gene could influence outcomes in AML patients receiving high-dose Ara-C treatment.

The catalytic conversion of UTP to CTP is accomplished by the CTPS enzyme encoded by *CTPS*, and increased Ara-C sensitivity results from decreased CTP/dCTP pools caused by inhibition of CTPS with cyclopentenyl cytosine in myeloid leukemia and T-lymphoblastic leukemia cell lines [19, 20]. Although Ara-C resistance caused by clustered mutations within the coding region of CTPS have been identified in Chinese hamster ovary cells, no mutations were identified in the regions indicated from recurrent or resistant acute leukemia in 36 patients [10]. In our study,

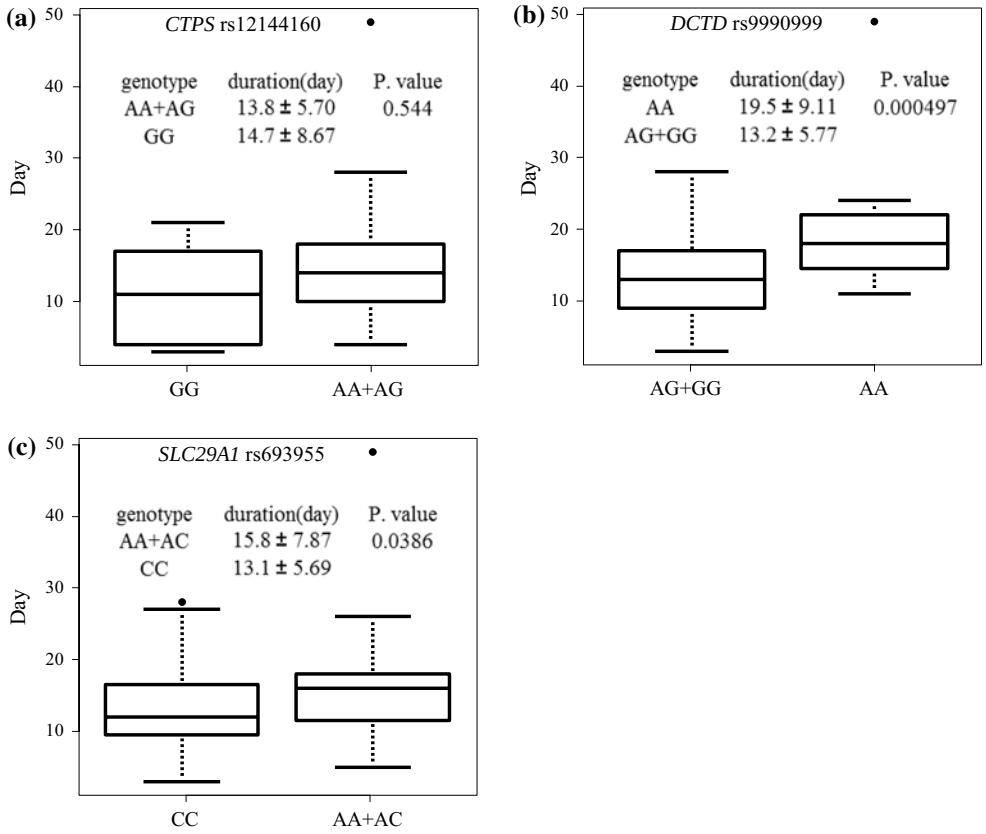

Fig. 3 Duration of neutropenia. Three SNPs associated with TTR are shown in this figure. **a** SNP effect of CTPS rs12144160. **b** SNP effect of DCTD rs9990999. **c** SNP effect of SLC29A1 rs693955. CTPS rs12144160 was not associated with hematological toxicity. The DCTD rs9990999 AA genotype was associated with a longer duration of neutropenia than the AA or CC genotype. The SLC29A1 rs693955 AA genotype was associated with a longer duration of both neutropenia and thrombocytopenia than the AA or CC genotype

the *CTPS* rs12144160 GG genotype was significantly associated with shorter TTR compared to the AA/AG genotype, suggesting that the GG genotype patients had higher levels of CTPS expression or activity than those with the AA/AG genotype. However, rs12144160 is located in an intronic region and therefore might affect RNA expression rather than enzyme activity.

SNP rs9990999 in the *DCTD* gene was a significant prognostic factor for TTR in this study, and the AG/GG genotype was significantly associated with shorter TTR compared to the AA genotypes. Interestingly, the patient with an AA genotype showed a long duration of neutropenia and did not experience relapse in our study. The protein encoded by the *DCTD* gene catalyzes the deamination of Ara-CMP to Ara-UMP and is allosterically activated by dCTP and inhibited by dTTP. Schröder et al. [9] reported that the expression level of DCTD was not associated with Ara-C sensitivity, while a non-synonymous SNP, the A172G mutation causing Asn58Asp, on the coding regions and causing loss of activity for gemcitabine monophosphate was identified in Caucasian and African ethnic groups in vitro assays [21], although the minor allele frequency was too low for meaningful association analysis with clinical response to Ara-C in this previous study [12]. However, nonsynonymous SNPs, including A172G, have not been observed in the DCTD gene in a Japanese population. There is also no evidence of functional SNPs in the *DCTD* gene, although our findings showed some kind of gene function for rs9990999 in TTR and neutrophil toxicity.

Our univariate and multivariate analysis found that the *SLC29A1* rs693955 CC genotype was significantly associated with shorter TTR and shorter duration of hematological toxicity. The *SLC29A1* gene encodes the human equivalent of nucleoside transporter 1 (hENT1), a protein that resides in the plasma membrane to mediate the cellular uptake of cytotoxic nucleosides as Ara-C from the surrounding medium. Although multiple alternatively spliced variants have been found for the *SLC29A1* gene, they all encode the same protein, and thus a deficiency in hENT1 expression might be the basis of cellular resistance to Ara-C [22]. SNPs have been previously detected in the *SLC29A1* gene from Japanese populations and some SNPs have been implicated in the efficacy of Ara-C [23] and the

mRNA expression [24, 25]. However, hENT1 is a limiting determinant of Ara-C efficacy, and the simple diffusion rate of Ara-C exceeds its pump-mediated transport in high plasma concentrations of Ara-C [26]. Although it is less likely that Ara-C is taken up into the cell by SLC29A1 at the 50-μM plasma concentration reached by high-dose Ara-C, rs693955 located in the *SLC29A1* gene might still influence clinical outcomes, based on our multivariate analysis identifying first induction failure and rs693955 CC genotype as independent prognostic factors. Suzuki et al. [25] reported that mRNA levels in the rs6932345 wild-type (A>C) and rs747199 wild-type (G>C) were higher than in the mutation carriers, and LD block analysis from the HapMap database linked the rs693955 C allele with the rs747199 C allele at a frequency of 14.8 %. Conversely, the rs693955 A allele was not linked with the rs747199 G allele. Thus, we proposed that patients with the rs693955 CC genotype have lower expression levels of hENT1 and consequently, shorter TTR and lower hematological toxicity. In addition, Pérez-Torras et al. [27] reported that overexpression of hENT1 in a relatively low transporter activity background increased the uridine uptake, resulting in a decreased amount of mRNA encoding key nucleotide metabolism enzymes, such as DCK and RR, and reduced cell cycle progression in the cell lines derived from human pancreatic adenocarcinomas. Nucleotide metabolism with the rs693955 CC genotype might be easy to change by the similar action of hENT1 overexpression. High intracellular concentrations of Ara-C or the product of Ara-C metabolism due to high-dose Ara-C therapy may have caused the decrease in nucleotide metabolism enzymes and cell cycle progression. The rs693955 CC genotype patient in this study might therefore have a phenotypic resistance to Ara-C, leading to the rapid recovery from cytopenia and the early relapse.

DCK is required for the first phosphorylation of deoxyribonucleosides and Ara-C is the most important enzyme in the activation pathway of Ara-C. However, in our study, the *DCK* rs12648166 was not associated with therapeutic outcomes. Our study does not include all SNPs on the *DCK* locus, but only one SNP was available based on our SNP selection criteria, and it is possible other SNPs on the *DCK* locus with a lower MAF might be functional polymorphisms.

Interestingly, the *DCTD* rs9990999 AG/GG and *SLC29A1* rs693955 CC were associated with shorter time to relapse and shorter duration of neutropenia. This finding suggested that the sensitivity to Ara-C of de novo leukemic cells is not very different from the sensitivity to Ara-C of normal hematopoietic stem cells. Braess et al. [28] reported CDA activities and Ara-C deamination in a variety of the most commonly used leukemic cell lines, fresh blasts, and normal bone marrow cells. However, the cell lines herein had different CDA activity profiles and degrade between 18.5 and 96.5 % of Ara-C to Ara-U. Formation of Ara-CTP is therefore significantly influenced by the differences in cell type-dependent cytidine deaminase activity. In contrast to the cell lines, fresh leukemic blasts and normal bone marrow mononuclear cells show low Ara-C degradation, and cultured cell lines are exposed to unknown selective pressure during a year or even several decades. Therefore, the biological reactions of cultured cells to Ara-C exposure seem to be relatively changed from the primary source leukemia cells. Conversely, the de novo leukemic cell without exposure to Ara-C might maintain a similar Ara-C metabolism to normal cells.

The results of our study suggested that SNP analysis could lead to better drug responsiveness and improved treatments for AML patients who benefit by receiving consolidation therapy with high-dose Ara-C. To our knowledge, this is the first report showing the relationship between SNPs and clinical outcomes in AML patient receiving high-dose Ara-C as single-agent therapy. Previous studies investigated the relationships between SNPs located on Ara-C metabolic genes and clinical response or toxicity with various doses of Ara-C based therapy including hematopoietic stem cell transplantation. *RRM1* rs1042919 and rs1561876 were related to intracellular Ara-CTP concentration, CR rate, and OS [29]. *CDA* rs2072671 and rs532545 were related to OS in a FLT3-ITD mutation-positive normal karyotype AML patient, and *NT5C2* rs10883841 was related to OS in a FLT3-ITD mutation-negative case [30]. In addition, the *SLC29A1* rs3734703 AA/AC genotype in combination with *TYMS* rs2612100 was significantly associated with relapse-free survival and *DCK* rs469436 was associated with OS in AML patients [13]. Nevertheless, few studies have determined SNP functions, and it is possible that *CDA* rs2072671 caused CDA protein variants (p.Lys27Gln) that may be related to the loss of CDA activity [31]. Our study did not include such SNPs because their MAF was lower than 0.25. For particular SNPs to be extracted as therapeutic surrogate markers, the functional meaning of these candidate SNPs must be determined and validated in future cohort studies. It might also be applicable to improve other nucleotide analog treatments which have similar pharmacokinetics system of Ara-C, such as gemcitabine, fluorouracil, and azacitidine by conducting SNP analysis associated with the Ara-C pharmacokinetics. However, our study was limited due to the small sample size and the inherent selection bias, since the patients examined here were already in the first remission state and were receiving high-dose Ara-C as a consolidation therapy. All the meaningful SNPs in our study were in introns. We could therefore not explore the SNP functions based on RNA expression, elongation, or splicing variants of the gene. It is therefore necessary to identify functional

SNPs that could be related to LD with the SNPs in our study by genome sequencing and thereby confirm the differences by RNA expression level or enzyme activity. Further studies are therefore needed to reveal the SNP functions and validation cohort studies are warranted.

Acknowledgments We thank the all physicians and nurses at the Hematology and Oncology Department of Tokai University Hospital and laboratory staff in the Department of Hematology and Oncology at Tokai University for their kind support; particularly T. I., E. M., and N. S. for assitance with the genotyping. We also appreciate valuable advice regarding this study from the Morishima research group on Allergic Disease and Immunology from the Ministry of Health, Labor, and Welfare of Japan.

Conflict of interest The authors declare that they have no conflict of interest.

References

1. Kumar CC. Genetic abnormalities and challenges in the treatment of acute myeloid leukemia. Genes Cancer. 2011;2:95–107.
2. Döhner H, Estey EH, Amadori S, Appelbaum FR, Büchner T, Burnett AK, European LeukemiaNet, et al. Diagnosis and management of acute myeloid leukemia in adults: recommendations from an international expert panel, on behalf of the European LeukemiaNet. Blood. 2010;115:453–74.
3. Miyawaki S, Ohtake S, Fujisawa S, Kiyoi H, Shinagawa K, Usui N, et al. A randomized comparison of 4 courses of standard-dose multiagent chemotherapy versus 3 courses of high-dose cytarabine alone in postremission therapy for acute myeloid leukemia in adults: the JALSG AML201 Study. Blood. 2011;117:2366–72.
4. Bullinger L, Döhner K, Bair E, Fröhling S, Schlenk RF, Tibshirani R, et al. Use of gene-expression profiling to identify prognostic subclasses in adult acute myeloid leukemia. N Engl J Med. 2004;350:1605–16.
5. Sakamaki H, Miyawaki S, Ohtake S, Emi N, Yagasaki F, Mitani K, et al. Allogeneic stem cell transplantation versus chemotherapy as post-remission therapy for intermediate or poor risk adult acute myeloid leukemia: results of the JALSG AML97 study. Int J Hematol. 2010;91:284–92.
6. Naoe T, Kiyoi H. Gene mutations of acute myeloid leukemia in the genome era. Int J Hematol. 2013;97:165–74.
7. Krivtsov AV, Figueroa ME, Sinha AU, Stubbs MC, Feng Z, Valk PJ, et al. Cell of origin determines clinically relevant subtypes of MLL-rearranged AML. Leukemia. 2013;27:852–60.
8. Wiley JS, Jones SP, Sawyer WH, Paterson AR. Cytosine arabinoside influx and nucleoside transport sites in acute leukemia. J Clin Investig. 1982;69:479–89.
9. Schröder JK, Seidelmann M, Kirch HC, Seeber S, Schütte J. Assessment of resistance induction to cytosine arabinoside following transfer and overexpression of the deoxycytidylate deaminase gene in vitro. Leuk Res. 1998;22:619–24.
10. Whelan J, Smith T, Phear G, Rohatiner A, Lister A, Meuth M. Resistance to cytosine arabinoside in acute leukemia: the significance of mutations in CTP synthetase. Leukemia. 1994;8:264–5.
11. Gamazon ER, Lamba JK, Pounds S, Stark AL, Wheeler HE, Cao X, et al. Comprehensive genetic analysis of cytarabine sensitivity in a cell-based model identifies polymorphisms associated with outcome in AML patients. Blood. 2013;121:4366–76.
12. Mahlknecht U, Dransfeld CL, Bulut N, Kramer M, Thiede C, Ehninger G, et al. SNP analyses in cytarabine metabolizing enzymes in AML patients and their impact on treatment response and patient survival: identification of CDA SNP C-451T as an independent prognostic parameter for survival. Leukemia. 2009;23:1929–32.
13. Kim KI, Huh IS, Kim IW, Park T, Ahn KS, Yoon SS, et al. Combined interaction of multi-locus genetic polymorphisms in cytarabine arabinoside metabolic pathway on clinical outcomes in adult acute myeloid leukaemia (AML) patients. Eur J Cancer. 2013;49:403–10.
14. Barrett JC, Fry B, Maller J, Daly MJ. Haploview: analysis and visualization of LD and haplotype maps. Bioinformatics. 2005;21:263–5.
15. Rha SY, Jeung HC, Choi YH, Yang WI, Yoo JH, Kim BS, et al. An association between RRM1 haplotype and gemcitabine-induced neutropenia in breast cancer patients. Oncologist. 2007;12:622–30.
16. Gray RJ. A class of k-sample tests for comparing the cumulative incidence of a competing risk. Annal Statist. 1988;16:1141–54.
17. Fine JP, Gray RJ. A proportional hazards model for the subdistribution of a competing risk. Am Statist Assoc. 1999;94:496–509.
18. Kanda Y. Investigation of the freely available easy-to-use software 'EZR' for medical statistics. Bone Marrow Transplant. 2013;48:452–8.
19. Verschuur AC, van Gennip AH, Leen R, Voûte PA, van Kuilenburg AB. Cyclopentenyl cytosine increases the phosphorylation and incorporation into dna of arabinofu-ranosyl cytosine in a myeloid leukemic cell-line. Adv Exp Med Biol. 2000;486:311–7.
20. Verschuur AC, Brinkman J, Van Gennip AH, Leen R, Vet RJ, Evers LM, et al. Cyclopentenyl cytosine induces apoptosis and increases cytarabine-induced apoptosis in a T-lymphoblastic leukemic cell-line. Leuk Res. 2001;25:891–900.
21. Gilbert JA, Salavaggione OE, Ji Y, Pelleymounter LL, Eckloff BW, Wieben ED, et al. Gemcitabine pharmacogenomics: cytidine deaminase and deoxycytidylate deaminase gene resequencing and functional genomics. Clin Cancer Res. 2006;12:1794–803.
22. Gati WP, Paterson AR, Larratt LM, Turner AR, Belch AR. Sensitivity of acute leukemia cells to cytarabine is a correlate of cellular es nucleoside transporter site content measured by flow cytometry with SAENTA-fluorescein. Blood. 1997;90:346–53.
23. Kim SR, Saito Y, Maekawa K, Sugiyama E, Kaniwa N, Ueno H, et al. Thirty novel genetic variations in the SLC29A1 gene encoding human equilibrative nucleoside transporter 1 (hENT1). Drug Metab Pharmacokinet. 2006;21:248–56.
24. Suzuki Y, Homma M, Abei M, Hyodo I, Kohda Y. Impact of solute carrier family 29 member 1 (SLC29A1) single nucleotide polymorphisms on mRNA expression in peripheral blood mononuclear cells. Biol Pharm Bull. 2013;36:144–6.
25. Myers SN, Goyal RK, Roy JD, Fairfull LD, Wilson JW, Ferrell RE. Functional single nucleotide polymorphism haplotypes in the human equilibrative nucleoside transporter 1. Pharmacogenet Genom. 2006;16:315–20.
26. Capizzi RL, Yang JL, Cheng E, Bjornsson T, Sahasrabudhe D, Tan RS, et al. Alteration of the pharmacokinetics of high-dose ara-C by its metabolite, high ara-U in patients with acute leukemia. J Clin Oncol. 1983;1:763–71.
27. Pérez-Torras S, García-Manteiga J, Mercadé E, Casado FJ, Carbó N, Pastor-Anglada M, et al. Adenoviral-mediated overexpression of human equilibrative nucleoside transporter 1 (hENT1) enhances gemcitabine response in human pancreatic cancer. Biochem Pharmacol. 2008;76:322–9.
28. Braess J, Pförtner J, Kern W, Hiddemann W, Schleyer E. Cytidine deaminase—the methodological relevance of AraC deamination for ex vivo experiments using cultured cell lines, fresh leukemic blasts, and normal bone marrow cells. Ann Hematol. 1999;78:514–20.

29. Cao X, Mitra AK, Pounds S, Crews KR, Gandhi V, Plunkett W, et al. RRM1 and RRM2 pharmacogenetics: association with phenotypes in HapMap cell lines and acute myeloid leukemia patients. Pharmacogenomics. 2013;14:1449–66.
30. Falk IJ, Fyrberg A, Paul E, Nahi H, Hermanson M, Rosenquist R, et al. Decreased survival in normal karyotype AML with single-nucleotide polymorphisms in genes encoding the AraC metabolizing enzymes cytidine deaminase and 5′-nucleotidase. Am J Hematol. 2013;88:1001–6.
31. Carpi FM, Vincenzetti S, Ubaldi J, Pucciarelli S, Polzonetti V, et al. CDA gene polymorphisms and enzyme activity: genotype–phenotype relationship in an Italian-Caucasian population. Pharmacogenomics. 2013;14:769–81.

Leukemia Research 39 (2015) 1405–1413

Contents lists available at ScienceDirect

Leukemia Research

journal homepage: www.elsevier.com/locate/leukres

FLT3-ITD drives Ara-C resistance in leukemic cells via the induction of RUNX3

Anar Damdinsuren[a,1], Hiromichi Matsushita[a,*,1], Masatoshi Ito[b,1], Masayuki Tanaka[b], Guilan Jin[a], Hideo Tsukamoto[b], Satomi Asai[a], Kiyoshi Ando[c], Hayato Miyachi[a]

[a] Department of Laboratory Medicine, Tokai University School of Medicine, Isehara, Kanagawa 259-1193, Japan
[b] Support Center for Medical Research and Education, Tokai University, Isehara, Kanagawa 259-1193, Japan
[c] Division of Hematology, Department of Internal Medicine, Tokai University School of Medicine, Isehara, Kanagawa 259-1193, Japan

ARTICLE INFO

Article history:
Received 31 December 2014
Received in revised form 23 August 2015
Accepted 6 September 2015
Available online 10 September 2015

Keywords:
FLT3-ITD
RUNX3
Chemotherapy-resistance
Ara-C

ABSTRACT

Internal tandem duplication (ITD) mutations of the *FLT3* gene (*FLT3*-ITD) are well known to correlate with a poor prognosis in acute myeloid leukemia (AML). We previously reported that *FLT3*-ITD confers resistance to cytosine arabinoside (Ara-C), a key cytotoxic agent in AML treatments. In order to elucidate the detailed molecular mechanisms underlying the Ara-C resistance induced by *FLT3*-ITD, we performed a microarray gene expression analysis of the human leukemic cell line K562 transduced with *FLT3*-ITD (K562/FLT3-ITD) and identified *RUNX3* as a downstream target of *FLT3*-ITD. The transcriptional induction of the *RUNX3* expression by FLT3-ITD was noted on a Luciferase assay. The knockdown of the *RUNX3* expression in the K562/FLT3-ITD cells increased the sensitivity to Ara-C, and the exogenous expression of *RUNX3 per se* resulted in the enhancement of Ara-C resistance in the K562 cells. A relationship between the *FLT3*-ITD-induced *RUNX3* expression and Ara-C resistance was also observed in AML cells with an endogenous *FLT3*-ITD expression. Collectively, these findings demonstrate that RUNX3 is a prerequisite for Ara-C resistance via FLT3-ITD signaling.

1. Introduction

Acute myeloid leukemia (AML) is a group of heterogeneous hematological malignancies that includes 24 subtypes according to the 2008 World Health Organization (WHO) classification. The current standard induction therapy for AML, except acute promyelocytic leukemia, is composed of Ara-C and anthracyclines such as daunorubicin and idarubicin [1]. These regimens are effective in eliminating the bulk of leukemic blasts and inducing AML remission in most cases; however, the disease often relapses in patients with certain cytogenetics. Therefore, chromosomal aberrations are thought to affect the AML prognosis [2,3].

Cytogenetically normal AML (CN-AML) represents approximately 45% of cases and is considered to have an intermediate risk. However, it is further divided by gene mutations into subsets with different outcomes [4–6]. For example, internal tandem duplication of the juxtamembrane domain of fms-related tyrosine kinase 3 (*FLT3*-ITD) is found in 25–35% of CN-AML patients and carries a poor prognosis, with a high risk of relapse after standard chemotherapy and a median survival of less than five months [7–10].

Class III receptor tyrosine kinase FLT3, expressed in the hematopoietic stem cell fraction, plays an important role in cellular survival and proliferation. Functional analyses have revealed that ITD mutations constitutively activate multiple downstream targets of FLT3, including PI3K/AKT, MAPK/ERK and STAT3/5 [11]. A number of tyrosine kinase inhibitors (TKIs) against FLT3 have been developed and introduced in clinical trials [12]. However, the treatment effectiveness has not yet reached satisfactory levels.

We previously reported Ara-C resistance in *FLT3*-ITD leukemic cells via reduced intracellular Ara-C uptake [13]. In order to clarify the detailed mechanisms, we performed a microarray gene expression analysis in *FLT3*-ITD-transduced K562 cells and found that *RUNX3* is upregulated by *FLT3*-ITD transduction. Moreover, *RUNX3* was found to play an important role as a downstream molecule in Ara-C resistance in leukemic cells with FLT3-ITD.

* Corresponding author at: Department of Laboratory Medicine, Tokai University School of Medicine, 143 Shimokasuya, Isehara, Kanagawa 259-1193, Japan. Fax: +81 463 93 8607
E-mail address: hmatsu@is.icc.u-tokai.ac.jp (H. Matsushita).
[1] These authors have contributed equally.

http://dx.doi.org/10.1016/j.leukres.2015.09.009
0145-2126/

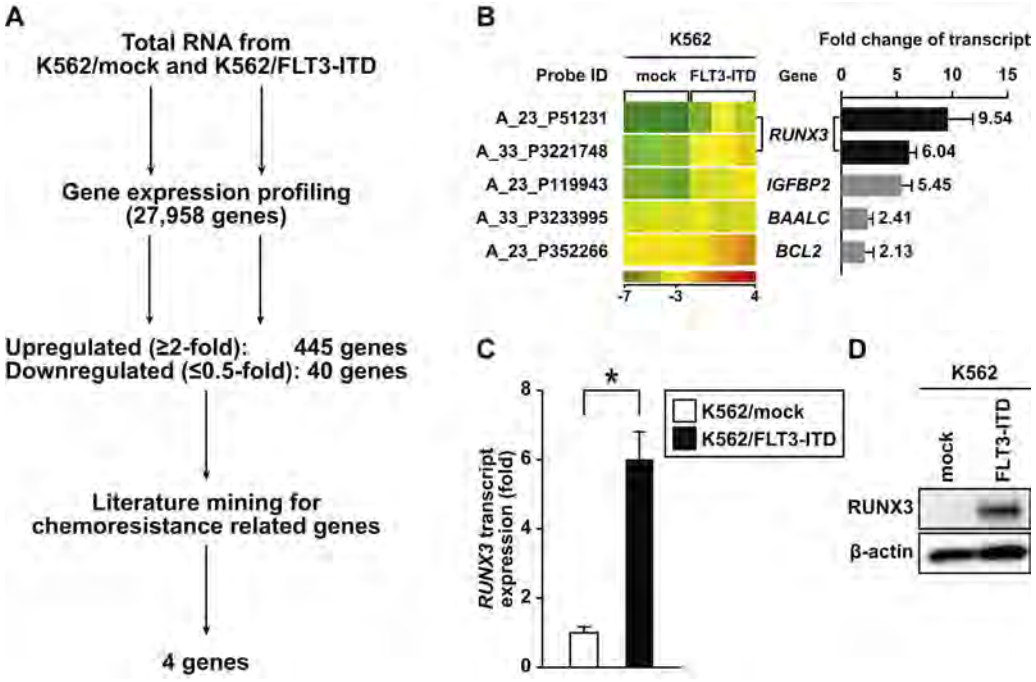

Fig. 1. *FLT3*-ITD upregulated the RUNX3 expression in the K562 cells.
(A) Selection strategy of the genes differently expressed in the K562/FLT3-ITD cells using a microarray gene expression analysis. (B) Heat-map representation and the quantitative expression levels of four identified genes associated with chemotherapy resistance in the K562/FLT3-ITD cells. The mean gene expression values were calculated using the data obtained from three independent experiments. (C), (D). The expression of RUNX3 in the K562/mock and K562/FLT3-ITD cells evaluated by RT-qPCR (C) and a Western blot analysis (D). * indicates $p < 0.01$.

2. Materials and methods

2.1. Cell lines and reagents

Human leukemia cell lines K562, MOLM-14 (kindly provided by Hayashibara Biochemical Laboratories, Okayama, Japan) [14] and MV4:11 (ATCC, Manassas, VA, USA) were cultured in RPMI-1640 medium (Wako, Osaka, Japan) containing 10% Fetal Bovine Serum (FBS; Wako) and 1% Penicillin/Streptomycin (PC/SM; Sigma–Aldrich, St. Louis, MO, USA) at 37 °C and 5% CO_2. PLAT-gp packaging cells (kindly provided by Dr. Toshio Kitamura) and HEK293T cells were cultured in DMEM medium (Wako) with 10% FBS, 1% PC/SM at 37 °C and 5% CO_2. Primary leukemic blasts were obtained from AML patients with *FLT3*-ITD (supplementary Table S1), after their written informed consent was provided, according to the Declaration of Helsinki and with approval from the Tokai University Committee on Clinical Investigation (Permit number: #13I-24). The blasts were cultured in StemPro-34 SFM medium (Life Technologies, Carlsbad, CA, USA), supplemented with StemPro-34 Nutrient Supplement (Life Technologies), 2 mM L-Glutamine (Life Technologies), 50 ng/ml recombinant human thrombopoietin (rhTPO; Kirin Brewery, Gunma, Japan), 50 ng/ml recombinant human stem cell factor (rhSCF; Wako), and 50 ng/ml recombinant human FLT3 ligand (rhFL; Wako).

Supplementary material related to this article found, in the online version, at http://dx.doi.org/10.1016/j.leukres.2015.09.009.

Stock solutions of 2 mM cytosine arabinofuranoside (cytarabine, Ara-C; Wako) and 20 mM vincristine (VCR; Wako) were prepared with physiological saline solution. Methotrexate (MTX; Wako) and idarubicin (IDR; Sigma–Aldrich) were diluted with RPMI-1640 and ethanol to prepare 20 mM and 0.5 nM stock solutions, respectively. Stock solutions of FLT3 inhibitors PKC412 (5 mM) (Alexis, Lausen, Switzerland) and Crenolanib (100 μM) (ChemieTek, Indianapolis, IN, USA) were prepared in DMSO.

2.2. Generation of FLT3-ITD, RUNX3-overexpressed and RUNX3-knockdown cells

The pMY-puro-FLT3-ITD plasmid was kindly provided by Dr. Tetsuya Nosaka (Mie University, Tsu, Japan) [15]. Human *RUNX3* cDNA (purchased from RIKEN Bioresource Center, Tsukuba, Japan) [16] was cloned into the pMY-puro vector (kindly provided by Dr. Toshio Kitamura), yielding pMY-puro-RUNX3. These retroviral vectors were used to generate recombinant retroviruses, as previously described [17]. K562 cells infected with these viruses were selected using 2 μg/ml of puromycin.

The pLKO.1 lentiviral vectors encoding two different target sequences of pre-designed shRNA for *RUNX3* and the negative control were obtained from Sigma–Aldrich. The puromycin resistance gene was replaced with the enhanced green fluorescent protein (*EGFP*) gene. After packaging, generated recombinant lentiviruses were infected into both K562/FLT3-ITD and MOLM-14 cells; EGFP-expressing cells were subsequently sorted via FACSAria (BD Biosciences, San Jose, CA, USA). The target sequences of shRNA were: negative control, 5′-GCGCGATAGCGCTAATAATTT-3′; RUNX3_KD-1, 5′-GGCTAGCAGCATGCGGTATTT-3′; RUNX3_KD-2, 5′-CGCCTTCAAGGTGGTGGCATT-3′.

2.3. RNA extraction, reverse transcription and quantitative real-time PCR

Total RNA was extracted using Isogen (Nippon Gene, Tokyo, Japan), and cDNA was generated from 2 μg of RNA using the VILO SuperScript cDNA synthesis kit (Life Technologies). PCR was performed using Phusion FLEX HS (New England Biolabs, Ipswich, MA, USA) polymerase, and quantitative real-time PCR (RT-qPCR) was performed with SYBR Premix Ex Taq II (Tli RNase H Plus) (Takara Bio, Otsu, Japan) on ABI StepOnePlus thermal cycler (Applied Biosystems, Foster City, CA, USA).

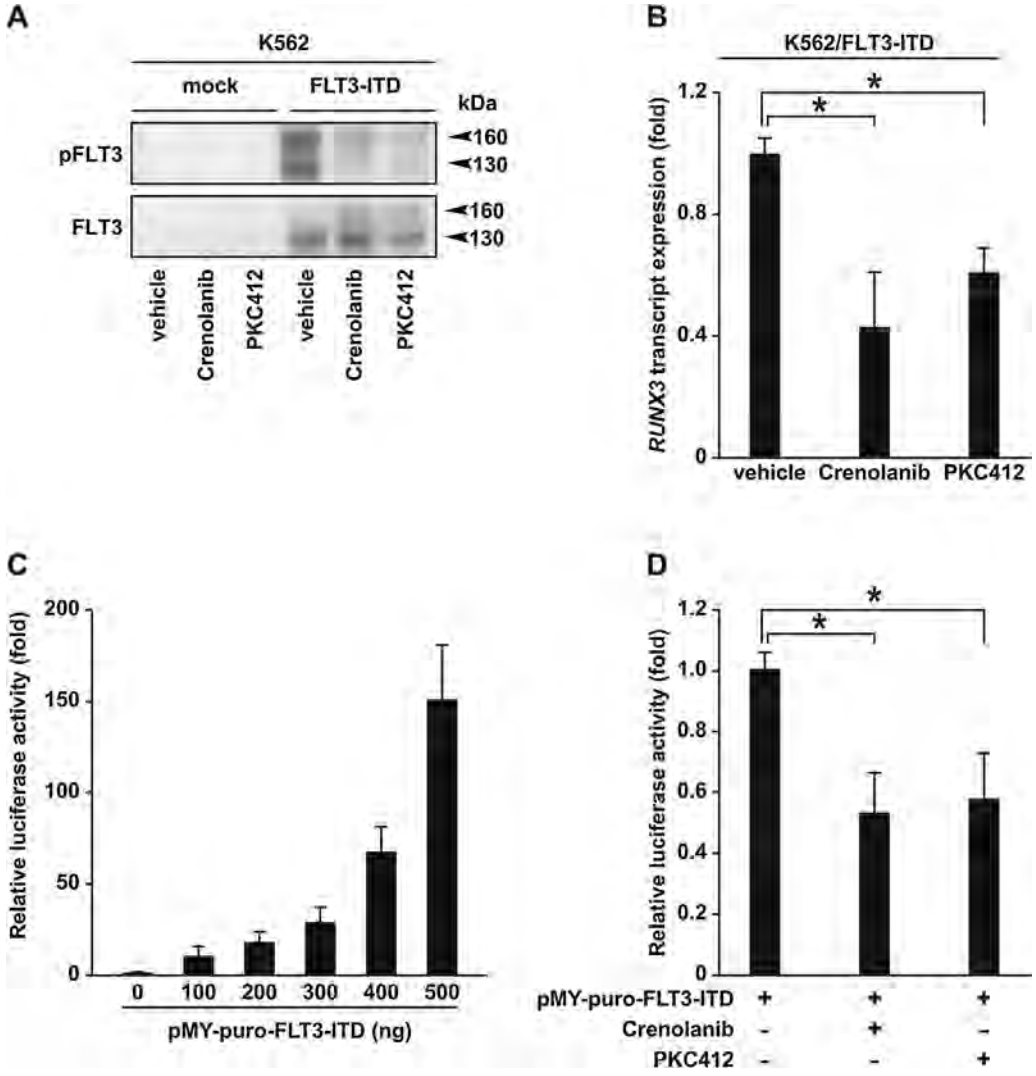

Fig. 2. FLT3-ITD phosphorylation induced the transcriptional expression of RUNX3.
(A) The phosphorylation status of FLT3-ITD in the K562/FLT3-ITD cells treated with the FLT3 inhibitors. The cells were cultured with PKC412 (10 nM) or Crenolanib (10 nM) for 3 h. (B) The quantitative comparison of the *RUNX3* transcript in the K562/FLT3-ITD cells treated with vehicle or FLT3 inhibitors. The cells were cultured with vehicle, PKC412 (10 nM) or Crenolanib (10 nM) for 24 h. * indicates $p < 0.01$. (C) Dose-dependent effect of *FLT3*-ITD on the *RUNX3* promoter activity. A luciferase assay was performed using HEK293T cells transfected with the *RUNX3* promoter-luciferase reporter and increasing doses of *FLT3*-ITD construct DNA. (D) *FLT3*-ITD-induced *RUNX3* promoter activity with FLT3 inhibition. A luciferase assay was performed using HEK293T cells transfected with the *RUNX3* promoter-luciferase reporter and 500 ng of pMY-puro-FLT3-ITD under culture with vehicle, Crenolanib (10 nM) or PKC412 (10 nM). * indicates $p < 0.05$.

The transcript levels of *RUNX3* were determined and expressed as the relative ratio to glyceraldehyde-3-phosphate dehydrogenase (*GAPDH*). The primer sequences were: *RUNX3* forward 5′-GCAGGCAATGACGAGAACTA-3′, reverse 5′-CAGTGATGGTCAGGGTGAAA-3′; *GAPDH* forward 5′-TTGCCATCAATGACCCCTTCA-3′, reverse 5′-CGCCCCACTTGATTTTGGA-3′. The primer sequences for *FLT3* were as previously described [13].

2.4. Microarray analysis

After confirming the total RNA quality using an Agilent Model 2100 Bioanalyzer (Agilent Technologies, Palo Alto, CA, USA), 200 ng of total RNA was subjected to a microarray analysis using Whole Human Genome Microarray 4 × 44 K v2 (Agilent). The microarray data were analyzed using the GeneSpring GX 12.1 program (Agilent). The fold-changes for each probe were calculated as the ratio of the signal intensity of the control and *FLT3*-ITD-overexpressing samples. Changes in the gene expression of more than 2-fold were considered to be significant. The microarray data were deposited into the Gene Expression Omnibus (Acc. No. GSE64330).

2.5. Western blot analysis

The Western blot analysis was performed as previously described [13]. The utilized antibodies were specific to total FLT3, phosphorylated FLT3 (Y589/591), RUNX3, total STAT5, phosphorylated STAT5 (Tyr694) (Cell Signaling Technology, Danvers, MA, USA) and ACTB (Sigma–Aldrich). Enhanced chemiluminescence signals were detected using the Immobilon Western Blotting Chemiluminescent HRP Substrate kit (Merck Millipore, Billerica, MA, USA).

2.6. Cellular proliferation and sensitivity to the cytotoxic agents

Ten thousand cells were cultured at 37 °C for 72 h with varying concentrations of the cytotoxic agents in 200 μl in 96-well plates and an MTT assay was performed as previously described [18]. The 50% inhibitory concentration for cellular growth (IC_{50}) was

determined as compared to the untreated controls. Each experiment was done in duplicate, and three independent experiments were performed.

2.7. Reporter assay

Five hundred and fifty nanograms of DNA, including pMY-puro-FLT3-ITD and luciferase reporter constructs, pLightSwitch_Prom-RUNX3 (ID S713138) (the *RUNX3* promoter-luciferase reporter) or empty control pLightSwitch_Prom (ID 790005) (SwitchGear Genomics, Carlsbad, CA, USA), were transfected into 1×10^5 HEK293T cells with FuGENE 6 transfection reagent (Promega, Madison, WI, USA). The luciferase activity was measured with LightSwitch Assay Reagent (SwitchGear) using a Turner Designs Luminometer Model TD-20/20 (Promega) at 48 h after transfection, according to each manufacturer's protocol.

2.8. Data analysis

The results are presented as the mean ± SD. Statistical differences were evaluated with the nonparametric independent Mann–Whitney U test using the SPSS v20.0 software program (IBM Corporation, Armonk, NY, USA).

3. Results

3.1. The RUNX3 expression was upregulated in the K562/FLT3-ITD cells

The gene expression profiles of the K562 cells transduced with pMY-puro-FLT3-ITD (K562/FLT3-ITD) were compared with the pMY-puro controls (K562/mock) to obtain a comprehensive understanding of the molecular mechanisms mediating *FLT3*-ITD-induced Ara-C resistance. The *FLT3*-ITD transcript and protein expression in the K562/FLT3-ITD cells were confirmed on RT-PCR (Fig. S1A) and Western blotting (Fig. S1B), respectively. The K562/FLT3-ITD exhibited 10-fold increased Ara-C resistance compared with K562/mock cells (1.72 ± 0.32 μM, 0.17 ± 0.01 μM respectively), with no changes in IDR, MTX or VCR (Fig. S1C), similar to our previous report [13].

Supplementary material related to this article found, in the online version, at http://dx.doi.org/10.1016/j.leukres.2015.09.009.

The cDNA microarray analysis identified 445 upregulated (496 probes) and 40 downregulated (43 probes) genes among 27,958 genes (44,000 probes) in the K562/FLT3-ITD cells. This gene list included four genes (5 probes), *RUNX3*, *IGFBP2*, *BAALC* and *BCL-2*, previously reported in clinical studies to be associated with chemoresistance in leukemia (Fig. 1A) [19–23]. The highest expressional fold change probes (9.54 ± 2.34, 6.04 ± 0.72-fold upregulation) targeted *RUNX3* (Fig. 1B). Six-fold upregulation of the *RUNX3* transcript in the K562/FLT3-ITD cells compared with K562/mock cells was verified on RT-qPCR ($p < 0.01$) (Fig. 1C). Western blotting showed the RUNX3 expression only in the K562/FLT3-ITD, not K562/mock, cells (Fig. 1D), suggesting RUNX3 to be positively related to the *FLT3*-ITD expression in K562 cells.

3.2. FLT3-ITD transcriptionally induced the RUNX3 expression

To examine the correlation between the *RUNX3* expression and FLT3-ITD activity, we used a potent small-molecule tyrosine kinase inhibitor of both wild-type and mutated FLT3 receptor, PKC412, and a highly selective FLT3 inhibitor, Crenolanib. As expected, phosphorylation of FLT3-ITD was remarkably inhibited by the addition of either 10 nM Crenolanib or 10 nM PKC412 in K562/FLT3-ITD cells (Fig. 2A). Compared to untreated K562/FLT3-ITD cells, inhibitor treatment reduced the *RUNX3* transcript expression to 43% and 61%, respectively ($p < 0.01$) (Fig. 2B). Furthermore, the luciferase assay showed that FLT3-ITD induced a dose-dependent increase in the *RUNX3* promoter activity in the HEK293T cells, which was strongly inhibited by either 10 nM Crenolanib or 10 nM PKC412 ($p < 0.01$) (Fig. 2C and D). These findings demonstrate that FLT3-ITD activation induces the *RUNX3* expression transcriptionally.

3.3. The RUNX3 expression promoted Ara-C resistance in the K562/FLT3-ITD cells

Crenolanib (10 nM) treatment substantially restored the Ara-C sensitivity to 0.84 ± 0.09 μM from 1.70 ± 0.08 μM in K562/FLT3-ITD cells ($p < 0.01$) (Fig. 3A). *RUNX3*-knockdown K562/FLT3-ITD cells were generated to directly evaluate the involvement of *RUNX3* in FLT3-ITD-induced Ara-C resistance. Two types of *RUNX3*-shRNA and a scramble shRNA control were transduced into K562/FLT3-ITD cells, designated K562/FLT3-ITD/RUNX3_KD-1, K562/FLT3-ITD/RUNX3_KD-2 and K562/FLT3-ITD/scramble cells. Compared to that induced by K562/FLT3-ITD/scramble, the expression levels of the *RUNX3* transcript in the K562/FLT3-ITD/RUNX3_KD-1 and K562/FLT3-ITD/RUNX3_KD-2 cells were suppressed to 17% and 26%, respectively ($p < 0.01$) (Fig. 3B). The Western blot analysis confirmed that the *RUNX3*-shRNAs suppressed the RUNX3 protein expression without affecting the phosphorylation status of FLT3-ITD and its major downstream target, STAT5 (Fig. 3C and Fig. S2A).

Supplementary material related to this article found, in the online version, at http://dx.doi.org/10.1016/j.leukres.2015.09.009.

Upon exposure to cytotoxic agents, the reduced expression of RUNX3 in the K562/FLT3-ITD cells correlated with an increased sensitivity to Ara-C. The 2.27 ± 0.27 μM Ara-C IC_{50} in the K562/FLT3-ITD/scramble cells was decreased in the K562/FLT3-ITD/RUNX3_KD-1 and K562/FLT3-ITD/RUNX3_KD-2 cells, at 0.51 ± 0.22 and 0.66 ± 0.29 μM, respectively ($p < 0.01$). *RUNX3* knockdown did not affect the IC_{50} values for the other cytotoxic agents (IDR, MTX and VCR). The IC_{50} values in the K563/FLT3-ITD/scramble, K562/FLT3-ITD/RUNX3_KD-1 and K562/FLT3-ITD/RUNX3_KD-2 cells were 51.92 ± 8.87, 44.32 ± 4.94 and 49.50 ± 6.15 nM for IDR, 8.00 ± 0.81, 8.47 ± 0.82 and 8.77 ± 0.32 nM for MTX, and 16.67 ± 0.86, 16.43 ± 1.40 and 17.70 ± 0.85 nM for VCR, respectively (Fig. 3D), indicating that RUNX3 specifically mediated FLT3-ITD-induced Ara-C resistance in the K562 cells

To investigate whether RUNX3 provides Ara-C resistance, pMY-puro-RUNX3 was transduced into K562 cells. The RUNX3 expression in K562/RUNX3 cells was confirmed on RT-qPCR and Western blotting ($p < 0.01$) (Fig. 3E and F). The IC_{50} for Ara-C was 0.22 ± 0.10 μM in the K562/mock control cells versus 2.51 ± 0.80 μM in the K562/RUNX3 cells ($p < 0.01$). To verify cross-resistance to other cytotoxic agents in these cells, we analyzed the sensitivity to IDR, MTX and VCR. The IC_{50} values for the K562/mock and K562/RUNX3 cells were 54.99 ± 1.77 and 48.87 ± 1.50 nM for IDR, 9.8 ± 0.5 and 8.9 ± 2.9 nM for MTX, and 15.77 ± 2.14 and 16.36 ± 3.94 nM for VCR, respectively (Fig. 3G). Crenolanib treatment, which inhibited the *RUNX3* expression and restored the Ara-C sensitivity in K562/FLT3-ITD cells, did not alter the *RUNX3* transcript level or the high IC_{50} value for Ara-C induced by the forced RUNX3 expression in K562/RUNX3 cells (2.04 ± 0.08 and 2.26 ± 0.27 μM with and without Crenolanib, respectively) (Fig. S3A and B).

Taken together, these findings demonstrate that RUNX3 is a key mediator of FLT3-ITD-induced Ara-C resistance in K562 cells, without affecting the sensitivity to other cytotoxic agents, such as IDR, MTX and VCR.

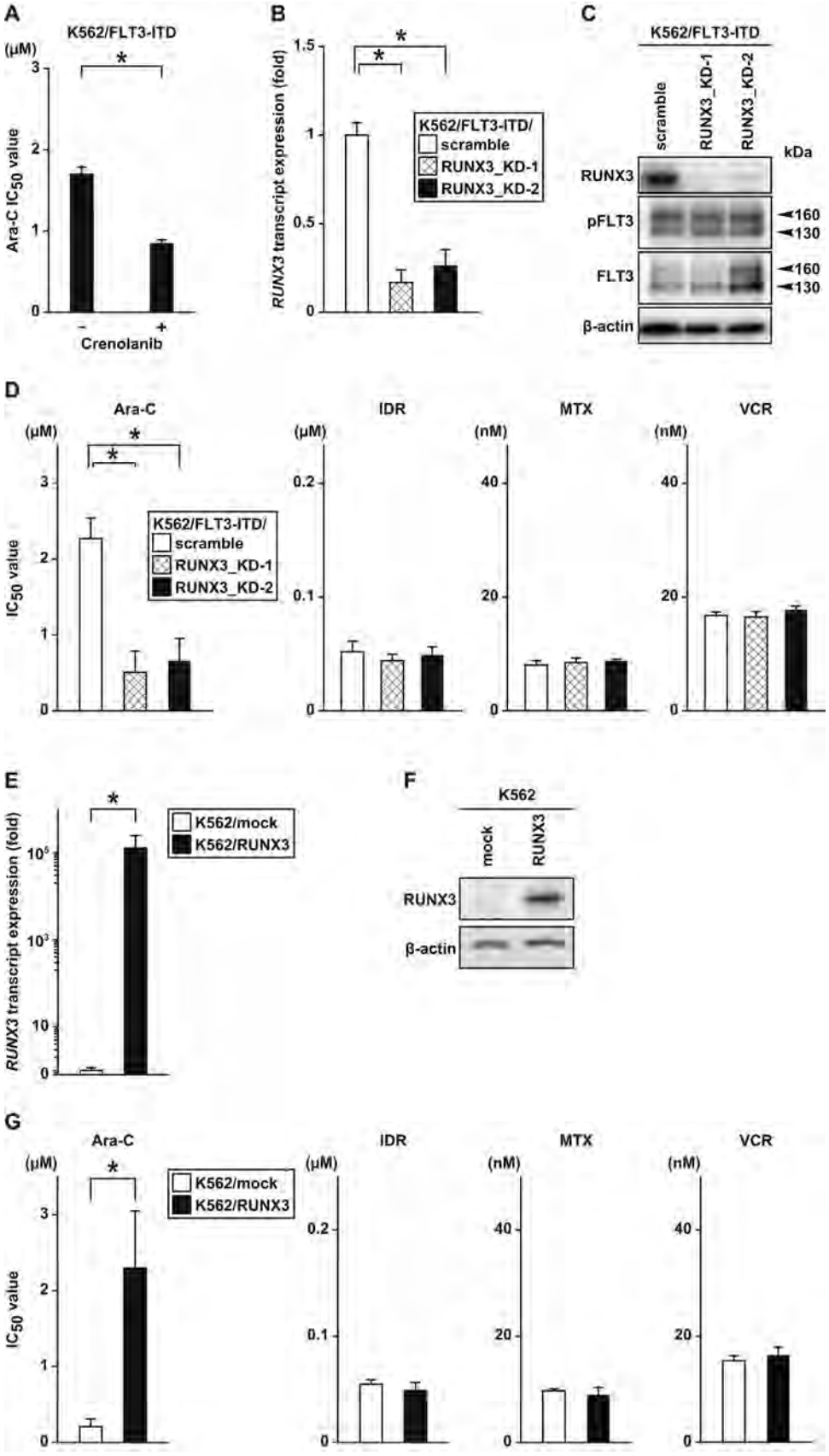

Fig. 3. RUNX3 is involved in *FLT3*-ITD-induced Ara-C resistance in K562 cells.
(A) Ara-C sensitivity of the K562/FLT3-ITD cells with FLT3-ITD inhibition. Crenolanib (10 nM) was added to the culture medium for the evaluation of IC_{50} for Ara-C. * indicates $p < 0.01$. (B), (C). The expression levels of RUNX3 in the K562/FLT3-ITD/RUNX3_KD-1, K562/FLT3-ITD/RUNX3_KD-2 and K562/FLT3-ITD/scramble cells evaluated by RT-qPCR (B) and a Western blot analysis (C). * indicates $p < 0.05$. (D) IC_{50} values for Ara-C, IDR, MTX and VCR in the K562/FLT3-ITD/RUNX3_KD-1, K562/FLT3-ITD/RUNX3_KD-2 and K562/FLT3-ITD/scramble cells. * indicates $p < 0.01$. (E), (F). The expression of RUNX3 in the K562/mock and K562/RUNX3 cells evaluated by RT-qPCR (E) and a Western blot analysis (F). * indicates $p < 0.01$. (G) IC_{50} values for Ara-C, IDR, MTX and VCR in the K562/mock and K562/RUNX3 cells. * indicates $p < 0.01$.

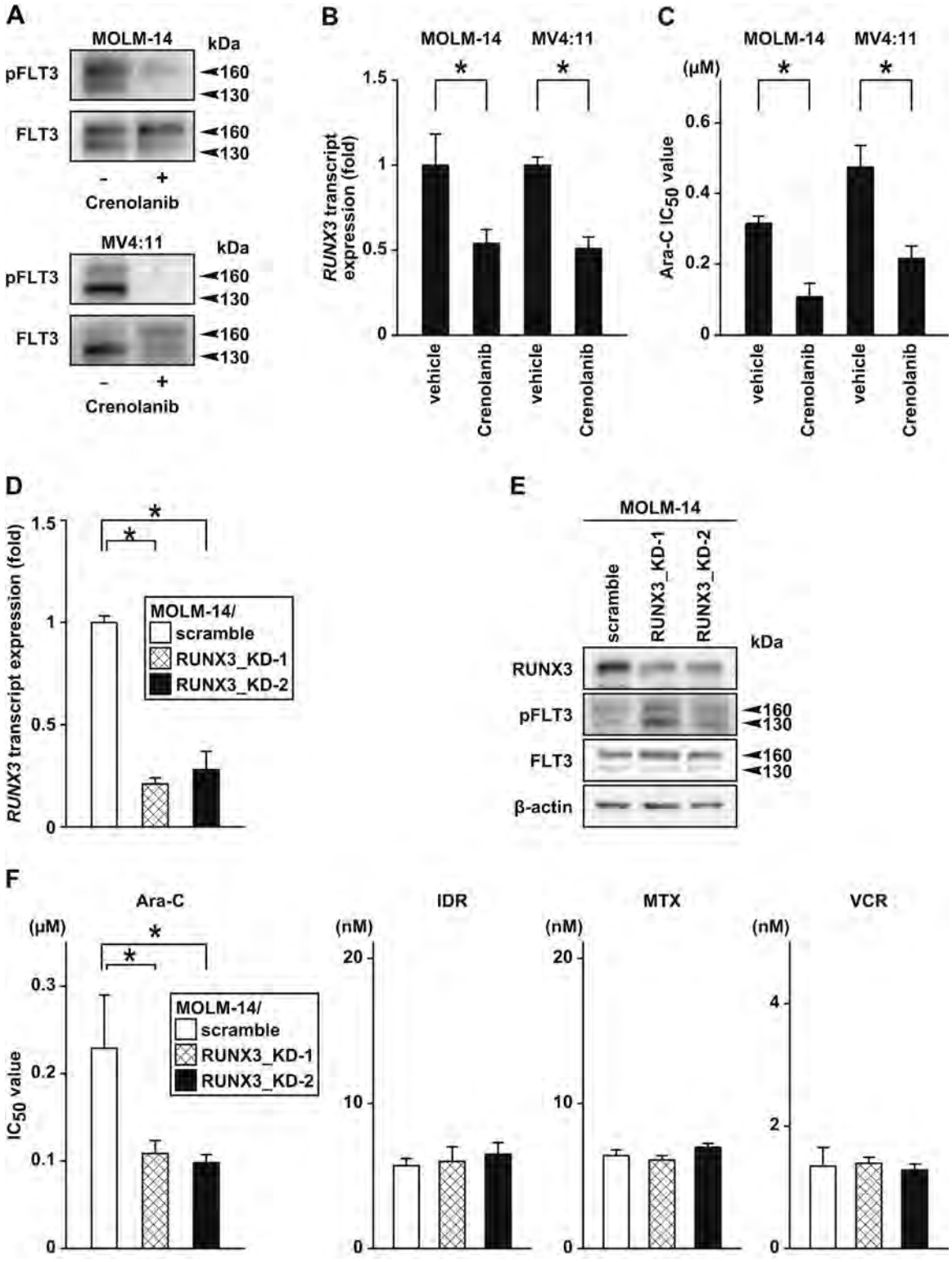

Fig. 4. RUNX3 inhibition confers increased sensitivity to Ara-C in AML cells with endogenous *FLT3*-ITD.
(A) The phosphorylation status of FLT3-ITD in the MOLM-14 and MV4:11 cells treated with Crenolanib. Crenolanib treatment for MOLM-14 and MV4:11 cells were 1 nM for 1 h and 2 nM for 6 h (upper and lower panels, respectively). (B) The expression levels of *RUNX3* transcript in MOLM-14 and MV4:11 cells treated with Crenolanib. The cells were cultured for 24 h with vehicle or 1 nM and 2 nM of Crenolanib, respectively. (C) Ara-C sensitivity in MOLM-14 and MV4:11 cells with FLT3-ITD inhibition. Crenolanib (1 nM for MOLM-14 and 2 nM for MV4:11) was added to the culture media for the evaluation of IC_{50} for Ara-C. * indicates $p < 0.01$. (D), (E) The expression levels of RUNX3 in the MOLM-14/RUNX3_KD-1, MOLM-14/RUNX3_KD-2 and MOLM-14/scramble cells evaluated by RT-qPCR (D) and a Western blot analysis (E). * indicates $p < 0.05$. (F) IC_{50} values for Ara-C, IDR, MTX and VCR in the MOLM-14/RUNX3_KD-1, MOLM-14/RUNX3_KD-2 and MOLM-14/scramble cells. * indicates $p < 0.01$.

Supplementary material related to this article found, in the online version, at http://dx.doi.org/10.1016/j.leukres.2015.09.009.

3.4. *RUNX3* mediates Ara-C resistance in AML cells with endogenous *FLT3*-ITD expression

FLT3-ITD-induced Ara-C resistance via the RUNX3 expression was analyzed in FLT3-ITD-overexpressing K562 cells. To validate the above observations, studies of *FLT3*-ITD inhibition were performed using the AML-derived MOLM-14 and MV4:11 human leukemia cell lines, which express endogenous *FLT3*-ITD. Crenolanib treatment abolished the phosphorylation of FLT3 in these cells (Fig. 4A) and significantly reduced *RUNX3* transcript expression to 56% in the MOLM-14 ($p < 0.01$) and 47% in the MV4:11 cells ($p < 0.01$) (Fig. 4B). Furthermore, Crenolanib decreased the IC_{50} for Ara-C from $0.31 \pm 0.02\,\mu M$ to $0.11 \pm 0.04\,\mu M$ in MOLM-14 and from $0.47 \pm 0.06\,\mu M$ to $0.22 \pm 0.03\,\mu M$ in MV4:11 cells, respectively ($p < 0.05$) (Fig. 4C).

To precisely validate the involvement of the *RUNX3* expression in *FLT3*-ITD-induced Ara-C resistance, MOLM-14 cells were transduced with *RUNX3*-shRNAs or scramble shRNA to generate MOLM-14/RUNX3_KD-1, MOLM-14/RUNX3_KD-2 and MOLM-14/scramble cells. RT-qPCR and Western blotting confirmed reduced RUNX3 transcript and protein levels in both MOLM-14/RUNX3_KD-1 and MOLM-14/RUNX3_KD-2 cells ($p < 0.05$) (Fig. 4D and E). The *RUNX3*-shRNA transduction did not affect the expression or phosphorylation status of FLT3-ITD and STAT5 in the MOLM-14 cells (Fig. 4E and S2B).

We then evaluated the effects of *RUNX3* knockdown on Ara-C sensitivity in the MOLM-14 cells. The IC_{50} was $0.23 \pm 0.06\,\mu M$ in the MOLM-14/scramble cells, compared to the decreased values of 0.12 ± 0.02 and $0.10 \pm 0.02\,\mu M$ in the MOLM-14/RUNX3_KD-1 and MOLM-14/RUNX3_KD-2 cells, respectively ($p < 0.01$). There were no significant changes in sensitivity to the other cytotoxic agents (IC_{50} in MOLM-14/RUNX3_KD-1, MOLM-14/RUNX3_KD-2 and MOLM-14/scramble cells: 6.0 ± 1.8 nM, 6.5 ± 1.5 nM and 5.7 ± 0.8 nM for IDR, 6.1 ± 0.5 nM, 7.5 ± 0.3 nM and 6.4 ± 0.8 nM for MTX, and 1.39 ± 0.1 nM, 1.28 ± 0.1 nM and 1.38 ± 0.7 nM for VCR, respectively) (Fig. 4F).

Finally, the effects of *FLT3*-ITD inhibition were analyzed in the leukemic blasts obtained from 2 AML patients with *FLT3*-ITD. Upon treatment of both samples with 1 nM Crenolanib, the *RUNX3* transcript expression was reduced to 54% and 26%, respectively ($p < 0.01$) (Fig. 5).

Collectively, these findings verify that *RUNX3* mediates Ara-C resistance in AML cells with an endogenous *FLT3*-ITD expression.

4. Discussion

The enhanced capacity for survival and proliferation dominance caused by *FLT3*-ITD is believed to confer a high risk of relapse and treatment failure, resulting in a poor prognosis of AML. However, our studies have revealed that FLT3-ITD induces resistance to Ara-C, but not other cytotoxic agents, in leukemic cells. In the current study, we newly identified RUNX3 as a downstream target of *FLT3*-ITD and demonstrated that RUNX3 mediates *FLT3*-ITD-induced Ara-C resistance in leukemic cells.

The leukemic cells utilized in the initial analysis in this study were K562 cells, which express another constitutively activated tyrosine kinase BCR-ABL1 fusion protein [24]. Due to the considerable overlap in BCR-ABL1 and FLT3-ITD signaling pathways, including RAS-MAPK, PI3K-AKT and STATs, the significance and function of RUNX3 identified in K562/FLT3-ITD cells were verified in AML cells without BCR-ABL1. The increased Ara-C sensitivity achieved via *FLT3*-ITD inhibition or *RUNX3* knockdown was also

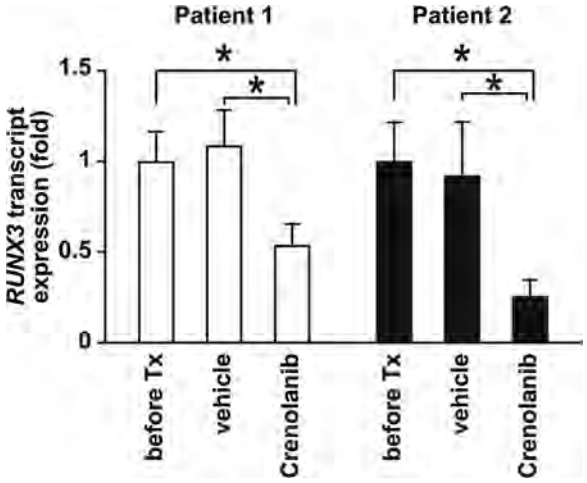

Fig. 5. FLT3-ITD inhibition suppresses RUNX3 expression in leukemic blasts. The expression of *RUNX3* transcript in the leukemic blasts before and after 12 h treatment with vehicle or 1 nM Crenolanib. The graph represents the results of triplicate real-time PCR experiments for single samples. Before Tx, before treatment. * indicates $p < 0.01$.

observed in MOLM-14 and MV4:11 cells, which express endogenous *FLT3*-ITD [25]. The transduction of *FLT3*-ITD in HEK293T cells triggered luciferase activation under the control of the *RUNX3* promoter in a dose-dependent manner and was hampered by either PKC412 or Crenolanib treatment. Furthermore, *FLT3*-ITD inhibition in the patient samples reduced the expression of *RUNX3*. These findings demonstrate that FLT3-ITD, but not BCR-ABL1, induces Ara-C resistance via the induction of the RUNX3 expression.

RUNX3 is a transcription factor containing the *runt* domain which forms a heterodimer with CBFB and acts as either a tumor suppressor or oncogene [26,27]. It is mainly expressed in the hematopoietic system, with high levels in the spleen, thymus and blood [28]. The importance of *RUNX3* in oncogenesis was initially described in gastric, colon and other cancers. Point mutations, inactivation by deletion, promoter hypermethylation and cytoplasmic mislocalization are frequently observed in these cancers, suggesting that *RUNX3* has a tumor suppressive role [29–31]. However, in light of several recent reports, this role has become controversial as *RUNX3* is overexpressed and functions as an oncogene in solid tumors, such as ovarian, skin and head and neck cancers [32–34].

Regarding the hematopoietic system, RUNX3 deficiency results in myeloproliferative neoplasms in older mice [35], whereas disruption of both Runx1 and Runx3 induces bone marrow failure and myeloproliferative neoplasms via DNA repair defects, suggesting that RUNX3 is not a simple tumor suppressor in the myeloid lineage and instead protects the bone marrow function from cellular exhaustion [15]. Clinically, a high *RUNX3* transcript level is associated with lower event-free survival in pediatric AML with FLT3 activating mutations, including *FLT3*-ITD [20]. In addition, the transcriptional repression of RUNX3 in AML with t(8;21) and inv(16) is associated with a good response to Ara-C-based chemotherapy and a favorable prognosis [19]. Such inverse correlation between the RUNX3 expression and prognosis of AML suggests that RUNX3 contributes to the survival of leukemic clones against chemotherapy supporting our findings.

Although we observed Ara-C resistance to be induced by the RUNX3 expression in this study, the exact mechanisms underlying the *FLT3*-ITD-induced RUNX3 expression and resulting Ara-C resistance must be clarified in detail. AML cases with *FLT3*-ITD display the constitutive activation of proliferative and anti-apoptotic signals via an enhanced kinase activity, including activation of the STAT3/5 pathway, which is related to short disease-free

survival [36,37]. Previous studies have identified the expression of pro-survival genes regulated by FLT3-ITD, including *PIM1*, *PIM2*, *Survivin*, *PRL-3*, contributing to the survival of leukemic cells [38–41]. Recently, FLT3-ITD-induced MYC activation via PIM1 has been reported to enhance the SIRT1 protein expression, which contributes to the maintenance of AML stem cells [42]. However, these observations do not explain the onset of chemotherapy resistance relative to Ara-C.

One possible mechanism may be the synergistic interaction of RUNX3 and SMADs to implement the signaling of transforming growth factor-β (TGFβ) [43]. The latter shows pro-survival and anti-apoptotic effects under Ara-C treatment, which are reversed by inhibitors or neutralizing antibodies against TGFβ [44,45]. Another target gene for TGFβ, *MCL1*, induced by TAK1/MEK and SMAD activation is upregulated by FLT3-ITD and confers resistance to Ara-C and daunorubicin in leukemic cells [46]. Although our microarray gene expression analysis did not show upregulation of *MCL1* (data not shown), the relationship with *RUNX3*, TGFβ/SMADs and *MCL1* in *FLT3*-ITD AML should be evaluated in detail.

In conclusion, our results demonstrate that *FLT3*-ITD induces *RUNX3* expression, resulting in Ara-C resistance in leukemic cells. Although the full details underlying this event remain undetermined, our results provide a rationale for the development of chemotherapy resistance and poor prognosis of AML with *FLT3*-ITD and validate *RUNX3* expression as a prognostic marker in AML. Further studies are required to explore the possibility of inhibiting the *RUNX3* expression and activity as a novel therapeutic target in AML with *FLT3*-ITD.

Acknowledgements

The authors thank Prof. Toshio Kitamura (Institute of Medical Science, University of Tokyo, Tokyo, Japan) for providing the pMY-puro retroviral vector and PLAT-gp packaging cells, Prof. Tetsuya Nosaka (Mie University, Tsu, Japan) for providing the pMY-Puro-FLT3-ITD plasmid DNA, and Hideyuki Matsuzawa, Hideki Hayashi, Yoshinori Okada and Yumi Iida (Support Center for Medical Research and Education, Tokai University, Japan) for their skill in the experimental techniques.

This work was supported by a School of Medicine Research Grant from Tokai University (A. D.), the Kurozumi Medical Foundation (Hi.M.), the Charitable Trust Laboratory Medicine Research Foundation of Japan (Hi. M.) and a Grant-in-Aid for Scientific Research from the Ministry of Education, Culture, Sports, Science and Technology of Japan (Ha. M.) (No. 24590709).

References

[1] M.S. Tallman, D.G. Gilliland, J.M. Rowe, Drug therapy for acute myeloid leukemia, Blood 106 (2005) 1154–1163.
[2] D. Grimwade, H. Walker, F. Oliver, K. Wheatley, C. Harrison, G. Harrison, et al., The importance of diagnostic cytogenetics on outcome in AML: analysis of 1612 patients entered into the MRC AML 10 trial. The medical research council adult and children's leukaemia working parties, Blood 92 (1998) 2322–2333.
[3] D. Grimwade, R.K. Hills, Independent prognostic factors for AML outcome. Hematology/the Education Program of the American Society of Hematology, Am. Soc. Hematol. Educ. Program (2009) 385–395.
[4] I. Khan, J.K. Altman, J.D. Licht, New strategies in acute myeloid leukemia: redefining prognostic markers to guide therapy, Clin. Cancer Res. 18 (2012) 5163–5171.
[5] J.P. Patel, M. Gonen, M.E. Figueroa, H. Fernandez, Z. Sun, J. Racevskis, et al., Prognostic relevance of integrated genetic profiling in acute myeloid leukemia, N. Engl. J. Med. 366 (2012) 1079–1089.
[6] O. Abdel-Wahab, R.L. Levine, Mutations in epigenetic modifiers in the pathogenesis and therapy of acute myeloid leukemia, Blood 121 (2013) 3563–3572.
[7] H. Kiyoi, M. Yanada, K. Ozekia, Clinical significance of FLT3 in leukemia, Int. J. Hematol. 82 (2005) 85–92.
[8] D. Small, FLT3 mutations: biology and treatment. Hematology/the Education Program of the American Society of Hematology, Am. Soc. Hematol. Educ. Program (2006) 178–184.
[9] F. Ravandi, H. Kantarjian, S. Faderl, G. Garcia-Manero, S. O'Brien, C. Koller, et al., Outcome of patients with FLT3-mutated acute myeloid leukemia in first relapse, Leukemia Res. 34 (2010) 752–756.
[10] M. Levis, F. Ravandi, E.S. Wang, M.R. Baer, A. Perl, S. Coutre, et al., Results from a randomized trial of salvage chemotherapy followed by lestaurtinib for patients with FLT3 mutant AML in first relapse, Blood 117 (2011) 3294–3301.
[11] S. Meshinchi, F.R. Appelbaum, Structural and functional alterations of FLT3 in acute myeloid leukemia, Clin. Cancer Res. 15 (2009) 4263–4269.
[12] R. Swords, C. Freeman, F. Giles, Targeting the FMS-like tyrosine kinase 3 in acute myeloid leukemia, Leukemia 26 (2012) 2176–2185.
[13] G. Jin, H. Matsushita, S. Asai, H. Tsukamoto, R. Ono, T. Nosaka, et al., FLT3-ITD induces ara-C resistance in myeloid leukemic cells through the repression of the ENT1 expression, Biochem. Biophys. Res. Commun. 390 (2009) 1001–1006.
[14] Y. Matsuo, R.A. MacLeod, C.C. Uphoff, H.G. Drexler, C. Nishizaki, Y. Katayama, et al., Two acute monocytic leukemia (AML-M5a) cell lines (MOLM-13 and MOLM-14) with interclonal phenotypic heterogeneity showing MLL-AF9 fusion resulting from an occult chromosome insertion, ins(11;9)(q23;p22p23), Leukemia 11 (1997) 1469–1477.
[15] C.Q. Wang, V. Krishnan, L.S. Tay, D.W. Chin, C.P. Koh, J.Y. Chooi, et al., Disruption of Runx1 and Runx3 leads to bone marrow failure and leukemia predisposition due to transcriptional and DNA repair defects, Cell Rep. 8 (2014) 767–782.
[16] T. Ota, Y. Suzuki, T. Nishikawa, T. Otsuki, T. Sugiyama, R. Irie, et al., Complete sequencing and characterization of 21,243 full-length human cDNAs, Nat. Genet. 36 (2004) 40–45.
[17] H. Matsushita, T. Yahata, Y. Sheng, Y. Nakamura, Y. Muguruma, H. Matsuzawa, et al., Establishment of a humanized APL model via the transplantation of PML-RARA-Transduced human common myeloid progenitors into immunodeficient mice, PLoS One 9 (2014) e111082.
[18] H. Miyachi, L. Ma, Y. Takemura, H. Kobayashi, I. Hirahara, H. Sonehara, et al., Microsatellite instability and clonal heterogeneity of MDR1 messenger RNA expression in trimetrexate-resistant human leukemia MOLT-3 cells developed in thymidine, Int. J. Cancer 82 (1999) 63–69, Journal international du cancer.
[19] C.K. Cheng, L. Li, S.H. Cheng, K.M. Lau, N.P. Chan, R.S. Wong, et al., Transcriptional repression of the RUNX3/AML2 gene by the t(8;21) and inv(16) fusion proteins in acute myeloid leukemia, Blood 112 (2008) 3391–3402.
[20] N.J. Lacayo, S. Meshinchi, P. Kinnunen, R. Yu, Y. Wang, C.M. Stuber, et al., Gene expression profiles at diagnosis in de novo childhood AML patients identify FLT3 mutations with good clinical outcomes, Blood 104 (2004) 2646–2654.
[21] A. Kuhnl, M. Kaiser, M. Neumann, L. Fransecky, S. Heesch, M. Radmacher, et al., High expression of IGFBP2 is associated with chemoresistance in adult acute myeloid leukemia, Leukemia Res. 35 (2011) 1585–1590.
[22] A. Kuhnl, N. Gokbuget, A. Stroux, T. Burmeister, M. Neumann, S. Heesch, et al., High BAALC expression predicts chemoresistance in adult B-precursor acute lymphoblastic leukemia, Blood 115 (2010) 3737–3744.
[23] M. Konopleva, S. Zhao, W. Hu, S. Jiang, V. Snell, D. Weidner, et al., The anti-apoptotic genes Bcl-X(L) and Bcl-2 are over-expressed and contribute to chemoresistance of non-proliferating leukaemic CD34+ cells, Br. J. Haematol. 118 (2002) 521–534.
[24] G. Grosveld, T. Verwoerd, T. van Agthoven, A. de Klein, K.L. Ramachandran, N. Heisterkamp, et al., The chronic myelocytic cell line K562 contains a breakpoint in bcr and produces a chimeric bcr/c-abl transcript, Mol. Cell. Biol. 6 (1986) 607–616.
[25] H. Quentmeier, J. Reinhardt, M. Zaborski, H.G. Drexler, FLT3 mutations in acute myeloid leukemia cell lines, Leukemia 17 (2003) 120–124.
[26] E.R. Cameron, K. Blyth, L. Hanlon, A. Kilbey, N. Mackay, M. Stewart, et al., The Runx genes as dominant oncogenes, Blood cells, Mol. Dis. 30 (2003) 194–200.
[27] K. Blyth, E.R. Cameron, J.C. Neil, The RUNX genes. gain or loss of function in cancer, Nat. Rev. Cancer 5 (2005) 376–387.
[28] C. Bangsow, N. Rubins, G. Glusman, Y. Bernstein, V. Negreanu, D. Goldenberg, et al., The RUNX3 gene-sequence, structure and regulated expression, Gene 279 (2001) 221–232.
[29] Q.C. Lau, E. Raja, M. Salto-Tellez, Q. Liu, K. Ito, M. Inoue, et al., RUNX3 is frequently inactivated by dual mechanisms of protein mislocalization and promoter hypermethylation in breast cancer, Cancer Res. 66 (2006) 6512–6520.
[30] H.F. Kang, Z.J. Dai, H.P. Bai, W.F. Lu, X.B. Ma, X. Bao, et al., RUNX3 gene promoter demethylation by 5-Aza-CdR induces apoptosis in breast cancer MCF-7 cell line, Onco Targets Ther. 6 (2013) 411–417.
[31] C.W. Lee, K. Ito, Y. Ito, Role of RUNX3 in bone morphogenetic protein signaling in colorectal cancer, Cancer Res. 70 (2010) 4243–4252.
[32] C.W. Lee, L.S. Chuang, S. Kimura, S.K. Lai, C.W. Ong, B. Yan, et al., RUNX3 functions as an oncogene in ovarian cancer, Gynecol. Oncol. 122 (2011) 410–417.
[33] M. Salto-Tellez, B.K. Peh, K. Ito, S.H. Tan, P.Y. Chong, H.C. Han, et al., RUNX3 protein is overexpressed in human basal cell carcinomas, Oncogene 25 (2006) 7646–7649.
[34] T. Tsunematsu, Y. Kudo, S. Iizuka, I. Ogawa, T. Fujita, H. Kurihara, et al., RUNX3 has an oncogenic role in head and neck cancer, PLoS One 4 (2009) e5892.
[35] C.Q. Wang, L. Motoda, M. Satake, Y. Ito, I. Taniuchi, V. Tergaonkar, et al., Runx3 deficiency results in myeloproliferative disorder in aged mice, Blood 122 (2013) 562–566.

[36] K. Spiekermann, K. Bagrintseva, R. Schwab, K. Schmieja, W. Hiddemann, Overexpression and constitutive activation of FLT3 induces STAT5 activation in primary acute myeloid leukemia blast cells, Clin. Cancer Res. 9 (2003) 2140–2150.
[37] D. Schmidt-Arras, S.A. Bohmer, S. Koch, J.P. Muller, L. Blei, H. Cornils, et al., Anchoring of FLT3 in the endoplasmic reticulum alters signaling quality, Blood 113 (2009) 3568–3576.
[38] K. Natarajan, Y. Xie, M. Burcu, D.E. Linn, Y. Qiu, M.R. Baer, Pim-1 kinase phosphorylates and stabilizes 130 kDa FLT3 and promotes aberrant STAT5 signaling in acute myeloid leukemia with FLT3 internal tandem duplication, PLoS One 8 (2013) e74653.
[39] M. Adam, V. Pogacic, M. Bendit, R. Chappuis, M.C. Nawijn, J. Duyster, et al., Targeting PIM kinases impairs survival of hematopoietic cells transformed by kinase inhibitor-sensitive and kinase inhibitor-resistant forms of Fms-like tyrosine kinase 3 and BCR/ABL, Cancer Res. 66 (2006) 3828–3835.
[40] S. Fukuda, P. Singh, A. Moh, M. Abe, E.M. Conway, H.S. Boswell, et al., Survivin mediates aberrant hematopoietic progenitor cell proliferation and acute leukemia in mice induced by internal tandem duplication of Flt3, Blood 114 (2009) 394–403.
[41] J. Zhou, C. Bi, W.J. Chng, L.L. Cheong, S.C. Liu, S. Mahara, et al., PRL-3, a metastasis associated tyrosine phosphatase, is involved in FLT3-ITD signaling and implicated in anti-AML therapy, PLoS One 6 (2011) e19798.
[42] L. Li, T. Osdal, Y. Ho, S. Chun, T. McDonald, P. Agarwal, et al., SIRT1 activation by a c-MYC oncogenic network promotes the maintenance and drug resistance of human FLT3-ITD acute myeloid leukemia stem cells, Cell Stem Cell 15 (2014) 431–446.
[43] Y. Ito, K. Miyazono, RUNX transcription factors as key targets of TGF-beta superfamily signaling, Curr. Opin. Genet. Dev. 13 (2003) 43–47.
[44] Y. Xu, Y. Tabe, L. Jin, J. Watt, T. McQueen, A. Ohsaka, et al., TGF-beta receptor kinase inhibitor LY2109761 reverses the anti-apoptotic effects of TGF-beta1 in myelo-monocytic leukaemic cells co-cultured with stromal cells, Br. J. Haematol. 142 (2008) 192–201.
[45] Y. Tabe, Y.X. Shi, Z. Zeng, L. Jin, M. Shikami, Y. Hatanaka, et al., TGF-beta-neutralizing antibody 1D11 enhances cytarabine-induced apoptosis in AML cells in the bone marrow microenvironment, PLoS One 8 (2013) e62785.
[46] S. Kasper, F. Breitenbuecher, F. Heidel, S. Hoffarth, B. Markova, M. Schuler, et al., Targeting MCL-1 sensitizes FLT3-ITD-positive leukemias to cytotoxic therapies, Blood Cancer J. 2 (2012) e60.

Int J Hematol (2016) 103:341–347
DOI 10.1007/s12185-015-1917-7

CASE REPORT

Successful bypass surgery for esophageal carcinoma under adequate factor XIII/13 replacement therapy in a case of intractable autoimmune hemorrhaphilia due to anti-Factor XIII/13 antibodies

Minoru Kojima[1] · Akitada Ichinose[2,3] · Masayoshi Souri[2,3] · Tsukasa Osaki[2,3] · Hidetsugu Kawai[1] · Jun Amaki[1] · Hiroki Numata[1] · Mitsuki Miyamoto[1] · Daisuke Ogiya[1] · Kosuke Tsuboi[4] · Yoshiaki Ogawa[1] · Soji Ozawa[5] · Kiyoshi Ando[1]

Received: 15 September 2015 / Revised: 16 November 2015 / Accepted: 18 November 2015 / Published online: 30 November 2015

Abstract Autoimmune hemorrhaphilia due to anti-factor XIII (FXIII) antibodies (AH13) is a life-threatening disease associated with high risk of surgical bleeding. Since AH13 occurs mainly in the elderly, patients of AH13 tend to be complicated with other life-threatening diseases that may require surgical procedures. During our nation-wide survey on AH13, supported by the Japanese Ministry of Health, Labor, and Welfare, patients with unexplained bleeding were examined for FXIII-related parameters and anti-FXIII autoantibodies. A 64-year-old man had previously been tentatively diagnosed with AH13 and received immunosuppressive therapies, as FXIII inhibitor was detected by functional cross-mixing studies. About 2 years later, he was definitively diagnosed with AH13, because our immunochromatographic test and enzyme-linked immuno-sorbent assay detected FXIII-bound anti-FXIII-A subunit autoantibodies. Since routine endoscopic examination revealed suspected esophageal carcinoma, a preparatory FXIII pharmacokinetic (PK) analysis was performed by infusing FXIII concentrates prior to biopsy. Consequently, biopsy of this lesion was done without bleeding complications. One month later, a second PK study was carried out before surgery, and esophageal bypass surgery was completed successfully under FXIII replacement therapy. Our experience with this case suggests that operations can be performed safely and with confidence even in patients with such life-threatening hemorrhagic diseases.

Keywords Autoimmune/acquired hemorrhaphilia · Anti-FXIII/13 antibodies · Factor XIII concentrates · Pharmacokinetic study · Immunosuppressive therapy

Introduction

Factor XIII (FXIII or FXIII/13 to avoid confusion with factor VIII/8 or factor XII/12) is a plasma pro-transglutaminase, which is activated to active transglutaminase, FXIIIa, by thrombin at the final stage of the blood coagulation reaction. FXIII is also called fibrin stabilizing factor because FXIIIa increases the strength of a fibrin clot by cross-linking fibrin monomers to themselves, α_2-plasmin inhibitor (α_2-PI; ISTH Nomenclature in 1972), or fibronectin [1]. Inherited FXIII deficiency is a rare life-long severe bleeding disorder including spontaneous intracranial hemorrhage, and female patients manifest recurrent miscarriage. Some patients also show abnormal wound healing [2].

In the twenty-first century, Japan has become a first super-aging society in the world (population ages 65 and above as a percentage of the total population is 25.1 % in 2013; source, The United Nations Population Division's World Population Prospects). Incidentally, "the number of diagnosed cases" with autoimmune hemorrhagic disease (hemorrhaphilia) due to anti-FXIII autoantibodies (termed AH13) has been on the rise in Japan (8 cases in the last

✉ Akitada Ichinose
aichinos@med.id.yamagata-u.ac.jp

1 Division of Hematology/Oncology, Department of Internal Medicine, Tokai University School of Medicine, Isehara, Japan

2 Department of Molecular Patho-Biochemistry and -Biology, Yamagata University School of Medicine, Yamagata, Japan

3 Japanese Collaborative Research Group on AHXIII/13 (Japanese Ministry of HLW), Yamagata, Japan

4 Department of Internal Medicine, Nagaoka Chuo General Hospital, Nagaoka, Japan

5 Department of Gastroenterological Surgery, Tokai University School of Medicine, Isehara, Japan

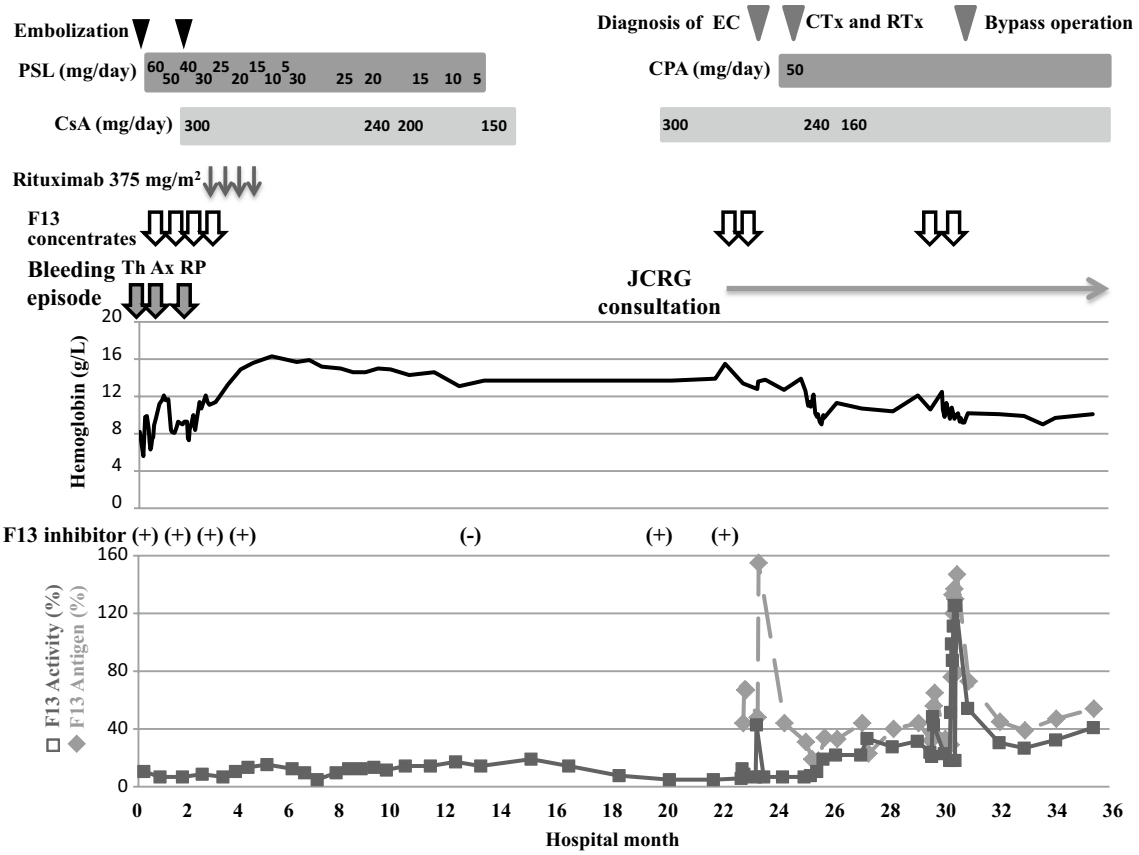

Fig. 1 Clinical course of the present patient. Hemoglobin levels (*black line*) corresponded to bleeding episodes (*arrows with bleeding sites*). Plasma-derived FXIII concentrates were given to arrest bleeding. The patient underwent immune-suppressive therapies first with prednisolone (PSL), then with cyclosporine A (CsA), and finally with rituximab. Although his FXIII activity (*filled squares*) remained low, the FXIII inhibitor (measured by 1:1 cross-mixing test) disappeared 1 year later, and thus CsA treatment was discontinued. Since his FXIII activity returned to 4 % and his FXIII inhibitor re-appeared, CsA treatment was re-started. Then esophageal carcinoma (EC) was suspected by an endoscopic examination. The Japanese collaborative research group (JRCG) was called into consultation and their detailed studies were carried out. He was definitely diagnosed as AH13 by immunological assays, and thus cyclophosphamide (CPA) was added. Under FXIII replacement therapy, biopsy of the esophageal lesion and then its bypass surgery were carried out without hemorrhagic complication, followed by cisplastin treatment (CTx) and radiation therapy (RTx). Both FXIII activity (*filled squares*) and antigen (*filled diamonds*) started to increase gradually. *Ty* thigh, *Ax* axillar, *RP* retroperitoneal hematoma

century vs. 47 case in this century; Refs. [3, 4] and unpublished data as of April 2015), mostly in the elderly [3–6]. It is very likely that our nation-wide survey and effort to diagnose AH13 identified more patients than former times [3, 4]. AH13 is a life-threatening hemorrhagic disease [7–9], and some patients are accidentally recognized and diagnosed after they manifest severe postoperative bleedings. Their hemorrhage pattern is also characterized as "delayed bleeding" that occurs 12–36 h after trauma or invasive procedures [1].

On the contrary, if AH13 cases were diagnosed beforehand, operations would be withheld by surgeons, in general, mainly because of the deliberation on excessive/abnormal bleeding. However, even female patients with inherited FXIII deficiency can safely deliver babies under FXIII replacement therapy [10, 11]. This holds true for surgery in cases with inherited FXIII deficiency [12, 13], so why is surgery not performed in AH13 cases? To the authors' best knowledge, there was a single AH13 case for which coronary artery bypass surgery was performed using off-pump, beating heart surgery to minimize risks of a postoperative coagulopathy [14].

Case presentation

A previously otherwise healthy 64-year-old Japanese man was hospitalized for a left femur hematoma after a bicycle accident a month earlier (Dec. 201X; Fig. 1, arrow with 'Th'). There was no personal or family history of bleeding diathesis. He underwent embolization of the left femoral artery, because computed tomography (CT; Fig. 2a)

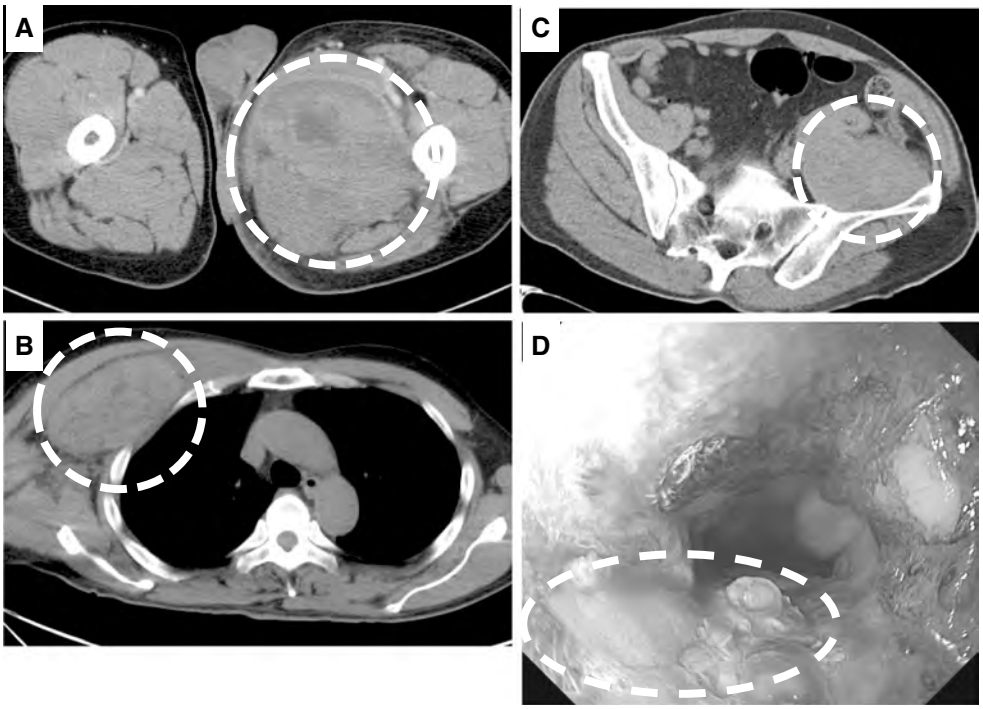

Fig. 2 Computed tomographic images and an endoscopic picture. **a** Left femoral hematoma at first visit (Jan. 201X + 1). **b** Right axillar hematoma at first visit (Jan. 201X + 1). **c** Retro-peritoneal hematoma during clinical exacerbation (Mar. 201X + 1). **d** Esophageal carcinoma suspected by upper gastrointestinal endoscopy (Dec. 201X + 2). Each lesion is enclosed by a *white broken circle/oval*

and angiography revealed its active bleeding. The patient noticed a hematoma at his right axilla 5 days after embolization (Fig. 1, arrow with 'Ax') and visited our hospital (Jan. 201X + 1; Fig. 2b). His height and body weight were 168 cm and 68 kg.

A physical examination revealed a hematoma of the right axilla as well as a huge hematoma of the left femur accompanied with purpura. Laboratory tests showed low levels of hemoglobin (71 g/L) and red blood cell count (2.3×10^{12}/L), while leukocyte and platelet numbers, C-reactive protein and fibrinogen levels were above the normal ranges (14.2 and 412×10^{9}/L, 81.3 and 426 mg/mL, respectively). D-Dimer (1.1 μg/mL) and fibrin/fibrinogen degradation products (FDP; 4.5 μg/mL), thrombin–antithrombin complex (>60 ng/mL), and von Willebrand factor (VWF; 323 %) activity levels were also increased slightly or moderately, reflecting the patient's severe bleeding condition. Antithrombin and plasmin–plasmin inhibitor complex (PIC) levels were within the normal limits. Routine coagulation screening tests also showed normal prothrombin time and activated partial thromboplastin time. However, his FXIII activity was as low as 10 % (normal range 70–140 %) on Jan. 30, 201X + 1. A cross-mixing study in which the patient's plasma was mixed at a 1:1 ratio with a healthy control's plasma demonstrated significantly low residual FXIII activity (10 %) on Feb. 1, 201X + 1 (FXIII activities of a healthy control and the patient; 108 and 11 %, respectively). He was therefore diagnosed with hemorrhagic acquired FXIII deficiency resulting from FXIII inhibitor, i.e., AH13, tentatively, and thus started to take prednisolone (PSL) at 1 mg/kg, cyclosporine A (CyA) at 5 mg/kg and received plasma-derived FXIII concentrates (Fibrogammin P®, CSL Behring, Tokyo, Japan; 240 U/vial according to the manufacturer's definition). Upper gastrointestinal endoscopic examination revealed no abnormal findings in Jan. 201X + 1, and tumor markers, such as carcino-embryonic antigen, carbohydrate antigen 19-9, and prostate-specific antigen, were not elevated in Jan. 201X + 1.

The patient's bleeding appeared to be temporarily stopped, but his blood pressure and hemoglobin level suddenly dropped a few days later. CT imaging revealed a retroperitoneal hematoma (Fig. 1, arrow with 'RP', Fig. 2c), and thus red cell concentrates (RCC) and FXIII concentrates were transfused, and embolization was performed. To reinforce immunosuppressive therapy, he was also treated with weekly rituximab, four times (Fig. 1). His FXIII activity increased to 15 %, but then decreased to 10 %. After 8 months, FXIII activity increased to 20 % and 1:1 cross-mixing test became negative for FXIII inhibitor, so that CyA was discontinued.

Four months later, FXIII activity decreased again to as low as 4 % and the 1:1 cross-mixing test returned to be

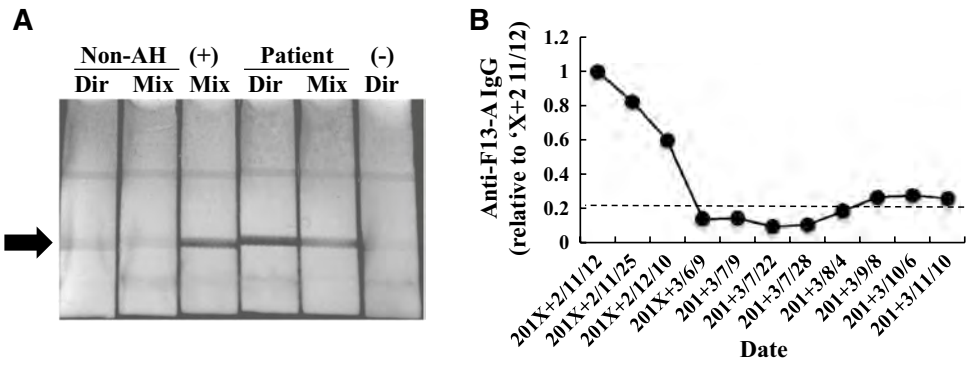

Fig. 3 Japanese collaborative research group (JCRG) analyses of the patient's plasma FXIII and detection of anti-FXIII antibodies (Nov 201X + 2). **a** ICTs to detect FXIII-A-bound anti-FXIII-A autoantibodies with (spiked) or without (direct) pre-mixing pooled normal plasma. From the *left to the right lanes* direct and spiked ICTs for a case with non-autoimmune hemorrhagic FXIII deficiency (Non-AH), spiked ICT for positive control [(+)], i.e., the plasma obtained from a previously diagnosed AH13 case, direct and spiked ICTs for the present AH13 case (patient), and direct ICT for negative control [(−)], i.e., the plasma obtained from a healthy control. **b** A fair amount of total anti-FXIII-A immunoglobulin G (IgG) was still clearly detected by the ELISA (*filled circles*). After the immunosuppressive therapy with CPA, his total anti-FXIII-A IgG had significantly decreased. A *dashed line* represents an average level of normal controls. *ICT* immuno-chromatography test, *Dir* direct, *Mix* spiked, *AH13* autoimmune hemorrhagic disease due to anti-FXIII autoantibodies, *ELISA* enzyme-linked immuno-sorbent assay, *CPA* cyclophosphamide

positive for FXIII inhibitor. Accordingly, the patient restarted CyA treatment. Because of the chronic intractable nature of his disease, the Japanese collaborative research group (JCRG; chair; Prof. Ichinose of Yamagata University) was called into consultation. When the patient was examined for the presence of anti-FXIII autoantibodies by an immuno-chromatography test (ICT) [15], anti-FXIII-A autoantibodies were positive (Fig. 3a). Our ELISA method also demonstrated the presence of (total) anti-FXIII-A antibodies (Fig. 3b) [16]. Consequently, he was definitely diagnosed as AH13 and reinforcement of immunosuppressive therapy was planned.

Unfortunately, an upper gastrointestinal endoscopy during a routine health checkup revealed suspected esophageal carcinoma in Dec. 201X + 2, about 2 years after the first endoscopic examination (Fig. 2d). Because of his severe FXIII deficiency, he was began cyclophosphamide (CPA) at 50 mg/day and underwent a pharmacokinetic (PK) analysis by infusing FXIII concentrates at 1200 U in preparation for biopsy (Fig. 4a). Because the recovery rate of the PK study was considerably low (about 25 %), a large dose of FXIII replacement therapy at 60 U/kg (equivalent to 120 % increase) was carried out. As a result, the biopsy was performed successfully without excessive/abnormal bleeding 2 weeks later. The patient was diagnosed as having squamous cell carcinoma of esophagus (UtMt, Type 2, T2, N0, M0, stage II; [17]).

He was treated with chemo-radiotherapy because his severe FXIII deficiency made him ineligible for a curative operation. He received 60 Gy/30 Fr radiotherapy with concurrent chemotherapy (5-FU at 700 mg/m^2 on days 1–4 and cisplatin at 70 mg/m^2; Fig. 1). His esophageal carcinoma went into complete remission and his FXIII activity rose to about 20 %. However, the carcinoma recurred 2 months later. His body weight suddenly decreased to 58 kg due to swallowing disturbance because of esophageal stricture. Accordingly, he required an esophageal bypass operation. In preparation for surgery, an FXIII PK study (dosing 1440 U) was again conducted 3 weeks before (Fig. 4b). Since a good recovery rate of 77 % was obtained, the patient was given 50 U/kg of FXIII concentrate before entering the operating room to achieve a goal of at least 100 % FXIII activity (Fig. 4c). Esophageal bypass and jejunostomy creation were performed. The operation lasted a total of 4 h and 7 min, and the total blood loss during the operation was 302 g, which was the same as that in patients without a bleeding disorder [18], and he received a blood transfusion of 4 units of RCC. There were no problems related to the surgery. FXIII concentrates were also infused during the postoperative period (Fig. 4c), in order to prevent possible "delayed bleeding". Immunosuppressive therapy with CPA alone was continued, whereas CyA was not administered on the day of operation until postoperative day 7.

No massive bleeding was observed after the surgery. No thrombotic events or problematic wound healing occurred. He was released from the hospital on postoperative day 24.

Discussion

Severe hemorrhagic tendency of AH13 patients seems to be quite a burden for surgeons because they have decision-making responsibilities. However, AH13 is a chronic intractable disease mainly in the elderly [7–9], who tend to

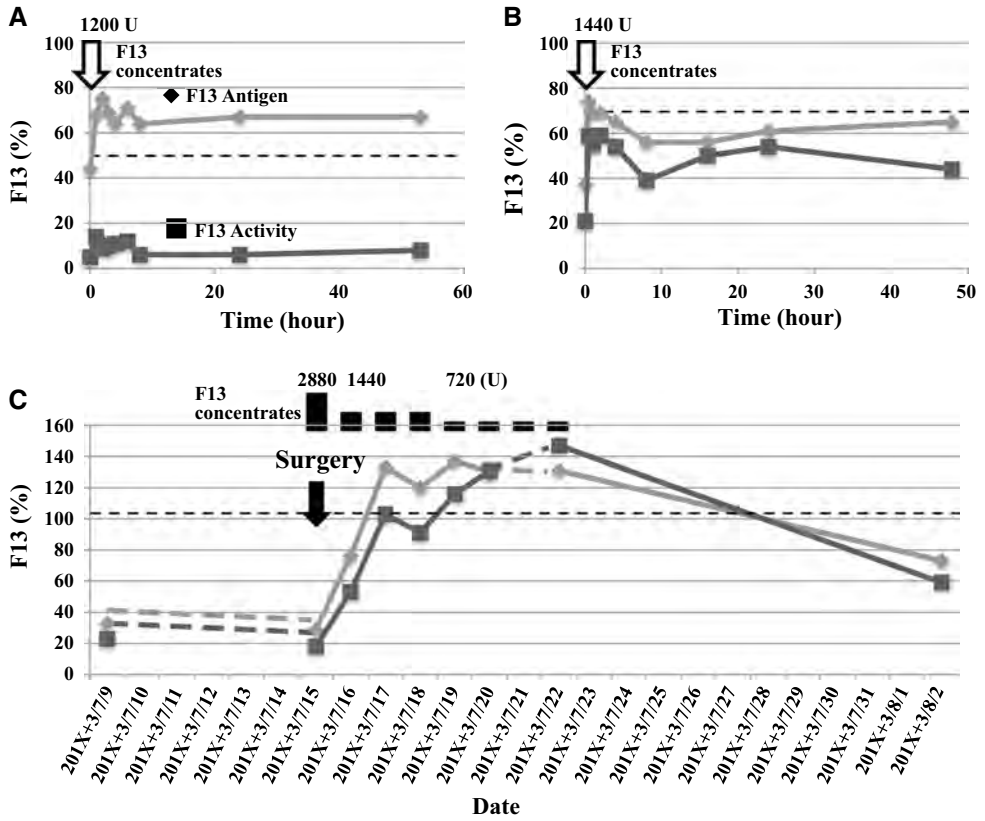

Fig. 4 Preparatory pharmacokinetic (PK) studies (**a**, **b**) and hemostatic treatment (**c**) by infusion of exogenous FXIII. Plasma-derived FXIII concentrates were infused at a dose of 1200 U in Nov. 201X + 2 (17.6 U/kg, equivalent to about 35 % increase) in preparation for biopsy (**a**) and 1440 U in June 201X + 3 (24.8 U/kg, equivalent to about 50 % increase) in preparation for bypass surgery (**b**), and during the perioperative period in July 201X + 3 (**c**). Both FXIII activity (*filled squares*) and antigen levels (*filled diamonds*) were measured before and at the indicated time intervals (**a**, **b**) or postoperation dates just before the daily exogenous FXIII infusions (at the *top*; **c**). *Broken lines* depict calculated FXIII activities after the infusion of exogenous FXIII concentrates. Discrepancies between FXIII activity and antigen levels indicate the formation and existence of FXIII antigen–antibody complexes between "free" anti-FXIII-A autoantibodies and exogenous FXIII concentrates (**c**). As expected, his FXIII activity reasonably increased from 18 to 53 % on the next day after FXIII concentrates infusion despite he underwent surgical procedure the day before (i.e., in spite of surgical bleeding in addition to the inhibition by anti-FXIII-A autoantibodies and the accelerated clearance of infused FXIII). His FXIII activity kept further increase to 103, 91, 116, 131, and 147 %, because about 30 U/kg FXIII concentrates were administered for the following 3 days and 15 U/kg for another 3 days. We tried to keep his FXIII activity around 100 % of normal at least for several days after surgery in order to prevent the notorious 'delayed bleeding' of severe FXIII deficiency. His FXIII activity then decreased to 59 % 10 days after the discontinuation of FXIII concentrates administration

suffer from other life-threatening diseases, such as cancer, aortic aneurysm, and myocardial infarction, which require surgical procedures. In other words, even if AH13 patients could survive the life-threatening acute stage by proper hemostatic and immunosuppressive treatments, they might be endangered next by aforementioned life-threatening diseases.

Thanks to surgeons, at least two AH13 patients' lives were saved, including a 73-year-old man with AH13 who actually underwent coronary bypass surgery for increasing angina and did well for more than 3 years [14]. Our 64-year-old man with AH13 has also been doing well more than 10 months after esophageal bypass surgery for carcinoma.

It is important to emphasize that malignancies were one of the leading underlying diseases among Japanese AH13 cases [3, 4]. There were 2 cases with gastric cancer, 2 cases with bladder cancer, 1 patient with seminoma, and 1 patient with skin cancer (11 % of all Japanese AH13 cases; Refs. [3, 4] and unpublished data of JCRG). Surgical treatments are indications for most of these malignancies, in general. This is also true in patients with acquired hemophilia A (AHA) caused by auto-antibodies against factor VIII/8, in which malignancies are one of the most common underlying diseases (14.7 % of 150 cases in Ref. [19]). These facts suggest that malignancies may be related to compromised immune reaction and, to some extent, to production of auto-antibodies against these coagulation factors. It was

reported that treatment of cancer with chemotherapy or surgery was followed by the eradication of the inhibitor in 5 out of 41 AHA patients with cancer [20].

We recommended an administration trial of FXIII for the diagnosis of AH13 [6]. It may be also useful to make a hemostatic plan in terms of subsequent dosage and dosing intervals. In fact, PK studies were performed in a 2.5-year-old boy and a 53-year-old man with severe inherited FXIII deficiency before epilepsy neurosurgery [12] and a surgery for aortic valve replacement [13], respectively. Furthermore, it was done in a 73-year-old man with AH13 before coronary artery bypass surgery for angina, although the timing of survival study was not specified [14]. In the present case of AH13, a PK analysis was carried out before esophageal bypass surgery for carcinoma. Surgeries for all four patients were completed successfully, regardless of whether the FXIII deficiency was inherited or acquired, in other words, with or without anti-FXIII autoantibodies. Thus, preparatory PK studies seemed to be very useful to predict the efficacy of FXIII replacement therapy during and after surgery.

There are no evidence-based guidelines on how to manage perioperative therapy for FXIII deficiency, regardless of whether it is inherited or acquired. In particular, few data are available on FXIII dosing perioperatively. In inherited FXIII deficiency, a surgery was performed under FXIII replacement therapy at a dose of 36 U/kg for intracranial surgery [12], and major or minor surgeries were conducted at preoperative doses ranging from 25 to 40 U/kg [13]. Among AH13 cases, a 73-year-old man was given 42 U/kg FXIII for coronary artery bypass surgery [14]. In the present AH13 case, we administered 50 U/kg FXIII concentrates for esophageal bypass surgery, and tried to keep the patient's FXIII level around 100 % of normal for several days after operation.

All these cases demonstrate that major surgeries can be quite safely performed in patients with severe FXIII deficiency, regardless of the presence or the absence of anti-FXIII antibodies.

Acknowledgments This study was approved by the institutional review board of Yamagata University School of Medicine. All procedures were conducted in accordance with the Declaration of Helsinki. Written informed consent was obtained from this patient. This study was supported in part by research aids from the Japanese Ministry of Health, Labor, and Welfare and a research grant from Yamagata University. We would like to thank all members of 'Japanese Collaborative Research Group (JCRG) on AH13' and Ms. Yuriko Shibue for their cooperation in conducting a nation-wide survey in Japan from 2009 through 2014. The authors also thank Drs. Koji Okamoto, Kento Sakon and Masahito Yano for their invaluable advices on surgical problems of the present case.

Compliance with ethical standards

Conflict of interest The authors declare no conflicts of interest in association with this study.

References

1. Ichinose A. Physiopathology and regulation of factor XIII. Thromb Haemost. 2001;86:57–65.
2. Kohler HP, Ichinose A, Seitz R, Ariens RA, Muszbek L, Factor XIII And Fibrinogen SSC Subcommittee Of The ISTH. Diagnosis and classification of factor XIII deficiencies. J Thromb Haemost. 2011;9:1404–6.
3. Ichinose A, Souri M, Japanese collaborative research group on "Acquired haemorrha-philia due to factor XIII deficiency". As many as 12 cases with haemorrhagic acquired factor XIII deficiency due to its inhibitors were recently found in Japan. Thromb Haemost. 2011;105:925–7.
4. Ichinose A, Osaki T, Souri M, Japanese collaborative research group on "Acquired haemorrha-philia due to factor XIII deficiency". Clinical features of 32 new Japanese cases with autoimmune haemorrha-philia due to anti-factor XIII antibodies. Haemophilia. 2015;21(5):653–8. doi:10.1111/hae.12677.
5. Ichinose A. Hemorrhagic acquired factor XIII (13) deficiency and acquired hemorrhaphilia 13 revisited. Semin Thromb Hemost. 2011;37:382–8.
6. Ichinose A, Japanese Collaborative Research Group (JCRG) on AH13 Hemorrhagic Acquired Coagulopathies. Inhibitors of factor XIII/13 in older patients. Semin Thromb Hemost. 2014;40:704–11.
7. Sugiyama H, Uesugi H, Suzuki S, Tanaka K, Souri M, Ichinose A. Aggressive fatal case of autoimmune hemorrhaphilia resulting from anti-Factor XIII antibodies. Blood Coagul Fibrinolysis. 2013;24:85–9.
8. Boehlen F, Casini A, Chizzolini C, Mansouri B, Kohler HP, Schroeder V, et al. Acquired factor XIII deficiency: a therapeutic challenge. Thromb Haemost. 2013;109:479–87.
9. Kotake T, Souri M, Takada K, Kosugi S, Nakata S, Ichinose A. Report of a patient with chronic intractable autoimmune hemorrhaphilia* due to anti-Factor XIII/13 antibodies who died of hemorrhage after sustained clinical remission† for three years. Int J Hematol. 2015;101:598–602.
10. Ichinose A. Factor XIII is a key molecule at the intersection of coagulation and fibrinolysis as well as inflammation and infection control. Int J Hematol. 2012;95:362–70.
11. Naderi M, Eshghi P, Cohan N, Miri-Moghaddam E, Yaghmaee M, Karimi M. Successful delivery in patients with FXIII deficiency receiving prophylaxis: report of 17 cases in Iran. Haemophilia. 2012;18:773–6.
12. Pernod G, Barro C, Arnutti B, Blanc-Jouvan F, Garrel S, Kahn P, et al. Surgery in severe factor XIII deficiency: report of a case of epilepsy neurosurgery and review. Haemophilia. 2003;9:121–4.
13. Janbain M, Nugent DJ, Powell JS, St-Louis J, Frame VB, Leissinger CA. Use of factor XIII (FXIII) concentrate in patients with congenital FXIII deficiency undergoing surgical procedures. Transfusion. 2015;55:45–50.
14. Lim W, Moffat K, Hayward CP. Prophylactic and perioperative replacement therapy for acquired factor XIII deficiency. J Thromb Haemost. 2004;2:1017–9.
15. Osaki T, Sugiyama D, Magari Y, Souri M, Ichinose A. Rapid immunochromatographic test for detection of anti-factor XIII A subunit antibodies can diagnose 90% of cases with autoimmune hemorrhaphilia XIII/13. Thromb Haemost. 2015;113:1347–56.
16. Souri M, Osaki T, Ichinose A. Anti-factor XIII A subunit (FXIII-A) autoantibodies block FXIII-A2B2 assembly and steal FXIII-A from native FXIII-A2B2. J Thromb Haemost. 2015;13:802–14.
17. Kuwano H, Nishimura Y, Oyama T, Kato H, Kitagawa Y, Kusano M, et al. Guidelines for diagnosis and treatment of carcinoma of the esophagus April 2012 edited by the Japan Esophageal Society. Esophagus. 2015;12:1–30.

18. Kimura M, Ishiguro H, Tanaka T, Takeyama H. Advanced esophageal cancer with tracheobronchial fistula successfully treated by esophageal bypass surgery. Int J Surg Case Rep. 2015;9:115–8.
19. Collins PW, Hirsch S, Baglin TP, Dolan G, Hanley J, Makris M, et al. Acquired hemophilia A in the United Kingdom: a 2-year national surveillance study by the United Kingdom Haemophilia Centre Doctors' Organisation. Blood. 2007;109:1870–7.
20. Sallah S, Wan JY. Inhibitors against factor VIII in patients with cancer. Analysis of 41 patients. Cancer. 2001;91:1067–74.

Int J Hematol (2016) 103:25–33
DOI 10.1007/s12185-015-1897-7

REVIEW ARTICLE

A phase I study of vorinostat combined with bortezomib in Japanese patients with relapsed or refractory multiple myeloma

Yoshiaki Ogawa[1] · Michinori Ogura[2] · Kensei Tobinai[3] · Kiyoshi Ando[1] · Tatsuya Suzuki[2] · Takashi Watanabe[3] · Ken Ohmachi[1] · Toshiki Uchida[2] · Mary E. Hanson[4] · Yoshinobu Tanaka[5] · Yasuhiro Koh[5] · Takashi Shimamoto[5] · Tomomitsu Hotta[6]

Received: 18 March 2015 / Revised: 30 October 2015 / Accepted: 4 November 2015 / Published online: 30 November 2015

Abstract This study was undertaken to evaluate safety and pharmacokinetics and to determine treatment doses of vorinostat plus bortezomib in Japanese patients with relapsed or refractory multiple myeloma (MM). Of 9 originally enrolled patients, 2 were refractory to bortezomib, and both experienced dose-limiting toxicity (DLT), prompting a protocol amendment to exclude bortezomib-refractory individuals. Patients not considered bortezomib refractory ($N = 7$) received 21-day cycles of 1.3 mg/m^2 intravenous bortezomib (Days 1, 4, 8, and 11) and oral vorinostat 400 mg (Days 1 through 14) and were further evaluated. Vorinostat and bortezomib treatment doses were determined by DLT and safety, tolerability, and treatment response were assessed. Of 7 enrolled patients, 6 were evaluated, and one developed DLTs. The most common adverse events were leukopenia, neutropenia, thrombocytopenia, diarrhea, nausea, decreased appetite, and vomiting. Combination of vorinostat plus bortezomib did not increase vorinostat exposure at Day 11 [$AUC_{0-24\ h}$ ratio (95 % CI) = 1.08 (0.80, 1.45)]; geometric mean $AUC_{0-24\ h}$ ratio for bortezomib (90 % CI) was 1.96 (1.24–3.12). Objective therapeutic response occurred in 3 patients, including 1 complete response and 2 partial responses. Vorinostat 400 mg plus bortezomib 1.3 mg/m^2 was safe and well-tolerated in Japanese patients with relapsed or refractory MM not considered bortezomib refractory (NCT00858234).

Keywords Vorinostat · Bortezomib · Multiple myeloma · Phase I study · HDAC inhibitor

Introduction

Multiple myeloma (MM) is a malignant hematopoietic disorder characterized by aberrant monoclonal proliferation of plasma cells. Approximately 102,000 new cases of MM worldwide were estimated for 2008, comprising approximately 0.8 % of all new cancer cases [1]. In spite of the availability of autologous stem cell transplantation and newer treatment drugs, MM remains an incurable disease with a high relapse rate and poor prognosis [2]. Therefore, an ongoing need for new treatment agents and therapeutic strategies to control MM progression and improve survival exists.

Bortezomib is a dipeptide proteasome inhibitor that suppresses the NF-κB signaling pathway, which controls cellular functions important for the malignant progression of MM, including cell proliferation and survival [3]. Bortezomib was approved by the US Food and Drug Administration in 2003 after a phase II trial that demonstrated a high overall response rate in patients with MM [4, 5]. Since then, bortezomib has become an important component of

Electronic supplementary material The online version of this article (doi:10.1007/s12185-015-1897-7) contains supplementary material, which is available to authorized users.

✉ Yoshiaki Ogawa
yoshioga@is.icc.u-tokai.ac.jp

1 Department of Hematology and Oncology, Tokai University School of Medicine, Shimokasuya 143, Isehara, Kanagawa 259-1193, Japan

2 Department of Hematology and Oncology, Nagoya Daini Red Cross Hospital, Nagoya, Japan

3 Department of Hematology, National Cancer Center Hospital, Tokyo, Japan

4 Merck and Co., Inc., Kenilworth, NJ, USA

5 MSD K.K., Tokyo, Japan

6 National Cancer Center, Tokyo, Japan

conventional MM treatment strategies. Clinical trials of bortezomib in Japanese patients demonstrated strong antitumor activity and greater efficacy over thalidomide in patients with relapsed or refractory MM [3, 6, 7]. Nevertheless, no standard treatment regimen has been established for patients who fail to respond to bortezomib or who have relapsed after bortezomib therapy.

Vorinostat is a hydroxamic acid-based inhibitor of histone deacetylases (HDACs), compounds which have emerged in recent years as an important target in MM [8]. High concentrations of a hydroxamic acid-based HDAC inhibitor have been shown to induce apoptosis in an acute T-cell leukemia cell line via a mechanism dependent on reactive oxygen species production [9]. Preclinical studies have shown that addition of vorinostat to cells previously exposed to bortezomib impaired mitochondrial function and induced apoptosis in drug-resistant as well as drug-sensitive human MM cell lines, suggesting that vorinostat and bortezomib may be a potent combination for inhibiting MM progression [10]. The safety and tolerability of vorinostat have subsequently been demonstrated in a phase I trial in patients with relapsed and/or refractory MM [11–14]. Trials evaluating safety and efficacy of vorinostat combined with bortezomib showed that this combination was generally well-tolerated and produced clinical responses in patients with relapsed and/or refractory MM, including patients refractory to bortezomib [12–14].

Building upon data from prior studies investigating maximum tolerated doses of vorinostat and bortezomib, a phase I trial was conducted with the primary goal of determining the clinical doses of vorinostat plus bortezomib that would be well-tolerated in Japanese patients with relapsed and/or refractory MM [12, 14]. Secondary objectives included evaluation of vorinostat and bortezomib pharmacokinetics and preliminary assessment of efficacy in these patients.

Patients and methods

Study design

This was a phase I open-label, multicenter study (clinicaltrials.gov identifier NCT00858234; Merck protocol number 098) to evaluate the safety, tolerability, pharmacokinetics, and efficacy of vorinostat combined with bortezomib in Japanese patients with MM. The study was conducted between March 2009 and April 2012 in accordance with the principles of Good Clinical Practice and the Declaration of Helsinki, and was approved by the institutional review boards and regulatory agencies at each study site. Each enrolled patient gave written consent prior to study participation.

Patients

Japanese patients at least 20 years of age with an established diagnosis of MM were enrolled in the study. A protocol amendment after study initiation restricted the study population to those not considered to be refractory to bortezomib therapy. Patients were considered refractory to bortezomib if they did not respond to prior bortezomib-containing regimens or had disease progression on or within 60 days of a bortezomib-containing regimen. Patients must have had an Eastern Cooperative Oncology Group (ECOG) performance status score of 0 or 1 and clinically measurable disease previously treated with 1–3 anti-myeloma regimens, with progressive disease after the most recent treatment based on European Group for Blood and Marrow Transplantation (EBMT) criteria.

Patients who had had any prior allogeneic or planned hematopoietic stem cell transplant were excluded from the study. Patients were also excluded if they had an active systemic infection requiring treatment or were receiving >10 mg/day prednisone or equivalent corticosteroid treatment. Prior treatment with vorinostat or other HDAC inhibitor drugs, inability to tolerate prior bortezomib treatment, or known hypersensitivity to bortezomib or vorinostat were also criteria for exclusion.

Treatment plan

Vorinostat and bortezomib were given over 21-day treatment cycles, during which patients were administered bortezomib intravenously on Days 1, 4, 8, and 11 and vorinostat orally once daily with food concurrently from Day 1 through Day 14. Dose level 1 consisted of vorinostat 400 mg plus bortezomib 1.3 mg/m^2, dose level 1 consisted of vorinostat 400 mg plus bortezomib 1.0 mg/m^2, and dose level-2 consisted of vorinostat 300 mg plus bortezomib 1.0 mg/m^2. On days when patients received both drugs, vorinostat was administered prior to bortezomib. To determine the optimal dose combination, treatment was initiated at dose level 1 in the first 3 enrolled patients. The initial dosing was based on results from a previous study of vorinostat combined with bortezomib in MM patients, which did not permit determination of the maximum tolerated dose [12, 14]. If 2 or fewer of the 3 patients developed DLT during the first cycle, up to 3 additional patients were enrolled and administered the study drugs at this dose level or the dose level was reduced without enrolling additional patients. If more patients were enrolled and 2 or fewer of the 6 patients who received a particular dose level developed a DLT, this dose level was considered to be tolerable. If 3 or more of the 6 patients developed DLT at a particular dose level, new patients were enrolled at the next lower dose level. If all 3 patients initially tested at dose level 1 developed a DLT, newly enrolled

patients were administered dose level 1. Decisions regarding whether to enroll more patients at a particular dose level or to reduce the dose were made by the investigator and sponsor in consultation with the independent Efficacy and Safety Evaluation Committee.

Toxicity was graded according to the National Cancer Institute Common Terminology Criteria for Adverse Events (NCI-CTCAE) Guidelines, version 3.0. Dose-limiting hematologic and non-hematologic toxicities were defined separately and were based on events during the first study drug cycle. To be considered a DLT, an adverse event (AE) must have been considered by the investigator to have a 'possible,' 'probable,' or 'definite' causal association with the study therapy. DLTs were defined as: (1) any Grade 3 or 4 non-hematologic event except for any toxicity manageable with supportive care or with non-prohibited therapies (e.g., nausea, vomiting, and/or fatigue), or a transient increase in alanine aminotransferase (ALT) or aspartate aminotransferase (AST); or (2) any Grade 4 hematologic toxicity except for neutropenia, decreased hemoglobin, or decreased lymphocyte count. Neutropenia was considered a DLT criteria if it was Grade 3 or 4 and accompanied by a fever of ≥38.5 °C or by infection requiring antibiotic or antifungal treatment, or if it was a Grade 4 neutropenia lasting at least 5 days.

Patients were evaluable if they had DLT in the first cycle or completed the first cycle without a DLT and received at least 11 of the 14 vorinostat doses and at least 3 of the 4 bortezomib doses. Depending on the cause of toxicity determined by the investigator, vorinostat could be omitted at any time, bortezomib could be omitted on Day 8 or 11, or both drugs could be omitted. All study drugs were administered under hospitalization during the first cycle; subsequent treatments were administered at an outpatient clinic.

Safety assessments

Safety assessments included DLT incidence during the first treatment cycle, the incidence of all AEs and drug-related AEs, and laboratory tests. Laboratory tests included those related to hematology, urinalysis, and hepatic function.

Pharmacokinetic assessments

Blood samples were obtained during the first treatment cycle to evaluate vorinostat and bortezomib pharmacokinetics. Blood volumes of 3 mL were collected on Days 1, 4, 8, and 11 predose (all days) and at the time points that included 5, 15, and 30 min, and 1, 1.5, 2, 3, 4, 6, 8, 10, 12, 24 h (Days 1 and 11) and 48 h (Day 11) post-dose.

Pharmacokinetic parameters evaluated for serum vorinostat included area under the plasma concentration time curve (AUC), peak concentration (C_{max}), time to reach C_{max} (t_{max}), and elimination half-life ($t_{1/2}$). Pharmacokinetic parameters evaluated for plasma bortezomib were AUC, $t_{1/2}$, clearance, and volume of distribution. Pharmacokinetic results were compared with those of bortezomib alone, as previously described [6, 15].

Efficacy assessments

Efficacy assessments included response rate, response duration, time to progression, and time to response. Response to therapy was assessed using EBMT criteria [16] and the International Myeloma Working Group criteria [17, 18], in which responses were graded as complete response (CR), partial response (PR), very good partial response, minor response, no change, or progressive disease; and was determined using quantitative measurements of serum immunoglobulin, serum protein electrophoresis, M-protein quantitation, 24-h urine protein electrophoresis, serum and urine immunofixation, bone marrow aspirate and biopsy, if applicable. Disease progression was monitored every 21 days after the baseline visit. For patients with extramedullary plasmacytoma at baseline, follow-up efficacy measurements were performed every 6 weeks during study treatment.

Statistical analysis

Since the total number of patients was dependent on the number of dose levels tested before the recommended clinical doses were established, formal calculation of sample size was not performed based on power analysis.

Summary statistics, including mean, standard deviation, median, and range for time to onset and duration of first AE of Grade 3 or higher were calculated for each dose level. All patients considered not refractory to bortezomib and receiving at least 1 study drug dose were included in the safety analysis. For the pharmacokinetic analysis, summary statistics (mean, standard deviation, and range) were calculated based on patients with available data. For the efficacy analysis, response rate, response duration, time to response, and time to progression were listed and described as appropriate. Patients who withdrew from the study due to disease progression were considered to have disease progression between the last visit and study withdrawal. Since the primary objective was to determine the recommended clinical doses of the vorinostat and bortezomib and evaluate the safety of the combination, no formal statistical hypothesis was tested, and therefore, no adjustments were made for multiplicity.

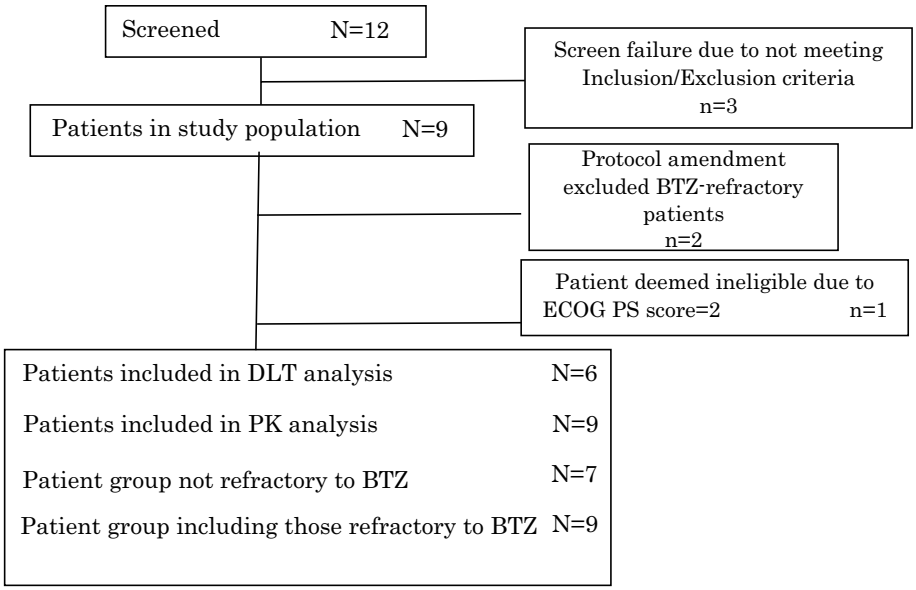

Fig. 1 Patients included in the study analyses

Results

Patient characteristics

A total of 12 patients were screened; 3 of these did not meet the inclusion/exclusion criteria, and 9 were enrolled in the study (Fig. 1). Of these 9 patients, 2 were refractory to bortezomib and both experienced Grade 4 thrombocytopenia after study initiation. These results raised concerns about tolerability in bortezomib-refractory patients with the combination treatment, prompting a protocol amendment to include only patients who were not considered refractory to bortezomib. Of the remaining 7 patients, 1 received inconsistent ECOG PS scores (score of 1 by the investigator and score of 2 by the independent Efficacy and Safety Evaluation Committee). As the study inclusion criteria required an ECOG PS score of 0 or 1, the patient was excluded.

Demographic and clinical characteristics of the enrolled patients are shown in Table 1. Patients ranged in age from 43 to 80 years, with the median age being 65 years, and 8 patients were male. Enrolled patients received a median of 1 prior chemotherapy regimen. Study treatment compliance was $\geq$75 % in the first treatment cycle for all patients except 1, who discontinued from Day 8 onward as a result of a DLT (Grade 3 tumor lysis syndrome and Grade 4 thrombocytopenia).

Safety

Safety was evaluated for 2 groups: the 9 patients originally enrolled (all enrolled patients) and the 7 patients who were considered not refractory to bortezomib (bortezomib-refractory group). Three patients developed 7 serious treatment-related clinical AEs (Grade 3 fatigue, Grade 3 anorexia and Grade 3 pneumonia in 1 patient; Grade 3 pneumonia in 1 patient, and Grade 3 sepsis, Grade 3 pyelonephritis and Grade 3 disseminated intravascular coagulation in another patient), and 6 patients discontinued therapy due to treatment-related clinical AEs. These included Grade 4 thrombocytopenia, 2 Grade 3 pneumonia, Grade 2 peripheral neuropathy, Grade 3 pyelonephritis resulting in Grade 3 sepsis and Grade 2 disseminated intravascular coagulation, and Grade 1 peripheral sensory neuropathy. The most commonly reported AEs in at least 50 % of patients (Table 2) in either group were leukopenia, neutropenia, thrombocytopenia and diarrhea (100 % or 9/9 patients and 100 % or 7/7 patients), nausea and decreased appetite (89 % or 8/9 patients and 86 % or 6/7 patients), vomiting (78 % or 7/9 patients and 71 % or 5/7 patients), lymphopenia and constipation (67 % or 6/9 patients and 57 % or 4/7 patients and fatigue and hypokalemia (56 % or 5/9 patients and 57 % or 4/7 patients). The most common Grade 3 or higher AE was thrombocytopenia, which occurred in all patients (Table 2).

All enrolled patients required dose reductions due to AEs, with the most frequent cause being thrombocytopenia in 67 % (6/9) of patients. All bortezomib-refractory patients also had AEs that led to dose reductions, the most common being thrombocytopenia in 57 % (4/7) of patients. One patient was excluded from the DLT evaluation; and of the remaining 6 patients, one developed DLTs consisting of Grade 3 tumor lysis syndrome (onset time of 8 days), and Grade 4 thrombocytopenia (onset time of 11 days).

For both groups (all enrolled patients and the bortezomib-refractory group), the most common laboratory AEs were increased liver enzymes. Elevated AST was seen in

Table 1 Patient characteristics

	Vorinostat + Bortezomib ($N = 9$)
Demographics	
Male sex	8 (89)
Median age, years (range)	65 (43–80)
Mean weight, kg (SD)	64.2 (8)
Disease characteristics	
Mean disease duration, years (SD)	5.3 (2)
Range	3.0–10.0
ECOG status	
0	6 (67)
1	3 (33)
ISS stage	
I	5 (56)
II	3 (33)
III	1 (11)
Immunoglobulin	
IgG kappa	5 (56)
IgG lambda	2 (22)
IgA kappa	1 (11)
IgA lambda	1 (11)
Plasma cell %[a], mean (SD)	0.2 (0.4)
Plasmocytomas	1 (11)
Bone lesion	1 (11)
Chromosome	
Deficiency 13q–	0
Deficiency 17p–	0
Translocation (11; 14)	1 (11)
Translocation (4; 14)	3 (33)
Translocation (14; 16)	0
Prior treatment	
Transplantation	
0	4 (44)
1	4 (44)
2	1 (11)
History of radiation	1 (11)
Number of prior chemotherapy regimens	
1	6 (67)
3	3 (33)

All values are *n* (%) unless otherwise noted

ISS, International staging system

[a] 5 patients with data

44 % (4/9) of all enrolled patients and elevated ALT and AST were each reported in 43 % (3/7) of bortezomib-refractory patients. A depressed lymphocyte count, the only laboratory AE of Grade 3 or higher, was reported in 11 % (1/9) of all enrolled patients. No laboratory AEs of Grade 3 or above were reported in the bortezomib-refractory group. None of the laboratory AEs were considered serious, and none led to study discontinuation.

Pharmacokinetics

Analysis of pharmacokinetic parameters was performed for all 9 patients enrolled with a few exceptions. Pharmacokinetic parameters were not calculated for 1 patient on Day 8 due to a lack of sample availability. Vorinostat pharmacokinetic data for 2 patients and bortezomib pharmacokinetic data for 3 patients were not included in the calculation of pharmacokinetic parameters on Day 11 since these patients did not receive the indicated drug.

Vorinostat pharmacokinetics are shown in Table 3. The least squares mean $AUC_{0-24\ h}$ for vorinostat was 5.41 μM h on Day 1 and 5.84 μM h on Day 11, while the least squares mean C_{max} was 1.23 μM on Day 1 and 1.81 μM on Day 11. Median t_{max} for vorinostat on Day 1 was 1.95 h (range 0.27–3.12 h) and that of Day 11 was 2.9 h (range 0.45–6.02 h). Vorinostat was eliminated quickly from the serum on Days 1 and 11, with a harmonic mean $t_{1/2}$ of 2.08 and 2.74 h, respectively. Vorinostat t_{max} and $t_{1/2}$ on Day 11 were not markedly different from Day 1, and no increase in vorinostat trough concentrations were observed after multiple dosing (Table 3; Fig. 2). Moreover, the combination of vorinostat and bortezomib at Day 11 did not significantly

Table 2 Most common drug-related AEs occurring in two or more patients

Events	Grade 1–2 *n* (%)	Grade ≥3 *n* (%)
Hematologic		
Thrombocytopenia	0 (0)	7 (100)
Neutropenia	5 (71)	2 (29)
Leukopenia	7 (100)	0 (0)
Anemia	1 (14)	2 (29)
Lymphopenia	1 (14)	3 (43)
Non-hematologic		
Diarrhea	6 (86)	1 (14)
Decreased appetite	5 (71)	1 (14)
Vomiting	5 (71)	0 (0)
Nausea	4 (57)	2 (29)
Constipation	4 (57)	0 (0)
Fatigue	3 (43)	1 (14)
Hypokalemia	3 (43)	1 (14)
Hypoesthesia	2 (29)	0 (0)
Weight decreased	2 (29)	0 (0)
Dehydration	0 (0)	2 (29)
Pneumonia	0 (0)	2 (29)

Only the highest reported grade of a given AE is counted for the individual patient. Grades are based on NCI-CTCAE version 3.0

Table 3 Pharmacokinetic parameters of serum vorinostat administered in combination with bortezomib

	$AUC_{0-\infty}$ (μM h)[a]	$AUC_{0-24\,h}$ (μM h)[a]	C_{max} (μM)[a]	T_{max} (h)[b]	$t_{1/2}$ (h)[c]	Accumulation Ratio Day 11/Day 1[d]	
						$AUC_{0-24\,h}$	C_{max}
Day 1 (*N*=9)	5.53 (4.42, 6.92)	5.41 (4.33, 6.77)	1.23 (0.909, 1.67)	1.95 (0.27, 3.12)	2.08 (1.23)	NA	NA
Day 11 (*N*=7)	5.68 (4.42, 7.30)	5.84 (4.48, 7.61)	1.81 (1.30, 2.52)	2.9 (0.45, 6.02)	2.74 (1.28)	1.08 (0.80, 1.45)	1.47 (1.13, 1.93)

Root mean square error on the log-scale from mixed effects model = 0.29 for AUC, 0.26 for C_{max}

[a] Back-transformed least squares mean and 95% CI from mixed effects model performed on natural log-transformed values

[b] Median; minimum, maximum based on actual times

[c] Harmonic mean; jackknife SD

[d] Back-transformed least squares mean difference and 90% CI from mixed effects model performed on natural log-transformed values

increase exposure to vorinostat compared with Day 1; the $AUC_{0-24\,h}$ ratio (95 % CI) for Day 11 to that of Day 1 was 1.08 (0.80–1.45), and the C_{max} accumulation ratio (95 % CI) was 1.47 (1.13, 1.93).

Bortezomib pharmacokinetic results are shown in Table 4. The plasma bortezomib concentration versus time profile demonstrated a biphasic elimination pattern (Fig. 3) characterized by a rapid distribution phase (α) followed by a slow elimination phase (β). There was a modest level of bortezomib accumulation over 11 days, which was suggested by the $AUC_{0-24\,h}$ and C_{max} accumulation ratios of 1.96 (range 1.24–3.12) and 1.29 (range 0.43–3.87), respectively.

Clinical response

The efficacy of the vorinostat 400 mg plus bortezomib 1.3 mg/m^2 combination was evaluated separately in the 9 originally enrolled patients, and the 7 patients not considered refractory to bortezomib. Of the 7 patients in the second group, 3 (43 %) displayed objective treatment response, including 1 CR and 2 PRs. One of the 2 patients with PR (14 %) was considered to have a "very good partial response" according to the International Myeloma Working Group criteria. Median time to response was 22 days, median time to progression was 215 days, and median response duration was 481.5+ days.

Analyses of responses of all 9 patients originally enrolled revealed that 4 (44 %) displayed a PR or better response as defined by EBMT criteria. Of responders, median time to response was 22 days, median time to progression was 211 days, and median response duration was 171.5 days.

Discussion

In this phase I study, safety, tolerability, and pharmacokinetic parameters were assessed, and the recommended doses of vorinostat in combination with bortezomib were

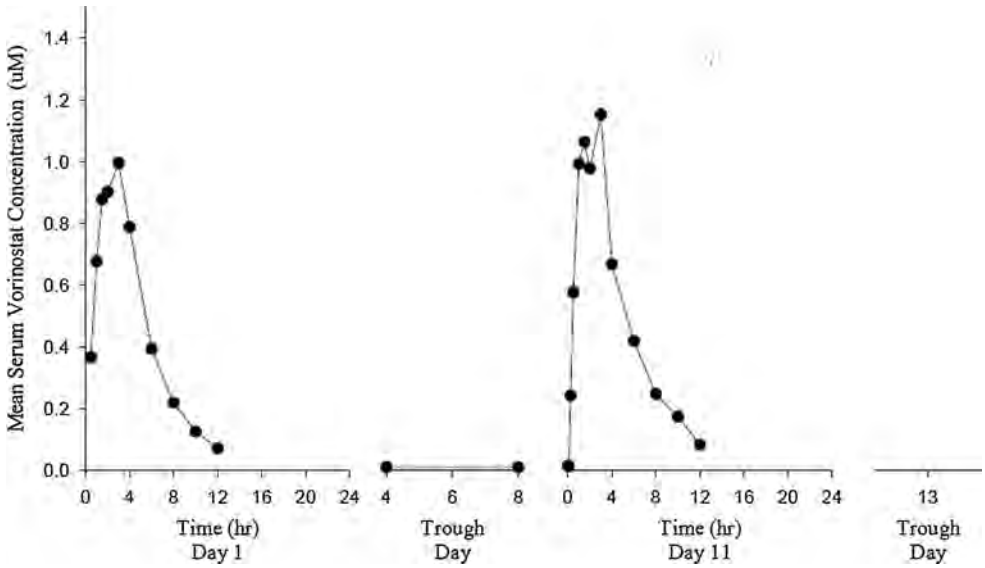

Fig. 2 Mean serum concentration* versus time profile of vorinostat following administration. *Values below the lower limit of quantification were not included in the calculation of mean concentration

Table 4 Pharmacokinetic parameters of plasma bortezomib administered in combination with vorinostat

	$AUC_{0-\infty}$ (ng h/mL)[a]	$AUC_{0-24\,h}$ (ng h/mL)[a]	C_{max} (ng/mL)[a]	C_0 (ng/mL)[a]	$t_{1/2}$ (h)[b]	Vz (L/m-)[a]	CL (L/h/m^2)[a]	Accumulation Ratio Day 11/ Day 1[c]
Day 1 ($N = 9$)	93.4 (73.0, 119)	36.1 (25.9, 50.2)	86.7 (42.3, 178)	199 (93.8, 422)	42.5 (39.9)	1005 (660, 1529)	13.9 (10.9, 17.8)	$AUC_{0-24\,h}$: 1.96 (1.24, 3.12)
Day 11 ($N = 6$)	216 (164, 285)	70.8 (46.3, 108)	112 (45.1, 279)	241 (97.9, 594)	29.4 (23.9)	370 (215, 639)	6.02 (4.56, 7.93)	C_{max}: 1.29 (0.43, 3.87) C_0: 1.21 (0.36, 4.03)

Root mean square error on the log-scale from mixed effects model = 0.46, 0.53 for AUC, 1.11, 1.11 for C_{max} and 1.25 for C_0

[a] Back-transformed least squares mean and 95% confidence interval from mixed effects model performed on natural log-transformed values

[b] Harmonic mean; jackknife SD

[c] Back-transformed least squares mean difference and 90% confidence interval from mixed effects model performed on natural log-transformed values

determined for Japanese patients with relapsed or refractory MM. The dose combination consisting of vorinostat at 400 mg administered orally on Days 1 through 14, with bortezomib at 1.3 mg/m^2 administered intravenously on Days 1, 4, 8, and 11 was generally safe and well-tolerated in these patients. However, in this phase I study of Japanese patients, 2 patients who were refractory to bortezomib experienced Grade 4 thrombocytopenia after study initiation and this result raised safety concerns about the treatment of bortezomib-refractory patients, prompting a protocol amendment to include only patients who were not considered refractory to bortezomib. These data suggested Japanese MM patients who were considered refractory to bortezomib were possibly intolerant to vorinostat combined with bortezomib at the recommended doses. The dose combination also elicited an objective clinical response in 3 of the 7 patients with relapsed and/or refractory MM who were considered not refractory to bortezomib. While the present study was ongoing, the same vorinostat and bortezomib dose combination was being evaluated and showed moderate efficacy in 2 international studies of patients with relapsed/refractory MM in which Japanese patients were not enrolled; the phase IIb open-label, single arm VANTAGE 095 study of bortezomib-refractory patients and the phase III randomized, double-blind, placebo-controlled VANTAGE 088 study of patients not refractory to bortezomib [13, 19]. Although Japanese patients had not been enrolled in the VANTAGE 095 study, enrollment was planned after the completion of the present phase I study.

The frequency and types of AEs commonly reported by the patients in the current study, including neutropenia, fatigue, diarrhea, nausea, and vomiting, correspond to the most frequently encountered AEs reported in previous trials of vorinostat and bortezomib as single agents and as combination therapies [13, 19–24]. High-grade thrombocytopenia was also seen in previous vorinostat and bortezomib trials and has been reported to be largely manageable in some [20–24]. The VANTAGE 088 study noted an increased rate of thrombocytopenia in the vorinostat plus bortezomib arm compared with the bortezomib monotherapy arm [19]. Although Grade ≥3 thrombocytopenia occurred in all patients in the present study, it was transient and manageable. The results of the present study support previously published findings that the combination of vorinostat with bortezomib, administered at the recommended dosing regimen, is generally safe and well-tolerated [12, 14].

In the present study, the vorinostat t_{max} and $t_{1/2}$ on Day 11 were not markedly different from the values for Day 1 and no increase in vorinostat trough concentration was observed after multiple dosing. These results suggested that serum vorinostat pharmacokinetics had reached steady-state by Day 11. Of note, vorinostat administered with bortezomib led to a somewhat lower t_{max} compared with t_{max}

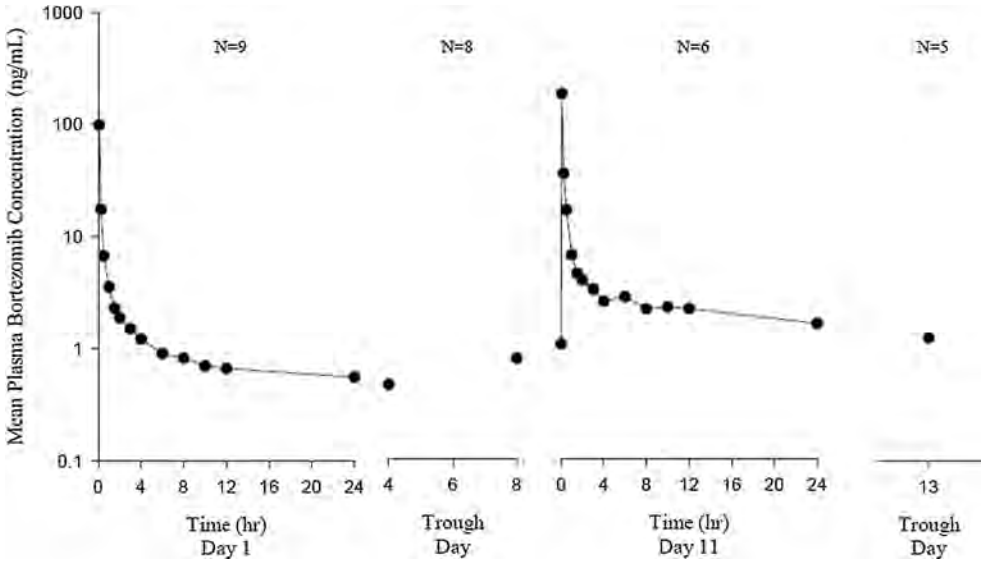

Fig. 3 Mean plasma concentration versus time profile of bortezomib following administration (semi-logarithmic scale)

values reported for vorinostat alone in previous studies [20, 21, 24]. However, the values obtained in the current study for $AUC_{0–24\ h}$ and C_{max} fell within the range of mean values reported in previous clinical studies with vorinostat administered alone, as did the mean $t_{1/2}$ [20, 21, 24]. Moreover, the geometric mean $AUC_{0–24\ h}$ and C_{max} accumulation ratios determined here for vorinostat were generally consistent with steady-state values previously reported for once daily administration of 400 mg vorinostat alone [20, 21, 24]. Collectively, these data suggest that bortezomib co-administration does not significantly affect vorinostat pharmacokinetics.

Conversely, the combination of vorinostat and bortezomib resulted in modest bortezomib accumulation, although the plasma bortezomib concentration versus time profile (i.e., the rapid distribution phase followed by a slow elimination phase) was consistent with that observed in previous trials in the absence of vorinostat [6, 12]. AUC values observed on Days 1 and 11 were consistent with those previously reported by Reece et al. [15] but higher than those reported by Ogawa et al. [6]. However, the high inter-subject variability in the bortezomib pharmacokinetic analysis combined with the small sample size of patients in the present study preclude any robust conclusion regarding whether the presence of vorinostat alters the plasma pharmacokinetics of bortezomib. Nevertheless, the volume distribution of bortezomib during the elimination phase also suggests good tissue penetration.

In conclusion, the results of this phase I clinical trial demonstrated that combination therapy with vorinostat and bortezomib was generally safe and well-tolerated in Japanese patients with relapsed and/or refractory MM who were not considered refractory to bortezomib. Based on the results of this study, the recommended dosing for this patient population is vorinostat 400 mg daily on Days 1 through 14 and bortezomib 1.3 mg/m^2 on Days 1, 4, 8, and 11 of each 21-day treatment cycle.

Acknowledgments The authors would like to thank the patients who participated in this study and their families, as well as the other treating physicians, clinical research coordinators, and operations staff. Medical writing and editorial assistance were provided by Susan Quiñones, PhD of ApotheCom, Yardley, PA, USA, which was funded by Merck and Co., Inc., Kenilworth, NJ, USA. Editorial assistance was provided by Kristen Lewis and Carol Zecca of Merck and Co., Inc., Kenilworth, NJ, USA.

Compliance with ethical standards

Funding Funding for this study was provided by MSD K.K., Tokyo, Japan.

Conflict of interest Dr. Watanbe reports personal fees from Takeda Pharmaceutical Co., Ltd., personal fees from Eisai Co., Ltd., personal fees from Daiichi Sankyo Co., Ltd., personal fees from Celgene K.K., personal fees from Nippon Shinyaku Co., Ltd., personal fees from Nippon Kayaku Co., Ltd., personal fees from Zenyaku Kogyo Co., Ltd., outside the submitted work. Drs. Ogawa, Ogura, Tobinai, Ando, Suzuki, Ohmachi, Uchida, and Hotta report no conflicts of interest. Mary E. Hanson is an employee of Merck and Co., Inc., and may own stock or hold stock options in the company. Yoshinobu Tanaka, Yasuhiro Koh, and Takashi Shimamoto are employees of MSD KK and may own stock or hold stock options in the company.

References

1. Ferlay J, Shin HR, Bray F, Forman D, Mathers C, Parkin DM. Estimates of worldwide burden of cancer in 2008: GLOBOCAN 2008. Int J Cancer. 2010;127:2893–917.
2. Kumar SK, Lee JH, Lahuerta JJ, Morgan G, Richardson PG, Crowley J, Haessler J, Feather J, Hoering A, Moreau P, LeLeu X, Hulin C, Klein SK, Sonneveld P, Siegel D, Blade J, Goldschmidt H, Jagannath S, Miguel JS, Orlowski R, Palumbo A, Sezer O,

Rajkumar SV, Durie BG. Risk of progression and survival in multiple myeloma relapsing after therapy with IMiDs and bortezomib: a multicenter international myeloma working group study. Leukemia. 2012;26:149–57.
3. Chen D, Frezza M, Schmitt S, Kanwar J, Dou QP. Bortezomib as the first proteasome inhibitor anticancer drug: current status and future perspectives. Curr Cancer Drug Targets. 2011;11:239–53.
4. Kapoor P, Ramakrishnan V, Rajkumar SV. Bortezomib combination therapy in multiple myeloma. Semin Hematol. 2012;49:228–42.
5. Richardson PG, Barlogie B, Berenson J, Singhal S, Jagannath S, Irwin D, Rajkumar SV, Srkalovic G, Alsina M, Alexanian R, Siegel D, Orlowski RZ, Kuter D, Limentani SA, Lee S, Hideshima T, Esseltine DL, Kauffman M, Adams J, Schenkein DP, Anderson KC. A phase 2 study of bortezomib in relapsed, refractory myeloma. N Engl J Med. 2003;348:2609–17.
6. Ogawa Y, Tobinai K, Ogura M, Ando K, Tsuchiya T, Kobayashi Y, Watanabe T, Maruyama D, Morishima Y, Kagami Y, Taji H, Minami H, Itoh K, Nakata M, Hotta T. Phase I and II pharmacokinetic and pharmacodynamic study of the proteasome inhibitor bortezomib in Japanese patients with relapsed or refractory multiple myeloma. Cancer Sci. 2008;99:140–4.
7. Satoh M, Oguro R, Yamanaka C, Takada K, Matsuura Y, Akiba T, Aotsuka N, Tani Y, Wakita H. Clinical assessment of bortezomib for multiple myeloma in comparison with thalidomide. J Pharm Pharm Sci. 2011;14:78–89.
8. Hideshima T, Richardson PG, Anderson KC. Mechanism of action of proteasome inhibitors and deacetylase inhibitors and the biological basis of synergy in multiple myeloma. Mol Cancer Ther. 2011;10:2034–42.
9. Ruefli AA, Ausserlechner MJ, Bernhard D, Sutton VR, Tainton KM, Kofler R, Smyth MJ, Johnstone RW. The histone deacetylase inhibitor and chemotherapeutic agent suberoylanilide hydroxamic acid (SAHA) induces a cell-death pathway characterized by cleavage of Bid and production of reactive oxygen species. Proc Natl Acad Sci USA. 2001;98:10833–8.
10. Pei XY, Dai Y, Grant S. Synergistic induction of oxidative injury and apoptosis in human multiple myeloma cells by the proteasome inhibitor bortezomib and histone deacetylase inhibitors. Clin Cancer Res. 2004;10:3839–52.
11. Richardson P, Mitsiades C, Colson K, Reilly E, McBride L, Chiao J, Sun L, Ricker J, Rizvi S, Oerth C, Atkins B, Fearen I, Anderson K, Siegel D. Phase I trial of oral vorinostat (suberoylanilide hydroxamic acid, SAHA) in patients with advanced multiple myeloma. Leuk Lymphoma. 2008;49:502–7.
12. Badros A, Burger AM, Philip S, Niesvizky R, Kolla SS, Goloubeva O, Harris C, Zwiebel J, Wright JJ, Espinoza-Delgado I, Baer MR, Holleran JL, Egorin MJ, Grant S. Phase I study of vorinostat in combination with bortezomib for relapsed and refractory multiple myeloma. Clin Cancer Res. 2009;15:5250–7.
13. Siegel DS, Dimopoulos MA, Yoon SS, Laubach JP, Goldschmidt H, Reece D, LeLeu X, Durrant S, Offner S, Cavo M, et al. Vantage 095: vorinostat in combination with bortezomib in salvage multiple myeloma patient: final study results of a global phase 2b trial (abstract). Blood. 2011;118:480.
14. Weber DM, Graef T, Hussein M, Sobecks RM, Schiller GJ, Lupinacci L, Hardwick JS, Jagannath S. Phase I trial of vorinostat combined with bortezomib for the treatment of relapsing and/or refractory multiple myeloma. Clin Lymphoma Myeloma Leuk. 2012;12:319–24.
15. Reece DE, Sullivan D, Lonial S, Mohrbacher AF, Chatta G, Shustik C, Burris H III, Venkatakrishnan K, Neuwirth R, Riordan WJ, Karol M, von Moltke LL, Acharya M, Zannikos P, Keith SA. Pharmacokinetic and pharmacodynamic study of two doses of bortezomib in patients with relapsed multiple myeloma. Cancer Chemother Pharmacol. 2011;67:57–67.
16. Blade J, Samson D, Reece D, Apperley J, Bjorkstrand B, Gahrton G, Gertz M, Giralt S, Jagannath S, Vesole D. Criteria for evaluating disease response and progression in patients with multiple myeloma treated by high-dose therapy and haemopoietic stem cell transplantation. Myeloma subcommittee of the EBMT. European Group for Blood and Marrow Transplant. Br J Haematol. 1998;102:1115–23.
17. International Myeloma Working Group. Criteria for the classification of monoclonal gammopathies, multiple myeloma and related disorders: a report of the International Myeloma Working Group. Br J Haematol. 2003;121:749–57.
18. Durie BG, Harousseau JL, Miguel JS, Blade J, Barlogie B, Anderson K, Gertz M, Dimopoulos M, Westin J, Sonneveld P, Ludwig H, Gahrton G, Beksac M, Crowley J, Belch A, Boccadaro M, Cavo M, Turesson I, Joshua D, Vesole D, Kyle R, Alexanian R, Tricot G, Attal M, Merlini G, Powles R, Richardson P, Shimizu K, Tosi P, Morgan G, et al. International uniform response criteria for multiple myeloma. Leukemia. 2006;20:1467–73.
19. Dimopoulos M, Siegel DS, Lonial S, Qi J, Hajek R, Facon T, Rosinol L, Williams C, Blacklock H, Goldschmidt H, Hungria V, Spencer A, Palumbo A, Graef T, Eid JE, Houp J, Sun L, Vuocolo S, Anderson KC. Vorinostat or placebo in combination with bortezomib in patients with multiple myeloma (VANTAGE 088): a multicentre, randomised, double-blind study. Lancet Oncol. 2013;14:1129–40.
20. Doi T, Hamaguchi T, Shirao K, Chin K, Hatake K, Noguchi K, Otsuki T, Mehta A, Ohtsu A. Evaluation of safety, pharmacokinetics, and efficacy of vorinostat, a histone deacetylase inhibitor, in the treatment of gastrointestinal (GI) cancer in a phase I clinical trial. Int J Clin Oncol. 2013;18:87–95.
21. Fujiwara Y, Yamamoto N, Yamada Y, Yamada K, Otsuki T, Kanazu S, Iwasa T, Hardwick JS, Tamura T. Phase I and pharmacokinetic study of vorinostat (suberoylanilide hydroxamic acid) in Japanese patients with solid tumors. Cancer Sci. 2009;100:1728–34.
22. Jagannath S, Barlogie B, Berenson J, Siegel D, Irwin D, Richardson PG, Niesvizky R, Alexanian R, Limentani SA, Alsina M, Adams J, Kauffman M, Esseltine DL, Schenkein DP, Anderson KC. A phase 2 study of two doses of bortezomib in relapsed or refractory myeloma. Br J Haematol. 2004;127:165–72.
23. Petrucci MT, Giraldo P, Corradini P, Teixeira A, Dimopoulos MA, Blau IW, Drach J, Angermund R, Allietta N, Broer E, Mitchell V, Blade J. A prospective, international phase 2 study of bortezomib retreatment in patients with relapsed multiple myeloma. Br J Haematol. 2013;160:649–59.
24. Wada H, Tsuboi R, Kato Y, Sugaya M, Tobinai K, Hamada T, Shimamoto T, Noguchi K, Iwatsuki K. Phase I and pharmacokinetic study of the oral histone deacetylase inhibitor vorinostat in Japanese patients with relapsed or refractory cutaneous T-cell lymphoma. J Dermatol. 2012;39:823–8.

Int J Hematol (2015) 101:286–294
DOI 10.1007/s12185-015-1743-y

ORIGINAL ARTICLE

Phase 1 study in Japan of siltuximab, an anti-IL-6 monoclonal antibody, in relapsed/refractory multiple myeloma

Kenshi Suzuki · Michinori Ogura · Yu Abe · Tatsuya Suzuki · Kensei Tobinai · Kiyoshi Ando · Masafumi Taniwaki · Dai Maruyama · Minoru Kojima · Junya Kuroda · Meguru Achira · Koho Iizuka

Received: 18 August 2014 / Revised: 8 January 2015 / Accepted: 15 January 2015 / Published online: 6 February 2015

Abstract Siltuximab, a chimeric monoclonal antibody with high affinity and specificity for interleukin-6, has been shown to enhance anti-multiple myeloma activity of bortezomib and corticosteroid in vitro. We evaluated the safety, pharmacokinetics, immunogenicity, and antitumor effect of siltuximab in combination with bortezomib and dexamethasone in Japanese patients with relapsed or refractory multiple myeloma. This open-label, phase 1, dose-escalating study used two doses of siltuximab: 5.5 and 11.0 mg/kg (administered on day 1 of each 21-day cycle). In total, nine patients were treated. The most common grade 3/4 adverse events, lymphopenia (89 %) and thrombocytopenia (44 %), occurred in patients receiving both doses of siltuximab; however, no dose-limiting toxicities (DLTs) were observed. Following intravenous administration of siltuximab at 5.5 and 11.0 mg/kg, the maximum serum concentration and the area under the curve from 0 to 21 days and from 0 to infinity increased in an approximately dose-proportional manner. Mean half-life, total systemic clearance, and volume of distribution were similar at doses of 5.5 and 11.0 mg/kg. Across both doses, six of the nine patients had complete or partial response (22 and 44 %, respectively). In conclusion, as no DLT was observed, the recommended dose for this combination is 11.0 mg/kg once every 3 weeks. The study is registered at http://www.clinicaltrials.gov as NCT01309412.

Keywords Bortezomib · Dexamethasone · Interleukin 6 · Multiple myeloma · Siltuximab

K. Suzuki (✉) · Y. Abe
Department of Hematology, Japanese Red Cross Medical Center, Hiroo 4-1-22 Shibuya-ku, Tokyo 1508935, Japan
e-mail: ken-suzuki@mtb.biglobe.ne.jp

M. Ogura · T. Suzuki
Department of Hematology and Oncology, Nagoya Daini Red Cross Hospital, Nagoya, Japan

K. Tobinai · D. Maruyama
Department of Hematology, National Cancer Center Hospital, Tokyo, Japan

K. Ando · M. Kojima
Department of Hematology and Oncology, Tokai University School of Medicine, Isehara, Japan

M. Taniwaki · J. Kuroda
Division of Hematology and Oncology, Department of Medicine, Kyoto Prefectural University of Medicine, Kyoto, Japan

M. Achira
Clinical Pharmacology Department, Quantitative Science Division, Research and Development, Janssen Pharmaceutical K.K., Tokyo, Japan

K. Iizuka
Oncology Department, Clinical Science Division, Research and Development, Janssen Pharmaceutical K.K., Tokyo, Japan

Introduction

Multiple myeloma is a B cell malignancy characterized by excessive malignant plasma cells in bone marrow as well as increased serum and urine monoclonal protein (M-protein) [1]. Clinical manifestations of multiple myeloma include bone disease, renal dysfunction, hypercalcemia, cytopenia, hyperviscosity, and peripheral neuropathy [2]. Proteasome inhibitors, such as bortezomib, have improved outcomes as induction and maintenance treatments, yet a majority of patients experience relapses and become refractory [3, 4].

The pleiotropic cytokine interleukin-6 (IL-6) is thought to play a central role in the pathogenesis of multiple myeloma. It is involved in the proliferation, differentiation, and

survival of malignant plasma cells [5–7]. Siltuximab is a chimeric, human–murine, monoclonal antibody with high affinity and specificity for IL-6. It has been investigated through clinical studies in patients with multiple myeloma, Castleman's disease, and other lymphomas. In multicentric Castleman's disease, siltuximab, with a recommended dose of 11 mg/kg every 3 weeks, has shown evidence of efficacy by blocking IL-6 activity [8–10].

In vitro preclinical studies have demonstrated that the combination of siltuximab and bortezomib has an additive to a synergistic effect in inducing apoptosis in multiple myeloma cell lines. The cancer cells respond to the proapoptotic effects of proteasome inhibitors with survival pathways that can include antiapoptotic myeloid cell leukemia (Mcl)-1 protein and heat shock proteins (HSPs). IL-6 upregulates these pathways in myeloma cells, and reduction of IL-6 could reduce their interference with bortezomib's proapoptotic effects [11]. Overcoming IL-6-mediated cell resistance by an IL-6 antagonist may also augment the effectiveness of corticosteroids in treating multiple myeloma. IL-6 can protect multiple myeloma cells from apoptosis induced by corticosteroids and chemotherapeutics [12–15]. Siltuximab increased the sensitivity of myeloma cells to dexamethasone in vitro, and in combination with dexamethasone, reduced patient tumor cell viability [12, 16].

Given the preclinical results, anti-IL-6-directed treatment is a logical addition to bortezomib and dexamethasone. The current study was conducted in Japan to evaluate the safety and tolerability of siltuximab up to 11.0 mg/kg in combination with bortezomib and dexamethasone in patients with relapsed/refractory multiple melanoma. Additionally, the pharmacokinetics (PK), immunogenicity, and preliminary efficacy of siltuximab were evaluated.

Materials and methods

Study design

This was a nonrandomized, open-label, dose-escalating, phase 1 study in patients who had relapsed/refractory multiple myeloma (http://www.clinicaltrials.gov; NCT01309412). The study was conducted in accordance with the Declaration of Helsinki and Good Clinical Practices and was approved by the institutional review board at each participating institution. Two doses of siltuximab were evaluated: 5.5 and 11.0 mg/kg. The initial siltuximab dose level of 5.5 mg/kg, which is lower than the maximum dose in earlier dose-finding studies [10, 17], was selected for this study from a safety standpoint. The rationale for selecting siltuximab 11.0 mg/kg every 3 weeks was due to previous findings of effective response rates in patients with Castleman's disease [4]. Siltuximab was administered intravenously over 1 h on day 1, after administration of bortezomib and dexamethasone during a 21-day cycle. Bortezomib was administered intravenously at 1.3 mg/m^2 on days 1, 4, 8, and 11 of each cycle, followed by a 10-day rest period. In the ninth or subsequent cycles of treatment, bortezomib was administered once weekly (days 1 and 8) followed by a 13-day rest period (days 9–21). Dexamethasone was administered orally at 20 mg four times weekly (days 1, 2, 4, 5, 8, 9, 11, and 12) with a 9-day rest period. In the ninth or subsequent cycles of treatment, the dosing regimen for dexamethasone was changed to twice-weekly oral administration of 10 mg (days 1, 2, 8, and 9) followed by a 12-day rest period (days 10–21). After the recommended dose of 11.0 mg/kg was determined, those patients whose starting dose was 5.5 mg/kg and who had not achieved complete response (CR) were escalated to 11.0 mg/kg in the next cycle based on the patient's willingness to proceed and the investigator's discretion. This study was not designed to estimate the maximum tolerated dose. Doses were withheld or reduced if patients could not tolerate therapy (Table 1). Administration was repeated in cycles of 21 days until disease progression. Up to 15 patients were planned for enrollment in the study: up to six patients were considered for the 5.5 mg/kg dose and up to nine patients were considered for the 11.0 mg/kg dose.

Eligibility

Eligible patients had to be 20 years of age or older, have symptomatic or nonsecretory multiple myeloma according to the International Myeloma Working Group criteria [18], have previously received 1–3 treatments for multiple

Table 1 Treatment withheld or reduced

Treatment	First dose reduction	Second dose reduction
Siltuximab (all cycles)	No dose reduction allowed*	–
Bortezomib 1.3 mg/m^2 (all cycles)	Bortezomib 1.0 mg/m^2	Bortezomib 0.7 mg/m^2
Dexamethasone 20 mg (cycles 1–8)	Dexamethasone 10 mg	No (further) dose reduction allowed*
Dexamethasone 10 mg (cycles ≥9)	No dose reduction allowed*	–

*As no dose reduction was allowed, protocol was to discontinue all the therapies (siltuximab, bortezomib, and dexamethasone)

myeloma and had relapsed or been refractory (less than minimal response, or disease progression within 2 months of last dose) after the most recent regimen. Patients were also included if they had a measurable lesion (generally, serum immunoglobulin G [IgG] or serum immunoglobulin M [IgM] M-protein ≥1.0 g/dL; serum immunoglobulin A [IgA] M-protein ≥0.5 g/dL; serum immunoglobulin D [IgD] M-protein ≥0.05 g/dL; or serum immunoglobulin E [IgE] M-protein ≥50 IU/mL). For nonsecretory multiple myeloma, measurable lesions were defined as patients with a soft tissue mass (plasmacytoma) that could be measured in two dimensions as longest diameter ≥2 cm with an appropriate diagnostic imaging technique (computed tomography or magnetic resonance imaging). Additionally, patients were eligible if they had an Eastern Cooperative Oncology Group performance status of 0–2; adequate hematologic function (absolute neutrophil count ≥1,000/mm^3, hemoglobin ≥8 g/dL, platelet count ≥50,000/mm^3); adequate hepatic function (aspartate aminotransferase and alanine aminotransferase ≤2.5 times the upper limit of normal, total bilirubin ≤1.5 mg/dL); corrected serum calcium <12.5 mg/dL; and adequate renal function (creatinine clearance [CrCL] ≥20 mL/min).

Patients were excluded if they had a condition in which M-protein was present in the absence of a clonal plasma cell infiltration with lytic bone lesions; peripheral neuropathy (grade 1 with pain or ≥ grade 2); previous IL-6 therapy; previous poor response to bortezomib due to its toxicity; an allogeneic stem cell transplantation within 28 days prior to study treatment; or major surgery, chemotherapy, plasmapheresis, or radiation therapy within 21 days before study treatment. Patients who had significant respiratory illnesses (pneumonitis, interstitial pneumonia, or pulmonary fibrosis); significant cardiac disease; significant concomitant illnesses (including human immunodeficiency virus); or any condition that the investigators found inappropriate were also excluded. Concomitant therapy with other anticancer therapies, live attenuated vaccines, systemic corticosteroids, or other therapies the investigators found unsuitable were not allowed. Informed consent was obtained from each patient before study enrollment.

Assessment of safety

Safety evaluations included adverse events (AEs); laboratory tests (hematology, blood chemistry, lipid panel, urinalysis, and blood coagulation); pregnancy test; electrocardiogram; chest X-ray; vital signs (body temperature, pulse rate, and blood pressure); and body weight. All AEs were graded according to National Cancer Institute Common Terminology Criteria for Adverse Events Version 4.0.

Definition of dose-limiting toxicity

Dose-limiting toxicity (DLT) was evaluated for 21 days after the first administration of siltuximab by the study evaluation team, which comprised all principal investigators and the sponsor's responsible medical officer. A DLT was defined as any nonhematologic toxicity of grade 3 or higher whose causal relationship to siltuximab could not be denied. Any toxicity thought to be controllable by supportive therapy (i.e., reversible to grade 1 or pretreatment grade within 3 days after any appropriate measure was taken) was not regarded as a DLT. Hematologic DLT included grade 4 neutropenia lasting more than 1 week, febrile neutropenia, and grade 4 thrombocytopenia lasting more than 1 week, or associated with hemorrhage. Thrombocytopenia with platelet transfusion, regardless of any grade, was also regarded as a DLT.

Siltuximab PK evaluation

During cycle 1, samples were collected predose and immediately, 4, and 6 h after administration on day 1 and on days 2, 4, 8, and 15. During cycles 2, 3, 4, and 5, samples were collected on day 1 before and immediately after siltuximab administration. During cycle 6, samples were collected on day 1 before administration. Serum concentrations of siltuximab were measured using a validated electro-chemiluminescence immunoassay method (lower limit of quantification: 0.045 μg/mL).

Noncompartmental analysis was conducted to calculate siltuximab PK parameters using Phoenix®WinNonlin® Version 6.2.1. (Pharsight Corp./Certara, St. Louis, MO, USA). In cycle 1, area under the serum concentration–time curve (AUC) from day 0 to 21 ($AUC_{0–21days}$) and AUC from 0 to infinity (AUC_{∞}) was calculated using the log-linear trapezoidal method. Terminal half-life ($t_{1/2}$) was determined using linear regression of log-transformed siltuximab concentration–time profile at the terminal phase of disposition. Maximum observed concentration (C_{max}), total systemic clearance (CL), and volume of distribution at terminal phase (Vd_z) were also calculated using standard noncompartmental analysis methods.

Immunogenicity evaluation

Serum samples for immunogenicity were collected predose on day 1 of cycle 1; at the time of discontinuation (end of treatment); and at 30 days, 8 weeks, and 12 weeks after the last administration of siltuximab. A validated and specific enzyme immunoassay method was used to detect anti-siltuximab antibodies in serum.

Assessment of efficacy

Antitumor response was assessed by the investigator based on findings obtained before the start of treatment and at the time of completion of an even number of cycles, or at the time of discontinuation, according to the European Group for Blood and Marrow transplantation (EBMT) criteria for assessment of multiple myeloma antitumor effect [19].

Statistical populations

Patients who received ≥1 dose of study drug were included in the safety population. The PK, immunogenicity, and efficacy population comprised all patients who received ≥1 administration of siltuximab and who had ≥1 appropriate postdose samples for serum concentration, immunogenicity, and efficacy evaluation, respectively.

Results

Patient demographics and characteristics

A total of 10 patients consented to participate in the study; nine patients were eligible and received ≥1 dose of siltuximab. Three patients received 5.5 mg/kg and the next six patients received 11.0 mg/kg of siltuximab (Fig. 1). All patients were Japanese with a median age of 66 years. Additional patient characteristics are summarized in Table 2. All patients had received one or two prior treatments for multiple myeloma, including proteasome inhibitors and immunomodulatory agents. No patients, however, received prior radiotherapy (Table 3).

Treatment compliance

Patients were 100 and >96 % compliant with siltuximab and all study treatments, respectively. The median exposure in days to siltuximab, bortezomib, and dexamethasone was 211 (range 22–549); 218 (range 29–556); and 219 (range 33–557), respectively.

Safety

There were no appreciable differences in the safety profiles between the two treatment groups for frequency (Table 4). There were no deaths during this study. Across all grades of severity, hematologic and gastrointestinal AEs were the most common, which all patients experienced. However, hematologic abnormalities were typically transient. The most common nonhematologic AEs across all grades included diarrhea and abnormal hepatic function (56 % each). One patient treated with 5.5 mg/kg of siltuximab experienced grade 3 pneumonia (confirmed to be caused due to *pseudomonas aeruginosa*) on day 22 of cycle 6, which was considered possibly related to siltuximab. After intravenous antibiotics, the pneumonia resolved, the patient's lung function improved, and clinical symptoms disappeared. Three patients treated with 11.0 mg/kg of siltuximab each had a serious AE (SAE): alveolitis allergic, interstitial lung disease, and colon cancer. The grade 1 interstitial lung disease abnormality occurred from

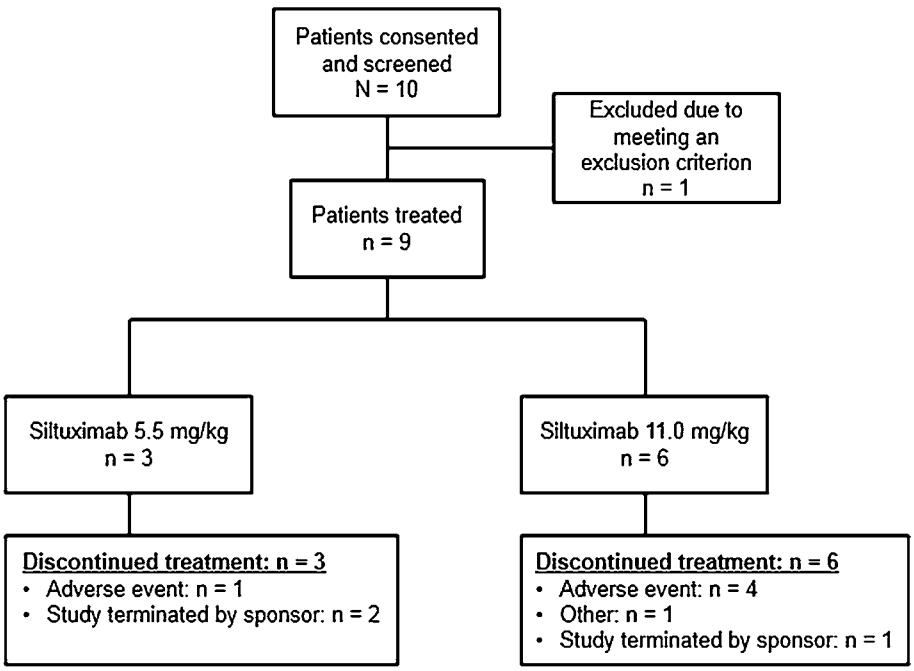

Fig. 1 CONSORT diagram

Table 2 Baseline characteristics and patient disposition

	Siltuximab 5.5 mg/kg ($n = 3$)	Siltuximab 11.0 mg/kg ($n = 6$)	All patients ($n = 9$)
Sex, *n* (%)			
Male	1 (33)	4 (67)	5 (56)
Female	2 (67)	2 (33)	4 (44)
Age (year)			
Mean ± SD	63.3 ± 8.1	65.8 ± 4.1	65.0 ± 5.3
Median (range)	67 (54, 69)	65 (61, 73)	66 (54, 73)
Type of myeloma, *n* (%)			
IgG	2 (67)	4 (67)	6 (67)
IgA	1 (33)	1 (17)	2 (22)
Bence Jones	0 (0)	1 (17)	1 (11)
Serum M-protein (g/dL)			
Mean ± SD	1.3 ± 0.1	2.3 ± 1.1	1.9 ± 1.0
Median (range)	1.3 (1.2, 1.3)	2.4 (0.5, 3.3)	1.8 (0.5, 3.3)
Duration since diagnosis (year)			
Mean ± SD	4.2 ± 2.7	1.9 ± 1.4	2.7 ± 2.1
Median (range)	4.8 (1.3, 6.6)	1.4 (0.2, 4.3)	1.5 (0.2, 6.6)
ECOG performance scale, *n* (%)			
0	3 (100)	3 (50)	6 (67)
1	0 (0)	3 (50)	3 (33)
β_2-microglobulin (mg/L)			
Mean ± SD	2.3 ± 0.4	3.8 ± 2.3	3.3 ± 2.0
Albumin, g/dL			
Mean ± SD	3.8 ± 0.2	3.7 ± 0.4	3.7 ± 0.3
KL-6, U/mL			
Mean ± SD	244.0 ± 102.3	207.8 ± 128.8	219.9 ± 115.4
ISS staging, *n* (%)			
I	3 (100)	2 (33)	5 (56)
II	0 (0)	2 (33)	2 (22)
III	0 (0)	2 (33)	2 (22)
Creatinine clearance (mL/min)			
Mean ± SD	75.5 ± 15.1	86.2 ± 30.7	82.6 ± 26.0

ECOG Eastern Cooperative Oncology Group, *Ig* immunoglobulin, *ISS* International Staging System, *KL-6* Krebs von den Lungen-6, *SD* standard deviation

Table 3 Prior multiple myeloma therapy

Prior therapy	Siltuximab 5.5 mg/kg ($n = 3$)	Siltuximab 11.0 mg/kg ($n = 6$)	All patients ($n = 9$)
Number of prior therapeutic MM regimens, *n* (%)			
1	2 (67)	3 (50)	5 (56)
2	1 (33)	3 (50)	4 (44)
Chemotherapy, *n* (%)			
Patients with any prior proteasome inhibitors	0 (0)	1 (17)	1 (11)
Patients with any prior immunomodulatory agents	0 (0)	1 (17)	1 (11)
Patients with any prior alkylating agents	3 (100)	4 (67)	7 (78)
Patients with any prior anthracyclines	2 (67)	4 (67)	6 (67)
Patients with any prior corticosteroids	3 (100)	6 (100)	9 (100)
Patients with any prior ASCT	1 (33)	1 (17)	2 (22)
Patients with any prior vinca alkaloid	2 (67)	4 (67)	6 (67)

ASCT autologous stem cell transplant, *MM* multiple myeloma

Table 4 Incidence and severity of adverse events of all grades (≥35 %) and grades 3/4 (≥35 %)

Adverse event	Siltuximab 5.5 mg/kg ($n = 3$)	Siltuximab 11.0 mg/kg ($n = 6$)	All patients ($n = 9$)
All adverse event			
All grades			
Hematologic			
Thrombocytopenia	3	6	9 (100)
Leukopenia	3	5	8 (89)
Lymphopenia	3	5	8 (89)
Neutropenia	2	5	7 (78)
Anemia	2	3	5 (56)
Leukocytosis	1	4	5 (56)
Neutrophilia	1	4	5 (56)
Nonhematologic			
Diarrhea	2	3	5 (56)
Hepatic function abnormal	2	3	5 (56)
Hyperlipidemia	1	3	4 (44)
Rash	1	3	4 (44)
Grades ≥3			
Hematologic			
Lymphopenia	3	5	8 (89)
Thrombocytopenia	1	3	4 (44)
Related to siltuximab*			
Hematologic			
Thrombocytopenia	3	6	9 (100)
Leukopenia	3	5	8 (89)
Lymphopenia	3	5	8 (89)
Neutropenia	2	5	7 (78)
Anemia	2	3	5 (56)
Nonhematologic			
Hepatic function abnormal	2	2	4 (44)

Data are presented as *n* or *n* (%)

*Adverse events whose relationship to siltuximab treatment was considered doubtful, possible, probably, or very likely

day 197 to the end of treatment. The investigator assessed the causal relationship between interstitial lung disease and bortezomib as probable, and between siltuximab and dexamethasone as possible. The alveolitis allergic event was considered grade 3 and probably related to siltuximab treatment. The alveolitis was treated with a prohibited concomitant drug (Solu-Cortef). Both events resolved, but led to treatment discontinuation. The colon cancer event was unrelated to the study drug and also led to treatment discontinuation. There were no infusion-related reactions. There was no DLT with either dose of siltuximab.

Pharmacokinetics and immunogenicity

Mean serum concentration–time profiles after administration of siltuximab 5.5 and 11.0 mg/kg during cycle 1 are shown in Fig. 2. The PK parameters of siltuximab are

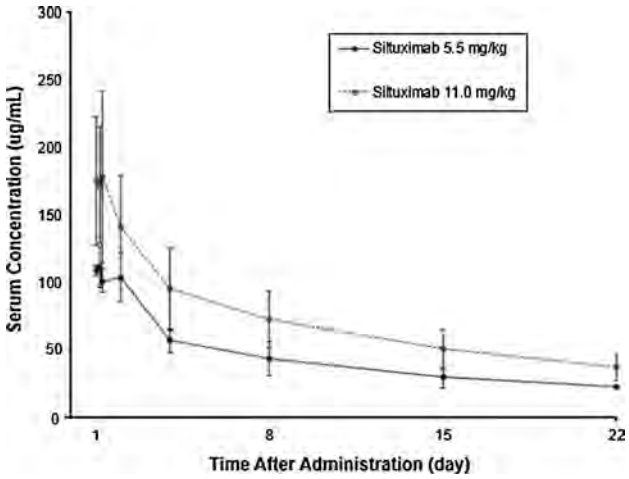

Fig. 2 Mean (± SD) serum concentration–time profiles of siltuximab by treatment in cycle 1

Table 5 Descriptive statistics for pharmacokinetic parameters of siltuximab by treatment

Parameter	Siltuximab 5.5 mg/kg ($n = 3$)	Siltuximab 11.0 mg/kg ($n = 6$)
C_{max} (μg/mL)	118.2 (8.78)	194.3 (52.46)
$AUC_{0–21days}$ (μg day/mL)	886.0 (197.75)	1,548.1 (324.14)†
AUC_{∞} (μg day/mL)	1347.0 (445.83)	2,273.9 (567.74)†
$t_{½}$ (day)	14.0 (2.73)	13.2 (3.86)†
CL (mL/day/kg)	4.406 (1.4922)	5.081 (1.2389)†
Vd_z (mL/kg)	84.90 (11.984)	94.29 (27.986)†

Data are presented as mean (standard deviation)

$AUC_{0-21\ days}$ area under the concentration time curve from time 0–21 days, *AUC_{∞}* area under the concentration time curve from time 0 to infinity, *CL* total systemic clearance of drug after intravenous administration, *C_{max}* maximum observed serum concentration, *$t_{½}$* terminal half-life, *Vd_z* volume of distribution at terminal phase

† $n = 5$

summarized in Table 5. Following the first intravenous administration of siltuximab at both 5.5 and 11.0 mg/kg, the C_{max}, $AUC_{0–21days}$, and AUC_{∞} increased in an approximate dose-proportional manner. Mean $t_{1/2}$, CL, and Vd_z values were similar in the dose range of 5.5 and 11.0 mg/kg. Steady state of siltuximab could not be adequately assessed, as samples were not collected appropriately for some cycles. None of the nine patients with appropriate samples were positive for antibodies to siltuximab.

Efficacy

Regarding the antitumor effect using EBMT criteria, one (33 %) patient had CR while two (67 %) patients had partial response (PR) with 5.5 mg/kg. At a dose of 11.0 mg/kg, one (17 %) and two (33 %) patients had CR and PR, respectively. The remaining patients in the siltuximab 11.0 mg/kg group had no change [three (50 %)].

Discussion

Multiple myeloma remains an incurable disease, despite improvements in therapy in recent years [20]. Most patients experience relapses and develop refractory disease [4]. Due to resistance conferred by IL-6, proteasome inhibitors and corticosteroid treatments alone result in a poor response [11, 14, 21]. The addition of an IL-6 inhibitor to proteasome inhibitors and corticosteroid treatments has shown synergy in reduction of multiple myeloma cells in preclinical and clinical studies [22]. This study was conducted to evaluate the safety and tolerability as well as the PK, immunogenicity, and preliminary efficacy of siltuximab.

While all patients in this study had treatment-related AEs, no DLT was observed in either dose of siltuximab. The most common AEs were hematological and gastroenterological disorders. This finding is in line with the results of a phase 2 study conducted in the United States and The Netherlands, where patients with relapsed or refractory multiple myeloma received siltuximab 6 mg/kg (actual dose of 5.5 mg/kg, based upon drug product vial) on days 1 and 15 of 28-day cycles with or without dexamethasone. Hematological AEs were of less severity in the phase 2 study [4]. Infections in the current study did not seem to be dose dependent, as there were more infection-related events in the treatment group receiving the lower dose of siltuximab. In the phase 2 study, infections including upper respiratory infection, cellulitis, and pneumonia occurred in 57 % of dexamethasone combination-treated patients, and 18 % of patients experienced ≥3 grade infections [4]. Results from another phase 2 study in patients with multiple myeloma treated with bortezomib plus either placebo or siltuximab demonstrated only a difference of 17 % in grade 3 and higher infections between the two treatment arms [23]. However, preclinical investigation showed minor and/or transient reductions in lymphocyte activities after treatment of cynomolgus monkeys with siltuximab (unpublished observations). IL-6 has an important role in immune response, and inhibition of IL-6 may further increase the risk of infection in patients immunocompromised by advanced multiple myeloma plus treatment with bortezomib or dexamethasone. Therefore, careful surveillance of infection-related toxicity during siltuximab-based therapy is warranted.

The PK parameters were similar to an earlier phase 1 study conducted in the United States in which patients received siltuximab 12 mg/kg (actual dose of 11 mg/kg, based upon drug product vial) every 3 weeks by 1-hour intravenous infusion [10]. Regarding immunogenicity, similar to the preceding phase 1 study [10], no antibodies to siltuximab were detected in any of the nine patient samples in this study.

Preliminary efficacy data were available as six of the nine patients, across both doses, had CR or PR (22 and

44 %, respectively) with the combination treatment. In the earlier phase 1 study, two of the 13 evaluable patients (17 %) with multiple myeloma achieved CR with siltuximab as a single agent [10]. A phase 2 study in which patients received siltuximab alone or in combination with dexamethasone did not produce any CRs; however, 8/47 patients had PR (17 %) [4]. The phase 2 study in patients with siltuximab plus bortezomib and bortezomib alone demonstrated an overall response rate of 55 (CR 11 %) and 47 % (CR 7 %), respectively [23]. Despite the numerically higher response rate, combination treatment did not lead to a statistically significant improvement in progression-free survival. However, siltuximab has been shown to provide long-lasting clinical activity [10] and durable tumor and symptomatic response in multicentric Castleman's disease, where IL-6 is also an important component of pathogenesis [24], at 11 mg/kg (34 % of patients had CR or PR) [9].

From our study we confirmed the tolerability of siltuximab up to 11.0 mg/kg in combination with bortezomib and dexamethasone as well as preliminary efficacy in Japanese patients with relapsed/refractory multiple myeloma. Based on the results, we established a recommended dose of 11 mg/kg of siltuximab in combination with bortezomib and dexamethasone. This is consistent with the global single-agent recommended dose of siltuximab in multicentric Castleman's disease [9]. Siltuximab is being further investigated in earlier myeloma settings, such as smoldering myeloma, as well as in other indications including multicentric Castleman's disease.

Acknowledgments The authors thank all the patients who participated in this study and their families, the investigators, the nursing staff and study support staff from their sites, Niigata Cancer Center Hospital led by Dr. Takaaki Chou, and the employees of Janssen who contributed to the design and implementation of this study. They would also like to thank Dr. Kiyohiko Hatake of Cancer Institute Hospital for his contribution as an independent expert and Hisaya Otani of the clinical pharmacology department, Janssen Pharmaceutical K.K., who contributed to PK and immunogenicity analyses. Editorial support was sponsored by Janssen and provided by Veejaye Sinha, PharmD, of AlphaBioCom, King of Prussia, PA, USA, and Miyuki Ueda of Janssen Pharmaceutical K.K.

Conflict of interest Janssen Pharmaceutical K.K. supported this study and supplied the investigational drugs. K. Suzuki, T. Suzuki, K. Anso, D. Maruyama, M. Kojima, M. Ogura, J. Kuroda, and Y. Abe have no conflicts of interest to disclose. M. Taniwaki has received grants from Janssen Pharma, Bristol-Myers Squibb, Chugai Pharmaceutical Co., Ltd., Celgene, and Kyowa Hakko Krin Co., Ltd. M. Achira and K. Iizuka are employees of Janssen Pharmaceutical K.K., Tokyo, Japan. H. Otani was an employee of Janssen Pharmaceutical K.K.M. Ogura was at Nagoya Daini Red Cross Hospital during the study conduct, and is now affiliated with Fujita Health University and Tohoku University as well as Nagoya Daini Red Cross Hospital. K. Iizuka was at Janssen Pharmaceutical K.K. during the study conduct, and is now affiliated with Janssen Diagnostics Inc., Raritan, NJ, USA.

References

1. Hideshima T, Mitsiades C, Tonon G, Richardson PG, Anderson KC. Understanding multiple myeloma pathogenesis in the bone marrow to identify new therapeutic targets. Nat Rev Cancer. 2007;7:585–98.
2. Kyle RA, Rajkumar SV. Multiple myeloma. N Engl J Med. 2004;351:1860–73.
3. Palumbo A, Rajkumar SV. Treatment of newly diagnosed myeloma. Leukemia. 2009;23:449–56.
4. Voorhees PM, Manges RF, Sonneveld P, Jagannath S, Somlo G, Krishnan A, et al. A phase 2 multicentre study of siltuximab, an anti-interleukin-6 monoclonal antibody, in patients with relapsed or refractory multiple myeloma. Br J Haematol. 2013;161:357–66.
5. Chauhan D, Pandey P, Hideshima T, Treon S, Raje N, Davies FE, et al. SHP2 mediates the protective effect of interleukin-6 against dexamethasone-induced apoptosis in multiple myeloma cells. J Biol Chem. 2000;275:27845–50.
6. Kawano M, Hirano T, Matsuda T, Taga T, Horii Y, Iwato K, et al. Autocrine generation and requirement of BSF-2/IL-6 for human multiple myelomas. Nature. 1988;332:83–5.
7. Klein B, Zhang XG, Lu ZY, Bataille R. Interleukin-6 in human multiple myeloma. Blood. 1995;85:863–72.
8. van Rhee F, Fayad L, Voorhees P, Furman R, Lonial S, Borghaei H, et al. Siltuximab, a novel anti-interleukin-6 monoclonal antibody, for Castleman's disease. J Clin Oncol. 2010;28:3701–8.
9. Wong RS, Casper C, Munshi N, et al. A multicenter, randomized, double-blind, placebo-controlled study of the efficacy and safety of siltuximab, an anti-interleukin-6 monoclonal antibody, in patients with multicentric Castleman's Disease. Blood. 2013;122:505. https://ash.confex.com/ash/2013/webprogram/Paper58548.html.
10. Kurzrock R, Voorhees PM, Casper C, Furman RR, Fayad L, Lonial S, et al. A phase I, open-label study of siltuximab, an anti-IL-6 monoclonal antibody, in patients with B-cell non-Hodgkin lymphoma, multiple myeloma, or Castleman disease. Clin Cancer Res. 2013;19:3659–70.
11. Voorhees PM, Chen Q, Kuhn DJ, Small GW, Hunsucker SA, Strader JS, et al. Inhibition of interleukin-6 signaling with CNTO 328 enhances the activity of bortezomib in preclinical models of multiple myeloma. Clin Cancer Res. 2007;13:6469–78.
12. Voorhees PM, Chen Q, Small GW, Kuhn DJ, Hunsucker SA, Nemeth JA, et al. Targeted inhibition of interleukin-6 with CNTO 328 sensitizes pre-clinical models of multiple myeloma to dexamethasone-mediated cell death. Br J Haematol. 2009;145:481–90.
13. Rowley M, Liu P, Van Ness B. Heterogeneity in therapeutic response of genetically altered myeloma cell lines to interleukin 6, dexamethasone, doxorubicin, and melphalan. Blood. 2000;96:3175–80.
14. Hardin J, MacLeod S, Grigorieva I, Chang R, Barlogie B, Xiao H, et al. Interleukin-6 prevents dexamethasone-induced myeloma cell death. Blood. 1994;84:3063–70.
15. Lichtenstein A, Tu Y, Fady C, Vescio R, Berenson J. Interleukin-6 inhibits apoptosis of malignant plasma cells. Cell Immunol. 1995;162:248–55.
16. Balmanno K, Cook SJ. Tumour cell survival signalling by the ERK1/2 pathway. Cell Death Differ. 2009;16:368–77.
17. Angevin E, Tabernero J, Elez E, Cohen SJ, Bahleda R, van Laethem JL, et al. A phase I/II, multiple-dose, dose-escalation study of siltuximab, an anti-interleukin-6 monoclonal antibody, in patients with advanced solid tumors. Clin Cancer Res. 2014;20:2192–204.

18. Durie BG, Harousseau JL, Miguel JS, Bladé J, Barlogie B, Anderson K, et al. International uniform response criteria for multiple myeloma. Leukemia. 2006;20:1467–73.
19. Blade J, Samson D, Reece D, Apperley J, Björkstrand B, Gahrton G, et al. Criteria for evaluating disease response and progression in patients with multiple myeloma treated by high-dose therapy and haemopoietic stem cell transplantation. Myeloma Subcommittee of the EBMT. European Group for Blood and Marrow Transplant. Br J Haematol. 1998;102:1115–23.
20. Shah JJ, Orlowski RZ. Proteasome inhibitors in the treatment of multiple myeloma. Leukemia. 2009;23:1964–79.
21. Liu T, Fei Z, Gangavarapu KJ, Agbenowu S, Bhushan A, Lai JC, et al. Interleukin-6 and JAK2/STAT3 signaling mediate the reversion of dexamethasone resistance after dexamethasone withdrawal in 7TD1 multiple myeloma cells. Leuk Res. 2013;37:1322–8.
22. Fulciniti M, Hideshima T, Vermot-Desroches C, et al. A high-affinity fully human anti-IL-6 mAb, 1339, for the treatment of multiple myeloma. Clin Cancer Res. 2009;15:7144–52.
23. Orlowski RZ, Gercheva L, Williams C, Sutherland HJ, Robak T, Masszi T, et al. Phase II, randomized, double blind, placebo-controlled study comparing siltuximab plus bortezomib versus bortezomib alone in pts with relapsed/refractory multiple myeloma. ASCO Meeting Abstracts. 2012;30: 8018. http://meetinglibrary.asco.org/content/96732-114.
24. El-Osta HE, Kurzrock R. Castleman's disease: from basic mechanisms to molecular therapeutics. Oncologist. 2011;16:497–511.

Jagged1-induced Notch activation is responsible for the acquisition of bortezomib resistance in myeloma cells

Yukari Muguruma[1,2], Takashi Yahata[1], Hiroyuki Warita[1], Katsuto Hozumi[3], Rikio Suzuki[2], Mamoru Ito[4], and Kiyoshi Ando[1,2]

[1]Center for Regenerative Medicine, Tokai University School of Medicine, Isehara, Japan
[2]Department of Hematology and Oncology, Tokai University School of Medicine, Isehara, Japan
[3]Department of Immunology, Tokai University School of Medicine, Isehara, Japan
[4]Central Institute for Experimental Animals, Kawasaki, Japan

Corresponding author: Yukari Muguruma mugu@is.icc.u-tokai.ac.jp
Kiyoshi Ando andok@keyaki.cc.u-tokai.ac.jp
Department of Hematology and Oncology, Tokai University School of Medicine,
143 Shimokasuya Isehara, Kanagawa, Japan, 259-1193
Tel.: +81-463-93-1121, Fax: +81-463-92-4750

Running head: Jagged1-Notch activation in bortezomib resistance in MM

Contract grant sponsor: Ministry of Education, Culture, Sports, Science and Technology of Japan, Basic Research Grant (c), Contract grant number: 26430094
Contract grant sponsor: Ministry of Education, Culture, Sports, Science and Technology of Japan, Strategic Research Foundation Grant-aided Project for Private University, Contract grant number: S1201001

Conflict of interest: The authors declare no conflicts of interest.

Word counts: Abstract: 200, Main text: 3435, Figures: 5, Supplementary materials: 3.

Abstract

Despite recent major advancements in therapy, multiple myeloma (MM) remains incurable largely due to the emergence and maintenance of drug-resistant myeloma cells, of which the interactions within the bone marrow (BM) niche are critical. Because Notch signaling, a pathway activated only through cell-cell contact, is implicated in the onset and progression of MM, we investigated how Notch activation in myeloma cells, specifically through the interactions with ligand-expressing niche cells, affected the pathophysiology of MM. We found that the Jagged1-induced activation of Notch is responsible for the emergence of bortezomib (BTZ)-resistant myeloma cells. Interestingly, Notch activation in myeloma cells caused a significant resistance to BTZ but not to melphalan or thalidomide *in vitro,* indicating a unique effect of the niche-induced Notch activation. Furthermore, Notch-activated myeloma cells in the BM demonstrated enhanced survival against BTZ treatment *in vivo*. Mechanistically, couplings between the niche-expressed Jagged1 and a specific Notch receptor expressed in myeloma cells, namely Notch2, activated a protein kinase C (PKC) pathway that led to sustained survival of myeloma cells; this is the first demonstration of a link between Notch and the PKC pathway in myeloma cells and provides a rationale for targeting a Notch-PKC pathway to overcome drug resistance in MM.

Introduction

Multiple myeloma (MM) is a hematologic malignancy characterized by the proliferation of malignant plasma cells in the bone marrow (BM)[1]. Since the introduction of bortezomib (BTZ), the first proteasome inhibitor approved for clinical application, survival of MM patients has substantially improved[2]. However, despite such major advancements in therapy, MM remains incurable due to the intrinsic and acquired ability of myeloma cells to resist conventional and novel therapies[3].

Myeloma cells are localized in the BM microenvironment (the BM niche) that consists of extracellular matrix (ECM) proteins and accessary cells, including hematopoietic cells, BM stromal cells, endothelial cells, osteoclasts, and osteoblasts. It is believed that the interactions of myeloma cells within the BM niche play key roles in the pathogenesis of MM[4, 5]. For example, the adhesion of myeloma cells to ECM through integrins induces a so called cell adhesion-mediated drug resistance (CAMDR) that causes growth arrest of myeloma cells, allowing them to escape from conventional chemotherapy[6]. Alternatively, binding of myeloma cells to the niche accessary cells through ligand-receptor couplings stimulates secretion of cytokines and growth factors that promote the proliferation and survival of myeloma cells against therapy as well as the development of bone disease that exacerbates clinical symptoms.

It has been shown that the activation of Notch in myeloma cells is

responsible for a number of cellular events that are critical for the onset and progression of MM[7, 8]. Notch activation affects the migration and localization of myeloma cells into the BM[9], subsequent proliferation and invasion of myeloma cells in the BM milieu, and the acquisition of resistance, even to the most advanced MM therapies, which is a major hurdle for the cure of this disease. In fact, Notch inhibition with the use of a γ-secretase inhibitor (GSI), a pan inhibitor for Notch signaling, can increase the sensitivity of human MM cell lines to the conventional chemotherapy[10, 11]. However, unlike other Notch-related hematologic malignancies that carry gain-of-function mutations in Notch itself, such mutations are not reported in MM[12-14]. Hence, in MM, Notch is activated through physical interactions between Notch receptor and its ligand.

Notch can be activated through the homotypic interaction of myeloma cells that simultaneously express both Notch and its ligand(s), or alternatively, activation can occur through the binding of Notch expressed in myeloma cells and the ligand(s) expressed in surrounding niche cells. Additionally, Notch activation can occur in cells that constitute the BM niche. Notch activation within the BM myeloma niche is a complicated process whereby it confers bilateral effects; it directly affects the activity of the cells where Notch is activated or indirectly affects neighboring cells through interactions with Notch-activated cells or through cytokines and growth factors produced by Notch-activated cells. These various and complex modes of action may account for the contradicttory outcomes reported in past studies regarding

the effects of Notch in MM[15-17]. As a result, the roles of Notch in MM pathophysiology are not yet clearly defined.

To clarify the roles of Notch and the molecular mechanisms that lead to specific events in the course of MM progression, we investigated the effects of Notch activation in myeloma cells, specifically through the interactions with surrounding niche cells. We demonstrated both *in vitro* and *in vivo* that the Jagged1-initiated Notch activation in myeloma cells induced the emergence of BTZ-resistant cells and that the sustained activation of myristoylated alanine-rich C-kinase substrate (MARCKS) was mechanistically responsible. This study identified a unique function of the niche-induced Notch activation in MM and provides a rationale for the modulation of a Notch-protein kinase C (PKC) pathway for better management of patients with refractory MM.

Materials and Methods

Mouse model of human myeloma

Non-obese diabetic/severe combined immunodeficient/IL2Rγnull (NOG) and NOG mice that express human *Jagged1* under the control of a 2.3-Kb osteoblast-specific promoter region of murine α1(I) collagen promotor (NOGJ) were obtained from Central Institute for Experimental Animals (Kawasaki, Japan)[18]. Mice were maintained in sterile microisolator cages in the animal facility of the Tokai University School of Medicine and were treated in accordance with the institutional guidelines. All animal experiments were approved by the Animal Care Committee of Tokai University. For experiments, 8- to 12-week-old mice were used. Mice were given an intravenous injection of 0.5-1.5X10^6 MM cells into the retro-orbital plexus in 100 μl of PBS and were humanely killed 5 to 6 weeks after transplantation. BM cells and bones were collected and used for analyses. The data obtained from transgenic mice were compared with sex-matched littermate control mice.

Drug administration

Three weeks after transplantation of myeloma cells, mice were assigned to the following 4 treatment groups. The BTZ group received 0.35 mg/kg or 0.5mg /kg of BTZ dissolved in saline, a concentration specifically determined for the purpose of the experiments, three times a week for three weeks. The GSI group received 7.5 mg/kg of a GSI dissolved in 10% DMSO 5 times a week for two weeks starting at 4 weeks after transplantation. The

combination group received both drugs, and the control group received the same volume of saline and DMSO.

Statistics

Statistical analyses were conducted with GraphPad Prism, version 5.0 (GraphPad Software). Student's two-tailed unpaired *t*-test was used to determine the significance of the difference between the mean values of two groups. One-way ANOVA, followed by Tukey's post hoc test, was used to compare the mean values among three or more independent groups. A normal distribution of the data was confirmed using the Kolmogorov-Smirnov test. The mean ± SD is presented in each graph. P values <.05 were considered significant. NS indicates not significant.

Results

Expression of Notch and its ligands in human MM cell lines

The cellular cross-talks within the BM niche, especially between myeloma cells and niche cells, are considered crucial in the progression of MM. As Notch is activated only through cell-cell contact, we decided to investigate the effects of the niche-induced Notch activation in myeloma cells. We first examined the expression of Notch and its ligands in 10 arbitrary selected human MM cell lines. Consistent with previous reports[16, 17, 19, 20], western blot analyses detected the presence of at least one Notch receptor in all of the human MM cell lines examined, indicating that Notch signaling can be activated and functions in human myeloma cells (Figure 1a). We then examined the expression of Jagged1 and Jagged2, two Notch ligands whose expression was previously reported in human myeloma cells[17, 19-21] (Figure 1a). While Jagged2 expression was not reported in cells constituting the BM niche[22, 23], Jagged1 is known to be abundantly expressed in many types of BM accessary cells in the BM myeloma niche, such as endothelial cells and osteoblasts[24-26]. Therefore, we investigated the effects of the niche-induced Jagged1-Notch activation in the biology of myeloma cells.

Effects of the niche-induced Notch signaling in the proliferation of myeloma cells

As Notch has previously been shown to regulate the proliferation of myeloma cells, either positively or negatively, depending on the context of cells[15-17], we

assessed the effect of Jagged1-Notch activation on the proliferation of myeloma cells. To isolate the niche-induced Notch activation from the homotypic activation of Notch in myeloma cells, MM cell lines that did not express Jagged1 or expressed it weakly, if at all, in our western blot analyses, namely U266, H929, KMM1, KMS11, and delta47, were selected and cultured in the presence of a recombinant human Jagged1-Fc chimera protein or control Fc fragment of human IgG. The presence of immobilized human Jagged1 did not significantly alter the proliferation of any of the 5 MM cell lines *in vitro* (Figure 1b).

To further investigate the roles of the niche-induced Notch signaling, we attempted to establish a clinically relevant animal model of human MM that allowed the examination of myeloma cells in the BM, the primary site of malignant plasma cell proliferation in patients with MM. The five MM cell lines used in the above *in vitro* studies were intravenously transplanted into NOG mice. U266 was the only cell line that resulted in consistent and substantial engraftment in the BM (Figure 1c), as determined by flow cytometric analyses performed 5 to 6 weeks after transplantation. Therefore, U266 cells were used in the following experiments. Of note, the expression of Jagged2, a Notch ligand implicated in the self-renewal of myeloma cells[19, 21], did not aid the engraftment and proliferation of myeloma cells in the BM, arguing against its importance *in vivo*.

To examine the effects of the niche-induced Jagged1-Notch signaling *in vivo*,

we utilized a transgenic mouse strain expressing human *Jagged1* in an osteoblast-specific manner (NOGJ)[18]. At 5 to 6 weeks after intravenous infusion of U266 cells, there was no significant difference between NOGJ and NOG recipients in the percentage of human MM cells engrafted in the BM (Figure 1d). Rather, the difference was more prominent among the independent experiments, probably due to the variations in the number and/or the conditions of the transplanted cells. The result was in agreement with the *in vitro* proliferation experiment, confirming that niche-induced Jagged1-Notch signaling is not specifically associated with the proliferation of myeloma cells.

Effect of Jagged1-Notch signal activation on the drug sensitivity of human myeloma cells

We then asked if the niche-induced Jagged1-Notch activation affects the sensitivity of myeloma cells to drugs clinically used for the treatment of MM. U266 cells co-cultured with BM stromal cells demonstrated a significant resistance to BTZ and melphalan compared to cells cultured without stroma, a phenomenon known as CAMDR (Figure 2a). As expected, treatment of myeloma cells with thalidomide in the absence of immunomodulatory cells did not alter the viability of cells. Transgenic expression of human *Jagged1* in stromal cells was found to upregulate Notch signaling in myeloma cells that was already increased when cells were co-cultured with BM stromal cells (Supplementary Figure S1a). Interestingly, the transgenic expression of human *Jagged1* in stromal cells increased the survival of U266 cells only

when cells were exposed to BTZ, which coincides with further upregulation of Notch signaling in myeloma cells (Figure 2a and Supplementary Figure S1a). Increased myeloma cell survival in the presence of *Jagged1*-expressing stromal cells was confirmed in 5 other MM cell lines (Supplementary Figure S1b), indicating the unique effect of the niche-induced Jagged1-Notch activation in the sensitivity of myeloma cells to BTZ.

To confirm whether the observed resistance to BTZ is a direct result of the Notch activation in myeloma cells, similar experiments were conducted in stroma-free conditions. Cells cultured on immobilized human Jagged1 demonstrated a significant resistance to 5 and 7.5 nM BTZ treatment (Figure 2b). In addition, a marked upregulation of *Hey1* and *Hes1* expression was detected in surviving cells, confirming the activation of Notch in cells exhibiting resistance to BTZ (Figure 2c). However, consistent with the experiment above, the presence of immobilized Jagged1 did not affect the survival of myeloma cells against melphalan (Supplementary Figure S1c). Therefore, the results suggest that the niche-induced Jagged1-Notch activation is uniquely responsible for the acquisition of resistance to BTZ in myeloma cells.

We therefore tested the *in vivo* effect of the niche-induced Jagged1-Notch activation in the sensitivity to myeloma therapy by treating human MM mice with BTZ. Mice that received U266 transplants were administered with the optimum dose of BTZ[27] or saline beginning at 3 weeks after

transplantation for 3 weeks (Figure 3a). At euthanasia, the BM was sectioned and stained for human CD138, a clinically established marker for the identification of malignant plasma cells. Immunohistochemical analyses revealed that the BM of NOGJ recipients was infused with human myeloma cells, in contrast to the BM of NOG mice where myeloma cells were effectively cleared by treatment with the same dose of BTZ (Figure 3a). These qualitative microscopic observations were quantitatively confirmed by flow cytometric analyses. Survival of myeloma cells in BTZ-treated NOGJ mice relative to saline-treated control NOGJ mice was enhanced approximately two-fold compared to NOG mice (41.91±16.63% in NOGJ and 18.93±12.60% in NOG, Figure 3b). Consistent with the earlier *in vitro* finding (Figure 2c and Supplementary Figure S1a), the expression of both *Hey1* and *Hes1* was significantly upregulated in human myeloma cells surviving after BTZ treatment in the NOGJ environment (Figure 3c), supporting our hypothesis that the niche-induced activation of Jagged1-Notch signaling was critical in the acquisition of resistance to BTZ.

Jagged1-Notch signaling is responsible for BTZ resistance

To confirm that the activation of Notch through interactions between myeloma cells and the niche is responsible for the acquisition of drug resistance in BM residing myeloma cells, we inhibited Notch activation by treating human MM mice with a GSI. NOG mice that received U266 transplants were treated with a suboptimum dose of BTZ alone, GSI alone, or a combination of the two drugs. Control mice received the same dose of

saline and/or DMSO (Figure 4a). Although injection of a GSI alone did not significantly alter the survival of human myeloma cells, administration of a suboptimum dose of BTZ reduced the survival of myeloma cells by approximately 50% (52.7±22.8%). Importantly, the combination of BTZ and a GSI further reduced the survival of myeloma cells by half (26.4±11.6%, Figure 4b), which is nearly equivalent to the extent observed in the earlier experiment using a higher dose of BTZ (Figure 3c), indicating that activation of Notch in myeloma cells through an interaction with physiologically expressed Notch ligands, quite possibly Jagged1, is critical to the survival of myeloma cells. Taken together, using a clinically relevant *in vivo* model, these results experimentally confirmed that the activation of Notch in myeloma cells through the interaction with Jagged1-expressing niche cells is responsible for the acquisition of BTZ resistance.

Notch activates a PKC-MARCKS pathway and enhances the survival of myeloma cells

To mechanistically determine how niche-induced Jagged1-Notch signaling protects human myeloma cells from BTZ treatment, we examined the expression and activation of MARCKS in BTZ treated cells. MARCKS is a substrate of PKC and has been found to be overexpressed in several cancers[28-30]. Furthermore, MARCKS overexpression and activation have been demonstrated in drug-resistant human MM cell lines and primary myeloma samples[31, 32], implicating its role(s) in the acquisition of drug resistance, plausibly by counteracting drug-induced cell-cycle arrest.

However, at present, how MARCKS is initially activated remains to be determined[33].

It has previously been shown that Jagged1-Notch signaling activates a PKC pathway in human mesenchymal stem cells[34]. When U266 cells were treated with BTZ or melphalan *in vitro*, the expression and activation of MARCKS were significantly downregulated, indicating an involvement of MARCKS in myeloma cell survival (Figure 5a and Supplementary Figure S2). Interestingly, MARCKS phosphorylation was maintained in cells treated with BTZ when they were cultured on immobilized human Jagged1, the first demonstration of a link between Notch activation and a PKC pathway that is involved in the acquisition of BTZ resistance in myeloma cells. In contrast, the presence of immobilized Jagged1 had no effect on the maintenance of MARCKS phosphorylation when cells were treated with melphalan (Supplementary Figure S2), which is consistent with the earlier experiments (Figure 2a, Supplementary Figure S1c) that showed no association between Jagged1-Notch activation and the acquisition of melphalan resistance.

We therefore asked if inhibitors of PKC signaling can counteract the Jagged1-induced survival of myeloma cells against BTZ treatment. As we anticipated, a combination of BTZ and PKC inhibitors attenuated the survival of myeloma cells *in vitro*. The addition of GF109203X, a pan-PKC inhibitor, effectively reduced the viability of myeloma cells and, at the same time, neutralized the Jagged1-induced enhanced survival of myeloma cells

(Figure 5b), an event consistently demonstrated in this study. In contrast, the effects of Gö6976, an inhibitor of PKCα and β, as well as enzastaurin, a specific inhibitor for PKCβ, were barely significant, and they did not affect the pro-survival effect of immobilized human Jagged1 against BTZ, suggesting that PKCα and β are not involved in the process of Jagged1-initiated acquisition of BTZ resistance. Importantly, the addition of a GSI to the culture abolished the sustained phosphorylation of MARCKS in the presence of Jagged1 (Figure 5c). The result is consistent with the earlier *in vivo* experiments (Figure 4b) and indicates that Jagged1-Notch signaling is indeed responsible for the activation of MARCKS. Altogether, our results demonstrate that niche-induced Jagged1-Notch signaling activates PKC, which then phosphorylates MARCKS and contributes to the survival of myeloma cells.

Discussion

Deregulated Notch signaling within the BM myeloma niche has been implicated in the pathogenesis and progression of MM[7, 8]. Despite having a seemingly simple signaling pathway, the outcomes of Notch activation in MM pathology can be quite diverse. In our attempt to delineate the heterogeneous and complex functions of Notch in MM pathophysiology, we focused on the niche-induced activation of Notch signaling and successfully demonstrated that Jagged1, expressed in niche cells, activated a Notch-PKC pathway in myeloma cells, where MARCKS plays an important role in the emergence of drug-resistant myeloma cells, which makes MM a fatal disease. Although MARCKS has been shown to be upregulated in multidrug resistant myeloma cell lines, this is the first study that demonstrates how MARCKS, a molecule important for myeloma cell survival, is continuously activated in the process of the acquisition of drug resistance.

Because of its causative association with many types of disease, including cancer[35], Notch signaling has been an attractive therapeutic target. However, severe adverse effects of pharmacological agents that inhibit Notch signaling preclude the development of drugs used clinically to treat patients[36, 37]. In the curent study, the addition of a pan-PKC inhibitor neutralized the Jagged1-induced survival of myeloma cells *in vitro*, which provides promising evidence for the use of PKC inhibitors as Notch signaling modulators in MM. However, unlike previous studies[31, 38-40], enzastaurin, a

366 specific inhibitor of PKCβ, and Gö6976, which inhibits α and β isoforms of
367 the PKC family, did not effectively inhibit the growth of U266 even when
368 used with BTZ. This is because the U266 cells that we used for most of this
369 study do not express PKCα, β, or γ ([41] and data not shown) and is consistent
370 with the notion that PKC isoforms that are responsible for the activation of
371 MARCKS differ depending on the types and the contexts of cells[42-44]. Thus,
372 while the modulation of a PKC pathway appears to be an attractive strategy
373 for overcoming drug resistance in MM, inhibitors ideal for treating
374 individual patients should be chosen carefully, given the heterogeneity in the
375 pathophysiology of individual MM patients.
376
377 Jagged1-Notch signaling has been implicated in the acquisition of resistance
378 to conventional chemotherapy, such as melphalan and mitoxantron, and
379 Notch1 was the receptor attributed to that effect[10, 11]. In this study, however,
380 Jagged1-induced Notch activation resulted in a significant resistance only to
381 BTZ treatment but not to melphalan treatments. Because the cell line that
382 we used in this experiment does not express Notch1, as shown in this study
383 and previous studies from other groups[11, 17, 19, 20], any effects on the biology of
384 myeloma cells must come through other Notch receptors, possibly Notch2,
385 which may be a reason that the Jagged1-induced Notch activation did not
386 change the sensitivity of myeloma cells to melphalan in our study.
387 Additionally, 5 additional MM cell lines expressing Notch2 demonstrated
388 enhanced resistance against BTZ in the presence of Jagged1-expressing
389 stromal cells. Consistent with our results, Xu et al. documented the

involvement of Notch2 activation in the acquisition of BTZ resistance in human and murine myeloma cells *in vitro*[45]. They also reported an increase in the sensitivity to BTZ when a GSI was added to the treatment using a murine, but not human, 5T33 myeloma model. Although several studies have reported the expression of Notch3 and Notch 4 in myeloma cells[11, 19, 20], whether they function in the pathobiology of myeloma cells is yet to be determined. According to our data, Notch signaling activation plays critical roles in the acquisition of drug resistance, and the combination of Notch receptors and ligands appears to determine the sensitivity of myeloma cells to a specific pharmacological agent.

Our study identified the unique role of the niche-induced Notch activation in the pathogenesis of MM. While the niche-induced Jagged1-Notch2 activation is responsible for the acquisition of BTZ resistance, it appeared not to be involved in the resistance to melphalan nor in the proliferation of myeloma cells. In addition, the current study presents experimental evidence that modulation of PKC signaling is an effective strategy for counteracting the emergence of drug-resistant cells induced by the activation of Notch signaling. Because MARKCS has been shown to be involved in the adhesion and metastatic invasion of tumor cells in solid tumors[29, 46], niche-induced Jagged1-Notch activation may also participate in the localization as well as the migration of malignant plasma cells into and from the BM milieu to extramedullary proliferation sites, which is critically involved in the progression of this disease. The study provides a rationale for the

PKC-MARCKS pathway as a druggable target in refractory MM.

Supplementary information is available at the *Leukemia* website.

Acknowledgements

This study was supported by a Grant-in-Aid from a Ministry of Education, Culture, Sports, Science and Technology of Japan, Basic Research Grant (c), (26430094) to YM and a Strategic Research Foundation Grant-aided Project for Private University (S1201001) to KA. The authors thank members of the Support Center for Medical Research and Education, and the Center for Regenerative Medicine at Tokai University for technical assistance.

Conflicts of Interest:

The authors declare that they have no conflicts of interest regarding this article.

Author Contribution:

YM designed the experiments and wrote the paper. YM and TY performed the experiments. HW and RS analyzed the gene expression data. KH and TY critically reviewed the manuscript. MI created the transgenic mice. KA approved data and supervised the study.

References

1. Palumbo A, Anderson K. Multiple myeloma. *The New England journal of medicine* 2011 Mar 17; **364**(11): 1046-1060.

2. Moreau P, Richardson PG, Cavo M, Orlowski RZ, San Miguel JF, Palumbo A*, et al.* Proteasome inhibitors in multiple myeloma: 10 years later. *Blood* 2012 Aug 02; **120**(5): 947-959.

3. Abdi J, Chen G, Chang H. Drug resistance in multiple myeloma: latest findings and new concepts on molecular mechanisms. *Oncotarget* 2013 Dec; **4**(12): 2186-2207.

4. Podar K, Chauhan D, Anderson KC. Bone marrow microenvironment and the identification of new targets for myeloma therapy. *Leukemia* 2009 Jan; **23**(1): 10-24.

5. Hideshima T, Mitsiades C, Tonon G, Richardson PG, Anderson KC. Understanding multiple myeloma pathogenesis in the bone marrow to identify new therapeutic targets. *Nature reviews Cancer* 2007 Aug; **7**(8): 585-598.

6. Damiano JS, Cress AE, Hazlehurst LA, Shtil AA, Dalton WS. Cell adhesion mediated drug resistance (CAM-DR): role of integrins and resistance to apoptosis in human myeloma cell lines. *Blood* 1999 Mar 1; **93**(5): 1658-1667.

7. Colombo M, Mirandola L, Platonova N, Apicella L, Basile A, Figueroa AJ*, et al.* Notch-directed microenvironment reprogramming in myeloma: a single path to multiple outcomes. *Leukemia* 2013 Apr; **27**(5): 1009-1018.

8. Colombo M, Galletti S, Garavelli S, Platonova N, Paoli A, Basile A*, et al.* Notch signaling deregulation in multiple myeloma: A rational molecular target. *Oncotarget* 2015 Sep 29; **6**(29): 26826-26840.

9. Mirandola L, Apicella L, Colombo M, Yu Y, Berta DG, Platonova N*, et al.* Anti-Notch treatment prevents multiple myeloma cells localization to the bone marrow via the chemokine system CXCR4/SDF-1. *Leukemia* 2013 Jul; **27**(7): 1558-1566.

10. Nefedova Y, Sullivan DM, Bolick SC, Dalton WS, Gabrilovich DI. Inhibition of Notch signaling induces apoptosis of myeloma cells and enhances sensitivity to

chemotherapy. *Blood* 2008 Feb 15; **111**(4): 2220-2229.

11. Nefedova Y, Cheng P, Alsina M, Dalton WS, Gabrilovich DI. Involvement of Notch-1 signaling in bone marrow stroma-mediated de novo drug resistance of myeloma and other malignant lymphoid cell lines. *Blood* 2004 May 01; **103**(9): 3503-3510.

12. Weng AP, Ferrando AA, Lee W, Morris JPt, Silverman LB, Sanchez-Irizarry C*, et al.* Activating mutations of NOTCH1 in human T cell acute lymphoblastic leukemia. *Science* 2004 Oct 08; **306**(5694): 269-271.

13. Chiaramonte R, Basile A, Tassi E, Calzavara E, Cecchinato V, Rossi V*, et al.* A wide role for NOTCH1 signaling in acute leukemia. *Cancer letters* 2005 Feb 28; **219**(1): 113-120.

14. Mutvei AP, Fredlund E, Lendahl U. Frequency and distribution of Notch mutations in tumor cell lines. *BMC cancer* 2015 Apr 25; **15**: 311.

15. Schwarzer R, Kaiser M, Acikgoez O, Heider U, Mathas S, Preissner R*, et al.* Notch inhibition blocks multiple myeloma cell-induced osteoclast activation. *Leukemia* 2008 Dec; **22**(12): 2273-2277.

16. Zweidler-McKay PA, He Y, Xu L, Rodriguez CG, Karnell FG, Carpenter AC*, et al.* Notch signaling is a potent inducer of growth arrest and apoptosis in a wide range of B-cell malignancies. *Blood* 2005 Dec 1; **106**(12): 3898-3906.

17. Jundt F, Probsting KS, Anagnostopoulos I, Muehlinghaus G, Chatterjee M, Mathas S*, et al.* Jagged1-induced Notch signaling drives proliferation of multiple myeloma cells. *Blood* 2004 May 1; **103**(9): 3511-3515.

18. Negishi N, Suzuki D, Ito R, Irie N, Matsuo K, Yahata T*, et al.* Effective expansion of engrafted human hematopoietic stem cells in bone marrow of mice expressing human Jagged1. *Experimental hematology* 2014 Jun; **42**(6): 487-494 e481.

19. Houde C, Li Y, Song L, Barton K, Zhang Q, Godwin J*, et al.* Overexpression of the NOTCH ligand JAG2 in malignant plasma cells from multiple myeloma patients and cell lines. *Blood* 2004 Dec 1; **104**(12): 3697-3704.

20. Ramakrishnan V, Ansell S, Haug J, Grote D, Kimlinger T, Stenson M*, et al.* MRK003, a gamma-secretase inhibitor exhibits promising in vitro pre-clinical activity in multiple myeloma and non-Hodgkin's lymphoma. *Leukemia* 2012 Feb; **26**(2): 340-348.

21. Chiron D, Maiga S, Descamps G, Moreau P, Le Gouill S, Marionneau S*, et al.* Critical role of the NOTCH ligand JAG2 in self-renewal of myeloma cells. *Blood cells, molecules & diseases* 2012 Apr 15; **48**(4): 247-253.

22. Kim TH, Shivdasani RA. Notch signaling in stomach epithelial stem cell homeostasis. *The Journal of experimental medicine* 2011 Apr 11; **208**(4): 677-688.

23. High FA, Zhang M, Proweller A, Tu L, Parmacek MS, Pear WS*, et al.* An essential role for Notch in neural crest during cardiovascular development and smooth muscle differentiation. *The Journal of clinical investigation* 2007 Feb; **117**(2): 353-363.

24. Li L, Milner LA, Deng Y, Iwata M, Banta A, Graf L*, et al.* The human homolog of rat Jagged1 expressed by marrow stroma inhibits differentiation of 32D cells through interaction with Notch1. *Immunity* 1998 Jan; **8**(1): 43-55.

25. High FA, Lu MM, Pear WS, Loomes KM, Kaestner KH, Epstein JA. Endothelial expression of the Notch ligand Jagged1 is required for vascular smooth muscle development. *Proceedings of the National Academy of Sciences of the United States of America* 2008 Feb 12; **105**(6): 1955-1959.

26. Fukushima H, Nakao A, Okamoto F, Shin M, Kajiya H, Sakano S*, et al.* The association of Notch2 and NF-kappaB accelerates RANKL-induced osteoclastogenesis. *Molecular and cellular biology* 2008 Oct; **28**(20): 6402-6412.

27. Deleu S, Lemaire M, Arts J, Menu E, Van Valckenborgh E, Vande Broek I*, et al.* Bortezomib alone or in combination with the histone deacetylase inhibitor JNJ-26481585: effect on myeloma bone disease in the 5T2MM murine model of myeloma. *Cancer research* 2009 Jul 1; **69**(13): 5307-5311.

28. Micallef J, Taccone M, Mukherjee J, Croul S, Busby J, Moran MF*, et al.* Epidermal

growth factor receptor variant III-induced glioma invasion is mediated through myristoylated alanine-rich protein kinase C substrate overexpression. *Cancer research* 2009 Oct 1; **69**(19): 7548-7556.

29. Estrada-Bernal A, Gatlin JC, Sunpaweravong S, Pfenninger KH. Dynamic adhesions and MARCKS in melanoma cells. *Journal of cell science* 2009 Jul 01; **122**(Pt 13): 2300-2310.

30. Chen CH, Cheng CT, Yuan Y, Zhai J, Arif M, Fong LW*, et al.* Elevated MARCKS phosphorylation contributes to unresponsiveness of breast cancer to paclitaxel treatment. *Oncotarget* 2015 Jun 20; **6**(17): 15194-15208.

31. Yang Y, Chen Y, Saha MN, Chen J, Evans K, Qiu L*, et al.* Targeting phospho-MARCKS overcomes drug-resistance and induces antitumor activity in preclinical models of multiple myeloma. *Leukemia* 2015 Mar; **29**(3): 715-726.

32. Micallef J, Dharsee M, Chen J, Ackloo S, Evans K, Qiu L*, et al.* Applying mass spectrometry based proteomic technology to advance the understanding of multiple myeloma. *Journal of hematology & oncology* 2010 Apr 07; **3**: 13.

33. Niewerth D, Jansen G, Assaraf YG, Zweegman S, Kaspers GJ, Cloos J. Molecular basis of resistance to proteasome inhibitors in hematological malignancies. *Drug resistance updates : reviews and commentaries in antimicrobial and anticancer chemotherapy* 2015 Jan; **18**: 18-35.

34. Zhu F, Sweetwyne MT, Hankenson KD. PKCdelta is required for Jagged-1 induction of human mesenchymal stem cell osteogenic differentiation. *Stem cells* 2013 Jun; **31**(6): 1181-1192.

35. Lobry C, Oh P, Aifantis I. Oncogenic and tumor suppressor functions of Notch in cancer: it's NOTCH what you think. *The Journal of experimental medicine* 2011 Sep 26; **208**(10): 1931-1935.

36. van Es JH, van Gijn ME, Riccio O, van den Born M, Vooijs M, Begthel H*, et al.* Notch/gamma-secretase inhibition turns proliferative cells in intestinal crypts and adenomas into goblet cells. *Nature* 2005 Jun 16; **435**(7044): 959-963.

37. Wong GT, Manfra D, Poulet FM, Zhang Q, Josien H, Bara T*, et al.* Chronic treatment with the gamma-secretase inhibitor LY-411,575 inhibits beta-amyloid peptide production and alters lymphopoiesis and intestinal cell differentiation. *The Journal of biological chemistry* 2004 Mar 26; **279**(13): 12876-12882.

38. Podar K, Raab MS, Zhang J, McMillin D, Breitkreutz I, Tai YT*, et al.* Targeting PKC in multiple myeloma: in vitro and in vivo effects of the novel, orally available small-molecule inhibitor enzastaurin (LY317615.HCl). *Blood* 2007 Feb 15; **109**(4): 1669-1677.

39. Baumann P, Armann J, Mandl-Weber S, Grun G, Oduncu F, Schmidmaier R. Inhibitors of protein kinase C sensitise multiple myeloma cells to common genotoxic drugs. *European journal of haematology* 2008 Jan; **80**(1): 37-45.

40. Rizvi MA, Ghias K, Davies KM, Ma C, Weinberg F, Munshi HG*, et al.* Enzastaurin (LY317615), a protein kinase Cbeta inhibitor, inhibits the AKT pathway and induces apoptosis in multiple myeloma cell lines. *Molecular cancer therapeutics* 2006 Jul; **5**(7): 1783-1789.

41. Ni H, Ergin M, Tibudan SS, Denning MF, Izban KF, Alkan S. Protein kinase C-delta is commonly expressed in multiple myeloma cells and its downregulation by rottlerin causes apoptosis. *British journal of haematology* 2003 Jun; **121**(6): 849-856.

42. Rombouts K, Lottini B, Caligiuri A, Liotta F, Mello T, Carloni V*, et al.* MARCKS is a downstream effector in platelet-derived growth factor-induced cell motility in activated human hepatic stellate cells. *Experimental cell research* 2008 Apr 15; **314**(7): 1444-1454.

43. Huse M, Kuriyan J. The conformational plasticity of protein kinases. *Cell* 2002 May 03; **109**(3): 275-282.

44. Ohno S, Mizuno K, Adachi Y, Hata A, Akita Y, Akimoto K*, et al.* Activation of novel protein kinases C delta and C epsilon upon mitogenic stimulation of quiescent rat 3Y1 fibroblasts. *The Journal of biological chemistry* 1994 Jul 01; **269**(26): 17495-17501.

45. Xu D, Hu J, De Bruyne E, Menu E, Schots R, Vanderkerken K*, et al.* Dll1/Notch activation contributes to bortezomib resistance by upregulating CYP1A1 in multiple myeloma. *Biochemical and biophysical research communications* 2012 Nov 30; **428**(4): 518-524.

46. Yang Z, Xu S, Jin P, Yang X, Li X, Wan D*, et al.* MARCKS contributes to stromal cancer-associated fibroblast activation and facilitates ovarian cancer metastasis. *Oncotarget* 2016 Jun 21; **7**(25): 37649-37663.

Figure Legends

***Figure 1: Effects of environmental Jagged1 expression on the proliferation of MM cell lines* in vitro *and* in vivo**

(a) Expressions of both Notch1 and Notch2 were detected in eight of the 10 MM cell lines. While Notch2 was expressed in the remaining two cell lines, Notch1 expression was detected only weakly in KMS11 but not in U266 cells. In addition to the major cleaved transmembrane region of the expected size for Notch1 and Notch2 (arrowheads), several smaller sized bands are seen. Jagged1 was expressed broadly at various intensities. However, Jagged2 expression was confined to five MM cell lines. Single bands of the expected size are shown for Jagged1 and Jagged2 (both 150 kDa). Representative images from two independent experiments are shown.

(b) Proliferation of Human MM cell lines. Representative results from three independent experiments are shown.

(c) Engraftment of human myeloma cells in the BM of NOG mice (n=5 for each cell line). Numbers above each bar represent the mean values of the engraftment results. (b and c) Error bars, mean ± SD.

(d) Engraftment of U266 cells in NOG or NOGJ hosts. Each symbol represents % of engraftment in the BM. Horizontal lines connect analytical pairs. Pooled data from six independent experiments are shown (n=10). NS, not significant.

Figure 2: Jagged1-induced Notch activation augmented human myeloma cell

survival against BTZ treatment in vitro

(a) Survival of U266 cells against the indicated concentration of drugs. Representative results from two to seven independent experiments are shown.

(b) Survival of U266 cells in the presence of immobilized recombinant human Jagged1-Fc chimera protein or control Fc fragment. Representative results from nine independent experiments are shown. (a and b) Bars represent % ATP activity relative to the control culture.

(c) The expression of *Hey1* and *Hes1* in the surviving cells. Representative results from two independent experiments are shown. 18SrRNA was used as a reference gene. (a-c) Error bars, mean ± SD; *, $P<0.05$; NS, not significant.

Figure 3: Jagged1-induced Notch activation augmented human myeloma cell survival against BTZ treatment in vivo

(a) Brown spots in the BM sections represent human myeloma cells expressing CD138. Representative images from five independent experiments are shown.

(b) Survival of human myeloma cells after BTZ treatment. Relative survival of myeloma cells was obtained by dividing the percentage of myeloma cells that remained after BTZ treatment by the percentage of myeloma cells in the BM of saline control mice. Each circle represents the calculated value of myeloma cell survival. Pooled data from five independent experiments are shown (n=11).

(c) The expression of *Hey1* and *Hes1* in the surviving cells. Representative

results from four independent experiments are shown. Human β–actin was used as a reference gene. (b and c) Error bars, mean ± SD; *, P<0.05; **, P<0.01

Figure 4: Inhibition of Notch signaling reduced BTZ-resistant myeloma cells in vivo

(a) Experimental scheme.

(b) Survival of human myeloma cells after drug treatment. Each circle represents the calculated value of an individual mouse. Pooled data from four independent experiments are shown (n=11 for control group, others n=6). Error bars, mean ± SD; *, P<0.05; **, P<0.01; NS, not significant.

Figure 5: Jagged1-induced Notch signaling is responsible for MARCKS-mediated survival of human myeloma cells.

(a) Expression and activation of MARCKS were reduced in the presence of BTZ. Jagged1-Notch signaling maintained MARCKS phosphorylation.

(b) Effects of PKC inhibitors on U266 cells survival. Representative results from five to seven independent experiments are shown. Error bars, mean ± SD; *, P>0.05; NS, not significant.

(c) Inhibition of Notch signaling abolished sustained MARCKS activation in the presence of immobilized Jagged1. Representative images of four (a) and two (c) independent experiments are shown.

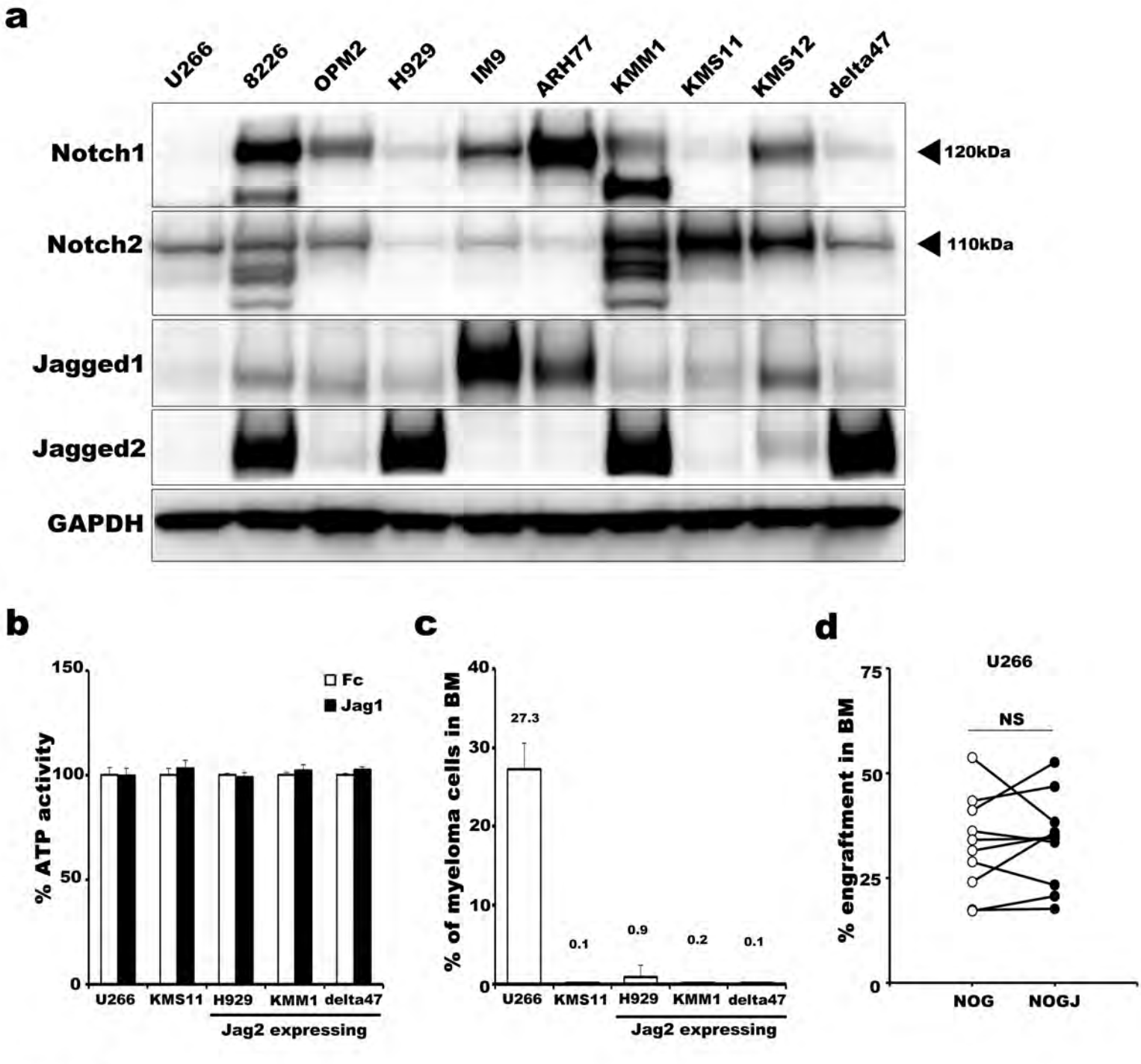
a
U266
8226
OPM2
H929
IM9
ARH77
KMM1
KMS11
KMS12
delta47
Notch1
Notch2
Jagged1
Jagged2
GAPDH
120kDa
110kDa
b
% ATP activity
150
100
50
0
Fc
Jag1
U266
KMS11
H929
KMM1
delta47
Jag2 expressing
c
% of myeloma cells in BM
40
30
20
10
0
27.3
0.1
0.9
0.2
0.1
U266
KMS11
H929
KMM1
delta47
Jag2 expressing
d
U266
NS
% engraftment in BM
75
50
25
0
NOG
NOGJ

Figure.1

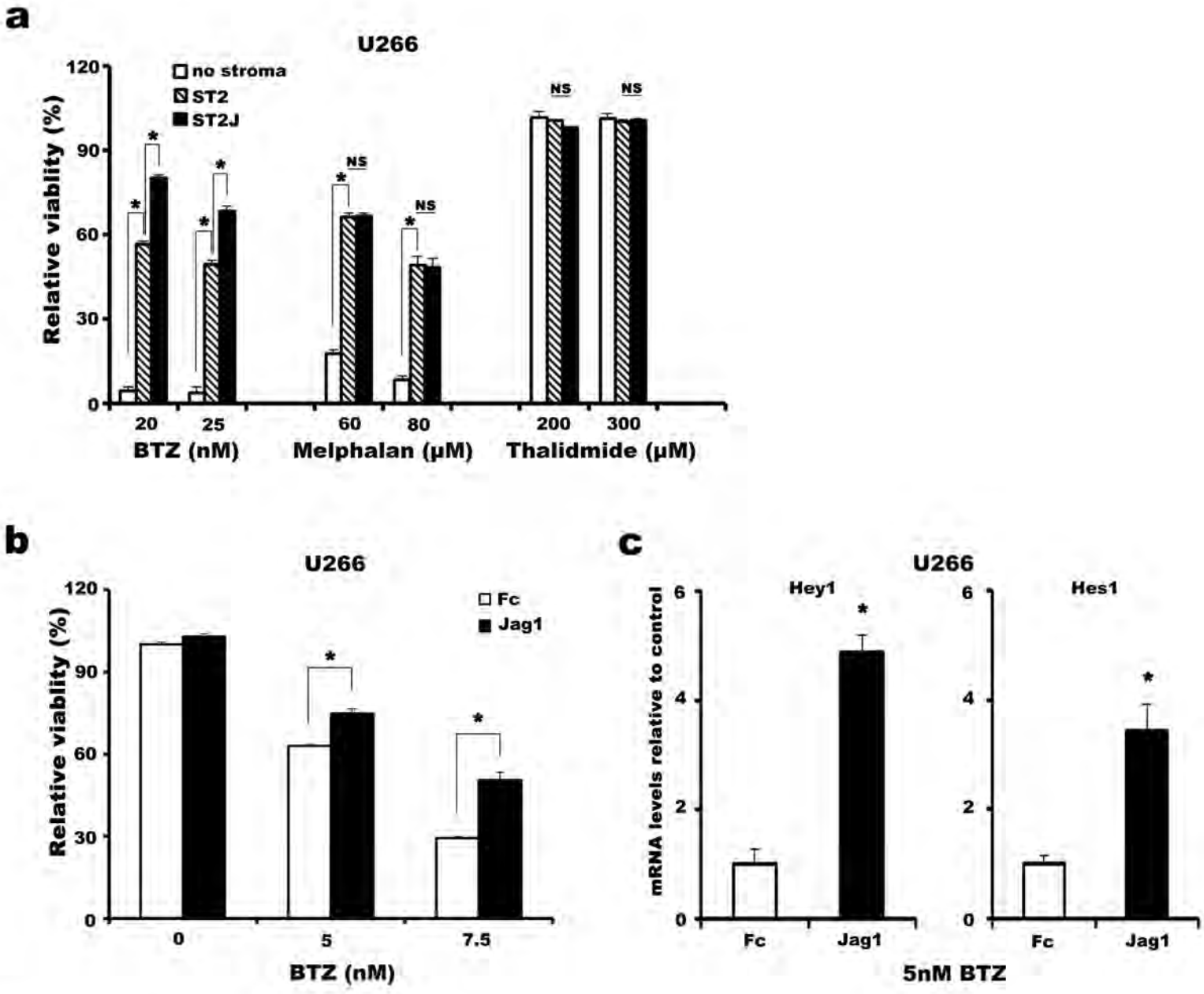
a
U266
no stroma
ST2
ST2J
Relative viability (%)
120
90
60
30
0
NS
NS
NS
20
25
60
80
200
300
BTZ (nM)
Melphalan (μM)
Thalidmide (μM)
b
U266
Fc
Jag1
Relative viability (%)
120
90
60
30
0
0
5
7.5
BTZ (nM)
c
U266
Hey1
Hes1
mRNA levels relative to control
6
4
2
0
Fc
Jag1
5nM BTZ

Figure. 2

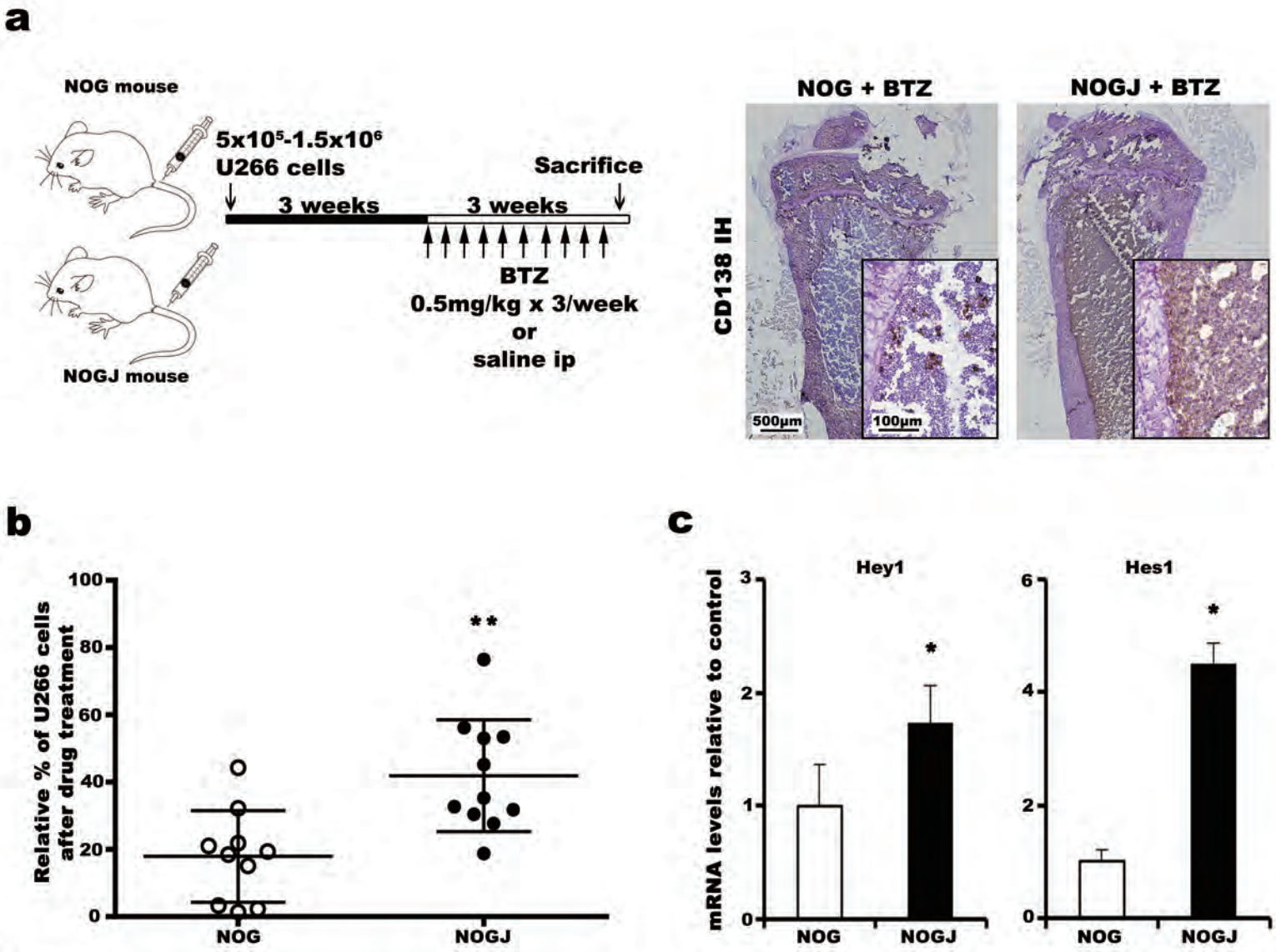
a
NOG mouse
NOGJ mouse
5x10⁵-1.5x10⁶
U266 cells
3 weeks
3 weeks
Sacrifice
BTZ
0.5mg/kg x 3/week
or
saline ip
NOG + BTZ
NOGJ + BTZ
CD138 IH
500μm
100μm
b
Relative % of U266 cells after drug treatment
100
80
60
40
20
0
**
NOG
NOGJ
c
mRNA levels relative to control
Hey1
Hes1
3
2
1
0
6
4
2
0
*
*
NOG
NOGJ
NOG
NOGJ

Figure. 3

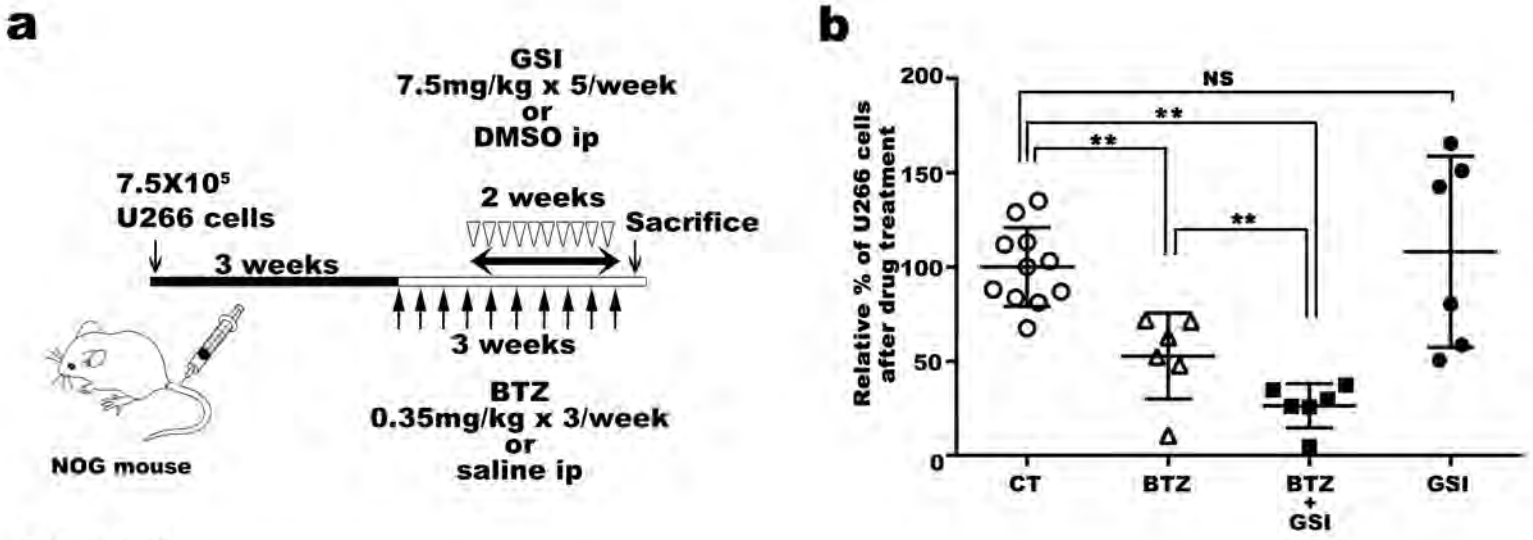
a
GSI
7.5mg/kg x 5/week
or
DMSO ip
7.5X10⁵
U266 cells
2 weeks
Sacrifice
3 weeks
3 weeks
BTZ
0.35mg/kg x 3/week
or
saline ip
NOG mouse
b
Relative % of U266 cells after drug treatment
200
150
100
50
0
NS
**
**
**
CT
BTZ
BTZ + GSI
GSI

Figure. 4

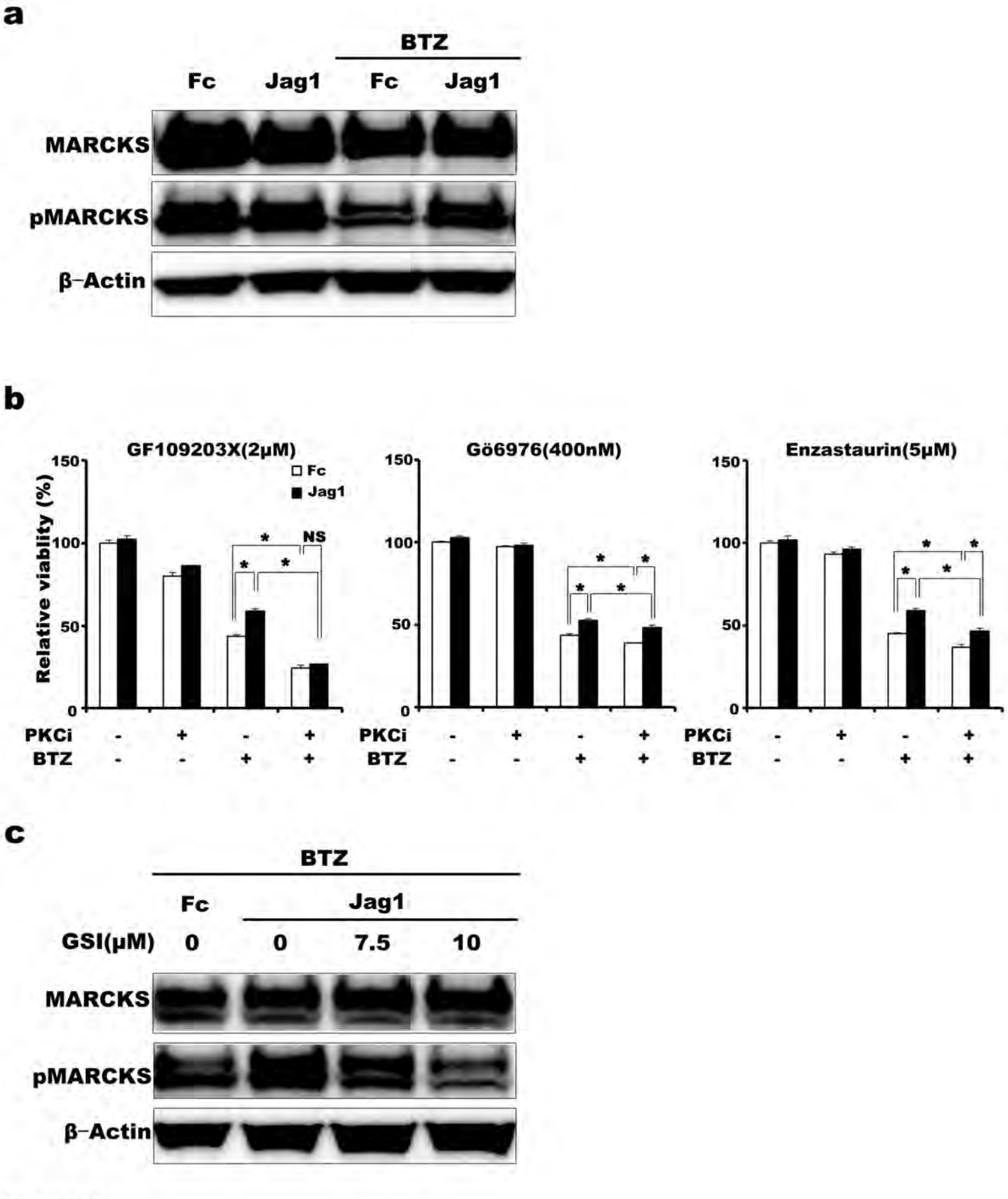
a
BTZ
Fc
Jag1
Fc
Jag1
MARCKS
pMARCKS
β-Actin
b
GF109203X(2μM)
Gö6976(400nM)
Enzastaurin(5μM)
Fc
Jag1
Relative viability (%)
150
100
50
0
NS
*
PKCi
BTZ
c
BTZ
Fc
Jag1
GSI(μM)
0
0
7.5
10
MARCKS
pMARCKS
β-Actin

Figure. 5

OPEN

Prospective Study on the Incidence of Bone Metastasis (BM) and Skeletal-Related Events (SREs) in Patients (pts) with Stage IIIB and IV Lung Cancer—CSP-HOR 13

Nobuyuki Katakami, MD, PhD, Hiroshi Kunikane, MD, PhD,† Koji Takeda, MD,‡ Koichi Takayama, MD, PhD,§ Toshiyuki Sawa, MD, PhD,‖ Hiroshi Saito, MD, PhD,¶ Masao Harada, MD, PhD,# Soichiro Yokota, MD, PhD,** Kiyoshi Ando, MD, PhD,†† Yuko Saito, MS,‡‡ Isao Yokota, MPH,§§ Yasuo Ohashi, PhD,§§ and Kenji Eguchi, MD, PhD‖‖*

Background: Bone metastasis (BM) is a frequent complication in patients with advanced lung cancer and it causes skeletal-related events (SREs). Our study aim is to prospectively investigate the incidence of BM, incidence and types of SRE, and predictive factors of BM and SREs.

Methods: Newly diagnosed, advanced non–small-cell lung cancer (NSCLC) or small-cell lung cancer (SCLC) patients were enrolled into the study. Patients were followed up every 4 weeks to monitor the development of SREs. Treatment for lung cancer was performed at the discretion of the investigator.

Results: Two hundred seventy-four patients were enrolled in this study between April 2007 and December 2009 from 12 institutions. Patients included 77 cases of SCLC and 197 of NSCLC (stage IIIB/IV = 73/124). Median follow-up time was 13.8 months. The incidence of BM at initial diagnosis was 48% in stage IV NSCLC and 40% in extensive stage (ED)-SCLC. Forty-five percent of patients who developed BM had SREs consisting of pathologic fracture (4.7%), radiation to bone (15.3%), spinal cord compression (1.1%), and hypercalcemia (2.2%). Multivariate analysis revealed that factors predicting BM are stage IV, performance status 1 or greater and higher bone alkaline phosphatase in NSCLC patients, higher lactate dehydrogenase, and lower parathyroid hormone–related peptide in SCLC patients. Factors predicting SREs were stage IV, age 64 or younger, and lower albumin in NSCLC patients. Multivariate analysis of SRE was not performed for SCLC because of the small number of events.

Conclusion: Predictive factors should be taken into consideration in future randomized studies evaluating BM and SREs.

Key Words: Bone metastasis, Skeletal-related event, Lung cancer, Predictive factor, Prospective study.

(*J Thorac Oncol.* 2014;9: 231–238)

Although the overall incidence of bone metastasis (BM) is unknown, BMs are a frequent complication in patients with advanced cancer. The most common human cancers such as breast, prostate, and lung have a great avidity for bone, leading to painful skeletal symptoms. How long patients live with a tumor is likely to influence whether BMs will occur. For example, in patients who quickly die of cancer because of an aggressively growing primary tumor, BMs will be relatively uncommon, simply because they have not adequate time to develop. This in no way implies that the tumor cells lacked the potential to grow in bone.[1,2] In the case of advanced non–small-cell lung cancer (NSCLC), the median survival time (MST) has increased from 8 to 12 months to 15 to 17 months, during the past 10 years.[3–6] Furthermore, when stage IIIB or stage IV NSCLC patients harboring a sensitive epidermal growth factor receptor (*EGFR*) gene mutation were treated with gefitinib, MST lengthened to 21.6 to 38.8 months.[7–9] On the other hand, for patients in limited stage (LD) small-cell lung cancer (SCLC), the MST is approximately 2 years.[10,11] For patients with extensive stage (ED) SCLC, survival is much more limited, ranging from 9.3 to 12.8 months.[12,13] Accordingly, the chance of developing BM has increased, both in advanced NSCLC and LD-SCLC.

BMs can be associated with skeletal-related events (SREs), which include pathologic fracture, the need for surgery or radiation to bone, spinal cord compression, and hypercalcemia of malignancy (HCM).[14–16] Because patient quality of life (QOL) deteriorates tremendously once SREs develop,

*Institute of Biomedical Research and Innovation, Kobe, Japan; †Yokohama Municipal Citizen's Hospital, Yokohama, Japan; ‡Osaka City General Hospital, Osaka, Japan; §Kyushu University Hospital, Fukuoka, Japan; ‖Gifu Municipal Hospital, Gifu, Japan; ¶Aichi Cancer Center Aichi Hospital, Okazaki, Japan; #National Hospital Organization Hokkaido Cancer Center, Sapporo, Japan; **Toneyama National Hospital, Toyonaka, Japan; ††Tokai University School of Medicine, University Hospital, Isehara, Japan; ‡‡Shizuoka Cancer Center, Shizuoka, Japan; §§The University of Tokyo, Tokyo, Japan; and ‖‖Teikyo University School of Medicine, Tokyo, Japan.

Disclosure: The authors declare no conflict of interest.

Address for correspondence: Nobuyuki Katakami, MD, PhD, Institute of Biomedical Research and Innovation, 2-2 Minatojima Minamimachi, Chuo-ku, Kobe, 650-0047, Japan. E-mail: nkatakami@kcho.jp

Previously presented at the 47th Annual Meeting of the American Society of Clinical Oncology, Chicago, IL, 3–7 June, 2011, and the 16th Congress of The European Multidisciplinary Cancer, Stockholm, Sweden, 23–27 September, 2011.

ISSN: 1556-0864/14/0902-0231

it is important for investigators to treat patients with BM with an appropriate treatment, as early as possible. To our knowledge, there have been no prospective studies investigating the incidence and predictive factors of BM and SREs in patients with advanced lung cancer. Accordingly, it is worthwhile to investigate how therapeutic interventions such as chemotherapy, radiotherapy, and bisphosphonate could affect the clinical course of lung cancer patients with BM and the development of SREs. The aim of this study is to prospectively investigate: (1) the incidence of BM at initial diagnosis in patients with SCLC and stage IV NSCLC, (2) the time interval for the development in BM in patients with SCLC and stage IIIB NSCLC who have no BM at initial diagnosis, (3) the time interval for the development of SRE from BM, and (4) the predictive factors of BM and SRE.

MATERIALS AND METHODS

Study Design

This study is a prospective multicenter cohort study. Adult patients (at least 20 years of age) with newly diagnosed SCLC in all stages and NSCLC in stage IIIB or stage IV were eligible.

All patients were required to have received no prior chemotherapy or bisphosphonate therapy, and were allowed to undergo palliative surgical or radiation treatment for skeletal complications before registration. Once patients were enrolled into the study, treatment for lung cancer and the use of zoledronate were at the discretion of the investigator. Zoledronate was administered only after the development of BMs. No patients received denosumab during the study period, because it had not been approved by the Japanese government. The study was approved by the institutional review boards of the respective institutions and was conducted in compliance with international guidelines regulating patient safety. All patients provided written informed consent. QOL assessment and other therapeutic factors affecting BM and SREs will be reported, separately.

Staging of Lung Cancer and Subsequent Follow-Up Schedule

Table 1 shows the study schedule. Before patient enrollment, a complete physical examination was performed and a medical history was taken, which included history of SREs, antineoplastic history, and Eastern Cooperative Oncology Group performance status (PS). Blood chemistry and bone turnover markers (parathyroid hormone–related peptide [PTHrP], bone alkaline phosphatase [BALP], and urine cross-linked N-telopeptide of type I collagen [NTx]) were obtained. Tumor assessment was undertaken using chest and abdominal computed tomography (CT), radionuclide bone scan, or integrated positron emission tomography (PET)-CT. Magnetic resonance imaging or enhanced CT of the brain was performed when patients were symptomatic. Bone survey was performed before enrollment, with thoracic and lumbar spine radiograph, pelvic radiograph, and bone scan or integrated PET-CT. When BM was suspected only with bone scan or PET-CT, its confirmation with bone magnetic resonance imaging, CT scan, or normal radiograph was mandatory.

After enrollment, tumor assessment, Eastern Cooperative Oncology Group PS, and SREs were assessed every 4 weeks. Bisphosphonate use, pain, and analgesic scores were recorded at each visit, every 4 weeks. Blood chemistry was measured at each visit, every 4 weeks. Bone scan or integrated PET-CT and skeletal survey were assessed every 6 months. After 12 months of follow-up, the above-mentioned assessments were repeated every 3 months. Patients were closely monitored for 24 months after enrollment into the study.

TABLE 1. Examination Schedule

	0	1	2	3	4	5	6	7	8	9–12
Visit	**Enrollment**	**1 mo**	**2 mos**	**3 mos**	**4 mos**	**5 mos**	**6 mos**	**9 mos**	**12 mos**	**24 mos**
Allowance	**≤1 mo**	**±2 wk**	**±2 wk**	**±2 wks**	**±2 wks**	**±2 wks**	**±2 wks**	**±6 wks**	**±6 wks**	**±6 wks**
Bone scintigram or PET	o						★		o	Repeat between 7 and 8
Radiograph (DV•L-Spine)	o									
Chest and abdominal CT	o			☆			☆	☆	☆	
Patient background	o									
PS	o	o	o	o	o	o	o	o	o	
Blood biochemistry	o	o	o	o	o	o	o	o	o	
Bone marker (blood and urine)	o									
Bone metastasis	o	o	o	o	o	o	o	o	o	
Metastasis extrabone	o	o	o	o	o	o	o	o	o	
Bisphosphonate	o	o	o	o	o	o	o	o	o	
Bone pain	o	o	o	o	o	o	o	o	o	
Analgesic use	o	o	o	o	o	o	o	o	o	
SRE	o	o	o	o	o	o	o	o	o	
QOL•ADL	o			☆					o	

SRE, skeletal-related event; QOL, quality of life; ADL, activity of daily living; PET, positron emission tomography; CT, computed tomography; PS, performance status; DV, ; ☆, ±4 wks; ★, ±6 wks.

Assessment of Outcome

SRE was defined as pathologic fracture, spinal cord compression, radiation or surgery to bone, or HCM. Fractures were identified by two expert radiologists at each institution. Spinal cord compression reported by investigators was confirmed by a neurologist and an orthopedic surgeon at each institution. Radiation to bone was given to control pain, treat or prevent pathologic fractures, or treat or prevent spinal cord compression. Surgery to bone included procedures to prevent imminent fractures or spinal cord compression or to set/stabilize fractures. Hypercalcemia was defined as a serum calcium concentration of greater than 11 mg/dl.

Statistical Analyses

The incidence provability rate was estimated for the time to the first occurrence of BM from diagnosis of lung cancer, and the time to the first occurrence of SREs from the diagnosis of lung cancer or from the first occurrence of BM, using the Kaplan–Meier method. Predictive factors for BMs and SREs were explored with Cox proportional hazard regression model for the following: Tumor type (stage IIIB NSCLC, stage IV NSCLC, LD-SCLC, and ED-SCLC), sex, age (65 or older/64 or younger), PS (PS1 or greater/PS0), and bone markers (lactate dehydrogenase [LDH], albumin, calcium, PTHrP, BALP, and urine NTx). The results were checked for consistency by conducting both a univariate Cox regression model, in which each factor was individually tested as an explanatory variable, and a multivariate Cox regression model, in which all variables were entered simultaneously into the model. To investigate whether the use of a chemotherapeutic agent and bisphosphonate inhibits the occurrence of SREs, Cox regression analysis was performed using these factors as time-dependent covariates. All analyses used the SAS statistical software package (version 9.1.3; SAS Institute, Cary NC).

The main purpose of this study is to survey lung cancer patients regarding the timing of elapsed events from onset to BM, to SRE, and is not intended as a comparison of treatment methods. Accordingly, the target number of cases was not designed for intergroup comparison, but to describe the time distribution until BM, search for predictors which affect metastasis to bone, describe what kind of SREs occur, and examine the effects on QOL, etc. The target number of cases was set at 50, as a number of cases for which descriptive statistics of some accuracy can be calculated, even for patients with stage IIIB NSCLC, which is anticipated to have comparatively small enrollment, for a total of approximately 400 cases from the percentage of each cancer type.

RESULTS

Patients

A total of 274 patients with lung cancer were enrolled in the study, between April 2008 and December 2009, from 12 institutions in Japan. Patient demographics and baseline characteristics are shown in Table 2. One hundred ninety-seven patients had NSCLC (stage IIIB, 73; stage IV, 124), and 77 patients had SCLC (LD, 30; ED, 47). The majority of patients were male (70.4%) and the median age was 68 years (range, 35–89). Ninety percent of patients had good PS (PS = 0, 27.7%; PS = 1, 62.4%). The number of patients with BM at initial diagnosis was 59 (47.6%) in stage IV NSCLC and 19 (40.4%) in ED-SCLC. Twenty patients of stage IV NSCLC (16.1%) and four patients in ED-SCLC (8.5%) already had SRE at the time of enrollment. The majority of patients (92.3%) were being treated with chemotherapy. The number of patients who received zoledronate was eight in stage IIIB NSCLC, 49 in stage IV NSCLC, two in LD-SCLC, and four in ED-SCLC after the development of BM during the study period. *EGFR* gene mutations were analyzed only in 92 (46.7%) of 197 NSCLC patients because it was not routinely tested during this period. Among these, 38 patients (19.3%) had *EGFR* gene mutations and 30 patients (15.2%) had active mutations (L858R or exon 19 deletion). Nine of 30 patients were treated with EGFR tyrosine kinase inhibitor (TKI) during the first regimen, 19 during the second regimen, and two during the third regimen. Eighteen patients (9.2%) were not treated with chemotherapy at all. One hundred fifty-two patients (77.2%) were treated with some kind of chemotherapy within 30 days of enrollment. The other patients (13.6%) were treated with chemotherapy after 31 days of enrollment.

During the treatment of SCLC, three patients (3.9%) were not treated with any kind of chemotherapy, 68 (88.3%) patients were treated with some kind of chemotherapy within 30 days of enrollment, whereas six patients (7.8%) were treated with chemotherapy after 31 days of enrollment. The number of patients with platinum plus CPT-11 and platinum and etoposide in the first regimen were 19 (24.7%) and 40 (51.9%), respectively. The median follow-up duration was 13.8 months (range, 0–28.5 months).

Time Interval of Development of BM and SREs

The incidence of BM and SREs at enrollment and during follow-up is presented in Figure 1 and Table 3. Among 274 lung cancer patients, BM was detected in 78 patients (28.5%) at enrollment and in another 34 patients (12.4%) during follow-up. SREs were reported in 24 patients (8.8%) at the time of enrollment and in another 26 patients (9.5%) during follow-up. Total number of patients who developed SREs was 52 (19.0%). The type of SRE was pathologic fracture in 14 (5.1%), radiation to bone in 45 (16.4%), spinal cord compression in three (1.1%), and HCM in six (2.2%). The median time to BM from diagnosis of lung cancer and to SRE from BM was 19.0 months (95% confidence interval [CI], 10.7 to not reached) and 9.5 months (95% CI, 5.1–16.9), respectively (Fig. 2*A* and *C*). However, the median time to SRE from diagnosis of lung cancer was not reached (Fig. 2*B*).

Predictive Factors of BM and SREs

We performed subgroup analysis by separating NSCLC and SCLC because their biological characteristics and clinical behavior differ. To identify the predictive factors of BM and SREs, Cox proportional hazard regression analysis was performed using stage (stage IIIB and stage IV in case of NSCLC, and ED and LD in case of SCLC), sex, age, PS, LDH, albumin, calcium, PTHrP, BALP, NTx, and treatment (chemotherapy

TABLE 2. Patient Characteristics

	NSCLC		SCLC		
	Stage IIIB	**Stage IV**	**LD**	**ED**	**Total**
N	73	124	30	47	274
Sex (male/female)	57/16	79/45	18/12	39/8	193/81
Age (median [range])	69.0 [35–86]	67.0 [41–89]	69.0 [53–80]	68.0 [45–82]	68.0 [35–89]
PS (ECOG)					
0	22 (30.1)	31 (25.0)	23 (29.9)	11 (23.4)	76 (27.7)
1	43 (58.9)	82 (66.1)	46 (59.7)	30 (63.8)	171 (62.4)
2	7 (9.6)	8 (6.5)	8 (10.4)	6 (12.89)	23 (8.4)
≥3	1 (1.4)	3 (2.4)	0 (0)	0 (0)	4 (1.5)
Bone metastasis					
−	73 (100.0)	65 (52.4)	30 (100)	28 (59.6)	196 (71.5)
+	0	59 (47.6)	0 (0)	19 (40.4)	78 (28.5)
SRE					
−	73 (100.0)	104 (83.9)	30 (100)	43 (91.5)	250 (91.2)
+	0	20 (16.1)	0 (0)	4 (8.5)	24 (8.8)
Chemotherapy					
−	9 (12.3)	9 (7.3)	1 (2.1)	2 (6.7)	21 (7.7)
≤30 days	54 (74.0)	98 (79.0)	41 (87.2)	27 (90.0)	220 (80.3)
>30 days	10 (13.7)	17 (13.7)	5 (10.6)	1 (3.3)	33 (12.0)
EGFR mutation					
+	10 (13.7)	28 (22.5)	1 (3.3)	0 (0.0)	39 (14.2)
−	16 (21.9)	44 (35.5)	1 (3.3)	2 (4.3)	63 (23.0)
NT	47 (64.4)	52 (42)	28 (93.6)	45 (95.7)	172 (62.8)
Zoledronate[a]					
+	8 (11.0)	49 (39.5)	4 (8.5)	2 (6.7)	63 (23.0)
−	65 (89.0)	75 (60.5)	43 (91.5)	28 (93.3)	211 (77.0)

[a]Zoledronate was administered after development of bone metastasis.

NSCLC, non–small-cell lung cancer; SCLC, small-cell lung cancer; LD, limited disease; ED, extensive disease; PS, performance status; ECOG, Eastern Cooperative Oncology Group; SRE, skeletal-related event; EGFR, epidermal growth factor receptor; NT, not tested.

and EGFR-TKI in case of NSCLC, chemotherapy and first-line platinum + etoposide or first-line platinum and CPT in case of SCLC) (Table 4). The multivariate analysis of the NSCLC patients demonstrated that stage IV (hazard ratio [HR] = 7.62; 95% CI, 3.76–15.46; $p < 0.001$), PS 1 or greater (HR = 1.82; 95% CI, 1.01–3.29; $p = 0.046$), and higher serum BALP level (HR = 10.36; 95% CI, 2.35–45.78; $p = 0.002$) were significant predictive factors for BM (Table 4). However, neither chemotherapy (HR = 0.51; 95% CI, 0.22–1.20; $p = 0.125$) nor EGFR-TKI (HR = 1.69; 95% CI, 0.76–3.75; $p = 0.196$) were predictive factors. The multivariate analysis of the SCLC patients revealed that ED stage (HR = 6.11; 95% CI, 1.69–22.05; $p = 0.006$), higher serum LDH at baseline (HR = 9.14; 95% CI, 1.51–55.14; $p = 0.016$), and higher serum PTHrP at baseline (HR = 0.38; 95% CI, 0.15–0.99; $p = 0.048$) were significant predictive factors, but chemotherapy (HR = 0.52; 95% CI, 0.14–1.87; $p = 0.340$) and first-line use of platinum + etoposide or platinum + CPT (HR = 0.44; 95% CI, 0.14–1.40; $p = 0.165$) were not predictive factors.

Regarding SREs, multivariate analysis of NSCLC patients demonstrated that stage IV (HR = 5.58; 95% CI, 2.21–14.10; $p < 0.001$), age 65 or older (HR = 0.50; 95% CI, 0.26–0.96; $p = 0.038$), and zoledronate use after BM (HR = 2.64; 95% CI, 1.25–5.57; $p = 0.011$) were predictive factors for SREs (Table 5). As for SCLC patients, multivariate analysis was not performed because of the small number of SRE events (only 9 events).

DISCUSSION

According to several studies published before 1991, the incidence of BM in NSCLC, as detected by bone scans, is between 8% and 34%, with a mean of 20%.[17] More recent reviews have reported incidences of 24% and 30% in American and Japanese patient populations, respectively.[18,19] Moreover, in retrospectively analyzed studies, the incidence of BM in patients with stage IV NSCLC was 41% to 54.8%.[19,20] Our prospective study demonstrated that the incidence of BM in stage IV NSCLC and ED-SCLC was 46.7% and 40.4%, respectively. As newer imaging modalities such as PET and bone scan have been developed, the incidence of BM may have increased.[21,22] However, it has been reported that the accuracies of PET and bone scan are 94% and 85% ($p < 0.05$), the sensitivity values were 91% and 75%, and the specificity values were 96% and 95%, respectively.[22]

The frequency of SREs among 274 patients in the current prospective study was in the order of frequency,

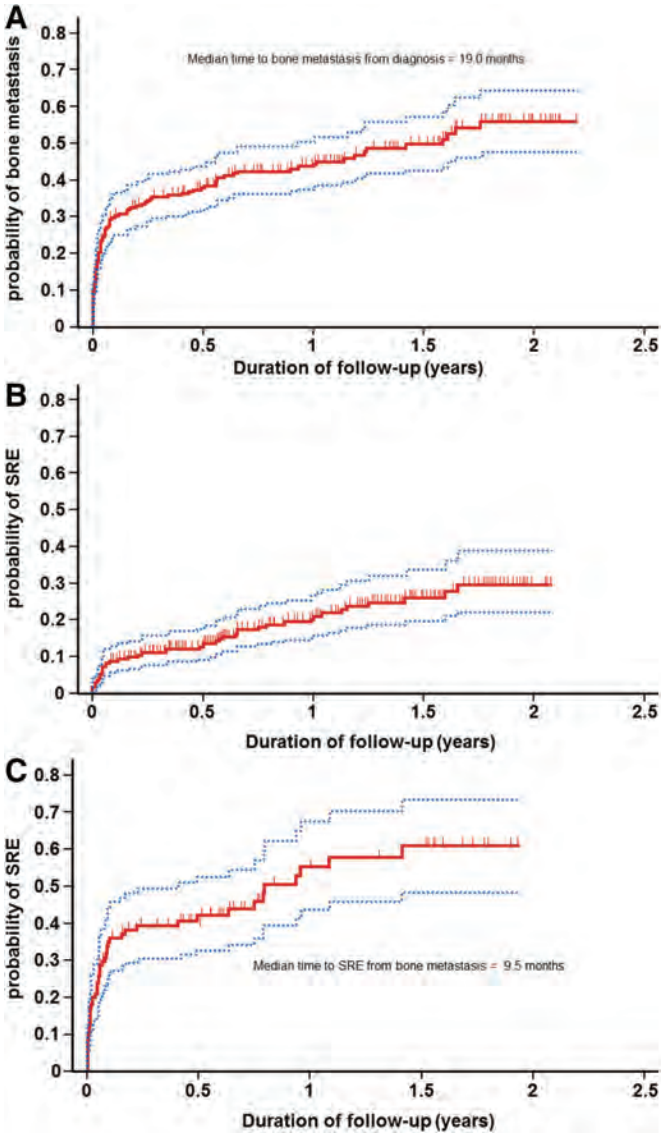

FIG. 1. *A,* Time to bone metastasis from diagnosis of lung cancer. *B,* Time to SRE from diagnosis of lung cancer. *C,* Time to SRE from bone metastasis. SRE, skeletal-related event.

radiation to bone (15.7%), pathologic fracture (4.7%), HCM (2.2%), and spinal cord compression (1.1%). Because spinal cord compression is considered an oncologic emergency, it requires urgent evaluation and treatment with corticosteroids and either radiotherapy or surgical decompression. Fortunately, we were able to reduce the incidence of spinal cord compression, as much as possible, because of close monitoring and appropriate treatment. A prospective study of 250 patients with a variety of solid tumors (120 of whom had NSCLC) complicated with BM found that the incidence of SRE was radiation to bone in 32%, pathologic fracture in 21%, surgery to bone in 4%, spinal cord compression in 4%, and HCM in 3% when patients were not treated prophylactically with zoledronate.[15] In a retrospective review of Japanese patients with NSCLC, among 135 stage IV patients, the most common SREs were the need for radiotherapy in 34.3% and hypercalcemia in 20%.[19]

Another retrospective study of 196 NSCLC patients with BM revealed that 47 of 110 patients without initial SRE eventually experienced their first SREs while receiving chemotherapy, whereas the accompanying type of SRE was radiotherapy in 39, pathologic fracture in 11, surgery to bone in six, and spinal cord compression in four patients.[23]

The median time to BM from diagnosis of lung cancer and to SREs from BM in our study was 19.0 and 9.5 months, respectively. To our knowledge, there seems to be no single prospective study which reports the interval to BM from diagnosis of stage IIIB NSCLC or LD-SCLC. Our result may be useful in future trials to prevent BM from lung cancer with bisphosphonate or denosumab, regarding the initiation of treatment. The median interval to SRE from BM was 9.5 months, compared with 171 days for NSCLC patients treated with 4 mg of zoledronate.[15] In a randomized phase III study comparing zoledronate with denosumab in the treatment of BMs in patients with advanced cancer (excluding breast and prostate cancer) or multiple myeloma, the median time to first on-study SRE was 20.6 months for denosumab and 16.3 months for zoledronate. The effect of denosumab on time to first on-study SRE relative to zoledronate by tumor stratification factors resulted in an HR of 0.84 for NSCLC (95% CI, 0.64 to 1.10; $p = 0.20$).[16] However, a direct comparison is not possible, as all of the patients in our study were not treated with zoledronate or denosumab, and were also treated with various types of anticancer drugs, including *EGFR*-TKIs, which were quite effective in *EGFR* mutation–positive patients.[8,9]

We evaluated the predictive factors of BM via multiple regression analysis separately in patients with SCLC and patients with NSCLC, because their biologic characteristics and clinical behavior differ. In case of NSCLC, stage IV (HR = 7.62; $p < 0.001$), PS 1 or greater at enrollment (HR = 1.82; $p = 0.046$), and high serum BALP at baseline (HR =10.36; $p = 0.002$) were found to be positive predictive factors. Two factors, excluding BALP, represent the tumor burden at the time of diagnosis of lung cancer. Therefore, the chance of developing BM increases with tumor progression. BALP has been investigated as a bone formation marker, but their association with clinical characteristics seems to vary depending on the tumor type, the nature of the BMs, and the effects of treatment. BALP measured in our study may represent active bone turnover as a result of subclinical metastasis to bone. Unexpectedly, EGFR-TKI treatment was not a negative predictive marker of BM. This may be related to the small number of active *EGFR* mutations (30 patients, 15.2%) and the fact that that most patients were treated with EGFR-TKI as a second- or third-line regimen (21 patients, 70%) instead of a first-line regimen. In SCLC, ED at enrollment (HR = 6.11; $p = 0.006$), higher serum LDH at baseline (HR = 9.14; $p = 0.016$), and higher serum PTHrP at baseline (HR = 0.38; $p = 0.048$) were found to be predictive factors. The former two factors represent the tumor burden at the time of diagnosis of lung cancer as in NSCLC while increasing the chance to develop BM. The reason why the higher serum PTHrP at baseline was a negative predictive factor of BM was not clear, but it may be acting

TABLE 3. Incidence and Type of SREs (N = 274)

	All SREs		New SREs during Follow-Up		Total	
	n	%	n	%	N	%
Any SRE	24	8.8	26	9.5	50	18.2
Pathologic fracture	9	3.3	4	1.5	13	4.7
Radiation to bone lesion	22	8	21	7.7	43	15.7
Surgery to bone	0	0	0	0	0	0
Spinal cord compression	2	0.7	1	0.4	3	1.1
Hypercalcemia of malignancy	1	0.4	5	1.8	6	2.2

SRE, skeletal-related event.

TABLE 4. Cox Regression Analysis for Bone Metastasis Incidence (Multivariable Analysis)

	NSCLC		SCLC	
Factor	**HR (95% CI)**	***p***	**HR (95% CI)**	***p***
NSCLC (stage IV/stage IIIB)	**7.62 (3.76–15.46**)	**<0.001**		
SCLC (ED/LD)			**6.11 (1.69–22.05)**	**0.006**
Sex (female/male)	1.02 (0.62–1.66)	0.952	0.90 (0.27–3.03)	0.875
Age (≥65/≤64)	0.69 (0.43–1.11)	0.124	0.74 (0.25–2.21)	9.585
PS (≥1/0)	**1.82 (1.01–3.29)**	**0.046**	1.87 (0.61–5.78)	0.276
LDH (1000 U)	1.07 (0.35–3.26)	0.911	**9.14 (1.51–55.14)**	**0.016**
Alb (g/dl)	0.82 (0.54–1.25)	0.362	0.70 (0.24–2.05)	0.513
Ca (mg/dl)	0.84 (0.60–1.16)	0.291	0.93 (0.54–1.60)	0.796
PTHrP (pmol/liter)	0.92 (0.76–1.11)	0.388	**0.38 (0.15–0.99)**	**0.048**
BALP (100 U/liter)	**10.36 (2.35–45.78)**	**0.002**	1.56 (0.60–4.05)	0.363
NTx (1000 nmol BCE/mmol CRE	0.67 (0.21–2.13)	0.499	0.29 (0.02–4.53)	0.374
Chemotherapy (yes/no)	0.51 (0.22–1.20)	0.125	0.52 (0.14–1.97)	0.340
EGFR-TKI (yes/no)	1.69 (0.76–3.75)	0.196		
First-line Plat + etoposide or Plat + CPT/other			0.44 (0.14–1.40)	0.165

HR, hazard ratio; CI, confidence interval; NSCLC, non–small-cell lung cancer; SCLC, small-cell lung cancer; ED, extensive disease; LD; limited disease, PS, performance status; Alb, albumin; PTHrP, parathyroid hormone–related peptide; BALP, bone alkaline phosphatase; NTx, cross-linked N-telopeptide of type 1 collagen; EGFR-TKI, epidermal growth factor receptor-tyrosine kinase inhibitor; Plat, platinum; LDH, lactate dehydrogenase; BCE, ; CRE, ; CPT,.

as a nonfunctioning tumor marker. A first-line regimen with platinum + CPT-11 or platinum + etoposide tended to be a negative predictive factor of BM (HR = 0.44; $p = 0.165$) but did not reach a significant level, probably because of the small sample size.

Another multiple regression analysis evaluating the predictive factors of SREs from initial documentation of BM demonstrated that stage IV NSCLC (HR = 5.58; $p < 0.001$) and zoledronate use after BM were positive factors, whereas age 65 or older (HR = 0.50; $p = 0.038$) was a negative predictive factor for SRE in NSCLC. Multiple regression analysis was not performed for SCLC, because the number of patients with SREs was only nine and all SREs occurred in ED-SCLC. The reason why an age of more than 65 years in NSCLC was a negative predictive factor for SREs is not clear in our study. This might be related to the physical activity of younger patients, as they enjoyed moving, without pain or limitation, and needed to receive radiation therapy more frequently than elder patients. Otherwise, older patients might have undergone single-agent chemotherapy for longer periods, or received molecular-targeted agents more often than younger patients. These factors need to be elucidated in a future trial. Surprisingly, zoledronate use after BM was a positive predictive factor of SREs. This may be because of the fact that zoledronate was used at the discretion of the investigators, and that they tended not to administer zoledronate at an early stage, but at a progressive stage of BM (bias due to the treatment by indication).

Serum albumin was a marginally significant negative predictive factor of SRE (HR = 0.59; $p = 0.070$) by multivariate analysis. High serum albumin reflects that patients have a good appetite, and can maintain good general condition, such as body weight. These two factors are also known as a good prognostic factor.[26–28] In contrast to other reports, NTx was not a predictive factor of SRE ($p = 0.758$) in our study.[29,30] Brown et al.[29] reported a statistically significant correlation between N-telopeptide levels at baseline and a range of skeletal complications in 121 bisphosphonate-treated patients with breast or prostate cancer with BM. Their definition of SRE was radiotherapy to bone, hypercalcemia, spinal cord compression, pathological fracture, surgery to bone, hospital admissions for control of bone pain, and/or

TABLE 5. Cox Regression Analysis for Skeletal-Related Event Incidence in Patients with NSCLC (Multivariate Analysis[a])

Factor	HR (95% CI)	*p*
Stage IV/stage IIIB	**5.58 (2.21–14.10)**	**<0.001**
Sex (female/male)	0.98 (0.49–1.95)	0.952
Age (≥65/≤64)	**0.50 (0.26–0.96)**	**0.038**
PS (≥1/0)	1.40 (0.61–3.22)	0.423
LDH (1000 U)	0.28 (0.04–2.17)	0.222
Alb (g/dl)	0.59 (0.33–1.05)	0.070
Ca (mg/dl)	0.89 (0.58–1.36)	0.589
PTHrP (pmol/liter)	0.88 (0.66–1.18)	0.407
BALP (100 U/liter)	1.21 (0.88–1.66)	0.246
NTx (1000 nmol BCE/mmol CRE)	0.68 (0.16–2.88)	0.605
Chemotherapy (yes/no)	0.64 (0.24–1.71)	0.371
EGFR-TKI (yes/no)	0.75 (0.27–2.04)	0.569
Zoledronate use after bone metastasis	2.64 (1.25–5.57)	0.011

[a]Multivariate analysis was not done because of small number of events (9 skeletal-related events).

NSCLC, non–small-cell lung cancer; HR, hazard ratio; CI, confidence interval; PS, performance status; LDH, lactate dehydrogenase; Alb, albumin; PTHrP, parathyroid hormone–related peptide; BALP, bone alkaline phosphatase; NTx, cross-linked N-telopeptide of type I collagen; EGFR-TKI, epidermal growth factor receptor-tyrosine kinase inhibitor; BCE, ; CRE, .

death due to metastatic bone disease. The total number of SREs was 111 in 121 patients during 6 months. In another report, which focused on metastatic NSCLC without zoledronate therapy, high NTx level at baseline was associated with an increased rate of first SRE, and this increased rate was maintained throughout the study period. Overall, there were a total of 110 SREs in 115 patients during 21 months.[30] However, there were only 50 SREs among 111 lung cancer patients with BM over a median follow-up duration of 13.8 months, and the number of SREs was relatively low in the current study, compared with these two reports. This may be the reason why NTx at baseline was not a predictive marker of SREs in our study.

CONCLUSIONS

The incidence of BM at initial diagnosis was 48% in patients with stage IV NSCLC and 40% in patients with ED-SCLC. Forty-six percent of the patients who developed BM had SREs at enrollment and during the follow-up period. Multivariate analysis revealed that the factors predicting BMs were stage IV, PS 1 or greater, higher serum BALP at baseline in case of NSCLC and ED, higher serum LDH at baseline, and higher serum PTHrP at baseline in case of SCLC, and that the factors predicting SRE in NSCLC were stage IV, age 64 or younger, and zoledronate use after BM. These factors should be taken into consideration in future randomized studies evaluating BM and SREs.

ACKNOWLEDGMENTS

The authors thank Mr. Hitoshi Inoue and other staff members of Comprehensive Support Project for Health Outcomes Research (CSP-HOR) data center for data management.

REFERENCES

1. Mundy GR. Metastasis to bone: causes, consequences and therapeutic opportunities. *Nat Rev Cancer* 2002;2:584–593.
2. Coleman RE. Metastatic bone disease: clinical features, pathophysiology and treatment strategies. *Cancer Treat Rev* 2001;27:165–176.
3. Schiller JH, Harrington D, Belani CP, et al; Eastern Cooperative Oncology Group. Comparison of four chemotherapy regimens for advanced non-small-cell lung cancer. *N Engl J Med* 2002;346:92–98.
4. Ohe Y, Ohashi Y, Kubota K, et al. Randomized phase III study of cisplatin plus irinotecan versus carboplatin plus paclitaxel, cisplatin plus gemcitabine, and cisplatin plus vinorelbine for advanced non-small-cell lung cancer: four-Arm Cooperative Study in Japan. *Ann Oncol* 2007;18:317–323.
5. Paz-Ares L, Marinis FD, Dediu M, et al: PARAMOUNT: final overall survival (OS) results of the phase III study of maintenance pemetrexed (pem) plus best supportive care (BSC) versus placebo (plb) plus BSC immediately following induction treatment with pem plus cisplatin (cis) for advanced nonsquamous (NS) non-small cell lung cancer (NSCLC). *ASCO Meeting Abstracts* 2012;30:7507
6. Katakami N, Gemma A, Sakai H, et al: Randomized phase III trial of S-1 plus cisplatin versus docetaxel plus cisplatin for advanced non-small-cell Lung cancer (TCOG0701)—CATS TRIAL (cisplatin and TS-1 TRIAL). *ASCO Meeting Abstracts* 2012;30:7515
7. Yang CH, Fukuoka M, Mok TS, et al: Final overall survival (OS) results from a phase III, randomised, open-label, first-line study of gefitinib (G) v carboplatin/paclitaxel (C/P) in clinically selected patients with advanced nonsmall cell lung cancer (NSCL) in Asia (IPASS). *Ann Oncol* 2010;21(Suppl 8):LBA 2
8. Inoue A, Kobayashi K, Maemondo M, et al; Final overall survival results of NEJ002, a phase III trial comparing gefitinib to carboplatin (CBDCA) plus paclitaxel (TXL) as the first-line treatment for advanced non-small cell lung cancer (NSCLC) with EGFR mutations. *ASCO Meeting Abstracts* 2011;29:7519
9. Mitsudomi T, Morita S, Yatabe Y, et al: Updated overall survival results of WJTOG 3405, a randomized phase III trial comparing gefitinib (G) with cisplatin plus docetaxel (CD) as the first-line treatment for patients with non-small cell lung cancer harboring mutations of the epidermal growth factor receptor (EGFR). *ASCO Meeting Abstracts* 2012;30:7521
10. Noda K, Nishiwaki Y, Kawahara M, et al; Japan Clinical Oncology Group. Irinotecan plus cisplatin compared with etoposide plus cisplatin for extensive small-cell lung cancer. *N Engl J Med* 2002;346:85–91.
11. Hanna N, Bunn PA Jr, Langer C, et al. Randomized phase III trial comparing irinotecan/cisplatin with etoposide/cisplatin in patients with previously untreated extensive-stage disease small-cell lung cancer. *J Clin Oncol* 2006;24:2038–2043.
12. Turrisi AT 3rd, Kim K, Blum R, et al. Twice-daily compared with once-daily thoracic radiotherapy in limited small-cell lung cancer treated concurrently with cisplatin and etoposide. *N Engl J Med* 1999;340:265–271.
13. Takada M, Fukuoka M, Kawahara M, et al. Phase III study of concurrent versus sequential thoracic radiotherapy in combination with cisplatin and etoposide for limited-stage small-cell lung cancer: results of the Japan Clinical Oncology Group Study 9104. *J Clin Oncol* 2002;20:3054–3060.
14. Hortobagyi GN, Theriault RL, Porter L, et al. Efficacy of pamidronate in reducing skeletal complications in patients with breast cancer and lytic bone metastases. Protocol 19 Aredia Breast Cancer Study Group. *N Engl J Med* 1996;335:1785–1791.
15. Rosen LS, Gordon D, Tchekmedyian S, et al. Zoledronic acid versus placebo in the treatment of skeletal metastases in patients with lung cancer and other solid tumors: a phase III, double-blind, randomized trial—the Zoledronic Acid Lung Cancer and Other Solid Tumors Study Group. *J Clin Oncol* 2003;21:3150–3157.
16. Henry DH, Costa L, Goldwasser F, et al. Randomized, double-blind study of denosumab versus zoledronic acid in the treatment of bone metastases in patients with advanced cancer (excluding breast and prostate cancer) or multiple myeloma. *J Clin Oncol* 2011;29:1125–1132.
17. Kosteva J, Langer C. The changing landscape of the medical management of skeletal metastases in nonsmall cell lung cancer. *Curr Opin Oncol* 2008;20:155–161.
18. Kosteva J, Langer CJ: Incidence and distribution of skeletal metastases in NSCLC in the era of PET [abstract]. *Lung Cancer* 2004;46 (Suppl 1):S45

19. Tsuya A, Kurata T, Tamura K, Fukuoka M. Skeletal metastases in non-small cell lung cancer: a retrospective study. *Lung Cancer* 2007;57:229–232.
21. Schumacher T, Brink I, Mix M, et al. FDG-PET imaging for the staging and follow-up of small cell lung cancer. *Eur J Nucl Med* 2001;28:483–488.
22. Cheran SK, Herndon JE 2nd, Patz EF Jr. Comparison of whole-body FDG-PET to bone scan for detection of bone metastases in patients with a new diagnosis of lung cancer. *Lung Cancer* 2004;44:317–325.
23. Bae HM, Lee SH, Kim TM, et al. Prognostic factors for non-small cell lung cancer with bone metastasis at the time of diagnosis. *Lung Cancer* 2012;77:572–577.
24. Coleman RE, Whitaker KB, Moss DW, Mashiter G, Fogelman I, Rubens RD. Biochemical prediction of response of bone metastases to treatment. *Br J Cancer* 1988;58:205–210.
25. Berruti A, Dogliotti L, Gorzegno G, et al. Differential patterns of bone turnover in relation to bone pain and disease extent in bone in cancer patients with skeletal metastases. *Clin Chem* 1999;45(8 Pt 1):1240–1247.
26. Finkelstein DM, Ettinger DS, Ruckdeschel JC. Long-term survivors in metastatic non-small-cell lung cancer: an Eastern Cooperative Oncology Group Study. *J Clin Oncol* 1986;4:702–709.
27. Hoang T, Xu R, Schiller JH, Bonomi P, Johnson DH. Clinical model to predict survival in chemonaive patients with advanced non-small-cell lung cancer treated with third-generation chemotherapy regimens based on eastern cooperative oncology group data. *J Clin Oncol* 2005;23:175–183.
28. Sculier JP, Chansky K, Crowley JJ, Van Meerbeeck J, Goldstraw P; International Staging Committee and Participating Institutions. The impact of additional prognostic factors on survival and their relationship with the anatomical extent of disease expressed by the 6th Edition of the TNM Classification of Malignant Tumors and the proposals for the 7th Edition. *J Thorac Oncol* 2008;3:457–466.
29. Brown JE, Thomson CS, Ellis SP, Gutcher SA, Purohit OP, Coleman RE. Bone resorption predicts for skeletal complications in metastatic bone disease. *Br J Cancer* 2003;89:2031–2037.
30. Brown JE, Cook RJ, Major P, et al. Bone turnover markers as predictors of skeletal complications in prostate cancer, lung cancer, and other solid tumors. *J Natl Cancer Inst* 2005;97:59–69.

Leukemia Research 38 (2014) 1451–1459

Contents lists available at ScienceDirect

Leukemia Research

journal homepage: www.elsevier.com/locate/leukres

Functional analysis of the *SEPT9-ABL1* chimeric fusion gene derived from T-prolymphocytic leukemia

Hidetsugu Kawai[a,b], Hiromichi Matsushita[a,c,e,*], Rikio Suzuki[b], Yin Sheng[a], Jun Lu[a], Hideyuki Matsuzawa[d], Takashi Yahata[a], Mitsuyo Tsuma-Kaneko[a,b], Hideo Tsukamoto[d], Hiroshi Kawada[a,b], Yoshiaki Ogawa[b], Kiyoshi Ando[a,b,e,**]

[a] *Research Center for Cancer Stem Cell, Tokai University School of Medicine, Isehara, Kanagawa, Japan*
[b] *Department of Hematology/Oncology, Tokai University School of Medicine, Isehara, Kanagawa, Japan*
[c] *Department of Laboratory Medicine, Tokai University School of Medicine, Isehara, Kanagawa, Japan*
[d] *Support Center for Medical Research and Education, Tokai University School of Medicine, Isehara, Kanagawa, Japan*
[e] *Medical Research Institute, Tokai University, Isehara, Kanagawa, Japan*

ARTICLE INFO

Article history:
Received 1 July 2014
Received in revised form 18 August 2014
Accepted 24 August 2014
Available online 30 August 2014

Keywords:
SEPT9-ABL1
ABL1 fusion gene
Tyrosine kinase inhibitors

ABSTRACT

We analyzed the function of a SEPT9-ABL1 fusion identified in a case of T-prolymphocytic leukemia with tyrosine kinase inhibitor (TKI) resistance. Five isoforms with different N-termini, including SEPT9a-ABL1, SEPT9b-ABL1, SEPT9d-ABL1, SEPT9e-ABL1 and SEPT9f-ABL1, were detected in the leukemic cells. All isoforms except SEPT9d-ABL1 are localized in the cytoplasm, undergo autophosphorylation and phosphorylate the downstream targets, STAT-5 and Crkl, and provided IL-3-independence and *in vivo* invasiveness to 32D cells. Additionally, these SEPT9-ABL1 isoforms were resistant to TKIs *in vitro* and *in vivo*, in comparison to BCR-ABL1. These findings demonstrated that SEPT9-ABL1 had oncogenic activity and conferred resistance to TKIs.

1. Introduction

The *Abelson* (*ABL1*) gene encoding a non-receptor tyrosine kinase is involved in protein networks that control cell proliferation, survival, migration and invasion [1]. To date, nine ABL1 fusion genes have been reported in various hematological malignancies [2]. They are thought to contribute to leukemogenesis through aberrant ABL1 signaling. *BCR-ABL1* is the most characterized of these fusion genes. The identification of *BCR-ABL1* is a criterion for the diagnosis of chronic myeloid leukemia (CML), and the fusion is also detected in 25–30% of adult cases of B-cell acute lymphoblastic leukemia (B-ALL) [3]. However, the other ABL1 fusion genes are detected in a relatively limited number of cases; *NUP214-ABL1* is detected only in 5% of T-cell acute lymphoblastic leukemias (T-ALL) and another seven ABL1 fusion genes have been described in case reports [2].

These fusion proteins are divided into two groups by their structure. The first group including *BCR-ABL1*, *ETV6-ABL1*, *EML1-ABL1*, *NUP214-ABL1* and *ZMIZ1-ABL1* has Src homology 2 (SH2) and 3 (SH3) domains of ABL1, and is found in various hematological malignancies, such as CML, B-ALL, T-ALL and acute myeloid leukemia (AML). The second group including *RCSD1-ABL1*, *SFPQ-ABL1*, *FOXP1-ABL1* and *SNX2-ABL1*, which were only identified in B-ALL, does not have the autoinhibitory SH3 domain [2,4]. Both groups of fusion gene products possess constitutive kinase activity, making them possible therapeutic targets for tyrosine kinase inhibitors (TKIs) such as imatinib, dasatinib and nilotinib.

We recently identified a novel chimeric fusion gene, *Septin9* (*SEPT9*)-ABL1, harboring SH3 and SH2 domains, in a patient with T-prolymphocytic leukemia (T-PLL). The patient was unresponsive to imatinib and dasatinib, and eventually died due to systemic infiltration of leukemic cells, suggesting that *SEPT9-ABL1* had oncogenic activities, as well as resistance to TKIs [5].

The SEPT9 product is a GTP-binding protein. It is ubiquitously expressed, and is considered to be a component of

* Corresponding author at: Department of Laboratory Medicine, Tokai University School of Medicine, 143 Shimokasuya, Isehara, Kanagawa 259-1193, Japan. Tel.: +81 463 93 1121; fax: +81 463 93 8607.
** Corresponding author at: Department of Hematology/Oncology, Tokai University School of Medicine, 143 Shimokasuya, Isehara, Kanagawa 259-1193, Japan. Tel.: +81 463 93 1121; fax: +81 463 92 4511.
E-mail addresses: hmatsu@is.icc.u-tokai.ac.jp (H. Matsushita), andok@keyaki.cc.u-tokai.ac.jp (K. Ando).

http://dx.doi.org/10.1016/j.leukres.2014.08.015
0145-2126/

cytoskeletal structures such as actin filaments, microtubules and cellular membranes [6]. SEPT9 possesses a proline rich region, a polybasic domain and a *p* loop-based GTP-binding domain (CDC/Septin domain with GTPase activity), which is important for hetero-oligomerization between SEPT9 and other proteins [7]. Whereas the C-terminus of SEPT9 with the CDC/Septin domain contributes to forming a MLL-SEPT9 fusion protein [8], the N-terminus of SEPT9 with the proline rich region forms SEPT9-ABL1. Because the six SEPT9 isoforms with different N-termini exhibit different intracellular distributions [9], it is expected that there are also six isoforms in SEPT9-ABL1, with different intracellular distribution and functions.

The current study was performed to evaluate the oncogenic activities and the sensitivity to TKIs of each isoform of *SEPT9-ABL1*. We found that SEPT9-ABL1 exhibited oncogenicity and conferred TKI resistance *in vitro* and *in vivo*, although the activities varied among the SEPT9-ABL1 isoforms.

2. Materials and methods

2.1. Reverse transcription (RT)-PCR analysis and cloning of SEPT9-ABL1 isoforms

The patient's sample was obtained after written informed consent was provided in accordance with the Declaration of Helsinki, and with approval from the Tokai University Committee on Clinical Investigation (Permit number: #12I-09). Total RNA was extracted from a sample using the RNeasy reagents (QIAGEN). The cDNA was synthesized using SuperScript VILO (Invitrogen), and was amplified by PCR using specific primers (Supplementary Table 1). After confirming the sequences of the PCR products, they were inserted into a MIGR1 retroviral vector [10].

Supplementary material related to this article can be found, in the online version, at http://dx.doi.org/10.1016/j.leukres.2014.08.015.

2.2. Cell culture, retroviral infection and cell proliferation assay

HEK293 T cells and a packaging cell line consisting Plat-gp cells were cultured in DMEM medium containing 10% fetal bovine serum (FBS) at 37 °C under 5% CO_2. The transduction of the plasmids into these attached cells was performed using Fugene HD (Promega), according to the manufacturer's protocol.

We cultured 32D cells, a murine interleukin3 (IL-3)-dependent hematopoietic cell line, in RPMI 1640 medium containing 10% fetal bovine serum (FBS) and recombinant murine IL-3 (5 ng/ml) at 37 °C under 5% CO_2. The cells were retrovirally transduced with *SEPT9-ABL1* isoforms (*SEPT9a-ABL1*, *SEPT9b-ABL1*, *SEPT9d-ABL1*, *SEPT9e-ABL1* and *SEPT9f-ABL1*) as described previously [11], and were sorted by their expression of EGFP using a FACSAria instrument (BD).

To evaluate the cell proliferation, the cells were cultured in 12-well plates at a density of 1×10^5 cells/ml, with or without murine IL-3 (5 ng/ml). The viable cells were counted after 48 h.

To evaluate the TKI sensitivity, ten thousand cells were cultured in 96-well plates with increasing concentrations of imatinib (Santa Cruz Biotechnology) or dasatinib (LC Laboratories). After 48 h, the cell proliferation was evaluated by the Cell Titer-Glo Luminescent cell viability assay (Promega).

2.3. Western blot analysis

Total cell lysates prepared using RIPA buffer were electrophoresed and transferred to polyvinylidene fluoride (PVDF) membranes. They were incubated with 2000- and 4000-fold diluted primary and secondary antibodies, respectively, and were visualized with Immobilon Western Chemiluminescent HRP Substrate (Millipore). The antibodies used were as follows: anti-β-actin from Sigma–Aldrich, anti-phospho-Abl (Tyr412), anti-Abl, anti-phospho-Stat5 (Tyr694), anti-Stat5, anti-phospho-Crkl (Tyr207), anti-Crkl and horseradish peroxidase (HRP)-conjugated anti-rabbit IgG from Cell Signaling, and HRP-conjugated anti-mouse IgG from GE Healthcare.

2.4. Immunocytochemistry

Cytospin slides with fifty thousand cells were fixed in ethanol, blocked by 5% normal goat serum (NGS) at room temperature (RT) for 1 h, and incubated with anti-Abl1 (1:200) (Sigma–Aldrich) and anti-SEPT9 (1:50) antibodies (Abcam). They were then incubated with secondary antibodies conjugated with Alexa 488 (1:200) or Alexa 594 (1:200) (Alexa Fluor). Nuclear staining was performed with Slow Fade Gold antifade reagent with DAPI (Life Technologies). Images were acquired using a confocal laser microscope (LSM510 META spectrometer, Carl Zeiss).

2.5. In vivo tumor models

We performed intravenous and subcutaneous syngeneic transplantation of 5×10^5 and 2×10^6 cells, respectively, into C3H/HeJ mice. To evaluate the TKI sensitivity, mice were orally treated with dasatinib. The treatment was started the day after the cell implantation. In the intravenous tumor model, mice were evaluated histopathologically to confirm the infiltration of transplanted cells into the bone marrow, spleen and liver using hematoxylin eosin staining and anti-EGFP antibody staining (Molecular Probes). In the subcutaneous tumor model, the diameters and heights of the subcutaneous tumors were measured twice a week.

All experiments using animals were approved by the animal care committee of Tokai University (Permit number: #132028).

2.6. Statistical analysis

The significance of the differences between two groups was determined using the Mann–Whitney test. A value of $p < 0.05$ was considered to be statistically significant.

3. Results

3.1. Identification of SEPT9-ABL1 isoforms

There have been six Septin 9 (SEPT9) isoforms reported with different N-termini. Fig. 1A shows the presumed structures of the six SEPT9-ABL1 isoforms, SEPT9a-ABL1 to SEPT9f-ABL1, corresponding to SEPT9a to SEPT9f. The SEPT9-ABL1 isoforms are thought to share the C-terminal structure with BCR-ABL1. In the N-termini, they possess only a small part of the CDC/Septin domain from SEPT9. SEPT9a-ABL1, SEPT9b-ABL1 and SEPT9c-ABL1 differed by a few amino acids in the N-terminal sequence. SEPT9d-ABL1 had a different structure in the N-terminal sequence compared to SEPT9a-ABL1 to SEPT9c-ABL1. SEPT9e-ABL1 and SEPT9f-ABL1 were translated from the second and fourth methionine present in SEPT9a-ABL1 to SEPT9c-ABL1, respectively (Fig. 1A).

To identify the *SEPT9-ABL1* isoforms expressed in the T-PLL patient, RT-PCR was performed. The transcripts of all SEPT9-ABL1 isoforms but SEPT9c-ABL1 were detected (Fig. 1B). All five detectable isoforms were cloned into MIGR1 retroviral vectors after sequencing, which revealed no point mutations. They were transduced into HEK293T cells to confirm their expression and size by a Western blot analysis. Three *SEPT9-ABL1* isoforms of different sizes were detected in the patient with T-PLL; 180, 170 and 150 kDa, which corresponded approximately to SEPT9a-ABL1 and SEPT9b-ABL1, SEPT9d-ABL1 and SEPT9e-ABL1 and SEPT9f-ABL1, respectively (Fig. 1C).

These findings suggested that five SEPT9-ABL1 isoforms, but not SEPT9c-ABL1, were expressed in the T-PLL patient.

3.2. Intracellular distribution of the SEPT9-ABL1 isoforms

In order to determine the functions of these SEPT9-ABL1 isoforms *in vitro*, their cellular distribution in 32D cells was first evaluated by immunocytochemistry. The 32D cells transfected with the MIGR1 control vector (32D/MIGR1) expressed wild-type SEPT9 in the both cytoplasm and nucleus, but did not express wild-type ABL1, suggesting that the anti-ABL1 antibody specifically recognized the SEPT9-ABL1 fusion proteins when they were exogenously expressed in 32D cells. SEPT9a-ABL1, SEPT9b-ABL1 and SEPT9e-ABL1 were mainly localized in the cytoplasm, with faint distribution in the nucleus. SEPT9f-ABL1 was localized predominantly in the cytoplasm. However, SEPT9d-ABL1 was weakly expressed only in the cytoplasm (Fig. 2A and B).

The anti-SEPT9 antibody recognized both wild-type and fusion SEPT9 products. 32D cells with SEPT9a-ABL1 (32D/SEPT9a-ABL1), SEPT9b-ABL1 (32D/SEPT9b-ABL1), SEPT9e-ABL1 (32D/SEPT9e-ABL1) and SEPT9f-ABL1 (32D/SEPT9f-ABL1) exhibited mainly cytoplasmic signals from the anti-SEPT9 antibody, in comparison to 32D/MIGR1. The 32D cells with SEPT9d-ABL1 (32D/SEPT9d-ABL1)

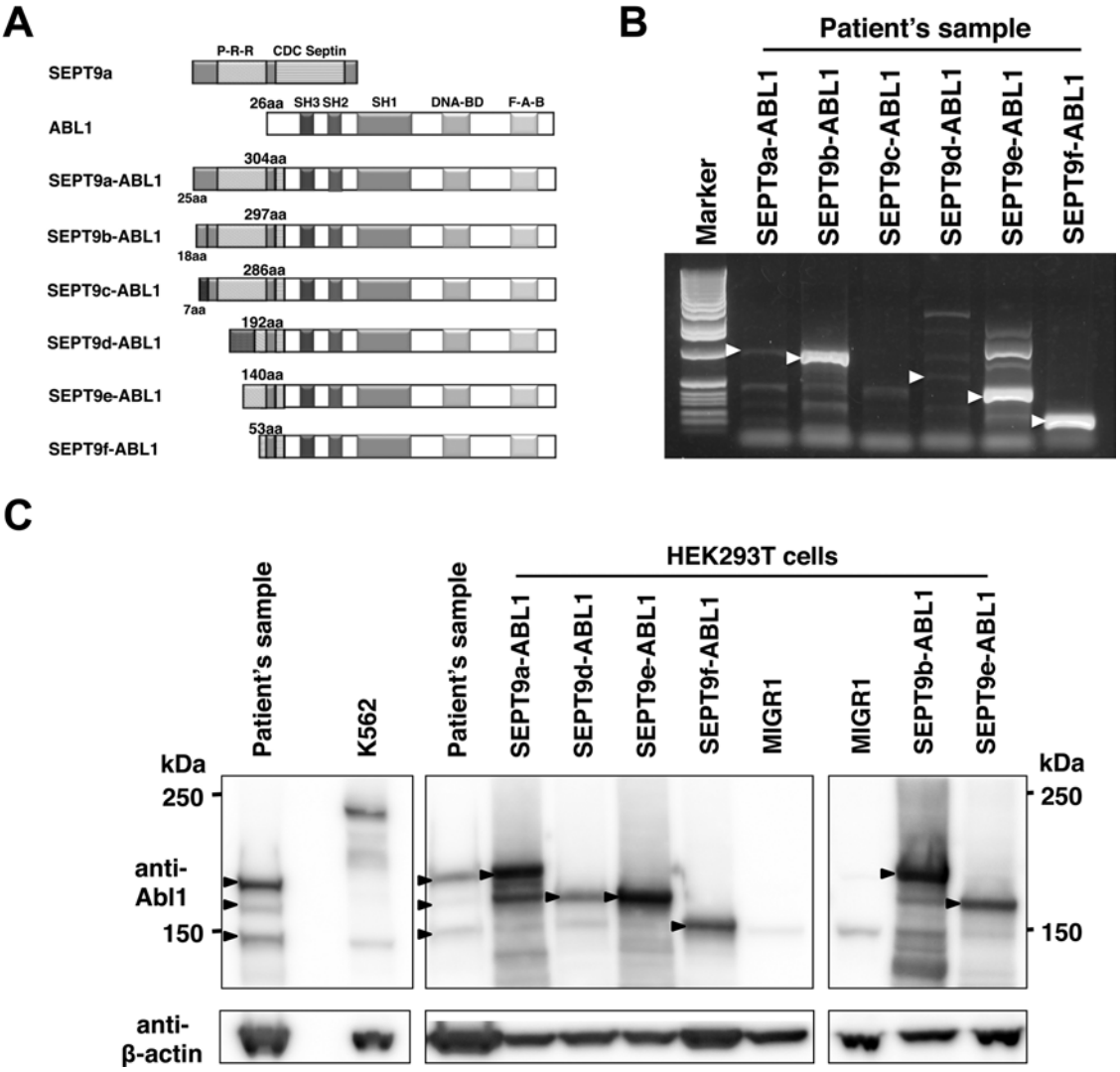

Fig. 1. Identification of *SEPT9-ABL1* isoforms. (A) The presumed structures of SEPT9-ABL1. The number of amino acids is also indicated. aa, amino acid; DNA-BD, DNA binding domain; F-A-B, F-actin binding; KD, kinase domain (SH1); P-R-R, proline-rich region; SH, SRC homology. (B) The mRNA expression analysis of the *SEPT9-ABL1* isoforms in the T-PLL patient using RT-PCR. (C) The overexpression of SEPT9-ABL1 isoforms in HEK293 T cells. The sizes were comparable among the three kinds of *SEPT9-ABL1* isoforms with different molecular weights in the T-PLL patient. K562 cells, which express p210 BCR-ABL1, were used as a positive control. The expression of β-actin was used as an internal control.

showed cytoplasmic, but not nuclear, signals generated by the anti-SEPT9 antibody.

These findings suggested that the SEPT9-ABL1 isoforms were localized preferentially in the cytoplasm, indicating the aberrant distribution of wild-type SEPT9 proteins.

3.3. Phosphorylation of SEPT9-ABL1 isoforms and their downstream targets

The phosphorylation status of exogenous SEPT9-ABL1 fusion products and their downstream targets in 32D cells was analyzed. IL-3 was deprived from the culture media to eliminate the effects of IL-3 signaling. All SEPT9-ABL1 isoforms but SEPT9d-ABL1 exhibited phosphorylation, which was the strongest in 32D/SEPT9f-ABL1 cells. Stat5, indispensable for BCR-ABL1-induced leukemogenesis [12], was phosphorylated most strongly in the 32D/SEPT9f-ABL1 cells. On the other hand, Crkl, a substrate of BCR-ABL in the cytoplasm [13], was phosphorylated in 32D cells with all of theSEPT9-ABL1 isoforms (Fig. 2C). These findings demonstrated that the phosphorylation of SEPT9-ABL1 and Stat5 was the highest in SEPT9f-ABL1, and was not detected in SEPT9d-ABL1.

3.4. Proliferation of 32D cells with the SEPT9-ABL1 isoforms

To evaluate the proliferation induced by SEPT9-ABL1, the cellular proliferation rates were examined in cells expressing the different isoforms. The 32D/MIGR1 cells only proliferated in culture with IL-3. The 32D cells with BCR-ABL1 (32D/BCR-ABL1) proliferated at the same rate as 32D/MIGR1 cells, regardless of the presence of IL-3. The 32D cells with SEPT9-ABL1 isoforms were less proliferative than 32D/BCR-ABL1 and 32D/MIGR1 cells in culture with IL-3. The 32D cells with all the isoforms, except 32/SEPT9d-ABL1 cells, were also able to proliferate in an IL-3-independent manner. The 32D/SEPT9d-ABL1 cells survived, but did not proliferate in culture without IL-3 (Fig. 2D). When the ratios of cell proliferation without/with IL-3 were compared for each isoform, that of the 32D/SEPT9f-ABL1 cells was the highest of all the isoforms and was equivalent to that of BCR-ABL1, suggesting that the cellular proliferation induced by SEPT9f-ABL1 was not affected by

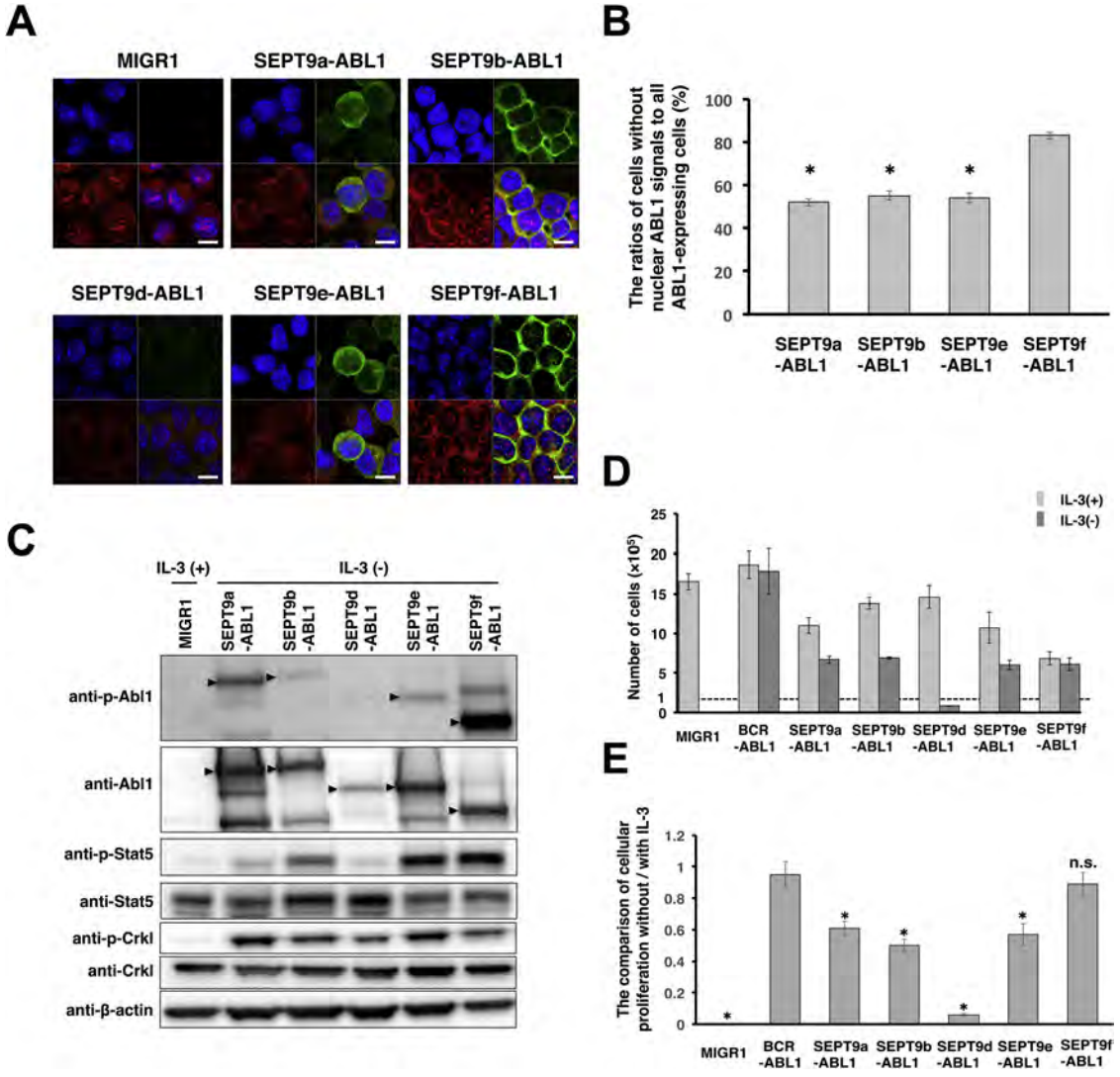

Fig. 2. The oncogenic activities of SEPT9-ABL1 *in vitro*. (A) The intracellular distributions of the SEPT9-ABL1 isoforms in 32D cells. Fluorescent immunohistochemical analyses were performed using anti-Abl1 (green, upper right) and anti-SEPT9 antibodies (red, lower left). Nuclear staining was performed using DAPI (blue, upper left). The merged images are shown in the lower right corner of each panel. The scale bars indicate 10 μM. (B) The ratios of cells without nuclear ABL1 signals to all ABL1-expressing cells for each SEPT9-ABL1 isoforms. Among all the cells with ABL1 signals (green) distributed in either nuclear or cytoplasmic regions, the cells with no co-localization of green and DAPI (blue) signals were counted. The averages of three independent experiments are shown. At least 30 cells were counted in each transfection. SEPT9f-ABL1 was localized significantly more often in the cytoplasm compared to SEPT9a-ABL1, SEPT9b-ABL1 and SEPT9e-ABL1. * Indicates p values < 0.05. (C) The phosphorylation status of the SEPT-ABL1 isoforms and their downstream targets, Stat5 (90 kDa) and Crkl (39 kDa), in 32D cells. The phosphorylated forms and total amounts of each protein were evaluated by an immunoblot analysis. The expression of β-actin was used as an internal control. (D) The proliferation of 32D cells with SEPT9-ABL1 isoforms *in vitro*. One hundred thousand cells were seeded, and the cell numbers in cultures with or without IL-3 were evaluated after 48 h. The averages of three independent experiments are shown. (E) A comparison of the cell proliferation rates without/with IL-3 in 32D cells harboring each SEPT9-ABL1 isoform. The values were calculated from the data presented in D. * Indicates p values < 0.05 compared with BCR-ABL1. n.s., not significant.

IL-3 signaling (Fig. 2E). These results revealed that 32D/SEPT9-ABL1 cells proliferated, to varying degrees, in an IL-3-independent manner.

3.5. Oncogenic activity in vivo

The oncogenic activity of SEPT9-ABL1 *in vivo* was examined using the 32D/SEPT9f-ABL1 cells, and was compared with 32D/MIGR1 and 32D/BCR-ABL1 cells used as negative and positive controls, respectively. All mice implanted with 32D/MIGR1 cells survived more than 100 days, whereas the mice with 32D/BCR-ABL1 cells died after 14–27 days (32D/MIGR1 *vs.* 32D/BCR-ABL1, $p < 0.05$). Mice with 32D/SEPT9f-ABL1 cells died from 21 to 47 days after the transplantation (32D/MIGR1 *vs.* 32D/SEPT9f-ABL1, $p < 0.05$) (Fig. 3A). All the dead mice had marked hepatosplenomegaly. A histological analysis showed the infiltration of 32D/SEPT9f-ABL1 cells in the bone marrow, spleen and liver (Fig. 3B). These findings revealed that 32D/SEPT9f-ABL1 cells infiltrated systemically in the transplanted mice.

3.6. TKIs sensitivity in vitro

Because the T-PLL patient with SEPT9-ABL1 was reported to be clinically resistant to TKIs, including imatinib and dasatinib [5], their 50% inhibitory concentration (IC_{50}) was analyzed using 32D cells with the SEPT9-ABL1 isoforms. Compared to 32D/BCR-ABL1 cells, the IC_{50} of imatinib and dasatinib were higher in 32D/SEPT9-ABL1-expressing cells except for 32D/SEPT9d-ABL1 cells; there were 4.3- to 11.1-fold resistance to imatinib (0.96–2.52 μM *vs.* 0.23 μM for BCR-ABL1) and 14.4- to 24.2-fold resistance to dasatinib (9.5–16.0 nM *vs.* 0.66 nM for BCR-ABL1) (Fig. 4A). These results revealed that all SEPT9-ABL1 isoforms, except for

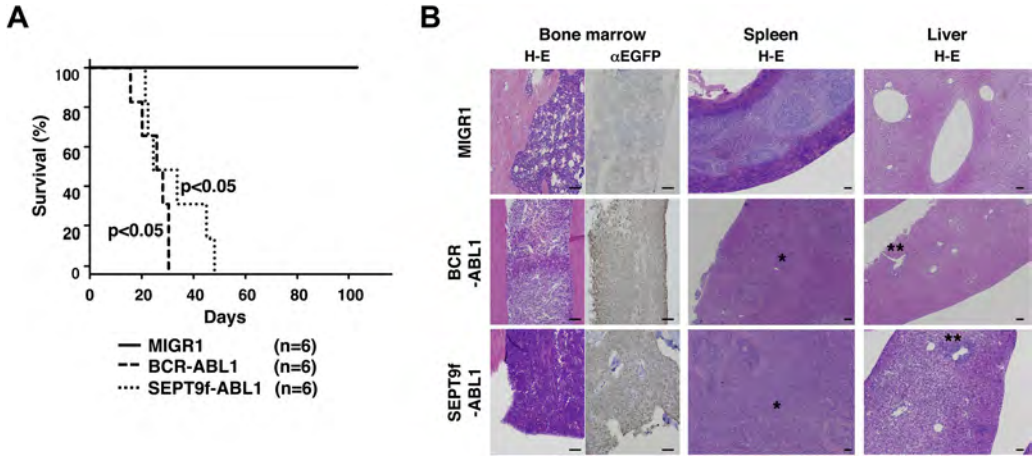

Fig. 3. The oncogenic activity of SEPT9f-ABL1 *in vivo*. (A) The Kaplan–Meier survival curves of mice transplanted with 32D/MIGR1, 32D/BCR-ABL1 and 32D/SEPT9f-ABL1 cells. The survival of mice with 32D/BCR-ABL1 and 32D/SEPT9f-ABL1 cells was significantly shortened compared to that of mice with 32D/MIGR1 (p values < 0.05). (B) The results of the histological analysis of the involved organs in leukemic mice with 32D/BCR-ABL1 and 32D/SEPT9f-ABL1 cells. The histological sections of the bone marrow, spleen and liver stained with hematoxylin and eosin and an anti-EGFP antibody are shown. 32D/BCR-ABL1 and 32D/SEPT9f-ABL1 cells infiltrated diffusely throughout the bone marrow in comparison to 32D/MIGR1 cells, as shown by EGFP staining. In the spleen, they dominantly infiltrated in the red pulp and the region thus became enlarged (*). In the liver, the cells also infiltrated the hepatic lobules, as well as around vessels and Glisson's sheath (**). The bars indicate 1 mm in the bone marrow and 0.4 mm in the spleen and liver.

SEPT9d-ABL1, were resistant to TKIs, especially to dasatinib, compared to BCR-ABL1.

To evaluate the changes in the phosphorylation status of the downstream targets of SEPT9-ABL1, such as Stat5 and Crkl, under treatment with TKIs, 32D/SEPT9f-ABL1 and 32D/BCR-ABL1 cells cultured with TKIs for 3 h were compared. Imatinib and dasatinib inhibited the phosphorylation of Stat5 and Crkl in 32D/SEPT9f-ABL1 and 32D/BCR-ABL1 cells in a concentration-dependent manner. In particular, the Stat5 phosphorylation was dramatically decreased in 32D/BCR-ABL1 cells. However, the phosphorylation was sustained in 32D/SEPT9f-ABL1 cells at higher concentrations of imatinib and dasatinib (Fig. 4B and C). These results suggested that the TKI resistance of SEPT9f-ABL1 was mainly due to the sustained phosphorylation of Stat5.

3.7. Dasatinib sensitivity in vivo

The TKI sensitivity of SEPT9f-ABL1 was then analyzed *in vivo*. Dasatinib was selected for the *in vivo* analysis due to the higher resistance of 32D/SEPT9f-ABL1 cells compared to imatinib *in vitro*. A subcutaneous tumor model was initially applied. The treatment with dasatinib at 30 mg/kg, but not 10 mg/kg, led to the regression of tumors composed of 32D/BCR-ABL1 cells 14 days after tumor implantation, in comparison to treatment with placebo ($p = 0.020$). In contrast, treatment with dasatinib (10 mg/kg or 30 mg/kg) did not inhibit the growth of 32D/SEPT9f-ABL1 tumors (Fig. 5A).

The dasatinib sensitivity of SEPT9f-ABL1 was also evaluated using an intravenous tumor model. The doses of dasatinib utilized in the study were 20 mg/kg and 30 mg/kg. Mice implanted with 32D/BCR-ABL1 cells died within 39 days in the placebo group. However, all mice with 32D/BCR-ABL1 cells survived during the administration of dasatinib at both doses ($p < 0.05$). In contrast, the survival of mice implanted with 32D/SEPT9f-ABL1 cells treated with 20 mg/kg of dasatinib was not prolonged in comparison to the placebo group ($p = 0.243$) (Fig. 5B). When they were treated with 30 mg/kg of dasatinib, two out of five mice with 32D/SEPT9f-ABL1 survived the 80 days of treatment, suggesting that this dose was partially effective ($p = 0.093$). Taken together, these results indicate that SEPT9f-ABL1 was resistant to dasatinib in both subcutaneous and intravenous tumor models.

4. Discussion

The current study identified five SEPT9-ABL1 isoforms with different N-terminal sequences, which exhibited different autonomous proliferation activities *in vitro* and *in vivo*. SEPT9f-ABL1, specifically localized in the cytoplasm, phosphorylated itself and Stat5 strongly, which might have been associated with the oncogenic activities of SEPT9-ABL1 *in vivo*. In addition, the SEPT9-ABL1 isoforms were resistant to TKIs in varying degrees, suggesting that the TKIs sensitivity of ABL1 fusion proteins are dependent on their N-terminal sequences.

BCR-ABL1 acts as an oncogene in the cytoplasm by activating multiple signals, including STAT5 and CRKL [14,15]. STAT5 can stimulate cell proliferation and enhance cell viability by upregulating anti-apoptotic genes, such as BCL-XL [12,16]. In contrast, CRKL binds directly to the SH2 domain of BCR-ABL1 and activates PI3 kinase directly or indirectly *via* CBL, inhibiting apoptosis [13]. Among the SEPT9-ABL1 isoforms, SEPT9f-ABL1 was localized in the cytoplasm and strongly phosphorylated Stat5 as well as BCR-ABL1, thus resulting in the strongest IL-3 independence. On the other hand, CRKL was phosphorylated almost equally in 32D cells with all isoforms, even in 32D/SEPT9d-ABL1 cells that only survived, but did not proliferate, without IL-3. This suggests that SEPT9-ABL1 also acts as an oncogene in the cytoplasm by recruiting STAT5 and CRKL, and that the activation of STAT5 is crucial for SEPT9-ABL1-induced cellular proliferation.

The N-terminal part of the ABL1 fusion proteins often has a coiled-coil or helix-loop-helix domain, which is associated with the oligomerization of fusion proteins and is required for the constitutive activation of the ABL1 tyrosine kinase [4]. Although SEPT9 does not have a coiled-coil or helix–loop–helix domain, it has a long N-terminal proline-rich region [17,18]. SEPT9f-ABL1 has a C-terminal proline-rich region that all the SEPT9-ABL1 isoforms shared. Our findings suggest that the C-terminal fragment might activate the ABL1 function, while the remaining N-terminal fragment regulates it.

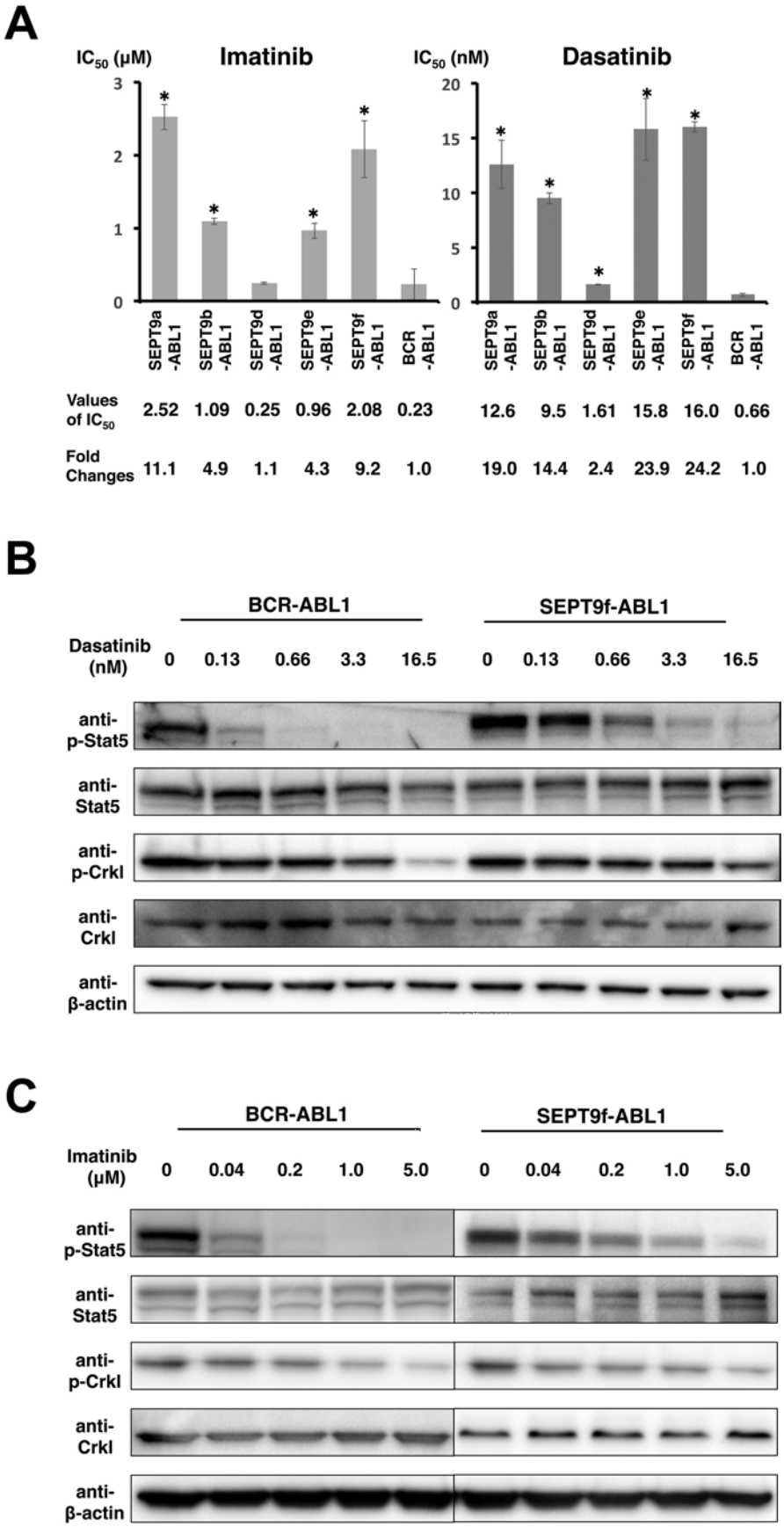

Fig. 4. The sensitivity of each SEPT9-ABL1 isoform to TKIs *in vitro*. (A) The IC_{50} of imatinib and dasatinib in 32D cells with the BCR-ABL1 and SEPT9-ABL1 isoforms. The cells were analyzed at 48 h after starting culture with various concentrations of each agent. The ratios of the IC_{50} values in 32D/SEPT9-ABL1 isoforms compared to 32D/BCR-ABL1 cells were shown as "Fold changes". * Indicates p values < 0.05 in comparison to BCR-ABL1. (B) and (C) The changes in the phosphorylation status of Stat5 and Crkl in 32D cells exposed to various concentrations of imatinib (B) and dasatinib (C).

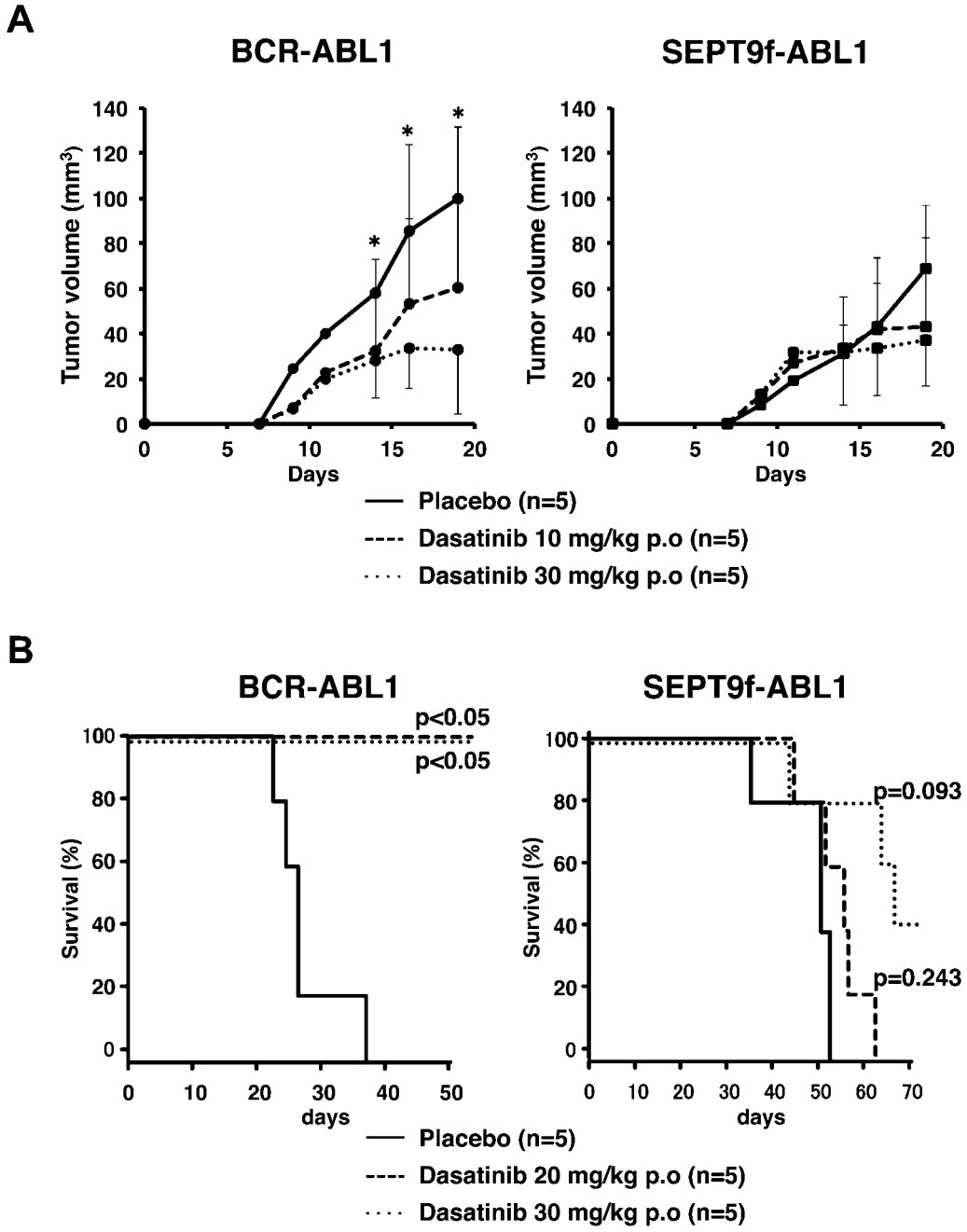

Fig. 5. The sensitivity of SEPT9f-ABL1 to dasatinib *in vivo*. (A) In the subcutaneous tumor model, dasatinib (at 10 mg/kg or 30 mg/kg) or placebo was administered daily to C3H/HeJ mice ($n = 5$ for each groups) with subcutaneously transplanted 32D/BCR-ABL1 or 32D/SEPT9f-ABL1 cells. The volume of the subcutaneous tumors is indicated. (Left panel) 30 mg/kg dasatinib, but not 10 mg/kg dasatinib, significantly inhibited the growth of 32D/BCR-ABL1 tumors compared to mice treated with placebo ($p = 0.020$, day 14; $p = 0.046$, day16; $p = 0.036$, day19). (Right panel) In contrast, neither 30 mg/kg nor 10 mg/kg dasatinib could inhibit the growth of 32D/SEPT9f-ABL1 tumors. * Indicates p values < 0.05. (B) (Left panel) In the intravenous tumor model, the Kaplan–Meier survival curves indicated that dasatinib at 20 mg/kg and 30 mg/kg significantly prolonged the survival of mice with 32D/BCR-ABL1 tumors compared to mice treated with placebo ($p < 0.05$). (Right panel) In contrast, dasatinib at 20 mg/kg did not significantly prolong the survival of mice with 32D/SEPT9f-ABL1 tumors ($p = 0.243$). The 30 mg/kg dose of dasatinib was partially effective for the mice with 32D/SEPT9f-ABL1 tumors ($p = 0.093$).

TKIs designed to target BCR-ABL1 have also been reported to be beneficial in the treatment of cases with other *ABL1* fusion genes; *EML1-ABL1*, *NUP214-ABL1* and *ETV6-ABL1* were sensitive to imatinib or dasatinib *in vitro* [19–21], and dasatinib reduced the subcutaneous tumor volume of *NUP214-ABL1*-positive cells *in vivo* [22]. In clinical case reports, *EML1-ABL1*, *RCSD1-ABL1*, *ETV6-ABL1* and *NUP214-ABL1* were sensitive to TKIs as monotherapy or combination chemotherapy [19,21,23,24]. On the other hand, *SNX2-ABL1* was resistant to dasatinib, and only partially sensitive to imatinib *in vitro* [25]. The IC_{50} values for imatinib and dasatinib of BCR-ABL1 in our analysis, 0.23 μM and 0.66 nM, were comparable with those in the previous studies [26]. In addition, the doses of dasatinib used in our *in vivo* experiments, 10–30 mg/kg, were consentient with previous analyses that required at least 2.5 mg/kg/day dasatinib to inhibit tumor growth in mice expressing BCR-ABL1 [27]. Therefore, our study proved that SEPT9-ABL1 is a TKIs-resistant ABL fusion.

SNX2-ABL1 and SEPT9-ABL1 had no point mutations in the ATP-binding site, phosphate binding site or activation loop of the *ABL1* gene, which were found to cause TKIs-resistance in

BCR-ABL1 fusion products [28]. SNX2-ABL1 had no SH3 domain and a partial SH2 domain which regulate the ABL1 function [29], but all the SEPT9-ABL1 isoforms, including SEPT9d-ABL1 and SEPT9f-ABL1, had SH3 and SH2 domains similar to BCR-ABL1. Although the absence of SH3 and SH2 may be associated with TKIs-resistance in SNX2-ABL1, these results demonstrated that the response of ABL1 fusion products to TKIs is dependent on the N-terminal structure. In addition, the findings that SEPT9-ABL1 and SNX2-ABL1 exhibited more resistance to dasatinib than imatinib should be mentioned. The mechanism of TKI-resistance of ABL1 fusion products might differ between imatinib and dasatinib.

The wild-type SEPT9 gene has also been reported to play a role in tumorigenesis [9]; however, this mechanism seems to be complicated because of the pleiotropic function of the wild-type SEPT9 gene. One report showed the deletion of *SEPT9* in sporadic epithelial ovarian tumors [30], whereas another study reported overexpression in breast cancer [31]. *SEPT9* mRNA is expressed ubiquitously, but the expression pattern of the isoforms is tissue-specific in both normal and malignant tissues [32]. Recent studies have shown the methylation of the SEPT9 promoter [33,34], specific expression patterns of SEPT9 isoforms in various cancers [35–37] and the tumorigenic functions of specific isoforms [38–41]. These findings suggest that dysregulated expression profiles of SEPT9 isoforms contribute to tumorigenesis, and that the SEPT9 isoforms responsible for tumorigenesis vary according to the type of tumors. In the formation of SEPT9-ABL1 in our T-PLL case [5], one allele of wild-type *SEPT9* might have been deleted coinstantaneously and recognized as SEPT9 haploinsufficiency, which might have contributed to leukemogenesis and TKI-resistance.

In conclusion, the SEPT9-ABL1 isoforms had different functions in terms of the cellular proliferation, and their N-terminal structures provided different levels of sensitivity to existing TKIs compared to BCR-ABL1. A recent comprehensive genetic analysis of tumors may uncover the various genetic mutations, including ABL1 fusions, in hematological or non-hematological malignancies. Although there have so far been a limited number of cases reported with various ABL1 fusion genes other than BCR-ABL1, the use of molecular targeting agents for hematological malignancies with ABL1 fusion genes should be optimized according to their structural features. Further refinement of ABL1-targeted therapy will be useful for the treatment of various malignancies in the future.

Conflict of interest

The authors declare no potential conflicts of interest.

Acknowledgments

We thank Dr. Warren S. Pear (University of Pennsylvania) for providing the MIGR1 retroviral vector, Dr. Toshio Kitamura (The University of Tokyo) for providing the PLAT-gp packaging cells, and Ms. Akemi Kamijo, Ms. Katsuko Naito, Ms. Yoshiko Ito and Mr. Masayuki Tanaka (Biological Science Support Center, Tokai University) for their professional technical assistance. This work was supported by a Grant-in-Aid for Scientific Research from the Ministry of Education, Culture, Sports, Science and Technology of Japan (Nos. 24390248 and 24591411), Tokai University School of Medicine Project Research in Japan.

References

[1] Colicelli J. ABL tyrosine kinases: evolution of function, regulation, and specificity. Sci Signal 2010;3:re6.
[2] Greuber EK, Smith-Pearson P, Wang J, Pendergast AM. Role of ABL family kinases in cancer: from leukaemia to solid tumours. Nat Rev Cancer 2013;13:559–71.
[3] Quintas-Cardama A, Cortes J. Molecular biology of bcr-abl1-positive chronic myeloid leukemia. Blood 2009;113:1619–30.
[4] De Braekeleer E, Douet-Guilbert N, Rowe D, Bown N, Morel F, Berthou C, et al. ABL1 fusion genes in hematological malignancies: a review. Eur J Haematol 2011;86:361–71.
[5] Suzuki R, Matsushita H, Kawai H, Matsuzawa H, Tsuboi K, Watanabe S, et al. Identification of a novel SEPT9-ABL1 fusion gene in a patient with T-cell prolymphocytic leukemia. Leuk Res Rep 2014;3:54–7.
[6] Hall PA, Russell SE. The pathobiology of the septin gene family. J Pathol 2004;204:489–505.
[7] Leipe DD, Wolf YI, Koonin EV, Aravind L. Classification and evolution of P-loop GTPases and related ATPases. J Mol Biol 2002;317:41–72.
[8] Cerveira N, Bizarro S, Teixeira MR. MLL-SEPTIN gene fusions in hematological malignancies. Biol Chem 2011;392:713–24.
[9] Connolly D, Abdesselam I, Verdier-Pinard P, Montagna C. Septin roles in tumorigenesis. Biol Chem 2011;392:725–38.
[10] Pear WS, Miller JP, Xu L, Pui JC, Soffer B, Quackenbush RC, et al. Efficient and rapid induction of a chronic myelogenous leukemia-like myeloproliferative disease in mice receiving P210 bcr/abl-transduced bone marrow. Blood 1998;92:3780–92.
[11] Harada Y, Inoue D, Ding Y, Imagawa J, Doki N, Matsui H, et al. RUNX1/AML1 mutant collaborates with BMI1 overexpression in the development of human and murine myelodysplastic syndromes. Blood 2013;121:3434–46.
[12] Warsch W, Grundschober E, Berger A, Gille L, Cerny-Reiterer S, Tigan AS, et al. STAT5 triggers BCR-ABL1 mutation by mediating ROS production in chronic myeloid leukaemia. Oncotarget 2012;3:1669–87.
[13] Feller SM, Posern G, Voss J, Kardinal C, Sakkab D, Zheng J, et al. Physiological signals and oncogenesis mediated through Crk family adapter proteins. J Cell Physiol 1998;177:535–52.
[14] Vigneri P, Wang JY. Induction of apoptosis in chronic myelogenous leukemia cells through nuclear entrapment of BCR-ABL tyrosine kinase. Nat Med 2001;7:228–34.
[15] McWhirter JR, Wang JY. Activation of tyrosinase kinase and microfilament-binding functions of c-abl by bcr sequences in bcr/abl fusion proteins. Mol Cell Biol 1991;11:1553–65.
[16] Warsch W, Grundschober E, Sexl V. Adding a new facet to STAT5 in CML: multitasking for leukemic cells. Cell Cycle 2013;12:1813–4.
[17] Peterson EA, Kalikin LM, Steels JD, Estey MP, Trimble WS, Petty EM. Characterization of a SEPT9 interacting protein, SEPT14, a novel testis-specific septin. Mamm Genome 2007;18:796–807.
[18] Landsverk ML, Ruzzo EK, Mefford HC, Buysse K, Buchan JG, Eichler EE, et al. Duplication within the SEPT9 gene associated with a founder effect in North American families with hereditary neuralgic amyotrophy. Hum Mol Genet 2009;18:1200–8.
[19] De Keersmaecker K, Graux C, Odero MD, Mentens N, Somers R, Maertens J, et al. Fusion of EML1 to ABL1 in T-cell acute lymphoblastic leukemia with cryptic t(9;14)(q34;q32). Blood 2005;105:4849–52.
[20] Graux C, Cools J, Melotte C, Quentmeier H, Ferrando A, Levine R, et al. Fusion of NUP214 to ABL1 on amplified episomes in T-cell acute lymphoblastic leukemia. Nat Genet 2004;36:1084–9.
[21] Gancheva K, Virchis A, Howard-Reeves J, Cross NC, Brazma D, Grace C, et al. Myeloproliferative neoplasm with ETV6-ABL1 fusion: a case report and literature review. Mol Cytogenet 2013;6:39.
[22] Quintas-Cardama A, Tong W, Manshouri T, Vega F, Lennon PA, Cools J, et al. Activity of tyrosine kinase inhibitors against human NUP214-ABL1-positive T cell malignancies. Leukemia 2008;22:1117–24.
[23] Mustjoki S, Hernesniemi S, Rauhala A, Kahkonen M, Almqvist A, Lundan T, et al. A novel dasatinib-sensitive RCSD1-ABL1 fusion transcript in chemotherapy-refractory adult pre-B lymphoblastic leukemia with t(1;9)(q24;q34). Haematologica 2009;94:1469–71.
[24] Deenik W, Beverloo HB, van der Poel-van de Luytgaarde SC, Wattel MM, van Esser JW, Valk PJ, et al. Rapid complete cytogenetic remission after upfront dasatinib monotherapy in a patient with a NUP214-ABL1-positive T-cell acute lymphoblastic leukemia. Leukemia 2009;23:627–9.
[25] Tomita O, Iijima K, Ishibashi T, Osumi T, Kobayashi K, Okita H, et al. Sensitivity of SNX2-ABL1 toward tyrosine kinase inhibitors distinct from that of BCR-ABL1. Leuk Res 2014;38:361–70.
[26] Soverini S, Rosti G, Iacobucci I, Baccarani M, Martinelli G. Choosing the best second-line tyrosine kinase inhibitor in imatinib-resistant chronic myeloid leukemia patients harboring Bcr-Abl kinase domain mutations: how reliable is the IC_{50}. Oncologist 2011;16:868–76.
[27] Luo FR, Yang Z, Camuso A, Smykla R, McGlinchey K, Fager K, et al. Dasatinib (BMS-354825) pharmacokinetics and pharmacodynamic biomarkers in animal models predict optimal clinical exposure. Clin Cancer Res 2006;12:7180–6.
[28] Cilloni D, Saglio G. Molecular pathways: BCR-ABL. Clin Cancer Res 2012;18:930–7.
[29] Barila D, Superti-Furga G. An intramolecular SH3-domain interaction regulates c-Abl activity. Nat Genet 1998;18:280–2.
[30] Russell SE, McIlhatton MA, Burrows JF, Donaghy PG, Chanduloy S, Petty EM, et al. Isolation and mapping of a human septin gene to a region on chromosome 17q, commonly deleted in sporadic epithelial ovarian tumors. Cancer Res 2000;60:4729–34.
[31] Montagna C, Lyu MS, Hunter K, Lukes L, Lowther W, Reppert T, et al. The Septin 9 (MSF) gene is amplified and overexpressed in mouse mammary gland adenocarcinomas and human breast cancer cell lines. Cancer Res 2003;63:2179–87.

[32] Scott M, Hyland PL, McGregor G, Hillan KJ, Russell SE, Hall PA. Multimodality expression profiling shows SEPT9 to be overexpressed in a wide range of human tumours. Oncogene 2005;24:4688–700.
[33] Wasserkort R, Kalmar A, Valcz G, Spisak S, Krispin M, Toth K, et al. Aberrant septin 9 DNA methylation in colorectal cancer is restricted to a single CpG island. BMC Cancer 2013;13:398.
[34] Dietrich D, Jung M, Puetzer S, Leisse A, Holmes EE, Meller S, et al. Diagnostic and prognostic value of SHOX2 and SEPT9 DNA methylation and cytology in benign, paramalignant and malignant pleural effusions. PLOS ONE 2013;8: e84225.
[35] Burrows JF, Chanduloy S, McIlhatton MA, Nagar H, Yeates K, Donaghy P, et al. Altered expression of the septin gene, SEPT9, in ovarian neoplasia. J Pathol 2003;201:581–8.
[36] Scott M, McCluggage WG, Hillan KJ, Hall PA, Russell SE. Altered patterns of transcription of the septin gene, SEPT9, in ovarian tumorigenesis. Int J Cancer 2006;118:1325–9.
[37] Connolly D, Hoang HG, Adler E, Tazearslan C, Simmons N, Bernard VV, et al Septin 9 amplification and isoform-specific expression in peritumoral and tumor breast tissue. Biol Chem 2014;395:157–67.
[38] Amir S, Mabjeesh NJ. SEPT9_V1 protein expression is associated with human cancer cell resistance to microtubule-disrupting agents. Cancer Biol Ther 2007;6:1926–31.
[39] Gonzalez ME, Makarova O, Peterson EA, Privette LM, Petty EM. Up-regulation of SEPT9_v1 stabilizes c-Jun-N-terminal kinase and contributes to its pro-proliferative activity in mammary epithelial cells. Cell Signal 2009;21:477–87.
[40] Golan M, Mabjeesh NJ. SEPT9_i1 is required for the association between HIF-1α and importin-α to promote efficient nuclear translocation. Cell Cycle 2013;12:2297–308.
[41] Chacko AD, McDade SS, Chanduloy S, Church SW, Kennedy R, Price J et al. Expression of the SEPT9_i4 isoform confers resistance to microtubule-interacting drugs. Cell Oncol 2012;35:85–93.

Experimental Hematology

Experimental Hematology 2014;42:487–494

Effective expansion of engrafted human hematopoietic stem cells in bone marrow of mice expressing human Jagged1

Naoko Negishi[a], Daisuke Suzuki[b,c], Ryoji Ito[d], Naoko Irie[e], Koichi Matsuo[e], Takashi Yahata[f], Kenichi Nagano[g], Kazuhiro Aoki[g], Keiichi Ohya[g], Katsuto Hozumi[b], Kiyoshi Ando[f], Norikazu Tamaoki[d], Mamoru Ito[d], and Sonoko Habu[a]

[a]*Department of Immunology, Juntendo University School of Medicine, Tokyo, Japan;* [b]*Department of Immunology, Tokai University School of Medicine, Kanagawa, Japan;* [c]*Department of Animal Biology, University of Pennsylvania School of Veterinary Medicine, Philadelphia, PA, USA;* [d]*Central Institute for Experimental Animals, Kanagawa, Japan;* [e]*Laboratory of Cell and Tissue Biology, Keio University School of Medicine, Tokyo, Japan;* [f]*Division of Hematopoiesis, Research Center for Regenerative Medicine and Department of Hematology, Tokai University School of Medicine, Kanagawa, Japan;* [g]*Section of Pharmacology, Department of Bio-Matrix, Tokyo Medical and Dental University, Tokyo, Japan*

(Received 2 November 2012; revised 4 December 2013; accepted 3 February 2014)

The human immune system can be reconstituted in experimental animals by transplanting human hematopoietic stem cells (hHSCs) into immunodeficient mice. To generate such humanized mice, further improvements are required, particularly to ensure that transplanted hHSCs are maintained in mice and proliferate long enough to follow prolonged immune responses to chronic diseases or monitor therapeutic effects. To prepare the relatively human bone marrow environment in mice, we generated nonobese diabetic/severe combined immunodeficiency/interleukin-2 receptor gamma chain null (NOG) mice expressing human Jagged1 (hJ1) in an osteoblast-specific manner (hJ1-NOG mice) to examine whether Notch signaling induced by hJ1 mediates hHSC proliferation and/or maintenance in mice. The established hJ1-NOG mice possess relatively larger bone marrow space and thinner cortical bone compared with nontransgenic littermates, but the number of c-kit$^+$ Sca-1$^+$ lineage$^-$ cells was not significantly different between hJ1-NOG and nontransgenic littermates. In the transplantation experiments of CD34$^+$ cells obtained from human cord blood, CD34$^+$CD38$^-$ cells (hHSCs) were more increased in hJ1-NOG recipient mice than in nontransgenic littermates in mouse bone marrow environment. In contrast, the transplanted mouse c-kit$^+$ Sca-1$^+$ lineage$^-$ cells did not show significant increase in the same hJ1-NOG mice. These results suggest that hJ1-NOG mice could contribute to the growth of transplanted human CD34$^+$ cells in a human-specific manner and be useful to study the in vivo behavior and/or development of human stem cells, including cancer stem cells and immune cells.

Humanized animals generated by transplantation of human cells or tissues into immunodeficient mice have been used for studying human-specific diseases and therapeutic interventions. Among engrafted cells, human cord blood (CB)-derived CD34$^+$ cells have been widely employed to establish a human immune system in mice to examine the in vivo behavior of human immune cells, including long-term immune responses to infections and tumor growth [1]. Efficient engraftment has been achieved by selection of recipients and the human hematopoietic stem cell (hHSC) injection route. However, the maintenance and proliferation of transplanted hHSCs in humanized mice have until now been insufficient to allow analysis of long-term processes including chronic diseases [2].

Hematopoietic stem cell (HSC) self-renewal and pluripotency are regulated primarily in the bone marrow (BM) niche, in part via Notch signaling. Notch signaling induced by specific binding of the Notch ligands (Delta-like 1–2, 4, and Jagged1–2 in mammals) to their receptors (Notch1–4 in mammals) determines cell fate [3]. Since Jagged1 (J1) is expressed on BM stromal cells, HSCs, which express

NN and DS contributed equally to this article.

Offprint requests to: Dr. Sonoko Habu, Department of Immunology, Juntendo University School of Medicine, 2-1-1 Hongo, Bunkyo-ku, Tokyo 113-8421, Japan; E-mail: sonoko-h@juntendo.ac.jp

Supplementary data related to this article can be found at http://dx.doi.org/10.1016/j.exphem.2014.02.001.

0301-472X/$ - see front matter.
http://dx.doi.org/10.1016/j.exphem.2014.02.001

Notch, may receive Notch signaling from the BM niche [4]. Many studies have revealed enhanced self-renewal capacity in HSCs expressing a constitutively active form of Notch or in those cocultured with stromal cells expressing Notch ligands [5,6]. Moreover, increased HSC proliferation has been reported in a transgenic mouse expressing an active form of parathyroid hormone-related protein receptor in osteoblasts, which drives high J1 expression [7]. Based on these studies, we generated a transgenic mouse expressing human J1 (hJ1) in osteoblasts of nonobese diabetic (NOD/Shi)-*scid*-IL2rγ^{null} (NOG) mice (hJ1-NOG mice) to create highly acceptable recipients for human cells. In these transgenic mice, high proportions of engrafted hHSCs relative to total BM cells were present after transplantation of human CB-derived CD34$^+$ cells. Thus, hJ1-NOG mice may be useful as humanized mice for maintaining the stem cell pool.

Materials and methods

Generation of hJ1 NOG mice

A DNA fragment containing the 2.3-Kb osteoblast-specific promoter region for the mouse α1(I) collagen (*Col1a1*) promoter [8] was provided by Dr. B. de Crombrugghe (University of Texas, Houston, TX). The chicken β-globin 5′ HS4 insulator (1.2 kb) [9,10] was provided by Dr. G. M. Lefevre (National Institutes of Health, Bethesda, MD). The DNA fragments of the *Col1a1* promoter, insulator, and human *jag1* (3.7kb) were inserted into the pCMVb vector (Clontech Laboratories, Inc., Mountain View, CA) (Fig. 1A). To generate transgenic mice, linearized DNA was injected into NOD/Shi mouse embryos, and transgenic offspring were further backcrossed to NOG mice [11]. Experiments using mice maintained under specific pathogen-free conditions were approved by the Institutional Animal Care and Use Committee of the Central Institute for Experimental Animals.

Bone analysis

The histological analysis was described previously [12]. For reverse transcriptase polymerase chain reaction (RT-PCR) analysis, the mRNA from femurs of hJ1-NOG and control nontransgenic NOG mice was isolated by RNA mini kit (QIAGEN, Hilden, Germany) and was transcribed with oligo-dT and Ominiscript reverse transcriptase (QIAGEN). The oligonucleotides used to hJ1 and osteocalcin (OCN) were the following: hJ1 sense, 5′-AGCTGTAAGGAGACCTCCCTG-3′; hJ1 antisense, 5′-TTCTGACACTGGCCAAGGCAGTC-3′; OCN sense, 5′-CTC TGTCTCTCTGACCTCACAG-3′; and OCN antisense, 5′-GGA GCTGCTGTGACATCCATAC-3′.

Three-dimensional imaging by microcomputed tomography (micro-CT)

Each isolated mouse femur was scanned by CT scanner (eXplore Locus CT System, GE Healthcare, *Buckinghamshire*, UK) operated at 80 kV and 450 μA using 400 projections over 88 min for half-scan reconstruction. Voxel resolution was 21 μm. The volume of bone marrow space was quantified using the three-dimensional image analysis software TRI/3DBON (Ratoc System Engineering, Tokyo, Japan).

Transplantation of CB-derived CD34$^+$ cells

For human CD34$^+$ cell transplantation, commercially available human CB-derived CD34$^+$cells (Lonza, Basel, Switzerland) were used. The purity of CD34$^+$ cells was more than 95%. Method of human CD34$^+$ cell transplantation was described previously [12]. Briefly, after 2.5 Gy X-ray irradiation, 5 x 10^4 human CD34$^+$ cells were intravenously transplanted into hJ1-NOG and control nontransgenic NOG mice. Eighteen weeks after transplantation of human CD34$^+$ cells, BM and spleen cells were stained with antihuman monoclonal antibodies and analyzed by flow cytometry.

Transplantation of mouse c-kit$^+$ sca-1$^+$ lineage$^-$ (KSL) cells

For mouse c-kit$^+$ sca-1$^+$ lineage$^-$ cell transplantation, c-kit-positive, sca-1-positive, lineage marker (Lin: TER119, CD3, CD19, Mac-1, Gr-1)-negative cells (KSL cells) were isolated from fetal liver of E15.5 green fluorescent protein (GFP) mouse embryos (Japan SLC, Shizuoka, Japan) or BM of 4-week-old GFP mice by sorting using a FACSAria (BD Biosciences, San Jose, CA). Mouse GFP$^+$KSL cells (2 x 10^4 cells) were injected into hJ1-NOG and control nontransgenic NOG mice receiving 2.5Gy irradiation before 24 hours. After 8 weeks, their BM cells were analyzed by flow cytometry.

Serial transplantation in NOG mice

Human CD34$^+$ cells were isolated from BM of initial CD34$^+$ transplanted hJ1-NOG or control nontransgenic NOG mice, 18 weeks after transplantation of human CB-derived CD34$^+$ cells (5 x 10^4 cells), by a magnetic cell sorting (MACS) system using biotinylated antihuman CD34 antibody (BioLegend, San Diego, CA) and avidin-conjugated magnetic beads (Milteny Biotec, Bergisch Gladbach, Germany). For the serial transplantation, 2 x 10^5 human CD34$^+$ cells from an each initial recipient were intravenously transplanted into NOG mice with 2.5 Gy irradiation. Eight weeks later, their BM cells were analyzed by flow cytometry.

Coculture assay with stromal cells

For establishment of OP9 cell lines expressing NotchL were obtained after transfection into the Plat-E ecotropic packaging cell line, as described previously [13]. *For coculture,* human CBCD34$^+$ cells were plated at 0.3 to 1×10^4 cells on a monolayer of stromal OP9 transfectants prepared in six-well culture plates for 3 to 7 weeks in the presence of recombinant cytokines: 50ng/mL hSCF, 50ng/mL hTPO and 50ng/mL Flt3L (Peprotech, London, UK). After two weeks of coculture, half of the cultured floating cells were re-cultured onto new OP9 monolayers with fresh medium containing growth factors weekly, to prevent overgrowth. After coculture, growing cells were harvested for flow cytometric analysis.

Flow cytometry

Both BM and spleen cell preparation and flow cytometric analysis have been described [14]. Antibodies used included: antihuman CD45-allophycocyanin-Cy7 (APC-Cy7), antihuman CD33-fluorescein isothiocyanate (FITC), and antihuman CD38-FITC antibodies (BD Biosciences); antihuman CD19-phycoerythrin (PE) and CD3-PE-Cy7 antibodies (Beckman Coulter, Brea, CA); antimouse c-kit-APC, antihuman lineage cocktail-PE, antimouse lineage cocktail-PE, antihuman CD34-PE-Cy7 antibodies, biotinylated antimouse Sca-1, and streptavidin-PE-Cy7 (BioLegend)

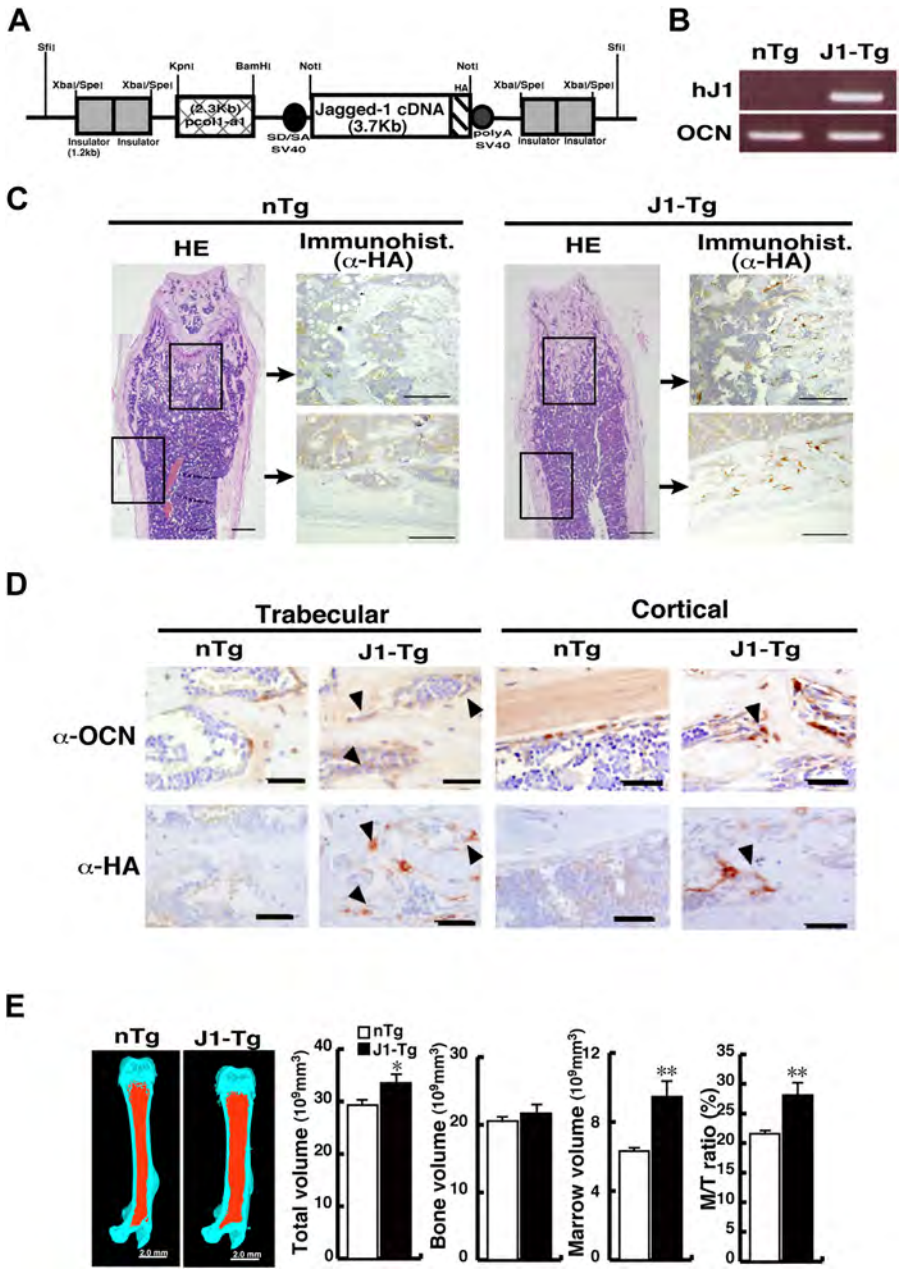

Figure 1. Generation and characterization of hJ1-NOG mice. (**A**) Schematic diagram of the *human Jag1* transgene. (**B**) RT-PCR analysis of hJ1 and OCN in femurs of 8-week-old hJ1-NOG (J1-Tg) mice and nTg littermates. (**C**) H&E staining of femurs of J1-Tg mice and nTg littermates (each of left, scale bars, 200 μm.), and higher magnification of immunohistochmical staining with anti-HA antibody of metaphyseal trabecular area (top) and diaphyseal cortical area (bottom). Scale bars, 100 μm. (**D**) Immunohistochemical staining of serial sections of femurs (metaphyseal trabecular regions: left, and diaphyseal cortical regions: right) from nTg and J1-Tg mice using antiosteocalcin antibody (α-OCN; top) and anti-HA antibody (α-HA; bottom). Arrowheads indicate positive cells. Scale bars, 20 μm. (**E**) Measurements of the BM cavity of femurs J1Tg and nTg mice ($n = 9$ each). Total volume (red and blue), bone volume (blue), and marrow volume (red) were quantified as described in article text, and M/T ratios were calculated based on them. Error bars represent SEM. $*p < 0.05$ and $**p < 0.01$ vs. nTg. Scale bars, 2mm.

and antimouse Sca-1-FITC antibody (eBioscience, San Diego, CA).

Immunohistochemistry

Femurs were fixed in 4% paraformaldehyde (PFA) and decalcified with 20% EDTA in phosphate-buffered saline. Bones were then embedded in paraffin and cut at 4-μm thickness. Sections were stained with anti-hemagglutinin (HA) (Serotec, Kidlington, U.K), antimouse osteocalcin (Enzo Life Sciences, Farmingdale, NY) and antihuman CD34 (DakoCytomation, Glostrup, Denmark). Secondary antibodies were horseradish peroxidase-labeled polymer-conjugated antirabbit immunoglobulin G (Nichirei, Tokyo, Japan). For color development, these sections were incubated with 0.02% 3,3'-diaminobenzidine (DAB)

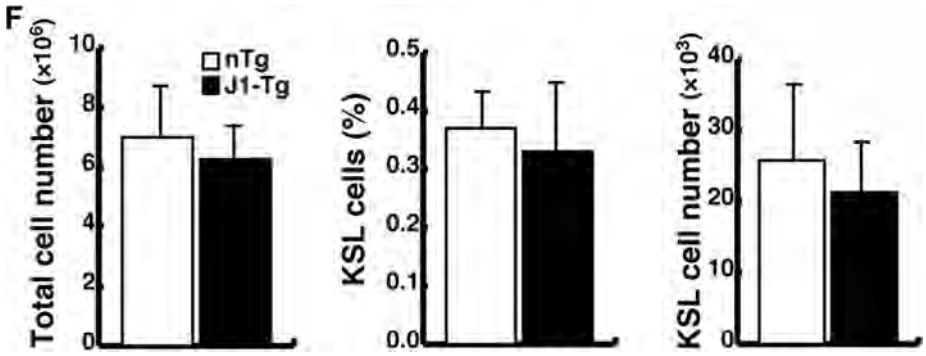

Figure 1. (*continued*) (**F**) Average number of total BM cells (left) of femurs in nTg (n = 3) and J1-Tg mice (n = 4) was counted under microscopy. The frequency (middle) and average number (right) of KSL cells in both mice. We determined KSL cells by staining BM cells with monoclonal antibodies to mouse lineage cocktail, c-Kit and Sca-1. Number of KSL cells was analyzed by flow cytometry. Error bars represent SEM. nTg = nontransgenic NOG; SEM = standard error of the mean.

(Dojindo, Kumamoto, Japan) substrate solution containing 0.006% H_2O_2. Immunostained sections were counterstained with hematoxylin (Sakura Finetek, Tokyo, Japan) for visualization of nuclei.

Statistical analysis

Mean values and standard deviations were computed using Excel (Microsoft, Redmond, WA). Significant differences were calculated by Student's t test.

Results and discussion

Generation and characteristics of transgenic mice expressing hJ1

To establish the experimental system that allows human hematopoietic stem cells to grow efficiently in mouse BM, we first examined the in vitro system in which human CB-derived $CD34^+$cells were cocultured on mouse OP9 stromal cells expressing human and mouse Notch ligands in the presence of growth factors for maintenance of HSCs. In preculture, the purity of $CD34^+$ cells was >95%, and, among them, the proportion of $CD34^+CD38^-$cells was about 10%. The coculture of $CD34^+$ cells on OP9 showed much greater proliferation of $CD34^+CD38^-$ cells (termed hHSCs in this study) in conditions employing hJ1 than in those with mouse J1 (Table 1). Based on this in vitro experimental result, we generated transgenic mice expressing human *Jag1* cDNA in osteoblasts under the control of the *COL1A1* promoter (Fig. 1A) to examine the in vivo effect of hJ1 in the mouse BM niche on hHSC. Of two transgenic lines (#115 and #116) we established, #116, expressing higher levels of hJ1 protein, was bred on an immunodeficient NOG mouse (hJ1-NOG mice) for further experiments of human cell transplantation.

In hJ1-NOG mice, hJ1 expression was detectable in femur by RT-PCR (Fig. 1B) in addition to the mouse J1 expression respectively. The immunohistochemical analysis showed hJ1 positive cells in both metaphyseal trabecular and diaphyseal

Table 1. Number of total cells and HSCs after co-culture of CB-derived $CD34^+$ cells on OP9 stromal cell lines

		No. of $CBCD34^+$cells (day 0)	No. of total cells ($\times10^6$ cells)			No. of $CD34^+$ $CD38^-$ cells ($\times10^6$ cells)		
	Stromal cell	($\times10^4$ cells)	3W	4W	7W	3W	4W	7W
Exp. 1	Control OP9	0.3	10.1	14.1	72.3	1.7	2.2	5.8
	hD1/OP9	0.3	4.6	11.5	60.8	1.5	4.2	22.7
	hJ1/OP9	0.3	10.6	28.6	232.0	4.9	4.9	62.9
Exp. 2	Control OP9	1.0	77.0	93.5	5667.0	6.8	3.9	561.6
	mD1/OP9	1.0	10.0	21.6	2100.0	0.1	1.7	59.4
	hD1/OP9	1.0	6.6	22.3	1123.0	1.2	1.6	112.6
	mJ1/OP9	1.0	99.0	115.5	3346.0	8.4	20.5	657.2
	hJ1/OP9	1.0	112.2	151.8	57024.0	8.9	30.7	16286.0

CB = cord blood; hD1 = human Delta-like1; hJ1 = human Jagged1; HSC = hematopoietic stem cell; mD1 = mouse Delta-like1; mJ1 = mouse Jagged1. Human $CBCD34^+$ cells were cultured for 3, 4, or 7 weeks (W) on a monolayer of OP9-derived transfectants expressing hD1, hJ1, mD1 or hJ1 in the presence of hSCF, hTPO and Flt3L. Each week, after washing the floating cells were re-cultured on a monolayer of OP9 transfectans. After culture, growing cells were harvested for flow cytometric analysis.

cortical areas in hJ1-NOG mice but not in nontransgenic NOG mice (Fig. 1C). In the same site of serial sections, osteocalcin positive cells were detectable (Fig. 1D). Bone sections of hJ1-NOG mice seem to have relatively larger marrow space and thinner trabecular bone in comparison to nontransgenic NOG littermates (Fig. 1C), which was confirmed in micro-CT analysis showing the increase of marrow volume and of marrow to total volume (M/T) ratio (Fig. 1E), as well as the decrease of trabecular bone volume fraction (BV/TV) (Supplementary Figure E1A, online only, available at www.exphem.org). In fact, tissue mineral density (TMD) of cortical area in hJ1-NOG mouse was decreased (Supplementary Figure E1A, online only, available at www.exphem.org). Although the marrow space of hJ1-NOG mice was enlarged, mouse total BM cells and c-kit$^+$ sca-1$^+$ lineage$^-$ (KSL) cells were not particularly increased (Fig. 1F). These characteristics of hJ1-NOG mice suggest that hJ1 expression on osteoblasts does not seem to enhance mouse stem cell proliferation. In addition to hJ1 expression, hJ1- NOG mice showed other BM phenotypes such as lower bone density and the increase of both osteoblasts and osteoclasts (Supplementary Figure E1B, online only, available at www.exphem.org), which might also be related to the enlargement of BM space and warrants further investigation.

Preferential increase of hHSC in hJ1-NOG mice post engraftment of CB-derived cells

These hJ1-NOG mice were then used to study whether hHSCs are efficiently maintained and/or proliferated in the mouse BM niche due to hJ1 expression. To accomplish this, human CB-derived CD34$^+$ cells were transplanted into hJ1-NOG and nontransgenic NOG mice, and then BM cells in the recipients were analyzed 18 weeks after transplantation. Immunohistochemical staining showed a higher proportion of CD34$^+$ cells in the marrow space (Fig. 2A). As shown in Figures 2B and 2C, the proportion and cell number of CD34$^+$ cells and CD34$^+$38$^-$ cells in CD45$^+$ cells were clearly increased in hJ1-NOG mice, while the number of human CD45$^+$ cells in BM was not significantly different between hJ1-NOG and nontransgenic NOG mice. Since both recipients were equally injected with 5x10^4 human CD34$^+$ cells containing around 10% of CD34$^+$CD38$^-$ cells, the mathematical estimation from Figure 2B indicates a 20-fold increase of CD34$^+$CD38$^-$ cells in hJ1-NOG mice and about a 4-fold increase in nontransgenic NOG mice. These results suggest that hHSC can be promoted to expand in hJ1 expressing BM niche, which is consistent with the observation in Table 1 showing that human CD34$^+$ cells greatly increased in coculture with hJ1$^+$ stromal cells. At the same time, it is also possible that the increased proportion of CD34$^+$ cells in BM may result from the suppression of the developing pathway from CD34$^+$ cells into CD34$^-$ cells by hJ1. However, this possibility requires further investigation, since our aim in this study is to establish a model mouse in which human CD34$^+$ cells grow efficiently.

In hJ1-NOG mouse spleen, lymphoid cells such as T and B cells and granulocytes were comparable in number and proportion between hJ1-NOG mice and nontransgenic NOG littermates (Fig. 2D), indicating that developing cells belonging to lineage committed cells may be released from BM comparably in both recipients.

To validate whether the above experimental results by transplantation of human CB-derived CD34$^+$ cells substantially occurs specifically in hHSC, mouse hematopoietic cells rather than human cells were transplanted into the same hJ1-NOG mice, and we examined their growth. To distinguish transplanted cells from recipient BM cells, donor cells were prepared from GFP transgenic mice. Then, the isolated GFP$^+$KSL cells were injected into non-GFP hJ1-NOG and nontransgenic NOG recipients. No significant difference was found in total GFP$^+$ cells and in the proportion of GFP$^+$KSL cells in both recipients, indicating that hJ1 expression did not significantly contribute to the growth of transplanted mouse KSL in BM (Table 2).

Altogether, transplantation experimental results of human and mouse hematopoietic stem cells clearly indicated that hJ1-expressing niche greatly contributes to the growth of transplanted hematopoietic precursor cells in a human cell specific manner.

Previous studies reported that both human and mouse Notch ligands support mouse KSL cell growth in the coculture system [15,16]. However, mouse KSL cell growth was not sufficiently enhanced in hJ1-NOG mice compared with control NOG mice, whereas hHSCs are clearly increased in the same BM niche. This disparity could be due, at least in part, to experimental differences between in vivo and in vitro cocultures, which may employ various types of HSC growth factors. Also, the pairing of combinations of Notch receptors and ligands in distinct species likely influences HSC growth because, as mentioned in the above-described culture system, hHSCs grew more rapidly in combination with hJ1 than with the mouse counterpart (Table 1).

Next, we examined whether the intramarrow expanded human CD34$^+$CD38$^-$ cells in hJ1-NOG mouse still maintain the original growing potentials of hHSC without retardation. For that, human CD34$^+$ cells grown in the first hJ1-NOG or in nontransgenic NOG recipient were isolated from each BM respectively, and then the same number of them was transplanted into the secondary recipient nontransgenic NOG mice but not hJ1-NOG mice. The flow cytometric analysis of BM cells from the secondary nontransgenic NOG recipient showed that the number and proportion of human CD34$^+$38$^-$ cells derived from hJ1-NOG mice were not statistically different, although they seem to be slightly enhanced in the hJ1-NOG–derived case (Table 3). These results suggest that enhancement of human CD34$^+$ cell growth is transiently induced as long as hJ1 exists, but restores without abrogation of their intrinsic growing potential in the absence of hJ1.

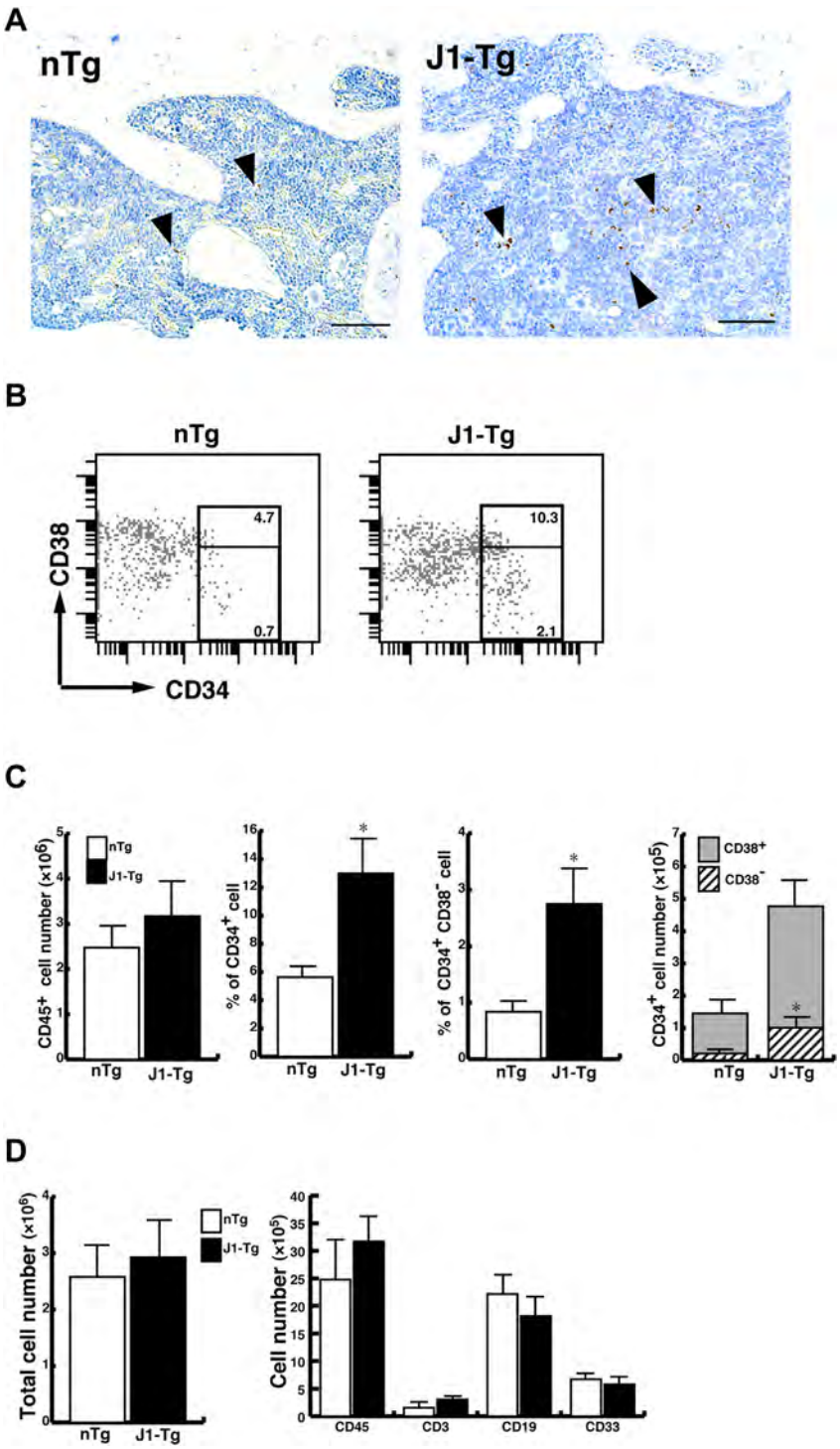

Figure 2. Characterization of hHSCs post transplantation in hJ1-NOG mice. Eighteen weeks after human $CD34^+$ cell transplantation (5 x 10^4 cells) into J1-Tg mice and nTg littermates, BM obtained from the femurs of each recipient was analyzed by immunohistochemistry and flow cytometry. (**A**) Immunohistochemical staining for human CD34 in femurs of J1-Tg and nTg mice. Arrowheads indicate positive cells. Scale bars; 100 μm. (**B**) Representative flow cytometric profiles of $CD34^+CD38^+$ and $CD34^+CD38^-$ cell proportion in $CD45^+$ BM cells. Numbers indicate the relative percentages of cells within indicated areas. (**C**) Histograms showed the number of engrafted $CD45^+$ cells in total BM cells, the proportion of $CD34^+$ cells and $CD34^+CD38^-$ cells in $CD45^+$ cells in five hJ1-Tg and nTg mice each. Error bars represent SEM ($n = 5$, $^*p < 0.05$). Total cell numbers of $CD34^+CD38^-$ cells (hatched bar), $CD34^+CD38^+$ cells (gray bar) and $CD34^+$ cells (hatched bar + grey bar) in J1-Tg and nTg mice. Error bars represent SEM ($n = 5$, $^* p < 0.05$). (**D**) Human-derived immune cells in spleen cells. Average number of total spleen cells (left), human CD45, CD3, CD19, and CD33 cells (right) in J1-Tg and nTg mice was determined by flow cytometer. J1-Tg = hJ1-NOG; nTg = nontransgenic NOG; SEM = standard error of the mean.

Table 2. Engrafted mouse GFP+ KSL cells in BM of hJ1-NOG or non-transgenic NOG recipient mice

		In recipient mice				
Mouse no.	Recipient	No. of total cells in BM (x 10^5)	% of GFP^+ cells in BM (x 10^5)	No. of GFP^+ cells in BM (x 10^5)	% of KSL cells in GFP^+ cells	No. of GFP^+KSL cells in BM (x 10^5)
1	J1-Tg	121.5	73.3	89.1	2.9	2.6
2	J1-Tg	69.3	73.7	51.1	4.9	2.5
3	J1-Tg	40.5	55.7	22.6	1.3	0.3
4	J1-Tg	102.6	96.5	990	3.3	3.3
5	J1-Tg	52.0	88.3	45.9	0.7	0.3
6	J1-Tg	73.0	94.0	68.9	2.3	1.6
mean ± SD		**76.5 ± 30.6**	**80.3 ± 15.6**	**72.8 ± 28.6**	**2.6 ± 1.5**	**1.8 ± 1.3**
7	nTg	104.4	55.3	57.7	1.9	1.1
8	nTg	137.7	86.4	119.0	1.4	1.7
9	nTg	63.0	89.2	56.2	0.2	0.1
10	nTg	62.5	95.0	59.4	2.5	1.5
11	nTg	71.0	94.3	67.0	2.4	1.6
12	nTg	55.0	73.5	40.4	0.2	0.1
mean ± SD		**82.3 ± 32.2**	**82.3 ± 15.3**	**66.6 ± 27.1**	**1.4 ± 1.0**	**1.0 ± 0.7**

Isolated BM KSL cells (2 x 10^4) from GFP mice were transplanted into J1-Tg or nTg mice, and, 8 weeks later, the number of BM cells and the percentage and number of GFP^+ and GFP^+ KSL cells in BM of the recipient mice were estimated based on the flow cytometric analysis. BM = bone marrow; GFP = green fluorescent protein; J1-Tg = hJ1-NOG; KSL = lineage-negative, c-kit-positive, sca-1-positove; nTg = nontransgenic NOG.

In conclusion, our established hJ1-NOG mouse is of use as an in vivo model to study human immune responses to various stimulants, such as pathogens or cancer cells, particularly of a chronic status, the study of which needs continuous and sufficient development of immune cells supplied by enhanced expansion and increased survival of hHSCs. At the same time, due to the longer maintenance and enhanced expansion of hHSCs in the mouse BM niche, the hJ1-NOG mouse could be a powerful tool for directly investigating the characterization of human-derived hematopoietic cancer stem cells and leukemogenesis and for developing therapeutic strategies.

Table 3. Human HSCs grown in J1Tg or nTg mice in the second nTg recipients

				In the recipient NOG mice transplanted after 8 weeks					
Mouse no.	Donor	Recipient	Injected $CD34^+$ cells (x 10^5)	% of $CD45^+$ cells in BM cells	No. of $CD45^+$ cells (x 10^5)	% of $CD34^+$ cells in $CD45^+$ cells	No. of $CD34^+$ cells (x 10^4)	% of $CD34^+$ $CD38^-$ cells in $CD45^+$ cells	No. of $CD34^+$ $CD38^-$ cells (x 10^3)
1	J1-Tg	nTg	2.0	5.8	3.4	3.5	1.2	2.0	6.9
2	J1-Tg	nTg	2.0	3.0	1.9	0.5	0.1	0.4	0.7
3	J1-Tg	nTg	2.0	5.5	3.5	0.3	0.1	0.1	0.4
4	J1-Tg	nTg	2.0	8.5	6.3	1.4	0.9	1.1	6.8
5	J1-Tg	nTg	2.0	17.7	6.5	5.0	3.3	0.6	4.0
6	J1-Tg	nTg	2.0	1.4	0.7	2.9	0.2	0.1	0.1
mean ± SD				**7.0 ± 5.8**	**3.7 ± 2.3**	**2.3 ± 1.9**	**1.0 ± 1.2**	**0.7 ± 0.7**	**3.1 ± 3.2**
7	nTg	nTg	2.0	2.0	1.0	2.9	0.3	1.1	1.2
8	nTg	nTg	2.0	37.5	26.7	1.1	2.9	0.4	10.4
9	nTg	nTg	2.0	3.0	1.8	1.7	0.3	0.2	0.3
10	nTg	nTg	2.0	1.8	1.0	1.0	0.1	0.2	0.2
11	nTg	nTg	2.0	3.3	1.3	0.8	0.1	0.3	0.4
12	nTg	nTg	2.0	10.3	3.4	1.8	0.6	0.8	2.8
mean ± SD				**9.7 ± 14.0**	**5.9 ± 10.2**	**1.5 ± 0.8**	**0.7 ± 1.1**	**0.5 ± 0.4**	**2.6 ± 4.0**

Human $CD34^+$ cells (2 x 10^5) obtained from the first recipients, J1-Tg or nTg mice, were transplanted into the nTg second recipients. The transplanted $CD34^+$ cells derived from hJ1-Tg and nTg contained $CD34^+CD38^-$ cells in average 10.3% and 9.9%, respectively. Eight weeks later, the percentage and the number of human $CD45^+$ and of $CD34^+$ or $CD34^+CD38^-$ cells in $CD45^+$ cell in BM were analyzed by flow cytometry. Difference between engrafted cells derived from J1-Tg and nTg was not significant. BM = bone marrow; HSC = hematopoietic stem cell; J1-Tg = hJ1-NOG; nTg = nontransgenic NOG.

Acknowledgments

We thank Tamaki Sasou of the Educational and Research Support Center, Tokai University School of Medicine; Dr. Toshimi Sato; and Mariko Takahashi of Tokyo Medical and Dental University for experimental support. This work was supported by a Grant-in-Aid for Scientific Research (B and S) from the Ministry of Education, Culture, Sports, Science and Technology (MEXT), Japan.

Conflict of interest disclosure

No financial interest/relationships with financial interest relating to the topic of this article have been declared.

References

1. Hiramatsu H, Nishikomori R, Heike T, et al. Complete reconstitution of human lymphocytes from cord blood CD34+ cells using the NOD/SCID/gammacnull mice model. Blood. 2003;102:873–880.
2. Ito M, Kobayashi K, Nakahata T. NOD/Shi-scid IL2rgamma(null) (NOG) mice more appropriate for humanized mouse models. Curr Top Microbiol Immunol. 2008;324:53–76.
3. Radtke F, Wilson A, Mancini SJ, MacDonald HR. Notch regulation of lymphocyte development and function. Nat Immunol. 2004;5:247–253.
4. Weber JM, Calvi LM. Notch signaling and the bone marrow hematopoietic stem cell niche. Bone. 2010;46:281–285.
5. Karanu FN, Murdoch B, Gallacher L, et al. The notch ligand jagged-1 represents a novel growth factor of human hematopoietic stem cells. J Exp Med. 2000;192:1365–1372.
6. Varnum-Finney B, Brashem-Stein C, Bernstein ID. Combined effects of Notch signaling and cytokines induce a multiple log increase in precursors with lymphoid and myeloid reconstituting ability. Blood. 2003;101:1784–1789.
7. Calvi LM, Adams GB, Weibrecht KW, et al. Osteoblastic cells regulate the haematopoietic stem cell niche. Nature. 2003;425:841–846.
8. Rossert J, Eberspaecher H, de Crombrugghe B. Separate cis-acting DNA elements of the mouse pro-alpha 1(I) collagen promoter direct expression of reporter genes to different type I collagen-producing cells in transgenic mice. J Cell Biol. 1995;129:1421–1432.
9. Chung JH, Whiteley M, Felsenfeld GA. 5' element of the chicken beta-globin domain serves as an insulator in human erythroid cells and protects against position effect in Drosophila. Cell. 1993;74:505–514.
10. Potts W, Tucker D, Wood H, Martin C. Chicken beta-globin 5'HS4 insulators function to reduce variability in transgenic founder mice. Biochem Biophys Res Commun. 2000;273:1015–1018.
11. Ito M, Hiramatsu H, Kobayashi K, et al. NOD/SCID/gamma(c)(null) mouse: an excellent recipient mouse model for engraftment of human cells. Blood. 2002;100:3175–3182.
12. Ito R, Negishi N, Irie N, et al. Osteosclerosis and inhibition of human hematopoiesis in NOG mice expressing human Delta-like 1 in osteoblasts. Exp Hematol. 2012;40:953–963.
13. Hozumi K, Abe N, Chiba S, et al. Active form of Notch members can enforce T lymphopoiesis on lymphoid progenitors in the monolayer culture specific for B cell development. J Immunol. 2003;170:4973–4979.
14. Hozumi K, Negishi N, Suzuki D, et al. Delta-like 1 is necessary for the generation of marginal zone B cells but not T cells in vivo. Nat Immunol. 2004;5:638–644.
15. Jones P, May G, Healy L, et al. Stromal expression of Jagged 1 promotes colony formation by fetal hematopoietic progenitor cells. Blood. 1998;92:1505–1511.
16. Han W, Ye Q, Moore MA. A soluble form of human Delta-like-1 inhibits differentiation of hematopoietic progenitor cells. Blood. 2000;95:1616–1625.

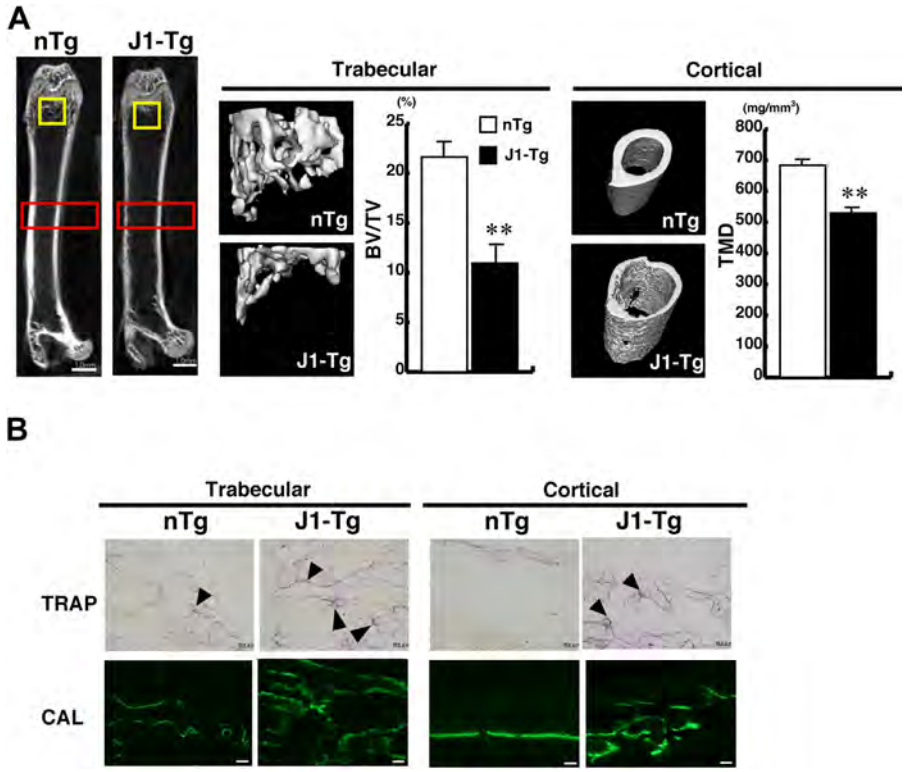

Supplementary Figure E1. Bone phenotypes of hJ1-NOG mice. (**A**) Three-dimensional microCT imaging (left) of femurs from 10-week-old female J1-Tg mice and nTg mice. Middle and right show three-dimensional reconstructions of metaphyseal trabecular regions and diaphyseal cortical regions. BV/TV and TMD were calculated using MicroView software. Yellow and red boxes indicate measurement regions corresponding to trabecular and cortical, respectively. Error bars represent SEM. $^{**}p < 0.01$ for nTg vs. J1-Tg mice ($n = 9$ each). (**B**) Histological analysis of femurs from 10-week-old female nTg and J1-Tg mice. Histological sections of trabecular (left) and cortical (right) bones. Top panels show TRAP staining indicative of osteoclast. Arrowheads indicate TRAP positive osteoclasts. Bottom panels show high-power fluorescent microscopy images of undecalcified femur sections labeled with calcein indicative of the newly formed bone. Scale bars: 20 μm. BV/TV = Trabecular bone volume fraction; J1-Tg = hJ1-NOG mice; nTg = nontransgenic NOG mice; SEM = standard error of the mean; TMD = tissue mineral density; TRAP = tartrate-resistant acid phosphatase.

Cancer Science
Japanese Cancer Association JCA
Open Access

Clinical outcome of Epstein–Barr virus-positive diffuse large B-cell lymphoma of the elderly in the rituximab era

Ai Sato,[1] Naoya Nakamura,[2] Minoru Kojima,[1] Ken Ohmachi,[1] Joaquim Carreras,[2] Yara Yukie Kikuti,[2] Hiroki Numata,[3] Daisuke Ohgiya,[4] Kei Tazume,[5] Jun Amaki,[1] Makiko Moriuchi,[6] Mitsuki Miyamoto,[1] Yasuyuki Aoyama,[1] Hidetsugu Kawai,[1] Akifumi Ichiki,[1] Ryujiro Hara,[1] Hiroshi Kawada,[1] Yoshiaki Ogawa[1] and Kiyoshi Ando[1]

Departments of [1]Hematology–Oncology, [2]Pathology,School of Medicine, Tokai University, Isehara; [3]Department of Hematology, Ozawa Hospital, Odawara; [4]Department of Hematology, Ebina General Hospital, Ebina; [5]Department of Hematology, Red Cross Hadano Hospital, Hadano; [6]Department of Hematology, Atsugi Satoh Hospital, Atsugi, Japan

Key words

Diffuse large B-cell lymphoma, Epstein–Barr virus (EBV), prognosis

Correspondence

Ai Sato, Department of Hematology–Oncology, School of Medicine, Tokai University, 143 Shimokasuya, Isehara, Kanagawa 259-1193, Japan.
Tel: +81-463-93-1121; Fax: +81-463-92-4511;
E-mail: mogumogu@is.icc.u-tokai.ac.jp

Funding Information
Tokai University.

Received February 10, 2014; Revised June 6, 2014; Accepted June 13, 2014

Cancer Sci **105** (2014) 1170–1175

doi: 10.1111/cas.12467

Diffuse large B-cell lymphoma (DLBCL) is the most common subtype of malignant lymphoma. The incidence of Epstein–Barr virus (EBV)-positive DLBCL in Asian and Latin American countries ranges from 8 to 10%. The prognosis of patients with EBV-positive DLBCL is controversial. To compare the clinical outcome of EBV-positive and EBV-negative patients with DLBCL in the rituximab era, we analyzed 239 patients with *de novo* DLBCL diagnosed between January 2007 and December 2011. The presence of EBV in lymphoma cells was detected using EBV-encoded RNA *in situ* hybridization, and it was found that 18 (6.9%) of 260 patients with diagnosed DLBCL tested positive. Among the 260 cases, 216 cases were treated with rituximab plus chemotherapy, as were 8 EBV-positive DLBCL patients. The median overall survival and progression-free survival times in patients with EBV-positive DLBCL were 8.7 months and 6.8 months, respectively. The median overall survival and progression-free survival could not be determined in EBV-negative DLBCL patients ($P = 0.0002$, $P < 0.0001$, respectively). The outcome of patients with EBV-positive DLBCL remains poor, even in the rituximab era.

Diffuse large B-cell lymphoma is the most common subtype of malignant lymphoma and accounts for 33% of all cases of malignant lymphoma in Japan.[1] Diffuse large B-cell lymphoma usually arises *de novo* in lymph nodes, but can also be derived from extranodal organs. The WHO classification describes various special types of DLBCL, and DLBCLs harboring EBV in patients older than 50 years are termed EBV-positive DLBCL of the elderly (EBV-DLBCL of the elderly) as a new category.[2,3] The EBV-DLBCL of the elderly category accounts for 8–10% of all DLBCL in Asian countries,[4] but <5% in Western countries.[5,6]

Epstein–Barr virus is the most common gamma herpes virus, and it has infected more than 90% of all adults. Most people are infected subclinically in childhood and maintain a latent infection throughout their life. During the process of infection, EBV attaches to B cells through the binding of viral gp350 protein to CD21 on the surface of B cells. Then, gp42 on EBV interacts with MHC class II molecules and triggers fusion with the host membrane.[7] The EBV is reactivated by various stimuli. Epstein–Barr virus-infected B cells are usually controlled by EBV-specific T cells, but they become uncontrolled when the host is immunodeficient. B cells infected with EBV sometimes become lymphoblastoid cell lines and obtain an unlimited ability to proliferate. Lymphoblastoid cell lines cause some lymphoid malignancies, including Burkitt lymphoma, extranodal natural killer/T-cell lymphoma, aggressive natural killer leukemia/lymphoma, angioimmunoblastic T-cell lymphoma, Hodgkin's lymphoma, immunodeficiency-associated lymphoproliferative disorders, and some DLBCLs.[8]

The standard treatment for DLBCL before the rituximab era was chemotherapy combined with CHOP. Since the introduction of rituximab into the clinic, R-CHOP has become the standard treatment for CD20-positive DLBCL.[9,10] The outcome of DLBCL patients is improved with R-CHOP, but the impact on the prognosis of EBV-positive DLBCL patients remains controversial.[11–15]

We investigated the clinical features of patients with EBV-positive DLBCL and showed that the outcome of elderly patients with EBV-positive DLBCL treated with R-CHOP was still worse than other groups in this study.

Materials and Methods

Patients. We reviewed the medical records of 289 patients who received a diagnosis of DLBCL at Tokai University Hospital (Isehara, Japan) and who were treated there and at affiliated hospitals between January 2007 and December 2011.

Table 1. Details of patients with diffuse large B-cell lymphoma (DLBCL) who were excluded from this analysis

	EBV-positive DLBCL	EBV-negative DLBCL
Total patients	18	242
Primary CNS DLBCL†	0	4
Immunodeficiency	3	2
Methotrexate	2	2
HIV infection	1	0
Unknown	1	11
No. of patients analyzed in this study	14	225

†Patients with primary central nervous system (CNS) DLBCL were excluded from analysis because rituximab plus cyclophosphamide, doxorubicin, vincristine, and prednisolone was not a treatment option. EBV, Epstein–Barr virus.

Among 289 patients, 29 patients were excluded because no paraffin-embedded samples were available. Therefore, 260 cases were examined for the presence of EBV using formalin-fixed paraffin-embedded tissue sections.

A suitably constituted Ethics Committee of our institution approved the protocol for this research project, and the work was carried out according to this protocol. Our study conformed to the provisions of the Declaration of Helsinki in 1995.

Epstein–Barr virus-encoded RNA *in situ* hybridization and IHC. Epstein–Barr virus-encoded RNA *in situ* hybridization was carried out using a fluorescein-conjugated EBER oligonucleotide probe and the purified IgG fraction of a mouse monoclonal anti-fluorescein antibody (Leica, Newcastle, UK). For IHC, mouse mAbs against CD3, CD5, CD10, CD15, CD20, CD79a, BCL-2, BCL-6, and MUM-1 (Novocastra, Newcastle upon Tyne, UK), and CD30 (Clone CON6D; Spanish National Cancer Research Centre (CNIO), Madrid, Spain) were used as primary antibodies. Detection of signals for EBER-ISH and IHC was carried out using the Leica BOND-MAX fully automatic IHC system with the BOND Polymer Refine detection kit according to the manufacturer's instructions using BOND Epitope Retrieval Solution for 20 min for antigen retrieval (DS9800 and AR9640; Leica Microsystems, Tokyo, Japan). For EBER-ISH-positive cases, LMP-1 (Novocastra) and EBNA-2 antibody (Novocastra) were examined with IHC.

When more than 30% of large-sized cells were positive, the case was deemed "EBV-positive". The DLBCL subtypes of GCB or non-GCB were categorized using CD10, BCL-6, and MUM-1 according to Hans' algorithm.[16] Cases that were unavailable for BCL-6 were categorized using CD10 and MUM-1 according to Chang's algorithm.[17] Epstein–Barr virus latency was classified as: latency I, LMP-1(−) EBNA-2(−); latency II, LMP-1(+) EBNA-2(−); and latency III, LMP-1(+) EBNA-2(+).

Clinical characteristics and statistical methods. Comparisons of characteristics between EBV-positive and EBV-negative cases were examined with Fisher's exact test or the non-parametric Mann–Whitney *U*-test, as appropriate. Tumor responses were assessed with computed tomography and PET. Patients were classified by the best tumor response according to the response criteria for malignant lymphoma.[18] Overall survival was defined as the duration from the date of diagnosis of DLBCL to the date of death of any cause. Progression-free survival was defined as the duration from the date of diagnosis to the date of progressive or relapsed disease. The OS and PFS probabilities were estimated using the Kaplan–Meier method, and patients who were alive at the last follow-up were censored. The log–rank test was used to compare pairs of subgroups regarding survival. Multivariate analyses were carried out using Cox's proportional hazards regression analysis. Statistical analyses were carried out using the GraphPad Prism 6.0 (GraphPad Software, San Diego, CA) and EZR version 3.0.2.[19]

Results

Patient selection, EBER-ISH, and IHC. The EBER-ISH analysis showed 18 cases of DLBCL that harbored EBV among the 260 cases examined (6.9%). Among these 260 cases, 21 cases were

Table 2. Summary of clinical data of patients with Epstein–Barr virus (EBV)-positive diffuse large B-cell lymphoma (DLBCL) (*n* = 14) and EBV-negative DLBCL (*n* = 225)

Variable	EBV-positive DLBCL (*n* = 14)	EBV-negative DLBCL (*n* = 225)	*P*-value
Age, years, median (range)	71.5 (55–84)	68.0 (22–92)	0.3379‡
Gender (male/female)	8/6	122/103	1.0000†
	No. of cases (%)	No. of cases (%)	*P*-value
Over 60 years of age	11 (78.6)	170 (75.6)	1.0000†
ECOG PS 2–4	6 (43.9)	38/214 (17.8)	0.0223†
Ann Arbor stage III/IV	9 (64.3)	114/216 (52.8)	0.5819†
B symptoms, presence	6 (43.9)	57/208 (27.4)	0.1067†
Extranodal involvement (>1 site)	12 (85.7)	121/204 (59.3)	0.0856†
IPI, High intermediate/High	9 (64.3)	96/202 (47.5)	0.2749†
LDH, IU/L, median (range)	339.5 (154–1798)	262.0 (132–5310)	0.1803‡
LDH ≥ facility upper limit of normal	11 (78.6)	135 (60.0)	0.2580†
IL2R, U/mL, median (range)	2740 (374–6780)	1300 (164–68 800)	0.1146‡
IL2R ≥1000 U/mL	10 (71.4)	128/219 (58.4)	0.2501†
IgG, mg/dL, median (range)	1501 (561–2510)	1275 (300–3644)	0.3785‡
IgA, mg/dL, median (range)	226 (128–1473)	251 (33–952)	0.8541‡
IgM, mg/dL, median (range)	78 (20–176)	72 (8–1203)	0.9227‡
Pathological subtype			
GCB type	1 (8.3)	54 (25.0)	0.3021†
Activated B-cell (non-GCB) type	11 (91.7)	162 (75.0)	
NA†	2	9	

†Fisher's exact test. ‡Mann–Whitney *U*-test. ECOG, Eastern Cooperative Oncology Group; GCB, germinal center B cell; IL2R, interleukin 2 receptor; IPI, international prognostic index; LDH, lactate dehydrogenase; NA, not available; PS, performance status.

excluded from analysis in this study for the following reasons: 1 case with HIV infection (EBV-positive); 4 cases with a history of methotrexate (EBV-positive, 2 cases; EBV-negative, 2 cases); 4 cases with primary large B-cell lymphoma of the central nervous system (EBV-negative); and 12 cases in which the clinical records were unavailable (EBV-positive, 1 case; EBV-negative, 11 cases). Finally, we analyzed 239 patients that included 14 cases of EBV-positive DLBCL and 225 cases of EBV-negative DLBCL, resulting in an EBV-positive rate of 6.0% (Table 1). Because all EBV-positive DLBCL patients were older than 50 years, they satisfied the criteria of EBV-DLBCL of the elderly.

Clinical data are summarized in Table 2. The median age was 71.5 years in EBV-positive patients and 68.0 years in EBV-negative patients ($P = 0.3379$). The percentages of patients aged over 60 years were 78.6% for EBV-positive and 75.6% for EBV-negative patients ($P = 1.0000$). The performance status was inferior in EBV-positive patients; the incidence of a performance status >2 in EBV-positive patients was higher than that in EBV-negative patients (43.9% *vs* 17.8%, respectively; $P = 0.0223$). Extranodal disease affecting more than two organs was found in 12/14 EBV-positive cases (85.7%) and 121/204 EBV-negative cases (59.3%) ($P = 0.0856$). Eleven out of 12 EBV-positive cases were non-GCB types (91.7%). In EBV-negative cases, GCB and non-GCB types were found in 54 patients (25.0%) and 162 patients (75.0%), respectively. In EBV-positive DLBCL, seven patients showed latency II and four showed latency III.

Table 3. Summary of therapy and treatment responses in patients with Epstein–Barr virus (EBV)-positive and EBV-negative diffuse large B-cell lymphoma (DLBCL)

	EBV-positive DLBCL	EBV-negative DLBCL	*P*-value
Immunocompetent	14	225	
No treatment	3	11	
Treatment	11	214	
Chemotherapy, no rituximab	3	8	
Radiation	0	3	
Rituximab only	0	5	
R plus chemotherapy	8	198	
R-CHOP	8	160	
R-CHOP-like	0	38	
R-COP	0	16	
R-THP-COP	0	14	
R-CHO	0	4	
R-CHP	0	2	
R-CO	0	2	
No. of chemotherapy cycles, median (range)	4.5 (1–8)	6 (1–8)	0.0201†
Response			
CR	2 (25.0%)	147 (74.2%)	0.0060‡
PR	2 (25.0%)	19 (9.6%)	
SD or PD	4 (50.0%)	29 (14.6%)	
NA	0	3	

†Mann–Whitney *U*-test. ‡χ2-test. C, cyclophospahmide; CR, complete remission; H, doxorubicin; NA, not available; O, vincristine; P, prednisolone; PD, progressive disease; PR, partial response; R, rituximab; SD, stable disease; THP, pirarubicin.

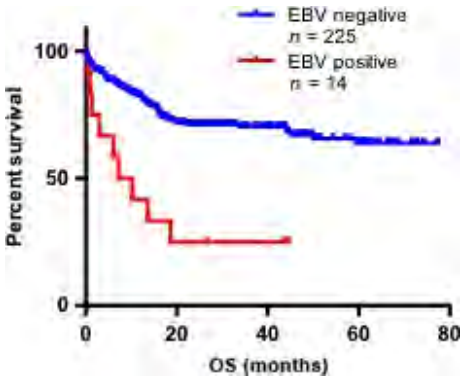

Fig. 1. Overall survival (OS) in immunocompetent Epstein–Barr virus (EBV)-positive versus EBV-negative patients with diffuse large B-cell lymphoma. The median OS in EBV-positive patients was 8.7 months; OS could not be determined in EBV-negative patients. Hazard ratio = 3.9; 95% confidence interval, 4.0–49.3; $P < 0.0001$.

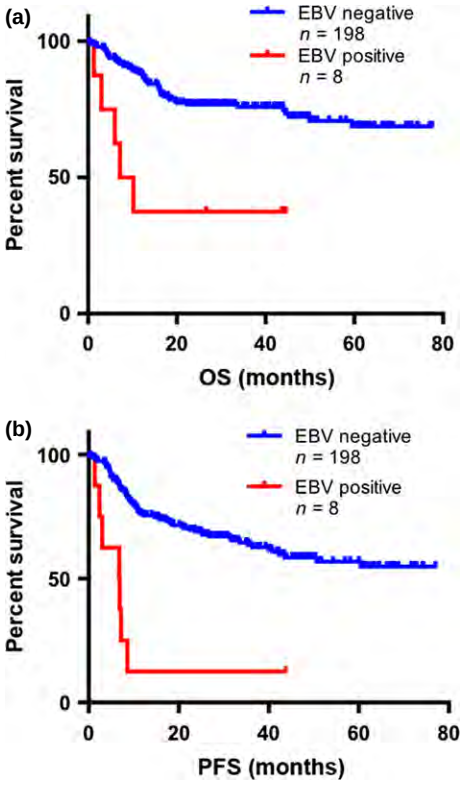

Fig. 2. Survival analysis in patients with diffuse large B-cell lymphoma (DLBCL) treated with chemotherapy regimens similar to rituximab plus cyclophosphamide, doxorubicin, vincristine, and prednisolone. (a) Overall survival (OS). The median OS in Epstein–Barr virus (EBV)-positive DLBCL patients was 8.7 months; OS could not be determined in EBV-negative patients. Hazard ratio = 4.3; 95% confidence interval, 3.6–121.6; $P = 0.0002$. (b) Progression-free survival (PFS). The median PFS in EBV-positive DLBCL patients was 6.8 months; median PFS could not be determined in EBV-negative patients. Hazard ratio = 5.6; 95% confidence interval, 13.0–384.6; $P < 0.0001$.

Treatment response. The various treatments are shown in Table 3. Both R-CHOP and R-CHOP-like regimens were used for chemotherapy.

The R-CHOP and R-CHOP-like regimens were given to 8/14 EBV-positive and 198/225 EBV-negative patients. The median number of R-CHOP cycles was 4 (range, 1–8) in

Table 4. Details of clinical data for patients with Epstein–Barr virus-positive diffuse large B-cell lymphoma (n = 14)

No.	Age, years/ gender	PS	CS	IPI	Extranodal disease	CD20	CD15	CD30	EBER-ISH	LMP1	EBNA2	Latency	GCB/non-GCB	Morphological subtype	Others	LDH (IU/L)	IL2R (U/mL)	IgG (mg/dL)	IgA (mg/dL)	IgM (mg/dL)	Therapy	No. of cycles	Response	OS (months)	PFS (months)	Outcome
1	59/F	3	IVA	HI	Lung	++	−	+	++	++	−	II	Non-GCB	Poly	Necrosis	154	1250	1069	190	176	R-CHOP	5	CR	44.6	8.6	Relapsed, treated with Bendamustine, alive, 2nd CR
2	80/F	1	IIIB	HI	Skin, pleurae	+++	−	+	+++	+	−	II	Non-GCB	Large	Plasma differentiation	293	1990	1501	226	88	R-CHOP	4	PR	26.6	6.9	Progressive, treated with CEPP/VP16/ rituximab, alive, 2nd CR
3	64/M	0	IIA	LI	Stomach	+++	−	−	++	++	−	II	Non-GCB	Poly	None	209	688	2510	396	78	R-CHO	6	CR	43.7	43.7	Alive, CR
4	78/F	0	IIA	LI	Intraoral ulcer	+++	−	−	+++	++	+	III	Non-GCB	Large	None	249	374	1279	238	119	R-CH (THP) OP	6	PD	10.2	6.7	Refractory to R-CPA-VP16/VP16/R-MIT-MCNU-VP16-Dex, died
5	77/F	1	IIIB	HI	Retroperitoneal tumor	+++	−	++	+++	+++	+	III	Non-GCB	Large	None	1677	3570	1421	149	52	R-CHOP	2	PD	6.0	2.4	Refractory to EPOCH/R-DeVIC, died
6	69/M	2	IIIB	LI	Liver	++	−	−	+	++	−	II	Non-GCB	Poly	HRS cell	219	6780	1573	1473	67	R-CHOP	3	PD	3.0	3.0	Sepsis, progressive disease, died
7	55/F	4	IIB	HI	Abdominal tumor (soft tissue)	+++	−	+++	+++	++	−	II	Non-GCB	Large	None	496	4520	634	174	71	R-CHOP	8	PR	7.2	7.2	Pneumonia, progressive disease, died
8	69/F	0	IA	LI	Intraoral ulcer	+++	−	−	+++	+++	+	III	Non-GCB	Large	None	363	1390	561	128	20	R-CHOP	1	PD	1.3	1.3	Pneumonia, alveolar hemorrhage, died
9	63/M	NA	IV*	H	None	++	−	++	+	++	−	II	Non-GCB	Poly	HRS cell	1798	9710	2001	189	113	No treatment	0	NA.	0.0	0.0	DIC, cerebral hemorrhage, died
10	76/M	4	IV*	H	Femur tumor	++	−	−	+++	++	+	III	Non-GCB	Poly	None	316	NA	NA	NA	NA	No treatment	0	NA.	0.4	0.4	Chose the best supportive care, died
11	79/M	0	IIA	LI	Left thoracic tumor, rib	−	NA	NA	+	NA	NA	NA	Non-GCB	Poly	None	370	952	2424	305	91	COP	8	PD	13.6	10.7	Relapse, chose the best supportive care after radiation, died
12	74/M	4	IVB	HI	Lung	−	+	+	+++	+	−	II	NA	Poly	Plasma differentiation	394	3530	1505	495	30	No treatment	0	NA.	0.0	0.0	Pneumonia by tumor invasion, died
13	59/M	4	IVA	H	Liver, small intestine	−	+	−	+++	NA	NA	NA	GCB	Large	None	768	12700	605	162	42	COP	1	PD	0.9	0.9	Progressive disease, died
14	84/M	1	IIIB	HI	None	++	−	+++	++	NA	NA	NA	NA	Poly	HRS cell	220	2740	2418	454	129	COP	6	CR	18.6	15.0	Relapse, chose the best supportive care, died

CEPP, cyclophosphamide, etoposide, procarbazine, prednisolone; CHO, cyclophosphamide, doxorubicin, vincristine; CHOP, cyclophosphamide, doxorubicin, vincristine, prednisolone; CPA, cyclophosphamide; CR, complete remission; CS, clinical stage; DeVIC, carboplatin, etoposide, interferon, dexamethasone, granulocyte-colony stimulating factor; Dex, dexamethasone; EBER-ISH, Epstein-Barr virus-encoded RNA *in situ* hybridization; EBNA, Epstein-Barr virus nuclear antigen antibody; EPOCH, rituximab, etoposide, doxorubicin, vincristine, cyclophosphamide, prednisolone; F, female; GCB, germinal center B cell; H, high; HI, high intermediate; IL2R, interleukin 2 receptor; IPI, international prognostic index; Large, large-cell type; LDH, lactate dehydrogenase; LI, low intermediate; LMP, latent membrane protein; M, male; MCNU, ranimustine; MIT, mitoxantrone; NA, not available; OS, overall survival; PD, progressive disease; PFS, progression-free survival; Poly, polymorphous type; PR, partial response; PS, performance status; R, rituximab; THP, piranubicin; VP16, etoposide.

EBV-positive patients and 6 (range, 1–8) in EBV-negative patients. Treatment was discontinued for various reasons in 5/8 EBV-positive patients and 30/198 EBV-negative patients (P = 0.0201). Among EBV-positive patients, two patients died of infection in the nadir phase during chemotherapy, one patient discontinued treatment due to PD, and one patient refused to continue chemotherapy due to an adverse drug reaction. Two EBV-positive patients showed CR (25%), two showed partial response (25%), and four showed stable disease/PD (50%). In contrast, 147 EBV-negative patients showed CR (74.2%), 19 patients showed partial response (9.6%), and 29 patients showed stable disease/PD (14.6%). The overall response rate was better in EBV-negative than EBV-positive patients (P = 0.0060).

Survival. The median follow-up time of surviving patients was 25.2 months (range, 0.8–71.3 months). Median OS was 8.7 months in EBV-positive patients and was not reached in EBV-negative patients (P < 0.0001; Fig. 1). Three EBV-positive patients could not receive chemotherapy because their general condition was poor and disease progression was rapid.

Median OS and PFS were 8.7 and 6.8 months, respectively, in EBV-positive patients treated with R-CHOP/R-CHOP-like regimens. Both OS and PFS were worse in EBV-positive patients than in EBV-negative patients (P = 0.0002, P < 0.0001, respectively; Fig. 2). Among eight patients who received R-CHOP/R-CHOP-like regimens, four died without achieving CR. All three patients with latency III died <1 year after diagnosis. Two of them were resistant to chemotherapy. No difference in OS or PFS was found between latency III and latency II (Table 4). We also did not find a difference in OS or PFS between the polymorphous type versus the large-cell type in EBV-positive DLBCL (Table 4). Among EBV-negative

Table 5. Summary of risk factors for prognosis in patients with diffuse large B-cell lymphoma, using multivariable analysis (n = 14)

	Univariate analysis†		Multivariate analysis‡	
	HR (95% CI)	P-value	HR (95% CI)	P-value
Age				
≥60 years	2.0 (1.1–3.8)	0.02039	1.6 (0.8–3.3)	0.1911
EBV				
Positive	4.2 (2.1–8.2)	<0.00010	4.6 (1.8–11.8)	0.0014
PS				
2–4	5.6 (3.4–9.1)	<0.00010	3.3 (1.7–6.7)	0.0007
Clinical stage				
III–IV	3.2 (1.9–5.5)	<0.00010	1.5 (0.7–3.1)	0.2616
B symptoms				
Present	2.5 (1.5–4.0)	0.00040	1.0 (0.5–2.0)	0.9379
Extranodal disease				
≥1 site	2.7 (1.6–4.7)	0.00030	1.0 (0.5–2.3)	0.9359
LDH levels				
≥Facility upper limit of normal	4.2 (2.6–6.7)	<0.00010	3.3 (1.4–7.7)	0.0070
IL2R levels				
≥1000 U/mL	4.2 (2.3–7.7)	<0.00010	1.2 (0.5–2.8)	0.6597
Subtype				
Non-GCB	2.2 (1.1–3.4)	0.02670	1.9 (0.8–4.2)	0.1324

†Log–rank test. ‡Cox's proportional hazards regression analysis. CI, confidence interval; GCB, germinal-center B cell; HR, hazard risk; IL2R, interleukin 2 receptor; LDH, lactate dehydrogenase; PS, performance status.

patients, 49 died and 149 were alive. Among the 149 alive patients, 115 maintained relapse-free survival after achieving the first CR.

Multivariate analyses. We carried out a Cox's proportional hazard regression analysis that included the following variables: age; EBV present; PS; clinical stage; B symptoms present; extranodal disease; LDH levels; interleukin-2 receptor levels; and GCB or non-GCB subtypes. The EBV, PS, and LDH levels were independent risk factors ($P = 0.0014$, 0.0007, and 0.0070, respectively). Among them, EBV had the highest hazard ratio (HR: 4.6. 95% confidence interval: 1.8–11.8) (Table 5).

Discussion

We carried out a clinicopathological analysis of DLBCL with special interest in EBV. The percentage of patients with EBV infection (6.9%) among all cases of DLBCL in our data was equivalent to previously reported data from Asian countries.[8,11,12] All patients with EBV-positive DLBCL met the criteria of EBV-DLBCL of the elderly, proposed by WHO.

In our analysis, patient characteristics between those who were EBV-positive and those who were EBV-negative were almost equivalent except for the performance status ($P = 0.0223$) and a trend towards extranodal disease ($P = 0.0856$). Epstein–Barr virus-positive DLBCL tends to develop extranodal involvement in 70% of patients;[11,20,21] DLBCL generally involves extranodal organs such as the gastrointestinal tract, skin, lungs, and tonsils.[22] Differences in extranodal organ involvement between EBV-positive and EBV-negative cases are unknown.

Several studies regarding the prognosis of EBV-positive DLBCL have been reported. Morales *et al.*[12] reported that EBV is an independent prognostic factor associated with *de novo* nodal DLBCL, before the rituximab era. This study analyzed six patients with EBV-positive DLBCL and 51 patients with EBV-negative DLBCL. The median OS rates in EBV-positive DLBCL and EBV-negative DLBCL patients were 6.5 and 47 months, respectively, and patients with EBV-positive DLBCL showed an inferior prognosis compared to those with EBV-negative DLBCL ($P = 0.001$). Park *et al.*[8] reported that DLBCL patients who are EBER-ISH-positive show a more rapidly deteriorating clinical course with poorer treatment response, survival, and PFS. They analyzed 34 patients with EBV-positive DLBCL and 346 patients with EBV-negative DLBCL. Epstein–Barr virus-encoded RNA positivity was significantly associated with age older than 60 years ($P = 0.005$), more advanced stage ($P < 0.001$), involvement of more than one extranodal site ($P = 0.009$), higher international prognostic index (the international prognostic index includes age >60 years, PS >2, number of extranodal sites >2, stage >III, and LDH level >normal) ($P = 0.015$), presence of B symptoms ($P = 0.004$), and poorer outcome following initial treatment ($P = 0.006$). The EBER-positive patients with DLBCL showed significantly poorer OS (EBER-positive *vs* EBER-negative, $P = 0.026$) and PFS (EBER-positive *vs* EBER-negative, $P = 0.018$). Both reports arrived at the same conclusion: that the presence of EBV leads to a more rapidly deteriorating clinical course with poorer treatment response and survival.

In contrast, Ahn *et al.* retrospectively analyzed 222 elderly patients (≥50 years) with DLBCL who received R-CHOP chemotherapy and evaluated the state of EBER. Eighteen cases (8.1%) were EBER-positive. At a median follow-up of 32.8 months, no significant difference was found in OS between the groups ($P = 0.627$). The EBV-positive DLBCL patients with early interruption of R-CHOP chemotherapy showed a trend toward a high EBV DNA titer (≥1000 copies/mL; $P = 0.091$). Thus, the EBV-positive tumoral status of elderly DLBCL patients who undergo R-CHOP chemotherapy may not predict their survival but their EBV status may contribute to the early interruption of R-CHOP chemotherapy.[15] In our study, we observed that OS and PFS of EBV-positive DLBCL patients were still lower than EBV-negative DLBCL, even after introduction of rituximab. Although the survival data are controversial between the two studies, they share some common features. For instance, both studies recognized that the overall response rate was worse in patients with EBV-positive DLBCL compared to those with EBV-negative DLBCL, and R-CHOP was interrupted early more frequently compared with EBV-negative DLBCL. Because the incidence of EBV-positive DLBCL of the elderly is low, a limitation is the small number of EBV-positive DLBCL patients in both studies. Based on these results, a multicenter study is needed to clarify the controversies regarding EBV-positive DLBCL.

Among 14 patients with EBV-positive DLBCL in our study, four patients showed latency III. Latency I is associated with EBV-related Burkitt lymphoma, latency II with classical Hodgkin's lymphoma and T-cell non-Hodgkin's lymphoma, and latency III occurs mainly in immunocompromised individuals suffering from post-transplant lymphoproliferative disorders and HIV-associated lymphoproliferative disorders and lymphoblastoid cell lines.[23] In general, a more intense immunosuppressive status is associated with a higher latency status. However, none of our patients was immunosuppressed. Patients with latency III died within 1 year of diagnosis, regardless of treatment with rituximab. Although no significant difference in survival was found, the outcome of latency III patients tended to be poor compared with that of latency II patients. Yoshino *et al.*[24] reported that EBV-positive DLBCL is resistant to standard chemotherapy. In this study, patients with latency III also showed resistance to chemotherapy.

In addition, we showed that the majority of patients classified as having EBV-positive DLBCL of the elderly were non-GCB types, which is a subtype with poor prognosis, and this may be another reason for the inferior prognosis. In EBV-positive DLBCL of the elderly, according to the WHO classification, age of more than 70 years and the presence of B symptoms are negative prognostic factors.[4,11,25] The proportion of the non-GCB type increases and reflects a change in the B-cell population during aging.[26] Thus, advanced age may lead to poor prognosis. Because age was not related to positive or negative EBV status in our study, we suggest that the latency status is a risk factor for developing the non-GCB type. Montes-Moreno *et al.*[27] reported that EBV infection may play a direct and additional role in activation of the nuclear factor-κB pathway. According to their report, EBV-positive DLBCL in the elderly is an aggressive and clonal B-cell neoplasm with prominent nuclear factor-κB pathway activation in the neoplastic cells. Epstein–Barr virus-encoded RNA positivity has an adverse impact on OS and PFS in patients with non-GCB DLBCL but not GCB DLBCL.[8] However, the detailed mechanism of conversion to more malignant clones in the presence of EBV is unknown. Infection with EBV in patients with non-GCB DLBCL may lead to further resistance to chemotherapy.

In summary, rituximab, which improved the outcome of DLBCL patients, did not show sufficient efficacy in EBV-

positive DLBCL patients. Patients with latency III were more resistant to chemotherapy. Further investigation of EBV-positive DLBCL patients based on their latency status and IHC phenotype is needed.

Acknowledgments

We thanks Mr. Akihiko Serizawa of Department of Pathology, Tokai University Hospital, for technical assistance.

Disclosure Statement

The authors have no conflict of interest.

Abbreviations

BCL	B-cell chronic lymphocytic leukemia/lymphoma
CHOP	cyclophosphamide, doxorubicin, vincristine, and prednisolone
CR	complete remission
DLBCL	diffuse large B-cell lymphoma
EBER	Epstein–Barr virus-encoded RNA
EBNA-2	Epstein–Barr virus nuclear antigen-2
EBV	Epstein–Barr virus
GCB	germinal center B cell
IHC	immunohistochemistry
ISH	*in situ* hybridization
LDH	lactate dehydrogenase
LMP-1	latent membrane protein-1
MUM-1	multiple myeloma oncogene-1
OS	overall survival
PD	progressive disease
PFS	progression-free survival
PS	performance status
R-CHOP	rituximab plus cyclophosphamide, doxorubicin, vincristine, and prednisolone
WHO	World Health Organization

References

1 Lymphoma Study Group of Japanese Pathologists. The World Health Organization classification of malignant lymphomas in Japan: incidence of recently recognized entities. *Pathol Int* 2000; **50**: 696–702.
2 Jaffe ES, Pittaluga S. Aggressive B-cell lymphomas: a review of new and old entities in the WHO classification. *Hematology Am Soc Hematol Educ Program* 2011; **2011**: 506–14.
3 Campo E, Swerdlow SH, Harris NL, Pileri S, Stein H, Jaffe ES. The 2008 WHO classification of lymphoid neoplasms and beyond: evolving concepts and practical applications. *Blood* 2011; **117**: 5019–32.
4 Swerdlow SH, Campo E, Harris NL *et al. WHO Classification of Tumours of Haematopoietic and Lymphoid Tissues*, 4th edn. Lyon, France: IARC Press, 2008.
5 Gibson SE, Hsi ED. Epstein-Barr virus-positive B-cell lymphoma of the elderly at a United States tertiary medical center: an uncommon aggressive lymphoma with a nongerminal center B-cell phenotype. *Hum Pathol* 2009; **40**: 653–61.
6 Hoeller S, Tzankov A, Pileri SA, Went P, Dirnhofer S. Epstein-Barr virus-positive diffuse large B-cell lymphoma in elderly patients is rare in Western populations. *Hum Pathol* 2010; **41**: 352–7. Epub 2009/11/17.
7 Odumade OA, Hogquist KA, Balfour HH Jr. Progress and problems in understanding and managing primary Epstein-Barr virus infections. *Clin Microbiol Rev* 2011; **24**(1): 193–209.
8 Park S, Lee J, Ko YH *et al.* The impact of Epstein-Barr virus status on clinical outcome in diffuse large B-cell lymphoma. *Blood* 2007; **110**(3): 972–8.
9 Feugier P, Van Hoof A, Sebban C *et al.* Long-term results of the R-CHOP study in the treatment of elderly patients with diffuse large B-cell lymphoma: a study by the Groupe d'Etude des Lymphomes de l'Adulte. *J Clin Oncol* 2005; **23**: 4117–26.
10 Coiffier B, Thieblemont C, Van Den Neste E *et al.* Long-term outcome of patients in the LNH-98.5 trial, the first randomized study comparing rituximab-CHOP to standard CHOP chemotherapy in DLBCL patients: a study by the Groupe d'Etudes des Lymphomes de l'Adulte. *Blood* 2010; **116**: 2040–5.
11 Oyama T, Yamamoto K, Asano N *et al.* Age-related EBV-associated B-cell lymphoproliferative disorders constitute a distinct clinicopathologic group: a study of 96 patients. *Clin Cancer Res* 2007; **13**: 5124–32.
12 Morales D, Beltran B, De Mendoza FH *et al.* Epstein-Barr virus as a prognostic factor in de novo nodal diffuse large B-cell lymphoma. *Leuk Lymphoma* 2010; **51**(1): 66–72.
13 Uner A, Akyurek N, Saglam A *et al.* The presence of Epstein-Barr virus (EBV) in diffuse large B-cell lymphomas (DLBCLs) in Turkey: special emphasis on 'EBV-positive DLBCL of the elderly'. *APMIS* 2011; **119**(4–5): 309–16.
14 Kuze T, Nakamura N, Hashimoto Y, Sasaki Y, Abe M. The characteristics of Epstein-Barr virus (EBV)-positive diffuse large B-cell lymphoma: comparison between EBV(+) and EBV(−) cases in Japanese population. *Jpn J Cancer Res* 2000; **91**(12): 1233–40.
15 Ahn JS, Yang DH, Choi YD *et al.* Clinical outcome of elderly patients with Epstein-Barr virus positive diffuse large B-cell lymphoma treated with a combination of rituximab and CHOP chemotherapy. *Am J Hematol* 2013; **88**: 774–9.
16 Hans CP, Weisenburger DD, Greiner TC *et al.* Confirmation of the molecular classification of diffuse large B-cell lymphoma by immunohistochemistry using a tissue microarray. *Blood* 2004; **103**(1): 275–82.
17 Chang CC, McClintock S, Cleveland RP *et al.* Immunohistochemical expression patterns of germinal center and activation B-cell markers correlate with prognosis in diffuse large B-cell lymphoma. *Am J Surg Pathol* 2004; **28**: 464–70.
18 Cheson BD, Pfistner B, Juweid ME *et al.* Revised response criteria for malignant lymphoma. *J Clin Oncol* 2007; **25**: 579–86.
19 Yoshinobu K. Investigation of the freely available easy-to-use software 'EZR' for medical statistics. *Bone Marrow Transplant* 2013; **48**: 452–8.
20 Shimoyama Y, Asano N, Kojima M *et al.* Age-related EBV-associated B-cell lymphoproliferative disorders: diagnostic approach to a newly recognized clinicopathological entity. *Pathol Int* 2009; **59**: 835–43.
21 Rooper L, Gocke CD, Belchis DA. Pleural fluid cytology of the polymorphous variant of EBV-positive diffuse large B-cell lymphoma: first report and distinction from a reactive process. *Case Rep Pathol* 2013; **2013**: 459279.
22 Moller MB, Pedersen NT, Christensen BE. Diffuse large B-cell lymphoma: clinical implications of extranodal versus nodal presentation – a population-based study of 1575 cases. *Br J Haematol* 2004; **124**: 151–9.
23 Carbone A, Gloghini A, Dotti G. EBV-associated lymphoproliferative disorders: classification and treatment. *Oncologist* 2008; **13**: 577–85.
24 Yoshino T, Nakamura S, Matsuno Y *et al.* Epstein-Barr virus involvement is a predictive factor for the resistance to chemoradiotherapy of gastric diffuse large B-cell lymphoma. *Cancer Sci* 2006; **97**: 163–6.
25 Oyama T, Ichimura K, Suzuki R *et al.* Senile EBV+ B-cell lymphoproliferative disorders: a clinicopathologic study of 22 patients. *Am J Surg Pathol* 2003; **27**(1): 16–26.
26 Mareschal S, Lanic H, Ruminy P, Bastard C, Tilly H, Jardin F. The proportion of activated B-cell like subtype among de novo diffuse large B-cell lymphoma increases with age. *Haematologica* 2011; **96**: 1888–90.
27 Montes-Moreno S, Odqvist L, Diaz-Perez JA *et al.* EBV-positive diffuse large B-cell lymphoma of the elderly is an aggressive post-germinal center B-cell neoplasm characterized by prominent nuclear factor-kB activation. *Mod Pathol* 2012; **25**(7): 968–82.

Leukemia Research Reports 3 (2014) 54–57

Contents lists available at ScienceDirect

Leukemia Research Reports

journal homepage: www.elsevier.com/locate/lrr

Case report

Identification of a novel *SEPT9-ABL1* fusion gene in a patient with T-cell prolymphocytic leukemia

Rikio Suzuki [a,e], Hiromochi Matsushita [b,c], Hidetsugu Kawai [a,c], Hideyuki Matsuzawa [c,d], Kosuke Tsuboi [a], Shigeki Watanabe [e], Hiroshi Kawada [a,c], Yoshiaki Ogawa [a], Kiyoshi Ando [a,c,*]

[a] Division of Hematology/Oncology, Department of Internal Medicine, Tokai University School of Medicine, Isehara, Kanagawa, Japan
[b] Department of Laboratory Medicine, Tokai University School of Medicine, Isehara, Kanagawa, Japan
[c] Research Center for Cancer Stem Cell, Tokai University School of Medicine, Isehara, Kanagawa, Japan
[d] Teaching and Research Support Center, Tokai University School of Medicine, Isehara, Kanagawa, Japan
[e] Division of Hematology, Ebina General Hospital, Ebina, Kanagawa, Japan

ARTICLE INFO

Article history:
Received 6 March 2014
Received in revised form
15 June 2014
Accepted 16 June 2014
Available online 28 June 2014

Keywords:
T-cell prolymphocytic leukemia
SEPT9-ABL1
Tyrosine kinase inhibitors

ABSTRACT

T-cell prolymphocytic leukemia (T-PLL), a rare type of peripheral T-cell leukemia, is characterized by marked splenomegaly with rapidly progressive lymphocytosis and a poor prognosis. Nine kinds of *ABL1* chimeric genes have been identified in various kinds of hematological malignancies, such as chronic myeloid leukemia and B- or T-lymphoblastic leukemia. However, there have been no reports describing T-PLL cases with *ABL1* rearrangements. We herein report a case of T-PLL with a novel *SEPT9-ABL1* fusion gene which induced strong resistance to tyrosine kinase inhibitors such as imatinib and dasatinib.

1. Introduction

T-cell prolymphocytic leukemia (T-PLL) is a rare type of peripheral T-cell leukemia with a naive T-cell phenotype [1]. The clinical features of T-PLL include marked hepatosplenomegaly and generalized lymphadenopathy with rapidly progressive lymphocytosis. The prognosis is generally poor due to resistance to chemotherapy, with a median survival ranging from 7.5 to 50 months [1–3]. Chromosomal abnormalities such as t(14;14)(q11;q32), inv(14)(q11;q32) and t(X;14)(q28;q11) have been identified in patients with T-PLL, which result in the rearrangement of the *TCL1* or *MTCP1* genes with the T-cell receptor loci, which were thought to contribute to the pathogenesis of T-PLL [3].

We herein report a case of T-PLL with a novel *ABL1* fusion gene which was fused to *SEPT9*, *SEPT9-ABL1*. The case exhibited strong resistance to the tyrosine kinase inhibitors (TKI) used against *BCR-ABL1*. This is the first report of T-PLL with an *ABL1* fusion gene, and additionally, only the second report of a hematological malignancy with an *ABL1* fusion gene that exhibited a poor response to TKI.

2. Case report

A 70-year-old male was admitted to our hospital due to leukocytosis. On a physical examination, lymphadenopathy extending from the bilateral cervical to supraclavicular regions with moderate hepatomegaly was noted. The laboratory data on admission were as follows: white blood cells (WBC), 248×10^9/L with 0% neutrophils, 1% lymphocytes, 1% monocytes, 0% eosinophils, 0% basophils and 98% atypical lymphocytes, which were medium-sized with pale cytoplasm and prominent nucleoli (Fig. 1A); red blood cells (RBC), 4110×10^9/L; hemoglobin (Hb), 12.4 g/dl; and platelets (Plt), 171×10^9/L. Blood biochemistry was normal, except for elevated levels of lactate dehydrogenase and hepatobiliary enzymes. Bone marrow aspirate smears showed marked proliferation of atypical lymphocytes with a similar morphology to that of the peripheral blood cells. Using a cytogenetic analysis, six of six metaphases examined were 46, XY. A flow cytometric analysis showed that the atypical lymphocytes were positive for CD2, CD4, CD5 and CD7. A *BCR-ABL* FISH analysis showed no *BCR-ABL* signals, although 79 of 100 bone marrow cells exhibited atypical signals (*ABL1*: three copies and *BCR*: two copies in each cell) (Fig. 1B). The three *ABL1* signals indicated either simple amplification of the *ABL1* gene or the presence of *ABL1* rearrangement. In order to examine these two possibilities, the 5′-terminal sequence of the *ABL1* gene was analyzed using the 5′ RACE PCR method (SMARTer

* Correspondence to: Department of Hematology/Oncology, Tokai University School of Medicine, 143 Shimokasuya, Isehara, Kanagawa, Japan.
Tel.: +81 463 93 1121; fax: +81 463 92 4511.
E-mail address: andok@keyaki.cc.u-tokai.ac.jp (K. Ando).

http://dx.doi.org/10.1016/j.lrr.2014.06.004

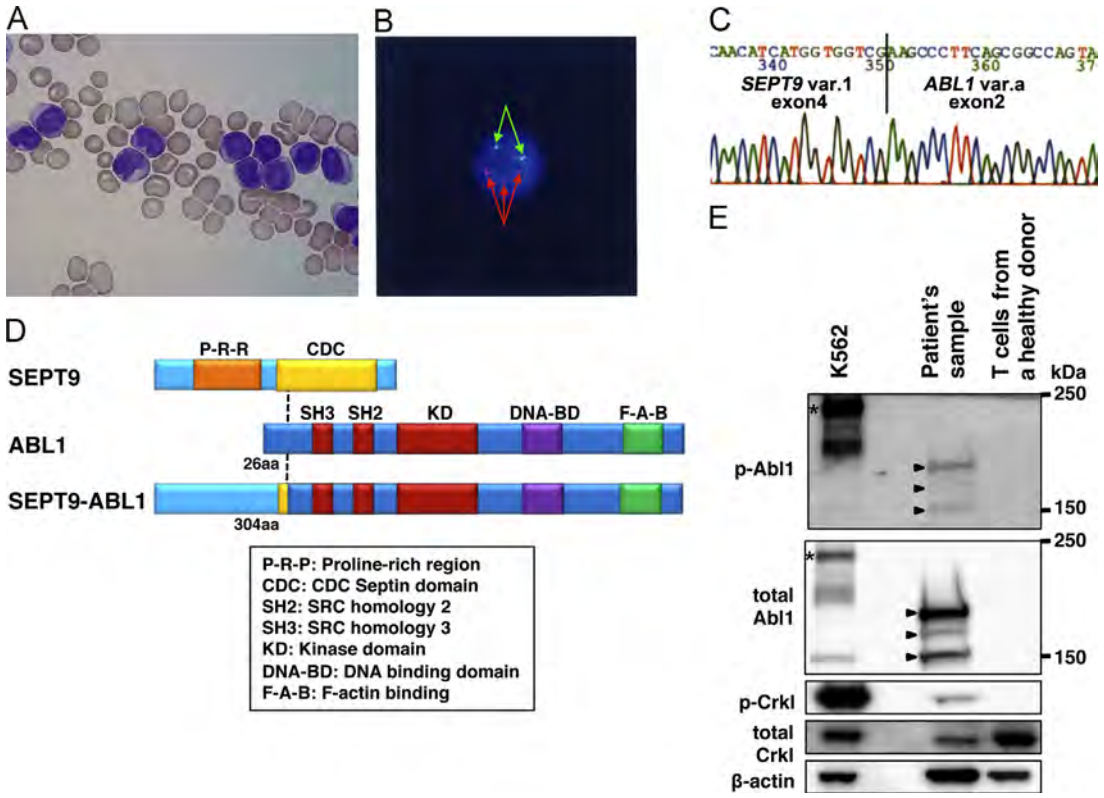

Fig. 1. Clinical and molecular characteristics of T-PLL harboring the *SEPT9-ABL1* fusion gene. (A) Cytology of the leukemic cells in the peripheral blood at diagnosis. The smear underwent Wright–Giemsa staining. (B) A FISH analysis of the bone marrow cells using the *BCR-ABL1* probe. The red signals show three *ABL1* signals, including one normal and two split signals (indicated by the lower arrows), while the green signals show normal biallelic *BCR* signals (indicated by the upper arrows). No *BCR-ABL1* fusion signals were detected. (C) Identification of *SEPT9-ABL1* fusion in the T-PLL cells. The PCR products of 5' RACE PCR using the ABL1 reverse primer were cloned into a cloning vector. Sequencing of the PCR products showed a fusion of exon 4 of *SEPT9* transcript variant 1 (GenBank accession number: NM_001113491.1) to exon 2 of *ABL1* transcript variant a (GenBank accession number: NM_005157.4). (D) The presumed structure of the SEPT9-ABL1 fusion product. (E) The phosphorylation of SEPT9-ABL1 and the downstream target CRKL in the T-PLL cells obtained from the patient. K562 cells and T-cells derived from a healthy donor were used as positive and negative controls for ABL1 fusion. Anti-ABL1 and anti-phosphorylated-ABL1 antibodies detected three SEPT9-ABL1 bands corresponding to 180, 170 and 150 KDa in the patient (arrowheads), as well as 210 KDa BCR-ABL1 in the K562 cells (asterisks), demonstrating the expression and phosphorylation of SEPT9-ABL1. CRKL was phosphorylated only in the cells harboring ABL1 fusion. The anti-phospho-Abl (Tyr412), anti-Abl, anti-phospho-Crkl (Tyr207) and anti-Crkl antibodies were purchased from Cell Signaling, and anti-β-actin was purchased from Sigma-Aldrich.

RACE cDNA Amplification Kit, Takara Bio, Shiga, Japan), according to the manufacturer's protocol. Sequencing of the PCR products demonstrated the fusion of exon 4 of *SEPT9* to exon 2 of *ABL1* (Fig. 1C), suggesting that the *SEPT9-ABL1* fusion gene had the same breakpoint in *ABL1* as that seen in *BCR-ABL1*. The presumed structure of the SEPT9-ABL1 fusion product is shown in Fig. 1D. A Western blot analysis revealed the expression and phosphorylation of SEPT9-ABL1, in addition to the phosphorylation of a downstream target CRKL, in the T-PLL cells obtained from the patient (Fig. 1E). Taking into account the patient's clinical, morphological, immunophenotypic and molecular features, he was diagnosed with T-PLL harboring *SEPT9-ABL1*. This is the first report of a novel *SEPT9-ABL1* fusion gene in a patient with malignancy, as well as T-PLL harboring *ABL1* fusion.

The patient received multiagent chemotherapy using cyclophosphamide, daunorubicin, vincristine, predonisolone and L-asparaginase, and high dose MTX/Ara-C, as well as the single-agent administration of nelarabine, hydroxyurea and tyrosine kinase inhibitors (TKIs) (imatinib and dasatinib). The conventional chemotherapies and cytotoxic agents effectively reduced the WBC count, however, TKIs were unable to do so. He finally died on day 223 after diagnosis (Fig. 2A). An autopsy was performed, and a macroscopic examination showed generalized lymphadenopathy with an enlarged lung, liver, spleen and kidney, while a microscopic examination disclosed leukemic cell infiltration throughout multiple organs (Fig. 2B). These findings suggested the occurrence of multiple organ failure due to a progression of leukemia which eventually caused the patient's death.

3. Discussion

ABL1 is a well-known oncogene that is often associated with the formation of fusion genes, such as *BCR-ABL1*, in human leukemia. The wild-type ABL1 product transduces diverse extracellular signals to protein networks that control proliferation, survival, migration and invasion [4]. Additionally, ABL1 modulates development and cytoskeletal remodeling processes in T-cells. To date, nine genes, including *BCR*, have been shown to fuse to *ABL1* [5]. These genes are divided into two groups according to their structure: one group has a breakpoint in exon 2 including the Src Homology (SH) 2 and SH3 domains in the fusion products and is found in various kinds of leukemia, while the other has a breakpoint in exon 4 excluding these domains and is primarily found in patients with B-lymphoblastic leukemia (B-ALL). Both groups share the C-terminus structure, including the SH1 tyrosine kinase domain. The N-terminal of the fusion proteins usually includes a coiled-coil or helix-loop-helix domain from the partner protein, which induces the oligomerization of the proteins, thus resulting in tyrosine kinase activation, cytoskeletal localization and neoplastic transformation [5].

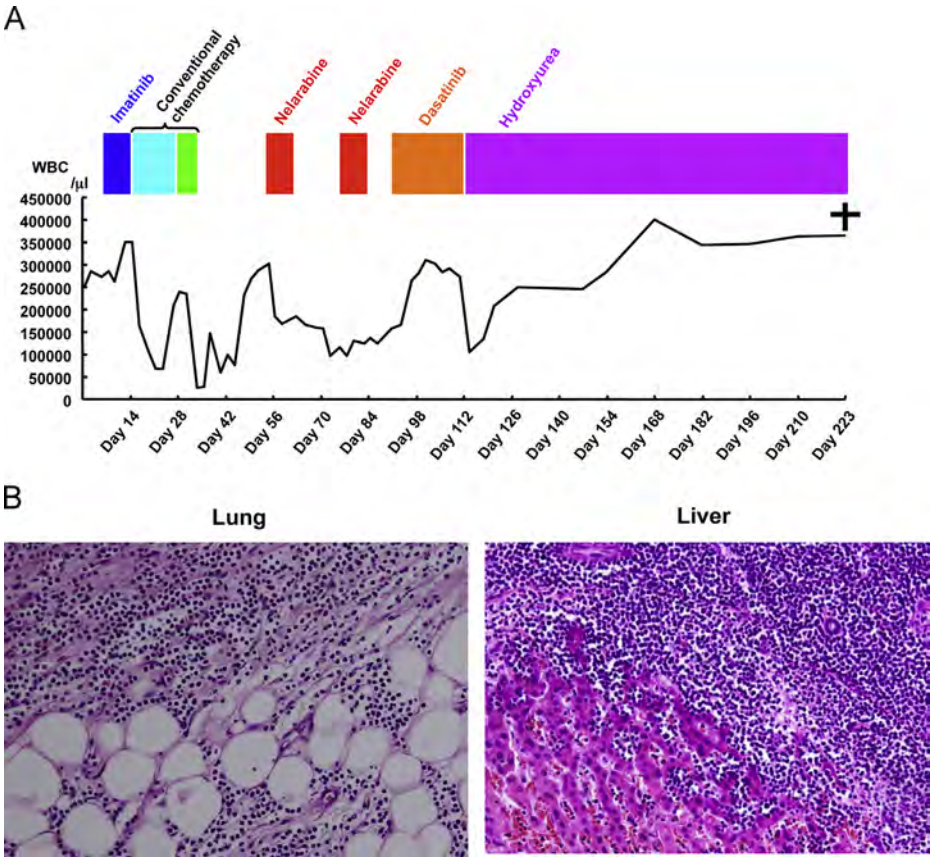

Fig. 2. The refractory clinical course of the patient. (A) The transitional changes in the WBC count in the present case. The administration of imatinib and dasatinib did not reduce the WBC count. (B) The histopathologic examination of the autopsy specimen stained with hematoxylin and eosin showed infiltration of T-PLL cells into the lungs and liver.

Septin proteins belong to a family of proteins that is highly conserved in eukaryotes [6]. These proteins are GTP-binding proteins that form hetero-oligomeric complexes. There are 13 septin genes in humans [6]. The *SEPT9* gene exists at chromosomal location 17q25 and exhibits a ubiquitous expression. SEPT9 plays a role in many cellular mechanisms, such as actin dynamics, axon growth, determination of the cell shape, chromosome segregation, cytokinesis, dendrite formation, DNA repair, membrane trafficking, microtubule regulation and T-cell motility [6]. Furthermore, SEPT9 is deeply associated with the development of various cancers (breast, colon, head, ovarian, neck, leukemia, lymphoma) [6]. In particular, it has been shown that *SEPT9* is a putative proto-oncogene involved in T-cell lymphomagenesis in mice [7].

In patients with hematological malignancies, *MLL* (*KMT2A*)-septin fusion has been repeatedly identified in cells exhibiting myeloid neoplasia in both children and adults. Five different septin genes (*SEPT2*, *SEPT5*, *SEPT6*, *SEPT9* and *SEPT11*) have been identified to be MLL fusion partners [8]. The C-terminal coiled-coil region of septin proteins is preserved in all MLL-septin fusion products, thus indicating that this region contributes to protein–protein interactions and ultimately oncogenesis. In contrast, the N-terminal of SEPT9 is fused to ABL1 in the SEPT9-ABL1 fusion product. It includes the Pro-rich region, which is necessary for binding with SH 3 regions [9]. Because the SH3 domain of ABL1 is preserved in SEPT9-ABL1, this Pro-rich region may contribute to an enhanced chimeric ABL1 kinase potential by promoting interaction with ABL1 SH3 regions, thereby synergistically inducing leukemogenesis.

Regarding the effectiveness of TKIs, some, but not all, patients carrying the *NUP214-ABL1* or *ETV6-ABL1* fusion gene respond to such therapy [5]. A recent report showed that B-ALL with *SNX2-ABL1* responds poorly to dasatinib but partially to imatinib [10,11]. In the present case, SEPT9-ABL1 exhibited a strong resistance to both imatinib and dasatinib. We confirmed that there were no point mutations in the *SEPT9-ABL1* fusion gene. These findings indicate that the TKI response in patients with hematological malignancies associated with various ABL1 fusion products is dependent on the ABL1-partner genes. Further examinations, including conformational analyses of ABL1 fusion products, such as SEPT9-ABL1, and genetic alteration screening of ABL1 fusion-expressing cells, will provide clues uncovering the mechanisms for determining sensitivity to TKI therapy in patients with hematological malignancies harboring *ABL1* fusion products.

Authorship

R.S. performed the experiments, analyzed the data and prepared the manuscript; Hir.M. designed the experiments, performed the experiments, analyzed the data and prepared the manuscript; Hid.K., K.T., Y.O. and Hir.K. analyzed the data; Hid.M. performed the experiments and analyzed the data; K.A. designed the experiments, analyzed the data and prepared the manuscript.

Conflict of interest disclosure

The authors declare no competing financial interests.

References

[1] Matutes E, Brito-Babapulle V, Swansbury J, Ellis J, Morilla R, Dearden C, et al. Clinical and laboratory features of 78 cases of T-prolymphocytic leukemia. Blood 1991;78(12):3269–74.

[2] Hoyer JD, Ross CW, Li CY, Witzig TE, Gascoyne RD, Dewald GW, et al. True T-cell chronic lymphocytic leukemia: a morphologic and immunophenotypic study of 25 cases. Blood 1995;86(3):1163–9.
[3] Dearden CE. T-cell prolymphocytic leukemia. Med Oncol 2006;23(1):17–22.
[4] Greuber EK, Smith-Pearson P, Wang J, Pendergast AM. Role of ABL family kinases in cancer: from leukaemia to solid tumours. Nat Rev Cancer 2013;13(8):559–71.
[5] De Braekeleer E, Douet-Guilbert N, Rowe D, Bown N, Morel F, Berthou C, et al. ABL1 fusion genes in hematological malignancies: a review. Eur J Haematol 2011;86(5):361–71.
[6] Mostowy S, Cossart P. Septins: the fourth component of the cytoskeleton. Nat Rev Mol Cell Biol 2012;13(3):183–94.
[7] Connolly D, Abdesselam I, Verdier-Pinard P, Montagna C. Septin roles in tumorigenesis. Biol Chem 2011;392(8–9):725–38.
[8] Cerveira N, Bizarro S, Teixeira MR. MLL-SEPTIN gene fusions in hematological malignancies. Biol Chem 2011;392(8–9):713–24.
[9] Boggon TJ, Eck MJ. Structure and regulation of Src family kinases. Oncogene 2004;23(48):7918–27.
[10] Masuzawa A, Kiyotani C, Osumi T, Shioda Y, Iijima K, Tomita O, et al. Poor responses to tyrosine kinase inhibitors in a child with precursor B-cell acute lymphoblastic leukemia with SNX2-ABL1 chimeric transcript. Eur J Haematol 2014;92(3):263–7.
[11] Tomita O, Iijima K, Ishibashi T, Osumi T, Kobayashi K, Okita H, et al. Sensitivity of SNX2-ABL1 toward tyrosine kinase inhibitors distinct from that of BCR-ABL1. Leuk Res 2014;38(3):361–70.

Published online 13 March 2014 *Nucleic Acids Research, 2014, Vol. 42, No. 8* ***5289–5301***
doi:10.1093/nar/gku137

Novel functional small RNAs are selectively loaded onto mammalian Ago1

Natsuko Yamakawa[1,†], Kazuki Okuyama[1,†], Jun Ogata[1,†], Akinori Kanai[2], Aleksandra Helwak[3], Masako Takamatsu[1], Ken-ichi Imadome[4], Kohei Takakura[1,5], Bidisha Chanda[1], Natsumi Kurosaki[1], Haruna Yamamoto[1,5], Kiyoshi Ando[6], Hirotaka Matsui[2], Toshiya Inaba[2] and Ai Kotani[1,7,*]

[1]Department of Regenerative Medicine, Division of Basic Clinical Science, Tokai University School of Medicine, Isehara, Kanagawa 259-1193, Japan, [2]Department of Molecular Oncology and Leukemia Program Project, Research Institute for Radiation Biology and Medicine, Hiroshima University, Hiroshima 734-8553, Japan, [3]Wellcome Trust Centre for Cell Biology, The University of Edinburgh, Edinburgh, EH9 3JR, UK, [4]Department of Infectious Diseases, National Research Institute for Child Health and Development, Tokyo 157-0074, Japan, [5]Department of Biosciences, School of Science, Kitasato University, Kanagawa 252-0373, Japan, [6]Research Center for Regenerative Medicine, Tokai University School of Medicine, Kanagawa 259-1193, Japan and [7]Precursory Research for Embryonic Science and Technology (PRESTO), Japan Science and Technology Agency (JST), Saitama 332-0012, Japan

Received August 25, 2013; Revised and Accepted January 23, 2014

ABSTRACT

Argonaute (Ago) proteins function in RNA silencing as components of the RNA-induced silencing complex (RISC). In lower organisms, the small interfering RNA and miRNA pathways diverge due in part to sorting mechanisms that direct distinct small RNA (sRNA) duplexes onto specific Ago-RISCs. However, such sorting mechanisms appear to be lost in mammals. miRNAs appear not to distinguish among Ago1–4. To determine the effect of viral infection on the sorting system, we compared the content of deep-sequenced RNA extracted from immunoprecipitation experiments with the Ago1 and Ago2 proteins using Epstein–Barr virus (EBV)-infected cells. Consistent with previous observations, sequence tags derived from miRNA loci in EBV and humans globally associate in approximately equivalent amounts with Ago1 and Ago2. Interestingly, additional sRNAs, which have not been registered as miRNAs, were associated with Ago1. Among them, some unique sequence tags derived from tandem loci in the human genome associate exclusively with Ago1 but not, or rarely, with Ago2. This is supported by the observation that the expression of the unique sRNAs in the cells is highly dependent on Ago1 proteins. When we knocked down Ago1, the expression of the Ago1-specific sRNAs decreased dramatically. Most importantly, the Ago1-specific sRNAs bound to mRNAs and regulated target genes and were dramatically upregulated, depending on the EBV life cycle. Therefore, even in mammals, the sorting mechanism in the Ago1–4 family is functional. Moreover, the existence of Ago1-specific sRNAs implies vital roles in some aspects of mammalian biology.

INTRODUCTION

miRNAs are a recently discovered class of small noncoding RNAs that are 18–24 nucleotides long and that downregulate target genes at the posttranscriptional level. The majority of miRNA genes are transcribed by RNA polymerase II into long primary miRNA transcripts, processed by the nuclear nuclease Drosha into ~60-bp hairpins, termed precursor (pre) miRNAs, and further cleaved in the cytosol by Dicer nuclease into mature miRNAs. Mature miRNAs are then incorporated into the multiprotein RNA-induced silencing complex (RISC), exerting posttranscriptional repression of target mRNAs, either by inducing mRNA cleavage and mRNA degradation or by blocking mRNA translation (1).

RNAi plays a critical role in innate cellular defence against viruses. In plants and invertebrates, viral RNA

*To whom correspondence should be addressed. Tel: +81 463 93 1121; Fax: +81 463 95 3522; Email: aikotani@tokai-u.jp

†These authors contributed equally to the paper as first authors.

genomes and mRNAs are targeted for destruction by the stimulated production of small interfering RNA (siRNAs) derived from viral double-stranded RNAs (2,3). Given the strong type I interferon-based antiviral response initiated by the intracellular double-stranded RNA sensors RNA-activated protein kinase (PKR), Retinoic acid-inducible gene-I (RIG-I) and Melanoma differentiation-associated gene 5 (MDA-5) in mammals, the siRNAi pathway may have been suppressed as a host protection mechanism against RNA viruses (4). Recently, analogous viral siRNAs were detected within the pool of small RNAs (sRNAs) isolated from RNA-virus–infected mammalian Embryonic stem (ES) cells that exhibited a low-level interferon-based antiviral response.

In lower organisms, the siRNA and miRNA pathways diverge in part due to sorting mechanisms that direct distinct sRNA duplexes into specific Argonaute (Ago)-RISCs (5). However, such sorting mechanisms appear to be lost in mammals. miRNAs appear not to distinguish among Ago1–4, while only Ago1 and Ago2 prefer siRNAs (6). In contrast, influenza A virus infected Ago 1 and 3 double-knockout mice exhibited increased mortality, consistent with more severe alveolitis and pneumonitis, indicating that optimal resistance to influenza requires Ago 1 and/or 3. Enhanced mortality of double-knockout mice was not associated either with increased viral replication or with differential pulmonary recruitment or function of innate and adaptive immune cells; therefore, its function in RNAi targeting against virus-coding RNAs has yet to be demonstrated. The results show that while miRNAs may not distinguish among Ago1–4, this may not be the case for other sRNAs (7). Epstein–Barr virus (EBV), a member of the γ-herpes virus family, was found to be widespread in all human populations and to persist in the vast majority of individuals as a lifelong, asymptomatic infection of the B-lymphocyte pool. It is usually the cause of infections that are not apparent, though it may cause infectious mononucleosis. The more severe, albeit rare, result of EBV infection is malignant transformation and cancer development in various forms, including Burkitt's lymphoma and nasopharyngeal carcinoma, one of the most common cancers in China. As a ubiquitous human pathogen, EBV-associated lymphoid malignancies include a subset of Burkitt's lymphoma, AIDS lymphoma, Hodgkin's lymphoma, posttransplant lymphoma, age-associated B-cell lymphoma and peripheral T- and NK-cell lymphoma (8).

Like other herpes viruses, EBV infection can exhibit two distinct patterns or states of gene expression. During acute EBV infection, the virus sequentially expresses its entire repertoire of genes, producing a lytic infection. In this lytic program, linear double-stranded genomes are produced and packaged as virions that spread the infection from cell to cell. In the latent program, few viral genes are transcribed, no viral progeny are produced and infected cells are protected from apoptotic stimuli and in some circumstances driven to proliferate (8).

EBV was the first human virus found to encode micro RNAs. EBV encodes 44 viral micro RNAs and one small-RNA. EBV-encoded micro RNAs originated from the Bam HI fragment H rightward open reading frame 1 (BHRF1) and Bam HI A region rightward transcript (BART) loci of the EB viral genome. These viral micro RNAs play a vital role in immunogenesis, host cell survival and proliferation, differentiation, lymphomagenesis and modulating the states of viral infection and latency (8).

To determine whether the viral-encoded RNAs are selectively sorted and if the sorting system is affected by viral infection, we compared the content of deep-sequenced RNA extracted from immunoprecipitation (IP) experiments with the Ago1 and Ago2 proteins using EBV-infected cells. The EBV-encoded miRNAs are incorporated equally into Ago1 and Ago2 and identified a novel class of sRNAs that are preferentially incorporated into Ago1 but not Ago2. In this study, we investigated the abundance, expression patterns, sequence characteristics and functions of the novel Ago1-specific–associated sRNAs.

MATERIALS AND METHODS

Cells

The EBV-positive and -negative Hodgkin's lymphoma cell lines, L591 and L1236 (9), and Akata (+) cells and acute monocytic leukemia cell lines, THP-1, were maintained in RPMI1640 medium (Nacalai tesque) supplemented with 10% (v/v) fetal bovine serum (FBS), 50 U/ml penicillin and 50 μg/ml streptomycin in a 50-ml flask (Sumilon). Human carcinoma of cervix cell line, HeLa, was maintained in Dulbecco's modified Eagle's medium (Nacalai tesque) supplemented with 10% (v/v) FBS, 50 U/ml penicillin and 50 μg/ml streptomycin in a 10-cm dish (Corning, Inc., Corning, NY, USA). Cells were passaged twice per week.

Immunoprecipitation

Small RNAs incorporated into Ago1 and Ago2 were immunoprecipitated from cell lysates using the microRNA Isolation Kit (human/mouse Ago1 and human Ago2) (Wako, Osaka, Japan) according to the manufacturer's protocol.

Next-generation sequencing

Immunoprecipitated sRNAs were converted to sequence libraries using the sRNA sample preparation kit (Illumina), according to the manufacturer's instructions.

The libraries were sequenced using an Illumina GA IIx with the single 36-bp read option. Adapter sequences were removed from the generated sequence data. The adapter-trimmed 20–24-bp sequences were mapped to the human hg19 genome assembly and EBV genome using the sequence alignment software Eland (Illumina).

Mapped sequences without any mismatches were used for further analysis. Redundantly mapped sequences that were <256 positions in the genomes were counted as 1 sequence at all possible mapped positions.

siRNA and transfection

siRNA targeting human *Ago1* and *DROSHA* was purchased from OriGene Technology, Inc. (MD, USA) and Cosmo Bio Co., Ltd. (Tokyo, Japan), respectively. siRNA against human *Ago2* was kindly provided by Dr N. Kosaka (National Cancer Center Research Institute, Tokyo, Japan). L591 cells, L1236 cells and Akata cells were suspended in resuspension buffer at a density of 2×10^7/ml and siRNA or the negative control synthetic RNA (Bioneer, Inc., CA, USA) was added at a final concentration of 1 μM (for Akata cells, 500 nM). The transfection of siRNA into cells was performed with the Neon® transfection system (Invitrogen, co., CA, USA) according to the manufacturer's protocol. Cells were cultured for 3 or 6 days in RPMI1640 medium supplemented with 10% (v/v) FBS.

Sequences of specific siRNAs were described in Supplementary Table S1.

Quantitative polymerase chain reaction for Agotaxis sRNAs

Total RNA was prepared from cells with Sepasol-RNA I Super G (Nakarai Tesque, Inc., Kyoto, Japan) and reverse-transcribed with the miScript II RT Kit (Qiagen, Hilden, Germany) to synthesize complementary DNA of sRNAs. The sRNAs were polyadenylated by poly(A) polymerase, then, bound by oligo-dT primer that have a 5′ universal tag sequence and 3′ degenerate anchor and reverse-transcribed by miScript Reverse Transcriptase. The cDNA with the universal tag was amplified by its complementary sequence and the gene-specific forward primers. Real-time polymerase chain reaction (PCR) was performed using the StepOne software and miScript SYBR Green PCR Kit (QIAGEN). Each of 2×SYBR Master Mix 5 μl, RNase-free water 2 μl, 5 μM target primer 1 μl and 1 μl of 10× universal primer mixture were added to 1 μl of water-soluble sample of cDNA. The reaction was run at 95°C for 10 min, followed by 40 cycles at 95°C for 15 s and 60°C for 1 min. miR-21, miR-155, RNU6 and candidate sRNAs were detected by quantitative PCR (qPCR) using the miScript SYBR Green PCR Kit (Qiagen). Sequences of specific primers were described in Supplementary Table S1.

Quantitative PCR for genes

For target gene detection, RT-PCR was performed using the High Capacity cDNA Reverse Transcription Kit (Applied Biosystems, Inc., CA, USA) and qPCR was carried out with the Fast SYBR Green Master mix. All real-time qPCR was conducted using the StepOnePlus real-time PCR system (Applied Biosystems). Threshold cycle (CT) values were calibrated to Glyceraldehyde-3-phosphate dehydrogenase (GAPDH) and analyzed by the 2-ΔΔCT method. Statistical analysis was done by student t-test. Sequences of specific primers were described in Supplementary Table S1.

Dual luciferase assay

In each well of a 96-well plate, 293T cells were cotransfected with 30 ng of psiCHECK-2 s (Promega) and 90 ng of siRNA. The siRNAs were purchased from Cosmo Bio Co., Ltd. (Tokyo, Japan). Sequences of the siRNAs for Dual luciferase assay were described in Supplementary Table S1.

After 48 h of transfection, the relative amounts of Renilla and firefly luciferase were determined by dual-luciferase assay (Promega). The Renilla/firefly luciferase ratio was calculated and normalized against the control.

Gene expression analysis

RNA from cells used for microarray analysis was isolated using the RNeasy Mini Kit (Qiagen, Hilden, Germany). For microarray analysis, splenocytes were cultured for 72 h with or without 10 μM IM. Gene expression microarray analysis was performed using two-colour microarray-based gene-expression analysis (Agilent Technologies, Santa Clara, CA, USA) according to the manufacturer's instructions. After scanning, expression values for the genes were determined using GeneSpringGX software. All experiments were performed in duplicate.

Analysis of CLASH data

Sequencing data generated with the CLASH technique and recently published (ref., GEO accession GSM1219490) were analyzed as previously reported (10) with the following modifications:

(1) Custom BLAST database was supplemented with the sequences of Agotaxis sRNAs (ASR1: gagaaagctca caagaactgct; ASR2: ccccccactgctaaatttgactg; ASR3: tcccactgcttcacttgactagc; ASR4: tcccccactgctaaatttgact gg; ASR5: aagcagggtcgggcctggt; ASR6: gggaataccggg tgctgtaggc).
(2) We selected all chimeras such that one bit was mapped to an ASR and the other bit was uniquely assigned to a protein coding gene (multiple transcripts allowed). Overview diagrams of ASRs-mRNA chimera preparation are presented in Figure 5b.

Lytic phase induction assay

Akata (+) cells were stimulated with rabbit anti-human IgG polyclonal antibody (final 20 μg/ml) (Dako) at 37°C in a CO_2 incubator for 15–40 h and induced into lytic phase. Cells were counted before and after stimulation and then the numbers of dead cells were calculated. For Ago1 knocked down experiments, siRNAs were electroporated into the cells by Neon® transfection system 2 days before anti-human IgG stimulation and the cells were cultured for 48 h. After stimulation, cells were harvested and total RNAs were prepared with Sepasol-RNA I Super G. To quantify sRNA expression, RT-PCR was performed using the miScript II RT kit, and qPCR using the miScript SYBR Green PCR kit. For

target gene detection, RT-PCR was performed using the high-capacity RNA-to-cDNA kit and qPCR was carried out with the Fast SYBR Green Master mix. All real-time qPCR was conducted using the StepOnePlus real-time PCR system.

RESULTS

Ago-associated sRNA libraries indicate that equivalent amounts of human and EBV-encoded miRNAs associated with Ago1 and Ago2

We analyzed the short RNAs from immunoprecipitated Ago1 and Ago2 proteins isolated from L591cells derived from EBV-positive Hodgkin's lymphoma cells. Raw tags from the generated data set were mapped to the hg19 human genome assembly using the procedures outlined in the 'Materials and Methods' section.

Notably, 30–40% of the total sRNAs in the latent-infected EBV cells were derived from the EBV genome, as was reported previously (4,11) (Figure 1a).

The majority of tags were mapped to regions annotated as both human and EBV miRNAs. Consistent with previous observations, the top 50 abundant sequence tags derived from the miRNA loci in both humans and EBV globally associate with Ago1 and Ago2 in approximately equivalent amounts (Figure 1b and c). Interestingly, tags that were derived from loci other than miRNA (non-miRNA loci) were found more often in the Ago1 than in the Ago2 IP sRNA library (26 versus 6%) (Figure 1d).

A new class of sRNAs selectively associated with Ago1

Interestingly, some unique sequence tags from non-miRNA loci, derived from tandem loci in the human genome, predominantly associate with Ago1 but not, or only rarely, with Ago2. The definition of tandem loci is as follows: when one locus has a read count of >10, both flanking loci located within 100 bases from the first locus also have >10 reads (Figure 2a). The typical loci are shown in Figure 2b. More than 2000 counted RNAs are listed in Figure 2c. We named the sRNAs as Agotaxis small RNAs (ASRs). The representative ASRs were further investigated (Figure 2d). The results for several of these sRNAs by next-generation sequencing were validated by real-time PCR, which showed that the sRNA levels were significantly higher in Ago1- than Ago2-immunoprecipitated samples (Figure 2e). The expression of the sRNAs in L591 cells was confirmed by the northern blot analysis (12) (Supplementary Figure).

Downregulation of DROSHA does not lead to the decrease of Agotaxis 2, 3 and 4 in L591 cells

From the registered sequence of ASRs transcripts shown in Figure 3a, we predicted their folding structures by the mfold web server (http://mfold.rna.albany.edu/?q=mfold/RNA-Folding-Form). Every ASR potentially form secondary hairpin loop structures (Figure 3b). We performed 5′ RACE and found only ASR1 transcript contained the flanking regions (data not shown). In the canonical pathway of miRNAs processing, the flanking regions of primary miRNAs are cleaved by DGCR8/DROSHA complex. We evaluated the expression of ASRs when DROSHA was knocked down in L591 cells by siRNA against DROSHA (siDROSHA). The expression of DROSHA was significantly decreased 3 days after the transfection (Figure 3c). The amounts of ASRs and mature miR-21 were evaluated with real-time PCR 6 days after the transfection (Figure 3d). While miR-21 was significantly decreased in siDROSHA-transfected L591 cells, the expressions of ASRs except ASR1 did not change (Figure 3d). About 30% reduction in ASR1 was confirmed (Figure 3d). The result suggested DROSHA is not involved in the processing of ASR2, 3 and 4.

Characteristic features of the first nucleotide preference

The 5′ ends of miRNAs and piRNAs are mostly uridine, which likely binds to Ago/Piwi proteins (13). The 5′ ends of the top 500 abundantly expressed ASRs were analyzed. A large proportion of the 5′ ends of the ASRs are C, G or A (82.2%), with uridine being a minor component (17.8%). Therefore, these binding proteins are different from those associated with canonical miRNAs (Figure 4a). The composition of the nucleotides of ASRs is slightly biased to C [A (23.7%):G (25.0%):C (26.9%):U (24.5%); Figure 4b]. We investigated the position-specific motif for the top 500 abundantly expressed ASRs using the MEM software (http://meme.sdsc.edu). The top consensus motif of 37 ASRs from the 500 ASRs was CACU at the 5′ end +2 and UUGACU at the 3′ end (Figure 4c). The alignment of 37 ASRs was shown in Supplementary Figure S1. We observed substantial sequence variation in ASRs. Some of the isoforms of ASRs had comparable abundances with major ASRs (Figure 2c).

Expression profiles of ASRs

Expression of ASRs in the peripheral blood mononuclear cell (PBMC), THP-1, HeLa and L1236 cells, which were derived from Hodgkin's lymphoma cells but were not EBV infected, were analyzed. All cells and cell lines express ASRs. The expression of ASRs is not restricted to EBV-infected cell lines, but seemed to be ubiquitous (Figure 4d). Moreover, the expression of ASRs in Ago1 IP and Ago2 IP L1236 cells by use of the next-generation sequencing demonstrated that ASRs were selectively incorporated into Ago1, indicating that selective incorporation of these sRNAs into Ago1 is not restricted to cells infected by EBV (Figure 4e), which was again confirmed by the real-time PCRs (Figure4e).

ASRs in cells are stabilized by Ago1 proteins

The expression of ASRs was not altered by RNase treatment after Ago1 IP, suggesting that ASRs bind specifically to Ago1 (data not shown). In addition, ASRs are highly dependent on Ago1. When Ago1 was knocked down, their expression decreased dramatically, while that of Ago2 was unchanged (Figure 4f left). In this condition, ASRs expression was determined by real-time PCR. In Figure 4f, right, the expression of miR-21, which is incorporated into Ago1 and Ago2 equally, was downregulated by half when Ago1

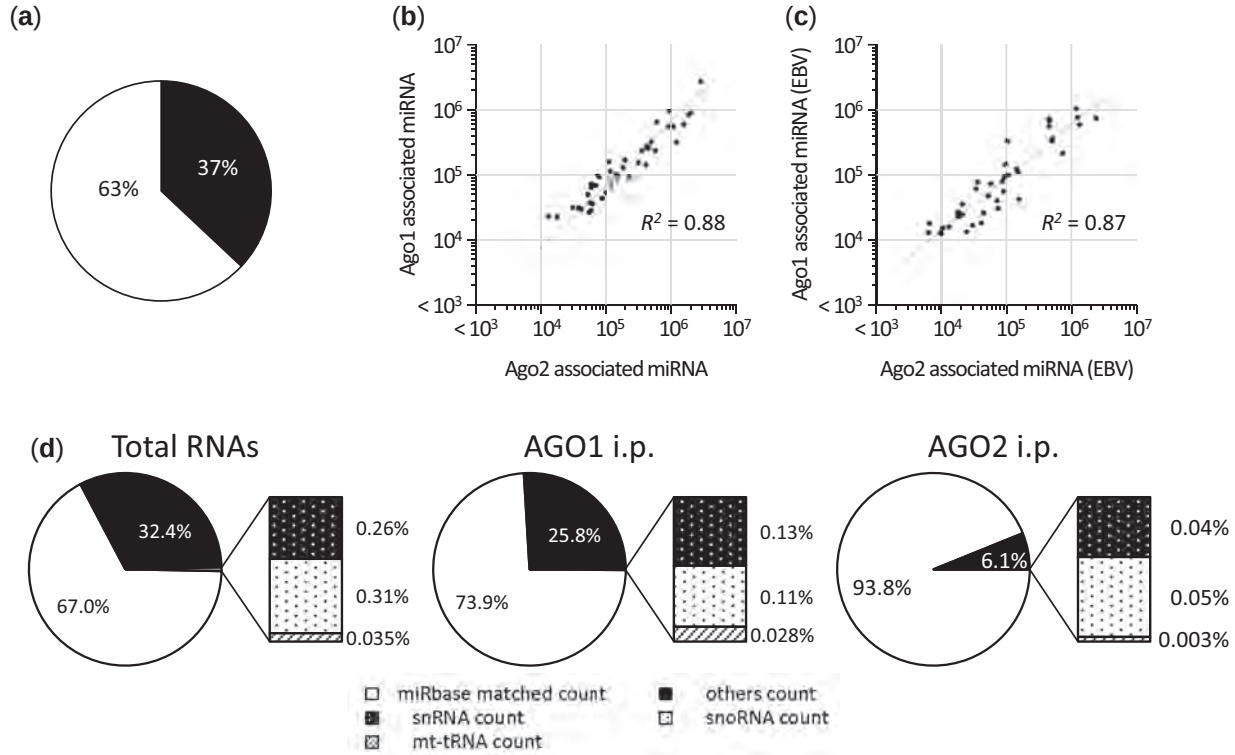

	Total RNAs	AGO1 i.p.	AGO2 i.p.
total read count	18,078,417 (100.0%)	18,757,434 (100.0%)	23,118,841 (100.0%)
├ miRbase matched count	12,107,482 (67.0%)	13,866,162 (73.9%)	21,693,070 (93.8%)
└ miRbase mismached	5,970,935 (33.0%)	4,891,272 (26.1%)	1,425,771 (6.2%)
├ snRNA count	46,948 (0.26%)	23,905 (0.13%)	8,994 (0.04%)
├ snoRNA count	56,654 (0.31%)	21,273 (0.11%)	12,009 (0.05%)
├ mt-tRNA count	6,350 (0.035%)	5,162 (0.028%)	701 (0.003%)
└ others count	5,860,983 (32.4%)	4,840,932 (25.8%)	1,404,067 (6.1%)

Figure 1. Equivalent amounts of human and EBV-encoded miRNAs associated with Ago1 and Ago2. The short RNAs that were co-immunoprecipitated with Ago1 and Ago2 derived from L591 cells were analyzed. (**a**) The ratio of sRNAs mapped to the human genome and the EBV genome. (**b**) Equivalent amounts of human miRNAs associated with Ago1 and Ago2. The top 50 highly associated human miRNAs were plotted. (**c**) Equivalent amounts of EBV-encoded miRNAs associated with Ago1 and Ago2. The EBV-encoded miRNAs, co-immunoprecipitated with Ago1 and Ago2, with reads of >10 000 counts (42 miRNAs) were plotted. (**d**) The ratio of sRNAs mapped to miRNA-registered loci, non-miRNA nonannotated loci, snRNA, snoRNA, mt-tRNA and the other noncording sRNA loci.

was knocked down. Expression of ASR2 and ASR3 in Ago1-knockdown cells was reduced to one-fifth that of the control. Most strikingly, the expression of ASR1 and ASR4 in Ago1-knockdown cells was reduced dramatically to almost below the detection limit. On the other hand, the amounts of ASRs did not change in mild Ago2 knocked down L591 cells (14) (Supplementary Figure S2). Free sRNAs are unstable in the cell and are digested rapidly (15). Therefore, ASRs are predominantly associated with Ago1 in a highly specific manner, which prevents ASRs incorporation by Ago2, 3 or 4. This was confirmed by determining the expression levels of sRNAs associated with Ago2 when Ago1 was knocked down. Expression levels of some were increased slightly in the Ago2 RISC complex, while others were unchanged (Supplementary Table S1). These results indicate that the majority of ASRs are incorporated preferentially into the Ago1–RISC complex.

ASRs can silence targets, suggesting that ASRs are potentially functional

To determine their regulatory roles, we searched for putative targets of four abundantly incorporated ASRs and isoforms. *In silico* prediction of the binding sites of the 3′ untranslated region (UTR) of ASR2 and ASR4 by miRanda v3.3, which are highly downregulated in Ago1-knockdown L591 cells, are listed in Supplementary Figure S4. Among them, Family with sequence similarity 22 (FAM22) and Myocyte enhancer factor 2B (MEF2B) expression in Ago1-knockdown L591 cells was upregulated 2- and 4-fold, respectively (Supplementary Figure S4). ASR2 and ASR4 target sequences of FAM22 and MEF2B were shown in Figure 5a. The results were validated by assessment of the capacity to direct functional repression, using a luciferase assay.

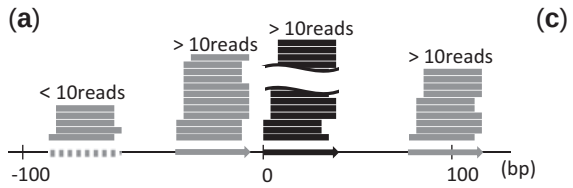

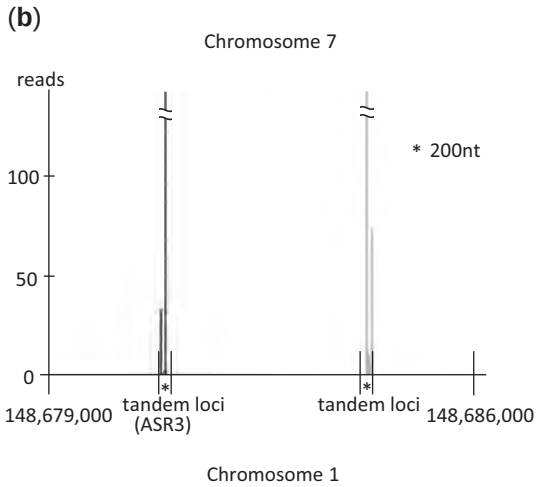

(c)

Chromo.	Start posi. (base)	Read count Ago1	Ago2
Chr.7	148,684,256	33,009	3,020
Chr.7	148,660,473	22,587	2,509
Chr.1.	228,781,808	13,091	377
Chr.12.	20,704,458	10,928	254
Chr.20.	62,550,904	8,641	3,139
Chr.1.	151,411,544	8,102	645
Chr.2.	133,012,403	7,753	186
Chr.6.	4,428,294	7,021	209
Chr.17.	33,478,275	6,999	314
Chr.7.	148,684,257	6,443	695
Chr.19.	7,951,883	5,680	181
Chr.1.	228,746,035	4,780	133
Chr.19.	21,295,954	4,770	133
Chr.7.	148,680,921	4,028	1,088
Chr.8.	93,179,766	3,932	534
Chr.14.	65,937,853	3,768	2,311
Chr.X.	68,892,419	3,531	109
Chr.6.	4,428,295	3,102	95
Chr.19.	7,951,882	2,225	77
Chr.3.	51,728,499	2,202	100
Chr.X.	68,892,423	2,199	100
Chr.mt.	12,208	2,112	342
Total read count		208,318	33,240

(d)

	Ago1 IP	Ago2 IP	Sequence
ASR1	2,112	342	5′- GAGAAAGCUCACAAGAACUGCU -3′
ASR2	22,587	2,509	5′- CCCCCCACUGCUAAAUUUGACUG -3′
ASR3	4,028	1,088	5′- UCCCACUGCUUCACUUGACUAG -3′
ASR4	8,102	645	5′- CCCCCACUGCUAAAUUUGACUG -3′

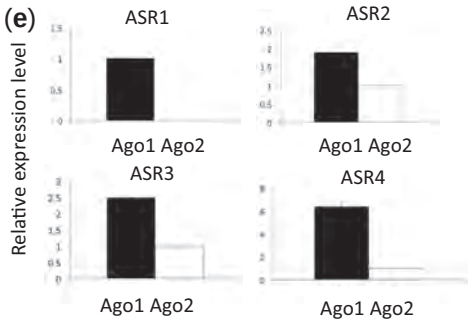

Figure 2. The sRNAs selectively associated with Ago1 are derived from tandem loci. (**a**) Definition of tandem loci and sRNA counts, which were mapped to the loci. When one locus (black arrow) with a read count of >10 reads and both flanking loci (gray arrows) located within 100 bases from the original locus also have >10 reads. (**b**) Representative loci are shown. Some Ago1 associating sRNAs are aligned to 228 776 000–228 783 000 bp area of chromosome 1 and 148 679 000–148 686 000 bp area of chromosome 7. The areas contain ASR3, ASR4 and many tandem locus. Black reads are aligned to forward strand, and gray reads to reverse strand. (**c**) Some unique sRNAs are selectively associated with Ago1. The counts of sRNAs associated with Ago1 and Ago2 (>2000 counts), derived from tandem loci, are listed. (**d**) The sequences of representative ASRs are shown. (**e**) Associations of ASR1, 2, 3 and 4 with Ago1 or Ago2 were determined by real-time PCR to validate the next-generation sequencing data. The data were normalized by the amount of RNA. Black bar indicates Ago1-associated RNA expression; white bar, Ago2.

We cloned the *FAM22* and *MEF2B* 3′ UTRs into a luciferase reporter vector and found that exogenous ASR2 and ASR4 repressed reporter activity, while the mutants had little or no effect (Figure 5a). This confirmed that ASR2 and ASR4 negatively regulate the mRNA expression of FAM22 and MEF2B directly through the 3′ UTR. The results indicate that these ASRs function in similar ways to miRNAs.

Moreover, the binding locus of ASRs in 293T cells was comprehensively investigated by use of the data sets previously reported (10). New technique for ligation and sequencing of miRNA-target RNA duplexes associated with human Ago1, known as 'CLASH', revealed that the majority of ASRs bind not only to mRNA 3′ UTRs but also to coding regions (CDS) and 5′ UTR (10). The library (~18 000 high-confidence miRNA–mRNA

(a)

ASRs	Sequence (5′ > 3′)
ASR1	GAGAAAGCTCACAAGAACTGCTAACTCATGCCCCCATGTCTAACAACATGGCTTTCTCA
ASR2	GGCTGGTCCGATGGTAGTGGGTTATCAGAACTTATTAACATTAGTGTCACTAAAGTTGGTATACAACCCCCCACTGCTAAATTTGACTGGCTTTTT
ASR3	GGCTGGTCCGAGTGCAGTGGTGTTTACAACTAATTGATCACAACCAGTTACAGATTTCTTTGTTCCTTCTCCACTCCCACTGCTTCACTTGACTAGCCTTTT
ASR4	GACTAGTCCTGTGGTAGTGGGTTATCAGAACTTATAAACATTAGTGTCACTAAAGTTGGTATACAACTCCCCCACTGCTAAATTTGACTGGCTTAA

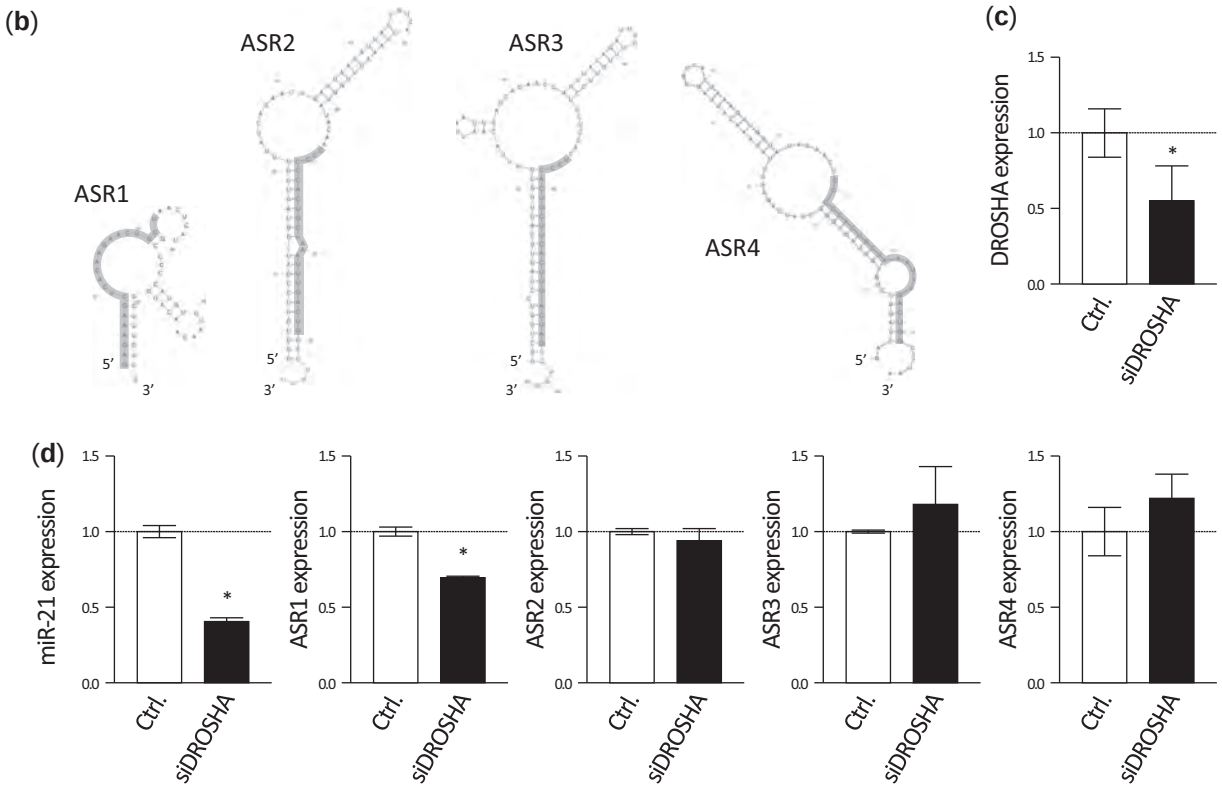

Figure 3. Processing of ASRs is independent of DROSHA. (**a**) Sequences of precursor of ASR transcripts are shown. That of ASR1 is ENST00000387449; ASR2, NR_004393.1; ASR2, NR_004392.1; ASR4, NG_032096.1. Underlined sequences indicate mature ASRs. (**b**) Structures of ASR1, 2, 3 and 4 were predicted with sequences indicated in Figure 3a by the mfold web server. Highlighted regions indicate mature ASRs sequences. (**c** and **d**) Control siRNA (Ctrl.) or siDROSHA were transfected into L591 cells by Neon^{TM} transfection system. (c) Expressions of DROSHA was evaluated by real-time PCR 3 days after the transfection. Expression levels relative to Ctrl. were normalized with GAPDH and shown. (d) Cells were cultured for 6 days, and then total RNAs were extracted. Amounts of ASRs and mature miR-21 were determined by real-time PCR. Data were shown as relative expression to the Ctrl. normalized with RNU6. Error bars indicate SD. $*P < 0.05$.

interactions) contained the binding locus of top 20 abundantly expressed ASRs, which revealed 90 loci. Among them, centromere protein B (CENPB), leptin receptor (LEPR), Muscleblind-like splicing regulator 1 (MBNL1), pygopus family PHD finger 2 (PYGO2)and Testis-specific kinase 2 (TESK2), which have the putative target binding sites of ASRs, were upregulated in Ago1 knockdown L591 cells (Figure 5b). These results suggest that it is highly possible that these five genes are regulated by ASRs in L591 cells as well.

Expression of ASRs in the EBV life cycle

We showed that many EBV-encoded miRNAs were expressed in EBV-latent-infected cells (Figure 1a). During acute EBV infection, the virus sequentially expresses its entire repertoire of genes, producing a lytic infection, while few genes are expressed during latent infection. Recently, it was reported that murine gammaherpesvirus 68 (MHV68) infection could induce and upregulate endo-siRNAs from short interspersed nuclear elements in murine cells during lytic infection (16). Therefore, linkage of the EBV life cycle with ASRs expression was investigated.

Akata is a type 3 latent-infected cell line derived from an EBV-positive Burkitt's lymphoma patient. The lytic phase was induced by Akata membrane IgG and anti-IgG cross-linking. When the lytic phase was induced, the cells underwent apoptosis. According to our results, expression level of ASR2, 3, 4 and 5 was linked with apoptotic cell numbers (Figure 6a). When the >60% Akata cells were dead, ASRs were increased >30-fold compared with latent-phase Akata cells. Moreover, when the lytic phase was induced with AGO1 knocked down cells, the expression of ASRs was decreased

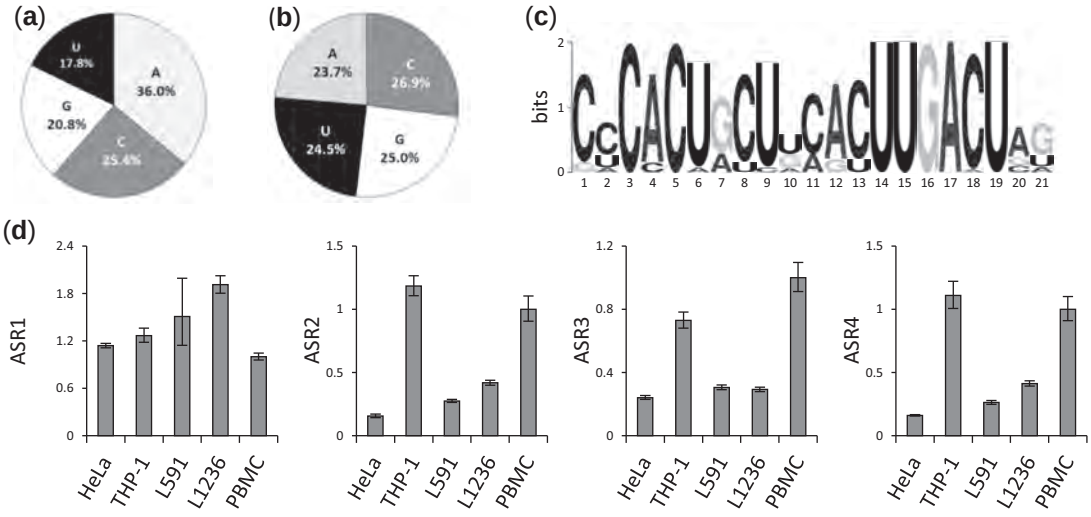

(e)

Chrom.	Start pos. (base)	Read count Ago1	Ago2
Chr.7	148,684,256	8,845	3,638
Chr.7	148,660,473	5,395	556
Chr.1	228,781,808	623,756	52,317
Chr.12	20,704,458	2,373	149
Chr.1	151,411,544	1,875	215
Chr.2	133,012,403	1,653	89
Chr.6	4,428,294	476,029	39,344
Chr.17	33,478,275	98,936	11,870
Chr.7	148,684,257	3,358	484
Chr.19	7,951,883	445,023	36,628
Chr.1	228,746,035	14,964	1,672
Chr.19	21,295,954	14,768	1,655
Chr.7	148,680,921	1,156	462
Chr.8	93,179,766	288	14
Chr.14	65,937,853	2,181	3,838
Chr.X	68,892,419	88,787	6,106
Chr.6	4,428,295	10,149	1,067
Chr.19	7,951,882	9,547	988
Chr.3	51,728,499	52,935	5,270
Chr.X	68,892,423	52,573	5,234
Chr.mt	12,208	34,286	2,075
Total read count		1,948,877	173,671

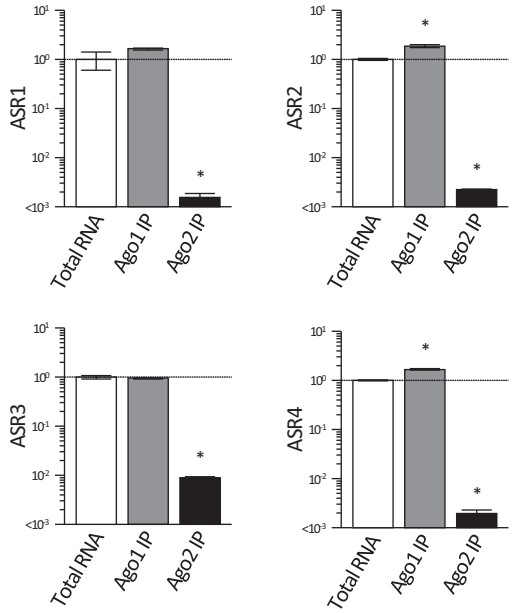

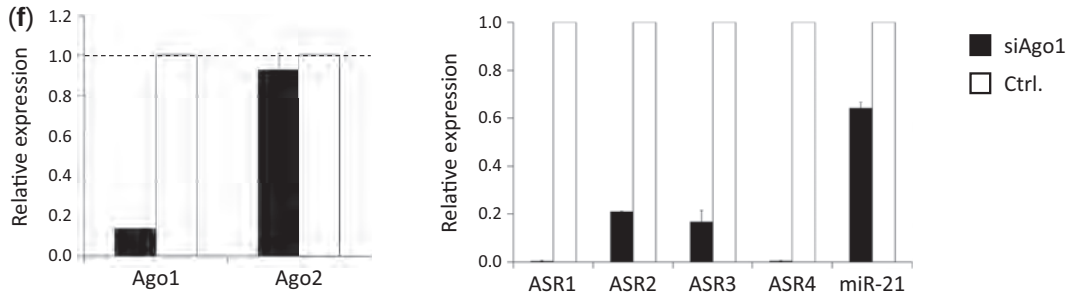

Figure 4. Characterization of ASRs. (**a**) The 5′ base of the top 500 abundantly expressed ASRs. (**b**) The composition of the top 500 abundantly expressed ASRs. (**c**) The consensus motif of top 500 abundantly expressed ASRs. (**d**) Expression of representative ASRs in HeLa, THP1, L591, L1236 and PBMCs were analyzed by real-time PCR, normalized by GAPDH ($n = 3$). (**e**) Associations of ASR1, 2, 3 and 4 with Ago1 or Ago2 in L1236 cells were determined by next-generation sequencing and real-time PCR normalized by the amount of RNAs. The read counts of the ASRs listed in Figure 2c in Ago1-IP and Ago2-IP L1236 cells are summarized. Error bars indicate SD. $*P < 0.05$. (**f**) mRNA expression of Ago1 and Ago2 in Ago1-knockdown (black bar) and control (white bar) L591 cells (left). Expression of representative ASRs under each condition. Both data were normalized by GAPDH.

(**a**)

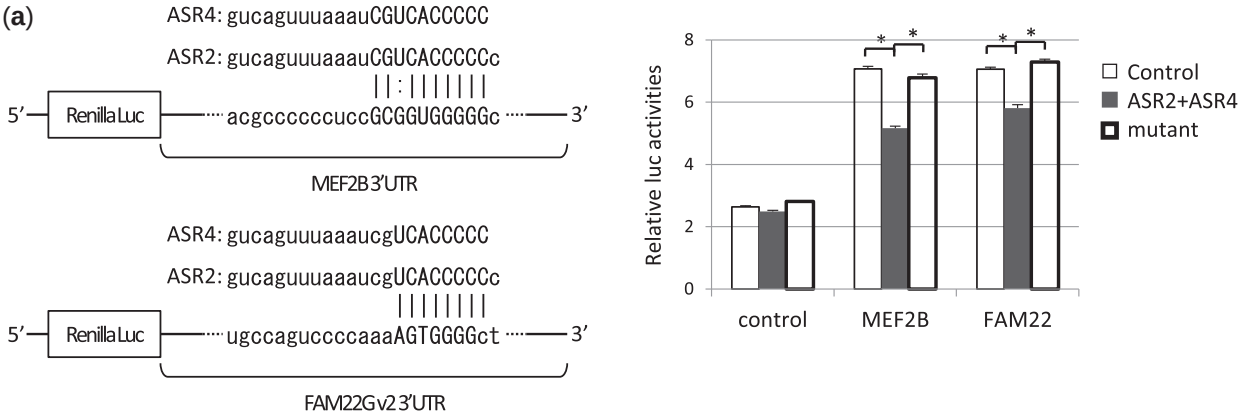

(**b**)

Fold change	Target gene symbol	Accession ID	mRNA region	mRNA sequence	ASRs	ASRs sequence
1.30	CENPB	NM_001810	3'UTR	ACGTCAGGTCTTTGGTGGGGGGACCCCAAA GCCATTCTGGGAAGGGCTCCAGAAGAAG	ASR4 isoform	TCCCCCACTGCTAAATTTGACTGG
1.62	LEPR	NM_002303	CDS	ATGGTCAGAAGATGTGGGAAATCACACGAA ATTCACTTTCCTGTGGAC	ASR3	TCCCACTGCTTCACTTGACTAGC
1.37	MBNL1	NM_021038	5'UTR	AAATTGGCACTGGGAAGGGGTTACTGAGAG CACAAGGCTGATACCAG	ASR2	CCCCCCACTGCTAAATTTGACTG
1.08	PYGO2	NM_138300	CDS	GGTGAGGATGGGGGGAAGCCCTTGAATCCA CCTGCTTCTACTGCTT	ASR4 isoform	TCCCCCACTGCTAAATTTGACTGG
1.69	TESK2	NM_007170	3'UTR	ACGGGAGGCAGCAGTGAGAGGCCTTCCTAG TTAGGGCCAACAG	ASR2	CCCCCCACTGCTAAATTTGACTG

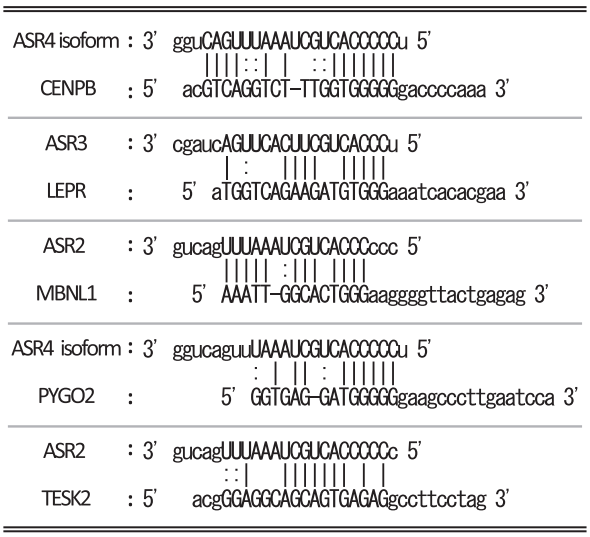

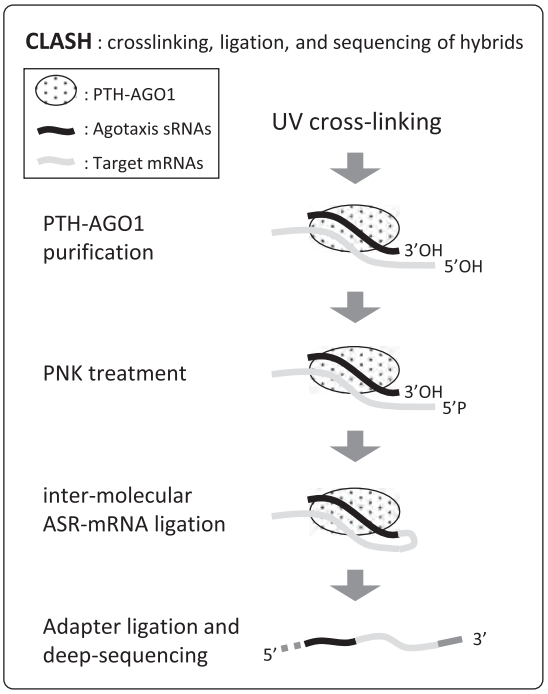

Figure 5. ASRs can bind and silence targets. (**a**) MEF2B and FAM 22 were regulated by ASR2 and ASR4 though their 3′ UTR. The putative target sequence of ASR2 and 4 in MEF2B and FAM22-3′ UTRs (left). Reporter vectors were constructed by inserting MEF2B and FAM22-3′ UTRs into Renilla luciferase in a psiCHECK2 vector. Renilla to firefly luciferase ratios are shown (right). All binding sites caused ASR2- and 4-dependent downregulation but not control or mutant (aggggacuaaaauuugacgg) (*$P < 0.05$). (**b**) The sequence-specific binding of ASRs at the CDS, 3′ UTR and 5′ UTR of the target mRNAs in 293T cells, which were revealed by CLASH and downregulated in Ago1 knockdown L591 cells. The five genes, which have putative target sequences of ASRs in the mRNAs, were bound by ASRs in 293T cells, and upregulated by Ago1 knockdown in L591 cells are listed (upper). The putative target sequences of ASRs in the target mRNAs are shown (lower left). Overview diagrams of ASRs-mRNA chimera preparation (lower right). AGO1-associated sRNAs including ASRs and target mRNAs were cross-linked to PTH-AGO1 by UV exposure. The protein–RNA complexes were purified. mRNA 5′ ends were phosphorylated with PNK treatment and ligated to associated ASRs. Finally, 5′ and 3′ adapters were ligated to the chimeric RNAs for next-generation sequencing.

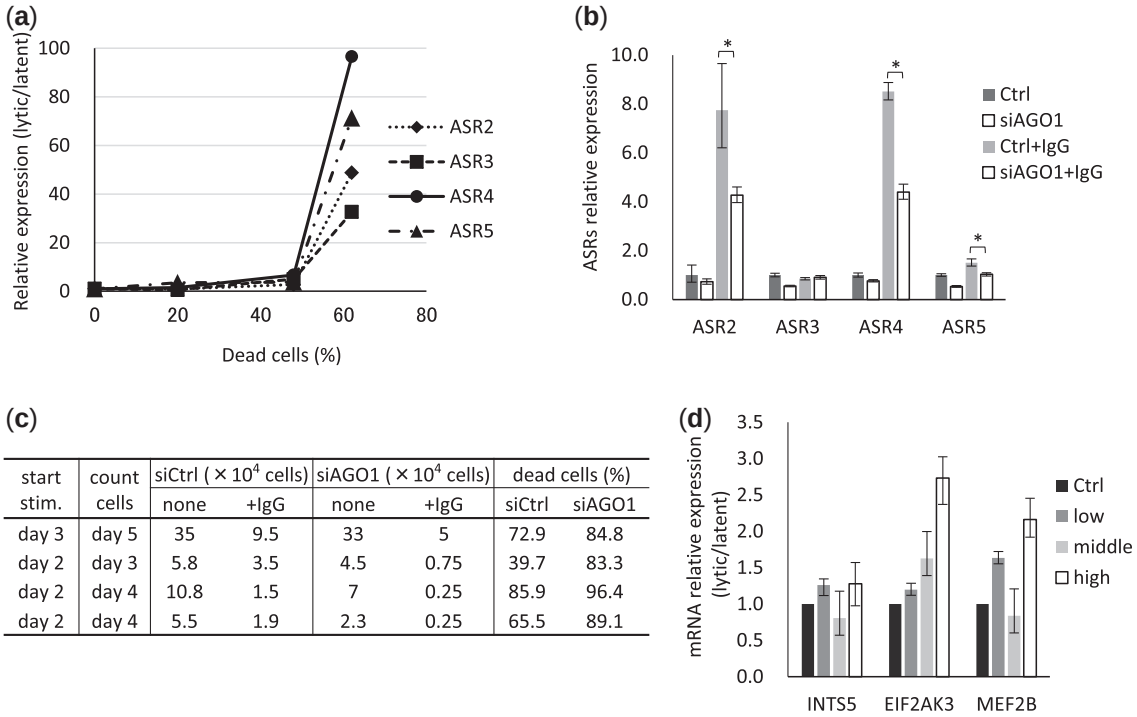

start stim.	count cells	siCtrl ($\times 10^4$ cells)		siAGO1 ($\times 10^4$ cells)		dead cells (%)	
		none	+IgG	none	+IgG	siCtrl	siAGO1
day 3	day 5	35	9.5	33	5	72.9	84.8
day 2	day 3	5.8	3.5	4.5	0.75	39.7	83.3
day 2	day 4	10.8	1.5	7	0.25	85.9	96.4
day 2	day 4	5.5	1.9	2.3	0.25	65.5	89.1

Figure 6. Expression of ASRs is correlated with the EBV life cycle. Akata cells were stimulated with anti-human IgG antibody and induced into the lytic phase. The cells were harvested at each point and total RNAs were purified. (**a** and **b**) The expression levels of total ASRs were measured by qPCR and calibrated with GAPDH. (a) ASRs relative expression levels are shown as fold-expression changes compared with that of the latent phase. (b) Akata cells were transfected with/without siRNA against AGO1 by Neon system (siAGO1 and Ctrl, respectively). After 2 days, cells were stimulated with/without anti-human IgG antibody to induce EBV lytic phase. After 2 more days in culture, cells were harvested and relative ASRs expression to Ctrl was measured by qPCR. Ctrl and siAgo1 indicate latent phase; Ctrl+IgG and siAgo1+IgG, lytic phase. $*P < 0.05$. (**c**) The cell numbers at harvested points were counted. The dead cell ratios were calculated by 1 – (IgG stimulated cell numbers/nonstimulated cell numbers). (**d**) The mRNA expression levels of ASRs' target genes were calculated by qPCR and calibrated with GAPDH. Relative expression levels are shown as fold-expression changes compared with that of the latent phase. Ctrl indicates latent phase; low, <40%; middle, 40–60%; high, >60% dead cell ratio. The data are shown as means and SD.

(Figure 6b). Under the condition, the apoptotic cell numbers tended to be upregulated (Figure 6c). These results indicated that in the lytic phase, the ASRs are significantly upregulated depending on AGO1.

The miRANDA predicted target genes of these sRNAs in L591 cells were listed (Supplementary Figure S4). Among them, we focused on INTS5, MEF2B and EIF2AK3, which are involved in viral reactivation, and analyzed their correlation with the EBV life cycle in Akata cells by qPCR (Figure 6d). The lytic phase was categorized by dead cell ratio into: low, <40%; middle, 40–60%; high, >60%. Expression of INTS5 and MEF2B showed a tendency to be decreased especially in middle level of the cell apoptosis. Interestingly, the expression of all these three genes tended to increase in high dead cell ratio (Figure 6d).

DISCUSSION

In *Drosophila*, siRNAs and miRNAs are actively sorted into functionally distinct Ago-RISCs based on differences in structure (17,18). Perfectly matched duplexes are preferentially incorporated into Ago2, whereas duplexes with central mismatched bulges (miRNA-like) are sorted to Ago1 (17,18). A similar sorting mechanism exists in *Caenorhabditis elegans*, whereby sRNA duplexes with perfectly matched or bulged stems are channelled into RNAi-defective 1 (RDE-1) or Argonaute (plant)-like gene 1 (ALG-1), respectively (19).

In mammals, the regularity of miRNA sorting onto distinct Ago proteins is poorly understood. Mammals have four Agos (Ago1–4) that are involved in the miRNA pathway. Among them, Ago2 is unique and possesses the slicer activity that mediates the cleavage of perfectly matched targets for miRNAs and siRNAs (20). When individual Agos are constitutively ablated in mice, only the loss of Ago2 causes embryonic lethality, whereas single loss of Ago1, Ago3 or Ago4 is dispensable for animal development. However, RNA-sequencing of Ago1-, Ago2- and Ago3-associated miRNAs revealed that some have a bias toward particular Ago proteins (21).

We investigated the effect of viral infection on the sorting of sRNAs onto Ago proteins and identified sRNAs derived from the human genome and incorporated exclusively into Ago1 (ASRs).

The 5′ ends of the ASRs in are mostly C, G or A; uridine represents only a minor portion, implying that their binding proteins differ from those associated with canonical miRNAs (16).

In *Drosophila*, several studies have demonstrated that miRNA sorting onto Ago proteins is coupled to strand

selection and depends on specific structural and sequence criteria, in which the sRNAs in the Ago1 protein complex with 5′ cytosine are more stable than those with 5′ uridine (13).The fate of a miRNA/miRNA* duplex, therefore, depends on multiple factors, including the structure of the duplex and the thermodynamic stability of the ends of the duplex (22). The importance of each factor in the sorting decision in mammals is as yet unknown.

We found that several ASRs harbor motifs that are preferred at locations on both their 5′ and 3′ ends.

The motifs on the 5′ ends of ASRs predict the target sequences that are commonly bound by ASRs. The common target sequence located in 3′ UTR of tumor suppressor genes has been recently reported, which is putatively bound by oncogenic miRNAs (23). The putative target sequence complementary to the motif on the 5′ ends of ASRs is completely different from the common target sequence bound by oncogenic miRNAs. It seems likely that the motif on the 5′ end of ASRs has some other regulatory functions.

The biogenesis of ASRs is independent from Drosha. They are incorporated in Ago1-RISC, bind mRNAs and work in similar way to miRNAs. Mirtrons also works as miRNA, which regulate RNA via a multistep process involving intron splicing and debranching, exosome-mediated trimming of the 3-tail and dicing. Top 20 highly expressed ASRs are coded within intergenic or transfer RNAs but not intron (24).

Accordingly, ASRs and Mirtron should be separately categorized. Still their biogenesis and functional mechanism seem to be overlapped. Further studies about the comparison of two kinds of sRNAs are needed.

Recently, 3′ motifs of miR-29 have been reported as nuclear transport signal (25). The 3′ common sequence of ASRs, which is not similar to the 3′ motif of miR-29, might be involved some other function such as transport and stability. Most importantly, whether both of the motifs are involved in the Ago1/Ago2 sorting decision needs further investigation.

ASRs regulate expression of their targets such as FAM22 and MEF2B by binding to the 3′ UTR in L591 cells. Therefore, ASRs have at least some functional similarity to miRNAs. Recent comprehensive analysis of sRNAs and their binding target RNAs, known 'CLASH', revealed that ASRs were incorporated into Ago1-RISC and bound to several mRNAs in 293T cells (10). Intriguingly, the data revealed that ASRs were also shown to bind mostly to CDS. Several genes, including CENPB, LEPR and PYGO2, bound by ASRs in Ago1-RISC in 293T cells had putative binding sites of ASRs and were upregulated by Ago1 knockdown in L591 cells, which suggest that these genes are highly possibly regulated by ASRs in L591 cells. CENPB, centromere protein B, is a DNA binding protein that recognizes CENP-B box in the centromeric alpha satellite DNA (26). The protein has an important role in assembly of kinetochore structure. In apoptotic cells, the protein is characterized as autoantigen that is cleaved to 60-kDa fragment and observed in blebs (27). It implies that ASRs may reduce autoimmune response in apoptotic phase.

By contrast, LEPR and PYGO2 are reported as anti-apoptotic elements. LEPR is known as the regulation of fat metabolism and hematopoiesis. Leptin activate Janus kinase/Signal transducer and activator of transcription (JAK/STAT) pathways via LEPR, which result in enhanced expression of anti-apoptotic factor, B-cell CLL/lymphoma 2 (BCL-2) (28). PYGO2 is a component of Wnt/beta-catenin transcriptional complex. Overexpression of PYGO2 reduces apoptotic activity in human carcinoma cell lines (29)

Together with our results in EBV lytic infection, ASRs might be involved in apoptosis. The significance and function of ASRs, including their binding to CDS warrants further investigation.

Finally, we analyzed the linkage of expression of ASRs with EBV infection status. Interestingly, the expression of ASRs was dramatically upregulated during lytic EBV infection. Small RNAs upregulations during lytic phase were consistent with the case of MHV68 infection (16). The gene expression pattern is dramatically changed between virus infectious latent and lytic phase. ASRs might be critical for this phase conversion. When Ago1 was knocked down, ASRs were downregulated and much more cells tended to be induced into apoptosis. ASRs depending on Ago1 might suppress apoptosis, terminal phase of lytic infection. The hypothesis was further evaluated by investigation of the target genes of ASRs involved in EBV reactivation. It is presumed that as more ASRs were expressed, there would be a corresponding decrease in the expression of the target genes. To the contrary, the general trend of the three genes supposed to be involved in EBV reactivation was upregulation correlatively to apoptosis levels (Figure 6d).

INTS5, integrator subunit 5, is a member of a multiprotein complex associated with the C-terminal repeats of RNA polymerase II, and mediates small nuclear RNA 3′-end processing (30). ASRs may reduce INTS5 function and suppress EBV-encoded miRNA processing. EIF2AK3, eukaryotic initiation factor 2-alpha kinase 3, is a type I endoplasmic reticulum (ER) transmembrane protein (31). It contains a stress-sensing domain. When unfolded proteins are sensed in the ER, protein synthesis is decreased, resulting in apoptosis (32). However, EIF2AK3 also has reported pro-tumorigenic properties (33). ASRs may function as a balancer of EIF2AK3 function, but further investigation is needed. MEF2B, myocyte enhancer factor 2B, is a transcriptional activator. A recent report showed that MEF2B (34) contributes to EBV-infected cell reactivation from the latent stage. Together with the upregulation of ASRs in the lytic infection, the result suggests that ASRs might have some functions through the posttranscriptional regulation of these target genes to prevent the lytic infection from 'overactivation'.

In mammals, the Ago1–4 family sorting mechanism is unknown. Still, the class of sRNAs selectively incorporated onto Ago1, 'ASRs', appear to play vital roles in some aspects of mammalian biology. A mechanistic analysis of their processing and stability, and an extended investigation of the function of the

ASRs in EBV-infected cells, needs thus further investigation.

SUPPLEMENTARY DATA

Supplementary Data are available at NAR Online.

ACKNOWLEDGEMENTS

The authors thank Dr Nobuyoshi Kosaka, Dr. Yukihide Tomari, Dr. Naomi Hirabayashi, Dr. Masayuki Tanaka, Dr. Hideki Hayashi and Educational Research Center of Tokai University School of Medicine for technical assistance. This work was supported by the Japan Society for the Promotion of Science (awarded to A.K.).

FUNDING

Japan Society for the Promotion of Science, Takeda Science Fundation, Mitsui Life Social Walfare Fundation, Mochida Memorial Fundation for Medical and Pharmaceutical Research, Banyu Life Science Foundation International, International Myeloma Foundation Sugi Memorial (Awarded to A.K.) and Japan Leukemia Research Fund (Awarded to K.O.). Funding for open access charge: PRESTO/JST.

Conflict of interest statement. None declared.

REFERENCES

1. Bartel,D.P. (2004) MicroRNAs: genomics, biogenesis, mechanism, and function. *Cell*, **116**, 281–297.
2. Deddouche,S., Matt,N., Budd,A., Mueller,S., Kemp,C., Galiana-Arnoux,D., Dostert,C., Antoniewski,C., Hoffmann,J.A. and Imler,J.L. (2008) The DExD/H-box helicase Dicer-2 mediates the induction of antiviral activity in drosophila. *Nat. Immunol.*, **9**, 1425–1432.
3. Deleris,A., Gallego-Bartolome,J., Bao,J., Kasschau,K.D., Carrington,J.C. and Voinnet,O. (2006) Hierarchical action and inhibition of plant Dicer-like proteins in antiviral defense. *Science*, **313**, 68–71.
4. Skalsky,R.L., Corcoran,D.L., Gottwein,E., Frank,C.L., Kang,D., Hafner,M., Nusbaum,J.D., Feederle,R., Delecluse,H.J., Luftig,M.A. *et al.* (2012) The viral and cellular microRNA targetome in lymphoblastoid cell lines. *PLoS Pathog.*, **8**, e1002484.
5. Ghildiyal,M., Xu,J., Seitz,H., Weng,Z. and Zamore,P.D. (2010) Sorting of *Drosophila* small silencing RNAs partitions microRNA* strands into the RNA interference pathway. *RNA*, **16**, 43–56.
6. Su,H., Trombly,M.I., Chen,J. and Wang,X. (2009) Essential and overlapping functions for mammalian Argonautes in microRNA silencing. *Genes Dev.*, **23**, 304–317.
7. Van Stry,M., Oguin,T.H., Cheloufi,S., Vogel,P., Watanabe,M., Pillai,M.R., Dash,P., Thomas,P.G., Hannon,G.J. and Bix,M. (2012) Enhanced susceptibility of Ago1/3 double-null mice to influenza A virus infection. *J. Virol.*, **86**, 4151–4157.
8. Lu,J., Chanda,B. and Kotani,A. (2012) *Hematology - Science and Practice*. Intech, pp. 409–425.
9. Kube,D., Holtick,U., Vockerodt,M., Ahmadi,T., Haier,B., Behrmann,I., Heinrich,P.C., Diehl,V. and Tesch,H. (2001) STAT3 is constitutively activated in Hodgkin cell lines. *Blood*, **98**, 762–770.
10. Helwak,A., Kudla,G., Dudnakova,T. and Tollervey,D. (2013) Mapping the human miRNA interactome by CLASH reveals frequent noncanonical binding. *Cell*, **153**, 654–665.
11. Okuyama,K., Ikawa,T., Gentner,B., Hozumi,K., Harnprasopwat,R., Lu,J., Yamashita,R., Ha,D., Toyoshima,T., Chanda,B. *et al.* (2013) MicroRNA-126-mediated control of cell fate in B-cell myeloid progenitors as a potential alternative to transcriptional factors. *Proc. Natl Acad. Sci. USA*, **110**, 13410–13415.
12. Dueck,A., Ziegler,C., Eichner,A., Berezikov,E. and Meister,G. (2012) microRNAs associated with the different human Argonaute proteins. *Nucleic Acids Res.*, **40**, 9850–9862.
13. Li,Z., Kim,S.W., Lin,Y., Moore,P.S., Chang,Y. and John,B. (2009) Characterization of viral and human RNAs smaller than canonical MicroRNAs. *J. Virol.*, **83**, 12751–12758.
14. Kosaka,N., Iguchi,H., Yoshioka,Y., Takeshita,F., Matsuki,Y. and Ochiya,T. (2010) Secretory mechanisms and intercellular transfer of microRNAs in living cells. *J. Biol. Chem.*, **285**, 17442–17452.
15. Modzelewski,A.J., Holmes,R.J., Hilz,S., Grimson,A. and Cohen,P.E. (2012) AGO4 regulates entry into meiosis and influences silencing of sex chromosomes in the male mouse germline. *Dev. Cell*, **23**, 251–264.
16. Xia,J. and Zhang,W. (2012) Noncanonical microRNAs and endogenous siRNAs in lytic infection of murine gammaherpesvirus. *PLoS One*, **7**, e47863.
17. Förstemann,K., Horwich,M.D., Wee,L., Tomari,Y. and Zamore,P.D. (2007) *Drosophila* microRNAs are sorted into functionally distinct argonaute complexes after production by dicer-1. *Cell*, **130**, 287–297.
18. Tomari,Y., Du,T. and Zamore,P.D. (2007) Sorting of *Drosophila* small silencing RNAs. *Cell*, **130**, 299–308.
19. Steiner,F.A., Hoogstrate,S.W., Okihara,K.L., Thijssen,K.L., Ketting,R.F., Plasterk,R.H. and Sijen,T. (2007) Structural features of small RNA precursors determine Argonaute loading in *Caenorhabditis elegans*. *Nat. Struct. Mol. Biol.*, **14**, 927–933.
20. Liu,X., Jin,D.Y., McManus,M.T. and Mourelatos,Z. (2012) Precursor microRNA-programmed silencing complex assembly pathways in mammals. *Mol. Cell*, **46**, 507–517.
21. Burroughs,A.M., Ando,Y., de Hoon,M.J., Tomaru,Y., Suzuki,H., Hayashizaki,Y. and Daub,C.O. (2011) Deep-sequencing of human Argonaute-associated small RNAs provides insight into miRNA sorting and reveals Argonaute association with RNA fragments of diverse origin. *RNA Biol.*, **8**, 158–177.
22. Gu,S., Jin,L., Zhang,F., Huang,Y., Grimm,D., Rossi,J.J. and Kay,M.A. (2011) Thermodynamic stability of small hairpin RNAs highly influences the loading process of different mammalian Argonautes. *Proc. Natl Acad. Sci. USA*, **108**, 9208–9213.
23. Hamilton,M.P., Rajapakshe,K., Hartig,S.M., Reva,B., McLellan,M.D., Kandoth,C., Ding,L., Zack,T.I., Gunaratne,P.H., Wheeler,D.A. *et al.* (2013) Identification of a pan-cancer oncogenic microRNA superfamily anchored by a central core seed motif. *Nat. Commun.*, **4**, 2730.
24. Ruby,J.G., Jan,C.H. and Bartel,D.P. (2007) Intronic microRNA precursors that bypass Drosha processing. *Nature*, **448**, 83–86.
25. Hwang,H.W., Wentzel,E.A. and Mendell,J.T. (2007) A hexanucleotide element directs microRNA nuclear import. *Science*, **315**, 97–100.
26. Cooke,C.A., Bernat,R.L. and Earnshaw,W.C. (1990) CENP-B: a major human centromere protein located beneath the kinetochore. *J. Cell Biol.*, **110**, 1475–1488.
27. Ramírez-Sandoval,R., Sánchez-Rodríguez,S.H., Herrera-van Oostdam,D., Avalos-Díaz,E. and Herrera-Esparza,R. (2003) Antinuclear antibodies recognize cellular autoantigens driven by apoptosis. *Joint Bone Spine*, **70**, 187–194.
28. Skibola,C.F., Holly,E.A., Forrest,M.S., Hubbard,A., Bracci,P.M., Skibola,D.R., Hegedus,C. and Smith,M.T. (2004) Body mass index, leptin and leptin receptor polymorphisms, and non-hodgkin lymphoma. *Cancer Epidemiol. Biomarkers Prev.*, **13**, 779–786.
29. De,D., Chen,A., Wu,Z., Lv,S., He,G. and Qi,Y. (2009) Overexpression of Pygopus2 protects HeLa cells from vinblastine-induced apoptosis. *Biol. Chem.*, **390**, 157–165.
30. Baillat,D., Hakimi,M.A., Näär,A.M., Shilatifard,A., Cooch,N. and Shiekhattar,R. (2005) Integrator, a multiprotein mediator of small nuclear RNA processing, associates with the C-terminal repeat of RNA polymerase II. *Cell*, **123**, 265–276.
31. Atkins,C., Liu,Q., Minthorn,E., Zhang,S.Y., Figueroa,D.J., Moss,K., Stanley,T.B., Sanders,B., Goetz,A., Gaul,N. *et al.* (2013)

Characterization of a novel PERK kinase inhibitor with antitumor and antiangiogenic activity. *Cancer Res.*, **73**, 1993–2002.
32. Su,Q., Wang,S., Gao,H.Q., Kazemi,S., Harding,H.P., Ron,D. and Koromilas,A.E. (2008) Modulation of the eukaryotic initiation factor 2 alpha-subunit kinase PERK by tyrosine phosphorylation. *J. Biol. Chem.*, **283**, 469–475.
33. Bobrovnikova-Marjon,E., Grigoriadou,C., Pytel,D., Zhang,F., Ye,J., Koumenis,C., Cavener,D. and Diehl,J.A. (2010) PERK promotes cancer cell proliferation and tumor growth by limiting oxidative DNA damage. *Oncogene*, **29**, 3881–3895.
34. Murata,T., Narita,Y., Sugimoto,A., Kawashima,D., Kanda,T. and Tsurumi,T. (2013) Contribution of myocyte enhancer factor 2 (MEF2) family transcription factors to BZLF1 expression in Epstein-Barr virus reactivation from latency. *J. Virol.*, **87**, 10148–10162.

OPEN ACCESS Freely available online

PLOS ONE

Establishment of a Humanized APL Model via the Transplantation of *PML-RARA*-Transduced Human Common Myeloid Progenitors into Immunodeficient Mice

Hiromichi Matsushita[1,2,3]*, Takashi Yahata[1,2,4], Yin Sheng[1], Yoshihiko Nakamura[1], Yukari Muguruma[1], Hideyuki Matsuzawa[1,5], Masayuki Tanaka[5], Hideki Hayashi[5], Tadayuki Sato[5], Anar Damdinsuren[3], Makoto Onizuka[6], Mamoru Ito[7], Hayato Miyachi[3], Pier Paolo Pandolfi[8], Kiyoshi Ando[1,2,6]*

1 Research Center for Cancer Stem Cell, Tokai University School of Medicine, Isehara, Kanagawa, Japan, **2** Medical Research Institute, Tokai University, Isehara, Kanagawa, Japan, **3** Department of Laboratory Medicine, Tokai University School of Medicine, Isehara, Kanagawa, Japan, **4** Department of Cell Transplantation, Tokai University School of Medicine, Isehara, Kanagawa, Japan, **5** Support Center for Medical Research and Education, Tokai University, Isehara, Kanagawa, Japan, **6** Division of Hematology and Oncology, Department of Internal Medicine, Tokai University School of Medicine, Isehara, Kanagawa, Japan, **7** Central Institute for Experimental Animals, Kawasaki, Kanagawa, Japan, **8** Cancer Research Institute, Beth Israel Deaconess Cancer Center, Departments of Medicine and Pathology, Beth Israel Deaconess Medical Center, Harvard Medical School, Boston, Massachusetts, United States of America

Abstract

Recent advances in cancer biology have revealed that many malignancies possess a hierarchal system, and leukemic stem cells (LSC) or leukemia-initiating cells (LIC) appear to be obligatory for disease progression. Acute promyelocytic leukemia (APL), a subtype of acute myeloid leukemia characterized by the formation of a PML-RARα fusion protein, leads to the accumulation of abnormal promyelocytes. In order to understand the precise mechanisms involved in human APL leukemogenesis, we established a humanized *in vivo* APL model involving retroviral transduction of *PML-RARA* into $CD34^+$ hematopoietic cells from human cord blood and transplantation of these cells into immunodeficient mice. The leukemia well recapitulated human APL, consisting of leukemic cells with abundant azurophilic abnormal granules in the cytoplasm, which expressed CD13, CD33 and CD117, but not HLA-DR and CD34, were clustered in the same category as human APL samples in the gene expression analysis, and demonstrated sensitivity to ATRA. As seen in human APL, the induced APL cells showed a low transplantation efficiency in the secondary recipients, which was also exhibited in the transplantations that were carried out using the sorted $CD34^-$ fraction. In order to analyze the mechanisms underlying APL initiation and development, fractionated human cord blood was transduced with *PML-RARA*. Common myeloid progenitors (CMP) from $CD34^+/CD38^+$ cells developed APL. These findings demonstrate that CMP are a target fraction for *PML-RARA* in APL, whereas the resultant $CD34^-$ APL cells may share the ability to maintain the tumor.

Citation: Matsushita H, Yahata T, Sheng Y, Nakamura Y, Muguruma Y, et al. (2014) Establishment of a Humanized APL Model via the Transplantation of *PML-RARA*-Transduced Human Common Myeloid Progenitors into Immunodeficient Mice. PLoS ONE 9(11): e111082. doi:10.1371/journal.pone.0111082

Editor: Marina Konopleva, University of Texas M.D. Anderson Cancer Center, United States of America

Received February 27, 2014; **Accepted** September 24, 2014; **Published** November 4, 2014

Funding: Hiromichi Matsushita received funding from a Grant-in-Aid for Scientific Research from The Ministry of Education, Culture, Sports, Science and Technology of Japan (#24591411, URL http://www.jsps.go.jp/english/e-grants/), Tokai University School of Medicine Project Research (http://www.med.u-tokai.ac.jp/web/international/about_us/message_from_the_dean.html), and the Takeda Science Foundation (http://www.takeda-sci.or.jp/index.html). Kiyoshi Ando received support from a Grant-in-Aid for Scientific Research from The Ministry of Education, Culture, Sports, Science and Technology of Japan (#24390248). The funders had no role in study design, data collection and analysis, decision to publish, or preparation of the manuscript.

Competing Interests: The authors have declared that no competing interests exist.

* Email: hmatsu@is.ic.cc.u-tokai.ac.jp (H. Matsushita); andok@keyaki.cc.u-tokai.ac.jp (KA)

Introduction

Acute myeloid leukemia (AML) constitutes a heterogeneous group of tumors in myeloid lineage cells characterized by the proliferation and accumulation of immature myeloblasts [1]. Recent advances in cancer biology have revealed that various genetic events result in the blockage of differentiation with subsequent uncontrolled cellular proliferation. In addition, *in vivo* analyses using a xenograft model with immunodeficient mice have shown that a very immature subset of AML cells called leukemic stem cells (LSC), which are typically characterized as $CD34^+/CD38^-$ cells, as observed in normal hematopoietic stem cells (HSCs), have been shown to slowly undergo cell division to both yield progenitor cells and sustain the LSC population, thus resulting in the maintenance of the tumor [2–6]. More recently, several reports have shown that $CD34^+/CD38^+$ hematopoietic progenitors are able to acquire the ability to maintain populations of LSC or leukemia-initiating cells (LIC) [7]. It is therefore possible that the phenotypes of LIC differ among the subtypes of AML.

Acute promyelocytic leukemia (APL) is a subset of AML defined by the formation of a chimeric gene, promyelocytic leukemia-retinoic acid receptor α (*PML-RARA*) [8]. It is characterized by the accumulation of abnormal promyelocytes with abundant large azurophilic granules, suggesting that APL cells undergo maturation arrest in the later steps of myeloid differentiation. The typical pattern of cellular surface markers of APL is positive for CD13,

CD33 and CD117, and negative for CD34, which is usually presumed to indicate cellular immaturity, and HLA-DR [9]. It is very difficult to engraft primary APL samples in immunodeficient mice. They did not become engrafted into the NOD/SCID mice to any degree [3]. In NOD/Shi-SCID/IL-2Rγ^{null} (NOG) mice, which are more profoundly immunocompromised than NOD/SCID mice [10,11], six out of eight APL samples were not engrafted or only very little engrafted [12]. It is therefore possible that the mechanisms underlying the development of APL differ from those involved in the pathogenesis of AML uncovered to date. Elucidating the pathogenesis of APL is important for improving the treatment of APL patients, and will provide clues to understand the development of other subtypes of AML.

In vivo analyses using transgenic APL mice models with *PML-RARA* have revealed that a population of committed myeloid progenitor cells ($CD34^+$, c-kit^+, FcγRIII/II^+, $Gr1^{int}$) was identified as the APL-LIC [13,14]. However, the cellular surface antigens and the gene expression pattern in humans are different from those in mice. In particularly, in transgenic systems, murine APL developed after a long latent period through a myelodysplastic/proliferative phase, which does not usually precede human APL [15–18]. There have been no *in vivo* models for exploring leukemogenesis of human APL to date; largely because human primary APL cells are difficult to engraft as a xenograft [3,12]. *PML-RARA*-retrovirally transduced human $CD34^+$ cells from cord blood have therefore only been evaluated *in vitro* [19].

Therefore, the aim of this study was to establish a humanized xenograft APL model using the retroviral transduction of *PML-RARA* into human $CD34^+$ cells and NOG mice in order to investigate the mechanisms of APL leukemogenesis, such as that involving disease initiation and maintenance in the model.

Materials and Methods

Fractionation of human hematopoietic cells from cord blood

Cord blood (CB) and patients' APL samples were obtained after written informed consent was provided in accordance with the Declaration of Helsinki and with approval from the Tokai University Committee on Clinical Investigation (Permit number: #12I-46 and #12I-49). CD34 positive and negative specimens were primarily prepared using the CD34 Progenitor Cell Isolation Kit (Miltenyi Biotec, Bergisch Gladbach, Germany). $CD34^+$ cells were then purified again using anti-human CD34 mAbs (Beckman Coulter, Brea, CA), in combination with or without an anti-CD38 antibody (BD, Franklin Lakes, NJ), with a FACS vantage instrument (BD). $CD34^-/CD33^+$ cells were also purified again using anti-human CD34 and CD33 mAbs (Beckman Coulter) and the FACS vantage instrument. The preparation of common myeloid progenitors (CMP), granulocyte-monocytic progenitors (GMP) and megakaryocyte-erythrocyte progenitors (MEP) was performed using an anti-CD123 antibody (BD) and anti-CD45RA (Biolegend, San Diego, CA) antibody, according to a previous report [20].

Retrovirus transduction of *PML-RARA* into human hematopoietic cells

The MIGR1 retroviral vector [21] or MIGR1-*PML-RARA* (bcr3/short form) [22] in combination with the vesicular stomatitis virus-G protein (VSV-G) envelope vector (pCMV-VSV-G) was transiently transfected into PLAT-gp cells using the Fugene 6 transfection reagent (Roche Diagnostics, Basel, Switzerland). The culture supernatant was concentrated 100 to 200 times by ultracentrifugation. After overnight culture of the fractionated cells in StemPro-34 (Life Technologies, Carlsbad, CA) with TPO, SCF, and FLT3 ligand (50 ng/ml each), they were incubated with the concentrated supernatant on retronectin-coated plates (Takara-Bio, Otsu, Japan). Retroviral transduction was performed twice, and then transplantation was performed the next day.

Colony-forming unit-cells assay

PML-RARA transduced cells were sorted by their EGFP, CD34 and CD38 expression by FACS vantage 48 h after infection. The colony-forming unit-cells (CFU-C) assay was performed as described previously [23]. The fluorescent images were captured using a HS All-in-One Fluorescence Microscope Biorevo 9000 (Keyence Corporation, Osaka, Japan) and were analyzed by the BZ II software program (Keyence Corporation).

RNA extraction and RT-PCR

Total RNA was isolated using the RNeasy micro kit (Qiagen, Hilden, Germany) or Isogen (Nippon gene, Tokyo, Japan), and the reverse-transcribed cDNA was amplified by qualitative PCR. The qualitative-PCR analysis was performed by SRL Inc. (Hachioji, Tokyo, Japan). The sequences of PCR primers and probes were shown in **Table S1**.

Transplantation, serial transplantation and ATRA treatment

Nine- to 20-week-old NOD/Shi-scid, IL-2Rγc^{null} (NOG) mice [10,11] were irradiated with 220 cGy of X-rays. On the following day, the whole infected cells or primary AML cells were intravenously injected. The EGFP-positive cells in the peripheral blood were monitored. The mice with induced APL were defined as those bearing more than 0.1% $EGFP^+$ cells which dominantly expressed CD33 (more than 70%) in their bone marrow at four months after transplantation. In the initial analysis, the occurrence of APL was confirmed by the morphological observations using cytospin slides after EGFP sorting. For serial transplantation, bone marrow cells were obtained from recipient mice, and the sorted EGFP-positive cells were injected intravenously or intramedullary into the irradiated mice [24]. The engrafted mice were treated intraperitoneally with 1.5 μg/g of body weight/day of all-*trans* retinoic acid (ATRA, Sigma) for 21 days [25], and were then sacrificed to collect the EGFP-positive cells in the bone marrow by sorting. All the experiments using animals were approved by the animal care committee of Tokai University (Permit number: #132028).

Flow cytometric analysis

The cells were stained with APC-conjugated anti-human CD45, CD33, CD34, HLA-DR (Beckman Coulter), CD13, and CD117 (BD) mAbs. They were subjected to flow cytometry using a FACSCalibur instrument (BD) and the CellQuest software program (BD).

Cell preparation, Wright-Giemsa staining and immunofluorescence microscopy

Cytospin slides were prepared using a Cytospin 4 Cytocentrifuge (Thermo Scientific, Waltham, MA) at 500 rounds per minute for 5 min. To observe the cellular morphology, Wright-Giemsa staining was performed. For the immunofluorescent study, cells were seeded onto poly-L-lysine coated slides and fixed with ice cold 70% ethanol for 15 min. After permeabilization with 0.2% Triton X-100 for 20 min, the slides were treated with PBS containing 5% normal goat serum for 1 hour to block the nonspecific binding of antibodies. The anti-PML antibody (Merck

Millipore, Billerica, MA) was applied overnight at 4°C. Cells were counterstained with DAPI. Images were captured with an LSM510 META confocal microscope (Carl Zeiss, Oberkochen, Germany) and processed using Adobe Photoshop 7.0 (Adobe Systems, San Jose, CA).

Southern blot analysis

Genomic DNA was extracted from the cells using a DNeasy kit (Qiagen). Ten micrograms of the DNA were electrophoresed and transferred to nylon membranes (Hybond-N+, GE Healthcare, Fairfield, CT). The DNA was then crosslinked to the membrane by ultraviolet light. The EGFP probe was prepared from MIGR1 vector by cutting it using NcoI and SalI, and was labeled with ^{32}P-dCTP using the Rediprime II DNA Labelling System (GE Healthcare). The membrane was hybridized with the probe in Rapid-hyb buffer (GE Healthcare), and was analyzed by a Phosphoimager (LAS1000, Fuji Film, Tokyo, Japan).

Microarray

Total RNA was labeled and hybridized to Affymetrix Human Genome U133 Plus 2.0 Array GeneChip microarrays (Affymetrix, Santa Clara, CA) using the manufacturer's protocols. The results were deposited in the Gene Expression Omnibus (GEO; http://www.ncbi.nlm.nih.gov/geo/; accession no. GSE49344). The microarray data from normal human promyelocytes and clinical samples bearing AML, including APL, were obtained from the deposited data on the GEO (GSE12662). The APL-specific expressed genes have been described in detail in a previous study [26]. The probe set data were generated using standard normalization algorithms included in the Affymetrix Microarray Suite software program, v.5 (MAS5.0). The clustering analysis was performed by the Gene spring GX software program, version 11 (Agilent technology, Santa Clara, CA).

To identify the genes that are differentially expressed in a specific cellular subset, all probe sets with fewer than 10% present calls in both groups and a coefficient of variation <0.5 across all samples were eliminated prior to the subsequent analysis; (i) The genes differently expressed in the induced APL cases among the AML cases were defined as genes whose expression change (upregulation or downregulation) was $\geq$2.0 fold in comparison to those in AML other than APL, (ii) The genes associated with immaturity in the induced APL cases were expressed at significantly higher levels in CD34$^+$ cells than the other normal cells (FDR <0.05, fold-change >2.0 upregulated), and were also expressed in the induced APL cells at similar levels (induced APL: CD34$^+$ $\geq$1:1), and moreover, these genes were expressed at higher levels in promyelocytes (induced APL: Pros $\geq$2:1). (iii) The genes upregulated during promyelocyte differentiation were expressed at significantly higher levels in promyelocytes than in the other normal cells (FDR <0.05, fold-change >2.0 upregulated), and were expressed at lower levels in the induced APL (induced APL: Pros $\leq$1:2), (iv) The genes induced by *PML-RARA* were expressed at higher levels in the induced APL than in all the normal cells (induced APL: normal $\geq$2:1), and were not expressed in any normal cells (more than 75% absent calls, as summarized by the MAS5.0). Statistical significance was assessed by the unpaired unequal variance Welch test ($P<0.05$), and correction for multiple testing was performed by the Benjamini and Hochberg False Discovery Rate (FDR), using a cutoff of 0.05.

The gene set specific for induced APL was defined to fulfill one or more of the above criteria (ii) to (iv) in the gene set identified in (i).

The integration site analysis of *PML-RARA* using linear amplification-mediated PCR

To identify the genomic-proviral junction sequence, linear amplification-mediated polymerase chain reaction (LAM-PCR) was performed as described previously, with minor modifications [27,28]. In brief, genomic DNA from bone marrow cells was first digested with Tsp509I. A linear amplification of target DNA in the digested genome was performed by repeated primer extension using a vector-specific 5′-biotinylated primer, LTR1.5, and Taq polymerase. After selection with Dynabeads MyOne Streptavidin C1 (Life Technologies), a double-stranded asymmetrical linker cassette was ligated to the Tsp509I-digested site using T4 DNA Ligase. The DNA products were then amplified by PCR using a vector-specific primer, LTR3, and linker cassette primer, LC1. The nested PCR was performed using internal primers LTR5 and LC2. The final products were sequenced after cloning them into the TOPO TA cloning vector (Life Technologies). The primer sequences are shown in **Table S1**.

Statistical analyses

The Kaplan-Meier method was used to estimate the leukemia-free survival (LFS) of mice. Log-rank p values were used for comparisons of the LFS among three subgroups. The analyses were conducted using the GraphPad Prism software package (GraphPad Software, La Jolla, CA). The other statistical analyses were performed using the Mann-Whitney U Test with the IBM SPSS Statistics software program (New York, NY). Values of $p<0.05$ were considered to be statistically significant.

Results

Functions of PML-RARα in human CD34 cells *in vitro*

To examine the functions of PML-RARα *in vitro*, a MIGR1-*PML-RARA* or MIGR1 control vector was retrovirally infected into human CD34$^+$ cells from cord blood. The transduction efficiency evaluated by EGFP positivity was 0.5% to 18.6% (n = 10, median: 5.7%) and 2.1% to 19.7% (n = 25, median: 6.8%), respectively. The expression of *PML-RARA* in these cells was confirmed by RT-PCR (**Figure S1**). The induction of *PML-RARA* in CD34$^+$ cells disrupted PML nuclear bodies by interacting with wild-type PML via the PML portion of the chimeric transcript, and the distribution of PML in the nucleus was altered to show a microspeckled pattern in these cells [29–31] (**Figure 1A**). Additionally, the induction of *PML-RARA* reduced all the colony formation capacity (**Figure 1B**). The *PML-RARA* expression was confirmed in these colonies by EGFP fluorescence (**Figure S1 and S2**) and RT-PCR, although the expression levels were 37 times lower compared to those in the CD34$^+$ cells 48 hours after *PML-RARA* transduction (**Figure S3**). Regarding the content of colonies, MIGR1-infected CD34$^+$ cells mainly generated the erythroid lineage-containing colonies, such as CFU-mix and BFU-E, whereas more than half of the colonies from the CD34$^+$ cells with *PML-RARA* were of the myeloid lineage, like CFU-GM (**Figures 1C**). These data demonstrate that *PML-RARA* induces the myeloid commitment of human CD34$^+$ cells.

Establishment of a humanized *in vivo* APL model

The cells transduced with *PML-RARA* or the MIGR1 control vector were then transplanted into NOG mice. The EGFP$^+$ cells survived and proliferated three to four months after transplantation only in the NOG mice transplanted with *PML-RARA*-, not control vector at all, infected human CD34$^+$ cells. The median proportion of EGFP$^+$/CD45$^+$ cells in the bone marrow obtained from the transplanted mice was 23.7% (0.95% to 96.5%, n = 24)

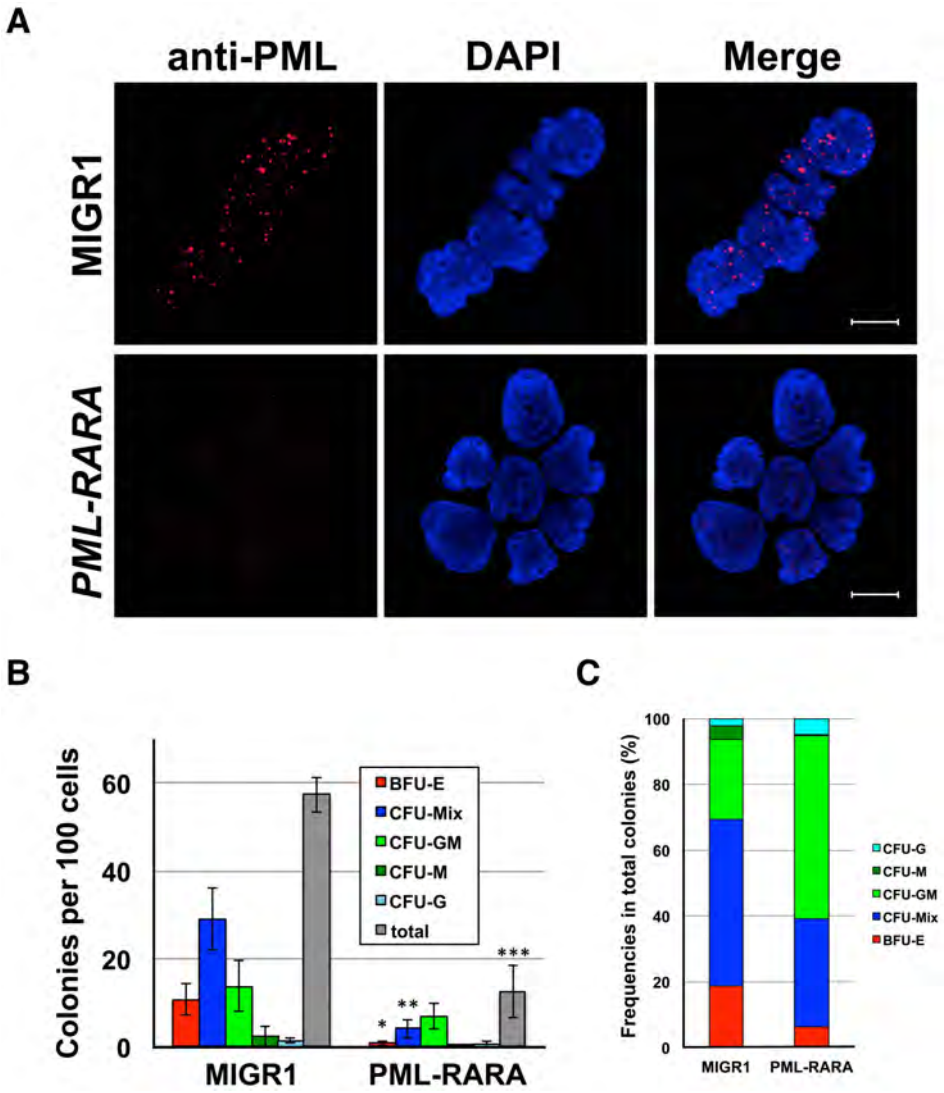

Figure 1. The function of *PML-RARA* in human CD34$^+$ cells *in vitro*. (**A**) The results of an immunofluorescent analysis of PML distribution in human CD34$^+$ cells transduced with *PML-RARA*. The images were captured with an LSM510 META confocal microscope (Carl Zeiss). The bars indicate 10 μm. (**B**) The colony-forming assay using *PML-RARA*-transduced CD34$^+$ cells. The cells were sorted by EGFP expression 48 h after infection. Colony formation was evaluated on days 10 to 12 after plating the cells. The average numbers of colonies from three independent experiments are shown. Data represent the means ± SD. The asterisks (*) indicate $p<0.05$. (**C**) The proportion of each kind of colony was calculated from the results of the colony-forming assay shown in (B). The percentages of CFU-GM are higher in *PML-RARA*-infected cells than in control (MIGR1) cells ($p = 0.013$).
doi:10.1371/journal.pone.0111082.g001

(**Figure 2A**). The majority of the engrafted EGFP$^+$/human CD45$^+$ cells expressed human CD33 (70.2% to 100%, median 90.6%, n = 24) (**Figure 2B**), thus suggesting that they were of the myeloid lineage. The *PML-RARA* expression was detected only in the EGFP$^+$ fraction and not in the EGFP$^-$ fraction of the sorted human CD45$^+$/CD33$^+$ cells from the NOG mice (**Figure 2C**). The expression levels of *PML-RARA* were decreased about 17-fold in comparison to those in the CD34$^+$ cells 48 hours after *PML-RARA* transduction (**Figure S3**), but the presence of P*ML-RARA* in the human myeloid cells, recognized as EGFP$^+$ cells, caused marked accumulation of promyelocytes, in comparison to the control EGFP$^-$ human myeloid cells (52.8% in EGFP$^+$ cells vs 19.4% EGFP$^-$ cells in the 13 paired samples, $p<0.0001$). On the other hand, the proportions of myeloblasts, mature neutrophils and monocytes were decreased (5.2% vs 14.4%, $p = 0.010$; 2.5% vs 12.7%, $p = 0.005$; 4.0% vs 10.1%, $p = 0.016$) (**Figure 2D**). These findings confirmed that the expression of *PML-RARA* induced the myeloid differentiation of human CD34$^+$ cells and blocked them at the promyelocytic stage. Morphologically, the promyelocytes had abundant large azurophilic granules and round nuclei with a high nucleocytoplasmic ratio. Some of them had a number of Auer bodies and looked like Faggot cells, which are the typical morphological features of APL cells, and were not seen in the previous murine models (**Figure 2E**). A Southern blot analysis using an EGFP probe revealed that the EGFP$^+$/CD45$^+$/CD33$^+$ cells oligoclonally proliferated *in vivo* (**Figure 2F**).

The induced APL cells were detected in 24 out of the 34 mice (71%) transplanted with *PML-RARA*-transduced CD34 cells ($p = 0.0184$ in comparison to the control). They were detected in all 16 mice when the calculated number of the transplanted EGFP$^+$/CD34$^+$ cells per mouse was more than 3,000 (4,655 to 29,728 cells, median: 11,085 cells) ($p = 0.0006$ in comparison to the control). On the other hand, they were only detected in eight out of 18 mice (44%) transplanted with EGFP$^+$/CD34$^+$ cells at a

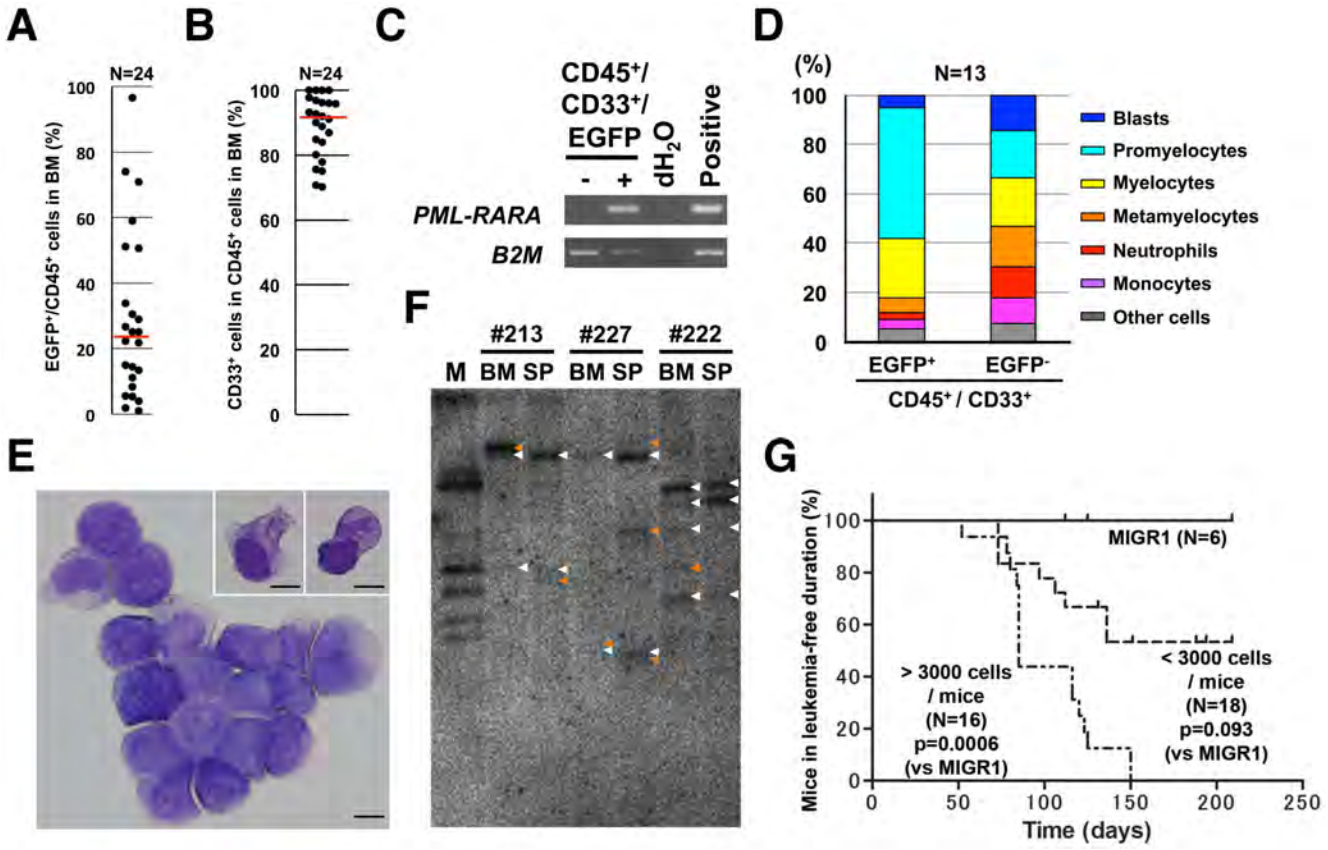

Figure 2. Establishment of humanized APL *in vivo*. (**A**) The proportion of EGFP$^+$/human CD45$^+$ cells in the bone marrow of leukemic NOG mice. Each dot represents a single mouse. The horizontal line represents the median value. (**B**) The proportion of CD33$^+$ cells among the EGFP$^+$/human CD45$^+$ cells in the bone marrow of the leukemic NOG mice. Each dot represents a single mouse. The horizontal line represents the median value. (**C**) The expression of *PML-RARA* in RT-PCR was detected only in the EGFP$^+$ fraction obtained from the engrafted human CD45$^+$/CD33$^+$ cells. The cells were obtained from bone marrow 16 weeks after transplantation. *B2M, beta 2 microglobulin*. The *PML-RARA* expression vector and human CD34$^+$ cells were used as a positive control for the *PML-RARA* and *B2M* analysis, respectively. (**D**) The differential counts of the engrafted CD45$^+$/CD33$^+$/EGFP$^+$ and EGFP$^-$ cells from the mice transplanted with *PML-RARA*-induced human CD34$^+$ cells. They were obtained from bone marrow 16 to 20 weeks after transplantation. The data represent the means. (**E**) A representative photograph of the resulting leukemic cells which morphologically recapitulated APL. Faggot cells were recognized, as seen in the right top corner. The images were captured with a BX41 microscope (Olympus). The bar indicates 10 μm. (**F**) The results of a Southern blot analysis of the genomic DNA from induced APL cells with an EGFP probe. Clonal bands are shown by arrow heads: white, seen in both BM and SP; orange, seen only in BM or SP. BM, bone marrow; SP, spleen. (**G**) The leukemia-free duration in NOG mice transplanted with *PML-RARA*-transduced CD34$^+$ cells.
doi:10.1371/journal.pone.0111082.g002

density of less than 3,000 (480 to 2,660 cells, median: 1,861 cells) ($p = 0.093$ in comparison to the control) (**Figure 2G**). This proportion was not dependent on the number of transplanted EGFP$^+$/CD34$^+$ cells.

These findings demonstrate that a humanized APL model can be successfully established by the transplantation of *PML-RARA*–transduced human CD34 cells into NOG mice.

Characteristics of the induced APL cells obtained from the humanized *in vivo* model

The induced APL cells were positive for human myeloid markers such as CD13, CD33 and CD117, and were negative for CD34 and HLA-DR, as seen in typical human APL [32]. *PML-RARA* did not contribute to the development of lymphocytes. Human CD19$^+$ B-cells in the spleen and human CD4$^+$/CD8$^+$ T-cells in the thymus were negative for EGFP (**Figure 3A**).

To evaluate the gene expression of the induced APL cells, a microarray analysis was performed, and the expression of the 510 APL-specific genes identified in a previous study was compared with that observed in the clinical AML samples [26]. Two clinical APL samples from our patients were simultaneously evaluated and were aligned in the APL category defined in the study, suggesting that our microarray results were comparable with those in the previous study. The induced APL cells from our models were also classified into the APL category when compared to normal promyelocytes and AML samples other than APL (**Figure 3B**).

In common with this previous study [26], the 3,439 probes (3278 genes) differentially expressed in the induced APL and the AML other than APL ((i) in the Materials and Methods) grouped the induced APL and human primary APL together, separately from the other types of AML (**Figure S4**). The gene sets whose expression in the induced APL cases was not dependent on the myeloid differentiation were also filtered by comparison with the data for normal myeloid cells. They included the genes for immaturity expressed in the induced APL (1,782 probes, including 1,720 genes), the genes upregulated in promyelocyte differentiation not in the induced APL (447 probes, including 427 genes) and the genes specifically induced by *PML-RARA* (466 probes, including 429 genes) ((ii), (iii) and (iv) in the Materials and Methods). Each gene set was analyzed using the DAVID website

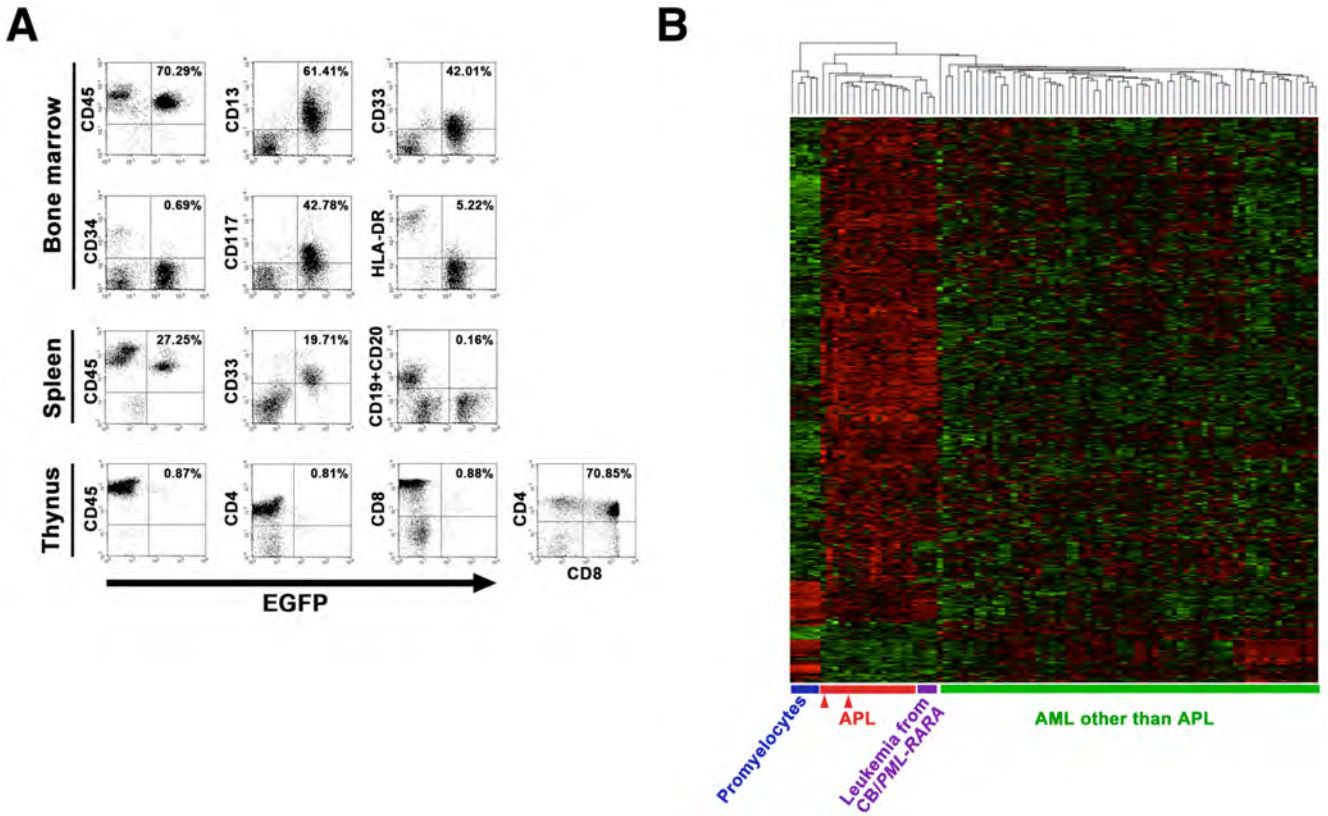

Figure 3. Characteristics of the induced APL *in vivo*. (**A**) The representative expression pattern of cell surface markers in the induced APL cells determined by a flow cytometric analysis. All the scatter plots show the relationships between the EGFP positivity and cell surface marker expression. The whole living cells gated as a propidium iodide-negative fraction in the bone marrow were analyzed. The induced APL cells were recognized as $EGFP^+$ cells. A few murine hematopoietic cells, recognized as a human $CD45^-$ fraction, were detected in this mouse. (**B**) The heat map of the microarray analysis using the 510 APL-specific genes for the comparison of the induced APL cells (purple, n = 3) with APL (red, n = 16), other types of AML (M0, 1, 2 and 4 in FAB classification, green, n = 62) and normal promyelocytes (blue, n = 5) in a previous study [26]. The red triangles (n = 2) for a total 16 APL cases show the clinical APL samples whose microarray data were obtained in this study.
doi:10.1371/journal.pone.0111082.g003

(david.abcc.ncifcrf.gov/). In the induced APL cases, the genes related to N-Glycan, steroid and heparan sulfate biosynthesis, the spliceosome and pyrimidine metabolism were expressed similar to the levels in normal $CD34^+$ cells, and those related to the MAPK signaling pathway were exclusively expressed in comparison to normal myeloid cells, including normal $CD34^+$ cells. On the other hand, the genes related to neurotrophin signaling and the cell cycle, as well as those associated with metabolic processes, such as glycolysis/gluconeogenesis, the pentose phosphate pathway and sphingolipid metabolism were downregulated (**Table S2**), thus suggesting that the induced APL exhibited dysregulated signaling and metabolism as differentiated myeloid cells. Additionally, the gene set composed of 573 probes including 547 genes, which fulfilled one or more above criteria (ii) to (iv) in the gene set identified in (i), clearly separated the normal and malignant promyelocytes, such as those of induced and human primary APL (**Figure S5 and Table S3**), as described in the previous study using primary APL cases [26].

To evaluate the additional genetic events that accompanied the integration of *PML-RARA* in the genome, the insertion sites of *PML-RARA* were analyzed. Some of the integration sites of *PML-RARA* were in the introns or exons of genes (**Table S4**). However, they were neither recurrent nor found in the previous whole genome sequence analysis of the APL patients [33]. These findings suggest that *PML-RARA* was a common key event, but that there were various additional genetic events in these induced APL cells, and this finding was compatible with the previous analysis using human primary APL [33].

The induced APL cells differentiated into mature neutrophils following treatment with all-*trans* retinoic acid (ATRA) *in vitro* (**Figures 4A and 4B**), which was accompanied by alterations in the PML distribution in the nucleus, from a microspeckled to a speckled pattern (**Figure 4C**). Similarly, ATRA induced transient myeloid differentiation *in vivo* (n = 4), as has been seen in APL patients (**Figures 4D and 4E**).

These findings demonstrate that our induced APL cells recapitulate human APL both phenotypically and functionally.

Re-transplantable cellular fraction in the induced APL cells

It is necessary to prove that the resultant induced APL cells possess the reproducibility of APL in the secondary recipients in order to demonstrate their capacity for leukemogenesis. However, previous studies have revealed that primary APL cells exhibit difficultly in engrafting in immunodeficient mice [3,12]. When the induced APL cells were transplanted into the second recipients, they were proven to be re-transplantable intravenously; 500,000 to 1,000,000 leukemic cells, but not 50,000 cells, were required, and the frequency of APL cells in the secondary recipients was low (0.04% to 1.41%, n = 6). The frequency was still low, even though

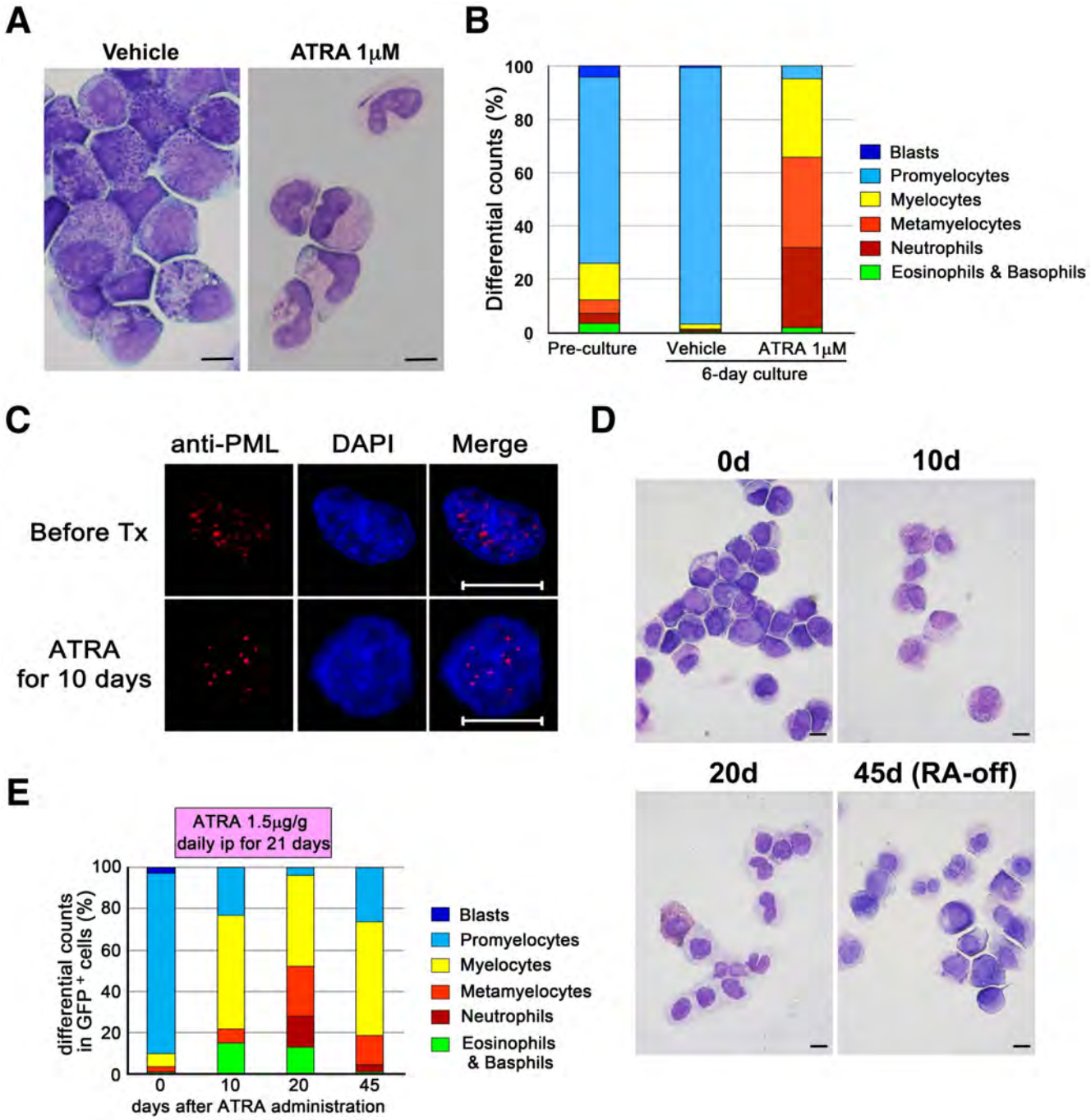

Figure 4. The induction of myeloid differentiation in the APL cells induced by ATRA treatment *in vitro* and *in vivo*. (**A**) Cytospin slides of the induced APL cells cultured with or without 1 μM ATRA for 6 days. The mature neutrophils with Auer rods are seen in the ATRA-treated group. The images were captured with a BX41 microscope (Olympus). The bar indicates 10 μm. (**B**) The differential cellular counts of the induced APL cells cultured with or without ATRA. The average leukocyte differentiation in three independent experiments is shown. (**C**) The results of an immunofluorescent analysis of the PML distribution in the induced APL cells before and after treatment with ATRA. The images were captured with an LSM510 META confocal microscope (Carl Zeiss). All the bars indicate 10 μm. (**D, E**) The induction of myeloid differentiation in the induced APL cells by ATRA *in vivo*. The secondary recipients transplanted with the induced APL cells were then intraperitoneally treated with ATRA for 21 days. Cytospin slides of $EGFP^+/hCD45^+/hCD33^+$ cells from the secondary recipients transplanted with the induced APL cells are shown (**D**). The images were captured with a BX41 microscope (Olympus). The bar indicates 10 μm. Their differentiated cellular counts were evaluated, and the representative series data are indicated (**E**).
doi:10.1371/journal.pone.0111082.g004

they were transplanted intramedullary (iBM, 2.00% to 5.98%, n = 2) (**Figure 5A**). The immunophenotype of the engrafted cells was the same as that seen in the primary induced APL cells: they were positive for CD13 and CD33, without the expression of CD34 or HLA-DR (**Figure 5B**), demonstrating that the induced APL retains self-renewal capacity with a low level of transplan-

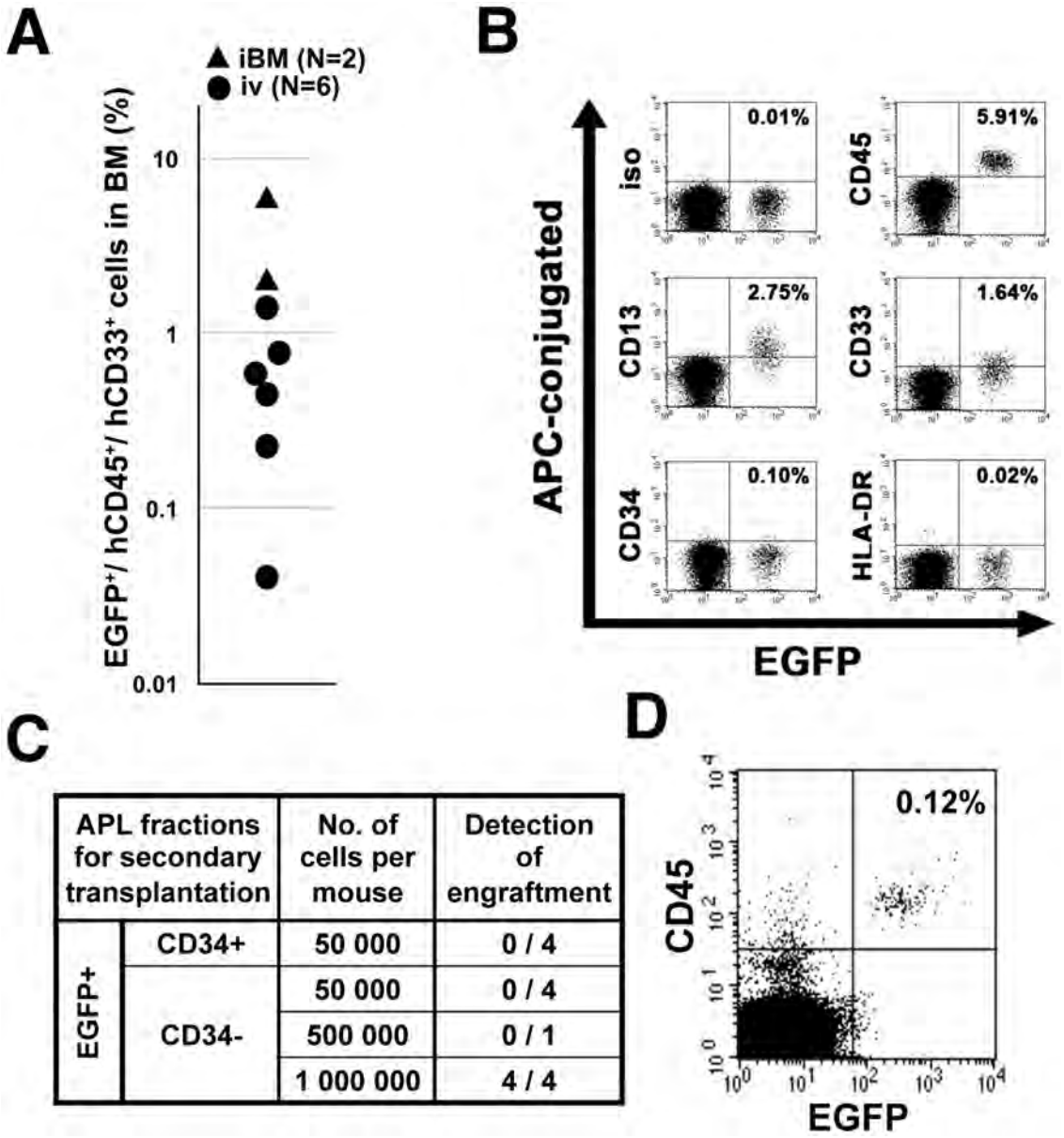

Figure 5. APL-LIC in the humanized APL *in vivo* model. (**A**) The engraftment of the induced APL cells in the secondary recipients. The bone marrow cells were obtained 16 weeks after transplantation and evaluated. Each dot represents a single mouse. (**B**) The immunophenotype of the induced APL cells in the secondary recipients. The representative pattern is shown. (**C**) The engraftment capacity in each fraction from the induced APL cells in the secondary recipients. The bone marrow cells were obtained 16 weeks after transplantation and evaluated. (**D**) The engraftment of the $CD34^-$ fraction in the secondary recipients. The engrafted cells are shown as $EGFP^+/CD45^+$ cells.
doi:10.1371/journal.pone.0111082.g005

tation efficiency. In addition, the results suggested that the capacity for engraftment in this xenograft model differed between the $CD34^+$ cells transduced with *PML-RARA* and the APL cells mostly composed of the $CD34^-$ fraction.

To identify a fraction responsible for the APL maintenance in the induced APL cases, $CD34^+$ and $CD34^-$ APL fractions were separately collected and transplanted intravenously. The $CD34^+$ fraction was pooled because there were very few $CD34^+$ cells in each induced APL case (**Figures 3A and 5B**). The $CD34^-$ fraction was sorted twice to exclude the $CD34^+$ fraction completely. Fifty thousand APL cells in both the $CD34^+$ and $CD34^-$ fractions failed to engraft in the secondary recipients (0 out of 4 mice in each fraction). Similar to the unsorted cells, one million $CD34^-$ fraction cells were able to engraft in recipient mice (4 out of 4 mice) (**Figures 5C and 5D**).

These findings revealed that $CD34^-$ induced APL cells exhibit the ability to function as APL-LIC *in vivo*, although the LIC function was not excluded in the $CD34^+$ APL fraction.

The $CD34^+/CD38^+$ progenitors trigger APL by *PML-RARA* induction *in vivo*

The findings that the *PML-RARA* transduced-$CD34^+$ cells developed APL while the resultant $CD34^-$ APL cells exhibited transplantability indicate the possibility that the initiation and maintenance of APL arise at different steps of differentiation, which are not likely to involve the $CD34^+/CD38^-$ fraction, as

originally reported in human AML. Therefore, in order to identify a cellular target for *PML-RARA* that effectively develops APL, *PML-RARA* was transduced into fractionated cells: $CD34^+/CD38^-$, $CD34^+/CD38^+$ and $CD34^-/CD33^+$ cells from the cord blood (**Figures 6A and 6B**). The transduction efficiency, as evaluated by EGFP expression, ranged from 1.9% to 5.0% (median: 3.53%, n = 6) in $CD34^+/CD38^-$ cells, 4.5% to 10.6% (median: 10.07%, n = 6) in $CD34^+/CD38^+$ cells and 19.1% to 22.1% (median: 20.63%, n = 4) in $CD34^-/CD33^+$ cells. Because the $CD34^+$ fraction from human cord blood possessed a higher proportion of $CD34^+/CD38^+$ (74.5% to 94.2%) than that of $CD34^+/CD38^-$ cells, the presumed absolute number of *PML-RARA* transplanted cells was higher in $CD34^+/CD38^+$ cells than in $CD34^+/CD38^-$ cells (3,430 to 31,800 cells vs 140 to 450 cells per mouse; 22,900 to 27,700 $CD34^-/CD33^+$ cells). One hundred unfractionated human $CD34^+$ cells, including both $CD34^+/CD38^-$ and $CD34^+/CD38^+$ cells, were engrafted with multilineage differentiation in our previous study [10], thus suggesting that the transplanted cell numbers were adequate for engraftment in the NOG mice. The induction of *PML-RARA* in $CD34^+/CD38^+$ cells reduced the colony formation capacity and favored the formation of myeloid colonies, as seen in $CD34^+$ cells (**Figures 1B and 1C**). On the other hand, the induction of *PML-RARA* in $CD34^+/CD38^-$ cells generated very few colonies in comparison to the MIGR1 control vector-infected $CD34^+/CD38^-$ cells (**Figures 6C and 6D**). Consistent with the results, the induced APL cells were detected mostly in the mice transplanted with $CD34^+/CD38^+$ cells (median, 16.4% in the whole bone marrow cells) (**Figure 6E**). These findings suggest that $CD34^+/CD38^+$ progenitors proliferate and survive more efficiently than $CD34^+/CD38^-$ cells *in vitro* and trigger APL *in vivo* by inducing *PML-RARA*.

Human common myeloid progenitors develop into APL by inducing *PML-RARA* among $CD34^+/CD38^+$ progenitors

In order to identify the detailed target fraction in $CD34^+/CD38^+$ cells that generates APL with *PML-RARA*, the $CD34^+/CD38^+$ cells were then divided into three fractions based on their expression of CD123 and CD45RA; CMP, GMP and MEP (**Figure 6F**). The retroviral transduction efficiencies of *PML-RARA* into CMP, GMP and MEP were 6.0% to 15.2% (median: 6.6%, n = 9), 3.3% to 8.8% (median: 7.1%, n = 8), and 7.8% to 24.6% (median: 8.5%, n = 7) (**Figure 6G**), and the presumed absolute numbers of *PML-RARA* transduced cells in CMP, GMP and MEP utilized for the transplantation were 5,850 to 15,200, 830 to 4,250, and 1,150 to 2,550 cells per mouse, respectively, which were deduced to directly reflect their proportion in the human cord blood. The frequency of induced APL cells in whole bone marrow cells from transplanted NOG mice was higher when using CMP (median, 25.2%) than GMP and MEP (median, 0.15% and 0.01%, respectively) (**Figure 6H**).

Taken together, these findings obtained using our humanized *in vivo* APL model demonstrate that CMP are a target fraction for *PML-RARA* in the development of APL.

Discussion

Our present study revealed that a humanized APL model was successfully established by transplantation of human $CD34^+$ cord blood transduced with *PML-RARA* into immunodeficient mice. Using this model, we demonstrated that the CMP develop into APL by transducing *PML-RARA* whereas the resultant $CD34^-$ APL cells had the ability to maintain the tumor. Our system improves in the following points: The induced APL cells were detected in all of the mice within 150 days if more than 3,000 human $CD34^+$ cells infected with *PML-RARA* were transplanted into NOG mice. The resultant leukemia well recapitulated the human disease phenotypically, genetically and functionally, including the presence of Auer rods and Faggot cells, and the expression pattern of cellular surface markers and transcripts, as well as ATRA sensitivity and low leukemia transplantability. These findings demonstrated that this humanized *in vivo* model is suitable for prospectively analyzing the process of APL development in humans.

The cellular subset from which the APL originates is still controversial. Several lines of evidence using *in vivo* experiments have suggested that APL arises in the committed myeloid progenitors, whereas several clinical observations using FISH and RT-PCR analyses suggest that APL arises in earlier progenitors [4]. A recent report using conditional knock-in mice showed that the induction of *PML-RARA* led to dominant proliferation in a stem cell compartment with multilineage potential, but did not result in myeloproliferation, as if the stem cell compartment would not support leukemogenesis in this model [34,35]. Our *in vitro* and *in vivo* findings are compatible with the previous findings which showed that the generation of *PML-RARA* transgenic mice was only possible by expressing *PML-RARA* in early myeloid cells using the human cathepsin G (hCG) and MRP8 promoters, not the promoters of β-actin, a housekeeping gene, and CD11b which is expressed at a later stage of myeloid differentiation [36].

The leukemogenic function of PML-RARα may require subtle myeloid differentiation, as seen in CMP in the present study; PML-RARα has been reported to possess the inhibitory or toxic effects on the cellular survival, senescence or apoptosis [18,37,38]. CMP are still immature enough to easily acquire stemness and are already committed to the myeloid lineage, which may allow *PML-RARA* to dysregulate RARα-dependent myelopoiesis, rather than hematopoietic stem cells, in agreement with the fact that *RARA* is implicated in the regulation of myelopoiesis, including both early stage and terminal differentiation. In this scenario, the expression of *PML-RARA* would induce differentiation of CMP to promyelocytes, but inhibit their terminal differentiation at the same time [19,39,40]. Therefore, if the CMP expressing *PML-RARA* acquires stemness, this can result in the development of APL. Our findings showed no engraftment of $CD34^+/CD38^-$ cells with *PML-RARA* transduction *in vivo*, although their leukemogenic activity cannot be denied, as fewer cells were transplanted in comparison to the $CD34^+/CD38^+$ cells. Further analyses are required to evaluate whether $CD34^+/CD38^-$ cells possess the ability to cause APL.

Xenograft models using immunodeficient mice are at present the only method for evaluating the maintenance of human leukemia as LIC. The induced APL generated in the NOG mice had a low engraftment efficiency; however, this biological feature well-reproduced the properties of APL cells found in human patients [3,12]. It is possible that the difficulty associated with engrafting APL cells, both primary samples and induced APL cells obtained from cord blood, into NOG mice may depend on the different preferences of human hematopoietic cells between humans and mice. The reconstitution of the human hematopoietic system in NOG mice is achieved with the dominant engraftment of B-cells, in comparison to the myeloid lineage cells [10]. This technical feature may affect the engraftment of each of the transplanted cellular subsets in our study. The slow progressive myeloid tumor cells, such as those involved in myelodysplastic syndromes and chronic myeloid leukemia in the chronic phase, were shown to be difficult to engraft in NOD/SCID-β2-

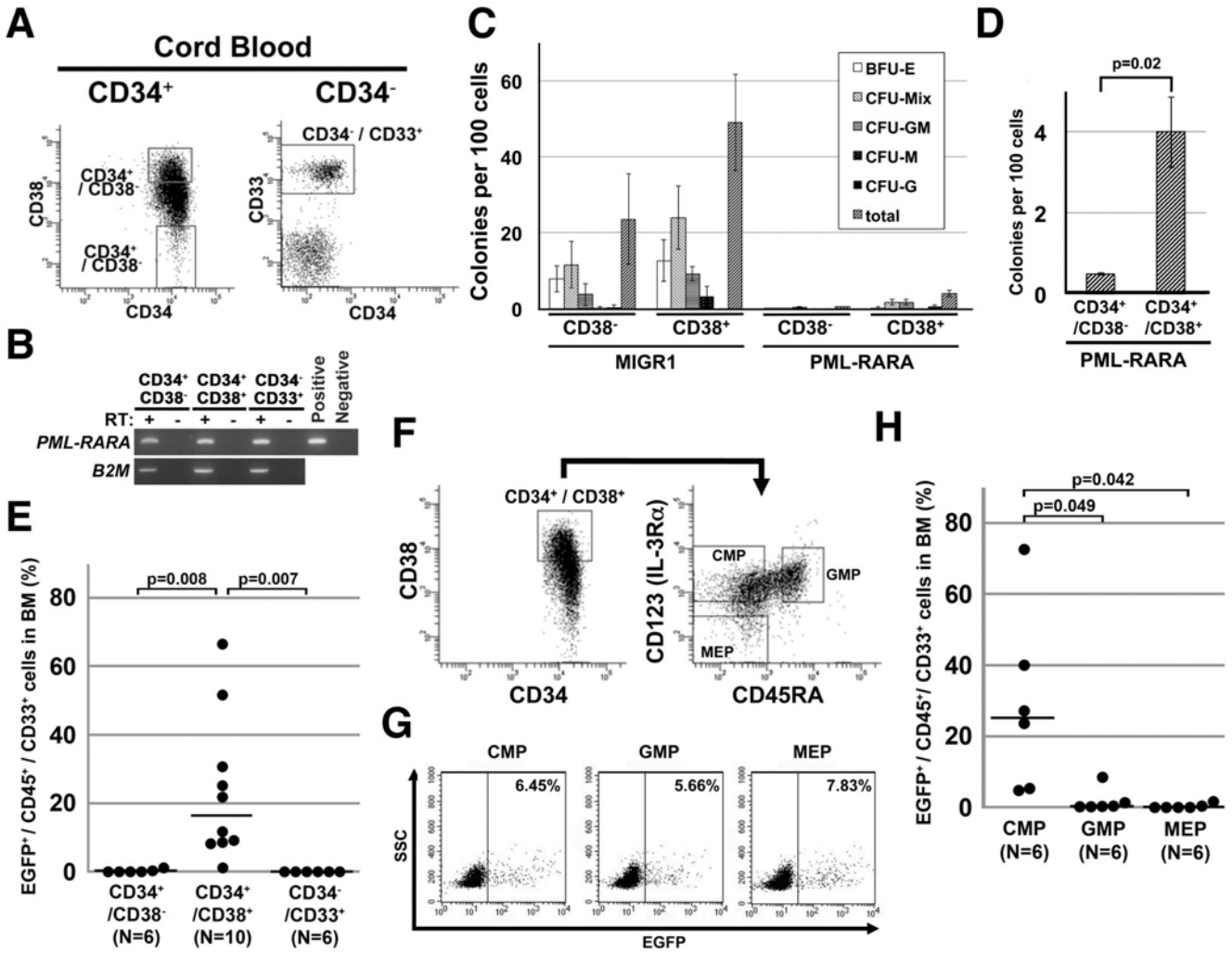

Figure 6. *PML-RARA* targeted human common myeloid progenitors for APL leukemogenesis. (**A**) The sorting strategy for $CD34^+/CD38^-$, $CD34^+/CD38^+$ and $CD34^-/CD33^+$ cells. Human cord blood was first separated into $CD34^+$ and $CD34^-$ cells by magnetic beads, and then sorted into three fractions by a FACS vantage instrument. (**B**) The expression of *PML-RARA* mRNA in each of the fractions after retroviral transfection. *B2M, beta 2 microglobulin*. The *PML-RARA* expression vector was used as a positive control for the *PML-RARA* analysis. (**C**) A colony-forming assay using *PML-RARA*-transduced $CD34^+/CD38^+$ and $CD34^+/CD38^-$ cells. The average of three independent experiments is shown. The data represent the means ± SD. (**D**) The total numbers of colonies of *PML-RARA*-transduced $CD34^+/CD38^+$ and $CD34^+/CD38^-$ cells shown in (C) are highlighted. The data represent the means ± SD (n = 3). (**E**) The development of the induced APL from $CD34^+/CD38^+$ cells in NOG mice. Each sorted fraction from human cord blood, as seen in (A), was retrovirally transduced with *PML-RARA* and transplanted into irradiated NOG mice. The percentages were determined by the frequency of $EGFP^+/CD45^+/CD33^+$ cells at 16 to 20 weeks after transplantation. Each dot represents a single mouse. The horizontal line represents the median value. (**F**) The sorting strategy for common myeloid progenitors (CMP), granulocyte-monocytic progenitors (GMP), and megakaryocyte-erythrocyte progenitors (MEP). Human cord blood was separated into $CD34^+$ cells by magnetic beads, $CD34^+/CD38^+$ cells were sorted out, and were finally divided into CMP, GMP and MEP by the FACS vantage instrument. (**G**) The transduction efficiency of *PML-RARA* in CMP, GMP and MEP. Representative data are shown. (**H**) The development of the induced APL from the human hematopoietic progenitors in NOG mice. Each sorted progenitor fraction from human cord blood, as seen in (F), was retrovirally transduced with *PML-RARA* and transplanted into irradiated NOG mice. The percentages were determined by the frequency of $EGFP^+/CD45^+/CD33^+$ cells at 16 to 20 weeks after transplantation. Each dot represents a single mouse. The horizontal line represents the median value.
doi:10.1371/journal.pone.0111082.g006

microglobulin-deficient or NOG mice (the previous reports [41–43] and our unpublished data), suggesting that the engraftment failure did not always indicate a lack of leukemogenecity of the transplanted cells. Therefore, our study confirmed the leukemogenic activity of the $CD34^-$ induced APL fraction, although it was not strong. These results are consistent with the previous *in vivo* reports which described the some primary $CD34^+/CD38^+$ and $CD34^-$ AML cells could function as LIC *in vivo* [44,45].

In conclusion, we demonstrated that the induction of *PML-RARA* targeted human $CD34^+$ cells, including CMP, and led to their ability to cause APL, and that $CD34^-$ APL cells have the capability of maintaining the disease. These findings suggest that it is not necessary that LIC are always consistent with a cellular fraction where leukemia-inducing events occur. Tumor-specific oncogenes, such as *PML-RARA*, effectively function to form tumors with specific characteristics in specific hierarchal stages of myelopoiesis. This model differs from the conventional hierarchal system of AML, in which LIC possess an immature phenotype as seen in hematopoietic stem cells. Since AML is a group of heterogeneous diseases with various causal genetic abnormalities,

the present findings will be helpful for the analysis of leukemogenesis in other types of AML which display differentiated leukemic blasts.

Supporting Information

Figure S1 The detection of *PML-RARA* expression in $CD34^+$ cells transduced with *PML-RARA* and their descendent colonies by qualitative RT-PCR. RT, reverse transcription.
(TIF)

Figure S2 Fluorescent images of the colonies derived from the $EGFP^+$ and $EGFP^-$ fractions of the $CD34^+$ cells transduced with *PML-RARA*.
(TIF)

Figure S3 The results of a quantitative analysis of the *PML-RARA* expression in the $CD34^+$ cells 48 hours after *PML-RARA* transduction, the differentiated cells from the resultant colonies and the induced APL cells. There were significant differences in the comparison of the expression level of *PML-RARA*. * indicates p values <0.05.
(TIF)

Figure S4 The heat map of the microarray analysis using the 3,439 probes (3,278 genes) that were differentially expressed in the induced APL (n = 3) and the AML other than APL (n = 62). The gene set separated the induced and human primary APL from the cases of AML other than APL. Red triangles (n = 2 from the total of 16 APL cases) show the clinical APL samples whose microarray data were obtained in this study.
(TIF)

Figure S5 The heat map of the microarray analysis performed using the gene set composed of 573 probes (547 genes), which were specifically expressed in the induced APL in comparison to cases of AML other than APL and normal promyelocytes. The gene set clearly clustered the malignant promyelocytes, such as the induced and human primary APL, apart from the normal promyelocytes. Red triangles (n = 2 of a total 16 APL cases) show the clinical APL samples whose microarray data were obtained in this study.
(TIF)

Table S1 The sequences of the PCR primers and probes.
(XLSX)

Table S2 KEGG pathway analysis with the gene sets aberrantly expressed in the induced APL.
(XLSX)

Table S3 The gene set apllied in Figure S5 (573 probes).
(XLSX)

Table S4 The integration sites of PML-RARA in the induced APL cells.
(XLSX)

Acknowledgments

We thank Dr. Warren S. Pear (University of Pennsylvania) for providing the MIGR1 retroviral vector, Dr. Toshio Kitamura (The University of Tokyo) for providing the PLAT-gp packaging cells, Dr. Guilherme Santos (Beth Israel Deaconess Medical Center, Harvard Medical School) for his valuable suggestions and comments, and Tomoko Uno and Tomomi Takanashi (Tokai University School of Medicine) for their expert technical assistance.

Author Contributions

Conceived and designed the experiments: H. Matsushita KA. Performed the experiments: H. Matsushita TY YS YN YM H. Matsuzawa TS AD H. Miyachi. Analyzed the data: H. Matsushita TY MT HH. Contributed reagents/materials/analysis tools: MO MI PPP. Wrote the paper: H. Matsushita TY KA.

References

1. Lowenberg B (2008) Acute myeloid leukemia: the challenge of capturing disease variety. Hematology Am Soc Hematol Educ Program: 1–11.
2. Lapidot T, Sirard C, Vormoor J, Murdoch B, Hoang T, et al. (1994) A cell initiating human acute myeloid leukaemia after transplantation into SCID mice. Nature 367: 645–648.
3. Bonnet D, Dick JE (1997) Human acute myeloid leukemia is organized as a hierarchy that originates from a primitive hematopoietic cell. Nat Med 3: 730–737.
4. Grimwade D, Enver T (2004) Acute promyelocytic leukemia: where does it stem from? Leukemia 18: 375–384.
5. Hope KJ, Jin L, Dick JE (2004) Acute myeloid leukemia originates from a hierarchy of leukemic stem cell classes that differ in self-renewal capacity. Nat Immunol 5: 738–743.
6. Dick JE (2008) Stem cell concepts renew cancer research. Blood 112: 4793–4807.
7. Becker MW, Jordan CT (2011) Leukemia stem cells in 2010: current understanding and future directions. Blood Rev 25: 75–81.
8. de The H, Chen Z (2010) Acute promyelocytic leukaemia: novel insights into the mechanisms of cure. Nat Rev Cancer 10: 775–783.
9. Paietta E (2003) Expression of cell-surface antigens in acute promyelocytic leukaemia. Best Pract Res Clin Haematol 16: 369–385.
10. Ito M, Hiramatsu H, Kobayashi K, Suzue K, Kawahata M, et al. (2002) NOD/SCID/gamma(c)(null) mouse: an excellent recipient mouse model for engraftment of human cells. Blood 100: 3175–3182.
11. Yahata T, Ando K, Nakamura Y, Ueyama Y, Shimamura K, et al. (2002) Functional human T lymphocyte development from cord blood CD34+ cells in nonobese diabetic/Shi-scid, IL-2 receptor gamma null mice. J Immunol 169: 204–209.
12. Patel S, Zhang Y, Cassinat B, Zassadowski F, Ferre N, et al. (2012) Successful xenografts of AML3 samples in immunodeficient NOD/shi-SCID IL2R-gamma(-/-) mice. Leukemia 26: 2432–2435.
13. Guibal FC, Alberich-Jorda M, Hirai H, Ebralidze A, Levantini E, et al. (2009) Identification of a myeloid committed progenitor as the cancer-initiating cell in acute promyelocytic leukemia. Blood 114: 5415–5425.
14. Wojiski S, Guibal FC, Kindler T, Lee BH, Jesneck JL, et al. (2009) PML-RARalpha initiates leukemia by conferring properties of self-renewal to committed promyelocytic progenitors. Leukemia 23: 1462–1471.
15. Brown D, Kogan S, Lagasse E, Weissman I, Alcalay M, et al. (1997) A PMLRARalpha transgene initiates murine acute promyelocytic leukemia. Proc Natl Acad Sci U S A 94: 2551–2556.
16. Grisolano JL, Wesselschmidt RL, Pelicci PG, Ley TJ (1997) Altered myeloid development and acute leukemia in transgenic mice expressing PML-RAR alpha under control of cathepsin G regulatory sequences. Blood 89: 376–387.
17. He LZ, Tribioli C, Rivi R, Peruzzi D, Pelicci PG, et al. (1997) Acute leukemia with promyelocytic features in PML/RARalpha transgenic mice. Proc Natl Acad Sci U S A 94: 5302–5307.
18. Westervelt P, Lane AA, Pollock JL, Oldfather K, Holt MS, et al. (2003) High-penetrance mouse model of acute promyelocytic leukemia with very low levels of PML-RARalpha expression. Blood 102: 1857–1865.
19. Grignani F, Valtieri M, Gabbianelli M, Gelmetti V, Botta R, et al. (2000) PML/RAR alpha fusion protein expression in normal human hematopoietic progenitors dictates myeloid commitment and the promyelocytic phenotype. Blood 96: 1531–1537.
20. Manz MG, Miyamoto T, Akashi K, Weissman IL (2002) Prospective isolation of human clonogenic common myeloid progenitors. Proc Natl Acad Sci U S A 99: 11872–11877.
21. Pear WS, Miller JP, Xu L, Pui JC, Soffer B, et al. (1998) Efficient and rapid induction of a chronic myelogenous leukemia-like myeloproliferative disease in mice receiving P210 bcr/abl-transduced bone marrow. Blood 92: 3780–3792.
22. Matsushita H, Scaglioni PP, Bhaumik M, Rego EM, Cai LF, et al. (2006) In vivo analysis of the role of aberrant histone deacetylase recruitment and RAR alpha blockade in the pathogenesis of acute promyelocytic leukemia. J Exp Med 203: 821–828.
23. Kawada H, Ando K, Tsuji T, Shimakura Y, Nakamura Y, et al. (1999) Rapid ex vivo expansion of human umbilical cord hematopoietic progenitors using a novel culture system. Exp Hematol 27: 904–915.
24. Yahata T, Takanashi T, Muguruma Y, Ibrahim AA, Matsuzawa H, et al. (2011) Accumulation of oxidative DNA damage restricts the self-renewal capacity of human hematopoietic stem cells. Blood 118: 2941–2950.

25. Rego EM, He LZ, Warrell RP Jr, Wang ZG, Pandolfi PP (2000) Retinoic acid (RA) and As2O3 treatment in transgenic models of acute promyelocytic leukemia (APL) unravel the distinct nature of the leukemogenic process induced by the PML-RARalpha and PLZF-RARalpha oncoproteins. Proc Natl Acad Sci U S A 97: 10173–10178.
26. Payton JE, Grieselhuber NR, Chang LW, Murakami M, Geiss GK, et al. (2009) High throughput digital quantification of mRNA abundance in primary human acute myeloid leukemia samples. J Clin Invest 119: 1714–1726.
27. Ando K, Yahata T, Sato T, Miyatake H, Matsuzawa H, et al. (2006) Direct evidence for ex vivo expansion of human hematopoietic stem cells. Blood 107: 3371–3377.
28. Schmidt M, Hoffmann G, Wissler M, Lemke N, Mussig A, et al. (2001) Detection and direct genomic sequencing of multiple rare unknown flanking DNA in highly complex samples. Hum Gene Ther 12: 743–749.
29. Dyck JA, Maul GG, Miller WH Jr, Chen JD, Kakizuka A, et al. (1994) A novel macromolecular structure is a target of the promyelocyte-retinoic acid receptor oncoprotein. Cell 76: 333–343.
30. Weis K, Rambaud S, Lavau C, Jansen J, Carvalho T, et al. (1994) Retinoic acid regulates aberrant nuclear localization of PML-RAR alpha in acute promyelocytic leukemia cells. Cell 76: 345–356.
31. Grignani F, Testa U, Rogaia D, Ferrucci PF, Samoggia P, et al. (1996) Effects on differentiation by the promyelocytic leukemia PML/RARalpha protein depend on the fusion of the PML protein dimerization and RARalpha DNA binding domains. EMBO J 15: 4949–4958.
32. Paietta E, Goloubeva O, Neuberg D, Bennett JM, Gallagher R, et al. (2004) A surrogate marker profile for PML/RAR alpha expressing acute promyelocytic leukemia and the association of immunophenotypic markers with morphologic and molecular subtypes. Cytometry B Clin Cytom 59: 1–9.
33. Welch JS, Ley TJ, Link DC, Miller CA, Larson DE, et al. (2012) The origin and evolution of mutations in acute myeloid leukemia. Cell 150: 264–278.
34. Welch JS, Yuan W, Ley TJ (2011) PML-RARA can increase hematopoietic self-renewal without causing a myeloproliferative disease in mice. J Clin Invest 121: 1636–1645.
35. Wartman LD, Welch JS, Uy GL, Klco JM, Lamprecht T, et al. (2012) Expression and function of PML-RARA in the hematopoietic progenitor cells of Ctsg-PML-RARA mice. PLoS One 7: e46529.
36. Puccetti E, Ruthardt M (2004) Acute promyelocytic leukemia: PML/RARalpha and the leukemic stem cell. Leukemia 18: 1169–1175.
37. Ferrucci PF, Grignani F, Pearson M, Fagioli M, Nicoletti I, et al. (1997) Cell death induction by the acute promyelocytic leukemia-specific PML/RARalpha fusion protein. Proc Natl Acad Sci U S A 94: 10901–10906.
38. Grignani F, Ferrucci PF, Testa U, Talamo G, Fagioli M, et al. (1993) The acute promyelocytic leukemia-specific PML-RAR alpha fusion protein inhibits differentiation and promotes survival of myeloid precursor cells. Cell 74: 423–431.
39. Collins SJ (2002) The role of retinoids and retinoic acid receptors in normal hematopoiesis. Leukemia 16: 1896–1905.
40. Du C, Redner RL, Cooke MP, Lavau C (1999) Overexpression of wild-type retinoic acid receptor alpha (RARalpha) recapitulates retinoic acid-sensitive transformation of primary myeloid progenitors by acute promyelocytic leukemia RARalpha-fusion genes. Blood 94: 793–802.
41. Thanopoulou E, Cashman J, Kakagianne T, Eaves A, Zoumbos N, et al. (2004) Engraftment of NOD/SCID-beta2 microglobulin null mice with multilineage neoplastic cells from patients with myelodysplastic syndrome. Blood 103: 4285–4293.
42. Kerbauy DM, Lesnikov V, Torok-Storb B, Bryant E, Deeg HJ (2004) Engraftment of distinct clonal MDS-derived hematopoietic precursors in NOD/SCID-beta2-microglobulin-deficient mice after intramedullary transplantation of hematopoietic and stromal cells. Blood 104: 2202–2203.
43. Muguruma Y, Matsushita H, Yahata T, Yumino S, Tanaka Y, et al. (2011) Establishment of a xenograft model of human myelodysplastic syndromes. Haematologica 96: 543–551.
44. Taussig DC, Vargaftig J, Miraki-Moud F, Griessinger E, Sharrock K, et al. (2010) Leukemia-initiating cells from some acute myeloid leukemia patients with mutated nucleophosmin reside in the CD34(-) fraction. Blood 115: 1976–1984.
45. Eppert K, Takenaka K, Lechman ER, Waldron L, Nilsson B, et al. (2011) Stem cell gene expression programs influence clinical outcome in human leukemia. Nat Med 17: 1086–1093.

Regular Article

MYELOID NEOPLASIA

RUNX1/AML1 mutant collaborates with BMI1 overexpression in the development of human and murine myelodysplastic syndromes

Yuka Harada,[1] Daichi Inoue,[2] Ye Ding,[3] Jun Imagawa,[3] Noriko Doki,[2] Hirotaka Matsui,[4] Takashi Yahata,[5] Hiromichi Matsushita,[5] Kiyoshi Ando,[5] Goro Sashida,[6] Atsushi Iwama,[6] Toshio Kitamura,[2] and Hironori Harada[3]

[1]Division of Radiation Information Registry, Research Institute for Radiation Biology and Medicine, Hiroshima University, Hiroshima, Japan; [2]Division of Cellular Therapy, Advanced Clinical Research Center, Institute of Medical Science, University of Tokyo, Tokyo, Japan; [3]Department of Hematology and Oncology and [4]Department of Molecular Oncology, Research Institute for Radiation Biology and Medicine, Hiroshima University, Hiroshima, Japan; [5]Division of Hematopoiesis, Research Center for Regenerative Medicine, Tokai University School of Medicine, Isehara, Japan; and [6]Department of Cellular and Molecular Medicine, Graduate School of Medicine, Chiba University, Chiba, Japan

Key Points

- BMI1 overexpression is one of the second hit partner genes of RUNX1 mutations that contribute to the development of MDSs.

RUNX1/AML1 **mutations have been identified in myelodysplastic syndromes (MDSs). In a mouse bone marrow transplantation model, a RUNX1 mutant, D171N, was shown to collaborate with Evi1 in the development of MDSs; however, this is rare in humans. Using enforced expression in human CD34$^+$ cells, we showed that the D171N mutant, the most frequent target of mutation in the *RUNX1* gene, had an increased self-renewal capacity, blocked differentiation, dysplasia in all 3 lineages, and tendency for immaturity, but no proliferation ability. *BMI1* overexpression was observed in CD34$^+$ cells from the majority of MDS patients with RUNX1 mutations, but not in D171N-transduced human CD34$^+$ cells. Cotransduction of D171N and BMI1 demonstrated that BMI1 overexpression conferred proliferation ability to D171N-transduced cells in both human CD34$^+$ cells and a mouse bone marrow transplantation model. Stepwise transduction of D171N followed by BMI1 in human CD34$^+$ cells resulted in long-term proliferation with a retained CD34$^+$ cell fraction, which is quite similar to the phenotype in patients with higher-risk MDSs. Our results indicate that *BMI1* overexpression is one of the second hit partner genes of *RUNX1* mutations that contribute to the development of MDSs. (*Blood*. 2013;121(17):3434-3446)**

Introduction

The *RUNX1/AML1* gene has been investigated in the pathogenesis of hematopoietic diseases, and point mutations of *RUNX1* have been frequently detected in patients with various types of myeloid neoplasms. A heterozygous germ line mutation of the *RUNX1* gene is known to cause familial platelet disorder with a predisposition to acute myeloid leukemia (FPD/AML),[1,2] which is regarded as familial myelodysplastic syndromes (MDSs).[3] *RUNX1* mutations have been detected with high frequency in MDSs, MDSs following AML,[4] minimally differentiated AML M0 subtypes,[2,5-7] de novo AML without recurrent or complex karyotype,[8,9] and myelodysplastic/myeloproliferative neoplasms.[10,11] Furthermore, *RUNX1* mutations are detected with high frequency in therapy-related or radiation-associated MDSs and AML,[4,12-15] and leukemic transformation from myeloproliferative neoplasms.[16-19]

It is intriguing how RUNX1 mutations contribute to the development of divergent hematologic neoplasms. Functionally, most of the RUNX1 mutants equally show a loss of normal RUNX1 *trans*-activation potential.[4,12,20,21] The amino acid residues in the runt homology domain (RHD) of the RUNX1 protein that directly interact with DNA have been found to be frequent targets of amino acid replacement.[20,21] Mutations on other amino acids close to these DNA-contact residues are also suspected to inhibit DNA binding by an obstructive side-chain or a structural change. Therefore, amino-replacement and in-frame insertion/deletion types of mutations confer loss of DNA-binding ability and *trans*-activation potential. *RUNX1* mutations have been shown to play a pivotal role in the pathogenesis of MDS/AML in mouse bone marrow transplantation (BMT) systems.[22] Mice transduced with the D171N mutant, which harbors a mutation in the RHD of the *RUNX1* gene, exhibited hyperproliferative AML with multilineage dysplasia in collaboration with *Evi1* overexpression. This impressive result indicates that *RUNX1* mutations may be a cause of MDSs with a leukemogenic potential. However, mouse phenotypes do not always correspond to the clinical features of patients with the mutations. This may be partly due to differential gene circumstances, such as retrovirus integration sites or collaborating gene alterations, between mouse and human.[23,24] As opposed to *EVI1*, overexpression of the polycomb group gene *BMI1* is more common in MDS patients and is associated with MDS progression.[25,26] Biological analysis using human hematopoietic cells is considered to be necessary to clarify the molecular mechanisms of the *RUNX1* mutations in the pathogenesis of MDSs. Enforced gene expression in human CD34$^+$ cells has been used to investigate the role of leukemogenic oncogenes in leukemogenesis.[27-35]

Submitted June 3, 2012; accepted February 16, 2013. Prepublished online as *Blood* First Edition paper, March 7, 2013; DOI 10.1182/blood-2012-06-434423.

Y.H., D.I., and Y.D. contributed equally to this study.

The online version of this article contains a data supplement.

The publication costs of this article were defrayed in part by page charge payment. Therefore, and solely to indicate this fact, this article is hereby marked "advertisement" in accordance with 18 USC section 1734.

In this study, using enforced gene expression in human CD34$^+$ cells, we demonstrated that the D171N mutant, the most frequent target of mutation in *RUNX1* gene, has an increased self-renewal capacity, blocked differentiation, dysplasia in all 3 lineages, and tendency for immaturity, but no proliferation ability. Moreover, we revealed that *BMI1* overexpression collaborates with *RUNX1* mutations and confers proliferation ability to D171N-mutated cells, which was confirmed in both human and mouse hematopoietic stem/progenitor cells. Our results indicate that *BMI1* overexpression is one of the second hit partner genes of *RUNX1* mutations in the development of MDSs.

Materials and methods

Patients

Patients with MDSs were divided into 2 groups using the International Prognostic Scoring System: lower-risk MDSs include low- or intermediate-1-risk MDSs, and higher-risk MDSs include intermediate-2- or high-risk MDSs. Mutation analysis of *RUNX1* was performed as described previously.[4] The study was approved by the institutional review board at Hiroshima University. Patients gave written informed consent for the study, according to the Declaration of Helsinki.

Quantitative reverse-transcription polymerase chain reaction (qRT-PCR)

CD34$^+$ cells were purified from patients using the CD34 MicroBead Kit and autoMACS system (Milteny Biotec, Bergisch Gladbach, Germany). Total RNA was harvested from the CD34$^+$ cells using the RNeasy Micro Kit (Qiagen, Hilden, Germany). The expression levels of *EVI1*, *BMI1*, *INK4A*, *ARF*, and *GAPDH* were quantified by the Applied Biosystems 7500 Real-Time PCR system using TaqMan Gene Expression Assays (Hs00602795_m1 for *EVI1*, Hs00180411_m1 for *BMI1*, Hs00923894_m1 for *INK4A*, Hs99999189_m1 for *ARF*, and Hs99999905_m1 for *GAPDH*) and TaqMan Universal PCR Master Mix (Applied Biosystems). qRT-PCR in mouse cells was performed as described previously[22] with the following forward/reverse primer pairs: p16 (aatctccgcgaggaaagc/gtctgcagcggactccat), p19 (gggttttcttg gtgaagttcg/ttgcccatcatcatcacct), Evi1 (atcggaagatcttagatgagttttg/cttcctacatctggt tgactgg), and Gapdh (gcattgtggaagggctcatg/ttgctgttgaagtcgcaggag).

Retroviral vectors and infection

RUNX1 (wild-type [WT] and D171N mutant) cDNA with FLAG tag was subcloned into the pMXs-internal ribosomal entry site (IRES)-enhanced green fluorescent protein (EGFP) (pMXs.IG). *BMI1* was subcloned into the pMXs-IRES-DsRed-Express (pMXs.IR), in which the IRES-DsRed-Express fragment from the pIRES2-DsRed-Express (Clontech, Mountain View, CA) was inserted into the pMXs. FLAG-tagged D171N was also subcloned into pMYs-IRES-puro (pMYs.IP) and pMYs-IRES-EGFP (pMYs.IG), and *BMI1* into pMYs-IRES-blasticidin (pMYs.IB) and pMYs-IRES-nerve growth factor receptor (NGFR) (pMYs.IN). Plat-GP and Plat-E packaging cells were transfected with retroviral constructs using FuGENE6 (Roche, Mannheim, Germany) as described previously.[16,22]

Retrovirus transduction of human CD34$^+$ primary cells

Cord blood cells (CBs) were collected with written informed consent. CD34$^+$ cells were purified from CBs by the CD34 MicroBead Kit using autoMACS. They were precultured for 3 to 4 days in Stemline II Hematopoietic Stem Cell Expansion medium (Sigma-Aldrich, St Louis, MO) supplemented with 100 ng/mL each of Fms-related tyrosine kinase (FLT-3) ligand, stem cell factor (SCF), and thrombopoietin (TPO) (PeproTech, London, UK) (expansion medium). The cells were resuspended in new expansion medium and placed in plates coated with RetroNectin (Takara, Otsu, Japan) preloaded with virus. At 3 to 4 days after transduction, green fluorescent protein (GFP$^+$) and/or DsRed$^+$ cells were sorted by FACS Aria (Becton Dickinson [BD], Franklin Lakes, NJ).

Cells were cultured continuously in Iscove modified Dulbecco medium containing 20% fetal bovine serum and 100 ng/mL each of FLT-3 ligand, SCF, and TPO. For long-term growth, Iscove modified Dulbecco medium was supplemented with 20% fetal bovine serum; 100 ng/mL each of FLT-3 ligand, SCF, and TPO; and 20 ng/mL each of interleukin (IL) 6 and IL-3 (Peprotech).

Colony-forming cell (CFC) replating assay

Ten thousand sorted cells were resuspended in MethoCult H4034$^+$ medium (StemCell Technologies, Vancouver, BC, Canada) containing SCF, granulocyte colony-stimulating factor (G-CSF), granulocyte macrophage (GM)–CSF, IL-3, and erythropoietin. After 14 days in culture, colonies were counted. Cells were then suspended in methylcellulose medium, and 10^4 cells were plated again for CFC replating assay. The remaining cells were used for cell number counting and cytospin centrifuge for morphologic and flow cytometry analyses.

Long-term culture-initiating cell (LTC-IC) assay

For bulk culture assay, 10 000 sorted cells were suspended in Myelocult H5100 medium (StemCell Technologies) with 1 μM hydrocortisone (StemCell Technologies). The cells were divided into 2 dishes precoated with MS5 stromal cells and cultured for 5 weeks. LTC-IC cultures were harvested, and clonogenic progenitors were assayed in Methocult GF$^+$ H4435 medium (StemCell Technologies) containing SCF, GM-CSF, IL-3, IL-6, G-CSF, and erythropoietin. After 20 days, LTC-IC–derived CFCs were counted. For limiting dilution assay, 100 to 800 sorted cells per well were plated on MS5 stromal cells in 96-well plates and cultured. Wells were scored as growth or no growth of colonies. LTC-IC frequency was calculated with L-Calc software (StemCell Technologies).

Retroviral transduction of 32Dcl3 cells and differentiation assay

The murine myeloid progenitor 32Dcl3 cells were infected with retrovirus as previously described.[36]

Mouse BMT

Mouse BMT was performed as described previously.[22] Bone marrow (BM) mononuclear cells were isolated from C57BL/6 (Ly-5.1) donor mice, and after stimulation with SCF, FLT-3 ligand, IL-6, and TPO (R&D Systems), the cells were transduced with retrovirus constructs. Then, 3×10^5 to 5×10^5 of the nonsorted cells were injected into sublethally γ-irradiated Ly-5.2 recipient mice. These studies were approved by the Animal Care Committee of the Institute of Medical Science at the University of Tokyo.

Flow cytometry

Human cells were stained with the indicated phycoerythrin (PE) or allophycocyanin–conjugated antibodies (BD). For the cell cycle analysis, the cells were stained with allophycocyanin BrdU Flow Kit (BD) or Hoechst 33342 (BD). Flow cytometry analysis was performed on a FACSCalibur (BD) or FACS Aria, and data were analyzed using CELLQuest. Mouse cells were stained with the indicated PE-conjugated antibodies (eBioscience) and analyzed using FACSCalibur equipped with FlowJo Version 7.2.4 software (TreeStar). Annexin V staining was carried out with the PE Annexin V Apoptosis Detection Kit I (BD).

Immunoblot analysis

Immunoblot analysis was performed as reported previously.[12] The primary antibodies used in this study were anti–FLAG M2 (Sigma-Aldrich), anti-Bmi1 (Upstate, Lake Placid, NY; or #05-637, Millipore), anti–β-actin (Santa Cruz), and anti–α-tubulin (Sigma-Aldrich) monoclonal antibodies.

Statistical analysis

For comparison of 2 independent samples, normally distributed variables were compared by the Student *t* test, and nonnormally distributed variables by the Mann-Whitney *U* test. For multiple pairwise comparisons, the data were analyzed by 1-way analysis of variance followed by Dunnett's multiple comparison test, or differences between individual groups were estimated using the Steel-Dwass test. Survival curves were estimated by the Kaplan-

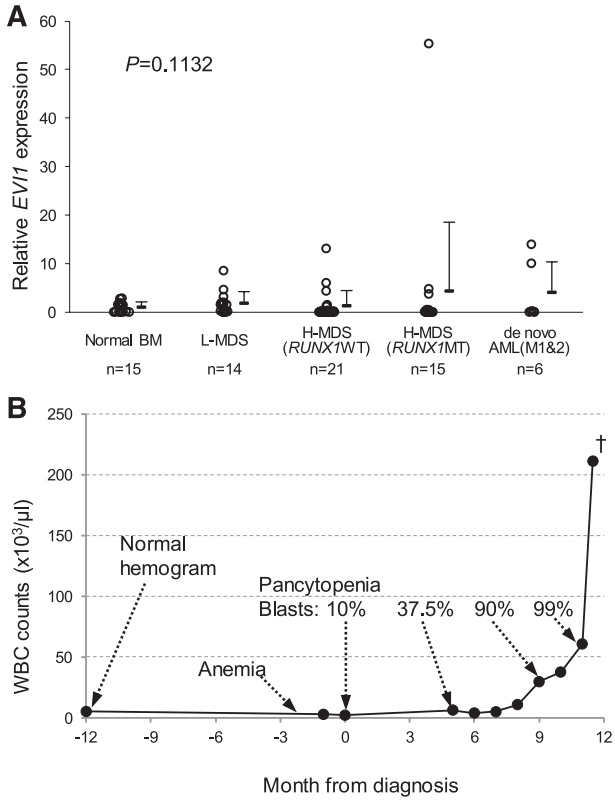

Figure 1. *EVI1* overexpression collaborates with *RUNX1* mutations in human MDSs. (A) *EVI1* expression levels by qRT-PCR in $CD34^+$ cells of clinical samples. Relative *EVI1* expression was calculated as the ratio of *EVI1* to *GAPDH* expression. RNA from normal BM $CD34^+$ cells served as a control, and the RNA level was defined as 1. Data are expressed as mean ± standard deviation (SD). L-MDS, lower-risk MDS; H-MDS, higher-risk MDS; MT, mutation. (B) White blood cell (WBC) count and clinical course of a patient with high *EVI1* expression. A 78-year-old male showed pancytopenia and blast cells in peripheral blood. BM examination showed hypocellular marrow with multilineage dysplasia and 16.5% of blast cells. Cytogenetic analysis showed 45,XY,add(3)(q13.2),-7. He was diagnosed with refractory anemia with excess blasts (RAEB-2) and received chemotherapy. However, his condition progressed to BM failure after chemotherapy and repeated severe infection. The blast population continued to increase gradually. Eight months after diagnosis, his WBC count started to increase, and he died with uncontrollable blast expansion 11.5 months after diagnosis.

Meier analysis and compared using the log-rank test. $P < .05$ was considered statistically significant.

Results

RUNX1 D171 amino acid is the most frequent target of mutations

We analyzed *RUNX1* mutations in various myeloid neoplasms, mostly MDSs and MDS-related AML including therapy-related cases. We found that 107 patients had *RUNX1* mutations, which were shown to be distributed throughout the full length of the RUNX1 protein (supplemental Table 1; see the *Blood* Web site). Replacement of the D171 amino acid (D171N and D171G) was the most frequent target of mutation in the *RUNX1* gene, which was detected in 8 (7.5%) patients. The D171 residue resides in the RHD and is one of the critical amino acid residues that directly contact DNA; however, small changes in the RHD do not influence the ability to bind core binding factor β.[20,21] Moreover, the carboxyl-terminal (C-terminal) region including the transactivation/repression domains is preserved in the mutations (supplemental Figure 1A), contrary to that in truncation-type mutations. Replacement or small in-frame insertions/deletions at or around critical amino acid residues involved in DNA binding were also detected, and 41.6% of the *RUNX1* mutations (45 of 107) had impaired DNA-binding but intact C-terminal transactivation/repression domains. The D171N mutant was localized to the nucleus (supplemental Figure 1B) and showed a loss of normal RUNX1 *trans*-activation potential for the macrophage-CSF receptor (supplemental Figure 1C). Furthermore, the mutant displayed a dominant-negative type of *trans*-activation suppression (supplemental Figure 1D), suggesting that the mutant may have some oncogenic potential in addition to the loss of normal RUNX1 function.

EVI1 overexpression collaborates with RUNX1 mutation in human MDSs

Because collaboration between *RUNX1* mutations and *Evi1* overexpression has been shown in a mouse BMT model,[22] we first checked *EVI1* expression levels in selected $CD34^+$ cells from MDS patients. Most of the examined patients showed very low *EVI1* expression (Figure 1A). However, 1 patient whose initial diagnosis was MDS with D171G mutation displayed an extremely high expression level of *EVI1*. The clinical course of the patient was unique in that a steep increase in blast cells was followed by a relatively short MDS period (Figure 1B), which was similar to that in the mouse BMT model.[22] Thus, expression of *EVI1* is generally not high in MDS patients. Then, we set out to elucidate the collaborating genes with *RUNX1* mutations in other patients.

Overexpression of D171N promotes inhibition of differentiation and increase in self-renewal capacity in human $CD34^+$ cells

To clarify the biological functions of the RUNX1 mutants and to identify their collaborating genes in hematopoietic stem/progenitor cells, we transduced a RUNX1 mutant into human $CD34^+$ cells to avoid the effect of *Evi1* overexpression. The D171N mutant, which was produced by a 1-bp replacement in exon 5, was transduced into $CD34^+$ cells from human CBs (Figure 2A). The efficiency of transduction was ~30% to 60% (Figure 2B), and RUNX1 expression was confirmed by Western blotting (Figure 2C).

To examine the effect of RUNX1 expression on cell differentiation, we performed CFC assay by plating sorted cells in methylcellulose medium. The number of burst-forming unit–erythroid (BFU-E) colonies was significantly decreased in both WT- and D171N-transduced cells, whereas the number of colony-forming unit GM (CFU-GM) colonies was not significantly different (Figure 2D). On the other hand, the individual BFU-E colonies in the WT plates and individual CFU-GM colonies in the D171N plates were larger in size (Figure 2E), in addition to the presence of significantly more growing cells as compared with the control (Figure 2F). Glycophorin A (GPA^+) erythroid cells were dominant in the WT group, whereas most of the D171N-transduced cells expressed myeloid lineage markers (Figure 2G). To determine whether D171N has a self-renewal advantage, we performed replating CFC assay. The plates of the D171N mutant contained approximately half the total number of colonies as the pMXs.IG plates in the first assay, whereas total cell numbers were comparable between the D171N and pMXs.IG plates (Figure 2H). Unlike pMXs.IG and WT, D171N showed replating capacity for 3 replatings. To confirm the presence of progenitors with long-term self-renewal capabilities, LTC-IC assay was conducted. Cells transduced with D171N showed a drastic increase in the number of colonies (Figure 2I).

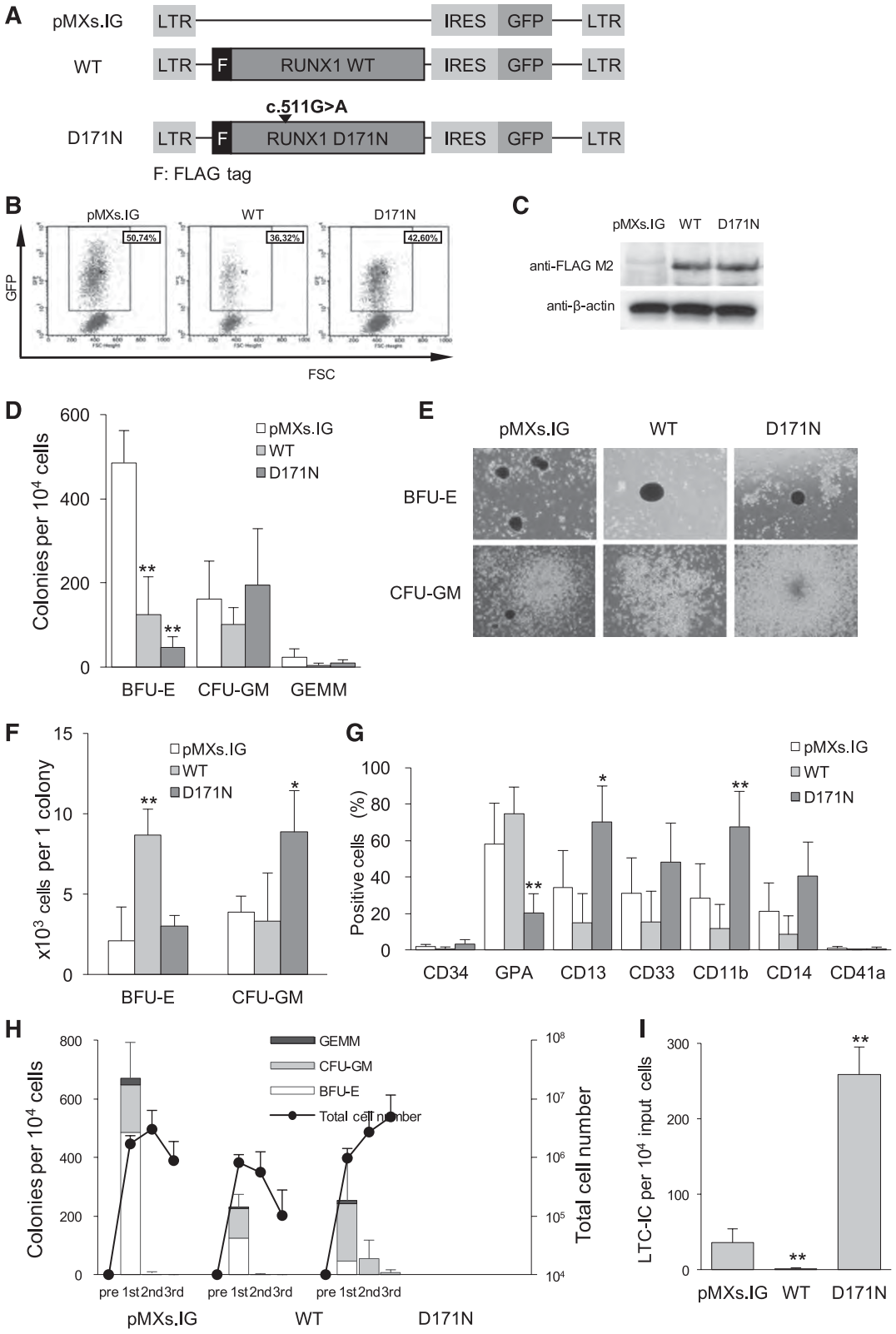

Figure 2. Overexpression of D171N promotes inhibition of differentiation and increase in self-renewal capacity. (A) Pictogram of pMXs.IG retroviral constructs of the FLAG-tagged RUNX1 WT and the D171N mutant (D171N). The difference in cDNA sequence of the mutant from the WT is indicated by an arrowhead. LTR, long terminal repeat. (B) Human CD34$^+$ CB cells were transduced with the indicated vector. A typical flow cytometry profile of cells retrovirally transduced with pMXs.IG, WT, or D171N shows the transduction efficiency. The GFP$^+$ cells shown within the gate were collected. (C) Anti-FLAG immunoblotting of sorted GFP$^+$ cells confirmed the expression of FLAG-tagged RUNX1 proteins. Anti–β-actin antibody was used as control. (D-H) Ten thousand cells were plated in methylcellulose culture dishes. GEMM, colony-forming unit–granulocyte, erythroid, macrophage, megalocyte. Data are expressed as mean ± SD of 6 independent experiments and compared with control (pMXs.IG). *$P < .05$; **$P < .01$. (D) Colony numbers were counted after 14 days. (E) Photomicrographs (×40) of representative colonies found in the plates with an IX71 microscope and a DP12 camera (Olympus). (F) The cell number per colony was calculated by total GPA$^+$ cells/total BFU-E colonies and total CD13$^+$ cells/total CFU-GM colonies. (G) GFP$^+$ cells were analyzed by flow cytometry for the indicated surface markers. (H) Colony number and cell proliferation fold in CFC replating assay. (I) LTC-IC assay in bulk was carried out in duplicate, and the average number of LTC-IC per 10 000 original input cells and SD of 4 independent experiments are indicated. **$P < .01$.

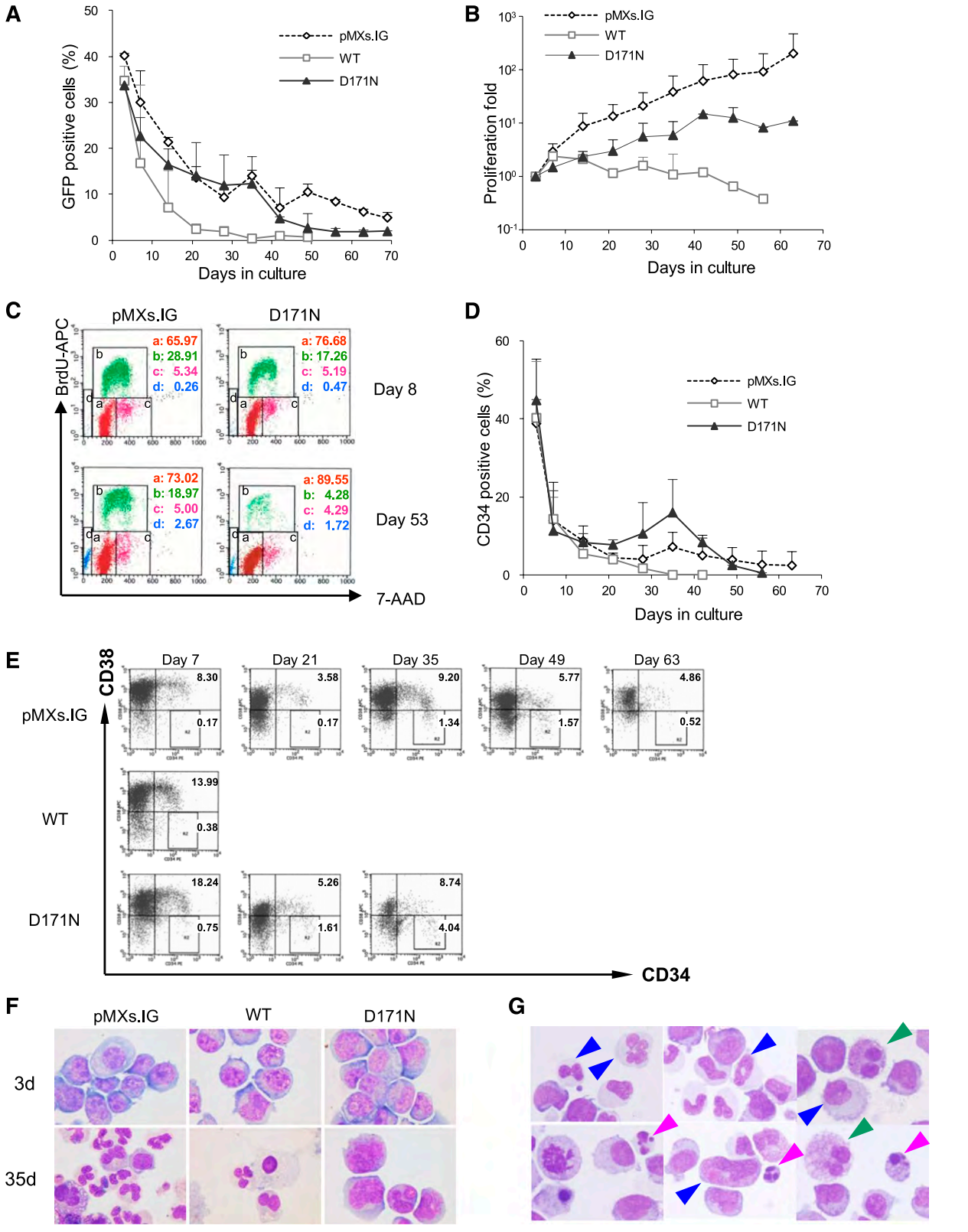

Figure 3. D171N-transduced cells lack long-term proliferation ability. Human CD34$^+$ CB cells were transduced with the indicated vectors and cultured in complete cytokine medium (without IL-3 and IL-6). To examine proliferation ability of each transduced cell type, the cells were sorted for GFP expression and cultured in complete cytokine medium. Four independent experiments were performed, and the error bars represent the SD. (A) Proliferation curve of GFP$^+$ RUNX1-transduced or control (empty vector-transduced) cells, nonsorted. (B) Growth patterns of the GFP-sorted transduced cells displayed as proliferation fold originating from 10° just after sorting. (C) Representative quantitative cell cycle analysis allowed the discrimination of cell subsets that were undergoing G0/G1 (a), S (b), or G2 + M (c) phases of the cell cycle, or apoptosis (d). (D) Percentage of CD34$^+$ cells was determined by flow cytometry. (E) Representative CD34/CD38 expression pattern in long-term culture. (F) Images of Wright-Giemsa–stained cytospins on days 3 and 35 obtained with a BX51 microscope and a DP12 camera (Olympus); original magnification ×1000. (G) Morphologic abnormalities observed in Wright-Giemsa–stained cytospins of the D171N cells on day 35 in culture, myeloid, erythroid, and megakaryocytic cells with dysplasia are indicated by blue, pink, and green arrows, respectively, as captured with a BX51 microscope and a DP12 camera (Olympus); original magnification ×1000.

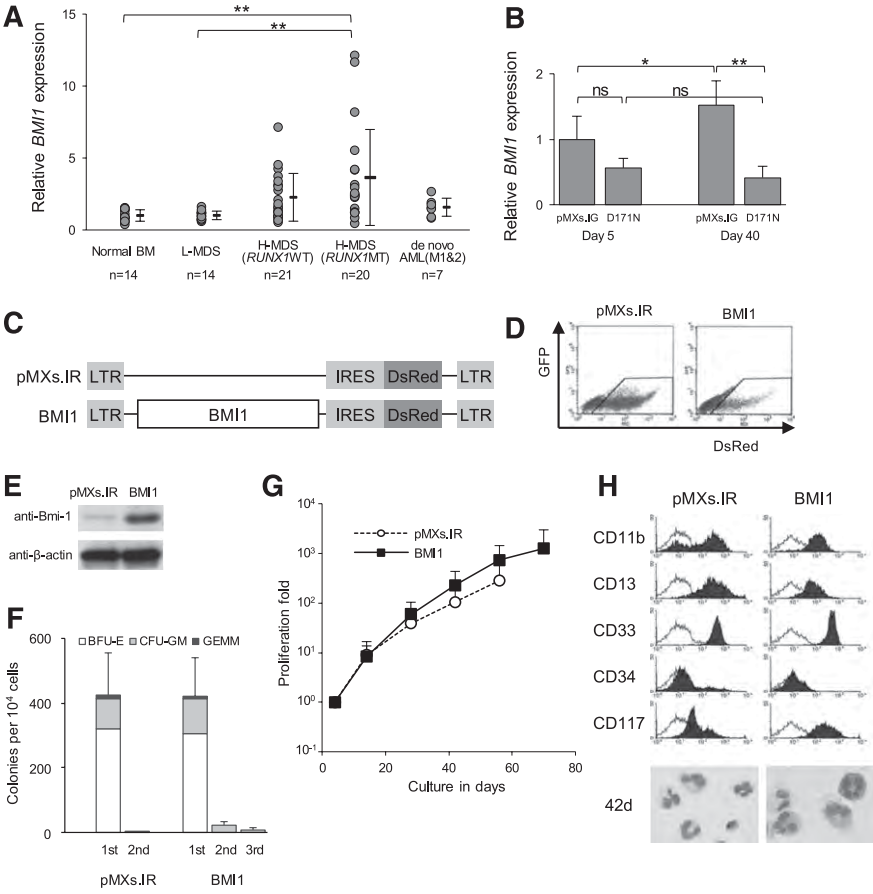

Figure 4. BMI1 expression pattern in human CD34$^+$ cells and enforced BMI1 expression in human CD34$^+$ cells. (A) BMI1 expression levels in CD34$^+$ cells of clinical samples. Relative BMI1 expression was measured by triplicated qRT-PCR and calculated as the ratio of BMI1 to GAPDH expression. Data are also expressed as mean ± SD of each patient group. $^{**}P < .01$. (B) BMI1 expression in transduced CD34$^+$ cells was confirmed by qRT-PCR. CD34$^+$ cells were repurified from GFP$^+$ sorted cells after 5 and 40 days of culture in complete cytokine medium. Bar chart represents the mean ± SD of 3 independent experiments. RNA from pMXs.IG-transduced cells on day 5 served as a control, and the RNA level was defined as 1. $^{*}P < .05$; $^{**}P < .01$. (C) pMXs.IRES-DsRed-Express (pMXs.IR) retroviral construct for the expression of BMI1. (D) Representative flow cytometry profile of cells retrovirally transduced with pMXs.IR or BMI1 shows the transduction efficiency. The DsRed$^+$ cells shown within the gate were collected. (E) Expression of BMI1 was confirmed by Western blotting using anti-Bmi1 antibody. Anti–β-actin antibody was used as the control. (F) Human CD34$^+$ cells transduced with the indicated vector and sorted for DsRed expression were analyzed by CFC replating assay. Ten thousand cells were plated in methylcellulose culture dishes. Data are expressed as mean ± SD of 3 independent experiments. (G) Growth pattern of the transduced cells cultured in complete cytokine medium displayed as proliferation fold originating from 10^0 just after sorting. The error bars represent the SD from 4 independent experiments. (H) The expression pattern of surface markers as shown by a typical flow cytometry profile, and Wright-Giemsa–stained cytospins of the DsRed$^+$ cells on day 42 culture in complete cytokine medium as captured with a BX51 microscope and a DP12 camera (Olympus); original magnification ×1000.

D171N-transduced cells lack long-term proliferation ability in human CD34$^+$ cells

To determine proliferative and survival advantages of RUNX1-mutated cells, transduced nonsorted human CD34$^+$ cells were cultured in liquid medium (Figure 3A). The percentage of GFP-expressing cells in the WT, D171N, and pMXs.IG-transduced control cultures gradually decreased over time in culture. For further evaluation of the proliferation ability of the transduced cells, we sorted GFP$^+$ cells and performed long-term culture. The WT-transduced cells hardly proliferated, whereas the D171N-transduced cells proliferated slightly, exhibiting lower proliferation ability than pMXs.IG cells (Figure 3B). These results indicate that the D171N cells have no proliferation ability. To determine whether these differences were due to increased apoptosis or cell cycle inhibition, we confirmed by cell cycle analysis. On day 53 when the D171N cells stopped proliferating, most of the cells accumulated in the G1 phase (Figure 3C). The percentage of CD34$^+$ cells among the D171N cell population increased slightly but gradually decreased with a maximum at approximately day 35 (Figure 3D). At this point, although the percentage of CD34$^+$/CD38$^+$ cells within the D171N cell population did not increase in comparison with the pMXs.IG group, the percentage of CD34$^+$/CD38$^-$ cells increased to a maximum at ~4% (Figure 3E). On day 35, a vast majority of the pMXs.IG cells and all the WT cells terminally differentiated into mature myeloid cells and monocytes, whereas the D171N cells contained a large number of immature cells (Figure 3F). The cells transduced with the D171N mutant displayed morphologic abnormalities in all 3 hematopoietic lineages (Figure 3G). These findings indicate that RUNX1 mutations probably give rise to the multilineage dysplasia of hematopoietic cells with increase in the number of blasts, which is the main characteristic of MDSs. However, the D171N-transduced cells did not expand in liquid media. Furthermore, the D171N mutant abrogated engraftment potential of human stem/progenitor cells in NOD/Shi-scid, IL2Rγc^{null} (NOG) mice[37] (supplemental Table 2). Thus, it is suspected that the mutant requires additional gene alterations for the development of MDSs.

BMI1 is overexpressed in CD34$^+$ cells from MDS patients with RUNX1 mutations, whereas it is repressed in D171N-transduced human CD34$^+$ cells

We focused on *BMI1* as a candidate of the additional partner gene alterations because this gene is known to be overexpressed in some MDS patients. *BMI1* expression levels were analyzed in selected CD34$^+$ cells from MDS patients (Figure 4A). Patients with *RUNX1* mutations displayed a significantly higher expression level of *BMI1* compared with normal control and lower-risk MDS patients, and 14 of 20 (70%) of the RUNX1-mutated patients showed *BMI1* overexpression that exceeded the range of normal control, as opposed to only 1 with *EVI1* overexpression. Next, we examined *BMI1* expression levels in the D171N-transduced CD34$^+$ cells over a time course. Unexpectedly, the cells with D171N mutation showed a lower expression level of *BMI1*, especially during a long culture period (Figure 4B). These results indicate that the high *BMI1* expression in patients with RUNX1 mutations is not induced by direct effects of the mutations, but rather, the RUNX1-mutated cells may require the acquisition of *BMI1* overexpression for the development of MDSs. To confirm the effects of additional *BMI1* overexpression on D171N-transduced cells, we antecedently analyzed BMI1-transduced CD34$^+$ cells.

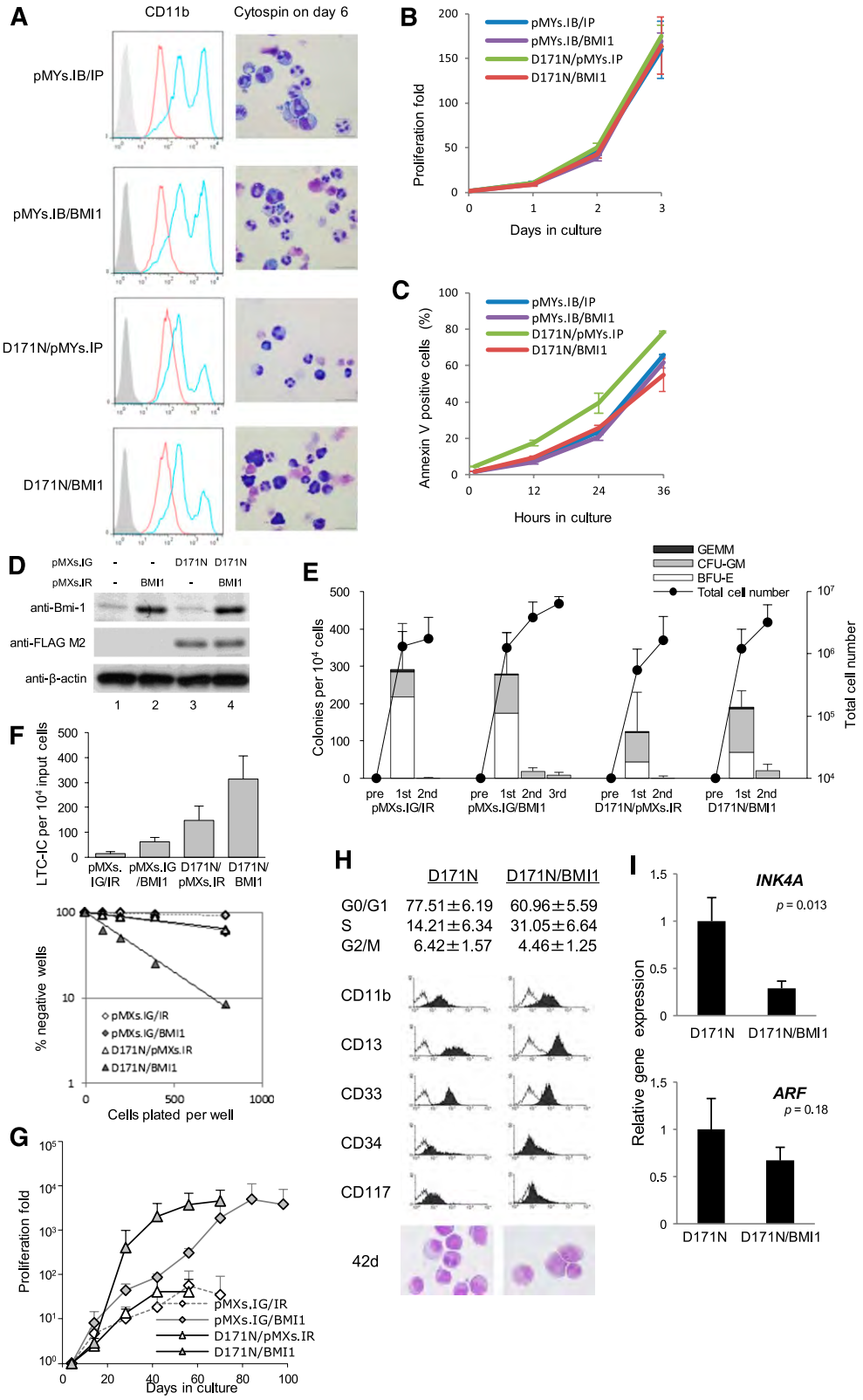

Figure 5. The effect of double expression of D171N and BMI1. (A-C) IL-3–dependent 32Dcl3 cells were stably transduced with pMYs.IP/IB, pMYs.IP/BMI1, D171N/pMYs.IB, or D171N/BMI1. Before the assay for proliferation and apoptosis, the transduced 32Dcl3 cells were subjected to drug selection with 1 μg/mL puromycin and 10 μg/mL blasticidin. (A) G-CSF–induced differentiation assay in indicated 32Dcl3 transfectants. Surface expression of CD11b after incubation for 6 days in the presence of 1 ng/mL IL-3 (red histograms) or 50 ng/mL G-CSF (blue histograms) was analyzed by flow cytometry. The result of control staining is shown as a filled histogram. Data are representative of 2 independent experiments. The cells cultured with G-CSF for 6 days were assessed by Giemsa staining. Images were obtained with a BX51 microscope and a DP12 camera (Olympus); objective lens, UplanFl (Olympus); original magnification ×1000. (B) Growth curve of the transduced 32Dcl3 cells cultured in the presence of 1 ng/mL of IL-3. Data are expressed as mean ± SD of 3 independent experiments. (C) Annexin V positivity in the transduced 32Dcl3 cells cultured without IL-3. Data are expressed as mean ± SD of 3 independent experiments. (D-G) Human $CD34^+$ cells were precultured for 3 to 4 days in expansion medium and transduced with both GFP-tagged D171N and

Enforced BMI1 expression shows no leukemogenic ability in human CD34$^+$ cells

To evaluate the biological significance of BMI1 overexpression in stem/progenitor cells, BMI1 was cloned into a retrovirus vector (Figure 4C) and transduced into CD34$^+$ cells (Figure 4D). BMI1 was endogenously expressed in cells transduced with pMXs.IR, whereas a strong upregulation of this protein was observed in the BMI1-transduced cells (Figure 4E). The number of colonies of the BMI1-transduced CD34$^+$ cells was almost equal to that of the pMXs.IR-transduced cells, whereas the replating efficiency of the BMI1 cells was slightly increased (Figure 4F). The BMI1-transduced cells exhibited greater proliferation than the pMXs.IR-transduced cells (Figure 4G), but the cells proliferated with myeloid terminal differentiation without dysplasia or increase in CD34$^+$ cells (Figure 4H). Thus, BMI1-overexpressed cells showed a slight increase in self-renewal capacity and an increase in proliferation ability. However, BMI1 did not block differentiation at all. Overexpression of BMI1 may have limited proliferation ability without differentiation inhibition, suggesting that BMI1 alone does not have enough potential for MDS genesis.

These results raised the possibility that BMI1 may be overexpressed by additional molecular abnormalities and may work as a proliferative activator in the stem/progenitor cells with RUNX1 mutations. Because the D171N mutation itself was not proliferogenic, our next investigation was undertaken to determine whether BMI1 is required for leukemogenesis in the D171N-mutated cells.

BMI1 overexpression confers survival advantage but does not inhibit G-CSF–induced differentiation of 32D cells

To confirm the collaboration of D171N with BMI1, we first transduced both the D171N mutant and BMI1 into 32Dcl3 cells. The 32Dcl3 cells were transduced with pMYs.IP/IB, pMYs.IP/BMI1, D171N/pMYs.IB, or D171N/BMI1, and the infected cells were subjected to drug selection by puromycin and blasticidin. G-CSF treatment induced terminal differentiation of 32Dcl3 cells transduced with pMYs.IP/IB, as indicated by the appearance of polymorphonucleated neutrophils and upregulation of CD11b on the surface, and pMYs.IP/BMI1-transduced cells were also terminally differentiated as well (Figure 5A). However, the differentiation was weakly inhibited by D171N/pMYs.IB, and D171N/BMI1 showed no additional effect on differentiation compared with D171N/pMYs.IB (Figure 5A), indicating that BMI1 did not block differentiation at all. Growth rate was comparable among the indicated transfectants after 3 days of culture with the presence of IL-3 (Figure 5B). However, annexin V positivity in the D171N/BMI1-transduced cells was at the same level as that in pMYs.IG/IB- or pMYs.IP/BMI1-transduced cells, and it was significantly lower than that in D171N/pMYs.IB-transduced cells after 36 hours of culture without IL-3 (Figure 5C). These data raised the possibility that BMI1 may add some survival effects to D171N-transduced cells.

Double transduction of D171N and BMI1 into human CD34$^+$ cells leads to proliferation with differentiation

To investigate whether BMI1 can add a growth advantage to RUNX1-mutated cells, we performed simultaneous double transduction of the D171N mutant with BMI1 into human CD34$^+$ cells. Human CB CD34$^+$ cells were transduced with pMXs.IG/IR, pMXs.IG/BMI1, D171N/pMXs.IR, or D171N/BMI1. BMI1 was endogenously expressed in cells transduced with pMXs.IG/IR or D171N/pMXs.IR, whereas a strong upregulation of this protein was observed in the BMI1-transduced cells (Figure 5D). In the CFC replating assay, all of the double-transduced cells formed fewer colonies than single-transduced cells (Figure 5E, compared with Figures 2H and 4F). Both colony number and replating ability were altered by the double transduction of D171N and BMI1 compared with D171N/pMXs.IR-transduced cells. The presence of stem/progenitor cells with long-term self-renewal capabilities was confirmed by the LTC-IC assay. In both limiting dilution and bulk assays, increased stem/progenitor cell frequencies were observed in D171N/BMI1-transduced cells (Figure 5F). In addition, a dramatic change was observed in the liquid culture. Double-transduced cells with pMXs.IG/IR or D171N/pMXs.IR hardly proliferated in the long-term culture medium, and their proliferation folds were <100 (Figure 5G). However, double-transduced cells containing BMI1 exhibited an altered effect on cell proliferation. In particular, the D171N/BMI1 double-transduced cells spontaneously started to proliferate at approximately day 20, a phenomenon that was earlier and greater than the cells with pMXs.IG/BMI1. The D171N/BMI1 cells markedly grew until day 70, resulting in the same proliferation ability when compared with pMXs.IG/BMI1-transduced cells (Figure 5G). Thus, the D171N/BMI1-transduced cells had a strong growth advantage compared with the D171N/pMXs.IR-transduced cells. The BMI1 double-transduced cells showed an increase in S phase; however, the cells did not harbor an expansion of a population of CD34$^+$ or blast cells, and most of the cells differentiated to various stages of myeloid cells with dysplasia (Figure 5H). These results indicate that BMI1 overexpression confers proliferation ability with differentiation to D171N-mutated cells. To assess the impact of BMI1 on the proliferation and survival of the progenitor cells, we analyzed the effect of *BMI1* expression on *INK4A/ARF* (*p16/p14*) locus expression in the CD34$^+$ cells. *INK4A/ARF* expression was downregulated by BMI1 (Figure 5I), which may have contributed to the proliferation and survival of D171N-transduced cells. Significant enrichments of BMI1 on *Ink4a/Arf* (*p16/p19*) promoter regions were detected in both BMI1-transduced 32D cells and BMI1/D171N-transduced 32D cells, but not on the β-actin promoter region (supplemental Figure 2A). A physical association in vivo between BMI1 and D171N was observed in 293T cells, which was comparable to that between BMI1 and WT RUNX1 (supplemental Figure 2B).

INK4A/ARF expression levels were also lower in MDS patients with RUNX1 mutations than in those without mutations in this gene (supplemental Figure 3A). To clarify the role of

Figure 5 (continued) DsRed-tagged BMI1. After 3 to 4 days, GFP$^+$/DsRed$^+$ cells were purified by sorting. The cells were cultured in methylcellulose or long-term culture medium. (D) Expression of BMI1 and RUNX1-D171N were confirmed by Western blotting using anti-Bmi1 and anti–FLAG M2 antibodies, respectively. Anti–β-actin antibody was used as control. (E) Double-transduced cells were analyzed by CFC replating assay. Data are expressed as mean ± SD from 4 independent experiments. (F) LTC-IC assay in bulk and limiting dilution was carried out. (G) Growth patterns of the transduced cells cultured in long-term culture medium displayed as proliferation fold. The error bars represent the SD from 4 independent experiments. The growth profiles of all cells with double transduction of GFP (empty or D171N) and DsRed (empty or BMI1) vectors are shown. (H) Cell cycle analysis and the expression pattern of surface markers as shown by a typical flow cytometry profile, and Wright-Giemsa–stained cytospins of D171N- and D171N/BMI1-transduced cells on day 42 as captured with a BX51 microscope and a DP12 camera (Olympus); original magnification ×1000. (I) *INK4A/ARF* (*p16/p14*) expression levels in D171N- and D171N/BMI1-transduced cells on day 42. Relative gene expression was measured by qRT-PCR performed in triplicate and calculated as the ratio of *INK4A/ARF* to *GAPDH* expression.

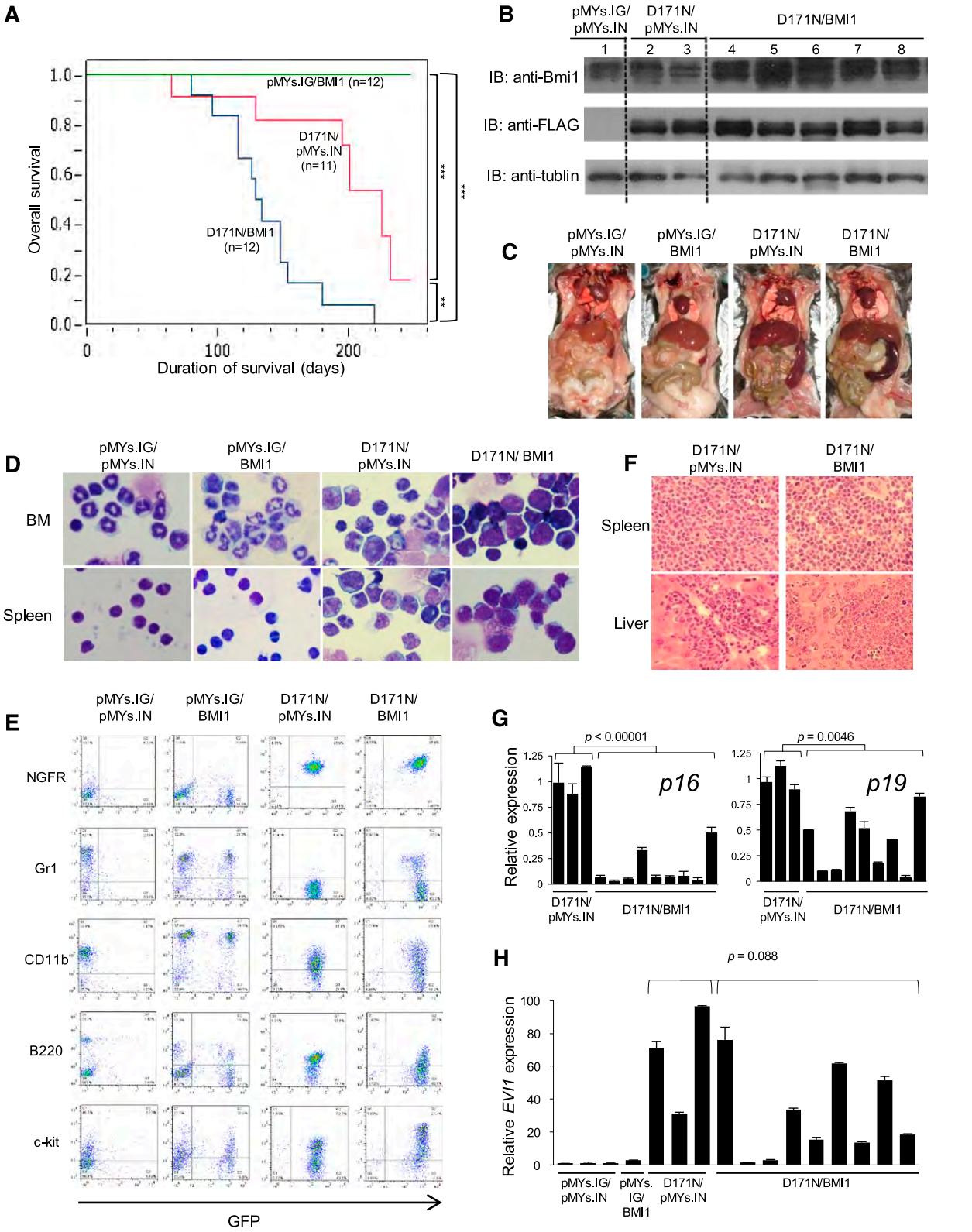

Figure 6. The effect of double expression of D171N and BMI1 in a mouse BMT model. (A) Kaplan-Meier analysis of the survival of mice that received transplants of BM cells transduced with pMYs.IG/BMI1 (n = 12, green line), D171N/pMYs.IN (n = 11, red line), or D171N/BMI1 (n = 12, blue line). *P* values were calculated using log-rank test. (B) Expression of RUNX1-D171N and BMI1 in BM cells derived from the BMT mice transduced with pMYs.IG/IN (lane 1), D171N/pMYs.IN (lanes 2, 3), or D171N/BMI1 (lanes 4-8). Cell lysates were immunoblotted with anti-Bmi1, anti–FLAG M2, or anti-tubulin antibody as control. Data are representative of 3 independent experiments. (C) Macroscopic findings of euthanized mice transplanted with BM cells transduced with the indicated construct. A representative photograph is shown. Mice with D171N/pMYs.IN or D171N/BMI1 died of MDS/AML with marked splenomegaly (right 2 panels), although mice with pMYs.IG/IN or pMYs.IG/BMI1 remained healthy without any organomegaly 8 months after BMT (left 2 panels). (D) Cytospin preparations of BM and spleen cells derived from indicated mice were stained with Giemsa. A representative photograph is shown. Images were obtained with a BX51 microscope and a DP12 camera (Olympus); objective lens, UplanFl (Olympus); original magnification ×1000. (E) Flow cytometric analysis of BM cells derived from each transduced mouse. In pMYs.IG/IN and pMYs.IG/BMI1, apparently healthy mice were euthanized for analysis of BM cells 8 months after BMT.

Table 1. Characteristics of AML mice caused by expression of D171N and BMI1

Characteristics	pMYs.IG/pMYs.IN (n = 3)	D171N/pMYs.IN (n = 5)	D171N/BMI1 (n = 10)
WBCs (/μL)	18 550 ± 1786	129 100 ± 68 089	70 838 ± 16 353
Hb (g/dL)	14.8 ± 0.4	7.3 ± 2.5	7.7 ± 2.3
PLTs ($\times 10^3$/μL)	291 ± 67	246 ± 80	134 ± 75
MCV (fL)	46.7 ± 0.6	53.6 ± 3.9	51.9 ± 9.3
BM count ($\times 10^7$ cells)	2.70 ± 0.78	7.05 ± 1.67	4.83 ± 1.14
Myeloblasts in BM (%)	1.8 ± 1.0	34.5 ± 16.0	59.6 ± 8.2
Liver weight (mg)	1668 ± 129	2008 ± 482	2015 ± 527
Spleen weight (mg)	98 ± 12	605 ± 242	531 ± 185

Averages and standard deviations are shown. BM cells were isolated from both tibias and femurs.

Hb, hemoglobin; MCV, mean corpuscular volume; PLTs, platelets.

micro RNAs (miRNAs) associated with BMI1 and polycomb-repressive complex (PRC) 1/2 in the patients with RUNX1 mutations, we analyzed miRNA levels in $CD34^+$ cells from MDS patients; however, no remarkable difference was detected between $CD34^+$ cells from patients and normal BM (supplemental Figure 3B). Furthermore, we analyzed the effects of BMI1 knockdown by short hairpin RNA in the $CD34^+$ cells from MDS/AML patients with RUNX1 mutations and high BMI1 expression. BMI1 knockdown resulted in impaired cell proliferation on MS5 stromal cells (supplemental Figure 3C). These results indicate that expansion of RUNX1-mutated $CD34^+$ cells depends on BMI1 expression, which coincides with repression of the cell cycle regulators INK4A/ARF.

Collaboration of the D171N mutant and BMI1 in a mouse BMT model

Nevertheless, even the D171N/BMI1-transduced human $CD34^+$ cells did not develop MDS/AML in NOG mice (supplemental Table 2). Therefore, to confirm the collaboration of BMI1 overexpression with the D171N mutant in vivo, we performed mouse BMT using BM cells transduced with both D171N and BMI1. We previously reported that most of the mice that received D171N-transduced BM cells died of MDS/AML, and collaboration between D171N and Evi1 overexpression was confirmed in a BMT model where coexpression of D171N and Evi1 induced MDS/AML with much shorter latencies.[22] To investigate whether high expression of BMI1 can also collaborate with D171N, Ly-5.1 murine BM mononuclear cells were infected with retrovirus harboring pMYs.IG/IN, pMYs.IG/BMI1, D171N/pMYs.IN, or D171N/BMI1. The efficiency of retrovirus infection was 35% to 45% of $GFP^+/NGFR^+$ cells (supplemental Figure 4A; supplemental Table 3), and nonsorted cells were transplanted into sublethally irradiated syngeneic Ly-5.2 mice. Each cell population was successfully engrafted (supplemental Figure 4B), and in time, the proportion of $GFP^+/NGFR^+$ cells gradually increased in the mice that were transplanted with D171N/BMI1-transduced cells (supplemental Figure 4C).

Mice that received transplants of pMYs.IG/BMI1-transduced cells remained healthy over the observation period (n = 12/12), as well as those that were transplanted with pMYs.IG/IN-transduced cells (n = 4/4). Most of the mice that received transplants of D171N/pMYs.IN-transduced cells developed MDS/AML mainly 6 to 8 months after transplantation (n = 6/11, $P < .0001$, Figure 6A), as observed in the previous report.[22] Of note, mice that received transplants of BM cells expressing D171N/BMI1 developed MDS/AML with significantly shorter latencies (mainly 3 to 5 months) compared with the D171N/pMYs.IN group (n = 12/12, $P = .001$, Figure 6A). Expression of the transduced D171N and BMI1 was confirmed by Western blot analysis, and endogenous Bmi1 expression could be detected in the D171N/pMYs.IN cohort (Figure 6B). Morbid mice with D171N/pMYs.IN or D171N/BMI1 exhibited similar phenotypes, characterized by leukocytosis, anemia, and marked splenomegaly, whereas the mice with pMYs.IG/BMI1 or pMYs.IG/IN, euthanized 8 months after BMT, showed none of these phenotypes (Table 1 and Figure 6C). In the leukemic mice with D171N/pMYs.IN or D171N/BMI1, BM and spleen were occupied by immature myeloid cells including myeloid blasts (Figure 6D). More myeloblasts in BM were observed in D171N/BMI1 mice than in D171N/pMYs.IN ones (Table 1). The leukemic cells displayed similar morphologic abnormalities and surface markers: $GFP^+/NGFR^+$ leukemic cells were $CD11b^{low\ to\ high}$, $Gr\text{-}1^{low}$, $B220^{low}$, and $c\text{-}kit^{low\ to\ high}$ (Figure 6E; supplemental Figure 4D; supplemental Table 2), although the expression level of c-kit tended to be higher in the D171N/BMI1 cohort than that in the D171N/pMYs.IN group. The normal structure of the spleen was completely destroyed with massive blast and immature myeloid cell infiltration, and these cells also invaded into the hepatic portal areas in the liver (Figure 6F). Meanwhile, $GFP^+/NGFR^+$ cells in pMYs.IG/BMI1-induced mice were very few, indicating that pMYs.IG/BMI1-transduced BM cells did not become dominant in vivo (Figure 6E). In addition, myeloid cells showed normal differentiation into segmented cells in the BM, and most of the nucleated cells in the spleen were found to be small lymphocytes as observed in the mice with pMYs.IG/IN (Figure 6D). Collectively, BMI1 overexpression has a strong potential to induce MDS/AML in concert with D171N in a mouse BMT model, although BMI1 overexpression by itself does not result in maturation block or leukemogenesis. Furthermore, *Ink4a/Arf* (*p16/p19*) expression in D171N/BMI1-transduced mice was significantly lower than that in the D171N/pMYs.IN-transduced mice (Figure 6G). However, most of the D171N/BMI1 mice still showed high expression of *Evi1*, which was relatively lower than that in the D171N/pMYs.IN group (Figure 6H). Therefore, *Evi1* overexpression is suspected to play a critical role along with the RUNX1 D171N mutation in the development of MDS/AML in the mouse system.

Stepwise transduction of the D171N mutant and BMI1 leads to MDS-like long-term proliferation in human $CD34^+$ cells

Our results showed that simultaneous transduction of D171N and BMI1 can induce MDS/AML, whereas FPD/AML patients who have congenital RUNX1 mutations develop MDS/AML after decades of latency period. This raises the possibility that additional gene abnormalities occur afterward in the RUNX1-mutated cells for the development of MDSs. To clarify the effect of BMI1 in RUNX1-mutated $CD34^+$ cells, we next performed stepwise transduction of the D171N mutant and BMI1 (Figure 7A).

Figure 6 (continued) The dot plots show staining for NGFR, Gr-1, CD11b, B220, or c-kit as detected with PE vs GFP. (F) Histopathological findings of spleen and liver from mice that died of MDS/AML in the indicated BMT model, as shown by hematoxylin and eosin staining. Images were obtained with a BX51 microscope and a DP12 camera (Olympus) with an UplanFL objective lens (Olympus) and are shown at an original magnification ×400. (G) *Ink4a/Arf* (*p16/p19*) expression levels in BM cells of mice. Relative *p16/p19* expression was measured by qRT-PCR performed in triplicate and calculated as the ratio of *p16/p19* to *Gapdh* expression. (H) *Evi1* expression levels in BM cells of mice. Relative *Evi1* expression was measured by qRT-PCR performed in triplicate and calculated as the ratio of *Evi1* to *Gapdh* expression. RNA from pMYs.IG/pMYs.IN mice served as a control, and the RNA level was defined as 1.

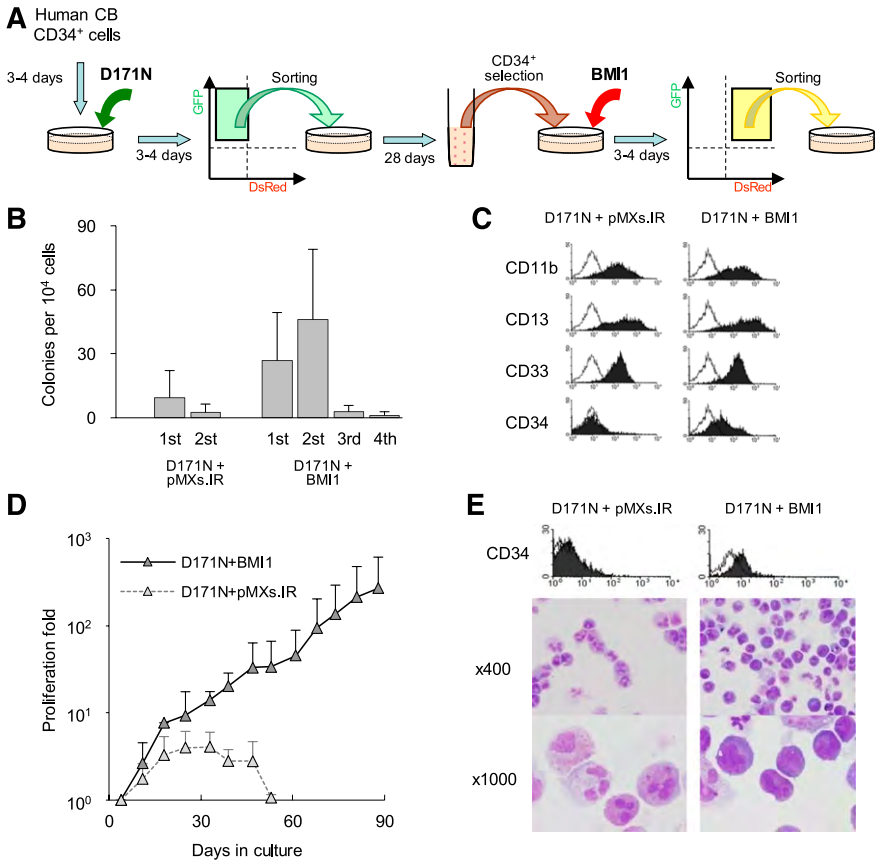

Figure 7. Stepwise transduction of the D171N mutant followed by BMI1 in human CD34$^+$ cells. (A) Human CD34$^+$ cells were precultured for 3 to 4 days in expansion medium and transduced with GFP-tagged D171N-mutant. After 3 or 4 days, GFP$^+$ cells were sorted and cultured in long-term culture medium for 28 days. Then, CD34$^+$ cells were reselected by the CD34 MicroBead Kit again and transduced with DsRed-tagged BMI1. We also transduced the DsRed vector as a control. Finally, 35 days after the D171N transduction, GFP$^+$/DsRed$^+$ cells were sorted and cultured in methylcellulose or long-term culture medium. (B) CFC replating assay in 3 independent experiments. (C) Representative flow cytometry analyses of the first colonies. (D) Proliferation fold in 3 independent experiments. Day 0 was the day of the second (DsRed vectors) transduction. (E) Flow cytometric analysis for CD34 expression, and Wright-Giemsa–stained cytospins on day 39 as captured with a BX51 microscope and a DP12 camera (Olympus) at ×400 and ×1000 original magnifications.

We first transduced D171N into CD34$^+$ cells. Sorted GFP$^+$ cells were cultured for 28 days more, until the percentage of the D171N-transduced CD34$^+$ cells, especially the CD34$^+$/CD38$^-$ population, was maximal (Figure 3D-E). Then, we selected for the CD34$^+$ cells again, followed by BMI1 transduction. GFP$^+$/DsRed$^+$ cells were sorted and cultured in methylcellulose or long-term culture medium. In the CFC assay, pMXs.IR-transduced cells seemed to have very low colony-forming ability, whereas the stepwise BMI1-transduced D171N cells displayed an increase in both colony-forming ability and replating capacity (Figure 7B). Moreover, the CD34$^+$ cell population remained in the stepwise BMI1-transduced D171N cells (Figure 7C). Furthermore, long-term proliferation with a retained CD34$^+$ cell fraction was observed in the stepwise BMI1-transduced D171N cells, and morphologic findings showed myeloid cell dysplasia with increased blast cells (Figure 7D-E). These findings are quite similar to those seen in human patients with higher-risk MDSs. Thus, our results demonstrate that the MDS phenotype could be reproduced in human hematopoietic cells by stepwise transduction of the D171N mutant followed by BMI1.

Discussion

RUNX1 mutations have been detected in nearly 20% patients with higher-risk MDSs. Biochemically, RUNX1 mutants show loss of normal RUNX1 function, and some mutants have dominant-negative *trans*-activation potential similar to leukemogenic chimeras such as CBFβ-MYH11. The biological functions of RUNX1 mutants, which have already been demonstrated using the mouse BMT model, include increase in leukemogenic potential.[22] In this model, however, the retrovirus frequently integrated into the chromosome near the *Evi1* locus, resulting in its high expression. We checked *EVI1* expression levels in MDS patients; however, most of the examined patients showed very low *EVI1* expression, except for only 1 patient with a *RUNX1* mutation, who rapidly progressed from MDS to AML with hyperblastcytosis. Because collaboration between *RUNX1* mutations and *EVI1* overexpression does not appear to be common in MDS patients, we tried to clarify the biological significance of RUNX1 mutants in stem/progenitor cells using human CBs without the effect of *Evi1* overexpression.

The cells transduced with WT RUNX1 quickly differentiated into mature myeloid/monocytoid cells without proliferation in both colony-forming and liquid culture assays. This result suggests that overexpression of WT RUNX1 in stem/progenitor cells promotes terminal differentiation without self-renewal, blocks cell proliferation, and has no oncogenic potential. These data can explain the reduction in WT RUNX1-transduced cells in a mouse BMT model.[22,38] On the other hand, the D171N mutant, the most common mutation in RUNX1 that is caused by only a 1-bp replacement in the RHD, has increased self-renewal capacity, mildly blocked differentiation, dysplasia in all 3 lineages, and a slight tendency for immaturity, but no proliferation ability. Although a stem/progenitor cell with the D171N mutation is suspected to have MDS-genic potential of cell dysplasia and self-renewal capacity, it induces G1 arrest and cannot develop MDS due to lack of proliferation ability. Thus, additional gene alterations that induce proliferation activity seem to be necessary for development of MDSs. *BMI1* overexpression was suspected as a candidate collaborator because upregulated BMI1 level was observed in higher-risk MDS patients with *RUNX1* mutations, even

though the D171N mutant itself does not induce BMI1 expression. The molecular mechanism of high BMI1 expression in RUNX1-mutated patients is not due to miRNAs either. A previous study showed that forced expression of the activated *N*-RAS mutant induced overexpression of Bmi1 in mouse c-Kit$^+$ cells, especially in Runx1$^{-/-}$ cells.[39] Thus, the gene mutations that induce activation of the RAS signaling pathway, which are frequently seen in patients with *RUNX1* mutations,[40] may result at least partly in *BMI1* overexpression. Furthermore, many gene mutations have been identified in MDS patients, including PRC2 complex proteins, and some of them showed positive associations with *RUNX1* mutations.[41] Our next investigation is to clarify the effects of both expression levels and mutations of PRC2 proteins in patients with RUNX1 mutations. There is a possibility that these gene expression patterns and mutations may act to elevate the *BMI1* expression level.

BMI1 is well known to be essential for self-renewal of hematopoietic stem cells,[42-44] in part via repression of genes involved in senescence,[45] and self-renewal of hematopoietic stem cells is enhanced by BMI1 expression in both mouse and human.[35,46] Our results showed that overexpression of BMI1 itself in human CD34$^+$ cells or a mouse BMT model does not appear to have MDS-genic potential, as reported previously.[35,46] When the CD34$^+$ cells were double-transduced simultaneously with D171N and BMI1, the cells could proliferate with differentiation and dysplasia. Cotransduction of D171N and BMI1 into BM cells resulted in faster induction of MDS/AML in BMT mice. It is suggested that BMI1 overexpression may act as one of the partner abnormalities collaborating with master gene mutations for MDS genesis. BMI1 affects *INK4A/ARF* expression, which has been sufficiently elucidated, involved in the leukemic phenotype. A previous report that showed that BMI1 collaborates with BCR-ABL in leukemic transformation also supports this idea.[47] We confirmed that significant enrichments of BMI1 were detected on *Ink4a/Arf* promoter regions in both BMI1-transduced cells and BMI1/D171N-transduced cells, suggesting that BMI1 overexpression may help cells transform, at least in part, due to suppressing the expression of the *Ink4a/Arf* tumor suppressor gene. Although a physical association in vivo between BMI1 and D171N, as well as WT RUNX1,[48] was observed, it is known that the D171N mutant has lost DNA-binding ability.[12] Therefore, the mechanism by which BMI1 coexpression with the D171N mutant induces proliferative effects seems to be independent of the direct physical association between RUNX1 and BMI1. Additionally, both BMI1-knockdown human CD34$^+$ cells and *Bmi1*-deficient mouse cells showed elevated levels of reactive oxygen species accumulation,[49,50] resulting in impairment of long-term expansion and apoptosis. It may be the reason why D171N-transduced human CD34$^+$ cells that showed reduced BMI1 expression could not proliferate. It may also explain the phenomenon in 32Dcl3 cells in which BMI1 transduction seemed to rescue D171N-transduced cells from apoptosis. However, the CD34$^+$ cells transduced with D171N/BMI1 did not develop MDS/AML in NOG mice, suggesting that other factors such as *EVI1* overexpression observed in a mouse BMT model may still be required for the development of MDS/AML in NOG mice.

Germ line mutations of *RUNX1* have been shown to occur in FPD/AML.[1,2] FPD/AML is regarded as familial MDS,[3] and the molecular mechanisms by which RUNX1 mutations promote the development of hematopoietic malignancies seem to be identical in both MDS and FPD/AML patients. Because decades-long asymptomatic latency periods do occur in patients with FPD/AML, it appears that RUNX1-mutated stem cells cannot promote the development of MDSs without other cooperative factors. It is suspected that additional gene abnormalities occur later on in the RUNX1-mutated cells for the development of MDSs. Therefore, we performed stepwise transduction of the D171N mutant followed by BMI1 into CD34$^+$ cells, which could reproduce continuous slow proliferation of a low percentage of blastoid cells, reflecting the hematologic features in higher-risk MDS patients. This result indicates that genetic alterations, such as EVI1 or BMI1 overexpression, which add proliferative advantage to cells, may occur as "second hits" after the master genetic alteration (ie, RUNX1 mutation) that has MDS-genic potential.

In the present study, we revealed the functional significance of the RUNX1 D171N mutant in the pathogenesis of MDSs using human CD34$^+$ cells. Thus, amino acid replacement–type mutations in the RHD, which comprise half of the RUNX1 mutations detected in patients, are suspected to have MDS-genic potential; however, the cells with this type of mutation lack proliferation ability. This may explain BM failure status, one of the phenotypes of MDSs. When the mutated cells gain partner gene abnormality (ie, *EVI1* or *BMI1* overexpression), they can acquire proliferation ability through alteration of the collaborating gene, which may explain the various clinical features of patients with RUNX1 mutations. On the other hand, the other half of the RUNX1 mutants may have different biochemical functions that remain unclear; in particular, mutants that lack the C-terminal functional domain but have an intact RHD may have other effects.[4,22] Our future investigations include the elucidation and clarification of the molecular mechanisms by which each type of RUNX1 mutant promotes the development of MDSs.

Acknowledgments

The authors thank the pregnant women, nursing staff, and Dr Hanioka at Yamashita Clinic for providing CB and Ryoko Matsumoto-Yamaguchi for providing excellent technical support in carrying out these experiments.

This work was supported in part by Grants-in-Aid for Scientific Research from the Ministry of Education, Culture, Sports, Science and Technology of Japan; grants from Hiroshima University; a grant from the Japan Leukaemia Research Fund; and a grant from Radiation Effects Association. This work was carried out in part at the Analysis Center of Life Science, Hiroshima University.

Authorship

Contribution: Y.H. designed the research, performed experiments, and wrote the manuscript; D.I. and Y.D. performed experiments and prepared the manuscript; J.I., N.D., H. Matsui, T.Y., H. Matsushita, and G.S. collected the data; K.A., A.I., and T.K. supervised the project and discussed the results; and H.H. conceived and designed the research, collected and interpreted the data, and revised the manuscript.

Conflict-of-interest disclosure: The authors declare no competing financial interests.

Correspondence: Hironori Harada, Department of Hematology and Oncology, Research Institute for Radiation Biology and Medicine, Hiroshima University, 1-2-3 Kasumi, Minami-ku, Hiroshima 734-8553, Japan; e-mail: herf1@hiroshima-u.ac.jp.

References

1. Song WJ, Sullivan MG, Legare RD, et al. Haploinsufficiency of CBFA2 causes familial thrombocytopenia with propensity to develop acute myelogenous leukaemia. *Nat Genet.* 1999; 23(2):166-175.
2. Osato M. Point mutations in the RUNX1/AML1 gene: another actor in RUNX leukemia. *Oncogene.* 2004;23(24):4284-4296.
3. Liew E, Owen C. Familial myelodysplastic syndromes: a review of the literature. *Haematologica.* 2011;96(10):1536-1542.
4. Harada H, Harada Y, Niimi H, Kyo T, Kimura A, Inaba T. High incidence of somatic mutations in the AML1/RUNX1 gene in myelodysplastic syndrome and low blast percentage myeloid leukemia with myelodysplasia. *Blood.* 2004; 103(6):2316-2324.
5. Preudhomme C, Warot-Loze D, Roumier C, et al. High incidence of biallelic point mutations in the Runt domain of the AML1/PEBP2 alpha B gene in Mo acute myeloid leukemia and in myeloid malignancies with acquired trisomy 21. *Blood.* 2000;96(8):2862-2869.
6. Dicker F, Haferlach C, Kern W, Haferlach T, Schnittger S. Trisomy 13 is strongly associated with AML1/RUNX1 mutations and increased FLT3 expression in acute myeloid leukemia. *Blood.* 2007;110(4):1308-1316.
7. Silva FPG, Swagemakers SMA, Erpelinck-Verschueren C, et al. Gene expression profiling of minimally differentiated acute myeloid leukemia: M0 is a distinct entity subdivided by RUNX1 mutation status. *Blood.* 2009;114(14):3001-3007.
8. Tang JL, Hou HA, Chen CY, et al. AML1/RUNX1 mutations in 470 adult patients with de novo acute myeloid leukemia: prognostic implication and interaction with other gene alterations. *Blood.* 2009;114(26):5352-5361.
9. Schnittger S, Dicker F, Kern W, et al. RUNX1 mutations are frequent in de novo AML with noncomplex karyotype and confer an unfavorable prognosis. *Blood.* 2011;117(8):2348-2357.
10. Kuo MC, Liang DC, Huang CF, et al. RUNX1 mutations are frequent in chronic myelomonocytic leukemia and mutations at the C-terminal region might predict acute myeloid leukemia transformation. *Leukemia.* 2009;23(8):1426-1431.
11. Ernst T, Chase A, Zoi K, et al. Transcription factor mutations in myelodysplastic/myeloproliferative neoplasms. *Haematologica.* 2010;95(9):1473-1480.
12. Harada H, Harada Y, Tanaka H, Kimura A, Inaba T. Implications of somatic mutations in the AML1 gene in radiation-associated and therapy-related myelodysplastic syndrome/acute myeloid leukemia. *Blood.* 2003;101(2):673-680.
13. Christiansen DH, Andersen MK, Pedersen-Bjergaard J. Mutations of AML1 are common in therapy-related myelodysplasia following therapy with alkylating agents and are significantly associated with deletion or loss of chromosome arm 7q and with subsequent leukemic transformation. *Blood.* 2004;104(5):1474-1481.
14. Zharlyganova D, Harada H, Harada Y, et al. High frequency of AML1/RUNX1 point mutations in radiation-associated myelodysplastic syndrome around Semipalatinsk nuclear test site. *J Radiat Res (Tokyo).* 2008;49(5):549-555.
15. Imagawa J, Harada Y, Shimomura T, et al. Clinical and genetic features of therapy-related myeloid neoplasms after chemotherapy for acute promyelocytic leukemia. *Blood.* 2010;116(26): 6018-6022.
16. Ding Y, Harada Y, Imagawa J, Kimura A, Harada H. AML1/RUNX1 point mutation possibly promotes leukemic transformation in myeloproliferative neoplasms. *Blood.* 2009; 114(25):5201-5205.
17. Beer PA, Delhommeau F, LeCouédic JP, et al. Two routes to leukemic transformation after a JAK2 mutation-positive myeloproliferative neoplasm. *Blood.* 2010;115(14):2891-2900.
18. Zhao LJ, Wang YY, Li G, et al. Functional features of RUNX1 mutants in acute transformation of chronic myeloid leukemia and their contribution to inducing murine full-blown leukemia. *Blood.* 2012; 119(12):2873-2882.
19. Grossmann V, Kohlmann A, Zenger M, et al. A deep-sequencing study of chronic myeloid leukemia patients in blast crisis (BC-CML) detects mutations in 76.9% of cases. *Leukemia.* 2011; 25(3):557-560.
20. Tahirov TH, Inoue-Bungo T, Morii H, et al. Structural analyses of DNA recognition by the AML1/Runx-1 Runt domain and its allosteric control by CBFbeta. *Cell.* 2001;104(5):755-767.
21. Bravo J, Li Z, Speck NA, Warren AJ. The leukemia-associated AML1 (Runx1)—CBF beta complex functions as a DNA-induced molecular clamp. *Nat Struct Biol.* 2001;8(4):371-378.
22. Watanabe-Okochi N, Kitaura J, Ono R, et al. AML1 mutations induced MDS and MDS/AML in a mouse BMT model. *Blood.* 2008;111(8): 4297-4308.
23. Cattoglio C, Facchini G, Sartori D, et al. Hot spots of retroviral integration in human CD34+ hematopoietic cells. *Blood.* 2007;110(6): 1770-1778.
24. Schwieger M, Löhler J, Fischer M, Herwig U, Tenen DG, Stocking C. A dominant-negative mutant of C/EBPalpha, associated with acute myeloid leukemias, inhibits differentiation of myeloid and erythroid progenitors of man but not mouse. *Blood.* 2004;103(7):2744-2752.
25. Xu F, Li X, Wu L, et al. Overexpression of the EZH2, RING1 and BMI1 genes is common in myelodysplastic syndromes: relation to adverse epigenetic alteration and poor prognostic scoring. *Ann Hematol.* 2011;90(6):643-653.
26. Mihara K, Chowdhury M, Nakaju N, et al. Bmi-1 is useful as a novel molecular marker for predicting progression of myelodysplastic syndrome and patient prognosis. *Blood.* 2006;107(1):305-308.
27. Mulloy JC, Cammenga J, MacKenzie KL, Berguido FJ, Moore MA, Nimer SD. The AML1-ETO fusion protein promotes the expansion of human hematopoietic stem cells. *Blood.* 2002; 99(1):15-23.
28. Tonks A, Pearn L, Tonks AJ, et al. The AML1-ETO fusion gene promotes extensive self-renewal of human primary erythroid cells. *Blood.* 2003; 101(2):624-632.
29. Mulloy JC, Cammenga J, Berguido FJ, et al. Maintaining the self-renewal and differentiation potential of human CD34+ hematopoietic cells using a single genetic element. *Blood.* 2003; 102(13):4369-4376.
30. D'Costa J, Chaudhuri S, Civin CI, Friedman AD. CBFbeta-SMMHC slows proliferation of primary murine and human myeloid progenitors. *Leukemia.* 2005;19(6):921-929.
31. Wunderlich M, Krejci O, Wei J, Mulloy JC. Human CD34+ cells expressing the inv(16) fusion protein exhibit a myelomonocytic phenotype with greatly enhanced proliferative ability. *Blood.* 2006;108(5): 1690-1697.
32. Shen SW, Dolnikov A, Passioura T, et al. Mutant N-ras preferentially drives human CD34+ hematopoietic progenitor cells into myeloid differentiation and proliferation both in vitro and in the NOD/SCID mouse. *Exp Hematol.* 2004;32(9):852-860.
33. Chou FS, Wunderlich M, Griesinger A, Mulloy JC. N-Ras(G12D) induces features of stepwise transformation in preleukemic human umbilical cord blood cultures expressing the AML1-ETO fusion gene. *Blood.* 2011;117(7):2237-2240.
34. Chung KY, Morrone G, Schuringa JJ, Wong B, Dorn DC, Moore MA. Enforced expression of an Flt3 internal tandem duplication in human CD34+ cells confers properties of self-renewal and enhanced erythropoiesis. *Blood.* 2005;105(1):77-84.
35. Rizo A, Dontje B, Vellenga E, de Haan G, Schuringa JJ. Long-term maintenance of human hematopoietic stem/progenitor cells by expression of BMI1. *Blood.* 2008;111(5):2621-2630.
36. Kato N, Kitaura J, Doki N, et al. Two types of C/EBPα mutations play distinct but collaborative roles in leukemogenesis: lessons from clinical data and BMT models. *Blood.* 2011;117(1):221-233.
37. Ito M, Hiramatsu H, Kobayashi K, et al. NOD/SCID/γ(c)(null) mouse: an excellent recipient mouse model for engraftment of human cells. *Blood.* 2002;100(9):3175-3182.
38. Tsuzuki S, Hong D, Gupta R, Matsuo K, Seto M, Enver T. Isoform-specific potentiation of stem and progenitor cell engraftment by AML1/RUNX1. *PLoS Med.* 2007;4(5):e172.
39. Motoda L, Osato M, Yamashita N, et al. Runx1 protects hematopoietic stem/progenitor cells from oncogenic insult. *Stem Cells.* 2007;25(12):2976-2986.
40. Niimi H, Harada H, Harada Y, et al. Hyperactivation of the RAS signaling pathway in myelodysplastic syndrome with AML1/RUNX1 point mutations. *Leukemia.* 2006;20(4):635-644.
41. Bejar R, Stevenson K, Abdel-Wahab O, et al. Clinical effect of point mutations in myelodysplastic syndromes. *N Engl J Med.* 2011; 364(26):2496-2506.
42. van der Lugt NM, Domen J, Linders K, et al. Posterior transformation, neurological abnormalities, and severe hematopoietic defects in mice with a targeted deletion of the bmi-1 proto-oncogene. *Genes Dev.* 1994;8(7):757-769.
43. Park IK, Qian D, Kiel M, et al. Bmi-1 is required for maintenance of adult self-renewing haematopoietic stem cells. *Nature.* 2003; 423(6937):302-305.
44. Lessard J, Sauvageau G. Bmi-1 determines the proliferative capacity of normal and leukaemic stem cells. *Nature.* 2003;423(6937):255-260.
45. Jacobs JJ, Kieboom K, Marino S, DePinho RA, van Lohuizen M. The oncogene and Polycomb-group gene bmi-1 regulates cell proliferation and senescence through the ink4a locus. *Nature.* 1999;397(6715):164-168.
46. Iwama A, Oguro H, Negishi M, et al. Enhanced self-renewal of hematopoietic stem cells mediated by the polycomb gene product Bmi-1. *Immunity.* 2004;21(6):843-851.
47. Rizo A, Horton SJ, Olthof S, et al. BMI1 collaborates with BCR-ABL in leukemic transformation of human CD34+ cells. *Blood.* 2010;116(22):4621-4630.
48. Yu M, Mazor T, Huang H, et al. Direct recruitment of polycomb repressive complex 1 to chromatin by core binding transcription factors. *Mol Cell.* 2012; 45(3):330-343.
49. Rizo A, Olthof S, Han L, Vellenga E, de Haan G, Schuringa JJ. Repression of BMI1 in normal and leukemic human CD34(+) cells impairs self-renewal and induces apoptosis. *Blood.* 2009; 114(8):1498-1505.
50. Liu J, Cao L, Chen J, et al. Bmi1 regulates mitochondrial function and the DNA damage response pathway. *Nature.* 2009;459(7245): 387-392.

2013 121: 3434-3446
doi:10.1182/blood-2012-06-434423 originally published online March 7, 2013

RUNX1/AML1 mutant collaborates with BMI1 overexpression in the development of human and murine myelodysplastic syndromes

Yuka Harada, Daichi Inoue, Ye Ding, Jun Imagawa, Noriko Doki, Hirotaka Matsui, Takashi Yahata, Hiromichi Matsushita, Kiyoshi Ando, Goro Sashida, Atsushi Iwama, Toshio Kitamura and Hironori Harada

Blood (print ISSN 0006-4971, online ISSN 1528-0020), is published weekly by the American Society of Hematology, 2021 L St, NW, Suite 900, Washington DC 20036.

Int J Hematol (2013) 98:406–416
DOI 10.1007/s12185-013-1404-y

ORIGINAL ARTICLE

Long-term efficacy and safety of eculizumab in Japanese patients with PNH: AEGIS trial

Yuzuru Kanakura · Kazuma Ohyashiki · Tsutomu Shichishima · Shinichiro Okamoto · Kiyoshi Ando · Haruhiko Ninomiya · Tatsuya Kawaguchi · Shinji Nakao · Hideki Nakakuma · Jun-ichi Nishimura · Taroh Kinoshita · Camille L. Bedrosian · Keiya Ozawa · Mitsuhiro Omine

Received: 19 April 2013 / Revised: 15 July 2013 / Accepted: 16 July 2013 / Published online: 11 August 2013

Abstract Paroxysmal nocturnal hemoglobinuria (PNH) is a rare, progressive hematopoietic stem cell disorder characterized by chronic complement-mediated hemolysis leading to life-threatening complications and early mortality. Eculizumab, a humanized anti-C5 monoclonal antibody, inhibits terminal complement activation, reduces hemolysis, decreases the risk of thrombosis, and improves renal function and quality of life in PNH patients. The long-term efficacy and safety of eculizumab in Japanese patients were assessed in a 2-year extension to a 12-week, open-label study (AEGIS). Eculizumab treatment led to an immediate and sustained reduction in intravascular hemolysis ($P < 0.001$) and red blood cell transfusions ($P = 0.0016$) compared with baseline levels. There were no reports of thromboembolism during eculizumab treatment. The majority of patients had stable (56 %) or improved (41 %) renal function and an improved quality of life ($P = 0.015$), with sustained reductions in fatigue and dyspnea. Eculizumab was well tolerated; no deaths or serious hemolytic events were reported, and the rate of infections declined over time. There were no significant differences in the response to eculizumab in patients with or without bone marrow dysfunction. These results demonstrate that eculizumab is an effective, well-tolerated

Y. Kanakura (✉)
Department of Hematology and Oncology, Osaka University Hospital, Suita, Japan
e-mail: kanakura@bldon.med.osaka-u.ac.jp

K. Ohyashiki
Tokyo Medical University, Tokyo, Japan

T. Shichishima
Department of Cardiology and Hematology, School of Medicine, Fukushima Medical University, Fukushima, Japan

S. Okamoto
Division of Hematology, Department of Internal Medicine, Keio University Hospital, Tokyo, Japan

K. Ando
Department of Hematology and Oncology, Tokai University School of Medicine, Isehara, Japan

H. Ninomiya
Institute of Clinical Medicine, University of Tsukuba, Tsukuba, Japan

T. Kawaguchi
Second Department of Internal Medicine, Kumamoto University School of Medicine, Kumamoto, Japan

S. Nakao
Department of Hematology and Oncology, Kanazawa University Hospital, Kanazawa, Japan

H. Nakakuma
Department of Hematology/Oncology, Wakayama Medical University, Wakayama, Japan

J. Nishimura
Department of Hematology and Oncology, Graduate School of Medicine, Osaka University, Suita, Japan

T. Kinoshita
Department of Immunoregulation, Research Institute for Microbial Diseases, Osaka University, Suita, Japan

C. L. Bedrosian
Alexion Pharmaceuticals, Cambridge, MA, USA

K. Ozawa
Division of Hematology, Jichi Medical University, Shimotsuke, Tochigi, Japan

M. Omine
Division of Hematology, Showa University Fujigaoka Hospital, Yokohama, Japan

long-term treatment for Japanese PNH patients and leads to continued amelioration of some hemolytic complications.

Keywords Paroxysmal nocturnal hemoglobinuria · Complement-inactivating agents · Hemolysis · Eculizumab · Hematopoietic stem cell

Introduction

Paroxysmal nocturnal hemoglobinuria (PNH) is a progressive and life-threatening disease characterized by chronic complement-mediated hemolysis resulting in severe morbidities that lead to end organ damage and early mortality [1–3]. Approximately 35 % of patients die within 5 years of diagnosis, a rate that increases to 50 % within 10–15 years of diagnosis [1, 2, 4]. The etiology of PNH stems from a somatic mutation in the X-chromosome-linked phosphatidylinositol glycan class A (*PIG-A*) gene that disrupts production of glycosylphosphatidylinositol (GPI)-linked anchors on the surface of blood cells [5, 6]. This results in the deficiency of the GPI-anchored complement inhibitor proteins CD55 and CD59, which leads to chronic complement-mediated hemolysis of the GPI-deficient red blood cells (RBCs) [3, 7], as well as activation of platelets, monocytes, and leukocytes [8, 9].

Although there is an established connection between PNH, an acquired clonal hematopoietic stem cell disorder, and bone marrow dysfunction conditions such as aplastic anemia (AA) [10], anemia is only one consequence of PNH. While many AA patients have blood cells phenotypically characteristic of PNH (i.e., cells deficient in cell-surface GPI anchors [11–13]), PNH is a distinct disease that requires specific therapeutic management to minimize its adverse clinical consequences.

As a result of chronic uncontrolled complement-mediated hemolysis and chronic complement activity, PNH patients are at risk of life-threatening complications such as thrombotic events, renal insufficiency, and other organ damage. Compared with the general population, patients with PNH have at least a 62-fold higher risk of venous thromboembolism (TE) [14] and up to a 6.6-fold higher risk of chronic kidney disease (CKD) [15, 16]. These heightened risks stem from increases in platelet aggregation and adhesion [9, 17], damage to the kidney tubule caused by microvascular thromboses [16], and accumulation of iron deposits [18], all consequences of uncontrolled complement activity. Up to two-thirds of PNH-related deaths are caused by TE, with renal failure accounting for up to 18 % of deaths in one large study of Japanese patients with PNH [3, 17, 19–22]. It is reported that the risk of death is increased 7- to 15-fold in patients who have experienced a TE [2, 23] and 3-fold in patients with renal impairment [24].

Patients with PNH also have an increased risk of experiencing symptoms such as severe fatigue disproportionate to levels of anemia, abdominal pain, dyspnea, dysphagia, chest pain, pulmonary hypertension, and, in men, erectile dysfunction [3, 17, 19, 20, 25]. These symptoms can manifest early in the course of the disease (often prior to a diagnosis of PNH being made), are frequently severe, and may be predictive of further clinical complications and death. One report determined that the odds of mortality are more than double in patients with abdominal pain [26]. The debilitating nature of these symptoms can be a cause of substantial suffering, with a detrimental impact on patients' quality of life.

Eculizumab, a humanized monoclonal antibody, specifically targets the terminal complement protein C5, thereby inhibiting chronic uncontrolled complement activity and complement-mediated hemolysis [27]. The efficacy and safety of eculizumab have been evaluated in two multinational phase III studies and a multinational extension study focusing primarily on Western patients [22, 28, 29]. We previously reported the results of a 12-week study of eculizumab in Japanese patients with PNH that confirmed the immediate efficacy and tolerability of the treatment in this patient population [30]. Here we report the results of a 2-year extension study in these patients, which evaluated the long-term efficacy and safety of eculizumab in patients with PNH.

Methods

AEGIS was an open-label, non-comparative study in 29 Japanese patients with a diagnosis of PNH who were recruited from nine centers in Japan [30]. Patients of either gender who were at least 12 years of age were enrolled in the study if they had been diagnosed with PNH for at least 6 months and had a PNH RBC clone size of at least 10 %, lactate dehydrogenase (LDH) levels $\geq$1.5 $\times$ the upper limit of normal (ULN) (240 U/L), and a platelet count $\geq 30 \times 10^9$/L. Patients were to have received at least one RBC transfusion over the past 2 years or, in the opinion of the investigator, could have benefited from one or more RBC transfusions during this period. Exclusion criteria included an absolute neutrophil count of $\leq$500/μL at screening, previous hematopoietic stem cell transplantation, a known or suspected hereditary complement deficiency, a history of meningococcal disease, an active or recurrent bacterial infection, pregnancy, or breastfeeding.

All patients received eculizumab, which was administered intravenously at a dose of 600 mg once per week for 4 weeks, 900 mg for 1 week, and then 900 mg every 2 weeks. The duration of the initial study was 12 weeks, following which all patients were offered participation in a

2-year extension study. At least 2 weeks prior to initiation of eculizumab therapy, all patients were vaccinated with a meningococcal vaccine.

Efficacy assessments performed during the extension study included changes from baseline in intravascular hemolysis (as measured by LDH), occurrence of TE, the Functional Assessment of Chronic Illness Therapy-Fatigue (FACIT-Fatigue) [31], PNH type III RBC count, number of units of packed RBCs (PRBCs) transfused, hemoglobin and plasma-free hemoglobin concentrations, CKD stage according to the Kidney Disease Outcomes Quality Initiative guidelines [32], and quality of life as assessed using the European Organisation for Research and Treatment of Cancer Quality of Life Questionnaire Core 30 (EORTC QLQ-C30) [33]. The safety of eculizumab treatment was assessed by recording adverse events (AEs) and routine laboratory investigations.

Statistical analysis

All analyses were based on the total duration of therapy with eculizumab, which included the initial 12-week study period. Accordingly, the start of the extension study was considered week 13, with the first assessment taking place in week 14. A Wilcoxon signed-rank test was used to assess changes from baseline in LDH, hemoglobin, RBC type III, free hemoglobin, and number of units of PRBCs transfused. Overall changes in FACIT-Fatigue and EORTC QLQ-C30 scores were analyzed using a linear mixed-effects model, with baseline scores as covariate, time as the fixed effect, and the patient as the random effect; changes from baseline in these parameters at individual assessments were analyzed using a signed-rank test. Chi-squared tests were used to assess changes from baseline in the percentage of patients with each CKD stage. The hypothesis tested the probability that treatment with eculizumab had an equal probability of worsening or improving CKD. A McNemar test was used to test changes in D-dimer levels from above the normal range at baseline to within the normal range at end of study, and Student's *t* tests were used to compare mean fatigue and quality-of-life scores at baseline between patients presenting with PNH plus AA/myelodysplastic syndrome (MDS) and those with PNH alone.

Results

Patient characteristics

A total of 27 Japanese patients (13 men and 14 women) completed the initial 12-week study [30] and entered into the extension period; a summary of baseline demographic and clinical data reported for these 27 patients at the start of the 12-week study is presented in Table 1. The mean age of this patient population was 48.3 years, with a range of 27–71 years. Only one patient was aged >65 years (age at screening was 70.8 years). Ten patients (37.0 %) had a history of AA, and two (7.4 %) had a history of MDS. At baseline, there were no statistically significant differences between the 15 patients with PNH and the 12 patients with PNH plus AA/MDS in the mean values of hemoglobin, LDH, PNH type III RBCs, FACIT-Fatigue score, EORTC QLQ-C30 scores, or the number of transfusions received over the previous 12 weeks. Mean baseline LDH levels for all patients (1827.6 U/L) were more than six-fold higher than the ULN (240 U/L).

Table 1 Baseline demographic and disease characteristics

Parameter	Eculizumab ($N = 27$)
Gender, female, *n* (%)	14 (51.9)
Age (years), mean (SD)	48.3 (12.35)
Range	26.8–70.8
Disease duration (years), mean (SD)	10.6 (6.37)
Range	1.2–22.4
History of aplastic anemia, *n* (%)	10 (37.0)
History of myelodysplastic syndrome, *n* (%)	2 (7.4)
PRBC units transfused in previous 12 months, median (range)	14.0 (0–70)
LDH levels (U/L), mean (SD)	1827.6 (638.65)
Hemoglobin (g/dL), mean (SD)	8.0 (1.69)
Plasma-free hemoglobin (mg/dL), mean (SD)	22.4 (14.50)
PNH RBC count ($\times 10^{12}$/L), mean (SD)	1.3 (0.76)
D-dimer (μg/L), mean (SD)	0.9 (0.78)
Granulocyte clone size (%), mean (SD)	
CD55/CD16	91.7 (9.92)
CD55/CD66b	91.1 (10.76)

SD standard deviation

Two of the 27 patients, one 47 years of age and the other 49 years of age and both females, had qualified for PRBC transfusions but had never received them. These two patients exhibited clinical signs and symptoms of PNH, with both having elevated LDH levels at baseline (1.3-fold and 1.6-fold above ULN, respectively) and one of the two having a history of deep vein thrombosis as well as stage 3 CKD.

Patient disposition

Overall mean exposure to eculizumab in the extension period was 24.9 months (range 4.2–27.1 months); the mean number of eculizumab infusions administered was 54.2 (range 10–58). No patients missed an infusion, and all administrations of eculizumab were at the protocol-specified 900-mg dose.

One of the 27 patients who entered the extension period requested that she be allowed to withdraw and did not complete the study. This patient was hospitalized on day 128 of treatment suffering with serious AEs (SAEs) of severe cellulitis and severe sepsis, as well as mild acute renal failure, though creatinine levels in this patient at study visits prior to and following hospitalization were within the normal range. The investigator considered both severe SAEs to probably be related to treatment. All AEs resolved without sequelae by 9 weeks after the last treatment administration.

Hemolysis and thrombosis

As previously reported, reduction in intravascular hemolysis, the primary endpoint of the original 12-week AEGIS study, was rapidly achieved; LDH levels were reduced by 62.8 % within 1 week of treatment initiation ($P < 0.001$) [30]. The reduction in LDH was sustained with continuous administration of eculizumab throughout the extension study; mean LDH levels were reduced by 86.7 % at the end of the extension period compared with baseline ($P < 0.001$; Table 2). Both of the never-transfused patients showed reductions in LDH levels to within the normal range. As seen in Table 3, there were no significant differences in the mean reduction in LDH from baseline at the end of the study between patients with AA/MDS as well as PNH and patients with PNH alone ($P = 0.876$).

Four patients (14.8 %) had a history of major adverse vascular events at baseline, and 9 patients (33.3 %) were treated with anticoagulation therapy during the extension period. No TEs were reported during the 2-year extension period. Ten patients (37.0 %) had elevated D-dimer levels ($\geq$0.72 mg/mL) at baseline. At the end of the study, D-dimer levels had returned to within normal limits in six of these patients, although no reductions were seen in either of the two patients with a history of major adverse vascular events.

CKD

At baseline, the majority of patients had either CKD stage 0 (37.0 %) or stage 1 (29.6 %). CKD stages 2, 3, and 4 were reported in six patients (22.2 %), two patients (7.4 %), and one patient (3.7 %), respectively. None of the patients had CKD stage 5. During the study, improvements in CKD were seen in 40.7–48.1 % of patients, with a further 48.1–59.3 % of patients showing no changes in CKD. Two patients (7.4 %) showed a worsening of one CKD stage during the study; in one of these patients, normal renal function was restored with continued treatment with eculizumab. Overall, at week 104, patients treated with eculizumab were significantly more likely to show improvement, rather than worsening, in renal function ($P < 0.0005$), with improvements from CKD stage 1, 2, and 3 to CKD stage 0 seen in six patients (22.2 %), four patients (14.8 %), and one patient (3.4 %), respectively. In the two never-transfused patients, one only showed signs of stage 1 CKD at a single assessment (week 44), and the second, with CKD stage 3 at baseline, showed an overall improvement, exhibiting stage 2 or lower CKD at most assessments. Throughout the extension period, mean increases from baseline in glomerular filtration rate were between 107.3 and 145.4 mL/min/1.73 m^2.

Table 2 Effects of eculizumab on mean (SE) changes in efficacy parameters

	Baseline ($n = 27$)	22 weeks ($n = 27$)	Change from baseline	40 weeks ($n = 26$)	Change from baseline	66 weeks ($n = 27$)	Change from baseline	Exit ($n = 26$)	Change from baseline
LDH ($\times 10^2$ U/L)	18.3 (1.23)	2.6 (0.16)	−15.7* (1.18)	2.9 (0.32)	−15.9* (1.20)	2.5 (0.15)	−15.8* (1.20)	2.5 (0.15)	−16.2* (1.15)
PNH type III RBC (%)	43.6 (4.79)	58.3 (5.59)	14.7* (3.64)	56.9 (5.50)	12.4* (4.29)	59.7 (5.88)	16.1* (4.10)	62.5 (5.54)	18.0* (4.28)
PNH RBC ($\times 10^{12}$/L)	1.28 (0.147)	1.81 (0.183)	0.53* (0.102)	1.83 (0.192)	0.51* (0.129)	1.92 (0.198)	0.64* (0.118)	1.99 (0.173)	0.68* (0.128)
Hemoglobin (g/dL)	7.9 (0.30)	9.5 (0.38)	1.6 (0.30)*	9.9 (0.36)	1.9 (0.26)*	10.0 (0.38)	2.1 (0.31)*	10.3 (0.41)	2.4 (0.37)*
Free hemoglobin (mg/dL)	22.4 (2.79)	3.3[a] (1.25)	−19.1* (3.13)	9.6 (8.26)	−13.5* (8.55)	2.3 (0.87)	−20.1* (3.13)	1.5 (0.14)	−21.6* (2.79)
D-dimer (μg/L)	0.9 (0.15)	1.1 (0.27)	0.2 (0.18)	0.8 (0.13)	−0.2 (0.11)	0.7 (0.07)	−0.3** (0.14)	0.8 (0.14)	−0.2 (0.18)
PRBC (U)[b]	5.2 (1.15)	1.7 (0.77)	−3.5*** (1.27)	1.4 (0.81)	−3.5*** (1.43)	0.2 (0.23)	−4.7* (1.20)	0.7 (0.37)	−4.2*** (1.30)
FACIT-Fatigue score	38.3 (2.02)		6.1[c]*** (1.88)		8.0* (1.95)		5.0**** (1.93)		5.2*** (1.84)

* $P < 0.001$; ** $P \leq 0.05$; *** $P < 0.01$; **** $P = 0.02$

[a] 28 weeks

[b] Mean (SE) number of units transfused in 3 months prior to baseline ($n = 27$) and in the 0–3 months ($n = 27$), 3–6 months ($n = 26$), 9–12 months ($n = 26$), and 21–24 months ($n = 26$) following initiation of treatment with eculizumab

[c] 20 weeks

Table 3 Effects of eculizumab on mean (SD) changes in efficacy parameters; comparison between PNH and PNH + AA/MDS groups

	Baseline			End-of-study change from baseline		
	PNH ($n = 15$)	PNH + AA/MDS ($n = 12$)	P value	PNH ($n = 15$)	PNH + AA/MDS ($n = 11$)	P value
LDH, U/L	1875.3 (568.09)	1767.3 (741.82)	0.558	−1634.1 (586.89)	−1610.6 (619.39)	0.876
PNH type III RBC (%)	37.7 (20.81)	50.4 (27.62)	0.294	18.0 (22.27)	18.7 (21.77)	0.836
Hemoglobin (g/L)	86.2 (21.95)	76.3 (13.96)	0.317	16.1 (22.69)	27.2 (19.23)	0.222
FACIT-Fatigue score	36.1 (11.61)	37.3 (9.65)	0.764	5.2 (1.84)	9.6 (2.14)	0.129

Hematological parameters

Inhibition of RBC hemolysis with eculizumab treatment led to a significant overall increase in the percentage of PNH type III RBCs, from a mean of 43.6 % at baseline to 58.3 % at 22 weeks, the first follow-up assessment ($P < 0.001$), and 62.5 % at the end of the extension period ($P < 0.001$; Table 2). In the majority of patients (17 of 27; 63.0 %), the percentage of PNH type III RBCs showed a sharp increase over the initial few months of treatment that then plateaued, with only gradual increases subsequently observed in the percentages of these cells during the remainder of the study. In the other 10 patients (37.0 %), the percentage of PNH type III RBCs either remained constant or showed small but continued decreases over time. In addition to the increase in the number of RBCs, there was an 85.7 % reduction in the mean number of units of PRBC transfused per patient, from 4.9 in the 3 months prior to initiation of treatment to 0.7 U in the last 3 months of the extension period ($P = 0.0016$; Table 2). The percentage of transfusion-independent patients increased rapidly, from 40.7 % at baseline to 70.4 % in the first 6 months of treatment with eculizumab, with 96 % of patients being transfusion free in the last 6 months of the extension period (Fig. 1). Both of the never-transfused patients and 10 of the 21 patients (47.6 %) who had received one or more transfusions in the 12 weeks prior to initiation of eculizumab therapy did not require any transfusions during the study.

Parallel with the decrease in transfusion requirement, there was a continuous improvement in average hemoglobin levels over time. Hemoglobin levels increased by 13.2 % ($P \leq 0.001$) at week 14 (the second week of the extension period) and by 30.8 % ($P < 0.001$) at the end of the study (Table 2). There were concomitant decreases in mean free hemoglobin of 85.3 and 93.3 % at week 14 and the end of the study, respectively ($P < 0.001$ in each case).

Eculizumab was equally effective in patients with both PNH and AA/MDS and in those with PNH alone; there

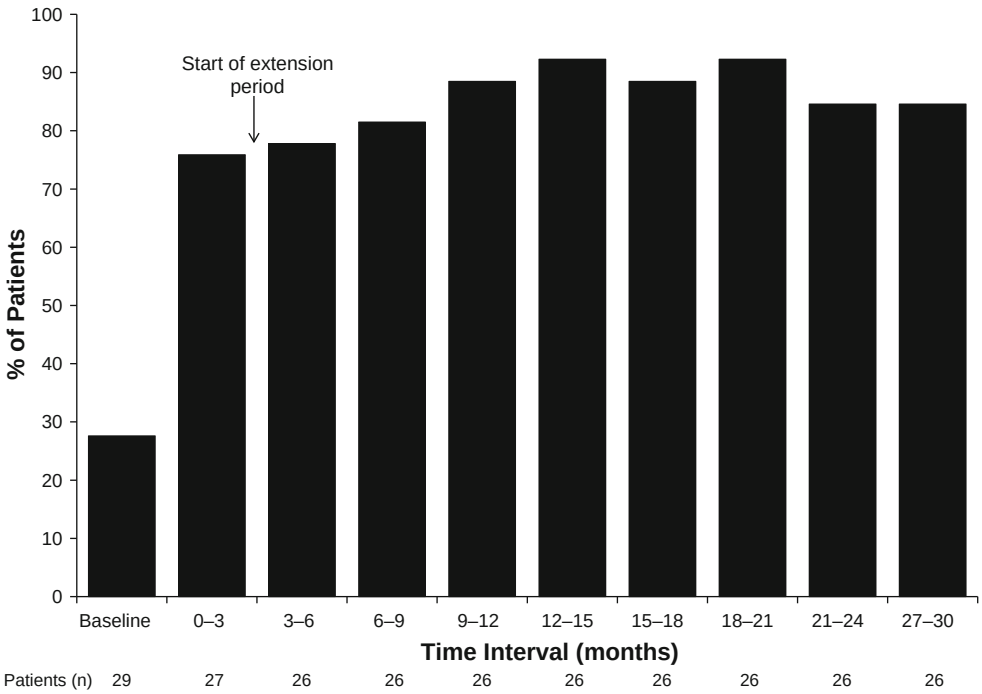

Fig. 1 Percentage of patients who did not require a blood transfusion (were transfusion independent) by time interval

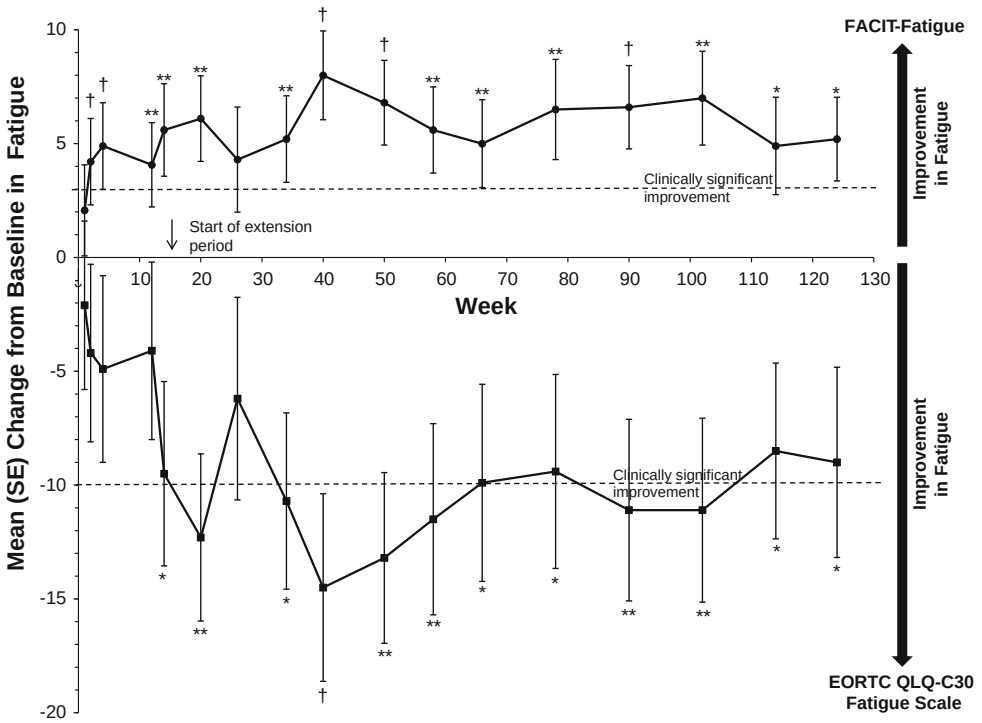

Fig. 2 Changes in FACIT-Fatigue and EORTC QLQ-C30 fatigue scores with long-term administration of eculizumab. $*P < 0.05$. $**P < 0.01$. $^{\dagger}P < 0.001$. *P* values are determined from Wilcoxon signed-rank test

were no statistically significant differences observed between the groups in the level of hemoglobin or percentage of PNH type III RBCs at baseline or in the change from baseline to end of study (Table 3).

Although changes in hematological parameters were not a specific study endpoint, preliminary comparisons in these parameters were made between patients with PNH and AA/MDS and those with only PNH. The presence of an underlying bone marrow failure did not appear to have any impact on recovery of platelet levels, but there was evidence to suggest that white blood cells and hemoglobin increased following initiation of treatment with eculizumab, particularly in patients with a history of AA/MDS. This was most evident for hemoglobin levels; mean (standard deviation) change from baseline to end of study was 16.1 (22.69) g/L in patients with no underlying bone marrow failure compared with 27.2 (19.23) g/L in patients with a history of AA/MDS. The difference between the groups was not statistically significant ($P = 0.222$), though this is perhaps not surprising, given the small number of patients in each group.

FACIT-Fatigue and quality of life

During the original 12-week study, a clinically meaningful improvement in fatigue, defined as at least a 3-point increase on the FACIT-Fatigue scale [31, 34], was observed after 2 weeks of eculizumab treatment [30]. Alleviation of fatigue was maintained throughout the extension period, as shown by both FACIT-Fatigue and EORTC QLQ-C30 fatigue assessments (Fig. 2), with the majority of patients showing clinically meaningful improvements. Although fluctuations were seen in the changes from baseline in fatigue, both assessments gave similar results and showed that there was a consistent improvement in fatigue throughout the study that achieved statistical significance at all but one assessment (week 26). Results from the linear mixed-effects model analysis showed that the reduction in FACIT-Fatigue was highly significant ($P < 0.00001$). FACIT-Fatigue scores at baseline and the change in scores at the end of the study were similar in patients with PNH plus AA/MDS and in those with PNH alone (Table 3). In the two patients who had never received any transfusions, FACIT-Fatigue scores were reduced by 26 % (from 19 to 14) and 41 % (from 46 to 27) between baseline and week 114.

Mean changes from baseline in EORTC QLQ-C30 assessments are shown in Fig. 3. Overall results from the linear mixed-effects model analysis showed that treatment with eculizumab was associated with significant improvements in global health status and quality of life ($P = 0.015$) and role and physical functioning (both $P < 0.001$), as well as the symptoms of fatigue ($P < 0.001$), dyspnea ($P < 0.001$), and appetite loss ($P = 0.015$). For the EORTC QLQ-C30 analysis of fatigue, a median improvement of 11.1 points was seen at each of the assessments throughout the extension period, except at 102 weeks (when there was a median improvement of 5.6 points). Using this scale, an

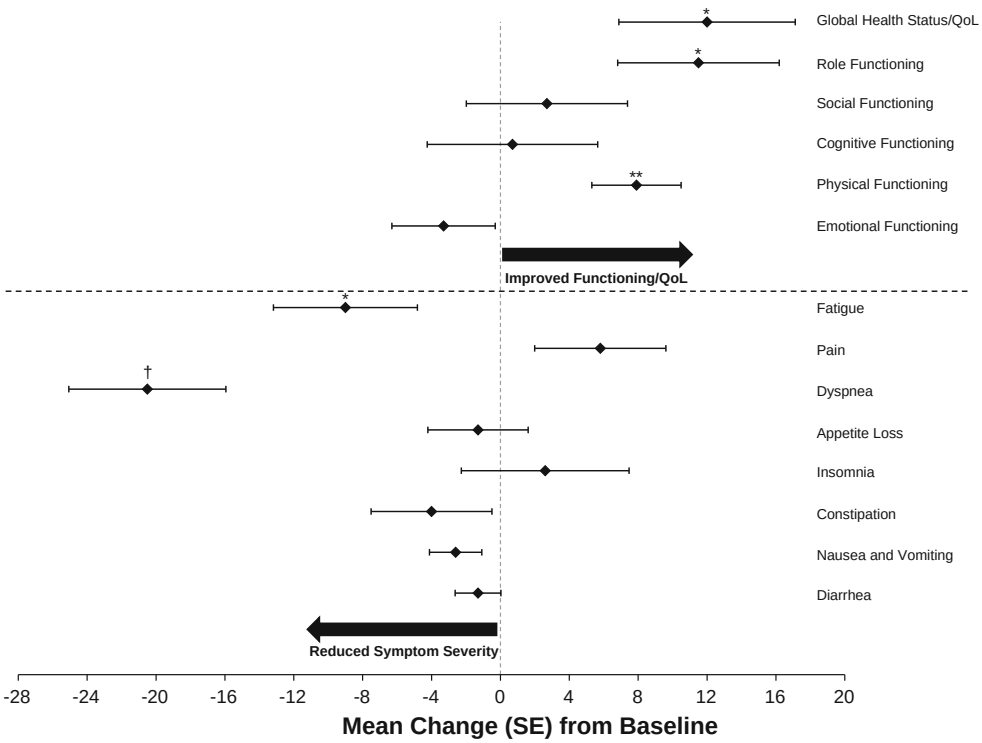

Fig. 3 Changes in EORTC QLQ-C30 scores with long-term administration of eculizumab. *$P < 0.05$. **$P < 0.01$. †$P < 0.001$. P values are determined from Wilcoxon signed-rank test (*QoL* quality of life)

Table 4 AEs reported in >10 % of patients during the extension study

Preferred term	Number (%) of patients ($N = 27$)		
	First 12 weeks of treatment[a]	Last 12 weeks of treatment	Overall
At least one AE	26 (96.3)	11 (40.7)	26 (96.3)
Nasopharyngitis	12 (44.4)	4 (14.8)	21 (77.8)
Upper respiratory tract infection	0	0	7 (25.9)
Headache	14 (51.9)	0	6 (22.2)
Gastroenteritis	0	0	5 (18.5)
Anemia	2 (7.4)	0	4 (14.8)
Diarrhea	4 (14.8)	0	4 (14.8)
Pneumonia	0	1 (3.7)	4 (14.8)
Pyrexia	2 (7.4)	2 (7.4)	4 (14.8)
Blood alkaline phosphatase increased	2 (7.4)	0	3 (11.1)
Contusion	0	0	3 (11.1)
Epistaxis	0	1 (3.7)	3 (11.1)
Pharyngitis	1 (3.7)	1 (3.7)	3 (11.1)

[a] As reported in the original 12-week study

improvement of at least 10 points in global health status is considered clinically meaningful [35]. All improvements in fatigue were statistically significant ($P < 0.05$), with the exception of the results at week 26.

Safety

Overall, 26 of 27 patients reported at least one AE. All AEs reported in three or more patients are presented in Table 4. The treatment-emergent AEs reported in the highest proportion of patients were nasopharyngitis (seen in 77.8 % of patients), upper respiratory tract infection (seen in 25.9 %), and headache (seen in 22.2 %). The majority of AEs (97.5 %) were mild to moderate in intensity. Seven AEs reported in five patients were considered severe, and all of the severe events were also considered serious. SAEs were reported by 12 of the 27 patients, with the majority of SAEs (75.0 %) being of mild or moderate intensity. No

Table 5 Serious infection-related treatment-emergent AEs reported during eculizumab therapy

AE	Number (%) of patients[a]
Pneumonia	4 (14.8)
Bronchitis	1 (3.7)
Cellulitis	1 (3.7)[b]
Herpes infection	1 (3.7)
Sepsis	1 (3.7)[b]
Upper respiratory tract infection	1 (3.7)
Viral gastroenteritis	1 (3.7)

[a] Patients may have experienced more than one infection. One of the pneumonia infections, along with the events of cellulitis and sepsis, was considered probably related to treatment; all of the other serious infections were considered possibly related to treatment

[b] Event leading to study discontinuation (both cellulitis and sepsis were reported in the same patient)

patients died during the study, there were no withdrawals as a result of an AE, and there were no major adverse vascular events or serious hemolytic events reported. The patient who did not complete the study was asked to withdraw because she no longer wished to continue the study; the SAEs experienced by this patient were not reported as reasons for withdrawal.

In order to investigate whether long-term treatment with eculizumab increased the incidence of any individual AE or category of AE or whether eculizumab was associated with cumulative toxicity, the incidence of AEs (irrespective of relation to treatment) during the first 12 weeks of eculizumab treatment was compared with the incidence during the last 12 weeks of treatment (Table 4). Overall, significantly fewer patients reported at least one AE in the last 12 weeks of treatment ($n = 11$) than in the first 12 weeks of treatment ($n = 26$; $P < 0.001$), and the majority of the most frequently reported AEs were not reported at all during the last 12 weeks of treatment. Treatment-emergent infections were reported in 25 patients (92.6 %), with 139 of the 159 reported infections (87.4 %) considered mild in severity. Six of the 159 infections (3.8 %) reported during the extension period were considered probably related to therapy with eculizumab, of which three (one case each of pneumonia, cellulitis, and sepsis) were severe. Besides nasopharyngitis and upper respiratory tract infection, the infection seen in the highest proportion of patients was gastroenteritis (seen in 18.5 % of patients). Serious treatment-emergent infections were reported in seven patients (25.9 %), with all considered possibly or probably related to treatment. Only one of these serious infections, pneumonia, was reported in more than one patient; all serious infection-related AEs are presented in Table 5. There were no staphylococcal or meningococcal infections reported.

Discussion

The results of this long-term efficacy and safety study demonstrate that eculizumab is effective and well tolerated over the long term in Japanese patients with PNH. The results for the primary endpoint of the study, decrease in serum LDH levels as a measure of reduced hemolysis, showed that eculizumab rapidly reduced complement-mediated hemolysis, with a significant decrease in LDH seen after 1 week of treatment. At the end of the original 12-week study, LDH levels had decreased by 78 % from baseline [30], which was sustained throughout the 2-year extension period, with LDH levels at the end of the study being 87 % lower than at baseline. Despite the effectiveness of eculizumab in reducing LDH levels, some patients still showed occasional assessments above the upper limit of normal (240 U/L), probably due to low-level extravascular hemolysis resulting from the binding of C3 to RBCs [36].

TE is the leading cause of mortality in PNH patients, and patients with a history of TE have a five-fold greater risk of developing further TEs [2]. It has been postulated that the clinical manifestations of PNH differ between Western and Asian populations, with TEs occurring less frequently in Asian patients [19]. In this study, 15 % of the 27 Japanese patients who entered the long-term extension study had a history of TE, which is slightly less than the 20 % of Western patients in the pivotal phase III eculizumab clinical trial (TRIUMPH) [37] and the 18 % of patients in the South Korean National PNH Registry [38]. Furthermore, 37 % of patients in the extension study had elevated D-dimer levels, which suggest subclinical, unreported TE [39]. During this long-term study, no TEs were reported during eculizumab treatment, which is consistent with results from previously published international studies, which demonstrated a 92 % reduction in TE rate [4, 22]. Although anticoagulant therapy has been used to reduce the risk of thrombosis in PNH patients [40], anticoagulation therapy alone may not effectively prevent the occurrence of TEs [4, 41–43], does not protect PNH patients from the adverse effects of hemolysis, and is associated with a small but significant risk of severe bleeding [44].

Even in PNH patients with no clinical signs of TE, subclinical emboli can still be present and may be associated with pulmonary hypertension and abdominal pain, which are frequently seen in PNH patients [45]. International studies in Western populations have shown that PNH patients have elevated levels of prothrombotic and proinflammatory markers, which have been effectively reduced following initiation of eculizumab therapy [9, 46]. Consistent with these results, the percentage of patients with elevated D-dimer levels was reduced from 37 % prior to

eculizumab therapy to 15 % at the end of the extension study.

Renal failure has been reported to occur in 11 % of Japanese patients with PNH and accounts for 18 % of PNH-related deaths in Japanese patients [19]. Long-term exposure to cell-free hemoglobin causes hemosiderin accumulation and tubule-interstitial inflammation [47], which, in association with microvascular thromboses [16], leads to renal dysfunction and failure. In the present study, we observed that 63 % of patients showed evidence of CKD at baseline (11 % with CKD stage 3 or 4) [30], which is consistent with the previously reported results in Western patients [16]. Sustained administration of eculizumab improved or stabilized renal function in 71 and 29 % of patients with CKD at baseline, respectively; one patient with normal renal function at the start of the study showed deterioration in kidney status. Improvements in renal function were observed in 88 % of patients with stage 1 CKD, 67 % of patients with stage 2 CKD, and 33 % of patients with stage 3–4 CKD. These results suggest that eculizumab can improve renal function, particularly if administered early in the course of disease and before the kidney is more severely impaired.

In contrast to the reported 5-year survival rate of 65 % in PNH patients prior to the introduction of eculizumab [1, 4], the 2-year survival rate in this study with eculizumab treatment was 100 %, despite the presence of known risk factors for poor outcomes amongst the patient population. This is consistent with results from a previously reported single-center, retrospective analysis of 79 PNH patients receiving eculizumab, who showed a 5-year survival rate of 96 %, which was similar to an age- and gender-matched normal population [4]. The 100 % survival of patients throughout this study demonstrates the importance of preventing TE and renal impairment, the leading causes of death in PNH patients.

In addition to reducing TE, the inhibition of intravascular hemolysis has led to a reduction in the total number of transfusions required and resulted in a 48 % reduction in the number of patients requiring any transfusions, with 96 % of patients being transfusion free in the final 6 months of the extension period. This is consistent with the results previously reported in the long-term, multinational phase III PNH clinical trials in Western patients [22, 29, 36]. However, the number of transfusions required does not provide a full reflection of the burden of disease in patients with PNH [48]. The role of hemolysis is important in determining the risk of morbidity and mortality in PNH patients. The two patients who had not received transfusions prior to the study had LDH 1.3- and 1.6-fold above normal and had a burden of disease at baseline similar to the rest of the patient population, including morbidities as severe as CKD stage 3 and deep vein thrombosis [30], and both patients showed a response to chronic eculizumab treatment comparable to patients receiving transfusions. Their hemoglobin concentrations remained stable or improved, and their fatigue levels were significantly improved. In addition, while one of the non-transfused patients had previously experienced a deep vein thrombosis, neither of the two experienced TEs during eculizumab therapy. These findings suggest that PNH patients with even slightly elevated LDH levels are at an increased risk for morbidity and mortality and such patients should be considered for treatment to reduce hemolysis to normal levels.

This study showed that the burden of PNH disease and baseline characteristics were similar in patients with and without a history of bone marrow dysfunction such as AA or MDS. Although it has been shown that the presence of minor populations of PNH-type cells in patients with AA is a reliable marker of a positive response to treatment with immunosuppressive therapy [49], PNH and AA are distinct diseases that require separate treatments. There were no significant differences between patients with PNH plus AA/MDS and those with PNH alone in any of the endpoints assessed, which confirm that patients with PNH and AA/MDS experience similar hemolysis-associated complications and can benefit from treatment with eculizumab.

The results from this study also confirm the effectiveness of eculizumab in alleviating clinical symptoms which contribute to the overall burden of disease in PNH. Fatigue, which is frequently debilitating in PNH patients, was alleviated by eculizumab treatment, and this improvement contributed to overall significant increases in global health status and quality of life. Results of the initial 12-week study [30] showed no association between level of fatigue and degree of anemia. Treatment with eculizumab resulted in a significant reduction in fatigue within 2 weeks of starting treatment, while recovery of hemoglobin levels was more gradual, with significant increases in hemoglobin to normal levels not seen until after 8 weeks of treatment. These results are in agreement with other international studies [25, 50]. Reduction in fatigue coincided with improvements in intravascular hemolysis; this suggests that the fatigue experienced by PNH patients is not just as a result of anemia but is associated with complement-mediated hemolysis or other hemoglobin-independent mechanisms. Significant improvements were also observed in dyspnea, which, along with symptoms of pulmonary hypertension and erectile dysfunction, results from nitric oxide consumption and subsequent smooth muscle dystonia and vascular constriction [25]. As with fatigue, the improvements in dyspnea were not dependent on improvement in hemoglobin.

The data collected over the 2-year extension study showed that long-term eculizumab treatment was well

tolerated. As would be expected in a study of this duration, most patients experienced at least one AE over 2 years. However, nearly 98 % of all AEs reported were of mild or moderate intensity, and only five patients had AEs that were considered to be severe. Most importantly, the incidence of AEs decreased over time, with significantly fewer AEs in the last 12 weeks of treatment than in the first 12 weeks of treatment. The data suggest that long-term treatment with eculizumab does not lead to increased susceptibility to infections.

A total of 159 infections were reported during the extension, with only seven of these infections (4 %) considered probably related to eculizumab. No patients withdrew from the study due to an AE, indicating that eculizumab is well tolerated over the long term. The safety profile was consistent with that reported in the multinational phase III trials of eculizumab [29, 37].

In summary, long-term administration of eculizumab to Japanese patients with PNH provided sustained clinical benefit by reducing terminal complement activation and chronic intravascular hemolysis, which is the cause of many of the disabling symptoms and life-threatening complications of PNH. These results were not only clinically meaningful and achieved against a background of known risk factors for poor outcomes in PNH patients, but were also reflected in the enhanced quality of life experienced by the patients and the 100 % survival of patients despite a mean duration of disease in excess of 10 years. The results from this study are consistent with those reported in Western PNH patient populations, showing that eculizumab is an effective and well-tolerated treatment for PNH across different ethnic populations.

Acknowledgments The authors would like to thank Gus Khursigara, PhD, for providing insightful comments on the manuscript; Masakazu Hase, PhD, for assistance with coordinating the manuscript preparation; and Mark Hughes, PhD, and Joshua Safran of Infusion Communications for writing and editorial support, which was funded by Alexion Pharmaceuticals.

Conflict of interest YK has received research funding and been a consultant and board member for Alexion Pharmaceuticals. H. Ninomiya has received honoraria for lectures from Alexion Pharmaceuticals. T. Kawaguchi has received honoraria for lectures from Alexion Pharmaceuticals and works for an institution that has received research funding from Alexion Pharmaceuticals. SN works for an institution that has received research support from Alexion Pharmaceuticals. H. Nakakuma has received honoraria for lectures from Alexion Pharmaceuticals. J-IN has received research grants from and been a consultant and board member for Alexion Pharmaceuticals. T. Kinoshita has received honoraria for lectures from Alexion Pharmaceuticals. CLB is an employee of and owns stock in Alexion Pharmaceuticals. MO has received consulting fees/honoraria, travel support, and payments for development of educational presentations from Alexion Pharmaceuticals. K. Ohyashiki, TS, SO, KA, and K. Ozama have no conflicts of interest to declare.

References

1. Hillmen P, Lewis SM, Bessler M, Luzzatto L, Dacie JV. Natural history of paroxysmal nocturnal hemoglobinuria. N Engl J Med. 1995;33319:1253–8.
2. Socié G, Mary JY, de Gramont A, Rio B, Leporrier M, Rose C, et al. Paroxysmal nocturnal haemoglobinuria: long-term follow-up and prognostic factors. French Society of Haematology. Lancet. 1996;3489027:573–7.
3. Parker C, Omine M, Richards S, Nishimura J, Bessler M, Ware R, et al. Diagnosis and management of paroxysmal nocturnal hemoglobinuria. Blood. 2005;10612:3699–709.
4. Kelly RJ, Hill A, Arnold LM, Brooksbank GL, Richards SJ, Cullen M, et al. Long-term treatment with eculizumab in paroxysmal nocturnal hemoglobinuria: sustained efficacy and improved survival. Blood. 2011;11725:6786–92.
5. Takeda J, Miyata T, Kawagoe K, Iida Y, Endo Y, Fujita T, et al. Deficiency of the GPI anchor caused by a somatic mutation of the PIG-A gene in paroxysmal nocturnal hemoglobinuria. Cell. 1993;734:703–11.
6. Yamada N, Miyata T, Maeda K, Kitani T, Takeda J, Kinoshita T. Somatic mutations of the PIG-A gene found in Japanese patients with paroxysmal nocturnal hemoglobinuria. Blood. 1995;854:885–92.
7. Bessler M, Mason PJ, Hillmen P, Miyata T, Yamada N, Takeda J, et al. Paroxysmal nocturnal haemoglobinuria (PNH) is caused by somatic mutations in the PIG-A gene. EMBO J. 1994;131:110–7.
8. Audebert HJ, Planck J, Eisenburg M, Schrezenmeier H, Haberl RL. Cerebral ischemic infarction in paroxysmal nocturnal hemoglobinuria report of 2 cases and updated review of 7 previously published patients. J Neurol. 2005;25211:1379–86.
9. Helley D, de Latour RP, Porcher R, Rodrigues CA, Galy-Fauroux I, Matheron J, et al. Evaluation of hemostasis and endothelial function in patients with paroxysmal nocturnal hemoglobinuria receiving eculizumab. Haematologica. 2010;954:574–81.
10. Lewis SM, Dacie JV. The aplastic anaemia–paroxysmal nocturnal haemoglobinuria syndrome. Br J Haematol. 1967;132:236–51.
11. Griscelli-Bennaceur A, Gluckman E, Scrobohaci ML, Jonveaux P, Vu T, Bazarbachi A, et al. Aplastic anemia and paroxysmal nocturnal hemoglobinuria: search for a pathogenetic link. Blood. 1995;855:1354–63.
12. Mortazavi Y, Merk B, McIntosh J, Marsh JC, Schrezenmeier H, Rutherford TR. The spectrum of PIG-A gene mutations in aplastic anemia/paroxysmal nocturnal hemoglobinuria (AA/PNH): a high incidence of multiple mutations and evidence of a mutational hot spot. Blood. 2003;1017:2833–41.
13. Galili N, Ravandi F, Palmero G, Bubis J, Illingworth A, Castro-Malaspina H, et al. Prevalence of paroxysmal nocturnal hemoglobinuria (PNH) cells in patients with myelodysplastic syndromes (MDS), aplastic anemia (AA), or other bone marrow failure (BMF) syndromes: Interim results from the EXPLORE trial. J Clin Oncol. 2009;27(Suppl 15):7082.
14. McKeage K. Eculizumab: a review of its use in paroxysmal nocturnal haemoglobinuria. Drugs. 2011;7117:2327–45.
15. Drey N, Roderick P, Mullee M, Rogerson M. A population-based study of the incidence and outcomes of diagnosed chronic kidney disease. Am J Kidney Dis. 2003;424:677–84.
16. Hillmen P, Elebute M, Kelly R, Urbano-Ispizua A, Hill A, Rother RP, et al. Long-term effect of the complement inhibitor eculizumab on kidney function in patients with paroxysmal nocturnal hemoglobinuria. Am J Hematol. 2010;858:553–9.
17. Rother RP, Bell L, Hillmen P, Gladwin MT. The clinical sequelae of intravascular hemolysis and extracellular plasma hemoglobin: a novel mechanism of human disease. JAMA. 2005;29313:1653–62.

18. Qian Q, Nath KA, Wu Y, Daoud TM, Sethi S. Hemolysis and acute kidney failure. Am J Kidney Dis. 2010;564:780–4.
19. Nishimura J, Kanakura Y, Ware RE, Shichishima T, Nakakuma H, Ninomiya H, et al. Clinical course and flow cytometric analysis of paroxysmal nocturnal hemoglobinuria in the United States and Japan. Medicine (Baltimore). 2004;833:193–207.
20. Hill A, Richards SJ, Hillmen P. Recent developments in the understanding and management of paroxysmal nocturnal haemoglobinuria. Br J Haematol. 2007;1373:181–92.
21. Parker CJ. The pathophysiology of paroxysmal nocturnal hemoglobinuria. Exp Hematol. 2007;354:523–33.
22. Hillmen P, Muus P, Dührsen U, Risitano AM, Schubert J, Luzzatto L, et al. Effect of the complement inhibitor eculizumab on thromboembolism in patients with paroxysmal nocturnal hemoglobinuria. Blood. 2007;11012:4123–8.
23. Kim JS, Lee JW, Yoon SS, Lee JH, Jo DY, Jang JH, et al. Association between elevated hemolysis at diagnosis and early mortality and risk of thrombosis in paroxysmal nocturnal hemoglobinuria (PNH) patients with cytopenia. Blood. 2010;11621: 4241.
24. Kim JS, Jang JH, Lee JW, Yoon SS, Lee JH, Kim YK, et al. Renal impairment ia a risk factor for early mortality in patients with paroxysmal nocturnal haemoglobinuria (PNH). Haematologica. 2011;96(Suppl 2):112.
25. Hill A, Rother RP, Wang X, Morris SM Jr, Quinn-Senger K, Kelly R, et al. Effect of eculizumab on haemolysis-associated nitric oxide depletion, dyspnoea, and measures of pulmonary hypertension in patients with paroxysmal nocturnal haemoglobinuria. Br J Haematol. 2010;1493:414–25.
26. Lee J, Jun Ho J, Sung Soo Y, Jin Seok K, Yeo Kyung K, Deog Yeon C, et al. High prevalence and mortality associated with thromboembolism in Asian patients with paroxysmal nocturnal hemglobinuria (PNH). Haematologica. 2010;95(Suppl 2):205–6.
27. Rother RP, Rollins SA, Mojcik CF, Brodsky RA, Bell L. Discovery and development of the complement inhibitor eculizumab for the treatment of paroxysmal nocturnal hemoglobinuria. Nat Biotechnol. 2007;2511:1256–64.
28. Hillmen P, Hall C, Marsh JC, Elebute M, Bombara MP, Petro BE, et al. Effect of eculizumab on hemolysis and transfusion requirements in patients with paroxysmal nocturnal hemoglobinuria. N Engl J Med. 2004;3506:552–9.
29. Brodsky RA, Young NS, Antonioli E, Risitano AM, Schrezenmeier H, Schubert J, et al. Multicenter phase 3 study of the complement inhibitor eculizumab for the treatment of patients with paroxysmal nocturnal hemoglobinuria. Blood. 2008;1114: 1840–7.
30. Kanakura Y, Ohyashiki K, Shichishima T, Okamoto S, Ando K, Ninomiya H, et al. Safety and efficacy of the terminal complement inhibitor eculizumab in Japanese patients with paroxysmal nocturnal hemoglobinuria: the AEGIS clinical trial. Int J Hematol. 2011;931:36–46.
31. Webster K, Cella D, Yost K. The Functional Assessment of Chronic Illness Therapy (FACIT) Measurement System: properties, applications, and interpretation. Health Qual Life Outcomes. 2003;1:79.
32. National Kidney Foundation. K/DOQI clinical practice guidelines for chronic kidney disease: evaluation, classification, and stratification. Am J Kidney Dis. 2002;392(Suppl 1):S1–266.
33. Aaronson NK, Ahmedzai S, Bergman B, Bullinger M, Cull A, Duez NJ, et al. The European Organization for Research and Treatment of Cancer QLQ-C30: a quality-of-life instrument for use in international clinical trials in oncology. J Natl Cancer Inst. 1993;855:365–76.
34. Cella D, Lai JS, Chang CH, Peterman A, Slavin M. Fatigue in cancer patients compared with fatigue in the general United States population. Cancer. 2002;942:528–38.
35. Cocks K, King MT, Velikova G, Fayers PM, Brown JM. Quality, interpretation and presentation of European Organisation for Research and Treatment of Cancer quality of life questionnaire core 30 data in randomised controlled trials. Eur J Cancer. 2008;4413:1793–8.
36. Risitano AM, Notaro R, Marando L, Serio B, Ranaldi D, Seneca E, et al. Complement fraction 3 binding on erythrocytes as additional mechanism of disease in paroxysmal nocturnal hemoglobinuria patients treated by eculizumab. Blood. 2009;113: 4094–100.
37. Hillmen P, Young NS, Schubert J, Brodsky RA, Socié G, Muus P, et al. The complement inhibitor eculizumab in paroxysmal nocturnal hemoglobinuria. N Engl J Med. 2006;35512:1233–43.
38. Kim JS, Jang JH, Lee JW, Yoon SS, Lee JH, Kim YK, et al. Renal impairment is a risk factor for early mortality in patients with paroxysmal nocturnal hemoglobinuria (PNH). 2011. Presented at the 16th Congress of the European Hematology Association (EHA); June 9–12, 2011; London, UK.
39. Pottier P, Fouassier M, Hardouin JB, Volteau C, Planchon B. D-dimers, thrombin-antithrombin complexes, and risk factors for thromboembolism in hospitalized patient. Clin Appl Thromb Hemost. 2009;156:666–75.
40. Hall C, Richards S, Hillmen P. Primary prophylaxis with warfarin prevents thrombosis in paroxysmal nocturnal hemoglobinuria (PNH). Blood. 2003;10210:3587–91.
41. Cheng KL, Brody J, Warshall CE, Sloand EM, Allen SL. Paroxysmal nocturnal hemoglobinuria following alemtuzumab immunosuppressive therapy for myelodysplastic syndrome and complicated by recurrent life-threatening thrombosis despite anticoagulation: successful intervention with eculizumab and fondaparinux. Leuk Res. 2010;344:e85–7.
42. Moyo VM, Mukhina GL, Garrett ES, Brodsky RA. Natural history of paroxysmal nocturnal haemoglobinuria using modern diagnostic assays. Br J Haematol. 2004;1261:133–8.
43. de Latour RP, Mary JY, Salanoubat C, Terriou L, Etienne G, Mohty M, et al. Paroxysmal nocturnal hemoglobinuria: natural history of disease subcategories. Blood. 2008;1128:3099–106.
44. Palareti G, Leali N, Coccheri S, Poggi M, Manotti C, D'Angelo A, et al. Bleeding complications of oral anticoagulant treatment: an inception-cohort, prospective collaborative study (ISCOAT). Italian Study on Complications of Oral Anticoagulant Therapy. Lancet. 1996;3489025:423–8.
45. Hill A, Sapsford RJ, Scally A, Kelly R, Richards SJ, Khurisgara G, et al. Under-recognized complications in patients with paroxysmal nocturnal haemoglobinuria: raised pulmonary pressure and reduced right ventricular function. Br J Haematol. 2012; 1583:409–14.
46. Weitz IC, Razavi P, Rochanda L, Zwicker J, Furie B, Manly D, et al. Eculizumab therapy results in rapid and sustained decreases in markers of thrombin generation and inflammation in patients with PNH independent of its effects on hemolysis and microparticle formation. Thromb Res. 2012;1303:361–8.
47. Nath KA, Vercellotti GM, Grande JP, Miyoshi H, Paya CV, Manivel JC, et al. Heme protein-induced chronic renal inflammation: suppressive effect of induced heme oxygenase-1. Kidney Int. 2001;591:106–17.
48. Jang JH, Lee JW, Kim JS, Yoon SS, Lee JH, Kim YK, et al. Poor clinical outcomes in non transfused patients with paroxysmal nocturnal hemoglobinuria (PNH). Haematologica. 2011;96(Suppl 2):595.
49. Sugimori C, Chuhjo T, Feng X, Yamazaki H, Takami A, Teramura M, et al. Minor population of CD55-CD59-blood cells predicts response to immunosuppressive therapy and prognosis in patients with aplastic anemia. Blood. 2006;1074:1308–14.
50. Brodsky RA. Advances in the diagnosis and therapy of paroxysmal nocturnal hemoglobinuria. Blood Rev. 2008;222:65–74.

OPEN ACCESS Freely available online

PLOS ONE

High Concentrations of L-Ascorbic Acid Specifically Inhibit the Growth of Human Leukemic Cells via Downregulation of *HIF-1α* Transcription

Hiroshi Kawada[1,2*☯], Mitsuyo Kaneko[1,2☯], Masakazu Sawanobori[1], Tomoko Uno[2], Hideyuki Matsuzawa[2], Yoshihiko Nakamura[2], Hiromichi Matsushita[2,3], Kiyoshi Ando[1,2]

1 Division of Hematology/Oncology, Department of Medicine, Tokai University School of Medicine, Isehara, Kanagawa, Japan, **2** Research Center for Regenerative Medicine, Tokai University School of Medicine, Isehara, Kanagawa, Japan, **3** Department of Laboratory Medicine, Tokai University School of Medicine, Isehara, Kanagawa, Japan

Abstract

We examined the antileukemic effects of high concentrations of L-ascorbic acid (high AA) on human leukemic cells. In vitro, high AA markedly induced apoptosis in various leukemic cell lines by generating hydrogen peroxide (H_2O_2) but not in normal hematopoietic stem/progenitor cells. High AA significantly repressed leukemic cell proliferation as well as neoangiogenesis in immunodeficient mice. We then noted that in leukemic cells, *HIF-1α* transcription was strongly suppressed by high AA and correlated with the transcription of *VEGF*. Our data indicate that exposure to high AA markedly increased the intracellular AA content of leukemic cells and inhibited the nuclear translocation of NF-κB, which mediates expression of HIF-1α. We next generated K562 cells that overexpressed *HIF-1α* (K562-HIF1α cells) and assessed the mechanistic relationship between inhibition of *HIF-1α* transcription and the antileukemic effect of high AA. The ability of high AA to induce apoptosis was significantly lower in K562-HIF1α cells than in K562 cells in vitro. We found that expression of HIF-1α-regulated antiapoptotic proteins of the Bcl-2 family, such as Mcl-1, Bcl-x_L, and Bcl-2, was significantly suppressed by high AA in K562 cells, but was sustained at higher levels in K562-HIF1α cells, regardless of high AA exposure. Moreover, repression of cell proliferation and neoangiogenesis by high AA was completely abrogated in mice receiving transplants of K562-HIF1α cells. These results indicate that, along with H_2O_2 generation, downregulation of *HIF-1α* transcription plays a crucial role in growth inhibition of human leukemic cells by high AA.

Citation: Kawada H, Kaneko M, Sawanobori M, Uno T, Matsuzawa H, et al. (2013) High Concentrations of L-Ascorbic Acid Specifically Inhibit the Growth of Human Leukemic Cells via Downregulation of *HIF-1α* Transcription. PLoS ONE 8(4): e62717. doi:10.1371/journal.pone.0062717

Editor: Amina Ann Qutub, Rice University, United States of America

Received July 10, 2012; **Accepted** March 25, 2013; **Published** April 23, 2013

Funding: This work was supported by grants from Tokai University and The Ministry of Education, Culture, Sports, Science, and Technology of Japan (MEXT)-Supported Program for the Strategic Research Foundation at Private Universities. The funders had no role in study design, data collection and analysis, decision to publish, or preparation of the manuscript.

Competing Interests: The authors have declared that no competing interests exist.

* E-mail: hkawada@is.icc.u-tokai.ac.jp

☯ These authors contributed equally to this work.

Introduction

Pauling and Cameron were the first to report that when L-ascorbic acid (AA) was given intravenously to human cancer patients for 10 days and then orally in pharmacologic doses of 10 g daily, it was effective in treating some cancers and in improving patient survival [1,2]. The same oral dose had no therapeutic effects on cancer patients in 2 subsequent double-blind placebo-controlled trials [3,4]. However, we thought that it was important to examine anew the role of AA in cancer treatment for the reasons that follow: (i) the route of AA administration leads to large differences in plasma concentrations, and intravenous administration results in 70-times higher plasma concentration than oral administration [5]; (ii) high concentrations of AA (high AA) administered intravenously exert remarkable anticancer effects by generating hydrogen peroxide (H_2O_2) in the extracellular fluid of tumor-bearing animals [6,7]; and (iii) recent clinical studies also demonstrate the antitumor effects of intravenous high AA in patients with different types of cancers [8,9]. Further, it is remarkable that the cytotoxic effects of high AA appear to be cancer cell-type specific [7].

In the present study, we attempted, therefore, to determine whether high AA exerts significant cytotoxic effects against human leukemic cells in vitro and in vivo. We confirm here that the leukemic cell-specific cytotoxic effects of high AA were caused by the generation of H_2O_2. Further, while HIF-1α plays an important role biologically and clinically in myeloid and lymphoid leukemias [10–15], we found that high AA strongly inhibited HIF-1α expression in leukemic cells.

HIF-1 is composed of an inducible (HIF-1α) and a constitutively expressed subunit (HIF-1β) [16]. HIF-1α contains an oxygen-dependent degradation domain, which when hydroxylated by specific prolyl hydroxylases, binds the von Hippel–Lindau protein, leading to the ubiquitination of HIF-1α and its degradation by the 26S proteasome. At low oxygen levels, the prolyl hydroxylases lose their activity, which prevents hydroxylation and subsequent binding to the von Hippel–Lindau protein [17,18]. This results in HIF-1α stabilization, nuclear translocation, dimerization with

the β-subunit, and binding to recognition elements in the promoters of target genes.

AA facilitates the hydroxylation of HIF-1α via the stimulation of the prolyl hydroxylases [19,20]. However, we have shown here that high AA markedly inhibit the expression of HIF-1α in leukemic cells at the level of transcription. We have further demonstrated that one important mechanism underlying this response is the transcriptional regulation of HIF-1α by the redox-sensitive transcription factor NF-κB, which has been shown to bind at a distinct element in the proximal promoter of *HIF-1α* under not only hypoxic but also non-hypoxic conditions and regulate *HIF-1α* transcription [21]. Most important, the inhibition of HIF-1α expression is considered to play a crucial role in the antileukemic effects of high AA.

Materials and Methods

Cells

The human leukemic cell lines, K562 (blast crisis of chronic myeloid leukemia), HL60 (promyelocytic leukemia), MOLM14 (monocytic leukemia), NB4 (promyelocytic leukemia), Jurkat (T-lymphoblastic leukemia), and Raji (B-lymphoblastic leukemia), were maintained in RPMI 1640 medium supplemented with 10% heat-inactivated fetal bovine serum (FCS) and antibiotics (100 U penicillin/ml and 100 μg streptomycin/ml) at 37°C in a humidified 5% CO_2 atmosphere. The MOLM-14 cell line [22] was kindly provided by the Cell Biology Institute, Research Center, Hayashibara Biochemical Laboratories. The NB4 cell line was purchased from the German Collection of Microorganisms and Cell Cultures. The remaining cell lines were purchased from the American Type Culture Collection. Human umbilical cord blood (CB) samples were harvested from subjects quickly after birth, after written informed consent was obtained in accordance with the Declaration of Helsinki and with approval from the Tokai University Committee on Clinical Investigation. The $CD34^+$ cell fraction was prepared using the CD34 Progenitor Cell Isolation Kit (Miltenyi Biotec) [23]. The CB-$CD34^+$ cells were frozen in a medium supplemented with dimethylsulfoxide and FCS using a step-down freezing procedure and placed in liquid nitrogen. Aliquots of frozen samples were thawed just before use. The thawed cells were washed twice and viability was determined using trypan blue. When cell viability was more than 95%, the samples were subjected to further studies. To prepare K562 cells that overexpressed HIF-1α, we transfected 293T cells with CSII-HIF1α-IRES-EGFP lentiviral vectors for 72 h and collected the supernatant. K562 cells were incubated with the highly concentrated viral supernatant at a multiplicity of infection of 50 for 24 h. Green fluorescent protein-positive K562 cells were then sorted using a FACSVantage cell sorter (Becton Dickinson).

AA

AA was buffered to pH 7.0 with sodium hydroxide and prepared immediately before use.

H_2O_2 assay

AA was added to the medium in 96-well culture plates at the concentrations indicated in the figures. H_2O_2 was quantitated using a Chemiluminescent H_2O_2 Detection Kit (Assay Designs) according to the manufacturer's protocol.

Cell viability assays

AA was added at varying concentrations to 96-well culture plates containing 5×10^3 cells/well. Saline solution was used as a vehicle control. One hour later, cells were washed and resuspended in the culture medium. Seventy-two hours later, the viability of the cells was measured with a nonradioactive cell proliferation assay using the Cell Counting Kit-8 (Dojindo) according to the manufacturer's protocol.

Measurement of apoptosis

Ten thousand cells were incubated with the vehicle, 2800 μM AA, or 2800 μM AA and 600 U/ml of catalase for 1 h and then washed and cultured in the medium. The cells were harvested 18 h later and stained with fluorescein isothiocyanate (FITC)- or allophycocyanin (APC)-labeled annexin V (BD Biosciences) and propidium iodide (PI) (Roche), or with primary anti-cleaved caspase-3 antibody (Cell Signaling) and secondary phycoerythrin (PE)-labeled antibody (eBioscience), according to the manufacturer's instructions. The treated cells were then analyzed using a FACScan flow cytometer (Becton Dickinson).

Measurement of intracellular catalase activity

The intracellular catalase activity of 2×10^4 cells was measured using a Fluorescent Catalase Detection Kit (Fluoro: Catalase^{TM}, Cell Technology) according to the manufacturer's instructions. Briefly, the kit utilizes a non-fluorescent substrate, 10-acetyl-3,7-dihydroxyphenoxazine, which is converted by residual H_2O_2 to the fluorescent molecule resorufin.

Histochemical catalase assay

Cell preparations (2×10^5) were placed on glass slides in a cytospin centrifuge and fixed with 4% paraformaldehyde (PFA) for 5 min. The slides were incubated with a rabbit anti-catalase antibody (Sigma Aldrich) overnight at 4°C and then with a horseradish peroxidase-conjugated anti-rabbit antibody (GE Healthcare, Japan) for 4 h at 4°C. After the slides were washed, they were stained with 3,3′-diaminobenzidine tetrahydrochloride, and images were acquired using a digital camera (AxioCam MRc5, Carl Zeiss).

Xenograft and Treatment Procedures

Leukemic cells (2×10^6) were mixed with 100 μl basement membrane matrix (BD Biosciences), and the mixture was transplanted subcutaneously into the right flank of 8-week-old nude mice. On day 8 after transplantation, the tumor volume was measured, and the mice were then injected intravenously with 100 μl of AA at a high concentration (0.5 mg/g body weight, which is similar to the pharmacologic doses for humans and rats [6,7,24–26]), or saline solution as a bolus twice daily for the designated periods. The tumor volume was measured at the times indicated in the figures. All experimental procedures and protocols involving animals were approved by the Animal Care Committee of Tokai University and were in compliance with the ARRIVE guidelines [27].

Immunohistochemical and immunocytochemical analyses

Isoflurane inhalation was used to anesthetize mice, and the tumor was perfused from the apex of the heart with phosphate-buffered saline (PBS) and fixed by perfusion with 4% PFA in PBS. The tumor was then dissected and immersed in 4% PFA overnight at 4°C, embedded in O.C.T. compound (Sakura Finetek, Japan), and then frozen in liquid nitrogen. Cryostat sections (6 μm thick) of the tumor or cytospin specimens of leukemic cells fixed with 4% PFA were stained with specific antibodies and incubated overnight at 4°C. Rat anti-mouse CD31 (BD Sciences) and rabbit anti-NF-κB p65 antibodies (Cell Signaling Technology) were used as

primary antibodies. The slides were then incubated with a secondary antibody conjugated with Alexa488 (Life Technologies). Nuclei were stained with 4′,6-diamidino-2-phenylindole (DAPI; Life Technologies). The slides were observed using a confocal laser-scanning microscope (LSM510 META spectrometer, Carl Zeiss).

Analysis of angiogenesis-related and antiapoptotic molecules

Cells were treated with a high AA (2800 μM). After 1 h, the cells were washed, cultured for 24 h, unless otherwise indicated, and then assayed.

Quantitative real-time polymerase chain reaction

RNA was isolated using the RNeasy Micro Kit (QIAGEN) and reverse transcribed. Each target cDNA was polymerase chain reaction (PCR)-amplified on the same plate by using the TaqMan(R) Gene Expression Assays (Life Technologies Corporation) and the ABI 7300 Real-Time PCR System (Applied Biosystems). The PCR primers used were derived from *HIF-1α* (Applied Biosystems, Assay ID; Hs00936376_m1) and *VEGF* (Applied Biosystems, Assay ID; Hs00900055_m1). The relative amounts of target genes were determined in reference to 18S rRNA. Comparative threshold cycle (C_T) analysis was used to quantify transcripts. The value was calculated by the expression $2^{-\Delta\Delta CT}$.

Western blotting

Cells were harvested and washed, and the pellets were suspended in 0.1 ml of ice-cold TNE buffer and incubated on ice for 10 min. When subcellular fractions were prepared, the Subcellular Proteome Extraction Kit (Calbiochem) was used according to the manufacturer's instructions. The lysates were then centrifuged, and the supernatants were boiled in SDS sample buffer. The proteins were separated on SDS-polyacrylamide gels, electroblotted onto a nitrocellulose membrane, and detected using the ECL Plus Western blotting analysis system (GE Lifesciences) using specific antibodies. Anti-HIF-1α and anti-β-actin antibodies were purchased from BD Biosciences and Sigma-Aldrich, respectively. Anti-p-IκB, anti-NF-κB, anti-Bcl-2, anti-Bcl-x_L, anti-caspase-3, and anti-lamin A/C antibodies were purchased from Cell Signaling Technology. Anti-Mcl-1, anti-Sp1, anti-Sp3, and anti-Sp4 were purchased from Santa Cruz Biotechnology, Inc.

Quantitative assays for intracellular AA content

Cells were treated with 2800 μM AA for 1 h, washed twice in PBS, and then assayed for AA content using a vitamin C assay kit (Shima Laboratories) according to the manufacturer's instructions. Briefly, AA in a given sample is converted by the oxidizing agent to dehydroascorbic acid. Dehydroascorbic acid is then derivatized with 2,4-dinitrophenylhydrazine. Total vitamin C (AA + dehydroascorbic acid) concentration is determined by the specific ultraviolet light (UV) absorption of the 2,4-dinitrophenylhydrazine derivative.

Statistics

All the experimental results have been expressed as the arithmetic mean and standard deviation (SD) values. Student's *t*-test was used to evaluate the statistical significance of the differences between unpaired groups.

Results

Cancer-specific cytotoxic effect of high AA on human hematopoietic cells

We first assessed the effect of high AA on the viability of various human leukemic cell lines as well as on normal hematopoietic stem/progenitor cells in vitro. Addition of 280 and 2800 μM of AA, which are approximately 6 and 60-times higher than the physiological level, produced significant amounts of H_2O_2 after 1 h incubation (34.4±4.1 and 134.0±11.8 μM, respectively) and reduced the viability of all myeloid and lymphoid leukemic cells tested but not that of CB-CD34$^+$ cells (Figure 1A). We further found that high AA induced apoptosis in leukemic cells and that this effect was almost completely abrogated by the addition of catalase (Figure 1B). It is important to note that the leukemic cell lines tested generally possessed lower catalase activities than did normal CB-CD34$^+$ cells (Figures 1C and 1D). Thus, we conclude that the induction of apoptosis by high AA was due to the generation of H_2O_2 and was specifically observed in leukemic cells that expressed relatively lower catalase activities.

Inhibitory effect of high AA on leukemic progression in vivo

We next examined the effect of high AA on the progression of leukemia by using an experimental transplantation model. We mixed HL60 cells and basement membrane matrix (BD Biosciences), transplanted the mixture subcutaneously into the right flank of nude mice, and injected high AA or vehicle intravenously. This procedure enabled a precise assessment of tumor burden over time. There were significant differences in tumor volumes between vehicle- and high AA-treated mice 4 days after the final injection (Figures 2A and 2B). We then killed the mice and found that tumor neoangiogenesis was less evident in high AA-treated mice than in vehicle-treated mice (Figures 2C and 2D).

Inhibitory effect of high AA on HIF-1α expression in leukemic cells

We next determined the expression of angiogenesis-related molecules in CB-CD34$^+$ and leukemic cells in the presence of vehicle or high AA. In CB-CD34$^+$ cells, there was no statistically significant difference in the expression of *HIF-1α* mRNA for the 2 conditions (Figure 3A). In contrast, in HL60 cells, expression of *HIF-1α* mRNA markedly decreased because of high AA (Figure 3A). The expression of HIF-1α in HL60 cells was significantly higher than that in CB-CD34$^+$ cells in the absence of high AA but markedly reduced in the presence of high AA (Figure 3B). Moreover, mRNA expression of *VEGF*, an HIF-1α-regulated gene, also reduced along with that of *HIF-1α* over time after incubation of HL60 cells with high AA (Figure 3C).

We then attempted to determine how *HIF-1α* mRNA expression was inhibited by high AA in leukemic cells. *HIF-1α* is known to be transcriptionally regulated by NF-κB, and AA inhibits phosphorylation of the NF-κB inhibitor (IκB) [28]. Therefore, we tested for the presence of phosphorylated IκB (p-IκB) and found that the p-IκB level in HL60 cells was significantly reduced by the addition of high AA (Figure 4A). These data indicate that high AA markedly inhibited the translocation of NF-κB into the nucleus of HL60 cells, but not CB-CD34$^+$ cells (Figure 4B). We demonstrated further that the intracellular content of AA was much higher in leukemic cells than in normal CB-CD34$^+$ cells after incubation with high AA (Figure 4C). These results suggest that the differences in the intracellular uptake of AA

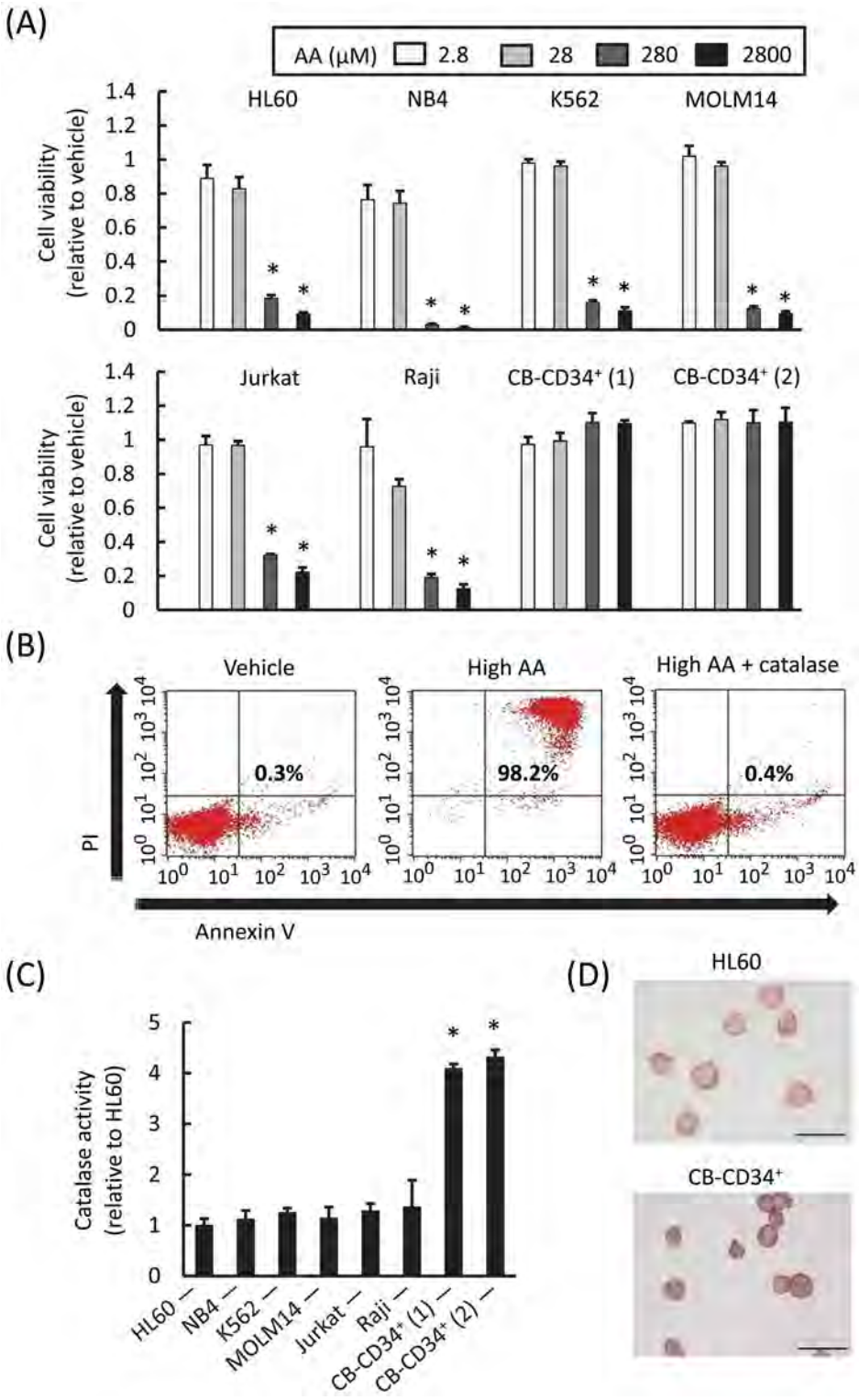

Figure 1. In vitro effects of AA on human leukemic and CB-CD34$^+$ cells, relative to catalase activity. A) Cell viability assay of various leukemic cell lines and 2 independent isolates of CB-CD34$^+$ cells. Cells were treated with different concentrations of AA for 1 h, and then washed, cultured, and analyzed after 72 h. The viability of all cell lines reduced significantly in the presence of 280 and 2800 μM AA (*$P<0.0001$, as compared with vehicle), but this finding was not obtained for CB-CD34$^+$ cells ($P>0.05$). The values represent the mean ± SD values of quadruplicate samples. B) Flow cytometric measurement of apoptosis of HL60 cells. Cells were treated with vehicle or AA for 1 h, and then washed, cultured, and analyzed after 18 h. Representative profiles are shown. The annexin V$^+$ propidium iodide (PI)$^+$ cell fraction indicates apoptotic cells. Note that AA-induced apoptosis was almost completely abrogated by the addition of catalase. C) Intracellular catalase activity. Leukemic cells generally expressed lower catalase activities than did CB-CD34$^+$ isolates (*$P<0.001$, as compared with each cell line). The values represent the mean ± SD values of quadruplicate samples. D) Histochemical analysis demonstrated lower catalase activity in HL60 cells than in CB-CD34$^+$ cells. The bars indicate 50 μm.
doi:10.1371/journal.pone.0062717.g001

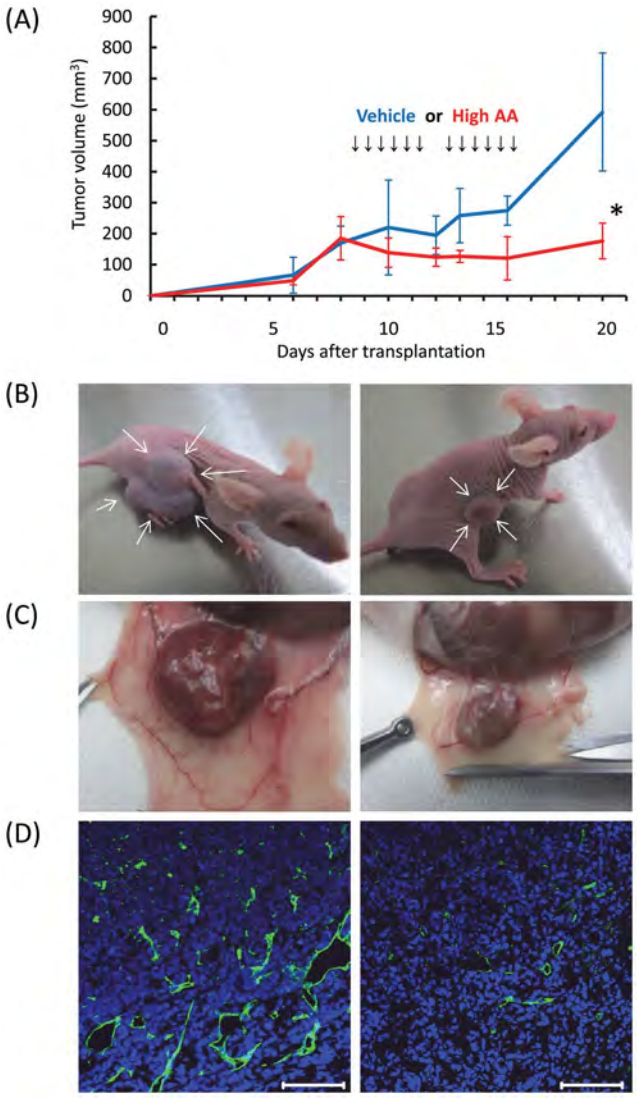

Figure 2. In vivo effects of high AA on progression of leukemia. A) High AA or the vehicle was injected intravenously for 6 days with a rest period of 2 days between 3 daily injections of mice transplanted with HL60 cells. Compared with vehicle (blue line), high AA (red line) significantly inhibited tumor growth (*$P<0.01$). The values represent the mean ± SD values of 5 mice. B) Appearance of mice treated with vehicle (left) and high AA (right), 4 days after the final injection. C) Representative macroscopic appearance of tumors of mice treated with the vehicle (left) and high AA (right). Note that the tumors of high AA-treated mice were smaller and less erythematous than those of vehicle-treated mice. D) Immunohistochemical analysis of tumor neoangiogenesis in mice treated with the vehicle (left) and high AA (right). The green and blue signals represent CD31 and 4′,6-diamidino-2-phenylindole (DAPI), respectively. The bars indicate 100 μm.
doi:10.1371/journal.pone.0062717.g002

reflected the differences seen between high AA-treated human leukemic cells and $CD34^+$ cells derived from normal CB in the presence of NF-κB translocation and following HIF-1α expression.

Relationship between the inhibitory effects of high AA on HIF-1α expression and leukemic progression

Next, we assessed the implications of the inhibition of HIF-1α expression by high AA on leukemic progression by generating *HIF-1α*-overexpressing K562 cells (K562-HIF1α) by using a lentiviral vector. High AA exposure significantly reduced the expression of *HIF-1α* mRNA in K562 but not in K562-HIF1α cells (Figure 5A). The level of HIF-1α in K562-HIF1α cells was also significantly higher than that in K562 cells after vehicle or high AA exposure (Figure 5B). We also found that the induction of apoptosis by high AA was significantly lower in K562-HIF1α than in K562 cells (Figure 5C and 5D). Therefore, we assessed the expression of antiapoptotic proteins of the Bcl-2 family (Mcl-1, Bcl-x_L, and Bcl-2) because their expression is regulated by HIF-1α in nonmalignant and malignant cells. Moreover, they play a key role in preventing apoptosis mediated by reactive oxygen species (ROS) [14,29–35]. We demonstrated that expression of Mcl-1, Bcl-x_L, and Bcl-2 was significantly inhibited by high AA in K562 cells but was sustained at a higher level in K562-HIF1α cells, regardless of high AA exposure (Figure 5E). We further assessed the involvement of the pro-oncogenic specificity protein (Sp) transcription factors Sp1, Sp3, and Sp4 in the antileukemic effect of high AA because high AA exhibits anticancer activity towards colon cancer cells. This is due in part to downregulation of Sp transcription factors and Sp-regulated genes, such as *VEGF* [36]. There were significant differences in the expression levels of these molecules between the vehicle-treated K562 and K562-HIF1α cells (Figure 5F). In K562 cells, the expression of Sp1, Sp3, and Sp4 as well as that of VEGF was reduced by high AA (Figure 5F). In K562-HIF-1α cells, the expression of Sp1, Sp3, and Sp4 was reduced by high AA, but the expression of VEGF was not (Figure 5F).

Finally, we mixed K562 or K562-HIF1α cells in basement membrane matrix, transplanted the mixture into mice, and injected the mice intravenously with the vehicle or high AA. We found that administration of high AA repressed tumor neoangiogenesis only in mice transplanted with K562 cells (Figure 6A). Further, administration of high AA significantly repressed the growth of K562 tumors but did not detectably inhibit the growth of K562-HIF1α tumors in mice (Figure 6B).

Discussion

AA plays a key role in protecting cells against oxidative damage. Paradoxically, in the presence of Fe^{3+} or Cu^{2+}, AA treatment generates ROS, such as H_2O_2 [37], and induces apoptosis or necrosis in various malignant cells but not in nonmalignant cells [38]. In the present study, we further investigated these findings and confirmed them using human leukemic and normal hematopoietic cells. We found that high AA induces apoptosis only in the leukemic cells, which we concluded reflects the increasing generation of H_2O_2 and relatively low catalase activities [24,39].

We also found that intravenous administration of high AA repressed proliferation of leukemic cells injected into nude mice. Although high AA are usually given by drip infusion in clinical settings [7,9,40,41], we injected mice with high AA in the form of a bolus, which might have weakened the effect of treatment because of more rapid clearance of AA than by drip infusion [42]. However, we observed a significant antileukemic effect of high AA in the present study. Further, the tumors showed markedly reduced neoangiogenesis. Our present findings demonstrate that high AA strongly inhibits expression of HIF-1α and one of HIF-1α-regulated molecules, VEGF, in leukemic cells. HIF-1α and VEGF are considered as potential targets for cancer therapy because they play an important role in the progression of many types of cancer, including leukemia, and are associated with resistance to therapy and poor prognosis [10–13,43–45]. Wang et al. demonstrated that HIF-1α signaling is selectively activated in human leukemic cells even under normoxic conditions [10]. AA

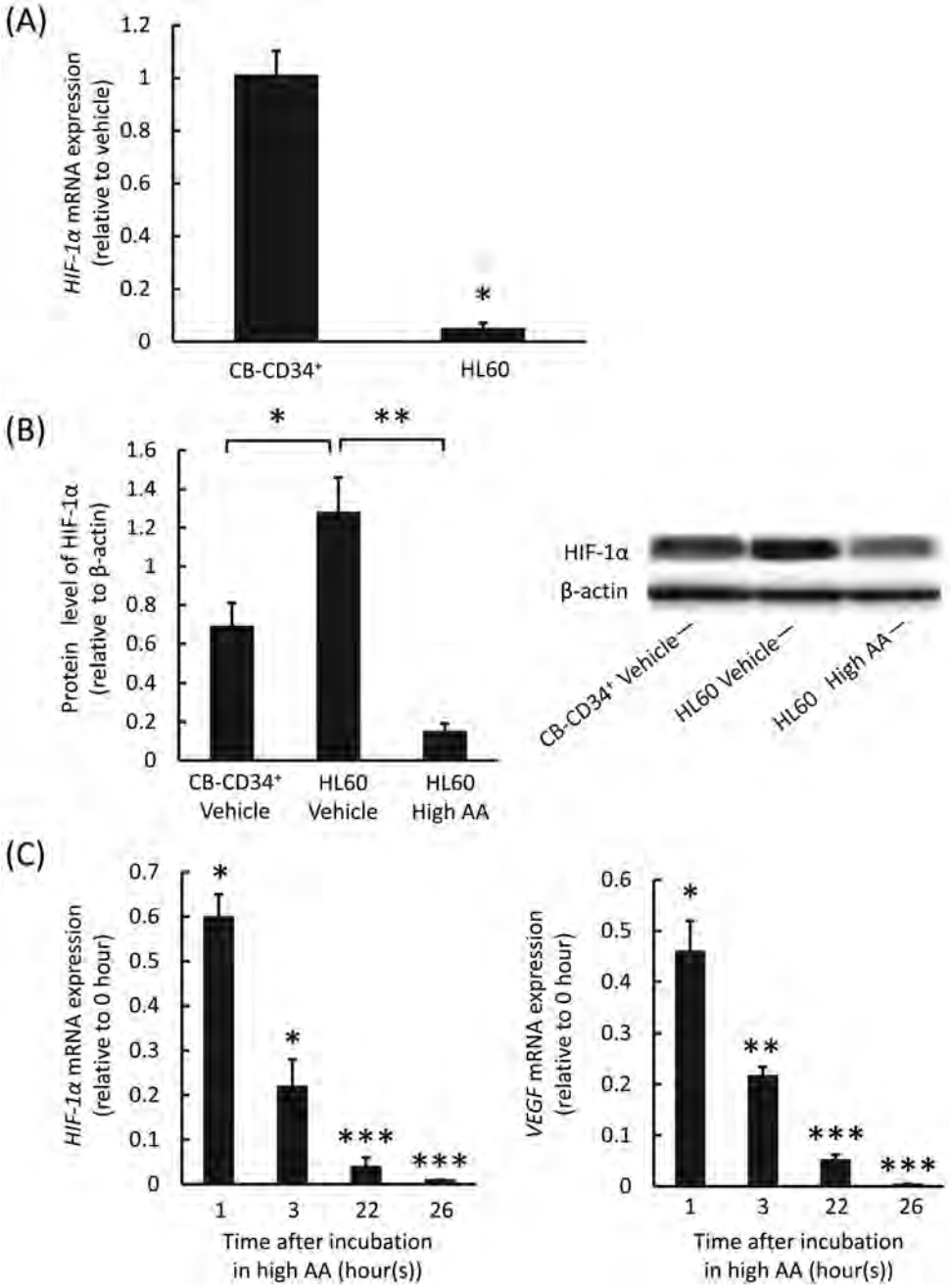

Figure 3. Expression of angiogenesis-related molecules in human leukemic and CB-CD34$^+$ cells exposed to the vehicle or to high AA. A) Quantitative real-time PCR (qRT-PCR) analysis of *HIF-1α* mRNA in CB-CD34$^+$ and HL60 cells. The cells were treated with vehicle or high AA for 1 h, and then washed, cultured, and analyzed after 24 h. There were no significant differences in the expression levels for the 2 conditions ($P>0.05$) in CB-CD34$^+$ cells. In contrast, there were significant differences in the expression levels between the 2 conditions (*$P<0.0001$) in HL60 cells. The values represent the mean ± SD values of triplicate samples. B) Western blotting analysis of HIF-1α in CB-CD34$^+$ and HL60 cells. The cells were treated with vehicle or high AA for 1 h, and then washed, cultured, and analyzed after 24 h. There were significant differences in the expression levels (*$P<0.01$, **$P<0.0005$). The values are mean ± SD values of triplicate samples. C) Sequential analysis of qRT-PCR results of *HIF-1α* and *VEGF* mRNA in HL60 cells. The cells were treated with high AA for 1 h, and then washed, cultured, and analyzed after 1, 3, 22, and 26 h. The expression of *VEGF* mRNA reduced along with that of *HIF-1α* over time. Compared with the expression levels at 0 h, there were significant differences in the expression levels (*$P<0.01$, **$P<0.001$, ***$P<0.0001$). The values represent the mean ± SD values of triplicate samples.
doi:10.1371/journal.pone.0062717.g003

facilitates the hydroxylation of HIF-1α via the stimulation of the Fe-dependent hydroxylases that mark this protein for polyubiquitination and subsequent proteosomal degradation [19,20]. Moreover, Knowles et al. reported that AA reduces HIF-1α protein levels in several human non-hematopoietic cancer cells under normoxic conditions [46]. We have shown here that high AA markedly inhibits the expression of HIF-1α at the level of transcription in leukemic cells.

We have also shown here that in the leukemic cells, high AA inhibited *HIF-1α* transcription by blocking transcriptional activa-

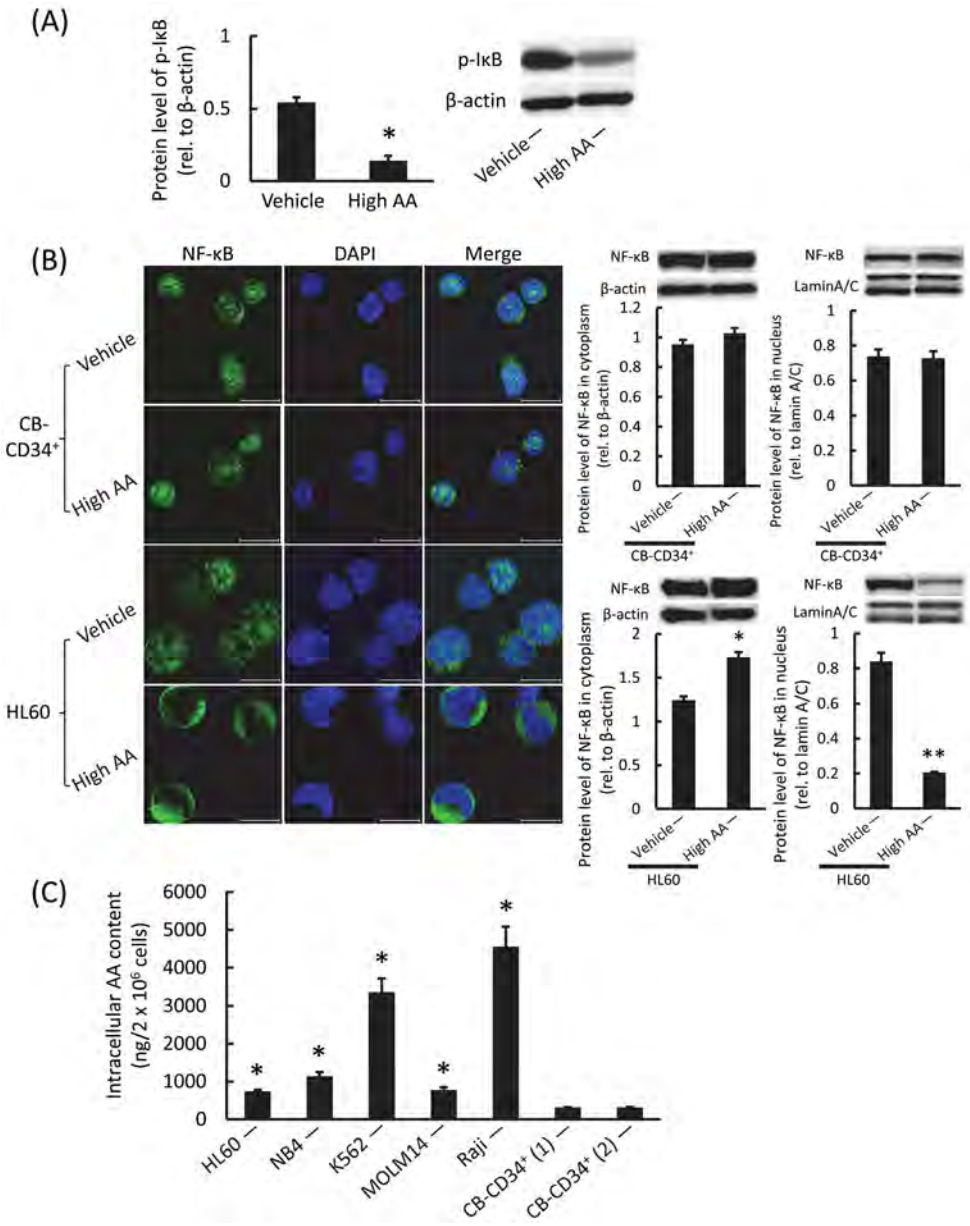

Figure 4. Differences in NF-κB activation and intracellular AA content between human leukemic and CB-CD34$^+$ cells in the presence of high AA. A) Western blotting analysis of p-IκB in HL60 cells. Cells were treated with the vehicle or with high AA for 1 h, and then washed, cultured, and analyzed after 24 h. There was a significant difference in the expression levels (*$P<0.001$). Values represent the mean ± SD of triplicate samples. B) Immunocytochemical (left) and Western blotting (right) analyses of NF-κB in CB-CD34$^+$ and HL60 cells. Cells were treated with vehicle or high AA for 1 h, then washed, cultured, and analyzed after 24 h. Note that translocation of NF-κB into the nucleus was markedly decreased in high AA-treated HL60 cells. Green and blue signals represent NF-κB and DAPI, respectively. Bars indicate 20 μm. There were significant differences in the expression levels (*$P<0.001$, **$P<0.0001$). The values represent the mean ± SD values of triplicate samples. C) Intracellular AA content of human leukemic cells and 2 different isolates of CB-CD34$^+$ cells. Cells were treated with high AA for 1 h, washed in PBS, and analyzed immediately. There were significant differences in the content between leukemic and CB-CD34$^+$ cells. *$P<0.001$, as compared with CB-CD34$^+$ cells (1) or (2). The values are mean ± SD values of triplicate samples.
doi:10.1371/journal.pone.0062717.g004

tion of NF-κB, which is also constitutively activated in many types of leukemia and is associated with leukemic progression [47–49]. Because the leukemic cells used in this study generally possessed significantly higher intracellular levels of AA than normal hematopoietic cells after incubation with high AA, we speculate that while H_2O_2 acts to activate NF-κB by increasing phosphorylation of IκB and *HIF-1α* expression [15,28], AA overcomes the effect of H_2O_2 on the regulation of NF-κB activation in the leukemic cells. Further, we conclude that the increased uptake of AA by leukemic cells, also observed by other investigators and possibly associated with an abnormality in AA transport [50–52], reflects the difference in HIF-1α expression levels between leukemic and normal CB-CD34$^+$ cells after high AA exposure. The levels of intracellular AA did not closely correlate with the cytotoxic effects of high AA, as shown in Figures 1A and 4C,

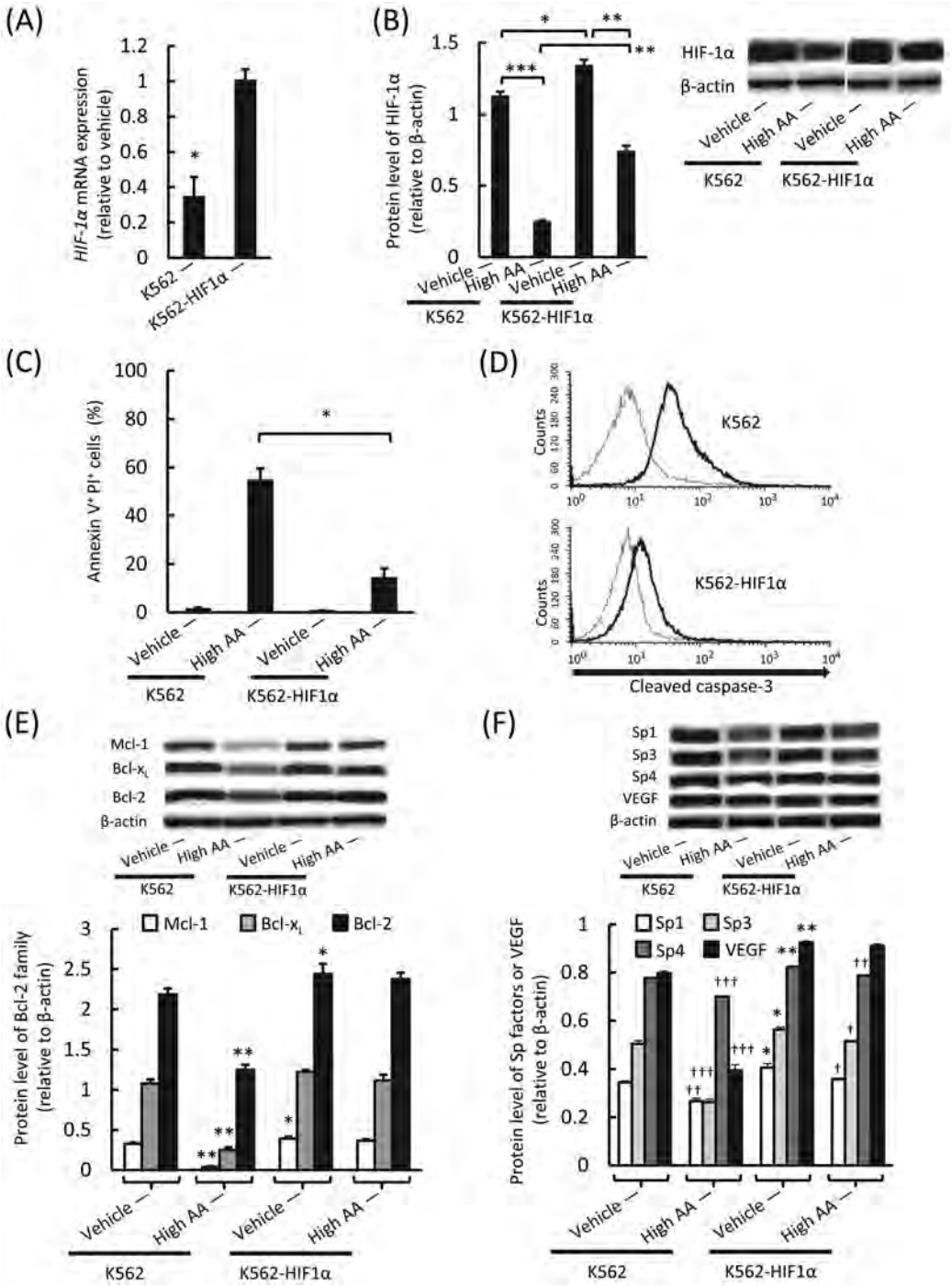

Figure 5. Relationship between antileukemic effects of high AA and HIF-1α expression. A) Quantitative real-time PCR analysis of *HIF-1α* mRNA expression in K562 and K562-HIF1α cells. Cells were treated with the vehicle or high AA for 1 h, washed, cultured in the medium, and analyzed after 24 h. After high AA exposure, *HIF-1α* mRNA expression significantly reduced in K562 (*$P<0.01$), but not in K562-HIF1α cells ($P>0.05$). The values represent the mean ± SD values of triplicate samples. B) Western blotting analysis of HIF-1α in K562 and K562-HIF1α cells. Cells were treated with vehicle or high AA for 1 h, washed, cultured in the medium, and analyzed after 24 h. High AA exposure significantly reduced the HIF-1α protein level in both types of cells. However, the HIF-1α protein level in K562-HIF1α cells was significantly higher than that in K562 cells after vehicle or high AA exposure. *$P<0.01$, **$P<0.0001$, ***$P<0.00001$. The values represent the mean ± SD values of triplicate samples. C) Flow cytometric measurement of apoptosis of K562 and K562-HIF1α cells. Cells were treated with vehicle or high AA for 1 h, washed, cultured in the medium, and analyzed after 18 h. There was a significant difference in the number of apoptotic (annexin V^+ propidium iodide $(PI)^+$) cells between high AA-treated K562 and K562-HIF1α cells (*$P<0.001$). The values represent the mean ± SD values of triplicate samples. D) Flow cytometric measurement of cleaved caspase-3 expressed by K562 and K562-HIF1α cells. Cells were treated with vehicle (gray lines) or high AA (black lines) for 1 h, washed, cultured, and analyzed after 24 h. Activation of caspase-3 by high AA was lower in K562-HIF1α than in K562 cells. E) Western blotting analysis of Mcl-1, Bcl-x_L, and Bcl-2 in K562 and K562-HIF1α cells. Cells were treated with vehicle or high AA for 1 h, washed, cultured, and analyzed after 24 h. There were significant differences in the expression levels between the vehicle-treated K562 and K562-HIF1α cells (*$P<0.05$) and between the vehicle-treated and high AA-treated K562 cells (**$P<0.0001$). There was no significant difference between the vehicle-treated and high AA-treated K562-HIF1α cells ($P>0.05$). The values

represent the mean ± SD values of triplicate samples. F) Western blotting analysis of Sp1, Sp3, Sp4, and VEGF. Cells were treated with vehicle or high AA for 1 h, washed, cultured, and analyzed after 24 h. There were significant differences in the expression levels of these molecules between the vehicle-treated K562 and K562-HIF1α cells (*$P<0.01$, ** $P<0.0001$). There were significant differences in the expression levels of Sp1, Sp3, and Sp4 between the vehicle-treated and high AA-treated K562 or K562-HIF1α cells ($^{\dagger}P<0.01$, $^{\dagger\dagger}P<0.001$, $^{\dagger\dagger\dagger}P<0.0001$). There was a significant difference in the expression level of VEGF between the vehicle-treated and high AA-treated K562 ($^{\dagger\dagger\dagger}P<0.0001$), but not between the vehicle-treated and high AA-treated K562-HIF1α cells ($P>0.05$).
doi:10.1371/journal.pone.0062717.g005

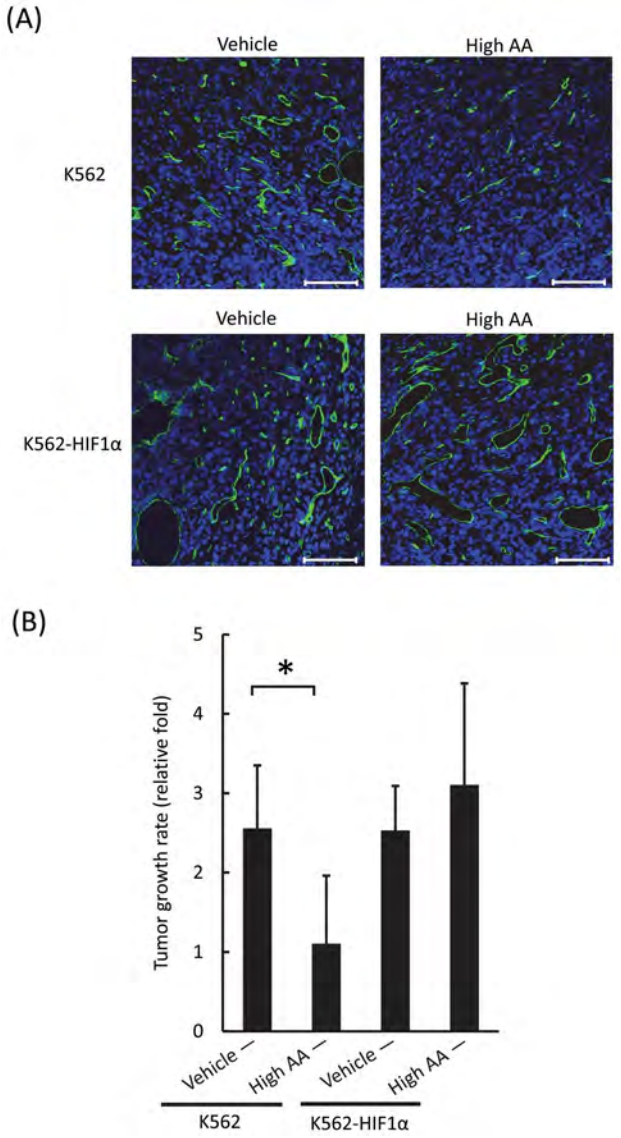

Figure 6. Effects of high AA on tumor growth in the presence or absence of overexpression of *HIF-1α*. A) Immunohistochemical analysis of tumor neoangiogenesis in vehicle-treated (left) and high AA-treated (right) mice transplanted with K562 (upper column) or K562-HIF1α cells (lower column). The green and blue signals represent CD31 and DAPI, respectively. The bars indicate 100 μm. Note that administration of high AA suppressed tumor neoangiogenesis in mice transplanted with K562 cells, but not in mice transplanted with K562-HIF1α cells. B) In the xenogeneic transplant model, high AA or vehicle was injected for 5 days. Administration of high AA significantly inhibited tumor growth of K562 cells (*$P<0.05$) but not of K562-HIF1α cells ($P>0.05$). Tumor growth rate was estimated using the following equation: tumor volume on day 4 after high AA treatment/tumor volume just before high AA treatment. The values represent the mean ± SD values for 4 mice.
doi:10.1371/journal.pone.0062717.g006

because the effects were caused largely by the H_2O_2 that was generated extracellularly by high AA (Figure 1B).

However, we found that *HIF-1α* overexpression completely abrogated the inhibitory effects of high AA on tumor growth and neoangiogenesis in vivo and significantly diminished the induction of apoptosis by high AA in the leukemic cells in vitro. HIF-1α regulates the expression of Bcl-2 family members such as Mcl-1, Bcl-x_L, and Bcl-2, which are essential for the growth and survival of leukemic cells because they prevent the induction of apoptosis by ROS [14,29,53–57]. Here, we demonstrated that high AA significantly suppressed expression of Mcl-1, Bcl-x_L, and Bcl-2, and induced apoptosis in K562 cells but not in K562 cells that overexpressed *HIF-1α*.

We further assessed the involvement of Sp1, Sp3, and Sp4 in the antileukemic effect of high AA because high AA exhibits anticancer activity towards colon cancer cells, which is due in part to downregulation of Sp transcription factors and Sp-regulated genes [58]. Similar results have been observed in bladder and pancreatic cancer cells treated with H_2O_2 or other ROS inducers [59–61]. Further, it has been reported that knockdown or downregulation of Sp1, Sp3, and Sp4 represses expression of Sp-regulated genes, including *VEGF* and *BCL-2*, inhibits cancer cell growth, and induces apoptosis [59–61]. In the present study, the expression levels of Sp1, Sp3, and Sp4 in K562-HIF1α cells were higher than those in K562 cells, suggesting some interaction between HIF-1α and Sp proteins. Further, the expression of Sp1, Sp3, and Sp4 was also downregulated by high AA in K562 cells, as was observed in colon cancer cells [58]. However, in K562-HIF1α cells, the expression of these factors was also downregulated by high AA, but the expression of VEGF and Bcl-2 was not. These results strongly suggest that marked inhibition of *HIF-1α* transcription and expression of HIF-1α-regulated molecules play a crucial role in the antileukemic effects of high AA along with the generation of H_2O_2. However, high AA do not specifically affect the transcription of *HIF-1α* because high AA block the activation of NF-κB, which acts as a transcription factor to regulate the expression of genes involved in the response of leukemic cells to extracellular signals such as *HIF-1α* [48,49]. Therefore, other molecular mechanisms might also play a role in the response to high AA treatment.

Because the use of high AA appears to be remarkably safe in clinical settings [40], it may provide an alternative option for cancer therapy. However, the anticancer effects of high AA vary among cancers or patients [7,9,41]. It is known that an increased number of leukemic cells, normal erythrocytes, or fibroblasts around leukemic cells inversely correlates with high AA-induced leukemic cell death because of increased catalase activity [62]. Therefore, the volume and localization of cancer cells should be considered to obtain more stable clinical effects of high AA. We think that it is reasonable to conclude that combinations with other drugs that compensate for H_2O_2 decomposition may also provide a new strategy for eliminating cancer cells [63].

Acknowledgments

The authors thank the members of the Research Center for Regenerative Medicine of Tokai University School of Medicine for the helpful

discussions and assistance. They also thank the members of the animal facility of Tokai University for the meticulous care of the experimental animals, the members of the Tokai Cord Blood Bank for their assistance, and Dr Eiichiro Nagata for kindly providing anti-Bcl-2 and anti-Bcl-x_L antibodies.

Author Contributions

Conceived and designed the experiments: HK MK. Performed the experiments: MK TU H. Matsuzawa YN. Analyzed the data: HK MK KA. Contributed reagents/materials/analysis tools: MS H. Matsushita KA. Wrote the paper: HK.

References

1. Cameron E, Pauling L (1976) Supplemental ascorbate in the supportive treatment of cancer: Prolongation of survival times in terminal human cancer. Proc Natl Acad Sci USA 73: 3685–3689.
2. Cameron E, Pauling L (1978) Supplemental ascorbate in the supportive treatment of cancer: reevaluation of prolongation of survival times in terminal human cancer. Proc Natl Acad Sci USA 75: 4538–4542.
3. Creagan ET, Moertel CG, O'Fallon JR, Schutt AJ, O'Connell MJ, et al. (1979) Failure of high-dose vitamin C (ascorbic acid) therapy to benefit patients with advanced cancer. A controlled trial. N Engl J Med 301: 687–690.
4. Moertel CG, Fleming TR, Creagan ET, Rubin J, O'Connell MJ, et al. (1985) High-dose vitamin C versus placebo in the treatment of patients with advanced cancer who have had no prior chemotherapy. A randomized double-blind comparison. N Engl J Med 312: 137–141.
5. Padayatty SJ, Sun H, Wang Y, Riordan HD, Hewitt SM, et al. (2004) Vitamin C pharmacokinetics: implications for oral and intravenous use. Ann Intern Med 140: 533–537.
6. Chen Q, Espey MG, Sun AY, Pooput C, Kirk KL, et al. (2008) Pharmacologic doses of ascorbate act as a prooxidant and decrease growth of aggressive tumor xenografts in mice. Proc Natl Acad Sci USA 105: 11105–11109.
7. Chen Q, Espey MG, Krishna MC, Mitchell JB, Corpe CP, et al. (2005) Pharmacologic ascorbic acid concentrations selectively kill cancer cells: action as a pro-drug to deliver hydrogen peroxide to tissues. Proc Natl Acad Sci USA 102: 13604–13609.
8. Padayatty SJ, Riordan HD, Hewitt SM, Katz A, Hoffer LJ, et al. (2006) Intravenously administered vitamin C as cancer therapy: three cases. CMAJ 174: 937–942.
9. Ohno S, Ohno Y, Suzuki N, Soma G, Inoue M (2009) High-dose vitamin C (ascorbic acid) therapy in the treatment of patients with advanced cancer. Anticancer Res 29: 809–815.
10. Wang Y, Liu Y, Malek SN, Zheng P, Liu Y (2011) Targeting HIF1α eliminates cancer stem cells in hematological malignancies. Cell Stem Cell 8: 399–411.
11. Deeb G, Vaughan MM, McInnis I, Ford LA, Sait SN, et al. (2011) Hypoxia-inducible factor-1α protein expression is associated with poor survival in normal karyotype adult acute myeloid leukemia. Leuk Res 35: 579–584.
12. Wellmann S, Guschmann M, Griethe W, Eckert C, von Stackelberg A, et al. (2004) Activation of the HIF pathway in childhood ALL, prognostic implications of VEGF. Leukemia 18: 926–933.
13. Abdel-Wahab O, Levine RL. (2010) Metabolism and the leukemic stem cell. J Exp Med 207: 677–680.
14. Piret JP, Minet E, Cosse JP, Ninane N, Debacq C, et al. (2005) Hypoxia-inducible factor-1-dependent overexpression of myeloid cell factor-1 protects hypoxic cells against tert-butyl hydroperoxide-induced apoptosis. J Biol Chem 280: 9336–9344.
15. Görlach A, Bonello S. (2008) The cross-talk between NF-kappaB and HIF-1: further evidence for a significant liaison. Biochem J 412: e17–19.
16. Semenza, G L (2000) HIF-1: mediator of physiological and pathophysiological responses to hypoxia. J Appl. Physiol 88, 1474–1480.
17. Maxwell PH (2005) Hypoxia-inducible factor as a physiological regulator. Exp Physiol 90, 791–797.
18. Ruas JL, Poellinger L (2005) Hypoxia-dependent activation of HIF into a ranscriptional regulator. Semin Cell Dev Biol 16, 514–522.
19. Myllyla R, Kuutti-Savolainen E-R, Kivirikko KI (1978) The role of ascorbate in the prolyl hydroxylase reaction. Biochem Biophys Res Commun 83: 441–448.
20. de Jong L, Albracht SPJ, Kemp A (1982) Prolyl 4-hydroxylase activity in relation to the oxidation state of enzyme-bound iron: the role of ascorbate in peptidyl proline hydroxylation. Biochim Biophys Acta 704: 326–332.
21. van Uden P, Kenneth NS, Rocha S (2008) Regulation of hypoxia-inducible factor-1α by NF-κB. Biochem J 412, 477–484.
22. Matsuo Y, MacLeod RA, Uphoff CC, Drexler HG, Nishizaki C, et al. (1997) Two acute monocytic leukemia (AML-M5a) cell lines (MOLM-13 and MOLM-14) with interclonal phenotypic heterogeneity showing MLL-AF9 fusion resulting from an occult chromosome insertion, ins(11;9)(q23;p22p23). Leukemia 11: 1469–1477.
23. Kawada H, Ando K, Tsuji T, Shimakura Y, Nakamura Y, et al. (1999) Rapid ex vivo expansion of human umbilical cord hematopoietic progenitors using a novel culture system. Exp Hematol 27: 904–915.
24. Riordan NH, Riordan HD, Meng X, Li Y, Jackson JA (1995) Intravenous ascorbate as a tumor cytotoxic chemotherapeutic agent. Med Hypotheses 44: 207–213.
25. Chen Q, Espey MG, Sun AY, Lee JH, Krishna MC, et al. (2007) Ascorbate in pharmacologic concentrations selectively generates ascorbate radical and hydrogen peroxide in extracellular fluid in vivo. Proc Natl Acad Sci USA 104: 8749–8754.
26. Drisko JA, Chapman J, Hunter VJ (2003) The use of antioxidants with first-line chemotherapy in two cases of ovarian cancer. J Am Coll Nutr 22: 118–123.
27. Kilkenny C, Browne WJ, Cuthill IC, Emerson M, Altman DG (2010) Improving bioscience research reporting: the ARRIVE guidelines for reporting animal research. PLoS Biol 8: e1000412.
28. Cárcamo JM, Pedraza A, Bórquez-Ojeda O, Zhang B, Sanchez R, et al. (2004) Vitamin C is a kinase inhibitor: dehydroascorbic acid inhibits IκBα kinase β. Mol Cell Biol 24: 6645–6652.
29. Lin MT, Juan CY, Chang KJ, Chen WJ, Kuo ML (2001) IL-6 inhibits apoptosis and retains oxidative DNA lesions in human gastric cancer AGS cells through up-regulation of anti-apoptotic gene mcl-1. Carcinogenesis 22: 1947–1953.
30. Chen N, Chen X, Huang R, Zeng H, Gong J, et al. (2009) BCL-xL is a target gene regulated by hypoxia-inducible factor-1α. J Biol Chem 284: 10004–10012.
31. Sasabe E, Tatemoto Y, Li D, Yamamoto T, Osaki T (2005) Mechanism of HIF-1alpha-dependent suppression of hypoxia-induced apoptosis in squamous cell carcinoma cells. Cancer Sci 96: 394–402.
32. Yang CC, Lin LC, Wu MS, Chien CT, Lai MK (2009) Repetitive hypoxic preconditioning attenuates renal ischemia/reperfusion induced oxidative injury via upregulating HIF-1 alpha-dependent bcl-2 signaling. Transplantation 88: 1251–1260.
33. Kowaltowski AJ, Fenton RG, Fiskum G (2004) Bcl-2 family proteins regulate mitochondrial reactive oxygen production and protect against oxidative stress. Free Radic Biol Med 37: 1845–1853.
34. Krishna S, Low IC, Pervaiz S (2011) Regulation of mitochondrial metabolism: yet another facet in the biology of the oncoprotein Bcl-2. Biochem J 435: 545–551.
35. Jung MS, Jin DH, Chae HD, Kang S, Kim SC, et al. (2004) Bcl-x_L and E1B-19K proteins inhibit p53-induced irreversible growth arrest and senescence by preventing reactive oxygen species-dependent p38 activation. J Biol Chem 279: 17765–17771.
36. Pathi SS, Lei P, Sreevalsan S, Chadalapaka G, Jutooru I, et al. (2011) Pharmacologic doses of ascorbic acid repress specificity protein (Sp) transcription factors and Sp-regulated genes in colon cancer cells. Nutr Cancer 63: 1133–1142.
37. Stadtman ER (1991) Ascorbic acid and oxidative inactivation of proteins. Am J Clin Nutr 54(6 Suppl): 1125S–1128S.
38. Du J, Cullen JJ, Buettner GR (2012) Ascorbic acid: Chemistry, biology and the treatment of cancer. Biochim Biophys Acta 1826: 443–457.
39. Nemoto S, Otsuka M, Arakawa N (1996) Inhibitory effect of ascorbate on cell growth: relation to catalase activity. J Nutr Sci Vitaminol (Tokyo) 42: 77–85.
40. Padayatty SJ, Sun AY, Chen Q, Espey MG, Drisko J, et al. (2010) Vitamin C: intravenous use by complementary and alternative medicine practitioners and adverse effects. PLoS One 5: e11414.
41. Hoffer LJ, Levine M, Assouline S, Melnychuk D, Padayatty SJ, et al. (2008) Phase I clinical trial of i.v. ascorbic acid in advanced malignancy. Ann Oncol 19: 1969–1974.
42. Padayatty SJ, Sun H, Wang Y, Riordan HD, Hewitt SM, et al. (2004) Vitamin C pharmacokinetics: implications for oral and intravenous use. Ann Intern Med 140: 533–537.
43. Semenza GL. (2003) Targeting HIF-1 for cancer therapy. Nat Rev Cancer 3: 721–732.
44. Aguayo A, Estey E, Kantarjian H, Mansouri T, Gidel C, et al. (1999) Cellular vascular endothelial growth factor is a predictor of outcome in patients with acute myeloid leukemia. Blood 94: 3717–3721.
45. Verstovsek S, Kantarjian H, Manshouri T, Cortes J, Giles FJ, et al. (2002) Prognostic significance of cellular vascular endothelial growth factor expression in chronic phase chronic myeloid leukemia. Blood 99: 2265–2267.
46. Knowles HJ, Raval RR, Harris AL, Ratcliffe PJ (2003) Effect of ascorbate on the activity of hypoxia-inducible factor in cancer cells. Cancer Res 63: 1764–1768.
47. Packham G. (2008) The role of NF-kappaB in lymphoid malignancies. Br J Haematol 143: 3–15.
48. Braun T, Carvalho G, Fabre C, Grosjean J, Fenaux P, et al. (2006) Targeting NF-kappaB in hematologic malignancies. Cell Death Differ 13: 748–758.
49. Reikvam H, Olsnes AM, Gjertsen BT, Ersvar E, Bruserud Ø (2009) Nuclear factor-kappaB signaling: a contributor in leukemogenesis and a target for pharmacological intervention in human acute myelogenous leukemia. Crit Rev Oncog 15: 1–41.
50. Liebes L, Krigel R, Kuo S, Nevrla D, Pelle E, et al. (1981) Increased ascorbic acid content in chronic lymphocytic leukemia B lymphocytes. Proc Natl Acad Sci USA 78: 6481–6484.
51. Vera JC, Rivas CI, Zhang RH, Farber CM, Golde DW (1994) Human HL-60 myeloid leukemia cells transport dehydroascorbic acid via the glucose transporters and accumulate reduced ascorbic acid. Blood 84: 1628–1634.

52. Wang Y, Mackenzie B, Tsukaguchi H, Weremowicz S, Morton CC, et al. (2000) Human vitamin C (L-ascorbic acid) transporter SVCT1. Biochem Biophys Res Commun 267: 488–494.
53. Glaser SP, Lee EF, Trounson E, Bouillet P, Wei A, et al. (2012) Anti-apoptotic Mcl-1 is essential for the development and sustained growth of acute myeloid leukemia. Genes Dev 26: 120–125.
54. Del Principe MI, Del Poeta G, Venditti A, Buccisano F, Maurillo L, et al. (2005) Apoptosis and immaturity in acute myeloid leukemia. Hematology 10: 25–34.
55. Broome HE, Yu AL, Diccianni M, Camitta BM, Monia BP, et al. (2002) Inhibition of Bcl-xL expression sensitizes T-cell acute lymphoblastic leukemia cells to chemotherapeutic drugs. Leuk Res 26: 311–316.
56. Gonzalez MS, De Brasi CD, Bianchini M, Gargallo P, Moiraghi B, et al. (2010) BAX/BCL-XL gene expression ratio inversely correlates with disease progression in chronic myeloid leukemia. Blood Cells Mol Dis 45: 192–196.
57. Del Principe MI, Del Poeta G, Maurillo L, Buccisano F, Venditti A, et al. (2003) P-glycoprotein and BCL-2 levels predict outcome in adult acute lymphoblastic leukaemia. Br J Haematol 121: 730–738.
58. Pathi SS, Lei P, Sreevalsan S, Chadalapaka G, Jutooru I, et al. (2011) Pharmacologic doses of ascorbic acid repress specificity protein (Sp) transcription factors and Sp-regulated genes in colon cancer cells. Nutr Cancer 63: 1133–1142.
59. Jutooru I, Chadalapaka G, Sreevalsan S, Lei P, Barhoumi R, et al. (2010) Arsenic trioxide downregulates specificity protein (Sp) transcription factors and inhibits bladder cancer cell and tumor growth. Exp Cell Res 316: 2174–2188.
60. Jutooru I, Chadalapaka G, Lei P, Safe S (2010) Inhibition of NFκB and pancreatic cancer cell and tumor growth by curcumin is dependent on specificity protein down-regulation. J Biol Chem 285: 25332–25344.
61. Jutooru I, Chadalapaka G, Abdelrahim M, Basha MR, Samudio I, et al. (2010) Methyl 2-cyano-3,12-dioxooleana-1,9-dien-28-oate decreases specificity protein transcription factors and inhibits pancreatic tumor growth: role of microRNA-27a. Mol Pharmacol 78: 226–236.
62. Sestili P, Brandi G, Brambilla L, Cattabeni F, Cantoni O (1996) Hydrogen peroxide mediates the killing of U937 tumor cells elicited by pharmacologically attainable concentrations of ascorbic acid: cell death prevention by extracellular catalase or catalase from cocultured erythrocytes or fibroblasts. J Pharmacol Exp Ther 277: 1719–1725.
63. Espey MG, Chen P, Chalmers B, Drisko J, Sun AY, et al. (2011) Pharmacologic ascorbate synergizes with gemcitabine in preclinical models of pancreatic cancer. Free Radic Biol Med 50: 1610–1619.

Int J Hematol (2013) 98:719–722
DOI 10.1007/s12185-013-1455-0

CASE REPORT

Deferasirox treatment improved hematopoiesis and led to complete remission in a patient with pure red cell aplasia

Minoru Kojima · Shinichiro Machida · Ai Sato · Mitsuki Miyamoto · Makiko Moriuchi · Yoshiaki Ohbayashi · Kiyoshi Ando

Received: 25 February 2013 / Revised: 18 September 2013 / Accepted: 16 October 2013 / Published online: 26 October 2013

Abstract A 64-year-old woman developed pure red cell aplasia (PRCA) 4 years after thymectomy for thymoma. During anti-thymocyte globulin treatment, the patient developed cytomegalovirus pneumonia and was thus unable to continue immunosuppressive therapy and became transfusion dependent. Deferasirox was started for treatment with iron overload when serum ferritin increased to >1000 ng/mL. Seven months after initiation of deferasirox treatment, serum ferritin level decreased the normal range and the patient has remained transfusion independent thereafter. Deferasirox was discontinued when serum ferritin level decreased below 500 ng/mL, and she has maintained in complete remission over the last 15 months. Hypotheses have been raised regarding the improvement of hematopoiesis by deferasirox treatment, but the mechanism whereby this might be achieved remains unclear. Deferasirox treatment may be clinically beneficial both by reducing iron overload and by improving hematopoiesis in patients with PRCA.

Keywords Pure red cell aplasia · Deferasirox · Iron chelation · Iron overload

M. Kojima (✉) · S. Machida · A. Sato · M. Miyamoto · M. Moriuchi · K. Ando
Division of Hematology/Oncology, Department of Internal Medicine, Tokai University School of Medicine, 143 Shimokasuya, Isehara, Kanagawa 259-1143, Japan
e-mail: kojima@tokai-u.jp

M. Kojima · S. Machida · M. Moriuchi · Y. Ohbayashi
Division of Internal Medicine, Hadano Red Cross Hospital, Hadano, Japan

Introduction

Pure red cell aplasia (PRCA) is characterized by normocytic anemia associated with reticulocytopenia in peripheral blood and severe erythroid hypoplasia in an otherwise normal bone marrow. PRCA can manifest as either a congenital or an acquired disease. Primary PRCA is treated as an immunologically mediated disease. The major objective in the treatment of PRCA is to induce remission and promote recovery of erythropoiesis, thus reducing the need for transfusions and avoiding the complications of transfusion-associated problems. The therapeutic plan typically consists of the sequential use of various immunosuppressive strategies, such as corticosteroids, cyclophosphamide, cyclosporine A (CyA), anti-thymocyte globulin (ATG), splenectomy, and plasma apheresis, until complete remission (CR) is achieved. Recent studies have also described the efficacies of the anti-CD20 monoclonal antibody, rituximab [1, 2], and the anti-CD52 monoclonal antibody, alemtuzumab [3, 4], to induce remission in patients with therapy-resistant PRCA.

Deferasirox is an oral iron chelator used for the management of transfusional iron overload [5, 6]. Several case reports and small studies of patients with myelodysplastic syndrome (MDS) and aplastic anemia (AA) have reported that iron chelation therapy (ICT) with deferasirox resulted in improvements in hematologic parameters and transfusion requirements [7–13] by mechanisms that remain unclear. However, no previous study has described hematologic improvement in response to deferasirox in patients with PRCA. The present report describes a case of a patient with transfusion-dependent PRCA and iron overload who was successfully treated with deferasirox, resulting in reduced serum ferritin, hematological improvement, and remission.

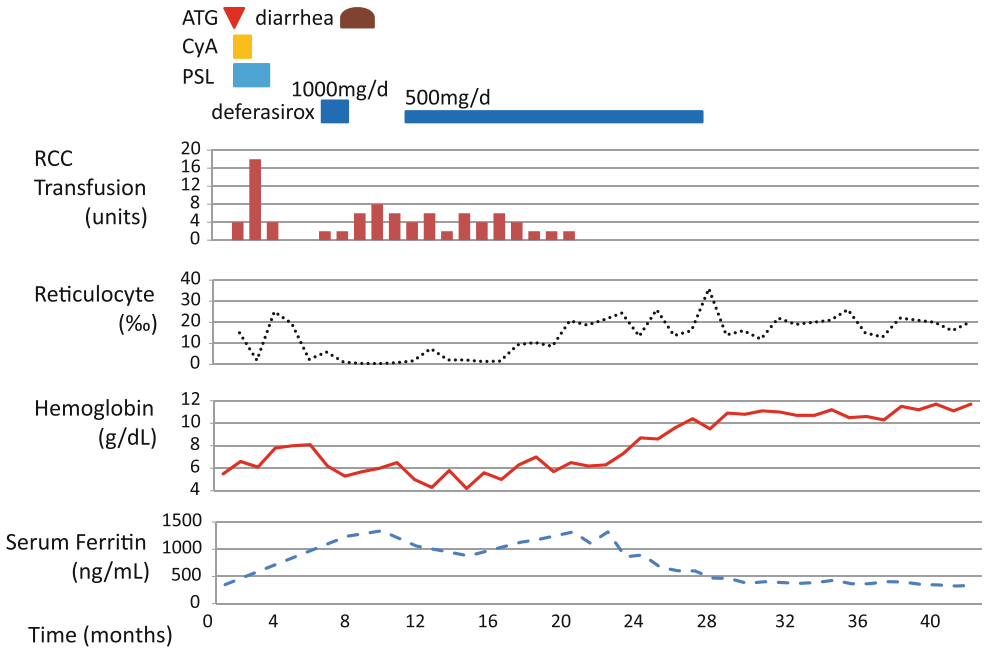

Fig. 1 Clinical course of the PRCA patient

Case report

A 64-year-old Japanese woman who underwent thymectomy for thymoma 4 years prior was diagnosed with lower hemoglobin of 5.0 g/dL, received four units of red cell concentrates (RCC) in local doctor and admitted to Hadano Red Cross Hospital due to anemia. Physical examination findings were non-specific. Laboratory examination at the first visit to our hospital showed normocytic anemia with a hemoglobin level of 7.9 g/dL and a hematocrit of 23.2 %, low reticulocyte count of 4 ‰, mild leukocytopenia, a leukocyte count of 3400/μl with normal differentials, and a normal platelet count. Blood chemistry was normal, except for a decreased serum total protein. Examination of a bone marrow aspiration specimen showed normal granulocytopoiesis and megakaryocytopoiesis with the absence of an erythroid component (M/E ratio of 86.4). Bone marrow presented normal morphology without MDS-related changes. The marrow karyotype was a normal female type. Based on these data, a diagnosis of PRCA was made.

The patient required more than 4U/month of RCC transfusion and underwent treatment with ATG and CyA. Twenty-two days after initiation of treatment, the patient developed dyspnea and fever, and chest X-ray showed bilateral interstitial lung disease. Serum cytomegalovirus (CMV) antigenemia was positive, consistent with a diagnosis of CMV pneumonia. CyA was immediately stopped, and ganciclovir and steroid pulse treatment were started, but the patient's respiratory condition deteriorated rapidly, and she was intubated for initiation of mechanical ventilation. She gradually recovered and was successfully extubated 29 days later. She temporarily achieved transfusion-free status, but became transfusion-dependent again on day 137 after ATG therapy. Since CMV antigenemia had been positive, she did not receive immunosuppressive therapy and was only supported by RCC transfusions. She was transfusion dependent but her organ damages were not observed. Deferasirox was started when serum ferritin increased to 1240 ng/mL, serum iron increased to 202 μg/dL and unsaturated iron-binding capacity decreased to 1 μg/dL and transferrin saturation was 100 %. The starting dose of deferasirox was 1000 mg/day, but she needed dose reduction after developing grade 3 diarrhea. She could continue 500 mg/day of deferasirox. Serum ferritin level decreased to 1000 ng/mL, and she was no longer RCC transfusion-dependent at 7 months after initiation of deferasirox treatment. Deferasirox was discontinued when serum ferritin level decreased below 500 ng/mL, and she has maintained in complete remission over the last 15 months (Fig. 1).

Discussion

In the present report, the patient was diagnosed with PRCA on the basis of anemia, low number of reticulocytes in the peripheral blood (PB) and low number of erythroblasts in the bone marrow (BM). This patient developed PRCA 4 years after thymectomy, and immunosuppressive therapy (IST) with ATG and CyA was effective. However, she had to terminate IST due to onset of CMV pneumonia, and PRCA subsequently recurred. Unexpectedly, deferasirox was effective in terms of iron chelation and also in terms of promoting erythropoiesis in this patient, and she was

ultimately able to attain CR without IST. This is the first report to describe the successful treatment of PRCA with deferasirox.

The pathophysiology of PRCA is not well understood but likely involves several distinct pathways that can lead to the clinical syndrome. Theories as to the etiology of the disease have included a humoral factor suppressing the erythroid lineage, antibodies against erythropoietin, cell-mediated suppression (including T cells, large granular lymphocytes, and natural killer cells), and direct toxic effects of viruses or drugs on erythroid precursors [14]. Studies of patients with PRCA have frequently found abnormal karyotypes; T-cell receptor gene rearrangement analyses have documented the presence of clonal cell populations [15]. Since IST was effective in the case, an immunological mechanism was likely involved in the pathophysiology of this case. A recent in vitro study showed that deferasirox is a potent inhibitor of nuclear factor kappa light-chain enhancer of activated B cells (NF-κB). Since exposure to deferoxamine or deferiprone has no effect on NF-κB activity, this effect is not simply related to a decrease in iron levels, but rather, seems to be a specific effect of deferasirox [16]. Therefore, the effect of deferasirox on PRCA in this case may be mediated by the suppression of autoreactive B or T cells through inhibition of NF-κB by deferasirox.

The second possible mechanism to explain the effect of deferasirox in this case is the stimulation of erythropoiesis. There are some reports of patients with lower risk myelodysplasia syndrome (MDS) that experienced an improvement of hematopoiesis while receiving ICT [7–10, 12]. Similar observations were made in patients with AA [11] and in those with Diamond-Blackfan anemia [13], but not in patients with PRCA. Although the underlying mechanism is unclear, there are some hypotheses. It is reported that iron chelators promote iron release from storage sites, facilitating its use by hematopoietic tissue; furthermore, the reduction of iron stores seems to upregulate erythropoietin, resulting in an increase in hemoglobin [17]. In patients with MDS, treatment with deferasirox significantly reduces reactive oxygen species, membrane lipid peroxidation and the labile iron pool and concomitantly increases glutathione in RBCs. Deferasirox also increases glutathione in platelets and neutrophils and decreases the labile iron pool in platelets [18]. Guariglia et al. [12] described a rapid improvement in erythroid and platelet counts after starting ICT, even when serum ferritin levels were still high, which suggests that deferasirox may have a direct effect on the activity of neoplastic cells. This observation is reminiscent of the rapid improvement in cardiac function that can be achieved with intensive chelation therapy in patients with beta-thalassemia major and heart failure. These observations suggest that the level of oxidative stress (rather than the level of tissue iron accumulation) is directly responsible for organ dysfunction, and we speculate that the hematopoietic system in the present patient was particularly sensitive to oxidative stress. Taher et al. [13] reported a case of patient with Diamond-Blackfan anemia who achieved transfusion independence after treatment with deferasirox, but Diamond-Blackfan anemia is a special subtype of PRCA, so it was not equal to the response mechanism of ICT between Diamond-Blackfan anemia and this case. Attributable mechanisms of such a response may be drug or disease specific [19]. Iron redistribution to the hematopoietic tissue, suppression of increased erythroblast apoptosis, and a decline in mitochondrial damage secondary to erythroblast iron deposition (as evident by decreased erythroblast membrane iron) have all been postulated [20–22].

Surgical resection is the primary mode of treatment for thymoma-associated PRCA and results in alleviation of anemia. Further, thymectomy has been reported to result in occasional improvement of PRCA [23]. Surgical resection of thymoma is recommended as the initial treatment of thymoma-associated PRCA and is associated with a hematological response rate of 25–38 % [23, 24]. However, in a more recent report of 13 patients who underwent thymectomy, thymectomy did not produce normalization of erythropoiesis in all cases [25]. Therefore, the effectiveness of thymectomy in PRCA is unclear.

In the present case, PRCA occurred 4 years after thymectomy. Hirokawa et al. [26] studied 36 patients who underwent surgical resection of thymoma and reported that 16 of those patients developed PRCA at a median of 80 months after thymectomy. The mechanism and difference between PRCA that develops pre-thymectomy versus PRCA that develops post-thymectomy is unclear. Masuda et al. [27] described a case of a patient with thymoma-associated PRCA and clonal T-cell expansion in both the thymoma and circulating blood. On the other hand, Fujishima et al. [28] described a patient with clonal T-cell expansions in the blood but not in the thymoma. Thus, the mechanism may be different for each case and may be influenced by cytotoxic T cells, and the role of thymoma in providing an environment for clonal expansions of pathogenic T cells may be different among individuals.

In conclusion, deferasirox treatment may be clinically beneficial in terms of reducing iron overload and in improving hematopoiesis in patients with PRCA. Further long-term studies in larger patient populations are needed to clarify the effect and safety of deferasirox-mediated restoration of hematopoiesis in patients with PRCA.

Conflict of interest The authors have no conflicts of interests or funding to disclose.

References

1. Zecca M, De Stefano P, Nobili B, Locatelli F. Anti-CD20 monoclonal antibody for the treatment of severe, immune-mediated, pure red cell aplasia and hemolytic anemia. Blood. 2001;97(12):3995–7.
2. Dungarwalla M, Marsh JC, Tooze JA, Lucas G, Ouwehand W, Pettengell R, Dearden CE, Gordon Smith EC, Elebute MO. Lack of clinical efficacy of rituximab in the treatment of autoimmune neutropenia and pure red cell aplasia: implications for their pathophysiology. Ann Hematol. 2007;86(3):191–7.
3. Willis F, Marsh JC, Bevan DH, Killick SB, Lucas G, Griffiths R, Ouwehand W, Hale G, Waldmann H, Gordon-Smith EC. The effect of treatment with Campath-1H in patients with autoimmune cytopenias. Br J Haematol. 2001;114(4):891–8.
4. Au WY, Lam CC, Chim CS, Pang AW, Kwong YL. Alemtuzumab induced complete remission of therapy-resistant pure red cell aplasia. Leuk Res. 2005;29(10):1213–5.
5. Cappellini MD, Porter J, El-Beshlawy A, Li CK, Seymour JF, Elalfy M, Gattermann N, Giraudier S, Lee JW, Chan LL, Lin KH, Rose C, Taher A, Thein SL, Viprakasit V, Habr D, Domokos G, Roubert B, Kattamis A. Tailoring iron chelation by iron intake and serum ferritin: the prospective EPIC study of deferasirox in 1744 patients with transfusion-dependent anemias. EPIC Study Investigators. Haematologica. 2010;95(4):557–66.
6. Miyazawa K, Ohyashiki K, Urabe A, Hata T, Nakao S, Ozawa K, Ishikawa T, Kato J, Tatsumi Y, Mori H, Kondo M, Taniguchi J, Tanii H, Rojkjaer L, Omine M. A safety, pharmacokinetic and pharmacodynamic investigation of deferasirox (Exjade, ICL670) in patients with transfusion-dependent anemias and iron-overload: a phase I study in Japan. Int J Hematol. 2008;88(1):73–81.
7. Messa E, Cilloni D, Messa F, Arruga F, Roetto A, Saglio G. Deferasirox treatment improved the hemoglobin level and decreased transfusion requirements in four patients with the myelodysplastic syndrome and primary myelofibrosis. Acta Haematol. 2008;120(2):70–4.
8. Capalbo S, Spinosa G, Franzese MG, Palumbo G. Early deferasirox treatment in a patient with myelodysplastic syndrome results in a long-term reduction in transfusion requirements. Acta Haematol. 2009;121(1):19–20.
9. Oliva EN, Ronco F, Marino A, Alati C, Praticò G, Nobile F. Iron chelation therapy associated with improvement of hematopoiesis in transfusion-dependent patients. Transfusion. 2010;50(7):1568–70.
10. Okabe H, Suzuki T, Omori T, Mori M, Uehara E, Hatano K, Ueda M, Matsuyama T, Toshima M, Qzaki K, Nagai T, Muroi K, Ozawa K. Hematopoietic recovery after administration of deferasirox for transfusional iron overload in a case of myelodysplastic syndrome. Rinsho Ketsueki. 2009;50(11):1626–9.
11. Lee SE, Yahng SA, Cho BS, Eom KS, Kim YJ, Lee S, Min CK, Kim HJ, Cho SG, Kim DW, Min WS, Park CW, Lee JW. Improvement in hematopoiesis after iron chelation therapy with deferasirox in patients with aplastic anemia. Acta Haematol. 2012;129(2):72–7.
12. Guariglia R, Martorelli MC, Villani O, Pietrantuono G, Mansueto G, Dâ€™Auria F, Grieco V, Bianchino G, Lerose R, Bochicchio GB, Musto P. Positive effects on hematopoiesis in patients with myelodysplastic syndrome receiving deferasirox as oral iron chelation therapy: a brief review. Leuk Res. 2011;35(5):566–70.
13. Taher AT, Musallam KM, Koussa S, Inati A. Transfusion independence in Diamond-Blackfan anemia after deferasirox therapy. Ann Hematol. 2009;88(12):1263–4.
14. Fisch P, Handgretinger R, Schaefer HE. Pure red cell aplasia. Br J Haematol. 2000;111(4):1010–22.
15. Lacy MQ, Kurtin PJ, Tefferi A. Pure red cell aplasia: association with large granular lymphocyte leukemia and the prognostic value of cytogenetic abnormalities. Blood. 1996;87(7):3000–6.
16. Messa E, Carturan S, Maffè C, Pautasso M, Bracco E, Roetto A, Messa F, Arruga F, Defilippi I, Rosso V, Zanone C, Rotolo A, Greco E, Pellegrino RM, Alberti D, Saglio G, Cilloni D. Deferasirox is a powerful NF-kappaB inhibitor in myelodysplastic cells and in leukemia cell lines acting independently from cell iron deprivation by chelation and reactive oxygen species scavenging. Haematologica. 2010;95(8):1308–16.
17. Vreugdenhil G, Smeets M, Feelders RA, Van Eijk HG. Iron chelators may enhance erythropoiesis by increasing iron delivery to haematopoietic tissue and erythropoietin response in iron-loading anaemia. Acta Haematol. 1993;89:57–60.
18. Ghoti H, Fibach E, Merkel D, Perez-Avraham G, Grisariu S, Rachmilewitz EA. Changes in parameters of oxidative stress and free iron biomarkers during treatment with deferasirox in iron-overloaded patients with myelodysplastic syndromes. Haematologica. 2010;95(8):1433–4.
19. Spivak JL. Polycythemia vera: myths, mechanisms, and management. Blood. 2002;100(13):4272–90.
20. Louache F, Testa U, Pelicci P, Thomopoulos P, Titeux M, Rochant H. Regulation of transferrin receptors in human hematopoietic cell lines. J Biol Chem. 1984;259(18):11576–82.
21. Kontoghiorghes GJ, May A. Uptake and intracellular distribution of iron from transferrin and chelators in erythroid cells. Biol Met. 1990;3(3–4):183–7.
22. Taoka K, Kumano K, Nakamura F, Hosoi M, Goyama S, Imai Y, Hangaishi A, Kurokawa M. The effect of iron overload and chelation on erythroid differentiation. Int J Hematol. 2012;95(2):149–59.
23. Zeok JV, Todd EP, Dillon M, DeSimone P, Utley JR. The role of thymectomy in red cell aplasia. Ann Thorac Surg. 1979;28(3):257–60.
24. Masaoka A, Hashimoto T, Shibata K, Yamakawa Y, Nakamae K, Iizuka M. Thymomas associated with pure red cell aplasia. Histologic and follow-up studies. Cancer. 1989;64(9):1872–8.
25. Thompson CA, Steensma DP. Pure red cell aplasia associated with thymoma: clinical insights from a 50-year single-institution experience. Br J Haematol. 2006;135(3):405–7.
26. Hirokawa M, Sawada K, Fujishima N, Nakao S, Urabe A, Dan K, Fujisawa S, Yonemura Y, Kawano F, Omine M, Ozawa K. Long-term response and outcome following immunosuppressive therapy in thymoma-associated pure red cell aplasia: a nationwide cohort study in Japan by the PRCA collaborative study group. PRCA Collaborative Study Group. Haematologica. 2008;93(1):27–33.
27. Masuda M, Arai Y, Okamura T, Mizoguchi H. Pure red cell aplasia with thymoma: evidence of T-cell clonal disorder. Am J Hematol. 1997;54(4):324–8.
28. Fujishima N, Hirokawa M, Fujishima M, Wada C, Toyoshima I, Watanabe S, Sawada K. Oligoclonal T cell expansion in blood but not in the thymus from a patient with thymoma-associated pure red cell aplasia. Haematologica. 2006;91(12 Suppl):ECR47.

Int J Hematol (2013) 98:143–144
DOI 10.1007/s12185-013-1381-1

IMAGES IN HEMATOLOGY

Atypical chronic myeloid leukemia harboring *NUP98-HOXA9*

Hiromichi Murayama · Hiromichi Matsushita · Kiyoshi Ando

Received: 24 April 2013 / Revised: 24 May 2013 / Accepted: 28 May 2013 / Published online: 11 June 2013

A previously healthy 67-year-old Japanese male visited our hospital to undergo a work up for leukocytosis. Laboratory tests showed a hemoglobin level of 11.9 g/dL, platelets 225×10^9/L, and leukocytes 23.0×10^9/L. The neutrophil alkaline phosphatase (NAP) score was 107 (control, 238). A peripheral blood smear showed neutrophilia (77.0 %) with a hypersegmented nucleus (Fig. 1a). Neither monocytosis (5.5 %), basophilia (0.0 %), nor eosinophilia (0.5 %) was seen. Bone marrow aspiration revealed marked myeloid proliferation without any differentiation block. Dysgranulopoiesis and dysmegakaryopoiesis were observed, including pseudo-Pelger-Huët anomaly, hypogranulation and bizarrely segmented nuclei in the neutrophils, and small megakaryocytes with hypolobulated nuclei (Fig. 1b, c). The erythroid lineage cells did not have apparent dysplasia. Karyotypic and molecular analysis of the bone marrow cells showed only one abnormality t(7;11)(p15;p15), and the resultant *NUP98-HOXA9* expression. Neither *BCR-ABL1* nor *JAK2V617F* was detected. The patient was diagnosed with atypical chronic myeloid leukemia (atypical CML) harboring t(7;11)(p15;p15)/*NUP98-HOXA9*.

t(7;11)(p15;p15)/*NUP98-HOXA9* is known to be a poor prognostic factor in acute myeloid leukemia, as well as an additional genetic event in CML progressing to blastic crisis [1]. Several reports have described Ph^1-negative CML or chronic myelomonocytic leukemia to harbor only t(7;11)(p15;p15)/*NUP98-HOXA9* [2, 3]. These cases were accompanied by dysgranulopoiesis and/or monocytosis, which are not usually seen in CML. A low NAP score cannot discriminate such patients from CML cases. To date, no treatment strategy or prognostic methods have yet been established for such cases. Our patient was followed up without any particular treatment, and his complete blood count and differentials have remained unchanged for more than 6 months.

Conflict of interest The authors declare no competing financial interests in association with this study.

References

1. Gough SM, Slape CI, Aplan PD. NUP98 gene fusions and hematopoietic malignancies: common themes and new biologic insights. Blood. 2011;118:6247–57.
2. Kaneko Y, Maseki N, Takasaki N, Sakurai M, Kawai K, Sakurai M. Possible association of a new translocation, t(7;11)(p15;p15), with Ph1 chromosome-negative chronic myelogenous leukemia. Int J Cancer. 1985;36:657–9.
3. Wong KF, So CC, Kwong YL. Chronic myelomonocytic leukemia with t(7;11)(p15;p15) and NUP98/HOXA9 fusion. Cancer Genet Cytogenet. 1999;115:70–2.

H. Murayama · K. Ando
Division of Hematology/Oncology, Department of Internal Medicine, Tokai University School of Medicine, 143 Shimokasuya, Isehara, Kanagawa 259-1193, Japan

H. Matsushita (✉)
Department of Laboratory Medicine, Tokai University School of Medicine, 143 Shimokasuya, Isehara, Kanagawa 259-1193, Japan
e-mail: hmatsu@is.icc.u-tokai.ac.jp

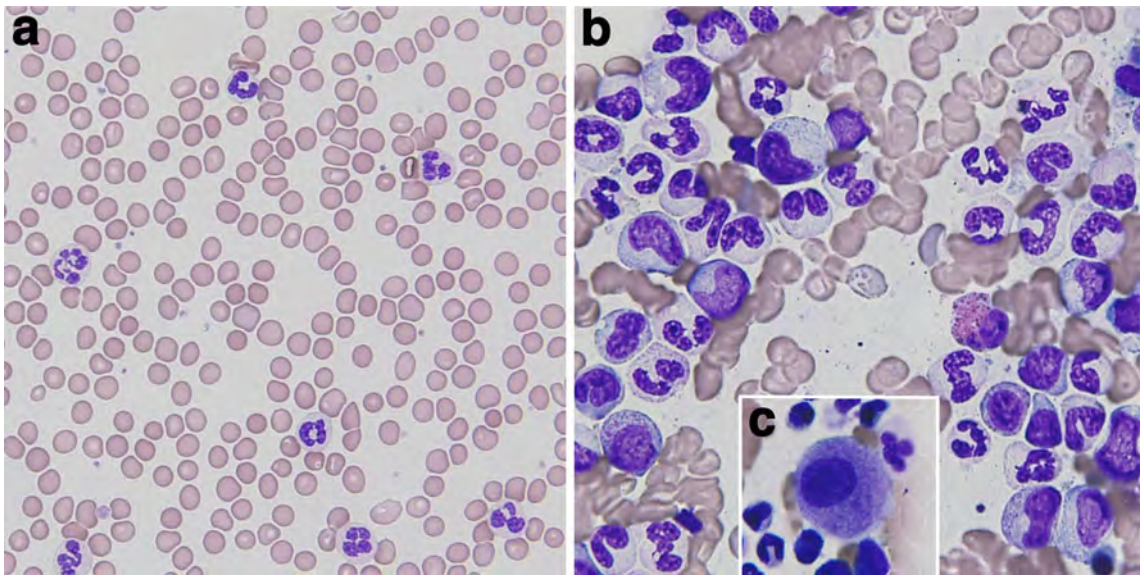

Fig. 1 **a** Peripheral blood smear showing neutrophilia with a hypersegmented nucleus. **b**, **c** Bone marrow smear (May–Giemsa staining). Marked myeloid proliferation with dysgranulopoiesis and dysmegakaryopoiesis were recognized

Int J Hematol (2013) 98:206–213
DOI 10.1007/s12185-013-1399-4

ORIGINAL ARTICLE

Unrelated allogeneic bone marrow-derived mesenchymal stem cells for steroid-refractory acute graft-versus-host disease: a phase I/II study

Kazuo Muroi · Koichi Miyamura · Kazuteru Ohashi · Makoto Murata · Tetsuya Eto · Naoki Kobayashi · Shuichi Taniguchi · Masahiro Imamura · Kiyoshi Ando · Shunichi Kato · Takehiko Mori · Takanori Teshima · Masaki Mori · Keiya Ozawa

Received: 27 May 2013 / Revised: 5 July 2013 / Accepted: 9 July 2013 / Published online: 17 July 2013

Abstract We conducted a multicenter phase I/II study using mesenchymal stem cells (MSCs) manufactured from the bone marrow of healthy unrelated volunteers to treat steroid-refractory acute graft-versus-host disease (aGVHD). Fourteen patients with hematological malignancies who suffered from grade II (9 patients) or III aGVHD (5) were treated. Affected organs were gut (10 patients), skin (9 patients), and liver (3 patients). Seven patients had two involved organs. The median age was 52. No other second-line agents were given. MSCs were given at a dose of 2×10^6 cells/kg for each infusion twice a week for 4 weeks. If needed, patients were continuously given MSCs weekly for an additional 4 weeks. By week 4, 13 of 14 patients (92.9 %) had responded to MSC therapy with a complete response (CR; $n = 8$) or partial response (PR; $n = 5$). At 24 weeks, 11 patients (10 with CR and 1 with PR) were alive. At 96 weeks, 8 patients were alive in CR. A total of 6 patients died, attributable to the following: underlying disease relapse (2 patients), breast cancer relapse (1), veno-occlusive disease (1), ischemic cholangiopathy (1), and

K. Muroi (✉)
Division of Cell Transplantation and Transfusion, Jichi Medical University Hospital, 3311-1 Yakushiji, Shimotsuke, Tochigi 329-0498, Japan
e-mail: muroi-kz@jichi.ac.jp

K. Miyamura
Department of Hematology, Japanese Red Cross Nagoya First Hospital, Nagoya, Japan

K. Ohashi
Hematology Division, Tokyo Metropolitan Komagome Hospital, Tokyo, Japan

M. Murata
Department of Hematology and Oncology, Nagoya University Graduate School of Medicine, Nagoya, Japan

T. Eto
Department of Hematology, Hamanomachi Hospital, Fukuoka, Japan

N. Kobayashi
Department of Internal Medicine, Sapporo Hokuyu Hospital, Sapporo, Japan

S. Taniguchi
Department of Hematology, Toranomon Hospital, Tokyo, Japan

M. Imamura
Department of Hematology, Hokkaido University Graduate School of Medicine, Sapporo, Japan

K. Ando
Division of Hematology/Oncology, Department of Internal Medicine, Tokai University School of Medicine, Isehara, Japan

S. Kato
Department of Cell Transplantation and Regenerative Medicine, Tokai University School of Medicine, Isehara, Japan

T. Mori
Division of Hematology, Keio University School of Medicine, Tokyo, Japan

T. Teshima
Center for Cellular and Molecular Medicine, Kyushu University Graduate School of Medicine, Fukuoka, Japan

M. Mori · K. Ozawa
Division of Hematology, Jichi Medical University, Shimotsuke, Japan

pneumonia (1). No clear adverse effects associated with MSC infusion were observed. Third party-derived bone marrow MSCs may be safe and effective for patients with steroid-refractory aGVHD.

Keywords Mesenchymal stem cells · GVHD · Steroid

Introduction

Allogeneic hematopoietic stem cell transplantation (AlloHSCT) is a curative therapy for hematological malignancies and hemopoietic stem cell disorders. Acute graft-versus-host disease (aGVHD), the most important complication associated with AlloHSCT, develops in a significant number of patients who receive AlloHSCT despite GVHD prophylaxis [1]. Levine et al. [2] showed using Cox regression analysis that GVHD grade had a significant impact on non-relapse mortality and overall survival (OS) in a phase II GVHD treatment trial. The relative risk of non-relapse mortality was 1.72 for patients with grade III–IV GVHD, compared to patients with grade 0–II GVHD. Significant factors on OS were aGVHD grade (0–II versus III–IV), donor type (related versus unrelated), and stem cell source (peripheral blood versus bone marrow versus cord blood).

In general, a steroid is first given to patients with aGVHD; however, about half of the patients do not respond to the therapy [3]. Unfortunately, second-line agents have not clearly shown effectiveness against steroid-refractory aGVHD, because they act as a non-specific immunosuppressant and reduce host immunity, leading frequently to infections caused by bacteria, fungi and viruses [4, 5]. Indeed, most patients with steroid-refractory aGVHD die of aGVHD itself, organ damage, and infections even if such second-line therapy is conducted. Recently, the American Society of Blood and Marrow Transplantation evaluated 29 studies in which agents were administered as secondary therapy in aGVHD [6]. Evaluated agents included mycophenolate mofetil, daclizumab, alemtuzumab, infliximab, etanercept, horse antithymocyte globulin, and so on, but excluded mesenchymal stem cells (MSCs). Importantly, the evaluation of complete response (CR) rates, overall response (OR) rates, and 6-month survival estimates did not support the choice of any specific agents for second-line therapy in aGVHD. Therefore, a new agent for steroid-refractory aGVHD is desirable.

MSCs have unique characteristics: specific immunosuppressive properties, no immunogenicity on its own, supportive activity for hemopoiesis, and differentiation abilities into fat cells, chondrocytes, and osteoblasts. Since the first dramatic report by LeBlanc et al., there have been several reports on the effectiveness of MSCs against steroid-refractory aGVHD [7–20]. However, there are several problems when evaluating MSCs against steroid-refractory aGVHD in these studies: before MSC administration, patients have already received one or more immunosuppressants other than for GVHD prophylaxis to steroid-refractory aGVHD and the follow-up time of the patients who received MSCs was relatively short. The source of MSCs used for steroid-refractory aGVHD in these studies was heterogeneous: HLA-identical siblings, HLA-haploidentical related donors, and HLA-mismatched unrelated (third-party) donors. The production of MSCs in different institutes leads to concern about purity and cell function. We report a phase I/II trial on steroid-refractory aGVHD using third party-derived bone marrow MSCs. Before MSC administration, patients only received steroids for aGVHD as a first-line therapy.

Materials and methods

Patients

During the period from January 2009 and November 2010, 14 patients were enrolled in a phase I/II trial using third party-derived bone marrow MSCs for steroid-refractory aGVHD across major transplant centers in Japan. This trial, sponsored by JCR Pharmaceuticals Co., Ltd (Ashiya, Japan) and designated JR-031-201, was approved by the ethics committee in each participating facility. Informed consent was obtained from all the patients.

The eligibility requirements included patients with steroid-refractory grade II to IV aGVHD and age over 6 months. Steroid-refractory aGVHD was defined as progression of aGVHD for 3 days with standard-dose steroid administration or no change in aGVHD for 5 days with the therapy. The standard steroid dose (prednisolone or methylprednisolone) was 1–2 mg/kg. Exclusion criteria were as follows: chemorefractory disease, severe infection, positive results of viral infections including human immunodeficiency virus, human T-lymphotropic virus type I, hepatitis B virus, and hepatitis C virus, severe organ damage including heart, lung, kidney, and liver except liver GVHD, uncontrolled hypertension, oxygen saturation at a steady state less than 94 %, and new immunosuppressive agents added other than steroids for aGVHD. In cases where attending physicians did not predict early relapse after AlloHSCT, no remission in acute leukemia, myelodysplastic syndrome, or hematological malignancies was included. All patients received prophylaxis against GVHD with a calcineurin inhibitor (tacrolimus or cyclosporine) alone or a combination of a calcineurin inhibitor and methotrexate or mycophenolate mofetil. The source of hemopoietic stem cell transplants was bone marrow, peripheral blood stem cells, or cord blood. Conditioning

was either myeloablative conditioning such as total body irradiation-based and intravenous busulfan-based regimens or non-myeloablative conditioning such as fludarabine-based regimens. aGVHD was defined according to the 1994 Consensus Conference on Acute GVHD Grading [21].

MSCs

MSCs were manufactured by JCR based on a license from Osiris Therapeutics Inc (Columbia, Merryland, USA) and named JR-031. JR-031 is almost the same as Prochymal produced by Osiris [12, 17]. Briefly, an aliquot of bone marrow obtained from healthy volunteers was cultured in a medium supplemented with 10 % fetal bovine serum from New Zealand (Life Technologies, New York, USA). The fetal bovine serum products were free of bacteria, viruses, mycoplasma, and endotoxins in the checking tests. The products met standards for Code of Federal Regulations 9CFR113.53 and the United States Department of Agriculture. Adherent cells were expanded by culture and used as MSCs. Before freezing, cells were examined in the terms of MSC characteristics [22]. Isolated cells showed positivity for CD73, CD90, CD105, and CD166 and negativity for CD34, CD45, and HLA-DR. The cells inhibited the mixed-lymphocyte reaction and differentiated to fat cells, chondrocytes, and osteoblasts. The cells had the ability to produce prostaglandin E2. Multicolor-fluorescence in situ hybridization showed that the cells had no chromosomal abnormalities. No infectious agents such as bacteria, mycoplasma, or viruses were detected in the supernatants of the cells or the cells themselves. No endotoxin was detected in the supernatant.

Treatment schedule and evaluation

Initially, patients received a dose of 2×10^6 MSCs/kg twice a week for 4 weeks. The first infusion of MSCs was given within 48 h of the diagnosis of steroid-refractory aGVHD. The interval between each MSC infusion was 3 or 4 days. The volume of one bag of JR-031 was 15 ml containing 100×10^6 MSC, 1.5 g DMSO, 750 mg of human albumin, and other electroride elements. A solution of 25 ml saline was added to thawed MSCs and they were infused at a speed of around 4 ml/min. Before infusion, either 100–200 mg of hydrocortisone or 5–10 mg of chlorpheniramine or both were given to prevent an infusion reaction. During the total course of MSC infusions, no increase in the dose of immunosuppressants given for GVHD prevention was allowed. As for the steroid dose for GVHD treatment, no increase of more than the initial dose of steroid was allowed. Steroid dose reduction including the start of tapering timing and the reduction dose was left to the physicians who took care of the patient.

Response to aGHVD was evaluated for each involved organ. CR was defined as the complete resolution of aGVHD; partial response (PR), as a decrease in organ stages of aGVHD; no response (NR), as no change in aGVHD; progression (PG), as progressive worsening of aGVHD; mixed response (MR), as a mixture of a decrease and increase in organ stages of aGVHD. Patients were dropped out of this JR-031-201 trial if there was PG after the infusion of 3 doses of MSCs or NR after the infusion of 5 doses of MSCs. After completing MSC infusion for 4 weeks, i.e., 8 doses of MSCs, the response was evaluated. When patients showed PR or MR, 2×10^6 MSCs/kg were further given weekly for 4 weeks. The response of MSC therapy to aGVHD was evaluated as follows: CR or PR by the end of 4, 12, and 24 weeks from the first MSC infusion, as wells as continuous CR for more than 28 days. Other evaluable factors associated with MSC therapy were survival, disease relapse, infection, chronic GVHD, and so on.

Monitoring of adverse effects

To monitor adverse effects associated with MSC therapy, laboratory studies, electrocardiogram (ECG), chest X-ray, and computed tomography (CT) of the chest and abdomen were done according to the schedule; ECG was conducted before the first MSC infusion, at 4, 12, and 24 weeks (the cessation of the study) from the first MSC infusion. Chest X-ray was performed before the first MSC infusion, at 4 and 24 weeks. CT was conducted before the first MSC infusion and at 24 weeks. Vital signs, including percutaneous oxygen saturation concentration, were measured before and after each MSC infusion.

Long-term follow-up

After completing JR-031-201, a long-term follow-up study, JR-031-202, was conducted. The observation period was from the week following the end of JR-031-201, i.e., 25 weeks after the first MSC infusion, to 96 weeks (2 years). Informed consent was obtained from each patient. Evaluated valuables included adverse effects associated with MSC therapy such as the status of aGVHD, development of chronic GVHD (cGVHD), disease relapse, ectopic tissue formation, and so on.

Statistical analysis

Survival was described as time from the first MSC infusion and calculated by the Kaplan–Meier method.

Results

Table 1 shows the characteristics of the patients who received MSCs. The median age was 52 years (range 4–62 years). Thirteen patients were adults, while only one was a child. All patients had hematological malignancies as follows: acute myeloid leukemia, 4 patients; acute lymphoblastic leukemia, 3; myelodysplastic syndrome, 3; chronic lymphocytic leukemia, 1; follicular lymphoma, 1; multiple myeloma, 1; and juvenile myelomonocytic leukemia, 1. Of these, 2 patients (no. 4 and 10) had MLL-related leukemia due to chemotherapy for breast cancer. Breast cancer in both patients was in complete remission before AlloHSCT. No patients with refractory disease to chemotherapy were included. Most patients received a transplant from HLA-mismatched unrelated donors after myeloablative or non-myeloablative conditioning. The source of hematopoietic stem cells for transplantation was bone marrow (9 patients), peripheral blood stem cells (1), and cord blood (4). HLA disparity was shown in the eight pairs. All except 3 patients received a combination of a calcineurin inhibitor and methotrexate as GVHD prophylaxis. All patients were first given either prednisolone or methylprednisolone to treat acute GVHD.

Table 2 shows the aGVHD severity and organ involvement before the first MSC infusion and response to aGVHD. The grade of aGVHD was grade II (9 patients) and III (5 patients). Grade IV aGVHD was not enrolled. The most affected organs were the skin (9 patients) and gut (10 patients). Seven patients had two involved organs. MSCs were first infused on the median 47 days after AlloHSCT. The median number of MSC infusions was eight. By 4 weeks after the first MSC infusion, 8 and 5 patients had achieved CR and PR, respectively. The OR rate was 92.9 % (13 of 14 patients). By 24 weeks, 4 of 5 patients with PR achieved CR. At 96 weeks, 8 patients were alive and in CR. As shown in Fig. 1, the estimated time to reach 50 % CR after the first MSC infusion was 3 weeks (MSC infusion six times). There was no difference in the time to reach CR between grade II and grade III aGVHD (data not shown). Relapse of aGVHD after MSC therapy occurred in one patient (no. 12). At 78 days after the first MSC infusion, he was admitted again because of bloody diarrhea. Endoscopic biopsy showed aGVHD in the cecum and colon. The patient was put on parenteral hyperalimentation with tacrolimus administration. His aGVHD gradually disappeared.

By the end of the follow-up (2 years), 6 patients had died (Table 2). Five of the 6 patients (no. 2, 3, 4, 9, and 10) died due to factors not directly related to aGVHD as follows: no. 9 patient, veno-occlusive disease on day 25; no. 7, hepatic failure on day 36; no. 2, pneumonia on day 82; no. 3 and 10, disease relapse on days 191 and 696, respectively; and no. 4, metastatic breast cancer on day

Table 1 Patient characteristics

Case no.	Age	Sex	Disease	HSCT				GVHD prophylaxis	First line therapy for acute GVHD
				Source	Donor	HLA disparity	Conditioning		
1	56	F	MDS/RCMD	BM	Unrelated	7/8	Myeloab	CyA + sMTX	mPSL
2	59	F	AML/2nd CR	BM	Unrelated	8/8	Myeloab	CyA	mPSL
3	44	M	AML/1st CR	BM	Unrelated	7/8	Myeloab	FK506	mPSL
4	36	F	ALL/2nd Rel	BM	Unrelated	6/8	Myeloab	FK506	mPSL
5	57	F	FL	PB	Sibling	8/8	Myeloab	CyA + sMTX	PSL
6	42	F	ALL/1st CR	BM	Unrelated	8/8	Myeloabl	FK506 + sMTX	PSL
7	29	M	MDS/RAEB	CB	Unrelated	4/8	Myeloab	FK506 + sMTX	mPSL
8	62	F	CLL/PR	CB	Unrelated	5/8	Non-myeloab	FK506 + sMTX	mPSL
9	55	M	ALL/1st CR	BM	Unrelated	8/8	Myeloab	CyA + sMTX	mPSL
10	49	F	AML/1st CR	BM	Unrelated	6/8	Myeloab	FK506 + sMTX	mPSL
11	4	M	JMML/1st CP	CB	Unrelated	5/6	Myeloab	CyA + sMTX	PSL
12	61	M	AML-MRC[a]	CB	Unrelated	4/6	Myeloab	FK506 + MMF	PSL
13	35	F	MM/1st CR	BM	Unrelated	8/8	Non-myeloab	FK506 + sMTX	PSL
14	61	F	MDS/RAEB	BM	Sibling	6/6	Non-myeloab	CyA + sMTX	PSL

HSCT hemopoietic stem cell transplantation, *GVHD* graft-versus-host disease, *F* female, *M* male, *MDS* myelodysplastic syndrome, *RCMD* refractory cytopenia with multilineage dysplasia, *AML* acute myeloid leukemia, *AML-MRC* acute myeloid leukemia with myelodysplasia-related changes, *ALL* acute lymphoblastic leukemia, *FL* follicular lymphoma, *RAEB* refractory anemia with excess of blasts, *CLL* chronic lymphocytic leukemia, *MM* multiple myeloma, *CR* complete remission, *PR* partial remission, *Rel* relapse, *BM* bone marrow, *PB* peripheral blood stem cell, *CB* cord blood, *Myeloab* myeloablative, *Non-myeloab* non-myeloablative, *CyA* cyclosporine, *FK506* tacrolimus, *sMTX* short-term methotrexate, *PSL* prednisolone, *mPSL* methylprednisolone

[a] No chemotherapy before HSCT

Table 2 GVHD and outcome

Case	GVHD				1st MSC infusion	No. of MSC infusions	Response		Survival/ death	Cause of death (days)
	Grade	Skin	Liver	Gut	Days after HSCT		By 4 weeks	By 24 weeks	At 96 weeks	
1	II	3	0	0	38	8	PR	PR	Alive in CR	N/A
2	II	1	0	1	50	10	PR	CR	Dead	Pneumonia (82)
3	II	3	0	0	43	12	PR	CR	Dead	Relapse (696)
4	III	1	0	2	51	12	CR	CR	Dead	Breast cancer (244)
5	II	3	0	1	46	8	CR	CR	Alive in CR	N/A
6	II	3	0	0	48	8	CR	CR	Alive in CR	N/A
7	III	0	1	2	33	5	PG	–	Dead	IC (36)
8	III	3	0	3	57	12	PR	CR	Alive in CR	N/A
9	II	1	0	1	38	3	CR	CR	Dead	VOD (25)
10	II	0	0	1	45	8	CR	CR	Dead	Relapse (191)
11	III	0	2	4	78	12	PR	CR	Alive in CR	N/A
12	II	0	1	0	52	8	CR	CR	Alive in CR	N/A
13	III	3	0	4	44	8	CR	CR	Alive in CR	N/A
14	II	0	0	1	108	7	CR	CR	Alive in CR	N/A

GVHD graft-versus-host disease, *MSC* mesenchymal stem cell, *HSCT* hemopoietic stem cell transplantation, *CR* complete response, *PR* partial response, *PG* progression, *VOD* veno-occlusive disease, *IC* ischemic cholangiopathy, *N/A* not applicable

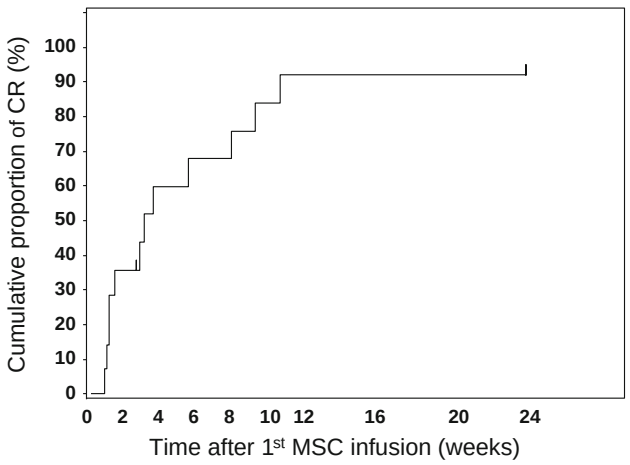

Fig. 1 Time to achieve complete response

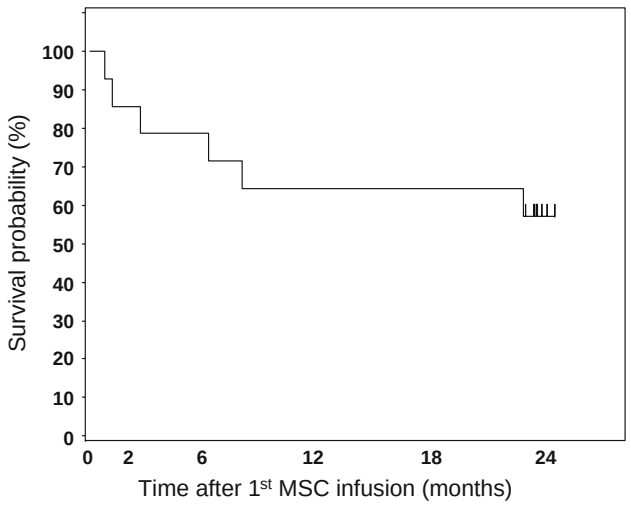

Fig. 2 Overall survival

244. The no. 2 patient showed pancytopenia caused by ganciclovir treatment for CMV antigenemia and died of pneumonia with massive pleural effusion. Autopsy findings showed pulmonary aspergillosis. Two patients with acute myeloid leukemia (no. 3 and 10) relapsed; the former received a second bone marrow transplant from another donor, but he died of sepsis. The latter died of septic shock after chemotherapy for disease relapse. Patient no. 4 maintained CR after MSC therapy, but a scheduled CT scan incidentally showed multiple low-density areas in both liver lobes on day 145. A liver biopsy demonstrated adenocarcinoma, leading to the suspicion of liver metastasis of breast cancer. Bone scintigraphy showed multiple isotope uptake regions in vertebrae and pelvic bone. The patient was diagnosed with recurrent breast cancer in the liver and bone and died of breast cancer. Patient no. 7 was evaluated as having PG of aGVHD. Serum liver enzyme levels and bilirubin values progressively worsened, leading to death. Necropsy of the liver showed ischemic cholangiopathy characterized by massive hepatocyte necrosis, marked congestion in the bile ducts, hyaline degeneration in the arterioles, disappearance of endothelial cells in the arterioles, and slight infiltration of lymphocytes. OS is shown in Fig. 2. There was no

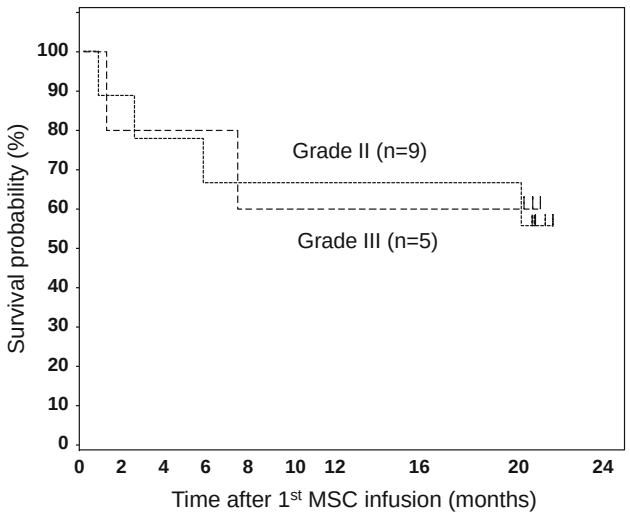

Fig. 3 Overall survival in the category of grade II and III acute GVHD. There was no difference between the two groups

difference in survival between groups of patients with grade II and grade III aGVHD (Fig. 3).

Adverse effects associated with MSC therapy were monitored. No infusion toxicity such as fever or decrease in oxygen saturation was observed. In the JCR-031-201 study, 27 events of infection episodes in 13 patients were collected as follows: bacteremia (3 events, 3 patients), pneumonia (4, 3), herpes zoster (3, 2), oral candidiasis (2, 2), infectious enterocolitis (2, 2), CMV antigenemia (2, 2), sepsis (1, 1), CMV colitis (1, 1), hemorrhagic cystitis (1, 1), and others (7, 7). In the JCR-031-202 study, 28 events in 9 patients were collected as follows: pneumonia (3 events, 3 patients), septic shock (3, 2), sinusitis (2, 2), upper respiratory tract infection (2, 2), oral herpes (4, 2), herpes zoster (1, 1), varicella (1, 1), infectious enterocolitis (1, 1), CMV antigenemia (1, 1), and others (8, 8). Ectopic tissue formation was not detected by scheduled CT scans. cGVHD developed in 7 patients; 4 patients (no. 8 at 24 weeks, 11 at 24 weeks, 12 at 48 weeks, and 14 at 36 weeks) with a limited form, and 3 patients (no. 1 at 24 weeks, 3 at 24 weeks, and 6 at 24 weeks) with an extensive form, of cGVHD.

Discussion

Reports of bone marrow MSCs used for steroid-refractory aGVHD are divided into two approaches; one approach used MSCs produced in the institution where patients were scheduled to receive the cells, while the another used MSCs manufactured in a company. In the former, the largest study was a phase II study conducted by the European Group for Blood and Bone Marrow [11]. Fifty-five patients with a median age of 22 years received MSCs for steroid-refractory aGVHD. Most patients had grade III or IV aGVHD. MSC donors were either HLA-identical, haploidentical, or HLA-mismatched unrelated donors. The median time from aGVHD onset to the first MSC infusion was 25 days. Of note, 33 patients had already received second-line therapy for aGVHD before MSC administration. Most patients received MSCs at a median dose of 1.4×10^6 MSCs/kg once or twice. The overall response rate was 71 % (CR, 30; PR, 9 patients). Twenty-four of these responders received MSCs from third-party donors. The overall estimated 2-year survival in this trial was 35 % and was significantly better in complete responders (53 %) versus non-complete responders (16 %). There was a better trend for 2-year estimated survival in the pediatric population compared to adults. No severe–adverse effects associated with MSC infusions were reported. Except for the report from the European Group for Blood and Bone Marrow, other reports were small-sized clinical studies including a phase I or a phase I/II study to treat steroid-refractory aGVHD with MSCs [7–10, 13–16, 18–20]. Importantly, in all of these studies, any second- or third-line immunosuppressive agent in combination with MSCs was allowed. Therefore, it is difficult to exactly evaluate the effects of MSCs on steroid-refractory aGVHD.

MSCs manufactured by Osiris, Prochymal, were given to steroid-refractory GVHD patients. Kebriaei et al. compared a dose of 2×10^8 Prochymal cells/kg with 8×10^8 Prochymal cells/kg in combination with steroids to treat patients with de novo aGVHD. Thirty-one patients were evaluated: there was no difference between the two groups in terms of safety and efficacy [12]. Prasad et al. [17] showed the efficacy of Prochymal for pediatric patients with severe refractory aGVHD. Most patients received Prochymal at a dose of 2×10^8 cells/kg. Following positive results in these two studies, Osiris conducted a phase III trial investigating Prochymal for steroid-refractory aGVHD across transplant centers in the United States, Canada, and Australia [23]. This was a double-blind placebo-controlled study. Patients were randomized at a 2:1 ratio for either Prochymal or the placebo. The dose of Prochymal was 2×10^8 cells/kg. Of note, most patients had already received a second-line therapy before MSC therapy. This trial enrolled 260 patients. The primary endpoint was durable CR for 28 days. The preliminary analysis did not show a statistical difference between Prochymal and the placebo for the primary endpoint (Prochymal 35 % versus placebo 30 %). However, subpopulation analysis showed that Prochymal significantly improved the response in liver aGVHD (76 versus 47 %) and gastrointestinal aGVHD (82 versus 68 %). Infection rates were not different between the two groups. Rates of severe–adverse effects associated with MSC administration were not different in the two arms. Now, Prochymal is approved for use

in pediatric steroid-refractory aGVHD in Canada and New Zealand as a cell-based medicine [24].

We confirmed that third party-derived bone marrow MSCs are safe and effective for patients with steroid-resistant aGVHD. In our study, only MSCs were given to patients with steroid-refractory GVHD as soon as possible after the diagnosis of steroid-refractory GVHD. Since the cell dose of infused MSCs was constant and the number of MSC infusions was strictly scheduled, our results are reliable to estimate the effects of MSCs on steroid-resistant aGVHD. A high CR rate and good OS were obtained. Of note, gut aGVHD comprised 71 % (10 of 14 patients) of our patients and all the patients except one showed CR. These results are consistent with others, i.e., MSCs have a favorable clinical effect on gut aGVHD [7, 12, 23]. Our trials did not include patients with grade IV aGVHD. Therefore, the good results in our studies may have been overestimated. As in other reports, no apparent adverse effects associated with MSC therapy were observed in short-term and long-term observations.

The presence of fetal bovine serum is necessary for standard conditions for MSC expansion [25]. However, it is better not to use animal products to avoid unknown infections and other complications. von Bonin et al. and Lucchini et al. showed the usefulness of platelet-lysate-expanded bone marrow MSCs for steroid-refractory aGVHD [13, 15]. Alternatively, MSC donor serum can be used for MSC expansion. Arima et al. and Pérez-Simon et al. successfully treated steroid-refractory aGVHD with bone marrow MSCs expanded in a medium supplemented with autologous serum [16, 18]. It is not known which MSC culture is the best in terms of the safety and growth of MSCs. Ideally, a serum-free culture of MSCs should be introduced in a clinical setting [26].

After the completion of the JCR-031-201 and JCR-031-202 trials, we started a phase III trial using JR-031 focusing on steroid-refractory grade III or IV aGVHD. In the near future, the results of this study will be published.

Conflict of interest K. Muroi and K. Ozawa received payment for consultancy from JCR Pharmaceuticals Co., Ltd. Other authors declare no conflicts of interest.

References

1. Bacigalupo A. Management of acute graft-versus-host disease. Br J Haematol. 2007;137:87–98.
2. Levine JE, Logan B, Wu J, Alousi AM, Ho V, Bolaños-Meade J, et al. Graft-versus-host disease treatment: predictors of survival. Biol Blood Marrow Transplant. 2010;16:1693–9.
3. Ferrara JL, Levine JE, Reddy P. Graft-versus-host disease. Lancet. 2009;373:1550–61.
4. Deeg HJ. How I treat refractory acute GVHD. Blood. 2007;109:4119–26.
5. Ho VT, Cutler C. Current and novel therapies in acute GVHD. Best Pract Res Clin Haematol. 2008;21:223–37.
6. Martin PJ, Rizzo JD, Wingard JR, Ballen K, Curtin PT, Cutler C, et al. First- and second-line systemic treatment of acute graft-versus-host disease: recommendations of the American Society of Blood and Marrow Transplantation. Biol Blood Marrow Transplant. 2012;18:1150–63.
7. Le Blanc K, Rasmusson I, Sundberg B, Götherström C, Hassan M, Uzunel M, et al. Treatment of severe acute graft-versus-host disease with third party haploidentical mesenchymal stem cells. Lancet. 2004;363:1439–41.
8. Ringdén O, Uzunel M, Rasmusson I, Remberger M, Sundberg B, Lönnies H, et al. Mesenchymal stem cells for treatment of therapy-resistant graft-versus-host disease. Transplantation. 2006;81:1390–7.
9. Fang B, Song Y, Liao L, Zhang Y, Zhao RC. Favorable response to human adipose tissue-derived mesenchymal stem cells in steroid-refractory acute graft-versus-host disease. Transplant Proc. 2007;39:3358–62.
10. Müller I, Kordowich S, Holzwarth C, Isensee G, Lang P, Neunhoeffer F, et al. Application of multipotent mesenchymal stromal cells in pediatric patients following allogeneic stem cell transplantation. Blood Cells Mol Dis. 2008;40:25–32.
11. Le Blanc K, Frassoni F, Ball L, Locatelli F, Roelofs H, Lewis I, et al. Mesenchymal stem cells for treatment of steroid-resistant, severe, acute graft-versus-host disease: a phase II study. Lancet. 2008;371:1579–86.
12. Kebriaei P, Isola L, Bahceci E, Holland K, Rowley S, McGuirk J, et al. Adult human mesenchymal stem cells added to corticosteroid therapy for the treatment of acute graft-versus-host disease. Biol Blood Marrow Transplant. 2009;15:804–11.
13. von Bonin M, Stölzel F, Goedecke A, Richter K, Wuschek N, Hölig K, et al. Treatment of refractory acute GVHD with third-party MSC expanded in platelet lysate-containing medium. Bone Marrow Transplant. 2009;43:245–51.
14. Lim JH, Lee MH, Yi HG, Kim CS, Kim JH, Song SU. Mesenchymal stromal cells for steroid-refractory acute graft-versus-host disease: a report of two cases. Int J Hematol. 2010;92:204–7.
15. Lucchini G, Introna M, Dander E, Rovelli A, Balduzzi A, Bonanomi S, et al. Platelet-lysate-expanded mesenchymal stromal cells as a salvage therapy for severe resistant graft-versus-host disease in a pediatric population. Biol Blood Marrow Transplant. 2010;16:1293–301.
16. Arima N, Nakamura F, Fukunaga A, Hirata H, Machida H, Kouno S, et al. Single intra-arterial injection of mesenchymal stromal cells for treatment of steroid-refractory acute graft-versus-host disease: a pilot study. Cytotherapy. 2010;12:265–8.
17. Prasad VK, Lucas KG, Kleiner GI, Talano JA, Jacobsohn D, Broadwater G, et al. Efficacy and safety of ex vivo cultured adult human mesenchymal stem cells (Prochymal) in pediatric patients with severe refractory acute graft-versus-host disease in a compassionate use study. Biol Blood Marrow Transplant. 2011;17:534–41.
18. Pérez-Simon JA, López-Villar O, Andreu EJ, Rifón J, Muntion S, Campelo MD, et al. Mesenchymal stem cells expanded in vitro with human serum for the treatment of acute and chronic graft-versus-host disease: results of a phase I/II clinical trial. Haematologica. 2011;96:1072–6.
19. Wernicke CM, Grunewald TG, Juenger H, Kuci S, Kuci Z, Koehl U, et al. Mesenchymal stromal cells for treatment of steroid-refractory GvHD: a review of the literature and two pediatric cases. Int Arch Med. 2011;4:27.
20. Herrmann R, Sturm M, Shaw K, Purtill D, Cooney J, Wright M, et al. Mesenchymal stromal cell therapy for steroid-refractory acute and chronic graft versus host disease: a phase 1 study. Int J Hematol. 2012;95:182–8.

21. Przepiorka D, Weisdorf D, Martin P, Klingemann HG, Beatty P, Hows J, et al. 1994 consensus conference on acute GVHD grading. Bone Marrow Transplant. 1995;15:825–8.
22. Sato K, Ozaki K, Mori M, Muroi K, Ozawa K. Mesenchymal stromal cells for graft-versus-host disease: basic aspects and clinical outcomes. J Clin Exp Hematop. 2010;50:79–89.
23. Martin P. Prochymal® improves response rates in patients with steroid-refractory acute graft-versus-host disease involving the liver and gut: results of a randomized, placebo-controlled, multicentre phase III trial in GvHD. Bone Marrow Transplant. 2010;45:S17.
24. Daly A. Remestemcel-L, the first cellular therapy product for the treatment of graft-versus-host disease. Drugs Today (Barc). 2012;48:773–83.
25. Aldahmash A, Haack-Sørensen M, Al-Nbaheen M, Harkness L, Abdallah BM, Kassem M. Human serum is as efficient as fetal bovine serum in supporting proliferation and differentiation of human multipotent stromal (mesenchymal) stem cells in vitro and in vivo. Stem Cell Rev. 2011;7:860–8.
26. Jung S, Panchalingam KM, Rosenberg L, Behie LA. Ex vivo expansion of human mesenchymal stem cells in defined serum-free media. Stem Cells Int. 2012;2012:123030.

Int J Hematol (2013) 98:164–170
DOI 10.1007/s12185-013-1393-x

ORIGINAL ARTICLE

A phase I/II study of ofatumumab (GSK1841157) in Japanese and Korean patients with relapsed or refractory B-cell chronic lymphocytic leukemia

Yoshiaki Ogawa · Michinori Ogura · Tatsuya Suzuki · Kiyoshi Ando · Toshiki Uchida · Yukari Shirasugi · Kensei Tobinai · Je Hwan Lee · Masazumi Kase · Koichi Katsura · Tomomitsu Hotta

Received: 17 October 2012 / Revised: 12 June 2013 / Accepted: 17 June 2013 / Published online: 12 July 2013

Abstract The tolerability, efficacy, safety and pharmacokinetic profile of a human anti-CD20 monoclonal antibody, ofatumumab, was evaluated in this phase I/II study in patients with relapsed or refractory B-cell chronic lymphocytic leukemia (B-CLL). This study consisted of two parts. Tolerability was assessed in phase I (Part A), while the overall response rate (ORR) was assessed in phase II (comprising Parts A and B). Three patients were enrolled in Part A, and another seven patients were enrolled in Part B. Ofatumumab 300 mg was given at the first infusion, followed by seven weekly and four monthly infusions of 2000 mg. No patients experienced dose-limiting toxicity, and tolerability was confirmed. The ORR was 70 %. The most commonly reported adverse events (AEs) were leukopenia, neutropenia, and lymphopenia. No patients discontinued the study due to AEs. Plasma concentrations of ofatumumab prior to the next weekly dose increased steadily over the 8 weeks and did not reach steady state; with monthly dosing, pre-dose ofatumumab concentrations decreased. Inter-patient variability of pharmacokinetic parameters was larger after the first dose than after the later dose. In conclusion, this phase I/II study suggests that ofatumumab provides favorable safety and efficacy in Japanese/Korean patients with relapsed or refractory B-CLL.

Keywords Ofatumumab · Phase I/II study · Relapsed or refractory chronic lymphocytic leukemia

Y. Ogawa and M. Ogura contributed equally to this work.

This study was registered at ClinicalTrials.gov (NCT01077622).

Y. Ogawa (✉) · K. Ando · Y. Shirasugi
Department of Hematology and Oncology, Tokai University School of Medicine, Shimokasuya 143, Isehara, Kanagawa 259-1193, Japan
e-mail: yoshioga@is.icc.u-tokai.ac.jp

M. Ogura · T. Suzuki · T. Uchida
Department of Hematology and Oncology, Nagoya Daini Red Cross Hospital, Nagoya, Japan

K. Tobinai
Department of Hematology, National Cancer Center Hospital, Tokyo, Japan

J. H. Lee
Department of Hematology, Asan Medical Center, Seoul, Korea

M. Kase · K. Katsura
GlaxoSmithKline K.K, Tokyo, Japan

T. Hotta
National Hospital Organization Nagoya Medical Center, Nagoya, Japan

Introduction

Ofatumumab (Genmab A/S, Denmark) is an IgG1κ human monoclonal antibody (mAb) that targets a unique epitope on the CD20 molecule that encompasses both small and large extracellular loops [1, 2]. Ofatumumab induce lysis of several B-cell lines and primary B-cell chronic lymphocytic leukemia (B-CLL) cells, including rituximab-resistant cells [1, 3]. Ofatumumab induces B-cell depletion via complement-dependent cytotoxicity (CDC) and antibody-dependent cell-mediated cytotoxicity (ADCC) [1].

Clinical studies of ofatumumab have been conducted in Western countries [4–11]. The safety and efficacy of ofatumumab monotherapy were initially evaluated in a phase I/II study in heavily pretreated patients with relapsed or refractory B-CLL. The study showed that first infusions of 100, 300, or 500 mg plus 3 weekly infusions of 500, 1000,

or 2000 mg were well tolerated, and at the highest dose administered, the overall response rate (ORR) was 50 % [10]. These promising results were confirmed in a pivotal phase II study of ofatumumab monotherapy in patients with B-CLL refractory to fludarabine and alemtuzumab (FA-ref) and in those with bulky lymphadenopathy refractory to fludarabine but not suitable for treatment with alemtuzumab. Patients received first infusion of 300 mg, followed by 7 weekly infusions of 2000 mg and 4 monthly infusions. The results were favorable for both efficacy and safety [8, 11] and resulted in approval of ofatumumab for the treatment of FA-ref B-CLL in the United States and Europe.

Furthermore, a phase I study in patients with small lymphocytic lymphoma and CLL in Japan has confirmed the tolerability of ofatumumab as monotherapy at 500 and 1000 mg [12].

To further determine the clinical significance of ofatumumab at 2000 mg in Japanese and Korean patients with B-CLL, a phase I/II study was conducted.

Materials and methods

Patients

Eligible patients were 20 years or older with relapsed or refractory B-CLL previously treated with any anti-CLL therapy. The diagnosis of B-CLL required the presence of at least 5000/μL B lymphocytes in the peripheral blood with positive findings for CD5, CD19, CD20, and CD23 tests according to the National Cancer Institute-Sponsored Working Group (NCI-WG) response guidelines [13].

This study was performed in accordance with Good Clinical Practice. The protocol was approved by the Institutional Review Board of each participating institution, and conformed to the provisions of the Declaration of Helsinki in 2008. All patients gave a written informed consent.

Study design

This study was planned as an open-label, non-randomized, multicenter phase I/II study, consisting of 2 parts (Part A and Part B).

The primary objective in Part A was to evaluate the tolerability of ofatumumab at 2000 mg in Japanese patients. In Part A and Part B, the primary objective was to assess the ORR to 2000 mg ofatumumab in Japanese and Korean patients.

Ofatumumab at 300 mg was given at the first infusion, followed by 7 weekly infusions of 2000 mg and then 4 monthly infusions of 2000 mg for a total of 12 infusions over 24 weeks. Safety and efficacy were evaluated until 48 weeks after the first infusion.

Thirty to 120 min prior to each infusion of the study drug, all patients received oral acetaminophen 400 mg or equivalent, and oral or intravenous antihistamine (e.g. cetirizine hydrochloride 10 mg, or equivalent). Before the first and second infusions, all patients also received intravenous glucocorticoid equivalent to 100 mg of prednisolone (30–120 min prior to infusion of the study drug). After the third infusion, glucocorticoid was given if clinically indicated in the opinion of the investigator.

Tolerability evaluation

Dose-limiting toxicity (DLT) was defined as grade 3 or greater non-hematological toxicity (excluding grade 3 nausea and vomiting and grade 3 infusion reaction), or grade 3 infusion reaction persisting until the next day despite pre-medication and appropriate management, or grade 4 hematological toxicity of neutropenia lasting $\geq$7 days and febrile neutropenia (fever for more than 2 days and grade 4 neutropenia).

DLT was monitored from the start of treatment until 7 days after the 8th infusion. DLT was evaluated in the first 3 patients. When 1/3 or 2/3 patients met one of the DLT criteria, additional 3 patients were enrolled to evaluate DLT. If 0/3 or $\leq$2/6 patients met one of the DLT criteria, the dose was judged as tolerable.

Efficacy evaluation

The primary efficacy endpoint was the ORR. Assessment of response was according to NCI-WG guidelines. Secondary efficacy endpoints included progression-free survival (PFS), duration of response, time to response, improvement in constitutional symptoms, and improvement in Eastern Cooperative Oncology Group (ECOG) performance status.

The efficacy was evaluated by an independent review committee (IRC).

Safety evaluation

Adverse events (AEs) were reported throughout the study period and graded according to the National Cancer Institute (NCI) Common Terminology Criteria for Adverse Events (CTCAE) version 3.0. The serum samples for the human anti-human antibody (HAHA) testing were collected at baseline prior to the treatment and at week 24 and week 48 post-treatment. The formation of HAHA against ofatumumab was assessed using a validated electro chemiluminescence bridging immunoassay method on a

Meso Scale Discovery 6000 plate reader (MSD, Gaithersburg, MD, USA).

The mean serum titers of IgA, IgG, and IgM antibody were assessed at baseline and at week 8, week 24, and week 48.

"Infusion reactions" were determined based on clinical judgment. All adverse events observed within 24 h after the end of infusion were reviewed by a clinical reviewer.

Pharmacokinetic parameters

Blood samples were collected from 8 patients enrolled in Part A and Part B of the study for pharmacokinetic (PK) examinations. PK parameters were derived by non-compartmental analysis, based on the time after the start of infusion. The following PK parameters were calculated for each patient, from available data from the first, 8, and 12th infusions: maximum plasma concentration (C_{max}), time to observed maximum drug concentration (t_{max}), plasma half-life at terminal phase ($t_{1/2}$), area under the concentration–time curve (AUC_{0-inf} and AUC_{0-tau}), clearance (CL), volume of distribution at steady state (V_{ss}), and mean residence time (MRT).

Statistical analysis

This study neither asserted nor tested any statistical hypotheses.

Results

Study population

A total of 10 patients with relapsed or refractory B-CLL were enrolled into this study and received ofatumumab at 3 centers in Japan and at 1 center in Korea. Three patients were enrolled in Part A and were evaluated for tolerability. After the tolerability of ofatumumab at 2000 mg was confirmed, 7 patients were enrolled in Part B. The median age of the patients was 67 years (range 55–74 years). The median number of prior anti-CLL therapy was 1 (range 1–3). Eight of 10 patients were treated with fludarabine or with fludarabine combination therapy as the prior therapy (Table 1). No patients were treated with rituximab. Seven of 10 patients completed study treatment, and 3 patients prematurely discontinued from the study (Table 2). Among 3 patients, one withdrew just before the administration of the 12th infusion. The patient refused further study treatment due to positional vertigo and tinnitus although the investigator considered withdrawal unnecessary. The remaining 2 withdrew during the follow-up period after the last infusion.

Table 1 Demographic characteristics

	$N = 10$ [n (%)]
Age in years at screening	
Median (range)	67 (55–74)
Age groups	
<65 years	2 (20)
≥65 years	8 (80)
≥75 years	0
Sex	
Female	3 (30)
Male	7 (70)
Regimen number of prior anti-CLL therapy	
Median (range)	1 (1–3)
Summary of prior anti-CLL therapy	
Fludarabine	8 (80)
Cyclophosphamide	5 (50)
Prednisolone	2 (20)
Chlorambucil	1 (10)
Vincristine	1 (10)
Rituximab	0 (0)
Time from diagnosis[a] (years)	
Median (range)	5.2 (1.4–7.8)
Binet staging at screening	
A	2 (20)
B	4 (40)
C	4 (40)
Modified Rai staging at screening	
Low risk (stage 0)	1 (10)
Intermediate (stage I, II)	5 (50)
High risk (stage III, IV)	4 (40)

CLL chronic lymphocytic leukemia

[a] Data in 8 patients

Table 2 Patients disposition

	$N = 10$ [n (%)]
Completed	7 (70)
Discontinued	3 (30)
Primary reason for discontinuation	
Investigator discretion	2 (20)[a]
Withdrew consent	1 (10)[b]

[a] Due to subsequent anti-CLL treatments

[b] Due to subject's willingness to discontinue study treatment

Tolerability

None of the patients experienced DLT. Ofatumumab at 2000 mg was well tolerated in Japanese patients.

Efficacy

Primary endpoint

The ORR was 70 % [95 % confidence intervals (CI), 35–93 %] as assessed by the IRC (Table 3). All of the 7 responders achieved partial remission (PR). Clinical improvements in components of the response are shown in Table 4.

Table 3 Overall Response Rate

Response	$N = 10$ [n (%)]
Complete remission	0
Partial remission	7 (70)
Stable disease	3 (30)
Progressive disease	0
Overall response rate	7 (70)
95 % Confidence interval (%)	(35–93)

Table 4 Improvement in each component

	$N = 10$ [n (%)]
Responders	7 (70)
Lymphadenopathy	
≥50 % reduction	2/9 (22)
Absence of lymphadenopathy (>1.5 cm in the greatest diameter)	1/9 (11)
Hepatomegaly	
≥50 % reduction in the size of the liver	3/5 (60)
No hepatomegaly	3/5 (60)
Splenomegaly	
≥50 % reduction in the size of the spleen	6/10 (60)
No splenomegaly	6/10 (60)
Blood lymphocytes	
≥50 % decrease in peripheral blood lymphocyte count from baseline	10/10 (100)
Peripheral lymphocyte <4000/μL	10/10 (100)
Marrow	
50 % reduction in marrow infiltrate, or B-lymphoid nodules	6/10 (60)
<30 % lymphocytes, no B-lymphoid nodules.	0/10 (0)
Platelet count	
>100000/μL or 50 % improvement from baseline	2/4 (50)
>100000/μL	1/4 (25)
Hemoglobin	
>11.0 g/dL or 50 % improvement from baseline	0/1 (0)
>11.0 g/dL	0/1 (0)
Neutrophils	
>1500/μL or 50 % improvement from baseline	–
>1500/μL	–
Constitutional symptoms	
Absence of constitutional symptoms	1/1 (100)

Secondary endpoints

The median duration of response and PFS could not be estimated with a median follow-up of 47.2 weeks. The median time to response was 8.1 weeks. One patient had constitutional symptoms at the baseline assessment, which resolved by week 5. The ECOG performance status remained unchanged from baseline in all patients.

Safety

AEs experienced by more than one patient are shown in Table 5.

Commonly reported AEs were leukopenia, lymphopenia, and neutropenia, each occurring in 6 of 10 patients (60 %). No deaths were reported. One patient (Korean) experienced a serious AE of enteritis with vomiting,

Table 5 Adverse events (adverse events experienced by ≥ two patients)

Adverse event	$N = 10$	
	Any grade n (%)	Grade 3/4 n (%)
Hematological		
Leukopenia	6 (60)	3 (30)
Lymphopenia	6 (60)	2 (20)
Neutropenia	6 (60)	4 (40)
Thrombocytopenia	4 (40)	0
Anemia	2 (20)	0
Non-hematological		
Increase of blood lactate dehydrogenase	5 (50)	0
Rash	5 (50)	0
Hyperglycemia	4 (40)	3 (30)
Infusion-related reaction	4 (40)	0
Nasopharyngitis	3 (30)	0
Peripheral sensory neuropathy	3 (30)	0
Increase of aspartate aminotransferase	2 (20)	0
Constipation	2 (20)	0
Diarrhea	2(20)	0
Eczema	2 (20)	0
Fatigue	2(20)	0
Herpes zoster	2 (20)	0
Influenza	2 (20)	0
Decrease of total protein	2 (20)	0
Pyrexia	2 (20)	0
Stomatitis	2 (20)	0
Positional vertigo	2 (20)	0

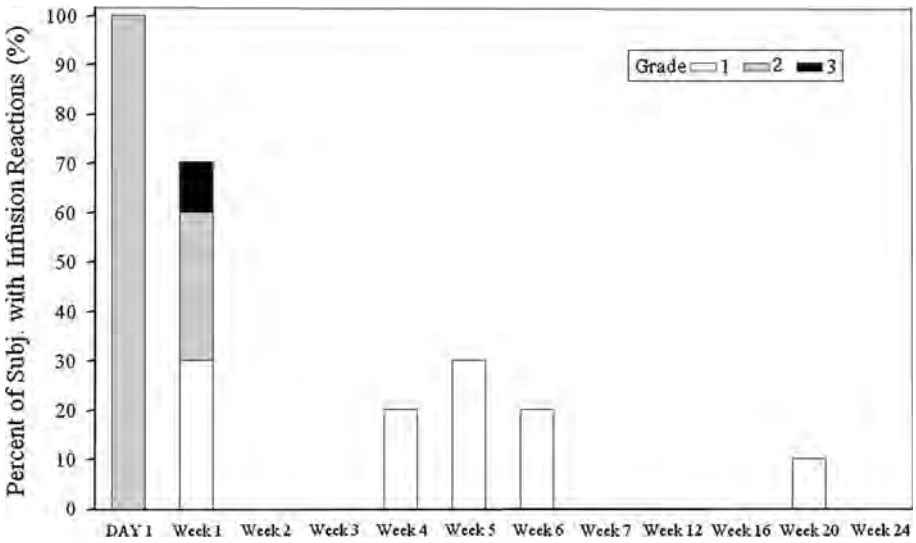

Fig. 1 Infusion reactions by grade

diarrhea, and fever (38.9 °C) during the study, but the event was considered to be unrelated to ofatumumab.

All 10 patients experienced "infusion reactions" (Fig. 1). All but one infusion reaction were of grade 1 or grade 2. One patient had grade 3 hypotension during the infusion. The most common "infusion reactions" were rash and infusion-related reaction, each reported in 4 of 10 patients (40 %), and pyrexia in 2 of 10 patients (20 %). The majority of the "infusion reactions" occurred on day 1 (first infusion) or week 1 (second infusion) and resolved within 24 h of onset. The percentage of patients experiencing "infusion reactions" decreased over the course of treatment.

Infections were reported in 7 of 10 patients; all but one infection were grade 1 or 2.

The most common infections were nasopharyngitis, reported in 3 of 10 patients (30 %), herpes zoster and influenza, each occurring in 2 of 10 patients (20 %); and gastroenteritis, oral herpes, pneumonia, and upper respiratory tract infection, each occurring in 1 of 10 patients (10 %).

The mean serum titers of IgA, IgG, and IgM antibody remained almost unchanged from the start of ofatumumab infusion until week 48.

Seven of 10 patients tested negative in the HAHA assay. The other 3 patients were not able to be evaluated.

Pharmacokinetic parameters

Mean (+SD) ofatumumab plasma concentration–time plot in all patients (7 Japanese and 1 Korean) who received ofatumumab 300 mg at the first infusion, followed by 7 weekly infusions of 2000 mg and then 4 infusions of 2000 mg every 4 weeks, is shown in Fig. 2. The summary of pharmacokinetic parameters is shown in Table 6.

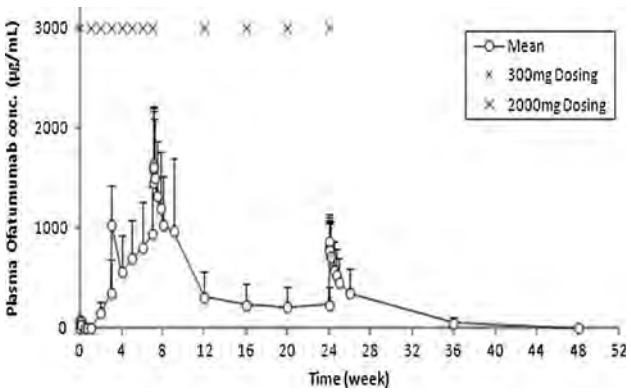

Fig. 2 Mean (+SD) plasma concentration of ofatumumab–time plots

Plasma concentration of ofatumumab prior to next weekly dose increased steadily over the 8 weeks but did not reach steady state; with monthly dosing, pre-dose ofatumumab concentrations decreased from 834 µg/mL prior to the 8th weekly infusion to 122 µg/mL prior to the fourth monthly infusion. Inter-patient variability of PK parameters was larger after the first dose when compared with later dose. Geometric mean of C_{max} of ofatumumab at the first infusion (300 mg), at the last weekly infusion (8th, 2000 mg), and at the last monthly infusion were 71, 1691 and 865 µg/mL, respectively. AUC was 1524 h µg/mL at the first infusion (300 mg, AUC_{0-inf}), 200904 h µg/mL at the last weekly infusion (8th infusion, 2000 mg, AUC_{0-168}), and 216678 h µg/mL at the last monthly infusion (12th infusion, 2000 mg, AUC_{0-672}).

In the patient in Korea, C_{max} was 76 µg/mL at the first infusion (300 mg), 1354 µg/mL at the last weekly infusion (8th infusion, 2000 mg), and 618 µg/mL at the last monthly interval infusion (12th infusion, 2000 mg). AUC was 1879 h µg/mL at the first infusion (300 mg, AUC_{0-inf}), 136612 h µg/mL at the last weekly infusion (8th infusion,

Table 6 Pharmacokinetic parameters of ofatumumab

	Day 1 300 mg ($N = 8$)	Week 7[a] 2000 mg ($N = 8$)	Week 24[b] 2000 mg ($N = 7$)
C_{max} (μg/mL)	71 (44–115)	1691 (1332–2146)	865 (659–1136)
C_{min} (μg/mL)	–	834 (539–1291)	122 (29–518)[c]
AUC[d] (h μg/mL)	1524 (599–3878)	200904 (139158–290046)	216678 (114238–410979)
$t_{1/2}$ (h)	9.6 (5.0–18.3)	332 (224–492)	300 (182–495)
CL (mL/h)	197 (77–501)	10.0 (6.9–14.4)	9.2 (4.9–17.5)
V_{ss} (mL)	3607 (2269–5735)	1333 (927–1917)	3069 (2123–4437)
MRT (h)	18.3 (10.4–32.3)	478 (333–686)	464 (264–817)

Geometric mean (95 % confidence interval)

[a] After final (8th) weekly dose

[b] After final (4th) monthly dose

[c] $N = 8$

[d] AUC_{0-inf} for day 1, AUC_{0-168} for week 7, AUC_{0-672} for week 24

2000 mg, AUC_{0-168}), and 90209 h μg/mL at the last monthly interval infusion (12th infusion, 2000 mg, AUC_{0-672}). C_{max} and AUC in the patient in Korea were within or just below the lower limit of the 95 % CI of all patients.

Discussion

This study was conducted to evaluate the tolerability, efficacy, safety, and PK profile of ofatumumab at 2000 mg in Japanese and Korean patients with relapsed or refractory B-CLL.

All 10 patients experienced "infusion reactions" such as rash and pyrexia. "Infusion reactions" were prevalent during the first 2 doses, but largely subsided with subsequent infusions (Fig. 1), as expected based on the previous Western clinical studies in patients with B-CLL [10, 11]. Most of the "infusion reactions" were of grade 1 or 2 and only one patient developed grade 3 hypotension. Dose interruption was required by 8 patients on day 1 and by 3 patients at week 1. However, all patients were able to recommence dosing and receive the complete planned ofatumumab infusion. These results suggest that the "infusion reactions" were manageable.

Infections were reported in 70 % of patients. The majority of the infections (86 %) were grade 1 or 2 in severity except for 1 patient who developed grade 3 pneumonia. Since the pneumonia occurred more than 4 months after the final administration of ofatumumab, it was judged unrelated to ofatumumab by the investigator. The incidence and severity of infections observed in this study were as expected based on experience in Western CLL patients. In the Western phase II study, infections were reported in 67 % of patients. The most infectious AEs (74 %) occurring during treatment were grade 1 or 2 in severity, and the incidence of grade 3 or 4 infections was reported at the expected level, considering prior treatment, extent of disease, and immunosuppression among these patients [11, 14].

The ORR of 70 % (95 % CI 35–93 %) in the present study is comparable with that of 47 % (95 % CI 40–54 %) in Western phase II study [8].

Clinical improvements for a minimum duration of 2 months, based on components of the NCI-WG guidelines, are shown in Table 4. The rates of complete resolution were 60 % (3 of 5 patients) for hepatomegaly and 60 % (6 of 10 patients) for splenomegaly, and the rate of substantial reduction in lymphadenopathy was 11 % (1 of 9 patients). These results were consistent with those in the Western phase II study; complete resolution of hepatomegaly in 20 of 39 patients (51 %), splenomegaly in 30 of 76 patients (39 %), and lymphadenopathy in 17 of 129 patients (13 %) [11]. The improvement rate for lymphadenopathy was lower than that for other components; however, all patients showed 8–82 % reductions in lymphadenopathy (Fig. 3), indicating activity.

Ofatumumab pharmacokinetics in this study in Japanese and Korean patients with CLL was consistent with ofatumumab pharmacokinetics in Western patients with CLL receiving the same dosing regimen [15]. At the eighth weekly infusion (2000 mg), geometric mean values of ofatumumab C_{max}, CL, and $t_{½}$ were 1482 μg/mL, 9.5 mL/h, and 15.8 days in Western patients [15] and were 1691 μg/mL, 10.0 mL/h, and 13.8 days in Japanese and Korean patients in this study.

The study population in this study was patients with CLL previously treated with any anti-CLL treatment, while that in the Western Phase II study mainly consisted of patients with CLL refractory to fludarabine and alemtuzumab, and CLL refractory to fludarabine with bulky (>5 cm) lymph nodes. Although the differences in the study population

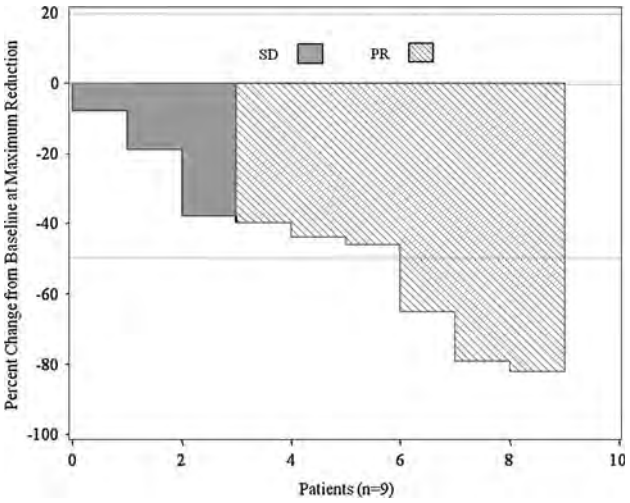

Fig. 3 Reduction of sum of products of the greatest diameters in lymphadenopathy

exist, no apparent differences in the profile of ofatumumab safety, efficacy and PK were suggested in this study.

In conclusion, Ofatumumab provided favorable safety and efficacy in Japanese and Korean patients with relapsed or refractory B-CLL. Although this was a small study, the results indicate that ofatumumab monotherapy is as clinically active and well tolerated in Asian patients as it is in non-Asian patients. This phase I/II study suggests that ofatumumab is a promising agent for the treatment of relapsed or refractory B-CLL.

Acknowledgments The authors would like to thank the patients, doctors, nurses, and staff members who participated in this multicenter study for their excellent cooperation. Participating institutions of this study included: Tokai University School of Medicine, Isehara, Nagoya Daini Red Cross Hospital, Nagoya, National Cancer Center Hospital, Tokyo, and Asan Medical Center, Seoul, National Hospital Organization Nagoya Medical Center, Nagoya.

Conflict of interest Yoshiaki Ogawa, Michinori Ogura, Tatsuya Suzuki, Kiyoshi Ando, Toshiki Uchida, Yukari Shirasugi have no conflicts of interest relevant to the subject matter or materials included in this manuscript. Kensei Tobinai has received honoraria from Genzyme Japan K.K., Janssen Pharmaceutical K.K., and Glaxo-SmithKline K.K. Je Hwan Lee has no conflict relevant to the subject matter or materials included in this manuscript. Masazumi Kase and Koichi Katsura are employees of GSK. Tomomitsu Hotta has no conflict relevant to the subject matter or materials included in this manuscript.

References

1. Teeling JL, French RR, Cragg MS, von den Brakel JH, Pluyter M, Huang H, et al. Characterization of new human CD20 monoclonal antibodies with potent cytolytic activity against non-Hodgkin lymphomas. Blood. 2004;104:1793–800.
2. Teeling JL, Mackus WJ, Wiegman LJ, von den Brakel JH, Beers SA, French RR, et al. The biological activity of human CD monoclonal antibodies is linked to unique epitopes on CD20. J Immunol. 2006;177:362–71.
3. Beum PV, Lindorfer MA, Beurskens F, Stukenberg PT, Lokhorst HM, Pawluczkowycz AW, et al. Complement activation on B lymphocytes opsonized with rituximab or ofatumumab produces substantial changes in membrane structure preceding cell lysis. J Immunol. 2008;181:822–32.
4. Hagenbeek A, Gadeberg O, Johnson P, Pedersen LM, Walewsk J, Hellmann A, et al. First clinical use of ofatumumab, a novel fully human anti-CD20 monoclonal antibody in relapsed or refractory follicular lymphoma: results of a phase 1/2 trial. Blood. 2008;111:5486–95.
5. Cheson BD. Ofatumumab, a novel anti-CD20 monoclonal antibody for the treatment of B-cell malignancies. J Clin Oncol. 2010;28:3525–30.
6. Coiffier B, Losic N, Rønn BB, Lepretre S, Pedersen LM, Gadeberg O, et al. Pharmacokinetics and pharmacokinetic/pharmacodynamic associations of ofatumumab, a human monoclonal CD20 antibody, in patients with relapsed or refractory chronic lymphocytic leukaemia: a phase 1–2 study. Br J Haematol. 2010;150:58–71.
7. Wierda WG, Kipps TJ, Dürig J, Griskevicius L, Stilgenbauer S, Mayer J, et al. Chemoimmunotherapy with O-FC in previously untreated patients with chronic lymphocytic leukemia. Blood. 2011;117:6450–8.
8. Wierda WG, Padmanabhan S, Chan GW, Gupta IV, Lisby S, Österborg A. Ofatumumab is active in patients with fludarabine-refractory CLL irrespective of prior rituximab: results from the phase 2 international study. Blood. 2011;118:5126–9.
9. Czuczman MS, Fayad L, Delwail V, Cartron G, Jacobsen E, Kuliczkowski K, et al. Ofatumumab monotherapy in rituximab-refractory follicular lymphoma: results from a multicenter study. Blood. 2012;119:3698–704.
10. Coiffier B, Lepretre S, Pedersen LM, Gadeberg O, Fredriksen H, van Oers MH, et al. Safety and efficacy of ofatumumab, a fully human monoclonal anti-CD20 antibody, in patients with relapsed or refractory B-cell chronic lymphocytic leukemia: a phase 1–2 study. Blood. 2008;111:1094–100.
11. Wierda WG, Kipps TJ, Mayer J, Stilgenbauer S, Williams CD, Hellmann A, et al. Ofatumumab as single-agent CD20 immunotherapy in fludarabine-refractory chronic lymphocytic leukemia. J Clin Oncol. 2010;28:1749–55.
12. Ogura M, Hatake K, Tobinai K, Uchida T, Suzuki T, Terui Y, et al. Phase 1 study of ofatumumab, a human anti-CD20 antibody, in Japanese patients with relapsed or refractory chronic lymphocytic leukemia and small lymphocytic lymphoma. Jpn J Clin Oncol. 2013;43:466–75.
13. Hallek M, Cheson BD, Catovsky D, Caligaris-Cappio F, Dighiero G, Döhner H, et al. Guidelines for the diagnosis and treatment of chronic lymphocytic leukemia: a report from the International Workshop on Chronic Lymphocytic Leukemia on Chronic Lymphocytic leukemia updating the National Cancer Institute-Working Group 1996 guidelines. Blood. 2008;111:5446–56.
14. Perkins JG, Flynn JM, Howard RS, Byrd JC. Frequency and type of serious infections in fludarabine-refractory B-cell chronic lymphocytic leukemia and small lymphocytic lymphoma: implications for clinical studies in this patient population. Cancer. 2002;94:2033–9.
15. Österborg A, Rønn BB, Jewell RC, Kipps TJ, Mayer J, Stilgenbauer S, et al. Correlation between serum ofatumumab concentrations, baseline patient characteristics, and clinical outcomes in patients with fludarabine-refractory chronic lymphocytic leukemia (CLL) treated with single-agent ofatumumab. Blood (ASH Annual Meeting Abstracts). 2009;114:3433.

Ann Hematol (2014) 93:719–720
DOI 10.1007/s00277-013-1874-2

LETTER TO THE EDITOR

Strong effect of mogamulizumab on splenic residual disease of adult T cell leukemia/lymphoma

Daisuke Ohgiya · Shinichiro Machida · Akihumi Ichiki · Jun Amaki · Yasuyuki Aoyama · Hidetsugu Kawai · Mitsuki Miyamoto · Hiromichi Murayama · Makoto Onizuka · Kiyoshi Ando

Received: 21 July 2013 / Accepted: 1 August 2013 / Published online: 15 August 2013

Dear Editor,

A 54-year-old female complained of multiple subcutaneous masses. A histological study and southern blotting for HTLV-1 proviral DNA led to a diagnosis of the acute type of ATLL. FDG accumulation was observed in the abdominal lymph nodes, liver, and spleen (Fig. 1, left panel). She received two cycles of multidrug chemotherapy, including vincristine, cyclophosphamide, doxorubicin, prednisone, ranimustine, vindesine, etoposide, and carboplatin (VCAP–AMP–VECP) [1]. A single residual ATLL lesion in the spleen remained following the administration of VCAP–AMP–VECP (Fig. 1, middle panel). Thereafter, the patient received intravenous infusions of mogamulizumab (1.0 mg/kg) once a week for 3 weeks and the splenic lesion completely disappeared (Fig. 1, right panel). The patient underwent umbilical cord blood transplantation (UCBT) following of cyclophosphamide (120 mg/kg) and total body irradiation (12 Gy). The HLA disparity was two loci mismatched at HLA-B and DR. The total nucleated cell and CD34-positive cell counts were 2.42×10^7/kg and 0.75×10^5/kg, respectively. Prophylaxis for graft-versus-host disease (GVHD) included tacrolimus and short-term methotrexate. Neutrophil engraftment was achieved on day 23. STR-based chimerism testing performed on day 28 revealed BM cells to be 100 % of the donor type [2]. A skin rash emerged on day 30, and the patient was diagnosed with grade II acute GVHD. The acute GVHD immediately disappeared following the dose escalation of tacrolimus. However, after elevation of the total bilirubin level and the development of massive ascites on day 40, she died due to multiple organ failure on day 110. The autopsy results revealed widespread omission of hepatic cells and acute tubular necrosis. No findings of relapse of ATLL, GVHD, microthromboembolism, or veno-occlusive disease were observed.

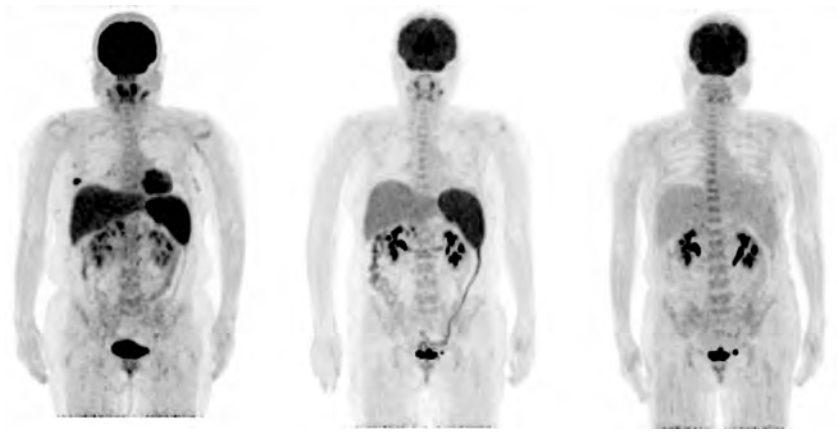

Fig. 1 Findings of PET imaging. FDG accumulation was observed in the abdominal lymph nodes, liver, and spleen at diagnosis of the acute type of ATLL (*left panel*). A single residual ATLL lesion in the spleen remained following two cycles of VCAP–AMP–VECP (*middle panel*). All ATLL lesions disappeared after three courses of mogamulizumab (*right panel*)

D. Ohgiya (✉) · S. Machida · A. Ichiki · J. Amaki · Y. Aoyama · H. Kawai · M. Miyamoto · H. Murayama · M. Onizuka · K. Ando
Department of Hematology and Oncology, Tokai University School of Medicine, 143 Shimokasuya, Isehara, Kanagawa 259-1193, Japan
e-mail: giya_pen_1213.0@triton.ocn.ne.jp

Adult T cell leukemia/lymphoma (ATLL) is a peripheral T cell neoplasm caused by human T cell leukemia/lymphotropic virus type 1 and has a poor prognosis [3]. Allogeneic hematopoietic stem cell transplantation (allo-HSCT) has been explored as a promising therapy for ATLL [4, 5]. However, the achievement of CR at transplantation is prerequisite for a successful outcome [6]. Recently, mogamulizumab, a next-generation humanized anti-CC chemokine receptor 4 (CCR4) monoclonal antibody, has become available in Japan for patients with CCR4 expressing ATLL [7]. We first showed that mogamulizumab has a strong effect on residual disease in the spleen, which resulted in CR at the time of UCBT. Motohashi et al. recently reported a case of a patient with ATLL who received mogamulizumab infusion before allogeneic HSCT and had a good clinical course [8]. However, it has also been reported that mogamulizumab decreases CCR4 expressing regulatory T cells [7] and a decreased level of regulatory T cells before allo-HSCT is associated with the onset and severity of acute GVHD [9]. In our case, grade II acute GVHD occurred after UCBT with death from multiorgan failure that was most likely induced by regimen-related toxicity and an obvious relapse of ATLL was not recognized. Since the safety of mogamulizumab treatment remains unclear, further studies are required to evaluate the optimal use of mogamulizumab before allo-HSCT.

Conflict of interest The authors declare no conflict of interest.

References

1. Tsukasaki K, Utsunomiya A, Fukuda H, Shibata T, Fukushima T, Takatsuka Y, Ikeda S, Masuda M, Nagoshi H, Ueda R, Tamura K, Sano M, Momita S, Yamaguchi K, Kawano F, Hanada S, Tobinai K, Shimoyama M, Hotta T, Tomonaga M (2007) VCAP–AMP–VECP compared with biweekly CHOP for adult T cell leukemia–lymphoma: Japan Clinical Oncology Group Study JCOG9801. J Clin Oncol 25(34):5458–5464
2. Kristt D, Stein J, Yaniv I, Klein T (2007) Assessing quantitative chimerism longitudinally: technical considerations, clinical applications and routine feasibility. Bone Marrow Transplant 39:255–268
3. Shimoyama M (1991) Diagnostic criteria and classification of clinical subtypes of adult T cell leukaemia–lymphoma. A report from the Lymphoma Study Group (1984–87). Br J Haematol 79(3):428–437
4. Utsunomiya A, Miyazaki Y, Takatsuka Y, Hanada S, Uozumi K, Yashiki S, Tara M, Kawano F, Saburi Y, Kikuchi H, Hara M, Sao H, Morishima Y, Kodera Y, Sonoda S, Tomonaga M (2001) Improved outcome of adult T cell leukemia/lymphoma with allogeneic hematopoietic stem cell transplantation. Bone Marrow Transplant 27(1):15–20
5. Fukushima T, Miyazaki Y, Honda S, Kawano F, Moriuchi Y, Masuda M, Tanosaki R, Utsunomiya A, Uike N, Yoshida S, Okamura J, Tomonaga M (2005) Allogeneic hematopoietic stem cell transplantation provides sustained long-term survival for patients with adult T cell leukemia/lymphoma. Leukemia 19(5):829–834
6. Ishida T, Hishizawa M, Kato K, Tanosaki R, Fukuda T, Taniguchi S, Eto T, Takatsuka Y, Miyazaki Y, Moriuchi Y, Hidaka M, Akashi K, Uike N, Sakamaki H, Morishima Y, Suzuki R, Nishiyama T, Utsunomiya A (2012) Allogeneic hematopoietic stem cell transplantation for adult T cell leukemia–lymphoma with special emphasis on preconditioning regimen: a nationwide retrospective study. Blood 120(8):1734–1741
7. Ishida T, Joh T, Uike N, Yamamoto K, Utsunomiya A, Yoshida S, Saburi Y, Miyamoto T, Takemoto S, Suzushima H, Tsukasaki K, Nosaka K, Fujiwara H, Ishitsuka K, Inagaki H, Ogura M, Akinaga S, Tomonaga M, Tobinai K, Ueda R (2012) Defucosylated anti-CCR4 monoclonal antibody (KW-0761) for relapsed adult T cell leukemia–lymphoma: a multicenter phase II study. J Clin Oncol 30(8):837–842
8. Motohashi K, Suzuki T, Kishimoto K, Numata A, Nakajima Y, Tachibana T, Ohshima R, Kuwabara H, Tanaka M, Tomita N, Ishigatsubo Y, Fujisawa S (2013) Successful treatment of a patient with adult T cell leukemia/lymphoma using anti-CC chemokine receptor 4 monoclonal antibody mogamulizumab followed by allogeneic hematopoietic stem cell transplantation. Int J Hematol. doi:10.1007/s12185-013-1387-8
9. Li Q, Zhai Z, Xu X, Shen Y, Zhang A, Sun Z, Liu H, Geng L, Wang Y (2010) Decrease of CD4(+)CD25(+) regulatory T cells and TGF-beta at early immune reconstitution is associated to the onset and severity of graft-versus-host disease following allogeneic haematogenesis stem cell transplantation. Leuk Res 34(9):1158–1168

Cell Adhesion & Migration

ISSN: 1933-6918 (Print) 1933-6926 (Online) Journal homepage: http://www.tandfonline.com/loi/kcam20

Regulation of cell shape and adhesion by CD34

Hiroe Ohnishi, Hiroyuki Sasaki, Yoshihiko Nakamura, Shunichi Kato, Kiyoshi Ando, Hisashi Narimatsu & Kouichi Tachibana

To cite this article: Hiroe Ohnishi, Hiroyuki Sasaki, Yoshihiko Nakamura, Shunichi Kato, Kiyoshi Ando, Hisashi Narimatsu & Kouichi Tachibana (2013) Regulation of cell shape and adhesion by CD34, Cell Adhesion & Migration, 7:5, 426-433, DOI: 10.4161/cam.25957

To link to this article: http://dx.doi.org/10.4161/cam.25957

Published online: 05 Aug 2013.

Cell Adhesion & Migration 7:5, 426–433; September/October 2013; © 2013 Landes Bioscience

Regulation of cell shape and adhesion by CD34

Hiroe Ohnishi[1,2,†], Hiroyuki Sasaki[3,‡], Yoshihiko Nakamura[4], Shunichi Kato[5], Kiyoshi Ando[4,6], Hisashi Narimatsu[1], and Kouichi Tachibana[1,2,*]

[1]Research Center for Medical Glycoscience; National Institute of Advanced Industrial Science and Technology (AIST); Umezono, Tsukuba, Ibaraki, Japan; [2]Health Research Institute; AIST; Nakouji, Amagasaki, Hyogo, Japan; [3]Department of Molecular Cell Biology; Institute of DNA Medicine; The Jikei University School of Medicine; Nishi-Shinbashi, Minato-ku, Tokyo 105, Japan; [4]Research Center for Regenerative Medicine; Tokai University School of Medicine; Bohseidai, Isehara, Kanagawa, Japan; [5]Department of Cell Transplantation and Regenerative Medicine; Tokai University School of Medicine; Bohseidai, Isehara, Kanagawa, Japan; [6]Department of Hematology/Oncology; Tokai University School of Medicine; Bohseidai, Isehara, Kanagawa, Japan

Current affiliation: [†]Department of Otolaryngology; Graduate School of Medicine; Kyoto University; Sakyo-ku, Kyoto, Japan; [‡]Department of Physical Therapy; Faculty of Community Health Care; Teikyo Heisei University; Ichihara, Chiba, Japan

Keywords: CD34, ERM proteins, cell adhesion, cell rounding, microvilli, phosphorylation, sialomucin

Abbreviations: HSCs, hematopoietic stem cells; HPCs, hematopoietic progenitor cells; AML, acute myelogenous leukemia; ERM, ezrin/radixin/moesin; p-ERM, phosphorylated-ERM; PLL, poly-L-lysine; BSA, bovine serum albumin; OSGEPase, O-sialoglycoprotein endopeptidase; SDF-1, stromal-derived factor-1; SEM, scanning electron microscopy

We previously reported that expression of CD43/leukosialin induces cell rounding and microvillus formation via inhibition of cell adhesion. Here, we found that CD34, a cell surface sialomucin and marker for hematopoietic progenitor cells, also inhibited cell adhesion and induced cell rounding and microvillus formation. Forced expression of CD34-induced cell rounding, microvillus formation, and phosphorylation of ezrin/radixin/moesin (ERM) proteins in HEK293T cells, while inhibiting integrin-mediated cell re-attachment. Furthermore, CD34+ blood cells and KG-1 cells, which express endogenous CD34 on their surface, were spherical in shape, surrounded by microvilli, and non-adherent to substrata. In addition, cleavage of *O*-sialomucin augmented integrin-mediated cell adhesion of KG-1 cells. These results suggest the involvement of CD34 in the inhibition of integrin-mediated cell adhesion and formation of the cell surface structure. The inhibitory function of CD34 in cell adhesion may affect cell shape organization via phosphorylation of ERM proteins. Cellular structures such as the spherical shape and microvilli of CD34+ cells may also contribute to regulation of cell adhesion.

Introduction

During studies of leukocyte sialomucin family members, we previously found that exogenous expression of CD43 induces cell rounding, microvillus formation, augments phosphorylation of ezrin/radixin/moesin (ERM) proteins, and inhibits integrin-mediated re-attachment of HEK293T cells.[1] CD43, also called leukosialin/sialophorin, belongs to the sialomucin family and is considered to be a potent inhibitory molecule of cell adhesion.[2,3] The highly *O*-glycosylated extracellular domain of CD43 is largely responsible for this phenomena. However, cleavage of the *O*-glycosylated extracellular domain of CD43 only partially reverses the inhibition of cell re-adhesion by CD43, suggesting there is another regulatory mechanism involving CD43.

In addition to CD43, other cell surface sialomucins are expressed in leukocytes. One of these sialomucins, CD34 shows restricted expression in a small population of bone marrow cells as well as endothelial cells.[4,5] The CD34+ cell population in bone marrow can fully reconstitute the hematopoietic system.[6,7] Although CD34+ bone marrow cells are considered as hematopoietic progenitor cells (HPCs) rather than hematopoietic stem cells (HSCs) in adult mice,[8] improved hematopoietic engraftment has been clinically achieved using sorted CD34+ human progenitor cells.[7,9] Thus, CD34 is a widely accepted marker for HPCs and HSCs.[4,7,9]

Despite its significance as a marker, the molecular functions of CD34 have not been fully revealed. Because *cd34*-null mice survive and have all hematopoietic lineage cells,[10,11] CD34 does not appear to be essential for the development of hematopoietic cells. However, *cd34*-null embryonic stem cells and cells from the hematopoietic organs of *cd34*-null mice exhibit a lower colony-forming ability than that of cells from wild-type mice.[10] This observation suggests the involvement of CD34 in the proliferation, differentiation, maturation, and/or adhesion of HPCs and HSCs. Furthermore, previous reports have demonstrated the involvement of CD34 in regulation of cell adhesion and mobilization. Bone marrow mast cells from *cd34*-null mice show higher homotypic adhesion than those from wild-type mice,[12] indicating an anti-adhesive function of CD34. Interestingly, *cd34*-null cells exhibit a significant defect in the contribution to peritoneal mast

*Correspondence to: Kouichi Tachibana; Email: kouichi-tachibana@aist.go.jp
Submitted: 05/13/2013; Revised: 07/28/2013; Accepted: 07/30/2013
http://dx.doi.org/10.4161/cam.25957

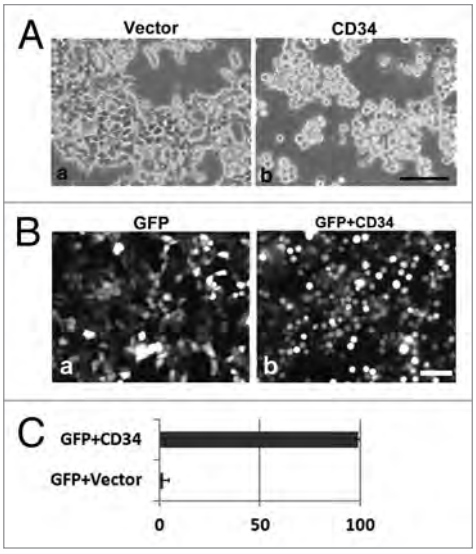

Figure 1. Cell rounding by CD34 in HEK293T cells. (**A**) Phase contrast images of HEK293T cells transfected with empty vector (HEK293T cells) or a CD34 expression vector (CD34-HEK293T cells). CD34-HEK293T cells were rounded and detached from the substrata (b), whereas HEK293T cells were flat (a) at 40 h after transfection. Scale bar: 100 μm. (**B**) Fluorescence images of HEK293T cells at 2 d after transfection of a GFP expression vector (a) or a GFP expression vector plus a CD34 expression vector (b). Scale bar: 100 μm. (**C**) Ratio of round cells among GFP+ cells shown in (**B**).

cells and reconstitution of bone marrow in competitive reconstitution assays.[12] These results suggest that the anti-adhesive function of CD34 is involved in the migration of mobilization of HSCs and HPCs or in fixation to the niche. On the other hand, ectopically expressed human CD34 increases murine hemopoietic cell adhesion to human bone marrow stromal cells,[13] suggesting that human CD34 functions in cell adhesion.

Structurally, CD34 is a single-pass type-I transmembrane glycoprotein.[4,5,14] Although the human *cd34* gene encodes multiple open reading frames generated by alternative splicing, each CD34 isoform consists of an N-terminal mucin domain followed by a globular domain and stalk, single-pass transmembrane region, and cytoplasmic tail. The mucin domain of CD34 is highly *O*-glycosylated,[4,14] and these *O*-glycans with many hydroxyl and carboxyl groups confer an extreme hydrophilicity and negative charge on the CD34 molecule. Such structural characteristics indicate potential functions of CD34 in the interactions with extracellular molecules or in the inhibition of these interactions.

We were interested in CD34 because (1) CD34 is a sialomucin, (2) CD34 appears to be involved in the regulation of cell adhesion, (3) CD34 localizes at the microvillus structure of endothelial cells,[15] and (4 podocalyxin, a CD34-related molecule, is a potent inducer of microvillus formation.[5,16,17] In this study, we found that ectopic expression of human CD34 induces cell rounding, microvillus formation, phosphorylation of ERM proteins, and inhibition of integrin-mediated re-attachment of HEK293T cells. Because these characteristics are observed in human cells that express endogenous CD34, we believe that CD34 functions in the formation and/or maintenance of cellular structure, and in the regulation of cell adhesion.

Results

Cell rounding by CD34 in HEK293T cells.

Previously, we found that ectopic expression of CD43 induces cell rounding, microvillus formation, and phosphorylation of ERM proteins, and inhibits integrin-dependent re-attachment of HEK293T cells.[1] Because CD43 is a cell surface sialomucin expressed in leukocytes, we performed similar analyses of another blood cell sialomucin, CD34. Endogenous CD34 is not expressed in HEK293T cells. HEK293T cells transfected with a CD34 expression vector (CD34-HEK293T) became round and detached from the substrata (**Fig. 1A**, b), whereas transfectants of mock vector (Vector-HEK293T) were flat and spread (**Fig. 1A**, a). Despite rounding and detachment, CD34-HEK293T cells were not dead or apoptotic, because these cells were not stained with trypan blue or contained fragmented nuclei (data not shown). To clarify the comparison, a green fluorescent protein (GFP) expression vector was co-transfected with the mock vector or CD34 expression vector into HEK293T cells. Compared with GFP expression alone, co-expression with CD34 clearly altered the shape of HEK293T cells to spherical (**Fig. 1B**). The ratio of round cells was about 99% among CD34 transfectants, whereas only 2% was observed among mock transfectants (**Fig. 1C**).

Microvillus formation by CD34 in HEK293T cells.

We further studied localization of CD34 by expression of GFP fused to the C-terminal of CD34 (CD34-GFP). At low magnification, CD34-GFP was detected mostly at the cell surface and as a dot-like structure in the cytoplasm, presumably an intracellular transport system such as the Golgi apparatus (**Fig. 2A**, a). At high magnification, CD34-GFP was detected as protrusions from cell bodies (**Fig. 2A**, b). Immunohistochemical analysis with an anti-CD34 antibody and phalloidin also demonstrated long protrusions with filamentous actin from the surface of CD34-HEK293T cells (**Fig. 2B**). Because ezrin, one of ERM proteins, has been detected in such protrusions, the protrusions may be microvilli.[18,19]

To ascertain augmentation of these protrusions by CD34, we examined Vector-HEK293T and CD34-HEK293T cells by electron microscopy. Many long protrusions from CD34-HEK293T cell bodies were observed by scanning electron microscopy (SEM) (**Fig. 2C**, b) and ultrathin section electron microscopy (**Fig. 2C**, d), whereas a few short protrusions were observed in Vector-HEK293T cells (**Fig. 2C**, a and c). Parallel fibers of filamentous actin were observed within the protrusions by ultrathin section electron microscopy (**Fig. 2C**, e and f, arrows), confirming these protrusions as microvilli. We also observed that the glycocalyx on the microvillar surface was thick in CD34-HEK293T cells, whereas it was thin in Vector transfectants (**Fig. 2C**, f and e, arrowheads).

To confirm augmentation of microvilli by CD34, we digitalized the number and length of cell surface protrusions from HEK293T transfectants by a method described previously.[1] In brief, mCherry with the myristoylation site of c-Src

(Myr-mCherry) or CD34-mCherry was expressed in HEK293T cells. Cell surface protrusions were then detected by mCherry fluorescence. Fluorescence images were captured at middle phases, but not at attachment phases, of transfectants to measure the number and length of microvilli. As summarized in **Table 1**, the number of microvillus protrusions per cell was 22 ± 11 (mean ± SD) for CD34-mCherry-HEK293T cells and 9 ± 8 for Myr-mCherry-HEK293T cells. The length of protrusions was 2.5 ± 1.3 μm for CD34-mCherry-HEK293T cells and 1.0 ± 0.8 μm for Myr-mCherry-HEK293T cells. These data indicated that the microvillus protrusions of HEK293T cells were augmented by CD34.

As a potential biochemical mechanism that leads to both cell rounding and microvillus formation, we previously found phosphorylation of ERM proteins in CD43-HEK293T cells.[1] Because phosphorylation of the C-terminal Thr residue is the activating mechanism for ERM proteins,[18,20] we investigated phosphorylation of ERM proteins in CD34-HEK293T cells. Immunoblotting with an anti-phosphorylated-ERM (p-ERM) antibody showed an increase of p-ERM by CD34 expression (**Fig. 2D**). Moreover, significant immunostaining of p-ERM was detected mostly at the microvillus protrusions of CD34-HEK293T cells (**Fig. 2E**). p-ERM was hardly detected in non-transfectant HEK293T cells (data not shown). Thus, phosphorylation of ERM proteins is augmented by CD34, and may be involved in the cell shape alterations observed in CD34-HEK293T cells.

Inhibition of integrin-mediated cell re-attachment by CD34.

When CD34 was expressed, HEK293T cells became spherical in shape, formed microvilli, and showed augmented phosphorylation of ERM proteins. We previously reported similar phenomena by expression of CD43/leukosialin, an inhibitory molecule of cell adhesion, and also showed that detachment of HEK293T cells by trypsin augments phosphorylation of ERM proteins.[1] These findings suggest that CD34 is an anti-adhesion molecule. To test the effect of CD34 on cell adhesion, we studied the effect of CD34 on integrin-mediated re-attachment of HEK293T cells. GFP or CD34-GFP were transiently expressed in α4-HEK293T cells that stably express α4 integrin.[1] In addition, tissue culture plates were coated with GST or a fusion protein of GST and fibronectin CS-1 peptide (GST-CS-1), a ligand of α4β1 integrin. The cells were detached by pipetting, incubated on the CS-1-coated substrata, and then evaluated for re-attachment. After incubation followed by washing, GFP-α4-HEK293T cells were mostly bound and spread (**Fig. 3A**, a), whereas CD34-GFP-α4-HEK293T cells were hardly attached to the CS-1-coated substrata (**Fig. 3A**, b). The numbers of bound fluorescent cells are shown in **Figure 3B**. The number of CD34-GFP transfectants bound to the CS-1-coated substrata was much lower than that of GFP transfectants. Flow cytometry showed that the expression level of CD34-GFP in unbound cells (**Fig. 3C**, continuous line) was higher than that in bound cells (dashed line), further suggesting that high expression of CD34-GFP inhibited integrin-mediated cell adhesion. Moreover, the GFP levels in unbound and bound GFP-HEK293T cells were indistinguishable. Thus, CD34 significantly inhibits α4β1 integrin-mediated cell re-attachment.

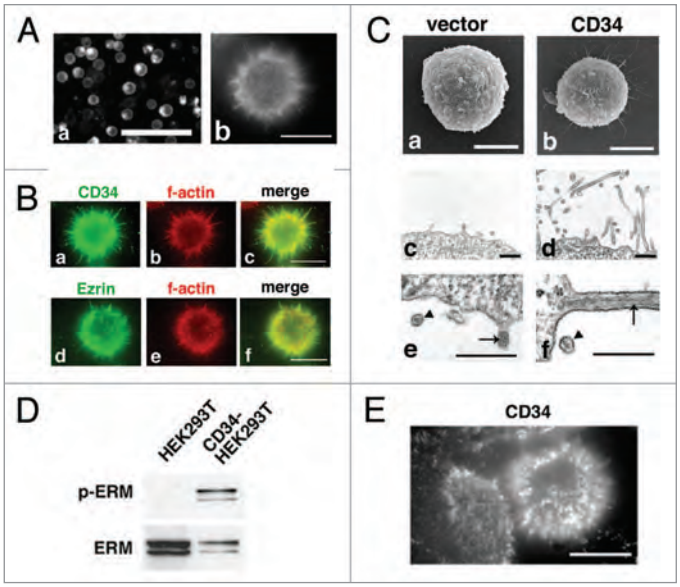

Figure 2. Formation of microvilli-like protrusions in CD34-HEK293T cells. (**A**) Subcellular localization of CD34-GFP in HEK293T cells. Images of HEK293T cells transfected with a CD34-GFP expression vector (CD34GFP-HEK293T cells) were captured at low magnification on a culture dish (a) or at high magnification on a glass coverslip (b). Scale bars: 100 μm (a) and 10 μm (b). (**B**) Subcellular localization of CD34 in CD34-HEK293T cells. CD34-HEK293T cells were double stained with anti-CD34 (a) or anti-Ezrin (d) antibodies and phalloidin (b and e). Staining was co-localized in microvilli-like protrusions from CD34-HEK293T cells. Merged images (c and f). Scale bars: 10 μm. (**C**) Electron microscopy of HEK293T transfectants. Scanning electron micrograph of Vector-HEK293T (a) and CD34-HEK293T (b) cells. Ultrathin section electron micrograph of Vector-HEK293T (c) and CD34-HEK293T (d) cells. Magnified images of microvilli-like protrusions from Vector-HEK293T (e) and CD34-HEK293T (f) cells. Arrowheads indicate lipid bilayer membranes. Arrows indicate actin filaments. Scale bars: 5 μm (a and b) and 500 nm (c–f). (**D**) Immunoblot analysis of ERM proteins in CD34-HEK293T cells. Alterations of ERM phosphorylation was detected by immunoblotting. (**E**) Immunofluorescence with an anti-p-ERM antibody. p-ERM proteins were observed at microvilli-like protrusions from CD34-HEK293T cells (b). Scale bars: 10 μm.

Table 1. Table of the length and number of microvilli

	CD34-mCherry	Myr-mCherry
Number of villi (per cell)	22 ± 11	9 ± 8
Length of microvilli (μm)	2.5 ± 1.3	1.0 ± 0.8

Identification of microvilli in CD34+ blood cells and the acute myelogenous leukemic cell line, KG-1.

Because ectopic expression of CD34 induced various cellular phenomena in HEK293T cells, we examined cells expressing endogenous CD34. CD34 is a marker for HPCs and HSCs. Therefore, we investigated CD34+ blood cells from bone marrow and cord blood. Using SEM, we observed microvillus protrusions at the surface of both types of CD34+ blood cells (**Fig. 4A**). Immunofluorescence further revealed protrusions with filamentous actin outgrown from the cell bodies (**Fig. 4B**, b and e) and co-localization of CD34 at these protrusions and the cell surface

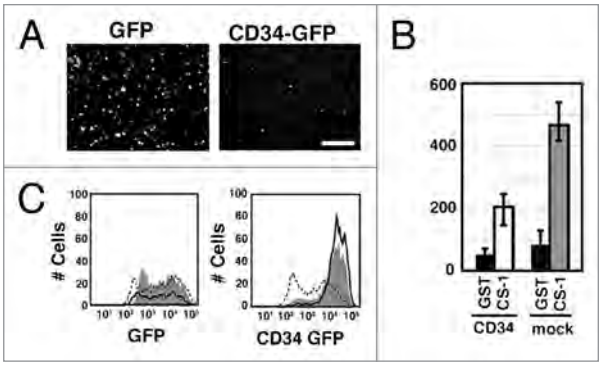

Figure 3. Inhibition of integrin-mediated cell adhesion by CD34. (**A**) Effect of CD34 on integrin-mediated re-attachment of α4-HEK293T cells. α4-HEK293T cells were transfected with a GFP expression vector (GFP-α4-HEK293T cells) or a CD34-GFP expression vector (CD34-GFP-α4-HEK293T cells). Cells were harvested, re-plated, and incubated in GST-CS1-coated wells, and then washed with medium. Adherent cells were evaluated by fluorescence microscopy. Scale bar: 200 μm. (**B**) Comparison of the number of bound cells. The average numbers of adherent cells with even weak fluorescence was calculated from three experiments. The histogram indicates the average numbers of adherent fluorescent cells on the coated surface. GFP-α4-HEK293T cells, CD34-GFP-α4-HEK293T cells, GST, and GST-CS1 are indicated as G, 34G, GST, and CS1, respectively. (**C**) Flow cytometric analysis of GFP in bound and unbound cells. The fluorescent intensity of GFP and CD34-GFP in cells bound (dashed line) or unbound (continuous line) to the GST-CS-1-coated substrata is shown. Cells prior to the binding assay are indicated by the shaded areas. The expression level of CD34-GFP in unbound CD34-GFP-α4-HEK293T cells in GST-CS1-coated wells was higher than that in bound cells.

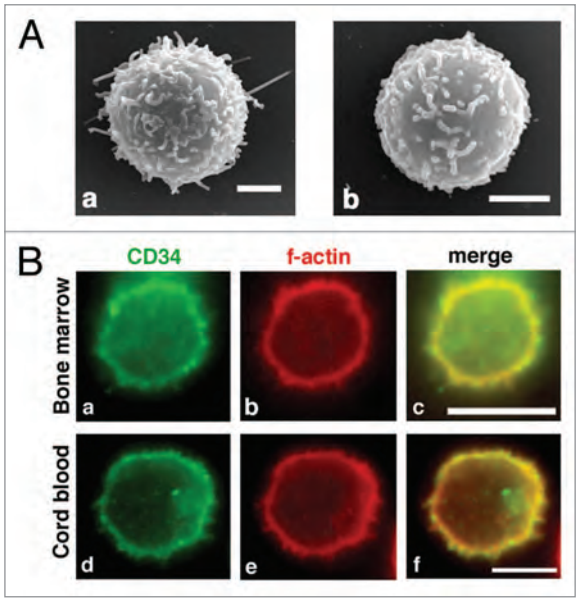

Figure 4. Microvilli in human CD34+ HPCs. (**A**) SEM of a CD34+ bone marrow cell (a) and CD34+ cord blood cell (b). Scale bars: 2 μm. (**B**) Immunofluorescence of a CD34+ bone marrow cell (a–c) and a CD34+ cord blood cell (d–f). CD34+ cells were double stained with an anti-CD34 antibody (a and d) and phalloidin (b and e). Merged images (c and f). Scale bars: 5 μm.

(**Fig. 4B**, a, c, d, and f). Thus, CD34+ primary blood cells possess microvilli on their surface, and CD34 is localized at these microvilli and the surface of spherical cells.

For a more precise analysis of the surface morphology of CD34+ cells, we investigated the surface structure of KG-1 cells by electron microscopy. KG-1 is an acute myelogenous leukemia (AML) cell line that abundantly expresses endogenous CD34.[21] As demonstrated by SEM (**Fig. 5A**, a), a KG-1 cell was spherical in shape and surrounded by microvilli-like protrusions. In ultrathin section electron microscopy, parallel fibers of filamentous actin were observed in these protrusions (**Fig. 5A**, b, arrow), indicating that the protrusions were indeed microvilli.

Immunofluorescence with an anti-CD34 antibody showed localization of CD34 on the protrusions from the cell surface (**Fig. 5B**, a), and co-localization of CD34 with filamentous actin (**Fig. 5B**, b and c). Co-localization of ezrin with filamentous actin at the protrusions further demonstrated the protrusions from KG-1 cells as microvilli (**Fig. 5B**, d–f). These data were consistent with the data obtained in CD34-HEK293T cells. We also observed β1 integrin (**Fig. 5B**, g–i) and α4 integrin (data not shown) at the protrusions. However, unlike immunostaining with anti-CD34 and anti-ERM antibodies or phalloidin, which showed homogenous staining of protrusions, immunostaining with anti-integrin antibodies showed a patchy staining pattern on the cell surface protrusions.

Augmented integrin-mediated KG-1 cell adhesion by *O*-sialoglycosylpeptide endopeptidase treatment.

KG-1 and CD34+ blood cells are non-adherent in culture with a spherical shape and microvilli. These characteristics suggest the involvement of CD34 in the inhibition of cell adhesion of these cells. Therefore, we tried to elucidate regulatory function of CD34 in cell adhesion of KG-1 cells. Because α4β1 integrin was observed on the surface of KG-1 cells, we investigated α4β1 integrin-mediated adhesion of KG-1 cells. As shown in **Figure 6A**, KG-1 cell adhesion to a GST-CS1-coated plate was marginally augmented compared with that to a GST-coated plate. However, pre-treatment of KG-1 cells with *O*-sialoglycoprotein endopeptidase (OSGEPase) largely augmented GST-CS1-dependent KG-1 cell adhesion. OSGEPase treatment significantly reduced the OSGEPase-sensitive class II epitope of CD34 (QBEnd10), while not affecting the OSGEPase-resistant class III epitope (581) (**Fig. 6B**). Thus, OSGEPase cleaves the *O*-sialoglycosylated N-terminal portion of the CD34 extracellular region.[22] Since other sialomucins can be also cleaved by OSGEPase, target molecule of OSGEPase in KG-1 cells is not limited to CD34. However, CD34 is cleaved by OSGEPase and abundantly expressed in KG-1 cells. Thus, the N-terminal mucin domain of CD34 can be involved in the inhibition of integrin-mediated adhesion of KG-1 cells.

At the same time, however, only some of the OSGEPase-treated KG-1 cells remained attached to the GST-CS-1-coated substrata after washing. This result suggests another mechanism for the regulation of cell adhesion other than direct inhibition by sialomucin domains. To better understand the integrin-mediated adhesion of OSGEPase-treated KG-1 cells, adherent cells in GST-CS-1-coated glass chambers were investigated by fluorescence

microscopy. As shown in **Figure 6C**, microvillus protrusions were observed at attachment sites to the substrata. Moreover, the area covered by each attached cell at the attachment phase was the same or less than the area at the middle phase, indicating that these attached KG-1 cells were not spread on the coated substrata. These data indicate that OSGEPase treatment is not sufficient for the collapse of microvilli, alteration of the spherical cell shape, and spreading of KG-1 cells. Moreover, interactions between GST-CS-1 and α4β1 integrin did not cause either the collapse of micorvilli or cell spreading. Given the rather weak attachment of OSGEPase-treated KG-1 cells to GST-CS-1-coated substrata, the collapse of microvilli and cell spreading may be important to establish strong cell adhesion. Therefore, the spherical cell shape and cell surface microvilli themselves function as regulators of cell adhesion.

Discussion

In this study, we have demonstrated that CD34, a leukocyte surface sialomucin and marker for HPCs and HSCs, has similar functions as those of CD43 when expressed in HEK293T cells. Expression of CD34 induced augmentation of microvilli, a switch from a polarized to spherical shape, and phosphorylation of ERM proteins. Integrin-mediated cell re-attachment was also inhibited in CD34-HEK293T cells. The cell shape and lack of cell adhesion of CD34+ blood cells and KG-1 cells, which express endogenous CD34, were consistent with the phenotypes of CD34-HEK293T cells. Treatment with OSGEPase resulted in augmented integrin-mediated KG-1 cell attachment to the substrata. Although other sialomucins can be also cleaved by OSGEPase, CD34 is abundantly expressed in KG-1 cells, and its mucin domain is cleaved off by OSGEPase. Thus, CD34 can be involved in the formation and/or maintenance of spherical cell morphology with microvilli and regulates integrin-mediated adhesion CD34+ cells. Then, how are these phenomena related each other?

We would like to start with a potential cause of cell shape alterations by CD34. Similar to CD43, CD34 augmented phosphorylation of ERM proteins. Recent studies have demonstrated that phosphorylated ERM proteins are essential for rounding of cells during mitosis.[23,24] Actin cortex is observed just under the plasma membrane in spherical cells, which is essential for the formation and maintenance of round cell shape. In addition, phosphorylated and activated ERM proteins function as a linker between the membrane component and actin cytoskeleton.[18,25] Thus, ERM proteins and their phosphorylation are critical elements for the formation and/or maintenance of a spherical cell shape during mitosis. In addition to mitotic cells, circulating lymphocytes and other leukocytes are spherical and relatively rigid. The spherical shape of leukocytes is also maintained by phosphorylated ERM proteins and an actin cortex.[26] Furthermore, phosphorylated ERM proteins and actin filaments are localized at microvilli.[18,19] Antisense oligonucleotides against ERM expression perturb microvilli,[27] indicating that ERM proteins are essential for microvillus formation and/or maintenance. Thus, phosphorylated ERM proteins are essential for cell

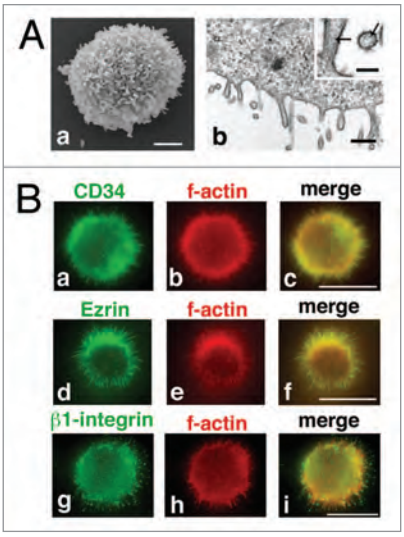

Figure 5. CD34 is localized at microvilli in KG-1 cells. (**A**) Electron microscopy of KG-1 cells. Scanning electron micrograph (a) and ultrathin section electron micrograph (b) of KG-1 cells. KG-1 cells were covered with numerous microvilli. Arrows indicate parallel filamentous actin. Scale bars: 2 μm (a), 500 nm (b), and 125 nm (inset). (**B**) Subcellular localization of CD34 in KG-1 cells. KG-1 cells were double stained with anti-CD34 (a), anti-ezrin (d), or anti-β1-integrin antibody (g) and phalloidin (b, e, and h). Merged images (c, f, and i). Scale bars: 10 μm.

rounding and microvillus formation. Our findings of phosphorylated ERM proteins in microvilli and at the surface of spherical CD34-HEK293T and CD34+ KG-1 cells are consistent with these previous reports.

Then, how does CD34 induce ERM phosphorylation? We have previously reported induction of ERM phosphorylation as a result of cell detachment either by expression of CD43 or by keeping cells swirling in BSA-coated dish after trypsinization.[1] Like CD43, CD34 was reported as an inhibitor of cell adhesion,[12] and expression of CD34 inhibited integrin-mediated HEK293T cell re-attachment (**Fig. 3**). Therefore, it is conceivable that CD34 induces ERM phosphorylation via inhibition of cell adhesion. Then, how does CD34 inhibit cell adhesion? CD34 has a highly *O*-glycosylated region in the N-terminal of its extracellular domain. In fact, a much thicker glycocalyx was observed in CD34-HEK293T cells than that in Vector transfectants (**Fig. 2C**), indicating augmented glycosylation on the surface of CD34-HEK293T cells. Cleavage of sialomucin by OSGEPase also augmented integrin-mediated adhesion of KG-1 cells (**Fig. 6A**) and in CD34-α4-HEK293T cells (data not shown). Taken together, these findings strongly suggest that large numbers of hydroxyl and carboxyl groups on the *O*-glycosylated region of CD34 affect other membrane proteins and/or modify the characteristics of the cell membrane to inhibit integrin-mediated cell adhesion.

Meanwhile, the function of CD34 as an anchor for ERM proteins remains unclear. Phosphorylated ERM proteins bind directly to the cytoplasmic domain of CD43,[28] and bind indirectly to that of podocalyxin, a CD34 family protein, via an interaction with another cytoplasmic protein, NHERF2.[5,16,17] However, CD34

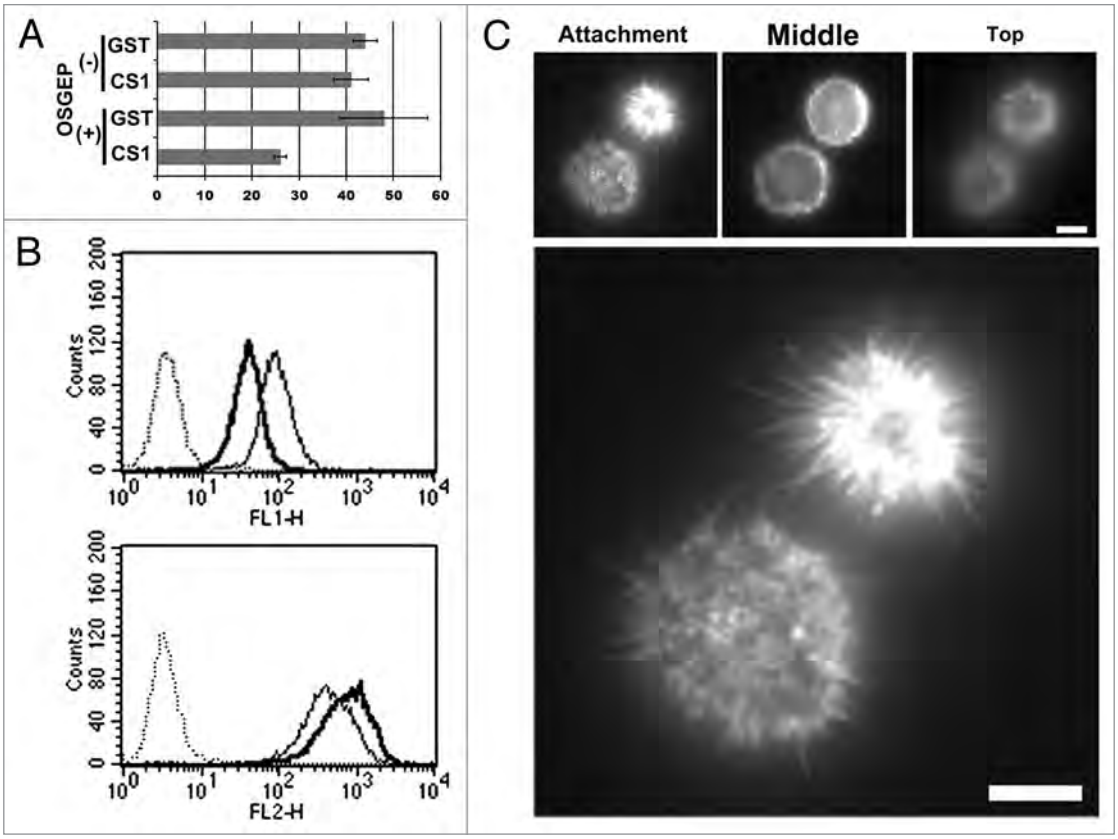

Figure 6. Effect of OSGEPase treatment on integrin-mediated adhesion of KG-1 cells. (**A**) Numbers of unattached KG-1 cells in GST-CS1-coated wells. KG-1 cells were treated with or without OSGEPase for 30 min. Cells were incubated in tissue culture plates coated with GST or GST-CS1, washed, and then the numbers of unattached cells were counted. (**B**) Flow cytometric analysis of OSGEPase-treated and untreated KG-1 cells. Cells were double immunostained with fluorophore-labeled anti-CD34 antibodies, 581 (PE) and QBEnd10 (FITC). OSGEPase treatment reduced QBEnd10 on KG-1 cells. (**C**) Phalloidin staining of KG-1 cells. OSGEPase-treated KG-1 cells were attached to GST-CS-1-coated glass chamber, fixed, permeabilized, and then stained with phalloidin. Images of attachment, middle, and top phases are shown. Scale bar: 1.25 μm.

does not bind to ERM proteins or NHERF family members.[5,17] Thus, no mechanism as a membrane anchor for phosphorylated ERM proteins has been established for CD34. However, because CD34 is localized at microvilli and the surface of spherical cells, it is reasonable to assume that CD34 functions as a membrane anchor for ERM proteins. Expression of human CD34 transcription variant 2, which has a different cytoplasmic tail from that of variant 1, caused similar phenomena in HEK293T cells (data not shown). Therefore, we believe the linkage to ERM proteins is within the common juxtamembrane sequence in the cytoplasmic domain or within extracellular-transmembrane domains.

Lastly, what is the potential function of microvilli and a spherical cell shape in regulation of cell adhesion? OSGEPase treatment augmented the attachment of many KG-1 cells to GST-CS1-coated substrata. However, the cell attachment was weak because sequential washing gradually washed out the cells. In addition, OSGEPase-treated KG-1 cells attached to GST-CS-1-coated or poly-l-lysine (PLL)-coated substrata maintained a spherical shape and cell surface microvilli, and did not spread on the substrata (**Fig. 6C** and data not shown). These findings indicate that (1) cleavage of sialomucins including the N-terminal sialomucin domain of CD34 does not induce microvillus collapse or alteration of the spherical shape of KG-1 cells at least over a few hours. (2) α4β1 integrin on the surface of KG-1 cells is active and can interact with its ligand, GST-CS1. (3) This integrin-ligand interaction does not induce a cell shape alteration and is not sufficient to support stable cell adhesion. Although it requires further study, our hypothesis for this limited cell adhesion is as follows. The spherical shape and surface microvilli of KG-1 cells restrict the attachment sites to a small area. Only limited numbers of adhesion molecules such as α4β1 integrin are exposed to the substrata because of the restriction of the attachment area. Because the number of adhesion molecules attached to the substrata is limited, cell adhesion to the substrata is vulnerable. If this is true, the spherical cell shape and microvilli themselves are the elements that regulate cell adhesion. For release from this regulation and formation of stable adhesion, alteration of the spherical cell shape and cell surface microvilli may be essential. Brown et al. reported microvillus collapse by stromal-derived factor-1 (SDF-1) in peripheral T lymphocytes,[29] suggesting that chemokines regulate cell shape. Taken together, these findings indicate a two-step mechanism for leukocyte adhesion, restructuring of the cell shape by chemokines, and then cell adhesion with spreading via adhesion molecule–ligand interactions.

Then, what can we infer as the functions of CD34 in HPCs and HSCs based on our findings? Cell adhesion, homing, and trafficking are all critical for HPCs and HSCs. Expression of CD34 alone inhibits integrin-mediated cell adhesion directly or indirectly via formation and/or maintenance of a spherical cell shape and cell surface microvilli. Considering the circulation of leukocytes, CD34 directly or indirectly inhibits cell adhesion of HPCs and HSCs with other blood cells and endothelial cells, while the spherical cell shape may promote HPC/HSC survival in the hemodynamic rigors of circulation. Furthermore, restructuring of the cytoskeleton and cell shape may be essential for stable cell adhesion such as that in the niche or during extravasation. It has been reported that the SDF-1-CXCR4 interaction is the major regulatory element for the trafficking, retention, and adhesion of HSCs and HPCs.[30,31] Taken together with the effect of SDF-1 on microvillus collapse of lymphocytes,[26,29] alterations of HPC/HSC morphology can be caused by the SDF-1-CXCR4 interaction. Thus, cell adhesion of HPCs and HSCs may be regulated by cell shape, and CD34 might play significant roles in the formation and/or maintenance of cell shape and adhesion.

Materials and Methods

Cells and reagents.

KG-1, HEK293T, and bone marrow CD34+ cells were purchased from RIKEN BioResource Center or Lonza. Cord blood CD34+ cells were purified with a CD34+ MicroBead kit (Miltenyi Biotec) from cord blood samples that were obtained from full-term deliveries according to the institutional guidelines approved by the Tokai University Committee on Clinical Investigation. HEK293T and KG-1 cells were cultured in Dulbecco's modified Eagle's medium (DMEM) and RPMI 1640, respectively, supplemented with 10% fetal calf serum (FCS). PLL, puromycin, paraformaldehyde, bovine serum albumin (BSA), and TRITC-labeled phalloidin were obtained from Sigma. Mowiol 4-88 Reagent was obtained from CALBIOCHEM. OSGEPase was purchased from CEDARLANE Laboratories. Anti-CD34 (clone 581), anti-β1 integrin (MAR4), and anti-Ezrin (clone 18) antibodies were obtained from BD Biosciences. Anti-p-ERM and anti-ERM antibodies were purchased from Cell Signaling Technologies. An anti-CD34 (QBEnd10) antibody was obtained from Santa Cruz Biotechnology. Alexa Fluor 488-labeled goat anti-mouse IgG was purchased from Invitrogen.

Plasmids and transfection.

The retroviral expression vector pCpuroCMVS and the expression vector with the myristoylation site of c-Src, pJ3SrcMS, have been described previously.[1] Human *cd34* transcription variant 1 cDNA was cloned by RT-PCR, fused to DNA fragments of EGFP or mCherry (Clontech) at the CD34 C terminus, and subcloned into pCpuroCMVS. Establishment of α4-HEK293T cells has been described previously.[1] Expression vectors were transfected with Lipofectamine 2000 (Invitrogen). pGEX-CS1 was a kind gift from Dr Kenjiro Kamiguchi.[32]

Electron and immunofluorescence microscopy.

Scanning and ultrathin section electron microscopy were preformed as described previously.[1]

For immunofluorescence microscopy, cells grown on glass coverslips were fixed with 4% paraformaldehyde in PBS for 10 min at room temperature, washed three times with PBS, permeabilized with 0.2% Triton X-100 in PBS for 5 min, and then washed three times with PBS. After blocking with 1% BSA in PBS for 10 min, samples were incubated with primary antibodies for 1 h, washed three times with PBS, incubated with the secondary antibody for 30 min, and then washed three times with PBS. After mounting with Mowiol 4-88, specimens were observed under a fluorescence microscope (IX70 or IX71; OLYMPUS).

Cell adhesion assays.

For the adhesion assay of HEK293T transfectants, tissue culture plates were coated with either 10 μg/ml GST or GST-CS1 in PBS at 37 °C for 3 h, washed three times with PBS, blocked with PBS containing 1% BSA, and then washed three times with PBS. HEK293T transfectants were harvested, washed, re-suspended in DMEM, and plated onto the coated plates. After incubation at 37 °C for 30 min in a CO_2 incubator, the cells were washed three times with DMEM and images were captured of the bound cells.

For OSGEPase treatment, 1×10^6 KG-1 cells were incubated with 36 μg OSGEPase in 0.5 ml RPMI 1640 at 37 °C in a CO_2 incubator for 30 min. Then, the cells were incubated in coated tissue culture plates in RPMI 1640 supplemented with FCS at 37 °C for 30 min, and then unbound cells were collected and counted. For immunohistochemistry, OSGEPase-treated KG-1 cells were incubated in GST-CS1-coated glass chambers (AGC Techno Glass Co., Ltd.).

Immunoblotting.

HEK293T cells and transfectants were washed with PBS, lysed in 1% Nonidet-P40 lysis buffer, and then subjected to immunoblot analysis as described previously.[1] After the first immunoblotting with an anti-phospho-ERM antibody, the membranes were stripped with WB Stripping Solution (Nacalai Tesque, Inc.), re-blocked, and then re-analyzed with an anti-ERM antibody.

Flow cytometry.

HEK293T transfectants were washed with RPMI 1640 and fixed with 0.5% paraformaldehyde in PBS. Cells were analyzed by a FACSCanto II (BD Biosciences).

Disclosure of Potential Conflicts of Interest

No potential conflicts of interest were disclosed.

Acknowledgments

We thank Dr Kenjiro Kamiguchi for providing the pGST-CS-1 vector and Mr Hideki Saito for technical assistance. This work was supported in part by Grants-in-Aid for Scientific Research (KAKENHI 10011601) and a grant from the New Energy and Industrial Technology Development Organization (NEDO) of Japan.

References

1. Yamane J, Ohnishi H, Sasaki H, Narimatsu H, Ohgushi H, Tachibana K. Formation of microvilli and phosphorylation of ERM family proteins by CD43, a potent inhibitor for cell adhesion: cell detachment is a potential cue for ERM phosphorylation and organization of cell morphology. Cell Adh Migr 2011; 5:119-32; PMID:21045567; http://dx.doi.org/10.4161/cam.5.2.13908
2. Carlsson SR, Fukuda M. Isolation and characterization of leukosialin, a major sialoglycoprotein on human leukocytes. J Biol Chem 1986; 261:12779-86; PMID:2943740
3. Rosenstein Y, Santana A, Pedraza-Alva G. CD43, a molecule with multiple functions. Immunol Res 1999; 20:89-99; PMID:10580634; http://dx.doi.org/10.1007/BF02786465
4. Krause DS, Fackler MJ, Civin CI, May WS. CD34: structure, biology, and clinical utility. Blood 1996; 87:1-13; PMID:8547630
5. Furness SGB, McNagny K. Beyond mere markers: functions for CD34 family of sialomucins in hematopoiesis. Immunol Res 2006; 34:13-32; PMID:16720896; http://dx.doi.org/10.1385/IR:34:1:13
6. Berenson RJ, Andrews RG, Bensinger WI, Kalamasz D, Knitter G, Buckner CD, Bernstein ID. Antigen CD34+ marrow cells engraft lethally irradiated baboons. J Clin Invest 1988; 81:951-5; PMID:2893812; http://dx.doi.org/10.1172/JCI113409
7. Berenson RJ, Bensinger WI, Hill RS, Andrews RG, Garcia-Lopez J, Kalamasz DF, Still BJ, Spitzer G, Buckner CD, Bernstein ID, et al. Engraftment after infusion of CD34+ marrow cells in patients with breast cancer or neuroblastoma. Blood 1991; 77:1717-22; PMID:1707696
8. Osawa M, Hanada K, Hamada H, Nakauchi H. Long-term lymphohematopoietic reconstitution by a single CD34-low/negative hematopoietic stem cell. Science 1996; 273:242-5; PMID:8662508; http://dx.doi.org/10.1126/science.273.5272.242
9. Yabe H, Yabe M, Hattori K, Hinohara T, Morimoto T, Nakamura Y, Noma M, Takei M, Kobayashi N, Tsuji K, et al. Successful engraftment of allogeneic CD34-enriched marrow cell transplantation from HLA-mismatched parental donors. Bone Marrow Transplant 1996; 17:985-91; PMID:8807104
10. Cheng J, Baumhueter S, Cacalano G, Carver-Moore K, Thibodeaux H, Thomas R, Broxmeyer HE, Cooper S, Hague N, Moore M, et al. Hematopoietic defects in mice lacking the sialomucin CD34. Blood 1996; 87:479-90; PMID:8555469
11. Suzuki A, Andrew DP, Gonzalo JA, Fukumoto M, Spellberg J, Hashiyama M, Takimoto H, Gerwin N, Webb I, Molineux G, et al. CD34-deficient mice have reduced eosinophil accumulation after allergen exposure and show a novel crossreactive 90-kD protein. Blood 1996; 87:3550-62; PMID:8611677
12. Drew E, Merzaban JS, Seo W, Ziltener HJ, McNagny KM. CD34 and CD43 inhibit mast cell adhesion and are required for optimal mast cell reconstitution. Immunity 2005; 22:43-57; PMID:15664158; http://dx.doi.org/10.1016/j.immuni.2004.11.014
13. Healy L, May G, Gale K, Grosveld F, Greaves M, Enver T. The stem cell antigen CD34 functions as a regulator of hemopoietic cell adhesion. Proc Natl Acad Sci USA 1995; 92:12240-4; PMID:8618877; http://dx.doi.org/10.1073/pnas.92.26.12240
14. Lanza F, Healy L, Sutherland DR. Structural and functional features of the CD34 antigen: an update. J Biol Regul Homeost Agents 2001; 15:1-13; PMID:11388737
15. Delia D, Lampugnani MG, Resnati M, Dejana E, Aiello A, Fontanella E, Soligo D, Pierotti MA, Greaves MF. CD34 expression is regulated reciprocally with adhesion molecules in vascular endothelial cells in vitro. Blood 1993; 81:1001-8; PMID:7679004
16. Nielsen JS, Graves ML, Chelliah S, Vogl AW, Roskelley CD, McNagny KM. The CD34-related molecule podocalyxin is a potent inducer of microvillus formation. PLoS One 2007; 2:e237; PMID:17311105; http://dx.doi.org/10.1371/journal.pone.0000237
17. Nielsen JS, McNagny KM. Novel functions of the CD34 family. J Cell Sci 2008; 121:3683-92; PMID:18987355; http://dx.doi.org/10.1242/jcs.037507
18. Niggli V, Rossy J. Ezrin/radixin/moesin: versatile controllers of signaling molecules and of the cortical cytoskeleton. Int J Biochem Cell Biol 2008; 40:344-9; PMID:17419089; http://dx.doi.org/10.1016/j.biocel.2007.02.012
19. Chhabra ES, Higgs HN. The many faces of actin: matching assembly factors with cellular structures. Nat Cell Biol 2007; 9:1110-21; PMID:17909522; http://dx.doi.org/10.1038/ncb1007-1110
20. Matsui T, Maeda M, Doi Y, Yonemura S, Amano M, Kaibuchi K, Tsukita S, Tsukita S. Rho-kinase phosphorylates COOH-terminal threonines of ezrin/radixin/moesin (ERM) proteins and regulates their head-to-tail association. J Cell Biol 1998; 140:647-57; PMID:9456324; http://dx.doi.org/10.1083/jcb.140.3.647
21. Simmons DL, Satterthwaite AB, Tenen DG, Seed B. Molecular cloning of a cDNA encoding CD34, a sialomucin of human hematopoietic stem cells. J Immunol 1992; 148:267-71; PMID:1370171
22. Sutherland DR, Marsh JCW, Davidson J, Baker MA, Keating A, Mellors A. Differential sensitivity of CD34 epitopes to cleavage by Pasteurella haemolytica glycoprotease: implications for purification of CD34-positive progenitor cells. Exp Hematol 1992; 20:590-9; PMID:1375160
23. Kunda P, Pelling AE, Liu T, Baum B. Moesin controls cortical rigidity, cell rounding, and spindle morphogenesis during mitosis. Curr Biol 2008; 18:91-101; PMID:18207738; http://dx.doi.org/10.1016/j.cub.2007.12.051
24. Carreno S, Kouranti I, Glusman ES, Fuller MT, Echard A, Payre F. Moesin and its activating kinase Slik are required for cortical stability and microtubule organization in mitotic cells. J Cell Biol 2008; 180:739-46; PMID:18283112; http://dx.doi.org/10.1083/jcb.200709161
25. Arpin M, Chirivino D, Naba A, Zwaenepoel I. Emerging role for ERM proteins in cell adhesion and migration. Cell Adh Migr 2011; 5:199-206; PMID:21343695; http://dx.doi.org/10.4161/cam.5.2.15081
26. Hao J-J, Liu Y, Kruhlak M, Debell KE, Rellahan BL, Shaw S. Phospholipase C-mediated hydrolysis of PIP2 releases ERM proteins from lymphocyte membrane. J Cell Biol 2009; 184:451-62; PMID:19204146; http://dx.doi.org/10.1083/jcb.200807047
27. Takeuchi K, Sato N, Kasahara H, Funayama N, Nagafuchi A, Yonemura S, Tsukita S, Tsukita S. Perturbation of cell adhesion and microvilli formation by antisense oligonucleotides to ERM family members. J Cell Biol 1994; 125:1371-84; PMID:8207064; http://dx.doi.org/10.1083/jcb.125.6.1371
28. Yonemura S, Hirao M, Doi Y, Takahashi N, Kondo T, Tsukita S, Tsukita S. Ezrin/radixin/moesin (ERM) proteins bind to a positively charged amino acid cluster in the juxta-membrane cytoplasmic domain of CD44, CD43, and ICAM-2. J Cell Biol 1998; 140:885-95; PMID:9472040; http://dx.doi.org/10.1083/jcb.140.4.885
29. Brown MJ, Nijhara R, Hallam JA, Gignac M, Yamada KM, Erlandsen SL, Delon J, Kruhlak M, Shaw S. Chemokine stimulation of human peripheral blood T lymphocytes induces rapid dephosphorylation of ERM proteins, which facilitates loss of microvilli and polarization. Blood 2003; 102:3890-9; PMID:12907449; http://dx.doi.org/10.1182/blood-2002-12-3807
30. Kucia M, Reca R, Miekus K, Wanzeck J, Wojakowski W, Janowska-Wieczorek A, Ratajczak J, Ratajczak MZ. Trafficking of normal stem cells and metastasis of cancer stem cells involve similar mechanisms: pivotal role of the SDF-1-CXCR4 axis. Stem Cells 2005; 23:879-94; PMID:15888687; http://dx.doi.org/10.1634/stemcells.2004-0342
31. Lapidot T, Dar A, Kollet O. How do stem cells find their way home? Blood 2005; 106:1901-10; PMID:15890683; http://dx.doi.org/10.1182/blood-2005-04-1417
32. Kamiguchi K, Tachibana K, Iwata S, Ohashi Y, Morimoto C. Cas-L is required for beta 1 integrin-mediated costimulation in human Tcells. J Immunol 1999; 163:563-8; PMID:10395641

MicroRNA-126–mediated control of cell fate in B-cell myeloid progenitors as a potential alternative to transcriptional factors

Kazuki Okuyama[a], Tomokatsu Ikawa[b], Bernhard Gentner[c], Katsuto Hozumi[d], Ratanakanit Harnprasopwat[e], Jun Lu[f], Riu Yamashita[e], Daon Ha[g], Takae Toyoshima[a], Bidisha Chanda[a], Toyotaka Kawamata[e], Kazuaki Yokoyama[e], Shusheng Wang[h], Kiyoshi Ando[f], Harvey F. Lodish[i], Arinobu Tojo[e], Hiroshi Kawamoto[b], and Ai Kotani[a,j,1]

[a]Division of Hematological Malignancy, Regenerative Medical Science, Tokai University School of Medicine, Kanagawa 259-1193, Japan; [b]RIKEN Research Center for Allergy and Immunology, Kanagawa 230-0045, Japan; [c]San Raffaele Scientific Institute, 20123 Milan, Italy; [d]Department of Immunology, Tokai University School of Medicine, Kanagawa 259-1193, Japan; [e]Institute of Medical Science, University of Tokyo, Tokyo 108-8639, Japan; [f]Department of Hematology, Tokai University, Kanagawa 259-1193, Japan; [g]Tufts University School of Medicine, Boston, MA 02111; [h]Tulane University, New Orleans, LA 70118; [i]Whitehead Institute for Biomedical Research, Cambridge, MA 02142; and [j]Precursory Research for Embryonic Science and Technology (PRESTO), Japan Science and Technology Agency (JST), Saitama 332-0012, Japan

Edited by Tasuku Honjo, Graduate School of Medicine, Kyoto University, Kyoto, Japan, and approved May 31, 2013 (received for review January 11, 2013)

Lineage specification is thought to be largely regulated at the level of transcription, where lineage-specific transcription factors drive specific cell fates. MicroRNAs (miR), vital to many cell functions, act posttranscriptionally to decrease the expression of target mRNAs. MLL-AF4 acute lymphocytic leukemia exhibits both myeloid and B-cell surface markers, suggesting that the transformed cells are B-cell myeloid progenitor cells. Through gain- and loss-of-function experiments, we demonstrated that microRNA 126 (miR-126) drives B-cell myeloid biphenotypic leukemia differentiation toward B cells without changing expression of E2A immunoglobulin enhancer-binding factor E12/E47 (E2A), early B-cell factor 1 (EBF1), or paired box protein 5, which are critical transcription factors in B-lymphopoiesis. Similar induction of B-cell differentiation by miR-126 was observed in normal hematopoietic cells in vitro and in vivo in uncommitted murine c-Kit$^+$Sca1$^+$Lineage$^-$ cells, with insulin regulatory subunit-1 acting as a target of miR-126. Importantly, in EBF1-deficient hematopoietic progenitor cells, which fail to differentiate into B cells, miR-126 significantly up-regulated B220, and induced the expression of B-cell genes, including recombination activating genes-1/2 and CD79a/b. These data suggest that miR-126 can at least partly rescue B-cell development independently of EBF1. These experiments show that miR-126 regulates myeloid vs. B-cell fate through an alternative machinery, establishing the critical role of miRNAs in the lineage specification of multipotent mammalian cells.

cell fate decision | lymphopoiesis

Lineage specification is critical in mammalian development, as well as in adult tissue maintenance. In mammals, this developmental hierarchy has been most extensively studied in the hematopoietic system, where well-characterized cell-surface markers allow the purification of distinct cell populations. Lineage specification has been thought to be largely regulated at the level of transcription, where lineage-specific transcriptional factors drive specific cell fates (1–4). Early B-cell factor 1 (EBF1) specifies B-cell differentiation (5), and GATA-3 drives Th2 lineage commitment of CD4 T cells (6). However, regulation of differentiation at the transcriptional level alone does not appear to explain all hematopoietic cell-fate decisions, suggesting the presence of other as-yet-unknown mechanisms for establishing cell fate. Ectopic expression of c-enhancer binding protein-α (c/EBPα) or knock-out of paired box protein 5 (PAX5) in B cells are both capable of reprogramming B cells to macrophages; however, down-regulation of c/EBPα or ectopic expression of PAX5 or E2A immunoglobulin enhancer-binding factor E12/E47 (E2A), both critical transcription factors for B-cell differentiation, fail to reprogram myeloid-committed cells to B cells (7). Therefore, we hypothesized that the developmental fate of mammalian multipotent cells may be guided, at least in part, by a different mechanism of gene regulation, namely, microRNAs (miRNAs).

miRNAs are recently discovered class of small, noncoding RNAs that are 18–24 nt long and that down-regulate target genes at the posttranscriptional level. The majority of miRNA genes are transcribed by RNA polymerase II into long primary (pri) miRNA transcripts, processed by the nuclear nuclease, Drosha, into ∼60-bp hairpins, termed precursor (pre) miRNAs, and further cleaved in the cytosol by the Dicer nuclease into mature miRNAs. Mature miRNAs are then incorporated into the multiprotein, RNA-induced silencing complex, exerting post-transcriptional repression of target mRNAs, either by inducing mRNA cleavage, mRNA degradation, or by blocking mRNA translation (8, 9).

Each miRNA is thought to have several target mRNAs, and computational predictions suggest that more than a third of all human genes are targets of miRNAs (10, 11). In animals, miRNAs control many developmental and physiological processes. In *Caenorhabditis elegans*, abnormal expression of certain miRNAs leads to developmental arrest (12). Many studies have revealed specific changes in miRNA expression profiles that correlate with particular human tumor phenotypes (13, 14). In the hematopoietic system, miR-181a down-regulates several phosphatases that regulate the sensitivity of T cells to antigens, and overexpression of miR-181 in hematopoietic stem/progenitor cells significantly increases B-cell production. In addition, overexpression of miR-150 leads to a block in B-cell formation at the proB-to-preB cell transition step by down-regulating c-myb, among other targets (15–18).

Down-regulation of specific miRNAs in certain cancers implies that some miRNAs may act as tumor suppressors. For example, let-7 family members directly down-regulate *Ras* and other protooncogenes. Reduced expression of let-7 family members has been previously characterized in lung cancer (19, 20). On the other hand, increased expression of miR-17–92 and miR-155 often occur in B-cell lymphomas (21), implying that these miRNAs can act as oncogenes (22, 23). Thus, miRNAs are capable of acting as either oncogenes or tumor suppressors.

Author contributions: A.K. designed research; K.O., T.I., B.G., R.H., J.L., R.Y., D.H., T.T., B.C., T.K., and K.Y. performed research; B.G., K.H., S.W., K.A., and H.F.L. contributed new reagents/analytic tools; A.T., H.K., and A.K. analyzed data; and K.O., R.H., and A.K. wrote the paper.

The authors declare no conflict of interest.

This article is a PNAS Direct Submission.

[1]To whom correspondence should be addressed. E-mail: ka102009@tsc.u-tokai.ac.jp.

This article contains supporting information online at www.pnas.org/lookup/suppl/doi:10.1073/pnas.1220710110/-/DCSupplemental.

The *myeloid/lymphoid leukemia* (*MLL*) gene is located at 11q23, a site frequently involved in chromosomal translocations that occur in aggressive human lymphoid and myeloid leukemias. MLL-AF4 acute lymphoblastic leukemia (ALL) is associated with steroid resistance, has a poor prognosis (24, 25), and is associated with "lineage fragility." MLL-AF4 ALL often expresses both B-cell and monomyelocytic surface antigens; hence, it is often described as "biphenotypic" leukemia. This characteristic suggests that early hematopoietic progenitors are transformed in MLL-AF4 ALL.

A recent survey of miRNAs in ALL showed that miRNA expression patterns differ among ALL subtypes (13). We analyzed publicly available raw data (www.broad.mit.edu/mpr/publications/projects/microRNA/ALL.gct) and discovered that many miRNAs were down-regulated in ALL with *MLL* rearrangements, compared with ALL that do not harbor *MLL* rearrangements (26). Importantly, some miRNAs that have been reported to be tumor suppressors were down-regulated to considerable degrees, raising the question whether these miRNAs are involved in the biology of *MLL*-rearranged ALL, especially in regard to its lineage fragility.

Here, we focused on miR-126, which is down-regulated in *MLL*-rearranged ALL compared with other types of ALL. Through gain- and loss-of-function experiments, we showed that miR-126 positively regulated B-cell fate without affecting expression of EBF1, E2A, and PAX5 by targeting insulin regulatory subunit-1 (IRS-1). Most importantly, miR-126 could partly rescued failed B-cell development in EBF1-deficient hematopoietic progenitor cells (HPCs). Our results elucidate a unique mechanism involved in cell fate, which can partially rescue B lymphopoiesis in EBF1 deficiency.

Results

miR-126 Is Down-Regulated in MLL-AF4 ALL, Compared with Other Types of ALL. We analyzed publicly available raw data (www.broad.mit.edu/mpr/publications/projects/microRNA/ALL.gct) and found that in *MLL*-rearranged ALL, many miRNAs were down-regulated, compared with other types of ALL (13, 26). Of the 10 miRNAs that showed the most dramatic down-regulation, we chose to further analyze miR-126, which has been reported to have tumor-suppressive activity in lung cancer (27) (Fig. 1*A*). We also analyzed other previously published raw data (28) and found that miR-126 is gradually down-regulated during B-cell differentiation (Fig. 1*B*). This result was confirmed by real-time PCR analysis of miR-126 expression in $CD43^+B220^+$, $CD43^-B220^+$, and IgM^+B220^+ mouse bone marrow (BM) cells, which correspond to proB, preB, and mature B cells, respectively (Fig. 1*C*). Therefore, we hypothesized that miR-126 is a tumor suppressive miRNA and potential regulator of B-cell development.

miR-126 Shifts the Balance of B-Cell/Monomyeloid Differentiation Toward B Cells in MLL-AF4 ALL Cells. To explore the role of miR-126 in hematopoietic cells, we designed a retroviral vector that expresses the miRNA gene together with GFP. The vector was transduced, via retroviral infection, into SEM cells established from an MLL-AF4 ALL patient. In agreement with the observations from other *MLL*-rearranged ALL cell lines, SEM cells endogenously express mature miR-126 at a low level (29).

To examine the functions of miR-126, we overexpressed it in SEM cells. The expression level of mature miR-126 was more than 600-times higher in miR-126–transduced cells than in control cells (29).

SEM cells were transduced with retrovirus vectors expressing either let-7b, miR-126, miR-128b, or no miRNA (negative control). The transduced cells were sorted for those expressing GFP (a marker gene on all of the retroviral vectors) and cultured in RPMI containing 10% (vol/vol) FCS. At 8 wk posttransduction, a significant up-regulation of CD20 (~16%) and CD19 (mean fluorescence intensity, ~600) was observed in SEM cells expressing miR-126, but control cells or cells expressing let-7b or miR-128b showed ~1–2% $CD20^+$ cells and a mean-fluorescence intensity of CD19 expression of 350–450 (Fig. 2). Furthermore, suppression of miR-126 promoted the differentiation of SEM cells into myeloid cells, inducing the down-regulation of CD19 and up-regulation of CD15 (Fig. S1). Accordingly, gain- and loss-of-function experiments in a cell line derived from an MLL-AF4 ALL patient suggested that miR-126 drives B-cell myeloid biphenotypic leukemia differentiation toward B cells, at the expense of myeloid cells.

miR-126 Shifts the Balance of B-Cell/Monomyeloid Differentiation Toward B Cells Without Up-Regulating Transcription Factors Critical for B-Cell Development. To confirm that miR-126 affects B-cell development beyond regulating the expression of CD19, CD20, and CD15, we performed a comprehensive analysis of the mRNA transcripts that were up-regulated or down-regulated in SEM cells that expressed miR-126. Using Agilent gene-expression arrays, we identified a set of B-cell genes and a set of monomyeloid genes, as defined by IPA software (Ingenuity Systems). B-cell genes in $miR\text{-}126^+$ SEM cells were significantly up-regulated compared with those in control SEM cells, but the monomyelocyte genes were not (Fig. 3 *A* and *B*, and Dataset S1). These results suggest that miR-126–expressing SEM cells up-regulated not only CD20 and CD19 but also the global expression of other B-cell genes in SEM cells. We concluded that miR-126 shifted the balance of B-cell/monomyeloid differentiation toward B cells in MLL-AF4 ALL cells. Interestingly, PAX5, EBF1, and E2A, critical transcription factors in B-lymphopoiesis, were not up-regulated. Instead, E2A was slightly down-regulated in miR-126–expressing cells (Fig. 3*C*). Expressions of non–B-cell genes targeted by E2A, EBF1, or PAX5 were not altered by the transduction of miR-126 (Figs. S2 and S3, and Dataset S2). This finding suggests that neither transcriptional nor functional activity of PAX5, EBF1, and

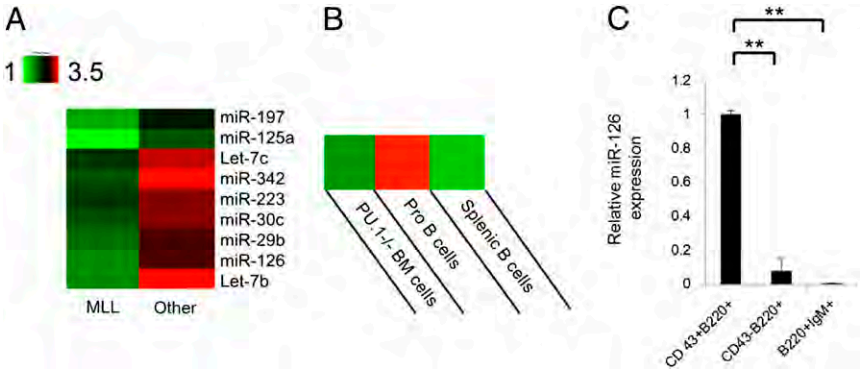

Fig. 1. Expression of miR-126 in acute lymphocytic leukemia and mouse hematopoietic cells. (*A*) The miRNAs that are most highly down-regulated in *MLL*-rearranged ALL compared with other types of ALL. These data were previously published and were reanalyzed here and presented as a heat map. (*B*) Expression of miR-126 in $PU.1^{-/-}$ BM cells, BM proB cells, and splenic B cells. These data were previously published and were reanalyzed here and presented as a heat map. (*C*) miRNA expression normalized by U6 expression in B-cell precursors detected by quantitative RT-PCR. B-cell precursor cells at various stages of differentiation were isolated from BM ($n = 3$) by FACS. ProB cells, $B220^+CD43^+IgM^-$; PreB cells, $B220^+CD43^-IgM^-$; immature B cells, $B220^+CD43^-IgM^+$. $^{**}P < 0.05$.

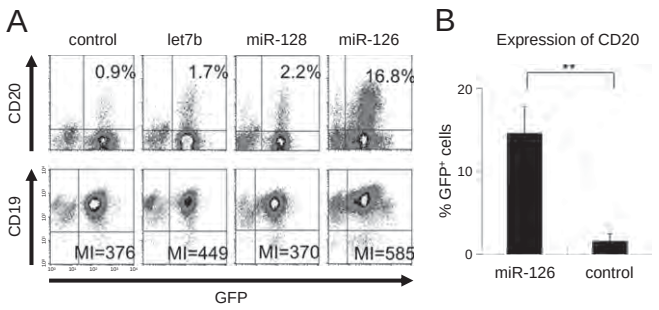

Fig. 2. Induction of B-cell differentiation by miR-126. (*A*) Representative flow plots of sorted SEM cells transduced with control, let-7b, miR-128b, or miR-126 vectors. The pregated live cells were analyzed. MI, mean intensity. (*B*) Percentages of $CD20^+$ cells among miR-126 or control vector-transduced SEM cells ($n = 3$).

E2A are enhanced by miR-126. Therefore, the shift toward B-cell lineage might be independent of PAX5, EBF1, and E2A.

miR-126 Regulates Lineage Fate in Lymphoid-Myeloid Progenitor Cells. To further analyze the B-cell differentiation caused by miR-126, we studied the effects of miR-126 transduction in a bilineage primary cell culture system. Mouse Lin^- HPCs isolated from fetal liver (FL), when cultured on thymic stromal (TSt)-4 cells, differentiate into monomyelocytic cells and B cells in vitro. This system allowed us to quantify the proportion of B cells and monomyelocytic cells derived from HPCs (30) following the perturbation of miR-126 expression. We transduced Lin^- cells with a retroviral construct harboring miR-126 or a control miRNA, and cultured them on TSt-4 cells. Then B cells were enumerated by flow cytometric analysis of the $CD19^+$ population. On day 5, in contrast to the control Lin^- cells, miR-126–expressing cells yielded an average fourfold enrichment of B cells (Fig. 4 *A* and *B*), and the proportion of $mac1^+$ monomyelocytic cells showed a reciprocal reduction (Fig. 4*B*). This result indicates that miR-126 shifts the balance of B-cell/monomyeloid differentiation toward B cells in normal HPCs.

To clarify which progenitor populations of Lin^- cells were affected by miR-126, we fractionated Lin^- cells into three groups: $Lin^-Flt3^+c\text{-}Kit^+Sca1^+IL\text{-}7R^-$ cells, $Lin^-c\text{-}Kit^{low}Sca1^{low}IL\text{-}7R^+$ cells, and $Lin^-c\text{-}Kit^+Sca1^-IL\text{-}7R^-$ cells. Although $Lin^-c\text{-}Kit^{low}Sca1^{low}IL\text{-}7R^+$ cells were slightly affected by miR-126, the most dramatic effect of miR-126 was on $Lin^-Flt3^+c\text{-}Kit^+Sca1^+IL\text{-}7R^-$ cells. Forced expression of miR-126 resulted in a statistically significant increase in $CD19^+$ cells in $Lin^-Flt3^+c\text{-}Kit^+Sca1^+IL\text{-}7R^-$ cells (Fig. 4*C* and Fig. S4). Next, we determined whether miR-126 had reprogrammed the myeloid-committed cells into B cells. To address this theory, we transduced miR-126 into $Lin^-c\text{-}Kit^+Sca1^-IL\text{-}7R^-$ cells, the majority of which were committed to the monomyelocyte lineage. miR-126 did not increase the proportion of $Lin^-c\text{-}kit^+Sca1^-IL\text{-}7R^-$ cells that were positive for CD19, indicating that miR-126 cannot reprogram monomyelocyte-committed cells (Fig. 4*C* and Fig. S4). Considering that $Lin^-c\text{-}Kit^{low}Sca1^{low}IL\text{-}7R^+$ cells are lymphoid-restricted progenitor cells, which still have potential to differentiate into myeloid cells although much less so than $Lin^-Flt3^+c\text{-}Kit^+Sca1^+IL\text{-}7R^-$ cells (7), these experiments suggest that miR-126 primarily regulates lymphoid versus myeloid lineage commitment in the multipotent cell population, and does not regulate the expansion of lymphoid- or myeloid-restricted progenitor cells.

miR-126 Increases B Cells in Vivo. Having established a functionally important role for miR-126 in an in vitro model of B-cell differentiation, we next examined the function of miR-126 in vivo. The competitive transplantation assays were performed in the Ptprc congenic mouse model, transducing $Ptprc^b$ (CD45.2) or $Ptprc^a$ (CD45.1) lin^- BM hematopoietic stem and progenitor cells, respectively, with either the miR126 or the control vector. The data were published in ref. 31.

Using flow cytometry, we characterized BM cells according to their expression of cell surface markers for B cells (CD19), T cells (CD3), or monomyeloid cells (Mac1). Remarkably, compared with control cells, the BM cells expressing miR-126 exhibited a significant expansion of $CD19^+$ B cells and reduction of $CD3^+$ T cells and $mac\text{-}1^+$ monomyeloid cells in the peripheral blood 4 wk after BM transplantation ($CD19^+$ cell frequency, $45.5 \pm 9.9\%$ vs. $70.7 \pm 05.4\%$; $P < 0.05$; $CD3^+$ cell frequency, $13.3 \pm 5.8\%$ vs. $5.5 \pm 2.0\%$; $P < 0.05$; $mac1^+$ cell frequency, $40.8 \pm 8.5\%$ vs. $23.1 \pm 6.1\%$; $P < 0.05$) (Fig. 5).

IRS-1 Is a Functional Target of miR-126 During B-Cell Expansion. The experiments described above establish an important role for miR-126 in B-cell development of HPCs. We next sought to determine the mRNA target of miR-126 that would explain its effect on B-lymphopoiesis. We initially focused on targets that were commonly predicted across multiple sequence-based prediction algorithms (10, 32–34). We chose *IRS-1* as a candidate because its gene expression was reduced in Lin^- FL cells overexpressing miR-126 (Fig. 6 *A* and *B* and Fig. S5). We focused on IRS-1 because it has known functions in cell proliferation and differentiation processes; higher expression of IRS-1 is associated with proliferation, and lower levels are associated with differentiation (35). First, we cloned the *IRS-1* 3′ UTR into a luciferase reporter vector and found that miR-126 repressed reporter activity by more than twofold, consistent with the predicted targeting of IRS-1 by miR-126 (34). This experiment confirmed that miR-126 negatively regulates the mRNA expression level of IRS-1 directly through its 3′ UTR (29). Then, we addressed whether the repression of IRS-1 could explain the B-cell differentiation observed with miR-126 overexpression using the in vitro mouse FL cell coculture system with TSt-4 cells. We tested whether complementation of IRS-1 by exogenous cDNA

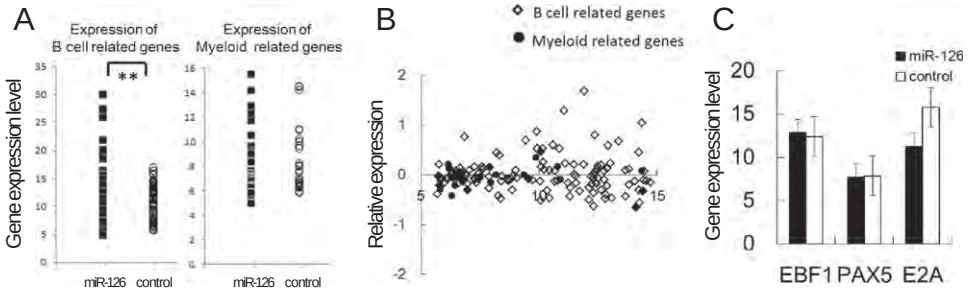

Fig. 3. miR-126 induces B-cell differentiation in MLL-AF4 ALL cells without up-regulating EBF1, PAX5, or E2A. (*A*) B-cell–related genes were significantly up-regulated in miR-126–transduced MLL-AF4 ALL cells compared with control-transduced MLL-AF4 ALL cells (*Left*), but monomyelocyte related genes were not (*Right*). The *y* axis shows log-transformed data. (*B*) Intensity scatter plot comparing miRNA profiles in miR-126–transduced and control-transduced MLL-AF4 ALL cells. The *x* axis shows log-transformed data, and the *y* axis shows the log ratio. (*C*) Intensity of E2A, PAX5, or EBF mRNA expression in miR-126– or control-transduced SEM cells. The *y* axis shows log-transformed data.

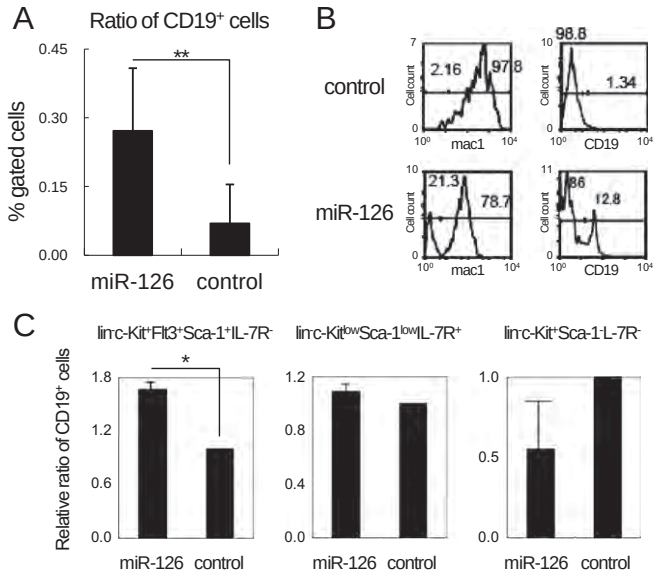

Fig. 4. miR-126 increases the proportion of B cells among progenitor FL cells cocultured with TSt-4 cells. Hematopoietic progenitors derived from mouse FL cells were sorted into Lin^- cells and transduced with control and miR-126–expressing viral constructions. The cells were then cocultured with TSt-4 cells to differentiate them into B cells or monocytes and analyzed after 5 d of differentiation using flow cytometric analysis with the lineage markers CD19 (B cells) and mac1 (monocytes). (*A*) Effects of the expression constructs on the percentage of $CD19^+$ cells. Error bars represent SD ($n = 3$). $^{**}P < 0.03$. (*B*) Representative flow histogram of control vector- and miR-126–transduced Lin^- FL cells. Expression of CD19 and mac1 were determined. These plots pregated on GFP^+ live cells. (*C*) Hematopoietic progenitors derived from mouse FL cells were sorted into $Lin^-Flt3^+c\text{-}Kit^+Sca1^+IL\text{-}7R^-$ cells, $Lin^-c\text{-}Kit^{low}Sca1^{low}IL\text{-}7R^+$ cells, and $Lin^-c\text{-}Kit^+Sca1^-IL\text{-}7R^-$ cells and transduced with control and miR-126-expressing viral constructs. Then, the cells were cocultured with TSt-4 cells to differentiate them into B cells or monocytes and analyzed by flow cytometry after 5 d of differentiation for the lineage markers CD19 (B cells). Effects of the expression constructs on the percentage of $CD19^+$ cells. The *y* axis represents the $CD19^+$ miR-126 transduced cells relative to the control. The error bars indicate SD ($n = 3$). $^*P < 0.03$.

that is not affected by miR-126 could reverse the observed increase in B-cell differentiation. Murine stem cell virus-based constructs containing the *IRS-1* coding sequence were generated with human nerve growth factor receptor (NGFR). Then, the IRS-1 coding sequence or a control vector was cotransduced with miR-126 into Lin^- cells to see whether IRS-1 expression could rescue the miR-126 phenotype. As shown in Fig. 6 *C* and *D*, $CD19^+$ B cells accounted for 2.34% of the 11.8% of Lin^- FL cells transduced with IRS-1 and miR-126, and 36.2% of the 56% cells transduced with control vector and miR-126. A total of 20% of IRS-1- and miR-126–transduced Lin^- FL cells and 70% of control vector- and miR-126–transduced cells were $CD19^+$, indicating that there were significantly fewer $CD19^+$ B cells among IRS-1–transduced Lin^- FL cells than among control cells (Fig. 6*D*). The opposite results were obtained for $mac1^+$ monomyelocytic cells (Fig. 6 *C* and *D*). These findings indicate that the influence of miR-126 on B-cell differentiation was abrogated by the introduction of IRS-1 lacking its 3′ UTR in murine FL cells, suggesting that the target genes of miR-126 in this system include *IRS-1*.

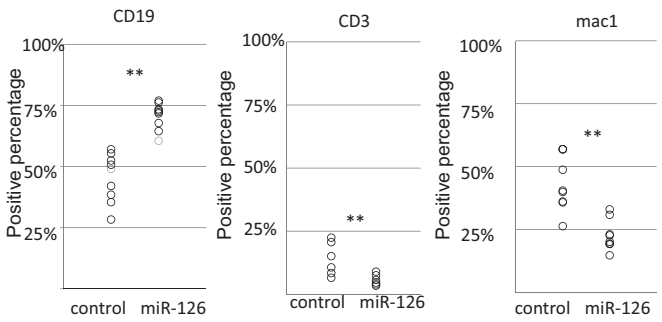

Fig. 5. miR-126 induces B-cell expansion in vivo. The competitive transplantation assays were performed in the Ptprc congenic mouse model, transducing $Ptprc^b$ (CD45.2) or $Ptprc^a$ (CD45.1) lin^- BM hematopoietic stem and progenitor cells, respectively, with either the miR126 or the control vector. The peripheral blood of recipient mice were analyzed 4 wk post-transplantation, when the hematopoietic system had largely recovered in the hosts. The data were published previously (31). Each dot represents data from one recipient mouse. $^{**}P < 0.01$.

miR-126 Can Rescue Failed B-Cell Differentiation in EBF1-Deficient HPCs. Mice lacking EBF1 fail to express most B-cell genes, including Cd79a and Cd79b, and do not undergo Igh V-to-DJ recombination in the BM. Neither E2A nor PAX5, which are critical transcriptional factors, can rescue the failure in EBF1-deficient HPCs. Ectopic expression of EBF1 is able to rescue B-lymphopoiesis in multipotent progenitors blocked at earlier stages of development because of targeted deletion of key lymphoid transcription factors such as E2A, PU.1, and PAX5. Taken together, these data indicate that EBF1 is an essential specification factor for the B-cell lineage. Accordingly, we tested whether failure of B-cell development because of EBF1 deficiency, can be rescued by miR-126. miR-126 induces B-cell differentiation in MLL-AF4 ALLs without affecting EBF1, PAX5, and E2A, suggesting that it may potentially induce B-cell differentiation by an alternative mechanism to transcriptional factors. We established EBF1-deficient HPCs expressing low amounts of B220 but not CD19. Retrovirus-mediated expression of miR-126 in these cells markedly up-regulated B220, but not CD19 (Fig. 7*A*). CD19 expression is contingent on EBF1. In the BM, B220 is up-regulated during the maturation of prepro B cells into mature B cells (36). Moreover, expression of B-cell genes, such as PAX5, CD79a/b, and recombination activating gene (RAG)1/2, is up-regulated (Fig. 7*B*). Although RAG1/2 was up-regulated by miR-126, V-DJ rearrangements were not induced by miR-126. miR-126 affected not only gene expression profiles, but the growth of EBF1-deficient HPCs. Although the proportion of control vector-carrying EBF1-deficient HPCs gradually decreased during 28-d culture, the proportion of EBF1-deficient HPCs carrying miR-126 increased (Fig. 7*C*). This finding suggested miR-126 promoted the proliferation or survival of EBF1-deficient HPCs. Next, we calculated the doubling time of them. The doubling time of control EBF1-deficient HPCs (26.6 ± 1.5 h) was comparable to that of the original EBF1-deficient HPCs (27.0 ± 2.0 h). In contrast, the doubling time of miR-126-transduced EBF1-deficient HPCs (21.4 ± 1.0 h) was significantly shorter than that of control cells. This result indicates that miR-126 enhanced the proliferation of EBF1-deficient HPCs. These results suggest that miR-126 can partly rescue failed B-cell lineage development and specification because of EBF1 deficiency.

Discussion

We found that miR-126 was down-regulated in MLL-AF4 ALL, a cancer with an immature B-cell phenotype, compared with other types of ALL. Furthermore, miR-126 expression strikingly decreased during successive stages of B-cell maturation in the BM, suggesting that this miRNA may participate in early B lymphopoiesis, and deregulation of its expression is involved in leukemogenesis. Indeed, inducing the re-expression of miR-126 promoted B-cell development in MLL-AF4 ALL, the mouse FL, and BM hematopoietic cells. miR-126, which was ectopically expressed in preB and immature B cells, did not affect B-cell

DEVELOPMENTAL BIOLOGY

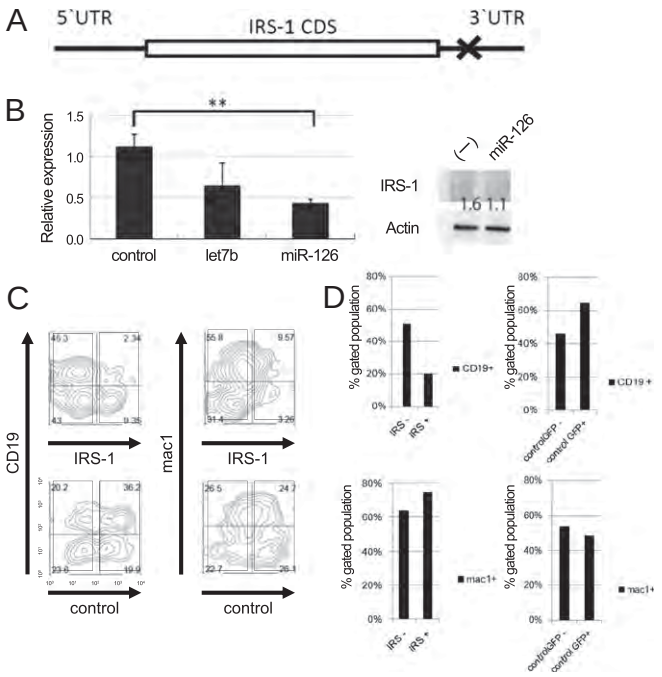

Fig. 6. IRS-1 is a functional target of miR-126 during B-cell expansion. (*A*) Location of the predicted (Pictar) miR-126 target sequence (X) in the 3′ UTR of the human IRS-1 mRNA. (*B*) Relative expression of IRS-1 mRNA normalized to U1A expression by quantitative PCR analysis of Lin$^-$ FL cells overexpressing miR-126, let-7, or control vector (n = 3, *Left*). $^{**}P < 0.05$. Western blot analysis of IRS-1 was performed with total protein extracts of miR-126–overexpressing or control Lin$^-$ FL cells (*Right*). The relative intensity of each band (indicated below the bands) was determined using Multigauge software and normalized to the GAPDH loading control. (*C* and *D*) Ectopic expression of IRS-1 in miR-126-expressing Lin$^-$ FL cells decreases B-cell numbers. (*C*) Representative plots for CD19 and mac1 expression in IRS-1$^+$/IRS-1$^-$ miR-126$^+$ and controlGFP$^+$/controlGFP$^-$ miR-126$^+$ Lin$^-$ FL cells. (*D*) Percentage of CD19$^+$ or mac1$^+$ cells in pregated IRS1$^+$, IRS1$^-$, control$^+$, or control$^-$ cells. Square indicates each pregated cells.

maturation, suggesting that its effect was limited to early B-cell development. Its effect was most dramatically observed in Lin$^-$c-Kit$^+$Sca1$^+$ uncommitted progenitor cells in the FL, suggesting miR-126 is involved in cell fate regulation. Notably, even though the expression of key transcription factors in B-cell development; E2A, EBF, and PAX5, were unchanged in miR-126–expressing cells, miR-126 plays a critical role in regulating the differentiation of B cells in leukemia, in which the deregulation of differentiation because of dysfunction of transcription factors is supposed to be involved in leukemogenesis (37). Moreover, expression of miR-126 in EBF1-deficient HPCs partly rescued B-lymphopoiesis, leading to the up-regulation of several B-cell genes and enhanced proliferation. Importantly, CD79a, which is critically regulated by EBF1, was up-regulated by miR-126 in EBF1-deficient cells. The stepwise expression and function of several factors is involved in cell fate determination. EBF1 can rescue B-cell development in E2A-, PU.1-, and PAX5-deficient hematopoietic stem cells. Conversely, these transcriptional factors cannot rescue B-cell development, indicating that EBF1 controls the minimal essential system for B-cell development. Our finding that miR-126 partly rescued B-cell development in EBF1-deficient HPCs suggests that miR-126, which is not a transcriptional factor, has critical roles in B-cell development. However, miR-126 is dispensable for B-cell development, because miR-126 deficiency does not cause any defects in B-lymphopoiesis. Taken together, our observations lead us to conclude that miR-126–mediated B-cell differentiation is at least partly independent of canonical assembly of a transcriptional factor regulatory network. miR-126 has the potential to compensate for the deregulation of cell fate caused by dysfunction of transcription factors in leukemia and is critically involved in B-cell lineage specification. These results challenge the view that miRNAs merely play fine-tuning roles in establishing lineage fate (8).

Surveying the predicted targets of miR-126, we found several genes that play important roles in myeloid development, including *IRS-1*, *v-crk sarcoma virus CT10 oncogene homolog* (*CRK*), and *homeobox A9* (*HOXA9*). Two highly conserved 8-nt sites in the 3′ UTR of IRS-1 mRNA, one conserved 7-nt site in the CRK 3′ UTR, and one conserved 7-nt site in the HOXA9 3′ UTR are complementary to the miR-126 "seed" region. Among these targets, we demonstrated that miR-126 targets IRS-1 during B-cell differentiation. IRS-1 is the main docking protein of both type 1 insulin-like growth factor I receptor and the insulin receptor. IRS-1 is a principal substrate of the insulin receptor tyrosine kinase. IRS-1 undergoes multisite tyrosine phosphorylation and mediates insulin signaling by associating with various signaling molecules containing Src homology 2 domains (38). Overexpression of *IRS-1* inhibits differentiation and promotes transformation of hematopoietic cells into a tumor-forming cell line (35). Although the function of IRS-1 in B-cell development has yet to be determined, it is reasonable that IRS-1, an inhibitor of differentiation, is down-regulated by miR-126 during B-cell differentiation.

Future investigations exploring the regulation of miR-126 expression are needed to understand its function; its expression is known to be greatest in highly vascularized tissues, such as the lung, heart, and kidney (39–41), and is also present in bronchial epithelium (27). miR-126 is located on chromosome 9q34.3 and is encoded within intron 5 of *epidermal growth factor like-7* (39). Recently, miR-126 was shown to function in angiogenesis, as miR-126–deficient mice are embryonic lethal because of vascular malformation (42). In the hematopoietic system, Landgraf et al. (43) reported qualitative detection of miR-126 in the CD34$^+$ pool containing hematopoietic stem cells, but they did not examine the function of miR-126 in this cell population. miR-126 has also

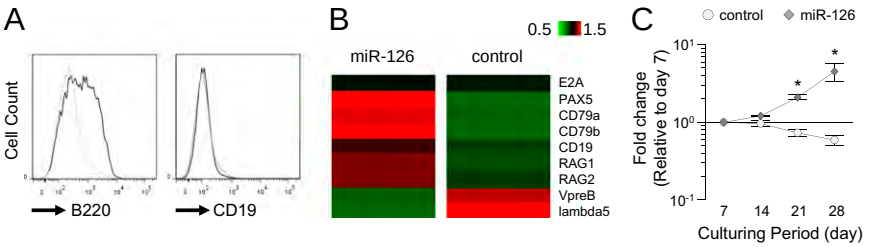

Fig. 7. miR-126 up-regulates B-cell markers and promotes cell proliferation in EBF1-deficient HPCs. (*A*) HPC lines derived from EBF1-deficient mouse FL were transduced with control and miR-126–expressing viral constructs. Cells were cocultured with TSt-4 cells in the presence of IL-7, stem cell factor, and Flt3 ligand and analyzed after 10 d of differentiation by flow cytometry for the B-cell lineage markers B220 and CD19. The black and gray lines indicate miR-126 and control vector-transduced pregated live cells, respectively. The same results were obtained three times. (*B*) cDNA analysis of B-lineage gene expression in the HPC lines derived from EBF1-deficient HPCs transduced with a viral construct expressing miR-126 (*Left*) or a control vector (*Rght*). (*C*) The proportion of miR-126–transduced EBF1-deficient HPCs in culture gradually increases, but that of control vector-transduced cells does not. The proportions of vector-carrying EBF1-deficient HPCs are shown as fold changes relative to day 7. $^*P < 0.05$.

been reported to be down-regulated during terminal megakaryocytopoiesis and up-regulated in megakaryocytic cell lines (44). We and others have found that miR-126 is down-regulated in B-cell differentiation. The regulation of miR-126 expression should be further investigated.

Finally, the observed function of miR-126 as an inducer of differentiation suggests miR-126 might be a promising therapeutic target. In acute promyelocytic leukemia, retinoic acid induces terminal differentiation of leukemic cells. This "differentiation induction" therapy has been tried in many types of tumors without much success. miR-126 may be an agent for differentiation induction therapy for ALL; thus, further studies are needed to evaluate its potential as a differentiation inducer.

Materials and Methods

Ebf1$^{-/-}$ Progenitor Cells. *Ebf1*$^{-/-}$ hematopoietic progenitor (Lin$^-$) cells were isolated from the *Ebf1*$^{-/-}$ livers of 14 d postcoitum embryos and cultured on TSt-4 stromal cells in IMDM containing 10% (vol/vol) FCS, 2-ME (5×10^{-5} M), penicillin (10 U/mL), and streptomycin (10 μg/mL) in the presence of stem cell factor, IL-7, and Flt3 ligand (10 ng/mL each), as described previously (45, 46).

Gene-Expression Analysis. RNA from cells used for microarray analysis was isolated using the RNeasy Mini Kit (Qiagen). For microarray analysis, splenocytes were cultured for 72 h with or without 10 μM IM. Gene-expression microarray analysis was performed using two-color microarray-based gene-expression analysis (Agilent Technologies) according to the manufacturer's instructions. After scanning, expression values for the genes were determined using GeneSpringGX software. All experiments were done in the duplicates.

Western Blot Analysis. FL cells transduced with either control or miR-126 vector were lysed in sample loading buffer and separated by SDS/PAGE and transferred to a polyvinylidene fluoride membrane. The membrane was incubated with primary antibody against IRS-1 (Cell Signaling Technology), followed by peroxidase-conjugated anti-rabbit Ig (GE Healthcare).

BM Transplantation. Lin- BM cells from congenic mice (Ptprca and Ptprcb, respectively) were transduced with a 126OE vector or with a CTRL vector, and injected in a 1:1 ratio into myeloablated recipients (31).

Peripheral blood analysis was performed 4 wk after the BM transplantation. Mononuclear cells were stained with various antibodies and analyzed on a FACSCalibur flow cytometer (BD Biosciences) and using FlowJo software (Tree Star).

Antibodies. Antibodies specific for CD3, CD19, CD20, Mac1, Gr-1, Flt3, c-kit, Sca1, and IL-7Rα were purchased from eBioscience.

Primer sequences, reagents, and more detailed methods are shown in *SI Materials and Methods*.

ACKNOWLEDGMENTS. We thank Mr. Keisuke Takahashi, and Drs. Masayuki Tanaka and Hideki Hayashi for technical assistance. We also thank Drs. Yoshio Katayama and Mari Sato for technical advice. This work was supported by the Japan Society for the Promotion of Science (to A.K.).

1. Cantor AB, Orkin SH (2002) Transcriptional regulation of erythropoiesis: An affair involving multiple partners. *Oncogene* 21(21):3368–3376.
2. Friedman AD (2002) Transcriptional regulation of myelopoiesis. *Int J Hematol* 75(5): 466–472.
3. Ye M, Graf T (2007) Early decisions in lymphoid development. *Curr Opin Immunol* 19(2):123–128.
4. Zhu J, Emerson SG (2002) Hematopoietic cytokines, transcription factors and lineage commitment. *Oncogene* 21(21):3295–3313.
5. Pongubala JM, et al. (2008) Transcription factor EBF restricts alternative lineage options and promotes B cell fate commitment independently of Pax5. *Nat Immunol* 9(2): 203–215.
6. Zheng W, Flavell RA (1997) The transcription factor GATA-3 is necessary and sufficient for Th2 cytokine gene expression in CD4 T cells. *Cell* 89(4):587–596.
7. Xie H, Ye M, Feng R, Graf T (2004) Stepwise reprogramming of B cells into macrophages. *Cell* 117(5):663–676.
8. Bartel DP (2004) MicroRNAs: Genomics, biogenesis, mechanism, and function. *Cell* 116(2):281–297.
9. Bagga S, et al. (2005) Regulation by let-7 and lin-4 miRNAs results in target mRNA degradation. *Cell* 122(4):553–563.
10. Lewis BP, Burge CB, Bartel DP (2005) Conserved seed pairing, often flanked by adenosines, indicates that thousands of human genes are microRNA targets. *Cell* 120(1): 15–20.
11. Miranda KC, et al. (2006) A pattern-based method for the identification of MicroRNA binding sites and their corresponding heteroduplexes. *Cell* 126(6):1203–1217.
12. Ambros V (2004) The functions of animal microRNAs. *Nature* 431(7006):350–355.
13. Lu J, et al. (2005) MicroRNA expression profiles classify human cancers. *Nature* 435(7043):834–838.
14. Volinia S, et al. (2006) A microRNA expression signature of human solid tumors defines cancer gene targets. *Proc Natl Acad Sci USA* 103(7):2257–2261.
15. Xiao C, et al. (2007) MiR-150 controls B cell differentiation by targeting the transcription factor c-Myb. *Cell* 131(1):146–159.
16. Chen CZ, Li L, Lodish HF, Bartel DP (2004) MicroRNAs modulate hematopoietic lineage differentiation. *Science* 303(5654):83–86.
17. Li QJ, et al. (2007) miR-181a is an intrinsic modulator of T cell sensitivity and selection. *Cell* 129(1):147–161.
18. Zhou B, Wang S, Mayr C, Bartel DP, Lodish HF (2007) miR-150, a microRNA expressed in mature B and T cells, blocks early B cell development when expressed prematurely. *Proc Natl Acad Sci USA* 104(17):7080–7085.
19. Johnson SM, et al. (2005) RAS is regulated by the let-7 microRNA family. *Cell* 120(5): 635–647.
20. Johnson CD, et al. (2007) The let-7 microRNA represses cell proliferation pathways in human cells. *Cancer Res* 67(16):7713–7722.
21. Metzler M, Wilda M, Busch K, Viehmann S, Borkhardt A (2004) High expression of precursor microRNA-155/BIC RNA in children with Burkitt lymphoma. *Genes Chromosomes Cancer* 39(2):167–169.
22. He L, et al. (2005) A microRNA polycistron as a potential human oncogene. *Nature* 435(7043):828–833.
23. Costinean S, et al. (2006) Pre-B cell proliferation and lymphoblastic leukemia/high-grade lymphoma in E(mu)-miR155 transgenic mice. *Proc Natl Acad Sci USA* 103(18): 7024–7029.
24. Pui CH, et al. (2003) Clinical heterogeneity in childhood acute lymphoblastic leukemia with 11q23 rearrangements. *Leukemia* 17(4):700–706.
25. Pieters R, et al. (2007) A treatment protocol for infants younger than 1 year with acute lymphoblastic leukaemia (Interfant-99): An observational study and a multicentre randomised trial. *Lancet* 370(9583):240–250.
26. Kotani A, et al. (2009) miR-128b is a potent glucocorticoid sensitizer in MLL-AF4 acute lymphocytic leukemia cells and exerts cooperative effects with miR-221. *Blood* 114(19):4169–4178.
27. Crawford M, et al. (2008) MicroRNA-126 inhibits invasion in non-small cell lung carcinoma cell lines. *Biochem Biophys Res Commun* 373(4):607–612.
28. Monticelli S, et al. (2005) MicroRNA profiling of the murine hematopoietic system. *Genome Biol* 6(8):R71.
29. Harnprasopwat R, et al. (2010) Alteration of processing induced by a single nucleotide polymorphism in pri-miR-126. *Biochem Biophys Res Commun* 399(2):117–122.
30. Lu M, Kawamoto H, Katsube Y, Ikawa T, Katsura Y (2002) The common myelolymphoid progenitor: a key intermediate stage in hemopoiesis generating T and B cells. *J Immunol* 169(7):3519–3525.
31. Lechman ER, et al. (2012) Attenuation of miR-126 activity expands HSC in vivo without exhaustion. *Cell Stem Cell* 11(6):799–811.
32. Krek A, et al. (2005) Combinatorial microRNA target predictions. *Nat Genet* 37(5): 495–500.
33. Xie X, et al. (2005) Systematic discovery of regulatory motifs in human promoters and 3′ UTRs by comparison of several mammals. *Nature* 434(7031):338–345.
34. Zhang J, et al. (2008) The cell growth suppressor, mir-126, targets IRS-1. *Biochem Biophys Res Commun* 377(1):136–140.
35. Prisco M, et al. (2004) Role of pescadillo and upstream binding factor in the proliferation and differentiation of murine myeloid cells. *Mol Cell Biol* 24(12):5421–5433.
36. Stehling-Sun S, Dade J, Nutt SL, DeKoter RP, Camargo FD (2009) Regulation of lymphoid versus myeloid fate 'choice' by the transcription factor Mef2c. *Nat Immunol* 10(3):289–296.
37. Gilliland DG (2002) Molecular genetics of human leukemias: New insights into therapy. *Semin Hematol* 39(4, Suppl 3)6–11.
38. Myers MG, Jr., Sun XJ, White MF (1994) The IRS-1 signaling system. *Trends Biochem Sci* 19(7):289–293.
39. Baskerville S, Bartel DP (2005) Microarray profiling of microRNAs reveals frequent coexpression with neighboring miRNAs and host genes. *RNA* 11(3):241–247.
40. Harris TA, Yamakuchi M, Ferlito M, Mendell JT, Lowenstein CJ (2008) MicroRNA-126 regulates endothelial expression of vascular cell adhesion molecule 1. *Proc Natl Acad Sci USA* 105(5):1516–1521.
41. Wang Y, et al. (2007) Identification of rat lung-specific microRNAs by micoRNA microarray: Valuable discoveries for the facilitation of lung research. *BMC Genomics* 8:29.
42. Wang S, et al. (2008) The endothelial-specific microRNA miR-126 governs vascular integrity and angiogenesis. *Dev Cell* 15(2):261–271.
43. Landgraf P, et al. (2007) A mammalian microRNA expression atlas based on small RNA library sequencing. *Cell* 129(7):1401–1414.
44. Garzon R, et al. (2006) MicroRNA fingerprints during human megakaryocytopoiesis. *Proc Natl Acad Sci USA* 103(13):5078–5083.
45. Ikawa T, Kawamoto H, Wright LY, Murre C (2004) Long-term cultured E2A-deficient hematopoietic progenitor cells are pluripotent. *Immunity* 20(3):349–360.
46. Lin YC, et al. (2010) A global network of transcription factors, involving E2A, EBF1 and Foxo1, that orchestrates B cell fate. *Nat Immunol* 11(7):635–643.

JJCO Japanese Journal of Clinical Oncology

Jpn J Clin Oncol 2013;43(12)1177–1183
doi:10.1093/jjco/hyt155
Advance Access Publication 14 October 2013

Phase I Study of Clofarabine in Adult Patients with Acute Myeloid Leukemia in Japan

Tatsuya Suzuki[1], Takahiro Yamauchi[2], Kiyoshi Ando[3], Tadashi Nagai[4], Kazuhiko Kakihana[5], Yasuhiko Miyata[6], Toshiki Uchida[1], Yasuhiro Tabata[7] and Michinori Ogura[1,*]

[1]Nagoya Daini Red Cross Hospital, Nagoya, [2]University of Fukui Hospital, Fukui, [3]Tokai University Hospital, Isehara, [4]Jichi Medical University Hospital, Shimotsuke-shi, [5]Tokyo Metropolitan Cancer and Infectious Diseases Center, Komagome Hospital, Tokyo, [6]National Hospital Organization Nagoya Medical Center, Nagoya and [7]Genzyme, Tokyo, Japan

*For reprints and all correspondence: Michinori Ogura, Department of Hematology and Oncology, Nagoya Daini Red Cross Hospital, 2-9 Myoken-cho, Showa-ku, Nagoya 466-8650 Japan. E-mail: mi-ogura@naa.att.ne.jp

Received July 10, 2013; accepted September 13, 2013

Objective: There are limited treatment options for relapsed/refractory acute myeloid leukemia patients or previously untreated elderly ($\geq$60 years) patients with acute myeloid leukemia. In Phase II studies from the USA and Europe, single-agent clofarabine demonstrated activity and acceptable toxicity in elderly patients with previously untreated acute myeloid leukemia. This Phase I, multicenter study assessed the maximum-tolerated dose, safety, pharmacokinetics and efficacy of clofarabine in Japanese adults with acute myeloid leukemia.
Methods: Intravenous clofarabine (20, 30 and 40 mg/m^2/day) was administered for 5 days to Japanese adult patients with relapsed or refractory acute myeloid leukemia or elderly patients with newly diagnosed acute myeloid leukemia.
Results: Fourteen patients, median age of 67.5 (59–72) years, were enrolled in this study. Eleven out of 14 patients had relapsed/refractory acute myeloid leukemia. Three patients received clofarabine at 20 mg/m^2, six at 30 mg/m^2 and five at 40 mg/m^2. Frequently reported treatment-related adverse events included thrombocytopenia (100%), anemia (93%), neutropenia (86%), nausea (86%), alanine aminotransferase increase (71%), headache (71%) and febrile neutropenia (57%). Three patients experienced reversible dose-limiting toxicities; two had increased alanine aminotransferase with 30 and 40 mg/m^2 and one had Grade 3 elevation of serum amylase with 40 mg/m^2. The maximum-tolerated dose was 30 mg/m^2/day. C_{max} and exposure area under the curve$_{0-24h}$ increased with increasing dose and were proportional to dose through the tested dose range. Among the 14 assessable patients, four (29%) achieved complete remission and two (14%) complete remission without platelet recovery. The overall remission rate was 43%.
Conclusions: These results demonstrate safety and preliminary, promising activity of clofarabine in Japanese patients with acute myeloid leukemia. Further investigation is warranted.

Key words: clofarabine – myeloid leukemia – acute – clinical trial – Phase I – aged

INTRODUCTION

Although the treatment of adult patients with newly diagnosed acute myeloid leukemia (AML) has improved, there are limited options for those with relapsed or refractory disease, and for elderly patients $\geq$60 years (1,2). The goal for treatment of patients with AML is to achieve complete remission (CR) because it has been shown to correlate with longer survival and better quality of life (3,4). Regimens including

anthracycline, such as daunorubicin or idarubicin, plus cytarabine have been the standard of care for induction therapy in patients with newly diagnosed AML (2,5). While 40–65% of previously untreated elderly patients with AML achieve remission, the vast majority (85%) relapse within ≤3 years and <10% achieve long-term survival (2,3,5). The median survival of patients ≥65 years has been reported to be 2 months for untreated patients, 6 months for treated patients and 22 months for the few who receive allogeneic hematopoietic stem cell transplantation (HSCT) (6).

There is no standard of care for patients with relapsed or refractory AML, and the only curative option for these patients is allogeneic HSCT after achieving remission with salvage chemotherapies. Options for physically fit elderly patients are more limited and include salvage chemotherapy followed by allogeneic HSCT, or treatment with the same successful induction for those patients who achieved an initial remission lasting at least 1 year (7). Alternatives for patients who cannot tolerate these options include best supportive care and low-dose cytarabine (5,7). There is a clear unmet medical need for more effective and safer treatment options for these patients.

Clofarabine, a purine nucleoside analog approved in the USA and European Union for the treatment of pediatric patients with relapsed or refractory acute lymphoblastic leukemia, was rationally designed to combine the cytotoxic properties of fludarabine and cladribine, and to avoid or reduce their characteristic dose-limiting toxicities (DLTs) (8). Thus, clofarabine inhibits both DNA polymerase and ribonucleotide reductase, inhibiting DNA replication and strand elongation, as well as RNA transcription (9). In a Phase II study from the USA, single-agent clofarabine showed activity and acceptable toxicity in patients older than 60 years of age with untreated AML and at least one unfavorable prognostic factor (10). Similarly, in two Phase II studies from Europe, clofarabine demonstrated activity and tolerability in patients at least 65 years of age who were considered not candidates for intensive chemotherapy (11).

We carried out this Phase I, multicenter study in Japan to determine the maximum-tolerated dose (MTD) and to evaluate safety and pharmacokinetics of clofarabine monotherapy in adult patients with relapsed or refractory AML and in previously untreated elderly patients with AML considered to be unlikely to benefit from standard induction therapy.

PATIENTS AND METHODS

Patient Criteria

Eligible patients had a diagnosis of relapsed or refractory AML according to the fourth World Health Organization classification of myeloid neoplasms criteria (12) or were elderly patients (60–74 years of age) with previously untreated AML who were deemed to be unlikely to benefit from standard induction chemotherapy. Additional inclusion criteria included Eastern Cooperative Oncology Group (ECOG) performance status (PS) 0–2; adequate hepatic [total bilirubin ≤1.5 × institutional upper limit of normal (ULN), aspartate aminotransferase (AST), alanine aminotransferase (ALT) ≤2.5 × ULN], renal (estimated glomerular filtration rate ≥60 ml/min/1.73 m^2), pancreatic (serum amylase level ≤1.5 ULN, serum lipase level within normal limit) and cardiac [left ventricular fractional shortening on echocardiography (ECHO) ≥22% or left ventricular ejection fraction (LVEF) on ECHO or multigated acquisition (MUGA) scan ≥40%] functions.

Exclusion criteria included diagnosis of acute promyelocytic leukemia, prior HSCT, prior radiation therapy to the pelvis, uncontrolled infection, severe concurrent disease that was difficult to control by drug therapies and history of serious organ dysfunction. Pregnant and lactating women were also ineligible.

All patients provided written informed consent. This study was conducted in accordance with the principles stipulated by the Declaration of Helsinki and by the standards stipulated by Good Clinical Practice. The Institutional Review Boards at each participating institution approved the study.

Treatment Plan

The study employed a 3 + 3 design (13). Three patients were enrolled in a dose cohort and assessed for DLTs during the first cycle. If none of the patients in a cohort experienced a DLT, three new patients were enrolled in the next dose cohort. If a patient developed a DLT, three new patients were added to that cohort for a total of six patients included in that cohort for tolerability assessment. If no additional patients developed a DLT, three new patients were enrolled in the next dose cohort. If two of the six patients developed a DLT, that dose level was deemed not to be tolerable. By definition, DLTs were any ≥Grade 3 non-hematologic toxicities (except for Grade 3 pyrexia, anorexia, nausea, vomiting, malaise and transient changes in laboratory values related to hepatic function) and severe Grade 4 myelosuppression that persisted until Day 42 from the start of therapy (an absolute neutrophil count (ANC) < 500/mm^3 and platelet count <25 000/mm^3 due to myelosuppression in the absence of persistent leukemia cell in bone marrow and peripheral blood). The MTD was defined to be the highest dose at which no more than one of six patients in the cohort developed DLTs during the first cycle.

Patients received once daily clofarabine 20 mg/m^2 in Cohort 1, 30 mg/m^2 in Cohort 2 and 40 mg/m^2 in Cohort 3 as a 1 h intravenous infusion for five consecutive days. Patients received one cycle, but patients with a hematologic remission after one cycle could receive up to a maximum of three cycles. Treatment had to be discontinued if patients did not achieve a CR or a CR without platelet recovery (CRp) after two cycles of treatment with clofarabine.

Patients in CR or CRp who did recover in peripheral blood cell count (ANC ≥1000/mm^3 and platelet count ≥50 000/mm^3 without the need for transfusion) from Days 57 to 84 proceeded to the next cycle with a 10 mg/m^2 dose reduction. Patients who did not show a recovery in peripheral blood cell count by Day 84 were withdrawn from the study. Only one dose reduction was allowed for delayed peripheral blood cell

count recovery. All patients who developed myelosuppression that met the definition of DLT were withdrawn from the study.

Prophylactic administration of antibacterial drugs, antifungal agents and antiviral agents was recommended, but not mandated.

Patient Evaluations

To assess response, bone marrow assessments and peripheral blood smear tests were performed on Day 21 in Cycles 1 and 2. Follow-up continued for 45 days after the last dose. If the results of the bone marrow test were inconclusive for determination of response, the bone marrow tests were repeated every 7–14 days. Efficacy assessments were made by the investigator using the International Working Group criteria for diagnosis and treatment of AML (14).

Patients were hospitalized during the DLT evaluation period. An independent Safety Data Monitoring Committee oversaw the study. Toxicities were assessed using the National Cancer Institute Common Terminology Criteria for Adverse Events (NCI-CTCAE version 3.0).

Pharmacokinetic Analyses

Blood samples for pharmacokinetic assessments were collected from patients before, during and at various time points after drug administration on Days 1–5 of Cycle 1. Urine samples were collected from patients before and after drug administration on Days 1 and 5 of Cycle 1. All blood and urine samples were analyzed by MicroConstants, Inc. (San Diego, USA) for measurement of clofarabine concentrations.

Clofarabine pharmacokinetic parameters were estimated using the times of drug administration and blood collection. All parameters were calculated using industry standard software for pharmacokinetics analyses. The following plasma pharmacokinetic parameters were calculated using non-compartmental methods: area under the curve (AUC_{0-24}) from time 0 up to 24 h calculated using the log trapezoidal method, the maximum observed plasma concentration (C_{max}) and time to maximum observed concentration (T_{max}). The relation of dose exposure with AUC_{0-24} and C_{max} was assessed using a Scatter plot.

Statistical Analysis

This was a Phase I dose-escalation study. The primary objectives of this study were to assess the MTD, safety and pharmacokinetics of clofarabine intravenously administered at 20, 30 and 40 mg/m^2/day for 5 days to Japanese adult patients with AML.

All patients who received clofarabine for five consecutive days in Cycle 1 at each dose level or patients who experienced a DLT in Cycle 1 were assessed for the development of DLTs to evaluate the tolerability of clofarabine. The full analysis set, which comprised of all patients who received at least one dose of clofarabine, was used for the primary safety and efficacy analyses.

RESULTS

Patient Characteristics

In total, 14 patients with a median age of 67.5 (range 59–72) years were enrolled at six study sites. Table 1 lists the patient demographics and baseline disease characteristics. Ten patients (71%) had refractory AML and most had an ECOG PS of 0.

Treatment Exposure

All enrolled patients ($n = 14$) received at least one dose of clofarabine: three patients in Cohort 1, six in Cohort 2 and five in Cohort 3. Overall, patients received a median of one (range 1–3) cumulative number of clofarabine cycles. Only two of 14 patients (14%) had a dose reduction or modification. One patient in Cohort 1 had a dose reduction due to neuralgia during the second cycle. A patient in Cohort 2 had the infusion time extended.

Toxicity and MTD

All patients experienced at least one adverse event (AE) regardless of the relationship to clofarabine treatment and all experienced at least one AE related to clofarabine treatment. Table 2 lists the treatment-related AEs experienced by at least three patients, according to the maximum NCI-CTCAE grade. The most frequently reported treatment-related hematologic AEs were thrombocytopenia (100%), anemia (93%), neutropenia (86%) and febrile neutropenia (57%). The most common treatment-related non-hematologic AEs were nausea (86%), headache (71%), increased ALT (71%) and increased AST (64%). Overall, the most common treatment-related Grade 4 AEs were thrombocytopenia (93%), neutropenia (86%), anemia (36%) and leukopenia (21%).

There was no major difference in the incidence of AEs or laboratory abnormalities between dose cohorts, with the exception of increases in Grade $\geq$3 of ALT and AST, which were reported more frequently in Cohort 3 than in the other cohorts (0, 17 and 100% in Cohorts 1, 2 and 3, respectively).

Three out of 14 patients experienced DLTs as assessed by the independent Safety Data Monitoring Committee. These DLTs included increased ALT in one patient in Cohort 2 (Grade 4) and prolongation of increased ALT in one in Cohort 3 (Grade 3) and Grade 3 elevation of serum amylase in one patient in Cohort 3. In this patient, the increase of laboratory test values was transient (reaching its worst level at Day 7 with recovery by Day 14) and occurred in the absence of any clinical symptoms suggestive of pancreatitis. Furthermore, the pattern of amylase isozyme values (for example, at Day 7, 43% for P-amylase and 57% for S-amylase) was not consistent with acute pancreatitis.

One patient in Cohort 2 and the one in Cohort 3 withdrew from the study due to DLTs. All the three patients recovered from their DLTs. Thus, the MTD was determined to be 30 mg/m^2/day.

One patient experienced a serious (Grade 3) herpes zoster deemed to be possibly related to clofarabine treatment. Once

Table 1. Patient demographics and baseline characteristics

Characteristic	Clofarabine (mg/m^2)			
	20 ($n = 3$)	30 ($n = 6$)	40 ($n = 5$)	Total ($n = 14$)
Median age (range), years	64.0 (61–69)	68.0 (59–72)	69.0 (59–70)	67.5 (59–72)
Sex, number				
Male	3	4	3	10
Female	0	2	2	4
AML state				
Previously untreated	2	0	1	3
Relapsed	0	1	0	1
Refractory	1	5	4	10
Secondary AML state				
Secondary AML[a]	2	0	2	4
AHD	2	0	2	4
Non-secondary AML	1	6	3	10
ECOG performance status				
0	3	4	3	10
1	0	2	1	3
2	0	0	1	1
Karyotype, number (%)				
Favorable	0	1	0	1
Intermediate	1	2	4	7
Unfavorable	2	3	1	6
Prior induction regimen for AML				
No	2	0	1	3
Yes	1	6	4	11
Other prior drug treatment for AML or AHD				
No	1	4	4	9
Yes	2	2	1	5

AHD, antecedent hematologic disorder; AML, acute myeloid leukemia; ECOG, Eastern Cooperative Oncology Group.
[a]All four patients were previously diagnosed with myelodysplastic syndromes; two were previously treated with azacitidine, one with decitabine and one had no prior treatment for AML or AHD.

Table 2. Treatment-related AEs experienced by ≥20% of patients ($n = 14$)

AE	Maximum NCI-CTC grade, no. of patients				
	1	2	3	4	All grades
Anemia	0	0	8	5	13
Neutropenia	0	0	0	12	12
Febrile neutropenia	0	0	8	0	8
Thrombocytopenia	0	0	1	13	14
Leukopenia	0	0	0	3	3
Diarrhea	3	0	0	0	3
Nausea	10	2	0	0	12
Vomiting	4	0	0	0	4
Chills	3	0	0	0	3
Fatigue	3	0	0	0	3
Malaise	5	0	0	0	5
Pyrexia	3	0	0	0	3
Pneumonia	0	2	3	0	5
ALT increased	6	0	3	1	10
AST increased	4	2	3	0	9
Blood bilirubin increased	2	2	0	0	4
Gamma-glutamyltransferase increased	2	1	0	0	3
Decreased appetite	3	0	2	0	5
Headache	6	4	0	0	10

AE, adverse event; ALT, alanine aminotransferase; AST, aspartate aminotransferase; NCI, National Cancer Institute.

diagnosed with this infection, this patient was admitted to the hospital and treated with antiviral medication and after discharge, he was maintained on aciclovir and vidarabine; he recovered from herpes zoster with neuralgia as a sequelae. There were no deaths during the study period. Six patients died after the study follow-up period, five of these deaths were due to disease progression and were considered not study related. For one death (reported as aggravated pneumonia), the relationship to clofarabine treatment was considered to be unlikely. This patient (a 66-year-old man) experienced drug-related pneumonia during the study period which improved at study completion, 10 days later. The pneumonia was reported to have been controlled 5 days later when the patient began an alternative treatment with aclarubicin hydrochloride, cytarabine and lenograstim. Almost 3 weeks after starting this new treatment, the patient's condition rapidly deteriorated and he died a week later. While the casual relationship between clofarabine treatment and the aggravated pneumonia that led to death appeared to be unlikely, it could not be ruled out given that no autopsy was performed.

Pharmacokinetics

After an intravenous infusion of clofarabine at doses of 20, 30 and 40 mg/m^2, maximum clofarabine concentrations were observed at the end of the infusion in the majority of patients (Table 3). C_{max} and exposure AUC_{0-24h} increased with increasing dose and were proportional to dose over the 20–40 mg/m^2 dose range tested (Fig. 1). The pharmacokinetics of clofarabine exhibited low-to-moderate inter-patient variability on both Days 1 and 5.

The elimination half-life ($t_{1/2}$) was not dependent on the dose or duration of treatment and was estimated consistently from each dose level, following either single or multiple dose regimens. Given the relatively short $t_{1/2}$ of clofarabine,

Table 3. Clofarabine plasma pharmacokinetics

Parameter, mean ± standard deviation	Clofarabine (mg/m^2)					
	20		30		40	
	Day 1 ($n = 3$)	Day 5 ($n = 3$)	Day 1 ($n = 6$)	Day 5 ($n = 5$)	Day 1 ($n = 5$)	Day 5 ($n = 5$)
C_{max} (ng/ml)	382.0 ± 68.51	479.0 ± 77.87	522.8 ± 85.11	615.8 ± 103.4	772.8 ± 122.9	966.2 ± 11.7
t_{max} (h)	0.917 ± 0.050	0.939 ± 0.025	1.006 ± 0.170	0.843 ± 0.242	0.893 ± 0.142	0.927 ± 0.043
$AUC_{0\text{-}24h}$ (ng h/ml)	1172.0 ± 157.4	1423.4 ± 349.2	2026.8 ± 918.7	1851.8 ± 356.1	2341.0 ± 397.1	2773.0 ± 688.1
$t_{1/2}$ (h)	5.561 ± 0.340	5.971 ± 0.796	6.804 ± 2.662	5.339 ± 0.375	5.838 ± 0.553	4.719 ± 0.542
CL (l/h)	27.62 ± 3.57	23.56 ± 6.60	26.18 ± 9.12	26.08 ± 5.34	27.10 ± 6.32	23.12 ± 5.20
Vd_{ss} (l/m^2)	103.50 ± 22.75	92.64 ± 22.80	111.99 ± 22.44	91.19 ± 13.74	103.11 ± 7.05	71.09 ± 11.13
Acc ratio	–	1.206 ± 0.194	–	1.007 ± 0.267	–	1.184 ± 0.173

Acc ratio, accumulation ratio; AUC, area under the drug-concentration curve; CL, total clearance; C_{max}, maximum drug plasma concentration; $t_{1/2}$, elimination half-life; t_{max}, time to maximum plasma concentration; Vd_{ss}, volume of distribution at a steady state.

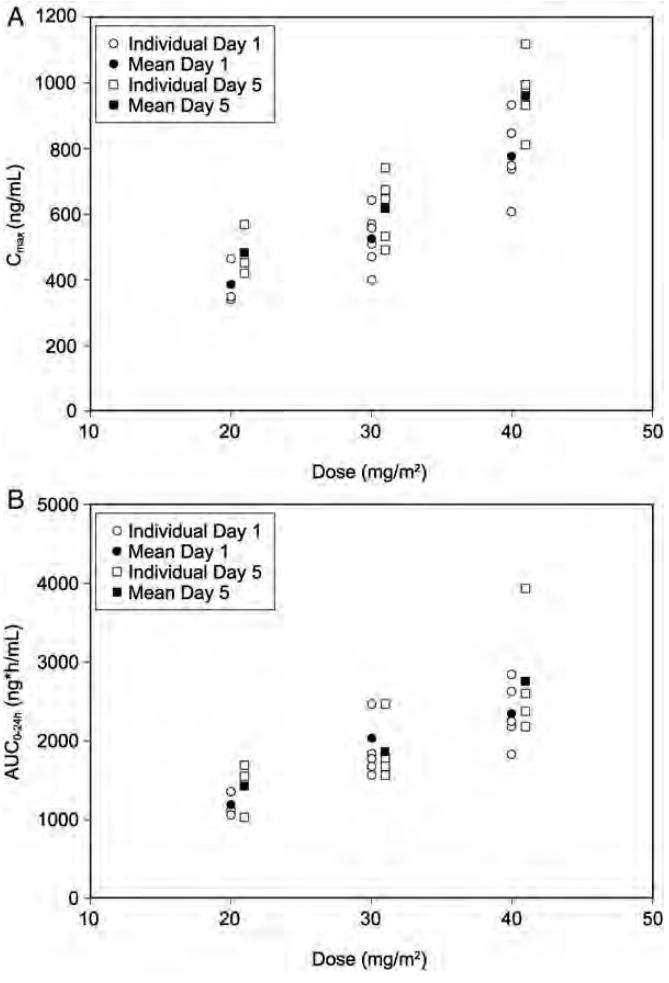

Figure 1. (**A**) Scatter plot of arithmetic mean C_{max} of clofarabine versus dose ($n = 3$ for 20 mg/m^2, $n = 6$ for 30 mg/m^2 on Day 1 and $n = 5$ on Day 5, $n = 5$ for 40 mg/m^2). (**B**) Scatter plot of arithmetic mean area under the curve $(AUC)_{0-24h}$ of clofarabine versus dose ($n = 3$ for 20 mg/m^2, $n = 6$ for 30 mg/m^2 on Day 1 and $n = 5$ on Day 5, $n = 5$ for 40 mg/m^2).

Table 4. Best response according to the investigator assessment

Best response category	Clofarabine (mg/m^2)			Total ($n = 14$)
	20 ($n = 3$)	30 ($n = 6$)	40 ($n = 5$)	
Complete remission, number (%)	1 (33)	1 (17)	2 (40)	4 (29)
Complete remission without platelet recovery, number (%)	1 (33)	1 (17)	0	2 (14)
Partial remission, number (%)	0	0	0	0
Overall remission (CR + CRp + PR)	2 (67)	2 (33)	2 (40)	6 (43)
Treatment failure, number (%)	1 (33)	4 (67)	3 (60)	8 (57)

CR, complete remission; CRp, complete remission without platelet recovery; PR, partial remission.

minimal drug accumulation was observed following daily intravenous infusion for 5 days.

Efficacy

All 14 patients were included in the efficacy assessment (Table 4). Four patients (29%) achieved CR, two (14%) achieved CRp and none had PR, leading to an overall remission rate (CR + CRp + PR) of 43%. Table 5 lists the characteristics of responding patients. Two of the three newly diagnosed patients achieved CR and the other achieved CRp. Among the 10 patients with relapse/refractory AML, two (20%) achieved CR and one (10%) achieved CRp.

DISCUSSION

The results from this multicenter Phase I study of clofarabine monotherapy show the MTD to be 30 mg/m^2 administered

Table 5. Characteristics of responding patients

Dose cohort	Sex and age (years)	AML state	Secondary AML state	FAB	No. of prior regimens	No. of clofarabine cycles	Best response	CR duration (days)
20	Male 64	New	AHD	M1	0	2	CR	61
20	Male 69	New	AHD	M2	0	1	CRp	NA
30	Female 72	Refractory	None	M0	1	2	CR	88+
30	Male 64	Refractory	None	M0	4	3	CRp	NA
40	Male 70	Refractory	None	Unknown	1	1	CR	1+
40	Female 70	New	AHD	Unknown	0	2	CR	36+

AHD, antecedent hematologic disorder; FAB, French–American–British classification; NA, not available.

intravenously daily for 5 days, and demonstrate preliminary but encouraging efficacy in 14 patients with AML, including 12 elderly patients. This MTD in Japanese patients is lower than the recommended Phase II doses of 40 mg/m^2 for adult patients and 52 mg/m^2 for pediatric patients with acute leukemia reported in two Phase I studies from the USA (13,15). However, this MTD of 30 mg/m^2 is identical to that used to treat elderly patients with AML in Phase II studies from Europe and the USA (10,11). The safety profile observed in the present study was similar to that reported in the previous studies.

One patient in our study experienced possibly drug-related Grade 3 herpes zoster; he recovered after treatment but withdrew from the study as per protocol. The study protocol recommended, but did not mandate prophylactic antiviral treatment. The use of prophylactic antiviral, antifungal and antibacterial agents in the USA (9,10) and EU (11) studies was as per institutional guidelines. Although cases of herpes zoster were not reported in these studies (10,11), prophylaxis against herpes is recommended for patients treated with T-cell depleting agents such as fludarabine (16), another purine analog, and should also be considered for patients undergoing clofarabine.

In the pharmacokinetic analysis, the C_{max} and AUC_{0-24h} of clofarabine increased dose proportionally over the dose range tested, with low-to-moderate inter-patient variability. The relative short $t_{1/2}$ was independent of dose or treatment duration; there was minimal drug accumulation. The pharmacodynamic analysis indicated that clofarabine did not have a significant impact on blood pressure, heart rate and electrocardiography parameters. There was no evident relationship between clofarabine concentration and the pharmacodynamic end points tested.

In addition to a tolerable safety profile, the results from this study show that clofarabine appears to have promising clinical activity, producing four CRs and two CRp, for an overall remission rate of 43%. This overall efficacy rate is consistent with that reported in the aforementioned studies from Europe (48%) (11) and the USA (46%) (10). The efficacy results obtained with clofarabine monotherapy in the treatment of elderly patients in these different studies appear to be higher than the rates reported in other studies of monotherapies in similar patient populations. For example, complete remission rates for single-agent decitabine ranged from 26% in a large Phase II study to 18% in a randomized Phase III study comparing it with best supportive care or low-dose cytarabine (which together had an 8% CR + CRp rate) (17,18). A subgroup analysis of a randomized study reported an 18% CR rate for azacitidine monotherapy in elderly patients with low bone marrow blast count AML (19). The primary analysis of this randomized trial found a survival benefit for azacitidine compared with the conventional regimens in the treatment of patients with intermediate-2 and high-risk myelodysplastic syndromes (MDS) (20). In another study, low-dose cytarabine treatment was associated with an 18% complete remission rate in patients with AML and high-risk MDS considered to be ineligible for intensive chemotherapy (18, 21).

In summary, this Phase I study showed that clofarabine monotherapy is well tolerated and has preliminary, promising activity in Japanese elderly patients with newly diagnosed AML and adult patients with relapsed/refractory disease. Further clinical study in a larger group of patients is warranted.

Acknowledgements

We are very grateful to the patients and their families who participated in this study. We thank the following colleagues for their contributions to this study: Ryuzo Ohno, MD (medical expert); Shuichi Miyawaki, MD (coordinating investigator), Tomoki Naoe, MD (Safety Data Monitoring Committee), and Keizo Horibe, MD (Safety Data Monitoring Committee). We also thank Monica Nicosia, PhD, and Angela Partisano, PharmD, for assistance in preparing and editing the manuscript.

Funding

This work was supported by Genzyme Corporation (now Sanofi), Cambridge, MA, USA.

Conflict of interest statement

Yasuhiro Tabata is an employee of Genzyme Corporation (now Sanofi).

References

1. Tallman MS, Gilliland DG, Rowe JM. Drug therapy for acute myeloid leukemia. *Blood* 2005;106:1154–63.
2. Yanada M, Naoe T. Acute myeloid leukemia in older adults. *Int J Hematol* 2012;96:186–93.
3. Roboz GJ. Novel approaches to the treatment of acute myeloid leukemia. *Hematol Am Soc Hematol Educ Program* 2011;2011:43–50.
4. Walter RB, Kantarjian HM, Huang X, et al. Effect of complete remission and responses less than complete remission on survival in acute myeloid leukemia: a combined Eastern Cooperative Oncology Group, Southwest Oncology Group, and MD Anderson Cancer Center Study. *J Clin Oncol* 2010;28:1766–71.
5. Burnett A, Wetzler M, Lowenberg B. Therapeutic advances in acute myeloid leukemia. *J Clin Oncol* 2011;29:487–94.
6. Oran B, Weisdorf DG. Survival for older patients with AML: a population based study. *Haematologica* 2012;97:1916–24.
7. National Comprehensive Cancer Network: NCCN Clinical Practice Guidelines in Oncology: Acute myeloid leukemia V.2. 2012. http://www.nccn.org/professionals/physician_gls/f_guidelines.asp (24 July 2012, date last accessed).
8. Montgomery JA, Shortnacy-Fowler AT, Clayton SD, Riordan JM, Secrist JA, III. Synthesis and biologic activity of 2′-fluoro-2-halo derivatives of 9-beta-D-arabinofuranosyladenine. *J Med Chem* 1992;35:397–401.
9. Tran H, Yang D. Clofarabine in the treatment of newly diagnosed acute myeloid leukemia in older adults. *Ann Pharmacother* 2012;46:89–96.
10. Kantarjian HM, Erba HP, Claxton D, et al. Phase II study of clofarabine monotherapy in previously untreated older adults with acute myeloid leukemia and unfavorable prognostic factors. *J Clin Oncol* 2010;28:549–55.
11. Burnett AK, Russell NH, Kell J, et al. European development of clofarabine as treatment for older patients with acute myeloid leukemia considered unsuitable for intensive chemotherapy. *J Clin Oncol* 2010;28:2389–95.
12. Vardiman JW, Thiele J, Arber DA, et al. The 2008 revision of the World Health Organization (WHO) classification of myeloid neoplasms and acute leukemia: rationale and important changes. *Blood* 2009;114:937–51.
13. Kantarjian HM, Gandhi V, Kozuch P, et al. Phase I clinical and pharmacology study of clofarabine in patients with solid and hematologic cancers. *J Clin Oncol* 2003;21:1167–73.
14. Cheson BD, Bennett JM, Kopecky KJ, et al. Revised recommendations of the International Working Group for Diagnosis, Standardization of Response Criteria, Treatment Outcomes, and Reporting Standards for Therapeutic Trials in acute myeloid leukemia. *J Clin Oncol* 2003;21:4642–9.
15. Jeha S, Gandhi V, Chan KW, et al. Clofarabine, a novel nucleoside analog, is active in pediatric patients with advanced leukemia. *Blood* 2004;103:784–9.
16. National Comprehensive Cancer Network: NCCN Guidelines Version 1. 2012. Prevention and Treatment of Cancer-Related Infections. http://www.nccn.org/professionals/physician_gls/f_guidelines.asp#infections. (12 November 2012, date last accessed).
17. Kantarjian HM, Thomas XG, Dmoszynska A, et al. Multicenter, randomized, open-label, phase III trial of decitabine versus patient choice, with physician advice, of either supportive care or low-dose cytarabine for the treatment of older patients with newly diagnosed acute myeloid leukemia. *J Clin Oncol* 2012;30:2670–7.
18. Lubbert M, Ruter BH, Claus R, et al. A multicenter phase II trial of decitabine as first-line treatment for older patients with acute myeloid leukemia judged unfit for induction chemotherapy. *Haematologica* 2012;97:393–401.
19. Fenaux P, Mufti GJ, Hellstrom-Lindberg E, et al. Azacitidine prolongs overall survival compared with conventional care regimens in elderly patients with low bone marrow blast count acute myeloid leukemia. *J Clin Oncol* 2010;28:562–9.
20. Fenaux P, Mufti GJ, Hellstrom-Lindberg E, et al. Efficacy of azacitidine compared with that of conventional care regimens in the treatment of higher-risk myelodysplastic syndromes: a randomised, open-label, phase III study. *Lancet Oncol* 2009;10:223–32.
21. Burnett AK, Milligan D, Prentice AG, et al. A comparison of low-dose cytarabine and hydroxyurea with or without all-trans retinoic acid for acute myeloid leukemia and high-risk myelodysplastic syndrome in patients not considered fit for intensive treatment. *Cancer* 2007;109:1114–24.

3、乳がん骨転移巣でのニッチ環境の解析および新規ワクチン療法の開発

分担研究者　乳腺内分泌外科　徳田裕
分子生命科学　亀谷美恵
研究協力者　乳腺内分泌外科　津田万里、宮本あすか

【研究の背景と目的】

乳癌は早期発見による完治の可能性が高い癌ではあるが、再発や転移したものを完治させることは今の治療法では困難である。再発腫瘍および骨転移腫瘍において HER2 蛋白の発現を解析すると原発腫瘍と再発および転移腫瘍でその発現が変化していることをわれわれは報告した。すなわち、腫瘍の進展に従ってその性格が分子レベルで変化することを示した。また乳癌で血中循環がん細胞：Circulating tumor cell（CTC），骨髄中に disseminated tumor cell（DTC）の出現している症例では予後が悪くなる傾向があるという報告がされているが,CTC や DTC が出現している症例すべてに転移を起こす訳ではない。従って、乳がん幹細胞と骨髄内ニッチの相互作用が骨転移巣形成のために重要であり、これを標的とする新規治療法の開発は患者生命予後と QOL を改善するために重要な課題である。

本研究の目的は、HER2 陽性乳癌患者の免疫系に関する解析を進め、がん幹細胞が転移、生着、増殖するために必要な免疫学的環境を調べ、標的となる細胞を同定することでワクチン療法を中心とした新規治療法の開発を促すことである。将来的には患者のテーラーメイド医療へのトランスレーションを目指した。

【研究方法と成果】

（1）　乳癌患者の HLA タイピングを行うと同時に in vitro でペプチド刺激を行い、IL-2 産生能、細胞増殖能、活性化抗原の発現を指標に HLA とペプチドの有効性を解析し、効果の得られる HLA を同定した。

（2）　実験動物中央研究所より提供されたヒト IL-4 産生重度免疫不全マウスである hIL4TgNOG マウスに様々な乳癌患者の末梢血単核球を移植し、申請者等が以前マウスで抗腫瘍効果を認めた HER2 の部分ペプチドである CH401MAP ペプチドをアジュバントと共に投与した。このマウス末梢血の上清について抗腫瘍効果の評価を行ったところ、健常者と比較して特異抗体産生能が低いことが示された。ペプチドに対する HLA 親和性をアルゴリズムで算出し、抗体産生能と比較したが、強い相関は観察されなかった。また、HER2/neu 抗原が発現していなくても HER2 抗体の産生が観察された。

（3）　乳癌における新規 Her2 ペプチドワクチン CH401MAP の患者末梢血における反応性を明らかにした(Tsuda et al. 2012)。CH401MAP が、大部分の日本人 HLA に提示されるモチーフを持つ事、末梢血を刺激する事によりリンパ球の反応性が得られる事が明らかになった。

【考察】

これらの結果より、改良NOGマウスであるNOG-IL-4-Tgマウスを用いて、ヒト免疫系をある程度再構築できること、また、これらのマウスを用いて、新規HER2ペプチドワクチン候補であるCH401MAPに対する乳がん患者の抗体産生能を評価することができることが明らかになった。この系を用いて、検体のHLAと抗体産生能について比較解析を行ったが、今まで汎用されてきたアルゴリズムと抗体産生能は必ずしも一致せず、アルゴリズムによるペプチド提示能予測は必ずしも抗体産生能の予測とはならないことが明らかとなった。しかし、我々が開発したヒト化マウスの系は、アルゴリズムを用いることなく抗体産生能を評価できるため、乳がん患者のHER2ペプチド反応生という免疫環境評価を可能とする優れた系であると考えられた。

Veterinary Immunology and Immunopathology 148 (2012) 252–259

Contents lists available at SciVerse ScienceDirect

Veterinary Immunology and Immunopathology

journal homepage: www.elsevier.com/locate/vetimm

Research paper

Porcine *MHC* classical class I genes are coordinately expressed in superantigen-activated mononuclear cells

Yoshie Kametani[a], Shino Ohshima[a,b], Yuki F. Kita[b], Shin Shimada[a], Hiroshi Kamiguchi[c], Takashi Shiina[b], Hidetoshi Inoko[b], Jerzy K. Kulski[b,d], Asako Ando[b,*]

[a] *Department of Immunology, Division of Basic Medical Science and Molecular Medicine, Tokai University School of Medicine, 143 Shimokasuya, Isehara, Kanagawa 259-1143, Japan*
[b] *Department of Molecular Life Science, Division of Basic Medical Science and Molecular Medicine, Tokai University School of Medicine, 143 Shimokasuya, Isehara, Kanagawa 259-1143, Japan*
[c] *Education and Research Support Center, Tokai University School of Medicine, 143 Shimokasuya, Isehara, Kanagawa 259-1143, Japan*
[d] *Centre for Forensic Science, The University of Western Australia, Nedlands, WA 6008, Australia*

ARTICLE INFO

Article history:
Received 7 October 2011
Received in revised form 18 April 2012
Accepted 2 May 2012

Keywords:
Swine
MHC
Expression
Superantigen
IRF-1

ABSTRACT

The expression of the major histocompatibility complex (MHC) classical class I genes is important for the adaptive immune response to target virus-infected cells and cancer cells. The up-regulation of the MHC is achieved by hormonal/cytokine signals including IFN-γ-inducible elements. The swine leukocyte antigen (SLA), the *MHC* class I region of pigs, consists of the duplicated classical class I genes, *SLA-1*, *SLA-2* and *SLA-3*, but the molecular mechanisms involved in their up-regulation after T cell stimulation have not been fully elucidated. In order to better understand some of the putative regulatory mechanisms of *SLA* class I gene expression in activated T cells, we examined the coordinated expression of the *SLA* classical class I, *IFN-γ* and interferon regulatory factor-1 (*IRF-1*) genes in the peripheral blood mononuclear cells (PBMCs) of *SLA* homozygous Clawn miniature swine stimulated for 72 h with either IFN-γ or an enterotoxin produced by *Staphylococcus aureus*. This enterotoxin, toxic shock syndrome-1 (TSST-1), is known to act as a superantigen (sAG) to activate the T cells in various vertebrate species. We showed by using mAbs and flow cytometry that the $CD4^+CD25^+$ cell number of swine PBMCs was also increased by TSST-1 and to a lesser degree by IFN-γ. Time course analyses of the expression of the *IFN-γ*, *IRF-1* and the three classical class I genes, *SLA-1*, *SLA-2*, and *SLA-3*, in PBMCs by quantitative real-time PCR revealed a transitory response to TSST-1 or IFN-γ stimulation. The *IFN-γ* mRNA levels in the PBMCs were continuously up-regulated over the first 48 h by TSST-1 or IFN-γ. In contrast, SLA class I expression moderately increased at 24 h and then decreased to a baseline level or less at 72 h of IFN-γ or TSST-1 stimulation. The three classical *SLA* class I genes showed similar expression kinetics, although *SLA-3* mRNA level was consistently lower than those of *SLA-1* and *-2*. The expression of *IRF-1*, a modulator of *SLA* expression, showed similar kinetics to those of the three classical *SLA* class I genes. The expression profiles detected by flow cytometry of the SLA molecules on the cell surface of PBMCs were maintained at a consistently high level during cell stimulation with either TSST-1 or IFN-γ, which was distinct from the kinetics of mRNA expression.

Abbreviations: FCS, fetal calf serum; FITC, fluorescein isothiocyanate; GAPDH, glyceraldehydes 3-phosphate dehydrogenase; Ig, immunoglobulin; Io, ionomycin; IRF-1, interferon regulatory factor-1; ISRE, interferon-stimulated response element; MFI, mean fluorescence intensity; MHC, major histocompatibility complex; PBMC, peripheral blood mononuclear cell; PBSA, bovine serum albumin-containing phosphate-buffered saline; PE, phycoerythrin; PMA, Phorbol 12-myristate13-acetate; SLA, swine leukocyte antigen; sAG, superantigen; TCR, T cell receptor; Th, helper T cell; TSST-1, toxic shock syndrome-1.

* Corresponding author. Tel.: +81 463 93 1121x2653; fax: +81 463 94 8884.
E-mail address: aando@is.icc.u-tokai.ac.jp (A. Ando).

0165-2427/$ – see front matter
http://dx.doi.org/10.1016/j.vetimm.2012.05.005

These results showed that miniature swine *SLA* class I mRNA expression was effectively and equally up-regulated among the three loci and coordinately with *IRF-1* gene expression after stimulation of T cell activation by sAG or IFN-γ.

1. Introduction

Major histocompatibility complex (MHC) molecules present pathogen or host protein-derived epitopes to T cell receptors (TCRs) and play an important role in inducing the antigen-specific immune response. The gene organization of the *MHC* region including the *MHC* class I genes is well characterized in various animals and at least three distinct class I gene duplication blocks, designated as alpha, beta and kappa blocks, are a common occurrence in the *MHC* class I regions of most mammals (Kulski et al., 2002). Examination of the entire sequence of the porcine *MHC* (swine leukocyte antigen, *SLA*) region of a Large White pig with an Hp-1a.1 haplotype that *SLA* class I genes also grouped into at least two separate genomic locations corresponding to the beta and kappa blocks. The beta block contains five non-classical *SLA* class I genes, *SLA-6*, *SLA*-7, and *SLA-8*, *MIC-1*, and *MIC-2* and the kappa block contains seven classical *SLA* class I genes, *SLA-1*, *SLA-2*, *SLA-3*, *SLA-4*, *SLA-5*, *SLA-9* and *SLA-11*. Of the seven classical *SLA* class I genes, *SLA-1*, *SLA-2*, and *SLA-3* are the constitutively expressed, whereas *SLA-4*, *SLA-9* and *SLA-11* are classified as pseudogenes (Smith et al., 2005). While there is no structural evidence that *SLA-5* is a pseudogene, no transcript for this gene has yet been identified (Ando and Chardon, 2006; Lunney et al., 2009; Renard et al., 2001, 2006). Recently, additional six and four expressible *SLA* class I loci were identified in the Hp-28.0 and Hp-62.0 haplotypes, respectively (Tanaka-Matsuda et al., 2009) and other studies have suggested that the number of expressed class I loci may vary among haplotypes (Ho et al., 2006; Lee et al., 2005; Smith et al., 2005; Soe et al., 2008).

The inbred miniature swine with defined *SLA* haplotypes is an useful experimental animal model in allo- and xeno-transplantation studies and also for association analyses between *SLA* haplotypes and immunological or physiological traits (Duran-Struuck et al., 2010; Mallard et al., 1989, 1991; Vallabhajosyula et al., 2007). We previously assigned two *SLA* class I haplotypes, Hp-16.0 (*SLA-1*0401*, *SLA-2*w09an02* and *SLA-3*0602*) and Hp-17.0 (*SLA-1 blank* (not assigned), *SLA-2*06an03* and *SLA-3*03an02*) in Clawn miniature swine population by sequencing analyses of RT-PCR products using allele group specific primer pairs (Ando et al., 2005). Therefore, at least three and two classical *SLA* class I loci are expressed in Clawn miniature swine with Hp-16.0 and Hp-17.0, respectively. However, the regulatory molecular mechanisms for the expression of *SLA* class I genes have yet to be elucidated, although putative regulatory elements in the promoter regions of the loci have been identified (Tennant et al., 2007).

Since its discovery in 1965, the regulatory role of IFN-γ in the transcription, expression and functions of the classical *MHC* class I genes has been extensively investigated and recently reviewed (Zhou, 2009). It was confirmed that IFN-γ induces the expression of the interferon regulatory factor-1 (*IRF-1*) that binds to the IRF-1-binding cis-element motif, called the interferon-stimulated response element (*ISRE*) in the *MHC* class I promoter region, resulting in the augmentation of class I *MHC* expression (Gobin et al., 1999). In swine, the putative IRF-binding motifs were identified on the proximal domain of the promoter regions in the three constitutively expressed classical class I genes, *SLA-1*, *SLA-2*, and *SLA-3*, suggesting a similar recruitment of regulatory elements in the promoter regions as seen in the *MHC* class I genes of human and mouse (Liu et al., 2011).

Bacterial superantigens (sAg) bind directly to MHC class II molecules and the specific Vβ domain of TCR on T cells independent of the presented peptide antigen (Fraser and Proft, 2008). Administration of sAg induces polyclonal T cell activation resulting in the secretion of a large amount of cytokines and a significant increase in T cell proliferation (Fraser and Proft, 2008; Sriskandan and Altmann, 2008; Sundberg et al., 2007). After intensive activation and proliferation, the T cells stop interleukin-2 production and proliferation, inducing cell death or T cell unresponsiveness to specific antigens. The enterotoxin, toxic shock syndrome-1 (TSST-1), is a sAG secreted by *Staphylococcus aureus* that can induce the overproduction of IFN-γ (Sriskandan and Altmann, 2008) and may enhance the expression of MHC. However, the up-regulation of *MHC* class I gene expression by this sAG, especially with respect to the *SLA* classical class I genes, has not been previously investigated.

The purpose of the present study was to examine whether T cell activation by sAG stimulation effectively up-regulates coordinated *SLA* class I gene expression at the protein and mRNA levels. In this study, we used *SLA* homozygous Clawn miniature swine with the haplotype Hp-16.16, (Ando et al., 2005), designed *SLA* class I allele-specific primer sets to amplify the three class I genes of the Hp-16.0 haplotype and compared transcription and protein expression levels among the loci in peripheral blood mononuclear cells (PBMCs) at different times after stimulation by either TSST-1 or IFN-γ for 72 h in cell culture. In addition, we analyzed the mRNA level of *IRF-1* to evaluate if this transcription factor for MHC expression is also involved in the regulation of SLA expression in PBMCs.

2. Materials and methods

2.1. Animal samples

SLA homozygous (Hp-16.0) Clawn miniature swine ($n = 6$, 11–30 months old) at the Japan Farm CLAWN Institute (Kagoshima, Japan) were bled in specific pathogen free conditions.

2.2. In vitro stimulation of PBMCs

Swine peripheral blood samples were collected into a heparinized tube and centrifuged on Lymphocepal (IBL Co.,

Fujioka, Japan) at 670 × *g* for 30 min. PBMCs were collected and washed with 10 ml of 1% (w/v) bovine serum albumin (BSA)-containing phosphate-buffered saline (PBSA). The blood mononuclear cells were collected by centrifuging at 350 × *g* for 5 min and the remaining erythrocytes were lysed osmotically. The white blood cells were washed and cultured (3×10^6/well) in RPMI1640 medium containing 10% fetal calf serum (FCS) in the presence of the toxic shock syndrome-1 (TSST-1) enterotoxin, (Toxin Tec., Sarasota, USA) at 1 μg/ml or IFN-γ (ITSI-Bioscience, PA, USA) at 1 ng/ml for 72 h at 37 °C 5% CO_2. After 24, 48 and 72 h the cells were collected, washed with PBSA and used for the analyses by flow cytometry and quantitative real-time PCR.

2.3. Flow cytometry

Swine PBMCs were re-suspended at a final concentration of 2×10^7 cells/ml in PBS containing 0.05% sodium azide (Wako, Tokyo, JPN). Ten microliter of three different primary monoclonal antibodies (mAb), (Fluorescein isothyanate (FITC)-conjugated anti-Porcine CD4a (clone number; 1974.12.4, Southern Biotech, Birmingham, AL), anti-class I major histocompatibility antigen (clone number; PT85A, Southern Biotech) and anti-pig CD25 (clone number; K231.3B2, AbD serotec, Kidington, UK)) were added to 50 μl of the cells at a final concentration between 1 and 5 μg/ml. For each mAb the concentration giving maximum labeling intensity without detectable background staining was determined in titration experiments. Cells were incubated at 4 °C for 15 min and then washed by adding 1 ml of PBSA/0.05% sodium azide. Fluorochrome-conjugated goat anti-mouse immunoglobulin (Ig) isotype-specific secondary antibodies were used at a final concentration of 1 μg/ml and cells incubated in the dark for 15 min at 4 °C. Anti-mouse IgG2a (L-MG2a-7, AbD serotec, Kidlington, UK) was added for anti-class I MHC mAb and anti-mouse IgG1-R-PE (Southern Biotech, AL, USA) was used for anti-pig CD25mAb. Cells were then washed with 1 ml of PBSA/0.05% sodium azide and were stored at 4 °C in the dark up to 1 h until analyzed with a FacsCalibur (Becton-Dickinson, Franklin Lakes, NJ) using CellQuest acquisition and analysis software (version 3.3, Becton-Dickinson). A minimum of 30,000 events was captured for each sample with data collected in the list-mode. Cells were gated to include only those that fell within 200–700 forward scatter and 50–900 side scatter. Compensation was FL1–0.9% FL2, FL2–33% FL1. FL1 used a 488 nm laser with a 530 nm filter to detect FITC and FL2 used a 488 nm laser with a 585 nm filter to detect phycoerythrin (PE). FL4 used a 635 nm laser with a 661 nm filter to detect allophycocyanin. The degree of cell membrane SLA class I expression was expressed as mean fluorescence intensity (MFI).

2.4. RNA extraction and quantitative real-time polymerase chain reaction

RNA was extracted from PBMCs using RNeasy Mini Kit (Qiagen, Germantown, MD) or Trizol (Invitrogen, Carlsbad, USA) according to manufacturer's instruction. Total RNA concentration was determined by measuring absorbance at 260 nm and 280 nm. The purity was estimated by the relative absorbance 260 nm/280 nm. Integrity was assayed by agarose gel electrophoresis. The purity and integrity of the RNA was more than 95%. cDNA was synthesized from the total RNA (2 μg) using High Capacity cDNA Reverse Transcription Kit (Life Technologies, CA).

Three previously published class I allele specific primer sets for the classical *SLA* class I genes, *SLA-2* (Kita et al., 2012), *SLA-1* and *SLA-3*, of the Hp-16.0 haplotype (Ando et al., 2005) were used for following the time course of gene expression levels in PBMCs of Clawn miniature swine by real-time PCR (Table 1). Another three sets of specific primers were designed to amplify porcine *IFN-γ*, *IRF-1* and the housekeeping gene glyceraldehydes 3-phosphate dehydrogenase (*GAPDH*) mRNA (Table 1). The *GAPDH* specific primer set was used as an internal control for the other five genes. Expression levels of the three classical *SLA* class I alleles, *IFN-γ*, *IRF-1* and *GAPDH* were measured by real-time PCR using an ABI PRISM 7500 Fast Sequence Detector System (Life Technologies, CA). The synthesized cDNAs were used as templates and were amplified using the allele specific primer sets for *IFN-γ*, *IRF-1* and *GAPDH*. cDNA was serially diluted and 3 μl of each dilution was amplified by real-time PCR using 0.5 μM of each gene-specific primer and Fast SYBR® Green Master Mix (Life Technologies, CA) in the 10 μl amplification reaction volume. The cycling parameters were as follows: 40 cycles of 98 °C/10 s, and 62 °C/30 s. Melting curve analysis showed that there was no primer dimer formation. The relative quantitative values were calculated by the comparative *C*(*T*) method (Livak and Schmittgen, 2001; Schmittgen and Livak, 2008). A plot of log cDNA concentration ratio *versus* threshold cycle (Ct) value gives an absolute value of the slope. The range of 100% ± 5% PCR efficiency was confirmed by the slope of the plot. To normalize relative cDNA amount of each gene, ΔCt value was calculated by [(target gene Ct) − (control gene Ct)]. The mean fold change in expression ratio of the target gene at each time point was calculated by $2-\Delta\Delta$Ct value that was calculated by [(target gene Ct) − (control gene Ct)] time × −[(target gene Ct) − (control gene Ct)] time 0. After stimulation with IFN-γ or TSST-1, the relative fold changes of the mRNA levels of the *SLA* class I genes, *IFN-γ* and *IRF-1* were compared with the mRNA level of the *GAPDH* gene. PBS was added to cells as a control stimulant instead of IFN-γ or TSST-1 at the same volume.

2.5. Statistical analysis

Results were presented as mean ± SE. Data from lymphocytes activation assay and real-time PCR were analyzed by Student's *t*-test to determine the significance of the treatment. In all statistical analyses a *P* value of <0.05 was considered significant.

3. Results

3.1. Activation of T cells by IFN-γ or TSST-1 and enhancement of IFN-γ gene expression

To define which cell types would respond to stimulation with IFN-γ and TSST-1 and to determine how many

Table 1
Primers for real time PCR.

Locus	Primer name	Primer sequence (5′–3′)	Annealing temp. (°C)	Product size (bp)
GAPDH	GAPDH-F1 GAPDH-R1	GGACCTGACCTGCCGTCTG TCCACCACCCTGTTGCTGTA	57	249
IFN-γ	IFN-γ-4F IFN-γ-4R	GCTCTGGGAAACTGAATGACTT TATTGCAGGCAGGATGACAA	53	199
SLA-1	SLA-1-PD1-1 SLA-1-PD1-2R	ACTCTCGCTTCATCGCCGTC CCCACTCCGTAAGTCTGTGC	60	175
SLA-2	SLA-2-w09ex3F1 SLA-2-w09ex3R1	ATCCAGAGCATGTTTGGCTG TGCAGGTAGCTCCTCCAGTG	62	200
SLA-3	SLA-3-031F SLA-3-032R	GGAAGCCCCGTTTCACCTC TCAGGTTCACTCGGAAAGTC	60	183
IRF-1	21 1114–1134 59 52 18 1161–1178 60 61	GATCTGAAGAAGAACGTGGACACC ATGGAGGGCAGCCTGACT	50	65

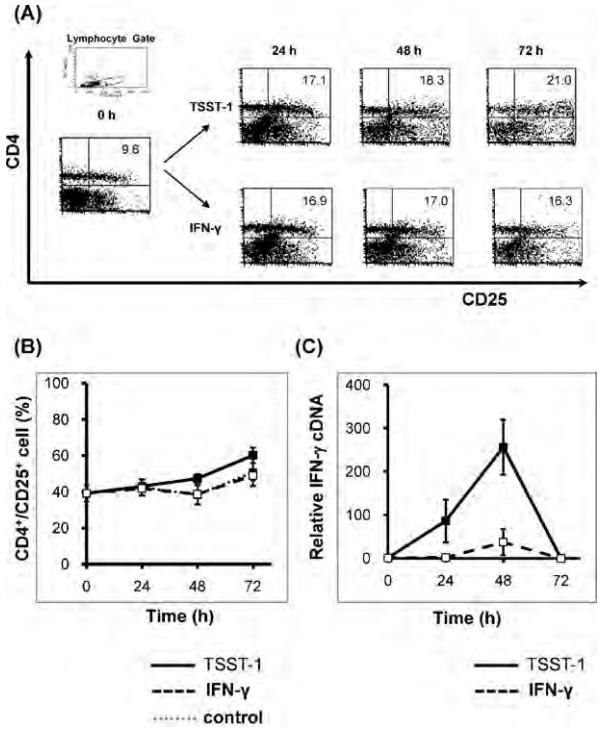

Fig. 1. Induction of IFN-γ expression in swine PBMC. Freshly prepared swine PBMCs were stimulated with TSST-1 or IFN-γ, and processed for staining with anti-CD4 and anti-CD25 mAb and analyzed by FACS. Representative FACS profiles are shown in (A). Mean % values of activated $CD4^+CD25^+$ Th cells from 0 to 72 h is shown in (B). Total RNA of PBMC was used for quantification of *IFN-γ* cDNA by real-time PCR (C). Data are shown as relative cDNA amount against *GAPDH* from 6 independent experiments and graphs show the mean ± SE ($n = 6$).

activated cells would be observed, PBMC of three Clawn miniature swine were cultured in the presence of TSST-1 or IFN-γ. After the stimulation, CD25 and CD4 expression of lymphocytes was analyzed by flow cytometry (Fig. 1(A)). Before the stimulation the $CD4^+CD25^+$ cells taken from the Clawn miniature swine peripheral blood occupied about 10% of lymphoid gated cells, which is higher than that found in mouse or human (Baecher-Allan et al., 2001; Wing et al., 2005). However, the level was similar to the swine $CD4^+CD25$dim cell subsets reported by Kaser et al. (2008). After 24 and 48 h of culture with IFN-γ in comparison with medium alone, the percentage of $CD4^+CD25^+$ cells in PBMCs was almost the same as that observed in the medium alone. In contrast, after 48 and 72 h of culture with TSST-1, the percentage of $CD4^+CD25^+$ cells in PBMCs increased relative to control (PBS). The percentage of $CD4^+CD25^+$ cells at 72 h of culture with TSST-1 stimulation was significantly higher than that at 72 h of IFN-γ stimulation (Fig. 1(B)). As CD25 is a marker of activated T cells and regulatory T cells, we cannot distinguish between the two subsets of T cells. However, since TSST-1 stimulation induced cell proliferation, this indicates that most of the increased cells were activated T cells.

We quantified *IFN-γ* cDNA by real-time PCR using the total RNA extracted from PBMCs and found that the quantitative level of the expressed *IFN-γ* gene in PBMCs stimulated with TSST-1 was significantly higher than that with PBS (Fig. 1(C)). Stimulation with IFN-γ also induced *IFN-γ* mRNA augmentation, although the quantitative level of the expressed *IFN-γ* gene in PBMCs stimulated with IFN-γ was lower than that with TSST-1 (0–1.8 for TSST-1 and 0–0.5 for IFN-γ). The highest *IFN-γ* cDNA level was observed by 48 h of stimulation with TSST-1. Furthermore, both of the relative cDNA levels in culture at 72 h of stimulation with TSST-1 or IFN-γ were decreased to 1.03 ± 0.47 (TSST-1) or 0.46 ± 0.33 (IFN-γ), respectively.

3.2. High level expression of SLA class I molecules on the surface of stimulated T cells

While TSST-1 and IFN-γ induced T cell activation, we quantified the SLA class I molecule expressed on the cell surface, by staining stimulated Clawn miniature swine PBMCs with a SLA class I-specific monoclonal antibody and analyzing with a flow cytometer. As shown in Fig. 2(A) and (B) constitutive levels of SLA class I protein expression on the PBMCs treated with either TSST-1- or IFN-γ continuously increased with time during the 72 h of cell culture. The MFI was (1545.21 ± 167.7) in TSST-1-treated cells, which was significantly higher than IFN-γ treated cells (1170 ± 180.8) (Fig. 2(A) and (B)). The cells with PBS

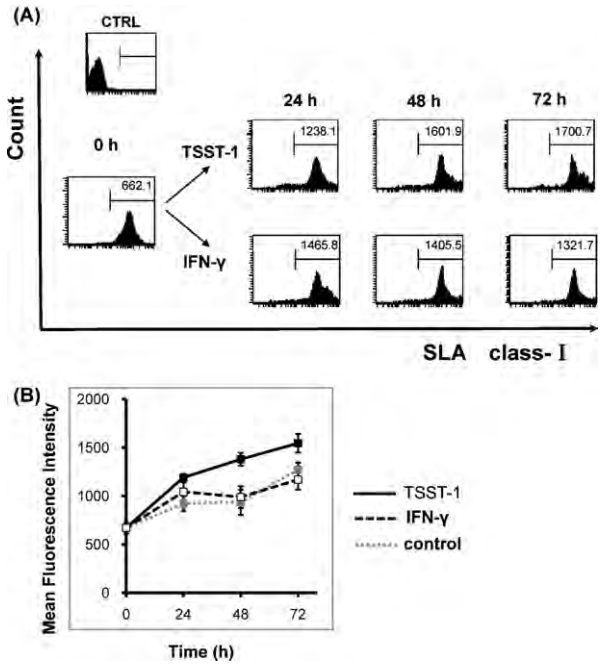

Fig. 2. Cell-surface expression of SLA class I molecules on stimulated swine PBMC. Swine PBMCs were stimulated with TSST-1 or IFN-γ, processed for staining with anti-class I Mab and analyzed by FACS. Representative FACS profiles are shown in (A). The mean fluorescence intensity values of cell surface expression of SLA class I molecules from 0 to 72 h is shown in (B). Data are shown as the mean fluorescein intensity (MFI) from 6 independent experiments and graphs show the mean ± SE ($n = 6$).

treatment showed the same kinetics of SLA class 1 expression as that with IFN-γ treatment.

3.3. Transient increase in the mRNA expression levels among SLA class I loci after stimulation of T cells

To define the locus-specific gene expression of *SLA* class I mRNA in Clawn miniature swine PBMCs, we analyzed the quantitative levels of mRNA expressed by the classical *SLA* class I genes (*SLA-1*, *SLA-2* and *SLA-3*) using three allele specific PCR primer sets and total RNA extracted from the PBMCs serially at 0, 24, 48 and 72 h of stimulation. As shown in Fig. 3(A–C), maximal fold changes when compared to the mRNA expression of the *GAPDH* gene were obtained from all three *SLA* class I genes loci, *SLA-1*, *SLA-2* and *SLA-3*, in PBMCs after 24 h of stimulation with either TSST-1 or IFN-γ, although the levels in TSST-1-stimulated cells were not significantly different ($P > 0.05$) than in the control culture treated with PBS. After 24 h the mRNA expression levels decreased gradually by 48 and 72 h of stimulation, showing no variation among the class I loci in the kinetics of expression. The mRNA expression levels in TSST-1-stimulated cells were lower than those in IFN-γ-stimulated cells throughout the culture periods. Notably, the expression levels stimulated with TSST-1 were lower than in the control cultures at 48 h and 72 h after stimulation (Fig. 3(A–C)). The mRNA level was also increased in control culture at 24 h, although the level was slightly lower than culture cells stimulated with TSST-1, except for the expression of *SLA-1* (24 h TSST-1, in which the level was nearly equal between control and stimulated cells). There was no significant difference between mRNA expression levels of *SLA-1* and *SLA-2*, whereas the *SLA-3* expression levels were consistently lower than those of the other two loci.

3.4. Parallel SLA class I and IRF-1 gene expression at the mRNA level

IRF-1 is a transcription factor expressed abundantly in the lymphoid organ (Liu et al., 2011). It binds to the *ISRE* in the promoter regions of *HLA* related genes to directly enhance MHC class I expression or to enhance *HLA*-related gene expression after IFN-γ stimulation (Zhou, 2009). Thus, we examined whether *IRF-1* gene expression is affected by IFN-γ and TSST-1 stimulation in Clawn miniature swine PBMCs. Quantitative RT-PCR was used to determine *IRF-1* mRNA levels and showed an increase during the first 24 h of stimulation and then a decrease at 48 h of stimulation with TSST-1. The expression profile was similar to that of the three *SLA* classical class I genes at 48 h of stimulation when the mRNA expression level of *IRF-1* decreased in the TSST-1-stimulated cells, although the mRNA expression level was still enhanced in IFN-γ-stimulated cells (Fig. 3(D)).

4. Discussion

sAG stimulation can cause a cytokine storm and immuno-suppression in effected human subjects (Sriskandan and Altmann, 2008). In experimental animals, the symptoms of immunosuppression is not always as clear as in humans, but the levels of various cytokines including IFN-γ increase, and T cell anergy can be induced by immunosuprressive agents (Lavoie et al., 1999). The up-regulation of *MHC* class I genes by sAG stimulation has not been previously reported. In order to mimic "the natural inflammatory condition", we used the sAG enterotoxin TSST-1 to stimulate a T-cell response of swine PBMCs *in vitro*. We first verified that TSST-1 stimulation enhanced *IFN-γ* mRNA expression of swine PBMC, followed by expression of the activation marker CD25. The expression level was higher in the TSST-1 stimulated cells than in the cells stimulated with recombinant swine IFN-γ (Fig. 1). Moreover, IFN-γ-stimulated PBMCs also enhanced *IFN-γ* gene expression. The IFN-γ receptor is expressed on naïve T cells and a B cell subset in response to IFN-γ and consequently IFN-γ is expressed in an autocrine manner (Girdlestone and Wing, 1996; Harris et al., 2005). As IFN-γ is a helper T cell type 1 (Th1) skewing cytokine, the Th subset might be shifted toward Th1 (Bowen et al., 2008).

IFN-γ and SLA class I mRNA levels both decreased substantially after 48 h of stimulation with either TSST-1 or IFN-γ, whereas the surface class I molecule continued to increase as a whole for 72 h of stimulation with either TSST-1 or IFN-γ. These results indicate that while IFN-γ produced by sAG stimulation affects the augmentation of class I expression, the kinetics of class I expression on the surface might be affected posttranscriptionally by some other regulatory systems such as peptide digestion by proteasome or transport to the endoplasm (Gao et al., in press). For example, IFN-γ was shown to control *HLA-A* expression

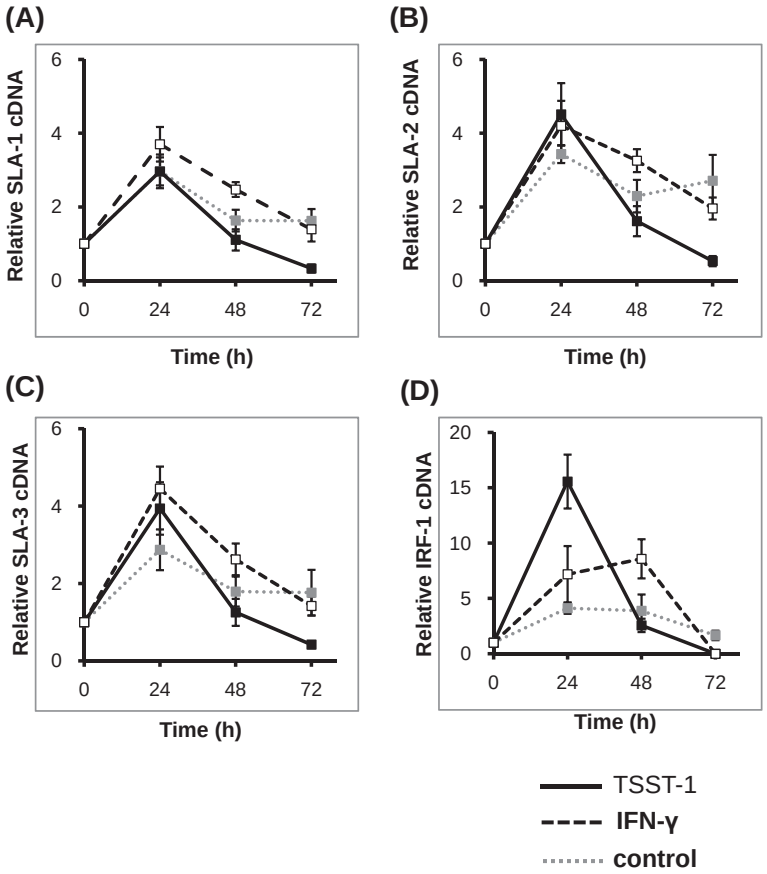

Fig. 3. Locus-specific expression of *SLA* class I and *IRF-1* genes in stimulated swine PBMC. Freshly prepared swine PBMCs were stimulated with TSST-1 or IFN-γ, and processed for quantification of *SLA-1* (A), *SLA-2* (B), *SLA-3* (C) and *IRF-1* (D) cDNA by real-time PCR. Data are shown as relative cDNA amount of stimulated cells/control culture cells against *GAPDH* from 5 independent experiments, and graphs show the mean ± SE ($n = 5$).

primarily at the posttranscriptional level through chromosome maintenance region 1-dependent nuclear RNA export (Browne et al., 2006).

There are few published studies on the coordinated regulation of the expression of the duplicated *SLA* classical class I genes to compare directly with our study. We found no major difference among the kinetics of the expression of three *SLA*-classical class I genes during either IFN-γ or TSST-1 stimulation, although the relative expression levels were approximately two to three times higher for *SLA-1* and *SLA-2* than for *SLA-3*. This result indicates that all three *SLA* loci possess the same regulatory system, which is not entirely compatible with the results of Tennant et al. (2007) who reported that the *SLA-1* promoter activity was 3 times or even higher than that of *SLA-2* in Max cells. However, we could not detect any substantial difference between the *SLA-1* and *SLA-2* cDNA levels by the detection method of real-time PCR. The discrepancy in cDNA levels and the promoter activities of *SLA-1* and *SLA-2* genes between the two studies might be attributable to differences in the cell types that were used in each study, where Tennant et al. (2007) used the established cell line Max, which are immortalized swine kidney cells with the *SLA* haplotype of Hp-4a.0, and we used freshly prepared PBMCs. In contrast, Gao et al. (in press), in a Tiling Alley analysis, reported that the mRNA expression of *SLA-1*, *SLA-2* and *SLA-3* decreased and the ability of antigen presentation was suppressed by Phorbol 12-myristate13-acetate (PMA) and Ionomycin (PMA/Io treatment for 24 h), suggesting different mechanisms of regulatory action between PMA/Io and either TSST-1 or IFN-γ. On the other hand, Browne et al. (2006) suggested that IFN-γ stimulation controls the *HLA* gene expression at the nuclear RNA export level. They defined that the nucleotide sequences in a 39-nt region in the *HLA-A* 3′-transcribed region are required for stimulation of *HLA-A* gene expression by IFN-γ. Similar regulation mechanism might exist in *SLA* class I gene expression.

In our results, sAG stimulation for 72 h caused a prolonged augmentation of the cell surface SLA proteins, while the enhancement of *SLA* mRNA expression was transient and the expression decreased after 24 h. Since the *IFN-γ* mRNA expression was enhanced for the first 48 h of sAG stimulation (Fig. 1(C)), the down-regulation of *SLA* mRNA might not depend on IFN-γ exhaustion. It was already reported that IRF-1 is induced by IFN-γ, binds to the *IRSE* region of the *SLA* promoter, and controls SLA expression (Liu et al., 2011; Tennant et al., 2007). In our results, *IRF-1* expression paralleled *SLA* class I mRNA expression. While the down regulation of *IRF-1* corresponded with the rapid down-regulation of the *SLA* gene expression after 24 h

of continuous TSST-1 stimulation, *IRF-1* was not down-regulated after 24 h in the presence of IFN-γ. The reason for this difference is not clear, but may be due in part to the many different regulatory molecules and pathways induced or suppressed by TSST-1 and IFN-γ, which in turn may effect *SLA* mRNA expression differently. On the other hand, the expression of SLA proteins on the cell surface might need other regulatory pathways such as peptide processing and presentation, which may affect the efficacy of SLA protein expression on the cell surface (Gao et al., in press). The reason why SLA mRNA was upregulated in control cells (PBS treatment) is not clear, but is probably due to the growth factors and interleukins present in 10% FCS as a medium supplement. For example, as previously reported, bovine serum albumin has some growth effect on primary culture (Rumley et al., 1984). Further comparative analyses concerning the antigen presenting ability of SLA and other molecules with sAG and IFN-γ stimulation might help to better clarify the regulatory pathway of antigen presentation and/or anergy induction.

In conclusion, we have shown that the sAG enterotoxin TSST-1 activated swine blood mononuclear cells and induced prolonged IFN-γ production and SLA class I protein expression. However, the *SLA* class I mRNA expression was transient and the level decreased after 48 h in the presence of the TSST-1 stimulant. The mRNA expression of three *SLA* class I loci was regulated coordinately along with the expression of the *IFN-γ* and *IRF-1* genes when cultured PBMCs were stimulated with TSST-1. In this regard, the freshly collected PBMCs from the inbred miniature swine with defined *SLA* haplotypes provided an useful experimental *in vitro* model for studying the regulatory factors and molecular mechanisms that are involved in the transcription, expression and functions of the classical *MHC* class I genes.

Conflict of interest statement

The authors declare that there is no conflict of interest.

Acknowledgments

We wish to thank Drs. Takehiro Iwanaga and Junichi Tottori (Japan Farm CLAWN Institute) for providing us with samples for Clawn miniature swine. The work was supported by Grant-in-Aid for Scientific Research (B) (22380172) from the Ministry of Education, Culture, Sports, Science and Technology of Japan (MEXT).

References

Ando, A., Chardon, P., 2006. Gene organization and polymorphism of the swine major histocompatibility complex. Animal Sci. J. 77, 127–137.

Ando, A., Ota, M., Sada, M., Katsuyama, Y., Goto, R., Shigenari, A., Kawata, H., Anzai, T., Iwanaga, T., Miyoshi, Y., Fujimura, N., Inoko, H., 2005. Rapid assignment of the swine major histocompatibility complex (SLA) class I and II genotypes in Clawn miniature swine using PCR-SSP and PCR-RFLP methods. Xenotransplantation 12, 121–126.

Baecher-Allan, C., Brown, J., Freeman, G., Hafler, D., 2001. $CD4^+CD25$high regulatory cells in human peripheral blood. J. Immunol. 167, 1245–1253.

Bowen, H., Kelly, A., Lee, T., Lavender, P., 2008. Control of cytokine gene transcription in Th1 and Th2 cells. Clin. Exp. Allergy 38, 1422–1431.

Browne, S., Roesser, J., Zhu, S., Ginder, G., 2006. Differential IFN-γ stimulation of HLA-A gene expression through CRM-1-dependent nuclear RNA export. J. Immunol. 177, 8612–8619.

Duran-Struuck, R., Cho, P.S., Teague, A.G.S., Fishman, B., Fishman, A.S., Hanekamp, J.S., Moran, S.G., Wikiel, k.J., Ferguson, K.K., Lo, D.P., Duggan, M., Arn, J.S., Billiter, B., Horner, B., Houser, S., Yeap, B.Y., Westmoreland, S.V., Spitzer, T.R., McMorrow, I.M., Sachs, D.H., Bronson, R.T., Huang, C.A., 2010. Myelogenous leukemia in adult inbred MHC defined miniature swine: a model for human myeloid leukemias. Vet. Immunol. Immunopathol. 135, 243–256.

Fraser, J., Proft, T., 2008. The bacterial superantigen and superantigen-like proteins. Immunol. Rev. 225, 226–243.

Gao, Y., Wahlberga, P., Martheya, S., DianeEsquerréa, D., Jaffrézic, F., Lecardonnela, J., Hugota, K., Rogel-Gaillarda, C. Analysis of porcine MHC using microarrays. Vet. Immunol. Immunopathol., http://dx.doi.org/10.1016/j.vetimm.2011.04.007, in press.

Girdlestone, J., Wing, M., 1996. Autocrine activation by interferon-gamma of STAT factors following T cell activation. Eur. J. Immunol. 26, 704–709.

Gobin, S., van Zutphen, M., Woltman, A., van den Elsen, P., 1999. Transactivation of classical and nonclassical HLA class I genes through the IFN-stimulated response element. J. Immunol. 163, 1428–1434.

Harris, D.P., Goodrich, S., Gerth, A.J., Peng, S.L., Lund, F.E., 2005. Regulation of IFN-gamma production by B effector 1 cells: essential roles for T-bet and the IFN-gamma receptor. J. Immunol. 174, 6781–6790.

Ho, C., Rochelle, E., Martens, G., Schook, L., Smith, D., 2006. Characterization of swine leukocyte antigen polymorphism by sequence-based and PCR-SSP methods in Meishan pigs. Immunogenetics 58, 873–882.

Kaser, T., Gerner, W., Hammer, S., Patzl, M., Saalmuller, A., 2008. Phenotypic and functional characterisation of porcine $CD4^+CD25^{high}$ regulatory T cells. Vet. Immunol. Immunopathol. 122, 153–158.

Kita, Y.F., Ando, A., Tanaka, K., Suzuki, S., Ozaki, Y., Uenishi, H., Inoko, H., Kulski, J.K., Shiina, T., 2012. Application of high-resolution, massively parallel pyrosequencing for estimation of haplotypes and gene expression levels of swine leukocyte antigen (SLA) class I genes. Immunogenetics 64, 187–199.

Kulski, J., Shiina, T., Anzai, T., Kohara, S., Inoko, H., 2002. Comparative genomic analysis of the MHC: the evolution of class I duplication blocks, diversity and complexity from shark to man. Immunol. Rev. 190, 95–122.

Lavoie, P., Thibodeau, J., Erard, F., Sekaly, R., 1999. Understanding the mechanism of action of bacterial superantigens from a decade of research. Immunol. Rev. 168, 257–269.

Lee, J., Simond, D., Hawthorne, W., Walters, S., AT, P., Smith, D., O'Connell, P., Moran, C., 2005. Characterization of the swine major histocompatibility complex alleles at eight loci in Westran pigs. Xenotransplantation 12, 303–307.

Liu, Y., Lu, X., Luo, Y.J.P., Zhou, J., Liu, X., Liu, J., Ding, X., Zhang, Q., 2011. Molecular characterization and association analysis of porcine interferon regulatory factor 1 gene. Mol. Biol. Rep. 38, 1901–1907.

Livak, K., Schmittgen, T., 2001. Analysis of relative gene expression data using real-time quantitative PCR and the $2(-\Delta\Delta C(T))$ method. Methods 25, 402–408.

Lunney, J., Ho, C., Wysocki, M., Smith, D., 2009. Molecular genetics of the swine major histocompatibility complex, the SLA complex. Dev. Comp. Immunol. 33, 362–374.

Mallard, B.A., Kennedy, B.W., Wilkie, B.N., 1991. The effect of swine leukocyte antigen haplotype on birth and weaning weights in miniature pigs and the role of statistical analysis in this estimation. J. Anim. Sci. 69, 559–564.

Mallard, B.A., Wilkie, B.N., Kennedy, B.W., 1989. Genetic and other effects on antibody and cell mediated immune response in swine leucocyte antigen (SLA)-defined miniature pigs. Anim. Genet. 20, 167–178.

Renard, C., Hart, b.E., Sehra, H.H., Beasley, H., Coggill, P., Howe, K., Harrow, J., Gilbert, J., Sims, S., Rogers, J., Ando, A., Shigenari, A.T., Shiina, T., Inoko, H., Chardon, P., Beck, S., 2006. The genomic sequence and analysis of the swine major histocompatibility complex. Genomics 88, 96–110.

Renard, C., Vaiman, M., Chiannilkulchai, N., Cattolico, L., Robert, C., Patrick Chardon, P., 2001. Sequence of the pig major histocompatibility region containing the classical class I genes. Immunogenetics 53, 490–500.

Rumley, R.L., Chapman, S.W., Hoover, M.L., Cuchens, M.A., 1984. Effects of different protein supplements on mitogen responses of human peripheral blood lymphocytes. J. Immunol. Methods 75, 339–349.

Schmittgen, T., Livak, K., 2008. Analyzing real-time PCR data by the comparative C(T) method. Nat. Protoc. 3, 1101–1108.

Smith, D., Lunney, J., Martens, G., Ando, A., Lee, J., Ho, C., Schook, L., Renard, C., Chardon, P., 2005. Nomenclature for factors of the SLA class-I system 2004. Tissue Antigens 65, 136–149.

Soe, O., Ohba, Y., Imaeda, N., Nishii, N., Takasu, M., Yoshioka, G., Kawata, H., Shigenari, A., Uenishi, H., Inoko, H., Ando, A., Kitagawa, H., 2008. Assignment of the SLA alleles and reproductive potential of selective breeding Duroc pig lines. Xenotransplantation 15, 390–397.

Sriskandan, S., Altmann, D., 2008. The immunology of sepsis. J. Pathol. 214, 211–223.

Sundberg, E., Deng, L., Mariuzza, R., 2007. TCR recognition of peptide/MHC class II complexes and superantigens. Semin. Immunol. 19, 262–271.

Tanaka-Matsuda, M., Ando, A., Claire Rogel-Gaillard, C., Chardon, P., Uenishi, H., 2009. Difference in number of loci of swine leukocyte antigen classical class I genes among haplotypes. Genomics 93, 261–273.

Tennant, L., Renard, C., Chardon, P., Powell, P., 2007. Regulation of porcine classical and nonclassical MHC class I expression. Immunogenetics 59, 377–389.

Vallabhajosyula, P., Griesemer, A., Yamada, K., Sachs, D.H., 2007. Vascularized composite islet-kidney transplantation in a miniature swine model. Cell Biochem. Biophys. 48, 201–207.

Wing, K., Suri-Payer, E., Rudin, A., 2005. $CD4^+CD25^+$-regulatory T cells from mouse to man. Scand. J. Immunol. 62, 1–15.

Zhou, F., 2009. Molecular mechanisms of IFN-gamma to up-regulate MHC class I antigen processing and presentation. Int. Rev. Immunol. 28, 239–260.

OPEN ACCESS Freely available online

PLOS ONE

Immune-Related Gene Expression Profile in Laboratory Common Marmosets Assessed by an Accurate Quantitative Real-Time PCR Using Selected Reference Genes

Yoshiki Fujii[1,2], Kazutaka Kitaura[1,2], Takaji Matsutani[3], Kenji Shirai[1,2], Satsuki Suzuki[4], Tomohiko Takasaki[2], Kenichi Kumagai[1,5], Yoshie Kametani[6], Takashi Shiina[7], Shuji Takabayashi[8], Hideki Katoh[8,9], Yoshiki Hamada[5], Ichiro Kurane[2], Ryuji Suzuki[1]*

1 Department of Rheumatology and Clinical Immunology, Clinical Research Center for Allergy and Rheumatology, Sagamihara National Hospital, National Hospital Organization, Kanagawa, Japan, **2** Department of Virology 1, National Institute of Infectious Diseases, Tokyo, Japan, **3** Laboratory of Immune Regulation, Wakayama Medical University, Osaka, Japan, **4** Section of Biological Science, Research Center for Odontology, Nippon Dental University, School of Life Dentistry, Tokyo, Japan, **5** Department of Oral and Maxillofacial Surgery, School of Dental Medicine, Tsurumi University, Kanagawa, Japan, **6** Department of Immunology, Division of Basic Medical Science and Molecular Medicine, Tokai University School of Medicine, Kanagawa, Japan, **7** Department of Molecular Life Science, Division of Basic Medical Science and Molecular Medicine, Tokai University School of Medicine, Kanagawa, Japan, **8** Experimental Animals Institute, Hamamatsu University School of Medicine, Shizuoka, Japan, **9** Laboratory of Animal Breeding and Genetics, Central Institute for Experimental Animals, Kawasaki, Japan

Abstract

The common marmoset (*Callithrix jacchus*) is considered a novel experimental animal model of non-human primates. However, due to antibody unavailability, immunological and pathological studies have not been adequately conducted in various disease models of common marmoset. Quantitative real-time PCR (qPCR) is a powerful tool to examine gene expression levels. Recent reports have shown that selection of internal reference housekeeping genes are required for accurate normalization of gene expression. To develop a reliable qPCR method in common marmoset, we used *geNorm* applets to evaluate the expression stability of eight candidate reference genes (*GAPDH*, *ACTB*, *rRNA*, *B2M*, *UBC*, *HPRT*, *SDHA* and *TBP*) in various tissues from laboratory common marmosets. *geNorm* analysis showed that *GAPDH*, *ACTB*, *SDHA* and *TBP* were generally ranked high in stability followed by *UBC*. In contrast, *HPRT*, *rRNA* and *B2M* exhibited lower expression stability than other genes in most tissues analyzed. Furthermore, by using the improved qPCR with selected reference genes, we analyzed the expression levels of CD antigens (CD3ε, CD4, CD8α and CD20) and cytokines (IL-1β, IL-2, IL-4, IL-5, IL-6, IL-10, IL-12β, IL-13, IFN-γ and TNF-α) in peripheral blood leukocytes and compared them between common marmosets and humans. The expression levels of CD4 and IL-4 were lower in common marmosets than in humans whereas those of IL-10, IL-12β and IFN-γ were higher in the common marmoset. The ratio of Th1-related gene expression level to that of Th2-related genes was inverted in common marmosets. We confirmed the inverted ratio of CD4 to CD8 in common marmosets by flow cytometric analysis. Therefore, the difference in Th1/Th2 balance between common marmosets and humans may affect host defense and/or disease susceptibility, which should be carefully considered when using common marmoset as an experimental model for biomedical research.

Citation: Fujii Y, Kitaura K, Matsutani T, Shirai K, Suzuki S, et al. (2013) Immune-Related Gene Expression Profile in Laboratory Common Marmosets Assessed by an Accurate Quantitative Real-Time PCR Using Selected Reference Genes. PLoS ONE 8(2): e56296. doi:10.1371/journal.pone.0056296

Editor: Guillermo López-Lluch, Universidad Pablo de Olavide, Centro Andaluz de Biología del Desarrollo-CSIC, Spain

Received November 6, 2012; **Accepted** January 7, 2013; **Published** February 25, 2013

Funding: This work was supported in part by Grants-in-Aid for Research on Emerging and Re-emerging Infectious Diseases from the Ministry of Health, Labor, and Welfare, Japan (Grants H20-shinkou-ippan-013 and H23-shinkou-ippan-010) as well as by Grant-in-Aid for Challenging Exploratory Research 23659237 from the Japan Society for the Promotion of Science. The funders had no role in study design, data collection and analysis, decision to publish, or preparation of the manuscript.

Competing Interests: The authors have declared that no competing interests exist.

* E-mail: r-suzuki@sagamihara-hosp.gr.jp

Introduction

The common marmoset (*Callithrix jacchus*) is a New World monkey and is considered potentially useful as an experimental animal model in research fields such as drug toxicology [1,2], neuroscience [3,4], autoimmune diseases [5,6] and infectious diseases [7,8], because of its size, availability and high genetic similarity with humans [9,10]. Compared with mice, common marmosets are more useful as an *in vivo* model to study immune function [11]. However, essential tools and gene information for conducting studies using common marmosets are in short supply or unavailable. For example, monoclonal antibodies specific for common marmosets have been only partially established. Although DNA microarray research for common marmoset brain has been reported [12], sufficient studies have not been performed in other research fields.

Quantitative real-time polymerase chain reaction (qPCR) is the dominant quantitative technique for gene expression analysis due to its broad dynamic range, accuracy, sensitivity, specificity and

speed [13]. Thus, qPCR is very useful for investigating physiological and pathological status from a small amount of sample. Normalization to reference genes such as housekeeping genes is usually required for qPCR analysis. However, expression levels of reference genes may vary between tissues, cell types and experimental conditions. Therefore, the validation of suitable reference genes in each experiment is critical for the accurate evaluation of qPCR data. Recently, a set of guidelines for evaluating qPCR experiments was developed [14] and a strict method for the selection of reference genes suitable for normalization was proposed [15]. A freely available program, *geNorm* applet (http://medgen.ugent.be/~jvdesomp/genorm/), can determine gene stability ranking and the number of reference genes required for normalization in a given panel of samples [15].

To develop an accurate and reliable qPCR method for common marmosets, we examined the expression stabilities of candidate reference genes in various tissues of laboratory common marmosets using *geNorm* applet. Then, we compared expression levels of immune-related genes in peripheral blood leukocytes between common marmosets and humans. To the best of our knowledge, this is the first such study for the selection of reference genes in common marmosets. The present data will contribute to future studies of gene expression analysis by qPCR for common marmosets.

Materials and Methods

Ethics statement

The study was conducted in accordance with the Act on Welfare and Management of Animals of Japanese government. All animals were housed, cared for, and used according to the principles set forth in the Guide for the Care and Use of Laboratory Animals: Eighth Edition (National Research Council, 2011). All experiments using common marmosets were approved by the committee for animal experiments at the National Institute of Infectious Diseases (Approval Number: 610,007). For humans, whole blood was obtained from eight healthy volunteers (mean age ± sd: 35.7±13.0 years old) after obtaining written informed consent. This study and the consent procedure were approved by the ethics committee of Tokai University School of Medicine (Approval Number: 10I-22).

Animals

Eight common marmosets (1.58±0.29 years old) were obtained from CLEA Japan, Inc. (Tokyo, Japan) and maintained in specific pathogen-free conditions at the National Institute of Infectious Diseases (Tokyo, Japan). Common marmosets were housed solely or in pairs in a single cages 39 cm (W)×55 (D)×70 (H) in size on 12:12 h light/dark cycles. Room temperature and humidity were maintained at 26–27°C and 40–50%, respectively. Filtered drinking water was delivered by an automatic watering system and total 40–50 g/individual of commercial marmoset chow (CMS-1M, CLEA Japan) were given in a couple of times per day. Dietary supplements (sponge cakes, eggs, banana pudding, honeys, vitamin C and D3) were also given to improve their health status. Machinery noise and dogs' barks were avoided to reduce stress. The cages were equipped with resting perches and a nest box as environmental enrichment. The marmosets were routinely tested to assure the absence of pathogenic bacteria, viruses, and parasite eggs in the animal facilities and did not exhibited abnormal external appearances. Four common marmosets were euthanized by cardiac exsanguinations under anesthesia with Ketamine hydrochroride (50 mg/kg, IM) and Xylazine (3.0 mg/kg, IM). After sacrifice, various tissues removed, and whole blood was obtained from all eight common marmosets.

RNA isolation

Heparinized venous blood samples from common marmosets were obtained before sacrifice and incubated in erythrocyte lysis buffer (155 mM NH_4Cl, 10 mM $KHCO_3$, and 0.1 mM EDTA). Following incubation on ice for 5 min, cells were centrifuged at 300×*g* for 10 min at 4°C and washed with lysis buffer and then PBS. Leukocytes were lysed with QIAzol® Lysis Reagent (Qiagen, Hilden, Germany) and total RNA was extracted using an RNeasy® Plus Universal Mini Kit (Qiagen) according to the manufacturer's instructions. Tissue samples (spleen, mesenteric lymph node, jejunum, ileum, descending colon, cerebrum, cerebellum, brainstem, heart, lung, liver and kidney) were excised from each animal and immediately submerged in RNAlater® RNA Stabilization Reagent (Qiagen). Then total RNA was extracted using RNeasy® Plus Universal Mini Kit (Qiagen). RNA concentration and integrity were assessed using the Agilent RNA 6,000 Nano Kit (Agilent Technologies, Inc., CA, USA) in an Agilent 2100 Bioanalyzer. All RNA samples were confirmed to have no degradation and were of optimal quality for downstream qPCR applications.

Candidate reference genes

Based on a literature search, eight commonly used candidate internal control genes were selected for analysis: *GAPDH* (glyceraldehyde-3-phosphate dehydrogenase), *ACTB* (actin, beta), *rRNA* (18S ribosomal RNA), *B2M* (beta-2-microglobulin), *UBC* (ubiquitin C), *HPRT* (hypoxanthine phosphoribosyltransferase 1), *SDHA* (succinate dehydrogenase complex, subunit A) and *TBP* (TATA-box binding protein). All genes chosen have independent cellular functions and are not thought to be co-regulated. The sequences of primers specific for each reference gene are shown in Table 1.

Quantitative real-time PCR

First-strand cDNA was synthesized using PrimeScript® RT reagent Kit (Takara Bio, Otsu, Japan) with attached random hexamers and oligo(dT) primers. Reactions were incubated at 37°C for 15 min followed by 85°C for 5 sec according to the manufacturer's instructions. Then each cDNA sample was diluted with RNase/DNase-free water to 25 ng/μL. The expression level of each gene was analyzed by qPCR using the Bio-Rad CFX96 system (Bio-Rad Laboratories, Inc., Hercules, CA, USA). PCR reactions consisted of 5 μL of SsoFast™ EvaGreen® Supermix (Bio-Rad), 3.5 μL of RNase/DNase-free water, 0.5 μL of 5 μM primer mix, 1 μL of cDNA in a total volume of 10 μL. The primer sequences are shown in Tables 1 and 2. Cycling conditions were as follows: 30 sec at 95°C followed by 45 rounds of 95°C for 1 sec and 60°C for 5 sec. Melting curve analysis to determine the dissociation of PCR products was performed between 65°C and 95°C. Data were expressed as mean values of experiments performed in triplicate. Seven points of a 10-fold serial dilution of standard DNA was used for absolute quantification. Standard DNA was generated by cloning PCR products into pGEM-T Easy Vector (Promega, WI, USA). Sequences of the cloned plasmid were confirmed by DNA sequencing using the CEQ8000 Genetic Analysis System (Beckman Coulter). Quality and concentration of the plasmid DNA were validated using Agilent DNA 7,500 Kit in an Agilent 2100 Bioanalyzer.

Table 1. Sequences of qPCR primers for housekeeping genes.

Target gene	Species	5′-primer sequence -3′[a),b)]		Product size (bp)	PCR efficiency	Reference
		Forward	Reverse			
GAPDH	Cj	TCGGAGTCAACGGATTTGGTC	TTCCCGTTCTCAGCCTTGAC	181	0.920	DD279474
	Hs	----------	----------	181	0.921	AF261085
ACTB	Cj	GATGGTGGGCATGGGTCAGAA	AGCCACACGCAGCTCGTTGT	163	0.901	DD279463
	Hs	----------	----------A----	163	0.883	NM_001101
HPRT	Cj	ATCCAAAGATGGTCAAGGTCG	GTATTCATTATAGTCAAGGGCATA	134	0.842	DD289567
	Hs	----------	----------	134	0.880	M31642
B2M	Cj	CTATTCAGCATGCTCCAAAGA	AAGACAAGTCTGAATGCTCCAC	168	0.928	AF084623
	Hs	----C----G-A---------	----------	168	0.950	AB021288
UBC	Cj	TCCCTTCTCGGCGGTTCTG	. TGCATTGTCAAGCGGCGAT	158	0.922	AB571242
	Hs	----------A-----	TC----------T-A----	160	0.936	NM_021009
rRNA	Cj	CGACCATAAACGATGCCGAC	GGTGGTGCCCTTCCGTCAAT	145	0.918	AB571241
	Hs	----------	----------	145	0.940	M10098
SDHA	Cj	TGGGAACAAGAGGGCATCTG	CCACCACGGCATCAAATTCATG	86	0.934	XM_002745154
	Hs	----------	-------T----------	86	0.948	BC001380
TBP	Cj	CCATGACTCCCGGAATCCCTAT	ATAGGCTGTGGGGTCAGTCCA	70	0.920	EU796973
	Hs	----------	----------	70	0.954	M55654

[a)]Hyphen indicates a nucleotide identical to human sequences.
[b)]Dot indicates a shift nucleotide to marmoset sequences.
doi:10.1371/journal.pone.0056296.t001

Analysis of gene expression stability

The expression stability of selected reference genes was evaluated using a publicly available program, *geNorm* applet [15]. *geNorm* calculates the stability of tested reference genes according to the similarity of their expression profiles by pairwise comparison and M value, where the gene with the highest value is the least stable one. It is possible to perform sequential elimination of the least stable gene in any given experimental group, thus resulting in the exclusion of all but the two most stable genes in each case.

Flow cytometry

Heparinized peripheral blood was collected from common marmosets and centrifuged in Lymphocepal (IBL Co. Takasaki, Japan) at 2,000 rpm for 30 min. Mononuclear cells were collected and re-suspended in RPMI1640 medium containing 10% fetal calf serum. Cells were stained with anti-common marmoset CD8 antibody (Mar8–10) [16] for 15 min at 4°C and washed with 1% (w/v) bovine serum albumin-containing PBS. Subsequently, cells were stained with phycoerythrin-labeled secondary antibody, peridinin chlorophyll protein cyanin5.5 (PerCPCy5.5)-conjugated anti-human CD3 (SP34-2) and Alexa488-conjugated anti-common marmoset CD4 (Mar4-33) antibodies [16]. Peripheral blood from healthy human volunteers was collected and mononuclear cells isolated by Ficoll-Paque (GE Healthcare Biosciences, Uppsala, Sweden) gradient centrifugation. The monoclonal antibodies used for cell staining were as follows: PerCPCy5.5-conjugated anti-human CD3 (SP34-2), allophycocyanin-conjugated anti-human CD4 (SK3), fluorescein isothiocyanate-conjugated anti-human CD8 (HIT8a) (BD PharMingen). Cells were analyzed by FACSCalibur (Becton Dickinson, Franklin Lakes, NJ, USA).

Statistical analysis

Student's *t*-test was used for statistical analysis to assess significant differences in qPCR assays. A P value<0.05 was considered to be statistically significant.

Results

The expression levels of candidate reference genes in tissues

Eight housekeeping genes were chosen as reference genes: *GAPDH*, *ACTB*, *rRNA*, *B2M*, *UBC*, *HPRT*, *SDHA* and *TBP*. We determined the transcription levels of these eight genes in 13 tissues (leukocyte, spleen, lymph node, jejunum, ileum, colon, cerebrum, cerebellum, brainstem, heart, lung, liver and kidney) from four individual common marmosets by qPCR. The sequences of primers specific for each reference gene are shown in Table 1. The expression level of each gene in each tissue is shown as the copy number per μg of purified total RNA (Figure 1). The most abundant gene was *rRNA* while the rarest gene was *UBC* and the difference in expression level between the two genes was more than 100,000-fold. For several genes, the expression levels were highly different among tissues. For example, *B2M* expression in heart and brain segments (cerebrum, cerebellum and brainstem) was markedly lower than in other tissues. *HPRT* expression also showed a large variability among tissues. In addition, the expression levels of *rRNA*, *B2M* and *HPRT* varied among individuals; the mean values of standard deviation were 0.224, 0.235 and 0.303, respectively, while those of the other genes were below 0.2.

Table 2. Sequences of qPCR primers for CD markers and cytokines.

Target gene	Species	5′-primer sequence -3′[a),b)]		Product size (bp)	PCR efficiency	Reference
		Forward	Reverse			
CD3ε	Cj	GGCTTGCTGCTGCTGGTTTAC	CCGGATGGGCTCATAGTCTG	150	0.865	DQ189218
	Hs	----------	----------	150	0.848	NM_000733
CD4	Cj	GGAAAACGGGAAAGTTGCATCA	GCCTTCTCCCGCTTAGAGAC	163	0.926	AF452616
	Hs	C------A----------	----------C-----	162	0.907	M35160
CD8α	Cj	TCTCCCAAACCAAGTCCAAGG	AGTTTCTCAGGGCCGAGCAG	144	0.940	DQ189217
	Hs	---------A----C------	. ---G----------	143	0.912	NM_001768
CD20	Cj	GGGCTGTCCAGATTATGAATG	GAGTTTTTCTCCGTTGCTGC	166	0.942	DQ189220
	Hs	----------	----------	166	1.002	X07203
IL-1β	Cj	TGCACCTGTACGATCCCTGAAC	TTGCACAAAGGACATGGAGAACAC	145	0.806	AB539804
	Hs	----------A------	---T----------	145	0.780	NM_000576
IL-2	Cj	CCCAAGAAGGCCAAAGAATTG	CTTAAGTGAAAGTTTTTGCTTTGAG	104	0.773	DQ826674
	Hs	----------C----C--	----------	103	0.797	BC070338
IL-4	Cj	CATTGTCACAGAGCAAAAGACTC	CTCAGTTGTGTTCTTGGAGGCA	79	0.910	XM_002744606
	Hs	. GCC----------G-------	----------	77	0.878	NM_000589
IL-5	Cj	AATCACCAACTGTGCACTGAAGAA	. TTTGGCGGTCAATGTGTTCCTT	130	0.871	DQ658152
	Hs	----------	TT------C--------A--T---	132	0.860	NM_000879
IL-6	Cj	GATTCAATGAGGAGACTTGCC	TGTTCTGGAGGTACTCTAGGTA	81	0.920	DQ658153
	Hs	----------	----------	81	0.990	NM_00600
IL-10	Cj	CTGCCTCACATGCTTCGAGA	TGGCAACCCAGGTAACCCTTA	134	0.970	DQ658154
	Hs	------A----------	----------	134	0.920	M57627
IL-12β	Cj	. GGACGGCAAGGAGTATGAGTA	TTGAGCTTGTGAACGGCATC	111	0.935	AB539805
	Hs	G----AA----------	----------	112	0.900	M65272
IL-13	Cj	TCCAGCTTGCTTGTCCGAG	CTGCAAATAATGATGCGTT-GATGT	127	0.916	AB571243
	Hs	----------A--------	. ----------T--C--A--	127	0.964	NM_002188
IFN-γ	Cj	GGGTTCTCTTGGCTGTTACTG	TGTCTAAGAAAAGAGTTCCATTATC	116	0.838	FJ598593
	Hs	----------	. -C----------	115	0.856	NM_000619
TNF-α	Cj	AGCCTGTAGCCCATGTTGTAG	CTCTCAGCTCCACGCCATTG	102	0.887	DQ520835
	Hs	----------	----------	102	0.817	NM_000594

[a)]Hyphen indicates a nucleotide identical to human sequences.
[b)]Dot indicates a shift nucleotide to marmoset sequences.
doi:10.1371/journal.pone.0056296.t002

A variety of gene expression stabilities among tissues

To evaluate the expression stability of selected reference genes, we used a publicly available program, *geNorm* applets. *geNorm* provides a ranking of tested genes based on the reference gene stability measure M, which is defined as the average pairwise variation of a particular gene compared with all other control genes. Thus, genes with higher M values have greater variations of expression. In addition, assessment of the pairwise variations ($V_{n/n+1}$) between each combination of sequential normalization factors allows identification of the optimal number of reference genes. In the original publication describing *geNorm* [15], a threshold of 0.15 for pairwise variation was established, below which the inclusion of additional reference genes was not necessary.

geNorm analysis produced line plots indicating the mean expression stability M of the remaining candidate reference genes in each round of the analysis (Figure 2A and 2B), the pairwise variation V (Figure 2C) and ranking of the candidate reference genes from the least stable to the two most stable genes (Figure 3). The stability score M indicated that gene expression in spleen, jejunum and cerebellum were relatively less stable than other tissues (Figure 2A and B). However, all tissues tested exhibited high stabilities, as M values were less than 1.5, which was the default limit even when all eight genes were analyzed. According to pairwise variation V (Figure 2C), the two most stable genes were sufficient for a stable and valid reference for each tissue analyzed by qPCR because V2/3 values were less than 0.15 in all tissues. Jejunum was the most variable tissue with a $V_{2/3}$ value of 0.139. Figure 3 shows ranking of gene expression stability based on M values. *GAPDH*, *ACTB*, *SDHA* and *TBP* had higher stability, while *HPRT*, *rRNA* and *B2M* were variable in most tissues. *TBP* in intestinal segments (jejunum, ileum and colon) and *SDHA* in brain segments (cerebrum, cerebellum and brain stem) were particularly stable. *HPRT* ranked as the worst of the eight genes in the 13 tissues tested.

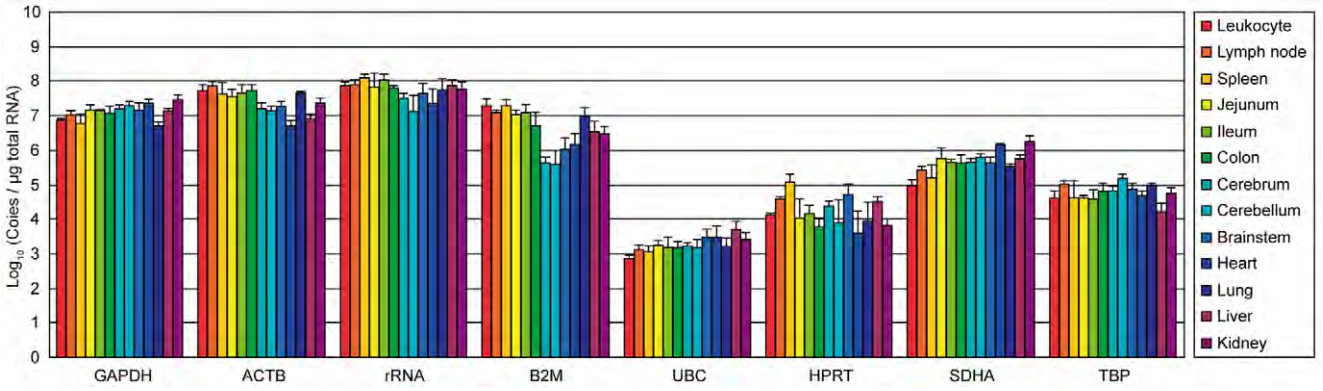

Figure 1. Absolute copy numbers of candidate reference genes. The expression level of each gene in 13 tissues is shown as a logarithmic histogram of absolute copy numbers per μg of total RNA. Means and standard deviations of four individuals are indicated. GAPDH: glyceraldehyde-3-phosphate dehydrogenase; ACTB: actin, beta; rRNA: 18S ribosomal RNA; B2M: beta-2-microglobulin; UBC: ubiquitin C; HPRT: hypoxanthine phosphoribosyltransferase 1; SDHA: succinate dehydrogenase complex, subunit A; TBP: TATA-box binding protein.
doi:10.1371/journal.pone.0056296.g001

Comparison of gene expression levels between human and common marmoset leukocytes

Subsequently, we analyzed gene expression levels of four CD antigens (CD3ε, CD4, CD8α, and CD20) and ten cytokines, interleukin (IL)-1β, IL-2, IL-4, IL-5, IL-6, IL-10, IL-12β, IL-13, interferon (IFN)-γ and tumor necrosis factor (TNF)-α, in peripheral blood leukocytes from humans and common marmosets (Figure 4). The sequences of primers specific for these

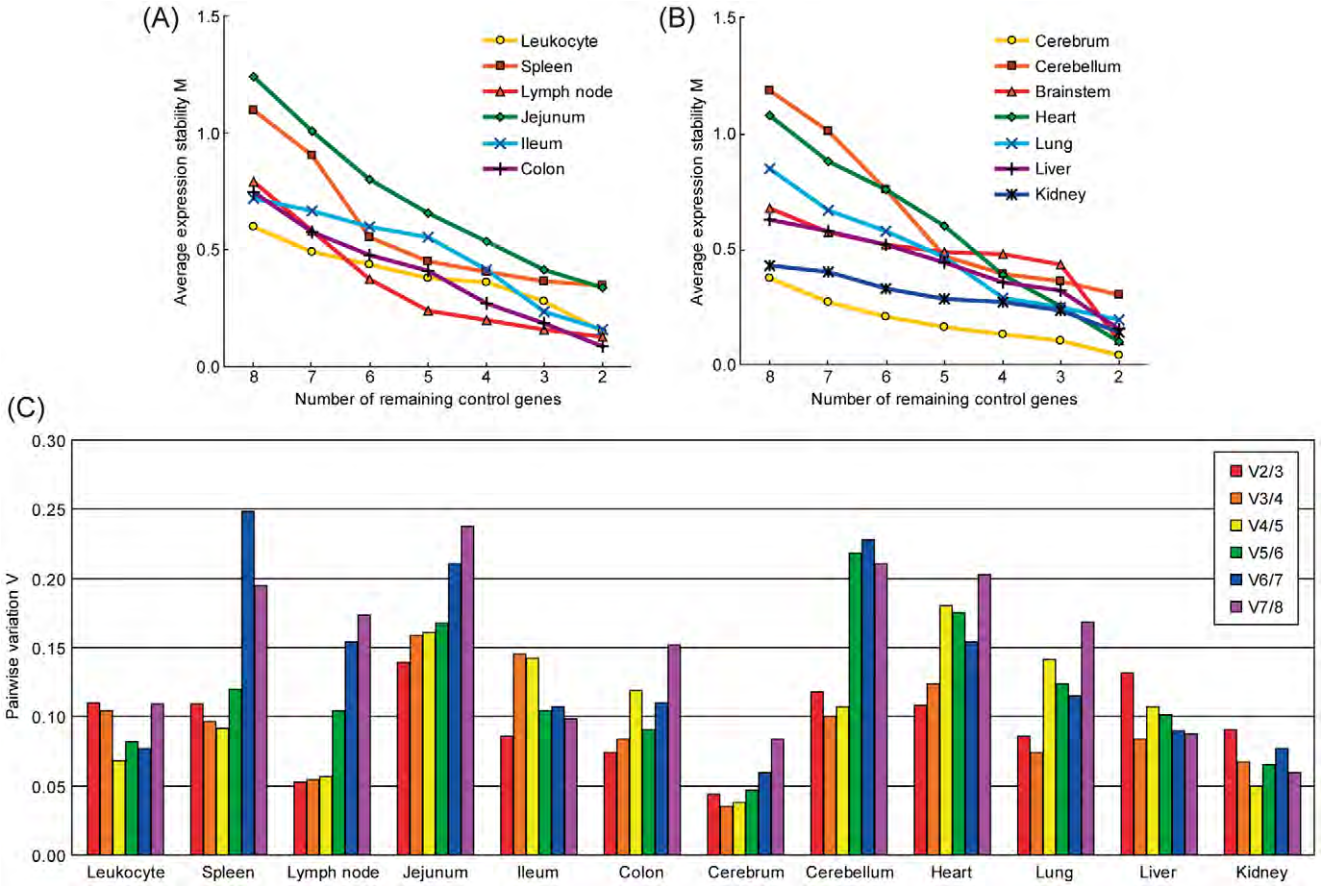

Figure 2. Gene expression stability and pairwise variation of candidate reference genes using *geNorm* analysis. (A) and (B): Average gene expression stability values M of the remaining reference genes during stepwise exclusion of the least stable gene in the different tissue panels are shown. Data are divided into two figures to avoid closely-packed lines. See also figure 3 for the ranking of genes according to their expression stability. (C) Pairwise variation analysis was used to determine the optimal number of reference genes for use in qPCR data normalization. The recommended limit for V value is 0.15, the point at which it is unnecessary to include additional genes in a normalization strategy.
doi:10.1371/journal.pone.0056296.g002

Stability	High						Low
Leukocyte	GAPDH-UBC	ACTB	SDHA	TBP	B2M	rRNA	HPRT
Spleen	GAPDH-SDHA	ACTB	TBP	UBC	rRNA	B2M	HPRT
Lymph node	rRNA-TBP	ACTB	SDHA	UBC	GAPDH	B2M	HPRT
Jejunum	UBC-TBP	GAPDH	B2M	SDHA	ACTB	rRNA	HPRT
Ileum	B2M-TBP	UBC	ACTB	HPRT	SDHA	GAPDH	rRNA
Colon	ACTB-TBP	SDHA	GAPDH	rRNA	UBC	HPRT	B2M
Cerebrum	GAPDH-SDHA	rRNA	ACTB	HPRT	UBC	TBP	B2M
Cerebellum	SDHA-TBP	GAPDH	ACTB	UBC	rRNA	B2M	HPRT
Brainstem	ACTB-SDHA	UBC	rRNA	HPRT	GAPDH	TBP	B2M
Heart	SDHA-TBP	GAPDH	ACTB	UBC	B2M	rRNA	HPRT
Lung	SDHA-TBP	ACTB	GAPDH	UBC	B2M	rRNA	HPRT
Liver	GAPDH-SDHA	HPRT	rRNA	ACTB	TBP	UBC	B2M
Kidney	GAPDH-SDHA	TBP	UBC	ACTB	B2M	rRNA	HPRT

Figure 3. Ranking of gene expression stability of candidate reference genes using *geNorm* analysis. Candidate reference genes are ranked in order of stability for each tissue with the two most stable genes at the left and the least stable at the right.
doi:10.1371/journal.pone.0056296.g003

immune-related genes are shown in Table 2. The normalization factor for common marmoset leukocytes was calculated using *GAPDH* and *UBC* based on the *geNorm* analysis as described above. For human leukocytes, we found that the expression of all eight genes were stable (M value = 0.363), of which *ACTB* and *HPRT* had the best score (M value = 0.163, $V_{2/3} = 0.062$) and were selected for use. The expression levels of CD4 and IL-4 were significantly lower in common marmosets than in humans while those of IL-10, IL-12β and IFN-γ were significantly higher in common marmosets compared with humans. Of interest, the expression level of IL-4 was notably lower in common marmosets than humans, and was close to the detection limit. There was no statistical difference in the expression levels of the other genes tested between common marmosets and humans.

Difference of CD4/CD8 ratio between humans and common marmosets

We calculated ratios of the expression levels of CD4 to CD8 (CD4/CD8 ratio) in human and common marmoset leukocytes (Figure 5, left panel). CD4/CD8 ratios were significantly higher in human leukocytes compared with common marmoset leukocytes (mean ± sd, 0.59±0.22 vs. −0.49±0.41, $P<0.01$). To confirm the difference in CD4/CD8 ratios, we examined the proportion of $CD4^+$ and $CD8^+$ in $CD3^+$ T cells by flow cytometric analysis. As shown in Figure 6, the rates of $CD3^+$ cells in the lymphocyte gate were similar between common marmosets (30%) and humans (38%). However, the rates of $CD4^+/CD3^+$ cells and $CD8^+/CD3^+$ cells was 36% and 61% in common marmosets, respectively, and 75% and 21% in humans, respectively. Similarly, the CD4/CD8 ratio was markedly different between common marmosets and humans (mean ± sd, 0.56±0.08 vs. 3.22±0.35, $P<0.01$) by qPCR. This indicated a good correlation between the results from FACS analysis and that of qPCR analysis. To examine whether the CD4/CD8 ratio is affected by age, we further performed FACS analyses with PBMCs from young and old marmosets (Table 3). The result showed that the inverted CD4/CD8 ratio was fairly constant among individuals and over ages.

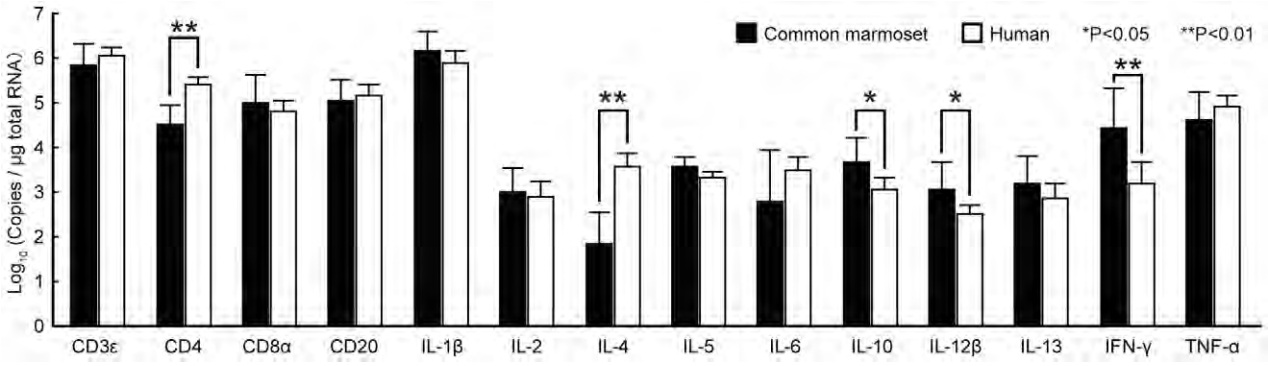

Figure 4. The expression levels of CD antigens and cytokine genes in common marmoset and human leukocytes. The expression level of each gene is shown as a logarithmic histogram of absolute copy numbers per μg of total RNA. Means and standard deviations of eight individuals are indicated. Asterisk indicates statistically significant differences between marmosets and humans by Student's *t*-test (*P value<0.05, **P value<0.01).
doi:10.1371/journal.pone.0056296.g004

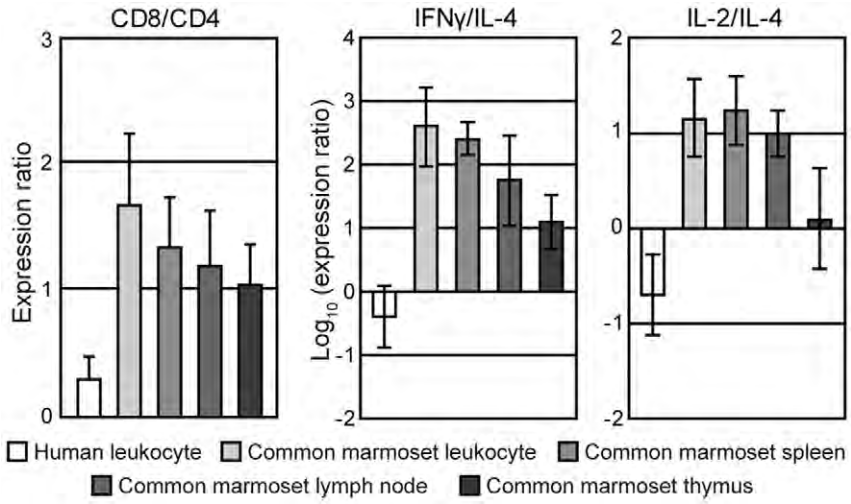

Figure 5. The expression ratios of CD8 to CD4 (CD8:CD4) and Th1-related genes to Th2-related genes. The ratio of CD8:CD4 (left panel), IFN-γ:IL-4 (middle panel) and IL-2:IL-4 (right panel) in human and common marmoset leukocytes, spleen, lymph node and thymus are shown. Significant differences in the CD8:CD4, IFN-γ:IL-4 and IL-2:IL-4 ratios were found between human leukocytes and common marmoset tissues (*$P<0.05$).
doi:10.1371/journal.pone.0056296.g005

Difference in T helper 1 (Th1)/T helper 2 (Th2) balance between humans and common marmosets

We compared the ratios of expression levels of Th1-related genes (IFN-γ or IL-2) and Th2-related genes (IL-4) (IFN-γ:IL-4 or IL-2:IL-4 ratio) (Figure 5, middle and right panels). Both logarithmic values of the IFN-γ:IL-4 and IL-2:IL-4 ratios were negative in human leukocytes whereas those of common marmoset leukocytes, spleen, lymph node and thymus indicated positive values, showing a clear difference in the Th1/Th2 balance between humans and common marmosets.

Discussion

In the present study, we evaluated the expression stability of common marmoset housekeeping genes in various tissues. To the best of our knowledge, this is the first report of a systematic evaluation of potential reference genes in common marmosets. We chose eight commonly used classical housekeeping genes. Of all genes tested, *rRNA* showed the most abundant expression and *UBC* showed the lowest expression. The *UBC* gene contains multiple directly repeated ubiquitin coding sequences (i.e., polyubiquitin precursor protein) [17]. However, the primer set we used enabled amplification of the unrepeated sequence at the 5′ region of the *UBC* gene only. Thus, low *UBC* expression in our data does not reflect the amount of ubiquitin C protein. *B2M* expression levels were markedly lower in brains and hearts than in other tissues. Resident brain cells normally express few or no MHC class I and B2M molecules [18–20]. In addition, *B2M* expression is upregulated by infection or autoimmune disease [21–23]. Therefore, in disorders with cellular infiltration such as inflammation (especially encephalitis) or cancer cell invasion, *B2M* expression levels may be significantly varied compared with normal tissue.

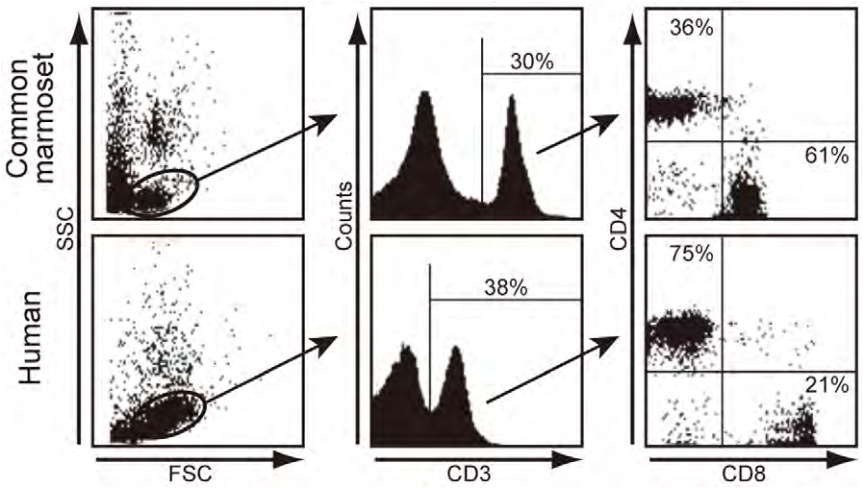

Figure 6. The ratio of $CD4^+$ to $CD8^+$ cells in common marmoset and human peripheral blood mononuclear cells (PBMCs) by flow cytometry. Representative scattered plots of FSC and SSC are shown in the left panels. Middle panels represent a histogram of CD3 analyzed in the lymphocyte gate. Gated $CD3^+$ cells were analyzed for CD4 and CD8 expression (right panels).
doi:10.1371/journal.pone.0056296.g006

Table 3. CD8/CD4 ratio in PBMCs from young and old marmosets.

Age	Sex	% positive		CD8/CD4 ratio
		CD8	CD4	
3 month*	male	58.3	38.4	1.52
1.5 year	female	60.7	36.1	1.68
1.5 year*	male	55.1	41.5	1.33
2.0 year	male	52.7	44.6	1.18
10 year*	female	58.6	37.8	1.55
Mean ± sd		57.1±3.2	39.7±3.4	1.45±0.20

*Only FACS analysis, but not qPCR, was done with PBMCs from these three marmosets.

doi:10.1371/journal.pone.0056296.t003

Thus, we predict that *B2M* may be unsuitable as a reference gene in many cases.

We assessed gene expression stability using the *geNorm* applet. As shown in Figure 2, *geNorm* analysis indicated that all tested genes were stable in each tissue. However, there were some trends in the stability ranking (Figure 3). For example, *TBP* in intestine segments and *SDHA* in brain segments represented prominently high stabilities. *GAPDH*, *ACTB*, *SDHA* and *TBP* were generally ranked high followed by *UBC*. In contrast, the stability of *rRNA* was generally low. This suggests the amount of mRNA is not always proportional to that of total RNA as reported by other studies [24,25]. In addition, *HPRT*, *rRNA* and *B2M* varied widely among tissues and rarely ranked high.

We analyzed the expression levels of CD antigens and cytokines by qPCR to compare the characteristics of peripheral blood leukocytes between common marmosets and humans (Figure 4). We observed that the expression levels of CD4 and IL-4 were lower in common marmosets than in humans. In contrast, the expression levels of IL-10, IL-12β and IFN-γ were higher in common marmosets. We calculated PCR efficiency of each primer set and found there was no great difference between primers for common marmosets and those for humans (Tables 1 and 2). Thus, the differences in the gene expression levels between common marmosets and humans are not attributable to the differences in PCR efficiency.

We also observed that the CD4:CD8 ratio and Th1/Th2 balance were inverted in common marmosets by qPCR analysis (Figure 5). In particular, we confirmed the inverted CD4:CD8 ratio by flow cytometric analysis (Figure 6 and Table 3). The inverted CD4:CD8 ratio was stable over age. Of interest, we noted that the Th1/Th2 balance is different between common marmosets and humans, although we can only speculate on the cause of the difference. First, intestinal parasite infections may affect the Th1/Th2 balance by regulating expression of genes encoding cytokines [26–28]. In particular, protozoan parasites are potent stimulators of IFN-γ expression and Th1 responses [29]. Moreover, humans living in poor hygienic conditions in developing countries had higher Th1 cytokine levels compared with people in developed countries [30]. Although the common marmosets used in this study were maintained in specific pathogen-free conditions, we cannot rule out that such infectious agents may be one of a number of factors responsible for the difference in Th1/Th2 balance.

A second possible reason may be a difference in the number of cells producing the respective cytokines. As shown in Figure 6, the ratio of $CD4^+$ to $CD8^+$ cells were markedly different in total leukocytes from common marmosets and humans. Since IL-4 is mainly produced by $CD4^+$ T cells [31,32], its expression level may be influenced by the CD4:CD8 ratio. However, this is not true for all the cytokines tested. For example, the expression levels of IL-2, IL-5 and IL-13, largely produced by T cells, were not significantly different between common marmosets and humans. Therefore, we suggest that the CD4:CD8 ratio has little effect on Th1/Th2 balance. IL-10 is produced by T cells and monocytes [33] and IL-12β is naturally produced by dendritic cells and macrophages [34,35]. However, we could not verify these cell numbers in the common marmoset. Further studies are required to determine whether the numbers of cytokine-producing cells influence the expression levels of IL-10 and IL-12β.

Another possibility is genetic variation. Bostik et al., reported distinct sequence differences in the promoter region or the proximal region of cytokine genes including IL-4, IL-10, IL-12β and TNF-γ among humans, macaque and mangabey monkeys, which affected regulation of cytokine synthesis [36]. Jeong et al., reported that the expression level of IL-4 was lower in monkeys (baboon and macaque) than in hominoids (human and chimpanzee) while the expression levels of IL-12β and the IFN-γ were higher in monkeys [37]. It is likely that Th1 dominant expression is common to primates other than hominoids and the difference in Th1/Th2 balance may be caused by genetic differences between common marmosets and humans.

The use of common marmoset is growing in popularity as a non-human primate model in many fields including autoimmune disease and infectious disease. In this study, we presented data regarding gene expression stabilities of common marmoset housekeeping genes and differences in the Th1/Th2 balance between common marmosets and humans. This difference may affect host defense and/or disease susceptibility, which should be carefully considered in biomedical research using common marmoset as an experimental model. We believe our data will contribute to future investigations using common marmoset models of various diseases.

Acknowledgments

We would like to acknowledge the efforts of Yasushi Ami in animal experiments. We also thank Ms. Hiro Yamada for technical assistance.

Author Contributions

Conceived and designed the experiments: YF TM K. Kitaura TS YH IK RS. Performed the experiments: YF K. Kitaura KS SS TT YK ST HK. Analyzed the data: YF RS. Contributed reagents/materials/analysis tools: K. Kumagai KS. Wrote the paper: TM K. Kitaura TS YH IK RS.

References

1. Klug S, Neubert R, Stahlmann R, Thiel R, Ryffel B, et al. (1994) Effects of recombinant human interleukin 6 (rhIL-6) in marmosets (Callithrix jacchus). 1. General toxicity and hematological changes. Arch Toxicol 68: 619–631.
2. Zühlke U, Weinbauer G (2003) The common marmoset (Callithrix jacchus) as a model in toxicology. Toxicol Pathol 31 Suppl: 123–127.
3. Yaguchi M, Tabuse M, Ohta S, Ohkusu-Tsukada K, Takeuchi T, et al. (2009) Transplantation of dendritic cells promotes functional recovery from spinal cord injury in common marmoset. Neurosci Res 65: 384–92.
4. Ando K, Maeda J, Inaji M, Okauchi T, Obayashi S, et al. (2008) Neurobehavioral protection by single dose l-deprenyl against MPTP-induced parkinsonism in common marmosets. Psychopharmacology (Berl) 195: 509–516.
5. Genain CP, Lee-Parritz D, Nguyen MH, Massacesi L, Joshi N, et al. (1994) In healthy primates, circulating autoreactive T cells mediate autoimmune disease. J Clin Invest 94: 1339–1345.
6. Genain CP, Hauser SL (1997) Creation of a model for multiple sclerosis in Callithrix jacchus marmosets. J Mol Med 75: 187–197.

7. Bright H, Carroll AR, Watts PA, Fenton RJ (2004) Development of a GB virus B marmoset model and its validation with a novel series of hepatitis C virus NS3 protease inhibitors. J Virol 78: 2062–2071.
8. Adams AP, Aronson JF, Tardif SD, Patterson JL, Brasky KM, et al. (2008) Common marmosets (Callithrix jacchus) as a nonhuman primate model to assess the virulence of eastern equine encephalitis virus strains. J Virol 82: 9035–9042.
9. Mansfield K (2003) Marmoset models commonly used in biomedical research. Comp Med 53: 383–392.
10. Abbott DH, Barnett DK, Colman RJ, Yamamoto ME, Schultz-Darken NJ (2003) Aspects of common marmoset basic biology and life history important for biomedical research. Comp Med 53: 339–350.
11. Quint DJ, Buckham SP, Bolton EJ, Solari R, Champion BR, et al. (1990) Immunoregulation in the common marmoset, Calithrix jaccus: functional properties of T and B lymphocytes and their response to human interleukins 2 and 4. Immunology 69: 616–621.
12. Fukuoka T, Sumida K, Yamada T, Higuchi C, Nakagaki K, et al. (2010) Gene expression profiles in the common marmoset brain determined using a newly developed common marmoset-specific DNA microarray. Neurosci Res 66: 62–85.
13. Bustin SA, Nolan T (2004) Pitfalls of quantitative real-time reverse-transcription polymerase chain reaction. J Biomol Tech 15: 155–166.
14. Bustin SA, Benes V, Garson JA, Hellemans J, Huggett J, et al. (2009) The MIQE guidelines: minimum information for publication of quantitative real-time PCR experiments. Clin Chem 55: 611–622.
15. Vandesompele J, De Preter K, Pattyn F, Poppe B, Van Roy N, et al. (2002) Accurate normalization of real-time quantitative RT-PCR data by geometric averaging of multiple internal control genes. Genome Biol 3: RESEARCH0034.
16. Kametani Y, Suzuki D, Kohu K, Satake M, Suemizu H, et al. (2009) Development of monoclonal antibodies for analyzing immune and hematopoietic systems of common marmoset. Exp Hematol 37: 1318–1329.
17. Wiborg O, Pedersen MS, Wind A, Berglund LE, Marcker KA, et al. (1985) The human ubiquitin multigene family: some genes contain multiple directly repeated ubiquitin coding sequences. EMBO J 4: 755–759.
18. Drezen JM, Babinet C, Morello D (1993) Transcriptional control of MHC class I and beta 2-microglobulin genes in vivo. J Immunol 150: 2805–2813.
19. Lampson LA (1995) Interpreting MHC class I expression and class I/class II reciprocity in the CNS: reconciling divergent findings. Microsc Res Tech 32: 267–285.
20. Daar AS, Fuggle SV, Fabre JW, Ting A, Morris PJ (1984) The detailed distribution of HLA-A, B, C antigens in normal human organs. Transplantation 38: 287–292.
21. Kimura T, Griffin DE (2000) The role of CD8(+) T cells and major histocompatibility complex class I expression in the central nervous system of mice infected with neurovirulent Sindbis virus. J Virol 74: 6117–6125.
22. Keskinen P, Ronni T, Matikainen S, Lehtonen A, Julkunen I (1997) Regulation of HLA class I and II expression by interferons and influenza A virus in human peripheral blood mononuclear cells. Immunology 91: 421–429.
23. Mátrai Z, Németh J, Miklós K, Szabó Z, Masszi T (2009) Serum beta2-microglobulin measured by immunonephelometry: expression patterns and reference intervals in healthy adults. Clin Chem Lab Med 47: 585–589.
24. Solanas M, Moral R, Escrich E (2001) Unsuitability of using ribosomal RNA as loading control for Northern blot analyses related to the imbalance between messenger and ribosomal RNA content in rat mammary tumors. Anal Biochem 288: 99–102.
25. Valente V, Teixeira SA, Neder L, Okamoto OK, Oba-Shinjo SM, et al. (2009) Selection of suitable housekeeping genes for expression analysis in glioblastoma using quantitative RT-PCR. BMC Mol Biol 10: 17.
26. Bentwich Z, Weisman Z, Moroz C, Bar-Yehuda S, Kalinkovich A (1996) Immune dysregulation in Ethiopian immigrants in Israel: relevance to helminth infections? Clin Exp Immunol 103: 239–243.
27. Sacks D, Sher A (2002) Evasion of innate immunity by parasitic protozoa. Nat Immunol 3: 1041–1047.
28. Sher A, Coffman RL (1992) Regulation of immunity to parasites by T cells and T cell-derived cytokines. Annu Rev Immunol 10: 385–409.
29. Denkers EY, Gazzinelli RT (1998) Regulation and function of T-cell-mediated immunity during Toxoplasma gondii infection. Clin Microbiol Rev 11: 569–588.
30. Malhotra I, Ouma J, Wamachi A, Kioko J, Mungai P, et al. (1997) In utero exposure to helminth and mycobacterial antigens generates cytokine responses similar to that observed in adults. J Clin Invest 99: 1759–1766.
31. Abbas AK, Murphy KM, Sher A (1996) Functional diversity of helper T lymphocytes. Nature 383: 787–793.
32. Mosmann TR, Sad S (1996) The expanding universe of T-cell subsets: Th1, Th2 and more. Immunol Today 17: 138–146.
33. de Waal Malefyt R, Abrams J, Bennett B, Figdor CG, de Vries JE (1991) Interleukin 10(IL-10) inhibits cytokine synthesis by human monocytes: an autoregulatory role of IL-10 produced by monocytes. J Exp Med 174: 1209–1220.
34. Hsieh CS, Macatonia SE, Tripp CS, Wolf SF, O'Garra A, et al. (1993) Development of TH1 CD4+ T cells through IL-12 produced by Listeria-induced macrophages. Science 260: 547–549.
35. Macatonia SE, Hosken NA, Litton M, Vieira P, Hsieh CS, et al. (1995) Dendritic cells produce IL-12 and direct the development of Th1 cells from naive CD4+ T cells. J Immunol 154: 5071–5079.
36. Bostik P, Watkins M, Villinger F, Ansari AA (2004) Genetic analysis of cytokine promoters in nonhuman primates: implications for Th1/Th2 profile characteristics and SIV disease pathogenesis. Clin Dev Immunol 11: 35–44.
37. Jeong AR, Nakamura S, Mitsunaga F (2008) Gene expression profile of Th1 and Th2 cytokines and their receptors in human and nonhuman primates. J Med Primatol 37: 290–296.

Original Article

DOI: 10.5582/bst.2014.01084

Differentiation ability of multipotent hematopoietic stem/progenitor cells detected by a porcine specific anti-CD117 monoclonal antibody

Shino Ohshima[1], Syuuya Mori[1], Atsuko Shigenari[1], Asuka Miyamoto[1], Masaki Takasu[2], Noriaki Imaeda[2], Satoshi Nunomura[3], Yoshimichi Okayama[3], Masafumi Tanaka[1], Hitoshi Kitagawa[3], Jerzy K. Kulski[1,4], Hidetoshi Inoko[1], Asako Ando[1], Yoshie Kametani[1,*]

[1] *Department of Molecular Life Science, Division of Basic Medical Science and Molecular Medicine, Kanagawa, Japan;*
[2] *Department of Veterinary Medicine, Faculty of Applied Biological Sciences, Gifu University, Gifu, Japan;*
[3] *Division of Molecular Cell Immunology, Nihon University Graduate School of Medical Science, Tokyo, Japan;*
[4] *Centre for Forensic Science, The University of Western Australia, Perth, Western Australia, Australia.*

Summary **CD117 is a cytokine receptor expressed on the surface of hematopoietic stem cells with a likely role in cell survival, proliferation and differentiation. In order to study the differentiation activity of porcine CD117 hematopoietic cells *in vitro* and *in vivo* we prepared an anti-swine CD117 Mab (2A1) with high specificity for flow-cytometrical analysis. The 2A1 Mab did not recognize mouse or human mast cells suggesting that 2A1 is species-specific. Swine bone marrow (BM) CD117$^+$ cells differentiated *in vitro* mainly into erythroid and monocyte lineages in the methylcellulose-based colony assay. When the swine BM CD117$^+$ cells were transplanted *in vivo* into immunodeficient NOG (NOD/SCID/IL-2gc-null) mice, a significant amount of swine CD45$^+$ leukocytes, including CD3 positive T cells, were developed in the mice. These results revealed that the swine BM CD117$^+$ cells possess hematopoietic stem/progenitor activity and when monitored in immunodeficient mice or *in vitro* they can develop into lymphoid, erythroid, and myeloid cells efficiently with the new monoclonal antibody.**

Keywords: Swine, CD117, hematopoietic cell, monoclonal antibody, xeno-transplantation

1. Introduction

In transplantation studies, stem cells from various tissues such as from the heart or bone marrow have become an important alternative source to using donor organs or whole tissue for engraftment (*1-5*). The development of new reagents and methods are needed for the identification of stem cell markers and for monitoring their purification, transplantation and differentiation in foreign environments such as with the xeno-transplantation of stem cells between different animal species, because most of the tools today are cross-reactive monoclonal antibodies prepared against human antigens and not species specific (*6*). The swine has been an useful animal model for human medical science research and transplantation studies (*7*). For example, organ transplantation was extensively studied with major histocompatibility complex (MHC)-defined swine lines, alpha 1, 3-galactosyltransferase gene-knockout and/or human decay-accelerating factor transgenic swine (*8*). However, in recent years, experimental organ transplantation in swine is also gradually being replaced by stem cell transplantation involving hematopoietic and other tissue stem cells (*9-11*). Concomitant with the development of the swine stem cell transplantation research there is a continued need to produce stem cell marker-specific monoclonal antibodies (Mabs) (*6*).

Recently, a hematopoietic stem cell (HSC)-transplanted severe-immunodeficient mouse system (known as humanized mice) was extensively investigated for its efficacy of engraftment of foreign hematopoietic cells (*12*). Although this and other

**Address correspondence to:*
Dr. Yoshie Kametani, Department of Immunology, Tokai University School of Medicine, 143, Shimokasuya, Isehara, Kanagawa 259-1193, Japan.
E-mail: y-kametn@is.icc.u-tokai.ac.jp

mouse systems have limitations, they have been used efficiently to clarify the development pathway of hematopoietic cells, the efficacy of vaccination or drugs (*13*), and an improved humanized hematopoietic mouse system, human leukocyte antigen (HLA)-expressing mice, was recently reported (*14,15*). However, other animal stem cell models such as those using non-human primates or the swine also may be useful for evaluating xeno-reconstituted systems.

CD117 is a cytokine receptor tyrosine kinase type III expressed on the surface of wide variety of tissue stem cells including HSC, mesenchymal stem cells and multipotent progenitors (*16*). This molecule is also known as mast/stem cell growth factor receptor, proto-oncogene c-Kit or tyrosine-protein kinase kit and when activated by binding to a stem cell factor may play a role in regulating cell survival, proliferation and differentiation. As a cell surface marker, CD117 can be detected by using specific antibodies to identify and monitor the hematopoietic/mesenchymal stem/progenitor cell types and their stage of differentiation and activity in mice, humans and non-human primates. We have studied the xeno-transplantation of hematopoietic stem/progenitor cells of human, common marmoset and mouse and found that the cellularity of the reconstituted immune system in the transplantation environment was different among these animals, suggesting a significant diversity of hematopoietic cell characteristics (*17-19*). Thus, the stem cells of swine may have unique and different developmental potential compared to the mouse and non-human primates. Alternatively, they may have similar characteristics to the human and potentially could be used in experimental transplantation models for studying the pathogenesis and treatments of some human diseases. In this regard, Le Guern *et al.* (*20*) reported on the effect of long-term engraftment of swine stem cell factor (SCF)-positive cells in immunodeficient mice. However, because there were no species-specific Mabs readily available against swine CD117, researchers have tended to use the stem cell factor as a detectable stem cell differentiation marker and not CD117 (*21*).

In this study, we prepared a porcine-specific CD117 Mab and constructed a xeno-transplantation system for the engraftment of swine $CD117^+$ hematopoietic progenitor cells into immunodeficient NOG (NOD/SCID/IL-2gc-null) mice. In addition, we studied the differentiation of the swine $CD117^+$ hematopoietic progenitor cells after transplantation into the mice recipients by flow-cytometrical analysis.

2. Materials and Methods

2.1. *Animals and cells*

Newborn triple hybrid swine ((Landrace x Large While) x Duroc) were purchased from a commercial hog firm in Gifu prefecture, Japan and used for collection of bone-marrow (BM) cells. NOD/Shi-scid, IL-2gc-null (NOD/SCID/gc-null; NOG) mice were provided by Central Institute for Experimental Animals (CIEA, Kawasaki, Japan) and kept under specific pathogen-free conditions. Experiments using mice were approved by the Institutional Committee for Animal Care and Use and performed at Tokai University following the University guidelines.

Newborn swine or adult Duroc pigs were sacrificed under anesthesia (0.02 mg/kg Medetomidine Domitor; Nihon Zenyaku Kogyo Co. Koriyama, Japan, 0.2 mg/kg Midazolam; Dormicum injection 10mg, Astellas, Tokyo, Japan, 0.04 mg/kg Butophanol; Vetophale, Meiji Seika Pharma Co. Tokyo, Japan, intramuscular administration). After the birth of the piglets, the umbilical cord blood (CB) cells were collected from the umbilical cords of the expelled uterus using a 5ml syringe with 21Gx1 1/2 needle. The cells were centrifuged on Lymphocepal (IBL Co. Takasaki, Japan) at 2,000 rpm for 30 min. Mononuclear cells (MNCs) were collected and the remaining red blood cells (RBCs) were lysed with low osmotic buffer (20 mM Tris-HCl, pH7.4, 0.15 M NH4Cl). Femurs of the BMs were taken from the newborn swine and the cells were released from the tissues. RBCs were lysed and the cell suspension, prepared as mentioned above, was suspended in RPMI1640 medium (Nissui, Tokyo, Japan) containing 10% (v/v) heat-inactivated fetal calf serum (FCS; SAFC Biosciences, Tokyo, Japan) and used for the cytometric analyses.

2.2. *Preparation of CD117 transfectant*

The cDNA sequence of the swine CD117 gene used in this study was based on Sus scrofa KIT mRNA sequence (AB250963). RNA was extracted from cells by Isogen (Nippon Gene Co. LTD., Tokyo, Japan) and reverse-transcribed to cDNA by using the Superscript system (Invitrogen, Carlsbad, CA). A 2966 bp portion of the cDNA sequence that corresponds to an extracellular domain of the protein was amplified by PCR using cDNA as a template and AccuPrime Pfx DNA Polymerase (Invitrogen, Tokyo, Japan). The set of forward and reverse primers for PCR amplification of the CD117 gene used were as follows:

F, 5'-TAGAATTCGGTCTCACCGGTCGCCACCATG AGAGGCGCTCGCCGCGCCTGGGATT-3',
R, 5'-ATGATATCGGTCTCGGATCCTCAGACGTCT TCGTGGACAAGCA-3'.

Modified S/MAR-based episomal vectors (*22*) expressing swine CD117 cDNA were transfected into HEK293 or a mouse lymphoma cell line, A20, by electroporation using Gene Pulser (Neon® invitrogen,

Oregon, USA) according to the manufacturer's instructions.

2.3. *Monoclonal antibody preparation*

We initially immunized BALB/c mice with mitomycin C (MMC, Kyowahakko-Kirin, Tokyo Japan)-treated swine cord blood (CB) MNCs (1×10^6 cells/animal). For booster treatments, MMC-treated A20 transfectant was used biweekly for 3-6 times with 4×10^5 cells/animal with each immunization. MMC (final, 0.04 mg/mL) was added to the culture and incubated at 37°C for 30 min in 5% CO_2. The serum antibody titers of immunized mice were checked by flow cytometry analyses using CD117 cDNA-transfected HEK293 cells as a source of antigen. After 4 days of the final boost, mice were sacrificed and splenocytes were fused with the mouse myeloma cell line, P3-X63-Ag8-U1, according to a standard procedure. Positive clones were identified by using flow cytometry or an Imaging Analyzer (Array Scan, Thermo scientific, MA, USA). Briefly, CD117 transfected HEK293 cells were plated into the wells of 96 well plates. Culture supernatants were added to each well, incubated for 15 min and washed twice. APC-labeled (APC: allophycocyanin) anti-mouse IgG polyclonal antibody (Poly4053; Bio Legend, San Diego, US) was added and incubated for 15 min. Plates were washed and stained with Hoechst (Invitrogen, Oregon, USA) for 30 min at room temperature and analyzed using the Imaging Analyzer. Positive cells were picked according to the fluorescent intensity of APC and the co-expressed mVenus fluorescent protein. The positive clones were then isolated, expanded and stocked.

2.4. *Preparation of primary murine and human mast cells*

Murine mast cells were prepared from the femurs of four- to six-week-old C57BL/6J mice. BM cells were cultured in RPMI1640 (Sigma-Adrich, St.Louis, US) supplemented with 10% (v/v) heat-inactivated FCS (SAFC Biosciences, Tokyo, Japan), and 4 ng/ml recombinant interleukin (IL)-3 (PeproTech, Rocky Hill, US). BM mast cells were used for experiments after they were cultured for six to eight weeks. We obtained approval of the ethical review boards to prepare primary human mast cells from CB-derived $CD34^+$ MNCs (RIKEN BioResource Center, Tsukuba, Japan). The $CD34^+$ cells were cultured in serum-free Iscove methylcellulose medium (Stem Cell Technologies Inc., Vancouver, BC, Canada) and Iscove modified Dulbecco medium containing SCF at 200 ng/mL, IL-6 at 50 ng/mL and IL-3 at 1 ng/mL as previously described (*23*). On day 42 of culture, methylcellulose was dissolved in phosphate-buffered saline (PBS) and the cells were resuspended and cultured in Iscove modified Dulbecco medium containing SCF at 100 ng/mL and IL-6 at 50 ng/mL with 2% FCS.

2.5. *Flow cytometry*

Cells were incubated with appropriately diluted, fluorescence-labeled primary Mab for 15 min at 4°C and washed with 1% (w/v) bovine serum albumin-containing PBS. In some cases, cells were re-incubated with labeled secondary antibody. The Mabs used were as follows: anti-mouse TER119-FITC (eBioscience, San Diego, CA), anti-swine CD45-FITC (clone # K252-1E4, AbD Serotec, Kidlington, UK), anti-swine CD3 (clone # 8E6, Monoclonal Antibody Center, WA, USA), anti-mouse CD117 (clone # 2B8, eBioscience) and anti-human CD117 (clone # YB5.B8, BD Bioscience), goat anti-mouse IgG1-RPE (Southern Biotech, Uden, Netherland) respectively. Cells were washed and further incubated with FITC-conjugated mouse anti-human IgE Mab (clone # BE5, eBioscience) on ice for 20 min. Stained cells were analyzed on FACS Calibur (Becton Dickinson, New Jersey, USA).

2.6. *Colony assay*

Newborn swine BM cells were washed and an aliquot was stained with 2A1 Mab as described above. After the staining with the Mab, cells were rewashed and sorted by employing a magnetic cell sorting system (AutoMACS, Miltenyi Biotec, Bergisch Gladbach, Germany) to separate $CD117^+$ cells from $CD117^-$ cells. The isolated cells were replated at 5×10^4/dish in 1 mL of methylcellulose-containing medium (StemCell technologies, Vancouver, Canada) in a 35 mm dish with mouse or human SCF (10 ng/mL), IL-3 (10 ng/mL), erythropoietin (2 U/mL) and granulocyte colony-stimulating factor (G-CSF) (10 ng/mL) and cultured at 37°C in a 5% CO_2 atmosphere. After 14 days of culture, the different types and numbers of hematopoietic colonies (colony-forming units (CFU)) were counted according to standard criteria. Samples from each animal were processed and assayed in triplicate with two different animals used for each of two separate experiments.

2.7. *Transplantation of swine hematopoietic cells into NOG mice*

$CD117^+$ cells were purified from newborn swine BMs by cell sorter as described above in section 2.6. Purity was more than 98% based on quantitation by flow cytometry. Nine-week-old NOG mice were irradiated with 2.5Gy X-ray prior to transplantation and swine cells were injected into mice intravenously (Suppl. Table 1, *http://www.biosciencetrends.com/docindex.php?year=2014&kanno=6*). Peripheral blood was collected *via* orbit under inhalation anesthesia at two and

four weeks after transplantation. MNCs were prepared and analyzed by flow cytomety.

2.8. *Transplantation of swine hematopoietic cells into NOG mice*

Student's *t*-test was performed, and data were expressed as mean ± S.D.

3. Results

3.1. *CD117 monoclonal antibody preparation*

The protocol used for CD117 monoclonal antibody preparation is shown in Suppl. Figure 1 (*http://www.biosciencetrends.com/docindex.php?year=2014&kanno=6*). First, swine CD117 cDNA was inserted into N576, an expression vector containing a monomer Venus yellow-green fluorescent protein (mVenus)-reporter gene, and the modified vector was transfected into the mouse lymphoma cell line A20 by electropolation. The expression of the mVenus gene was observed in more than 50% of the transfected cells 18-24 hr after transfection (Suppl. Figure 1A). Second, BALB/c mice were injected intraperitoneally initially with mitomycin C (MMC)-treated swine cord blood (CB) mononuclear cells (MNCs) and then with MMC treated N576-A20 cells as the booster immunizations (Suppl. Figure 1B). Third, the titer of the antiserum was checked against the CD117 expressed by the N576-HEK293 cells. The crossreactivity between N576-HEK293 and the antisera was confirmed by flow cytometry (Suppl. Figure 1C).

We selected a specific 2A1 subclone (Figure 1 and Suppl. Figure 2, *http://www.biosciencetrends.com/docindex.php?year=2014&kanno=6*) for further use because this clone secreted a Mab that reacted with the transfectants expressing CD117 and the mVenus fluorescent protein with similar or identical staining patterns (Figures 1B and 1C). All of the 2A1 subclones showed similar staining patterns, suggesting that they were stable expression products.

As CD117 is expressed on mast cells, we examined if the 2A1 Mab could also interact with the human and mouse CD117 molecules using cell lines derived from human or mouse primary mast cells. As shown in Figure 1D, neither human nor mouse mast cells were stained with 2A1. These results suggest that the 2A1 Mab is specific to swine CD117.

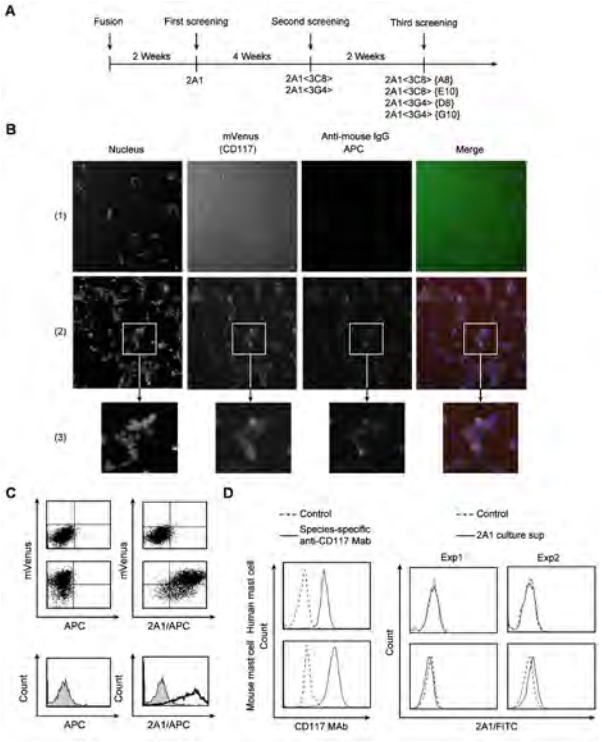

Figure 1. CD117-specific monoclonal antibody 2A1 specifically stains swine CD117. (A) Protocol for the cloning of swine CD117-specific Mab. Three screenings were performed after hybridoma fusion by limiting dilution of 2A1 hybridomas. **(B)** Imaging Analyzer image of the HEK293 parent cells **(1)** and CD117-HEK293 cells **(2)**. CD117 expression was monitored by mVenus expression. Screening of the hybridoma supernatants was performed by staining with the secondary antibody, anti-mouse IgG-APC. The encircled CD117-HEK293 cells in **(2)** are shown at a higher magnification (5×) in **(3)**. **(C)** The positive hybridoma supernatant submitted for the reactivity to the transfectant cells and analyzed by flow cytometry. The percentage of the cell numbers in the respective gates is shown in the quadrant panels. Control means the anti-mouse IgG-APC reactivity without the supernatants. **(D)** The reactivity of 2A1 Mab and species-specific anti-CD117 Mabs with human and mouse mast cells. As shown in the left panels, the human and mouse mast cells reacted with their respective species-specific anti-CD117 Mabs (anti-human CD117 or anti-mouse CD117 antibodies, respectively). Right panels; mast cells were stained with 2A1 and the dotted and solid curves are overlays of the control and 2A1 culture supernatants, respectively. Representative data of five independent assays are shown.

3.2. *CD117 expression in swine bone marrow (BM) cells*

To better clarify the existence of the swine CD117$^+$ cells in the lymphoid tissue, we examined their presence in the adult and newborn BMs, as hematopoietic stem/progenitor cells are abundant in the BM. Figure 2 shows that the newborn BM cells included a high level of 2A1-positive cells (ca.10%) compared to the ten fold lower levels (1.9%) in the adult BM cells. In addition, the ratio of CD117$^+$ cells is very low (0.5%) in the CB and no CD117$^+$ cells were detected in the spleen, lymph nodes and peripheral blood monocytes. These results suggest that CD117$^+$ cells and hematopoietic stem/progenitor cells exist in the swine bone marrow and other lymphoid tissues at a ratio that is comparable with human and mouse.

3.3. *Colony assay for the multipotency of CD117$^+$ cells*

To analyze the multipotency of CD117$^+$ BM cells *in vitro*, the swine BM MNCs were collected and stained

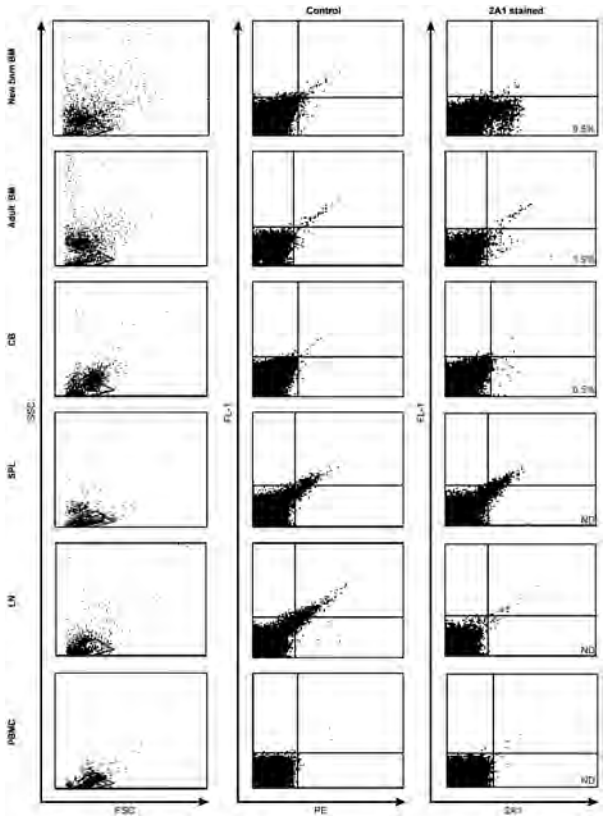

Figure 2. Abundance of swine CD117$^+$ cells in newborn BM relative to five other lymphoid tissue cells (adult BM, CB, SPL, LN and PBMC). Lymphoid tissue cells were stained with 2A1 Mabs. Control means the secondary antibody-stained cells. The percentage of 2A1 stained CD117$^+$ cells within the lymphoid-gate are shown in each panel. ND; not detected. Representative data of five independent assays are shown.

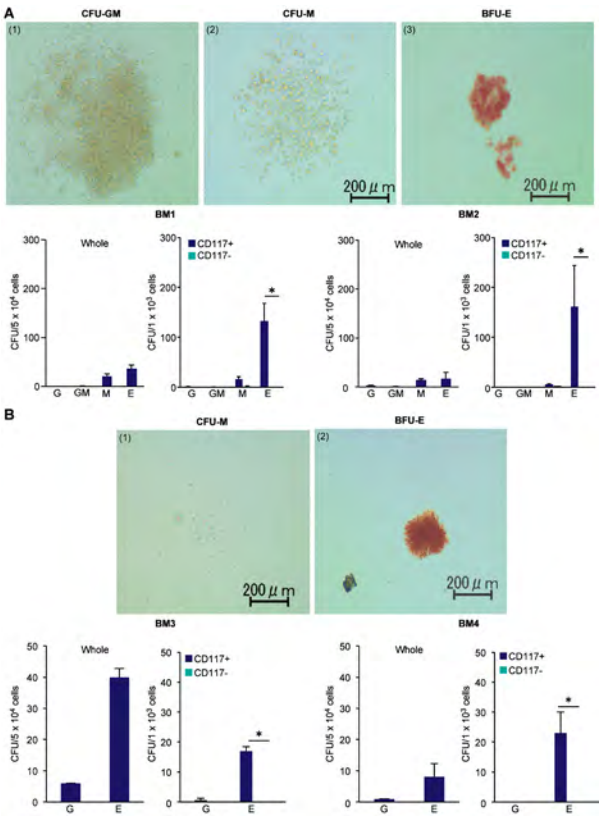

Figure 3. Swine CD117+ cells extensively develop into erythroid-lineage cells *in vitro*. BM cells were sorted as shown in Supplementary Figure 3 and the sorted cells were used in the colony assay. **(A)** Colony assay using the human cytokines SCF, IL-3, erythropoietin and G-CSF. **(1)** CFU-GM, **(2)** CFU-M, **(3)** BFU-E. (G; granulocyte, GM; granulocyte and monocyte, M; monocyte, E; erythrocyte). The data were obtained from two separate swine BM experiments, BM1 and BM2, for the human cytokine environment. Three independent cultures were performed for both of the two BMs and the colonies were counted and compared. The mark * represents the significant difference by *t*-test ($p < 0.05$). Two independent assays and representative photographs are shown here. **(B)** Colony assay using the mouse cytokines SCF, IL-3, erythropoietin and G-CSF. **(1)** CFU-G, **(2)** BFU-E. All pictures were taken by KEYENCE BIOREVO BZ-90000, Object lens: ×10 Plan Fluor NA 0.30 Ph1. The data were obtained from two separate swine BM experiments, BM3 and BM4, for the human cytokine environment. Three independent cultures were performed for both of the two BMs and the colonies were counted and compared. The mark * represents the significant difference by *t*-test ($p < 0.05$). Two independent assays and representative photographs are shown here.

with 2A1. The CD117$^+$ cells were purified as shown in Suppl. Figure 3 (*http://www.biosciencetrends.com/docindex.php?year=2014&kanno=6*). CD117$^+$ cells and CD117- cell fractions were partially purified by magnetic beads sorting at first and then to over 98% purity levels by additional sorting using a FACSaria (Suppl. Figure 3A). Both of the CD117 positive and negative cell fractions were then used in a colony assay by culturing the cells in the presence of the human cytokines, SCF, IL-3, erythropoietin and G-CSF. As a result of the cellular purifications and colony assays four types of cellular clones were identified in the BM cell cultures. These were granulocytes (G), granulocytes/monocytes (GM), monocytes (M) and erythrocytes (E). Notably, CD117$^+$ cells in the colony assay generated erythroid burst-forming units (BFU-E) with significantly higher efficiency than either the BM cells or CD117$^-$ cells. The generation of colony forming units (CFU) were also observed for G, M and GM, but at significantly lower levels for the CD117$^+$ cell fraction (Figure 3A). Similar results were obtained when the cells were cultured in the colony assay using the mouse instead of the human cytokines (Suppl. Figure 3B). In two of these experiments, the frequency of BFU-E in the CD117$^+$ cell fraction was significantly higher than in the CFU-M assay or in the CD117$^-$ cell fraction. The CFU of the other cell types, G and GM, were low or undetectable (Figure 3B and Suppl. Figure 3B). Compared to human cytokine conditions, the colony forming ability of BM cells was less effective with the mouse cytokines.

Overall, these results suggest that the swine CD117$^+$ BM cells have the potential to develop into erythroid-monocyte lineage *in vitro*.

3.3. *Development of swine hematopoietic cells in immunodeficient NOD/SCID/IL-2gc-null (NOG) mouse*

While mouse cytokines can support the development of swine erythroid cells and monocytes, other cell lineages

could not be detected by the *in vitro* colony assay. Therefore, we transplanted the swine hematopoietic cells into severely immunodeficient NOG mice to examine if lymphoid lineage cells could be developed from the CD117$^+$ cells *in vivo*. Swine CD117$^+$ cells were purified and transplanted into irradiated NOG mice and analysed by cytometry using different gate settings to detect erythroid cells, lymphoid cells and monocytes (Figure 4A). After 2 and 12 weeks post transplantation, lymphoid organs were collected and the presence of swine blood cells were examined by flow cytometry using the lymphoid gate setting. As a result,

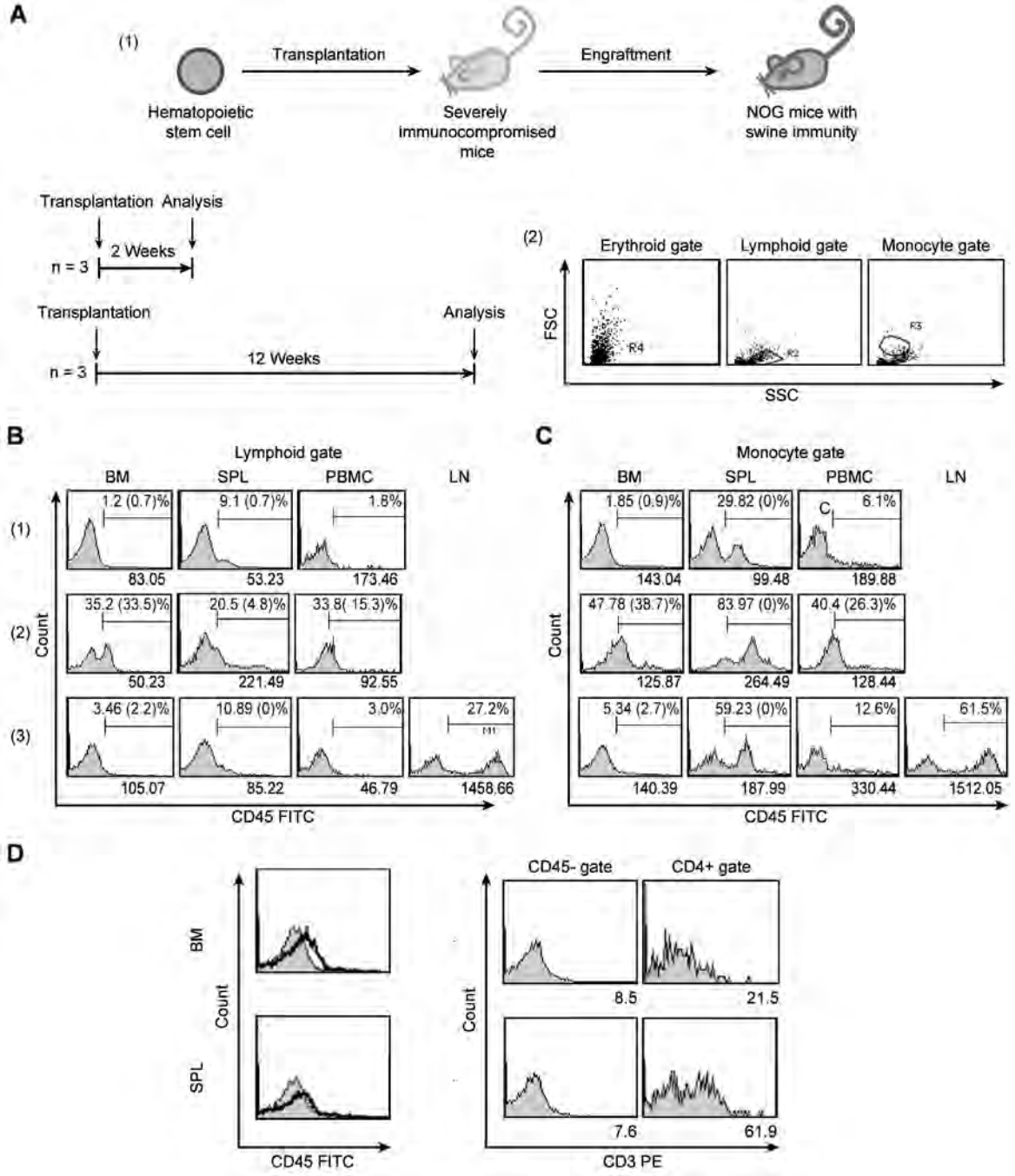

Figure 4. Repopulation of CD117$^+$ swine BM cells in immunodeficient NOG mice. (A) (1) Protocol for CD117$^+$ cell transplantation into NOG mice. In short term (2 w) and long term (12 w) analysis after the transplantation, lymphoid cells were analyzed for the swine cell engraftment either two weeks or twelve weeks after transplantation. **(2)** Flow cytometrical gates used for the analyses of erythroid (R4), lymphoid (R2) and monocyte (R3) cells were set by FSC and SSC. **B** and **C**. Flow cytometrical analysis of engrafted swine cells. Swine leukocytes were detected by swine CD45 expression using an anti-swine CD45-FITC antibody. Lymphoid-gated cells are shown in **B** and monocyte-gated cells in **C**. **(B) (1)** Non-transplanted control mice. **(2)** Two weeks after the transplantation. **(3)** Twelve weeks after the transplantation. Some of the SPL cells are stained with CD45-FITC. These are some non-specific binding of the antibodies to the cells as we analyzed by 2D-flow cytometry analysis (data not shown). The numbers show the shifted cell percentages compared to control mice without transplantation. In the brackets, shifted percentages of no-stain controls are shown. **(D)** Lymphoid-gated cells were analyzed for the expression of CD3. Swine CD45-FITC and CD3-PE double staining of the BM and SPL cells are shown in the panels. The mean fluorescent intensity (MFI) is shown below the panels. Representative data of three independent assays are shown.

swine $CD45^+$ cells were observed in BM, spleen (SPL) and the peripheral blood of NOG mice transplanted with $CD117^+$ cells 2 weeks after the transplantation (Figure 4B). Higher amounts of the $CD45^+$ cells were observed through the monocyte gate of the SPL cells 2 weeks after transplantation (Figure 4C). $CD45^+$ cells were also observed in the lymph node 12 weeks after transplantation. These results indicate that the engrafted swine white blood cells had developed successfully in the NOG mice. We used a TER119 antibody, which recognizes mouse erythrocyte to distinguish between the mouse and swine erythrocytes, and found that the NOG mice included $TER119^-$ cells in the erythrocyte gate, and that the swine $CD117^+$ cells might be differentiated into erythrocytes, which were TER119 (mouse erythroid marker) negative, *in vivo* (Suppl. Figure 4, *http://www.biosciencetrends.com/docindex.php?year=2014&kanno=6*).

The $CD45^+$ cells of the mice SPL were examined for the CD3 expression in lymphoid gate 12 weeks after the transplantation. As shown in Figure 4D, significant amount of $CD3^+$ cells were observed in the SPL.

These results show that the transplanted swine $CD117^+$ cells had developed into erythroid, myeloid and lymphoid cells in NOG mice and suggest that the swine $CD117^+$ cells are hematopoietic stem/progenitor cells that can be transplanted successfully to a different species under the right conditions of engraftment.

4. Discussion

CD117 is a cytokine receptor tyrosine kinase type III expressed on the surface of hematopoietic stem cells and when activated by the cytokine SCF can regulate the maintenance, proliferation, migration and differentiation of HSCs in the BM. In the swine, the stem cell activity of $CD117^+$ cells have been previously evaluated by using SCF to activate their stem cell potential to differentiate into various cellular lineages (*20,21*). Although a swine CD117 Mab has been developed and characterized (*24*), the species specificity of the Mab and xeno-transplantation of $CD117^+$ cells have not been reported. They checked *in vitro* development of erythroid and myeloid cells from Mab-enriched cells, but they could not detect lymphoid cell development. Swine SCF-reacting cells previously reported could not develop lymphoid cells, either (*25*). Because the species specificity of both tools was unclear, xeno-transplantation experiments using a species specific CD117 Mab might not be undertaken until we prepared our own highly species-specific anti-CD117 Mab clone. This Mab clone, 2A1, enabled us to evaluate the multipotency of swine $CD117^+$ cells *in vitro* and *in vivo*. The Mab reacted against the swine CD117 receptor expressed by a recombinant DNA vector N576 in HEK293 or A2 cells, was specific for the detection of CD117 in swine and did not cross react with the CD117 cells of mice or humans. This specificity allowed us to develop the *in vivo* xeno-transplantation system using NOG mice because the porcine specific CD117 antibody did not cross-react with other cells examined. In this *in vivo* system, we demonstrated that $CD117^+$ cells could develop into T cells, which indicate that the $CD117^+$ cells involve hematopoietic stem cells.

Consequently, on the basis of the specificity of Mab 2A1, we found that $CD117^+$ cells were abundant in the newborn swine BM, but not in CB or adult BM. Moreover, the $CD117^+$ cells from the newborn BM were found to develop into erythroid cells or monocytes using the *in vitro* colony assay and into lymphoid cells by the xeno-transplantation *in vivo* system. Thus, both the *in vitro* and the *in vivo* experiments confirmed that the $CD117^+$ cells from the newborn swine BM are hematopoietic stem/progenitor cells.

The similarity between our *in vitro* data for $CD117^+$ cells from the newborn BM and the data reported by Dor *et al*. (*25*) in the spleen or BM of young pigs less than 1 year old suggests a high efficiency of $CD117^+$ cell purification with SCF-binding affinity in their system. In our *in vitro* study, we also confirmed that the $CD117^+$ cells differentiated into the erythrocytes in the presence of mouse or human cytokines SCF, IL-3, erythropoietin and G-CSF. While the swine $CD117^+$ cells developed into erythroid colonies in our *in vitro* studies and those of others (24), we could not definitely conclude the potential of the $CD117^+$ cells to develop into erythroid cells in the mouse transplantation system because of the absence of a good erythrocyte monitoring system. We could only suggest that the TER119-negative erythroid gated cells were observed early after the $CD117^+$ cell transplantation. On the other hand, we found white blood cells including $CD3^+$ cells in the peripheral lymph organs of the transplanted NOG mice, suggesting that the $CD117^+$ cells had differentiated into the monocyte and lymphoid lineages. Human HSC that were transplanted into NOG mice developed into myeloid and lymphoid lineages, but not into erythroid lineage cells *in vivo* (*13,26*). The cytokine, erythropoietin, is a known requirement for the differentiation of CD117 stem cells into erythroid precursor cells and erythrocytes (*27*). The contrary results obtained in the *in vitro* and the *in vivo* systems respectively may be due to the presence of sufficient amount of erythropoietin in the *in vitro* system and its reduced amount in the *in vivo* system. Alternatively, other synergistic factors are missing or inhibitory factors are in play preventing the CD117 stem cells from developing into erythrocytes in the xeno-transplantation environment.

In conclusion, we produced a highly specific anti-swine CD117 Mab and used it to confirm that the swine $CD117^+$ stem cells have a multipotency that can differentiate into erythroid cells, monocytes and lymphoid cells depending on the *in vitro* or *in vivo* system chosen for analysis. The swine-NOG mouse transplantation system in conjunction with

specific detection reagents like the Mabs 2A1 shows an important experimental potential for the study of hematopoietic cells *in vivo*, especially for understanding the factors required in erythroid cell development from hematopoietic stem/progenitor cells.

Acknowledgements

This work was supported by JSPS KAKENHI Grant number 22380172 and MEXT-Supported Program for the Strategic Research Foundation at Privated Universities (2012-2016). We thank the members of Teaching and Research Support Center in Tokai University School of Medicine for their technical skills. We also thank Yumiko Nakagawa for her excellent animal care skills.

References

1. Smith KP, Luong MX, Stein GS. Pluripotency: Toward a gold standard for human ES and iPS cells. J Cell Physiol. 2009; 220:21-29.
2. Gokhale PJ, Andrews PW. The development of pluripotent stem cells. Curr Opin Genet Dev. 2012; 22:403-408.
3. Oberritter Z, Rolle U, Juhasz Z, Cserni T, Puri P. Altered expression of c-kit-positive cells in the ureterovesical junction after surgically created vesicoureteral reflux. Pediatr Surg Int. 2009; 25:1103-1107.
4. Leri A, Kajstura J, Anversa P. Role of cardiac stem cells in cardiac pathophysiology: A paradigm shift in human myocardial biology. Circ Res. 2011; 109:941-961.
5. Kawachi K, Iso Y, Sato T, Wakabayashi K, Kobayashi Y, Takeyama Y, Suzuki H. Effects of erythropoietin on angiogenesis after myocardial infarction in porcine. Heart Vessels. 2012; 27:79-88.
6. Rozemuller H, Prins H, Naaijkens B, Staal J, Bühring H, Martens A. Prospective isolation of mesenchymal stem cells from multiple mammalian species using cross-reacting anti-human monoclonal antibodies. Stem Cells Dev. 2010; 19:1911-1921.
7. Lunney JK. Advances in swine biomedical model genomics. Int J Biol Sci. 2007; 3:179-184.
8. d'Apice AJ, Cowan PJ. Xenotransplantation: The next generation of engineered animals. Transpl Immunol. 2009; 21:111-115.
9. Tseng YL, Sachs DH, Cooper DK. Porcine hematopoietic progenitor cell transplantation in nonhuman primates: A review of progress. Transplantation. 2005; 79:1-9.
10. He JQ, Vu DM, Hunt G, Chugh A, Bhatnagar A, Bolli R. Human cardiac stem cells isolated from atrial appendages stably express c-kit. PLoS One. 2011; 6:e27719.
11. Ezashi T, Telugu BP, Roberts RM. Induced pluripotent stem cells from pigs and other ungulate species: An alternative to embryonic stem cells? Reprod Domest Anim. 2012; 47 (Suppl 4):92-97.
12. Shultz LD, Brehm MA, Garcia-Martinez JV, Greiner DL. Humanized mice for immune system investigation: Progress, promise and challenges. Nat Rev Immunol. 2012; 12:786-798.
13. Ito M, Kobayashi K, Nakahata T. NOD/Shi-scid IL2rγ^{null} (NOG) mice more appropriate for humanized mouse models. Curr Top Microbiol Immunol. 2008; 324:53-76.
14. Suzuki M, Takahashi T, Katano I, Ito R, Ito M, Harigae H, Ishii N, Sugamura K. Induction of human humoral immune responses in a novel HLA-DR-expressing transgenic NOD/Shi-scid/γc^{null} mouse. Int Immunol. 2012; 24:243-252.
15. Sato Y, Nagata S, Takiguchi M. Effective elicitation of human effector CD8$^+$ T Cells in HLA-B*51:01 transgenic humanized mice after infection with HIV-1. PLoS One. 2012; 7:e42776.
16. Lennartsson J, Ronnstrand L. Stem cell factor receptor/c-Kit: From basic science to clinical implications. Physiol Rev. 2012; 92:1619-1649.
17. Saito Y, Kametani Y, Hozumi K, Mochida N, Ando K, Ito M, Nomura T, Tokuda Y, Makuuchi H, Tajima T, Habu S. The *in vivo* development of human T cells from CD34$^+$ cells in the murine thymic environment. Int Immunol. 2002; 14:1113-1124.
18. Kametani Y, Shiina M, Katano I, *et al*. Development of human-human hybridoma from anti-Her-2 peptide-producing B cells in immunized NOG mouse. Exp Hematol. 2006; 34:1240-1248.
19. Nunomura S, Shimada S, Kametani Y, *et al*. Double expression of CD34 and CD117 on bone marrow progenitors is a hallmark of the development of functional mast cell of Callithrix jacchus (common marmoset). Int Immunol. 2012; 24:593-603.
20. Le Guern AC, Giovino MA, Abe M, Theodore PR, Qi J, Down JD, Sachs DH, Sykes M, Yang YG. Stem cell activity of porcine c-kit$^+$ hematopoietic cells. Exp Hematol. 2003; 31:833-840.
21. Summerfield A, Horn M, Lozano G, Carrasco C, Atze K, McCullough K. C-kit positive porcine bone marrow progenitor cells identified and enriched using recombinant stem cell factor. J Immunol Methods. 2003; 280:113-123.
22. Mizutani A, Kikkawa E, Matsuno A, Shigenari A, Okinaga H, Murakami M, Ishida H, Tanaka M, Inoko H. Modified S/MAR episomal vectors for stably expressing fluorescent protein-tagged transgenes with small cell-to-cell fluctuations. Anal Biochem. 2013; 443:113-116.
23. Fukunaga M, Nunomura S, Nishida S, Endo K, Gon Y, Hashimoto S, Hashimoto Y, Okayama Y, Makishima M, Ra C. Mast cell death induced by 24(S),25-epoxycholesterol. Exp Cell Res. 2010; 316:3272-3281.
24. Perez C, Moreno S, Summerfield A, Domenech N, Alvarez B, Correa C, Alonso F, Ezquerra A, Dominguez J, Revilla C. Characterisation of porcine bone marrow progenitor cells identified by the anti-c-kit (CD117) monoclonal antibody 2B8/BM. J Immunol Methods. 2007; 321:70-79.
25. Dor FJ, Ramirez ML, Parmar K, Altman EL, Huang CA, Down JD, Cooper DK. Primitive hematopoietic cell populations reside in the spleen: Studies in the pig, baboon, and human. Exp Hematol. 2006; 34:1573-1582.
26. Ito M, Hiramatsu H, Kobayashi K, Suzue K, Kawahata M, Hioki K, Ueyama Y, Koyanagi Y, Sugamura K, Tsuji K, Heike T, Nakahata T. NOD/SCID/γ_c^{null} mouse: An excellent recipient mouse model for engagement of human cells. Blood. 2002; 100:3175-3182.
27. Agosti V, Karur V, Sathyanarayana P, Besmer P, Wojchowski DM. A KIT juxtamembrane PY567 -directed pathway provides nonredundant signals for erythroid progenitor cell development and stress erythropoiesis. Exp Hematol. 2009; 37:159-171.

(Received July 30, 2014; Revised November 11, 2014; Accepted December 13, 2014)

PLOS ONE

RESEARCH ARTICLE

Production of a Locus- and Allele-Specific Monoclonal Antibody for the Characterization of SLA-1*0401 mRNA and Protein Expression Levels in MHC-Defined Microminipigs

Yoshie Kametani[1,2]*, Shino Ohshima[1], Asuka Miyamoto[1], Atsuko Shigenari[1], Masaki Takasu[3], Noriaki Imaeda[3], Tatsuya Matsubara[3], Masafumi Tanaka[1], Takashi Shiina[1], Hiroshi Kamiguchi[4], Ryuji Suzuki[5], Hitoshi Kitagawa[3], Jerzy K. Kulski[1,6], Noriaki Hirayama[7], Hidetoshi Inoko[1], Asako Ando[1]

1 Department of Molecular Life Science, Division of Basic Medical Science, Tokai University School of Medicine, Isehara, Kanagawa, Japan, **2** Institute of Advanced Biosciences, Tokai University, Kanagawa, Japan, **3** Department of Veterinary Medicine, Faculty of Applied Biological Sciences, Gifu University, Gifu, Gifu, Japan, **4** Teaching and Research Support Center, Tokai University School of Medicine, Isehara, Japan, **5** Department of Rheumatology and Clinical Immunology, Clinical Research Center for Allergy and Rheumatology, Sagamihara National Hospital, National Hospital Organization, Sagamihara, Kanagawa, Japan, **6** School of Psychiatry and Clinical Neurosciences, The University of Western Australia, Crawley WA, Australia, **7** Institute of Glycoscience, Tokai University, Hiratsuka, Kanagawa, Japan

* y-kametn@is.icc.u-tokai.ac.jp

OPEN ACCESS

Citation: Kametani Y, Ohshima S, Miyamoto A, Shigenari A, Takasu M, Imaeda N, et al. (2016) Production of a Locus- and Allele-Specific Monoclonal Antibody for the Characterization of SLA-1*0401 mRNA and Protein Expression Levels in MHC-Defined Microminipigs. PLoS ONE 11(10): e0164995. doi:10.1371/journal.pone.0164995

Editor: Michelle L. Baker, CSIRO, AUSTRALIA

Received: March 21, 2016

Accepted: October 4, 2016

Published: October 19, 2016

Data Availability Statement: All relevant data are within the paper and its Supporting Information files.

Funding: This work was supported in part by Japan Society for the Promotion of Science (JSPS) KAKENHI Grant Number 23500502, Tokai University grant Kametani (2015-2017) and MEXT-Supported Program for the Strategic Research Foundation at Private Universities (2012-2016).

Competing Interests: The authors have declared that no competing interests exist.

Abstract

The class I major histocompatibility complex (MHC) presents self-developed peptides to specific T cells to induce cytotoxity against infection. The MHC proteins are encoded by multiple loci that express numerous alleles to preserve the variability of the antigen-presenting ability in each species. The mechanism regulating MHC mRNA and protein expression at each locus is difficult to analyze because of the structural and sequence similarities between alleles. In this study, we examined the correlation between the mRNA and surface protein expression of swine leukocyte antigen *(SLA)-1*0401* after the stimulation of peripheral blood mononuclear cells (PBMCs) by *Staphylococcus aureus* superantigen toxic shock syndrome toxin-1 (TSST-1). We prepared a monoclonal antibody (mAb) against a domain composed of Y102, L103 and L109 in the α2 domain. The Hp-16.0 haplotype swine possess only *SLA-1*0401*, which has the mAb epitope, while other haplotypes possess 0 to 3 SLA classical class I loci with the mAb epitopes. When PBMCs from *SLA-1*0401* homozygous pigs were stimulated, the *SLA-1*0401* mRNA expression level increased until 24 hrs and decreased at 48 hrs. The kinetics of the interferon regulatory transcription factor-1 (IRF-1) mRNA level were similar to those of the *SLA-1*0401* mRNA. However, the surface protein expression level continued to increase until 72 hrs. Similar results were observed in the Hp-10.0 pigs with three mAb epitopes. These results suggest that TSST-1 stimulation induced both mRNA and surface protein expression of class I SLA in the swine

PBMCs differentially and that the surface protein level was sustained independently of mRNA regulation.

Introduction

The class I major histocompatibility complex (MHC) antigens are constitutively expressed cellular membrane-bound glycoproteins that associate non-covalently with β-hamicroglobulin (β2M) to present intracellularly processed peptide antigens to T-cell receptors of specific CD8+ T cells [1–3]. MHC class I proteins are encoded by polymorphic genes at multiple loci, and they also act as ligands for killer-cell immunoglobulin-like receptors (KIRs) [4–6]. This polymorphism results in numerous alleles in a population, presumably to preserve the variability of the antigen presenting ability and help the species to defend against various infectious agents, although MHC variability may also cause autoimmune responses [7–9]. The main function of the classical class I MHC is the activation of cytotoxic T (Tc) cells, whereas the loss of MHC expression induces the activation of natural killer (NK) cells. In contrast, the down-regulation of classical HLA-A and HLA-B expression and up-regulation of non-classical HLA expression, such as HLA-G, negatively regulates the system of MHC-mediated immunity [10–12]. Therefore, it is important to distinguish between the classical and non-classical HLA alleles and their regulation at the level of expressed mRNAs and allele-specific surface proteins, as these different classes of MHC molecules have contrary functions. However, there are relatively few studies on the surface expression of MHC alleles, probably because of the lack of allele-specific monoclonal antibodies due to the similarity of the alleles among the MHC sequences.

The pig is an important animal model for the study of MHC function in response to infections, transplantation, and autoimmune disease [13–16]. Although the MHC molecules are known to be important for controlling infections, research on the regulation of the expression of the pig MHC genomic region, defined in pigs as the Swine Leukocyte Antigen (SLA) region, has received little or no attention to date. Most pigs have three classical SLA class I loci distributed within their MHC genomic region, and more than 100 classical SLA class I alleles have been identified [17–20]. We deduced the haplotypes in two types of mini-pig, Clawn and microminipig, and in the larger Duroc pig [21–23]. The SLA class I allele, *SLA-1*0401*, is one of the most frequently found alleles in various swine breeds such as Microminipig, Clawn, NIH, Yucatan, Mexican hairless mini-pigs and Meishan pigs [19, 20]. Moreover, the three-dimensional structure of this allele in complex with peptides derived from 2009-pandemic H1N1 swine-origin influenza A virus and Ebola virus has been determined in crystallographic studies [24]. Therefore, we decided to prepare a specific domain-recognizing monoclonal antibody against *SLA-1*0401* and analyze its specificity using the peripheral blood mononuclear cells (PBMCs) of SLA homozygous pigs.

Swine are known to be a reservoir for methicillin-resistant *Staphylococcus aureus* (MRSA) [25–30]. Superantigens secreted by *Staphylococcus aureus* are one set of virulence factors that can induce the T cell hyper-immune response and MHC gene expression. The induction of a systemic cytokine storm by superantigens is known to create life-threatening symptoms, such as toxic-shock syndrome in newborn babies [31]. Toxic shock syndrome toxin-1 (TSST-1) is an enterotoxin of *Staphylococcus aureus* and one of the superantigens that is used to activate antigen-specific T cell clones and polyclonal T cells irrespective of the peptide presented by MHC [32, 33]. The TSST-1-reacting T cell receptor (TCR) Vβ induces a large amount of cytokine

secretion containing interferon-γ (IFN-γ)Fto induce the cytotoxicity of T cells [34]. We previously reported that TSST-1 enhanced locus-specific SLA mRNA expression [35]. However, the locus-specific expression of surface SLA protein could not be detected because the only monoclonal antibodies available for the study were anti-HLA antibodies, and although they crossreact with SLA, they cannot distinguish between the different SLA loci and/or alleles [36].

Therefore, the purpose of the present study was (1) to produce and characterize a mAb that specifically recognizes *SLA-1*0401*, and (2) to distinguish the protein and mRNA expression levels of *SLA-1*0401* using the new mAb in TSST-1 in n TSST-1 PBMCs from Microminipigs.

Materials and Methods

Animals and tissues

Experiments using mice for monoclonal antibody production were approved by the Institutional Animal Care and Use Committee at Tokai University and performed at Tokai University following the University guidelines. Eight-week-old female BALB/c mice were purchased from CLEA Japan (Tokyo, Japan) and maintained under specific pathogen-free conditions. Peripheral blood from adult Microminipigs was provided by Fuji Micra Inc (Fujinomiya, Japan). The blood of healthy human donors was collected at the Tokai University Hospital with informed consent, and marmoset blood was purchased from CLEA Japan. The animal health check was performed once a week. No swine or mice became ill or died prior to the experimental endpoint. For blood collection, the mice were either euthanized by inhalation of 4 to 5% isoflurane or sacrificed by cervical dislocation. Since the swine were used only for blood collection (<50 ml), no euthanasia was applied before or after bleeding them with a fine-point needle and syringe.

Genotyping

The peripheral blood samples from Microminipigs with eight SLA haplotypes previously assigned by nucleotide sequence determination of RT-PCR products and low-resolution SLA genotyping using sequence-specific PCR primers (SSP) for the three SLA classical class I genes, SLA-1, SLA-2 and SLA-3 [21], were used in this study. Another twenty Microminipigs were genotyped for their SLA class I alleles using SSP [37], and their SLA class I haplotypes were deduced from their class I alleles and parental class I haplotypes. Of the genotyped alleles, *SLA-1*0501* and *SLA-1*1104* were used to predict the tertiary structure of the epitope, and *SLA-1*0401* was used for the immunization of mice.

Transfection

The transfected cDNA sequence of the swine *SLA-1*0401* gene was derived from SLA-defined Clawn and Yucatan mini-pigs and based on the *Sus scrofa SLA-1*0401* mRNA sequence (AB185317, AB847434, AF464002). The primers used to generate the cDNA sequences are shown in Table 1A (SLA1 N53: SLA1 C35: Table 1A). RNA was extracted from cells using TRIzol (Invitrogen, Carlsbad, CA, USA) and reverse-transcribed to cDNA using the High Capacity cDNA Reverse Transcription Kit (Life Technologies, Carlsbad, CA, USA). The sequence of the *ß2-microglobulin (ß 2M)* gene (Accession number: L13854) in GenBank was used for the design of primer sequences for *ß2M* cDNA synthesis. The primer sequences for preparation of SLA-1, SLA-2, SLA-3, SLA-6 and ß2M transfectants are summarized in Table 1A. The modified S/MAR (scaffold/matrix attachment region) episomal vectors [38] expressing SLA and β2M were used for the transfection.

HEK293 cells, a cell line derived from human embryonic kidney cells, were cultured in D-MEM (GE Healthcare, Buckingham, UK)-10% FCS (Sigma-Aldrich, Co. St. Louis, MO,

Table 1. Primer sequences.

Locus	Allele	Primer name	Primer sequence (5' to 3')	Annealing temp. (°C)	Length of PCR products (bp)	Reference
(A) For preparation of SLA-1, SLA-2, SLA-3, SLA-6 and β2M transfectants						
SLA-1	*SLA-1*0401*	1066: SLA1 N53	TAGATATCGGTCTCATATGGGGCCTGGAGCCCTCTT	60	1,110	This study
		1067: SLA1 C35	TAGGATCCTCACACTCTAGGGTCCTTGGTAAGGGACACATCGGA			This study
SLA-2	*SLA-2*0901*	2174: SLA2 N53	TAGAATTCGAAGACAACCGGTCGCCACCATGCGGGTCAGGGGCCCTCAAGCCATC	60	1,144	This study
		2175: SLA2 C35	ATGATATCGAAGACTGGATCCTCACACTCTAGGATCCTTGGTAAG			This study
SLA-3	*SLA-3*0602*	2176: SLA3 N53	TAGAATTCGAAGACAACCGGTCGCCACCATGGGGCCTGGAGCCCTCTTCTTG	60	1,135	This study
		2177: SLA3 C35	ATGATATCGAAGACTGGATCCTCACACTCTAGGATCCTTGGTGAGAG			This study
SLA-6	*SLA-6*0101*	1068: SLA6 N53	TAGATATCGGTCTCATATGCAGGTCACGGAGCCTCG	60	1,134	This study
		1071: SLA6 C35	TAGGATCCTCAGCTTGCAGCCTGAACATAGT			This study
β2M		1072: β2M PIG N53	TAGATATCGGTCTCATATGGCTCCCCTCGTGGCCTT	60	380	This study
		1073: β2M PIG C35	AGGATCCTTAGTGATCTCGATCCCACTTAACTATCTT			This study
(B) For real-time PCR assay						
SLA-1	*SLA-1*0501*	SLA-1-051F	GACTCCCGCTTCATCGCCGT	60	160	This study
		SLA-1-052R	GTGAGGTGTCCCTTTGTTTCC			This study
	*SLA-1*1104*	SLA-1-114F	AGCCCCGTTTCATCGAAGTC	60	156	This study
		SLA-1-115R	CGCTGCCCATGACACGCCG			This study
IFNγ		IFN-γ-4F	GCTCTGGGAAACTGAATGACTT	53	199	Kametani et al. 2012
		IFN-γ-4R	TATTGCAGGCAGGATGACAA			Kametani et al. 2012
IRF1		21 1114–1134 59 52	GATCTGAAGAAGAACGTGGACACC	50	65	Kametani et al. 2012
		18 1161–1178 60 61	ATGGAGGGCAGCCTGACT			Kametani et al. 2012
G3PDH		G3PDH-F	GGACCTGACCTGCCGTCTG	60	450	Kametani et al. 2012
		G3PDH-R	TCCACCACCCTGTTGCTGTA			Kametani et al. 2012
(C) For sequence-based typing (SBT) method						
SLA-1		SLA1-9/1,2R	CCTCTTCCTGCTGCTGTCG	65	585	Ando et al. 2003
			AGCGTGTCCTTCCCCATCT			Ando et al. 2003
		SLA1-15/1,2R	GGAGCCCTCTTCCTGCTGC	61	590	Ando et al. 2014
			AGCGTGTCCTTCCCCATCT			Ando et al. 2014
		SLA1-18/1,2R	TTCCTGCTGCTGTCGGGGGC	61	581	Ando et al. 2014
			AGCGTGTCCTTCCCCATCT			Ando et al. 2003
		SLA1-3#92/r#119	CCAGACCCCGAGGCTGAGGAT	61	1,512	Ho et al. 2006
			TTCTCAATCCTTCCATTTATTTCCTC			Ho et al. 2006
SLA-2		SLA2-3/1,2R	GCCATCCTCATTCTGCTGTC	65	587	Ando et al. 2003
			AGCGTGTCCTTCCCCATCT			Ando et al. 2003
		SLA2-8/1.2GR	CCCTCAAGCCATCCTCATTCTG	63	596	Ando et al. 2014
			GCAGCGTGTCCTTCCCCATC			Ando et al. 2014

(*Continued*)

Table 1. (*Continued*)

Locus	Allele	Primer name	Primer sequence (5' to 3')	Annealing temp. (°C)	Length of PCR products (bp)	Reference
		SLA2-f#55/r#56R	CCACAGAATCTCCGCAGATTC	60	1,232	Ho et al. 2006
			CCGACACAGACACATTCAAATGCT			Ho et al. 2006
SLA-3		SLA3-5/3-6R	CCCGAGCCCTCTTCTTGCT	65	566	Ando et al. 2003
			TTTCTGGAGCCACACCACA			Ando et al. 2003
		SLA3-8/3-9R	CCGAGCCCTCTTCCTGCTG	66	565	Ando et al. 2003
			TTTCTGGAGCCACTCCACA			Ando et al. 2003
		SLA3-10/3-11R	GACCCTGGCCCTGACTGGT	68	533	Ando et al. 2003
			GGAGCCACTCCACACACGC			Ando et al. 2003
		SLA3-f#923/ r#121	CCAGACTCCGAGGCTGAGGAT	61	1,494	Ho et al. 2006
			TAGGCTCTTTTCCCTTGGTTAGG			Ho et al. 2006

doi:10.1371/journal.pone.0164995.t001

USA) medium and A20 cells, a BALB/c B cell lymphoma line derived from a spontaneous reticulum cell neoplasm, were cultured in RPMI 1640 (Nissui Pharmaceutical co. Ltd. Tokyo, Japan)-10% FCS medium. The cells were transfected with the cDNA sequence inserted in the N576 expression vector using the Invitrogen Neon transfection system (HEK293 cells: 1100 V, 10 ms 3 pulses; A20 cells: 1500 V, 10 ms, 3 pulses) and cultured in 5% CO_2 at 37°C for 18 ~24 hrs. Cultured cells were collected and the expression of the mVenus reporter gene was measured by flow cytometry (Becton Dickinson, NJ, USA).

Preparation of the peripheral blood mononuclear cells (PBMCs)

Swine peripheral blood samples were collected into a heparinized tube and centrifuged on Lymphoprep (Axis-Shield, Oslo, Norway) at 670 x g for 30 min. PBMCs were collected and washed with 10 ml of 1% (w/v) bovine serum albumin (BSA)-containing phosphate-buffered saline (PBS). The blood cells were collected by centrifuging at 350 x g for 5 min, and the remaining erythrocytes were lysed osmotically. The white blood cells were washed with PBS and used for further experiments. Human PBMC samples were purified using Ficoll Paque (GE Healthcare UK Ltd.), and mouse and marmoset PBMCs were purified using Lymphocepal.

Monoclonal antibody preparation

We initially immunized BALB/c mice with mitomycin C (MMC, Kyowahakko-Kirin, Tokyo Japan)-treated swine PBMCs (2.2×10^6 cells/animal). For booster treatments, MMC-treated A20 transfectants were used biweekly for 7 times with 6.8×10^5 cells/animal at each immunization. MMC (final, 0.04 mg/ml) was added to the culture and incubated at 37°C for 30 min in 5% CO_2. The mice were anesthetized with 20% isoflurane, and the blood was collected from the orbit. The serum antibody titers of immunized mice were checked by flow cytometry analyses using SLA-1/β2M cDNA-transfected HEK293 cells as a source of antigen. After 4 days of the final boost, mice were anesthetized with 20% isoflurane and sacrificed by blood removal; subsequently, splenocytes were fused with the mouse myeloma cell line P3-X63-Ag8-U1 according to a standard procedure [39]. Positive clones were identified by flow cytometry or by using an Imaging Analyzer (Array Scan, Thermo scientific, MA, USA). Briefly, SLA-1/β2M transfected HEK293 cells were plated in the wells of 96-well plates. Culture supernatants were added to each well, incubated for 15 min and washed twice. APC-labeled (APC: allophycocyanin) anti-mouse IgG polyclonal antibody (Poly4053; Bio Legend, San Diego, US) was added and incubated for 15 min. Plates were washed and stained with Hoechst dye (Invitrogen, Oregon, USA) for 30 min at room temperature and analyzed using the Imaging Analyzer. Positive cells were picked according to the fluorescence intensity of APC and the co-expressed mVenus fluorescent protein. The positive clones were then isolated, expanded and stocked. The mAb isotype was determined using a mouse monoclonal antibody isotyping kit (Iso Strip, Roche, Basel Schweiz).

Flow cytometry

Cells were incubated with appropriately diluted, fluorescently-labeled primary mAb for 15 min at 4°C and washed with 1% (w/v) BSA-containing PBS. In some cases, cells were re-incubated with labeled secondary antibody. The mAbs used were as follows: anti-class-I major histocompatibility antigen (Monoclonal Antibody Center Co. Ltd, clone #PT85A), goat anti-mouse IgG1-RPE (Southern Biotech, Uden, the Netherlands). Stained cells were analyzed using the FACSVerse system (Becton Dickinson, New Jersey, USA) and FlowJo software (Tomy

biochemical, Tokyo, Japan). The culture supernatant of X2F6 was also used for the primary antibody.

Primary sequence and structure analysis of the X2F6 mAb and model building of the 3D structure

Total RNA was extracted from specific hybridoma X2F6, and the cDNA was checked for the amplification of immunoglobulin heavy- and light-chain-specific genes. Sequence reactions were performed with a GenomeLab DTCS Quick Start Kit (Beckman Coulter) and analyzed using a CEQ8000 Genetic Analysis System (Beckman Coulter). The software Genetyx was used for sequence prediction. The 3D model of the Fab fragment of X2F6 was constructed using protocols for antibody homology modeling [40] implemented in a software system, Molecular Operating Environment (MOE) (http://www.chemcomp.com, last accessed April 2014). The Protein Data Bank [41] ID code (PDB ID) of the template structure used for modeling is 3V7A [42].

Model-building of the SLA-1 3D structure

The protein structures of SLA-1*0501 and SLA-1*1104 were constructed by the use of homology modeling protocols implemented in MOE. The X-ray crystal structure of SLA-1*0401 (PDB ID: 3QQ4) [24] was used as the template structure and the bound antigenic peptide was used to construct the 3D structures of SLA-1*0501 and SLA-1*1104.

Stimulation of PBMCs

Swine peripheral blood samples were collected into a heparinized tube and centrifuged on Lymphocepal (IBL Co. Fujioka, Japan) at 670 x g for 30 min. PBMCs were collected and washed with 10 ml of 1% (w/v) BSA-containing PBS (PBSA) by centrifuging at 350 x g for 5 min and the remaining erythrocytes were lysed osmotically. The PBMCs were washed and cultured ($2.4x10^6$/well) in RPMI 1640 medium containing 10% FCS in the presence of the toxic shock syndrome-1 (TSST-1) enterotoxin, (Toxin Tec. Sarasota, USA) at 1 μin τ ορ ΙΦΝ-γ (ITSI-Bioscience, PA, USA) at 1 ng/ml for up to 72 h at 37°C, 5% CO_2. After 24, 48 and 72 hrs the cells were collected, washed with PBSA and used for the analyses by flow cytometry and quantitative real-time PCR.

RNA extraction and quantitative real-time PCR

RNA was extracted from PBMCs with TRIzol (Invitrogen, Carlsbad, USA) according to manufacturer's instructions. Total RNA concentration was determined by measuring the absorbance at 260 nm and 280 nm. The purity was estimated by the relative absorbance at 260 nm/280 nm. Integrity was assayed by agarose gel electrophoresis. The purity and integrity were greater than 95%. cDNA was synthesized from the total RNA (2 μtha σψντηa High Capacity cDNA Reverse Transcription Kit (Applied Biosystems, CA, USA).

Three sets of previously published specific primers against the swine genes *IFN-γ*, *IRF-1* and the housekeeping gene *glyceraldehyde 3-phosphate dehydrogenase* (*GAPDH*) were used to determine the time course of gene expression levels in PBMCs of Microminipigs by real-time PCR [35]; Table 1). Another two sets of *SLA-1*0401* and *SLA-1*1104* allele-specific primers were designed to amplify *SLA-1*0401* and *SLA-1*1104* alleles mRNA (Table 1). The *GAPDH*-specific primer set was used as an internal control for the other three genes. The expression levels of the two *SLA-1* alleles, *IFN-γ*, *IRF-1* and *GAPDH* were measured by real-time PCR using an ABI PRISM 7500 Fast Sequence Detector System (Applied Biosystems, CA) with Fast SYBR® Green Master Mix (Applied Biosystems, CA, USA). The synthesized cDNAs were used

as templates and were amplified using the allele specific primer sets of *SLA* and *IFN-γ*, *IRF-1* and *GAPDH*. The 10 μl amplification reaction volume contained 50 ng of cDNA, 0.5 units of high fidelity Gold *Taq* polymerase (Applied Biosystems, CA, USA), 10 x PCR buffer, 2.5 mM $MgCl_2$, 2 mM of each dNTP and 0.5 mM of each primer. The cycling parameters were as follows: 25 cycles of 98°C/10 sec, 62°C/30 sec and 68°C/30 sec. Melting curve analysis showed that there was no primer dimer formation. The relative quantitative values were calculated by the comparative C(T) method, also referred to as the 2(-DeltaDeltaC(T)) method [43, 44]. Serial dilutions of cDNA were amplified by real-time PCR using gene-specific primers. A plot of log cDNA dilution versus delta threshold cycle (Ct) value gives an absolute value of the slope. The absolute value of the slope (z) was calculated using an approximate formula, y = -3.32x+z. The 2-<DELTA><DE LTA>Ct value is given by [(Ct target gene—Ct internal control) Time X—(Ct target gene—Ct internal control) Time 0]]. Each Ct value was determined in the optimal cDNA dilution condition with the range of 100%±5% PCR efficiency.

Statistical analysis

Results were presented as the means ± SE. Data from the lymphocyte activation assay and real-time PCR were analyzed using Student's *t*-test to determine the significance of the treatment. In all statistical analyses, a *P* value of <0.05 was considered significant.

Results

Preparation of the monoclonal antibody X2F6

Swine *SLA-1*0401* and *β2 microglobulin* cDNAs were inserted into N576, an expression vector containing a monomer Venus yellow—green fluorescent protein (mVenus)-reporter gene, and the modified vector was transfected into A20 cells. The expression of the mVenus gene was observed in more than 50% of the transfected cells at 18 to 24 hrs after transfection. BALB/c mice were injected with mitomycin C (MMC)-treated swine PBMCs and then with MMC-treated N576-A20 cells as the booster immunizations. The titer of the antiserum against the *SLA-1*0401* expressed by the N576-HEK293 cells was increased successfully after the second booster. The crossreactivity between N576-HEK293 and the antisera was confirmed by flow cytometry, and the mice with sera that achieved a peak mean fluorescence intensity (MFI) of more than 30 were selected and used for monoclonal antibody preparation.

We selected a specific X2F6 subclone (Fig 1 and S1 Fig) for further use because this clone secreted a monoclonal antibody (mAb) that reacted with the HEK293 transfectants expressing *SLA-1*0401* (with an MFI greater than 3x10e3) and the *mVenus* fluorescent protein with similar or identical staining patterns. All of the X2F6 subclones showed similar staining patterns, suggesting that the cross-reacting proteins were stable expression products. The staining pattern was compared with that of PT-85A, a commercial pan-specific mAb against MHC. PT-85A stained not only classical class I SLA but also SLA-6, a non-classical class I SLA. The pattern of SLA-1-transfectant staining by the selected X2F6 clone was similar to that seen with the commercial PT-85A clones (Fig 1A). The isotype of this mAb was IgG2aκ.

Characterization of X2F6 specificity

We checked the species specificity of the X2F6 mAb using swine, human and common marmoset PBMCs. X2F6 recognized only the swine PBMCs, and no reactivity was observed with the human and common marmoset PBMCs, suggesting that the mAb was swine specific (Fig 1B). Next, we examined the locus specificity of the mAb using classical class I SLA, SLA-2*0901, and SLA-3*0602 and non-classical class-I SLA, and SLA-6*0101, which are contained in the

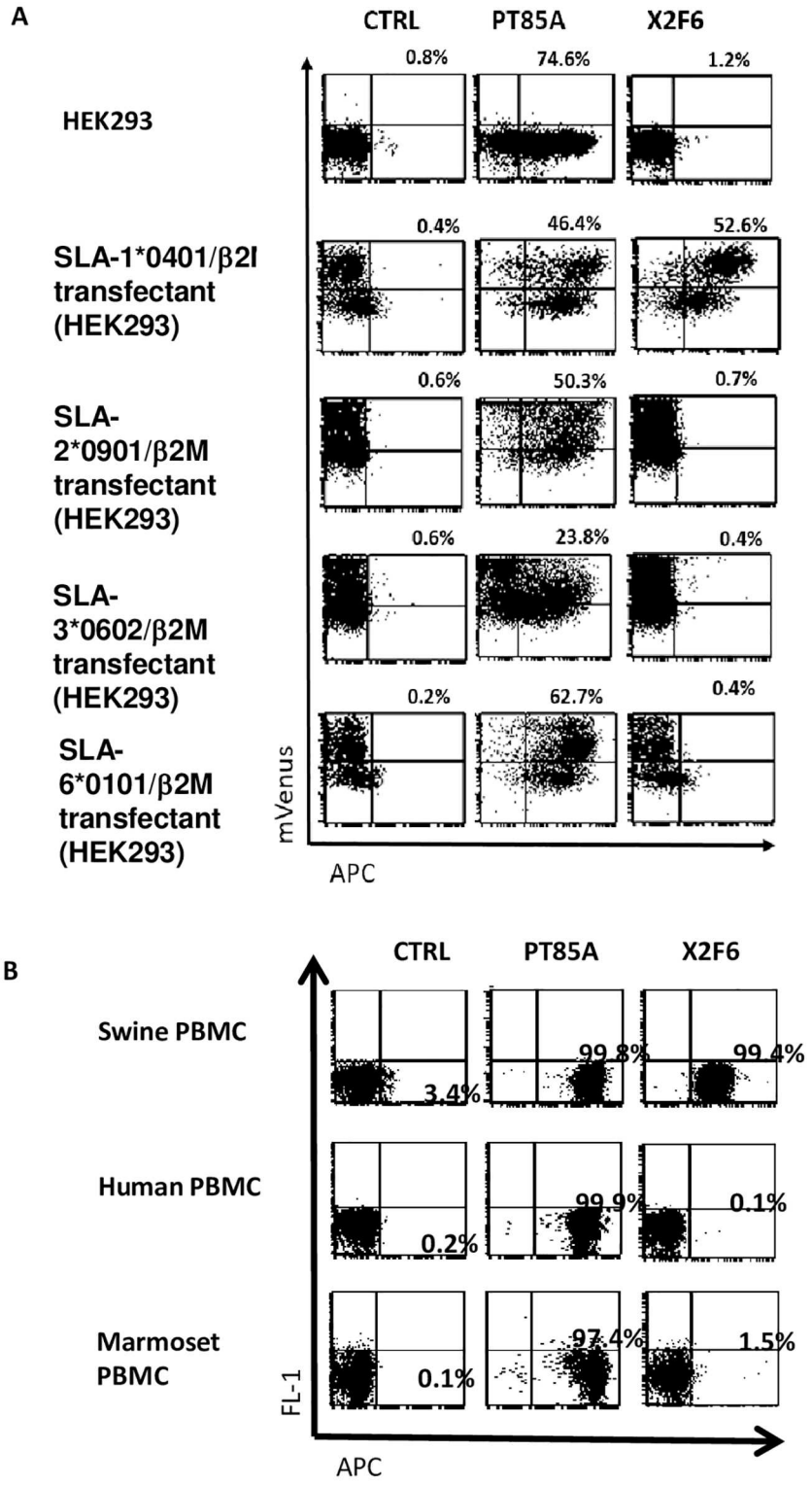

Fig 1. Specificity of the X2F6 mAb. (A) *SLA-1*0401*, *SLA-2*0901*, and *SLA-3*0602*, which are the classical class-I SLA alleles of Haplotype Hp-16.0, and *SLA-6*0101*, which is a non-classical class-I SLA allele of Hp-16.0, were transfected into HEK293 parent cells, and the reactivity of X2F6 (right panels) was examined by flow cytometry (FCM). Propidium iodide (PI) positive-dead cells were avoided for the gating. PT-85A, the pan-specific MHC class-1 antibody, was used for the positive control (middle panels). (B) The species specificity was examined using swine (Hp-16.0), human, and common marmoset PBMCs. Lymphoid

gate was used for the analysis. The percentages shown above the panels are the double-positive cell percentages.

doi:10.1371/journal.pone.0164995.g001

same haplotype (Hp-16.0) as the SLA-1*0401 antigen, using transfectants expressing each of these genes. The flow cytometry analysis revealed that SLA-2*0901, SLA-3*0602 and SLA-6*0101 transfectants were not recognized by X2F6, whereas the SLA-1*0401 transfectant was recognized by X2F6 (Fig 1A). These results suggest that X2F6 is specific for the SLA-1 locus in Hp-16.0.

To examine the allele specificity of X2F6 for haplotypes other than Hp-16.0, we tested the reactivity of X2F6 against the PBMCs of four other swine homozygous haplotypes that are shown in Table 2. The swine PBMCs collected from each of the duplicate homozygous haplotypes were stained with X2F6 or the pan-specific anti-class-I MHC mAb PT85A followed by fluorescently-labeled anti-mouse IgG and analyzed by flow cytometry. All five haplotypes showed different staining intensities (Fig 2A). The X2F6 antibody reacted with Hp-10.0 to produce the highest MFI, whereas Hp-35.0 showed the second highest MFI. The haplotypes Hp-16.0, which contained the immunized antigen SLA-1*0401, and Hp-17.0 both had an intermediate MFI. No reactivity was observed for Hp-43.0 (Table 2). On the other hand, the Hp-43.0 and Hp-10.0 heterozygous pigs reacted with X2F6 to produce an intermediate intensity that was lower than that in the Hp-10.0 homozygous pigs and higher than that in the Hp-43.0 homozygous pigs (Fig 2B). These results showed that X2F6 was specific to swine PBMCs and that it recognized different classical class I SLA alleles at different loci in a haplotypic manner.

Sequence analysis and SLA epitope recognition of X2F6

The amino acid sequences and variable regions of the X2F6 antibody are shown in Fig 3A for both the heavy and light chains. The protein database sequence 3V7A is shown above the X2F6 sequence. The tertiary structure of X2F6 was also predicted (Fig 3B). To predict the SLA epitope recognized by X2F6, we aligned the amino acid sequences of SLA-1, SLA-2 and SLA-3 alleles for each of the five haplotypes (Fig 4). We compared the antigenic sequence of SLA-1*0401 with the non-antigenic sequences of SLA-2*0901, SLA-3*0602, Hp-43.0 SLA-1*1104, SLA-2*040202 and SLA-3*0401 that did not react with X2F6. Amino acid sequence differences

Table 2. SLA class I genotypes and haplotypes deduced from SBT and sequence-specific primer (SSP) methods and MFI scores for Microminipigs.

Breed	Sample No.	Class I haplotype (Hp-)	class I			MFI (X2F6)[1]
			SLA-1	*SLA-3*	*SLA-2*	
Microminipig	320, 831, 2303, 2316, 2567,1083	10.0	*0501	*0801	*0302	1897
	807, 982	35.0	*1201, *1301	*0502	*1001	767
	965, 1938	16.0	*0401	*0602	*0901	182
	1003	17.0	*0804	*0305	*0603	122
	1173, 1495, 2024, 2030, 2259	43.0	*1104	*0401	*040202	11.7
	1599, 1810, 1932	10.0/43.0	*0501, *1104	*0801, *0401	*0302, *040202	—

[1]MFI scores for PBMCs of Microminipigs with each of the SLA class I haplotypes that were reacted with X2F6 Mab.

doi:10.1371/journal.pone.0164995.t002

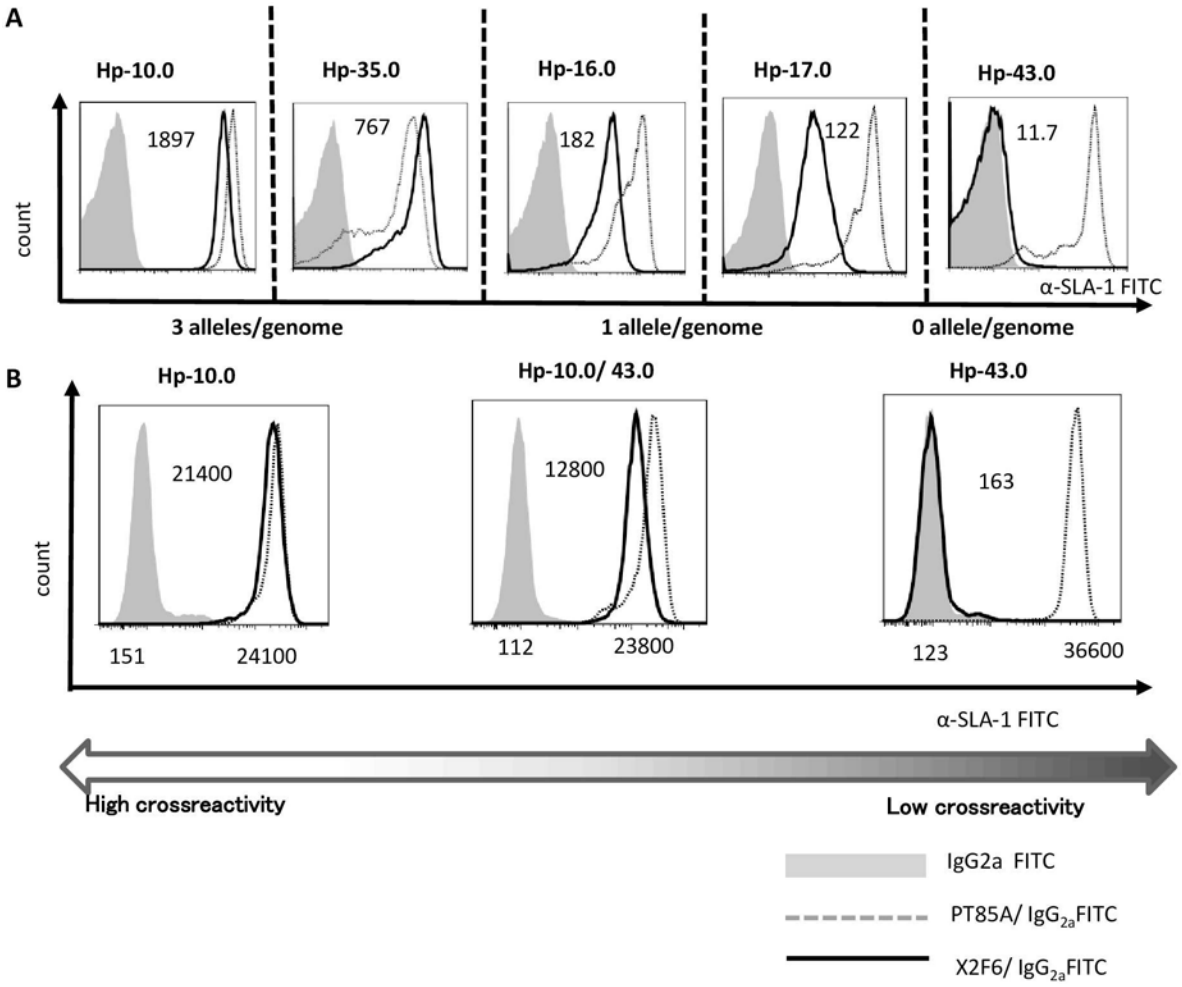

Fig 2. Haplotype-specific reactivity of the X2F6 mAb. (A) Microminipig PBMCs of each haplotype were stained with X2F6 or PT85A followed by anti-mouse IgG-FITC and analyzed by FCM. Lymphoid gate was used for the analysis. Solid lines represent the X2F6-stained patterns. Broken lines represent PT85A-stained patterns. Filled lines represent the isotype-control-stained patterns. MFI scores for each haplotype are shown in the panels. The YLL type-allele number is also shown. (B) The MFIs of Hp-10.0 and Hp-43.0 haplotypes were selected and the homozygous pig PBMCs and heterozygous pig PBMCs were compared. The upper panels are the data from FACSCalibur, and the MFI score is significantly lower than in the lower panels, whereas the relative levels of the surface protein are comparable.

doi:10.1371/journal.pone.0164995.g002

were found in the α2 domain, specifically, Y102, L103, and L109 (YLL set) in SLA-1*0401 compared to D102, V103, and F109 (DVF set) in the other alleles. Hp-10.0 and Hp-35.0, which reacted with X2F6, also had alleles with the YLL set. Interestingly, the allelic YLL set number and MFI exhibited strict correlation (Fig 2). The predicted 3D structures of SLA-1*0501 and SLA-1*1104 clearly show that the amino acids of the YLL and DVF sets are exposed and clustered near a loop region on the surface of these SLA molecules, respectively. As shown in Fig 3C, the structures and the surface characters of the YLL and DVF sets are significantly different.

These results predict that the antibody X2F6 will only recognize the SLA region composed of Y102, L103 and L109 residues. Thus, in the case of the Hp-16.0 haplotype, the antibody will only recognize the SLA-1 locus and the antigenic allele SLA-1*0401 that contains the YLL epitope.

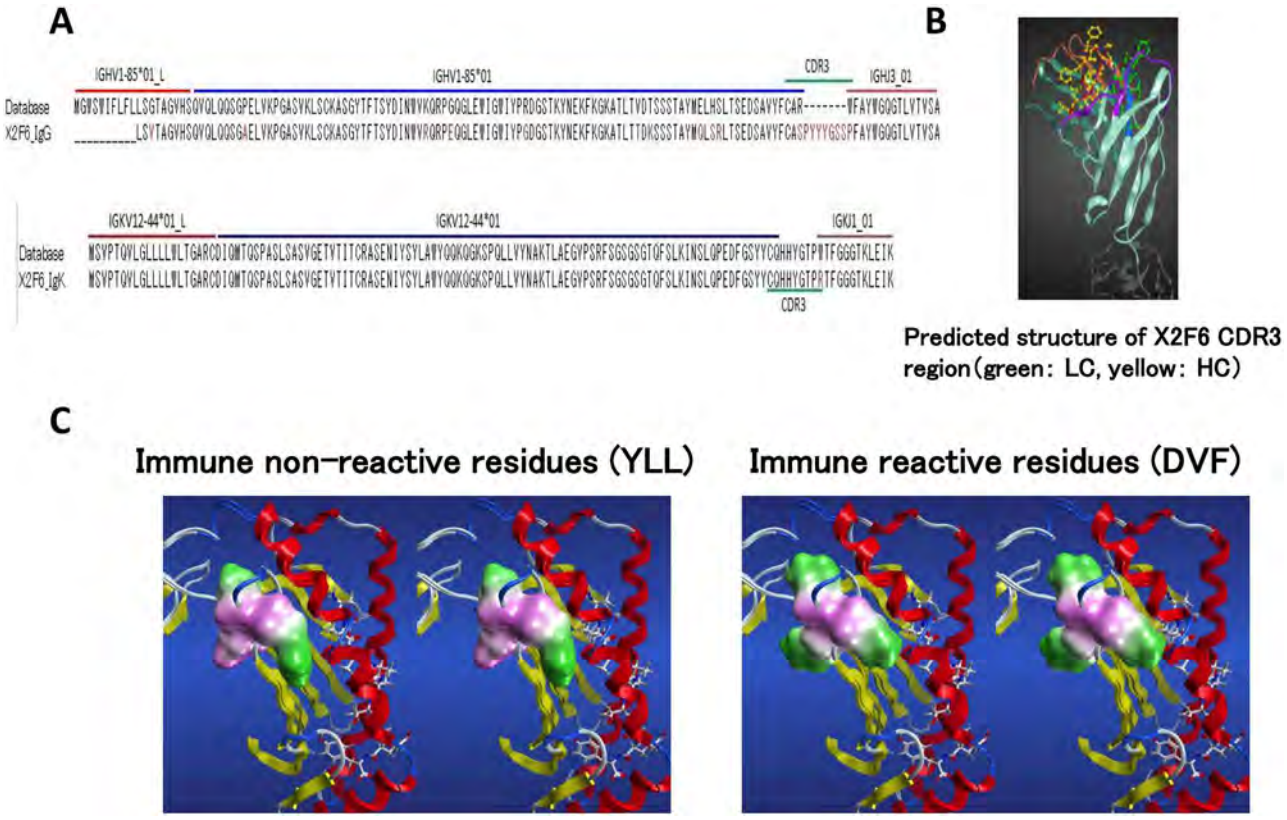

Fig 3. Tertiary structure of X2F6 mAb and the predicted antibody epitope. (A) Amino acid sequences of heavy and light chains of the X2F6 variable region. The database sequence PDB ID 3V7A is shown as the control sequence. (B) The predicted tertiary structure of the X2F6 mAb. (C) The tertiary structures of the YLL set in SLA-1*0501, which reacts with X2F6 with high reactivity (left panel), and the DVF set in SLA-1*1104, which cannot react with X2F6 (right panel), are shown. Pink (hydrophobic) and green (hydrophilic) colors represent the amino acid character. The structure is largely different, and the binding affinity is predicted to be different.

doi:10.1371/journal.pone.0164995.g003

Correlation of the mRNA and surface protein expression of SLA

To analyze the surface protein level of the SLA allele, we used X2F6 and homozygous Microminipigs with Hp-16.0 (n = 2) to detect the SLA-1*0401 protein level on the TSST-1-stimulated PBMC surface. The SLA-2 and SLA-3 alleles of Hp-16.0 have the DVF set, D102, V103, and F109, in their α2 domains, as mentioned above. These domains are predicted not to react with X2F6 (Fig 4). We also examined Hp-43.0, whose classical class-I SLA alleles have the DVF and not the YLL set. Both *SLA-1*0401* and *SLA-1*1104* mRNA were analyzed by real-time-PCR after stimulation.

First, PBMCs from each haplotype were stimulated with TSST-1 or IFN-γ, Fand the surface expression of SLA was analyzed serially. IFN-γ or TSST-1 stimulation enhanced the surface protein expression of SLA-1 in the PBMCs (Fig 5). However, while the protein expression peaked at 24 hrs and was down-regulated thereafter during IFN-γ treatment, the surface protein expression was sustained at near-maximum levels for up to 72 hrs during TSST-1 stimulation. In contrast, no cross-reactivity was detected in homozygous pigs with *SLA-1*1104*, irrespective of the stimulation (S2 Fig). When PT85A, a pan-specific anti-class-I MHC antibody, which crossreacts with human and swine, was used for the detection of surface SLA molecules, the peak was at 24 to 48 hrs and decreased slowly thereafter. As for Hp-10.0 (n = 3), which possesses three YLL sets, a similar complement of surface level SLA molecules was

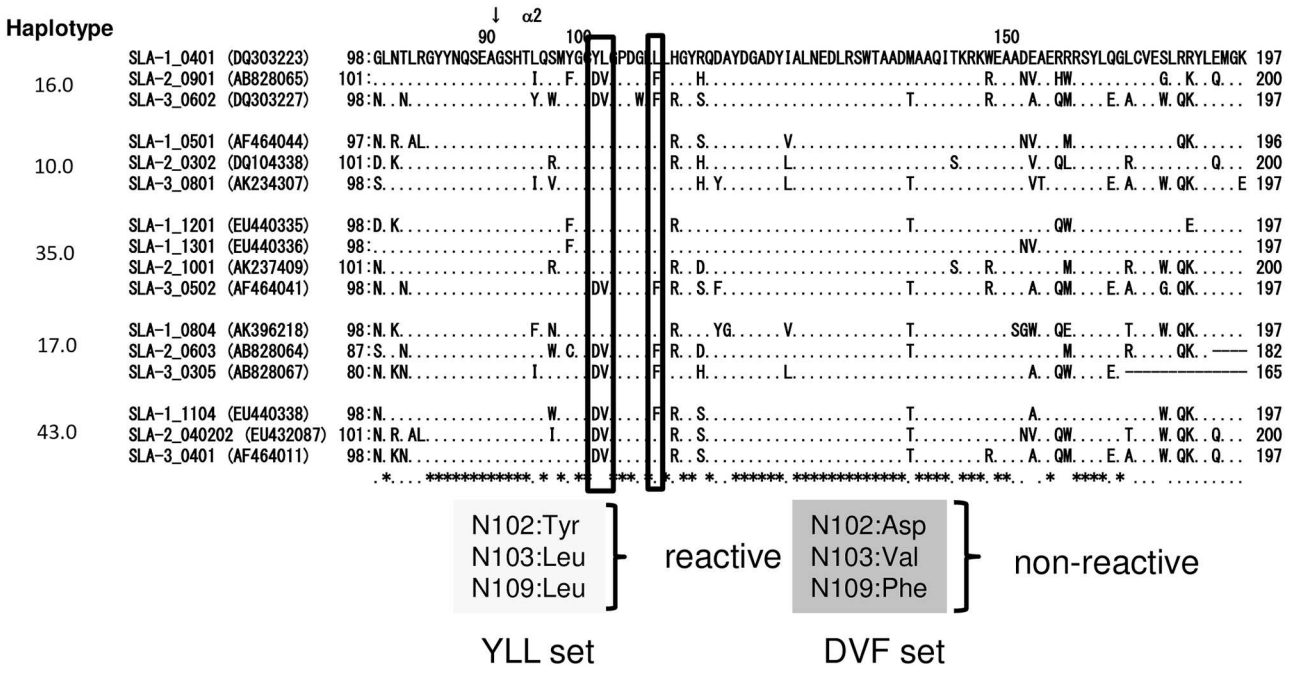

Fig 4. Amino acid alignment of each classical class I allele in five SLA class I haplotypes. The amino acid sequence alignment of the alleles of each SLA locus is shown. For the haplotypes with a specific set of amino acids (Y102, L103, L109; the YLL set), in which each allele reacted with X2F6, the number of YLL sets determined the level of reactivity. The MFI for X2F6 reactivity was highest in the Hp-10.0 PBMCs that possessed three YLL sets in the SLA-1, SLA-2 and SLA-3 loci.

doi:10.1371/journal.pone.0164995.g004

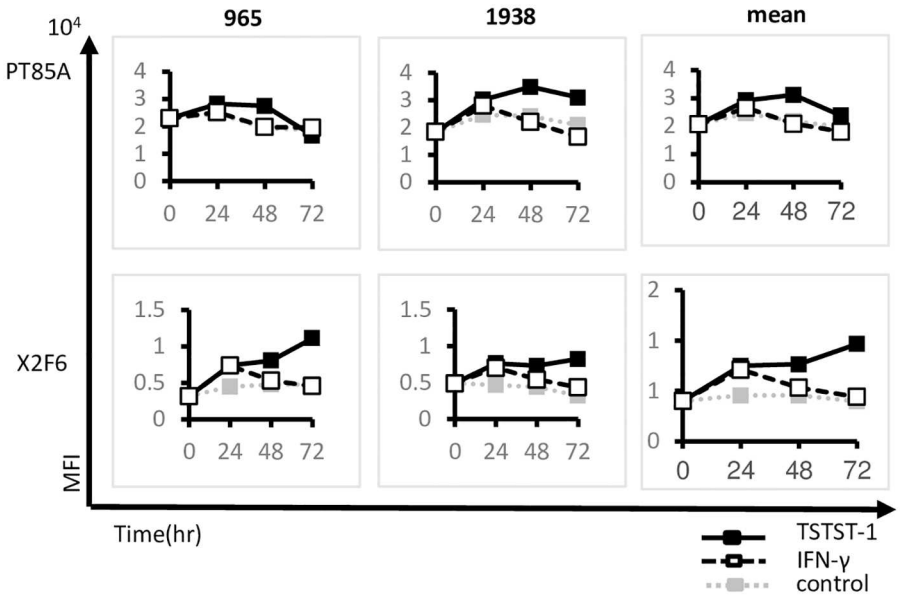

Fig 5. The quantification of the SLA-1*0401 protein after TSST-1 stimulation. The PBMCs of two pigs with the Hp-16.0 haplotype (individuals #965 and #1938) were examined for the surface protein level of SLA after the stimulation. X2F6 mAb was used to determine the SLA-1*0401 surface protein level (upper panels). PT-85A was used for the positive control (lower panels). Closed squares with a solid line show TSST-1-stimulated PBMCs, open squares with a broken line show IFN-γ stimulation. Closed squares with a dotted line show the negative control.

doi:10.1371/journal.pone.0164995.g005

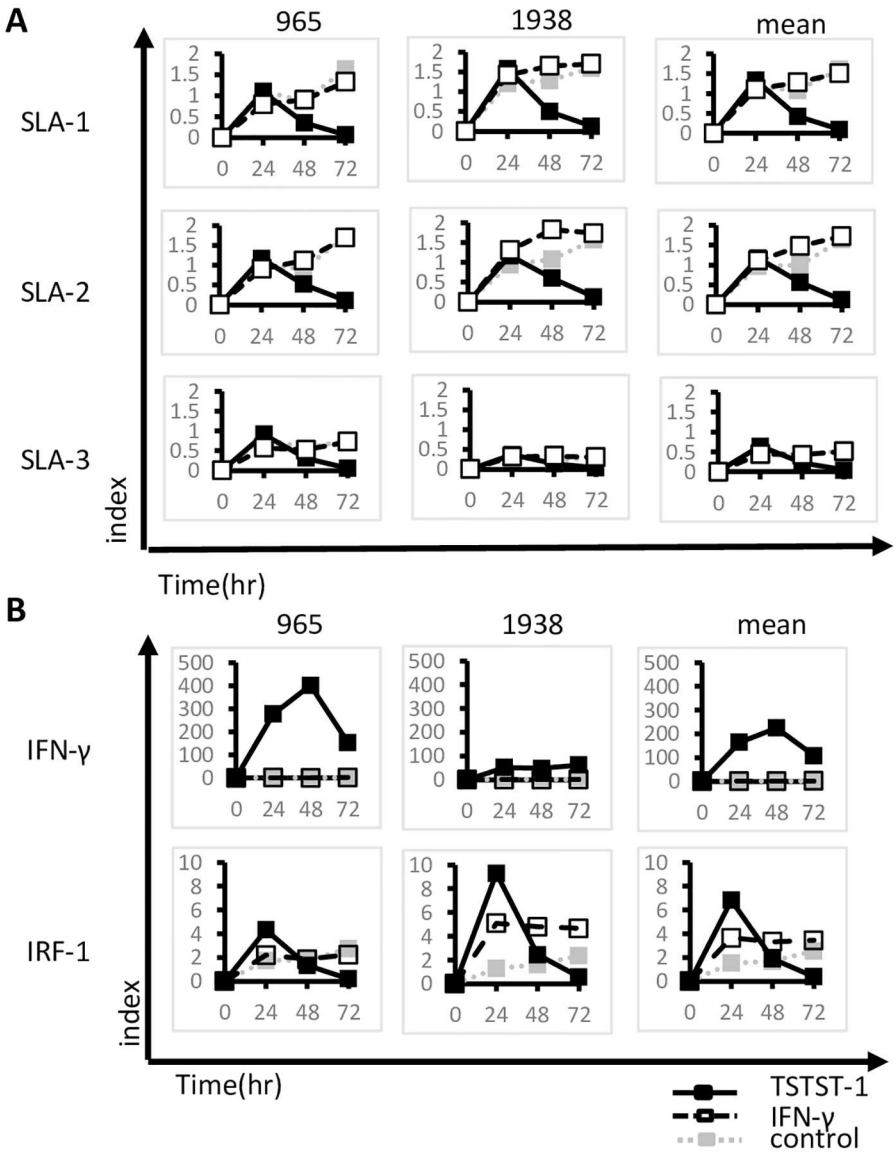

Fig 6. Class I SLA-related mRNA expression after TSST-1 stimulation. The PBMCs of two pigs with the Hp-16.0 haplotype (individuals #965 and #1938) were examined for classical class I SLA (A) and related mRNA (B) expression after stimulation. Closed squares with a solid line show TSST-1-stimulated PBMCs, open squares with a broken line show IFN-γ stimulation, and closed squares with a dotted line show the negative control.

doi:10.1371/journal.pone.0164995.g006

observed (S2 Fig). As for the heterozygotes of Hp-10.0 and Hp-43.0, intermediate reactivity was observed, but the kinetics were similar to those observed for Hp-10.0 homozygotes.

We also analyzed the mRNA level by real-time PCR with allele-specific primers and found that with TSST-1 stimulation, the *SLA-1*0401* and *SLA-1*1104* mRNA expression levels peaked at 24 hrs and decreased thereafter to reach base-line levels at 72 hrs after TSST-1 treatment (Fig 6A). The mRNA expression results obtained for the IFN-γ stimulation study were diverse among individuals and did not correlate strictly with *SLA-1*0401* expression (Fig 6B and data not shown). In addition, the *IRF-1* mRNA expression levels basically correlated with the *SLA-1*0401* mRNA expression (Fig 6B). Additionally, the mRNA expression levels of *SLA-1*0501*

and *SLA-1*1104* were similar to that of *SLA-1*0401* (S3 Fig). However, a strict correlation between SLA-1 and IRF-1 mRNA was not observed for the alleles *SLA-1*0501* and *SLA-1*1104* (data not shown). Contrary to this, as observed for IFN-γ stimulation, the *SLA-1*0401*, *SLA-1*0501* and *SLA-1*1104* mRNA levels did not differ significantly, and the expression levels increased or were maintained at maximum levels from 24 hrs to 72 hrs after treatment (Fig 6A and S3 Fig). In contrast, IFN-γ stimulation did not induce IFN-γ and IRF-1 mRNA expression above the levels stimulated by TSST-1, except for the IRF-1 mRNA expression level at 72 hrs (Fig 6B).

Collectively, these results suggest that the kinetics of *SLA-1*0401* allele expression were different at the mRNA and protein levels. In particular, TSST-1 stimulation induced quite different features of SLA-1 mRNA expression and surface protein expression compared to IFN-γ stimulation, although the SLA-1 mRNA level correlated with IRF-1 mRNA level.

Discussion

As the pig is recognized to be a useful experimental animal, we genotyped and haplotyped a number of different breeds to use SLA-defined pigs for infection and transplantation studies involving SLA-related reactions [21–23]. In this regard, immunodeficient pigs [45], iPS cells from the SLA-defined minipig [46], and transplantation of human iPS cells into the pigs [47] were established to advance a breakthrough for these types of studies on middle-sized experimental animals. However, the development of tools and reagents to distinguish SLA alleles is still urgently needed to drive progress in studies of the role of polymorphisms in the regulation and function of SLA gene expression.

In this study, we prepared and characterized a specific mAb that recognized a unique amino acid cluster, YLL, in the classical class I SLA tertiary structure and not the allelic DVF cluster. This was validated using a panel of SLA transfectants, human and common marmoset PBMCs and haplotype-defined Microminipig PBMCs. We undertook a predictive analysis of the alleles of three classical class I loci, SLA-1, SLA-2 and SLA-3, that might be recognized by X2F6 based on the sequences available at the IPD-MHC SLA website and those that were submitted recently to public DNA sequence databases [http://www.ebi.ac.uk/ipd/mhc/sla/index.html, 19, 20]. Of the 60 known SLA-1 alleles, 43 alleles were identified to have a unique amino acid cluster, YLL, that could be expected to react with the X2F6 antibody. In contrast, only 19 alleles and one allele of the 82 SLA-2 and 31 SLA-3 alleles, respectively, were found to have the unique amino acid cluster. Therefore, X2F6 might recognize most of the SLA-1 alleles and only a few of the SLA-2 and SLA-3 alleles.

In our previous study, the correlation of SLA allele mRNA and protein expression was not clear because of the lack of specificity of the mAb, PT85A. To use our new mAb, we selected a haplotype that could be used to examine the expression of a single locus and allele encoding a class I SLA protein, as the number of YLL and DVF sets in the class I SLA alleles were different among the haplotypes. This mAb possessed high specificity and recognized a specific locus and allele when we selected the haplotype Hp-16.0. Collectively, these tools enabled us to specifically analyze the kinetics of surface SLA protein expression.

Using this combination of tools, we characterized the kinetics of the surface protein levels of the *SLA-1*0401* allele after stimulating the haplotyped PBMCs for 72 hrs with TSST-1 or with IFN-γ. Both stimulants enhanced the surface protein expression, but after 48 hrs of TSST-1 stimulation, the mRNA expression was decreased. In contrast, the surface protein level was maintained until 72 hrs after the stimulation. The IFN-γ mRNA level was not closely correlated with the *SLA-1*0401* mRNA level, suggesting that the TSST-1 stimulation modified the expression of SLA-1 mRNA not only by inducing a large amount of translatable IFN-γ but also

through other complex regulatory systems. This result regarding the differential expression of the mRNAs and proteins of different MHC alleles is not controversial and was previously observed for the HLA-A and HLA-B molecules expressed by the HEK293T cell line [48]. Another haplotype, Hp-10.0, with plural YLL sets showed similar kinetics, suggesting that the surface protein level of three classical SLA class I loci may be similarly regulated by TSST-1 stimulation.

Although the reason why the mRNA level was not directly correlated with the surface protein expression is not clear, the regulatory systems for transcription, translation and post-translation processes are complicated, and the SLA-1 molecules may be affected at various steps during protein translation or during recruitment on the cell surface [49]. Because IFN-γ is reported to play a role in the expression of the antigen-processing machinery (APM) [10], the mRNA and surface SLA protein expression is usually thought to be induced by signals downstream of the IFN-γ signal, such as Janus activating kinase 2 (JAK2) suppression. Otherwise, structural modification of Tapasin and related molecules may be induced and the peptide loading complex may change its peptide-binding affinity [50]; alternatively, the recruitment of SLA molecules by cargo proteins such as Bap31 may be changed [51]. However, our results show that IFN-γ expression is not directly correlated with the surface expression of SLA. As for the interferon stimulated response element (IRSE), which is a target of IFN-γ, the sequence is different among the loci, and for example, HLA-A is reported to not easily respond to IFN-γ [52, 53]. Therefore, we may need to consider mechanisms other than IFN-γ modification to explain the discrepancy between mRNA and surface protein expression. After activation, T cells can induce IFN-γ expression along with the closing of the interleukin 2 (IL-2) promoter, as we reported previously [54]. Such an anergic state may be induced along with MHC down-regulation in the cells. Otherwise, by the extensive internalization of the SLA molecules after active TCR signal transduction, intracellular SLA proteins might be increased and the surface protein level might be decreased. Such specific modifications of cell surface expression may be clarified using our system in future studies.

Allele-specific transcription of classical class I MHC is mainly correlated with Enhancer A, ISRE and SXY, for which allele-specific transcriptional regulation was reported [55, 56]. The SXY module contains binding motifs for activating transcription factors (ATF)/cyclic AMP response element binding protein (CREB) [57], class-II trans-activator (CIITA) [58], and nuclear factor Y (NFY) [59]. Previous studies on polymorphisms in HLA regulatory regions have demonstrated that the correlation between diseases and HLA haplotype-specific gene expression is due to 3'-UTR sequence diversity and mRNA stability. However, these reports have not considered the differences in mRNA and protein expression regulation after stimulation by TSST-1 or IFN-γ. In this regard, our experimental system may help in the future to clarify these observed differences.

In our study, the X2F6 and PT85A antibodies detected different kinetics of SLA surface expression. While X2F6 detected only the SLA-1*0401 molecule, PT85A might have detected other class I SLA molecules and non-classical molecules, such as SLA-6 (Fig 1). As non-classical class I MHC is reported to have a different regulation system from classical class I MHC in human and mouse species [60], the swine non-classical class I MHC might also have a different regulation system. The different regulation of each class I SLA might affect the kinetics of the X2F6- and PT-85A-recognized surface SLA molecules.

Superantigens such as TSST-1 may induce a cytokine storm, which is life threatening for newborns and the old [31]. If the surface protein expression of MHC class I is maintained after mRNA down-regulation, the cells may continue to stimulate CD8 T cells to secrete Th1 cytokines and attack specific target cells. Moreover, the large amount of cytokines may induce tissue damage in the host and cause sepsis. Therefore, it is critical to monitor MHC class I

expression at the protein level. Moreover, if the mechanism for sustained surface protein expression is elucidated, it may help to develop molecular targeting reagents for the treatment of such deleterious cytokine storms.

In conclusion, we established a new SLA-1*0401 allele-recognizing monoclonal antibody, X2F6, and used it to find marked differences between mRNA and surface protein expression of the SLA-1*0401 allele during stimulation with TSST-1 of *staphylococcus aureus*. The X2F6 mAb and haplotype-defined Microminipigs in combination with next generation sequencing [61] may help to clarify the regulation of MHC gene expression in more detail in future studies.

Supporting Information

S1 Fig. Array Scan Images of the Specificity of the X2F6 mAb. Hybridoma screening was performed by Array Scan (Thermo Fisher co. Ltd). Upper panels show the crossreactivity of the X2F6 clone culture supernatant with either HEK293 or SLA-1/βmVenus (transfected gene expression) and APC-labeled secondary antibody (surface SLA recognition) are also shown. Lower panels show the same patterns using PT-85A, a pan-specific MHC class I antibody.
(TIF)

S2 Fig. Surface expression of Class I SLA of Hp10.0. Stimulated PBMCs of Hp-10.0 homozygous pigs (n = 3) and Hp-10.0 and Hp-43.0 heterozygous pigs (n = 3) were examined for surface class I SLA protein expression after TSST-1 or IFN-γ stimulation. Closed squares with solid lines show TSST-1 stimulated PBMCs, open squares with broken lines show IFN-γ, and closed squares with dotted lines show the negative control.
(TIF)

S3 Fig. mRNA Expression of the SLA-1 gene. Stimulated PBMCs of Hp-10.0 homozygous pigs (n = 3) and Hp-10.0 and Hp-43.0 heterozygous pigs (n = 3) were examined for the expression of the SLA-1*0501 and SLA-1*1104 mRNAs after TSST-1 or IFN-γ. Closed squares with solid lines show TSST-1-stimulated PBMCs, open squares with broken lines show IFN-γ, and closed squares with dotted lines show the negative control.
(TIF)

Acknowledgments

We thank the members of the Teaching and Research Support Center at Tokai University School of Medicine for their technical skills.

Author Contributions

Conceptualization: YK H. Kitagawa AA.

Formal analysis: NH.

Funding acquisition: YK AA H. Kitagawa.

Investigation: YK SO AM AS.

Methodology: YK M. Tanaka H. Kamiguchi RS.

Resources: M. Takasu NI TM H. Kitagawa.

Software: NH.

Supervision: AA.

Validation: YK TS.

Visualization: SO.

Writing – original draft: YK.

Writing – review & editing: HI JKK.

References

1. Groothuis T, Griekspoor A, Neijssen J, Herberts C, Neefjes J. MHC class I alleles and their exploration of the antigen-processing machinery. Immunol Rev. 2005; 207:60–76. PMID: 16181327, doi: 10.1111/j.0105-2896.2005.00305.x
2. Vyas J, Van der Veen A, Ploegh H. The known unknowns of antigen processing and presentation. Nat Rev Immunol 2008; 8:607–18. doi: 10.1038/nri2368 PMID: 18641646
3. Neefjes J, Jongsma M, Paul P, Bakke O. Towards a systems understanding of MHC class I and MHC class II antigen presentation. Nat Rev Immunol. 2011; 11:823–36. Review.
4. Parham P. MHC class I molecules and KIRs in human history, health and survival. Nat Rev Immunol. 2005; 5:201–14. PMID: 15719024 doi: 10.1038/nri1570
5. Thielens A, Vivier E, Romagné F. NK cell MHC class I specific receptors (KIR): from biology to clinical intervention. Curr Opin Immunol. 2012; 24:239–45. PMID: 22264929 doi: 10.1016/j.coi.2012.01.001
6. Long E, Kim H, Liu D, Peterson M, Rajagopalan S. Controlling natural killer cell responses: integration of signals for activation and inhibition. Annu Rev Immunol. 2013; 31:227–58. PMID: 23516982 PMCID: PMC3868343 doi: 10.1146/annurev-immunol-020711-075005
7. Satta Y, Li Y, Takahata N. The neutral theory and natural selection in the HLA region. Front Biosci. 1998; 3:d459–67. PMID: 9556500
8. Fernando M, Stevens C, Walsh E, De Jager P, Goyette P, Plenge R, et al. Defining the role of the MHC in autoimmunity: a review and pooled analysis. PLoS Genet. 2008; 4:e1000024. PMID: 18437207 PMCID: PMC2291482 doi: 10.1371/journal.pgen.1000024
9. Sollid L, Pos W, Wucherpfennig K. Molecular mechanisms for contribution of MHC molecules to autoimmune diseases. Curr Opin Immunol. 2014; 31:24–30. PMID: 25216261 PMCID: PMC4254370 doi: 10.1016/j.coi.2014.08.005
10. Bukur J, Jasinski S, Seliger B. The role of classical and non-classical HLA class I antigens in human tumors. Semin Cancer Biol. 2012; 22:350–8. PMID: 22465194 doi: 10.1016/j.semcancer.2012.03.003
11. Amodio G, Sales de Albuquerque R, Gregori S. New insights into HLA-G mediated tolerance. Tissue Antigens. 2014; 84:255–63. PMID: 25132109 doi: 10.1111/tan.12427
12. Carosella E, Rouas-Freiss N, Roux D, Moreau P, LeMaoult J. HLA-G: An Immune Checkpoint Molecule. Adv Immunol. 2015; 127:33–144. PMID: 26073983 doi: 10.1016/bs.ai.2015.04.001
13. Cameron A, Wesson R, Ahmadi A, Singer A, Hu X, Okabayashi T, et al. Chimeric Allografts Induced by Short-Term Treatment with Stem Cell Mobilizing Agents Result in Long-term Kidney Transplant Survival without Immunosuppression: II Study in Miniature Swine. Am J Transplant 2016. doi: 10.1111/ajt.13703 PMID: 26748958
14. Fernández-Rodríguez O, Ríos A, Palenciano C, Ramírez P, Navarro J, Martínez-Alarcón L, et al. A hemodynamic, metabolic and histopathological study of a heterotopic auxiliary swine liver graft with portal vein arterialization. Cir Esp. 2016; 94:77–85. PMID: 26615737 doi: 10.1016/j.ciresp.2015.09.007
15. Avsar M, Jansson K, Sommer W, Kruse B, Thissen S, Dreckmann K, et al. Augmentation of Transient Donor Cell Chimerism and Alloantigen-Specific Regulation of Lung Transplants in Miniature Swine. Am J Transplant. 2015. PMID: 26602894 doi: 10.1111/ajt.13629
16. Abud M, Baranov P, Hicks C, Patel S, Lieppman B, Regatieri C, et al. The Effect of Transient Local Anti-inflammatory Treatment on the Survival of Pig Retinal Progenitor Cell Allotransplants. Transl Vis Sci Technol. 2015; 4(5):6 eCollection PMID: 26425402 PMCID: PMC4585327 doi: 10.1167/tvst.4.5.6
17. Renard C, Sehra H, Beasley H, Coggill P, Howe K, Harrow J, et al. The genomic sequence and analysis of the swine major histocompatibility complex. Genomics. 2006; 88:96–110. PMID: 16515853 doi: 10.1016/j.ygeno.2006.01.004
18. Tanaka-Matsuda M, Ando A, Rogel-Gaillard C, Chardon P, Uenishi H. Difference in number of loci of swine leukocyte antigen classical class I genes among haplotypes. Genomics. 2009; 93:261–73. PMID: 18996466 doi: 10.1016/j.ygeno.2008.10.004

19. Smith D, Lunney J, Martens G, Ando A, Lee J-H, Ho C-S, et al. Nomenclature for factors of the SLA class I system, 2004. Tissue antigens. 2005; 65:136–49. PMID: 15713212 doi: 10.1111/j.1399-0039.2005.00337.x

20. Ho C, Lunney J, Ando A, C R-G, JH L, Schook L, et al. Nomenclature for factors of the SLA system, update 2008. Tissue Antigens. 2009; 73:307–15. PMID: 19317739 doi: 10.1111/j.1399-0039.2009.01213.x

21. Ando A, Imaeda N, Ohshima S, Miyamoto A, Kaneko N, Takasu M, et al. Characterization of swine leucocyte antigen alleles and haplotypes on a novel miniature pig line, Microminipig. Animal Genetics. 2014; 45:791–8. PMID: 25118109 doi: 10.1111/age.12199

22. Soe O, Ohba Y, Imaeda N, Nishii N, Takasu M, Yoshioka G, et al. Assignment of the SLA alleles and reproductive potential of selective breeding Duroc pig lines. Xenotransplantation. 2008; 15:390–7. PMID: 19152667 doi: 10.1111/j.1399-3089.2008.00499.x

23. Ando A, Ota M, Sada M, Katsuyama Y, Goto R, Shigenari A, et al. Rapid assignment of the swine major histocompatibility complex (SLA) class I and II genotypes in Clawn miniature swine using PCR-SSP and PCR-RFLP methods. Xenotransplantation. 2005; 12:121–6. PMID: 15693842 doi: 10.1111/j.1399-3089.2005.00204.x

24. Zhang N, Qi J, Feng S, Gao F, Liu J, Pan X, et al. Crystal structure of swine major histocompatibility complex class I SLA-1 0401 and identification of 2009 pandemic swine-origin influenza A H1N1 virus cytotoxic T lymphocyte epitope peptides. JVirol. 2009; 85:11709–24. PMID: 21900158 PMCID: PMC3209268 doi: 10.1128/JVI.05040-11

25. Voss A, Loeffen F, Bakker J, Klaassen C, Wulf M. Methicillin-resistant Staphylococcus aureus in pig farming. Emerg Infect Dis. 2005; 11(1965–1966). PMCID: PMC3291345

26. Cuny C, Nathaus R, Layer F, Strommenger B, Altmann D, Witte W. Nasal colonization of humans with methicillin-resistant Staphylococcus aureus (MRSA) CC398 with and without exposure to pigs. PLoS One. 2009; 4:e6800. PMID: 19710922 PMCID: PMC2728842 doi: 10.1371/journal.pone.0006800

27. Broens E, Graat E, Van der Wolf P, Van de Giessen A, De Jong M. De Jong MC. Prevalence and risk factor analysis of livestock associated MRSA-positive pig herds in The Netherlands. Prev Vet Med. 2011; 2011(102):41–9. PMID: 21733585 doi: 10.1016/j.prevetmed.2011.06.005

28. Crombé F, Willems G, Dispas M, Hallin M, Denis O, Suetens C, et al. Prevalence and antimicrobial susceptibility of methicillin-resistant Staphylococcus aureus among pigs in Belgium. Microb Drug Resist. 2012; 18(2):125–31. PMID: 22088147 doi: 10.1089/mdr.2011.0138

29. Alt K, Fetsch A, Schroeter A, Guerra B, Hammerl J, Hertwig S, et al. Factors associated with the occurrence of MRSA CC398 in herds of fattening pigs in Germany. BMC Vet Res. 2011; 7:69. PMID: 22074403 PMCID: PMC3260235 doi: 10.1186/1746-6148-7-69

30. Boost M, Ho J, Guardabassi L, O'Donoghue M. High meticillin-resistant Staphylococcus aureus carriage in intensive pig farms in southern China. Vet Rec. 2012; 171:156, 1–2. PMID: 22791521 doi: 10.1136/vr.100779

31. Kulhankova K, King J, Salgado-Pabón W. Staphylococcal toxic shock syndrome: superantigen-mediated enhancement of endotoxin shock and adaptive immune suppression. Immunol Res. 2014; 59:182–7. PMID: 24816557 doi: 10.1007/s12026-014-8538-8

32. Krakauer T. Immune response to staphylococcal superantigens. Immunol Res. 1999; 20:163–73. PMID: 10580640

33. Dinges M, Orwin P, Schlievert P. Exotoxins of Staphylococcus aureus. Clin Microbiol Rev. 2000; 13:16–34. PMID: 10627489 PMCID: PMC88931

34. Stach C, Herrera A, Schlievert P. Staphylococcal superantigens interact with multiple host receptors to cause serious diseases. Immunol Res. 2014; 59:177–81. PMID: 24838262 PMCID: PMC4125451 doi: 10.1007/s12026-014-8539-7

35. Kametani Y, Ohshima S, Kita Y, Shimada S, Kamiguchi H, Shiina T, et al. Porcine MHC classical class I genes are coordinately expressed in superantigen-activated mononuclear cells. Vet Immunol Immunopathol. 2012; 148:252–9. PMID: 22640570 doi: 10.1016/j.vetimm.2012.05.005

36. Mulder A, Kardol M, Arn J, Eijsink C, Franke M, Schreuder G, et al. Human monoclonal HLA antibodies reveal interspecies crossreactive swine MHC class I epitopes relevant for xenotransplantation. Mol Immunol. 2009; 47:809–15. PMID: 19931911 doi: 10.1016/j.molimm.2009.10.004

37. Ho C, Lunney J, Franzo-Romain M, Martens G, Lee Y, Lee J, et al. Molecular characterization of swine leucocyte antigen class I genes in outbred pig populations. Animal Genetics. 2009; 40:468–78. PMID: 19392823 doi: 10.1111/j.1365-2052.2009.01860.x

38. Mizutani A, Kikkawa E, Matsuno A, Shigenari A, Okinaga H, Murakami M, et al. Modified S/MAR episomal vectors for stably expressing fluorescent-protein tagged transgenes with small cell-to-cell fluctuations. Anal Biochem. 2013; 443(1):113–6. PMID: 23969013 doi: 10.1016/j.ab.2013.08.009

39. Ohshima S, Mori S, Shigenari A, Miyamoto A, Takasu M, Imaeda N, et al. Differentiation ability of multipotent hematopoietic stem/progenitor cells detected by a porcine specific anti-CD117 monoclonal antibody. Biosci Trends. 2014; 8:308–15. PMID: 25641176 doi: 10.5582/bst.2014.01084

40. Maier J, Labute P. Assessment of fully automated antibody homology modeling protocols in molecular operating environment. Proteins. 2014; 82:1599–610. PMID: 24715627 PMCID: PMC4284016 doi: 10.1002/prot.24576

41. Bernstein F, Koetzle T, Williams G, Meyer E Jr., Brice M, Rodgers J, et al. The Protein Data Bank: A Computer-based Archival File For Macromolecular Structures. J Mol Biol. 1977; 112:535. PMID: 875032

42. Hansman G, Taylor D, McLellan J, Smith T, Georgiev I, Tame J, et al. Structural Basis for Broad Detection of Genogroup II Noroviruses by a Monoclonal Antibody That Binds to a Site Occluded in the Viral Particle. J Virol. 2012; 86:3635–46. PMID: 22278249 PMCID: PMC3302548 doi: 10.1128/JVI.06868-11

43. Livak K, Schmittgen T. Analysis of relative gene expression data using real-time quantitative PCR and the 2(-Delta Delta C(T)) Method. Methods. 2001; 25:402–8. PMID: 11846609 doi: 10.1006/meth.2001.1262

44. Schmittgen T, Livak K. Analyzing real-time PCR data by the comparative C(T) method. Nat Protoc. 2008; 3:1101–8. PMID: 18546601

45. Ito T, Sendai Y, Yamazaki S, Seki-Soma M, Hirose K, Watanabe M, et al. Generation of recombination activating gene-1-deficient neonatal piglets: A model of T and B cell deficient severe combined immune deficiency. PLoS One. 2014; 9:e113833. PMID: 25437445 PMCID: PMC4249935 doi: 10.1371/journal.pone.0113833

46. Mizukami Y, Abe T, Shibata H, Makimura Y, Fujishiro S, Yanase K, et al. MHC-matched Induced pluripotent stem cells can attenuate cellular and humoral immune responses but are still susceptible to innate immunity in pigs. PLoS One. 2014; 13:e98319. PMID: 24927426 PMCID: PMC4057111 doi: 10.1371/journal.pone.0098319

47. Lee K, Kwon D-N, Ezashi T, Choi Y-J, Park C, Ericsson A, et al. Engraftment of human iPS cells and allogeneic porcine cells into pigs with inactivated RAG2 and accompanying severe combined immunodeficiency. Proc Natl Acad Sci USA. 2014; 111:7260–5. PMID: 24799706 PMCID: PMC4034252 doi: 10.1073/pnas.1406376111

48. Dellgren C, Nehlin J, Barington T. Cell surface expression level variation between two common Human Leukocyte Antigen alleles, HLA-A2 and HLA-B8, is dependent on the structure of the C terminal part of the alpha 2 and the alpha 3 domains. PLoS One. 2015; 10:e0135385. PMID: 26258424 PMCID: PMC4530957 doi: 10.1371/journal.pone.0135385

49. Cano F, L PJ. A novel post-transcriptional role for ubiquitin in the differential regulation of MHC class I allotypes. Mol Immunol. 2012; 55:135–8. PMID: 23140835 PMCID: PMC3625108 doi: 10.1016/j.molimm.2012.10.015

50. Harris M, Lybarger L, Myers N, Hilbert C, Solheim J, Hansen T, et al. Interactions of HLA-B27 with the peptide loading complex as revealed by heavy chain mutations. Int Immunol. 2001; 13:1275–82. PMID: 11581172

51. Spiliotis E, Manley H, Osorio M, Zúñiga M, Edidin M. Selective export of MHC class I molecules from the ER after their dissociation from TAP. Immunity. 2000; 13:841–51. PMID: 11163199

52. van den Elsen P, Gobin S, van Eggermond M, Peijnenburg A. Regulation of MHC class I and II gene transcription: differences and similarities. Immunogenetics. 1998; 48:208–21. PMID: 9683666

53. Gobin S, van Zutphen M, Woltman A, van den Elsen P. Transactivation of classical and nonclassical HLA class I genes through the IFN-stimulated response element. J Immunol. 1999; 163:1428–34. PMID: 10415043

54. Kametani Y, Wang L, Koduka K, Sato T, Katano I, Habu S. Rapid histone deacetylation and transient HDAC association in the IL-2 promoter region of TSST-1-stimulated T cells. Immunol Lett. 2008; 119:97–102. PMID: 18606456 doi: 10.1016/j.imlet.2008.05.006

55. van den Elsen P. Transcriptional regulation of the MHC class Ib genes HLA-E, HLA-F, and HLA-G. Frontiers Immunol. 2011; 2:2–9. PMID: 11137213

56. van den Elsen P, Holling T, Kuipers H, van der Stoep N. Transcriptional regulation of antigen presentation. Curr Opin Immunol. 2004; 16:67–75. PMID: 14734112

57. Gobin S, Biesta P, de Steenwinkel J, Datema G, van den Elsen P. HLA-G transactivation by cAMP-response element-binding protein (CREB). An alternative transactivation pathway to the conserved major histocompatibility complex (MHC) class I regulatory routes. J Biol Chem. 2002; 277:39525–31. PMID: 12183445 doi: 10.1074/jbc.M112273200

58. Hake S, Masternak K, Kammerbauer C, Janzen C, Reith W, Steimle V. CIITA leucine-rich repeats control nuclear localization, in vivo recruitment to the major histocompatibility complex (MHC) class II enhanceosome, and MHC class II gene transactivation. Mol Cell Biol. 2000; 20:7716–25. PMID: 11003667 PMCID: PMC86349

59. Gobin S, van Zutphen M, Westerheide S, Boss J, van den Elsen P. The MHC-specific enhanceosome and its role in MHC class I and beta(2)-microglobulin gene transactivation. J Immunol. 2001; 167:5175–84. PMID: 11673530

60. Pratheek B, Nayak T, Sahoo S, Mohanty P, Chattopadhyay S, Chakraborty N, et al. Mammalian non-classical major histocompatibility complex I and its receptors: Important contexts of gene, evolution, and immunity. Indian J Hum Genet. 2014; 20(2):129–41. PMID: 25400340 PMCID: PMC4228563 doi: 10.4103/0971-6866.142855

61. Vogel C, Marcotte E. Insights into the regulation of protein abundance from proteomic and transcriptomic analyses. Nat Rev Genet. 2013; 13(4):227–32. PMID: 22411467 doi: 10.1038/nrg3185

International Immunology, Vol. 27, No. 11, pp. 567–577
doi:10.1093/intimm/dxv031
Advance Access publication 14 May 2015

Common marmoset CD117$^+$ hematopoietic cells possess multipotency

Shin Shimada[1], Satoshi Nunomura[2], Shuya Mori[1,3], Hiroshi Suemizu[4], Toshio Itoh[4], Shuji Takabayashi[5], Yoshinori Okada[6], Takashi Yahata[3], Takashi Shiina[1], Hideki Katoh[5], Ryuji Suzuki[7], Kenzaburo Tani[8], Kiyoshi Ando[6], Hideo Yagita[9], Sonoko Habu[9], Erika Sasaki[4] and **Yoshie Kametani[1]**

[1]Department of Molecular Life Science, Tokai University School of Medicine, Isehara, Japan
[2]Division of Molecular Cell Immunology, Advanced Medical Research Center, Nihon University Graduate School of Medical Science, Tokyo, Japan
[3]Department of Hematology, Tokai University School of Medicine, Isehara, Japan
[4]Central Institute for Experimental Animals, Kawasaki, Japan
[5]Experimental Animals Institute, Hamamatsu University School of Medicine, Shizuoka, Japan
[6]Support Center for Medical Research and Education, Tokai University School of Medicine, Isehara, Japan
[7]Department of Rheumatology and Clinical Immunology, Clinical Research Center for Allergy and Rheumatology, Sagamihara National Hospital, National Hospital Organization, Sagamihara, Japan
[8]Division of Molecular and Clinical Genetics, Department of Molecular Genetics, Medical Institute of Bioregulation, Kyushu University, Fukuoka, Japan
[9]Department of Immunology, Juntendo University School of Medicine, Tokyo, Japan

Correspondence to: Y. Kametani, E-mail: y-kametn@is.icc.u-tokai.ac.jp

Received 7 January 2015, *accepted* 10 May 2015

Abstract

Analysis of the hematopoiesis of non-human primates is important to clarify the evolution of primate-specific hematopoiesis and immune regulation. However, the engraftment and development of the primate hematopoietic system are well-documented only in humans and are not clear in non-human primates. *Callithrix jacchus* (common marmoset, CM) is a New World monkey with a high rate of pregnancy and small size that lives in closed colonies. As stem cell factor (SCF) is an essential molecule for hematopoietic stem cell development in mice and humans, we focused on CD117, the SCF receptor, and examined whether CD117-expressing cells possess the hematopoietic stem/progenitor cell characteristics of newborn marmoset-derived hematopoietic cells that can develop into T cells and B cells. When CD117$^+$ cell fractions of the bone marrow were transplanted into immunodeficient NOD (non-obese diabetic)/Shi-scid, common γc-null (NOG) mice, these cells engrafted efficiently in the bone marrow and spleens of the NOG mice. The CD117$^+$ cells developed into myeloid lineage cells, CD20$^+$ B cells and CD3$^+$ T cells, which could express CM cytokines *in vivo*. The development of B cells did not precede that of T cells. The development of CD8$^+$ T cells was dominant in NOG mice. The engraftment was comparable for both CD117$^+$CD34$^+$ cells and CD117$^+$CD34$^-$ cells. These results suggest that the CD117$^+$ cell fraction can differentiate into all three cell lineages, and the development of marmoset immunity in the xenogeneic environment follows diverse developmental pathways compared with human immunity.

Keywords: common γc-null mice, lymphoid lineage, NOD/Shi-scid, xeno-transplantation

Introduction

Although primate hematopoiesis has been thoroughly investigated for humans, hematopoiesis in non-human primates (NHPs) has not been clarified. While NHPs are expected to possess hematopoietic systems more similar to humans than to mice, unique characteristics may have evolved. *Callithrix jacchus*, conventionally called the common marmoset (CM) (1, 2), is a New World monkey for which colonies have been established via planned breeding and maintenance in Japan for 50 years. Transgenic CM individuals carrying the green fluorescein protein transgene through multiple generations have been successfully generated (3). The MHC gene structure of CMs was previously determined (4, 5). Furthermore, the

amino acid sequences of immune molecules are 86% identical on average between human and CM orthologs, whereas the identities are 60% identical between mouse and human orthologs (6). This phylogenetic situation and recent technological advances may increase the likelihood of the CM being a candidate experimental animal for studying the primate hematopoietic system. For this purpose, identification of CM hematopoietic stem cells (HSCs) is essential. While human HSCs possess a $CD34^+CD117^{lo}$ phenotype and mouse HSCs possess a $CD34^-CD117^+$ phenotype, the expression of CD34 and CD117 must be determined for CM HSCs (7–12).

To analyze human hematopoiesis, a repopulation assay using a humanized mouse has been developed and improved (13–15). In this system, HSCs or progenitors of human HSCs have been transferred into immunodeficient mice, such as NOD (non-obese diabetic)/Shi-scid, common γc-null (NOD/SCID/γc-null; NOG) mice (16–19). Then, in these mice, T cells and B cells of human origin have been successfully regenerated to a certain extent. Currently, the xeno-transplantation system using immunodeficient mice is popular for analyzing the development of blood cells in experimental animals (15).

Previous studies by Izawa *et al.* and our group have reported the repopulation ability of CM bone marrow (BM) cells into the myeloid lineage (20–22). Izawa *et al.* developed an anti-marmoset CD34 mAb, isolated $CD34^+$ cells from CM BM, and transplanted them into immunodeficient NOD-SCID mice (20). The mice developed $CD11b^+CD14^+$ cells cross-reacting to antihuman CD11b and CD14 mAbs (23). However, the authors could not detect lymphoid cells, partially because they used NOD-SCID mice, which cannot develop human T cells. Subsequently, our group established an anti-marmoset CD117 mAb and showed that the $CD34^+CD117^+$ fraction contained differentiation activity for mast cells (MCs) using NOG mice, which is an improved immunodeficient mouse line to achieve higher engraftment and to develop human T cells (22). However, both Izawa *et al.* and our group could not develop a CM lymphoid lineage in these previous systems.

Thus, the aims of the present study were to determine whether CM hematopoietic cells that express CD117 can develop into the lymphoid lineage and to clarify their potential for differentiation into T cells and B cells.

Methods

Animals

CM animals were obtained from CLEA Japan (Tokyo, Japan) and kept at the Central Institute for Experimental Animals (CIEA, Kawasaki, Japan) or Hamamatsu Medical University during the experiments. Experiments using CMs were approved by the Institutional Committee for Animal Care and Use and performed at CIEA or Hamamatsu Medical University according to institutional guidelines. The CMs were aged 0–4 years, and the sex was arbitrary. With regard to newborn individuals, newborn pups that were actively rejected or neglected by their parents were provided from the laboratory animal facility at Hamamatsu University School of Medicine and used in the experiments according to the institutional guidelines as reported previously (24). Two newborn animals, eight adult (3–9 year old) animals, four young (1–2 year old) animals and four cord blood (CB) samples were used for the experiments. All animals were unrelated healthy animals. This study adhered to the legal requirements of Japan and to the American Society of Primatologist Principles for the Ethical Treatment of Non-Human Primates.

NOG mice were provided by CIEA and kept under specific pathogen-free conditions. Experiments using mice were approved by the Institutional Committee for Animal Care and Use and performed at Tokai University following university guidelines.

Preparation of human and marmoset cells

Human umbilical CB was obtained from full-term, healthy newborns immediately after vaginal delivery. Informed consent was obtained according to the institutional guidelines, and this work was approved by the Tokai University Human Research Committee. Mononuclear cells (MNCs) were separated by Ficoll-Paque gradient centrifugation. $CD34^+$ cells were purified from MNCs using a two-step magnetic bead sorting method (Miltenyi Biotec, Gladbach, Germany), and the purity was >95%. Marmoset CB cells were collected from the cord of the placenta just after the delivery of the baby with heparin. MNCs were separated in Lymphocepal (IBL Co., Takasaki, Japan) at 670 × *g* for 30 min. MNCs were collected, and the remaining erythrocytes were lysed. With regard to the marmoset tissue cells, spleens were removed from marmosets, and cells were isolated from tissues. After red blood cells were lysed with low osmotic buffer (20 mM Tris–HCl, pH 7.4, 0.15 M NH_4Cl), they were suspended in RPMI1640 medium (Nissui, Tokyo, Japan) containing 10% (v/v) heat-inactivated FCS (SAFC Biosciences, Tokyo, Japan). BM cells of CMs were collected into heparinized tubes and centrifuged in Lymphocepal. MNCs were collected, and the remaining erythrocytes were lysed.

Flow cytometry

Cells were incubated with appropriately diluted, fluorescence-labeled primary mAbs for 15 min at 4°C and washed with 1% (w/v) BSA-containing PBS. In some cases, the cells were re-incubated with a labeled secondary antibody. The mAbs used were as follows: anti-marmoset CD117-APC (allophycocyanin), anti-marmoset CD34-PE (phycoerythrin) and anti-marmoset CD4-Alexa488 (Oriental Yeast Co., Tokyo, Japan); antihuman CD3-PerCPCy5.5 (SP34-2), antihuman CD20 (B-Ly1), antihuman CD8-FITC (HIT8a), streptavidin-PE and streptavidin-APC (BD Biosciences, Franklin Lakes, NJ, USA) and antihuman CD14-FITC (61D3), human IgE (HE1) and antihuman IgE (BE5) purchased from e-Bioscience, BioPorto Diagnostics (Gentofte, Denmark) and Abcam Japan (Tokyo, Japan), respectively. An anti-marmoset CD45 mAb was prepared as reported previously (25).

Histological analyses

Tissues were fixed with 20%-buffered formalin and embedded in paraffin. A paraffin block was micro-sectioned, deparaffinized and post-fixed. Cells or tissue sections on glass slides were conventionally stained with hematoxylin–eosin. The primary antibody was the antihuman-HLA clone EMR8-5 (Hokudo, Sapporo, Japan). Sections were examined using a DP71 microscope (Olympus, Tokyo, Japan).

Reverse transcription–polymerase chain reaction (RT–PCR)

RNA was extracted from cells using the RNeasy Mini Kit (Qiagen, Germantown, MD, USA). RNA (50 ng) was reverse transcribed, and the generated cDNA was amplified using primers and a OneStep RT–PCR kit (Qiagen). Reverse transcription was performed at 50°C for 30 min and polymerase activation at 95°C for 15 min with 33 cycles of PCR, each cycle consisting of denaturation at 94°C for 1 min, annealing at 60°C for 1 min, and extension at 72°C for 1 min. PCR products were subjected to agarose gel electrophoresis. The primers used are summarized in Table 1.

Transplantation of marmoset and human hematopoietic cells into NOG mice

Lineagenegative [Lin(–)] cells were prepared via the depletion of CD3⁺/CD20⁺/CD14⁺ cells with magnetic bead sorting (AutoMACS, Miltenyi Biotec, Bergisch Gladbach, Germany). Afterwards, Lin(–), CD34⁻CD117⁻ (DN, double-negative), CD34⁺CD117⁺ (DP, double-positive) and CD34⁻CD117⁺ (SP, single-positive) cells were stained as described above and purified from CM BMs with a cell sorter (FACS Aria, Becton Dickinson, Franklin Lakes, NJ, USA). Purity was >95% based on flow cytometry. Eight- to nine-week-old NOG mice were sub-lethally irradiated with 2.5 Gy x-rays prior to transplantation, and CM cells were injected into the mice intravenously. The transplanted cell numbers are summarized in Table 2. Human CB CD34⁺ cells were purified via two-step magnetic bead sorting (AutoMACS, Miltenyi Biotec, Bergisch Gladbach, Germany), as mentioned in 'Preparation of human and marmoset cells'. Purified cells (5×10^5 per head) were transplanted into NOG mice intravenously as described previously (18). Two to twelve weeks after transplantation, peripheral blood (PB) was collected via the orbit under inhalation anesthesia. MNCs were prepared and analyzed by flow cytometry. After confirmation of the engraftment, the mice were sacrificed, and the lymphoid tissues were analyzed. The numbers of mice used were as follows: eight (DP), three (SP), three (DN), one (CD34SP) and four (control, CTR) in the experiments with CD45⁺ cells and monocytes (adult BM was used); five (DP) and six (SP) in the experiments with lymphocytes 4–12 weeks after transplantation (newborn BM was used) and four in the experiments with secondary transplantation. For human CB CD34⁺ cell-transplanted NOG mice (CB-NOG), CB from two neonates and nine NOG mice were used.

Confocal microscopy

To detect the surface expression of FcεRI, marmoset-derived MC cultures (2×10^5) were incubated with 5 μg ml^{-1} of human IgE overnight. The cells were washed and further incubated with an FITC-conjugated mouse antihuman IgE mAb on ice for 20 min. CM cells stained with APC-labeled anti-CD14, CD34 and CD117 mAbs as above were placed on glass slides pre-treated with 3-aminopropylethoxysilane (Digene, Beltsville, MD, USA), incubated in a 5% (v/v) CO_2 atmosphere at 37°C in a humidified chamber for 30–40 min, and centrifuged at 100 × *g* for 15 min using a Cytospin 3 (Shandon, Pittsburgh, PA, USA). The cells were washed, re-treated with 4% paraformaldehyde and analyzed by confocal laser microscopy (META 510, Carl Zeiss, Hertfordshire, UK).

Colony-forming assay using bone marrow and cord blood-derived mononuclear cells

Cells were collected, washed and plated at 2×10^4 cells in 1 ml of methylcellulose-containing medium (Methocult GF⁺ H4435: Stem Cell Technologies, Vancouver, Canada) in a 35-mm dish with human stem cell factor (SCF) (10 ng ml^{-1}), IL-3 (10 ng ml^{-1}), Epo (2 U ml^{-1}) and G-CSF (10 ng ml^{-1}) and cultured at 37°C in a 5% CO_2 atmosphere. After 14 days of culture, types and numbers of hematopoietic colonies (colony-forming units) were counted according to the standard criteria. Samples from one animal were processed for the assay in triplicate, and eight different animals were used (M1-M4 for CB, M5-M8 for BM of adult animals mentioned above).

Table 1. RT–PCR primers

Genes	Forward strand primer	Reverse strand primer
IL-2	5′-ATGTACAGCATGCAGCTCGC-3′	5′-GCTTTGACAGAAGGCTATCC-3′
IL-4	5′-TGTCCACGGACACAAGTGCGA-3′	5′-CATGATCGTCTTTAGCCTTTCC-3′
IL-5	5′-GCCAAAGGCAAACGCAGAACGTTTCAGAGC-3′	5′-AATCTTTGGCTGCAACAAACCAGTTTAGTC-3′
IL-6	5′-ATGAACTCCTTCTCCACAAGCGC-3′	5′-GAAGAGCCCTCAGGCTGGACTG-3′
IL-10	5′-GGTTACCTGGGTTGCCAAGCCT-3′	5′-CTTCTATGTAGTTGATGAAGATGTC-3′
IL-17A	5′-CTCCTGGGAAGACCTCATTG-3′	5′-CAGACGGATATCTCTCAGGG-3′
IL-17F	5′-CAAAGCAAGCATCCAGCGCA-3′	5′-CATTGGGCCTGTACAACTTCTG-3′
IFN-γ	5′-CTGTTACTGCCAGGACCCAT-3′	5′-CGTCTGACTCCTTCTTCGCTT-3′
TNF-α	5′-GAGTGACAAGCCTGTAGCCCATGTTGTAGCA-3′	5′-GCAATGATCCCAAAGTAGACCTGCCCAGACT-3′
CD11c	5′-CCCAGTGTCTATGCAGGAGT-3′	5′-CCCATTTGAGGCAAGGAACA-3′
CD13	5′-GTACATGGAGGGCAATGTCA-3′	5′-GTGGAACTCAGTGACATTCC-3′
CD14	5′-ATCCACTTATGTCAGCGCTC-3′	5′-CCACTTAGAACGTTCTCCAG-3′
HPRT	5′-TGACCAGTCAACAGGGGAC-3′	5′-GCTCTACTAAGCAGATGGC-3′
β-Actin[a]	5′-TCTCCCCAAGTTAGGTTTTGTC-3′	5′-ATCATGTTTGAGACCTTCAACAC-3′

HPRT, hypoxanthine-guanine phosphoribosyltransferase.

[a]β-Actin is a mouse internal control.

Table 2. List of marmoset WBC-transplanted NOG mice

Cell fraction	Tx No.	Tx period	BM hCD45(%)	
			Lymph gate	Mono gate
CTR	0	3 W	<0.1	<0.1
Lin(−)	1.5×10^5	3 W	<0.1	<0.1
Lin(−)	1.5×10^5	3 W	0.61	<0.1
CD34SP	4.6×10^4	3 W	<0.1	<0.1
DN	1.0×10^5	3 W	<0.1	<0.1
DN	1.0×10^5	3 W	<0.1	<0.1
DN	1.0×10^5	3 W	<0.1	<0.1
DP	1.0×10^5	2 W	15.2	58.2
DP	1.6×10^5	3 W	5.83	74.5
DP	1.0×10^5	3 W	6.21	42.5
DP	1.0×10^5	3 W	10.3	69.1
DP	1.0×10^5	5 W	3.64	34.8
DP	1.0×10^5	8 W	13.1	12.8
DP	1.0×10^5	8 W	5.15	17.3
DP	1.0×10^5	12 W	0.99	3.8
SP	1.7×10^5	3 W	2.13	60.5
SP	1.7×10^5	3 W	12.4	73.8
SP	1.0×10^5	3 W	7.01	78.3

Tx, transplantation; WBC, white blood cell.

Statistical analyses

Statistical analysis was performed using a two-tailed Student's *t*-test, and the data are expressed as the mean ± SD. Significant differences are indicated with asterisks: $^*P < 0.05$.

Results

Engraftment of CD117⁺ CM cells in NOG mice

In humans, CD34 is an HSC marker, while in mice, CD117 is an HSC marker. Thus, we focused on the repopulation ability of CD117⁺ cells with and without CD34 expression. First, we attempted to transplant whole BM MNCs from adult CMs. However, the BM MNCs could not repopulate in NOG mice up to 5×10^6 per head (data not shown). Therefore, we fractionated the BM cells into Lin(−), CD34⁺CD117⁺ (DP), CD34⁻CD117⁺ CD117 SP) CD34⁺CD117⁻ (CD34 SP) and CD34⁻CD117⁻ (DN) cells using anti-marmoset CD34 and anti-marmoset CD117 mAbs and FACS sorting, as reported previously (21) (Supplementary Figure 1). Then, Lin(−), DP, CD117 SP, CD34 SP and DN fractions were injected intravenously into irradiated NOG mice. As shown in Table 2, cells, Lin(−) CD34 SP cells and DN cells did not engraft in NOG mice, when the PB MNCs were examined for CD45 expression. Moreover, as in most CM BMs, the CD34 SP cell numbers were very low, and it was very difficult to administer 1×10^5 cells into one mouse. The mouse lymphoid organs and PB were collected, and the detected engraftment was confirmed. Thus, we concentrated on analyzing CD117⁺ cells in further experiments.

To assess short-term HSCs (ST-HSCs), BM cells and splenocytes were prepared from NOG mice 3 weeks after the transplantation of DN (negative control), DP and SP CM cells. The CM CD45⁺ cells were detected by flow cytometry. We set monocyte and lymphocyte gates for the preparation of BM cells and splenocytes on the basis of forward scatter (FSC) and side scatter (SSC; Supplementary Figure 2). Figure 1A shows the CD45 expression of monocyte-gated fractions. CM MNCs have high auto-fluorescence, and false-positive cells appear substantially more frequently than in human cells.

In contrast, when a lymphocyte gate was employed as shown in Fig. 1(B), only a small CD45⁺ population was detected, specifically 10–13% among BM cells and 7% among splenocytes. Therefore, the development of CM CD117⁺ cells in NOG mice early after transplantation was far more prominent in the direction of the myeloid lineage compared with the lymphoid lineage during this period, which is similar to the results observed for the transplantation of human and mouse HSCs into immunodeficient mice.

Next, we calculated the positive cells by subtracting the autofluorescence⁺ cells. As a result, BM cells and splenocytes contained similar levels of the CD45⁺ fraction when DP and SP cells were transplanted into NOG mice. BM or spleens of non-transplanted NOG mice exhibited no CD45⁺ cells. Figure 1C shows the mean percentages of the CD45⁺ fraction. Both DP and CD117 SP (but not DN) BM cells generated similar levels of CD45⁺ leukocytes in the BM and spleens of transplanted NOG mice.

Expansion of class-I⁺ marmoset cells in NOG mice

Unfortunately, a marmoset-specific CD45 antibody is not available for immunohistochemistry (IHC); therefore, we used an antihuman MHC antibody to recognize CM-derived cells. Spleens were collected 3 weeks after transplantation, and paraffin-embedded thin sections were processed for IHC staining with an anti-HLA-class I mAb recognizing a common epitope present in the heavy chains of HLA-A, -B and -C but not mouse MHC. As shown in Fig. 2, almost all cells from CM spleens were stained with the antibody, showing that this antibody reacted with the CM MHC. Positively stained cells were found in the spleens of DP- or SP-transplanted NOG mice but not in non-transplanted NOG mice. Thus, DP and SP BM cells of CM could engraft in the spleens of NOG mice.

At higher magnification, the CM cells diffusely dispersed around the blood vessels in the mouse spleen, and no B-cell follicles or germinal centers were observed, as reported in human HSC-transplanted NOG mice (17). These results suggest that CM CD117⁺ cells can engraft in NOG mice irrespective of CD34 expression, although the tissue structure is barely reconstituted when the purified cells are transplanted.

Differentiation of marmoset CD117⁺ cells into myeloid lineage cells

We then examined whether CM DP progenitors could differentiate into various myeloid cells in addition to the MCs that we reported previously (22). We examined the expression of CD13, CD14 and CD11c because these are markers for myeloid cells other than MC myeloid markers. Because CM-specific antibodies were not available or their specificity has not been validated, we used RT–PCR for the analysis. We designed primers for transcripts of these genes based on cDNA and genome databases and used them in RT–PCR analyses (Table 1, Fig. 3A). The DP and SP cells sorted from CM BM and splenocytes of non-transplanted NOG mice did

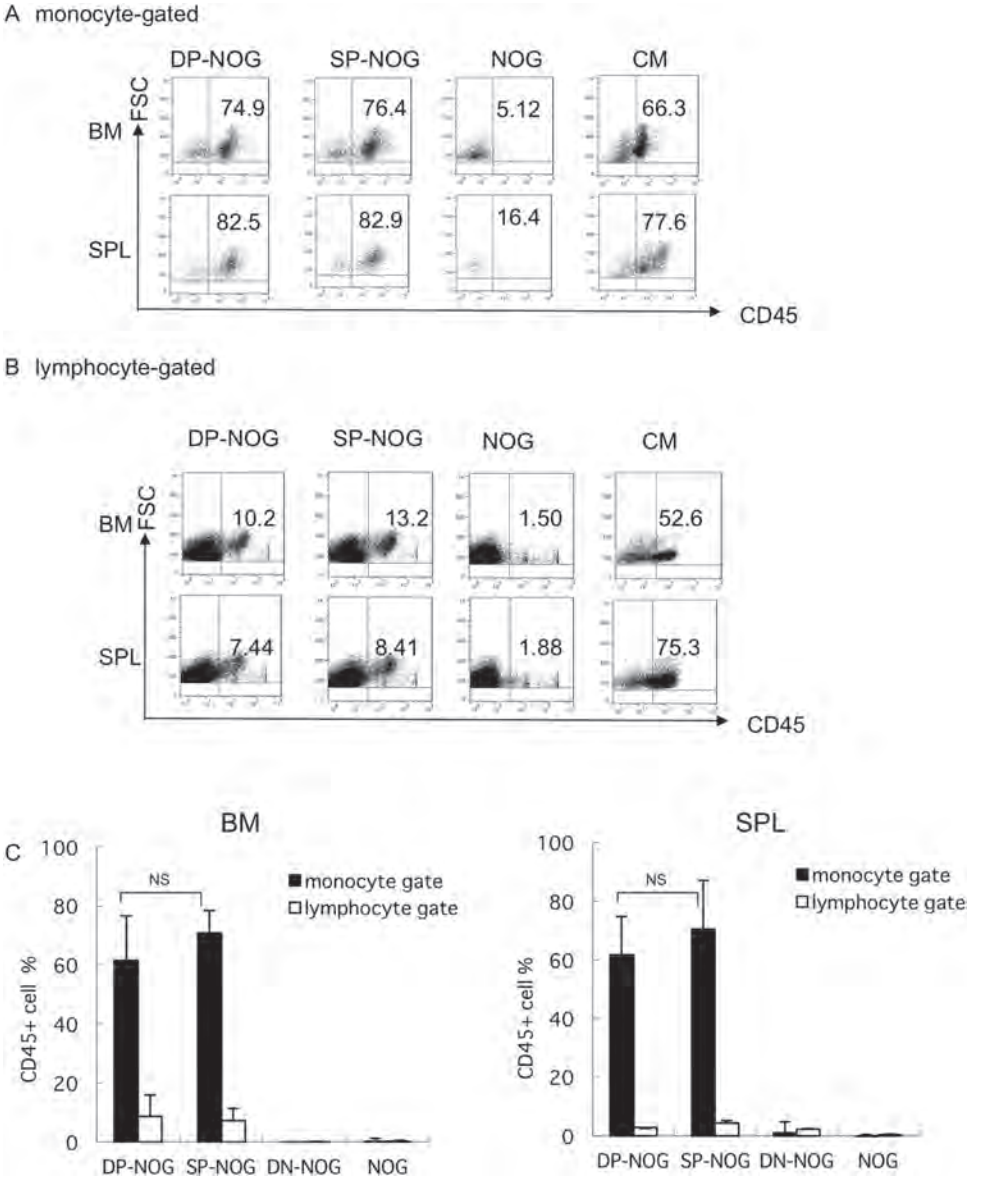

Fig. 1. Expansion of CD45⁺ marmoset cells in transplanted NOG mice. CD117⁺CD34⁺ (DP), CD117⁺CD34⁻ (SP) and CD117⁻CD34⁻ (DN) cells were isolated from marmoset bone marrow (BM) and transplanted into NOG mice intravenously. After 3 weeks, BM cells as well as splenocytes (SPL) were collected from the mice and processed for flow cytometry with an anti-marmoset CD45 mAb. (A) The monocyte-gated fraction as defined by SSC and FSC (see Supplementary Figure 2) is displayed for the CD45 fluorescence intensity. Cells from non-transplanted NOG mice were used as a negative control, whereas cells from CMs were used as a positive control. In the marmoset spleen, a fraction in the control sample exhibited auto-fluorescence. (B) The mean ± SD was calculated for the percentages of the CD45⁺ sub-fractions from more than three independent experiments as in (A). NOG indicates cells from non-transplanted NOG mice. (C) Experiments were performed as in (A), and the lymphocyte-gated fractions were analyzed. The data are shown as the mean ± SD. Significant differences were not detected between DP and SP ($P < 0.05$). Filled lines represent the negative control stained with isotype control, and the solid lines represent anti-CD45 antibody-stained cells. The number shown in each panel is an index calculated as the margin of the percentages of the cell fractions stained and un-stained cells gated for FL2CD45-hi and FSC-hi.

not express any of these three transcripts, suggesting that the myeloid cells were not contaminated in the transplanted cells. After transplantation of CD117⁺ cells into NOG mice, transcripts of CD11c, CD13 and CD14 were clearly detected. As we reported previously, CM MCs were observed in the mouse spleen (Fig. 3B) (22). These results indicate that the DP and SP progenitors of CM were capable of developing into cells of myeloid lineages.

Differentiation of marmoset CD117⁺ cells into lymphoid cells

We next examined whether T cells and B cells developed from CM CD117⁺ cells and compared with human HSC development in NOG mice. Because there were very few adult CD117⁻CD34⁺ cells, only one NOG mouse was transplanted with the cells, and CM cell engraftment was not detected (Table 2), whereas adult CD117⁺ cell fractions

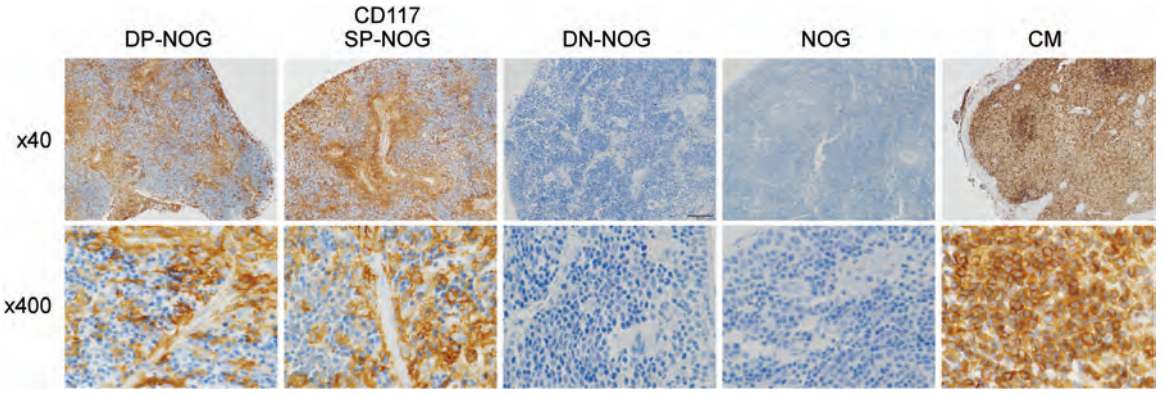

Fig. 2. Expansion of transplanted marmoset cells in the spleens of NOG mice. CD117⁺CD34⁺ (DP), CD117⁺CD34⁻ (SP) and CD117⁻CD34⁻ (DN) fractions were isolated from the BM of the CM and injected intravenously into NOG mice as mentioned in Fig. 1. Spleens were collected after 3 weeks, and paraffin-embedded thin sections were processed for immunohistochemical staining with an antihuman HLA class I mAb. Deposition of brown dye indicates positive staining. Spleens from non-transplanted NOG mice and the CM served as negative and positive controls, respectively. Representative data for each transplanted mouse are shown. The ×400 data show that the positive cells are dispersed from the blood vessels of NOG spleens.

achieved the reconstitution of CM cells, as we reported previously (22). However, they did not maintain CM cells until 12 weeks after transplantation *in vivo*, and lymphoid cells were not observed. Because human CB HSCs possess a higher repopulation ability compared with adult BM HSCs (17), we speculated that newborn HSCs possess higher multipotency. Therefore, we used newborn CM BM cells for further xeno-transplantation. Both SP and DP cell-transplanted NOG mice were analyzed at 8 and 12 weeks after transplantation. After 12 weeks, the engraftment was compared. In this newborn system, both DP-NOG and SP-NOG showed CM cell engraftment in both BM and spleen, although the percentage of human CD45 cells in BM (CB-NOG in Fig. 4A) was not significantly higher than that of older marmosets (CM in Fig. 4A). CD3 and CD19 mRNA was already detected 8 weeks after transplantation in DP- and SP-NOG spleen cells (Fig. 4B), while a few lymphocytes were detected by flow cytometry. After 12 weeks, the surface expression of both markers on the lymphoid cells was evident (Fig. 4C and D). Developed CD3⁺ cells contained CD8⁺ T cells, but CD4⁺ T cells were not detected in these mice (Table 3). As reported previously, when human HSCs were transplanted into NOG mice, the B-cell ratio was higher in the mice during the early period (16, 17, 19). Moreover, both CD4⁺ and CD8⁺ T cells were detected in the mice. Thus, the cellularity of reconstituted lymphoid cells was different between CMs and humans. The PB MNCs of CMs contained equal amounts of CD4 and CD8 T cells, while that of humans contained substantially higher amounts of CD4 T cells, suggesting that CD8 T-cell-dominant differentiation in NOG mice reflects a unique characteristic of the CM hematopoietic immune system (Supplementary Figure 3). When TCR repertoire analysis was employed (24), the CD3⁺ cells contained detectable Vα9-1 and Vβ24, the most frequent Vα and Vβ in CM peripheral lymphoid organs, which exist equally in CD4 T cells and CD8 T cells in the thymus, indicating the existence of functional TCR-expressing T cells (R. Suzuki, personal communication). No thymic T cells were observed in the NOG mice, indicating the extra-thymic differentiation of the CD8⁺ cells.

We also examined the expression of cytokines in the differentiated CM cells to determine whether the lymphocytes have any bias regarding cytokine production. Primers specific for CM cytokine transcripts were set and used for RT–PCR analyses (Table 1). The sorted DP cells of CM and the splenocytes of non-transplanted NOG mice did not express detectable amounts of cytokine transcripts, except for transforming growth factor (*TGF*)-β in DP cells (Fig. 5). The DP and SP cells cultured *in vitro* expressed large amounts of *TGF*-β and small amounts of *IL-4* and *IL-17F*. Interestingly, the transcripts of T_h2, T_h17 and Treg-related cytokines, including IL-4, IL-5, IL-6, IL-10, IL-17A, IL-17F, IFN-gamma, TGF-beta and tumour necrosis factor TNF-alpha, were detected in the DP-NOG and SP-NOG spleens 8 weeks after transplantation. Of note, cells of the CD4 lineage were not detected in the spleens of NOG mice. Therefore, it is possible that myeloid cells, B cells and CD8⁺ T cells might be producing these various cytokine transcripts in the CM CD117⁺ cell-transplanted NOG spleen.

Collectively, newborn CD117⁺ cells can differentiate into lymphoid cells in the NOG environment. B cells and CD8⁺ T cells were involved in the differentiated lymphoid cells. The cells express T-cell cytokines, suggesting that the immune system is at least partially functional for cytokine production.

Maintenance of newborn marmoset CD117⁺ cells

To evaluate the characteristics of newborn CD117⁺ cells, we examined the ratio of CD117⁺ cells and their colony-forming ability (CFA) in CB MNCs of four independent newborn marmosets (Supplementary Figure 4). The results showed that all CBs contained CD117⁺ cells, and the ratio was different among the individuals. High CFA was evident in the samples that contained high ratios of CD117⁺ cells (M2). These included erythroid and myeloid colonies, but monocyte and megakaryocyte lineages were not detected.

Next, we examined whether aged BM MNCs contained CD117⁺ cells and CFA. Similar levels of CD117⁺ cells were found among 5-year-old BM MNC fractions, while 9-year-old marmoset BM contained fewer CD117⁺ cells. These BM cells possessed comparable CFA to the erythroid and myeloid

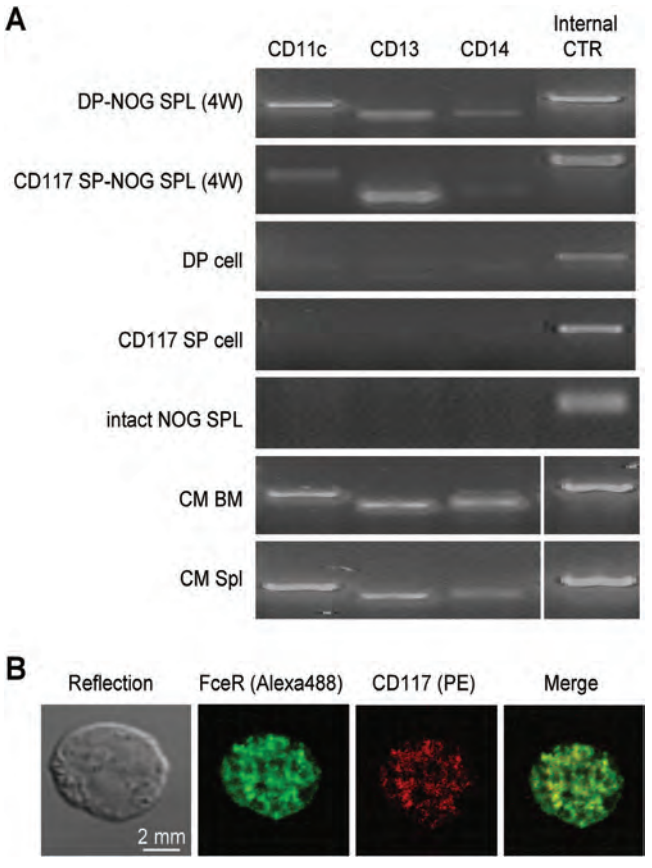

Fig. 3. Myeloid lineage cells were developed from marmoset BM cell fractions. CD117⁺CD34⁺ (DP) and CD117⁺CD34⁻ (SP) cells were prepared from marmoset bone marrow BM and transplanted into NOG mice. After 4 weeks, BM cells as well as splenocytes (SPL) were collected from mice and purified based on CD34 and CD117 expression. Cells were processed for RT–PCR or confocal microscopy. (A) RNA was prepared from the indicated samples including cultures of CD117⁺CD34⁺ (DP) or CD117⁺CD34⁻ (SP) cells, spleens of DP- or SP-transplanted or non-transplanted NOG mice, or bone marrow or spleens of CM. Transcripts of myeloid lineage-markers were examined. Internal controls: hypoxanthine-guanine phosphoribosyltransferase (*HPRT)* served as a control for CM, β-*actin* served as a control for NOG mice. (B) MCs developed in NOG mice. The monocyte-gated fractions were sorted out and analyzed by confocal microscopy after CD117 and FcεR staining.

lineages. These results demonstrate that CFA was present in both newborn and adult hematopoietic cells of the CM, and their differentiation ability was somewhat decreased among CB hematopoietic stem/progenitor cells in terms of myeloid and erythroid cells. Younger marmosets tended to possess more CD117⁺ cells in the BM, but the CD117⁺ cell ratio was not strictly correlated with the colony number.

As lymphocytes developed in the NOG mice transplanted with newborn BM cells, we examined whether the transplanted mouse BM still contained transplantable stem cells. As a result, DP cells were detected in the BM of transplanted NOG mice 12 weeks after newborn BM transplantation (Table 3), irrespective of the CD34 expression of transplanted CD117⁺ cells (Fig. 6). However, when the BM cells of these transplanted NOG mice were prepared and transplanted into new NOG mice, they could not be engrafted in the second group of NOG mice (Table 4).

Collectively, CD117⁺ cells of newborn BM had the ability to repopulate, but their LT-HST characteristics could not be evaluated with this system.

Discussion

The initial trial to identify hematopoietic progenitors in the CM was reported by Izawa *et al.* in 2004 (20). The results of this study demonstrated the differentiation potential of CM CD34⁺ cells into the myeloid lineage. Subsequently, our group established an anti-marmoset CD117 mAb and showed that the CD117⁺ fraction contained differentiation activity for the erythroid and myeloid lineages in colony-forming assays and developed into CD45⁺ leukocytes, including MCs, in transplanted NOG mice. However, the development of CM BM cells into the lymphoid lineage has not been achieved. In the present study, we extended the analysis of CM hematopoietic progenitors to lymphocyte differentiation by utilizing newborn BM CD117⁺ cells.

On the basis of extensive studies of hematopoiesis in humans, CD34⁺CD117^{lo} cells represent HSCs (11, 12), whereas CD34⁺CD117^{hi} cells contain myeloid progenitor activity that can develop lineages of MCs and monocytes (9, 26, 27). In CMs, while the development of myeloid lineage cells was also observed with CD34⁺CD117^{hi} cells, CD34⁺CD117⁻ cells could not achieve engraftment themselves (Table 2). This evidence suggests that in CMs, CD34 is not a definitive marker of CM HSCs. In humans and rhesus macaques, Lin(–) CD34⁺ cells are conveniently used as HSCs. Although most human and NHP CD34⁺ cells express CD117 (28, 29), CD117 is not an HSC marker, as the expression is maintained in myeloid cells such as MCs (30). In our results, a large portion of the CD117⁺ cells were also CD34⁺ cells, which have hematopoietic characteristics. On the other hand, mouse HSCs express no or very low levels of CD34. Thus, although CD34 SP cells cannot repopulate, and CD117 SP cells can also repopulate, their characteristics may not be more similar to mouse. This may represent an intermediate between mice and humans.

In our results, only newborn BM CD117⁺ cells developed into lymphoid cells (Fig. 4). The reason may be the BM aging of HSCs in adult CM BM or the difficulty in purifying stem cells from the BM matrix that aggregates in adult BM (data not shown). As BM MNCs had a higher CFA for the myeloid lineage than CB MNCs, their repopulation ability for the myeloid lineage was not decreased in older CMs. On the basis of previous evidence in mice and humans (31), aged BM CD117⁺ cells may possess a higher repopulation ability for the myeloid lineage compared with CB CD117⁺ cells because younger CD117⁺ cells may possess more lymphoid-committed cells than aged BM. This should be analyzed more extensively in the future.

Apart from MC development, we also observed additional remarkable phenomena in NOG mice transplanted with CM CD117⁺ cells. First was the appearance of CD13⁺, CD14⁺ and/or CD11c⁺ cells, whose expression was verified at the transcriptional level through RT–PCR analysis. It is probable that these cells correspond to mature myeloid cells, including

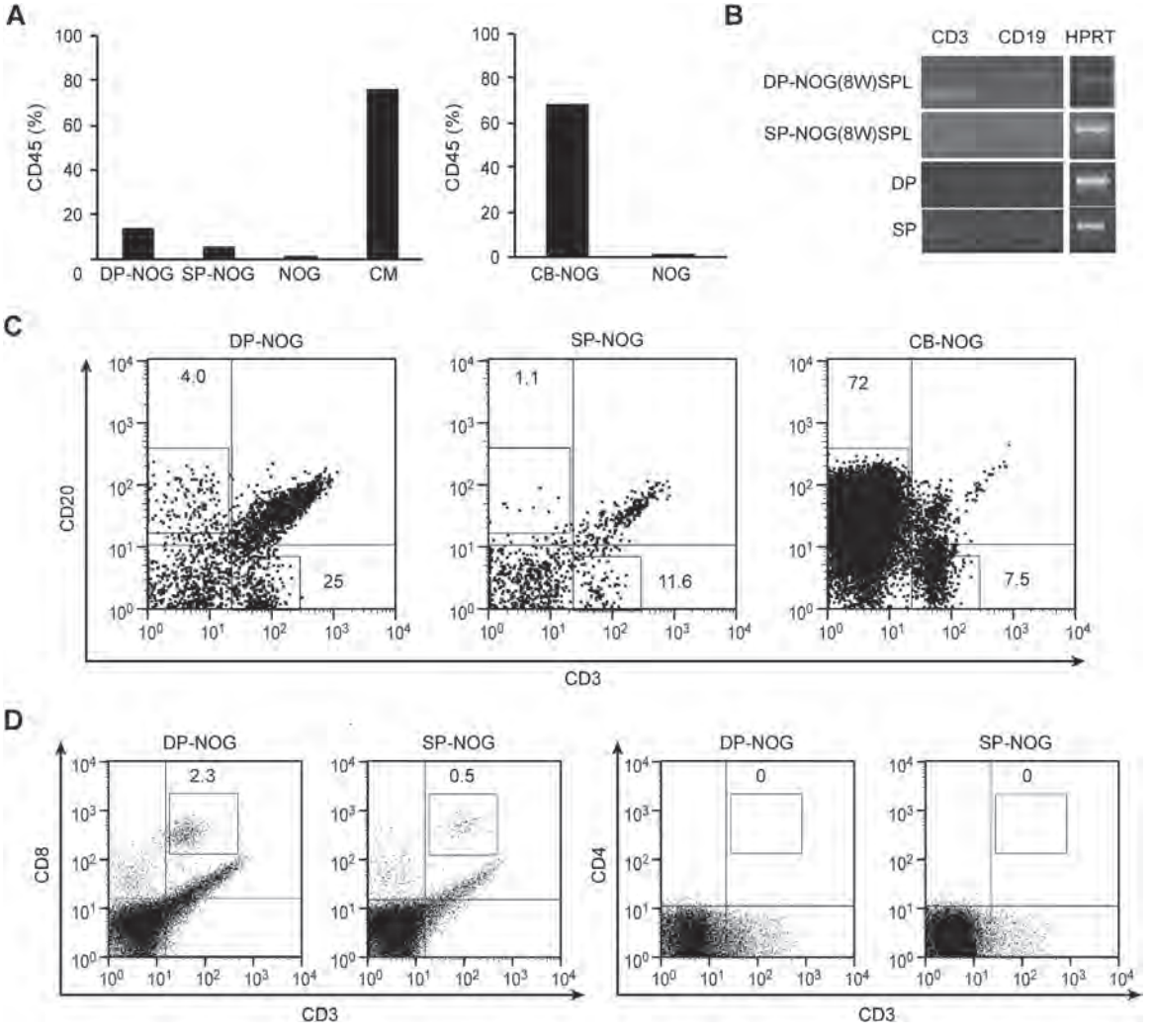

Fig. 4. Lymphoid lineage cells were developed from newborn CD117⁺ marmoset BM cell fractions. CD117⁺CD34⁺ (DP) and CD117⁺CD34⁻ (SP) cells were prepared from marmoset BM. Human CD34⁺ cells were prepared from CB. These cell fractions were transplanted into NOG mice. After 8 and 12 weeks, splenocytes (SPL) were taken from mice and analyzed for lymphocyte marker expression by RT–PCR or flow cytometry. (A) The average CD45⁺ lymphoid gate cell numbers from two mice (12 weeks) are shown in the figure. As the number of mice was only two, statistical analysis could not be performed. The mean % of the SPL from CM (n = 4, young adults), NOG (n = 3) and NOG mice transplanted with human CB HSCs (CB-NOG) (n = 9) are also shown. (B) RNA was prepared from the spleens of DP- or SP-transplanted NOG mice and assayed for mRNA expression. Transcripts of lymphoid lineage markers were examined. (C) CD20 and CD3 expression was analyzed for DP-NOG, SP-NOG and CB-NOG SPL. NOG, non-transplanted NOG spleen. (D) CD3⁺ T cells were analyzed for CD4 and CD8 expression. CD45⁺ lymphoid-gated cells were stained for CD3, CD4 and CD8. The percentages of the CD45-gated cell fractions further gated in the squares are shown in each panel.

Table 3. NOG-derived marmoset cells transplanted with newborn marmoset CD117⁺ cells

Cell fraction	Tx no.	Tx period	BM CD45 (%)		SPL cell no.	CD3⁺ (%)			CD20
			L gate	M gate		CD8⁺	CD4⁺	DN	
Newborn DP	1.35×10^5	4 W	0.193	0.928	1.0×10^7	<0.01	<0.01	0.017	0.042
Newborn DP	1.0×10^5	5 W	33.7	45.7	4×10^6	<0.01	<0.01	4.93	0.318
Newborn DP	1.0×10^5	8 W	54.7	71.9	5.0×10^7	2.04	<0.01	<0.01	0.177
Newborn DP	1.35×10^5	12 W	12.4	9.21	6×10^6	2.42	<0.01	<0.01	1.86
Newborn DP	1.3×10^4	12 W	1.8	44	1.25×10^7	6.34	<0.01	<0.01	1.25
Newborn SP	1.7×10^5	4 W	0.237	0.775	1.1×10^7	<0.01	<0.01	0.114	0.061
Newborn SP	1.0×10^5	5 W	0.139	0.551	4×10^6	<0.01	<0.01	0.416	0.68
Newborn SP	1.0×10^5	5 W	0.196	9.18	9×10^7	<0.01	<0.01	0.716	0.367
Newborn SP	1.0×10^5	8 W	14	39	7.5×10^6	0.476	<0.01	<0.01	0.127
Newborn SP	1.0×10^5	8 W	60.8	13.9	3.5×10^7	3.55	<0.01	<0.01	0.037
Newborn SP	1.7×10^5	12 W	25.2	52	1.0×10^7	0.498	<0.01	<0.01	0.749

monocytes (26, 27). It is most likely that the transplanted CM DP cells are capable of differentiating not only into MCs but also into other myeloid cells. Furthermore, these cells appeared to expand and massively infiltrate into the spleen (and liver, data not shown), as judged by staining with an antihuman HLA class I antibody. Second, the expression of various cytokines was detected at the transcriptional level (Fig. 4). The types of cells transcribing these cytokines could not be identified due to the lack of anti-marmoset cytokine monoclonal antibodies. Considering the differentiation profiles of the CD117⁺ cells described above, MCs and/or other myeloid cells might be the source of these cytokine transcripts. Because human and NHPs share many common characteristics with regard to the immune system, CM cytokine-producing cells might mimic the human cells (32–34).

Most importantly, newborn CM CD117⁺ cells developed into CD20⁺ cells and CD3⁺ cells in NOG mice (Table 3 and Fig. 4). In human HSC-transplanted NOG mice, B cells are dominant in the BM and periphery 2 months after the transplantation (17). CD3⁺ T cells appear in the periphery several weeks after B cells appear (35). Contrary to this phenomenon, in our study, CM T cells appeared simultaneously with B cells, and the amount of B cells was substantially lower than in humanized mice. Moreover, DN T cells dominated in the early period (4–5 weeks), and CD8⁺ T cells were dominant in the late period (8–12 weeks) among the CD3⁺ cells. While a similar ratio of CD4⁺ T cells and CD8⁺ T cells is observed in the PB of wild-type CMs (21), these results indicate that CD8⁺ cells are prone to developing in CM under lymphopenic conditions. CD4⁺ T cells were not observed in the thymus and periphery of this mouse system. We observed neither mouse nor marmoset thymocytes in the mice. Thus, marmoset CD8⁺ T cells might have developed extrathymically. Although we could not clarify the underlying reason, marmoset helper T-cell development in the thymus might require extra factors other than those from mice. This may be a unique characteristic of the CM or other NHPs. Otherwise, the mouse environment cannot develop conventional CD4⁺ T cells of CMs.

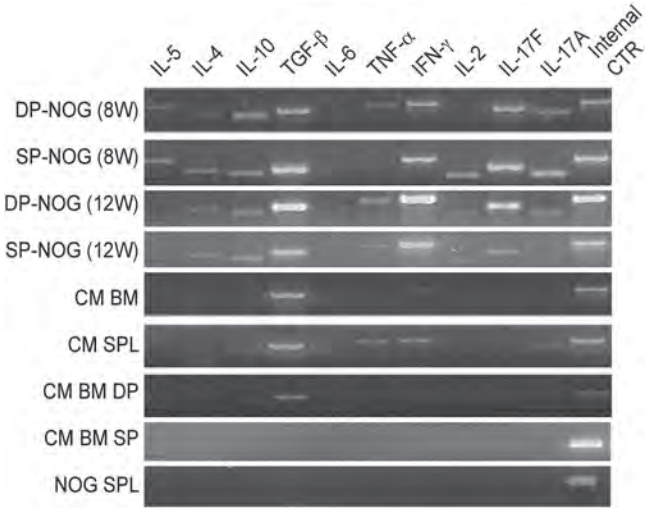

Fig. 5. The mRNA expression of marmoset cytokines. The mRNA expression of cytokines (*IL-5, IL-4, IL-10, TGF-β, IL-6, TNF-α, IFN-γ, IL-2, IL-17F* and *IL-17A*; internal controls: hypoxanthine-guanine phosphoribosyltransferase served as a control for CM, *β-actin* served as a control for NOG mice) was examined by semi-quantitative RT–PCR using DP-NOG and SP-NOG spleen cells (SPL) 8 and 12 weeks after transplantation, CM whole BM cells, whole SPL, purified DP cells, purified SP cells from CM BM and non-treated NOG SPL.

On the basis of the results indicating the development of CM T cells and B cells in NOG mice, CD117⁺ cells are multipotent because they can develop into erythroid cells (colony assay) (21), myeloid cells (colony assay and xeno-transplantation assay) (22) and lymphoid cells (xeno-transplantation assay). However, they could not maintain their repopulation ability after the secondary transplantation. While human CD34⁺ cells can engraft after a second transplantation in NOG mice (19). The NOG environment for the hematopoiesis of CM is different from humans and might be incompatible for long-term HSC repopulation.

In this study, we first demonstrated the development of CM lymphoid lineage cells in immunodeficient mice. This is an important finding because detailed marmoset immunity should be clarified not only for the sake of determining the evolution of immunology but also to evaluate this primate as an experimental animal for the development of immune-related molecular targeting reagents for human beings.

Supplementary data

Supplementary data are available at *International Immunology* Online.

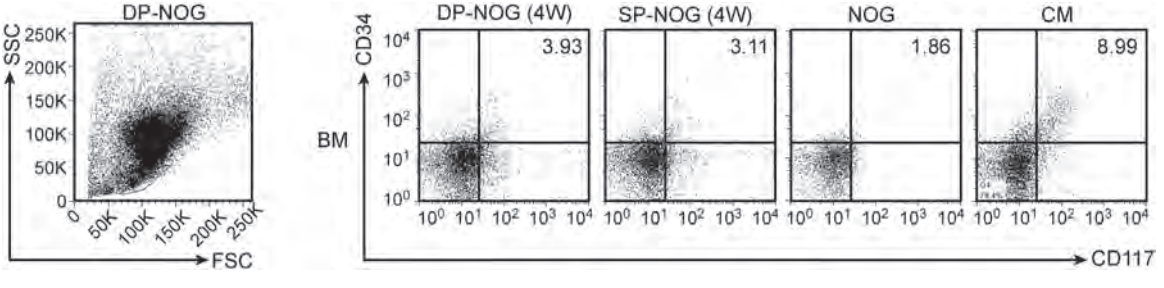

Fig. 6. Self-renewal of HSCs. DP-NOG and SP-NOG BM cells were prepared 4 weeks after transplantation and analyzed by flow cytometry for CD34 and CD117 expression.

Table 4. List of NOG mice used for re-transplantation

Mouse no.	Tx cell no.	Weeks after Tx	Engraftment
#1 (SP)	2×10^4	12 W (dead)	<0.01
#2 (DP)	1.3×10^5	12 W	<0.01
#3 (SP)	9×10^3	12 W	<0.01
#4 (DP)	1.2×10^4	12 W	<0.01

The BM MNCs of DP-NOG and SP-NOG were re-transplanted into NOG mice. Tx cell no.: number of MNCs transplanted into NOG mice. Mouse #1 died before analysis. None of the mice with secondary transplantation demonstrated the engraftment of marmoset cells.

Funding

Japan Society for the Promotion of Science (KAKENHI(C)22500391 to Y.K.); MEXT-Supported Program for the Strategic Research Foundation at Private Universities [2012–202016]; 2013 Tokai University School of Medicine Research Aid to Y.K.

Acknowledgements

The authors thank Dr J. Itoh (Teaching and Research Support Center, Tokai University School of Medicine) and M. Kuronuma (Central Institute for Experimental Animals) for their technical assistance and suggestions.

Conflict of interest statement: Y.K. and S.S designed the research, analyzed the data and wrote the paper. H.S. and S.N. analyzed the data and R.S. performed RT–PCR. H.S. supplied the NOG mice. E.S. supplied the CMs. Others contributed to the research design and the writing of the manuscript. The authors declare no competing financial interests.

References

1 Mansfield, K. 2003. Marmoset models commonly used in biomedical research. *Comp. Med.* 53:383.
2 Mansfield, K., Tardif, S. and Eichler, E. 2004. White paper for complete sequencing of the common marmoset (*Callithrix jacchus*) genome. https://www.genome.gov/Pages/Research/Sequencing/SeqProposals/MarmosetSeq.pdf.
3 Sasaki, E., Suemizu, H., Shimada, A. *et al.* 2009. Generation of transgenic non-human primates with germline transmission. *Nature* 459:523.
4 Shiina, T., Kono, A., Westphal, N. *et al.* 2011. Comparative genome analysis of the major histocompatibility complex (MHC) class I B/C segments in primates elucidated by genomic sequencing in common marmoset (Callithrix jacchus). *Immunogenetics* 63:485.
5 Kono, A., Brameier, M., Roos, C. *et al.* 2014. Genomic sequence analysis of the MHC class I G/F segment in common marmoset (Callithrix jacchus). *J. Immunol.* 192:3239.
6 Kohu, K., Yamabe, E., Matsuzawa, A. *et al.* 2008. Comparison of 30 immunity-related genes from the common marmoset with orthologues from human and mouse. *Tohoku J. Exp. Med.* 215:167.
7 Papayannopoulou, T., Brice, M., Broudy, V. C. and Zsebo, K. M. 1991. Isolation of c-kit receptor-expressing cells from bone marrow, peripheral blood, and fetal liver: functional properties and composite antigenic profile. *Blood* 78:1403.
8 Okada, S., Nakauchi, H., Nagayoshi, K., Nishikawa, S., Miura, Y. and Suda, T. 1992. In vivo and in vitro stem cell function of c-kit- and Sca-1-positive murine hematopoietic cells. *Blood* 80:3044.
9 Gunji, Y., Nakamura, M., Osawa, H. *et al.* 1993. Human primitive hematopoietic progenitor cells are more enriched in KITlow cells than in KIThigh cells. *Blood* 82:3283.
10 Mestas, J. and Hughes, C. C. 2004. Of mice and not men: differences between mouse and human immunology. *J. Immunol.* 172:2731.
11 Shizuru, J. A., Negrin, R. S. and Weissman, I. L. 2005. Hematopoietic stem and progenitor cells: clinical and preclinical regeneration of the hematolymphoid system. *Annu. Rev. Med.* 56:509.
12 Weissman, I. L. and Shizuru, J. A. 2008. The origins of the identification and isolation of hematopoietic stem cells, and their capability to induce donor-specific transplantation tolerance and treat autoimmune diseases. *Blood* 112:3543.
13 Pflumio, F., Izac, B., Katz, A., Shultz, L. D., Vainchenker, W. and Coulombel, L. 1996. Phenotype and function of human hematopoietic cells engrafting immune-deficient CB17-severe combined immunodeficiency mice and nonobese diabetic-severe combined immunodeficiency mice after transplantation of human cord blood mononuclear cells. *Blood* 88:3731.
14 Wermann, K., Fruehauf, S., Haas, R. and Zeller, W. J. 1996. Human-mouse xenografts in stem cell research. *J. Hematother.* 5:379.
15 Shultz, L. D., Brehm, M. A., Garcia-Martinez, J. V. and Greiner, D. L. 2012. Humanized mice for immune system investigation: progress, promise and challenges. *Nat. Rev. Immunol.* 12:786.
16 Ito, M., Hiramatsu, H., Kobayashi, K. *et al.* 2002. NOD/SCID/gamma©(null) mouse: an excellent recipient mouse model for engraftment of human cells. *Blood* 100:3175.
17 Matsumura, T., Kametani, Y., Ando, K. *et al.* 2003. Functional CD5+ B cells develop predominantly in the spleen of NOD/SCID/gammac(null) (NOG) mice transplanted either with human umbilical cord blood, bone marrow, or mobilized peripheral blood CD34+ cells. *Exp. Hematol.* 34:1240.
18 Kametani, Y., Shiina, M., Katano, I. *et al.* 2006. Development of human-human hybridoma from anti-Her-2 peptide-producing B cells in immunized NOG mouse. *Exp. Hematol.* 34:1240.
19 Ito, M., Kobayashi, K. and Nakahata, T. 2008. NOD/Shi-scid IL2rgamma(null) (NOG) mice more appropriate for humanized mouse models. *Curr. Top. Microbiol. Immunol.* 324:53.
20 Izawa, K., Tani, K., Nakazaki, Y. *et al.* 2004. Hematopoietic activity of common marmoset CD34 cells isolated by a novel monoclonal antibody MA24. *Exp. Hematol.* 32:843.
21 Kametani, Y., Suzuki, D., Kohu, K. *et al.* 2009. Development of monoclonal antibodies for analyzing immune and hematopoietic systems of common marmoset. *Exp. Hematol.* 37:1318.
22 Nunomura, S., Shimada, S., Kametani, Y. *et al.* 2012. Double expression of CD34 and CD117 on bone marrow progenitors is a hallmark of the development of functional mast cell of Callithrix jacchus (common marmoset). *Int. Immunol.* 24:593.
23 Prasad, S., Kireta, S., Leedham, E., Russ, G. R. and Coates, P. T. 2010. Propagation and characterisation of dendritic cells from G-CSF mobilised peripheral blood monocytes and stem cells in common marmoset monkeys. *J. Immunol. Methods* 352:59.
24 Kitaura, K., Fujii, Y., Matsutani, T. *et al.* 2012. A new method for quantitative analysis of the T cell receptor V region repertoires in healthy common marmosets by microplate hybridization assay. *J. Immunol. Methods* 384:81.
25 Ito, R., Maekawa, S., Kawai, K. *et al.* 2008. Novel monoclonal antibodies recognizing different subsets of lymphocytes from the common marmoset (Callithrix jacchus). *Immunol. Lett.* 121:116.
26 Doulatov, S., Notta, F., Eppert, K., Nguyen, L. T., Ohashi, P. S. and Dick, J. E. 2010. Revised map of the human progenitor hierarchy shows the origin of macrophages and dendritic cells in early lymphoid development. *Nat. Immunol.* 11:585.
27 Geissmann, F., Manz, M. G., Jung, S., Sieweke, M. H., Merad, M. and Ley, K. 2010. Development of monocytes, macrophages, and dendritic cells. *Science* 327:656.
28 Simmons, P. J., Aylett, G. W., Niutta, S., To, L. B., Juttner, C. A. and Ashman, L. K. 1994. c-kit is expressed by primitive human hematopoietic cells that give rise to colony-forming cells in stroma-dependent or cytokine-supplemented culture. *Exp. Hematol.* 22:157.
29 Kawashima, I., Zanjani, E. D., Almaida-Porada, G., Flake, A. W., Zeng, H. and Ogawa, M. 1996. CD34+ human marrow cells that

express low levels of Kit protein are enriched for long-term marrow-engrafting cells. *Blood* 87:4136.
30 Edling, C. E. and Hallberg, B. 2007. c-Kit–a hematopoietic cell essential receptor tyrosine kinase. *Int. J. Biochem. Cell Biol.* 39:1995.
31 Wang, J., Geiger, H. and Rudolph, K. L. 2011. Immunoaging induced by hematopoietic stem cell aging. *Curr. Opin. Immunol.* 23:532.
32 Genain, C. P. and Hauser, S. L. 1996. Allergic encephalomyelitis in common marmosets: pathogenesis of a multiple sclerosis-like lesion. *Methods* 10:420.
33 't Hart, B. A., Laman, J. D., Bauer, J., Blezer, E., van Kooyk, Y., and Hintzen, R. Q. 2004. Modelling of multiple sclerosis: lessons learned in a non-human primate. *Lancet Neurol.* 3:588.
34 Hibino, H., Tani, K., Ikebuchi, K. *et al.* 1999. The common marmoset as a target preclinical primate model for cytokine and gene therapy studies. *Blood* 93:2839.
35 Yahata, T., Ando, K., Nakamura, Y. *et al.* 2002. Functional human T lymphocyte development from cord blood CD34+ cells in nonobese diabetic/Shi-scid, IL-2 receptor gamma null mice. *J. Immunol.* 169:204.

Breast Cancer Res Treat (2016) 160:163–172
DOI 10.1007/s10549-016-3984-8

EPIDEMIOLOGY

Young adult breast cancer patients have a poor prognosis independent of prognostic clinicopathological factors: a study from the Japanese Breast Cancer Registry

Akemi Kataoka[1] · Takayuki Iwamoto[2] · Eriko Tokunaga[3] · Ai Tomotaki[4] · Hiraku Kumamaru[4] · Hiroaki Miyata[4] · Naoki Niikura[5] · Masaaki Kawai[6] · Keisei Anan[7] · Naoki Hayashi[8] · Shinobu Masuda[9] · Koichiro Tsugawa[10] · Kenjiro Aogi[11] · Takanori Ishida[12] · Hideji Masuoka[13] · Kotaro Iijima[14] · Takayuki Kinoshita[15] · Seigo Nakamura[16] · Yutaka Tokuda[5]

Received: 13 September 2016 / Accepted: 15 September 2016 / Published online: 19 September 2016

Abstract

Purpose The aim of this study was to investigate whether young age at onset of breast cancer is an independent prognostic factor in patients from the Japanese Breast Cancer Registry, after adjustment of known clinicopathological prognostic factors.

Methods Of the 53,670 patients registered between 2004 and 2006 and surveyed after a 5-year follow-up prognosis, 25,898 breast cancer patients (48.3 %), who were obtained prognostic data, were examined. Clinicopathological factors were compared between young adult (YA; <35 years), middle-aged adult (MA; 35–50 years), and older adult (OA; >50 years) patients. Five-year disease-*free* survival (DFS) and overall survival (OS) rates were studied.

Results YA patients were associated with an advanced TNM stage and aggressive characteristics (e.g. human epidermal growth factor receptor 2 (HER2)-positive or oestrogen receptor (ER)-negative breast cancers) compared to MA and OA patients ($P < 0.001$). The 5-year DFS and OS rates were 79.4 % and 90.8, 88.5 and 95.0 %, and 87.8 % and 91.6 % for YA, MA, and OA patients, respectively. From the multivariable regression analysis, young age at onset was confirmed as an independent prognostic factor for both DFS (hazard ratio 1.73, 95 % confidence interval 1.42–2.10; $P < 0.001$) and OS (hazard ratio 1.58, 95 % confidence interval 1.16–2.15; $P = 0.004$).

Electronic supplementary material The online version of this article (doi:10.1007/s10549-016-3984-8) contains supplementary material, which is available to authorized users.

✉ Takayuki Iwamoto
tiwamoto@cc.okayama-u.ac.jp

[1] Breast Surgical Oncology Department, Cancer Institute Hospital of Japanese Foundation for Cancer Research, Tokyo, Japan

[2] Department of Breast and Endocrine Surgery, Okayama University Hospital, 2-5-1 Shikata-cho, Kitaku, Okayama City, Okayama 700-8558, Japan

[3] Department of Breast Oncology, National Hospital Organization Kyushu Cancer Center, Fukuoka, Japan

[4] Department of Healthcare Quality Assessment, Graduate School of Medicine, Tokyo University, Tokyo, Japan

[5] Department of Breast and Endocrine Surgery, Tokai University School of Medicine, Kanagawa, Japan

[6] Department of Breast Surgery, Miyagi Cancer Center, Natori, Japan

[7] Department of Surgery, Kitakyushu Municipal Medical Center, Kitakyushu, Japan

[8] Department of Breast Surgery, St. Luke's International Hospital, Tokyo, Japan

[9] Department of Pathology, Nihon University School of Medicine, Tokyo, Japan

[10] Division of Breast and Endocrine Surgery, Department of Surgery, St. Marianna University School of Medicine, Kawasaki, Japan

[11] Department of Breast Surgery, Shikoku Cancer Center, Matsuyama, Japan

[12] Department of Surgical Oncology, Graduate School of Medicine, Tohoku University, Sendai, Japan

[13] Sapporo-kotoni Breast Clinic, Sapporo, Japan

[14] Department of Breast Oncology, Juntendo University School of Medicine, Tokyo, Japan

[15] Department of Breast Surgery, National Cancer Center Hospital, Tokyo, Japan

[16] Division of Breast Surgical Oncology, Department of Surgery, Showa University, Tokyo, Japan

Conclusions Young age at onset is an independent negative prognostic factor in breast cancer. Further studies are required to develop new therapeutic strategies for YA breast cancer patients.

Keywords Breast cancer · Young women · Surveillance data · Prognosis · Multivariable analysis

Introduction

Young adult (YA) cancers are relatively rare and represent a minority of cases. Consequently, data are lacking concerning intellectual and other psychosocial issues affecting this specific patient population [1]. YA cancer patients are significantly more likely to indicate unmet needs for supportive care services [2]. Moreover, fewer clinical trials have been conducted for YA cancers compared to other adult cancers, suggesting that there may be little evidence of high impact. Among YA cancers in women, breast cancer has the highest incidence rates (30–34 years, 13.3 per 100,000 population, and 35–39 years, 31.6 per 100,000 population [3]. However, even breast cancers account for a very small proportion (approximately 7 %) of the total number of breast cancers in these age groups [4–6].

YA breast cancer patients diagnosed in their twenties or thirties tend to have a poorer prognosis than women diagnosed in middle age (MA) [7]. Differences in survival may reflect clinical and biological variations. Indeed, YA breast cancer patients are reported to present with more aggressive biological characteristics and to behave more poorly compared to older breast cancer patients [8]. Previously, we reported the clinicopathological features of YA patients as having advanced TNM staging and human epidermal growth factor receptor 2 (HER2)-positive/oestrogen receptor (ER)-negative breast cancers compared to older patients [6]. Similarly, aggressive and unfavourable characteristics, including TNM classification, ER status, and HER2 status for YA patients with breast cancer have been reported [9–13].

However, to our knowledge, most of the data on the biological characteristics and treatment to evaluate these patients were derived from older and relatively smaller cohort studies. Moreover, whether age remains an independent predictive prognostic factor, after adjustment of breast cancer subtype (ER, PR, and HER2 status), as well as, other known prognostic factors (TNM classification, adjuvant systemic therapy, etc.) has yet to be determined, given YA patients are at risk of developing more aggressive and more advanced breast cancers.

The aim of this study was to investigate whether young age at onset of breast cancer is an independent negative prognostic factor in patients from the Japanese Breast Cancer Registry (which includes >25,000 newly treated breast cancers between 2004 and 2006).

Materials and methods

Patients

This study was conducted using the Japanese Breast Cancer Registry database, the details of which have been reported previously by Kurebayashi et al. [14]. Briefly, it is a registry managed by the Registration Committee of the Japanese Breast Cancer Society with support from the Public Health Research Foundation (Tokyo, Japan). Data on newly operated primary breast cancer patients are reported from affiliated institutes throughout Japan, which included 741 facilities in 2011, through a web-based system that collects information on >50 demographic and clinicopathological characteristics. Pathological TNM classification is registered based on the Unio Internationalis Contra Cancrum staging system (sixth edition) [15]. Histological classification is registered according to the General Rules for Clinical and Pathological Recording of Breast Cancer [16], which has been translated into the Classification of Tumours of the Breast and Female Genital Organs [17]. Age at onset was defined as the age of the beginning of treatment.

HER2 positivity was defined as immunohistochemical staining of 3+ or a positive fluorescent in situ hybridisation test according to the manufacturer's criteria. Hormone receptor (ER/progesterone receptor [PR]) positivity was determined if ≥1 % of nuclei in the tumour stained positive for ER/PR on immunohistochemical analysis. Of the 53,670 patients registered in the Japanese Breast Cancer Registry between 2004 and 2006 and surveyed after a 5-year follow-up prognosis, 25,898 patients (48.3 %) were obtained follow-up data and used for further examinations. Cases with connective tissue properties and mixed epithelial or unclassified tumours ($n = 385$) were excluded, as were male cases and cases of unknown age or sex ($n = 211$). A patient flow chart is depicted in Fig. 1. In total, 25,302 patients were analysed in this study. YA breast cancer patients ($n = 736$; 2.9 %) were defined as <35 years of age, MA patients ($n = 6905$; 27.3 %) as between 35 and 50 years of age at onset, and OA patients ($n = 17{,}661$; 69.8 %) as >50 years of age at onset. Clinicopathological and prognostic factors were compared between the three groups. For the analysis of survival, patients who did not undergo surgery ($n = 312$; 1.2 %), patients who had Stage IV or an unknown disease stage

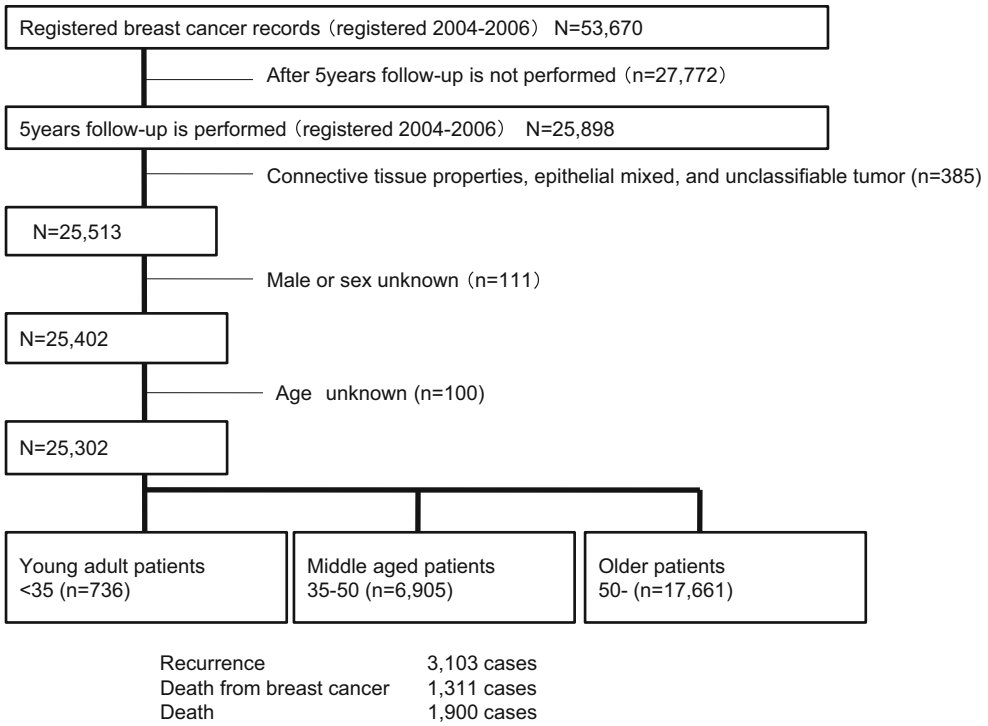

Fig. 1 Patient flow chart

($n = 987$; 3.9 %), and patients with unavailable event data ($n = 212$; 0.8 %) were excluded.

Statistical analyses

Fisher's exact tests were used to compare various prevalence rates among the three patient groups. Unpaired Student's *t*-tests were used for inter-group comparisons of continuous variables. Survival curves were constructed using the Kaplan–Meier method with and without stratification on known prognostic factors, and were compared using a log-rank test. Multivariable analyses for disease-*free* survival (DFS), breast cancer-specific survival (BCSS), and overall survival (OS) were performed using a Cox proportional hazards model to estimate the hazard ratios and 95 % confidence intervals for survival. We considered the following variables as potential confounders in the Cox model; age, TNM classification, breast cancer subtype, and neo-adjuvant/adjuvant therapy. Patients with any missing or unknown data were excluded from analysis of the Cox model. DFS was defined as the time interval between the date of surgery and the point of local or distant recurrence. BCSS and OS were defined as the time intervals between the date of surgery and the date of breast cancer-related death or death from any cause. A P value of <0.05 was considered statistically significant. All statistical analyses were conducted using SAS software version 9.4 (SAS Institute, Inc., Cary, NC, USA).

Results

Clinicopathological characteristics

Prognostic information was available for 736 YA patients (2.9 %), 6905 MA patients (27.3 %), and 17,661 OA patients (69.8 %), indicating that the minority of all breast cancers are YA cases, as previously reported (Table 1) [4–6].

YA patients were more likely to be diagnosed with a larger tumour (e.g., T3: YA patients, 12.6 %; MA patients, 8.4 %; and OA patients, 7.0 %; $P < 0.001$), Tis (ductal carcinoma in situ) occurred most frequently in MA patients (11.5 %) and T1 occurred more frequently in MA (38.5 %) and OA patients (38.9 %) compared to YA patients (31.1 %; $P < 0.001$). A greater proportion of YA patients (28.5 %) had a positive nodal status compared to MA (22.4 %) and OA patients (21.7 %; $P < 0.001$). Distant metastasis (M status) also occurred significantly more frequently in YA patients compared to MA and OA patients ($P < 0.001$). Moreover, an advanced TNM classification (Stage III/IV) occurred more frequently in YA patients (14.5 %) compared to MA (9.6 %) and OA patients (11.2 %; $P < 0.001$). YA patients were also associated with an aggressive breast cancer receptor status. Specifically, the proportion of ER-negative tumours was higher in YA patients compared to MA and OA patients ($P < 0.001$), although the difference in frequencies

Table 1 Patient characteristics[a]

	Patients' age at onset						
	<35 ($n = 736$)		35–50 ($n = 6905$)		50– ($n = 17,661$)		
	N	%	*N*	%	*N*	%	*P* value
T stage							
Tis	73	9.9	795	11.5	1580	9.0	**<.001**
T0	5	0.7	97	1.4	233	1.3	
T1	229	31.1	2655	38.5	6870	38.9	
T2	301	40.9	2434	35.3	6475	36.7	
T3	93	12.6	579	8.4	1243	7.0	
T4	26	3.5	280	4.1	1109	6.3	
Unk	9	1.2	65	0.9	151	0.9	
Nodal status							
Negative	515	70.0	5281	76.5	13,625	77.2	**<.001**
Positive	210	28.5	1547	22.4	3825	21.7	
Unk	11	1.5	77	1.1	211	1.2	
M							
M0	692	94.0	6640	96.2	16848	95.4	**<.001**
M1	29	3.9	128	1.9	461	2.6	
Unknown	15	2.0	137	2.0	352	2.0	
Stage							
0	73	9.9	795	11.5	1576	8.9	**<.001**
1	202	27.5	2468	35.7	6354	36.0	
2	338	45.9	2886	41.8	7499	42.5	
3	78	10.6	535	7.8	1511	8.6	
4	29	3.9	128	1.9	461	2.6	
Unknown	16	2.2	93	1.4	260	1.5	
ER							
Negative	195	26.5	1307	18.9	4578	25.9	**<.001**
Positive	517	70.2	5353	77.5	12544	71.0	
Unknown	24	3.3	245	3.6	539	3.1	
PR							
Negative	263	335.7	1647	23.9	7594	43.0	**<.001**
Positive	447	60.7	4997	72.4	9460	53.6	
Unknown	26	3.5	261	3.8	607	3.4	
HER2							
Negative	554	75.3	5231	75.8	12961	73.4	**<.001**
Positive	101	13.7	806	11.7	2582	14.6	
Unknown	81	11.0	868	12.9	2118	12.0	
Surgery							
None	1	0.1	4	0.1	18	0.1	**<.001**
BCT	456	62.0	4070	58.9	9092	51.5	
Mastectomy	256	34.8	2671	38.7	8115	45.9	
Others	16	2.2	97	1.4	217	1.2	
Unknown	7	1.0	63	0.9	219	1.2	

Table 1 continued

	Patients' age at onset						
	<35 ($n = 736$)		35–50 ($n = 6905$)		50– ($n = 17,661$)		
	N	%	*N*	%	*N*	%	*P* value
Adjuvant therapy							
None	126	17.1	1036	15.0	3414	19.3	**<.001**
ET	252	34.2	2899	42.0	7725	43.7	
ET + CT	197	26.8	1834	26.6	3133	17.7	
CT	122	16.6	879	12.7	2701	15.3	
Unknown	39	5.3	257	3.7	688	3.9	

Bold *P* value <0.05

[a] TNM classification is shown based on the sixth edition of the Unio Internationalis Contra Cancrum staging system; *ER* estrogen receptor, *PR* progesteron receptor, *HER2* human epidermal growth factor-receptor 2, *BCT* breast conserving therapy, *ET* endocrine therapy, *CT* Chemo therapy

between YA (26.5 %) and OA patients (25.9 %) was small. A similar trend was observed in the HER2-positive group in which YA patients (13.7 %) were more frequent than MA patients (11.7 %) ($P < 0.001$; Table 1).

In regard to the type of surgery conducted, YA patients (62.0 %) underwent BCT more frequently compared to MA (58.9 %) and OA patients (51.5 %; $P < 0.001$). Adjuvant systemic therapies (endocrine therapy alone, combination chemo-endocrine therapy, chemotherapy alone, and no adjuvant therapy) were also compared. The uptake of adjuvant endocrine therapy alone was significantly lower in YA patients compared to MA and OA patients ($P < 0.001$). Conversely, YA patients were administered chemotherapy and combination chemo-endocrine therapy more frequently compared to MA and OA patients ($P < 0.001$; Table 1).

Prognosis

At 5-year follow-up, 3103 cases (12.3 %) of breast cancer recurrence, 1311 cases (5.2 %) of breast cancer-related death, and 1900 cases (7.5 %) of all-cause death were reported. The 5-year DFS rates were 79.4, 88.5, and 87.8 % for YA, MA, and OA patients, respectively. The 5-year BCSS and OS rates were 92.1 and 90.8 % for YA, 95.8 and 95.0 % for MA, and 94.6 and 91.6 % for OA patients.

YA patients were associated with a significantly poorer prognosis in relation to DFS, BCSS, and OS ($P < 0.001$; Fig. 2) in the univariate analysis, indicating that these results are consistent with previously reported data [9–13]. We subsequently assessed the prognostic value of young age at onset in breast cancer, stratifying on known clinicopathological prognostic factors. Stratifying on breast cancer receptor status (HER2-positive/ER-positive, HER2-positive/ER-negative, HER2-negative/ER-positive, and triple receptor negative breast cancer), YA patients were found to be significantly associated with a poorer prognosis in all breast cancer receptor subtypes ($P < 0.05$; Fig. 3). In ER-positive cases, there was no difference on recurrence pattern by age at onset in the early phase during this study period, and YA cases had poorer prognosis than the older cases in the late phase(Fig. 3a, b). Conversely, in ER-negative cases, the distinct pattern of the recurrence by age at onset was seen only in the early phase and no difference in the late phase(Fig. 3c, d). TNM stage, another well-known clinicopathological prognostic factor, was also stratified. YA patients were associated with a significantly poorer prognosis in the Stage I and Stage II groups ($P < 0.001$; Fig. S1). In the Stage 0 group, YA, MA, and OA patients with ductal carcinoma in situ were associated with similarly favourable prognoses with statistically marginal effect ($P = 0.053$; Fig. S1). Conversely, in the Stage III group, YA patients exhibited a trend towards a poorer prognosis. However, this was not statistically significant ($P = 0.121$; Fig. S1).

Finally, multivariable Cox regression analysis was performed using a young age at onset adjusted by known breast cancer prognostic factors, including T/N status, breast cancer subtypes, and adjuvant therapies. YA patients were significantly associated with the poorest prognosis for all three endpoints, 5-year DFS, BCSS, and OS. Specifically, both comparisons between YA and MA patients (hazard ratio 1.58, 95 % confidence interval 1.16–2.15; $P < 0.01$) and between YA and OA patients (hazard ratio: 1.52, 95 % confidence interval 1.33–1.75; $P < 0.001$) were significant for OS (Table 2).

Discussion

YA breast cancer accounts for a minority of breast cancer cases [6].

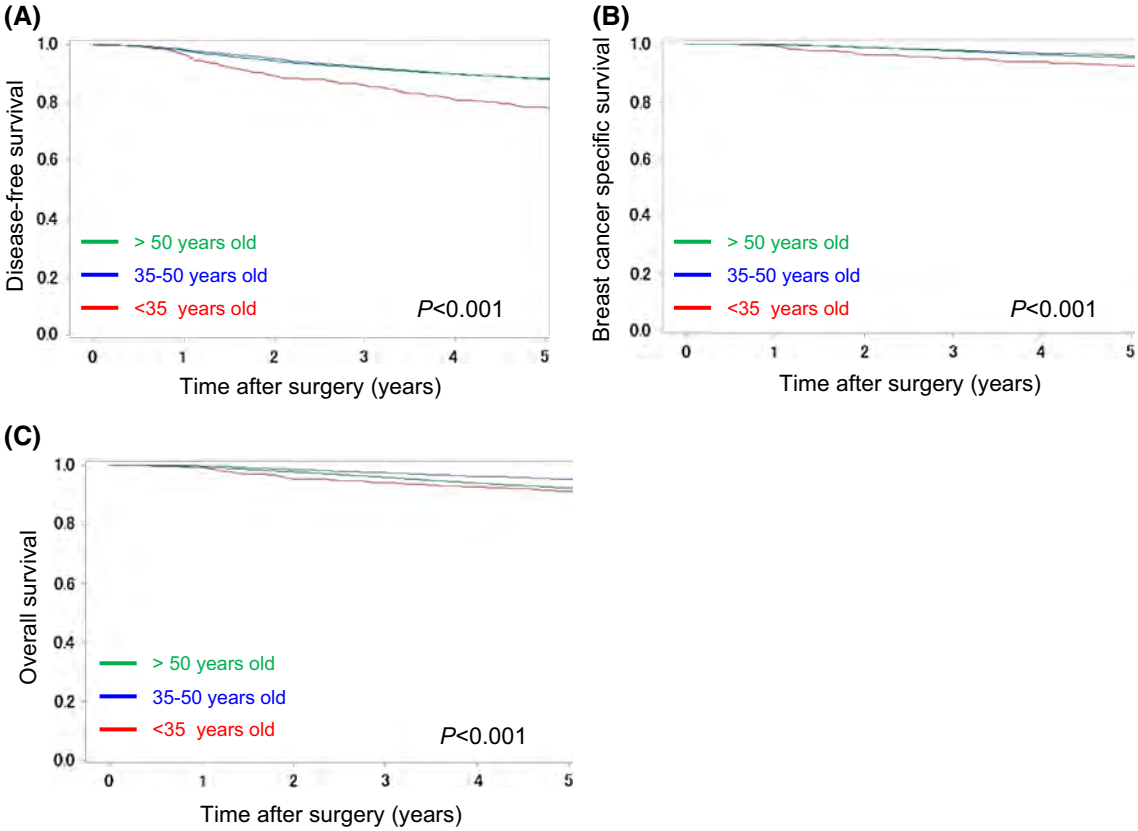

Fig. 2 Kaplan–Meier curves for **a** disease-*free* survival, **b** breast cancer-specific survival, and **c** overall survival between young adult (<35 years; *red line*), middle-aged adult (35–50 years; *blue line*), and older adult (>50 years; *green line*) breast cancer patients. *P*-values were calculated using a log-rank test

Consequently, it is unlikely that a prospective clinical trial would ever be conducted to define the optimal treatment strategy for this disease subset.

We analysed data from a large number of breast cancer patients registered by the Japanese Breast Cancer Registry database in order to characterise and advance our understanding of YA breast cancer. Using nationwide, population-based data representing approximately 70 % of all newly diagnosed breast cancer patients in Japan between 2004 and 2006, we were able to circumvent many problems associated with single institutional experiences or limited sample sizes. Our study demonstrated that a young age at onset was an independent predictive factor for poor prognosis in patients with breast cancer, after adjustment of well-known clinicopathological factors, including breast cancer receptor status, tumour size, and nodal status. Classically, it has been suggested that YA breast cancer patients are associated with a poorer prognosis because of delayed diagnosis at an advanced stage, a larger tumour size, and higher incidences of HER2-positive/ER-negative tumours [6, 9]. These reports proved consistent with our findings in the present study. Some previously published studies have already established a poorer prognosis in YA breast cancer patients as independent from other clinicopathological factors, such as tumour size, nodal status, histological grade, and hormone receptor status [8, 18, 19]. However, these reports are relatively old, have smaller sample sizes, and patients may have been treated with a classical adjuvant chemotherapy and endocrine therapy regimen. Recently, some studies using large databases have also reported similarly poor prognostic outcomes in YA breast cancer patients after stratifying on multiple prognostic factors [20–23]. Conversely, a single study has found that a young age at onset has no influence on the prognosis of individual breast cancer patients from a database of almost 3000 cases [24]. Partridge et al. [12] also reported no effect of age on breast cancer outcomes in patients with HER2-positive breast cancer from a large, randomised controlled trial. At the St Gallen International Expert Consensus meetings, a younger age at onset had been considered a high-risk factor from the 1990s to 2009. Later, a younger age at onset was no longer considered to be a poor prognostic factor and treatment strategies were recommended based on biological subtype or the concept of a ‘threshold for indication’ of each systemic treatment modality to be respected without a young age at onset [25].

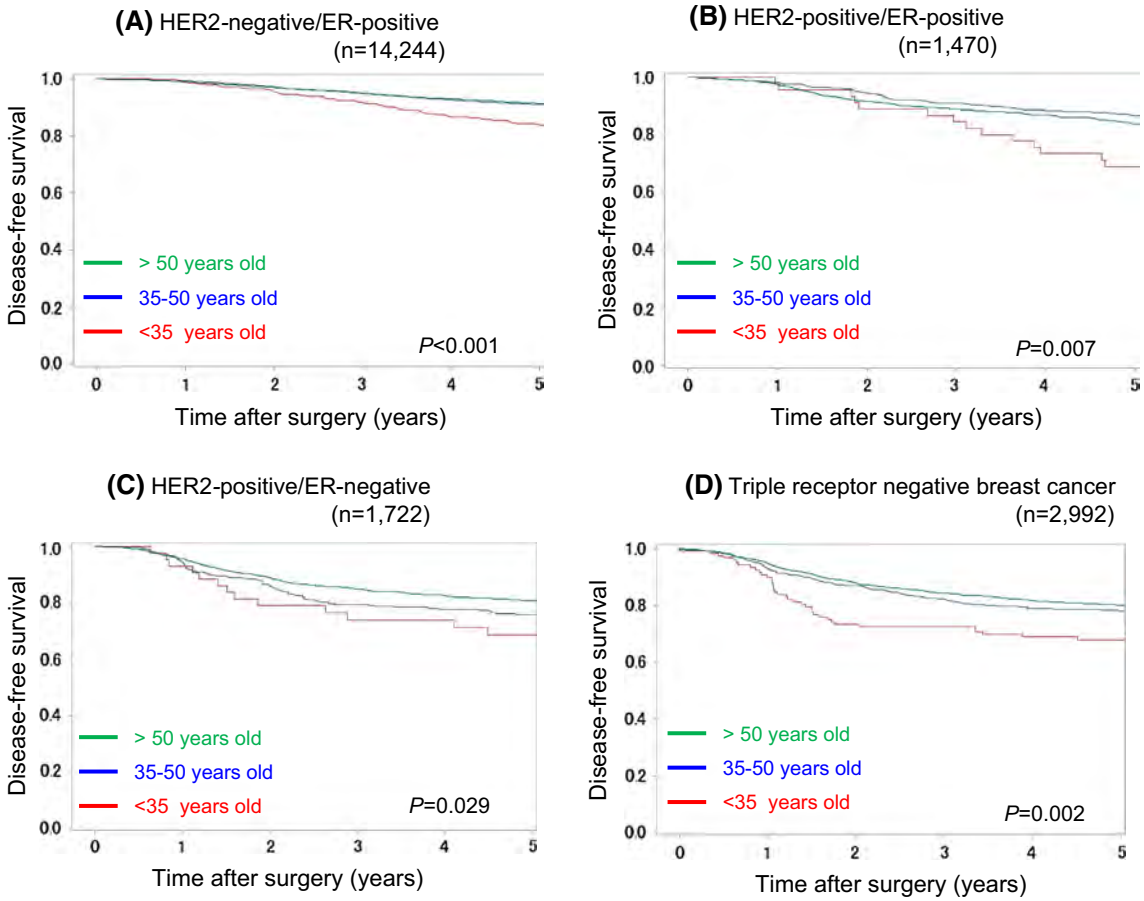

Fig. 3 Kaplan–Meier curves for disease-*free* survival between young adult (<35 years; *red line*), middle-aged adult (35–50 years; *blue line*), and older adult (>50 years; green line) patients with **a** HER2-negative/ER-positive, **b** HER2-positive/ER-positive, **c** HER2-positive/ER-negative, and **d** triple receptor negative breast cancer. *P*-values were calculated using a log-rank test

Then, YA patients were treated according to various predictive factors and the subtype of the tumour, including ER, PR, and HER2 status, proliferation markers, and TNM classification and a young age itself had no impact on the treatment strategy. Based on our findings and the results of several previously published reports of large cohorts [20–23], YA breast cancer patients have a poor prognosis independent of other aggressive breast cancer features.

Another interesting finding was distinct recurrence pattern between ER-positive and -negative entities according to age at onset (Fig. 3). These differences between age at onset and ER status may lead to the distinct biological and molecular processes of age at onset by ER status. Research highlighting the genetic differences between YA and other breast cancer entities by ER status is lacking. Anders et al. [11] reported that YA breast cancer represents a unique biological entity driven by unifying a higher probability of phosphoinositide 3-kinase and Myc pathway dysregulation. Investigating how high-risk genetic mutations affect age at onset, Ford et al. [26] observed that 5.3 % of breast cancers in <40 year olds are attributable to *BRCA1* mutations compared 2.2 % and 1.1 % in 40- to 49-year olds and 50- to 70-year olds, respectively. It has been established that patients with *BRCA1* mutations are more likely to develop basal-like breast cancers, including the triple-negative subtype [27, 28] [29, 30]. Further research to elucidate the development of disease in this high-risk YA population and to determine the prognosis following a diagnosis of breast cancer is clearly warranted. An improved understanding of breast cancer genetics through molecular profiling may provide information that can be applied to patients with YA breast cancer.

Efficacy to adjuvant therapy in YA breast cancer patients remains controversial. Ahn et al. [10] reported that the survival differences according to age in hormone receptor-positive breast cancer patients were significant in patients who received hormone therapy as well as those who did not. This suggests YA breast cancer patients may need another strategy of treatment instead of conventional adjuvant hormone and chemo therapy. A similarly insufficient efficacy to chemotherapy has also been reported. YA breast cancer patients treated with adjuvant

Table 2 Multivariate analysis for 5 year survival[a]

	Hazard ratio	95 % C.I.	*P value*	Hazard ratio	95 % C.I.	*P value*	Hazard ratio	95 % C.I.	*P value*
Age at diagonosis									
<35 versus 35–50	1.73	1.42–2.10	**<.001**	1.52	1.09–2.13	0.098	1.58	1.16–2.15	**0.004**
Over 50 versus 35–50	0.99		0.821	1.14	0.98–1.34	**0.015**	1.52	1.33–1.75	**<.001**
T									
T2–4 versus T0, 1	2.22	0.90–1.09	**<.001**	3.04	2.49–3.70	**<.001**	2.25	1.96–2.59	**<.001**
N									
Positive versus negative	2.81	2.01–2.46	**<.001**	4.01	3.46–4.64	**<.001**	3.05	2.72–3.43	**<.001**
Breast cancer subtype									
ER+HER2+ versus ER+HER2−	1.52	2.58–3.07	**<.001**	1.73	1.35–2.23	**<.001**	1.39	1.13–1.72	**0.002**
ER−HER2+ versus ER+HER2−	1.86	1.65–2.11	**<.001**	2.33	1.89–2.88	**<.001**	1.75	1.47–2.07	**<.001**
Triple negative versus ER + HER2−	2.06	1.86–2.28	**<.001**	4.48	3.84–5.23	**<.001**	3.08	2.72–3.50	**<.001**
Adjuvant therapy									
Any versus none	0.87	0.76–1.00	**0.041**	1.32	1.03–1.71	**0.032**	0.70	0.60–0.81	**<.001**

Bold P value < 0.05

[a] *DFS* disease-*free* survival, *BCSS* breast cancer specific survival, *OS* overall survival; TNM classification is shown based on the 6th edition of the Unio Internationalis Contra Cancrum staging system; *ER* estrogen receptor, *HER2* human epidermal growth factor receptor 2

cyclophosphamide, methotrexate, and fluorouracil are at a higher risk of relapse and death compared to older breast cancer patients [31].

These distinct genetic patterns and clinical outcomes may lead to individual management of breast cancer patients. Previous studies reported significantly higher rates of local recurrence in YA patients who received BCT compared to OA patients who underwent a mastectomy [32, 33]. Freedoman et al. [34] reported that YA breast cancer patients were significantly more likely to have a mastectomy than BCT compared to older breast cancer patients. Efforts are required to confirm whether different types of surgery effect not only local recurrence rates but also OS rates. [35].

This study had several limitations. First, the relatively short follow-up period (median 4.5 years), which limited the power of the survival analysis. Nevertheless, prognostic analyses from this database that have previously been published were relatively consistent with the well-known consensus and clinical outcomes [36–38]. Second, during the study period, trastuzumab (which should exert a favourable effect on HER2-positive breast cancers) had not been widely prescribed as the standard agent and was only partially received. Third, we have no proliferation data, such as grade and genomic signatures. They are primarily prognostic and secondary predictive markers to chemotherapy response especially in ER-positive cases.

In conclusion, the present study confirmed that YA breast cancer patients have a poor prognosis independent of well-known clinicopathological prognostic factors. The different prognoses between YA, MA, and OA patients may require different screening algorithms, therapies, and follow-up. In order to establish an optimal strategy for YA breast cancer patients, further studies will need to be conducted.

Acknowledgments The authors thank the Public Health Research Foundation for their data collection and analysis. They also thank the affiliated institutes participating in the Breast Cancer Registry of the JBCS for their efforts to register patients' data.

Funding This work was supported by the research fund from the JBCS and JSPS KAKENHI Grant Numbers 15H04796.

Compliance with ethical standards

Conflict of Interest AT, HK, and HM are affiliated with the Department of Healthcare Quality Assessment at the University of Tokyo, and the department is endowed by Johnson & Johnson K.K., Nipro Corporation, Teijin Pharma Ltd., Kaketsuken K.K., St. Jude Medical Japan Co., Ltd., Novartis Pharma K.K., Taiho Pharmaceutical Co., Ltd., W. L. Gore & Associates, Co., Ltd., Olympus Corporation, and Chugai Pharmaceutical Co., Ltd. The other authors declare that they have no conflict of interest.

Ethical approval All procedures performed in studies involving human participants were in accordance with the ethical standards of the institutional and/or JBCS and with the 1964 Helsinki Declaration and its later amendments or comparable ethical standards.

Informed consent The study was approved by the review boards of JBCS. The study used only unidentifiable patient information, and no informed consent was required.

Research involving human and animal rights This article does not contain any studies with animals performed by any of the authors.

References

1. Soliman H, Agresta SV (2008) Current issues in adolescent and young adult cancer survivorship. Cancer Control 15(1):55–62
2. Zebrack B (2008) Information and service needs for young adult cancer patients. Support Care Cancer 16(12):1353–1360. doi:10.1007/s00520-008-0435-z
3. http://seer.cancer.gov/archive/csr/1975_2011/ [Accessed 19 April 2016]
4. Yankaskas BC (2005) Epidemiology of breast cancer in young women. Breast Dis 23:3–8
5. Siegel R, Naishadham D, Jemal A (2013) Cancer statistics, 2013. CA Cancer J Clin 63(1):11–30. doi:10.3322/caac.21166
6. Kataoka A, Tokunaga E, Masuda N, Shien T, Kawabata K, Miyashita M (2014) Clinicopathological features of young patients (<35 years of age) with breast cancer in a Japanese Breast Cancer Society supported study. Breast cancer 21(6):643–650. doi:10.1007/s12282-013-0466-2
7. Kroman N, Jensen MB, Wohlfahrt J, Mouridsen HT, Andersen PK, Melbye M (2000) Factors influencing the effect of age on prognosis in breast cancer: population based study. BMJ 320(7233):474–478
8. Nixon AJ, Neuberg D, Hayes DF, Gelman R, Connolly JL, Schnitt S, Abner A, Recht A, Vicini F, Harris JR (1994) Relationship of patient age to pathologic features of the tumor and prognosis for patients with stage I or II breast cancer. J Clin Oncol 12(5):888–894
9. Gonzalez-Angulo AM, Broglio K, Kau SW, Eralp Y, Erlichman J, Valero V, Theriault R, Booser D, Buzdar AU, Hortobagyi GN, Arun B (2005) Women age ≤35 years with primary breast carcinoma: disease features at presentation. Cancer 103(12):2466–2472. doi:10.1002/cncr.21070
10. Ahn SH, Son BH, Kim SW, Kim SI, Jeong J, Ko SS, Han W, Korean Breast Cancer S (2007) Poor outcome of hormone receptor-positive breast cancer at very young age is due to tamoxifen resistance: nationwide survival data in Korea–a report from the Korean Breast Cancer Society. J Clin Oncol 25(17):2360–2368. doi:10.1200/JCO.2006.10.3754
11. Anders CK, Hsu DS, Broadwater G, Acharya CR, Foekens JA, Zhang Y, Wang Y, Marcom PK, Marks JR, Febbo PG, Nevins JR, Potti A, Blackwell KL (2008) Young age at diagnosis correlates with worse prognosis and defines a subset of breast cancers with shared patterns of gene expression. J Clin Oncol 26(20):3324–3330. doi:10.1200/JCO.2007.14.2471
12. Partridge AH, Gelber S, Piccart-Gebhart MJ, Focant F, Scullion M, Holmes E, Winer EP, Gelber RD (2013) Effect of age on breast cancer outcomes in women with human epidermal growth factor receptor 2-positive breast cancer: results from a herceptin adjuvant trial. J Clin Oncol 31(21):2692–2698. doi:10.1200/JCO.2012.44.1956
13. McGuire A, Brown JA, Malone C, McLaughlin R, Kerin MJ (2015) Effects of age on the detection and management of breast cancer. Cancers 7(2):908–929. doi:10.3390/cancers7020815
14. Kurebayashi J, Miyoshi Y, Ishikawa T, Saji S, Sugie T, Suzuki T, Takahashi S, Nozaki M, Yamashita H, Tokuda Y, Nakamura S (2015) Clinicopathological characteristics of breast cancer and trends in the management of breast cancer patients in Japan: based on the Breast Cancer Registry of the Japanese Breast Cancer Society between 2004 and 2011. Breast Cancer 22(3):235–244. doi:10.1007/s12282-015-0599-6
15. Greene F (2002) TNM classification of malignant tumours, 6th edn. Wiley, New York, pp 131–141
16. The Japanese Breast Cancer Society (ed) (2012) General rules for clinical and pathological recording of breast cancer, 17th edn. Kanehara Shuppan, Tokyo
17. Lakhani S, Ellis I, Schnitt S, Tan P, van de Vijver M (2012) WHO classification of tumours of the breast, 4th edn. IARC Press, Lyon
18. de la Rochefordiere A, Asselain B, Campana F, Scholl SM, Fenton J, Vilcoq JR, Durand JC, Pouillart P, Magdelenat H, Fourquet A (1993) Age as prognostic factor in premenopausal breast carcinoma. Lancet 341(8852):1039–1043
19. Albain KS, Allred DC, Clark GM (1994) Breast cancer outcome and predictors of outcome: are there age differentials? J Natl Cancer Inst Monogr 16:35–42
20. Gnerlich JL, Deshpande AD, Jeffe DB, Sweet A, White N, Margenthaler JA (2009) Elevated breast cancer mortality in women younger than age 40 years compared with older women is attributed to poorer survival in early-stage disease. J Am Coll Surg 208(3):341–347. doi:10.1016/j.jamcollsurg.2008.12.001
21. Cancello G, Maisonneuve P, Rotmensz N, Viale G, Mastropasqua MG, Pruneri G, Veronesi P, Torrisi R, Montagna E, Luini A, Intra M, Gentilini O, Ghisini R, Goldhirsch A, Colleoni M (2010) Prognosis and adjuvant treatment effects in selected breast cancer subtypes of very young women (<35 years) with operable breast cancer. Ann Oncol 21(10):1974–1981. doi:10.1093/annonc/mdq072
22. Han W, Kang SY, Korean Breast Cancer S (2010) Relationship between age at diagnosis and outcome of premenopausal breast cancer: age less than 35 years is a reasonable cut-off for defining young age-onset breast cancer. Breast Cancer Res Treat 119(1):193–200. doi:10.1007/s10549-009-0388-z
23. Azim HA Jr, Michiels S, Bedard PL, Singhal SK, Criscitiello C, Ignatiadis M, Haibe-Kains B, Piccart MJ, Sotiriou C, Loi S (2012) Elucidating prognosis and biology of breast cancer arising in young women using gene expression profiling. Clin Cancer Res 18(5):1341–1351. doi:10.1158/1078-0432.CCR-11-2599
24. Kollias J, Elston CW, Ellis IO, Robertson JF, Blamey RW (1997) Early-onset breast cancer–histopathological and prognostic considerations. Br J Cancer 75(9):1318–1323
25. Goldhirsch A, Ingle JN, Gelber RD, Coates AS, Thurlimann B, Senn HJ, Panel m (2009) Thresholds for therapies: highlights of the St Gallen International Expert Consensus on the primary therapy of early breast cancer 2009. Ann Oncol 20(8):1319–1329. doi:10.1093/annonc/mdp322
26. Ford D, Easton DF, Peto J (1995) Estimates of the gene frequency of BRCA1 and its contribution to breast and ovarian cancer incidence. Am J Hum Genet 57(6):1457–1462
27. Honrado E, Benitez J, Palacios J (2005) The molecular pathology of hereditary breast cancer: genetic testing and therapeutic implications. Mod Pathol 18(10):1305–1320. doi:10.1038/modpathol.3800453
28. Cancer Genome Atlas N (2012) Comprehensive molecular portraits of human breast tumours. Nature 490(7418):61–70. doi:10.1038/nature11412
29. Balmana J, Domchek SM, Tutt A, Garber JE (2011) Stumbling blocks on the path to personalized medicine in breast cancer: the case of PARP inhibitors for BRCA1/2-associated cancers. Cancer Discov 1(1):29–34. doi:10.1158/2159-8274.CD-11-0048
30. Azim HA Jr, Partridge AH (2014) Biology of breast cancer in young women. Breast Cancer Res 16(4):427. doi:10.1186/s13058-014-0427-5

31. Aebi S, Gelber S, Castiglione-Gertsch M, Gelber RD, Collins J, Thurlimann B, Rudenstam CM, Lindtner J, Crivellari D, Cortes-Funes H, Simoncini E, Werner ID, Coates AS, Goldhirsch A (2000) Is chemotherapy alone adequate for young women with oestrogen-receptor-positive breast cancer? Lancet 355(9218): 1869–1874
32. Voogd AC, Nielsen M, Peterse JL, Blichert-Toft M, Bartelink H, Overgaard M, van Tienhoven G, Andersen KW, Sylvester RJ, van Dongen JA, Danish Breast Cancer Cooperative Group. Breast Cancer Cooperative Group of the European Organization for R, Treatment of C (2001) Differences in risk factors for local and distant recurrence after breast-conserving therapy or mastectomy for stage I and II breast cancer: pooled results of two large European randomized trials. Journal of Clin Oncol 19(6): 1688–1697
33. de Bock GH, van der Hage JA, Putter H, Bonnema J, Bartelink H, van de Velde CJ (2006) Isolated loco-regional recurrence of breast cancer is more common in young patients and following breast conserving therapy: long-term results of European Organisation for Research and Treatment of Cancer studies. Eur J Cancer 42(3):351–356. doi:10.1016/j.ejca.2005.10.006
34. Freedman RA, Virgo KS, Labadie J, He Y, Partridge AH, Keating NL (2012) Receipt of locoregional therapy among young women with breast cancer. Breast Cancer Res Treat 135(3):893–906. doi:10.1007/s10549-012-2156-8
35. Ohuchi N, Suzuki A, Sobue T, Kawai M, Yamamoto S, Zheng YF, Shiono YN, Saito H, Kuriyama S, Tohno E, Endo T, Fukao A, Tsuji I, Yamaguchi T, Ohashi Y, Fukuda M, Ishida T, groups JSi (2016) Sensitivity and specificity of mammography and adjunctive ultrasonography to screen for breast cancer in the Japan strategic anti-cancer randomized trial (J-START): a randomised controlled trial. Lancet 387(10016):341–348. doi:10.1016/S0140-6736(15)00774-6
36. Kinoshita T, Fukui N, Anan K, Iwamoto T, Niikura N, Kawai M, Hayashi N, Tsugawa K, Aogi K, Ishida T, Masuoka H, Masuda S, Iijima K, Nakamura S, Tokuda Y (2015) Comprehensive prognostic report of the Japanese Breast Cancer Society Registry in 2004. Breast Cancer. doi:10.1007/s12282-015-0644-5
37. Anan K, Fukui N, Kinoshita T, Iwamoto T, Niikura N, Kawai M, Hayashi N, Tsugawa K, Aogi K, Ishida T, Masuoka H, Masuda S, Iijima K, Nakamura S, Tokuda Y (2015) Comprehensive prognostic report of the Japanese Breast Cancer Society Registry in 2005. Breast Cancer. doi:10.1007/s12282-015-0645-4
38. Iwamoto T, Fukui N, Kinoshita T, Anan K, Niikura N, Kawai M, Hayashi N, Tsugawa K, Aogi K, Ishida T, Masuoka H, Masuda S, Iijima K, Nakamura S, Tokuda Y (2015) Comprehensive prognostic report of the Japanese Breast Cancer Society registry in 2006. Breast Cancer. doi:10.1007/s12282-015-0646-3

Cancer Science
Japanese Cancer Association JCA
Open Access

Comparison of tumor-infiltrating lymphocytes between primary and metastatic tumors in breast cancer patients

Rin Ogiya,[1] Naoki Niikura,[1] Nobue Kumaki,[2] Giampaolo Bianchini,[3] Shigehisa Kitano,[4] Takayuki Iwamoto,[5] Naoki Hayashi,[6] Kozue Yokoyama,[1] Risa Oshitanai,[1] Mayako Terao,[1] Toru Morioka,[1] Banri Tsuda,[1] Takuho Okamura,[1] Yuki Saito,[1] Yasuhiro Suzuki[1] and Yutaka Tokuda[1]

Departments of [1]Breast and Endocrine Surgery; [2]Pathology, School of Medicine, Tokai University, Isehara, Japan; [3]Department of Medical Oncology, Ospedale San Raffaele, Milan, Italy; [4]Department of Experimental Therapeutics, Exploratory Oncology Research and Clinical Trial Center, National Cancer Center Hospital, Tokyo, Japan; [5]Department of Breast and Endocrine Surgery, Okayama University Hospital, Okayama, Japan; [6]Department of Breast Surgical Oncology, St. Luke's International Hospital, Tokyo, Japan

Key words

Immune microenvironment, immunohistochemistry, metastatic breast tumor, primary breast tumor, tumor-infiltrating lymphocytes

Correspondence

Naoki Niikura, Department of Breast and Endocrine Surgery, Tokai University School of Medicine, 143 Shimokasuya, Isehara, Kanagawa 259-1193, Japan.
Tel: +81-463-93-1121; Fax: +81-463-95-6491;
E-mail: niikura@is.icc.u-tokai.ac.jp

Funding Information

Ministry of Education, Culture, Sports, Science and Technology, Japan.

Received July 25, 2016; Revised September 29, 2016; Accepted October 2, 2016

Cancer Sci **107** (2016) 1730–1735

doi: 10.1111/cas.13101

The presence of tumor-infiltrating lymphocytes (TILs) is associated with favorable long-term outcome in breast cancer. However, little is known about changes in TILs during metastatic progression. To confirm our hypothesis that malignant tumors escape from the host immune system during metastasis, we evaluated the percentage of TILs in paired samples of primary and metastatic breast tumors. We retrospectively identified 25 patients with human epidermal growth factor receptor-2 (HER2$^+$, $n = 14$) and triple negative (TN, $n = 11$) early breast cancer diagnosed between 1990 and 2009 at Tokai University Hospital (Isehara, Japan) and who subsequently experienced regional or distant recurrence confirmed by tumor biopsy/resection. Hematoxylin–eosin-stained slides of these paired samples were evaluated for stromal TILs. Immunohistochemical staining was carried out using primary antibodies against CD4, CD8, Foxp3, programmed cell death ligand 1 (PD-L1), PD-L2, and HLA class I for characterizing the TILs and breast tumors. The percentage of TILs in the primary tumors was significantly higher (average 34.6%) than that in metastatic tumors (average 15.7%) (paired *t*-test, $P = 0.004$) and that of CD8$^+$ and CD4$^+$ T cells significantly decreased from primary to metastatic tumors (paired *t*-test, $P = 0.008$ and $P = 0.026$, respectively). The PD-L1, PD-L2, and HLA class I antibody expression changed from positive to negative and vice versa from the primary to the metastatic tumors. Tumors at first metastatic recurrence in HER2$^+$ and TN breast cancers have a lower percentage of TILs and CD8$^+$ and CD4$^+$ T cells compared to primary tumors, which indicates that immune escape plays a role in tumor progression.

The presence of tumor-infiltrating lymphocytes (TILs) is associated with favorable long-term outcome in breast cancer.[1,2] Previous studies have reported that immune activation at the baseline, as assessed by pathology or gene expression arrays, is associated with a higher likelihood of pathological complete response after neoadjuvant chemotherapy (NAC), particularly in human epidermal growth factor receptor-2 (HER2)-positive and triple negative (TN) breast cancers.[3–10] Furthermore, trastuzumab has been predicted to have beneficial effects.[11] Increased expression of a subset of immune function genes may provide a means of predicting the benefits of adjuvant trastuzumab treatment.[12] Tumor-infiltrating lymphocytes in breast tumors mainly comprise cytotoxic (CD8$^+$) T cells, followed by helper (CD4$^+$) T cells and natural killer cells.[13] A high CD8$^+$/Foxp3$^+$ ratio in the TILs of biopsy specimens was found to be a strong predictor of pathological complete response after NAC in TN breast cancers.[14] In addition, the presence of TILs in residual disease after NAC is associated with better prognosis in TN breast cancers patients. This suggests that chemotherapy could convert low-TIL tumors into high-TIL tumors. This finding supports the concept that chemotherapy could partly exert its antitumor effect through the immune system.[15] Preclinical studies have also suggested that cytotoxic agents may partly exert their antitumor activity by inducing immune responses against tumor cells.[16]

However, little is known about the change in TILs during metastatic progression and the prognostic impact of TILs in metastatic sites.[17,18] The current concept of cancer immunoediting leading from immune surveillance to immune escape is proposed to comprise three essential phases: (i) elimination; (ii) equilibrium; and (iii) escape.[19] In the elimination phase, tumor cells undergo angiogenesis and stromal remodeling, resulting in tumor cell variants with low immunogenicity and resistance to immune attack. These tumor cell variants then proceed to the equilibrium phase but the elimination phase continues through immune selection pressure. Tumor progression then leads to the release of tumor-derived soluble factors

that are involved in several mechanisms of immune evasion in the escape phase.[20]

We hypothesized that malignant tumors escape from the immune system of the host during the process of metastasis. We therefore aimed to study the immune escape by evaluating TILs in paired samples from primary and metastatic breast tumors. We also evaluated the prognostic impact of TILs in the metastatic sites.

Methods

Patients. This study was reviewed and approved by the Institutional Review Board for Clinical Research, Tokai University (Isehara, Japan). We retrospectively identified 25 patients with TN or $HER2^+$ early breast cancer diagnosed between 1990 and 2009 at Tokai University Hospital and who subsequently experienced a regional or distant recurrence confirmed by tumor biopsy/resection. Patients who had only local events were excluded because it is difficult to determine whether the tumor has recurred or is a new primary tumor.[21] The clinical characteristics of all the patients were obtained from their medical records.

Pathological assessment. All the tumor specimens were fixed in 10% formalin and embedded in paraffin, and 4-μm-thick sections were prepared for H&E staining and immunohistochemistry (IHC) and were reviewed by a pathologist. Immunohistochemistry was carried out using the following primary antibodies: anti-estrogen receptor (ER) (–2009, clone 1D5; Dako, Carpinteria, CA, USA; 2010–, clone SP1; Roche Diagnostics, Basel, Switzerland), anti-HER2 (–2009, polyclonal, HercepTest II, Dako; 2010–, clone 4B5, Roche Diagnostics), anti-CD4 (clone SP35; Spring Bioscience, Pleasanton, CA, USA), anti-CD8 (clone C8/144B; Nichirei, Tokyo, Japan), anti-Foxp3 (clone 236A/E7; Abcam, Cambridge, MA, USA), anti-programmed cell death ligand 1 (PD-L1) (polyclonal, ab58810; Abcam), anti-Pdcd-1L2 (PD-L2, clone XX19; Santa Cruz Biotechnology, Dallas, TX, USA), and anti-HLA class I A, B, C (clone EMR8-5; Hokudo, Sapporo, Japan). The specimens were considered positive for hormone receptor if ≥1% of the cancer cells expressed ER. For the patients determined as $HER2^+$ by IHC, FISH (PathVysion kit; Abbott, Des Plaines, IL, USA) was used to confirm $HER2^+$ disease. The breast cancer subtypes were classified using IHC as previously described:[22] HER2-positive or HER2-overexpressing ($HER2^+$) and TN (ER^- and $HER2^-$). Hematoxylin–eosin-stained slides for the paired match cases were evaluated for stromal TILs using full sections in 10% increments (<10%, 10%–100%) by a pathologist (N.K.) blinded to the clinicopathological characteristics of the patients, as recommended.[23] The specimens were classified into three groups: low TIL (<10%), intermediate TIL (10–<60%), and lymphocyte-predominant breast cancer (LPBC) (≥60%).

To quantify the TILs in each antibody-stained slide, we used a NanoZoomer 2.0 HT (Hamamatsu Photonics, Hamamatsu, Japan) at ×40 magnification. Three non-overlapping fields with high numbers of TILs on the H&E-stained slides were selected.[14] CD4, CD8, and PD-L1 positivity was determined by membranous lymphocyte staining, and Foxp3 and PD-L2 positivity was determined by nuclear lymphocyte staining. The expression of CD4, CD8, Foxp3, PD-L1, and PD-L2 by TILs was recorded in 10% increments, and the score of three fields was averaged. The expression of PD-L1, PD-L2, and HLA class I in the tumors was scored as 0 (negative), 1 (weak), or 2 (strong).

Statistical analyses. Associations of the percentage of TILs with the positivity for each antibody between the primary and metastatic tumors were evaluated using Fisher's exact test for categorical variables and using the two-sided *t*-tests for continuous variables. Overall survival (OS) was defined as the time from date of the first biopsy of metastatic tissue to the date of death resulting from any cause. Patients who were alive and disease-free were censored at the date of last contact. Post-progression OS curves of the patients were drawn using the Kaplan–Meier method, and the statistical difference between two survival curves was calculated using the log–rank test. The correlation between the percentage of TILs and the expression of each of the antibodies was calculated using Spearman's rank correlation coefficient test. In all the analyses, the differences were considered significant at $P < 0.05$. Statistical analyses were carried out using SPSS, version 23 (Armonk, New York, USA).

Results

Comparison of TILs between primary and metastatic tumors. The characteristics of the 25 breast cancer patients ($HER2^+$, $n = 14$; TN, $n = 11$) at the time of diagnosis of the primary breast cancer are presented in Table 1. Six primary tumors and one metastatic tumor were core needle biopsy specimens, and the rest were surgical specimens. We evaluated the core needle biopsy specimens before chemotherapy in the patients who received neoadjuvant therapy for excluding the possibility of alterations in the immune microenvironments of the tumors caused by the neoadjuvant therapy. The first biopsy sites of the metastatic tumors were the skin ($n = 7$), brain ($n = 6$), lymph node ($n = 4$), lung ($n = 3$), bone ($n = 2$), and bone marrow/liver/muscle ($n = 1$). The median follow-up time after the first biopsy of recurrent tumors was 54 months (range, 2–176 months). Ten (40%) patients had died of metastatic disease at the last follow-up.

The TILs of the primary and metastatic tumors are shown in Table 2. Of the primary tumors, 28% were LPBC, 52% were intermediate TIL tumors, and 20% were low TIL tumors. Among the corresponding first metastatic tumors, 44% were intermediate TIL tumors and 56% were low TIL tumors (Table 3). Overall, the percentage of TILs in the primary tumors was significantly higher (average, 34.6%) than that in the metastatic tumors (average, 15.7%) (paired *t*-test, $P = 0.004$). This difference was similar in the $HER2^+$ ($P = 0.036$) and TN ($P = 0.06$) breast cancer groups. The percentage of TILs decreased in 13 of the 25 cases (66%) and increased in 3 of the 25 cases (12%) from the primary tumors to the metastatic tumors (difference >10%). We next undertook an exploratory analysis of the post-progression OS according to the percentage of TILs at a distant site of recurrence ($n = 17$). The group with low TILs had a significantly lower OS than that with intermediate TILs (hazard ratio = 3.77; 95% confidence interval, 0.99–14.9; log–rank test, $P = 0.038$) (Fig. S1).

Characteristics of TILs. Immunohistochemical evaluations could not be carried out in five primary tumors and two metastatic tumors because of the small quantity of the specimens. The results of the comparison of the expression of antibodies between the primary and metastatic tumors are shown in Table 4 and Figures S2–S4. Representative photographs of each antibody in the primary and metastatic tumors from the same patient are shown in Figure 1. The median percentage of $CD8^+$ T cells was 15.8% (range, <10–37%) and 10.0% (range,

Table 1. Clinicopathological characteristics of primary surgical breast tumor specimens

Characteristics	Total patients (n = 25)	HER2$^+$ (n = 14)	TN (n = 11)
Age, years			
Median (range)	48 (28–64)	46 (28–61)	49 (40–63)
T			
1	7 (28)	4 (29)	3 (27)
2	12 (48)	8 (57)	3 (27)
3	2 (8)	1 (7)	1 (9)
4	2 (8)	0 (0)	2 (18)
Unknown	2 (8)	1 (7)	2 (18)
N			
0	14 (56)	8 (57)	6 (55)
1	6 (24)	5 (36)	1 (9)
2	0 (0)	0 (0)	0 (0)
3	3 (12)	1 (7)	2 (18)
Unknown	2 (8)	0 (0)	2 (18)
Stage			
1	5 (20)	2 (14)	3 (27)
2	13 (52)	10 (71)	3 (27)
3	4 (16)	1 (7)	3 (27)
4	0 (0)	0 (0)	0 (0)
Unknown	3 (12)	1 (7)	2 (18)
Histological grade			
1	5 (20)	2 (14)	3 (27)
2	13 (52)	8 (57)	5 (45)
3	7 (28)	4 (29)	3 (27)
ER			
Positive	11 (44)	11 (79)	0 (0)
Negative	14 (56)	3 (21)	11 (100)
Chemotherapy			
No	5 (20)	4 (29)	1 (9)
Neoadjuvant	6 (24)	3 (21)	3 (27)
Adjuvant	13 (52)	7 (50)	6 (55)
Unknown	1 (4)	0 (0)	1 (9)
Trastuzumab			
No	21 (84)	12 (86)	9 (82)
Yes	3 (12)	2 (14)	1 (9)
Unknown	1 (4)	0 (0)	1 (9)
Endocrine therapy			
No	11 (44)	4 (29)	7 (64)
Yes	13 (52)	10 (71)	3 (27)
Unknown	1 (4)	0 (0)	1 (9)
Radiotherapy			
No	16 (64)	10 (71)	6 (55)
Adjuvant	8 (32)	4 (29)	4 (36)
Unknown	1 (4)	0 (0)	1 (9)
Alive at last follow-up			
No	10 (40)	6 (43)	4 (36)
Yes	15 (60)	8 (57)	7 (64)

Data are shown as *n* (%) unless otherwise indicated. ER, estrogen receptor; HER2, human epidermal growth factor receptor 2; TN, triple negative.

Table 2. Comparison of tumor-infiltrating lymphocytes (TILs) between primary and metastatic breast cancer tumors for each subtype

Subtype	First site of biopsy	Primary tumor TILs, %	Metastatic tumor TILs, %	Comparison
HER2$^+$	Bone marrow	10	<10	→
	Brain	20	<10	▼
	Brain	<10	<10	→
	Brain	80	10	▼
	Brain	<10	10	→
	Brain	30	50	△
	Liver	60	10	▼
	LN (Ax)	50	20	▼
	LN (rotter)	70	20	▼
	LN (SCLN)	70	10	▼
	Lung	10	<10	→
	Muscle (pectoralis)	<10	30	△
	Skin (thoracic wall)	30	<10	▼
	Skin (thoracic wall)	<10	<10	→
TN	Bone	10	20	→
	Bone	20	20	→
	Brain	50	<10	▼
	LN (rotter)	70	<10	▼
	Lung	10	50	△
	Lung	30	<10	▼
	Skin (abdominal wall)	80	30	▼
	Skin (head)	10	<10	→
	Skin (thoracic wall)	<10	<10	→
	Skin (thoracic wall)	50	20	▼
	Skin (thoracic wall)	80	10	▼

The percentage of TILs in the primary tumors was significantly higher (average, 34.6%) than in the metastatic tumors (average, 15.7%) (paired *t*-test, $P = 0.004$). This difference was similar in the human epidermal growth factor receptor 2 (HER2)$^+$ ($P = 0.036$) and triple negative (TN) ($P = 0.06$) breast cancer groups. Ax, axillary lymph node; SCLN, supraclavicular fossa lymph node.

Table 3. Comparison of tumor-infiltrating lymphocytes (TILs) between primary and metastatic breast cancer tumors

	Primary	Rate, %	Metastatic	Rate, %
Low TIL	5	20	11	44
Intermediate TIL	13	52	14	56
LPBC	7	28	0	0

LPBC, lymphocyte-predominant breast cancer.

<10–37%) and that of CD4$^+$ T cells was 40.0% (range, <10–77%) and 25% (range, <10–83%) in the primary and metastatic tumors, respectively. The percentages of CD8$^+$ and CD4$^+$ T cells in the primary tumors were significantly higher than those in the metastatic tumors (paired *t*-test, $P = 0.008$ and $P = 0.026$, respectively). Moreover, there was a strong correlation between the percentage of CD4$^+$ T cells and CD8$^+$ T cells in both the primary and the metastatic tumors ($r = 0.607$ and 0.656, $P = 0.005$ and 0.001, respectively). The percentage of Foxp3$^+$ T cells was very low (approximately <10%) and stable in the primary and metastatic tumors.

With regard to the TILs, the median percentage of PD-L1$^+$ TILs was <10% (range, <10–90%) and <10% (range, <10–15%) and that of PD-L2$^+$ TILs was 42% (range, <10–80%) and 30% (range, <10–80%) in the primary and metastatic

Table 4. Comparison of positivity rate between primary and metastatic breast cancer tumors for each antibody

	Primary tumor	Metastatic tumor	*P*-value
Total breast tumors, *n* (%)	20 (100)	23 (100)	
CNB specimens	5 (25)	1 (4)	
Surgical specimens	15 (75)	22 (96)	
TIL positivity rate, median % (range)			
CD4	40 (<10–77)	25 (<10–83)	0.03
CD8	16 (<10–37)	10 (<10–37)	0.01
Foxp3	<10 (<10–10)	<10 (<10)	0.16
PD-L1	<10 (<10–90)	<10 (<10–15)	0.21
PD-L2	42 (<10–80)	30 (<10–80)	0.09
Expression in tumor cells, n (%)			
PD-L1			
Strong: 2	8 (40)	5 (25)	0.46
Weak: 1	10 (50)	15 (75)	
Negative: 0	2 (10)	3 (15)	
PD-L2			
Strong: 2	6 (30)	9 (45)	0.78
Weak: 1	10 (50)	11 (55)	
Negative: 0	4 (20)	3 (15)	
HLA			
Strong: 2	4 (20)	6 (30)	0.89
Weak: 1	14 (70)	15 (75)	
Negative: 0	2 (10)	2 (10)	

CNB, core needle biopsy; PD-L1/2, programmed cell death ligand 1/2; TIL, tumor-infiltrating lymphocyte.

tumors, respectively. There was no significant difference in the percentage of PD-L1$^+$ and PD-L2$^+$ TILs between the primary and metastatic tumors.

The expression of PD-L1, PD-L2, and HLA class I antibodies changed from strong or weakly positive to negative and vice versa from the primary to the metastatic tumor cells. There was a strong correlation between the expression of PD-L1 and PD-L2 ($r = 0.602$, $P = 0.005$) and between the percentage of PD-L2$^+$ TILs and the expression of PD-L2 in the primary tumor cells ($r = 0.788$, $P < 0.001$). There was no strong correlation between the primary and metastatic tumors; the results of the correlation test for the antibody expression between the primary and metastatic tumors were: PD-L1, $r = 0.28$; PD-L2, $r = -0.13$; and HLA class I, $r = 0.43$. We next undertook an exploratory analysis of the post-progression OS according to the expression score for PD-L1, PD-L2, and HLA class I of the tumors at a distant site of recurrence ($n = 17$), but no significance was observed (log–rank test: PD-L1, $P = 0.13$; PD-L2, $P = 0.00012$; and HLA class I, $P = 0.35$. The *P*-value for PD-L2 was <0.05, but the order of the survival curve was not theoretical (upper, score 1; middle, score 2; and lower, score 0).

Discussion

Previous studies have shown that a loss of concordance in the status of biomarkers such as ER, Progesterone receptor (PR), and HER2 can occur between primary and metastatic breast tumors.[24–27] According to the concept of cancer immunoediting, the possibility of discordance of immune microenvironments between primary and metastatic breast tumors should also be considered. In this study, we found that tumors at the first metastatic recurrence in HER2$^+$ and TN breast cancers

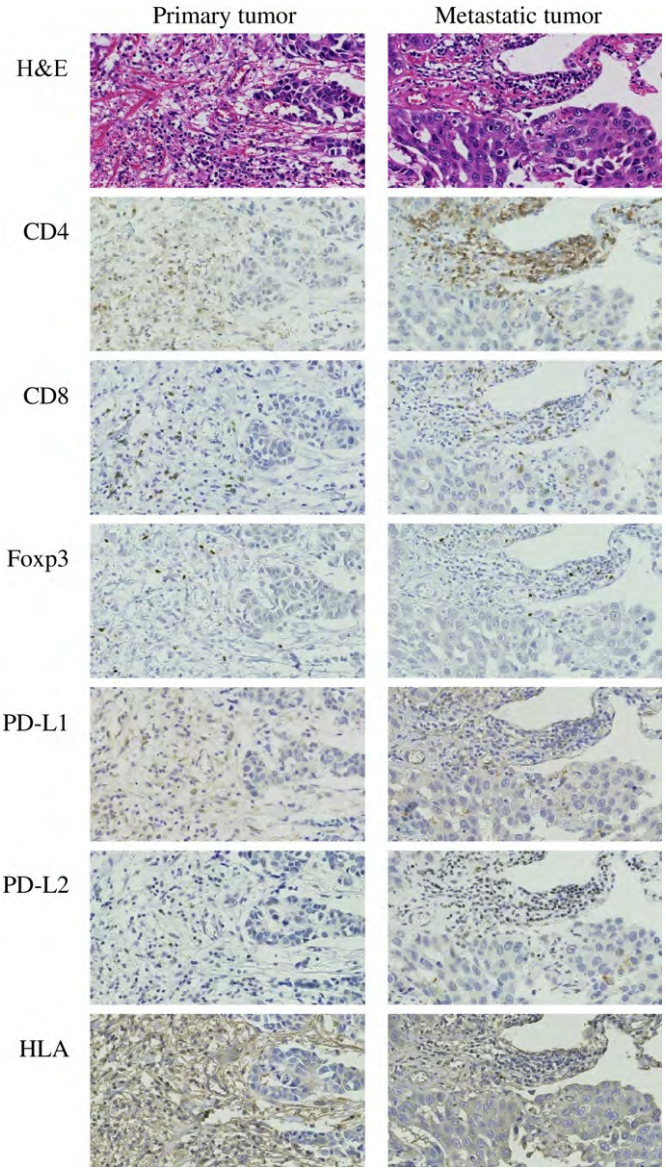

Fig. 1. Immunohistochemical staining for primary antibodies against CD4, CD8, Foxp3, programmed cell death ligand 1 (PD-L1), PD-L2, and HLA class I to characterize tumor-infiltrating lymphocytes. Representative photographs are shown from the same patient who had human epidermal growth factor receptor-2-positive primary breast tumor (left column) and lung metastasis (right column). Original magnification, × 400.

have a lower percentage of TILs and CD8$^+$ and CD4$^+$ T cells compared to primary tumors, suggesting that immune escape plays a role in tumor progression. To the best of our knowledge, this is one of the first studies to evaluate changes in the tumor microenvironment during the process of metastasis using pair-matched specimens. Our study was similar to previous articles in reporting that TILs and the subset percentages of metastatic sites was lower than that of primary sites;[17,18] however, we focused on HER2$^+$ and TN breast cancers, because TILs are a reliable predictive and prognostic biomarker in these subtypes. Furthermore, we found that the expression of PD-L1, PD-L2, and HLA class I were changeable between primary and metastatic breast cancer tumors.

The clinical utility of TILs in most patients is limited because the determination of the potential of TILs as a specific immune

marker or their ability to facilitate the prediction of the use of T-cell checkpoint inhibitors is a major challenge and because no methods to successfully modulate immunity to reduce mortality have been established so far.[28] Antibodies targeting cytotoxic T-lymphocyte-associated antigen 4/programmed death 1/PD-L1 have resulted in clinical responses in multiple tumor types including advanced melanomas, advanced non-small-cell lung cancers, and advanced renal cell carcinomas.[29–31] These treatment methods are expected to slow cancer progression and significantly prolong the survival of patients with advanced cancer. Given that immune checkpoint therapy only benefits a fraction of patients, there are ongoing efforts being made to identify predictive biomarkers that could be used to select patients that will respond well to such treatment.[32]

There are many candidates for biomarkers, such as PD-L1 expression in tumors, the percentage of TILs, the percentage of $CD8^+$ T cells in the TILs, the level of cytokines and chemokines produced by lymphocytes in the peripheral blood, and myeloid-derived suppressor cells in tumor lesions.[9,33] However, sometimes these biomarkers are also detected in primary tumors. These biomarkers could also be influenced by metastatic processes and cytotoxic chemotherapy.[34] In our study, the expression of PD-L1, PD-L2, and HLA class I antigen was also found to change from primary to metastatic tumors. Therefore, the evaluation of targeted lesions just before the start of immunotherapy might be needed in future clinical trials.

Although many adjuvant and neoadjuvant studies have assessed infiltrating lymphocytes and stromal lymphocytic infiltration has been found to constitute a robust prognostic factor in primary $HER2^+$ tumors or TN breast cancers,[8,9,35] whether lymphocytic infiltration in metastatic tumors could be a prognostic factor has not yet been evaluated. In our study, the group with low TILs in metastatic tumors had a significantly lower OS than the group with intermediate TILs. Thus, our results indicate that a higher percentage of TILs could have a prognostic impact, even in metastatic tumors.

Previous studies showed that the results of evaluation of the stromal compartment were more reproducible than those of the evaluation of intratumoral TILs.[23] We evaluated TILs within the borders of the invasive tumor and found that it was quite difficult to distinguish the invasive margin TILs clearly from stromal TILs. Although there are few studies involving the evaluation of the invasive edge, there is currently no evidence indicating that TILs at the invasive edge are functionally different from stromal TILs. We therefore evaluated stromal TILs of the breast tissue and other organs. Recommendations for TIL evaluation have been published previously,[23] and guidelines for the same will be standardized in the years ahead. However, we encountered some difficulties in the evaluation of TILs from other tissues. In some cases, there was very little stromal area in the biopsy specimens, which was not the case in the surgical specimens. It was also difficult to precisely detect TILs among the background lymphocytes in the recurrent tumors in the lymph nodes or the bone marrow on the H&E-stained slides. The TILs were differentiated from the background lymphocytes based on the structural patterns of infiltration in the case of bone marrow tumors, and in case of the tumors in the lymph nodes, the lymph node structure had been totally replaced by the tumor in our study.

One limitation of this study was the small number of patients; in particular, patients with LPBCs were few, which limited our ability to determine the prognostic value of lymphocyte predominance in breast cancer. The reason for the small number of cases is that metastatic biopsy samples were very rare. Previous articles that compared primary and metastatic breast tumors consisted of $ER^+/HER2^-$ cases and the number of $HER2^+$ and TN cases was approximately 30–40 in their cohorts.[17,18] Tumor-infiltrating lymphocytes are associated with a better neoadjuvant chemotherapy response and prognosis in $HER2^+$ and TN breast cancers. Therefore, we focused only on $HER2^+$ and TN breast cancers, which resulted in a small number of cases.

In summary, we found that tumors at the first metastatic recurrence in $HER2^+$ and TN breast cancer patients have a lower percentage of TILs and $CD8^+$ and $CD4^+$ T cells compared to primary tumors, suggesting a role for immune escape in tumor progression. These differences could occur in a time-, site-, and therapy- (chemotherapy, radiotherapy, and surgery) dependent manner; therefore, the evaluation of targeted lesions just before the start of immunotherapy might be needed in future clinical trials. Furthermore, a low percentage of TILs at the recurrence sites seemed to be associated with poor OS, suggesting a more aggressive phenotype. These findings warrant independent confirmation in future studies.

Acknowledgments

We would like to thank Toshiya Tanaka, Division of Diagnostic Pathology and Support Center for Medical Research and Education for technical assistance with staining. This research was supported in part by the Japanese Ministry of Education, Culture, Sports, Science and Technology's Supported Program for the Strategic Research Foundation at Private Universities, 2012–2016. The authors thank Editage for providing editorial assistance.

Disclosure Statement

The authors have no conflict of interest.

References

1 DeNardo DG, Coussens LM. Inflammation and breast cancer. Balancing immune response: crosstalk between adaptive and innate immune cells during breast cancer progression. *Breast Cancer Res* 2007; **9**(4): 212.
2 Schmidt M, Bohm D, von Torne C *et al.* The humoral immune system has a key prognostic impact in node-negative breast cancer. *Cancer Res* 2008 (Jul 1); **68**: 5405–13.
3 Denkert C, Loibl S, Noske A *et al.* Tumor-associated lymphocytes as an independent predictor of response to neoadjuvant chemotherapy in breast cancer. *J Clin Oncol* 2010 (Jan 1); **28**(1): 105–13.
4 West NR, Milne K, Truong PT, Macpherson N, Nelson BH, Watson PH. Tumor-infiltrating lymphocytes predict response to anthracycline-based chemotherapy in estrogen receptor-negative breast cancer. *Breast Cancer Res* 2011; **13**(6): R126.
5 Ono M, Tsuda H, Shimizu C *et al.* Tumor-infiltrating lymphocytes are correlated with response to neoadjuvant chemotherapy in triple-negative breast cancer. *Breast Cancer Res Treat* 2012 (Apr); **132**: 793–805.
6 Yamaguchi R, Tanaka M, Yano A *et al.* Tumor-infiltrating lymphocytes are important pathologic predictors for neoadjuvant chemotherapy in patients with breast cancer. *Hum Pathol* 2012 (Oct); **43**: 1688–94.
7 Lee HJ, Seo JY, Ahn JH, Ahn SH, Gong G. Tumor-associated lymphocytes predict response to neoadjuvant chemotherapy in breast cancer patients. *J Breast Cancer* 2013 (Mar); **16**(1): 32–9.
8 Loi S, Sirtaine N, Piette F *et al.* Prognostic and predictive value of tumor-infiltrating lymphocytes in a phase III randomized adjuvant breast cancer trial in node-positive breast cancer comparing the addition of docetaxel to doxorubicin with doxorubicin-based chemotherapy: BIG 02-98. *J Clin Oncol* 2013 (Mar 1); **31**: 860–7.

9 Adams S, Gray RJ, Demaria S *et al.* Prognostic value of tumor-infiltrating lymphocytes in triple-negative breast cancers from two phase III randomized adjuvant breast cancer trials: ECOG 2197 and ECOG 1199. *J Clin Oncol* 2014 (Jul 28); **32**: 2959–66. PubMed PMID: 25071121. Epub 2014/07/30. Eng.
10 Denkert C, von Minckwitz G, Brase JC *et al.* Tumor-infiltrating lymphocytes and response to neoadjuvant chemotherapy with or without carboplatin in human epidermal growth factor receptor 2-positive and triple-negative primary breast cancers. *J Clin Oncol* 2014 (Dec 22); **33**: 983–91. PubMed PMID: 25534375. Epub 2014/12/24. Eng.
11 Loi S, Michiels S, Salgado R *et al.* Tumor infiltrating lymphocytes are prognostic in triple negative breast cancer and predictive for trastuzumab benefit in early breast cancer: results from the FinHER trial. *Ann Oncol* 2014 (Aug); **25**: 1544–50.
12 Perez EA, Thompson EA, Ballman KV *et al.* Genomic analysis reveals that immune function genes are strongly linked to clinical outcome in the north central cancer treatment group N9831 adjuvant trastuzumab trial. *J Clin Oncol* 2015 (Jan 20); **33**: 701–8. PubMed PMID: 25605861. Epub 2015/01/22. Eng.
13 Leong PP, Mohammad R, Ibrahim N *et al.* Phenotyping of lymphocytes expressing regulatory and effector markers in infiltrating ductal carcinoma of the breast. *Immunol Lett* 2006 (Feb 15); **102**: 229–36.
14 Miyashita M, Sasano H, Tamaki K *et al.* Tumor-infiltrating CD8+ and FOXP3+ lymphocytes in triple-negative breast cancer: its correlation with pathological complete response to neoadjuvant chemotherapy. *Breast Cancer Res Treat* 2014 (Dec); **148**: 525–34.
15 Dieci MV, Criscitiello C, Goubar A *et al.* Prognostic value of tumor-infiltrating lymphocytes on residual disease after primary chemotherapy for triple-negative breast cancer: a retrospective multicenter study. *Ann Oncol* 2014 (Mar); **25**: 611–8.
16 Burstein HJ, Lacchetti C, Anderson H *et al.* Adjuvant endocrine therapy for women with hormone receptor-positive breast cancer: American Society of Clinical Oncology Clinical Practice Guideline Update on Ovarian Suppression. *J Clin Oncol* 2016 (Feb 16); **34**: 1689–701. PubMed PMID: 26884586.
17 Cimino-Mathews A, Ye X, Meeker A, Argani P, Emens LA. Metastatic triple-negative breast cancers at first relapse have fewer tumor-infiltrating lymphocytes than their matched primary breast tumors: a pilot study. *Hum Pathol* 2013 (Oct); **44**: 2055–63.
18 Sobottka B, Pestalozzi B, Fink D, Moch H, Varga Z. Similar lymphocytic infiltration pattern in primary breast cancer and their corresponding distant metastases. *Oncoimmunology* 2016 (Jun); **5**(6): e1153208.
19 Dunn GP, Bruce AT, Ikeda H, Old LJ, Schreiber RD. Cancer immunoediting: from immunosurveillance to tumor escape. *Nat Immunol* 2002 (Nov); **3**: 991–8.
20 Kim R, Emi M, Tanabe K. Cancer immunoediting from immune surveillance to immune escape. *Immunology* 2007 (May); **121**(1): 1–14.
21 Moossdorff M, van Roozendaal LM, Strobbe LJ *et al.* Maastricht Delphi consensus on event definitions for classification of recurrence in breast cancer research. *J Natl Cancer Inst* 2014 (Dec); **106**(12): dju288. PubMed PMID: 25381395. Epub 2014/11/09. Eng.
22 Goldhirsch A, Wood WC, Coates AS, Gelber RD, Thurlimann B, Senn HJ. Strategies for subtypes–dealing with the diversity of breast cancer: highlights of the St. Gallen International Expert Consensus on the Primary Therapy of Early Breast Cancer 2011. *Ann Oncol* 2011 (Aug); **22**: 1736–47.
23 Salgado R, Denkert C, Demaria S *et al.* The evaluation of tumor-infiltrating lymphocytes (TILs) in breast cancer: recommendations by an International TILs Working Group 2014. *Ann Oncol* 2015 (Feb); **26**: 259–71.
24 Amir E, Miller N, Geddie W *et al.* Prospective study evaluating the impact of tissue confirmation of metastatic disease in patients with breast cancer. *J Clin Oncol* 2012 (Feb 20); **30**: 587–92.
25 Simmons C, Miller N, Geddie W *et al.* Does confirmatory tumor biopsy alter the management of breast cancer patients with distant metastases? *Ann Oncol* 2009 (Sep); **20**: 1499–504.
26 Thompson AM, Jordan LB, Quinlan P *et al.* Prospective comparison of switches in biomarker status between primary and recurrent breast cancer: the Breast Recurrence In Tissues Study (BRITS). *Breast Cancer Res* 2010; **12**(6): R92.
27 Niikura N, Liu J, Hayashi N *et al.* Loss of human epidermal growth factor receptor 2 (HER2) expression in metastatic sites of HER2-overexpressing primary breast tumors. *J Clin Oncol* 2012 (Feb 20); **30**: 593–9.
28 Loi S, MacCallum P. Host antitumor immunity plays a role in the survival of patients with newly diagnosed triple-negative breast cancer. *J Clin Oncol* 2014 (Sep 20); **32**: 2935–7.
29 Borghaei H, Paz-Ares L, Horn L *et al.* Nivolumab versus docetaxel in advanced nonsquamous non-small-cell lung cancer. *N Engl J Med* 2015 (Oct 22); **373**: 1627–39.
30 Weber JS, D'Angelo SP, Minor D *et al.* Nivolumab versus chemotherapy in patients with advanced melanoma who progressed after anti-CTLA-4 treatment (CheckMate 037): a randomised, controlled, open-label, phase 3 trial. *Lancet Oncol* 2015 (Apr); **16**: 375–84.
31 Motzer RJ, Escudier B, McDermott DF *et al.* Nivolumab versus everolimus in advanced renal-cell carcinoma. *N Engl J Med* 2015 (Nov 5); **373**: 1803–13.
32 Sharma P, Allison JP. The future of immune checkpoint therapy. *Science* 2015 (Apr 3); **348**(6230): 56–61.
33 Arato T, Daimon T, Heike Y *et al.* Guidance on cancer immunotherapy development in early-phase clinical studies. *Cancer Sci* 2015 (Dec);**106**(12):1761–71. PubMed PMID: 26767933. Pubmed Central PMCID: 4714668. Epub 2016/01/16. eng.
34 Champiat S, Ileana E, Giaccone G *et al.* Incorporating immune-checkpoint inhibitors into systemic therapy of NSCLC. *J Thorac Oncol* 2014; **9**: 144–53.
35 Salgado R, Denkert C, Campbell C *et al.* Tumor-infiltrating lymphocytes and associations with pathological complete response and event-free survival in HER2-positive early-stage breast cancer treated with lapatinib and trastuzumab: a secondary analysis of the NeoALTTO trial. *JAMA Oncol* 2015 (Jul); **1**: 448–54.

Supporting Information

Additional Supporting Information may be found online in the supporting information tab for this article:

Fig. S1. Overall survival after first recurrence. The group with low tumor-infiltrating lymphocytes (TILs; <10%) had a significantly lower overall survival than the intermediate TIL group (≥10% TILs) (hazard ratio = 3.77; 95% confidence interval, 0.99–14.9; log–rank, $P = 0.038$).

Fig. S2. Comparison of positivity rate between primary and metastatic tumor-infiltrating lymphocytes for each antibody. CD4, CD8, and programmed cell death ligand 1 (PD-L1) positivity was defined by membranous lymphocyte staining, and FoxP3 and PD-L2 positivity was defined by nuclear lymphocyte staining. CD4, CD8, Foxp3, PD-L1, and PD-L2 expression by the tumor-infiltrating lymphocytes was recorded in 10% increments and the score of three fields was averaged.

Fig. S3. Comparison of expression score between primary and metastatic tumor cells for each antibody. The expression of programmed cell death ligand 1 (PD-L1), PD-L2, HLA class I A, B, and C in the tumor cells was scored as 0 (negative), 1 (weak), or 2 (strong). The number of cases is noted above the bars and each bar without annotation represents only one case.

Fig. S4. Representative photographs. The expression of programmed cell death ligand 1 (PD-L1), PD-L2, and HLA class I in the tumors was scored as 0 (negative), 1 (weak), or 2 (strong).

A Case of Giant Borderline Phyllodes Tumor of the Breast Associated with Hypoglycemia

Yuki SAITO[*1], Yasuhiro SUZUKI[*2], Chie INOMOTO[*3], Nobue KUMAKI[*4], Kozue YOKOYAMA[*2], Rin OGIYA[*2] , Risa OSHITANAI[*1], Mayako TERAO[*2], Banri TSUDA[*2], Tooru MORIOKA[*2], Naoki NIIKURA[*2], Takuho OKAMURA[*2], Shinobu MASUDA[*5] and Yutaka TOKUDA[*2]

[*1]*Department of Endocrine-Breast Surgery, Tokai University School of Medicine, Hachioji Hospital*
[*2]*Department of Endocrine-Breast Surgery, Tokai University School of Medicine*
[*3]*Department of Pathology, Tokai University School of Medicine, Oiso Hospital*
[*4]*Department of Pathology, Tokai University School of Medicine*
[*5]*Department of Pathology, Nihon University School of Medicine*

(Received May 26, 2016; Accepted June 11, 2016)

We report a patient with a giant phyllodes tumor of the right breast associated with a hypoglycemic attack. A 48-year-old woman experienced a loss of consciousness and was transferred via ambulance to our hospital emergency department. Upon arrival, her blood glucose level was 26 mg/dl, and a giant tumor (> 20 cm in diameter) with skin ulceration was observed on the right breast. Core needle biopsy led to a histological diagnosis of a phyllodes tumor of the breast. Ultrasonography and computed tomography detected neither distant metastasis nor a pancreatic endocrine tumor. Her preoperative serum insulin-like growth factor (IGF)-II and insulin levels were 1,330 ng/ml (normal range, 519−1067 ng/ml) and < 1.0 μU/ml, respectively. Following a simple mastectomy, the 24-h postoperative serum IGF-II and insulin levels were 496 ng/ml and 10.0 μU/ml, respectively. The IGF-II levels detected in the phyllodes tumor and normal breast tissue were 10,600 ng/Wg (wet weight in grams) and 855 ng/Wg. We conclude from these findings that the hypoglycemic attack was related to the elevated IGF-II level in the giant phyllodes tumor of the breast.

Key words: phyllodes tumor, IGF-II, hypoglycemic attack

INTRODUCTION

Phyllodes tumor of the breast is a rare, often benign (> 50%) type of fibroepithelial tumor that accounts for less than 1% of breast tumors [1]. Phyllodes tumors are generally first identified during routine breast medical examination and/or on mammography.

There have been a few reports of tumor-induced hypoglycemia, which is an infrequent condition occurring most often due to insulin secretion by pancreatic islet beta-cell tumors (insulinomas) or rarely due to excess secretion of insulin-like growth factor (IGF)-II from a tumor, leading to insulin receptor stimulation and increased glucose utilization. This latter condition is called non-islet cell tumor hypoglycemia (NICTH), which is a serious complication. In this report, we describe a rare case of a giant phyllodes tumor of the breast that induced NICTH consequent to excess IGF-II secretion.

CASE REPORT

In December 2004, a 48-year-old woman was brought to our emergency department after losing consciousness. Her past medical history and family history were unremarkable. Physical examination revealed a giant (> 20 cm in diameter), hard, elastic bleeding mass with skin ulceration in the right breast (Fig. 1). The axillary, supraclavicular, and cervical lymph nodes were not palpable. No neurological disorders were noted.

Blood studies indicated severe hypoglycemia (20 mg/dl), hypokalemia (2.4 mEq/L), hypernatremia (151 mEq/L), and hypoinsulinemia (1.0 μIU/ml) (Table 1). Imaging findings (X-ray of the chest and abdomen and computed tomography (CT) of the head) were unremarkable. The patient was administered 160 ml of a 40% glucose solution (6.4 g), which restored her serum blood sugar level and consciousness, and was discharged from the hospital the same day.

However, the next day after discharge, she again experienced a loss of consciousness and was brought to the emergency department. Because of hypoglycemia (29 mg/dl), she received another infusion of 40% glucose (40 ml, 1.6 g), which alleviated the hypoglycemic symptoms. However, her case was considered urgent with respect to examination and therapy because she had experienced continuous hypoglycemic attacks on 2 consecutive days. Consequently, she was administered continuous infusion of glucose (100 g/day) to alleviate the hypoglycemia.

Ultrasonographic evaluation of the breast mass indicated a heterogeneous internal echo and internal structures containing small cystic components, calcification, and hyperechoic separations. The mass had a nearly smooth margin with a somewhat irregular contour (Fig. 2). No axillary lymphadenopathy was observed. CT showed a giant mass in the right breast, with no tumor infiltration into the pectoral muscle fascia. Areas of high density observed within the tumor

Yuki SAITO, Department Endocrine Breast Surgery, Tokai University School of Medicine Hachioji Hospital, 1838 Ishikawa-machi, Hachioji, Tokyo 192-0032, Japan Tel: +81-42-639-1111 Fax: +81-42-639-1144 E-mail: yu-ki@is.icc.u-tokai.ac.jp

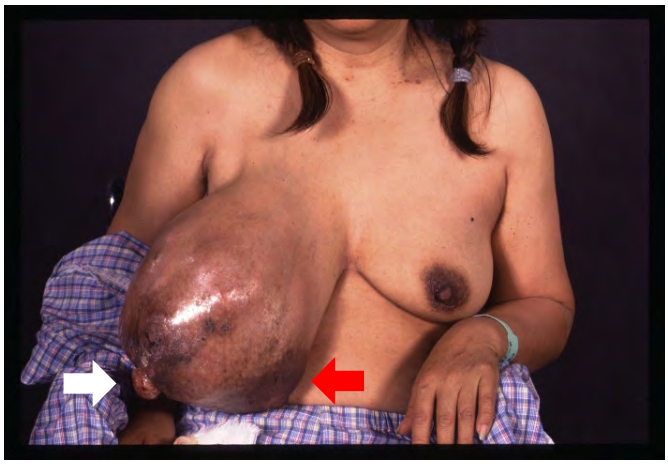

Fig. 1 Physical examination findings.
A giant right breast tumor, measuring approximately 20 cm in diameter with skin ulceration (white arrow), was observed. The red arrow indicates the right nipple. The tumor was hard and elastic, with good mobility, and bled easily from the skin ulcer. The axillary lymph node was not palpable.

Table 1 Blood analyses conducted upon arrival or before surgery

White blood cell	$10.1 \times 10^3/mm^3$ (4.0–8.0)
Red blood cell	$4.6 \times 10^6/mm^3$ (3.8–4.8)
Hemoglobin	13.8 g/dl (11.5–15.5)
Hematocrit	40.8% (34.0–42.0)
Platelet	$30.0 \times 10^4/mm^3$ (14.0–40.0)
Total protein	7.3 g/dl (6.5–8.0)
Albumin	4.1 g/dl (4.1–5.0)
AST	27 U/L (< 30)
ALT	14 U/L (< 35)
LDH	266 U/L (110–219)
ALP	252 U/L (100–300)
BUN	6 mg/ml (8–20)
Creatinine	0.4 mg/ml (0.5–0.8)
Sodium	151 mEq/L (136–145)
Potassium	2.4 mEq/L (3.5–4.8)
Chlorine	107 mEq/L (98–108)
Blood sugar	20 mg/dl (70–110)
Insulin	< 1.0 μIU/ml (1.5–13.3)
CEA	1.4 ng/ml (< 5)
CA15-3	27.7 U/ml (< 30)
IGF-I (serum)	210 ng/ml (46–282) (preoperatively)
IGF-II (serum)	1330 ng/ml (519–1067) (preoperatively)
IGFBP-3	3.57 μg/ml (2.17–4.05) (preoperatively) (normal ranges)

AST: aspartate aminotransferase, ALT: alanine aminotransferase, LDH: lactate dehydrogenase, ALP, alkaline phosphatase, BUN: blood urea nitrogen CEA: carcinoembryonic antigen, CA15-3: carbohydrate antigen 15-3, IGF: insulin-like growth factor, IGFBP-3: insulin-like growth factor binding protein-3

on plain CT images (Fig. 3A) were thought to be calcifications. Contrast-enhanced CT (Fig. 3B) indicated heterogeneous enhancement within the mass, with no cystic component. T1-weighted, fat-saturated magnetic resonance imaging (MRI) (Fig. 4A) indicated relative homogeneity within the tumor; an area of high signal intensity was thought to indicate a possible focal hemorrhage. Furthermore, contrast-enhanced T2-weighted, fat-saturated MRI (Fig. 4B) revealed a giant, lobulated mass with heterogeneous high signal intensity, as well as septa and well-circumscribed margins. These findings were typical of a phyllodes tumor.

A subsequent core needle biopsy (CNB) revealed that the tumor comprised both epithelial and stromal elements. Although high stromal cellularity was not observed, the stromal elements were abundant. These histological findings suggested a fibroepithelial lesion, including phyllodes tumor. The patient's baseline serum IGF-II level was high at 1330 ng/ml (normal range, 519–1067 ng/ml), whereas IGF-I and insulin growth factor binding protein-3 (IFGBP-3) levels were normal (210 ng/ml [normal, 46–282 ng/ml) and 3.57 mg/ml [normal, 2.17–4.05 mg/ml)]. The serum insulin level was low, at < 1.0 μU/ml (Table 1). The patient was

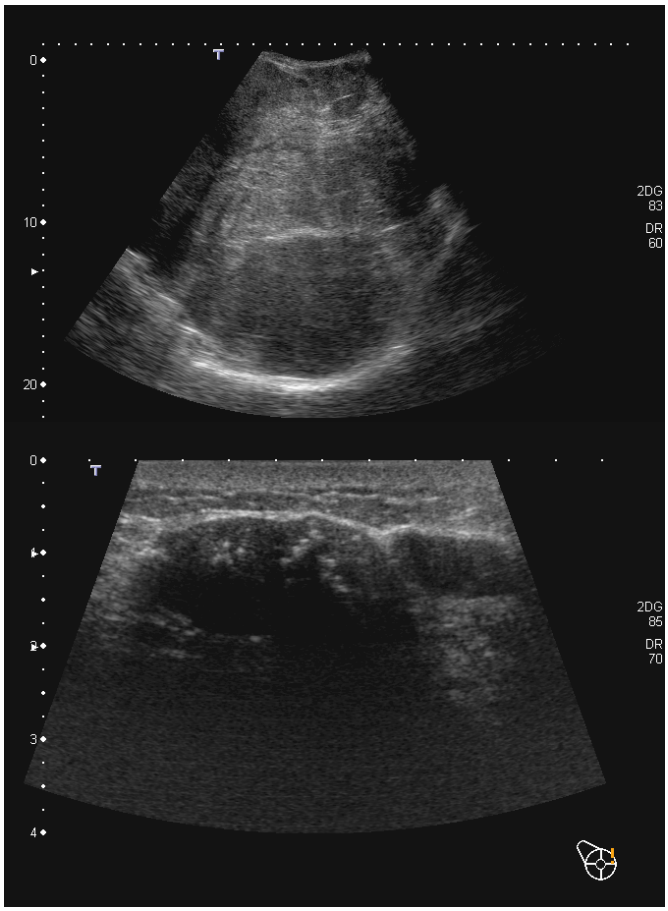

Fig. 2 Ultrasonography findings.
The right giant breast mass appeared as an area of heterogeneous internal echo, with had internal structures comprising small cystic parts, calcification and hyperechoic separations. The mass exhibited a nearly smooth, partially irregular contour.

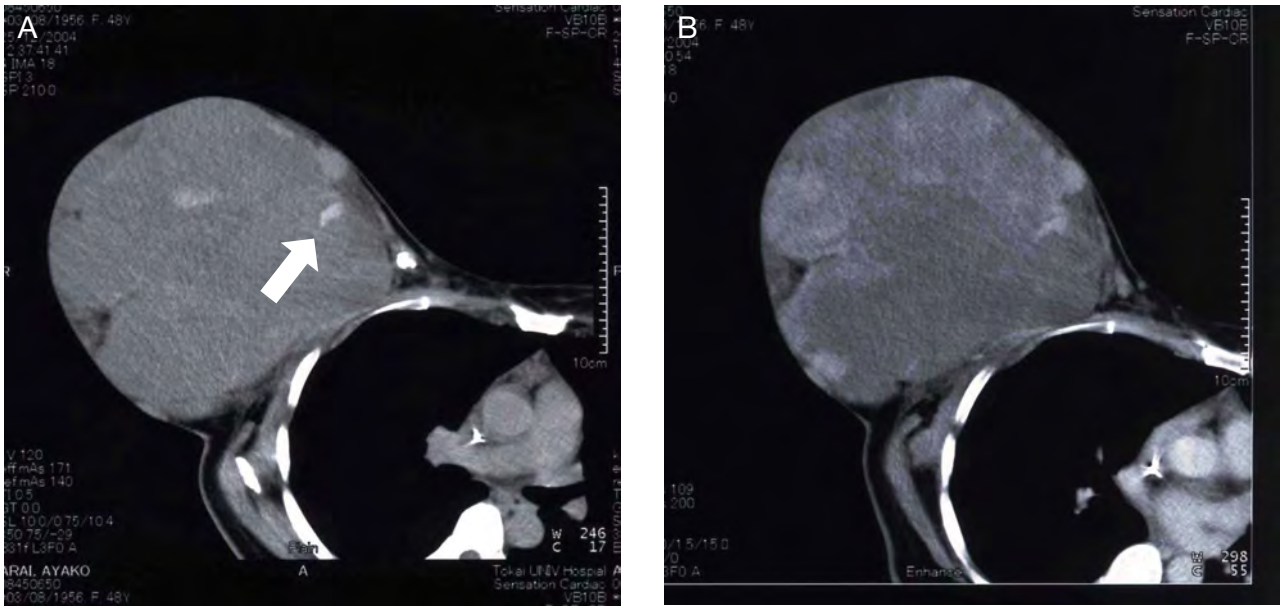

Fig. 3 CT findings.
Computed tomography (CT) revealed a giant mass in the right breast. (A) Areas of high density within the tumor on plain CT were thought to be calcifications (arrow). (B) Contrast-enhanced CT indicated heterogeneous enhancement within the mass.

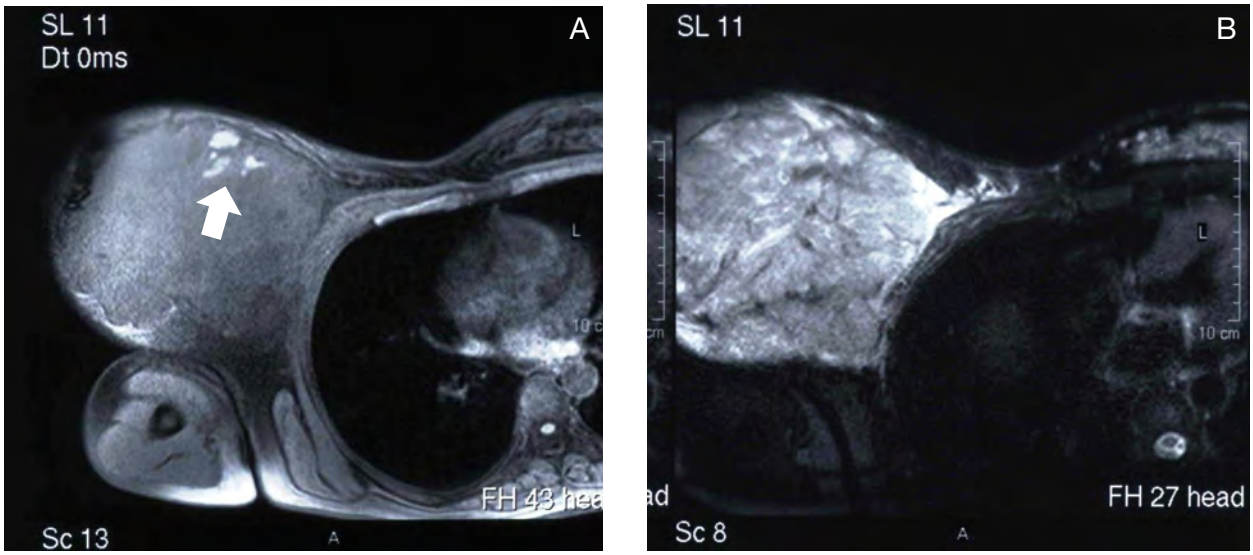

Fig. 4 MRI findings.
Magnetic resonance imaging (MRI) of the giant tumor in the right breast. (A) T1-weighted, fat-saturated MRI indicated relative homogeneity within the tumor, with an area of high signal intensity, possibly indicative of focal hemorrhage (arrow). (B) Contrast-enhanced, T2-weighted, fat-saturated MRI showed a lobulated giant mass with heterogeneous high signal intensity. The tumor contained some septa and well-circumscribed margins.

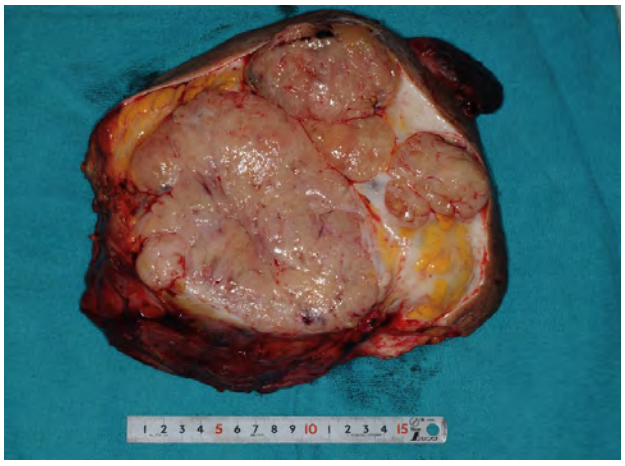

Fig. 5 Gross appearance of the cut surface of the tumor.
The cut surface of the tumor was white-to-gray with hemorrhagic foci.

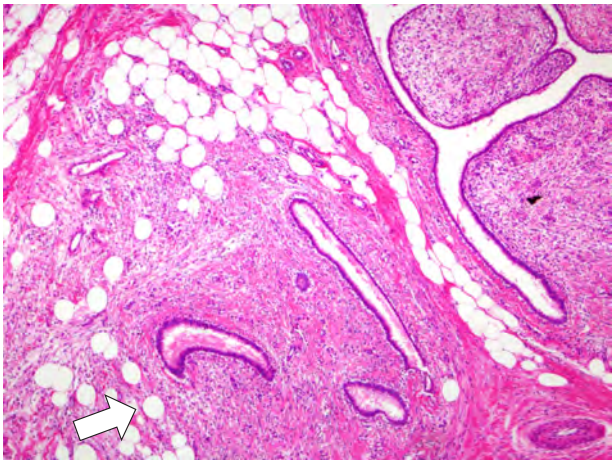

Fig. 6 Histopathological findings (Hematoxylin eosin stain; low magnification).
The stromal cells exhibited nuclear hyperchromasia and mild pleomorphism.
Invasive growth patterns were focally detected (arrow).

diagnosed with an IGF-II-secreting phyllodes tumor.

A simple mastectomy was performed to remove the tumor. The approximate size and weight of the removed tumor were 25 × 18 × 17 cm and > 5 kg, respectively. The cut surface of the tumor was white-to-gray with hemorrhagic foci (Fig. 5). The tumor was relatively well defined, and a phylloid pattern with cystic lumina was focally detected at the periphery of the tumor. As indicated by the CNB findings, the tumor comprised abundant stromal and epithelial elements. The stromal cells exhibited nuclear hyperchromasia and mild pleomorphism, with few mitotic figures (1–2/10 high-powered field), and a focal invasive growth pattern was identified. These histological features were consistent with a borderline phyllodes tumor (Fig. 6). Furthermore, the IGF-II concentration in the tumor was 10600 ng/Wg, compared with the normal tissue value of 855 ng/Wg (Table 2). Thus, this phyllodes tumor produced a large quantity of IGF-II to which the recurring hypoglycemic attacks were attributed.

The patient's post-operative serum IGF-II levels decreased to within the normal range over time—with values of 921 ng/ml at 1 h, 790 ng/ml at 3 h, 666 ng/ml at 6 h, 521 ng/ml at 12 h, and 496 ng/ml at 24 h (Table 3). Her blood sugar level accordingly increased after surgery without requiring an intravenous administration of high-concentration glucose, and her postoperative serum insulin level consistently exceeded 10.0 μU/ml. The borderline phyllodes tumor as well as the hypoglycemic attacks did not recur within a 10-year postoperative follow-up period.

Table 2 IGF-II concentration in the phyllodes tumor relative to the normal breast tissue.

IGF-II concentrations in tissue extracts	
Phyllodes tumor	10,600 ng/Wg
Normal breast tissue	855 ng/Wg

IGF: insulin-like growth factor

Table 3 Changes over time in serum IGF-II, glucose, and insulin levels and the concentration of administered glucose after tumor resection.

		Time after resection					
	Before surgery	1 h	3 h	6 h	12 h	24 h	72 h
Serum IGF-II (ng/ml)	1,330	921	790	666	521	496	680
Serum glucose (mg/ml)	122	145	202	159	-	144	145
Insulin (μU/ml)	<1.0	12.2	11.0	-	-	10.0	-
Administration glucose (%)	50	5	5	5	5	5	-

IGF: insulin-like growth factor

DISCUSSION

Breast phyllodes tumor was reported for the first time in 1838 by Johannes Muller, and was originally designated "cystosarcoma phyllodes" [2]. Histologically, these uncommon fibroepithelial tumors are classified as benign, borderline, or malignant according to the presence of stromal cellular atypia, cell density, mitotic activity, infiltrative vs. circumscribed tumor margins, and the presence of an interstitial one-sided increase [3]. In the present case, the tumor stromal cells exhibited nuclear hyperchromasia and mild atypia, along with mitotic activity and a circumscribed infiltrative tumor margin. These pathological features were consistent with a borderline phyllodes tumor.

NICTH, which was first reported in 1929 [4], is usually associated with large tumors of mesodermal or epithelial origin [5]. Notably, the first report of hypoglycemia associated with a phyllodes tumor was published in 1983 [6]. The most common cause of NICTH is tumoral overproduction of IGF-II, a single-chain peptide that shares approximately 50% sequence homology with proinsulin. Hypoglycemia appears to be consequent to increased glucose utilization and inhibited release of glucose from the liver consequent to the tumoral secretion of incompletely processed IGF-II. The laboratory evaluation for hypoglycemia includes episodic measurements of glucose, insulin, proinsulin, C-peptide, beta-hydroxybutyrate, and sulfonylurea/meglitinide levels [7]; in addition, measurements of serum IGF-I and IGF-II levels might be diagnostically useful. Accordingly, a diagnosis of NICTH is based upon both clinical and biochemical findings, and is not usually difficult. When a patient with a known tumor presents with hypoglycemia, the cause is typically apparent from the history and physical examination. Furthermore, a healthy person who experiences hypoglycemia is less likely to have NICTH, although in some cases, hypoglycemia is the initial event that leads to the diagnosis of a tumor. Although we were unable to measure the serum C-peptide, proinsulin, and beta-hydroxybutyrate levels, the current patient was a typical case in which the measured high serum IGF-II level led to a preoperative diagnosis.

Complete resection of the IGF-producing tumor is the most effective treatment for NICTH [8]. However, if surgery is delayed, ongoing management of hypoglycemia might include an increased caloric intake and intravenous glucose administration. In the present case, the patient received a continuous intravenous administration of 50% glucose before surgery to remove the tumor, which had a very high IGF-II concentration relative to that of the normal breast tissue. Following mastectomy, her serum IGF-II concentration decreased over time, resulting in an increase in her blood sugar level without intravenous glucose.

In summary, we have reported our experience with a rare case of a giant borderline phyllodes tumor with hypoglycemic attacks caused by tumor-secreted IGF-II. This is the first report in which the IGF-II concentration has been measured in the tumor and corresponding normal tissues.

REFERENCES

1) Calhoun K, Lawton TJ, Kim JM, *et al*. Phyllodes tumors. In: Diseases of the breast, Harris J, Lippman ME, Osborne CK, Morrow M (Eds), Lippincott Williams and Wilkins, 2010 2010. p.781.
2) Muller J. Ueber den Feinern Bau und die Formen der Krankhaften Geschwulste. Berlin G Reimer 1838: 54–60.
3) The Japanese Breast Cancer Society. Japanese Classification of Breast cancer. 17th Edition: Kanahara & Co., Ltd., Tokyo, 2012: 25–26.
4) Nadler WH, Wolfer JA. Hepatogenic hypoglycemic associated with primary liver cell carcinoma. Arch Intern Med. 1929; 44: 701.
5) Zepf J. Insulinlike growth factor binding proteins and tumor hypoglycemia.Trends Endocrinol Metab. 1995; 6: 37–42.
6) Li TC, Reed CE, Stubenbord WT Jr, *et al*. Surgical cure of hypoglycemia associated with cystosarcoma phyllodes and elevated non-suppressible insulin-like protein. Am J Med 1983; 74: 1080–1084.
7) Service FJ. Diagnostic approach to adults with hypoglycemic disorders. Endocrinol Metab Clin North Am. 1999; 28: 519–532.
8) Bodnar TW, Acevedo MJ, Pietropaolo M. Management of non-islet-cell tumor hypoglycemia: a clinical review. J Clin Endocrinol Metab. 2014; 99: 713–722.

ORIGINAL PAPER

Nagoya J. Med. Sci. **77**. 265 ~ 273, 2015

IMPACT OF THE INTRAOPERATIVE USE OF FIBRINOGEN CONCENTRATE FOR HYPOFIBRINOGENEMIA DURING THORACIC AORTIC SURGERY

YOSHIMORI ARAKI, MD, PhD; AKIHIKO USUI, MD, PhD; HIDEKI OSHIMA, MD, PhD; TOMONOBU ABE, MD, PhD; KAZURO FUJIMOTO, MD, PhD; MASATO MUTSUGA, MD, PhD; YOSHIYUKI TOKUDA, MD, PhD; SACHIE TERAZAWA, MD, PhD; KEI YAGAMI, MD, PhD; and HIDEKI ITO, MD

Department of Cardiac Surgery, Nagoya University Graduate School of Medicine, Nagoya, Japan

ABSTRACT

Thoracic aortic surgery often causes massive bleeding due to coagulopathy. Hypofibrinogenemia is one of the major causative factors, but the utility of the intraoperative administration of fibrinogen concentrate has not yet been proven. The aim of this study was to estimate incidence of hypofibrinogenemia and to evaluate efficacy of using fibrinogen concentrate intraoperatively. The perioperative serum fibrinogen levels (SFL) had routinely been measured in consecutive 216 thoracic aortic surgeries performed from 2010 to 2012. Fibrinogen concentrate was principally used for hypofibrinogenemia (< 150 mg/dl of SFL) at cardiopulmonary bypass (CPB) termination. The patients who received fibrinogen concentrate (FIB group) were compared with the patients who did not received (non Fib group). There were 147 patients (68%) in FIB group at a dose of 5.5±3.5 g. The SFL were dramatically decreased with values of 164±71 mg/dl at CPB termination, compared to the preoperative SFL of 352±131 mg/dl. In the FIB group, the intraoperative and postoperative SFLs were 139±53 and 262±75 (mg/dl), respectively. Thus the SFL was recovered quickly by the administration. 110 cases (51%) showed hypofibrinogenemia at the termination of CPB. The predictors of hypofibrinogenemia were preoperative SFL < 250 mg/dl, emergency surgery and thracoabdominal aortic surgery. Hypofibrinogenemia frequently was observed at the termination of CPB during thoracic aortic surgery. Administering intraoperative fibrinogen concentrate appears to be a useful option to treat coagulopathy.

Key Words: fibrinogen concentrate, coagulopathy, thoracic aortic surgery

INTRODUCTION

The management of massive bleeding due to intraoperative coagulopathy is a major concern during thoracic aortic surgery. The bleeding tendency is associated with numerous factors; however, the consumption of coagulation factors and platelets is one of the main factors. In particular, hypofibrinogenemia is an important factor associated with coagulopathy during thoracic

Received: November 19, 2014; accepted: January 22, 2015

Corresponding Author; Yoshimori Araki

Department of Cardiac Surgery, Nagoya University Graduate School of Medicine, 65 Tsurumai-cho, Showa-ku, Nagoya, Aichi, 466-8650, Japan

Tel: +81 52 744 2375, Fax: +81 52 744 2383, E-mail: yaraki@med.nagoya-u.ac.jpIntroduction

aortic surgery. Fibrinogen concentrate is a useful blood product that can help to improve hypofibrinogenemia when intraoperative coagulopathy occurs. However, it is not yet approved for the treatment of intraoperative hypofibrinogenemia in Japan. The use of fibrinogen concentrate has been limited to only cases of congenital hypofibrinogenemia or other congenital coagulopathy disorders. These clinical limitations of fibrinogen concentrate in Japan are probably the same as in Western countries. Therefore, the use of fibrinogen concentrate to manage intraoperative coagulopathy has not been approved, even during thoracic aortic surgery. In the literature,[1,2] the transfusion of fibrinogen concentrate during cardiac surgery reduced the amount of intraoperative blood transfusion required. The advantage of the administration of fibrinogen products is that they can raise the serum fibrinogen levels (SFL) quickly without volume loading, unlike fresh frozen plasma (FFP) products.

At our institute, fibrinogen concentrate was approved to treat intraoperative coagulopathy due to hypofibrinogenemia by our institutional ethics committee, not only for thoracic aortic surgery, but also all other highly invasive surgeries. We have routinely measured the SFL during cardiac and thoracic aortic surgery and have aggressively used fibrinogen concentrate intraoperatively when patients showed hypofibrinogenemia. There are no definite guidelines regarding when to administer fibrinogen concentrate during thoracic aortic surgery at our institute, however, fibrinogen concentrates are principally used for patients who show the SFL under 150 mg/dl and/or patients who show a massive bleeding tendency, regardless of the values of SFL.

In this study, we measured the changes in the SFL during thoracic aortic surgery and clarified the incidence and predictors of hypofibrinogenemia. We also evaluated the clinical efficacy of fibrinogen concentrate for the management of hypofibrinogenemia during thoracic aortic surgery.

PATIENTS AND METHODS

This retrospective survey was performed on consecutive patients surgically treated for diseases of the thoracic aorta at our institution from 2010 to 2012. Excluding stent grafting therapy (TEVAR; Thoracic Endovascular Aortic Repair), hybrid therapy without cardiopulmonary bypass and wrapping of the ascending aorta, there were 216 thoracic aortic surgeries performed between January 2010 and December 2012. The patient characteristics are shown in Table 1. The mean age of the patients was 64.0±12.7 years. There were 25 patients who underwent emergency surgery and 33 patients who underwent urgent operations. The details of the surgical procedures were as follows: 23 patients underwent root reconstruction, 59 ascending aortic replacement, 92 arch replacement, 22 descending aortic replacement and 19 patients underwent thoracoabdominal surgery. The other surgeries included descending aorta tailoring in one case, anti-anatomical arch reconstruction in one and descending aorta formation in one case.

Hypothermia, which may be related to coagulopathy,[3,4] has been applied for brain protection. Selective cerebral perfusion is mainly used for total aortic arch replacement under moderate hypothermia around 25°C. Retrograde cerebral perfusion is routinely used for hemiarch replacement in patients with acute aortic dissection under deep hypothermia around 20°C. When aortic cross-clamping could be applied, the root surgery or proximal ascending aorta replacement required no intentional hypothermia. Descending and/or thoracoabdominal replacement was mainly performed with partial bypass under mild hypothermia.

Informed consent for the intraoperative use of fibrinogen concentrate was obtained from all patients undergoing thoracic aortic surgery before the operation. The retrospective review of the medical records for this study was also approved by the institutional ethics committee. The administration of fibrinogen concentrate was decided by discussions between surgeons and

Table 1 The Patient Characteristics

Patient number	216
Age (years)	64 ±12.7
Male gender	146 (67.6%)
DM	26 (12.0%)
Hypertension	156 (72.2%)
Hyperlipidemia	64 (29.6%)
CKD	22 (10.1%)
HD	7 (3.2%)
COPD	8 (3.7%)
Current smoking	131 (60.6%)
Surgery	
Elective	158
Urgent	33
Emergency	25
Surgical extent	
Root	23
(Root + Asc + Arch)	(5)
(Root + Asc)	(4)
Asc	59
(Asc + Arch)	(4)
Arch	92
Desc	22
Desc + Thoracoabdominal	6
Thoracoabdominal	13
Hypothermia	163
No BTF	14
Fibrinogen concentrate	147 (68.1%)
Platelet products	168 (77.8%)
Intraoperative RBC (U)	14.2±12.7
Intraoperative FFP (U)	20.5±17.0
Intraoperative PC (U)	25.4±12.4

Asc Ascending Aorta, Desc Descending Aorta, BTF Blood Transfusion
Values are expressed as *n* (%), mean ±SD

anesthetists, based on the SFL and/or aspects of the bleeding tendency. Fibrinogen concentrates are principally administrated for patients who show hypofibrinogenemia (< 150 mg/dl) or patients who show a serious bleeding tendency, regardless of the values of the SFL. There were 147 patients (68%) who received fibrinogen concentrates, with an average dose of 5.6±3.5 g (FIB group), and the other 69 patients underwent surgery without fibrinogen products (non-FIB group).

The average usage of the red blood cells (RBC), FFP and platelet concentrate (PC) were 18±13, 25±18 and 25±14 (U) in the FIB group, which were significantly higher than those of 6±7, 10±8 and 8±10 (U), respectively, in the non-FIB group.

A quick blood test was routinely performed about 20 minutes before the termination of cardiopulmonary bypass. It included the hemoglobin (Hb) level, platelet (PLT) counts, prothrombin time (PT), activated partial thromboplastin time (aPTT) and fibrinogen levels. Furthermore, additional measurements were performed during the operation according to the visual aspect of surgical bleeding or the formation of clots, and were routinely done upon the admission to the intensive care unit.

The SFL was measured by the Clauss method[5] at our institute. The results of the quick blood test were promptly reported within 30 minutes. The administration of blood products, including fibrinogen concentrate, was considered before reversing the heparin with protamine sulfate.

In this study, the incidence and predictors of hypofibrinogenemia were also studied. For this purpose, the patients were divided into three groups according to their SFLs at the termination of CPB as follows: patients with SFLs < 100 mg/dl were defined as group 100, those with levels of 101–150 mg/dl were group 150 and those with levels of 151–200 was group 200. The intraoperative use of blood products was also compared among the groups.

All data were expressed as the means ± standard deviation. Differences between two groups were analyzed by means of a t-test. Comparisons between groups were done using the Chi square test or Fisher's exact test. Correlations among data were analyzed by determining Pearson's coefficients. A factor analysis was done by performing a univariate logistic regression analysis. A p value < 0.05 was considered to be statistically significant. These statistical analyses were performed with the SPSS version 22 software program.

RESULTS

1. Serum fibrinogen levels (SFL)

The serum fibrinogen levels (SFL) were dramatically decreased to half of the preoperative value (352±131 mg/dl to 164±71 mg/dl) at the termination of CPB, and recovered gradually up to 265±68 mg/dl at ICU admission. More than half (110 cases, 51%) of the patients showed hypofibrinogenemia (< 150 mg/dl) at the termination of CPB, including 28 cases (13%) who showed values < 100 mg/dl, and the lowest value noted was 25 mg/dl.

The SFL dropped more dramatically at CPB termination and had recovered almost fully by ICU admission in the FIB group (333±121, 139±53 and 262±75 mg/dl), while the non-FIB group showed a decrease by nearly half at CPB termination, but slight recovery at ICU admission (402±120, 228±81 and 286±98 mg/dl) (Fig. 1). The SFL at the termination of CPB were significantly lower in the FIB group ($p>0.05$) than those in the non-FIB group, while there were no significant differences between the preoperative values and values at ICU admission between the groups. Two-thirds (69%) of the FIB group showed hypofibrinogenemia under 150 mg/dl at the termination of CPB, whereas the majority of the non-FIB group (81.4%) showed the SFL over 150 mg/dl.

The SFL at the termination of CPB showed a strong correlation with the preoperative values ($r=0.64$); however, they showed a moderate negative correlation with the CPB time ($r=–0.25$) and no correlation with the lowest nasopharyngeal temperature ($r=0.09$). Preoperative values under 250 mg/dl resulted in hypofibrinogenemia under 150 mg/dl at the termination of CPB in 40 of the 42 cases (95%), however, 18 of the 26 cases (69%) with perfusion lasting more than six hours, and 41 of 68 cases (69%) with hypothermia less than 24°C showed hypofibrinogenemia

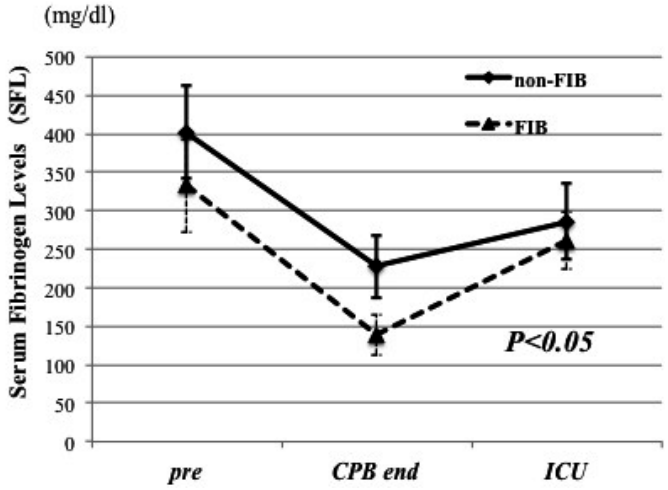

Fig. 1 The perioperative serum fibrinogen levels in the FIB group and non-FIB group

under 150 mg/dl at CPB termination. The predictors of hypofibrinogenemia under 150 mg/dl at the termination of CPB were preoperative SFL less than 250 mg/dl, emergency surgery and thoracoabdominal aortic replacement, as identified by a univariate logistic regression analysis, while acute aortic dissection or aortic rupture were not significant predictors.

2. Usage of blood products

Based on the SFL at the termination of CPB, there were 28 cases in group 100, 71 cases in group 150 and 32 cases in group 200 in the FIB group. The average SFL at CPB termination of group 100, group 150 and group 200 were 72±22, 127±15 and 173±15 mg/dl, respectively.

Fibrinogen concentrate was administered to recover the SFL with a dose of 9.5±4.5 g in group 100, 4.8±2.5 g in group 150 and 4.4±2.5 g in group 200. However, the SFL recovered to 226±79, 258±67 and 271±66 mg/dl, respectively, in these groups. Group 100 showed lower SFL at ICU admission despite the use of more fibrinogen concentrate (Fig. 2).

The intraoperative use of RBC, FFP and PC were 28±16, 36±24 and 33±16 U in group 100, 16±12, 22±16 and 25±14 U in group 150 and 14±9, 22±12 and 21±11 U in group 200, respectively. Group 100 required significantly larger amount of blood products, however, there were no significant differences between group 150 and group 200 in terms of the amount of blood products administered (Fig. 3).

There were no cases categorized as belonging to group 100, 11 cases in group 150 and 22 cases in group 200 in the non-FIB group. The SFL in group 150 and group 200 were 131±15 and 179±12 mg/dl at CPB termination, and recovered to 177±34 and 254±71 mg/dl at ICU admission, respectively.

The intraoperative use of RBC, FFP and PC were 6±8, 10±10 and 7±8 U in group 150 and 5±6, 10±8 and 9±11 U in group 200, respectively. There were no significant differences between the two groups in terms of the amount of blood products used (Fig. 3).

3. Surgical results and clinical safety

Among the 25 emergency surgeries, the fibrinogen concentrate was used in 18 cases (72%). In thoracoabdominal aortic surgeries, fibrinogen concentrate was used in but one case (17 patients,

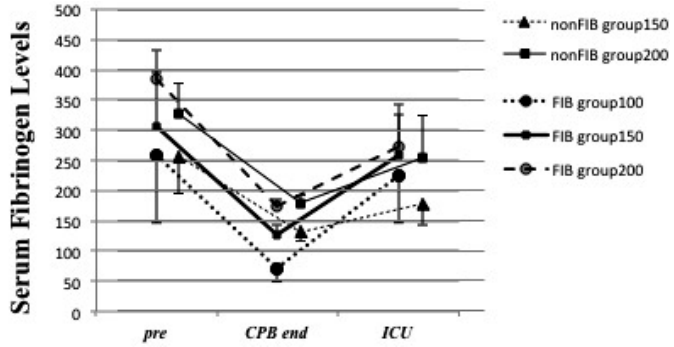

Fig. 2 The perioperative changes in the serum fibrinogen levels between the FIB group and the non-FIB group. The FIB group included three subgroups divided by the minimum fibrinogen values after CPB termination, and the non FIB group included two subgroups.

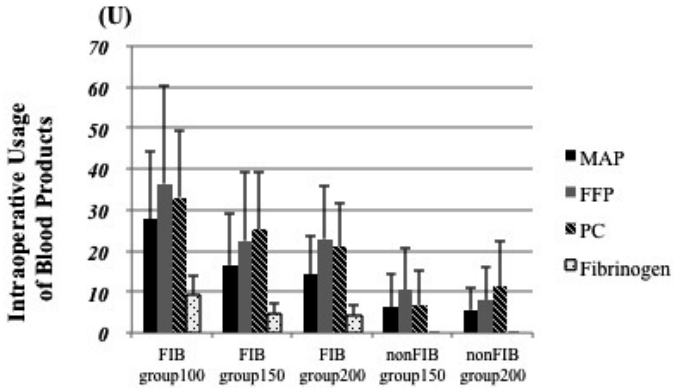

Fig. 3 The intraoperative use of blood products in the FIB group and the non-FIB group. The patients in Group 100 of the FIB group required a large amount of blood products. RBC: Red Blood Cells, FFP: Fresh Frozen Products, PC: Platelet Concentrate.

94%). The rate of fibrinogen concentrate use was higher in patients who required a long CPB time (> 6 hours; 92.0%) and patients who were exposed to hypothermia less than 24□ (75.3%). Fibrinogen concentrate was generally used in complex and long surgeries.

There were 14 cases (10%) that required re-exploration for bleeding in the FIB group and two such cases (3%) in the non-FIB group. Stroke was a complicating condition in 12 cases (8%) in the FIB group and seven cases (10%) in the non-FIB group. Hemodialysis was required in nine cases (6%) in the FIB group and one case (1%) in the non-FIB group. Postoperative atrial fibrillation was observed in 40 cases (27%) in the FIB group and 12 cases (17%) in the non-FIB group. There were no significant differences between the groups in each of these factors.

There were five cases of 30-day mortality (2.3%). There were four deaths (2.7%) in the FIB group and one death (1.4%) in the non-FIB group. There were also no significant differences between the groups in terms of the 30-day mortality rate. The causes of death were sepsis in three patients, ischemic colitis due to malperfusion in one and MRSA pneumonia in one. There were no deaths related to massive bleeding. There were also no serious allergic complications associated with fibrinogen concentrate.

DISCUSSION

The management of coagulation disorders has still been a major concern in thoracic aortic surgery. Most thoracic aortic surgeries, such as aortic arch surgery, require hypothermia for brain protection, which is associated with a long CPB time and may cause dysfunction of the platelets and coagulation system. Surgery for the thoracoabdominal aorta is performed via a large spiral incision, which makes a large and invasive surgical field, and creates a large foreign body surface for blood. The long cardiopulmonary bypass, hypothermia and large invasive surgical fields are all associated with the consumption of coagulation factors and dysfunction of the coagulation system, and may lead to intraoperative coagulopathy. Therefore, maintaining coagulation is mandatory to ensure that a safe surgery can be performed and to reduce the amount of blood transfusion required during thoracic aortic surgery.

The causes of coagulopathy during thoracic aortic surgery are numerous ; [6] however, hypofibrinogenemia is one of the major factors leading to coagulopathy. The present study demonstrated that more than half of the enrolled cases showed hypofibrinogenemia (< 150 mg/dl SFL) at CPB termination. Of note, 13% of all cases showed severe hypofibrinogenemia under 100 mg/dl, which generally causes critical coagulopathy.

Many studies have reported the perioperative fibrinogen levels during cardiac surgery[7-9] and have indicated that lower postoperative fibrinogen levels were associated with more extensive intraoperative blood loss. However, there have been few studies that have reported the intraoperative fibrinogen levels during surgery, especially during aortic surgery.[10,11] In these points, the present study contributes new information.

The administration of fibrinogen concentrate appears to be an optimal way to treat hypofibrinogenemia; however, the intraoperative use of fibrinogen concentrate for hypofibrinogenemia has not yet been approved in most countries. Therefore, FFP is a realistic alternative for fibrinogen products. To improve the coagulation under hypofibrinogenemia, however, a large volume of FFP transfusion would be necessary; furthermore, it takes a longer time for a full recovery of the SFL to be reached after the administration of FFP. Therefore, fibrinogen concentrate is the best way to increase the SFL promptly, and without volume loading. A quick recovery of the coagulation system should result in better surgical hemostasis and reduce the total amount of blood transfusion required. It may thus result in a reduction of the total medical expenses.

The criteria for when to administer fibrinogen products for intraoperative coagulopathy have not been determined. Based on the guidelines for blood transfusion proposed by the Ministry of Health, Labour and Welfare of Japan, the use of FFP is recommended for hypofibrinogenemia less than 100 mg/dl due to DIC or after a large amount of blood transfusion. In the present study, patients who showed hypofibrinogenemia with a value < 100 mg/dl required a significantly larger amount of fibrinogen products and blood transfusion than did the patients with higher levels. Hypofibrinogenemia under 100 mg/dl must be considered a critical coagulopathy, and should be treated with fibrinogen concentrate to achieve surgical hemostasis.

However, there are still no criteria for the administration of fibrinogen concentrate even at our institution. In fact, surgeons and anesthesiologists discussed the use of fibrinogen products not only based on the serum fibrinogen level, but also the blood clot formation in the surgical field. We generally administer fibrinogen concentrate for hypofibrinogenemia less than 150 mg/dl at the termination of CPB as a temporary criterion. Because the SFL at the termination of CPB are not the lowest value and they generally decreased during surgical hemostasis, it may be necessary to identify different cut-off values or to measure the levels at another time point. There were no significant differences in the total amount of blood products used between patients who showed fibrinogen values of 101–150 mg/dl and 151–200 mg/dl. This may indicate that

fibrinogen concentrate achieved sufficient hemostasis and reduced the use of blood products even in patients with SFL of 101–150 mg/dl. Hypofibrinogenemia less than 150 mg/dl may be a useful value as a cut-off criterion for when to administer fibrinogen concentrate.

The next concern is how much fibrinogen concentrate is required to achieve sufficient surgical hemostasis. The average SFL at ICU admission were 250 mg/dl, which may be the optimal target value for sufficient surgical hemostasis, because a sufficient SFL is necessary upon the neutralization of heparin. When the SFL are restored effectively and promptly at this point, the subsequent coagulation failure could be avoided. However, in cases without sufficient hemostasis, the surgical bleeding is prolonged, and the consumption of coagulation factors continues. This leads to a gradual decrease in the SFL, and leads to a vicious cycle of coagulopathy. Therefore, sufficient SFLs are mandatory before protamine injection, especially after complex and difficult surgeries. A dose of one gram of fibrinogen concentrate theoretically will increase the SFL by 20 mg/dl in a 65 kg patient with 5L of intravascular blood volume. When patients show a SFL of 150 mg/dl at CPB termination, 5 g of fibrinogen concentrate is therefore theoretically required to achieve the target SFL of 250 mg/dl.

The guidelines for blood transfusion also recommend that blood examinations, including fibrinogen, PT and APTT, are mandatory before the use of FFP. We have a quick measurement system to examine the coagulation in our laboratory, and can obtain a prompt response within 30 minutes even at night. We propose that such a quick measurement of the coagulation is mandatory for deciding whether to administer fibrinogen concentrate. The information obtained by this quick measurement of the coagulation is important for the surgical team to understand the patients' coagulation condition. A lack of factors such as fibrinogen or platelets should be noted and remedied before the neutralization of heparin and during surgical hemostasis. When the bleeding tendency is predicted to continue in the surgical field, additional measurements should be performed. Surgeons must understand the mechanisms underlying coagulopathy in order to achieve sufficient surgical hemostasis.

As noted above, fibrinogen concentrate has not been approved for hypofibrinogenemia during surgery in Japan. This situation is similar in many Western countries. Fibrinogen concentrate will be approved in the near future for intraoperative coagulopathy. Prior to this, the safety of the intraoperative use of fibrinogen concentrate should be confirmed. The present study was a retrospective observational study; however, there were observed no complications related to the fibrinogen concentrate. In addition, there is no evidence that fibrinogen concentrate increased the risk of major complications or mortality.

In conclusion, hypofibrinogenemia frequently was observed at the termination of CPB during thoracic aortic surgery. Hypofibrinogenemia is one of the major factors associated with intraoperative coagulopathy. Quick measurement of the coagulation status is mandatory for deciding whether to administer fibrinogen concentrate, and should provide important information to understand the patients' coagulation condition as well. Hypofibrinogenemia of < 150 mg/dl SFL may be a useful criterion to decide whether to administer fibrinogen concentrate. The intraoperative administration of fibrinogen concentrate appears to be an optimal strategy to increase the SFLs effectively and promptly. It can treat coagulopathy and reduce the need for a large blood transfusion, and can help to avoid massive bleeding during thoracic aortic surgery.

DISCLOSURE

All the authors have declared no competing interest.

REFERENCES

1) Tanaka KA, Egan K, Szlam F, Ogawa S, Roback JD, Sreeram G, Guyton RA, Chen EP. Transfusion and hematologic variables after fibrinogen or platelet transfusion in valve replacement surgery: preliminary data of purified lyophilized human fibrinogen concentrate versus conventional transfusion. *Transfusion*, 2014; 54: 109–118.
2) Karlsson M, Ternstrom L, Hyllner M, Baghaei F, Flinck A, Skrtic S, Jeppsson A. Prophylactic fibrinogen infusion reduces bleeding after coronary artery bypass surgery. A prospective randomised pilot study. *Thromb Haemost*, 2009; 102: 137–144.
3) Ellis PR, Jr., Kleinsasser LJ, Speer RJ. Changes in coagulation occurring in dogs during hypothermia and cardiac surgery. *Surgery*, 1957; 41: 198–210.
4) Dirkmann D, Hanke AA, Gorlinger K, Peters J. Hypothermia and acidosis synergistically impair coagulation in human whole blood. *Anesth Analg*, 2008; 106: 1627–1632.
5) Clauss A. [Rapid physiological coagulation method in determination of fibrinogen]. *Acta Haematol*, 1957; 17: 237–246.
6) Williams JB, Phillips-Bute B, Bhattacharya SD, Shah AA, Andersen ND, Altintas B, Lima B, Smith PK, Hughes GC, Welsby IJ. Predictors of massive transfusion with thoracic aortic procedures involving deep hypothermic circulatory arrest. *J Thorac Cardiovasc Surg*, 2011; 141: 1283–1288.
7) Bilecen S, Peelen LM, Kalkman CJ, Spanjersberg AJ, Moons KG, Nierich AP. Fibrinogen concentrate therapy in complex cardiac surgery. *J Cardiothorac Vasc Anesth*, 2013; 27: 12–17.
8) Gielen C, Dekkers O, Stijnen T, Schoones J, Brand A, Klautz R, Eikenboom J. The effects of pre- and postoperative fibrinogen levels on blood loss after cardiac surgery: a systematic review and meta-analysis. *Interact Cardiovasc Thorac Surg*, 2014; 18: 292–298.
9) Walden K, Jeppsson A, Nasic S, Backlund E, Karlsson M. Low preoperative fibrinogen plasma concentration is associated with excessive bleeding after cardiac operations. *Ann Thorac Surg*, 2014; 97: 1199–1206.
10) Rahe-Meyer N, Hanke A, Schmidt DS, Hagl C, Pichlmaier M. Fibrinogen concentrate reduces intraoperative bleeding when used as first-line hemostatic therapy during major aortic replacement surgery: results from a randomized, placebo-controlled trial. *J Thorac Cardiovasc Surg*, 2013; 145: S178–185.
11) Rahe-Meyer N, Solomon C, Winterhalter M, Piepenbrock S, Tanaka K, Haverich A, Pichlmaier M. Thromboelastometry-guided administration of fibrinogen concentrate for the treatment of excessive intraoperative bleeding in thoracoabdominal aortic aneurysm surgery. *J Thorac Cardiovasc Surg*, 2009; 138: 694–702.

15. Azria D, Ozsahin M, Kramar A et al. Single nucleotide polymorphisms, apoptosis, and the development of severe late adverse effects after radiotherapy. Clin Cancer Res 2008; 14: 6284–6288.
16. Allen PB, Greenfield AT, Svenningsson P et al. Phactrs 1–4: a family of protein phosphatase 1 and actin regulatory proteins. Proc Natl Acad Sci USA 2004; 101: 7187–7192.
17. Sagara J, Higuchi T, Hattori Y et al. Scapinin, a putative protein phosphatase-1 regulatory subunit associated with the nuclear nonchromatin structure. J Biol Chem 2003; 278: 45611–45619.
18. Guo CY, Brautigan DL, Larner JM. Ionizing radiation activates nuclear protein phosphatase-1 by ATM-dependent dephosphorylation. J Biol Chem 2002; 277: 41756–41761.
19. Bollen M, Peti W, Ragusa MJ, Beullens M. The extended PP1 toolkit: designed to create specificity. Trends Biochem Sci 2010; 35: 450–458.
20. Edvardsen H, Landmark-Hoyvik H, Reinertsen KV et al. SNP in TXNRD2 associated with radiation-induced fibrosis: a study of genetic variation in reactive oxygen species metabolism and signaling. Int J Radiat Oncol Biol Phys 2013; 86: 791–799.

Annals of Oncology 27: 480–487, 2016
doi:10.1093/annonc/mdv611
Published online 23 December 2015

Changes in tumor expression of HER2 and hormone receptors status after neoadjuvant chemotherapy in 21 755 patients from the Japanese breast cancer registry

N. Niikura[1]*, A. Tomotaki[2], H. Miyata[2], T. Iwamoto[3], M. Kawai[4], K. Anan[5], N. Hayashi[6], K. Aogi[7],T. Ishida[8], H. Masuoka[9], K. Iijima[10], S. Masuda[11], K. Tsugawa[12], T. Kinoshita[13], S. Nakamura[14] & Y. Tokuda[1]

[1]Department of Breast and Endocrine Surgery, Tokai University School of Medicine, Isehara; [2]Department of Healthcare Quality Assessment, Graduate School of Medicine, The University of Tokyo, Tokyo; [3]Department of Breast and Endocrine Surgery, Okayama University Hospital, Okayama; [4]Department of Breast Surgery, Miyagi Cancer Center, Natori; [5]Department of Surgery, Kitakyushu Municipal Medical Center, Kitakyushu; [6]Department of Breast Surgery, St Luke's International Hospital, Tokyo; [7]Department of Breast Surgery, Shikoku Cancer Center, Matsuyama; [8]Department of Surgical Oncology, Graduate School of Medicine, Tohoku University, Sendai; [9]Sapporo-kotoni Breast Clinic, Sapporo; [10]Department of Breast Oncology, Cancer Institute Hospital, Tokyo; [11]Department of Pathology, Nihon University School of Medicine, Tokyo; [12]Division of Breast and Endocrine Surgery, Department of Surgery, St Marianna University School of Medicine, Kawasaki; [13]Department of Breast Surgery, National Cancer Center Hospital, Tokyo; [14]Division of Breast Surgical Oncology, Department of Surgery, Showa University School of Medicine, Tokyo, Japan

Received 21 August 2015; revised 28 October 2015; accepted 28 November 2015

Background: We investigate rates of pathologic complete response (pCR) and tumor expression of ER, PgR, HER2 discordance after neoadjuvant chemotherapy using Japanese breast cancer registry data.

Patients and methods: Records of more than 300 000 breast cancer cases treated at 800 hospitals from 2004 to 2013 were retrieved from the breast cancer registry. After data cleanup, we included 21 755 patients who received neoadjuvant chemotherapy and had no distant metastases. pCR was defined as no invasive tumor in the breast detected during surgery after neoadjuvant chemotherapy. HER2 overexpression was determined immunohistochemically and/or using fluorescence *in situ* hybridization.

Results: pCR was achieved in 5.7% of luminal tumors ($n = 8730$), 24.6% of HER2-positive tumors ($n = 4403$), and 18.9% of triple-negative tumors ($n = 3660$). Among HER2-positive tumors, pCR was achieved in 31.6% of ER-negative tumors ($n = 2252$), 17.0% of ER-positive ones ($n = 2132$), 31.4% of patients who received trastuzumab as neoadjuvant chemotherapy ($n = 2437$), and 16.2% of patients who did not receive trastuzumab ($n = 1966$). Of the 2811 patients who were HER2-positive before treatment, 601 (21.4%) had HER2-negative tumors after neoadjuvant chemotherapy, whereas 340 (3.4%) of the 9947 patients with HER2-negative tumors before treatment had HER2-positive tumors afterward. Of the 10 973 patients with ER-positive tumors before treatment, 499 (4.6%) had ER-negative tumors after neoadjuvant chemotherapy, whereas 519 (9.3%) of the 5607 patients who were ER-negative before treatment had ER-positive tumors afterward.

Correspondence to: Dr Naoki Niikura, Department of Breast and Endocrine Surgery, Tokai University School of Medicine, 143 Shimokasuya, Isehara, Kanagawa 259-1193, Japan. Tel: +81-463-93-1121; Fax: +81-463-95-6491; E-mail: niikura@is.icc.u-tokai.ac.jp

Conclusion: We confirmed that loss of HER2-positive status can occur after neoadjuvant treatment in patients with primary HER2-positive breast cancer. We also confirmed that in practice, differences in pCR rates between breast cancer subtypes are the same as in clinical trials. Our data strongly support the need for retest ER, PgR, HER2 of surgical sample after neoadjuvant therapy in order to accurately determine appropriate use of targeted therapy.

Key words: breast cancer, chemotherapy, HER2, *in situ* hybridization, neoadjuvant therapy

introduction

In breast cancer patients, neoadjuvant chemotherapy (i.e. presurgical systemic chemotherapy) is associated with rates of disease-free survival and overall survival comparable with those for adjuvant (post-surgical) chemotherapy [1]. It is standard in locally advanced and operable breast cancer, being intended to shrink the tumor and improve the chance for breast-conserving surgery [2]. Pathologic complete response (pCR) is the best predictor of patient outcome after neoadjuvant chemotherapy [2–4]; it is generally defined as the absence of residual invasive cancer in the breast [5]. Clinical trials have found that different breast cancer subtypes have different rates of pCR and that patients who show pCR have a different prognosis in each subtype. However, in an attempt to improve pCR, clinical trial investigators may use more frequent or standard doses of chemotherapeutic agents than would be used in a routine clinical setting.

The *HER2/neu* gene is amplified in 10%–20% of primary breast cancer cases. In HER2-positive patients, HER2-targeting therapies such as neoadjuvant trastuzumab result in better rates of pCR than non-HER2-targeting therapies [6, 7], as might be expected, HER2-positive patients who show pCR have a better prognosis than those who do not. In the latter, HER2 status may be discordant between the primary breast tumor and those remaining after chemotherapy [8–12]. Some studies suggest that trastuzumab in particular can convert disease status from HER2-positive in a primary tumor to HER2-negative in residual tumors [13–15]. Mittendorf et al. found that according to fluorescence *in situ* hybridization (FISH) analysis, approximately one-third of their patients with sufficient residual disease to warrant repeat HER2 testing had lost *HER2* gene amplification. Furthermore, patients who have lost *HER2* gene amplification have significantly lower relapse-free survival than those whose tumors retain *HER2* gene amplification [15]. Patients with such HER2 status discordance between primary tumors and residual or metastatic ones may also have shorter survival than those without [15, 16]. However, the prevalence of such discordance in patients who have undergone neoadjuvant chemotherapy has not been conclusively established, and it is unclear if trastuzumab increases its likelihood; if so, the treatment may not be suitable for such patients. Using data from the Japanese national breast cancer registry, we aimed to investigate pCR and discordance rates after neoadjuvant chemotherapy in relation to positivity for estrogen receptor (ER), progesterone receptor (PgR), and HER2.

materials and methods

data collection

The Breast Cancer Registry (BCR) in Japan's National Clinical Database (NCD) contains records on more than 300 000 cases of breast cancer from more than 800 hospitals. Affiliated institutes voluntarily provide the BCR with data on newly diagnosed primary breast cancer patients through a Web-based system, covering more than 50 demographic and clinicopathological categories. TNM classification is registered according to the 6th edition of the Unio Internationalis Contra Cancrum (UICC) staging system [17].

The BCR was originally maintained by the Registration Committee of the Japanese Breast Cancer Society (JBCS) and supported by the Public Health Research Foundation (Tokyo). Until 2012, annual reports on this registry were published in Japanese and made accessible to active JBCS members through the JBCS homepage (http://www.jbcs.gr.jp/Member/tourokusyukei.html). Since 2012, this dataset has been part of the NCD, a nationwide project managed in cooperation with the certification board of the Japan Surgical Society [18]. For the year 2011 alone, data from more than 1.2 million surgical cases were collected from more than 3500 hospitals. The NCD is continuously updated by the data management departments of participating institutions and is evaluated annually using a Web-based data management system to ensure data traceability. All variables, definitions, and inclusion criteria for the NCD are accessible to participating institutions on its web site (http://www.ncd.or.jp); the database administrators also provide e-learning systems to teach participants how to input data consistently [18]. The administrators answer all inquiries regarding data entry, having taken ~80 000 inquiries in 2011, and a list of frequently asked questions is displayed on the web site.

For our study, we used the BCR to review 238 840 breast cancer cases treated between 2004 and 2011 and selected 21 755 patients who received neoadjuvant chemotherapy and had no distant metastases (Figure 1). Male patients, those with bilateral tumors, those who did not undergo surgery, and those with tumor stages of Tis or T0, were excluded. pCR was defined as no invasive tumor in the breast found during surgery after neoadjuvant chemotherapy. HER2 overexpression was defined as immunohistochemically 3+ and/or a positive FISH result. Hormone receptor positivity (ER or PgR positivity) was diagnosed if at least 1% of nuclei in the tumor were stained on immunohistochemical tests for ER or PgR. Immunohistochemical tests for ER, PgR, and HER on core biopsies were carried out before neoadjuvant therapy. Cases were categorized on the basis of their immunohistochemical status as follows: luminal (ER+ and HER2−); HER2-overexpressing (HER2+, regardless of ER status); and triple-negative (ER− and HER2−).

statistical analysis

The median and standard deviations were calculated for age at diagnosis. Associations between clinical categorical variables and HER2 status were analyzed using Pearson's χ^2. Fisher's exact test was also used to determine differences between patients who showed HER2 status discordance and those who did not. All analyses were carried out using SAS 9.3 (SAS Institute, Cary, NC).

results

A total of 21 755 patients who received neoadjuvant chemotherapy and developed no distant metastases were listed in Table 1. More than 80% of patients had a tumor of stage T2 or worse, and more than 60% were node-positive. Almost 70% received anthracyclines and taxanes as neoadjuvant chemotherapy.

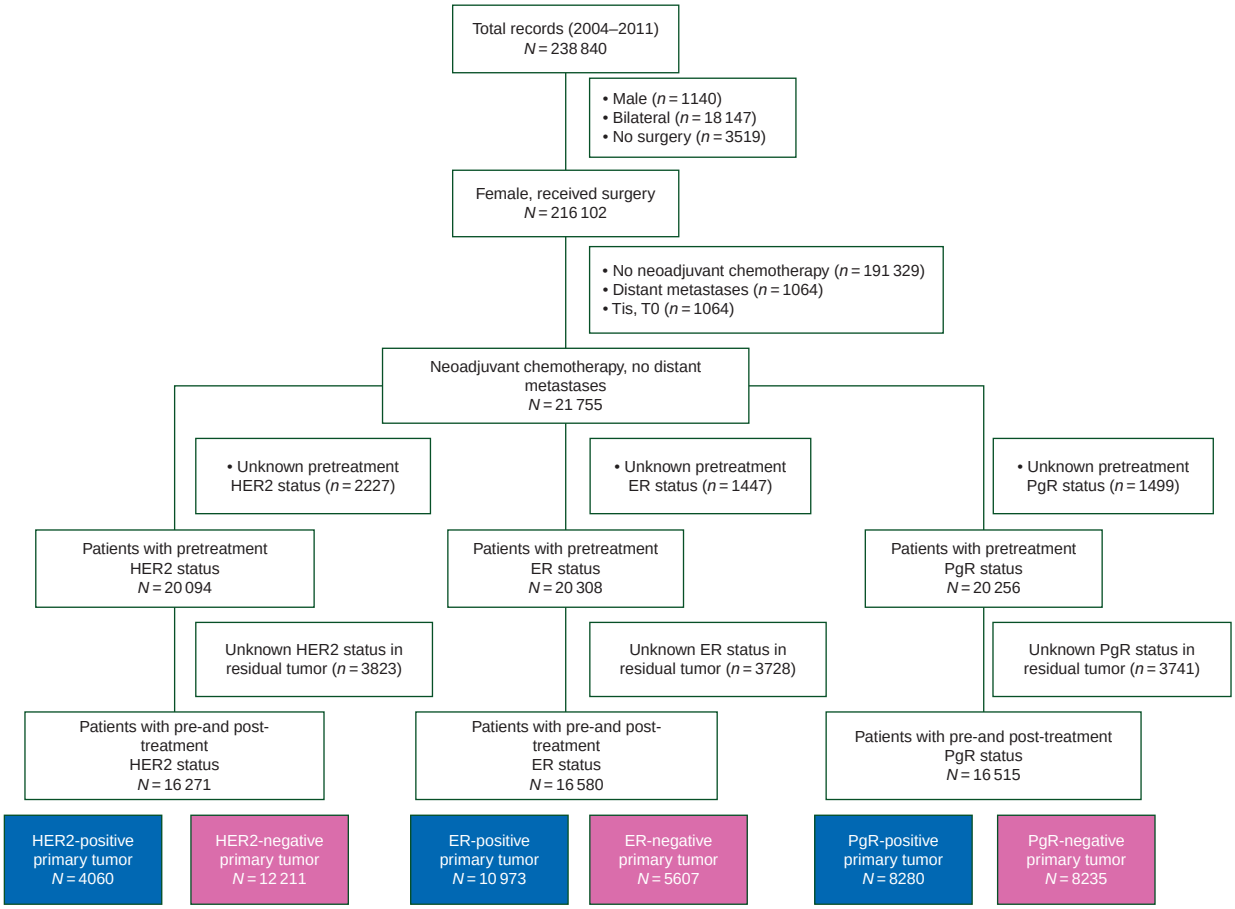

Figure 1. Study flow.

rate of pCR

The rate of pCR was 5.7% for luminal cancer ($n = 8730$), 24.6% for HER2-positive ($n = 4403$), and 18.9% for triple-negative ($n = 3660$) (Figure 2). Thus, HER2-overexpressing tumors had a higher rate of pCR than triple-negative or luminal ones; however, within this category, the rate was 31.6% for ER-negative tumors ($n = 2252$), 17.0% for ER-positive ones ($n = 2132$), 31.4% for those who received trastuzumab as neoadjuvant chemotherapy ($n = 2437$), and 16.2% for those who did not receive trastuzumab ($n = 1966$) (Figure 2). In addition, HER2-positive patients who were ER-negative had a higher rate of pCR than those who were ER-positive ($P < 0.0001$), and those treated with trastuzumab had a higher rate of pCR than those not so treated ($P < 0.0001$).

rate of discordance after chemotherapy

Of the 2811 patients who were HER2-positive before treatment, 601 (21.4%) had tumors that showed HER2 negativity after neoadjuvant chemotherapy, whereas only 340 (3.4%) of the 9947 patients with HER2-negative pretreatment tumors developed HER2-positive tumors after neoadjuvant chemotherapy (Table 2). According to immunohistochemical testing, 499 (20.4%) of the 2447 patients with HER2-positive tumors lost HER2 positivity after neoadjuvant chemotherapy; with FISH, the rate was 8.4% (17/203). Of 342 patients whose tumors converted from HER2-positive to HER2-negative, who received neoadjuvant trastuzumab, 96 (28%) did not receive adjuvant trastuzumab therapy. Conversely, of 340 patients whose tumors converted from HER2-negative to HER2-positive, 206 (60%) received adjuvant trastuzumab therapy.

Of the 10 973 patients with ER-positive tumors before treatment, 499 (4.6%) had ER-negative tumors after neoadjuvant chemotherapy, whereas 519 (9.3%) of the 5607 patients with ER-negative tumors before treatment had ER-positive ones after neoadjuvant chemotherapy. Of the 499 patients whose tumors converted from ER-positive to ER-negative, 280 (56%) did not receive adjuvant endocrine therapy. Conversely, of 519 patients whose tumors converted from ER-negative to ER-positive, 333 (64%) received adjuvant endocrine therapy.

Of the 8280 patients with PgR-positive tumors before treatment, 1545 (18.7%) had PgR-negative ones after neoadjuvant chemotherapy, whereas 766 (9.3%) of the 8235 patients with PgR-negative tumors before treatment had PgR-positive tumors after neoadjuvant chemotherapy (Table 3).

clinicopathologic features associated with discordance

We evaluated HER2 concordance and discordance rates in relation to various clinical factors (Table 4). There were statistically significant differences in HER2 discordance rates between patients

Table 1. Patients Characteristic

		With pretreatment HER2 status (n = 20 094)				With pretreatment ER status (n = 20 308)				With pretreatment PgR status (n = 20 256)			
		Positive (n = 5535)		Negative (n = 14 559)		Positive (n = 12 938)		Negative (n = 7370)		Positive (n = 9720)		Negative (n = 10 536)	
		n	%	n	%	n	%	n	%	n	%	n	%
Age	Median		54		51		51		55		49		55
Menopausal status													
	Premenopausal	2079	37.6	6928	47.6	6429	49.7	2679	36.4	5302	54.6	3779	35.9
	Post-menopausal	3289	59.4	7260	49.9	6183	47.8	4468	60.6	4152	42.7	6472	61.4
	Unknown	167	3.0	371	2.6	326	2.5	223	3.0	266	2.7	285	2.7
T stage													
	T1	587	10.6	1772	12.2	1578	12.2	804	10.9	1222	12.6	1157	11.0
	T2	3197	57.8	8288	56.9	7472	57.8	4112	55.8	5673	58.4	5876	55.8
	T3	893	16.1	2071	14.2	1837	14.2	1173	15.9	1346	13.9	1660	15.8
	T4	858	15.5	2428	16.7	2051	15.9	1281	17.4	1479	15.2	1843	17.5
N stage													
	N0	1725	31.2	4793	32.9	4304	33.3	2288	31.0	3353	34.5	3217	30.5
	N1	2807	50.7	7513	51.6	6805	52.6	3631	49.3	5116	52.6	5296	50.3
	N2	582	10.5	1356	9.3	1100	8.5	849	11.5	779	8.0	1169	11.1
	N3	411	7.4	859	5.9	699	5.4	583	7.9	452	4.7	825	7.8
	Unknown	10	0.2	38	0.3	30	0.2	19	0.3	20	0.2	29	0.3
Neoadjuvant chemotherapy													
	CMF alone	2	0.0	12	0.1	9	0.1	5	0.1	7	0.1	7	0.1
	Anthracycline regimen alone	547	9.9	1765	12.1	1502	11.6	851	11.6	1106	11.4	1235	11.7
	TC alone	81	1.5	265	1.8	265	2.1	82	1.1	219	2.3	127	1.2
	Taxane alone	532	9.6	586	4.0	634	4.9	510	6.9	464	4.8	681	6.5
	Anthracycline regimen and taxane	3891	70.3	10 191	70.0	9118	70.5	5097	69.2	6856	70.5	7316	69.4
	Others	482	8.71	1740	11.95	1410	10.90	825	11.19	1068	10.99	1170	11.10

doi:10.1093/annonc/mdv611 | 483

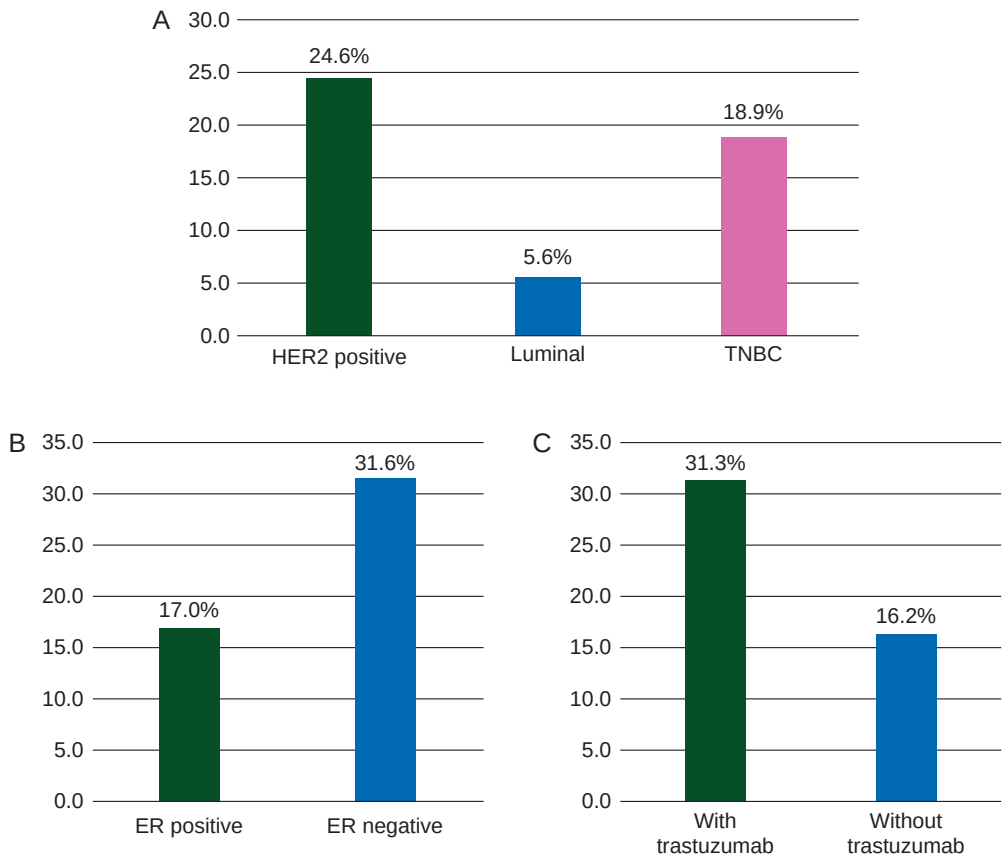

Figure 2. Rates of pathologic complete in response by (A) subtype (HER2-positive, luminal, triple-negative), (B) ER status (for HER2-positive tumors), and (C) treatment with trastuzumab as neoadjuvant therapy (HER2-positive tumors).

Table 2. Change in HER2 status of the primary tumor after neoadjuvant therapy

Primary tumor		Residual tumor	
HER2 status	n	HER2 status	n
Positive	2811	Positive	2210 (78.6%)
		Negative	601 (21.4%)
Negative	9947	Positive	340 (3.4%)
		Negative	9607 (96.6%)
Immunohistochemical analysis			
HER2 3+	2447	HER2 3+	1948 (79.6%)
		HER2 2+	203 (8.3%)
		HER2 1+	163 (6.6%)
		HER2 0	133 (5.4%)
HER2 2+	2077	HER2 3+	128 (6.2%)
		HER2 0, 1+, 2+	1949 (93.8%)
HER2 1+	3741	HER2 3+	68 (1.8%)
		HER2 0, 1+, 2+	3673 (98.2%)
HER2 0	4196	HER2 3+	45 (1.1%)
		HER2 0, 1+, 2+	4151 (98.9%)
FISH analysis			
Positive	203	Positive	186 (91.6%)
		Negative	17 (8.4%)
Negative	572	Positive	28 (4.9%)
		Negative	544 (95.1%)

who received trastuzumab and those who did not ($P < 0.0001$). Of the 1385 patients who received trastuzumab as neoadjuvant therapy, 342 (24.7%) showed HER2 discordance. Similarly, of the 1426 patients who did not receive trastuzumab as neoadjuvant therapy, 259 (18.2%) showed HER2 discordance. Furthermore, there were statistically significant differences in discordance rates in relation to pretreatment ER status ($P < 0.0001$) and PgR status ($P < 0.0001$). In contrast, there were no statistically significant differences in HER2 discordance rates between premenopausal and menopausal women ($P = 0.440$) or among patients with residual tumors of different volumes ($P = 0.345$).

discussion

To the best of our knowledge, we use largest dataset to compare tumor expression of ER, PgR, HER2 discordance after neoadjuvant chemotherapy. Our pCR rates, obtained in a setting of clinical practice, were lower than those reported in clinical trials. One reason may be that in our study, almost 70% of patients were treated with anthracyclines and taxanes, whereas in clinical trials with a focus on pCR, investigators often test new agents and higher doses, patients in the real world have higher age, and poor performance status than in clinical trials. Another may be that 44% of HER-positive patients did not receive trastuzumab as neoadjuvant therapy; it was not until 2008 that trastuzumab was approved as an adjuvant therapy by the Ministry of Health, Labour and Welfare in Japan. However, differences in pCR rates in our study with regard to cancer subtype and trastuzumab treatment were similar to those reported in clinical trials. For

instance, patients with luminal tumors had lower pCR rates than those with HER2-positive or triple-negative tumors. Among HER2-positive tumors, tumors negative for hormonal receptors had higher pCR rates after neoadjuvant chemotherapy than those positive for hormonal receptors. HER2-positive, tumors that are negative for hormonal receptors are highly dependent on the *HER2* gene and respond well to therapies targeted against HER2 such as trastuzumab and pertuzumab [19]. As might be expected, HER2-positive, ER-negative patients who show pCR have better prognosis than those who do not [3, 4]. A previous study found that the use of trastuzumab as a neoadjuvant increased pCR rate (43% with trastuzumab, 26% without) in HER2-positive cancer [6]. Our data also showed this.

Table 3. Change in ER and PgR status of the primary tumor after neoadjuvant therapy

Primary tumor		Residual tumor	
ER status	*n*	ER status	*n*
Positive	10 973	Positive	10 474 (95.5%)
		Negative	499 (4.5%)
Negative	5607	Positive	519 (9.3%)
		Negative	5088 (90.7%)
PgR status			
Positive	8280	Positive	6735 (81.3%)
		Negative	1545 (18.7%)
Negative	8235	Positive	766 (9.3%)
		Negative	7469 (90.7%)

Our results also showed that HER2 status does not necessarily carry over between the original tumor and residual tumors. In 21.4% of HER2-positive patients, the tumor converted to HER2-negative; further, according to immunohistochemistry, 635 (17.9%) of the 3548 patients with HER2-positive tumors before neoadjuvant chemotherapy had HER2-negative tumors afterward. However, inconsistencies in immunohistochemical testing, for example, in antigen retrieval methods, fixation, and observer analysis, may affect the results [20]. Another study [14, 15] using FISH found a loss of HER2 amplification in paired pre- and post-treatment specimens from patients treated with neoadjuvant trastuzumab. FISH data are more easily reproducible than immunohistochemical data [21, 22], and in our study, although the sample size for FISH analysis was small, FISH data were less likely to show discordance than immunohistochemical data.

We previously reported that trastuzumab therapy is not associated with an increased chance of loss of HER2 positivity in metastases, whereas chemotherapy is associated with an increase in the loss of such positivity [16]. Likewise, in a previous study of patients with residual disease treated with either chemotherapy alone or chemotherapy plus an anti-HER2 agent, HER2 expression loss was observed in 40% of the former group and 14.7% of the latter group [23]. We demonstrated that trastuzumab therapy is associated with increased odds of loss of HER2 positivity in residual tumors.

Nevertheless, it is unclear whether loss of HER2 amplification reflects response to therapy or a resistance mechanism and

Table 4. Discordance rates by clinical factors

	Post-treatment HER2 status ($N = 2811$)				*P*-value
	Negative (discordance)		Positive (concordance)		
	n	%	*n*	%	Pearson's χ^2
Pretreatment ER status					
Negative	169	13.0	1130	87.0	<0.0001
Positive	427	28.4	1075	71.6	
Pretreatment PgR status					
Negative	263	14.9	1501	85.1	<0.0001
Positive	330	32.0	701	68.0	
Menopausal status					
Pre	245	22.5	846	77.5	0.4626
Post	337	20.6	1301	79.4	
Unknown	19	23.2	63	76.8	
Neoadjuvant trastuzumab					
No	259	18.2	1167	81.8	<0.0001
Yes	342	24.7	1043	75.3	
Volume of residual tumor					
<50%	265	22.3	923	77.7	0.3436
>50%	313	20.8	1192	79.2	
Year of registration					
2004–2007	159	18.95	680	81.05	0.0405
2008–2011	442	22.41	1530	77.59	
Surgical cases at institution					
>100 cases/year	277	19.74	1126	80.26	0.0346
<100 cases/year	324	23.01	1084	76.99	

Volume of residual tumor: size of residual tumor divided by size of primary tumor.

whether chemotherapy can promote clonal selection of *HER2/neu*-amplified cancers. In our study, 28% of patients whose cancer lost HER2 expression after neoadjuvant therapy did not receive trastuzumab, and 60% patients whose cancer developed HER2 expression after therapy did receive it. Possible explanations include true biological change, treatment-induced clonal selection, pre-analytical and analytical pitfalls, sampling errors, and tumor heterogeneity [24]. It is unclear if patients with HER2-negative tumors after neoadjuvant chemotherapy should receive anti-HER2 treatment, as sampling by core needle biopsy in pretreatment settings may not be representative of the character of the whole tumor. If the core needle biopsy proves to be a false positive, discontinuing the drug will avoid risking unnecessary treatment after loss of HER2 amplification after neoadjuvant therapy. However, if the core needle biopsy gives a false-negative result, anti-HER2 treatment should be started as soon as post-therapy HER2 amplification is detected.

We acknowledge several important limitations of this study. First, this study is retrospective, incurring the possibility of selection bias and precluding the determination of causal relationships. However, Japanese BCR data cover more than 50% of patients diagnosed with breast cancer in Japan [25], and therefore, we do not feel that this possibility would have substantially affected our findings. Secondly, our data were obtained through a web database, with no centralized reassessment of ER, PgR or HER2 status. Thirdly, several studies reported discordance ER, PgR, HER2 status between core needle biopsy, and resection specimens without neoadjuvant chemotherapy [26]. Finally, our registry data did not include sufficient survival data to fully analyze the effects of pCR and tumor expression discordance on survival. However, the strength of our study is that it draws from more than 20 000 patients treated with neoadjuvant chemotherapy in a 'real-world' setting.

In conclusion, our findings demonstrate that although pCR rates in the real world have the same differences with regard to subtypes and trastuzumab treatment that are seen in clinical trials, they are also lower than those in clinical trials. Further, we have shown that HER2 status does not always carry over from the original tumor to residual tumors. In our study, more than 20% of patients with residual tumors after neoadjuvant therapy showed loss of HER2 expression. Our data strongly support the need for retest ER, PgR, HER2 of surgical sample after neoadjuvant therapy in order to accurately determine appropriate use of targeted therapy. Additional research should be conducted on biology and treatment in breast cancer patients whose tumors lose HER2 expression after neoadjuvant chemotherapy.

acknowledgments

We would like to thank Editage (www.editage.jp) for English language editing.

funding

This research was supported in part by MEXT KAKENHI grant number 26870597 (2014–2015) JSPS KAKENHI grant numbers 15H04796 and Tokai University School of Medicine Research Aid (2013–2015).

disclosure

The authors have declared no conflicts of interest.

references

1. Mauri D, Pavlidis N, Ioannidis JP. Neoadjuvant versus adjuvant systemic treatment in breast cancer: a meta-analysis. J Natl Cancer Inst 2005; 97: 188–194.
2. Bonadonna G, Valagussa P, Brambilla C, Ferrari L. Preoperative chemotherapy in operable breast cancer. Lancet 1993; 341: 1485.
3. Cortazar P, Zhang L, Untch M et al. Pathological complete response and long-term clinical benefit in breast cancer: the CTNeoBC pooled analysis. Lancet 2014; 384: 164–172.
4. von Minckwitz G, Untch M, Blohmer JU et al. Definition and impact of pathologic complete response on prognosis after neoadjuvant chemotherapy in various intrinsic breast cancer subtypes. J Clin Oncol 2012; 30: 1796–1804.
5. Berruti A, Brizzi MP, Generali D et al. Presurgical systemic treatment of nonmetastatic breast cancer: facts and open questions. Oncologist 2008; 13: 1137–1148.
6. Gianni L, Eiermann W, Semiglazov V et al. Neoadjuvant chemotherapy with trastuzumab followed by adjuvant trastuzumab versus neoadjuvant chemotherapy alone, in patients with HER2-positive locally advanced breast cancer (the NOAH trial): a randomised controlled superiority trial with a parallel HER2-negative cohort. Lancet 2010; 375: 377–384.
7. Buzdar AU, Ibrahim NK, Francis D et al. Significantly higher pathologic complete remission rate after neoadjuvant therapy with trastuzumab, paclitaxel, and epirubicin chemotherapy: results of a randomized trial in human epidermal growth factor receptor 2-positive operable breast cancer. J Clin Oncol 2005; 23: 3676–3685.
8. Simon R, Nocito A, Hubscher T et al. Patterns of her-2/neu amplification and overexpression in primary and metastatic breast cancer. J Natl Cancer Inst 2001; 93: 1141–1146.
9. Gancberg D, Di Leo A, Cardoso F et al. Comparison of HER-2 status between primary breast cancer and corresponding distant metastatic sites. Ann Oncol 2002; 13: 1036–1043.
10. Simmons C, Miller N, Geddie W et al. Does confirmatory tumor biopsy alter the management of breast cancer patients with distant metastases? Ann Oncol 2009; 20: 1499–1504.
11. Thompson AM, Jordan LB, Quinlan P et al. Prospective comparison of switches in biomarker status between primary and recurrent breast cancer: the Breast Recurrence in Tissues Study (BRITS). Breast Cancer Res 2010; 12: R92.
12. Lower EE, Glass E, Blau R, Harman S. HER-2/neu expression in primary and metastatic breast cancer. Breast Cancer Res Treat 2008; 113: 301–306.
13. Burstein HJ, Harris LN, Gelman R et al. Preoperative therapy with trastuzumab and paclitaxel followed by sequential adjuvant doxorubicin/cyclophosphamide for HER2 overexpressing stage II or III breast cancer: a pilot study. J Clin Oncol 2003; 21: 46–53.
14. Hurley J, Doliny P, Reis I et al. Docetaxel, cisplatin, and trastuzumab as primary systemic therapy for human epidermal growth factor receptor 2-positive locally advanced breast cancer. J Clin Oncol 2006; 24: 1831–1838.
15. Mittendorf EA, Wu Y, Scaltriti M et al. Loss of HER2 amplification following trastuzumab-based neoadjuvant systemic therapy and survival outcomes. Clin Cancer Res 2009; 15: 7381–7388.
16. Niikura N, Liu J, Hayashi N et al. Loss of human epidermal growth factor receptor 2 (HER2) expression in metastatic sites of HER2-overexpressing primary breast tumors. J Clin Oncol 2012; 30: 593–599.
17. Fl G. TNM Classification of Malignant Tumours. 6th ed. New York: Wiley 2002; 131–141.
18. Miyata H, Gotoh M, Hashimoto H et al. Challenges and prospects of a clinical database linked to the board certification system. Surg Today 2014; 44: 1991–1999.
19. Nagayama A, Hayashida T, Jinno H et al. Comparative effectiveness of neoadjuvant therapy for HER2-positive breast cancer: a network meta-analysis. J Natl Cancer Inst 2014; 106.

20. Sauter G, Lee J, Bartlett JMS et al. Guidelines for human epidermal growth factor receptor 2 testing: biologic and methodologic considerations. J Clin Oncol 2009; 27: 1323–1333.
21. Press MF, Sauter G, Bernstein L et al. Diagnostic evaluation of HER-2 as a molecular target: an assessment of accuracy and reproducibility of laboratory testing in large, prospective, randomized clinical trials. Clin Cancer Res 2005; 11: 6598–6607.
22. Paik S, Bryant J, Tan-Chiu E et al. Real-world performance of HER2 testing—national surgical adjuvant breast and bowel project experience. J Natl Cancer Inst 2002; 94: 852–854.
23. Guarneri V, Dieci MV, Barbieri E et al. Loss of HER2 positivity and prognosis after neoadjuvant therapy in HER2-positive breast cancer patients. Ann Oncol 2013; 24: 2990–2994.
24. Pusztai L, Viale G, Kelly CM, Hudis CA. Estrogen and HER-2 receptor discordance between primary breast cancer and metastasis. Oncologist 2010; 15: 1164–1168.
25. Kurebayashi J, Miyoshi Y, Ishikawa T et al. Clinicopathological characteristics of breast cancer and trends in the management of breast cancer patients in Japan: based on the Breast Cancer Registry of the Japanese Breast Cancer Society between 2004 and 2011. Breast Cancer 2015; 22: 235–244.
26. Dekker TJ, Smit VT, Hooijer GK et al. Reliability of core needle biopsy for determining ER and HER2 status in breast cancer. Ann Oncol 2013; 24: 931–937.

Annals of Oncology 27: 487–493, 2016
doi:10.1093/annonc/mdv608
Published online 17 December 2015

Prospective phase II trial of trabectedin in BRCA-mutated and/or BRCAness phenotype recurrent ovarian cancer patients: the MITO 15 trial

D. Lorusso[1*], G. Scambia[2], S. Pignata[3], R. Sorio[4], G. Amadio[2], S. Lepori[1], A. Mosconi[5], C. Pisano[3], G. Mangili[6], G. Maltese[1], R. Sabbatini[7], G. Artioli[8], T. Gamucci[9], M. Di Napoli[3], E. Capoluongo[10], V. Ludovini[11], F. Raspagliesi[1] & G. Ferrandina[2]

[1]Gynecologic Oncology Unit, Fondazione IRCCS National Cancer Institute, Milan; [2]Department of Obstetrics and Gynecology, Catholic University of Rome; [3]Department of Gynecologic and Urologic Oncology, Fondazione Pascale, National Cancer Institute of Naples; [4]Department of Oncology, CRO Aviano, Aviano; [5]Medical Oncology Unit, University Hospital S. Maria della Misericordia, Perugia; [6]Department of Obstetrics and Gynecology, San Raffaele Hospital, Milan; [7]Department of Oncology Haematology and Respiratory Disease, AOU Policlinico di Modena, Modena; [8]Medical Oncology Unit, Hospital of Mirano, Mirano; [9]Medical Oncology Unit, Hospital 'SS. Trinità', Sora; [10]Department of Molecular Biology, Catholic University of Rome; [11]Molecular Biology Unit, University Hospital S. Maria della Misericordia, Perugia, Italy

Received 5 August 2015; revised 7 December 2015; accepted 9 December 2015

Background: Current evidence suggest that trabectedin is particularly effective in cells lacking functional homologous recombination repair mechanisms. A prospective phase II trial was designed to evaluate the activity of trabectedin in the treatment of recurrent ovarian cancer patients presenting BRCA mutation and/or BRCAness phenotype.

Patients and methods: A total of 100 patients with recurrent *BRCA*-mutated ovarian cancer and/or BRCAness phenotype (≥2 previous responses to platinum) were treated with trabectedin 1.3 mg/mq i.v. q 3 weeks. The activity of the drug with respect to BRCA mutational status and to a series of polymorphisms [single-nucleotide polymorphisms (SNPs)] involved in DNA gene repair was analyzed.

Results: Ninety-four were evaluable for response; in the whole population, 4 complete and 33 partial responses were registered for an overall response rate (ORR) of 39.4. In the platinum-resistant (PR) and -sensitive (PS) population, an ORR of 31.2% and 47.8%, and an overall clinical benefit of 54.2% and 73.9%, respectively, were registered. In the whole series, the median progression-free survival (PFS) was 18 weeks and the median overall survival (OS) was 72 weeks; PS patients showed a more favorable PFS and OS compared with PR patients. BRCA gene mutational status was available in 69 patients. There was no difference in ORR, PFS and OS according to BRCA 1–2 status nor any association between SNPs of genes involved in DNA repair and NER machinery and response to trabectedin was reported.

Conclusions: Our data prospectively confirmed that the signature of 'repeated platinum sensitivity' identifies patients highly responsive to trabectedin. In this setting, the activity of trabectedin seems comparable to what could be obtained using platinum compounds and the drug may represent a valuable alternative option in patients who present

*Correspondence to: Dr Domenica Lorusso, Gynecologic Oncology Unit, Fondazione IRCCS National Cancer Institute of Milan, Via Venezian 1, 20133 Milan, Italy. Tel: +39-0223903697; E-mail: domenica.lorusso@istitutotumori.mi.it

4、婦人科系腫瘍の維持機構を標的とした癌免疫療法の開発

分担研究者　産婦人科学　　三上幹男
分子生命科学　亀谷美恵
分子生命科学　椎名隆
再生医療科学　中村雅登
研究協力者　分子生命科学　大島志乃・小島美香・木南理仁・
大野裕介
産婦人科学　　後藤優美子・柏木寛史

【研究の背景と目的】

我々のグループは胎盤と癌との類似性に着目し、がん幹細胞ニッシェが胎盤形成・維持機構を模倣すると仮定してヒト胎盤と癌の比較解析を行うとともに、妊娠免疫と腫瘍免疫がニッシェ形成にどのように関わるのかを明らかにする為に免疫系の比較解析も行った。また、この研究に必須の in vivo 霊長類モデルとしてコモンマーモセットが使用できるのかについての評価も行った。その結果、以下の知見を得た。

（1）　マーモセット免疫系解析ツールの開発を行い、基本的な免疫系の解析を行った(Fujii et al. 2013, Kitaura et al. 2012, Kametani et al. 2012)。種々のサイトカインおよび TCR の発現を定量的に測定できる事を可能とし、マーモセット CD117+細胞が機能的なマスト細胞に分化する事を報告した。さらに、これらの細胞が T 細胞にも分化すること、ヒトと異なり、B 細胞分化は先行しないことを明らかにした(Shimada et al. 2015)。また、IL-2Rg 遺伝子をゲノム編集によりノックアウトしたマーモセットのリンパ球を解析し、ヒトと異なり、IL-2Rg を KO しても T 細胞が分化することを明らかにした(Sato et al. 2016)。

（2）　担癌状態で亢進する調節性 T 細胞に発現する HLA-G のマーモセットオーソログ遺伝子構造を明らかにした(Kono et al. 2014)。また、ブタ MHC(SLA)については、遺伝子上の3種類の class-I 遺伝子が活性化とともに連動して発現亢進する事が明らかになった(Kametani et al.2012)。さらに SLA のアロタイプ特異的なモノクローナル抗体を作製し、遺伝子座特異的な mRNA 発現とタンパク質発現の間に相違があることを明らかにした(Kametani et al. 2016)。

（3）　神経栄養因子受容体であり、卵胞の生育にも重要な役割を果たす癌遺伝子 TrkB アイソフォームの発現が、明細胞腺癌で異なる事を明らかにした(Goto et al. 2014)。また、この遺伝子の発現をヒトおよびマーモセット胎盤で確認し、そのアイソフォームの発現が、胎盤局所において変化することについても明らかにした。これらの結果は、ヒト・マ

ーモセットのいずれの動物種でも観察され、マーモセットがこの現象に関しては動物モデルとなりうることが示唆された（**ISPGRS・2016 で発表・優秀賞を受賞、日本生殖免疫学会にて発表・学会賞ノミネート、マイクロナノ研究会・ポスター賞受賞**）。

さらに、胎盤および癌の免疫学的ニッシェの同定に必要なマーモセットNK 細胞の性状を明らかにした(Watanabe et al. 2014,)。

（4） マーモセットおよびヒトの妊娠初期・中期・後期の末梢血より血漿を採取し、これらの血漿成分の LC/MS 解析を行った。その結果、ヒトでは妊娠中期に血漿中で亢進するPZP が、マーモセットでは亢進しないこと、代わりに、同じ arpha-2-macrogulobulin (A2M)ファミリーである arpha-2-macroblobulin-like 1 (A2ML1)が亢進することが明らかとなった。一方、ヒトでは末梢血中の A2ML1 は発現が確認できなかった(上右図)。また、ヒト・およびマーモセット胎盤組織には、両者の mRNA が発現していた（**柏木（東海大学医学部大学院生）：ISPGRS で発表・最優秀賞を受賞**）

【考察】

以上の結果、本研究において、マーモセットは免疫学的には異なる部分も多いが、浸潤性などの胎盤の性状については類似しており、ヒトを模倣できることが示された。特に、ヒトではPZPが妊娠関連タンパク質として妊娠中期に血清中濃度が上昇するが、マーモセットでも同一ファミリー分子であるA2ML1が上昇することから、このようなプロテアーゼインヒビターが、妊娠免疫で重要な役割を果たすことが示唆された。

Possible role of thymidine phosphorylase in gynecological tumors as an individualized treatment strategy

MASAKO SHIDA[1], MASANORI YASUDA[2], MARIKO FUJITA[1], MASAKI MIYAZAWA[1], HIROSHI KAJIWARA[3], TAKESHI HIRASAWA[1], MASAE IKEDA[1], NARUAKI MATSUI[4], TOSHINARI MURAMATSU[5] and MIKIO MIKAMI[1]

[1]Department of Obstetrics and Gynecology, Tokai University School of Medicine, Isehara, Kanagawa 259-1193;
[2]Department of Pathology, Saitama Medical University International Medical Center, Hidaka, Saitama 350-1298;
[3]Department of Pathology, Tokai University School of Medicine, Isehara, Kanagawa 259-1193;
[4]Department of Pathology, Tokai University Oiso Hospital, Oiso, Kanagawa 259-0198;
[5]Department of Obstetrics and Gynecology, Tokai University Hachioji Hospital, Hachioji, Tokyo 192-0032, Japan

Received March 13, 2015; Accepted April 1, 2016

DOI: 10.3892/ol.2016.5082

Abstract. Thymidine phosphorylase (TP) is structurally similar to platelet-derived endothelial cell growth factor, and it activates 5-fluorouracil (5-FU) prodrugs and also promotes angiogenesis. In the present study, the possibility of using TP expression as a biomarker for 5-FU prodrugs, and the significance of TP as an angiogenic factor, were investigated in patients with gynecological tumors. The subjects enrolled in the study were 188 patients with gynecological tumors who provided informed consent and underwent tumor resection at the Department of Obstetrics and Gynecology of Tokai University Hospital between February 2002 and January 2010. Measurement of the enzymatic activity of TP and dihydropyrimidine dehydrogenase (DPD) was performed by enzyme-linked immunosorbent assay. In addition, immunohistochemistry (IHC) analysis of microvessels by monochrome imaging, western blotting and reverse transcription-polymerase chain reaction were performed. The mean TP activity and the TP/DPD ratio were increased in squamous cell carcinoma of the cervix (306.9 and 2.2 U/mg protein, respectively) and adenosquamous carcinoma (317.6 and 1.4 U/mg protein, respectively) compared with benign tumors and other malignancies, including endometrial (uterine) carcinoma, ovarian serous adenocarcinoma and ovarian mucinous adenocarcinoma. However, these parameters were also elevated in other histological types of cancer such as clear cell adenocarcinoma of the ovary (115.2 and 2.1 U/mg protein, respectively), in which the microvessel area was the largest of all the histological types analyzed. Since high TP expression and a high TP/DPD ratio were identified in other tumors besides cervical cancer, it is possible that patients for whom 5-FU prodrugs are indicated could be selected appropriately if their TP activity is determined and their TP expression is analyzed by IHC prior to initiation of the treatment.

Correspondence to: Professor Masanori Yasuda, Department of Pathology, Saitama Medical University International Medical Center, 1397-1 Yamane, Hidaka, Saitama 350-1298, Japan
E-mail: mmikami0603@gmail.com

Key words: gynecological tumor, thymidine phosphorylase, dihydropyrimidine dehydrogenase, 5-FU prodrug

Introduction

Pyrimidine nucleoside phosphorylase is the collective name for enzymes involved in the metabolism of pyrimidine nucleosides, which convert thymidine to thymine and participate in the biosynthesis of pyrimidine nucleosides, angiogenesis and activation of anti-neoplastic drugs (1). There are two thymidine phosphorylases: Uridine phosphorylase (UP), which belongs to the family of glycosyltransferases, specifically the pentosyltransferases; and thymidine phosphorylase (TP), which belongs to the family of glycosyltransferases, specifically the pentosyltransferases (2). UP has uridine and thymidine as its substrates, and is abundant in mice and rats (2), while TP only has thymidine as its substrate, and is abundant in humans (2). TP is involved in the synthesis of nucleic acids, and its activity is increased in cancer cells due to the additional nucleic acid synthesis required for active cell proliferation (2). TP has a similar structure to that of the angiogenic factor platelet-derived endothelial cell growth factor (PD-ECGF), and promotes vascular endothelial migration (3).

Another tumor-associated action of TP that has attracted attention is the activation of 5-fluorouracil (5-FU) prodrugs (2). 5-FU was first synthesized by Dushinsky *et al* (4) in 1957, and its efficacy as an anti-cancer agent was subsequently established by the fundamental and clinical studies of Heidelberger *et al* (5). Since then, its use has been approved for a variety of tumors, including breast and gastrointestinal cancers (6-10). Once incorporated into cells by nucleotide transporters, 5-FU is largely degraded and inactivated by dihydropyrimidine dehydrogenase (DPD), prior to be excreted in the urine as α-fluoro-β-alanine, while unchanged 5-FU is phosphorylated and activated via the same pyrimidine metabolic pathway that processes uracil (11). The anti-neoplastic effect of 5-FU generally depends on the following mechanism:

When 5-FU is metabolized to fluorodeoxyuridine monophosphate (FdUMP) by TP, it forms a strong ternary complex with thymidylate synthetase and 5,10-methylenetetrahydrofolate (a reduced folic acid coenzyme), thus inhibiting the conversion of dUMP to thymidine 5'-monophosphate and interfering with DNA synthesis (11). 5-FU also causes RNA dysfunction when it is incorporated into intracellular RNA by orotate phosphoribosyltransferase (11). Development of 5-FU prodrugs with various mechanisms of action has enabled the availability of a number of drugs, including doxifluridine, capecitabine, uracil plus tegafur (UFT) and titanium silicate-1 (Fig. 1). These prodrugs are designed to reduce adverse reactions to 5-FU or to exhibit enhanced activity against tumors with elevated TP expression, since these agents display an anti-tumor effect upon being converted to 5-FU by TP in tumor cells (12).

TP is an important enzyme that activates 5-FU. However, there are a limited number of studies on TP expression in gynecological cancer, with the exception of cervical cancer, for which 5-FU prodrugs have already been approved (12), and no studies have been performed to date to compare TP expression among all gynecological tumors. In the present study, the expression of TP was analyzed in various types of gynecological cancer, and the expression of TP in these tumors was compared with the tumor characteristics to explore the possibility of individualized treatment.

Materials and methods

Patients and tissue specimens. A total of 188 patients who underwent surgery for gynecological tumors at the Department of Obstetrics and Gynecology of Tokai University Hospital (Isehara, Kanagawa, Japan) between February 2002 and January 2010 were enrolled in the present study (Table I). At the time of surgery for the benign tumors, samples that were considered normal tissues, including myometrium, endometrium and ovary in 33 patients, were resected. The samples were confirmed to be free from gynecological neoplasm and pathologically diagnosed as normal tissue. The Institutional Review Board (IRB) for Clinical Research of Tokai University School of Medicine (Isehara, Kanagawa, Japan) approved the present study (IRB no. 09R-082). Written informed consent was obtained from all patients for the use of the resected specimens at the time of enrollment. The present study was performed in accordance with the Declaration of Helsinki. Clinicopathological staging was performed according to the International Federation of Gynecology and Obstetrics classification (13).

Enzyme-linked immunosorbent assay (ELISA) for TP and DPD activity. TP and DPD activities were measured by a sandwich ELISA using a Protein Detector ELISA kit (KPL, Inc., Gaithersburg, MD, USA), according to the manufacturer's protocol. A 96-well plate was incubated for 1 h at room temperature (RT) with 10 µg/ml monoclonal mouse anti-TP (catalog no., 1C6-203; Roche Diagnostics GmbH, Mannheim, Germany) and 10 µg/ml monoclonal mouse anti-DPD antibodies (Nippon Roche Research Center, Kamakura, Kanagawa, Japan). Then, the plasmatic compartment was added to each well and incubated with the antibodies for 1 h. Upon washing the plate with PBS containing 0.05% Tween-20 (Wako Pure Chemical Industries, Ltd., Osaka, Osaka, Japan), incubation was conducted with anti-TP and anti-DPD antibodies overnight at 4˚C. Next, peroxidase-linked species-specific $F(ab')_2$ fragments of anti-rabbit immunoglobulin (Ig)G (dilution, 1:10,000; catalog number NA9340; GE Healthcare Life Sciences, Chalfont, UK) were added to each well for 1 h. Subsequently, a reaction was conducted at RT for 15 min with substrate solution containing 3,3',5,5'-tetramethylbenzidine and H_2O_2 (TMB Microwell Peroxidase Substrate system; KPL), and the absorbance at 450 nm was measured using a microplate reader (3550; Bio-Rad Laboratories, Inc., Hercules, CA, USA).

Immunohistochemistry (IHC). The expression of TP and cluster of differentiation (CD)34 in gynecological tumors was determined by IHC analysis and hematoxylin (Merck, Ltd., Tokyo, Japan) and eosin (Muto Pure Chemicals, Co., Ltd, Tokyo, Japan) staining in all 188 patients. Tumor sections were deparaffinized in xylene (3 times for 5 min each) and ethanol (4 times for 5 min each) and heated in 0.01 M citrate buffer (pH 6.0; Dako, Glostrup, Denmark) for 13 min in a microwave oven at 99˚C. Then, endogenous peroxidase was blocked by incubation in methanol (Wako Pure Chemical Industries, Ltd.) containing 0.3% H_2O_2 (Wako Pure Chemical Industries, Ltd.) for 30 min at RT. Next, the sections were washed in 0.01 M phosphate-buffered saline (PBS; Wako Pure Chemical Industries, Ltd.) for 10 min, prior to be incubated overnight at 4˚C with anti-TP (dilution, 1:400) and monoclonal mouse anti-CD34 antibodies (dilution, 1:100; product code, END-L-CE; Novocastra; Leica Microsystems, Ltd., Milton Keynes, UK). Subsequently, the sections were washed in 0.01 M PBS and incubated with goat anti-mouse/rabbit IgG conjugated to a horseradish peroxidase-labeled dextran polymer (EnVision kit; catalog no., K1491; Dako) for 60 min at RT. Upon being washed 20 times in 0.01 M PBS, the sections were developed in a 3'3-diaminobenzidine solution (Dojindo Laboratories, Kamimashiki, Kumamoto, Japan) containing 0.006% H_2O_2 for 3-5 min at RT, and counterstained with hematoxylin. Protein expression was assessed semiquantitatively as negative (0% positive, 0), weak (<10% positive, 1+), intermediate (10-50% positive, 2+) or strong (>50% positive, 3+).

Analysis of microvessels by monochrome imaging. The distribution of microvessels was analyzed by monochrome imaging of sections immunostained with anti-CD34 antibody and mounted on glass slides (Muto Pure Chemicals, Co., Ltd). Tumor stromal microvessels with a longer and shorter diameter of ≤5 mm were counted in five fields (magnification, x200; Axiophot; Carl Zeiss, Oberkochen, Germany) for each patient, and the area occupied by the vessels was measured. Microvessels were only counted in fields without necrosis that were completely filled by tissue.

Western blotting. To confirm the results of TP expression detected by IHC, western blot analysis was performed in four representative tumors of squamous cell carcinoma (SCC) and clear cell adenocarcinoma (CCA) of ovary (OV). Total protein from whole tissue lysates was separated by electrophoresis on NuPAGE Novex 4-12% Bis-Tris Protein Gels (1.0 mm; 12-well; Thermo Fisher Scientific, Inc., Waltham, MA, USA) and transferred to Immobilon-P polyvinylidene

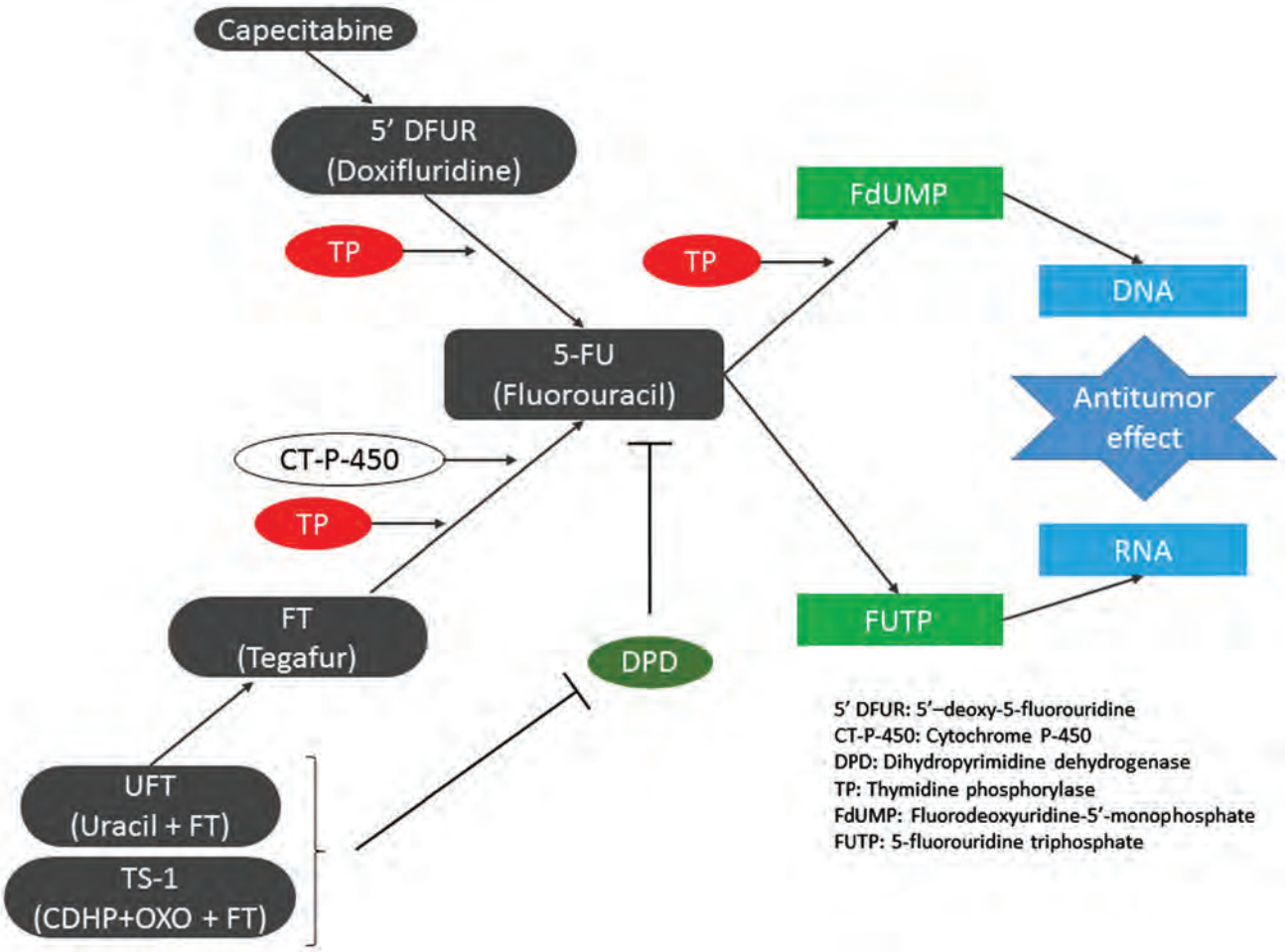

Figure 1. Effects, summary of metabolic pathways and antitumor activity of 5-FU and fluorinated pyrimidines. Capecitabine is absorbed from the gastrointestinal tract, transformed into doxifluridine in the tumor tissue and subsequently transformed into 5-FU by TP to exert an antitumor effect. FT was developed to reduce gastrointestinal toxicity, and is transformed into 5-FU by cytochrome P-450 mainly in the liver and by TP in the tumor tissue, where its concentration remains stable for a long period. Uracil plus FT contains uracil, which has an inhibitory effect on the degradation of 5-FU. TS-1 contains 5-chloro-2,4-dihydroxypyridine, which has a stronger inhibitory effect on dihydropyrimidine dehydrogenase than that of uracil. Oxonate is distributed to the gastrointestinal tract at a high concentration, and reduces gastrointestinal toxicity by inhibiting the phosphorylation of 5-FU. 5-FU is transformed into fluorodeoxyuridine monophosphate in tumor cells, which inactivates TS-1 and inhibits the synthesis of DNA. It also causes dysfunction of RNA through 5-fluorouridine 5'-triphosphate. 5'-DFUR, 5'-deoxy-5-fluorouridine; CT-P-450, cytochrome P-450; DPD, dihydropyrimidine dehydrogenase; TP, thymidine phosphorylase; FdUMP, fluorodeoxyuridine monophosphate; FUTP, 5-fluorouridine 5'-triphosphate; 5-FU, fluorouracil; OXO, oxonate; CDHP, 5-chloro-2,4-dihydroxypyridine; FT, tegafur; UFT, uracil plus tegafur; TS-1, titanium silicate.

difluoride membranes (EMD Millipore, Billerica, MA, USA). The running buffer was 20X NuPAGE MES SDS Running Buffer (Thermo Fisher Scientific, Inc.) and the blotting buffer consisted of Trizma base (Sigma-Aldrich, St. Louis, MO, USA), glycine (Nacalai Tesque, Inc., Kyoto, Kyoto, Japan) and methanol. Precision Plus Protein Standards All Blue (Bio-Rad Laboratories, Inc.) was used as a marker. Membranes were blocked with 5% skim milk (Wako Pure Chemical Industries, Ltd.) in PBS containing 0.5% Tween-20 (PBS-T) at RT for 1 h, followed by overnight incubation at 4˚C with anti-TP antibody diluted 1:500 in PBS-T containing 5% skim milk. Horseradish peroxidase-conjugated anti-mouse/rabbit complexes were visualized with an ECL Plus kit (GE Healthcare Life Sciences). Cultured HeLa whole-cell lysates served as positive control. The HeLa cells were grown and maintained in 75 cm^2 tissue culture flasks in a humidified 5% CO_2 atmosphere at 37˚C. The cells were cultured in Minimum Essential Media (Gibco; Thermo Fisher Scientific, Inc.) supplemented with 10% heat-incubated fetal bovine serum (Gibco; Thermo Fisher Scientific, Inc.), 1% penicillin-streptomycin (10,000 U/ml penicillin; 10,000 µg/ml streptomycin; Gibco; Thermo Fisher Scientific, Inc.).

Reverse transcription-polymerase chain reaction (RT-PCR) analysis. To verify the close association between TP protein and messenger (m)RNA expression in the limited cases of gynecological cancer evaluated in the present study, RT-PCR analysis was performed. TRIzol (500 µl) was used to homogenize the samples. Subsequently, the samples were centrifuged at 20,379 x g and 4˚C for 15 min, and the aqueous layer was transferred to a different tube. After performing DNase treatment with DNAse I (RQ1 RNase-Free DNase; Promega Corporation, Madison, WI, USA) overnight at 37˚C, the quantity of total RNA dissolved in DEPC-DW was measured using an absorbance measuring instrument, and total RNA was calculated as 5 µg. Complementary DNA was prepared from four representative tumors using a Ready-To-Go T-primed First-Strand kit (GE Healthcare Life Sciences). The sequences of the TP primers

Table I. Patient characteristics and TP and DPD activities.

Classification (total cases, n=188)	Histology	Cases, n	TP average, U/mg protein (SD)	DPD average, U/mg protein (SD)	TP/DPD ratio
Uterine cervical tumors (18)	SCC	11	306.9 (106.9)	138.2 (66.6)	2.2
	AA	2	317.6 (183.7)	222.4 (205.3)	1.4
	MUA	2	52.7 (1.2)	17.8 (15.0)	3.0
	SMCC	3	23.1 (8.0)	10.4 (2.6)	2.2
Uterine body tumors (53)	EMA-G1	22	68.6 (30.0)	48.7 (40.0)	1.4
	EMA-G2	5	63.3 (61.6)	42.1 (33.1)	1.5
	EMA-G3	6	63.0 (79.3)	34.6 (20.2)	1.8
	SEA	2	52.4 (19.2)	45.9 (21.9)	1.2
	Adenomyosis	2	26.2 (15.6)	33.1 (10.6)	0.8
	Leiomyoma	14	12.9 (7.7)	48.1 (17.5)	0.3
	Leiomyosarcoma	2	41.1 (21.4)	54.9 (26.9)	0.7
Ovarian tumors (84)	SEA	9	98.6 (65.8)	82.7 (70.2)	1.2
	CCA	16	115.2 (59.3)	54.2 (109.6)	2.1
	MUA	16	54.4 (44.4)	63.3 (47.1)	0.9
	EMA	8	74.8 (47.9)	37.2 (12.8)	2.0
	Serous BT	1	42.2	59.1	0.7
	Mucinous BT	19	17.3 (10.4)	52.4 (24.2)	0.3
	Mucinous adenoma	6	21.0 (16.9)	58.7 (19.2)	0.4
	Yolk sac tumor	4	24.4 (17.6)	73.2 (84.5)	0.3
	Dysgerminoma	2	109.5 (41.2)	41.9 (1.2)	2.6
	Endometriosis cyst	1	77.5	121.8	0.6
	Mature teratoma	1	69.5	84.7	0.8
	Adenofibroma	1	6.4	142.9	0.0
Non-neoplastic lesions (33)	Myometrium	12	32.4 (38.4)	62.5 (19.5)	0.5
	Endometrium	8	27.5 (35.2)	40.5 (16.3)	0.7
	Ovary	13	19.5 (14.7)	89.3 (55.3)	0.2

SCC, squamous cell carcinoma; AA, adenosquamous carcinoma; MUA, mucinous adenocarcinoma; SMCC, small cell carcinoma; EMA, endometrioid adenocarcinoma; SEA, serous adenocarcinoma; CCA, clear cell adenocarcinoma; BT, borderline tumor; TP, thymidine phosphorylase; DPD, dihydropyrimidine dehydrogenase.

used were as follows: 5'-CTGCTGTATCGTGGGTCAGA-3' and 5'-CAGCGTCTTTGCCAGCTC-3' (Greiner Bio-One International GmbH, Tokyo, Japan). In addition, β-actin was amplified with another pair of primers (5'-TCATGAAGTGTG ACGTTGACATCCGT-3' and 5'-CCTAGAAGCATTTGCGGT GCACGATG-3'; Promega Corporation), and served as internal standard. PCR was initiated with denaturation at 95˚C for 10 min, followed by 30 cycles of 95˚C for 20 sec, 59˚C for 30 sec and 72˚C for 60 sec, with a final elongation at 72˚C for 10 min. PCR products were analyzed by 2% agarose gel electrophoresis (Wako Pure Chemical Industries, Ltd.), and the gels were stained with ethidium bromide (Invitrogen; Thermo Fisher Scientific, Inc.). Tris-acetate-EDTA (50X; Sigma-Aldrich) was used as the running buffer and 100 bp DNA Ladder (New England Biolabs Japan, Inc., Tokyo, Japan) was used as a marker. Mupid (Advance Co., Ltd., Tokyo, Japan) was used for electrophoresis. Visualization was performed using High Performance UV Transilluminator (UVP, Inc., Upland, CA, USA). Leiomyoma samples were used as negative controls and an RT- control (no reverse transcription) was also performed.

Statistical and prognosis analysis. The overall survival ratios were calculated by the Kaplan-Meier method, and the significance of difference in survival was analyzed by the log-rank test. Quantitative variables are presented as the mean ± standard deviation. Data were analyzed using SPSS software version 21.0 (IBM SPSS, Armonk, NY, USA). $P<0.05$ was considered to indicate a statistically significant difference.

Results

TP and DPD activity in various tumors

Cervical tumors. The mean TP activity was elevated in SCC (306.9 U/mg protein) and adenosquamous carcinoma (AA) (317.6 U/mg protein) of the cervix, although it was not very high in mucinous adenocarcinoma (MUA) (52.7 U/mg protein) or small cell carcinoma (SMCC) (23.1 U/mg protein). The mean DPD activity was also elevated in SCC (138.2 U/mg protein) and AA (222.4 U/mg protein). However, the TP/DPD ratios of all cervical tumors did not exhibit major differences (2.2 for SCC, 1.4 for AA, 3.0 for MUA and 2.2 for SMCC).

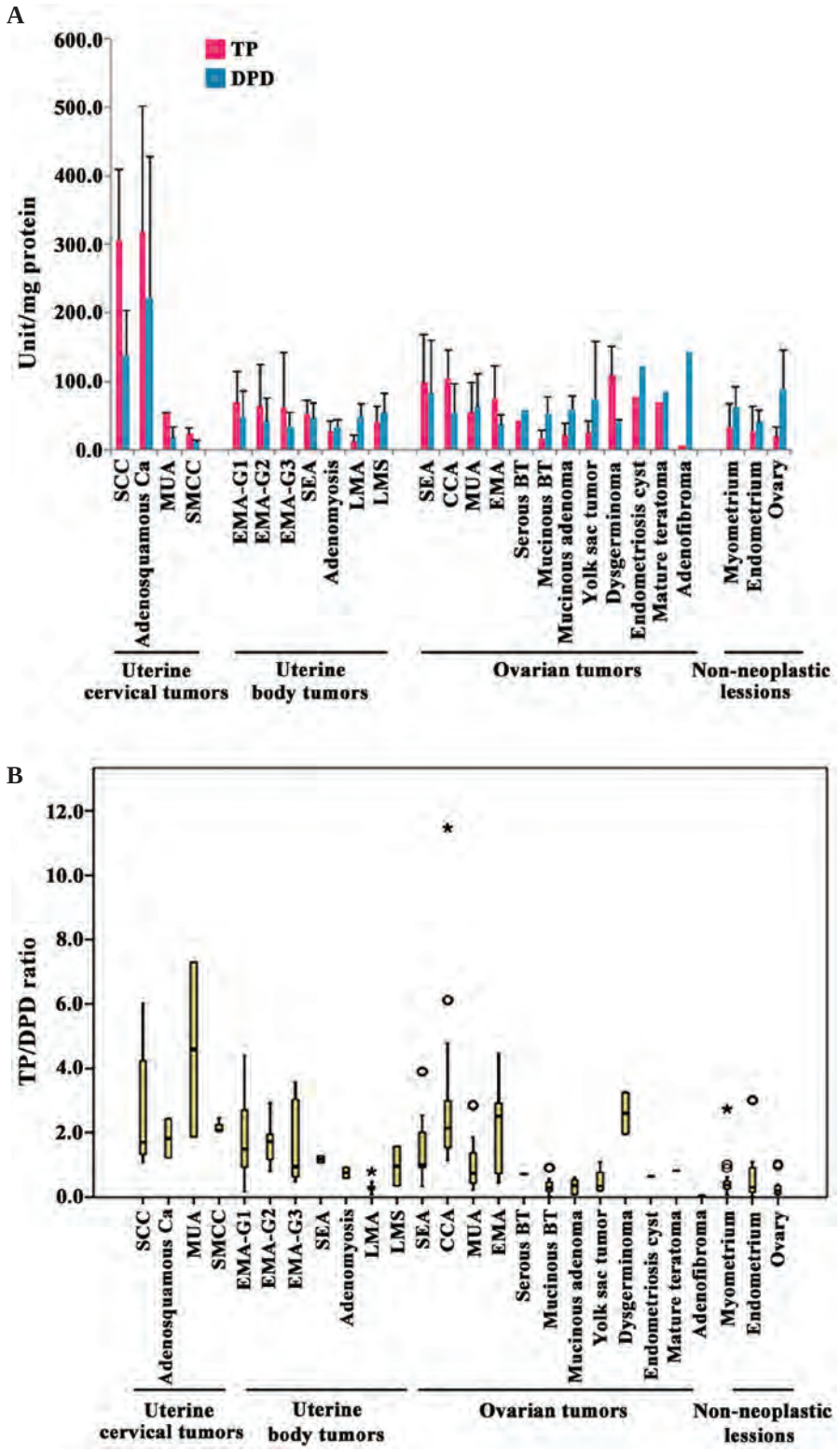

Figure 2. (A) Enzymatic activity of TP and DPD (mean levels stratified by histological type) and (B) TP/DPD ratio in gynecological tumors. The mean enzymatic activity of TP and DPD was higher in SCC of the cervix and adenosquamous carcinoma compared with other tumor types. In patients with tumors of other histological types, the TP levels were often higher than the DPD levels. As observed in SCC of the cervix, the median TP/DPD ratio was also high in other malignant tumors, and a number of patients exhibited a very high TP/DPD ratio. *Outlier point ≥3 x IQR; °Outlier point 1.5 x IQR - 3 x IQR. SCC, squamous cell carcinoma; AA, adenosquamous carcinoma; MUA, mucinous adenocarcinoma; SMCC, small cell carcinoma; EMA, endometrioid adenocarcinoma; SEA, serous adenocarcinoma; LMA, leiomyoma; LMS, leiomyosarcoma; CCA, clear cell adenocarcinoma; BT, borderline tumor; TP, thymidine phosphorylase; DPD, dihydropyrimidine dehydrogenase; IQR, interquartile range.

Tumors of the uterine corpus. There were no significant differences in TP activity among the different grades of endometrioid adenocarcinoma (EMA), with the mean TP activity being 68.6, 63.3 and 63.0 U/mg protein in G1, G2 and G3 tumors, respectively. In contrast, DPD activity decreased as EMA became progressively less differentiated, with the mean

levels being 48.7, 42.1 and 34.6 U/mg protein in G1, G2 and G3 tumors, respectively. DPD activity was significantly higher than TP activity in leiomyoma (P=0.048), where the mean TP activity was 12.9 U/mg protein, while the mean DPD activity was 48.1 U/mg protein, with a TP/DPD ratio of 0.3. DPD activity was also higher than TP activity in leiomyosarcoma, with a TP/DPD ratio of 0.7.

Ovarian tumors. Comparison of the TP/DPD ratios among four histological types of epithelial ovarian cancer [serous adenocarcinoma (SEA)-OV, CCA-OV, EMA-OV and MUA-OV] revealed that the TP/DPD ratio was highest for CCA-OV (2.1), followed by EMA-OV (2.0) and SEA-OV (1.2). Mean TP activity was the highest in CCA-OV (115.2 U/mg protein), followed by SEA-OV (98.6 U/mg protein) and EMA-OV (74.8 U/mg protein) and MUA-OV (54.4 U/mg protein). Among non-epithelial ovarian tumors, the mean TP activity was 109.5 U/mg protein in dysgerminoma, where the TP/DPD ratio was also high (2.6), while the TP/DPD ratios of the other non-epithelial tumors were ≤1.0.

Non-tumor tissues. In normal tissues, including myometrium, endometrium and ovary, the mean DPD activity (64.4 U/mg protein) was higher than the mean TP activity (19.7 U/mg protein), and the TP/DPD ratio was ≤0.7 (Table I and Fig. 2).

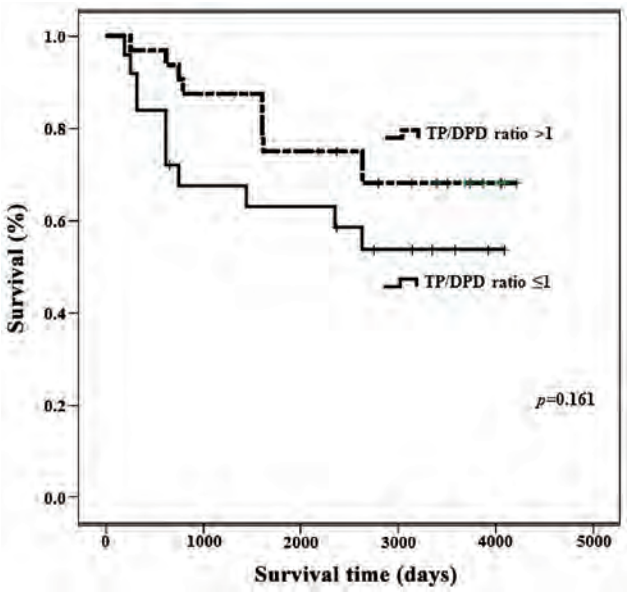

Figure 3. Prognosis analysis. Ovarian tumors with a thymidine phosphorylase/dihydropyrimidine dehydrogenase ratio >1.0 exhibited poor prognosis (P=0.161). TP, thymidine phosphorylase; DPD, dihydropyrimidine dehydrogenase.

Prognosis analysis. The ovarian tumors with a TP/DPD ratio >1.0 demonstrated poor prognosis (P=0.161; Fig. 3). There were no significant differences among uterine cervical tumors and uterine body tumors (data not shown).

IHC analysis of TP expression and localization. TP expression was observed in a wide range of uterine tumors, but it was generally strongest in MUA, SCC and AA.

In tumors of the uterine corpus, TP expression was strongest in G1 EMA, and TP expression decreased as these tumors became less differentiated. There were significant differences in TP expression among G1, G2 and G3 tumors (P<0.01). TP expression could not be detected by IHC in >50% of leiomyoma cases.

Among ovarian tumors, ELISA also revealed high levels of TP expression in EMA-OV, CCA-OV and SEA-OV. In CCA-OV, TP expression was detected in both the nucleus and cytoplasm of tumor cells, and was stronger than in the other histological types. TP expression was not observed in the normal tissues of the majority of patients. Although TP was predominantly localized to the cytoplasm, it was often detected in the nucleus when the tumor exhibited strong expression (Figs. 4 and 5).

Monochrome imaging of microvessel distribution. When the area occupied by microvessels in a section was measured in each type of ovarian cancer, the part of the vasculature defined as microvessels had an area of 116.6 μm^2 in CCA-OV, 71.8 μm^2 in SEA-OV and 56.8 μm^2 in EMA-OV (Table II and Fig. 6). There were no significant differences among uterine cervical tumors and uterine body tumors (data not shown).

Western blotting analysis. Western blotting revealed dense bands for TP protein expression in patients with SCC and CCA-OV, who exhibited high TP activity and TP positive reaction on immunostaining (Fig. 7).

RT-PCR analysis. Analysis of TP mRNA expression in patients with prominent TP protein bands in western blot analysis revealed that TP mRNA expression was closely associated with TP protein expression (Fig. 7).

Discussion

TP activity, which was the focus of the present study, could be measured in fresh tissue specimens and serum, and could also be evaluated by IHC. Therefore, the efficacy of 5-FU prodrugs may be predicted if the activity and expression of TP are investigated prior to initiation of the treatment. While TP activity is known to be increased in cervical cancer (14), the present study demonstrated that TP activity is also high in certain patients with CCA-OV and malignant epithelial ovarian tumors.

DPD acts to degrade TP, and may weaken the therapeutic effect of oral pyrimidine fluoride-based drugs (5). UFT, which contains an oral pyrimidine fluoride-based drug combined with uracil to inhibit DPD, was designed to overcome this problem, even when both TP and DPD activities are high in a tumor (15,16). UFT is a 5-FU prodrug that was developed in Japan as a catabolic enzyme for tegafur and 5-FU (16). Since the response rate to this drug was high (16%) in a previous phase II study performed in 25 patients with advanced/recurrent cervical cancer, the use of UFT for the treatment of cervical cancer is already covered by national health insurance in Japan (14). The usefulness of UFT as adjuvant chemotherapy for various other types of cancer has also been established (6-9). These findings suggest that UFT may be useful as adjuvant chemotherapy for gynecological tumors. In a previous phase III study comparing radiotherapy combined with low- or high-dose Z-100 and maintenance therapy, oral pyrimidine fluoride-based drugs such as 5-FU and UFT were used as adjuvant chemotherapy, and comparison was

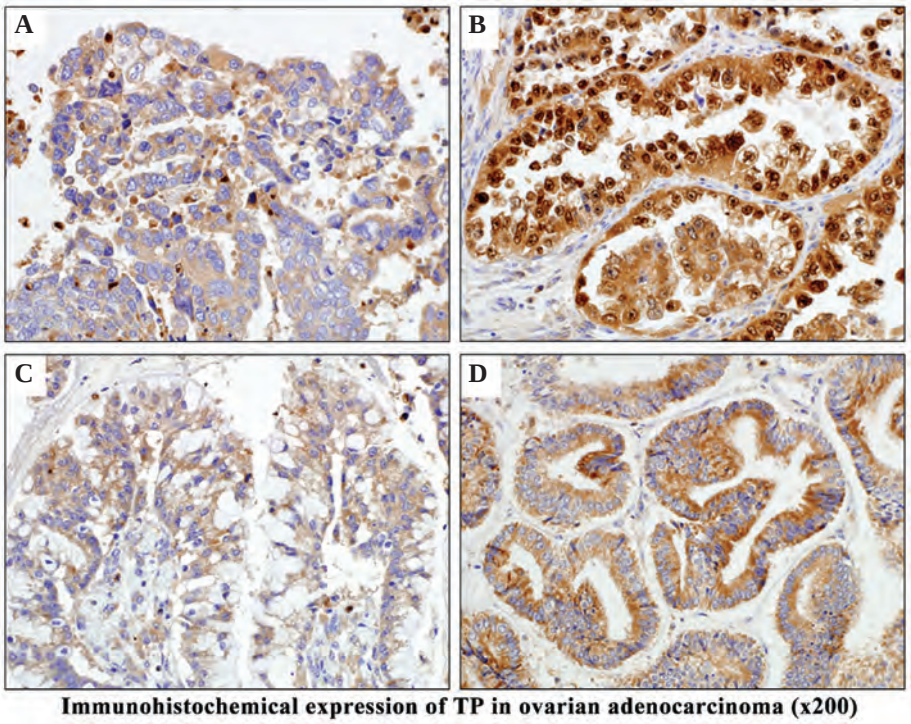

Figure 4. Immunohistochemical analysis of TP expression in various types of ovarian adenocarcinoma. The expression levels of TP varied among (A) serous adenocarcinoma-OV, (B) mucinous adenocarcinoma-OV, (C) CCA-OV and (D) endometrioid adenocarcinoma-OV. TP was detected both in the nucleus and cytoplasm of tumor cells, particularly in CCA-OV, and stronger staining was observed in CCA-OV than in the other histological types analyzed. Magnification, x200. TP, thymidine phosphorylase; CCA, clear cell adenocarcinoma; OV, of ovary.

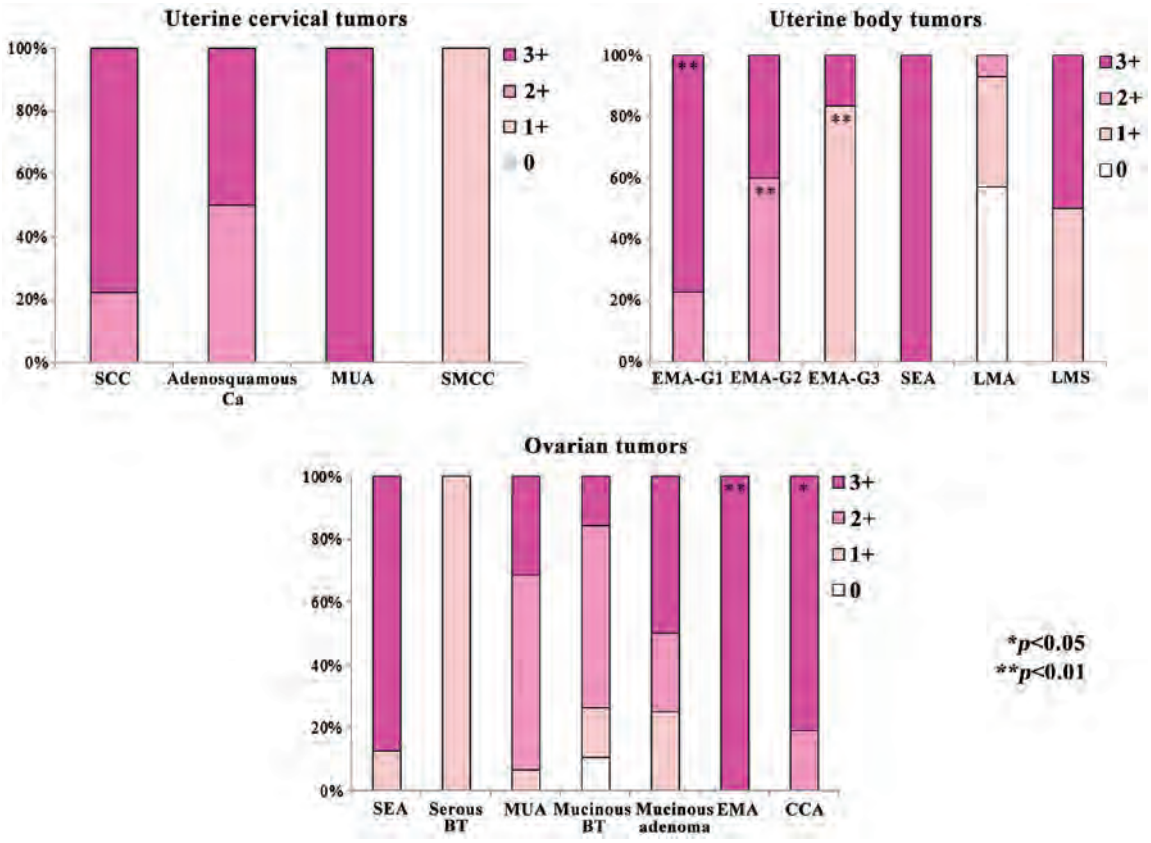

Figure 5. Comparison of immunohistochemical findings. All malignant tumors exhibited expression of TP at different levels, whereas benign tumors were often negative for TP expression. Significant differences in positive expression rate were observed among G1, G2 and G3 EMA tumors of the uterus ($^{**}P<0.01$). Strong TP expression (3+) was detected in numerous patients with ovarian tumors such as clear cell adenocarcinoma-OV and EMA-OV ($^{*}P<0.05$, $^{**}P<0.01$). SCC, squamous cell carcinoma; AA, adenosquamous carcinoma; MUA, mucinous adenocarcinoma; SMCC, small cell carcinoma; EMA, endometrioid adenocarcinoma; SEA, serous adenocarcinoma; LMA, leiomyoma; LMS, leiomyosarcoma; BT, borderline tumor; CCA, clear cell adenocarcinoma; TP, thymidine phosphorylase; OV, of ovary.

Table II. Analysis of vascularity on monochrome images of ovarian carcinoma.

Histology	Microvessel area, μm^2
CCA-OV	116.6
SEA-OV	71.8
EMA-OV	56.8
MUA-OV	43.6

CCA, clear cell adenocarcinoma; SEA, serous adenocarcinoma; EMA, endometrioid adenocarcinoma; MUA, mucinous adenocarcinoma; OV, of ovary.

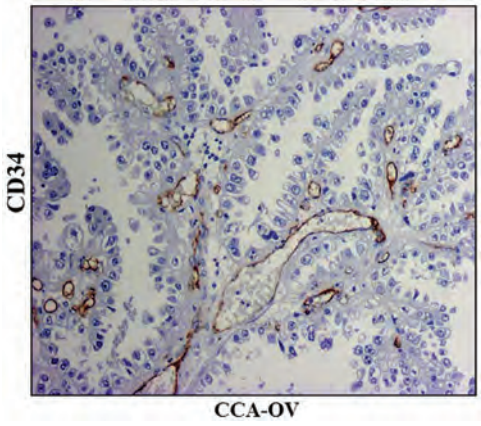

Figure 6. Immunohistochemical expression of CD34 in CCA and analysis of vascularity on monochrome images of ovarian carcinoma. Evaluation of the total microvascular area within tumors revealed that it was largest in clear cell adenocarcinoma-OV, followed by serous adenocarcinoma-OV, endometrioid adenocarcinoma-OV and mucinous adenocarcinoma-OV. Magnification, x200. OV, of ovary; CD, cluster of differentiation; CCA, clear cell adenocarcinoma.

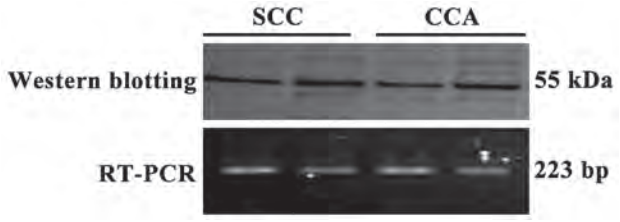

Figure 7. Western blot and reverse transcription-polymerase chain reaction analyses. Western blotting revealed a strong band corresponding to TP protein expression in two patients with squamous cell carcinoma and two patients with clear cell adenocarcinoma of ovary, in whom immunohistochemical expression of TP was also high. Expression of TP messenger RNA was also detected in these patients. SCC, squamous cell carcinoma; CCA, clear cell adenocarcinoma; RT-PCR, reverse transcription-polymerase chain reaction; TP, thymidine phosphorylase.

performed with patients not receiving adjuvant chemotherapy. In that study, the 3- and 5-year survival rates were respectively 22.5 and 15.8% higher in the adjuvant chemotherapy group than in the group without adjuvant chemotherapy (17). Based on those results, a phase III, randomized, comparative study of UFT in patients with locally advanced cervical cancer receiving radical radiotherapy (termed LUFT trial) is currently ongoing in Japan, whereby radiotherapy and chemotherapy are administered simultaneously to patients with stage IB2-IVA cervical cancer. By July 2014, 180 subjects were enrolled in that study, whose results have not been published thus far. However, exploration of biomarkers was not performed during the LUFT trial (18).

It is known that TP activates 5-FU prodrugs and is also structurally similar to PD-ECGF, an angiogenic factor that enhances the migration of vascular endothelial cells (19). In the present study, IHC demonstrated that TP was strongly positive in three types of epithelial ovarian cancer, including CCA-OV, SEA-OV and EMA-OV (Figs. 4 and 5). Suzuki *et al* (20) reported that TP was probably closely associated with the mechanism of angiogenesis in CCA-OV, unlike MUA-OV, since TP expression was higher in this type of adenocarcinoma than in other histological types, and was significantly lower in MUA-OV than in other histological types. However, TP expression in different types of cancer remains a matter of controversy. For example, TP expression was reported to be low in CCA-OV, but high in MUA-OV (19), while another study demonstrated high TP expression in SEA-OV and EMA-OV, but not in CCA-OV (21). It was observed in the present study that TP activity could vary considerably within each tumor, and TP expression may depend on the local growth pattern characterized by the histological structure, including papillary, tubular and solid nests. At present, there is little information concerning the association between TP expression and prognosis, due to the insufficient number of patients and duration of observations. However, Fujimoto *et al* (21) reported that the treatment outcome was significantly worse for ovarian cancer patients with high TP expression than for those with low TP expression. In the present study, the ovarian tumors with a TP/DPD ratio >1.0 presented poor prognosis (Fig. 3).

The present study also revealed that TP expression was increased compared with other histological types, and the number of microvessels was larger than other histological types, in CCA-OV and SEA-OV patients, presumably because papillary proliferation is characteristic of these two tumors (22). Ogawa *et al* (23) also reported that the prognosis was better for CCA-OV patients with a high microvessel density than those with a low microvessel density. Since the present study also demonstrated that CCA-OV tumors exhibited the largest vascular area (Fig. 6) of all the gynecological tumors analyzed, the association between TP expression and angiogenesis or long-term prognosis will be further analyzed in future studies.

The localization of TP was investigated by IHC in the present study, and TP expression was detected in both tumor cells and stromal cells. It has been previously reported that the production of TP by colorectal cancer cells is limited, with the majority of TP being produced by stromal cells around the tumor, particularly activated macrophages (24). It has also been reported that the number of TP^+ activated macrophages is positively correlated with the number of stromal microvessels, and that activated macrophages producing TP are involved in angiogenesis in colorectal cancer (24). In addition, Konishi (25) reported that TP expression was more common in the stroma of ovarian cancer than in tumor cells, and was closely correlated with the presence of $CD68^+$ cells and microvessels, particularly at sites of cancer cell infiltration or metastasis associated with a stromal reaction and angiogenesis (25). These findings

suggest that macrophages may be activated by the tumor cells via certain mechanism to increase TP expression and promote angiogenesis. Thus, the significance of TP expression may depend on its location (in the tumor cells or in the stroma, particularly at sites of infiltration). Accordingly, the significance of TP localization in patients with gynecological tumors requires further investigation.

In recent years, attempts have been made to transiently increase TP activity by administration of cytokines or other anti-neoplastic drugs, so that pyrimidine fluoride-based drugs could also be used in patients with low TP activity (26). As a result, drugs that inhibit angiogenesis by directly blocking TP activity have been developed (27,28). Phase I clinical studies of these drugs in patients with colorectal and breast cancer have already commenced in the USA (29). While awaiting the results of these studies, research on the development of novel treatments must continue, focusing on TP activity, the significance of TP as a biomarker and the utility of UFT maintenance therapy for gynecological cancer.

References

1. Haraguchi M, Miyadera K, Uemura K, Sumizawa T, Furukawa T, Yamada K, Akiyama S and Yamada Y: Angiogenic activity of enzymes. Nature 368: 198, 1994.
2. Miwa M, Ura M, Nishida M, Sawada N, Ishikawa T, Mori K, Shimma N, Umeda I and Ishitsuka H: Design of a novel oral fluoropyrimidine carbamate, capecitabine, which generates 5-fluorouracil selectively in tumours by enzymes concentrated in human liver and cancer tissue. Eur J Cancer 34: 1274-1281, 1998.
3. Furukawa T, Yoshimura A, Sumizawa T, Haraguchi M, Akiyama S, Fukui K, Ishizawa M and Yamada Y: Angiogenic factor. Nature 356: 668, 1992.
4. Dushinsky R, Pleven E and Heidelberger C: The synthesis of 5-fluoropyrimidines. J Am Chem Soc 79: 4559-4560, 1957.
5. Heidelberger C, Chaudhuri NK, Danneberg P, Mooren D, Griesbach L, Duschinsky R, Schnitzer RJ, Pleven E and Scheiner J: Fluorinated pyrimidines, a new class of tumour-inhibitory compounds. Nature 179: 663-666, 1957.
6. Nakajima T, Kinoshita T, Nashimoto A, Sairenji M, Yamaguchi T, Sakamoto J, Fujiya T, Inada T, Sasako M and Ohashi Y; National Surgical Adjuvant Study of Gastric Cancer Group: Randomized controlled trial of adjuvant uracil-tegafur versus surgery alone for serosa-negative, locally advancer gastric cancer. Br J Surg 94: 1468-1476, 2007.
7. Kato H, Ichinose Y, Ohta M, Hata E, Tsubota N, Tada H, Watanabe Y, Wada H, Tsuboi M, Hamajima N and Ohta M; Japan Lung Cancer Research Group on Postsurgical Adjuvant Chemotherapy: A randomized trial of adjuvant chemotherapy with uracil-tegafur for adenocarcinoma of the lung. N Engl J Med 350: 1713-1721, 2004.
8. Akasu T, Moriya Y, Ohashi Y, Yoshida S, Shirao K and Kodaira S; National Surgical Adjuvant Study of Colorectal Cancer: Adjuvant chemotherapy with uracil-tegafur for pathological stage III rectal cancer after mesorectal excision with selective lateral pelvic lymphadenectomy: A multicenter randomized controlled trial. Jpn J Clin Oncol 36: 237-244, 2006.
9. Kato T, Ohashi Y, Nakazato H, Koike A, Saji S, Suzuki H, Takagi H, Nimura Y, Hasumi A, Baba S, *et al*: Efficacy of oral UFT as adjuvant chemotherapy to curative resection of colorectal cancer: Multicenter prospective randomized trial. Langenbecks Arch Surg 386: 575-581, 2002.
10. Kasumi F, Yoshimoto M, Uchino J, Abe R, Nomura Y, Sugimachi K, Nakazato H and Abe O: Meta-analysis of five studies on tegafur plus uracil (UFT) as post-operative adjuvant chemotherapy for breast cancer. Oncology 64: 146-153, 2003.
11. Hirashima Y and Shirao K: Predicting drug efficacy-fluorinated pyrimidines (fluorouracil, S-1 and capecitabine). Gan To Kagaku Ryoho 39: 1603-1607, 2012 (In Japanese).
12. Yamamoto K, Noda K, Hatae M, Kudo T, Hasegawa K, Nishimura R, Honjo H, Yajima A, Sato S, Mizutani K, *et al*: Effects of concomitant use of doxifluridine, radiotherapy and immunotherapy in patients with advanced cervical cancer. Oncol Rep 8: 273-277, 2001.
13. Piver MS, Rose PG, Freedman MF: Change in International Federation of Gynecology and Obstetrics staging. Am J Obstet Gynecol. 1988 Mar;158 (3 Pt 1):678-9.
14. Noda K, Teshima K, Ikeda M, Sugawa T, Yamagata S, Sekiba K, Kohno I, Kaneshige E, Sawaragi I, Matsuoka I, *et al*: Phase II study of UFT in cancer of the uterine cervix. Gan To Kagaku Ryoho 12: 900-906, 1985 (In Japanese).
15. Fujii S, Kitano S, Ikenaka K and Shirasaka T: Effect of coadministration of uracil or cytosine on the anti-tumor activity of clinical doses of 1-(2-tetrahydrofuryl)-5-fluorouracil and level of 5-fluorouracil in rodents. Gan 70: 209-214, 1979.
16. Ikenaka K, Shirasaka T, Kitano S and Fujii S: Effect of uracil on metabolism of 5-fluorouracil in vitro. Gan 70: 353-359, 1979.
17. Noda K, Ohashi Y, Sugimori H, Ozaki M, Niibe H, Ogita S, Kohno I, Hasegawa K, Kikuchi Y, Takegawa Y, *et al*: Phase III double-blind randomized trial of radiation therapy for stage IIIb cervical cancer in combination with low- or high-dose Z-100: Treatment with immunomodulator, more is not better. Gynecol Oncol 101: 455-463, 2006.
18. Gynecologic Oncology Trial and Investigation Consortium: LUFT Trial: A randomized phase III trial of long UFT administration following curative radiation therapy for locally advanced cervical cancer. Version 1.20, 2010. http://www.gotic.jp. Accessed April 4, 2016.
19. Nakanishi Y, Kodama J, Tokumo K, Seki N, Miyagi Y, Yoshinouchi M, Okuda H and Kudo T: The expression of platelet-derived endothelial cell growth factor/thymidine phosphorylase associates with angiogenesis in epithelial ovarian cancer. Int J Clin Oncol 2: 19-23, 1997.
20. Suzuki M, Usui N, Furugen Y and Mitsuhasi N: Pyrimidine nucleoside phosphorylase activity in normal tissues of the uterus and ovary and in benign and malignant lesions of these organs. Int J Clin Oncol 6: 19-24, 2001.
21. Fujimoto J, Ichigo S, Sakaguchi H, Hirose R and Tamaya T: Expression of platelet-derived endothelial cell growth factor (PD-ECGF) and its mRNA in ovarian cancers. Cancer Lett 126: 83-88, 1998.
22. Seidman JD, Cho KR, Ronnett BM and Kurman RJ: Surface epithelial tumors of the ovary. In: Blaustein's Pathology of the Female Genital Tract. Kurman RJ, Ellenson LH and Ronnett BM (eds). 6th edition. Springer US, New York, NY, pp701-758, 2011.
23. Ogawa S, Kaku T, Kobayashi H, Hirakawa T, Ohishi Y, Kinukawa N and Nakano H: Prognostic significance of microvessel density, vascular cuffing and vascular endothelial growth factor expression in ovarian carcinoma: A special review for clear cell adenocarcinoma. Cancer Lett 176: 111-118, 2002.
24. Satou S, Nakajima A and Koyanagi Y: PhNPase-expressing macrophage and angiogenesis in colorectal cancer. Nippon Daicho Komonbyo Gakkai Zasshi 51: 267-275, 1998.
25. Konishi I: Angiogenic factors in gynecological cancer. Acta Obstet Gynaecol Jpn 52: 1222-1227, 2000.
26. Ogawa K, Katsube T, Konno S, Miura K, Wakasugi S, Watanabe T, Shimakawa T, Ishikawa S, Naritaka Y, Yagawa H, *et al*: Influence of intratumor administration of OK-432 on the tumor selectivity of 5'-DFUR. Gan To Kagaku Ryoho 22: 2095-2100, 1995 (In Japanese).
27. Takao S, Akiyama SI, Nakajo A, Yoh H, Kitazono M, Natsugoe S, Miyadera K, Fukushima M, Yamada Y and Aikou T: Suppression of metastasis by thymidine phosphorylase inhibitor. Cancer Res 60: 5345-5348, 2000.
28. Mori S, Takao S, Ikeda R, Noma H, Mataki Y, Wang X, Akiyama S and Aikou T: Thymidine phosphorylase suppresses Fas-induced apoptotic signal transduction independent of its enzymatic activity. Biochem Biophys Res Commun 295: 300-305, 2002.
29. Overman MJ, Varadhachary G, Kopetz S, Thomas MB, Fukushima M, Kuwata K, Mita A, Wolff RA, Hoff PM, Xiong H and Abbruzzese JL: Phase 1 study of TAS-102 administered once daily on a 5-day-per-week schedule in patients with solid tumors. Invest New Drugs 26: 445-454, 2008.

J Gynecol Oncol. 2016 May;27(3):e29
http://doi.org/10.3802/jgo.2016.27.e29
pISSN 2005-0380 · eISSN 2005-0399

JOURNAL OF GYNECOLOGIC ONCOLOGY

Original Article

Practice patterns of adjuvant therapy for intermediate/high recurrence risk cervical cancer patients in Japan

Yuji Ikeda,[1,2] Akiko Furusawa,[3] Ryo Kitagawa,[4] Aya Tokinaga,[5] Fuminori Ito,[6] Masayo Ukita,[7] Hidetaka Nomura,[8] Wataru Yamagami,[9] Hiroshi Tanabe,[10] Mikio Mikami,[11] Nobuhiro Takeshima,[8] Nobuo Yaegashi[12]

[1]Department of Obstetrics and Gynecology, The University of Tokyo, Tokyo, Japan
[2]Department of Gynecologic Oncology, Saitama Medical University International Medical Center, Saitama, Japan
[3]Department of Obstetrics and Gynecology, Tokyo Medical and Dental University, Tokyo, Japan
[4]Department of Obstetrics and Gynecology, NTT Medical Center Tokyo, Tokyo, Japan
[5]Department of Obstetrics and Gynecology, Yokohama City University Graduate School of Medicine, Yokohama, Japan
[6]Department of Obstetrics and Gynecology, Nara Medical University, Nara, Japan
[7]Department of Obstetrics and Gynecology, Kinki University Faculty of Medicine, Osakasayama, Japan
[8]Department of Gynecology, Cancer Institute Hospital, Tokyo, Japan
[9]Department of Obstetrics and Gynecology, Keio University School of Medicine, Tokyo, Japan
[10]Department of Obstetrics and Gynecology, Jikei University Kashiwa Hospital, Kashiwa, Japan
[11]Department of Obstetrics and Gynecology, Tokai University School of Medicine, Isehara, Japan
[12]Department of Obstetrics and Gynecology, Tohoku University Graduate School of Medicine, Sendai, Japan

Received: Nov 23, 2015
Revised: Dec 26, 2015
Accepted: Jan 5, 2016

Correspondence to
Ryo Kitagawa
Department of Obstetrics and Gynecology, NTT Medical Center Tokyo, 5-9-22 Higashi-Gotanda Shinagawa-ku, Tokyo 141-8625, Japan.
E-mail: ryokitagawajp@yahoo.co.jp

The contents of this study was partially presented at 57th Meeting of the Japan Society of Gynecologic Oncology.

ORCID
Yuji Ikeda
http://orcid.org/0000-0003-1633-5385
Akiko Furusawa
http://orcid.org/0000-0003-1279-4971
Ryo Kitagawa
http://orcid.org/0000-0003-3679-8168
Aya Tokinaga
http://orcid.org/0000-0002-7134-7437
Fuminori Ito
http://orcid.org/0000-0002-0437-0979

ABSTRACT

Objective: Although radiation therapy (RT) and concurrent chemoradiotherapy (CCRT) are the global standards for adjuvant therapy treatment in cervical cancer, many Japanese institutions choose chemotherapy (CT) because of the low frequency of irreversible adverse events. In this study, we aimed to clarify the trends of adjuvant therapy for intermediate/high-risk cervical cancer after radical surgery in Japan.
Methods: A questionnaire survey was conducted by the Japanese Gynecologic Oncology Group to 186 authorized institutions active in the treatment of gynecologic cancer.
Results: Responses were obtained from 129 facilities. Adjuvant RT/CCRT and intensity-modulated RT were performed in 98 (76%) and 23 (18%) institutions, respectively. On the other hand, CT was chosen as an alternative in 93 institutions (72%). The most common regimen of CT, which was used in 66 institutions (51%), was a combination of cisplatin/carboplatin with paclitaxel. CT was considered an appropriate alternative option to RT/CCRT in patients with risk factors such as bulky tumors, lymph node metastasis, lymphovascular invasion, parametrial invasion, and stromal invasion. The risk of severe adverse events was considered to be lower for CT than for RT/CCRT in 109 institutions (84%).
Conclusion: This survey revealed a variety of policies regarding adjuvant therapy among institutions. A clinical study to assess the efficacy or non-inferiority of adjuvant CT is warranted.

Keywords: Adjuvant Therapy; Drug Therapy; Radiation; Uterine Cervical Neoplasms

JOURNAL OF GYNECOLOGIC ONCOLOGY

Masayo Ukita
http://orcid.org/0000-0002-1660-1834
Hidetaka Nomura
http://orcid.org/0000-0002-2742-5282
Wataru Yamagami
http://orcid.org/0000-0003-3925-6057
Hiroshi Tanabe
http://orcid.org/0000-0002-8445-8558
Mikio Mikami
http://orcid.org/0000-0002-7496-3518
Nobuo Yaegashi
http://orcid.org/0000-0003-2521-039X

Conflict of Interest
No potential conflict of interest relevant to this article was reported.

INTRODUCTION

Cervical cancer is the third most common cause of death among gynecologic cancers [1]. Women with stage IA2 to IIA lesions require radical hysterectomy with bilateral pelvic lymph-node dissection, radiation therapy (RT), or concurrent chemoradiotherapy (CCRT) [2,3]. In Japan, more than 80% of institutions choose radical hysterectomy as the primary therapy for patients with stage IB1 and IIA1 tumors [4]. After the surgical procedure, the recurrence risk is evaluated by pathological criteria such as lymph node metastasis, lymphovascular space invasion, depth invasion, parametrial invasion, nonsquamous histology, and positive surgical margins [5-8]. Subsequently, adjuvant therapy is considered for patients with an intermediate/high risk of recurrence.

RT decreases the incidence of local recurrence when used as an adjuvant therapy [9,10]; however, there is little or no effect on overall survival [11,12]. On the other hand, CCRT improves progression-free and overall survival for high-risk and early-stage patients who undergo radical hysterectomy and pelvic lymphadenectomy [13]. The National Comprehensive Cancer Network (NCCN) recommends pelvic RT/CCRT for high-risk patients [2]. The Japan Society of Gynecologic Oncology treatment guidelines for cervical cancer also follow the NCCN policy with minor modifications [14]. However, 37% to 48% of recurrences in cervical cancer occur in the extra-pelvic area, and their prognosis is extremely poor [15,16]. In addition, patients who undergo RT may still experience late adverse events and toxicity because of the anatomic locations such as the bladder, bowel, vagina, and ovary [17]. In terms of the quality of life, RT has a disadvantage about sexual function in young women with cervical cancer [18]. Since complications exist over a long time and the mean age at diagnosis of cervical cancer is 48 years, many patients and physicians hesitate to choose RT/CCRT [19,20]. Although some institutions adopt an approach using intensity-modulated radiation therapy (IMRT) to reduce the adverse events, a longer follow-up is required to evaluate the benefit of this treatment [21].

Our previous study showed that many institutions in Japan use chemotherapy (CT) as an adjuvant therapy in patients with intermediate and high risk of recurrence [22]. However, to the best of our knowledge, no clinical study has been conducted to evaluate the efficacy or inferiority of CT as an adjuvant therapy for cervical cancer. In this study, we first aimed to clarify the current trends for adjuvant therapy in different institutions, then evaluated the need for a prospective study to assess CT as an adjuvant therapy for postoperative cervical cancer.

MATERIALS AND METHODS

A questionnaire was designed by a gynecological oncology clinical fellow who attended an educational seminar conducted by the Japanese Gynecologic Oncology Group (JGOG) in August 2013. The details of the questionnaire are listed in **Appendix**. Briefly, the questionnaire included the following questions:

(1) What kind of therapy is routinely selected as an adjuvant therapy for intermediate/high risk postoperative cervical cancer?
(2) What kind of regimen is used for adjuvant CT?
(3) What kind of chemotherapeutic agents are used for CCRT?

http://doi.org/10.3802/jgo.2016.27.e29

JOURNAL OF GYNECOLOGIC ONCOLOGY

(4) Does your institute perform IMRT?
(5) What do you select as a most appropriate adjuvant therapy for patients with risk factors such as bulky tumor, lymph node metastasis, lymphovascular invasion, parametrial invasion, stromal invasion, and vaginal stump invasion?
(6) Will you conduct or support a clinical study to evaluate appropriate adjuvant therapies for cervical cancer?

In August 2014, we mailed the questionnaire to all 186 JGOG member institutions. All the chosen hospitals treated gynecologic cancer and were authorized by the JGOG membership committee. Responses were accepted until December 2014.

RESULTS

1. Characteristics of responders' institutions

In total, 129 of the 199 JGOG member institutions replied to our questionnaire. The characteristics of responding institutions are shown in **Table 1**. Since JGOG membership extended only to institutions active in the treatment of gynecologic cancer, 69 (53%) and 14 (11%) of the 129 institutions were academic hospitals and cancer centers, respectively. Furthermore, 65 (50%) and 52 (40%) institutions had one and two (or more) gynecologic oncologists on the board of the Japanese Society of Gynecologic Oncology, respectively. The average number of radical hysterectomies performed annually was 5 to 15 and >15 in 64 (50%) and 48 (37%) institutions, respectively.

2. Practice patterns of adjuvant therapy for cervical cancer in Japan

First, current adjuvant therapy policies in each institution were analyzed. Our questionnaire allowed multiple answers because many institutions may have multiple therapeutic strategies based on the histological subtypes and/or number of risk factors. According to Japanese guidelines, CCRT/RT was performed in 98 institutions (76%) (**Fig. 1A**). On the other hand, 93 institutions (72%) also had the option to perform CT alone (**Fig. 1A**). IMRT was performed in 18% of institutions (**Fig. 1B**). The CCRT regimen was simple; 83% of institutions used cisplatin alone (**Fig. 1C**). However, multiple CT regimen were used; the most popular regimen, which was used in 46% of institutions, was a combination of carboplatin and paclitaxel, followed by irinotecan with nedaplatin (20%), and cisplatin with paclitaxel (17%) (**Fig. 1D**).

Table 1. Background of responding institutions

Variable	Institution (%)
Responder	129
Academic hospital	69 (53)
Cancer center	14 (11)
General hospital	46 (36)
Physicians with board of Japan Society of Gynecologic Oncology	
0	12 (10)
1	65 (50)
≥2	52 (40)
No. of radical hysterectomy per year	
<5	17 (13)
5–15	64 (50)
>15	48 (37)

http://doi.org/10.3802/jgo.2016.27.e29

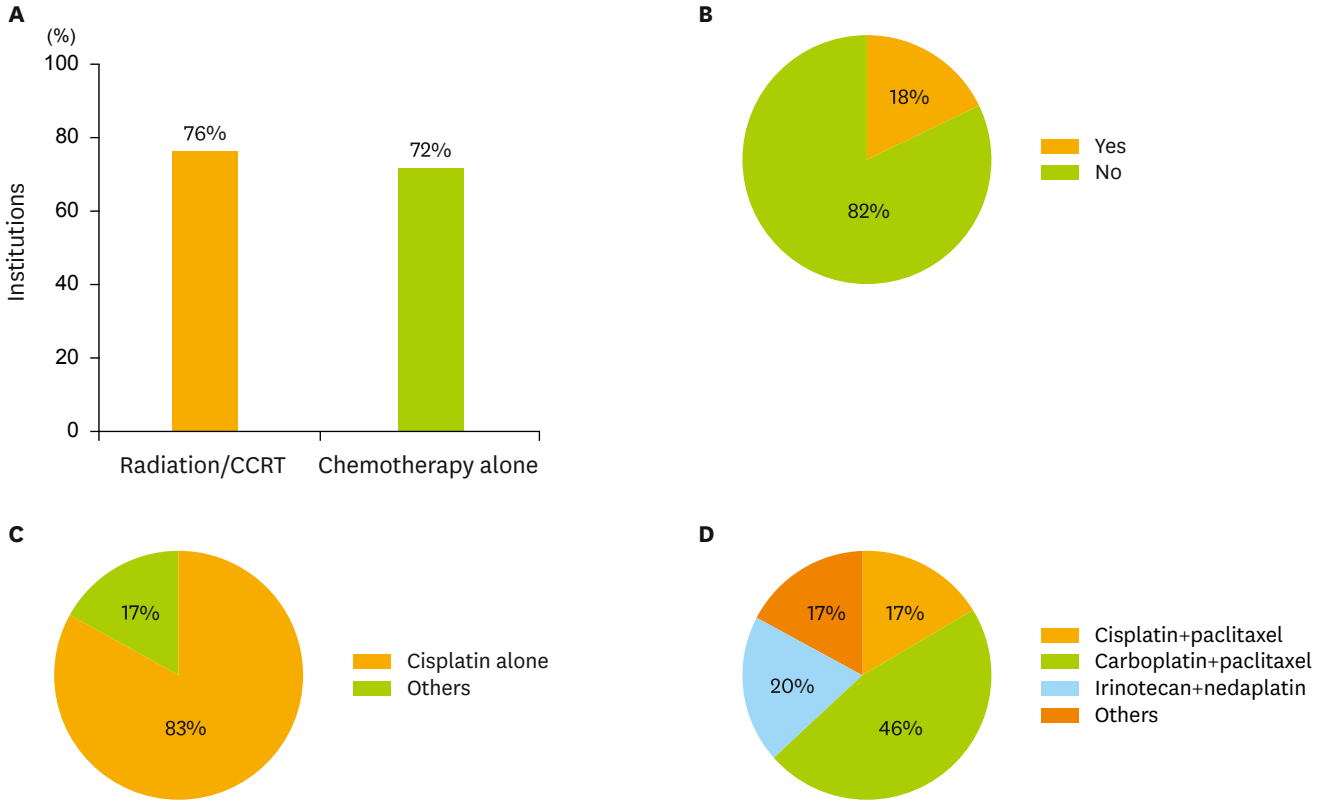

Fig. 1. Variety of adjuvant therapy policies for cervical cancer in Japan. The policy for adjuvant therapy was investigated in each institution (multiple answers allowed). (A) Therapeutic options considered for adjuvant therapy. (B) Percentage of institutions performing intensity-modulated radiation therapy. (C) Regimen for concurrent chemoradiotherapy (CCRT). (D) Regimen for adjuvant chemotherapy.

3. Risk assessment for clinicopathological factors

Next, we assessed risk assessment for clinicopathological factors which might be one of the reasons for the variety of adjuvant therapies. As shown in **Fig. 2**, RT was revealed to be the most appropriate adjuvant therapy for vaginal stump invasion cases, but not for other factors such as bulky tumor, lymph node metastasis, lymphovascular invasion parametrial invasion, and stromal invasion. CCRT was appropriate especially in cases of lymph node metastasis and parametrial invasion. Interestingly, CT ranked highly as an adjuvant therapy for all risk factors except vaginal stump invasion, and even for factors where observation was frequently chosen, for example, bulky tumors, lymphovascular invasion, and stromal invasion. These results indicate that the type of risk factor might affect the selection of adjuvant therapy.

4. Expectation of randomized controlled trial to evaluate the efficacy of CT as an adjuvant therapy in cervical cancer

Finally, we focused on how gynecologic oncologists evaluate the complications of each therapeutic option and the necessity of a trial to evaluate the efficacy or non-inferiority of CT as an adjuvant therapy in cervical cancer. The result showed that 85% of institutions evaluated CT as an adjuvant therapy with fewer incidences of severe complications (**Fig. 3A**). On the other hand, only 4% of institutions chose RT and 5% rated both CT and RT equally. Moreover, 87% of institutions were supportive of a clinical study to evaluate the efficacy or non-inferiority of CT as an adjuvant therapy in cervical cancer (**Fig. 3B**). Approximately 13% of institutions did not support a future clinical study because of the lack of radiation facilities or fewer cases for adjuvant therapy than expected (not shown in figure).

http://doi.org/10.3802/jgo.2016.27.e29

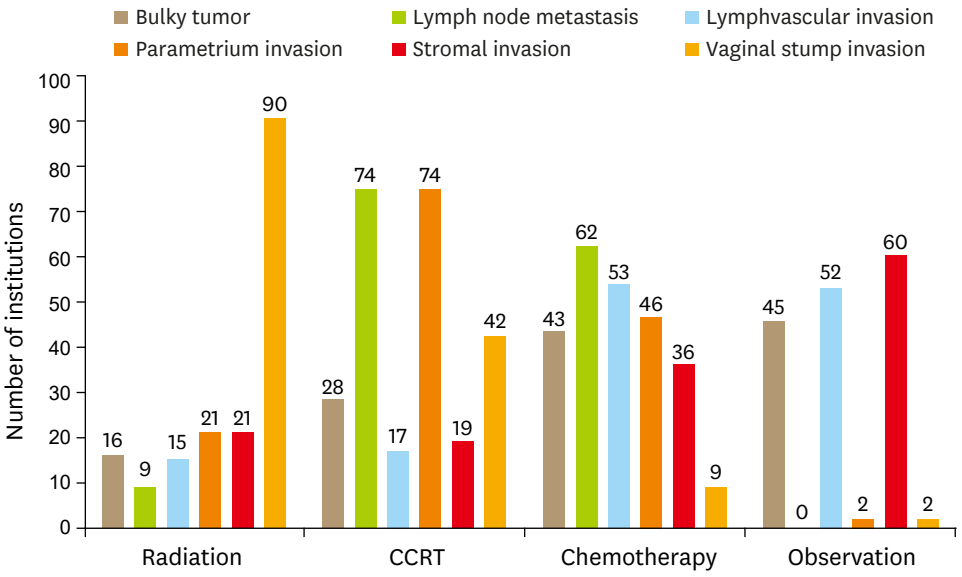

Fig. 2. Risk assessment for clinicopathological factors. Appropriate therapeutic options are chosen from among radiation, concurrent chemoradiotherapy (CCRT), chemotherapy, and observation (multiple answers allowed).

DISCUSSION

In this survey, we showed (1) the variety of adjuvant therapies for cervical cancer in Japan, (2) that the combination of risk factors might affect the selection of adjuvant therapy, and (3) that a clinical study is required to evaluate the efficacy or non-inferiority of CT as an adjuvant therapy in cervical cancer.

Previous retrospective studies had revealed the efficacy of CT as an adjuvant therapy for cervical cancer. A large-scale retrospective study in 2,268 patients comparing efficacy and adverse effects indicated no significant differences between CT and RT/CCRT in both the 5-year overall survival and disease-free survival [23]. Notably, the increased 5-year overall survival and disease-free survival rates of CT compared to RT were seen in patients with early-stage disease, clinical response, and younger age [23]. These results motivate gynecologic oncologists to use CT as an adjuvant therapy. Our survey also revealed that CT was a wise choice for adjuvant therapy in Japan.

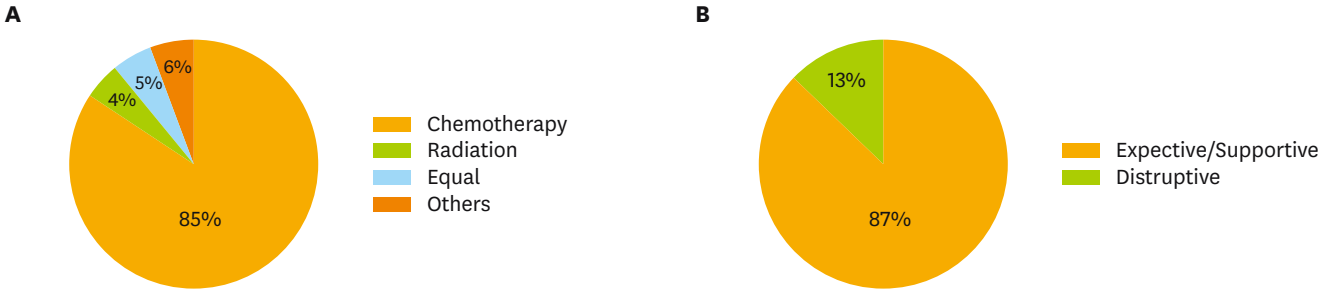

Fig. 3. Recognition of complications and requirement for a clinical study to assess adjuvant therapy. (A) Identification of the most reduced complication of adjuvant therapy. (B) The approach of your institution for clinical study to assess the efficacy or non-inferiority of chemotherapy as an adjuvant therapy.

http://doi.org/10.3802/jgo.2016.27.e29

In our survey, the regimen for CCRT generally involved only cisplatin because previous meta-analysis including 4,580 randomized patients showed an improved overall survival (hazard ratio, 0.71; p<0.001) in CCRT compared to RT, and cisplatin was the most commonly used agent in the study [24]. However, the regimen for CT alone showed variety, for example, cisplatin with paclitaxel, carboplatin with paclitaxel, and irinotecan with nedaplatin. These regimens come from clinical studies of cervical cancer in Japan. Previously, a combination of paclitaxel and cisplatin was considered the standard CT for cervical cancer [25,26]. Recently, we reported the non-inferiority of the paclitaxel and carboplatin regimen compared to paclitaxel and cisplatin in patients with recurrent or metastatic cervical cancer [27].

Risk criteria should be considered before the selection of adjuvant therapy. Currently, recurrence risk is evaluated according to the number of risk factors found in the patient. However, our survey revealed that gynecologists assess the recurrence risk according to the kind of risk factors the patient has, and then choose the appropriate therapeutics. Radiation was supported by the majority of institutions for the adjuvant therapy of vaginal stump invasion. This is reasonable because RT such as brachytherapy can directly approach the tumor. In fact, the 10-year survival rate of non-palpable recurrence at the vaginal stump is reported to be more than 70% following brachytherapy alone [28]. On the other hand, postoperative CCRT was used for lymph node metastasis and parametrial invasion because previous randomized studies proved the efficacy of CCRT in these patients [13]. However, lymph node metastasis is considered as a significant risk factor for prognosis, even after CCRT/RT [29]. Notably, the 3-year survival rate of adjuvant CT was more than 78% and superior to that of radiotherapy (67%), even though 34% of patients had multiple lymph node metastases. In addition, CT has an equivalent therapeutic effect to RT with fewer postoperative complications [30,31]. Our results showed that many gynecologic oncologists in Japan also evaluate the superiority of CT according to the complication. These results support the need for evaluation of CT as an adjuvant therapy for cervical cancer. In fact, almost 90% of the institutions supported such a clinical study.

Our survey has several limitations. First, this study was performed for selected institutions. Since treatment for cervical cancer is generally performed in front-line medical centers and most of them belong to JGOG, we conducted this survey only in these institutions. Therefore, our result might not reflect the opinions in a small institution. Second, in this survey, we evaluated all institutions equally. Since the number of patients is different in each institution, some of the results might have to be evaluated considering the scale of the institution. In fact, some institutions in our survey have no radiation facility in their hospital. However, if the efficacy or non-inferiority of CT for adjuvant therapy is proven, these institutions can choose CT without any hesitation.

In conclusion, our study showed that a variety of adjuvant therapy policies for cervical cancer are currently in use in each institution. Clinical study to assess the efficacy or non-inferiority of adjuvant CT is required.

ACKNOWLEDGMENTS

We thank JGOG for support and assistance since our survey was conducted by members who participated in a JGOG education seminar in August 2013. We also thank all the doctors and institutions who responded to our questionnaire survey.

http://doi.org/10.3802/jgo.2016.27.e29

REFERENCES

1. Siegel RL, Miller KD, Jemal A. Cancer statistics, 2015. CA Cancer J Clin 2015;65:5-29.
PUBMED | CROSSREF
2. Kokka F, Bryant A, Brockbank E, Powell M, Oram D. Hysterectomy with radiotherapy or chemotherapy or both for women with locally advanced cervical cancer. Cochrane Database Syst Rev 2015;4:CD010260.
PUBMED
3. Rosa DD, Medeiros LR, Edelweiss MI, Pohlmann PR, Stein AT. Adjuvant platinum-based chemotherapy for early stage cervical cancer. Cochrane Database Syst Rev 2012;6:CD005342.
PUBMED
4. Mikami M, Aoki Y, Sakamoto M, Shimada M, Takeshima N, Fujiwara H, et al. Current surgical principle for uterine cervical cancer of stages Ia2, Ib1, and IIa1 in Japan: a survey of the Japanese Gynecologic Oncology Group. Int J Gynecol Cancer 2013;23:1655-60.
PUBMED | CROSSREF
5. Ho CM, Chien TY, Huang SH, Wu CJ, Shih BY, Chang SC. Multivariate analysis of the prognostic factors and outcomes in early cervical cancer patients undergoing radical hysterectomy. Gynecol Oncol 2004;93:458-64.
PUBMED | CROSSREF
6. Lai CH, Hong JH, Hsueh S, Ng KK, Chang TC, Tseng CJ, et al. Preoperative prognostic variables and the impact of postoperative adjuvant therapy on the outcomes of Stage IB or II cervical carcinoma patients with or without pelvic lymph node metastases: an analysis of 891 cases. Cancer 1999;85:1537-46.
PUBMED | CROSSREF
7. Park TK. Adjuvant therapy in cervical cancer patients with high risk factors. Yonsei Med J 1997;38:255-60.
PUBMED | CROSSREF
8. Rushdan MN, Tay EH, Khoo-Tan HS, Lee KM, Low JH, Ho TH, et al. Tailoring the field and indication of adjuvant pelvic radiation for patients with FIGO stage Ib lymph nodes-negative cervical carcinoma following radical surgery based on the GOG score--a pilot study. Ann Acad Med Singapore 2004;33:467-72.
PUBMED
9. Atkovar G, Uzel O , Ozşahin M, Koca S, Sahinler I, Okkan S, et al. Postoperative radiotherapy in carcinoma of the cervix: treatment results and prognostic factors. Radiother Oncol 1995;35:198-205.
PUBMED | CROSSREF
10. Uno T, Ito H, Itami J, Sato T, Minoura S, Yasuda S, et al. Adjuvant pelvic irradiation in patients with pathologic T2b carcinoma of the uterine cervix. Int J Gynecol Cancer 2002;12:187-91.
PUBMED | CROSSREF
11. Kinney WK, Alvarez RD, Reid GC, Schray MF, Soong SJ, Morley GW, et al. Value of adjuvant whole-pelvis irradiation after Wertheim hysterectomy for early-stage squamous carcinoma of the cervix with pelvic nodal metastasis: a matched-control study. Gynecol Oncol 1989;34:258-62.
PUBMED | CROSSREF
12. Monk BJ, Cha DS, Walker JL, Burger RA, Ramsinghani NS, Manetta A, et al. Extent of disease as an indication for pelvic radiation following radical hysterectomy and bilateral pelvic lymph node dissection in the treatment of stage IB and IIA cervical carcinoma. Gynecol Oncol 1994;54:4-9.
PUBMED | CROSSREF
13. Peters WA, Liu PY, Barrett RJ, Stock RJ, Monk BJ, Berek JS, et al. Concurrent chemotherapy and pelvic radiation therapy compared with pelvic radiation therapy alone as adjuvant therapy after radical surgery in high-risk early-stage cancer of the cervix. J Clin Oncol 2000;18:1606-13.
PUBMED
14. Japan Society of Gynecologic Oncology. Treatment guidelines for cervical cancer 2007 edition. Tokyo: Kanehara & Co.; 2007.
15. Larson DM, Copeland LJ, Stringer CA, Gershenson DM, Malone JM, Edwards CL. Recurrent cervical carcinoma after radical hysterectomy. Gynecol Oncol 1988;30:381-7.
PUBMED | CROSSREF
16. Samlal RA, Van Der Velden J, Van Eerden T, Schilthuis MS, Gonzalez Gonzalez D, Lammes FB. Recurrent cervical carcinoma after radical hysterectomy: an analysis of clinical aspects and prognosis. Int J Gynecol Cancer 1998;8:78-84.
PUBMED | CROSSREF
17. Viswanathan AN, Lee LJ, Eswara JR, Horowitz NS, Konstantinopoulos PA, Mirabeau-Beale KL, et al. Complications of pelvic radiation in patients treated for gynecologic malignancies. Cancer 2014;120:3870-83.
PUBMED | CROSSREF
18. Frumovitz M, Sun CC, Schover LR, Munsell MF, Jhingran A, Wharton JT, et al. Quality of life and sexual

functioning in cervical cancer survivors. J Clin Oncol 2005;23:7428-36.
PUBMED | CROSSREF

19. Matsuura Y, Kawagoe T, Toki N, Tanaka M, Kashimura M. Long-standing complications after treatment for cancer of the uterine cervix--clinical significance of medical examination at 5 years after treatment. Int J Gynecol Cancer 2006;16:294-7.
PUBMED | CROSSREF

20. Eifel PJ, Levenback C, Wharton JT, Oswald MJ. Time course and incidence of late complications in patients treated with radiation therapy for FIGO stage IB carcinoma of the uterine cervix. Int J Radiat Oncol Biol Phys 1995;32:1289-300.
PUBMED | CROSSREF

21. Mundt AJ, Mell LK, Roeske JC. Preliminary analysis of chronic gastrointestinal toxicity in gynecology patients treated with intensity-modulated whole pelvic radiation therapy. Int J Radiat Oncol Biol Phys 2003;56:1354-60.
PUBMED | CROSSREF

22. Mikami M, Aoki Y, Sakamoto M, Shimada M, Takeshima N, Fujiwara H, et al. Surgical principles for managing stage IB2, IIA2, and IIB uterine cervical cancer (Bulky Tumors) in Japan: a survey of the Japanese Gynecologic Oncology Group. Int J Gynecol Cancer 2014;24:1333-40.
PUBMED | CROSSREF

23. Li S, Hu T, Chen Y, Zhou H, Li X, Cheng X, et al. Adjuvant chemotherapy, a valuable alternative option in selected patients with cervical cancer. PLoS One 2013;8:e73837.
PUBMED | CROSSREF

24. Green JA, Kirwan JM, Tierney JF, Symonds P, Fresco L, Collingwood M, et al. Survival and recurrence after concomitant chemotherapy and radiotherapy for cancer of the uterine cervix: a systematic review and meta-analysis. Lancet 2001;358:781-6.
PUBMED | CROSSREF

25. Moore DH, Blessing JA, McQuellon RP, Thaler HT, Cella D, Benda J, et al. Phase III study of cisplatin with or without paclitaxel in stage IVB, recurrent, or persistent squamous cell carcinoma of the cervix: a gynecologic oncology group study. J Clin Oncol 2004;22:3113-9.
PUBMED | CROSSREF

26. Monk BJ, Sill MW, McMeekin DS, Cohn DE, Ramondetta LM, Boardman CH, et al. Phase III trial of four cisplatin-containing doublet combinations in stage IVB, recurrent, or persistent cervical carcinoma: a Gynecologic Oncology Group study. J Clin Oncol 2009;27:4649-55.
PUBMED | CROSSREF

27. Kitagawa R, Katsumata N, Shibata T, Kamura T, Kasamatsu T, Nakanishi T, et al. Paclitaxel plus carboplatin versus paclitaxel plus cisplatin in metastatic or recurrent cervical cancer: the Open-Label Randomized Phase III Trial JCOG0505. J Clin Oncol 2015;33:2129-35.
PUBMED | CROSSREF

28. Ito H, Shigematsu N, Kawada T, Kubo A, Isobe K, Hara R, et al. Radiotherapy for centrally recurrent cervical cancer of the vaginal stump following hysterectomy. Gynecol Oncol 1997;67:154-61.
PUBMED | CROSSREF

29. Bradbury M, Founta C, Taylor W, Kucukmetin A, Naik R, Ang C. Pathological risk factors and outcomes in women with stage IB2 cervical cancer treated with primary radical surgery versus chemoradiotherapy. Int J Gynecol Cancer 2015;25:1476-83.
PUBMED | CROSSREF

30. Hosaka M, Watari H, Takeda M, Moriwaki M, Hara Y, Todo Y, et al. Treatment of cervical cancer with adjuvant chemotherapy versus adjuvant radiotherapy after radical hysterectomy and systematic lymphadenectomy. J Obstet Gynaecol Res 2008;34:552-6.
PUBMED | CROSSREF

31. Jung PS, Kim DY, Lee SW, Park JY, Suh DS, Kim JH, et al. Clinical role of adjuvant chemotherapy after radical hysterectomy for FIGO stage IB-IIA cervical cancer: comparison with adjuvant RT/CCRT using inverse-probability-of-treatment weighting. PLoS One 2015;10:e0132298.
PUBMED | CROSSREF

Appendix. Questionnaire on the cervical cancer treatment policy of Japanese Gynecologic Oncology Group medical institutions

This questionnaire survey should be answered by the Head or responsible person of each institution.

1. Does your institution have criteria for performing adjuvant therapy for intermediate/high risk cervical cancer after surgery?
   1) According to the Japanese guidelines
   2) Almost the same as the Japanese guidelines
   3) Unique criteria, specific to the institution
   4) Other criteria

2. What according to you is the most appropriate adjuvant therapy for each of the recurrent risk factors listed below? (multiple answers allowed)
   1) Bulky tumor:
      (a) Observation, (b) Radiotherapy, (c) Chemotherapy, (d) Other

   2) Lymph node metastasis:
      (a) Observation, (b) Radiotherapy, (c) Chemotherapy, (d) Other

   3) Lymphovascular invasion:
      (a) Observation, (b) Radiotherapy, (c) Chemotherapy, (d) Other

   4) Parametrial invasion:
      (a) Observation, (b) Radiotherapy, (c) Chemotherapy, (d) Other

   5) Stromal invasion:
      (a) Observation, (b) Radiotherapy, (c) Chemotherapy, (d) Other

   6) Vaginal invasion:
      (a) Observation, (b) Radiotherapy, (c) Chemotherapy, (d) Other

3-1. What should be performed as an adjuvant therapy for intermediate/high risk postoperative cervical cancer? (multiple answers allowed)
   1) Chemotherapy
   2) Radiation
   3) Concurrent chemoradiotherapy (CCRT)
   4) Other

3-2. Why did you select this (these) therapy (therapies)?

4. What kind of regimen do you use for adjuvant chemotherapy?
   Agents:
   Dose:

5-1. What is total dose in Gy you use for adjuvant radiation therapy?

5-2. What kind of chemotherapeutic agents do you use for CCRT?
   Agents:
   Dose:

6. Does your institution perform Intensity-Modulated Radiation Therapy (IMRT)?
   1) Yes
   2) No, but we can perform IMRT.
   3) No. We can only perform conventional radiation therapy.
   4) No. We cannot perform radiation therapy.

7. Which therapy do you think has the fewest adverse events?
   1) Radiation
   2) Chemotherapy
   3) Equal
   4) Other

http://doi.org/10.3802/jgo.2016.27.e29

Int J Clin Oncol (2016) 21:419–434
DOI 10.1007/s10147-016-0981-1

SPECIAL ARTICLE

Japan Society of Gynecologic Oncology guidelines 2013 for the treatment of uterine body neoplasms

Yasuhiko Ebina[1] · Hidetaka Katabuchi[2] · Mikio Mikami[3] · Satoru Nagase[4] · Nobuo Yaegashi[5] · Yasuhiro Udagawa[6] · Hidenori Kato[7] · Kaneyuki Kubushiro[8] · Kiyoshi Takamatsu[9] · Kazuhiko Ino[10] · Hiroyuki Yoshikawa[11]

Received: 25 March 2016 / Accepted: 3 April 2016 / Published online: 26 April 2016

Abstract The third version of the Japan Society of Gynecologic Oncology guidelines for the treatment of uterine body neoplasms was published in 2013. The guidelines comprise nine chapters and nine algorithms. Each chapter includes a clinical question, recommendations, background, objectives, explanations, and references. This revision was intended to collect up-to-date international evidence. The highlights of this revision are to (1) newly specify costs and conflicts of interest; (2) describe the clinical significance of pelvic lymph node dissection and para-aortic lymphadenectomy, including variant histologic types; (3) describe more clearly the indications for laparoscopic surgery as the standard treatment; (4) provide guidelines for post-treatment hormone replacement therapy; (5) clearly differentiate treatment of advanced or recurrent cancer between the initial treatment and the treatment carried out after the primary operation; (6) collectively describe fertility-sparing therapy for both atypical endometrial hyperplasia and endometrioid adenocarcinoma (corresponding to G1) and newly describe relapse therapy after fertility-preserving treatment; and (7) newly describe the treatment of trophoblastic disease. Overall, the objective of these guidelines is to clearly delineate the standard of care for uterine body neoplasms in Japan with the goal of ensuring a high standard of care for all Japanese women diagnosed with uterine body neoplasms.

Keywords Clinical practice guidelines · Endometrial cancer · Treatment · Trophoblastic disease · Uterine sarcoma

Introduction

Endometrial cancer is one of the most common malignancies of the female genital tract. In Japan, the age-adjusted incidence rate of endometrial cancer was 17.2 (per 100,000 women) in 2011, indicative of a four- to five-fold increase over the past three decades [1]. It is estimated

This article originally appeared in Japanese as *Shikyu taigan chiryo gaidorain 2013 nen ban*, published by Kanehara, Tokyo, 2013.

✉ Yasuhiko Ebina
ebiyas@med.kobe-u.ac.jp

1 Department of Obstetrics and Gynecology, Kobe University Graduate School of Medicine, Kobe, Japan

2 Department of Obstetrics and Gynecology, Faculty of Life Sciences, Kumamoto University, Kumamoto, Japan

3 Department of Obstetrics and Gynecology, Tokai University School of Medicine, Isehara, Japan

4 Department of Obstetrics and Gynecology, Yamagata University Faculty of Medicine, Yamagata, Japan

5 Department of Obstetrics and Gynecology, Tohoku University Graduate School of Medicine, Sendai, Japan

6 Fujita Health University School of Medicine, Toyoake, Japan

7 Division of Gynecologic Oncology, National Hospital Organization, Hokkaido Cancer Center, Sapporo, Japan

8 Department of Obstetrics and Gynecology, Toho University School of Medicine, Toho University Medical Center Ohashi Hospital, Tokyo, Japan

9 Department of Obstetrics and Gynecology, Tokyo Dental College Ichikawa General Hospital, Ichikawa, Chiba, Japan

10 Department of Obstetrics and Gynecology, Wakayama Medical University, Wakayama, Japan

11 Department of Obstetrics and Gynecology, Faculty of Medicine, University of Tsukuba, Tsukuba, Japan

that 10,300 new uterine cancer cases occurred in 2014 [2], with 2,243 deaths resulting from the disease [1]. Surgery, chemotherapy, radiation, and hormone therapy are used either alone or sequentially to treat endometrial cancer. Surgery is recommended for medically operable disease. When the disease is limited to the uterus, then hysterectomy, bilateral salpingo-oophorectomy, and pelvic/para-aortic lymph node dissection are recommended. However, whether to add para-aortic lymphadenectomy to pelvic node dissection remains controversial. Furthermore, there are differences in the adjuvant therapies employed in Japan and in Western countries. In Western countries, radiation therapy is the mainstay of postoperative adjuvant therapy, whereas in Japan, chemotherapy is more frequently performed. These differences are one reason why evidence from Western countries cannot be directly applied to the development of recommendations for Japanese patients. Under such circumstances, the first edition of the Japan Society of Gynecologic Oncology (JSGO) guidelines for the treatment of endometrial cancer was published in 2006 and revised in 2009 [3]. The second revised version contained two new sections—the treatment of mesenchymal tumors such as leiomyosarcoma and the treatment of serous and clear-cell adenocarcinoma [3].

The third edition of the JSGO guidelines for the treatment of uterine body neoplasms was published in 2013. The guidelines comprise nine chapters and nine algorithms. The highlights of this revision are indicated below.

1. Chapter 1: Overview of guidelines. New specification of costs and conflicts of interests are identified.
2. Chapter 2: Initial treatment for endometrial cancer. The clinical significance of pelvic lymph node dissection and para-aortic lymphadenectomy, including variant histologic types, are described in detail. An additional indication for laparoscopic surgery as the standard treatment is also described more clearly. Finally, the optimal treatment for patients in whom it is evident that endometrial cancer is present after hysterectomy is also described.
3. Chapter 3: Postoperative adjuvant therapy for endometrial cancer. Chemotherapy is described as having priority over radiation therapy in line with the present conditions in Japan, including the above-mentioned variant histologic type.
4. Chapter 4: Post-treatment surveillance for endometrial cancer. The guidelines for hormone replacement therapy after treatment are described first based on "The Guidelines for Hormone Replacement Therapy 2012," edited by the Japan Society of Obstetrics and Gynecology (JSOG) and the Japan Society for Menopause and Women's Health.
5. Chapter 5: Treatment for advanced or recurrent endometrial cancer. The difference between the initial treatment and the treatment carried out after the primary operation is clearly described.
6. Chapter 6: Fertility-sparing therapy. Two diseases, namely atypical endometrial hyperplasia and endometrioid adenocarcinoma (corresponding to G1), are collectively described. Relapse therapy after the fertility-preserving treatment is also newly described.
7. Chapter 7: Treatment of uterine carcinosarcoma and uterine sarcoma. This chapter was first included in the 2009 version. In addition, chapter 8 "Treatment of trophoblastic disease" is newly described to support "the general roles for clinical and pathological management of trophoblastic diseases (the third edition)".

Chapter 1: Overview of guidelines

1. How to use these guidelines

These guidelines are intended for doctors (general practitioners and specialists) who provide medical care for patients with uterine tumors and are meant to provide useful treatment methods by integrating previous evidence of benefit. However, the guidelines are not intended to be limited to the therapies listed. The main purposes of the guidelines are (1) to indicate current treatment that is considered appropriate for endometrial cancer, carcinosarcoma/sarcoma, and trophoblastic diseases; (2) to reduce differences in therapy among institutions; (3) to improve the prognosis and safety of treatments; (4) to reduce the economic and psychosomatic burden of patients by promoting the performance of appropriate treatment; and (5) to aid mutual understanding of healthcare professionals and patients.

2. Intended audience

These guidelines are intended for practicing physicians engaged in the treatment of patients with endometrial cancer, carcinosarcoma/sarcoma, and trophoblastic diseases.

3. Diseases addressed by these guidelines

Endometrial cancer was mainly described in the first edition. Variant histologic types of uterine cancer and carcinosarcoma/sarcoma were added in the revised edition. Trophoblastic disease was added to the latest revised edition, and these tumors and their recurrence are described in these guidelines. The characteristics of these guidelines are as follows. Initial, postoperative and advanced/recurrent treatment of variant histologic type was discussed

Table 1 Classification of evaluation criteria for evidence quality

Level I Evidence from meta-analyses of multiple randomized controlled trials or evidence from multiple randomized controlled trials
Level II Evidence from at least one randomized controlled trial or evidence from multiple well-designed controlled studies without randomization
Level III Evidence obtained from at least one other type of well-designed quasi-experimental study, or evidence obtained from well-designed, nonexperimental descriptive studies such as comparative studies, correlation studies, or case studies
Level IV Expert committee reports or opinions and/or clinical experiences of respected authorities

Table 2 Classification of recommendation categories

Grade A Treatment is strongly recommended if there is at least one piece of level I evidence indicating validity
Grade B Treatment is recommended if there is at least one piece of level II evidence indicating validity
Grade C1 Treatment can be considered, but the evidence is insufficient; for example, there are several reports of level III evidence, which shows validity with generally consistent results
Grade C2 Treatment is not recommended without sufficient scientific evidence
Grade D Treatment is not recommended because utility and effectiveness have not been shown and the treatment may be harmful

in two separate chapters. Lymph node dissection and laparoscopic surgery are described in detail. In addition, postoperative hormone adjuvant therapy is described in the chapter regarding post-treatment follow-up. Atypical endometrial hyperplasia is included in the chapter regarding fertility-sparing therapy. The chapter regarding treatment of trophoblastic disease is based on the third edition of the general rules for clinical anc pathological management of trophoblastic diseases by Japan society of obstetrics and gynecology and the Japanese pathological society.

4. Basic policies in creating the guidelines

To create these guidelines, the Guidelines Formulation Committee and Evaluation Committee were independently established within the Committee for Treatment Guidelines for Uterine Body Neoplasms. The initial draft was created after a thorough evaluation. Opinions from within and outside the JSGO were incorporated into the final draft. The guidelines were published after approval by the JSGO. Much of the evidence that formed the basis for the Japanese guidelines was obtained from clinical trials in Western countries. However, given the differences between practice in Japan and other countries, the consensus regarding clinical practice in Japan took priority in the event of discrepancies. Wherever possible, high-level Japanese evidence was used to formulate these guidelines. The following items are assumed to underlie the basic policy of the guidelines:

(1) These guidelines were created in accordance with the principles of evidence-based medicine, considered to be the international standard for creating clinical practice guidelines.
(2) Searches were performed of data and literature published until December 2011, including Japanese and non-Japanese studies in Japan and overseas.
(3) The collected evidence was evaluated for quality using the criteria of the Japan Society of Clinical Oncology and its Formulation Committee of Clinical Practice Guidelines for the Use of Anticancer Agents [4, 5]. However, some of the contents were modified in line with these guidelines (Table 1).
(4) The strengths of the recommendations in our guidelines were also determined by the recommendation criteria of the Japan Society of Clinical Oncology and its Formulation Committee of Clinical Practice Guidelines for the Use of Anticancer Agents. These were modified while referring to the "Minds clinical practice guidelines 2007" [6] (Table 2).
(5) The surgical staging criteria described in the 2013 edition were based on the surgical staging system developed in 2008 by the International Federation of Gynecology and Obstetrics (FIGO). In the text, we did not use clinical stage (JSOG 1983, FIGO 1982), but used a description 'considered to be stage X preoperatively' instead.
(6) Therapy is often difficult to administer under the Japanese medical care insurance system. In this regard, the present guidelines follow the Formulation Committee of Clinical Practice Guidelines for the Use of Anticancer Agents.

5. Disclosure of information

These guidelines are published as a pamphlet and are shown on the homepage of JSCO to facilitate widespread use.

6. Responsibility for treatment

The JSGO bears the responsibility for the content and descriptions of these guidelines. However, the final decision to use these guidelines should be made by the individual user. Thus, the responsibility for the treatment outcomes should be directly attributed to the person in charge.

7. Revision

(1) These guidelines are continuously being revised by the Committee for Treatment Guidelines for Uterine Body Neoplasms with medical advances and medical changes.
(2) Newly accumulated evidence after publishing these guidelines is saved in a database.
(3) Any associated information regarding clinical inconvenience occurring with the use of these guidelines is collected.
(4) Revision work is conducted by the Guidelines Formulation Committee and Evaluation Committee based on new evidence and information. Opinions from associated academic societies, groups or JSGO members are widely gained.
(5) After the above-mentioned process, the Committee for Treatment Guidelines for Uterine Body Neoplasms provides a revised version with the approval of the JSGO.

8. Funding

Preparation of these guidelines was funded by the JSGO. We also acknowledge support by grants from the Ministry of Health, Labour and Welfare and H24-Clinical Cancer Research-001 (chief researcher, Koichi Hirata). The expense incurred had no influence on the contents of these guidelines.

9. Conflicts of interest

The Board of the Society Conflict of Interest Committee confirmed the absence of any conflicts of interest. Although some committees had conflicts of interest through study or lecture activity with the company, the contents of these guidelines are based on scientific evidence and thus unaffected by any interest with specific groups or products.

10. Summary of recommendations

In general, each chapter comprises a clinical question (CQ), recommendations, background, objectives, explanations, and references. This article summarizes the guidelines in a question-and-answer format. Recommendations from each chapter are listed below under their respective chapter titles.

11. Algorithms

These guidelines contain the following nine algorithms:

1. Initial treatment for patients with endometrial cancer considered to be stage I or II preoperatively (Fig. 1).
2. Initial treatment for patients who are confirmed as having endometrial cancer after hysterectomy (Fig. 2).
3. Initial treatment for patients with endometrial cancer considered to be stage III or IV preoperatively (Fig. 3).
4. Postoperative adjuvant treatment for endometrial cancer (Fig. 4, Table 3).
5. Treatment of recurrent endometrial cancer (Fig. 5).
6. Strategies for fertility-sparing therapy (atypical endometrial hyperplasia and endometrioid adenocarcinoma; corresponding to G1) (Fig. 6).
7. Treatment for uterine carcinosarcoma (Fig. 7).
8. Treatment for uterine sarcoma (Fig. 8).
9. Treatment for choriocarcinoma (Fig. 9).

Chapter 2: Initial treatment for endometrial cancer (including histologic variant type)

CQ01 Which surgical techniques for hysterectomy are recommended for patients considered to be stage I preoperatively?

Recommendations:

1. Abdominal total hysterectomy (extrafascial technique) is recommended (Grade B).
2. Modified radical (extended) hysterectomy is also considered (Grade C1).

[See Fig. 1].

CQ02. Which surgical hysterectomy techniques are recommended for patients considered to be stage II?

Recommendations:

Either radical hysterectomy or modified radical hysterectomy should be considered for patients with clinically apparent cervical stromal involvement (Grade C1).
[See Fig. 1].

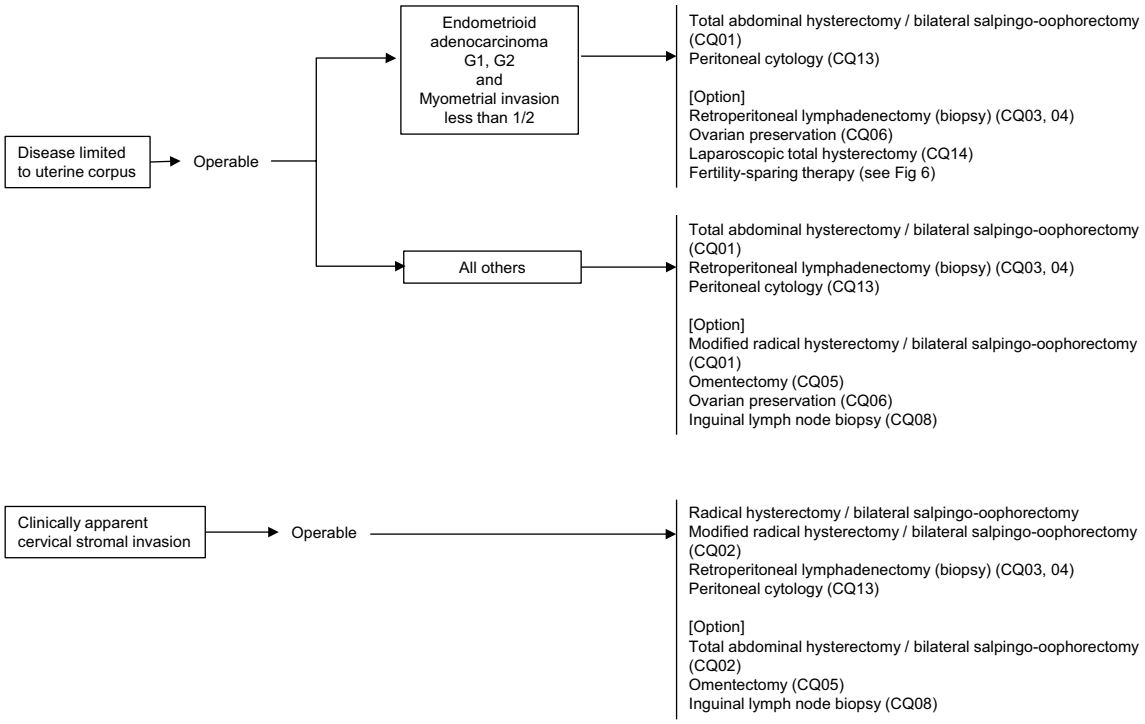

Fig. 1 Initial treatment for patients with endometrial cancer considered to be stage I or II preoperatively. **a** Radiation therapy or chemotherapy are considered when surgery is impossible. **b** Pelvic and paraaortic lymphadenectomy/lymph node biopsy and omentectomy are considered in addition to total hysterectomy with bilateral salpingo-oophorectomy for patients with serous adenocarcinoma or clear-cell adenocarcinoma. *CQ* clinical question

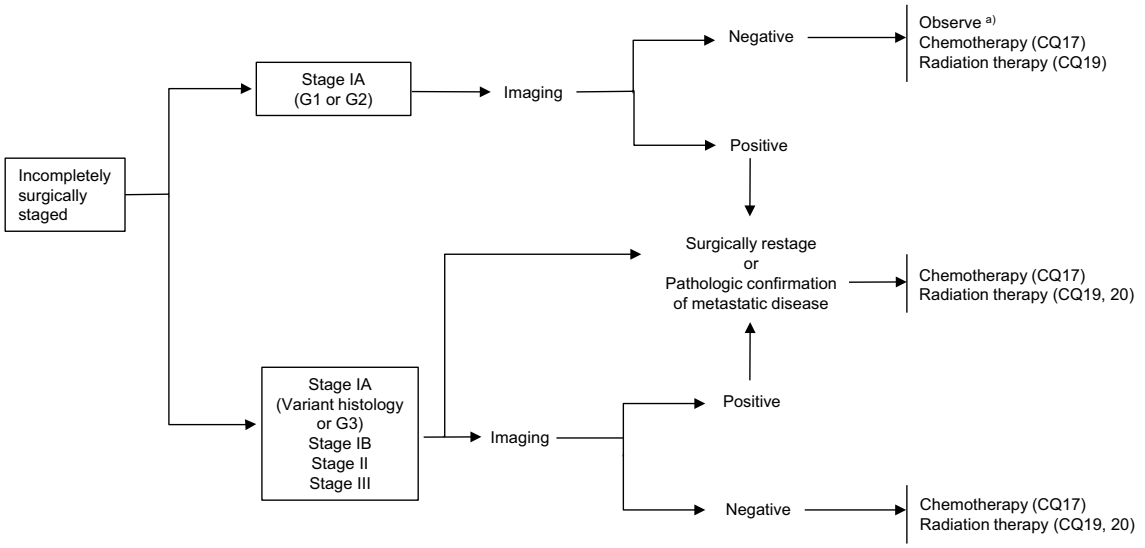

Fig. 2 Initial treatment for patients who are confirmed as having endometrial cancer after hysterectomy. **a** Postoperative chemotherapy is considered for positive lymphovascular space invasion

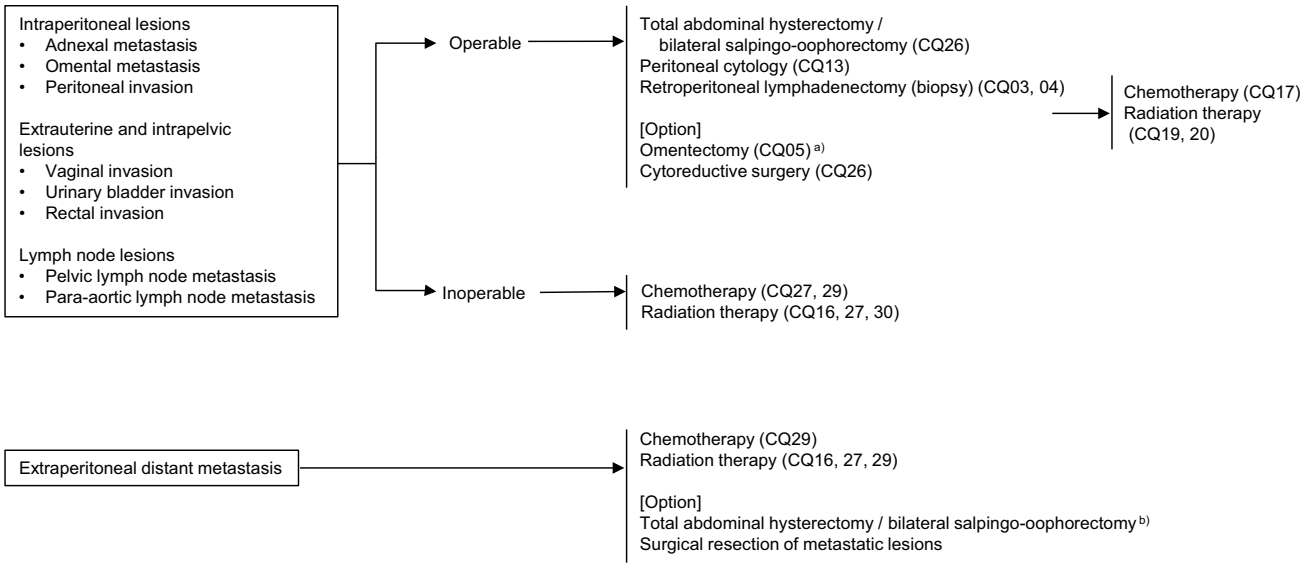

Fig. 3 Initial treatment for patients with endometrial cancer considered to be stage III or IV preoperatively. **a** Because serous adenocarcinoma/clear cell adenocarcinoma is likely to become disseminated, the omentectomy is useful for a diagnosis. **b** Surgery is considered for the purpose of hemostasis even if there is extra-peritoneal metastasis or liver metastasis

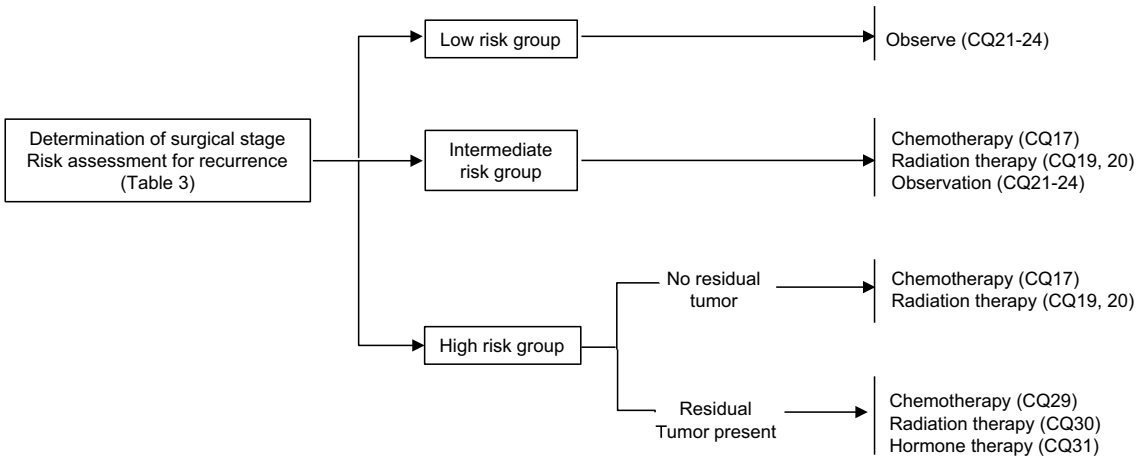

Fig. 4 Postoperative adjuvant treatment for endometrial cancer

CQ03 What are the benefits of pelvic lymphadenectomy?

Recommendations:

1. The diagnostic significance of pelvic lymph node dissection in the determination of correct surgical staging has been established (Grade A).
2. The therapeutic benefits of pelvic lymphadenectomy are not established. However, this procedure should be considered in intermediate-risk or high-risk patients (Grade C1).

[See Fig. 1].

CQ04 What are the benefits of para-aortic lymphadenectomy (biopsy)?

Recommendations:

1. Para-aortic lymphadenectomy (biopsy) is necessary to determine correct surgical staging (Grade A).
2. The therapeutic benefits of para-aortic lymphadenectomy (lymph node biopsy) are not established. How-

Table 3 Classification of postoperative recurrence risk of endometrial cancer

Low-risk group
Endometrioid adenocarcinoma G1 or G2 and <1/2 myometrial invasion
No cervical involvement
No lymphovascular invasion
No distant metastasis
Intermediate-risk group
Endometrioid adenocarcinoma G1 or G2 and ≥1/2 myometrial invasion
Endometrioid adenocarcinoma G3 and <1/2 myometrial invasion
Serous adenocarcinoma, clear-cell adenocarcinoma and no myometrial invasion
No cervical involvement
Positive lymphovascular invasion
No distant metastasis
High-risk group
Endometrioid adenocarcinoma G3 and ≥1/2 myometrial invasion
Serous adenocarcinoma, clear-cell adenocarcinoma and myometrial invasion
Spread to the uterine adnexa, serosa, or cardinal ligament
Invasion of the vaginal wall
Pelvic or para-aortic lymph node metastasis
Vesical or rectal invasion
Peritoneal dissemination
Distant metastasis

There is the opinion to think that positive peritoneal cytology is a poor prognostic factor. (extracted from refs. [7, 8] with some modification)

ever, this procedure should be considered in intermediate-risk or high-risk patients (Grade C1).

[See Fig. 1].

CQ05 Is omentectomy necessary?

Recommendations:

1. Searching the omentum by careful ocular inspection and palpation is necessary in all cases. When metastasis is suspected, omentectomy should be performed to determine the correct stage (Grade A).
2. Omentectomy is considered when deep myometrial invasion, positive intraoperative peritoneal cytology, Grade 3 endometrial carcinoma, serous or clear cell adenocarcinoma, or macroscopic extrauterine disease is present, even if no gross abnormalities are detected in the omentum (Grade C1).

[See Fig. 1].

CQ06 Is ovarian preservation possible?

Recommendations:

1. In principle, bilateral adnexectomy is conducted to determine the correct surgical stage during initial treatment (Grade A).

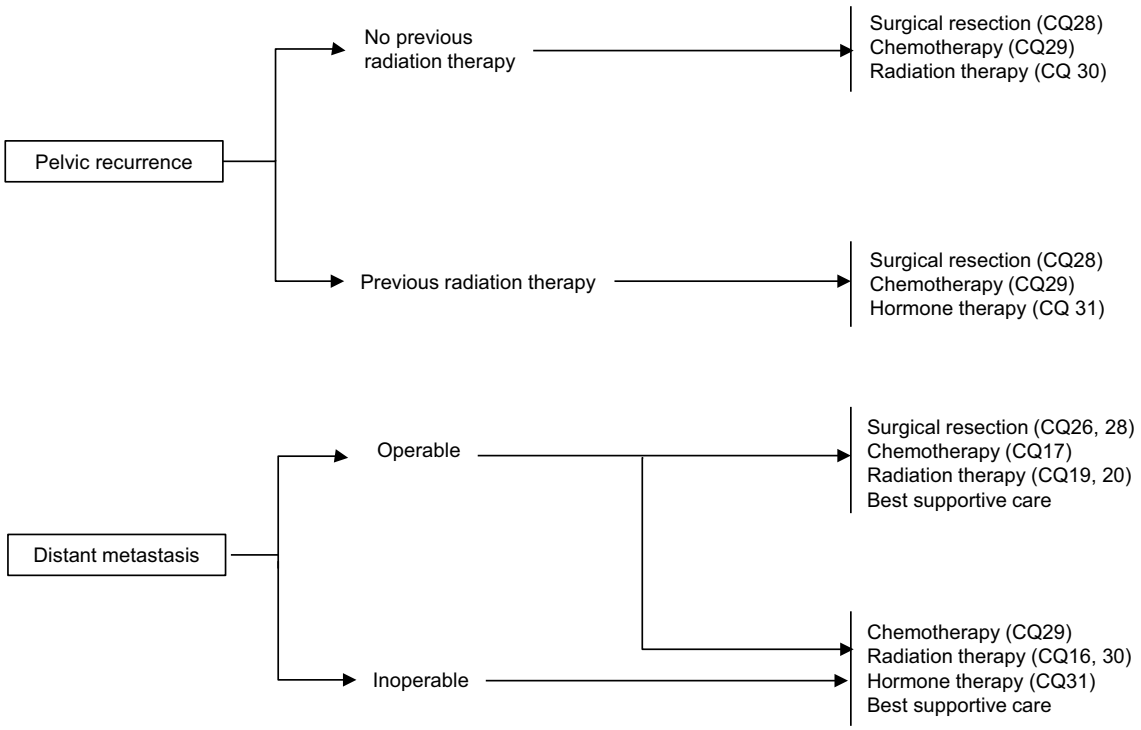

Fig. 5 Treatment of recurrent endometrial cancer

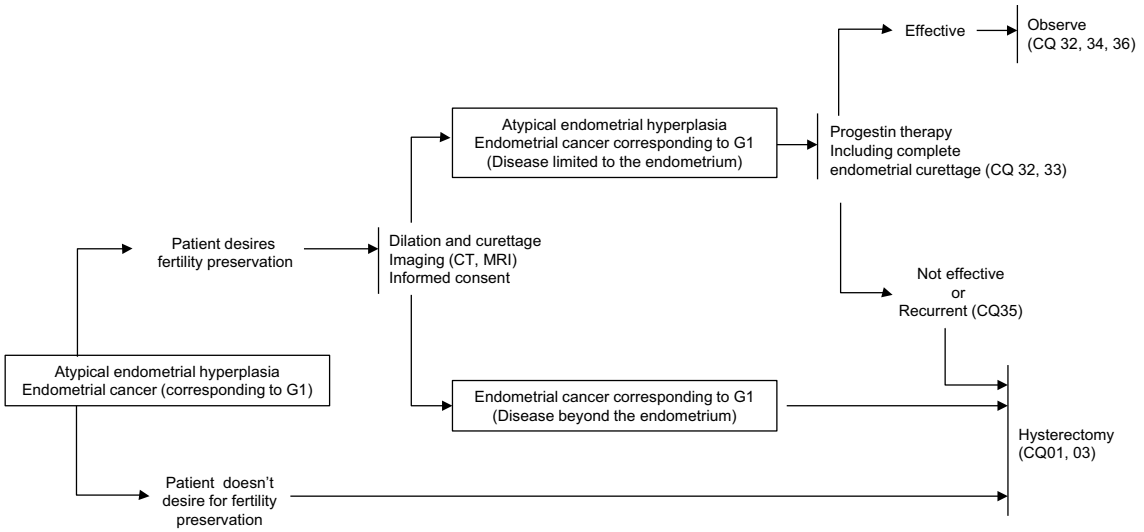

Fig. 6 Strategies for fertility-sparing therapy (atypical endometrial hyperplasia and endometrioid adenocarcinoma; corresponding to G1)

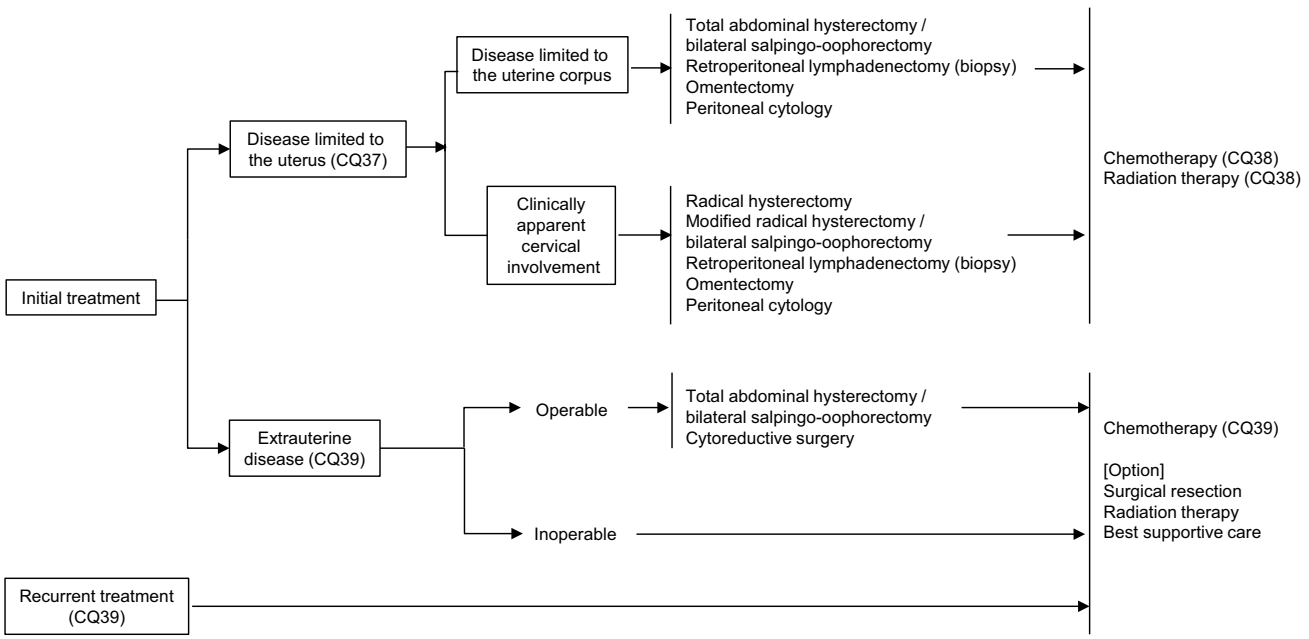

Fig. 7 Treatment for uterine carcinosarcoma

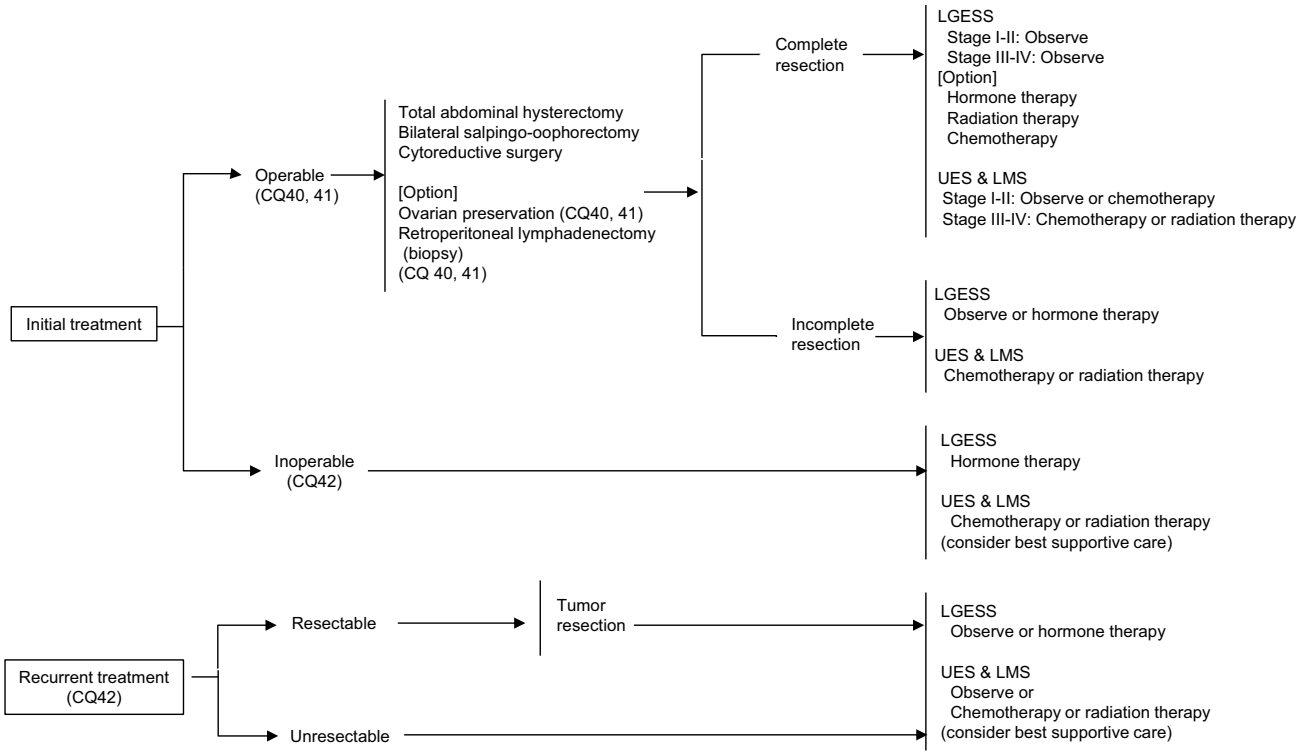

Fig. 8 Treatment for uterine sarcoma. *LGESS* low-grade endometrial stromal sarcoma, *UES* undifferentiated endometrial sarcoma, *LMS* leiomyosarcoma

2. Ovarian preservation is considered after having explained the risks to young patients with well-differentiated tumors and shallow myometrial invasion (Grade C1).

[See Fig. 1].

CQ07 What surgical technique is recommended for serous adenocarcinoma and clear-cell adenocarcinoma?

Recommendations:

1. Total hysterectomy with bilateral salpingo-oophorectomy is recommended (Grade B).
2. Additionally, pelvic and para-aortic lymphadenectomy (lymph node biopsy) and omentectomy are considered (Grade C1).

[See Fig. 1].

CQ08 Is an inguinal lymph node biopsy noted in the surgical staging guidelines necessary?

Recommendations:

1. When an enlarged inguinal lymph node is detected in preoperative imaging such as a computed tomography (CT) scan, then a biopsy is recommended to determine the surgical stage (Grade A).
2. When an enlarged inguinal lymph node is not detected, the benefits of biopsy are not evident. Therefore, routine inguinal lymph node biopsy is not recommended (Grade C2).

[See Fig. 1].

CQ09 What is the significance of preoperative diagnostic imaging?

Recommendations:

1. Evaluation for myometrial invasion and cervical invasion by preoperative magnetic resonance imaging (MRI) is recommended (Grade A).
2. Evaluation for lymph node metastases or distant metastases by preoperative imaging such as CT scan or MRI is recommended (Grade C1).

[See Figs. 1, 3, and 6].

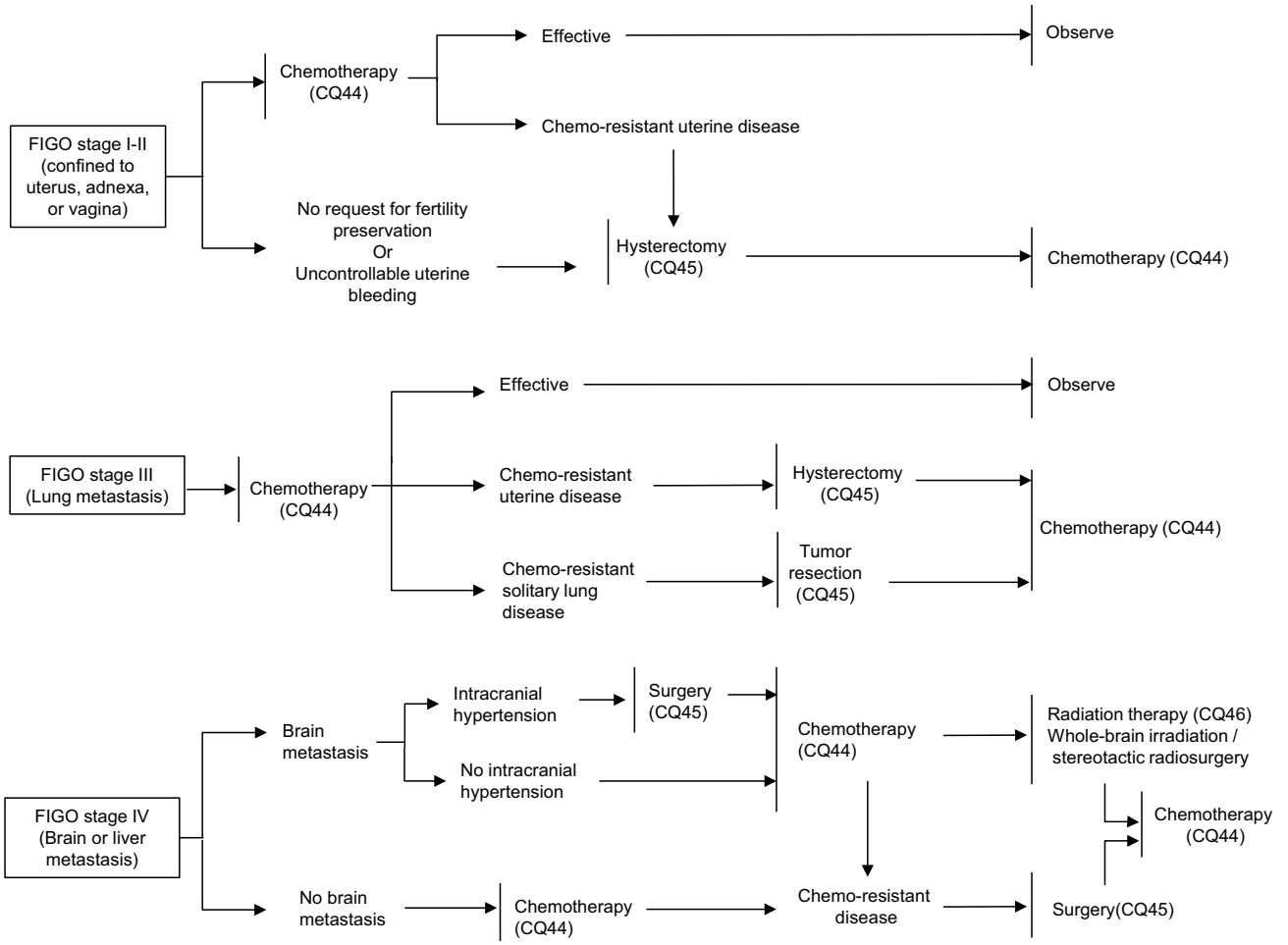

Fig. 9 Treatment for choriocarcinoma

CQ10 Is intraoperative frozen-section diagnosis useful to determine the optimal operative method?

Recommendations:

1. Intraoperative frozen-section diagnosis may be useful for predicting high-risk disease for which pelvic and para-aortic lymphadenectomy or omentectomy would be appropriate (Grade C1).
2. Intraoperative frozen-section diagnosis is not recommended for a definite diagnosis in terms of histological type, histologic differentiation, and myometrial invasion (Grade C2).

CQ11 Should intraoperative frozen-section diagnosis be performed to detect lymph node metastases?

Recommendations:

1. Intraoperative frozen-section diagnosis is useful in the diagnosis of metastasis when apparent lymph node enlargement is detected (Grade C1).
2. There is insufficient evidence to recommend modification of the surgical technique based on the lymph node metastasis status assessed with intraoperative frozen sections. It is not recommended in daily practice (Grade C2).

CQ12 Can lymphadenectomy be omitted if a sentinel node biopsy is performed?

Recommendations:

There is insufficient evidence to omit retroperitoneal lymphadenectomy (lymph node biopsy) based on the sentinel lymph node status. It is not recommended in daily practice (Grade C2).

CQ13 Should peritoneal cytology be performed at the same time as surgery?

Recommendations:

The performance of peritoneal cytology should be continued regardless of whether it is a prognostic factor. Positive cases should be reported separately from surgical staging (Grade A).

[See Figs. 1 and 3].

CQ14 Can laparoscopic surgery become a standard surgical technique?

Recommendations:

1. Laparoscopic surgery is considered for patients with atypical endometrial hyperplasia or an early endometrial cancer limited to the uterus (stage I) (Grade B).
2. Laparoscopic surgery is not recommended for patients with advanced endometrial cancer (Grade C2).

[See Fig. 1].

Additional statement

- It is advisable to decide upon the appropriate surgical procedure and to use a surgical team which includes a qualified surgeon of the Japan Society of Gynecologic and Obstetric Endoscopy and Minimally Invasive Therapy or the Japan Society for Endoscopic Surgery, and board-certified gynecologic oncologists of the JSGO. Otherwise, it is recommended that the surgery be performed according to the instructions of these physicians.
- The decision regarding the appropriate surgical procedure for laparoscopic surgery is carried out according to a basic policy described in CQ01, CQ03, and CQ04.

CQ15 How should patients be treated who are confirmed as having endometrial cancer after hysterectomy?

Recommendations:

1. Follow-up is possible when an extrauterine lesion is negative for myometrial invasion <1/2, G1, or G2. However, adjuvant therapy is considered when vascular invasion is detected (Grade C1).
2. Reoperation is considered when an extrauterine lesion is suspected or when G3, a variant histologic type, or stage >IB disease is present, even if myometrial invasion is <1/2. Based on the results, restaging is recommended, metastasis is confirmed, and the necessity for adjuvant therapy should be discussed.

[See Fig. 2].

CQ16 What are the indications for definitive radiation therapy?

Recommendations:

Radiation therapy is considered when surgery is undesirable because of advanced age, complications, or when patients have unresectable tumors (Grade C1).
[See Fig. 3].

Chapter 3: Postoperative adjuvant therapy for endometrial cancer (including histologic variant type)

CQ17 What are the indications and drugs recommended for postoperative chemotherapy?

Recommendations:

1. Chemotherapy with adriamycin (doxorubicin hydrochloride) and cisplatin is recommended for high-risk patients (Grade B).
2. Taxane-based and platinum-based drug combination therapy (e.g., paclitaxel/carboplatin) is also considered (Grade C1).
3. Postoperative adjuvant chemotherapy is considered for intermediate-risk patients (Grade C1).
4. Postoperative adjuvant chemotherapy is not recommended for low-risk patients (Grade D).

[See Figs. 2, 3 and 4].

CQ18 Is hormone therapy effective as postoperative adjuvant therapy?

Recommendations:

Postoperative progesterone therapy is not recommended (Grade D).

CQ19 What are the indications for postoperative whole-pelvis external-beam irradiation?

Recommendations:

1. Postoperative whole-pelvis external-beam irradiation is considered for patients with risk factors for recurrence (Grade C1).

2. Postoperative vaginal brachytherapy is considered to reduce the risk of vaginal recurrence (Grade C1).

[See Figs. 2, 3 and 4].

CQ20 What are the indications for postoperative irradiation of the para-aortic lymph node region and whole abdomen?

Recommendations:

1. Postoperative irradiation of the para-aortic lymph node region is considered for patients with advanced diseases (Grade C1).
2. Postoperative whole-abdominal irradiation may be used in patients with a variant histologic type, but it is not common in daily practice in Japan (Grade C2).

[See Figs. 2, 3 and 4].

Chapter 4: Post-treatment surveillance for endometrial cancer

CQ21 What intervals are recommended for post-treatment surveillance?

Recommendations:

Standard intervals between routine follow-up appointments are shown below (Grade C1):

1. Every 1−3 months for the first 1–3 years after treatment.
2. Every 6 months for the fourth and fifth years after treatment.
3. Annually from the sixth year after treatment.

[See Fig. 4].

CQ22 Should pelvic examinations and vaginal vault smears be performed at post-treatment follow-up?

Recommendations:

1. Pelvic examination should be performed to diagnose recurrence in the pelvis (Grade A).
2. Vaginal vault smears are considered to detect vaginal stump recurrence (Grade C1).

[See Fig. 4].

CQ23 Should serum tumor markers be measured at post-treatment follow-up?

Recommendations:

Measurement of CA-125 or CA19-9 is considered in post-treatment follow-up (Grade C1).

[See Fig. 4].

CQ24 Should diagnostic imaging be performed in post-treatment follow-up?

Recommendations:

1. Annual chest X-rays are considered for early detection of recurrence (Grade C1).
2. Diagnostic imaging methods such as MRI or CT scan are recommended when recurrence is clinically suspected (Grade B).

[See Fig. 4].

CQ25 Is hormone replacement therapy recommended after treatment?

Recommendations:

Hormone replacement therapy after treatment is carefully considered after having explained the advantages and disadvantages to the patient (Grade C1).

Chapter 5: Treatment for advanced or recurrent endometrial cancer

CQ26 What are the indications for surgery for clinical stages III and IV?

Recommendations:

Surgery is considered whenever a hysterectomy and cytoreduction are possible (Grade C1).

[See Fig. 3].

CQ27 Should neoadjuvant chemotherapy or preoperative radiation therapy be conducted for advanced cancer?

Recommendations:

1. Preoperative chemotherapy is considered in patients with peritoneal dissemination (Grade C1).

2. Preoperative radiation therapy may be conducted for patients with cervical invasion and enlargement; however, it is not common in daily practice in Japan (Grade C2).

[See Fig. 3].

CQ28 What are the indications for surgery for recurrent cancer?

Recommendations:

1. Surgical resection is considered for patients with pelvic recurrence without obvious distant metastasis (Grade C1).
2. Partial resection of the lung is also considered for patients with a few small lung metastases (Grade C1).

[See Fig. 5].

CQ29 Should chemotherapy be conducted for advanced cancer of imperfect resection and recurrent cancer?

Recommendations:

1. Chemotherapy is recommended (Grade B).
2. Paclitaxel/carboplatin, doxorubicin/cisplatin, or paclitaxel/doxorubicin/cisplatin is considered for patients with advanced diseases (Grade C1).
3. Paclitaxel/carboplatin, doxorubicin/cisplatin, or monotherapy is considered for patients with recurrent cancer by taking the situation of the patient and the initial treatment into consideration (Grade C1).

[See Figs. 3, 4, and 5].

CQ30 Should radiation therapy be conducted for recurrent and inoperable advanced cancer?

Recommendations:

1. Radiation therapy is recommended for patients with recurrence at the vaginal cuff (Grade B).
2. Radiation therapy is considered as a palliative option for recurrent cancer, unresectable advanced cancer, and metastatic cancer (Grade C1).

[See Figs. 3, 4, and 5].

CQ31 Should hormone therapy be conducted for advanced and recurrent cancer?

Recommendations:

Progesterone therapy is considered for patients with endometrioid adenocarcinoma (G1) and advanced or recurrent cancer with positive progesterone receptors (Grade C1).

[See Figs. 4 and 5].

Chapter 6: Fertility-sparing therapy

CQ32 When patients with atypical endometrial hyperplasia desire fertility preservation, is progesterone therapy recommended?

Recommendations:

Progesterone therapy is considered in patients with atypical endometrial hyperplasia (Grade C1).

[See Fig. 6].

CQ33 When patients with endometrioid adenocarcinoma (corresponding to G1) desire fertility preservation, is progesterone therapy recommended?

Recommendations:

Progesterone therapy is considered for patients with endometrioid adenocarcinoma (corresponding to G1) suspected to be confined to the endometrium (Grade C1).

[See Fig. 6].

CQ34 What are suitable follow-up periods and examinations?

Recommendations:

Endometrial biopsy and transvaginal ultrasonography are considered every 3 months after completion of progesterone therapy (Grade C1).

[See Fig. 6].

CQ35 What treatments are recommended for patients with recurrence after fertility preservation therapy?

Recommendations:

1. Total hysterectomy is recommended for patients with recurrent disease, an incomplete response, or progressive disease (Grade B).
2. The effectiveness of retreatment with progesterone has not been established in patients with recurrent disease. Retreatment with progesterone is not recommended in routine practice (Grade C2).

[See Fig. 6].

CQ36 Is ovulation induction permissible in patients after fertility preservation therapy?

Recommendations:

Induction of ovulation for pregnancy is considered (Grade C1).

[See Fig. 6].

Chapter 7: Treatment of uterine carcinosarcoma and uterine sarcoma

CQ37 What surgical techniques are recommended for uterine carcinosarcoma?

Recommendations:

1. Total hysterectomy with bilateral salpingo-oophorectomy should be performed (Grade B).
2. In addition to the surgical method mentioned above, pelvic and para-aortic lymphadenectomy (biopsy) are recommended (Grade C1).
3. Radical hysterectomy or modified radical hysterectomy is considered for patients with obvious cervical stromal invasion in whom complete resection is anticipated (Grade C1).

[See Fig. 7].

CQ38 What postoperative adjuvant therapy is recommended for uterine carcinosarcoma?

Recommendations:

1. When postoperative chemotherapy is selected, regimens including ifosfamide, platinum-based drugs, and paclitaxel are considered (Grade C1).
2. Radiation therapy (whole-pelvis external-beam irradiation) is also considered (Grade C1).

[See Fig. 7].

CQ39 What treatments are recommended for advanced and recurrent uterine carcinosarcoma?

Recommendations:

1. If total hysterectomy and cytoreductive surgery are possible, surgical treatment is recommended (Grade C1).
2. Regimens including ifosfamide, platinum-based drugs, and paclitaxel are recommended for chemotherapy in patients with advanced or recurrent disease (Grade C1).

[See Fig. 7].

CQ40 What surgical techniques and postoperative adjuvant therapy are recommended for uterine leiomyosarcoma?

Recommendations:

1. Complete extraction including total hysterectomy with bilateral salpingo-oophorectomy is recommended (Grade B).
2. Chemotherapy is considered as postoperative adjuvant therapy (Grade C1).
3. Postoperative radiation is less efficacious and is therefore not recommended in routine practice (Grade C2).

[See Fig. 8].

CQ41 What surgical techniques and postoperative adjuvant therapy are recommended for endometrial stromal sarcoma (ESS)?

Recommendations:

1. Total hysterectomy with bilateral salpingo-oophorectomy is recommended as a standard surgical procedure (Grade B).
2. Pelvic and para-aortic lymphadenectomy (biopsy) or cytoreductive surgery is also considered (Grade C1).
3. For stage I or II low-grade ESS, follow-up without postoperative adjuvant therapy is recommended (Grade B).
4. When adjuvant therapy is necessary for high-grade ESS, chemotherapy is recommended (Grade C1).

[See Fig. 8].

CQ42 What treatments are recommended for unresectable or recurrent ESS/leiomyosarcoma?

Recommendations:

1. Surgery is considered for recurrence if the tumor is resectable (Grade C1).
2. Chemotherapy is also considered (Grade C1).
3. Hormonal therapy is also considered for low-grade ESS (Grade C1).
4. Radiation therapy for the purpose of palliative care is considered (Grade C1).

[See Fig. 8].

Chapter 8: Treatment of trophoblastic disease

CQ43 What chemotherapy is recommended for an invasive mole, clinical invasive mole, or post-molar persistent human chorionic gonadotropin (hCG)?

Recommendations:

Monotherapy with methotrexate or actinomycin D is recommended (Grade B).

CQ44 What chemotherapy is recommended for choriocarcinoma?

Recommendations:

A multidrug regimen including methotrexate, actinomycin D, and etoposide is recommended (Grade C1).

[See Fig. 9].

CQ45 What are the indications for surgery for choriocarcinoma?

Recommendations:

1. Surgical resection is considered for patients with a uterine lesion or metastatic lesion associated with chemoresistance (Grade C1).
2. Surgical resection is also considered for patients with a uterine lesion in which hemorrhage is difficult to control or those who have brain metastasis with symptoms of intracranial hypertension (Grade C1).

[See Fig. 9].

CQ46 What are the indications for radiation therapy for choriocarcinoma?

Recommendations:

Whole-brain irradiation and/or stereotactic radiosurgery are considered to treat brain metastasis (Grade C1).

[See Fig. 9].

CQ47 What treatments are recommended for cases with placental site trophoblastic disease or epithelioid trophoblastic tumor?

Recommendations:

1. Total hysterectomy is recommended for patients with disease limited to the uterus (Grade B).
2. Combination therapy with surgical treatment including total hysterectomy and chemotherapy are desirable for patients with metastasis (Grade C1).

CQ48 How should patients with persistent low-positive hCG be treated?

Recommendations:

After every gestation including hydatidiform mole or after treatment of trophoblastic disease, strict follow-up is recommended when 'real' low-unit hCG persists long term without an obvious lesion (Grade C1).

Acknowledgments We thank the Japan Society of Obstetrics and Gynecology, the Japan Association of Obstetricians and Gynecologists, the Japanese Gynecologic Oncology Group, the Japan Society of Clinical Oncology, and the Japanese Society for Therapeutic Radiology and Oncology for their comments and contributions throughout the project. We also acknowledge the support by grants from the Ministry of Health, Labour and Welfare and H24-Clinical Cancer Research-001 (chief researcher, Koichi Hirata).

Members of guidelines formulation committee Yasuhiko Ebina, Hisaya Fujiwara, Shinji Fukunaga, Yasuyuki Hasuo, Atsushi Hongo, Kazuhiko Ino, Yuko Kaneyasu, Hidenori Kato, Naoki Kawamura, Yoichi Kobayashi, Kaneyuki Kubushiro, Masataka Kudo, Hideo Matsui, Koji Matsumoto, Yoshiki Mikami, Toshinari Muramatsu, Shoji Nagao, Satoru Nagase, Takafumi Nakamura, Toru Nakanishi, Satoru Nakayama, Hideyuki Ohtake, Yoshikazu Ozaki, Nobuyuki Susumu, Tsutomu Tabata, Kiyoshi Takamatsu, Masashi Takano, Satoshi Takeuchi, Yoshito Terai, Takafumi Toita, Akiko Tozawa, Takashi Uno, Hidemichi Watari, Tetsuro Yahata, Hideko Yamamoto, Koji Yamazawa, Nozomu Yanaihara, Masami Yasuda, Yoshihito Yokoyama.

Members of guidelines evaluation committee Daisuke Aoki, Yoichi Aoki, Makoto Emoto, Takayuki Enomoto, Toru Hachisuga, Seiryu Kamoi, Takahiro Kasamatsu, Noriyuki Katsumata, Junzo Kigawa, Hiroaki Kobayashi, Takeshi Kodaira, Junichi Kodama, Shinichi Komiyama, Hiroyuki Kuramoto, Makoto Kuroda, Masaki Mandai, Etsuko Miyagi, Takashi Nakano, Kaei Nasu, Fumitaka Numa, Kazunori Ochiai, Tsuyoshi Saito, Toshiaki Saito, Masaru Sakamoto, Noriaki Sakuragi, Nobuhiro Takeshima, Toshimitsu Toya, Satoshi Umezawa, Yoh Watanabe, Hiroyuki Yanai.

Compliance with ethical standards

Conflict of interest Kiyoshi Takamatsu received lecture fees from Bayer Yakuhin, Ldt, and Pfizer Japan Inc.

References

1. Matsuda A, Matsuda T, Shibata A et al (2014) Cancer incidence and incidence rates in Japan in 2008: a study of 25 population-based cancer registries for the Monitoring of Cancer Incidence in Japan (MCIJ) project. Jpn J Clin Oncol 44(4):388–396

2. For act on anti-cancer measures based on the data of statistics white paper 2012 (Shinoharashinsha Publishers Inc.) Cancer Information Service, National Cancer Center, Japan
3. Nagase S, Katabuchi H, Hiura M et al (2010) Evidence-based guidelines for treatment of uterine body neoplasmin Japan: Japan Society of Gynecologic Oncology (JSGO) 2009 edition. Int J Clin Oncol 15:531–542
4. Ariyoshi H (2002) Guideline for correct use of antineoplastic agents (draft). General theory. Gan To Kagaku Ryoho 29(6):970–977 **(in Japanese)**
5. Ochiai K, Okamoto A, Katsumata N (2002) Guidelines for proper use of antineoplastic agents. Gynecologic cancer. Gan To Kagaku Ryoho 29(6):1047–1054 **(in Japanese)**
6. Fukui T, Yoshida M, Yamaguchi N (2007) Minds clinical practice guideline. Igaku-Shoin, Tokyo, p 40 (**in Japanese**)
7. Dowdy SC, Mariani A, Lurain JR (2012) Uterine cancer. In: Berek JS (ed) Berek and Novak's gynecology, 15th edn. Lippincot Williams & Wilkins, Philadelphia, PA, pp 1250−1303
8. Miller DS, Creasman WT (2012) Adenocarcinoma of the uterine corpus. In: DiSaia PJ, Creasman WT (eds) Clinical gynecologic oncology, 8th edn. Elsevier Saunders, Philadelphia, pp 141–174

Aggressive Angiomyxoma of the Vulva with No Recurrence on a 5-year Follow up: A Case Report

Chisa NARAYAMA, Masae IKEDA, Miwa YASAKA, Yu-suke SAGARA, Yasuhira KAN-NO, Io HAYASHI, Atuya NARITA, Satoshi ASAI, Toshiki TAJIMA, Masako SHIDA, Takeshi HIRASAWA and Mikio MIKAMI

Department of Obstetrics and Gynecology, Tokai University School of Medicine

(Received January 27, 2016; Accepted February 16, 2016)

We report a case of vulvar aggressive angiomyxoma (AA) which is a rare, slow growing and benign tumor of mesenchymal origin, but has a high risk of local recurrence.
A 49-year-old Japanese female was referred to us with a large mass of the left vulva, measuring 15×9.5×9 centimeters. She underwent surgical excision of the tumor with no evidence of recurrence on a 5-year follow up. In this case, histopathological examination and immunohistochemical staining after excision revealed a diagnosis of vulvar AA with estrogen and progesterone receptors positive.
Aggressive angiomyxoma of the vulva needs to be distinguished from benign myxoid tumor with a low risk of local recurrence as well as from malignant neoplasma. The first line treatment of AA is complete surgical excision with tumor free margins, it will reduce the recurrence.

Key words: aggressive angiomyxoma, mesenchymal tumor, vulva, slow growing, local recurrence

INTRODUCTION

Aggressive angiomyxoma (AA), a rare soft tissue tumor of mesenchymal origin, predominantly occurs in the pelvic peritoneum, vulvo-vaginal, perineal and groin region of female in reproductive age. The female-to-male ratio is 6.6/1 [1]. Although AA is a slow growing and benign neoplasm, it has a high risk of local recurrence after many years but usually does not metastasize.

AA was first described by Steeper and Rosai in 1983 as a rare mesenchymal tumor of reproductive-age women [2]. AA is often clinically misdiagnosed as a malignancy, such as mixed mesodermal tumor, malignant fibrous histiocytoma, botyroid pseudosarcoma, embryonal rhabdomyosarcoma and squamous cell carcinoma by primary care providers. Misdiagnosis is seen in 80% of the cases [3]. Imaging is important to diagnose and to determine the extent of the lesion for surgery as the first line of treatment.

We describe a case report of AA of the vulva in a 49-year-old female who underwent complete surgical excision of the tumor with no evidence of recurrence on a 5-year follow up.

CASE REPORT

A 49-year-old, Gravida 5 Para 2, Japanese female referred to the gynecology outpatient unit of our hospital with a complaint of a large left vulvar mass, measuring 15 × 9.5 × 9 centimeters (Fig. 1). It was an elongated, non-mobile, non-tender and painless mass extending longitudinally between the mons pubis and the anal verge along the left labial fold. The patient noticed the small mass 5 years ago and it has been gradually increased in size. As the increasing, she has complained of progressively worsening her quality of life. She was previously healthy, her past medical and family histories were normal. She had smoked 15 cigarettes per day for 35 years in her personal history. Her physical examination and laboratory tests were within normal limits.

Magnetic Resonance Imaging (MRI) revealed a bulky well circumscribed subcutaneous mass lesion in the left vulva. The mass demonstrated isointensity to the muscle on T1-weighted images (Fig. 2-1). On T2-weighted images high signal intensity relative to the muscle with "swirled" low signals intensity bands within the hyperintense tumor was noted (Fig. 2-2). Computed tomography (CT) showed no pelvic lymphadenopathy and ascites.

With informed consent, she underwent a surgical excision of the tumor (Fig. 3-1, 2). The final pathological diagnosis was AA of the vulva.

Macroscopically, the bulky mass was a solid and soft tumor, measuring 15 cm in longitudinal diameter and well circumscribed (Fig. 4-1). The cut surface showed a fleshy glistening myxoid mass with a mixed white and yellow tone (Fig. 4-2). Microscopically, short spindle-shaped tumor cells proliferate in a myxoid, edematous background (Fig. 5). The tumor cells have scant eosinophilic cell bodies and mildly enlarged nuclei. Mitoses are rarely seen. Blood vessels are occasionally found. In immunohistochemical stain, tumor cells are positive for desmin, SM-actin, estrogen receptor and

Masae IKEDA, Department of Obstetrics and Gynecology, Tokai University School of Medicine, 143 Shimokasuya, Isehara, Kanagawa 259-1193, Japan
Tel: +81-463-93-1121 Fax: +81-463-91-4343 E-mail: ikedam@tokai-u.jp

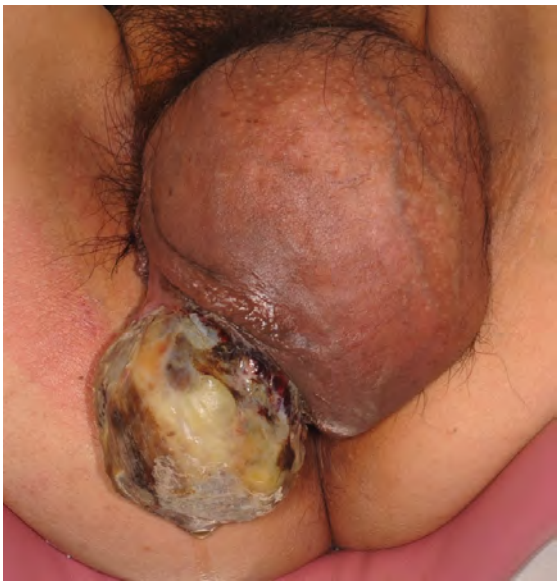

Fig. 1 a large left vulvar mass, measuring 15 × 9.5 × 9 centimeters.

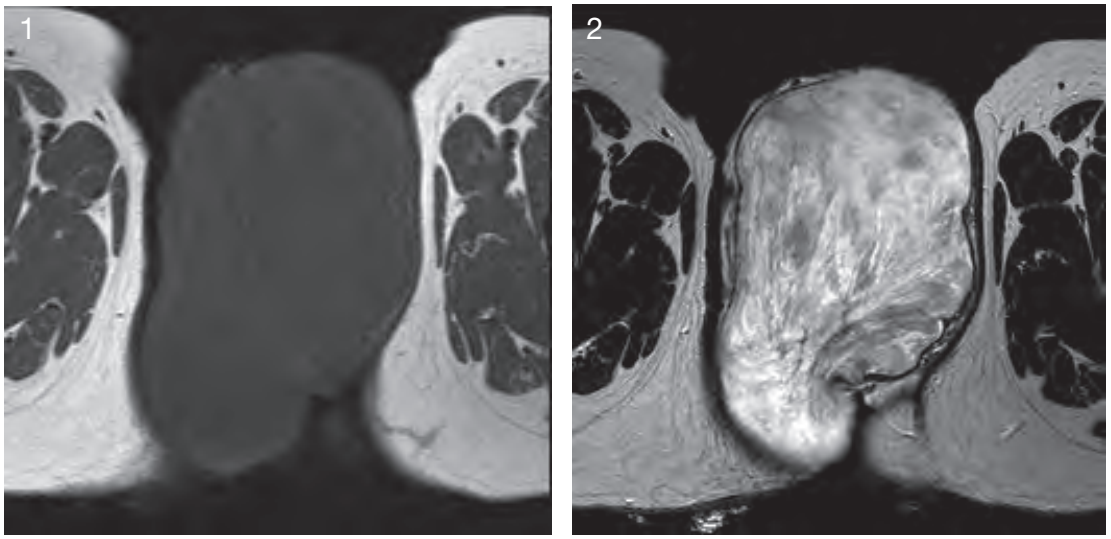

Fig. 2 (1) Axial MRI: T1-weighted images showing vulvar mass with isointensity to the muscle.
(2) Axial MRI: T2-weighted images showing vulvar aggressive angiomyxoma with the swirled appearance.

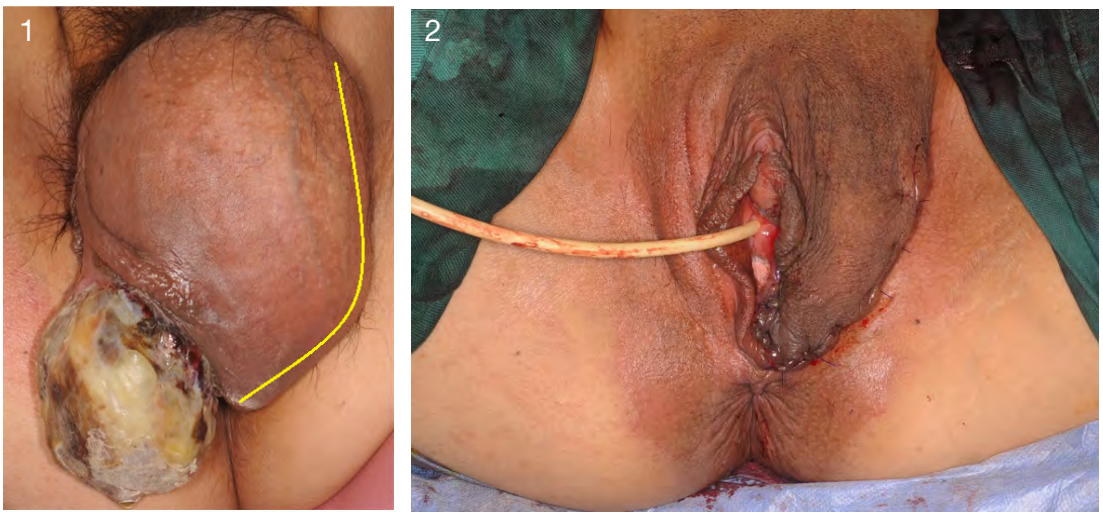

Fig. 3 (1) Surgery of vulvar aggressive angiomyxoma. (Preoperative)
(2) Surgery of vulvar aggressive angiomyxoma. (Postoperative)

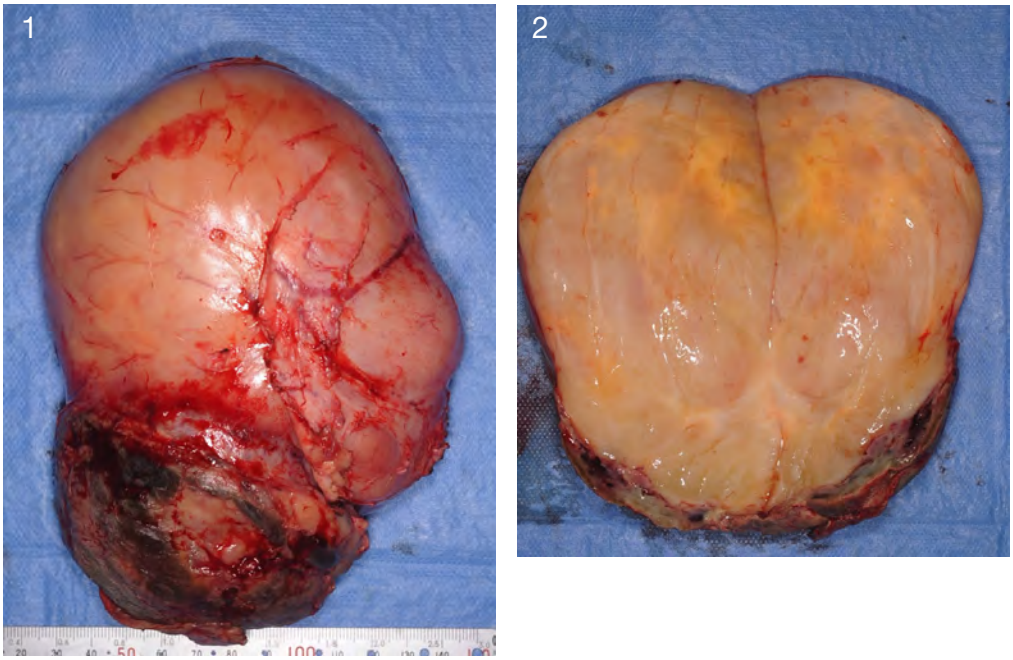

Fig. 4 (1) Gross vulvar aggressive angiomyxoma: the solid tumor, measuring 15 cm in longitudinal diameter and almost encapsulated with the exception of the self-destructive part. (2) Cut surface: fleshy glistening myxoid mass mixed white and yellow tone.

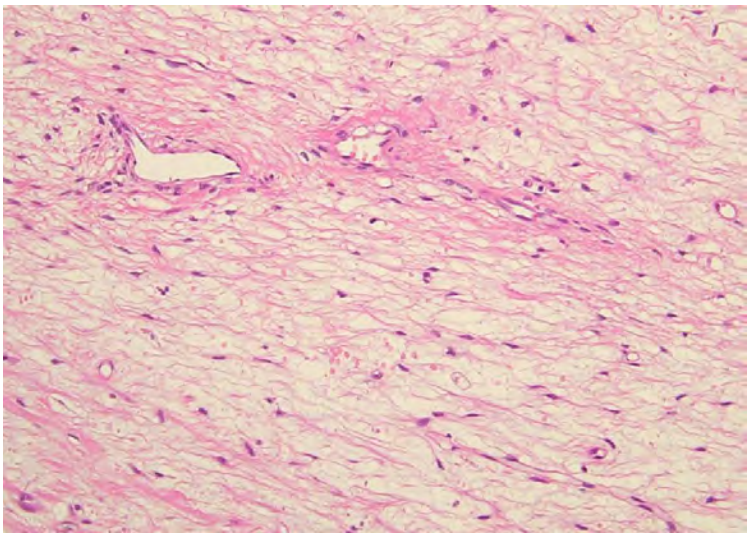

Fig. 5 short spindle-shaped tumor cells proliferate in a hypocellular myxoid stroma. (HE stain, x100)

progesterone receptor. No expression of CD34, S-100 protein, caldesmon and myoglobin is seen.

No relapse has occurred by the time of follow-up at 5 years after surgery.

DISCUSSION

The vulvar AA is a benign mesenchymal tumor but with a high local recurrence rate up to 72%, and relapse occurs months to several years after surgery [4, 5]. That is why differential diagnosis is pivotal for the prognosis from other benign myxoid neoplasms.

Several imaging modalities are useful in primary and recurrent diagnosing and surgical treatment of AA. Particularly, MRI and CT are recommended to diagnose and identify the extent of the tumor for making surgical approach. Relative to muscle signals on MRI, AA shows an isointense signal on T1-weighted images and a hyperintense one on T2-weighted images. A swirled appearance retaining the enhancing layered appearance on MRI and CT is characteristic and often present in 83% of cases [5]. CT also shows a tumor with well-defined moderately enhanced margins with attenuation less than that of muscle [6]. The attenuation on CT and high signal intensity on MRI are likely related to the loose myxoid matrix and high water content of angiomyxoma [2].

In our patient, a gynecological exam revealed a self-destructive fleshy mass in the left vulva, and MRI

and CT confirmed the superficial nature of this lesion with respect to the pelvic diaphragm and provided a proper surgical route. To obtain a successful result in surgical treatment, it is important to completely excise a tumor with tumor-free margins. The excised lesion of our case had negative margins on pathological evaluation. AA of the external surface is smooth and usually appears not to be encapsulated. They typically have finger-like projections that extend into neighboring tissues [1]. Our case, unlike most AA, was almost encapsulated by a fibrofatty layer with the exception of the self-destructive part, and there was no evident infiltration into neighboring tissues in this case. This may explain why there has been no recurrence in the last 5 years.

There are various treatments, however if it is possible, complete surgical excision with a clear margin should be sought. While lesion recurrence is frequent, hormonal treatment with gonadotropin-releasing hormone analogs (GnRHa) or anti-hormonal therapy is sometimes needed for primary and recurrent AA. This can be attributed to the fact that most of AA express estrogen and progesterone receptors and are sensitive to hormonal therapy [7, 8]. Han-Guerts *et al*. [9] proposes the following guidelines in treating AA: (1) complete excision of the lesion when possible and avoiding mutilating surgery, (2) adjunct therapy when partial resection is performed is acceptable using arterial embolization and/or hormonal treatment, and (3) radiotherapy is reserved to cases that are resistant to embolization and/or hormonal therapy and still symptomatic. There are no standard treatments for recurrence in the postoperative management of vulvar AA. Our patient required no additional treatment postoperatively because of complete excision with negative margins and an almost encapsulated tumor.

The pathogenesis of vulvar AA is poorly understood, but a translocation at chromosome 12 with a consequent aberrant expression of the high-mobility group protein isoform I-C (HMGI-C) protein involved in DNA transcription has been demonstrated. Detection of inappropriate HMGI-C expression using immunoperoxidase technique with anti HMG1-C antibody may be a useful marker for microscopic residual disease [10].

In conclusion, AA is a rare locally aggressive mesenchymal tumor. When complete resection with tumor-free margins is possible, it will offer the lowest recurrence rate. Even if the AA is resected completely, it is clear that it requires close and long-term follow up for recurrence.

ACKNOWLEDGMENTS

The authors express the sincere gratitude to Dr. Hiroshi Kajiwara, and Dr. Nobue Kumaki, Departmentbof Pathology, Tokai School of Medicine, for their cooperation.

REFERENCES

1) Dahiya K, Jain S, Duhan N, Nanda S, Kundu P. Aggressive angiomyxoma of vulva and vagina: a series of three cases and review of literature. Archives of Gynecology and Obstetrics 2011; 283(5): 1145–1148.
2) Steeper TA, Rosai J. Aggressive angiomyxoma of the female pelvis and perineum. Report of nine cases of a distinctive type of gynecologic soft-tissue neoplasm. American Journal of Surgical Pathology 1983; 7(5): 463–475.
3) Güngör T, Zengeroğlu S, Kaleli A, Kuzey GM. Aggressive angiomyxoma of the vulva and vagina — a common problem: misdiagnosis. European Journal of Obstetrics Gynecology and Reproductive Biology 2004; 112(1): 114–116.
4) Dierickx I, Deraedt K, Poppe W, Verguts J. Aggressive angiomyxoma of the vulva: a case report and review of literature. Archives of Gynecology and Obstetrics 2008; 277(6): 483–487.
5) Kiran G, Yancar S, Sayar H, Kiran H, Coskun A, Arikan DC. Late recurrence of aggressive angiomyxoma of the vulva. Journal of Lower Genital Tract Disease 2013; 17(1): 85–87.
6) Outwater EK, Marchetto BE, Wagner BJ, Siegelman ES. Aggressive angiomyxoma: findings on CT and MR imaging. American Journal of Roentgenology 1999; 172(2): 435–438.
7) Fine BA, Munoz AK, Litz CE, Gershenson DM. Primary medical management of recurrent aggressive angiomyxoma of the vulva with a gonadotropin-releasing hormone agonist. Gynecologic Oncology 2001; 81(1): 120–122.
8) McCluggage WG, Jamieson T, Dobbs SP, Grey A. Aggressive angiomyxoma of the vulva: dramatic response to gonadotropin-releasing hormone agonist therapy. Gynecol Oncol 2006; 100: 623–625.
9) Han-Geurts IJM, van Geel AN, van Doorn L, M. den Bakker MDB, Eggermont AMM, Verhoef C. Aggressive angiomyxoma: multimodality treatments can avoid mutilating surgery. European Journal of Surgical Oncology 2006; 32(10): 1217–1221.
10) Nucci MR, Fletcher CDM. Vulvovaginal soft tissue tumours: update and review. Histopathology 2000; 36(2): 97–108.

J Gynecol Oncol. 2016 May;27(3):e29
http://doi.org/10.3802/jgo.2016.27.e29
pISSN 2005-0380 · eISSN 2005-0399

JOURNAL OF GYNECOLOGIC ONCOLOGY

Original Article

Practice patterns of adjuvant therapy for intermediate/high recurrence risk cervical cancer patients in Japan

Yuji Ikeda,[1,2] Akiko Furusawa,[3] Ryo Kitagawa,[4] Aya Tokinaga,[5] Fuminori Ito,[6] Masayo Ukita,[7] Hidetaka Nomura,[8] Wataru Yamagami,[9] Hiroshi Tanabe,[10] Mikio Mikami,[11] Nobuhiro Takeshima,[8] Nobuo Yaegashi[12]

[1]Department of Obstetrics and Gynecology, The University of Tokyo, Tokyo, Japan
[2]Department of Gynecologic Oncology, Saitama Medical University International Medical Center, Saitama, Japan
[3]Department of Obstetrics and Gynecology, Tokyo Medical and Dental University, Tokyo, Japan
[4]Department of Obstetrics and Gynecology, NTT Medical Center Tokyo, Tokyo, Japan
[5]Department of Obstetrics and Gynecology, Yokohama City University Graduate School of Medicine, Yokohama, Japan
[6]Department of Obstetrics and Gynecology, Nara Medical University, Nara, Japan
[7]Department of Obstetrics and Gynecology, Kinki University Faculty of Medicine, Osakasayama, Japan
[8]Department of Gynecology, Cancer Institute Hospital, Tokyo, Japan
[9]Department of Obstetrics and Gynecology, Keio University School of Medicine, Tokyo, Japan
[10]Department of Obstetrics and Gynecology, Jikei University Kashiwa Hospital, Kashiwa, Japan
[11]Department of Obstetrics and Gynecology, Tokai University School of Medicine, Isehara, Japan
[12]Department of Obstetrics and Gynecology, Tohoku University Graduate School of Medicine, Sendai, Japan

Received: Nov 23, 2015
Revised: Dec 26, 2015
Accepted: Jan 5, 2016

Correspondence to
Ryo Kitagawa
Department of Obstetrics and Gynecology, NTT Medical Center Tokyo, 5-9-22 Higashi-Gotanda Shinagawa-ku, Tokyo 141-8625, Japan.
E-mail: ryokitagawajp@yahoo.co.jp

The contents of this study was partially presented at 57th Meeting of the Japan Society of Gynecologic Oncology.

ORCID
Yuji Ikeda
http://orcid.org/0000-0003-1633-5385
Akiko Furusawa
http://orcid.org/0000-0003-1279-4971
Ryo Kitagawa
http://orcid.org/0000-0003-3679-8168
Aya Tokinaga
http://orcid.org/0000-0002-7134-7437
Fuminori Ito
http://orcid.org/0000-0002-0437-0979

ABSTRACT

Objective: Although radiation therapy (RT) and concurrent chemoradiotherapy (CCRT) are the global standards for adjuvant therapy treatment in cervical cancer, many Japanese institutions choose chemotherapy (CT) because of the low frequency of irreversible adverse events. In this study, we aimed to clarify the trends of adjuvant therapy for intermediate/high-risk cervical cancer after radical surgery in Japan.
Methods: A questionnaire survey was conducted by the Japanese Gynecologic Oncology Group to 186 authorized institutions active in the treatment of gynecologic cancer.
Results: Responses were obtained from 129 facilities. Adjuvant RT/CCRT and intensity-modulated RT were performed in 98 (76%) and 23 (18%) institutions, respectively. On the other hand, CT was chosen as an alternative in 93 institutions (72%). The most common regimen of CT, which was used in 66 institutions (51%), was a combination of cisplatin/carboplatin with paclitaxel. CT was considered an appropriate alternative option to RT/CCRT in patients with risk factors such as bulky tumors, lymph node metastasis, lymphovascular invasion, parametrial invasion, and stromal invasion. The risk of severe adverse events was considered to be lower for CT than for RT/CCRT in 109 institutions (84%).
Conclusion: This survey revealed a variety of policies regarding adjuvant therapy among institutions. A clinical study to assess the efficacy or non-inferiority of adjuvant CT is warranted.

Keywords: Adjuvant Therapy; Drug Therapy; Radiation; Uterine Cervical Neoplasms

JOURNAL OF GYNECOLOGIC ONCOLOGY

Masayo Ukita
http://orcid.org/0000-0002-1660-1834
Hidetaka Nomura
http://orcid.org/0000-0002-2742-5282
Wataru Yamagami
http://orcid.org/0000-0003-3925-6057
Hiroshi Tanabe
http://orcid.org/0000-0002-8445-8558
Mikio Mikami
http://orcid.org/0000-0002-7496-3518
Nobuo Yaegashi
http://orcid.org/0000-0003-2521-039X

Conflict of Interest
No potential conflict of interest relevant to this article was reported.

INTRODUCTION

Cervical cancer is the third most common cause of death among gynecologic cancers [1]. Women with stage IA2 to IIA lesions require radical hysterectomy with bilateral pelvic lymph-node dissection, radiation therapy (RT), or concurrent chemoradiotherapy (CCRT) [2,3]. In Japan, more than 80% of institutions choose radical hysterectomy as the primary therapy for patients with stage IB1 and IIA1 tumors [4]. After the surgical procedure, the recurrence risk is evaluated by pathological criteria such as lymph node metastasis, lymphovascular space invasion, depth invasion, parametrial invasion, nonsquamous histology, and positive surgical margins [5-8]. Subsequently, adjuvant therapy is considered for patients with an intermediate/high risk of recurrence.

RT decreases the incidence of local recurrence when used as an adjuvant therapy [9,10]; however, there is little or no effect on overall survival [11,12]. On the other hand, CCRT improves progression-free and overall survival for high-risk and early-stage patients who undergo radical hysterectomy and pelvic lymphadenectomy [13]. The National Comprehensive Cancer Network (NCCN) recommends pelvic RT/CCRT for high-risk patients [2]. The Japan Society of Gynecologic Oncology treatment guidelines for cervical cancer also follow the NCCN policy with minor modifications [14]. However, 37% to 48% of recurrences in cervical cancer occur in the extra-pelvic area, and their prognosis is extremely poor [15,16]. In addition, patients who undergo RT may still experience late adverse events and toxicity because of the anatomic locations such as the bladder, bowel, vagina, and ovary [17]. In terms of the quality of life, RT has a disadvantage about sexual function in young women with cervical cancer [18]. Since complications exist over a long time and the mean age at diagnosis of cervical cancer is 48 years, many patients and physicians hesitate to choose RT/CCRT [19,20]. Although some institutions adopt an approach using intensity-modulated radiation therapy (IMRT) to reduce the adverse events, a longer follow-up is required to evaluate the benefit of this treatment [21].

Our previous study showed that many institutions in Japan use chemotherapy (CT) as an adjuvant therapy in patients with intermediate and high risk of recurrence [22]. However, to the best of our knowledge, no clinical study has been conducted to evaluate the efficacy or inferiority of CT as an adjuvant therapy for cervical cancer. In this study, we first aimed to clarify the current trends for adjuvant therapy in different institutions, then evaluated the need for a prospective study to assess CT as an adjuvant therapy for postoperative cervical cancer.

MATERIALS AND METHODS

A questionnaire was designed by a gynecological oncology clinical fellow who attended an educational seminar conducted by the Japanese Gynecologic Oncology Group (JGOG) in August 2013. The details of the questionnaire are listed in **Appendix**. Briefly, the questionnaire included the following questions:

(1) What kind of therapy is routinely selected as an adjuvant therapy for intermediate/high risk postoperative cervical cancer?
(2) What kind of regimen is used for adjuvant CT?
(3) What kind of chemotherapeutic agents are used for CCRT?

http://doi.org/10.3802/jgo.2016.27.e29

JOURNAL OF GYNECOLOGIC ONCOLOGY

(4) Does your institute perform IMRT?
(5) What do you select as a most appropriate adjuvant therapy for patients with risk factors such as bulky tumor, lymph node metastasis, lymphovascular invasion, parametrial invasion, stromal invasion, and vaginal stump invasion?
(6) Will you conduct or support a clinical study to evaluate appropriate adjuvant therapies for cervical cancer?

In August 2014, we mailed the questionnaire to all 186 JGOG member institutions. All the chosen hospitals treated gynecologic cancer and were authorized by the JGOG membership committee. Responses were accepted until December 2014.

RESULTS

1. Characteristics of responders' institutions

In total, 129 of the 199 JGOG member institutions replied to our questionnaire. The characteristics of responding institutions are shown in **Table 1**. Since JGOG membership extended only to institutions active in the treatment of gynecologic cancer, 69 (53%) and 14 (11%) of the 129 institutions were academic hospitals and cancer centers, respectively. Furthermore, 65 (50%) and 52 (40%) institutions had one and two (or more) gynecologic oncologists on the board of the Japanese Society of Gynecologic Oncology, respectively. The average number of radical hysterectomies performed annually was 5 to 15 and >15 in 64 (50%) and 48 (37%) institutions, respectively.

2. Practice patterns of adjuvant therapy for cervical cancer in Japan

First, current adjuvant therapy policies in each institution were analyzed. Our questionnaire allowed multiple answers because many institutions may have multiple therapeutic strategies based on the histological subtypes and/or number of risk factors. According to Japanese guidelines, CCRT/RT was performed in 98 institutions (76%) (**Fig. 1A**). On the other hand, 93 institutions (72%) also had the option to perform CT alone (**Fig. 1A**). IMRT was performed in 18% of institutions (**Fig. 1B**). The CCRT regimen was simple; 83% of institutions used cisplatin alone (**Fig. 1C**). However, multiple CT regimen were used; the most popular regimen, which was used in 46% of institutions, was a combination of carboplatin and paclitaxel, followed by irinotecan with nedaplatin (20%), and cisplatin with paclitaxel (17%) (**Fig. 1D**).

Table 1. Background of responding institutions

Variable	Institution (%)
Responder	129
Academic hospital	69 (53)
Cancer center	14 (11)
General hospital	46 (36)
Physicians with board of Japan Society of Gynecologic Oncology	
0	12 (10)
1	65 (50)
≥2	52 (40)
No. of radical hysterectomy per year	
<5	17 (13)
5–15	64 (50)
>15	48 (37)

http://doi.org/10.3802/jgo.2016.27.e29

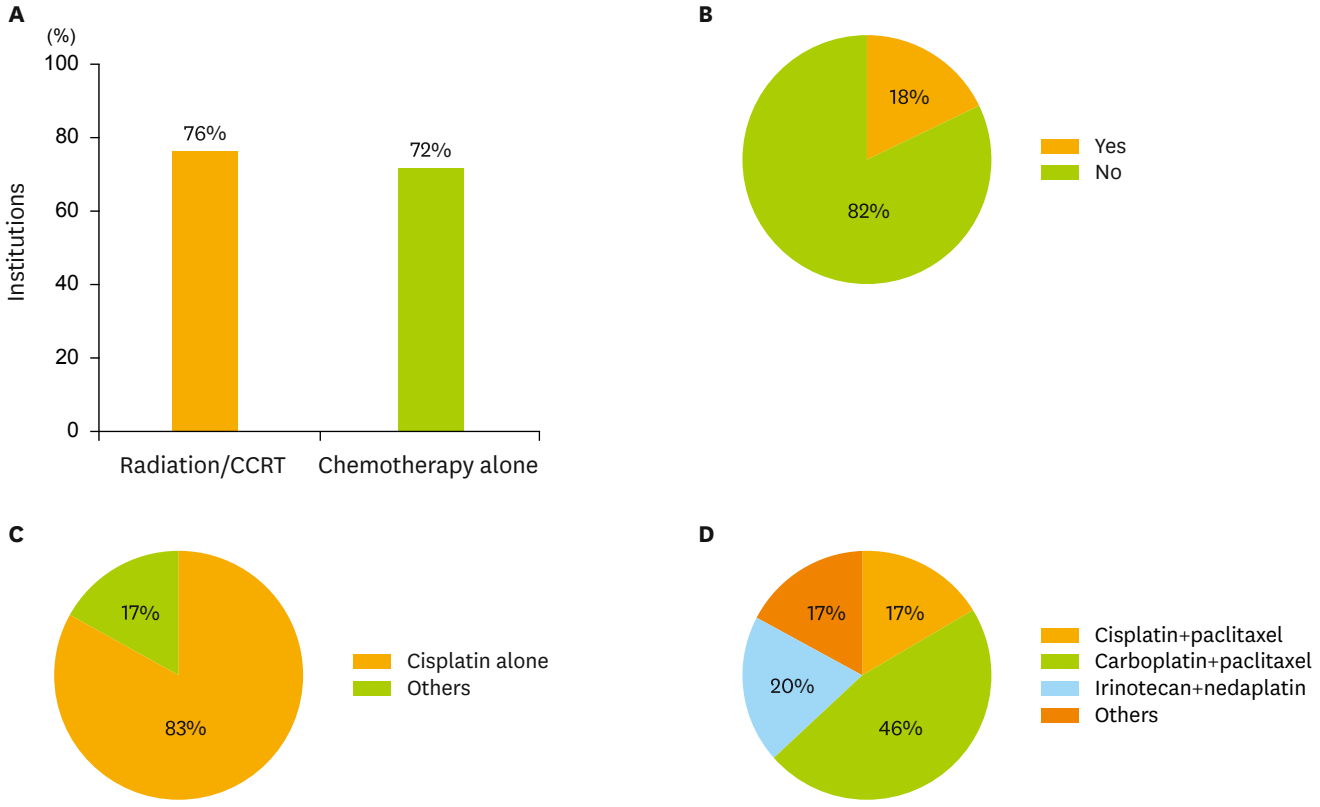

Fig. 1. Variety of adjuvant therapy policies for cervical cancer in Japan. The policy for adjuvant therapy was investigated in each institution (multiple answers allowed). (A) Therapeutic options considered for adjuvant therapy. (B) Percentage of institutions performing intensity-modulated radiation therapy. (C) Regimen for concurrent chemoradiotherapy (CCRT). (D) Regimen for adjuvant chemotherapy.

3. Risk assessment for clinicopathological factors

Next, we assessed risk assessment for clinicopathological factors which might be one of the reasons for the variety of adjuvant therapies. As shown in **Fig. 2**, RT was revealed to be the most appropriate adjuvant therapy for vaginal stump invasion cases, but not for other factors such as bulky tumor, lymph node metastasis, lymphovascular invasion parametrial invasion, and stromal invasion. CCRT was appropriate especially in cases of lymph node metastasis and parametrial invasion. Interestingly, CT ranked highly as an adjuvant therapy for all risk factors except vaginal stump invasion, and even for factors where observation was frequently chosen, for example, bulky tumors, lymphovascular invasion, and stromal invasion. These results indicate that the type of risk factor might affect the selection of adjuvant therapy.

4. Expectation of randomized controlled trial to evaluate the efficacy of CT as an adjuvant therapy in cervical cancer

Finally, we focused on how gynecologic oncologists evaluate the complications of each therapeutic option and the necessity of a trial to evaluate the efficacy or non-inferiority of CT as an adjuvant therapy in cervical cancer. The result showed that 85% of institutions evaluated CT as an adjuvant therapy with fewer incidences of severe complications (**Fig. 3A**). On the other hand, only 4% of institutions chose RT and 5% rated both CT and RT equally. Moreover, 87% of institutions were supportive of a clinical study to evaluate the efficacy or non-inferiority of CT as an adjuvant therapy in cervical cancer (**Fig. 3B**). Approximately 13% of institutions did not support a future clinical study because of the lack of radiation facilities or fewer cases for adjuvant therapy than expected (not shown in figure).

http://doi.org/10.3802/jgo.2016.27.e29

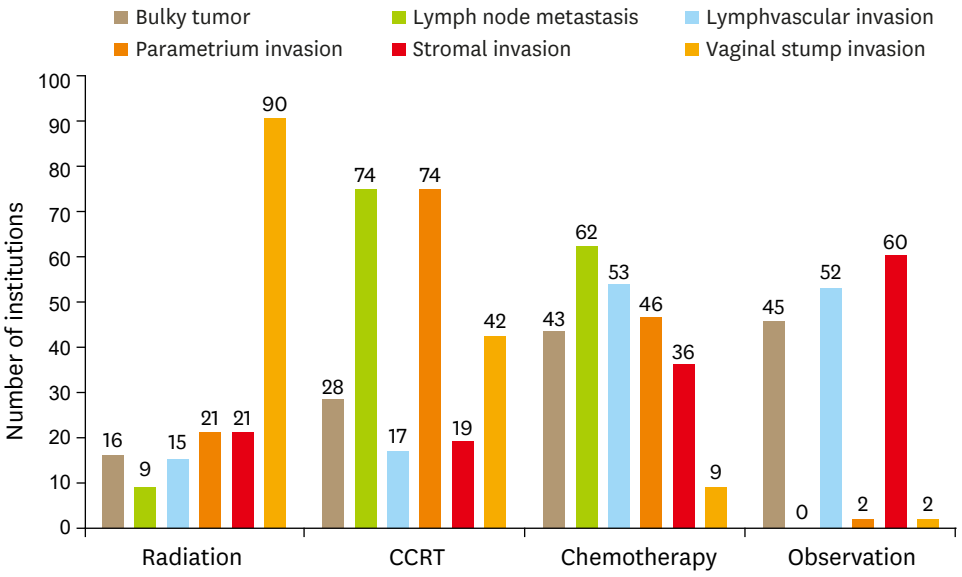

Fig. 2. Risk assessment for clinicopathological factors. Appropriate therapeutic options are chosen from among radiation, concurrent chemoradiotherapy (CCRT), chemotherapy, and observation (multiple answers allowed).

DISCUSSION

In this survey, we showed (1) the variety of adjuvant therapies for cervical cancer in Japan, (2) that the combination of risk factors might affect the selection of adjuvant therapy, and (3) that a clinical study is required to evaluate the efficacy or non-inferiority of CT as an adjuvant therapy in cervical cancer.

Previous retrospective studies had revealed the efficacy of CT as an adjuvant therapy for cervical cancer. A large-scale retrospective study in 2,268 patients comparing efficacy and adverse effects indicated no significant differences between CT and RT/CCRT in both the 5-year overall survival and disease-free survival [23]. Notably, the increased 5-year overall survival and disease-free survival rates of CT compared to RT were seen in patients with early-stage disease, clinical response, and younger age [23]. These results motivate gynecologic oncologists to use CT as an adjuvant therapy. Our survey also revealed that CT was a wise choice for adjuvant therapy in Japan.

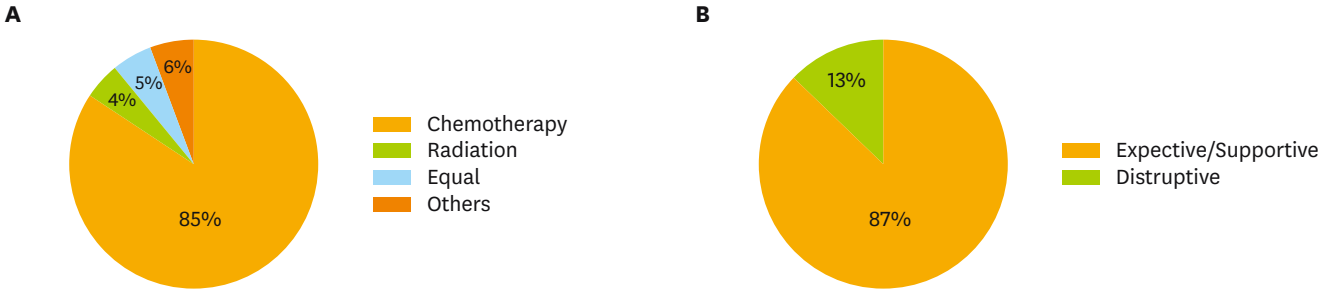

Fig. 3. Recognition of complications and requirement for a clinical study to assess adjuvant therapy. (A) Identification of the most reduced complication of adjuvant therapy. (B) The approach of your institution for clinical study to assess the efficacy or non-inferiority of chemotherapy as an adjuvant therapy.

http://doi.org/10.3802/jgo.2016.27.e29

In our survey, the regimen for CCRT generally involved only cisplatin because previous meta-analysis including 4,580 randomized patients showed an improved overall survival (hazard ratio, 0.71; p<0.001) in CCRT compared to RT, and cisplatin was the most commonly used agent in the study [24]. However, the regimen for CT alone showed variety, for example, cisplatin with paclitaxel, carboplatin with paclitaxel, and irinotecan with nedaplatin. These regimens come from clinical studies of cervical cancer in Japan. Previously, a combination of paclitaxel and cisplatin was considered the standard CT for cervical cancer [25,26]. Recently, we reported the non-inferiority of the paclitaxel and carboplatin regimen compared to paclitaxel and cisplatin in patients with recurrent or metastatic cervical cancer [27].

Risk criteria should be considered before the selection of adjuvant therapy. Currently, recurrence risk is evaluated according to the number of risk factors found in the patient. However, our survey revealed that gynecologists assess the recurrence risk according to the kind of risk factors the patient has, and then choose the appropriate therapeutics. Radiation was supported by the majority of institutions for the adjuvant therapy of vaginal stump invasion. This is reasonable because RT such as brachytherapy can directly approach the tumor. In fact, the 10-year survival rate of non-palpable recurrence at the vaginal stump is reported to be more than 70% following brachytherapy alone [28]. On the other hand, postoperative CCRT was used for lymph node metastasis and parametrial invasion because previous randomized studies proved the efficacy of CCRT in these patients [13]. However, lymph node metastasis is considered as a significant risk factor for prognosis, even after CCRT/RT [29]. Notably, the 3-year survival rate of adjuvant CT was more than 78% and superior to that of radiotherapy (67%), even though 34% of patients had multiple lymph node metastases. In addition, CT has an equivalent therapeutic effect to RT with fewer postoperative complications [30,31]. Our results showed that many gynecologic oncologists in Japan also evaluate the superiority of CT according to the complication. These results support the need for evaluation of CT as an adjuvant therapy for cervical cancer. In fact, almost 90% of the institutions supported such a clinical study.

Our survey has several limitations. First, this study was performed for selected institutions. Since treatment for cervical cancer is generally performed in front-line medical centers and most of them belong to JGOG, we conducted this survey only in these institutions. Therefore, our result might not reflect the opinions in a small institution. Second, in this survey, we evaluated all institutions equally. Since the number of patients is different in each institution, some of the results might have to be evaluated considering the scale of the institution. In fact, some institutions in our survey have no radiation facility in their hospital. However, if the efficacy or non-inferiority of CT for adjuvant therapy is proven, these institutions can choose CT without any hesitation.

In conclusion, our study showed that a variety of adjuvant therapy policies for cervical cancer are currently in use in each institution. Clinical study to assess the efficacy or non-inferiority of adjuvant CT is required.

ACKNOWLEDGMENTS

We thank JGOG for support and assistance since our survey was conducted by members who participated in a JGOG education seminar in August 2013. We also thank all the doctors and institutions who responded to our questionnaire survey.

http://doi.org/10.3802/jgo.2016.27.e29

REFERENCES

1. Siegel RL, Miller KD, Jemal A. Cancer statistics, 2015. CA Cancer J Clin 2015;65:5-29.
PUBMED | CROSSREF
2. Kokka F, Bryant A, Brockbank E, Powell M, Oram D. Hysterectomy with radiotherapy or chemotherapy or both for women with locally advanced cervical cancer. Cochrane Database Syst Rev 2015;4:CD010260.
PUBMED
3. Rosa DD, Medeiros LR, Edelweiss MI, Pohlmann PR, Stein AT. Adjuvant platinum-based chemotherapy for early stage cervical cancer. Cochrane Database Syst Rev 2012;6:CD005342.
PUBMED
4. Mikami M, Aoki Y, Sakamoto M, Shimada M, Takeshima N, Fujiwara H, et al. Current surgical principle for uterine cervical cancer of stages Ia2, Ib1, and IIa1 in Japan: a survey of the Japanese Gynecologic Oncology Group. Int J Gynecol Cancer 2013;23:1655-60.
PUBMED | CROSSREF
5. Ho CM, Chien TY, Huang SH, Wu CJ, Shih BY, Chang SC. Multivariate analysis of the prognostic factors and outcomes in early cervical cancer patients undergoing radical hysterectomy. Gynecol Oncol 2004;93:458-64.
PUBMED | CROSSREF
6. Lai CH, Hong JH, Hsueh S, Ng KK, Chang TC, Tseng CJ, et al. Preoperative prognostic variables and the impact of postoperative adjuvant therapy on the outcomes of Stage IB or II cervical carcinoma patients with or without pelvic lymph node metastases: an analysis of 891 cases. Cancer 1999;85:1537-46.
PUBMED | CROSSREF
7. Park TK. Adjuvant therapy in cervical cancer patients with high risk factors. Yonsei Med J 1997;38:255-60.
PUBMED | CROSSREF
8. Rushdan MN, Tay EH, Khoo-Tan HS, Lee KM, Low JH, Ho TH, et al. Tailoring the field and indication of adjuvant pelvic radiation for patients with FIGO stage Ib lymph nodes-negative cervical carcinoma following radical surgery based on the GOG score--a pilot study. Ann Acad Med Singapore 2004;33:467-72.
PUBMED
9. Atkovar G, Uzel O , Ozşahin M, Koca S, Sahinler I, Okkan S, et al. Postoperative radiotherapy in carcinoma of the cervix: treatment results and prognostic factors. Radiother Oncol 1995;35:198-205.
PUBMED | CROSSREF
10. Uno T, Ito H, Itami J, Sato T, Minoura S, Yasuda S, et al. Adjuvant pelvic irradiation in patients with pathologic T2b carcinoma of the uterine cervix. Int J Gynecol Cancer 2002;12:187-91.
PUBMED | CROSSREF
11. Kinney WK, Alvarez RD, Reid GC, Schray MF, Soong SJ, Morley GW, et al. Value of adjuvant whole-pelvis irradiation after Wertheim hysterectomy for early-stage squamous carcinoma of the cervix with pelvic nodal metastasis: a matched-control study. Gynecol Oncol 1989;34:258-62.
PUBMED | CROSSREF
12. Monk BJ, Cha DS, Walker JL, Burger RA, Ramsinghani NS, Manetta A, et al. Extent of disease as an indication for pelvic radiation following radical hysterectomy and bilateral pelvic lymph node dissection in the treatment of stage IB and IIA cervical carcinoma. Gynecol Oncol 1994;54:4-9.
PUBMED | CROSSREF
13. Peters WA, Liu PY, Barrett RJ, Stock RJ, Monk BJ, Berek JS, et al. Concurrent chemotherapy and pelvic radiation therapy compared with pelvic radiation therapy alone as adjuvant therapy after radical surgery in high-risk early-stage cancer of the cervix. J Clin Oncol 2000;18:1606-13.
PUBMED
14. Japan Society of Gynecologic Oncology. Treatment guidelines for cervical cancer 2007 edition. Tokyo: Kanehara & Co.; 2007.
15. Larson DM, Copeland LJ, Stringer CA, Gershenson DM, Malone JM, Edwards CL. Recurrent cervical carcinoma after radical hysterectomy. Gynecol Oncol 1988;30:381-7.
PUBMED | CROSSREF
16. Samlal RA, Van Der Velden J, Van Eerden T, Schilthuis MS, Gonzalez Gonzalez D, Lammes FB. Recurrent cervical carcinoma after radical hysterectomy: an analysis of clinical aspects and prognosis. Int J Gynecol Cancer 1998;8:78-84.
PUBMED | CROSSREF
17. Viswanathan AN, Lee LJ, Eswara JR, Horowitz NS, Konstantinopoulos PA, Mirabeau-Beale KL, et al. Complications of pelvic radiation in patients treated for gynecologic malignancies. Cancer 2014;120:3870-83.
PUBMED | CROSSREF
18. Frumovitz M, Sun CC, Schover LR, Munsell MF, Jhingran A, Wharton JT, et al. Quality of life and sexual

functioning in cervical cancer survivors. J Clin Oncol 2005;23:7428-36.
PUBMED | CROSSREF

19. Matsuura Y, Kawagoe T, Toki N, Tanaka M, Kashimura M. Long-standing complications after treatment for cancer of the uterine cervix--clinical significance of medical examination at 5 years after treatment. Int J Gynecol Cancer 2006;16:294-7.
PUBMED | CROSSREF

20. Eifel PJ, Levenback C, Wharton JT, Oswald MJ. Time course and incidence of late complications in patients treated with radiation therapy for FIGO stage IB carcinoma of the uterine cervix. Int J Radiat Oncol Biol Phys 1995;32:1289-300.
PUBMED | CROSSREF

21. Mundt AJ, Mell LK, Roeske JC. Preliminary analysis of chronic gastrointestinal toxicity in gynecology patients treated with intensity-modulated whole pelvic radiation therapy. Int J Radiat Oncol Biol Phys 2003;56:1354-60.
PUBMED | CROSSREF

22. Mikami M, Aoki Y, Sakamoto M, Shimada M, Takeshima N, Fujiwara H, et al. Surgical principles for managing stage IB2, IIA2, and IIB uterine cervical cancer (Bulky Tumors) in Japan: a survey of the Japanese Gynecologic Oncology Group. Int J Gynecol Cancer 2014;24:1333-40.
PUBMED | CROSSREF

23. Li S, Hu T, Chen Y, Zhou H, Li X, Cheng X, et al. Adjuvant chemotherapy, a valuable alternative option in selected patients with cervical cancer. PLoS One 2013;8:e73837.
PUBMED | CROSSREF

24. Green JA, Kirwan JM, Tierney JF, Symonds P, Fresco L, Collingwood M, et al. Survival and recurrence after concomitant chemotherapy and radiotherapy for cancer of the uterine cervix: a systematic review and meta-analysis. Lancet 2001;358:781-6.
PUBMED | CROSSREF

25. Moore DH, Blessing JA, McQuellon RP, Thaler HT, Cella D, Benda J, et al. Phase III study of cisplatin with or without paclitaxel in stage IVB, recurrent, or persistent squamous cell carcinoma of the cervix: a gynecologic oncology group study. J Clin Oncol 2004;22:3113-9.
PUBMED | CROSSREF

26. Monk BJ, Sill MW, McMeekin DS, Cohn DE, Ramondetta LM, Boardman CH, et al. Phase III trial of four cisplatin-containing doublet combinations in stage IVB, recurrent, or persistent cervical carcinoma: a Gynecologic Oncology Group study. J Clin Oncol 2009;27:4649-55.
PUBMED | CROSSREF

27. Kitagawa R, Katsumata N, Shibata T, Kamura T, Kasamatsu T, Nakanishi T, et al. Paclitaxel plus carboplatin versus paclitaxel plus cisplatin in metastatic or recurrent cervical cancer: the Open-Label Randomized Phase III Trial JCOG0505. J Clin Oncol 2015;33:2129-35.
PUBMED | CROSSREF

28. Ito H, Shigematsu N, Kawada T, Kubo A, Isobe K, Hara R, et al. Radiotherapy for centrally recurrent cervical cancer of the vaginal stump following hysterectomy. Gynecol Oncol 1997;67:154-61.
PUBMED | CROSSREF

29. Bradbury M, Founta C, Taylor W, Kucukmetin A, Naik R, Ang C. Pathological risk factors and outcomes in women with stage IB2 cervical cancer treated with primary radical surgery versus chemoradiotherapy. Int J Gynecol Cancer 2015;25:1476-83.
PUBMED | CROSSREF

30. Hosaka M, Watari H, Takeda M, Moriwaki M, Hara Y, Todo Y, et al. Treatment of cervical cancer with adjuvant chemotherapy versus adjuvant radiotherapy after radical hysterectomy and systematic lymphadenectomy. J Obstet Gynaecol Res 2008;34:552-6.
PUBMED | CROSSREF

31. Jung PS, Kim DY, Lee SW, Park JY, Suh DS, Kim JH, et al. Clinical role of adjuvant chemotherapy after radical hysterectomy for FIGO stage IB-IIA cervical cancer: comparison with adjuvant RT/CCRT using inverse-probability-of-treatment weighting. PLoS One 2015;10:e0132298.
PUBMED | CROSSREF

Appendix. Questionnaire on the cervical cancer treatment policy of Japanese Gynecologic Oncology Group medical institutions

This questionnaire survey should be answered by the Head or responsible person of each institution.

1. Does your institution have criteria for performing adjuvant therapy for intermediate/high risk cervical cancer after surgery?
   1) According to the Japanese guidelines
   2) Almost the same as the Japanese guidelines
   3) Unique criteria, specific to the institution
   4) Other criteria

2. What according to you is the most appropriate adjuvant therapy for each of the recurrent risk factors listed below? (multiple answers allowed)
   1) Bulky tumor:
      (a) Observation, (b) Radiotherapy, (c) Chemotherapy, (d) Other

   2) Lymph node metastasis:
      (a) Observation, (b) Radiotherapy, (c) Chemotherapy, (d) Other

   3) Lymphovascular invasion:
      (a) Observation, (b) Radiotherapy, (c) Chemotherapy, (d) Other

   4) Parametrial invasion:
      (a) Observation, (b) Radiotherapy, (c) Chemotherapy, (d) Other

   5) Stromal invasion:
      (a) Observation, (b) Radiotherapy, (c) Chemotherapy, (d) Other

   6) Vaginal invasion:
      (a) Observation, (b) Radiotherapy, (c) Chemotherapy, (d) Other

3-1. What should be performed as an adjuvant therapy for intermediate/high risk postoperative cervical cancer? (multiple answers allowed)
   1) Chemotherapy
   2) Radiation
   3) Concurrent chemoradiotherapy (CCRT)
   4) Other

3-2. Why did you select this (these) therapy (therapies)?

4. What kind of regimen do you use for adjuvant chemotherapy?
   Agents:
   Dose:

5-1. What is total dose in Gy you use for adjuvant radiation therapy?

5-2. What kind of chemotherapeutic agents do you use for CCRT?
   Agents:
   Dose:

6. Does your institution perform Intensity-Modulated Radiation Therapy (IMRT)?
   1) Yes
   2) No, but we can perform IMRT.
   3) No. We can only perform conventional radiation therapy.
   4) No. We cannot perform radiation therapy.

7. Which therapy do you think has the fewest adverse events?
   1) Radiation
   2) Chemotherapy
   3) Equal
   4) Other

http://doi.org/10.3802/jgo.2016.27.e29

Int J Clin Oncol (2016) 21:435–446
DOI 10.1007/s10147-016-0985-x

SPECIAL ARTICLE

Japan Society of Gynecologic Oncology guidelines 2015 for the treatment of ovarian cancer including primary peritoneal cancer and fallopian tube cancer

Shinichi Komiyama[1] · Hidetaka Katabuchi[2] · Mikio Mikami[3] · Satoru Nagase[4] · Aikou Okamoto[5] · Kiyoshi Ito[6] · Kenichiro Morishige[7] · Nao Suzuki[8] · Masanori Kaneuchi[9] · Nobuo Yaegashi[10] · Yasuhiro Udagawa[11] · Hiroyuki Yoshikawa[12]

Received: 16 April 2016 / Accepted: 20 April 2016 / Published online: 3 May 2016

Abstract The fourth edition of the Japan Society of Gynecologic Oncology guidelines for the treatment of ovarian cancer including primary peritoneal cancer and fallopian tube cancer was published in 2015. The guidelines contain seven chapters and six flow charts. The major changes in this new edition are as follows—(1) the format has been changed from reviews to clinical questions (CQ), and the guidelines for optimal clinical practice in Japan are now shown as 41 CQs and answers; (2) the 'flow charts' have been improved and placed near the beginning of the guidelines; (3) the 'basic points', including tumor staging, histological classification, surgical procedures, chemotherapy, and palliative care, are described before the chapter; (4) the FIGO surgical staging of ovarian cancer, fallopian tube cancer, and primary peritoneal cancer was revised in 2014 and the guideline has been revised accordingly to take the updated version of this classification into account; (5) the procedures for examination and management of hereditary breast and ovarian cancer are described; (6) information on molecular targeting therapy has been added; (7) guidelines for the treatment of recurrent cancer based on tumor markers alone are described, as well as guidelines for providing hormone replacement therapy after treatment.

Keywords Guideline · Ovarian cancer · Primary peritoneal cancer · Fallopian tube cancer · Japan Society of Gynecologic Oncology

Introduction

The number of patients with ovarian cancer is increasing in Japan and 8,631 cases were reported in 2007 [1]. Deaths due to ovarian cancer are also increasing and 4,705 patients died of this disease in 2011 [1]. Ovarian cancer is the most

This article originally appeared in Japanese as Ransougan Chiryo guideline 2015 nen-ban, published by Kanehara & Co., Ltd, Tokyo, Japan.

✉ Shinichi Komiyama
komiyama@med.toho-u.ac.jp

1 Department of Gynecology, Toho University Ohashi Medical Center, 2-17-6 Ohashi, Meguro-ku, Tokyo 153-8515, Japan

2 Department of Obstetrics and Gynecology, Faculty of Life Sciences, Kumamoto University, Kumamoto, Japan

3 Department of Obstetrics and Gynecology, Tokai University School of Medicine, Kanagawa, Japan

4 Department of Obstetrics and Gynecology, Faculty of Medicine, Yamagata University, Yamagata, Japan

5 Department of Obstetrics and Gynecology, Jikei University School of Medicine, Tokyo, Japan

6 Department of Disaster Obstetrics and Gynecology, Tohoku University Graduate School of Medicine, Sendai, Japan

7 Department of Obstetrics and Gynecology, Gifu University Graduate School of Medicine, Gifu, Japan

8 Department of Obstetrics and Gynecology, School of Medicine St. Marianna University, Kawasaki, Japan

9 Department of Obstetrics and Gynecology, Nagasaki University Graduate School of Medicine, Nagasaki, Japan

10 Department of Obstetrics and Gynecology, Tohoku University Graduate School of Medicine, Sendai, Japan

11 Department of Obstetrics and Gynecology, Fujita Health University School of Medicine, Aichi, Japan

12 Ibaraki Prefectural Central Hospital, Ibaraki, Japan

Table 1 Criteria for evaluating the quality of evidence (levels of evidence)

Level I	Evidence from meta-analyses of multiple randomized controlled trials
Level II	Evidence from randomized controlled trials, or evidence from well-designed nonrandomized controlled trials
Level III	Evidence from well-designed quasi-experimental studies, or evidence from well-designed non-experimental descriptive studies, such as comparative studies, correlation studies, and case–control studies
Level IV	Expert committee reports and opinions, or clinical experiences of respected authorities

common cause of death among malignant tumors of the female genital tract. Tumor stage is thought to be an important prognostic factor, with stage III and IV cancer having a poor prognosis [2]. Since the ovary is a pelvic organ, an ovarian tumor may not cause any early symptoms, and approximately 40–50 % of patients with ovarian cancer have stage III or IV disease (with a poor prognosis) at the time of first presentation [3]. Thus, an important challenge is to improve the outcome of treatment in patients with advanced ovarian cancer.

In order to improve the prognosis of ovarian cancer and reduce regional differences in the management of ovarian cancer in Japan, the first edition of the guidelines for the treatment of ovarian cancer was published by the Japan Society of Gynecologic Oncology in 2004. It has since been revised several times, and the fourth edition was published in April 2015. The new guidelines include seven chapters and six flow charts. The major changes in the new edition are as follows:

(1) The format has been changed from a review format to a clinical question (CQ) format, so the guidelines for optimal clinical practice in Japan are now shown as 41 CQs and answers.
(2) The 'flow charts' have been improved and are placed near the beginning of the guideline.
(3) The 'basic points', including staging, histological classification, surgical procedures, chemotherapy, and palliative care are included before the chapter.
(4) The FIGO surgical staging of ovarian cancer, fallopian tube cancer, and primary peritoneal cancer was revised in 2014 and the guideline has been revised accordingly to take the updated version of this classification into account.
(5) Procedures for the examination and management of hereditary breast and ovarian cancer (HBOC) are described.
(6) Information on molecular targeting therapy has been added.
(7) Guidelines for the treatment of recurrent cancer based on tumor markers alone and for providing hormone replacement therapy (HRT) after treatment are described.

Chapter 1: Overview

The aims of this guideline are to describe current optimal treatment for ovarian cancer (epithelial tumors, germ cell tumors, and sex cord stromal tumors), primary peritoneal cancer, and fallopian tube cancer, to reduce differences in management between medical institutions, to improve the safety of therapy and the prognosis, to reduce the burden (physical, mental, and economic) on patients by promoting optimal treatment, and to improve communication between patients and healthcare professionals.

Much of the evidence adopted in this guideline was obtained from clinical studies performed in Europe, the USA, and Japan. However, some evidence from Europe and the USA does not apply in Japan because of differences in background factors between Europe/USA and Japan. Conversely, some treatments used widely in Japan are uncommon in Europe and the USA. In such cases, the current consensus for disease management in Japan is prioritized in this guideline.

This guideline was created according to the principles of 'evidence-based medicine', which is a standard method for producing clinical practice guidelines. The quality of evidence was evaluated using the criteria shown in Table 1 [4, 5]. In addition, the grade of each recommendation in the guideline was determined using the criteria set out in Table 2 [4–6].

Chapter 2: Epithelial ovarian cancer

Treatment of epithelial ovarian cancer is summarized as flow chart 1 (Fig. 1).

CQ 01: What is the optimal surgical procedure for ovarian cancer when the tumor seems to be localized to the ovary?

Recommendations

(1) In addition to bilateral salpingo-oophorectomy + total hysterectomy + omentectomy, peritoneal cytol-

Table 2 Grading of recommendations

Grade A	The proposed treatment is strongly recommended
	In principle, there is at least one source of Level I evidence showing efficacy of the treatment
Grade B	The proposed treatment is recommended
	In principle, there is at least one source of Level II evidence showing efficacy of the treatment
Grade C1	The proposed treatment may be considered. However, there is not enough scientific evidence
	(or the treatment may have efficacy, although sufficient scientific evidence has not been obtained)
	There are multiple sources of Level III evidence showing efficacy of the treatment and the outcomes are roughly consistent
Grade C2	There is not enough scientific evidence, and the treatment is not recommended in routine clinical practice
Grade D	The treatment is not recommended (usefulness or efficacy have not been shown, and the treatment may be harmful)

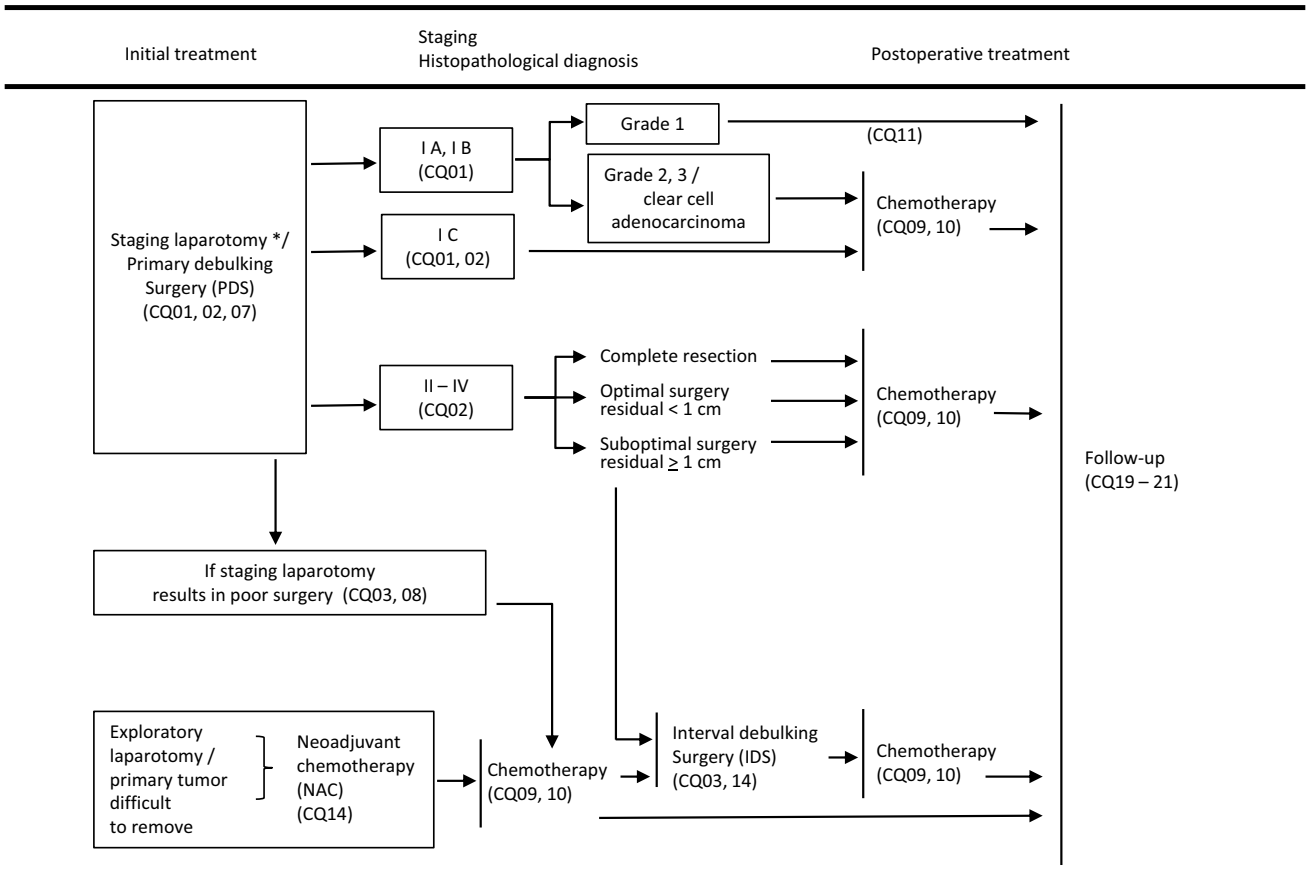

Fig. 1 Flow chart 1: treatment of epithelial ovarian cancer. *Staging laparotomy—bilateral salpingo-oophorectomy + total hysterectomy + omentectomy + peritoneal cytology + pelvic/para-aortic lymph node dissection (biopsy) + biopsies from sites in the abdominal cavity

ogy + pelvic/para-aortic lymph node dissection (biopsy) + biopsies from sites in the abdominal cavity are recommended (Grade B).

(2) When biopsies are obtained from sites in the abdominal cavity, sampling from the following sites should be considered—pouch of Douglas, parietal peritoneum, surface of the diaphragm, intestinal tract, mesentery, and suspected lesions (Grade C1).

CQ 02: What is the optimal surgical procedure for ovarian cancer that is thought to be stage II or a more advanced stage preoperatively?

Recommendations

Maximal debulking surgery to accomplish complete resection (no gross residual tumor) is strongly recommended (Grade A).

CQ 03: Is interval debulking surgery (IDS) recommended for advanced ovarian cancer if primary debulking surgery (PDS) had a suboptimal outcome?

Recommendations

As a treatment option, IDS should be considered during chemotherapy for patients with advanced cancer if previous surgery had a suboptimal outcome (Grade C1).

CQ 04: What is the optimal management if a patient wishes to preserve fertility?

Recommendations

(1) Detailed informed consent about preservation of fertility is necessary (Grade A).
(2) As the basic operative procedure to preserve fertility, affected-side salpingo-oophorectomy + omentectomy + peritoneal cytology is recommended (Grade B).
(3) In addition to the above-mentioned basic procedure, biopsy of the contralateral ovary, biopsy (dissection) of the pelvic/para-aortic lymph nodes, and biopsies from sites in the abdominal cavity should be considered as part of staging laparotomy (Grade C1).

CQ 05: Is risk-reducing salpingo-oophorectomy (RRSO) recommended for patients with the *BRCA1* or *BRCA2* gene mutation?

Recommendations

It is recommended that RRSO only be performed by a gynecologic oncologist who is a member of the Japan Society of Gynecologic Oncology in cooperation with a clinical geneticist at a medical facility with an established genetic counseling system and cooperative pathologists, after review and approval by the institutional ethics committee (Grade B).

CQ 06: Is laparoscope-assisted surgery possible?

Recommendations

(1) Currently, laparoscope-assisted surgery is not recognized as a standard procedure that can be substituted for laparotomy (Grade C2).
(2) However, in patients with advanced cancer, laparoscope-assisted surgery may be substituted for laparotomy to observe the abdominal cavity and collect tissue samples (Grade C1).

CQ 07: For which patients is intraoperative rapid pathological examination recommended?

Recommendations

For patients in whom judgment between benign/borderline malignancy/malignancy is difficult based on preoperative evaluation and intraoperative findings, intraoperative rapid pathological examination is recommended for selecting the optimal surgical procedure (Grade B).

CQ 08: What is the recommended management of a patient in whom ovarian cancer is diagnosed after surgery?

Recommendations

Staging laparotomy (re-laparotomy) is recommended (Grade B).

CQ 09: What chemotherapy regimen is recommended as first-line therapy?

Recommendations

(1) Paclitaxel + carboplatin (conventional TC therapy) is strongly recommended (Grade A).
(2) Dose-dense TC therapy is also recommended (Grade B).

CQ 10: What chemotherapy regimens other than TC therapy are recommended as first-line therapy?

Recommendations

(1) Docetaxel + carboplatin (DC therapy) is recommended (Grade B).
(2) Cisplatin monotherapy or carboplatin monotherapy can be considered (Grade C1).

CQ 11: Which patients do not need postoperative chemotherapy?

Recommendations

It can be omitted for patients with stage I A/I B, Grade 1 disease confirmed by staging laparotomy (Grade B).

CQ 12: Should first-line chemotherapy be selected by considering tumor histology?

Recommendations

This is not recommended because there is insufficient evidence to show that standard treatment should be changed depending on tumor histology (Grade C2).

CQ 13: Is intraperitoneal chemotherapy recommended as the first-line therapy?

Recommendations

Intraperitoneal chemotherapy should be considered for patients with advanced cancer who have undergone optimal surgery (Grade C1).

CQ 14: Are neoadjuvant chemotherapy (NAC) and IDS recommended for advanced ovarian cancer if optimal surgery is thought to be impossible?

Recommendations

For patients with advanced cancer in whom it is thought that primary surgery will not result in an optimal outcome, preoperative chemotherapy and debulking surgery (NAC + IDS) are recommended as a treatment option (Grade B).

CQ 15: Is maintenance chemotherapy recommended after complete remission is achieved?

Recommendations

It is not recommended, because usefulness of maintenance chemotherapy has not been demonstrated (Grade C2).

CQ 16: What management approach is recommended if complete remission is not achieved by initial treatment?

Recommendations

Additional treatment (second-line chemotherapy and radiotherapy), participation in a clinical trial, or best supportive care should be considered (Grade C1).

CQ 17: What is the recommended management of serious adverse events associated with chemotherapy?

Recommendations

Hypersensitivity reactions (*HSR*)

(1) Premedication should be provided because taxanes, such as paclitaxel, are associated with a risk of HSR (Grade A).
(2) When carboplatin causes HSR, premedication alone cannot reduce the risk of recurrence. Therefore, switching to another drug or desensitization therapy should be considered (Grade C1).

Gastrointestinal symptoms (*nausea, diarrhea*)

(1) For nausea, refer to the relevant guideline [7], and provide adequate antiemetic therapy (Grade A).
(2) For mild diarrhea, antidiarrheal agents should be administered orally. For severe diarrhea complicated by other symptoms, early aggressive treatment should be performed, such as fluid replacement and administration of an antibacterial agent (Grade A).

Myelosuppression/febrile neutropenia
Refer to the relevant guideline [8], and provide adequate treatment with an antibacterial agent and/or a granulocyte-colony stimulating factor (G-CSF) preparation (Grade A).

CQ 18: Are any molecular targeting drugs recommended as first-line therapy or as treatment for recurrence?

Recommendations

Bevacizumab should be considered in combination with chemotherapy and as subsequent maintenance therapy. However, careful patient selection and appropriate monitoring for adverse events are required when bevacizumab is used (Grade C1).

CQ 19: What is the optimal follow-up interval after treatment?

Recommendations

After the start of initial treatment,

Years 1–2: an interval of 1–3 months
Years 3–5: an interval of 3–6 months
Year 6 onward: an interval of 1 year

The above-mentioned intervals are only intended as a guide (Grade C1).

CQ 20: What examinations/tests should be performed for follow-up after treatment?

Recommendations

(1) Taking a history and performing and pelvic examination at every visit should be considered (Grade C1).
(2) Measurement of CA125, transvaginal ultrasonography, or computed tomography scanning should be considered as required (Grade C1).

CQ 21: Is intervention for recurrence recommended if the patient only has elevation of CA125 without any symptoms?

Recommendations

Early intervention in response to elevation of CA125 alone is not necessarily recommended (Grade C2).

CQ 22: Is HRT recommended?

Recommendations

After informing the patient about its merits and demerits, HRT should be considered carefully for individual patients (Grade C1).

Chapter 3: Borderline epithelial ovarian tumors

Treatment of borderline epithelial ovarian tumors is summarized as flow chart 2 (Fig. 2).

CQ 23: What is the optimal surgical procedure for borderline epithelial ovarian tumors?

Recommendations

(1) In addition to bilateral salpingo-oophorectomy + total hysterectomy + omentectomy + peritoneal cytology, detailed intra-abdominal examination is recommended (Grade B).
(2) If suspected peritoneal lesions are found by intra-abdominal examination, removing such lesions should be considered, or taking peritoneal biopsies from several sites should be considered if there are no suspected peritoneal lesions (Grade C1).
(3) For patients who wish to preserve fertility, in addition to salpingo-oophorectomy on the affected side + omentectomy + peritoneal cytology, detailed intra-abdominal examination should be considered (Grade C1).

CQ 24: What are the indications for chemotherapy and the recommended regimens?

Recommendations

For patients with gross residual tumors and patients with invasive peritoneal implants, performing postoperative chemotherapy with platinum agents and taxanes according to the treatment regimens for ovarian cancer should be considered (Grade C1).

CQ 25: What is important for follow-up after treatment of a borderline epithelial ovarian tumor?

Recommendations

In patients with borderline epithelial tumors, long-term follow-up for at least 10 years after treatment should be considered (Grade C1).

Chapter 4: Recurrent epithelial ovarian cancer

Treatment of recurrent ovarian cancer is summarized as flow chart 3 (Fig. 3).

CQ 26: What chemotherapy regimen is recommended for recurrence after a disease-free interval (DFI) of <6 months?

Recommendations

Monotherapy that avoids cross-resistance to previous treatment is recommended (Grade B).

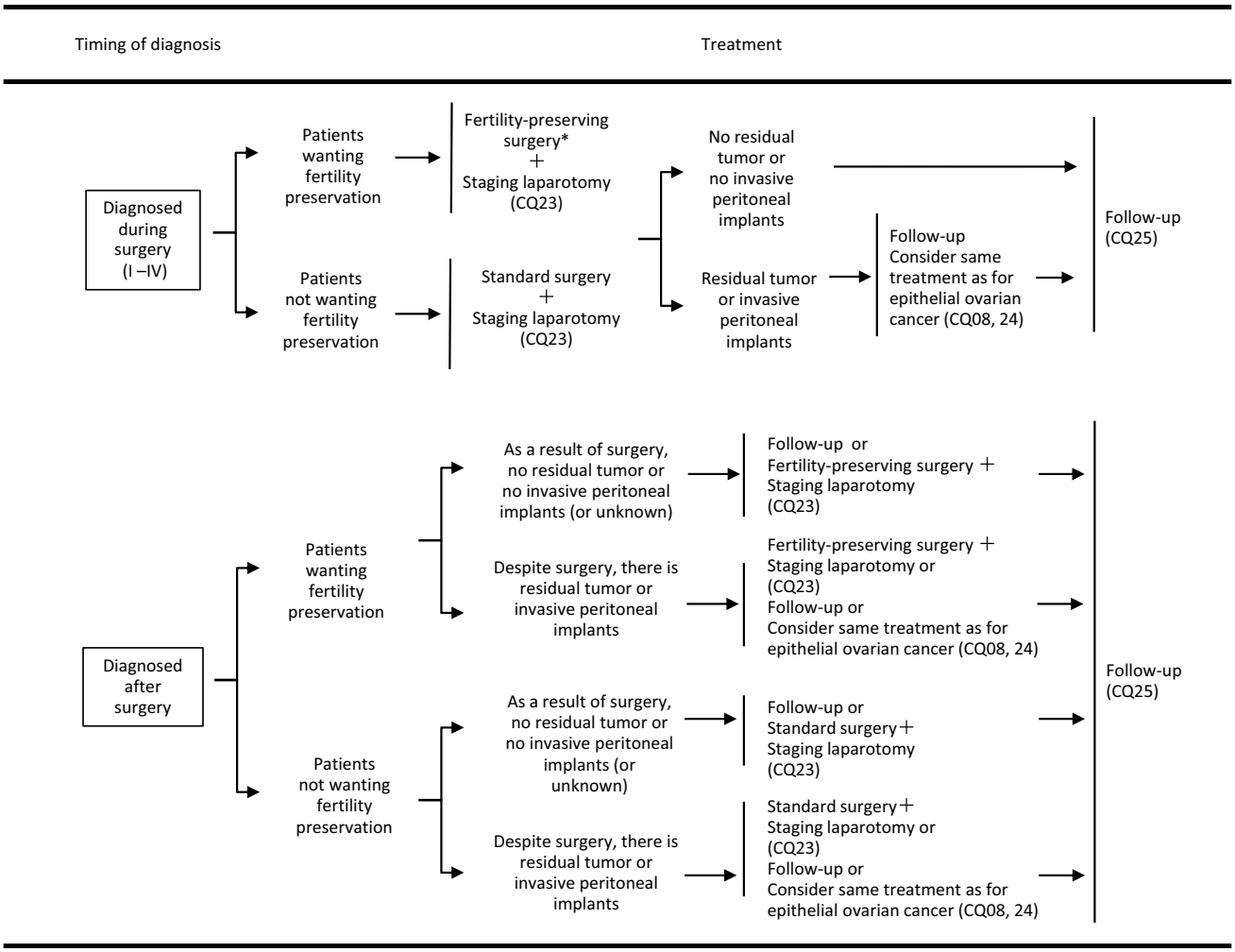

Fig. 2 Flow chart 2: treatment of borderline epithelial ovarian tumors. *Fertility-preserving surgery—affected-side salpingo-oophorectomy + omentectomy + peritoneal cytology + detailed intra-abdominal examination

CQ 27: What chemotherapy regimen is recommended for recurrence after a DFI of ≥6 months?

Recommendations

Combination therapy including a platinum agent is strongly recommended (Grade A).

CQ 28: What are the indications and strategy for secondary debulking surgery (SDS) in patients with recurrence?

Recommendations

(1) Whether or not SDS is worth performing should be carefully determined by evaluating the timing of recurrence, the primary surgical procedure, the site of recurrence, the number of lesions, and the performance status of the patient in a comprehensive manner (Grade C1).
(2) When SDS is performed, the objective should be complete resection of the tumor when possible (Grade C1).

CQ 29: What are the indications for radiation therapy in patients with recurrence?

Recommendations

(1) Radiation therapy should be considered in order to relieve symptoms, such as pain and bleeding (Grade C1).
(2) Radiation therapy should be considered for brain metastasis, not only to relieve symptoms, but also to prolong survival (Grade C1).

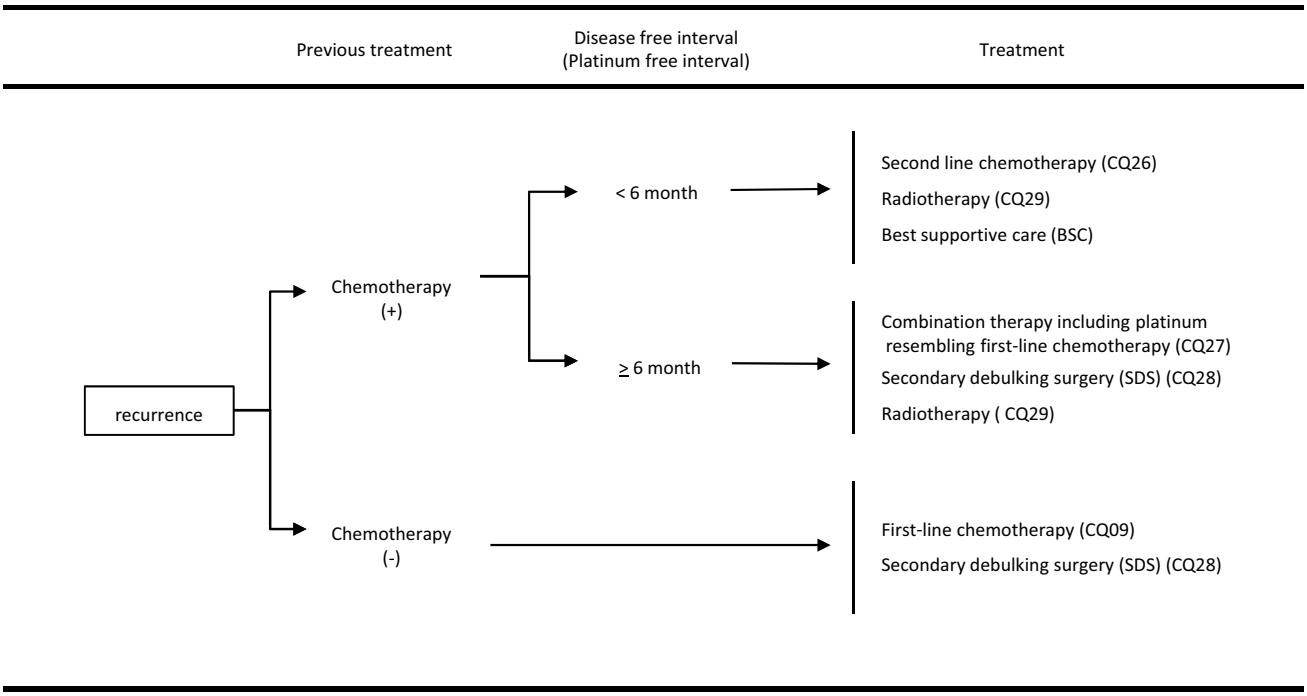

Fig. 3 Flow chart 3: treatment of recurrent epithelial ovarian cancer

CQ 30: What is the recommended management strategy for intestinal obstruction and accumulation of ascites?

Recommendations

Intestinal obstruction

(1) Administration of octreotide is strongly recommended for nausea/vomiting (Grade A).
(2) Correcting physical obstruction by palliative surgery is recommended for relieving nausea/vomiting (Grade B).
(3) Administration of corticosteroids should be considered to relieve nausea/vomiting (Grade C1).

Accumulation of ascites

(1) In patients with terminal cancer whose life expectancy is estimated to be ≤1–2 months, the volume of infusion solution should be limited to ≤1,000 mL/day if the patient has pain due to accumulation of ascites (Grade C1).
(2) Taking the underlying pathological state into consideration, administration of diuretics, drainage of ascitic fluid (paracentesis), creation of a peritoneovenous shunt, and cell-free and concentrated ascites reinfusion therapy should be considered for relieving pain due to accumulation of ascites (Grade C1).

Chapter 5: Primary peritoneal cancer/fallopian tube cancer

Treatment of primary peritoneal cancer or fallopian tube cancer is summarized as flow chart 4 (Fig. 4).

CQ 31: What is the optimal surgical procedure for primary peritoneal cancer?

Recommendations

Maximal debulking surgery to accomplish complete resection (no gross residual tumor) should be considered (Grade C1).

CQ 32: What chemotherapy regimen is recommended for primary peritoneal cancer?

Recommendations

(1) Either conventional TC therapy or dose-dense TC therapy should be considered (Grade C1).

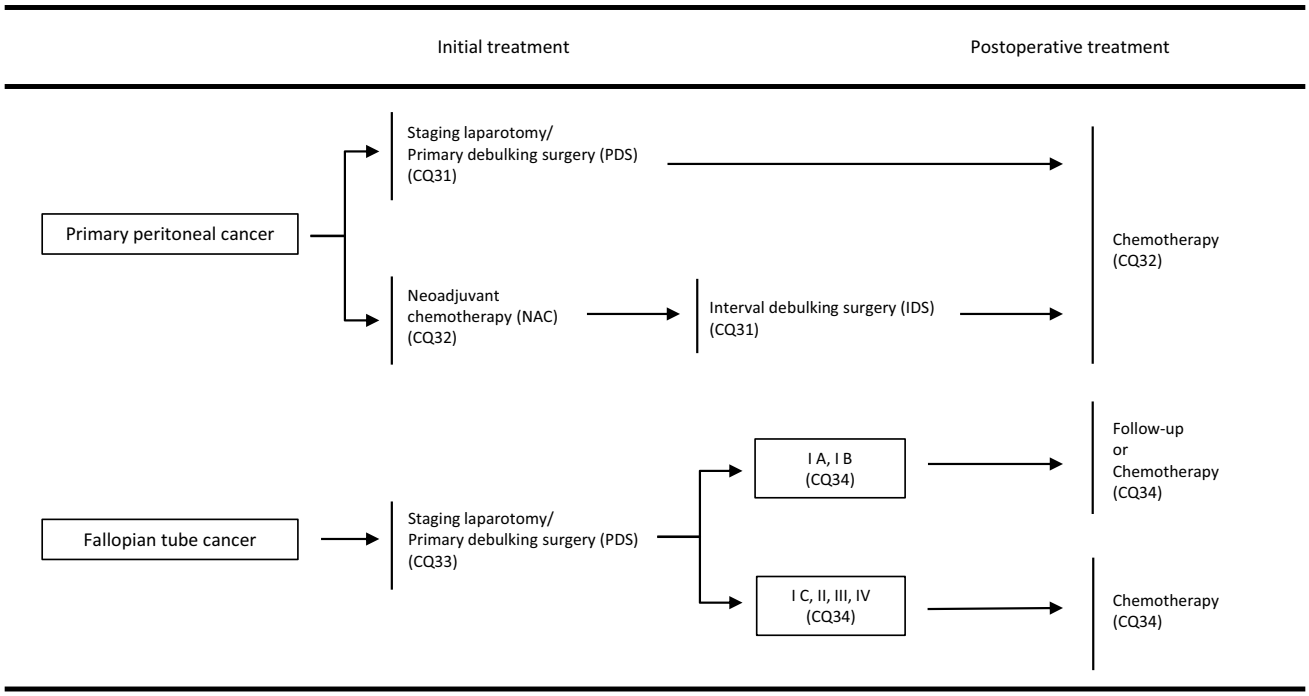

Fig. 4 Flow chart 4: treatment of primary peritoneal cancer and fallopian tube cancer

(2) Neoadjuvant chemotherapy should also be considered (Grade C1).

CQ 33: What is the optimal surgical procedure for fallopian tube cancer?

Recommendations

(1) According to the procedure for treating ovarian cancer, bilateral salpingo-oophorectomy + total hysterectomy + omentectomy are recommended together with peritoneal cytology + pelvic/para-aortic lymph node dissection (biopsy) + biopsies from sites in the abdominal cavity (Grade B).
(2) Maximal debulking surgery to accomplish complete resection (no gross residual tumor) is recommended for patients with advanced cancer (Grade B).

CQ 34: What chemotherapy regimen is recommended for fallopian tube cancer?

Recommendations

Conventional TC therapy or dose-dense TC therapy should be considered (Grade C1).

Chapter 6: Malignant ovarian germ cell tumors

Treatment of malignant ovarian germ cell tumors is summarized as flow chart 5 (Fig. 5).

CQ 35: What is the optimal surgical procedure for malignant ovarian germ cell tumors?

Recommendations

(1) For patients who wish to preserve fertility, in addition to salpingo-oophorectomy on the affected side + omentectomy + peritoneal cytology, detailed intra-abdominal examination is recommended (Grade B).
(2) For patients who do not require preservation of fertility, according to the procedure for treating ovarian cancer, bilateral salpingo-oophorectomy + total hysterectomy + omentectomy are recommended together with peritoneal cytology, pelvic/para-aortic lymph node dissection (biopsy), and biopsies from sites in the abdominal cavity. However, lymph node dissection (biopsy) can be omitted (Grade B).
(3) For patients with advanced cancer, maximal debulking surgery to accomplish complete resection (no

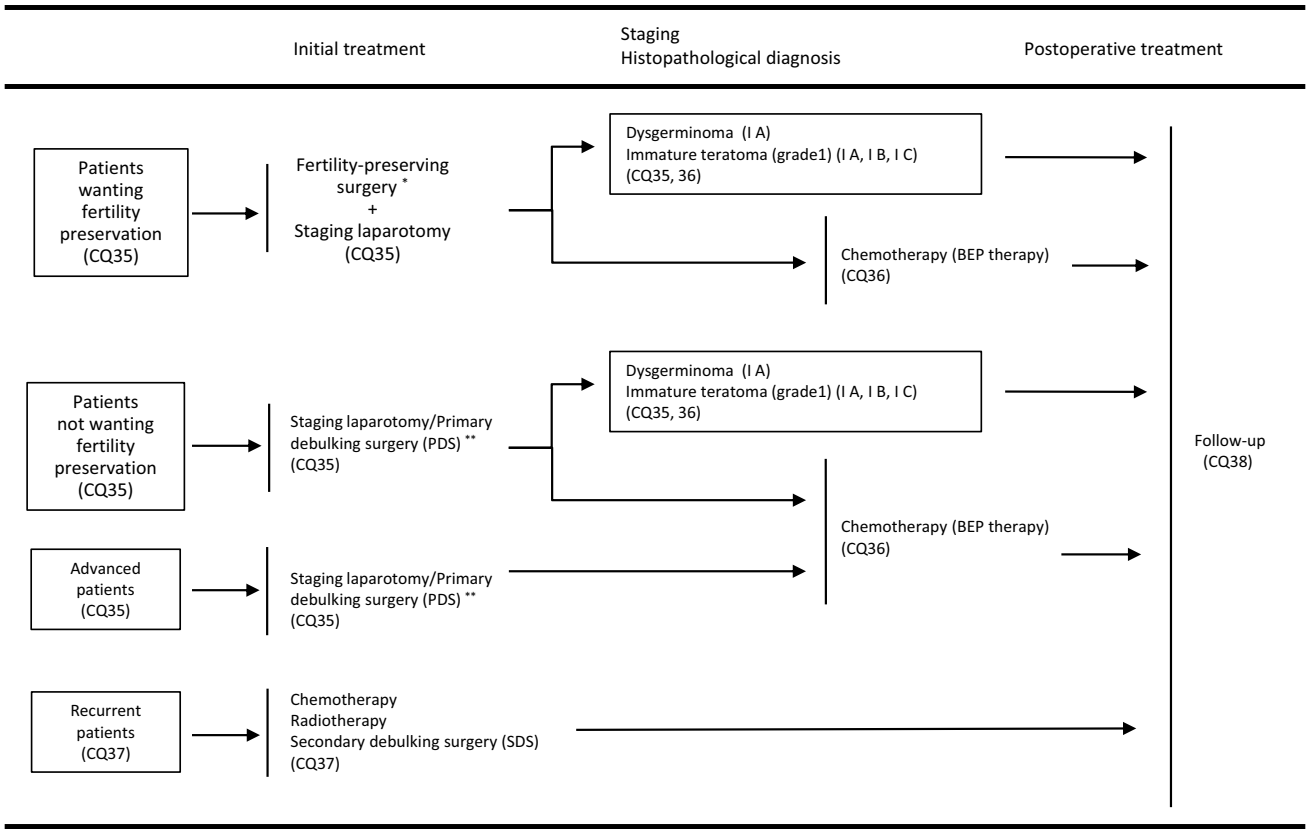

Fig. 5 Flow chart 5: treatment of malignant germ cell tumors. *Fertility-preserving surgery—affected-side salpingo-oophorectomy + omentectomy + peritoneal cytology + detailed intra-abdominal examination. **Lymph node dissection (biopsy) can be omitted

gross residual tumor) is recommended. However, lymph node dissection (biopsy) can be omitted (Grade B).

CQ 36: What postoperative treatment is recommended for malignant ovarian germ cell tumors?

Recommendations

Chemotherapy using bleomycin, etoposide, and cisplatin (BEP therapy) is strongly recommended (Grade A).

CQ 37: What treatment is recommended for recurrence of malignant ovarian germ cell tumors after first-line chemotherapy?

Recommendations

(1) Combination chemotherapy using cisplatin, such as a triple-drug combination of cisplatin with two other drugs (from among ifosfamide, etoposide, vinblastine, and/or paclitaxel), should be considered (Grade C1).
(2) SDS can be considered for some patients (Grade C1).

CQ 38: What should be kept in mind during follow-up after treatment of malignant ovarian germ cell tumors?

Recommendations

(1) You should be mindful that ovarian dysfunction may occur (Grade C1).
(2) When etoposide has been administered, you should consider that secondary cancer may occur (Grade C1).

Chapter 7: Malignant sex cord-stromal tumors

Treatment of malignant sex cord-stromal tumors is summarized as flow chart 6 (Fig. 6).

CQ 39: What is the optimal surgical procedure for malignant sex cord-stromal tumors?

Recommendations

(1) According to the procedure for treating ovarian cancer, bilateral salpingo-oophorectomy + total hysterec-

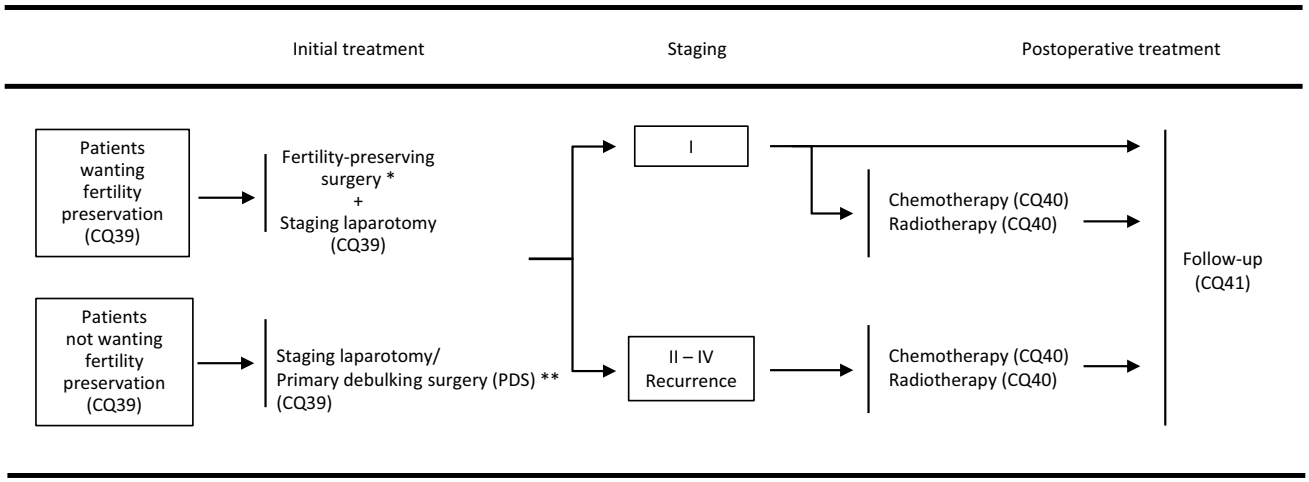

Fig. 6 Flow chart 6: treatment of malignant sex cord-stromal tumors. *Fertility-preserving surgery—affected-side salpingo-oophorectomy + omentectomy + peritoneal cytology + detailed intra-abdominal examination. **Lymph node dissection (biopsy) can be omitted

tomy + omentectomy are recommended together with peritoneal cytology, pelvic/para-aortic lymph node dissection (biopsy), and biopsies from sites in the abdominal cavity. However, lymph node dissection (biopsy) can be omitted (Grade C1).

(2) For patients who wish to preserve fertility, in addition to affected-side salpingo-oophorectomy + omentectomy + peritoneal cytology, detailed intra-abdominal examination should be considered (Grade C1).

CQ 40: What postoperative treatment is recommended for malignant sex cord-stromal tumors?

Recommendations

(1) With regard to chemotherapy, a platinum-containing regimen should be considered (Grade C1).
(2) Radiotherapy should also be considered (Grade C1).

CQ 41: What is important during follow-up after treatment of malignant sex cord-stromal tumors?

Recommendations

Management should be performed according to the protocol for ovarian cancer. Additionally, long-term follow-up for at least 10 years after treatment should be considered for granulosa cell tumors (Grade C1).

Acknowledgments Creation of this guideline was supported by the Japan Society of Gynecologic Oncology with contributions from "Encouragement of wider use of practice guidelines for cancer and their effects, as well as investigation of guideline projects" (chief investigator: Koichi Hirata), Research for Promotion of Cancer Control Programmes (2014), and a Health and Labour Sciences Research Grant. The funding sources did not influence the contents of this guideline.

Conflict of interest The conflict-of-interest committee of the Japan Society of Gynecologic Oncology checked conflicts of interest for the people involved in creating and evaluating this guideline and their associates (i.e., marital partner, first-degree relatives, or people sharing income/assets), according to the "Guidelines for conflict of interest issues in clinical studies on cancer" (http://www.jsgo.or.jp/topics/index01.html) published by the Japan Society of Gynecologic Oncology. Although there were conflicts of interest for some contributors through research/lecture activities supported by companies, the recommendations in this guideline are based on scientific evidence and have not been influenced by the interests of a specific organization and are not biased in recommending or products or techniques.

Guidelines for treatment of ovarian cancer including primary peritoneal cancer and fallopian tube cancer 2015 (4th edition)

Guideline development committee

Mitsuya Ishikawa, Fumiaki Isohashi, Yoshio Itani, Kimihiko Ito, Masahiro Iwasaki, Yasuhiko Ebina, Yoshihiro Ohishi, Hideyuki Ohtake, Tatsuru Oohara, Hiroaki Kajiyama, Noriyuki Katsumata, Kazuyoshi Kato, Shingo Kato, Masanori Kanemura, Kei Kawana, Takako Kiyokawa, Keisuke Kurose, Shinichi Komiyama, Kimiko Sato, Morio Sawada, Tadahiro Shoji, Masashi Takano, Hiroshi Tanabe, Hiroshi Tsubamoto, Fumitoshi Terauchi, Yasuhisa Terao, Kimihiro Nagai, Yoshifumi Nakao, Satoru Nagase, Kentaro Nakayama, Koji Nishino, Hiroyuki Nomura, Kazuhiko Hayashi, Eiji Hirata, Kiyoshi Fujiwara, Hiroyuki Fujiwara, Masayuki Futagami, Yusuke Matsuura, Noriomi Matsumura, Koji Matsumoto, Yoshiki Mikami, Yo Miyahara, Toshinari

Muramatsu, Hidekazu Yamada, Kiyoshi Yoshino, Yoshimitsu Ryo, and Hidemichi Watari (in order of the Japanese syllabary).

Guideline review committee

Satomi Aihara, Daisuke Aoki, Yoichi Aoki, Seiji Isonishi, Hiroaki Itamochi, Kazuhiko Ino, Osamu Iwanari, Kimio Ushijima, Masahide Ohmichi, Kazunori Ochiai, Takashi Onda, Hidenori Kato, Junzo Kigawa, Satoru Kyo, Hiroyuki Kuramoto, Hiroaki Kobayashi, Tsuyoshi Saito, Noriaki Sakuragi, Toyomi Satoh, Kiyosumi Shibata, Toru Sugiyama, Mitsuaki Suzuki, Kazuhiro Takehara, Shinichi Tate, Tsutomu Tabata, Katsuhiro Teramoto, Takafumi Toita, Takafumi Nakamura, Kaei Nasu, Toru Hachisuga, Kenichi Harano, Fumiki Hirahara, Ichio Fukasawa, Keiichi Fujiwara, Satoru Makinoda, Koji Miyazaki, Masanori Yasuda, Yoshihito Yokoyama, Hiroyuki Yoshikawa, and Kosuke Yoshinaga (in order of the Japanese syllabary).

References

1. Cancer Mortality in Japan (2012) Center for Cancer Control and Information Services. National Cancer Center, Japan. http://ganjoho.jp/professional/statistics/statistics.html. Accessed 15 Sept 2014
2. Heintz AP, Odicino F, Maisonneuve P et al (2006) Carcinoma of the ovary. FIGO 26th annual report on the results of treatment in gynecological cancer. Int J Gynaecol Obstet 95(Suppl 1):S161–S192
3. Gynecologic Cancer Committee (2012) Gynecologic cancer committee report in 2011. Acta Obstet Gynaecol Jpn 66:1024–1038
4. Ariyoshi H (2002) Guideline for correct use of antineoplastic agents (draft). General theory. Gan To Kagaku Ryoho 29:970–977
5. Ochiai K, Okamoto A, Katsumata N (2002) Guidelines for proper use of antineoplastic agents. Gynecologic cancer. Gan To Kagaku Ryoho 29:1047–1054
6. Fukui T, Yoshida M, Yamaguchi N (2007) Minds Guidance of practice guidelines 2007. Igakushoin, Tokyo
7. Takeuchi H, Saeki T, Aiba K et al (2016) Japanese Society of Clinical Oncology clinical practice guidelines 2010 for antiemesis in oncology: executive summary. Int J Clin Oncol 21:1–12
8. Japanese Society of Clinical Oncology clinical practice guidelines 2013 for G-CSF. http://www.jsco-cpg.jp/item/30/index.html

Aggressive Angiomyxoma of the Vulva with No Recurrence on a 5-year Follow up: A Case Report

Chisa NARAYAMA, Masae IKEDA, Miwa YASAKA, Yu-suke SAGARA, Yasuhira KAN-NO, Io HAYASHI, Atuya NARITA, Satoshi ASAI, Toshiki TAJIMA, Masako SHIDA, Takeshi HIRASAWA and Mikio MIKAMI

Department of Obstetrics and Gynecology, Tokai University School of Medicine

(Received January 27, 2016; Accepted February 16, 2016)

We report a case of vulvar aggressive angiomyxoma (AA) which is a rare, slow growing and benign tumor of mesenchymal origin, but has a high risk of local recurrence.
A 49-year-old Japanese female was referred to us with a large mass of the left vulva, measuring 15×9.5×9 centimeters. She underwent surgical excision of the tumor with no evidence of recurrence on a 5-year follow up. In this case, histopathological examination and immunohistochemical staining after excision revealed a diagnosis of vulvar AA with estrogen and progesterone receptors positive.
Aggressive angiomyxoma of the vulva needs to be distinguished from benign myxoid tumor with a low risk of local recurrence as well as from malignant neoplasma. The first line treatment of AA is complete surgical excision with tumor free margins, it will reduce the recurrence.

Key words: aggressive angiomyxoma, mesenchymal tumor, vulva, slow growing, local recurrence

INTRODUCTION

Aggressive angiomyxoma (AA), a rare soft tissue tumor of mesenchymal origin, predominantly occurs in the pelvic peritoneum, vulvo-vaginal, perineal and groin region of female in reproductive age. The female-to-male ratio is 6.6/1 [1]. Although AA is a slow growing and benign neoplasm, it has a high risk of local recurrence after many years but usually does not metastasize.

AA was first described by Steeper and Rosai in 1983 as a rare mesenchymal tumor of reproductive-age women [2]. AA is often clinically misdiagnosed as a malignancy, such as mixed mesodermal tumor, malignant fibrous histiocytoma, botyroid pseudosarcoma, embryonal rhabdomyosarcoma and squamous cell carcinoma by primary care providers. Misdiagnosis is seen in 80% of the cases [3]. Imaging is important to diagnose and to determine the extent of the lesion for surgery as the first line of treatment.

We describe a case report of AA of the vulva in a 49-year-old female who underwent complete surgical excision of the tumor with no evidence of recurrence on a 5-year follow up.

CASE REPORT

A 49-year-old, Gravida 5 Para 2, Japanese female referred to the gynecology outpatient unit of our hospital with a complaint of a large left vulvar mass, measuring 15 × 9.5 × 9 centimeters (Fig. 1). It was an elongated, non-mobile, non-tender and painless mass extending longitudinally between the mons pubis and the anal verge along the left labial fold. The patient noticed the small mass 5 years ago and it has been gradually increased in size. As the increasing, she has complained of progressively worsening her quality of life. She was previously healthy, her past medical and family histories were normal. She had smoked 15 cigarettes per day for 35 years in her personal history. Her physical examination and laboratory tests were within normal limits.

Magnetic Resonance Imaging (MRI) revealed a bulky well circumscribed subcutaneous mass lesion in the left vulva. The mass demonstrated isointensity to the muscle on T1-weighted images (Fig. 2-1). On T2-weighted images high signal intensity relative to the muscle with "swirled" low signals intensity bands within the hyperintense tumor was noted (Fig. 2-2). Computed tomography (CT) showed no pelvic lymphadenopathy and ascites.

With informed consent, she underwent a surgical excision of the tumor (Fig. 3-1, 2). The final pathological diagnosis was AA of the vulva.

Macroscopically, the bulky mass was a solid and soft tumor, measuring 15 cm in longitudinal diameter and well circumscribed (Fig. 4-1). The cut surface showed a fleshy glistening myxoid mass with a mixed white and yellow tone (Fig. 4-2). Microscopically, short spindle-shaped tumor cells proliferate in a myxoid, edematous background (Fig. 5). The tumor cells have scant eosinophilic cell bodies and mildly enlarged nuclei. Mitoses are rarely seen. Blood vessels are occasionally found. In immunohistochemical stain, tumor cells are positive for desmin, SM-actin, estrogen receptor and

Masae IKEDA, Department of Obstetrics and Gynecology, Tokai University School of Medicine, 143 Shimokasuya, Isehara, Kanagawa 259-1193, Japan
Tel: +81-463-93-1121 Fax: +81-463-91-4343 E-mail: ikedam@tokai-u.jp

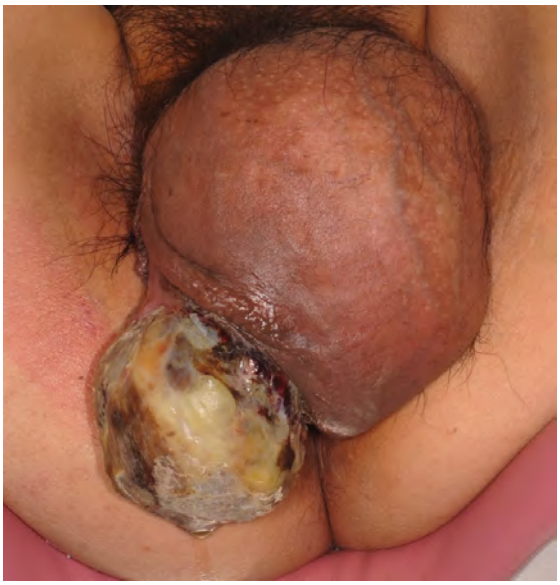

Fig. 1 a large left vulvar mass, measuring 15 × 9.5 × 9 centimeters.

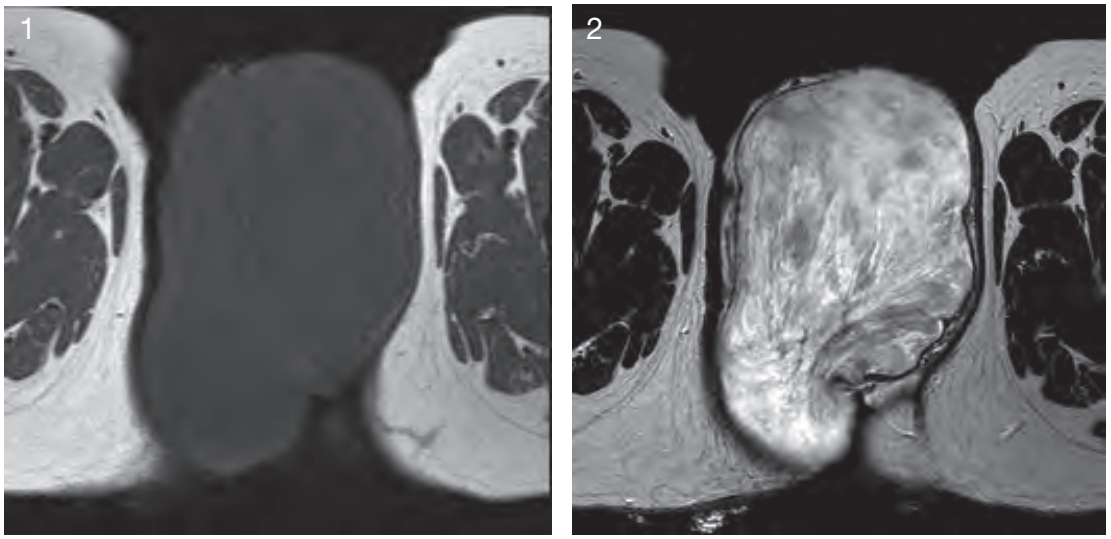

Fig. 2 (1) Axial MRI: T1-weighted images showing vulvar mass with isointensity to the muscle.
(2) Axial MRI: T2-weighted images showing vulvar aggressive angiomyxoma with the swirled appearance.

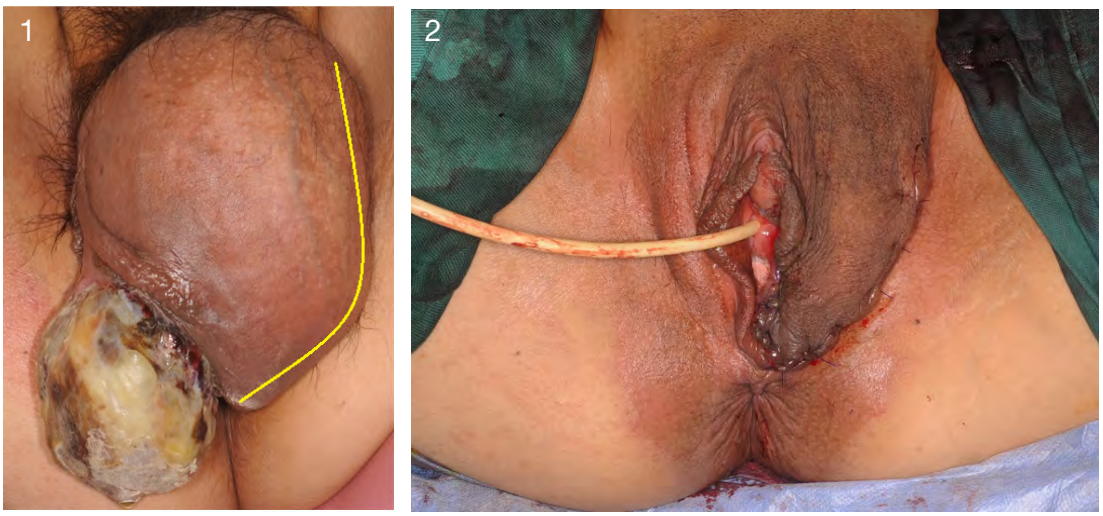

Fig. 3 (1) Surgery of vulvar aggressive angiomyxoma. (Preoperative)
(2) Surgery of vulvar aggressive angiomyxoma. (Postoperative)

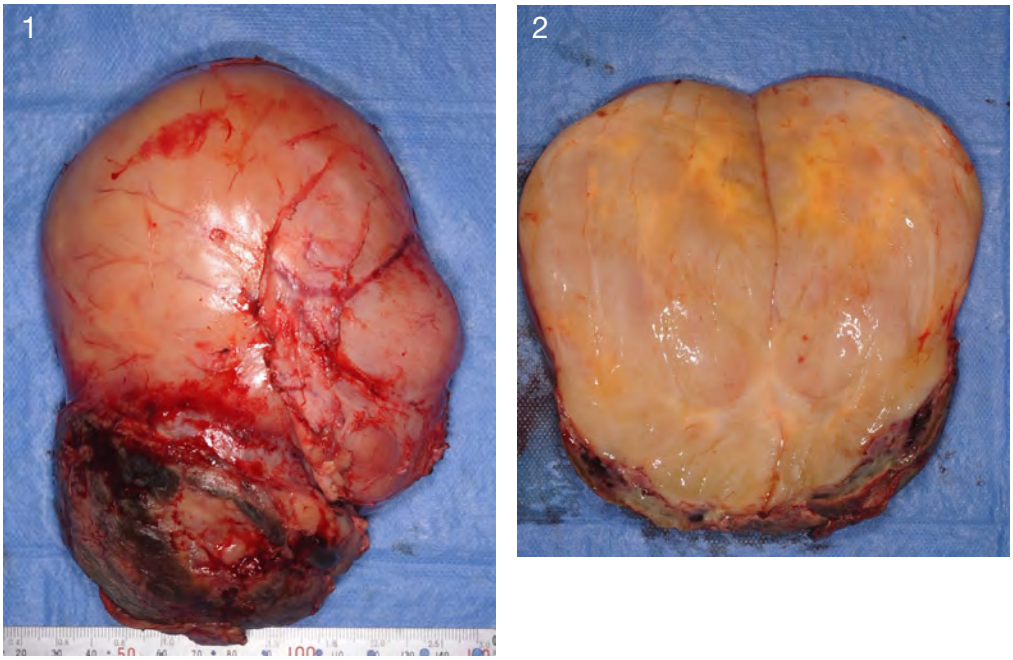

Fig. 4 (1) Gross vulvar aggressive angiomyxoma: the solid tumor, measuring 15 cm in longitudinal diameter and almost encapsulated with the exception of the self-destructive part. (2) Cut surface: fleshy glistening myxoid mass mixed white and yellow tone.

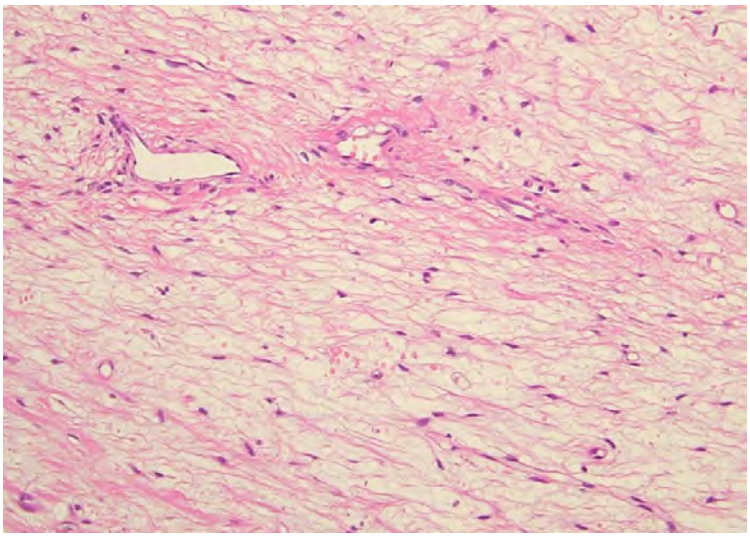

Fig. 5 short spindle-shaped tumor cells proliferate in a hypocellular myxoid stroma. (HE stain, x100)

progesterone receptor. No expression of CD34, S-100 protein, caldesmon and myoglobin is seen.

No relapse has occurred by the time of follow-up at 5 years after surgery.

DISCUSSION

The vulvar AA is a benign mesenchymal tumor but with a high local recurrence rate up to 72%, and relapse occurs months to several years after surgery [4, 5]. That is why differential diagnosis is pivotal for the prognosis from other benign myxoid neoplasms.

Several imaging modalities are useful in primary and recurrent diagnosing and surgical treatment of AA. Particularly, MRI and CT are recommended to diagnose and identify the extent of the tumor for making surgical approach. Relative to muscle signals on MRI, AA shows an isointense signal on T1-weighted images and a hyperintense one on T2-weighted images. A swirled appearance retaining the enhancing layered appearance on MRI and CT is characteristic and often present in 83% of cases [5]. CT also shows a tumor with well-defined moderately enhanced margins with attenuation less than that of muscle [6]. The attenuation on CT and high signal intensity on MRI are likely related to the loose myxoid matrix and high water content of angiomyxoma [2].

In our patient, a gynecological exam revealed a self-destructive fleshy mass in the left vulva, and MRI

and CT confirmed the superficial nature of this lesion with respect to the pelvic diaphragm and provided a proper surgical route. To obtain a successful result in surgical treatment, it is important to completely excise a tumor with tumor-free margins. The excised lesion of our case had negative margins on pathological evaluation. AA of the external surface is smooth and usually appears not to be encapsulated. They typically have finger-like projections that extend into neighboring tissues [1]. Our case, unlike most AA, was almost encapsulated by a fibrofatty layer with the exception of the self-destructive part, and there was no evident infiltration into neighboring tissues in this case. This may explain why there has been no recurrence in the last 5 years.

There are various treatments, however if it is possible, complete surgical excision with a clear margin should be sought. While lesion recurrence is frequent, hormonal treatment with gonadotropin-releasing hormone analogs (GnRHa) or anti-hormonal therapy is sometimes needed for primary and recurrent AA. This can be attributed to the fact that most of AA express estrogen and progesterone receptors and are sensitive to hormonal therapy [7, 8]. Han-Guerts *et al*. [9] proposes the following guidelines in treating AA: (1) complete excision of the lesion when possible and avoiding mutilating surgery, (2) adjunct therapy when partial resection is performed is acceptable using arterial embolization and/or hormonal treatment, and (3) radiotherapy is reserved to cases that are resistant to embolization and/or hormonal therapy and still symptomatic. There are no standard treatments for recurrence in the postoperative management of vulvar AA. Our patient required no additional treatment postoperatively because of complete excision with negative margins and an almost encapsulated tumor.

The pathogenesis of vulvar AA is poorly understood, but a translocation at chromosome 12 with a consequent aberrant expression of the high-mobility group protein isoform I-C (HMGI-C) protein involved in DNA transcription has been demonstrated. Detection of inappropriate HMGI-C expression using immunoperoxidase technique with anti HMG1-C antibody may be a useful marker for microscopic residual disease [10].

In conclusion, AA is a rare locally aggressive mesenchymal tumor. When complete resection with tumor-free margins is possible, it will offer the lowest recurrence rate. Even if the AA is resected completely, it is clear that it requires close and long-term follow up for recurrence.

ACKNOWLEDGMENTS

The authors express the sincere gratitude to Dr. Hiroshi Kajiwara, and Dr. Nobue Kumaki, Departmentbof Pathology, Tokai School of Medicine, for their cooperation.

REFERENCES

1) Dahiya K, Jain S, Duhan N, Nanda S, Kundu P. Aggressive angiomyxoma of vulva and vagina: a series of three cases and review of literature. Archives of Gynecology and Obstetrics 2011; 283(5): 1145–1148.
2) Steeper TA, Rosai J. Aggressive angiomyxoma of the female pelvis and perineum. Report of nine cases of a distinctive type of gynecologic soft-tissue neoplasm. American Journal of Surgical Pathology 1983; 7(5): 463–475.
3) Güngör T, Zengeroğlu S, Kaleli A, Kuzey GM. Aggressive angiomyxoma of the vulva and vagina — a common problem: misdiagnosis. European Journal of Obstetrics Gynecology and Reproductive Biology 2004; 112(1): 114–116.
4) Dierickx I, Deraedt K, Poppe W, Verguts J. Aggressive angiomyxoma of the vulva: a case report and review of literature. Archives of Gynecology and Obstetrics 2008; 277(6): 483–487.
5) Kiran G, Yancar S, Sayar H, Kiran H, Coskun A, Arikan DC. Late recurrence of aggressive angiomyxoma of the vulva. Journal of Lower Genital Tract Disease 2013; 17(1): 85–87.
6) Outwater EK, Marchetto BE, Wagner BJ, Siegelman ES. Aggressive angiomyxoma: findings on CT and MR imaging. American Journal of Roentgenology 1999; 172(2): 435–438.
7) Fine BA, Munoz AK, Litz CE, Gershenson DM. Primary medical management of recurrent aggressive angiomyxoma of the vulva with a gonadotropin-releasing hormone agonist. Gynecologic Oncology 2001; 81(1): 120–122.
8) McCluggage WG, Jamieson T, Dobbs SP, Grey A. Aggressive angiomyxoma of the vulva: dramatic response to gonadotropin-releasing hormone agonist therapy. Gynecol Oncol 2006; 100: 623–625.
9) Han-Geurts IJM, van Geel AN, van Doorn L, M. den Bakker MDB, Eggermont AMM, Verhoef C. Aggressive angiomyxoma: multimodality treatments can avoid mutilating surgery. European Journal of Surgical Oncology 2006; 32(10): 1217–1221.
10) Nucci MR, Fletcher CDM. Vulvovaginal soft tissue tumours: update and review. Histopathology 2000; 36(2): 97–108.

Int J Clin Oncol (2016) 21:435–446
DOI 10.1007/s10147-016-0985-x

SPECIAL ARTICLE

Japan Society of Gynecologic Oncology guidelines 2015 for the treatment of ovarian cancer including primary peritoneal cancer and fallopian tube cancer

Shinichi Komiyama[1] · Hidetaka Katabuchi[2] · Mikio Mikami[3] · Satoru Nagase[4] · Aikou Okamoto[5] · Kiyoshi Ito[6] · Kenichiro Morishige[7] · Nao Suzuki[8] · Masanori Kaneuchi[9] · Nobuo Yaegashi[10] · Yasuhiro Udagawa[11] · Hiroyuki Yoshikawa[12]

Received: 16 April 2016 / Accepted: 20 April 2016 / Published online: 3 May 2016

Abstract The fourth edition of the Japan Society of Gynecologic Oncology guidelines for the treatment of ovarian cancer including primary peritoneal cancer and fallopian tube cancer was published in 2015. The guidelines contain seven chapters and six flow charts. The major changes in this new edition are as follows—(1) the format has been changed from reviews to clinical questions (CQ), and the guidelines for optimal clinical practice in Japan are now shown as 41 CQs and answers; (2) the 'flow charts' have been improved and placed near the beginning of the guidelines; (3) the 'basic points', including tumor staging, histological classification, surgical procedures, chemotherapy, and palliative care, are described before the chapter; (4) the FIGO surgical staging of ovarian cancer, fallopian tube cancer, and primary peritoneal cancer was revised in 2014 and the guideline has been revised accordingly to take the updated version of this classification into account; (5) the procedures for examination and management of hereditary breast and ovarian cancer are described; (6) information on molecular targeting therapy has been added; (7) guidelines for the treatment of recurrent cancer based on tumor markers alone are described, as well as guidelines for providing hormone replacement therapy after treatment.

Keywords Guideline · Ovarian cancer · Primary peritoneal cancer · Fallopian tube cancer · Japan Society of Gynecologic Oncology

Introduction

The number of patients with ovarian cancer is increasing in Japan and 8,631 cases were reported in 2007 [1]. Deaths due to ovarian cancer are also increasing and 4,705 patients died of this disease in 2011 [1]. Ovarian cancer is the most

This article originally appeared in Japanese as Ransougan Chiryo guideline 2015 nen-ban, published by Kanehara & Co., Ltd, Tokyo, Japan.

✉ Shinichi Komiyama
komiyama@med.toho-u.ac.jp

1 Department of Gynecology, Toho University Ohashi Medical Center, 2-17-6 Ohashi, Meguro-ku, Tokyo 153-8515, Japan

2 Department of Obstetrics and Gynecology, Faculty of Life Sciences, Kumamoto University, Kumamoto, Japan

3 Department of Obstetrics and Gynecology, Tokai University School of Medicine, Kanagawa, Japan

4 Department of Obstetrics and Gynecology, Faculty of Medicine, Yamagata University, Yamagata, Japan

5 Department of Obstetrics and Gynecology, Jikei University School of Medicine, Tokyo, Japan

6 Department of Disaster Obstetrics and Gynecology, Tohoku University Graduate School of Medicine, Sendai, Japan

7 Department of Obstetrics and Gynecology, Gifu University Graduate School of Medicine, Gifu, Japan

8 Department of Obstetrics and Gynecology, School of Medicine St. Marianna University, Kawasaki, Japan

9 Department of Obstetrics and Gynecology, Nagasaki University Graduate School of Medicine, Nagasaki, Japan

10 Department of Obstetrics and Gynecology, Tohoku University Graduate School of Medicine, Sendai, Japan

11 Department of Obstetrics and Gynecology, Fujita Health University School of Medicine, Aichi, Japan

12 Ibaraki Prefectural Central Hospital, Ibaraki, Japan

Table 1 Criteria for evaluating the quality of evidence (levels of evidence)

Level I	Evidence from meta-analyses of multiple randomized controlled trials
Level II	Evidence from randomized controlled trials, or evidence from well-designed nonrandomized controlled trials
Level III	Evidence from well-designed quasi-experimental studies, or evidence from well-designed non-experimental descriptive studies, such as comparative studies, correlation studies, and case–control studies
Level IV	Expert committee reports and opinions, or clinical experiences of respected authorities

common cause of death among malignant tumors of the female genital tract. Tumor stage is thought to be an important prognostic factor, with stage III and IV cancer having a poor prognosis [2]. Since the ovary is a pelvic organ, an ovarian tumor may not cause any early symptoms, and approximately 40–50 % of patients with ovarian cancer have stage III or IV disease (with a poor prognosis) at the time of first presentation [3]. Thus, an important challenge is to improve the outcome of treatment in patients with advanced ovarian cancer.

In order to improve the prognosis of ovarian cancer and reduce regional differences in the management of ovarian cancer in Japan, the first edition of the guidelines for the treatment of ovarian cancer was published by the Japan Society of Gynecologic Oncology in 2004. It has since been revised several times, and the fourth edition was published in April 2015. The new guidelines include seven chapters and six flow charts. The major changes in the new edition are as follows:

(1) The format has been changed from a review format to a clinical question (CQ) format, so the guidelines for optimal clinical practice in Japan are now shown as 41 CQs and answers.
(2) The 'flow charts' have been improved and are placed near the beginning of the guideline.
(3) The 'basic points', including staging, histological classification, surgical procedures, chemotherapy, and palliative care are included before the chapter.
(4) The FIGO surgical staging of ovarian cancer, fallopian tube cancer, and primary peritoneal cancer was revised in 2014 and the guideline has been revised accordingly to take the updated version of this classification into account.
(5) Procedures for the examination and management of hereditary breast and ovarian cancer (HBOC) are described.
(6) Information on molecular targeting therapy has been added.
(7) Guidelines for the treatment of recurrent cancer based on tumor markers alone and for providing hormone replacement therapy (HRT) after treatment are described.

Chapter 1: Overview

The aims of this guideline are to describe current optimal treatment for ovarian cancer (epithelial tumors, germ cell tumors, and sex cord stromal tumors), primary peritoneal cancer, and fallopian tube cancer, to reduce differences in management between medical institutions, to improve the safety of therapy and the prognosis, to reduce the burden (physical, mental, and economic) on patients by promoting optimal treatment, and to improve communication between patients and healthcare professionals.

Much of the evidence adopted in this guideline was obtained from clinical studies performed in Europe, the USA, and Japan. However, some evidence from Europe and the USA does not apply in Japan because of differences in background factors between Europe/USA and Japan. Conversely, some treatments used widely in Japan are uncommon in Europe and the USA. In such cases, the current consensus for disease management in Japan is prioritized in this guideline.

This guideline was created according to the principles of 'evidence-based medicine', which is a standard method for producing clinical practice guidelines. The quality of evidence was evaluated using the criteria shown in Table 1 [4, 5]. In addition, the grade of each recommendation in the guideline was determined using the criteria set out in Table 2 [4–6].

Chapter 2: Epithelial ovarian cancer

Treatment of epithelial ovarian cancer is summarized as flow chart 1 (Fig. 1).

CQ 01: What is the optimal surgical procedure for ovarian cancer when the tumor seems to be localized to the ovary?

Recommendations

(1) In addition to bilateral salpingo-oophorectomy + total hysterectomy + omentectomy, peritoneal cytol-

Table 2 Grading of recommendations

Grade A	The proposed treatment is strongly recommended
	In principle, there is at least one source of Level I evidence showing efficacy of the treatment
Grade B	The proposed treatment is recommended
	In principle, there is at least one source of Level II evidence showing efficacy of the treatment
Grade C1	The proposed treatment may be considered. However, there is not enough scientific evidence
	(or the treatment may have efficacy, although sufficient scientific evidence has not been obtained)
	There are multiple sources of Level III evidence showing efficacy of the treatment and the outcomes are roughly consistent
Grade C2	There is not enough scientific evidence, and the treatment is not recommended in routine clinical practice
Grade D	The treatment is not recommended (usefulness or efficacy have not been shown, and the treatment may be harmful)

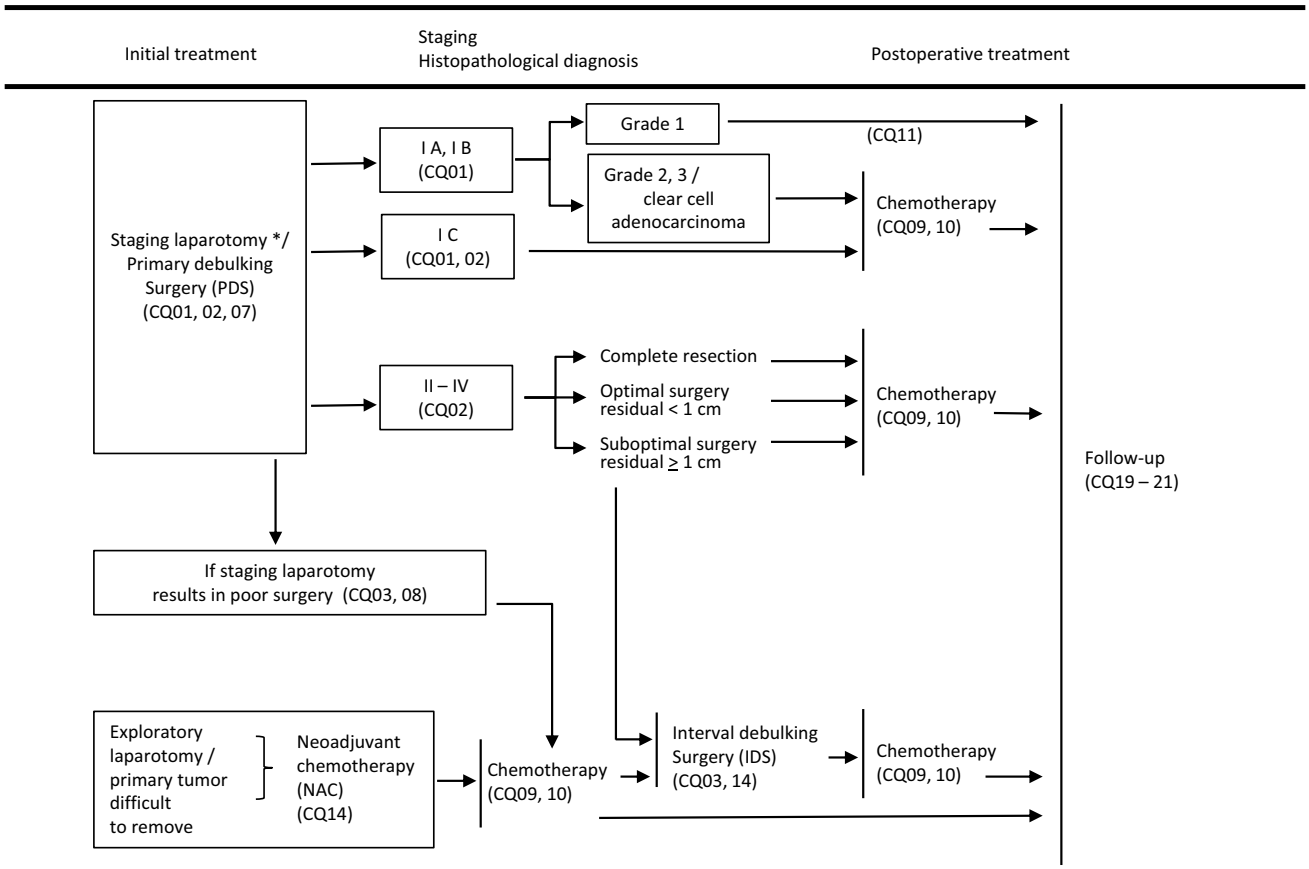

Fig. 1 Flow chart 1: treatment of epithelial ovarian cancer. *Staging laparotomy—bilateral salpingo-oophorectomy + total hysterectomy + omentectomy + peritoneal cytology + pelvic/para-aortic lymph node dissection (biopsy) + biopsies from sites in the abdominal cavity

ogy + pelvic/para-aortic lymph node dissection (biopsy) + biopsies from sites in the abdominal cavity are recommended (Grade B).

(2) When biopsies are obtained from sites in the abdominal cavity, sampling from the following sites should be considered—pouch of Douglas, parietal peritoneum, surface of the diaphragm, intestinal tract, mesentery, and suspected lesions (Grade C1).

CQ 02: What is the optimal surgical procedure for ovarian cancer that is thought to be stage II or a more advanced stage preoperatively?

Recommendations

Maximal debulking surgery to accomplish complete resection (no gross residual tumor) is strongly recommended (Grade A).

CQ 03: Is interval debulking surgery (IDS) recommended for advanced ovarian cancer if primary debulking surgery (PDS) had a suboptimal outcome?

Recommendations

As a treatment option, IDS should be considered during chemotherapy for patients with advanced cancer if previous surgery had a suboptimal outcome (Grade C1).

CQ 04: What is the optimal management if a patient wishes to preserve fertility?

Recommendations

(1) Detailed informed consent about preservation of fertility is necessary (Grade A).
(2) As the basic operative procedure to preserve fertility, affected-side salpingo-oophorectomy + omentectomy + peritoneal cytology is recommended (Grade B).
(3) In addition to the above-mentioned basic procedure, biopsy of the contralateral ovary, biopsy (dissection) of the pelvic/para-aortic lymph nodes, and biopsies from sites in the abdominal cavity should be considered as part of staging laparotomy (Grade C1).

CQ 05: Is risk-reducing salpingo-oophorectomy (RRSO) recommended for patients with the *BRCA1* or *BRCA2* gene mutation?

Recommendations

It is recommended that RRSO only be performed by a gynecologic oncologist who is a member of the Japan Society of Gynecologic Oncology in cooperation with a clinical geneticist at a medical facility with an established genetic counseling system and cooperative pathologists, after review and approval by the institutional ethics committee (Grade B).

CQ 06: Is laparoscope-assisted surgery possible?

Recommendations

(1) Currently, laparoscope-assisted surgery is not recognized as a standard procedure that can be substituted for laparotomy (Grade C2).
(2) However, in patients with advanced cancer, laparoscope-assisted surgery may be substituted for laparotomy to observe the abdominal cavity and collect tissue samples (Grade C1).

CQ 07: For which patients is intraoperative rapid pathological examination recommended?

Recommendations

For patients in whom judgment between benign/borderline malignancy/malignancy is difficult based on preoperative evaluation and intraoperative findings, intraoperative rapid pathological examination is recommended for selecting the optimal surgical procedure (Grade B).

CQ 08: What is the recommended management of a patient in whom ovarian cancer is diagnosed after surgery?

Recommendations

Staging laparotomy (re-laparotomy) is recommended (Grade B).

CQ 09: What chemotherapy regimen is recommended as first-line therapy?

Recommendations

(1) Paclitaxel + carboplatin (conventional TC therapy) is strongly recommended (Grade A).
(2) Dose-dense TC therapy is also recommended (Grade B).

CQ 10: What chemotherapy regimens other than TC therapy are recommended as first-line therapy?

Recommendations

(1) Docetaxel + carboplatin (DC therapy) is recommended (Grade B).
(2) Cisplatin monotherapy or carboplatin monotherapy can be considered (Grade C1).

CQ 11: Which patients do not need postoperative chemotherapy?

Recommendations

It can be omitted for patients with stage I A/I B, Grade 1 disease confirmed by staging laparotomy (Grade B).

CQ 12: Should first-line chemotherapy be selected by considering tumor histology?

Recommendations

This is not recommended because there is insufficient evidence to show that standard treatment should be changed depending on tumor histology (Grade C2).

CQ 13: Is intraperitoneal chemotherapy recommended as the first-line therapy?

Recommendations

Intraperitoneal chemotherapy should be considered for patients with advanced cancer who have undergone optimal surgery (Grade C1).

CQ 14: Are neoadjuvant chemotherapy (NAC) and IDS recommended for advanced ovarian cancer if optimal surgery is thought to be impossible?

Recommendations

For patients with advanced cancer in whom it is thought that primary surgery will not result in an optimal outcome, preoperative chemotherapy and debulking surgery (NAC + IDS) are recommended as a treatment option (Grade B).

CQ 15: Is maintenance chemotherapy recommended after complete remission is achieved?

Recommendations

It is not recommended, because usefulness of maintenance chemotherapy has not been demonstrated (Grade C2).

CQ 16: What management approach is recommended if complete remission is not achieved by initial treatment?

Recommendations

Additional treatment (second-line chemotherapy and radiotherapy), participation in a clinical trial, or best supportive care should be considered (Grade C1).

CQ 17: What is the recommended management of serious adverse events associated with chemotherapy?

Recommendations

Hypersensitivity reactions (*HSR*)

(1) Premedication should be provided because taxanes, such as paclitaxel, are associated with a risk of HSR (Grade A).
(2) When carboplatin causes HSR, premedication alone cannot reduce the risk of recurrence. Therefore, switching to another drug or desensitization therapy should be considered (Grade C1).

Gastrointestinal symptoms (*nausea, diarrhea*)

(1) For nausea, refer to the relevant guideline [7], and provide adequate antiemetic therapy (Grade A).
(2) For mild diarrhea, antidiarrheal agents should be administered orally. For severe diarrhea complicated by other symptoms, early aggressive treatment should be performed, such as fluid replacement and administration of an antibacterial agent (Grade A).

Myelosuppression/febrile neutropenia
Refer to the relevant guideline [8], and provide adequate treatment with an antibacterial agent and/or a granulocyte-colony stimulating factor (G-CSF) preparation (Grade A).

CQ 18: Are any molecular targeting drugs recommended as first-line therapy or as treatment for recurrence?

Recommendations

Bevacizumab should be considered in combination with chemotherapy and as subsequent maintenance therapy. However, careful patient selection and appropriate monitoring for adverse events are required when bevacizumab is used (Grade C1).

CQ 19: What is the optimal follow-up interval after treatment?

Recommendations

After the start of initial treatment,

Years 1–2: an interval of 1–3 months
Years 3–5: an interval of 3–6 months
Year 6 onward: an interval of 1 year

The above-mentioned intervals are only intended as a guide (Grade C1).

CQ 20: What examinations/tests should be performed for follow-up after treatment?

Recommendations

(1) Taking a history and performing and pelvic examination at every visit should be considered (Grade C1).
(2) Measurement of CA125, transvaginal ultrasonography, or computed tomography scanning should be considered as required (Grade C1).

CQ 21: Is intervention for recurrence recommended if the patient only has elevation of CA125 without any symptoms?

Recommendations

Early intervention in response to elevation of CA125 alone is not necessarily recommended (Grade C2).

CQ 22: Is HRT recommended?

Recommendations

After informing the patient about its merits and demerits, HRT should be considered carefully for individual patients (Grade C1).

Chapter 3: Borderline epithelial ovarian tumors

Treatment of borderline epithelial ovarian tumors is summarized as flow chart 2 (Fig. 2).

CQ 23: What is the optimal surgical procedure for borderline epithelial ovarian tumors?

Recommendations

(1) In addition to bilateral salpingo-oophorectomy + total hysterectomy + omentectomy + peritoneal cytology, detailed intra-abdominal examination is recommended (Grade B).
(2) If suspected peritoneal lesions are found by intra-abdominal examination, removing such lesions should be considered, or taking peritoneal biopsies from several sites should be considered if there are no suspected peritoneal lesions (Grade C1).
(3) For patients who wish to preserve fertility, in addition to salpingo-oophorectomy on the affected side + omentectomy + peritoneal cytology, detailed intra-abdominal examination should be considered (Grade C1).

CQ 24: What are the indications for chemotherapy and the recommended regimens?

Recommendations

For patients with gross residual tumors and patients with invasive peritoneal implants, performing postoperative chemotherapy with platinum agents and taxanes according to the treatment regimens for ovarian cancer should be considered (Grade C1).

CQ 25: What is important for follow-up after treatment of a borderline epithelial ovarian tumor?

Recommendations

In patients with borderline epithelial tumors, long-term follow-up for at least 10 years after treatment should be considered (Grade C1).

Chapter 4: Recurrent epithelial ovarian cancer

Treatment of recurrent ovarian cancer is summarized as flow chart 3 (Fig. 3).

CQ 26: What chemotherapy regimen is recommended for recurrence after a disease-free interval (DFI) of <6 months?

Recommendations

Monotherapy that avoids cross-resistance to previous treatment is recommended (Grade B).

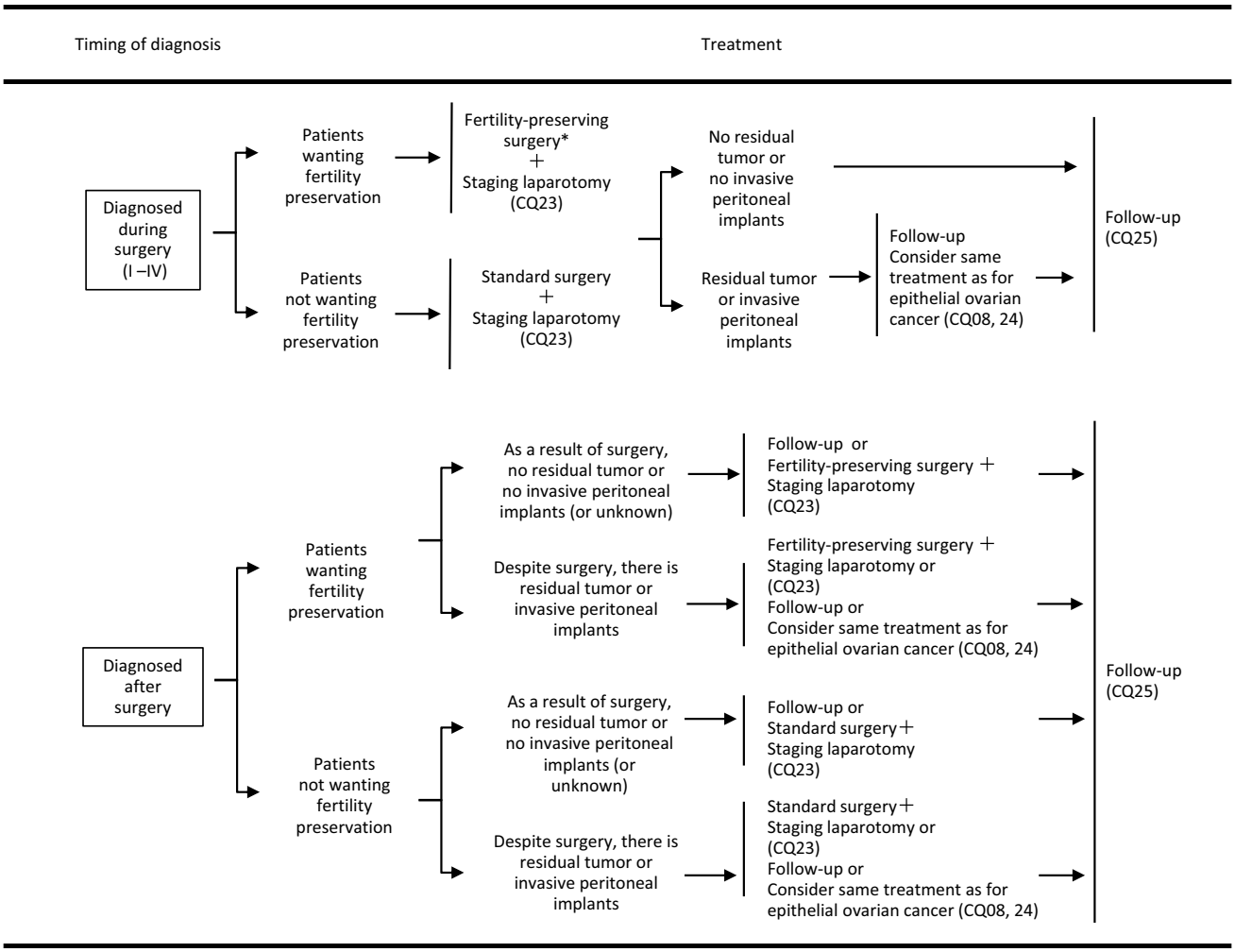

Fig. 2 Flow chart 2: treatment of borderline epithelial ovarian tumors. *Fertility-preserving surgery—affected-side salpingo-oophorectomy + omentectomy + peritoneal cytology + detailed intra-abdominal examination

CQ 27: What chemotherapy regimen is recommended for recurrence after a DFI of ≥6 months?

Recommendations

Combination therapy including a platinum agent is strongly recommended (Grade A).

CQ 28: What are the indications and strategy for secondary debulking surgery (SDS) in patients with recurrence?

Recommendations

(1) Whether or not SDS is worth performing should be carefully determined by evaluating the timing of recurrence, the primary surgical procedure, the site of recurrence, the number of lesions, and the performance status of the patient in a comprehensive manner (Grade C1).
(2) When SDS is performed, the objective should be complete resection of the tumor when possible (Grade C1).

CQ 29: What are the indications for radiation therapy in patients with recurrence?

Recommendations

(1) Radiation therapy should be considered in order to relieve symptoms, such as pain and bleeding (Grade C1).
(2) Radiation therapy should be considered for brain metastasis, not only to relieve symptoms, but also to prolong survival (Grade C1).

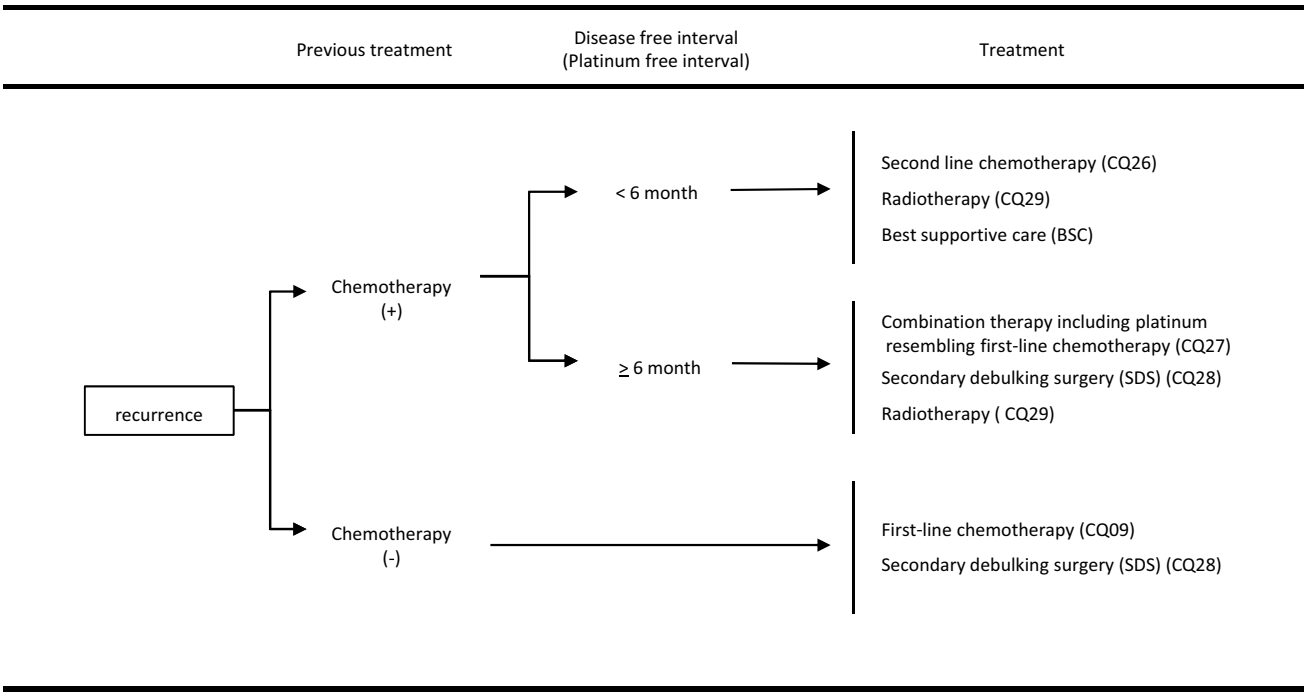

Fig. 3 Flow chart 3: treatment of recurrent epithelial ovarian cancer

CQ 30: What is the recommended management strategy for intestinal obstruction and accumulation of ascites?

Recommendations

Intestinal obstruction

(1) Administration of octreotide is strongly recommended for nausea/vomiting (Grade A).
(2) Correcting physical obstruction by palliative surgery is recommended for relieving nausea/vomiting (Grade B).
(3) Administration of corticosteroids should be considered to relieve nausea/vomiting (Grade C1).

Accumulation of ascites

(1) In patients with terminal cancer whose life expectancy is estimated to be ≤1–2 months, the volume of infusion solution should be limited to ≤1,000 mL/day if the patient has pain due to accumulation of ascites (Grade C1).
(2) Taking the underlying pathological state into consideration, administration of diuretics, drainage of ascitic fluid (paracentesis), creation of a peritoneovenous shunt, and cell-free and concentrated ascites reinfusion therapy should be considered for relieving pain due to accumulation of ascites (Grade C1).

Chapter 5: Primary peritoneal cancer/fallopian tube cancer

Treatment of primary peritoneal cancer or fallopian tube cancer is summarized as flow chart 4 (Fig. 4).

CQ 31: What is the optimal surgical procedure for primary peritoneal cancer?

Recommendations

Maximal debulking surgery to accomplish complete resection (no gross residual tumor) should be considered (Grade C1).

CQ 32: What chemotherapy regimen is recommended for primary peritoneal cancer?

Recommendations

(1) Either conventional TC therapy or dose-dense TC therapy should be considered (Grade C1).

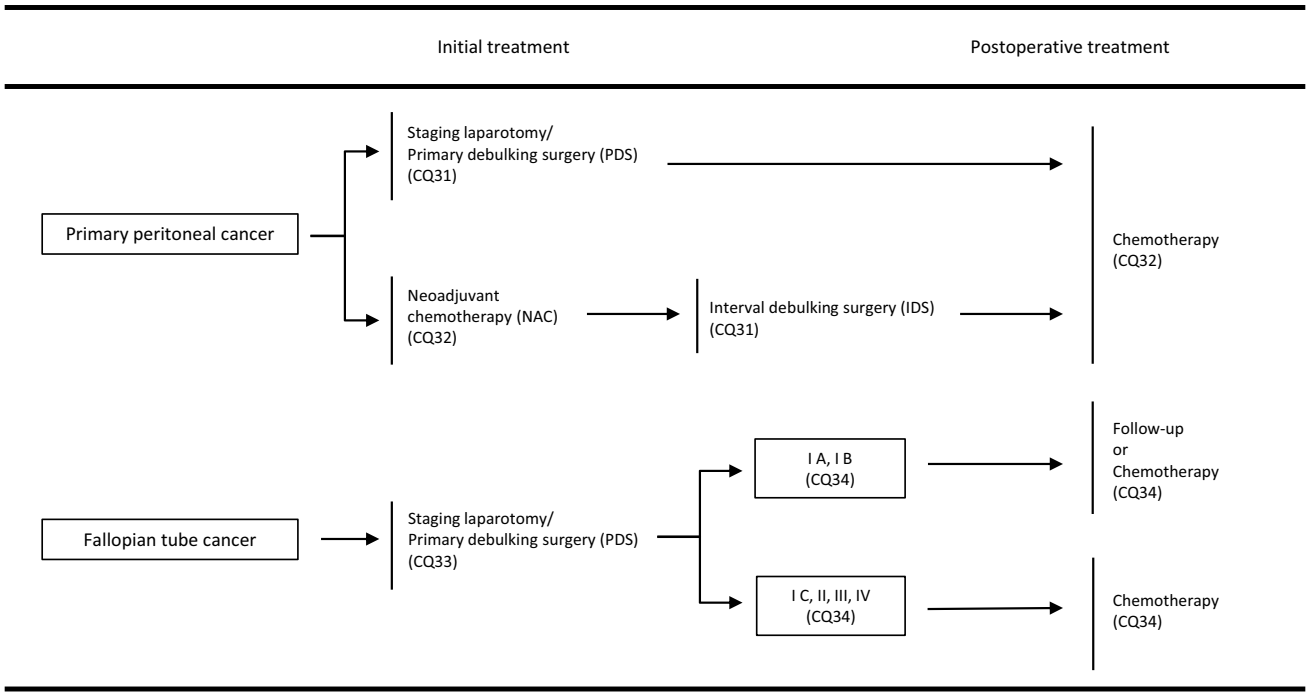

Fig. 4 Flow chart 4: treatment of primary peritoneal cancer and fallopian tube cancer

(2) Neoadjuvant chemotherapy should also be considered (Grade C1).

CQ 33: What is the optimal surgical procedure for fallopian tube cancer?

Recommendations

(1) According to the procedure for treating ovarian cancer, bilateral salpingo-oophorectomy + total hysterectomy + omentectomy are recommended together with peritoneal cytology + pelvic/para-aortic lymph node dissection (biopsy) + biopsies from sites in the abdominal cavity (Grade B).
(2) Maximal debulking surgery to accomplish complete resection (no gross residual tumor) is recommended for patients with advanced cancer (Grade B).

CQ 34: What chemotherapy regimen is recommended for fallopian tube cancer?

Recommendations

Conventional TC therapy or dose-dense TC therapy should be considered (Grade C1).

Chapter 6: Malignant ovarian germ cell tumors

Treatment of malignant ovarian germ cell tumors is summarized as flow chart 5 (Fig. 5).

CQ 35: What is the optimal surgical procedure for malignant ovarian germ cell tumors?

Recommendations

(1) For patients who wish to preserve fertility, in addition to salpingo-oophorectomy on the affected side + omentectomy + peritoneal cytology, detailed intra-abdominal examination is recommended (Grade B).
(2) For patients who do not require preservation of fertility, according to the procedure for treating ovarian cancer, bilateral salpingo-oophorectomy + total hysterectomy + omentectomy are recommended together with peritoneal cytology, pelvic/para-aortic lymph node dissection (biopsy), and biopsies from sites in the abdominal cavity. However, lymph node dissection (biopsy) can be omitted (Grade B).
(3) For patients with advanced cancer, maximal debulking surgery to accomplish complete resection (no

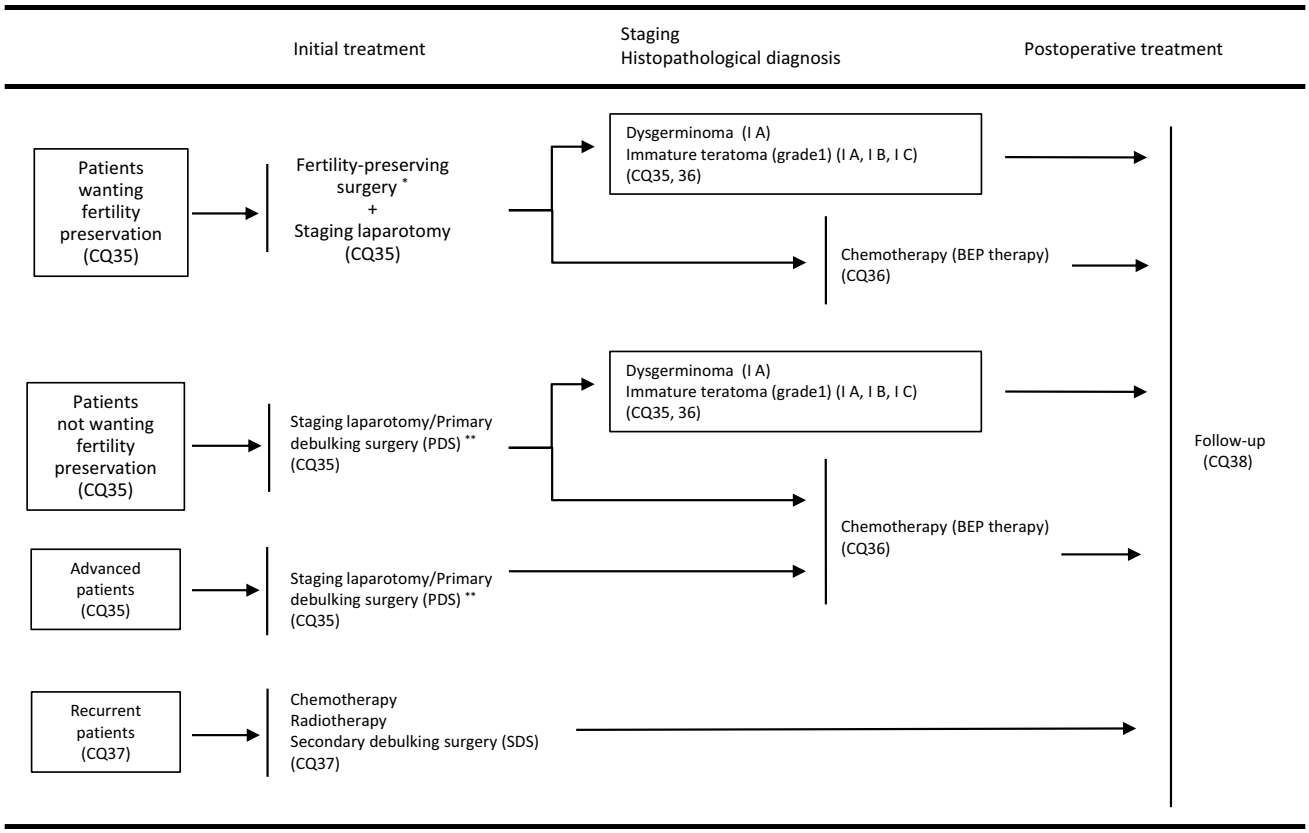

Fig. 5 Flow chart 5: treatment of malignant germ cell tumors. *Fertility-preserving surgery—affected-side salpingo-oophorectomy + omentectomy + peritoneal cytology + detailed intra-abdominal examination. **Lymph node dissection (biopsy) can be omitted

gross residual tumor) is recommended. However, lymph node dissection (biopsy) can be omitted (Grade B).

CQ 36: What postoperative treatment is recommended for malignant ovarian germ cell tumors?

Recommendations

Chemotherapy using bleomycin, etoposide, and cisplatin (BEP therapy) is strongly recommended (Grade A).

CQ 37: What treatment is recommended for recurrence of malignant ovarian germ cell tumors after first-line chemotherapy?

Recommendations

(1) Combination chemotherapy using cisplatin, such as a triple-drug combination of cisplatin with two other drugs (from among ifosfamide, etoposide, vinblastine, and/or paclitaxel), should be considered (Grade C1).
(2) SDS can be considered for some patients (Grade C1).

CQ 38: What should be kept in mind during follow-up after treatment of malignant ovarian germ cell tumors?

Recommendations

(1) You should be mindful that ovarian dysfunction may occur (Grade C1).
(2) When etoposide has been administered, you should consider that secondary cancer may occur (Grade C1).

Chapter 7: Malignant sex cord-stromal tumors

Treatment of malignant sex cord-stromal tumors is summarized as flow chart 6 (Fig. 6).

CQ 39: What is the optimal surgical procedure for malignant sex cord-stromal tumors?

Recommendations

(1) According to the procedure for treating ovarian cancer, bilateral salpingo-oophorectomy + total hysterec-

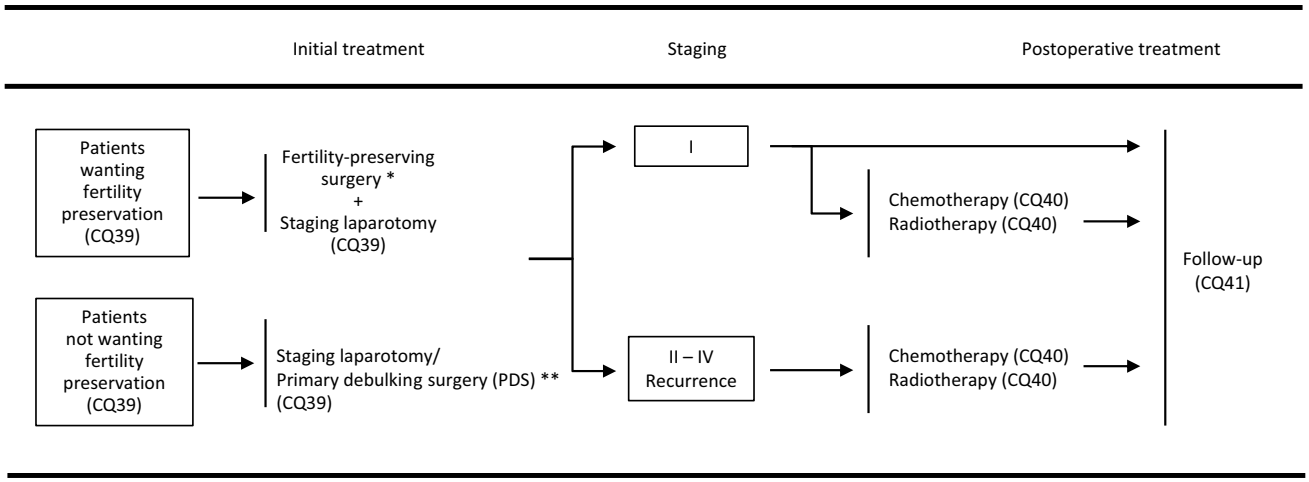

Fig. 6 Flow chart 6: treatment of malignant sex cord-stromal tumors. *Fertility-preserving surgery—affected-side salpingo-oophorectomy + omentectomy + peritoneal cytology + detailed intra-abdominal examination. **Lymph node dissection (biopsy) can be omitted

tomy + omentectomy are recommended together with peritoneal cytology, pelvic/para-aortic lymph node dissection (biopsy), and biopsies from sites in the abdominal cavity. However, lymph node dissection (biopsy) can be omitted (Grade C1).

(2) For patients who wish to preserve fertility, in addition to affected-side salpingo-oophorectomy + omentectomy + peritoneal cytology, detailed intra-abdominal examination should be considered (Grade C1).

CQ 40: What postoperative treatment is recommended for malignant sex cord-stromal tumors?

Recommendations

(1) With regard to chemotherapy, a platinum-containing regimen should be considered (Grade C1).
(2) Radiotherapy should also be considered (Grade C1).

CQ 41: What is important during follow-up after treatment of malignant sex cord-stromal tumors?

Recommendations

Management should be performed according to the protocol for ovarian cancer. Additionally, long-term follow-up for at least 10 years after treatment should be considered for granulosa cell tumors (Grade C1).

Acknowledgments Creation of this guideline was supported by the Japan Society of Gynecologic Oncology with contributions from "Encouragement of wider use of practice guidelines for cancer and their effects, as well as investigation of guideline projects" (chief investigator: Koichi Hirata), Research for Promotion of Cancer Control Programmes (2014), and a Health and Labour Sciences Research Grant. The funding sources did not influence the contents of this guideline.

Conflict of interest The conflict-of-interest committee of the Japan Society of Gynecologic Oncology checked conflicts of interest for the people involved in creating and evaluating this guideline and their associates (i.e., marital partner, first-degree relatives, or people sharing income/assets), according to the "Guidelines for conflict of interest issues in clinical studies on cancer" (http://www.jsgo.or.jp/topics/index01.html) published by the Japan Society of Gynecologic Oncology. Although there were conflicts of interest for some contributors through research/lecture activities supported by companies, the recommendations in this guideline are based on scientific evidence and have not been influenced by the interests of a specific organization and are not biased in recommending or products or techniques.

Guidelines for treatment of ovarian cancer including primary peritoneal cancer and fallopian tube cancer 2015 (4th edition)

Guideline development committee

Mitsuya Ishikawa, Fumiaki Isohashi, Yoshio Itani, Kimihiko Ito, Masahiro Iwasaki, Yasuhiko Ebina, Yoshihiro Ohishi, Hideyuki Ohtake, Tatsuru Oohara, Hiroaki Kajiyama, Noriyuki Katsumata, Kazuyoshi Kato, Shingo Kato, Masanori Kanemura, Kei Kawana, Takako Kiyokawa, Keisuke Kurose, Shinichi Komiyama, Kimiko Sato, Morio Sawada, Tadahiro Shoji, Masashi Takano, Hiroshi Tanabe, Hiroshi Tsubamoto, Fumitoshi Terauchi, Yasuhisa Terao, Kimihiro Nagai, Yoshifumi Nakao, Satoru Nagase, Kentaro Nakayama, Koji Nishino, Hiroyuki Nomura, Kazuhiko Hayashi, Eiji Hirata, Kiyoshi Fujiwara, Hiroyuki Fujiwara, Masayuki Futagami, Yusuke Matsuura, Noriomi Matsumura, Koji Matsumoto, Yoshiki Mikami, Yo Miyahara, Toshinari

Muramatsu, Hidekazu Yamada, Kiyoshi Yoshino, Yoshimitsu Ryo, and Hidemichi Watari (in order of the Japanese syllabary).

Guideline review committee

Satomi Aihara, Daisuke Aoki, Yoichi Aoki, Seiji Isonishi, Hiroaki Itamochi, Kazuhiko Ino, Osamu Iwanari, Kimio Ushijima, Masahide Ohmichi, Kazunori Ochiai, Takashi Onda, Hidenori Kato, Junzo Kigawa, Satoru Kyo, Hiroyuki Kuramoto, Hiroaki Kobayashi, Tsuyoshi Saito, Noriaki Sakuragi, Toyomi Satoh, Kiyosumi Shibata, Toru Sugiyama, Mitsuaki Suzuki, Kazuhiro Takehara, Shinichi Tate, Tsutomu Tabata, Katsuhiro Teramoto, Takafumi Toita, Takafumi Nakamura, Kaei Nasu, Toru Hachisuga, Kenichi Harano, Fumiki Hirahara, Ichio Fukasawa, Keiichi Fujiwara, Satoru Makinoda, Koji Miyazaki, Masanori Yasuda, Yoshihito Yokoyama, Hiroyuki Yoshikawa, and Kosuke Yoshinaga (in order of the Japanese syllabary).

References

1. Cancer Mortality in Japan (2012) Center for Cancer Control and Information Services. National Cancer Center, Japan. http://ganjoho.jp/professional/statistics/statistics.html. Accessed 15 Sept 2014
2. Heintz AP, Odicino F, Maisonneuve P et al (2006) Carcinoma of the ovary. FIGO 26th annual report on the results of treatment in gynecological cancer. Int J Gynaecol Obstet 95(Suppl 1):S161–S192
3. Gynecologic Cancer Committee (2012) Gynecologic cancer committee report in 2011. Acta Obstet Gynaecol Jpn 66:1024–1038
4. Ariyoshi H (2002) Guideline for correct use of antineoplastic agents (draft). General theory. Gan To Kagaku Ryoho 29:970–977
5. Ochiai K, Okamoto A, Katsumata N (2002) Guidelines for proper use of antineoplastic agents. Gynecologic cancer. Gan To Kagaku Ryoho 29:1047–1054
6. Fukui T, Yoshida M, Yamaguchi N (2007) Minds Guidance of practice guidelines 2007. Igakushoin, Tokyo
7. Takeuchi H, Saeki T, Aiba K et al (2016) Japanese Society of Clinical Oncology clinical practice guidelines 2010 for antiemesis in oncology: executive summary. Int J Clin Oncol 21:1–12
8. Japanese Society of Clinical Oncology clinical practice guidelines 2013 for G-CSF. http://www.jsco-cpg.jp/item/30/index.html

Int J Clin Oncol (2015) 20:240–248
DOI 10.1007/s10147-015-0806-7

SPECIAL ARTICLE

Japan Society of Gynecologic Oncology guidelines 2011 for the treatment of uterine cervical cancer

Yasuhiko Ebina · Nobuo Yaegashi · Hidetaka Katabuchi · Satoru Nagase · Yasuhiro Udagawa · Toru Hachisuga · Tsuyoshi Saito · Mikio Mikami · Yoichi Aoki · Hiroyuki Yoshikawa

Received: 5 February 2015 / Accepted: 17 February 2015 / Published online: 24 March 2015

Abstract The second edition of the Japan Society of Gynecologic Oncology guidelines for the treatment of uterine cervical cancer was published in 2011. The guidelines comprise eight chapters and five algorithms. They were prepared by consensus among the members of the Japan Society of Gynecologic Oncology Guidelines Formulation Committee and Evaluation Committee and are based on a careful review of the evidence obtained from the literature, health insurance system, and actual clinical settings in Japan. The highlights of the 2011 revision are (1) the recommended grades have been changed to five stages—A, B, C1, C2, and D; (2) the revisions are consistent with the new International Federation of Gynecology and Obstetrics staging system; (3) the roles are shared between the 'Japanese classification of cervical cancer' and the new guidelines; (4) clinical questions related to adenocarcinoma have been revised; and (5) a clinical question regarding cervical cancer in pregnant patients has been added. Each chapter includes a clinical question, recommendations, background, objectives, explanations, and references. Each recommendation is accompanied by a classification of recommendation categories. The objective of these guidelines is to update the standard treatment strategies for cervical cancer, thus eliminating unnecessary and insufficient treatment.

Keywords Uterine cervical cancer · Clinical practice guidelines · Surgery · Chemotherapy · Irradiation · Recurrence

This article originally appeared in Japanese as *Shikyu keigan chiryo gaidorain 2011 nen ban*, published by Kanehara, Tokyo, 2011.

Y. Ebina (✉)
Department of Obstetrics and Gynecology, Kobe University Graduate School of Medicine, 7-5-1 Kusunoki-cho, Chuo-Ku, Kobe 650-0017, Japan
e-mail: ebiyas@med.kobe-u.ac.jp

N. Yaegashi
Department of Obstetrics and Gynecology, Tohoku University Graduate School of Medicine, Sendai, Japan

H. Katabuchi
Department of Obstetrics and Gynecology, Faculty of Life Sciences, Kumamoto University, Kumamoto, Japan

S. Nagase
Department of Obstetrics and Gynecology, Faculty of Medicine, Yamagata University, Yamagata, Japan

Y. Udagawa
Department of Obstetrics and Gynecology, Fujita Health University School of Medicine, Toyoake, Japan

T. Hachisuga
Department of Obstetrics and Gynecology, University of Occupational and Environmental Health School of Medicine, Kitakyusyu, Japan

T. Saito
Department of Obstetrics and Gynecology, Sapporo Medical University School of Medicine, Sapporo, Japan

M. Mikami
Department of Obstetrics and Gynecology, Tokai University School of Medicine, Isehara, Japan

Y. Aoki
Department of Obstetrics and Gynecology, Graduate School of Medical Science, University of the Ryukyus, Nishihara, Japan

H. Yoshikawa
Department of Obstetrics and Gynecology, Faculty of Medicine, University of Tsukuba, Tsukuba, Japan

Introduction

An estimated 6,000 new cases of invasive cervical cancer were diagnosed in Japan in 2011 [1], and 2,737 women died of the disease [2]. The mortality rate associated with cervical cancer in Japan decreased from the 1960s until 1995; however, the incidence of cervical cancer has slightly increased [2].

The first edition of the Japan Society of Gynecologic Oncology (JSGO) guidelines for the treatment of uterine cervical cancer was published in 2007 [3]; however, some clinical questions (CQs) in the first edition remained unanswered. The second edition, published in 2011, was intended to represent an aggregation of domestic evidence while collecting up-to-date international evidence without providing a new section. For the first time, we accepted specialist physicians engaged in clinical practice in cancer centers or university hospitals as candidates for the committee. Radiation oncologists and pathologists were also members of the guideline committee.

The highlights of the 2011 revision are indicated below.

1. The recommended grades have been changed to five stages—A, B, C1, C2, and D.
2. The revisions are consistent with the new International Federation of Gynecology and Obstetrics (FIGO) staging system. The new FIGO staging system was revised during the creation of these updated guidelines. The new FIGO classification excludes stage 0 carcinoma in situ; however, stage 0 still has high importance in the guidelines because many people, especially young people, have stage 0 disease. Therefore, stage 0 is present in the guidelines. Additionally, stage IIA has been reclassified to stage IIA1 and stage IIA2 in the new FIGO classification. This revision from the Japan Society of Obstetrics and Gynecology 'Japanese classification of cervical cancer' has been adopted, and the reclassification to stage IIA1 and IIA2 is present in the new guidelines.
3. Roles are shared between the 'Japanese classification of cervical cancer' and the new guidelines. A specific radiotherapy technique is detailed in the guidelines.
4. CQs related to adenocarcinoma have been revised. Few clinical trials on adenocarcinoma alone have been conducted; thus, the chapter on adenocarcinoma was deleted and a CQ related to adenocarcinoma is described in each chapter.
5. A CQ regarding cervical cancer in pregnant patients has been added. Because of the increasing incidence of cervical cancer in younger patients and of pregnancy in older patients, the treatment of cervical cancer and its complications owing to pregnancy should be addressed. Therefore, these treatment guidelines are described in detail by increasing the CQs relevant to this topic.

Treatment guidelines for cervical cancer

Chapter 1: Overview of guidelines

1. How to use these guidelines

These guidelines are intended for doctors (general practitioners and specialists) who provide medical care for patients with cervical cancer. The guidelines aim to provide useful treatment methods by integrating previous evidence of treatment benefits. However, the guidelines are not intended to be limited to the therapies listed. Their main purposes are (1) to indicate the current cervical cancer treatments that are considered appropriate, (2) to reduce differences in therapy among various institutions, (3) to improve the prognosis and safety of treatments, (4) to reduce the economic and psychosomatic burden on patients by performing appropriate treatment, and (5) to promote mutual understanding between healthcare professionals and patients.

The JSGO bears the responsibility for the content and descriptions of these guidelines. However, the final decision to use these guidelines should be made by the individual user. Thus, the physicians in charge of treatment are responsible for the outcome of treatment.

2. Method used to prepare these guidelines

To create these guidelines, the Guidelines Formulation Committee and Evaluation Committee were established independently from the Committee for the Treatment Guidelines for Cervical Cancer. The initial draft was created by thoroughly evaluating the various opinions from within and outside the JSGO prior to incorporating them into the final draft. The guidelines were published after approval by the JSGO.

(1) Classification of evidence

1. The guidelines were created in accordance with the international standard procedures of evidence-based medicine used for the creation of clinical practice guidelines.
2. In principle, searches of data and published literature were performed prior to December 2009 in Japan and overseas, and evidence was collected.
3. This collected evidence was evaluated for quality using the criteria of the Japan Society of Clinical Oncology and its Formulation Committee on clinical practice guidelines for the use of anticancer agents [4, 5]; however, it was modified to allow some of it to fit into the guidelines (Table 1).

Table 1 Classification of evaluation criteria for evidence quality

Level I Evidence from multiple randomized controlled trials or meta-analyses of multiple randomized controlled trials
Level II Evidence from at least one randomized controlled trial or multiple well-designed controlled studies without randomization
Level III Evidence from at least one other type of well-designed quasi-experimental study or from well-designed nonexperimental descriptive studies, such as comparative studies, correlation studies, or case studies
Level IV Expert committee reports, or opinions and/or clinical experiences of respected authorities

Table 2 Classification of recommendation categories

Grade A The treatment is strongly recommended if at least one level I evidence indicates validity
Grade B The treatment is recommended if at least one level II evidence indicates validity
Grade C1 The treatment can be considered, but the evidence is insufficient; for example, there are several reports of level III evidence that show validity with generally consistent results
Grade C2 The treatment is not recommended without sufficient scientific evidence
Grade D The treatment is not recommended because neither utility nor effectiveness has been shown and because the treatment may be harmful

(2) Clinical questions and classification of recommendation categories

As a result of the discussions held by the Guideline Committee, controversial issues were selected as CQs and associated recommendations were made. Each recommendation in response to a CQ is accompanied by a classification of the evidence and a classification of the recommendation categories based on the consensus reached by the Guideline Committee members.

The strengths of the recommendations in our guidelines were also determined by the recommendation criteria of the Japan Society of Clinical Oncology and its Formulation Committee of Clinical Practice Guidelines for the Use of Anticancer Agents [6]. These were modified while referring to the 'Guide 2007 Minds practice guidelines' (Tables 2, 3).

Chapter 2: Primary treatment for stage 0 to IA cervical cancer (Fig. 1)

CQ01. What treatments are recommended for carcinoma in situ?

Recommendations A cervical cone biopsy is recommended (grade B).

Table 3 Classification of risk of postoperative recurrence of cervical cancer

Low-risk group: patients who meet all of the following criteria
Small cervical tumor
Negative pelvic nodes
Negative parametrical invasion
Shallow cervical stromal invasion
No venous or lymphatic infiltration
Intermediate-risk group: patients with negative pelvic nodes and negative parametrical invasion but who meet one of the following criteria
Large cervical tumor
Deep cervical stromal invasion
Positive venous or lymphatic infiltration
High-risk group: patients who meet one of the following criteria
Positive pelvic nodes
Positive parametrical invasion

CQ02. What treatments are recommended for recurrence following conservative treatment?

Recommendations (1) For recurrence following laser cone biopsy or the loop electrosurgical excision procedure, the same procedure should be repeated or a total hysterectomy considered, depending on the patient (grade B). (2) For recurrence following laser ablation or cryotherapy, either a cone biopsy or total hysterectomy is recommended (grade B).

CQ03. What treatments are recommended for stage IA1 disease?

Recommendations (1) It is possible to preserve the uterus by performing a cervical cone biopsy in patients who strongly desire fertility preservation; however, these patients must have no vascular or lymphatic infiltration, negative resection margins, and negative histological results from endocervical curettage (grade B). (2) A total hysterectomy without pelvic lymphadenectomy is recommended for patients with no evidence of vascular or lymphatic infiltration (grade B). (3) Both a modified radical hysterectomy and pelvic lymphadenectomy are sometimes performed for patients with vascular or lymphatic infiltration (grade C1).

CQ04. What treatments are recommended for stage IA2 disease?

Recommendations (1) A modified radical hysterectomy or a more extensive procedure with lymphadenectomy should be considered for stage IA2 disease (grade C1). (2) After thorough histopathological examination of a specimen obtained by diagnostic conization, omission of

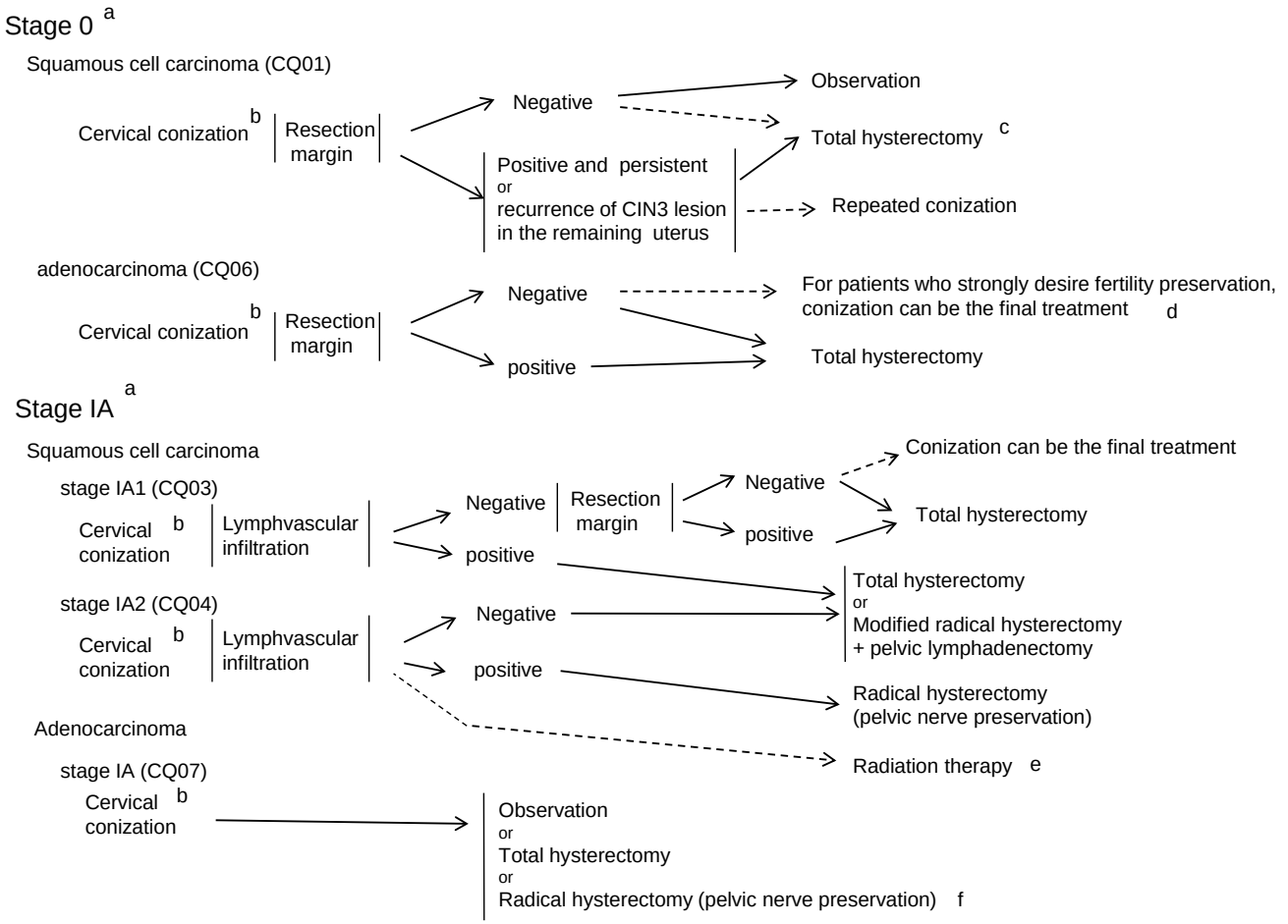

Fig. 1 Primary treatment for stage 0 to IA cervical cancer. **a** If cervical conization is difficult because of atrophy of the cervix, such as in older patients, omission of the conization may be considered. However, prior to surgery, it is necessary to carefully review the cytology, colposcopy, and biopsy tissue findings; this allows for the performance of a hysterectomy suitable for the estimated lesion. **b** Cervical canal curettage should be performed at the time of cervical conization. If cervical curettage is positive, the patient should be treated as if they have positive margins. **c** Hysterectomy may be considered if the patient does not wish to preserve her fertility. **d** Residual lesions are reportedly found in about 20 % of cases involving negative margins. Careful inspection is required to preserve the uterus. **e** In the NCCN clinical practice guidelines in oncology, radiation therapy is also an option for patients with cervical cancer. **f** Operative procedures should be individualized according to the histopathological findings of the conization specimens, namely the extent of invasion and the presence or absence of lymphovascular infiltration

lymphadenectomy in patients with no vascular or lymphatic infiltration can be considered (grade C1).

CQ05. What treatments are recommended if the disease is upstaged to stage IB or higher following total hysterectomy?

Recommendations Adjuvant radiotherapy or concurrent chemoradiotherapy (CCRT) should be considered (grade C1).

CQ06. What treatments are recommended for adenocarcinoma in situ?

Recommendations (1) A total hysterectomy is recommended (grade B). (2) Uterus preservation can be considered with cervical cone biopsy in patients who strongly desire fertility preservation. However, careful management is required (grade C1).

CQ07. What treatments are recommended for stage IA adenocarcinoma?

Recommendations (1) In cases involving deep invasion, a radical hysterectomy or modified radical hysterectomy with pelvic lymphadenectomy should be considered (grade C1). (2) In cases involving shallow invasion, a hysterectomy without pelvic lymphadenectomy (total hysterectomy or modified radical hysterectomy) can also be considered (grade C1). (3) If the patient strongly desires fertility preservation, a cervical cone biopsy can be performed

to preserve the uterus. Careful case selection is required (grade C1).

Chapter 3: Primary treatment for stage IB to II cervical cancer (Fig. 2)

CQ08. What treatments are recommended for stage IB1 and IIA1 squamous cell carcinoma?

Recommendations A radical hysterectomy or radiation therapy is recommended (grade B).

CQ09. What treatments are recommended for stage IB2 and IIA2 squamous cell carcinoma?

Recommendations A radical hysterectomy (+ adjuvant therapy) or CCRT is recommended (grade B).

CQ10. What treatments are recommended for stage IIB squamous cell carcinoma?

Recommendations A radical hysterectomy (+adjuvant therapy) or CCRT is recommended (grade B).

CQ11. Is neoadjuvant chemotherapy recommended for stage IB and II squamous cell carcinoma?

Recommendations Neoadjuvant chemotherapy can be considered depending on the extent and size of the tumor (grade C1).

CQ12. Is pelvic nerve preservation recommended in radical hysterectomy?

Recommendations Pelvic nerve preservation can be considered when curability is not impaired (grade C1).

CQ13. Is ovary preservation possible in radical hysterectomy?

Recommendations (1) Ovary preservation is possible without compromising curability if appropriate case selection is performed by considering the patient's histological type or stage (grade B). (2) If the ovaries are to be preserved, ovarian transposition and fixation outside of the pelvic radiation field can be considered (grade C1).

CQ14. Is para-aortic lymphadenectomy recommended in radical hysterectomy?

Recommendations If diagnostically useful, para-aortic lymphadenectomy can be considered to search for metastasis or determine the irradiation field (grade C1).

CQ15. What treatments are recommended for stage IB and II adenocarcinoma?

Recommendations In principle, surgery should be considered for stage IB and II disease (grade C1).

Chapter 4: Postoperative therapy for stage IB to II cervical cancer (Fig. 3)

CQ16. What is the recommended postoperative adjuvant therapy?

Recommendations (1) CCRT is recommended for patients at high risk of recurrence (grade B). (2) Radiation therapy is recommended for patients at intermediate risk of recurrence. However, CCRT can be considered depending on the number and extent of risk factors (grade C1).

CQ17. What irradiation methods are recommended when performing postoperative adjuvant radiotherapy for a patient at high risk of relapse?

Recommendations (1) Whole-pelvis irradiation is recommended (grade B). (2) Three-dimensional treatment planning is recommended (grade B). (3) The addition of intracavitary irradiation is not recommended with the exception of cases involving positive margins (grade C2).

CQ18. For whom is prophylactic para-aortic irradiation indicated?

Recommendations Para-aortic irradiation can be considered for patients with a high risk of recurrence in the para-aortic lymph nodes (grade C1).

CQ19. Are oral anticancer drugs and immunotherapy recommended as maintenance therapies?

Recommendations (1) Oral anticancer agents are not recommended because their usefulness is unclear (grade C2). (2) Immunotherapy is not recommended because its usefulness has not been fully verified (grade C2).

Chapter 5: Primary therapy for stage III to IV cervical cancer (Fig. 4)

CQ20. Which is the recommended radiotherapy for stage III and IVA disease: definitive radiotherapy or CCRT?

Recommendations CCRT is recommended rather than radiation monotherapy (grade B).

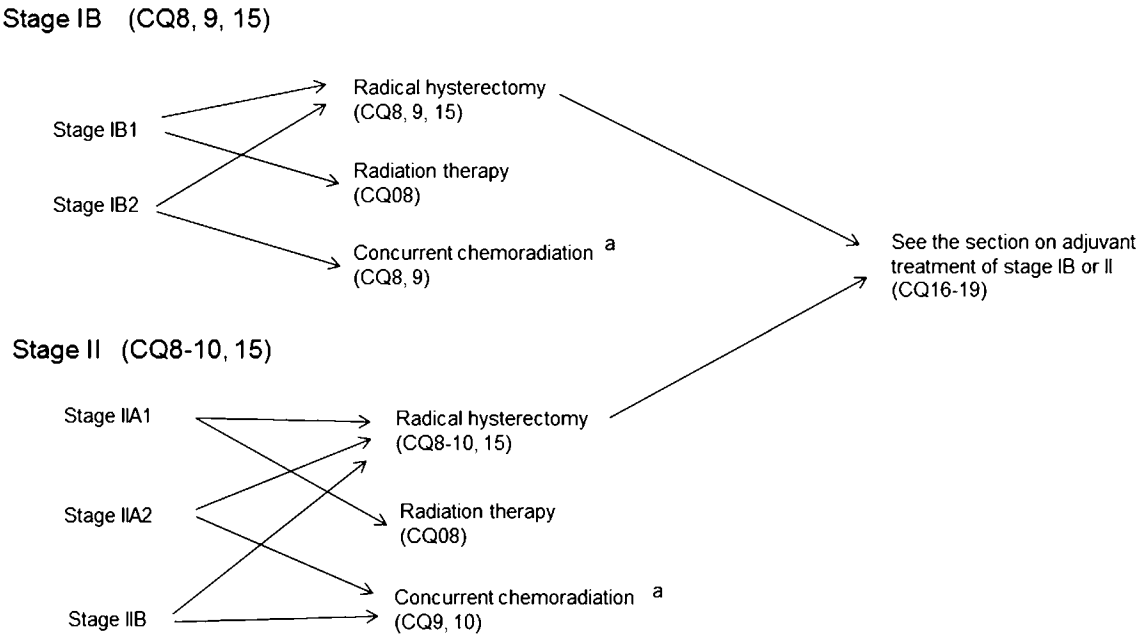

Fig. 2 Primary treatment for stage IB to II cervical cancer (including squamous cell carcinoma and adenocarcinoma). **a** Primary treatment for stage IB to II cervical cancer should be performed with caution because the tolerability of concurrent chemoradiation therapy among Japanese women has not been sufficiently tested

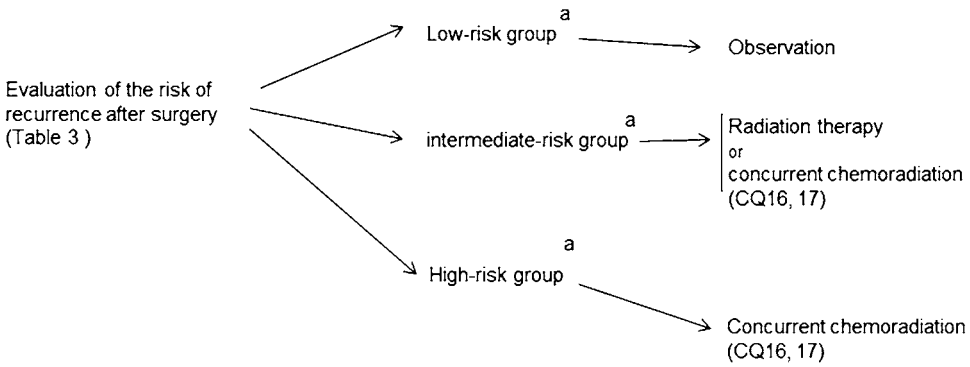

Fig. 3 Postoperative therapy for stage IB to II cervical cancer (including squamous cell carcinoma and adenocarcinoma). **a** There are many discussions and various reports on risk assessment for postoperative recurrence. Postoperative therapy must be considered according to the individual case

CQ21. What CCRT regimens are recommended for stage III and IVA disease?

Recommendations Regimens that include cisplatin are recommended (grade A).

CQ22. Is chemotherapy recommended prior to principal treatment for stage III and IVA disease?

Recommendations (1) Chemotherapy is not recommended before radiotherapy (grade D). (2) Chemotherapy is not recommended before surgery (grade C2). (3) For adenocarcinoma, chemotherapy is not recommended before primary treatment (grade C2).

CQ23. Is surgery recommended for stage III and IVA disease?

Recommendations Surgery is not recommended (grade C2).

CQ24. What treatments are recommended for stage IVB disease?

Recommendations (1) Systemic chemotherapy can be considered for patients with a good performance status and preserved organ function (grade C1). (2) Surgery, radiotherapy, chemotherapy, or a combination of these treatments can be selected for patients with distant metastatic lesions, such as resectable lung metastases, or with lymph

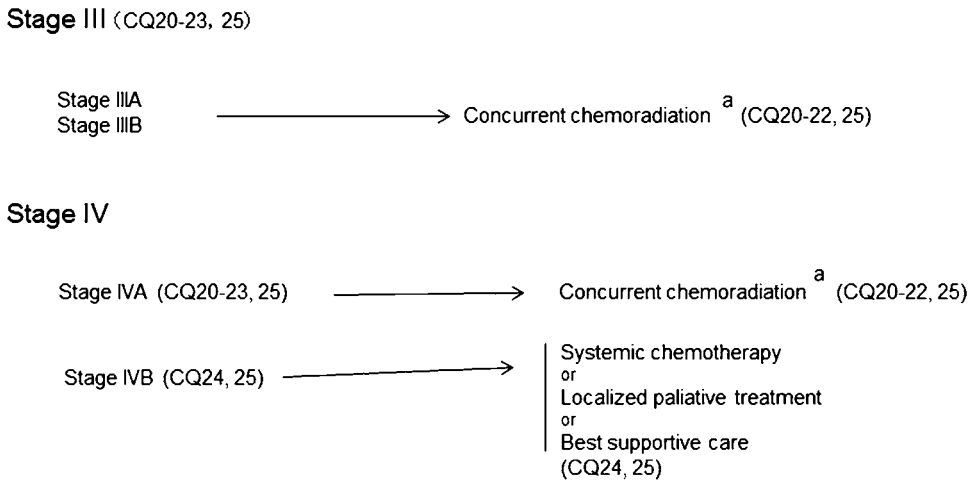

Fig. 4 Primary treatment for stage III to IV cervical cancer (including squamous cell carcinoma and adenocarcinoma). **a** Primary treatment for stage III to IV cervical cancer should be performed with caution because the tolerability of concurrent chemoradiation therapy among Japanese women has not been sufficiently tested

node metastases only (grade C1). (3) If the patient has severe symptoms accompanying oncological complications, palliative radiotherapy of the causal lesion is recommended (grade B).

CQ25. What treatments are recommended for stage III and IV adenocarcinoma?

Recommendations CCRT involving external irradiation and intracavitary irradiation is recommended for stage III or VIA adenocarcinoma (grade B). (2) A platinum-based agent other than cisplatin, either as monotherapy or as part of combination chemotherapy, can also be considered for patients with stage IVB adenocarcinoma with preserved organ function (grade C1).

Chapter 6: Therapies for relapsed cervical cancer (Fig. 5)

CQ26. What treatment methods are recommended for recurrence confined to the pelvis if radiotherapy has not been previously performed?

Recommendations (1) Radiotherapy is recommended (grade B). (2) CCRT can also be considered (grade C1).

CQ27. What treatments are recommended for recurrence within the radiation field?

Recommendations (1) Palliative treatment for symptomatic relief is the general rule for treatment (grade C1). (2) Chemotherapy can also be considered, keeping in mind that the response rate is low for recurrence within the radiation field (grade C1). (3) Localized radiotherapy or pelvic exenteration can also be considered for central recurrence in the vaginal stump after a thorough preoperative evaluation (grade C1). (4) Re-irradiation is not recommended (grade C2).

CQ28. What treatments are recommended for recurrence outside the radiation field or for extrapelvic recurrence if radiotherapy has not been previously performed?

Recommendations (1) Para-aortic metastasis: radiation therapy or CCRT can be considered for solitary metastasis (grade C1). (2) Brain metastasis: (a) stereotaxic radiosurgery along with whole-brain radiation therapy (WBRT) or WBRT alone is recommended for metastases of up to three sites (grade B). (b) WBRT is recommended for more than four metastases (grade B). (3) Bone metastasis: (a) single-fraction or multi-fraction radiotherapy is recommended for pain relief (grade B). (b) Bisphosphonates are recommended for symptom relief (grade B). (c) Strontium chloride can be considered for multiple bone metastases if medical therapy is ineffective (grade C1). (4) Lung metastasis: resection or stereotactic body radiotherapy can be considered for one to three localized metastases (grade C1).

CQ29. Is systemic chemotherapy recommended for recurrence?

Recommendations Systemic chemotherapy is recommended for patients with disease that is difficult to control by surgery or radiotherapy as well as for patients with a good performance status and preserved organ function (grade B).

CQ30. What systemic chemotherapy regimens are recommended to treat recurrent disease?

Recommendations (1) Cisplatin as either monotherapy or part of two-drug combination chemotherapy is

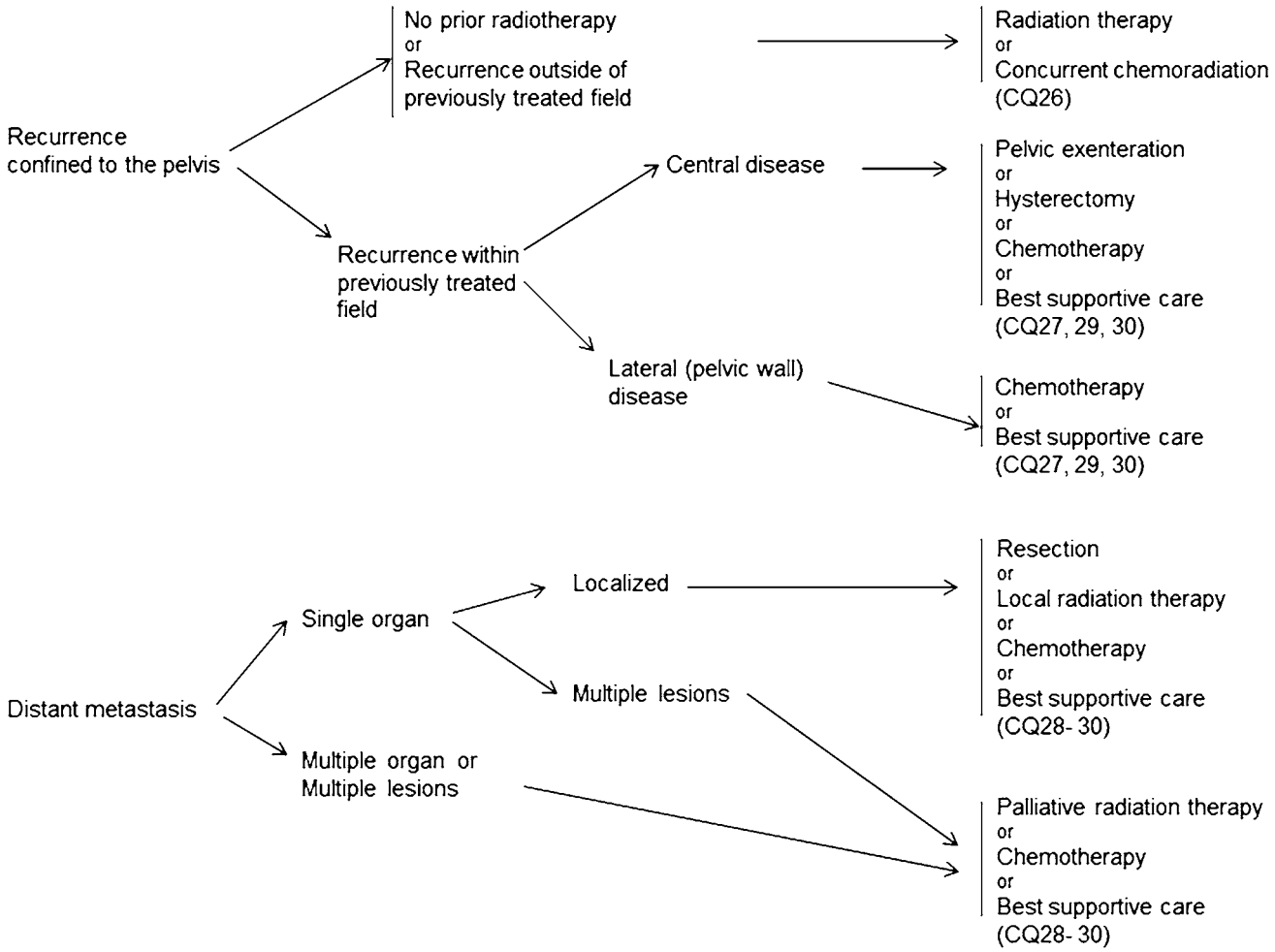

Fig. 5 Therapy for relapsed cervical cancer (including squamous cell carcinoma and adenocarcinoma)

recommended (grade B). (2) A platinum-based agent other than cisplatin, as either monotherapy or part of two-drug combination chemotherapy, can also be recommended (grade B). (3) Cisplatin as either monotherapy or part of two-drug combination chemotherapy is preferable for recurrent adenocarcinoma (grade C1).

Chapter 7: Management of cervical cancer during pregnancy

CQ31. What treatments are recommended for stage 0 disease during pregnancy?

Recommendations (1) Cone biopsy may be delayed until after delivery as long as the diagnosis is stage 0 disease based on consistent cytology, colposcopy, or biopsy analysis results (grade C1). (2) If adenocarcinoma in situ is suspected, a cone biopsy should be performed to determine the diagnosis during pregnancy (grade C1).

CQ32. What treatments are recommended for stage IA disease during pregnancy?

Recommendations If stage IA or higher disease is suspected, a cervical cone biopsy should be considered to determine the diagnosis during pregnancy (grade C1).

CQ33. What treatments are recommended for invasive cancer during pregnancy?

Recommendations If the diagnosis made during the gestational period (usually during the 3rd trimester) indicates that the fetus can survive outside the uterus, standard treatment after delivery can be considered (grade C1).

Chapter 8: Surveillance after treatment for cervical cancer

CQ34. What intervals are recommended for post-treatment surveillance?

Recommendations The following intervals are recommended for standard surveillance (grade C1):

For the first 1–2 years: every 1–3 months
For the 3rd year: every 3–6 months
For the 4th and 5th years: every 6 months
From the 6th year: every 12 months

CQ35. What investigations and examinations should be performed during post-treatment surveillance?

Recommendations (1) A physical examination (including pelvic and rectal examination), cytological examination, chest radiography, measurement of tumor markers, and diagnostic imaging should be performed (grade C1). (2) Any complications associated with surgery, radiotherapy, or chemotherapy should be noted (grade C1).

Acknowledgments We thank the Japan Society of Obstetrics and Gynecology, the Japan Association of Obstetricians and Gynecologists, the Japanese Gynecologic Oncology Group, the Japan Society of Clinical Oncology, and the Japanese Society for Therapeutic Radiology and Oncology for their comments and contributions throughout the project. We also acknowledge support by grants from the Ministry of Health, Labour and Welfare; H24-Clinical Cancer Research-001 (chief researcher, Koichi Hirata).

Conflicts of interest None of the members of the committee in charge of the preparation of these guidelines has any conflict of interest with entities such as a specific profit or nonprofit organization. The board of the Society Conflict of Interest Committee confirmed the self-reported absence of any conflicts of interest by the Guideline Committee members.

Members of guidelines formulation committee (alphabetical order)

Yoichi Aoki, Yasuhiko Ebina, Takayuki Enomoto, Hisaya Fujiwara, Toru Hachisuga, Yasuyuki Hasuo, Atsushi Hongo, Seiryu Kamoi, Takahiro Kasamatsu, Hidetaka Katabuchi, Naoki Kawamura, Hiroaki Kobayashi, Yoichi Kobayashi, Takeshi Kodaira, Junichi Kodama, Kaneyuki Kubushiro, Masaki Mandai, Mikio Mikami, Yoshiki Mikami, Etsuko Miyagi, Toshinari Muramatsu, Tetsuro Nagasaka, Satoru Nagase, Toru Nakanishi, Kaei Nasu, Hideyuki Ohtake, Tsuyoshi Saito, Toshiaki Saito, Masaru Sakamoto, Muneaki Shimada, Nao Suzuki, Tsutomu Tabata, Masashi Takano, Nobuhiro Takeshima, Takafumi Toita, Yasuhiro Udagawa, Takashi Uno, Yoh Watanabe, Nobuo Yaegashi, Masanori Yasuda, Yoshihito Yokoyama

Members of guidelines evaluation committee (alphabetical order)

Daisuke Aoki, Masaki Fujimura, Keiichi Fujiwara, Masayuki Hatae, Masamichi Hiura, Yoshiki Inoue, Kiyoshi Ito, Hisao Ito, Tsuyoshi Iwasaka, Toshiko Jobo, Tsunehisa Kaku, Toshiharu Kamura, Noriyuki Katsumata, Junzo Kigawa, Eizo Kimura, Tsunekazu Kita, Hiroyuki Kuramoto, Yoshinari Matsumoto, Takashi Nishida, Kazunori Ochiai, Yujiro Ota, Aikou Okamoto, Isao Otsuka, Satoru Sagae, Noriaki Sakuragi, Mayumi Sugiura, Toru Sugiyama, Mitsuaki Suzuki, Hironori Tashiro, Hiroshi Tsuda, Masatsugu Ueda, Naohiko Umesaki, Masato Yamasaki, Hiroyuki Yoshikawa

References

1. Gynecologic cancer committee (2012) Gynecologic cancer committee report in 2011. Acta Obstetrica et Gynaecologica Japonica 64:2340–2388
2. Cancer mortality in Japan (1958–2012) Center for cancer control and information services, National Cancer Center, Japan. http://ganjoho.jp/professional/statistics/statistics.html. Accessed 15 Sep 2014
3. Nagase S, Inoue Y, Umesaki N et al (2010) Evidence-based guidelines for treatment of cervical cancer in Japan: Japan Society of Gynecologic Oncology (JSGO) 2007 edition. Int J Clin Oncol 15:117–124
4. Ariyoshi H (2002) Guideline for correct use of antineoplastic agents (draft). General theory. Gan To Kagaku Ryoho 29:970–977
5. Ochiai K, Okamoto A, Katsumata N (2002) Guidelines for proper use of antineoplastic agents. Gynecologic cancer. Gan To Kagaku Ryoho 29:1047–1054
6. Fukui T, Yoshida M, Yamaguchi N (2007) Minds Guidance of practice guidelines 2007. Igakushoin, Tokyo

Journal of proteome research

Article

pubs.acs.org/jpr

Novel Glycobiomarker for Ovarian Cancer That Detects Clear Cell Carcinoma

Maki Sogabe,[†,#] Hirofumi Nozaki,[†,#] Nana Tanaka,[†] Tomomi Kubota,[†] Hiroyuki Kaji,[†] Atsushi Kuno,[†] Akira Togayachi,[†] Masanori Gotoh,[†] Hayao Nakanishi,[‡] Toru Nakanishi,[§] Mikio Mikami,[∥] Nao Suzuki,[⊥] Kazushige Kiguchi,[⊥] Yuzuru Ikehara,[†] and Hisashi Narimatsu*[,†]

[†]Research Center for Medical Glycoscience (RCMG), National Institute of Advanced Industrial Science and Technology (AIST), Central-2, 1-1-1 Umezono, Tsukuba 305-8568, Japan

[‡]Division of Oncological Pathology, Aichi Cancer Center Research Institute and [§]Department of Gynecologic Oncology, Aichi Cancer Center Hospital, 1-1 Kanokoden, Chikusa-ku, Nagoya 464-8681, Japan

[∥]Department of Obstetrics and Gynecology, School of Medicine, Tokai University, 143 Shimokasuya, Isehara 259-1193, Japan

[⊥]Department of Obstetrics and Gynecology, St. Marianna University School of Medicine, 2-16-1 Sugao, Miyamae-ku, Kawasaki 216-8511, Japan

Supporting Information

ABSTRACT: Epithelial ovarian cancer (EOC) is often asymptomatic and thus diagnosed at advanced stages with a poor prognosis. False-negative results for the conventional marker CA125 frequently occur in cases of clear cell carcinoma (CCC), a type of EOC; therefore, it is necessary to develop biomarkers with greater sensitivity. We previously reported a strategy to discover glycobiomarker candidates by combined lectin microarray and IGOT−LC/MS analysis. We have now optimized this strategy for discovering EOC biomarkers. Glycopeptides possessing cancerous glycans were enriched from the ascites fluids and culture supernatants of cancer cell lines with a fucose-binding lectin, AAL. IGOT−LC/MS analysis of CCC samples yielded 144 candidate glycoproteins. We selected WFA by lectin microarray as the optimal lectin to distinguish EOC from gastric and colon cancer. The candidates were narrowed by Western analysis of the WFA-bound fraction of ascites fluids. One of the final candidates, WFA-reactive ceruloplasmin, produced higher signals in the ascites fluids of EOC patients, including CCC, in comparison with the benign samples, while CA125 levels were comparable in the sandwich ELISA. Thus, our glycoproteomic strategy featuring efficient enrichment of glycans with disease-related alterations is applicable to various diseases.

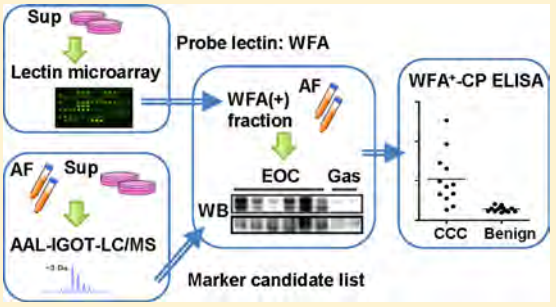

KEYWORDS: *glycoprotein, glycoproteomics, glycan alteration, epithelial ovarian cancer, clear cell carcinoma, WFA, ceruloplasmin, lectin microarray*

INTRODUCTION

Glycosylation is a major post-translational modification of secreted and cell surface proteins; it is often altered by changes in the cellular environment that are coincident with the progress of various diseases, including cancer.[1−4] A promising approach to discovering novel reliable biomarkers is to focus on such qualitative, not quantitative, changes of disease-specific glycan structures. Changes in the glycosylation pattern can be represented as altered lectin reactivity such as LCA (*Lens culinaris* agglutinin)-reactive alpha-fetoprotein (AFP).[5]

We developed a highly sensitive lectin microarray system optimized for comparative analysis in the discovery and development of disease-specific biomarkers.[6] To develop a cholangiocarcinoma marker, we first identified the probe lectins that specifically distinguish diseased from nondiseased specimens by using the lectin microarray system with pathological tissue samples and body fluids from patients.[7] After selection of the probe lectins, we enriched glycopeptides with the respective lectin-bound glycoepitopes. These glycopeptides were analyzed to identify the core proteins through lectin−IGOT (isotope-coded glycosylation site-specific tagging)−LC/MS technology, which identifies protein molecules and their *N*-glycosylated sites.[8]

It is essential to identify glycoprotein disease markers with high specificity and sensitivity. Each glycoprotein undergoes various glycan modifications, and disease progression is reflected by various glycoproteins and their glycan motifs. We established an analytical flow for comprehensive and reliable biomarker development with glycoproteomic study of clinical specimens.[9] We previously reported the discovery of new candidate biomarkers for liver fibrosis and hepatocarcinoma using this strategy.[10,11]

Received: November 13, 2013
Published: February 5, 2014

dx.doi.org/10.1021/pr401109n | *J. Proteome Res.* 2014, 13, 1624−1635

It is difficult to discover novel candidate cancer markers directly from serum samples, except in the case of hepatocarcinoma. Because most serum proteins are secreted by the liver, serum proteins secreted by other organs are relatively minor and difficult to detect.[12,13] Therefore, we modified the strategy to utilize ascites fluids instead of serum and added lectin column enrichment prior to analysis for discovery of novel candidate glycoproteins as ovarian cancer markers.

Ovarian cancer is asymptomatic and insensible; most cases are diagnosed when the disease is advanced, and the 5 year survival rate is <30%.[14] Epithelial ovarian cancer (EOC) accounts for 90% of all ovarian cancers and is classified into four major tissue types (serous, mucinous, endometrioid, and clear cell) and two minor types (undifferentiated and mixed epithelial), each of which shows different response rates to chemotherapy. Serous carcinoma is the most frequent diagnosis and shows good response rates. In contrast, clear cell carcinoma (CCC) is relatively resistant to standard chemotherapy, and its prognosis in the advanced stage is often worse in comparison with other tissue types.[15−18] Early detection is needed to improve prognosis in CCC. The ovarian cancer marker CA125 often yields a false-negative result in CCC, although its diagnostic performance is good in serous type EOC.[19,20] Moreover, CA125 frequently yields a false-positive result under non-neoplastic conditions such as pregnancy, menstruation, and endometriosis. Endometriosis is associated with risk of CCC and endometrioid ovarian cancer; therefore, it is clinically important to discriminate CCC from endometriosis, which cannot be achieved by CA125.[21] To improve diagnostic accuracy in ovarian cancer, we searched for a reliable marker for CCC by employing a modified strategy for glycobiomarker exploration.

MATERIALS AND METHODS

Cancer Cell Lines

Human ovarian cancer cell lines RMG-V (CCC) and RTSG (undifferentiated carcinoma) were previously established;[22,23] RMG-I, RMG-II (CCC), and RMUG-S (mucinous carcinoma) were kindly provided by Dr. Daisuke Aoki at Keio University (Tokyo, Japan).[24−26] Other cell lines were purchased: gastric cancer cell lines KATOIII and NUGC-4 (Japanese Collection of Research Bioresources Cell Bank, Japan); hepatoma cell lines HuH-7 and Hep G2, gastric cancer cell line GCIY (RIKEN Cell Bank, Japan); and colon cancer cell lines COLO 201 and COLO 205 (American Type Culture Collection, USA).

The serum-free cell culture supernatants were used for all analyses. As previously described, fucosylated AFP, a well-known glycan structure associated with hepatic cancer progression, was identified from the serum-free culture supernatants after 48 h of incubation.[27] In other words, serum-free supernatants can provide information regarding glycan alterations in cancer. RMG-I, RMG-II, RMG-V, RTSG, and RMUG-S were grown in 90% Ham's F-12 medium with 10% fetal bovine serum (FBS), KATOIII, NUGC-4, GCIY, COLO 201, and COLO 205 were grown in 90% RPMI1640 medium with 10% FBS, and HuH-7 and Hep G2 were grown in 90% Dulbecco's modified Eagle medium with 10% FBS. All growth media were supplemented with 50 unit/mL penicillin and 50 μg/mL streptomycin as antibiotics. After reaching ∼90% confluence, the cells were washed and cultured in serum-free (i.e., protein-free) and antibiotic-free media for 48 h; culture supernatants were harvested for analysis.

Biological Specimens

Peritoneal washings were collected from nine ovarian cancer patients and two peritoneal disseminated gastric cancer patients at Aichi Cancer Center Hospital (Nagoya, Japan); the supernatants were used as ascites fluid samples for lectin−IGOT−LC/MS, lectin fractionation, and lectin−antibody sandwich ELISA analyses. Ascites fluids were also collected from 44 EOC and 38 other gynecological disease patients at Tokai University Hospital (Isehara, Japan) and used for the ELISA verification study. Tissue samples were collected from patients diagnosed with clear cell adenocarcinoma at St. Marianna University School of Medicine Hospital (Kawasaki, Japan) and used for immunohistochemistry. All biological samples were collected with the approval of each institutional ethics committee and the informed consent of each subject for the use of clinical specimens. All diagnoses were established histologically, and the tumors were staged according to the current classification of the International Federation of Gynecology and Obstetrics (FIGO).[14] Clinical characteristics are presented in Supplementary Table 1a−c in the Supporting Information.

Antibodies

Antibodies against target proteins were purchased and used in their unconjugated or biotinylated forms. Biotinylation was performed by the manufacturer or in the laboratory with a biotin labeling kit (Dojindo, Japan) if required. Antibody details are listed in Supplementary Table 2 in the Supporting Information.

Lectin−IGOT−LC/MS

Samples included cancer cell culture supernatants (RMG-I, RMG-V, RMUG-S, KATOIII, NUGC-4, GCIY, COLO 201, COLO 205) and ascites fluids from patients with ovarian cancer (three CCC, three serous carcinoma, one endometrioid carcinoma) and two patients with gastric cancer (Supplementary Table 1a in the Supporting Information). Proteins in the supernatants of culture media (concentrated 10-fold by ultrafiltration using YM-10) and ascites fluids were precipitated with 10% trichloroacetic acid on ice, recovered by centrifugation, and washed with ice-cooled acetone. The precipitates were dissolved in 0.5 M Tris-HCl, pH 8.5, containing 7 M guanidine-HCl and 10 mM ethylenediamine tetraacetic acid, reduced with dithiothreitol (equivalent to protein weight) for 2 h in a nitrogen atmosphere and alkylated with iodoacetamide (at 2.5-fold protein weight) for 2 h in the dark. After dialysis, the proteins were digested with trypsin (2% weight) at 37 °C overnight, and the digestion was stopped with 5 μM phenylmethylsulfonyl fluoride. An aliquot of the tryptic digest was applied to an AAL column (LA-AAL, *Aleuria aurantia* lectin, Seikagaku Biobusiness, Japan; 4.6 mm inner diameter [i.d.] × 150 mm) equilibrated with 10 mM HEPES-NaOH, pH 7.5. Glycopeptides were eluted in the same buffer with 5 mM fucose. The eluate was purified by hydrophilic interaction chromatography (HILIC) on a Sepharose CL-4B column (GE Healthcare, USA) as previously described,[28] where the HILIC procedure was found to not result in a bias of glycopeptide populations by a test using tryptic digest of ovalbumin and transferrin (data not shown). Purified glycopeptides were treated with PNGase (2.5 mU, 37 °C overnight) in stable isotope ^{18}O-labeled water to remove the glycan moiety, and the

dx.doi.org/10.1021/pr401109n | J. Proteome Res. 2014, 13, 1624−1635

glycosylated Asn of glycopeptides was labeled with the isotope, as previously described.[28] This step is referred to as "isotope-coded glycosylation site-specific tagging (IGOT)". The labeled peptides were analyzed by LC−MS, as previously described.[11] In brief, the peptide mixture was injected into a C18 trap column (0.5 mm i.d. × 1 mm). After washing, the column was connected to a nanoflow LC system (flow rate: 100 nL/min), and the peptides were separated on a reverse-phase (C18) tip column (150 μm i.d. × 70 mm) using a linear gradient of MeCN (0−35% in 0.1% formic acid) for 70 min. The eluted peptides were sprayed directly into a quadrupole time-of-flight hybrid mass spectrometer (Q-TOF Ultima; Waters-Micromass, USA). The spectrometer was operated in the data-dependent MS/MS mode.

MS/MS spectra were processed using MassLynx software (ver. 4.0, Micromass) to create peak list files with smoothing by the Savitzky−Golay method (window channels, ± 3). The files were processed by the MASCOT algorithm (ver. 2.1, Matrix Science) to assign peptides using the refseq protein sequence database (34 276 entries, downloaded on July 2007). The database search was performed by the MS/MS ion search method with the following parameters. Enzyme: trypsin + Lys-C; fixed modification: carbamidomethyl (Cys); variable modifications: Gln > pyro-Glu (N-term Gln), oxidation (Met), pyro-carbamidomethyl (N-term Cys), IGOT (Asn > Asp +^{18}O = +2.988261 Da, custom-made) (Asn); peptide mass tolerance: 200 ppm; fragment mass tolerance: 0.5 Da; max missed cleavage: 2. The false discovery rates of the Mascot search were <1%. Results were exported as CSV files and processed by Microsoft Excel. First, we selected the peptides with rank 1 and an expectation value <0.05. Then, we selected the peptides that contained one or more aspartic acids labeled with ^{18}O atoms (IGOT) at the position of Asn in the consensus sequence for *N*-glycosylation, Asn-Xaa-(Ser/Thr), where Xaa is any residue except Pro.

Lectin Microarray

The Cy3-labeled supernatants of cancer cell lines RMG-I, RMG-II, RMG-V, KATO-III, COLO 201, and COLO 205 were applied to slide glasses spotted with 45 lectins and subjected to lectin microarray analysis by GlycoStation (Moritex, Japan).[27]

AAL and WFA Fractionation of Ascites Fluids

AAL and *Wisteria floribunda* lectin (WFA)−agarose (Vector Laboratories) were packed into columns in the laboratory. Ascites fluids (0.25 mg protein) from CCC patients were applied to the 1 mL AAL-agarose column, and AAL-bound [AAL(+)] proteins eluted by 50 mM fucose were Western blotted for verification. For WFA fractionation, ascites fluids (5 mg protein) from two samples of each EOC type (clear cell, endometrioid, and serous types) and gastric cancer patients (Supplementary Table 1b in the Supporting Information) were applied to the 0.5 mL WFA-agarose column. WFA-bound [WFA(+)] proteins were eluted by 10 mM GalNAc and Western blotted for candidate selection.

Western Blotting

Crude samples and AAL(+) and WFA(+) fractions of ascites fluids were Western blotted and visualized with the enhanced chemiluminescence (ECL) system (Western Lightning, PerkinElmer, USA).

Lectin-Antibody Sandwich ELISA

WFA-coated (0.1 μg/well) ELISA plates (MaxiSorp, Thermo Scientific, USA) were blocked with 3% BSA in PBS. Serially diluted ascites fluids and RMG-I culture supernatants were applied to the plates and incubated for 2 h at room temperature. The plates were washed with PBS containing 0.05% Tween 20, and captured protein was detected by biotinylated antibody and horseradish peroxidase (HRP)-conjugated streptavidin (Jackson ImmunoResearch, USA). The substrate 3,3′,5,5′-tetramethylbenzidine (1-Step Ultra TMB-ELISA, Thermo Scientific) was applied, and absorbance was measured at 450 nm.

WFA-Ceruloplasmin ELISA for Verification

To establish the sandwich ELISA system with WFA and anti-ceruloplasmin (CP) antibody (WFA-CP ELISA), biotinylated WFA (Vector Laboratories, 0.1 μg/well) was immobilized on the streptavidin-coated ELISA plates (NUNC Immobilizer, Thermo Scientific) by overnight incubation at 4 °C. Ascites fluid samples (10 μL) were mixed with an equal amount of TBS (50 mM Tris-pH 8.0, 0.15 M NaCl, 0.1% NaN_3) containing 2% SDS and denatured at 98 °C for 5 min. The resulting solutions were diluted five-fold with TBS and 0.1% Tween 20, added to the wells, and incubated 3 h at room temperature. After the solution was removed, the plates were washed four times with wash buffer (0.05% Tween 20, PBS) and incubated with anti-human CP (0.1 μg/well, Bethyl Laboratories, USA) in wash buffer for 2 h. The plates were washed four times and incubated with a secondary antibody, HRP-conjugated anti-goat IgG (Jackson ImmunoResearch, 1:3000 in wash buffer) at room temperature for 1 h. The plates were washed four times; then, the substrates (1-Step Ultra TMB-Blotting Solution, 100 μL/well) were added. The reactions were stopped by adding 50 μL/well of 1 N H_2SO_4, and absorbance was measured at 450 nm on a plate reader.

Sample Quantification

Protein concentrations were measured with the Pierce BCA Protein Assay Kit (Thermo Scientific). CA125 was measured with the CA125 (Human) ELISA Kit (Abnova, U.K.). Ascites fluids were diluted 10- or 40-fold with the diluent provided by the manufacturer.

CP concentrations were measured by the sandwich ELISA system. The ELISA plate (MaxiSorp) was coated with mouse monoclonal anti-CP (0.1 μg/well, clone 3B11, Santa Cruz Biotechnology, CA) and blocked with 3% BSA in PBS. CP purified from human plasma (Merck, Germany) was serially diluted from 1.25 to 160 ng/mL with wash buffer (PBS containing 0.05% Tween20) and used as standards. The standards and 1000- to 10 000-fold diluted ascites fluids were applied to the plate and incubated for 2 h at room temperature. The plate was washed, and captured CP was reacted with biotinylated polyclonal anti-human CP (0.01 μg/well, Bethyl Laboratories) by incubation for 1.5 h. The plate was washed and reacted with HRP-conjugated streptavidin (Jackson ImmunoResearch), followed by reaction with the substrate (1-Step Ultra TMB-ELISA); absorbance was measured at 450 nm.

Immunoprecipitation and PNGase Treatment

Serum-free culture supernatants (2 to 20 mL) of RMG-I, RMG-II, RMG-V, Hep G2, and HuH-7 were concentrated about 20-fold and incubated with 10 μL of anti-CP (clone 3B11) conjugated agarose (CNBr-activated Sepharose 4B, GE Healthcare) for 4 h at 4 °C. After washing, CP was eluted with 0.1 M glycine, pH 2.5. Of the 40 μL eluate, 12 μL aliquots were denatured and incubated with 2 μL of PNGase (1 mU, Takara,

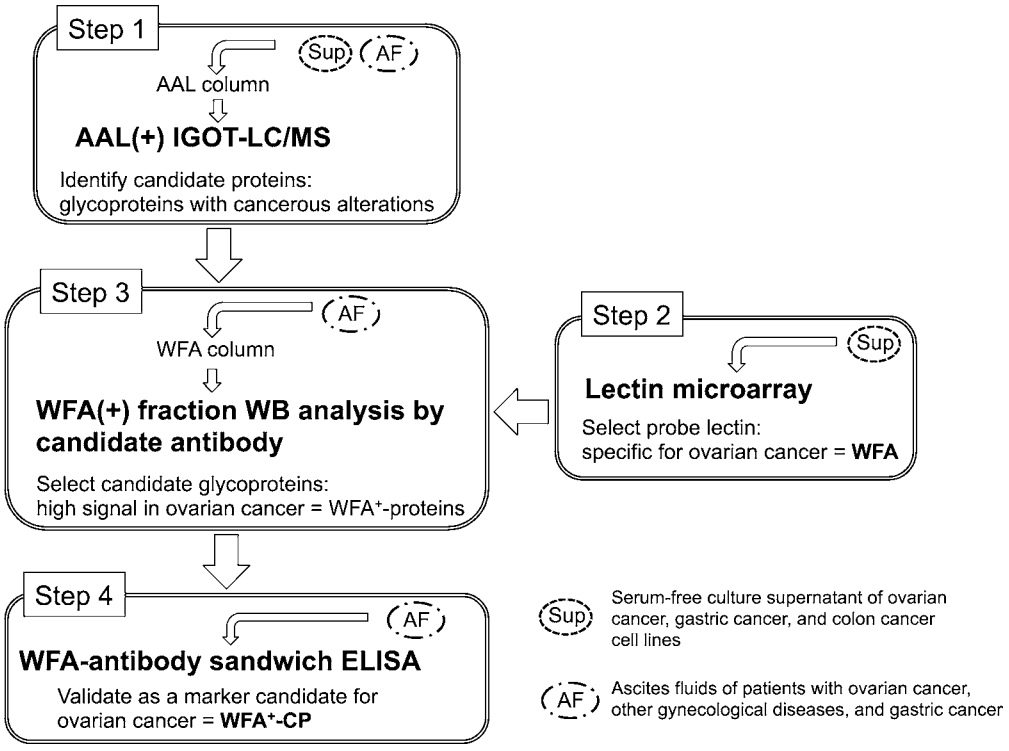

Figure 1. Strategy to discover glycobiomarker candidates optimized for ovarian cancer. This study includes the experimental work from Steps 1−4.

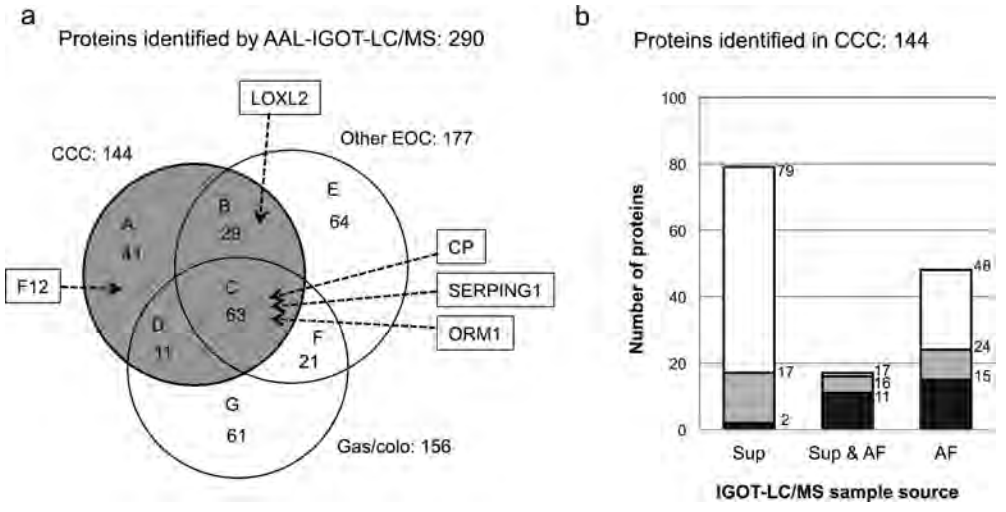

Figure 2. Profiling of the glycoproteins identified by AAL−IGOT−LC/MS. Glycopeptides from Sup and AF were captured by the AAL column and identified by IGOT−LC/MS. (a) Profiles of AAL(+) glycoproteins categorized by disease [CCC (gray circle), other EOC, and Gas/colo]. Each group included proteins identified in Sup or AF. Arrows indicate the attribution of five potential EOC marker candidates (F12, LOXL2, CP, SERPING1, and ORM1) selected through the subsequent steps. (b) Profiles of AAL(+) glycoproteins categorized by sample sources. Attribution of the 144 glycoproteins identified in CCC samples was categorized by sample source (Sup, AF, and Sup&AF). Candidate glycoproteins were tested by Western blotting of ascites fluids. Numbers of proteins are indicated by bar height. Proteins in white regions were not subjected to Western blotting, proteins in gray regions were blotted but not detected, and proteins in black regions were detected by Western blotting.

Japan) or with 2 μL of H_2O as an untreated sample for 20 h at 37 °C. The anti-CP eluate, purified CP (Merck), and PNGase-treated samples were separated by SDS-PAGE, followed by silver staining, anti-CP Western blotting, and WFA blotting. Silver staining was performed by EzStain (ATTO, Japan). Anti-CP (Bethyl) antibody directly labeled with HRP (Dojindo) was used for anti-CP Western blotting. For WFA blotting, the SDS-PAGE gels were transferred to a nitrocellulose membrane (Protran, GE Healthcare) and blocked with 3% BSA in PBS, followed by incubation with HRP-labeled (Dojindo) WFA (Vector Laboratories). Both membranes were visualized with the ECL system.

Immunohistochemistry

Fluorescent triple staining was performed with Hoechst 33342 (Dojindo) for nucleus, fluorescein (FITC)-labeled WFA (Vector Laboratories), and anti-human CP (Bethyl) with Alexa 546-labeled anti-goat IgG (Life Technologies, USA) as a secondary antibody. The slides were washed with PBS, mounted in Prolong Gold antifade reagent (Life Technologies),

dx.doi.org/10.1021/pr401109n | J. Proteome Res. 2014, 13, 1624−1635

Table 1. EOC Marker Candidates Tested by Western Blotting of Ascites Fluids[b]

group[a]	gene symbol	description	AAL−IGOT−LC/MS		Western blotting		
			Sup	AF	crude	AAL(+)	WFA(+)
A	FSTL1	follistatin-like 1	+	−	+	±	→
A	L1CAM L1	cell adhesion molecule	+	−	f	NT	NT
A	PSG5	pregnancy-specific beta-1-glycoprotein 5	+	−	−	NT	NT
A	PSG9	pregnancy-specific beta-1-glycoprotein 9	+	−	f	NT	NT
A	TFPI2	tissue factor pathway inhibitor 2	+	−	f	NT	NT
A	COL6A1	collagen, type VI, alpha 1	+	+	+	+	→
A	BGN	biglycan	−	+	−	NT	NT
A	CSF1R	colony stimulating factor 1 receptor	−	+	+	+	→
A	DCN	decorin	−	+	±	±	NT
A	F12	coagulation factor XII (Hageman factor)	−	+	+	+	↑
B	ATRN	attractin	+	−	f	NT	NT
B	CEACAM6	carcinoembryonic antigen-related cell adhesion molecule 6 (nonspecific cross-reacting antigen)	+	−	−	NT	NT
B	CTSD	cathepsin D	+	+	±	±	NT
B	CTSH	cathepsin H	+	+	+	+	−
B	ECM1	extracellular matrix protein 1	+	+	+	+	−
B	LOXL2	lysyl oxidase-like 2	+	+	+	+	↑
B	FBN1	fibrillin 1	−	+	f	NT	NT
B	MMRN2	multimerin 2	−	+	−	NT	NT
B	PLXDC2	plexin domain containing 2	−	+	+	+	−
B	PPIB	peptidylprolyl isomerase B (cyclophilin B)	−	+	−	NT	NT
C	AGRN	agrin	+	−	+	+	−
C	HYOU1	hypoxia up-regulated 1	+	−	−	NT	NT
C	ICOSLG	inducible T-cell costimulator ligand	+	−	f	NT	NT
C	IGFBP3	insulin-like growth factor binding protein 3	+	−	f	NT	NT
C	LCN2	lipocalin 2	+	−	+	+	→
C	MET	met proto-oncogene (hepatocyte growth factor receptor)	+	−	f	NT	NT
C	PRNP	prion protein	+	−	f	NT	NT
C	SPINT2	serine protease inhibitor, Kunitz type, 2	+	−	f	NT	NT
C	ADAM9	ADAM metallopeptidase domain 9	+	+	−	NT	NT
C	CP	ceruloplasmin (ferroxidase)	+	+	+	+	↑
C	GOLM1	Golgi membrane protein 1	+	+	f	NT	NT
C	HP	haptoglobin	+	+	f	NT	NT
C	ICAM1	intercellular adhesion molecule 1	+	+	+	+	−
C	LAMP1	lysosomal-associated membrane protein 1	+	+	−	NT	NT
C	LGALS3BP	lectin, galactoside-binding, soluble, 3 binding protein	+	+	+	+	→
C	QSOX1	quiescin Q6 sulfhydryl oxidase 1	+	+	+	+	−
C	SERPINA1	serpin peptidase inhibitor, clade A (alpha-1 antiproteinase, antitrypsin), member 1	+	+	+	+	→
C	TIMP1	TIMP metallopeptidase inhibitor 1	+	+	−	NT	NT
C	A1BG	alpha-1-B glycoprotein	−	+	+	+	−
C	A2M	alpha-2-macroglobulin	−	+	+	+	→
C	AHSG	alpha-2-HS-glycoprotein	−	+	+	±	NT
C	APOD	apolipoprotein D	−	+	f	NT	NT
C	AZGP1	alpha-2-glycoprotein 1, zinc-binding	−	+	+	+	−
C	BCHE	butyrylcholinesterase	−	+	−	+	→
C	CLU	clusterin	−	+	±	±	NT
C	HPX	hemopexin	−	+	+	+	→
C	KNG1	kininogen 1	−	+	f	NT	NT
C	LRG1	leucine-rich alpha-2-glycoprotein 1	−	+	f	NT	NT
C	ORM1	orosomucoid 1	−	+	+	+	↑
C	PIGR	polymeric immunoglobulin receptor	−	+	+	+	→
C	PTGDS	prostaglandin D2 synthase 21 kDa (brain)	−	+	−	NT	NT
C	SERPINC1	serpin peptidase inhibitor, clade C (antithrombin), member 1	−	+	−	NT	NT
C	SERPING1	serpin peptidase inhibitor, clade G (C1 inhibitor), member 1	−	+	+	+	↑
C	TF	transferrin	−	+	+	+	→
D	LAMC1	laminin, gamma 1 (formerly LAMB2)	+	−	−	NT	NT
D	LAMP2	lysosomal-associated membrane protein 2	+	−	−	NT	NT
D	VCAN	versican	+	−	f	NT	NT

[a]Group in Venn diagram of Figure 2a. [b]Symbols: +, identified (AAL−IGOT−LC/MS) or detected (Western blotting); −, not identified (AAL−IGOT−LC/MS) or not detected (Western blotting); ±, detected but weak; f, fuzzy band detected; NT, not tested; ↑, enhanced in EOC; →, not

dx.doi.org/10.1021/pr401109n | J. Proteome Res. 2014, 13, 1624−1635

Table 1. continued

enhanced in EOC. Detected: Western blot pattern was matched to the reference blot for each antibody provided by the manufacturer. Enhanced: stronger appearance of the bands in EOC than gastric cancer by comparison within the same membrane (Figure 3).

and examined with an LSM 510 confocal laser microscope (Carl Zeiss, Germany).

Statistics

Student's *t* test (unpaired *t* test with Welch's correction) was performed to evaluate the differences between groups.

RESULTS

IGOT−LC/MS Analysis of AAL-bound Glycopeptides

Our strategy is summarized in Figure 1. Fucosylation is enhanced in many cancers including ovarian cancer.[10,11,29] Therefore, the target proteins were first enriched by the AAL column, which binds fucosylated glycoproteins (Figure 1, Step 1). Supernatants from ovarian, gastric, and colon cancer cell lines (Sup) and ascites fluids from ovarian and gastric cancer patients (AF) were applied to the AAL column. Supernatants from cultured cell lines can provide specific cancer-derived glycoproteins other than human serum proteins, and the patients' ascites fluids contain glycoproteins secreted from the actual cancerous tissues. The glycoproteins with cancer-related glycans were captured from both sample sources. IGOT−LC/MS analysis was performed on the AAL(+) fractions (AAL−IGOT−LC/MS) prepared from Sup and AF. The AAL−IGOT−LC/MS-analyzed samples were categorized by disease: (1) CCC, including Sup and AF of CCC; (2) other EOC, including Sup and AF of non-CCC EOC; and (3) Gas/colo, including Sup and AF of gastric and colon cancer (Supplementary Table 1a in the Supporting Information). We identified 290 proteins (423 glycopeptides, Supplementary Tables 3, 4a, and 5a in the Supporting Information), of which 144 were found in CCC (Figure 2a, groups A−D), 177 in other EOC (Figure 2a, group B,C,E,F), and 156 in Gas/colo (Figure 2a, group C,D,F,G). Within the AAL(+) proteins identified in CCC, 41 were exclusive to CCC (Figure 2a, group A), 29 were also found in other EOC (Figure 2a, group B), 63 were found in all categories (Figure 2a, group C), and 11 were found in CCC and Gas/colo (Figure 2a, group D). The largest number of AAL(+) proteins was found in all categories (group C), suggesting that AAL recognizes cancer-related glycans, regardless of the tissue origin. The 144 glycoproteins identified in CCC were studied as candidate markers for EOC that are also sensitive to CCC. Representative MS/MS spectra of IGOT-labeled candidate peptides from CP are shown in Supplementary Figure 1a−c in the Supporting Information.

The RCA120 column was used to obtain relatively abundant glycopeptides based on the knowledge that RCA120 recognizes Galβ1,4GlcNAc-terminated glycans, which are found in the majority of glycoproteins after neuraminidase treatment.[11] The glycopeptides identified in RCA120(+) fractions in this study, which were assumed to be abundant in comparison with unidentified, potentially minor glycopeptides from ascites fluids, or culture supernatant of ovarian, gastric, and colon cancer, are listed in Supplementary Tables 4b and 5b in the Supporting Information.

Western Blotting of Candidate Proteins

Of the 144 candidate proteins, antibodies against 57 were commercially available and tested by Western blotting of the ascites fluids of CCC, and proteins not detected or identified were eliminated from further testing (Table 1, Western blotting, Crude column, (−, f)). The results showed 28 proteins in the crude ascites fluids (Table 1, Western blotting, Crude column, (+, ±)) and those were also detected in the AAL(+) fraction of the ascites fluids, consistent with the AAL−IGOT−LC/MS results (Table 1, Western blotting, AAL(+) column). Thus, the 28 proteins present in the ascites fluids were sufficient for detection by Western blotting and were studied further for their specificity as EOC markers.

Of the 144 candidate proteins, 79 and 48 were identified exclusively in Sup and AF, respectively, and 17 were identified in both sample sources (Sup&AF) (Figure 2b). The 57 antibody-tested proteins and the 28 proteins detected were classified by sample sources, where 2 of 17 (12%), 11 of 16 (69%), and 15 of 24 (63%) antibody-tested proteins from Sup, Sup&AF, and AF were detectable in Western blots of ascites fluids, respectively (Figure 2b, gray and black bars). Thus, ascites fluids are more suitable than the culture supernatants as a sample source for efficient discovery of marker candidates by IGOT−LC/MS.

Selection of the Optimal Probe Lectin to Distinguish EOC

We performed the lectin microarray analysis of serum-free culture supernatants of ovarian, gastric, and colon cancer cell lines to select a lectin probe that detects glycan alterations specific to the onset of ovarian cancer (Figure 1, Step 2). Ascites fluids were considered to be inappropriate for this step because it contains serum proteins and proteins secreted from inflammatory sites. Maximum normalized signal intensities for each cell line were compared (Table 2, intensity values are in Supplementary Table 6 in the Supporting Information). AAL, DSA (*Datura stramonium* lectin), and ABA (*Agaricus bisporus* lectin) yielded high signal intensity in almost all supernatants, indicating that our strategy featuring glycoprotein enrichment with cancer-related glycosylation using AAL is appropriate. WFA, PSA (*Pisum sativum* lectin), and LCA showed stronger signals in EOC than in gastric and colon cancer, while the signals of LEL (*Lycopersicon esculentum* lectin), EEL (*Euonymus europaeus* lectin), PWM (*Phytolacca americana* lectin), and PTL-I (*Psophocarpus tetragonolobus* lectin) were stronger in gastric and colon cancer (Table 2). Of the 45 tested lectins, the signal intensity of WFA provided the greatest contrast between CCC and gastric or colon cancer (Table 2, ratio of the mean column). This remarkable difference in signal intensity indicates the feasibility of WFA as a probe to distinguish ovarian cancer with sensitivity to CCC. Thus, WFA was selected as the probe lectin for further investigations.

Selection of Candidate Proteins by Western Blotting of WFA(+) Fraction

Subsequent selections from the 28 candidate proteins were performed with ascites fluid samples to evaluate the sensitivity and specificity for ovarian cancer (Figure 1, Step 3). Ascites fluids from ovarian and gastric cancer patients were fractionated with the WFA column, and the WFA(+) fraction was analyzed by Western blotting with antibodies against the candidate proteins. Sixteen proteins were detected in the WFA(+) fraction (Table 1, Western blotting, WFA(+) column), of which five proteins, ceruloplasmin (CP), serpin peptidase inhibitor, clade G, member 1 (SERPING1), lysyl oxidase-like 2

dx.doi.org/10.1021/pr401109n | J. Proteome Res. 2014, 13, 1624−1635

Table 2. Lectin Microarray Analysis of Culture Supernatants[a]

Signal Intensity (%, MAX normalized)

Cancer Cell Line								Lectin	Ratio of the Mean*	
CCC			Other EOC		Gastric	Colon				
RMG-I	RMG-II	RMG-V	RMUG-S	RTSG	KATO-III	COLO205	COLO201		CCC/GasColo	EOC/GasColo
								LTL	0.80	0.81
								PSA	1.81	1.61
								LCA	1.53	1.47
								UEAI	0.82	0.85
								AOL	0.84	0.66
								AAL	0.87	0.74
								MAL	0.69	0.74
								SNA	0.68	0.70
								SSA	0.78	0.79
								TJAI	0.66	0.69
								PHAL	0.73	0.77
								ECA	1.28	1.24
								RCA120	1.50	1.37
								PHAE	1.06	1.11
								DSA	1.03	1.05
								GSLII	0.52	0.70
								NPA	0.70	0.81
								ConA	0.82	0.84
								GNA	0.92	1.00
								HHL	0.89	1.02
								BPL	1.44	1.08
								TJAII	1.64	1.42
								EEL	0.32	0.38
								ABA	0.84	0.84
								LEL	0.71	0.73
								STL	0.82	0.83
								UDA	1.06	1.10
								PWM	0.26	0.34
								Jacalin	0.83	0.87
								PNA	0.57	0.62
								WFA	4.57	3.83
								ACA	1.09	0.93
								MPA	0.97	1.15
								HPA	0.42	0.44
								VVA	0.74	0.74
								DBA	0.33	0.39
								SBA	1.44	1.23
								GSLI	0.40	0.39
								PTLI	0.27	0.33
								MAH	0.41	0.51
								WGA	1.35	1.23
								GSL-IA4	0.43	0.47
								GSL-IB4	0.38	0.46

[a]Gray scale represents signal intensity: white (minimum, 0) to black (maximum, 100). *Ratio of the Mean: ratios of the mean signal intensity of each disease group were calculated; CCC/GasColo: ratio of [CCC] to [gastric and colon], and EOC/GasColo: ratio of [CCC and other EOC] to [gastric and colon].

(LOXL2), orosomucoid 1 (ORM1), and coagulation factor XII (F12), were present in high concentrations in the EOC versus gastric cancer samples (Figure 3). The volumes of the WFA-bound fractions required for Western blotting were about 75 to 4000 times the volumes of the crude samples, indicating that the content of WFA-bound proteins was about 0.025 to 1.3% of the respective total protein contents in the ascites fluids. It should be noted that the content of each candidate protein in the crude samples did not correlate with the content in the WFA(+) fraction. This suggests that the differences in band intensity for the WFA(+) fractions were due to differences in glycans not protein concentrations.

Although WFA-reactive CP (WFA$^+$-CP), SERPING1 (WFA$^+$-SERPING1), LOXL2 (WFA$^+$-LOXL2), ORM1 (WFA$^+$-ORM1), and F12 (WFA$^+$-F12) showed quantitative differences between EOC samples, their band intensities in the gastric cancer samples were extremely low. Therefore, the five glycoproteins were considered to be promising marker candidates for EOC and studied further.

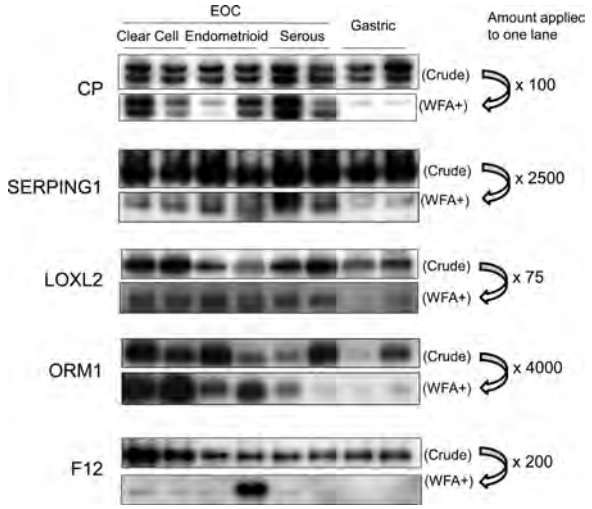

Figure 3. Western blot of the WFA(+) fractions from ascites fluids of EOC and gastric cancer. Ascites fluid samples (clear cell, endometrioid, and serous of EOC and gastric cancer; n = 2 each) were fractionated with the WFA column and blotted with antibodies against candidate proteins (CP, SERPING1, LOXL2, ORM1, and F12). Blots of untreated samples (crude; above) and WFA(+) fraction (WFA+; below) are indicated. Numbers indicate relative amounts applied to one lane for (WFA+) with (crude) set as 1.

Verification of Candidate Proteins by Lectin–Antibody Sandwich ELISA

Candidate proteins WFA$^+$-CP, WFA$^+$-SERPING1, WFA$^+$-LOXL2, WFA$^+$-ORM1, and WFA$^+$-F12 were examined by WFA–antibody sandwich ELISA (Figure 1, Step 4). The RMG-I supernatant and ascites fluid of an ovarian cancer patient were serially diluted and analyzed by ELISA (Supplementary Figure 1a in the Supporting Information). Dose dependency was observed in WFA$^+$-CP and WFA$^+$-SERPING1 but not in WFA$^+$-LOXL2, WFA$^+$-ORM1, and WFA$^+$-F12. Thus, WFA$^+$-CP was selected for further analysis because it showed the highest reactivity in both the supernatants and ascites fluids.

WFA-CP ELISA was evaluated by drawing a dose–response curve for the pooled, serially diluted ascites fluids of CCC patients (Supplementary Figure 3a in the Supporting Information). WFA$^+$-CP content was measured by ELISA in the same sample set used for Western blotting of the WFA(+) fraction; high signal intensity was observed in ovarian cancer samples, and a similar pattern was maintained after normalization to the total protein concentration (Supplementary Figure 3b–d in the Supporting Information), consistent with the Western blotting result (Figure 3a).

WFA$^+$-CP was then measured by WFA-CP ELISA in the ascites fluids from patients with EOC (n = 38) and other gynecological diseases including chocolate cyst, leiomyoma, uterine corpus cancer, and uterine sarcoma (n = 44). Signal intensity was significantly higher in the EOC samples (P < 0.0001, Figure 4a), and the ROC curve was drawn with an AUC of 0.843 (Figure 4b). It is worth noting that CCC, endometrioid carcinoma, and serous carcinoma showed significantly high signals in comparison with the endometriosis samples (i.e., chocolate cyst), and the signal in CCC tended to be higher (Figure 4c). The ability to distinguish CCC and endometrioid carcinoma from endometriosis is important for the marker's clinical utility. The CP concentration was also

dx.doi.org/10.1021/pr401109n | J. Proteome Res. 2014, 13, 1624–1635

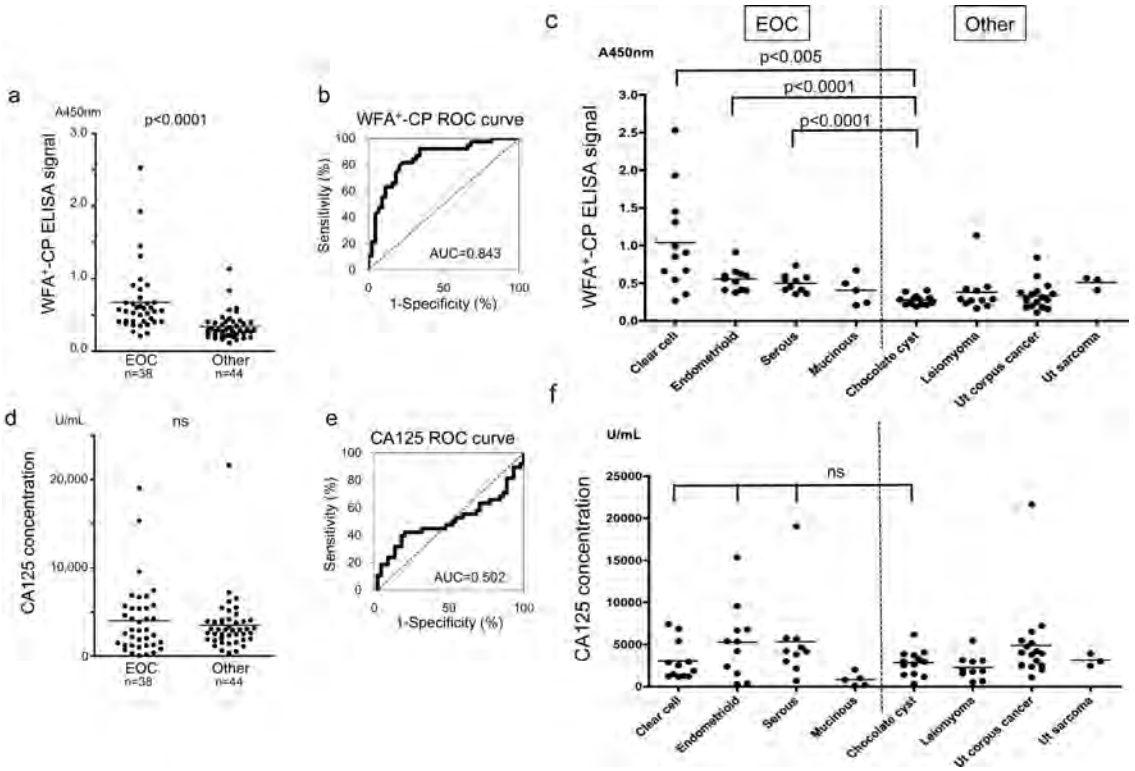

Figure 4. Sandwich ELISA of WFA$^+$-CP and CA125 in the ascites fluids of patients with EOC and other gynecological diseases. WFA$^+$-CP was measured by WFA-CP ELISA and CA125 was measured by a commercial kit. Statistical analysis was performed by Student's *t* test. (a) Distribution of WFA$^+$-CP in the ascites fluids of EOC and other gynecological diseases significantly differed ($p < 0.0001$). (b) ROC curve of WFA$^+$-CP with an AUC value of 0.843. (c) WFA$^+$-CP distribution in each tissue type of EOC and other gynecological diseases; significant differences ($p < 0.005$ to $p < 0.0001$) were observed between chocolate cyst and clear cell, endometrioid, and serous carcinoma of EOC. (d) Distribution of CA125 levels in the ascites fluids of EOC and other gynecological diseases did not significantly differ. (e) ROC curve of CA125 with an AUC value of 0.502. (f) CA125 distribution in each tissue type of EOC and other gynecological diseases. No significant difference was observed.

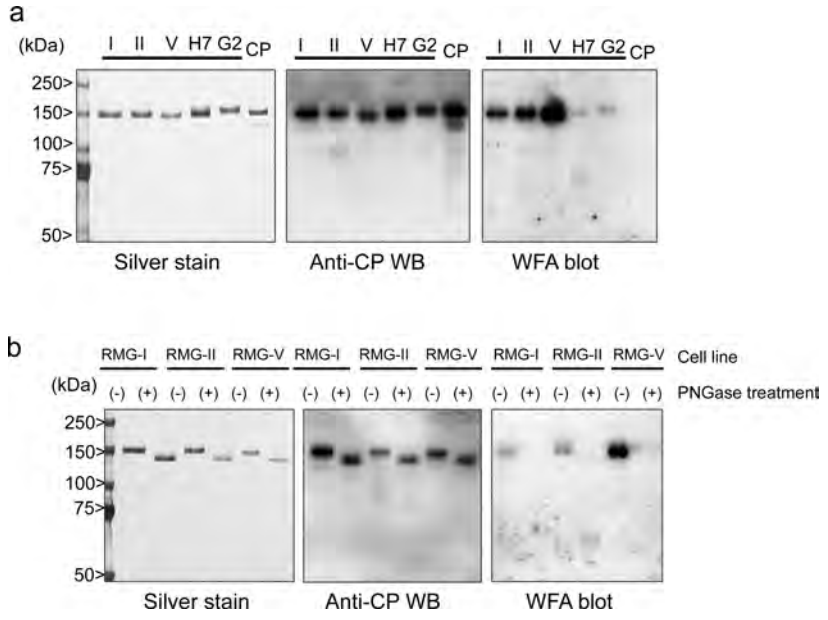

Figure 5. Immunoprecipitation of CP from culture supernatants followed by silver staining, anti-CP Western blotting, and WFA blotting. (a) CP was immunoprecipitated from supernatants of CCC (Lane I: RMG-I, Lane II: RMG-II, Lane V: RMG-V) and hepatoma (Lane H7: HuH-7, Lane G2: Hep G2) cell lines. CP from human plasma (Merck) was applied to Lane CP. (b) PNGase treatment of CP from supernatants of CCC cell lines. Immunoprecipitated CP from CCC cell lines (RMG-I, RMG-II, RMG-V) was analyzed without treatment (−) or after PNGase treatment (+).

elevated in EOC than other gynecological diseases, but the significance level was lower than WFA$^+$-CP (Supplementary Figure 4a in the Supporting Information). The total protein distributions of EOC and other gynecological diseases were comparable (Supplementary Figure 4b in the Supporting Information).

dx.doi.org/10.1021/pr401109n | J. Proteome Res. 2014, 13, 1624−1635

To evaluate the diagnostic performance of WFA$^+$-CP, we measured CA125 in the same sample set. Although the CA125 level in the ascites fluids was 20 to 100 times higher than the cutoff for serum CA125 (35 U/mL), the level was also high in benign samples (leiomyoma, chocolate cyst), and no significant difference was found between them and EOC (Figure 4d–f). This was similar to the serum CA125 results in the same patients from whom ascites fluids were collected. No significant difference was observed between chocolate cyst and CCC, endometrioid, or serous carcinoma (Supplementary Figure 5 in the Supporting Information). In contrast, the WFA$^+$-CP level was high in CCC and low with small deviation in endometriosis, thereby resulting in fewer false-negative and false-positive results. This shows the advantage of WFA$^+$-CP over CA125.

Verification of WFA$^+$-CP by Immunoprecipitation, Lectin Blot, and PNGase Treatment

To confirm the ability of WFA to recognize glycans on CP molecules secreted from ovarian cancer cells, we compared WFA reactivity of CP in three CCC cell lines (RMG-I, RMG-II, and RMG-V) and hepatoma cell lines (HuH-7, Hep G2) as well as CP from normal plasma (Merck). CP was immunoprecipitated in the supernatants (Figure 5a, silver stain, anti-CP WB). WFA blotting of these samples produced a band at the position of CP in the CCC cell lines, but the band was very weak in hepatoma cell lines and was not detectable in normal plasma (Figure 5a, WFA blot). Thus, the CCC cell lines secrete CP molecules with glycans specifically recognized by WFA (WFA$^+$-CP), and the ratio of WFA$^+$-CP against WFA-unbound CP (WFA$^-$-CP) was high in comparison with hepatoma cells or normal plasma.

CP was immunoprecipitated from RMG-I, RMG-II, and RMG-V and treated with PNGase to release N-glycans, followed by silver staining and anti-CP western and WFA blotting. The band corresponding to CP migrated at a smaller molecular weight (Figure 5b, silver stain and anti-CP WB), and the PNGase-treated sample was not detected in the WFA blot (Figure 5b, WFA blot). These results suggest that WFA recognizes N-glycans of CP molecules.

Verification of WFA$^+$-CP by Histological Staining of Tissue Samples

Histology of tissue specimens obtained from CCC patients yielded clear stains with anti-CP antibody and WFA in the cancer lesion (Figure 6a–c). The merged images indicated some colocalization of CP and WFA-reactive glycans (Figure 6d).

DISCUSSION

We demonstrated a new strategy for discovery of a novel ovarian cancer marker based on the cancerous alteration of glycans. This strategy is remarkable for three reasons. (1) We enriched samples for glycoproteins with cancer-related glycosylation by AAL column separation prior to IGOT–LC/MS. (2) We used ascites fluids rather than serum from patients for candidate selection and verification because the ascites fluids contain cancer-derived biomarkers at higher concentrations than serum. (3) We used cultured cell supernatants for lectin microarray analysis to select the lectin probe that recognizes ovarian cancer-specific glycoproteins. These methods allowed us to identify the glycoprotein accompanied by cancer-specific aberrant glycans as a candidate marker for ovarian cancer.

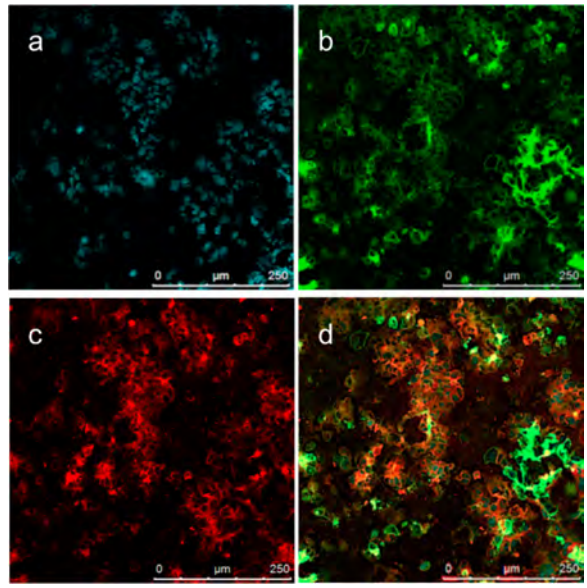

Figure 6. Fluorescent triple staining of nuclei, WFA, and anti-CP antibody in CCC tissues. (a) Nuclei were stained with Hoechst 33342 (blue fluorescence). (b) WFA-reactive glycans were stained with WFA-FITC (green fluorescence). (c) CP was stained with anti-CP polyclonal antibody followed by Alexa 546-labeled antigoat IgG (red fluorescence). (d) Merged image shows colocalization of WFA and CP staining in orange to yellow.

Enrichment of the biological samples and IGOT–LC/MS analysis identified 144 candidate CCC-sensitive EOC markers. In a proteomic analysis, Gortzak-Uzan et al. identified more than 2500 proteins in the ascites fluids of ovarian cancer patients.[30] We tested 57 of the original 144 candidates and efficiently identified five potential EOC marker candidates. In this study, we used the AAL column to enrich potential target glycopeptides derived from cancerous cells because various types of cancer cells express enhanced fucosyl glycans.[9,27,29]

The amount of the final candidate WFA$^+$-CP in the ascites fluids was <1% of the total CP, and it would be far lower in serum. Therefore, it is unlikely that our candidate could have been identified in patient serum, as is often done in conventional methods. The use of ascites fluids improved the efficiency of our selection and identification of marker candidates. As shown in Table 1, candidate selection depends on the amount of target protein in the ascites fluids as well as antibody performance or optimization of the Western blotting system. Glycoproteins excluded because of low performance on Western blots may also have potential as candidates.

The relationships between the glycan alterations that occur with canceration and the lectins that recognize them have been proposed in many studies and include branching and DSA, fucosylation and LCA or AAL, and sialylation and SNA (*Sambucus nigra* lectin).[31−33] However, those glycans are also abundant in normal serum, so it is difficult to identify ectopic alterations of glycans as cancer-specific glycans in serum. The signals of LCA and AAL, which bind fucosylated glycoproteins, were reduced in lectin microarrays of sera from ovarian cancer patients.[34] In our lectin microarray of serum-free culture supernatants, strong AAL reactivity was confirmed in all tested cell lines. In addition, weak but specific WFA reactivity was observed in ovarian cancer cell lines versus gastric and colon cancer cell lines. Thus, we selected WFA as the probe lectin candidate. Of the five candidates, three (CP, SERPING1, and

ORM1) were detected in all categories tested by AAL−IGOT−LC/MS (i.e., CCC, other EOC, Gas/colo) (Figure 2a, group C). This means that the glycoproteins commonly found in other organs may also serve as an EOC marker by using WFA as the probe. Our lectin microarray of the supernatants suggested the possibility of WFA-reactive proteins other than those we verified as ovarian cancer marker candidates. Because the WFA signal in the lectin microarray was relatively weak in comparison with AAL, IGOT−LC/MS analysis of samples enriched with a WFA column was not applicable in this study. Further technical modification is necessary for comprehensive identification of candidate markers with WFA as the capturing lectin.

Appropriate usage of the samples in each process is important. For instance, we selected the disease-specific probe by lectin microarray using serum-free culture supernatants, which eliminates proteins that do not originate from cancer cells. Meanwhile, IGOT−LC/MS analysis can yield a reliable list of candidate molecules from biological samples containing irrelevant proteins, as long as preliminary target enrichment is performed, such as the AAL capture in our study. Moreover, the use of ascites fluids in addition to culture supernatants provided efficient selection of marker candidates.

WFA recognizes the GalNAcβ1,4GlcNAc (LacdiNAc) motif[35] and reacts to the glycans on proteins associated with diseases.[7,36] In our study, WFA recognized the N-glycan structures of WFA$^+$-CP from ovarian cancer cells (Figure 5b). In contrast, CP from normal plasma has four N-glycans, and no LacdiNAc structure was found.[37] Thus, we conclude that ovarian cancer cells may produce CP with the LacdiNAc structure on N-glycans.

CP is a serum glycoprotein secreted from the liver; the blood of healthy adults contains abundant CP (200−400 μg/mL). CP is a multicopper transporter with oxidase activity as a radical scavenger, and its expression is elevated as an acute phase protein. Serum CP is positively correlated with the acute phase reaction activated by inflammation, infection, and diseases including cancer[30,38,39] due to enhanced secretion from the liver and up-regulation of cytokine signaling.[38,39] CP expression has been reported in ovarian cancer tissues but not in normal ovarian tissues.[40,41] In our study, the levels of total CP in the ascites fluids were elevated in EOC compared with other gynecological diseases (Supplementary Figure 2 in the Supporting Information), but the WFA$^+$-CP level differed between groups. The CP in the ascites fluids was considered to be a mixture of CP from serum (liver) and ovarian cancer tissue. In the immunoprecipitation study of CP, WFA reactivity was positive in CP derived from ovarian cancer cell lines but was very weak in CP from hepatoma cell lines and negative in CP purified from normal plasma (Figure 5a). We therefore speculate that the increase in WFA$^+$-CP in the ascites fluids of EOC patients was due to alteration or abnormality of the glycosylation process that accompanies canceration and which is not affected by CP expression in the liver.

The immunohistochemical study indicated that CP and WFA-reactive glycans were expressed and partially colocalized on the ovarian cancer tissues (Figure 6). Thus, CP expression occurs in ovarian cancer tissues, and some proteins with WFA-reactive glycans are expressed simultaneously, one of which is WFA$^+$-CP.

For further verification of the marker candidates, it is important to use samples from patient groups that need differential diagnosis. Especially for cancer, comparative analysis using samples obtained from patients with cancer and background diseases is essential to evaluate the feasibility of clinical diagnostic markers. CCC of the ovary is characterized by its association with endometriosis.[42,43] In our study, the WFA$^+$-CP level was higher in CCC than in chocolate cyst, a type of endometriosis. This emphasizes the possible utility of WFA$^+$-CP as a specific marker for EOC with sensitivity to CCC. Although measuring serum WFA$^+$-CP level is difficult due to interference by a large amount of CP secreted from the liver, WFA$^+$-CP has potential as a serum marker for simple screening of patients with CCC, facilitating early treatment decisions and improved prognosis of patients with CCC of the ovary.

■ ASSOCIATED CONTENT

Supporting Information

Supplementary Table 1. Clinical characteristics of biological specimens from EOC and gastric cancer patients. Supplementary Table 2. Antibodies applicable for Western blot of ascites fluids. Supplementary Table 3. Groups of the identified glycoproteins (AAL(+)). Supplementary Table 4a. Information on glycopeptides identified from each sample (AAL(+)). Supplementary Table 4b. Information on glycopeptides identified from each sample (RCA120(+)). Supplementary Table 5a. Glycoproteins identified from each sample (AAL(+)). Supplementary Table 5b. Glycoproteins identified from each sample (RCA120(+)). Supplementary Table 6. Lectin microarray signal intensity. Supplementary Figure 1. MS/MS spectra of IGOT-peptides derived from the candidate glycoprotein (ceruloplasmin) verified in this study. Supplementary Figure 2. Lectin-antibody sandwich ELISA for five candidate glycoproteins. Supplementary Figure 3. Evaluation of WFA-CP ELISA. Supplementary Figure 4. Supporting measurements for the verification study. Supplementary Figure 5. CA125 in the serum of EOC and other gynecological diseases. This material is available free of charge via the Internet at http://pubs.acs.org.

■ AUTHOR INFORMATION

Corresponding Author

*Tel: +81-29-861-3253. Fax: +81-29-861-3252. E-mail: h.narimatsu@aist.go.jp.

Author Contributions

#Maki Sogabe and Hirofumi Nozaki contributed equally to this work.

Notes

The authors declare no competing financial interest.

■ ACKNOWLEDGMENTS

This work was partially supported by a grant under the "Medical Glycomics Project" by the New Energy and Industrial Technology Development Organization (NEDO). We thank T. Ohkura for lectin−IGOT−LC/MS analysis; M. Fujita and N. Tetsura for large-scale MS data processing; N. Ohmichi, A. Matsuda, and S. Unno for lectin microarray analysis; and M. Hashimoto for immunohistochemical analysis. We also thank A. Takahashi for assistance with manuscript preparation. All persons acknowledged here are members of the Research Center for Medical Glycoscience.

REFERENCES

(1) Dube, D. H.; Bertozzi, C. R. Glycans in cancer and inflammation–potential for therapeutics and diagnostics. *Nat. Rev. Drug Discovery* **2005**, *4* (6), 477−488.

(2) Comunale, M. A.; Lowman, M.; Long, R. E.; Krakover, J.; Philip, R.; Seeholzer, S.; Evans, A. A.; Hann, H. W.; Block, T. M.; Mehta, A. S. Proteomic analysis of serum associated fucosylated glycoproteins in the development of primary hepatocellular carcinoma. *J. Proteome Res.* **2006**, *5* (2), 308−315.

(3) Yang, Z.; Harris, L. E.; Palmer-Toy, D. E.; Hancock, W. S. Multilectin affinity chromatography for characterization of multiple glycoprotein biomarker candidates in serum from breast cancer patients. *Clin. Chem.* **2006**, *52* (10), 1897−1905.

(4) Olewicz-Gawlik, A.; Korczowska-Lacka, I.; Lacki, J. K.; Klama, K.; Hrycaj, P. Fucosylation of serum alpha1-acid glycoprotein in rheumatoid arthritis patients treated with infliximab. *Clin. Rheumatol.* **2007**, *26* (10), 1679−1684.

(5) Taketa, K.; Endo, Y.; Sekiya, C.; Tanikawa, K.; Koji, T.; Taga, H.; Satomura, S.; Matsuura, S.; Kawai, T.; Hirai, H. A collaborative study for the evaluation of lectin-reactive alpha-fetoproteins in early detection of hepatocellular carcinoma. *Cancer Res.* **1993**, *53* (22), 5419−5423.

(6) Uchiyama, N.; Kuno, A.; Tateno, H.; Kubo, Y.; Mizuno, M.; Noguchi, M.; Hirabayashi, J. Optimization of evanescent-field fluorescence-assisted lectin microarray for high-sensitivity detection of monovalent oligosaccharides and glycoproteins. *Proteomics* **2008**, *8* (15), 3042−3050.

(7) Matsuda, A.; Kuno, A.; Kawamoto, T.; Matsuzaki, H.; Irimura, T.; Ikehara, Y.; Zen, Y.; Nakanuma, Y.; Yamamoto, M.; Ohkohchi, N.; Shoda, J.; Hirabayashi, J.; Narimatsu, H. Wisteria floribunda agglutinin-positive mucin 1 is a sensitive biliary marker for human cholangiocarcinoma. *Hepatology* **2010**, *52* (1), 174−182.

(8) Kaji, H.; Saito, H.; Yamauchi, Y.; Shinkawa, T.; Taoka, M.; Hirabayashi, J.; Kasai, K.; Takahashi, N.; Isobe, T. Lectin affinity capture, isotope-coded tagging and mass spectrometry to identify N-linked glycoproteins. *Nat. Biotechnol.* **2003**, *21* (6), 667−672.

(9) Narimatsu, H.; Sawaki, H.; Kuno, A.; Kaji, H.; Ito, H.; Ikehara, Y. A strategy for discovery of cancer glyco-biomarkers in serum using newly developed technologies for glycoproteomics. *FEBS J.* **2010**, *277* (1), 95−105.

(10) Kuno, A.; Ikehara, Y.; Tanaka, Y.; Angata, T.; Unno, S.; Sogabe, M.; Ozaki, H.; Ito, K.; Hirabayashi, J.; Mizokami, M.; Narimatsu, H. Multilectin assay for detecting fibrosis-specific glyco-alteration by means of lectin microarray. *Clin. Chem.* **2011**, *57* (1), 48−56.

(11) Kaji, H.; Ocho, M.; Togayachi, A.; Kuno, A.; Sogabe, M.; Ohkura, T.; Nozaki, H.; Angata, T.; Chiba, Y.; Ozaki, H.; Hirabayashi, J.; Tanaka, Y.; Mizokami, M.; Ikehara, Y.; Narimatsu, H. Glycoproteomic Discovery of Serological Biomarker Candidates for HCV/HBV Infection-Associated Liver Fibrosis and Hepatocellular Carcinoma. *J. Proteome Res.* **2013**, *12* (6), 2630−2640.

(12) Klein, A.; Michalski, J. C.; Morelle, W. Modifications of human total serum N-glycome during liver fibrosis-cirrhosis, is it all about immunoglobulins? *Proteomics. Clin. Appl.* **2010**, *4* (4), 372−378.

(13) Zhang, Q.; Faca, V.; Hanash, S. Mining the plasma proteome for disease applications across seven logs of protein abundance. *J. Proteome Res.* **2011**, *10* (1), 46−50.

(14) Heintz, A. P. M.; Odicino, F.; Maisonneuve, P.; Quinn, M. A.; Benedet, J. L.; Creasman, W. T.; Ngan, H. Y. S.; Pecorelli, S.; Beller, U. Carcinoma of the Ovary. *Int. J. Gynecol. Obstet.* **2006**, *95*, S161−S192.

(15) Anglesio, M. S.; Carey, M. S.; Kobel, M.; Mackay, H.; Huntsman, D. G. Vancouver Ovarian Clear Cell Symposium, Clear cell carcinoma of the ovary: a report from the first Ovarian Clear Cell Symposium, June 24th, 2010. *Gynecol. Oncol.* **2011**, *121* (2), 407−415.

(16) Lee, Y. Y.; Kim, T. J.; Kim, M. J.; Kim, H. J.; Song, T.; Kim, M. K.; Choi, C. H.; Lee, J. W.; Bae, D. S.; Kim, B. G. Prognosis of ovarian clear cell carcinoma compared to other histological subtypes: a meta-analysis. *Gynecol. Oncol.* **2011**, *122* (3), 541−547.

(17) Sugiyama, T.; Kamura, T.; Kigawa, J.; Terakawa, N.; Kikuchi, Y.; Kita, T.; Suzuki, M.; Sato, I.; Taguchi, K. Clinical characteristics of clear cell carcinoma of the ovary: a distinct histologic type with poor prognosis and resistance to platinum-based chemotherapy. *Cancer* **2000**, *88* (11), 2584−2589.

(18) del Carmen, M. G.; Birrer, M.; Schorge, J. O. Clear cell carcinoma of the ovary: a review of the literature. *Gynecol. Oncol.* **2012**, *126* (3), 481−490.

(19) Behbakht, K.; Randall, T. C.; Benjamin, I.; Morgan, M. A.; King, S.; Rubin, S. C. Clinical characteristics of clear cell carcinoma of the ovary. *Gynecol. Oncol.* **1998**, *70* (2), 255−258.

(20) Nossov, V.; Amneus, M.; Su, F.; Lang, J.; Janco, J. M.; Reddy, S. T.; Farias-Eisner, R. The early detection of ovarian cancer: from traditional methods to proteomics. Can we really do better than serum CA-125? *Am. J. Obstet. Gynecol.* **2008**, *199* (3), 215−223.

(21) Pearce, C. L.; Templeman, C.; Rossing, M. A.; Lee, A.; Near, A. M.; Webb, P. M.; Nagle, C. M.; Doherty, J. A.; Cushing-Haugen, K. L.; Wicklund, K. G.; Chang-Claude, J.; Hein, R.; Lurie, G.; Wilkens, L. R.; Carney, M. E.; Goodman, M. T.; Moysich, K.; Kjaer, S. K.; Hogdall, E.; Jensen, A.; Goode, E. L.; Fridley, B. L.; Larson, M. C.; Schildkraut, J. M.; Palmieri, R. T.; Cramer, D. W.; Terry, K. L.; Vitonis, A. F.; Titus, L. J.; Ziogas, A.; Brewster, W.; Anton-Culver, H.; Gentry-Maharaj, A.; Ramus, S. J.; Anderson, A. R.; Brueggmann, D.; Fasching, P. A.; Gayther, S. A.; Huntsman, D. G.; Menon, U.; Ness, R. B.; Pike, M. C.; Risch, H.; Wu, A. H.; Berchuck, A. Association between endometriosis and risk of histological subtypes of ovarian cancer: a pooled analysis of case-control studies. *Lancet Oncol.* **2012**, *13* (4), 385−394.

(22) Aoki, D.; Suzuki, N.; Susumu, N.; Noda, T.; Suzuki, A.; Tamada, Y.; Higashiguchi, A.; Oie, S.; Nozawa, S. Establishment and characterization of the RMG-V cell line from human ovarian clear cell adenocarcinoma. *Human Cell* **2005**, *18* (3), 143−146.

(23) Udagawa, Y.; Nozawa, S.; Chin, K.; Sakayori, M.; Mikami, M.; Ohta, K.; Tsukazaki, K.; Kiguchi, K.; Iizuka, R. Establishment and characterization of a human chorionic gonadotropin (hCG) producing cell line (RTSG) from an ovarian epithelial cancer. *Human Cell* **1990**, *3* (1), 70−75.

(24) Nozawa, S.; Tsukazaki, K.; Sakayori, M.; Jeng, C. H.; Iizuka, R. Establishment of a human ovarian clear cell carcinoma cell line (RMG-I) and its single cell cloning—with special reference to the stem cell of the tumor. *Human Cell* **1988**, *1* (4), 426−435.

(25) Nozawa, S.; Yajima, M.; Sasaki, H.; Tsukazaki, K.; Aoki, D.; Sakayori, M.; Udagawa, Y.; Kobayashi, T.; Sato, I.; Furusako, S.; et al. A new CA125-like antigen (CA602) recognized by two monoclonal antibodies against a newly established ovarian clear cell carcinoma cell line (RMG-II). *Jpn. J. Cancer Res.* **1991**, *82* (7), 854−861.

(26) Sakayori, M.; Nozawa, S.; Udagawa, Y.; Chin, K.; Lee, S. G.; Sakuma, T.; Iizuka, R.; Wada, Y.; Yoshida, S.; Takeda, Y. Biological properties of two newly established cell lines (RMUG-S, RMUG-L) from a human ovarian mucinous cystadenocarcinoma. *Human Cell* **1990**, *3* (1), 52−56.

(27) Ito, H.; Kuno, A.; Sawaki, H.; Sogabe, M.; Ozaki, H.; Tanaka, Y.; Mizokami, M.; Shoda, J.; Angata, T.; Sato, T.; Hirabayashi, J.; Ikehara, Y.; Narimatsu, H. Strategy for glycoproteomics: identification of glyco-alteration using multiple glycan profiling tools. *J. Proteome Res.* **2009**, *8* (3), 1358−1367.

(28) Kaji, H.; Yamauchi, Y.; Takahashi, N.; Isobe, T. Mass spectrometric identification of N-linked glycopeptides using lectin-mediated affinity capture and glycosylation site-specific stable isotope tagging. *Nat. Protoc.* **2006**, *1* (6), 3019−3027.

(29) Alley, W. R., Jr.; Vasseur, J. A.; Goetz, J. A.; Svoboda, M.; Mann, B. F.; Matei, D. E.; Menning, N.; Hussein, A.; Mechref, Y.; Novotny, M. V. N-linked glycan structures and their expressions change in the blood sera of ovarian cancer patients. *J. Proteome Res.* **2012**, *11* (4), 2282−2300.

(30) Gortzak-Uzan, L.; Ignatchenko, A.; Evangelou, A. I.; Agochiya, M.; Brown, K. A.; St. Onge, P.; Kireeva, I.; Schmitt-Ulms, G.; Brown, T. J.; Murphy, J.; Rosen, B.; Shaw, P.; Jurisica, I.; Kislinger, T. A proteome resource of ovarian cancer ascites: integrated proteomic and bioinformatic analyses to identify putative biomarkers. *J. Proteome Res.* **2008**, *7* (1), 339−351.

(31) Abbott, K. L.; Nairn, A. V.; Hall, E. M.; Horton, M. B.; McDonald, J. F.; Moremen, K. W.; Dinulescu, D. M.; Pierce, M. Focused glycomic analysis of the N-linked glycan biosynthetic pathway in ovarian cancer. *Proteomics* **2008**, *8* (16), 3210−3220.
(32) Abbott, K. L.; Lim, J. M.; Wells, L.; Benigno, B. B.; McDonald, J. F.; Pierce, M. Identification of candidate biomarkers with cancer-specific glycosylation in the tissue and serum of endometrioid ovarian cancer patients by glycoproteomic analysis. *Proteomics* **2010**, *10* (3), 470−481.
(33) Shetty, V.; Hafner, J.; Shah, P.; Nickens, Z.; Philip, R. Investigation of ovarian cancer associated sialylation changes in N-linked glycopeptides by quantitative proteomics. *Clin. Proteomics* **2012**, *9* (1), 10.
(34) Wu, J.; Xie, X.; Liu, Y.; He, J.; Benitez, R.; Buckanovich, R. J.; Lubman, D. M. Identification and confirmation of differentially expressed fucosylated glycoproteins in the serum of ovarian cancer patients using a lectin array and LC-MS/MS. *J. Proteome Res.* **2012**, *11* (9), 4541−4552.
(35) Ikehara, Y.; Sato, T.; Niwa, T.; Nakamura, S.; Gotoh, M.; Ikehara, S. K.; Kiyohara, K.; Aoki, C.; Iwai, T.; Nakanishi, H.; Hirabayashi, J.; Tatematsu, M.; Narimatsu, H. Apical Golgi localization of N,N′-diacetyllactosediamine synthase, beta4GalNAc-T3, is responsible for LacdiNAc expression on gastric mucosa. *Glycobiology* **2006**, *16* (9), 777−785.
(36) Kuno, A.; Ikehara, Y.; Tanaka, Y.; Ito, K.; Matsuda, A.; Sekiya, S.; Hige, S.; Sakamoto, M.; Kage, M.; Mizokami, M.; Narimatsu, H. A serum "sweet-doughnut" protein facilitates fibrosis evaluation and therapy assessment in patients with viral hepatitis. *Sci. Rep.* **2013**, *3*, 1065.
(37) Harazono, A.; Kawasaki, N.; Itoh, S.; Hashii, N.; Ishii-Watabe, A.; Kawanishi, T.; Hayakawa, T. Site-specific N-glycosylation analysis of human plasma ceruloplasmin using liquid chromatography with electrospray ionization tandem mass spectrometry. *Anal. Biochem.* **2006**, *348* (2), 259−268.
(38) Banks, R. E.; Forbes, M. A.; Storr, M.; Higginson, J.; Thompson, D.; Raynes, J.; Illingworth, J. M.; Perren, T. J.; Selby, P. J.; Whicher, J. T. The acute phase protein response in patients receiving subcutaneous IL-6. *Clin. Exp. Immunol.* **1995**, *102* (1), 217−223.
(39) Shannahan, J. H.; Alzate, O.; Winnik, W. M.; Andrews, D.; Schladweiler, M. C.; Ghio, A. J.; Gavett, S. H.; Kodavanti, U. P. Acute phase response, inflammation and metabolic syndrome biomarkers of Libby asbestos exposure. *Toxicol. Appl. Physiol.* **2012**, *260* (2), 105−114.
(40) Lee, C. M.; Lo, H. W.; Shao, R. P.; Wang, S. C.; Xia, W.; Gershenson, D. M.; Hung, M. C. Selective activation of ceruloplasmin promoter in ovarian tumors: potential use for gene therapy. *Cancer Res.* **2004**, *64* (5), 1788−1793.
(41) Chen, Y.; Lim, B. K.; Peh, S. C.; Abdul-Rahman, P. S.; Hashim, O. H. Profiling of serum and tissue high abundance acute-phase proteins of patients with epithelial and germ line ovarian carcinoma. *Proteome Sci.* **2008**, *6*, 20.
(42) Kobayashi, H.; Kajiwara, H.; Kanayama, S.; Yamada, Y.; Furukawa, N.; Noguchi, T.; Haruta, S.; Yoshida, S.; Sakata, M.; Sado, T.; Oi, H. Molecular pathogenesis of endometriosis-associated clear cell carcinoma of the ovary (review). *Oncol. Rep.* **2009**, *22* (2), 233−240.
(43) Kurman, R. J.; Shih, I.-M. Molecular pathogenesis and extraovarian origin of epithelial ovarian cancer–shifting the paradigm. *Human Pathol.* **2011**, *42* (7), 918−931.

Gynecologic Oncology 126 (2012) 211–216

Contents lists available at SciVerse ScienceDirect

Gynecologic Oncology

journal homepage: www.elsevier.com/locate/ygyno

Phase II study of concurrent chemoradiotherapy with high-dose-rate intracavitary brachytherapy in patients with locally advanced uterine cervical cancer: Efficacy and toxicity of a low cumulative radiation dose schedule ☆

Takafumi Toita [a,*], Ryo Kitagawa [b], Tetsutaro Hamano [c], Kenji Umayahara [d], Yasuyuki Hirashima [e], Yoichi Aoki [f], Masahiko Oguchi [g], Mikio Mikami [h], Ken Takizawa [d] and Cervical Cancer (Vulva Cancer) Committee of the Japanese Gynecologic Oncology Group (JGOG)

[a] Department of Radiology, Graduate School of Medical Science, University of the Ryukyus, Okinawa, Japan
[b] Department of Obstetrics and Gynecology, NTT Medical Center Tokyo, Tokyo, Japan
[c] Division of Biostatistics, School of Pharmaceutical Sciences, Kitasato University, Tokyo, Japan
[d] Department of Gynecology, Cancer Institute Hospital, Tokyo, Japan
[e] Department of Gynecology, Shizuoka Cancer Center Hospital, Shizuoka, Japan
[f] Department of Obstetrics and Gynecology, Graduate School of Medical Science, University of the Ryukyus, Okinawa, Japan
[g] Department of Radiation Oncology, Cancer Institute Hospital, Tokyo, Japan
[h] Department of Obstetrics and Gynecology, Tokai University School of Medicine, Kanagawa, Japan

ARTICLE INFO

Article history:
Received 5 March 2012
Accepted 24 April 2012
Available online 30 April 2012

Keywords:
Cervix cancer
Chemotherapy
Radiotherapy

ABSTRACT

Objective. A multicenter phase II trial was conducted to assess the efficacy and toxicity of concurrent chemoradiotherapy (CCRT) with high-dose-rate intracavitary brachytherapy (HDR-ICBT) using a low cumulative prescribed dose schedule in patients with locally advanced uterine cervical cancer.

Methods. The Japanese Gynecologic Oncology Group (JGOG) study JGOG1066 enrolled patients with FIGO stages III–IVA uterine cervical cancer who had no para-aortic lymphadenopathy (>10 mm) assessed by CT. Patients received definitive radiotherapy (RT) consisting of external beam whole pelvic RT and HDR-ICBT. The cumulative linear quadratic equivalent dose (EQD2) was 62–65 Gy prescribed at point A. Cisplatin 40 mg/m^2 weekly was administered concurrently with RT for 5 courses.

Results. Of the 72 patients registered, 71 were eligible. With a median follow-up of 28 months, the 2-year progression-free survival rate and pelvic disease progression-free rate were 66% (95% CI, 54% to 76%) and 73% (95% CI, 61% to 82%), respectively. Progression-free survival decreased significantly with increased central tumor size (P = 0.036). The 2-year cumulative late complication rates were 24% for all grades, 9% for grade 1, 12% for grade 2, 3% for grade 3, and 0 for grades 4/5.

Conclusions. The JGOG1066 demonstrated that CCRT using HDR-ICBT with a low cumulative RT dose schedule achieved comparable outcome as those achieved with global dose schedules (EQD2 = 85 Gy) with a lower incidence of late toxicity for locally advanced uterine cervical cancer in a Japanese population.

Introduction

Concurrent chemoradiotherapy (CCRT) has been shown to be superior to definitive radiotherapy (RT) alone in several randomized controlled trials (RCTs), and is now the standard of care for locoregionally advanced uterine cervical cancer [1]. Standard definitive RT consists of whole pelvic external beam RT (EBRT) and either high or low dose rate intracavitary brachytherapy (ICBT). The previously mentioned RCTs utilized only low dose-rate ICBT (LDR-ICBT) [1]. High dose-rate ICBT (HDR-ICBT) has become widely used in Japan [2], and many centers worldwide are also shifting to HDR-ICBT [3].

Several RCTs have demonstrated clinical equivalence in terms of both local control and toxicity between HDR-ICBT and LDR-ICBT in the setting of definitive RT (without chemotherapy) [4]. In CCRT, many investigators also reported favorable treatment results using HDR-ICBT in single institutional retrospective series [5–13]. The Gynecologic Oncology Group (GOG) and the Radiation Therapy Oncology Group (RTOG) now allow the use of HDR-ICBT as well as LDR-ICBT in recent clinical trials of CCRT for cervical cancer [14–18]. In these

☆ Presented in part at the 2012 Annual Meeting on Women's Cancer, Austin, Texas, March 24–27, 2012, and World Congress of Brachytherapy, Barcelona, Spain, 10–12 May, 2012.

* Corresponding author at: Department of Radiology, Graduate School of Medical Science, University of the Ryukyus, 207 Uehara, Nishihara-cho, Okinawa, 903-0215, Japan. Fax: +81 98 895 1420.
E-mail address: b983255@med.u-ryukyu.ac.jp (T. Toita).

0090-8258/$ – see front matter © 2012 Elsevier Inc. All rights reserved.
doi:10.1016/j.ygyno.2012.04.036

trials, however, the patients treated with HDR-ICBT were not evaluated separately. It is unclear whether concurrent chemotherapy delivery with RT increases late complications [19]. In view of potential narrow therapeutic window of HDR-ICBT, the optimum RT dose should be carefully determined especially in the CCRT setting. Late RT complications, even when mild to moderate (i.e., Grades 1–2), significantly reduce quality of life [20]. Recently, image-guided brachytherapy (IGBT) using CT/MRI has been investigated in order to decrease late toxicity as well as improve local control [21].

Japanese centers use lower cumulative dose schedules than those of the US and Europe [2,3]. Favorable local control results have been obtained with these lower dose schedules in retrospective series of RT alone [22,23]. However, these lower dose schedules have not been accepted in the US and Europe given the lack of prospective data. In this situation, prospective clinical trials on the efficacy and safety of the CCRT using HDR-ICBT with the low cumulative dose schedules are encouraged.

Based on this background, we conducted a phase II multi-institutional clinical trial on CCRT for locally advanced cervical cancer patients. Herein, we report the data of outcomes and late toxicity observed in the trial.

Materials and methods

Study design

The JGOG1066 trial was a multicenter phase II prospective study aimed at evaluating the efficacy and late toxicity of CCRT using HDR-ICBT for locally advanced uterine cervical cancer patients. This study was designed by the JGOG Cervical Cancer Committee in collaboration with the Japanese radiation oncologists with expertise in the cervical cancer treatment. The study was approved by the JGOG Clinical Trial Review Committee, and the local institutional review boards (IRB) of the participating institutions. This trial is registered in the University Hospital Medical Information Network Clinical Trials Registry (UMIN-CTR; number 000001042).

Patients

Patients with histologically proven squamous cell carcinoma, adenocarcinoma, or adenosquamous carcinoma of the uterine cervix with International Federation of Gynecology and Obstetrics (FIGO) stages IIIA, IIIB, or IVA disease with no para-aortic lymphadenopathy (<10 mm) assessed by computed tomography (CT), performed within 4 weeks prior to entry were eligible. Histopathological evaluation of the para-aortic nodes (e.g., retroperitoneal surgical exploration) was not required. Eligibility criteria also included patient age between 20 and 70 years and Eastern Cooperative Oncology Group (ECOG) performance status (PS)<2. Patients with prior therapy (radiotherapy, surgery or chemotherapy) for cervical cancer were ineligible. Patients were also required to have abdomen-pelvic CT, pelvic MRI (T2 weighted image), chest X-ray/CT, within 28 days before entry. All patients were required to give written informed consent prior to enrollment in this study.

Radiotherapy

Protocol radiotherapy (RT) consisted of a combination of whole pelvic (WP) EBRT and HDR-ICBT. Interstitial brachytherapy was not allowed.

WP-EBRT was delivered with a photon beam of 6 MV or greater. Both anteroposterior (AP)–posteroanterior (PA) and a four-field technique were permitted. Intensity modulated radiation therapy (IMRT) was not allowed. When the four-field technique was utilized, the portal arrangement was changed to the AP–PA technique after the midline block (MB) was inserted. A tissue heterogeneity correction was not applied in the dose calculation. WP-EBRT was delivered for 5 days during a week to achieve a total dose of 50 Gy/25 fractions or 50.4 Gy/28 fractions. The WP-EBRT was initially delivered without a MB. Subsequently, the next phase of WP-EBRT was administered through the same WP field with a MB width of 3 or 4 cm. The MB was formed with multileaf collimators (MLC) or a custom cerrobend block. Four radiotherapy schedules were provided for the protocol (Table 1). Because these schedules are biologically nearly equivalent, the choice of schedule was left to the treating radiation oncologist. The upper boarder of the pelvic field was L4–5, and the lower border was a transverse line below the obturator foramen or pubic symphysis or 2 cm inferior from caudal end of the tumor. The lateral borders of the AP/PA portals were 1.5 to 2 cm beyond the lateral margin of the bony pelvis. For the lateral field, the anterior border was placed at a horizontal line drawn 0.5 cm anterior to the symphysis pubis anteriorly and the posterior border was placed at least 1.5 cm posterior from the surface of the sacrum. Boost EBRT of 6–10 Gy/3–5 fractions was indicated for patients with nodular parametrial involvement to the pelvic walls and/or nodal metastases (≥10 mm in shortest diameter).

The first HDR-ICBT was performed within 7 days after the MB insertion. HDR-ICBT was performed once a week with a fraction dose of 6 Gy prescribed at point A using Ir-192 afterloading machines. HDR-ICBT was not allowed on the same day as the EBRT. The total HDR-ICBT dose was determined by the timing of the MB insertion (Table 1). The cumulative linear quadratic equivalent doses (EQD2) [24] at point A, which were the summation of the EBRT doses without the MB and HDR-ICBT doses, ranged from 62 to 65 Gy. For patients who had an inadequate response to EBRT or failed tandem insertion, additional WP EBRT without the MB was allowed to a total dose of 50 or 50.4 Gy. The total HDR-ICBT dose was 11 Gy per 2 fractions (i.e., 6 Gy + 5 Gy or 5.5 Gy × 2) at point A for this situation. A tandem and ovoid combination was recommended except as restricted by the vaginal anatomy (e.g., narrow vagina) or significant (>1/2) vaginal disease. For these patients, a vaginal cylinder could be utilized. Source dwell patterns (i.e., times and positions) were determined according to the Manchester system [25]. A dose calculation was performed for each application, using two orthogonal radiographs. The isodose curves were plotted, and doses at the rectum and bladder were calculated according to the International Commission on Radiation Units and Measurements (ICRU) 38 criteria [26]. Three dimensional planning using CT and/or MRI was not applied.

For patients who could not receive HDR-ICBT appropriately even after the additional EBRT without MB to 50/50.4 Gy, a boost EBRT with reduced portals was given to a total dose ranging from 64.8 to 72 Gy. Treatment was to be completed within 56 days.

To maintain RT quality, the protocol included an integrated QA process. Credentialing of participating institutions and individual case reviews for all patients were performed. The details of the QA process and its results have been published elsewhere [27].

Table 1
Radiotherapy schedules.

External beam radiotherapy		HDR-ICBT	Total EQD2 at point A
WP	WP + MB		WP + HDR-ICBT
30 Gy/15 fs	20 Gy/10 fs	24 Gy/4 fs	62 Gy
30.6 Gy/17 fs	19.8 Gy/11 fs	24 Gy/4 fs	62 Gy
40 Gy/20 fs	10 Gy/5 fs	18 Gy/3 fs	64 Gy
41.4 Gy/23 fs	9 Gy/5 fs	18 Gy/3 fs	65 Gy

WP: whole pelvic radiotherapy, MB: midline block.
HDR-ICBT: high-dose-rate intracavitary brachytherapy.
EQD2: equivalent dose in 2 Gy per fraction.

Chemotherapy

Weekly cisplatin at a dose of 40 mg/m^2 (maximum dose of 70 mg/body) was administered for 5 courses during the radiotherapy period. The first course of cisplatin was administered on day 1 of radiotherapy. Cisplatin could be given on the same day of HDR-ICBT as well as EBRT.

Follow-up

Response was assessed by MRI T2 weighted images 3 months after the completion of treatment according to the RECIST criteria. Patients were followed every 3 months for the first 2 years. Follow-up included a pelvic examination with PAP smear and monitoring of tumor markers if initially elevated. CT scans of the abdomen and pelvis, and chest X-ray (or CT scan) were performed annually. Pelvic disease progression was defined as follows: pelvic recurrence after assessment of CR, pelvic disease progression with a >20% increase in the size of target lesions assessed by MRI T2WI, or initiation of salvage treatment (regardless of pathological findings) for pelvic disease.

Statistical design

This was a phase II trial with the primary endpoint of estimating 2-year cumulative progression-free survival rate (PFS). The secondary endpoints included the treatment completion rate (all, chemotherapy, and radiotherapy), adverse events (acute and late), compete response rate, 2-year cumulative overall survival rate (OS), 2-year cumulative pelvic disease progression-free rate (PDPF), and 2-year cumulative distant metastasis rate (DM). Details of feasibility and acute adverse events will be reported elsewhere (manuscript submitted for publication).

The sample size was initially calculated based on the following assumptions: an expected 2-year PFS rate of 60% versus the threshold value of 40% from the previous published data of RT alone series [28,29] and data of the US RCT's control arms [1]. CCRT would be considered superior to RT alone if the lower limit of the 95% confidence interval of the 2-year PFS rate exceeded the threshold value of 40%. To attain 90% power with a two-sided α error of 0.05, the minimum required sample size was estimated to be 68 patients. After the sample size was adjusted to allow for patient ineligibility or loss, the total sample size was 70 patients. We also performed a Monte-Carlo simulation to examine the effect of censoring on the power. We generated the exponential and Weibull random numbers to simulate censoring times, assumed the recruiting time and follow-up time of 2 years, and set the expected 2-year PFS rate to 60%. In various scenarios, we confirmed the lower limits of the 95% confidence intervals for 2-year PFS rates that exceeded the threshold value of 40% with the probability of more than 80%.

The cumulative outcomes and late complication curves were estimated by the Kaplan-Meier method. Differences in outcomes were compared using a log-rank test. PFS was measured from the time of registration until disease progression or death resulting from any cause. OS was measured from the time of registration until death resulting from any cause. Late adverse events were graded according to the National Cancer Institute Common Toxicity Criteria version 3.0. Complete response was assessed following the Response Evaluation Criteria in Solid Tumors. All analyses were performed with SAS software, version 9.2.

Results

Patient characteristics

Seventy-two patients were enrolled from 25 institutions between March 2008 and January 2009. One patient was ineligible because she had para-aortic lymphadenopathy of 10 mm in the shortest diameter assessed on pretreatment abdominal CT. She never received treatment on protocol and was not included into the following analyses. Therefore, 71 patients formed the patient cohort for this report. The clinical characteristics of the 71 patients are listed in Table 2.

Feasibility

Sixty-three of the 71 patients (89%) completed the protocol treatment as planned. Chemotherapy was administered for the planned 5 courses in 65 patients (92%). Planned radiotherapy was completed in 68 patients (96%). One patient could not receive HDR-ICBT due to uterine perforation that occurred after 4 Gy of EBRT was delivered and the first administration of cisplatin. Subsequently, she was discontinued from the protocol treatment and received EBRT irradiation as a salvage treatment. Individual case reviews on RT QA revealed favorable compliance with the RT protocol [27]. The median total EQD2 (WP-EBRT + HDR-ICBT) at point A was 62 Gy (range, 49–65 Gy). Prescribed point A doses per protocol were delivered in 63 patients (89%): WP-EBRT 30 Gy + HDR-ICBT 24 Gy in 10 patients, WP-EBRT 30.6 Gy + HDR-ICBT 24 Gy in 30 patients, WP-EBRT 40 Gy + HDR-ICBT 18 Gy in 15 patients, WP-EBRT 41.4 Gy + HDR-ICBT 18 Gy in 6 patients, and WP-EBRT 50 Gy + HDR-ICBT 11 Gy in 2 patients. Boost EBRT was delivered to the parametrium in 28 patients, enlarged nodes in 22 patients, and both in 11 patients.

The rectal and bladder dose calculation according to the ICRU 38 definition was performed for every fraction in 66 patients (93%). Median doses were 4.4 Gy (range, 2.6–9.4 Gy) for the bladder, and 4.3 Gy (range, 2.8–11.1 Gy) for the rectum. Median cumulative biologically effective doses (BEDs) (EBRT + HDR-ICBT) were 95 Gy_3 (range, 68–184 Gy_3) for the bladder, and 96 Gy_3 (range, 71–199 Gy_3) for the rectum. Nine out of 66 patients (14%) received over 120 Gy_3 for the rectum. The median overall treatment time was 50 days (range, 37 to 66 days) for 68 patients who completed the planned radiotherapy.

Table 2
Patient characteristics.

Clinical variable	n	%
Median age (range)	57 years (32–70 years)	
PS		
0	63	89
1	8	11
FIGO stage		
IIIA	3	4
IIIB	64	90
IVA	4	6
Histological diagnosis		
Squamous cell carcinoma	66	93
Adenosquamous carcinoma	2	3
Adenocarcinoma	3	4
Parametrial involvement (fixed to pelvic wall)		
No	4	6
Yes	67	94
Unilateral	47	66
Bilateral	20	28
Maximum tumor diameter (mm)[a]		
<40	16	22.5
40≤, <50	10	14
50≤, <60	16	22.5
60≤, <70	16	22.5
70≤, <80	6	8.5
80≤	7	10
Pelvic node enlargement[b]		
Yes	41	58
No	30	42

[a] Assessed by MRI T2WI.
[b] ≥10 mm in shortest diameter assessed by CT/MRI.

Efficacy and late toxicity

The median follow-up for the 71 patients was 28 months (range, 12 to 35 months). Fifty-six patients (79%) achieved a complete response and 25 patients had disease progression. Twenty-one patients had a pelvic recurrence: primary lesion in 14; pelvic node in 6; and pelvic peritoneum in 1. Seventeen patients developed distant metastases: para-aortic node in 11; lung in 4; bone in 2; liver in 1; and supraclavicular node in 1. The 2-year PFS rate was 66% (95% CI, 54% to 76%; Fig. 1). The 2-year OS, PDPF, and DM were 90% (95% CI, 80% to 95%), 73% (95% CI, 61% to 82%), and 25% (95% CI, 16% to 37%), respectively.

There were decreases in both PFS (P = 0.036) and PDPF (P = 0.24) with increased tumor diameter as assessed by MRI. The 2-year PFS and PDPF were, respectively, 77% and 85% for tumors <50 mm, 69% and 72% for tumors 50–70 mm, and 39% and 54% for tumors ≥70 mm. The 2-year DM was higher for patients with large diameter tumors (47% for ≥70 mm) compared with those with smaller diameter tumors (19% for <50 mm, 20% for 50–70 mm) (P = 0.067). Patients with enlarged pelvic nodes (≥10 mm in the shortest diameter assessed by CT/MRI) had poorer PFS and PDPF, and higher DM than those with no enlarged nodes. The 2-year PFS, PDPF and DM were, respectively, 60%, 67% and 31% for the node positive patients and 71%, 78% and 20% for the node negative patients. There were no significant differences between these two groups for these endpoints.

Table 3 lists late adverse events. Only 3 patients (4%) suffered severe (≥grade 3) late toxicity. The 2-year cumulative late complication rates by grades were 24% for all grades, 9% for grade 1, 12% for grade 2, 3% for grade 3, and 0 for grades 4/5.

Table 3
Reported late adverse events (n = 71).

Events	Grade (n)				3≤(%, 95% CI)
	1	2	3	4	
Gastrointestinal					
Colitis	2	5	0	0	0
Enteritis	1	1	0	0	0
Proctitis	3	2	0	0	0
Nausea	1	0	0	0	0
Vomiting	1	0	0	0	0
Other (hemorrhage, upper GI)	1	0	0	0	0
Renal/genitourinary					
Cystitis	2	5	1	0	1 (0–8)
Incontinence	0	1	0	0	0
Obstruction (ureter)	0	0	1	0	1 (0–8)
Urinary retention	0	1	0	0	0
Other					
Edema: limb	3	0	0	0	0
Creatinine	0	0	1	0	1 (0–8)
Pain (pelvis)	0	1	0	0	0

Discussion

This prospective multi-institutional phase II study (JGOG1066) demonstrated that CCRT using HDR-ICBT with a low cumulative dose schedule (EQD2 = 62–65 Gy prescribed at point A) achieved a 2-year PFS rate of 66% with a low incidence (4%) of severe late toxicity in stage III and IVA uterine cervical cancer patients. The lower limit of the 95% CI for PFS was 54%, which was higher than the threshold of 40%, confirming the superiority of CCRT over historical outcomes of RT alone, although the eligibility criteria regarding para-aortic node evaluation were different from the prior RCTs [1].

Although the cumulative doses prescribed at point A adopted in this study were remarkably lower than those used in global schedules, the pelvic control rate appeared to be comparable to previously reported data (Table 4). However, there remains room for improvement in local control, particularly for patients with large tumors (≥70 mm in the largest diameter) who frequently developed pelvic recurrences in this study. The data from previously published papers suggested that higher prescribed doses had no apparent impact for improving local control, but probably did increase the risk of severe late complications (Table 4).

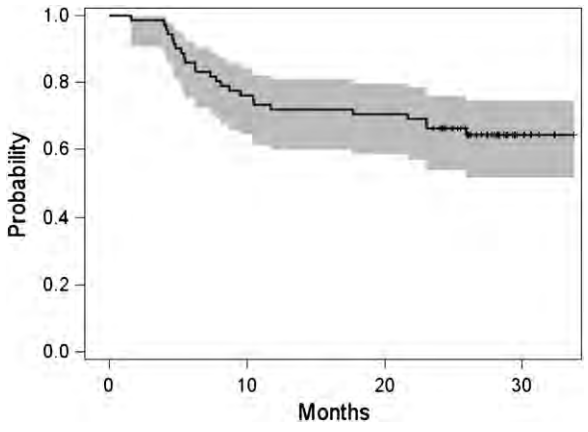

Fig. 1. Progression-free survival (PFS) of 71 eligible patients enrolled in JGOG1066.

In this study, 14% of the patients received over 120 Gy_3 at the ICRU38 rectal point, which is considered to be the threshold for developing severe proctitis [1]. We must bear in mind that these data, including those from our study, were for patients who were treated with ICBT that was planned only by a classical 2-dimensional (2-D) method, which prescribes doses at a single point A. Recently, 3-dimensional (3-D) image-guided brachytherapy (IGBT) using CT/MRI has become popular in clinical practice [30]. With IGBT, the actual tumor volume can be sufficiently covered with adequate prescribed doses while limiting the doses to surrounding organs at risk (OAR).

Dimopoulos et al. analyzed the dose–effect relationship between tumor diameter (at diagnosis and at time of HDR-ICBT) and local control for cases that were treated with IGBT [31]. They found a significant dose–effect relationship for local control within a dose range of 68 to 91 Gy using D90 HR-CTV for patients with large pretreatment tumor diameters and those with poor responses to EBRT [31]. A simple dose escalation for a single point A is an inappropriate approach to provide additional improvements in the therapeutic ratio. It is essential to investigate the therapeutic value of dose escalation using IGBT with careful monitoring of the doses to OAR, particularly for patients with large central tumors or, perhaps, those who responded poorly to prior EBRT.

In contrast, in this study, local control for patients with non-bulky tumors (<50 mm) was favorable (85%). Dimopoulos et al. showed excellent local control (97%) with no dose–effect relationship in patients with small tumors (2–5 cm) and those who had good responses to EBRT. Based on these results, they suggested that dose de-escalation with IGBT for these patient subsets might be appropriate [31]. Narayan et al. reported their experience with IGBT for cervical cancer [32]. Their goal with IGBT was to treat residual disease in the cervix and uterus after EBRT to a total dose of 80 Gy_{10}. They showed excellent local control with an average target dose of 79.2 Gy_{10} (resulting in 72 Gy_{10} at point A) for patients who had good responses to EBRT before ICBT and proper application of tandem applicator (i.e., inserted through the center of a cervical tumor) [32]. Unfortunately, for our study, we could not analyze local control based on both the response to EBRT and applicator laterality within a tumor, as we did not have a planned response evaluation or 3-D planning. A prospective study with IGBT to investigate local control with the prescribed doses used in this study is encouraged to determine whether dose de-escalation from global schedules is feasible for patients with

Table 4
Treatment results of cisplatin-based CCRT using HDR-ICBT for locally advanced cervical cancer.

Authors	n	Stage	III, IVA/all	EBRT (Gy) at point A	HDR-ICBT (Gy/fr) at point A	Total EQD2 (Gy) at point A	Median OTT	Median F/U	PC[a]	PFS[a]	Late toxicity[a] G3 <=	Subject for PC, and comments
Retrospective study												
Toita et al. [5]	40	IIB–IIIB	65%	40	18/3	64	48d	37 m	91% (3y)	67% (3y)	3%[b]	All stages
Novetsky et al. [6]	77	IB2–IV	40%	45	18/2	73	–	3.5y	68% (5y)	61% (5y)	6%[b]	Stages III and IVA
Ozsaran et al. [7]	81	IB–IVA	19%	50.4	18/3	73	–	42 m	78% (5y)	77% (5y)	0	>4 cm tumors
Parker et al. [8]	92	IB1–IVA	30%	45	24/4	77	61d	26 m	67% (5y)	–	4%[b]	All stages
Chen et al. [9]	70	IIB–IIIB	31%	45	24/4	77	–	43 m	87% (4y)	–	14%	All stages
Lim et al. [10]	69	IB1–IVA	26%	45	27.5/5, 30/5[c]	80, 84	8.4w	27 m	70% (2y)	59% (2y)	6%[b]	All stages
Anker et al. [11]	65	IB1–IVA	20%	45	30/5	84	–	25 m	97% (3y)	76% (3y)	17% (3y)	All stages, including RT alone cases (8%)
Forrest et al. [12]	122	IB–IV	25%	45	30/5	84	51d	18 m	86%[b]	70% (2y)	14% (2y)	All stages, including RT alone cases (16%)
Souhami et al. [13]	50	IIA–IVA	60%	46	30/3	96	–	27 m	68%[b]	–	26%[b]	Stage IIIB
Prospective study												
RTOG0128 [14]	77	IB1–IVA	21%	45	30/5	85	45d	24 m	74% (2y)	69% (4y)	16%[b]	All stages, HDR-ICBT was used in 35% of cases
Present study	71	III–IVA	100%	30–40	18/3, 24/4	62–65	50d	28 m	73% (2y)	66% (2y)	3% (2y)	Stages III and IVA

Abbreviations: CCRT = concurrent chemoradiotherapy; EBRT = external beam radiotherapy; HDR-ICBT = high dose-rate intracavitary brachytherapy; EQD2 = linear quadratic equivalent dose; PC = pelvic control rate; PFS = progression-free survival; d = days; w = weeks; m = months; y = year; NS = not stated; RT = radiotherapy.
[a] Actuarial rate.
[b] Crude rate.
[c] Point H.

non-bulky tumors or those with tumors that show good response. We believe that dose de-escalation has the potential to decrease the incidence of lower grade complications as well as high grade complications, which would contribute to improving patients' quality of life [20].

Distant failures, including para-aortic node metastases were frequently observed in this study. The incidence of distant failure increased with increased tumor size as well. In this study, histopathological examinations and PET/CT were not done to rule out para-aortic node metastases. This might have been one of the causes for frequent distant failures, including PAN recurrences. Reducing distant failures is another challenge that must be faced in order to improve the outcomes of patients with locoregionally advanced cervical cancer. A meta-analysis suggested that there might be therapeutic value with additional systemic chemotherapy after CCRT [19]. A phase I study to determine the optimum dose for adjuvant chemotherapy after definitive CCRT is now underway (JGOG1068).

One limitation of this study was that all of the patients were Japanese. Japanese women are generally smaller than Western women. This might have affected the toxicity incidences and grades. In addition, possible genetic differences between Japanese and Westerners cannot be completely ruled out. As mentioned previously, another limitation was that we did not use IGBT. For future multi-institutional prospective studies with IGBT, another quality assurance program on RT will be necessary [27].

In conclusion, despite the limited follow-up periods, the results of this study demonstrated that CCRT using HDR-ICBT with low cumulative RT dose schedules achieved comparable outcomes to those attained with global dose schedules with a lower incidence of late toxicity for locally advanced uterine cervical cancer patients in a Japanese population. If the presented RT dose schedules presented here are integrated into the current global standards, it would encourage the participation of Japanese patients in ongoing global studies. To further improve these outcomes, investigations on appropriate RT dose with IGBT and additional systemic treatment are warranted.

Conflict of interest statement
No conflict of interest.

Acknowledgments

This study was supported in part by grants from the Ministry of Health, Labor and Welfare (Grants-in-Aid for Cancer Research nos. 16-12, 20S-5 and 23-A-21), and a Grant-in-Aid for Scientific Research from the Japan Society for the Promotion of Science (Nos. 18591387 and 21591614). We thank all staff of the Kitasato University Research Center for Clinical Pharmacology, especially Ms. Miki Fukutani, for their assistance in data management.

The following Japanese Gynecologic Oncology Group institutions participated in the study: Cancer Institute Hospital, Shizuoka Cancer Center Hospital, Ryukyu University Hospital, Mie University Hospital, Shikoku Cancer Center, Kitasato University Hospital, Yamaguchi University Hospital, Yokohama City University Hospital, Gifu University Hospital, Gunma University Hospital, Hyogo Cancer Center, Chiba University Hospital, Kyushu University Hospital, Keio University Hospital, Iwate Medical University Hospital, Osaka Medical Center for Cancer and Cardiovascular Disease, Kyoto University Hospital, St. Marianna University School of Medicine Hospital, Fukuoka University Hospital, Hyogo College of Medicine Hospital, Nara Medical University Hospital, National Institute of Radiological Sciences, Niigata Cancer Center Hospital, Hiroshima University Hospital, and Kumamoto University Hospital.

References

[1] Monk BJ, Tewari KS, Koh WJ. Multimodality therapy for locally advanced cervical carcinoma: state of the art and future directions. J Clin Oncol 2007;25:2952–65.
[2] Toita T, Kodaira T, Shinoda A, et al. Patterns of radiotherapy practice for patients with cervical cancer (1999–2001): patterns of care study in Japan. Int J Radiat Oncol Biol Phys 2008;70:788–94.
[3] Viswanathan AN, Creutzberg CL, Craighead P, et al. International brachytherapy practice patterns: a survey of the Gynecologic Cancer Intergroup (GCIG). Int J Radiat Oncol Biol Phys 2012;82:250–5.
[4] Stewart AJ, Viswanathan AN. Current controversies in high-dose-rate versus low-dose-rate brachytherapy for cervical cancer. Cancer 2006;107:908–15.
[5] Toita T, Moromizato H, Ogawa K, et al. Concurrent chemoradiotherapy using high-dose-rate intracavitary brachytherapy for uterine cervical cancer. Gynecol Oncol 2005;96:665–70.
[6] Novetsky AP, Einstein MH, Goldberg GL, et al. Efficacy and toxicity of concomitant cisplatin with external beam pelvic radiotherapy and two high-dose-rate brachytherapy insertions for the treatment of locally advanced cervical cancer. Gynecol Oncol 2007;105:635–40.
[7] Ozsaran Z, Kamer S, Yalman D, et al. Treatment results and prognostic factors for cervical cancer patients treated by radiochemotherapy with weekly cisplatin. Eur J Gynaecol Oncol 2007;28:196–200.

[8] Parker K, Gallop-Evans E, Hanna L, et al. Five years' experience treating locally advanced cervical cancer with concurrent chemoradiotherapy and high-dose-rate brachytherapy: results from a single institution. Int J Radiat Oncol Biol Phys 2009;74:140–6.
[9] Chen SW, Liang JA, Hung YC, et al. Concurrent weekly cisplatin plus external beam radiotherapy and high-dose rate brachytherapy for advanced cervical cancer: a control cohort comparison with radiation alone on treatment outcome and complications. Int J Radiat Oncol Biol Phys 2006;66:1370–7.
[10] Lim A, Sia S. Outcomes of chemoradiotherapy in cervical cancer—the Western Australian experience. Int J Radiat Oncol Biol Phys 2012;82:1431–8.
[11] Anker CJ, Cachoeira CV, Boucher KM, et al. Does the entire uterus need to be treated in cancer of the cervix? Role of adaptive brachytherapy. Int J Radiat Oncol Biol Phys 2010;76:704–12.
[12] Forrest JL, Ackerman I, Barbera L, et al. Patient outcome study of concurrent chemoradiation, external beam radiotherapy, and high-dose rate brachytherapy in locally advanced carcinoma of the cervix. Int J Gynecol Cancer 2010;20:1074–8.
[13] Souhami L, Seymour R, Roman TN, et al. Weekly cisplatin plus external beam radiotherapy and high dose rate brachytherapy in patients with locally advanced carcinoma of the cervix. Int J Radiat Oncol Biol Phys 1993;27:871–8.
[14] Lanciano R, Calkins A, Bundy BN, et al. Randomized comparison of weekly cisplatin or protracted venous infusion of fluorouracil in combination with pelvic radiation in advanced cervix cancer: a gynecologic oncology group study. J Clin Oncol 2005;23:8289–95.
[15] Thomas G, Ali S, Hoebers FJ, et al. Phase III trial to evaluate the efficacy of maintaining hemoglobin levels above 12.0 g/dL with erythropoietin vs above 10.0 g/dL without erythropoietin in anemic patients receiving concurrent radiation and cisplatin for cervical cancer. Gynecol Oncol 2008;108:317–25.
[16] DiSilvestro PA, Walker JL, Morrison A, et al. Gynecologic Oncology Group. Radiation therapy with concomitant paclitaxel and cisplatin chemotherapy in cervical carcinoma limited to the pelvis: a phase I/II study of the Gynecologic Oncology Group. Gynecol Oncol 2006;103:1038–42.
[17] Walker JL, Morrison A, DiSilvestro P, et al. Gynecologic Oncology Group. A phase I/II study of extended field radiation therapy with concomitant paclitaxel and cisplatin chemotherapy in patients with cervical carcinoma metastatic to the para-aortic lymph nodes: a Gynecologic Oncology Group study. Gynecol Oncol 2009;112:78–84.
[18] Gaffney DK, Winter K, Dicker AP, et al. A phase II study of acute toxicity for Celebrex (celecoxib) and chemoradiation in patients with locally advanced cervical cancer: primary endpoint analysis of RTOG 0128. Int J Radiat Oncol Biol Phys 2007;67:104–9.
[19] Chemoradiotherapy for Cervical Cancer Meta-Analysis Collaboration. Reducing uncertainties about the effects of chemoradiotherapy for cervical cancer: a systematic review and meta-analysis of individual patient data from 18 randomized trials. J Clin Oncol 2008;26:5802–12.
[20] Vale C, Nightingale A, Spera N, et al. Late complications from chemoradiotherapy for cervical cancer: reflections from cervical cancer survivors 10 years after the national cancer institute alert. Clin Oncol (R Coll Radiol) 2010;22:588–9.
[21] Viswanathan AN, Dimopoulos J, Kirisits C, Berger D, Pötter R. Computed tomography versus magnetic resonance imaging-based contouring in cervical cancer brachytherapy: results of a prospective trial and preliminary guidelines for standardized contours. Int J Radiat Oncol Biol Phys 2007;68:491–8.
[22] Toita T, Kakinohana Y, Ogawa K, et al. Combination external beam radiotherapy and high-dose-rate intracavitary brachytherapy for uterine cervical cancer: analysis of dose and fractionation schedule. Int J Radiat Oncol Biol Phys 2003;56:1344–53.
[23] Nakano T, Kato S, Ohno T, et al. Long-term results of high-dose rate intracavitary brachytherapy for squamous cell carcinoma of the uterine cervix. Cancer 2005;103:92–101.
[24] Pötter R, Haie-Meder C, Van Limbergen E, et al. Recommendations from gynaecological (GYN) GEC ESTRO working group (II): concepts and terms in 3D image-based treatment planning in cervix cancer brachytherapy-3D dose volume parameters and aspects of 3D image-based anatomy, radiation physics, radiobiology. Radiother Oncol 2006;78:67–77.
[25] Tod M, Meredith W. A dosage system for use in the treatment of cancer of the uterine cervix. Br J Radiol 1938;11:809–24.
[26] International Commission on Radiation Units and Measurements. Dose and volume specification for reporting intracavitary therapy in gynecology. ICRU report 38. Washington: ICRU; 1985. p. 11–2.
[27] Toita T, Kato S, Ishikura S, et al. Radiotherapy quality assurance of the Japanese Gynecologic Oncology Group study (JGOG1066): a cooperative phase II study of concurrent chemoradiotherapy for uterine cervical cancer. Int J Clin Oncol 2011;16:379–86.
[28] Coia L, Won M, Lanciano R, et al. The Patterns of Care Outcome Study for cancer of the uterine cervix. Results of the Second National Practice Survey. Cancer 1990;66:2451–6.
[29] The 38th annual report of gynecologic tumors committee. Acta Obstet Gynaecol Jpn 2004;56:751–65.
[30] Viswanathan AN, Erickson BA. Three-dimensional imaging in gynecologic brachytherapy: a survey of the American Brachytherapy Society. Int J Radiat Oncol Biol Phys 2010;76:104–9.
[31] Dimopoulos JC, Pötter R, Lang S, et al. Dose–effect relationship for local control of cervical cancer by magnetic resonance image-guided brachytherapy. Radiother Oncol 2009;93:311–5.
[32] Narayan K, van Dyk S, Bernshaw D, et al. Comparative study of LDR (Manchester system) and HDR image-guided conformal brachytherapy of cervical cancer: patterns of failure, late complications, and survival. Int J Radiat Oncol Biol Phys 2009;74:1529–35.

JSHC
Japan Society of Histochemistry and Cytochemistry
Established 1959

Acta Histochem. Cytochem. 45 (2): 147–154, 2012
doi:10.1267/ahc.11063

Long Term Prognostic Implications of Expression of Glucose Transporter-1 and Hexokinase II in Patients with Stage I Uterine Leiomyosarcoma

Hitomi Tsukada[1], Toshinari Muramatsu[1], Masaki Miyazawa[1], Tetsuji Iida[1], Masae Ikeda[1], Masako Shida[1], Takeshi Hirasawa[1], Hiroshi Kajiwara[2], Masaru Murakami[3], Masanori Yasuda[4] and Mikio Mikami[1]

[1]Department of Obstetrics and Gynecology, Tokai University School of Medicine, [2]Department of Pathology, Tokai University School of Medicine, Shimokasuya 143, Isehara, Kanagawa 259–1193, Japan, [3]Department of Obstetrics and Gynecology, Tokai University Oiso Hospital, Kanagawa 259–0198, Japan and [4]Department of Pathology, Saitama Medical University International Medical Center, Saitama 350–1298, Japan

Received December 21, 2011; accepted February 21, 2012; published online April 21, 2012

Many malignant epithelial tumors show increased expression of glucose transporter-1 (GLUT-1) and hexokinase II (HK-II), both of which are involved in glucose metabolism. GLUT-1 levels are often correlated with prognosis in these tumors. The current retrospective study was conducted to evaluate the importance of GLUT-1 and HK-II expression in leiomyosarcoma (LMS), a malignant uterine non-epithelial tumor with a poor prognosis. The subjects were 23 patients with stage I LMS. Expression of GLUT-1 and HK-II was evaluated immunohistochemically in samples removed surgically, and the MIB-1 index was evaluated as a measure of cell proliferation. The association of these results with prognosis was examined. Twenty samples of leiomyoma (LOM), a benign non-epithelial tumor, were used as controls. Immunohistochemical expression was defined as negative staining (–), weak to sporadic staining (1+), and strong staining (2+) per microscopic field, respectively. Malignancy was evaluated in 2000 cells and the MIB-1 index was calculated. Overall survival for LMS was estimated using the Kaplan-Meier method. Of the LMS cases, 12 were GLUT-1-positive (52.2%; 2+: 2, 1+: 10) and 15 were HK-II-positive (65.2%; 2+: 1, 1+: 14). GLUT-1 expression in LMS was significantly correlated with the MIB1 index. The 10-year survival rates were 90.9% and 58.3% in GLUT-1-negative and GLUT-1-positive cases, respectively, and 75.0% and 73.3% in HK-II-positive and HK-II-negative cases, respectively. GLUT-1 expression was significantly correlated with prognosis. Cases of stage I LMS showed a significant correlation between the expression level of GLUT-1 and the MIB-1 index, an indicator of malignancy. GLUT-1-negative cases had a better prognosis than GLUT-1-positive cases, suggesting that GLUT-1 expression is an effective prognostic marker.

Key words: uterine leiomyosarcoma, immunoexpression, glucose transporter-1, hexokinase II

I. Introduction

Leiomyosarcoma (LMS) is a malignant uterine non-epithelial tumor that accounts for 1% to 3% of all malignant tumors in women. LMS has a poor prognosis, since the primary tumor is likely to undergo recurrence and metastasis [7]. Tissue necrosis and higher mitotic rates are important indicators for malignancy and prognosis [18, 29, 40]. More than 80% of cases of stage III LMS show recurrence and metastasis and the 5-year survival rate in cases of stages II–IV is approximately 8%, indicating an extremely poor prognosis [9, 33]. Surgery is the first option for LMS treatment; however, even if LMS is in the early stage and

Correspondence to: Toshinari Muramatsu, M.D., Department of Obstetrics and Gynecology, Tokai University School of Medicine, Shimokasuya 143, Isehara, Kanagawa 259–1193, Japan.
E-mail: mura-to@is.icc.u-tokai.ac.jp

can be completely removed, distant metastasis to the lung often occurs and results in a poor long-term prognosis [22]. Radiotherapy and combination chemotherapy with doxorubicin have also been used for LMS, but treatment outcomes remain poor [22, 34].

Many malignant epithelial tumors show increased glucose uptake [42]. Expression of glucose transporter-1 (GLUT-1) is often increased in malignant hypoxic cells and hexokinase II (HK-II) expression also increases. This causes resistance to radiotherapy and chemotherapy and enhanced recurrence and metastasis, which underlie the close relationship of GLUT-1 expression with prognosis [2, 10, 15, 28, 37]. In a clinicopathologic study of epithelial ovarian cancer, we found increased GLUT-1 expression and strong expression of hypoxia inducible factor-1 (HIF-1α), with a clear increase in glucose uptake. Similarly, high expression levels of HIF-1α and GLUT-1 have been shown in clear cell carcinoma, which also has a poor prognosis and is common in Japanese patients [16, 43]. Thus, the current study was performed to examine expression of GLUT-1 and HK-II and the relationship of these data with the long term prognosis of LMS, which has not been examined in previous studies.

II. Materials and Methods

Patients and treatments

The subjects were 23 patients (mean age: 51.5 years old; range: 35–70 years old) with clinical stage I LMS who underwent hysterectomy between March 1987 and May 2005 in our hospital. Adjuvant chemotherapy were performed in 14 patients (61%) (CYVADIC, n=12, 86%; cyclophosphamide 500 mg/m^2 and doxorubicin 50 mg/m^2 on day 1, vincristine sulfate 1.5 mg/m^2 on days 1 and 5, and dacarbazine 250 mg/m^2 on days 1 through 5 for three to five monthly cycles); IAP, n=1, 7%; doxorubicin 50 mg/m^2 and cisplatin 50 mg/m^2 on day 1 and ifosfamide 1000 mg/m^2 on days 1 through 5 for three monthly cycles; and weekly TC, n=1, 7%; paclitaxel 60 mg/m^2 and carboplatin AUC 1.7 on day 1 for 16 weekly cycles). The benign controls were 20 specimens of uterine leiomyomas that were removed surgically in the same period. At least 2 sections were isolated from each tumor and a tumor with at least one stained section was judged to be positive. The study was approved by the institutional review board and informed consent was obtained from all patients.

Immunohistochemistry and histological examination

Formalin-fixed and paraffin-embedded tissue blocks were cut into 4-μm sections for immunohistochemistry and hematoxylin and eosin staining.

The presence of a malignant mesenchymal tumors was examined based on positive staining for SMA (Sigma 1A4, Sigma Chemical Co., St. Louis, MO), vimentin (clone V9, DakoCytomation, Glostrup, Denmark), desmin (clone D33, DakoCytomation, Glostrup, Denmark) and MIB-1 (Ki-67/clonal MIB1, DakoCytomation, Glostrup, Denmark), and negative staining for CD34 (QBEnd/10, Novocastra, Newcastle, UK) in an initial histological examination.

GLUT-1 expression was evaluated immunohistochemically using rabbit polyclonal anti-human GLUT-1 antibody (DAKO, Carpinteria, CA, USA) at a dilution of 1:50. HK-II expression was evaluated with a polyclonal rabbit anti-HK-II antibody (Chemicon International, Inc., Temecula, CA) diluted at 1:500. The sections were washed and then incubated with anti-rabbit IgG conjugated to horseradish peroxidase-labeled-dextran polymer (EnVision Kit, DAKO) for 60 min at room temperature. The extent of GLUT-1 and HK-II expression was assessed semi-quantitatively according to the following scoring scheme: negative staining (–), weak to sporadic staining (1+), and strong staining (2+). In judging the staining level, erythrocytes and pancreatic tissue were used as positive controls for GLUT-1 and HK-II, respectively.

The histological grade of LMS was evaluated by two expert pathologists by counting of 2000 cells, with >20 mitosis events in 10 microscopic fields judged to be positive. These data were used to calculate the MIB-1 index for cell proliferation.

Statistical analysis

The relationship between immunohistochemical scores and MIB-1 index was determined by linear regression for the GLUT-1 and HK-II data. Survival curves related to immunoreactivity were constructed using the Kaplan-Meier method and assessed by log-rank test. $P<0.05$ was considered to indicate significance in all analyses.

III. Results

Hematoxylin & eosin and immunohistochemical staining

Malignant mesenchymal tumors identified from positive staining for SMA, vimentin, desmin and MIB-1 and negative staining for CD34 were excluded from the study (Fig. 1).

GLUT-1 and HKII expression, and MIB-1 index

Of the 23 cases of stage I LMS, 12 (52.2%) were GLUT-1-positive, including 2 2+ and 10 1+ cases; and 15 (65.2%) were HK-II-positive, including 1 2+ and 14 1+ cases (Table 1, Figs. 2, 3). The MIB-1 index was ≥5% in 10 cases and <5% in 13 (Fig. 4). Of the 20 benign controls, 2 (10%) were GLUT-1-positive, 4 (20%) were HK-II-positive, and all showed 1+ staining. MIB-1 was negative in all control specimens (Table 2).

Relationships of GLUT-1 and HK-II expression with the MIB-1 index

GLUT-1 expression levels showed a significant correlation with the MIB-1 index ($R^2=0.403$, $p=0.0011$, Fig. 4). In contrast, there was no correlation between HK-II expression and the MIB-1 index ($p=0.703$, Fig. 5).

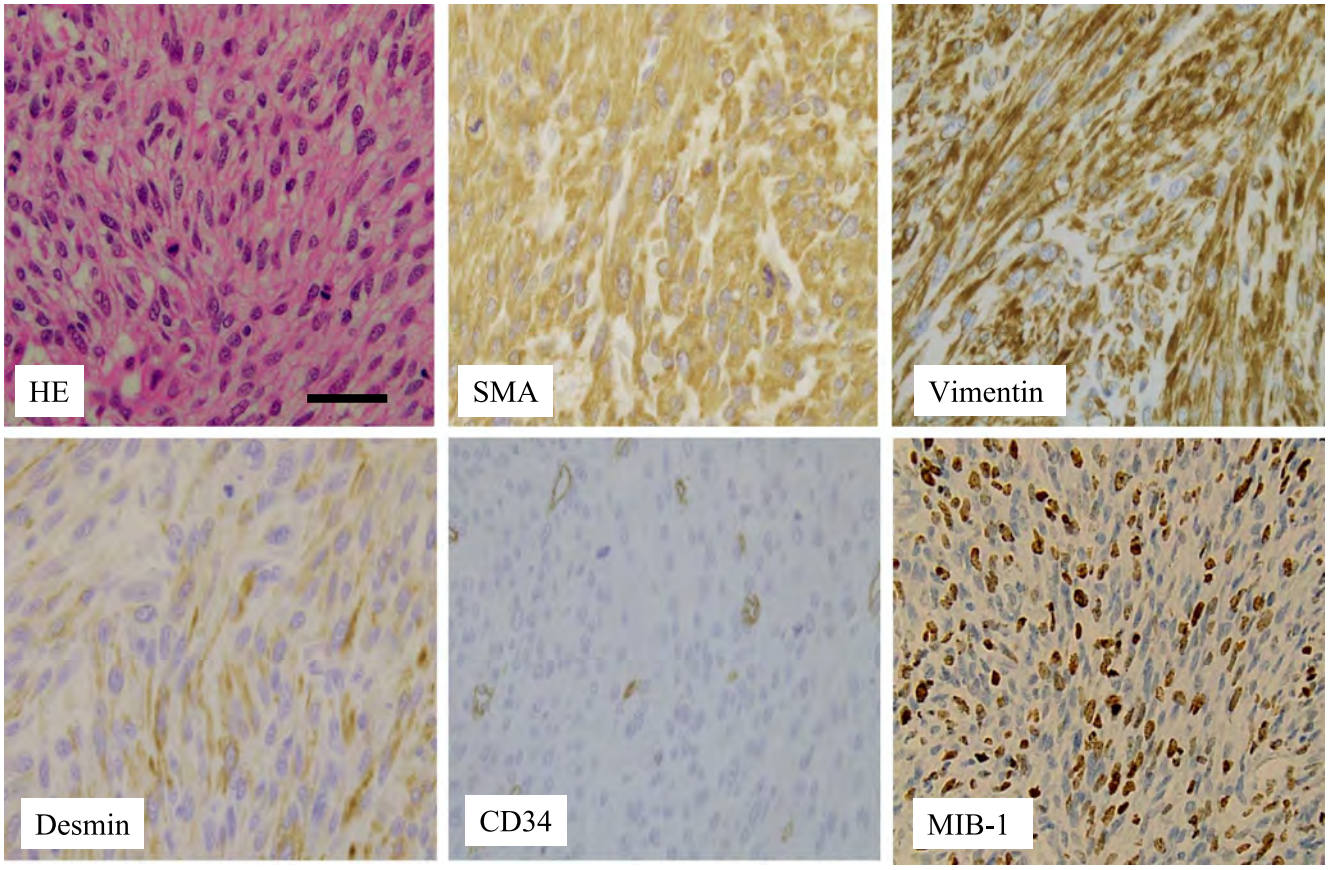

Fig. 1. Malignant mesenchymal tumors detected with hematoxylin-eosin (HE) staining, positive immunostaining for SMA, vimentin, desmin and MIB-1, and negative immunostaining for CD34. Bar=100 μm.

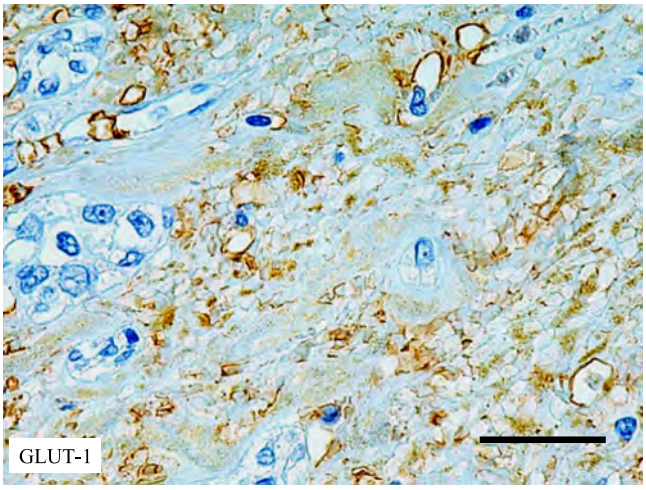

Fig. 2. Immunohistochemical staining showed strong GLUT-1 expression in sarcoma cell membranes. Bar=100 μm.

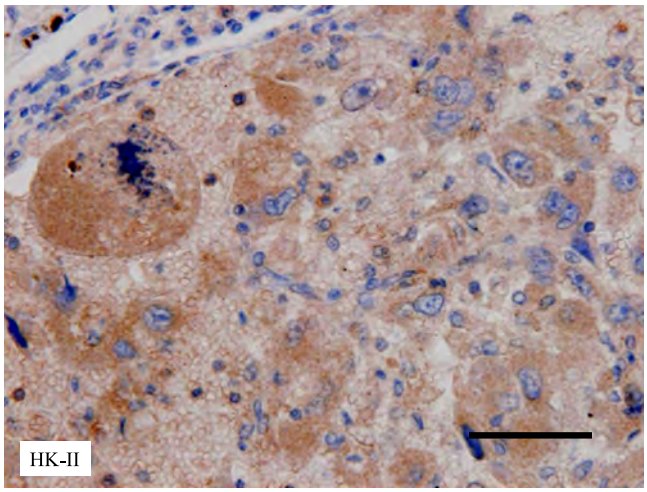

Fig. 3. Immunohistochemical staining was strongly positive for hexokinase (HK)-II in sarcoma cells. Bar=100 μm.

Survival curves based on GLUT-1 expression and HK-II expression

The Kaplan-Meier estimates of overall survival (OS) at 10 years for LMS were 90.9% in the GLUT-1-negative group and 58.3% in the GLUT-1-positive group, showing a significant difference in prognosis (Fig. 6). The Kaplan-Meier estimates of OS at 10 years were 75.0% and 73.3% in the HK-II-negative and HK-II-positive groups, with no significant difference between these groups (Fig. 7).

Table 1. *Characteristics of patients with stage I uterine leiomyosarcoma*

Case	Age	Operation	Chemotherapy	Expression		MIB-1 Index	Tumor size maximum (cm)
				GLUT-1	HK II		
1.	48	ATH+RSO	N	(–)	(–)	0.2	3
2.	36	Myomec → ATH+BSO	CYVADIC	(–)	(1+)	0.4	5
3.	38	Myomec → ATH+BSO+PLN	CYVADIC	(–)	(1+)	0.8	10
4.	59	ATH+BSO	CYVADIC	(–)	(1+)	1.1	5
5.	35	ATH+BSO	N	(–)	(1+)	0.1	5
6.	62	ATH+BSO	CYVADIC	(–)	(–)	2.7	6
7.	52	ATH+BSO	CYVADIC	(–)	(–)	3.3	10
8.	42	ATH	N	(–)	(1+)	2.8	6
9.	52	ATH+BSO	N	(–)	(–)	1.6	13
10.	61	ATH+BSO	N	(1+)	(1+)	0.3	8
11.	57	ATH+BSO+PLN	CYVADIC	(1+)	(–)	5.2	11
12.	64	ATH+BSO+PLN	N	(1+)	(–)	37.8	7
13.	58	ATH+BSO	CYVADIC	(2+)	(1+)	23.7	8
14.	70	ATH+BSO	N	(1+)	(1+)	1.9	8
15.	44	ATH+BSO	CYVADIC	(2+)	(1+)	20.0	6
16.	66	ATH+BSO	IAP	(1+)	(1+)	15.0	12
17.	48	ATH+BSO	CYVADIC	(1+)	(1+)	31.9	7
18.	56	ATH+BSO+PLN+OMT	Weekly TC	(1+)	(2+)	3.1	4
19.	45	ATH+BSO	N	(–)	(–)	0.4	5
20.	54	ATH+BSO	N	(–)	(1+)	6.3	8
21.	44	ATH+BSO+PLN	CYVADIC	(1+)	(1+)	30.3	11
22.	45	ATH+BSO	CYVADIC	(1+)	(–)	9.7	7
23.	53	ATH+BSO	CYVADIC	(1+)	(1+)	29.2	10

Myomec, myomectomy; ATH, abdominal total hysterectomy; BSO, bilateral salpingo-oophorectomy; RSO, right salpingo-oophorectomy; PLN, pelvic lymph adenectomy; OMT, omentectomy; N, no treatment; CYVADIC, cyclophosphamide, vincristine, doxorubicin and dacarbazine; TC, paclitaxel and carboplatin.

Table 2. *Characteristics of patients with uterine leiomyoma*

Case	Age	Expression		MIB-1 Index	Tumor size maximum (cm)
		GLUT-1	HK II		
1.	56	(–)	(1+)	0.0	8 (mu)
2.	39	(–)	(–)	0.0	8 (mu)
3.	49	(–)	(–)	0.0	6 (mu)
4.	38	(–)	(–)	0.0	14 (mu)
5.	46	(–)	(–)	0.0	3 (mu)
6.	47	(1+)	(1+)	0.0	14 (mu)
7.	73	(–)	(–)	0.0	4 (mu)
8.	36	(–)	(–)	0.0	25 (mu)
9.	69	(–)	(1+)	0.0	5
10.	66	(–)	(–)	0.0	4 (mu)
11.	27	(–)	(–)	0.0	10 (mu)
12.	61	(1+)	(–)	0.0	15 (mu)
13.	44	(–)	(1+)	0.0	3 (mu)
14.	48	(–)	(–)	0.0	6 (mu)
15.	52	(–)	(–)	0.0	6
16.	50	(–)	(–)	0.0	11 (mu)
17.	47	(–)	(–)	0.0	25 (mu)
18.	46	(–)	(–)	0.0	8 (mu)
19.	46	(–)	(–)	0.0	8 (mu)
20.	47	(–)	(–)	0.0	17

(mu): multiple myomas.

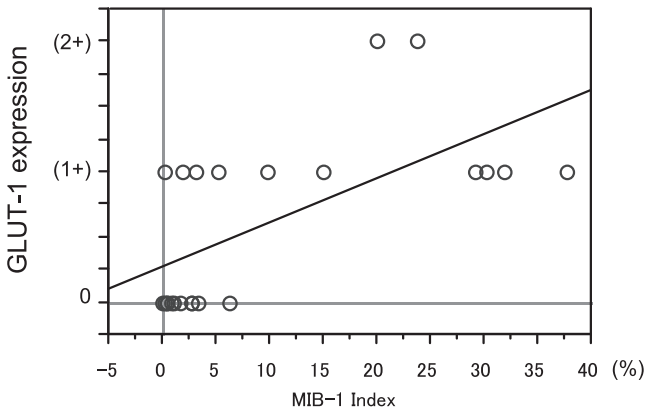

Fig. 4. Simple regression analysis of GLUT-1 expression and the MIB-1 index.

IV. Discussion

Uterine LMS is likely to show recurrence and metastasis, even in the early stage, and effective treatment has not been established. In 1985, Omura *et al.* evaluated 48 cases of stage I and II uterine LMS in a randomized comparative study, and found recurrence rates of 44% in

patients given adjuvant chemotherapy of 8 cycles of doxorubicin after resection and 61% in those who underwent observation only, with no significant difference between the groups [27]. A more recent randomized phase III trial of adjuvant pelvic radiotherapy versus observation for stage I and II uterine sarcomas (carcinosarcoma, leiomyosarcoma or endometrial stromal sarcoma) indicated that radiotherapy did not contribute to control of local metastasis or survival rate [32]. Hensley *et al.* conducted a prospective study in 23 cases (stage I: 15, II: 3, III: 1, and IV: 4) of high grade uterine LMS for a mean period of 49 months after complete resection, and found that progression free survival (PFS) at 2 years was 45% after treatment with gemcitabine 900 mg/m^2 (on days 1 and 8 i.v.) plus docetaxel 75 mg/m^2 (on day 8 i.v.) for 4 cycles at 3-week intervals. The PFS in stage I and II cases at 2–3 years was 59%, which suggested that adjuvant chemotherapy with gemcitabine plus docetaxel after complete resection may improve the prognosis of early stage LMS [13]. Several pilot studies of adjuvant therapies, including CYVADIC (cyclophosphamide, vincristine, doxorubicin, and dacarbazine) therapy, ifosfamide single therapy, and API (doxorubicin, cisplatin and ifosfamide) plus radiotherapy have been conducted for early stage LMS [21, 26, 30], with 3- and 5-year survival rates ranging from 67% to 89% (one study with CYVADIC therapy had a 15-year survival rate of 69%).

There is currently no established surgical procedure or anticancer treatment for uterine sarcoma. This may be because of the relatively small number of cases of uterine sarcoma and because the disease is often not diagnosed before surgery. Cases 1 and 2 were young patients who underwent myomectomy and were diagnosed with uterine sarcoma in a postoperative pathologic examination. Consequently, these patients underwent hysterectomy in an

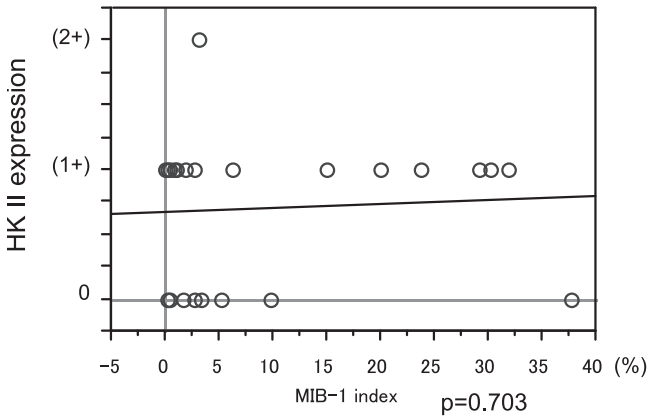

Fig. 5. Simple regression analysis of HK-II expression and the MIB-1 index.

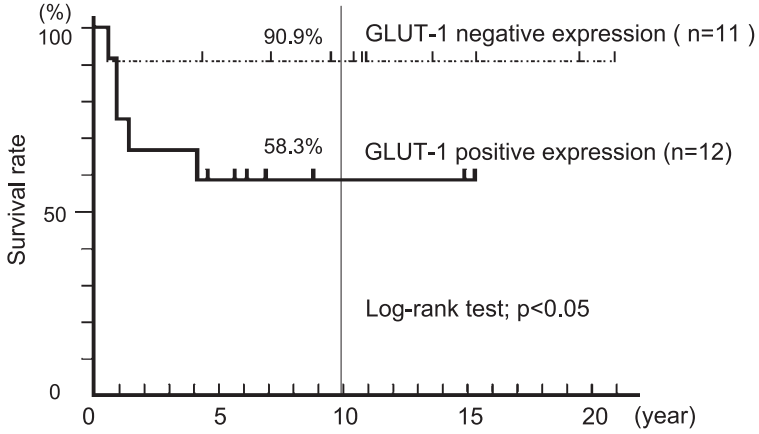

Fig. 6. Survival curves for GLUT-1-positive and GLUT-1-negative cases of LMS.

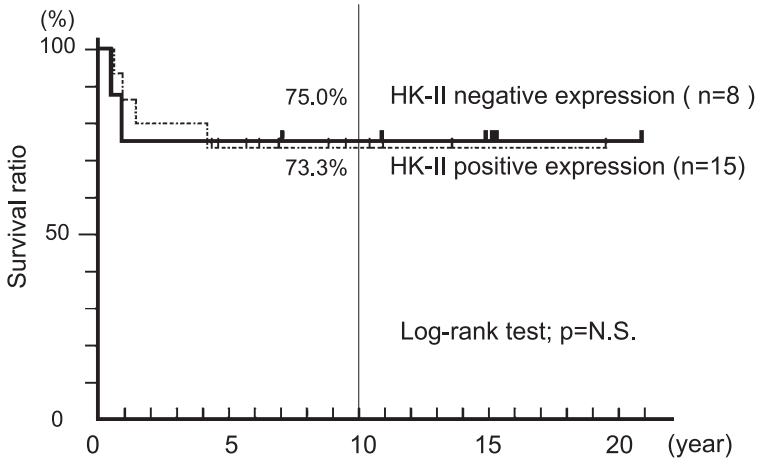

Fig. 7. Survival curves of HK-II-positive and HK-II-negative cases of LMS.

abdominal reoperation. Several small-scale studies have indicated that CYVADIC chemotherapy improves prognosis after total hysterectomy and adnexectomy [12, 31, 41]. In our study, no gross residual tumor was found during lymph node dissection. Twelve patients (52%) were treated with CYVADIC chemotherapy and 9 (39%) did not receive this chemotherapy. Three patients died in each of these groups. Most previous studies and the current study were performed at single centers and with a limited number of patients. Therefore, multicenter randomized clinical trials are required to establish more reliable evidence of the efficacy of treatment.

In our previous investigation of different histological types (serous, mucous, endometrioid and clear cell) of epithelial ovarian cancer, we found that expression levels of GLUT-1 and HIF1α were correlated in the respective histological types. Expression of both proteins was especially high in serous adenocarcinoma, which is frequently found in epithelial ovary cancer, and clear cell adenocarcinoma, which is chemoresistant and associated with recurrence and metastasis. Histopathologically, these two tumors have fewer vascular vessels, but have papillary proliferation and a stratified structure, and cause extensive necrosis in progression. Therefore, hypoxia is induced as the cancer progresses, and this leads to strong expression of GLUT-1 and HIF-1α [16, 43].

Many studies have evaluated the relationship between the expression level of GLUT-1 and progression of epithelial and gynecologic cancers, with the general finding that strong GLUT-1 expression is associated with a poorer prognosis [1, 6, 11, 17, 19, 44, 45]. In a study of 67 patients with bone and soft tissue sarcoma or non-epithelial carcinoma (stage IA–IVB, 15 different histological types), Endo *et al.* found a correlation of prognosis with therapy including surgical resection and adjuvant chemotherapy ($p<0.0001$), tumor differentiation ($p=0.017$), necrotic grade ($p=0.04$), mitotic grade ($p=0.0198$), MIB-1 grade ($p=0.031$), and GLUT-1 expression ($p=0.029$) in univariate analysis of 3-year survival; but found that metastasis ($p=0.031$) was the only significant prognostic factor in multivariate analysis of overall survival. However, Kaplan-Meier estimates of overall survival at 5 years were <40% in the GLUT-1-positive group and 90% in the GLUT-1-negative group, showing a significant difference in prognosis [8].

In the present study, all the cases of non-epithelial carcinoma were in clinical stage I, involved uterine LMS with a single histological type, and were completely resectable in surgery. Thus, there was less variation in the subjects in this study in comparison with Endo *et al.*, which included cases of different histological types and progression. The 5-year OS of all LMS patients was approximately 74%, and the MIB-1 index and expression level of GLUT-1 had a significant positive correlation. The 5-year survival rates were 90.9% and 58.3% in GLUT-1-negative and GLUT-1-positive cases, respectively. Thus, GLUT-1 expression was significantly correlated with prognosis in uterine LSM, as found in previous studies of malignant epithelial tumors. In contrast, there was no relationship of HK-II expression with the MIB-1 index or prognosis, and no significant difference in survival between HK-II-positive and HK-II-negative cases.

Previous studies have shown that expression of GLUT-1 and HK-II in epithelial cancer cells, including breast, esophageal, and lung cancer cells, plays a pivotal role in glucose metabolism and that the expression levels of GLUT-1 and HK-II are correlated with malignancy [5, 14, 17, 23, 28, 38]. The subjects of the current study were 23 patients with LMS associated with non-epithelial malignancy and the prognosis correlated with the presence or absence of expression of GLUT-1 in malignant cells, but not with expression of HK-II. Therefore, it is possible that the occurrence of malignant cells depends on glucose metabolism, glucose enzyme activity and phosphorylation, but not on epithelial cell malignancy.

The recent development of [^{18}F]-fluorodeoxyglucose positron emission tomography (FDG-PET) allows imaging based on the difference in glucose metabolism between malignant and normal cells. Thus, FDG-PET is effective for detection of early stage malignant tumors, and has high sensitivity for detection of recurrence and metastasis in malignant gynecological epithelial tumors [3, 4, 20, 35]. In the first study of non-epithelial bone and soft tissue sarcomas using FDG-PET, Tateishi *et al.* showed an association between higher GLUT-1 expression and a higher standardized uptake value (SUV) of [^{18}F]fluorodeoxyglucose, thereby suggesting the efficacy of FDG-PET diagnostic imaging for non-epithelial tumors, as well as MIB-1 grade, mitotic grade, and tumor differentiation [36].

We have also evaluated FDG-PET for early detection of recurrence and metastasis of advanced ovary cancer after treatment. The rates of detection of intraperitoneal and retroperitoneal metastasis by FDG-PET were 93.9% and 92.9%, respectively, and metastasis was detected in 14 (50%) of 28 metastatic lymph nodes of normal size. FDG-PET detected recurrence in 87.5% of CA125-positive patients with no symptoms and negative results in conventional CT and ultrasonography [24]. The efficacy of follow-up FDG-PET was evaluated in patients with uterine LMS, and early-stage minimal recurrent lesions were detected in patients in whom conventional CT and ultrasonography did not show intraperitoneal recurrence. Two of 5 patients underwent reoperation for a recurrent tumor and survived for one year or more after surgery.

Benign non-epithelial tumors such as uterine leiomyomas are rarely positive in PET, but such cases should be followed up carefully because some may be false-positives [39]. However, FDG-PET is effective for detection of early-stage intraperitoneal recurrence that may be overlooked in conventional diagnostic imaging [25]. The clinicopathological results reported here show that malignant non-epithelial tumors have high glucose metabolic activity and high GLUT-1 expression, and these findings support the use of FDG-PET for detection of malignant lesions.

V. Acknowledgments

This work was supported in part by Grants-in-aid for scientific research from the Ministry of Education, Japan (No. 23592465), and Tokai University Research Aid.

VI. References

1. Airley, R., Loncaster, J., Davidson, S., Bromley, M., Roberts, S., Patterson, A., Hunter, R., Stratford, I. and West, C. (2001) Glucose transporter glut-1 expression correlates with tumor hypoxia and predicts metastasis-free survival in advanced carcinoma of the cervix. *Clin. Cancer Res.* 7; 928–934.
2. Airley, R. E., Phillips, R. M., Evans, A. E., Double, J., Burger, A. M., Feibig, H. H., West, C. M. and Stratford, I. J. (2005) Hypoxia-regulated glucose transporter Glut-1 may influence chemosensitivity to some alkylating agents: results of EORTC (First Translational Award) study of the relevance of tumour hypoxia to the outcome of chemotherapy in human tumour-derived xenografts. *Int. J. Oncol.* 26; 1477–1484.
3. Bristow, R. E., del Carmen, M. G., Pannu, H. K., Cohade, C., Zahurak, M. L., Fishman, E. K., Wahl, R. L. and Montz, F. J. (2003) Clinically occult recurrent ovarian cancer: patient selection for secondary cytoreductive surgery using combined PET/CT. *Gynecol. Oncol.* 90; 519–528.
4. Bristow, R. E., Giuntoli, R. L. 2nd, Pannu, H. K., Schulick, R. D., Fishman, E. K. and Wahl, R. L. (2005) Combined PET/CT for detecting recurrent ovarian cancer limited to retroperitoneal lymph nodes. *Gynecol. Oncol.* 99; 294–300.
5. Brown, R. S. and Wahl, R. L. (1993) Overexpression of Glut-1 glucose transporter in human breast cancer. An immunohistochemical study. *Cancer* 72; 2979–2985.
6. Cantuaria, G., Fagotti, A., Ferrandina, G., Magalhaes, A., Nadji, M., Angioli, R., Penalver, M., Mancuso, S. and Scambia, G. (2001) GLUT-1 expression in ovarian carcinoma: association with survival and response to chemotherapy. *Cancer* 92; 1144–1150.
7. Echt, G., Jepson, J., Steel, J., Langholz, B., Luxton, G., Hernandez, W., Astrahan, M. and Petrovich, Z. (1990) Treatment of uterine sarcomas. *Cancer* 66; 35–39.
8. Endo, M., Tateishi, U., Seki, K., Yamaguchi, U., Nakatani, F., Kawai, A., Chuman, H. and Beppu, Y. (2007) Prognostic implications of glucose transporter protein-1 (glut-1) overexpression in bone and soft-tissue sarcomas. *Jpn. J. Clin. Oncol.* 37; 955–960.
9. Gadducci, A., Landoni, F., Sartori, E., Zola, P., Maggino, T., Lissoni, A., Bazzurini, L., Arisio, R., Romagnolo, C. and Cristofani, R. (1996) Uterine leiomyosarcoma: analysis of treatment failures and survival. *Gynecol. Oncol.* 62; 25–32.
10. Griffiths, E. A., Pritchard, S. A., Welch, I. M., Price, P. M. and West, C. M. (2005) Is the hypoxia-inducible factor pathway important in gastric cancer? *Eur. J. Cancer* 41; 2792–2805.
11. Haber, R. S., Rathan, A., Weiser, K. R., Pritsker, A., Itzkowitz, S. H., Bodian, C., Slater, G., Weiss, A. and Burstein, D. E. (1998) GLUT1 glucose transporter expression in colorectal carcinoma: a marker for poor prognosis. *Cancer* 83; 34–40.
12. Hempling, R. E., Piver, M. S. and Baker, T. R. (1995) Impact on progression-free survival of adjuvant cyclophosphamide, vincristine, doxorubicin (adriamycin), and dacarbazine (CYVADIC) chemotherapy for stage I uterine sarcoma. A prospective trial. *Am. J. Clin. Oncol.* 18; 282–286.
13. Hensley, M. L., Ishill, N., Soslow, R., Larkin, J., Abu-Rustum, N., Sabbatini, P., Konner, J., Tew, W., Spriggs, D. and Aghajanian, C. A. (2009) Adjuvant gemcitabine plus docetaxel for completely resected stages I–IV high grade uterine leiomyosarcoma: Results of a prospective study. *Gynecol. Oncol.* 112; 563–567.
14. Higashi, T., Saga, T., Nakamoto, Y., Ishimori, T., Mamede, M. H., Wada, M., Doi, R., Hosotani, R., Imamura, M. and Konishi, J. (2002) Relationship between retention index in dual-phase (18)F-FDG PET, and hexokinase-II and glucose transporter-1 expression in pancreatic cancer. *J. Nucl. Med.* 43; 173–180.
15. Hockel, M., Schlenger, K., Aral, B., Mitze, M., Schaffer, U. and Vaupel, P. (1996) Association between tumor hypoxia and malignant progression in advanced cancer of the uterine cervix. *Cancer Res.* 56; 4509–4515.
16. Iida, T., Yasuda, M., Miyazawa, M., Fujita, M., Osamura, R. Y., Hirasawa, T., Muramatsu, T., Murakami, M., Saito, K. and Mikami, M. (2008) Hypoxic status in ovarian serous and mucinous tumors: relationship between histological characteristics and HIF-1alpha/GLUT-1 expression. *Arch. Gynecol. Obstet.* 277; 539–546.
17. Kato, H., Takita, J., Miyazaki, T., Nakajima, M., Fukai, Y., Masuda, N., Fukuchi, M., Manda, R., Ojima, H., Tsukada, K., Kuwano, H., Oriuchi, N. and Endo, K. (2003) Correlation of 18-F-fluorodeoxyglucose (FDG) accumulation with glucose transporter (Glut-1) expression in esophageal squamous cell carcinoma. *Anticancer Res.* 23; 3263–3272.
18. Kempson, R. L. and Hendrickson, M. R. (1988) Pure mesenchymal neoplasms of the uterine corpus: selected problems. *Semin. Diagn. Pathol.* 5; 172–198.
19. Kunkel, M., Reichert, T. E., Benz, P., Lehr, H. A., Jeong, J. H., Wieand, S., Bartenstein, P., Wagner, W. and Whiteside, T. L. (2003) Overexpression of Glut-1 and increased glucose metabolism in tumors are associated with a poor prognosis in patients with oral squamous cell carcinoma. *Cancer* 97; 1015–1024.
20. Kurokawa, T., Yoshida, Y., Kawahara, K., Tsuchida, T., Okazawa, H., Fujibayashi, Y., Yonekura, Y. and Kotsuji, F. (2004) Expression of GLUT-1 glucose transfer, cellular proliferation activity and grade of tumor correlate with [F-18]-fluorodeoxyglucose uptake by positron emission tomography in epithelial tumors of the ovary. *Int. J. Cancer* 109; 926–932.
21. Kushner, D. M., Webster, K. D., Belinson, J. L., Rybicki, L. A., Kennedy, A. W. and Markman, M. (2000) Safety and efficacy of adjuvant single-agent ifosfamide in uterine sarcoma. *Gynecol. Oncol.* 78; 221–227.
22. Major, F. J., Blessing, J. A., Silverberg, S. G., Morrow, C. P., Creasman, W. T., Currie, J. L., Yordan, E. and Brady, M. F. (1993) Prognostic factors in early-stage uterine sarcoma. A Gynecologic Oncology Group study. *Cancer* 71; 1702–1709.
23. Mamede, M., Higashi, T., Kitaichi, M., Ishizu, K., Ishimori, T., Nakamoto, Y., Yanagihara, K., Li, M., Tanaka, F., Wada, H., Manabe, T. and Saga, T. (2005) [18F]FDG uptake and PCNA, Glut-1, and Hexokinase-II expressions in cancers and inflammatory lesions of the lung. *Neoplasia* 7; 369–379.
24. Murakami, M., Miyamoto, T., Iida, T., Tsukada, H., Watanabe, M., Shida, M., Maeda, H., Nasu, S., Yasuda, S., Yasuda, M. and Ide, M. (2006) Whole-body positron emission tomography and tumor marker CA125 for detection of recurrence in epithelial ovarian cancer. *Int. J. Gynecol. Cancer* 16; 99–107.
25. Murakami, M., Tsukada, H., Shida, M., Watanabe, M., Maeda, H., Koido, S., Hirasawa, T., Muramatsu, T., Miyamoto, T., Nasu, S., Yasuda, S., Kajiwara, H., Yasuda, M. and Ide, M. (2006) Whole-body positron emission tomography with F-18 fluorodeoxyglucose for the detection of recurrence in uterine sarcomas. *Int. J. Gynecol. Cancer* 16; 854–860.
26. Odunsi, K., Moneke, V., Tammela, J., Ghamande, S., Seago, P., Driscoll, D., Marchetti, D., Baker, T. and Lele, S. (2004) Efficacy of adjuvant CYVADIC chemotherapy in early-stage uterine sarcomas: results of long-term follow-up. *Int. J. Gynecol. Cancer* 14; 659–664.
27. Omura, G. A., Blessing, J. A., Major, F., Lifshitz, S., Ehrlich, C. E., Mangan, C., Beecham, J., Park, R. and Silverberg, S. (1985) A randomized clinical trial of adjuvant adriamycin in uterine sarcomas: a Gynecologic Oncology Group Study. *J. Clin. Oncol.*

3; 1240–1245.
28. Paudyal, B., Oriuchi, N., Paudyal, P., Higuchi, T., Nakajima, T. and Endo, K. (2008) Expression of glucose transporters and hexokinase II in cholangiocellular carcinoma compared using [18F]-2-fluro-2-deoxy-D-glucose positron emission tomography. *Cancer Sci.* 99; 260–266.
29. Pautier, P., Genestie, C., Rey, A., Morice, P., Roche, B., Lhommé, C., Haie-Meder, C. and Duvillard, P. (2000) Analysis of clinicopathologic prognostic factors for 157 uterine sarcomas and evaluation of a grading score validated for soft tissue sarcoma. *Cancer* 88; 1425–1431.
30. Pautier, P., Rey, A., Haie-Meder, C., Kerbrat, P., Dutel, J. L., Gesta, P., Bryard, F., Morice, P., Duvillard, P. and Lhommé, C. (2004) Adjuvant chemotherapy with cisplatin, ifosfamide, and doxorubicin followed by radiotherapy in localized uterine sarcomas: results of a case-control study with radiotherapy alone. *Int. J. Gynecol. Cancer* 14; 1112–1117.
31. Piver, M. S., Lele, S. B., Marchetti, D. L. and Emrich, L. J. (1988) Effect of adjuvant chemotherapy on time to recurrence and survival of stage I uterine sarcomas. *J. Surg. Oncol.* 38; 233–239.
32. Reed, N. S., Mangioni, C., Malmström, H., Scarfone, G., Poveda, A., Pecorelli, S., Tateo, S., Franchi, M., Jobsen, J. J., Coens, C., Teodorovic, I., Vergote, I. and Vermorken, J. B. (2008) Phase III randomised study to evaluate the role of adjuvant pelvic radiotherapy in the treatment of uterine sarcomas stages I and II: an European Organization for Research and Treatment of Cancer Gynaecological Cancer Group Study (protocol 55874). *Eur. J. Cancer* 44; 808–818.
33. Salazar, O. M., Bonfiglio, T. A., Patten, S. F., Keller, B. E., Feldstein, M., Dunne, M. E. and Rudolph, J. (1978) Uterine sarcomas: natural history, treatment and prognosis. *Cancer* 42; 1152–1160.
34. Sutton, G., Blessing, J. A. and Malfetano, J. H. (1996) Ifosfamide and doxorubicin in the treatment of advanced leiomyosarcomas of the uterus: a Gynecologic Oncology Group study. *Gynecol. Oncol.* 62; 226–229.
35. Takekuma, M., Maeda, M., Ozawa, T., Yasumi, K. and Torizuka, T. (2005) Positron emission tomography with 18F-fluoro-2-deoxyglucose for the detection of recurrent ovarian cancer. *Int. J. Clin. Oncol.* 10; 177–181.
36. Tateishi, U., Yamaguchi, U., Seki, K., Terauchi, T., Arai, Y. and Hasegawa, T. (2006) Glut-1 expression and enhanced glucose metabolism are associated with tumour grade in bone and soft tissue sarcomas: a prospective evaluation by [18F]fluorodeoxyglucose positron emission tomography. *Eur. J. Nucl. Med. Mol. Imaging* 33; 683–691.
37. Tian, M., Zhang, H., Higuchi, T., Oriuchi, N., Nakasone, Y., Takata, K., Nakajima, N., Mogi, K. and Endo, K. (2005) Hexokinase-II expression in untreated oral squamous cell carcinoma: comparison with FDG PET imaging. *Ann. Nucl. Med.* 19; 335–338.
38. Tohma, T., Okazumi, S., Makino, H., Cho, A., Mochiduki, R., Shuto, K., Kudo, H., Matsubara, K., Gunji, H. and Ochiai, T. (2005) Relationship between glucose transporter, hexokinase and FDG-PET in esophageal cancer. *Hepatogastroenterology* 52; 486–490.
39. Tsukada, H., Murakami, M., Shida, M., Kikuchi, K., Watanabe, M., Yasuda, S. and Suzuki, Y. (2009) 18F-fluorodeoxyglucose uptake in uterine leiomyomas in healthy women. *Clin. Imaging* 33; 462–467.
40. Van Dinh, T. and Woodruff, J. D. (1982) Leiomyosarcoma of the uterus. *Am. J. Obstet. Gynecol.* 144; 817–823.
41. van Nagell, J. R., Hanson, M. B., Donaldson, E. S. and Gallion, H. H. (1986) Adjuvant vincristine, dactinomycin, and cyclophosphamide therapy in stage I uterine sarcomas. A pilot study. *Cancer* 57; 1451–1454.
42. Warburg, O. (1956) On the origin of cancer cells. *Science* 123; 309–314.
43. Yasuda, M., Miyazawa, M., Fujita, M., Kajiwara, H., Iida, T., Hirasawa, T., Muramatsu, T., Murakami, M., Mikami, M., Saitoh, K., Shimizu, M., Takekoshi, S. and Osamura, R. Y. (2008) Expression of hypoxia inducible factor-1alpha (HIF-1alpha) and glucose transporter-1 (GLUT-1) in ovarian adenocarcinomas: difference in hypoxic status depending on histological character. *Oncol. Rep.* 19; 111–116.
44. Younes, M., Lechago, L. V., Somoano, J. R., Mosharaf, M. and Lechago, J. (1996) Wide expression of the human erythrocyte glucose transporter Glut1 in human cancers. *Cancer Res.* 56; 1164–1167.
45. Younes, M., Juarez, D., Lechago, L. V. and Lerner, S. P. (2001) Glut 1 expression in transitional cell carcinoma of the urinary bladder is associated with poor patient survival. *Anticancer Res.* 21; 575–578.

5、消化器癌進行における癌幹細胞血管ニッチを標的とした治療法開発
癌ニッチを標的とした新規制癌治療法開発

分担研究者　再生医療科学　増田治史
研究協力者　再生医療科学　志津野朋子、佐藤敦子、宮崎幸造、小山田晃

【研究の背景】

癌による腫瘍増大及び癌転移において重要な役割を担う癌ニッチの血液細胞群の修飾による癌ニッチ崩壊戦略を提案し、その基礎研究を実施した。癌ニッチは、炎症性血管を構築し、制御性 T 細胞や M2 マクロファージなどの抗炎症性および免疫制御性細胞を動員し、炎症性および免疫賦活化 CD8+T 細胞、NK 細胞、M1 マクロファージなどの癌細胞傷害性細胞浸潤が抑制された環境として、いわば「癌バリアー」を獲得し、癌細胞増殖、腫瘍増大を容易にしている。この癌ニッチにおけるを炎症性および免疫賦活性環境の表現型に変換することによる癌ニッチの「癌バリアー」崩壊を抗癌戦略として提案した。

【方法と結果】

1）抗 VEGF 抗体(Avastin)による炎症環境の修飾による癌ニッチの炎症環境および抗血管新生環境への変換効果、2）マウス担癌モデルを用いて、炎症性・抗血管形成性培養細胞(Inflammatory Anti-vasculogenic Cell= InAVC)あるいは抗炎症・血管形成性培養細胞(Anti-inflammatory Vasculogenic Cell= AInVC)の移植による抗腫瘍効果について検討した。Avastin を添加したヒト末梢血単核球の培養において、TNF-alpha の存在及び非存在下のいずれにおいても血管内皮前駆細胞(Endothelial Progenitor Cell= EPC)の増幅及び抗炎症性 M2 マクロファージの増殖を抑制した。さらに、制御性 T 細胞(Treg)の誘導をも抑制した。これは、抗腫瘍血管新生薬が癌組織の癌ニッチ環境を癌増大に都合の良い血管新生、抗炎症・免疫抑制環境から抗癌性のニッチ環境に変換させる可能性を示し、抗血管新生薬の癌ニッチ破壊効果が確認された。2）InAVC 及び AInVC のいずれの細胞が抗腫瘍効果を有するかを検討したところ、InAVC は腫瘍増大を促進したが、AInVC は血管の成熟及び腫瘍の壊死を誘導し腫瘍組織内の炎症を抑制していた。また、腫瘍の退縮効果は軽度であったが、生存率において上昇する効果が認められた。

【考察】

1）Avastin は、腫瘍組織内癌ニッチを炎症性に改変させ、腫瘍免疫を活性化させることが示唆

される。しかしながら、臨床では、Avastin の投与初期におけいて抗腫瘍効果は認められるが、持続投与ではその効果が減弱することが、報告されている。2）InAVC 及び AInVC の移植実験に用いた担癌モデルは異なるが、InAVC による腫瘍の増大、逆に、AInVC による血管成熟を伴う腫瘍退縮傾向が認められた。

これらの Avastin の初期の限定的効果、InAVC の腫瘍増大効果及び AInVC の抗腫瘍効果について、癌ニッチの誘導と維持において癌細胞の増殖による腫瘍増大における中心部虚血に伴う炎症環境が重要な役割を担うことが考えられた。したがって、AInVC は、この癌ニッチの特性に対して抑制的に作用したと考えられる。

【結論】

今後の抗癌戦略として、癌細胞の増殖抑制による抗癌剤投与のみならず、癌ニッチを抗炎症性環境及び血管成熟化環境に改変させることにより、「癌バリアー」を崩壊させる治療法の開発が重要と考えられた。

（研究方法および結果）

1）抗 VEGF 抗体(Avastin)による炎症環境の修飾による癌ニッチに及ぼす影響に関する in vitro における検討

Avastin による EPC の血管形成能力に及ぼす影響について（図1、2）:ヒト末梢血単核球を用いた TNF-alpha 添加 AInVC の EPC コロニーアッセイを行い、Avastin の EPC 血管形成能力に及ぼす影響を評価した。EPC コロニー数は、TNF-alpha 存在下では対照の 75%程度に減

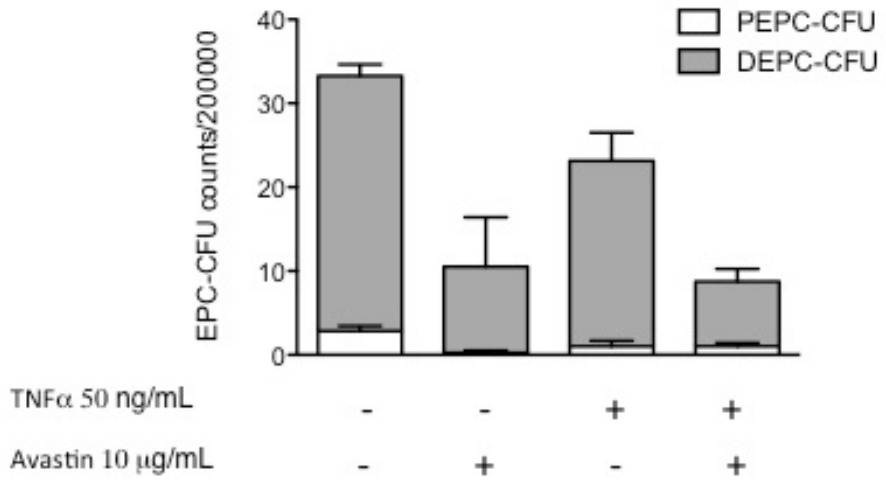

図1. AvastinによるEPCコロニー形成能抑制作用。
AvastinまたはTNF-alpha添加を添加したヒト末梢血単核球の抗炎症性・血管形成性培養細胞(AInVC)のEPCコロニー産生能。

少した。また、Avastin は、TNF-alpha 存在の有無にかかわらず対照の 30%程度に減少させた**(図1)**。

さらに、同様の培養細胞においてコロニー形成機能のない分化した EPC 産生能力を EPC 培

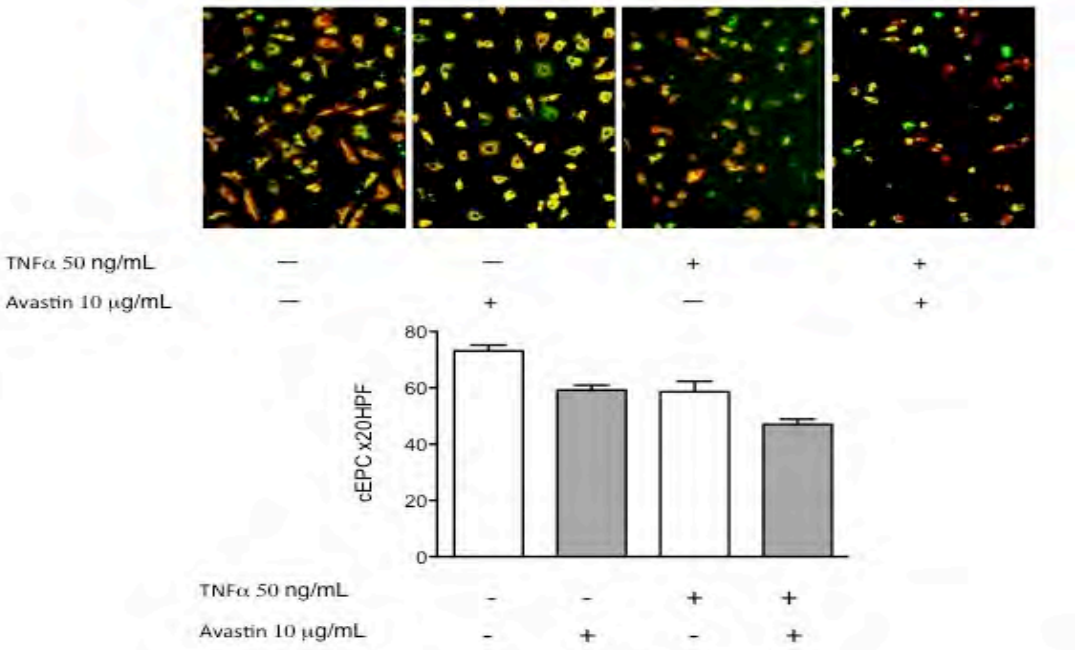

図2. Avastinによるコロニー非形成性EPC産生抑制作用。
AvastinまたはTNF-alpha添加を添加した末梢血単核球のEPC培養アッセイ。

養アッセイにより評価した。TNF-alpha 存在下では、EPC の産生数は減少し、Avastin 添加培養細胞では、さらに減少した**(図2)**。

Avastin は、癌幹細胞において炎症性、抗炎症性細胞群のいずれにおいても EPC の血管形成能力を低下させると考えられ、腫瘍血管新生に抑制的に働く一方で、腫瘍の壊死を促進し、癌ニッチの炎症を促進する可能性が示唆された。

Avastin による炎症性、抗炎症性血液細胞に及ぼす影響について(図3):

AInVC 培養において、Avastin は、未分化な EPC(CD133+細胞)の含有率を低下させた。また、TNF-alpha の存在に関わらず、M2 マクロファージ(CD206+細胞)の含有率を低下させた。さらに、Avastin は、Treg (CD4+CD25+Foxp3+細胞)の含有率を低下させたが、TNF-alpha 存在下ではさらに低下させ、AInVC の抗炎症性培養環境においても、培養細胞群を炎症環境に変化させることが判明した。以上、Avastin は、癌ニッチにおいて腫瘍血管形成を抑制するが、その腫瘍虚血に伴う炎症環境を誘導させると考えられた。

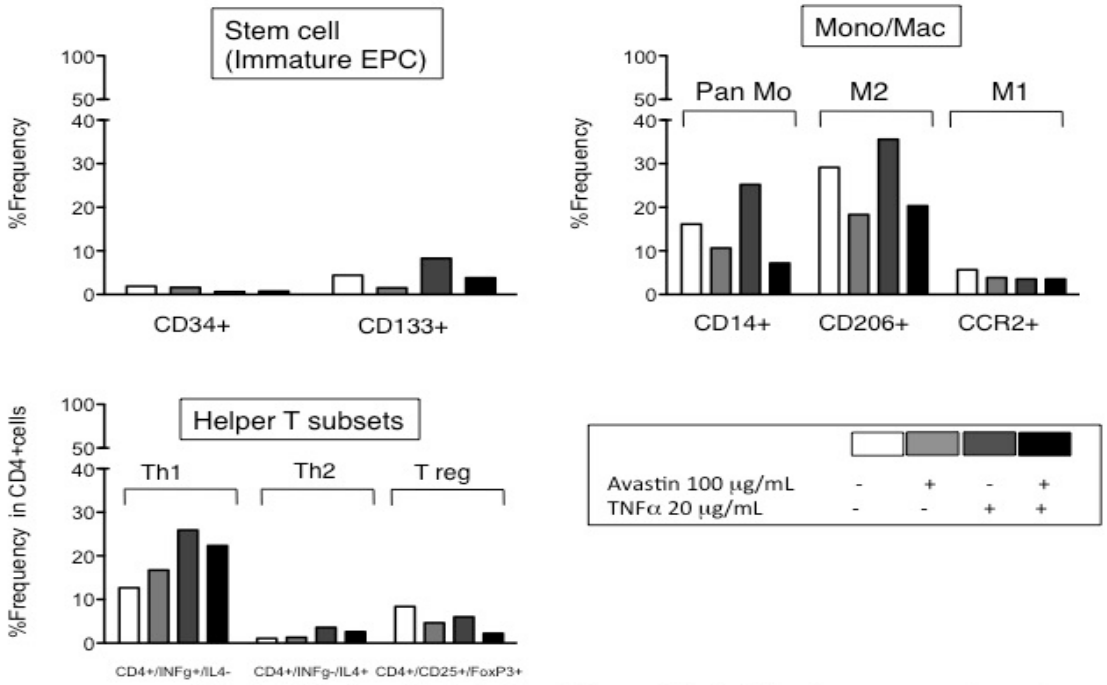

図3.ヒト末梢血単核球の抗炎症性・血管形成性培養細胞(AInVC)における Avastinの効果。

2)担癌マウスの炎症性および抗炎症性環境に関する検討

担癌マウスにおける癌ニッチ環境の検討:C57BL6 マウス由来 B16-F10 メラノーマ細胞株を C57BL6 マウスの側腹部皮下に移植(1x10^6 個/マウス)し担癌モデルとした。移植後、9日、21日後に屠殺し、末梢血単核球(perpheral blood mononuclear cell=PBMNC)および腫瘍組織を採取し、M1(CD11b+CCR7+細胞)および M2 (CD11b+CD206+細胞)マクロファージを Flow cytometry を用いて解析した。PBMNC においては、M1 の含有率が腫瘍増大に伴い上昇したが、逆に腫瘍組織内では M2 マクロファージの含有率が上昇した。この結果は、腫瘍の増大に伴い、全身性には炎症性環境に、腫瘍部では抗炎症性環境に偏位することを示す**(図4)**。

癌細胞そのものが、M2 マクロファージを誘導するか否かを in vitro 培養系にて検討した**(図5)**。BALB/c マウスから脾臓細胞を採取し、BALB/c マウス由来 C26 大腸癌株と RPMI1640 培地を用いて共培養(脾臓細胞 : C26 癌細胞= 20 : 1 の細胞数にて)を実施した。3日後に Flow cytometry を用いて M2 マクロファージの含有率を検討した。M2 マクロファージ細胞数は増加し**(図5a)**、総細胞数に占める M2 マクロファージの含有率も上昇した**(図5b)**。

この結果は、癌細胞が抗炎症ニッチを自ら構築し、宿主側からの炎症性細胞による攻撃を免れていることを示している。

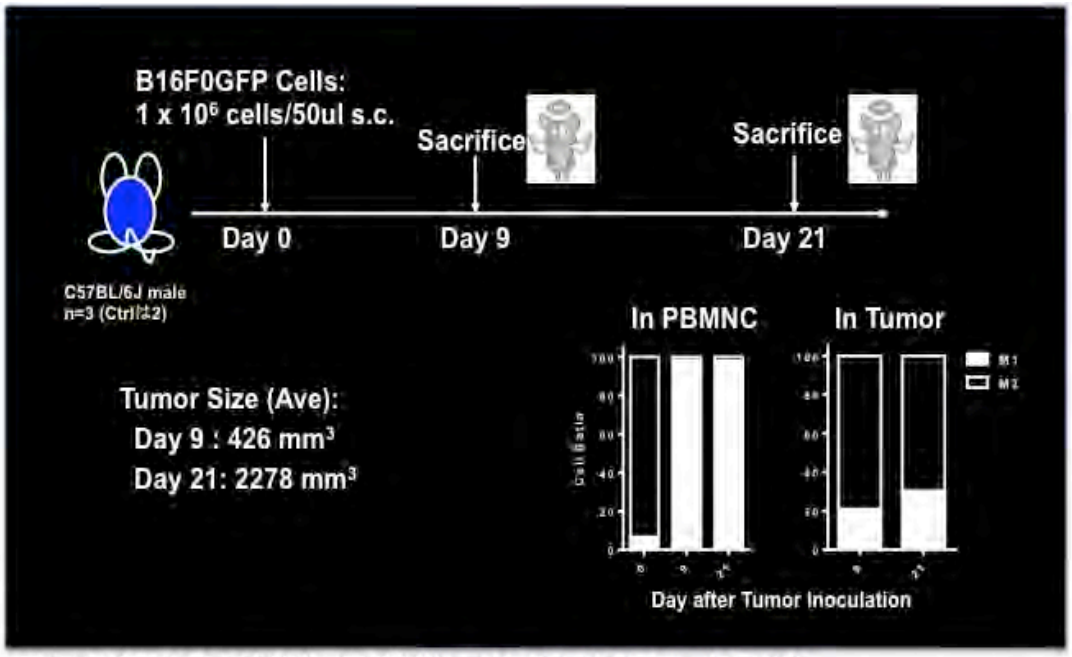

図4. 担癌マウスの末梢血、腫瘍組織内M1, M2マクロファージの分布。
末梢血(PBMNC)中には、M1マクロファージ(CD11b+CCR7+)、癌組織内(Tumor)にはM2マクロファージ(CD11b+CD206+)が優位に存在していた。腫瘍の増大に伴い、腫瘍組織内のM2マクロファージ含有率が上昇した。

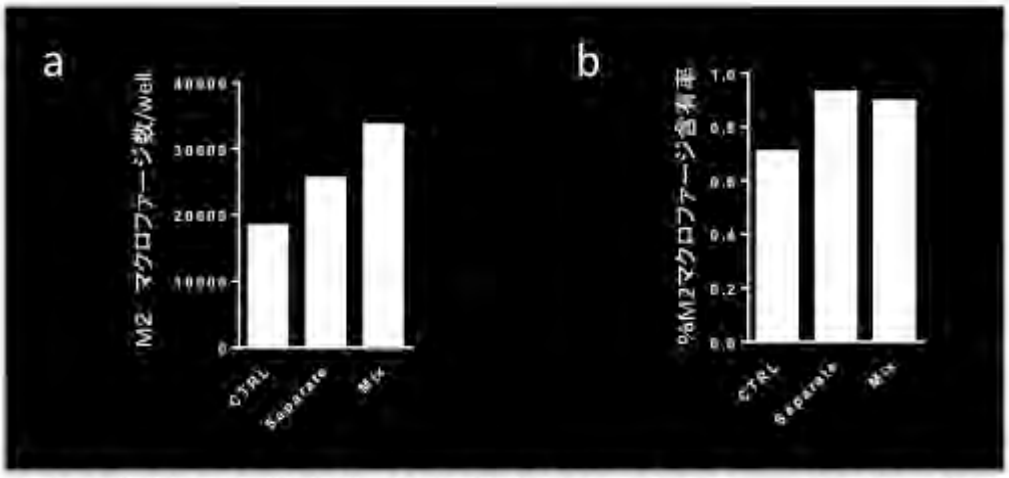

図5.癌細胞の抗炎症性・免疫寛容性M2マクロファージの増加作用。
(a) M2マクロファージ(CD11b+CD206+細胞)数/well、
(b) M2マクロファージ含有率。

3)癌ニッチ制御による新たな制癌戦略の検討;

次に、癌ニッチを制御することによる細胞治療による新たな制癌戦略を発案した。基礎的実験方法として、マウス脾臓細胞あるいは血液単核球から炎症性・抗血管形成性培養細胞を調整した。我々は、独自にヒトの単核球やマウスの血液単核球、脾臓細胞を用いた抗炎症性・血管形成性培養法(AInVC)を開発してきた(Masuda et al., 2014)。この培養法を改変して新たに炎

症性・血管形成抑制性培養系(InAVC)を確立し、これらを各々、B16 メラノーマ細胞株または C26 大腸癌細胞株の側腹部皮下移植による担癌マウスに移植した。腫瘍退縮効果、M1/M2 マクロファージを指標にした癌ニッチの炎症、抗炎症環境の改変、組織学的検討を行った。

InAVC 培養系の確立:5つの Grwoth factor/Cytokine(5G; SCF,Flt3-ligand, TPO, VEGF, IL-6)コンビネーションよる AInVC 培養系に INF-gamma を添加することによる血管形成機能を EPC コロニーアッセイにより評価した。INF-gamma の添加により濃度依存性にコロニー産生能は抑制された(**図6**)。

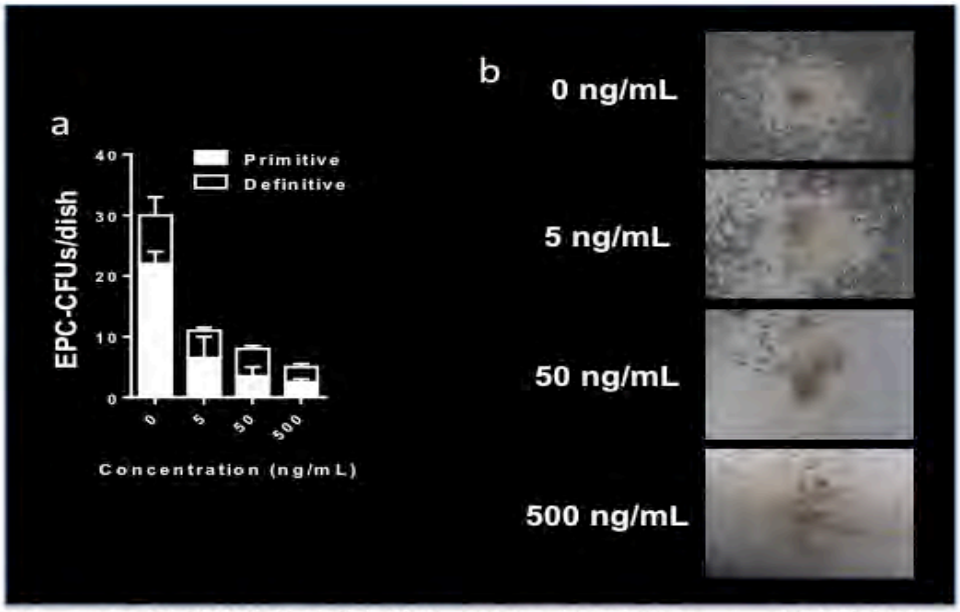

図6. マウス脾臓炎症性培養細胞(InAVC)におけるINF-gammaの血管新生抑制効果 。
(a) INF-gamma添加QQ培養細胞のEPCコロニーアッセイ、
(b) INF-gammaの各濃度添加QQ培養細胞からのEPCコロニー。

また、5G+INF-gamma 培地、4G(SCF,Flt3-ligand, TPO, IL-6)、4G+INF-gamma 培地の各培養条件において、BALB/c マウスの脾臓細胞を3日間培養し、Flow cytometry を用いて、M1 及び M2 の総マクロファージに占める比率と対照の 5G 培養細胞に対する増減率を評価した。5G 及び 4G 培養細胞のいずれにおいても M1 比率は 60%程度であったが、INF-gamma の添加により M1 の比率は 90%以上に上昇した(**図7**)。これは、5G+INF-gamma あるいは 4G+INF-gamma 培養系により AInVC 培養系から InAVC の表現型に変化させることが可能であることが示唆された。

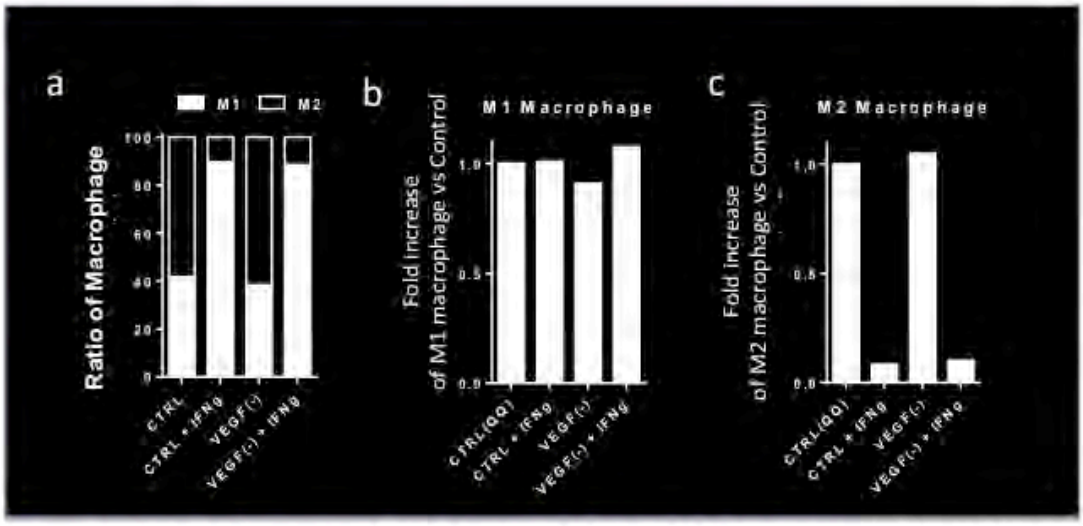

図7. VEGFまたはINF-gamma添加によるマウス脾臓炎症性培養細胞(InAVC)におけるM1及びM2マクロファージ動態 。
(a) QQ培養細胞に含有されるマクロファージにおけるM1(CD11b+CCR7+細胞)、M2(CD11b+CD206+細胞)の比率。Control細胞(INF-gamma及びVEGF非添加のQQ培養細胞)に対する各条件の培養細胞のM1マクロファージ数の比率 (b)、M2マクロファージ数の比率 (c)。VEGFの有無にかかわらず、M2マクロファージ数はINF-gammaにより減少した。

C26 大腸癌の担癌マウスの癌ニッチに対する InAVC 移植の影響に関する検討:

BALB/c マウスの脾臓細胞を用いて 4G+INF-gamma 培養系による InAVC を調整し、C26 大腸癌の担癌マウスの尾静脈移植(全身性投与)または腫瘍部移植(局所性投与)について腫瘍増大に与える影響を検討した。$1x10^6$ 個/マウスの癌細胞を側腹部皮下に移植した。InAVC を各々のアプローチにて、癌細胞移植後7日後から1週間ごとに3週間に渡り移植した(合計4回、$1x10^6$ 個/マウス/回 x 4 回)。結果、いずれのアプローチにおいても、腫瘍退縮効果は認められず、逆に腫瘍増大が認められた。炎症性細胞の移植では、癌ニッチ機能の促進効果をもたらすことが判明した(**図8**)。

B16 メラノーマ担癌マウスの癌ニッチに対する AInVC 移植の影響に関する検討:

$1x10^6$ 個/マウスの B16 メラノーマ細胞を側腹部皮下に移植し担癌マウスを作製した。
AInVC を癌細胞移植後4日目に尾静脈から移植した($1x10^6$ 個/マウス)。結果、対照の非細胞移植群に比較して、腫瘍の増大遅延効果が認められた(**図9a**)。また、生存率において、28 日後の生存率の上昇が認められた(**図9b**)。
さらに、B16 メラノーマ細胞移植後の組織像においては、AInVC 移植マウスにおいて、iNOS 陽性領域、壊死領域は減少し(**図10a**)、腫瘍内壊死組織領域が拡大した(**図10b**)。

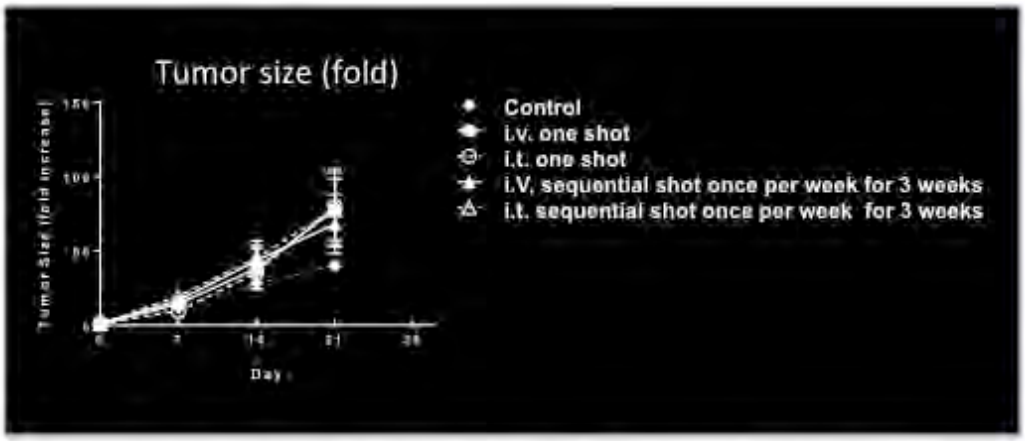

図8. INF-gamma添加によるマウス脾臓炎症性培養細胞(InAVC)の移植による抗腫瘍効果の検討。
C26　マウス大腸癌株をBALB/cマウスの皮下に移植(1x10^{6}個/マウス)。7日後(day0)に培養細胞を尾静脈又は腫瘍内に直接移植した。
また、day0から1週間に1回ずつ2週間に渡ってInAC細胞を移植した。
InAC細胞は、全身性、局所性移植いずれにおいても腫瘍退縮効果は認められなかった。

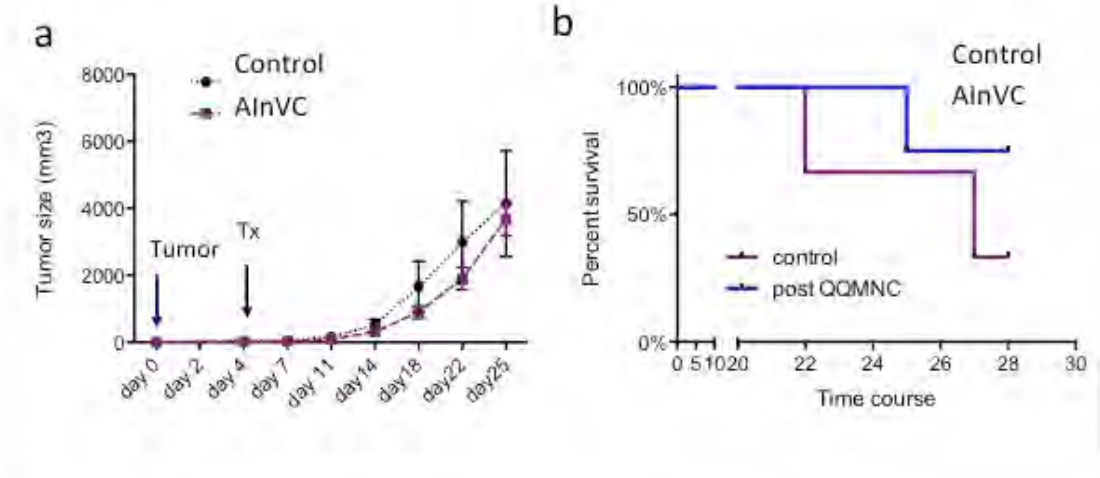

図9. マウス血液単核球由来AIVC細胞の移植によるB16メラノーマの腫瘍退縮効果及び生存率の検討。
C57BL6マウスの腹部皮下に7x10^{4}個/マウスのB16-F10メラノーマ細胞株を移植。移植後4日目でAIVC細胞を尾静脈から投与(1x106個/マウス)。経時的に腫瘍径及び生存率を測定した。腫瘍移植後28日に屠殺。

また、腫瘍内組織内血管は、pericyte(alpha SM actin+細胞)に裏打ちされた血管が増加した(**図10c**)。結果として、AInVC による抗炎症効果は、癌ニッチを抗炎症・血管成熟化を誘導し、癌細胞の壊死を誘導する効果があると考えられた。

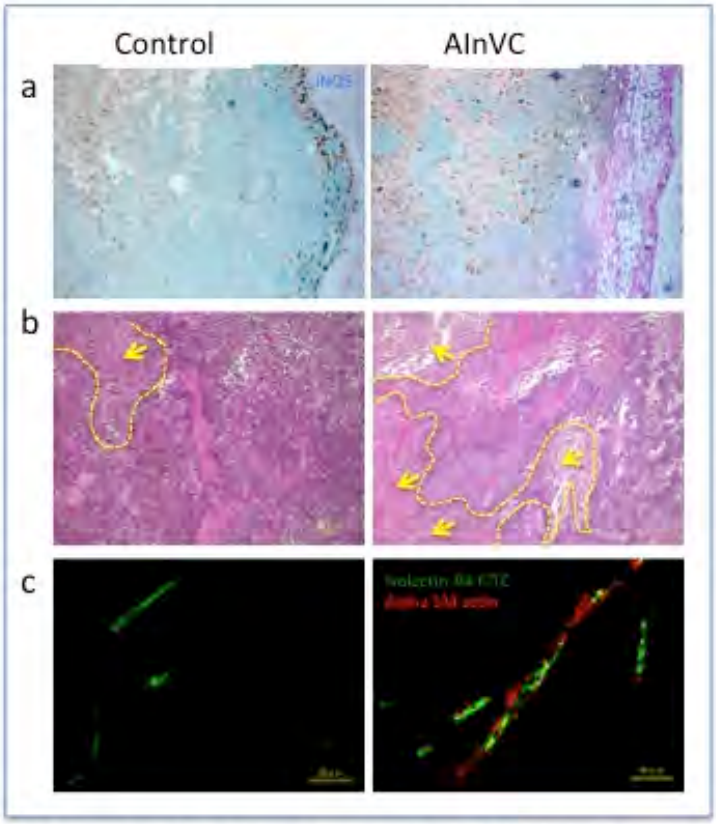

図10　マウス血液単核球のAInVC細胞の移植によるB16メラノーマの組織像（腫瘍移植後28日の腫瘍組織像）。
(a)　iNOS抗体による免疫組織染色像(x10)。iNOS発現領域は　light blueに染色されている。(b) H&E　染色による腫瘍壊死領域。Yellow dot　linelに囲まれた領域。(c　)腫瘍組織内血管。AIVC移植マウスの腫瘍血管はpericytelに囲まれて成熟している(vascular normalization)。Scale bar = 50 μm。

（研究考察）

癌ニッチにおける免疫寛容・抗炎症性細胞の動員は、癌細胞傷害性の免疫賦活細胞から癌細胞を保護し、腫瘍増大に重要な役割を担うこと、したがって、癌ニッチに免疫賦活細胞を浸潤させ、炎症環境にすることが癌制御において重要であることが報告されている。しかしながら、今回の研究により、癌ニッチにおいて、炎症環境ではなく抗炎症環境を整備し、血管成熟化を誘導することが制癌戦略として重要であることが判明した。実際、臨床において、Avastin　の効果が投与初期に限定される。これは、腫瘍血管形成抑制により結果的に腫瘍組織の虚血を促進し、炎症を遷延させることによるサイトカインの産生亢進による腫瘍増大、免疫寛容担当細胞(M2　マクロファージ、制御性　T　細胞など)の動員を促進してしまうことによると考えられる。また、InAVC　移植細胞ではなく、AInVC　移植細胞が腫瘍退縮及び生存率延長効果を示したことは、傷害組織の再生と同様に、癌組織においても抗炎症及び血管の成熟化による機能性血管の構築が抗癌において重要であると考えられた。以上、新たな制癌戦略として、抗炎症

性環境及び機能性血管の構築による癌ニッチの崩壊促進療法の開発が期待される。

REVIEW ARTICLE doi: 10.2176/nmc.ra.2016-0027

Neurol Med Chir (Tokyo) 56, 302–309, 2016 Online April 4, 2016

Recent Progress in Endothelial Progenitor Cell Culture Systems: Potential for Stroke Therapy

Shunya TAKIZAWA,[1] Eiichiro NAGATA,[1] Taira NAKAYAMA,[1] Haruchika MASUDA,[2] and Takayuki ASAHARA[2]

Departments of Neurology[1] and Regenerative Medicine Science,[2] Tokai University School of Medicine, Isehara, Kanagawa

Abstract

Endothelial progenitor cells (EPCs) participate in endothelial repair and angiogenesis due to their abilities to differentiate into endothelial cells and to secrete protective cytokines and growth factors. Consequently, there is considerable interest in cell therapy with EPCs isolated from peripheral blood to treat various ischemic injuries. Quality and quantity-controlled culture systems to obtain mononuclear cells enriched in EPCs with well-defined angiogenic and anti-inflammatory phenotypes have recently been developed, and increasing evidence from animal models and clinical trials supports the idea that transplantation of EPCs contributes to the regenerative process in ischemic organs and is effective for the therapy of ischemic cerebral injury. Here, we briefly describe the general characteristics of EPCs, and we review recent developments in culture systems and applications of EPCs and EPC-enriched cell populations to treat ischemic stroke.

Key words: endothelial progenitor cells, neuroregeneration, neurorepair, cerebral ischemia

Introduction

Current treatments for acute ischemic stroke rely mainly on vascular recanalization, including intravenous thrombolysis and interventional treatments, which have a narrow therapeutic time window after onset. The radical scavenger edaravone has been approved for acute ischemic stroke and is in clinical use, but only in Japan.[1)] On the other hand, therapeutic strategies for neurorepair following ischemic stroke are limited at present. Numerous studies have demonstrated beneficial neurorepair effects of various stem/progenitor cells, including bone marrow (BM) stem cells,[2)] mesenchymal stem cells,[3)] neural stem cells,[4)] induced neuronal cells directly converted from human skin fibroblasts,[5)] and endothelial progenitor cells (EPCs).[6)] In particular, EPCs are considered to have a great potential for neurorepair following ischemic stroke, based on their abilities to differentiate into endothelial cells and to secrete protective cytokines and growth factors.[7–9)]

In this review, we first briefly summarize recent work on identification and characterization of EPCs, together with the results of biological studies aimed at defining the roles of circulating EPCs in postnatal neovascularization. We then review the current status of culture systems for EPCs and EPCs-enriched cell populations, focusing on the therapeutic potential of EPCs, especially for cerebrovascular disease. Finally, we discuss current and planned clinical trials of EPC transplantation.

Received January 26, 2016; Accepted February 25, 2016

I. Development of the concept of EPC transplantation therapy

The EPCs were first isolated from peripheral blood (PB) of adults by one of the present authors, Asahara et al. in 1997.[10)] Circulating EPCs were derived from the BM, and they were shown to contribute to postnatal physiological and pathological neovascularization,[11,12)] which is consistent with a role in vasculogenesis. This opened the door to the epoch-making concept of "therapeutic vasculogenesis" by EPC transplantation, targeting ischemic diseases. As first-generation EPC transplantation therapy, unfractionated mononuclear cells (MNCs) from BM and PB were practically applied for patients with critical limb ischemia (CLI) (Fig. 1).

Subsequently, a second-generation approach was developed, involving exogenous mobilization of EPCs by stimulating hematopoietic progenitor

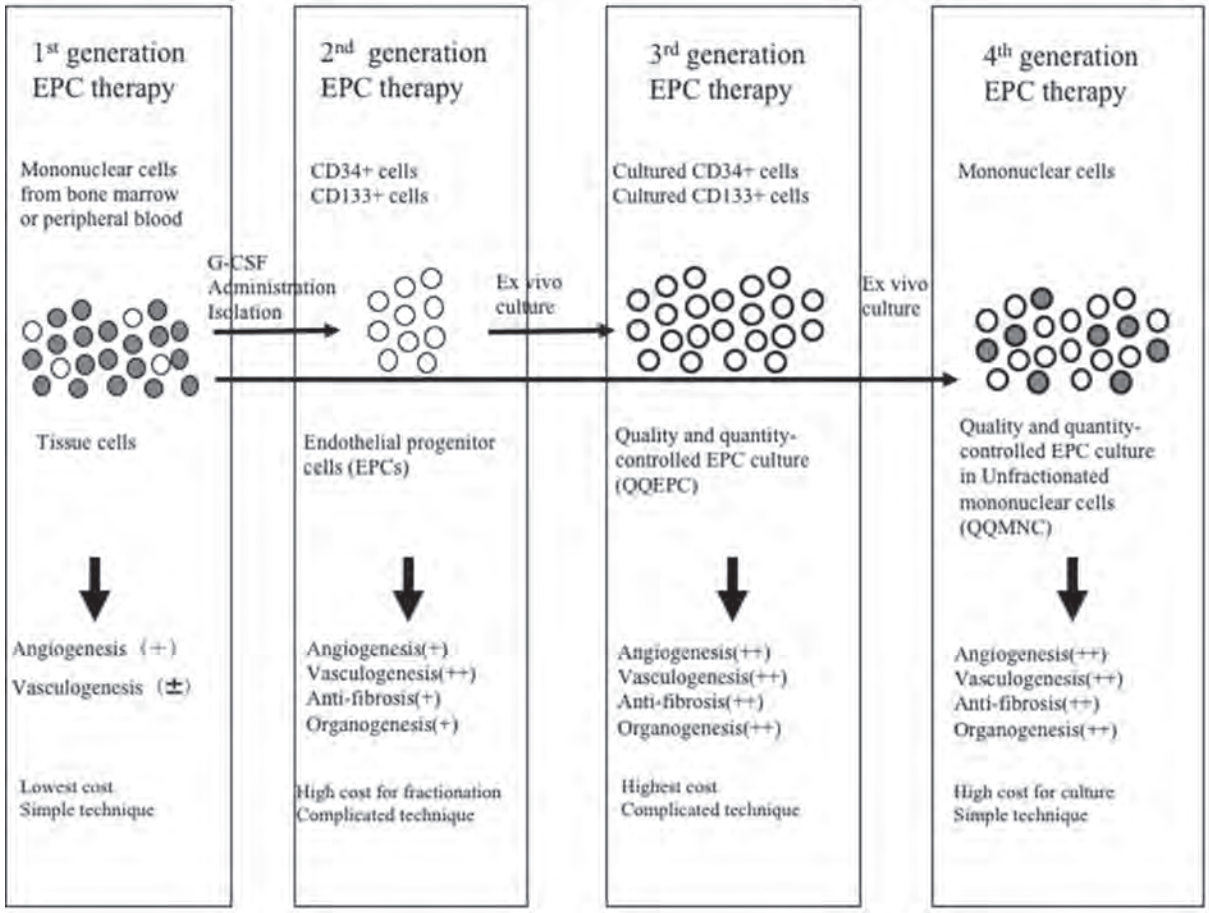

Fig. 1 Chronological development of EPC-based cell therapies. Since EPCs were first isolated from peripheral blood, various EPC-based cell therapies have been developed. The latest fourth-generation EPC therapy utilizes QQMNCs with mainly angiogenic and anti-inflammatory phenotypes. QQMNCs promote the regenerative process in ischemic organs, and offer the advantages of relatively low cost and simple culture technique. EPC: endothelial progenitor cell, QQMNCs: quality and quantity culture system to obtain mononuclear cells.

cells (Fig. 1) with granulocyte macrophage colony-stimulating factor or granulocyte colony-stimulating factor (G-CSF) to induce EPC mobilization and enhanced neovascularization of ischemic tissues.[13] However, this approach is more costly and requires more complicated techniques, compared to first-generation therapy.

Circulating EPCs can be subdivided into hematopoetic and non-hematopoetic lineages, which especially in human give rise to "early and late EPCs" depending on time duration after endothelial culture of PB- or umbilical cord blood (UCB)-MNCs.[14,15] Hematopoetic EPCs are derived from a pro-vasculogenic subpopulation of hematopoietic stem cells in the BM.[14] Hematopoetic EPCs can be defined as circulating cell populations bearing cell-surface markers such as $CD34^+$, $CD133^+$, and vascular endothelial growth factor receptor-2 (VEGFR-2),[14] or as "EPC colonies" obtained by conventional EPC culture methods that produce spindle-shaped adherent cells from PB, BM, or UCB MNCs in the presence of endothelial growth factors and cytokines.[16]

A novel EPC colony-forming assay (EPC-CFA) system to evaluate vasculogenic potential of EPCs[17–20] has recently been developed. Application of this system to progenitor-enriched populations, such as c-Kit+/Sca-1+/lineage negative cells in mouse[18–20] and $CD34^+$ or $CD133^+$ cells in human,[17] resulted in the identification of two morphologically distinct types of cell colony, each derived from a single cell: small EPC colonies and large EPC colonies. Based on their *in vitro* and *in vivo* characteristics, small EPCs are considered to represent "primitive EPCs," which are immature and have high proliferative capacity, whereas large EPCs

are considered to represent "definitive EPCs," having differentiating and vasculogenic capabilities. Considering the functional differences associated with the EPC differentiation cascade, "definitive EPCs" should be more suitable for clinical application, because of their potent vasculogenic and angiogenic activities.

At present, methods for fractionation of "definitive EPCs," have yet to be established, owing to the absence of any clinically based antibodies defining an attractive population for EPC therapy. An alternative approach is to develop culture systems to expand definitive EPCs from fractionated EPC populations ($CD133^+$ or $CD34^+$ cells). Based on this idea, a quality and quantity (QQ)-controlled culture system has been developed to obtain EPCs with vasculogenic potential for use as third-generation EPC therapy (Fig. 1).[21] However, the cost is still high and complicated techniques are required.

To overcome this practical difficulty, a QQ culture system skipping the EPC fractionation step, i.e., using unfractionated MNCs, has also been developed (Fig. 1).[22] This can be regarded as a fourth-generation culture system, and is discussed in "Fourth-generation EPC culture system."

II. Direct and indirect contributions of EPCs to neovascularization

A direct contribution of BM-derived EPCs to neovascularization has been demonstrated in various animal models. One well-established model uses transplantation of BM cells from transgenic mice in which LacZ is expressed under the regulation of an endothelial cell lineage specific promoter, such as Flk-1 or Tie-2 (Flk-1/LacZ/BMT, Tie-2/LacZ/BMT), into wild-type control mice, which are then exposed to various types of ischemic injury. In this model, BM-derived Flk-1- and/or Tie-2-expressing endothelial lineage cells can localize to vascular structures during tumor growth,[23,24] wound healing,[25] skeletal[23] or cardiac ischemia,[26,27] corneal neovascularization,[28] and endometrial remodeling following hormone-induced ovulation.[23,24] Regardless of the origin of EPCs, they make a significant contribution to neovascularization via vasculogenesis in ischemic tissues.

On the other hand, tissue-bound "resting EPCs" produce a variety of proangiogenic cytokines and growth factors, promoting proliferation and migration of pre-existing endothelial cells, activating angiogenesis, and contributing indirectly to vascular regeneration and the re-establishment of tissue homeostasis. Thus, EPCs not only work via the activation and support of vasculogenesis, but may also be major players in activation and mediation of angiogenesis[29] by promoting in situ proliferation and migration of pre-existing endothelial cells. This indirect contribution of EPCs to neovascularization is supported by several reports demonstrating the secretion by EPCs of various cytokines and other proangiogenic factors: VEGF, hepatic growth factor (HGF), angiopoietin-1 (Ang-1), stroma-derived factor-1α (SDF-1α), insulin-like growth factor-1 (IGF-1), and endothelial nitric oxide synthase (eNOS)/inducible nitric oxide synthase (iNOS).[26,30,31]

III. Fourth-generation EPC culture system

Masuda et al.[21,22] have recently established an improved QQ culture system to obtain mononuclear cells (QQMNCs) enriched in EPCs from unfractionated MNCs (fourth-generation culture system; Fig. 1). The QQ culture medium of Stem Line II (Sigma-Aldrich, St. Louis, Missouri, USA) contains five human recombinant proteins: stem cell factor (SCF), thrombopoietin, Flt-3 ligand, VEGF, and interleukin-6 (IL-6). Isolated PBMNCs were cultured in this system for 7 days at the cell density of 2×10^6 cells/2 mL QQ culture medium.

Fig. 2 illustrates the cell populations and characteristics of PBMNCs and QQMNCs. The cell numbers of QQMNCs were approximately half than those of PBMNCs, mainly due to a significant reduction of B lymphocytes ($CD19^+$), NK cells ($CD16^+$ and $CD56^+$), and pro-inflammatory monocytes and macrophages ($CD14^+$ and $CCR2^+$). In contrast, populations of

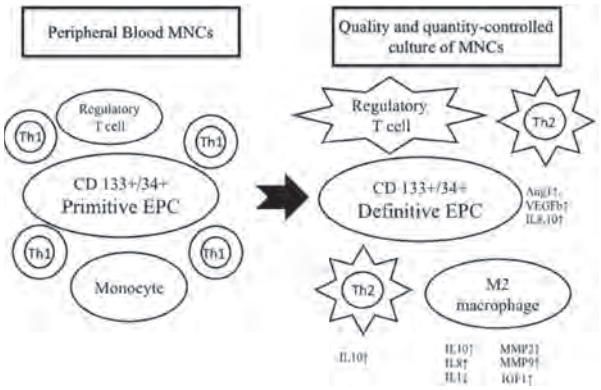

Fig. 2 Comparison of cell populations and characteristics of PBMNCs and QQMNCs. QQMNCs contain large EPCs, which are classified as definitive EPCs, with differentiating and vasculogenic capabilities. In addition, M2 macrophages are induced by anti-inflammatory cytokines and control adaptive immunity. Secreted anti-inflammatory cytokines promote and regulate type 2 immune responses, angiogenesis, and tissue repair. EPC: endothelial progenitor cell, PBMNC: peripheral blood mononuclear cell, QQMNCs: quality and quantity culture system to obtain mononuclear cells.

progenitor cells ($CD34^+$ and $CD133^+$) and of anti-inflammatory monocytes and macrophages ($CD206^+$) were greatly expanded in QQMNCs, while populations of endothelial cells ($CD105^+$ and $CD146^+$) and helper T cells ($CD4^+$) were expanded moderately. The increase in $CD34^+$ or $CD133^+$ cell populations indicates an expanded population of immature EPCs, while the increase in $CD105^+$ or $CD146^+$ cell populations is indicative of EPC expansion and differentiation. The extent in the increase of $CD206^+$ cells and decrease of $CCR2^+$ cells indicate conversion of the monocyte/macrophage phenotype from M1 to M2. Monocytes/macrophages differentiate toward a pro-inflammatory, classically activated M1 state or toward an anti-inflammatory, alternatively activated M2 state in response to different environments and stimuli. M2 macrophages are induced by anti-inflammatory cytokines, such as IL-4, IL-13, and IL-10, and they ameliorate type 1 inflammatory responses and control adaptive immunity. Furthermore, their secreted anti-inflammatory cytokines promote and regulate type 2 immune responses, angiogenesis, and tissue repair. Thus, monocyte/macrophages in QQMNCs mainly exhibit angiogenic and anti-inflammatory phenotypes, and are expected to contribute to the regenerative process in ischemic organs. QQMNCs offer the advantages of lower cost, simpler techniques, and faster culture, compared with the original third-generation EPC therapy.

IV. EPC-based cell therapies for ischemic stroke

Currently, there is no gold standard treatment that is available outside the acute therapeutic window to improve outcome in stroke patients. However, there is increasing evidence that transplantation of EPCs can promote recovery of ischemic cerebral injury. Table 1 summarizes the results of basic experiments of EPC-based cell therapies in ischemic stroke models.

Taguchi et al.[32] demonstrated that systemic administration of human UCB-derived $CD34^+$ cells to immune-compromised mice subjected to stroke 48 hours earlier induces neovascularization and provides a favorable environment for neuronal regeneration. Endogenous neurogenesis is accelerated as a result of enhanced migration of neuronal progenitor cells to the damaged area, followed by maturation, leading to functional recovery. Ohta et al.[33] demonstrated that autologous intra-arterial transplantation of BM-derived EPCs at 90 minutes after ischemia reduced infarct volume and improved motor function. Interestingly, administration of EPCs significantly reduced the number of myeloperoxidase-immunoreactive cells in the ischemic lesion at 24 hours and increased regional cortical blood flow at 48 hours. The EPCs expressing eNOS were observed in the ischemic hemisphere and around the endothelial layer of pial arteries. Fan et al.[7] demonstrated that acute intravenous administration of human PB-derived EPCs reduced infarct volume at day 3 after transient middle cerebral artery occlusion (MCAO) and reduced brain atrophy at 1 month, accompanied with improvement of neurobehavioral outcomes, and increased vessel density. Furthermore, expression of SDF-1, which mediates BM cell homing to brain ischemic regions,[34] was increased in ischemic brain from 24 hours after MCAO. Moubarik et al.[8] reported that administration of human UCB-derived EPCs improved neurological function in a rat model of ischemia-reperfusion. This improvement occurred along with an increase in capillary density, a decrease in apoptosis in peri-infarct areas and an increase in neurogenesis in the subventricular zone. Iskander et al.[35] found that intravenous administration of human UCB-$CD133^+$ EPCs reduced infarct volume in rat MCAO models and improved endogenous proliferation, angiogenesis, and neurogenesis. Magnetic resonance imaging (MRI) with *in vivo* magnetically labeled cells confirmed accumulation of transplanted cells in stroke-affected hemispheres. Thus, EPCs originated from any cell source appear to be beneficial for neurorepair in both permanent and transient ischemic stroke models.

The direct effect of EPCs on angiogenesis and the indirect effect of multiple EPC-secreted factors are both relevant to the treatment of ischemic stroke. Rosell et al.[36] demonstrated the angiogenic potential of EPC-secreted factors, such as VEGF, fibroblast growth factor-basic (FGF-b), and platelet-derived growth factor-b (PDGF-b) to safely treat cerebral ischemia beyond the hyperacute phase, using a cell-free approach. Both EPCs and EPC-cell-free treatments significantly increased angiogenesis in peri-infarct areas. Functional improvement at 2 weeks after MCAO was enhanced in mice receiving either EPCs or EPC-cell-free treatment. Chen et al.[37] reported that astrocytic-high mobility group box1 (HMGB1) modulates the paracrine function of endogenous human PB-derived EPCs. Transplantation of EPCs improved neurobehavioral outcomes, reduced brain atrophy volume, and enhanced neovascularization in a transient MCAO model. The HMGB1 inhibitor glycyrrhizin blocked the beneficial effect of human PB-EPC transplantation and blocked integration of green fluorescent protein-labeled human PB-EPCs with microvessels, suggesting that HMGB1 upregulation in postischemic brain could promote exogenous EPCs-mediated stroke recovery by modulating the paracrine function of EPCs.

It may be controversial whether EPCs through systemic administration reach to the injured organs. Hofmann et al.[38] confirmed CD34-enriched cells

Table 1 Basic experiments of endothelial progenitor cell-based cell therapy for ischemic stroke

Author/year	Ischemic stroke model	Cell sources of EPC therapy	Timing and route of administration	Outcome
Taguchi et al. (2004)[32]	Permanent occlusion of distal MCA in mice	Human UCB-derived $CD34^+$ cells (non cultured $CD34^+$ cells from UCBMNCs)	i.v. (48 hours after occlusion) from tail vein of SCID mice	Enhanced neovascularization followed by endogenous neurogenesis
Ohta et al. (2006)[33]	90-min transient occlusion of MCA in rat	Autologous rat BM-derived EPCs (cultured EPCs from BMCs of Sprague-Dawley rat)	i.a. at 2 hours after occlusion from ICA of Sprague-Dawley rat	Reduced infarct volume and improved neurological deficits
Fan et al. (2010)[7]	60-min transient occlusion of MCA in adult nude CD-1 mice	Human PB-derived EPCs (cultured EPCs from PBMNCs; late EPCs, i.e., EOCs or ECFCs)	i.v. (1 hour after occlusion) from a jugular vein of nude CD-1 mice	Reduced infarct volume, and upregulated SDF-1
Moubarik et al. (2011)[8]	60-min transient occlusion of MCA in rats	Human UCB-derived EPCs (cultured EPCs from UCBMNCs; late EPCs, i.e., EOCs or ECFCs)	i.v. (24 hours after occlusion) from a femoral vein of Sprague-Dawley rat	Improved neurological deficits, increased capillary density, decreased apoptosis
Iskander et al. (2013)[35]	2-hour transient occlusion of MCA in rats	Human UCB-derived AC $(CD)133^+$ EPCs (suspension cultured EPCs from AC $(CD)133^+$ cells of UCBMNCs)	i.v. (24 hours after occlusion) to Wistar rats	Reduced infarct volume, and affected endogenous proliferation, angiogenesis, and neurogenesis
Rosell et al. (2013)[36]	Permanent occlusion of distal MCA in mice	Mouse spleen-derived EPCs (cultured EPCs from splenic MNCs of BALB/c mice) or EPC-cell-free medium	i.v. (1 day after occlusion) to BALB/c mice	Increased angiogenesis in peri-infarct areas by EPCs, as well as EPC-cell-free medium
Chen et al. (2014)[37]	90-min transient occlusion of MCA in mice	Human PB-derived EPCs (cultured EPCs from PBMNCs; late EPCs, i.e., EOCs or ECFCs)	i.v. (just after occlusion) from a jugular vein of ICR mice	Improved neurobehavioral outcomes, reduced brain atrophy volume, and enhanced neovascularization
Hecht et al. (2014)[39]	Bilateral vertebral arteries and the right common carotid artery in rats	Mouse embryo-derived EPCs (cultured EPCs from 129Sv mouse E7.5 embryos)	i.v. (just after, and days 7 and 14 after occlusion) from a tail vein of Sprague-Dawley rats	Restored hemodynamic impairment, increased collateralization and parenchymal capillary density

BALB/c: Bagg Albino (inbred research mouse strain) named by Jackson's laboratory, BMC: bone marrow cell, ECFC: endothelial colony forming cell, EOC: endothelial outgrowth cell, EPC: endothelial progenitor cell, i.a.: intra-arterial infusion, ICA: internal carotid artery, ICR: Institute of Cancer Research, i.v.: intra-venous infusion, PBMNC: peripheral blood mononuclear cell, SCID: severe combined immunodeficiency, SFD: stroma-derived factor, UCB: umbilical cord blood.

predominantly homed in the border zone of myocardial infarction after intravenous injection of ^{16}F-FDG-labeled BMC. As shown in Table 1, seven out of eight animal studies,[7,8,32,35–37,39] in which cell therapies were given through intravenous administration, indicated favorable outcome in cerebral ischemia. Although EPCs may be partly trapped in lung, liver, and spleen, favorable outcome may be explained by the direct effect of EPC such as angiogenesis, as well as the indirect effect of EPC, EPC-secreted factors such as VEGF, HGF, Ang-1, SDF-1α, IGF-1, eNOS, FGF-b, PDGF-b, etc.[26,30,31,36]

As mentioned above, several EPC cell therapies have been investigated in models of acute cerebral ischemia, but it remains unclear whether EPCs are effective on chronic cerebral hypoperfusion. Hecht et al.[39] found that embryonic EPCs restored hemodynamic impairment and increased the basal and leptomeningeal collateralization and parenchymal capillary density in a rat model of chronic cerebral hypoperfusion. Thus, EPCs appear to have potential for therapeutic stimulation of collateral vessel growth in chronic cerebrovascular hypoperfusion.

Dual effect of VEGF, microvascular hyperpermeability, and angiogenesis has been presented in many different pathological and physiological settings.[40] Zhang et al.[41] demonstrated that VEGF in the ischemic core may mediate blood-brain barrier leakage 2–4 hours after embolic MCA occlusion, whereas upregulation of VEGF/VEGF receptors at the boundary zone may regulate neovascularization in ischemic brain 2–28 days after the onset. Although EPCs also appear to have potential for blood-brain barrier leakage and angiogenesis, our preliminary data suggest that QQMNC-mediated anti-inflammatory and immune-modulatory cytokines may conceal the adverse effect of VEGF at early phase of cerebral ischemia.

As described above, QQMNCs have potential to activate anti-inflammatory and angiogenic monocytes/helper T lymphocytes, as well as expanding vasculogenic EPCs. Our preliminary study demonstrated that intra-arterial administration of human QQMNCs (1×10^5 cells) improved cerebral blood flow in nude mice with permanent MCAO, and increased VEGF-positive cells in the peri-infarct area, compared with the vehicle-treated group (Fig. 3). These results indicate that QQMNCs may promote repair and regeneration of neurovascular units, and is considered as the best candidate for clinical trial against ischemic stroke.

V. Clinical trials of EPC transplantation

A phase II clinical trial of intramuscular transplantation of autologous $CD34^+$ cells in patients with intractable CLI has been reported.[42] No-option CLI patients underwent intramuscular transplantation of G-CSF-mobilized $CD34^+$ cells isolated by magnetic sorting. Ischemic resting pain scales and physiological parameters improved relatively early after cell therapy, and subsequently plateaued, accompanied with recovery from the CLI state. Rutherford's category and CLI-free ratio at week 36 or later may be suitable endpoints in clinical trials of cell therapy for CLI. On the basis of these results, Asahara et al. are preparing a larger phase III, randomized controlled clinical trial to evaluate $CD34^+$ cell therapy versus standard care. In addition, we are currently planning a clinical trial of intra-arterial QQMNCs administration in atherothrombotic patients within a week after onset. This may provide a new option for treatment of acute ischemic stroke, in addition to conventional thrombolytic therapies.

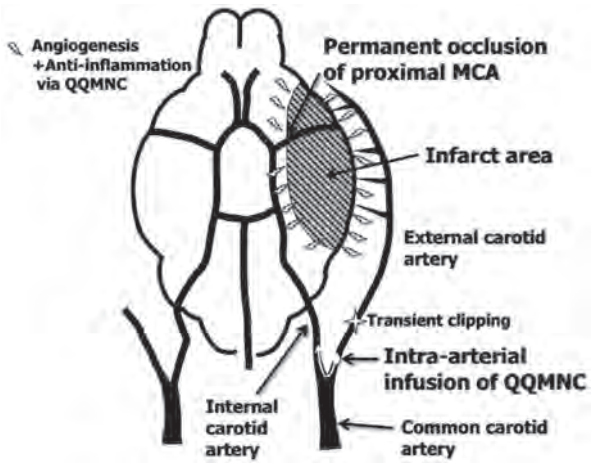

Fig. 3 Study to examine the effect of human QQMNCs in mice with permanent MCAO. This figure schematically illustrates our study to examine the effect of intra-arterial administration of human QQMNCs in nude mice with permanent MCAO. Preliminary results indicate that QQMNCs promote repair and regeneration of neurovascular units after ischemic stroke. QQMNCs: quality and quantity culture system to obtain mononuclear cells.

Conclusion

The EPCs participate in endothelial repair and angiogenesis in various animal models through their abilities to differentiate into endothelial cells and to secrete protective cytokines and growth factors. Thus, EPCs and EPC-enriched cell populations, especially QQMNCs, are considered promising for the treatment of ischemic stroke. The results of clinical trials are expected to become available in the near future.

Acknowledgments

This work was partly supported by Grant-in-Aid for Scientific Research (C) 26461320 from the Japan Society for the Promotion of Science.

Conflicts of Interest Disclosure

The authors report no conflict of interest.

References

1) Abe K, Yuki S, Kogure K: Strong attenuation of ischemic and postischemic brain edema in rats by a novel free radical scavenger. *Stroke* 19: 480–485, 1988
2) Shichinohe H, Kuroda S, Yano S, Hida K, Iwasaki Y: Role of SDF-1/CXCR4 system in survival and migration of bone marrow stromal cells after transplantation into mice cerebral infarct. *Brain Res* 1183: 138–147, 2007
3) Lee JS, Hong JM, Moon GJ, Lee PH, Ahn YH, Bang OY; STARTING collaborators: A long-term follow-up study of intravenous autologous mesenchymal stem cell transplantation in patients with ischemic stroke. *Stem Cells* 28: 1099–1106, 2010
4) Gage FH: Mammalian neural stem cells. *Science* 287: 1433–1438, 2000
5) Vierbuchen T, Ostermeier A, Pang ZP, Kokubu Y, Südhof TC, Wernig M: Direct conversion of fibroblasts to functional neurons by defined factors. *Nature* 463: 1035–1041, 2010
6) Zhang ZG, Zhang L, Jiang Q, Chopp M: Bone marrow-derived endothelial progenitor cells participate in cerebral neovascularization after focal cerebral ischemia in the adult mouse. *Circ Res* 90: 284–288, 2002
7) Fan Y, Shen F, Frenzel T, Zhu W, Ye J, Liu J, Chen Y, Su H, Young WL, Yang GY: Endothelial progenitor cell transplantation improves long-term stroke outcome in mice. *Ann Neurol* 67: 488–497, 2010
8) Moubarik C, Guillet B, Youssef B, Codaccioni JL, Piercecchi MD, Sabatier F, Lionel P, Dou L, Foucault-Bertaud A, Velly L, Dignat-George F, Pisano P: Transplanted late outgrowth endothelial progenitor cells as cell therapy product for stroke. *Stem Cell Rev* 7: 208–220, 2011
9) Chen J, Chen S, Chen Y, Zhang C, Wang J, Zhang W, Liu G, Zhao B, Chen Y: Circulating endothelial progenitor cells and cellular membrane microparticles in db/db diabetic mouse: possible implications in cerebral ischemic damage. *Am J Physiol Endocrinol Metab* 301: E62–E71, 2011
10) Asahara T, Murohara T, Sullivan A, Silver M, van der Zee R, Li T, Witzenbichler B, Schatteman G, Isner JM: Isolation of putative progenitor endothelial cells for angiogenesis. *Science* 275: 964–967, 1997
11) Shi Q, Rafii S, Wu MH, Wijelath ES, Yu C, Ishida A, Fujita Y, Kothari S, Mohle R, Sauvage LR, Moore MA, Storb RF, Hammond WP: Evidence for circulating bone marrow-derived endothelial cells. *Blood* 92: 362–367, 1998
12) Asahara T, Masuda H, Takahashi T, Kalka C, Pastore C, Silver M, Kearne M, Magner M, Isner JM: Bone marrow origin of endothelial progenitor cells responsible for postnatal vasculogenesis in physiological and pathological neovascularization. *Circ Res* 85: 221–228, 1999
13) Takahashi T, Kalka C, Masuda H, Chen D, Silver M, Kearney M, Magner M, Isner JM, Asahara T: Ischemia- and cytokine-induced mobilization of bone marrow-derived endothelial progenitor cells for neovascularization. *Nat Med* 5: 434–438, 1999
14) Asahara T, Kawamoto A, Masuda H: Concise review: circulating endothelial progenitor cells for vascular medicine. *Stem Cells* 29: 1650–1655, 2011
15) Fadini GP, Losordo D, Dimmeler S: Critical reevaluation of endothelial progenitor cell phenotypes for therapeutic and diagnostic use. *Circ Res* 110: 624–637, 2012
16) Hill JM, Zalos G, Halcox JP, Schenke WH, Waclawiw MA, Quyyumi AA, Finkel T: Circulating endothelial progenitor cells, vascular function, and cardiovascular risk. *N Engl J Med* 348: 593–600, 2003
17) Masuda H, Alev C, Akimaru H, Ito R, Shizuno T, Kobori M, Horii M, Ishihara T, Isobe K, Isozaki M, Itoh J, Itoh Y, Okada Y, McIntyre BA, Kato S, Asahara T: Methodological development of a clonogenic assay to determine endothelial progenitor cell potential. *Circ Res* 109: 20–37, 2011
18) Kwon SM, Eguchi M, Wada M, Iwami Y, Hozumi K, Iwaguro H, Masuda H, Kawamoto A, Asahara T: Specific Jagged-1 signal from bone marrow microenvironment is required for endothelial progenitor cell development for neovascularization. *Circulation* 118: 157–165, 2008
19) Tanaka R, Wada M, Kwon SM, Masuda H, Carr J, Ito R, Miyasaka M, Warren SM, Asahara T, Tepper OM: The effects of flap ischemia on normal and diabetic progenitor cell function. *Plast Reconstr Surg* 121: 1929–1942, 2008
20) Kamei N, Kwon SM, Alev C, Ishikawa M, Yokoyama A, Nakanishi K, Yamada K, Horii M, Nishimura H, Takaki S, Kawamoto A, Ii M, Akimaru H, Tanaka N, Nishikawa S, Ochi M, Asahara T: Lnk deletion reinforces the function of bone marrow progenitors in promoting neovascularization and astrogliosis following spinal cord injury. *Stem Cells* 28: 365–375, 2010
21) Masuda H, Iwasaki H, Kawamoto A, Akimaru H, Ishikawa M, Ii M, Shizuno T, Sato A, Ito R, Horii M, Ishida H, Kato S, Asahara T: Development of serum-free quality and quantity control culture of colony-forming endothelial progenitor cell for vasculogenesis. *Stem Cells Transl Med* 1: 160–171, 2012
22) Masuda H, Tanaka R, Fujimura S, Ishikawa M, Akimaru H, Shizuno T, Sato A, Okada Y, Iida Y, Itoh J, Itoh Y, Kamiguchi H, Kawamoto A, Asahara T: Vasculogenic conditioning of peripheral blood mononuclear cells promotes endothelial progenitor cell expansion and phenotype transition of anti-inflammatory macrophage and T lymphocyte to cells with regenerative potential. *J Am Heart Assoc* 3: e000743, 2014
23) Asahara T, Masuda H, Takahashi T, Kalka C, Pastore C, Silver M, Kearne M, Magner M, Isner JM: Bone marrow origin of endothelial progenitor cells responsible for postnatal vasculogenesis in physiological and pathological neovascularization. *Circ Res* 85: 221–228, 1999

24) Masuda H, Kalka C, Takahashi T, Yoshida M, Wada M, Kobori M, Itoh R, Iwaguro H, Eguchi M, Iwami Y, Tanaka R, Nakagawa Y, Sugimoto A, Ninomiya S, Hayashi S, Kato S, Asahara T: Estrogen-mediated endothelial progenitor cell biology and kinetics for physiological postnatal vasculogenesis. *Circ Res* 101: 598–606, 2007
25) Bauer SM, Goldstein LJ, Bauer RJ, Chen H, Putt M, Velazquez OC: The bone marrow-derived endothelial progenitor cell response is impaired in delayed wound healing from ischemia. *J Vasc Surg* 43: 134–141, 2006
26) Ii M, Nishimura H, Iwakura A, Wecker A, Eaton E, Asahara T, Losordo DW: Endothelial progenitor cells are rapidly recruited to myocardium and mediate protective effect of ischemic preconditioning via "imported" nitric oxide synthase activity. *Circulation* 111: 1114–1120, 2005
27) Iwakura A, Shastry S, Luedemann C, Hamada H, Kawamoto A, Kishore R, Zhu Y, Qin G, Silver M, Thorne T, Eaton L, Masuda H, Asahara T, Losordo DW: Estradiol enhances recovery after myocardial infarction by augmenting incorporation of bone marrow-derived endothelial progenitor cells into sites of ischemia-induced neovascularization via endothelial nitric oxide synthase-mediated activation of matrix metalloproteinase-9. *Circulation* 113: 1605–1614, 2006
28) Murayama T, Tepper OM, Silver M, Ma H, Losordo DW, Isner JM, Asahara T, Kalka C: Determination of bone marrow-derived endothelial progenitor cell significance in angiogenic growth factor-induced neovascularization in vivo. *Exp Hematol* 30: 967–972, 2002
29) Folkman J, Shing Y: Angiogenesis. *J Biol Chem* 267: 10931–10934, 1992
30) Jujo K, Ii M, Losordo DW: Endothelial progenitor cells in neovascularization of infarcted myocardium. *J Mol Cell Cardiol* 45: 530–544, 2008
31) Miyamoto Y, Suyama T, Yashita T, Akimaru H, Kurata H: Bone marrow subpopulations contain distinct types of endothelial progenitor cells and angiogenic cytokine-producing cells. *J Mol Cell Cardiol* 43: 627–635, 2007
32) Taguchi A, Soma T, Tanaka H, Kanda T, Nishimura H, Yoshikawa H, Tsukamoto Y, Iso H, Fujimori Y, Stern DM, Naritomi H, Matsuyama T: Administration of CD34+ cells after stroke enhances neurogenesis via angiogenesis in a mouse model. *J Clin Invest* 114: 330–338, 2004
33) Ohta T, Kikuta K, Imamura H, Takagi Y, Nishimura M, Arakawa Y, Hashimoto N, Nozaki K: Administration of ex vivo-expanded bone marrow-derived endothelial progenitor cells attenuates focal cerebral ischemia-reperfusion injury in rats. *Neurosurgery* 59: 679–686; discussion 679–686, 2006
34) Hill WD, Hess DC, Martin-Studdard A, Carothers JJ, Zheng J, Hale D, Maeda M, Fagan SC, Carroll JE, Conway SJ: SDF-1 (CXCL12) is upregulated in the ischemic penumbra following stroke: association with bone marrow cell homing to injury. *J Neuropathol Exp Neurol* 63: 84–96, 2004
35) Iskander A, Knight RA, Zhang ZG, Ewing JR, Shankar A, Varma NR, Bagher-Ebadian H, Ali MM, Arbab AS, Janic B: Intravenous administration of human umbilical cord blood-derived AC133+ endothelial progenitor cells in rat stroke model reduces infarct volume: magnetic resonance imaging and histological findings. *Stem Cells Transl Med* 2: 703–714, 2013
36) Rosell A, Morancho A, Navarro-Sobrino M, Martínez-Saez E, Hernández-Guillamon M, Lope-Piedrafita S, Barceló V, Borrás F, Penalba A, García-Bonilla L, Montaner J: Factors secreted by endothelial progenitor cells enhance neurorepair responses after cerebral ischemia in mice. *PLoS One* 8: e73244, 2013
37) Chen C, Lin X, Wang J, Tang G, Mu Z, Chen X, Xu J, Wang Y, Zhang Z, Yang GY: Effect of HMGB1 on the paracrine action of EPC promotes post-ischemic neovascularization in mice. *Stem Cells* 32: 2679–2689, 2014
38) Hofmann M, Wollert KC, Meyer GP, Menke A, Arseniev L, Hertenstein B, Ganser A, Knapp WH, Drexler H: Monitoring of bone marrow cell homing into the infarcted human myocardium. *Circulation* 111: 2198–2202, 2005
39) Hecht N, Schneider UC, Czabanka M, Vinci M, Hatzopoulos AK, Vajkoczy P, Woitzik J: Endothelial progenitor cells augment collateralization and hemodynamic rescue in a model of chronic cerebral ischemia. *J Cereb Blood Flow Metab* 34: 1297–1305, 2014
40) Dvorak HF, Brown LF, Detmar M, Dvorak AM: Vascular permeability factor/vascular endothelial growth factor, microvascular hyperpermeability, and angiogenesis. *Am J Pathol* 146: 1029–1039, 1995
41) Zhang ZG, Zhang L, Tsang W, Soltanian-Zadeh H, Morris D, Zhang R, Goussev A, Powers C, Yeich T, Chopp M: Correlation of VEGF and angiopoietin expression with disruption of blood-brain barrier and angiogenesis after focal cerebral ischemia. *J Cereb Blood Flow Metab* 22: 379–392, 2002
42) Fujita Y, Kinoshita M, Furukawa Y, Nagano T, Hashimoto H, Hirami Y, Kurimoto Y, Arakawa K, Yamazaki K, Okada Y, Katakami N, Uno E, Matsubara Y, Fukushima M, Nada A, Losordo DW, Asahara T, Okita Y, Kawamoto A: Phase II clinical trial of CD34+ cell therapy to explore endpoint selection and timing in patients with critical limb ischemia. *Circ J* 78: 490–501, 2014

Address reprint requests to: Shunya Takizawa, MD, PhD, Department of Neurology, Tokai University School of Medicine, 143 Shimokasuya, Isehara, Kanagawa 259-1193, Japan.
e-mail: shun@is.icc.u-tokai.ac.jp

Cell Transplantation, Vol. 23, pp. 167–179, 2014

0963-6897/14 $90.00 + .00
DOI: http://dx.doi.org/10.3727/096368912X658007
E-ISSN 1555-3892
www.cognizantcommunication.com

Autologous G-CSF-Mobilized Peripheral Blood CD34$^+$ Cell Therapy for Diabetic Patients With Chronic Nonhealing Ulcer

Rica Tanaka,*† Haruchika Masuda,† Shunichi Kato,† Kotaro Imagawa,‡ Kazuo Kanabuchi,§ Chie Nakashioya,¶ Fumiaki Yoshiba,¶ Tsuyoshi Fukui,‡ Rie Ito,† Michiru Kobori,† Mika Wada,† Takayuki Asahara,† and Muneo Miyasaka‡

*Department of Plastic and Reconstructive Surgery, Juntendo University School of Medicine, Tokyo, Japan
†Department of Regenerative Medicine, Tokai University School of Medicine, Isehara, Kanagawa, Japan
‡Department of Plastic and Reconstructive Surgery, Tokai University School of Medicine, Isehara, Kanagawa, Japan
§Department of Cardiovascular Surgery, Tokai University School of Medicine, Isehara, Kanagawa, Japan
¶Department of Blood Transfusion Service, Cell Transplantation and Regenerative Medicine, Tokai University School of Medicine, Isehara, Kanagawa, Japan

Recently, animal studies have demonstrated the efficacy of endothelial progenitor cell (EPC) therapy for diabetic wound healing. Based on these preclinical studies, we performed a prospective clinical trial phase I/IIa study of autologous G-CSF-mobilized peripheral blood (PB) CD34$^+$ cell transplantation for nonhealing diabetic foot patients. Diabetic patients with nonhealing foot ulcers were treated with 2×10^7 cells of G-CSF-mobilized PB CD34$^+$ cells as EPC-enriched population. Safety and efficacy (wound closure and vascular perfusion) were evaluated 12 weeks posttherapy and further followed for complete wound closure and recurrence. A total of five patients were enrolled. Although minor amputation and recurrence were seen in three out of five patients, no death, other serious adverse events, or major amputation was seen following transplantation. Complete wound closure was observed at an average of 18 weeks with increased vascular perfusion in all patients. The outcomes of this prospective clinical study indicate the safety and feasibility of CD34$^+$ cell therapy in patients with diabetic nonhealing wounds.

Key words: Nonhealing diabetic wound; Endothelial progenitor cells (EPC); Autologous cell therapy; Vasculogenesis; Wound healing

INTRODUCTION

Diabetic patients with nonhealing chronic ulcer are increasing yearly. Most nonhealing diabetic ulcers with peripheral vascular disease are difficult to cure, and once all conventional treatment modalities are exhausted, amputation is the final solution. More than 40–60% of nontraumatic lower extremity amputations are related to diabetic foot. It is also reported that individuals with diabetes have 15 to 46 times greater risk of high-level lower extremity amputations than those without diabetes (29). In addition, 5-year mortality rates after lower extremity amputation for diabetics, critical limb ischemia, and peripheral artery disease range from 39% to 68% (15). Furthermore, the economic burden of diabetic foot ulcer is estimated to be $98 billion per year (26). These data suggest the importance and necessity of alternative and more effective treatment option for diabetic patients with nonhealing ulcers.

After the discovery of endothelial progenitor cells (EPCs) in 1997, these vascular stem cells became the subject of intense experimental and clinical investigation for angiogenesis and wound healing. EPCs are an immature cell population that possesses an enhanced potential to differentiate into mature endothelial cells (2). EPCs can be isolated as cluster of differentiation 34-positive cells (CD34$^+$) and CD133$^+$ mononuclear cells (MNCs) from adult bone marrow (BM) and peripheral blood (2,9). EPCs mainly reside in the bone marrow and are mobilized into the peripheral blood with tissue ischemia or systematic administration of granulocyte colony-stimulating factor (G-CSF), vascular endothelial growth factor (VEGF), or estrogen (22,31). Mobilized EPCs will be home to ischemic sites for vascular repair. Preliminary studies support the potential of EPC therapy for angiogenesis and wound healing, and systemic (27) and local transplantation of EPCs (30) has become an alternative

Received March 22, 2012; final acceptance October 9, 2012. Online prepub date: October 25, 2012.
Address correspondence to Rica Tanaka, M.D., Ph.D., Department of Plastic and Reconstructive Surgery, Juntendo University School of Medicine, 2-1-1 Hongo Bunkyo-ku, Tokyo, 113-8421, Japan. Tel: +81-03-8313-3111; E-mail: rtanaka@juntendo.ac.jp

therapeutic option for diabetic ulcers. In murine diabetic ulcer, human EPCs are incorporated into the wound bed of diabetic mice following local injection and participate in neovascularization with recipient's endothelial cells, resulting in enhancement of wound vascular density and higher wound closure rate (28). Lin et al. also demonstrated that topical application of bone marrow-derived progenitor cells accelerates diabetic wound healing and increases wound vasculogenesis (19). These promising results encouraged clinical application of EPC transplantation for improvement of nonhealing diabetic ulcer. Until now, several researchers have investigated and reported the efficacy of autologous bone marrow and peripheral blood MNCs on patients with diabetic ulcers; however, the efficacy of purified EPC transplantation is not yet investigated (13,18).

Here we report a phase I/IIa clinical trial of transplantation of autologous and G-CSF-mobilized $CD34^+$ cells in patients with intractable diabetic ulcer. G-CSF was used to efficiently mobilize bone marrow-derived EPCs to peripheral blood, and the mobilized $CD34^+$ cells were isolated as the EPC-enriched fraction.

MATERIALS AND METHODS

Ethical Conduct of Research

The authors have obtained appropriate institutional review board approval or have followed the principles outlined in the Declaration of Helsinki for all human experimental investigation. In addition, appropriate informed consent has been obtained from all patients by the investigator in charge.

Study Design

This phase I/IIa study was conducted from July 2005 to March 2010 at Tokai University School of Medicine Department of Plastic and Reconstructive Surgery. The protocol was reviewed and approved by the Ethics Committee of the Tokai University School of Medicine, Kanagawa, Japan. The primary end point of this trial is safety, and the secondary end point is primary efficacy. Patients providing informed consent had type 2 diabetes with a nonhealing chronic ulcer. If wounds were on both feet, the foot with a more severe wound was treated with autologous G-CSF-mobilized peripheral blood $CD34^+$ cells. Inclusion criteria included (1) type 2 diabetic patients of ages 20 to 70 years with a nonhealing chronic wound deeper than the subcutaneous layer of the skin. The wound was determined as nonhealing and chronic when the wound was treated with current standard care for diabetic foot ulcer by a wound care specialist for at least 3 months prior to the therapy with less than 40% of wound closure. There were no limitations of the wound size. (2) Patients with strict diabetic control of glycated hemoglobin (HbA1c) below 6.5%. The exclusion criteria included (1) collagen tissue disease or malignant disease, (2) an ejection fraction lower than 50%, (3) interventional treatment required for coronary or cerebral artery stenosis within 6 months, (4) diabetic retinal bleeding, (5) hematological disorder, (6) onset of myocardial infarction or cerebral infarction within the last 6 months, (7) side effects arising from G-CSF pharmaceutical or apheresis procedures, and (8) wound infection. Written informed consent for participation was obtained from all subjects. All patients did not receive any medication changes pre- and post-EPC injection therapy. Since the study was a phase I/IIa clinical trial, controls for the study were not established.

Study Procedures

Screening assessments within 14 days before treatment included medical history, review of inclusion and exclusion criteria, review of medications, vital signs, physical examination, chest X-ray (Shimadzu, Kyoto, Japan), urinalysis, blood collections for hematology [complete blood count (CBC) and differential], clinical chemistry [bilirubin, alkaline phosphatase, alanine aminotransferase (ALT), aspartate aminotransferase (AST), lactate dehydrogenase (LDH), urea nitrogen, creatinine, glucose, uric acid, calcium, phosphorus, total protein, albumin, electrolytes, amylase, cholesterol, triglycerides], and HbA1c. All blood-related measurements were performed by the blood testing central laboratory at the Hospital of Tokai University, Kanagawa, Japan. Patients underwent cardiac echography, abdominal echography (Toshiba, Tokyo, Japan), and cerebral, chest, and abdominal computed tomography (CT; Siemens, Tokyo, Japan) to rule out any conditions listed in the exclusion criteria. During the 3-month screening period, patients continued to receive the standard care for diabetic feet. Foot ulcers were photographed using a digital camera with a 1-cm^2 size sticker marked near the wound. The area of the ulcer was calculated by measuring the size of the photographed ulcer divided by the photographed 1-cm^2 size marker using VH analyzer (Keyence Corp, Osaka, Japan). Vascular perfusion was evaluated by using the following parameters: ankle brachial pressure index (ABI), skin perfusion pressure (SPP), and transcutaneous oxygen pressure (TcO_2). Angiographic analysis was performed for cases with severe peripheral vascular disease. TcO_2 was measured with an oxymonitor (PO-850, Sumitomo-Hightechs, Tokyo, Japan). The probe was placed at the dorsum pedis, and the skin was heated to 42°C (4). SPP was measured with the PAD3000 (Vasamedics, St. Paul, MN, USA) proximal to the wound with an exclusive cuff (5,6). These physiological examinations were performed while the patient was in a supine position after more than 30 min of rest in a temperature-controlled room. Angiographic examinations were performed with the intra-arterial digital subtraction angiography (IA-DSA) technique. The

standard Seldinger approach was used as follows: the top of the 4 Fr catheters was placed at the external iliac artery, and iohexol (Omnipaque, 300 mg of iodine/ml; Daiichi Pharmaceutical, Tokyo, Japan) was injected automatically using an infusion pump at a speed of 20 ml/s for 2 s. Wound care was standardized throughout the entire study by using several different dressing types dependent on the type of the wound (e.g., dry, wet, and intermediate) with daily dressing changes and use of an offloading device by a wound care specialist. Minor debridement of necrotic tissue without general anesthesia was performed as regular wound care. Major debridement was performed only at the time of cell transplantation under general anesthesia.

Treatment Period

Collection of Peripheral Blood CD34+ Cells. Patients who met the criteria were admitted to the hospital, and 10 μg/kg/day of G-CSF (Filgrastim; Gran®, Kyowa Hakko Kirin, Co. Ltd., Tokyo, Japan) was injected subcutaneously for 5 days. Blood counts, peripheral leukocyte differential counts, and peripheral CD34+ cell counts were determined daily. If leukocyte count exceeded 50,000/μl, the dose of G-CSF was reduced to one half. On day 5, peripheral blood MNC collection was performed with the COBE SPECTRA apheresis system (Gambro BCT, Lakewood, CO, USA). MNC collection was followed by purification of CD34+ cells by means of a magnetic-activated cell sorting system (CliniMACS, Milteny Biotech, Bergisch Gladbach, Germany).

Administration of Isolated CD34+ Cells. Debridement and transplantation of CD34+ cells were performed under general anesthesia on the same day of cell isolation. After debridement and irrigation of the wound, CD34+ cells were injected intramuscularly within 20 cm surrounding the wound with a 26-gauge needle (Nipro Corporation, Osaka, Japan). A total of 2×10^7 CD34+ cells/patient was administered by 20 injections, each injection containing 1×10^6 cells/0.25 ml saline (0.25 ml×20 sites, 1.5–2.0 cm deep). Saline gauze dressing was placed over the treated wound immediately after the treatment to avoid cell damage, and standard of wound care was continued starting postoperative day 1. The patient was discharged from the hospital the following day unless any side effects due to the CD34+ cell therapy were seen. Current standard of care for diabetic foot was performed starting on the day of discharge.

End Points

The primary end point of this study is to evaluate the safety, and the secondary end point is to evaluate efficacy 12 weeks posttherapy. No gold standard efficacy end points have been established for small size, early phase clinical trials in patients with diabetic foot, so we originally prespecified the efficacy score as a surrogate end point so that we could simultaneously evaluate subjective and objective parameters in the study. Twelve weeks posttherapy was determined as the time point of evaluation in reference to other clinical trial reports assessing diabetic wound healing because all patients included in the study had nonhealing wound for more than 3 months (20,37). The adverse effects were evaluated according to the National Cancer Institute Common Terminology Criteria for Adverse Events (NCI CTCAE version 3 http://ctep.cancer.gov/protocolDevelopment/electronic_applications/docs/ctcaev3.pdf). Full physical examination, blood collection for hematology, clinical chemistry, chest X-ray, abdominal echo, cardiac echo, cerebral CT, chest CT, and abdominal CT were performed to find if any conditional change existed after the therapy. C-Reactive protein was measured by latex-enhanced immunoturbidimetric assay (Eiken Chemical Co. Ltd., Tokyo, Japan). The efficacy score was defined as the sum of four scores, each of which measured a difference in the parameters between baseline and 12 weeks after cell therapy: (1) percent wound closure calculated by VH analyzer as previously mentioned in the study procedure section (wound needing minor or major amputation was evaluated and performed at 12 weeks posttherapy; major amputation is an amputation of below the knee or above the knee or a procedure proximal to this level, whereas minor

Table 1. Efficacy Score

Parameter	Score Value
Wound closure at post-12 weeks score according to from baseline	
76–100% wound closure	2
36–75% wound closure	1
0–35% wound closure	0
Minor amputation	−1
Major amputation	−2
SPP score 12 weeks after treatment	
>40 mmHg	2
30–40 mmHg	1
<30 mmHg	0
No change	−1
Worsening	−2
Wong-Baker FACES Pain Rating Scale score	
Improvement by ≥2 steps	2
Improvement by 1 step	1
No change	0
Worsening by 1 step	−1
Worsening by ≥2 steps	−2
Recurrence	
No recurrence more than a year	2
No recurrence within a year	1
Recurrence but healed	0
Recurrence but nonhealing	−1
Recurrence with amputation	−2

The efficacy score = (wound closure + SPP + Wong-Baker FACES Pain Scale) post-12 weeks therapy + Recurrence. Range: −2 to 2 for each category. SPP, skin perfusion pressure.

Table 2. Exposure and Outcome for All Patients Treated With Autologous G-CSF-Mobilized Peripheral Blood $CD34^+$ Cell Therapy

Case	Age/ Sex	PMH	Location of Ulcer	Nonhealing Time Pretherapy (Weeks)	Ulcer Size at Baseline (cm)	HbA1C	Time of Complete Wound Closure (Weeks)	Amputation	SPP	ADL Posttherapy	Time Posttherapy	Ulcer Recurrence	Adverse Effects
1	41/M	DM CRF on HD PAD	Rt 1st, 2nd, 3rd toe	22	4.4×3.6	5.6	12	None	↑	Ambulant	4.8	None	None
2	70/F	DM CRF on HD PAD	Rt foot	74	2×1.5	5.4	12	None	↑	Ambulant	4	Within 1 year/ nonhealing	None
3	63/M	DM CRF on HD PAD CVD	Lt. 5th toe	100	2.7×1.5	4.7	18	Minor	↑	Ambulant	3	Within 1 year/ healed	None
4	53/M	DM CRF on HD PAD	Rt. 1st toe	33	3×2	4.9	26	Minor	↑	Ambulant	2	Within 1 year/ healed	None related/ restenosis of Pop. A
5	63/M	DM CRF on HD PAD	Lt foot	26	4.5×6.0	5.8	16	None	↑	Ambulant	2	None	None

G-CSF, granulocyte colony-stimulating factor; CD34, cluster of differentiation 34; PMH, past medical history; HbA1c, glycated hemoglobin; SPP, skin perfusion pressure; ADL, activities of daily living; DM, diabetes mellitus; CRF, chronic renal failure; HD, hemodialysis; PAD, peripheral artery disease; Pop. A, popliteal artery.

Table 3. Outcome of Mobilization, Harvest, and Isolation of CD34⁺ Cells

Case	% CD34⁺ Cells in PB by Flow Cytometry	Total MNCs After Apheresis	Total CD34⁺ Cells After Apheresis	Total Isolated CD34⁺ Cells	Total Isolated CD34⁺ Cells/kg	Purity of CD34⁺ Cells
1	0.31%	4.02E + 10	1.19E + 08	7.21E + 07	9.01E + 05	80%
2	0.08%	1.16E + 10	1.23E + 07	6.14E + 06	1.23E + 05	50%
3	0.40%	2.31E + 10	8.59E + 07	4.60E + 07	7.67E + 05	83%
4	0.33%	2.59E + 10	8.86E + 07	4.28E+07	5.35E + 05	82%
5	0.28%	3.34E + 10	9.23E + 07	4.04E + 07	5.05E + 05	56%
Average	0.28%	2.68E + 10	7.96E + 07	4.15E + 07	5.66E + 05	70%
SD	0.12%	1.08E + 10	3.99E + 07	2.35E + 07	3.29E + 05	15.82%

The frequency of CD34⁺ cells in the peripheral blood at day 5 post-G-CSF injection was 0.28 ± 0.1% by flow cytometry. The average apheresis product number was $2.68 \pm 1 \times 10^{10}$, and the average of total CD34⁺ cells obtained after magnetic sorting was $7.96 \pm 4.0 \times 10^{7}$. Flow cytometry revealed that the purity and viability of the CD34⁺ cell fraction following magnetic sorting were 70 ± 15.8%. PB, peripheral blood; MNCs, mononuclear cells.

amputation is classified as all other partial foot or toe resection) (10); (2) skin perfusion pressure (SPP) in the treated foot; (3) Wong–Baker FACES Pain Rating Scale score (http://www.wongbakerfaces.org/), evaluation of pain in the treated leg; and (4) recurrence of the treated wound. Each score is given a range of plus 2 to minus 2 points; the best response is assigned plus 2, and the worst outcome is assigned minus 2. The efficacy score sum is in the range of +8 to 8 (Table 1). The patients visited the clinic 2 weeks, 4 weeks, 8 weeks, and 12 weeks postoperatively to evaluate safety and efficacy. The patients were still followed every 4 weeks when complete wound closure was not seen at 12 weeks posttherapy. The photographs were taken for percent wound closure, and ABI, SPP, and TcO_2 were tested for vascular perfusion at each visit. Angiographic analysis was performed for cases with severe peripheral vascular disease 12 weeks postoperatively. Each patient evaluated pain level at baseline and at 12 weeks after transplantation using the Wong–Baker FACES Pain Rating Scale (7). A clinical research coordinator interviewed each patient regarding the level of psychroesthesia, paresthesia, and the required quantity of analgesic drugs at baseline and at 12 weeks after transplantation. Recurrence of the wound was evaluated every 4 weeks posttherapy at each clinical visit. The recurred wounds were treated by standard of wound care and evaluated for time of wound closure. The efficacy score was validated by two individual physicians not included in the study.

Quality Analysis of CD34⁺ Cells

CD34⁺ cells isolated for transplantation were labeled with fluorescein isothiocyanate (FITC)-conjugated anti-CD34 (BD Biosciences, San Jose, CA, USA) and phycoerythrin (PE)-conjugated anti-KDR [kinase insert domain receptor or vascular endothelial growth factor receptor 2 (VEGFR2); BD Biosciences] antibodies for 20-min incubation at 4°C. Cells were then analyzed

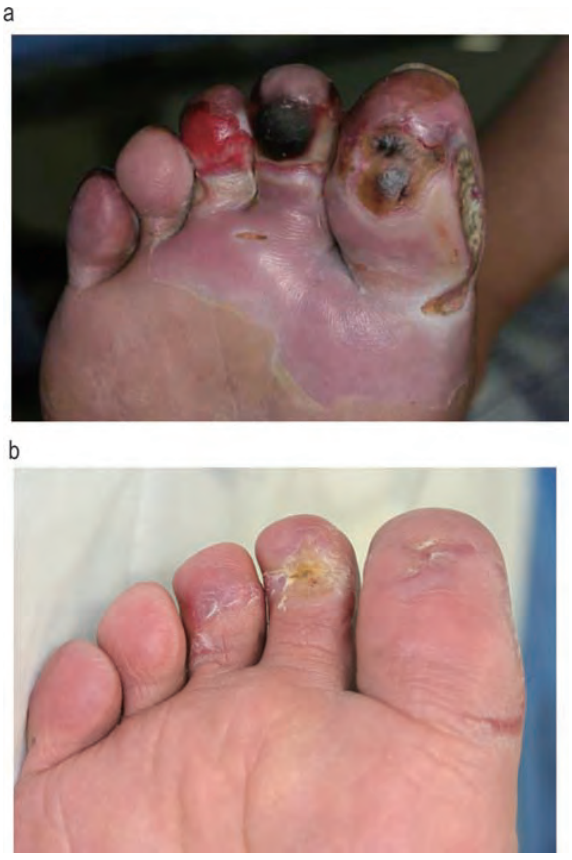

Figure 1. Case 1: A 41-year-old male who was diagnosed with diabetes at age 30 and currently undergoing dialysis. **(**a) Pretherapy: the ulcer seen in the picture was not healing for 22 weeks. (b) Three months posttherapy. After cluster of differentiation 34-positive (CD34⁺) cell therapy, the wound healed rapidly, and wound closure had occurred by 12 weeks after the therapy. No recurrence was seen for 4.8 years posttherapy. Skin perfusion pressure (SPP) measured proximal to the wound showed 13 mmHg pretherapy and 75 mmHg 12 weeks posttransplant.

using FACSCalibur and CellQuest Pro software (Becton Dickinson, Franklin Lakes, NJ, USA).

EPC Colony-Forming Assay

The vasculogenic potential of isolated peripheral blood $CD34^+$ cells was assessed using the EPC colony-forming assay (EPC-CFA) as previously described (17,21,32). Briefly, isolated 3,000 $CD34^+$ cells were suspended in 300 µl of 30% fetal bovine serum (FBS; Nichirei Bioscience Inc., Tokyo, Japan)/Iscove's modified Dulbecco's media (IMDM; Gibco) and mixed with 3 ml of previously stored EPC-CFA working medium (Methocult, Stem Cell Technologies, Vancouver, BC, Canada). A total of 1,000 $CD34^+$ cells/dish were seeded into a 35-mm hydrophilic tissue culture dish (BD Falcon, Bedford, MA, USA; 1 ml working medium to one dish, a total of three dishes per sample). After 18 days, the number of total EPC colony-forming units (EPC-CFU) was counted by two investigators who were blinded to the experimental conditions.

Statistical Analysis

All data are presented as the mean ± standard deviation. Student's *t* test was performed to assess statistical significance between the two groups.

A Kruskal–Wallis one-way ANOVA with Tukey–Kramer post hoc analysis was performed when comparisons involved more than two groups. Significance was considered to be $p < 0.05$. The statistical program used for the analysis of all data was Graph Pad Prism 5 (Graph pad Software, Inc., La Jolla, CA, USA).

RESULTS

Patient Characteristics

A total of five patients were enrolled in the trial. The characteristics of all patients enrolled in the trial are listed in Table 2. The age ranged from 41 to 70 years old. All patients had diabetes and chronic renal failure with hemodialysis as past medical history. Blood sugar levels were controlled for all patients, and hbA1C was below 6.5%. All of the wounds extended into bone or tendon and were located in the digits of the foot. The average size of the wound was 3.3 ± 1.1 cm^2 $\times$ 2.92 ± 1.9 cm^2. The average wound history prior to EPC therapy was 34 ± 23 weeks (240 days). Average ABI was 0.9 ± 0.17. All patients had low skin perfusion pressure (SPP: 14.8 ± 5.3) proximal to the wound, indicating peripheral vascular disease. Cases 4 and 5 had percutaneous transluminal angioplasty (PTA) 3 months prior to the therapy.

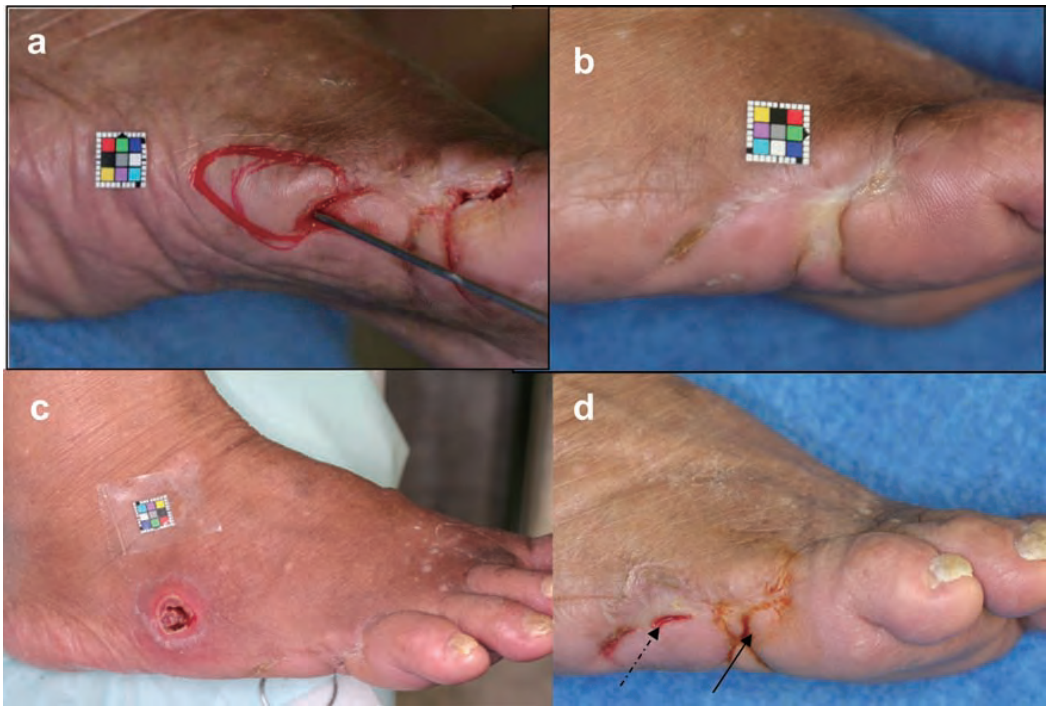

Figure 2. Case 2: A 70-year-old female with 48 years of diabetes and 28 years of chronic renal failure (CRF) on hemodialysis. (a) Pretherapy: the ulcer with a deep pocket reaching to the fifth metatarsal bone located in the lateral side of the right foot was nonhealing for 74 weeks. SPP was 10 mmHg pretherapy. (b) Posttherapy: the ulcer healed completely, and SPP increased to 45 mmHg after 12 weeks posttherapy. (c) One year posttherapy. (d) The dotted arrow shows cured heterotrophic ulcer 2 years posttherapy. The solid arrow shows ulcer recurrence.

Outcome of Mobilization, Harvest, and Isolation of CD34+ Cells

G-CSF was administered 10 μg/kg/day for 5 days for all patients. The frequency of $CD34^+$ cells in the peripheral blood at day 5 post-G-CSF injection was $0.3 \pm 0.1\%$ by flow cytometry analysis. The average apheresis product number was $2.7 \pm 1 \times 10^{10}$, and the average of total $CD34^+$ cells obtained after magnetic sorting by CliniMACS was $8.0 \pm 4.0 \times 10^7$. Flow cytometry revealed that the purity and viability of the $CD34^+$ cell fraction following magnetic sorting were $70 \pm 15.8\%$. The number of $CD34^+$ cells isolated was significantly low for Case 2 (1.23×10^5/kg) and high for Case 1 (9.0×10^5/kg) (Table 3).

Safety Evaluation

Neither death (NCI CTCAE grade 5) nor life-threatening adverse events (grade 4) were observed during the 12-week follow-up after cell therapy. In contrast, mild to moderate adverse events (grades 1–2) were observed as G-CSF-related events in all patients. Symptoms such as bone pain ($n = 5$), headache ($n = 1$), fever ($n = 1$), and C-reactive protein (CRP) elevation ($n = 1$) seen were transient and disappeared without permanent damage. There were no adverse events following general anesthesia. No episodes of site infection following cell injections were noted. There was no incidence of pathogenic angiogenesis after serial examination of fundus oculi.

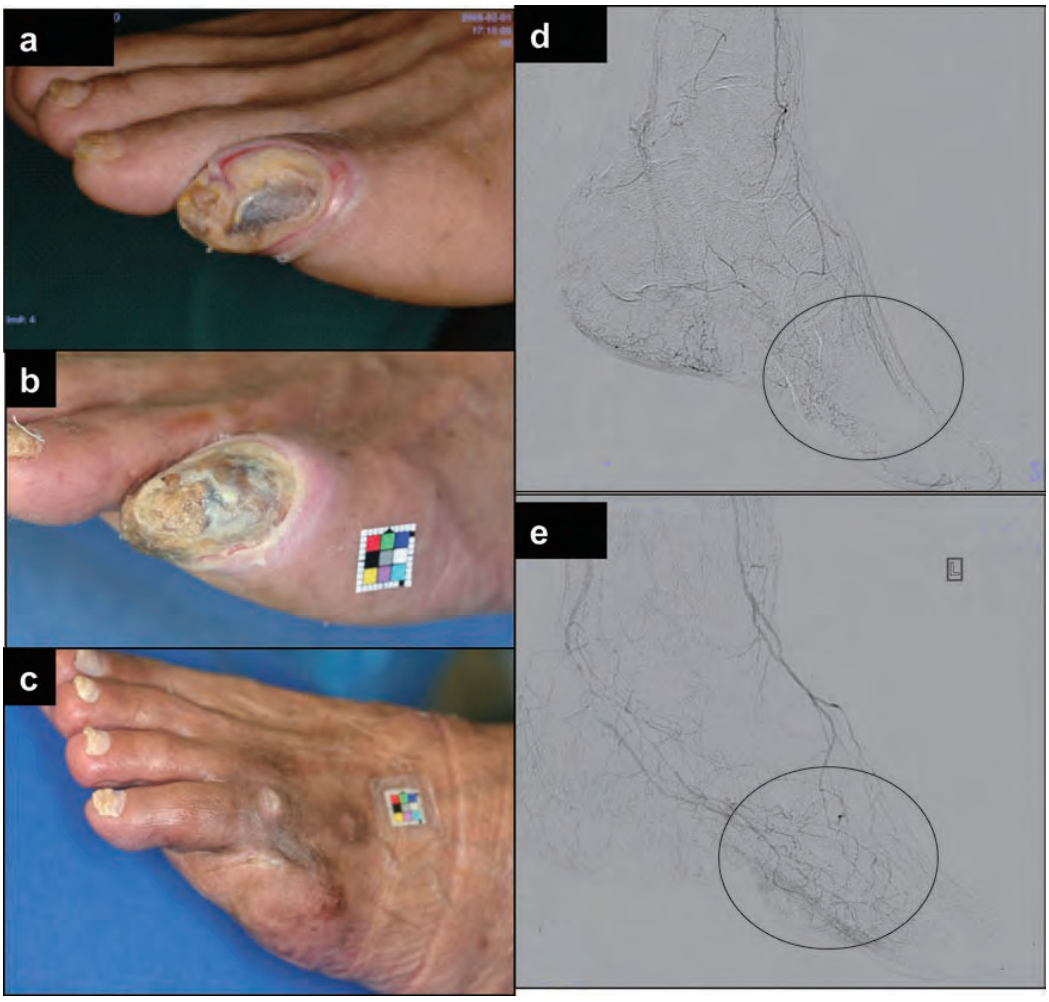

Figure 3. Case 3: A 63-year-old male with diabetes and CRF on hemodialysis. (a) The ulcer on the left fifth toe seen in the picture was nonhealing for 14 weeks. Dorsal SPP was 10 mmHg at this point. (b) The ulcer after 12 weeks posttherapy; the ulcer did not heal at this point, but SPP increased to 45 mmHg. (c) The patient underwent minor amputation of the fifth toe, and the wound completely healed 28 weeks after the therapy. (d) Angiography pretherapy; circled area is avascular. (e) Angiography 12 weeks posttherapy showed increased vascularity in the avascular area pretherapy.

Efficacy Evaluation

The efficacy score at 12 weeks was more than or equal to 2 in all patients, indicating the efficacy of transplantation of $CD34^+$ cells.

Wound Closure. Only two out of five patients (Case 1 and Case 2; Figs. 1 and 2) had complete wound closure within 12 weeks of evaluation. Since the remaining sequestrum was obstructing wound healing, two out of five patients (Case 3 and Case 4; Figs. 3 and 4) received further debridement resulting as minor amputation. In Case 5, the patient had the largest wound pretherapy, which had healed within 16 weeks posttherapy (Fig. 5). Although only two had complete wound closure by 12 weeks posttherapy and two resulted as minor amputation, all patients had complete wound closure without any major amputation at an average of 18.8 weeks (131.6 days) (Fig. 6). During the trial, Case 4 had sudden stenosis of popliteal artery after 8 weeks of therapy, which had healed after percutaneous transluminal angioplasty (PTA).

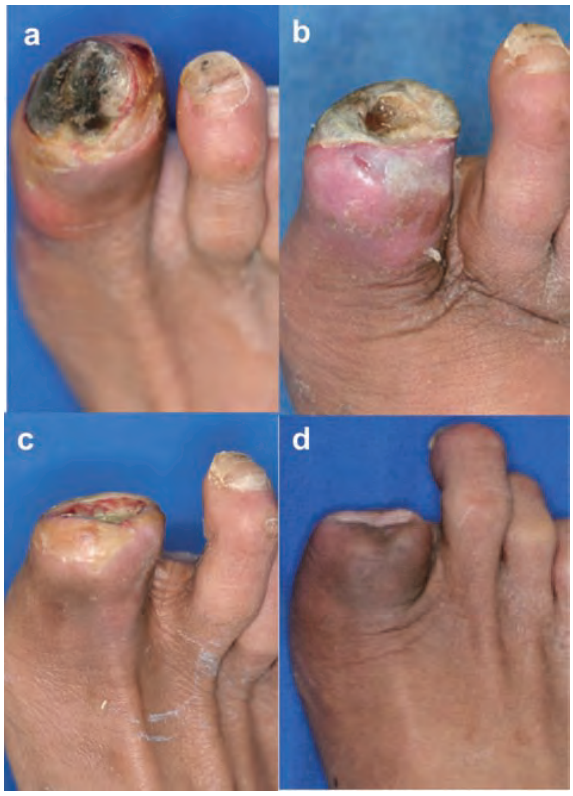

Figure 4. Case 4: A 53-year-old male with 15 years of diabetes and 9 years of CRF on hemodialysis. (a) The ulcer on the right toe pretherapy, which did not heal for 33 weeks. (b) Eight weeks after the therapy, SPP proximal to the wound, which was 14 mmHg, suddenly dropped to 2 mmHg. Angiogram showed stenosis of popliteal artery, and emergency percutaneous transluminal angioplasty (PTA) was performed. (c) At 12 weeks posttherapy. SPP increased to 58 mmHg with increased granulation. (d) At 26 weeks posttherapy. The wound completely healed at this point, and the patient was wound free for more than 2 years with an average SPP of 42 ± 11 mmHg.

Peripheral Vascular Perfusion. There was no significant change in resting ABI pretherapy and posttherapy (0.9 ± 0.2 vs. 0.9 ± 0.2), but SPP (14.5 ± 5.3 vs. 53.6 ± 16.3; $p < 0.01$) and TcO_2 (27.8 ± 8.2 vs. 56.0 ± 7.2; $p < 0.01$) proximal to the wound showed a significant increase 12 weeks after the therapy in all patients (Fig. 6). Angiography performed 12 weeks posttherapy showed increased vascularity in the deep plantar artery for Cases 3 and 5 (Figs. 3 and 5).

Pain Scale. Four out of five patients had limb and foot pain before the therapy, which began to be relieved 4 weeks after the therapy. The average pain level evaluated using the Wong–Baker FACES Pain Rating Scale of 3.2 ± 2.1 at baseline decreased to 0.6 ± 0.9 at 3 months after therapy ($p < 0.05$) (Fig. 6).

Recurrence. The ulcer of Cases 1 and 5 had not yet recurred after more than 2 years of cell therapy. Cases 3 and 4 showed recurrence of the ulcer within 1 year after the therapy, but it was rapidly cured in a few weeks (3 weeks for Case 3 and 2 weeks for Case 4) after standard care. However, the recurred ulcer for Case 2 did not heal even after 3 years of standard care (Fig. 2).

Vasculogenic Potential of Transplanted $CD34^+$ Cells

Case 1 with wound closure at 12 weeks posttherapy and no incidence of heterotopic ulcers or recurrence demonstrated a significantly higher number of total EPC-CFU compared to the other four cases (Case 1: 25 ± 6 vs. Case 2: 4 ± 2, Case 3: 11 ± 1, Case 4: 11 ± 1.5, Case 5: 16 ± 1; $p < 0.01$) (Fig. 7). Flow cytometry of CD34 and KDR double-positive cell percentages within the transplanted $CD34^+$ cells showed similar results to EPC-CFU. Case 1 showed a significantly higher number of CD34/KDR double-positive cell percentage compared to the other four cases (2.8 vs. 0.5, 0.37, 1.49, 1.67), suggesting that transplanted $CD34^+$ cells with higher vasculogenic potential exhibit accelerated wound healing and better prognosis (Fig. 7).

DISCUSSION

To the best of our knowledge, the present study is the first clinical trial of transplantation of autologous and purified $CD34^+$ cells into diabetic patients on hemodialysis who were suffering from nonhealing chronic wounds for more than 3 months. Previous studies on autologous transplantation of bone marrow or peripheral blood stem cells for diabetic ulcers were focused on administrating mononuclear cells to more acute or subacute wounds as cell population including EPCs (13). Since application of peripheral blood or bone marrow mononuclear cells

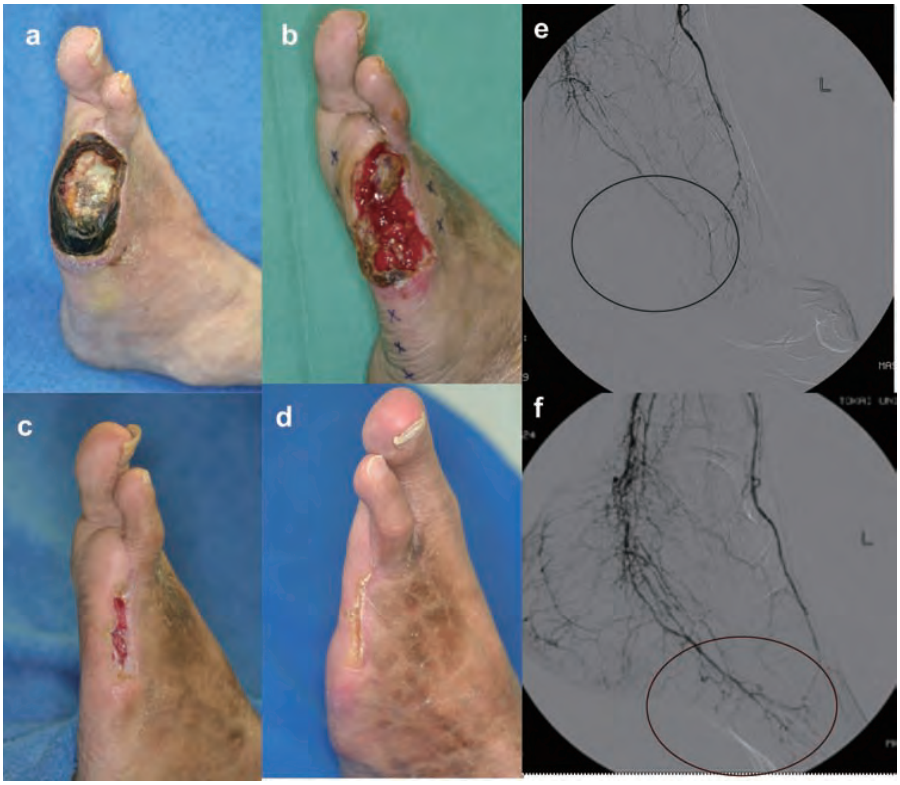

Figure 5. Case 5: A 63-year-old male with 20 years of diabetes and 4 years of CRF on hemodialysis. (a) Pretherapy: The ulcer located on the left third, fourth, and fifth toes to metatarsus did not heal for 26 weeks. SPP was 10 mmHg at this point. (b) The ulcer at time of debridement and $CD34^+$ cell transplant. (c) At 12 weeks posttherapy with an SPP of 67 mmHg. (d) At 16 weeks posttherapy; time of complete wound closure. Currently, patient is ambulant for 2 years posttherapy without any recurrence and heterotopic ulcer with stable SPP of 66 ± 23 mmHg. (e) Angiography pretherapy; avascular area is marked with circle. (f) Angiography 12 weeks posttherapy; avascular area pretherapy has increased vascular perfusion after $CD34^+$ cell therapy.

may contain cells not related to angiogenesis and wound healing, we believe that purified $CD34^+$ cells are a more suitable source of stem cell therapy for angiogenesis and wound healing. Regarding this, although many investigators identify $CD34^+/CD133^+/KDR^+$ cells as EPCs in basic research (5), isolating the rare cell population is clinically impractical due to the absence of a clinical-grade anti-KDR antibody. Therefore, we have chosen $CD34^+$ cells as an enriched population of EPCs for cell isolation that was technically and clinically applicable.

Furthermore, animal studies have reported that purified $CD34^+$ cells exhibit improved healing and vasculogenesis compared to nonpurified mononuclear cell transplantation (33). In a clinical randomized trial of direct intramyocardial injection of autologous mononuclear bone marrow cells during coronary artery bypass graft (CABG) to improve left ventricle function, it was reported that the "responder" group was transplanted with a cell population containing a significantly higher percentage and absolute number of $CD34^+$ cells than nonresponders (11). Recently, Kawamoto et al. reported the safety and efficacy of G-CSF-mobilized $CD34^+$ cell transplant to patients with critical limb ischemia (16). Therefore, we hypothesized that the autologous transplantation of purified $CD34^+$ cells as enriched population of EPCs may be effective in the treatment of nonhealing chronic diabetic wounds with peripheral vascular disease. Since uncontrolled diabetes and high blood sugar level influence diabetic wound healing, our trial confirmed that the wounds were untreatable even after diabetic control and standard wound care. We designed this small size, phase I/IIa clinical trial as a prospective, uncontrolled, single-blinded study to obtain useful information for a future phase IIb/III trial. In this pilot study, we observed many clinical manifestations that significantly improved after autologous peripheral blood $CD34^+$ cell transplant, such as wound closure, SPP, TcO_2, and lower limb pain. Measurements of ambulatory blood pressure (ABP) are reported to fail to reflect the severity of

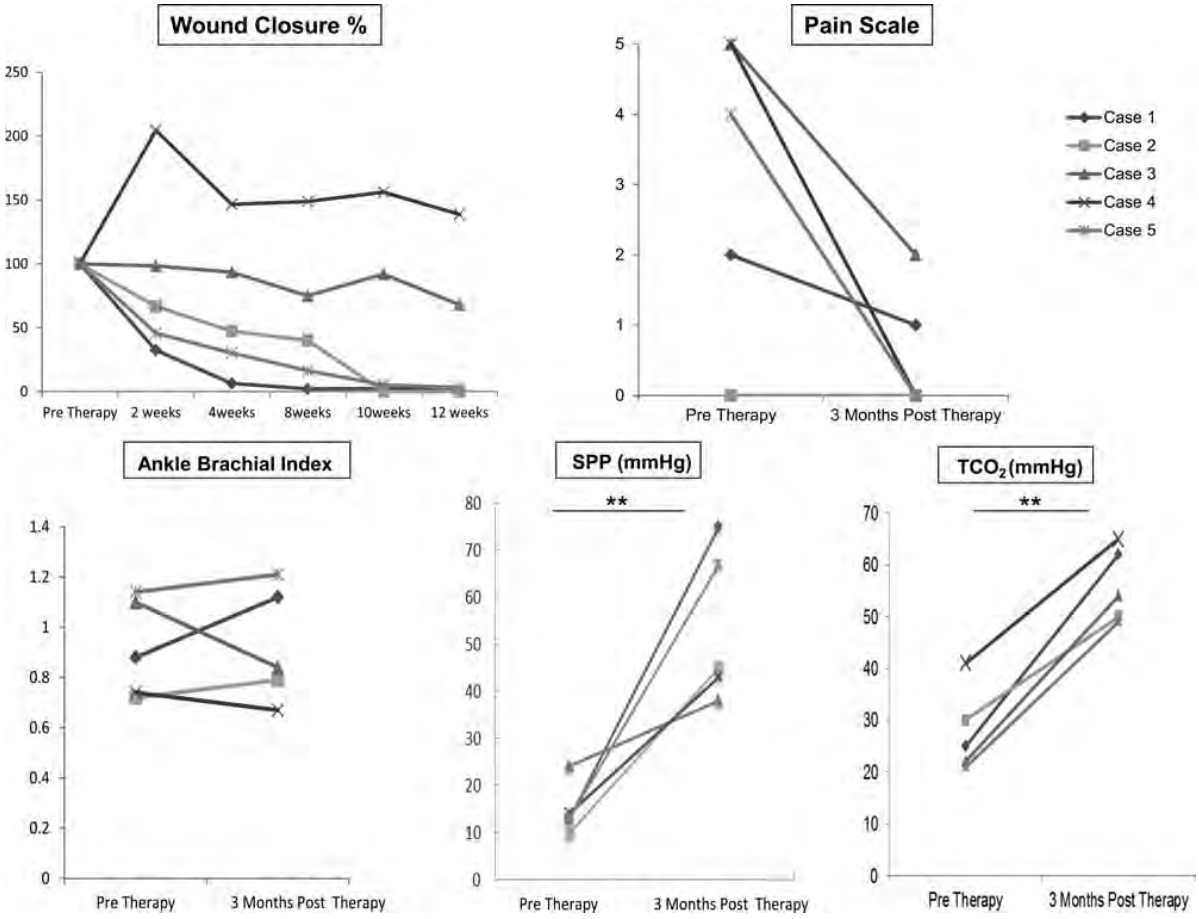

Figure 6. Improvement of efficacy parameters following $CD34^+$ therapy. Serial changes of subjective and objective parameters of wound healing and vascular perfusion of the treated foot. Percent wound closure was calculated by VH analyzer. Cases 1, 2, and 5 had near-complete wound closure after 12 weeks. Ankle brachial pressure index (ABI), SPP, and transcutaneous partial oxygen pressure (TcO_2) were performed to evaluate peripheral vascular perfusion. There was no significant change in resting ABI pretherapy and posttherapy (0.9 ± 0.2 vs. 0.9 ± 0.2), but SPP (14.5 ± 5.3 vs. 53.6 ± 16.3; $p < 0.01$) and TcO_2 (27.8 ± 8.2 vs. 56.0 ± 7.2; $p < 0.01$) proximal to the wound showed significant increase 12 weeks after the therapy in all patients. Pain level was evaluated using the Wong–Baker FACES Pain Rating Scale. All patients with pain pretransplantation showed a significant decrease in Pain Rating Scale (3.2 ± 2.1 vs. 0.6 ± 0.9; $p < 0.05$). SPP, skin perfusion pressure.

peripheral ischemia if the underlying vessels are calcified in patients who have diabetes or are receiving hemodialysis (25,35). In contrast to ABP, measurements of SPP and TcO_2 provide more accurate information even in noncompressive vessels, and false-positive results are rare (4,12). Since all patients in this trial were receiving hemodialysis due to chronic renal failure, skin perfusion pressure and TcO_2 measurements were used as a more reliable evaluator of peripheral vascular perfusion. Consequently, we did not observe significant changes in ABP in our cases, but a significant increase in SPP and TcO_2 was observed after receiving the therapy. Furthermore, patients of peripheral vascular disease with end-stage renal failure are reported to be less responsive to peripheral or bone marrow mononuclear cell therapy (24). Although all patients included in our trial were receiving hemodialysis, all patients had complete wound closure at an average of 18 weeks posttherapy and increased peripheral perfusion with no major amputations. This result suggests that purified $CD34^+$ cells may be the feasible cell therapy of these patients.

The role of G-CSF administration in the healing process in diabetic patients is not clear. There have been reports that G-CSF administration itself may accelerate wound healing (8). Some investigators reported that treatment by G-CSF improves symptoms but not signs of ischemic heart disease (36). However, in our cases, increase in SPP and TcO_2 was

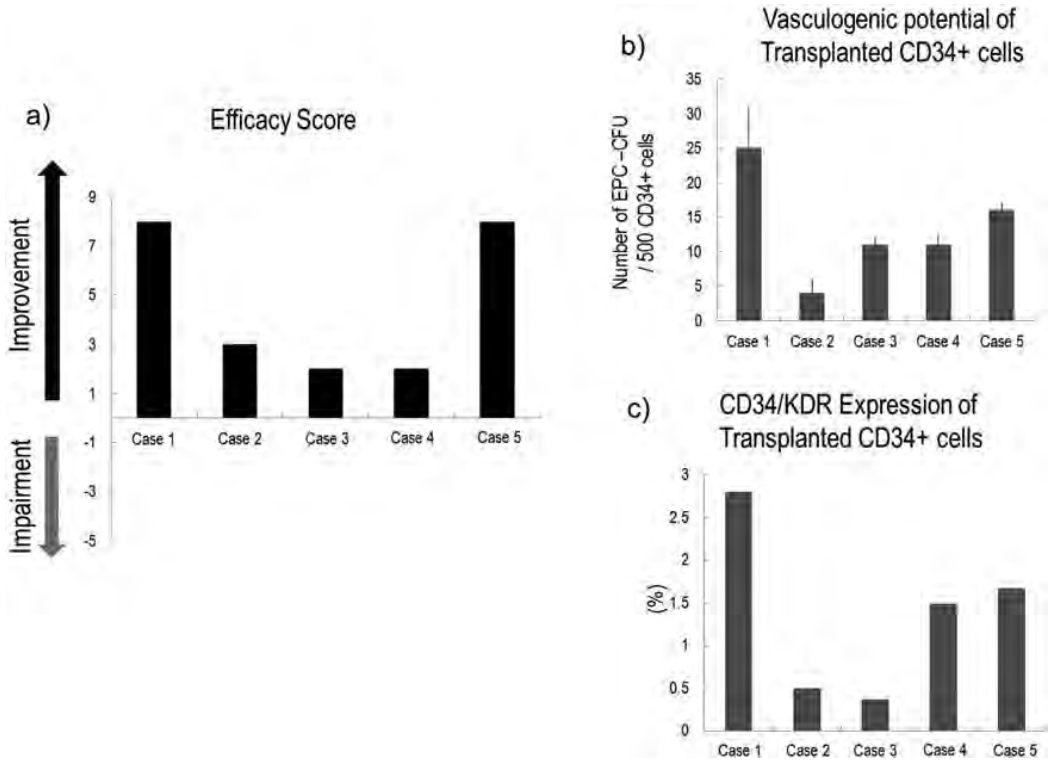

Figure 7. Efficacy score and vasculogeneic potential of transplanted CD34+ cells. (a) Efficacy score at 12 weeks following CD34+ transplantation. Efficacy score was positive for all cases indicating efficacy of the therapy. However, Cases 2, 3, and 4 showed less improvement compared to Cases 1 and 5. (b) Vasculogenic potential of transplanted CD34+ cells was evaluated by endothelial progenitor cell colony-forming assay (EPC-CFA). Number of total EPC colonies were counted per well of 500 CD34+ cells; $n = 3$ per patient. The total colonies for all cases were as follows: Case 1: 25 ± 6, Case 2: 4 ± 2, Case 3: 11 ± 1, Case 4: 11 ± 1.5, Case 5: 16 ± 1. CFU, colony-forming units. (c) Flow cytometry of CD34+ and kinase insert domain receptor [KDR or vascular endothelial growth factor receptor 2 (VEGFR2)] double-positive cell percentage of transplanted EPCs is graphed. Similar to EPC-CFU, Case 1 demonstrated the highest CD34+/KDR percentage. Cases 1 and 5 with high efficacy score demonstrated a significantly higher number of total EPC-CFUs and CD34 and KDR double positivity, indicating that transplanting EPCs with higher vasculogenic function leads to better therapeutic outcome.

not seen in the nontreated side of the foot. In addition, the velocity measurement of dorsal artery by Doppler showed an increase only in the treated side of the foot (data not shown). The contralateral foot could be identified as an internal control; therefore, this observation suggests that CD34+ cells might have an improved neovascularization effect regardless of G-CSF administration.

One of the limitations of autologous EPC therapy for diabetic patients is impaired mobilization and function of diabetic EPCs (7). We and others have previously reported that both bone marrow and circulating diabetic EPCs have significantly lower vasculogenic potential compared to healthy EPCs (6,34). For that reason, the number of isolated peripheral blood CD34+ cells in our trial was lower compared to the number reported in a similar trial conducted by Kawamoto et al. with nondiabetic patients (16). In our trial, the vasculogenic potential of isolated and transplanted CD34+ cells was evaluated by EPC-CFU and a number of CD34/KDR double-positive cells. The patient with accelerated wound healing and positive prognosis without recurrence or heterotopic ulcers had a higher total number of EPC-CFU and CD34/KDR double-positive cells, indicating that the vasculogenic potential of transplanted cells is an important factor of effective autologous EPC therapy. These outcomes suggest the necessity to future investigate the relationship between patient background, EPC potential, and its efficacy.

The role of transplanted CD34+ cells in wound healing and postnatal neovascularization was not investigated in our study; however, we believe that accelerated wound healing and increased vascular perfusion were promoted with involvement of direct and indirect CD34+ cell contribution to neovascularization. In the context of EPC biology, CD34+ cells that contain enriched population

of EPCs can promote vasculogenesis by migration, proliferation, differentiation, and/or incorporation of bone marrow-derived EPCs into newly forming vasculature (1). This has been previously demonstrated by several studies using a well-established model using tunica interna endothelial cell kinase-dependent -galactosidase reporter gene (Tie-2/LacZ) transgenic mice, allowing the detection of bone marrow EPCs in the targeted tissue (14,22). Transplantation of bone marrow-derived EPCs from Tie-2/LacZ mice accelerated wound healing and hind limb perfusion in wounded hind limb ischemia model by direct incorporation of EPCs into the neovessels in the granulation tissue using transgenic mice (3). We believe that not all EPCs incorporate into vasculature formation, but many of these cells greatly contribute to indirect contribution to vascular regeneration. EPCs activate the preexisting endothelial cells by producing various cytokines and other secreting proangiogenic factors in EPCs, such as VEGF, hepatocyte growth factor (HGF), insulin-like growth factor-1 (IGF-1), endothelial and induced nitric oxide synthase (eNOS/iNOS), angiopoietin 1 (Ang-1), and stem cell-derived factor-1 (SDF-1) (14,23).

As for the safety evaluation, there were no severe adverse events seen during and after cell therapy. Although mild adverse events were frequent, these were transient and expected. Exacerbation of diabetic retinopathy caused worry due to pathogenic angiogenesis such as arteriovenous shunt due to G-CSF administration and stem cell therapy. However, fundus oculi examinations demonstrated no pathogenic angiogenesis following $CD34^+$ cell transplant. There was no malignant tumor or angina pectoris and embolism identified during this trial. These results indicate that the autologous transplantation of mobilized peripheral blood $CD34^+$ cells is an effective and safe therapeutic approach for nonhealing chronic diabetic wounds.

In conclusion, we demonstrated that this prospective clinical trial of autologous peripheral blood $CD34^+$ cell transplant may be an alternative therapeutic option for nonhealing chronic diabetic wound for patients with peripheral vascular disease and chronic renal failure with hemodialysis. Future studies are needed to reveal its safety and efficacy in a larger number of patients and by comparison with an appropriate control group receiving G-CSF only or placebo.

CONCLUSIONS

Autologous peripheral blood $CD34^+$ cell transplant is a safe and effective therapy for nonhealing diabetic wound patients. Patients treated with $CD34^+$ cells with higher vasculogenic potential tend to have higher efficacy score and better prognosis. Furthermore, larger clinical studies with appropriate control groups are necessary to establish the safety and efficacy of this procedure.

ACKNOWLEDGMENTS: This work was supported by Health and Labor Sciences Research grants from the Japanese Ministry of Health, Labor, and Welfare (20890227, 22791737), Funding Program for Next Generation World Leading Researchers LS113, and Tokai University Research Aid grant awarded to Rica Tanaka. The authors declare no conflict of interest.

REFERENCES

1. Asahara, T.; Masuda, H.; Takahashi, T.; Kalka, C.; Pastore, C.; Silver, M.; Kearne, M.; Magner, M.; Isner, J. M. Bone marrow origin of endothelial progenitor cells responsible for postnatal vasculogenesis in physiological and pathological neovascularization. Circ. Res. 85(3):221–228; 1999.
2. Asahara, T.; Murohara, T.; Sullivan, A.; Silver, M.; van der Zee, R.; Li, T.; Witzenbichler, B.; Schatteman, G.; Isner, J. M. Isolation of putative progenitor endothelial cells for angiogenesis. Science 275(5302):964–967; 1997.
3. Bauer, S. M.; Goldstein, L. J.; Bauer, R. J.; Chen, H.; Putt, M.; Velazquez, O. C. The bone marrow-derived endothelial progenitor cell response is impaired in delayed wound healing from ischemia. J. Vasc. Surg. 43(1):134–141; 2006.
4. Brooks, B.; Dean, R.; Patel, S.; Wu, B.; Molyneaux, L.; Yue, D. K. TBI or not TBI: That is the question. Is it better to measure toe pressure than ankle pressure in diabetic patients? Diabet. Med. 18(7):528–532; 2001.
5. Brunner, S.; Schernthaner, G. H.; Satler, M.; Elhenicky, M.; Hoellerl, F.; Schmid-Kubista, K. E.; Zeiler, F.; Binder, S.; Schernthaner, G. Correlation of different circulating endothelial progenitor cells to stages of diabetic retinopathy: First in vivo data. Invest. Ophthalmol. Vis. Sci. 50(1):392–398; 2009.
6. Capla, J. M.; Grogan, R. H.; Callaghan, M. J.; Galiano, R. D.; Tepper, O. M.; Ceradini, D. J.; Gurtner, G. C. Diabetes impairs endothelial progenitor cell-mediated blood vessel formation in response to hypoxia. Plast. Reconstr. Surg. 119(1):59–70; 2007.
7. Ceradini, D. J.; Kulkarni, A. R.; Callaghan, M. J.; Tepper, O. M.; Bastidas, N.; Kleinman, M. E.; Capla, J. M.; Galiano, R. D.; Levine, J. P.; Gurtner, G. C. Progenitor cell trafficking is regulated by hypoxic gradients through HIF-1 induction of SDF-1. Nat. Med. 10(8):858–864; 2004.
8. Fang, Y.; Shen, J.; Yao, M.; Beagley, K. W.; Hambly, B. D.; Bao, S. Granulocyte-macrophage colony-stimulating factor enhances wound healing in diabetes via upregulation of proinflammatory cytokines. Br. J. Dermatol. 162(3):478–486; 2010.
9. Friedrich, E. B.; Walenta, K.; Scharlau, J.; Nickenig, G.; Werner, N. $CD34^-/CD133^+/VEGFR\text{-}2^+$ endothelial progenitor cell subpopulation with potent vasoregenerative capacities. Circ. Res. 98(3):e20–e25; 2006.
10. Griffin, K. J.; Rashid, T. S.; Bailey, M. A.; Bird, S. A.; Bridge, K.; Scott, J. D. Toe Amputation: A predictor of future limb loss? J. Diabetes Complications 26(3):251–254; 2012.
11. Hendrikx, M.; Hensen, K.; Clijsters, C.; Jongen, H.; Koninckx, R.; Bijnens, E.; Ingels, M.; Jacobs, A.; Geukens, R.; Dendale, P.; Vijgen, J.; Dilling, D.; Steels, P.; Mees, U.; Rummens, J. L. Recovery of regional but not global contractile function by the direct intramyocardial autologous bone marrow transplantation: Results from a randomized controlled clinical trial. Circulation 114(1 Suppl):I101–I107; 2006.
12. Holstein, P.; Lassen, N. A. Healing of ulcers on the feet correlated with distal blood pressure measurements in occlusive arterial disease. Acta Orthop. Scand. 51(6):995–1006; 1980.

13. Huang, P.; Li, S.; Han, M.; Xiao, Z.; Yang, R.; Han, Z. C. Autologous transplantation of granulocyte colony-stimulating factor-mobilized peripheral blood mononuclear cells improves critical limb ischemia in diabetes. Diabetes Care 28(9):2155–2160; 2005.
14. Ii, M.; Nishimura, H.; Iwakura, A.; Wecker, A.; Eaton, E.; Asahara, T.; Losordo, D. W. Endothelial progenitor cells are rapidly recruited to myocardium and mediate protective effect of ischemic preconditioning via "imported" nitric oxide synthase activity. Circulation 111(9):1114–1120; 2005.
15. Izumi, Y.; Satterfield, K.; Lee, S.; Harkless, L. B.; Lavery, L. A. Mortality of first-time amputees in diabetics: A 10-year observation. Diabetes Res. Clin. Pract. 83(1):126–131; 2009.
16. Kawamoto, A.; Katayama, M.; Handa, N.; Kinoshita, M.; Takano, H.; Horii, M.; Sadamoto, K.; Yokoyama, A.; Yamanaka, T.; Onodera, R.; Kuroda, A.; Baba, R.; Kaneko, Y.; Tsukie, T.; Kurimoto, Y.; Okada, Y.; Kihara, Y.; Morioka, S.; Fukushima, M.; Asahara, T. Intramuscular transplantation of G-CSF-mobilized CD34(+) cells in patients with critical limb ischemia: A phase I/IIa, multicenter, single-blinded, dose-escalation clinical trial. Stem Cells 27(11):2857–2864; 2009.
17. Kwon, S. M.; Lee, Y. K.; Yokoyama, A.; Jung, S. Y.; Masuda, H.; Kawamoto, A.; Lee, Y. M.; Asahara, T. Differential activity of bone marrow hematopoietic stem cell subpopulations for EPC development and ischemic neovascularization. J. Mol. Cell. Cardiol. 51(3):308–317; 2011.
18. Lawall, H.; Bramlage, P.; Amann, B. Stem cell and progenitor cell therapy in peripheral artery disease. A critical appraisal. Thromb. Haemost. 103(4):696–709; 2010.
19. Lin, C. D.; Allori, A. C.; Macklin, J. E.; Sailon, A. M.; Tanaka, R.; Levine, J. P.; Saadeh, P. B.; Warren, S. M. Topical lineage-negative progenitor-cell therapy for diabetic wounds. Plast. Reconstr. Surg. 122(5):1341–1351; 2008.
20. Margolis, D. J.; Kantor, J.; Berlin, J. A. Healing of diabetic neuropathic foot ulcers receiving standard treatment. A meta-analysis. Diabetes Care 22(5):692–695; 1999.
21. Masuda, H.; Alev, C.; Akimaru, H.; Ito, R.; Shizuno, T.; Kobori, M.; Horii, M.; Ishihara, T.; Isobe, K.; Isozaki, M.; Itoh, J.; Itoh, Y.; Okada, Y.; McIntyre, B. A.; Kato, S.; Asahara, T. Methodological development of a clonogenic assay to determine endothelial progenitor cell potential. Circ. Res. 109(1):20–37; 2011.
22. Masuda, H.; Kalka, C.; Takahashi, T.; Yoshida, M.; Wada, M.; Kobori, M.; Itoh, R.; Iwaguro, H.; Eguchi, M.; Iwami, Y.; Tanaka, R.; Nakagawa, Y.; Sugimoto, A.; Ninomiya, S.; Hayashi, S.; Kato, S.; Asahara, T. Estrogen-mediated endothelial progenitor cell biology and kinetics for physiological postnatal vasculogenesis. Circ. Res. 101(6):598–606; 2007.
23. Miyamoto, Y.; Suyama, T.; Yashita, T.; Akimaru, H.; Kurata, H. Bone marrow subpopulations contain distinct types of endothelial progenitor cells and angiogenic cytokine-producing cells. J. Mol. Cell. Cardiol. 43(5):627–635; 2007.
24. Onodera, R.; Teramukai, S.; Tanaka, S.; Kojima, S.; Horie, T.; Matoba, S.; Murohara, T.; Matsubara, H.; Fukushima, M. Bone marrow mononuclear cells versus G-CSF-mobilized peripheral blood mononuclear cells for treatment of lower limb ASO: Pooled analysis for long-term prognosis. Bone Marrow Transplant. 46(2):278–284; 2011.
25. Quigley, F. G.; Faris, I. B.; Duncan, H. J. A comparison of Doppler ankle pressures and skin perfusion pressure in subjects with and without diabetes. Clin. Physiol. 11(1):21–25; 1991.
26. Saar, W. E.; Lee, T. H.; Berlet, G. C. The economic burden of diabetic foot and ankle disorders. Foot Ankle Int. 26(1):27–31; 2005.
27. Sander, A. L.; Jakob, H.; Henrich, D.; Powerski, M.; Witt, H.; Dimmeler, S.; Barker, J.; Marzi, I.; Frank, J. Systemic transplantation of progenitor cells accelerates wound epithelialization and neovascularization in the hairless mouse ear wound model. J. Surg. Res. 165(1):165–170; 2011.
28. Sivan-Loukianova, E.; Awad, O. A.; Stepanovic, V.; Bickenbach, J.; Schatteman, G. C. CD34+ blood cells accelerate vascularization and healing of diabetic mouse skin wounds. J. Vasc. Res. 40(4):368–377; 2003.
29. Snyder, R. J.; Hanft, J. R. Diabetic foot ulcers—Effects on QOL, costs, and mortality and the role of standard wound care and advanced-care therapies. Ostomy Wound Manage. 55(11):28–38; 2009.
30. Suh, W.; Kim, K. L.; Kim, J. M.; Shin, I. S.; Lee, Y. S.; Lee, J. Y.; Jang, H. S.; Lee, J. S.; Byun, J.; Choi, J. H.; Jeon, E. S.; Kim, D. K. Transplantation of endothelial progenitor cells accelerates dermal wound healing with increased recruitment of monocytes/macrophages and neovascularization. Stem Cells 23(10):1571–1578; 2005.
31. Takahashi, T.; Kalka, C.; Masuda, H.; Chen, D.; Silver, M.; Kearney, M.; Magner, M.; Isner, J. M.; Asahara, T. Ischemia- and cytokine-induced mobilization of bone marrow-derived endothelial progenitor cells for neovascularization. Nat. Med. 5(4):434–438; 1999.
32. Tanaka, R.; Wada, M.; Kwon, S. M.; Masuda, H.; Carr, J.; Ito, R.; Miyasaka, M.; Warren, S. M.; Asahara, T.; Tepper, O. M. The effects of flap ischemia on normal and diabetic progenitor cell function. Plast. Reconstr. Surg. 121(6):1929–1942; 2008.
33. Tei, K.; Matsumoto, T.; Mifune, Y.; Ishida, K.; Sasaki, K.; Shoji, T.; Kubo, S.; Kawamoto, A.; Asahara, T.; Kurosaka, M.; Kuroda, R. Administrations of peripheral blood CD34-positive cells contribute to medial collateral ligament healing via vasculogenesis. Stem Cells 26(3):819–830; 2008.
34. Tepper, O. M.; Galiano, R. D.; Capla, J. M.; Kalka, C.; Gagne, P. J.; Jacobowitz, G. R.; Levine, J. P.; Gurtner, G. C. Human endothelial progenitor cells from type II diabetics exhibit impaired proliferation, adhesion, and incorporation into vascular structures. Circulation 106(22):2781–2786; 2002.
35. Tsai, F. W.; Tulsyan, N.; Jones, D. N.; Abdel-Al, N.; Castronuovo, J. J., Jr.; Carter, S. A. Skin perfusion pressure of the foot is a good substitute for toe pressure in the assessment of limb ischemia. J. Vasc. Surg. 32(1):32–36; 2000.
36. Wang, Y.; Tagil, K.; Ripa, R. S.; Nilsson, J. C.; Carstensen, S.; Jorgensen, E.; Sondergaard, L.; Hesse, B.; Johnsen, H. E.; Kastrup, J. Effect of mobilization of bone marrow stem cells by granulocyte colony stimulating factor on clinical symptoms, left ventricular perfusion and function in patients with severe chronic ischemic heart disease. Int. J. Cardiol. 100(3):477–483; 2005.
37. Zimny, S.; Schatz, H.; Pfohl, M. Determinants and estimation of healing times in diabetic foot ulcers. J. Diabetes Complications 16(5):327–332; 2002.

J. Cell. Mol. Med. Vol 16, No 10, 2012 pp. 2413-2421

Up-regulation of miR-210 by vascular endothelial growth factor in *ex vivo* expanded CD34+ cells enhances cell-mediated angiogenesis

Mohamad Amer Alaiti [a, #], Masakazu Ishikawa [a, #], Haruchika Masuda [b], Daniel I. Simon [a], Mukesh K. Jain [a], Takayuki Asahara [b], Marco A. Costa [a, *]

[a] *Department of Medicine, Case Cardiovascular Research Institute, Harrington-McLaughlin Heart & Vascular Institute, University Hospital Case Medical Center, Case Western Reserve University School of Medicine, Cleveland, OH, USA*
[b] *Department of Regenerative Medicine Science, Tokai University School of Medicine, Isehara, Kanagawa, Japan*

Received: September 21, 2011; Accepted: January 31, 2012

Abstract

Ex vivo culture has been proposed as a means to augment and repair autologous cells in patients with chronic diseases, but the mechanisms governing improvement in cell function are not well understood. Although microRNAs (miRs) are increasingly appreciated as key regulators of cellular function, a role for these factors in CD34+ cell-mediated angiogenesis has not been elucidated. Vascular endothelial growth factor (VEGF) was previously shown to induce expression of certain miRs associated with angiogenesis in endothelial cells and promote survival and number of vascular colony forming units of haematopoietic stem cells (HSCs). We sought to evaluate the role of VEGF in expansion and angiogenic function of CD34+ cells and to identify specific miRs associated with angiogenic properties of expanded cells. Umbilical cord blood CD34 + cells were effectively expanded (18- to 22-fold) in culture medium containing stem cell factor (SCF), Flt-3 ligand (Flt-3), thrombopoietin (TPO) and interleukin-6 (IL-6) with (postEX/+VEGF) and without VEGF (postEX/noVEGF). Tube formation in matrigel assay and tissue perfusion/capillary density in mice ischaemic hindlimb were significantly improved by postEX/+VEGF cells compared with fresh CD34+ and postEX/noVEGF cells. MiR-210 expression was significantly up-regulated in postEX/+VEGF cells. MiR-210 inhibitor abrogated and 210 mimic recapitulated the pro-angiogenic effects by treatment of postEX/+VEGF and postEX/noVEGF cells respectively. Collectively, these observations highlight a critical role for VEGF in enhancing the angiogenic property of expanded cells, and identify miR-210 as a potential therapeutic target to enhance CD34+ stem cell function for the treatment of ischaemic vascular disease.

Keywords: CD34+ cells • VEGF • miR-210 • angiogenesis

Introduction

The CD34+ cell population is an important target for therapeutic angiogenesis [1], but limited cell number and impaired function hinder its clinical application in patients with chronic diseases [2]. *Ex vivo* culture has been proposed as a means to augment and repair autologous cells, but the mechanisms governing improvement in cell function are not well understood. Although microRNAs (miRs), ~21 nucleotide non-coding RNAs, are increasingly appreciated as key regulators of cellular function [3], a role for these factors in CD34+ cell-mediated angiogenesis remains largely unexplored. Certain miRs are promoted by VEGF in a Dicer-dependent fashion and have been implicated in endothelial cell-mediated post-natal angiogenesis [4–6]. The addition of VEGF to conventional haematopoietic stem cell expansion media [7] is appealing because of its positive role in cell survival and angiogenesis [8,9], but the effects of such an approach to augment CD34+ cells are unknown. Therefore, we conducted a study to: (*i*) evaluate the impact of VEGF in *ex vivo* expansion of CD34+ cells, and (*ii*) identify specific miRs associated with angiogenic properties of *ex vivo* expanded CD34+ cells.

[#]These authors contributed equally to this paper.
*Correspondence to: Marco A. COSTA, M.D., Ph.D.,
Professor of Medicine, Director, Research & Innovation Center
Harrington-McLaughlin Heart & Vascular Institute, University Hospitals Case Medical Center, 11100 Euclid Avenue – Lakeside 3001, Cleveland, OH 44106-5038, USA.
Tel.: +216-844-5840
Fax: 216-844-8954
E-mail: marco.costa@uhhospitals.org

doi: 10.1111/j.1582-4934.2012.01557.x

Materials and methods

Collection of CD34+ cells

Human cord blood (CB) was obtained from the University Hospitals Case Medical Center after IRB approval and written consent from donors. Total cord blood mononuclear cells were isolated by Histopaque 1077 (Sigma-Aldrich, Oakville, Ontario, Canada) density-gradient centrifugation. CD34+ cells were separated from mononuclear cells using CD34-bound microbeads and a magnetically activated cell sorter (autoMACS™; Miltenyi Biotec, Bergisch-Gladback, Germany) following the manufacturer's protocol. After separation, purity was determined by flow cytometry as described below.

Ex vivo expansion of CD34+ cells

5×10^4 CB-CD34+ cells in 2 ml of media were plated into each well of the six-well tissue culture dish (Primaria™; BD Falcon, Bedford, MA, USA) and cultured in a suspension manner using a serum-free expansion culture medium (CellGro® SCGM medium; CellGenix USA, Portsmouth, NH, USA) for 7 days. Expansion medium contained the four growth factors/cytokines: SCF (100 ng/ml), Flt-3 (100 ng/ml), TPO (20 ng/ml) and IL-6 (20 ng/ml), with or without VEGF (50 ng/ml). All growth factors and cytokines were purchased from Peprotech Inc. (Rocky Hill, NJ, USA).

Characterization of fresh and post-expansion CD34+ cells

To confirm the purity and to characterize pre- and post- expansion cells, fluorescence-activated cell sorting (FACS) analysis was performed with BD™ LSR Cell Analyser (BD Biosciences, San Jose, CA, USA) and Cell Quest™ software (BD Biosciences) after staining with mouse anti-human monoclonal antibodies against surface markers: CD133-APC (clone 293C3; Miltenyi Biotec), CD34-PE (clone 581; Pharmingen, San Diego, CA, USA), CD45-FITC (Biolegend, San Diego, CA, USA), CXCR4-PE (Pharmingen), CD11b-PE (Biolegend), CD3-PE (Biolegend), CD19-PE (Biolegend). Dead cells were excluded from the plots on the basis of 7-AAD staining (Pharmingen). Cells were stained with monoclonal antibodies for 20 min. at 4°C following FcR blocking, washed twice using Hank's buffer containing 2% FBS, and analysed. Relevant isotype controls (IgG1-PE isotype control (Biolegend), IgG1-FITC (Biolegend), IgG2b-APC (Biolegend), and IgG1-APC (Biolegend)) were also included. In all samples, 10,000 events were acquired.

MiRs expression analysis

Expression of miRs that have been previously associated with endothelial-mediated angiogenesis was determined in fresh and post-expansion cells ($n = 3$ in each group) using quantitative RT PCR. A quantity of 10 ng of total RNA was used for RT reactions from each sample following manufacturer's protocol (ABI kit). Reaction mixtures (15 μl) were incubated in a thermal cycler (Veriti® 96-Well Thermal Cycler; Applied Biosystems, Foster City, CA, USA) for 30 min. at 16°C, 30 min. at 42°C and 5 min. at 85°C and then maintained at 4°C. Quantitative PCR assays were performed using a TaqMan microRNA assay kit (Applied Biosystems). Real-time PCR was performed with a StepOnePlus™ Real-Time PCR System (Applied Biosystems). All reactions were incubated at 95°C for 10 min., followed by 40 cycles of 95°C for 15 sec., and 60°C for 1 min.; all were performed in triplicate. The RNU48 was used as a control to normalize differences in total RNA levels in each sample. A threshold cycle (Ct) was observed in the exponential phase of amplification, and quantification of relative expression levels was performed using standard curves for target genes and the endogenous control. Geometric means were used to calculate the ΔΔCt values and were expressed as $2^{-\Delta\Delta Ct}$. The value of each control sample was set at 1 and was used to calculate the fold of difference in the target gene.

Transfection of expanded cells with miR-210 inhibitor and mimic

To silence or up-regulate miR-210, cells were transfected with specific Anti-miR™ miRNA Inhibitor or Pre-miR™ miRNA mimic, hsa-miR-210 (Applied Biosystems). On day 5 of expansion, cells were seeded in antibiotic-free expansion media and transfected with miRs at a final concentration of 160 nM using Lipofectamine 2000 (Invitrogen, Carlsbad, CA, USA). After 48 hrs incubation, cells were collected and washed twice with sterile phosphate-buffered saline (PBS). As a negative control of transfection, we used non-targeting scrambled oligonucleotide following same transfection method. To evaluate miR transfection efficiency, cells were transfected with FITC-conjugated miR-210 inhibitor (mercury LNA™ micro RNA Power inhibitor, hsa-miR-210, EXIQON, Woburn, MA, USA) and analysed using flow cytometry to count transfected cells. After transfection, obtained cells proceeded for gene expression analysis, flow cytometric analysis, tube formation assay and animal experiments as described.

In vitro HUVEC tube formation assay

Pre- and post- expansion cells were applied to the tube formation assay by co-culturing with human umbilical vein endothelial cells (HUVECs) on Matrigel™ (BD Biosciences) to investigate their functional angiogenic contribution. 1×10^3 cells from each group (preEX, postEX/+VEGF, and postEX/noVEGF) were co-cultured with 1.5×10^4 HUVECs in 50 μl of EBM-2 complete medium with 2% FBS. A quantity of 50 μl of the cell suspension incubated at 37°C for 5 min. was applied onto Matrigel™ (50 μl/well) in 96-well plate. To evaluate miR-210 effect on angiogenic function of expanded cells, miR-210 inhibitor or mimic transfected cells were incubated with HUVEC following the same cell density. As a control, only HUVEC was cultured. After incubation for 18 hrs, a photomicrograph per well was taken under light microscopy (Leica DM IL LED with EC3 camera system,

Buffalo Grove, IL, USA), then the number of tube formation was counted using Photoshop software.

Mouse model of unilateral hind limb ischaemia and cell transplantation

The protocol was approved by the Case Western Reserve University School of Medicine Institutional Animal Care and Use Committee. Unilateral hind limb ischaemia was surgically induced as previously described [10]. Under anaesthesia with intraperitoneal xylazine (40 mg/kg) and ketamine (100 mg/kg), male 8- to 10-week-old NOD/SCID mice underwent left femoral artery ligation and transection at two points: proximally at inguinal ligament level and distally before bifurcation of popliteal and saphenous arteries. Two to six hours after surgery, 2.5×10^4 cells of preEX, postEX/noVEGF, postEX/+VEGF, and cells transfected with miR-210 inhibitor, mimic or scrambled miRs suspended in 30 μl of PBS, were injected into adductor muscles. As a vehicle control, only PBS (30 μl) was injected into adductor muscles in the same manner ($n = 5$–6 per group).

Perfusion imaging

Hind limb perfusion was measured with a laser Doppler perfusion imager system (Moor Instruments Ltd., Axminster, England) immediately and on day 14 after surgery. To account for variables, such as ambient light and temperature, the results were expressed as the mean flux ratio of perfusion in the left (ischaemic) *versus* the right (non-ischaemic) hind limb.

Tissue preparation for histological immunofluorescent analysis

After completing blood flow measurements at 14 days, left calf muscles (ischaemic side) were harvested and immediately embedded in freezing compound (Triangle Biomedical Sciences, Inc., Durham, NC, USA). Transverse sections of 5-μm thick were made using the middle portion of calf muscle for subsequent staining procedures. For capillary density evaluation, samples were stained with anti-CD31 antibody, PECAM-1 (Santa Cruz Biotechnology, Santa Cruz, CA, USA) and labelled with fluorescent conjugated 2nd antibody (Alexafluora; Invitrogen). Capillaries, stained by CD31 with green fluorescent, were counted under a 200× magnification to determine the capillary density (number of capillaries per muscle bundle). Serial sections were cut at three different levels, and representative fields were analysed by counting the number of capillaries in each field. All samples were observed under a fluorescent microscope and images were taken using a digital camera system (Leica).

Statistical analysis

Values were presented as mean ± S.E.M. One-way ANOVA with Newman–Keuls *post-hoc* test were used to compare the experimental groups. Unpaired *t*-test was used for comparing two groups. A $P < 0.05$ was considered statistically significant.

Results

Ex vivo expansion and characterization of human CD34+ cells

We first determined the expansion yield of CD34+ cells in medium containing four cytokines TPO, Flt3 ligand, SCF, and IL6 with (postEX/+VEGF) and without VEGF (postEX/noVEGF). CD34+ cell expansion was similar in both groups (Fold increase: 18.26 ± 2.24 *versus* 21.87 ± 5.85, respectively, $P = 0.655$) (Fig. 1). To characterize cells after expansion, we performed FACS analysis for CD34 positivity and other HSC/progenitor, monocytic and lymphocytic lineage markers (Fig. 2). CD34 positivity was 46% and 49% (P = n.s.) for postEX/+VEGF and postEX/no VEGF groups respectively (91% for freshly isolated cells) (Fig. 2). *Ex vivo* culture also resulted in significantly decreased CD133 and c-Kit positivity. There was modestly higher expression of c-Kit in the postEX/+VEGF group. FACS analysis suggested no differentiation into monocytic or lymphocytic lineages as indicated by the extremely low or absent expression of CD11b, CD3 and CD19.

Ex vivo expansion in VEGF-enriched medium enhances neovascularization

We first preformed the *in vitro* HUVEC tube formation assay to evaluate the effect of VEGF on the pro-angiogenic response by expanded cells. PostEX/+VEGF cells significantly improved *in vitro* tube formation in matrigel compared to both preEX and postEX/noVEGF groups (Fig. 3). We next compared the three cell groups in the mouse hind limb ischaemia model to further determine their *in vivo* neovascularization. Transplantation of postEX/+VEGF cells in the ischaemic hind-

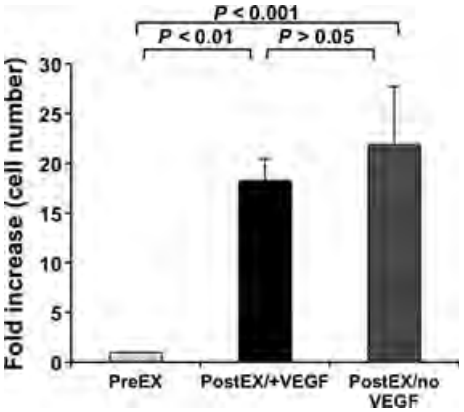

Fig. 1 Fold increase in cell number after expansion with and without VEGF. Data presented as fold increase in cell number compared to preEX cells (adjusted to 1); $P = 0.001$.

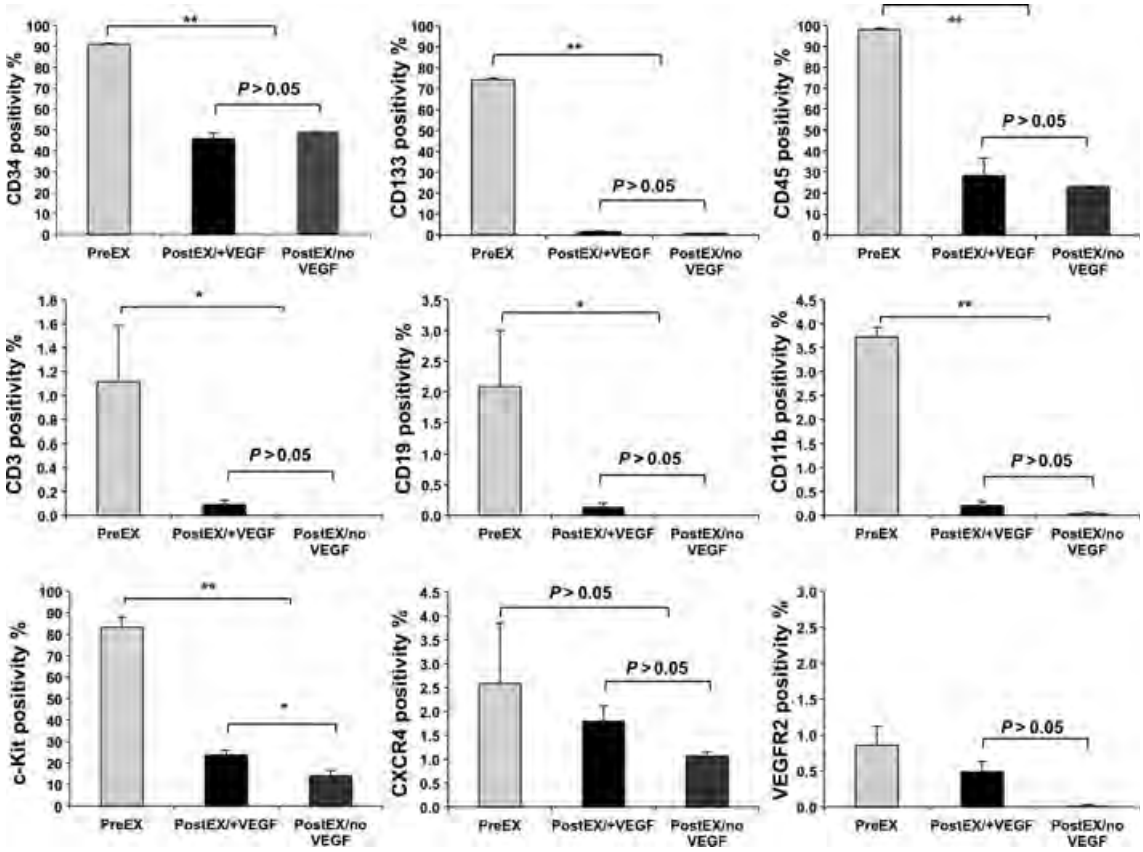

Fig. 2 Representative flow cytometry data of preEX (fresh CD34+), postEX/+ VEGF, and postEX/noVEGF cells. Comparison of flow cytometry data showed decrease in CD34, CD133, and c-Kit in post-expansion cells, but no indication of differentiation into monocytic or lymphocytic lineages (CD11b, CD3 or CD19). There was low expression of CXCR4 and VEGFR2 in preEX cells and further decrease in both expansion groups. $P < 0.01$ for CD34, CD133, c-Kit, CD11b, CD14 and CD45, $P < 0.05$ for CD3, CD19, and VEGFR2, and $P > 0.05$ for CXCR4. * and ** represents *post-hoc P* values of <0.05 and <0.01, respectively.

limb significantly improved tissue perfusion and increased capillary density compared to preEX and postEX/noVEGF cells (Fig. 4).

VEGF augments miR-210 expression in expanded CD34+ cells

MiRs are increasingly appreciated as essential regulators of numerous cellular processes; however, their role in CD34+ cell-induced angiogenesis is not completely understood. VEGF was previously reported to induce expression of certain miRs associated with endothelial angiogenesis [6]. We therefore sought to identify specific miRs associated with angiogenic properties of *ex vivo* expanded CD34+ cells. Cells expanded in VEGF-containing medium altered the expression levels of various miRs (Fig. 5). VEGF treatment enhanced the expression of miRs, such as 17-92 cluster and -296 in expanded cells, similarly to previously reported effects in endothelial cells [6]. We found no change in miR-126 and -130a expression; miRs that were shown to be pro- angiogenic [11–13]. However, we found significant and robust increase in miR-210 level in postEX/+VEGF cells (Fig. 5). We focused our attention on miR-210 given its known anti-apoptotic and pro-angiogenic effects [14], but heretofore-unrecognized role in CD34+ cells.

miR-210 silencing reduced postEX/+VEGF cell-mediated angiogenesis

To test whether up-regulation of miR-210 is required for the enhanced angiogenic properties of postEX/+VEGF cells, we transfected cells with miR-210 silencing inhibitor on day 5 of *ex vivo* culture. Transfection efficiency was ~60% (Fig. S1A), with specific ~70% reduction in miR-210 level (Fig. S1B and C). Minimal effects of transfection with miRs on cell viability were confirmed by trypan blue dye exclusion test (~87% *versus* ~93% with no transfection). Additional control experiments were performed to exclude a deleterious effect of transfection procedure on cell function and expression of surface markers (Figs. S2 and S3). Inhibition of miR-210 in

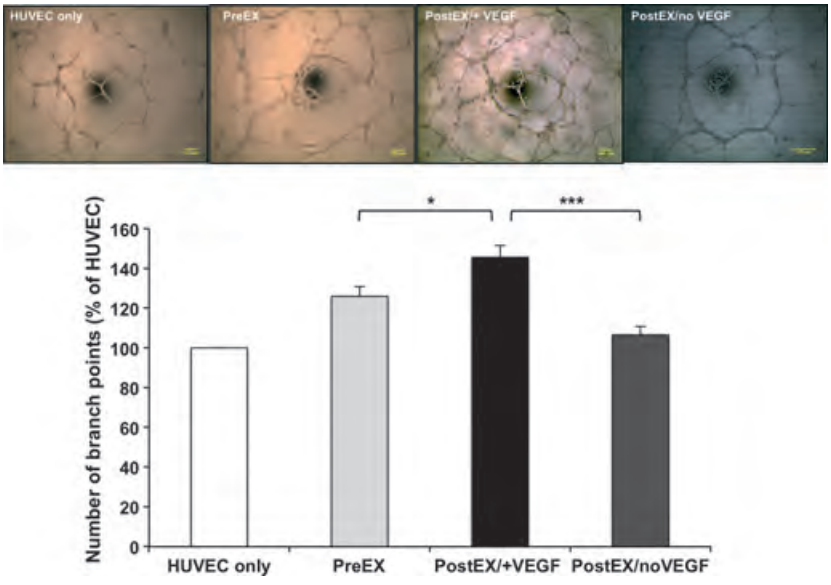

Fig. 3 Enhanced HUVEC *in vitro* tube formation by CD34+ cells expanded in VEGF-enriched medium. Pre-or post- expanded CD34+ cells were washed and incubated with HUVEC in 96-well plate coated with matrigel. Upper panel shows representative images of different groups (×40; scale bar = 100 μm). Lower panel represents percentage increase in number of branch points compared to HUVEC alone. Data show significant increase in tube formation in postEX/+VEGF group ($P < 0.0001$). *, *** represents *post-hoc P* values of <0.05, and <0.001 respectively.

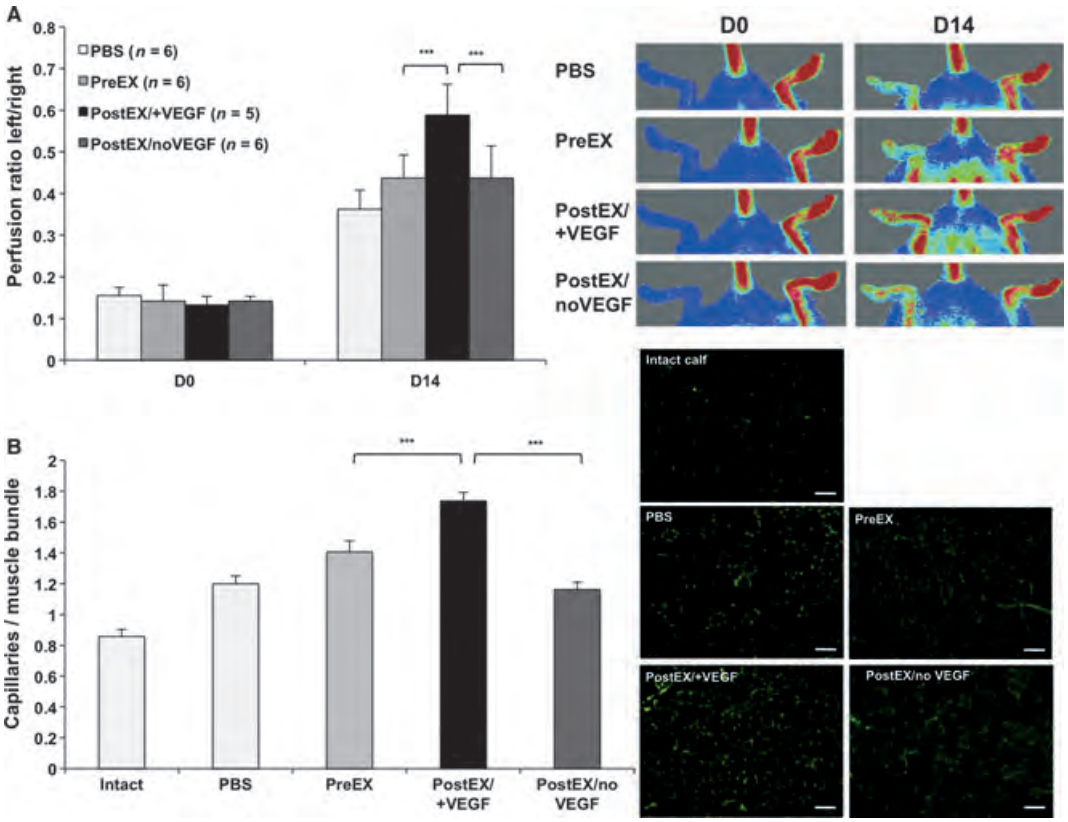

Fig. 4 CD34+ cells expanded in VEGF-enriched medium promote tissue perfusion and capillary density in mice ischaemic hindlimb. PBS or 2.5×10^4 cells were injected into ischaemic limb. Graphs show significant increase in tissue perfusion (**A**; $P < 0.0001$) and capillary density (**B**; $P < 0.0001$) in postEX/+VEGF group. Representative images of tissue perfusion and capillary density in calf muscle assessed by CD31staining (×200; scale bar = 200 μm) are shown in the right upper and lower panels, respectively. *** represents *post-hoc P* value of <0.001.

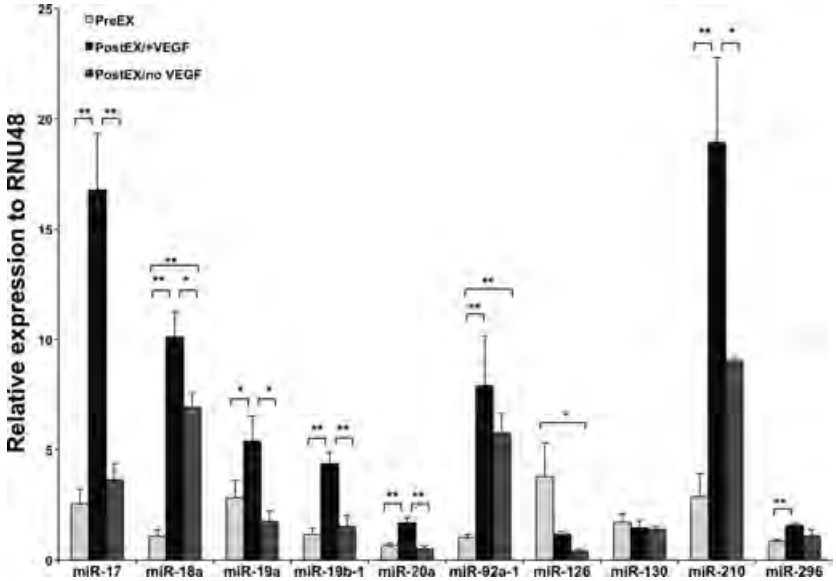

Fig. 5 Expression profile of various miRs associated with angiogenesis. Representative graph of quantitative PCR data for selected miRs in PreEX (fresh CD34+), PostEX/+VEGF, and PostEX/noVEGF cell groups ($n = 3$ donors). $P < 0.01$ for miR-17, 18a, 19b-1, 20a, 92a-1 and 210, $P < 0.05$ for miR-19a, 126 and 296 and $P > 0.05$ for miR-130. * and ** represents *post-hoc P* values of <0.05 and <0.01 respectively. RNU48 used as reference gene.

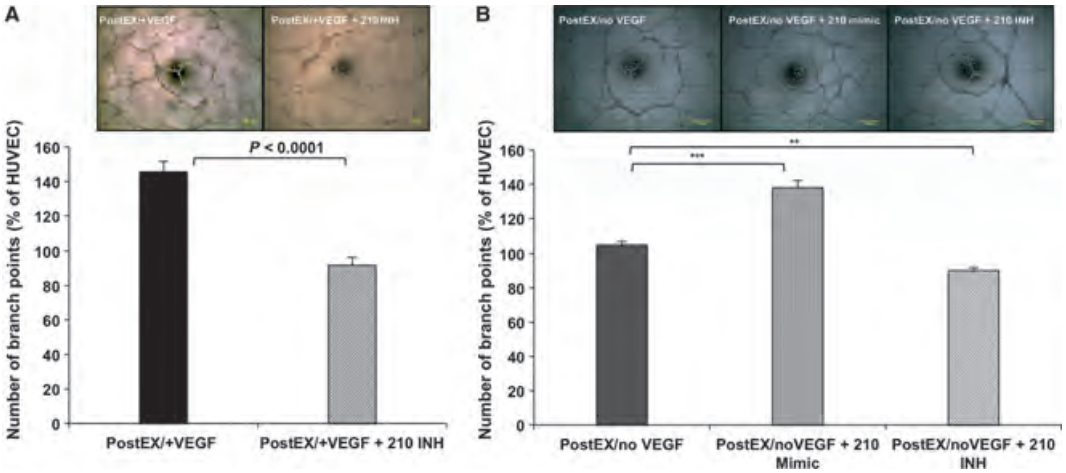

Fig. 6 MiR-210 is essential for the pro-angiogenic effects of expanded CD34+ cells on HUVEC *in vitro* tube formation assay. Post-expansion cells were transfected with miR-210 inhibitor or mimic, washed and incubated with HUVEC in matrigel coated 96-well plate. MiR-210 inhibitor resulted in significant decrease in number of branch points by cells expanded with or without VEGF (**A**: $P < 0.0001$ and **B**: $P < 0.0001$), whereas 210-mimic enhanced tube formation by postEX/noVEGF cells. Upper panel shows representative images of different groups (×40; scale bar = 100 μm). Lower panel represents percentage increase in number of branch points compared to HUVEC alone. **, *** represents *post-hoc P* values of <0.01, and <0.001 respectively.

postEX/+VEGF cells was associated with reduced tube formation *in vitro* (Fig. 6A) and decreased tissue perfusion and capillary density *in vivo* (Fig. 7A).

miR-210 mimic enhanced postEX/noVEGF cell-mediated angiogenesis

To further determine whether miR-210 is specifically involved in CD34+ cell-mediated angiogenesis independent of VEGF treatment, we transfected miR-210 mimic to CD34+ cells expanded in medium containing no VEGF. Similarly, 210-mimic was associated with enhanced *in vitro* tube formation (Fig. 6B) and increased tissue perfusion and capillary density *in vivo* (Fig. 7B).

Discussion

Our study demonstrates an important role of VEGF in *ex vivo* augmentation of CD34+ cells that is miR-210-dependent. The addition of

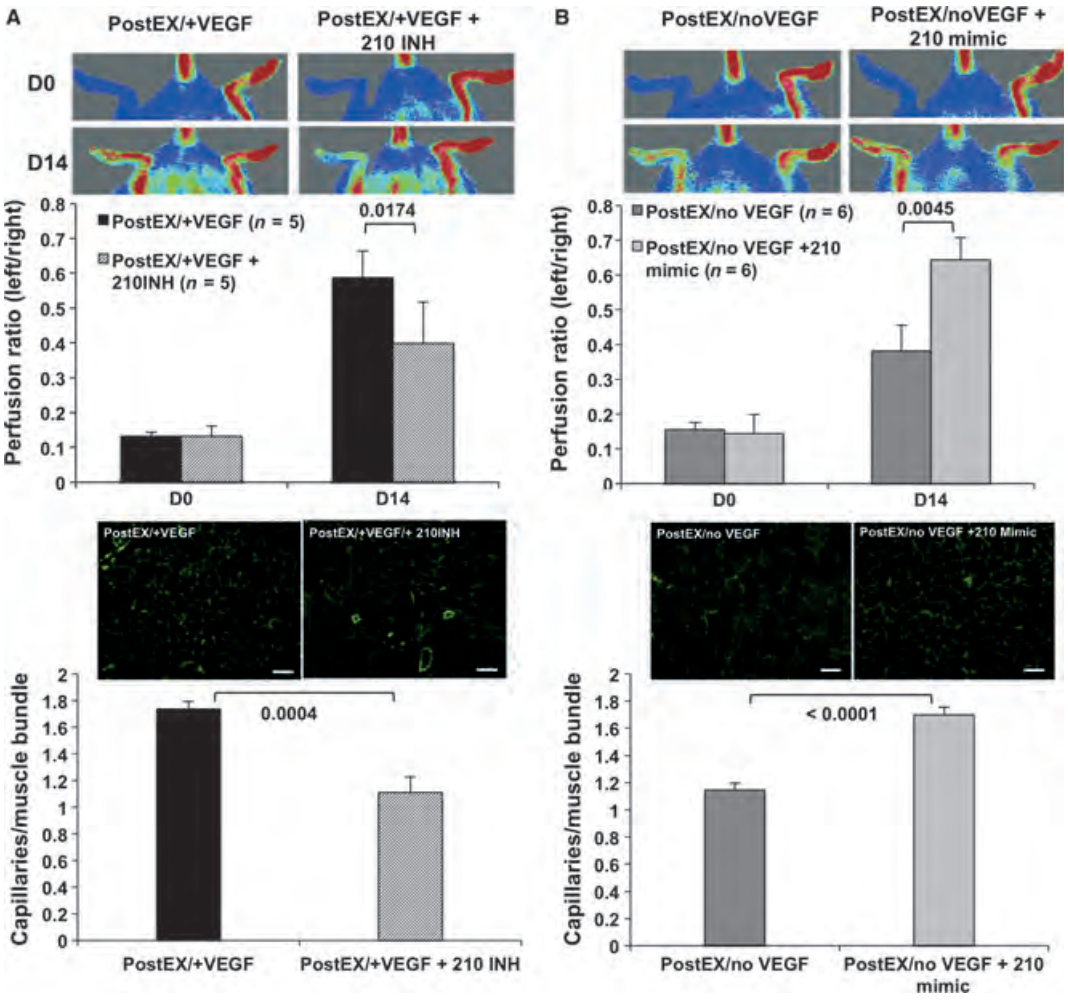

Fig. 7 MiR-210 promotes tissue perfusion and capillary density by expanded CD34+ cells in mice ischaemic hindlimb. Expanded cells were transfected for 48 hrs with either miR-210 inhibitor or mimic on day 5. After washing, 2.5×10^4 cells were injected into ischaemic limb. MiR-210 inhibition abrogated tissue re-perfusion (**A**, upper panel) and capillary density (**A**, lower panel) in postEX/+VEGF group, whereas mimic significantly improved tissue re-perfusion (**B**, upper panel) and capillary density (**B**, lower panel) in postEX/noVEGF. Representative images of tissue perfusion and capillary density in calf muscle assessed by CD31staining (×200; scale bar = 200 μm) are shown in the right upper and lower panels, respectively.

VEGF to a medium containing four cytokines commonly used for HSCs culture resulted in improved *in vitro* and *in vivo* angiogenesis, while preserving cell expansion yield. Importantly, cells expanded in VEGF-containing medium had a significant up-regulation in miR-210 expression (Fig. 5). Inhibition of miR-210 abrogated the pro-angiogenic effects of these cells (Figs 6A and 7A), and miR-210 mimic promoted cell-induced angiogenesis by cells expanded in VEGF-deficient medium (Figs 6B and 7B).

The importance of miRs in regulating the differentiation and fate of haematopoietic progenitor CD34+ cells has been previously described [15–18]. However, their role in angiogenic properties of *ex vivo* expanded CD34+ cells remains largely unexplored. VEGF is a central regulator of angiogenesis during development and ischaemia [19] and was shown to stimulate postnatal angiogenesis through enhancing expression of certain miRs in endothelial cells (EC) [6]. MiR17-92 cluster (17, 18a, 19a, 19b-1, 20a, 92a-1) was induced by VEGF, and it rescued EC proliferation and angiogenesis under VEGF stimulation after the loss of Dicer, an endoribonuclease required for generation and maturation of miRs [6]. In our study, we found significantly increased expression of this cluster after CD34+ cell expansion and VEGF treatment. Although this cluster has an important role in angiogenesis, cell survival and proliferation [20], its function is still incompletely understood. Individually, miR-17 has anti-proliferative properties [21, 22], whereas miR-92 is demonstrated to have anti-angiogenic effects [23], and miRs 18 and 19 are considered pro-angiogenic [24]. Additional studies are needed to explore the orchestrated mechanisms of this cluster in CD34+ cells and cell-induced angiogenesis.

We focused our attention on miR-210 given its established anti-apoptotic and pro-angiogenic effects [14], but heretofore-unrecognized role in CD34+ cells. MiR-210 regulates mitochondrial metabolism, cellular apoptosis and stem cell survival, as well as EC-mediated angiogenesis *in vitro* by regulating numerous targets, such as caspase-8-associated protein 2, protein-tyrosine phosphatase 1B, iron-sulphur cluster assembly proteins and ephrin-A3 mRNAs [14, 25]. MiR-210 also promotes migration of ECs in response to VEGF [5]. The expression of miR-210 in ECs was increased by hypoxia [5], but was not altered after VEGF exposure for 9 hrs [6]. Our study provides the first observation of increased levels of miR-210 induced by VEGF in CD34+ cells, and a new role for miR-210 in promoting CD34 + cell-mediated therapeutic angiogenesis *in vivo*.

Although CD34+ cells were cultured under normoxic conditions, it is possible that a state of relative hypoxia after 7-day culture led to the observed small increase in expression of miR-210 in postEX/no-VEGF cells. These cells showed similar angiogenic capacity compared to pre-expanded CD34+ cells, suggesting the importance of VEGF exposure in augmenting pro-angiogenic properties of expanded CD34+ cells and raising the possibility that induction of miR-210 targets by VEGF may be required. It is possible that this increase in miR-210 expression may insufficiently compensate for the lack of other positive effects of VEGF stimulation, or for the phenotypic changes after *ex vivo* culture of CD34+ cells as demonstrated by FACS data (decreased expression of CD34, CD133 and c-Kit) (Fig. 2). Nonetheless, miR-210 silencing virtually eliminated whereas miR-210 mimic recapitulated the pro-angiogenic effects of VEGF stimulation on expanded cells (Figs 6 and 7). Collectively, these observations identify miR-210 as an important regulator of CD34+ cell-induced angiogenesis.

The number of cells transplanted into mice ischaemic hindlimbs in the present study was similar to weight-adjusted cell doses used in humans [26]. The 20–40 times lower number (2.5×10^4 cells) compared to effective cell doses reported in previous pre-clinical studies [1, 27, 28] may explain the observed relative lower efficacy of pre-expanded (fresh) CD34+ cell transplantation. Importantly, postEX/+VEGF cell-induced *in vitro* and *in vivo* neovascularization was enhanced in spite of relatively low expression of CD34 and other known HSC and endothelial progenitor cell markers (Fig. 2).

Future investigation is warranted to dissect these pathways and explore whether the observed pro-angiogenic effects of miR-210 are cell-intrinsic [29] or operate through a paracrine exosome-mediated transfer of miR-210 from transplanted cells to the ischaemic tissue [30, 31]. Given the meaningful and sustained clinical benefit of CD34 cells in recent clinical trials [26], efforts to augment CD34+ cell function by targeting miR-210 are likely to be clinically impactful.

Acknowledgements

This study was supported by Wolf Family Fund at University Hospitals, GCIC Ohio Cell-based Therapy Consortium, Bio-Heart Discretionary Fund for Stem Cell Research at Case Western Reserve University, and the Cytometry & Imaging Microscopy Core Facility of the Case Comprehensive Cancer Center (P30 CA43703).

Author contributions

MAM: conception and design, collection and assembly of data, data analysis and interpretation, manuscript writing.

MI: conception and design, collection and assembly of data, data analysis and interpretation, manuscript writing.

HM: conception and design.

DIS: data analysis and interpretation, final approval of manuscript.

MKJ: data analysis and interpretation, final approval of manuscript.

TA: conception and design, final approval of manuscript.

MAC: conception and design, data analysis and interpretation, manuscript writing, final approval of manuscript.

Conflict of interest

Masuda H and Asahara T are co-founders of StemMed. Inc.

Supporting information

Additional Supporting Information may be found in the online version of this article:

Figure S1 miR210 inhibitor transfection efficiency. Representative flow cytometric analysis of CD34+ cells transfected with unconjugated (control) or FITC-conjugated miR-210 inhibitor at 160 nM on day 5 of *ex vivo* expansion. Percentage of FITC-positive cells indicating ~60% transfection efficiency after 48 hrs (**A**). Quantitative PCR data demonstrated specific (~70%) inhibition of miR-210 (**B**), and no inhibition of other miRs (**C**). PostEX/+VEGF cells with (210INH) or without (control) specific miR-210 inhibitor were used for this experiment.

Figure S2 Representative flow cytometry data showing no significant effect of miR-210 modulation on CD34, CD133, c-Kit or CXCR4 expression. PostEX/noVEGF cells were used as control (no transfection), or transfected with scramble miRs, miR-210 mimic, or miR-210 inhibitor. This data suggests that miR-210 is not involved in expression of these markers. Representative *P* values by ANOVA are shown.

Figure S3 Representative data for *in vitro* tube formation matrigel assay (**A**) and tissue perfusion 14 days post hind ischaemic hindlimb (**B**) showing no significant effect of transfection procedure on angiogenic properties of expanded cells. PostEX/noVEGF cells with and without (control) scramble miRs transfection were used for this experiment. (×40; scale bar = 100 μm for tube formation assay images).

Please note: Wiley-Blackwell are not responsible for the content or functionality of any supporting materials supplied by the authors. Any queries (other than missing material) should be directed to the corresponding author for the article.

References

1. **Asahara T, Murohara T, Sullivan A, *et al.*** Isolation of putative progenitor endothelial cells for angiogenesis. *Science.* 1997; 275: 964–7.
2. **Shantsila E, Watson T, Lip GYH.** Endothelial progenitor cells in cardiovascular disorders. *J Am Coll Cardiol.* 2007; 49: 741–52.
3. **Bushati N, Cohen SM.** microRNA functions. *Annu Rev Cell Dev Biol.* 2007; 23: 175–205.
4. **Suárez Y, Fernández-Hernando C, Pober JS, *et al.*** Dicer dependent microRNAs regulate gene expression and functions in human endothelial cells. *Circ Res.* 2007; 100: 1164–73.
5. **Fasanaro P, D'Alessandra Y, Di Stefano V, *et al.*** MicroRNA-210 modulates endothelial cell response to hypoxia and inhibits the receptor tyrosine kinase ligand Ephrin-A3. *J Biol Chem.* 2008; 283: 15878–83.
6. **Suárez Y, Fernández-Hernando C, Yu J, *et al.*** Dicer-dependent endothelial microRNAs are necessary for postnatal angiogenesis. *Proc Natl Acad Sci USA.* 2008; 105: 14082–7.
7. **Boitano AE, Wang J, Romeo R, *et al.*** Aryl hydrocarbon receptor antagonists promote the expansion of human hematopoietic stem cells. *Science.* 2010; 329: 1345–8.
8. **Gerber H-P, Malik AK, Solar GP, *et al.*** VEGF regulates haematopoietic stem cell survival by an internal autocrine loop mechanism. *Nature.* 2002; 417: 954–8.
9. **Masuda H, Alev C, Akimaru H, *et al.*** Methodological development of a clonogenic assay to determine endothelial progenitor cell potential. *Circ Res.* 2011; 109: 20–37.
10. **Niiyama H, Huang NF, Rollins MD, *et al.*** Murine model of hindlimb ischemia. *J Vis Exp.* 2009; pii: 1035.
11. **Fish JE, Santoro MM, Morton SU, *et al.*** miR-126 regulates angiogenic signaling and vascular integrity. *Dev Cell.* 2008; 15: 272–84.
12. **van Solingen C, Seghers L, Bijkerk R, *et al.*** Antagomir-mediated silencing of endothelial cell specific microRNA-126 impairs ischemia-induced angiogenesis. *J Cell Mol Med.* 2009; 13: 1577–85.
13. **Chen Y, Gorski DH.** Regulation of angiogenesis through a microRNA (miR-130a) that down-regulates antiangiogenic homeobox genes GAX and HOXA5. *Blood.* 2008; 111: 1217–26.
14. **Hu S, Huang M, Li Z, *et al.*** MicroRNA-210 as a novel therapy for treatment of ischemic heart disease. *Circulation.* 2010; 122: S124–31.
15. **Tenedini E, Roncaglia E, Ferrari F, *et al.*** Integrated analysis of microRNA and mRNA expression profiles in physiological myelopoiesis: role of hsa-mir-299-5p in CD34+ progenitor cells commitment. *Cell Death Dis.* 2010; 1: e28.
16. **Lu J, Guo S, Ebert BL, *et al.*** MicroRNA-mediated control of cell fate in megakaryocyte-erythrocyte progenitors. *Dev Cell.* 2008; 14: 843–53.
17. **Labbaye C, Spinello I, Quaranta MT, *et al.*** A three-step pathway comprising PLZF/miR-146a/CXCR4 controls megakaryopoiesis. *Nat Cell Biol.* 2008; 10: 788–801.
18. **Zhao H, Kalota A, Jin S, *et al.*** The c-myb proto-oncogene and microRNA-15a comprise an active autoregulatory feedback loop in human hematopoietic cells. *Blood.* 2009; 113: 505–16.
19. **Coultas L, Chawengsaksophak K, Rossant J.** Endothelial cells and VEGF in vascular development. *Nature.* 2005; 438: 937–45.
20. **Mendell JT.** miRiad roles for the miR-17-92 cluster in development and disease. *Cell.* 2008; 133: 217–22.
21. **Shan SW, Lee DY, Deng Z, *et al.*** MicroRNA MiR-17 retards tissue growth and represses fibronectin expression. *Nat Cell Biol.* 2009; 11: 1031–8.
22. **Hossain A, Kuo MT, Saunders GF.** Mir-17-5p regulates breast cancer cell proliferation by inhibiting translation of AIB1 mRNA. *Mol Cell Biol.* 2006; 26: 8191–201.
23. **Bonauer A, Carmona G, Iwasaki M, *et al.*** MicroRNA-92a controls angiogenesis and functional recovery of ischemic tissues in mice. *Science.* 2009; 324: 1710–3.
24. **Dews M, Homayouni A, Yu D, *et al.*** Augmentation of tumour angiogenesis by a Myc-activated microRNA cluster. *Nat Genet.* 2006; 38: 1060–5.
25. **Fasanaro P, Greco S, Lorenzi M, *et al.*** An integrated approach for experimental target identification of hypoxia-induced miR-210. *J Biol Chem.* 2009; 284: 35134–43.
26. **Losordo DW, Henry TD, Davidson C, *et al.*** Intramyocardial, Autologous CD34+ Cell Therapy for Refractory Angina. *Circ Res.* 2011; 109: 724–8.
27. **Schatteman GC, Hanlon HD, Jiao C, *et al.*** Blood-derived angioblasts accelerate blood-flow restoration in diabetic mice. *J Clin Invest.* 2000; 106: 571–8.
28. **O E, Lee BH, Ahn H-Y, *et al.*** Efficient nonadhesive *ex vivo* expansion of early endothelial progenitor cells derived from CD34+ human cord blood fraction for effective therapeutic vascularization. *FASEB J.* 2011; 25: 159–69.
29. **Doebele C, Bonauer A, Fischer A, *et al.*** Members of the microRNA-17-92 cluster exhibit a cell-intrinsic antiangiogenic function in endothelial cells. *Blood.* 2010; 115: 4944–50.
30. **Valadi H, Ekström K, Bossios A, *et al.*** Exosome-mediated transfer of mRNAs and microRNAs is a novel mechanism of genetic exchange between cells. *Nat Cell Biol.* 2007; 9: 654–9.
31. **Sahoo S, Klychko E, Thorne T, *et al.*** Exosomes from human CD34+ stem cells mediate their proangiogenic paracrine activity. *Circ Res.* 2011; 109: 724–8.

ORIGINAL RESEARCH

American Heart Association | American Stroke Association

Vasculogenic Conditioning of Peripheral Blood Mononuclear Cells Promotes Endothelial Progenitor Cell Expansion and Phenotype Transition of Anti-Inflammatory Macrophage and T Lymphocyte to Cells With Regenerative Potential

Haruchika Masuda, MD, PhD; Rica Tanaka, MD, PhD; Satoshi Fujimura, PhD; Masakazu Ishikawa, MD, PhD; Hiroshi Akimaru, PhD; Tomoko Shizuno, BS; Atsuko Sato, BS; Yoshinori Okada, PhD; Yumi Iida, BS; Jobu Itoh, PhD; Yoshiko Itoh, PhD; Hiroshi Kamiguchi, BS; Atsuhiko Kawamoto, MD, PhD; Takayuki Asahara, MD, PhD

***Background*—**Cell-based therapies involving mononuclear cells (MNCs) have been developed for vascular regeneration to treat ischemic diseases; however, quality control of therapeutic MNCs has not been evaluated. We investigated the therapeutic potential of peripheral blood (PB) MNCs, operated by recently developed quality and quantity (QQ) culture of endothelial progenitor cells (EPCs).

***Methods and Results*—**PBs were collected from healthy volunteers; peripheral blood mononuclear cells (PBMNCs) isolated from these PBs were subjected to QQ culture for 7 days with medium containing stem cell factor, thrombopoietin, Flt-3 ligand, vascular endothelial growth factor, and interleukin-6. The resulting cells (QQMNCs) in EPC colony-forming assay generated significantly more definitive EPC colonies than PBMNCs. In flow cytometry, macrophages and helper T lymphocytes of QQMNCs became phenotypically polarized into angiogenic, anti-inflammatory, and regenerative subsets: classical M1 to alternative M2; T helper (Th) 1 to Th2; angiogenic or regulatory T-cell expansion. Quantitative real-time polymerase chain reaction (qRT-PCR) assay revealed the predominant proangiogenic gene expressions in QQMNCs versus PBMNCs. Using murine ischemic hindlimb models, the efficacy of QQMNC intramuscular transplantation (Tx) was compared to that of PBMNCTx, cultured "early EPC" Tx (eEPCTx), and granulocyte colony-stimulating factor mobilized $CD34^+$ cell Tx (GmCD34Tx). Laser Doppler imaging revealed the blood perfusion recovery in ischemic hindlimbs after QQMNCTx superior to after PBMNCTx and eEPCTx, but also earlier than after GmCD34Tx. Histological evaluations and qRT-PCR assays in ischemic hindlimbs demonstrated that QQMNCTx, similarly to GmCD34Tx, enhanced angiovasculogenesis and myogenesis, whereas it preponderantly inhibited inflammation and fibrosis versus PBMNCTx and eEPCTx.

***Conclusions*—**QQ culture potentiates the ability of PBMNCs to promote regeneration of injured tissue; considering the feasible cell preparation, QQ culture-treated PBMNCs may provide a promising therapeutic option for ischemic diseases.

***Clinical Trial Registration*—**URL: irb.med.u-tokai.ac.jp/d/2/monthly/2010.html; IRB No.: 10R-020.URL: irb.med.u-tokai.ac.jp/d/2/monthly/201312.html; IRB No.: 13R228. **(*J Am Heart Assoc*.2014;3:e000743 doi: 10.1161/JAHA.113.000743)**

Key Words: anti-inflammation • cell-based therapy • peripheral blood mononuclear cells • serum-free culture • vascular regeneration

Based on the isolation of bone marrow (BM)-derived endothelial progenitor cells (EPCs),[1–3] autologous total mononuclear cells (MNCs) freshly isolated from BM or peripheral blood (PB) have been applied to clinical vascular regenerative therapy in patients with severe ischemic heart or limb diseases.

From the Department of Regenerative Medicine Science (H.M., T.S., A.S., T.A.) and Teaching and Research Support Core Center (Y.O., Y. Iida., J.I., Y. Itoh, H.K.), Tokai University School of Medicine, Isehara, Japan; Department of Plastic and Reconstructive Surgery, Juntendo University School of Medicine, Tokyo, Japan (R.T., S.F.); Department of Orthopedic Surgery, Graduate School of Biomedical Science, Hiroshima University, Hiroshima, Japan (M.I.); Vascular Regeneration Research Group, Institute of Biomedical Research and Innovation IBRI, Kobe, Japan (H.A., A.K., T.A.).

An accompanying Video S1 is available at http://jaha.ahajournals.org/content/3/3/e000743/suppl/DC1

Correspondence to: Haruchika Masuda, MD, PhD, or Takayuki Asahara, MD, PhD, Division of Basic Clinical Science, Department of Regenerative Medicine Science, Tokai University School of Medicine, Shimokasuya, Isehara, Kanagawa 259-1143, Japan. E-mails: masu3510@is.icc.u-tokai.ac.jp, asa777@is.icc.u-tokai.ac.jp

Received January 8, 2014; accepted April 7, 2014.

These initial clinical experiences indicate that cell-based therapy for vascular regenerations is safe, feasible, and effective.[4–7] However, the translational and clinical trials have also demonstrated insufficient or contradictory effectiveness on recovery from ischemic diseases.[8–11]

Peripheral blood and bone marrow MNCs (PBMNCs and BMMNCs) constitute hematopoietic lineage cells; most are lymphoid cells or myeloid monocytes, and very few are stem/progenitor cell types, such as hematopoietic stem/progenitor cells, EPCs, or other mesenchymal stem cells. The scarcity of EPCs in MNC populations is a main reason for failure of constant and potent contributions in clinical cases.

Enriched EPCs, such as $CD34^+$ or $CD133^+$ cells, constitute <0.01% of PBMNCs and 0.1% of BMMNCs, and the frequency of colony-forming EPCs is 0.005% in PBMNCs.[12]

Taking into account the majority in MNCs, we need to issue the critical functions of monocyte/macrophages. Monocytes are precursors of macrophages; monocytes play key roles in both proinflammatory and regenerative processes by phenotype alterations after tissue infiltrations.[13] Macrophages are a heterogeneous cell population that adapts and responds to a large variety of microenvironmental signals. For example, the cytokines and growth factors in some microenvironments induce macrophages to adopt regenerative phenotypes, whereas the inflammatory deterioration and fibrosis in uncontrolled inflammatory environment in tissues induce proinflammatory macrophage transitions and suppress regenerative processes.

Also, the inflammatory environment is interacted by major lymphoid phenotypes simultaneously stimulated by proinflammatory signals and controlled macrophage phenotype transition for proinflammatory drive.[13,14]

To suppress unproductive inflammatory process and enhance vasculogenic regeneration, purified EPCs have been transplanted into patients with severe ischemic heart or limb diseases, and these initial clinical experiences indicate that this cell-based therapy is safe and effective.[15–19] Nevertheless, the problems caused by EPC scarcity must be overcome for EPC-mediated therapy to become reproducible and effective. To this end, the following 3 step-wise strategies have been used: (1) leukapheresis; (2) daily administration of granulocyte colony-stimulating factor (G-CSF); and (3) isolation of machinery $CD34^+$ or $CD133^+$ cells. Such an isolation process of autologous EPC sources burdens the patients to be treated with "EPC therapy," in terms of medical invasiveness and costs.

More important, the number and functionality of EPCs decline as patients age[20] and in patients with cardiovascular (CV) risk factors.[21,22]

Here, we describe a method for MNC culture that enhances the vasculogenic potential of EPCs and facilitates the preparation of monocytes for regenerative phenotype activation.

Our method for quality and quantity-control culture (QQ culture) of MNCs (QQMNCs) is based on an established culture method that increases the quality and quantity of EPCs derived from enriched EPC populations, such as $CD34^+$ and $CD133^+$ cells. Notably, the therapeutic potential of QQ culture is demonstrably greater than that of naïve EPCs for CV regeneration after infarcted myocardia in rats.[23] Interestingly, we found that the vasculogenic signaling condition of MNCs in QQ culture potentiates the vascular and tissue regeneration ability of naïve PBMNCs. The regenerative function of QQMNCs turned out to be operated through activation of anti-inflammatory and angiogenic monocytes/helper T lymphocytes as well as vasculogenic EPC expansion.

Moreover, the present experimental study demonstrated that therapeutic efficacy of QQMNC transplantation (QQMNCTx) is equal to and greater than that of G-CSF mobilized $CD34^+$ cell Tx (GmCD34Tx).

Therefore, in cell-based therapy for ischemic diseases, QQMNC provides a practical option of cell sources, including PBMNC and GmCD34.

Methods

Collection of PBMNCs Cells or $CD34^+$ Cells From Healthy Volunteers

Experiments using human samples were performed with institutional approval and guidelines from the Clinical Investigation Committee at Tokai University School of Medicine (institutional review board [IRB] No.: 10R-020; irb.med.u-tokai.ac.jp/d/2/monthly/2010.html and IRB No.: 13R228; irb.med.u-tokai.ac.jp/d/2/monthly/201312.html). The whole healthy human volunteers between the ages of 20 and 55 years gave informed consent.

PB (20 to 100 mL per subject) was drawn by heparinized venous puncture at the forearm. PBMNCs were isolated by density gradient centrifugation using Lymphocyte Separation Solution (d=1.077; Nakalai Tesque, Kyoto, Japan), as previously reported.[24] $CD34^+$ cells were purified by an autoMACS separator (Miltenyi Biotec, Lund, Sweden), using magnetic beads-coated mouse anti human CD34 antibody (Ab) and a CD34 Cell isolation kit (Miltenyi Biotec), according to the manufacturer's instructions.

QQ Culture and Early EPC Culture of PBMNCs

QQ culture condition for PBMNCs

QQ culture medium of Stem Line II (Sigma-Aldrich, St. Louis, MO) contained the 5 human recombinant proteins: stem cell factor (SCF); thrombopoietin (TPO); Flt-3 ligand; vascular endothelial growth factor (VEGF); and interleukin (IL)-6.

Then, isolated PBMNCs were cultured for 7 days at the cell density of 2×10^6 cells/2 mL QQ culture medium per well of 6-well Primaria tissue culture plate (BD Falcon; BD Biosiences, San Jose, CA). Cell density in QQ culture was corresponded to the approximate density of 1×10^6 MNCs in 1 mL of PB. Culture well plates and the contents of QQ culture medium are listed in Tables 1 and 2.

Early EPC culture of PBMNCs

As previously reported,[24,25] early EPCs (eEPCs) were acquired after 7 days of culture of isolated PBMNCs using the EGM-2-MV SingleQuots kit (Lonza Walkersville, Inc., Walkersville, MD). In brief, EGM-2-MV complete medium was adjusted by adding 5% FBS (SAFC Biosciences Inc., Lenexa, KS) and supplemented growth factors, except hydrocortisone, to EBM-2 basal medium. PBMNCs were adjusted to the similar cell density (1×10^6 cells/mL) with 5% FBS/EGM-2-MV complete medium to that in QQ culture of PBMNCs. Cells were then plated on a human fibronectin-coated 6-well Primaria tissue culture plate (2×10^6 cells/2 mL per well) and cultured. The medium was changed 4 days after seeding, then cultured for 3 more days. Seven days later, nonattaching cells were removed; adherent cells were harvested with 2 mmol/L of EDTA/PBS after washing with PBS. Harvested eEPCs were suspended in Iscove's Modified Dulbecco's Medium (IMDM) (Sigma Aldrich), adjusted the cell density (1×10^4 cells/40 μL or 2×10^5 cells/40 μL), cells were then transplanted into skeletal muscle of murine ischemic hindlimb, as described below.

EPC Colony-Forming Assay

To investigate the vasculogenic potential of PBMNCs or QQMNCs, we used semisolid culture medium and 35-mm Primaria dishes (BD Falcon; BD Biosciences) to grow and then counted the adhesive EPC colonies by EPC colony-forming assay (EPC-CFA) (MethoCult SF[BIT]; STEMCELL Technologies Inc., Vancouver, BC, Canada) with proangiogenic growth factors/cytokines, as previously reported (Table 3).[12] Aliquots of those cells were seeded at 2×10^5 cells/dish (3 dishes per volunteer) for EPC-CFA. Sixteen to 18 days after initiation of the culture, the number of adherent colonies per dish was measured using a gridded scoring dish (STEMCELL Technologies) under phase-contrast light microscopy (Eclipse TE300; Nikon, Tokyo, Japan). Primitive EPC colony-forming units (pEPC-CFUs) and definitive EPC-CFUs (dEPC-CFUs) were separately counted.

Table 1. Materials for QQ Culture and EPC-CFA

	Company, Catalaog No.	Application
6-well Primaria tissue culture plate	BD Biosciences, #353846	QQ culture
35-mm Primaria tissue culture dish	BD Biosciences, #353801	EPC-CFA
Blunt-end needle	STEMCELL Technologies, #28110	Applying semisolid medium
Gridded scoring dish	STEMCELL Technologies, #27500	Guide when counting EPC-CFU

EPC-CFA indicates endothelial progenitor cell colony-forming assay; EPC-CFU, endothelial progenitor cell colony-forming units; QQ, quality and qunatity.

Table 2. Contents of QQ Culture Medium

	Company, Catalog No.	Final Concentration
Stemline II™ Hematopoietic Stem Cell Expansion Medium	Sigma-Aldrich, #S0192	
rh SCF	Peprotec, #300-07	100 ng/mL
rh Flt-3 ligand	Peprotec, #300-19	100 ng/mL
rh TPO	Peprotec, #300-18	20 ng/mL
rh VEGF	Peprotec, #100-20	50 ng/mL
rh IL-6	Peprotec, #200-06	20 ng/mL

IL indicates interleukin; rh, recombinant human; SCF, stem cell factor; TPO, thrombopoietin; VEGF, vascular endothelial growth factor.

Flow Cytometry

Performance of flow cytometry for lineage cell populations

Freshly isolated PBMNCs and the QQMNCs were subjected to flow cytometry (FCM) to detect surface antigen positivities

Table 3. Contents in Semisolid Culture for EPC-CFA

	Company, Catalog No.	Final Concentration
MethoCult™ SF[BIT] H4236	STEMCELL Technologies, #04236	
rh SCF	Peprotec, #300-07	66.7 ng/mL
rh VEGF	Peprotec, #100-20	33.3 ng/mL
rh basic FGF	Peprotec, #100-18B	33.3 ng/mL
rh EGF	Peprotec, #100-15	33.3 ng/mL
rh IGF-1	Peprotec, #100-11	33.3 ng/mL
rh IL-3	Peprotec, #200-03	13.3 ng/mL
Heparin	Shimizu Pharmaceutical Co	1.33 IU/mL
FBS	SAFC Biosciences, #12303	30% (vol/vol)

EGF indicates epidermal growth factor; FGF, fibroblast growth factor; IGF, insulin-like growth factor; IL, interleukin; rh, recombinant human; VEGF, vascular endothelial growth factor.

of hematopoietic stem or lineage committed cells as well as endothelial lineage cells. The Abs were listed in Tables 4 through 6. Cells suspended in 2 mmol/L of EDTA/0.2% BSA/PBS buffer (5×10^5 cells/200 μL) were incubated after the addition of 10 μL of FcR blocking reagent at 4°C for 30 minutes and then equally dispensed into reaction tubes for subsequent staining (100 μL/tube). Each aliquot was incubated with 2 μL of each first Ab at 4°C for 20 minutes and then washed twice with 1 mL of 2 mmol/L of EDTA/0.2% BSA/PBS buffer. Cells were suspended in 2 mmol/L of EDTA/0.2% BSA/PBS buffer (2×10^5 cells/200 μL). FCM analysis was performed using the LSRFortessa cell analyzer (BD Biosciences) and FlowJo software (Tomy Digital Biology Co., Ltd., Tokyo, Japan). When staining for von Willebrand factor (vWF), after incubation with each first Ab, cells were incubated with biotin conjugated rat anti-mouse immunoglobulin G (IgG)1 and then conjugated to streptavidin/phycoerythrin/cyanine 7 (PE/Cy7).

Table 4. Antibodies Recognizing Hematopoietic Cell Populations for Flow Cytometry

Antibody	Clone	Isotype	Company, Catalog No.
CD34-FITC	581	Mouse IgG1 κ	BD Pharmingen, #555821
CD133-APC	AC133	Mouse IgG1	Miltenyi Biotec, #130-090-826
VEGFR-2-PE	89106	Mouse IgG1	R&D Systems, #FAB357P
CD31-FITC	WM59	Mouse IgG1 κ	BD Pharmingen, #555445
vWF	4F9	Mouse IgG1 κ	Abcam, #ab20435
CD105-APC	SN6	Mouse IgG1 κ	eBioscience, #17-1057-42
CD146-PE	P1H12	Mouse IgG1 κ	BD Pharmingen, #550315
CD3-Alexa700	HIT3a	Mouse IgG2a κ	BioLegend, #300324
CD4-APC/Cy7	RPA-T4	Mouse IgG1 κ	BioLegend, #300518
CD8-Pacific Blue	SK1	Mouse IgG1 κ	BioLegend, #344718
CD11c-PE	S-HCL-3	Mouse IgG2b κ	BD Biosciences, #347637
CD14-Pacific Blue	M5E2	Mouse IgG2a κ	BioLegend, #301828
CD16-APC/Cy7	3G8	Mouse IgG1 κ	BioLegend, #302018
CD19-PE/Cy7	HIB19	Mouse IgG1 κ	BioLegend, #302215
CD56-APC	HCD56	Mouse IgG1 κ	BioLegend, #318309
CD192(CCR2)-PerCP/Cy5.5	TG5/CCR2	Mouse IgG2b κ	BioLegend, #335303
CD206-APC/Cy7	15-2	Mouse IgG1 κ	BioLegend, #321119
CD235a-FITC	GA-R2 (HIR2)	Mouse IgG2b κ	BD Pharmingen, #559943
CD184(CXCR4)-PE/Cy7	12G5	Mouse IgG2a κ	BioLegend, #306514

APO indicates allophycocyanin; CCR2, CC chemokine receptor 2; CXCR4, C-X-C chemokine receptor type 4; PE, phycoerythrin; VEGFR, vascular endothelial growth factor receptor; vWF, von Willebrand factor.

Table 5. Antibodies Recognizing Helper T-Cell Subsets for Flow Cytometry

Antibody	Clone	Isotype	Company, Cat No.
CD4-PerCP/Cy5.5	OKT4	Mouse IgG2b κ	BioLegend, #317428
CD25-PE	BC96	Mouse IgG1 κ	BioLegend, #302606
INF-γ-Pacific Blue	4S.B3	Mouse IgG1 κ	BioLegend, #502522
IL-4-APC	8D4-8	Mouse IgG1 κ	BioLegend, #500713
Foxp3-FITC	206D	Mouse IgG1 κ	BioLegend, #320105

Foxp3 indicates forkhead box P3; IL, interleukin; INF, interferon.

Table 6. Isotype Antibodies and Reagents for Flow Cytometry

Antibody	Clone	Company, Catalog No.
Mouse IgG1 κ-FITC	MOPC-21	BD Pharmingen, #555748
Mouse IgG1 κ-APC	679.1Mc7	Beckman Coulter, #IM2475
Mouse IgG1 κ-PE	MOPC-21	BD Pharmingen, #555749
Mouse IgG1 κ	MOPC-21	BD Pharmingen, #555746
Mouse IgG1 κ-Pacific Blue	MOPC-21	BioLegend, #400131
Mouse IgG1 κ-PE/Cy7	MOPC-21	BioLegend, #400125
Mouse IgG1 κ-APC/Cy7	MOPC-21	BioLegend, #400127
Mouse IgG2a κ-Pacific Blue	MOPC-173	BioLegend, #400235
Mouse IgG2a κ-Alexa700	MOPC-173	BioLegend, #400247
Mouse IgG2b κ-FITC	27-35	BD Pharmingen, #555742
Mouse IgG2b κ-PE	27-35	BD Pharmingen, #555743
Mouse IgG2 κ-PerCP/Cy5.5	MPC-11	BioLegend, #400337
Mouse IgG2a κ-PE/Cy7	MOP-173	BioLegend, #400232
Biotin-rat anti-mouse IgG1	A85-1	BD Pharmingen, #553441
Streptavidin-PE/Cy7		BioLegend, #405206
Fc blocking reagent, human		Miltenyi Biotec, #130-059-901

Performance of FCM for activated helper T-lymphocyte subsets

PBMNCs or QQMNCs in 10% FBS/RPMI 1640 medium (1×10^6 cells/mL) were treated with 25 ng/mL of phorbol-12-myristate-13-acetate (PMA; Promega, Madison, WI) and 1 μg/mL of ionomycin (Wako Pure Chemical Industries, Ltd., Osaka, Japan) for 12 hours at 37°C. Subsequently, for the last 3 hours, cells were incubated with 2 μmol/L of monensin (BioLegend, San Diego, CA). Thereafter, cells were washed and suspended with 2 mmol/L of EDTA/PBS buffer and stained for cell surface markers with CD4-PerCP/Cy5.5 and CD25-PE before fixation. Stained cells were washed, resuspended with 2 mmol/L of EDTA/PBS buffer, and distributed into aliquots for each staining. After treatment with fixation buffer (BioLegend) and permeabilization buffer (BioLegend), cells underwent intracellular staining with interferon-gamma (INF-γ)-Pacific Blue and IL-4/allophycocyanin (APC). Alternatively, after treatment with the FOXP3 Fix/Perm Buffer Set (BioLegend), cells underwent intranuclear staining with forkhead box protein 3/fluorescein isothiocyanate (Foxp3-FITC). Intracellular or intranuclear staining was performed, according to the supplemental protocol for each buffer. The cellular frequency of $CD4^+/INF\text{-}\gamma^+/IL\text{-}4^-$, $CD4^+/INF\text{-}\gamma^-/IL\text{-}4^+$, or $CD4^+/CD25^+/Foxp3^+$ in $CD4^+$ helper lymphocytes was evaluated as that of T helper (Th)1, Th2, or regulatory T cells.

FCM analysis

The scatter diagram of each PBMNC, or the QQ cultured cell (QQMNC) population in an individual, was gated into 3 cell-sized populations of lymphocytes, monocytes, and the larger cells. The percent (%) positivity of a hematopoietic cell population per each gate in PBMNCs or QQMNCs was evaluated and then calculated to that in the whole cells of the 3 gates. The ratio of the % positivity in the whole cells of QQMNCs to that in PBMNCs was further calculated for each cell population. Similarly, the % positivity of each helper T subset (Th1, Th2, or regulatory T cell) was calculated in $CD4^+$ T cells of the 3 gates of PBMNCs or QQMNCs; the ratio of the % positivity in $CD4^+$ T cells of QQMNCs to that in PBMNCs was calculated.

Quantitative Real-Time Polymerase Chain Reaction In Vitro

Using Trizol (Invitrogen, Carlsbad, CA), total RNA was isolated from PBMNCs or QQMNCs. Contaminated genomic DNA was digested by DNase I treatment (Invitrogen) at 37°C for 15 minutes. DNase I-treated total RNA was purified by phenol extraction and ethanol precipitation. One hundred nanograms of purified total RNA was used for cDNA synthesis with the SuperScript VILO cDNA synthesis kit (Invitrogen). cDNA mixture was diluted by 10-fold after first-strand cDNA synthesis. Using ABI Prism 7700 (Applied Biosystems, Foster City, CA), quantitative real-time polymerase chain reaction (qRT-PCR) for diluted cDNA was performed with EagleTaq Master Mix (Roche Diagnostics, Tokyo, Japan), 0.3 μmol/L of forward and reverse primers used for cDNA amplification, and 0.25 μmol/L of probe (Sigma-Aldrich), according to the manufacturer's protocol. The relative mRNA expression was calculated by ΔΔCt method with normalization against human GAPDH (hGAPDH). All primers and probes used are listed in Table 7.

In Vitro Angiogenesis Assay Using Matrigel

As previously reported,[12] PBMNCs and QQMNCs were respectively incubated in 500 μL of 2% FBS/EBM-2 with 20 μg/mL of acetylated low-density lipoprotein, labeled with 1,1′-dioctadecyl-3,3,3′,3′-tetramethyl-indocarbocyanine perchlorate (acLDL-DiI; Biomedical Technologies Inc., Stoughton, MA) (4×10^4 cells/500 μL) in a 1.5-mL tube for 30 minutes at 37°C in a CO_2 incubator. After centrifugation at 400*g* for 10 minutes at 4°C, and aspirating the supernatant, the cell pellets were washed by 1 mL of PBS and suspended with EBM-2/2% FBS (1.0×10^3 cells/50 μL). Labeled cells were resuspended together with human umbilical vain endothelial cells (HUVECs; EPCs: HUVECs=1×10^3:1.5×10^4 in 100 μL of 2% FBS/EBM-2). The mixed cell suspension was incubated at 37°C in a water bath and applied at 100 μL each onto preincubated Matrigel (BD Falcon) (50 μL/well) in each 96-well plate (BD Falcon; BD Biosciences). After incubation for 12 hours, the numbers of closed areas formed by HUVECs were counted using Photoshop software in the pictures taken at ×2 high power field (HPF) by a phase-contrast light microscope (Eclipse TE300; Nikon). Furthermore, acLDL-DiI-labeled PBMNCs or QQMNCs incorporated into a tube were also counted using ImageJ software in the pictures taken at ×4 HPF by a fluorescence microscope (IX70; Olympus, Tokyo, Japan). The tube and cellular numbers were counted independently by 2 blinded investigators.

In Vivo Assessment of Blood Flow Recovery and Tissue Regeneration by Cell Tx Using Murine Ischemic Hindlimb Model

Guideline for animal experiment

All animal studies conformed to national and institutional guidelines. The protocols were approved by the guidelines of the Institutional Animal Care and Use Committee of the Isehara Campus, Tokai University School of Medicine (Isehara, Japan), based on Guide for the Care and Use of Laboratory Animals (National Research Council). The experimental animal protocols for making ischemic models and laser Doppler

Table 7. Human PCR Primers and Probes for qRT-PCR in PBMNC and QQMNC

Gene	Forward Primer	Reverse Primer	TaqMan Probe (5′-FAM, 3′-BHQ)
VEGF-A	5′-CCCAGGAGACCT 5′-GGTTGTGT-3′	5′-TGGATCCTGCCCTGT CTCTCT-3′	5′-AGTGGTTGACCTTCC TCCATCCCC-3′
VEGF-B	5′-AGGTGACACATG GCTTTTCAG A-3′	5′-GTTCCCCCACTGGGA TATAGC-3′	5′-TCAGCAGGGTGACTT GCCTCAGA-3′
Ang-1	5′-AAGCTACTGGGC CTCCTCTCA-3′	5′-CCATTAAGGCAT AGTGGATCAAGTC-3′	5′-AAAAGAGACAGTTGT TGGCAAGGTAGCAA-3′
Ang-2	5′-GCAGGGAGTGG TGAGACAGTT-3′	5′-TGCAGGTGCTATGGT CTTTAGAAT-3′	5′-ACGGCTCCTCAGAAA TCCAGTGACC-3′
IGF-1	5′-GCCCAAAATGCA CTGATGTAAA-3′	5′-AGTGACTTTGCTATGAGTTGGTGAGT-3′	5′-CTCTAAAATCCCTTT CAAGCCACCCAT-3′
Leptin	5′-TCACTAGATGGCGAGCATCCT-3′	5′-CACGCTCAGCTAACTTTTGTGTTT-3′	5′-CCAACATGGTGAAACCCCGTCTCTAC-3′
IL-8	5′-TTTGATACTCCCAGTCTTGTCATTG-3′	5′-CAAGTTTCAACCAGCAAGAAATTACT-3′	5′-TTAGAACTATTAAAACAGCCAAAACTCCACA-3′
IL-10	5′-GCCTGACCACGCTTTCTAGCT-3′	5′-CCAAGCCCAGAGACAAGATAAATT-3′	5′-TTGAGCTGTTTTCCCTGACCTCCC-3′
IL-1 β	5′-CGGCCACATTTGGTTCTAAGA-3′	5′-AGGGAAGCGGTTGCTCATC-3′	5′-ACCCTCTGTCATTCGCTCCCACA-3′
TGF-β	5′-CCCTGCCCCTACATTTGGA-3′	5′-CCGGGTTATGCTGGTTGTACA-3′	5′-TGGACACGCAGTACAGCAAGGTCCT-3′
TNF-α	5′-GAGACCAGGGAGCCTTTGGT-3′	5′-TGTGTCAATTTCTAGGTGAGGTCTTC-3′	5′-CTGGCCAGAATGCTGCAGGACTT-3′
MMP-2	5′-GGTTCCCCTGTTCACTCTACTTAGC-3′	5′-CGGCTTGGTTTTCCTCCAT-3′	5′-TGTCCCTACCGAGTCTCTTCTCCACTG-3′
MMP-9	5′-CCCGGAGTGAGTTGAACCA-3′	5′-AGGGCACTGCAGGATGTCA-3′	5′-TGGACCAAGTGGGCTACGTGACCT-3′
GAPDH	5′-GGTGGTCTCCTCTGACTTCAACA-3′	5′-GTGGTCGTTGAGGGCAATG-3′	5′-ACACCCACTCCTCCACCTTTGACG-3′

Ang indicates angiopoietin; GAPDH, glyceraldehyde-3-phosphate dehydrogenase; IGF, insulin-like growth factor; IL, interleukin; MMP, matrix metalloproteinase; PBMNCs, peripheral blood mononuclear cells; QQMNCs, quality and quantity control culture of mononuclear cells; qRT-PCR, quantitative real-time polymerase chain reaction; TGF, transforming growth factor; TNF, tumor necrosis factor; VEGF, vascular endothelial growth factor.

perfusion imaging (LDPI; Moor Instruments, Axminster, UK) were performed under adequate anesthetization by 1.5% to 2.0% isoflurane (Dainippon Sumitomo Pharma Co., Ltd., Osaka, Japan) to minimize pain to mice by regarding the 3Rs (replacement, reduction, and refinement). After surgery, mice were subcutaneously injected with buprenorphine (Repetan, 0.1 mg/kg body weight; Otsuka Pharmaceutical Co., Ltd., Tokyo, Japan) once a day for 3 days to relieve pain or discomfort. At sacrifice, pentobarbital sodium (Somnopentyl, 60 to 70 mg/kg body weight; Kyouritu Seiyaku Co., Ltd., Tokyo, Japan) was intraperitoneally injected.

Making ischemic hindlimb model and cell Tx

Eight- to 10-week-old male BALB/c nu/nu mice (CAnN.Cg-Foxn1^{nu}/CrlCrlj; Charles River Laboratories Japan, Inc., Tokyo, Japan) were used, as reported elsewhere.[26] The proximal portion of the left femoral artery, including the superficial and the deep branch, was suture-ligated, and the proximal and distal portions of the saphenous artery were occluded with a bipolar forcep electric coagulator (MERA N3-14; SENKO MEDICAL INSTRUMENT mfg. Co., Ltd., Tokyo, Japan). The overlying skin was closed with a 6-0 silk suture. The next day, cells were suspended in IMDM medium and intramuscularly injected into ischemic hindlimbs.

The cell injection sites and the doses for assays were as follows: each one site of anterior tibial muscle (ATM) and gastrocunemius muscle (GCM) for blood flow analysis and histology, that is, hematoxylin and eosin (H&E) staining, Azan staining, and inducible nitric oxide synthase (iNOS) immunohistochemistry (IHC) (5.0×10^3 cells/20 μL per site: total 1×10^4 cells/mouse), 2 sites of ATM for qRT-PCR (5.0×10^3 cells/20 μL per site: total 1×10^4 cells/mouse), or for histological assessment by confocal images (1.0×10^5 cells/20 μL per site: total 2×10^5 cells/mouse).

Assessment of blood flow

LDPI was used to record serial blood flow measurements for 3 weeks after surgery; these data were analyzed using Moor Idi Main software (Laser Doppler Imager ver 5.2; Moor Instruments). The blood flow in identical toe regions of interest (ROIs) between ischemic and contralateral hindlimbs per mouse was measured by LDPI; the blood-flow ratio of ischemic versus contralateral hindlimb was calculated. Mice with toe necrosis or limb salvage were only involved in the calculation, whereas those with foot necrosis or autoamputation were excluded.

Tissue preparation of histochemical assessment

Three weeks after surgery, 40 μL of Isolectin B4-FITC (Fluorescein Griffonia Simplicifolia Lectin I, Isolectin B4; Vector Laboratories Inc., Burlingame, CA) was injected into the tail vein using a insulin syringe, and then 20 minutes later, mice were sacrificed under adequate anesthetization. Immediately after sacrifice, mice were perfused with 20 mL of PBS and then with the equivalent volume of 4% paraformaldehyde (PFA)/PBS by cardiac puncture. Subsequently, hindlimbs were resected and incubated in 4% PFA/PBS at 4°C overnight. Thereafter, ATMs, after QQMNCTx and PBMNCTx, were

excised and embedded into paraffin for the tissue sample preparation. Alternatively, the muscles, after QQMNCTx, GmCD34Tx, and eEPCTx, were coated with optimal cutting temperature (O.C.T.) compound (Tissue-Tek; Sakura Finetek Japan Co., Ltd., Tokyo, Japan), immediately frozen in liquid nitrogen, and refrigerated until use at −80°C. Cross-sectional tissue samples with the thickness at 6 to 8 μm for paraffin section or at 10 μm for frozen sections, were sliced from tissue blocks of muscles and then subjected to assessments as described below.

Microvasculature and pericyte recruitment

For alpha-smooth muscle actin (α-SMA) staining, paraffin tissue sections, after deparaffinization or the frozen ones, were washed with PBS, blocked with 10% goat serum for 30 minutes at room temperature (RT), then, incubated with Cy3-conjugated anti-α-SMA Ab (Sigma-Aldrich) and prediluted (1:200 ratio) with 1% BSA/PBS for 2 hours at RT. After washing with PBS, sections were mounted with 1.25% (w/v) DABCO (Sigma-Aldrich)/90% (v/v) glycerol/10% (v/v) PBS, then observed using a fluorescent microscope (Biorevo; Keyence Corporation, Osaka, Japan). The same protocol, without using the Ab, was performed as the negative control. Also, the negative control for Isolectin B4-FITC staining was in advance, prepared from the mice without in vivo injecting Isolectin B4-FITC into the tail vein.

Using software (VH analyzer; Keyence), microvascular densities were evaluated by counting the microvessels stained with Isolectin B4-FITC. Simultaneously, pericyte recruitment to the vascularures was evaluated by counting the α-SMA-positive microvessels.

Myogenesis and interstitial fibrosis

Centrally nucleated muscle fibers stained with H&E were photographed with an automatic research photomicroscope (AX80; Olympus) and were then counted as regenerating muscle fibers implying fusion of myoblasts[27] by VH analyzer (Keyence). Limb interstitial fibrosis detected by Azan staining was morphometrically assessed by the same photomicroscope and software.[28,29]

Tissue inflammation

Paraffin tissue sections were deparaffinized, autoclaved in citrate buffer at 121°C for 10 minutes to retrieve the target antigen, incubated with the primary Ab of rabbit polyclonal anti-iNOS Ab (Abcam, Cambridge, MA) prediluted with 1% BSA/PBS (1:100 ratio) at 4°C overnight (Table 8). Thereafter, samples were treated with 0.3% H_2O_2/methanol and Histofine Simple Stain MAX PO (Nichirei Biosciences Inc., Tokyo, Japan) and then dyed with 3,3′-diaminobenzidine, tetrahydrochloride (DAB; Dojindo, Kumamoto, Japan). Furthermore, the samples were stained with hematoxylin, dehydrated, and then mounted with malinol. Frozen tissue sections were also stained with the anti-iNOS Ab in the same way, after similar autoclave and subsequent treatment with 0.5% Triton X-100/PBS. Control samples were prepared under the same procedure, using rabbit immunoglobulin fraction (DAKO, Tokyo, Japan).

Table 8. Primary and Isotype Antibodies to Detect iNOS for Immunohistochemistry

Antibodies	Company, Catalog No.	Final Dilution Ratio or Concentration
Anti-iNOS antibody	Abcam, #ab15323	1:100 in 1% BSA/PBS
Rabbit immunoglobulin fraction (solid-phase absorbed)	Dako, #X0936	2 μg/mL in 1% BSA/PBS

iNOS indicates inducible nitric oxide synthase.

Vasculogenesis by transplanted cells

The cross-sections at 10 μm from frozen tissues, after washing with PBS, were microwaved in target retrieval solution (Dako) diluted with distilled water (1:10 ratio) at 98°C for 10 minutes. Then, after treatment with a streptavidin/biotin blocking kit (Vector Laboratories) to block endogenous biotin, sections were incubated with 5% goat serum/1% BSA/PBS for 30 minutes at RT. For the preparation of primary Ab to human CD31, mouse anti-human CD31 Ab and biotinylated goat anti-mouse IgG (Fitzgerald Industries International Inc., Acton, MA) were, respectively, diluted in 1% BSA/PBS (1:8 and 1:48 ratio), that is, adjusted to the concentration of 25 and 60 μg/mL. The prediluted reagents were mixed in the equal volume and reacted at RT for 1 hour. The prereacted reagent was further mixed with mouse serum (2:1 ratio; Rockland Immunochemicals, Inc., Gilbertsville, PA) and incubated at RT for 1 hour. The primary Ab reagent for human CD31 was incubated with the tissue sections at 4°C overnight. Sections were washed with PBS and subsequently incubated with streptavidin and Alexa Fluor 594 conjugate prediluted in 1% BSA/PBS (1:90 ratio) at RT for 1 hour. Tissue sections were washed with PBS and finally mounted with 1 μmol/L of TOTO-3 iodide (Invitrogen) in 1.25% (w/v) DABCO/90% (v/v) glycerol/10% (v/v) PBS. Tissue sections were observed by a confocal laser-scanning microscope (LSM510META; Carl Zeiss GmbH, Jena, Germany). Mouse anti-human CD31 Ab and reagents are detailed in Table 9. The acquired images at 0.8 μm z interval (11 sliced images by 10 intervals at total 8-μm thickness) were reconstructed three-dimensional (3D) structures using the function of 3D spectrum analysis. Furthermore, to quantify "vasculogenic properties" in their images, the surface of a volume object in the ROI, was visualized, using an Imaris iso-surface function of 4D Image analysis software (Imaris 6.2.0; Carl Zeiss): murine

Table 9. Primary and Secondary Antibodies for Immunohistochemistry to Detect Vascular Structures Formed by Transplanted Human Cells

Antibodies	Company, Catalog No.	Final Dilution Ratio
Mouse anti-human CD31	Dako, #M0823	1:24 in 1% BSA/PBS
Goat anti-mouse IgG (H+L) (biotin)	Fitzgerald, #43C-CB1533	1:144 in 1% BSA/PBS
Purified mouse IgG1, isotype control	Dako Cytomation, #X0931	1:6 in 1% BSA/PBS
Streptavidin, Alexa Fluor 594 conjugate	Molecular Probes, #S-11227	1:90 in 1% BSA/PBS

vessels stained with Isolectin B4-FITC (green) and transplanted cell-derived microvessels stained with Alexa 594–conjugated human specific anti-CD31 Ab (red). The values of microvascular density in 2D image and % volume per image cube in 3D were respectively calculated for the green- or red-colored microvessels.

Murine qRT-PCR of ischemic hindlimb

Mice were sacrificed under adequate anesthetization on day 6 after cell Tx. GCMs of ischemic hindlimbs were harvested for total RNA isolation, mice were perfused with 20 mL of PBS by cardiac puncture to remove circulating blood, and GCMs were resected out and incubated into 1 mL of RNA later at 4°C overnight. After homoginization of GCMs with 1 mL of Trizol (Invitrogen), total RNA was isolated and genomic DNA was digested by DNase I treatment (Invitrogen) at 37°C for 15 minutes. DNase I–treated total RNA was purified by phenol extraction and ethanol precipitation. Two micrograms of purified total RNA was used for cDNA synthesis with the High Capacity cDNA Reverse Transcription kit (Applied Biosystems). cDNA mixture was sequentially diluted by 20- to 160-fold with Milii-Q water (Millipore Corporation, Billerica, MA) after first-strand cDNA synthesis. Using ABI Prism 7700 (Applied Biosystems), TaqMan gene expression assays for diluted cDNA were performed with TaqMan Fast Universal PCR Master Mix (Applied Biosystems), according to the manufacturer's protocol. The amplification of cDNA was as follows: denaturation at 95°C for 3 seconds, annealing/extension at 62°C for 30 seconds, and 40 cycles. The relative mRNA expression was calculated by the ΔΔCt method with normalization to mouse 18S rRNA. All primers and TaqMan probes used are listed in Table 10.

Statistical Analysis

Prism5 software (GraphPad Software Inc., Cary, NC) was used to conduct all statistical analyses. Wilcoxon's signed-rank test

Table 10. Murine PCR Primers and TaqMan Probes for qRT-PCR

Gene	Catalog No.	Company
MyoD1	Mm01203489_g1	Applied Biosystems
Myogenin	Mm00446195_g1	Applied Biosystems
IGF-1	Mm00439560_m1	Applied Biosystems
IL-1β	Mm00434228_m1	Applied Biosystems
TGF-β	Mm01227699_m1	Applied Biosystems
18S rRNA	Mm03928990_g1	Applied Biosystems

IGF indicates insulin-like growth factor; IL, interleukin; qRT-PCR, quantitative real-time polymerase chain reaction; TGF, transforming growth factor.

or linear regression analysis was used to analyze quantitative variation or correlation of cells and EPC-CFUs between PBMNCs and QQMNCs in each individual. To assess the variation of each hematopietic cell or helper T subset through QQ culture, Wilcoxon's signed-rank test was also applied for comparison of the ratio of % cell positivity in the whole cells or $CD4^+$ T cells of QQMNCs to that of PBMNCs in each individual. Mann-Whitney's U test and Kruskal-Wallis' test were applied to compare the data between 2 groups and among 3 to 4 groups. The experiment to assess angiovasculogenic properties by transplanted human cells using a confocal fluorescence microscope was performed simultaneously on the whole groups: IMDM control, PBMNCTx, eEPCTx, QQMNCTx, and GmCD34Tx. The data were separately analyzed in the following comparisons: QQMNCTx versus PBMNCTx or IMDM control and QQMNCTx versus GmCD34Tx, eEPCTx, or IMDM control. Especially, vasculogenic properties by transplanted human cells were compared in the groups, excludingd IMDM control. qRT-PCR assay to evaluate mRNA expression in ischemic hindlimbs was also implemented simultaneously on the whole groups; the data were analyzed and compared in the same manner as those in the former experiment. Furthermore, in the assay, the ratio of relative mRNA expression of ischemic-to-contralateral (healthy) hindlimbs in IMDM control was compared by Mann-Whitney's U test to confirm the ischemic response. In histological assays, 2 tissue sections per mouse were prepared, and 4 to 6 fields per tissue section were evaluated. Probability values of $P<0.05$ were deemed statistically significant. All values are expressed as mean±SE.

Results

Decrease in Cell Counts in QQMNCs

The fold increase of QQMNCs to PBMNCs per well declined in the whole subjects with an average of 0.54-fold (Table 11). The calculated total QQMNCs derived from 100 mL of PB

Table 11. The Cell and EPC Colony Counts in QQMNC Versus PBMNC

	PB-MNC	QQ-MNC	*P* Value
Cell counts$\times 10^5$/well	20.00±0	10.88±1.19***	0.0003
Cell counts$\times 10^5$/100 mL PB	831.3±75.3	399.2±43.1***	0.0004
pEPC-CFU counts/ 2×10^5 cells/dish	1.58±0.34	2.89±0.60*	0.0393
dEPC-CFU counts/ 2×10^5 cells/dish	0.71±0.22	29.41±2.34***	0.0002
Total EPC-CFU counts/ 2×10^5 cells/dish	2.31±0.53	31.63±2.66***	0.0002
pEPC-CFU counts$\times 10^5$/100 mL PB	644.7±125.2	500.4±106.2	0.4331
dEPC-CFU counts$\times 10^5$/100 mL PB	285.1±78.4	5407±790.0***	0.0002
Total EPC-CFU counts$\times 10^5$/100 mL PB	934.3±190.8	5839±855.2***	0.0002

Each value indicates a mean±SE. N=18 volunteers. dEPC-CFU indicates definitive endothelial progenitor cells colony-forming units; PBMNC, peripheral blood mononuclear cell; pEPC-CFU, primitive endothelial progenitor cells colony-forming units; QQMNC, quality and quantity control culture of mononuclear cell.
*P<0.05; ***P<0.001 versus PBMNC.

decreased from original cells (cell counts$\times 10^5$=831.3±75.3 to 399.2±43.1), on average, by 0.48-fold (Figure 1A; Table 11).

Interestingly, the fold increase of QQMNCs per well exhibited the negative correlation with total cells of PBMNCs from 100 mL of PB in healthy subjects (Figure 1B, left). Taken together, these findings indicate that even using higher PBMNC densities per 100 mL of PB resulted in constant relative yields of QQMNCs per the PB volume (Figure 1B, right).

Increase of Colony-Forming EPCs in QQMNCs

To assess vasculogenic activities between PBMNCs and QQMNCs, EPC-CFA was used to monitor 2 different types of EPC-CFUs, pEPC-CFUs, and dEPC-CFUs, which comprised small cells and large cells, respectively. pEPCs had high cell proliferation activity; in contrast, dEPCs had high vasculogenic potential.[12]

Briefly, for in vitro assays, dEPCs had higher cell adhesion activity than did pEPCs, and dEPCs formed tube-like structures; additionally, dEPCs extensively formed blood vessel de novo after Tx into ischemic hindlimbs of mice, but pEPCs did less.

Therefore, pEPCs derive from relatively immature, highly proliferative EPCs, whereas dEPCs are relatively mature, differentiated, and able to promote EPC-mediated cell functions required for vasculogenesis.

The pEPC and dEPC colony-forming cells (CFCs) each constituted a small proportion of the cells in primary PBMNC populations (8×10^{-4}% and 3.5×10^{-4}%, respectively; Figure 1C and 1D, left; Table 11). These colony assays demonstrated that QQMNCs have much greater vasculogenic potential than do PBMNCs. After QQ culture, the frequency of total EPC-CFUs from 2×10^5 cells per dish in QQMNCs was significantly enhanced by 13.7-fold of that in PBMNCs. Especially, the frequency of dEPC-CFUs increased by 41.4-fold of that in PBMNCs.

The present data indicate that the vascular regenerative capacity of QQMNCs was superior to that of PBMNCs (Figure 1D, left).

Although QQ culture reduced the count of cells in each individual culture, dEPC-CFCs, and total EPC-CFCs in QQMNCs, derived from the even blood volume were enriched 19.0- and 6.2-fold, relative to those in PBMNCs (Figure 1D, middle; Table 11). Not only were QQ culture enriched with dEPC-CFCs, but also the EPC-CFCs in QQMNCs had a 2.7-fold greater differentiation potential than those in PBMNCs, considering the percentage of dEPC-CFUs to total EPC-CFUs per dish in PBMNCs and QQMNCs (Figure 1D, right).

We also used a linear regression analysis to compare between PBMNCs and QQMNCs with regard to both the quantity and quality of EPC-CFUs (Figure 1E).

Notably, dEPC-CFU and total EPC-CFU counts in QQMNCs were positively correlated with pEPC-CFU counts in PBMNCs, but pEPC-CFU counts in QQMNCs were not (Figure 1E, left). In contrast, neither pEPC-CFU counts nor total EPC-CFU counts in QQMNCs were positively correlated with dEPC-CFU counts in PBMNCs (Figure 1E, middle).

In summary, the frequency of EPC-CFCs in QQMNCs depended on that in PBMNCs (Figure 1E, right). Importantly, the frequency of dEPC-CFCs in QQMNCs was positively correlated with that of pEPC-CFCs in PBMNCs; these correlations indicate that the differentiation during QQ culture of pEPC-CFCs in PBMNCs contributed to formation of dEPC-CFCs in QQMNCs.

Collectively, assays of colony formation demonstrated that the quantitative and qualitative vasculogenic potential of QQMNCs is drastically enhanced, relative to that of PBMNCs, when evaluated even by blood volume.

Moreover, we assessed the functional relationship between $CD34^+$ cells and $CD34^+$ cell-depleted MNCs (CD34-MNCs) in PBMNCs during QQ culture (Figure 1F). CD34-MNCs after QQ culture (QQ-34-MNCs) did not yield EPC colony, whereas $CD34^+$ cells after QQ culture (QQ-34^+ cells) encompassed pEPC-CFCs. This means that EPC-CFCs were basically derived from $CD34^+$ cells. When $CD34^+$ cells were cocultured with CD34-MNCs (QQ-34^+/34-MNC) at a 1:500 ratio, mimicking the proportion of $CD34^+$ cells involved in naïve PBMNCs, the dEPC population expanded significantly, relative to the QQ-34^+ population, even though the original $CD34^+$ cell count was equal. The result suggests that CD34-MNCs included some cell population to accelerate EPC expansion and differentiation in $CD34^+$ cells through QQ culture.

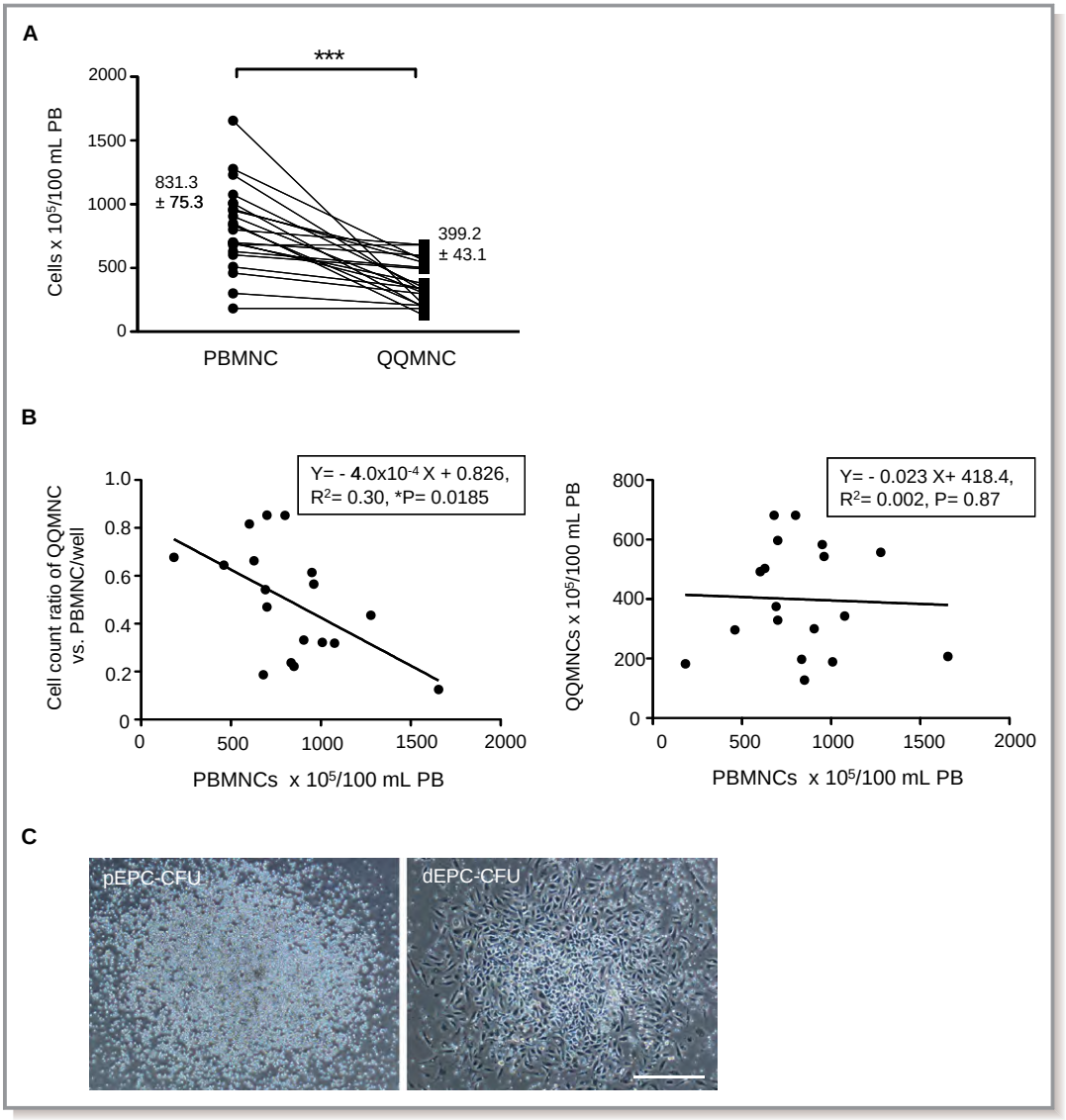

Figure 1. Characteristics of QQMNCs versus PBMNCs. A, The graph shows total cell counts of PBMNCs isolated from 100 mL of PB and the respective QQMNC counts. B, The left graph indicates linear regression analysis between the cell-count ratio of QQMNCs versus PBMNCs (2×10^6 cells/well) and PBMNC counts isolated from 100 mL of PB. The right indicates linear regression analysis of cell counts between PBMNCs and QQMNCs per 100 mL of PB. C, Representative pictures of pEPC-CFU and dEPC-CFU. Scale bar=500 μm. D, The left and middle graphs are EPC-CFU counts generated from PBMNCs or QQMNCs per dish (2×10^5 cells/dish) and in 100 mL of PB. The right graph shows the percentage of each EPC-CFU count versus total EPC-CFU count per dish. Each column in the graph represents a mean±SE. The white and gray areas in the bar graphs indicate the values of pEPC-CFU and dEPC-CFU. E, Linear regression graphs on the interrelation of each EPC-CFU count per dish in QQMNCs to that in PBMNCs. **P*<0.05; ****P*<0.001. N=18 volunteers. F, Comparison of EPC colony forming activities of post-QQ cultured cells among $CD34^+$ cells, CD34-MNCs, and their repopulated cells. QQ-34-MNC: QQ cultured cells of CD34-MNCs (2×10^6 cells/2 mL of QQ culture medium), QQ-34^+: QQ cultured cells of $CD34^+$ cells alone (4×10^3 cells/2 mL of QQ culture medium); QQ-34^+/34-MNC: QQ cultured cells of $CD34^+$ cells repopulated CD34-MNCs (4×10^3 cells for $CD34^+$ cells with 2×10^6 cells for CD34-MNCs/2 mL of QQ culture medium). **P*<0.05; ***P*<0.01; ****P*<0.001 versus QQ-34-MNC. $^{\#}P$<0.05; $^{\#\#\#}P$<0.001 versus QQ-34^+. Each column in the graph represents a mean±SE. N=3 volunteers. Aliquots of each cell cultured in the equal volume of QQ culture medium were applied to EPC-CFA; the aliquots were respectively seeded at 2×10^5 cells/dish (3 dishes each for 3 volunteers) for QQ-34-MNC and QQ-34^+/34-MNC, and at the ratio of 2×10^5 cells to the QQ-34^+/34-MNCs for QQ-34^+. dEPC-CFU indicates definitive endothelial progenitor cells colony-forming units; PBMNCs, peripheral blood mononuclear cells; pEPC-CFU, primitive endothelial progenitor cells colony-forming units; QQMNCs, quality and quantity control culture of mononuclear cells.

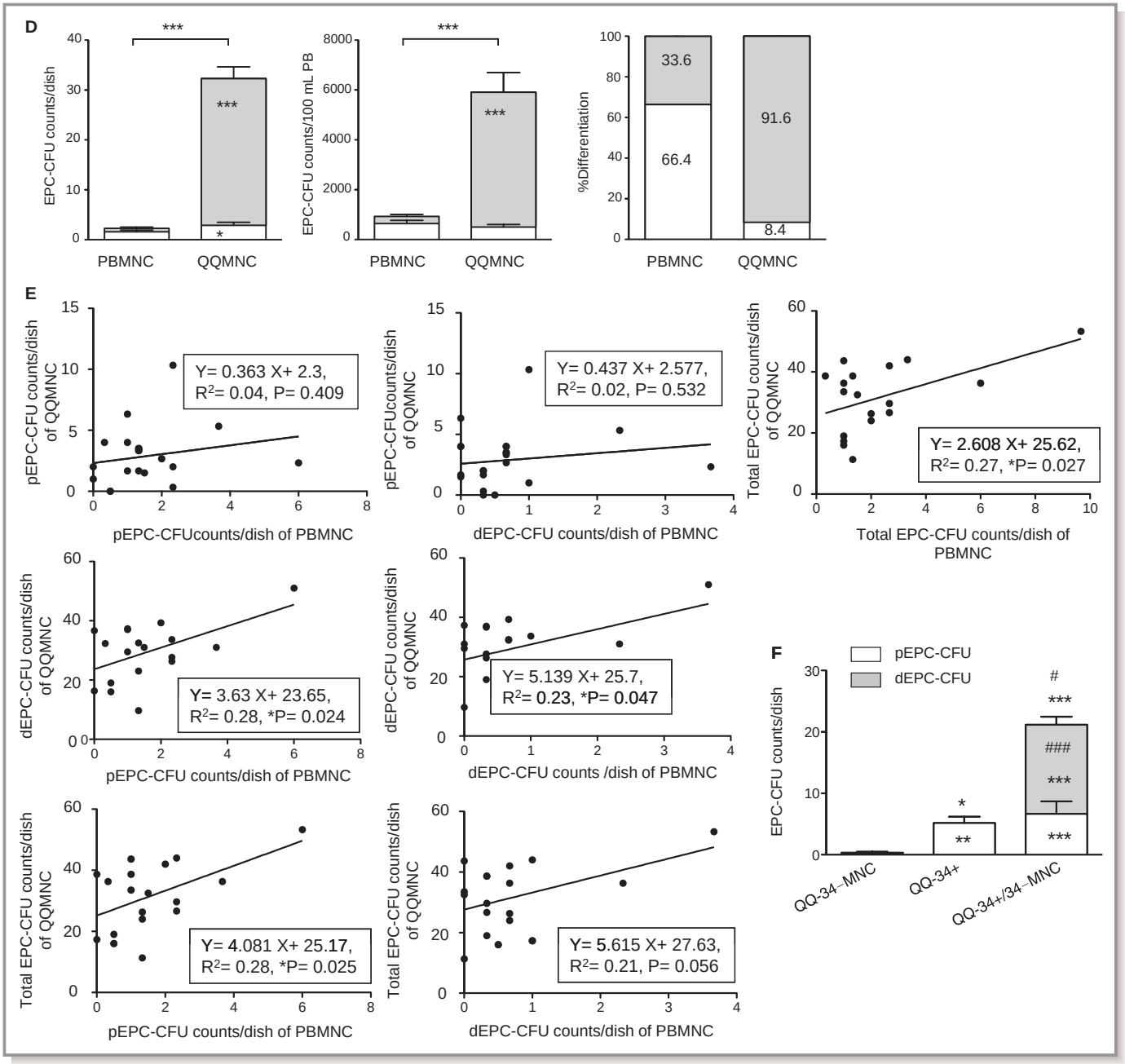

Figure 1. (Continued).

Cell Population Transition in QQMNCs

Based on microscopy and fluorescent cell sorting, large cells were proportionally more common in QQMNC than in PBMNC samples (Figure 2A and 2B). In FCM, the proportion of each positive cell involved in the whole cells of (a), (b), and (c) gates separated with red lines was estimated (Figure 2B).

QQMNCs exhibited the enrichment of $CD34^+$ and $CD133^+$ stem cell populations, compared to PBMNCs (5.97-fold in $CD34^+$ cells; 3.59 in $CD133^+$ cells; Figure 2C; Table 12).

In contrast, the proportion of many hematopoietic cell types, including B lymphoid cells ($CD19^+$ cells), proinflammatory monocytes/macrophages (CC chemokine receptor 2^+ cells; $CCR2^+$ cells), and natural killer (NK) cells ($CD56^+$ cells) was lower in QQMNC than in PBMNC samples.

The proportion of endothelial lineage cells was slightly increased in CD105, whereas it was not changed in CD31 and slightly decreased in vWF. Although not significant, the proportion was slightly increased in CD146, while decreased in VEGF receptor (VEGFR)-2.

In the T-lymphoid cell population, and particularly in the angiogenic T-cell subpopulation, C-X-C chemokine receptor

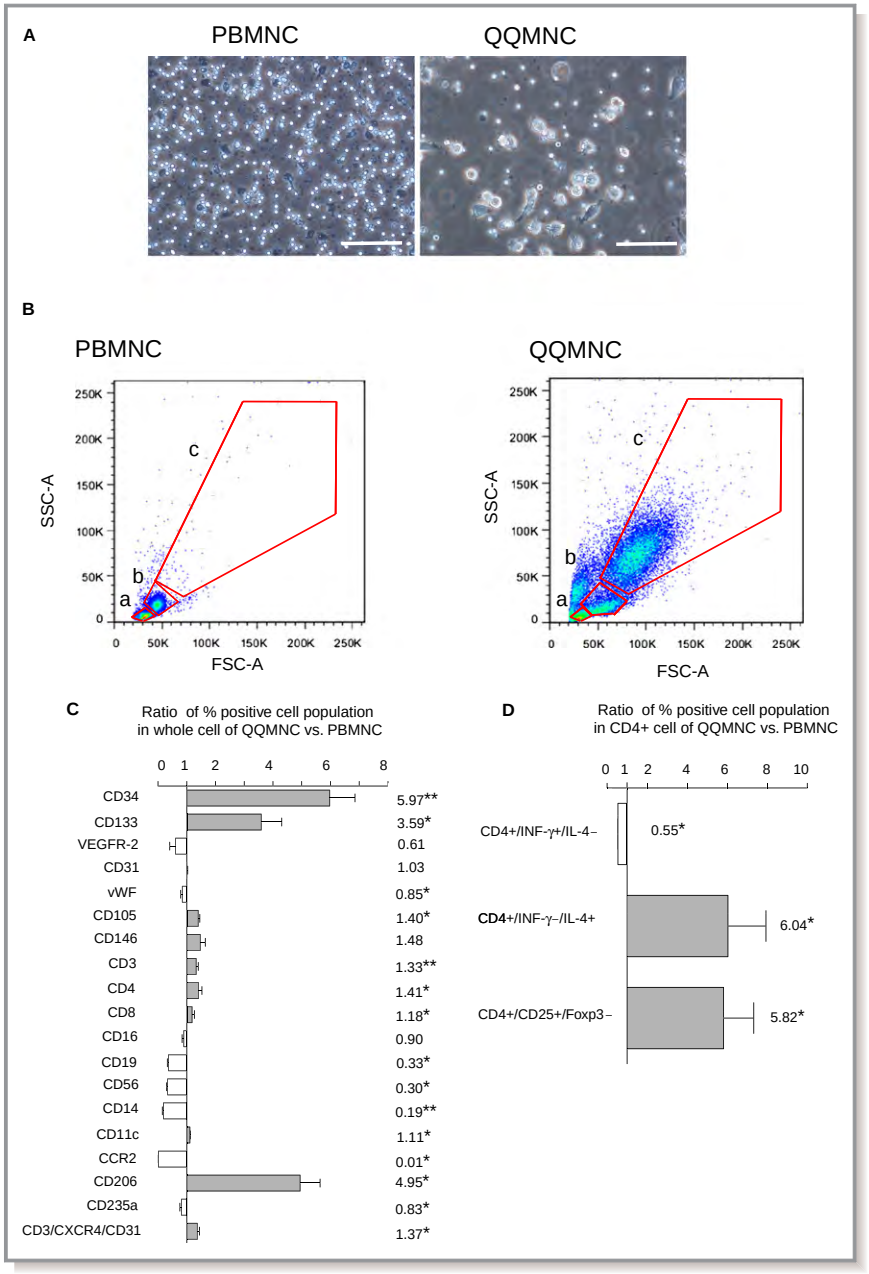

Figure 2. Flow cytometry analysis of PBMNCs and QQMNCs. A, Representative features of PBMNCs at 3 hours after seeding and QQMNCs after 7 days. Scale bar=100 μm. B, Scatter diagrams of PBMNCs and QQMNCs in flow cytometry. The red lines indicate the cellular-sized gates of lymphocyte (a), monocyte (b), or the larger cell (c). C, The bar graph shows the ratio of each percent (%) cell positivity in QQMNCs to that in PBMNCs. N=4 to 6 volunteers. The investigated cell surface markers were as follows: hematopoietic stem cell (CD34, CD133), endothelial cell (VEGFR-2, CD31, vWF, CD105, and CD146), T cell (CD3, CD4, CD8, and CD3/CXCR4/CD31), NK cell (CD16 and CD56), B cell (CD19), monocyte (CD14), dendritic cell (CD11c), M1 macrophage (CCR2), M2 macrophage (CD206), and erythroid progenitor (CD235a). D, The bar graph indicates the ratio of each % helper T subset positivity in $CD4^+$ cells of QQMNCs to that of PBMNCs. N=6 volunteers. *P<0.01; **P<0.01 in (C and D). The gray or white column represents a mean±SE in each increase or decrease. The number associated with each graph column shows the mean value. CCR2 indicates CC chemokine receptor 2; Foxp3, forkhead box P3; FSC-A, forward scatter-area; IL, interleukin; INF, interferon; NK, natural killer; PBMNCs, peripheral blood mononuclear cells; QQMNCs, quality and quantity control culture of mononuclear cells; SSC-A, side scatter-area; VEGFR, vascular endothelial growth factor receptor; vWF, von Willebrand factor.

Table 12. Percent Positivities of Hematopoietic Cell Populations in QQMNC Versus PBMNC

	% in PBMNC	% in QQMNC	*P* Value	Ratio	*P* Value
$CD34^+$	0.21±0.03	1.25±0.26**	0.0078	5.97±0.88**	0.0078
$CD133^+$	0.23±0.08	0.48±0.08	0.0977	3.59±0.71*	0.0195
$VEGFR\text{-}2^+$	1.07±0.15	0.67±0.28	0.2500	0.61±0.21	0.2500
$CD31^+$	39.60±1.93	40.66±1.89	0.2969	1.03±0.02	0.2969
vWF^+	10.52±3.63	10.33±4.07	0.7422	0.85±0.06*	0.0391
$CD105^+$	22.65±1.37	32.05±2.84*	0.0313	1.40±0.05*	0.0313
$CD146^+$	1.57±0.20	2.09±0.16	0.1094	1.48±0.17	0.1094
$CD3^+$	55.16±4.12	71.30±2.61**	0.0078	1.33±0.08**	0.0078
$CD4^+$	34.38±4.27	46.38±3.28*	0.0350	1.41±0.12*	0.0313
$CD8^+$	19.54±2.70	22.03±1.80*	0.0345	1.18±0.08*	0.0313
$CD16^+$	35.66±1.73	31.76±0.88	0.2500	0.90±0.06	0.2500
$CD19^+$	22.00±2.27	6.98±0.16*	0.0350	0.33±0.03*	0.0313
$CD56^+$	24.50±1.17	7.63±1.11*	0.0350	0.30±0.03*	0.0313
$CD14^+$	19.80±1.73	3.47±0.57**	0.0078	0.19±0.04**	0.0078
$CD11c^+$	35.81±2.19	39.57±2.39*	0.0391	1.11±0.03*	0.0391
$CCR2^+$	15.70±1.48	0.22±0.06*	0.0350	0.01±0.004*	0.0355
$CD206^+$	5.53±0.33	26.28±2.69*	0.0350	4.95±0.70*	0.0355
$CD235a^+$	0.88±0.09	0.71±0.03*	0.0211	0.83±0.05*	0.0223
$CD3^+/CXCR4^+/CD31^+$	30.28±1.75	41.01±2.07*	0.0350	1.37±0.07*	0.0350

"% in PBMNC" and "% in QQMNC" indicate the % positivity of each cell population in the whole cell of QQMNC and PBMNC. "Ratio" means the ratio of the % positivity in the whole cell of QQMNC to that of PBMNC, corresponding to Figure 2C. The left *P* values indicate the comparison of % cell positivities between QQMNC and PBMNC; the right ones indicate that of the ratios. N=4 to 6 volunteers. CCR2 indicates CC chemokine receptor 2; CXCR4, C-X-C chemokine receptor type 4; PBMNC, peripheral blood mononuclear cell; QQMNC, quality and quantity control culture of mononuclear cell; VEGFR, vascular endothelial growth factor receptor; vWF, von Willebrand factor.
*$P<0.05$; **$P<0.01$ versus PBMNC.

type 4 $(CXCR4)^+/CD31^+/CD3^+$ cells[30] increased significantly after QQ culture. Notably, the proportion of anti-inflammatory M2-type (CD206) cells increased significantly (4.95-fold) in the 2 categories of macrophages; inversely, the proportion of proinflammatory M1-type (CCR2) cells decreased significantly (0.01-fold).[31,32]

More interestingly, when activated T lymphocytes of QQMMCs or PBMNCs by PMA and ionomycin, the proportion of Th1 cells $(CD4^+/INF\text{-}\gamma^+/IL\text{-}4^-)$ in helper T $(CD4^+)$ cells in QQMNCs declined 0.55-fold of that in PBMNCs. In contrast, the proportions of Th2 cells $(CD4^+/INF\text{-}\gamma^-/IL\text{-}4^+)$ and regulatory T cells $(CD4^+/CD25^+/Foxp3^+)$ increased 6.04- and 5.82-fold (Figure 2D; Table 13).

These data indicate that QQ culture conditions specifically selected for and/or promote proliferation of stem/progenitor cell populations of EPCs as well as anti-inflammatory and angiogenic monocytes/T-lymphocytes in primary PBMNC cultures.

Table 13. Percent Positivities of Helper T-Cell Subsets in $CD4^+$ T Cells of QQMNC Versus PBMNC

	% in $CD4^+$ Cell				
	PBMNC	QQMNC	*P* Value	Ratio	*P* Value
$CD4^+/INF\text{-}\gamma^+/IL\text{-}4^-$	10.34±3.71	5.90±2.28*	0.0355	0.55±0.02*	0.0355
$CD4^+/INF\text{-}\gamma^-/IL\text{-}4^+$	2.94±0.53	14.91±3.10*	0.0355	6.04±1.90*	0.0350
$CD4^+/CD25^+/Foxp3^+$	3.40±0.82	15.00±1.96*	0.0355	5.82±1.51*	0.0355

"% in $CD4^+$ cell" indicates the percent (%) positivity of each helper T subset in $CD4^+$ T cell of QQMNC and PBMNC. "Ratio" means the ratio of the % positivity in $CD4^+$ T cell of QQMNC to that of PBMNC, corresponding to Figure 2D. The left *P* values indicate the comparison of % cell positivities between QQMNC and PBMNC; the right ones indicate that of the ratios. Foxp3 indicates forkhead box P3; IL, interleukin; INF, interferon; PBMNC, peripheral blood mononuclear cell; QQMNC, quality and quantity control culture of mononuclear cell. N=6 volunteers.
*$P<0.05$ versus PBMNC.

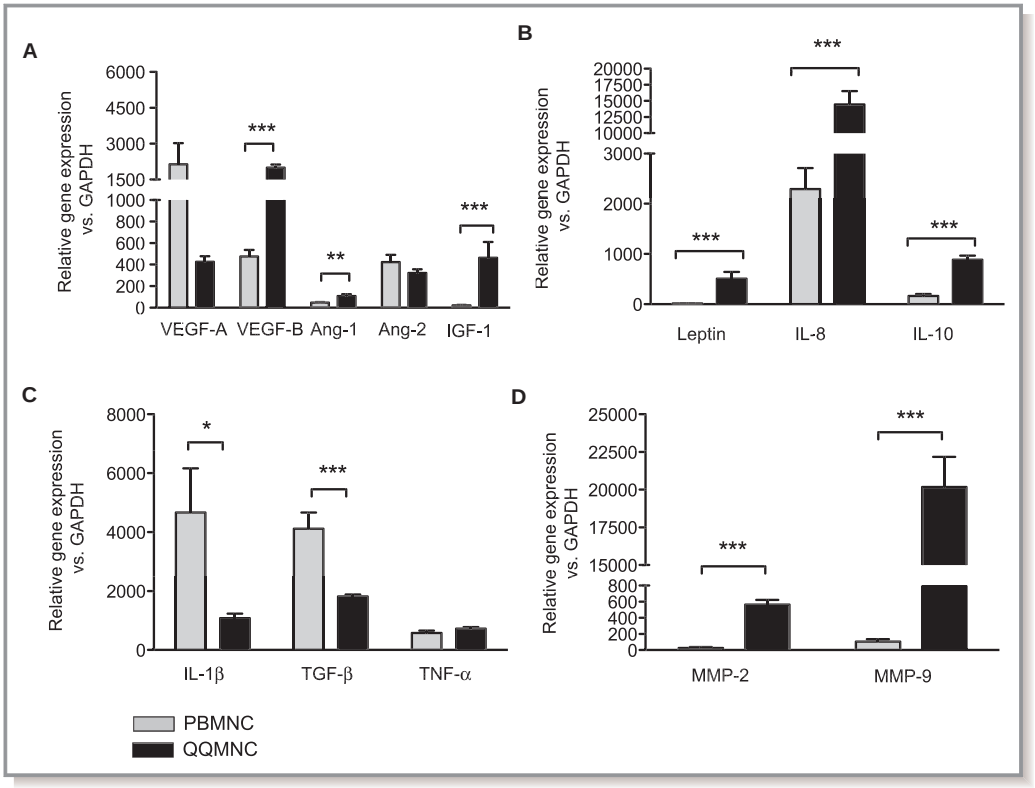

Figure 3. qRT-PCR assay of PBMNCs and QQMNCs. A, Proangiogenic growth factors. B, Proangiogenic cytokines. C, Pro- or anti-inflammatory cytokines. D, MMPs. **P*<0.05; ***P*<0.01; ****P*<0.001. Each graph column represents a mean±SE. N=8 volunteers. Ang indicates angiopoietin; GAPDH, glyceraldehyde-3-phosphate dehydrogenase; IGF, insulin-like growth factor; IL, interleukin; MMPs, matrix metalloproteinases; PBMNCs, peripheral blood mononuclear cells; QQMNCs, quality and quantity control culture of mononuclear cells; qRT-PCR, quantitative real-time polymerase chain reaction; TGF, transforming growth factor; TNF, tumor necrosis factor; VEGF, vascular endothelial growth factor.

Enhanced Gene Expression for Vascular Regeneration and Anti-Inflammation in QQMNCs

Expression of genes encoding vascular regeneration factors, including VEGF-B, angiopoietin-1 (Ang-1), leptin, IL-8, IL-10, and insulin-like growth factor 1 (IGF-1), was much higher in QQMNCs than in PBMNCs; the fold increases in QQMNCs versus PBMNCs were 4.2 for VEGF-B, 2.4 for Ang-1, 35.9 for leptin, 6.3 for IL-8, 5.4 for IL-10, and 21.2 for IGF-1 (Figure 3A and 3B). Especially, VEGF-B and Ang-1 also induce vascular maturation,[33,34] and IGF-1 exerts myogenic potential.[35]

Additionally, expression of the gene encoding IL-1β, a proinflammatory cytokine, in QQMNCs decreased by 0.23-fold of that in PBMNCs, with the increase of the gene encoding the anti-inflammatory IL-10 (Figure 3C). These expressional profiles indicate that QQMNCs preferred to arrange an anti-inflammatory environment in injured tissue. Furthermore, the expression of genes encoding to matrix metalloproteinases (MMPs) of MMP-2 and -9 was significantly higher in QQMNCs than in PBMNCs; the fold increases were 22.1 for MMP-2 and 189.4 for MMP-9 (Figure 3D). MMP-2 and -9 have antifibrotic activity that plays critical roles during neovascularization and tissue remodeling.[36,37]

QQMNCs Promote Angiogenesis In Vitro

Using an in vitro Matrigel assay, we found that QQMNCs promoted tube formation of cocultured HUVECs for 12 hours, but PBMNCs did not (tube counts/×2 HPF=63.3±1.43 for HUVEC+QQMNC versus 55.1±1.45 for HUVEC+PBMNC or 55.3±1.39 for HUVEC alone; Figure 4A and 4B).

Moreover, QQMNCs were readily incorporated into the tubes formed by HUVECs; in contrast, PBMNCs were rarely incorporated into such tubes (incorporated Dil-uptaking cells in tubes/×4 HPF=38.5±8.30 for QQMNC versus 8.72±1.89 for PBMNC; Figure 4C and 4D).

These findings indicate that in vitro QQMNCs had more angiogenic- and EPC-incorporating activity than did PBMNCs.

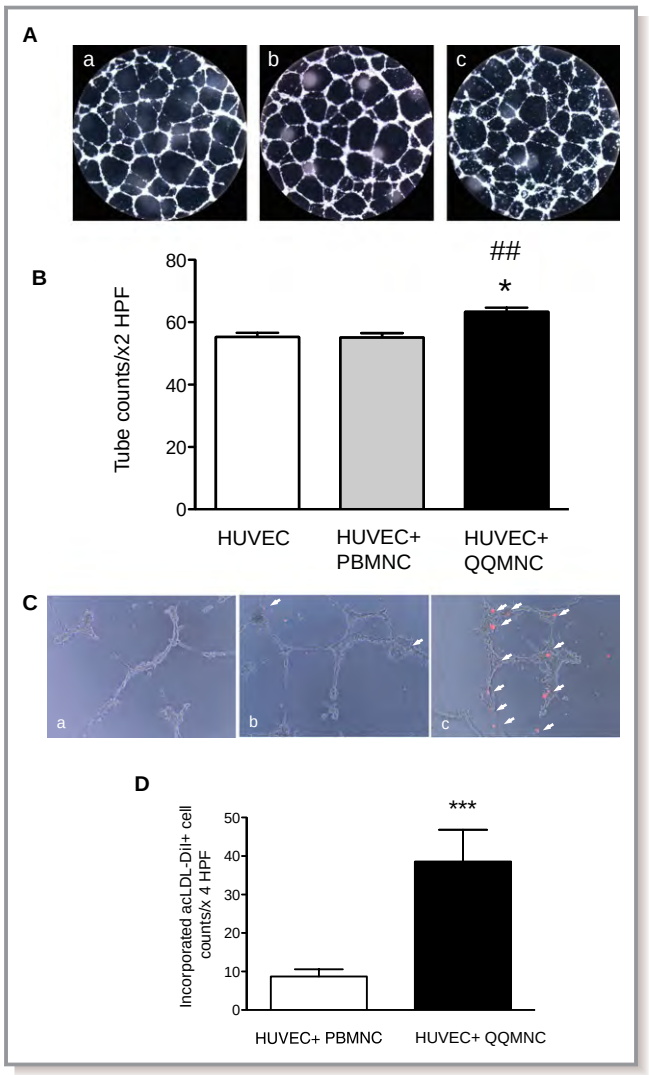

Figure 4. In vitro angiogenic assay of HUVECs cocultured with QQMNCs. A, Features of tubes formed by HUVECs. B, The bar graphs represent the number of tubes counted under ×2 HPF. $^{*}P<0.05$ versus HUVEC; $^{\#\#}P<0.01$ versus HUVEC+PBMNC. C, Incorporation of acLDL-DiI uptaking PBMNCs or QQMNCs into tubes of HUVECs. Arrow heads indicate PBMNCs or QQMNCs that are labeled with acLDL-DiI and incorporated into tubes formed by HUVECs. (a) HUVEC alone, (b) HUVEC+PBMNC, and (c) HUVEC+QQMNC in (A and C). D, The bar graphs show numbers of incorporated PBMNCs or QQMNCs, counted under ×4 HPF. $^{***}P<0.001$. Each graph column represents a mean±SE. N=10 wells/group. acLDL-DiI indicates acetylated low density lipoprotein, labeled with 1,1′-dioctadecyl-3,3,3′,3′-tetramethyl-indocarbocyanine perchlorate; HPF, high power field; HUVECs, human umbilical vein endothelial cells; PBMNCs, peripheral blood mononuclear cells; QQMNCs, quality and quantity control culture of mononuclear cells.

Physiological Recovery of Blood Perfusion in Ischemic Hindlimb After QQMNCTx

We investigated the potential of QQMNCs to treat ischemia, using a mouse ischemic hindlimb model; the effect was evaluated by blood flow measurement for 21 days after ischemic surgery. We compared the effect of QQMNCTx with that of no-cell Tx (IMDM medium-injected mice:IMDM control) or PBMNCTx (Figure 5A).

For each mouse, we measured blood flow in the ischemic and contralateral hindlimb; we then calculated the ratio of ischemic blood flow to contralateral flow: % blood flow ratio in the QQMNCTx, PBMNCTx, and control groups=at day 14, 48.8±4.25, 32.3±5.53, and 28.9±4.52: at day 21, 50.7±5.50, 28.1±6.19, and 27.4±6.98, respectively. The ratio in the QQMNCTx was significantly higher after day 14 than that in PBMNCTx and control, indicating that QQMNCTx recovered ischemic blood flow greater than the others.

Comparing to other EPC transplantations (Figure 5B), QQMNCTx improved the blood-flow ratio earlier than GmCD34Tx, eEPCTx, and control: % blood flow ratio in QQMNCTx, GmCD34Tx, eEPCTx, and control=at day 14, 52.8±6.13, 37.6±3.48, 24.8±2.83, and 24.1±5.13; at day 21, 62.1±6.61, 53.9±6.18, 31.8±1.57, and 27.7±3.86, respectively.

The % ratios of autoamputation in the QQMNCTx, PBMNCTx, and control groups were 4.3, 9.5, and 15.8, respectively; conversely, those of limb salvage were 21.7, 9.5, and 10.5, respectively. These findings indicate that QQMNCTx potentiated physiological recovery in hindlimb ischemia more so than did PBMNCTx or control (Figure 5C).

When compared to GmCD34Tx and eEPCTx, the % ratios of autoamputation in QQMNCTx, GmCD34Tx, and eEPCTx were 4.5, 26.3, and 37.5, respectively. In contrast, those of limb salvage in QQMNCTx, GmCD34Tx, and eEPCTx were 27.3, 21.1, and 25.0, respectively.

Regarding these findings, the earlier blood flow recovery by QQMNCTx might favorably rescue the ischemic foot from injury, compared to other treatments (Figure 5D).

QQMNCTx Potentiates Vascular and Muscle Regeneration in Ischemic Hindlimb

Angiogenesis and arteriogenesis

For each animal, we used histological methods to measure Isolectin B4-FITC stained microvessel density and assess angiogenic capacity in the ATM of ischemic hindlimbs; the mean densities (microvessel counts/mm^2) for the QQMNCTx, PBMNCTx, and control groups were 400.7±37.9, 118.9±20.1, and 98.7±15.8, respectively (Figure 6A and 6B).

We also evaluated pericyte-recruited (α-SMA$^+$) microvessel densitiy in the ATM to assess arteriogenesis for vascular maturation: The mean densities (pericyte-recruited microvessel counts/mm^2) for the QQMNCTx, PBMNCTx, and control groups were 38.7±5.5, 19.8±4.3, and 15.0±2.7, respectively (Figure 6A and 6C).

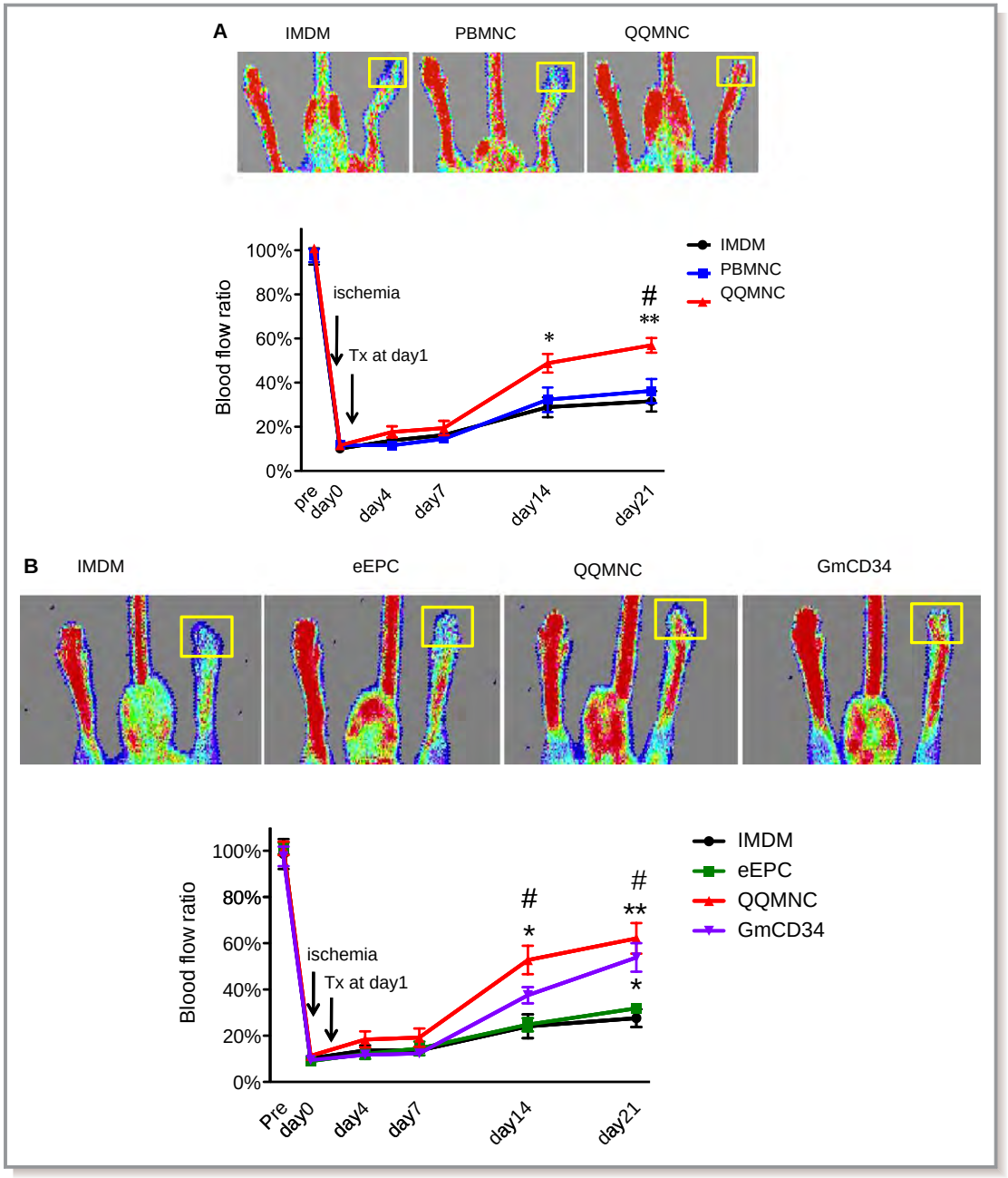

Figure 5. Blood flow and distribution of limb salvage patterns in ischemic hindlimbs. A and B, Laser Doppler imaging was used to analyze blood flow 21 days after ischemia. Cells were transplanted at 1×10^4/mouse (5×10^3 cells/each of ATM and GCM). The top panels show the representative features in each group. ROI for blood flow measurement is shown by a yellow square. The bottom line graph presents percent (%) blood-flow ratio of ischemic-to-contralateral hindlimb during the observation period for 21 days. **P*<0.05; ***P*<0.01 versus IMDM control. #*P*<0.05 versus PBMNCTx in (A) or eEPCTx in (B). Each line graph represents a mean±SE. N=12 mice/group. C and D, Limb salvage features of QQMNCTx versus PBMNCTx day 21 after ischemia. The top pictures in (C) show the representative features of ischemic leg patterns; the severity of the phenotypes are graded from the left to the right. The column graphs in (C and D) show the respective % distributions of severity for each group. N=19 mice for IMDM control, 21 for PBMNCTx, and 23 for QQMNCTx in (C). N=10 mice per each group in (D). LS, limb salvage; TN, toe necrosis; FN, foot necrosis; AA, autoamputation in (C and D). ATM indicates anterior tibial muscle; eEPCTx, early endothelial progenitor cell transplantation; GCM, gastrocunemius muscle; GmCD34, granulocyte colony-stimulating factor mobilized $CD34^+$ cell; IMDM, Iscove's Modified Dulbecco's Medium; PBMNCTx, peripheral blood mononuclear cell transplantation; QQMNCTx, quality and quantity control culture of mononuclear cell transplantation; ROI, regions of interest.

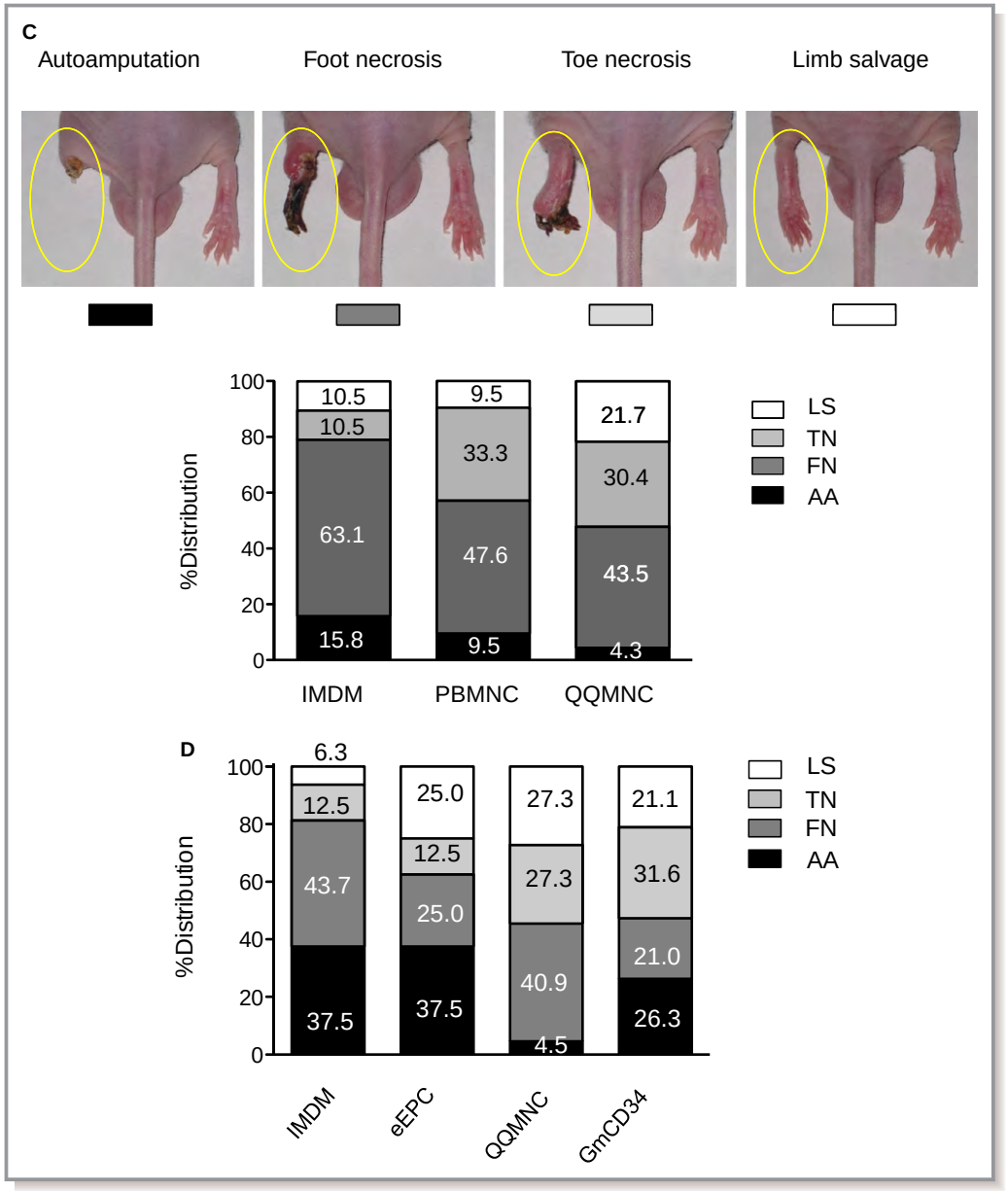

Figure 5. (Continued).

Likewise, the mean microvessel densities (microvessel counts/mm^2) for the QQMNCTx, GmCD34Tx, eEPCTx, and control groups were 510.7±30.0, 430.6±29.8, 347.9±36.5, and 210.5±16.8 respectively (Figure 6D and 6E). The mean pericyte-recruited microvessel densities (pericyte-recruited microvessel counts/mm^2) for the QQMNCTx, GmCD34Tx, eEPCTx, and control groups were 42.6±4.3, 39.5±3.8, 29.8±2.0, and 23.2±2.9, respectively (Figure 6D and 6F). These findings demonstrate that QQMNCTx promoted angiogenesis and arteriogenesis for vascular maturation.

Vasculogenesis

We performed in vivo experimenents to assess vasculogenic properties of transplanted cells (2×10^5 cells/mouse): to investigate whether and to what extent transplanted cells differentiate into endothelial cell forming vascular structure in the host tissue, using a confocal fluorescence microscope (Figure 7A; Video S1).

IHC stainings demonstrated the significantly higher vasculogenic microvessel counts in QQMNCTx muscles than those in PBMNCTx (Figure 7B through 7D; Table 14).

The average vasculogenic microvessel densities in 2D image (vasculogenic microvessel counts/mm^2) for the QQMNCTx and PBMNCTx groups were 811.6±178.6 and 202.9±97.3 (Figure 7C); the % ratios of vasculogenic microvessel volume per image cube for the respective groups were 0.76±0.17 and 0.05±0.04 (Figure 7D).

The potential of QQMNCTx was also markedly superior to that of eEPCTx, whereas it was equal to or greater than that of

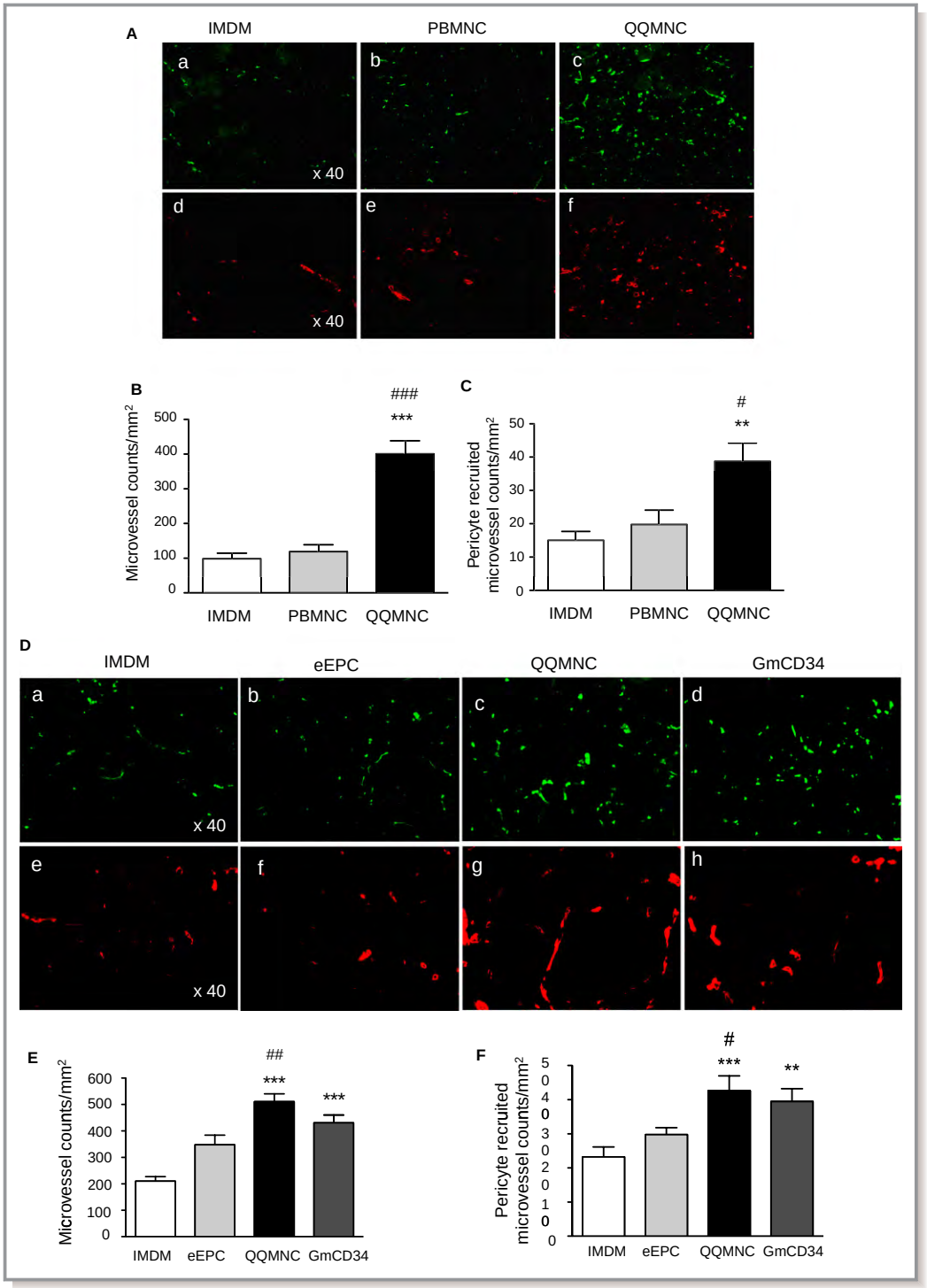

Figure 6. Assessment of angiogenesis and arteriogenesis in ischemic hindlimbs. A and D, Representative pictures of angiogenesis and arteriogenesis in ATM in each group. (a through c) in (A) and (a through d) in (D): mouse microvessels stained with isolectin B4-FITC. (d through f) in (A) and (e through h) in (D): pericyte recruited microvessels stained with Cy3-conjugated anti-α-SMA antibody. The graphs present the counts of microvessels in (B and E) and pericyte recruited microvessels in (c and f). $^{*}P<0.05$; $^{**}P<0.01$; $^{***}P<0.001$ versus IMDM control in (B, C, E, and F). $^{\#}P<0.05$; $^{\#\#\#}P<0.001$ versus PBMNCTx in (B and C). $^{\#}P<0.05$; $^{\#\#}P<0.01$ versus eEPCTx in (E and F). ×40 HPF. Each column in the graph represents a mean±SE. N=6 mice per group. ATM indicates anterior tibial muscle; eEPCTx, early endothelial progenitor cell transplantation; FITC, fluorescein isothiocyanate; GmCD34, granulocyte colony stimulating factor mobilized $CD34^{+}$ cell; HPF, high power field; PBMNCTx, peripheral blood mononuclear cell transplantation; QQMNC, quality and quantity control culture of mononuclear cells; α-SMA, alpha-smooth muscle actin.

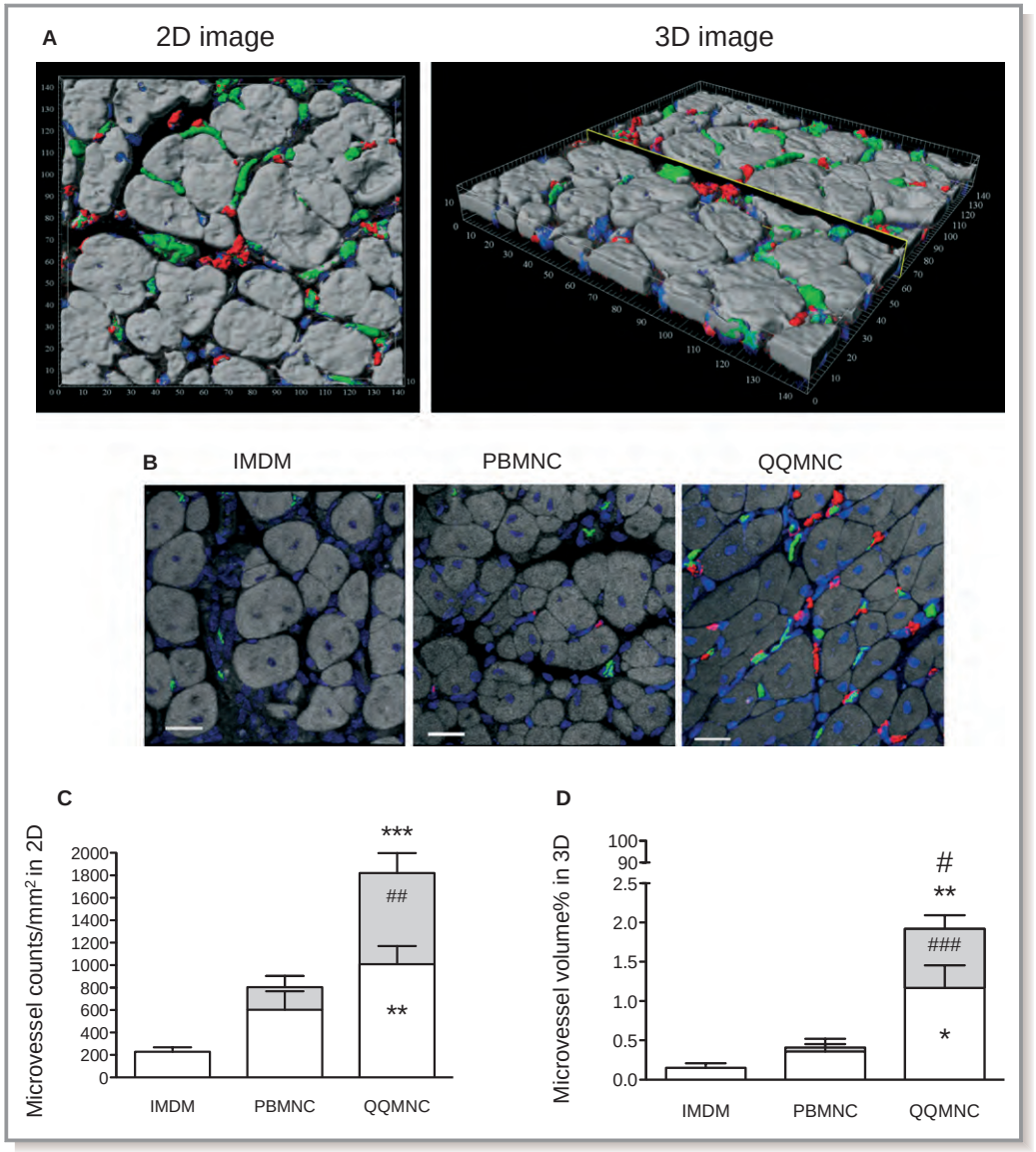

Figure 7. Evaluation of vasculogenesis by transplanted cells in ischemic hindlimbs. A, The representative 2D and 3D images to assess vasculogenesis and angiogenesis in cell (GmCD34) transplanted ATM by 3D spectrum analysis using a confocal microscope. (Green) Mouse microvessels stained with isolectin B4-FITC, (red) vasculogenic microvessels by transplanted human cells, stained with human specific anti-CD31 antibody/Alexa 594, and (blue) nuclei stained with TOTO-3. The unit of numbers in their images indicates micrometers (μm). B and E, The panels show the representative similar images in each treatment group. Cells were transplanted at 2×10^5 cells per ATM. Scale bar=20 μm. C and F, Microvessel counts/mm^2 in each group. D and G, Percent (%) microvessel volume per 3D image cube ($142.58\times142.58\times8$ μm) in each group. $^*P<0.05$; $^{**}P<0.01$; $^{***}P<0.001$ versus IMDM control in (C, D, F, and G). $^{\#}P<0.05$; $^{\#\#}P<0.01$; $^{\#\#\#}P<0.001$ versus PBMNCTx in (C and D) or eEPCTx in (F and G). Each column on the graph represents a mean±SE. N=3 to 4 mice per group. ATM indicates anterior tibial muscle; eEPCTx, early endothelial progenitor cell transplantation; GmCD34, granulocyte colony-stimulating factor mobilized CD34$^+$ cell; PBMNCTx, peripheral blood mononuclear cell transplantation; QQMNC, quality and quantity control culture of mononuclear cells.

GmCD34Tx. The average vasculogenic microvessel densities (vasculogenic microvessel counts/mm^2) for the GmCD34Tx and eEPCTx groups were 662.2±98.6 and 203.8±50.8, respectively (Figure 7E and 7F; Table 14); the % ratios of vasculogenic microvessel volume per image cube for the groups were 0.53±0.15 and 0.06±0.02 (Figure 7E and 7G; Table 14).

Similarly, the angiogenic properties of transplanted cells, here evaluated by the confocal microscopic analysis, exhibited the compatible feature with those in the aforementioned

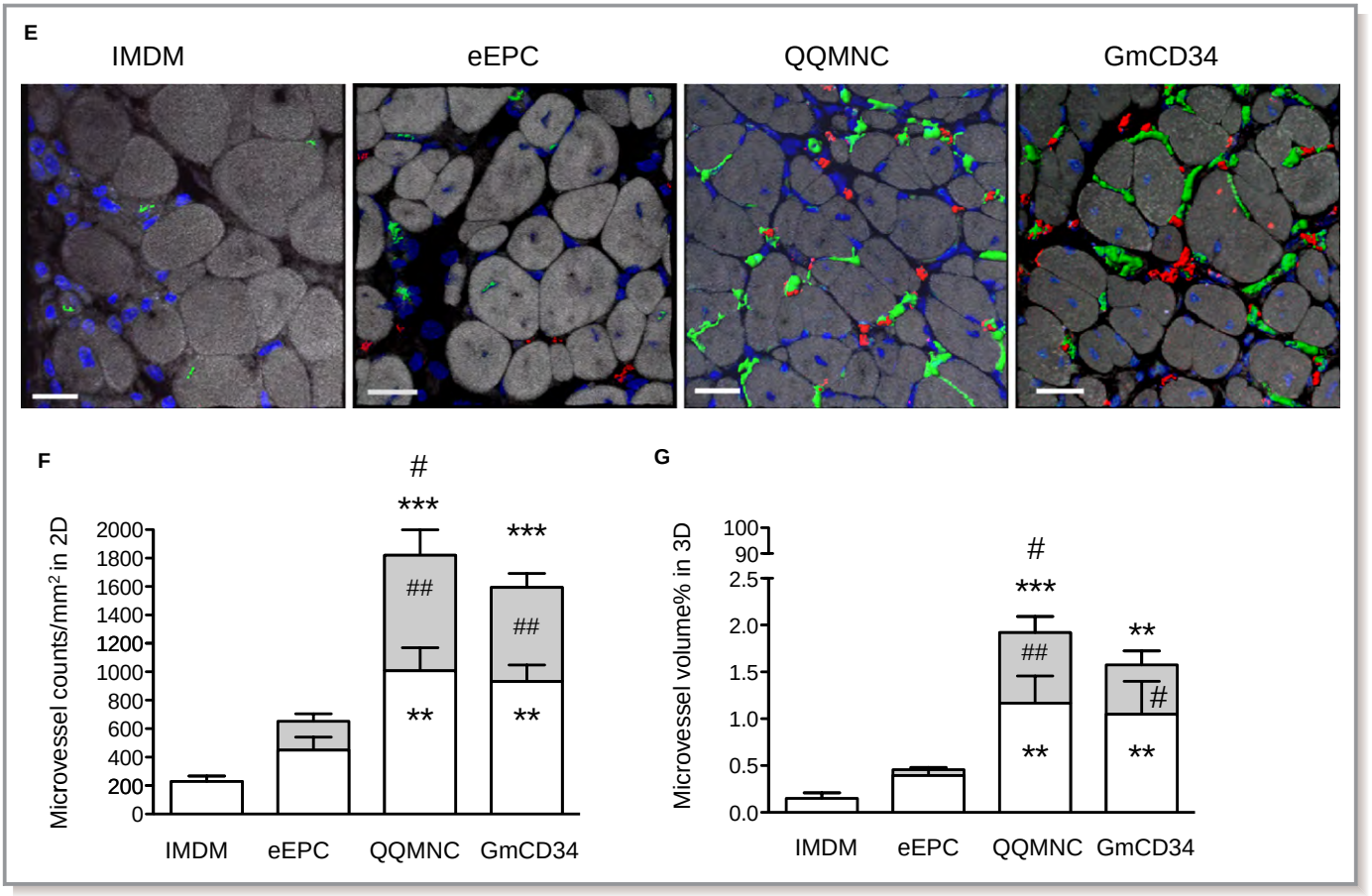

Figure 7. (Continued).

experiments of the low-dose cellular Tx (1×10^4 cells/mouse).

The findings indicate that transplanted cells of QQMNCs, as well as GmCD34, exerted vasculogenic properties in ischemic hindlimbs superior to those of PBMNCs or eEPCs.

Myogenesis

Muscle fibers with centrally located nuclei indicate myogenesis mediated by fusion of myoblasts in ATM of ischemic hindlimbs; therefore, we determined that the average densities of such regenerating muscle fibers (regenerating muscle fibers/mm^2) for the QQMNCTx, PBMNCTx, and control groups were 775.6±113.3, 424.2±47.12, and 398.6±48.42, respectively (Figure 8A and 8B).

In the respective experiments to compare myogenesis among the QQMNCTx, GmCD34Tx, eEPCTx, and control groups, we also determined that the average densities of regenerating muscle fibers (regenerating muscle fiber counts/

Table 14. The Angiogenic and Vasculogenic Microvessels in Ischemic ATMs 21 Days After Surgery

	Microvessel counts/mm^2 in 2D			Microvessel Volume % in 3D		
Tx Cells	Angio	Vasculo	Total	Angio	Vasculo	Total
IMDM	229.6±37.4	0±0	229.6±37.4	0.15±0.06	0±0	0.15±0.06
PBMNC	602.6±165.4	202.9±97.3	805.5±220.6	0.36±0.16	0.05±0.04	0.41±0.19
eEPC	449.7±90.7	203.8±50.8	653.5±115.5	0.39±0.07	0.06±0.02	0.46±0.07
QQMNC	1008.0±162.1	811.6±178.6	1820.0±191.0	1.17±0.29	0.76±0.17	1.92±0.37
GmCD34	930.8±118.2	662.2±98.6	1593.0±168.7	1.05±0.35	0.53±0.15	1.58±0.46

Each value indicates a mean±SE. N=3 to 4 mice per group. Angio indicates angiogenic microvessel; ATM, anterior tibial muscle; eEPC, early endothelial progenitor cell; GmCD34, granulocyte colony-stimulating factor mobilized CD34$^+$ cell; PBMNC, peripheral blood mononuclear cell; QQMNC, quality and quantity control culture of mononuclear cell; Tx cells=2×10^5 cells/mouse transplanted into ischemic ATM; Vasculo, vasculogenic microvessel.

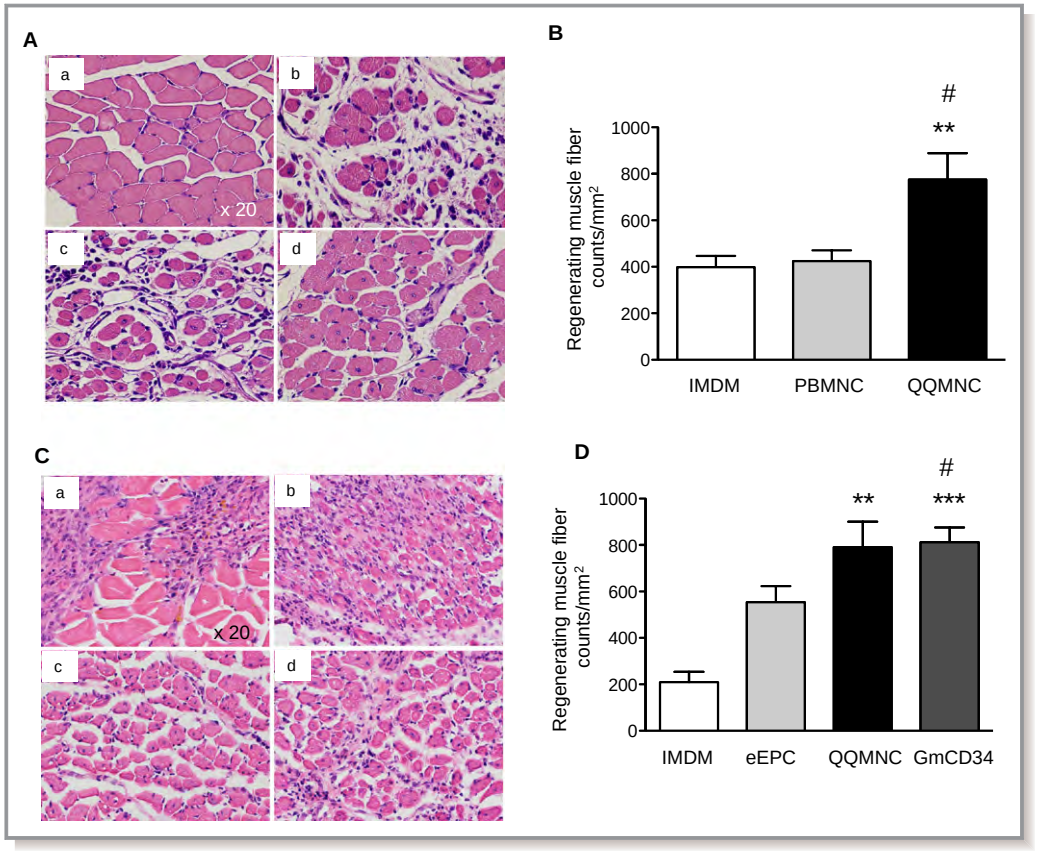

Figure 8. Histological evaluation of myogenesis in ischemic hindlimbs. A and C, Representative images of muscle tissues in ATM by H&E staining. (a) Normofused tissue with normal morphology of skeletal muscle fibers with the subsarcolemmal nuclei in contralateral hindlimb of IMDM control, (b) ischemic hindlimbs from IMDM control, (c) PBMNCTx, or (d) QQMNCTx in (A). (a) IMDM control, (b) eEPCTx, (c) QQMNCTx, and (d) GmCD34Tx in (C). Note that the smaller size of the fibers in combination with centrally located nuclei indicated that a muscle fiber had been actively regenerating. B and D, The graphs present the counts of regenerating muscle fibers in each group. $^{**}P<0.01$; $^{***}P<0.001$ versus IMDM control in (B and D). $^{\#}P<0.05$ versus PBMNCTx in (B) or eEPCTx in (D). Each column in the graph represents a mean±SE. ×20 HPF. N=6 mice per group. ATM indicates anterior tibial muscle; eEPCTx, early endothelial progenitor cell transplantation; GmCD34, granulocyte colony-stimulating factor mobilized $CD34^+$ cell; H&E, hematoxylin and eosin; HPF, high power field; PBMNCTx, peripheral blood mononuclear cell transplantation; QQMNCTx, quality and quantity control culture of mononuclear cell transplantation.

mm^2) for the respective groups were 790.7±110.1, 811.8±63.6, 553.6±69.25, and 209.4±44.01, respectively (Figure 8C and 8D). These findings indicate that QQMNCTx potentiated myogenesis greater than PBMNCTx and control, or equal to GmCD34Tx in ischemic hindlimbs, although did not compare to eEPCTx.

Inhibitory Effects of QQMNCTx to Fibrosis and Inflammation in Hindlimb Ischemia

To evaluate anti-inflammatory and -fibrotic potential of QQMNCTx, fibrotic area in ischemic ATM was detected by Azan staining on day 21 after treatment. The mean fibrotic area (% fibrotic area/×40 HPF) for the QQMNCTx, PBMNCTx, and control groups were 2.78±0.61, 8.41±1.51, and 11.94±3.59. These findings indicate that QQMNCTx exerted greater antifibrotic effects than did PBMNCTx (Figure 9A and 9B).

In the respective comparison among the QQMNCTx, GmCD34Tx, eEPCTx, and control groups, the mean fibrotic areas (% fibrotic area/×40 HPF) for each group were 5.89±1.12, 8.06±1.05, 11.07±1.19, and 17.04±1.75 (Figure 9C and 9D). QQMNCTx as well as GmCD34Tx featured superior antifibrotic effects to control and further exerted greater effects than eEPCTx.

We performed IHC of iNOS in ischemic ATM to assess inflammation. The mean iNOS-expressing areas (% iNOS-expressing area/×20 HPF) for the QQMNCTx, PBMNCTx, and control groups were 3.16±0.58, 6.26±0.89, and 21.31±2.26 (Figure 10A and 10B). These findings indicate that QQMNCTx inhibited inflammation more markedly than PBMNCTx.

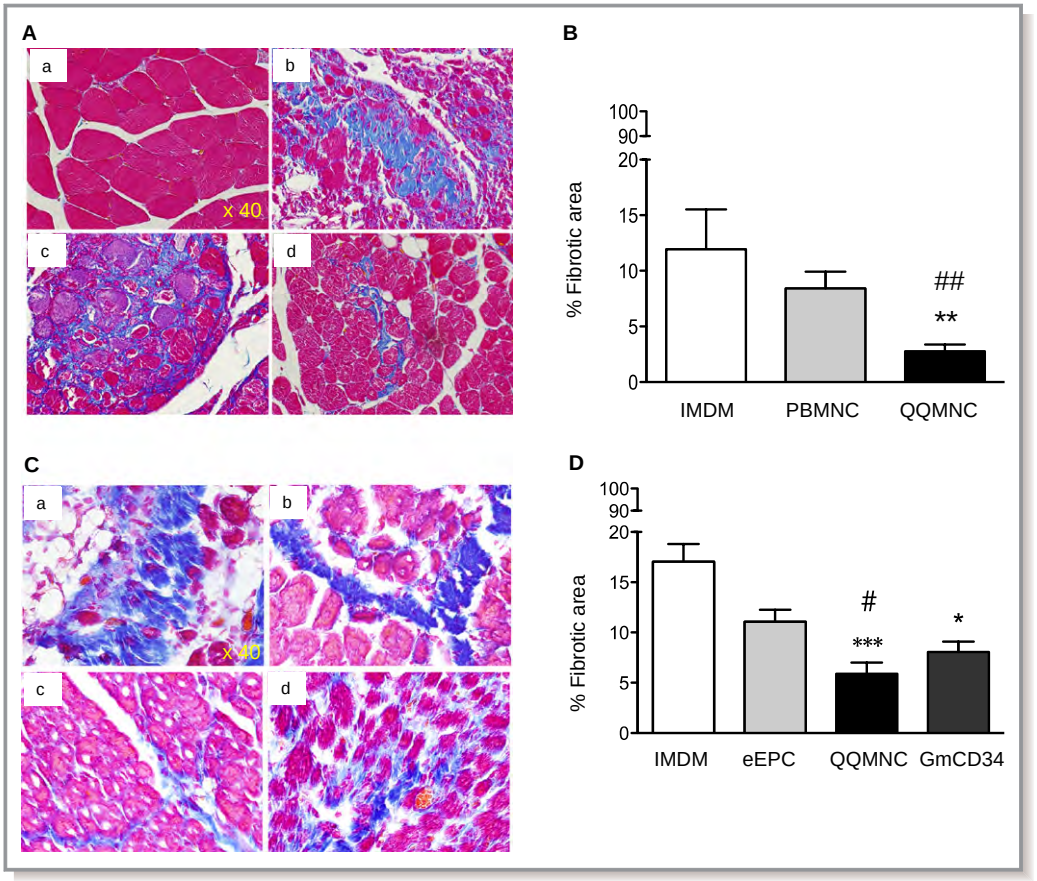

Figure 9. Histological evaluation of fibrosis in ischemic hindlimbs. A and C, Representative pictures of fibrosis in ATM assessed by Azan staining (blue) in each group. ×40 HPF. (a) Contralateral hindlimb of IMDM control (b, c, and d) and ischemic hindlimbs of IMDM control, PBMNCTx, and QQMNCTx in (A). (a, b, c, and d) Ischemic hindlimbs of IMDM control, eEPCTx, QQMNCTx, and GmCD34Tx in (C). B and D, The graphs show percent (%) fibrotic area in each group. $^{*}P<0.05$; $^{**}P<0.01$; $^{***}P<0.001$ versus IMDM control in (B and D). $^{\#\#}P<0.01$ versus PBMNCTx in (B). $^{\#}P<0.05$ versus eEPCTx in (D). Each column in the graph represents a mean±SE. N=6 mice per group. ATM indicates anterior tibial muscle; eEPCTx, early endothelial progenitor cell transplantation; GmCD34, granulocyte colony-stimulating factor mobilized $CD34^{+}$ cell; HPF, high power field; PBMNCTx, peripheral blood mononuclear cell transplantation; QQMNCTx, quality and quantity control culture of mononuclear cell transplantation.

In the respective comparison among the QQMNCTx, GmCD34Tx, eEPCTx, and control groups, the mean iNOS-expressing areas (% iNOS-expressing area/×20 HPF) for the respective groups were 4.97±0.95, 6.07±0.81, 9.75±1.09, and 18.15±1.44 (Figure 10C and 10D). In the same manner as antifibrotic aspects, QQMNCTx as well as GmCD34Tx featured superior anti-inflammation effects to control and further displayed greater effects than eEPCTx.

These findings indicate that QQMNCTx, similarly to GmCD34Tx, potentiated protective effects against inflammation and fibrosis in the ischemic hindlimb.

QQMNCTx Enhances Gene Expression for Tissue Regeneration in Ischemic Muscle

The qRT-PCR assay was implemented for murine mRNA transcripts encoding the following factors: IL-1β (proangiogenic/-inflammatory), transforming growth factor beta (TGF-β; proangiogenic/anti-inflammatory), IGF-1 (proangiogenic/-myogenic), or MyoD1 and myogenin (promyogenic transcription).

In the comparison of the murine transcripts among the QQMNCTx, PBMNCTx, and control groups, gene expression of MyoD1, myogenin, and IGF-1 was significantly augmented by responding to QQMNCTx, but not to PBMNCTx.

Likewise, in the comparison among the QQMNCTx, GmCD34Tx, and eEPCTx groups, gene expression of MyoD1, myogenin, and IGF-1 was significantly enhanced by responding to QQMNCTx, equally to GmCD34Tx, but not to eEPCTx.

The relative ratio of each gene expression in PBMNCTx, QQMNCTx, GmCD34Tx, and eEPCTx versus that in IMDM control was as follows: 1.22±0.05, 2.58±0.63, 2.94±0.61, and 1.06±0.08 in MyoD1; 1.90±0.10, 2.94±0.49, 2.69±0.41, and 0.84±0.06 in myogenin; and 1.17±0.11,

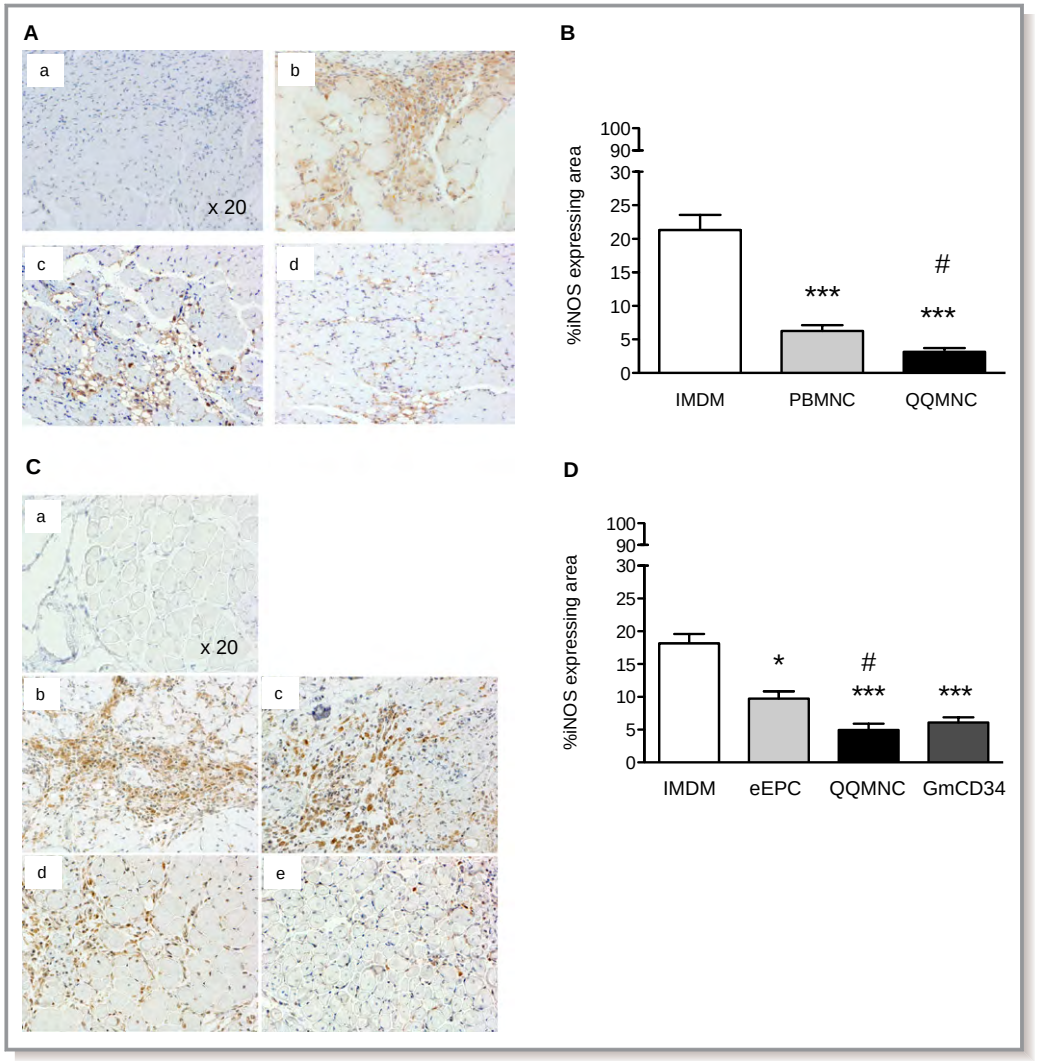

Figure 10. Histological evaluation of inflammation in ischemic hindlimbs. A and C, Representative pictures of inflammation in ATM by immunohistochemistry using anti-iNOS antibody (brown color) in each group. ×20 HPF. (a) Control of rabbit polyclonal IgG, (b) IMDM control, (c) PBMNCTx, and (d) QQMNCTx in (A). (a) Control of rabbit polyclonal IgG, (b) IMDM control, (c) eEPCTx, (d) QQMNCTx, and (e) GmCD34Tx in (C). B and D, The graphs show percent (%) iNOS expressing area in each group. *P<0.05; ***P<0.001 versus IMDM control in (B and D). $^{\#}P$<0.05 versus PBMNCTx in (B) or eEPCTx in (D). Each graph column represents a mean±SE. N=6 mice per group. ATM indicates anterior tibial muscle; eEPCTx, early endothelial progenitor cell transplantation; GmCD34, granulocyte colony-stimulating factor mobilized CD34^{+} cell; HPF, high power field; iNOS, inducible nitric oxide synthase; PBMNCTx, peripheral blood mononuclear cell transplantation; QQMNCTx, quality and quantity control culture of mononuclear cell transplantation.

2.06±0.40, 2.20±0.56, and 1.00±0.11 in IGF-1, respectively (Figure 11A and 11B).

The gene expression of TGF-β was fairly promoted by responding to QQMNCTx, rather than to PBMNCTx, and also enhanced equal to or higher than that in GmCD34Tx, although not in eEPCTx. The relative ratio of TGF-β gene expression in PBMNCTx, QQMNCTx, GmCD34Tx, and eEPCTx, control, was 3.14±0.42, 4.35±0.60, 3.52±0.36, and 0.52±0.04 (Figure 11A and 11B).

Thus, gene expressions of the potent factors for angiogenesis, myogenesis, and anti-inflammation reacting to QQMNCTx as well as GmCD34Tx were similarly up-regulated, when compared with those to PBMNCTx or eEPCTx.

Above all, the gene expression encoding IGF-1 to QQMNCTx was unambiguously enhanced, compared with that to the other Tx groups of PBMNCTx and eEPCTx. The findings correspond with the histological results to show the multifunctional mechanisms of QQMNCTx as superior to those of PBMNCTx or eEPCTx.

Notably, Tx of all cell sources, more or less, up-regulated gene expression of IL-1β, a proinflammatory factor, whereas unpurified EPC Tx of QQMNCs as well as PBMNCs tended to

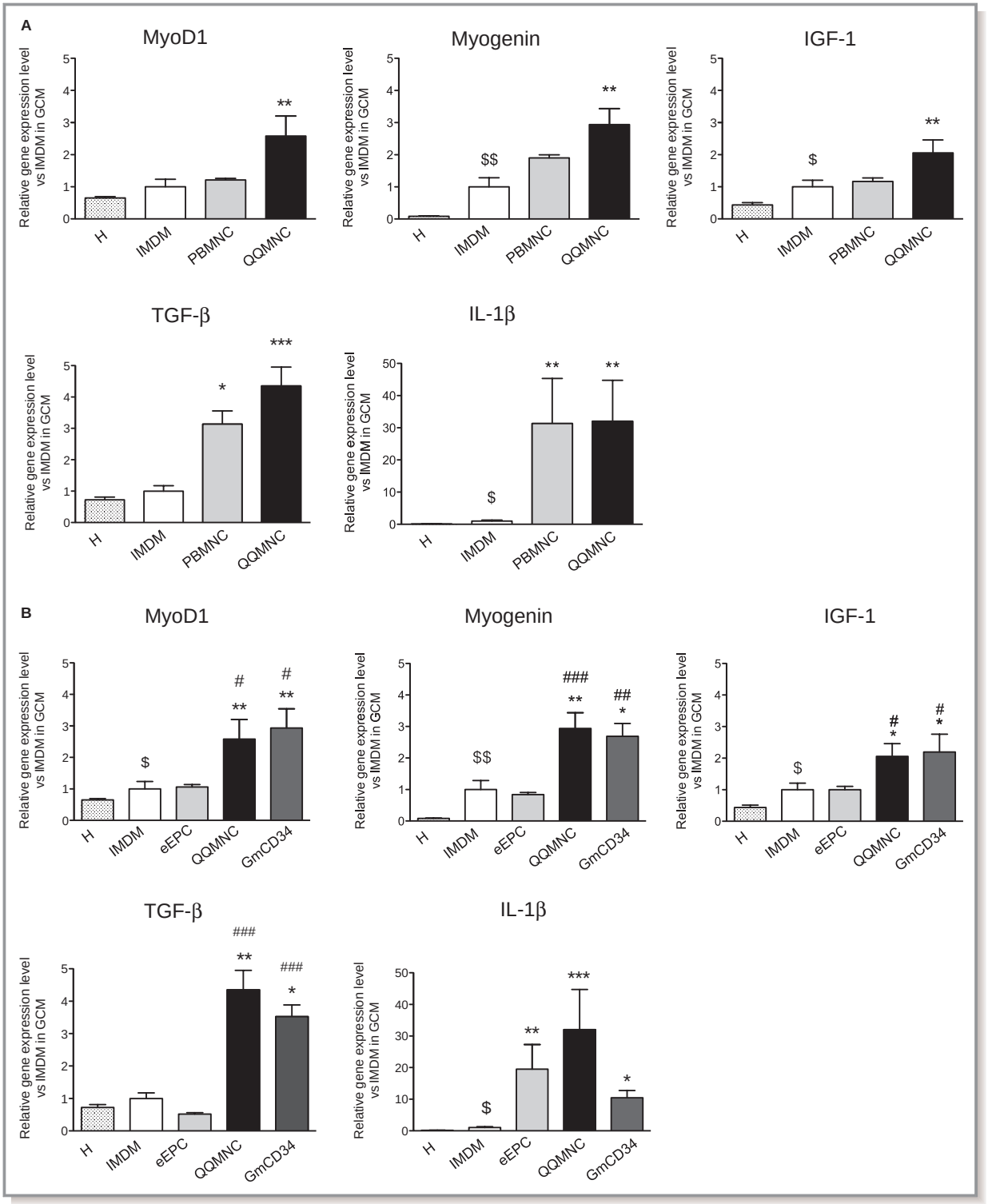

Figure 11. qRT-PCR assay of murine gene expression in ischemic hindlimbs. The graphs show the relative gene expression levels of promyogenic (MyoD1, myogenin, and IGF-1), anti-inflammation (TGF-β), and proangiogenic (IL-1β) factors. The comparison of the levels in QQMNCTx to those in IMDM control or PBMNCTx in (A) and in IMDM control, eEPCTx, and GmCD34Tx in (B). H, healthy (contralateral) hindlimb of IMDM control mice. $^{*}P<0.05$; $^{**}P<0.01$; $^{***}P<0.001$ versus IMDM control. $^{\$}P<0.0.5$; $^{\$\$}P<0.01$ versus H. $^{\#}P<0.05$ in (A and B). $^{\#\#}P<0.01$; $^{\#\#\#}P<0.001$ versus eEPCTx in (B). Each graph column represents a mean±SE. N=4 to 6 mice per group. eEPCTx indicates early endothelial progenitor cell transplantation; GCM, gastrocunemius muscle; GmCD34, granulocyte colony-stimulating factor mobilized $CD34^{+}$ cell; IGF, insulin-like growth factor; IL, interleukin; PBMNCTx, peripheral blood mononuclear cell transplantation; QQMNCTx, quality and quantity control culture of mononuclear cell transplantation; qRT-PCR, quantitative real-time polymerase chain reaction; TGF, transforming growth factor.

produce the transcript more drastically than the purified EPC Tx of GmCD34 or eEPCs. The relative ratio of IL-1β gene expression in QQMNCTx, GmCD34Tx, and eEPCTx versus that in IMDM control was 32.00±12.74, 10.47±2.27, and 19.53±7.78, respectively.

In the present experiments, PBMNCTx, despite the fairly high expression of IL-1β, did not exert angiogenic ability, whereas GmCD34Tx, even in the lesser expression, did so favorably. In other words, IL-1β production in ischemic tissue responding to any cell Tx did not seemingly contribute to angiogenesis for vascular regeneration.

Discussion

Here, we developed and characterized QQMNCs (novel therapeutic cells), QQMNCs derived from PBMNCs that were subjected to QQ culture, and this QQ culture promoted expansion of EPCs and adoption of regenerative phenotypes by macrophages and T lymphocytes. The QQ culture that we used to generate QQMNCs was based on a well-established QQ culture that increases the quality and quantity of EPCs from enriched EPC populations, such as $CD34^+$ and $CD133^+$ cells; this established QQ culture was used to generate therapeutic stem cells for CV regeneration in rat infarcted myocardia.[23]

We found here that the vasculogenic signaling condition of this QQ culture potentiated the vascular regeneration ability of naïve PBMNCs to produce QQMNCs. QQMNCs were superior to PBMNCs, and equal to or greater than GmCD34 cells, in terms of regeneration abilities, including vascular regeneration (angiogenesis, arteriogenesis, and vasculogenesis), myogenesis, anti-inflammation, and antifibrosis.

EPC Expansion and Differentiation in QQMNCs

EPC-CFA of QQMNCs demonstrated intensive expansion potential of colony-forming EPCs, especially dEPCs (Figure 1D). The concept of colony-forming EPCs was recently introduced.[12,38] pEPCs in small-sized EPC colonies showed a higher rate of proliferation and a higher percentage of cells in S-phase, when compared to dEPCs in large-sized EPC colonies. In contrast, dEPCs had a significantly higher capacity for vasculogenic activity than did pEPCs; similarly, dEPCs also had a greater overall potential for cell adhesion and formation of tube-like structures in vitro; importantly, dEPCs had a greater capacity than pEPCs to support de novo blood vessel formation in vivo after transplantation into ischemic models.

Therefore, pEPCs are defined as very immature, highly proliferative EPCs; in contrast, dEPCs are believed to derive from pEPCs and represent cells prone to differentiation and promotion of vasculogenesis. These dEPCs are proven to play a key role in vasculogenesis, and to be suitable for vascular regeneration therapy. In this regard, QQ culture promoted significant expansion and commitment of colony-forming EPCs with vasculogenic potential.

To confirm colony-forming EPC expansion in QQ culture of naïve PBMNCs, we evaluated EPC colony-forming activity before and after QQ culture (Figure 1E). Total EPC-CFU count in QQMNC samples was correlated with that in PBMNC samples. For example, pEPC-CFU count in PBMNC samples correlated with dEPC-CFU count and with total EPC-CFU count in QQMNC samples, but not with pEPC-CFU count in QQMNC samples. The dEPC-CFU count in PBMNC samples did not correlate to any EPC-CFU count in QQMNC samples. These data indicate that signals in QQ culture probably induced concurrent expansion and differentiation of pEPC-CFCs, resulting in an increase in the dEPC-CFC population instead of the pEPC-CFC population. Consequently, the enhanced vasculogenic potential of post QQ culture-treated cells, compared with the precursor PBMNCs, explained the preferential vascular regeneration.

Cell Populations in QQ Cultures

The cell numbers of QQMNCs were, on average, approximately half of those in the respective PBMNCs. The cellular density of PBMNCs per blood volume is inversely correlated with the ratio of cellular density per well between PBMNCs and QQMNCs. Therefore, the QQMNC numbers are rather dependent on the original blood volume per se (Figure 1B).

From the view of cell populations, the decrease in total cell count is mainly derived from significant reduction of B lymphocytes ($CD19^+$), NK cells ($CD16^+$ and $CD56^+$), cytotoxic T cells ($CD8^+$), and proinflammatory monocytes and macrophages ($CD14^+$ and $CCR2^+$). In contrast, populations of progenitor cells ($CD34^+$ and $CD133^+$) and of anti-inflammatory monocytes and macrophages ($CD206^+$) expanded greatly, but populations of endothelial cells ($CD105^+$ and $CD146^+$) and helper T cells ($CD4^+$) expanded only moderately.

The increase in $CD34^+$ or $CD133^+$ cell populations indicates the expanded population of immature EPCs. The increase in $CD105^+$ or $CD146^+$ cell populations was also indicative of EPC expansion and differentiation; notably, differentiating EPCs express these markers.[39,40]

The extent of the increase in $CD206^+$ cells and of the decrease in $CCR2^+$ cells indicates the conversion of the monocyte/macrophage phenotype from M1 to M2 type. Monocytes/macrophages differentiate toward a proinflammatory, classically activated M1 state or toward an anti-inflammatory, alternatively activated M2 state according to different environments and stimuli. M1 macrophages are induced by proinflammatory cytokines and microbial products, such as INF-γ, tumor necrosis factor alpha (TNF-α), and lipopolysaccharide; these macrophages are mainly associated with pathologic inflammations. M2 macrophages are induced

by anti-inflammatory cytokines, such as IL-4, IL-13, and IL-10, to ameliorate type 1 inflammatory responses and control adaptive immunity. Furthermore, their anti-inflammatory cytokines promote and regulate type 2 immune responses, angiogenesis, and tissue repair.[41]

In this regard, monocyte/macrophages in QQMNCs mainly adopt angiogenic and anti-inflammatory phenotypes and are contributing to regenerative process in ischemic organs.

Among lymphocyte lineage cells, B lymphocytes, NK cells, and cytotoxic T cells significantly decrease or fade away. Instead, helper T cells are the last surviving lymphocyte population in QQ cultures. The phenotype identification of $CD4^+$ cells disclosed the significant increase in $CD4^+$/$CD25^+$/$Foxp3^+$ regulatory T lymphocytes as well as $CD4^+$/$IL\text{-}4^+$ Th2 lymphocytes. In recent years, the interaction between monocytes/macrophages and T lymphocytes has been investigated. IFN-γ produced by Th1 lymphocytes induce monocytes to become classical activated M1 macrophages, whereas IL-4, IL-13, and IL-10 that are produced by Th2 and regulatory T lymphocytes induce differentiation of regenerative M2 macrophages. IL-12 and IL-6 produced by M1 macrophages activate Th1 lymphocytes, whereas IL-10 and TGF-β produced by M2 macrophages encourage Th2 and regulatory T-lymphocyte functions.[41,42]

Therefore, the cell-cell interactions among M2 macrophages, Th2, and regulatory T cells are considered to accelerate QQMNCs function as angiogenic and anti-inflammatory tools.

Of note, the majority of T lymphocytes in QQ cultures are $CXCR4^+$/$CD31^+$/$CD3^+$ cells. This population is called "angiogenic T cells" in the vascular biology field; these T cells deliver proangiogenic cytokines in tissues for neovascularization.[30] The finding also encourages that the phenotype of T lymphocytes is conducible to angiogenic preference of QQMNCs.

Therefore, QQMNCs signal regenerative switches on PBMNCs not only by EPC expansion and differentiation, but also through collaborative M2 macrophage polarization and Th2 and regulatory T-cell activation in QQ culture.

Cross-Talk of Cell Populations in QQMNCs

The finding shown in Figure 1F indicates that $CD34^+$ cell-depleted PBMNCs included some cell population to accelerate EPC expansion and differentiation in $CD34^+$ cells through QQ culture. As demonstrated in Figure 2C and 2D, EPCs, M2 macrophage, Th2, and regulatory T lymphocytes were mainly activated in QQMNCs. Increasingly, researches are focused on the interaction between macrophages and T lymphocytes to elucidate the collaborative mechanism of inflammation and immunity. Although we do not have any evidence to indicate that EPCs are involved in this collaboration, the developed culture for EPC expansion, QQ culture, regulates phenotypes of macrophages and T lymphocytes and, consequently, exerts EPC expansion and differentiation. Therefore, any cellular or molecular mechanism responsible for the effects of $CD34^+$ cell-depleted PBMNCs needs to be identified in the future for scientific and therapeutic interests.

Factors Expressed From QQMNCs

In order to further examine the vasculogenic potential of QQMNCs, qRT-PCR was used to determine gene expression profiles. In QQMNCs, the expression of mRNAs encoding anti-inflammatory and proangiogenic factors was enhanced, whereas that of mRNAs encoding proinflammatory cytokines declined (Figure 3).

Expression of mRNAs encoding proangiogenic cytokines and growth factors (eg, IL-10,[43] leptin,[44,45] IGF-1,[46] and IL-8[47]) was greatly elevated. Leptin[45] and IL-10[48] promote the vasculogenic and angiogenic potentials of EPCs and ECs. IGF-1[49] and IL-8[50] are also related factors responsible for angiogenic properties of EPCs. Furthermore, IGF-1 promotes muscle fiber regeneration[35]; this phenomenon may be reflected in the findings of enhanced myogenesis after QQMNCTx. VEGF-B and Angn-1 were up-regulated in QQMNCs, and they potentiate vascular survival and maturation relating to arteriogenesis induced by pericyte recruitment.[33,34] However, expression of mRNA encoding VEGF-A, one of the main proangiogenic growth factors, was not elevated, but rather reduced in QQMNCs, relative to PBMNCs. The reduction of VEGF-A expression might be explained by a negative feedback mechanism through high dose of VEGF-A protein in QQ culture conditioning.

In contrast, expression of mRNA encoding TGF-β, one of the potent anti-inflammatory factors, was lower in QQMNCs. However, expression of mRNAs encoding TNF-α and IL-1β, the important proinflammatory mediators, was similarly mitigated between QQMNCs and PBMNCs for TNF-α while prominently down-regulated in QQMNCs and in PBMNCs for IL-1β.

The findings indicate that QQMNCs may not, at least, bring proinflammatory cell populations more than PBMNCs.

Moreover, the expression of mRNAs encoding MMP-2 or -9, which, playing a critical role in neovascularization and tissue remodeling for antifibrosis,[36] were highly up-regulated.

Taken together, QQMNCTx, compared to PBMNCTx, resulted in more favorable conditions for vascular regeneration or tissue repair because of the orchestration of dynamic expression of multiple cytokines and growth factors.

Therapeutic Potential of QQMNCs for Hindlimb Ischemia Models

QQMNCs have therapeutic potential because transplantation of the cells into ischemic hindlimb tissue was associated with

increased blood flow, limb survival, and neovascularization in tissues (Figure 5). Moreover, histological findings indicate that transplanted human QQMNCs contributed to new microvessel formation composed of human cells derived from EPCs in QQMNCs, as well as mouse microvessel formation and arteriogenesis supported by pericytes (Figures 6 and 7). The latter effects were presumably the result of angiogenic paracrine effects by accelerated phenotypes of macrophages and T lymphocytes as well as EPCs.

The other categorical finding of this transplantation treatment was decreased fibrosis and inflammation as well as enhanced myogenesis (Figures 8 through 10). As indicated by cell population study and gene expression analyses, QQMNCs included many anti-inflammatory M2 macrophages; the cells had enhanced expression of the anti-inflammatory cytokine, IL-10, and the anti-fibrotic proteases, MMP-2 and -9, as well as decreased expression of the proinflammatory cytokine, IL-1β. This anti-inflammatory effect by QQMNCs conceivably protected against fibrosis, even in severe ischemic muscles. Moreover, skeletal myogenesis was also augmented by transplantation of QQMNCs with enhanced expression of mRNA encoding IGF-1.

Thus, we demonstrated that transplanted QQMNCs per se provide the favorable microenvironment for injured tissue regeneration by exerting vascularization as well as anti-inflammatory and myogenic effects.

As recently reported,[7] autologous PBMNCs isolated by apheresis and then transplanted into patients had vascular therapeutic potential, when the largest cell dose (over 1×10^{10} cells of human subject) was implanted. Here, we transplanted only 1×10^{4} cells (PBMNCs and/or QQMNCs) per mouse subject; this dose corresponds to $\approx$2.0 to 2.5×10^{7} cells in a human subject of 50 kg body weight. We implanted far fewer cells than are generally used for clinical treatments. Therefore, the effect of PBMNCs on ischemic hindlimbs was minimal, whereas QQMNCTx had extensive therapeutic effects on vascular regeneration and tissue repair.

On the other hand, the cell dose of 1×10^{4} cells per mouse subject also corresponds to that used at transplantation of G-CSF-mobilized $CD34^{+}$ cells in patients with critical limb ischemia.[17,19] Of note, in the present study, QQMNCTx exerted the experimental efficacy equal to or in part greater than that of GmCD34Tx.

The count of transplanted QQMNCs (1×10^{4} cells/mouse) for therapeutic activity of tissue regeneration corresponds to cell quantity, on average, acquired from <100 mL of PB of human subjects. The isolation and preparation of QQMNCs require only the MNC isolation and a week culture in QQ culture conditions that included recombinant factors without any manipulation. Furthermore, the process avoids invasive procedures for isolation, such as BM cell isolation or leukapheresis, and expensive costs for mobilization and target cell isolation, such as G-CSF administration or $CD34^{+}/CD133^{+}$ cell isolation using magnetic beads.

Collectively, the QQMNC is expected to be an advantageous and feasible cell source for cell-based therapy targeting ischemic diseases.

Responsive Mechanism in Ischemic Hindlimb for Tissue Regeneration After QQMNCTx

Histochemistry (Figures 8 through 10) and qRT-PCR assay (Figure 11) demonstrated that QQMNCTx, as well as GmCD34Tx, provides the preferential environment for tissue regeneration of myogenesis, antifibrosis, and anti-inflammation in the ischemic hindlimb.

With respect to qRT-PCR assay, IL-1β, a proinflammatory cytokine, has been reported to function as a proangiogenic factor derived from regenerating myoblasts responding to PBMNC implantation in the ischemic hindlimb.[51] In the present study, implantation of PBMNCs highly induced the expression of mRNA encoding IL-1β in ischemic tissue, similarly to that of QQMNCs, whereas it did not demonstrate great angiogenic potential. The causes of the dissimilar response might be presumably attributed to the distinct animal experiments using different murine strains with various cell doses for transplantation: immunodeficient BALB/c nu/nu nude mice (1×10^{4} cells/mouse) in our study and C57BL/6 mice (1×10^{6} cells/mouse) elsewhere.[51]

Notably, QQMNCTx, similarly to GmCD34Tx, up-regulated the gene expression of mRNAs encoding promyogenic factors of IGF-1,[52] MyoD1, and myogenin in the ischemic hindlimb; Tx of those cell types induced preferential myogenesis, unlike Tx of the other cell candidates, in histological evaluation.

This means that the effective myogenesis by cell transplantation may primarily require in situ IGF-1 production, which also signifies a myogenic biomarker in the ischemic hindlimb. Regarding the results, skeletal muscle-restricted expression of IGF-1 in transgenic mice has been reported to not only accelerate muscle regeneration, but also to exert the protective effects against inflammation and fibrosis in the injured skeletal muscle.[53] Moreover, IGF-1 has been reported to inhibit nuclear factor kappa B activation through TNF-α[54] or proapoptotic miRNA expression[55] in ischemic cardiomyocytes. Therefore, IGF-1 supplied to ischemic tissue by local QQMNCTx is adequately conceived to exert the protective effect on inflammation, fibrosis, or tissue injury. Also, QQMNCs per se exhibited enhanced expression of mRNA encoding human IGF-1 (Figure 3A).

Likewise, QQMNCTx, as well as GmCD34Tx, up-regulated expression of mRNA encoding TGF-β, a potent inhibitory factor of inflammation, in transplanted tissue, although

QQMNC in vitro exhibited lesser expression than PBMNCs. Unlike the aspect of IGF-1, the responsive tissue expression in situ of TGF-β after cell transplantations, might contribute to protecting against inflammation, rather than the expression by the transplanted cells.

Take together, expression of IGF-1 or TGF-β by injured tissue responsive to QQMNCTx, as well as that of IGF-1 and other tissue regeneration mediators by the transplanted cells per se, are expected to reveal the mechanism underlying the preferential efficacy of cell Tx.

Limitation of the Present Study

In the present study, recipients' T-lymphocyte-deficient condition in athymic BALB/c nu/nu nude mice limits the insight into regeneration mechanism by regulatory effects on host immune response through regulatory T cells increased in QQMNCs. Therefore, the relevant animal model studies are required to elucidate the essential effect of QQMNCTx in future experiments.

Conclusion

The QQ culture system for whole PBMNCs that we described here may lead to an effective cell-based therapy to alleviate the physical burdens in patients as one feasible strategy for vascular regeneration or tissue repair.

Acknowledgments

The authors thank the staves of Teaching and Research Support Core Center of Tokai University School of Medicine for outstanding technical support as well as Sachie Ota for her secretarial assistance.

Sources of Funding

This work was supported by grants from the Riken Center for Developmental Biology Collaborative Research Fund, Kobe (08001475), Japan, the Ministry of Health, Labor and Welfare (25280401), Japan, and the Ministry of Education, Culture, Sports, Science and Technology (Academic Frontier Promotion Program), Japan. H.M. is personally supported by the Ministry of Education, Culture, Sports, Science and Technology (Basic Research Grant No. 25461091), Japan, Tokai University School of Medicine Research Aid, and Research and Study Project of Tokai University Education System General Research Organization, Japan.

Disclosures

None.

References

1. Asahara T, Murohara T, Sullivan A, Silver M, van der Zee R, Li T, Witzenbichler B, Schatteman G, Isner JM. Isolation of putative progenitor endothelial cells for angiogenesis. *Science*. 1997;275:964–967.
2. Shi Q, Rafii S, Wu MH, Wijelath ES, Yu C, Ishida A, Fujita Y, Kothari S, Mohle R, Sauvage LR, Moore MA, Storb RF, Hammond WP. Evidence for circulating bone marrow-derived endothelial cells. *Blood*. 1998;92:362–367.
3. Asahara T, Masuda H, Takahashi T, Kalka C, Pastore C, Silver M, Kearne M, Magner M, Isner JM. Bone marrow origin of endothelial progenitor cells responsible for postnatal vasculogenesis in physiological and pathological neovascularization. *Circ Res*. 1999;85:221–228.
4. Tateishi-Yuyama E, Matsubara H, Murohara T, Ikeda U, Shintani S, Masaki H, Amano K, Kishimoto Y, Yoshimoto K, Akashi H, Shimada K, Iwasaka T, Imaizumi T; Therapeutic Angiogenesis using Cell Transplantation Study I. Therapeutic angiogenesis for patients with limb ischaemia by autologous transplantation of bone-marrow cells: a pilot study and a randomised controlled trial. *Lancet*. 2002;360:427–435.
5. Assmus B, Schachinger V, Teupe C, Britten M, Lehmann R, Dobert N, Grunwald F, Aicher A, Urbich C, Martin H, Hoelzer D, Dimmeler S, Zeiher AM. Transplantation of progenitor cells and regeneration enhancement in acute myocardial infarction (TOPCARE-AMI). *Circulation*. 2002;106:3009–3017.
6. Schachinger V, Tonn T, Dimmeler S, Zeiher AM. Bone-marrow-derived progenitor cell therapy in need of proof of concept: design of the REPAIR-AMI trial. *Nat Clin Pract Cardiovasc Med*. 2006;3(suppl 1):S23–S28.
7. Moriya J, Minamino T, Tateno K, Shimizu N, Kuwabara Y, Sato Y, Saito Y, Komuro I. Long-term outcome of therapeutic neovascularization using peripheral blood mononuclear cells for limb ischemia. *Circ Cardiovasc Interv*. 2009;2:245–254.
8. Yoon YS, Park JS, Tkebuchava T, Luedeman C, Losordo DW. Unexpected severe calcification after transplantation of bone marrow cells in acute myocardial infarction. *Circulation*. 2004;109:3154–3157.
9. Lunde K, Solheim S, Aakhus S, Arnesen H, Abdelnoor M, Egeland T, Endresen K, Ilebekk A, Mangschau A, Fjeld JG, Smith HJ, Taraldsrud E, Grogaard HK, Bjornerheim R, Brekke M, Muller C, Hopp E, Ragnarsson A, Brinchmann JE, Forfang K. Intracoronary injection of mononuclear bone marrow cells in acute myocardial infarction. *N Engl J Med*. 2006;355:1199–1209.
10. Miyamoto K, Nishigami K, Nagaya N, Akutsu K, Chiku M, Kamei M, Soma T, Miyata S, Higashi M, Tanaka R, Nakatani T, Nonogi H, Takeshita S. Unblinded pilot study of autologous transplantation of bone marrow mononuclear cells in patients with thromboangiitis obliterans. *Circulation*. 2006;114:2679–2684.
11. Moazzami K, Majdzadeh R, Nedjat S. Local intramuscular transplantation of autologous mononuclear cells for critical lower limb ischaemia. *Cochrane Database Syst Rev*. 2011;12:CD008347.
12. Masuda H, Alev C, Akimaru H, Ito R, Shizuno T, Kobori M, Horii M, Ishihara T, Isobe K, Isozaki M, Itoh J, Itoh Y, Okada Y, McIntyre BA, Kato S, Asahara T. Methodological development of a clonogenic assay to determine endothelial progenitor cell potential. *Circ Res*. 2011;109:20–37.
13. Mosser DM, Edwards JP. Exploring the full spectrum of macrophage activation. *Nat Rev Immunol*. 2008;8:958–969.
14. Mosser DM, Zhang X. Interleukin-10: new perspectives on an old cytokine. *Immunol Rev*. 2008;226:205–218.
15. Bartunek J, Vanderheyden M, Vandekerckhove B, Mansour S, De Bruyne B, De Bondt P, Van Haute I, Lootens N, Heyndrickx G, Wijns W. Intracoronary injection of CD133-positive enriched bone marrow progenitor cells promotes cardiac recovery after recenyocardial infarction: feasibility and safety. *Circulation*. 2005;112:I178–I183.
16. Losordo DW, Schatz RA, White CJ, Udelson JE, Veereshwarayya V, Durgin M, Poh KK, Weinstein R, Kearney M, Chaudhry M, Burg A, Eaton L, Heyd L, Thorne T, Shturman L, Hoffmeister P, Story K, Zak V, Dowling D, Traverse JH, Olson RE, Flanagan J, Sodano D, Murayama T, Kawamoto A, Kusano KF, Wollins J, Welt F, Shah P, Soukas P, Asahara T, Henry TD. Intramyocardial transplantation of autologous CD34+ stem cells for intractable angina: a phase I/IIa double-blind, randomized controlled trial. *Circulation*. 2007;115:3165–3172.
17. Kawamoto A, Katayama M, Handa N, Kinoshita M, Takano H, Horii M, Sadamoto K, Yokoyama A, Yamanaka T, Onodera R, Kuroda A, Baba R, Kaneko Y, Tsukie T, Kurimoto Y, Okada Y, Kihara Y, Morioka S, Fukushima M, Asahara T. Intramuscular transplantation of G-CSF-mobilized CD34(+) cells in patients with critical limb ischemia: a phase I/IIa, multicenter, single-blinded, dose-escalation clinical trial. *Stem Cells*. 2009;27:2857–2864.
18. Losordo DW, Henry TD, Davidson C, Sup Lee J, Costa MA, Bass T, Mendelsohn F, Fortuin FD, Pepine CJ, Traverse JH, Amrani D, Ewenstein BM, Riedel N, Story K, Barker K, Povsic TJ, Harrington RA, Schatz RA; Investigators AC. Intramyocardial, autologous CD34+ cell therapy for refractory angina. *Circ Res*. 2011;109:428–436.

19. Kinoshita M, Fujita Y, Katayama M, Baba R, Shibakawa M, Yoshikawa K, Katakami N, Furukawa Y, Tsukie T, Nagano T, Kurimoto Y, Yamasaki K, Handa N, Okada Y, Kuronaka K, Nagata Y, Matsubara Y, Fukushima M, Asahara T, Kawamoto A. Long-term clinical outcome after intramuscular transplantation of granulocyte colony stimulating factor-mobilized CD34 positive cells in patients with critical limb ischemia. *Atherosclerosis*. 2012;224:440–445.
20. Scheubel RJ, Zorn H, Silber RE, Kuss O, Morawietz H, Holtz J, Simm A. Age-dependent depression in circulating endothelial progenitor cells in patients undergoing coronary artery bypass grafting. *J Am Coll Cardiol*. 2003;42:2073–2080.
21. Vasa M, Fichtlscherer S, Aicher A, Adler K, Urbich C, Martin H, Zeiher AM, Dimmeler S. Number and migratory activity of circulating endothelial progenitor cells inversely correlate with risk factors for coronary artery disease. *Circ Res*. 2001;89:E1–E7.
22. Hill JM, Zalos G, Halcox JP, Schenke WH, Waclawiw MA, Quyyumi AA, Finkel T. Circulating endothelial progenitor cells, vascular function, and cardiovascular risk. *N Engl J Med*. 2003;348:593–600.
23. Masuda H, Iwasaki H, Kawamoto A, Akimaru H, Ishikawa M, Ii M, Shizuno T, Sato A, Ito R, Horii M, Ishida H, Kato S, Asahara T. Development of serum-free quality and quantity control culture of colony-forming endothelial progenitor cell for vasculogenesis. *Stem Cells Transl Med*. 2012;1:160–171.
24. Kalka C, Masuda H, Takahashi T, Kalka-Moll WM, Silver M, Kearney M, Li T, Isner JM, Asahara T. Transplantation of ex vivo expanded endothelial progenitor cells for therapeutic neovascularization. *Proc Natl Acad Sci USA*. 2000;97:3422–3427.
25. Hur J, Yoon CH, Kim HS, Choi JH, Kang HJ, Hwang KK, Oh BH, Lee MM, Park YB. Characterization of two types of endothelial progenitor cells and their different contributions to neovasculogenesis. *Arterioscler Thromb Vasc Biol*. 2004;24:288–293.
26. Sasaki K, Heeschen C, Aicher A, Ziebart T, Honold J, Urbich C, Rossig L, Koehl U, Koyanagi M, Mohamed A, Brandes RP, Martin H, Zeiher AM, Dimmeler S. Ex vivo pretreaent of bone marrow mononuclear cells with endothelial NO synthase enhancer AVE9488 enhances their functional activity for cell therapy. *Proc Natl Acad Sci USA*. 2006;103:14537–14541.
27. Pesce M, Orlandi A, Iachininoto MG, Straino S, Torella AR, Rizzuti V, Pompilio G, Bonanno G, Scambia G, Capogrossi MC. Myoendothelial differentiation of human umbilical cord blood-derived stem cells in ischemic limb tissues. *Circ Res*. 2003;93:e51–e62.
28. Napoli C, Williams-Ignarro S, de Nigris F, de Rosa G, Lerman LO, Farzati B, Matarazzo A, Sica G, Botti C, Fiore A, Byrns RE, Sumi D, Sica V, Ignarro LJ. Beneficial effects of concurrent autologous bone marrow cell therapy and metabolic intervention in ischemia-induced angiogenesis in the mouse hindlimb. *Proc Natl Acad Sci USA*. 2005;102:17202–17206.
29. Sica V, Williams-Ignarro S, de Nigris F, D'Armiento FP, Lerman LO, Balestrieri ML, Maione C, Palagiano A, Rossiello L, Ignarro LJ, Napoli C. Autologous bone marrow cell therapy and metabolic intervention in ischemia-induced angiogenesis in the diabetic mouse hindlimb. *Cell Cycle*. 2006;5:2903–2908.
30. Hur J, Yang HM, Yoon CH, Lee CS, Park KW, Kim JH, Kim TY, Kim JY, Kang HJ, Chae IH, Oh BH, Park YB, Kim HS. Identification of a novel role of T cells in postnatal vasculogenesis: characterization of endothelial progenitor cell colonies. *Circulation*. 2007;116:1671–1682.
31. Fadini GP, Albiero M, Boscaro E, Menegazzo L, Cabrelle A, Piliego T, Federici M, Agostini C, Avogaro A. Rosuvastatin stimulates clonogenic potential and anti-inflammatory properties of endothelial progenitor cells. *Cell Biol Int*. 2010;34:709–715.
32. Sica A, Larghi P, Mancino A, Rubino L, Porta C, Totaro MG, Rimoldi M, Biswas SK, Allavena P, Mantovani A. Macrophage polarization in tumour progression. *Semin Cancer Biol*. 2008;18:349–355.
33. Zhang F, Tang Z, Hou X, Lennartsson J, Li Y, Koch AW, Scotney P, Lee C, Arjunan P, Dong L, Kumar A, Rissanen TT, Wang B, Nagai N, Fons P, Fariss R, Zhang Y, Wawrousek E, Tansey G, Raber J, Fong GH, Ding H, Greenberg DA, Becker KG, Herbert JM, Nash A, Yla-Herttuala S, Cao Y, Watts RJ, Li X. VEGF-B is dispensable for blood vessel growth but critical for their survival, and VEGF-B targeting inhibits pathological angiogenesis. *Proc Natl Acad Sci USA*. 2009;106:6152–6157.
34. Gluzman Z, Koren B, Preis M, Cohen T, Tsaba A, Cosset FL, Shofti R, Lewis BS, Virmani R, Flugelman MY. Endothelial cells are activated by angiopoeitin-1 gene transfer and produce coordinated sprouting in vitro and arteriogenesis in vivo. *Biochem Biophys Res Commun*. 2007;359:263–268.
35. Borselli C, Storrie H, Benesch-Lee F, Shvartsman D, Cezar C, Lichan JW, Vandenburgh HH, Mooney DJ. Functional muscle regeneration with combined delivery of angiogenesis and myogenesis factors. *Proc Natl Acad Sci USA*. 2010;107:3287–3292.
36. Johnson C, Sung HJ, Lessner SM, Fini ME, Galis ZS. Matrix metalloproteinase-9 is required for adequate angiogenic revascularization of ischemic tissues: potential role in capillary branching. *Circ Res*. 2004;94:262–268.
37. Shao H, Tan Y, Eton D, Yang Z, Uberti MG, Li S, Schulick A, Yu H. Statin and stromal cell-derived factor-1 additively promote angiogenesis by enhancement of progenitor cells incorporation into new vessels. *Stem Cells*. 2008;26:1376–1384.
38. Tsukada S, Kwon SM, Matsuda T, Jung SY, Lee JH, Lee SH, Masuda H, Asahara T. Identification of mouse colony-forming endothelial progenitor cells for postnatal neovascularization: a novel insight highlighted by new mouse colony-forming assay. *Stem Cell Res Ther*. 2013;4:20.
39. Rohde E, Malischnik C, Thaler D, Maierhofer T, Linkesch W, Lanzer G, Guelly C, Strunk D. Blood monocytes mimic endothelial progenitor cells. *Stem Cells*. 2006;24:357–367.
40. Delorme B, Basire A, Gentile C, Sabatier F, Monsonis F, Desouches C, Blot-Chabaud M, Uzan G, Sampol J, Dignat-George F. Presence of endothelial progenitor cells, distinct from mature endothelial cells, within human CD146+ blood cells. *Thromb Haemost*. 2005;94:1270–1279.
41. Mosser DM, Zhang X. Activation of murine macrophages. *Curr Protoc Immunol*. 2008;Chapter 14:Unit 14.2.
42. Liu G, Yang H. Modulation of macrophage activation and programming in immunity. *J Cell Physiol*. 2013;228:502–512.
43. Dace DS, Khan AA, Kelly J, Apte RS. Interleukin-10 promotes pathological angiogenesis by regulating macrophage response to hypoxia during development. *PLoS One*. 2008;3:e3381.
44. Goetze S, Bungenstock A, Czupalla C, Eilers F, Stawowy P, Kintscher U, Spencer-Hansch C, Graf K, Nurnberg B, Law RE, Fleck E, Grafe M. Leptin induces endothelial cell migration through Akt, which is inhibited by PPARgamma-ligands. *Hypertension*. 2002;40:748–754.
45. Heida NM, Leifheit-Nestler M, Schroeter MR, Muller JP, Cheng IF, Henkel S, Limbourg A, Limbourg FP, Alves F, Quigley JP, Ruggeri ZM, Hasenfuss G, Konstantinides S, Schafer K. Leptin enhances the potency of circulating angiogenic cells via src kinase and integrin (alpha)vbeta5: implications for angiogenesis in human obesity. *Arterioscler Thromb Vasc Biol*. 2010;30:200–206.
46. Rabinovsky ED, Draghia-Akli R. Insulin-like growth factor I plasmid therapy promotes in vivo angiogenesis. *Mol Ther*. 2004;9:46–55.
47. Schomig K, Busch G, Steppich B, Sepp D, Kaufmann J, Stein A, Schomig A, Ott I. Interleukin-8 is associated with circulating CD133+ progenitor cells in acute myocardial infarction. *Eur Heart J*. 2006;27:1032–1037.
48. Krishnamurthy P, Thal M, Verma S, Hoxha E, Lambers E, Ramirez V, Qin G, Losordo D, Kishore R. Interleukin-10 deficiency impairs bone marrow-derived endothelial progenitor cell survival and function in ischemic myocardium. *Circ Res*. 2011;109:1280–1289.
49. Hynes B, Kumar AH, O'Sullivan J, Klein Buneker C, Leblond AL, Weiss S, Schmeckpeper J, Martin K, Caplice NM. Potent endothelial progenitor cell-conditioned media-related anti-apoptotic, cardiotrophic, and pro-angiogenic effects posyocardial infarction are mediated by insulin-like growth factor-1. *Eur Heart J*. 2013;34:782–789.
50. Medina RJ, O'Neill CL, O'Doherty TM, Knott H, Guduric-Fuchs J, Gardiner TA, Stitt AW. Myeloid angiogenic cells act as alternative M2 macrophages and modulate angiogenesis through interleukin-8. *Mol Med*. 2011;17:1045–1055.
51. Tateno K, Minamino T, Toko H, Akazawa H, Shimizu N, Takeda S, Kunieda T, Miyauchi H, Oyama T, Matsuura K, Nishi J, Kobayashi Y, Nagai T, Kuwabara Y, Iwakura Y, Nomura F, Saito Y, Komuro I. Critical roles of muscle-secreted angiogenic factors in therapeutic neovascularization. *Circ Res*. 2006;98:1194–1202.
52. Musaro A, McCullagh K, Paul A, Houghton L, Dobrowolny G, Molinaro M, Barton ER, Sweeney HL, Rosenthal N. Localized IGF-1 transgene expression sustains hypertrophy and regeneration in senescent skeletal muscle. *Nat Genet*. 2001;27:195–200.
53. Pelosi L, Giacinti C, Nardis C, Borsellino G, Rizzuto E, Nicoletti C, Wannenes F, Battistini L, Rosenthal N, Molinaro M, Musaro A. Local expression of IGF-1 accelerates muscle regeneration by rapidly modulating inflammatory cytokines and chemokines. *FASEB J*. 2007;21:1393–1402.
54. Wang M, Tsai B, Brown JW, Meldrum DR. Insulin-like growth factor-1 in myocardial tissue: interaction with tumor necrosis factor. *Crit Care*. 2003;7:417–419.
55. Iekushi K, Seeger F, Assmus B, Zeiher AM, Dimmeler S. Regulation of cardiac microRNAs by bone marrow mononuclear cell therapy in myocardial infarction. *Circulation*. 2012;125:1765–1773, S1761–S1767.

Vasculogenic Conditioning of Peripheral Blood Mononuclear Cells Promotes Endothelial Progenitor Cell Expansion and Phenotype Transition of Anti-Inflammatory Macrophage and T Lymphocyte to Cells With Regenerative Potential

Haruchika Masuda, Rica Tanaka, Satoshi Fujimura, Masakazu Ishikawa, Hiroshi Akimaru, Tomoko Shizuno, Atsuko Sato, Yoshinori Okada, Yumi Iida, Jobu Itoh, Yoshiko Itoh, Hiroshi Kamiguchi, Atsuhiko Kawamoto and Takayuki Asahara

J Am Heart Assoc. 2014;3:e000743; originally published June 25, 2014;
doi: 10.1161/JAHA.113.000743
The *Journal of the American Heart Association* is published by the American Heart Association, 7272 Greenville Avenue, Dallas, TX 75231
Online ISSN: 2047-9980

ORIGINAL ARTICLE

Quality-Control Culture System Restores Diabetic Endothelial Progenitor Cell Vasculogenesis and Accelerates Wound Closure

Rica Tanaka,[1,4] Max Vaynrub,[2] Haruchika Masuda,[1] Rie Ito,[1] Michiru Kobori,[1] Muneo Miyasaka,[3] Hiroshi Mizuno,[4] Stephen M. Warren,[2] and Takayuki Asahara[1]

Delayed diabetic wound healing is, in part, the result of inadequate endothelial progenitor cell (EPC) proliferation, mobilization, and trafficking. Recently, we developed a serum-free functional culture system called the quality and quantity culture (QQc) system that enhances the number and vasculogenic potential of EPCs. We hypothesize that QQc restoration of diabetic EPC function will improve wound closure. To test this hypothesis, we measured diabetic c-kit$^+$Sca-1$^+$lin$^-$ (KSL) cell activity in vitro as well as the effect of KSL cell–adoptive transfer on the rate of euglycemic wound closure before and after QQc. KSL cells were magnetically sorted from control and streptozotocin-induced type I diabetic C57BL6J bone marrow. Freshly isolated control and diabetic KSL cells were cultured in QQc for 7 days and pre-QQc and post-QQc KSL function testing. The number of KSL cells significantly increased after QQc for both diabetic subjects and controls, and diabetic KSL increased vasculogenic potential above the fresh control KSL level. Similarly, fresh diabetic cells form fewer tubules, but QQc increases diabetic tubule formation to levels greater than that of fresh control cells ($P < 0.05$). Adoptive transfer of post-QQc diabetic KSL cells significantly enhances wound closure compared with fresh diabetic KSL cells and equaled wound closure of post-QQc control KSL cells. Post-QQc diabetic KSL enhancement of wound closure is mediated, in part, via a vasculogenic mechanism. This study demonstrates that QQc can reverse diabetic EPC dysfunction and achieve control levels of EPC function. Finally, post-QQc diabetic EPC therapy effectively improved euglycemic wound closure and may improve diabetic wound healing. ***Diabetes*** **62:3207–3217, 2013**

Although blood supply is essential for tissue viability, new blood vessel formation is critical for tissue recovery, regeneration, and repair. Postnatal new blood vessel formation was long thought to be restricted to angiogenesis, the sprouting of new blood vessels from existing vascular structures. However, in 1997, we demonstrated that the de novo formation of new blood vessel derived from bone marrow (BM)-derived cells (i.e., vasculogenesis) is an important part of postnatal healing (1–3). The BM-derived endothelial progenitor cells (EPCs) are precursors of endothelial cells (ECs) and are characterized by their surface expression of KDR, CD133, and CD34 for humans and of lineage-negative c-kit$^+$Sca-1$^+$ (KSL) cells for murine BM cells (4–6).

After injury, locally derived circulating factors mobilize EPCs from their endosteal BM niche. Circulating BM-derived EPCs traffic to the site of injury, experience diapedesis, cluster, tubulize, and canalize to form nascent vessels that inosculate with the existing vasculature (7,8). EPCs have been shown to revascularize numerous ischemic tissues, including myocardium (i.e., myocardial infarction), brain (i.e., cerebral infarction), and skin (i.e., cutaneous wounding) (9,10). Whereas BM-derived EPCs contribute to only 25% of newly formed endothelium in healing tissues, when EPC function is impaired there are marked deficits in tissue repair mechanisms (11,12).

Compared with nondiabetic patients, diabetic EPCs have impaired proliferation, adhesion, migration, and differentiation (13–15). Although the pathogenesis of impaired diabetic wound healing is multifactorial, EPC dysfunction plays a central role (16,17). These intrinsic diabetic EPC vasculogenic impairments may result in >83,000 amputations each year and a postamputation 3-year mortality rate of 75.9% (18). In preclinical studies, the administration of exogenous EPCs has improved ventricular function after myocardial ischemia (19,20), enhanced neuronal recovery after cerebral vascular occlusion, and accelerated restoration of blood flow to ischemic limbs (13,16,17,21–23). Based on these exciting results, we have conducted a phase 3 clinical trial of autologous granulocyte colony-stimulating factor–mobilized peripheral blood EPC therapy for nonhealing diabetic foot patients (24). The results demonstrated that more successful therapeutic results were seen in patients receiving high-vasculogenic EPCs. From these results, we hypothesize that successful autologous diabetic EPC therapy relies on the vasculogenic function of transplanted EPCs and speculate that the intrinsic diabetic EPC dysfunction will limit the efficacy of the therapeutic strategy (25,26).

Recently, our group established a serum-free quality and quantity culture (QQc) system (containing stem cell factor, thrombopoietin, vascular endothelial growth factor, interleukin-6, and Flt-3 ligand) that enhances the vasculogenic potential of EPCs (27). We hypothesize that QQc can reverse the detrimental effects of diabetes-induced EPC dysfunction and can supply a sufficient number of functional EPCs for adoptive autologous cell–based therapy for diabetic patients. In the current study, we tested this hypothesis.

RESEARCH DESIGN AND METHODS

Diabetic mouse model. C57BL/6J male mice aged 8–10 weeks and weighing 20–25 g were purchased from Crea Japan (Kawasaki, Japan) and The Jackson

From the [1]Division of Regenerative Medicine, Department of Basic Clinical Science, Tokai University School of Medicine, Kanagawa, Japan; the [2]Department of Plastic Surgery, Institute of Reconstructive Plastic Surgery Laboratories, New York University Medical Center, New York, New York; the [3]Department of Plastic and Reconstructive Surgery, Juntendo University School of Medicine, Tokyo, Japan; and the [4]Department of Plastic Surgery, Tokai University School of Medicine, Kanagawa, Japan.
Corresponding authors: Takayuki Asahara, asa777@is.icc.u-tokai.ac.jp, and Stephen M. Warren, stephen.warren.md@gmail.com.
Received 28 November 2012 and accepted 7 May 2013.
DOI: 10.2337/db12-1621

Laboratory (Bar Harbor, ME). Obliteration of pancreatic β-cells was achieved with intraperitoneal injections of 50 mg/kg streptozotocin (STZ; Sigma-Aldrich, St. Louis, MO) in 50 mmol/L sodium citrate buffer (pH 4.5) for 5 consecutive days (28). Ten days after the initial injection, mice with a blood glucose level >300 mg/dL were deemed diabetic, whereas those with a level <300 mg/dL received an additional 3 days of STZ injections (50 mg/kg). Mice were considered diabetic if they maintained glucose levels >300 mg/dL for at least 4 weeks before the date of wounding. Control mice received intraperitoneal injections at the same time points with an equal volume of 50 mmol/L sodium citrate buffer. A total of 200 mice were used in this experiment (n = 100 per group). All procedures were conducted in accordance with the guidelines set forth by the committee of Ethical Animal Care and Use at Tokai University School of Medicine and the Institutional Animal Care and Use Committee at New York University Medical Center.

BM progenitor cell isolation. BM cells were harvested from diabetic and control mouse femurs and tibias as previously described (7). Mononuclear cells were washed with PBS-EDTA, and erythrocytes were removed by ammonium chloride hemolyzation and stained with a lineage-positive antibody cocktail containing CD45R/B220, TER119, CD3e, CD11b, Ly-6G, and Ly6C (Gr-1) for 20 min at 4°C (all antibodies obtained from BD PharMingen, San Diego, CA). After labeling the lineage-positive antibodies with biotin-labeled magnetic beads, cells underwent a negative selection process with a magnetic cell sorting system. Lineage-negative cells were counted and then incubated with rat fluorescein isothiocyanate antimouse Ly-6A/E (Sca-1; BD PharMingen) and rat phycoerythrin CD117 (c-kit; BD PharMingen) for 20 min at 4°C, washed three times, and resuspended in 20% Iscove modified Dulbecco medium (Gibco, Carlsbad, CA). Fluorescein isothiocyanate–conjugated Sca-1 and phycoerythrin-conjugated c-kit double-positive cells (KSL cells) then were obtained by fluorescent-activated cell sorting.

Serum-free QQc. Diabetic and control BM KSL cells were isolated as described, and 1×10^3 cells were placed in each well of a 24-well plate (BD Falcon, Bedford, MA) and cultured in QQc for 7 days as previously described (27). Briefly, QQc is an optimized growth factor/cytokine combination (20 ng/mL thyroid peroxidase, 20 ng/mL interleukin-6, 100 ng/mL SCF, 100 ng/mL Flt-3 ligand, and 50 ng/mL vascular endothelial growth factor; all from Peprotech, Rocky Hills, NJ) serum-free stem span (Stem Cell Technologies) media. After 7 days of QQc, control KSL cells were termed C_{QQc} and diabetic KSL cells were termed DM_{QQc}. Growth in QQc has been shown to dramatically expand and enhance the vasculogenic potential of EPCs.

EPC colony-forming assay of KSL population. The vasculogenic potential of diabetic and control BM KSL cells was assessed using the EPC colony-forming assay as previously described (6,29,30). EPC colony-forming assay is designed to distinguish total EPC colony-forming units (tEPC-CFUs) into two different types of EPC-CFUs: primitive (small cell) and definitive (large cell). The primitive EPC-CFU (pEPC-CFUs) is a predominantly proliferative population of cells and the definitive EPCs-CFU (dEPC-CFU) is a predominantly vasculogenic population with greater adhesion, migration, and differentiation and tabularization potential. Briefly, a total of 500 BM KSL cells per dish were seeded into a 35-mm hydrophilic tissue culture dish. Seven days later, tEPC-CFUs, pEPC-CFUs, and dEPC-CFUs were counted by two investigators who were blinded to the experimental conditions. Experiments were performed in triplicate.

Tube formation assay. Tubule formation assay was performed by adding Biocoat Matrigel (Becton Dickinson; Franklin Lakes, NJ) into 24-well plates and incubating in a CO_2-free incubator at 37°C for 30 min. The same lot of Matrigel was used for all experiments. The gels were then overlaid with 3×10^3 fresh and expanded diabetic and control cells cocultured with 1×10^4 endothelial cells suspended in culture medium and incubated at 37°C in an atmosphere of 5% CO_2. The well cultured with endothelial cells only was used as a control. After 12 h of incubation, gels were examined by using a phase-contrast microscope equipped with a digital camera (Nikon eclipse TE2000-U; Nikon, Melville, NY). A blinded observer measured the total number of tube-like structures per high-power field (HPF) in five random fields.

Quantitative real-time PCR. Total RNA from 2×10^4 diabetic and control KSL cells was extracted using the RNeasy Micro kit (Qiagen, Basel, Switzerland) based on the manufacturer's protocol, and reverse-transcription was performed using high-capacity cDNA reverse-transcription kit (Applied Biosystems, Foster City, CA). The transcription reaction was performed at 37°C for 2 h. The obtained cDNA was amplified using the reaction mixture of TaqMan FAST Universal PCR Master Mix (Applied Biosystems). The following TaqMan probes (Applied Biosystems) were used: 18S rRNA (ribosomal RNA control reagents 4308329), endothelial growth factor (Mm00438696_m1; Egf), hepatocyte growth factor (Mm01135193_m1; Hgf), fibroblast growth factor-2 (Mm00433287_m1; Fgf2), fibroblast growth factor-7 (Mm00433291_m1; Fgf7), von Willebrand factor (Mm00550376_m1; vWF), CD29 (Mm0125320_m1; Itgb1), and Flk-1 (Mm0122419_m1; Kdr). The PCR mixtures were preincubated at 95°C for 20 s, followed by 40 cycles of 95°C for 3 s and 62°C for 30 s by ABI 7500 FAST (Applied Biosystems). The real-time data were analyzed by change (Δ) in threshold cycle (Ct) method. The ΔCt was calculated as (gene of target Ct) − (18S rRNA Ct). The relative quantity of mRNA of the target gene was determined by the ΔCt calculation $2^{-\Delta Ct}$.

Wound model and KSL adoptive cellular therapy. To reduce the confounding variables that would affect KSL function in a diabetic wound, we first used 8- to 10-week-old euglycemic C57BL/6J male mice (n = 45; 3 per experimental group in triplicates) as recipients for diabetic and control KSL therapy (31). To verify the efficacy of QQc diabetic cells in diabetic wound healing, a diabetic STZ mouse wound model was similarly prepared. Briefly, each mouse was anesthetized and depilated, and one set of bilateral 6-mm punch biopsy specimens was excised on the dorsum. Excisions were full-thickness, including the hypodermis and panniculus carnosum. India ink was applied intradermally at the margins to permanently mark the wound edge. A silicone stent (Grace Bio-Laboratories, Bend, OR) with an 8-mm inner diameter was sutured with 5–0 nylon (Ethicon, Somerville, NJ) around each wound to minimize skin contracture and to ensure healing by secondary intention. On postoperative day 3, a 1-mL syringe with a 30-gauge needle was used to inject 25 μL saline, 2×10^4 freshly isolated control KSL, 2×10^4 freshly isolated diabetic KSL, 2×10^4 post-QQc control KSL, or 2×10^4 post-QQc diabetic KSL (QD) into the center of the muscle at the base of the wound. The wounds were covered with Tegaderm to prevent the cells from leaking and drying.

Wound photographs were acquired with a 7-megapixel digital camera (Canon USA, Lake Success, NY) from a distance of 6.5 cm, with the lens oriented parallel to the wound. Wound area was measured digitally (Photoshop CS3; Adobe Systems, San Jose, CA) and calibrated against the internal diameter of the silicon stent to correct for magnification, perspective, or parallax effects. Percent wound closure {1 − [(wound area)/(original wound area)]} was measured photogrammetrically on days 0, 3, 7, 10, 14, 18, and 21.

Wound harvest. Wounds were harvested from killed animals at postoperative days 7, 14, and 21 (n = 4 per group at each time point). A full-thickness excision including 3 mm beyond the margin of the original wound edge (demarcated with India ink) was performed. Each wound was bisected, and one-half of the wound was frozen in optimal cutting temperature compound for cryosectioning. The other half was fixed in 100% methanol and embedded in paraffin. Sections were cut from the central region of the wound at a thickness of 5 μm. Before staining, paraffin sections were deparaffinized and rehydrated by successive passages through xylene and decreasing concentrations of ethanol.

Van Gieson stain for wound maturity. Wound maturity can be quantified with Van Gieson staining protocol, which simultaneously stains mature collagen deep red and stains immature collagen pink (32). Horizontal sections were cut from each specimen at each time point. Paraffin sections were processed with staining solution as described previously (33). Sections were imaged and digitized in their entirety at 200× resolution with an Aperio ScanScope GL scanning optical microscope (Aperio Technologies, Vista, CA). Images were then analyzed with Adobe Photoshop CS3 (Adobe Systems). Percentage mature collagen was quantified by measuring the total pixel area of the wound and the percentage of pixels therein that were consistent in color with mature collagen. Lateral wound margins were identified at the border of the panniculus carnosum layer.

CD31 staining for vascularity and proliferating cell nuclear antigen staining for cellular proliferation. Paraffin sections were incubated in either CD31 (an endothelial marker) or proliferating cell nuclear antigen (PCNA; a nuclear marker for proliferation) (both from Cell Signaling Technology, Danvers, MA) antibodies, washed, and stained with DAB (Vector Laboratories, Burlingame, CA). Slides were examined under 200× magnification and captured as digital images (Olympus BX51 microscope and DP12 camera). In CD31-labeled sections, patent vessels were tallied, and numeral density was reported as vessels per 200× field. Cross-sectional area of each vessel was obtained with Adobe Photoshop CS3 and reported as total cross-sectional area normalized to wound area as well as average cross-sectional area per vessel. In PCNA-labeled sections, nuclei exhibiting positive PCNA staining were tallied and reported as cells per 200× field.

Green fluoroscent protein and vWF costaining. To follow the adoptively transferred cell trafficking, BM-KSL cells from diabetic and controls were isolated from 8- to 10-week-old green fluorescent protein (GFP)-expressing C57BL6 mice (CLEA Japan) as described. The KSL cells were cultured in QQc medium for 1 week as described; 2×10^4 GFP-KSL cells were injected into 8- to 10-week-old euglycemic C57BL/6J male mice as described. Wounds were harvested from killed animals at postoperative days 7, 14, and 21 (n = 4 per group at each time point) as described. Tissue sections were fixed in 4% paraformaldehyde overnight at 4°C, processed through 100% ethanol and xylenes, and embedded in paraffin. To enhance GFP expression, samples were incubated with a 1:300 dilution of anti-GFP mouse polyclonal antibody (Invitrogen) for 1 h at room temperature, washed, and stained with DAB (DOTITE). For vWF staining, the sections were further treated with 1:300 dilution anti-vWF rabbit polyclonal antibody (DAKO) for 4°C overnight and washed and blocked in 5% normal sheep serum for 5 min followed by anti-rabbit IgG alkaline phosphatase-streptavidin

complex (NICHIREI). The double-stained images with vWF images were obtained with the same equipment as described. Dual-filter images were superimposed to illustrate GFP trafficking and wound vascular architecture.

Statistical analysis. All data are presented as the mean ± SD. A Kruskal-Wallis one-way ANOVA with Tukey-Kramer post hoc analysis was performed when comparisons involved more than two groups. Mann-Whitney test was used for pairwise comparisons. Significance was considered at $P < 0.05$. The number of animals in each group was determined with an a priori power analysis using a standard for adequacy of 80% to reject the null hypothesis of zero correlation using G*Power.

RESULTS

QQc restores growth and vasculogenic potential of diabetic EPCs. Because ex vivo expansion is an important step in adoptive cellular therapy, we measured the effects of QQc on KSL proliferation. After 7 days of QQc, the C_{QQc} population increased 338.2- ± 260.7-fold (Fig. 1*A*). Similarly, after 7 days of QQc, the DM_{QQc} population increased 329.0- ± 125.7-fold (Fig. 1*A*). There was no

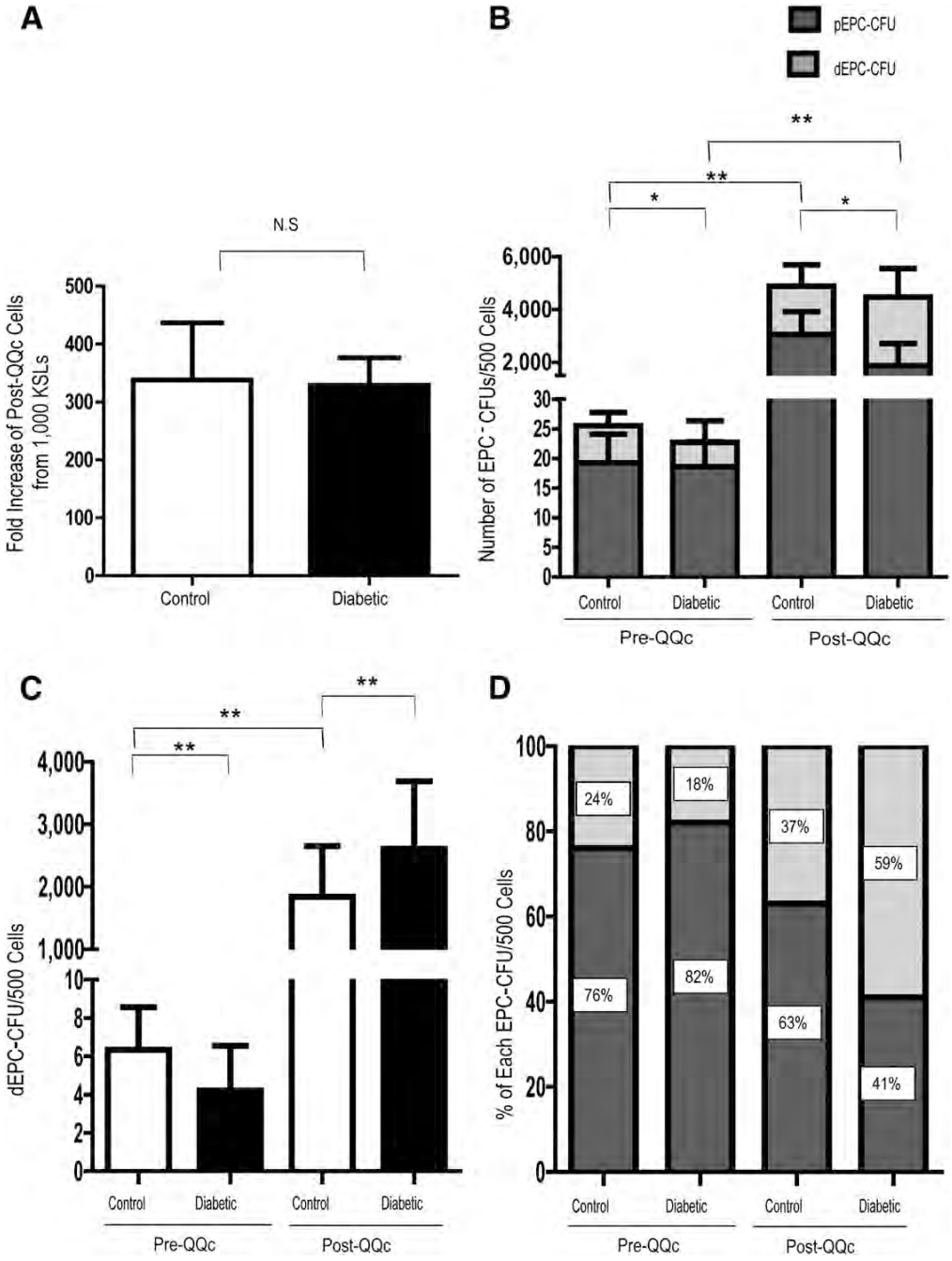

FIG. 1. QQc restores growth and vasculogenic potential of diabetic progenitor cells to more than the level of controls. *A*: Fold increase of control and diabetic post-QQc cells. *B*: The frequency of EPC-CFU production from pre-QQc and post-QQc control and diabetic KSL cells. *C*: The frequency of DEPC-CFU production from pre-QQc and post-QQc control and diabetic KSL cells. *D*: The percent of pEPC-CFUs and dEPC-CFUs from total EPC-CFUs. *$P < 0.05$; **$P < 0.01$. $n = 3$ dishes/group for 4 trials. NS, not significant.

significant difference ($P = 0.6$) in the QQc cellular expansion of diabetic and control KSL cells.

Because QQc restored ex vivo diabetic KSL expansion to control rates, we assessed the effects of QQc on the vasculogenic potential of diabetic KSL cells using EPC colony-forming assay. Before expansion, diabetic KSL cells had similar numbers of pCFUs (19.2 ± 4.9 vs. 18.6 ± 04.2; $P = 0.5$) but significantly fewer tCFUs (22.7 ± 5.2 vs. 25.0 ± 3.8; $P < 0.01$) and dEPC-CFUs (4.2 ± 2.3 vs. 6.3 ± 2.2; $P < 0.01$) compared with control KSL cells. After QQc, the number of diabetic tEPC-CFUs (4,469 ± 1,593; $P < 0.01$), pEPC-CFUs (1,862 ± 842; $P < 0.01$), and dEPC-CFUs (2,607 ± 1,084; $P < 0.01$) increased significantly from pre-QQc levels, as did the number of diabetic tEPC-CFUs (4,469 ± 1,593 vs. 4,884 ± 1,495; $P = 0.4$), and dEPC-CFUs (2,607 ± 1,084 vs. 1,839 ± 813; $P = 0.06$) were restored to control levels (Fig. 1*B*). Importantly, QQc increased the percentage of diabetic dEPC-CFUs (the EPC population that most readily forms new vessels) more than three-fold (17.8 ± 8.8 vs. 58.2 ± 12.7%; $P < 0.01$) (Fig. 1*C* and *D*).

QQc restores tubular formation of diabetic progenitor cells. Organization of endothelial cells in a three-dimensional network of tubes is the final step of angiogenesis. Because QQc increased the rate of diabetic KSL proliferation as well as differentially increased the proportion of diabetic dCFUs, we tested the effects of QQc on diabetic KSL tubule formation in vitro. Before QQc, on matrigel, diabetic KSL cells had significantly fewer tubules per HPF than controls (17.55 ± 7.4 vs. 28.53 ± 15.4; $P < 0.01$) (Fig. 2). Moreover, the tube formation with diabetic KSL cells demonstrated significantly less tubules per HPF compared with human umbilical vein endothelial cells with no cell group, suggesting that diabetic KSL may have a negative effect on augmenting angiogenesis (21.5 ± 6.5 vs. 17.55 ± 7.4; $P < 0.05$). Although the number of tubules per HPF with DM_{QQc} KSL cells was still significantly lower (33.3 ± 8. vs. 47.1 ± 15.3; $P < 0.05$) than C_{QQc} KSL cells tubules per HPF, diabetic KSL tube formation significantly increased (17.55 ± 7.4 vs. 33.3 ± 8.0; $P < 0.01$) after QQc, and it significantly increased compared with pre-QQc control KSL cells (33.3 ± 8.0 vs. 28.53 ± 15.4; $P < 0.05$)

QQc enhances expression of vasculogenic and wound healing factors. Because QQc increased the rate of diabetic KSL proliferation, differentially increased the proportion of diabetic dEPC-CFUs, and increased the tubule-forming potential of diabetic KSL cells, we tested the effects of

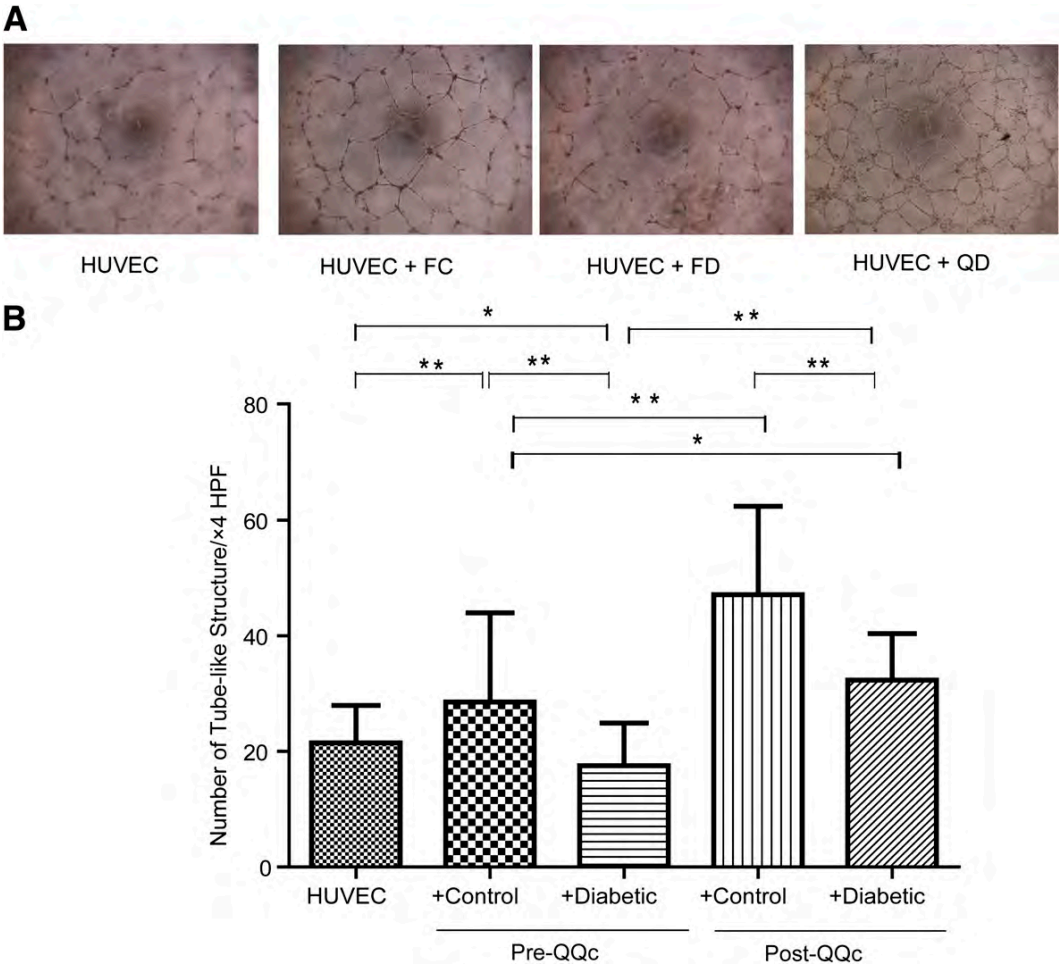

FIG. 2. QQc restores tubular formation of diabetic progenitor cells. *A*: Representative features of tube formation assay of human umbilical vein endothelial cells (HUVECs) by coculturing with presence or absence of pre-QQc and post-QQc control and diabetic cells (4× magnification). The ratio of HUVEC:KSL cells is 1×10^4:3×10^3 (10:3). *B*: Graph of the numbers of tubules formed in each group. $n = 10$ wells/group. *$P < 0.05$; **$P < 0.01$. FC, freshly isolated control cells; FD, freshly isolated diabetic cells.

QQc on diabetic KSL gene expression. After QQc, diabetic KSL cells increased their expression of wound healing–related growth factor genes endothelial growth factor, fibroblast growth factor-2, and fibroblast growth factor-7 and vasculogenesis-related genes vWF, CD29, and Flk-1 (Fig. 3). Although all key wound healing–related factors increased after QQc, endothelial growth factor production increased 3.5-fold in control KSL cells and 8.3-fold in diabetic KSL. Among the vasculogenesis-related genes, the expression of vWF increased by 8.3-fold and 6.7-fold in control and diabetic KSL, respectively, post-QQc. The expression of Flk-1 in C_{QQc} KSL remarkably increased (32.7-fold), and in DM_{QQc} KSL cells were increased 2.5-fold.

In addition to the upregulation of key wound healing and vasculogenic genes, KSLs also increase their expression of CD29/integrin β-1, an integrin unit associated with the angioblastic growth cone during vasculogenesis. After QQc, *CD29* expression in both C_{QQc} and DM_{QQc} KSL cells increased significantly (2.3-fold for control and 1.9-fold for diabetic; $P < 0.05$). Moreover, the expression of *CD29* in DM_{QQc} KSL cells was not significantly different from *CD29* expression in C_{QQc} KSL cells.

Post-QQc diabetic progenitor cell therapy accelerates wound closure. To reduce the number of confounding variables that might affect EPC function during wound closure, we tested pre-QQc and post-QQc diabetic and control KSL-adoptive cellular therapy in wounded euglycemic mice. Adoptive cellular therapy with pre-QQc diabetic KSL cells had little impact on wound healing compared with PBS treatment on day 7 (26.1 ± 3.0 vs. 30.7 ± 1.9%; $P < 0.05$), day 14 (61.5 ± 5.6 vs. 70.1 ± 3.5%; $P = 0.50$), day 18 (70.0 ± 13.6 vs. 87.4 ± 11.1%; $P = 0.6$), or day 21 (83.5 ± 5.0 vs. 89.7 ± 5.5%; $P = 0.05$) (Fig. 4*A* and *B*). In marked contrast, adoptive transfer of DM_{QQc} KSL cells accelerated the percent wound closure compared with pre-QQc diabetic treatment on day 14 (81.3 ± 8.7 vs. 61.5 ± 20.3%; $P < 0.05$), day 18 (70.0 ± 13.6 vs. 97.7 ± 4.0%; $P < 0.01$), or day 21 (83.5 ± 5.0 vs. 89.7 ± 5.5%; $P < 0.05$) (Fig. 4*A* and *B*). Moreover, the percent wound closure achieved with adoptive transfer of DM_{QQc} KSL cells was not significantly different than the percent wound closure achieved with adoptive transfer of C_{QQc} KSL on day 14 (81.3 ± 7.2 vs. 89.98 ± 7.7%; $P < 0.05$), but it was not significantly different on day 18 (97.7 ± 4.0 vs. 99.1 ± 1.5%; $P = 0.9$) or day 21 (94.4 ± 1.6 vs. 100 ± 0%; $P = 0.3$) (Fig. 4*A* and *B*).

Post-QQc adoptive diabetic progenitor therapy enhances wound vascularization and collagen maturation. To understand how QQc improved diabetic KSL-mediated wound closure, we measured wound vascularization and collagen maturation. Interestingly, wounds injected with QD KSL cells showed significantly higher CD31 counts compared with the freshly isolated diabetic KSL treatment group and PBS (13.8 ± 1.8 vs. 8.6 ± 0.9 vs. 7.2 ± 0.8; $P < 0.01$) starting at day 7. On day 21, the vascularity in the post-QQc diabetic KSL treatment groups significantly increased compared with freshly isolated control and diabetic KSL treatment groups, as well as compared with the PBS control group (25.5 ± 1.7 vs. 15.0 ± 1.8 vs. 18.0 ± 1.2 vs. 11.5 ± 1.0; $P < 0.05$). Interestingly, post-QQc KSL treatment groups showed a rapid increase in vascularity after injection, as compared with the relatively delayed response in the freshly isolated KSL treatment group (Fig. 5*A* and *B*).

On day 21, the percentage of mature collagen as assessed by Van Gieson staining in the wounds treated with post-QQc diabetic KSL cells (58 ± 11%) was greater compared with wounds treated with freshly isolated control (43 ± 14%) and diabetic KSL cells (38 ± 3%) and PBS (33 ± 7%; $P < 0.01$ and $P < 0.01$, respectively) (Fig. 6*A* and *B*).

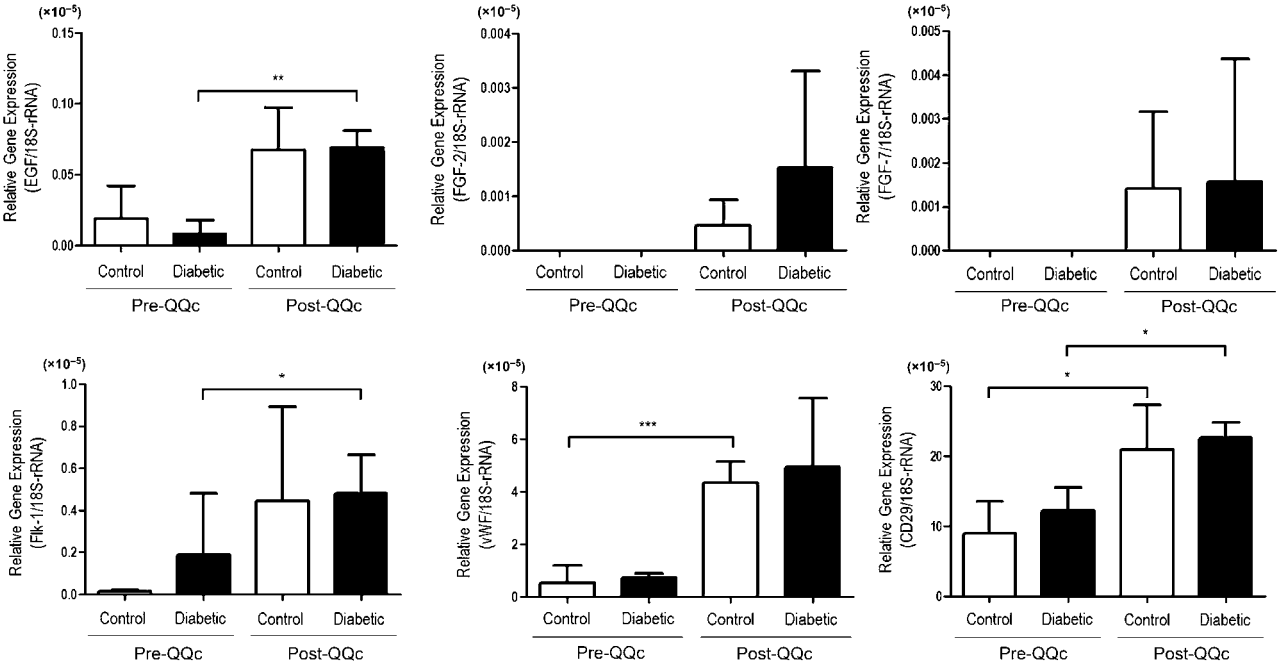

FIG. 3. QQc enhances expansion of vasculogenic and wound healing factors. The total RNA were prepared from pre-QQc and post-QQc cells from control and diabetic mice KSL cells. The gene expression levels of proangiogenic growth factors were estimated by real-time PCR, and the data were shown as the relative gene expression of the target genes vs. 18S rRNA. The target genes of quantitative PCR were EGF, FGF-2, FGF-7, vWF, CD29, and Flk-1. The data are shown as means ± SD. $n = 4$. *$P < 0.05$; **$P < 0.01$; ***$P < 0.001$. Flk-1, VEGFR-2 (KDR/Flk-1).

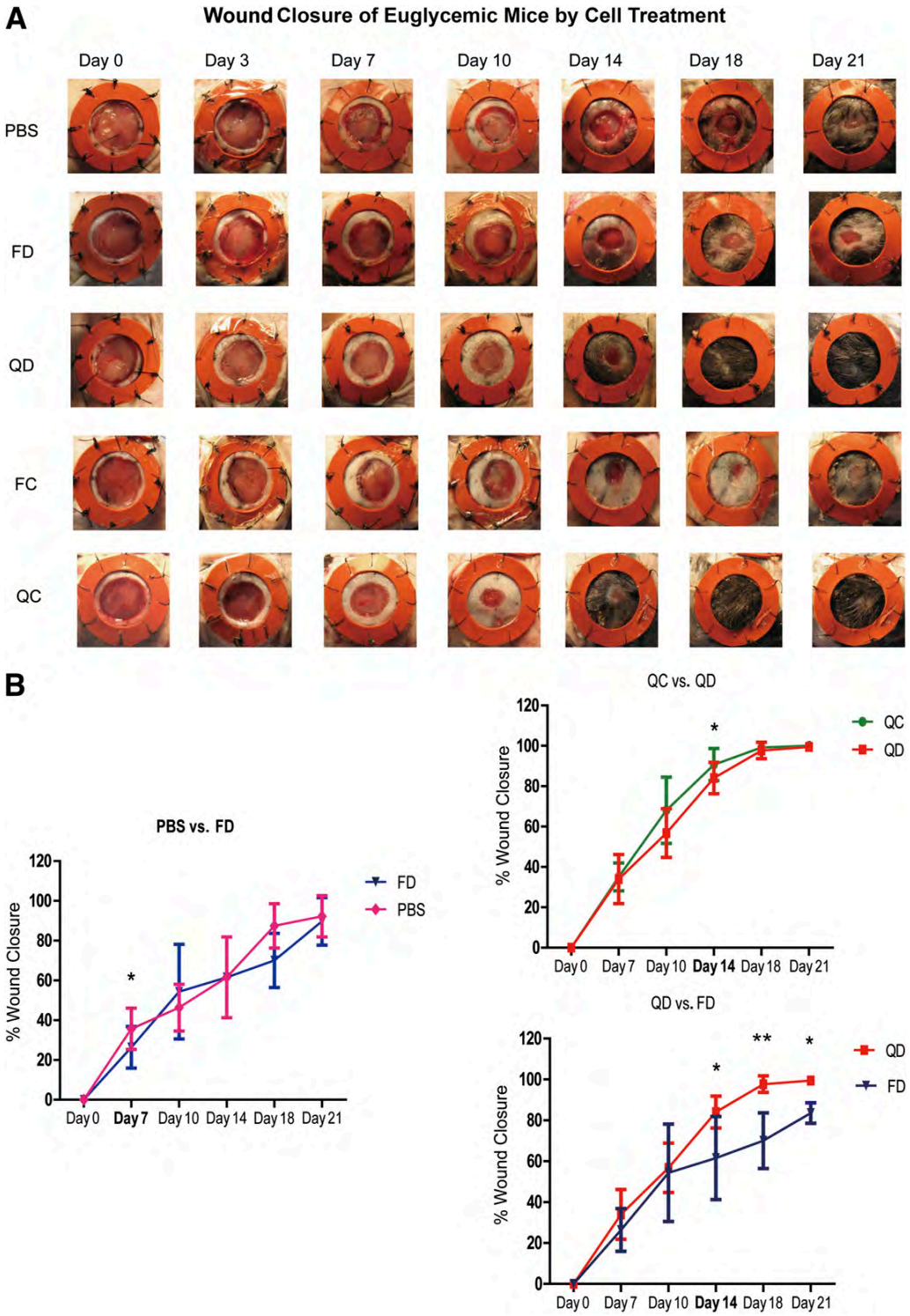

FIG. 4. Post-QQc adoptive diabetic progenitor cell therapy accelerates wound healing. *A*: Representative images show wound healing in euglycemic mice treated with PBS, pre-QQc, and post-QQc control and diabetic cells. Wounds were photographed at the times indicated from day 0 to day 21. *B*: The graphs show the comparison of percent wound closure between PBS and freshly isolated diabetic cell (FD)-treated group (*left*), post-QQc control cell (QC)-treated group, QD-treated group (*top right*), and QD-treated and FD-treated group (*bottom right*). *P < 0.05; **P < 0.01. FC, freshly isolated control cell.

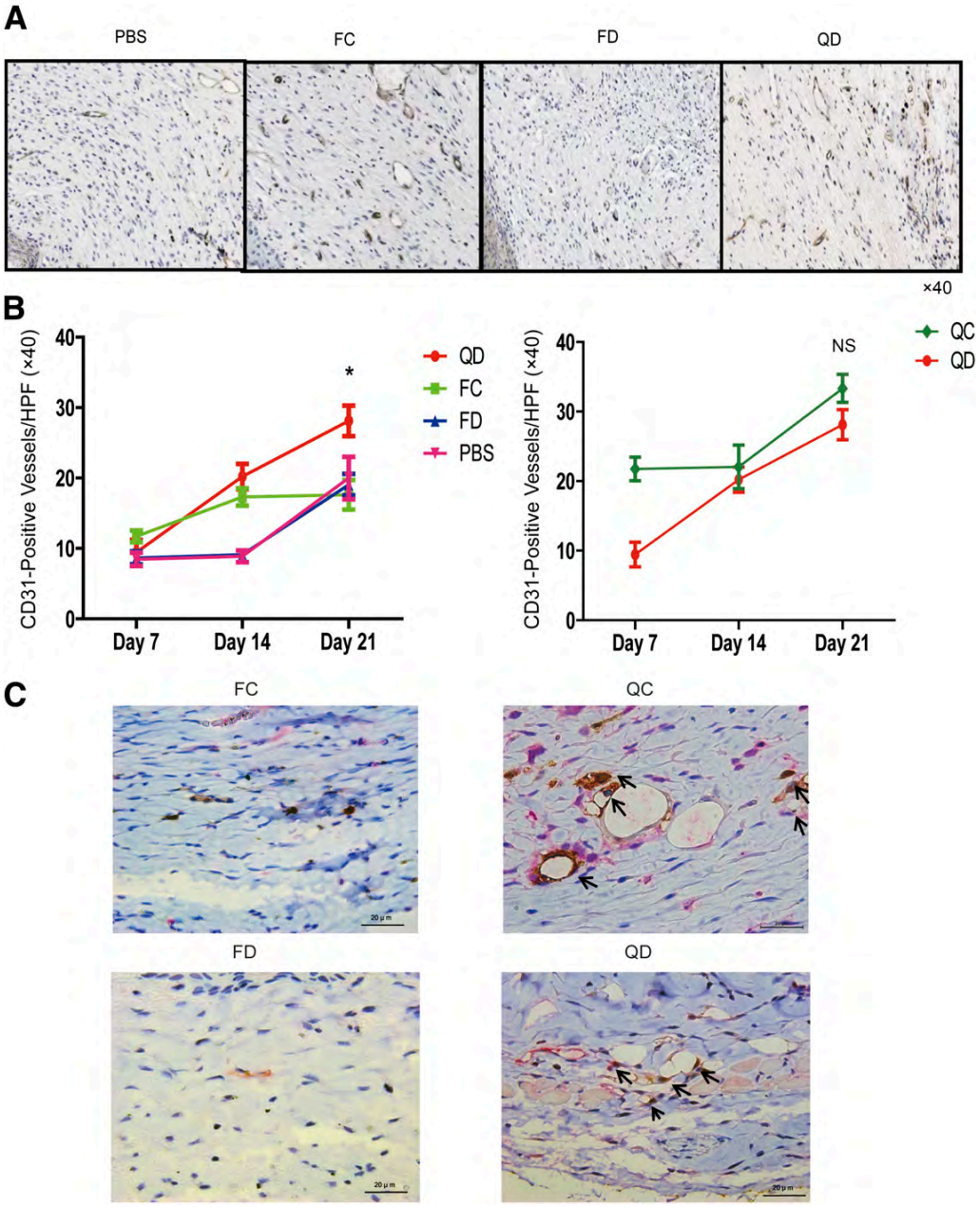

FIG. 5. Post-QQc diabetic progenitor cell therapy enhances wound vascularization. *A*: **Representative immunohistochemistry staining of CD31 to evaluate vascular density in the wounds of PBS-treated, freshly isolated control cell (FC)-treated, freshly isolated diabetic cell (FD)-treated, and QD-treated groups at day 21 (×40).** *B*: **The graphs show the CD31-positive vessels per HPF at days 7, 14, and 21.** ***Left graph*** **shows the comparison between QD-treated and FC-treated, FD-treated, and PBS-treated groups.** ***Right graph*** **shows the comparison between post-QQc control cell (QC)-treated and QD-treated groups.** $*P < 0.05$. *C*: **Representative immunohistochemistry double staining of GFP (brown) and vWF (red). The arrows point to the vessels with positive double staining. ×60 scale bar = 20 μm. The staining demonstrates that GFP/vWF double-stained vessels are only observed in the post-QQc control- and diabetic cell-treated wounds. GFP-positive cells observed more in the QC treated group. NS, not significant.**

Post-QQc diabetic progenitor cells have high potential for direct vasculogenesis. To identify whether the increased vascularity is attributable to differentiation of injected post-QQc KSL cells or is attributable to increased numbers of resident endothelial cells, we injected pre-QQc and post-QQc GFP control and diabetic KSL cells in the wound and identified the GFP and vWF costaining cells. As a result, GFP-positive cells costained with vWF were only identified in the post-QQc control and the diabetic cell-treated groups at day 21. Comparing post-QQc control and diabetic cell-treated groups, the post-QQc control cell-treated group showed higher numbers of GFP cells incorporated into the vasculature, suggesting higher vasculogenesis of post-QQc control KSL cells (Fig. 5C).

Post-QQc diabetic progenitor cell therapy increases cellular proliferation in the wound. To study the effects

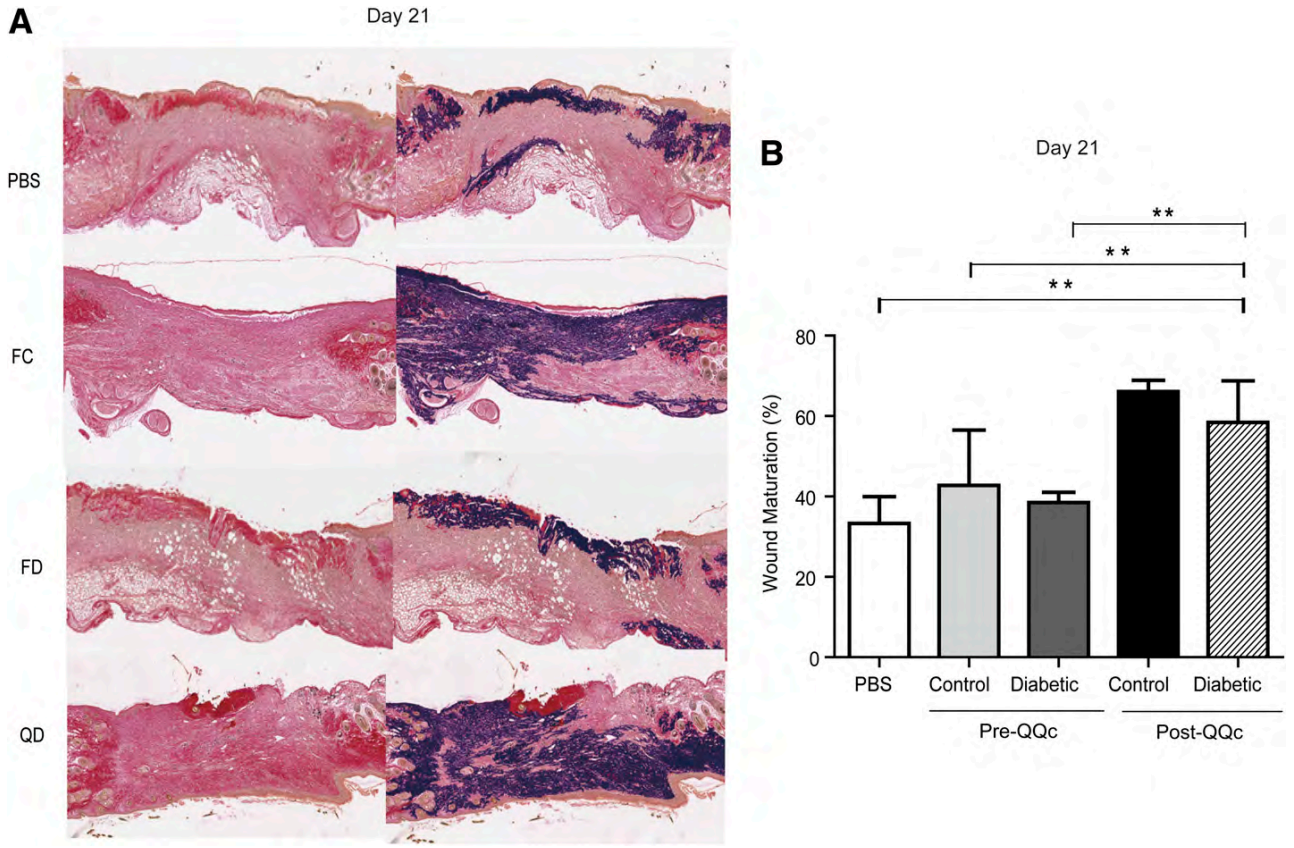

FIG. 6. Post-QQc diabetic progenitor cell therapy enhances the percentage of mature collagen in the wound. *A*: Representative Van Gieson staining demonstrating mature collagen staining in PBS-treated, freshly isolated control cell (FC)-treated, freshly isolated diabetic cell (FD)-treated, and QD-treated groups on day 21 (×10). *B*: The graph shows the percentage of mature collagen in wounds treated with PBS, FC, FD, and QD cells on day 21. **$P < 0.01$.

of QQc-expanded diabetic KSL cells on native cells in the wound, we measure fibroblastic proliferation in situ. After adoptive QD KSL treatment, wound fibroblastic proliferation peaked early and declined significantly from day 7 to day 21 in the groups treated with freshly isolated control KSL cells (795 ± 221 vs. 247 ± 86 cells/field; $P = 0.044$) and post-QD KSL cells (761 ± 171 vs. 238 ± 141 cells/field; $P = 0.011$). Contrarily, there was no increase in cellular proliferation in wounds treated with freshly isolated diabetic KSL cells (664 ± 321 vs. 534 ± 116 cells/field; $P = 0.41$) or PBS (621 ± 122 vs. 672 ± 278 cells/field; $P = 0.31$) (Fig. 7).

Function of post-QQc diabetic progenitor cells is deteriorated in glycemic diabetic wounds. The in vivo efficacy of post-QQc diabetic KSL cells also was tested in STZ-induced glycemic murine diabetic wounds. As a result, post-QQc KSL cells indicated significant percent wound closure compared with pre-QQc KSL cells and PBS on day 14 (73.60 ± 3.69 vs. 55.02 ± 3.61 vs. 58.98 ± 5.86%; $P < 0.05$) and day 21 (96.34 ± 1.52 vs. 82.29 ± 4.72 vs. 84.01 ±2.28%; $P < 0.05$) (Fig. 8). However, there was no significant difference between the wound closures between pre-C_{QQc} KSL, pre-DM_{QQc} and post-DM_{QQc} KSL, and PBS at all times. Although post-DM_{QQc} KSL can accelerate wound healing and possess the restored vasculogenic potential in euglycemic in vivo conditions, these data suggest functional limitation of post-DM_{QQc} KSL function in glycemic diabetic condition.

DISCUSSION

Current diabetic wound treatment hinges on patient education, prevention, and early diagnosis. Once a wound has developed, however, invasive therapies are costly and noninvasive therapies are less effective. Ultimately, because current treatments do not correct the underlying pathophysiology, many patients experience untoward complications and require amputations. Although investigators have long focused on the detrimental effects of elevated blood glucose on diabetic wound healing, recent data suggest that diabetic impairment of EPC function has a secondary effect on diabetic wound healing (5,34). This latter point is highlighted in the results of our recent clinical trial (24). By injecting autologous granulocyte colony-stimulating factor–mobilized peripheral blood EPCs into the nonhealing wounds of diabetic patients, we found that successful wound healing correlated with the vasculogenic function of transplanted EPCs. Moreover, we discovered that autologous EPC therapy has two inherent limitations: low EPC cell number and low vasculogenic function.

In an effort to overcome the limitations of autologous EPC therapy in diabetic patients, we studied the effect of QQc diabetic EPC ex vivo expansion on wound healing. In our study, mouse BM KSL cells were used as an EPC-enriched population based on a recent study reported by

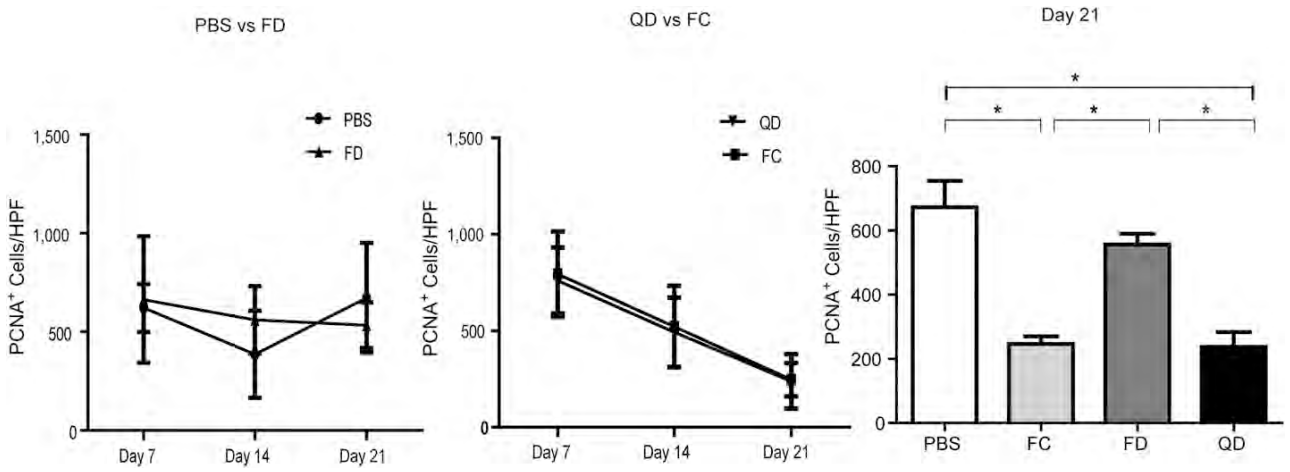

FIG. 7. Post-QQc diabetic progenitor cell therapy increases cellular proliferation in the wound. The *left* and *middle graphs* show the number of PCNA-positive cells in the wound per HPF on day 7, day 14, and day 21 in the following treated groups: PBS vs. freshly isolated diabetic cells (FD; *left*), QD vs. FC (*middle*). The *right bar graph* shows the number of PCNA-positive cells in the wound per HPF on day 21. *$P < 0.05$.

Kwon et al. (6) QQc is a serum-free culture system recently developed and reported by our group (27). QQc is a functional culture system that not only increases the number of EPCs but also increases the population of differentiated colony-forming EPCs (i.e., vasculogenic EPCs). Our in vitro experiments demonstrate that QQc significantly increases diabetic EPC cell number, definitive colony formation, and tubulization. Because QQc not only increased the number of diabetic EPCs but also restored their function to the level of control EPCs, we tested the effects of QQc diabetic EPCs ex vivo–expanded cells on wound closure. We used a stented wound closure model to minimize the effects of wound contracture (35). To focus our investigation on the function and efficacy of post-QQc diabetic EPCs compared with fresh healthy allogeneic EPCs, we selected a euglycemic wound closure mice model. We hypothesized that the use of a euglycemic recipient would eliminate the effect of confounding variables present in a diabetic recipient model.

Because new blood vessel formation is crucial for successful wound healing, we hypothesize that DM_{QQc} therapy leads to accelerated wound closure by enhancing vasculogenesis (36). CD31 staining demonstrated that post-QQc diabetic EPC treatment increased wound vascularity compared with freshly isolated diabetic EPC treatment and control groups at all time points. Moreover, as demonstrated previously by Masuda et al. (27,29), because QQc increases the number of dEPC-CFUs (i.e., vasculogenic EPCs) and dEPCs more readily form new vessels (compared with pEPCs), we hypothesize that they are the vitally important EPC fraction mediating the therapeutic vasculogenesis observed in our in vivo experiments. Collectively, our findings suggest a potential mechanism by which DM_{QQc} EPCs accelerate wound closure; transplanted post-QQc EPCs accelerate wound closure by forming tubules and inosculating with existing vasculature. This idea is further supported by the finding that GFP-labeled KSL cells incorporated into the native vascular network.

Enhanced new blood vessel formation may accelerate wound closure in a number of different ways. We found that DM_{QQc} therapy significantly enhanced the percentage of mature collagen in the wound. Interestingly, post-QQc diabetic EPCs exhibit significantly higher CD29mRNA expression compared with fresh diabetic EPCs. Recently, it was reported that CD29 directly influences growth factor signaling and promotes fibroblast migration (37). Together with the PCNA data, we hypothesize that DM_{QQc} stimulates fibroblast migration to the wound and accelerates wound closure.

To confirm the efficacy of QQc therapy in diabetic mice, we injected pre-QQc and post-QQc control and diabetic KSL cells to a full-thickness wound in STZ-induced glycemic diabetic mice. The results indicated that accelerated wound healing was seen only in post-QQc control KSL cell–treated group. The pre-diabetic and post-diabetic QQc KSL cells group, pre-QQc control KSL cells group, and the PBS-treated group demonstrated the same percent wound closure at all times from day 3 to day 21. In other words, the healing of post-QQc diabetic KSL cells in eugylcemic wounds was not seen in a diabetic condition. We assume from this result that hyperglycemic conditions of diabetic mice may have deteriorated the function of post-QQc diabetic KSL cells. Because post-QQc diabetic KSL cells have a highly therapeutic effect in euglycemic conditions, we believe that QQc therapy may be effective in euglycemic diabetic patients, i.e., patients with controlled blood glucose levels (blood glucose <8 mmol/L or <140 mg/dL) according to the practical guidelines on the management and prevention of diabetic foot (38). Our data are similar, and we daily treat diabetic patients with chronic wounds and high blood glucose. Many previous reports have shown that one of the standards of care for diabetic wounds involves systemic glucose control, and effective wound healing cannot be expected for uncontrolled diabetes even with highly effective therapy. Our results for EPC therapy for uncontrolled diabetic mice show that the condition of the host has a great impact on deterioration of the cells being administered, and we believe that "metabolic memory" and epigenetic modification by hyperglycemia are possibilities for why this is. In euglycemic diabetic patients the efficacy of EPC therapy for wound healing is limited because of autologous EPC vasculogenic dysfunction, as shown in our previous report (24). We believe that present EPC therapy with application of autologous dysfunctional EPC may not be effective even for diabetic patients with controlled glucose. The application of QQc in these patients may be the key for highly therapeutic autologous

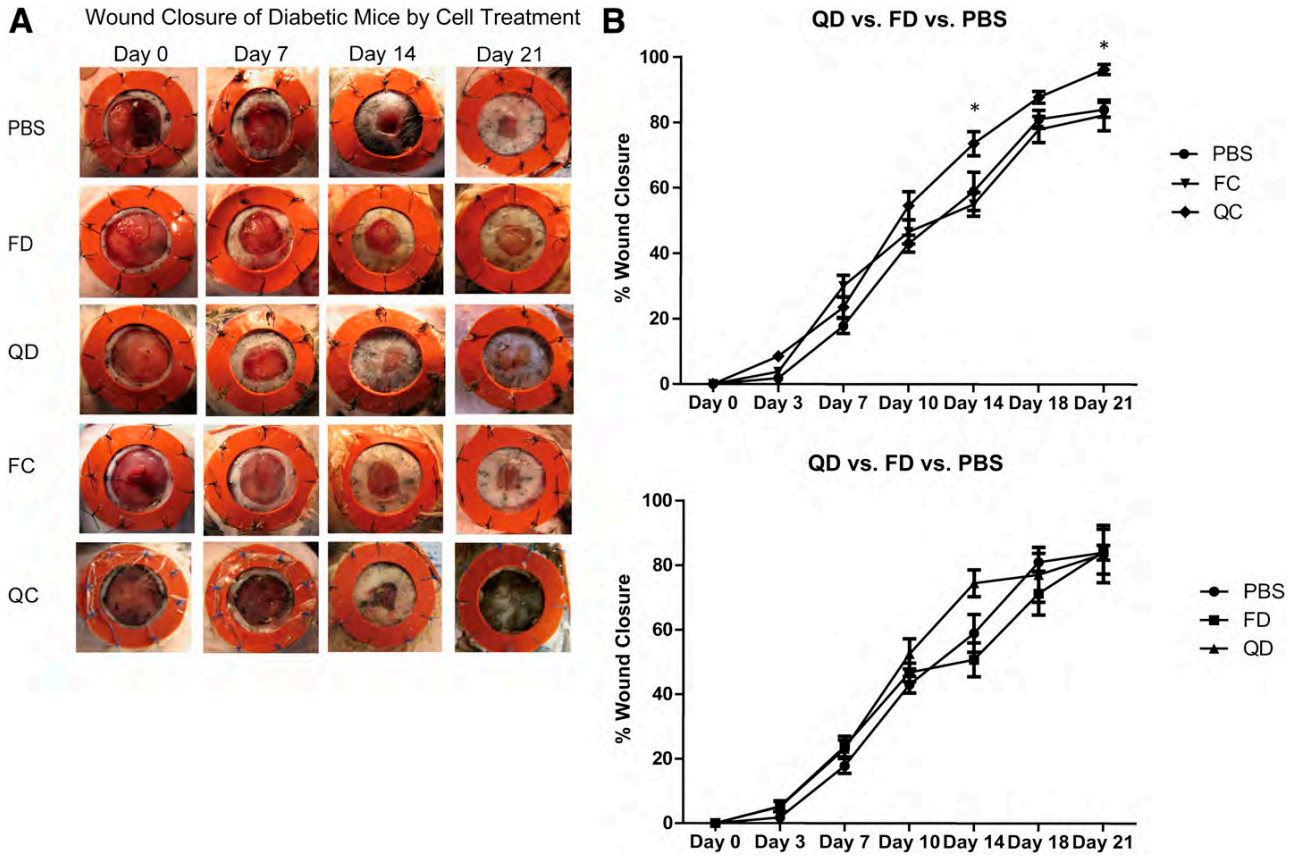

FIG. 8. Efficacy of post-QQc diabetic progenitor cell therapy is deteriorated by diabetic condition. *A*: Representative images show wound healing in STZ-induced diabetic mice treated with PBS, before and after control, and treated with diabetic QQc cells. Wounds were photographed at the times indicated, from day 0 to day 21. *B*: The graph shows the comparison of percent wound closure between post-QQc control cell (QC)-treated vs. freshly isolated control cell (FC)-treated vs. PBS-treated groups. QC indicated significant percent wound closure compared with FC and PBS on day 14 (QC: 73.60 ± 3.69 vs. FC: 55.02 ± 3.61 vs. PBS: 58.98 ± 5.86%; $P < 0.05$) and day 21 (QC: 96.34 ± 1.52 vs. FC: 82.29 ± 4.72 vs. PBS: 84.01 ± 2.28%; $P < 0.05$). The wound closure between FC and PBS was similar without any significance. *C*: The graph shows the comparison of percent wound closure between QD-treated vs. freshly isolated diabetic cell (FD)-treated vs. PBS-treated groups. There was no significant difference between the three compared groups at all time points. *$P < 0.05$.

diabetic EPC therapy. To test our hypothesis, we have tried to establish a stented wound healing model of insulin-treated STZ diabetic mice with controlled glucose levels and treated these mice with diabetic pre-QQc and post-QQc KSL cells. Unfortunately, the model was difficult to establish because of the many interventions on the mice. Therefore, this hypothesis remains to be proven.

Another limitation of our study includes not knowing the exact mechanism of how QQc restores the vasculogenic dysfunction of diabetic EPCs. We recently have looked into the effect of QQc on oxidative stress of control and diabetic BM KSL cells and found that QQc relieves oxidative stress on both control and diabetic BM KSL cells (data not shown). However, this was not the specific mechanism for restoring diabetic BM KSL dysfunction. We plan to investigate further in a future study.

In summary, we have demonstrated that QQc not only restores diabetic EPC function but also achieves supraphysiologic EPC vasculogenic function in vitro and in vivo. Because QQc is serum-free and rapidly expands the number of diabetic EPCs, this system may facilitate cell-based therapies for diabetic patients. Although this study has limitations regarding future clinical applications for diabetic patients, this study can be considered the first step in establishing an ideal cell-based therapy for diabetic patients. Moreover, the rapidly expanded post-QQc EPC population could be aliquoted, cryopreserved, and used again for metachronous wounds or other ischemic conditions (e.g., myocardial ischemia).

Conclusions. Here, we demonstrate that a novel serum-free QQc system expands the number of cells and enhances the vasculogenic and therapeutic potential of diabetic EPCs. We hypothesize that adoptive post-QQc diabetic EPC therapy may be an effective cell-based therapy for nonhealing diabetic wounds.

ACKNOWLEDGMENTS

This work was supported by a Health and Labor Sciences research grant from the Japanese Ministry of Health, Labor, and Welfare (20890227, 22791737), a funding program for Next Generation World Leading Researchers LS113, a Tokai University research aid grant, and Plastic Surgery Research Award 2007 (awarded to R.T.).

No potential conflicts of interest relevant to this article were reported.

R.T. conceived and designed the study, obtained financial support, wrote the manuscript, provided the study

material, collected data, analyzed data, and interpreted data. M.V. collected data, analyzed data, interpreted data, and wrote the manuscript. H.M. conceived and designed the study and wrote the manuscript. R.I. collected and assembled data, analyzed data, and interpreted data. M.K. collected data, assembled data, analyzed data, and interpreted data. M.M. provided administrative support. H.M. wrote the manuscript. S.M.W. obtained financial support, provided administrative support, wrote the manuscript, and approved the final manuscript. T.A. obtained financial support, provided administrative support, wrote the manuscript, and approved the final manuscript. T.A. is the guarantor of this work and, as such, had full access to all of the data in the study and takes responsibility for the integrity of the data and the accuracy of the data analysis.

The authors acknowledge the contributions of Christopher C. Chang, Dan Bassiri, Clarence Lin, Oren M. Tepper, and Anthony L. Rios (all from Institute of Reconstructive Plastic Surgery Laboratories, Department of Plastic Surgery, New York University Medical Center, New York, New York), Mika Wada (from Tokai University School of Medicine, Department of Regenerative Medicine), and Satoshi Fujimura, Kayo Okada, and Kayoko Arita (from Juntendo University School of Medicine, Department of Plastic and Reconstructive Surgery) for their kind technical assistance. The authors also thank Dr. Yoshinori Okada, Dr. Hiroshi Kamiguchi, and Yoko Kameyama (from Tokai University School of Medicine) for their outstanding technical support regarding flow cytometry, real-time PCR, and immunohistochemistry.

REFERENCES

1. Drake CJ. Embryonic and adult vasculogenesis. Birth Defects Res C Embryo Today 2003;69:73–82
2. Asahara T, Murohara T, Sullivan A, et al. Isolation of putative progenitor endothelial cells for angiogenesis. Science 1997;275:964–967
3. Shi Q, Rafii S, Wu MH, et al. Evidence for circulating bone marrow-derived endothelial cells. Blood 1998;92:362–367
4. Hristov M, Erl W, Weber PC. Endothelial progenitor cells: isolation and characterization. Trends Cardiovasc Med 2003;13:201–206
5. Tanaka R, Wada M, Kwon SM, et al. The effects of flap ischemia on normal and diabetic progenitor cell function. Plast Reconstr Surg 2008;121:1929–1942
6. Kwon SM, Lee YK, Yokoyama A, et al. Differential activity of bone marrow hematopoietic stem cell subpopulations for EPC development and ischemic neovascularization. J Mol Cell Cardiol 2011;51:308–317
7. Asahara T, Masuda H, Takahashi T, et al. Bone marrow origin of endothelial progenitor cells responsible for postnatal vasculogenesis in physiological and pathological neovascularization. Circ Res 1999;85:221–228
8. Tepper OM, Capla JM, Galiano RD, et al. Adult vasculogenesis occurs through in situ recruitment, proliferation, and tubulization of circulating bone marrow-derived cells. Blood 2005;105:1068–1077
9. Ii M, Nishimura H, Iwakura A, et al. Endothelial progenitor cells are rapidly recruited to myocardium and mediate protective effect of ischemic preconditioning via "imported" nitric oxide synthase activity. Circulation 2005;111:1114–1120
10. Ceradini DJ, Kulkarni AR, Callaghan MJ, et al. Progenitor cell trafficking is regulated by hypoxic gradients through HIF-1 induction of SDF-1. Nat Med 2004;10:858–864
11. Murayama T, Tepper OM, Silver M, et al. Determination of bone marrow-derived endothelial progenitor cell significance in angiogenic growth factor-induced neovascularization in vivo. Exp Hematol 2002;30:967–972
12. Tepper OM, Carr J, Allen RJ Jr, et al. Decreased circulating progenitor cell number and failed mechanisms of stromal cell-derived factor-1alpha mediated bone marrow mobilization impair diabetic tissue repair. Diabetes 2010;59:1974–1983
13. Schatteman GC, Hanlon HD, Jiao C, Dodds SG, Christy BA. Blood-derived angioblasts accelerate blood-flow restoration in diabetic mice. J Clin Invest 2000;106:571–578
14. Loomans CJ, de Koning EJ, Staal FJ, et al. Endothelial progenitor cell dysfunction: a novel concept in the pathogenesis of vascular complications of type 1 diabetes. Diabetes 2004;53:195–199
15. Li Calzi S, Neu MB, Shaw LC, Grant MB. Endothelial progenitor dysfunction in the pathogenesis of diabetic retinopathy: treatment concept to correct diabetes-associated deficits. EPMA J 2010;1:88-100
16. Albiero M, Menegazzo L, Boscaro E, Agostini C, Avogaro A, Fadini GP. Defective recruitment, survival and proliferation of bone marrow-derived progenitor cells at sites of delayed diabetic wound healing in mice. Diabetologia 2011;54:945–953
17. Fadini GP, Sartore S, Albiero M, et al. Number and function of endothelial progenitor cells as a marker of severity for diabetic vasculopathy. Arterioscler Thromb Vasc Biol 2006;26:2140–2146
18. Neukomm LJ, Frei AP, Cabello J, et al. Loss of the RhoGAP SRGP-1 promotes the clearance of dead and injured cells in Caenorhabditis elegans. Nat Cell Biol 2011;13:79–86
19. Kawamoto A, Gwon HC, Iwaguro H, et al. Therapeutic potential of ex vivo expanded endothelial progenitor cells for myocardial ischemia. Circulation 2001;103:634–637
20. Kocher AA, Schuster MD, Szabolcs MJ, et al. Neovascularization of ischemic myocardium by human bone-marrow-derived angioblasts prevents cardiomyocyte apoptosis, reduces remodeling and improves cardiac function. Nat Med 2001;7:430–436
21. Taguchi A, Soma T, Tanaka H, et al. Administration of CD34+ cells after stroke enhances neurogenesis via angiogenesis in a mouse model. J Clin Invest 2004;114:330–338
22. Lin CD, Allori AC, Macklin JE, et al. Topical lineage-negative progenitor-cell therapy for diabetic wounds. Plast Reconstr Surg 2008;122:1341–1351
23. Sivan-Loukianova E, Awad OA, Stepanovic V, Bickenbach J, Schatteman GC. CD34+ blood cells accelerate vascularization and healing of diabetic mouse skin wounds. J Vasc Res 2003;40:368–377
24. Tanaka R, Masuda H, Kato S, et al. Autologous G-CSF mobilized peripheral blood CD34(+) cell therapy for diabetic patients with chronic non-healing ulcer. Cell Transplant. 25 October 2012 [Epub ahead of print]
25. Jarajapu YP, Grant MB. The promise of cell-based therapies for diabetic complications: challenges and solutions. Circ Res 2010;106:854–869
26. Tan Q, Qiu L, Li G, et al. Transplantation of healthy but not diabetic outgrowth endothelial cells could rescue ischemic myocardium in diabetic rabbits. Scand J Clin Lab Invest 2010;70:313–321
27. Masuda H, Iwasaki H, Kawamoto A, et al. Development of serum-free quality and quantity control culture of colony-forming endothelial progenitor cell for vasculogenesis. Stem Cells Transl Med 2012;1:160–171
28. Westermann D, Rutschow S, Van Linthout S, et al. Inhibition of p38 mitogen-activated protein kinase attenuates left ventricular dysfunction by mediating pro-inflammatory cardiac cytokine levels in a mouse model of diabetes mellitus. Diabetologia 2006;49:2507–2513
29. Masuda H, Alev C, Akimaru H, et al. Methodological development of a clonogenic assay to determine endothelial progenitor cell potential. Circ Res 2011;109:20–37
30. Tanaka R, Wada M, Kwon S, et al. The effects of flap ischemia on normal and diabetic progenitor cell function. Plast Reconstr Surg 2008;121:1929–1942
31. Park S, Tepper OM, Galiano RD, et al. Selective recruitment of endothelial progenitor cells to ischemic tissues with increased neovascularization. Plast Reconstr Surg 2004;113:284–293
32. Pugazhenthi K, Kapoor M, Clarkson AN, Hall I, Appleton I. Melatonin accelerates the process of wound repair in full-thickness incisional wounds. J Pineal Res 2008;44:387–396
33. Carson FL. *Histotechnology: A Self-Instructional Text*. Chicago, ASCP Press, 1997
34. Fadini GP, Avogaro A. Potential manipulation of endothelial progenitor cells in diabetes and its complications. Diabetes Obes Metab 2010;12:570–583
35. Michaels J, Churgin SS, Blechman KM, Greives MR, Aarabi S, Galiano RD, Gurtner GC. db/db mice exhibit severe wound-healing impairments compared with other murine diabetic strains in a silicone-splinted excisional wound model. Wound Repair Regen 2007;15:665–670
36. Glotzbach JP, Levi B, Wong VW, Longaker MT, Gurtner GC. The basic science of vascular biology: implications for the practicing surgeon. Plast Reconstr Surg 2010;126:1528–1538
37. King SJ, Worth DC, Scales TM, Monypenny J, Jones GE, Parsons M. β1 integrins regulate fibroblast chemotaxis through control of N-WASP stability. EMBO J 2011;30:1705–1718
38. Bakker K, Apelqvist J, Schaper NC; International Working Group on Diabetic Foot Editorial Board. Practical guidelines on the management and prevention of the diabetic foot 2011. Diabetes Metab Res Rev 2012;28 (Suppl. 1):225–231

Tsukada et al. Stem Cell Research & Therapy 2013, 4:20
http://stemcellres.com/content/4/1/20

stem cell research&therapy

RESEARCH Open Access

Identification of mouse colony-forming endothelial progenitor cells for postnatal neovascularization: a novel insight highlighted by new mouse colony-forming assay

Shizu Tsukada[1†], Sang-Mo Kwon[2†], Takenori Matsuda[3], Seok-Yun Jung[2], Jun-Hee Lee[2], Sang-Hun Lee[2], Haruchika Masuda[1] and Takayuki Asahara[1,3*]

Abstract

Introduction: Endothelial progenitor cells (EPCs) play a critical role in restoration of ischemic diseases. However, the actual status of EPC development and the mechanisms of EPC dysfunctions in patients with various ischemic diseases remain unknown.

Methods: To investigate the detailed function of EPCs in experimental murine models, we have established an EPC colony forming assay (EPC-CFA) in murine EPCs. The abilities of murine EPCs in differentiation, adhesive capacity, proliferative potency, and transplantation *in vitro* and *in vivo* were then examined.

Results: Peripheral blood mononuclear cells (PB-MNCs), bone marrow mononuclear cells (BM-MNCs) or bone marrow c-Kit$^+$/Sca-1$^+$ lineage negative (BM-KSL) cells differentiated into two types of EPC colony forming units (EPC-CFUs), large sized EPC (large-EPC)-CFUs and small sized EPC (small-EPC)-CFUs. Gene expression analysis demonstrated that both EPC-CFU-derived cells expressed eNOS, Flk-1 and VE-cadherin, markers of endothelial cells (ECs), although the small-EPCs derived from small-EPC-CFU were higher in number and showed more immature features (higher population of KSL cells). Functionally, the large-EPCs derived from large-EPC-CFU had higher adhesive capacity but lower proliferative potency than small-EPCs, showing improved tubular forming capacity and incorporation potency into primary EC-derived tube formation. Importantly, hindlimb ischemia increased the frequencies of large-EPC-CFUs differentiated from PB-MNCs and bone marrow. Actually, transplantation of large-EPCs into ischemic hindlimb enhanced neovascularization in hindlimb ischemia model, although small-EPCs or murine ECs did not, suggesting that large-EPC-CFUs might play an important role in restoration of ischemic diseases.

Conclusions: We demonstrated, using a murine ischemia model, that the EPC-CFA could be a useful way to investigate the differentiation levels of murine EPCs, further providing a crucial clue that large-EPC-CFU status may be more functional or effective EPCs to promote neovascularization.

Introduction

Endothelial progenitor cells (EPCs) [1-3] play an important role in the restoration of ischemic vascular diseases [2-5]. Recently, several independent groups have shown that transplantation of EPCs into ischemic hindlimb or myocardial tissue improves organ function following the growth of new vessels [6-11]. In clinical aspects, the frequency of circulating EPCs may also serve as a biomarker for vascular function, and the number of circulating EPCs has been reported to be reduced in patients with diabetes mellitus or risk factors for coronary artery disease and to negatively correlate with the Framingham cardiovascular risk score [12-15]. However, the actual mechanical status of EPC development and the 'evaluation system' for EPC

* Correspondence: asa777@is.icc.u-tokai.ac.jp
† Contributed equally
[1]Department Regenerative Medicine, Tokai University of Medicine, Kanagawa, 259-1193, Japan
Full list of author information is available at the end of the article

dysfunctions in patients with various ischemic diseases remain to be disclosed.

Because EPCs accumulate in ischemic injured tissues and repair injured tissue following cluster formation [1,2,9], not only the number of EPCs identified by uptake of acetylated-low density lipoprotein (acLDL) and lectin reactivity but also the colony-forming potential of EPCs is important for angiogenic therapy. Thus, the assay system in which colony-forming potential of EPCs can be assessed is important. EPCs should encompass a group of cells existing in a variety of stages, ranging from hemangioblastic hematopoietic stem cells to fully differentiated endothelial cells (ECs), and EPCs can be classified into stages according to differentiation levels in each circulating EPC and tissue EPC [16]. Recently, the methods to culture colony-forming unit-endothelial cells (CFU-ECs) [14] or to culture endothelial colony-forming cells (ECFCs) were established on mononuclear cells from peripheral blood or cord blood [17-20]. However, it was reported that CFU-ECs were not EPCs but were myeloid cells that differentiate into phagocytic macrophages and that T cells could mimic the morphology of CFU-ECs [19,21]. Besides, the culture of ECFCs enables us to evaluate the EPC colony-forming potential change as EPCs differentiated during culture *in vitro*. In these assay systems, each EPC at different differentiation levels could not be discriminated at the same time, and the differentiation capacities of immature stem cells could not be tested. In our laboratory, EPC-CFA, a novel method to assess the colony-forming potential of EPCs at different differentiation levels, was recently established and enables us to investigate the commitment of each cell [22-24].

In the present study, we aimed to methodologically establish the murine EPC-CFA on PB-MNCs, BM-MNCs, or BM-KSL cells by analyzing the functions of each EPC-CFU at different differentiation levels and to clarify the roles of each EPC-CFU at different differentiation levels *in vivo* by using hindlimb ischemic mice. By EPC-CFA, we investigated the status of EPC differentiation in response to ischemic signals and the effects of two types of EPC-CFUs - small-EPC-CFUs or large-EPC-CFUs - in a hindlimb ischemia model on *in vivo* neovascularization.

Materials and methods

Animals

Experiments were performed on male 8- to 10-week-old C57BL/6J mice and BALB/CA-nu/nu mice (Japan Clea, Tokyo, Japan) maintained under a 12-hour light/dark cycle and in accordance with the regulations of Tokai University. Standard laboratory chow and water were available *ad libitum*. The protocols were approved by guidelines of the Institutional Animal Care and Use Committee of the Isehara Campus, Tokai University School of Medicine, based on the Guide for the Care and Use of Laboratory Animals (National Research Council) (Institutional Review Board ID number 083005).

Preparation

Peripheral blood was obtained from the heart immediately before sacrifice and was separated by Histopaque-1083 (Sigma-Aldrich, St. Louis, MO, USA) density gradient centrifugation, as previously described [25]. Briefly, low-density mononuclear cells were harvested and washed twice with Dulbecco's phosphate-buffered saline (PBS) supplemented with 2 mmol/L ethylenediaminetetraacetic acid (EDTA). Contaminated red blood cells were hemolyzed by using ammonium chloride solution. BM-MNCs were obtained by flushing the femurs and tibias and reacted with a mixture of biotinylated monoclonal antibodies against B220 (RA3-6B2), CD3 (145-2C11), CD11b (M1/70), TER-119 (Ly-76), and Gr-1 (RB6-8C5) (all from BD Pharmingen, San Diego, CA, USA) as lineage markers to deplete lineage-positive cells from BM-MNCs by using AutoMACS (Becton Dickinson, Franklin Lakes, NJ, USA). Lineage-negative bone marrow cells (BM-LNneg) were incubated with saturating concentrations of directly labeled anti-c-Kit (at 1:25 dilution) (BD Biosciences, Franklin Lakes, NJ, USA) and anti-Sca-1 antibodies (at 1:25 dilution) (BD Biosciences) for 30 minutes on ice, and then the c-Kit$^+$/Sca-1$^+$ lineage-negative cells (BM-KSL) were isolated with live sterile cell sorting (FACSVantage SE; Becton Dickinson).

Endothelial progenitor cell colony-forming assay

Various cells were cultured in methylcellulose-containing medium M3236 (StemCell Technologies, Vancouver, BC, Canada) with 20 ng/mL stem cell-derived factor (Kirin, Tokyo, Japan), 50 ng/mL vascular endothelial (VE) growth factor (R&D Systems, Minneapolis, MN, USA), 20 ng/mL interleukin-3 (Kirin), 50 ng/mL basic fibroblast growth factor (Wako, Osaka, Japan), 50 ng/mL epidermal growth factor receptor (Wako), 50 ng/mL insulin-like growth factor-1 (Wako), 2 U/mL heparin (Ajinomoto, Tokyo, Japan), and 10% fetal bovine serum (FBS) on a 35-mm dish for 8 days. Cell densities for each sample were as follows: PB-MNCs 7×10^5 cells per dish, BM-MNCs 1×10^4 cells per dish, BM-LNneg 2.5×10^3 cells per dish, and BM-KSL 500 cells per dish. The EPC-CFUs were identified as large-EPC-CFUs or small-EPC-CFUs by visual inspection with an inverted microscope under 40× magnification. Large-EPC-CFUs were composed of spindle-shaped cells, and small-EPC-CFUs were composed of round adhesive cells.

Endothelial progenitor cell-colony-forming unit staining

After 8 days in culture, the EPC-CFU cultures were treated with 0.4 μg/mL 1,1'-dioctadecyl-3,3,3',3-tetramethyl-indocarbocyanine perchlorate-labeled acLDL

(acLDL-DiI; Biomedical Technologies Inc., Stoughton, MA, USA) for 1 hour and fixed by application of 1 mL of 2% paraformaldehyde (PFA) for 1 hour at room temperature. After a wash of the methylcellulose-containing medium with PBS, the cultures were reacted with fluorescein isothiocyanate (FITC)-conjugated BS-1 lectin (Sigma-Aldrich) for 1 hour at room temperature. After a wash with PBS, the cultures were observed under a fluorescence microscope (IX70; Olympus, Tokyo, Japan).

Large-endothelial progenitor cell or small-endothelial progenitor cell isolation

Cells composed of small-EPC-CFUs were collected with a pipette under a microscope as small-EPCs. Then the cultures were washed with PBS, and large-EPCs were harvested after treatment with 2 mmol/L EDTA/PBS. For the purpose of cell transplantation into a hindlimb ischemia model, non-attached cells were isolated as small-EPCs by washing with PBS, whereas attached cells were harvested as large-EPCs by treatment with EDTA/PBS (5 mmol/L) for 5 minutes at 37°C.

Adhesive assay

Culture plates (24-well) were coated with human fibronectin (100 μg/mL; Gibco, now part of Invitrogen Corporation, Carlsbad, CA, USA). Large-EPCs or small-EPCs (2×10^4 cells per well) were allowed to attach in EGM-2 (Cambrex Bio Science Walkersville, Walkersville, MD, USA) for 20 minutes at 37°C, and the non-adherent cells were aspirated. The adherent population was fixed with 1% PFA for 20 minutes and stored in PBS. The numbers of adherent cells were quantified from counts in six random microscopic fields per well.

Proliferation assay

At day 7, EPC-CFU cultures were treated with 10 μmol/L bromodeoxyuridine (BrdU) (Sigma-Aldrich) and incubated for 24 hours. BrdU positivities of large-EPCs or small-EPCs were analyzed by using BrdU flow kits (BD Pharmingen) and a fluorescence-activated cell sorter, as previously described [26].

Tubular formation assay

Two-week derived $CD133^-$ mononuclear cells of human cord blood were used as ECs. These cells were confirmed to be ECs by tubular formation and immunocytochemistry of endothelial nitric oxide synthase (eNOS), kinase insert domain receptor (KDR), and VE-cadherin (data not shown) [5]. Each small-EPC or large EPC was labeled with acLDL-DiI for 1 hour. After washing of the labeled small-EPCs or large-EPCs with PBS, the 1×10^3 cells were mixed together with 1.2×10^4 ECs in 50 μL of 2% FBS/EBM-2. Cell suspension (50 μL) was applied onto 50 μL of Matrigel (BD, Franklin Lakes, NJ, USA) per well of a 96-well plate (BD Falcon, Franklin Lakes, NJ, USA) and then incubated for 8 hours. After incubation, the numbers of tubular formation were counted on a display of Photoshop software (Adobe, San Jose, CA, USA) after a picture per well was taken at 40× magnification under a light microscope (Eclipse TE300; Nikon, Tokyo, Japan). The numbers of incorporated labeled cells into tubes were also counted on a display of Photoshop software after a picture per well was taken at 100× magnification under a fluorescence microscope.

Secondary culture

Isolated small-EPCs (5×10^4) were suspended in 50 μL of Iscove's modified Dulbecco's medium (IMDM) (Gibco) and applied onto 100 μL of methylcellulose-containing medium per well of a 96-well plate (BD Falcon). After 2 days of incubation, methylcellulose-containing medium was changed to IMDM containing acLDL-DiI and BS-1 lectin-conjugated FITC and then incubated for 1 hour. After a wash with PBS, cultures were observed under a fluorescence microscope.

Reverse transcription-polymerase chain reaction

Total RNA of small-EPCs or large-EPCs was prepared with an RNeasy Micro/Mini kit (Qiagen, Valencia, CA, USA). Reverse transcription-polymerase chain reaction (RT-PCR) was performed by using Superscript III Reverse Transcriptase (Invitrogen Corporation) with 1 μg of total RNA. PCR amplification was then performed with synthetic gene-specific primers for eNOS (forward primer, 5'-GGATTGTGTCACTTCGTTCGGT-3'; reverse primer, 5'-CAGCAGGATGCCCTAACTACCA-3'; product length, 183 base pairs (bp)), Flk-1 (forward primer, 5'-AAAGAG AGGAACGTCGGCAGA-3'; reverse primer, 5'-AAGC ACACAGGCAGAAACCAGT-3'; product length, 376 bp), VE-cadherin (forward primer, 5'-AGATTCACGAGC AGTTGGTCA-3'; reverse primer, 5'-GATGTCAG AGTC GGAGGAATT-3'; product length, 355 bp), and β-actin (forward primer, 5'-AACACCCCAGCCATGTACGTA-3'; reverse primer, 5'-AAGGAAGGCTGGAAAAGA GCC-3'; product length, 416 bp) by using exTaq polymerase (Takara, Kyoto, Japan). To quantify transcripts, semi-quantitative RT-PCRs were performed and normalized to Actb, which encodes β-actin. PCRs were performed at 94°C for 45 seconds, 64°C for 1 minute, and 72°C for 1 minute for 35 or 33 or 22 cycles and analyzed on 2% agarose gels.

Flow cytometry

For flow cytometry analysis, we used monoclonal antibodies specific to Sca-1 and c-Kit. BM-LNneg- or EPC-CFU-derived cells were incubated with directly labeled anti-Sca-1 (at 1:100 dilution) and anti-c-Kit (at 1:100 dilution) antibodies for 30 minutes on ice. The cells

were analyzed by two-color flow cytometry by using a FACS caliber (Becton Dickinson).

Animal model of ischemic hindlimb

Unilateral hindlimb ischemia was created in C57BL/6J mice or BALB/CA-nu/nu as previously described [27]. Briefly, the animals were anesthetized with Nembutal (60 mg/kg intraperitoneally; Dainippon Sumitomo Pharma Co., Osaka, Japan) and then an incision in the skin overlying the middle portion of the left hindlimb was performed. After ligation of the proximal end of the femoral artery, the distal portion of the saphenous artery was ligated and the artery, as well as all side branches, was dissected free and excised. The skin was closed by using a surgical stapler.

Monitoring of hindlimb blood flow

After anesthesia, hindlimb perfusion was measured by using a laser Doppler perfusion imaging system (LDPI; Moor Instruments, Wilmington, DE, USA). The stored perfusion values behind the color-coded pixels representing the microvascular blood flow distribution are available for analysis. Color photographs were recorded and analysis performed by calculating the average perfusion of the ischemic and non-ischemic foot. To account for variables such as ambient light and temperature, the results are expressed as the ratio of perfusion in the left (ischemic) versus right (normal) limb. In the EPC transplantation experiment, isolated small-EPCs, large-EPCs, or murine ECs (2.5×10^5) derived from the aorta of C57BL/6J were transplanted into hindlimb induced nude mice by intramuscular injection, respectively ($n = 8$).

Measuring of capillary density

Twenty-eight days after ischemia, capillary density was determined in tissue sections from the lower calf muscles of ischemic and healthy limbs by expressed as number of $CD31^+$ cells as ECs per myocyte. To stain the capillary, we performed a staining procedure with rat anti-mouse CD31 antibodies (BD Biosciences) or Alexa-fluor 594 (Molecular Probes, now part of Invitrogen Corporation) anti-iso-lectin B4 reagents (Sigma-Aldrich).

Statistical analysis

All data were presented as mean ± standard deviation. *P* values were calculated by using the unpaired Student *t* test. For the analysis of *in vivo* ischemia experiments, the Scheffe's test was performed for the multiple comparisons after analysis of variance between each group. A *P* value of less than 0.05 was considered statistically significant.

Results

Development of murine endothelial progenitor cell colony-forming assay

To address the detail functions and actual status of *in vivo* EPCs, we have first established a novel EPC-CFA in murine EPCs. After culture of PB-MNCs, BM-MNCs, or BM-KSL of C57BL/6J mice in growth factor-containing methylcellulose medium, these primitive cells differentiated into two types of EPC colony clusters: large-EPC-CFUs and small-EPC-CFUs (Figure 1a, data not shown). Morphologically, these cells are large-EPC-CFUs, which were composed mainly of spindle/round-shaped cells, whereas cells composed of small-EPC-CFUs were round. Both EPC-CFUs differentiated from primary PB-MNCs or primary BM-derived cells were identified as EPCs by acLDL uptake and BS-1 lectin reactivity, a typical feature of characterization of endothelial lineage cells (Figure 1b-d, data not shown). The frequencies of large-EPC-CFUs or small-EPC-CFUs differentiated from 7×10^5 PB-MNCs were 2.8 ± 1.3 and 6.0 ± 2.0 per dish, respectively. The normalized frequencies of large-EPC-CFUs or small-EPC-CFUs differentiated from 7×10^5 BM-MNCs were 665 ± 309 and 852 ± 82 per dish, respectively (Figure 1e). These results revealed that BM-MNCs had higher EPC colony-forming capacity than PB-MNCs. In this EPC-CFA, EPCs from primary murine cells could be classified into two types of EPC-CFUs and the colony-forming potential could be assessed by the frequency of EPC-CFUs. To check the commitment of each EPC-CFU-derived cell, eNOS, Flk-1, and VE-cadherin, markers of ECs, were examined. Gene expression profiles revealed that large-EPCs and small-EPCs expressed eNOS, Flk-1, and VE-cadherin gene in both PB-MNCs and BM-MNCs (Figure 1f), showing that large-EPCs strongly expressed VE-cadherin, a typical EC marker, although small-EPCs also expressed eNOS or Flk-1, each of which is a committed marker of endothelial lineage cells.

Characterization of large endothelial progenitor cells or small endothelial progenitor cells

To characterize these two types of EPC-CFUs (large-EPC-CFUs or small-EPC-CFUs), we separately collected EPC-CFU-derived cells and investigated the functions of both EPC-CFUs. To determine the proliferation potency of each EPC-CFU-derived cell, we performed a proliferation assay. In PB-MNCs-derived EPC-CFUs, 24.5% ± 15.6% of large-EPCs and 51.2% ± 8.8% of small-EPCs incorporated BrdU. In BM-MNCs-derived EPC-CFUs, 17.1% ± 13.9% of large-EPCs and 46.4% ± 23.0% of small-EPCs incorporated BrdU (Figure 2a). More small-EPCs incorporated BrdU than large-EPCs, suggesting that large-EPCs have lower proliferation potency than small-EPCs. From observation of EPC-CFUs under a microscope, small-EPC-CFUs were constituted of more cells than large-EPC-CFUs and the areas of small-EPC-CFUs were significantly larger than those of large-EPC-CFUs (data not shown). We next defined an adhesive capacity of these two types of EPC-CFUs. The numbers of adherent large-EPCs or small-EPCs from PB-MNCs

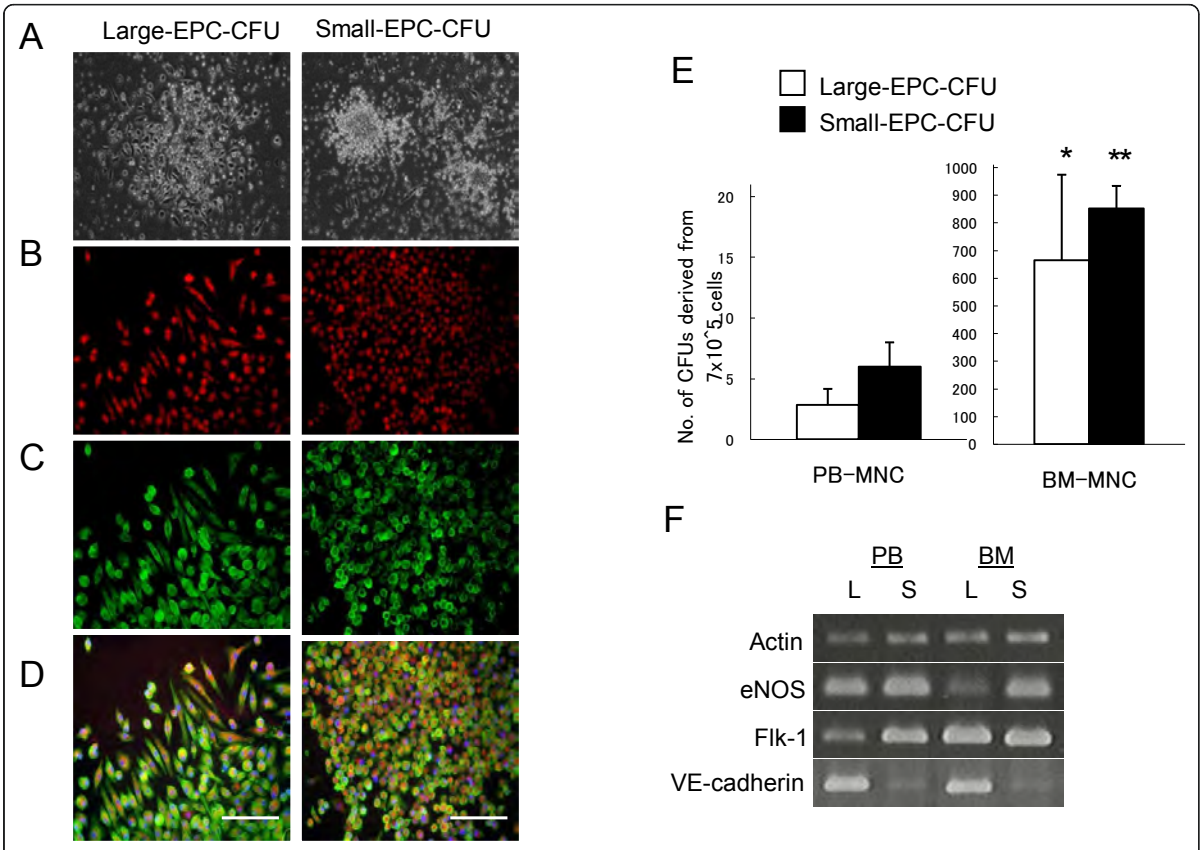

Figure 1 Murine endothelial progenitor cell colony-forming units (EPC-CFUs). **(a)** Representative micrographs of large-EPC-CFUs or small-EPC-CFUs cultured from bone marrow mononuclear cells (BM-MNCs) for 8 days. Large-EPC-CFUs and small-EPC-CFUs were defined according to cell morphology as spindle-shaped cells or round cells, respectively. **(b-d)** EPC-CFUs were identified as double-positive cells due to 1,1′-dioctadecyl-3,3,3′,3-tetramethyl-indocarbocyanine perchlorate-labeled acetylated-low density lipoprotein (acLDL-DiI) uptake (red) and BS-1 lectin reactivity (green). Scale bar represents 100 μm. **(e)** EPC colony-forming assay in murine peripheral blood mononuclear cells (PB-MNCs) or BM-MNCs. The frequencies of large-EPC-CFUs (white columns) or small-EPC-CFUs (black columns) from PB-MNCs or BM-MNCs (7×10^5 cells) were counted after 8 days of culture. *$P < 0.05$, **$P < 0.01$ versus PB-MNC-derived EPC-CFUs. **(f)** Expression patterns of endothelial nitric oxide synthase (eNOS), Flk-1, and vascular endothelial (VE)-cadherin genes in large-EPCs (L) or small-EPCs (S) from PB-MNCs or BM-MNCs. Both EPC-CFU-derived cells expressed markers of endothelial cells.

were 40.5 ± 7.6 and 26.3 ± 5.6 per field, respectively, and those from BM-MNCs were 63.7 ± 12.0 and 27.2 ± 8.0 per field, respectively (Figure 2b), proving that the large-EPCs have higher adhesive capacity than small-EPCs by 1.5-fold in PB-MNCs and 2.3-fold in BM-MNCs. To check tube-forming ability, large-EPCs or small-EPCs derived from BM were labeled with acLDL-DiI and cocultured with ECs, which were 2-week derived $CD133^-$ mononuclear cells of human cord blood, on Matrigel. Fluorescent tagging of each EPC-CFU-derived cell with DiI enabled delineation from ECs (Figure 2c). The number of tubes in coculture with large-EPCs increased significantly compared with small-EPCs (large-EPCs; 78.3 ± 5.8, small-EPCs; 70.7 ± 8.4) (Figure 2d, left). Moreover, more large-EPCs were incorporated into tubes compared with small-EPCs (large-EPCs; 8.3 ± 2.7, small-EPCs; 4.2 ± 1.7) (Figure 2d, right), implying that large-EPCs made a substantial contribution to tubular networks with ECs, although small-EPCs showed minimal incorporation into the developing vascular network. Taken together, three independent results strongly indicated that large-EPCs and small-EPCs had different functions and that large-EPCs might be more mature EPCs with respect to adhesion ability and functional contribution of tubule networks of ECs.

Importance of small-endothelial progenitor cells as large-endothelial progenitor cell-colony-forming unit sprouting cells

To determine whether small-EPCs are real immature cells, we performed FACS analysis on EPC-CFU-derived cells, which developed from fresh isolated BM-KSL ($c\text{-}Kit^+/Sca\text{-}1^+/LNneg$, purity of greater than 99.5%) cells.

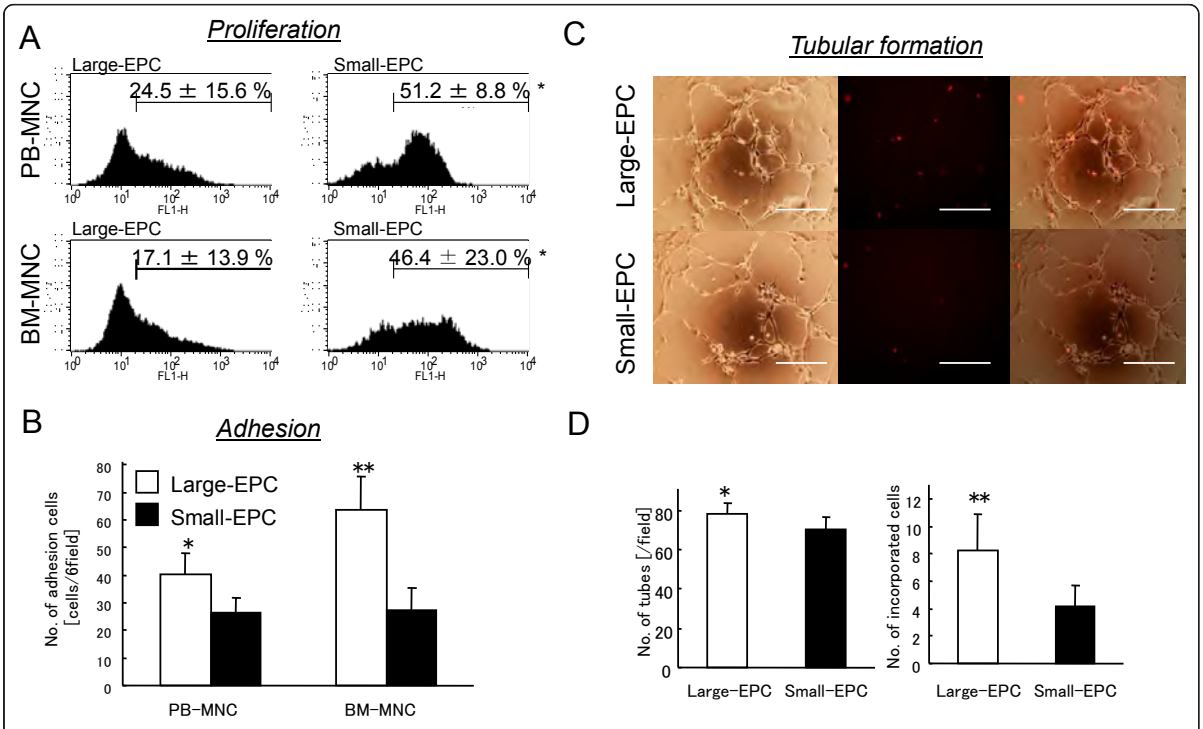

Figure 2 Characterization of large-EPCs or small-EPCs. **(a)** Proliferation assay of large-EPCs or small-EPCs from peripheral blood mononuclear cells (PB-MNCs) (upper) or bone marrow mononuclear cells (BM-MNCs) (bottom). After 7 days of culture, large-EPC-CFUs or small-EPC-CFUs were allowed to incorporate bromodeoxyuridine (BrdU) for 24 hours and analyzed by flow cytometry. Large-EPCs had significantly lower proliferative potency than small-EPCs in both PB-MNCs and BM-MNCs (*P < 0.05 versus large-EPCs). **(b)** Adhesion assay of large-EPCs or small-EPCs from PB-MNCs or BM-MNCs. Large-EPCs (white columns) or small-EPCs (black columns) were allowed to adhere to a fibronectin-coated plate for 20 minutes. More large-EPCs had adhesive capacity than small-EPCs. *P < 0.05, **P < 0.01 versus small-EPCs. **(c)** Tubular formation assay of large-EPCs or small-EPCs from BM-MNCs. Large-EPCs or small-EPCs labeled with 1,1′-dioctadecyl-3,3,3′,3-tetramethyl-indocarbocyanine perchlorate-labeled acetylated-low density lipoprotein (acLDL-DiI) (red) were cocultured with endothelial cells (ECs) to form tubular structures within Matrigel. Representative light and fluorescent micrographs of ECs cocultured with large-EPCs (upper) and small-EPCs (bottom) are shown. Scale bar represents 500 μm. **(d)** Quantification of the number of tubes (left). Large-EPCs made a substantial contribution to tubular networks with ECs. *P < 0.05 versus small-EPCs. (d) Quantification of the number of cells incorporated into tubes (right). Small-EPCs showed minimal incorporation into the developing vascular network. **P < 0.01 versus small-EPCs. EPC, endothelial progenitor cell.

As shown in Figure 3a, we observed the higher population of KSL cells in small-EPCs, providing us a clue that small-EPCs contained actual progenitors. Therefore, to check whether small-EPCs can differentiate into large-EPCs, isolated small-EPCs were reseeded in methylcellulose-containing medium. PB-MNC-, BM-MNC-, or BM-KSL cell-derived-small-EPCs could differentiate into spindle-shaped cells, large-EPCs and could represent positivity of acLDL uptake and BS-1 lectin binding (Figure 3b, data not shown). To characterize small-EPCs-derived large-EPCs, we examined the gene expression of VE-cadherin, Flk-1, and eNOS; adhesion capacity; and incorporation potential of small-EPC-derived large-EPCs (large EPCs-1) compared with small-EPCs and large-EPCs (large EPCs-2). Gene expression profiles by RT-PCR revealed that large EPCs-1 strongly expressed VE-cadherin and Flk-1 compared with small-EPCs (Figure 3c). In the adhesion assay, the numbers of adherent small-EPCs, large EPCs-1, and large EPCs-2 were 23.2 ± 5.1, 52 ± 5.3, and 61.5 ± 8.3 per field, respectively (Figure 3d). In the tubular formation assay, more large EPCs-1 were incorporated into tubes compared with small-EPCs (Figure 3e). These results revealed that the large-EPCs derived from small-EPCs showed a higher potential of VE-cadherin expression, adhesion, and tube formation compared with those of small-EPCs, suggesting that small-EPCs might be more immature EPCs and be early EPCs, which could differentiate into large-EPCs.

Kinetics of endothelial progenitor cell-colony-forming units in response to ischemia

EPCs play a critical role in restoration of ischemic diseases. To explore the effects of hindlimb ischemia on differentiation of BM into EPC-CFUs, we examined PB-MNCs and

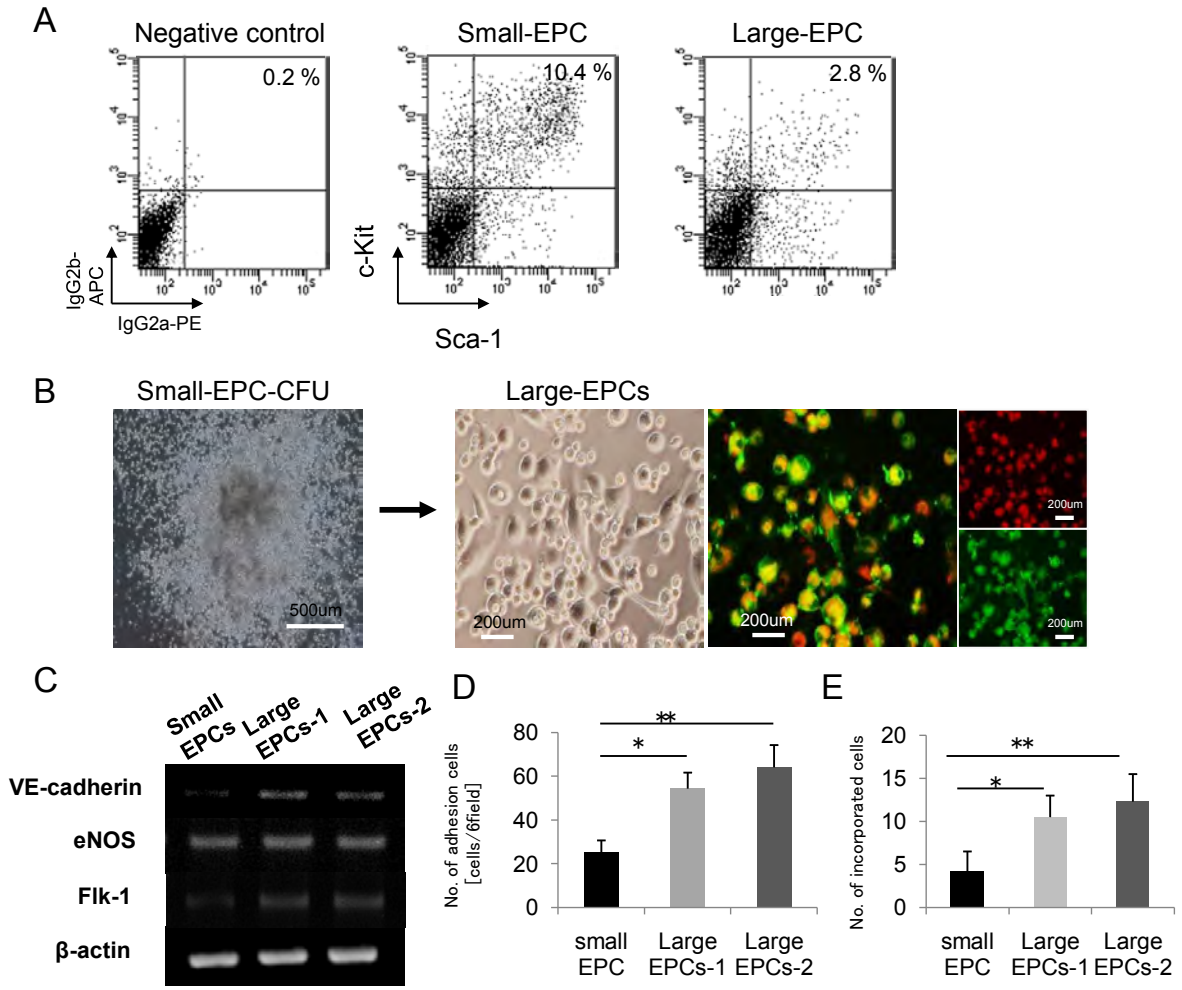

Figure 3 Importance of small-EPCs as large-EPC-CFU-sprouting cells. **(a)** Flow cytometry analysis of small-EPCs or large-EPCs after culturing for 10 days from freshly isolated bone marrow c-Kit$^+$/Sca-1$^+$ lineage-negative cells (BM-KSL). **(b)** Secondary culture assay of small-EPC-CFUs from bone marrow mononuclear cells (BM-MNCs). Representative micrographs of small-EPC-CFUs from BM-MNCs before reseeding are shown on the left, and representative light and fluorescent micrographs of small-EPCs cultured secondarily in methylcellulose-containing medium are shown on the right. Secondary cultured cells were identified as double-positive cells due to 1,1′-dioctadecyl-3,3,3′,3-tetramethyl-indocarbocyanine perchlorate-labeled acetylated-low density lipoprotein (acLDL-Dil) uptake (red) and BS-1 lectin reactivity (green). Small-EPCs could differentiate into large-EPCs. **(c)** The expression of vascular endothelial (VE)-cadherin, Flk-1, and endothelial nitric oxide synthase (eNOS) was measured in small-EPCs, small-EPCs-derived large-EPCs (Large EPCs-1), and large-EPCs (Large EPCs-2) by reverse transcription-polymerase chain reaction analysis. **(d)** Adhesion assay of small-EPCs, Large EPCs-1, and Large EPCs-2. *P < 0.05, **P < 0.01 versus small-EPCs. **(e)** Quantification of the number of cells incorporated into tubes in small-EPCs, Large EPCs-1, and Large EPCs-2. *P < 0.05, **P < 0.01 versus small-EPCs.

BM of hindlimb ischemic mice in EPC-CFA. This experiment could enable us to elucidate the roles of each EPC-CFU *in vivo*. First, hindlimb perfusion was evaluated by serial LDPI studies at day 5 after surgery. The ratio of blood flow between the ischemic and the normal limb was 0.19 ± 0.16, which was a significant difference compared with 0.98 ± 0.21 in the normal mice (data not shown). To explore the *in vivo* change in BM, we estimated the percentage of KSL population in BM by FACS analysis. The percentage of BM-LNneg did not change, but that of the KSL population in BM-LNneg was 6.6% ± 2.0% in ischemic mice, which was significantly increased compared with the normal mice: 3.8% ± 1.2% (Figure 4a, b). These data demonstrated that BM-KSL cells, which produced more EPC-CFUs, were induced by hindlimb ischemia. To check the differentiation capacities of EPCs from PB-MNCs and various fractions of BM-MNCs, the frequencies of EPC-CFUs from each population were counted. In all populations, the frequencies of large-EPC-CFUs and the ratios of large-EPC-CFUs

were significantly increased in hindlimb ischemic mice (Figure 4c). These results indicated that hindlimb ischemia induced the differentiation of PB-MNCs and various populations of BM, implying that large-EPC-CFUs might play an important role in the restoration of ischemic diseases.

Contribution of large-endothelial progenitor cells or small-endothelial progenitor cells to postnatal/adult neovascularization

To determine the functional importance of *in vivo* EPC status in a pathological situation, we transplanted large-EPCs or small-EPCs and murine ECs as controls into hindlimb ischemia models. As shown in Figure 5a, b, we observed limb salvage in large-EPC transplantation groups, although small-EPC, EC, or PBS transplantation groups did not operate as useful limb therapy cells. These macroscopical observations were further supported by monitoring of real blood flow by using a laser Doppler perfusion imaging system because the recovery of limb perfusion was significantly improved in large-EPCs transplantation groups only (Figure 5c) compared with those of small-EPC, EC, or PBS transplantation groups. Moreover, immunohistochemical analysis clearly showed that capillary density in large-EPC transplantation groups was markedly increased (Figure 5d, e), suggesting that large-EPC-CFUs are more functional EPC status for vascular regeneration *in vivo*.

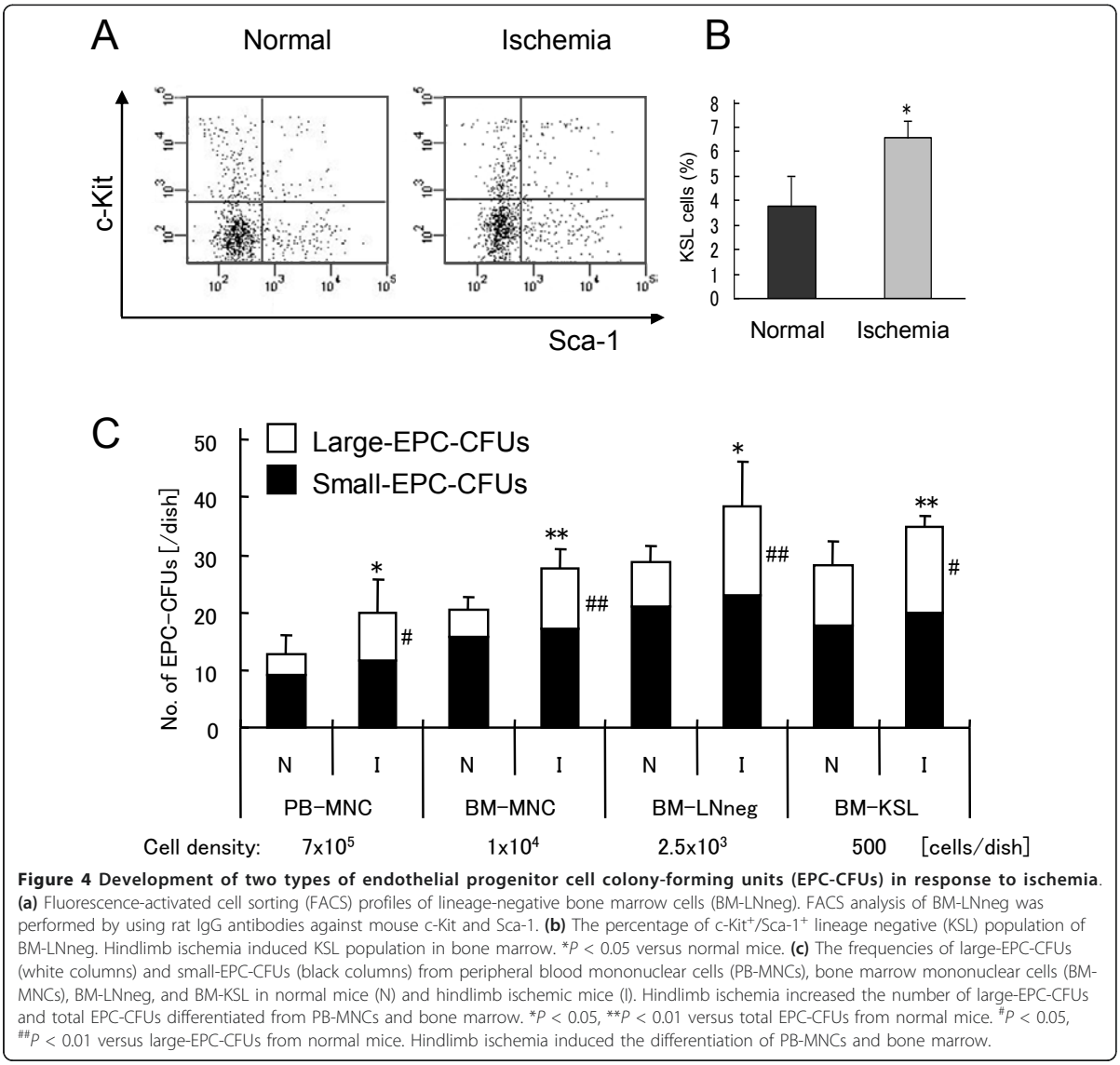

Figure 4 Development of two types of endothelial progenitor cell colony-forming units (EPC-CFUs) in response to ischemia. **(a)** Fluorescence-activated cell sorting (FACS) profiles of lineage-negative bone marrow cells (BM-LNneg). FACS analysis of BM-LNneg was performed by using rat IgG antibodies against mouse c-Kit and Sca-1. **(b)** The percentage of c-Kit$^+$/Sca-1$^+$ lineage negative (KSL) population of BM-LNneg. Hindlimb ischemia induced KSL population in bone marrow. *P < 0.05 versus normal mice. **(c)** The frequencies of large-EPC-CFUs (white columns) and small-EPC-CFUs (black columns) from peripheral blood mononuclear cells (PB-MNCs), bone marrow mononuclear cells (BM-MNCs), BM-LNneg, and BM-KSL in normal mice (N) and hindlimb ischemic mice (I). Hindlimb ischemia increased the number of large-EPC-CFUs and total EPC-CFUs differentiated from PB-MNCs and bone marrow. *P < 0.05, **P < 0.01 versus total EPC-CFUs from normal mice. $^{\#}P$ < 0.05, $^{\#\#}P$ < 0.01 versus large-EPC-CFUs from normal mice. Hindlimb ischemia induced the differentiation of PB-MNCs and bone marrow.

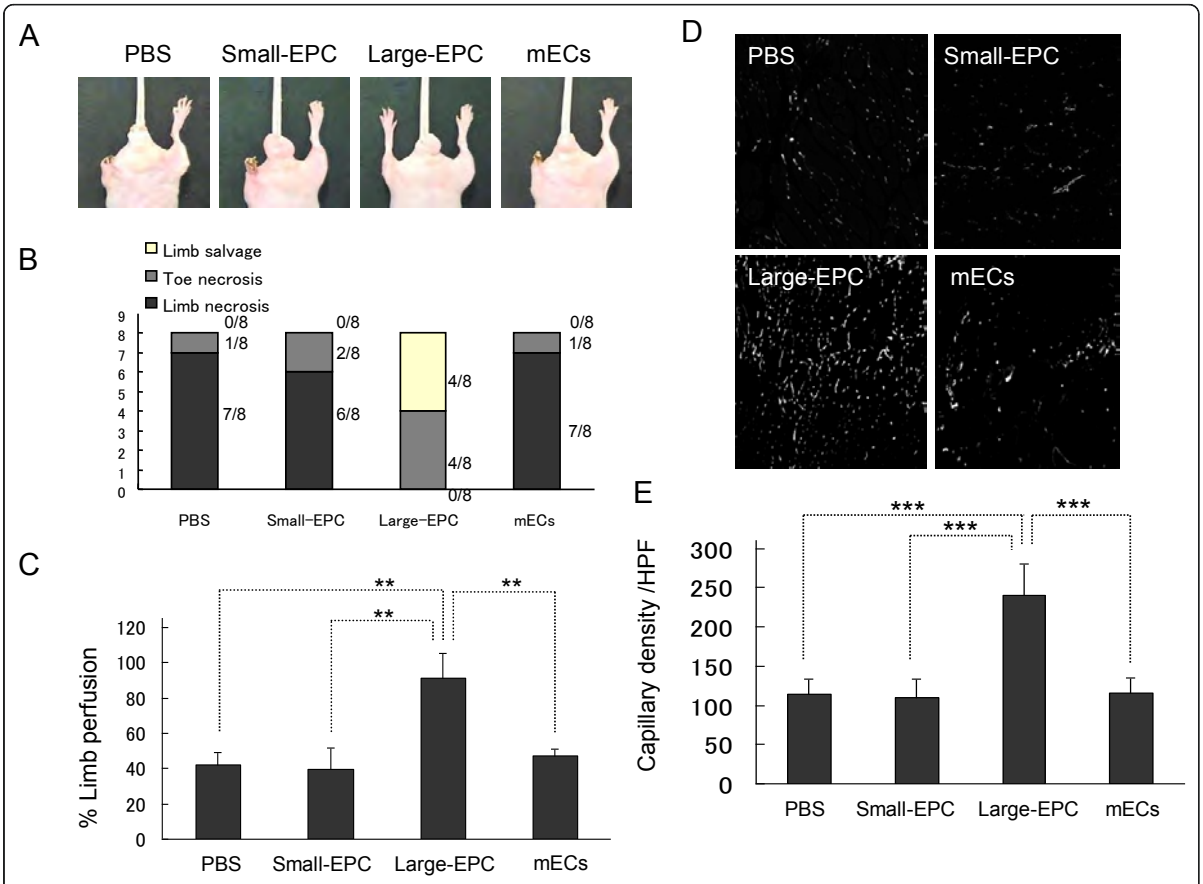

Figure 5 Effect of two types of endothelial progenitor cell colony-forming units (EPC-CFUs) on neovascularization. **(a)** Macroscopical observation of ischemic hindlimb 28 days after transplantation of large-EPCs and small-EPCs, which are derived from bone marrow c-Kit$^+$/Sca-1$^+$ lineage-negative (BM-KSL) cells, and murine endothelial cells (mECs) into hindlimb ischemia. **(b)** The ratios of the above outcomes in each group. **(c)** Laser Doppler perfusion imaging showing reduction of blood flow at day 28 after surgery. Quantification data of blood flow as the ratio of perfusion in ischemic hindlimb to that in normal hindlimb are shown. In hindlimb ischemic mice, blood flow of hindlimb kept to be low in small-EPCs transplanted and other control groups at day 28 after surgery. Transplantation of large-EPCs recovered the limb perfusion in hindlimb ischemic mice. $^{**}P < 0.01$ versus mice transplanted with large-EPCs ($n = 8$). **(d)** Representative images of iso-lectin B4-positive tissue 28 days after transplantation of large-EPCs, small-EPCs, and mECs into hindlimb ischemia. **(e)** The statistical data of (a). Transplantation of large-EPC-CFUs into hindlimb ischemia model enhanced neovascularization. $^{***}P < 0.001$ versus mice transplanted with large-EPCs ($n = 8$). HPF, high-powered field; PBS, phosphate-buffered saline.

Discussion

EPCs can be classified into various differentiation levels in both circulating EPCs and tissue EPCs [16]. Here, we first defined *in vivo* EPC status by establishing the novel murine EPC-CFA, in which the colony-forming potential of EPCs at different differentiation levels can be assessed. We demonstrated, for the first time, that hindlimb ischemia induced onsets of large-EPCs, which might be the accelerated differential status of EPCs. The observation was further supported by an *in vivo* experiment in which transplantation of more mature large-EPCs into a hindlimb ischemia model enhanced neovascularization, implying the contribution of large-EPC-CFUs in a pathogenic situation as 'cells ready to operate'.

Previously, Hur and colleagues [20] reported that they found two types of EPCs - early EPCs and late EPCs - from a source of adult PB-MNCs; attached cells that appeared after 3 to 5 days of culture were defined as early EPCs, and cells that appeared in 2 to 4 weeks after plating were defined as late EPCs [20]. However, these classifications gave us some limitation for a full understanding of the EPC status. First, as these two types of EPCs were defined by different assays, two types of EPCs could not be assayed synchronously. Second, these assays failed to provide enough information about the differential cascade from immature stem cells, such as BM-KSL, into real EPC status. In our study, we redefined EPC status in response to a pathogenic situation. Small-EPC-CFUs had greater

proliferative activity, suggesting that small-EPC-CFUs contained more immature clonogenic cells (KSL cells) derived from hematopoietic stem cells which preserve hemagioblastic potentials. Large-EPC-CFUs are sequentially differentiated from small-EPC-CFUs in response to ischemic signals (Figure 6). That is, small-EPC-CFUs are 'primitive EPCs' and large-EPC-CFUs are 'definitive EPCs'. Importantly, in regard to the vasculogenic potential *in vivo*, our study clearly demonstrated that transplantation of definitive EPCs (large-EPCs), not primitive EPCs (small-EPCs), markedly increased limb perfusion and capillary density and that small-EPC-CFUs have pro-vasculogenic potential and large-EPC-CFUs have vasculogenic potential, although early and late EPCs were reported to contribute equally to neovasculogenesis in a previous study [20]. Regarding the fact that small-EPCs did not show any therapeutic effect in Figure 5, we speculated three possibilities due to the low adhesion and incorporation potentials of small-EPCs: (a) transplanted small-EPCs could not survive in a hypoxic tissue environment, (b) transplanted small-EPCs could not differentiate into large-EPCs in a hypoxic tissue environment, and (c) transplanted small-EPCs could not show their function as secretion of growth factors in a hypoxic tissue environment.

Two types of EPC-CFUs represented distinct functional differences in both *in vitro* EPC colony study and *in vivo* EPC transplantation study. The adhesive potential and the incorporation into tubes formed by EC-like cells of large-EPCs were superior to those of small-EPCs, and small-EPCs had higher proliferation capacity than large-EPCs, which was consistent with the data on EPC-CFUs from BM-LNneg and BM-KSL (data not shown). In these points, definitive large-EPCs had similar functions to ECs compared with primitive small-EPCs. Besides, the secondary culture revealed that small-EPCs could differentiate into adherent cell, large-EPCs; in contrast, large-EPCs could not differentiate into round cell, small-EPCs (data not shown). These data showed that definitive large-EPCs are well-differentiated EPCs compared with primitive small-EPCs (Figure 1e). VE-cadherin is specifically expressed in adherent junctions of ECs and exerts important functions in cell-cell adhesion [28]. The different expression level of VE-cadherin between large-EPCs and small-EPCs might explain the better potential of adhesion, incorporation into tubes, and migration (data not shown) of definitive large-EPCs than those of primitive small-EPCs, which were consistent with our recent findings using human cord blood $AC133^+$ cells [29]. Gene expression profiles revealed that both EPC-CFUs were committed to endothelial lineage because both definitive large-EPCs and primitive small-EPCs expressed eNOS, Flk-1, and VE-cadherin, which are EC-specific markers [5]. However, both EPC-CFUs would be different from mature ECs in terms of colony formation capacity, tubular formation ability, and contribution of *in vivo* neovascularization, demonstrated by ischemia model, because ECs could not form colonies and did not have an effect on the restoration of blood vessels, and EPC-CFU-derived cells could not form tubes on Matrigel in a culture without ECs.

In this EPC-CFA, to compare the potentials to produce EPC-CFUs of three populations in BM (BM-MNCs, BM-LNneg, and BM-KSL), we calculated the numbers of cells producing one EPC-CFU in BM-MNC, BM-LNneg, and BM-KSL populations. It was revealed that one large-EPC-CFU was derived from $1.1 \times 10^3 \pm 0.2 \times 10^3$ BM-MNCs or $3.6 \times 10^2 \pm 1.1 \times 10^2$ BM-LNneg or 57 ± 34 BM-KSL (Figure 1b). One small-EPC-CFU was derived from $5.5 \times 10^2 \pm 0.7 \times 10^2$ BM-MNCs or $1.2 \times 10^2 \pm 0.2 \times 10^2$ BM-LNneg or 28 ± 3 BM-KSL (Figure 1b). These data demonstrated that BM-LNneg had 3- or 4.6-fold higher potential to produce large- or small-EPC-CFUs than BM-MNCs, respectively, and this suggested that more immature EPCs were contained mainly in the BM-LNneg population. In addition, it was demonstrated that BM-KSL had the highest potential to produce EPC-CFUs in any other populations in BM, and those potentials to produce large- or small-EPC-CFUs were 6.3- or 4.3-fold higher than BM-LNneg, respectively, and this suggested that immature EPCs were highly enriched in the BM-KSL population. In this study, using EPC-CFA, we determined that BM-KSL was the major population which highly enriched immature EPCs. We concluded, in this paper, that small-EPCs differentiated into large-EPCs because BM-KSL grew into small-EPCs about 5 days after plating and then those small-EPCs derived from BM-KSL could differentiate into large-EPCs in further culture. In our study, it remained unclear which niche component does small- or large-EPC differentiate from'. This should be definitely addressed in further issues.

In a clinical setting, the frequency of circulating EPCs serves as a biomarker for vascular function, and the number of circulating EPCs has been reported to be reduced in patients with diabetes mellitus or risk factors for coronary artery disease and to negatively correlate with the Framingham cardiovascular risk score [12-15]. Transplantation of EPCs into ischemic hindlimb or myocardial tissue improves organ function following new vessel growth [6-10]. Thus, EPCs play an important role in the restoration of ischemic vascular diseases. But essential molecular events that control the differentiation to EPCs and changes in EPCs in response to ischemia had not been clarified yet. Then we investigated the changes of EPCs in response to hindlimb ischemia in EPC-CFA and revealed that the population of KSL, which enriched immature EPC populations in BM, increased by ischemia. In previous studies, it was demonstrated that BM-derived EPCs were mobilized in response to tissue ischemia [26]. In this study, we showed, for the first time, that the ischemic signals could promote the differentiation of PB-MNCs,

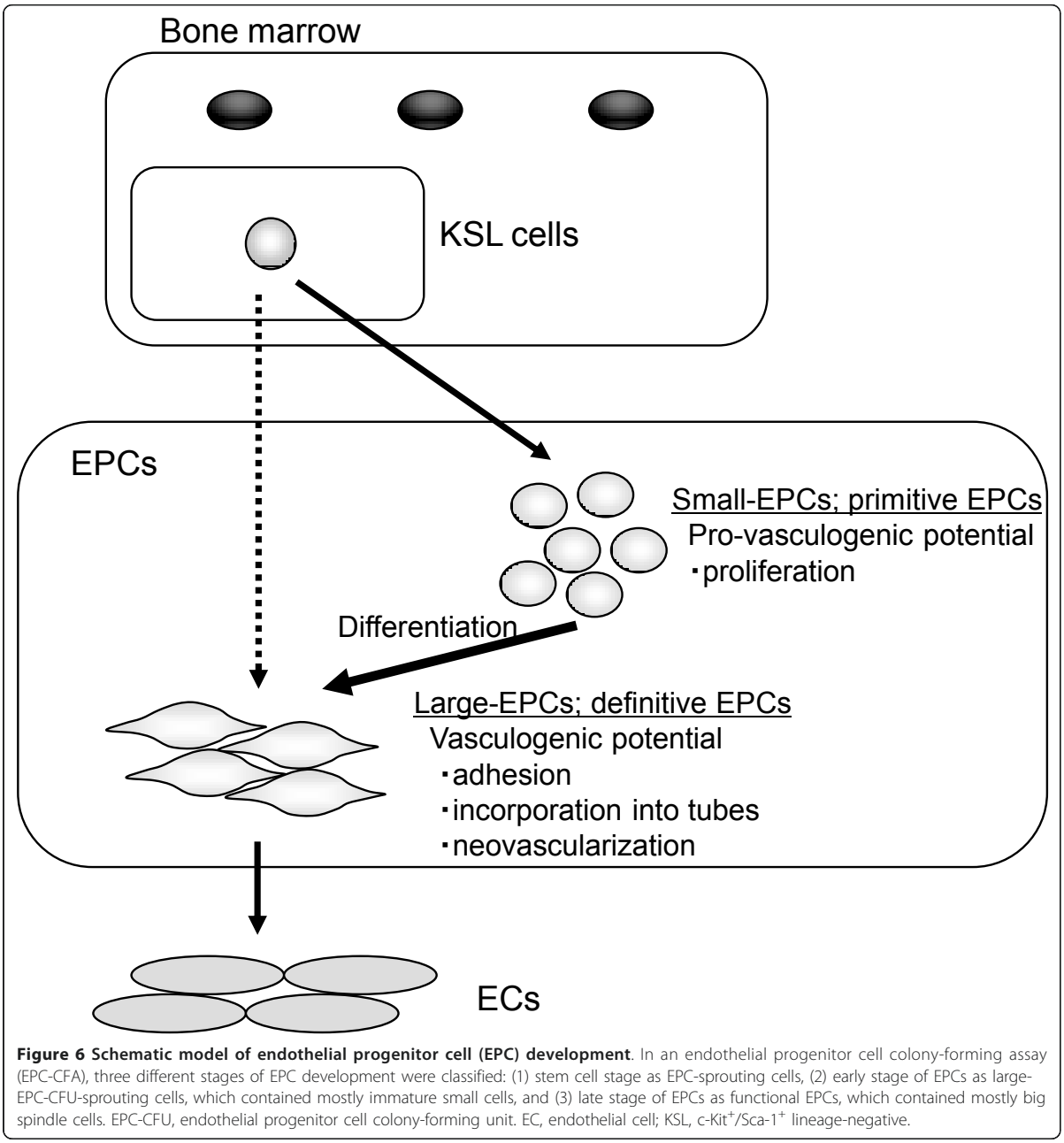

Figure 6 Schematic model of endothelial progenitor cell (EPC) development. In an endothelial progenitor cell colony-forming assay (EPC-CFA), three different stages of EPC development were classified: (1) stem cell stage as EPC-sprouting cells, (2) early stage of EPCs as large-EPC-CFU-sprouting cells, which contained mostly immature small cells, and (3) late stage of EPCs as functional EPCs, which contained mostly big spindle cells. EPC-CFU, endothelial progenitor cell colony-forming unit. EC, endothelial cell; KSL, c-Kit$^+$/Sca-1$^+$ lineage-negative.

BM-MNCs, or BM-KSL cells into mature EPC-CFUs. Ischemia-induced differentiation into large-EPC-CFUs suggested that definitive large-EPC-CFUs as more mature EPCs might play an important role in the restoration of ischemic tissue, and this possibility was supported by the recovery of limb perfusion by transplantation of BM-KSL-derived large-EPCs into a hindlimb ischemia model compared with small-EPCs. In ischemic tissue, the expression of stromal cell-derived factor-1 (SDF-1) was induced by transcription factor hypoxia-inducible factor-1 (HIF-1) according to hypoxic gradients [27,28]. SDF-1 enhances differentiation of BM-derived c-Kit$^+$ stem cells into EPCs [29]. Thus, the EPC differentiation presented above might be promoted by SDF-1, which is induced by HIF-1 after ischemia.

Conclusions

Our novel findings highlighted the actual status of EPCs via a redefinition of the differential stages of EPCs

through BM-derived stem cells using our established murine EPC-CFA. The understanding of molecular cascades of EPC development from primitive small-EPC-CFUs to definitive large-EPC-CFUs will provide us some useful therapeutic advantages to solve the quantitative or qualitative problems for EPCs therapy.

Abbreviations

acLDL: acetylated-low density lipoprotein; acLDL-DiI: 1,1′-dioctadecyl-3,3,3′,3-tetramethyl-indocarbocyanine perchlorate-labeled acetylated-low density lipoprotein; BM: bone marrow; BM-KSL: bone marrow c-Kit$^+$/Sca-1$^+$ lineage-negative; BM-LNneg: lineage-negative bone marrow cell; BM-MNC: bone marrow mononuclear cell; bp: base pairs; BrdU: bromodeoxyuridine; CFU-EC: colony-forming unit-endothelial cell; EC: endothelial cell; ECFC: endothelial colony-forming cell; EDTA: ethylenediaminetetraacetic acid; eNOS: endothelial nitric oxide synthase; EPC: endothelial progenitor cell; EPC-CFA: endothelial progenitor cell colony-forming assay; EPC-CFU: endothelial progenitor cell colony-forming unit; FBS: fetal bovine serum; FITC: fluorescein isothiocyanate; IMDM: Iscove's modified Dulbecco's medium; large EPC-1: large endothelial progenitor cell derived from small endothelial progenitor cell; PB-MNC: peripheral blood mononuclear cell; PBS: phosphate-buffered saline; PCR: polymerase chain reaction; PFA: paraformaldehyde; RT-PCR: reverse transcription-polymerase chain reaction; VE: vascular endothelial.

Authors' contributions

ST and S-MK participated in study conception and design, collection or assembly of data (or both), data analysis and interpretation, and manuscript writing. TM, S-YJ, S-HL J-HL, and HM participated in collection, assembly, analysis, and interpretation of data. TA drafted and revised the manuscript. All authors read and approved the final manuscript.

Competing interests

The authors declare that they have no competing interests.

Acknowledgements

We thank Rie Ito and Michiru Kobori for providing technical assistance and Sachie Ota for secretarial assistance. We thank all of our colleagues for helpful discussions and encouragement. This work was supported by the Academic Frontier Promotion Program of the Ministry of Education, Culture, Sports, Science, and Technology in Japan; a National Research Foundation grant funded by the Korean government (MEST) (2010-0020260); and the Basic Science Research Program of the National Research Foundation of Korea (NRF), funded by the Ministry of Education, Science and Technology (2010-0003132).

Author details

[1]Department Regenerative Medicine, Tokai University of Medicine, Kanagawa, 259-1193, Japan. [2]Department of Physiology, School of Medicine, Medical Research Institute, Pusan National University Beomeo-ri, Mulgeum-eup, Yangsan, Gyeongsangnam-do, 626-870, Republic of Korea. [3]Kobe Institute of Biomedical Research and Innovation, 2-2 Minatojima-minamimachi, Chuo-ku, Kobe, Hyogo, 650-0047, Japan.

Received: 14 June 2012 Revised: 24 October 2012
Accepted: 9 January 2013 Published: 28 February 2013

References

1. Asahara T, Murohara T, Sullivan A, Silver M, van der Zee R, Li T, Witzenbichler B, Schatteman G, Isner JM: **Isolation of putative progenitor endothelial cells for angiogenesis.** *Science* 1997, **275**:964-967.
2. Asahara T, Masuda H, Takahashi T, Kalka C, Pastore C, Silver M, Kearne M, Magner M, Isner JM: **Bone marrow origin of endothelial progenitor cells responsible for postnatal vasculogenesis in physiological and pathological neovascularization.** *Circ Res* 1999, **85**:221-228.
3. Naiyer AJ, Jo DY, Ahn J, Mohle R, Peichev M, Lam G, Silverstein RL, Moore MA, Rafii S: **Stromal derived factor-1-induced chemokinesis of cord blood CD34(+) cells (long-term culture-initiating cells) through endothelial cells is mediated by E-selectin.** *Blood* 1999, **94**:4011-4019.
4. Isner JM, Asahara T: **Angiogenesis and vasculogenesis as therapeutic strategies for postnatal neovascularization.** *J Clin Invest* 1999, **103**:1231-1236.
5. Rafii S, Lyden D: **Therapeutic stem and progenitor cell transplantation for organ vascularization and regeneration.** *Nat Med* 2003, **9**:702-712.
6. Gunsilius E, Petzer AL, Duba HC, Kahler CM, Gastl G: **Circulating endothelial cells after transplantation.** *Lancet* 2001, **357**:1449-1450.
7. Cho HJ, Kim HS, Lee MM, Kim DH, Yang HJ, Hur J, Hwang KK, Oh S, Choi YJ, Chae IH, Oh BH, Choi YS, Walsh K, Park YB: **Mobilized endothelial progenitor cells by granulocyte-macrophage colony-stimulating factor accelerate reendothelialization and reduce vascular inflammation after intravascular radiation.** *Circulation* 2003, **108**:2918-2925.
8. Murohara T, Ikeda H, Duan J, Shintani S, Sasaki K, Eguchi H, Onitsuka I, Matsui K, Imaizumi T: **Transplanted cord blood-derived endothelial precursor cells augment postnatal neovascularization.** *J Clin Invest* 2000, **105**:1527-1536.
9. Kalka C, Masuda H, Takahashi T, Kalka-Moll WM, Silver M, Kearney M, Li T, Isner JM, Asahara T: **Transplantation of *ex vivo* expanded endothelial progenitor cells for therapeutic neovascularization.** *Proc Natl Acad Sci USA* 2000, **97**:3422-3427.
10. Kawamoto A, Tkebuchava T, Yamaguchi J, Nishimura H, Yoon YS, Milliken C, Uchida S, Masuo O, Iwaguro H, Ma H, Hanley A, Silver M, Kearney M, Losordo DW, Isner JM, Asahara T: **Intramyocardial transplantation of autologous endothelial progenitor cells for therapeutic neovascularization of myocardial ischemia.** *Circulation* 2003, **107**:461-468.
11. Kawamoto A, Gwon HC, Iwaguro H, Yamaguchi JI, Uchida S, Masuda H, Silver M, Ma H, Kearney M, Isner JM, Asahara T: **Therapeutic potential of *ex vivo* expanded endothelial progenitor cells for myocardial ischemia.** *Circulation* 2001, **103**:634-637.
12. Loomans CJ, de Koning EJ, Staal FJ, Rookmaaker MB, Verseyden C, de Boer HC, Verhaar MC, Braam B, Rabelink TJ, van Zonneveld AJ: **Endothelial progenitor cell dysfunction: a novel concept in the pathogenesis of vascular complications of type 1 diabetes.** *Diabetes* 2004, **53**:195-199.
13. Tepper OM, Galiano RD, Capla JM, Kalka C, Gagne PJ, Jacobowitz GR, Levine JP, Gurtner GC: **Human endothelial progenitor cells from type II diabetics exhibit impaired proliferation, adhesion, and incorporation into vascular structures.** *Circulation* 2002, **106**:2781-2786.
14. Hill JM, Zalos G, Halcox JP, Schenke WH, Waclawiw MA, Quyyumi AA, Finkel T: **Circulating endothelial progenitor cells, vascular function, and cardiovascular risk.** *N Engl J Med* 2003, **348**:593-600.
15. Vasa M, Fichtlscherer S, Aicher A, Adler K, Urbich C, Martin H, Zeiher AM, Dimmeler S: **Number and migratory activity of circulating endothelial progenitor cells inversely correlate with risk factors for coronary artery disease.** *Circ Res* 2001, **89**:E1-7.
16. Asahara T, Kawamoto A: **Endothelial progenitor cells for postnatal vasculogenesis.** *Am J Physiol Cell Physiol* 2004, **287**:C572-579.
17. Lin Y, Weisdorf DJ, Solovey A, Hebbel RP: **Origins of circulating endothelial cells and endothelial outgrowth from blood.** *J Clin Invest* 2000, **105**:71-77.
18. Ingram DA, Mead LE, Tanaka H, Meade V, Fenoglio A, Mortell K, Pollok K, Ferkowicz MJ, Gilley D, Yoder MC: **Identification of a novel hierarchy of endothelial progenitor cells using human peripheral and umbilical cord blood.** *Blood* 2004, **104**:2752-2760.
19. Yoder MC, Mead LE, Prater D, Krier TR, Mroueh KN, Li F, Krasich R, Temm CJ, Prchal JT, Ingram DA: **Redefining endothelial progenitor cells via clonal analysis and hematopoietic stem/progenitor cell principals.** *Blood* 2007, **109**:1801-1809.
20. Hur J, Yoon CH, Kim HS, Choi JH, Kang HJ, Hwang KK, Oh BH, Lee MM, Park YB: **Characterization of two types of endothelial progenitor cells and their different contributions to neovasculogenesis.** *Arterioscler Thromb Vasc Biol* 2004, **24**:288-293.
21. Rohde E, Bartmann C, Schallmoser K, Reinisch A, Lanzer G, Linkesch W, Guelly C, Strunk D: **Immune cells mimic the morphology of endothelial progenitor colonies *in vitro*.** *Stem Cells* 2007, **25**:1746-1752.
22. Asahara T, Takahashi T, Masuda H, Kalka C, Chen D, Iwaguro H, Inai Y, Silver M, Isner JM: **VEGF contributes to postnatal neovascularization by mobilizing bone marrow-derived endothelial progenitor cells.** *Embo J* 1999, **18**:3964-3972.
23. Aicher A, Heeschen C, Mildner-Rihm C, Urbich C, Ihling C, Technau-Ihling K, Zeiher AM, Dimmeler S: **Essential role of endothelial nitric oxide synthase for mobilization of stem and progenitor cells.** *Nat Med* 2003, **9**:1370-1376.

24. Couffinhal T, Silver M, Zheng LP, Kearney M, Witzenbichler B, Isner JM: **Mouse model of angiogenesis.** *Am J Pathol* 1998, **152**:1667-1679.
25. Drake CJ, Fleming PA: **Vasculogenesis in the day 6.5 to 9.5 mouse embryo.** *Blood* 2000, **95**:1671-1679.
26. Takahashi T, Kalka C, Masuda H, Chen D, Silver M, Kearney M, Magner M, Isner JM, Asahara T: **Ischemia- and cytokine-induced mobilization of bone marrow-derived endothelial progenitor cells for neovascularization.** *Nat Med* 1999, **5**:434-438.
27. Ceradini DJ, Kulkarni AR, Callaghan MJ, Tepper OM, Bastidas N, Kleinman ME, Capla JM, Galiano RD, Levine JP, Gurtner GC: **Progenitor cell trafficking is regulated by hypoxic gradients through HIF-1 induction of SDF-1.** *Nat Med* 2004, **10**:858-864.
28. Fadini GP, Sartore S, Schiavon M, Albiero M, Baesso I, Cabrelle A, Agostini C, Avogaro A: **Diabetes impairs progenitor cell mobilisation after hindlimb ischaemia-reperfusion injury in rats.** *Diabetologia* 2006, **49**:3075-3084.
29. De Falco E, Porcelli D, Torella AR, Straino S, Iachininoto MG, Orlandi A, Truffa S, Biglioli P, Napolitano M, Capogrossi MC, Pesce M: **SDF-1 involvement in endothelial phenotype and ischemia-induced recruitment of bone marrow progenitor cells.** *Blood* 2004, **104**:3472-3482.

doi:10.1186/scrt168
Cite this article as: Tsukada *et al.*: Identification of mouse colony-forming endothelial progenitor cells for postnatal neovascularization: a novel insight highlighted by new mouse colony-forming assay. *Stem Cell Research & Therapy* 2013 **4**:20.

TRENDS IN CARDIOVASCULAR MEDICINE 23 (2013) 99–103

Available online at www.sciencedirect.com

SciVerse ScienceDirect

www.elsevier.com/locate/tcm

Review article

Clonogenic assay of endothelial progenitor cells

Haruchika Masuda[a], *and Takayuki Asahara*[a,b,*]

[a]*Department of Regenerative Medicine Science, Division of Basic Clinical Science, Tokai University School of Medicine, Shimokasuya, Kanagawa 259-1143, Isehara, Japan*
[b]*Vascular Regeneration Research Group, Institute of Biomedical Research and Innovation IBRI, Kobe, Japan*

ARTICLE INFO

Article history:
Received 22 June 2012
Received in revised form
12 September 2012
Accepted 13 September 2012
Available online 1 February 2013

ABSTRACT

In stem cell biology, $CD34^+$ or $CD133^+$ hematopoietic stem cells (HSCs) give rise to two types of endothelial progenitor cell (EPC) colonies: primitive and definitive EPC-colony forming units (*primitive* EPC-CFU and *definitive* EPC-CFU), which can be morphologically defined. Based on their morphology, an evaluation of the number or the ratio of each EPC colony constitutes the Endothelial Progenitor Cell Clonogenic Forming Assay (EPC-CFA), a novel assay to quantify the differentiation of colony forming EPCs. This assay system allows us to practically evaluate the vasculogenic potential of primary or cultured stem cell populations, i.e., mononuclear cells or fractionated stem cells ($CD34^+$ or $CD133^+$ cells) in peripheral blood, bone marrow, or umbilical cord blood. EPC-CFA can be used not only for basic research in vascular biology but also for evaluating the vascular reparative activity of patients with cardiovascular diseases. This review summarizes the underlying concepts and significance of the EPC-CFA in vascular biology.

Introduction

Circulating endothelial progenitor cells (EPC) can be subdivided into two categories, *hematopoietic* and *non-hematopoietic lineage* EPCs (hEPCs and non-hEPCs), after the controversy during the decade following their initial isolation (Asahara et al., 1997, 2011), as there is no definitive delineation of EPCs, no clear differentiation hierarchy, and no defined isolation protocol. hEPCs have been revealed to be derived from a pro-vasculogenic subpopulation of hematopoietic stem cells (HSCs) in the bone marrow (BM) (Asahara et al., 2011).

hEPCs have been quantified and qualified as either circulating cell populations identified by cell surface markers such as CD34, CD133, and Vascular Endothelial Growth Factor Receptor-2 (VEGFR-2) (Asahara et al., 2011), or as 'colonies' (Hill et al., 2003) using conventional EPC culture methods to produce spindle adherent cells from peripheral blood (PB), BM, or umbilical cord blood (UCB) mononuclear cells (MNCs) with endothelial growth factors and cytokines.

These assays, using conventional EPC culture protocols, are simple and satisfactory for estimating the vasculogenic properties of EPC-enriched fractions, but have recently been criticized with respect to the quality and quantity of EPCs derived from primary cells. These assays further group heterogeneous EPCs into one qualitative category, "adhesive cultured EPCs", without any hierarchical discrimination or proper characterization of contaminating cell populations, consisting mainly of hematopoietic cells (Rohde et al., 2007). Ingram et al. (2005) have demonstrated circulating endothelial differential stages, with high- and low proliferative potential-endothelial colony forming cells (HPP-ECFCs and LPP-ECFCs), using their original

*Corresponding author at: Department of Regenerative Medicine Science, Division of Basic Clinical Science, Tokai University School of Medicine, Shimokasuya, Isehara, Kanagawa 259-1143, Japan. Tel.: +11 81 463 93 1121x2521; fax: +11 81 463 95 0961.
E-mail address: asa777@is.icc.u-tokai.ac.jp (T. Asahara).

1050-1738/$ - see front matter © 2013 Elsevier Inc. All rights reserved.
http://dx.doi.org/10.1016/j.tcm.2012.09.007

culture parameters, demonstrating clonal CFUs in outgrowth EPCs, cultured adhesive EPCs, or differentiated endothelial cells (ECs). This carefully conceived culture assay system, which demonstrates thorough insight into stem cell biology, has contributed significantly to the development of EPC biology via the introduction of a differential hierarchy system for ECs.

However, this system does not identify primary circulating EPCs from PB, BM, or UCB, i.e., hEPCs, but instead isolates CFUs from cultured adhesive cells of tissue-derived ECs or EPCs, which is to say, non-hematopoietic EPCs (Asahara et al., 2011). Considering the necessity to create a defined assay to detect hEPCs qualitatively and quantitatively from primary blood samples, we have developed a new colony assay system, modifying the conventional methylcellulose assay used for stem/progenitor cell identification (Benndorf et al., 2007; Eichmann et al., 1997; Rustemeyer et al., 2007).

As we have recently reported, the present assay system discriminates two types of EPC-CFUs, morphologically identified by their respective colony cells with their specific features (Masuda et al., 2011). The first group of colony cells presents proliferative capabilities, and in a secondary semi-solid colony assay system, they are converted into the latter cell type with vasculogenic properties. The two types are defined as primitive EPC-CFUs and definitive EPC-CFUs, respectively.

The concept of EPC-CFA in hEPC differentiation cascade

Over the last decade, there have been a couple of reported EPC culture methods to identify hEPCs in circulation by the quantification of 'adhesive EPCs' from PBMNCs. These are known as the 'cultured EPC assay' and 'Hill's assay' that use endothelial cell-conditioned medium. Since then, these culture methods have been revealed to present the adhesive or aggregation features of circulating angiogenic cells (CACs), i.e., T-lymphocytes (Hur et al., 2007), monocytes/macrophages (Rehman et al., 2003), or 'early EPC' (Duan et al., 2006), indicating that these assay systems are insufficient to investigate the hEPC differentiation activity from HSCs. In contrast to conventional culture methods, EPC-CFA has been demonstrated to be a clonogenic culture system that accurately assesses the differentiation of hEPCs from HSCs. In fact, the $CD133^{+}$ cells of the HSC fraction in UCB in EPC-CFA generate EPC-CFUs, but not 'adhesive EPCs', as they appear in conventional culture assays. On the other hand, colony cells of definitive EPC-CFUs show the cellular phenotype of 'adhesive EPCs' in the EPC culture assay. These findings indicate that there exists a hierarchical EPC differentiation

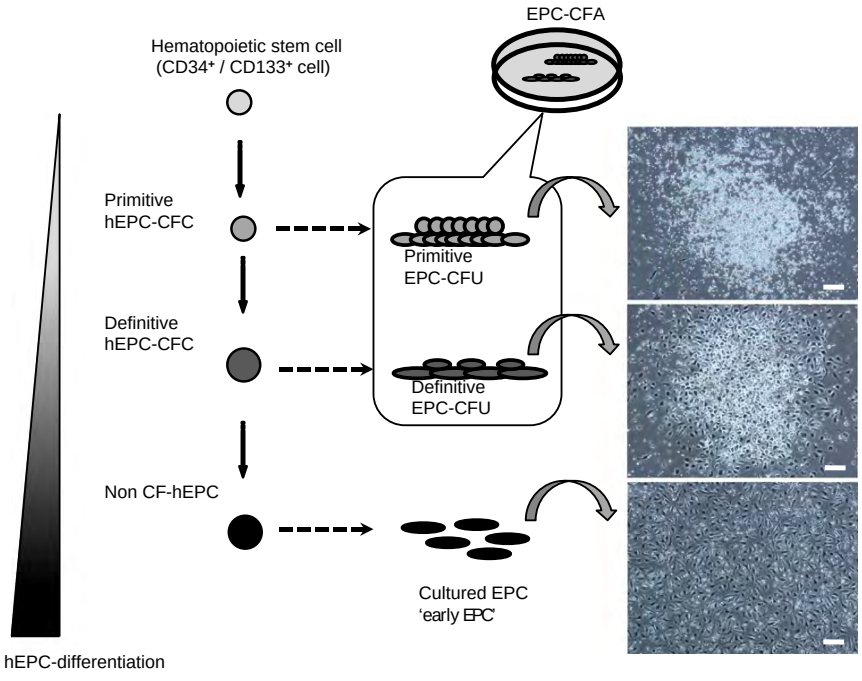

Fig. 1 – Concept of EPC-CFA to assess the hEPC differentiation cascade. hEPCs originate from HSCs. During hEPC differentiation, hEPCs loose their colony forming potential and become vasculogenic. Based on this, hEPCs exhibit individual colony forming features: primitive EPC-CFUs or definitive EPC-CFUs, which are morphologically defined as small round colony cells or spindle-like colony cells; these are respectively pro-vasculogenic or vasculogenic, thereby providing the significance to evaluate the number or frequency of each colony for the assessment of vasculogenic potential of investigated cell populations. HSC: hematopoietic stem cell; hEPC-CFC: hematopoietic EPC colony forming cell; non CF-hEPC: non colony forming hematopoietic EPC. The upper, middle, and lower pictures indicate primitive EPC-CFU, definitive EPC-CFU, or cultured EPC, respectively. Scale bar = 200 μm.

cascade in circulation that consists of each EPC colony forming cell type, primitive EPC-CFUs or definitive EPC-CFUs, at an immature phase, and then non-colony forming EPCs, i.e., 'early EPCs' at a more differentiated phase (Fig. 1).

EPC-CFA to assess colony forming EPC kinetics in hematopoietic cell population

The present assay system differentiates the two types of EPC-CFUs morphologically by identifying their respective colony cells as having small (10–20 μm) round cells and large (50–200 μm) spindle-like cells (Masuda et al., 2011). The former small round colony cells are proliferative, and in a secondary semi-solid colony assay system, the cells convert into the latter vasculogenic type, and are defined as primitive EPC-CFUs and definitive EPC-CFUs, respectively. Our findings indicate that there is a hierarchical differentiation cascade of EPC colony forming cells, allowing for quantitative enumeration of colonies and calculation of the ratio of the number of definitive EPC-CFUs to total EPC-CFUs (Fig. 2). In other words, the fundamental concept of EPC-CFA allows us to quantitatively assess each colony in terms of hEPC differentiation kinetics.

Application for basic research in vascular biology

EPC-CFA is available for primary or cultured cell populations of MNCs, and single or bulky stem cells in hematological cell populations (PB, BM, and CB), except for BM-MNCs, which include stromal cells that disturb the growth of EPC-CFUs. This universal application allows for investigation of the EPC bioactivity of proliferation or differentiation in cell populations of interest. In particular, the single stem cell fate can be analyzed by a hematopoietic and/or endothelial cell lineage commitment assay (HELIC assay) (Masuda et al., 2011), where hematopoietic CFA can be performed simultaneously with EPC-CFA in expansion cultured cells from single stem cells. The HELIC assay provides better information concerning the relationship between hematopoietic and endothelial lineages committed from HSCs (Fig. 3).

Clinical applications

Additionally, EPC-CFA is available for the evaluation of vasculogenic potential of target cells isolated from patients with cardiovascular disorders who have been reported to have a

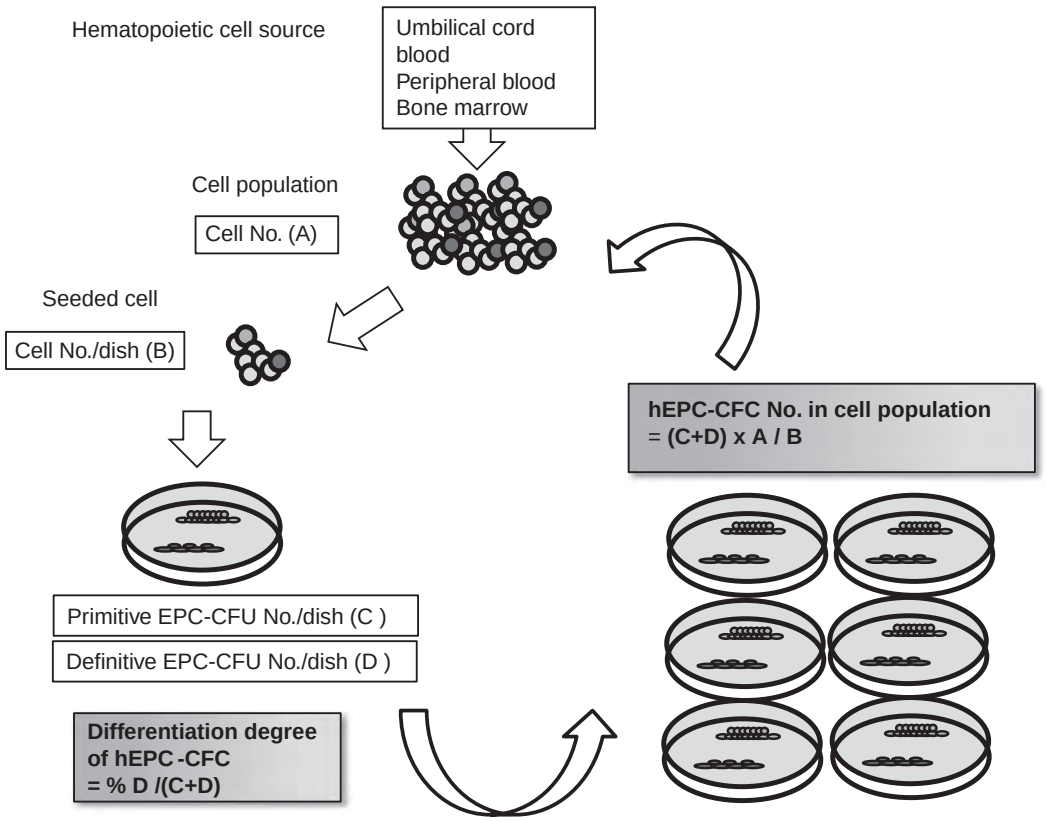

Fig. 2 – EPC-CFA to evaluate the degree of differentiation and number of hEPC-CFCs in a hematopoietic cell population. EPC-CFA allows us to evaluate the differentiation degree and number of hEPC-CFCs in investigated cell population from hematopoietic cell sources. (1) When performing EPC-CFA, the cell number (A) and seeded cell number per dish (B) of the cell population are first determined. (2) Using the counted numbers of primitive and definitive EPC-CFUs/dish (C and D), the differentiation degree is calculated as the %ratio of D to total EPC-CFUs (C + D). Further, total hEPC-CFCs in the whole cell population are simply estimated by the equation (C + D) × A/B.

reduction in EPC kinetics, i.e., mobilization, proliferation, or differentiation (Fadini et al., 2006; Hill et al., 2003). The assessment of vascular repair or regenerative capabilities in patients can thus be performed practically. Alternatively, under EPC therapy using autologous PBMNCs (Moriya et al., 2009), or PB-$CD34^+$ cells mobilized after G-CSF administration (Kawamoto et al., 2006), etc., EPC-CFA using cells from patients permits the evaluation of vasculogenic potential at the pre- or post-transplantation stage, enabling prognosis of therapeutic efficacy.

Future perspectives

For basic research into vascular biology, EPC-CFA can detect the differentiation of HSCs into the vasculogenic phase. In particular, EPC-CFA may help clarify the specific surface antigens of circulating EPC-colony forming cells, which are still elusive. Moreover, cell surface marker profiling of EPC-colony forming cells enables the direct identification of those cells in circulation by flow cytometry, thereby leading to the complete elucidation of the EPC differentiation cascade from colony forming to non-colony forming EPCs. Such a direct analysis of the EPC differentiation cascade by flow cytometry, based on EPC-CFA, would result in a more objective and time-saving methodology, whereas EPC-CFA requires the time-consuming need to grow EPC-CFUs, it eliminates the training needed for quantification of those colonies under present circumstances.

Conclusion

EPC-CFA permits the determination of the fate of circulating hEPCs, based on a numerical assessment of their hierarchical adhesive clonogenicity, providing a novel and powerful tool not only to investigate the significance of EPC differentiation in vascular biology but also to evaluate the vasculogenic potential of patients in clinical situations.

Disclosures

None.

Acknowledgments

We thankfully accepted the outstanding technical supports from the Teaching and Research Support Center of Tokai University School of Medicine and Ms. Tomoko Shizuno, as well as

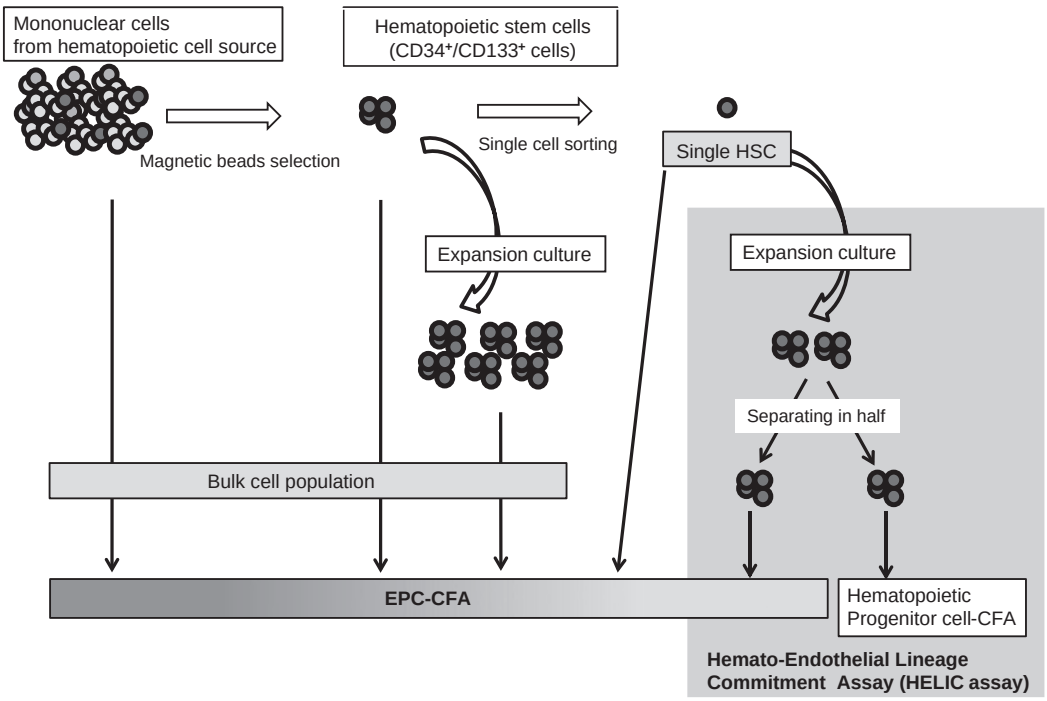

Fig. 3 – Application of EPC-CFA for primary or expansion cultured cell populations. EPC-CFA is applicable for primary or expansion cultured cells, not only for bulk non-selected MNCs or selected $CD34^+/CD133^+$ cells, but also for single selected $CD34^+/CD133^+$ cells. In particular, the Hemato-Endothelial lineage commitment assay (HELIC assay), which is applicable for EPC-CFA, uses single hematopoietic stem cells to analyze their commitment into hematopoietic and/or endothelial lineages. In brief, EPC-CFA and a conventional hematopoietic progenitor cell-CFA can be performed practically by using half of each expansion of the cultured cells from a single hematopoietic stem cell. Subsequently, the cell fate of the single stem cells into endothelial and/or hematopoietic cell lineages is quantitatively evaluated by analyzing the frequency of the stem cell generating EPC-CFUs in EPC-CFA and/or hematopoietic lineage-CFUs (e.g., erythrocyte-CFU, granulocyte/macrophage-CFU and monocyte/macrophage-CFU) in hematopoietic progenitor cell-CFA.

Ms. Sachie Ota for her secretarial assistance. This work was supported by grants from the Riken Center for Developmental Biology Collaborative Research Fund (08001475), Kobe for T.A.; National Institutes of Health (HL53354 and HL57516), Bethesda, MD for T.A.; the Ministry of Health, Labor and Welfare (H14-trans-001, H14-trans-002, H17-trans-002, H17-trans-014, and H20-regenerative medicine-general-001), Japan for T.A.; the Ministry of Education, Culture, Sports, Science and Technology (Basic Research Grant 22590796 for H.M., and Program for the Strategic Research Foundation at Private Universities, S1201001 for T.A. and H.M.), Japan.

REFERENCES

Asahara T, Kawamoto A, Masuda H. Concise review: circulating endothelial progenitor cells for vascular medicine. Stem Cells 2011;29(11):1650–5.

Asahara T, Murohara T, Sullivan A, Silver M, van der Zee R, Li T, et al. Isolation of putative progenitor endothelial cells for angiogenesis. Science 1997;275(5302):964–7.

Benndorf RA, Gehling UM, Appel D, Maas R, Schwedhelm E, Schlagner K, et al. Mobilization of putative high-proliferative-potential endothelial colony-forming cells during antihypertensive treatment in patients with essential hypertension. Stem Cells and Development 2007;16(2):329–38.

Duan HX, Cheng LM, Wang J, Hu LS, Lu GX. Angiogenic potential difference between two types of endothelial progenitor cells from human umbilical cord blood. Cell Biology International 2006;30(12):1018–27.

Eichmann A, Corbel C, Nataf V, Vaigot P, Breant C, Le Douarin NM. Ligand-dependent development of the endothelial and hemopoietic lineages from embryonic mesodermal cells expressing vascular endothelial growth factor receptor 2. Proceedings of the National Academy of Sciences of the United States of America 1997;94(10):5141–6.

Fadini GP, de Kreutzenberg SV, Coracina A, Baesso I, Agostini C, Tiengo A, et al. Circulating $CD34^+$ cells, metabolic syndrome, and cardiovascular risk. European Heart Journal 2006;27(18):2247–55.

Hill JM, Zalos G, Halcox JP, Schenke WH, Waclawiw MA, Quyyumi AA, et al. Circulating endothelial progenitor cells, vascular function, and cardiovascular risk. New England Journal of Medicine 2003;348(7):593–600.

Hur J, Yang HM, Yoon CH, Lee CS, Park KW, Kim JH, et al. Identification of a novel role of T cells in postnatal vasculogenesis: characterization of endothelial progenitor cell colonies. Circulation 2007;116(15):1671–82.

Ingram DA, Caplice NM, Yoder MC. Unresolved questions, changing definitions, and novel paradigms for defining endothelial progenitor cells. Blood 2005;106(5):1525–31.

Kawamoto A, Iwasaki H, Kusano K, Murayama T, Oyamada A, Silver M, et al. CD34-positive cells exhibit increased potency and safety for therapeutic neovascularization after myocardial infarction compared with total mononuclear cells. Circulation 2006;114(20):2163–9.

Masuda H, Alev C, Akimaru H, Ito R, Shizuno T, Kobori M, et al. Methodological development of a clonogenic assay to determine endothelial progenitor cell potential. Circulation Research 2011;109(1):20–37.

Moriya J, Minamino T, Tateno K, Shimizu N, Kuwabara Y, Sato Y, et al. Long-term outcome of therapeutic neovascularization using peripheral blood mononuclear cells for limb ischemia. Circulation. Cardiovascular Interventions 2009;2(3)245–54.

Rehman J, Li J, Orschell CM, March KL. Peripheral blood "endothelial progenitor cells" are derived from monocyte/macrophages and secrete angiogenic growth factors. Circulation 2003;107(8):1164–9.

Rohde E, Bartmann C, Schallmoser K, Reinisch A, Lanzer G, Linkesch W, et al. Immune cells mimic the morphology of endothelial progenitor colonies in vitro. Stem Cells 2007;25(7):1746–52.

Rustemeyer P, Wittkowski W, Greve B, Stehling M. Flow-cytometric identification, enumeration, purification, and expansion of $CD133^+$ and $VEGF\text{-}R2^+$ endothelial progenitor cells from peripheral blood. Journal of Immunoassay and Immunochemistry 2007;28(1):13–23.

STEM CELLS TRANSLATIONAL MEDICINE℠

PROTOCOLS AND MANUFACTURING FOR CELL-BASED THERAPIES

Development of Serum-Free Quality and Quantity Control Culture of Colony-Forming Endothelial Progenitor Cell for Vasculogenesis

HARUCHIKA MASUDA,[a]* HIROTO IWASAKI,[b]* ATSUHIKO KAWAMOTO,[c] HIROSHI AKIMARU,[c] MASAKAZU ISHIKAWA,[d] MASAAKI II,[e] TOMOKO SHIZUNO,[a] ATSUKO SATO,[a] RIE ITO,[a] MIKI HORII,[c] HIDEYUKI ISHIDA,[f] SHUNICHI KATO,[g] TAKAYUKI ASAHARA[a,c]

Departments of [a]Regenerative Medicine Science, [f]Physiology, and [g]Cell Transplantation and Regenerative Medicine, Tokai University School of Medicine, Isehara, Japan; [b]Department of Cardiovascular Surgery, Osaka City University Graduate School of Medicine, Osaka, Japan; [c]Vascular Regeneration Research Group, Institute of Biomedical Research and Innovation, Kobe, Japan; [d]Case Cardiovascular Research Institute, Department of Medicine, Case Western Reserve University, Cleveland, Ohio, USA; [e]Department of Pharmacology, Osaka Medical College, Takatsuki, Japan

*Contributed equally as first authors.

Correspondence: Takayuki Asahara, M.D., Ph.D., Department of Regenerative Medicine Science, Division of Basic Clinical Science, Tokai University School of Medicine, Shimokasuya, Isehara, Kanagawa 259-1143, Japan. Telephone: 11-81-463-93-1121, ext. 2521; Fax: 11-81-463-95-0961; e-mail: asa777@is.icc.u-tokai.ac.jp

Received September 7, 2011; accepted for publication January 4, 2012; first published online in SCTM *EXPRESS* February 6, 2012.

1066-5099/2012/$30.00/0

http://dx.doi.org/10.5966/sctm.2011-0023

Key Words. Angiogenesis • Cellular therapy • Human cord blood • Serum-free medium • Stem/progenitor cell

ABSTRACT

Quantitative and qualitative impairment of endothelial progenitor cells (EPCs) limits the efficacy of autologous cell therapy in patients with cardiovascular diseases. Here, we developed a serum-free quality and quantity control culture system for colony-forming EPCs to enhance their regenerative potential. A culture with serum-free medium containing stem cell factor, thrombopoietin, vascular endothelial growth factor, interleukin-6, and Flt-3 ligand was determined as optimal quality and quantity culture (QQc) in terms of the most vasculogenic colony-forming EPC expansion, evaluated by the newly established EPC colony formation assay. The QQc of umbilical cord blood-CD133$^+$ cells for 7 days produced a 52.9-fold increase in total cell number and 3.28-fold frequency in definitive EPC colony development, resulting in a 203.9-fold increase in estimated total definitive EPC colony number in vitro. Pre- or post-QQc cells were intramyocardially transplanted into nude rats with myocardial infarction (MI). Echocardiographic and micromanometer-tipped conductance catheter examinations 28 days post-MI revealed significant preservation of left ventricular (LV) function in rats receiving pre- or post-QQc cells compared with those receiving phosphate-buffered saline. Assessments of global LV contractility indicated a dose-dependent effect of pre- or post-QQc cells and the superior potency of post-QQc cells over pre-QQc cells. Furthermore, immunohistochemistry showed more abundant formation of both human and rat endothelial cells and cardiomyocytes in the infarcted myocardium following transplantation of post-QQc cells compared with pre-QQc cells. Our optimal serum-free quality and quantity culture may enhance the therapeutic potential of EPCs in both quantitative and qualitative aspects for cardiovascular regeneration. STEM CELLS TRANSLATIONAL MEDICINE *2012;1:160–171*

INTRODUCTION

Several translational researchers have demonstrated that CD34$^+$ or CD133$^+$ cells in umbilical cord blood (CB), bone marrow (BM), or peripheral blood (PB), previously defined as hematopoietic stem/progenitor cells, also serve as the enriched source of endothelial progenitor cells (EPCs) [1, 2], inducing neovascularization for functional recovery from ischemic injury [3–10]. Particularly autologous CD34$^+$ or CD133$^+$ stem/progenitor cells have been therapeutically transplanted in patients with severe ischemic heart or limb diseases, and these initial clinical experiences indicate the safety and feasibility as well as the effectiveness of cell-based therapy [3, 11–19].

However, a limitation of stem/progenitor cell therapy has been also reported. EPC-enriched populations (CD34$^+$, CD133$^+$, CD34$^+$/vascular endothelial growth factor receptor 2$^+$ [VEGFR-2$^+$], or CD133$^+$/VEGFR-2$^+$) are scarce even in the BM and PB. Moreover, the EPC fraction numerically and functionally declines in patients with aging [20] or cardiovascular risk factors [21, 22]. These reports suggest that poor responses to cellular therapy are due to quantitative and/or qualitative impairment of the EPC fraction. To further augment the efficacy of EPC transplantation, several methodological approaches to enhance EPC bioactivities are currently being developed [5, 23–28].

Initially, the EPC expansion culture has been established in terms of an increase in attached endothelial lineage cells following the conditioning of PB or BM mononuclear cells with endothelial growth factor-supplemented medium [4, 29–31]. Although high performances for vasculogenesis are represented in animal models, the quality and quantity culture control for medical

Table 1. Investigated combinations of growth factors/cytokines for quality and quantity culture

Comb	Comb 1	Comb 2	Comb 3	Comb 4	Comb 5	Comb 6
TPO/VEGF	−	+	+	+	+	+
SCF	+	−	+	+	+	+
Flt-3 ligand	+	+	−	+	+	+
IL3	+	+	+	−	+	+
IL6	+	+	+	+	−	+

Abbreviations: Comb, combination; IL, interleukin; SCF, stem cell factor; TPO, thrombopoietin; VEGF, vascular endothelial growth factor.

EPCs is limited by less proliferative activity and progressive senescence during the culture in attached EPC phenotype. In this regard, the several culture systems of suspended EPC phenotype have been developed and demonstrated the significance of EPC expansions ex vivo and the efficiency of cultured $CD34^+$ or $CD133^+$ cell transplant for neovascularization in ischemic animal models [5, 23–28].

However, despite the effective results for therapeutic strategy in many researches, EPCs remain a controversial topic among researchers as there is no definitive delineation of EPCs, no clear differentiation hierarchy, and no unambiguously defined isolation protocol. Therefore, the methodological development of EPC culture has lacked the definitive EPC evaluation methodology.

Considering the necessity of creating a defined assay, a novel adhesive clonogenic assay for the quantitative and qualitative analysis of EPCs based on differentiation hierarchy has been developed recently [32–37]. The new EPC colony-forming assay (EPC-CFA) enabled the distinction and the definition of two different types of EPC-colony-forming units (EPC-CFUs), that is, primitive and definitive EPC-CFUs, composed of small and large cells, respectively. Primitive EPC-CFUs (PEPC-CFUs) revealed a predominant potential for proliferation. The other kind, definitive EPC-CFUs (DEPC-CFUs), demonstrated a predominantly vasculogenic potential, including cell adhesion and tube-like structure formation in vitro, as well as a high in vivo activity toward de novo blood vessel formation following transplantation into an ischemic hind limb model, as compared with PEPC-CFUs. Therefore, PEPC-CFUs are possibly derived from further immature and proliferative EPCs, and DEPC-CFUs generating EPCs are more prone to differentiation and promoting EPC-mediated cell functions required for vasculogenesis. The definitive colony-forming EPCs are capable of differentiating into a noncolonizing large-cell EPC phenotype, similar to cultured EPCs or early EPCs derived via conventional EPC culture, and are speculated to represent further differentiating EPCs, departed from the niche of colony-forming EPCs.

These findings indicate EPC-CFA would be an ideal tool to develop EPC culture system by qualifying and quantifying the repopulating colony-forming EPCs to expand ex vivo for therapeutic vasculogenesis. In the present study, we optimized the growth factor/cytokine combination (Comb) in a serum-free, quality and quantity culture (QQc) of $CB\text{-}CD133^+$ cells as an EPC-enriched population for vasculogenesis using EPC-CFA and further evaluated the therapeutic potential of the optimal QQc cells for cardiac repair post-myocardial infarction (MI) versus $CB\text{-}CD133^+$ cells in pre-QQc.

Materials and Methods

Preparation of $CB\text{-}CD133^+$ Cells by Magnetic Cell Sorting

CB was used for isolation of $CB\text{-}CD133^+$ cells under the approval of the ethical committees of the Cord Blood Bank and Clinical Investigation of the Tokai University School of Medicine. The protocol of $CB\text{-}CD133^+$ cell isolation is described in supplemental online Methods 1.

Serum-Free Culture Trials of $CB\text{-}CD133^+$ Cells

At first, 10,000 $CB\text{-}CD133^+$ cells in 500 μl of medium were plated into each well of a 24-well tissue culture dish (Primaria, BD Biosciences, San Diego, http://www.bdbiosciences.com) and cultured in a suspension manner using serum-free culture medium (StemSpan SFEM; StemCell Technologies, Vancouver, BC, Canada, http://www.stemcell.com) containing six Combs of several growth factors/cytokines for 7 days (Table 1). Furthermore, $CB\text{-}CD133^+$ cells were similarly cultured by Comb 4 medium, named QQc medium, for 2, 4, or 7 days (Table 2).

EPC-CFA

To investigate the vasculogenic potential of pre- or post-QQc cells, we quantified adhesive EPC colonies by EPC-CFA using semi-solid culture medium (MethoCult SF^{BIT}; StemCell Technologies) with pro-angiogenic growth factors in 35-mm Primaria dishes (BD Biosciences), as described in supplemental online Methods 2 [32–35, 37]. Eighteen days after initiation of the culture, the number of adherent colonies per dish was measured using a gridded scoring dish (StemCell Technologies) under light

Table 2. Endothelial progenitor cell (EPC) CFU production of $CB\text{-}CD133^+$ cells in QQc

EPC-CFU no.	Day 0	Day 2	Day 4	Day 7
Per 500 cells				
PEPC-CFU (no.)	18.9 ± 1.0	19.9 ± 0.9	14.6 ± 0.6	11.0 ± 0.7
DEPC-CFU (no.)	5.8 ± 1.0	15.3 ± 0.9	21.2 ± 1.6	19.0 ± 1.7
TEPC-CFU (no.)	24.7 ± 1.5	35.2 ± 1.5	35.8 ± 1.6	30.0 ± 1.6
Per 1×10^4 $CB\text{-}CD133^+$ cells				
PEPC-CFU (no.)	503.3 ± 45.7	608.6 ± 55.3	3,083.2 ± 200.1	12,396.1 ± 981.4
DEPC-CFU (no.)	116.7 ± 24.8	455.1 ± 48.0	3,012.6 ± 200.1	23,793.2 ± 2,399
TEPC-CFU (no.)	620.0 ± 65.6	1063.7 ± 91.8	6,095.8 ± 38.0	36,189.3 ± 2,117

The top three rows are counted EPC-CFU numbers per 500 QQc cells in each period. The bottom three rows are estimated EPC-CFU numbers per whole QQc cell at each period from 1×10^4 pre-QQc cells ($CB\text{-}CD133^+$ cells) at day 0. The values indicated are mean ± SE in 3 dishes per each time point per sample × 6 CB samples.

Abbreviations: CB, umbilical cord blood; CFU, colony-forming unit; DEPC, definitive endothelial progenitor cell; PEPC, primitive endothelial progenitor cell; QQc, quality and quantity culture; TEPC, total endothelial progenitor cell (PEPC-CFU plus DEPC-CFU).

microscopy. PEPC-CFUs and DEPC-CFUs were counted separately [32–35, 37].

Characterization of EPC Colonies

To confirm the endothelial characterization of the colonized cells, we measured biochemical binding with *Ulex europaeus* agglutinin I-conjugated fluorescein isothiocyanate (UEA-I-FITC), (Vector Laboratories, Burlingame, CA, http://www.vectorlabs.com) and uptake of acetylated low-density lipoprotein-conjugated 1,1′-dioctadecyl-3,3,3′,3′-tetramethylindo-carbocyanine perchlorate (acLDL-DiI) (Biomedical Technologies, Inc., Stoughton, MA, http://www.btiinc.com) , and we also examined immunocytochemistry for endothelial cell (EC)-specific markers, as described in supplemental online Methods 3.

Flow Cytometry Analysis

To characterize pre- and post-QQc cells, cells were analyzed by flow cytometry using a FACSCalibur flow cytometry system (BD Biosciences) after staining with mouse anti-human antibodies against surface markers listed in the supplemental online Material List. The data were analyzed by FlowJo, a flow cytometry analysis software (Tomy Digital Biology Co., Ltd., Tokyo, http://www.digital-biology.co.jp).

Real-Time Polymerase Chain Reaction Assay

The gene expression of proangiogenic growth factors and a cell proliferation marker, Ki67, in pre- and post-QQc cells was quantitatively analyzed by real-time polymerase chain reaction (PCR) assay as described in supplemental online Methods 4.

In Vitro Tube Formation and Incorporation Assay in Matrigel

To investigate the functional contribution of pre- or post-QQc cells to neovascular formation, the cells were applied to a tube formation and incorporation assay by coculturing with human umbilical vein endothelial cells (HUVECs) on Matrigel, as described in supplemental online Methods 5.

In Vitro Sprouting Assay in Matrigel

A colony cell fraction of PEPC- or DEPC-CFUs from pre- or post-QQc cells was isolated, and then each colony cell fraction was applied to Matrigel assay as described in supplemental online Methods 6.

In Vitro Induction of Functional Cardiomyocytes

The methods used to investigate the trans-differentiation of post-QQc cells into functional cardiomyocytes (CMCs) are detailed in supplemental online Methods 7.

In Vivo Assessment of Vascular and Cardiac Repair by Transplanted Pre- or Post-QQc Cells in the Rat Myocardial Ischemic Model

Vascular and cardiac repair by transplantation of pre- or post-QQc cells was investigated in rat myocardial ischemic model, as described in supplemental online Methods 8.

Statistical Analysis

The results were statistically analyzed as described in supplemental online Methods 9.

RESULTS

Optimization of Growth Factor/Cytokine Comb for QQc

To identify the QQc, we evaluated EPC colony producing potential among the six kinds of growth factor/cytokine Combs using EPC-CFA (Table 1). The cell numbers postculture for 7 days in six kinds of Combs varied from 26.0-fold in Comb 2 to 95.8-fold in Comb 6, compared with precultured cells (1×10^4 CB-CD133$^+$ cells) (Fig. 1A).

Of note, stem cell factor (SCF) exhibited the most potent factor to increase cell number because of the comparison of Comb 2 versus Comb 6. In EPC-CFA of cultured cells in all Combs, as previously indicated in mouse or human EPC-CFA [32–37], two types of EPC colonies were morphologically detected: PEPC-CFU, formed of small, round cells, and DEPC-CFU, formed of large, spindle-like cells (supplemental online Fig. 1A). These colonies showed biological features of endothelial lineage—that is, intracellular uptake of acLDL-DiI, cell surface binding of UEA-I-FITC (supplemental online Fig. 1B), and immunohistochemical positivities of endothelial antigens, such as endothelial nitric oxide synthase, VEGFR-2, and vascular endothelial (VE) cadherin (supplemental online Fig. 1C) [37].

The numerical assessment of EPC-CFA revealed a different pattern of EPC colony-forming potentials among the Comb groups from cultured cell numbers (Fig. 1B, 1C). The amount of PEPC-CFU, DEPC-CFU, or total EPC-CFU per 500 post-QQc cells was significantly higher in Comb 4 compared with the other Combs (Fig. 1B). In particular, the production of DEPC-CFU, indicating further vasculogenic capability superior to that of PEPC-CFU, was highest in Comb 4 (from 1.65-fold vs. Comb 3 to 2.65-fold vs. Comb 6). The estimated number of DEPC-CFUs produced from postculture of 1×10^4 CB-CD133$^+$ cells in Comb 4 significantly increased by 1.77-fold (vs. Comb 6) to 4.44-fold (vs. Comb 2) (Fig. 1C).

Together, EPC-CFA disclosed that Comb 4 (SCF, thrombopoietin [TPO], Flt3-ligand, interleukin-6 [IL-6], and vascular endothelial growth factor [VEGF]) provides the QQc system, compared with the other Comb candidates, based on vasculogenic potential of EPC colony production. On the basis of this, the following experimental data were found under the QQc.

EPC Quality and Quantity During and Post-QQc

The total cell expansion during QQc was measured. The cell number in culture did not increase by day 2 but gradually increased, from 7.4-fold at day 4 post-QQc up to 52.9-fold at day 7 post-QQc (Fig. 2A). To evaluate the quality of vasculogenic potential during QQc, we performed EPC-CFA at each time point (Fig. 2B–2D; Table 2).

Total EPC-CFU number post-QQc did not exhibit a significant difference versus pre-QQc at day 7, although it was slightly increased at days 2 and 4 versus pre-QQc (Fig. 2B). On the other hand, the frequency of PEPC-CFU per 500 cells at each time point gradually decreased from day 2, finally reaching 0.58-fold of pre-QQc at day 7 post-QQc. Inversely, DEPC-CFU increased and reached a peak level of 3.66-fold at day 4 and 3.28-fold at day 7 post-QQc, compared with pre-QQc (Fig. 2B). Further, the ratio of DEPC-CFU number in total EPC-CFU number increased gradually (Fig. 2C).

On the basis of the expansion ratio at each time point of QQc, the estimated quantity of EPC-CFUs produced from pre-QQc was

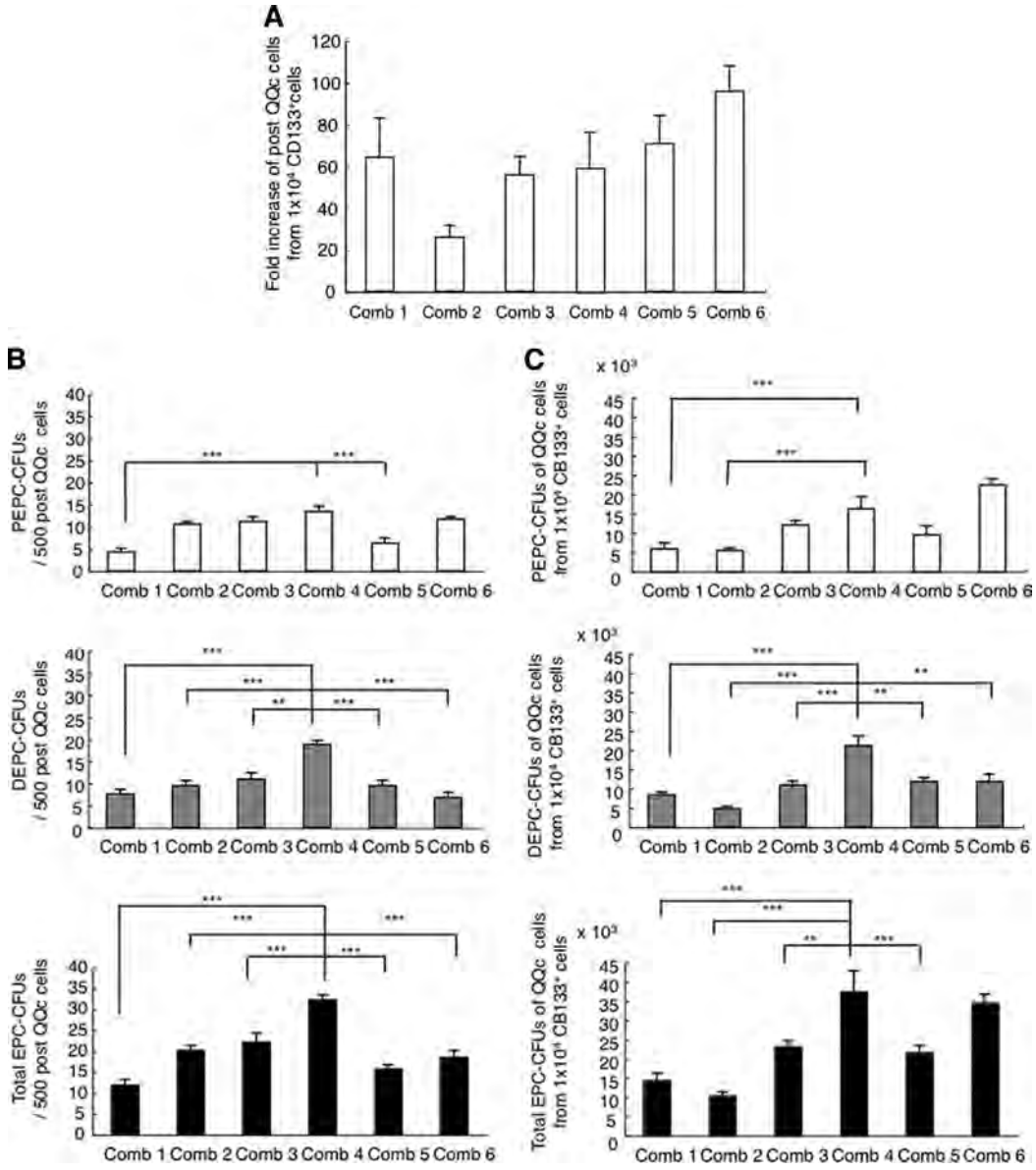

Figure 1. Optimization of the Combs of growth factors/cytokines for QQc to acquire optimal EPC-CFU production. **(A):** Fold increase of post-QQc cells versus CB-CD133$^+$ cells pre-QQc. **(B):** The frequency of EPC-CFU production from the Combs of growth factors/cytokines for QQc. **(C):** Estimated EPC-CFU numbers produced from an initial 10,000 CB-CD133$^+$ cells pre-QQc. **(B, C):** ∗, $p < .05$; ∗∗, $p < .01$; ∗∗∗, $p < .001$. $n = 3$ dishes per Comb per CB sample × 4 CB samples. Abbreviations: CFU, colony-forming unit; Comb, combination; DEPC, definitive endothelial progenitor cell; EPC, endothelial progenitor cell; PEPC, primitive endothelial progenitor cell; QQc, quality and quantity culture.

calculated. Numbers of PEPC-CFU, DEPC-CFU, and total EPC-CFU increased drastically and reached a maximal level at day 7 post-QQc (24.6-fold for PEPC-CFU, 203.9-fold for DEPC-CFU, and 58.4-fold for total EPC-CFU) (Fig. 2D). These findings indicate that QQc is superior at the quantity control culture to increase in EPC number, and at the quality control culture to potentiate EPC vasculogenic capability in terms of preferential increase in DEPC-CFUs.

Characterization of Pre- and Post-QQc Cells In Vitro

Flow cytometry was performed to estimate the positivities for endothelial lineage markers in pre- and post-QQc cells. The percentage of positivity for endothelial-specific markers of VEGFR-2, CD146 (P1H12), or von Willebrand factor (vWF) increased in post-QQc cells versus pre-QQc cells, although CD33$^+$ cells decreased (Fig. 3A). Concomitantly, the different positive ratio of the other hematopoietic lineage marker antigens between pre- and post-QQc cells could be detected (supplemental online Figure 2). T- or B-lymphocytes (CD3 or CD19) or dendritic cells (CD83) were rather predominant in pre-QQc cells, compared with post-QQc cells. On the other hand, the number of monocytes (CD14) or macrophages (CD68) was higher in post-QQc cells than in pre-QQc cells, concurrent with endothelial-specific

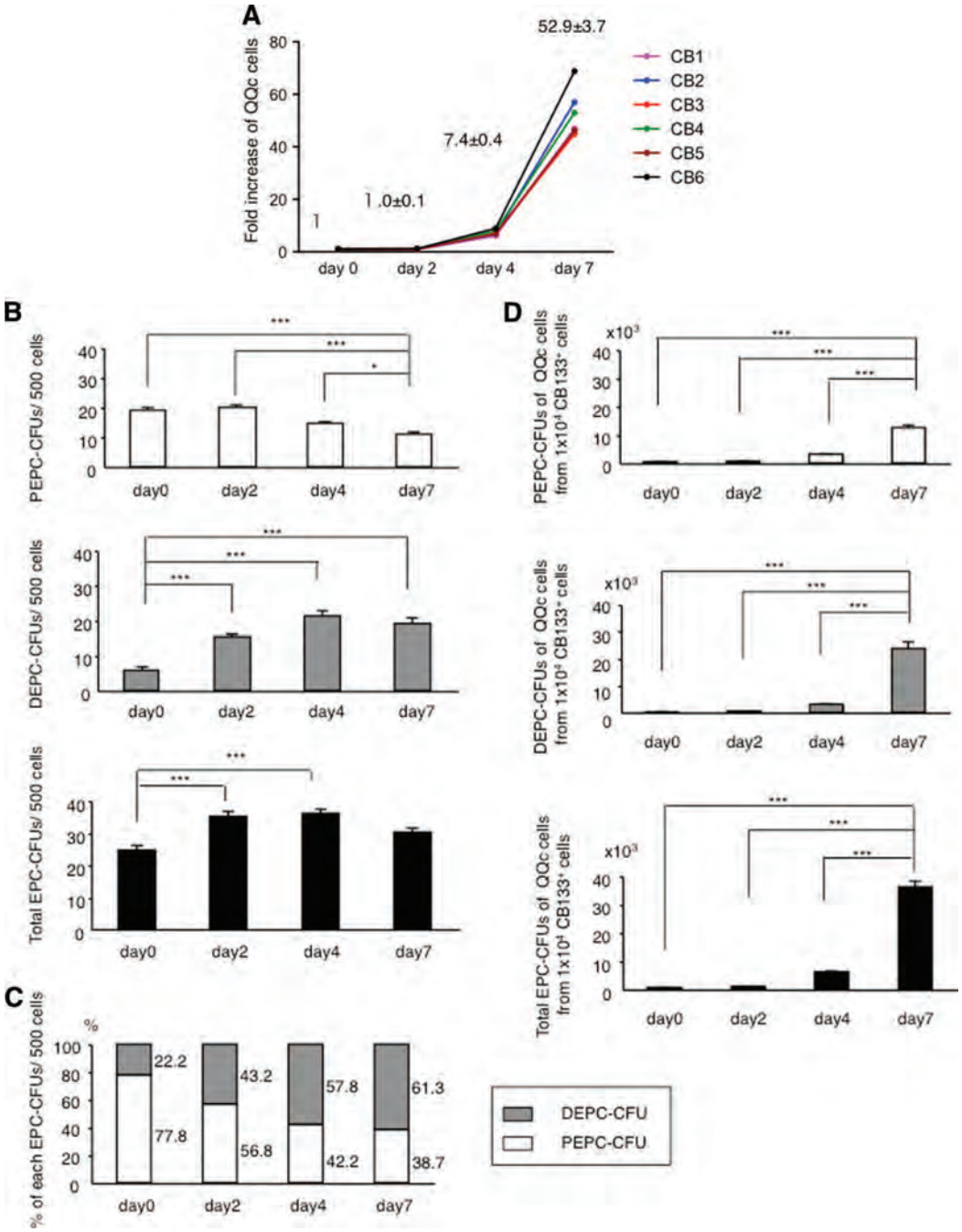

Figure 2. Profile of EPC-CFU production from CB-CD133$^+$cells in QQc. **(A):** Fold increase of cell numbers during QQc in six CB samples. The value at each QQc period indicates the fold increase of QQc cells versus CB-CD133$^+$ cells pre-QQc. **(B):** Frequency of EPC-CFU production per 500 cells at each time point of QQc. **(C):** Percentage of each EPC-CFU in produced total EPC-CFU. The adjacent values of shaded columns indicate the averaged percentages at each time point. **(D):** Estimated EPC-CFU numbers produced from an initial 10,000 CB-CD133$^+$cells. **(B–D):** *, $p < .05$; **, $p < .01$; ***, $p < .001$. $n = 3$ dishes per CB sample $\times$ 6 CB samples. Abbreviations: CB, umbilical cord blood; CFU, colony-forming unit; DEPC, definitive endothelial progenitor cell; EPC, endothelial progenitor cell; PEPC, primitive endothelial progenitor cell; QQc, quality and quantity culture.

markers. Above all, the augmented frequency for VEGFR-2 or vWF was considerably higher in post-QQc cells compared with monocyte/macrophages (CD14) or macrophages (CD68). These findings indicate that QQc predominantly promotes the commitment and differentiation of CD133$^+$ stem cells into EPCs.

Real-time PCR revealed upregulated gene expression of proangiogenic growth factors VEGF (8.3-fold) and hepatocyte

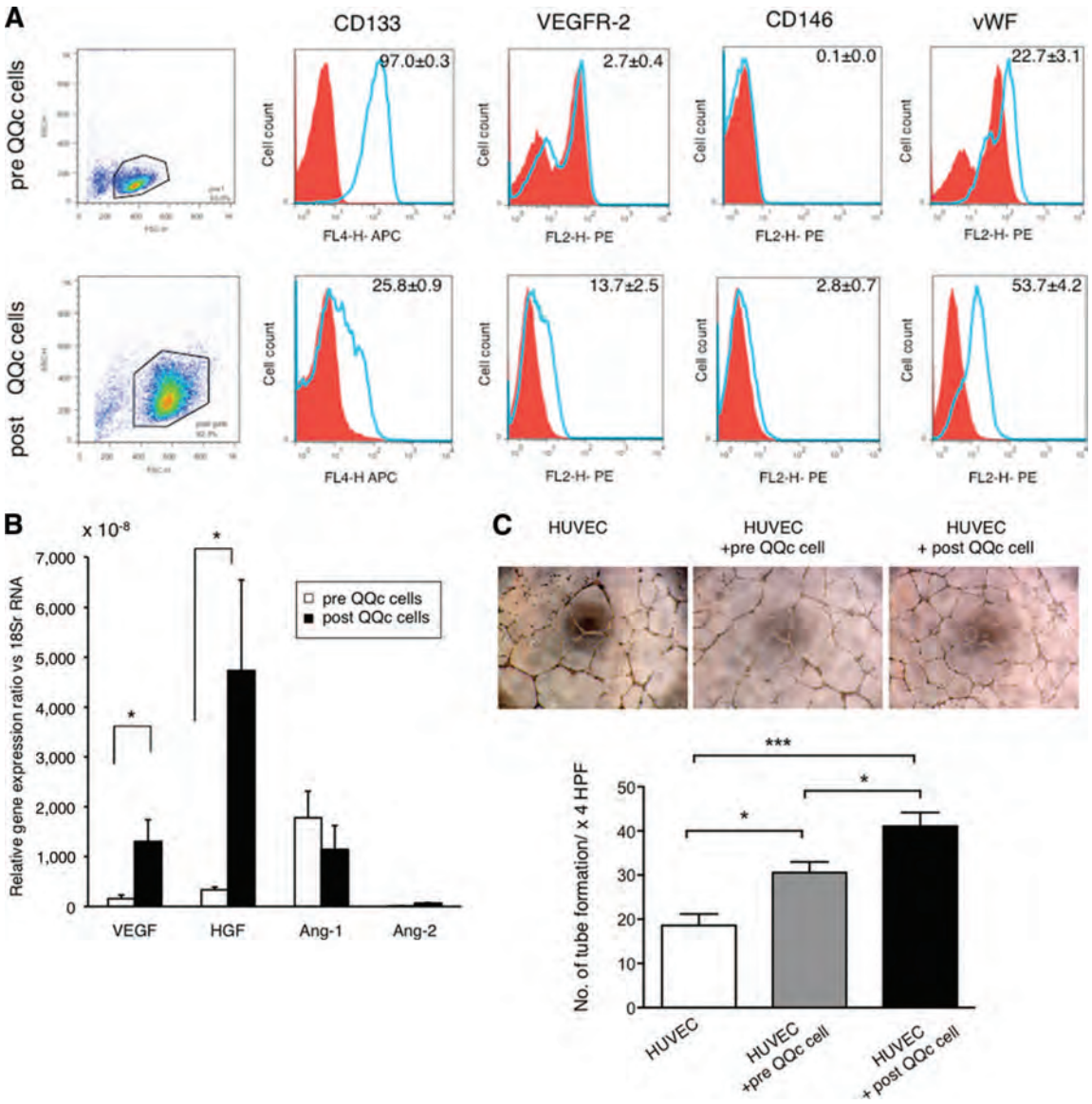

Figure 3. Profile of pre- and post-QQc cells. **(A):** Flow cytometry of pre- and post-QQc cells. $n = 4$ umbilical cord blood (CB) samples. **(B):** Relative gene expression ratio of proangiogenic growth factors versus 18S rRNA in pre- or post-QQc cells assessed by quantitative real-time polymerase chain reaction. $n = 6$ CB samples. **(C):** Matrigel tube formation assay of HUVECs by coculturing with pre- and post-QQc cells. The top panels show representative features of tube formation by HUVECs in the presence or absence of pre- or post-QQc cells (magnification, ×4). The graph indicates the numbers of tube formation in each group. $n = 10$ wells per group. **(B, C):** *, $p < .05$; **, $p < .01$; ***, $p < .001$. Abbreviations: Ang, angiopoietin; APC, allophycocyanin; FL, fluorescence; HGF, hepatocyte growth factor; HPF, high power field; HUVEC, human umbilical vein endothelial cell; PE, phycoerythrin; QQc, quality and quantity culture; VEGF, vascular endothelial growth factor.

growth factor (HGF) (14.1-fold) in post-QQc cells compared with pre-QQc cells. On the other hand, angiopoietin-1 did not show statistical significance, although it tended to decline. Alternatively, angiopoietin-2 remained at a very low expression level (Fig. 3B). These data indicate that post-QQc cells are more angiogenic cells, which predominantly express VEGF or HGF, compared with pre-QQc cells.

In vitro Matrigel assay revealed that post-QQc cells cocultured with HUVECs predominantly promoted tube formation 12 hours after cell seeding by 2.28-fold over HUVECs alone and 1.45-fold over pre-QQc cells cocultured with HUVECs (Fig. 3C). These findings showed that post-QQc cells preferentially possess the capability of augmenting angiogenesis compared with those pre-QQc cells.

Therapeutic Evaluation of Post-QQc Cells Following Cell Transplantation into Infarcted Myocardium

We transplanted pre- and post-QQc cells into myocardial ischemia animal models in vivo and then evaluated microvascular density (MVD) in the infarcted myocardium assessed by *Griffonia* (*Bandeiraea*) *simplicifolia* lectin I (isolectin B4; Vector Laboratories) staining. MVD was significantly greater in rats receiving high

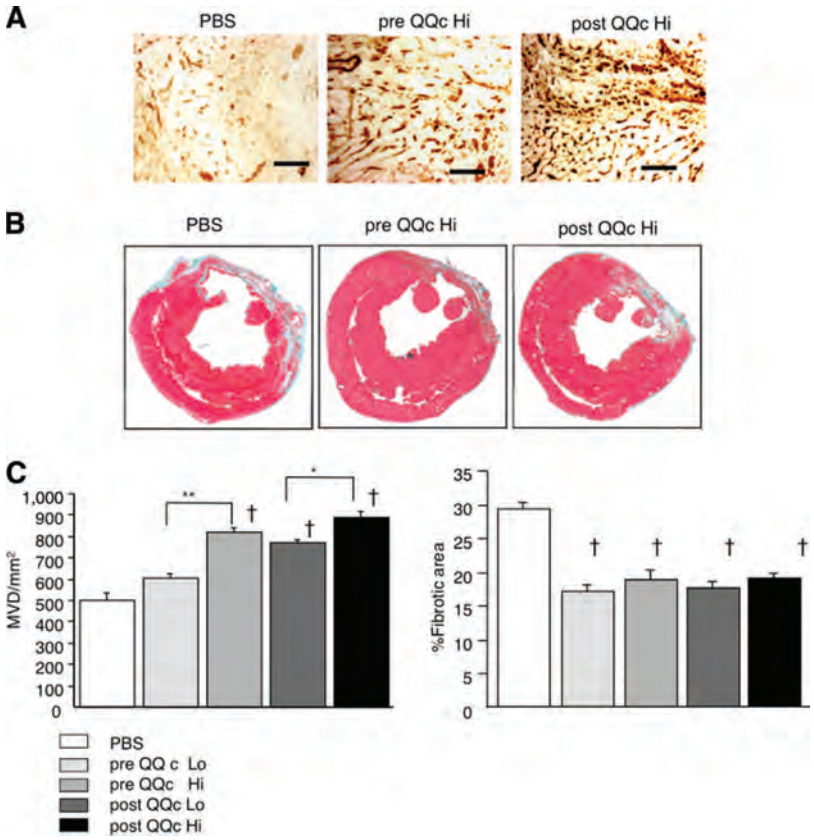

Figure 4. Promotion of neovascularization and inhibition of left ventricular remodeling by transplantation of pre- or post-QQc cells. **(A):** Representative chemical staining with *Griffonia* (*Bandeiraea*) *simplicifolia* lectin I in each group. Scale bars = 100 μm. **(B):** Representative Masson-trichrome staining to evaluate the fibrotic area in each group. **(C):** Bar graphs showing MVD (left) and percentage of fibrosis (right). *, $p < .05$; **, $p < .01$; ***, $p < .001$. Six sections per rat × 10 rats per group. Abbreviations: Hi, high dose in pre- or post-QQc group; Lo, low dose in pre- or post-QQc group; MVD, microvascular density; PBS, phosphate-buffered saline; QQc, quality and quantity culture.

doses of pre-QQc and both doses of post-QQc, compared with phosphate-buffered saline (PBS) (PBS, 501.7 ± 32.2; low dose of pre-QQc, 601.1 ± 21.4; high dose of pre-QQc, 820.6 ± 23.0; low dose of post-QQc, 770.0 ± 15.9; high dose of post-QQc, 889.1 ± 28.9/mm^2; $p < .001$). Also, MVD increased dose-dependently in pre- and post-QQc ($p < .01$ for pre-QQc and $p < .05$ for post-QQc) (Fig. 4A, 4C).

Percentage of left ventricular (LV) fibrosis area assessed by Masson-trichrome staining, in the same manner, was significantly smaller in rats receiving low and high doses of pre- or post-QQc, compared with those receiving PBS (PBS, 29.1 ± 1.1; low dose of pre-QQc, 16.6 ± 1.0; high dose of pre-QQc, 16.7 ± 1.0; low dose of post-QQc, 19.0 ± 1.4; high dose of post-QQc, 19.8 ± 0.9; $p < .001$) (Fig. 4B, 4C). These results suggest that transplantation of pre- and post-QQc cells may have equivalent potentials for inhibiting LV fibrosis following MI.

Autocrine and Paracrine Effects of Pre- or Post-QQc Cells for Vasculogenesis and Myocardiogenesis in the Infarcted Myocardium

Immunohistochemistry with a human-specific marker revealed that the histological density of human ECs was significantly greater in rats receiving low and high doses of pre- or post-QQc cells than in those receiving PBS (PBS, 0 ± 0; low dose of pre-QQc, 76.3 ± 7.5; high dose of pre-QQc, 111.5 ± 13.7; low dose of post-QQc, 148.3 ± 16.0; high dose of post-QQc, 226.3 ± 16.7/mm^2; $p < .001$). Human EC density was significantly greater in the high dose of pre- or post-QQc than in low dose of each cell group, respectively ($p < .05$ for pre-QQc and $p < .001$ for post-QQc). Furthermore, human EC density was significantly higher in the low and high doses of post-QQc than in the same doses of pre-QQc ($p < .001$). The effect of pre- or post-QQc on rat EC density was similar to that observed on human EC density (Fig. 5A, 5C).

The histological density of human CMCs was greater in the high dose of pre-QQc cells and both the low and high doses of post-QQc cells than the PBS group (PBS, 0 ± 0; low dose of pre-QQc, 17.8 ± 1.9; high dose of pre-QQc, 83.1 ± 11.6; low dose of post-QQc, 32.3 ± 4.1; high dose of post-QQc, 134.0 ± 14.3/mm^2; $p < .001$). Human CMC density was dose-dependently greater in pre- and post-QQc groups ($p < .001$). Human CMC density was also greater in the high dose of post-QQc group than in that of pre-QQc ($p < .01$). The effect of CB-CD133$^+$ cells pre- or post-QQc on rat CMC density was almost the same as that on human CMC density. (Fig. 5B, 5C).

These data demonstrate dose-dependent autocrine and paracrine effects of pre- and post-QQc from CB-CD133$^+$ cells on vasculogenesis and cardiomyogenesis. The potency for cardiovascular regeneration seems superior in post-QQc cells over pre-QQc.

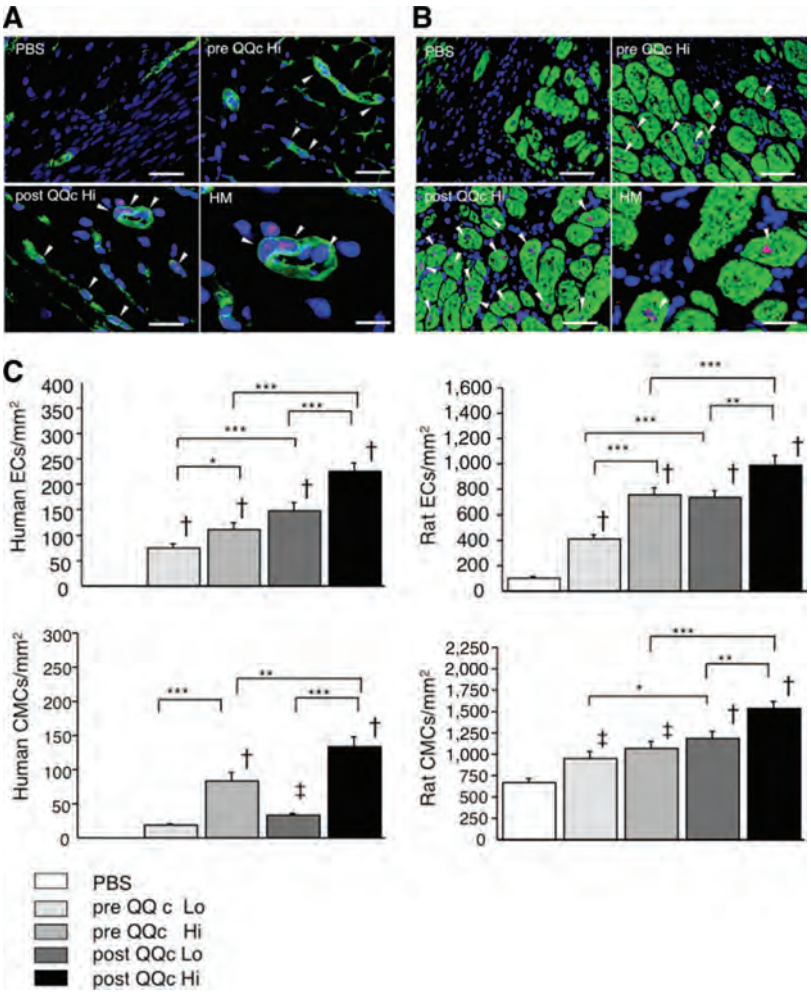

Figure 5. In vivo vasculogenesis and cardiomyogenesis dose-dependently augmented by engraftment of pre- or post-QQc cells. **(A, B):** Representative double immunohistochemistry for human transplanted cells differentiating into ECs or CMCs stained by *Griffonia* (*Bandeiraea*) *simplicifolia* lectin I-fluorescein isothiocyanate (green) or anti-cardiac troponin I antibody (green) with human nuclear antigen (HNA) (red), using infarcted heart samples. HNA appears pink with 4′,6-diamidino-2-phenylindole (blue) overlay. The arrows indicate human nuclei of transplanted cells differentiating into ECs **(A)** or CMCs **(B)**. **(C):** Quantification of ECs (top left) and CMCs (bottom left) differentiated from the transplanted cells in each group. Scale bars = 25 μm **(A)** or 50 μm **(B)** in HM panels and 50 μm **(A)** or 100 μm **(B)** in the others. **(C):** ∗, $p < .05$; ∗∗, $p < .01$; ∗∗∗, $p < .001$. ‡, $p < .01$ versus PBS; †, $p < .001$ versus PBS. Six sections per rat × 10 rats per group. Abbreviations: CMC, cardiomyocyte; EC, endothelial cell; Hi, high dose in pre- or post-QQc group; HM, higher magnification of the corresponding pictures in post-QQc Hi group; Lo, low dose in pre- or post-QQc group; PBS, phosphate-buffered saline; QQc, quality and quantity culture.

Preservation of LV Function Post-MI by Transplantation of CB-CD133$^+$ Cells Pre- or Post-QQc

The invasive hemodynamic assessment of LV function in each group showed that positive pressure and its derivative (+dP/dt) were significantly greater in all cell therapy groups than in the PBS group ($p < .001$). +dP/dt was significantly greater in the high dose of pre- or post-QQc than in the low dose of each group ($p < .001$). +dP/dt was similar in the low dose of pre- or post-QQc group and the high dose of each group. −dP/dt was significantly smaller (better preserved) in all cell therapy groups except the low dose of pre-QQc cells than in the PBS group ($p < .001$ for high dose of pre- and post-QQc groups vs. PBS; $p < .01$ for low dose of post-QQc vs. PBS). −dP/dt was significantly smaller in the high dose of post-QQc than in the low dose of post-QQc group ($p < .001$). −dP/dt was significantly better preserved in the high or low dose of post-QQc groups than in the same dose of pre-QQc groups ($p < .01$ for high-dose and $p < .05$ for low-dose groups) (Fig. 6A). Echocardiography performed 4 weeks after cell therapy demonstrated that fractional shortening (FS) was greater in all cell therapy groups than in the PBS group ($p < .001$). FS was greater in the high dose of pre- or post-QQc cells than in the low dose of each group ($p < .001$). FS was also higher in the low or high dose of post-QQc group than in the same dose of pre-QQc ($p < .05$ for low dose and $p < .01$ for high dose) (Fig. 6B).

These results suggest that transplantation of CB-CD133$^+$ cells either pre- or post-QQc may be beneficial for preservation of LV function post-MI. The present data also show a dose-dependent effect of each cell therapy and the superior potency of post-QQc cells over pre-QQc cells for functional

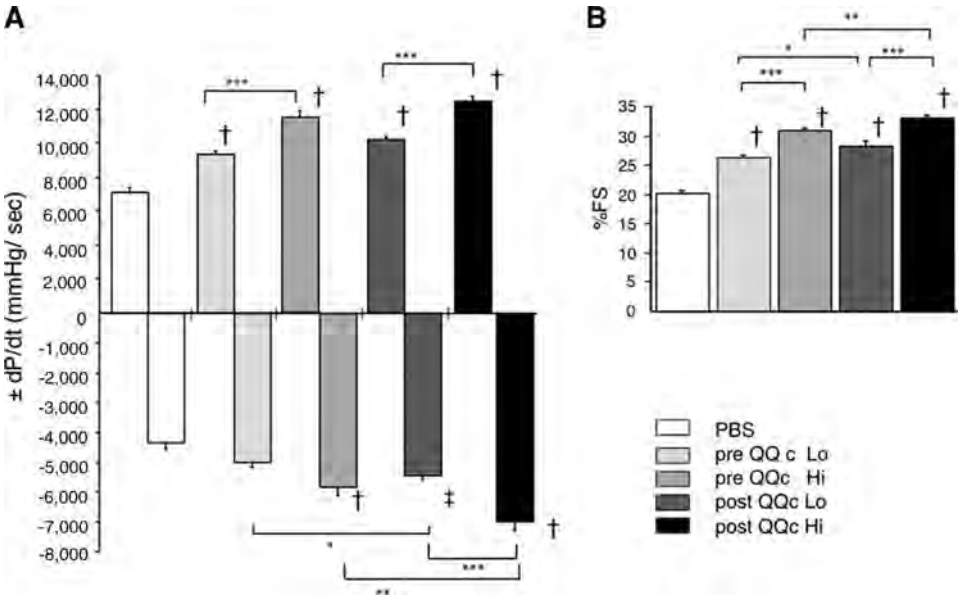

Figure 6. Improvement of left ventricular (LV) function following transplantation of pre- or post-QQc cells. **(A):** Hemodynamic assessment of LV function by micromanometer-tipped conductance catheter. **(B):** Quantitative assessment of LV function by echocardiography. *, $p < .05$; **, $p < .01$; ***, $p < .001$. ‡, $p < .01$ versus PBS; †, $p < .001$ versus PBS. $n = 10$ rats per group. Abbreviations: FS, fractional shortening; Hi, high dose in pre- or post-QQc group; Lo, low dose in pre- or post-QQc group; PBS, phosphate-buffered saline; QQc, quality and quantity culture.

recovery. The echocardiographic data of LV function post-MI by transplantation of pre- or post-QQc cells are shown in supplemental online Table 1 and supplemental online Figure 3.

Discussion

In the present study, we disclosed optimal serum-free QQc for quantitative and qualitative control of colony-forming EPCs by recently defined EPC-CFA. The optimal QQc system augmented the potential of CB-CD133$^+$ cells not only by specific augmentation of provasculogenic colony-forming EPCs producing DEPC-CFUs but also by upregulating autocrine or paracrine effects of proangiogenic growth factors in produced cells. Furthermore, in vivo experiments using a rat model of MI showed predominant cardiac repair postintramyocardial transplantation of post-QQc cells compared with CB-CD133$^+$ cells as pre-QQc cells.

Clinical Significance of the Serum-Free Quality and Quantity System Optimized in This Study

In the hematology field, serum-free expansion cultures for hematopoietic stem cells (i.e., CD133$^+$ cells or CD34$^+$ cells in CB) have so far been developed to reconstitute hematopoiesis following BM ablation by chemotherapy for malignancies [38, 39]. On the basis of these ex vivo hematopoietic expansion cultures, the development of EPC expansion culture has also been attempted, because EPCs share common surface markers, such as CD34 and CD133, with hematopoietic stem cells. First of all, Pesce et al. [5] expanded CB-CD34$^+$ cells for 7 days using a serum-free cytokine cocktail of SCF, Flt-3 ligand, interleukin-3 (IL-3), and IL-6, which was also used by Bonanno et al. [40], included as Comb 1 (Table 1), and successfully increased the number of CB-CD34$^+$ cells by 10-fold. Although the arteriole length density in ischemic adductor muscles was significantly greater following transplantation of CB-CD34$^+$ cells postexpansion compared with saline injection, the angiogenic parameter was similar in the CB-CD34$^+$ cell pre- and postexpansion groups. Skeletal myogenesis was also less enhanced in the CB-CD34$^+$ cell postexpansion group than in the pre-expansion group [5]. Other groups have also developed growth factor cocktails to test EPC expansions from CB-CD34$^+$ or CD133$^+$ cell populations and demonstrated significant increases in total cell number and EPC marker-positive cell number [25, 41]. All studies demonstrated the efficacy of transplantation into myocardial ischemic models by the equivalent or better improvement of cardiac function or vascular incorporation compared with pre-expansion EPCs.

However, there was a crucial limitation to establish the scientific and clinical culture system by conventional EPC biological methodologies. EPC origin and differentiation biology have remained a major concern among researchers for years, as there is still no definitive concept and methodology for EPCs. In this regard, researchers have long resisted the lack of qualitative and quantitative measures of regenerative EPCs to establish the culture for EPCs.

Here we used the newly established methodology of EPC-CFA to develop the culture system to increase in number and function of colony-forming EPCs for vascular regeneration. We have recently demonstrated EPC-CFA using semisolid medium and single or bulk CD133$^+$ or CD34$^+$ cord blood cell exhibited the formation of two types of attaching cell colonies made of small or large cells featuring endothelial lineage potential and properties, termed small-cell EPC-CFU and large-cell EPC-CFU, respectively [37]. In vitro and in vivo assays of colony cells of each EPC-CFU revealed a differentiation hierarchy ranging from PEPC-CFU, with highly proliferative activity, to DEPC-CFU, with vasculogenic properties, respectively. In particular, the transplantation of each colony cell represented not only the therapeutic potential of both EPC-CFUs for neovascular formation in ischemic animals

but the priority of the regenerative property of DEPC-CFU compared with that of PEPC-CFU. Therefore, numerical evaluation of both EPC-CFUs generated from any stem cell sources permits estimation of their vasculogenic property. In the present study, we have tried to optimize growth factor and cytokine combinations for colony-forming EPC expansion, to detect the best combination to especially increase the frequency of DEPC-CFU and total number of both EPC-CFUs in culture.

In our recent report, analysis of EPC-CFA revealed that VEGF added to the combination of early acting growth factors (SCF, TPO, Flt-3 ligand, IL-6) [42] for hematopoietic stem cell expansion promotes the EPC commitment and differentiation of single CB-CD133$^+$ cells [43]. Given this finding, we investigated the productivities of EPC-CFU in the several combinations, including the previously reported ones [5, 40], in comparison with the combination (VEGF, SCF, TPO, Flt-3 ligand, IL-6) named Comb 4. For example, Comb 6 (SCF, TPO, Flt-3 ligand, IL-3, IL-6, VEGF) represented the most increase in cell number after culture but resulted in a significantly lower frequency of DEPC-CFU, whereas Comb 4 demonstrated the highest total EPC-CFU frequency and, in particular, the highest DEPC-CFU frequency postculture among the groups (Fig. 1B, 1C). Of interest, Comb 4 exhibited greater EPC-CFU productivity, especially in DEPC-CFU, compared with the previously reported Comb 1 (SCF, Flt-3 ligand, IL-3, IL-6) for EPC expansion [5, 40]. Collectively, we determined that the Comb 4 growth factors are the most effective culture system for vasculogenic colony-forming EPC expansion, and we named them the QQc control system.

On the other hand, differing from a conventional culture of total mononuclear cells for adhesive EPC expansion [29, 43], the present QQc enabled suspended EPCs to robustly expand even from a scarce stem cell fraction (CB-CD133$^+$ cells) under serum-free conditions. The lack of requirement for either serum, with its possible risk of viral/bacterial infection, or a cellular detachment procedure using chemical substances (e.g., trypsinization) would support the safety of stem cell therapy in clinical applications.

Superior Vasculogenenic Potential of Post-QQc Cells over Pre-QQc

The specific increase in DEPC-CFUs in EPC-CFA and enhanced endothelial expressions, such as VEGFR-2, CD146, and vWF, was demonstrated in CB-CD133$^+$ cells post-QQc compared with those pre-QQc. These findings indicate that the QQc system may augment differentiation of CB-CD133$^+$ cells into the EC lineage. On the other hand, the capacity of tube-like structure formation with HUVECs and sprouting capability were also enhanced in post-QQc cells, compared with pre-QQc (supplemental online Fig. 4A, 4B). Moreover, post-QQc cells exhibited the predominant potential not only of incorporation into the tubes (supplemental online Fig. 4C) but also of proliferation (supplemental online Fig. 4D). Production of critical proangiogenic growth factors, such as VEGF or HGF, was also enhanced in post-QQc cells versus pre-QQc.

These data indicate another mechanism underlying the enhanced vasculogenic potential of post-QQc cells: upregulation of proangiogenic cytokine secretion for autocrine and paracrine actions, besides the performance of post-QQc cells per se. Given this evidence, the QQc system may possess not only quantitative but also qualitative advantages in acquiring an optimal EPC resource for therapeutic applications.

Enhanced Cardiac Repair by Engraftment of Post-QQc Cells

The histological density of both rat and human ECs in the infarcted myocardium was greater in rats receiving human post-QQc cells than in animals receiving pre-QQc cells. These favorable results in vivo may reflect the autocrine and paracrine effects of post-QQc cells on angiovasculogenesis shown in the in vitro studies.

In the present study, the density of both rat and human CMCs was also higher in the post-QQc group than in the pre-QQc group. The increase in host CMCs may have been due to the cardioprotective effects of post-QQc by attenuation of myocardial ischemia through angiovasculogenesis. Dai et al. [44] reported that VEGF, the expression of which was upregulated in post-QQc in our study, has antiapoptotic effects on CMCs. Transplanted cells post-QQc may secrete cytokines directly, protecting ischemic or apoptotic CMCs. Furthermore, the increase in human CMCs may be due to trans-differentiation of the cells into the CMC lineage, although trans-differentiation of endothelial or hematopoietic stem/progenitor cells (CD34$^+$cells or CD133$^+$cells) into CMCs remains controversial [8, 10, 45–47].

Also of scientific interest is the effect of EPC culture on the induction of cardiomyogenesis. Park et al. reported that CB-CD133$^+$ cells cocultured with rat CMCs after pretreatment with platelet-derived growth factor and epidermal growth factor feature cardiomyocytic phenotypes in terms of morphology and expression of lineage-specific markers [48]. Bonanno et al. [40] also demonstrated that a specific differentiation culture system after preconditioning of CB-CD133$^+$ cells with SCF, Flt-3 ligand, IL-3, and IL-6 for 2 days promoted differentiation into EC or CMC lineages in vitro.

These reports indicate that preconditioning with the appropriate growth factors may favorably promote the commitment of an EPC-enriched fraction into the CMC lineage. In fact, as shown in supplemental online Figure 5 and supplemental online Video Image 1, the cultured cells from post-QQc cells performed synchronized beating with fetal mouse CMCs under the coculture system, indicating that post-QQc cells possess trans-differentiation potential into functional CMC lineage. Further investigation is warranted to evaluate cardiomyogenic induction of EPCs by the QQc system.

Prospective Clinical Application of Stem/Progenitor Cells Post-QQc

Considering stem/progenitor cell therapy for ischemic diseases by CD34$^+$ or CD133$^+$ stem cells isolated from CB or autologous BM or PB, a serum-free QQc system may reduce the physical burden of patients, that is, decreasing the dose of granulocyte-colony stimulating factor for stem cell mobilization and minimizing the number of stem cells to be isolated. The expansion of aliquoted, cryopreserved stem cells permits patients to be treated repeatedly without invasive cell harvesting procedures at each treatment. As described above, in terms of safety, suspended stem cells in serum-free conditions may be readily applicable in the clinic.

Conclusion

The present study demonstrates that our novel evaluation method for serum-free expansion provides a transplantable EPC

source with quantitative and qualitative advantages for cardiovascular regeneration in ischemic disease.

Acknowledgments

We thank Dr. Yoshinori Okada (Department of Cell Biology and Histology) and Dr. Hiroshi Kamiguchi (Department of Molecular Biology) for their outstanding technical support of flow cytometry and real-time PCR, and we thank the Department of Animal Care in the Education and Research Support Center, Tokai University School of Medicine. We also thank Sachie Ota for secretarial assistance. This work was supported by grants from the Riken Center for Developmental Biology Collaborative Research Fund, Kobe, Japan (08001475); National Institutes of Health, Bethesda, MD (HL53354 and HL57516); the Ministry of Health, Labor and Welfare (H14-Trans-001, H14-Trans-002, H17-Trans-002, H17-Trans-014, H20-Regenerative Medicine-General-001); and the Ministry of Education, Culture, Sports, Science and Technology, Japan (Academic Frontier Promotion Program and Basic Research Grant 22590796).

Author Contributions

H.M.: conception and design, collection and assembly of data, data analysis and interpretation, financial support, manuscript writing; H. Iwasaki: collection and assembly of data, data analysis and interpretation; A.K.: assembly of data, data analysis, interpretation, manuscript writing; H.A.: collection and assembly of data, data analysis, interpretation; M. Ishikawa, M. Ii, T.S., A.S., R.I., M.H., and H. Ishida: assembly of data, data analysis and interpretation; S.K.: providing cord blood, financial support; T.A.: conception and design, financial support, data analysis and interpretation, manuscript writing, final approval of manuscript.

Disclosure of Potential Conflicts of Interest

The authors indicate no potential conflicts of interest.

References

1 Asahara T, Murohara T, Sullivan A et al. Isolation of putative progenitor endothelial cells for angiogenesis. Science 1997;275:964–967.

2 Shi Q, Rafii S, Wu MH et al. Evidence for circulating bone marrow-derived endothelial cells. Blood 1998;92:362–367.

3 Yang C, Zhang ZH, Li ZJ et al. Enhancement of neovascularization with cord blood CD133+ cell-derived endothelial progenitor cell transplantation. Thromb Haemost 2004;91:1202–1212.

4 Murohara T, Ikeda H, Duan J et al. Transplanted cord blood-derived endothelial precursor cells augment postnatal neovascularization. J Clin Invest 2000;105:1527–1536.

5 Pesce M, Orlandi A, Iachininoto MG et al. Myoendothelial differentiation of human umbilical cord blood-derived stem cells in ischemic limb tissues. Circ Res 2003;93:e51–e62.

6 Agbulut O, Vandervelde S, Al Attar N et al. Comparison of human skeletal myoblasts and bone marrow-derived CD133+ progenitors for the repair of infarcted myocardium. J Am Coll Cardiol 2004;44:458–463.

7 Botta R, Gao E, Stassi G et al. Heart infarct in NOD-SCID mice: Therapeutic vasculogenesis by transplantation of human CD34+ cells and low dose CD34+KDR+ cells. FASEB J 2004;18:1392–1394.

8 Iwasaki H, Kawamoto A, Ishikawa M et al. Dose-dependent contribution of CD34-positive cell transplantation to concurrent vasculogenesis and cardiomyogenesis for functional regenerative recovery after myocardial infarction. Circulation 2006;113:1311–1325.

9 Untergasser G, Koeck R, Wolf D et al. CD34+/CD133− circulating endothelial precursor cells (CEP): Characterization, senescence and in vivo application. Exp Gerontol 2006;41:600–608.

10 Leor J, Guetta E, Feinberg MS et al. Human umbilical cord blood-derived CD133+ cells enhance function and repair of the infarcted myocardium. Stem Cells 2006;24:772–780.

11 Kudo FA, Nishibe T, Nishibe M et al. Autologous transplantation of peripheral blood endothelial progenitor cells (CD34+) for therapeutic angiogenesis in patients with critical limb ischemia. Int Angiol 2003;22:344–348.

12 Bartunek J, Vanderheyden M, Vandekerckhove B et al. Intracoronary injection of CD133-positive enriched bone marrow progenitor cells promotes cardiac recovery after recent myocardial infarction: Feasibility and safety. Circulation 2005;112:I178–I183.

13 Klein HM, Ghodsizad A, Marktanner R et al. Intramyocardial implantation of CD133+ stem cells improved cardiac function without bypass surgery. Heart Surg Forum 2007;10:E66–E69.

14 Manginas A, Goussetis E, Koutelou M et al. Pilot study to evaluate the safety and feasibility of intracoronary CD133(+) and CD133(-) CD34(+) cell therapy in patients with nonviable anterior myocardial infarction. Catheter Cardiovasc Interv 2007;69:773–781.

15 Losordo DW, Schatz RA, White CJ et al. Intramyocardial transplantation of autologous CD34+ stem cells for intractable angina: A phase I/IIa double-blind, randomized controlled trial. Circulation 2007;115:3165–3172.

16 Yerebakan C, Kaminski A, Westphal B et al. Autologous bone marrow stem cell therapy for the ischemic myocardium during coronary artery bypass grafting. Minim Invasive Ther Allied Technol 2008;17:143–148.

17 Ahmadi H, Baharvand H, Ashtiani SK et al. Safety analysis and improved cardiac function following local autologous transplantation of CD133(+) enriched bone marrow cells after myocardial infarction. Curr Neurovasc Res 2007;4:153–160.

18 Schots R, De Keulenaer G, Schoors D et al. Evidence that intracoronary-injected CD133(+) peripheral blood progenitor cells home to the myocardium in chronic postinfarction heart failure. Exp Hematol 2007;35:1884–1890.

19 Kawamoto A, Katayama M, Handa N et al. Intramuscular transplantation of G-CSF-mobilized CD34(+) cells in patients with critical limb ischemia: A phase I/IIa, multicenter, single-blinded, dose-escalation clinical trial. Stem Cells 2009;27:2857–2864.

20 Scheubel RJ, Zorn H, Silber RE et al. Age-dependent depression in circulating endothelial progenitor cells in patients undergoing coronary artery bypass grafting. J Am Coll Cardiol 2003;42:2073–2080.

21 Vasa M, Fichtlscherer S, Aicher A et al. Number and migratory activity of circulating endothelial progenitor cells inversely correlate with risk factors for coronary artery disease. Circ Res 2001;89:E1–E7.

22 Hill JM, Zalos G, Halcox JP et al. Circulating endothelial progenitor cells, vascular function, and cardiovascular risk. N Engl J Med 2003;348:593–600.

23 Ott I, Keller U, Knoedler M et al. Endothelial-like cells expanded from CD34+ blood cells improve left ventricular function after experimental myocardial infarction. FASEB J 2005;19:992–994.

24 Schlechta B, Wiedemann D, Kittinger C et al. Ex-vivo expanded umbilical cord blood stem cells retain capacity for myocardial regeneration. Circ J 2010;74:188–194.

25 Senegaglia AC, Barboza LA, Dallagiovanna B et al. Are purified or expanded cord blood-derived CD133+ cells better at improving cardiac function? Exp Biol Med (Maywood) 2010;235:119–129.

26 Janic B, Guo AM, Iskander AS et al. Human cord blood-derived AC133+ progenitor cells preserve endothelial progenitor characteristics after long term in vitro expansion. PLoS One 2010;5:e9173.

27 O E, Lee BH, Ahn HY et al. Efficient non-adhesive ex vivo expansion of early endothelial progenitor cells derived from CD34+ human cord blood fraction for effective therapeutic vascularization. FASEB J 2011;25:159–169.

28 Lippross S, Loibl M, Hoppe S et al. Platelet released growth factors boost expansion of bone marrow derived CD34(+) and CD133(+) endothelial progenitor cells for autologous grafting. Platelets 2011;22:422–432.

29 Kalka C, Masuda H, Takahashi T et al. Transplantation of ex vivo expanded endothelial progenitor cells for therapeutic neovascularization. Proc Natl Acad Sci U S A 2000;97:3422–3427.

30 Vasa M, Fichtlscherer S, Adler K et al. Increase in circulating endothelial progenitor cells by statin therapy in patients with stable coronary artery disease. Circulation 2001;103:2885–2890.

31 Sharpe EE 3rd, Teleron AA, Li B et al. The origin and in vivo significance of murine and human culture-expanded endothelial progenitor cells. Am J Pathol 2006;168:1710–1721.

32 Tanaka R, Wada M, Kwon SM et al. The effects of flap ischemia on normal and diabetic progenitor cell function. Plast Reconstr Surg 2008;121:1929–1942.

33 Kwon SM, Eguchi M, Wada M et al. Specific Jagged-1 signal from bone marrow microenvironment is required for endothelial progenitor cell development for neovascularization. Circulation 2008;118:157–165.

34 Kwon SM, Suzuki T, Kawamoto A et al. Pivotal role of lnk adaptor protein in endothelial progenitor cell biology for vascular regeneration. Circ Res 2009;104:969–977.

35 Kamei N, Kwon SM, Alev C et al. Lnk deletion reinforces the function of bone marrow progenitors in promoting neovascularization and astrogliosis following spinal cord injury. STEM CELLS 2010;28:365–375.

36 Kwon SM, Lee YK, Yokoyama A et al. Differential activity of bone marrow hematopoietic stem cell subpopulations for EPC development and ischemic neovascularization. J Mol Cell Cardiol 2011;51:308–317.

37 Masuda H, Alev C, Akimaru H et al. Methodological development of a clonogenic assay to determine endothelial progenitor cell potential. Circ Res 2011;109:20–37.

38 Yao CL, Feng YH, Lin XZ et al. Characterization of serum-free ex vivo-expanded hematopoietic stem cells derived from human umbilical cord blood CD133(+) cells. Stem Cells Dev 2006;15:70–78.

39 Piacibello W, Sanavio F, Severino A et al. Engraftment in nonobese diabetic severe combined immunodeficient mice of human CD34(+) cord blood cells after ex vivo expansion: Evidence for the amplification and self-renewal of repopulating stem cells. Blood 1999;93:3736–3749.

40 Bonanno G, Mariotti A, Procoli A et al. Human cord blood CD133+ cells immunoselected by a clinical-grade apparatus differentiate in vitro into endothelial- and cardiomyocyte-like cells. Transfusion 2007;47:280–289.

41 Zhang Y, Wong S, Lafleche J et al. In vitro functional comparison of therapeutically relevant human vasculogenic progenitor cells used for cardiac cell therapy. J Thorac Cardiovasc Surg 2010;140:216–224, 224 e211–e214.

42 Bruno S, Gammaitoni L, Gunetti M et al. Different growth factor requirements for the ex vivo amplification of transplantable human cord blood cells in a NOD/SCID mouse model. J Biol Regul Homeost Agents 2001;15:38–48.

43 Jang JH, Kim SK, Choi JE et al. Endothelial progenitor cell differentiation using cryopreserved, umbilical cord blood-derived mononuclear cells. Acta Pharmacol Sin 2007;28:367–374.

44 Dai Y, Xu M, Wang Y et al. HIF-1α induced-VEGF overexpression in bone marrow stem cells protects cardiomyocytes against ischemia. J Mol Cell Cardiol 2007;42:1036–1044.

45 Badorff C, Brandes RP, Popp R et al. Transdifferentiation of blood-derived human adult endothelial progenitor cells into functionally active cardiomyocytes. Circulation 2003;107:1024–1032.

46 Zhang S, Wang D, Estrov Z et al. Both cell fusion and transdifferentiation account for the transformation of human peripheral blood CD34-positive cells into cardiomyocytes in vivo. Circulation 2004;110:3803–3807.

47 Yeh ET, Zhang S, Wu HD et al. Transdifferentiation of human peripheral blood CD34+-enriched cell population into cardiomyocytes, endothelial cells, and smooth muscle cells in vivo. Circulation 2003;108:2070–2073.

48 Park J, Setter V, Wixler V et al. Umbilical cord blood stem cells: Induction of differentiation into mesenchymal lineages by cell-cell contacts with various mesenchymal cells. Tissue Eng Part A 2009;15:397–406.

6、幹細胞ニッチ分子：Notchリガンドを標的とした新規抗癌剤開発
Notchリガンドの解析と基礎技術供与

分担研究者　基礎医学系生体防御学　穂積　勝人
血液腫瘍内科　六車　ゆかり
研究協力者　基礎医学系生体防御学　平野　健一
基礎医学系生体防御学　横山　和明

【研究の背景と目的】

Notch 系は種を越えて広く保存され、細胞膜上に発現した Notch 分子（哺乳類では Notch1-4）がそのリガンド（NotchL；哺乳類では Dll1、Dll4、Jag1、Jag2）と結合することで誘導されるシグナルが種々の細胞の系列決定に寄与する、広く共有されたシステムである。Notch シグナルが基本的作用機構として分化抑制と増殖誘導を有することから、未分化細胞の「多能性」を保持するニッチ分子として NotchL の関与が想定されてきたが、哺乳動物では組織に固有な幹細胞集団の同定が明確にされた例はまだ少なく（造血幹細胞、腸管幹細胞など）、その生理的寄与は明瞭でなかった。2011 年、マウス腸管幹細胞（Lgr5+）の維持に NotchL:Dll1/Dll4 が必須であることが報告され、幹細胞ニッチとしての NotchL の機能が始めて示された。また、肝実質細胞と胆管細胞の系列決定に肝動脈に付随する周皮細胞上の Jag1 が機能し、Jag1 遺伝子変異に起因する Alagile 症候群に固有の胆管形成不全に関与することが知られており、肝臓での分化ニッチとして Jag1 の重要性が示されている。我々は Dll1、Dll4、Jag1 各遺伝子の誘導型遺伝子欠損マウスを独自に樹立し、その生理的意義について報告してきた（Nat Immunol, 2004; Development, 2006; J Exp Med, 2008）。

本研究では各組織に固有のニッチ分子として NotchL を想定し、特に骨髄、胸腺、膵臓での幹・前駆細胞ニッチとしての機能を追求した。また、増殖や生存維持、腫瘍化との関連における NotchL の機能について、血液腫瘍と NotchL 改変マウスを用い、NotchL の機能について検証した。さらに、NotchL 機能発現に重要な細胞外ドメインの NotchL 特異性について精査し、pan-Notch シグナル阻害薬（gamma-secretase inhibitor）に認められる腸管上皮細胞不全の誘導を回避し、Notch/NotchL の各分子相互作用に特異的な抑制薬の開発に向けた情報の整理を目指した。

【研究方法】

Notch リガンド（NotchL）の骨髄における幹・前駆細胞あるいは腫瘍細胞の環境要因（ニッチ）としての役割を解析するため、ヒト Jag1、Dll1 を骨芽細胞に強制発現させた超免疫不全マウス

(NOG マウス)を作製した。同マウスへヒト多発性骨髄腫(MM)細胞を静注することで、腫瘍細胞の正着や抗癌剤耐性能について検証した。

また、独自に作製した NotchL(Dll1、Dll4、Jag1)誘導型遺伝子欠損(floxed)マウスを、様々な細胞系列あるいは誘導型 Cre 発現マウスと交配し、NotchL 遺伝子欠損状態におけるニッチの状態を調べた。

【研究成果】

1. 多発性骨髄腫(Multiple Myeloma、MM)のボルテゾミブ耐性を促す腫瘍ニッチ分子としての Notch リガンド:Jagged1 の役割

多発性骨髄腫(MM)は、形質細胞の異常増殖を示す難治性の血液腫瘍であり、いまだに治療法は確立されていない。近年開発されたプロテアソーム阻害剤:ボルテゾミブ(BTZ)により、ようやくその治療が可能になりつつあるが、依然として治療抵抗性の MM が一定頻度存在し、その予後は不良である。MM の治療抵抗性は、細胞自身の性状に加えて、腫瘍ニッチと呼ばれる環境要因の存在が指摘されている。すなわち、環境から付与される刺激によって、MM が性状を変化させ、抗癌剤治療抵抗性を獲得する可能性が推察される。最近、その一部として、骨髄環境にて Notch シグナルが発生し、MM の増殖性や挙動に影響を与えることが示され、MM の治療抵抗性との関連が想定された。

そこで我々は、ヒト MM 細胞における Notch 分子の発現を詳細に調べ、Notch リガンド存在下での MM 細胞への挙動の変化について確認した。また、我々が独自に作製したヒト NotchL 発現 NOG マウスを用いて、Notch シグナル誘導環境における MM の振る舞いを、in vivo モデルにて検討した。さらに、BTZ 存在下での MM 細胞の治療抵抗性について精査した。

その結果、10種類のヒト MM 細胞株すべてにおいて、Notch1 あるいは Notch2(または両者)の顕著な発現を認めた。しかし、いずれの細胞についても、Jag1 を介して誘導される Notch シグナルがその細胞増殖に、in vitro、in vivo いずれについても影響しなかった。一方、Jag1 誘導 Notch シグナルの存在は、BTZ 処理による細胞死を in vitro にて抑制することを見出した。これは BTZ 処置に特徴的な効果であり、他の抗癌剤処置(サリドマイド、メルファラン)に対しては認められなかった。同様の効果は、in vivo での Jag1 発現 NOG マウスへの MM 細胞移植と BTZ 処置による in vivo の実験系でも示された。さらに、Notch シグナル発生を抑制する gamma-secretase 阻害剤を BTZ と併用することにより、BTZ 耐性能獲得が抑制され、相乗効果が発揮されることが示された。また、Jag1 を介した Notch シグナルが、BTZ 処理によって抑制される MARCKS を、PKC を介して誘導し、腫瘍細胞の生存維持に寄与する可能性を示唆した。

以上の結果は、MM 治療に際し大きな問題となる BTZ 耐性が、腫瘍環境要因としての Jag1 を介して誘導される Notch シグナルによってもたらされることを、初めて明確にした。
（本研究成果は、現在、国際学術誌へ投稿中である）

2. Notch リガンド機能発現に寄与する細胞外ドメインの重要性

Notch リガンドとして機能する Dll1、Dll4、Jag1、Jag2 は、Notch 受容体へのシグナル誘導能を共有し、個々の機能的差異については明確ではない。腫瘍環境要因としての Notch リガンドの重要性やその新たな制御法を探索するにあたり、Notch リガンド個々の特徴を明らかにすることはきわめて重要である。

我々はこれまで、Dll1、Dll4、Jag1 の floxed マウスを独自に樹立し、各 Notch リガンドの in vivo での生理的役割について調べてきた。その過程で、Dll1 と Dll4 の間に、それまで予想されていなかった機能的差異があることを見出したが、その分子的詳細は不明であった。Dll4 分子は、Dll1 と異なり、Notch リガンドの重要な共通構造である DOS モチーフを有しておらず、これを含む DOS 領域が、両分子の機能的差異を生み出していると考え、それを Dll4/1 間で置換したキメラ分子をそれぞれ作製し、その機能について調べた。その結果、Dll4 の DOS 領域は、Dll1 分子内ではまったく機能せず、Notch1 シグナル誘導能が消失することがわかった。一方、Dll1 由来の DOS 領域（DOS モチーフを有する）は、Dll4 分子内でも機能し、野生型 Dll4 に比べ、明らかに強い活性を発揮した。これらの結果は、Dll 分子における DOS モチーフの重要性を示したものの、Dll4 の機能的優位性については、DOS 領域以外の部位が重要であることを意味した。

そこで、これまで機能的意義が不明瞭であった Dll 分子 N 末（MNNL）領域に着目し、先と同様にキメラ分子を作製し、その機能を調べた。その結果、Dll4 分子の MNNL 領域がきわめて機能的に重要であることが判明し、逆に、Dll1 分子の MNNL 領域はほとんどその機能に寄与していないことが示唆された。以上の結果は、2つの Dll 分子は、少なくとも Notch1 を介したシグナル発動に際し、それぞれ異なる領域を中心として機能していることを示している。この結論は、これまでの Notch リガンド研究からはまったく想定されてこなかったものであり、より詳細な分子機構の解明が待たれる。
（本研究成果は、現在、国際学術誌へ投稿中である）

3. Notch リガンドによる幹細胞・未分化細胞の分化制御における役割

Notch リガンドの環境要因としての役割を in vivo にて明らかにするため、独自に作製した

Notch リガンド floxed マウスを用い、以下の知見を得た。

（1）胸腺・T 前駆細胞（DN 期）

T 細胞の分化決定には、胸腺環境を担う上皮細胞上の Dll4 と、胸腺に移行してきた T 前駆細胞上の Notch1 の相互作用によって生じる Notch シグナルが、必須の役割を担う。一方、それ以降の胸腺内での T 細胞分化における Dll4/Notch1 の生理的意義については不明な点が多かった。すでに知られているヒト T 型急性リンパ性白血病（T-ALL）発症への Notch シグナルの関与がきわめて大きいことの分子基盤を理解するためにも、本課題の解明は重要である。

胸腺以降後の未分化 T 細胞では、DN 期の細胞に特に Notch1 の発現が高く、これに付随して、Notch1 細胞内断片（Intracellular Notch1 fragment、N1ICD）が観察された。DN1/2 期あるいは DN3 期細胞を分取し、Dll4 欠失あるいは対照マウス胎仔胸腺に導入後に器官培養することで、Dll4 の各未分化細胞分化における役割を調べると、前者は完全な分化停滞、後者は DP 期への分化は起こるものの増殖不全を示すことが判明した。この結果は、胸腺内での T 細胞分化にも Dll4 が重要であることを示している。また、DN3/DP 分化に伴う増殖不全は、c-Myc の強制発現によりほぼ回復することから、Notch シグナル標的分子としての c-Myc による増殖制御が DN/DP 期にて機能することが示唆された。c-Myc の過剰発現によるヒト T 細胞腫瘍が、特に DN/DP 形質を伴い高頻度に認められることは、本研究成果とよく一致することから、Notch シグナル過剰と c-Myc の協働による T 細胞増殖異常が、同ステージでの腫瘍化の本態であることが予想される。

（本研究成果は、Eur J Immunol 45:2252, 2015、にて公表された）

（2）膵臓・腺房中心細胞

膵発生期における Notch シグナルの役割については、膵組織の形成期であるマウス胎生9日前後にて必須の役割を担うことが知られている。しかし、膵臓を構成する主たる細胞系列である外分泌、内分泌および管細胞の系列決定およびその幹細胞が出現する胎生 14 日前後における役割は明確ではなかった。また、膵癌発生に先行して認められる異形成（metaplasia）および上皮内腫瘍性病変（Pancreatic intraepithelial neoplasia）については、これまで支持されていた膵管細胞の異常形質ではなく、外分泌細胞からの分化転換に伴う形質発現と考えられ、特に外分泌前駆細胞の増殖・細胞生存維持の分子機構は、膵癌発生機構を理解するうえできわめて重要と考えられた。

我々は、マウス胎仔膵臓での免疫組織学的解析から、①胎齢 14 日前後から外分泌細胞様の細胞集団内に、Notch シグナルを受容した増殖性の細胞が出現すること、②同細胞が外分泌組織の中央部に移行し腺房中心細胞（Centroacinar cells、CA）に分化すること、③Notch リ

ガンド：Dll1/Jag1 が CA を含む管系列細胞に発現すること、④Dll1/Jag1 欠失膵臓では、CA 細胞が消失し、外分泌組織の基本構造が破綻すること、⑤CA 細胞が、外分泌・管細胞分化能を有する未分化細胞として機能すること、を見出した。この成果は、Dll1/Jag1 を介した Notch シグナルが、外分泌・管細胞系列分化を制御し、その前駆細胞としての CA 細胞の増殖・細胞生存を支持する重要な環境要因であることを示している。ヒト膵癌あるいはその前癌状態において、Notch シグナルの発動が高頻度に認められることは、膵癌発生における Notch シグナルの重要性を示す結果として興味深い。また、膵癌治療において、Notch シグナルあるいはその関連分子を標的とすることの有用性を示唆している。
（本研究成果は、Genes to Cells 20:500, 2015、にて公表された）

(3)骨髄・骨芽細胞

骨芽細胞を含む間葉系細胞（軟骨細胞、脂肪細胞）は、間葉系幹細胞を起源として分化し、その系列決定に Notch シグナルが関与することが知られている。しかし、各細胞系列に分化した後、成熟期までの分化過程における Notch シグナルの役割については不明な点が多い。また、骨芽細胞は骨髄環境を構成する主要な細胞系列であり、既述した多発性骨髄腫をはじめとした造血系腫瘍の環境を構築する細胞として、その機能が注目されている。

我々が独自に作製した a1Col-hDll1（D1 Tg）マウスは、マウス a1-collagen プロモーター制御下にヒト Dll1 を配した遺伝子改変マウスであり、未分化骨芽細胞を含む骨芽細胞系列にてヒト Dll1 の発現が確認できる。D1 Tg マウスでは、出生直後より、過剰な骨化が進行する一方、骨代謝回転は著しく低下していた。同マウス骨髄内では、胎齢後期より Osterix 陽性未分化骨芽細胞の異常増殖を認め、その結果、幼若な骨組織の拡大と骨髄腔の縮小が観察された。この形質は、Dll1 に特徴的であり、同様に作製した hJag1 発現マウスでは、そうした形質は見出されなかった。D1 Tg マウスでは、Osterix 陽性細胞の異常増殖に伴い、Osteocalcin 陽性の骨細胞への分化が抑制されており、未分化骨芽細胞期にて分化が停滞しているものと推測された。また、骨芽細胞分化不全に付随して破骨細胞分化が抑制されており、結果として、骨代謝回転が大きく低下していた。同マウス骨間葉系細胞の培養から、そうした形質が再現される一方、本培養系での Dll1 遺伝子欠損の誘導により、未分化骨芽細胞が減少するとともに骨細胞への分化が促進される、Dll1 過剰発現系とは逆の形質を認め、Dll1 が Notch リガンドとして生理的重要性を有することが示唆された。以上の結果から、Dll1 が、未分化骨芽細胞期の増殖・分化を精密に制御し、骨組織形成のバランスを維持していることが推察された。
（本研究成果は、J Cell Physiol 2016 Oct 13. Doi:10.1002/jcp.25647、にて公表された）

4．ヒト Notch1 細胞内断片と変異型 IL7Ra 鎖の発現による T 細胞白血病（T acute

lymphoblastic leukemia、T-ALL）発症の分子機構

我々は、独自にヒト T-ALL 細胞株より変異型 IL7Ra 鎖（細胞膜領域挿入型）を単離し、同変異が造血細胞に IL7 非依存的な増殖能を付与することを見出した。本研究では、変異 IL7Ra 鎖を様々なマウス造血未分化細胞に導入することにより、その造腫瘍性について調べた。その結果、同遺伝子を造血幹細胞画分に導入すると、骨髄増殖症（myeloproliferative disorder）を促し、さらに Notch 細胞内断片との協働により、悪性度の高い T-ALL を発症することを示した。また、リンパ性前駆細胞（common lymphoid progenitors、CLP）への導入では、B-ALL 様の症状を呈した。以上の結果は、ヒト T-ALL にて比較的高頻度に認められる細胞膜領域挿入型 IL7Ra 鎖変異は、明らかな造腫瘍性を有し、発現時期に依存した細胞系列の血液腫瘍を誘導した。すなわち、血液腫瘍に共通するシグナル伝達機構として、JAK3-STAT5 系が機能する可能性が示唆された。また、その中で、Notch シグナルにより、明確な T-ALL 誘導を認め、ヒト T-ALL 発生要因における Notch シグナルの役割が注目された。今後、Notch シグナル発生要因として、骨髄・骨芽細胞上に発現する Notch リガンド：Dll4 の関与を明確にする必要がある。

（本研究成果は、Blood 122:4259, 2013、にて公表された）

【研究考察】

腫瘍の増殖・維持に腫瘍を取り巻く環境要因が寄与する可能性は、特に腫瘍幹細胞の存在と相まって、想定されるようになった。幹細胞環境（ニッチ）による幹細胞の維持については造血幹細胞に関する知見が先行したことから、造血幹細胞と血液系腫瘍幹細胞の維持環境の相違や、抗癌剤耐性との関連が注目されている。しかし、多くの解析はマウス血液腫瘍モデルの検証であり、ヒト血液腫瘍の環境要因についてはほとんど解析がなされていない。

我々は、ヒト多発性骨髄腫（MM）細胞が正着可能なマウスモデルの作製を試みる過程で、ヒト Jag1 の環境要因としての可能性を追求した。当初、想定していた Jag1 を介した Notch シグナルによる腫瘍生存あるいは増殖の向上については、有意な差を確認できなかったが、一方で、ヒト MM 治療薬として使用されるボルテゾミブに対する耐性能の獲得に、Jag1 由来 Notch シグナルの寄与を新たに見出した。この成果は、ヒト腫瘍細胞の環境要因を標的としたきわめて重要な知見であり、現在、MM 治療の大きな課題であるボルテゾミブ耐性能の分子機構を探るうえでも貴重な情報を提示している。

近年、腫瘍環境因子として機能することが明らかになった骨髄ニッチ分子として、CXCL12 が挙げられる。血液細胞上の CXCR4 に結合するリガンドとしてケモカイン様作用を有するだけ

でなく、造血幹・前駆細胞の未分化性や生存維持に重要な役割を担うが、AML や B-ALL の腫瘍環境因子として寄与することが報告されている。さらに 2015 年には、T-ALL の骨髄中への移動と生存維持に必須であること、CXCR4 アンタゴニストの投与により T-ALL の効率的な治療が可能であることが示された。我々がすでに変異型ヒト IL7Ra 鎖を用いて示した結果から、強い Notch シグナルは T 細胞系腫瘍の造成を助ける可能性が高く、骨髄中の NotchL は、CXCL12 とともに、T-ALL の腫瘍ニッチを形成することが推察される。Jag1 と比較し、骨芽細胞上での発現が知られる Dll4 は、T 細胞系列への priming を担うことが報告されていることから、T-ALL 腫瘍環境としては、Dll4 の関与が想定される。未分化 T 細胞型腫瘍として高い抗癌剤耐性能を有することが知られる ETP-ALL の治療標的として、Dll4/Notch1 を介したシグナルは有望と考えられる。

しかし、すべての Notch/NotchL を介したシグナルを抑制する pan-Notch inhibitor は、Notch シグナル依存的な腸管上皮細胞の分化を抑制（杯細胞などの粘液分泌細胞が過剰に誘導される）するなどの副作用が強く、臨床上、問題となる場合が多い。よって、Notch/NotchL の組み合わせを特異的に制御する方策を実現する必要がある。我々は、Dll4 と Dll1 の機能的差異を特定する過程で、両 NotchL が、異なる領域を用いて Notch 受容体と結合・シグナル誘導を行うことを初めて明らかにした（投稿中）。こうした取り組みから得られる情報を整理し、Dll4 特異的な抑制を実現できれば、ETP-ALL の効果的治療薬の開発に有用と考えられる。

blood

2013 122: 4259-4263
Prepublished online October 30, 2013;
doi:10.1182/blood-2012-08-451278

In vivo leukemogenic potential of an interleukin 7 receptor α chain mutant in hematopoietic stem and progenitor cells

Kazuaki Yokoyama, Nozomi Yokoyama, Kiyoko Izawa, Ai Kotani, Akira Harashima, Katsuto Hozumi and Arinobu Tojo

Blood (print ISSN 0006-4971, online ISSN 1528-0020), is published weekly by the American Society of Hematology, 2021 L St, NW, Suite 900, Washington DC 20036.

Brief Report

LYMPHOID NEOPLASIA

In vivo leukemogenic potential of an interleukin 7 receptor α chain mutant in hematopoietic stem and progenitor cells

Kazuaki Yokoyama,[1,2] Nozomi Yokoyama,[3] Kiyoko Izawa,[1] Ai Kotani,[4] Akira Harashima,[5] Katsuto Hozumi,[2] and Arinobu Tojo[1]

[1]Division of Molecular Therapy, Advanced Clinical Research Center, Institute of Medical Science, University of Tokyo, Tokyo, Japan; [3]Department of Laboratory Medicine, Research Hospital, Institute of Medical Science, University of Tokyo, Tokyo, Japan; [2]Department of Immunology and [4]Institute of Innovation Science and Technology, Tokai University School of Medicine, Kanagawa, Japan; and [5]Cell Biology Institute, Research Center, Hayashibara Biochemical Laboratories, Okayama, Japan

Key Points

- Gain-of function mutation of IL7Rα induces lymphoid leukemia as well as myeloproliferative disease.
- In vivo oncogenicity of mutant IL7Rα is influenced by the differentiation stage at which it occurs.

Somatic gain-of-function mutations in interleukin 7 receptor α chain (IL7Rα) have been described in pediatric T and B acute lymphoblastic leukemias (T/B-ALLs). Most of these mutations are in-frame insertions in the extracellular juxtamembrane-transmembrane region. By using a similar mutant, a heterozygous in-frame transmembrane insertional mutation (INS), we validated leukemogenic potential in murine hematopoietic stem/progenitor cells, using a syngeneic transplantation model. We found that ectopic expression of INS alone in hematopoietic stem/progenitor cells caused myeloproliferative disorders, whereas expression of INS in combination with a Notch1 mutant led to the development of much more aggressive T-ALL than with wild-type IL7Rα. Furthermore, forced expression of INS in common lymphoid progenitors led to the development of mature B-cell ALL/lymphoma. These results demonstrated that INS has significant in vivo leukemogenic activity and that the lineage of the resulting leukemia depends on the developmental stage in which INS occurs, and/or concurrent mutations. (*Blood*. 2013;122(26):4259-4263)

Introduction

Interleukin 7 (IL7) is essential for T-cell development and homeostasis.[1] Its cognate receptor (IL7R) forms a heterodimer composed of the α chain (IL7Rα) and common γ chain; binding of IL7 to IL7R triggers activation of Janus kinase (JAK)/signal transducer and activator of transcription signaling and the PI3K/v-akt murine thymoma viral oncogene homolog 1 (Akt) pathways.[1]

Accumulating evidence has demonstrated that dysregulation of the IL7 signaling axis may be implicated in lymphoid malignancies. For example, IL7 transgenic mice develop T- and B-cell lymphomas,[1] and human primary T-cell acute lymphoblastic leukemia (T-ALL) cells respond to IL7 in vitro[1] and in vivo.[2] Moreover, recent findings describing IL7Rα gain-of-function mutations in pediatric ALL and a T-ALL cell line have provided direct evidence that the IL7-IL7R axis plays a crucial role in the pathogenesis of human ALL.[3-6]

Although the gain-of-function properties of these mutants have been precisely studied in vitro,[3-5] their leukemogenic potential in vivo has not been well studied. One study reported that T-cell leukemogenesis was triggered by an IL7Rα mutant.[5] However, they used murine IL7-dependent D1 progenitor T-cell lines derived from p53-knockout mice,[7] which spontaneously develop T-cell lymphoma,[8,9] and this specific animal model may not be generally applicable.

To extend these observations, we demonstrate the in vivo leukemogenic potential of such a mutant when expressed in primary hematopoietic stem and progenitor cells by using a IL7Rα mutant, which was previously identified in a T-ALL cell line.[6]

Methods

Mice

Six- to 12-week-old Balb/c mice were used for all experiments. Lineage depletion of bone marrow (BM) or embryonic day 14.5 (E14.5) fetal liver was performed by the EasySep Mouse Hematopoietic/Progenitor Cell Enrichment Kit (StemCell Technologies). Via tail vein injection, 1×10^6 Lineage$^-$ BM/fetal liver cells (lin$^-$ cells), pro-B, or Thy1$^+$T cell progenitors were injected into lethally (8 Gy) or sublethally (4 Gy) irradiated recipients. Mice were maintained in accordance with institutional animal care guidelines (Institute of Medical Science, University of Tokyo). Detailed methods are provided in the supplemental Methods.

Submitted August 20, 2012; accepted October 10, 2013. Prepublished online as *Blood* First Edition paper, October 30, 2013; DOI 10.1182/blood-2012-08-451278.

K.Y. and N.Y. contributed equally to this study.

The online version of this article contains a data supplement.

There is an Inside *Blood* commentary on this article in this issue.

The publication costs of this article were defrayed in part by page charge payment. Therefore, and solely to indicate this fact, this article is hereby marked "advertisement" in accordance with 18 USC section 1734.

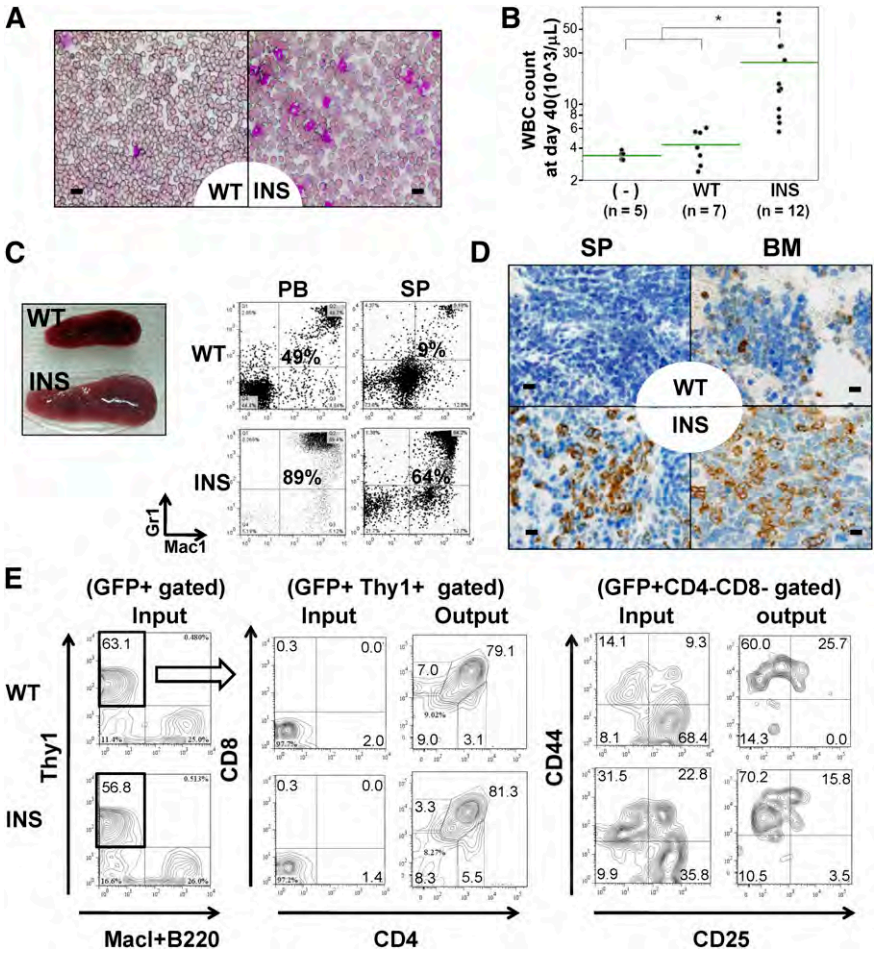

Figure 1. In vivo transforming activity of INS. (A-D) Lin$^-$ cells were retrovirally transduced with mock vectors (mock), WT, or INS, followed by injection into lethally irradiated congenic mice. (A) May-Giemsa staining of PB smears at day 40, showing marked leukocytosis consisting predominantly of mature myeloid cells. (B) White blood cell count at day 40. *$P < .05$ (analysis of variance; INS vs WT or mock recipient mice). (C) FACS of the PB and SP at day 40, showing an increase in Mac-1$^+$/Gr-1$^+$ myeloid cells. (D) Immunohistochemical analysis (IHC) of SP and BM specimens by anti-myeloperoxidase, indicating an increase in the number of myeloid cells in INS recipient mice. Bars represent (A) 10 μm and (D) 20 μm. (E) Demonstration of in vivo reconstitutive capacity of hIL7R (WT/INS) transduced T-cell progenitors. Lin$^-$ kit$^+$ stem/progenitor cells were cultured on OP9-DL1 stromal layer for 7days, supplemented with mIL7$^+$ human Fms-like tyrosine kinase 3-ligand, which allowed them to differentiate into Thy1$^+$CD25$^-$CD44$^+$DN1 immature T-cell progenitor fractions. These cells were retrovirally transduced with WT/INS vector. The resultant cells were allowed to expand on OP9-DL1 stroma for additional 7 to 10 days, and developed into CD25$^+$CD44$^-$ DN3 immature T-cell progenitor fractions. These Thy1$^+$ cells were green fluorescent protein (GFP)-sorted and intravenously injected into sublethally irradiated mice. The resultant GFP$^+$ thymic seeding progenitors (denoted as "input") in recipient mice of WT and INS at day 52 was shown (denoted as "output").

Results and discussion

In vitro transforming activity of the mutant IL7Rα, INS

Consistent with previous report, sequencing analysis of exon 6 of the IL7Rα gene, mainly encoding the transmembrane domain, identified a heterozygous in-frame transmembrane insertional mutation (INS) in the T-ALL cell line DND-41.[6] Forced expression of INS exerted transforming activity in Ba/F3 cells, as revealed by acquisition of cytokine-independent growth (supplemental Figure 1A-C, found on the *Blood* website) as well as the autonomous phosphorylation of Stat1, Stat3, Stat5, and Akt (supplemental Figure 1D). In addition, transient expression of IL7Rα in human embryonic kidney 293 cells leads to autonomous tyrosine phosphorylation of Jak1 only in those expressing INS (supplemental Figure 1D, *left*), suggesting that INS constitutively activated IL7R downstream signals via Jak1. As INS falls within the same category of reported mutation of IL7Rα,[3-6] we decided to use INS as a representative gain-of-function IL7Rα mutation for further experiments.

INS in stem/progenitor cells caused myeloproliferative disorders

The leukemogenic activity of INS and wild-type (WT) IL7Rα was assessed by retroviral transduction of Lin$^-$ cels. Within 6 to 9 weeks after transplantation, recipient mice transplanted with INS Lin$^-$ cells, but not WT Lin$^-$ cells, developed myeloproliferative disorders (MPDs) characterized by splenomegaly, leukocytosis, and polycythemia (Figure 1A-C, *right*; supplemental Figures 1D and 3C-D). Fluorescence-activated cell sorter (FACS) and morphological analysis revealed a marked increase in Mac1^{++} Gr-1^{++} mature myeloid cells in the peripheral blood (PB), spleen (SP), and BM (Figure 1C-D; supplemental Figures 2 and 4). An increase of Ter119$^+$ CD71$^+$ immature erythroblast was also noted in SP and BM (supplemental Figure 4, SP; data not shown). INS-induced MPD was oligoclonal, as evidenced by Southern blot analysis (supplemental Figure 5, *left*). A similar disease phenotype was also observed in mice transplanted with Lin$^-$c-Kit^{++}Sca1^{++} (KSL) fractions transduced with INS (supplemental Figures 3A-B,E and 4). Both B- and T-cell development were severely perturbed in INS recipient mice (supplemental Figure 4). As transplantation of INS-transduced KSL cells resulted in preferential expansion of myeloid progenitor–enriched Lin$^-$c-Kit^{++}Sca1$^-$ fraction (supplemental Figure 6), we speculate that in vitro transforming activity of INS skewed myeloid progenitor expansion at the expense of common lymphoid progenitor Lin–c-kit^{low}Sca1$^+$ IL7Rα$^+$ (CLP) expansion, through which normal lymphopoiesis might be perturbed. This was also supported by the fact that INS exerted transforming activity in input KSL cells, as well as resultant myeloid progenitors ex vivo, as revealed by colony-forming cell assay (supplemental Figure 7). It was previously reported that forced expression of wild-type murine IL7Rα into IL7Rα knockout BM progenitors induces a very similar MPD phenotype, including

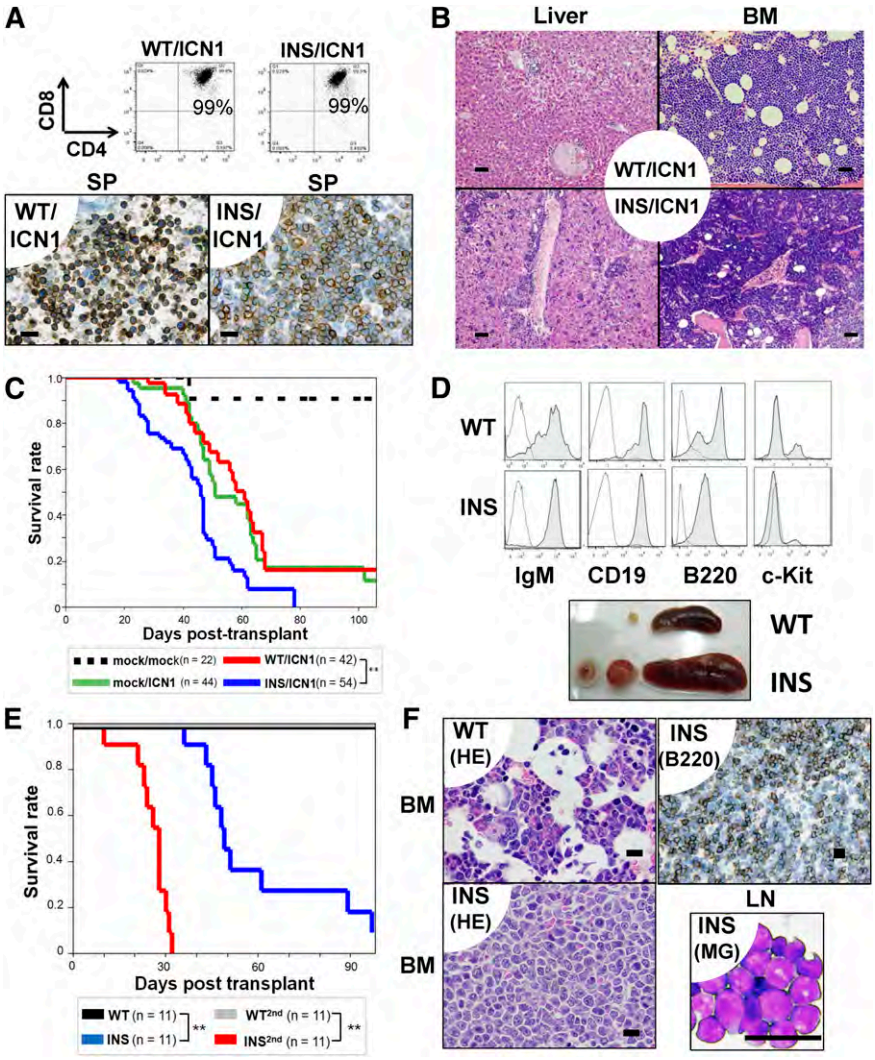

Figure 2. INS synergized with active Notch1 (A-C) and exerted transforming activity in CLPs (D-F) in vivo. (A-C) Lin$^-$ cells were cotransfected with vectors encoding the ICN1 gene (mock, ICN1) and the hIL7R gene (mock, WT, INS), followed by injection into lethally irradiated congenic mice. (A, *upper*) FACS analysis of the SP from WT/ICN1 or INS/ICN1 recipient mice at day 40. Data were obtained from GFP$^+$ (marker for the ICN1 gene) and rat CD2$^+$ (marker for the hIL7R gene) fractions. (A, *lower*) IHC of SP specimens using anti-CD3 antibodies from WT/ICN1 (*left*) and INS/ICN1 (*right*) recipient mice. Bar represents 20 μm. (B) Histological findings of liver (*left 2 panels*) and BM (*right 2 panels*) from WT/ICN1 (*upper*) and INS/ICN1 (*lower*) recipient mice (hematoxylin and eosin stain). Bar represents 50 μm. (C) Survival curves of recipient mice (mock/mock, n = 22; mock/ICN1, n = 44; WT/ICN1, n = 42; INS/ICN1, n = 54) $^{**}P < .01$ (log-rank test). (D-F) CLPs transfected with hIL7R constructs were expanded in vitro for 18 days and injected into sublethally irradiated congenic mice. (D, *top 2 panels*) FACS analysis of the BM: WT recipient mice at day 60 (WT) and INS recipient mice at day 60 (INS). Data are obtained from GFP$^+$ gated fractions. Open histogram, isotype control; shaded histogram, specific staining. (D, *lower*) Splenomegaly and lymphadenopathy developed in CLPs-INS recipient mice at day 60 (denoted as "INS"). (E) Survival curves of recipient mice (n = 11 for each condition). $^{**}P < .01$ (log-rank test, INS vs WT or INS vs INS^{2nd}). (F) Histological findings: BM specimens from WT recipient mice (*upper left*) and INS recipient mice at day 60 by hematoxylin and eosin stain (*lower left*) or by IHC of B220$^+$ cells (*upper right*). Lymph node cytospin from INS recipient mice at day 60 by May-Giemsa stain (*lower right*). Bar represents 20 μm. WT, WT primary recipients; INS, INS primary recipients; WT-2nd, WT day 30 BM secondary recipients; INS-2nd, INS day 30 BM secondary recipients.

splenomegaly resulting from neutrophilia.[10] Consistent with this report, transduced WT appeared to induce some degree of increase in myeloid fraction and neutrophilia in PB and SP compared with that of mock increase of myeloid fraction and neutrophilia in PB (supplemental Figure 4). Importantly, the magnitude was quite different, as we could not find a statistically significant difference of SP weight in mock and WT (n = 4 each; $P = .61$, 1-way analysis of variance; supplemental Figure 3C). This is in contrast to the difference of INS (n = 4) and WT ($P < .01$; supplemental Figure 3C). WT-induced mild myeloid expansion was accompanied by concomitant increase in lymphoid subset in PB, SP, and BM, specifically CD19$^+$ B-cell fractions (supplemental Figure 4). Considering the fact that the phenotype of WT-recipient mice was different from that of mock (supplemental Figure 4), it should be mentioned that we could not rule out the possibility that the phenotype elicited by INS is in part a result of the effect of IL7R overexpression per se, irrespective of its mutational status. The major difference from the previous report was that they rescued the loss-of-function phenotype of IL7Rα by ectopic expression of IL7Rα.[10]

Neither of these recipient mice developed overt leukemia throughout the median follow-up period of 5 months (WT, n = 28; INS, n = 22), suggesting that additional transforming events are required for clonal evolution to aggressive leukemia. Considering the fact that recipient mice for hematopoietic stem cells transduced with constitutively active Akt or signal transducer and activator of transcription-5 also developed similar diseases together,[11,12] this MPD phenotype is likely to be induced by stem cells ectopically expressing INS.

Nononcogenic consequence of INS in T-cell progenitors

Next, we wished to test the effect of INS on T-cell precursors. Toward this aim, we cocultured Lin$^-$ kit$^+$ stem/progenitor cells for 7 days, which allowed the emergence of Thy1$^+$CD25$^-$CD44$^+$DN1 immature T-cell-progenitor fractions (data not shown). These cells were transduced by retroviral transduction of the WT/INS vector. The resultant transduced cells were allowed to expand on OP9 expressing the Notch ligand Delta-like 1 (OP9-DL1) stroma for an additional 7 to 10 days, which allowed them to develop Thy1$^+$ CD4$^-$CD8$^-$CD25$^-$CD44$^+$DN1 to DN3 CD25$^+$CD44$^-$DN3 immature T-cell-progenitor fractions (Figure 1E). The resultant Thy1$^+$ cells were GFP sorted and injected into sublethally irradiated mice. As a result, we could detect stable engraftment of GFP$^+$ T-cell progenitors in recipient mice from day 40 to day 50 in thymus (Figure 1E) and CD4 or CD8 single-positive cells in the periphery, such as SP or PB (data not shown). Neither of these recipient mice

developed overt leukemia throughout the median follow-up period of 106 days (WT and INS, n = 12 each). We speculate that this might be partly attributable to the limited engraftment of WT/INS-transduced T-cell progenitors in thymus (data not shown).

INS exacerbates the in vivo oncogenic activity of Notch1

INS-like mutations were reported to occur in 10% of T-ALL patients.[3,4] In contrast, Notch1 mutations were more frequently found in T-ALL patients and were equally distributed between patients with WT and INS.[4,] The DND-41 cell line carries both INS and Notch1 mutations.[6,13] Moreover, IL7 signaling coordinates with Notch1 in proper T-cell developmental programming.[14,15] We hypothesized that INS may cooperate with active Notch1 mutants in T-cell leukemogenesis. Therefore, Lin^- cells were transduced with mock or IL7Rα-WT/INS along with an active form of intracellular Notch1 (ICN1), followed by syngeneic transplantation. As reported previously,[16] within 4 to 6 weeks after transplantation, all mice developed T-ALL, characterized by extrathymic expansion of leukemic cells (Figure 2A-B; supplemental Figure 8B). Clonality of INS/ICN1-induced leukemia was confirmed by Southern blot analysis around day 35 (supplemental Figure 5, *right*). Despite similar immunophenotypes ($CD3^+CD4^+CD8^+TCR\text{-}\beta^+$) between WT/ICN1 and INS/ICN1 cells (Figure 2A, *Upper*; supplemental Figures 8A and 9), histological examinations of the liver, SP, and BM in recipient mice revealed that systemic expansion of INS/ICN1-Lin^- cells was much more aggressive than that of WT/$ICN1^-$ and mock/$ICN1^-Lin^-$ cells (Figure 2A, *Lower*, and 2B). Furthermore, the median survival time of INS/ICN1 mice (44 days; n = 54) was significantly shorter than that of mock/ICN1 (60 days; n = 44) and WT/ICN1 (57 days; n = 42) mice ($P < .001$ by log-rank test; Figure 2C). Taken together, INS clearly exaggerated ICN1-induced T-ALL.

Forced expression of INS in B-cell progenitors caused mature B-ALL/lymphoma

Because the IL7Rα gene is transcriptionally active in common lymphoid progenitors (CLPs; $Lin^-c\text{-}kit^{low}Sca1^+$ $IL7R\alpha^+$) and their progenies and not expressed in stem cell compartments,[17] the INS allele could target the same cell populations. Then, CLPs were transduced with INS or WT IL7Rα and cultured on the OP9 stromal layer with a cytokine cocktail for 18 days, followed by transplantation of resulting pro-B cells into syngeneic recipient mice (supplemental Figure 10A). All but 1 of the INS-CLP recipients died of mature B-ALL/lymphoma, whereas no WT-CLP recipients died ($P < .01$; Figure 2D-E). Autopsy specimens revealed massive infiltration of $B220^+$ leukemic blasts into the BM, SP, and lymph nodes (Figure 2F; data not shown). This mature B-cell ALL/lymphoma was transplantable to secondary recipients, resulting in more aggressive mature B-ALL/lymphoma with much shorter survival periods (Figure 2E). INS-induced mature B-ALL/lymphoma was biclonal, as evidenced by Southern blot analysis (supplemental Figure 5, *right*). Under these experimental conditions, INS-CLPs had already committed to the cytokine-independent clonogenic pro-B cells before transplantation (supplemental Figure 10B-C; data not shown).

Finally, we wished to identify the downstream signals involved in INS-induced leukemogenesis. Using microarray analysis (Gene Expression Omnibus accession number GSE51211) of the resultant transformed cells in vitro and in vivo, we performed a comparative analysis of gene expression profiles from WT and INS-transduced hematopoietic stem/progenitor cells, as well as resultant leukemia cells that developed in vivo. As a result, we found a list of candidate genes (n = 6133) that were up- or downregulated by INS in comparison with WT. Among those genes, by reviewing hierarchical clustering analysis, several genes could be candidate mediators downstream of INS in comparison with WT, including hairy and enhancer of split-1 (*HES1*) for MPD, proviral insertion site in Moloney murine leukemia virus 1 (*PIM1*) for B-ALL, and insulin-like growth factor 1 receptor (*IGF1R*) for T-ALL (supplemental Figure 11). Quantitative RT-PCR verified their differential expression in comparison with WT (supplemental Figure 12). Putative involvement of these genes in INS-induced leukemogenesis was supported by previous data reporting the significance of *HES1* overexpression reported in advanced chronic myelogenous leukemia,[18] *PIM1* activation involved in pre-B-cell transformation,[19] *PIM1* overexpression reported in B-ALL,[20] and high-level expression of *IGF1R* in T-ALL.[20,21] In addition, we performed gene set enrichment analysis[22] to find significant overlaps between INS/ICN1 (in comparison with WT/ICN1) gene expression signature and gene sets present in the public database (supplemental Discussion). As a result, we found that in vivo INS/ICN1 was characterized by overexpression of interferon (IFN)-stimulated genes[23] and IGF1-signal-related genes,[24] suggesting constitutive activation of IFN^- as well as the $IGF1^-$ signal pathway (supplemental Figures 13 and 14; supplemental Tables 2 and 3). These are consistent with the previous report that JAK1-mutated T-ALL samples were characterized by the IFN-pathway[23] signature, as well as our findings of a higher *IGF1R* transcript level in INS/ICN1 cells compared with that of WT/ICN1 (supplemental Figures 11 and 12).

In conclusion, we provided evidence that INS has significant in vivo leukemogenic activity and that determination of the lineage of resulting leukemias depends on the developmental stage during which they occur and/or concurrent mutations. In addition, as far as we know, this is the first report in which transformation of CLP leading to in vivo malignancy is shown. This is also of general relevance for the field of lymphoid malignancies. Given that either IL7Rα or Jak1 gain-of-function mutations have been found in approximately 10%[3-5] or 19%[25] of T-ALL patients and that IFN-pathway signatures have been associated with Jak1-mutated T-ALL,[23] it is fairly certain that IFN-pathway signatures induced by aberrant IL7R/Jak1 axis might substantially contribute to the pathogenesis of T-ALL in close association with activating mutations in the Notch pathways.

Acknowledgment

We thank Kana Minegishi and Kazuo Ogami for their help.

Authorship

Contribution: K.Y., N.Y., and K.I. performed experiments; K.Y. wrote the manuscript; A.H., A.K., and K.H. provided vital reagents; and A.T. supervised the research.

Conflict-of interest disclosure: The authors declare no competing financial interests.

Correspondence: Arinobu Tojo, Department of Hematology-Oncology, Research Hospital, Institute of Medical Science, the University of Tokyo, 4-6-1 Shirokanedai, Minato-ku, Tokyo 108-8639, Japan; e-mail: a-tojo@ims.u-tokyo.ac.jp.

References

1. Barata JT, Cardoso AA, Boussiotis VA. Interleukin-7 in T-cell acute lymphoblastic leukemia: an extrinsic factor supporting leukemogenesis? *Leuk Lymphoma.* 2005;46(4): 483-495.
2. Silva A, Laranjeira AB, Martins LR, et al. IL-7 contributes to the progression of human T-cell acute lymphoblastic leukemias. *Cancer Res.* 2011;71(14):4780-4789.
3. Shochat C, Tal N, Bandapalli OR, et al. Gain-of-function mutations in interleukin-7 receptor-α (IL7R) in childhood acute lymphoblastic leukemias. *J Exp Med.* 2011;208(5):901-908.
4. Zenatti PP, Ribeiro D, Li W, et al. Oncogenic IL7R gain-of-function mutations in childhood T-cell acute lymphoblastic leukemia. *Nat Genet.* 2011; 43(10):932-939.
5. Zhang J, Ding L, Holmfeldt L, et al. The genetic basis of early T-cell precursor acute lymphoblastic leukaemia. *Nature.* 2012;481(7380):157-163.
6. Porcu M, Kleppe M, Gianfelici V, et al. Mutation of the receptor tyrosine phosphatase PTPRC (CD45) in T-cell acute lymphoblastic leukemia. *Blood.* 2012;119(19):4476-4479.
7. Kim K, Khaled AR, Reynolds D, Young HA, Lee CK, Durum SK. Characterization of an interleukin-7-dependent thymic cell line derived from a p53 (-/-) mouse. *J Immunol Methods.* 2003;274(1-2): 177-184.
8. Harvey M, McArthur MJ, Montgomery CA Jr, Butel JS, Bradley A, Donehower LA. Spontaneous and carcinogen-induced tumorigenesis in p53-deficient mice. *Nat Genet.* 1993;5(3):225-229.
9. Haines BB, Ryu CJ, Chang S, et al. Block of T cell development in P53-deficient mice accelerates development of lymphomas with characteristic RAG-dependent cytogenetic alterations. *Cancer Cell.* 2006;9(2):109-120.
10. Jiang Q, Li WQ, Aiello FB, Klarmann KD, Keller JR, Durum SK. Retroviral transduction of IL-7Ralpha into IL-7Ralpha-/- bone marrow progenitors: correction of lymphoid deficiency and induction of neutrophilia. *Gene Ther.* 2005;12(24): 1761-1768.
11. Kharas MG, Okabe R, Ganis JJ, et al. Constitutively active AKT depletes hematopoietic stem cells and induces leukemia in mice. *Blood.* 2010;115(7):1406-1415.
12. Kato Y, Iwama A, Tadokoro Y, et al. Selective activation of STAT5 unveils its role in stem cell self-renewal in normal and leukemic hematopoiesis. *J Exp Med.* 2005;202(1):169-179.
13. Weng AP, Ferrando AA, Lee W, et al. Activating mutations of NOTCH1 in human T cell acute lymphoblastic leukemia. *Science.* 2004; 306(5694):269-271.
14. Magri M, Yatim A, Benne C, et al. Notch ligands potentiate IL-7-driven proliferation and survival of human thymocyte precursors. *Eur J Immunol.* 2009;39(5):1231-1240.
15. García-Peydró M, de Yébenes VG, Toribio ML. Notch1 and IL-7 receptor interplay maintains proliferation of human thymic progenitors while suppressing non-T cell fates. *J Immunol.* 2006; 177(6):3711-3720.
16. Pear WS, Aster JC, Scott ML, et al. Exclusive development of T cell neoplasms in mice transplanted with bone marrow expressing activated Notch alleles. *J Exp Med.* 1996;183(5): 2283-2291.
17. Miller JP, Izon D, DeMuth W, Gerstein R, Bhandoola A, Allman D. The earliest step in B lineage differentiation from common lymphoid progenitors is critically dependent upon interleukin 7. *J Exp Med.* 2002;196(5):705-711.
18. Nakahara F, Sakata-Yanagimoto M, Komeno Y, et al. Hes1 immortalizes committed progenitors and plays a role in blast crisis transition in chronic myelogenous leukemia. *Blood.* 2010;115(14): 2872-2881.
19. Guo G, Qiu X, Wang S, et al. Oncogenic E17K mutation in the pleckstrin homology domain of AKT1 promotes v-Abl-mediated pre-B-cell transformation and survival of Pim-deficient cells. *Oncogene.* 2010;29(26): 3845-3853.
20. Haferlach T, Kohlmann A, Wieczorek L, et al. Clinical utility of microarray-based gene expression profiling in the diagnosis and subclassification of leukemia: report from the International Microarray Innovations in Leukemia Study Group. *J Clin Oncol.* 2010;28(15): 2529-2537.
21. Medyouf H, Gusscott S, Wang H, et al. High-level IGF1R expression is required for leukemia-initiating cell activity in T-ALL and is supported by Notch signaling. *J Exp Med.* 2011;208(9): 1809-1822.
22. Subramanian A, Tamayo P, Mootha VK, et al. Gene set enrichment analysis: a knowledge-based approach for interpreting genome-wide expression profiles. *Proc Natl Acad Sci USA.* 2005;102(43):15545-15550.
23. Hornakova T, Chiaretti S, Lemaire MM, et al. ALL-associated JAK1 mutations confer hypersensitivity to the antiproliferative effect of type I interferon. *Blood.* 2010;115(16): 3287-3295.
24. Creighton CJ, Casa A, Lazard Z, et al. Insulin-like growth factor-I activates gene transcription programs strongly associated with poor breast cancer prognosis. *J Clin Oncol.* 2008;26(25): 4078-4085.
25. Flex E, Petrangeli V, Stella L, et al. Somatically acquired JAK1 mutations in adult acute lymphoblastic leukemia. *J Exp Med.* 2008;205(4): 751-758.

 DOI: 10.1002/eji.201445123 Eur. J. Immunol. 2015. 45: 2252–2262

European Journal of Immunology

Delta-like 4-mediated Notch signaling is required for early T-cell development in a three-dimensional thymic structure

Ken-ichi Hirano[1], Naoko Negishi[3], Masaki Yazawa[1,2], Hideo Yagita[3], Sonoko Habu[3] and Katsuto Hozumi[1]

[1] Department of Immunology, Tokai University School of Medicine, Isehara, Kanagawa, Japan
[2] Department of Biochemistry, Tokai University, Hiratsuka, Kanagawa, Japan
[3] Department of Immunology, Juntendo University School of Medicine, Bunkyo-ku, Tokyo, Japan

Delta-like 4 (Dll4)-mediated Notch signaling is critical for specifying T-cell fate, but how Dll4-mediated Notch signaling actually contributes to T-cell development in the thymus remains unclear. To explore this mechanism in the thymic three-dimensional structure, we performed fetal thymus organ culture using Dll4-deficient mice. DN1a/b+DN2mt cells, which had not yet committed to either the αβ T or γδ T/NK cell lineage, did not differentiate into the αβ T-cell lineage in Dll4-deficient thymus despite the lack of cell fate conversion into other lineages. However, DN3 cells efficiently differentiated into a later developmental stage of αβ T cells, the double-positive (DP) stage, although the proliferation was significantly impaired during the differentiation process. These findings suggest that the requirement for Notch signaling differs between the earliest and pre-TCR-bearing precursors and that continued Notch signaling is required for proper differentiation with active proliferation of αβ T lineage cells. Furthermore, we showed that Notch signaling increased the c-Myc expression in DN3 cells in the thymus and that its overexpression rescued the proliferation and differentiation of DN3 cells in the Dll4-null thymus. Therefore, c-Myc plays a central role in the transition from stage DN3 to DP as a downstream target of Notch signaling.

Keywords: c-Myc · Dll4 · Notch signal · Thymus · T-cell development

Additional supporting information may be found in the online version of this article at the publisher's web-site

Introduction

Lateral inhibition theory suggests that during embryonic development, Notch signaling occurs between two equivalent progenitors and causes them to adopt distinct developmental fates [1]. In the thymus, however, we demonstrated that Notch signaling, which is critical for the determination of T-cell fate, is triggered by the interaction between Notch1 on hematopoietic progenitors and a Notch ligand (NotchL), Delta-like 4 (Dll4), on the thymic epithelium [2, 3]. This evidence was the first to show that the Notch–NotchL interaction by direct contact between cells with distinct origins contributes to the determination of cell fate. On the basis of this background, how and when the Notch–NotchL system is involved in the consecutive steps of the T-cell differentiation pathway can be further investigated.

Previously, it was reported that Notch signaling is necessary to advance the differentiation of immature thymocytes from

Correspondence: Dr. Katsuto Hozumi
e-mail: hozumi@is.icc.u-tokai.ac.jp

CD4/CD8 double-negative (DN) to double-positive (DP) stages by using gene-modified mice with the *Notch1*- or *Rbpj-floxed* alleles and the *lck-Cre* transgene [4, 5]. In these mice, Notch1 or Rbpj was deleted after the DN2t stage, resulting in severe perturbation of αβ but not γδ T-cell development with impaired rearrangement of the *TCR*β gene. However, the role of Notch signaling in earlier differentiation stages, such as the DN1a/b and DN2mt stages, or in $CD44^+CD117^{high}$ pro-T cells [6, 7] in maintaining the multilineage differentiation potential [8–10] has remained unclear because the appropriate *Cre* transgenic mice were not available. Another step for further investigation is the transition from the DN3 to the DP stage in which the role of Notch signaling remains obscure. From the monolayer culture system with DN3 thymocytes and Dll1-expressing stromal cells [11], Notch signaling is reported to be necessary for the transition process [12, 13], whereas the gene deletion of *Notch1*- or *Rbpj-floxed* alleles during the late DN3 stage in *CD4-Cre* transgenic mice showed no phenotype in the thymus [5, 14]. The reason for the discrepancy is not clear.

In this study, we purified thymocytes at specific differentiation stages and cultured them in Dll4-deficient thymic lobes with 3D structure, focusing on the significance of Notch signaling for the differentiation into the following stage. This measurement is clearly advantageous over the experiments with intrinsic thymocyte gene deletion using the *Cre* transgene driven by the *lck* or *CD4* promoter/enhancer [4, 5, 14] because Notch signaling can be completely disrupted in any defined differentiation stage in our system. Furthermore, Dll4-deficient thymic lobes with intact 3D structure provide a suitable experimental tool, enabling us to elucidate physiological downstream targets of Notch signaling.

We separately prepared $CD44^+CD117^{high}$ and $CD44^-CD25^+$ populations as DN1a/b+DN2mt and DN3 cells, respectively, from fetal thymi and monitored their development in the presence or absence of Dll4 in FTOC (fetal thymus organ culture) with 3D thymic structure. We showed that these immature thymocytes differently required Notch signaling for their differentiation and proliferation, which had not yet been observed in a monolayer culture system. Furthermore, we found that for the signaling that is downstream of Notch, c-Myc, but not active Akt, plays central roles in the differentiation from the DN3 to the DP stage with proper proliferation in the thymus.

Results

Active Notch signaling occurs during early T-cell development

Dll4-mediated Notch signaling is absolutely necessary to determine the T-cell fate of thymic immigrants [2], but its physiological significance for successive developmental stages in the thymus remains to be elucidated. We directly examined actual Notch signaling at each developmental stage by the intracellular detection of the cleaved fragment of Notch1 (N1ICD). As we have previously shown [2], N1ICD was frequently detected in fetal thymocytes before the DP stage, especially the cells in earlier stages, DN1a/b plus DN2mt or DN3 (Fig. 1A). Considering the instability of N1ICD due to Fbxw7-mediated ubiquitination and degradation [15], this result suggested that before β-selection, almost all cells received signaling via Notch1, which is supported by the remarkable expression of Notch1 on the cell surface (Fig. 1B), as shown previously [16, 17]. Notch2 and Notch3 were also detected (Fig. 1B), but they were incompetent for supporting the T-cell appearance in the Notch1-deficient condition [18]. In fact, the expression of CD25 on thymocytes at the DN2/3 stages, a potential target of Notch signaling in T cells [19–21], decreased after the depletion of Notch1 but not Notch2 (Supporting Information Fig. 1). Therefore, the induced Notch signaling via Notch1 into immature thymocytes possibly contributes to early T-cell development in the thymus.

In addition, the unexpected presence of N1ICD was detected in CD8 single-positive cells of the neonatal (8SP) but not the adult (8SP*) thymus (Fig. 1A). This result might be related to the recent finding that Notch signaling is also significant for the commitment of DP precursors to the CD8 T-cell lineage [22].

Dll4 on the thymic epithelium is necessary for T-cell development from the earliest stage

To examine the physiological significance of the Dll4-induced Notch signaling on the thymic environment for T-cell development from the earliest stage of thymocytes, we prepared thymic lobes from *Dll4-floxed* fetuses with or without the *FoxN1-Cre* transgene [2] and performed thymic organ culture (FTOC) with $CD44^+CD117^{high}$ murine fetal thymocytes as DN1a/b and DN2mt (Fig. 1B), which were shown to be pro-T cells without the gene rearrangement of the TCRβ or γ chain [6, 7] that also retained the potential to differentiate into the NK cell lineage [8–10]. These thymocytes did not fully differentiate into the DP stage in the Dll4-deficient condition (Fig. 2A); the total cell number after the culture was reduced to approximately 1/10, and almost all cells remained in the DN stage. The density of CD25 on the surface of DN cells decreased in the Dll4-deficient condition (Fig. 2A). In addition, the development of γδ T cells was significantly impaired, but that of DP cells was more severely affected (Fig. 2B). The development of NK cells was not significantly influenced (Fig. 2B). In some cases, an increase in the $CD19^+$ B lineage cells was observed without Notch signaling, as shown previously [2]; the cells that contributed to this increase seemed to be derived from B-committed progenitors (Fig. 2A). These results indicated that the most immature thymocytes absolutely require Dll4 on the thymic epithelium for further development into the αβ T-cell lineage, but these immature thymocytes are not redirected to alternative cell fates without Notch signaling.

It was argued that thymic epithelial cells without Dll4 could be different from normal ones in some aspects other than Dll4 expression because they did not exhibit cross-talk with developing thymocytes. To overcome the effect, we prepared two groups of DN1a/b plus DN2mt cells transduced with mock or the active form of Notch1, intracellular active form of Notch1 (ICN1); the

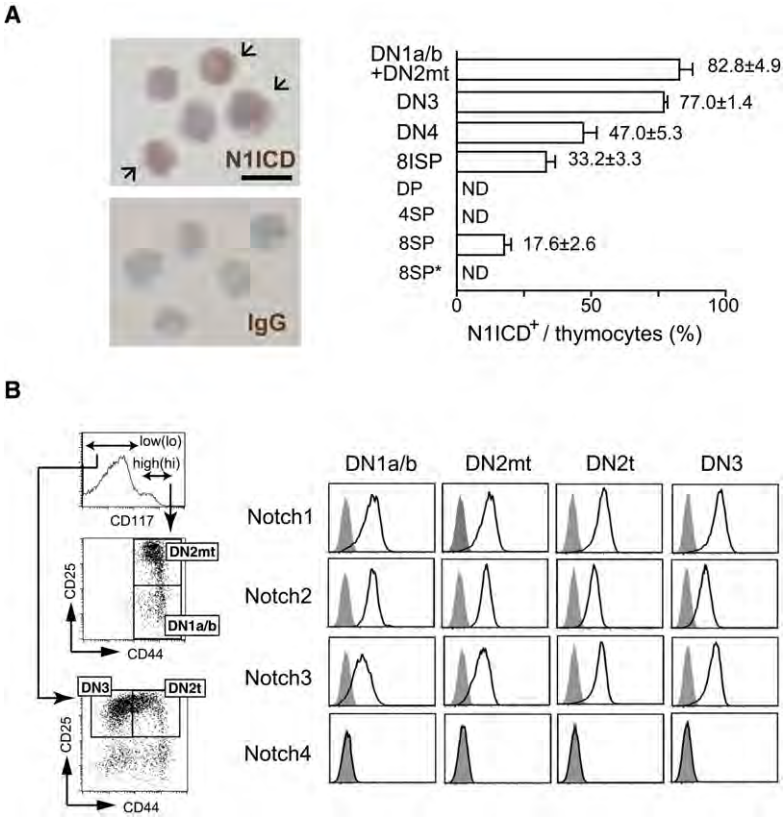

Figure 1. Thymocytes bearing Notch receptors in the DN stages frequently possess the cleaved Notch1 fragment. (A) Fetal thymocytes (e15.5) were fixed and stained with Ab that recognizes the cleaved Notch1 fragment (N1ICD, upper-left panel) or control rabbit IgG (IgG, lower-left panel) as described in the Materials and methods. Stained cells are depicted by arrows. Original magnification, 400×. Bar: 10 μm. The frequencies of N1ICD-bearing thymocytes at various differentiation stages are shown (mean % ± SD, $n = 5$, five random fields; right panel). Two populations (DN1a/b+DN2mt as $CD44^{+}CD117^{hi}$, DN3 as $CD44^{-}CD25^{+}CD117^{lo}$) and others were isolated from e15.5 fetal and neonatal thymi, respectively, other than CD8 single-positive cells that were also obtained from adult thymi (8W, 8SP*), as described in the Materials and methods. (B) Expression of Notch family members (Notch1-4) on immature thymocytes. Thymocytes from e15.5 fetuses were subdivided into four populations as DN1a/b, DN2mt, DN2t, and DN3 stages (left panels), and analyzed for their expression by flow cytometry (right panels). Open histograms indicate staining with anti-Notch1, anti-Notch2, anti-Notch3, and anti-Notch4 mAb. Filled histograms indicate staining with control hamster IgG. These profiles are representative of at least three independent experiments.

cells were monitored using different markers (rat CD2 and GFP) and then mixed for FTOC (Supporting Information Fig. 2). As expected, ICN1-transduced cells could progress toward the DP stage in the Dll4-deficient condition; these cells had retained their cross-talk with epithelial cells, but the mock-transduced cells still arrested at the DN stage without proper proliferation. These results indicated that the impairment in supporting the T-cell development of Dll4-deficient thymic epithelial cells was mainly due to the disappearance of Dll4 on thymic epithelial cells and not to an alteration other than the lack of Dll4.

To determine what molecular machinery is downstream of Notch signaling at this stage, we tried to overcome the defect by retrovirus-mediated induction of exogenous molecules—the rearranged TCRβ chain, pTα or Hes1 (Supporting Information Fig.

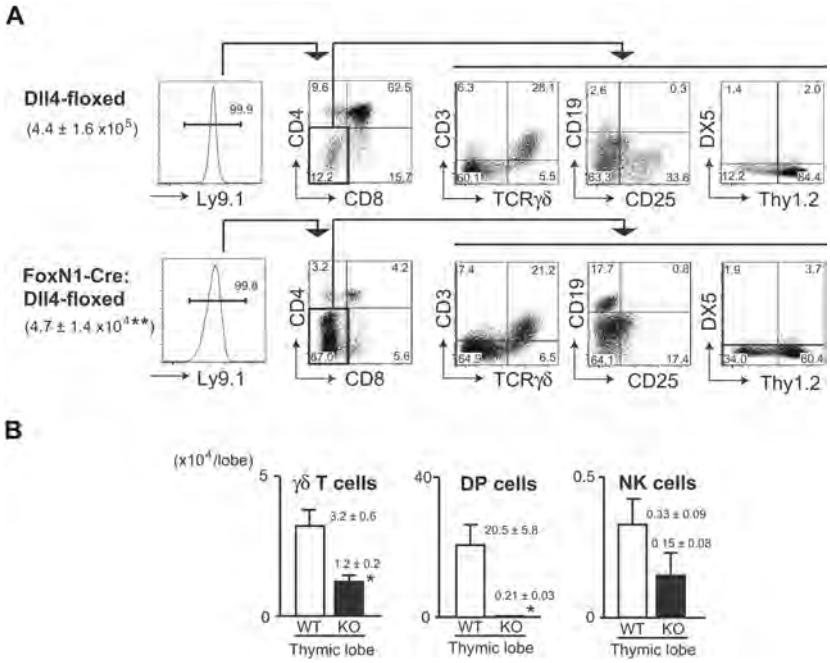

Figure 2. Differentiation arrest of DN1/2 pro-T cells in the thymus with Dll4-null epithelial cells. (A) $CD44^{+}CD117^{hi}$ DN1a/b+DN2mt cells were isolated from an e16.5 fetal thymus (BALB/c, $Ly9.1^{+}$) and cultured with deoxyguanosine-treated thymic lobes from *Dll4-floxed* mice with (FoxN1-Cre, Dll4-floxed; Dll4-deficient) or without (Dll4-floxed, control) *FoxN1-Cre* transgene for 9 days as hanging-drop FTOC. After the cultures, live cells were counted (mean ± SD, obtained from six independent experiments) and analyzed for the expression of CD4 and CD8 in $Ly9.1^{+}$ cells and TCRγδ, CD3, CD19, CD25, Thy1.2, and DX5 in $Ly9.1^{+}CD4^{-}CD8^{-}$ fraction. Numbers in the dot-plot represent the relative percentages for each corresponding quadrant. (B) Absolute cell numbers of γδ T cells ($TCR\gamma\delta^{+}CD3^{+}$), DP cells ($CD4^{+}CD8^{+}$), and NK cells ($CD3^{-}DX5^{+}$) in a thymic lobe of control (Dll1-floxed; WT) or Dll4-deficient (FoxN1-Cre, Dll4-floxed; KO) fetuses after the cultures are shown (mean ± SD, obtained from three independent experiments). $^{*}p < 0.05$; $^{**}p < 0.01$; paired Student's *t* test.

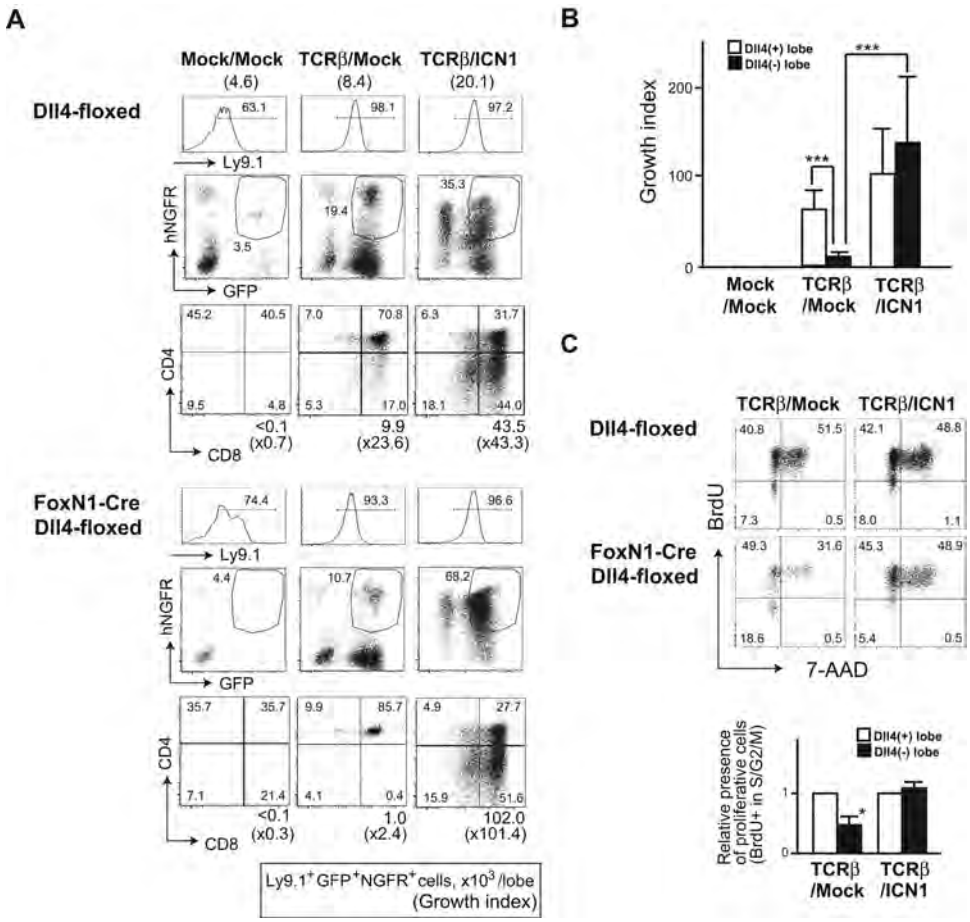

Figure 3. Proliferation defect during the transition from the DN3 to the DP stage with Dll4-null epithelial cells. RAG2-deficient DN3 cells from fetal thymi (e17.5–e18.5, Ly9.1$^+$) were infected with retroviruses encoding TCRβ (monitored by GFP or rat CD2) plus empty vector (TCRβ/Mock), TCRβ plus intracellular active form of Notch1 (ICN1, monitored by hNGFR) (TCRβ/ICN1) or two empty vectors (Mock/Mock) with GFP or rat CD2 and human NGFR. Cells were cultured with control ((A) Dll4-floxed; (B and C) white columns, Dll4(+) lobe) or Dll4-deficient ((A) FoxN1-Cre, Dll4-floxed; (B and C) black columns, Dll4(-) lobe) thymic lobes as shown in Fig. 2 for 7 days without any enrichment of infected cells. (A and C) Cultures were pulsed with BrdU for the last 18 h for cell-cycle analysis. (A, lower panels) Expression of CD4 and CD8 in (upper panels) Ly9.1$^+$ and (middle panels) GFP$^+$hNGFR$^+$ fraction was measured by flow cytometry. (C) DNA content was analyzed by 7-AAD staining and BrdU incorporation in the fraction of Ly9.1$^+$rCD2$^+$hNGFR$^+$ cells. (A) The frequencies of infection before the culture are shown at the top of the panels in brackets. Numbers in the histogram and dot-plot represent the relative percentages for each corresponding fraction and quadrant. Numbers under the profiles represent the number of Ly9.1$^+$GFP$^+$NGFR$^+$ cells obtained after the cultures ($\times 10^3$/lobe) and the growth index as fold times compared to the infected cells before the culture. (B) Growth indexes obtained from seven independent experiments are presented (mean ± SD ($n = 7$); $^{***}p < 0.001$, paired Student's *t* test). (C) Presence of proliferative cells (BrdU-incorporated cells in S/G2/M stages) in the Dll4-deficient condition relative to those in control is shown (mean ± SD ($n = 3$), three independent experiments; $^{*}p < 0.01$, paired Student's *t* test.

3). However, none of these candidates could advance the development without Dll4, although ICN1 completely overcame the defect. These findings suggested that other target(s) can substitute for the Dll4-mediated Notch signaling in thymocytes at the earliest stage.

DN3 cells can differentiate into the DP stage with reduced proliferation in the Dll4-null thymus

Then, we prepared a CD44$^-$CD25$^+$ population defined as DN3 cells from RAG2-deficient fetal thymi and cultured in FTOC with or without Dll4. After the introduction of the exogenous rearranged TCRβ chain by a retrovirus vector, RAG2-deficient DN3 cells could differentiate into the DP stage with proper cell proliferation (Fig. 3A and B, TCRβ/Mock), while few DP cells appeared without the TCRβ chain as the background (Fig. 3A and B, Mock/Mock). This finding was consistent with the dependency of the transition from the DN3 stage to the DP stage on pre-TCR [23]. Under the Dll4-deficient condition, TCRβ-transduced DN3 cells efficiently became DP cells, while their proliferation was impaired (Fig. 3A and B). We have never detected any induction of Dll1 in Dll4-deficient thymus (data not shown), negating its contribution. The reduced proliferation was restored by the enforced co-expression of ICN1, and the expression profiles of CD4 and CD8 were indistinguishable (Fig. 3A and B, TCRβ/ICN1). To monitor the status of their proliferation directly, we measured the DNA content and synthesis (Fig. 3C), and we confirmed the decrease in proliferation without

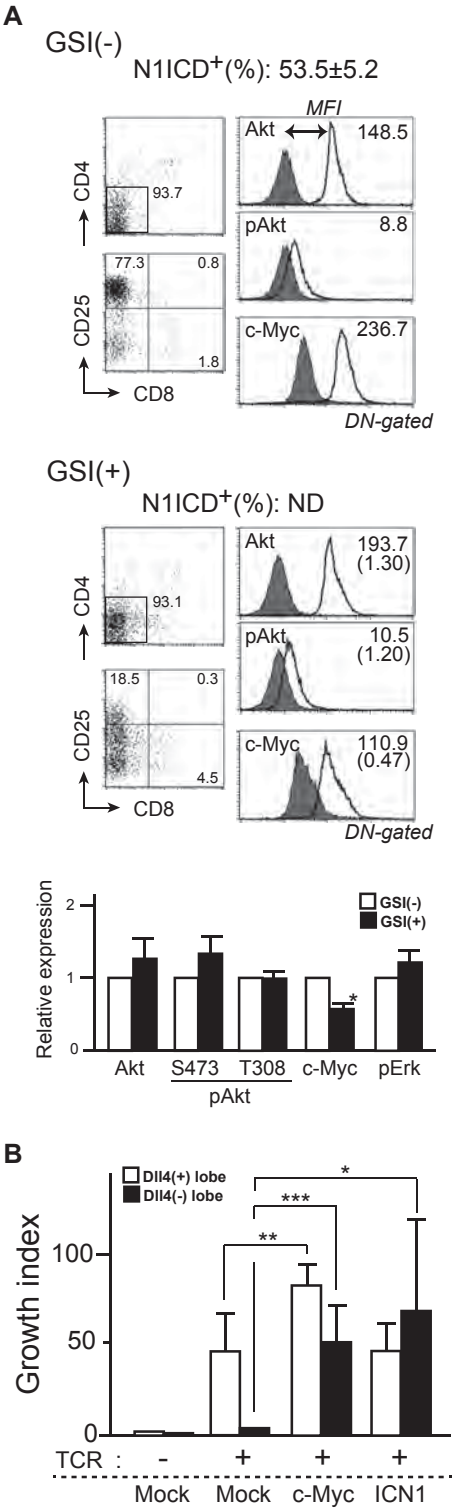

Dll4-mediated Notch signaling. In contrast, the viability after the cultures was not altered without Dll4 (data not shown). These findings suggested that the reduction in the cell number after the culture without Dll4 is mainly due to the impaired proliferation.

c-Myc is a target of Notch signaling and promotes proliferation in the Dll4-deficient condition

Previous reports showed that c-Myc and phosphorylation of Akt at Ser473 were maintained by Notch signaling [24, 25], but these results were obtained from cultured thymocytes on a monolayer of stromal cells with or without NotchL, Dll1. To confirm this finding in the more physiological 3D architecture of the thymus directly, we performed FTOC of RAG2-deficient thymi with or without gamma-secretase inhibitor (GSI), pan-Notch signal inhibitor, and examined the amount of c-Myc, phosphorylated Akt, and total Akt after the culture using flow cytometry. The specificity of the mAb that recognizes phosphorylated Akt (Ser473) was confirmed by staining of a transfectant that expressed the constitutive active form of Akt and cultured immature B cells with or without IL7 (Supporting Information Fig. 4). Coincidentally with the disappearance of cytoplasmic N1ICD (Fig. 4A, Supporting Information Fig. 5), the expression of both c-Myc and CD25 was significantly decreased after the culture with GSI (GSI(+)) (Fig. 4A). This result indicated that similar to CD25, c-Myc is also a potential target of Notch signaling in the thymus before pre-TCR signaling occurs. In contrast, the amount of both phosphorylated (Ser473) and total Akt did not diminish without Notch signaling (Fig. 4A). It is noteworthy that in the monolayer culture system, the expression, and phosphorylation of Akt (Ser473) were reduced, as was the expression of c-Myc, in the absence of Dll4-mediated Notch signaling (Supporting Information Fig. 4), as previously reported [25]. In addition, another phosphorylation of Akt at Thr308, which is mediated by PDK1 [26], was similarly retained after GSI treatment in FTOC (Fig. 4A and Supporting Information Fig. 4). These findings suggested that c-Myc expression, but not Akt phosphorylation, was controlled mainly by Notch signaling in the

Figure 4. c-Myc is a downstream target of Notch signaling at the DN stage and rescues the proliferation defect in the Dll4-deficient condition. (A) RAG2-deficient thymic lobes (e17.5) were cultured as FTOC for 2 days in the presence (GSI(+)) or absence (GSI(-)) of gamma-secretase inhibitor (DAPT). Cells were then stained with anti-CD4, anti-CD8, and anti-CD25 mAbs. Analysis of total Akt, phosphorylated Akt (pAkt, Ser473) and c-Myc expression in the intracellular regions was measured by flow cytometry. Active Notch signaling was monitored by detection of N1ICD in the cells after the cultures (N1ICD$^+$ (%); mean % ± SD, n = 5). ND, not detected. (Left panels) Surface expression of CD4, CD8, and CD25. Numbers in left panels refer to the percentages of populations in each square or quadrant. (Right panels) Open histograms indicate the staining with mAbs for Akt, pAkt (Ser473), and c-Myc, and filled histograms indicate staining with control rabbit IgG. Profiles of DN cells are shown, and differences of MFI (ΔMFI), with fold changes of ΔMFI by GSI treatment in parentheses. (Lower panel) Relative expression of Akt, phosphorylated Akt (pAkt; Ser473, S473; Thr308, T308), c-Myc, and pErk (control) with (black) or without (white) GSI treatment is shown; $^*p < 0.01$, paired Student's t test. (B) RAG2-deficient DN3 cells (e17.5) were infected with retrovirus encoding c-Myc, ICN1, or empty vector (Mock) with that encoding TCRβ (+) or with empty vector (-, mock control) and cultured in control (white, Dll4(+) lobe) or Dll4-deficient (black, Dll4(-) lobe) thymic lobes as described in Fig. 3. Growth indexes, as fold times compared to the infected cells before the culture are shown for each lobe; $^*p < 0.05$; $^{**}p < 0.01$; $^{***}p < 0.001$; unpaired Student's t-test. (A and B) Data are shown as mean ± SD of (A) $n = 3$ or (B) $n = 4$–5 samples and are representative of three independent experiments.

physiological condition, although Notch signaling seemed to be essential for the maintenance of Akt phosphorylation in the monolayer culture system.

To examine whether c-Myc, as a potential target of Notch signaling, is involved in cell proliferation, we introduced c-Myc into RAG2-deficient DN3 cells with a rearranged TCRβ chain that were cultured in a Dll4-deficient thymus (Fig. 4B). The enforced expression of c-Myc fully sustained the proliferation potential for FTOC without Dll4 at a level comparable to that of ICN1. These results suggested that Dll4-mediated Notch signaling actually maintains the expression of c-Myc, which leads to their cell expansion during the DN3 to DP stages in the thymus.

Dll4-mediated Notch signaling is necessary for the transition to the DP stage

Endogenous cleaved Notch1 in DN3 cells was obviously diminished by the 2-day GSI treatment in FTOC (Fig. 4A). Thus, we examined whether preexisting Notch signaling affects the potential of DN3 cells to differentiate into the DP stage. To remove the preexisting Notch signaling, we introduced RAG2-deficient DN3 cells into thymic lobes without Dll4 expression in a hanging-drop organ culture for 2 days, and we then triggered pre-TCR signaling by the addition of anti-CD3 mAb into the FTOC (Fig. 5A). Of course, the concentration of anti-CD3 mAb was critical. In the FTOC experiment, under the 3D condition, differentiation to the DP stage with proper proliferation was induced most effectively when a 100-fold lower dose of anti-CD3 mAb (0.1 μg/mL) was used compared to the standard condition (more than 10 μg/mL) in 2D monolayer culture systems [12], again arguing for the difference between 3D and 2D culture systems (Supporting Information Fig. 6). Although DP cell differentiation accompanied by vigorous proliferation occurred in the presence of Dll4-mediated Notch signaling, both differentiation and cell proliferation were abolished in the absence of Dll4 (Fig. 5B and C). This result indicated that DN3 cells absolutely require Notch signaling not only for cell expansion but also for their differentiation into the DP stage.

These defects were also recovered by the enforced expression of c-Myc (Fig. 5B and C), suggesting the significance of c-Myc for both their differentiation and proliferation. In contrast, active Akt, another candidate for the downstream target of Notch signaling in this stage, did not contribute to their proliferation at all but suppressed it (Fig. 5B and C). However, enforced expression of active Akt promoted the transition of DN3 cells to the DP stage (Fig. 5B), while a few cells were collected in the absence of Dll4. Therefore, the effect of Akt signaling on T-cell development seemed to differ between 3D and monolayer culture systems.

We confirmed the effects of active Akt and c-Myc on 2D cultures for comparison with the effects in previous reports (Supporting Information Fig. 7 and Supporting Information Table). Freshly isolated RAG2-deficient DN3 cells could differentiate into the DP stage with α-CD3 mAb-mediated pre-TCR signaling and Dll4-mediated Notch signaling and with active Akt and Notch signaling; these findings were consistent with previous reports [25, 27–29]. These results indicated that the construct for active Akt used in this study was effective in promoting their proliferation and expression of CD4 on their surface, as observed in the previous report [25]. However, these DN3 cells could not undergo this differentiation with pre-TCR signaling and c-Myc or active Akt instead of Notch signaling; these conditions were sufficient for the differentiation in a few previous reports [25, 29]. These discrepancies seemed to be due to the cellular context of DN3 cells that were proliferative in the culture for their preparation or expressed transgenic Bcl2 (Supporting Information Table).

Discussion

Using a thymic organ culture system, we demonstrated that the distinct developmental stages of DN thymocytes have different requirements for Dll4-mediated Notch signaling. Although the most immature $CD44^{+}CD117^{high}$ population (DN1a/b+DN2mt) did not develop at all without continuous Notch signaling, $CD44^{-}CD25^{+}$ cells (DN3) fully differentiated into DP cells using the Dll4-deficient epithelium in the thymus. However, using a monolayer culture system, differentiation from the DN3 to the DP stage had not been observed in the absence of Notch signaling [24, 25, 27–29]. Moreover, we validated the functions of possible downstream molecules of Notch signaling and demonstrated that c-Myc, but not Akt, plays important roles in the proliferation of thymocytes accompanied by the DN3 to DP stage transition, although the results shown in previous reports using the monolayer culture system have remained obscure.

Previous reports showed that the rearrangement of the *TCR*β gene and its protein synthesis were impaired in the thymi of *lck-Cre*, *Notch1*-floxed mice [4] in which gene deletion occurs after the DN2t stage. It was also shown that the transcript of the *Ptcra* gene is induced by Notch signaling; this gene encodes pTα, the partner of the TCRβ chain in pre-TCR [30]. Moreover, another target of Notch signaling, Hes1, was reported to be necessary for the efficient expansion of thymocytes at an early stage [31]. In this study, we never observed any recovery of the development from $CD44^{+}CD117^{high}$ cells by enforced expression of TCRβ, pTα, or Hes1 in the Dll4-deficient condition. As Notch signaling induced at the earliest stage of thymocytes, DN1a/b and DN2mt, should have multiple targets other than those molecules to advance their development, these combined inductions seem to be effective.

Because Notch signaling contributes to the determination of various cell fates, it is expected that Notch signaling will affect the ratio of cell populations. Although a preceding study reported an increase in γδ and a reciprocal decrease in αβ T cells in Rbpj-deficient thymocytes [5], the former was not observed in Notch1-deficient thymocytes [4]. In addition, ICN1-transfected hematopoietic progenitors gave rise to a considerable amount of γδ T cells [32]. It was also reported that Notch signaling does not antagonize γδ T-cell development; rather, it supports the expansion of γδ T-cell progenitors, especially at the DN2 stage in monolayer cultures [33]. These findings, as well as recent reports [34, 35], suggested that Notch signaling does not contribute to the

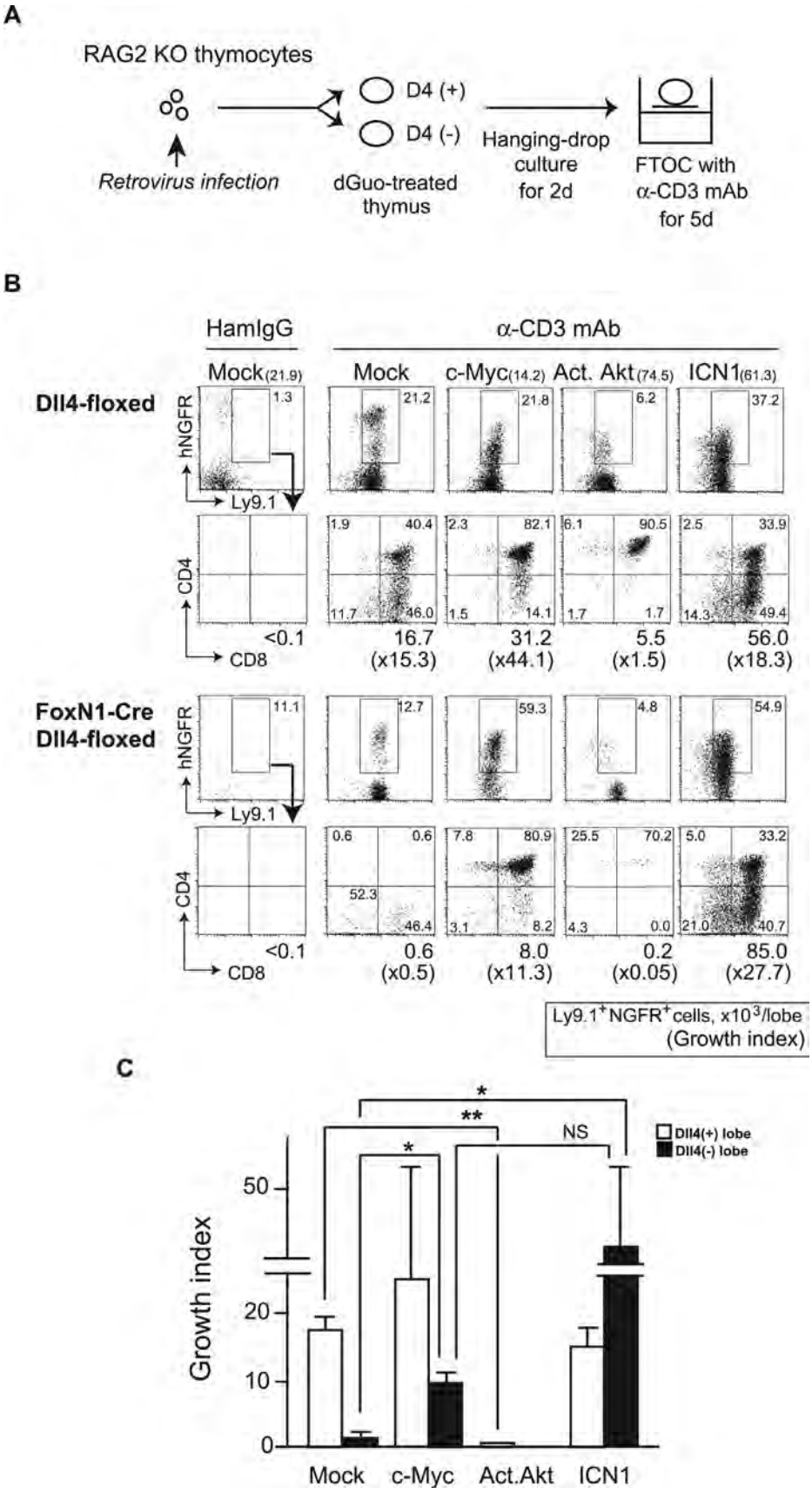

Figure 5. Dll4-mediated Notch signaling is absolutely required for differentiation from the DN3 to the DP stage induced by delayed pre-TCR signaling. (A) Experimental procedures schema. RAG2-deficient DN3 cells (e17.5–e18.5) were infected with various retroviruses indicated in (B) with NGFR and cultured in aliquot with deoxyguanosine-treated thymic lobes from control (Dll4-floxed; D4(+)) or Dll4-deficient (FoxN1-Cre, Dll4-floxed; D4(-)) fetuses as hanging-drop culture for 2 days. The lobes were then transferred onto filter and cultured as FTOC for 5 days in the presence of anti-CD3 mAb (145–2C11; α-CD3 mAb) or isotype-matched control Ab (Hamster IgG; HamIgG). (B) Expression of CD4 and CD8 in the $Ly9.1^+hNGFR^+$ fraction was measured by flow cytometry. The frequencies of infection before the culture are shown in the parentheses at the top of the panels. The numbers under the profiles represent the number of $Ly9.1^+hNGFR^+$ cells obtained from the cultures ($\times 10^3$/lobe) and the growth index as fold times compared to the infected cells before the culture (parentheses). The numbers in the profiles indicate the relative percentages for each corresponding square and quadrant. Data are representative of three independent experiments. (C) Growth indexes with anti-CD3 mAb are shown as mean ± SD ($n = 3$) and are pooled from three independent experiments; $^*p < 0.05$; $^{**}p < 0.01$; NS, not significant; paired Student's *t*-test.

determination of αβ/γδ T-cell lineages. The substantial reduction in the amount of γδ T cells after FTOC without Dll4 in the present study seems to be consistent with these findings. However, the appearance of NK lineage cells was not affected under the Dll4-deficient condition. These results suggested that almost all cells in the DN1a/b and DN2mt stages have their cell fates already determined or are not critically regulated by Dll4-mediated Notch signaling for their differentiation into the γδ T or NK cell lineages.

Molecular dissection of Notch signaling during the transition from the DN3 to the DP stage had been previously reported using the monolayer culture system of OP9 stromal cells with or without Dll1. In these studies, c-Myc and active Akt were shown to be Notch signal targets and to substitute for Notch signaling [24, 25, 27]. However, in these studies, this function was only shown in thymocytes on stromal cells in vitro, and the significance was never confirmed in a thymus with 3D structure.

How c-Myc acts downstream of Notch signaling remains controversial, and these functions have only been examined in a monolayer culture system (Supporting Information Table, underlined). It was shown that overexpression of c-Myc with pre-TCR signaling was not sufficient to induce the differentiation of DN3 cells to the DP stage without Notch signaling on the monolayer cultures [28], which was consistent with our result here and that of a previous report [27]. In contrast, it was also demonstrated that only c-Myc was sufficient for that differentiation [29]. Notably, the former studies used normal DN3 cells, whereas the cells in the latter study were prepared from Bcl2 transgenic mice to sustain their cell viability. Thus, differences in the anti-apoptotic properties of DN3 cells might affect the dependency of the differentiation on molecular events other than the expression of c-Myc; such events are entirely induced by Notch signaling in monolayer cultures, and these differences may lead to an overestimation of the significance of c-Myc. In the present study, we found that the maintenance of c-Myc was precisely dependent on Notch signaling in the thymus, and its enforced induction rescued the defect of the differentiation and proliferation during the transition from the DN3 to the DP stage in Dll4-deficient thymic lobes. These findings indicated that c-Myc is a critical target of Notch signaling during this transition in the thymus and suggested that the thymic 3D environment is more advantageous than the 2D condition for maintaining cell survival.

Moreover, the preexisting Notch signaling before pre-TCR signaling occurs was essential and sufficient for the differentiation to the DP stage in Dll4-deficient thymic lobes, suggesting that the Notch signaling induced at the DN3 stage is required for the maintenance of the competence of the pre-TCR signaling that triggers the differentiation. Moreover, continuous Notch signaling during the DN3/DP transition was essential for efficient proliferation, which was also mediated by c-Myc.

Using the 3D culture system, we revealed that the maintenance of phosphorylated Akt was not dependent on Notch signaling in DN3 cells before β-selection. It was well known that Akt signaling increases the uptake of glucose and activates glycolysis [25]. In this study, excessive activation of Akt seemed to influence the cellular state, including the regulation of metabolism, which might be adaptable for development in a 2D monolayer culture but not in the thymus. We realize that Akt and its signaling cascade, including PTEN and PI3K, are important for development [36], but these molecules are not mainly or directly connected with Notch signaling in the thymic environment with a 3D structure. The molecular details of Akt activation in the thymus should be further investigated.

Materials and methods

Mice

C57BL6 and BALB/c mice were purchased from Japan Clea (Kawasaki, Japan) and Japan SLC (Shizuoka, Japan), respectively. RAG2-deficient mice (BALB/c background, Ly9.1$^+$) were provided by the Central Institute of Experimental Animals (Kawasaki, Japan) and maintained in our animal facility. *FoxN1-Cre*, *Dll4-floxed* (C57BL/6 × 129, Ly9.1$^-$) mice were described previously [2]. All mice were maintained in specific pathogen-free conditions, and all mouse experiments were approved by the Animal Experimentation Committee (Tokai University, Kanagawa, Japan).

mAb and flow cytometry

FITC-conjugated CD44, FITC-CD229.1 (Ly9.1), PerCP/Cy5.5-CD4, PE/Cy7-CD4, PerCP/Cy5.5-CD19, Pacific Blue-CD8, biotinylated CD229.1 mAbs, and streptavidin-APC/Cy7 were purchased from BD Bioscience. FITC-rat CD2, PE-Notch1, PE-Notch2, PE-Notch3, PE-Notch4, PE-Hamster IgG, PE-human NGFR, Alexa Fluor700-CD8, and Pacific Blue-CD90.2 (Thy1.2) mAbs were purchased from BioLegend. Anti-Notch mAbs were originally established and characterized by ourselves [37]. FITC-CD3, PE-TCRβ, PE-TCRγδ, PE-CD25, PerCP/Cy5.5-CD25, allophycocyanin-CD3, allophycocyanin-CD8, allophycocyanin-CD44, allophycocyanin-CD117, allophycocyanin-DX5, allophycocyanin/eFluor780-CD3, and allophycocyanin/AlexaFluor750-CD25 mAbs were purchased from eBioscience. Streptavidin-Pacific Orange was obtained from Life Technologies. Flow cytometric analysis was conducted as described previously [7] and performed using a FACS Calibur equipped with CellQuest^{TM} Pro ver. 6, a FACS Verse or a FACS LSRFortessa (BD Bioscience) with FlowJo ver. 9. The PMT voltages were adjusted using unstained cells for all parameters. The mean autofluorescence values of unstained cells were adjusted to approximately 100 for all fluorochromes. For cytoplasmic staining, 5 × 10^5 cells were fixed and permeabilized with IntraStain (DAKO) and stained with Alexa Fluor488-conjugated rabbit anti-Akt (Cell Signaling, #5084), Alexa Fluor488-conjugated anti-phosphorylated Akt (Ser473; Cell Signaling, #4071) mAbs or Alexa Fluor488-conjugated isotype control (#2975), or anti-c-Myc (#5605), anti-phosphorylated Erk1/2 (Thr202/204, #4370) mAbs, or isotype control (#3900), followed by treatment with Dylight488-conjugated donkey anti-rabbit Ab (BioLegend). For

the detection of incorporated BrdU, an APC BrdU Flow Kit (BD Bioscience) was used according to the manufacturer's instructions.

To isolate the thymocytes at various stages, they were stained with CD3, CD4, CD8, TCRβ, CD44, CD25, CD117, and Thy1.2 and defined as DN1a/b ($CD44^+CD25^-CD117^{hi}$) [38, 39], DN2mt ($CD44^+CD25^+CD117^{hi}$) [8, 9], DN2t ($CD44^+CD25^+CD117^{lo}$) [8, 9], DN3 ($CD44^-CD25^+CD117^{lo}$), DN4 ($CD44^-CD25^-CD3^-CD4^-CD8^-CD90.2^+$), CD8 intermediate single-positive (8ISP) ($CD3^-CD4^-CD8^+$), DP ($CD4^+CD8^+$), CD4 single-positive (4SP) ($TCR\beta^+CD4^+CD8^-$), and CD8 single-positive (8SP) ($TCR\beta^+CD4^-CD8^+$) cells, respectively. These thymocytes were sorted from fetal (e15.5, DN1a/b-DN3), neonatal (DN4-8SP), or adult (8W, 8SP) thymi using a FACSAria (BD Bioscience). All methods for flow cytometry were described along MIATA guideline.

Detection of the cleaved Notch1 fragment

Thymocytes (5×10^4) were fixed in PBS containing 4% PFA at 4°C for 7 min. Antigen retrieval was accomplished by autoclave treatment in Target Retrieval Solution (DAKO) at 105°C for 5 min. These slides were stained with rabbit anti-cleaved Notch1 mAb (Cell signaling, #4147) or control rabbit IgG. The signals were visualized using Simplestain (Nichirei) and DAB (Sigma). Five random fields were digitally photographed and printed so that the number of cells with or without cleaved Notch1 could be counted.

Retroviral infections

$CD44^+CD117^{hi}$ or $CD44^-CD25^+$ fetal thymocytes, as DN1a/b plus DN2mt or DN3 cells, were sorted from e16.5 BALB/c ($Ly9.1^+$) or e17.5-e18.5 RAG2-deficient (BALB/c background, $Ly9.1^+$) fetal thymi and were infected with the retrovirus encoding the intracellular active form of human Notch1 (ICN1) [32], a rearranged murine TCRβ chain (Vβ8.2) derived from a cytotoxic T-cell clone 2C [40], c-Myc [41], constitutively active human Akt1 (myristylated Akt lacking the PH domain, residues 4–125) [42] or empty vectors (MIGR1, pMR2, or GCDN) [40, 43, 44], as described previously [32]. The infected cells could be identified by the detection of GFP (MIGR1), rat CD2 (pMR2), or human NGFR (GCDN).

Fetal thymus organ cultures

cRPMI-10 consisted of RPMI-1640 medium supplemented with 10% fetal bovine serum, penicillin/streptomycin (Meiji Seika Pharma), L-glutamine (Wako Pure Chemical Industries), 2-ME (Invitrogen), sodium pyruvate (Sigma), and HEPES buffer (Sigma). FBS was from a single lot previously qualified for low background and supporting T-cell development efficiently from fetal liver-derived hematopoietic progenitors.

The retrovirus-infected thymocytes ($Ly9.1^+$) were aliquoted at 2000 cells/well in Terasaki plates (NUNC), and one deoxyguanosine-treated lobe per well was added. The cells and lobes were incubated as hanging-drop cultures for 48 h, and then the lobes were removed, rinsed, and cultured on floating filters with cRPMI-10 for 5 or 7 days as FTOC. After the cultures, live cells were harvested and counted using trypan blue staining, and analyzed as $Ly9.1^+$ cells by flow cytometry. The remaining cells outside of the lobes after the hanging-drop cultures were used to check for infection efficiencies. To monitor DNA synthesis during FTOC, BrdU (10 μM) was pulsed for the last 18 h. For the detection of intracellular molecules without endogenous Notch signaling, RAG2-deficient thymic lobes (e17.5) were simply cultured on the filter with or without a gamma-secretase inhibitor, DAPT (10 μM, CALBIOCHEM), for 2 days. For the induction of pre-TCR signaling after the hanging-drop cultures, anti-CD3 mAb (145-2C11, #14-0031, eBioscience), or hamster IgG (#14-4888, eBioscience) was added to the culture medium for FTOC. All methods for the culture were described along MIATA guideline.

Acknowledgments: We thank Drs. W. Pear, M. Onodera, T. Kitamura, T. Sato, and Y. Gotoh for providing ICN1/MIGR1, the GCDN vector, packaging cells, c-Myc, and active Akt cDNAs; Y. Okada and Y. Iida for cell sorting; Y. Ishikawa, S. Ogiwara, Y. Nakano, and Y. Sakurai for producing murine embryos; and Dr. T. Sato for valuable discussion and comments on this manuscript.
This work was supported by a Grant-in-Aid for Scientific Research (JSPS KAKENHI Grant Number 21390121), a Grant-in-Aid for Scientific Research on Priority Areas (MEXT, 22021040) and Takeda Science Foundation to K. Hozumi.

Conflict of interest: The authors declare no financial or commercial conflict of interest.

References

1 **Lewis, J.**, Notch signaling and the control of cell fate choices in vertebrates. *Semin. Cell Dev. Biol.* 1998. **9**: 583–589.

2 **Hozumi, K., Mailhos, C., Negishi, N., Hirano, K., Yahata, T., Ando, K., Zuklys, S. et al.**, Delta-like 4 is indispensable in thymic environment specific for T cell development. *J. Exp. Med.* 2008. **205**: 2507–2513.

3 **Koch, U., Fiorini, E., Benedito, R., Besseyrias, V., Schuster-Gossler, K., Pierres, M., Manley, N. R. et al.**, Delta-like 4 is the essential, nonredundant ligand for Notch1 during thymic T cell lineage commitment. *J. Exp. Med.* 2008. **205**: 2515–2523.

4 **Wolfer, A., Wilson, A., Nemir, M., MacDonald, H. R. and Radtke, F.**, Inactivation of Notch1 impairs VDJβ rearrangement and allows pre-TCR-independent survival of early αβ lineage thymocytes. *Immunity* 2002. **16**: 869–879.

5 **Tanigaki, K., Tsuji, M., Yamamoto, N., Han, H., Tsukada, J., Inoue, H., Kubo, M. and Honjo, T.**, Regulation of αβ/γδ T cell lineage commitment and peripheral T cell responses by Notch/RBP-J signaling. *Immunity* 2004. **20**: 611–622.

6 **Hozumi, K., Kobori, A., Sato, T., Nozaki, H., Nishikawa, S., Nishimura, T. and Habu, S.**, Pro-T cells in fetal thymus express c-kit and RAG2 but do not rearrange the gene encoding the T cell receptor β chain. *Eur. J. Immunol.* 1994. **24**: 1339–1344.

7 **Hozumi, K., Kobori, A., Sato, T., Nishimura, T. and Habu, S.**, Transcription and demethylation of TCR β gene initiate prior to the gene rearrangement in c-kit+ thymocytes with CD3 expression: evidence of T cell commitment in the thymus. *Int. Immunol.* 1996. **8**: 1473–1481.

8 **Li, L., Leid, M. and Rothenberg, E. V.**, An early T cell lineage commitment checkpoint dependent on the transcription factor Bcl11b. *Science* 2010. **329**: 89–93.

9 **Ikawa, T., Hirose, S., Masuda, K., Kakugawa, K., Satoh, R., Shibano-Satoh, A., Kominami, R. et al.**, An essential developmental checkpoint for production of the T cell lineage. *Science* 2010. **329**: 93–96.

10 **Li, P., Burke, S., Wang, J., Chen, X., Ortiz, M., Lee, S., Lu, D. et al.**, Reprogramming of T cells to natural killer-like cells upon Bcl11b deletion. *Science* 2010. **329**: 85–89.

11 **Schmitt, T. M. and Zúñiga-Pflücker, J. C.**, Induction of T cell development from hematopoietic progenitor cells by Delta-like 1 in vitro. *Immunity* 2002. **17**: 749–756.

12 **Ciofani, M., Schmitt, T. M., Ciofani, A., Michie, A. M., Çuburu, N., Aublin, A., Maryanski, J. L. and Zúñiga-Pflücker, J. C.**, Obligatory role for cooperative signaling by pre-TCR and Notch during thymocyte differentiation. *J. Immunol.* 2004. **172**: 5230–5239.

13 **Tussiwand, R., Engdahl, C., Gehre, N., Bosco, N., Ceredig, R. and Rolink, A. G.**, The preTCR-dependent DN3 to DP transition requires Notch signaling, is improved by CXCL12 signaling and is inhibited by IL-7 signaling. *Eur. J. Immunol.* 2011. **41**: 3371–3380.

14 **Wolfer, A., Bakker, T., Wilson, A., Nicolas, M., Ioannidis, V., Littman, D. R., Wilson, C. B. et al.**, Inactivation of Notch1 in immature thymocytes does not perturb CD4 or CD8 T cell development. *Nat. Immunol.* 2001. **2**: 235–241.

15 **Onoyama, I., Tsunematsu, R., Matsumoto, A., Kimura, T., de Alborán, I. M., Nakayama, K. and Nakayama, K. I.**, Conditional inactivation of Fbxw7 impairs cell-cycle exit during T cell differentiation and results in lymphomatogenesis. *J. Exp. Med.* 2007. **204**: 2875–2888.

16 **Koyanagi, A., Sekine, C. and Yagita H.**, Expression of Notch receptors and ligands on immature and mature T cells. *Biochem. Biophys. Res. Commun.* 2012. **418**: 799–805.

17 **Fiorini, E., Merck, E., Wilson, A., Ferrero, I., Jiang, W., Koch, U., Auderset, F., E. et al.**, Dynamic regulation of Notch1 and Notch2 surface expression during T cell development and activation revealed by novel monoclonal antibodies. *J. Immunol.* 2009. **183**: 7212–7222.

18 **Radtke, F., Wilson, A., Stark, G., Bauer, M., van Meerwijk, J., MacDonald, H. R. and Aguet, M.**, Deficient T cell fate specification in mice with an inducible inactivation of Notch1. *Immunity* 1999. **10**: 547–558.

19 **Maillard, I., Tu, L., Sambandam, A., Yashiro-Ohtani, Y., Millholland, J., Keeshan, K., Shestova, O. et al.**, The requirement for Notch signaling at the β-selection checkpoint in vivo is absolute and independent of the pre-T cell receptor. *J. Exp. Med.* 2006. **203**: 2239–2245.

20 **Adler, S. H., Chiffoleau, E., Xu, L., Dalton, N. M., Burg, J. M., Wells, A. D., Wolfe, M. S. et al.**, Notch signaling augments T cell responsiveness by enhancing CD25 expression. *J. Immunol.* 2003. **171**: 2896–2903.

21 **Del Real, M. and Rothenberg, E. V.**, Architecture of a lymphomyeloid developmental switch controlled by PU.1, Notch and Gata3. *Development* 2013. **140**: 1207–1219.

22 **Dervovi´c, D. D., Liang, H. C.-Y., Cannons, J. L., Elford, A. R., Mohtashami, M., Ohashi, P. S., Schwartzberg, P. L. and Zúñiga-Pflücker, J. C.**, Cellular and molecular requirements for the selection of in vitro-generated CD8 T cells reveal a role for Notch. *J. Immunol.* 2013. **191**: 1704–1715.

23 **Yamasaki, S. and Saito, T.**, Molecular basis for pre-TCR-mediated autonomous signaling. *Trends Immunol.* 2006. **28**: 39–43.

24 **Weng, A. P., Millholland, J. M., Yashiro-Ohtani, Y., Arcangeli, M. L., Lau, A., Wai, C., del Bianco, C. et al.**, c-Myc is an important direct target of Notch1 in T-cell acute lymphoblastic leukemia/lymphoma. *Gene. Dev.* 2006. **20**: 2096–2109.

25 **Ciofani, M. and Zúñiga-Pflücker, J. C.**, Notch promotes survival of pre-T cells at the β-selection checkpoint by regulating cellular metabolism. *Nat. Immunol.* 2005. **6**: 881–888.

26 **Downward, J.**, Mechanisms and consequences of activation of protein kinase B/Akt. *Cur. Biol.* 1998. **10**: 262–267.

27 **Wong, G. W., Knowles, G. C., Mak, T. W., Ferrando, A. A. and Zúñiga-Pflücker, J. C.**, HES1 opposes a PTEN-dependent check on survival, differentiation, and proliferation of TCRβ-selected mouse thymocytes. *Blood* 2012. **120**: 1439–1448.

28 **Liu, H., Chi, A. W. S., Arnett, K. L., Chiang, M. Y., Xu, L., Shestova, O., Wang, H. et al.**, Notch dimerization is required for leukemogenesis and T-cell development. *Gene. Dev.* 2010. **24**: 2395–2407.

29 **Kreslavsky, T., Gleimer, M., Miyazaki, M., Choi, Y., Gagnon, E., Murre, C., Sicinski, P. and von Boehmer, H.**, β-selection-induced proliferation is required for αβ T cell differentiation. *Immunity* 2012. **37**: 840–853.

30 **Reizis, B. and Leder, P.**, Direct induction of T lymphocyte-specific gene expression by the mammalian Notch signaling pathway. *Gene. Dev.* 2002. **16**: 295–300.

31 **Wendorff, A. A., Koch, U., Wunderlich, F. T., Wirth, S., Dubey, C., Brüning, J. C., MacDonald, H. R. and Radtke, F.**, Hes1 is a critical but context-dependent mediator of canonical Notch signaling in lymphocyte development and transformation. *Immunity*. 2010. **33**: 1–14.

32 **Hozumi, K., Abe, N., Chiba, S., Hirai, H. and Habu, S.**, Active form of Notch members can enforce T lymphopoiesis on lymphoid progenitors in the monolayer culture specific for B cell development. *J. Immunol.* 2003. **170**: 4973–4979.

33 **Ciofani, M., Knowles, G. C., Wiest, D. L., von Boehmer, H. and Zúñiga-Pflücker J. C.**, Stage-specific and differential Notch dependency at the alphabeta and gammadelta T lineage bifurcation. *Immunity* 2006. **25**: 105–116.

34 **Van de Walle, I., Waegemans, E., De Medts, J., De Smet, G., De Smedt, M., Snauwaert, S., Vandekerckhove, B. et al.**, Specific Notch receptor-ligand interactions control human TCR-αβ/γδ development by inducing different Notch signal strength. *J. Exp. Med.* 2013. **210**: 683–697.

35 **Ferrero, I., Koch, U., Claudinot, S., Favre, S., Radtke, F., Luther, S. A. and MacDonald, H. R.**, DL4-mediated Notch signaling is required for the development of fetal αβ and γδ T cells. *Eur. J. Immunol.* 2013. **43**: 2845–2853.

36 **Hagenbeek, T. J., Naspetti, M., Malergue, F., Garçon, F., Nunès, J. A., Cleutjens, K. B. J. M., Trapman, J. et al.**, The loss of PTEN allows TCR αβ lineage thymocytes to bypass IL-7 and pre-TCR-mediated signaling. *J. Exp. Med.* 2004. **200**: 883–894.

37 **Moriyama, Y., Sekine, C., Koyanagi, A., Koyama, N., Ogata, H., Chiba, S., Hirose, S. et al.**, Delta-like 1 is essential for the maintenance of marginal zone B cells in normal mice but not in autoimmune mice. *Int. Immunol.* 2008. **20**: 763–773.

38 **Porritt, H. E., Rumfelt, L. L., Tabrizifard, S., Schmitt, T. M., Zúñiga-Pflücker, J. C. and Petrie, H. T.**, Heterogeneity among DN1 prothymocytes reveals multiple progenitors with different capacities to generate T cell and non-T cell lineages. *Immunity* 2004. **20**: 735–745.

39 **Sambandam, A., Maillard, I., Zediak, V. P., Xu, L., Gerstein, R. M., Aster, J. C., Pear, W. S. and Bhandoola, A.**, Notch signaling controls the generation and differentiation of early T lineage progenitors. *Nat. Immunol.* 2005. **6**: 663–670.

40 **Hozumi, K., Ohtsuka, R., Suzuki, D., Ando, K., Ito, M., Nishimura, T., Merkenschlager, M. and Habu, S.**, Establishment of efficient reaggregation culture system for gene transfection into immature T cells by retroviral vectors. *Immunol. Lett.* 2000. **71**: 61–66.

41 **Sato, T., Chiba, T., Ohno, S., Sato, C., Sugoh, T., Miyashita, K., Akatsuka, H. et al.**, Reciprocal control of G1-phase progression is required for Th-POK/Runx3-mediated CD4/8 thymocyte cell fate decision. *J. Immunol.* 2012. **189**: 4426–4436.

42 **Tsuruta, F., Masuyama, N. and Gotoh, Y.**, The phosphatidylinositol 3-kinase (PI3K)-Akt pathway suppresses Bax translocation to mitochondria. *J. Biol. Chem.* 2002. **277**: 14040–14047.

43 **Pui, J. C., Allman, D., Xu, L., DeRocco, S., Karnell, F. G., Bakkour, S., Lee, J. Y. et al.**, Notch1 expression in early lymphopoiesis influences B versus T lineage determination. *Immunity* 1999. **11**: 299–308.

44 **Nabekura, T., Otsu, M., Nagasawa, T., Nakauchi, H. and Onodera, M.**, Potent vaccine therapy with dendritic cells genetically modified by the gene-silencing-resistant retroviral vector GCDNsap. *Mol. Ther.* 2006. **13**: 301–308.

Abbreviations: **Dll**: delta-like · **DN**: double-negative · **DP**: double-positive · **FTOC**: fetal thymus organ culture · **ICN1**: intracellular active form of Notch1 · **N1ICD**: intracellular cleaved fragment of Notch1 · **NotchL**: Notch ligand

Full correspondence: Dr. Katsuto Hozumi, Department of Immunology, Tokai University School of Medicine, 143 Shimokasuya, Isehara, Kanagawa 259-1193, Japan
E-mail: hozumi@is.icc.u-tokai.ac.jp
Fax: +81-463-94-2976

Received: 13/8/2014
Revised: 5/5/2015
Accepted: 12/5/2015

Original Research Article

Maintenance of bone homeostasis by DLL1-mediated Notch signaling†

Yukari Muguruma[1,2*], Katsuto Hozumi[3], Hiroyuki Warita[1], Takashi Yahata[1], Tomoko Uno[1], Mamoru Ito[4], Kiyoshi Ando[2*]

[1]Center for Regenerative Medicine, Tokai University School of Medicine, Isehara, Japan
[2]Department of Hematology-Oncology, Tokai University School of Medicine, Isehara, Japan
[3]Department of Immunology, Tokai University School of Medicine, Isehara, Japan
[4]Central Institute for Experimental Animals, Kawasaki, Japan

*Corresponding author: Yukari Muguruma mugu@is.icc.u-tokai.ac.jp
Kiyoshi Ando andok@keyaki.cc.u-tokai.ac.jp
Department of Hematology-Oncology, Tokai University School of Medicine,
143 Shimokasuya Isehara, Kanagawa, Japan, 259-1193
Tel: +81-463-93-1121, Fax: +81-463-92-4750

Running head: DLL1-Notch signal regulates bone remodeling

Key words: DLL1-Notch signaling, bone remodeling, osteoblast-osteoclast coupling

Contract grant sponsor: Ministry of Education, Culture, Sports, Science and Technology of Japan, Basic Research Grant (c), Contract grant number: 26430094
Contract grant sponsor: Ministry of Education, Culture, Sports, Science and Technology of Japan, Strategic Research Foundation Grant-aided Project for Private University, Contract grant number: S1201001

Additional Supporting Information may be found in the online version of this article.

Received 18 March 2016; Revised 8 October 2016; Accepted 10 October 2016
Journal of Cellular Physiology

DOI 10.1002/jcp.25647

Abstract

Adult bone mass is maintained through a balance of the activities of osteoblasts and osteoclasts. Although Notch signaling has been shown to maintain bone homeostasis by controlling the commitment, differentiation, and function of cells in both the osteoblast and osteoclast lineages, the precise mechanisms by which Notch performs such diverse and complex roles in bone physiology remain unclear. By using a transgenic approach that modified the expression of *delta-like 1* (*DLL1*) or *Jagged1* (*JAG1*) in an osteoblast-specific manner, we investigated the ligand-specific effects of Notch signaling in bone homeostasis. This study demonstrated for the first time that the proper regulation of *DLL1* expression, but not *JAG1* expression, in osteoblasts is essential for the maintenance of bone remodeling. DLL1-induced Notch signaling was responsible for the expansion of the bone-forming cell pool by promoting the proliferation of committed but immature osteoblasts. However, DLL1-Notch signaling inhibited further differentiation of the expanded osteoblasts to become fully matured functional osteoblasts, thereby substantially decreasing bone formation. Osteoblast-specific expression of *DLL1* did not alter the intrinsic differentiation ability of cells of the osteoclast lineage. However, maturational arrest of osteoblasts caused by the *DLL1* transgene impaired the maturation and function of osteoclasts due to a failed osteoblast-osteoclast coupling, resulting in severe suppression of bone metabolic turnover. Taken together, DLL1-mediated Notch signaling is critical for proper bone remodeling as it regulates the differentiation and function of both osteoblasts and osteoclasts. Our study elucidates the importance of ligand-specific activation of Notch signaling in the maintenance of bone homeostasis.

Introduction

Integrity of the mammalian skeleton is maintained through two distinct mechanisms. Bone modeling during fetal and early postnatal life, in which osteoblasts and osteoclasts act independently in response to physiological stress, determines the shape and size of bone. In bone remodeling that occurs throughout life, old bone is removed by osteoclasts and then replaced with bone newly formed by osteoblasts, thereby maintaining the proper bone mass. An imbalance in this coupled activity of osteoclasts and osteoblasts leads to pathologic conditions, such as osteosclerosis, osteopetrosis, and osteoporosis (Feng and McDonald, 2011).

Notch signaling is an evolutionarily conserved signaling pathway and plays a central role in cell fate decisions and maintenance of tissue homeostasis in various organs during embryonic development as well as in postnatal life. Although the importance of Notch signaling in bone homeostasis has long been suggested through a number of *in vitro* studies (Deregowski et al., 2006; Sciaudone et al., 2003; Sekine et al., 2012; Tezuka et al., 2002; Vujovic et al., 2007; Yamada et al., 2003), Notch signal modifications in target cells have often produced conflicting results regarding the differentiation and/or function of the respective cell types. Recently, a series of *in vivo* murine genetic studies, in which Notch signaling was specifically activated or abolished at the various and specific stages of osteoblast lineage development, confirmed that Notch signaling regulates skeletal development as well as adult bone mass (Chen et al., 2014; Engin and Lee, 2010; Tao et al., 2010). These studies established the idea that the effects of Notch signaling in bone physiology are cell-context dependent, meaning that Notch exerts different effects depending on the differentiation status of target cells. However, how Notch carries out such diverse roles in bone cells remains elusive. Notch can be activated only through cell-cell contact, and in theory, binding of Notch to any one of the

at least 4 Notch ligands, namely Jagged1, Jagged2, delta-like ligand 1 (DLL1), and DLL4, can trigger the Notch signaling cascade. Nevertheless, whether any or all of the Notch ligands can elicit identical cellular events in bone cells has not yet been investigated. Since Jagged1 and DLL1 had been shown to be upregulated at the site of bone regeneration (Nobta et al., 2005), we decided to investigate how these two Notch ligands participate in bone homeostasis. To assess the roles of Jagged1 and DLL1 in bone metabolism *in vivo*, we utilized two transgenic mouse strains expressing either human *Jagged1 (JAG1)* or *DLL1* under the control of the osteoblast-specific *col1a1* promoter. It has been shown that while *JAG1*-expression in osteoblasts resulted in slightly decreased trabecular bone mass without altering total bone volume (Negishi et al., 2014), *DLL1*-expressing transgenic mice demonstrated abnormally dense bone (Ito et al., 2012), indicating that Jagged1 and DLL1 induce distinct cellular responses in bone cells. Since *DLL1*-expressing mice recapitulated the phenotypes of osteoblast-specific Notch gain-of-function mice (Engin and Lee, 2010), we sought to determine the roles of DLL1-mediated Notch signaling activation in the maintenance of bone homeostasis.

Here, we report that DLL1-mediated Notch signaling regulates the differentiation and function of both osteoblast and osteoclast lineage cells during bone remodeling. A primary role of DLL1-mediated Notch signaling is to induce proliferation of osteoblast progenitors to expand the pool of bone-forming cells. In addition, DLL1-Notch signaling regulates osteoblast-osteoclast coupling by controlling the differentiation of osteoblast progenitors into mature osteoblast/osteocytes, which are responsible for local production of RANK ligand (RANKL) and osteoprotegerin (OPG), thus maintaining the integrity of bone.

Materials and Methods

Mice

Transgenic mice that express human *DLL1* or *JAG1* under the control of a 2.3-kb osteoblast-specific promoter region of mouse *Col1a1* promoter were generated initially on a non-obese diabetic/severe combined immunodeficient/IL2Rγ^{null} (NOG) background. More than three founder mice were obtained in each transgenic line. Each founder mouse within the same transgenic line demonstrated a similar bone phenotype (Ito et al., 2012; Negishi et al., 2014). The NOG-DLL1-Tg and NOG-Jagged1-Tg mice were backcrossed with C57BL/6 mice more than ten times before being used for this study. Conditional knockout mice for the *DLL1* gene were created by crossing the *DLL1*-floxed mice with the *RosaCreER^{T2}* mice (Hozumi et al., 2004; Seibler et al., 2003). The *DLL1* gene was removed by treating mice with tamoxifen (2 mg/20 g) for 4 consecutive days. Mice, between E15.5 and 8 weeks old, were used at the time points specified in individual experiments. Both male and female mice were used. All experiments were performed using age- and sex-matched littermates. Mice were maintained in the animal facility of the Tokai University School of Medicine under specific-pathogen-free conditions with *ad libitum* access to sterilized food and water. All animal experiments were approved by the Animal Care Committee of Tokai University.

Bone histomorphometric analysis and microcomputed tomography analysis

Both static and dynamic histomorphometry and CT scanning were conducted independently at the Kureha Special Laboratory (Fukushima, Japan). Briefly, femurs and tibiae were fixed and dehydrated in ethanol. Femurs were subjected to CT scanning using Scan Xmate-A09S (Comscantechno, Kanagawa, Japan). Three-dimensional microstructural image data were reconstructed, and structural indices were calculated using 3D-BON software (Ratoc Systems Inc, Tokyo, Japan). Dehydrated and degreased tibiae were embedded undecalcified in glycol methacrylate

acrylic resin, sliced to 3 μm in thickness, and stained with Toluidine blue. Bone formation and resorption parameters were measured in a defined area of secondary spongiosa between 600 and 2100 μm from the growth plate using an OsteoPlan II morphometry system (Carl Zeiss, Thornwood, NY). Double labeling was performed via intraperitoneal calcein (Nacalai Tesque, Kyoto, Japan) injection twice at an interval of 3 days. Mice were sacrificed one day after the last injection. The terminology and units recommended by the American Society for Bone and Mineral research were used in this study (Parfitt et al., 1987).

Skeletal preparation, histology, immunohistochemistry, and image analysis

Whole-mount skeletal preparations were established using a standard protocol described elsewhere. For histology, bones were fixed overnight in 4% paraformaldehyde at 4°C and decalcified in 0.2 M EDTA for 1 to 4 weeks depending on the age of the animals. Bones were embedded in paraffin, and 3 μm longitudinal sections were obtained. For immunohistochemical staining, sections were dewaxed, rehydrated, and subjected to an antigen-retrieval procedure. Endogenous peroxidase and nonspecific binding of antibody were blocked by treating sections with 0.3% H_2O_2 in methanol and 5% normal sera, respectively. Sections were incubated overnight at 4°C with the antibodies listed below. The specific binding of primary antibodies was detected using a standard avidin-biotin peroxidase method (Vector Laboratories, Burlingame, CA), the universal immunoenzyme polymer method (Nichirei, Tokyo, Japan), or a tyramid signal amplification system (DakoCytomation, Denmark), followed by visualization with DAB. In some experiments, sections were stained for tartrate-resistant acid phosphatase (TRAP) to identify osteoclasts. The number of osterix-positive osteoblasts or TRAP-positive osteoclasts in the secondary spongiosa was obtained by using Image J software (http://rsbweb.nih.gov/ij/).

Antibodies

For immunostaining, the following antibodies were used at the indicated concentrations: anti-DLL1 (1:50, goat polyclonal, Santa Cruz Biotechnology, Dallas, Texas), anti-Jagged1 (1:100, goat polyclonal, Santa Cruz Biotechnology), anti-DLL4 (1:50, rabbit polyclonal, BioRad, Hercules, CA; Novus Biologicals, Littleton, CO), anti-Hes1 (1:250, rabbit polyclonal, Abcam, Cambridge, UK), anti-osterix (1:5000, rabbit polyclonal, Abcam), anti-RANK ligand (RANKL) (1:100, goat polyclonal, Santa Cruz), anti-Runx2 (1:100, mouse monoclonal, clone 8G5, MBL, Nagoya, Japan), anti-CD31 (1:10, rat monoclonal, clone MEC13.3, BD Biosciences, San Jose, California).

Preparation of BM cells

For *in vitro* culture of osteoblasts and osteoclasts, bone marrow (BM) cell fractions were prepared as described previously with slight modifications (Morikawa et al., 2009). Briefly, femurs, tibiae, and humeri were dissected and ground in 1 mL phosphate-buffered saline (PBS) using a mortar and pestle. PBS that contained BM cells, including both hematopoietic and non-hematopoietic cells, was transferred to a small tube. After centrifugation, cell-free PBS, hereafter called BM liquid, was collected and saved for protein quantification. Following treatment with 0.15 M NH_4Cl cell lysis buffer, cells, hereafter called BM cells, were resuspended in α-MEM containing 10% FBS (10%MEM) and used for osteoclast culture. Bone fragments were digested with 0.2% collagenase (Wako Chemicals, Osaka, Japan) for 1 h at 37°C. Liquid cell suspension was passed through a 0.45 μm filter, centrifuged, treated with 1 mL of sterile distilled water to remove hematopoietic cells, and washed with PBS containing 2% FBS. The remaining cells, hereafter called mesenchymal stem cell (MSC)-enriched BM cells, were used for osteoblast culture.

In vitro *osteoblast culture*

MSC-enriched BM cells were plated at a density of $5X10^4$ cells/cm^2 in 10%MEM. Cells were harvested at several time points for gene expression analyses, alkaline phosphatase (ALP) staining, and ALP activity analyses. ALP enzyme activity was measured using the LabAssay ALP kit (Wako chemical).

In vitro *osteoclast culture*

BM cells plated at a density of $5X10^4$ cells/cm^2 were cultured with 20 ng/mL each of macrophage-colony stimulating factor (M-CSF) and RANKL (both from R&D systems, Minneapolis, MN) for 6-7 days. For mixed culture, BM cells were plated at a density of $3X10^6$ cells/cm^2 and stimulated with 10^{-7} M dexamethasone (Dex) and 10^{-8} M 1α,25-dihydroxhy vitamin D_3 (VD_3) for 11-13 days. Culture supernatant of this mixed culture was saved for cytokine quantification analyses. Co-culture experiments were conducted as described previously (Xing et al., 2002) with slight modifications. Briefly, primary osteoblasts were isolated from calvariae of 4- to 6-day-old DLL1 and non-transgenic littermates using a sequential collagenase/dispase digestion, propagated, and plated on to 24-well tissue culture plates ($2.5X10^4$ cells/well). BM cells obtained as described above were cultured overnight in 10%MEM containing 10 ng/mL M-CSF. Non-adherent BM cells ($2X10^5$ cells/well) were seeded onto a monolayer of primary osteoblasts and cultured for 9 to 13 days in the presence of 10^{-7} M Dex and 10^{-8} M VD_3. At the end of the culture, wells were fixed with 3.7% formaldehyde/PBS and stained for TRAP. TRAP-positive cells containing 3 or more nuclei were designated as osteoclasts and counted under the microscope.

RNA purification and gene expression analysis

Total RNA was purified from cultured cells and calvariae using Isogen II solution (Nippon Gene Co, Toyama, Japan) according to the manufacturer's instructions and was reverse transcribed into cDNA. Expression levels of osteoblast differentiation

markers, Notch signaling molecules, and osteoclast differentiation markers were quantified using appropriate Taqman® probes, listed below (Applied Biosystems, Foster City, CA). Jagged2: Mm01325629_m1, Hes1: Mm01342805_m1, Hey1: Mm00468865_m1, Col1a1: mm0080166_g1, ALP: Mm00475834_m1, osteocalcin (bglap3): Mm03413826_m1, Runx2: Mm00501580_m1, osterix (sp7): Mm04209856_m1, RANKL (tnfsf11): Mm00441906_m1, Sema3b: Mm00436477_m1.

Enzyme-linked immunosorbent assay (ELISA)

The concentration of RANKL, osteoprotegerin (OPG), M-CSF in plasma, BM liquid, and culture supernatant was determined using Quantikine kits (R&D systems). The concentrations of carboxylated osteocalcin (Gla-osteocalcin), an indicator of bone formation, and undercarboxylated osteocalcin (Glu-osteocalcin), an indicator of bone resorption, were determined using High Sensitive EIA kits (Takara, Shiga, Japan).

Statistics

Data were analyzed using GraphPad Prism, version 5.0 (GraphPad Software). Student's two-tailed unpaired (or paired, when applicable) *t*-test was used to determine the significance of the difference between the means of two groups. A normal distribution of the data was confirmed using the Kolmogorov-Smirnov test. The mean ± SD is presented in each graph. P values < .05 were considered significant. NS stands for not significant.

Results

Phenotypes of Notch ligand transgenic mice

In our attempt to determine the ligand-specific effects of Notch signaling in the physiology of bone in normal immune environment, previously described NOG-DLL1-Tg and NOG-Jagged1-Tg mice, in which human *DLL1* or *JAG1* was expressed under the control of the osteoblast-specific 2.3 kb *col1a1* promoter on NOG background, were backcrossed with C57BL/6 mice. In the bone marrow (BM) of both non-transgenic mice and DLL1-C57BL/6 transgenic mice, hereafter called DLL1 mice, endogenous murine Jagged1 and DLL4 were prominently expressed both the bone lining and the matrix embedded osteoblasts. Meanwhile, endogenous expression of DLL1 was detected only weakly in osteoblasts of non-transgenic mice. The *col1a1*-driven upregulation of *DLL1* augmented the expression of DLL1 in the BM stoma as well as in osteoblasts without affecting DLL4 or Jagged1 expression levels (supplementary figure 1a). It did not affect the expression of *Jagged2* in calvaria either (supplementary figure 1b). The results indicate the specificity of the transgene expression in our experimental system. DLL1 mice, both male and female, were smaller than their non-transgenic littermates and exhibited a general feature of osteosclerosis (Fig. 1a and supplementary figure 1c). In analyses of skeletal preparations, both the proximal and distal portions of limbs appeared short and thick, and the calvaria was also short (Fig. 1b and supplementary figure 1d). These osteosclerotic phenotypes were confirmed by histological analyses in 3- and 6-week-old mice and μCT analysis of 6-week-old mice (Fig. 1c and supplementary figure 1e). Unexpectedly, despite their abnormally high bone mass, bone metabolic turnover in DLL1 mice was severely compromised. Quantitative histomorphometry revealed substantial decreases in the mature osteoblast surface area and the bone formation rate

as well as in the osteoclast surface area and eroded surface area in both 3- and 6-week-old DLL1 mice (Fig. 1d and supplementary figure 1f). Consistent with these histological measurements, plasma levels of both carboxylated (Gla-Ocn) and undercarboxylated (Glu-Ocn) osteocalcin were markedly decreased (Fig. 1e). Gla-Ocn has a high affinity for bone minerals and is often considered a biochemical marker for bone formation. On the other hand, the acidic pH in resorption lacunae decarboxylates Gla-Ocn bound to calcium in the bone; hence, the circulating level of Glu-Ocn reflects bone-resorption activity (Karsenty and Ferron, 2012). The significant decreases in these biomarkers confirmed that the osteosclerotic phenotype of DLL1 mice was caused by functional suppression of both osteoblasts and osteoclasts. In contrast to this pathological bone phenotype in DLL1 mice, osteoblast-specific expression of *JAG1* on a C57BL/6 background had a mild effect on bone. The cortical bone of *JAG1*-expressing mice was thick but porous, resembling cancellous bone, suggesting an enhancement in bone-resorption activity (supplementary figure 1g). These results are consistent with our hypothesis that particular Notch ligands are responsible for distinct biological events in bone physiology.

Effects of DLL1-mediated Notch signaling on osteoblast differentiation in vivo

Because *DLL1* overexpression produced a stronger effect on the postnatal bone phenotype than did *JAG1* overexpression, we evaluated the roles of DLL1-mediated Notch signal activation in bone physiology. We asked whether DLL1-mediated Notch signaling functioned in perinatal bone formation. Using routine histological observation, no distinct morphological differences were noted in the endochondral ossification of DLL1 and non-transgenic littermates at E15.5 (Fig. 2a and supplementary figure 2a). The difference between the two groups first became noticeable at E18.5. Non-hematopoietic fibroblast-like cells progressively dominated

in the BM of DLL1 mice, and at 1 week after birth, fibroblastic cells with the morphology of early osteoblasts outnumbered hematopoietic cells. This was in stark contrast to the BM of non-transgenic mice, in which hematopoietic cells migrating through the vascular network proliferated vigorously, making BM a primary site of adult hematopoiesis. Since immunohistochemical staining using a CD31 antibody revealed a similar level of vascular invasion into the BM cavity at the beginning of BM hematopoiesis, the abnormally high content of fibroblast-like cells in the BM of DLL1 mice was due not to poor migration of hematopoietic cells from other embryonic hematopoietic sites but rather to *in situ* proliferation of immature osteoblast-like cells, as confirmed by positive staining with a Ki67 antibody (Fig. 2b). In addition, activation of Notch signaling was detected by Hes1 immunostaining of BM sections (Fig. 2b) as well as by quantitative analyses of *Hes1* and *Hey1* expression in calvaria and adherent BM cells obtained from DLL1 mice (Fig. 2c). These results indicate that expression of the *DLL1* transgene in osteoblasts induces marked proliferation of Notch signal-activated non-hematopoietic cells.

To unequivocally characterize the fibroblast-like cells proliferating in the BM of DLL1 mice, hind limbs of embryos and neonates were stained for osteoblast differentiation markers. In non-transgenic mice, Runx2- and osterix-positive osteoblasts were easily detected around primary spongiosa of developing bone at E15.5 and 18.5, but their expressions became restricted in cells on the surface or embedded in the bone at later time points (Fig. 3a). In contrast, those osteoblast marker-positive cells were ubiquitously distributed in the BM of DLL1 mice throughout the time points analyzed (Fig. 3b). Even at 6 weeks of age, the number of Runx2- and osterix-positive immature osteoblasts per bone surface was significantly higher in DLL1 mice (Fig. 3c and supplementary figure 2b) than in their non-transgenic littermates. This result did not contradict our earlier histomorphometric analyses, i.e., fewer mature osteoblasts on

bone surface and a concomitant decrease in bone formation, but rather indicated perturbations in osteoblast maturation in DLL1 mice. Consistently, osteoid thickness and cortical bone mineral density, key parameters for matrix production and mineralization, respectively, were both markedly decreased in DLL1 mice at 3 and 6 weeks (Fig. 3d and supplementary figure 2c), another indication of reductions in functional osteoblasts. These results indicate that DLL1-Notch signaling plays diverse roles in osteoblast development.

Roles of DLL1 mediated Notch signal activation in osteoblast development in vitro

To determine the endogenous function of DLL1-mediated Notch signaling in the physiology of osteoblast development, *in vitro* osteoblast differentiation experiments were conducted without adding any cytokines or osteogenic agents using MSC-enriched BM cells obtained from DLL1 mice, mice with conditional deletion of the *DLL1* gene (Dll1-floxed), and their respective littermates. In a classical colony forming unit (CFU) assay that identified both fibroblast-like (CFU-F) and alkaline phosphatase (ALP)-expressing osteoblast colonies (CFU-ALP), DLL1 mice showed approximately 4 times as many osteoblast progenitors as their littermates(Fig. 4a). Consistent with this, MSC-enriched BM cells obtained from DLL1 mice demonstrated significantly higher expression levels of *Collagen 1*, a marker for committed osteoblast progenitors, at days 3, 7, and 10 and of *Alp*, an early osteoblast marker, at days 3 and 7 (Fig. 4b). In contrast, the expression levels of *Collagen 1* and *Alp*, as well as the number of colonies, were all reduced in Dll1-floxed cultures (Fig. 4c and supplementary figure 3a), indicating the physiological importance of DLL1 during the early phase of osteoblast differentiation. ALP histochemistry and enzyme activity analyses confirmed the gene expression analyses (supplementary figure 3a and b). Conversely, the expression of *Osteocalcin*, a marker for mature functional osteoblasts, was severely reduced in the

DLL1 culture while mildly elevated in Dll1-floxed culture at days 7 and 10 (Fig. 4b and c). These results indicate that *DLL1* expression in osteoblasts must be regulated properly to ensure both the early and late phases of the physiological development of osteoblast

To further delineate the mechanisms by which DLL1-mediated Notch signaling regulates osteoblast differentiation and maturation, expression levels of transcriptional regulators were analyzed. The transcription factors Runx2 and osterix govern the commitment to osteoblast-lineage cells from mesenchymal stem cells (MSCs), subsequent differentiation, and further maturation into functional osteoblasts. At the beginning of culture, the expression of *Osterix* was more than 3-fold higher in DLL1 culture than in the controls, whereas *Osterix* expression was decreased by half in Dll1-floxed culture compared to the controls (Fig 4d), implicating the involvement of DLL-Notch signaling in osterix-dependent proliferation of osteoblast progenitors. On the contrary, no significant changes were detected in *Runx2* transcription in either DLL1 or Dll1-floxed mice compared with their respective littermates, implying that DLL1-mediated Notch signaling was not involved in a *Runx2* transcription-dependent process of osteoblast commitment from MSCs. These results delineated the mechanisms underlying the pathological bone phenotype seen in DLL1 mice at the cellular and molecular level: transgenic expression of *DLL1* drove the proliferation of early osteoblast cells but caused a maturational arrest of those cells.

Effects of DLL1-mediated Notch signal activation on osteoclast differentiation in vivo *and* in vitro

We have thus far determined the cause of the suppression of bone formation as a maturational arrest in osteoblast differentiation. In addition, severely compromised

bone turnover was a distinct feature of our DLL1 mice. To gain further insight into the processes suppressing bone-resorption activity in DLL1 mice, we examined the differentiation of cells in the osteoclast lineage. Until late stages of embryonic development (E15.5 and E18.5), there were no noticeable changes in the number or morphology of osteoclasts: Relatively small tartrate-resistant acid phosphatase (TRAP)-positive osteoclasts were observed in similar numbers in the BM of DLL1 mice and non-transgenic littermates. However, the difference between the two groups became apparent immediately after birth (Fig. 5a). As early as P0.5, multinucleated large osteoclasts covering the bone surface formed resorption lacunae, an indicator of active osteoclast function, in the BM of non-transgenic littermates. In contrast, osteoclasts in DLL1 mice were smaller and were not particularly associated with the bone surface. In addition, consistent with the earlier histomorphometric analyses of adult mice, microscopic quantification of TRAP-stained BM sections showed a marked reduction in the number of osteoclasts per bone surface in DLL1 mice even at 1 week after birth (Fig. 5b) without substantial changes in the total number of TRAP-positive cells in the observed fields. These results revealed that down-regulation of bone-resorption activity began at the beginning of bone remodeling.

To identify the cause of defective bone-resorption activity at the cellular level, we first examined the ability of hematopoietic cells to form osteoclasts *in vitro*. Stimulation of hematopoietic cells with macrophage colony-stimulating factor (M-CSF) and RANK ligand (RANKL) can produce osteoclasts. When BM hematopoietic cells of DLL1 mice and non-transgenic littermates were cultured in the presence of M-CSF and RANKL, osteoclasts were formed in similar numbers (Fig. 6a), confirming that the number and the functionality of osteoclast precursors within the hematopoietic population were not altered by osteoblast-specific activation of DLL1-mediated Notch signaling. Since osteoblasts are the major source of cytokines regulating osteoclast differentiation

during bone remodeling *in vivo*, we examined osteoclast differentiation in the context of osteoblast-osteoclast coupling. When whole BM cells were stimulated with 1,25-dihydroxyvitamin D_3 (VD_3) and dexamethasone, a condition known to promote osteoclast formation via osteoblast-derived factors (Muguruma and Lee, 1998; Takahashi et al., 1988a; Takahashi et al., 1988b), considerably fewer osteoclasts were detected in DLL1 cultures (Fig. 6b), indicating alterations in osteoblast-osteoclast coupling. To identify the cause of this defective osteoblast-osteoclast coupling, we conducted co-culture experiments using calvarial primary osteoblasts and BM hematopoietic cells obtained from DLL1 and non-transgenic littermates. Consistent with our results described above, there were no differences between DLL1 and non-transgenic mice in the numbers of osteoclasts formed from BM hematopoietic cells. On the contrary, significantly fewer numbers of osteoclasts were formed when BM hematopoietic cells were cultured with osteoblasts obtained from DLL1 mice (Fig. 6c), confirming that the defective osteoclast differentiation and function observed in DLL1 mice were indeed due to the defect in osteoblasts.

To further clarify the roles of DLL1-mediated Notch signaling in osteoblast-osteoclast coupling, we measured the concentrations of cytokines important for osteoclastogenesis in the plasma, BM liquid, and culture supernatant of DLL1 and non-transgenic littermates. Although the concentration of M-CSF in the supernatant did not differ between the DLL1 and non-transgenic cultures, the DLL1 cultures showed a significant reduction in RANKL production and a slight elevation in osteoprotegerin (OPG), a decoy receptor for RANKL that acts as an inhibitor of osteoclast differentiation, which resulted in a considerably smaller RANKL/OPG ratio, an important determinant of skeletal integrity (Table 1). Reductions in RANKL production were confirmed by quantitative gene expression analyses as well as immunohistochemical staining of BM specimens with RANKL antibody followed by TRAP staining, revealing a lack of

RANKL production in osteoblasts/osteocytes and concomitant poor osteoclast differentiation in DLL1 mice (Fig. 6d and e). In contrast, the systemic levels of RANKL, OPG, and M-CSF did not differ between DLL1 and non-transgenic littermates (supplementary Fig. 4), highlighting the importance of local, i.e., osteoblast/osteocyte-specific, production of RANKL in osteoclast differentiation during bone remodeling. Also interesting was a significant decrease in *Semaphorin 3B* (*Sema3B*) expression in DLL1 cultures (Fig. 6f). Sema3B is expressed in osteoblasts and induces osteoclastogenesis in response to VD_3 stimulation (Sutton et al., 2008). Although, a previous study indicated that transgenic expression of *Sema3B* did not alter the expression levels of any cytokines critical for osteoclastogenesis, we observed an association of the transgenic expression of *DLL1* in osteoblasts with marked down-regulation of both *Sema3B* and *Rankl* transcriptional activity. These results demonstrated that the abnormal osteoclast differentiation and function observed in DLL1 mice were not due to a cell-autonomous defect in osteoclast lineage but instead to a defective environment that could not properly supply osoteclastogenic cytokines. In other words, a direct effect of transgenic expression of *DLL1* in osteoblast was a blockage in osteoblast maturation, which in turn inhibited the differentiation and maturation of osteoclasts, thereby resulting in severe suppression of bone metabolism. Altogether, our results demonstrate the significance of DLL1-mediated Notch signaling in osteoblast-osteoclast coupling during bone remodeling.

Discussion

Although the importance of Notch signaling in bone physiology has been shown by a number of *in vivo* and *in vitro* studies, the mechanisms by which Notch signaling regulates bone homeostasis remain elusive. Since Notch regulates many types of

cellular events, we hypothesized that the effects of Notch signal activation are determined by the ligands that bind to Notch at particular times and places. In this study, we investigated the effects of DLL1-induced Notch signaling in the differentiation and function of bone cells.

Mice expressing human *DLL1* under the control of a *col1a1* promoter on C57BL/6 background exhibited severe osteosclerosis that was caused by the proliferation of Notch-activated osterix-positive immature osteoblasts. Importantly, postnatal deletion of *DLL1* resulted in a decrease in the expression of *Osterix* and the number of osteoblast progenitors, leading to a significant inhibition of osteoblast differentiation, indicating that DLL1-Notch signaling is indispensable in the osterix-dependent proliferation of osteoblasts, an event necessary for the expansion of bone-forming cells. On the contrary, transgenic expression or deletion of *DLL1* in osteoblasts did not affect *Runx2* transcription in our experiments. Notch has been shown to negatively control two important Runx2-dependent events in osteoblast development (Hilton et al., 2008, Kalajzic et al., 2002; Rossert et al., 1995, Zanotti et al., 2008). One is the inhibition of osteoblast commitment from MSCs through the downregulation of *Runx2* transcriptional activity, which did not appear to involve DLL1-Notch signaling, suggesting that other Notch ligands are responsible for this process. The other is the negative effect on the differentiation and maturation of immature osteoblasts into functional osteoblasts, plausibly through physical interaction with Runx2. In this study, *DLL1* expression in osteoblasts caused substantial decreases in the numbers of mature osteoblasts both *in vitro* and *in vivo*, while deletion of *DLL1* slightly upregulated the maturation of cells already committed to the osteoblast lineage *in vitro*. Interestingly, histological analyses detected markedly higher numbers of Runx2-positive osteoblasts in the BM of DLL1 mice. Since *Runx2* expression was unaffected by the *DLL1* transgene, the persistence of Runx2-positive osteoblasts was

not due to the increase in transcription but may be due in part to the suppression of Runx2 degradation, as seen in mice lacking the zinc finger adapter protein Schnurri-3, a protein important for the maintenance of adult bone mass (Glimcher et al., 2007; Jones et al., 2006). As overexpression of *Runx2* in osteoblasts has been shown to inhibit osteoblast differentiation at a later stage (Liu et al., 2001), the continuous expression of Runx2 protein is likely to be a cause of the maturational arrest of osteoblasts in our DLL1 mice. Taken together, DLL1-mediated Notch signaling appeared to act as a regulatory switch for at least two critical points in the osteoblast differentiation: a positive regulator for the expansion of bone-forming cells and a negative regulator for the functional maturation of osteoblasts.

A profound loss of bone-resorbing osteoclasts is another pathologic feature of DLL1 bone. DLL1 mice demonstrated severely suppressed bone metabolic turnover, a phenotype quite similar to a dentin matrix protein 1 promoter-specific gain-of-Notch-function mouse (Dmp-1 mouse), in which Notch signaling was preferentially activated in osteocytes (Canalis et al., 2013). Unlike the Dmp-1 mouse, in which a systemic upregulation of OPG production is a main cause of the osteosclerosis, the circulating levels of all of the cytokines important for maintaining bone homeostasis, including OPG, were unchanged in the DLL1 mice. Even in the *in vitro* experiment that demonstrated a substantial decrease in osteoclast formation, no meaningful change was noted in the OPG level compared to non-transgenic culture. In contrast, a significant reduction in RANKL production was confirmed at both the gene expression and protein levels in DLL1 osteoblasts/osteocytes. Furthermore, a substantial decrease in *Sema3B* expression was detected in DLL1 culture. Semaphorins are secreted and membrane-bound proteins that regulate developmental processes in many organs. As proteins expressed by both osteoblasts and osteoclasts, semaphorins have recently been identified as critical regulators of the coupling process in bone remodeling

(Jongbloets and Pasterkamp, 2014; Sims and Martin, 2014). Sema3B is a soluble semaphorin produced by osteoblasts and induces osteoclastogenesis upon VD_3 treatment. Transgenic expression of *Sema3B* was shown to promote osteoclast formation by enhancing the action of RANKL without changing the levels of *Rankl* transcript (Sutton et al., 2008). Although *Sema3B* knockout mice have yet to be described, we demonstrated that consistent activation of DLL1-Notch signaling simultaneously reduced the expression levels of *Sema3B* and *Rankl*. Based upon these observations, it is evident that DLL1-Notch signaling regulates the production of RANKL from matrix-embedded osteoblasts, a critical determinant of bone remodeling (Nakashima et al., 2011; Xiong et al., 2011), conceivably by controlling the maturation of osteoblasts into RANKL-producing osteoblasts/osteocytes, or possibly by directly modulating *Rankl* expression through a Notch-semaphorin cascade, thus maintaining the proper bone mass.

Our study revealed unique roles of DLL1-mediated Notch signaling in the process of bone remodeling. DLL1-Notch signaling directly controls the physiological expansion and differentiation of osteoblasts and indirectly affects the maturation and function of osteoclasts, thereby ensuring the homeostasis of bone mass. Deregulations in Notch signaling have been implicated in the development of bone cell neoplasia (Zhang et al., 2008). Given the importance of DLL1-Notch signaling in the proliferation and differentiation of osteoblast cells, we plan to investigate the relationship between *DLL1* expression and bone neoplasia.

Acknowledgements: We would like to thank Dr. Y. Nakano, Mr. K. Hirano, members of the Support Center for Medical Research and Education, and the Center for Regenerative Medicine at Tokai University for technical assistance.

Conflict of Interest: The authors declare no conflicts of interest regarding this article.

Author Contribution: YM and KH designed the experiments and wrote the paper. YM and TY performed the experiments. HW and TU analyzed the gene expression data. KH and MI created transgenic mice. KA approved data.

References

Canalis E, Parker K, Feng JQ, Zanotti S. 2013. Osteoblast lineage-specific effects of notch activation in the skeleton. Endocrinology 154(2):623-634.

Chen S, Lee BH, Bae Y. 2014. Notch signaling in skeletal stem cells. Calcif Tissue Int 94(1):68-77.

Deregowski V, Gazzerro E, Priest L, Rydziel S, Canalis E. 2006. Notch 1 overexpression inhibits osteoblastogenesis by suppressing Wnt/beta-catenin but not bone morphogenetic protein signaling. J Biol Chem 281(10):6203-6210.

Engin F, Lee B. 2010. NOTCHing the bone: insights into multi-functionality. Bone 46(2):274-280.

Engin F, Yao Z, Yang T, Zhou G, Bertin T, Jiang MM, Chen Y, Wang L, Zheng H, Sutton RE, Boyce BF, Lee B. 2008. Dimorphic effects of Notch signaling in bone homeostasis. Nat Med 14(3):299-305.

Feng X, McDonald JM. 2011. Disorders of bone remodeling. Annu Rev Pathol 6:121-145.

Glimcher LH, Jones DC, Wein MN. 2007. Control of postnatal bone mass by the zinc finger adapter protein Schnurri-3. Ann N Y Acad Sci 1116:174-181.

Hilton MJ, Tu X, Wu X, Bai S, Zhao H, Kobayashi T, Kronenberg HM, Teitelbaum SL, Ross FP, Kopan R, Long F. 2008. Notch signaling maintains bone marrow mesenchymal progenitors by suppressing osteoblast differentiation. Nat Med 14(3):306-314.

Hozumi K, Negishi N, Suzuki D, Abe N, Sotomaru Y, Tamaoki N, Mailhos C, Ish-Horowicz D, Habu S, Owen MJ. 2004. Delta-like 1 is necessary for the generation of marginal zone B cells but not T cells in vivo. Nat Immunol 5(6):638-644.

Ito R, Negishi N, Irie N, Matsuo K, Suzuki D, Katano I, Hayakawa E, Kawai K, Kamisako T, Eto T, Ogura T, Hozumi K, Ando K, Aiso S, Tamaoki N, Habu S, Ito M. 2012. Osteosclerosis and inhibition of human hematopoiesis in NOG mice expressing human Delta-like 1 in osteoblasts. Exp Hematol 40(11):953-963 e953.

Jones DC, Wein MN, Oukka M, Hofstaetter JG, Glimcher MJ, Glimcher LH. 2006. Regulation of adult bone mass by the zinc finger adapter protein Schnurri-3. Science 312(5777):1223-1227.

Jongbloets BC, Pasterkamp RJ. 2014. Semaphorin signalling during development. Development 141(17):3292-3297.

Kalajzic I, Kalajzic Z, Kaliterna M, Gronowicz G, Clark SH, Lichtler AC, Rowe D. 2002. Use of type I collagen green fluorescent protein transgenes to identify subpopulations of cells at different stages of the osteoblast lineage. Journal of bone and mineral research : the official journal of the American Society for Bone and Mineral Research 17(1):15-25.

Karsenty G, Ferron M. 2012. The contribution of bone to whole-organism physiology. Nature 481(7381):314-320.

Liu W, Toyosawa S, Furuichi T, Kanatani N, Yoshida C, Liu Y, Himeno M, Narai S, Yamaguchi A,

Komori T. 2001. Overexpression of Cbfa1 in osteoblasts inhibits osteoblast maturation and causes osteopenia with multiple fractures. J Cell Biol 155(1):157-166.

Morikawa S, Mabuchi Y, Kubota Y, Nagai Y, Niibe K, Hiratsu E, Suzuki S, Miyauchi-Hara C, Nagoshi N, Sunabori T, Shimmura S, Miyawaki A, Nakagawa T, Suda T, Okano H, Matsuzaki Y. 2009. Prospective identification, isolation, and systemic transplantation of multipotent mesenchymal stem cells in murine bone marrow. J Exp Med 206(11):2483-2496.

Muguruma Y, Lee MY. 1998. Isolation and characterization of murine clonogenic osteoclast progenitors by cell surface phenotype analysis. Blood 91(4):1272-1279.

Nakashima T, Hayashi M, Fukunaga T, Kurata K, Oh-Hora M, Feng JQ, Bonewald LF, Kodama T, Wutz A, Wagner EF, Penninger JM, Takayanagi H. 2011. Evidence for osteocyte regulation of bone homeostasis through RANKL expression. Nat Med 17(10):1231-1234.

Negishi N, Suzuki D, Ito R, Irie N, Matsuo K, Yahata T, Nagano K, Aoki K, Ohya K, Hozumi K, Ando K, Tamaoki N, Ito M, Habu S. 2014. Effective expansion of engrafted human hematopoietic stem cells in bone marrow of mice expressing human Jagged1. Exp Hematol 42(6):487-494 e481.

Nobta M, Tsukazaki T, Shibata Y, Xin C, Moriishi T, Sakano S, Shindo H, Yamaguchi A. 2005. Critical regulation of bone morphogenetic protein-induced osteoblastic differentiation by Delta1/Jagged1-activated Notch1 signaling. J Biol Chem 280(16):15842-15848.

Parfitt AM, Drezner MK, Glorieux FH, Kanis JA, Malluche H, Meunier PJ, Ott SM, Recker RR. 1987. Bone histomorphometry: standardization of nomenclature, symbols, and units. Report of the ASBMR Histomorphometry Nomenclature Committee. Journal of bone and mineral research : the official journal of the American Society for Bone and Mineral Research 2(6):595-610.

Rossert J, Eberspaecher H, de Crombrugghe B. 1995. Separate cis-acting DNA elements of the mouse pro-alpha 1(I) collagen promoter direct expression of reporter genes to different type I collagen-producing cells in transgenic mice. J Cell Biol 129(5):1421-1432.

Sciaudone M, Gazzerro E, Priest L, Delany AM, Canalis E. 2003. Notch 1 impairs osteoblastic cell differentiation. Endocrinology 144(12):5631-5639.

Seibler J, Zevnik B, Kuter-Luks B, Andreas S, Kern H, Hennek T, Rode A, Heimann C, Faust N, Kauselmann G, Schoor M, Jaenisch R, Rajewsky K, Kuhn R, Schwenk F. 2003. Rapid generation of inducible mouse mutants. Nucleic Acids Res 31(4):e12.

Sekine C, Koyanagi A, Koyama N, Hozumi K, Chiba S, Yagita H. 2012. Differential regulation of osteoclastogenesis by Notch2/Delta-like 1 and Notch1/Jagged1 axes. Arthritis Res Ther 14(2):R45.

Sims NA, Martin TJ. 2014. Coupling the activities of bone formation and resorption: a multitude of signals within the basic multicellular unit. Bonekey Rep 3:481.

Sutton AL, Zhang X, Dowd DR, Kharode YP, Komm BS, Macdonald PN. 2008. Semaphorin 3B is a 1,25-Dihydroxyvitamin D3-induced gene in osteoblasts that promotes osteoclastogenesis and induces osteopenia in mice. Mol Endocrinol 22(6):1370-1381.

Takahashi N, Akatsu T, Udagawa N, Sasaki T, Yamaguchi A, Moseley JM, Martin TJ, Suda T. 1988a. Osteoblastic cells are involved in osteoclast formation. Endocrinology 123(5):2600-2602.

Takahashi N, Yamana H, Yoshiki S, Roodman GD, Mundy GR, Jones SJ, Boyde A, Suda T. 1988b. Osteoclast-like cell formation and its regulation by osteotropic hormones in mouse bone marrow cultures. Endocrinology 122(4):1373-1382.

Tao J, Chen S, Lee B. 2010. Alteration of Notch signaling in skeletal development and disease. Ann N Y Acad Sci 1192:257-268.

Tezuka K, Yasuda M, Watanabe N, Morimura N, Kuroda K, Miyatani S, Hozumi N. 2002. Stimulation of osteoblastic cell differentiation by Notch. Journal of bone and mineral research : the official journal of the American Society for Bone and Mineral Research 17(2):231-239.

Vujovic S, Henderson SR, Flanagan AM, Clements MO. 2007. Inhibition of gamma-secretases alters both proliferation and differentiation of mesenchymal stem cells. Cell Prolif 40(2):185-195.

Xing L, Bushnell TP, Carlson L, Tai Z, Tondravi M, Siebenlist U, Young F, Boyce BF. 2002. NF-kappaB p50 and p52 expression is not required for RANK-expressing osteoclast progenitor formation but is essential for RANK- and cytokine-mediated osteoclastogenesis. Journal of bone and mineral research : the official journal of the American Society for Bone and Mineral Research 17(7):1200-1210.

Xiong J, Onal M, Jilka RL, Weinstein RS, Manolagas SC, O'Brien CA. 2011. Matrix-embedded cells control osteoclast formation. Nat Med 17(10):1235-1241.

Yamada T, Yamazaki H, Yamane T, Yoshino M, Okuyama H, Tsuneto M, Kurino T, Hayashi S, Sakano S. 2003. Regulation of osteoclast development by Notch signaling directed to osteoclast precursors and through stromal cells. Blood 101(6):2227-2234.

Zanotti S, Smerdel-Ramoya A, Stadmeyer L, Durant D, Radtke F, Canalis E. 2008. Notch inhibits osteoblast differentiation and causes osteopenia. Endocrinology 149(8):3890-3899.

Zhang P, Yang Y, Zweidler-McKay PA, Hughes DP. 2008. Critical role of notch signaling in osteosarcoma invasion and metastasis. Clin Cancer Res 14(10):2962-2969.

Figure legends

Figure 1: Phenotypes of DLL1 mice

(a) Body weights of non-transgenic and DLL1 littermates at 3 to 8 weeks of age. Horizontal lines indicate analytical pairs. A total of 12 non-transgenic and DLL1 littermate pairs were analyzed.

(b) Representative pictures of skeletal preparations at 4 weeks of age. Eight non-transgenic and three DLL1 mice were analyzed. Bars indicate the lengths of the distal portions of limbs.

(c) Representative H&E staining of bone section and μCT analysis at 6 weeks of age. Six non-transgenic and DLL1 littermate pairs were analyzed. At least two slides were stained in each littermate.

(d) Static bone morphometric analysis at 6 weeks of age (n=8). Error bars, mean ± SD; **P<0.01.

(e) ELISA analyses of carboxylated and decarboxylated osteocalcin in plasma of 4-week-old mice. n=8.

Figure 2: Effects of osteoblast-specific DLL1 expression in BM histomorphology

(a) Representative H&E staining of hind limbs of non-transgenic and DLL1 littermates between E15.5 and 1 week. Beginning at E18.5, fibroblast-like cells are evident in DLL1 specimens. An insert at 1 week of DLL1 image shows higher magnification. Two to 6 littermate pairs were analyzed at each time point. At least two slides were stained for each sample.

(b) Representative images of immunostaining for CD31 at E15.5 and for Ki67 and Hes1 at P5.5. Note that numerous Ki67- and Hes1-positive fibroblastic cells are evident in DLL1 BM, whereas in the non-transgenic littermate, the majority of Ki67- and Hes1-positive cells appear to be round hematopoietic cells. Arrowheads indicate CD31

positive endothelial cells of vasculature. Two littermate pairs were analyzed at each time point. At least two independent staining procedures were performed for each antibody.

(c) Representative quantitative-PCR analyses for *Hes1* and *Hey1* expression in calvaria and adherent BM cells. RNA purified from calvaria (n=7) and adherent BM cells (n=3) obtained from non-transgenic and DLL1 littermates was analyzed. All analyses were performed in quadruplicate wells. Gene expression levels are shown relative to non-transgenic controls. Error bars, mean ± SD; *P<0.05.

Figure 3: ***Effects of osteoblast-specific DLL1 expression in osteoblast differentiation*** **in vivo**

Immunostaining for Runx2 and osterix. Representative images of BM samples from non-transgenic (a) and DLL1 mice (b) are shown. Arrowheads at P5.5 of non-transgenic specimens indicate Runx2-positive cells. Two to 3 littermate pairs were analyzed at each time point. At least two independent staining procedures were performed for each sample.

(c) Quantification of osterix-positive cells in bone surface of the 6-week-old BM specimen. Osterix-positive cells in 20 random fields were counted for each mouse. Pooled data obtained from three independent littermate pairs were used for analyses. Error bars, mean ± SD; **P<0.01.

(d) Osteoid thickness and mineral density of non-transgenic and DLL1 mice at 6 weeks of age (n=8). Error bars, mean ± SD; *P<0.05, **P<0.01.

Figure 4: Roles of DLL1 in osteoblast differentiation **in vitro.**

(a) CFU assays for quantifying fibroblast and osteoblast colonies formed from the BM cells of non-transgenic and DLL1 mice. Representative data from 7 independent experiments are shown. All experiments were performed in triplicate wells. Error

bars, mean ± SD; *P<0.05.

(b), (c) Time course analyses of the expression levels of osteoblast markers during cultures of DLL1 and Dll1-floxed mice, as indicated. Col1: C*ollagen 1*, ALP: *Alkaline phosphatase*, Ocal: *Osteocalcin*.

Osterix (d) and *Runx2* (e) expression in MSC-enriched BM cells. In (b)-(e), representative data from 3 independent experiments are shown. All analyses were performed in triplicate wells. Bars in each graph represent relative levels of mRNA compared to non-transgenic controls. Error bars, mean ± SD; *P<0.05.

***Figure 5: Effects of osteoblast-specific DLL1 expression in osteoclast differentiation* in vivo.**

(a) Representative TRAP staining pictures of BM specimens from E15.5 to 1 week. Arrowheads in DLL1 images indicate osteoclasts. Inserts in non-transgenic images are higher magnification. Two littermate pairs were analyzed at each time point. At least two slides were stained for each sample.

(b) Microscopic quantification of the number of TRAP(+) cells on the bone surface and in the entire field at 1-week-old samples. Seven random fields were counted for each sample. Pooled data from two independent littermate pairs were used for analyses. Error bars, mean ± SD; *P<0.05.

***Figure 6: Effects of osteoblast-specific DLL1 expression in osteoclast differentiation* in vitro.**

(a) The numbers of TRAP(+) osteoclasts formed in cytokine-induced culture, (b) mixed culture, and (c) osteoblast-osteoclast co-culture *in vitro*. (a) and (b) Representative data from six independent experiments are shown. (c) Representative data from three independent experiments using calvarial osteoblasts obtained from a total of 3

non-transgenic and 6 DLL1 littermates. Experiments were performed at least in triplicate wells. Error bars, mean ± SD; *P<0.05.

Quantitative PCR analyses of *Rankl* (d) and *Semaphorin 3B* (f) expression in non-transgenic and DLL1 osteoclast culture. Representative data from 5 independent experiments are shown. Analyses were performed at least in triplicate wells. Error bars, mean ± SD; *P<0.05.

(e) Immunostaining of 4-week-old mice. BM specimens were stained for RANKL and then for TRAP. Brown staining in the cytoplasm of bone-lining and matrix-embedded osteoblasts demonstrates RANKL expression. Arrowheads indicate RANKL-positive cells. Four independent littermate pairs at the ages of 2 to 4 weeks were stained.

Table 1

	M-CSF (pg/mL)	RANKL (pg/mL)	OPG (pg/mL)	RANKL/OPG
Non-transgenic	45.0 ± 10.5	298.3 ± 46.7	83.9 ± 6.4	3.6 ± 0.5
DLL1	42.9 ± 6.4	165.2 ± 8.2*	87.1 ± 3.7	1.9 ± 0.01*

BM cells of non-transgenic and DLL1 mice were stimulated with Dex and VD_3. ELISA analyses were performed on culture supernatant collected at Day8 of culture. Representative data from three independent experiments are shown. All experiments were performed in at least triplicate wells. Mean ± SD is shown. *$p<0.05$

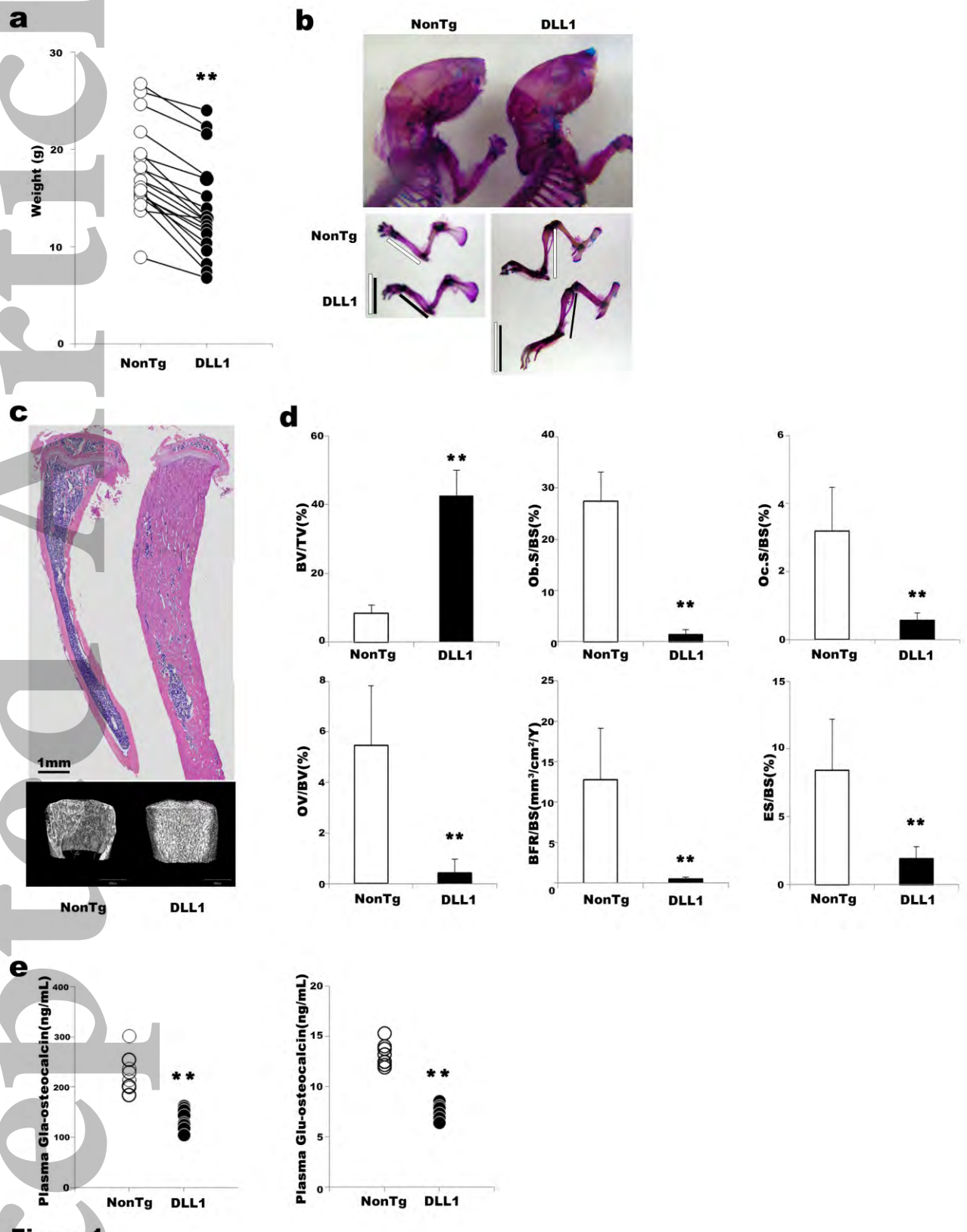

Figure1

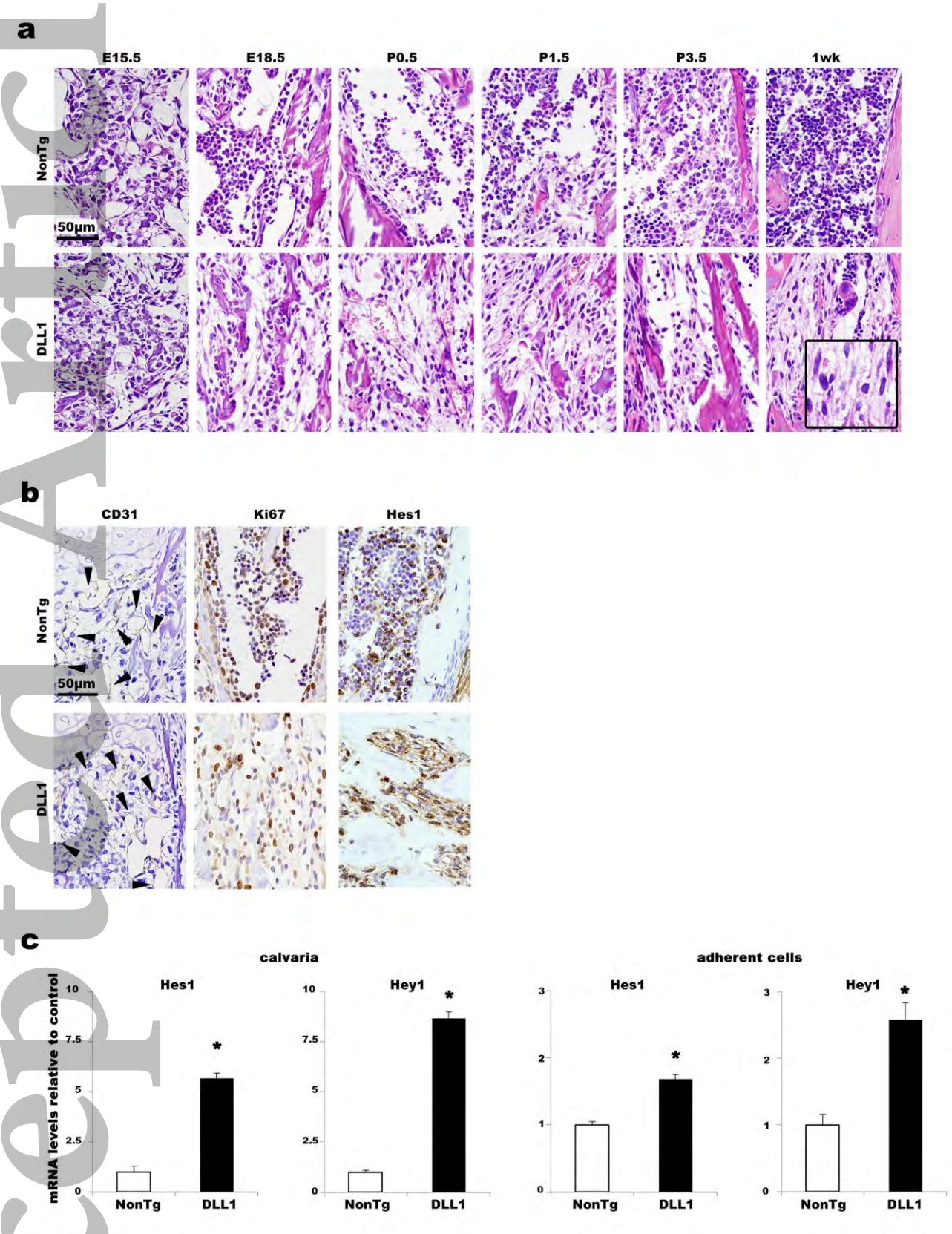

Figure.2

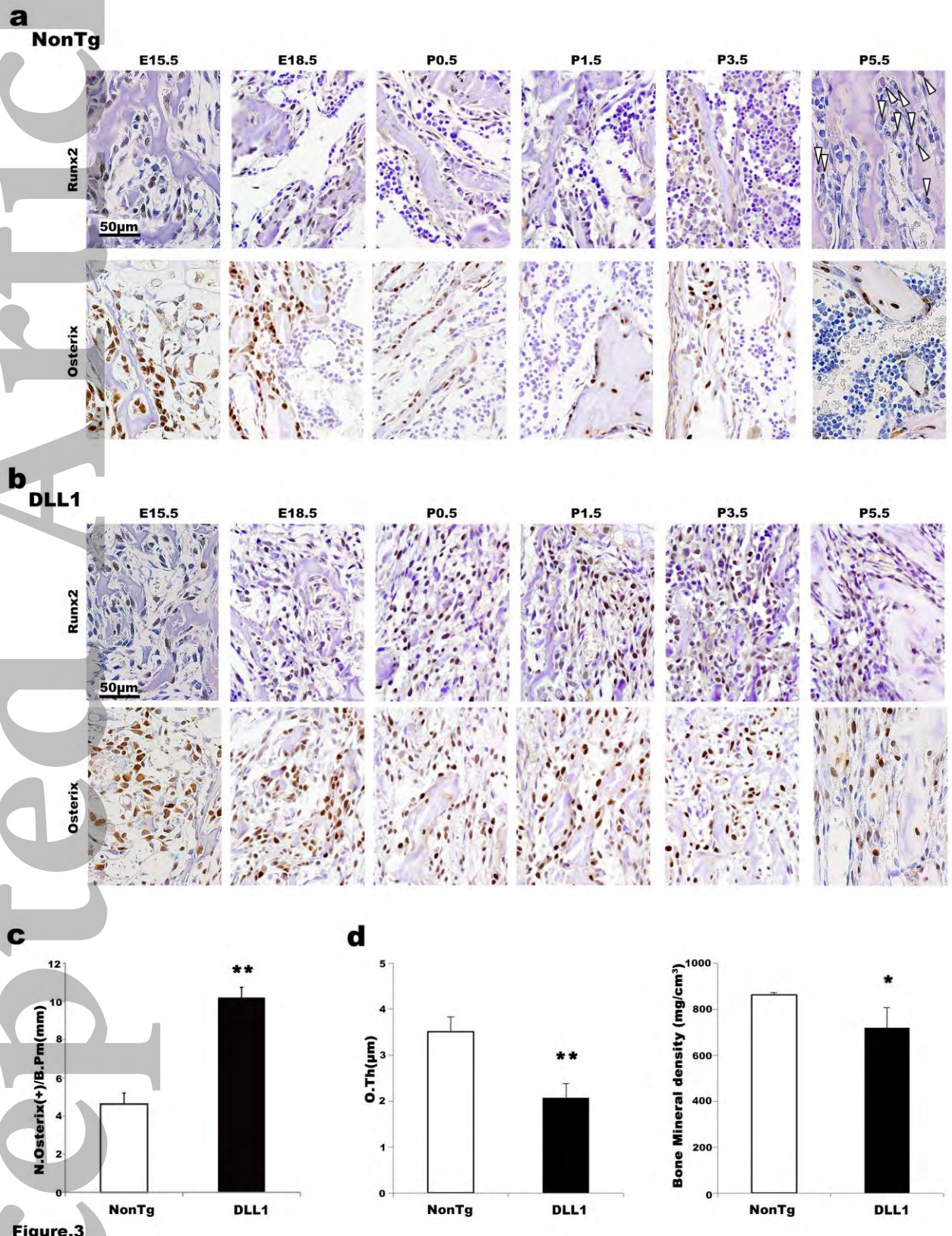

Figure.3

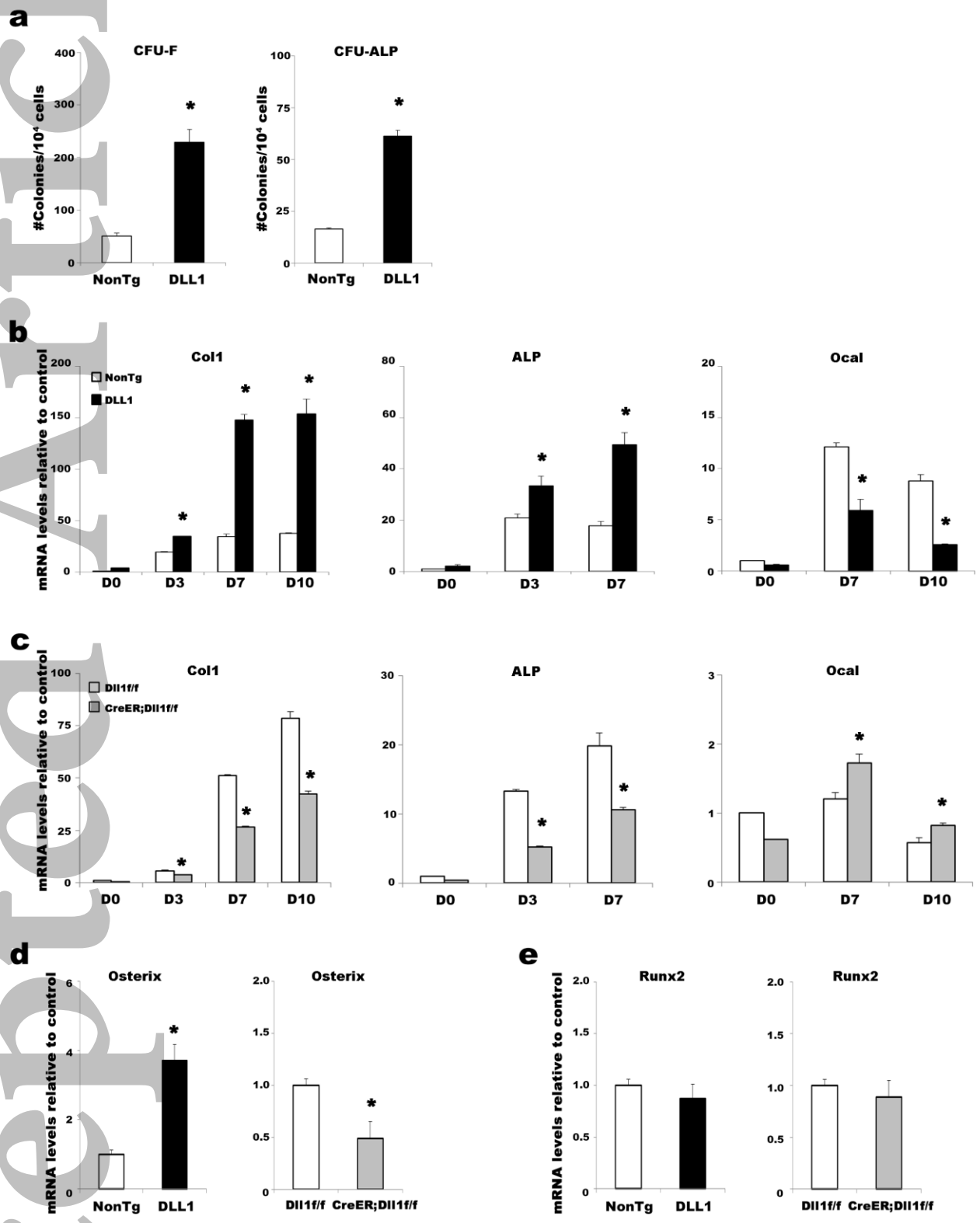

Figure.4

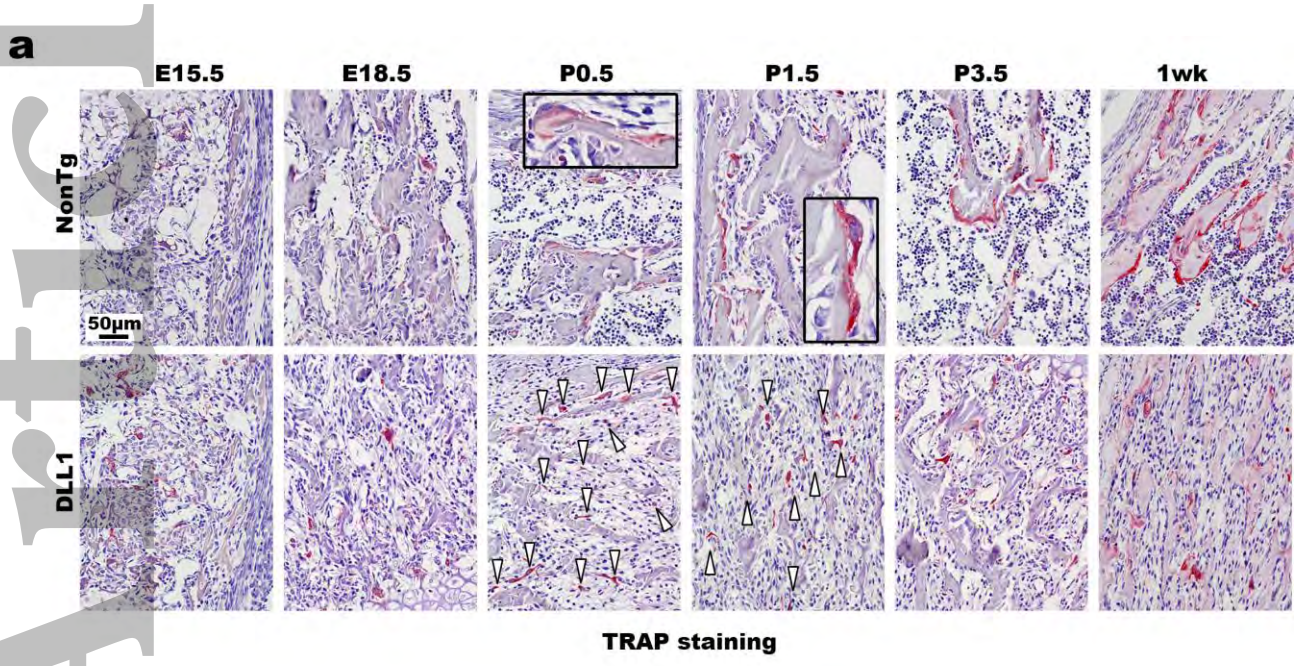

Figure.5

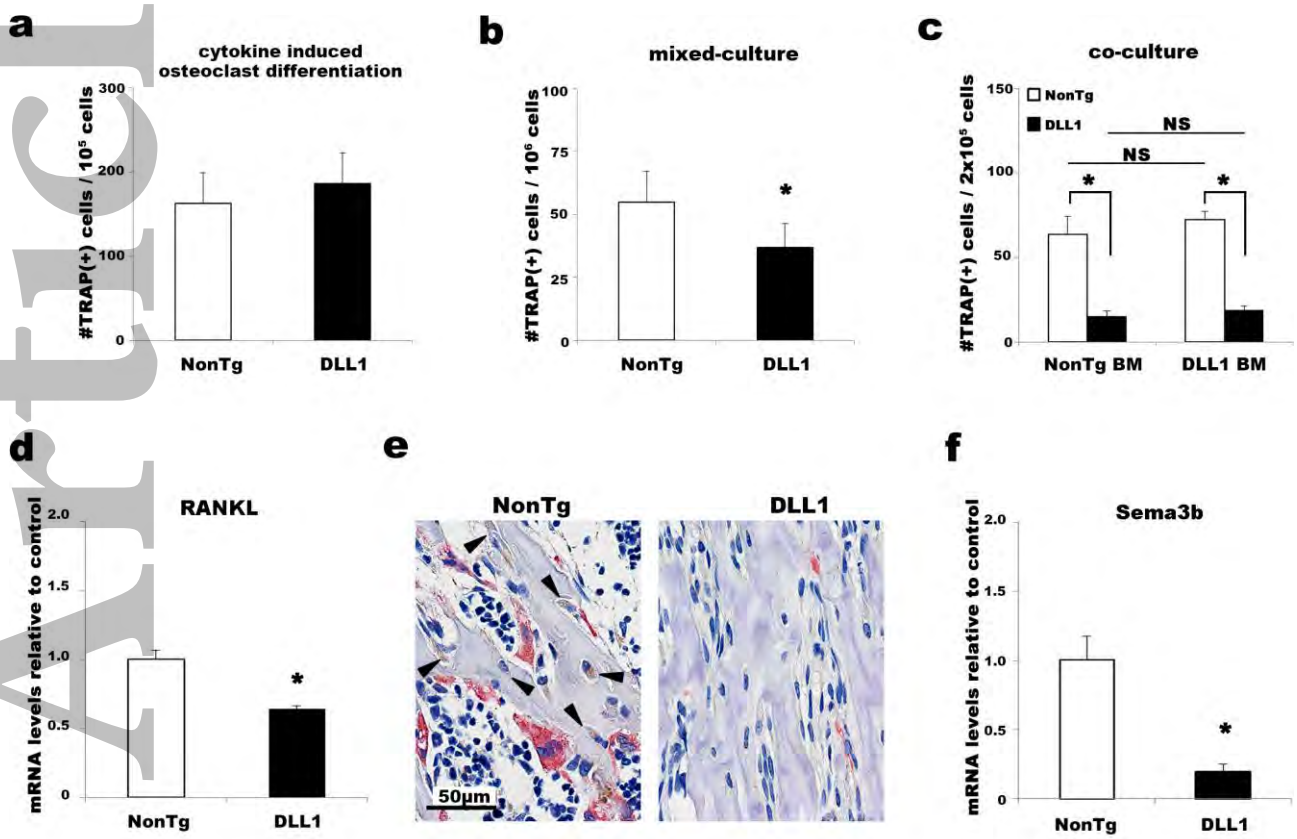

Figure.6

Genes to Cells

Disappearance of centroacinar cells in the Notch ligand-deficient pancreas

Yasuhiro Nakano[1,2], Naoko Negishi[1,3], Seiho Gocho[4], Tetsuya Mine[4], Yuri Sakurai[1], Masaki Yazawa[1], Koichiro Abe[5], Hideo Yagita[3], Sonoko Habu[3], Ryoichiro Kageyama[6], Yoshiya Kawaguchi[2]* and Katsuto Hozumi[1]*

[1]*Department of Immunology and Research Center for Regenerative Medicine, Tokai University School of Medicine, 143 Shimokasuya, Isehara 259-1193, Japan*
[2]*Department of Clinical Application, Center for iPS Cell Research and Application, Kyoto University, 53 Kawahara-cho, Shogoin Sakyo-ku, Kyoto 606-8507, Japan*
[3]*Department of Immunology, Juntendo University School of Medicine, 2-1-1 Hongo, Bunkyo-ku 113-0033, Japan*
[4]*Department of Internal Medicine, Tokai University School of Medicine, 143 Shimokasuya, Isehara, Kanagawa 259-1193, Japan*
[5]*Division of Basic Medical Science and Molecular Medicine, Tokai University School of Medicine,143 Shimokasuya, Isehara 259-1193, Japan*
[6]*Institute of Virus Research, Kyoto University, 53 Kawahara-cho, Kyoto 606-8507, Japan*

Notch signaling has been shown to contribute to murine pancreatic development at various stages. Delta-like 1 (Dll1) or Jagged1 (Jag1) are the Notch ligands that solely function to trigger this signaling during the pancreatic bud stage (~e9.5) or after birth, respectively. However, it has not been elucidated whether these Notch ligands are required at the later stage (e10.5–18.5) when the particular pancreas structures form. Here, we detected the dual expression of Dll1 and Jag1 in the epithelium after e10.5, which was restricted to the ductal cell lineage, including centroacinar cells expressing Sox9, CD133 and Hes1 but not the ductal cell markers Hnf1β and DBA, at e18.5. To evaluate the significance of the Notch ligands during this period, we established double-floxed mice of *Dll1* and *Jag1* genes with *Ptf1a-Cre* knock-in allele and examined the effects on development. The abrogation of both ligands but not a single one led to the loss of centroacinar cells, which was due to the decrease in cell proliferation and the increase in cell death, as well as to the reduction of Sox9. These results suggested that Dll1 and Jag1 function redundantly and are necessary to maintain the centroacinar cells as an environmental niche in the developing pancreas.

Introduction

The formation of tissue structures is crucial to obtaining organ functions. The exocrine pancreas is composed of enzyme-producing acini and ductal structures that channel the pancreatic fluid into the duodenum. The exocrine acinus is composed of enzyme-secreting acinar cells and of centroacinar cells located in the center of the acinar structure (Ashizawa *et al.* 2005). The branched ductal tree is subdivided into the main, interlobular and terminal ducts, the latter of which connects to the acini (Reichert & Rustgi 2011). Previous studies identified genes involved in the specification and differentiation of acinar and duct cells, but the precise mechanisms underlying the construction of the exocrine pancreatic architecture during the embryonic stages are largely unknown. At approximately embryonic day 9.5 (e9.5) in mice, pancreatogenesis begins with the evagination of endodermal cells from the primitive foregut tube to form the dorsal and ventral pancreatic buds. At first, no obvious ductal structures are observed within the buds, but segregated epithelial cells gradually form the branching ductal tree (Pan & Wright 2011). As development proceeds, at e13.5–15.5, amylase-expressing exocrine acinar cells appear in the 'tip' region of the ductal trees, whereas endocrine cells formed in the ductal 'trunk' region (Zhou

Communicated by: Yukiko Gotoh
**Correspondence:* yoshiyak@cira.kyoto-u.ac.jp or hozumi@is.icc.u-tokai.ac.jp

DOI: 10.1111/gtc.12243

et al. 2007). During these stages, lines of acinar cells are observed adjacent to the ductal structures and acinar and centroacinar cells cannot be distinguished by H&E staining. The branching structure of the ducts becomes more complex after that stage, and mature acinar structures are completed at e18.5, when identifiable centroacinar cells appear at the center of the acini.

Previous studies suggested that centroacinar cells function as progenitor cells; inducible Cre-based cell-tracking experiments showed that Sox9-expressing cells differentiated into all types of pancreatic cells during the embryonic and neonatal stages, including exocrine, endocrine and ductal lineages (Furuyama *et al.* 2011; Kopp *et al.* 2011). Considering their location at the junction of ductal tree and the acini, $Sox9^+$ centroacinar cells are thought to be the best candidate for the source of new acinar cell populations at the perinatal stages. Moreover, ALDH1-expressing centroacinar/terminal duct cell populations in adult mouse possess multidifferentiation capacity toward endocrine and exocrine pancreatic cells *in vitro* (Rovira *et al.* 2010). However, the lack of specific markers has prevented the elucidation of how centroacinar cells are formed and maintained in the developing exocrine tissue.

The construction of an acinar structure appears to be associated with the formation of a boundary between acinar cells and the ductal network during pancreatic development. Previous studies showed the pivotal role of Notch signaling in the formation of a boundary between different cell types, such as that in the *Drosophila* wing margin and vertebrate somite (Artavanis-Tsakonas *et al.* 1999). Thus, we speculated that Notch signaling is likely involved in the proper construction of exocrine pancreatic tissue, including the acinar structures. Although recent reports showed that Notch signaling functions in controlling endocrine cell and ductal differentiation in the 'trunk' domain (Afelik *et al.* 2012; Horn *et al.* 2012; Shih *et al.* 2012) and that its signaling confines centroacinar cells to the ductal lineage during adulthood (Kopinke *et al.* 2012; Hosokawa *et al.* 2015), the details of how Notch signaling functions in exocrine pancreatic development remain unknown. In this study, we showed that centroacinar cells comprise the $Sox9^+Hnf1\beta^-CD133^+ALDH1^+DBA^-$ population that expressed the Notch ligands, Delta-like 1 (Dll1) and Jagged1 (Jag1), as well as Hes1, a target of Notch signaling, at e18.5 in mice. Depleting Dll1 and Jag1 in pancreatic progenitor cells in the Ptf1a-Cre line, in which the recombinase becomes active as early as e10.5, reduced the level of Hes1 expression and caused the loss of centroacinar cells and some of the terminal duct cells at e18.5. These results showed the pivotal role of Dll1/Jag1-mediated Notch signaling in maintaining the centroacinar/terminal duct cells during the construction of the exocrine structure *in vivo*.

Results

Delta-like 1 and Jagged1 are expressed in the developing ductal tree and the centroacinar region during murine pancreatogenesis

As several previous reports showed, the Notch ligands Dll1 and Jag1 exhibited dynamically changing expression patterns during the construction of the pancreatic architecture; Dll1 was expressed in Sox9-expressing epithelial cells in pancreatic buds as early as e9.5, whereas Jag1 expression was not detected at this stage (Fig. 1A,E; Ahnfelt-Rønne *et al.* 2012). From e10.5 to e13.5, almost all of the pancreatic epithelial cells expressed both Dll1 and Jag1 (Fig. 1B,C, F,G; Golson *et al.* 2009a). As cell differentiation and branching of the ductal tree proceeded, different levels of Dll1 expression were detected throughout the Sox9-expressing trunk region and in acinar cells, and Jag1 expression was retained in duct cells but was reduced in acinar cells at e15.5 (Fig. 1D,H; Shih *et al.* 2012). At e18.5, centroacinar cells were identified as the most distal cells with a high N/C ratio in the center of the mature acinar structures (Fig. 1I–M, arrowheads). At this stage, the branching ductal structure was fully developed and could be divided into the following two components based on H&E staining: the main/interlobular and terminal ducts. The former cells were found outside the acini (Fig. 1I,J, thick arrows), and the latter cells were found near the centroacinar cells at the near side of the duct within an acinus (Fig. 1I,J, thin arrows). All of the cells that composed the ductal structures as well as the centroacinar cells expressed Sox9, but we found differential expression of the Notch ligands (Fig. 1I,J,L,M; Table S1 in Supporting Information). Dll1 was expressed in the centroacinar regions and a subset of the terminal ducts but not in the interlobular/main ducts, whereas Jag1 was detected throughout the ductal tree and in the centroacinar cells at e18.5 (Fig. 1I,J,L,M; Table S1 in Supporting Information). Thus, the centroacinar cells at this stage expressed both of the Notch ligands and Sox9, whereas the acinar cells expressed neither of the Notch ligands or Sox9. Hes1, the main effector of Notch signaling, was occasionally detected in centroacinar cells, terminal ducts and interlobular/

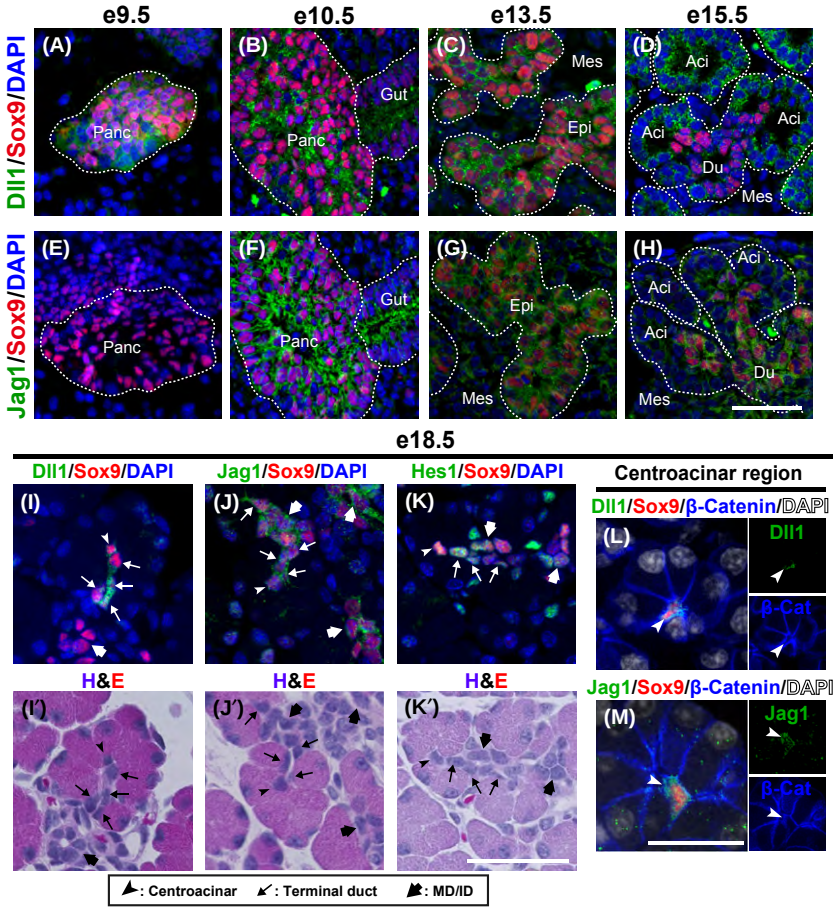

Figure 1 Expression of the Notch ligands and Sox9 during murine pancreatogenesis. (A–H) Immunofluorescence analysis of pancreatic tissue from e9.5 to e15.5 mice was carried out using anti-Dll1 (green; A–D), anti-Jag1 (green; E–H) and anti-Sox9 (red) Abs. The dotted lines indicate the pancreatic or gut epithelium (Panc, Gut) at e9.5 or e10.5, the boundary between the epithelial (Epi) and mesenchymal (Mes) regions at e13.5, and the primitive acinar structures (Aci) and ductal (Du) regions at e15.5. (I–K) The co-expression of Dll1, Jag1 or Hes1 (green) and Sox9 was also observed (red) at e18.5. Centroacinar cells (arrowheads) were identified in the center of the mature acinar structures. The branching ductal structures were fully developed and could be divided into two components: the main/interlobular ducts (MD/ID, thick arrows) and the terminal ducts (thin arrows). The same sections were used for H&E staining (I'–K'). (L, M) Expression of Dll1 and Jag1 (green) in the centroacinar region was confirmed, with the cellular boundary identified through anti-β-catenin staining (blue). Centroacinar cells are indicated by arrowheads. All of the sections were also stained using DAPI. Original magnification, 400×. Bars: 50 μm (A–K), 20 μm (L,M).

main ducts but not in acinar cells (Fig. 1K; Table S1 in Supporting Information), suggesting that a subset of the centroacinar and duct cells received Notch signaling at this stage.

Characterization of the epithelial cells in the centroacinar region at e18.5 in mice

For a more detailed characterization of the centroacinar cells at e18.5, we carried out additional immunostaining assays. Our immunofluorescence analyses using two independent antibodies showed that Hnf1β was expressed in the main/interlobular ducts but that its expression was remarkably reduced in the terminal ducts and was lost in centroacinar cells (Fig. 2A; Table S1 in Supporting Information). DBA, a well-known ductal marker, was also expressed strongly in the main/interlobular ducts and weakly in the terminal ducts but not in the centroacinar and acinar cells, thereby having an expression pattern similar to that of Hnf1β at this stage (Fig. 2A,C,D; Fig. S1 and Table S1 in Supporting

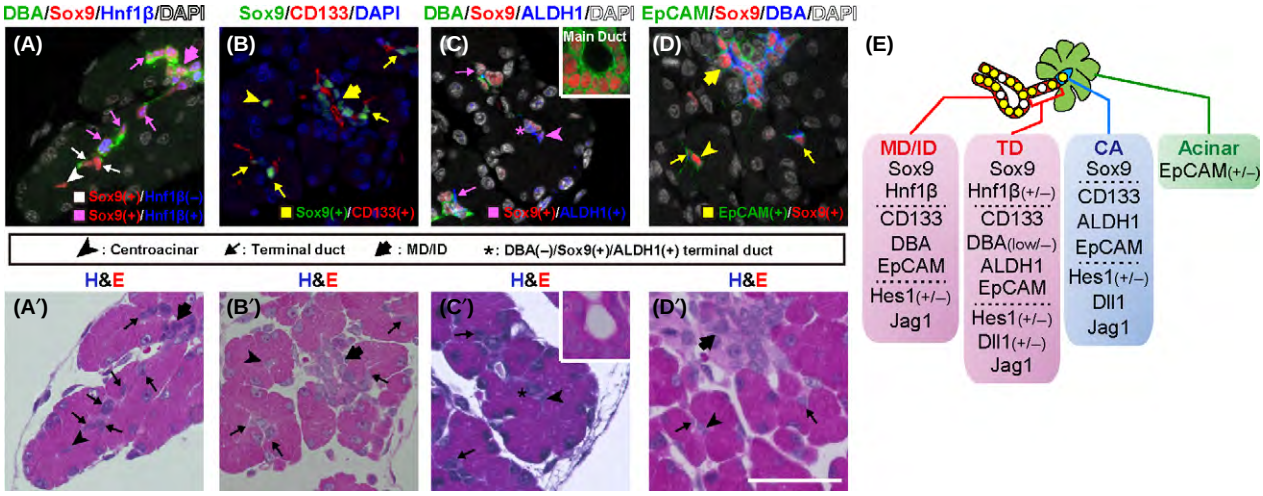

Figure 2 Characterization of the epithelial cells in the centroacinar region. (A–D) Epithelial cells residing in the centroacinar regions of the fetal pancreas (e18.5) were identified by their expression of various cellular markers: DBA (green in A, C; blue in D), Sox9 (red in A, C, D; green in B), Hnf1β (blue, A), CD133 (red, B), ALDH1 (blue, C) or EpCAM (green, D). Centroacinar, terminal duct and main/interlobular duct cells are indicated by arrowheads and thin and thick arrows, respectively, as shown in Fig. 1. Cells with red staining (Sox9 or CD133) and with or without blue staining (Hnf1β or ALDH1) are indicated by purple or white arrowheads/arrows, respectively, and those stained with red and green (Sox9 or EpCAM) are indicated by yellow arrowheads/arrows. The asterisk in C indicates DBA-negative terminal duct cells. The expression of ALDH1 was also observed in the main ducts (Main Duct, inset in C). The same sections were used for H&E staining (A'–D'). Original magnification, 400×. Bar: 50 μm. (E) Exocrine tissue was completed and composed of branching duct structure with centroacinar (CA), terminal duct (TD) and main/interlobular duct (MD/ID) cells and acinar cells at e18.5. These cell populations were identified with various cell markers described.

Information). We also detected rare DBA-negative terminal duct cells (Fig. 2C, asterisk; Fig. S1C, green arrows in Supporting Information). We found that the expression of CD133, a marker of multipotent progenitors in the developing pancreas *in vitro* (Oshima *et al.* 2007; Immervoll *et al.* 2011), overlapped with that of Sox9 (Fig. 2B; Table S1 in Supporting Information) in that both were expressed throughout the ductal tree and in the centroacinar cells but not in acinar cells. ALDH1, another marker of multipotent progenitors during adulthood (Rovira *et al.* 2010), was restrictively expressed in the centroacinar and terminal ductal regions, and thus, the ALDH1-expressing epithelial cells could be divided into two populations, as follows: $Sox9^{+}ALDH1^{+}DBA^{-}$ centroacinar cells (Fig. 2C, arro-whead) and $Sox9^{+}ALDH1^{+}DBA^{+}$ (Fig. 2C, arrows) with rare $Sox9^{+}ALDH1^{+}DBA^{-}$ (Fig. 2C, asterisk) cells in the terminal ductal region (Rovira *et al.* 2010). Taken together, the centroacinar cells could be defined as $Sox9^{+}Hnf1\beta^{-}CD133^{+}ALDH1^{+}DBA^{-}$ with Dll1 and Jag1 expression at e18.5 in mice (Fig. 2E; Table S1 in Supporting Information). In contrast, EpCAM was expressed in Sox9-positive duct cells and a few Sox9-negative acinar cells (Fig. 2D), which could be useful at this stage for concentrating amylase-negative epithelial cells in flow cytometric analysis.

Reduced proliferation and accelerated apoptosis accompany reduced Sox9 expression in Dll1/Jag1-deficient mice

To determine the significance of Notch ligands in the construction of the pancreatic architecture, we first analyzed $Ptf1a^{Cre/+}$; $Dll1^{lox/lox}$ mice and $Ptf1a^{Cre/+}$; $Jag1^{lox/lox}$ mice, in which the Cre-mediated recombination appropriately occurs at e10.5 (Kawaguchi *et al.* 2002; Fujikura *et al.* 2007). In these single knockout mice, no apparent related phenotype of the pancreatic structure was observed during the embryonic stages (Y. Nakano, *et al.* unpublished data), which might be explained by the redundant expression of the Notch ligands from e10.5 to the perinatal stage (Fig. 1). We then analyzed $Ptf1a^{Cre/+}$; $Dll1^{lox/lox}$; $Jag1^{lox/lox}$ doubly deficient mice (Dll1/Jag1 cKO mice). Until e15.5, we did not observe any related structural phenotype, even when using electron microscopy (Fig. 3A,B and Fig. S2A,B in Supporting Information). Despite no apparent structural defects, we found that the overall level of Sox9 expression was reduced at e15.5 in Dll1/

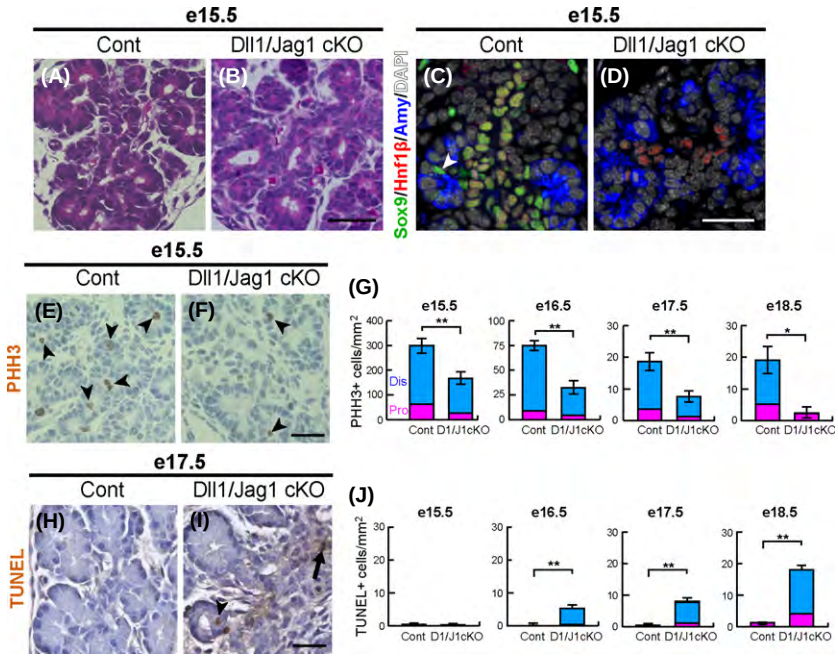

Figure 3 Reduction of Sox9 expression accompanied with the decrease of proliferation and the increase of apoptosis in Dll1/Jag1-deficient pancreas. (A–D) H&E staining and the expression of Sox9 (green), Hnf1β (red) and amylase (blue) were examined in control (Cont; A, C) and Dll1/Jag1-deficient (Dll1/Jag1 cKO; B, D) pancreatic tissues at e15.5. Arrowhead indicates $Sox9^{+}Hnf1\beta^{-}amylase^{-}$ cell in the primitive acinar structure. (E–G) The cell proliferation status in control (Cont; E) and Dll1/Jag1-deficient (Dll1/Jag1 cKO; F) pancreatic tissues at e15.5 was monitored using PHH3 immunohistochemistry (arrowheads; E, F). The number of $PHH3^{+}$ cells in the epithelial areas (1 mm^2) in sections of the pancreata of e15.5 to e18.5 embryos was counted (G). The values are the mean values ± SD (n = 3–4; ⋆, $P < 0.05$; ⋆⋆, $P < 0.01$). Dis, distal region; Pro, proximal region. (H–J) Apoptotic cells were detected using TUNEL staining in control (Cont; H) and Dll1/Jag1-deficient (Dll1/Jag1 cKO; I) pancreatic tissues at e17.5. The $TUNEL^{+}$ cells in Dll1/Jag1-deficient tissue are indicated by arrowheads (distal area, I) or thick arrows (proximal area, I). The number of $TUNEL^{+}$ cells in the epithelial areas (1 mm^2) in the sections of pancreata from e15.5 to e18.5 embryos (J) was counted, as shown in G. Original magnification for all of the images, 400×; bars: 50 μm.

Jag1 cKO mice but not in the single mutant mice (Fig. 3C,D), which is consistent with previous reports that Notch signaling regulates Sox9 expression (Notch–Sox9 axis) (Zong *et al.* 2009; Shih *et al.* 2012). Furthermore, reduced cell proliferation and accelerated apoptosis were observed in the mutants, predominantly in the distal region of the branching ductal tree, including in the primitive acinar structure (Fig. 3E–J). Our PHH3 staining analysis showed that the cells in the distal ductal epithelium were proliferating more rapidly than those in the proximal ducts from e15.5 to e18.5 in the control mice (Fig. 3E–G). As normal development proceeded, the cell proliferation rate decelerated overall, as reflected by the reduction in the number of $PHH3^{+}$ cells (e15.5: 298 cells/mm^2, e16.5: 76 cells/mm^2, e17.5: 19 cells/mm^2, e18.5: 20 cells/mm^2; Fig. 3G). In the Dll1/Jag1 cKO mice, the number of $PHH3^{+}$ cells was significantly lower than that of control mice in both the distal and proximal ducts at all of the stages evaluated (e15.5: 169 cells/mm^2, e16.5: 33 cells/mm^2, e17.5: 7.5 cells/mm^2, e18.5: 2.5 cells/mm^2; Fig. 3G). In addition, we observed accelerated apoptosis, predominantly in the distal region of the ductal tree, in the Dll1/Jag1 cKO mice after e16.5 (Fig. 3H–J). Consistent with this finding, the expression of anti-apoptotic genes, such as *Bcl2* and *Bcl2a*, was significantly down-regulated in the pancreata of the Dll1/Jag1 cKO mice (Fig. S3 in Supporting Information). These results showed that Dll1/Jag1-mediated Notch signaling supports the proliferation and survival of cells in the distal portion of the branching ducts, presumably via the Notch–Sox9 axis.

Loss of centroacinar cells and abrogated acinar construction in Dll1/Jag1-deficient pancreas

Reduced proliferation and accelerated cell death in the distal region of the branching tree (Fig. 3)

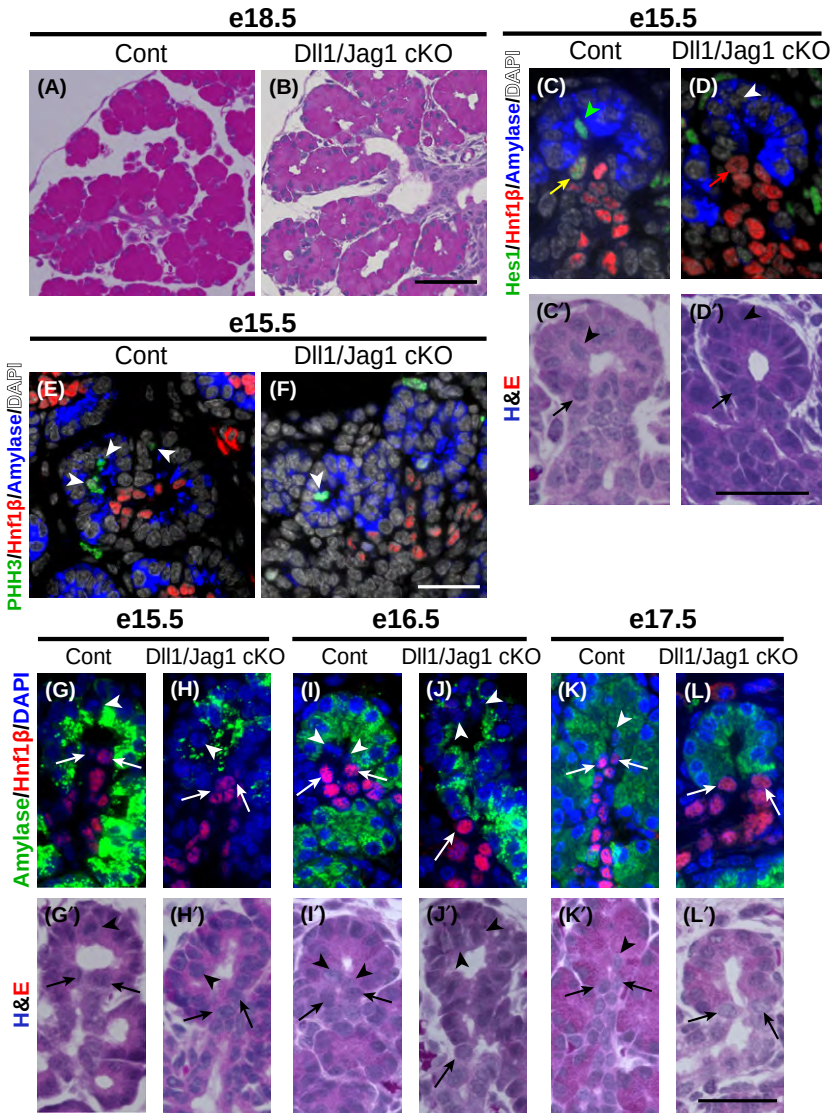

Figure 4 Construction of the acinar structures in Dll1/Jag1-deficient embryos. (A, B) H&E staining of control (Cont; A) and Dll1/Jag1-deficient (Dll1/Jag1 cKO; B) fetal pancreata at e18.5. (C, D) The expression of Hes1 (green in C and D), Hnf1β (red) and amylase (blue) was examined in control (Cont; C) and Dll1/Jag1-deficient (Dll1/Jag1 cKO; D) pancreata at e15.5. Hnf1β^{-}amylase^{-} cells that expressed or did not express Hes1 are indicated by green (C) or white (D) arrowheads, respectively. Hnf1β^{+} cells that expressed or did not express Hes1 are also indicated by yellow (C) or red (D), respectively. The same sections were used for H&E staining (C', D'). (E, F) PHH3 was also detected with Hnf1β and amylase as shown in C and D. PHH3^{+}Hnf1β^{-}amylase^{-} cells were depicted by white arrowheads. (G–L) Immunofluorescence analysis of pancreatic tissues from e15.5 to e17.5 mice was carried out using anti-amylase (green) and anti-Hnf1β Abs. Hnf1β^{-}amylase^{-} cells were represented by arrowheads. Hnf1β^{+} cells connected to the cell layer of amylase-expressing cells (green) were depicted by arrows. The same sections were used for H&E staining (G'–L'). Original magnification of all of the images, 400×; bars: 50 μm.

resulted in abrogated acinar construction in the Dll1/Jag1 cKO mice at e18.5 (Fig. 4A,B). In the primitive acinar structure at e15.5, the amylase-expressing acinar cells were aligned (blue in Fig. 4C,D) but left a vacant space in the center of the primitive acini, which contained Hnf1β-expressing cells (red in Fig. 4C,D) in linear pattern contiguous to the primitive acinar structures in either the control or the Dll1/Jag1 mutant pancreata. It should be noted that Hnf1β^{-}amylase^{-} cells existed within the primitive acinar structures (arrowhead in Fig. 4C,D) and that they also expressed Sox9, Dll1 and Jag1 (arrowhead in

Fig. 3C; Fig. S4 in Supporting Information). Hes1 expression was detected in a subset of amylase-negative cells regardless of the status of Hnf1β expression in the control mice but was not detected in the Dll1/Jag1 cKO mice (Fig. 4C,D), indicating that Hnf1β$^-$amylase$^-$ cells in the primitive acinar structures of the control mice receive Notch signaling. In fact, PHH3$^+$ cells were observed among the Hnf1β$^-$amylase$^-$ cells in the primitive acinar structures of the control mice, but they were sparse in the Dll1/Jag1 cKO mice (Fig. 4E,F).

During the normal construction of the acinar structures (e15.5–e17.5, Fig. 4G,I,K), the vacant spaces were gradually occupied, and very few vacant spaces were detected in the mature acini of the control mice at e18.5 (Fig. 4A; Fig. S2C,D in Supporting Information). However, in the Dll1/Jag1 cKO mice, the Hnf1β$^-$amylase$^-$ cells gradually disappeared (Fig. 4H,J,L) and vacant spaces still existed at e18.5 (Fig. 4B; Fig. S2E, F in Supporting Information). In addition to the reduction of Sox9 expression, a similar defect was also observed in the Hes1-deficient pancreas at e17.5 (Fig. S5 in Supporting Information). Because the acinar cells were normal in shape and size, with the nucleus localized on the basal side (Fig. 4A,B; Fig. S2C–F in Supporting Information), we speculated that the abrogated acinar structures in the Dll1/Jag1 cKO mice were due to the loss of a certain cellular population, most likely the Hnf1β$^-$amylase$^-$ cells, in the centroacinar region, rather than the shrinkage or disorganized localization of acinar cells.

To test this hypothesis, we carried out additional immunostaining and flow cytometric analyses using the pancreata of e18.5 mice (Fig. 5). We found that, although ALDH1$^-$DBA$^+$ main/interlobular duct cells (see Fig. 2C,E) had been preserved, ALDH1$^+$DBA$^-$ centroacinar/terminal duct cells (see Fig. 2C,E) were lost in the Dll1/Jag1 cKO mice (Fig. 5A,B). In fact, flow cytometry analyses showed that ALDH1$^+$DBA$^-$ cells, which were identified as an Aldefluor$^+$DBA$^-$ population (Rovira *et al.* 2010), accounted for 11.3% of the EpCAM-positive epithelial cells in the control mice, whereas this population was markedly decreased to 1.6% in the mutants (Fig. 5E,F,H). Furthermore, we found that CD133-expressing cells co-expressing ALDH1 in the centroacinar/terminal duct region of the control mice (Fig. 5C) were absent in the mutant mice (Fig. 5D). Consistently, another set of flow cytometry showed that the CD133$^+$DBA$^{-/low}$ population was reduced to 3.7% of the EpCAM-positive contingent in the mutant mice, whereas this cells accounted for 33.6% of that contingent in the control mice (Fig. 5E,G,I). Notably, cytospin analysis showed that the sorted CD133$^+$DBA$^{-/low}$ cells expressed Sox9 but not Hnf1β or amylase (Fig. S6A–O in Supporting Information), indicating that the lost cell types in the mutant acinar structures were Hnf1β$^-$amylase$^-$ cells. It was reported that Aldefluor-positive centroacinar/terminal ductal populations of adult mice exhibit multidifferentiation ability *in vitro* (Rovira *et al.* 2010); thus, we next questioned whether the cell population that was lost in the mutants at e18.5 possess a similar ability as adult Aldefluor-positive cells. We found that the sorted CD133$^+$DBA$^{-/low}$ cells from the e18.5 control mice were capable of forming cell sphere and then differentiating into both endocrine and exocrine lineages

Figure 5 Loss of centroacinar/terminal duct cells in the Dll1/Jag1-deficient pancreas**.** (A–D) Immunofluorescence analysis of the expression of DBA (green in A and B, red in C and D) and ALDH1 (red in A and B) or CD133 (green in C and D) in control (Cont; A, C) or Dll1/Jag1-deficient (Dll1/Jag1 cKO; B, D) pancreata from e18.5 embryos was carried out. Arrowheads, thick and thin arrows indicate centroacinar, terminal duct and main/interlobular duct cells, respectively, as shown in Figs 1 and 2. Intact ducts (CD133$^+$DBA$^+$) were observed in the double-deficient pancreas (inset in H). The asterisks indicate the loss of centroacinar cells; the cross indicates an enlarged ductal lumen in a Dll1/Jag1-deficient pancreas. The same sections were used for H&E staining (A'–D'). Original magnification, 400×. Bars: 50 μm. (E–G) The cells of fetal pancreata from e18.5 control (Cont) and Dll1/Jag1-deficient (Dll1/Jag1 cKO) embryos were dissociated, and single-cell suspensions were prepared. The cells were stained using a DBA (F, G), Aldefluor (F) or an anti-CD133 mAb (G) and an anti-EpCAM mAb (E) and were analyzed using flow cytometry. To determine the population negative for ALDH activity, the relevant profiles (upper panels) were compared with those representing control staining with a specific inhibitor of ALDH, DEAB (lower panels), and the boundaries were adjusted according to the frequencies of the Aldefluor$^+$ populations that were provided with the inhibitor, which were fewer than 1% (F). The immature epithelial cells of the e18.5 pancreas could be enriched using EpCAM-positive gating in the assay (E). The numbers in the plots represent the frequency of cells lying in the indicated regions within the gate (n = 5, % ±SD). (H, I) The absolute number of cells in the indicated fractions of EpCAM$^+$ cells from the control (Cont) and Dll1/Jag1-deficient (D1/J1cKO) e18.5 embryos was calculated (n = 5, mean ± SD). CA, centroacinar cells; TD, terminal duct cells; MD/ID, main/interlobular duct cells. *** indicates differences determined using unpaired Student's t-test at $P < 0.001$.

(Fig. S6P–S in Supporting Information). From these findings, we concluded that the lost cell types in Dll1/Jag1 cKO mice, which were identified as Hnf1β^{-}amylase^{-}, ALDH1^{+}DBA^{-} or CD133^{+}DBA$^{-/low}$ cells in the control mice, are centroacinar and a part of terminal duct cells that share a differentiation capacity that is similar to that of adult Aldefluor^{+} cells.

Dilated ducts in Dll1/Jag1-deficient pancreas

In addition to the disappearance of centroacinar/terminal duct cells, we observed that the lumens of the main/interlobular ducts were dilated. As early as e18.5, some of DBA-positive duct cells had an abnormal cuboidal shape, 66% of the duct cells lacked CD133, and the ductal lumens were dilated in the

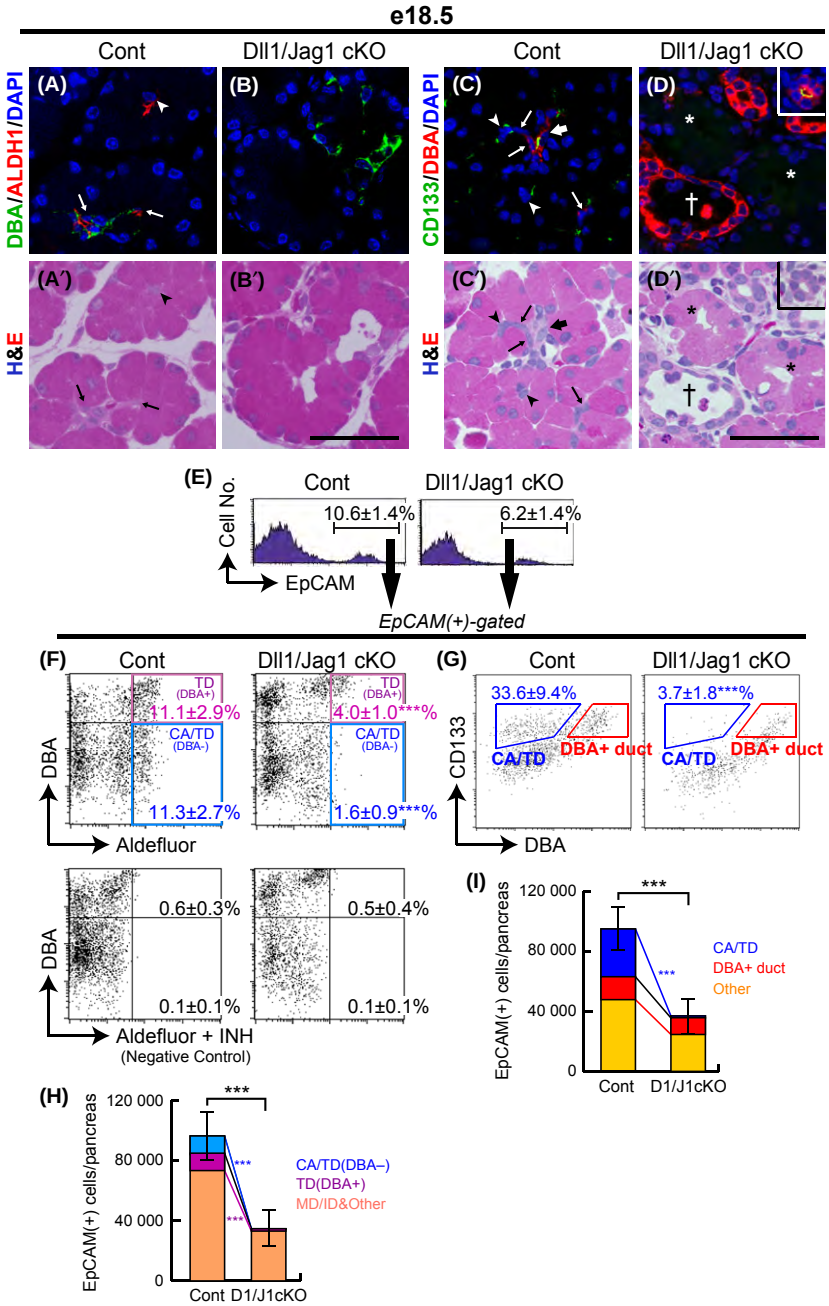

mutant mice (Figs 4B, 5D). The mutant phenotypes, including the hypoplastic pancreas, the loss of centroacinar/terminal duct cells and ductal dilatation, were progressive at e18.5 (Fig. 5) and were more severe at P3 (Fig. S7 in Supporting Information).

Discussion

The dynamically changing patterns of expression of the Notch-related genes during the construction of the exocrine pancreatic architecture suggested that the strength of Notch signaling is spatiotemporally determined in the developing pancreas, thereby regionally controlling cell differentiation and the development of tissue structures. Consistent with this hypothesis, modulating the expression of Notch-related genes produced different phenotypes, depending on the timing of gene activation or inactivation. Thus, interpreting each experimental result requires careful attention. For example, the conditional depletion of Mib1, which is indispensable for the endocytosis of Notch ligands to trigger Notch signaling, beginning at the anterior definitive endoderm stage (e7.5~) in a FoxA2-Cre line leads to the reduction and complete disappearance of the progenitor cells in trunk region at e12.5 and e15.5 (Horn *et al.* 2012), respectively, whereas the number of these cells was the same at e13.5 as at e12.5 and were slightly reduced at e15.5 in the Dll1/Jag1 cKO mice produced using the Ptf1a-Cre line compared to the control mice (Y. Nakano, *et al.* unpublished data). These results suggested that the trunk/tip patterning of the ductal tree was not severely impaired depleting Dll1/Jag1-mediated Notch signaling as early as e10.5. Although the strong expression of Dll1 and Jag1 and the high incidence of Hes1-positive cells at the later developmental stages indicated that Notch activity remained strong in the tip region, including in the centroacinar/terminal duct cells, Notch signaling appeared to be negatively regulated in the acinar cells; no Hes1-expressing cells were detected at this stage and the Notch inhibitor Numb/Numb1 was preferentially observed in acinar cells (Yoshida *et al.* 2003). Thus, the formation of a boundary between the Notch-active and Notch-inactive cell types potentially plays a pivotal role in the determination of the distal ductal and acinar cell fates, thereby maintaining the acinar structures. Based on this hypothesis, we focused on the centroacinar cells located at the junction between the acinar and ductal structures. In this study, we believe that we have provided the first evidence supporting the indispensable role of the Notch ligands in the maintenance of centroacinar cells and acinar structures.

The lack of specific markers has prevented us from elucidating how centroacinar cells are formed and maintained and how the acinar structures are constructed during embryogenesis; however, we defined the centroacinar cells as the $Sox9^{+}Hnf1\beta^{-}CD133^{+}ALDH1^{+}DBA^{-}$ cells expressing the Notch ligands Dll1 and Jag1 at e18.5 and showed that these cells were lost in Dll1/Jag1 cKO mice. We found that the $Hnf1\beta^{-}amylase^{-}$ epithelial cells in primitive acinar structures at e15.5, during the construction of acinar structures, were highly proliferative. Notably, they frequently exhibited the expression of Hes1, a typical target of Notch signaling. In the Dll1/Jag1 cKO mice at e15.5, we detected a considerable number of $Hnf1\beta^{-}amylase^{-}$ cells, suggesting that the formation of primitive acinar structures could be initiated in the absence of the Notch ligands. However, the $Hnf1\beta^{-}amylase^{-}$ cells did not proliferate efficiently and were eliminated through apoptosis, leading to abrogated acinar structures associated with the loss of centroacinar cells in the mutant mice. Although the lack of specific cell markers makes it currently impossible to precisely trace the fate of the $Hnf1\beta^{-}amylase^{-}$ cells, we speculated that this cell population is the best candidate for the centroacinar/terminal ductal cell progenitors.

We showed that the expression of Sox9 was reduced in the Notch ligand-deficient mice, which was consistent with the results of a previous report concerning the Notch–Sox9 axis (Shih *et al.* 2012). Although this has not been clearly delineated, the acinar structures of the Sox9-depleted mutant obtained using the Pdx1-Cre line, in which genetic deletion is mediated by Cre recombinase driven by the Pdx1 promoter, appeared very similar to those of the Dll1/Jag1 cKO mice or the Hes1-deficient mice, in which vacant spaces remained at e18.5 (Seymour *et al.* 2007). Considering that the expression of the Notch ligands remained strong in the centroacinar cells, one may naturally assume that the activated Notch–Sox9 axis in this region, particularly that of the $Hnf1\beta^{-}amylase^{-}$ cells, functions in proper acinar construction and the maintenance of centroacinar cells. In addition, another mutant phenotype of the Dll1/Jag1 cKO mice was the progressive dilatation of the main/interlobular ducts. This condition was detected at e18.5 and was more severe at P3. The inducible Cre-mediated Sox9 knockout caused defects in the formation of ductal cell cilia (Shih *et al.* 2012), resulting in a dilated ductal phenotype similar to that found in the current study. Thus, the reduc-

tion of Sox9 expression is also likely the key mechanism underlying the ductal dilatation phenotype in the Dll1/Jag1 cKO mice.

Experimental procedures

Mice

The protocol for generating mice bearing a floxed allele of *Dll1* (*Dll1*^{lox}) or *Jag1* (*Jag1*^{lox}) was described previously (Hozumi *et al.* 2004; Brooker *et al.* 2006). To obtain the conditional deletion of the *Dll1* and/or *Jag1* genes within the pancreatic epithelial cells, we used *Ptf1a-Cre* knock-in mice (Kawaguchi *et al.* 2002). The expression of neither Dll1 nor Jag1 was detected in the developing pancreas of the Dll1/Jag1 cKO mice, resulting in the disappearance of the cleaved fragments of Notch receptors. Mice lacking the *Ptf1a-Cre allele* were used as controls for the *Notch ligand* cKO mice, except in the experiment in which X-gal staining was used to monitor gene deletion by the Cre recombinase encoded by the CAG-CAT-lacZ transgene (Araki *et al.* 1995). The generation of the *Hes1* heterozygote mice was described previously (Ishibashi *et al.* 1995), and these mice were inbred to obtain knockout embryos (Fukuda *et al.* 2006). All of the mice were maintained in specific pathogen-free conditions, and all of the mouse experiments were approved by the university's Animal Experimentation Committee (Tokai University, Kanagawa, Japan).

Immunolabeling and statistical analysis

Immunolabeling was carried out as previously described (Furuyama *et al.* 2011). Briefly, dissected tissues were fixed using ice-cold 4% paraformaldehyde, paraffin-embedded and cut into 2- to 3-μm-thick sections. Immunolabeling was conducted using the primary antibodies listed in Table S2 in Supporting information. For immunofluorescent staining, the bound antibodies were visualized using fluorescent secondary antibodies (Table S3 in Supporting Information), and the samples were examined using fluorescence microscopy (BZ-9000, Keyence). TUNEL staining (Promega) was carried out according to the manufacturer's instructions. To estimate the frequency of PHH3- or TUNEL-positive cells in the pancreatic epithelium, whole pancreatic tissues obtained from embryos were cut into 2-μm-thick serial sections, the PHH3^{+} or TUNEL^{+} cells were counted, and their ratios to all of the epithelial cells were calculated for every section. The data were expressed as the mean values ± SD.

Flow cytometry

The PE-conjugated anti-CD133 antibody and biotinylated DBA lectin were purchased from eBioscience and Vector, respectively. APC-conjugated anti-EpCAM antibodies were purchased from BioLegend. The Aldefluor kit (StemCell Technologies) was used according to the manufacturer's instructions. Pancreatic buds obtained from e18.5 embryos were dissociated using 0.05% trypsin/0.53 mM EDTA (Wako) for 20 minutes at 37 °C and were triturated gently using a pipette. Single-cell suspensions were incubated with several antibodies for 15 minutes on ice. After washing, flow cytometric analysis and sorting were conducted using a FACSCalibur system and a FACSAria system, respectively (BD Biosciences).

Acknowledgements

We are grateful to T. Sudo and J. Miyazaki for the generous gifts of the anti-Hes1 antibody and the CAG-CAT-lacZ mice and to M. Tsujimoto, A. Fukuda, K. Hirano, A. Sakai, M. Tanigawa, K. Ishikawa, Y. Okada, N. Kawabe, T. Saso, K. Okamoto-Furuta, H. Kohda, K. Tokunaga, T. Shirao and K. Mitsunaga for their technical assistance. We also thank Y. Inagaki, K. Furuyama and T. Masui for helpful discussions.

Author contributions

YN, YK and KH conceived the concept and design of the study; YN, NN, SG, YS, MY, KA and KH performed the experiments and acquired the data; KA, HY and RK provided materials; TM and SH contributed to supervising the study; and YK and KH wrote the manuscript, with contributions from all of the authors.

References

Afelik, S., Qu, X., Hasrouni, E., Bukys, M.A., Deering, T., Nieuwoudt, S., Rogers, W., Macdonald, R.J. & Jensen, J. (2012) Notch-mediated patterning and cell fate allocation of pancreatic progenitor cells. *Development* **139**, 1744–1753.

Ahnfelt-Rønne, J., Jørgensen, M.C., Klinck, R., Jensen, J.N., Füchtbauer, E.M., Deering, T., MacDonald, R.J., Wright, C.V., Madsen, O.D. & Serup, P. (2012) Ptf1a-mediated control of Dll1 reveals an alternative to the lateral inhibition mechanism. *Development* **139**, 33–45.

Araki, K., Araki, M., Miyazaki, J. & Vassalli, P. (1995) Site-specific recombination of a transgene in fertilized eggs by transient expression of Cre recombinase. *Proc. Natl Acad. Sci. USA* **92**, 160–164.

Artavanis-Tsakonas, S., Rand, M.D. & Lake, R.J. (1999) Notch signaling: cell fate control and signal integration in development. *Science* **284**, 770–776.

Ashizawa, N., Sakai, T., Yoneyama, T., Naora, H. & Kinoshita, Y. (2005) Three-dimensional structure of peripheral exocrine gland in rat pancreas: reconstruction using transmission electron microscopic examination of serial sections. *Pancreas* **31**, 401–404.

Brooker, R., Hozumi, K. & Lewis, J. (2006) Notch ligands with contrasting functions: Jagged1 and Delta1 in the mouse inner ear. *Development* **133**, 1277–1286.

Fujikura, J., Hosoda, K., Kawaguchi, Y., *et al.* (2007) Rbp-j regulates expansion of pancreatic epithelial cells and their differentiation into exocrine cells during mouse development. *Dev. Dyn.* **236**, 2779–2791.

Fukuda, A., Kawaguchi, Y., Furuyama, K., Kodama, S., Horiguchi, M., Kuhara, T., Koizumi, M., Boyer, D.F., Fujimoto, K., Doi, R., Kageyama, R., Wright, C.V. & Chiba, T. (2006) Ectopic pancreas formation in Hes1 -knockout mice reveals plasticity of endodermal progenitors of the gut, bile duct, and pancreas. *J. Clin. Invest.* **116**, 1484–1493.

Furuyama, K., Kawaguchi, Y., Akiyama, H., *et al.* (2011) Continuous cell supply from a Sox9-expressing progenitor zone in adult liver, exocrine pancreas and intestine. *Nat. Genet.* **43**, 34–41.

Golson, M.L., Le Lay, J., Gao, N., Brämswig, N., Loomes, K.M., Oakey, R., May, C.L., White, P. & Kaestner, K.H. (2009) Jagged1 is a competitive inhibitor of Notch signaling in the embryonic pancreas. *Mech. Dev.* **126**, 687–699.

Horn, S., Kobberup, S., Jørgensen, M.C., Kalisz, M., Klein, T., Kageyama, R., Gegg, M., Lickert, H., Lindner, J., Magnuson, M.A., Kong, Y.Y., Serup, P., Ahnfelt-Rønne, J. & Jensen, J.N. (2012) Mind bomb 1 is required for pancreatic β-cell formation. *Proc. Natl Acad. Sci. USA* **109**, 7356–7361.

Hosokawa, S., Furuyama, K., Horiguchi, M., Aoyama, Y., Tsuboi, K., Sakikubo, M., Goto, T., Hirata, K., Tanabe, W., Nakano, Y., Akiyama, H., Kageyama, R., Uemoto, S. & Kawaguchi, Y. (2015) Impact of Sox9 dosage and Hes1-mediated notch signaling in controlling the plasticity of adult pancreatic duct cells in mice. *Sci. Rep.* **5**, 8518.

Hozumi, K., Negishi, N., Suzuki, D., Abe, N., Sotomaru, Y., Tamaoki, N., Mailhos, C., Ish-Horowicz, D., Habu, S. & Owen, M.J. (2004) Delta-like 1 is necessary for the generation of marginal zone B cells but not T cells *in vivo*. *Nat. Immunol.* **5**, 638–644.

Immervoll, H., Hoem, D., Steffensen, O.J., Miletic, H. & Molven, A. (2011) Visualization of CD44 and CD133 in normal pancreas and pancreatic ductal adenocarcinomas: non-overlapping membrane expression in cell populations positive for both markers. *J. Histochem. Cytochem.* **59**, 441–455.

Ishibashi, M., Ang, S.L., Shiota, K., Nakanishi, S., Kageyama, R. & Guillemot, F. (1995) Targeted disruption of mammalian hairy and Enhancer of split homolog-1 (HES-1) leads to up-regulation of neural helix-loop-helix factors, premature neurogenesis, and severe neural tube defects. *Genes Dev.* **9**, 3136–3148.

Kawaguchi, Y., Cooper, B., Gannon, M., Ray, M., MacDonald, R.J. & Wright, C.V. (2002) The role of the transcriptional regulator Ptf1a in converting intestinal to pancreatic progenitors. *Nat. Genet.* **32**, 128–134.

Kopinke, D., Brailsford, M., Pan, F.C., Magnuson, M.A., Wright, C.V. & Murtaugh, L.C. (2012) Ongoing Notch signaling maintains phenotypic fidelity in the adult exocrine pancreas. *Dev. Biol.* **362**, 57–64.

Kopp, J.L., Dubois, C.L., Schaffer, A.E., Hao, E., Shih, H.P., Seymour, P.A., Ma, J. & Sander, M. (2011) Sox9+ ductal cells are multipotent progenitors throughout development but do not produce new endocrine cells in the normal or injured adult pancreas. *Development* **138**, 653–665.

Oshima, Y., Suzuki, A., Kawashimo, K., Ishikawa, M., Ohkohchi, N. & Taniguchi, H. (2007) Isolation of mouse pancreatic ductal progenitor cells expressing CD133 and c-Met by flow cytometric cell sorting. *Gastroenterology* **132**, 720–732.

Pan, F.C. & Wright, C. (2011) Pancreas organogenesis: from bud to plexus to gland. *Dev. Dyn.* **240**, 530–565.

Reichert, M. & Rustgi, A.K. (2011) Pancreatic ductal cells in development, regeneration, and neoplasia. *J. Clin. Invest.* **121**, 4572–4578.

Rovira, M., Scott, S.G., Liss, A.S., Jensen, J., Thayer, S.P. & Leach, S.D. (2010) Isolation and characterization of centroacinar/terminal ductal progenitor cells in adult mouse pancreas. *Proc. Natl Acad. Sci. USA* **107**, 75–80.

Seymour, P.A., Freude, K.K., Tran, M.N., Mayes, E.E., Jensen, J., Kist, R., Scherer, G. & Sander, M. (2007) SOX9 is required for maintenance of the pancreatic progenitor cell pool. *Proc. Natl Acad. Sci. USA* **104**, 1865–1870.

Shih, H.P., Kopp, J.L., Sandhu, M., Dubois, C.L., Seymour, P.A., Grapin-Botton, A. & Sander, M. (2012) A Notch-dependent molecular circuitry initiates pancreatic endocrine and ductal cell differentiation. *Development* **139**, 2488–2499.

Yoshida, T., Tokunaga, A., Nakao, K. & Okano, H. (2003) Distinct expression patterns of splicing isoforms of mNumb in the endocrine lineage of developing pancreas. *Differentiation* **71**, 486–495.

Zhou, Q., Law, A.C., Rajagopal, J., Anderson, W.J., Gray, P.A. & Melton, D.A. (2007) A multipotent progenitor domain guides pancreatic organogenesis. *Dev. Cell* **13**, 103–114.

Zong, Y., Panikkar, A., Xu, J., Antoniou, A., Raynaud, P., Lemaigre, F. & Stanger, B.Z. (2009) Notch signaling controls liver development by regulating biliary differentiation. *Development* **136**, 1727–1739.

Received: 20 January 2015
Accepted: 3 March 2015

Supporting Information

Additional Supporting Information may be found in the online version of this article at the publisher's web site:

Figure S1 Centroacinar cells are located in the most distal $Sox9^{+}$ ductal-tree by whole-mount immunofluorescence at e18.5.

Figure S2 Electron microscopic analysis of fetal pancreas.

Figure S3 Quantitative analysis of anti-apoptotic gene transcripts in Notch ligand-deficient fetal pancreas.

Figure S4 $Hnf1\beta^{-}amylase^{-}$ cells in acinar structure at e15.5 expressed both Dll1 and Jag1.

Figure S5 Construction of acinar structure in Hes1-deficient pancreas.

Figure S6 Characterization of sorted pancreatic epithelial cells of the control mice at e18.5.

Figure S7 Impairment of newborn pancreas in Dll1- and Jag1-deficient condition.

Appendix S1 Experimental procedures

Table S1 Quantification of cells expressing Notch-related molecules and cell-surface markers in the $Sox9^{+}$ expression domains at e18.5

Table S2 Primary antibodies and lectin used for immunolabeling

Table S3 Secondary antibodies used for immunolabeling

Table S4 Primers used for real-time PCR